frontiers | Research Topics

Meta-scenario computation for social-geographical sustainability

Edited by
Jun Yang, Bing Xue, Xiangming Xiao, Jianhong Xia and Xinli Ke

Published in
Frontiers in Environmental Science
Frontiers in Ecology and Evolution
Frontiers in Earth Science

FRONTIERS EBOOK COPYRIGHT STATEMENT

The copyright in the text of individual articles in this ebook is the property of their respective authors or their respective institutions or funders. The copyright in graphics and images within each article may be subject to copyright of other parties. In both cases this is subject to a license granted to Frontiers.

The compilation of articles constituting this ebook is the property of Frontiers.

Each article within this ebook, and the ebook itself, are published under the most recent version of the Creative Commons CC-BY licence. The version current at the date of publication of this ebook is CC-BY 4.0. If the CC-BY licence is updated, the licence granted by Frontiers is automatically updated to the new version.

When exercising any right under the CC-BY licence, Frontiers must be attributed as the original publisher of the article or ebook, as applicable.

Authors have the responsibility of ensuring that any graphics or other materials which are the property of others may be included in the CC-BY licence, but this should be checked before relying on the CC-BY licence to reproduce those materials. Any copyright notices relating to those materials must be complied with.

Copyright and source acknowledgement notices may not be removed and must be displayed in any copy, derivative work or partial copy which includes the elements in question.

All copyright, and all rights therein, are protected by national and international copyright laws. The above represents a summary only. For further information please read Frontiers' Conditions for Website Use and Copyright Statement, and the applicable CC-BY licence.

ISSN 1664-8714
ISBN 978-2-83251-590-7
DOI 10.3389/978-2-83251-590-7

About Frontiers

Frontiers is more than just an open access publisher of scholarly articles: it is a pioneering approach to the world of academia, radically improving the way scholarly research is managed. The grand vision of Frontiers is a world where all people have an equal opportunity to seek, share and generate knowledge. Frontiers provides immediate and permanent online open access to all its publications, but this alone is not enough to realize our grand goals.

Frontiers journal series

The Frontiers journal series is a multi-tier and interdisciplinary set of open-access, online journals, promising a paradigm shift from the current review, selection and dissemination processes in academic publishing. All Frontiers journals are driven by researchers for researchers; therefore, they constitute a service to the scholarly community. At the same time, the *Frontiers journal series* operates on a revolutionary invention, the tiered publishing system, initially addressing specific communities of scholars, and gradually climbing up to broader public understanding, thus serving the interests of the lay society, too.

Dedication to quality

Each Frontiers article is a landmark of the highest quality, thanks to genuinely collaborative interactions between authors and review editors, who include some of the world's best academicians. Research must be certified by peers before entering a stream of knowledge that may eventually reach the public - and shape society; therefore, Frontiers only applies the most rigorous and unbiased reviews. Frontiers revolutionizes research publishing by freely delivering the most outstanding research, evaluated with no bias from both the academic and social point of view. By applying the most advanced information technologies, Frontiers is catapulting scholarly publishing into a new generation.

What are Frontiers Research Topics?

Frontiers Research Topics are very popular trademarks of the *Frontiers journals series*: they are collections of at least ten articles, all centered on a particular subject. With their unique mix of varied contributions from Original Research to Review Articles, Frontiers Research Topics unify the most influential researchers, the latest key findings and historical advances in a hot research area.

Find out more on how to host your own Frontiers Research Topic or contribute to one as an author by contacting the Frontiers editorial office: frontiersin.org/about/contact

Meta-scenario computation for social-geographical sustainability

Topic editors

Jun Yang — Northeastern University, China

Bing Xue — Research Institute for Sustainability – Helmholtz Centre Potsdam, Germany

Xiangming Xiao — University of Oklahoma, United States

Jianhong Xia — Curtin University, Australia

Xinli Ke — Huazhong Agricultural University, China

Citation

Yang, J., Xue, B., Xiao, X., Xia, J., Ke, X., eds. (2023). *Meta-scenario computation for social-geographical sustainability*. Lausanne: Frontiers Media SA.

doi: 10.3389/978-2-83251-590-7

Table of contents

09 Editorial: Meta-scenario computation for social-geographical sustainability
Bing Xue, Yaotian Xu, Xiangming Xiao, Jianhong (Cecilia) Xia, Xinli Ke and Jun Yang

15 Spatiotemporal Pattern Evolution of Urban Ecosystem Resilience Based on "Resistance-Adaptation-Vitality": A Case Study of Nanchang City
Linghua Duo, Yanan Li, Ming Zhang, Yuxi Zhao, Zhenhua Wu and Dongxue Zhao

35 Spatial Distribution and Evolution of Ancient Settlements From the Neolithic to the Bronze Age in Dalian Area, China
Liang Liu, Fangfang Liu, Wei Zhang and Zhaofeng Xu

48 Spillover Effects of Built-Up Land Expansion Under Ecological Security Constraint at Multiple Spatial Scales
Dan Yang, Yuanyuan Lou, Pengyan Zhang and Ling Jiang

60 Spatial-Temporal Patterns of Network Structure of Human Settlements Competitiveness in Resource-Based Urban Agglomerations
Wenbo Yu, Jun Yang, Dongqi Sun, Huisheng Yu, Yao Yao, Xiangming Xiao and Jianhong(Cecilia) Xia

76 Research on the Regional Environmental Impact and Risk Assessment Affected by Mineral Resource Development: A Case Study of the Taojia River Watershed in Hunan
Hongying Cao, Ziwei Wang, Xiaoyong Liao, You Li and Yongbing Zhu

89 Impact of Rapid Transit Development on Urban Economic Growth: An Empirical Study of the Urban Agglomerations in China
Jinhuang Mao, Qianwen Tian and Chengpeng Lu

104 Spatio-Temporal Evolution and Quality Analysis of Construction Land in Urban Agglomerations in Central China
Qimeng Ning, Xiao Ouyang and Shaobo Liu

115 Dynamic Change of Vegetation Index and Its Influencing Factors in Alxa League in the Arid Area
Peng Zhou, Dongxue Zhao, Xiao Liu, Linghua Duo and Bao-Jie He

129 Evaluation of Cropland System Resilience to Climate Change at Municipal Scale Through Robustness, Adaptability, and Transformability: A Case Study of Hubei Province, China
Mingyan Yan, Bohan Yang, Siyu Sheng, Xiangyu Fan, Xiaoyun Li and Xinhai Lu

144 How Does Different Cropland Expansion Trajectories Affect Cropland Fragmentation? Insights From Three Urban Agglomerations in Yangtze River Economic Belt, China
Liye Wang, Siyu Zhang, Yifan Xie, Yanfang Liu and Yaolin Liu

157 Spatiotemporal Variations of Human Pressure on Key Biodiversity Areas in the Qinghai–Tibet Plateau: A Comparative Analysis
Yuxi Zeng, Ling-en Wang and Linsheng Zhong

169 Exploring Spatial Distributions and Formation Factors of Brownfields in China: From Macro-Scales
Xinjia Zhang, Yang Song, Sitong Qian, Shijun Wang and Donghang Wu

181 Energy Consumption Connection of Industrial Sector Based on Industrial Link Theory: A Case Study of China
Jinwen Xia, Xiaojun Liu, Dongqi Sun, Chenxi Li and Zhaofei Wang

193 Exotic Food, Food Environment, and Geographical Patterns: Big Data Analytics From Japanese Cuisine in China
Chuang Tian, Weixin Luan and Hui Wang

204 Impacts of Water Bodies on Microclimates and Outdoor Thermal Comfort: Implications for Sustainable Rural Revitalization
Yanyan Cheng, Xiao Liu, Zhi Zeng, Shengshuai Liu, Zhaoyu Wang, Xu Tang and Bao-Jie He

217 Quantifying the Temporal and Spatial Patterns of Ecosystem Services and Exploring the Spatial Differentiation of Driving Factors: A Case Study of Sichuan Basin, China
Chunguang Hu, Ziyi Wang, Jiaming Li, Huan Liu and Dongqi Sun

231 Education Equality and Its Influencing Factors for Migrant Children in the Compulsory Education Stage Based on Multi-Source Data: A Case Study of Dalian, China
Zhenchao Zhang, Weixin Luan, Chuang Tian, Min Su and Zeyang Li

241 On the Contributions of the Northeast Cold Vortex to the Formation and Evolution of Backflow Blizzard
Qi Yan, Jin Cui, Zhenghua Tan and Bao-Jie He

254 Analysis of the spatiotemporal mechanism of high temperature on residents' irritability in Beijing based on multiscale geographically weighted regression model
Huanchun Huang, Xuan Liu and Lijian Ren

269 Spatiotemporal relationship characteristic of climate comfort of urban human settlement environment and population density in China
Dahao Zhang, Chunshan Zhou, Yi Zhou and Bahram Zikirya

281 Spatial impact of urban expansion on lake surface water temperature based on the perspective of watershed scale
Linfeng Tang, Kun Yang, Chunxue Shang, Zongqi Peng and Yi Luo

293 Research on temporal and spatial evolution of land use and landscape pattern in Anshan City based on GEE
Yanhua Fu and Yalin Zhang

310 Commercial gentrification in China and its distribution, development, and correlates: The case of Chengdu
Qinran Yang, Yang Liu and Linchuan Yang

325 Combining spatial planning and ecosystem services value to assist ecological compensation decision-making—A case study of Yangtze River Delta ecological barrier, China
Ziyi Wang, Yu Wang, Zihang Zhou, Fan Yu, Debin Ma and Jiaming Li

340 Resource-based cities: Spatial structure and evolutionary identification based on nighttime light images
Shuo Lu, Wenzhong Zhang, Jiaming Li and Shaohua Wang

356 Optimization of low-carbon land use in Chengdu based on multi-objective linear programming and the future land use simulation model
Ran Wu, Haifeng Lan, Yuxin Cao and Pingyi Li

373 Theoretical framework and research prospect of the impact of China's digital economic development on population
Chunshan Zhou, Dahao Zhang and Yu Chen

384 Seasonal differences in the dominant factors of surface urban heat islands along the urban-rural gradient
Jiaxing Xin, Jun Yang, Ling-en Wang, Cui Jin, Xiangming Xiao and Jianhong (Cecilia) Xia

400 Spatio–temporal evolution and factors of climate comfort for urban human settlements in the Guangdong–Hong Kong–Macau Greater Bay Area
Chunshan Zhou, Dahao Zhang, Yongwang Cao, Yunzhe Wang and Guojun Zhang

418 Study on the dynamic evolution and synergistic relationship between urbanization and eco-efficiency through the selection of 76 agricultural counties and districts in Liaoning province as research units
Yanpeng Gao, Chunyao Guo and Ye Wei

435 Towards innovation resilience through urban networks of co-invention: A case study of cities in China
Haitao Ma, Xuanfang Xu, Xiaozhen Li and Jingyu Liu

450 Node-place model extended by system support: Evaluation and classification of metro station areas in Tianfu new area of Chengdu
Jiexi Ma, Zhongwei Shen, Yi Xie, Pengpeng Liang, Bingjie Yu and Li Chen

467 Spatiotemporal changes of ecosystem service trade-offs under the influence of forest conservation project in Northeast China
Guangliang Jia, Yulin Dong, Siyu Zhang, Xingyuan He, Haifeng Zheng, Yujie Guo, Guoqiang Shen and Wei Chen

480 Spatiotemporal mechanism of urban heat island effects on human health—Evidence from Tianjin city of China
Yifang Dai and Tongtong Liu

489 Spatiotemporal heterogeneity of primary and secondary school student distribution in Liaoning Province, China from 2010 to 2020
Wanbo Liu, Zhenghui Zhu and Ling-en Wang

506 Research on the spatial correlation and drivers of industrial agglomeration and pollution discharge in the Yellow River Basin
Yuming Qin, Hao Zhang, Huimin Zhao, Di Li, Ye Duan and Zenglin Han

523 Spatiotemporal analysis of land use changes and their trade-offs on the northern slope of the Tianshan Mountains, China
Haitao Ma

538 TOD and vibrancy: The spatio-temporal impacts of the built environment on vibrancy
Bingjie Yu, Xu Cui, Hong Li, Pinyang Luo, Runze Liu and Tian Yang

555 Spatiotemporal differences of land use pattern between mountainous areas and basin areas at township scale: A case study of Yuxi City
Li Wu, Jing Zhou, Binggeng Xie, Sizhong Yang and Jingzhong Li

570 Spatially varying impacts of the built environment on physical activity from a human-scale view: Using street view data
Pinyang Luo, Bingjie Yu, Pengfei Li and Pengpeng Liang

589 Exploring the cooling effect of urban parks based on the ECOSTRESS land surface temperature
Yihui Liu, Xinliang Xu, Fei Wang, Zhi Qiao, Hongmin An, Dongrui Han and Jie Luo

604 Spatio-temporal distribution characteristics and influencing factors of drought in the Liaohe river basin, China
Yuanshan Gong

615 Spatial-temporal changes of land use/cover change and habitat quality in Sanjiang plain from 1985 to 2017
Shanhe Jin, Xin Liu, Jiajia Yang, Junchao Lv, Yuchao Gu, Jishun Yan, Ruiyang Yuan and Yudi Shi

627 Quantitative estimation of sentinel-1A interferometric decorrelation using vegetation index
Jianping Pan, Ruiqi Zhao, Zhengxuan Xu, Zhuoyan Cai and Yuxin Yuan

643 Eco-environmental constraints, economic incentives, and spatiotemporal variations of construction land use efficiency in regional China
Jiawei Wu, Chonggang Liu and Wei Sun

660 Built environment and travel behavior in rural areas: A scientometric literature review
Yibin Ao, Mingyang Li, Xuan Ding, Junjie Zheng, Shan Xiao, Shulin Deng, Zijun Zhang, Yan Wang, Tong Wang and Igor Martek

672 Period-oriented spatial comparative evaluation of biodiversity conservation effectiveness in China
Ziqi Chen, Zhaoli Liu, Guanglei Hou, Kaikai Dong, Yanhong Zhang and Changbao Yang

683 A quantitative model based on grey theory for sea surface temperature prediction
Fanyu Meng, Jilin Gu, Ling-en Wang, Zhibin Qin, Mingyao Gao, Junhong Chen and Xueming Li

700 Spatial distribution and influencing factors of mountainous geological disasters in southwest China: A fine-scale multi-type assessment
Bo Shu, Yang Chen, Majid Amani-Beni and Ruizhi Zhang

715 Do hospital and rail accessibility have a consistent influence on housing prices? Empirical evidence from China
Kaida Chen, Hanliang Lin, Fangxiao Cao, Yan Han, Shuying You, Oliver Shyr, Yichen Lu and Xiaodi Huang

739 High-speed rail effects on station area-level business commercial agglomeration: Evidence from 110 stations in China
Pengpeng Liang, Xu Cui, Mao Lin, Tian Yang and Bo Wu

755 Historical reconstruction of aquatic vegetation of typical lakes in Northeast China based on an improved CA-Markov model
Guanglei Hou, Haobin Zhang, Zhaoli Liu, Ziqi Chen and Yakun Cao

770 Evaluation on the urban green space layout in the central city of Yuxi based on big data
Jing Zhou, Maoxiao Yang, Jing Chai and Li Wu

785 Evaluating the performance of different thermal indices on quantifying outdoor thermal sensation in humid subtropical residential areas of China
Kunming Li, Xiao Liu and Ying Bao

797 Mapping the grassland quality of the flooded plain based on Jilin-01 images with a red-edge spectral band
Ziqi Chen, Yanhong Zhang, Peng Zang, Zhaoli Liu and Wenbin Zhao

807 A quantitative enhanced assessment for ancient landslide reactivation risk considering cross-time scale joint response mechanism
Zixi Yang, Tingchen Wu, Chao E, Xiao Xie, Leiqi Tan and Xinxi Jiang

826 Construction of the Hainan Free Trade Port from the perspective of regional cultural development
Chunliang Xiu and Tong Li

839 Classifying the surrounding rock of tunnel face using machine learning
Shubao Song, Guangchun Xu, Liu Bao, Yalong Xie, Wenlong Lu, Hongfeng Liu and Wanqi Wang

849 The inversion modeling and aboveground biomass mapping of withered grass changes in the western grassland of Northeast China
Peng Zang, Yanhong Zhang, Ziqi Chen, Guanglei Hou, Zhaoli Liu and Xingchang Lu

frontiers | Frontiers in Environmental Science

TYPE Editorial
PUBLISHED 23 January 2023
DOI 10.3389/fenvs.2023.1143374

Check for updates

OPEN ACCESS

EDITED AND REVIEWED BY
Alexander Kokhanovsky,
German Research Centre for Geosciences, Germany

*CORRESPONDENCE
Bing Xue,
xuebing@iae.ac.cn
Jun Yang,
yangjun8@mail.neu.edu.cn

SPECIALTY SECTION
This article was submitted to Environmental Informatics and Remote Sensing, a section of the journal Frontiers in Environmental Science

RECEIVED 12 January 2023
ACCEPTED 13 January 2023
PUBLISHED 23 January 2023

CITATION
Xue B, Xu Y, Xiao X, Xia JC, Ke X and Yang J (2023), Editorial: Meta-scenario computation for social-geographical sustainability.
Front. Environ. Sci. 11:1143374.
doi: 10.3389/fenvs.2023.1143374

COPYRIGHT
© 2023 Xue, Xu, Xiao, Xia, Ke and Yang. This is an open-access article distributed under the terms of the Creative Commons Attribution License (CC BY). The use, distribution or reproduction in other forums is permitted, provided the original author(s) and the copyright owner(s) are credited and that the original publication in this journal is cited, in accordance with accepted academic practice. No use, distribution or reproduction is permitted which does not comply with these terms.

Editorial: Meta-scenario computation for social-geographical sustainability

Bing Xue[1,2]*, Yaotian Xu[1,3], Xiangming Xiao[4], Jianhong (Cecilia) Xia[5], Xinli Ke[6] and Jun Yang[7,8]*

[1]Institute of Applied Ecology, Chinese Academy of Sciences, Shenyang, China, [2]Institute for Advanced Sustainability Studies (IASS) Potsdam, Potsdam, Germany, [3]University of the Chinese Academy of Sciences, Beijing, China, [4]Department of Microbiology and Plant Biology, University of Oklahoma, Norman, OK, United States, [5]School of Earth and Planetary Sciences (EPS), Curtin University, Perth, WA, Australia, [6]College of Public Administration, Huazhong Agricultural University, Wuhan, China, [7]Human Settlements Research Center, Liaoning Normal University, Dalian, China, [8]Jangho Architecture College, Northeastern University, Shenyang, China

KEYWORDS

social-geographical system, sustainability, human-natural system, geo-computation, scenario analysis, data-driven

Editorial on the Research Topic
Meta-scenario computation for social-geographical sustainability

Introduction

A socio-geographical system is a highly complex, coupled, open, and giant system (Pickett et al., 2011; Cui et al., 2019). In this system, both the space of human economic production and social life activities and the space of the natural environment form a diverse flow-based network of elements and system structures through material, information, capital, and value flows (Luo et al., 2021). With the development of information technology, especially in the context of rapid development of industrialization, urbanization, and digitalization, the organization of material circulation, energy consumption, and information flow of the social-geographic system also undergo different degrees of changes (Cui, 2022; Su et al., 2022), and the multi-dimensional, multi-structural, multi-level, and multi-element relationships within and among the system become more complex (Moore et al., 2022). The social geographic system exhibited a high level of complexity in both space and time, and the dynamics of its changes and mutations reveal non-linear behavior (Moroni and Cozzolino, 2019; Zhang et al., 2022). These changes and mutations could further impact the geographical setting, which serves as the foundation for economic and production activities (Magalhães et al., 2023). Similarly, the organizational form, strategic path, and goal vision of industrial activities react to the operation and performance of the social-geographical system, which brings about a series of socioeconomic and environmental effects that extend across time and space scales, and they have a profound impact on the government decision-making process and the efficiency with which it operates (Gambarotto et al., 2022; Wang et al., 2022). For example, the trend of urbanization leads to the loss of agriculture and ecological land, which creates danger for both the preservation of ecosystems and the ability to ensure adequate food supplies (Qiao and Huang, 2022; Shi et al., 2022).

Today, understanding the interactive coupling between social systems dominated by human activities and geographical systems dominated by environmental and ecological evolution is a key scientific component for advancing and achieving sustainable development (Mackinnon et al., 2019). Therefore, sustainable development in the perspective of complex social geographic systems requires the promotion of cross-innovation and integration research of multidisciplinary technological approaches in the context of new and changing times (He et al., 2022). In particular, we need to conduct interdisciplinary and method integration research based on data-driven technologies, so as to promote integrated system development of disciplinary knowledge and decision support (Kim et al., 2022; Liu et al., 2023). For example, to build a new knowledge system that is based on spatio-temporal big data, with computational science as the core, combined with new technologies such as geographic cloud, artificial intelligence, deep learning, and digital twinning, and is compatible with cross-disciplinary methods such as information science, and industrial ecology (Stratigea et al., 2015; Ahad et al., 2020; Said and Tolba, 2021). In addition, there is also an urgent need to carry out case experience summaries and refine new development directions to promote the cognitive and adaptive management of the complexity of social geographic systems and support the construction of a community for a shared future of humanity (Xue et al., 2020; Aigwi et al., 2023).

Therefore, we organized the Research Topic "Meta-Scenario Computation for Social-Geographical Sustainability", under which a total of 59 articles from 248 authors were published and have received more than 47 k views till 10 Jan 2023, which shows the broad interest of scholars and readers in this Research Topic. In the following section, we will summarize the key contributions of this Research Topic, and then present the conclusions and outlook.

Contributions and highlights

Data mining, modeling, and methodology development in new data contexts

The continuous development of digital technology and information technology provides new possibilities to re-observe and better understand the socio-geographical system (Xue et al., 2022), therefore, the development of new data sets, the development of new models, and the innovation and development of new methodologies in the new data context is a fundamental and critical area of socio-geographical system research. Under this research theme, we find more than ten valuable and interesting research papers. For example, Zhang et al. develop the first comprehensive dataset of known brownfield sites and their distributions in China, which contains 816 georeferenced brownfield records from 255 cities. Lu et al. use the new data generated from the nighttime light images to identify the spatial structure and evolutionary trends of the resource-based cities, which provides a fresh viewpoint on the stages of urban life cycle development. Yang et al. propose a mapping relationship between the POI data (points of interest) and commercial gentrification and then explain the development process and spatial correlations of commercial gentrification in Chengdu, Sichuan Province. In terms of modeling studies, Meng et al. propose a GM(1,1|sin) power model-based prediction approach for predicting sea surface temperature in conjunction with the genetic algorithm and the least-squares method; Pan et al. establish the two two-order linear quantitative models between Landsat8-derived normalized difference vegetation index and Sentinel-1A interferometric coherence in co- and cross-polarization, which solves the problem that Sentinel-1A decorrelation in the vegetated area is difficult to estimate prior to single-look complex interference. Chen et al. develop the grassland quality index (GQI) and map the grassland quality of the flooded plain based on Jilin-01 images with a red-edge spectral band, and this study is of practical significance for the timely and accurate monitoring of grassland growth, which is beneficial for the development of livestock husbandry and the protection of the ecological environment in northern China. Other interesting research was done by Zang et al. , they establish a remote-sensing estimation model for withered AGB (the aboveground biomass) in the dry-grass season, which could contribute to rapidly acquiring the amount of withered-grass biomass and improve the fire-warning efficiency. While Hou et al.'s study focus on aquatic vegetation models of lakes, they establish an improved CA-Markov model to reconstruct the historical potential distribution of aquatic vegetation in the two typical lakes in Northeast China during 1950s to 1960s. Machine learning is an important tool for data analysis in the new era, herein, Song et al. propose a machine learning-based automatic classification and dynamic prediction method of the surrounding rocks of the tunnel face using the data monitored by a computerized rock drilling trolley based on the intelligent mechanized construction process for drilling and blasting tunnels. Through a summary analysis of this theme, we find that with the new technology support, the analysis data of the social geographic system is more diversified, but also needs innovative and integrated analysis methods, and further form a new series of methodological analysis systems. Although there are many data analysis methods at present, the integrated analysis methods for complex systems still need to be further developed and improved at the application level.

Land use and change, land functions and their influencing factors and responses

The study of land use and its associated systems has been a traditional yet new topic in social geography systems, and it is not only an important scientific topic, but also a topic that involves development decisions, spatial planning, and other practical issues (Foley et al., 2005; Song et al., 2021). Under this research theme, our Research Topic has also attracted a large number of intriguing articles with diverse discussions based on various research viewpoints, spatial dimensions, and research methodologies. For instance, concerning urban land use and its related issues, Yang et al. quantitatively analyze the landscape ecological effects under the expansion of built-up land in the Yellow River basin based on multi-period Landsat satellite image data, and their study emphasizes the importance of spatial heterogeneity at different zoning scales in identifying the dynamic relationships between land expansion in built-up areas and ecological security, scientific planning of land resources, and mitigation of ecological and environmental crises. Ning et al. use remote sensing images combined with statistical methods to analyze the spatial and temporal patterns and quality levels of construction land expansion at different scales, taking the middle reaches of the Yangtze River urban agglomeration as the research object. Fu and Zhang focus on the main urban area of Anshan city of Liaoning province, where mining areas

are concentrated, and map the land use in 2008, 2014, and 2020 by using the Landsat TM/OLI surface reflectance data from the Google Earth Engine (GEE) platform and the random forest algorithm. One of the important values of their study is that the GEE-based random forest algorithm is found to exhibit high accuracy in land use classification; in contrast, Wu et al. study the change characteristics of carbon emissions from land use in Chengdu from 1990 to 2020 and then develop four low-carbon land use scenarios based on multi-objective linear programming and the future land use simulation model. In recent years, rural land systems have also gradually become a hot topic, especially in the context of rural revitalization as well as reverse urbanization (Trenberth, 2004; Gawith and Hodge, 2019). Under our Research Topic, we also received several valuable contributions concerning either land use in rural areas or arable land issues. Wang et al. evaluate the arable land expansion trajectories of three urban agglomerations in the Yangtze River Economic Zone and their impact on arable land fragmentation, emphasizing that arable land protection policies should pay attention to arable land expansion trajectories rather than just requiring the total arable land area to be in dynamic equilibrium. Using 75 townships in Yuxi City, Yunnan Province as an example, Wu et al. use an integrated land use/land cover change evaluation model and related analysis methods to analyze the changes in land use patterns in mountainous areas and basins during 1995–2018 and reveal the spatial differences and their influencing factors. Of course, there are also studies that focus on ecological land use or land structure and changes in natural systems. For example, to fully comprehend the dynamic dynamics of land use, Ma quantifies the spatiotemporal pattern of land use change and estimated trade-offs and synergies between dominant and recessive morphologies. Jin et al. use multi-source land use data and Google remote sensing data to explore land use change, spatial-temporal evolution of habitat quality, and driving variables impacting habitat quality change in Sanjiang Plain from 1985 to 2017. In summary, we would like to point out that the study of regional spillover effects and coupling relationships of different land use transformations should be strengthened in the future. Existing studies still focus more on single systems, such as urban systems, rural systems, or natural ecosystems, while the issue of cross-system land-use transitions and functions needs to be further strengthened.

Ecosystem, ecological resilience, and ecosystem-economic system interactions and relationships

Ecosystem services are a key reliance for sustainable human development, and the relationship between ecosystems and economic systems forms one of the cognitive foundations of the socio-geographic system (Sonter et al., 2020; Mandle et al., 2021). Within this research theme, Duo et al. explain the complex dynamic evolutionary mechanism of urban ecosystem resilience and develop a framework for quantitative measurement of urban ecological resilience in three dimensions (resistance, resilience, and vitality) which aims to provide a comprehensive evaluation of urban ecosystem resilience. Hu et al. construct a PCA-MGWR (principal component analysis - multi-scale geographically weighted regression) model to explore the temporal and spatial patterns of ecosystem services in the Sichuan Basin from 2000 to 2015 and explore the spatial variability of the driving factors. Trade-offs between ecosystem services are measures of the degree to which the differences between individual ecosystem services are changing (Bennett et al., 2009). Thus, Jia et al. investigate the spatiotemporal changes and determinants of ecosystem service trade-offs in various forest types after the implementation of the natural forest conservation project, using the Greater Khingan Mountains as an example. Ecological compensation is an important tool for optimizing ecosystem management from an economic policy perspective and an important tool for situational governance of socio-geographic systems (Wei et al., 2022; Xing et al., 2022). With this in mind, Wang et al. design a decision-making framework of ecological compensation by combining spatial planning and ecosystem service value accounting, which includes “Subject choice, Value accounting, Priority evaluation, Policy supply”, and they select 32 counties (districts) in the Yangtze River Delta region to test the framework and find that the implementation of ecological compensation slows down the urbanization process and promotes the increase of ecological space. However, given that the period-oriented comparative evaluation of biodiversity conservation success is the primary foundation for executing the transfer payment policy of ecological compensation (Gantioler et al., 2014; Hayes et al., 2022). Chen et al. propose a method to construct the period conservation effectiveness index and apply it to the spatial comparative assessment of Chinese biodiversity conservation effectiveness in three periods from 1990 to 2015. Such a study could provide a reference for global large-scale ecological compensation. In addition to this, we have received some studies on the evolution of natural ecosystems and climate systems. For example, Yan et al., analyze the characteristics of a backflow blizzard in Liaoning, China, and reveal the reasons behind the spatial heterogeneity of snowstorm intensity and duration. Zhou et al. uncover the dynamic change of vegetation index and its influencing factors in Alxa League in the Arid Area. It is worth mentioning that we have an article discussing the spatial and temporal variation of human pressures faced by key biodiversity areas; Zeng et al. analyze the spatiotemporal variation of human pressure on key biodiversity areas from 1990 to 2017 and compare it with the human pressure on national natural reserves through a case study of the Qinghai–Tibet Plateau, and the findings are expected to serve as a reference to formulate policies for the improvement of the effectiveness of conservation.

Built environment, habitat, and the mechanisms on human health, ecosystems, and climate change

The built environment and habitat system are the core dominant forces of the socio-geographic system and have the most complex system composition (Liu et al., 2022). Within this research theme, we collected several interesting an d inspired articles which combine detailed and reliable technical analysis with decision-support applicability. For example, Zhang et al. explore the spatiotemporal evolution characteristics of the climate comfort of the urban human settlement environment in China from 2000 to 2015, based on a three-level time scale of a year, a month, and a day using the temperature and humidity index and wind efficiency index, and their findings imply that the population density in the country is generally concentrated in the climate comfort areas. Xin et al. assess the seasonal differences in surface UHI (urban heating island), normalized differences in

vegetation index, built-up index, and water index and their relationships in Dalian City, Northeast China, and their findings could facilitate the rational layout of cities. Further, Dai and Liu establish an appraisal system to assess how and to what extent UHIs affect resident health, by taking Tianjin during 2006–2020 as an example, and their findings offer some decision-making guidance for the planning of healthy cities. A study done by Huang et al. shows us the spatiotemporal pattern of temperature's impact on residents' irritability using data from summer high-temperature measurements and an emotional health survey in Beijing, combined with remote sensing images and statistical yearbooks, while Li et al. evaluate the performance of different thermal indices on quantifying outdoor thermal sensation in humid subtropical residential areas of China. The authors argue that it is necessary to establish the thermal sensation ranges of humid subtropical areas of China. Zhou et al. investigate the spatiotemporal evolution and factors of climate comfort for urban human settlements in the Guangdong–Hong Kong–Macau Greater Bay Area, which provide data-driven guidelines for improving the climate comfort of urban human settlements, while Ao et al. focus on the rural built environment, performing a scientometrics literature review to understand the state-of-the-art interplay between the rural built environment and travel behaviors and to identify future research directions. We also include several articles that discuss microclimate and ecosystem or health responses. For example, Cheng et al. demonstrate the positive impact of water bodies on improving the thermal environment of a village and regulating its microclimate by quantifying the impact of morphological elements of the settlement on its microclimate, while Tang et al. uncover the spatial impact of urban expansion on lake surface water temperature base on the perspective of watershed scale, and Liu et al. explore the cooling effect of urban parks based on the ECOSTRESS (ECOsystem Spaceborne Thermal Radiometer Experiment on Space Station) land surface temperature data. We also note that there are other studies that focus on urban green spaces, the built environment, and their relationship to vitality. For example, Zhou et al. conduct a thermal analysis of crowd activities, service pressure analysis, and demand evaluation for the layout of green park space in the central urban area of Yuxi City in Yunnan province, Yu et al. study the spatial-temporal impacts of the built environment on vibrancy, and Luo et al. uncover the spatially varying impacts of the built environment on physical activity from a human-scale view by using the street view data. The above studies not only provide good intellectual contributions and discussion on their topics but also, it is particularly important to note that they have tried to introduce new data systems, such as POI big data, to enrich their studies, which reflects the new trend of current research (Xue et al., 2023).

Human activities, socio-cultural and environmental impacts and their sustainable development mechanisms

Human activities are the core dominant force of socio-geographical systems, and culture is an important driving force influencing the evolution of socio-geographical systems (Campari and Frank, 1995). At the same time, we also note that it remains an important research proposition to quantify the environmental and climate impacts of human socio-economic activities under socio-geographical systems. As the only article with archaeological ideas under this research theme, Liu et al. investigate the spatial distribution and evolution of ancient settlements from the Neolithic to the Bronze Age in the Dalian area, --China, and they find that such spatial distribution and evolution are influenced by the contemporary climate. Gao et al. study the dynamic evolution and synergistic relationship between urbanization and eco-efficiency through the selection of 76 agricultural counties and districts in Liaoning province as research units. In contrast, Wu et al. investigate the eco-environmental constraints, economic incentives, and spatiotemporal variations of construction land use efficiency in the Yangtze River Delta, China between 2000 and 2020, and they argue that proper policies should be tailored to specific places to coordinate construction land use, economic growth, and eco-environmental sustainability. We also received two valuable articles that discuss educational inequality and equity using multiple sources of data. One of them was done by Zhang et al., who discuss education equality and its influencing factors for migrant children in the compulsory education stage by taking Dalian City as a case study, and they call for attention to be paid to the spatial balance of educational resource allocation. Another article, done by Liu et al., discusses the spatiotemporal heterogeneity of primary and secondary school student distribution in Liaoning Province, China from 2010 to 2020, which provides important insights into the population and educational geography. We also received articles focusing on themes such as urban transportation, innovation networks, digital economy, industrial ecology, and regional culture. They either focus on methodological innovation or are problem-oriented and present some valuable conclusions and recommendations. For example, Mao et al. analyze the impact of rapid transit development on the urban economic growth of 220 cities in 19 urban agglomerations in China from 2008 to 2019 and examined the heterogeneity of the difference in market integration capability in promoting urban economic growth, Ma et al. constructed a theoretical analytical framework for intercity innovation network resilience and conducted a case study of 338 prefecture-level cities in China from 2017–2019, finding that the systemic resilience of Chinese urban innovation networks exhibits relatively low hierarchical and decreasing mismatch characteristics year by year. Zhou et al. propose a framework to discuss the impact of China's digital economic development on the population and find that the digital economy has a bidirectional influence on the population, and the digital economy can indirectly affect the spatial layout of the population attributes by giving digital connotations to regional elements. Xiu and Li summarize the internal relationship and mechanism of industrialization, business culture, and higher education that affect the development of modern industrial and commercial culture, and they argued that it is necessary to continue cultural construction, adapt to the requirements of the highest level of openness and realize the healthy development of the Hainan Free Trade Port. Furthermore, Qin et al. study the spatial correlation and drivers of industrial agglomeration and pollution discharge in the Yellow River basin. In contrast, Xia et al. investigate the energy consumption connection of the industrial sector based on the industrial link theory. In general, we find that the research on social subsystems is still not particularly adequate, and existing studies still focus on the economic-environmental system, while research on the socio-cultural system and its interaction with the geographical-environmental system is obviously lacking, and the data

accumulation and research in this area should be strengthened in the future.

Conclusion and outlook

Under this Research Topic, more than 59 articles have been published, ranging from technical articles on data methods and modeling studies to thematic articles focusing on land use, ecosystems, built environment, and society and culture, which fully illustrates the frontier and topicality of this research theme. However, we also note that there are still many challenges and difficulties to be overcome in the future, including but not limited to 1) strengthening data and methodological research, further developing new data systems with modern technical support, and creating more advanced analytical methodologies to achieve visualization and modeling interpretation of research processes and results; 2) strengthening research on the integration of socio-cultural themes with environmental-geographic themes, establishing a comprehensive analysis system for different time scales, different spatial scales, and different organizational scales of professional research system comprehensive analysis system, to realize the collaborative innovation research under the socio-geographic system and 3) strengthening using international case studies and promotion. The authors in this Research Topic are predominately Chinese authors, which reflects the popularity of this research theme in China, but international cooperation should be strengthened in the future to establish a broader academic community and jointly promote academic development.

Author contributions

BX, YX, and JY wrote the first version of this editorial. All the editors contributed to the final version of this editorial.

Acknowledgments

All the editors also thank the reviewers for their service, insight, and comments during the revisions of this Research Topic. The following grants are sincerely acknowledged: National Natural Science Foundation of China (41971166).

Conflict of interest

The authors declare that the research was conducted in the absence of any commercial or financial relationships that could be construed as a potential conflict of interest.

Publisher's note

All claims expressed in this article are solely those of the authors and do not necessarily represent those of their affiliated organizations, or those of the publisher, the editors and the reviewers. Any product that may be evaluated in this article, or claim that may be made by its manufacturer, is not guaranteed or endorsed by the publisher.

References

Ahad, M., Paiva, S., Tripathi, G., and Feroz, N. (2020). Enabling technologies and sustainable smart cities. *Sustain. Cities. Soc.* 61, 102301. doi:10.1016/j.scs.2020.102301

Aigwi, I., Duberia, A., and Nwadike, A. (2023). Adaptive reuse of existing buildings as a sustainable tool for climate change mitigation within the built environment. *Sustain. Energy. Technol. Assess.* 56, 102945. doi:10.1016/j.seta.2022.102945

Bennett, E. M., Peterson, G. D., and Gordon, L. J. (2009). Understanding relationships among multiple ecosystem services. *Ecol. Lett.* 12, 1394–1404. doi:10.1111/j.1461-0248.2009.01387.x

Campari, I., and Frank, A. (1995). "Cultural differences and cultural aspects in geographical information systems," in *Cognitive aspects of human-computer interaction for geographic information systems. NATO ASI series*. Editors T. L. Nyerges, D. M. Mark, R. Laurini, and M. J. Egenhofer (Dordrecht: Springer). doi:10.1007/978-94-011-0103-5_18

Cui, X., Fang, C., Liu, H., and Liu, X. (2019). Assessing sustainability of urbanization by a coordinated development index for an urbanization-resources-environment complex system: A case study of jing-jin-ji region, China. *Ind* 96, 383–391. doi:10.1016/j.ecolind.2018.09.009

Cui, Y. (2022). The coordinated relationship among industrialization, environmental carrying capacity and green infrastructure: A comparative research of beijing-tianjin-hebei region, China. *Environ. Dev.* 44, 100775. doi:10.1016/j.envdev.2022.100775

Foley, J. A., Defries, R., Asner, G. P., Barford, C., Bonan, G., Carpenter, S. R., et al. (2005). Global consequences of land use. *Science* 309 (5734), 570–574. doi:10.1126/science.1111772

Gambarotto, F., Magrini, C., Pedrini, G., and Stamboglis, N. (2022). How to map industrial waste metabolism at a geographical level? A proposal for a composite indicator. *J. Clean. Prod.* 379, 134681. doi:10.1016/j.jclepro.2022.134681

Gantioler, S., Rayment, M., ten Brink, P., McConville, A., Kettunen, M., and Bassi, S. (2014). The costs and socio-economic benefits associated with the Natura 2000 network. *Int. J. Sustain. Soc.* 6, 135. doi:10.1504/IJSSOC.2014.057894

Gawith, D., and Hodge, I. (2019). Focus rural land policies on ecosystem services, not agriculture. *Nat. Ecol. Evol.* 3, 1136–1139. doi:10.1038/s41559-019-0934-y

Hayes, T., Murtinho, F., Wolff, H., Salazar, J., López-Sandoval, M. F., and Salazar, J. (2022). Effectiveness of payment for ecosystem services after loss and uncertainty of compensation. *Nat. Sustain* 5, 81–88. doi:10.1038/s41893-021-00804-5

He, C., He, S., Mu, E., and Peng, J. (2022). Environmental economic geography: Recent advances and innovative development. *Geogr. Sustain.* 3 (2), 152–163. doi:10.1016/j.geosus.2022.05.002

Kim, B., Ogwal, M., Sande, E., Kiyingi, H., Serwada, D., and Hladik, W. (2022). Using geographical data and rolling statistics for diagnostics of respondent-driven sampling. *Soc. Netw.* 69, 74–83. doi:10.1016/j.socnet.2020.05.001

Liu, Q., Zhao, P., Zhang, Y., Zhang, Z., and Yang, J. (2022). Estimating the non-linear effects of urban built environment at residence and workplace on carbon dioxide emissions from commuting. *Front. Public Health* 10, 1077560. doi:10.3389/fpubh.2022.1077560

Liu, Z., Guo, Z., Chen, Q., Song, C., Shang, W., Yuan, M., et al. (2023). A review of data-driven smart building-integrated photovoltaic systems: Challenges and objectives. *Energy* 263, 126082. doi:10.1016/j.energy.2022.126082

Luo, D., Liang, L., Wang, Z., Chen, L., and Zhang, F. (2021). Exploration of coupling effects in the economy–society–environment system in urban areas: Case study of the Yangtze River Delta urban agglomeration. *Ind* 128, 107858. doi:10.1016/j.ecolind.2021.107858

Mackinnon, D., Dawley, S., Steen, M., Menzel, M., Karlsen, A., Sommer, P., et al. (2019). Path creation, global production networks and regional development: A comparative international analysis of the offshore wind sector. *Prog. Plan.* 130, 1–32. doi:10.1016/j.progress.2018.01.001

Magalhães, L., Kuffer, M., Schwarz, N., and Haddad, M. (2023). Bringing economic complexity to the intra-urban scale: The role of services in the urban economy of belo horizonte, Brazil. *Appl. Geogr.* 150, 102837. doi:10.1016/j.apgeog.2022.102837

Mandle, L., Shields-Estrada, A., Chaplin-Kramer, R., Bremer, L. L., Gourvitch, J. D., Hawthorne, P., et al. (2021). Increasing decision relevance of ecosystem service science. *Nat. Sustain* 4, 161–169. doi:10.1038/s41893-020-00625-y

Moore, F., Lacasse, K., Mach, K., Shin, Y., Gross, L., and Beckage, B. (2022). Determinants of emissions pathways in the coupled climate–social system. *Nature* 603, 103–111. doi:10.1038/s41586-022-04423-8

Moroni, S., and Cozzolino, S. (2019). Action and the city: Emergence, complexity. *Plan. Cities* 90, 42–51. doi:10.1016/j.cities.2019.01.039

Pickett, S., Cadenasso, M., Grove, J., Boone, C., Groffman, P. M., Irwin, E., et al. (2011). Urban ecological systems: Scientific foundations and a decade of progress. *J. Environ. Manag.* 92 (3), 331–362. doi:10.1016/j.jenvman.2010.08.022

Qiao, W., and Huang, X. (2022). The impact of land urbanization on ecosystem health in the Yangtze River Delta urban agglomerations, China. *Cities* 130, 103981. doi:10.1016/j.cities.2022.103981

Said, O., and Tolba, A. (2021). Accurate performance prediction of IoT communication systems for smart cities: An efficient deep learning based solution. *Sustain. Cities. Soc.* 69, 102830. doi:10.1016/j.scs.2021.102830

Shi, X., Matsui, T., Machimura, T., Haga, C., Hu, A., and Gan, X. (2022). Impact of urbanization on the food–water–land–ecosystem nexus: A study of shenzhen, China. *Sci. Total. Environ.* 808, 152138. doi:10.1016/j.scitotenv.2021.152138

Sonter, L. J., Simmonds, J. S., Watson, J. E. M., Jones, J. P. G., Kiesecker, J. M., Costa, H. M., et al. (2020). Local conditions and policy design determine whether ecological compensation can achieve No Net Loss goals. *Nat. Commun.* 11, 2072. doi:10.1038/s41467-020-15861-1

Stratigea, A., Papadopoulou, C., and Panagiotopoulou, M. (2015). Tools and technologies for planning the development of smart cities. *J. Urban Technol.* 22 (2), 43–62. doi:10.1080/10630732.2015.1018725

Su, M., Wang, Q., Li, R., and Wang, L. (2022). Per capita renewable energy consumption in 116 countries: The effects of urbanization, industrialization, GDP, aging, and trade openness. *Energy* 254, 124289. doi:10.1016/j.energy.2022.124289

Trenberth, K. (2004). Rural land-use change and climate. *Nature* 427, 213. doi:10.1038/427213a

Wang, W., Wang, H., Ortiz, J., Alidaee, B., and Sun, B. (2022). The role of economic development on the effectiveness of industrial pollution reduction policy in Chinese cities. *J. Clean. Prod.* 339, 130709. doi:10.1016/j.jclepro.2022.130709

Wei, C., Zhou, Y., and Kong, J. (2022). Evidence regarding the ecological benefits of payment for ecological services programs from China's grassland ecological compensation policy. *Front. Environ. Sci.* 10, 989897. doi:10.3389/fenvs.2022.989897

Winkler, K., Fuchs, R., Rounsevell, M., and Gerold, M. (2021). Global land use changes are four times greater than previously estimated. *Nat. Commun.* 12, 2501. doi:10.1038/s41467-021-22702-2

Xing, Q., Gang, H., and Yao, W. (2022). Research of mining area ecological compensation from the perspective of knowledge innovation. *Front. Environ. Sci.* 10, 838146. doi:10.3389/fenvs.2022.838146

Xue, B., Han, B., Huang, B., Wang, H., Zhao, X., Fang, K., et al. (2022). Approach and evidence-based study of provincial eco-economic development planning. *Chin. J. Appl. Ecol.* 33 (12), 3169–3176. (in Chinese). doi:10.13287/j.1001-9332.202212.039

Xue, B., Xiao, X., and Li, J. (2020). Identification method and empirical study of urban industrial spatial relationship based on POI big data: A case of shenyang city, China. *Geogr. Sustain.* 1 (2), 152–162. doi:10.1016/j.geosus.2020.06.003

Xue, B., Xiao, X., Li, J., Zhao, B., and Fu, B. (2023). Multi-source data-driven identification of urban functional areas: A case of shenyang, China. *Chin. Geogr. Sci.* 33 (1), 21–35. doi:10.1007/s11769-022-1320-2

Zhang, J., Li, J., Yang, X., Yin, S., and Chen, J. (2022). Rural social-ecological systems vulnerability evolution and spatial-temporal heterogeneity in Arid environmental change region: A case study of minqin oasis, northwestern China. *Appl. Geogr.* 145, 102747. doi:10.1016/j.apgeog.2022.102747

frontiers | Frontiers in Earth Science

ORIGINAL RESEARCH
published: 10 May 2022
doi: 10.3389/feart.2022.902444

Spatiotemporal Pattern Evolution of Urban Ecosystem Resilience Based on "Resistance-Adaptation-Vitality": A Case Study of Nanchang City

Linghua Duo[1,2,3], *Yanan Li*[2], *Ming Zhang*[2], *Yuxi Zhao*[2], *Zhenhua Wu*[4] *and Dongxue Zhao*[5]*

[1]Jiangxi Ecological Civilization Construction System Research Center, East China University of Technology, Nanchang, China, [2]Faculty of Geomatics, East China University of Technology, Nanchang, China, [3]Key Laboratory of Mine Environmental Monitoring and Improving Around Poyang Lake, Ministry of Natural Resources, Nanchang, China, [4]School of Economics and Management, China University of Mining and Technology, Xuzhou, China, [5]Queensland Alliance for Agriculture and Food Innovation, The University of Queensland, Brisbane, QLD, Australia

OPEN ACCESS

Edited by:
Jun Yang,
Northeastern University, China

Reviewed by:
Xiao Liu,
South China University of Technology, China
Zhi Qiao,
Tianjin University, China
Yang Liu,
Zhongnan Hospital, Wuhan University, China

***Correspondence:**
Dongxue Zhao
mailto:zhaodx08@gmail.com

Specialty section:
This article was submitted to Environmental Informatics and Remote Sensing, a section of the journal Frontiers in Earth Science

Received: *23 March 2022*
Accepted: *11 April 2022*
Published: *10 May 2022*

Citation:
Duo L, Li Y, Zhang M, Zhao Y, Wu Z and Zhao D (2022) Spatiotemporal Pattern Evolution of Urban Ecosystem Resilience Based on "Resistance-Adaptation-Vitality": A Case Study of Nanchang City. Front. Earth Sci. 10:902444. doi: 10.3389/feart.2022.902444

With the rapid development of the economy and society in recent years, the ecological environment has deteriorated significantly. The governments at all levels, departments, and relevant scholars have begun to pay attention to urban ecological construction and research on urban disaster prevention and mitigation. The concept of resilience has gained widespread attention in this context. However, at present, urban ecological resilience research is still in its infancy, and there are many qualitative but few quantitative studies in terms of assessment methods. This study explores the complex dynamic evolution mechanism of urban ecosystem resilience based on the three resilience characteristics and selects Nanchang, an important ecological barrier in the middle and lower reaches of the Yangtze River and a model area for integrated management of the Great Lakes basin, as an assessment target. This study establishes a quantitative measurement and evaluation framework for urban ecological resilience in three dimensions (resistance, adaptation, and vitality) and conducts a comprehensive evaluation of urban ecosystem resilience. The results show that the trend of land-use change from 1990 to 2020 is mainly characterized by the continuous decrease in arable land and ecological land (forestland, grassland, and water) and the continuous increase in construction land, among which the land-use dynamic attitude of construction land is the largest, reaching 5.33% from 1990 to 2005. During the study period, the overall ecosystem resilience of Nanchang showed a gradual decline and was always at a moderate-to-low level, with a long-term distribution pattern of "low in the middle and high in the surrounding areas" and clear spatial heterogeneity. This study helps clarify the security status of the regional ecosystem and provides a reference for exploring the complex dynamic evolution mechanism of ecological resilience.

Keywords: ecological resilience, spatial-temporal pattern evolution, landscape patterns, integrated assessment, Nanchang city

1 INTRODUCTION

Natural ecosystems are not only the basis and conditions for human survival and development but also an important prerequisite for the sustainable development of human society. The stability of their structure and function is an effective guarantee for the development of human society (Ma et al., 2001). However, as urbanization continues and the number of people grows, human interference with natural ecosystems is intensifying and the burden on ecosystems is becoming heavier (Jin et al., 2018), resulting in more ecological problems such as global warming (He et al., 2022), heat island effect (Yang et al., 2019; He et al., 2021), and deterioration of human habitat. Cities are the most complex social and ecological systems, which are inevitably subject to various disturbances and intrusions from human activities, especially since the 20th century, when modern societies have become more densely populated, urban social environments and conflicts have become more complex, urban economic structures have become more diverse, the risks and unknown threats to urban development have further increased, and their possible malignant consequences have gradually become apparent (He et al., 2018). Therefore, to cope with shocks and threats, how to enhance the ability of cities to resist ecological risks has attracted the close attention of many countries and regions, and the construction of resilient cities has gradually become a major hot spot of academic research.

The historical changes in resilience have evolved considerably under the tireless research of scholars. The concept of resilience was first applied to ecology by the Canadian scholar Holling and referred to the ability of a system to resist risk, restore equilibrium, and adapt to new environments (Holling, 1996). Since then, experts and scholars in urban science research have referred to this concept and explored urban resilience to improve the buffering capacity and resistance of cities in the face of external threats with the help of resilience thinking. As an important aspect of urban resilience, the assessment of urban ecological resilience has also received attention from governments, departments, and relevant scholars at all levels (Chen W. X. et al., 2022). The New Urban Agenda adopted at the United Nations Conference on Housing and Sustainable Urban Development, launched in Ecuador in October 2016, included "urban ecological resilience" as the material for the eighth policy cluster and set the ecological goal of sustainable urban development as building "environmentally sustainable and resilient cities" (He, 2017). In China, on 3 November 2020, the "Proposal of the Central Committee of the Communist Party of China on Formulating the 14th Five-Year Plan for National Economic and Social Development and the Visionary Goals for 2035" was proposed to "promote a new-type urbanization with people-oriented." We will strengthen historical and cultural protection, shape the urban landscape, strengthen urban renovation of old neighborhoods and community construction, enhance urban flood control and drainage capacity, and build sponge cities and resilient cities. We will improve the level of urban governance and strengthen the prevention and control of risks in the governance of megacities (Xia et al., 2022). These elaborated that the implementation of resilient cities has a key role in the sustainable development construction of China's cities that should not be underestimated (Yang et al., 2021; Ren et al., 2022). The domestic attention to and international influence of resilient cities show that resilience is of considerable importance in promoting harmonious urban and ecological development (Yu et al., 2022; Xie et al., 2022).

The scientific research on ecological resilience has accumulated some rich experiences by domestic and foreign scholars. In 2001, the adaptive cycle theory was created, shifting the starting point of research from an ecological resilience perspective to evolutionary resilience and using this theory to define resilience (Ostrom, 2004). By reviewing the origins and expansion of the definition of resilience, Manyena (2006) elucidated the strong link between urban resilience and urban vulnerability and revealed the important role played by resilience theory when cities are subjected to shocks. Abdrabo and Hassaan (2015) constructed a comprehensive framework for urban resilience using four entry points: urban, peri-urban, urban networks, and adjacent rural areas. Suárez et al. (2016) creatively proposed an urban resilience index for the construction of a framework system to measure urban resilience, using 50 provincial capitals in Spain as the study area. Gimenez et al. (2017) explored the need for multiple interests to join in the construction of urban resilience and discussed how policy-makers could lead the process of building urban resilience (Gimenez et al., 2017). Bozza et al. (2017) argued that resilience evaluation models should be differentiated according to the different natural threats that ecosystems resist, based on which they developed a resilience evaluation framework with the ability to assess different ecological threats in the same city, starting from a time-series perspective (Bozza et al., 2017).

However, most of the current studies focus on the nature of resilience theory, development history, component units, basic categories, and other basic principles and the overall planning of resilient city construction, with more qualitative and fewer quantitative studies, making it difficult to make a deep and objective quantitative evaluation of urban resilience. This study focuses on the long time series resilience process and constructs a quantitative evaluation framework of ecological resilience from the three dimensions of "resistance-adaptation-vitality" to address the shortcomings of the current qualitative evaluation. A comprehensive evaluation of urban ecosystem resilience is conducted to understand the complex dynamic evolutionary mechanisms of ecological resilience, thus clarifying the state of regional ecosystem security.

This study takes Nanchang city as the study area, constructs a quantitative evaluation framework for urban ecological resilience from three aspects "resistance-adaptation-vitality," and conducts a comprehensive assessment of ecosystem resilience in Nanchang city to investigate the impact of landscape pattern evolution on ecological resilience. Specifically, this study can achieve the following three objectives: 1) a framework for quantitative measurement and evaluation of urban ecological resilience is established; 2) trends and characteristics of ecological resilience are assessed from the perspective of three major characteristics of resilience; and 3) new ideas and measures to optimize the

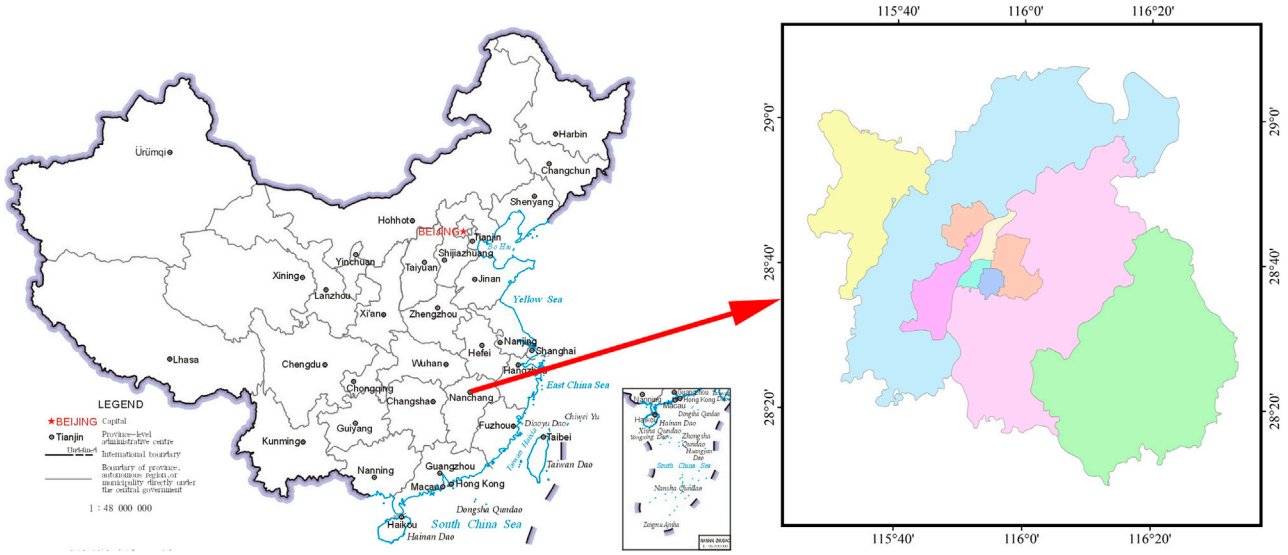

FIGURE 1 | The study area.

landscape pattern and improve ecological resilience in Nanchang city are obtained.

The main contributions of this study are as follows. Theoretically, the introduction of a quantitative description of the urban ecosystem resilience evaluation index system under the trend of rapid urbanization allows a multidimensional and comprehensive analysis of ecological resilience, providing a new approach and perspective for the diversification of ecological resilience assessment systems. Practically speaking, exploring the influence of landscape pattern evolution on ecological resilience helps people understand the complex mechanisms of ecological resilience changes, better optimizes landscape patterns, improves the current ecological environment, and provides references for the implementation of territorial spatial planning and ecological control strategies.

2 MATERIALS AND METHODS

2.1 Study Area

Nanchang is located in the middle and lower reaches of the Yangtze River, close to the first freshwater lake in China-Poyang Lake (**Figure 1**), rich in water resources, and connected to numerous rivers and lakes, with a forest coverage rate of 21.96%. The unique natural resource endowment makes Nanchang an important ecological barrier in the middle and lower reaches of the Yangtze River and a model area for comprehensive management of the Great Lakes basin (Ypa et al., 2020). However, what cannot be ignored is that, as the core city of the Poyang Lake city cluster, Nanchang city has experienced rapid population growth and construction land expansion in recent years, which has resulted in a series of urban ecological environment problems, such as water pollution, air pollution, and deterioration of the human living environment. If left unaddressed and uncorrected, these problems will not only adversely affect the quality of the urban habitat but also hinder socioeconomic progress, making it particularly important to quantify the resilience of Nanchang's ecosystem.

2.2 Data Sources and Pre-Processing

The main data used in this study are remote sensing images of Nanchang in 1990, 2005, and 2020, digital elevation data of Nanchang (resolution 30 × 30 m), township vector data of Nanchang, population data, GDP data, road data, soil type, average annual temperature, annual precipitation, and other data. Among them, Landsat TM/ETM+ is selected for remote sensing images with a resolution of 30 m (Zhao et al., 2021), the time periods are 1990, 2005, and 2020, the months are July–August, the cloudiness is less than 10%, and the geographic coordinate system is WGS84. The specific description and main sources of the above data are shown in **Table 1**.

Firstly, the remote sensing image processing software ENVI was used to pre-process the image data of 1990, 2005, and 2020, including a series of operations such as radiation calibration, atmospheric correction, de-clouding, image stitching, and cropping. According to the actual situation of Nanchang city, the land-use types of Nanchang city were classified into the following six categories: arable land, forest land, grassland, water, construction land, and unused land concerning the classification standards in the Classification of Current Land Use (GB/T21010-2017), combined with the computer supervised classification method and manual visual

TABLE 1 | Data description and source.

Data type	Filename	Data description	Data source
Land-use data	LUCC1990	Land-use classification data of Nanchang city in 1990	USGS Platform (https://earthdata.nasa.gov/)
	LUCC2005	Land-use classification data of Nanchang city in 2005	
	LUCC2020	Nanchang city 2020 land-use classification data	
Climate and environmental data	DEM	Elevation	Geospatial Data Cloud (http://www.gscloud.cn/)
	SLOPE	Slope	Calculated from DEM
	Soil	Soil type data	CAS Resource and Environmental Science and Data Center (http://www.resdc.cn/) Spatial distribution data of soil types in China
	Temp	Average annual temperature data	CAS Resource and Environmental Science and Data Center (http://www.resdc.cn/)
	Rain	Average annual precipitation data	China Meteorological Background Dataset
	Dis_water	Distance to water bodies	Water bodies were extracted from land-use data using the Euclidean distance tool
Socioeconomic data	GDP	Gross national product data	CAS Resource and Environmental Science and Data Center (http://www.resdc.cn/) China GDP spatial distribution km grid dataset
	POP	Population density data	CAS Resource and Environmental Science and Data Center (http://www.resdc.cn/) Chinese population spatial distribution km grid dataset
	Dis_highway	Distance to highways	The road data are obtained from the OSM data (https://www.openhistoricalmap.org/) using the Euclidean distance tool
	Dis_railway	Distance to railroad	

interpretation. The specific operations are as follows: firstly, based on the field survey and reference to the land-use data of Nanchang city in known years, the interpretation samples of each land-use type are obtained using the supervised classification method; then, the classification template for interpretation is created according to the distribution characteristics and spectral characteristics of the interpretation samples, and when the accuracy of the classification template is higher than 85%, the accuracy is considered to meet the requirements and the template can be interpreted. After that, the supervised classification results are subjected to post-classification processing, including operations such as spot error correction and topology checking. Those that do not meet the requirements for supervised classification accuracy are modified and improved by manual visual interpretation. Finally, to evaluate the accuracy of the classification results, the high-definition historical images of Google Earth were used as a reference, and the sample points were selected to verify the results of supervised classification. In this study, the Kappa coefficient was used for quantitative evaluation, and the Kappa coefficients of 1990, 2005, and 2020 were calculated to be above 80%, according to the conclusion of Eike's study (Eike and Andeas, 2008). The interpretation accuracy can meet the needs of this study and can be used as the base data for the follow-up study.

2.3 Methodology

2.3.1 Urban Ecosystem Assessment Model Construction

The concept of resilience has been defined in different fields, but at its core, it emphasizes the resistance, adaptation, and vitality of systems in the face of disturbances and uncertainties (Xia et al., 2022). The following three essential characteristics of resilience can be summarized (Peng et al., 2015): first, the ability of the system to self-organize in response to external changes (resistance); second, the ability of the system to establish and increase learning and self-adaptation (adaptation); and third, the ability of the system to restore normal order promptly after the basic structure of the system has been damaged (vitality). Compared with the early warning characteristics of risk (Zhang et al., 2011), resilience can be used for ex-ante assessment or retrospective analysis, so some risk prevention and control management in resilient cities can achieve "twice the result with half the effort" (Xiu et al., 2018). Therefore, this study constructs an urban ecological resilience assessment model from three aspects: resistance, adaptation, and vitality (**Figure 2**).

2.3.1.1 Ecosystem Resistance Model Construction

Resistance indicates the ability of urban ecosystems to resist external disturbances. Habitat quality is the ability of an ecosystem to provide the conditions required for the continued survival and reproduction of individual species, populations, communities, and humans (Gong et al., 2014). It can be used to characterize the good or bad ecological suitability of regional land class land-scape patches, and its numerical magnitude can reflect the resistance of each landscape patch to habitat degradation (Liu, 2014). Areas with high habitat quality are more stable on their own when subjected to external disturbances (i.e., threat factors) and therefore provide a better characterization of ecosystem resilience. Therefore, habitat quality can be used as a proxy for "resilience" to characterize the ability of urban ecosystems to resist external disturbances (Zhang, 2018).

Habitat quality is generally obtained through the InVEST model, the full name of which is the Integrated Valuation of Ecosystem Services and Trade-offs. The focus is on applying the sensitivity of stressors and the intensity of external threats for various land cover categories and considering habitat quality as a continuous variable to measure biodiversity based on the distance of influence of stressors, spatial weights, and other factors. The specific calculation procedure is as follows (Huang et al., 2020):

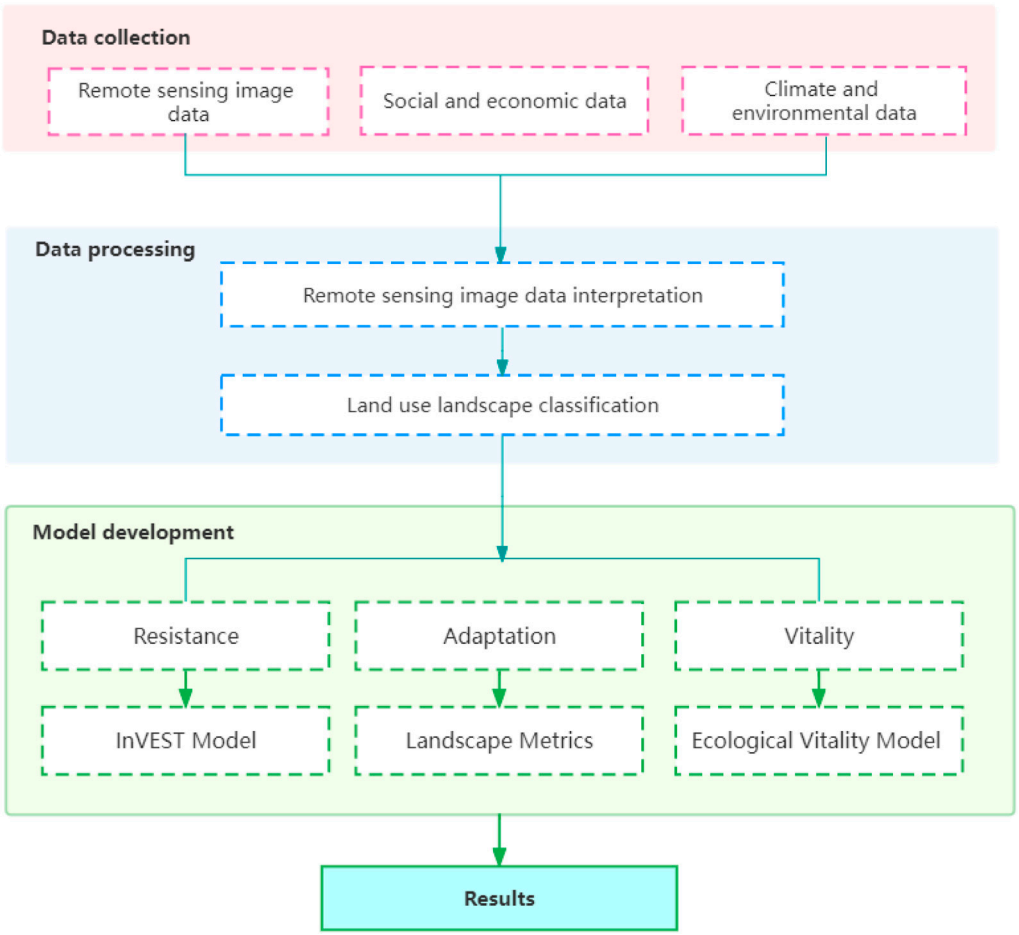

FIGURE 2 | Framework diagram for resilience evaluation of urban ecosystems based on "resistance-adaptation-vitality."

$$Q_{xj} = H_j\left[1 - \left(\frac{D_{xj}^z}{D_{xj}^z + k^z}\right)\right] \quad (1)$$

$$D_{xj} = \sum_{r=1}^{R}\sum_{y=1}^{Y_r}\left(\frac{w_r}{\sum_{R=1}^{R} w_r}\right) r_y i_{rxy} \beta_x S_{jr} \quad (2)$$

Q_{xj} is the habitat quality of raster cell x in land cover type j. H_j is the habitat suitability of land cover type j. D_{xj}^z is the level of habitat stress for raster cell x in land cover type j. k is the half-saturation factor, which is usually half of the maximum value of D_{xj}^z. x is a constant. R is the number of stress factors. y denotes all raster cells of stressor r. Y_r is the total number of raster cells occupied by the stressor r. r_y is the stressor r in the raster cell y. The stressor $r(r_y)$ in the raster cell y has a stressing effect on the habitat raster cell x as i_{rxy}. The formula is as follows:

$$i_{rxy} = 1 - \left(\frac{d_{xy}}{d_{r\max}}\right) \quad (3)$$

$$i_{rxy} = \exp\left[-\left(\frac{2.99}{d_{r\max}}\right) d_{xy}\right] \quad (4)$$

d_{xy} is the straight line distance between raster cell x and raster cell y. w_r is the maximum distance of influence of stressor r. β_x is the legal reachability of raster cell x, and 1 indicates that it is extremely easy to reach. S_{jr} is the sensitivity of land cover type j to stressor r, it takes the value 0–1, and the closer the value is to 1, the more sensitive it is.

The main parameters needed to run the habitat quality model include the distance of threat factor effects and their weights, the suitability, and the sensitivity of the habitat to each threat factor. Combining with relevant studies (Gong et al., 2014; Chen et al., 2016), arable land, settlements, other construction lands, urban land, railroads, and roads, which have a greater impact on the ecological landscape, were selected and defined as ecological stressors, and assigning values to the suitability and sensitivity of each threat factor concerning previous studies (Chen et al., 2016; Zheng et al., 2018), as shown in **Tables 2**, **3**.

2.3.1.2 Ecosystem Adaptation Model Construction

The more stable an ecosystem is, the more adaptable it is (Ren et al., 2000). Therefore, this study uses the indicators of the landscape pattern index related to the stability of ecosystem landscape structure to express its adaptation.

TABLE 2 | The attribute of threat factor.

Threat factor	Maximum impact distance (km)	Weights	Type of spatial recession
Arable land	1.5	0.6	Linear
Rural settlement	2.5	0.4	Exponential
Urban land	6	0.8	Exponential
Other construction lands	1	0.5	Exponential
Highways	6	0.6	Linear
Railroad	5	0.3	Linear

TABLE 3 | Landscape types and their sensitivity to threats.

Land-use type	Habitat suitability	Arable land	Rural settlement	Urban land	Other construction lands	Highways	Railroad
Arable land	0.4	0	0.35	0.5	0.3	0.5	0.5
Forest land	1	0.8	0.85	1	0.8	0.9	0.8
Grassland	0.6	0.5	0.35	0.6	0.5	0.7	0.7
Water area	1	0.7	0.75	0.9	0.9	0.75	0.6
Construction land	0	0	0	0	0	0	0
Unused land	0	0	0	0	0	0	0

TABLE 4 | Landscape pattern index, weight, and meaning.

Landscape structure	Landscape pattern index	Abbreviation	Weights	Significance
Landscape heterogeneity	Shannon's diversity	SHDI	0.25	This indicator is sensitive to the non-equilibrium distribution of each type in the landscape and can better reflect the heterogeneity of the landscape
	Area-weighted average patch fractal dimension	AWMPFD	0.25	Used to characterize the spatial shape complexity of patches and landscapes, reflecting the impact of human activities on landscape patterns
Landscape connectivity	Landscape fragmentation	FN	0.5	The total number of patches per unit area, the magnitude of the value is positively correlated with the fragmentation of the landscape

The landscape pattern index is a quantitative analysis index that summarizes and describes landscape pattern information, such as landscape patch shape, patch density, landscape fragmentation, landscape heterogeneity, and landscape connectivity. Generally, landscape connectivity and landscape spatial heterogeneity can describe landscape pattern changes in terms of aggregation, connectivity, fragmentation, distribution structure, and diversity of landscape patches, respectively, which provides a more comprehensive analysis of the dynamic changes of land-use change on landscape patterns and their functions (Xie and Li, 2008).

Landscape structural stability of ecosystems depends on landscape pattern indices related to spatial heterogeneity and landscape connectivity (Ou et al., 2014; Peng et al., 2015). Generally, landscape connectivity is characterized by the connectivity of the entire landscape and habitat (Turner, 2003), specifically quantified using landscape fragmentation (FN) (Yuan et al., 2019; Chen Y. et al., 2022). This study proposes to use the Shannon diversity index and area-weighted average patch fractal index to characterize the spatial heterogeneity of the landscape. In terms of weight setting, landscape heterogeneity and landscape connectivity describe two aspects of ecosystem landscape structure, respectively, and are not substitutable for each other, so their weights can be assumed to be equal (Peng et al., 2015), as shown in **Table 4**.

Based on **Table 4**, the formula for ecosystem adaptation is as follows (Xia et al., 2022):

$$A = 0.25 \times SHDI + 0.25 \times AWMPFD + 0.5 \times FN \quad (5)$$

A denotes connectivity, SHDI indicates Shannon diversity index, AWMPFD denotes the area-weighted average patch fractal dimension, and FN indicates landscape fragmentation.

2.3.1.3 Ecosystem Vitality Model Construction

Ecosystem vitality emphasizes the ability and potential of an ecosystem to return to its original state after being harmed. This section portrays and evaluates the resistance and adaptation of landscape patches to external disturbances in ecosystem processes and provides an in-depth analysis of them in terms of spatial and temporal evolution patterns and spatial association patterns.

Ecosystem vitality is the ability of a system to gradually bounce back after the disappearance of a stressor, reflecting the resistance and adaptation of landscape patches to external disturbances

TABLE 5 | Coefficient of vitality for different land-use types.

Land-use type	Arable land	Forest land	Grassland	Water area	Construction land	Unused land
RC	0.3	0.8	0.6	0.8	0.2	1

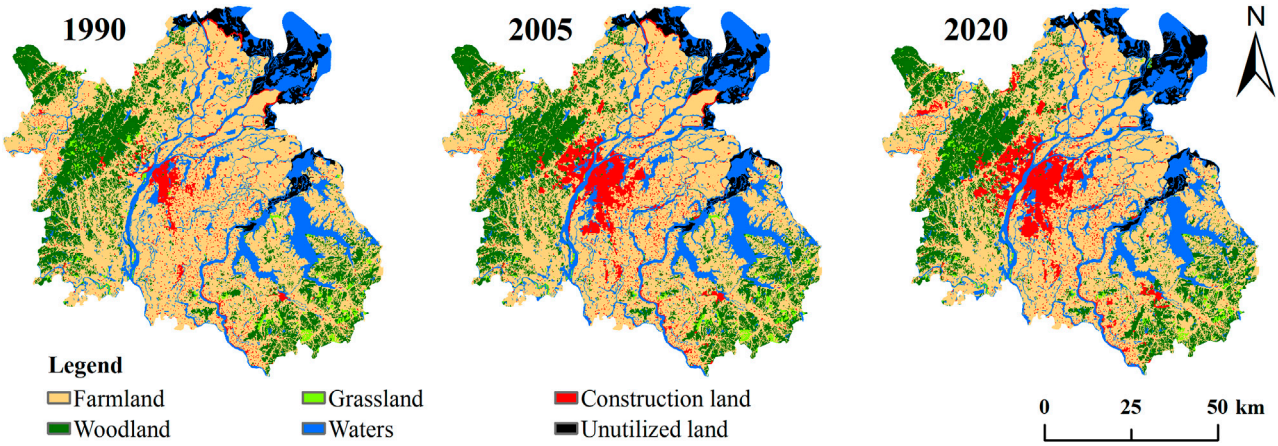

FIGURE 3 | Spatial distribution of landscape types in Nanchang city in 1990, 2005, and 2020.

during the ecosystem process. It is difficult to measure ecosystem vitality directly. Therefore, this study refers to the ecological vitality model and coefficients proposed according to Peng et al., where land-use types that are closer to natural ecosystems in terms of attributes are relatively easier to recover when subjected to external disturbances. The vitality coefficients (RC) of different land-use types are set according to their restoration difficulty (**Table 5**).

Based on the grid sampling method, the ecological vitality index was constructed by calculating the proportion of land area within each grid to describe the relative size of the integrated ecological resilience within a sample site. Thus, the land-use structure is transformed into ecological vitality values by sampling, and an ecosystem vitality model is constructed. The specific calculation formula is as follows:

$$R = \sum_{i=1}^{n} A_i \times RC_i \tag{6}$$

R is ecosystem vitality. A_i is the area ratio of type i land-use types. RC_i is the ecosystem vitality coefficient for type i land-use type. n is the number of land-use types.

2.3.1.4 Comprehensive Evaluation Model Construction

The scale of each evaluation index in the indicator system varies, and even for the same scale, its actual quantity varies greatly. In order to eliminate the differences in scale and quantity among the evaluation indices, the variables should be normalized when constructing the ecosystem health evaluation system. In this study, the variables are first treated using the extreme value normalization method. The formula is as follows:

$$Y_i = \frac{X_i - \min(X_i)}{\max(X_i) - \min(X_i)} \tag{7}$$

Y_i is the standard value of the index. X_i is the value of the i indicator. $max(X_i)$ and $min(X_i)$ are the maximum and minimum values of the i index. i is in the range of 1-n, and n indicates the number of raster cells.

On this basis, the resilience index of the Nanchang ecosystem was calculated based on the framework of "resistance-vitality-adaptation" concerning previous research results. The calculation formula is as follows:

$$Resilience = \sqrt[3]{A \times P \times R}. \tag{8}$$

Resilience is the ecosystem resilience index. A is adaptability, P is resistance, and R is resilience.

2.3.2 Spatial Autocorrelation Model

Spatial autocorrelation is a statistical method used to reveal the spatially correlated characteristics of spatial reference units and neighboring units in terms of attribute feature values by describing whether there is a significantly correlated relationship between the attribute values of an element and its spatially adjacent attribute values of each element (Wu et al., 2015). The global and local coefficients of spatial autocorrelation can be used to determine the spatial correlation and the degree of correlation of the study variables. The global auto-correlation coefficient is mainly used to verify the spatial pattern of the whole study area and measure the distribution trend and clustering status of the attribute values over the geographical space. There are many indicators and methods to express the global spatial autocorrelation, mainly including Moran's I, Geary's C, and Getis, among which Moran's I is the most

commonly used. Local Moran's I and Getis-Ord G indices are used to reflect the similarity or correlation between spatial geographical units and their neighboring spatial units' attribute characteristics, mainly to identify "hot spots" and test the heterogeneity of the data.

2.3.2.1 Global Autocorrelation

The global autocorrelation Moran I index is used to examine the spatial correlation of the attribute values of a given element across the study area. The formula was calculated as follows (Liu and Wang, 2018):

$$GlobalMorans'I = \frac{\sum_{i=1}^{n}\sum_{j=1}^{m} W_{ij}(x_i - \bar{x})}{S^2 \sum_{i=1}^{n}\sum_{j=1}^{m} W_{ij}} \tag{9}$$

$$S^2 = \frac{1}{n}\sum_{i=1}^{n}(x_i - \bar{x})^2 \tag{10}$$

$$\bar{x} = \frac{1}{n}\sum_{i=1}^{n} x_i \tag{11}$$

x_i is the observed value in the region. n is the number of grids. W denotes the binary adjacency space weight matrix, reflecting the adjacency relationship of spatial objects, i = 1, 2...n, j = 1, 2...m. W_{ij} = 1 when regions i and j are adjacent to each other.

2.3.2.2 Local Autocorrelation

1) Moran's I Index

This index is used to portray the correlation between the attribute values of an element and the adjacent spatial units. The formula was calculated as follows (Feng et al., 2015):

$$Local Moran's\ \mathrm{I} = \left(\frac{(x_i - \bar{x})}{m}\right)\sum_{j=1}^{n} w_{ij}(x_i - \bar{x}), \tag{12}$$

$$m = \left(\sum_{j=i, j\neq i}^{n} x_j^2\right) \Big/ (n-1) - x^2, \tag{13}$$

Moran's I between −1 and 1. When Moran's I > 0, it indicates a positive correlation in the study area and that the attribute values of the study units exhibit convergent clustering. While when Moran's I < 0, it represents a negative correlation, indicating a discrete distribution of the attribute values of the study unit. When Moran's I = 0, then there is no spatial correlation.

2) Getis-Ord Gi Index

The Getis-Ord Gi index analyzes the information in a region to reveal the similarity or correlation between the spatial units and the attribute values of their neighboring spatial units to identify the spatial distribution of the "hot and cold spot areas" and test the heterogeneity of the data. The formula was calculated as follows (Anselin, 1995):

$$G_i(d) = \frac{\sum_{j=1}^{n} w_{ij}(d)x_j}{\sum_{j=1}^{n} x_j} \ (i \neq j) \tag{14}$$

$$Z(G_i) = \frac{G_i - E(G_i)}{\sqrt{Var(G_i)}} \tag{15}$$

w_{ij} denotes the elements of the spatial weight matrix w, 1 when spatially contiguous and 0 when not contiguous. $E(G_i)$ and $Var(G_i)$ are the mathematical expectation and variance of G_i, respectively. If $Z(G_i)$ is positive and significant, it indicates that the values around the position i are relatively high, and it behaves spatially as a high-value agglomeration area (hot spot area). On the contrary, it behaves spatially as a low-value agglomeration area (cold spot area).

3 RESULTS

3.1 Land Use and Its Transfer Changes

As can be seen from **Figures 3**, **4**, the land-use types in the study area are mainly cropland, forest land, and water surface, which together account for about 90% of the total study area, with cropland accounting for relatively large and wide distribution in the region, accounting for about 55%. From 1995 to 2005, the evolution of the landscape pattern in the region is very obvious, where the most obvious growth is in construction land, showing a steady increase from 279.09 km^2 in 1990 to 712.14 km^2 in 2020, an increase of 155.17% in 30 years, with an area of 433.05 km^2, indicating that with urbanization, population and economy all continuing to advance, the demand for expansion of construction land is increasing. The area of idle land is also gradually increasing, from 308.14 km^2 initially in 1990 to 318.28 km^2 in 2019. Arable land, forest land, grassland, and water area continue to decline from 1990 to 2020, with the largest decline in the area of arable land from 4,089.13 hm^2 to 3,796.97 km^2 in 2020. Forest land, grassland, and water area decreases from 1,212.94, 97.76, and 1,197.57 km^2 in 1990 to 1,149.47, 75.34, and 1,132.44 km^2 in 2020, decreasing by 0.88%, 0.31%, and 0.31% respectively. The proportion of total land use will decrease by 0.88%, 0.31%, and 0.91%, respectively.

Analyzing the reasons for the above changes, the land-use types that show an increasing trend are construction land and unused land, while the area of arable land, forest land, grassland, and water area decreases year by year. The increase in construction land is mainly concentrated in Honggutan, Donghu, Xihu, and Qingshanhu Districts on both sides of Ganjiang River in central Nanchang, mainly due to the accelerated industrialization and urbanization process and the sharp increase in population leading to the increase in construction land demand. The construction of Jiulonghu New Area proposed in 2010 and Ganjiang New Area proposed in 2016 has promoted the urbanization process more, and the urban development and expansion require a large amount of occupied arable land and ecological lands such as woodland and grassland, causing a continuous reduction in the area of arable land, woodland, and grassland. The main reason for the decrease in water area is that the water level of Poyang Lake decreases and the shoreline shrinks in recent years, which leads to the exposure of unused land such as marshland, so the unused land increases slightly. By analyzing and compiling the information on land-use change in the study area over 30 years, it is important to grasp the rule and direction of regional land-use change, which is of

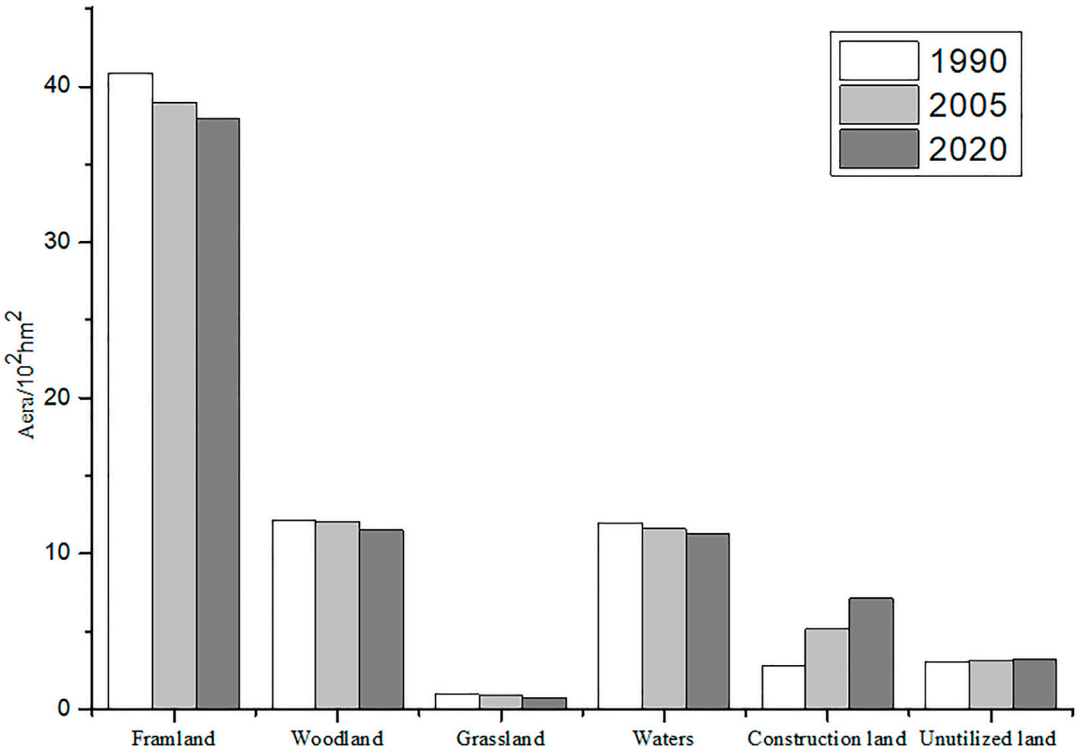

FIGURE 4 | Land-use area of the first classes in 1995, 2005, and 2020.

strategic significance for future land-use planning and ecological environmental protection of the study area.

In **Table 6**, the land-use transfer matrix of the study area shows that, from 1990 to 2005, cropland was the most transferred land use category in the study area, with a net transfer of 188.65 km^2, mainly shifted to construction land (213.50 km^2), and the expansion of urban construction land was the main reason for the transfer of cropland. The second-largest land-use category to be transferred out is water, with a net transfer of 26.89 km^2. The majority of the decrease in water area comes from arable land (92.69 km^2) and construction land (23.66 km^2). The net transfer of forest land is 16.28 km^2, with a net shift to arable land (59.32 km^2) and construction land (22.88 km^2), indicating that the phenomenon of deforestation still exists. The most obvious land-use category to expand is construction land, with an increase of 303.34 km^2. The most obvious category of land expansion is construction land, with an increase of 303.34 km^2, and 70.38% of the area transferred to construction land comes from arable land, reflecting that the expansion of construction land is mainly achieved by encroaching on arable land. The area of grassland and unused land fluctuates slightly.

From the land-use transfer matrix of the study area, it can be seen that, from 2005 to 2020, the largest area transferred out is still arable land, with a net transfer out of 103.54 km^2 and a net reduction of 85.11 km^2 compared to 1990–2005, mostly to construction land (182.75 km^2), followed by forest land (40.99 km^2) and water (35.60 km^2). The reduction in water area also tends to be smaller, with a total reduction of 14.99 km^2 and a reduction of 11.90 km^2 compared with the previous period, mainly shifting to arable land (47.87 km^2) and unused land (40.43 km^2). The area of grassland slightly decreases. The water area changes significantly; compared with the previous period, the shrinkage of the water surface of Poyang Lake is the primary reason, which never makes the area transferred out to unused land increase. The construction land continues to expand, the net transfer is 45.30 km^2, the growth rate is basically the same as the previous period, and the primary source of construction land is still arable land. The net transfer of unused land was 6.06 km^2, an increase of 3.39 km^2 from the previous period, and there was a significant mutual transfer between waters.

3.2 Evaluation System of Urban Ecosystem Resilience

3.2.1 Evaluation Unit Division

The quantification and spatial representation of evaluation objects can improve the accuracy and visualization of evaluation and facilitate the analysis of their spatial and temporal distribution characteristics. Among them, the division of evaluation units is the basic work to realize spatial representation. Commonly used methods include 1) dividing risk units by administrative boundaries, used in areas with a large degree of human interference; 2) dividing risk units by topography and geomorphology, watersheds, and other natural geographical boundaries, determining the division of evaluation

TABLE 6 | Land-use transfer matrix of the study area.

Period	Landscape types	Farmland	Woodland	Grassland	Waters	Construction land	Unutilized land	Transfer out	Net transfer out
1990–2005	Farmland	3,721.98	64.61	3.08	81.69	213.5	4.27	367.15	188.65
	Woodland	59.32	1,122.86	3.41	4.34	22.88	0.13	1,153.62	16.28
	Grassland	3.2	5.02	84.55	1.49	3.51	0	94.57	4.84
	Waters	92.69	8.07	1.71	1,060.85	23.66	10.59	1,104.88	26.89
	Construction land	20.86	1.35	0.06	1.85	252.29	2.46	258.01	−45.33
	Unutilized land	2.44	0.05	0	9.46	1	295.19	305.7	−2.67
	Transfer in	178.5	1,137.34	89.73	1,077.99	303.34	308.37		
2005–2020	Farmland	3,637.84	40.99	2.37	35.6	182.75	0.2	261.91	103.54
	Woodland	69.31	1,085.58	3.53	3.34	39.78	0.02	1,132.25	24.25
	Grassland	7.72	14.93	68.28	1.21	0.64	0	85.06	12.12
	Waters	47.87	5.75	0.71	1,043.89	20.34	40.43	1,111.11	14.99
	Construction land	32.79	1.74	0.18	13.74	468.26	0.11	484.02	−45.3
	Unutilized land	0.67	0.01	0.24	33.94	0.3	277.31	311.8	−6.06
	Transfer in	158.37	1,108	72.94	1,096.12	529.33	317.86		

units within a relatively complete ecological region, and the ecosystems and landscape structures within the evaluation units have a high degree of homogeneity; and 3) grid method, dividing the study area into grids of equal size according to certain granularity and using the grids as evaluation units to analyze their spatial and temporal distribution characteristics. This method is convenient for spatial interpolation to obtain a continuous spatial distribution map, so it is more commonly used at present (Gong et al., 2014). In this study, the study area was divided into 0.1, 0.5, 1, and 5 km granularity according to the actual situation of Nanchang city, and the final comparison revealed that the most suitable granularity size for the study area is 1 km. A 1 km grid is not too dense and leads to too much workload, but it also can well distinguish and portray spatial homogeneity and heterogeneity. Therefore, according to the extent of the study area, the study area was divided into 1 × 1 km square evaluation units with a total of 7,536 sampling areas.

3.2.2 Spatial and Temporal Evolutionary Characteristics of Ecosystem Resistance

Habitat quality can be used as a proxy for "resilience" to characterize the ability of urban ecosystems to withstand external disturbances (Zhang, 2018). The habitat quality index refers to the magnitude of the ability of the environment to provide the conditions and resources needed for species and populations to survive and reproduce sustainably. The habitat quality index ranges from 0 to 1. The larger the value, the higher the habitat quality, the higher the biodiversity, and the higher the stability and resistance of the system itself. The ArcGIS regional statistical tool showed that the mean values of habitat quality in Nanchang in 1990, 2005, and 2020 were 0.487144, 0.47363, and 0.458934, respectively, indicating that the regional habitat quality had an overall downward trend.

In order to explore the role of the evolution of land-use patterns in the region in habitat quality in depth and conduct a comprehensive assessment of habitat quality in Nanchang city (Chen W. X. et al., 2022), drawing on the grading methods of relevant experts and scholars (Rong et al., 2016; Zhong and Wang, 2017; Chu et al., 2018) on habitat quality, and based on field research in the study area, the habitat quality results obtained from running the model for the three periods were classified into five classes: lower (0–0.2), low (0.2–0.3), medium (0.3–0.4), high (0.4–0.8), and higher (0.8–1). The area of habitat quality at each level and its percentage were calculated for the three periods (**Table 7**). In 1990, the study area had the largest proportion of low-grade habitats, 53.48%, and the proportion of higher-, lower-, medium-, and high-grade habitats decreased in order, 33.54%, 8.20%, 3.43%, and 1.36%, respectively. In 2005, except for the percentage of lower-grade habitats, which increased significantly to 11.57%, low-, medium-, high-, and higher-grade habitats all decreased slightly to 52.17%, 2.11%, 1.29%, and 32.86%, respectively. In 2020, the percentage of low-, high-, and higher-grade habitats continued to decrease to 50.54%, 1.05%, and 31.76%, respectively, based on the 2005 level. Unlike the previous period, the proportion of medium-grade habitats increased slightly and showed a fluctuating decrease overall, while the proportion of lower-grade habitats maintained a steady increase at 14.34%. Overall, lower and low-grade habitats quality has been dominant for a long time, and the proportion of lower-grade habitats has been increasing over the past 30 years, indicating that the overall habitat quality level in Nanchang is at a low level, while the continuous decrease in the proportion of high- and higher-grade habitats further indicates the habitat quality is deteriorating, mainly due to rapid urbanization and expansion of urban construction land in recent years, resulting in the proportion of lower-grade habitats and the rapid increase in the proportion of low-grade habitats. It is urgent to take measures to improve the ecological environment in Nanchang to prevent habitat degradation and achieve healthy ecosystem development.

Combined with the spatial distribution pattern of the three phases in **Figure 5**, the spatial variation in habitat quality in

TABLE 7 | Area and percentage of habitat quality for each grade.

Grade	Value range	1990		2005		2020	
		Area (km^2)	Percentage (%)	Area (km^2)	Percentage (%)	Area (km^2)	Percentage (%)
Lower	0–0.2	589.13	8.20	831.51	11.57	1,030.38	14.34
Low	0.2–0.3	3,842.13	53.48	3,748.09	52.17	3,630.82	50.54
Medium	0.3–0.4	246.24	3.43	151.65	2.11	166.15	2.31
High	0.4–0.8	97.56	1.36	92.60	1.29	75.13	1.05
Higher	0.8–1	2,409.54	33.54	2,360.73	32.86	2,282.11	31.76

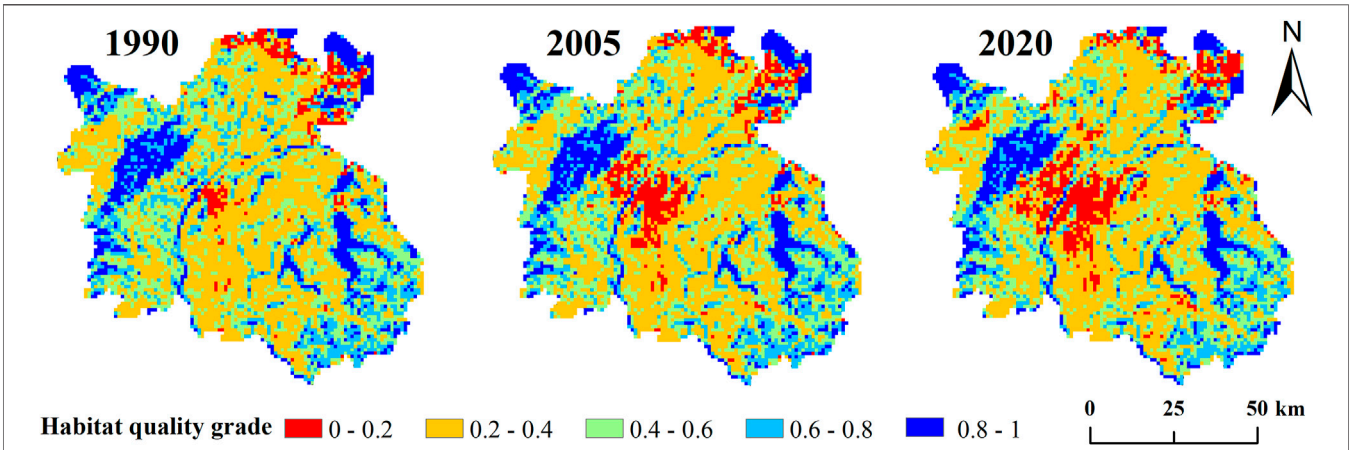

FIGURE 5 | Spatial distribution pattern of habitat quality in 1990, 2005, and 2020.

Nanchang was obvious during the study period, showing an overall low-grade pattern in the central part, gradually increasing in the surrounding area, and there was a significant correlation between habitat quality and land-use types in the study area. The habitat quality of forestland, grassland, water, and other ecological land distribution areas was higher, while the habitat quality of construction land and cultivated land was lower.

Lower habitat quality areas are mainly located in the urban built-up areas mainly on both sides of the Ganjiang River in the central part of the city, represented by Honggutan, Donghu, Xihu, and Qingshanhu Districts, which are closely connected with the center of Nanchang city and are the economically prosperous areas of Nanchang city, with rapid urban development, high urbanization levels, and rapid expansion of land for construction, whose disorderly spreading engulfs ecological space such as woodlands and grasslands, which in turn threatens the surrounding habitats and destroys the ecological integrity of the habitats on which living organisms depend, resulting in poor habitat quality in the area and a significant decline in habitat quality. Areas with poor habitat quality are scattered in most of the plain areas, where the main land-use category is arable land, and many rural settlements are gathered here, which are subject to great human interference and low biodiversity, resulting in increased habitat fragmentation, poor connectivity, and serious ecological destruction. The habitat quality in this area is mainly poor. The area proportion of high habitat quality is small, mainly scattered in Meiling in northwestern Nanchang, Poyang Lake in the northeast, and Junshan Lake and Qinglan Lake in the southeast. The famous Meiling National Forest Park is located in Meiling, which is mainly woodland, with rich biodiversity due to its overlapping mountains and scarce inhabitants, so its habitat quality is high. Poyang Lake, Junshan Lake, and Qinglan Lake have the role and advantages of protecting landscape biodiversity and replenishing groundwater, and the habitat quality in this area is also good under the protection of the local government. In general, the most significant spatial changes were observed in lower-grade habitats. From 1990 to 2005, the areas with lower habitat quality expanded in a circle around the Xihu, Donghu, Qingyunpu, and Qingshanhu Districts on the east bank of the Ganjiang River as the origin, with the most significant expansion spreading to the Meiling Mountains in the northwest and to Nanchang County in the south. The change in the area with higher habitat quality was not obvious. From 2005 to 2020, the expansion of the area with lower habitat quality in Honggutan District, Xinjian County and Nanchang County was significant. Unlike in the previous period, the area with higher habitat quality in the Poyang Lake area in the northeast of the study area experienced large-scale shrinkage because of human exploitation of resources in the Poyang Lake basin, which led to a series of human activities such as enclosing the lake for farming and urban expansion that engulfed the lake body. The habitat degradation of the Poyang Lake basin intensified, while the habitat quality of Junshan Lake and

TABLE 8 | Area and percentage of ecosystem adaptation at each level.

Grade	Value range	1990		2005		2020	
		Area	Percentage	Area	Percentage	Area	Percentage
Lower	0–20	1,185	15.73	1,276	16.94	1,251	16.60
Low	20–40	1,882	24.98	1,871	24.83	1,859	24.67
Medium	40–60	2,140	28.40	2,023	26.85	2,095	27.81
High	60–80	1,618	21.48	1,664	22.09	1,695	22.50
Higher	80–100	709	9.41	700	9.29	634	8.42

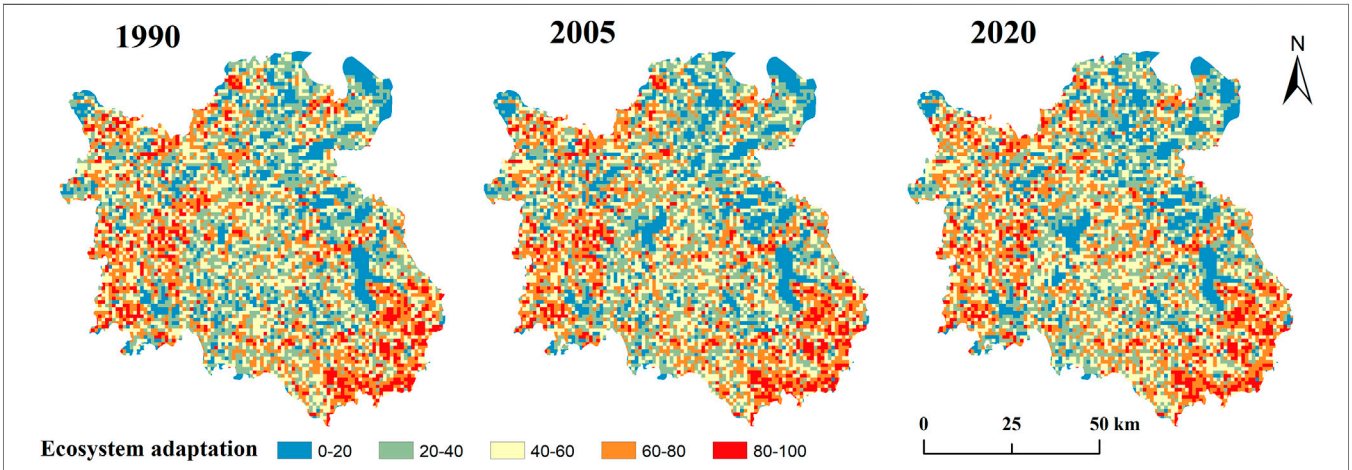

FIGURE 6 | Spatial distribution pattern of ecosystem adaptation in 1990, 2005, and 2020.

Qinglan Lake in the east was consistently maintained at a high level because they are closed water bodies with stable water levels, and the government has been effective in protecting them.

3.2.3 Spatial and Temporal Evolutionary Characteristics of Ecosystem Adaptation

To deeply explore and compare the changing trend of the ecosystem adaptation level, based on the Natural Hiatus Grading Method (Bai, 2019), ecosystem adaptation was divided into five levels using 20, 40, 60, 80, and 100 as critical values: lower ecosystem adaptation zone ($0 \leq A < 20$), low ecosystem adaptation zone ($20 \leq A < 40$), medium ecosystem adaptation zone ($40 \leq A < 60$), high ecosystem adaptation zone ($60 \leq A < 80$), and higher ecosystem adaptation zone ($80 \leq A < 100$). The area and proportion of each ecosystem adaptation zone were calculated (**Table 8**). The results show that, from 1990 to 2005, the trend of change in the adaptation level was mainly reflected in the lower ecosystem adaptation zone and the medium ecosystem adaptation zone, whose changed area reached 91 and 117 km^2, respectively, among which the area of the medium ecosystem adaptation zone showed a trend of shrinkage, the proportion of which decreased from 28.4% to 26.85%, while the lower ecosystem adaptation zone showed a trend of expansion, the proportion of which increased from 15.73% to 16.94%. The other classes showed less change. The trend of change in the adaptation level from 2005 to 2020 was the opposite. The main trend was the change in the medium ecosystem adaptation zone and higher ecosystem adaptation zone. In other words, the area of the medium ecosystem adaptation zone showed an upward trend, and the area of the higher ecosystem adaptation zone decreased. The area of the medium-level zone increased by 72 km^2, and the area of the higher-level zone decreased by 66 km^2. Specifically, the overall trend of the adaptation level from 1990 to 2005 decreased, the proportion of lower- and medium-level ecosystem adaptation gradually increased, and the level of ecosystem adaptation in the study area gradually decreased. On average, there was a medium level of adaptation from 2005 to 2020, the level of both higher and lower adaptation decreased, and the degree of differentiation of the adaptation level was moderated. In general, from the whole study period, the high and higher levels of adaptation changed significantly, with the area of higher-level adaptation decreasing from 9.41% to 8.42% and the high level increasing from 21.48% to 22.50%, but the medium level of adaptation was dominant during the study period, indicating that the adaptation level in the study area was mostly at the medium level.

The spatial distribution pattern of adaptation of urban ecosystems was analyzed (**Figure 6**) to compare the characteristics of their spatial distribution differences. From the spatial distribution, the levels of ecosystem adaptation in 1990, 2005, and 2020 showed similar distribution patterns with significant spatial heterogeneity characteristics. The areas with high values of adaptation are scattered in the west and southeast of the study area, where the main landscape type is woodland, with better natural ecological protection and a higher degree of

TABLE 9 | Area and percentage of ecosystem vitality at each level.

Ecological Vitality Grade	1990		2005		2020	
	Area/Km^2	Percentage (%)	Area/Km^2	Percentage (%)	Area/Km^2	Percentage (%)
Lower ecological vitality zone	292.74	4.07	320.47	4.46	342.75	4.77
Low ecological vitality zone	2,794.63	38.90	2,902.63	40.40	3,052.63	42.49
Medium ecological vitality zone	2,093.26	29.14	1,992.53	27.73	1,875.25	26.10
High ecological vitality zone	1,401.37	19.51	1,382.64	19.24	1,337.28	18.61
Higher ecological vitality zone	602.63	8.39	586.36	8.16	576.72	8.03

connectivity. The areas with low values of adaptation are clustered in the urban built-up areas in the central part of the study area, the plains with arable land as the main type of land in the east, and the water areas such as lakes and reservoirs. The proportion of low- and medium-grade adaptation dominated during the study period and showed a basal distribution pattern, and the distribution of low- and medium-grade adaptation was generalized in the region, which played a decisive role in the adaptation level, indicating that the adaptation level in the study area was mostly at the middle to lower level.

Further analysis of the changes in the spatial distribution of adaptation reveals that the levels of adaptation changed significantly from 1990 to 2005, and the area that experienced significant changes was the central urban built-up area in a circle-like ring clustering, mainly because of the rapid increase in population and socioeconomic status at the early stage of urban development and the expansion of urbanization, which required a large amount of construction land, significantly reducing the forestland, arable land, grassland, and other ecological lands around the city. At the same time, as the intensity of human activities increased, dominant artificial patches with excellent connectivity were formed, landscape homogeneity was serious, landscape heterogeneity and species diversity decreased, and landscape heterogeneity and landscape connectivity, which characterize ecosystem resilience, declined significantly at the same time during this period, so the area with a low value of adaptation during the expansion from 1990 to 2005 is obvious. The change in adaptation from 2005 to 2020 is not obvious, mainly because the policies of "returning farmland to forest" and "returning farmland to grassland" were put forward in 2002 and 2003, and the 17th Party Congress put forward the concept of ecological civilization in 2007, when the government began to pay attention to ecology. However, the mathematical analysis of adaptation in shows that the overall level of adaptation in 2020 is still lower than that in 1990, and the change in patch morphology caused by urban expansion has led to the decline in landscape connectivity and landscape heterogeneity. In the process of rapid urban development, how to use existing regional conditions to increase the stability of landscape structure and thus enhance ecosystem adaptation is a question that urban builders need to seriously consider.

3.2.4 Spatial and Temporal Evolutionary Characteristics of Ecosystem Vitality

The average ecological vitality of Nanchang in 1990, 2005, and 2020 was 0.474561, 0.468409, and 0.460525, respectively, which shows that, with the development of urbanization, some unreasonable development and utilization behaviors have broken the ecological space, and the ecosystem processes are less resistant and adaptive to external disturbances. The resistance and adaptation of ecosystem processes to external disturbances are reduced.

To explore the characteristics of ecosystem vitality changes in depth, based on the Natural Hiatus Grading Method (Bai, 2019), ecosystem risk was classified into five levels using 0.20, 0.40, 0.55, and 0.75 as critical values: lower ecological vitality zone ($R < 0.20$), low ecological vitality zone ($0.20 \leq R < 0.40$), medium ecological vitality zone ($0.40 \leq R < 0.55$), high ecological vitality zone ($0.55 \leq R < 0.75$), and higher ecological vitality zone $R \geq 0.75$. The area and proportion of each vitality zone were calculated (**Table 9**). The results show that, from 1990 to 2020, the ecosystem vitality of Nanchang was mainly dominated by low ecological vitality zones and medium ecological vitality zones, and the sum of the two was more than 60% in each period. The city was in a rapid development stage, the overall ecosystem vitality was at a low level, and the resistance and adaptive ability of the urban ecosystem to external risks still needed to be strengthened.

The study area had the largest share of low ecological vitality areas in 1990, with 38.90%, and the share of areas with medium, high, higher, and lower ecological vitality decreased by 29.14%, 19.51%, 8.39%, and 4.07%, respectively. In 2005, the areas with medium, high, and higher ecological vitality showed a continuous downward trend during the study period, except for the percentage of lower ecological vitality zones and low ecological vitality zones, which increased to 4.46% and 40.40%, respectively. In 2020, the share of areas with medium, high, and higher ecological vitality continued to decrease to 26.10%, 18.61%, and 8.03%, respectively, from the 2005 level, while the share of lower and low ecological vitality zones continued to increase, indicating that the ability of ecosystems to maintain their structure and pattern has not improved. It is noteworthy that the area with lower ecological vitality gradually expanded from 4.07% in 1990 to 4.77% in 2020, with an increase of 17.20%. This area needs to be closely monitored to prevent further reduction in ecological vitality. Overall, the ecosystem vitality response to disturbance and self-regulation in the study area has been decreasing, mainly due to the rapid urbanization and expansion of urban construction land in recent years, resulting in a rapid increase in the proportion of the area with low ecological vitality. Nanchang city urgently needs to adopt means to improve the ecological environment to prevent the

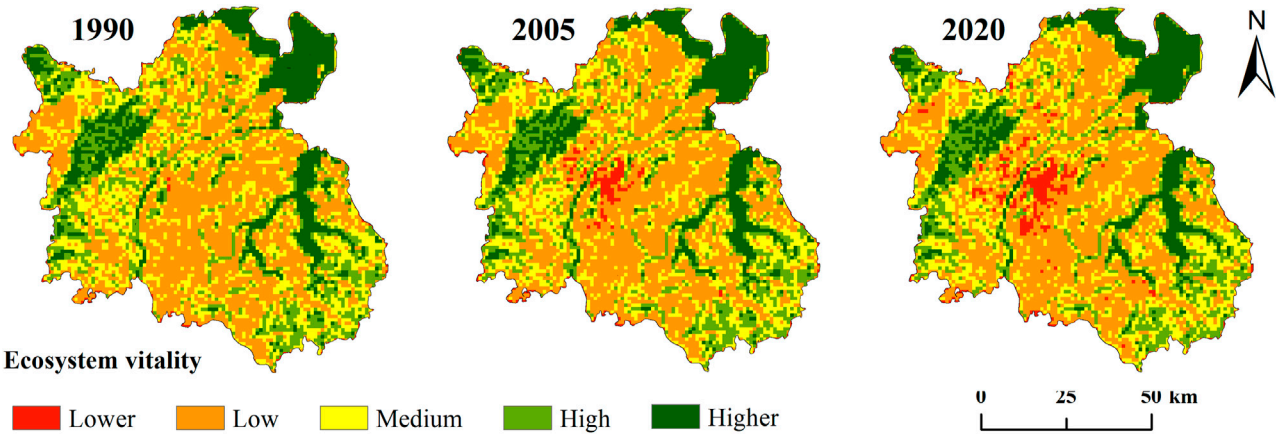

FIGURE 7 | Spatial distribution pattern of ecological elasticity in 1990, 2005, and 2020.

decline in ecosystem vitality to achieve healthy ecosystem development.

The spatial pattern of ecosystem vitality in Nanchang was obtained using the ArcGIS 10.7 software to calculate the ecological vitality index and classify 7,536 grid plots in 1990, 2005, and 2020 using the natural break method (**Figure 7**). From 1990 to 2020, the spatial divergence of ecosystem vitality was significant, showing low vitality in the middle of the decade and high vitality in the fourth year.

From **Figure 7**, it can be seen that the low ecological vitality areas occupy the main part of the spatial distribution of Nanchang, dominated by arable land, which is widely distributed and forms the substrate because there is more human activity interference in arable land and lower biodiversity because of its lower vitality level. The areas with higher ecological vitality are distributed in clusters, with woodland, water, and other land types with high biodiversity as the main areas. The areas with lower ecological vitality are distributed in the urban built-up areas on both sides of the Ganjiang River in the central part of the study area. The medium and high ecological vitality areas are scattered in Jinxian County in the southeast and Xinjian County in the southwest of the study area, and the main land types are woodland and grassland. In 1990, the area with lower ecological vitality was very small and concentrated in the old urban areas, such as Donghu and Xihu Districts. From 1990 to 2005, the area with lower ecological vitality began to expand to the west bank of the Ganjiang River and Nanchang County, and t. This expansion led to concentrated and continuous urban construction land, which was disturbed by high-intensity human activities. Ecological vitality showed concentrated and continuous drastic changes in the urban expansion zone. From 2005 to 2020, the area with lower ecological vitality continued to maintain a significant expansion trend because the northwest expansion straddled the Meiling Mountains. The development and utilization of mountainous areas are difficult, and development is blocked, so the expansion of the area with lower ecological vitality expanded in a "southwest-northeast" direction. The southwest direction is represented by the rapid development of the Honggutan District, and the spread to Xinjiang County represents the northeast direction. In general, the distribution of lower ecological vitality areas is significantly influenced by urban expansion, and the growth trend is approximately the same as the expansion of construction land, which has a greater correlation with economic development and human activities, on which the expansion of construction land and economic development have had certain ecological and environmental impacts. From 1990 to 2020, although the area with higher ecological vitality showed a slight decrease, its distribution pattern was relatively stable, mainly distributed in the Poyang Lake basin in the northeast, the Meiling Mountains in the northwest, and Junshan Lake and Qinglan Lake in the east, which are also part of the Poyang Lake basin, thanks to the ecological pattern structure of Nanchang city of "eastern lake and western mountains, mountains and lakes reflecting each other" and "the ecological pattern structure of Nanchang city and the planning of two ecological barriers of "Poyang Lake—Qinglan Lake in the east and Meiling–Mengshan–Xishan in the west." Other levels of areas with ecological vitality have fewer changes in spatial distribution.

3.3 Resilience Level and Spatial Analysis of Urban Ecosystem Resilience Based on "Resistance-Adaptation-Vitality"

3.3.1 Spatial and Temporal Evolutionary Characteristics of Urban Ecosystem Resilience

In the context of continuous urban expansion, the mean value of urban ecosystem resilience declined from 0.491496 in 1990 to 0.475469 in 2005 and to 0.454988 in 2020, indicating a gradual decrease in ecosystem resilience during the 30-year period from 1990 to 2020, which indicates that human activities have gradually increased the consumption of ecosystems and caused a gradual decrease in ecosystem resilience. This indicates that human activities have gradually increased the consumption of ecosystems, resulting in the decreasing level of ecosystem

TABLE 10 | Area and proportion of each grade of comprehensive resilience level of the ecosystem in Nanchang.

Grade	Value range	1990		2005		2020	
		Area (km^2)	Percentage (%)	Area (km^2)	Percentage(%)	Area (km^2)	Percentage(%)
Lower	0–0.2	300	3.98	384	5.34	464	6.45
Low	0.2–0.4	1,965	26.07	1,852	25.74	2014	27.99
Medium	0.4–0.5	2,472	32.80	2,428	33.75	2,239	31.12
High	0.5–0.6	1,633	21.67	1,631	22.67	1,604	22.29
Higher	0.6–0.85	825	10.95	900	12.51	874	12.15

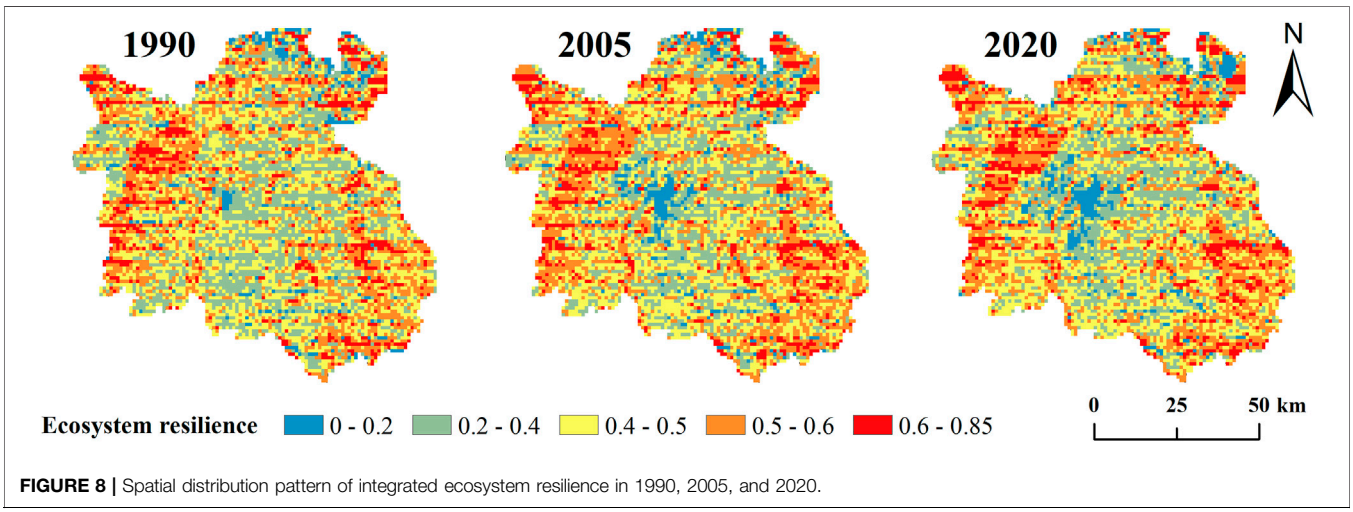

FIGURE 8 | Spatial distribution pattern of integrated ecosystem resilience in 1990, 2005, and 2020.

resilience and the gradual reduction of the city's ability to address risks. In order to compare the trends of urban ecosystem resilience, the ecosystem resilience index was classified into five levels: lower, low, medium, high, and higher using natural breaks (Jenks) classification (**Table 10**).

The results show that from 1990 to 2020, the ecosystem resilience level of Nanchang was mainly dominated by low and medium ecological resilience levels. The sum of the two was more than 55% in all three periods, and ecosystem resilience contributed a great deal to the overall resilience level. As the city is in a rapid development stage, the overall ecosystem resilience level is at a lower median level, and the resistance and adaptation capacity of the urban ecosystem to external risks still needs to be strengthened. During the study period, low-grade resilience showed a continuous upward trend, and the area with lower-grade resilience expanded significantly from 1990 to 2005, with an increase of 28% during the 15 years, while lower-grade resilience increased slightly from 2005 to 2020 to 20.78%. The area with a low ecological resilience level first decreased and then increased, with an overall "V"-shaped fluctuating upward trend. From 1990 to 2005, the area decreased slightly, and the proportion decreased by 0.33%, while from 2005 to 2020, the low resilience area increased by 2.25% and reached 27.99%. The area with a medium ecological resilience level first increased and then decreased, showing an overall inverted V-shaped fluctuating decline with a plateau at a moderate level, accounting for more than 30% of the three periods and contributing significantly to the overall resilience level. The area with a high-level ecological resilience level increased overall during the study period, but the magnitude of change was relatively small. The area with a higher-level ecological resilience showed an upward trend, with a good regional resilience level trend (Yu et al., 2022).

From **Figure 8**, the spatial distribution pattern of urban ecosystem resilience based on "resistance-vitality-adaptation" was analyzed, and ecosystem resilience was classified into five levels (lower, low, medium, high, and higher) using 0.2, 0.4, 0.5, and 0.6 as cutoff points to compare their spatial differences. From the spatial distribution of resilience levels, the overall spatial distribution of ecosystem resilience from 1990 to 2020 shows a pattern of "low in the middle and high around," with significant spatial differentiation. The areas with lower ecological resilience are mainly distributed in the central urban built-up areas, while the higher-grade ecological resilience areas are located in Meiling National Forest Park, the mountainous and hilly areas in the northwest of Anyi County, most of Jinxian County and the Poyang Lake area in the northeast of the study area. The medium-grade resilience areas occupy the base of urban spatial distribution, are widely distributed, and are the main body of the study, among which the resilience of the built-up areas of central cities is distributed in a piecemeal manner, and the expansion trend is obvious during the study period.

Exploring the changes in the spatial distribution of urban ecosystem resilience, from 1990 to 2005, the areas with lower resilience expanded in a circle around the old urban areas such as Xihu, Donghu, and Qingyunpu Districts as the origin; the low resilience areas immediately adjacent to the urban areas were

TABLE 11 | Spatial autocorrelation analysis results of ecosystem resilience in Nanchang city.

Year	Moran's I	Z-score	*p*-value	Result
1990	0.414918	50.440,827	0.000000	Cluster
2005	0.472387	57.424,714	0.000000	Cluster
2020	0.516780	62.818,151	0.000000	Cluster

transformed into lower resilience areas, and the proportion of low resilience areas shrank slightly. From 2005 to 2020, except for the spread of lower resilience areas in the central part of the city, another more significant expansion appeared in the northeastern Poyang Lake area in the form of clumps, and many high- and higher-grade resilience areas were transformed into lower-grade resilience areas. The land type in this area is mainly wetland mudflats, and the loss of lake wetlands caused by factors such as lake reclamation is an important reason for the decline in ecosystem resilience in this area. At the same time, low resilience areas were also transformed from medium-level resilience areas because most areas in Nanchang are medium-level ecological resilience areas, and arable land is the main landscape of the area. However, the continuous promotion of urbanization makes the rural settlements continue to gather, integrate, and expand, resulting in the gradual shrinkage of arable land in the area. Coupled with the great improvement in transportation infrastructure in recent years, the crisscrossing road network leads to higher fragmentation of arable land patches and increasing pressure on the landscape, which gradually has a negative effect on the ecosystem, thus making the ecosystem resilience level in the area transform from a medium to a low level. From 1990 to 2020, the area with higher resilience increased in Jinxian County in the southeastern part of the study area, mainly transformed from high-grade ecological resilience areas, which are located in the lakeside plain with dense water networks, numerous lakes, abundant water resources, and superior ecological conditions. Coupled with the vigorous development of woodland-dependent derivative industries in the area in recent years to further increase biodiversity, the level of ecosystem resilience has increased.

3.3.2 Spatial and Temporal Evolutionary Characteristics of Urban Ecosystem Resilience

As shown in **Table 11**, the global Moran index of ecosystem resilience in Nanchang from 1990 to 2020 was above 0.40, among which the lowest global Moran index was 0.414918 in 1990 and gradually increased from 1990 to 2020, with the highest value of 0.516780 in 2020. The standardized *z*-values were all greater than 1.96 and all were statistically significant. All of them passed the significance level test of $p = 0.05$, indicating that there was a positive spatial correlation and a high correlation in the level of ecosystem resilience in Nanchang during the study period. The growth of the Moran index and the increasing standardized z-score indicate that the spatial clustering of regional landscape ecosystem security indices is further evidence.

The distribution pattern of cold hot spots in Nanchang city during 1990–2020 was obtained by hot spot analysis in ArcGIS 10.7. The results are shown in **Figure 9**. The cold spots during the study period are mainly located in the urban area in the middle of the study area, and the hot spots are mainly distributed in three places in the western, northeastern, and southeastern parts of the study area, except for the western part. The other two places are far from the main urban area, the primary land-use types are water, woodland, and grassland, and the land-use intensity is low.

In 1990, the area with cold spots was widely distributed, in which the larger cold spot patches were located in the central Donghu, Xihu, and Qingyunpu Districts, and the rest of the finer cold spot patches were scattered in the northern Poyang Lake basin and southern counties. By 2005, the area with cold spots experienced a significant expansion, and the direction and rate of its expansion were consistent with the spreading characteristics of urban construction land. During the period 1990–2005, most of

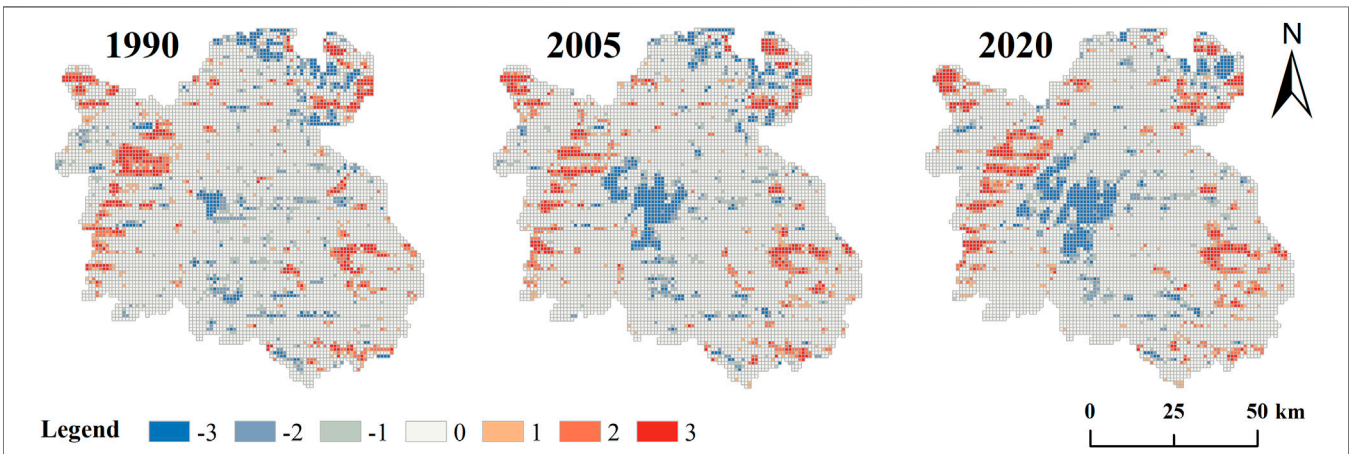

FIGURE 9 | Distribution patterns of cold/hot spots of ecosystem resilience in 1990, 2005, and 2020. Note: 3/3 represents the cold spot/hot spot with a 99% confidence level; –2/2 represents the cold spot/hot spot with a 95% confidence level; –1/1 indicates the cold spot/hot spot with a 90% confidence level; and 0 indicates no statistical significance.

the hotspot areas of ecosystem resilience in Nanchang remained unchanged from the previous period, with significant changes occurring in the Meiling area of the study area, where high values of ecosystem resilience were originally clustered by human activities and urban expansion, becoming insignificant.

4 DISCUSSION

4.1 Findings

The medium and low levels of resilience of the Nanchang ecosystem dominated for a long time, and the growth rate of the low level of resilience was the most significant, indicating that the overall level of resilience of the Nanchang ecosystem is relatively low, and the overall level of resilience of the urban ecosystem still needs to be further improved. In the face of external threats (i.e., increasing risks), cities need to continuously improve the level of ecosystem resilience to cope with shocks, strengthen the ecological environment, gradually improve the overall level of habitat quality and biodiversity richness, and enhance ecosystem integrity and stability, thus contributing to a certain extent to the increase in ecosystem resilience. In general, the spatial distribution of ecosystem resilience based on "resistance-vitality-adaptation" is influenced by the quality of habitat, stability of landscape structure and ecological resilience. On the one hand, we protect and reasonably utilize the ecological space with woodland, grassland, lakes, and wetland as the main types of land to enhance the stability of the ecosystem and improve ecosystem resilience. On the other hand, the intensive use of construction land and three-dimensional development should be promoted to avoid the negative impact on ecological space caused by the expansion of the urban "disorderly state."

From 2005 to 2020, the cold spots of ecosystem resilience in Nanchang County east of the main urban area tended to gather, indicating that the difference in ecosystem resilience between the regions was narrowing, mainly because Nanchang County is so close to Nanchang city that the two areas have undergone colocation development and the urban construction sites have been connected. Meanwhile, the rapid socioeconomic development in the Honggutan District on the west bank of the Ganjiang River inevitably has some impact on the ecology, so new cold spot patches appeared in this area. In addition, in the Poyang Lake basin in the northeast of the study area, the originally scattered cold spot areas were gathered into larger cold spot patches, which indicates that the ecological function of the land in this area is reduced compared with the previous area and needs to be considered. The change in hot spot areas is less significant. In summary, the area with higher ecosystem resilience is mainly located in the area dominated by natural ecological land, especially the mountainous, hilly area dominated by woodland and water landscape types, while the area with lower ecosystem resilience is mainly located in the plains area dominated by construction land and other landscape types. During 1990–2020, Nanchang still needed to increase investment in ecological environmental protection and management to promote regional ecological security.

4.2 Implications

The implications of this study can be described from both theoretical and practical aspects.

In terms of theory, at present, the study of urban ecosystem resilience is still in its initial stage, and there are still many theories that need to be improved, but there is a lack of systematic research. In this study, based on the basic characteristics of resilience, with reference to previous research results, the urban ecological resilience evaluation index model is constructed from the three dimensions of "resistance-adaptation-vitality," which not only provides a quantitative evaluation framework for the ecosystem resilience theory of Nanchang city but also provides a qualitative evaluation framework for the ecosystem resilience theory of Nanchang city. The model also provides theoretical guidance and application demonstration for ecological resilience assessment of other similar cities in China and the world.

In terms of practice, as the key city of the Poyang Lake city cluster, Nanchang plays an important role in the economic development strategy of central China. However, with the rapid economic development in recent years, the accelerated urbanization process has posed a threat to the ecological environment and even endangered regional ecological security. Urban ecosystem resilience is an anticipatory, goal-oriented risk management model that aims to enhance the defensive capacity of urban ecosystems against ecological risks, their ability to restore normalcy after threats, and their adaptation to similar threats. Thus, there is a significant problem-response mechanism between ecological risk and urban ecological resilience, which are closely linked and interlocking and are two aspects that must be considered holistically in urban ecological protection. Therefore, taking Nanchang city as an example to carry out research on urban ecosystem resilience, it is of great significance to establish a sound mechanism for the green development of the urban ecosystem and realize the coordinated development of the urban social economy and ecological protection.

4.3 Limitations

The city is a huge system consisting of many subsystems, such as social, cultural, economic, ecological, and political subsystems. Although this study is innovative in constructing an indicator system based on the feasibility of empirical research and the quantifiability of data, it is still necessary to acknowledge that the indicators used in this study can hardly cover all the characteristics of urban resilience. It is imperative to systematize the framework of urban ecological resilience indicators, and the coupling of social, economic, ecological, cultural, and other urban subsystems into the ecological resilience evaluation system is also the focus of future research in the academic community.

At this stage, research on the resilience of urban ecosystems is just beginning and is still immature. By considering the limitation of data acquisition, this study uses the parametric substitution method to construct the evaluation framework, which makes the ecosystem resilience evaluation more convenient. However, it should be noted that the establishment of the urban ecosystem resilience evaluation model in this study may lack the

quantification of some risk factors and disaster prevention culture. Uncertainty risk data should be incorporated into the integrated assessment framework in the future to improve the accuracy of ecosystem resilience assessment results.

5 CONCLUSION

This study constructs an urban ecological resilience assessment model from the three aspects of the basic characteristics of resilience (resistance, adaptation, and vitality). Second, taking Nanchang as an example, we summarize its ecological resilience evolution law and characteristics by quantitatively measuring its ecosystem resilience and use the patch-level landscape simulation PLUS model to conduct a multiscenario simulation and ecological resilience assessment of the urban expansion of Nanchang in 2035. Based on the above study, this study obtained the following conclusions:

1) Land-use types in Nanchang are mainly arable land, forestland, and water area, which together occupy approximately 90% of the total area of the study area. The 1990–2020 land-use change trend was mainly characterized by the continuous decrease in arable land and ecological land (forestland, grassland, and water area) and the continuous increase in construction land. Cultivated land is the largest land type transferred out, and the mutual transfer between it and construction land is remarkable. The largest dynamic attitude of construction land reaches 5.33% from 1990 to 2005, and the transfer from natural ecological landscapes (woodlands, grasslands, waters, etc.) to human landscapes (construction land, cultivated land, etc.) is the general trend and main feature of land-use transfer in the study area over the 3 decades.
2) From 1995 to 2020, the ecosystem resilience level of Nanchang city was at a medium-to-low level for a long time, and the overall trend is decreasing. The spatial distribution of ecosystem resilience shows a stable pattern of "high in the east and low in the west," with a stable distribution pattern of higher and lower resilience and significant spatial heterogeneity, in which the higher resilience areas are mainly located in the hilly areas dominated by natural ecological land, and the lower resilience areas are mainly located in the plain areas dominated by construction land, arable land, and other landscape types.
3) By changing the probability of land-use transfer and designating prohibited development zones, three land-use scenarios of ecological protection, natural development, and urban development are set, and the PLUS model, a patch-level landscape simulation model, is used to simulate and predict the expansion hotspots of urban construction land in 2035 under multiple scenarios, mainly in Donghu, Xihu, Qingyunpu, Qingshanhu, and Xinjian Districts. In addition, the Honggutan District and the Changbei area located in Ganjiang New District are important directions for future urban development. A large area of arable plains in central Nanchang County, the Poyang Lake area in the northeast, Meiling National Forest Park in the southwest, and woodlands and lakes and reservoirs in Jinxian County in the southeast are threatened by the expansion of urban construction land and encroachment of human activities, and ecological security is under threat.
4) Comparing the level of ecosystem resilience under three scenarios in 2035, the relationship between the ecological conservation scenario, the normal development scenario, and the high-speed development scenario is presented. Under different scenario simulations, there are significant differences between construction land expansion and ecological land protection. The conflict between the two is most prominent in the high-speed development scenario, and ecological land is the most threatened. In general, a large amount of ecological space (mountains, water, forests, and fields) in the periphery of urban areas is the main provider of ecosystem resilience. The contiguous expansion of urban areas and towns along transportation routes intensifies the fragmentation of natural ecological space, reduces ecosystem connectivity, and has a direct impact on ecosystem resilience impairment.

DATA AVAILABILITY STATEMENT

The raw data supporting the conclusions of this article will be made available by the authors without undue reservation.

AUTHOR CONTRIBUTIONS

LD, DZ, and YL: conceptualization, methodology, and visualization. LD: software and funding acquisition. DZ, YL, and MZ: validation. YZ and ZW: formal analysis and supervision. MZ and ZW: investigation. LD, DZ, and YL: writing—review and editing.

FUNDING

This research was funded by the Jiangxi Provincial Social Science Foundation "the 14th Five-Year Plan" (2021) regional projects (21DQ44), Institutional Research Centers of Jiangxi Provincial of Ecological Civilization Construction (JXST2103), Science and Technology Research Project of Jiangxi Provincial Department of Education (GJJ210723), the Doctoral Research Initiation fund of East China University of Technology (DHBK2019184).

ACKNOWLEDGMENTS

The authors are grateful to the editor and reviewers for their valuable comments and suggestions.

REFERENCES

Abdrabo, M. A., and Hassaan, M. A. (2015). An Integrated Framework for Urban Resilience to Climate Change - Case Study: Sea Level Rise Impacts on the Nile Delta Coastal Urban Areas. *Urban Clim.* 14, 554–565. doi:10.1016/j.uclim.2015.09.005

Anselin, L. (1995). Local Indicators of Spatial Association-LISA. *Geogr. Anal.* 27, 93–115.

Bai, L. M. (2019). "Evaluation and Optimization of Urban Ecological Resilience in Changchun Based on Landscape Pattern," (Changchun, China: Northeast Normal University). PhD Thesis. doi:10.27011/d.cnki.gdbsu.2019.000089

Bozza, A., Asprone, D., Parisi, F., and Manfredi, G. (2017). Alternative Resilience Indices for City Ecosystems Subjected to Natural Hazards. *Computer-Aided Civ. Infrastructure Eng.* 32, 527–545. doi:10.1111/mice.12275

Chen, W. X., Zhao, X. L., Zhong, M. X., Li, J. F., and Zeng, J. (2022a). Spatiotemporal Evolution Patterns of Ecosystem Health in Middle Reaches of the Yangtze River Urban Agglomerations. *Acta Ecol. Sin.* 42 (1), 138–149. doi:10.5846/stxb202012093142

Chen, Y., Qiao, F., and Jiang, L. (2016). Effects of Land Use Pattern Change on Regional Scale Habitat Quality Based on InVEST Model—A Case Study in Beijing. *Acta Sci. Nat. Univ. Pekin.* 52 (3), 553–562. doi:10.13209/j.0479-8023.2016.057

Chen, Y., Yang, J., Yang, R., Xiao, X., and Xia, J. (2022b). Contribution of Urban Functional Zones to the Spatial Distribution of Urban Thermal Environment. *Build. Environ.* 216, 109000. doi:10.1016/j.buildenv.2022.109000

Chu, L., Zhang, X. R., Wang, T. W., Li, Z. X., and Cai, C. F. (2018). Spatial-temporal Evolution and Prediction of Urban Landscape Pattern and Habitat Quality Based on CA-Markov and InVEST Model. *Ying Yong Sheng Tai Xue Bao* 29 (12), 4106–4118. doi:10.13287/j.1001-9332.201812.013

Feng, X. H., Zhong, Y. X., Li, J. X., and Huang, J. (2015). Causal Analysis on Economic Disparity in Yangtze River Basin. *World Reg. Stud.* 24 (3), 100–109. doi:10.3969/j.issn.1004-9479.2015.03.012

Gimenez, R., Labaka, L., and Hernantes, J. (2017). A Maturity Model for the Involvement of Stakeholders in the City Resilience Building Process. *Technol. Forecast. Soc. Change* 121, 7–16. doi:10.1016/j.techfore.2016.08.001

Gong, J., Zhao, C. X., Xie, Y. C., and Gao, Y. J. (2014). [Ecological Risk Assessment and its Management of Bailongjiang Watershed, Southern Gansu Based on Landscape Pattern],southern Gansu Based on Landscape Pattern. *Ying Yong Sheng Tai Xue Bao* 25 (7), 2041–2048. doi:10.13287/j.1001-9332.20140425.005

He, B.-J., Wang, J., Zhu, J., and Qi, J. (2022). Beating the Urban Heat: Situation, Background, Impacts and the Way Forward in China. *Renew. Sustain. Energy Rev.* 161, 112350. doi:10.1016/j.rser.2022.112350

He, B.-J., Zhao, D.-X., Zhu, J., Darko, A., and Gou, Z.-H. (2018). Promoting and Implementing Urban Sustainability in China: An Integration of Sustainable Initiatives at Different Urban Scales. *Habitat Int.* 82, 83–93. doi:10.1016/j.habitatint.2018.10.001

He, B.-J., Zhao, D., Xiong, K., Qi, J., Ulpiani, G., Pignatta, G., et al. (2021). A Framework for Addressing Urban Heat Challenges and Associated Adaptive Behavior by the Public and the Issue of Willingness to Pay for Heat Resilient Infrastructure in Chongqing, China. *Sustain. Cities Soc.* 75, 103361. doi:10.1016/j.scs.2021.103361

He, Y. (2017). Ecology and Resilience in the New Urban Agenda: Report on Habitat III. *World Archit.* 4, 24–29. doi:10.16414/j.wa.2017.04.004

Holling, C. S. (1996). *Engineering Resilience versus Ecological Resilience.Engineering within Ecological Constraints*. Canada: National Academies Press.

Huang, Y., Feng, Z., Yue, W. Z., Feng, S. R., and Zhang, J. H. (2020). Spatial-temporal Evolution of Habitat Quality and Analysis of Landscape Patterns in Dabie Mountain Area of West Anhui Province Based on InVEST Model. *Acta Eco Sin.* 40 (9), 2895–2906. doi:10.5846/stxb201904260858

Jin, G., Deng, X. Z., Zhao, X. D., Guo, B. S., and Yang, J. (2018). Spatio-temporal Patterns of Urban Land Use Efficiency in the Yangtze River Economic Zone during 2005-2014. *Acta Geogr. Sin.* 73 (07), 1242–1252. doi:10.11821/dlxb201807005

Liu, C. F., and Wang, C. (2018). Spatio-temporal Evolution Characteristics of Habitat Quality in the Loess Hilly Region Based on Land Use Change: a Case Study in Yuzhong County. *Acta Eco Sin.* 38 (20), 7300–7311. doi:10.5846/stxb201710101800

Liu, Z. W. (2014). "Ecological Response to Wetland Landscape Pattern Change Based on InVEST Model: A Case Study in Southern Hangzhou Bay Area," (Hangzhou, China: Zhejiang University). Master's Thesis.

Luedeling, E., and Buerkert, A. (2008). Typology of Oases in Northern Oman Based on Landsat and SRTM Imagery and Geological Survey Data. *Remote Sens. Environ.* 112 (3), 1181–1195. doi:10.1016/j.rse.2007.08.007

Ma, K. M., Kong, H. M., Guan, W. B., and Fu, B. J. (2001). Ecosystem Health Assessment: Methods and Directions. *Acta Ecol. Sin.* 21 (12), 2106–2116. doi:10.3321/j.issn:1000-0933.2001.12.020

Manyena, S. B. (2006). The Concept of Resilience Revisited. *Disasters* 30 (4), 434–450. doi:10.1111/j.0361-3666.2006.00331.x

Ostrom, E. (2004). Panarchy: Understanding Transformations in Human and Natural Systems. *Ecol. Econ.* 49 (4), 488–491. doi:10.1016/j.ecolecon.2004.01.010

Ou, W. X., Zhao, L. N., and Li, R. (2014). Simulation on Regional Ecological Land Demand Based on Coordination of the Eco-Environmental Stress – Acase Study of Jiangsu Province. *Res. Soil Water Conservation* 21 (4), 274–278. doi:10.13869/j.cnki.rswc.2014.04.053

Peng, J., Liu, Y., Wu, J., Lv, H., and Hu, X. (2015). Linking Ecosystem Services and Landscape Patterns to Assess Urban Ecosystem Health: A Case Study in Shenzhen City, China. *Landsc. Urban Plan.* 143, 56–68. doi:10.1016/j.landurbplan.2015.06.007

Ren, H., Wu, J. G., and Peng, S. L. (2000). Evaluation and Monitoring of Ecosystem Health. *Trop. Geo* 20 (4), 310–316. doi:10.3969/j.issn.1001-5221.2000.04.018

Ren, J., Yang, J., Zhang, Y., Xiao, X., Xia, J. C., Li, X., et al. (2022). Exploring Thermal Comfort of Urban Buildings Based on Local Climate Zones. *J. Clean. Prod.* 340, 130744. doi:10.1016/j.jclepro.2022.130744

Rong, Y. J., Zhang, H., and Wang, Y. S. (2016). Assessment on Land Use and Biodiversity in Nanjing City Based on logistic-CA-Markov and InVEST Model. *Res. Soil Water Conservation* 23 (3), 82–89. doi:10.13869/j.cnki.rswc.2016.03.015

Suárez, M., Gómez-Baggethun, E., Benayas, J., Tilbury, D., Benayas, J, Tilbury, D, et al. (2016). Towards an Urban Resilience Index: A Case Study in 50 Spanish Cities. *Sustainability* 8 (8), 774. doi:10.3390/su8080774

Turner, M. G. (2003). Landscape Ecology: The Effect of Pattern on Process. *Annu. Rev. Ecol. Syst.* 20, 171–197. doi:10.1146/annurev.es.20.110189.001131

Wu, J. S., Cao, Q. W., Shi, S. Q., Huang, X. L., and Lu, Z. Q. (2015). Spatio-temporal Variability of Habitat Quality in Beijing-Tianjin-Hebei Area Based on Land Use Change. *Ying Yong Sheng Tai Xue Bao* 26 (11), 3457. doi:10.13287/j.1001-9332.20150915.008

Xia, C., Dong, Z. Y. Z., and Chen, B. (2022). Spatio-temporal Analysis and Simulation of Urban Ecological Resilience: A Case Study of Hangzhou. *Acta Eco Sin.* 42 (1), 116–126. doi:10.5846/stxb202101030007

Xie, H. L., and Li, B. (2008). Driving Forces Analysis of Land-Use Pattern Changes Based on Logistic Regression Model in the Farming-Pastoral Zone: A Case Study of Ongiud Banner, Inner Mongolia. *Geogr. Res-Aust* 27 (2), 294–304. doi:10.3321/j.issn:1000-0585.2008.02.007

Xie, P., Yang, J., Sun, W., Xiao, X., and Cecilia Xia, J. (2022). Urban Scale Ventilation Analysis Based on Neighborhood Normalized Current Model. *Sustain. Cities Soc.* 80, 103746. doi:10.1016/j.scs.2022.103746

Xiu, C. L., Wei, Y., and Wang, Q. (2018). Evaluation of Urban Resilience of Dalian City Based on the Perspective of Size-Density-Morphology. *Acta Geogr. Sin.* 73 (12), 2315–2328. doi:10.11821/dlxb201812004

Yang, J., Wang, Y., Xiao, X., Jin, C., Xia, J., and Li, X. (2019). Spatial Differentiation of Urban Wind and Thermal Environment in Different Grid Sizes. *Urban Clim.* 28, 100458. doi:10.1016/j.uclim.2019.100458

Yang, J., Yang, Y., Sun, D., Jin, C., and Xiao, X. (2021). Influence of Urban Morphological Characteristics on Thermal Environment. *Sustain. Cities Soc.* 72, 103045. doi:10.1016/j.scs.2021.103045

Ypa, B., Li, L., Hxa, B., Rza, B., and Hx, A. (2020). *Spatial Variability of Inhalable Fungal Communities in Airborne Pm 2.5 across Nanchang*. china: Science of The Total Environment, 746.

Yu, H., Yang, J., Li, T., Jin, Y., and Sun, D. (2022). Morphological and Functional Polycentric Structure Assessment of Megacity: An Integrated Approach with

Spatial Distribution and Interaction. *Sustain. Cities Soc.* 80, 103800. doi:10.1016/j.scs.2022.103800

Yuan, M. N., Liu, Y. X., Wang, M., Tian, L., and Peng, J. (2019). Ecosystem Health Assessment Based on the Framework of Vigor, Organization, Resilience and Contribution in Guangzhou City. *Chin. J. Ecol.* 38 (4), 1249. doi:10.13292/j.1000-4890.201904.026

Zhang, L. J. (2018). "A Land-Cover-Based Approach to Assessing the Spatio-Temporal Dynamics of Ecosystem Health in the Yangtze River Delta Region," (Nanjing,China: Nanjing Agricultural University). Master's Thesis. doi:10.27244/d.cnki.gnjnu.2018.000040

Zhang, X. F., Wang, R. S., Li, Z. G., Li, F., Wu, J. S., Huang, J. L., et al. (2011). Comprehensive Assessment of Urban Ecological Risks: the Case of Huaibei City. *Acta Ecol. Sin.* 31 (20), 6204–6214. doi:10.1016/j.chnaes.2011.07.006

Zhao, Z., Sharifi, A., Dong, X., Shen, L., and He, B.-J. (2021). Spatial Variability and Temporal Heterogeneity of Surface Urban Heat Island Patterns and the Suitability of Local Climate Zones for Land Surface Temperature Characterization. *Remote Sens.* 13 (21), 4338. doi:10.3390/rs13214338

Zheng, Y., Zhang, P. T., Zhao, L., and Zhao, X. (2018). The Effects of Land Use Change on Habitat Quality in Changli Country Based on Invest Model. *Chin. J. Agric. Resour. Regional Plan.* 39 (7), 121–128.

Zhong, L. N., and Wang, J. (2017). Evaluation on Effect of Land Consolidation on Habitat Quality Based on InVEST Model. *Trans. CSAE* 33 (1), 250–255. doi:10.11975/j.issn.1002-6819.2017.01.034

Conflict of Interest: The authors declare that the research was conducted in the absence of any commercial or financial relationships that could be construed as a potential conflict of interest.

Publisher's Note: All claims expressed in this article are solely those of the authors and do not necessarily represent those of their affiliated organizations or those of the publisher, the editors, and the reviewers. Any product that may be evaluated in this article, or claim that may be made by its manufacturer, is not guaranteed or endorsed by the publisher.

Copyright © 2022 Duo, Li, Zhang, Zhao, Wu and Zhao. This is an open-access article distributed under the terms of the Creative Commons Attribution License (CC BY). The use, distribution or reproduction in other forums is permitted, provided the original author(s) and the copyright owner(s) are credited and that the original publication in this journal is cited, in accordance with accepted academic practice. No use, distribution or reproduction is permitted which does not comply with these terms.

frontiers | Frontiers in Earth Science

ORIGINAL RESEARCH
published: 25 May 2022
doi: 10.3389/feart.2022.917520

Spatial Distribution and Evolution of Ancient Settlements From the Neolithic to the Bronze Age in Dalian Area, China

Liang Liu[1,2]*, *Fangfang Liu*[1], *Wei Zhang*[1] and *Zhaofeng Xu*[3]

[1]School of Geography, Liaoning Normal University, Dalian, China, [2]Postdoctoral Research Station of Chinese History, Liaoning Normal University, Dalian, China, [3]School of History, Culture and Tourism, Liaoning Normal University, Dalian, China

The research on the spatial distribution and evolution of ancient settlements from the Neolithic Age to the Bronze Age in Dalian area is of great significance for a profound understanding of the prehistoric human-land relationship in Dalian area. The results showed that: ① The number of settlement sites in Dalian area showed an overall upward trend from the Mid-Neolithic to the Bronze Age. Most sites during the three periods studied were to be found 0–50 m above sea level (asl), with a significant increase in the number of sites located >50 m asl during the Bronze Age. In terms of gradient of slope, all settlements were concentrated on coastal plains or in low-altitude, hilly areas on relatively gentle slopes ranging between 0 and 6°. Settlements from each period faced in all directions, and were mainly located in river valleys or low-altitude mountain valleys with low terrains.② The proximity of ancient settlements to river courses during the Mid Holocene evolved, with Mid and Late Neolithic settlements usually distributed in the range beyond 3 km of the river buffer zone; the distribution of Bronze Age sites was relatively uniform, reflecting an increasing demand for water resources; the density of settlements was clustered between the Mid Neolithic and the Bronze Age, Neolithic sites being both the smallest in number and the most concentrated. ③ The spatiotemporal distribution and evolution of settlements in the Dalian area were influenced by the contemporary climate: the Mid Neolithic climate was warm and humid, and settlements were distributed principally on the various islands near present-day Dalian, and especially Guanglu Island; the Late Neolithic climate became increasingly drier and cooler, stimulating cultural advances and a slight increase in the number of ancient settlements, which gradually developed in the areas in and around present-day Dalian; during the cold and dry Bronze Age, the number of settlements across the Dalian region reached their peak, and it is widely distributed in various areas of Dalian. To a certain extent, this reflected a continuous improvement in the ability of the human population to adapt to the natural environment.

Keywords: Dalian area, ancient settlements, Mid Holocene, spatiotemporal distribution, evolution

OPEN ACCESS

Edited by:
Bing Xue,
Institute of Applied Ecology (CAS), China

Reviewed by:
Li Wu,
Anhui Normal University, China
Chun Mei Ma,
Nanjing University, China
Zhigang Zhang,
Nanjing Normal University, China

***Correspondence:**
Liang Liu
liuliangdm@126.com

Specialty section:
This article was submitted to Geoscience and Society, a section of the journal Frontiers in Earth Science

Received: *11 April 2022*
Accepted: *05 May 2022*
Published: *25 May 2022*

Citation:
Liu L, Liu F, Zhang W and Xu Z (2022) Spatial Distribution and Evolution of Ancient Settlements From the Neolithic to the Bronze Age in Dalian Area, China. Front. Earth Sci. 10:917520. doi: 10.3389/feart.2022.917520

1 INTRODUCTION

As the core of geography research, human-natural relationship run through each stage of geographical development (Xue et al., 2018). Ancient settlements are places where ancient humans lived, produced and socialized; their spatiotemporal distribution presents a rich archive of geographical and spatial features, all of which were significantly affected by the environment (Guo et al., 2013; Wang et al., 2015). The spatial distribution and evolution of ancient Holocene human settlements have become an important focus within environmental archeological research. Such environmental archeological research (Goude and Fontugne, 2016; Wang et al., 2021; Zhang et al., 2021) covers three main areas (Zhu, 2015; Wu et al., 2021): 1) research into the evolutionary rules governing the spatiotemporal distribution of human sites in the particular study area; 2) research into the archeological stratigraphy of typical sites in the particular study area; and 3) research into the environmental evolution of a particular study area, based on the typical natural sediments found in that area. Information contained within an archeological site can aid the spatiotemporal understanding of such ancient settlements, and can help delineate the roles played by altitude, gradient and river proximity on the cultural development and evolution of these settlements. This can help us comprehend the ancient human-land dynamic and analyze the relationship between the development of settlements and the surrounding environment (Gu and Zhu, 2005). Understanding and interpreting the development and evolution of ancient human cultures, At the same time, it is of great scientific significance to the coordinated development of modern man and land, and that China and the world take the road of sustainable development (Xue and Mario, 2015).

Non-Chinese research into ancient settlements has principally employed GIS for site prediction (Garcia, 2013; 2013; Nsanziyera et al., 2018). Scientists have explored the relationship between settlements, their natural stratigraphy and their climatic environment, etc. (Turney and Brown, 2007; Guo et al., 2018; Huang et al., 2020; Parker et al., 2020). Such research has also focused on quantitative analyses of the range of ancient human activity, using technical approaches (Kidder et al., 2008). Chinese research has mainly focused on Neolithic and Bronze Age sites (An et al., 2006; Deng et al., 2009; Wu et al., 2012b), studying the numbers of ancient settlements from different periods within the Neolithic and Bronze Age, and the sites of such settlements and how they may have been affected by different natural and environmental constraints. GIS spatial analyses have also therefore been widely used in the regional studies of ancient settlements. Chen et al. (2018) established a database of Neolithic cultural sites in the middle reaches of the Yangtze River. The scale, altitude, gradient of slope, distance from river courses and other characteristics of these cultural sites were also systematically analyzed. The number, scale and spatial distribution of these sites constantly expanded during the Neolithic period, with settlements usually found at low altitudes, on gentle terrain and closer to rivers. Yuan (2018) studied the spatial distribution of Lower and Upper Xiajiadian cultural sites in the western Liao River Basin. Bronze Age settlements in the area reached their peak, and were concentrated in the plain and hilly interactive zone between the Liao River and the Daling River Basin. Ren et al. (2021) systematically sorted the distribution of ancient settlements in the Min River Basin using a GIS spatial analysis tool. This analysis indicated that Bronze Age settlements were the most widely distributed, covering the entire watershedAlthough settlements were centered on riversides, they did expand outwards, and there were also sites 15 km away from a river course. It is clear from the above, therefore, that ancient humans made different choices about where to live during different historical periods, often in response to different topographic conditions and geographical locations.

To conclude, Chinese research has principally focused on northwestern China (An et al., 2006;; Chen et al., 2016), its Central Plains (Li et al., 2013; Zhao et al., 2021) and its eastern regions (Wu et al., 2012a; Wu et al., 2012b; Chen et al., 2018). In northeastern China, preliminary studies have been conducted into ancient settlements in northeastern Liaoning Province and the western Liao River Basin (Wang et al., 2016; Zhao et al., 2019). The Dalian area is located in the southern part of the Liaodong Peninsula, where the marine sedimentary environment transitions to a continental sedimentary environment. Research has shown that many cultures and civilizations have arisen in ecological transition zones where there are significant marginal impacts (Wang and Lei, 2002). The Dalian area has, in this regard, nurtured a wealth of Neolithic and Bronze Age cultures, of which the Xiaozhushan and Shuangtuozi cultures are the most representative (Zhang, 2011). However, there have been few studies into the spatial distribution and evolution of Mid Holocene settlements in the Dalian area, meaning that the close relationships between the origins of ancient human civilization, paleogeography and the paleoclimatic environment in this area have not yet been systematized. This paper has therefore taken the Dalian area as its study area. ArcGIS 10.2 software was used to analyze the spatial distribution of Mid Holocene settlements in the Dalian area. this research will help reveal the relationship of Cultural evolution, settlement distribution patterns and environment and climate change.

2 STUDY AREA

The Dalian area (**Figure 1**) is located on the eastern coast of the Eurasian continent, at the southernmost tip of the Liaodong Peninsula, between 120°53′E-123°31′E and 38°43′-40°10′N. It is flanked by the Yellow Sea and the Bohai Sea to the east and west, respectively, and faces the Shandong Peninsula across the sea to its south. The Dalian Sub-Peninsula is wide in the north and narrow in the south, bordered by the sea on both sides, and surrounded by islands. Its landforms are principally composed of low mountains and a hilly peninsula environment. The remnant spines of the Changbai and Qianshan mountain ranges traverse the area along the trend of the Peninsula, forming a ridge terrain with a high center, low east-west flanks, a high northern, and a

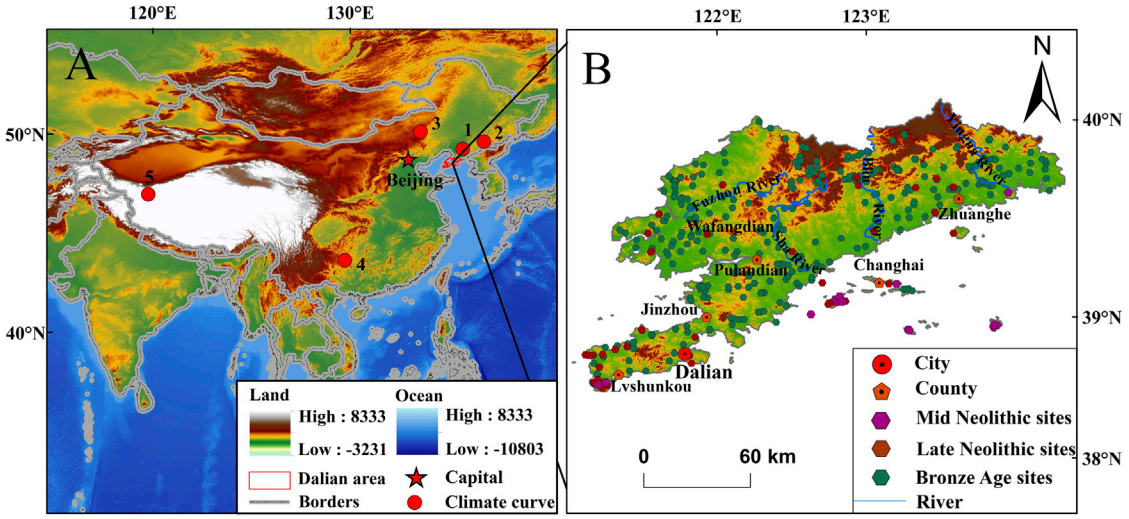

FIGURE 1 | Geographical location of the study area, with sites of ancient settlements. **(A)** The location of Dalian area and climatic curves. (1) The Benxi Nuanhe Cave (Wu et al., 2011; Zhang and Wu, 2012). (2) Sihailongwan (Stebich et al., 2017; Wang et al., 2020). (3) Dali Lake (Wen et al., 2017; Wang et al., 2020). (4) Dongge Cave (Dykoski et al., 2005). (5) Guliya Ice Core (Thompson et al., 1997). **(B)** Distribution of Sites from the Mid Neolithic to the Bronze Age in Dalian area (Heritage, 2009; Zhang et al., 2016; Xu, 2019a).

TABLE 1 | Cultural sequences of different periods in the study area.

Period	Number of sites	Cultural period	Time (ka BP)
Mid Neolithic	15	Lower Xiaozhushan	6.7–6.3
		Middle Xiaozhushan	6.5–5.3
Late Neolithic	43	Upper Xiaozhushan	4.8–4.1
Bronze Age	315	Shuangtuozi I	4.1–3.9
		Shuangtuozi II	3.9–3.6
		Shuangtuozi III	3.4–3.1

low southern aspect (Li et al., 2008). The Dalian area lies in a temperate, monsoonal climatic zone, with marine climatic characteristics. Mean annual precipitation (MAP) is ~610 mm, and the mean annual temperature (MAT) is 10°C (http://data.cma.cn/). The Dalian area has a dense river network; the largest river is the Biliu River, which flows into the Yellow Sea. In addition, there are Yingna River and Sha River into the Yellow Sea and Fuzhou River into the Bohai Sea (Xu, 2019a).

3 MATERIALS AND METHODS

3.1 Materials

The site data presented in this paper were derived from cultural and historical documents, archeological excavation reports from the Dalian area (Zhang et al., 2016; Xu, 2019b), and "The Atlas of Chinese Cultural Relics - Liaoning Volume" (Heritage, 2009). A total of 15 in the Mid Neolithic, 43 in the Late Neolithic and 315 settlements in the Bronze Age were documented and summarized. For the sake of completeness, this study excluded tomb sites with incomplete relevant data, and siters with scattered data (Zhao, 2011), and then sorted out the ancient settlements in the Dalian area as they belong to each cultural period, *i.e.*, the cultural periods that existed during the Mid Neolithic, Late Neolithic and Bronze Age (**Table 1**). A digital elevation model (DEM) image of the Dalian area, with a horizontal resolution of 30 × 30 m, was extracted from the Geospatial Data Cloud (http://www.gcloud.cn). Using this DEM data, the altitude asl, gradient of slope, aspect and distance from a river course of each ancient site in the study area were extracted. Representative Holocene climatic index data was taken from the NOAA (https://www.ncdc.noaa.gov/paleo-search/) database.

3.2 Methods

3.2.1 Voronoi Diagram

A Voronoi diagram (VD) is a continuous polygon formed by the vertical bisector of the line connecting two adjacent points in the study area. The target area is cut by the plane of the Thiessen polygon, and each center corresponds to a polygon. The distance from any point in the polygon to the center of the area is smaller than the position between this point and the center point of other areas. Since the area of the Thiessen polygon changes with the distribution of the point set, the coefficient of variation (CV) value can be used to measure the relative change in the area of the convex polygon, so as to analyze the spatial distribution of the sample points. The CV is equal to the ratio of the standard deviation of the area of the Thiessen polygon to the mean, and is calculated as:

$$R = \sqrt{\sum \frac{(S_i - S)^2}{n}} (i = 1, 2, \cdots, n) \quad (1)$$

$$CV = R/S \quad (2)$$

where R is the standard deviation of the polygon; S_i is the area of the *i*th polygon; *S* is the mean value of the polygon area; and *n* is the number of polygons. When the point set is evenly distributed in the space, the area variability of the Thiessen polygon is small, and the CV value is low; when the point set is densely distributed in the space, the Thiessen polygon exhibits a significant variability and a high CV value. Duyckaerts *et al.* proposed three values: when the CV is 0.29 (<0.33), the spatial point data are uniformly distributed; when the CV is 0.57 (including within the range 0.33–0.64), the spatial point data are characterized by a random distribution; when the CV is 0.92 (>0.64), the spatial point data exhibit a clustered distribution (Xiao, 2019).

3.2.2 Average Nearest Neighbor

The Nearest-Neighbor analysis tool embedded in the ArcGIS software program was used to analyze the cluster characteristics of the sites in the study area using the average nearest neighbor (ANN) index (http://resources.arcgis.com/en/help/main/10.1/index.html). Nearest neighbor analysis was performed on the settlement sites of each cultural period by analyzing the relationship between the distance between the points and the corresponding Thiessen polygons. ANN analysis has three modes of expression: clustered distributions; random distributions; and uniform distributions. The value of the ANN index indicates whether points are clustered (<1), random (= 1), or scattered (>1) in space. It is calculated using the average distance of each point to its nearest neighbor; the formulae are as follows:

$$ANN = \frac{\bar{D}_o}{\bar{D}_e} \tag{3}$$

$$\bar{D}_o = \frac{\sum_{i=1}^{n} d_i}{n} \tag{4}$$

$$\bar{D}_e = \frac{0.5}{\sqrt{n/A}} \tag{5}$$

where $\bar{D}_o$ is the observed average distance between each point and its nearest neighbor, and $\bar{D}_e$ is the expected average distance for a given point in a random pattern. d_i is the distance between point i and its nearest neighbor, A is the smallest enclosed area, and n is the total number of points. The Average Nearest-Neighbors tool in ArcGIS not only calculates the Nearest Neighbor Ratio for each cultural period, but also calculates a *p*-value representing probability and a Z-score representing standard deviation. The *p*-value and Z-score are measures of statistical significance used to determine whether to rule out the assumption of complete spatial randomness. The smaller the *p*-value and the larger the absolute value of the Z-score, the less likely the observed spatial pattern is the result of a random process. If the *p* value is <0.01 and the absolute value of the Z score is >2.58 (i.e., < -2.58 or > +2.58), the confidence level will exceed 99% (Yuan, 2019).

4 RESULTS

4.1 Topography and Settlements Distribution in the Dalian Area

The distribution of Neolithic to Bronze Age settlements in the Dalian area evinces a certain regularity. This study analyzed 15 sites Mid Neolithic, 43 Late Neolithic and 315 Bronze Age sites in the Bronze Age in the Dalian area. In terms of their altitude (**Figure 2**; **Table 2**), from the Mid (**Figure 2A**) to the Late Neolithic (**Figure 2B**), to the Bronze Age (**Figure 2C**), settlements were concentrated in the range of 0–50 m asl, accounting for 86.6%, 72% and 58.1% of the total number of sites from each period, respectively. In the Mid Neolithic period, ~6.7% of the sites were distributed in low-altitude, hilly areas at altitudes of 50–100 m asl, and >100 m asl.

When considering gradient of slope (**Table 3**), Mid Neolithic, Late Neolithic and Bronze Age settlements in the Dalian area were found to be concentrated within the 0–2° and 2–6° ranges, with nine, 31 and 197 sites respectively, accounting for 59.7%, 72.1% and 62.5% of the total number of settlements for each of the three periods. There were also a certain number of sites in the 6~15° range for each period, accounting for 40%, 23.3% and 30.5% of the total number of settlements for the Mid Neolithic, Late Neolithic and Bronze Age, respectively. When considering any potential relationship between the location of ancient settlements and agriculture, the suitability of the area around each settlement to agricultural development must be taken into account. This is why the gradient of the slope of any cultivated land, as defined by "The Technical Regulations for the Investigation of Land Use Status" (Qiu and Li, 1982), was adopted. Slopes were divided into three grades, based on the ranges of their gradients: slopes of gradient 0–6° were considered of an excellent, 6–15° a good, and >15° a poor, grade. **Figure 3A** shows that the slopes of Neolithic and Bronze Age sites in the Dalian area were biased towards excellent and good grades.

Investigations into the aspects of the Mid Neolithic, Late Neolithic and Bronze Age settlement sites in the Dalian area (**Figure 4**; **Table 4**) showed that they faced in all directions, except for three Bronze Age settlements situated on flat land. No Mid Neolithic settlements faced south. During the Mid Neolithic period, sites were mainly distributed on north-, northeast-, east-, southeast-, southwest- and northwest-facing slopes (13 sites, accounting for 86.6% of the total). During the Late Neolithic and the Bronze Age, the distribution of the aspects of sites was generally uniform, inclined usually to the northeast, east, south, southwest and southeast. 28 sites in the Late Neolithic, and 202 sites in the Bronze Age, faced in these directions, accounting for 65.1% and 64.2% of the total sites of the two periods, respectively. 7 and 51 sites faced west, accounting for 16.3% and 16.2% of the total number of Late Neolithic and Bronze Age settlements, respectively. The aspects of settlements in the study area were divided into those which received poor solar illumination (0~45°, 45~90°, 270~315° and 315~360°) and those with better illumination (90~270°) (Liu et al., 2021). The number and proportion of archeological remains from each of the three periods distributed on different slopes in the Dalian area were then counted (**Figure 3B**). During the Mid Neolithic period, more settlements were distributed in areas with good light than in areas with poor light, accounting for 66.7% and 33.3% of the total, respectively. During the Late Neolithic and Bronze Age, more settlements were distributed in areas with poor light.

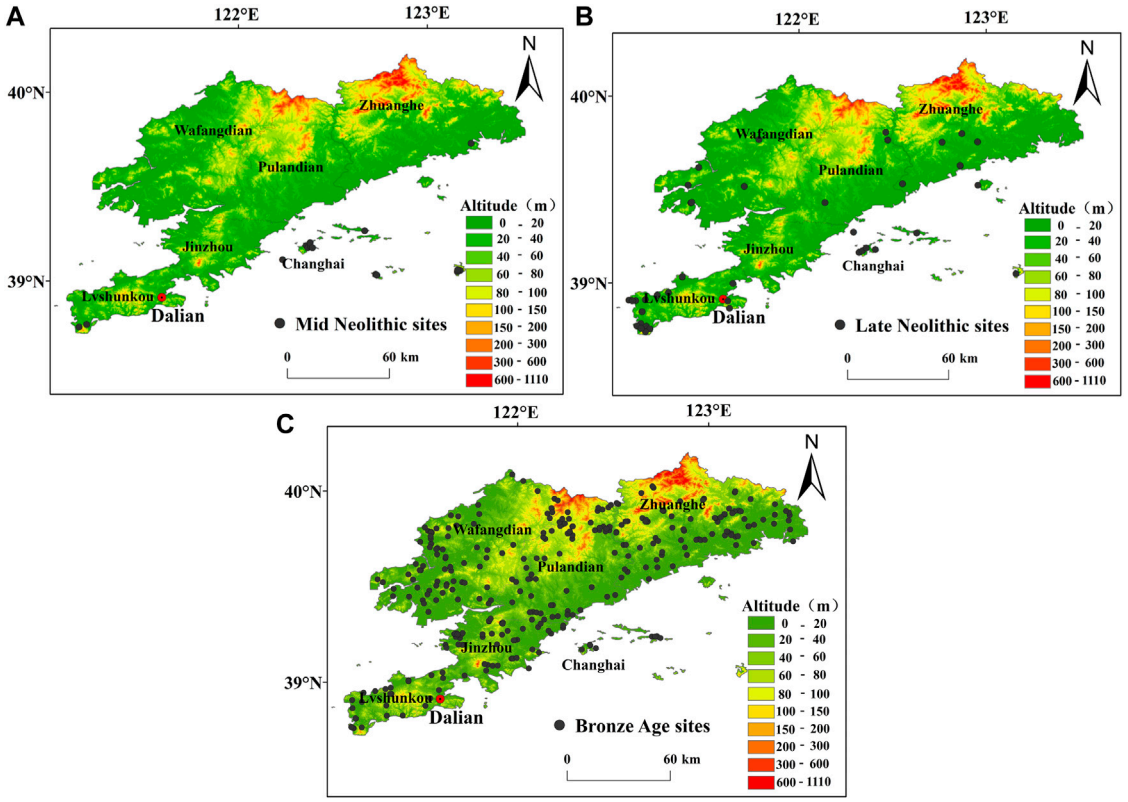

FIGURE 2 | Topographic map, with ancient settlement sites in the Dalian area (by period). **(A)** Mid Neolithic sites. **(B)** Late Neolithic sites. **(C)** Bronze Age sites.

TABLE 2 | Spatial distribution of, and altitudinal relationship between, ancient settlements in the Dalian area.

Altitude (m asl)	Period					
	Mid Neolithic		Late Neolithic		Bronze age	
	Number	Proportion (%)	Number	Proportion (%)	Number	Proportion (%)
<50	13	86.6	31	72	183	58.1
50–100	1	6.7	5	11.7	79	25.1
>100	1	6.7	7	16.3	53	16.8

TABLE 3 | Relationship between the spatial distribution and gradients of slope for ancient settlements in the Dalian area.

Slope (°)	Period					
	Mid Neolithic		Late Neolithic		Bronze age	
	Number	Proportion (%)	Number	Proportion (%)	Number	Proportion (%)
0–2	4	26.7	11	25.6	59	18.7
2–6	5	33.3	20	46.5	138	43.8
6–15	6	40	10	23.3	96	30.5
15–25	0	0	1	2.3	21	6.7
>25	0	0	1	2.3	1	0.3

4.2 Proximity of Ancient Settlements to River Courses in the Dalian Area

Human life is impossible without access to water. Accessibility to river water would therefore have had an impact on the selection of settlement sites by ancient humans. The distance between any settlement and the nearest river course therefore reflects the degree of utilization of water resources by ancient people, as well as the judged safe distance from a river and flood

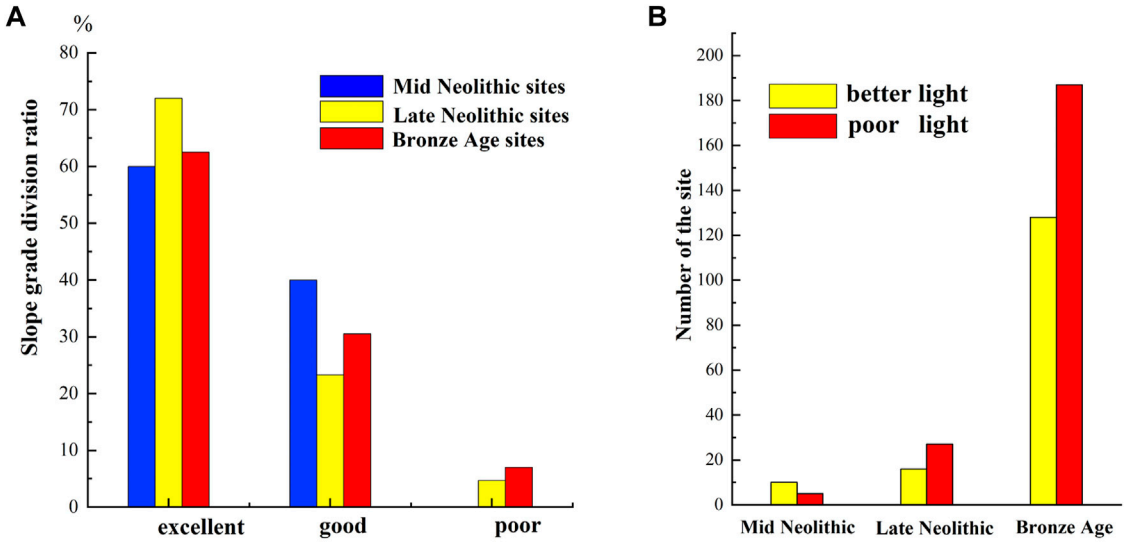

FIGURE 3 | (A) Slope hierarchy of ancient settlement sites in the Dalian area, by period. **(B)** Degree of solar illumination of ancient settlement sites in the Dalian area, by period.

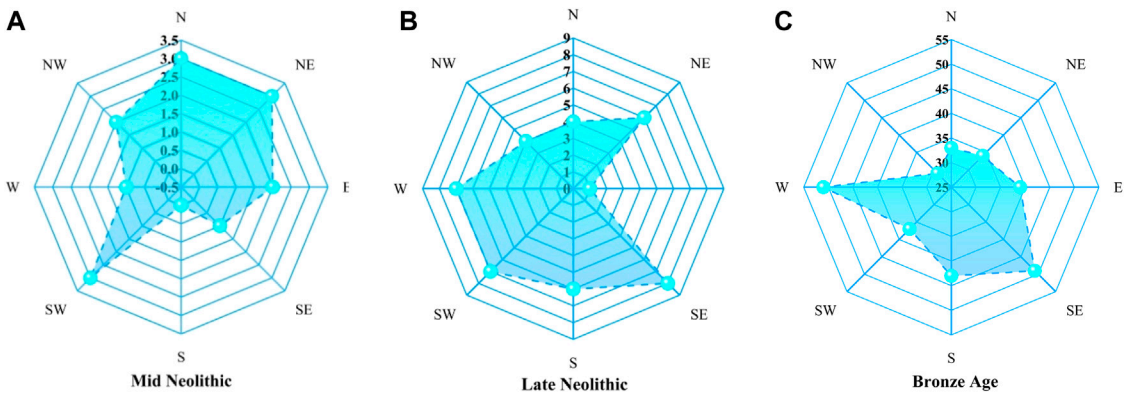

FIGURE 4 | Aspects of ancient settlement sites in the Dalian area, by period**. (A)** Mid Neolithic sites. **(B)** Late Neolithic sites. **(C)** Bronze Age sites.

TABLE 4 | Relationship between spatial distribution and aspect for ancient settlements in the Dalian area, by period.

Aspect	Period					
	Mid Neolithic		Late Neolithic		Bronze age	
	Number	Proportion (%)	Number	Proportion (%)	Number	Proportion (%)
Flat	0	0	0	0	3	0.9
N	3	20	4	9.3	30	9.5
NE	3	20	6	14	34	10.8
E	2	13.3	1	2.3	39	12.4
SE	1	6.7	8	18.5	49	15.6
S	0	0	6	14	43	13.7
SW	3	20	7	16.3	37	11.7
W	1	6.7	7	16.3	51	16.2
NW	2	13.3	4	9.3	29	9.2

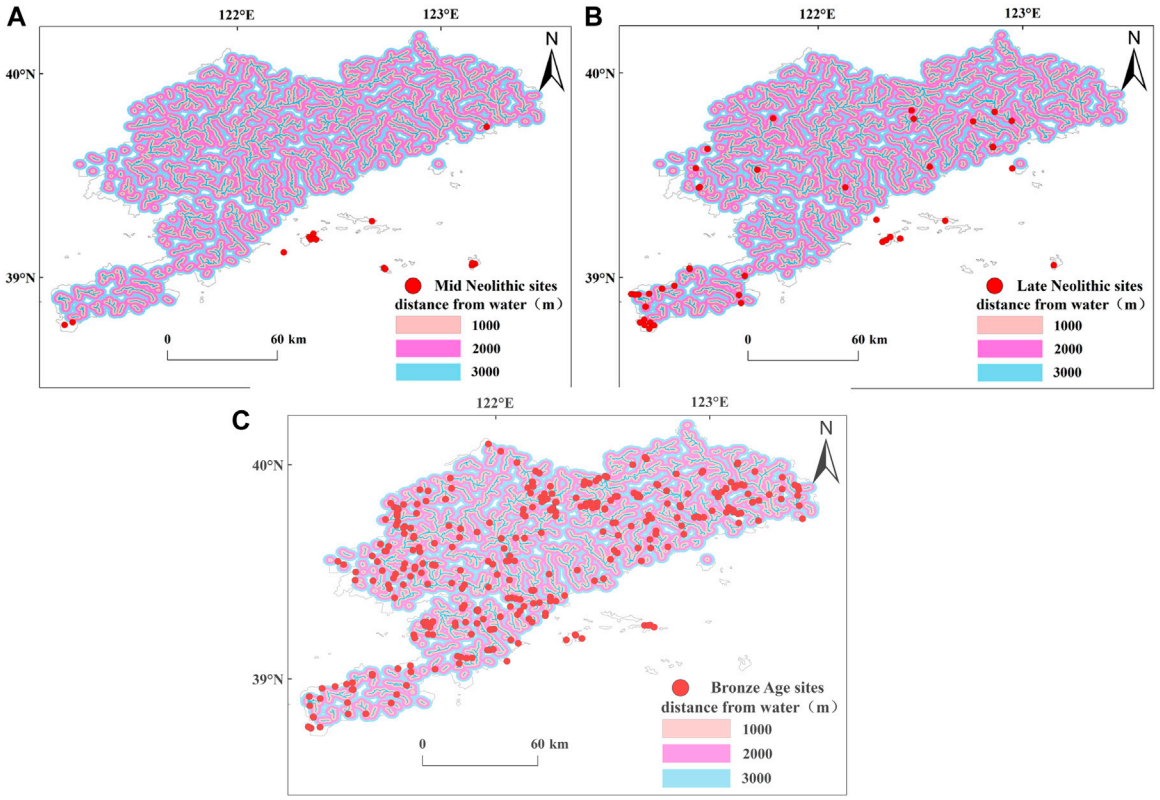

FIGURE 5 | Distances between ancient settlements and river courses in the Dalian area, by period. **(A)** Mid Neolithic sites. **(B)** Late Neolithic sites. **(C)** Bronze Age sites.

TABLE 5 | Relationship between the spatial distribution of ancient settlements in the Dalian area and river buffer zones, by period.

Distance from river (km)	Period					
	Mid Neolithic		Late Neolithic		Bronze age	
	Number	Proportion (%)	Number	Proportion (%)	Number	Proportion (%)
0–1	0	0	5	11.6	75	23.8
1–2	1	6.7	8	18.6	85	27
2–3	1	6.7	12	28	66	21
>3	13	86.6	18	41.8	89	28.2

preventative considerations. In this study, a DEM was used to map river systems. Considering that river courses can change significantly over a millennial timeframe, and that the Dalian area's modern river systems are denser and therefore do not conform to the actual hydrological conditions that would have been present during the three periods studied, the river threshold was set to 10,000 (Chen, 2014). Then, using ArcGIS v10.2 software, a river buffer zone was delineated within a 3 km range from any river system, at intervals of 1 km, and the distance from any settlements to a river course, as well as the distribution ratio of any settlements in the river buffer zone, were counted for each of the three periods.

Figure 5 and **Table 5** show the spatial distribution of settlements in the Mid Neolithic, Late Neolithic and Bronze Age in the Dalian area in relation to river systems. Mid Neolithic sites were not distributed within 1 km of rivers (**Figure 5A**), but mainly (*i.e.*, 86.6%) in a range >3 km beyond water courses. Late Neolithic sites were principally distributed 2–3 km and >3 km away from rivers (**Figure 5B**) (28% and 41.8%, respectively). Bronze Age settlements were located fairly equally within the ranges of 0–1 km, 1–2 km, 2–3 km, and >3 km from a river course (23.8%, 27%, 21%, and 28.2%, respectively) (**Figure 5C**). The number of ancient settlements located within 0–3 km of the river system buffer zone in the three periods accounted for 13.4%, 58.2%, and 71.8% of the totals for each period, respectively, indicating that the Neolithic to Bronze Age settlements tended to move closer to river courses.

Based on analyses of VDs and CVs, the spatial distributions of ancient settlements in the Dalian area during the three studied

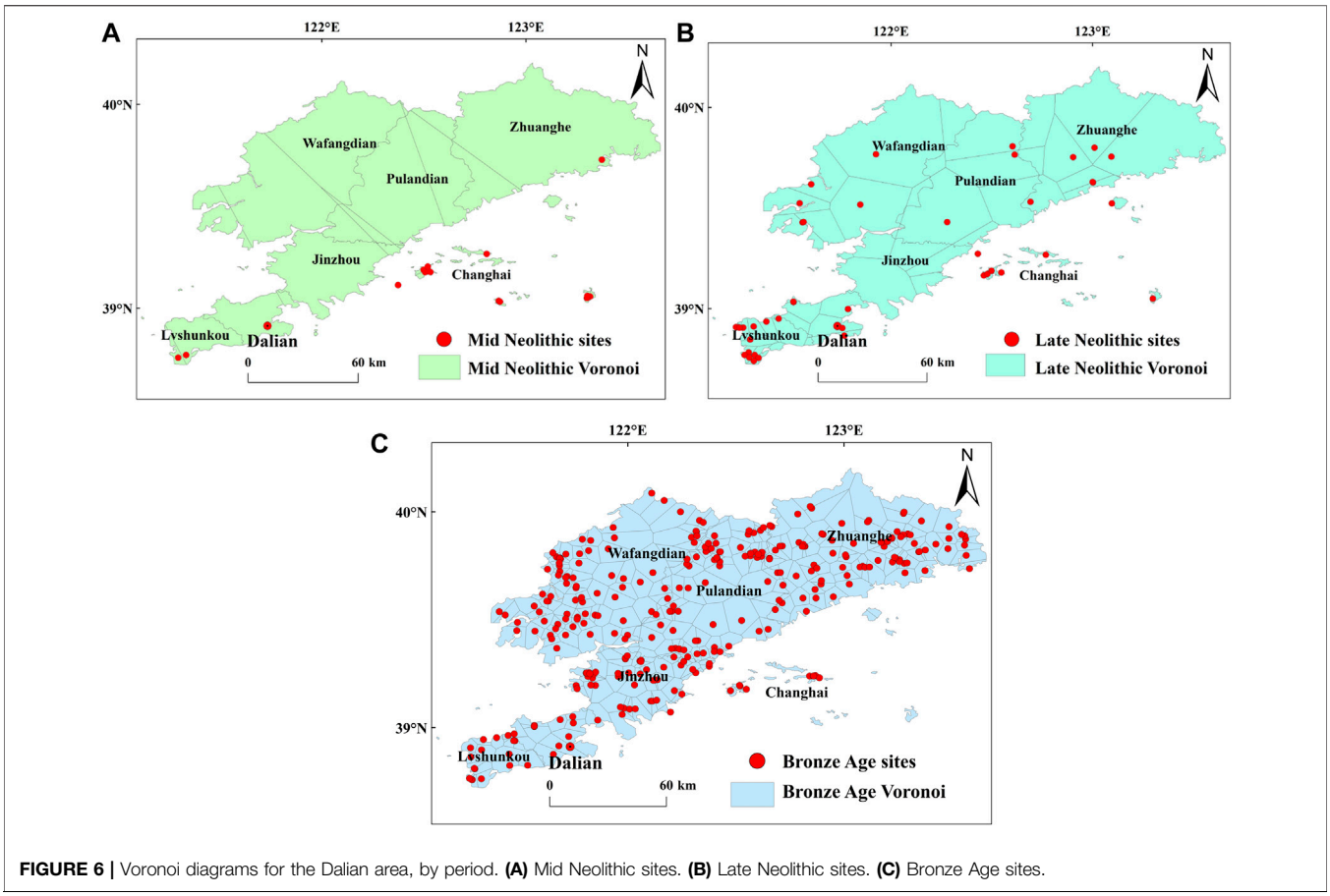

FIGURE 6 | Voronoi diagrams for the Dalian area, by period. **(A)** Mid Neolithic sites. **(B)** Late Neolithic sites. **(C)** Bronze Age sites.

TABLE 6 | CV and ANN indices for the Dalian area, by period.

Period	Mid Neolithic	Late Neolithic	Bronze age
Sample points	15	43	315
CV(%)	159.46	141.18	88.39
ANN	0.562	0.723	0.599
p-Value	0.001	0.000	0.000
Z-Score	–3.247	–3.480	–13.626

periods can be seen to be essentially clustered (**Figure 6**). ArcGIS v10.2 software was used to generate VDs for the Mid Neolithic (**Figure 6A**), Late Neolithic (**Figure 6B**) and Bronze Age (**Figure 6C**). It can be seen from **Figure 6** that although the number of sites in the Mid and Late Neolithic period was small, they were generally clustered close to one another. The number of Bronze Age settlements increased significantly, but their distribution remained relatively clustered. By calculating the polygon area of each cultural period in ArcGIS, and using the formulae outlined in this research, the CV values for the different cultural periods in the Dalian area were obtained. It can be seen from **Table 6** that the CV values for the Mid Neolithic, Late Neolithic and Bronze Age were 159.46%, 141.18% and 88.39%, respectively, indicating that settlements from the Mid Neolithic to the Bronze Age were spatially clustered, with Mid Neolithic sites having the highest degree of aggregation.

Using analyses of the ANN index for the Dalian area, it was found that the ancient settlements in each period also showed a degree of aggregation. The ANN indices for the Mid Neolithic, Late Neolithic and Bronze Age were 0.562, 0.723 and 0.599 respectively, all <1, indicating aggregation. This was consistent with the VD and CV results, confirming that the distribution of settlements in the Dalian area from the Mid Neolithic to the Bronze Age presents a generally clustered distribution.

5 DISCUSSION

Pollen is a surrogate paleoenvironmental indicator that has played an important role in paleovegetation and paleoclimatic reconstructions (Innes et al., 2014; Shen et al., 2017; Zhao et al., 2021a; Zhao et al., 2021b). In recent years, sporopollen analysis has also been widely used in environmental archaeological research (Xu et al., 2002; Peng et al., 2011; Liu et al., 2018), and is therefore of great significance when discussing regional climate change. Due to a lack of complete sporopollen sequences in the Dalian area, the sporopollen archive from the adjacent Liao River Basin area was used (Stebich et al., 2015; Wen et al., 2017; Wang et al., 2020), then combined with stalagmite $\delta^{18}O$ records from Benxi Nuanhe Cave (Wu et al., 2011; Zhang and Wu, 2012), Guliya Ice Core $\delta^{18}O$ records (Thompson et al., 1997), North

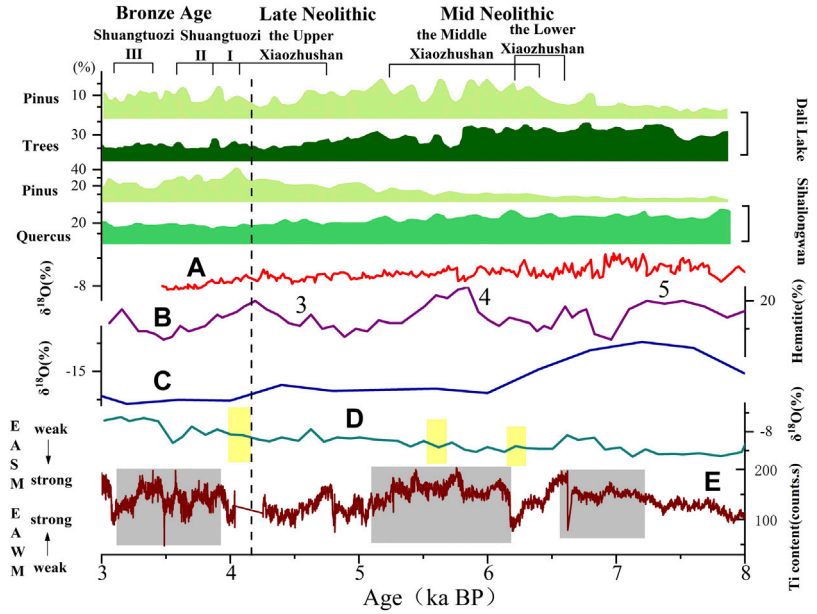

FIGURE 7 | Comparison of palynological records from the Liao River Basin (Stebich et al., 2015; Wen et al., 2017; Wang et al., 2020) and other high resolution records. **(A)** Stalagmite $\delta^{18}O$ record, Benxi Nuanhe Cave (Wu et al., 2011; Zhang and Wu, 2012). **(B)** Hematite-stained grains, North Atlantic (Dong et al., 2015). **(C)** Guliya Ice Core (Thompson et al., 1997). **(D)** Stalagmite $\delta^{18}O$ record, Dongge Cave (Dykoski et al., 2005). **(E)** Ti content record, Lake Huguangyan Maar (Yancheva et al., 2007). Note: The yellow bars represent weak East Asian summer Monsoon (EASM) events; the light grey bars represent strong East Asian winter Monsoon events; the figures represent North Atlantic climatic event (Bond event); EASM, East Asian summer monsoon; EAWM, East Asian winter monsoon.

Atlantic stained hematite particles (Dong et al., 2015), the stalagmite $\delta^{18}O$ records from Dongge Cave (Dykoski et al., 2005) and the Ti content records of Huguangyan Maar Lake (Yancheva et al., 2007), in order to explore the impact of regional climate change on the spatiotemporal evolution of ancient settlements.

5.1 Mid Neolithic (7.5–5.0 ka BP)

According to the sporopollen records from the Liao River Basin and its surrounding areas (Stebich et al., 2015; Wen et al., 2017; Wang et al., 2020) (**Figure 7**), the broadleaved tree sporopollen content of this temperate zone, when climatic conditions were warm and humid, gradually increased, indicating that the climate became gradually warmer and more humid. At ~8.4–4.3 ka BP, the broadleaved tree sporopollen content reached its highest Holocene value. Stalagmite $\delta^{18}O$ values from the Benxi Nuanhe Cave also show high-frequency fluctuations (Wu et al., 2011; Zhang and Wu, 2012) (**Figure 7A**). Other climatic records (Dykoski et al., 2005; Yancheva et al., 2007; Yao, 2000; Dong et al., 2015) reflect a gradually intensifying East Asian Summer Monsoon (EASM), during which period precipitation began to increase, reflecting a warmer and more humid climate. This period marked the Holocene Climatic Optimum; the Lower Xiaozhushan (6.7–6.3 ka BP) and Middle Xiaozhushan (6.3–5.3 ka BP) cultures arose within this suitably warm climatic environment. At this time, the number of settlements was relatively small and mainly distributed on various islands, principally Guanglu Island, where the Xiaozhushan Culture settlement was the most representative. The Donggang and Guojiacun ancient settlements were also found in the Lüshunkou area (Xu and Su, 1980; Xu, 2019b), and the Beiwutun site (Xu, 1994) in the Zhuanghe area. However, the nomenclature of these sites has remained controversial. In this study, they were tentatively determined as belonging to the Middle Xiaozhushan Culture (Xu and Jin, 1986; Xu, 1994; Xu, 2019b). All of the above ancient settlements were concentrated in coastal areas at an altitude of 50 m asl, on slopes of gradient <6°, and with good solar illumination. Coastal terraces, estuarine deltas and low-altitude hills provided the principal living environments for ancient peoples. Overall, during this period, human beings were less able to adapt to harsher natural environments, and preferred to live in environments with lower altitudes, gentler slopes and better sunlight.

The river buffer zone delineated by ArcGIS indicated that, during the Mid Neolithic period, Lower Xiaozhushan (6.7–6.3 ka BP) and Middle Xiaozhushan (6.3–5.3 ka BP) culture settlements were generally distributed in area beyond 3 km from the river. Because the Xiaozhushan settlements scattered in low-altitude areas on the northwestern and eastern coasts of Guanglu Island were all close to the sea, we judged that there was no shortage of water resources for human survival during this cultural period. Based on the determined ^{14}C ages of the Dagushan peat layer and the Qianyang gray-green silt deposits (Yang and Lin, 1985), the Liaodong Peninsula was at the peak of its climatic transgression at 6.0–5.0 ka BP, and the sea level was 2–4 m higher than now. However, since Guanglu Island is shaped like a turtle's back and has a raised topography (Li, 2017), we judged that the extent of seawater intrusion into the land during this period was not large,

and that any threat to human settlements was therefore limited. The Xiaozhushan settlements are shell mound sites, where a large number of shells have accumulated. Production tools unearthed here have mainly included grinding discs, grinding sticks, and a small number of stone balls and net sinkers. These tools reflect the contemporary fishing and hunting economy (Liu, 2009), with only minor agricultural production.

The degree of aggregation, or cluster, of ancient settlements can reflect the potential communication and interaction between sites. In the Mid Neolithic period, there were not many settlements; Xiaozhushan Culture settlements were mainly located on Guanglu Island, with just a few on the Dalian Sub-Peninsula. Perhaps because of the limitations in the geographical scope of the island and the mainland, these settlements appear to have had little connection with the surrounding land. This was the time of the Holocene Climatic Optimum (8.4–4.3 ka BP), though the island environment also exerted some impact upon the local climate, meaning that ancient humans had to adapt their living environment to the climatic environment; this helps explain why settlements in the Dalian area appear clustered.

5.2 Late Neolithic (5.0–4.0 ka BP)

The Late Neolithic sporopollen records for the Liao River Basin and its surrounding areas (Wang et al., 2020) show that (**Figure 7**), at ~4.3 ka BP, broadleaved trees sporopollen contents, and sporopollens from other trees that like warm and wet conditions, decreased rapidly, and that the climate began to change from being warm and wet, to dry and cool. Globally, a sudden cooling occurred ~4.3 ka BP; a cold event at ~4.5 ka BP was recorded in the North Atlantic (**Figure 7C**) (Dong et al., 2015). The Dongge Cave $\delta^{18}O$ stalagmite record (**Figure 7B**) records a weak EASM at ~4.2 ka B.P. (Dykoski et al., 2005), and the Huguangyan Maar Lake Ti content archive (**Figure 7D**) records a weak EAWM at ~4.5 ka B.P. (Yancheva et al., 2007). Climate change also had an impact on the ancient settlements in the Dalian area. At this time, the Upper Xiaozhushan Culture (4.8–4.1 ka BP) developed. Ancient settlements were initially concentrated in island areas, then gradually expanded to various districts of the mainland Dalian area. These were principally distributed on coastal marine plains at altitudes of <50 m asl, and on slope of gradients <6°, or in low-altitude, hilly areas. The population density also increased. None of these ancient settlements faced south. This would indicate that the population was small at this time, and that human agricultural production was not a major means of food production. The impact of light on agricultural development had not yet been fully realized. Settlements were generally sited on flat terrain, so as to facilitate human travel and water extraction.

The remains of Late Neolithic settlements have been excavated within 1 km of river courses. Although small in number, this perhaps reflects a gradual increase in the human demand for water resources. At this time, most settlements were still located at fixed distances away from river courses. Human beings appear to have been more afraid of flooding than needing greater accessibility to water. The total number of Late Neolithic production tools excavated increases sharply, but felling tools decrease. A large number of pig and dog bones have also been found at the Guojiacun site (Shi, 2008), indicating that, during this period, agriculture and animal husbandry were gradually increasing in importance.

During the Late Neolithic, the degree of aggregation of ancient settlements decreased slightly. In addition to the Xiaozhushan settlement, the number of settlements in the Lüshunkou area of Dalian also increased, and the Santang and the Dapanjia village sites appeared (Liu, 1994; Chen, 1996). This increase in the number of settlements and the expansion in their spatial distribution would indicate that traveling had become gradually easier, hence a relatively lower degree of cluster. This may also be because, at that time, the number of settlements was relatively small, there was less communication with the outside world, and the technical ability to build new settlements was not advanced.

5.3 Bronze Age (4.0–3.0 ka BP)

In the Bronze Age, according to the sporopollen archive, arboreal pollens gradually decreased, pine species within broadleaved forest environments increased, and the climatic conditions were significantly drier and colder (Dai et al., 2007). This was a period of regression and stagnation, when Holocene sea levels remained high (Shi, 2006). However, Bronze Age cultures continued to grow and flourish in the Dalian area, mainly including the first, second and third phases of the Shuangtuozi Culture. The number of ancient settlements also increased significantly, and their distribution ranges experienced a period of unprecedented expansion. This might indicate that the climatic deterioration suffered during the Bronze Age did not have a significant impact on the rise of such cultures. This may be explained by population migration, the spread of regional settlements, or the development of agricultural civilization or the rise of social civilization, etc. (Zhang, 2011), promoting a rapid increase in population. At this time, settlements spread from their sporadic spatial distribution in various districts of the Dalian area to a more extensive distribution. Many settlements were located in areas with altitudes of >100 m asl, and slopes of gradients 6–25°, principally low-altitude hills or platforms near piedmont plains or water systems. This may have been to guard against flooding and attacks from wild animals. The ability of ancient humans to adapt their production capabilities and capacity with regard to the natural environment improved. Furthermore, the increase in the number of settlements would suggest that people were eager to build new settlements to meet human survival needs. Bronze Age settlements faced in all directions; the predominance of south- and north-facing sites may have been due to the topographical orientation of the Dalian Peninsula, which can play a certain role in providing shelter from the wind. West-facing settlements may reflect the human use of marine resources along the Bohai Sea (Li, 2017). Ancient humans had clearly begun to adapt gradually to changes in the natural environment; their ability to protect themselves from adverse natural conditions clearly strengthened, thus promoting cultural development.

The number of settlements increased significantly compared with the Neolithic Age, and more and more of these ancient settlements moved further away from river courses. At this time, most settlements were within 3 km of a water course, in river valleys or valleys in low-altitude mountain areas with low terrains. Such a fixed distance from river courses provided not

only a close enough distance to allow access to a sufficient water supply, but also protected inhabitants from the threat of flooding. Furthermore, unearthed Shuangtuozi Culture agricultural production tools and grain seeds indicate a continuously heightening human dependence on, and utilization of, water resources, promoting a rapid development in the agricultural economy.

The Bronze Age marks the heyday of ancient settlements, in terms of their number and spatial distribution. Combining the ANN index with VD and CV analyses, we can see that settlements remained relatively clustered. Settlements were widely distributed in the Dalian area and were relatively compact, showing a certain degree of clustering (**Figure 1**). During Shuangtuozi Culture Phase I (4.1–3.9 ka BP), as settlements and the population increased, stoves came to be extensively used, and have been found in all housing sites (Chen et al., 1996). Life appears not have been based upon the individual unit, and there may have been small family organizations with members as units. During Shuangtuozi Culture Phase II (3.9–3.6 ka BP), although ancient human culture developed, the social organization of settlements did not change greatly. The Shuangtuozi Culture and the Yueshi Culture in Shandong Province belonged to the same period, but the Shuangtuozi Culture was deeply influenced by the Yueshi Culture (Zhao, 2010), showing that settlements in the Dalian area had already communicated with external advanced cultures. During Shuangtuozi Culture Phase III (3.4–3.1 ka BP), settlements were more widely distributed, and the number of housing sites doubled, indicating that the population was also increasing. Investigations into existing housing sites (i.e., the Shuangtuozi and Dazuizi settlements) (Chen et al., 2011) have proven that our ancestors' made purposeful choices when it came to selecting sites in which to settle. These sites not only required close distances between settlements to reduce communication costs, but also needed to be in locations conducive to agricultural production and the development of fishing, so as to maximize the chances of human survival.

6 CONCLUSION

1) On the whole, the number of ancient settlements in the Dalian area increased over time, with the greatest increase during the Bronze Age, the most prosperous period of material civilization in the ancient Dalian area. Each of the three periods' settlements were mainly distributed in low-altitude, hilly areas at altitudes of 0–100 m asl, on relatively gentle slopes of gradients between 0 and 6°. Settlements from each period faced in all directions, and were mainly located in river valleys or low-altitude mountain valleys with low terrains.
2) In terms of proximity to river courses, the number of Neolithic sites distributed within 3 km of a river course was very small. In the Bronze Age, with an expansion in the spatial distribution of settlements, the number of sites distributed within 3 km of a river gradually increased, and their spatial distribution became relatively uniform, perhaps reflecting the continuous development of the agricultural economy and the increasing dependence of the ancient human population on water resources. The density of settlement sites in each of the three periods shows a certain degree of aggregation from the Mid Neolithic to the Bronze Age; Mid Neolithic sites were the fewest in number, and the most clustered.
3) The spatiotemporal distribution and evolution of ancient settlements in the Dalian area clearly responded to developments in human activity, and to climatic and environmental change, mainly reflected by the impact of the warm and humid climate prevalent during the Mid Neolithic period. Then, settlements were mainly distributed in various island areas. Coastal terraces, estuarine deltas and low-altitude hills provided the main living spaces for ancient humans. During the Late Neolithic, the climate gradually became drier and cooler, but this did not exert a significant impact on human survival. To a certain extent, indeed, it stimulated cultural development, and settlements expanded to various other areas on the Dalian Sub-Peninsula, principally coastal marine plains and low-altitude, hilly areas. During the Bronze Age, the number of settlements peaked; these ancient settlements were widely distributed in various districts of the Dalian Sub-Peninsula, mainly in low-altitude, hilly areas near the foothills of more mountainous districts, and near and water systems. At this time, the climate was mainly cold and dry, indicating the improving ability of ancient humans to adapt to their natural environments.

DATA AVAILABILITY STATEMENT

The data in this article were mainly acquired from National Meteorological Science Data Center (http://data.cma.cn/), Geospatial Data Cloud (http://www.gscloud.cn) and Nation Centers for Environmental Information (https://www.ncdc.noaa.gov/paleo-search/).

AUTHOR CONTRIBUTIONS

LL: contributed to all aspects of this work; FL: wrote the main manuscript text. WZ and ZX: pro-vided modifications for this study. All authors have read and agreed to the published version of the manuscript.

FUNDING

This research was funded by Social Science Foundation of Liaoning Province (L21BKG005).

ACKNOWLEDGMENTS

The author of this article thanks the School of Geography of Liaoning Normal University for their assistance in developing this research.

REFERENCES

An, C. B., Wang, L., Ji, D. X., Chen, F. H., and Wang, P. (2006). The Temporal and Spatial Changes of Neolithic Cultures in Gansu-Qinghai Region and Possible Environmental Forcing. *Quat. Sci.* 26 (6), 923–927. doi:10.3321/j.issn:1001-7410.2006.06.006

Chen, F., Wu, D., Chen, J., Zhou, A., Yu, J., Shen, J., et al. (2016). Holocene Moisture and East Asian Summer Monsoon Evolution in the Northeastern Tibetan Plateau Recorded by Lake Qinghai and its Environs: A Review of Conflicting Proxies. *Quat. Sci. Rev.* 154, 111–129. doi:10.1016/j.quascirev.2016.10.021

Chen, G. Q. (1996). Excavation of the Dazuizi Bronze Age Site in Dalian City. *Liaoning Prov. Archaeol.* 17, 35+99–100.

Chen, M. H. (2014). *Preliminary Study on the Interaction between Human-Environment in the Western-Central Northeastern China from Xia Dynasty to Warring States Period via Geographic Information System (GIS)*. Jilin, China: Jilin University.

Chen, R., Li, F. Q., Wang, T. Y., Zhu, L. D., Ye, W., and Zhou, G. C. (2018). The Size Distribution of Neolithic Sites in the Middle Reaches of the Yangtze River. *Acta Geogr. Sin.* 73 (3), 474–486. doi:10.11821/dlxb201803007

Chen, S., Xu, S. G., and Zhang, G. X. (2011). Brief Report on the Excavation of the Pingdingshan Bronze Age Site in Zhuanghe, Dalian. *North Cult. relics* 3, 113–115. doi:10.16422/j.cnki.1001-0483.2011.01.014

Dai, X. L., Ji, K., and Yin, H. N. (2007). Relationship Between Economic Form Transit of Neolithic Culture and Environmental Change in Liaodong Peninsula. *J. Shenyang Norm. Univ. Nat. Sci. Ed.* 25(1), 95–98. doi:10.3969/j.issn.1673-5862.2007.01.026

Deng, H., Chen, Y. Y., Jia, J. Y., Mo, D. W., and Zhou, K. S. (2009). Distribution Patterns of the Ancient Cultural Sites in the Middle Reaches of the Yangtze River since 8500 a BP. *Acta Geogr. Sin.* 64 (9), 1113–1125. doi:10.3321/j.issn:0375-5444.2009.09.009

Dong, J., Shen, C.-C., Kong, X., Wang, H.-C., and Jiang, X. (2015). Reconciliation of Hydroclimate Sequences from the Chinese Loess Plateau and Low-Latitude East Asian Summer Monsoon Regions over the Past 14,500years. *Palaeogeogr. Palaeoclimatol. Palaeoecol.* 435, 127–135. doi:10.1016/j.palaeo.2015.06.013

Dykoski, C., Edwards, R., Cheng, H., Yuan, D., Cai, Y., Zhang, M., et al. (2005). A High-Resolution, Absolute-Dated Holocene and Deglacial Asian Monsoon Record from Dongge Cave, China. *Earth Planet. Sci. Lett.* 233, 71–86. doi:10.1016/j.epsl.2005.01.036

Garcia, A. (2013). GIS-based Methodology for Palaeolithic Site Location Preferences Analysis. A Case Study from Late Palaeolithic Cantabria (Northern Iberian Peninsula). *J. Archaeol. Sci.* 40, 217–226. doi:10.1016/j.jas.2012.08.023

Goude, G., and Fontugne, M. (2016). Carbon and Nitrogen Isotopic Variability in Bone Collagen during the Neolithic Period: Influence of Environmental Factors and Diet. *J. Archaeol. Sci.* 70, 117–131. doi:10.1016/j.jas.2016.04.019

Gu, W. W., and Zhu, C. (2005). Distribution Feature of Neolithic Sites in North Jiangsu Province and EnvironmentalArchaeology Researth on its Relation with Environmental Variation. *Sci. Geogr. Sin.* 25 (2), 239–243. doi:10.3969/j.issn.1000-0690.2005.02.018

Guo, L., Xiong, S., Ding, Z., Jin, G., Wu, J., and Ye, W. (2018). Role of the Mid-Holocene Environmental Transition in the Decline of Late Neolithic Cultures in the Deserts of NE China. *Quat. Sci. Rev.* 190, 98–113. doi:10.1016/j.quascirev.2018.04.017

Guo, Y., Mo, D., Mao, L., Wang, S., and Li, S. (2013). Settlement Distribution and its Relationship with Environmental Changes from the Neolithic to Shang-Zhou Dynasties in Northern Shandong, China. *Acta Geogr. Sin.* 23 (4), 679–694. doi:10.1007/s11442-013-1037-3

Huang, J., Lei, S., Tang, L., Wang, A. H., and Wang, Z. H. (2020). Mid-Holocene Environmental Change and Human Response at the Neolithic Wuguishan Site in the Ningbo Coastal Lowland of East China. *News. Sci.* 30, 1591–1605. doi:10.1177/0959683620941070

Innes, J. B., Zong, Y. Q., Wang, Z. H., and Chen, Z. Y. (2014). Climatic and Palaeoecological Changes during the Mid- to Late Holocene Transition in Eastern China: High-Resolution Pollen and Non-pollen Palynomorph Analysis at Pingwang, Yangtze Coastal Lowlands. *Quat. Sci. Rev.* 99, 164–175. doi:10.1016/j.quascirev.2014.06.013

Kidder, T. R., Adelsberger, K. A., Arco, L. J., and Schilling, T. M. (2008). Basin-scale Reconstruction of the Geological Context of Human Settlement: an Example from the Lower Mississippi Valley, USA. *Quat. Sci. Rev.* 27, 1255–1270. doi:10.1016/j.quascirev.2008.02.012

Li, J. (2017). *Elementary Analysis of Man-Land Relationship of Liaodong Peninsula from Neolithic to Bronze Age Based on GIS – A Case Study on Xiaozhushan Site Catchment Area*. Jilin, China: Jilin University.

Li, L., Zhang, W., Li, Y. Y., Ding, M., and Yang, C. Y. (2008). A Preliminary Study on the Magnetic Susceptibility Feature Sand the Paleo Environment Changes of Qi Ding Shan Loess Profile in Dalian. *Resour Ind* 10 (6), 112–118. doi:10.3969/j.issn.1673-2464.2008.06.028

Li, Z. X., Zhu, C., Wu, G. X., Zheng, C. G., Shao, S. X., Feng, F. F., et al. (2013). Spatial and Temporal Distribution of Prehistoric Human Sites and its Driving Factors in Henan Province. *Acta Geogr. Sin.* 68 (11), 1527–1537. doi:10.11821/dlxb201311008

Liu, J. Y. (2009). On the Economic Form of the Prehistoric Liaodong Peninsula. *J. Liaoning Norm. Univ. (Nat.Sci).* 32, 110–119. doi:10.3969/j.issn.1000-1751.2009.06.026

Liu, J. Y. (1994). *The Neolithic Site of Dapanjia Village*. Dalian: Liaoning Province. Archaeol, 877–894.

Liu, S., Zou, C. H., Mao, L. J., Jia, X., and Mo, D. W. (2021). The Spatial and Tempo Raldist Ribution of Archaeological Settlemant Sites in Shandong Province from the Paleolithic to Shang and Zhou Periods and its Relationship with Hyd Rology and Geomorphology. *Quat. Sci.* 41 (5), 1394–1407. doi:10.11928/j.issn.1001-7410.2021.05.14

Liu, Z. Y., Ma, C. M., Zhu, C., Shang, G. C., and Sun, Z. B. (2018). A Preliminary Study of Sporo Pollen Record on the Zhongba Site in the Three Gorges. *Yangtze River, China* 35 (3), 250–259. doi:10.16087/j.cnki.1000-0674.2018.03.003

Nsanziyera, A. F., LechgarFal, H. S., Maanan, M., Saddiqi, O., and Oujaa, A. (2018). Remote-sensing Data-Based Archaeological Predictive Model (APM) for Archaeological Site Mapping in Desert Area, South Morocco. *C. R. Geosci.* 350, 319–330. doi:10.1016/j.crte.2018.06.010

Parker, A. G., Morley, M. W., Armitage, S. J., Engel, M., Parton, A., Preston, G. W., et al. (2020). Palaeoenvironmental and Sea Level Changes during the Holocene in Eastern Saudi Arabia and Their Implications for Neolithic Populations. *Quat. Sci. Rev.* 249, 106618. doi:10.1016/j.quascirev.2020.106618

Peng, F., Fan, X. C., and Xia, Z. K. (2011). Prelim Inary Study on the Paleo Enviroment of the Lianhuachishan Palaeolithic Site, Fujian Province,China. *Quat. Sci.* 31 (4), 705–714. doi:10.3969/j.issn.1001-7410.2011.04.14

Qiu, S. W., and Li, F. H. (1982). On the Problem of Geomorphological Classification in China. *Sci. Geogr. Sin.* 2 (4), 327–335.

Ren, Y. Q., Jin, J. H., Zuo, X. X., Huang, Y. M., and Li, Z. Z. (2021). Spatial and Temporal Distribution of Prehistoric Settlement Sites in Minjiang River Basin and Their Relationship with Environmental Factors. *J. Earth Environ.* 12 (1), 68–83. doi:10.7515/JEE202012

Shen, W., Xu, Q. H., Li, J. Y., Li, M. Y., Zhang, P. P., and Lu, J. Y. (2017). Relationship of Pollen-Vegetation-Land Use in Small Watersheds of Mountain Area: A Tentative Study of Quantitative Detecting Human Activities on Environment. *Adv. Earth Sci.* 32 (9), 972–982. doi:10.11867/j.issn.1001-8166.2017.09.0962

Shi, B. H. (2006). Archaeological Observation on the Largest Holocene Transgression in the Liaodong Peninsula. *Sichuan Cult. Relics* 7, 37–41. doi:10.3969/j.issn.1003-6962.2006.06.006

Shi, B. H. (2008). The Transformation of the Ancient Subsistence Economic Model of the Liaodong Peninsula and its Environmental Background. *Chin. Archaeol.* 4, 59–72. doi:10.3969/j.issn.1001-9928.2008.04.008

State Administration of Cultural Heritage (2009). *Atlas of Chinese Cultural Relics: Liaoning Volume*. Xian: Xi'an Map Press, 61–94.

Stebich, M., Rehfeld, K., Schlütz, F., Tarasov, P. E., Liu, J. Q., et al. (2015). Holocene Vegetation and Climate Dynamics of NE China Based on the Pollen Record from Sihailongwan Maar Lake. *Quat. Sci. Rev.* 124, 275–289. doi:10.1016/j.quascirev.2015.07.021

Thompson, L. G., Yao, T., Davis, M. E., Henderson, K. A., Mosley-Thompson, E., Lin, P.-N., et al. (1997). Tropical Climate Instability: the Last Glacial Cycle from a Qinghai-Tibetan Ice Core. *Science* 276, 1821–1825. doi:10.1126/science.276.5320.1821

Turney, C. S. M., and Brown, H. (2007). Catastrophic Early Holocene Sea Level Rise, Human Migration and the Neolithic Transition in Europe. *Quat. Sci. Rev.* 26, 2036–2041. doi:10.1016/j.quascirev.2007.07.003

Wang, F., Yang, X. L., Yang, Z. P., Luan, F. M., Xiong, H. G., Wang, Z. G., et al. (2015). Spatiotemporal Characteristics of Cultural Sites and Their Driving Forces in the Ili River Valley during Historical Periods. *Acta Geogr. Sin.* 25 (9), 1089–1108. doi:10.1007/s11442-015-1221-8

Wang, J. F., and Lei, R. D. (2002). On Progress of T Heoretical Research on Ecotone. *J Northwest For. Univ.* 17 (4), 24–28+37. doi:10.3969/j.issn.1001-7461.2002.04.007

Wang, K., Ma, Y. Z., Li, D. D., Meng, H. W., and Guo, C. (2020). The Relationship between Ecological Environments Recorded by Pollen and Neolithic Cultures in the Representative Areas of China during the Holocene: A Review. *Chin. J. Ecol.* 39 (8), 2467–2477. doi:10.13292/j.1000-4890.202008.022

Wang, L. B., Wang, X. H., Wang, L. S., Diao, Y. D., Zhang, L. N., and Jiang, C. (2021). Temporal and Spatial Distribution Characteristics and Driving Factors of the Mid-Holocene Settlements in the Weihai Area. *J. Earth Environ.* 12 (6), 605–614. doi:10.7515/JEE212014

Wang, L., Wu, H., and Jia, X. (2016). Study on the Temporal-Spatial Evolution of Prehistoric Settlements and its Correlation with Subsistence Strategy and Climate History in the Western Liao River Area. *Adv. Earth Sci.* 31 (11), 1159–1171. doi:10.11867/j.issn.1001-8166.2016.11.1159

Wen, R. L., Xiao, J. L., Fan, J. W., Zhang, S. R., and Yamagata, H. (2017). Pollen Evidence for a Mid-Holocene East Asian Summer Monsoon Maximum in Northern China. *Quat. Sci. Rev.* 176, 29–35. doi:10.1016/j.quascirev.2017.10.008

Wu, J. Y., Wang, Y. J., and Dong, J. G. (2011). Changes in East Asian Summer Monsoon During the Holocene Recorded by Stalagmite $\delta^{18}O$ Records from Liaoning Province. *Quat. Sci.* 31 (6), 990–998. doi:10.3969/j.issn.1001-7410.2011.06.06

Wu, L., Li, F., Zhu, C., Li, L., and Li, B. (2012a). Holocene Environmental Change and Archaeology, Yangtze River Valley, China: Review and Prospects. *Geosci. Front.* 3 (6), 875–892. doi:10.1016/j.gsf.2012.02.006

Wu, L., Lu, S. G., Zhu, C., Ma, C. M., Sun, X. L., Li, X. X., et al. (2021). Holocene Environmental Archaeology of the Yangtze River Valley in China: A Review. *Land* 3, 302. doi:10.3390/LAND10030302

Wu, L., Zhu, C., Zheng, C. G., Li, F., Ma, C. M., Sun, W., et al. (2012b). Response of Prehistoric Culture to Climatic Environmental Changes since Holocene in Zhejiang, East China. *Acta Geogr. Sin.* 67 (7), 903–916. doi:10.11821/xb201207004

Xiao, Y. (2019). *Spatial Distribution and Influencing Factors of the Neolithic Sites in the Taihu Basin*. Zhejiang, China: Zhejiang Normal University. doi:10.27464/d.cnki.gzsfu.2019.000390

Xu, Q. H., Yang, Z. J., Cui, Z. J., Yang, X. L., and Liang, W. D. (2002). A Study on Pollen Analysis of Qiguoshan Section and Ancestor Living Environment in Chifeng Area, Nei Mongol. *Sci. Geogr. Sin.* 22 (4), 453–457. doi:10.3969/j.issn.1000-0690.2002.04.014

Xu, Y. L., and Jin, S. Z. (1986). The Right Bank of the Yalu River and its Neolithic Remains of Tributaries. *Archaeol* 10, 865–872.

Xu, Y. L., and Su, X. X. (1980). A Brief Talk on the Neolithic Site of Guojiacun. *J. Liaoning Univ. Philos. Soc. Sci. Ed.)* 1, 43–46+2.

Xu, Y. L. (1994). The Neolithic Site at Beiwutun,Dalian City. *Acta. Archaeol. Sin.* 3, 343–380.

Xu, Z. F. (2019a). *A Study on Archaeological Culture from Neolithic Age to Bronze Age in Liaodong Peninsula*. Beijing, China: Zhong huas hu jv.

Xu, Z. F. (2019b). The Chronology and Genealogy of the Archaeological Cultures in the South of Liaodong Peninsula. *Acta. Archaeol. Sin.* 2, 143–162.

Xue, B., Li, J., Xiao, X., and Li, J. (2018). A Big-Data-Based Platform for Man-Land Relationship Analysis and Application in Urban Areas. *J. Glob. Change Data & Discov.* 35 (6), 51–60.

Xue, B., and Mario, T. (2015). Sustainability in China: Bridging Global Knowledge with Local Action. *Sustainability* 7, 3714–3720. doi:10.3390/su7043714

Yancheva, G., Nowaczyk, N. R., Mingram, J., Dulski, P., Schettler, G., Negendank, J. F. W., et al. (2007). Influence of the Intertropical Convergence Zone on the East Asian Monsoon. *Nat* 445, 74–77. doi:10.1038/nature05431

Yang, W. C., and Lin, J. X. (1985). Preliminary Notes on Holocene Transgression in the Southeast Coast of Liaodong Peninsula. *Chin. J. Geol. Sci. Geol. Sin.* 2, 196–201.

Yuan, Y. Y. (2018). Characteristics and Genesis of Spatial Distribution of Settlements in the West Liaohe River Basin During the Mid-Holocene. *Sci. Geogr. Sin.* 38 (5), 773–779. doi:10.13249/j.cnki.sgs.2018.05.015

Yuan, Y. Y. (2019). Cultural Evolution and Spatial-Temporal Distribution of Archaeological Sites from 9.5–2.3 ka BP in the Yan-Liao Region, China. *Sci. Geogr. Sin.* 29 (3), 449–464. doi:10.1007/s11442-019-1609-y

Zhang, C. M. (2011). Cause of Formation of Early Bronze Cultural Pattern in Dalian Area. *East Asia Archaeol.*, 195–210.

Zhang, W. H., and Wu, J. Y. (2012). Ecological Response of $\delta^{13}C$ to Holocene Climate Changes from Stalagmite Record in Nuanhe Cave. *Mar. Geol. Quat. Geol.* 32 (3), 147–154.

Zhang, X. L., Jin, Y. X., and Jia, X. B. (2016). Archaeological and Cultural Studies of the Xiaozhushan Site in Changhai. *Liaoning Chronology. Archaeol.* 5, 110–120.

Zhang, Z. P., Liu, J. B., Chen, J., Chen, S. Q., Shen, Z. W., Liu, X. K., et al. (2021). Holocene Climatic Optimum in the East Asian Monsoon Region of China Defined by Climatic Stability. *Earth-Sci. Rev.* 212, 103450. doi:10.1016/j.earscirev.2020.103450

Zhao, B. F. (2011). Archaeology of the Northeast Region during the Summer Solstice and Warring States Periods The Construction of Cultural Space-Time Framework. *Soc. Sci. Front.* 7, 118–122.

Zhao, B. F. (2010). Three New Understandings on the First and Second Phases of Shuangtuozi Culture. *Northeast Hist.* 6, 3–8. doi:10.16435/j.cnki.cn22-1273/c.2010.06.019

Zhao, J., Feng, Q., and Wang, Y. (2021). Research on the Cultural Gravity Migration and Environmental Archaeology of Xi'an Neolithic Settlement Sites. *J. Arid. Land Resour. Environ.* 35 (5), 87–93. doi:10.13448/j.cnki.jalre.2021.13210.1080/15324982.2020.1832159

Zhao, L., Ma, C. M., Wen, Z. M., Ye, W., Shang, G. C., and Tang, L. Y. (2021b). Vegetation Dynamics and Their Response to Holocene Climate Change Derived from Multi-Proxy Records from Wangdongyang Peat Bog in Southeast China. *Veg Hist Archaeobot* 31, 247–260. doi:10.1007/S00334-021-00852-Z

Zhao, L., Ma, C. M., XuDeng, Q. M. Y. K., Shang, C. G., and Tang, L. Y. (2021a). Vegetation Evolution in Response to Climate Change and Rapid Sea-Level Rise during 8.2–7.0 Cal ka BP: Pollen Evidence from the Northwest Coast of Bohai Bay, North China. *Catena* 196. doi:10.1016/j.catena.2020.104869

Zhao, Q., Yao, T., Lu, D., Zou, C. H., and Gao, Q. (2019). Spatial and Temporal Distribution Characteristics and Natural Environmental Background of the Middle Holocene Settlements in the Northeastern Liaoning Province. *Sci. Geogr. Sin.* 39 (9), 1516–1524. doi:10.13249/j.cnki.sgs.2019.09.017

Zhu, C., Zheng, C. G., and Wu, L. (2015). *Environmental Archaeology Since the Neolithic Age in the Yangtze River Valley, China*. Beijing, China: Science Press.

Conflict of Interest: The authors declare that the research was conducted in the absence of any commercial or financial relationships that could be construed as a potential conflict of interest.

Publisher's Note: All claims expressed in this article are solely those of the authors and do not necessarily represent those of their affiliated organizations, or those of the publisher, the editors and the reviewers. Any product that may be evaluated in this article, or claim that may be made by its manufacturer, is not guaranteed or endorsed by the publisher.

Copyright © 2022 Liu, Liu, Zhang and Xu. This is an open-access article distributed under the terms of the Creative Commons Attribution License (CC BY). The use, distribution or reproduction in other forums is permitted, provided the original author(s) and the copyright owner(s) are credited and that the original publication in this journal is cited, in accordance with accepted academic practice. No use, distribution or reproduction is permitted which does not comply with these terms.

frontiers | Frontiers in Ecology and Evolution

ORIGINAL RESEARCH
published: 26 May 2022
doi: 10.3389/fevo.2022.907691

Spillover Effects of Built-Up Land Expansion Under Ecological Security Constraint at Multiple Spatial Scales

Dan Yang[1], Yuanyuan Lou[1], Pengyan Zhang[1,2,3] and Ling Jiang[4]**

[1] College of Geography and Environmental Science, Henan University, Kaifeng, China, [2] Key Laboratory of Geospatial Technology for the Middle and Lower Yellow River Regions, Ministry of Education, Henan University, Kaifeng, China, [3] Regional Planning and Development Center, Henan University, Kaifeng, China, [4] School of Government, Central University of Finance and Economics, Beijing, China

OPEN ACCESS

Edited by:
Jun Yang,
Northeastern University, China

Reviewed by:
Shaohua Wang,
Aerospace Information Research Institute (CAS), China
Xiao Xie,
Key Lab for Environmental Computation and Sustainability of Liaoning Province, Institute of Applied Ecology (CAS), China
Bao-Jie He,
Chongqing University, China

***Correspondence:**
Pengyan Zhang
pengyanzh@126.com
Ling Jiang
cufejiangling@126.com

Specialty section:
This article was submitted to Environmental Informatics and Remote Sensing, a section of the journal Frontiers in Ecology and Evolution

Received: *30 March 2022*
Accepted: *26 April 2022*
Published: *26 May 2022*

Citation:
Yang D, Lou Y, Zhang P and Jiang L (2022) Spillover Effects of Built-Up Land Expansion Under Ecological Security Constraint at Multiple Spatial Scales. Front. Ecol. Evol. 10:907691. doi: 10.3389/fevo.2022.907691

Land-use change is a global issue, and the built-up land expansion has affected the ecological landscape patterns of the major river basins in the world. However, measurement of the ecological risks of potential landscape and identification of the dynamic relationships by natural and human-driven built-up land expansion at different zoning scales are still less understood. Based on multi-period Landsat satellite image data, we combined remote sensing (RS) and geography information systems (GIS) technologies with Spatial Durbin Panel Model to quantitatively analyze the landscape ecological effects under the built-up land expansion in the Yellow River Basin. The results showed that there is spatial heterogeneity in the built-up land expansion and ecological security patterns, with the expansion gravity center gradually spreading from the downstream to the middle and upstream areas, and the most dramatic change in landscape patches of ecological safety patterns occurring around the year 2000. At different zoning scales, there is a spatial spillover effect on the interaction between built-up land expansion and ecological security, with the significance of the regression estimates decreasing from large sample sizes to small sample sizes. Our findings highlighted the importance of spatial heterogeneity at different zoning scales in identifying the dynamic relationship between built-up land expansion and ecological security, scientific planning of land resources, and mitigation of ecological and environmental crises.

Keywords: spillover effect, Spatial Durbin Panel Model, built-up land expansion, ecological constraint, Yellow River Basin

INTRODUCTION

The impact of human activities on ecosystems has gradually increased in the Anthropocene era and has become a dominant factor in ecosystem evolution (Best, 2019). In the past few decades, the world's built-up land expansion has exceeded the population growth rate (Flörke et al., 2018), with far-reaching implications for biodiversity and water, carbon, and nitrogen cycles in local and global climate systems (Chen et al., 2020). In 2018, the global built-up land

area was nearly 8 km × 10^5 km, which is 1.5 times of that in 1990 (Gong et al., 2020). In the future, built-up land is expected to continue to expand globally, reaching three times its 2000 level by 2030 (Seto et al., 2012). Nearly 60% of the population lives in urban built-up areas (Narducci et al., 2019). Although the built-up land expansion provides opportunities for human, social, and economic development, the expansion also leads to the loss of more than 80% of natural habitats (Li et al., 2021), threatening the sustainability of human survival (Elmqvist et al., 2019; Zhang et al., 2020b). Therefore, in this "urban age," understanding how the expansion of built-up land will affect other land covers and how to protect and optimize the pattern of ecological security is essential for resolving social and environmental problems that challenge the sustainable development of human society (Zhou et al., 2020).

Ecological security is considered a basic component of regional security (Ghosh et al., 2021). Global competition for multiple land use has led to a sharp decrease in ecologically safe land (Lambin and Meyfroidt, 2011), which has a significant negative impact on ecosystem services and terrestrial biodiversity (Newbold et al., 2015). In particular, the loss of natural habitats, such as woodlands and water bodies, has significantly increased global greenhouse gas emissions (Tubiello et al., 2015). Land-use change is one of the important factors leading to the loss of ecological security land (Cayuela et al., 2015). The impact of built-up land expansion on ecological processes is currently gaining an increasing amount of attention and debate (Lausch et al., 2015; Guo et al., 2020; Zhang et al., 2020c). Between 1982 and 2016, global land-use change resulted in significant woodland loss: Paraguay lost 34% of its total area of 7.9 km × 10^4 km; Argentina lost 25% of its total area of 11.3 km × 10^4 km; and Brazil lost 8% of the forest area of its total area of 38.5 km × 10^4 km (Song et al., 2018). It is expected that natural habitats will be reduced by 26–58% (Jantz et al., 2015), 39% of ecological security land will be occupied by built-up land and cropland, and 37% will be degraded and segmented from 2005 to 2100 (Ellis et al., 2010). Alcamo et al. (2005) pointed out that by 2050, 10–20% of woodlands and water bodies will be occupied by built-up land and cropland. Therefore, it is increasingly important to explore the impact of built-up land change on natural habitats.

Exploring the impact of past and future built-up land expansion on ecological security has become a key link in landscape analysis (Yang et al., 2020; Stoica et al., 2021). Wihbey (2017) predicted that global built-up land will increase to nearly 300 km × 10^4 km by 2050. The built-up land not only occupies natural habitats but also threatens local food security and biodiversity (d'Amour et al., 2017; Van Vliet, 2019; McDonald et al., 2020). Furthermore, it affects the regional and global biogeochemical cycles (Huang et al., 2019), resulting in increased pollutant emissions and natural disaster risks (Güneralp et al., 2015). The methods for balancing economic development and the ecological environment in regions experiencing rapid expansion are also being discussed. McDonald et al. (2018) believe that the establishment of ecological priority zones can effectively mitigate biodiversity loss due to the built-up land expansion. To avoid placing more economic assets at risk, it is necessary to prevent and control floods and other disasters within the basin (Mård et al., 2018). Although most scholars have discussed the impact of built-up land expansion on the ecological environment at different levels, it is mostly at the macro level, and studies focused on forest land and water bodies are limited.

The river basin is an important unit for studying the coupling of natural and human processes (Gleeson et al., 2020). Nearly 40% of the global built-up land expansion occurs near river basins, such as the Mississippi River Basin and the Yangtze River Basin (Huang et al., 2021). In addition, built-up land expansion at most of the world's watershed scales is in line with the S Northam curve model of urbanization (Xu et al., 2020). The model helps developed economies to reduce the changes in the biogeochemical cycle, while the impact of the model on developing economies cannot be overlooked (Wiedmann and Lenzen, 2018). The Yellow River Basin is not only an important ecological barrier area in China, but also, at the same time, an area lagging in economic and social development and the current fight against poverty. The region is facing regional development imbalance, ecological function degradation, ecosystem connectivity, and integrity weakening (Rong et al., 2020). The transformation and development of the region have become an urgent problem that can be solved by finding ways to meet the needs of regional green development with limited land resources.

The issue of scale is central to landscape ecology, and because differences in the physical geography and socioeconomic conditions of regions at different scales can lead to large differences and even reverse outputs, it is necessary to make multiscale attempts to enhance the reliability of research results (Xiao et al., 2022). The expansion of built-up land and its impacts are not limited to the boundaries of administrative divisions but are reflected in different natural ecological backgrounds. Existing studies have examined the expansion of built-up land from the perspective of administrative divisions but lacked a comprehensive understanding of different divisions. Our study investigated the characteristics of built-up land expansion and its impact on ecological security patterns from three zoning perspectives: administrative zoning, eco-geographical zoning, and agricultural natural zoning, and then revealed the spatial spillover effects of the complex relationship between built-up land expansion and ecological security patterns in different regions. New methods and perspectives for studying this relationship are necessary to avoid conflicting and inconsistent outcomes in research, which can lead to the formulation of inappropriate policies. The aim of our research is to examine the relationship between human activities and regional ecological security patterns at the watershed scale using a perspective that provides more confidence and reliable results than traditional perspectives in the field. We argue that regional governance should move from administrative boundaries to multiple zoning perspectives; thus, it is necessary to resolve land-use conflicts through scientific land use planning and management to achieve ecological civilization.

MATERIALS AND METHODS

Overview of the Study Area

The Yellow River Basin is located in the central and eastern regions of China. It is the birthplace of Chinese civilization (Zhang et al., 2021). In 2019, the ecological protection and high-quality development strategy in the Yellow River Basin provide new directions for watershed management and protection. Promoting the construction of an ecological civilization in the Yellow River Basin is a long-term goal.

The terrain of Yellow River Basin is high in the west and low in the east, with a total area of approximately 79.5 km $\times$ 10^4 km. Among them, the built-up land area increased from 3.9 km $\times$ 10^4 km in 1980 to 6.2 km $\times$ 10^4 km in 2018 (**Figure 1**). By the end of 2018, the per capita GDP was 60,000 yuan, which was lower than the national average GDP (64,000 yuan). The vegetation coverage of the basin decreased significantly due to climate change and soil erosion, with threatened species accounting for 15–20%, which is higher than the world average (10–15%) (Jing et al., 2020). Since the 1990s, a series of major ecological security protection projects launched by government departments have curbed the degradation trend of ecosystem in some regions. However, the gradual improvement of the ecological environment does not imply that the previous development methods can be restored. We need to pay attention to the ecological security of the basin and seek sustainable land development strategies.

Regional Division

Regional development may have an impact on adjacent areas (Kopp and Allen, 2021). This study aims to analyze the interactive relationship between multiple spatial zoning scales to test the spatial spillover effect of the relationship between built-up land expansion and ecological security.

First, the use of administrative division data improves the accuracy of spatial dependence capture (Liu and Wu, 2021). Prefecture-level cities were chosen as the analysis scale (**Figure 2A**).

Second, the Yellow River Basin spans the eastern, central, and western parts of China, with a wide range of climatic, geomorphological, and geological conditions and resource endowments. We selected the eco-geographical zoning scale based on geographic relativity (i.e., geographical differences in nature are not absolute, and geographical changes are often in a state of development and gradual transition) and the main ecosystem elements (i.e., the spatial location of various ecosystem factors changes over time, and their manifestations are diverse, e.g., encompassing plains, hills, and basins) (**Figure 2B**).

Third, the Yellow River Basin is the largest agricultural base in China, spanning all climate zones in northern China. The agricultural natural zoning scale was selected based on differences in natural climatic conditions and temperatures (**Figure 2C**).

Variables Selection

The aim of this study was to analyze the impact of built-up land expansion on the ecological security pattern in the Yellow River Basin. Therefore, it is necessary to define variables, introduce data sources, and provide empirical models. The following specific variables were selected for the study:

(1) Explained variables: Built-up land to correlate the surface area variables of built-up land and polygon landscape pattern variables, according to different spatial scales. The area calculated by ArcGIS 10.2 software spatial statistical

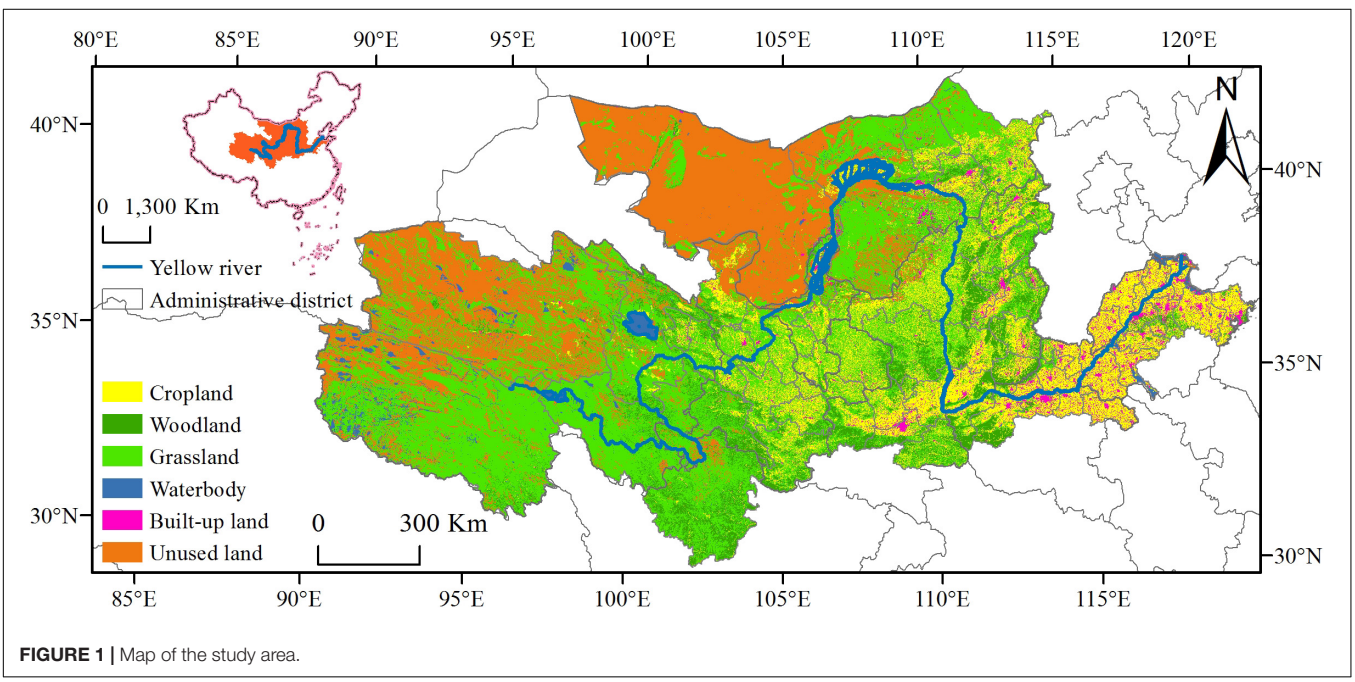

FIGURE 1 | Map of the study area.

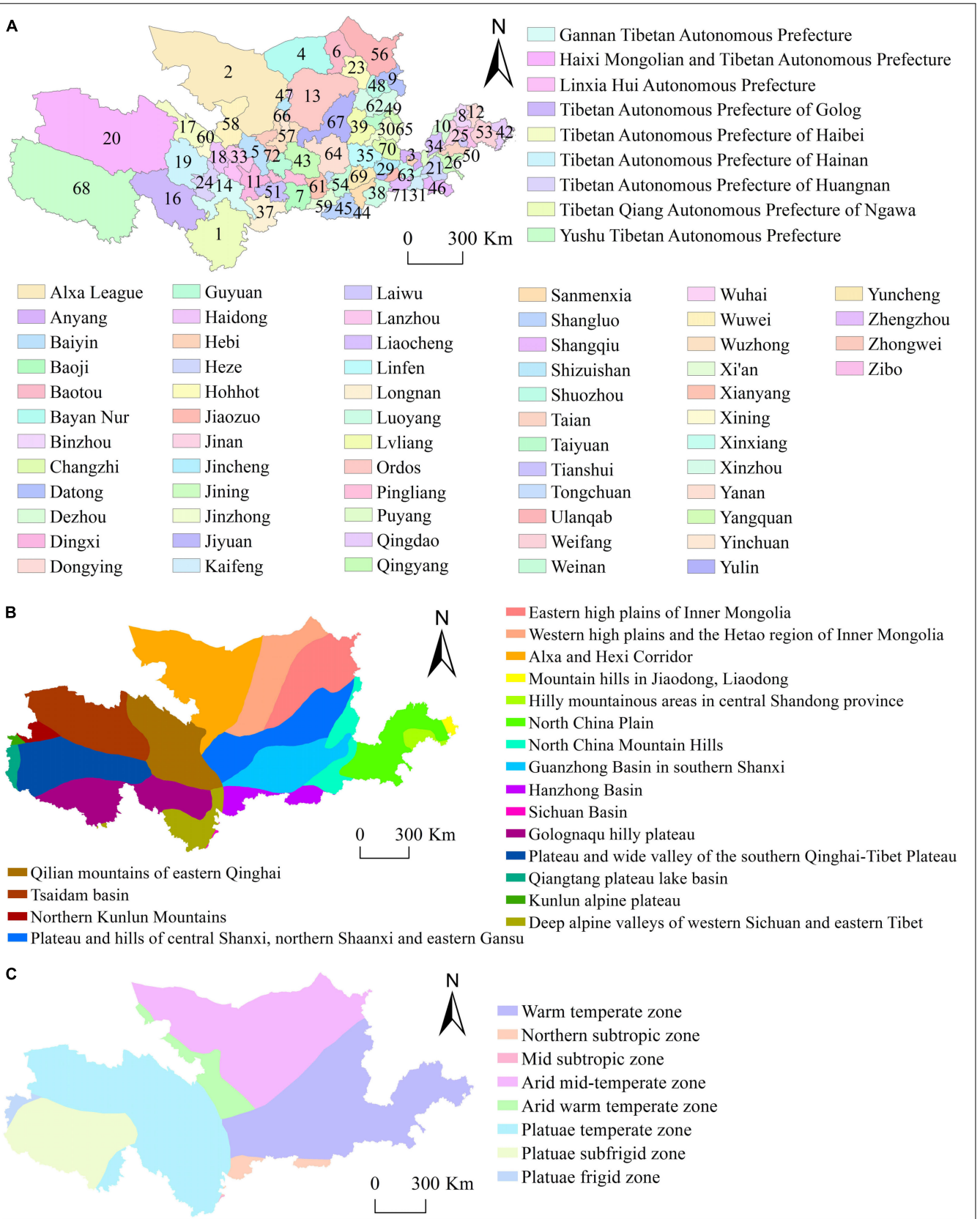

FIGURE 2 | Regional delineation of the study area. **(A)** Administrative zoning; **(B)** eco-geographical zoning; **(C)** agricultural natural zoning.

tool was used as the expansion level of built-up land (referred to as LUE).

(2) Core explanatory variables: The study comprehensively considers the spatial resolution of data and refers to relevant studies (Yang et al., 2018; Bosch et al., 2020) selected five landscape pattern indexes from patch and landscape types to comprehensively characterize the landscape ecological effect of built-up land expansion (Riitters et al., 1995; **Table 1**).

Model Establishment

Transfer Matrix of Land Use

The land use transfer matrix is a quantitative description of the state and state transfer in a specific period and uses the transfer matrix to measure the dynamic information of land use in that period (Anees et al., 2019). This method is considered one of the most commonly used landscape change detection methods (Ghosh et al., 2016). The calculation formula is as follows:

$$S_{ab} = \begin{vmatrix} S_{11} & S_{12} & \cdots & S_{1n} \\ S_{21} & S_{22} & \cdots & S_{2n} \\ \cdots & \cdots & \cdots & \cdots \\ S_{n1} & S_{n2} & \cdots & S_{nn} \end{vmatrix} \quad (1)$$

where S is the land area, a and b are pre-transfer and post-transfer land-use types, respectively (a, b = 1, 2, . . ., n), and n is the total number of land-use types.

Landscape Expansion Index

Landscape indices are used to express landscape heterogeneity within a region (Kowe et al., 2021). To comprehensively reflect the landscape pattern and characteristics and reduce information redundancy, this study used the traditional landscape index calculation method, based on the Fragstats 4.2 software, to depict the landscape status and landscape pattern fragmentation, heterogeneity, and connectivity from a macro perspective. The specific landscape pattern index is summarized in **Table 1**. According to the scope of the research area, it has been determined through multiple debugging that the land use data of the Yellow River Basin should be resampled to 200 m to better reflect the changes in the study area.

Spatial Durbin Panel Model

To future reveal the spatial spillover effect of built-up land expansion, we introduced the Spatial Durbin Panel Model (SDPM) for referring to the research results of Elhorst (2014) and Chen et al. (2017). The maximum likelihood method was used to estimate the parameters, which tests the spatial, temporal, and spatiotemporal correlations of the explained variables (Anselin et al., 2008). Based on this, the initial model was set to the SDPM with the following formula:

$$y_{it} = \rho \sum_{j=1}^{N} w_{ij} y_{jt} + \alpha + x_{it}\beta + \theta \sum_{j=1}^{N} w_{ij} x_{ijt} + \mu_i + \lambda_t + \varepsilon_{it} \quad (2)$$

where y_{it} is the built-up land expansion of region i in period t, and i and j are regional individuals, N is the number of sample units, w_{ij} is the spatial weight matrix, α is a constant term, x_{it} is the explanatory variable, β is the regression coefficient of each variable, ρ is a space regression coefficient, $w_{ij}x_{it}$ is the spatial lag term, θ is the coefficient of the spatial lag term, μ_i and λ_t are individual fixed effects and individual time effects, respectively, and ε_{it} is a random error term.

The Likelihood Ratio test and the Wald test are used to verify the original hypothesis: when $\theta = 0$, SDPM is the same as the spatial lag panel model (SLPM), and when $\theta = -\rho\beta$, SDPM is the same as the spatial error panel model (SEPM). According to this model, spatial econometric regression estimations were conducted for different zoning variables.

The spatial weight matrix (w_{ij}) is the core element of the spatial econometric model (Feng et al., 2019). This study selected the adjacency matrix (w) as the benchmark space matrix referring to the study of Lesage and Pace (2014), as follows:

$$w_{ij} = \begin{cases} 1 & (i \text{ is adjacent to } j) \\ 0 & (i \text{ is not adjacent to } j) \end{cases} \quad (3)$$

Data Source

To study the impact of built-up land expansion on regional ecological security patterns, the Yellow River Basin panel data (covering 73 prefecture-level and above cities in China) from 1980 to 2018 were selected. **Figure 3** shows the overview chart of the article. The basic data used in the study were 100 m resolution land-use datasets from 1980, 1990, 2000, 2010, and 2018. The zoning data were derived from http://www.resdc.cn. The production of the land use data set was based on the remote sensing images of Landsat TM/ETM of each period as the main data source. The built-up land, ecological security pattern land (woodland, water body), and transition land (cropland, grassland, and unused land) at each time point were generated by manual visual interpretation based on the "source–sink" theory (Chen et al., 2006). Among them, the built-up land is the interference source area, the ecological security pattern land is the sink area disturbed by the source area, and the other land is the source-sink transition area. At the same time, to avoid the potential heteroscedasticity of the data and the dependence on the setting of the regression model, all variables were converted into natural logarithms (**Table 2**).

RESULTS

Evolutionary Characteristics of Spatiotemporal

Spatiotemporal Evolutionary Characteristics of Built-Up Land Expansion

The built-up land in the Yellow River Basin expanded rapidly from 1980 to 2018, with significant spatial and temporal variations (**Figure 4**). In terms of land-use change (**Table 3**), the built-up land area expanded by 58.83% from 39,061.56 km^2 in 1980 to 62,042.20 km^2 in 2018. The difference in the expansion level was greatly affected by the location. The expansion level in the eastern plains was significantly higher than in the western region, and the remaining areas were concentrated in

TABLE 1 | Description and significance of landscape pattern indicators.

Indicator type	Landscape pattern indicators	Unit	Ecological significance
Class metrics	Percentage of landscape (PLAND)	%	Reflects the area percentage of a certain landscape type, it can help to identify the dominant elements
	Largest patch index (LPI)	–	Reflects the proportion of the largest patches in the entire landscape and reveals the concentration of patches
	Landscape shape index (LSI)	%	Reflects the characteristics of the patch shape in the landscape, and the higher the value, the greater the area exchanged with external energy
Landscape metrics	Patch density (PD)	–	Reflects heterogeneity and fragmentation per unit area of the landscape
	Patch cohesion index (COHESION)	%	Measures physical connectivity between patches, reflects the corridor connections between the patches

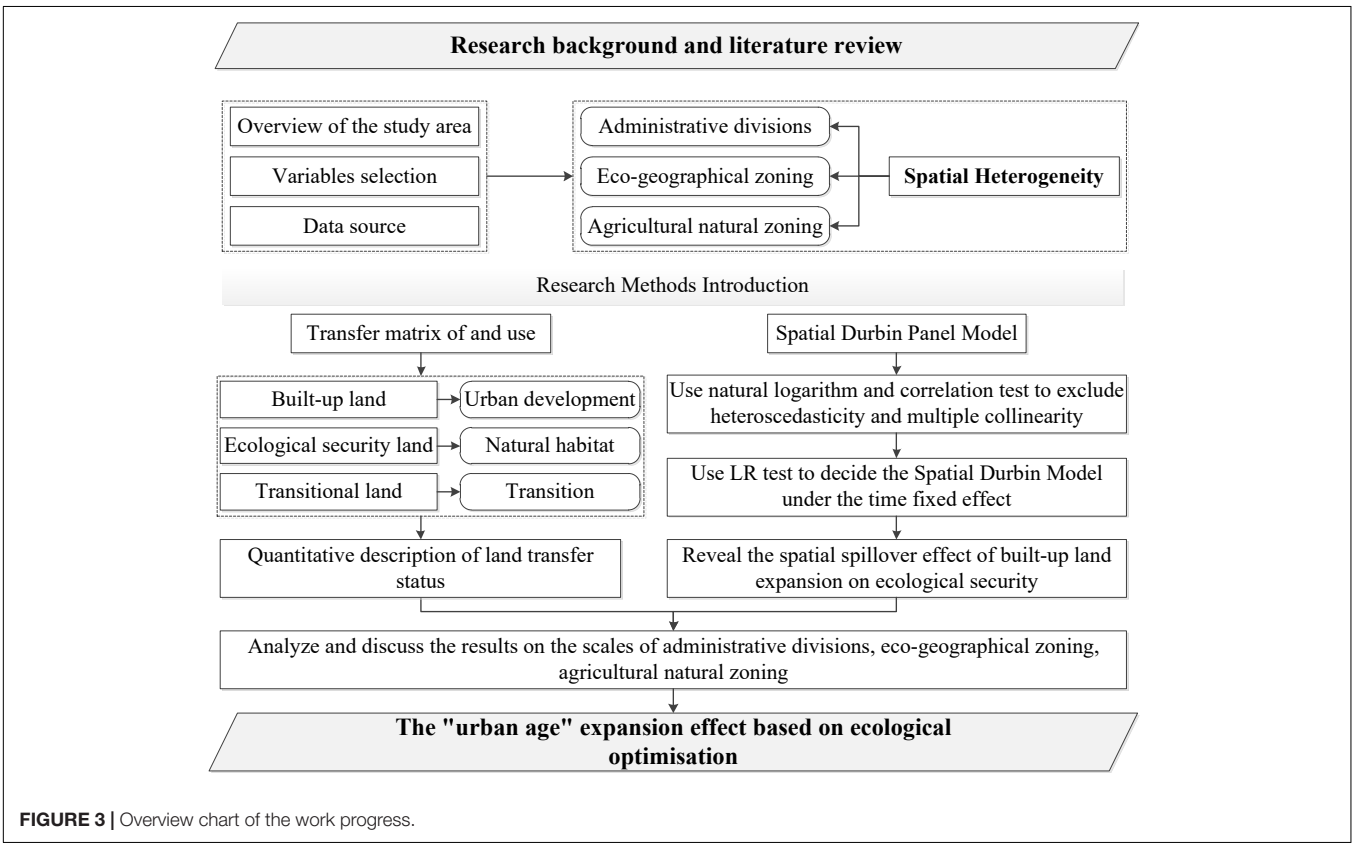

FIGURE 3 | Overview chart of the work progress.

the provincial capital. The expansion was mainly concentrated in provinces of the Lower Yellow River Basin, with the most significant increase between 2010 and 2018 and gradually spreading to the middle and upper regions. Thus, the rapid development of built-up land in the downstream plains was the main feature during this period.

Spatiotemporal Evolutionary of Ecological Security Pattern

The variation range of ecological security land was not significant, and the overall decrease was dominated by patches (**Figure 5**). The ecological security land increased from 246,358.87 km^2 in 1980 to 247,421 km^2 in 2018. In space, ecological security land shows a trend of gradual increase from east to west. The western region was mainly characterized by scattered patches reduction, while the eastern region had a relatively significant reduction along the river channel, and the rest of the region had fewer local

TABLE 2 | Descriptive statistics of all variables.

Variables	Obs	Mean	Standard deviation (SD)	Minimum	Maximum
LUE	365	5.973	1.086	2.519	7.838
PLAND	365	1.674	0.974	−0.932	3.302
LPI	365	0.0312	1.452	−3.180	3.011
LSI	365	4.158	0.546	2.927	5.386
PD	365	−2.961	0.856	−6.812	−1.301
COHESION	365	4.605	0.000	4.603	4.605

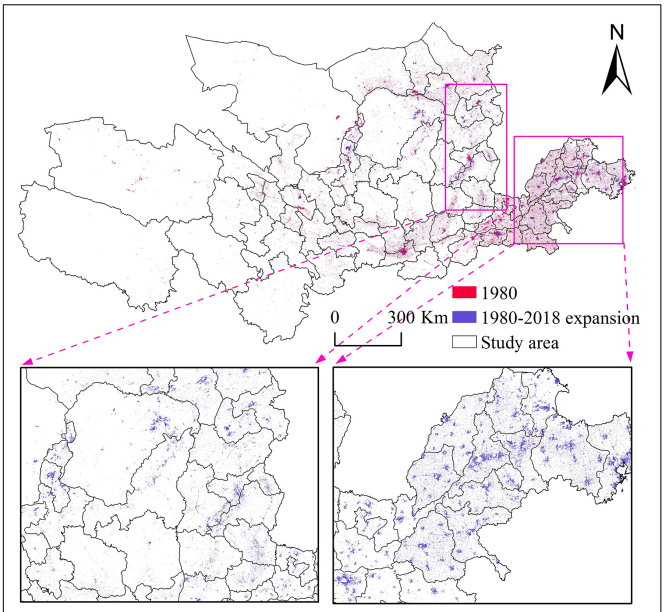

FIGURE 4 | Spatial changes of built-up land, 1980–2018.

patches. It was observed that the ecological environment in the basin is still relatively fragile, the ecological security pattern in the upper and middle region is significantly degraded, and the wetland in the downstream area is shrinking.

The landscape is a comprehensive reflection of environmental and anthropogenic activities, revealing the succession law of landscape elements and ecological security patterns in the study area (Keita et al., 2021). In this study, COHESION, LSI, PLAND, LPI, and PD were selected to reflect the landscape characteristics of the ecological security pattern in the basin (**Figure 6**). During the study period, COHESION was in a horizontal state, indicating a good overall spatial connectivity of the ecological security pattern in the basin. Although the change was minimal, it showed a decreasing trend year by year, indicating that the landscape patches of the ecological security pattern had a potential trend of dispersion. The LSI and COHESION indices trends were basically the same, but the LSI value was always high, indicating a complex landscape shape in the basin. PLAND, LPI, and PD decreased sharply around 2000 and then gradually stabilized, indicating that the ecological security pattern in the basin has gradually decreased since 2000. The most significant change in the pattern of ecological security in the basin was observed around 2000.

Impact of Built-Up Land Expansion on Ecological Security Patterns

The spatial agglomeration state of expansion level was observed to be increasing through a horizontal comparison of the relationship between built-up land expansion and the ecological security pattern index at the city level. Based on this, the SDPM under the time-fixed effect was further determined by combining the significance LR test. The variables with collinearity were eliminated and the four explanatory variables (PLAND, LPI, LSI, and PD) were retained to eliminate the possibility of multiple collinearities among variables (**Table 4**). In terms of the total effect, the response degree of each variable was: LSI > PLAND > LPI > PD.

In terms of the direct effect, the LPI and LSI coefficients were significantly negative at the 1% level, implying that the LPI and LSI of ecological security pattern significantly slowed down the built-up land expansion. The impact of LPI on ecological security pattern was opposite to that of built-up land expansion, which further verified that the estimation results of this study are highly feasible and reliable. The PD coefficient was significantly positively correlated at the 1% level and belonged to the index describing the overall pattern change in landscape types, implying that the explanatory variable significantly increased the built-up land expansion. The coefficient of PLAND was positive but not significant, indicating that the proportion of patches in the ecological security pattern has little effect on the built-up land expansion. The mutual transformation between built-up land expansion and transition land is higher than that of ecological security land, whereas the relevant measures to protect the ecological security pattern have different impacts on the built-up land. In terms of indirect effects, the coefficients of PLAND, LPI, and LSI were significantly correlated at the levels of 5, 1, and 1%, respectively, indicating that the land-use expansion will affect the local ecological security pattern as well as the ecological security pattern of adjacent areas.

The time lag coefficient of built-up land in the model was significantly positive at the 1% level, that is, the time dependence of built-up land significantly accelerated the expansion in the basin. Although the built-up land expansion in surrounding areas will intensify the expansion of local built-up land in the current stage, it will also force the local government to strengthen land expansion control and improve land-use level in the next stage.

TABLE 3 | Land-use changes in the Yellow River Basin, 1980–2018 (km^2).

1980/2018	Built-up land	Ecological security land	Transitional land	Total
Built-up land	32,408.99	502.51	6,150.06	39,061.56
Ecological security land	1,980.89	207,794.78	36,583.20	246,358.87
Transitional land	27,652.32	39,123.71	1,671,904.97	1,738,681
Total	62,042.20	247,421	1,714,638.23	2,024,101.43
Change	22,980.64	1,062.13	−24,042.77	–
Rate of change (%)	58.83	0.43	−1.38	–

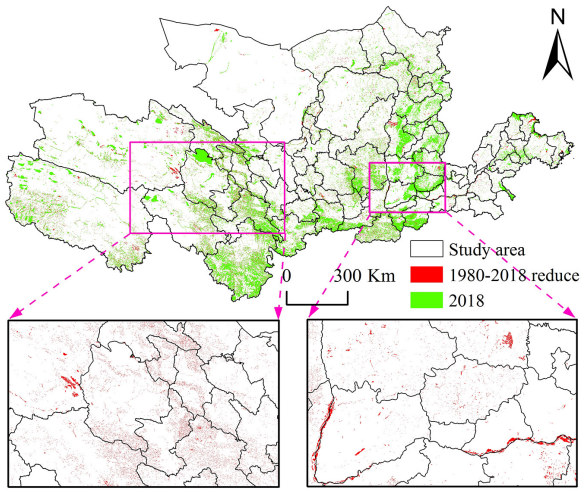

FIGURE 5 | Spatial change in ecological security land, 1980–2018.

Regional Differences in the Effect of Built-Up Land Expansion on Ecological Safety Patterns

The difference in responses of variables cannot be further identified due to the uncertainty of human factors and natural conditions in administrative divisions. This study used two geographical divisions (i.e., eco-geographical zoning and agricultural natural zoning) to re-estimate and to further explore whether the expansion process of built-up land and ecological security pattern have established spatial heterogeneity at the regional level.

Differences in Eco-Geographic Zoning

Table 5 summarizes the estimation results of the SDPM for the time-fixed effect in eco-geographical zoning. The significance of each variable decreased when compared with the results for the entire watershed (**Table 4**). However, it is worth noting that the results (coefficients and symbols) of PLAND, LSI, and PD were different from those of the entire basin. First, the direct effect coefficient of PLAND was positive but not significant. The indirect and total effect coefficients were significantly negative at the 1% level, indicating that the proportion of patches in the ecological security pattern effectively slows down the expansion process. Although the patch shape is relatively complex, its effect on inhibiting the disorderly expansion of built-up land is significantly enhanced.

Second, the indirect effect and the total effect coefficient of LSI were significantly positively correlated at the 1 and 5% levels, respectively. The direct effect coefficient was also positive, but not significant, indicating that the more complex the patch shape under eco-geographical zoning, the faster the expansion of surrounding built-up land; the spatial spillover effect is relatively poor on the local area. Third, the direct effect coefficient of PD was positive, the indirect effect and the total effect coefficients were negative, and the three effects were not significant, indicating that the number of landscape patches per unit area was helpful in protecting the local ecological security pattern, but had less effect on the surrounding areas. The direct effect of LPI on the local was higher than that of the whole basin, and the indirect effect and total effect were not significant. The spatial spillover effect was not significant because of the significant regional differences under eco-geographical zoning. Moreover, the time-dependent positive impact of built-up land expansion is no longer as significant as that of the entire basin.

Differences in Agricultural Natural Zoning

Table 6 summarizes the estimation results of the SDPM with time-fixed effects in agricultural natural zoning. Compared with the estimation results presented in **Table 4**, the regression coefficient of variables improved, whereas the coefficient symbols of PLAND and LSI were inconsistent with the results of the whole basin. In terms of the indirect and total effects, only the PLAND and LSI coefficients were significant at the 5 and 1% levels, respectively, which is consistent with the eco-geographical zoning results, indicating that the effect of built-up land expansion on

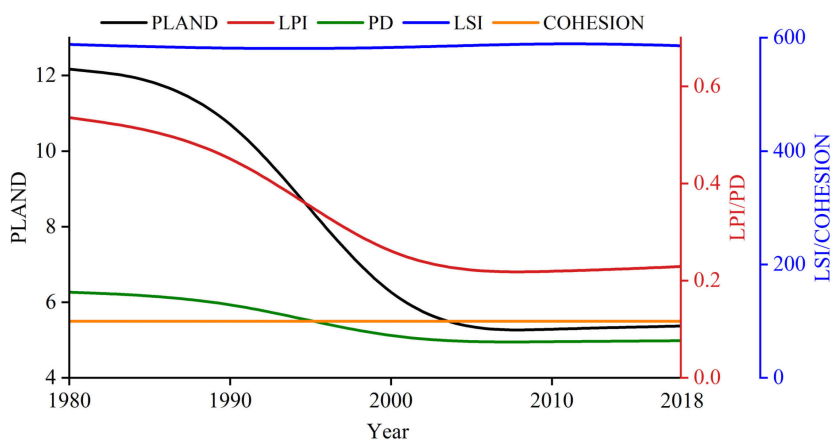

FIGURE 6 | Trends in the ecological security landscapes index, 1980–2018.

TABLE 4 | Estimating results across all cities.

Variables	LR_Direct	LR_Indirect	LR_Total
v2 (PLAND)	0.172	1.010**	1.181**
v3 (LPI)	−0.268***	−0.734***	−1.002***
v4 (LSI)	−1.402***	−1.395***	−2.797***
v5 (PD)	0.624***	0.297	0.921***
Observations			365
R-squared			0.592

****p < 0.01, **p < 0.05.*

TABLE 5 | Estimating results of eco-geographical zoning.

Variables	LR_Direct	LR_Indirect	LR_Total
v2 (PLAND)	0.459	−7.308***	−6.848***
v3 (LPI)	−0.936**	1.937	1.001
v4 (LSI)	1.430	11.353***	12.783**
v5 (PD)	0.543	−0.894	−0.351
Observations			95
R-squared			0.897

****p < 0.01, **p < 0.05.*

TABLE 6 | Estimation results of agricultural natural zoning.

VARIABLES	LR_Direct	LR_Indirect	LR_Total
v2 (PLAND)	−0.546	−3.122**	−3.668**
v3 (LPI)	−1.904***	1.003	−0.901
v4 (LSI)	2.319***	3.146***	5.465***
v5 (PD)	2.016***	−1.423	0.593
Observations			40
R-squared			0.991

****p < 0.01, **p < 0.05.*

regional landscape patterns under the agricultural natural zoning differs at different stages of built-up land expansion compared with administrative zoning.

In terms of direct effect, the coefficients of PLAND and LPI were negative, but PLAND was not significant, indicating that the proportion of patches in agricultural natural zoning had no significant effect on the ecological security pattern. However, the effect of the proportion of the largest patch area in the total area is the highest among the three zonings, indicating that this variable had a strong impact on regional ecological security pattern. The LSI and PD coefficients were significantly positively correlated at the 1% level. It was observed that the impact of built-up land expansion on ecological security pattern existed in the change in patch area.

DISCUSSION

Understanding Built-Up Land Expansion From a Watershed Perspective

Rivers around the world provide various ecosystem services and commodities for human livelihoods and are also important bases for global biodiversity (Zipper et al., 2020). Although the Yellow River is only 15% smaller than the Amazon River and the Nile River, the annual discharge and flow rates are relatively low (Wohlfart et al., 2016). We found ecosystem degradation, landscape fragmentation, and increasing landscape diversity and structural complexity in the watershed after years of intensive economic development and natural resources exploitation, which were consistent with the findings of Liu et al. (2018). In addition, the rapid expansion of built-up land in the area will easily trigger the heat island effect (Zhao et al., 2021), which will seriously hinder the high-quality development of the region (Chi et al., 2021; Song et al., 2021). Therefore, there is an urgent need to strengthen the ecological civilization of watersheds and scientifically control the total amount of built-up land to maintain a balance between economic development and ecological security. Our results at the watershed scale were useful for understanding the dynamics of built-up land expansion under different zoning levels on the watershed scale.

Many natural ecological patches have been occupied by urban activities, particularly in the last 10 years, driven by urban development and limited by national arable land protection policies (Zhang et al., 2020d), and some areas are extremely vulnerable to overexploitation of groundwater and large-scale logging (Fang et al., 2020; Lin et al., 2020). Due to the influence of human activities, the density of patches in the basin was significantly and positively correlated with the built-up land expansion (Kuenzer et al., 2014), which is closely related to the long-term maintenance of the artificial environment-dominated mode in traditional planning in China (Zhang et al., 2020a). The most significant areas of built-up land expansion were located in the eastern part of the basin, and the conversion between built-up land and ecological security land is most notable along the river, which is consistent with the trend of urban sprawl in other countries (Middleton and Sternberg, 2013; Berdugo et al., 2020). This implies that the expansion trend of built-up land may have a greater ecological impact on inland river basins. Therefore, more attention should be paid to the built-up land expansion in inland river basins with different types of situations through developmental policy control. In contrast, filling expansion and vertical growth are encouraged to improve land-use efficiency.

Effects of Built-Up Land Expansion on Ecological Security Patterns

In recent years, spatial issues have been extensively explored in regional development (Ertur and Koch, 2007; Cheng et al., 2021). Therefore, it is necessary to consider possible spatial correlations. Studies have shown that when built-up land expansion reaches a certain stage, it accelerates the expansion of adjacent landscape patches and merges into larger patches (Qian et al., 2015). Our study also confirms that the different landscape pattern indexes in different stages of built-up land expansion have different trends. Since the beginning of the 21st century, there have been varying degrees of disorderly development and illegal buildings in the north and south of the Qinling Mountains, resulting in a decrease in PLAND and LPI. In this process, plaque density and connectivity also change accordingly.

The proportion of built-up land in the study area has increased from 1.93 to 3.07% in the past 40 years, which is the most prominent change among the three land-use types based on the "source–sink" theory. However, the contribution of expansion to the loss of ecological security land was very small (0.80%). This is mainly due to the current urban planning scheme implemented by local governments, which correctly guides the direction of spatial development and protects most of the ecological security land (Xiao, 2021). However, because of the influence of the geographical environment, most of the ecological security land does not have the suitability factors for built-up land, which inhibits the expansion in the region (Jiang et al., 2021).

The ecological security model is mainly based on the development of ecosystem service functions and ecological carrying capacity (Liang et al., 2018; Liang et al., 2020). Built-up land expansion has been identified as the most important direct cause of the loss of natural landscape areas (McDonald et al., 2020; Winkler et al., 2021). The landscape pattern changes of ecological security through human activities (urban expansion, zoning creation, agricultural mechanization, etc.) can affect the ecological processes within the natural landscape area (Tanner and Fuhlendorf, 2018) and change the relationship between human beings and the natural environment (Pickard et al., 2017). The changes in landscape types and proportions are mainly reflected in the conversion of ecological land, such as woodlands and water bodies, to built-up land and cropland (Dadashpoor et al., 2019). At the same time, the landscape pattern of the rapid expansion area showed significant and highly dispersed characteristics. Single and continuous natural areas have gradually evolved into complex and discontinuous landscape patches (Li et al., 2017). Therefore, it is important to study the spatiotemporal variation characteristics of ecological security landscape patterns.

CONCLUSION

Land-use change is a global problem, and the built-up land expansion affects the ecological landscape pattern of the world's major river basins. In our study, we consider that the development of one region may have an effect on the neighboring regions and that there is spatial heterogeneity between different zones. Therefore, we break away from the limitations of previous studies, which have mostly used administrative zones as boundaries, and explore the spatial spillover effects of the built-up land expansion in the Yellow River Basin on ecological security patterns based on three scales: Administrative zoning, Eco-geographical zoning, and Agricultural natural zoning. We found that the built-up land expanded rapidly, and spread from the downstream region to the middle and upper reaches, and the landscape patches of the ecological security pattern gradually decreased. At different zoning scales, the interactive relationship between built-up land expansion and ecological security showed a certain spatial spillover effect, and the significance of regression estimation gradually decreases from large sample size to small sample size. However, the underlying mechanisms controlling the complex relationship between the built-up land expansion and ecological security patterns within the basin are not elucidated yet and need further research. To optimize the ecological security pattern, in the future basin management, land use planning, and policy should break the limitations of administrative boundaries. Our research provides reference and significance for land development and urban planning regulation of the Yellow River Basin, as well as for other basins in China and other large river basins in developing countries, to seek sustainable urban planning and alleviate environmental pressure.

DATA AVAILABILITY STATEMENT

The original contributions presented in the study are included in the article/supplementary material, further inquiries can be directed to the corresponding authors.

AUTHOR CONTRIBUTIONS

PZ, DY, and LJ contributed to the conceptualization and writing, reviewing, and editing the manuscript. DY contributed to the methodology and writing the original draft. PZ and YL contributed to the supervision. PZ contributed to project administration and funding acquisition. All authors have read and agreed to the published version of the manuscript.

FUNDING

This research was funded by the National Natural Science Foundation of China, grant numbers 41601175 and 41801362, the Young Backbone Teachers Foundation from Henan Province, grant numbers 2018GGJS019 and 2020GGJS114, the Program for Innovative Research Talent in University of Henan Province, grant number 20HASTIT017, 2021 Project of Henan Soft Science Funds, grant number 212400410250 and 2020 Philosophy and Social Science Planning Project of Henan Province, grant number 2020BJJ020.

ACKNOWLEDGMENTS

We thank the Geographical Science Data Center of The Greater Bay Area for providing the relevant data in this study.

REFERENCES

Alcamo, J., Van Vuuren, D., and Cramer, W. (2005). Changes in ecosystem services and their drivers across the scenarios. *Ecosystems Hum. Well Being* 2, 297–373.

Anees, M. M., Sajjad, S., and Joshi, P. K. (2019). Characterizing urban area dynamics in historic city of Kurukshetra, India, using remote sensing and spatial metric tools. *Geocartol. Int.* 34, 1584–1607. doi: 10.1080/10106049.2018.1499819

Anselin, L., Gallo, J. L., and Jayet, H. (2008). "Spatial Panel Econometrics," in *The Econometrics of Panel Data. Advanced Studies in Theoretical and Applied Econometrics*, eds L. Mátyás and P. Sevestre (Berlin: Springer), 625–660. doi: 10.1007/978-3-540-75892-1_19

Berdugo, M., Delgado-Baquerizo, M., and Soliveres, S. (2020). Global ecosystem thresholds driven by aridity. *Science* 367, 787–790. doi: 10.1126/science.aay5958

Best, J. (2019). Anthropogenic stresses on the world's big rivers. *Nat. Nanotechnol.* 12, 7–21. doi: 10.1038/s41561-018-0262-x

Bosch, M., Jaligot, R., and Chenal, J. (2020). Spatiotemporal patterns of urbanization in three Swiss urban agglomerations: insights from landscape metrics, growth modes and fractal analysis. *Landsc. Ecol.* 35, 879–891. doi: 10.1007/s10980-020-00985-y

Cayuela, H., Lambrey, J., and Vacher, J. P. (2015). Highlighting the effects of land-use change on a threatened amphibian in a human-dominated landscape. *Popul. Ecol.* 57, 433–443. doi: 10.1007/s10144-015-0483-4

Chen, G. Z., Li, X., and Liu, X. P. (2020). Global projections of future urban land expansion under shared socioeconomic pathways. *Nat. Commun.* 11:537. doi: 10.1038/s41467-020-14386-x

Chen, L. D., Fu, B. J., and Zhao, W. W. (2006). Source-sink landscape theory and its ecological significance. *Acta Ecol. Sin.* 26, 1444–1449.

Chen, W. Y., Hu, F. Z. Y., Li, X., and Hua, J. (2017). Strategic interaction in municipal governments' provision of public green spaces: a dynamic spatial panel data analysis in transitional China. *Cities* 71, 1–10. doi: 10.1016/j.cities.2017.07.003

Cheng, C., Yang, X., and Cai, H. (2021). Analysis of spatial and temporal changes and expansion patterns in mainland Chinese urban land between 1995 and 2015. *Remote Sens.* 13:2090. doi: 10.3390/rs13112090

Chi, Q., Zhou, S., and Wang, L. (2021). Exploring on the eco-climatic effects of land use changes in the influence area of the Yellow River Basin from 2000 to 2015. *Land* 10:601. doi: 10.3390/land10060601

Dadashpoor, H., Azizi, P., and Moghadasi, M. (2019). Land use change, urbanization, and change in landscape pattern in a metropolitan area. *Sci. Total Environ.* 655, 707–719. doi: 10.1016/j.scitotenv.2018.11.267

d'Amour, C. B., Reitsma, F., and Baiocchi, G. (2017). Future urban land expansion and implications for global croplands. *PNAS* 114, 8939–8944. doi: 10.1073/pnas.1606036114

Elhorst, J. P. (2014). "Dynamic Spatial Panels: Models, Methods and Inferences," in *Spatial Econometrics. Springer Briefs in Regional Science*, ed. Springer (Berlin: Springer), 95–119. doi: 10.1007/978-3-642-40340-8_4

Ellis, E. C., Goldewijk, K. K., and Siebert, S. (2010). Anthropogenic transformation of the biomes, 1700 to 2000. *Global Ecol. Biogeogr.* 19, 589–606. doi: 10.1111/j.1466-8238.2010.00540.x

Elmqvist, T., Andersson, E., and Frantzeskaki, N. (2019). Sustainability and resilience for transformation in the urban century. *Nat. Sustain.* 2, 267–273. doi: 10.1038/s41893-019-0250-1

Ertur, C., and Koch, W. (2007). Growth, technological interdependence and spatial externalities: theory and evidence. *J. Appl. Economet.* 22, 1033–1062. doi: 10.1002/jae.963

Fang, F., Ma, L., and Fan, H. (2020). The spatial differentiation of quality of rural life based on natural controlling factors: a case study of Gansu Province. *China J. Environ. Manage.* 264:110439. doi: 10.1016/j.jenvman.2020.110439

Feng, Y., Wang, X., and Du, W. (2019). Effects of environmental regulation and FDI on urban innovation in China: a spatial Durbin econometric analysis. *J. Clean. Prod.* 235, 210–224. doi: 10.1016/j.jclepro.2019.06.184

Flörke, M., Schneider, C., and McDonald, R. I. (2018). Water competition between cities and agriculture driven by climate change and urban growth. *Nat. Sustain.* 1, 51–58. doi: 10.1038/s41893-017-0006-8

Ghosh, M. K., Kumar, L., and Roy, C. (2016). Mapping long-term changes in mangrove species composition and distribution in the Sundarbans. *Forests* 7:305. doi: 10.3390/f7120305

Ghosh, S., Chatterjee, N. D., and Dinda, S. (2021). Urban ecological security assessment and forecasting using integrated DEMATEL-ANP and CA-Markov models: a case study on Kolkata Metropolitan Area, India. Sustain. *Cities Soc.* 68:102773. doi: 10.1016/j.scs.2021.102773

Gleeson, T., Wang-Erlandsson, L., and Zipper, S. C. (2020). The water planetary boundary: interrogation and revision. *One Earth* 2, 223–234. doi: 10.1016/j.oneear.2020.02.009

Gong, P., Li, X., and Wang, J. (2020). Annual maps of global artificial impervious area (GAIA) between 1985 and 2018. *Remote Sens. Environ.* 236:111510. doi: 10.1016/j.rse.2019.111510

Güneralp, B., Güneralp, I., and Liu, Y. (2015). Changing global patterns of urban exposure to flood and drought hazards. *Global Environ. Chang.* 31, 217–225. doi: 10.1016/j.gloenvcha.2015.01.002

Guo, A. D., Yang, J., and Sun, W. (2020). Impact of urban morphology and landscape characteristics on spatiotemporal heterogeneity of land surface temperature. *Sustain. Cities Soc.* 63:102443. doi: 10.1016/j.scs.2020.102443

Huang, Q., Zhang, H., and van Vliet, J. (2021). Patterns and distributions of urban expansion in global watersheds. *Earth's Future* 9:e2021EF002062.

Huang, Q. X., Zhao, X., and He, C. Y. (2019). Impacts of urban expansion on wetland ecosystem services in the context of hosting the Winter Olympics: a scenario simulation in the Guanting Reservoir Basin. *China Reg. Environ. Change.* 19, 2365–2379. doi: 10.1007/s10113-019-01552-1

Jantz, S. M., Barker, B., and Brooks, T. M. (2015). Future habitat loss and extinctions driven by land-use change in biodiversity hotspots under four scenarios of climate-change mitigation. *Conserv. Biol.* 29, 1122–1131. doi: 10.1111/cobi.12549

Jiang, L., Zuo, Q., and Ma, J. (2021). Evaluation and prediction of the level of high-quality development: a case study of the Yellow River Basin. *China Ecol. Indic.* 129:107994. doi: 10.1016/j.ecolind.2021.107994

Jing, M. X., Cai, Fu, Wang, X. J., and Zhao, X. J. (2020). The vegetation coverage spatial characteristics in the Three River source region. *J. Arid Land Res. Environ.* 34, 141–147.

Keita, M. A., Ruan, R. Z., and An, R. (2021). Spatiotemporal change of urban sprawl patterns in Bamako district in Mali based on time series analysis. *J. Urban Sci.* 5:4. doi: 10.3390/urbansci5010004

Kopp, D., and Allen, D. (2021). Scaling spatial pattern in river networks: the effects of spatial extent, grain size and thematic resolution. *Landsc. Ecol.* 36, 2781–2794. doi: 10.1007/s10980-021-01270-2

Kowe, P., Mutanga, O., and Dube, T. (2021). Advancements in the remote sensing of landscape pattern of urban green spaces and vegetation fragmentation. *Int. J. Remote Sens.* 42, 3797–3832. doi: 10.1080/01431161.2021.1881185

Kuenzer, C., Ottinger, M., and Liu, G. (2014). Earth observation-based coastal zone monitoring of the Yellow River Delta: dynamics in China's second largest oil producing region over four decades. *Appl. Geogr.* 55, 92–107. doi: 10.1016/j.apgeog.2014.08.015

Lambin, E. F., and Meyfroidt, P. (2011). Global land use change, economic globalization, and the looming land scarcity. *PNAS* 108, 3465–3472. doi: 10.1073/pnas.1100480108

Lausch, A., Blaschke, T., and Haase, D. (2015). Understanding and quantifying landscape structure–A review on relevant process characteristics, data models and landscape metrics. *Ecol. Model.* 295, 31–41. doi: 10.1016/j.ecolmodel.2014.08.018

Lesage, J., and Pace, R. (2014). The biggest myth in spatial econometrics. *Econometrics* 2, 217–249. doi: 10.3390/econometrics2040217

Li, H., Peng, J., and Yanxu, L. (2017). Urbanization impact on landscape patterns in Beijing City. *China* 82, 50–60. doi: 10.1016/j.ecolind.2017.06.032

Li, S., Sun, Z. Q., Wang, Y. F., and Wang, Y. X. (2021). Understanding urban growth in Beijing-Tianjin-Hebei region over the past 100 years using old maps and landsat data. *Remote Sens.* 13:3264. doi: 10.3390/rs13163264

Liang, X., Liu, X., Li, X., Chen, Y., Tian, H., Yao, Y., et al. (2018). Delineating multi-scenario urban growth boundaries with a CA-based FLUS model and morphological method. *Landsc. Urban Plan.* 177, 47–63. doi: 10.1016/j.landurbplan.2018.04.016

Liang, Z., Wu, S., and Wang, Y. (2020). The relationship between urban form and heat island intensity along the urban development gradients. *Sci. Total Environ.* 708:135011. doi: 10.1016/j.scitotenv.2019.135011

Lin, M., Biswas, A., and Bennett, E. M. (2020). Socio-ecological determinants on spatiotemporal changes of groundwater in the Yellow River Basin. *China. Sci. Total Environ.* 731:138725. doi: 10.1016/j.scitotenv.2020.138725

Liu, L. M., and Wu, J. G. (2021). Ecosystem services-human wellbeing relationships vary with spatial scales and indicators: the case of China. *Resour. Conserv. Recycl.* 172:105662. doi: 10.1016/j.resconrec.2021.105662

Liu, P., Jia, S. J., Han, R. M., and Zhang, H. W. (2018). Landscape pattern and ecological security assessment and prediction using remote sensing approach. *J. Sens.* 2018, 1–14. doi: 10.1155/2018/1058513

Mård, J., Baldassarre, D. G., and Mazzoleni, M. (2018). Nighttime light data reveal how flood protection shapes human proximity to rivers. *Sci. Adv.* 4:eaar5779. doi: 10.1126/sciadv.aar5779

McDonald, R. I., Güneralp, B., and Huang, C. W. (2018). Conservation priorities to protect vertebrate endemics from global urban expansion. *Biol. Conserv.* 224, 290–299. doi: 10.1016/j.biocon.2018.06.010

McDonald, R. I., Mansur, A. V., and Ascensão, F. (2020). Research gaps in knowledge of the impact of urban growth on biodiversity. *Nat. Sustain.* 3, 16–24. doi: 10.1038/s41893-019-0436-6

Middleton, N. J., and Sternberg, T. (2013). Climate hazards in drylands: a review. *Earth Sci. Rev.* 126, 48–57. doi: 10.1016/j.earscirev.2013.07.008

Narducci, J., Quintas-Soriano, C., and Castro, A. (2019). Implications of urban growth and farmland loss for ecosystem services in the western United States. *Land Use Policy* 86, 1–11. doi: 10.1016/j.landusepol.2019.04.029

Newbold, T., Hudson, L. N., and Hill, S. L. L. (2015). Global effects of land use on local terrestrial biodiversity. *Nature* 520, 45–50. doi: 10.1038/nature14324

Pickard, B. R., Van Berkel, D., and Petrasova, A. (2017). Forecasts of urbanization scenarios reveal trade-offs between landscape change and ecosystem services. *Landsc. Ecol.* 32, 617–634. doi: 10.1007/s10980-016-0465-8

Qian, M., Pu, L. J., and Zhang, J. (2015). Urban spatial morphology evolution in Suzhou-Wuxi-Changzhou region based on improved landscape expansion index. *Sci. Geol. Sin.* 35, 314–321.

Riitters, K. H., O'Neill, R. V., and Hunsaker, C. T. (1995). A factor analysis of landscape pattern and structure metrics. *Landsc. Ecol.* 10, 23–39. doi: 10.1007/bf00158551

Rong, T. Q., Zhang, P. Y., and Jing, W. L. (2020). Carbon dioxide emissions and their driving forces of land use change based on Economic Contributive Coefficient (ECC) and Ecological Support Coefficient (ESC) in the Lower Yellow River Region (1995–2018). *Energies* 13:2600. doi: 10.3390/en13102600

Seto, K. C., Guneralp, B., and Hutyra, L. R. (2012). Global forecasts of urban expansion to 2030 and direct impacts on biodiversity and carbon pools. *PNAS* 109, 16083–16088. doi: 10.1073/pnas.1211658109

Song, X. P., Hansen, M. C., and Stehman, S. V. (2018). Global land change from 1982 to 2016. *Nature* 560, 639–643. doi: 10.1038/s41586-018-0411-9

Song, Y., Wang, M., and Sun, X. (2021). Quantitative assessment of the habitat quality dynamics in Yellow River Basin. *China Environ. Monit. Assess.* 193:614. doi: 10.1007/s10661-021-09404-4

Stoica, I.-V., Zamfir, D., and Vîrghileanu, M. (2021). Evaluating the territorial impact of built-up area expansion in the surroundings of Bucharest (Romania) through a multilevel approach based on landsat satellite imagery. *Remote Sens.* 13:3969. doi: 10.3390/rs13193969

Tanner, E. P., and Fuhlendorf, S. D. (2018). Impact of an agri-environmental scheme on landscape patterns. *Ecol. Indic.* 85, 956–965. doi: 10.1016/j.ecolind.2017.11.043

Tubiello, F. N., Salvatore, M., and Ferrara, A. F. (2015). The contribution of agriculture, forestry and other land use activities to global warming, 1990–2012. *Glob Chang Biol.* 21, 2655–2660. doi: 10.1111/gcb.12865

Van Vliet, J. (2019). Direct and indirect loss of natural area from urban expansion. *Nat. Sustain.* 2, 755–763. doi: 10.1038/s41893-019-0340-0

Wiedmann, T., and Lenzen, M. (2018). Environmental and social footprints of international trade. *Nat. Geosci.* 11, 314–321. doi: 10.1038/s41561-018-0113-9

Wihbey, J. (2017). Boundary Issues: the 2016 atlas of urban expansion indicates global dedensification. *City Scape.* 19, 21–30.

Winkler, K., Fuchs, R., and Rounsevell, M. (2021). Global land use changes are four times greater than previously estimated. *Nat. Commun.* 12:2501. doi: 10.1038/s41467-021-22702-2

Wohlfart, C., Kuenzer, C., and Chen, C. (2016). Social–ecological challenges in the Yellow River basin (China): a review. *Environ. Earth Sci.* 75:1066. doi: 10.1007/s12665-016-5864-2

Xiao, F. J. (2021). Impact of climate change on ecological security of the Yellow River Basin and its adaptation countermeasures. *J. Landsc. Res.* 13, 51–56. doi: 10.16785/j.issn1943-989x.2021.4.012

Xiao, R., Cao, W., Liu, Y., and Lu, B. (2022). The impacts of landscape patterns spatio-temporal changes on land surface temperature from a multi-scale perspective: a case study of the Yangtze River Delta. *Sci. Total Environ.* 821:153381. doi: 10.1016/j.scitotenv.2022.153381

Xu, Z., Li, Y., and Chau, S. (2020). Impacts of international trade on global sustainable development. *Nat. Sustain.* 3, 964–971. doi: 10.1038/s41893-020-0572-z

Yang, J., Zhan, Y. X., and Xiao, X. M. (2020). Investigating the diversity of land surface temperature characteristics in different scale cities based on local climate zones. *Urban Clim.* 34:100700. doi: 10.1016/j.uclim.2020.100700

Yang, Y., Liu, Y., and Li, Y. (2018). Quantifying spatio-temporal patterns of urban expansion in Beijing during 1985–2013 with rural-urban development transformation. *Land Use Policy* 74, 220–230. doi: 10.1016/j.landusepol.2017.07.004

Zhang, P. Y., Li, Y. Y., and Jing, W. L. (2020b). Comprehensive assessment of the effect of urban built-up land expansion and climate change on net primary productivity. *Complexity* 2020, 1–12. doi: 10.1155/2020/8489025

Zhang, P. Y., Yang, D., and Qin, M. Z. (2020c). Spatial heterogeneity analysis and driving forces exploring of built-up land development intensity in Chinese prefecture-level cities and implications for future Urban Land intensive use. *Land Use Policy* 99:104958. doi: 10.1016/j.landusepol.2020.104958

Zhang, Y., Geng, W. L., and Zhang, P. Y. (2020d). Dynamic changes, spatiotemporal differences and factors influencing the urban eco-efficiency in the lower reaches of the Yellow River. *Int. J. Env. Res. Pub. He.* 17:7510. doi: 10.3390/ijerph17207510

Zhang, J. Q., Luo, T., Xu, M., and Wang, Y. Y. (2020a). Influence of urban spatial expansion on the regionally ecological security pattern in Min-Delta region. *J. Ecol.* 40, 5113–5123.

Zhang, Y., Lyu, X., Liu, B., and Wu, D. (2021). Spatial relationships between ecosystem services and socioecological drivers across a large-scale region: a case study in the Yellow River Basin. *Sci. Total Environ.* 766:142480. doi: 10.1016/j.scitotenv.2020.142480

Zhao, Z. Q., Sharifi, A., Dong, X., Shen, L. S., and He, B. J. (2021). Spatial Variability and Temporal Heterogeneity of Surface Urban Heat Island Patterns and the Suitability of Local Climate Zones for Land Surface Temperature Characterization. *Remote Sens.* 13:4338. doi: 10.3390/rs13214338

Zhou, L., Dang, X. W., and Mu, H. W. (2020). Cities are going uphill: slope gradient analysis of urban expansion and its driving factors in China. *Sci. Total Environ.* 775, 1–10. doi: 10.1016/j.scitotenv.2021.145836

Zipper, S. C., and Jaramillo, F., and Wang-Erlandsson, L. (2020). Integrating the water planetary boundary with water management from local to global scales. *Earth's Future* 8:e2019EF001377. doi: 10.1029/2019EF001377

Conflict of Interest: The authors declare that the research was conducted in the absence of any commercial or financial relationships that could be construed as a potential conflict of interest.

Publisher's Note: All claims expressed in this article are solely those of the authors and do not necessarily represent those of their affiliated organizations, or those of the publisher, the editors and the reviewers. Any product that may be evaluated in this article, or claim that may be made by its manufacturer, is not guaranteed or endorsed by the publisher.

Copyright © 2022 Yang, Lou, Zhang and Jiang. This is an open-access article distributed under the terms of the Creative Commons Attribution License (CC BY). The use, distribution or reproduction in other forums is permitted, provided the original author(s) and the copyright owner(s) are credited and that the original publication in this journal is cited, in accordance with accepted academic practice. No use, distribution or reproduction is permitted which does not comply with these terms.

frontiers | Frontiers in Environmental Science

ORIGINAL RESEARCH
published: 30 May 2022
doi: 10.3389/fenvs.2022.893876

Spatial-Temporal Patterns of Network Structure of Human Settlements Competitiveness in Resource-Based Urban Agglomerations

Wenbo Yu[1], *Jun Yang*[1,2,3]*, *Dongqi Sun*[4]*, *Huisheng Yu*[1], *Yao Yao*[5], *Xiangming Xiao*[6] *and Jianhong(Cecilia) Xia*[7]

[1]School of Humanities and Law, Northeastern University, Shenyang, China, [2]Jangho Architecture College, Northeastern University, Shenyang, China, [3]Human Settlements Research Center, Liaoning Normal University, Dalian, China, [4]Key Laboratory of Regional Sustainable Development Modeling, Institute of Geographic Sciences and Natural Resources Research, CAS, Beijing, China, [5]School of Geography and Information Engineering, China University of Geosciences, Wuhan, China, [6]Department of Microbiology and Plant Biology, Center for Spatial Analysis, University of Oklahoma, Norman, OK, United States, [7]School of Earth and Planetary Sciences (EPS), Curtin University, Perth, WA, Australia

OPEN ACCESS

Edited by:
Edyta Laszkiewicz,
University of Łódź, Poland

Reviewed by:
Haozhi Pan,
Shanghai Jiao Tong University, China
Adam Radzimski,
Adam Mickiewicz University, Poland

***Correspondence:**
Jun Yang
yangjun8@mail.neu.edu.cn
Dongqi Sun
sundq@igsnrr.ac.cn

Specialty section:
This article was submitted to Environmental Informatics and Remote Sensing, a section of the journal Frontiers in Environmental Science

Received: 11 March 2022
Accepted: 27 April 2022
Published: 30 May 2022

Citation:
Yu W, Yang J, Sun D, Yu H, Yao Y, Xiao X and Xia J (2022) Spatial-Temporal Patterns of Network Structure of Human Settlements Competitiveness in Resource-Based Urban Agglomerations. Front. Environ. Sci. 10:893876. doi: 10.3389/fenvs.2022.893876

Resource-based urban agglomerations often encounter greater challenges in the sustainable development of human settlements. The aim of this study is to propose an approach to the coordinated development of competitiveness by analyzing the interaction of human settlements competitiveness (HSC) in resource-based urban agglomerations. Through the compound evaluation model of HSC and urban network analysis, this study finds: 1) the HSC measure increased from 35.12 in 1990 to 52.15 in 2015 and showed a downward trend from 2015 to 2019, with an average value of 47.82 in 2019; 2) The change trend of the relevance network density is the same as that of the HSC, while the difference network density reaches the lowest value of 0.441 when the HSC is the highest, indicating that the HSC of the urban agglomerations has improved to a certain extent but is more unsustainable, and 3) Communities in the relevance network are obviously bounded by the borders of provinces or urban agglomerations, while the communities in the difference network are differentiated into two types: high-competitiveness and low-competitiveness. Using the theory of "co-opetition" to analyze the sustainable development path of resource-based urban agglomerations, the study believes that a coordination mechanism and a guarantee mechanism for benefit distribution should be established between urban agglomerations to curb local protectionism, and promote regional dislocation development. The development gradient level also should be established within the urban agglomeration to narrow the gap between HSC of cities, and innovative development should be the core of promoting industrial transformation and upgrading.

Keywords: urban network analysis, compound evaluation model, relevance and difference coefficient, network evolution analysis, northeast China urban agglomerations

1 INTRODUCTION

In the process of trade liberalization and economic globalization, urban agglomeration is a new regional unit for countries to participate in global competition and international division of labor (Ma et al., 2019), and its agglomeration benefit has become the key factor of economic development (Meijers and van der Wouw, 2019). As a spatial form with high concentration of resources, urban agglomeration has caused great pressure on regional land and ecosystem. Building compact cities is an effective way to improve land efficiency and curb disorderly spread (Yao et al., 2022). High-density and intensive model has a positive impact on economic sustainability, but has a negative impact on environmental and social sustainability (Lin and Yang, 2006). Therefore, it is necessary to consider the quality of human settlements in order to achieve three sustainable considerations (Westerink et al., 2013). In addition, the economic hinterland of cities within urban agglomerations must overlap with each other, the large demand for production factors such as free capital and high-level labor makes the competition between cities inevitable (Wang and Shen, 2017). However, under the guidance of "co-opetition" theory and "positive sum game" thinking, cities tend to establish a regional coordinated development model of cooperation in competition (Esty and Geradin, 2000; Li and Zhong, 2020). To understand the important role of human settlements in urban competition and promote the cooperation of urban agglomerations in competition to maximize regional interests, it is necessary to clarify the relationship between urban comparative competitive advantage and regional competition based on human settlements science.

Competitiveness was originally conceived as an economic concept to understand the competitive relationship between firms, whereas in urban studies, competitiveness is defined as a city's comparative advantage relative to other cities, and a city's ability to optimize its allocation to promote development (Song and Xie, 2021). In 1990s, the "Diamond model" (Portergoff, 1990) was developed to measure the relationship between national competitiveness and national economy and then to evaluate urban competitiveness (Rogerson, 1999). Ni et al. (2014), Ni et al. (2017) also regarded the economic performance of cities as a core factor to evaluate competitiveness and analyzed the driving factors of competitiveness using urban hard and soft factors. Since the ecological environment has a significant effect on human survival and development (Li et al., 2021; Liu D et al., 2021), competition between cities depends on the attractiveness of the urban environment, and thus ecological factors have started to be included in the construction of theoretical urban competitiveness models. Webster and Muller (2000) added territorial endowment factors to their competitiveness model, and Oensel et al. (2008) introduced environmental factors into their nation competitiveness model. Rapid and extensive urbanization and industrialization create severe problems for megacities, while small and medium-sized cities are facing population loss and lack of economic vitality (Bell and Gonzalez, 2011)The urban quality of life has become an important factor affecting the population's willingness to stay in cities (Sørensen and Sørensen, 2015; Zhao et al., 2021) as reflected by the livability of cities (Liu et al., 2017). There is a symbiotic relationship between the urban quality of life and urban competitiveness (Esmaeilpoorarabi et al., 2016), and improving the quality of life has become the ultimate goal of enhancing urban competitiveness (Zhang and Corrie, 2018). Creating livable cities is the main goal of modern urban development (Liu and Wang, 2013), and the basis of urban competition has gradually shifted from economic strength to the sustainable development of human settlements. However, there is limited research on urban competitiveness based on the science of human settlements.

The high concentration of population and the rapid development of social economy in urban agglomerations lead to problems such as resource depletion, environmental pollution, traffic congestion and housing difficulties (Li et al., 2009), so in the long-term development planning, more attention should be paid to its sustainability (Ma et al., 2019). Human settlements refer to the unity of natural, humanistic, and spatial elements and to the geographical spaces where residents live, work, study, and carry out other activities (Mamat, 2012). The Sustainable Development Goals put forward the construction of sustainable cities and human settlements, which also causes global scholars to pay more attention to the human settlement environment. Wu (2001) first advocated human settlement science in China, and studied the spatial structure of human settlements from systematic and hierarchical points of view. Quantitative evaluation of human settlements is an important part of human settlement research, and data sources are key factors for evaluation. Statistical data reflect the macro-scale development of cities, and comprehensive evaluation of human settlements can be realized using the panel data of statistical yearbooks. Zhang and Fan, (2020) analyzed the driving mechanism of human settlements at the township level, and Tian et al. (2016) established a risk model to analyze the spatial-temporal evolution of human settlements at the provincial level in China. Multi-source big data, including remote sensing and meteorological data, can reflect the complex characteristics of human settlements, and grid-based accurate assessment of human settlements can be realized with the support of geographic information systems and spatial analysis methods. Based on this method, the natural suitability of urban human settlement environment has been effectively evaluated (Chen et al., 2021; Luo et al., 2021). The adjustment and optimization of urban internal structure can also effectively improve the living environment (Guo et al., 2020; Yang Y.et al., 2020; Ren et al., 2022). Yang Z. et al. (2020) found that residents seem to attach the greatest importance to quality of life facilities when choosing their residence. Patias et al. (2021) thought that the increase of urban walking space was the main reason for the improvement of urban structural sustainability. In addition, questionnaire data can directly reflect the subjective feelings of urban residents about their living environment, and quantitative analysis of the questionnaire results can reveal the livability score of human settlements (Simis et al., 2016; Yu et al., 2019). Current research on human settlement assessment reflects the spatial and temporal characteristics of human settlements but

cannot directly measure the external impact of urban human settlements (Zachary, 2012). In this study, an urban network model was developed to explore the competitiveness of urban human settlements. Network models are popular in urban attraction and diffusion studies (Yuan et al., 2017). The GaWC research team was committed to establishing the network of major cities in the world and revealing the hierarchical characteristics of the global economy by analyzing changes in network integrity and node centrality caused by changes in urban competitiveness (Derudder and Taylor, 2016; Taylor and Derudder, 2021). Network modeling and analysis are widely used to describe the relative attractiveness of cities in terms of local economy (Huang et al., 2020), population growth (Yang et al., 2020), and transportation infrastructure (Wang et al., 2020).

Resource-based and industrial-based urban agglomerations are facing more severe problems in the process of sustainable development of human settlements. Urban agglomerations in Northeast China used to be the most important heavy industry base of China, with the most complete industrial system in Northeast Asia. With the advancement of economic and trade globalization, planned economic systems, and imbalance between supply and demand, the urban agglomerations have gradually produced "northeast problems," including land disputes and societal conflicts (You et al., 2021), transformation of resource-based cities (Fu et al., 2020; Chen and Zhang, 2021), and urban environmental pollution, resulting in great resistance to the development of human settlements (H. Zhao et al., 2021; Zhao et al., 2013).

To help solve the "northeast problem" and enhance the attractiveness of human settlements in the urban agglomerations, we aim to address the following two research questions with empirical data: 1) how to establish a competitiveness model to reflect the attraction of human settlement environment to population and capital? and 2) how to understand the impact of the relevance and difference of human settlements on sustainable development in urban agglomerations and the wider region? Specifically, 1) a compound evaluation model was constructed to quantify the HSC of urban agglomerations over a long period, and spatial and temporal differentiation of human settlements in urban agglomerations was analyzed based on the evaluation results; and 2) a social network model was constructed to describe interactions between cities, and the relevance and difference coefficients of HSC were determined to explore the network spatial structure and evolution process of urban HSC in urban agglomerations. The study has reference value for promoting resource-based and industrial urban agglomerations to enhance their competitiveness of human settlements.

2 DATA AND METHODS

2.1 Data

2.1.1 Study Area

The urban agglomerations in Northeast China are located at 38.72–49.44°N and 119.21°–135.09°E and cover a total area of 5.372×10^{11} km^2. The area consists of five regional-level urban agglomerations and 29 prefecture-level cities, and the terrain is primarily plain and mountainous. The five regional urban agglomerations in Northeast China are Liaoning Coastal Urban Agglomeration, including Dalian, Dandong, Yingkou, Panjin, Jinzhou, and Huludao; Central Liaoning Urban Agglomeration, including Shenyang, Anshan, Fushun, Benxi Liaoyang, Tieling, and Fuxin; Central Jilin Urban Agglomeration, including Changchun and surrounding cities Jilin, Liaoyuan, Songyuan, and Siping; Harbin-Daqing-Qiqihar Urban Agglomeration including Harbin, Daqing, Qiqihar, and Suihua; and the planned Eastern Heilongjiang Urban Agglomeration including Mudanjiang, Jiamusi, Qitaihe Jixi, Shuangyashan, Hegang, and Yichun. As of 2019, the population of the region was 9.085×10^7, and per capita gross domestic product was 5.15×10^4 yuan. The administrative division map of the region is shown in **Figure 1**.

2.1.2 Index System

The scientific of human settlements proposed by Wu (2001) includes five subsystems: population, social, environmental, supporting, and housing. Based on these subsystems, we constructed an evaluation index system of HSC composed of multiple indices (**Table 1**). The population subsystem reflects changes in the urban population and employment structure, the social subsystem reflects urban economic growth and expansion, the environmental subsystem reflects urban greening and control of industrial pollution, the supporting subsystem reflects the development and construction of urban infrastructure and public services, and the residential subsystem reflects housing density and support.

2.1.3 Data Sources

We evaluated the HSC of the urban agglomerations in Northeast China for the years 1990, 1995, 2000, 2005, 2010, 2015, and 2019. The sources of statistical data, nighttime light data, and administrative division data are listed in **Table 2**. The statistical data were obtained from the China Urban Statistical Yearbook, Liaoning Statistical Yearbook, Jilin Statistical Yearbook, and Heilongjiang Statistical Yearbook from 1990 to 2020, which were downloaded from the National Bureau of Statistics of China. The nighttime light data were obtained from the National Oceanic and Atmospheric Administration (NOAA) National Centers for Environmental Information (NCEI) (formerly National Geophysical Data Center, NGDC). Administrative boundary data were obtained from the Resources and Environmental Science and Data Center, Institute of Geographical Sciences and Resources, Chinese Academy of Sciences, and the collection year was 2015.

2.2 Methods

2.2.1 Evaluation Model of HSC

In this study, we constructed a compound HSC evaluation model whose architecture is shown in **Figure 2**. Principal component analysis was used to reduce the number of initial indices and generate principal component indices (Meng and Chen, 2021). Using SPSS 26 software, 30 original indices were classified and dimensional reduction of

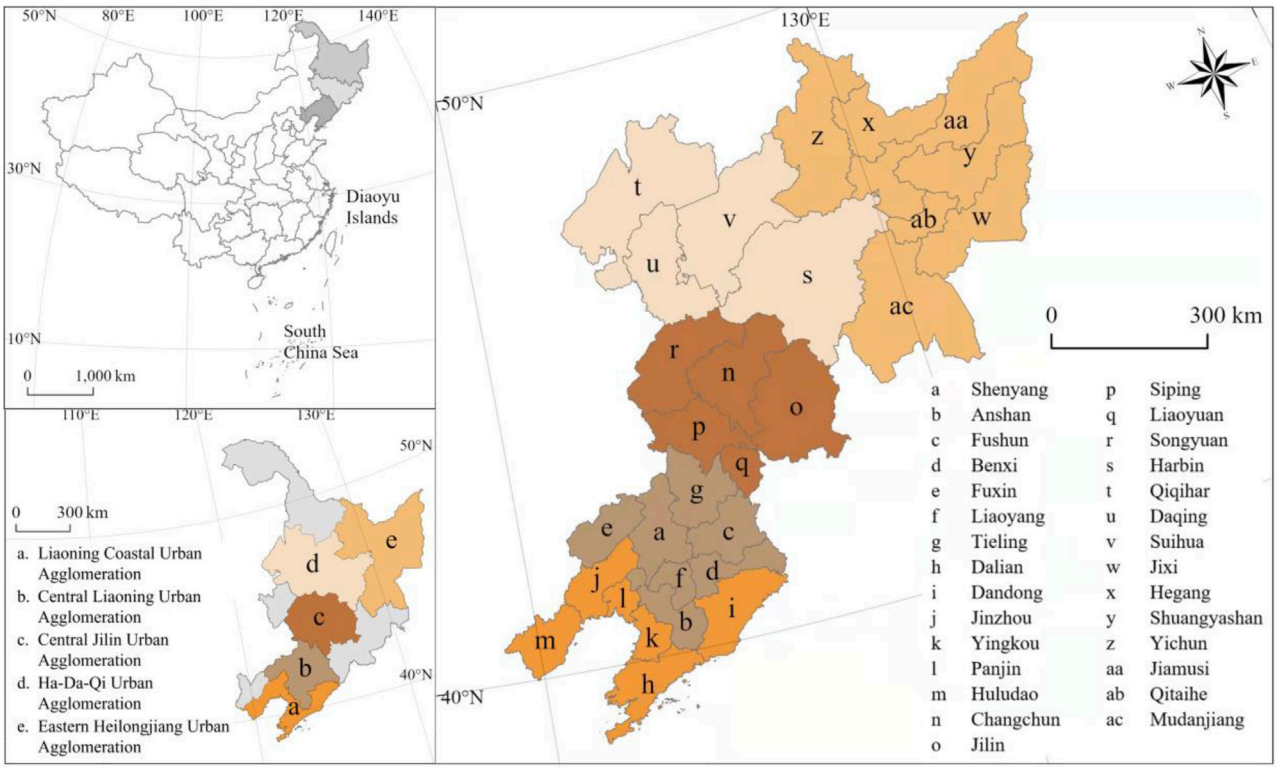

FIGURE 1 | Administrative division map of the urban agglomerations.

TABLE 1 | Competitive index system of the HSC.

Target layer	Criterion layer	Evaluation index layer
HSC indices based on The scientific of human settlements	Population subsystem Y_{01}	Natural population growth rate, X_{01} (%); roportion of non-agricultural population, X_{02} (%); Sexual proportion, X_{03} (%); Unemployment rate, X_{04} (%); Proportion of students, X_{05} (%); Proportion of workers in the primary industry, X_{06} (%)
	Social subsystem Y_{02}	Per capita GDP, X_{07}(Yuan); Average employee wages, X_{08}(Yuan); Per capita social commodity sales, X_{09}(Yuan); Percentage of primary industry GDP, X_{10} (%); Average Nighttime light index, X_{11} (nano-Wcm^{-2}sr^{-1}); Per capita investment in fixed assets, X_{12}(Yuan); Proportion of built-up area to urban area, X_{13} (%)
	Environmental subsystem Y_{03}	Industrial wastewater treatment rate, X_{14} (%); Industrial waste gas treatment rate, X_{15} (%); Industrial solid waste recovery rate, X_{16} (%); Per capita green area, X_{17} (m^2); Green coverage rate of built-up area, X_{18} (%)
	Supporting subsystem Y_{04}	Number of buses per 10,000 people, X_{19} (units); Hardened road area per capita, X_{20} (m^2); Number of cultural facilities per 10,000 people, X_{21} (units); of doctors per 10,000 people, X_{22} (person); Collection of books per 1,000 people, X_{23} (units); Number of teachers per 10,000 people, X_{24} (person)
	Housing subsystem Y_{05}	Population density, X_{25} (person/km^2); Per capita housing area of residents, X_{26} (m^2/person); Tap water usage, X_{27} (%); Liquefied petroleum gas usage, X_{28} (%); Domestic water consumption per capita, X_{29} (m^3); Electricity consumption per capita, X_{30} (kWh)

the five subsystems was performed in the scientific of human settlements. Each subsystem formed two principal components, and then the original 30 indices were synthesized into 10 principal components. By analyzing the proportion of compound index components, the 10 principal components were named Z_{01} population change; Z_{02} employment structure; Z_{03} economic growth; Z_{04} urban expansion; Z_{05} urban greening; Z_{06} pollution control; Z_{07} infrastructure construction; Z_{08} public service; Z_{09} housing support; Z_{10} housing density.

Subsequently, the constant weight of the principal component set Z was determined using the subjective and objective variable weight determination method, and the constant weight was further revised according to the index

TABLE 2 | Data sources and descriptions.

Data Types	Data sources	Descriptions	Date
Statistical data	China Urban Statistical Yearbook Liaoning Statistical Yearbook Jilin Statistical Yearbook Heilongjiang Statistical Yearbook	https://data.cnki.net/Yearbook/	1991; 1996; 2001; 2006; 2011; 2016; 2020
Night-lighting Data	DMSP-OLS VIRS-NPP	http://www.ngdc.noaa.gov/dmsp/download.html	1990; 1995; 2000; 2005; 2010 2015; 2018
Administrative boundary	—	https://www.resdc.cn/	2015

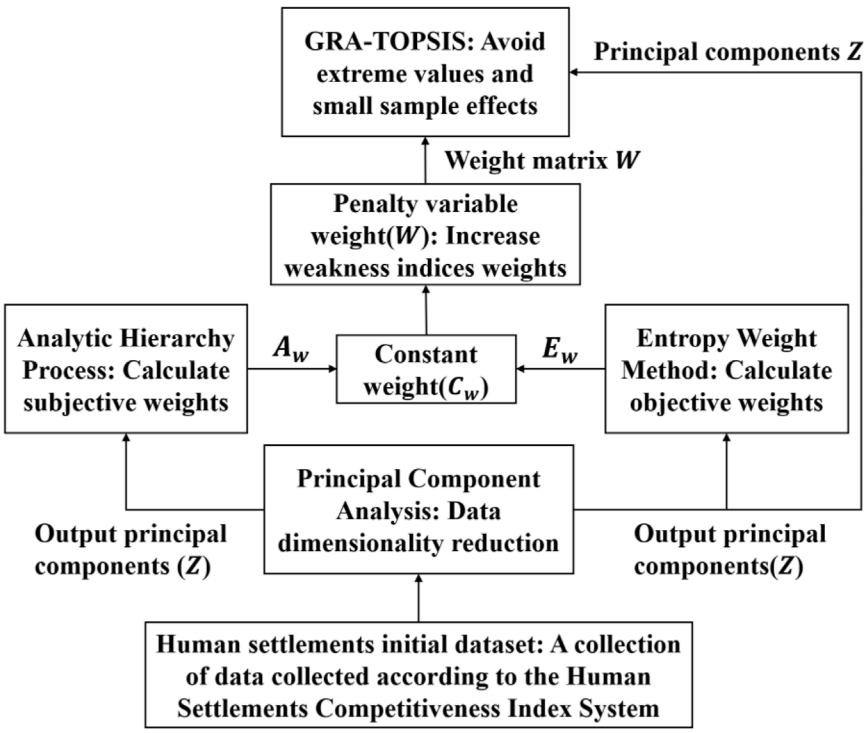

FIGURE 2 | HSC evaluation process.

TABLE 3 | Constant weight of the principal component of HSC.

Weight (%)	Z_{01}	Z_{02}	Z_{03}	Z_{04}	Z_{05}	Z_{06}	Z_{07}	Z_{08}	Z_{09}	Z_{10}
A_w	3.60	7.10	24.90	18.80	11.60	11.60	7.30	7.00	4.80	3.30
E_w	3.90	10.56	18.02	8.77	8.39	14.91	9.00	14.42	8.06	3.99
C_w	3.85	8.89	21.74	13.18	10.12	13.50	8.32	10.31	6.38	3.72

data using the penalty incentive variable weight method. Using the analytic hierarchy process to calculate the subjective weight *Aw* and consulting relevant literature (Cong et al., 2010; Xu et al., 2012), we determined the principal component contrast relationship as economic growth > urban expansion > urban greening = pollution control > infrastructure > employment structure > public service > residential support > residential density. The formed relationship matrix passed the consistency test. The entropy method was used to calculate the objective weight *Ew*, and the weight of each principal component was determined by the data (Khorrami et al., 2021), in which the weight of economic growth, public service, and pollution control accounted for more than 14%, indicating that these principal components showed significant changes over time. The weights are listed in **Table 3**.

The Lagrange multiplier method was used to combine the subjective and objective weights. The obtained constant weight Cw can be expressed by using **Eq. 1**.

$$Cw = \sqrt{Aw_jEw_j} \Big/ \sum_{j=1}^{q} \sqrt{Aw_jEw_j}. \quad (1)$$

Considering the influence of index data on index weight, the penalty incentive variable weighting method was adopted to increase the weight of the principal component indices that are lower than the average value. The obtained variable weight matrix W can be expressed by using **Eq. 2** (Liu et al., 2018):

$$W = Cw_jS \Big/ \sum_{j=1}^{q} Cw_jS, \quad (2)$$

where Cw is a constant weight and S is the variable weight vector of the penalty state, which is determined by the average value of the index and penalty level. Through related calculations, we found the punishment strength was greater for employment structure, urban expansion, and infrastructure indices. Using the constant and variable weighting methods, a variable weight matrix W was formed.

The GRA-TOPSIS method was used to evaluate the HSC (Shi and Gan, 2020). The method can be used to reduce the influence of small sample size and extreme value effect on the evaluation results.

$$HSC_i = k_{gr}GR_i + k_{ts}TS_i, \quad (3)$$

where GR_i and TS_i represent the GRA and TOPSIS evaluation results of city i, respectively, and k_{gr} and k_{ts} represent the weights of the two methods evaluated by decision-makers.

2.2.2 Urban Network Analysis

2.2.2.1 Network Metrics

The relevance coefficient of HSC (HSCR) constructed in this study is an extension of the economic gravity model (Fan et al., 2018). For any two cities in the network, the HSCR can be expressed by using **Eq. 4**:

$$HSCR_{ij} = k_C \cdot \frac{HSC_i \cdot HSC_j}{D_{ij}^2}, \quad (4)$$

where $HSCR_{ij}$ is the relevance coefficient between cities i and j, k_C is the correction coefficient, which is taken as 10e-6 in this research, and D_{ij} is the Euclidean distance between the administrative centers of cities i and j.

The difference coefficient of HSC (HSCD) constructed in this study is based on the Gini coefficient, considering the spatial distance (Zhang et al., 2020). For any two cities in the network, HSCD can be expressed by using **Eq. 5**:

$$HSCD_{ij} = \frac{\left|HSC_i - HSC_j\right| \cdot D_{ij}}{\left(\lambda_i + \lambda_j\right) \cdot n_i n_j}, \quad (5)$$

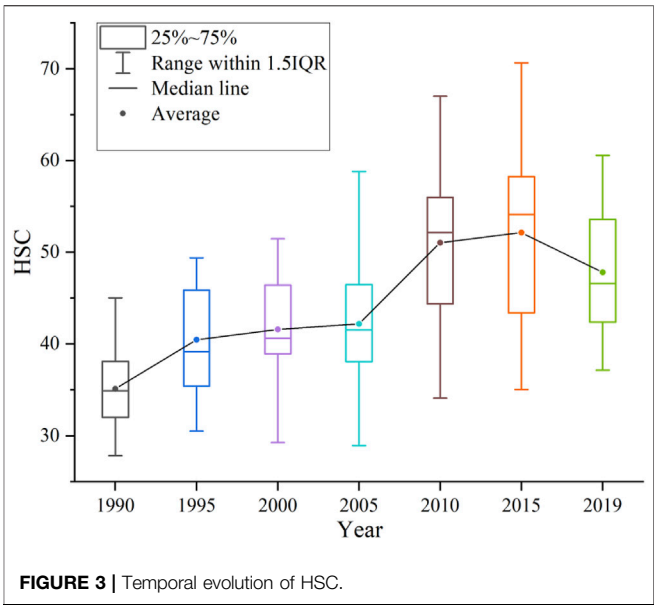

FIGURE 3 | Temporal evolution of HSC.

where λ_i and λ_j are the average values of the HSC of cities i and j, respectively, n_i and n_j are the number of cities in the urban agglomerations to which cities i and j belong.

2.2.2.2 Characteristic Network Parameters

The complete social network was processed using the binary method, and the median of HSCR and HSCD in all time nodes was calculated as basis for screening. There will be a connection between the two cities, if either the HSCR between two cities is greater than the median, or if the HSCD between the two cities is lesser than the median.

The spatial-temporal patterns of the network structure are analyzed by calculating the network density, centrality, and community characteristics of social networks (Fan et al., 2018). Network density describes the closeness of connections between nodes in a social network and can be expressed as the ratio of the number of connections in the network to the maximum number of connections possible. Centrality is used to describe the central characteristics of nodes, including degree centrality, closeness centrality, and betweenness centrality, which represent the direct, indirect, and intermediary degrees between nodes, respectively. Community detection can measure the aggregation behavior of nodes in social networks and is used here to detect the aggregation patterns of cities in the HSC network.

3 RESULTS

3.1 HSC

The HSC was evaluated using the GRA-TOPSIS comprehensive evaluation method combined with the weight matrix W. Based on the annual changes in human settlements characteristics, the HSC continued to rise from 35.12 in 1990 to 52.15 in 2015 and showed

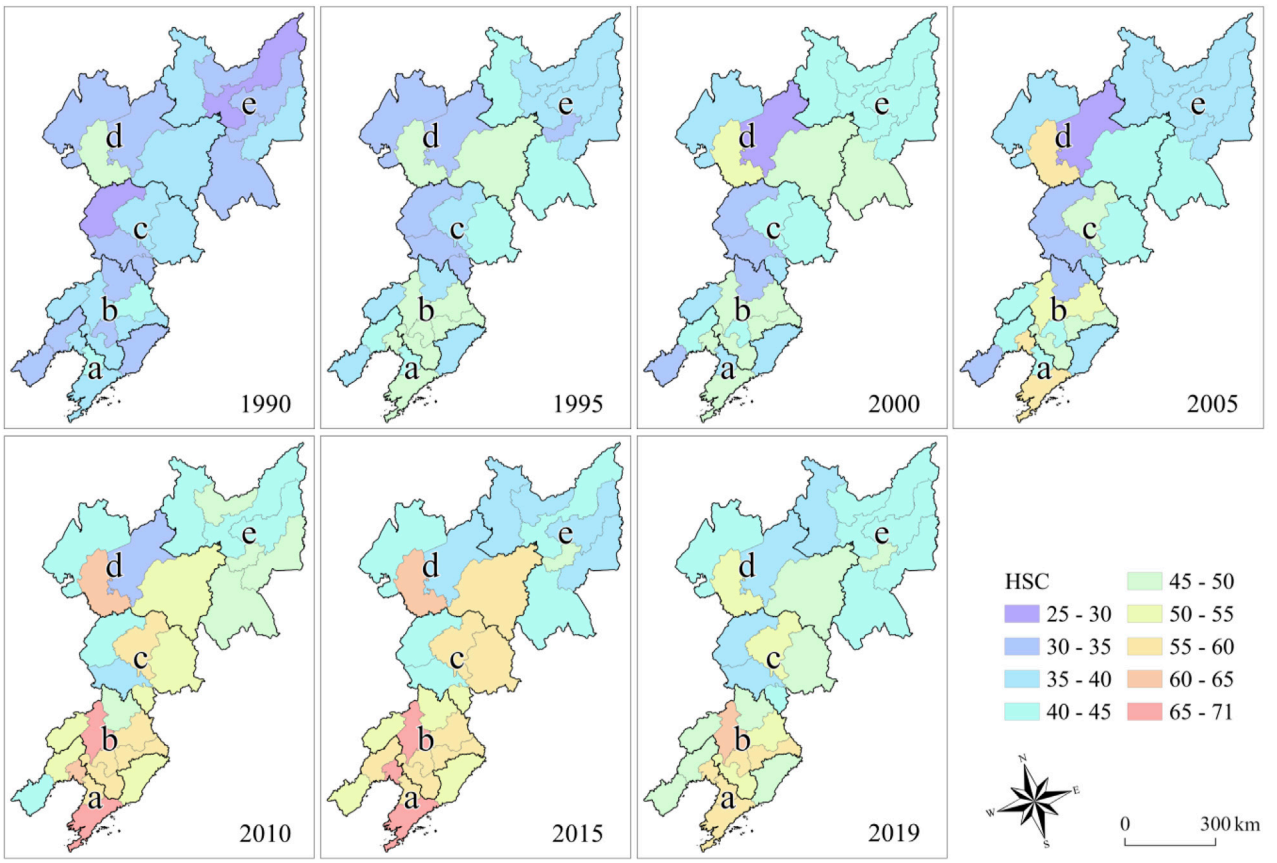

FIGURE 4 | Spatial and temporal patterns of human settlement competitiveness.

a downward trend from 2015 to 2019, with an average value of 47.82 in 2019 (**Figure 3**). From 1990 to 2010, the growth rate of HSCs gradually increased by 20.96% from 2005 to 2010. After 2010, the upward trend of HSC slowed, and the average value of HSC decreased by 8.31% from 2015 to 2019. In addition, we found that although the HSC of the urban agglomerations showed an overall upward trend, the standard deviation of the HSC also showed an upward trend. 2015 was the highest year for HSC, with the highest standard deviation of 9.76.

Each urban agglomeration showed different development trends of HSC. As shown in **Figure 4**, the HSC of each city in the Eastern Heilongjiang Urban Agglomeration grew slowly, and the difference in HSC among cities was small; the polarization effect between Harbin-Daqing-Qiqihar Urban Agglomeration and Central Jilin Urban Agglomeration was evident. Daqing and Changchun were dominant in terms of HSC, whereas Suihua and Siping were in the inferior position in terms of HSC. Liaoning Coastal Urban Agglomeration and Central Liaoning Urban Agglomeration gradually developed into HSC hot spots, and the coordinated development ability of human settlements in urban agglomerations was satisfactory, Dalian and Shenyang have the highest HSC in their urban agglomerations.

3.2 Relevance Network Characteristics

The relevance coefficient matrix of HSC is shown in **Figure 5**. The relevance coefficient within urban agglomerations was higher than that between urban agglomerations. Central Liaoning Urban Agglomeration had high relevance of HSC with Liaoning Coastal Urban Agglomeration and Central Jilin Urban Agglomeration due to its location and competitive advantage. The structural characteristics of the relevance network of the HSC are shown in **Figure 6**. The density of the HSC relevance network showed an upward trend, reflecting that the relevance of the urban human settlements in northeastern cities was getting closer, but the upward trend gradually slowed down, and even negative growth occurred. The years with a density higher than the average of 0.5 include 2010, 2015, and 2019. The network density was the highest in 2015 (0.569). The average values of degree centrality, closeness centrality, and betweenness centrality of the HSC relevance network were 14, 0.72, and 9.45, respectively. The order of relevance of urban agglomerations was Central Jilin Urban Agglomeration > Central Liaoning Urban Agglomeration > Liaoning Coastal Urban Agglomeration > Harbin-Daqing-Qiqihar Urban Agglomeration > Eastern Heilongjiang Urban Agglomeration,

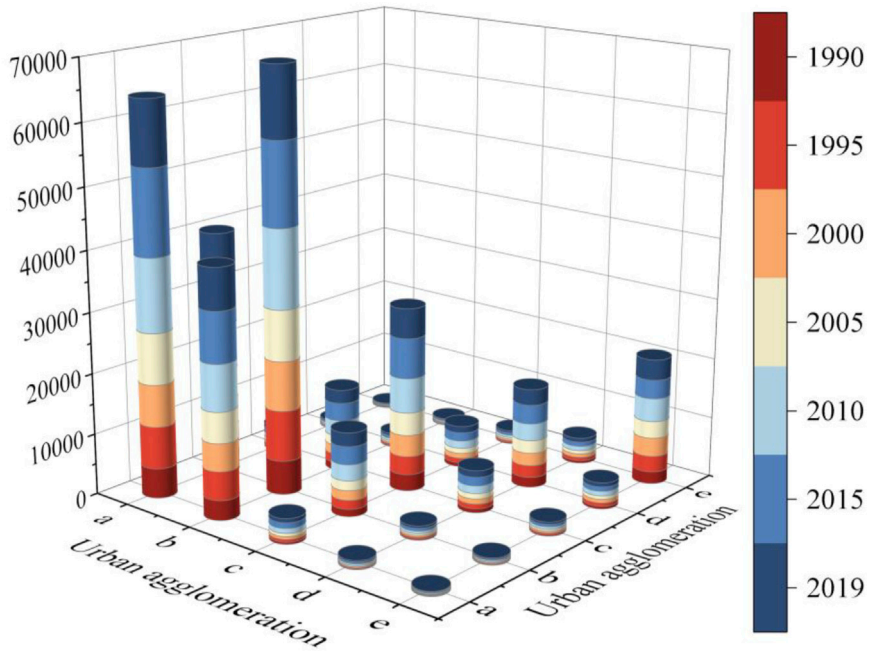

FIGURE 5 | Relevance coefficient matrix between urban agglomerations.

and betweenness centrality measure showed that Central Jilin Urban Agglomeration and Harbin-Daqing-Qiqihar Urban Agglomeration had significant intermediary capabilities, with averages of 21.23 and 22.49, respectively. Central Liaoning Urban Agglomeration, Liaoning Coastal Urban Agglomeration, and Eastern Heilongjiang Urban Agglomeration had low intermediary capabilities (for Liaoning Coastal Urban Agglomeration, it is only 0.67). Community detection was carried out on the relevance network of HSC with the resolution of 1.0. The results showed that there are two main communities in the HSC relevance network, and the community boundaries coincided with the boundaries of urban agglomerations and provinces to a great extent, indicating that the association between HSC were significant in urban agglomerations within the same province, but not significant among inter-provincial urban agglomerations.

The relevance network of HSC in each urban agglomeration presents the following characteristics. 1) The degree centrality and closeness centrality of cities in Liaoning Coastal Urban Agglomeration were close to the average value, but the intermediary ability was lacking. Cities were closely related to HSC within urban agglomerations, while the HSC relevance between urban agglomerations was relatively low. 2) The cities in Central Liaoning Urban Agglomeration showed the central characteristics of high point-high closeness-low betweenness, and the competitiveness of human settlements was highly correlated, but the role of cities as a "bridge" for human settlements was weak; Fushun had the highest average degree centrality and closeness centrality among all cities, which were 19 and 0.833, respectively. 3) The cities in Central Jilin Urban Agglomeration showed the centrality characteristics of high degree-high closeness-high betweenness, and the centrality of cities was average. The betweenness centrality values of Changchun and Jilin were 29.10 and 29.51, respectively, which are important intermediary nodes. 4) The centrality polarization of cities in Harbin-Daqing-Qiqihar Urban Agglomeration was significant: the values for Harbin and Daqing were slightly higher than the average value, whereas those for Suihua and Qiqihar were lower than the average value. The betweenness centrality in Harbin was 61.85, which was the core intermediary node of the relevance network. 5) The cities in Eastern Heilongjiang Urban Agglomeration showed the centrality characteristics of low degree-low closeness-low betweenness, and Mudanjiang had the strongest centrality in this urban agglomeration and played the role of an intermediary node.

3.3 Difference Network Characteristics

The difference coefficient matrix of HSC is shown in **Figure 7**. The difference coefficient within urban agglomerations was lower than that between urban agglomerations, and HSC in Liaoning Coastal Urban Agglomeration was different from that of Harbin-Daqing-Qiqihar Urban Agglomeration and Eastern Heilongjiang Urban Agglomeration. The structural characteristics of the difference network of HSC are shown in

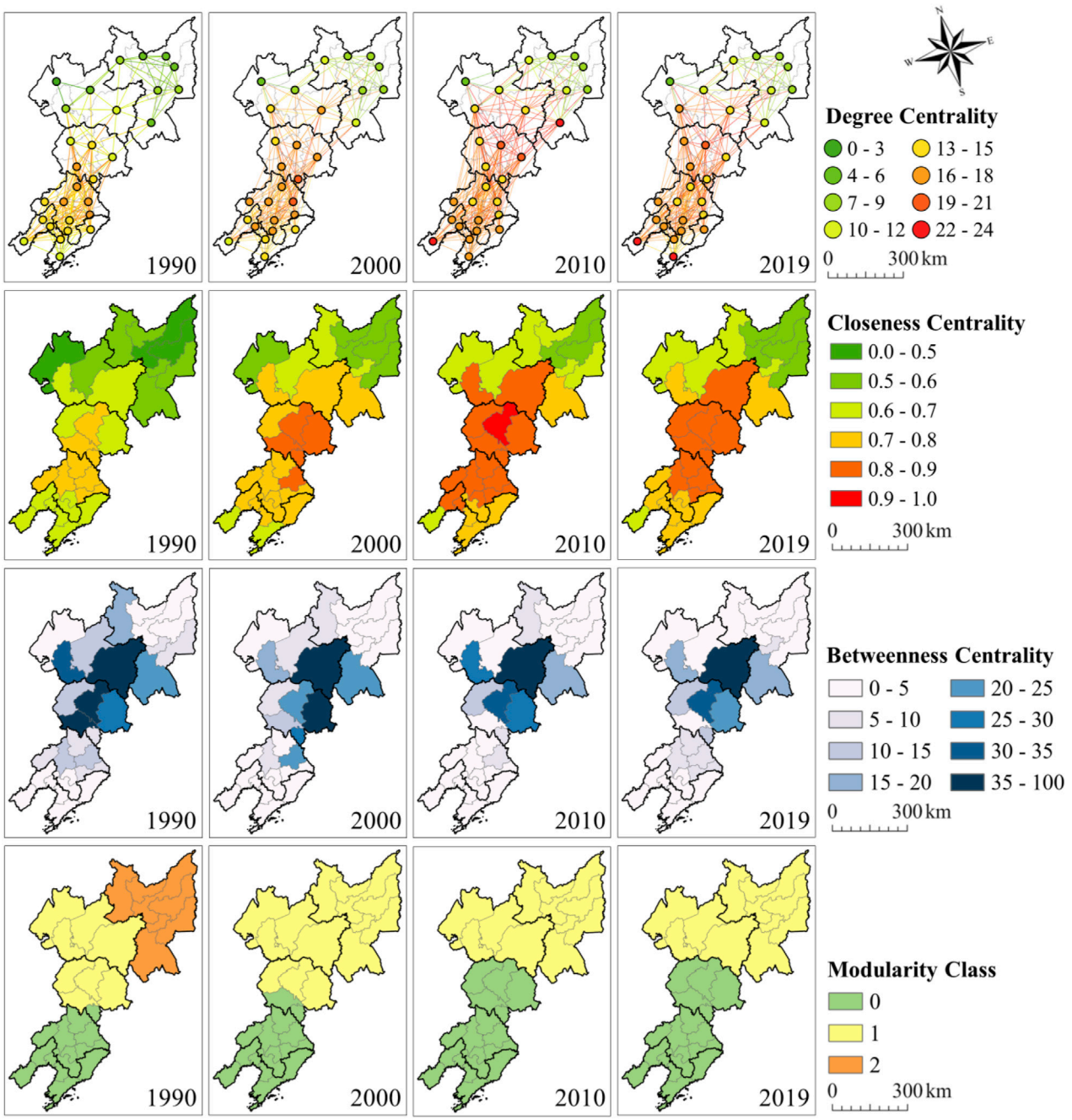

FIGURE 6 | Relevance network structure characteristics.

Figure 8, and the difference in network density shows a wavy downward trend. The lowest network density value of 0.441 was achieved in 2015 with the highest average value of HSC, reflecting the uncoordinated development of HSC in urban agglomerations, with average values of degree centrality, closeness centrality, and betweenness centrality of the difference network were 14, 0.72, and 9.45, respectively. The order of difference of urban agglomerations was Harbin-Daqing-Qiqihar Urban Agglomeration > Eastern Heilongjiang Urban Agglomeration > Central Jilin Urban Agglomeration > Liaoning Coastal Urban Agglomeration > Central Liaoning Urban Agglomeration; Central Jilin Urban Agglomeration and Central Liaoning Urban Agglomeration had significant intermediary ability with average values of 14.74 and 13.13, respectively, whereas Harbin-Daqing-Qiqihar Urban Agglomeration, Eastern Heilongjiang Urban Agglomeration, and Liaoning Coastal Urban Agglomeration showed low intermediary ability. Community detection was

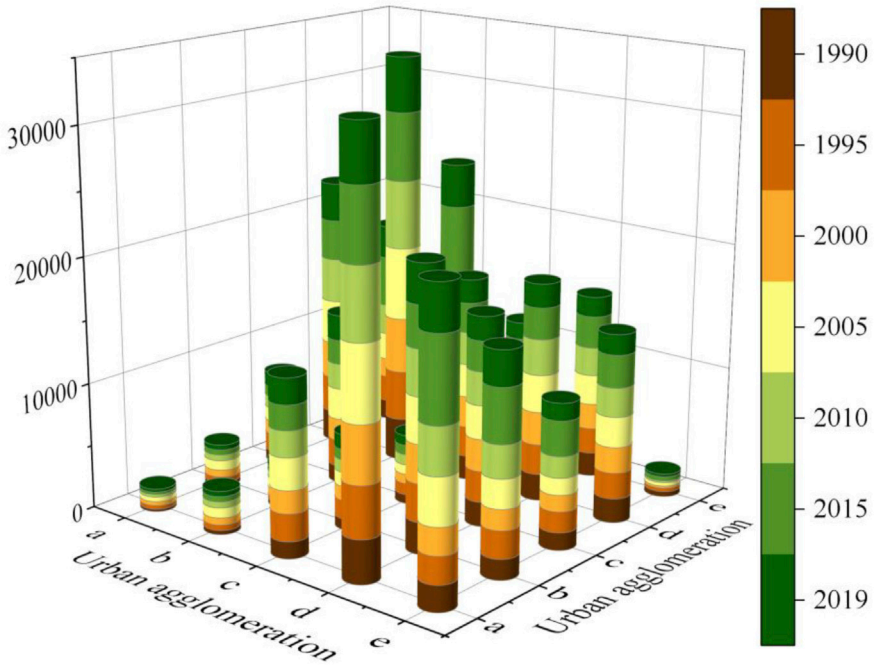

FIGURE 7 | Difference coefficient matrix between urban agglomerations.

carried out on the difference network of HSC with a resolution of 1.0. The results show two main communities in urban agglomerations (high-competitiveness and low-competitiveness communities). Overall, the number of cities in highly competitive communities increased.

The difference network of HSC in each urban agglomeration presents the following characteristics. 1) The degree centrality and closeness centrality of each city in the Central Liaoning Urban Agglomeration were higher than the average value, showing the centrality characteristics of high degree-high closeness-high betweenness; degree centrality, closeness centrality, betweenness centrality of Tieling were 21, 0.87, and 23.15, respectively, which were higher than those of other cities. 2) In the Liaoning Coastal Urban Agglomeration, the degree centrality and closeness centrality of Dandong, Jinzhou, Panjin, and Yingkou were higher than the average, whereas Dalian and Panjin had lower centrality than the average because of their high HSC. Dandong is an important intermediary node with betweenness centrality of 11.39. 3) The Central Jilin Urban Agglomeration shows the centrality characteristic of high degree-high closeness-high betweenness. The centrality of Changchun and Liaoyuan was higher than the average and showed a characteristic of low difference. All cities in the urban agglomeration except Jilin had significant intermediary function. 4) The cities in Harbin-Daqing-Qiqihar Urban Agglomeration showed the centrality characteristics of low degree-low closeness-low betweenness, and there were differences in human settlements inside and outside the urban agglomeration, where Suihua and Daqing experienced solitary point, and Harbin had the highest centrality in the urban agglomeration, with degree centrality, closeness centrality, and betweenness centrality values of 12.29, 0.70, and 2.48, respectively. 5) The cities in the Eastern Heilongjiang Urban Agglomeration showed the central characteristics of low degree-low closeness-low betweenness, and the urban agglomeration showed the characteristics of low internal difference and high external difference. Mudanjiang was the city with the highest centrality in the urban agglomeration, with degree centrality, closeness centrality, and betweenness centrality values of 16.29, 0.78, and 12.64, respectively.

4 DISCUSSION

4.1 Scientificity and Accuracy of HSC

In terms of scientificity, different research frameworks have diversified the index system that reflects human settlements. Based on the scientific of human settlements proposed by Wu, (2001), we constructed a “five-in-one” index system of HSC, which takes “human” as its internal core factor, “economy” as its key factor, and “environment” as its important influencing factor. While considering natural factors, we highlight the key role played by social and economic factors in urban competition. Compared with previous research that mainly focused on the

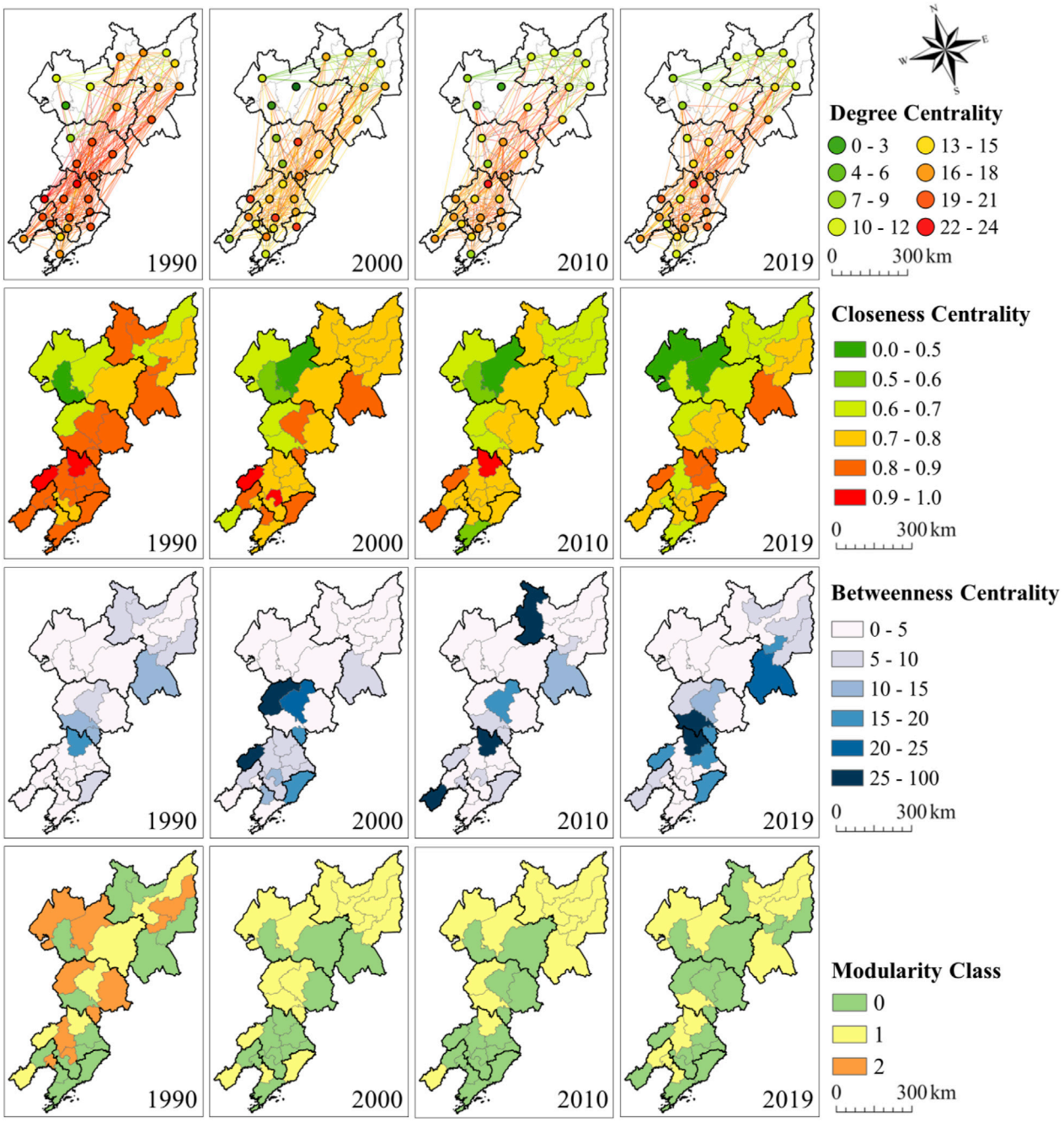

FIGURE 8 | Difference network structure characteristics.

suitability and risk of human settlements (Tian et al., 2016; Li et al., 2018; Luo et al., 2021), the index system of HSC in our study reflects the attraction of human settlements to population and capital. In terms of accuracy, the evaluation model of HSC constructed in this study is an organic combination of the methods widely used in human settlement evaluation (Ma et al., 2016; Tang et al., 2017). We applied principal component analysis to reduce the overlapping effect of indices, the analytic hierarchy process and entropy weight method to realize the comprehensive consideration of subjective and objective decision-making factors, and the positive and negative ideal solutions and gray correlation degree to explore the synchronous changes in human settlements among cities to form HSC evaluation results.

In order to further prove the accuracy of HSC evaluation model, we used the floating population in the sixth national census of China (2010) to verify the extent to which HSC could reflect the attraction effect of cities on population. Specifically,

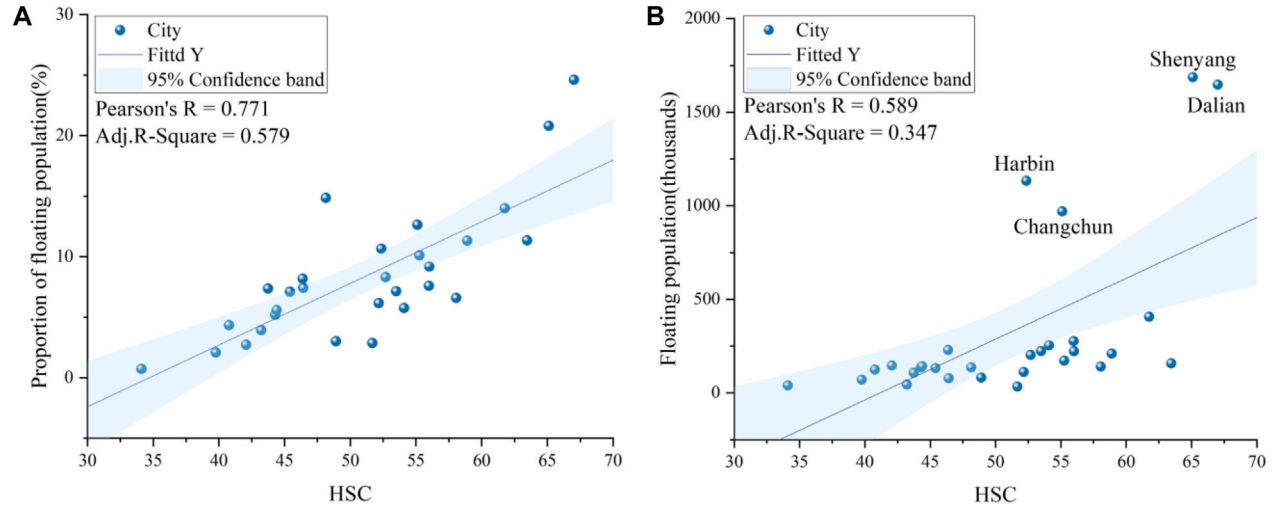

FIGURE 9 | Correlation between floating population and HSC. **(A)** correlation between HSC and the proportion of floating population; **(B)** correlation between HSC and the number of floating population.

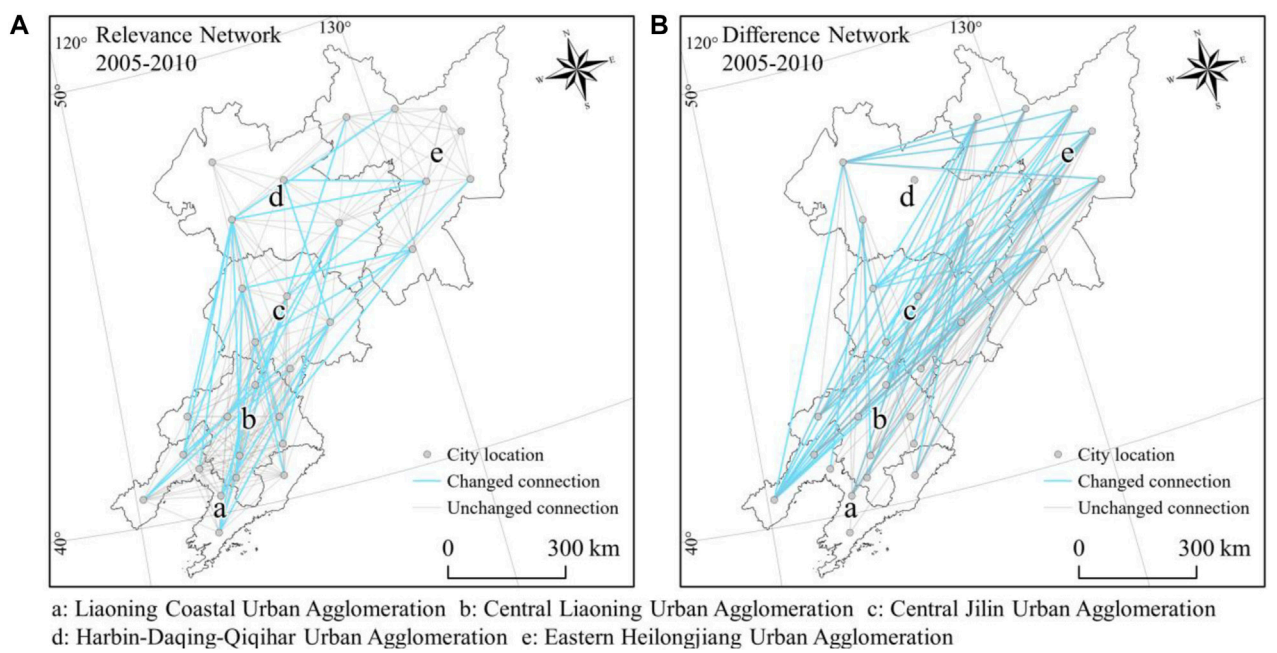

FIGURE 10 | HSC networks evolution. **(A)** HSC relevance networks evolution; **(B)** HSC difference networks evolution.

the proportion of floating population to resident population was used to represent the relative population attraction capacity of cities based on their population carrying capacity, **Figure 9A** showed the correlation between HSC and the proportion of floating population. Pearson correlation coefficient of HSC and floating population was 0.771, showing a significant positive correlation between HSC and floating population, and R square was 0.579, indicating that there was a good linear correlation between HSC and floating population proportion. To sum up, the evaluation results of HSC by the evaluation model established in this study can significantly reflect the influence of the advantages or disadvantages of urban living environment on the residence willingness of floating population.

In addition, this study used the number of floating population to represent the absolute population attraction of cities.

Figure 9B showed the correlation between HSC and the number of floating population. Pearson correlation coefficient between them was 0.589, and R square was 0.347. Although the correlation between HSC and the number of floating population also verified the effectiveness of HSC evaluation results to a certain extent, compared with the proportion of floating population, the interpretation strength declined. The reason lies in the existence of Changchun, Harbin, Dalian and Shenyang, which actually attract more floating population than their HSC should attract. These four cities are the core cities in the urban agglomeration where they are located, and they are also the provincial capitals and sub-provincial cities of the Northeast China. The advantages of employment, medical care and education resources brought by their political status are obviously more attractive to the floating population than those embodied by HSC, which attaches importance to the quality of ecological environment.

4.2 HSC Networks Evolution Mechanism

For HSC relevance networks, the network structure was most obviously improved between 2005–2010 (**Figure 10A**). This is mainly due to the implementation of the strategy of revitalizing the old industrial bases in Northeast China in 2003. Due to the promotion of policies, the social and economic development of cities in the Northeast region has been rapid, and the infrastructure has been further improved. Between 2010–2015, the upgrading rate of HSC network structure in Northeast urban agglomeration slowed down, and there was even a contraction between 2015–2019. This is because after the implementation of the strategy, most of the urban development in the urban agglomerations is still highly dependent on the development and utilization of resources and lacks the ability to innovate. The urban agglomerations pursue the rapid growth of the regional economy through over-exploitation of resources, resulting in a sharp decline in resource stock and extraction efficiency, and has not achieved the transformation and upgrading of the industrial structure. At the same time, this development model leads to rising costs and environmental degradation, which finally caused the global financial crisis in 2008 to have a serious impact on its development.

In addition, we found that all the cities at both ends of the newly connected of relevance network have come from different urban agglomerations since 1995. Community detection results of relevance network showed that the influence of the two urban agglomerations in Liaoning province was increasing. This is mainly due to the fact that the Central Liaoning Urban Agglomeration and the Liaoning Coastal Urban Agglomeration have gradually developed into a window for the northeast region to communicate with the south of China and foreign countries. Especially, the coastal cities represented by Dalian have made great efforts to improve the ecological environment and develop diversified economy, and the competitive advantages brought by their human settlement environment have gradually enhanced the radiation ability. This result is similar to the related research on the evolution of the economic network structure of the urban agglomerations in Northeast China (Li, 2019; Jia, 2021).

For HSC difference network, we found that there were huge HSC differences inside and outside urban agglomerations. Moreover, HSC difference connection was more unstable (**Figure 10B**), indicating that the core cities in urban agglomerations failed to form a stable radiation-driven effect, and the development of human settlements in urban agglomerations was uncoordinated and unsustainable. The reason is that there are many resource-based cities in urban agglomerations, which are highly dependent on resources and weak in driving the surrounding cities. Restricted by regional economic development level, talents, labor and other factors, the overall differences in HSC between cities are huge. Shenyang, Dalian, Changchun and Harbin, the core cities of the four urban agglomerations in Northeast China, have strong regional influence and gather a lot of resources. Under the long-term effect of siphon effect in the four cities, Matthew effect is formed, in which the stronger the strong and the weaker the weak.

4.3 Sustainable Development of Human Settlements

From the evolution mechanism of HSC networks, we found that the relationship between human settlements in Northeast urban agglomerations at present was mostly competition rather than competition and cooperation, which was not conducive to the sustainable development of resource-based urban agglomerations. But in fact, the Northeast urban agglomeration has many competing conditions, but it has not been well utilized. First of all, the resources of each urban agglomeration are rich and complementary. Among them, Harbin-Daqing-Qiqihar and Eastern Heilongjiang urban agglomerations are rich in forest, cultivated land and oil resources, Central Jilin urban agglomeration are rich in natural gas, water and mountain resources, and Liaoning Coastal and Central Liaoning urban agglomerations are rich in marine resources and non-ferrous metal resources; Secondly, the industrial development pattern has made the infrastructure of the Northeast urban agglomerations increasingly perfect, especially the Northeast urban agglomeration has formed a comprehensive transportation system with staggered water, land and air, which has laid a good foundation for the urban agglomeration to enhance cooperation; Finally, the Northeast urban agglomerations is being supported by the second round of national policies such as “Revitalizing the Old Industrial Base in Northeast China,” and the policy opportunities are obvious.

Based on the theory of “co-opetition,” we believe that the competitiveness of human settlements in Northeast urban agglomerations can be promoted synergistically from the following aspects. First of all, coordination mechanism and benefit distribution guarantee mechanism should be established among urban agglomerations to curb local protectionism. The theory of “co-opetition” emphasizes that conflicts do not necessarily occur between different regions. As long as the interests of both sides are improved and local governments can make profits from such competition and cooperation, there are inherent incentives for competition and

cooperation. In the early development process of Northeast urban agglomerations, the planning positioning was highly overlapping, which not only increased the cost, but also reduced the efficiency of resource allocation. Good division of labor and coordination can reduce the conflicts of interests among urban agglomerations, so that all urban agglomerations can obtain higher benefits, and then realize the sustainable development model.

Secondly, from the perspective of internal development of urban agglomerations, all urban agglomerations in Northeast China had different degrees of HSC polarization. The analysis of competition and cooperation shows that the agglomeration of cities with low HSC is not conducive to the improvement of competitiveness, and polarization will also have a negative impact on the balanced pattern (Liu R et al., 2021). For urban agglomerations in Northeast China, it is necessary to gradually narrow the HSC gap within urban agglomerations by establishing urban development gradient levels. In addition, considering the long-term competition and cooperation between cities, urban agglomerations should take innovation and development as the core, promote industrial transformation and upgrading, improve labor efficiency and factor allocation efficiency, and pay attention to ecological protection and environmental sustainable development, so as to drive regional HSC promotion.

4.4 Limitations

In this study, the urban agglomerations in Northeast China were taken as the research area, and the competitiveness of the urban human settlements was quantitatively evaluated from 1990 to 2019. The characteristics of the HSC network structure and its driving factors were analyzed. However, this study has some limitations. 1) The research time scale of this study is relatively macro, which reduces the availability of data. A better index system can be constructed in the future to cover the scientific of human settlements. 2) In this study, the Euclidean distance between urban administrative centers was used to express the urban interaction ability, and follow-up research can describe the interaction ability between cities more accurately.

5 CONCLUSION

In this study, a HSC compound evaluation model is established. Compared with the existing models, this model introduces the penalty variable weight method to increase the penalty for extreme disadvantage index, and introduces GRA-TOPSIS method to reduce the influence of small sample size and extreme value effect on the basis of considering subjective and objective factors. Using this model, this study evaluates the HSC in the urban agglomerations in Northeast China from 1990 to 2019 and quantifies the temporal and spatial patterns of the relevance and difference network structure based on the overall characteristics, node characteristics, and community characteristics. The main conclusions are as follows.

1) The HSC increased from 35.12 in 1990 to 52.15 in 2015 and showed a downward trend from 2015 to 2019, with an average value of 47.82 in 2019. The HSC of cities in the Eastern Heilongjiang Urban Agglomeration grew slowly, the difference in HSC among cities was small, and the polarization effect between Harbin-Daqing-Qiqihar Urban Agglomeration and Central Jilin Urban Agglomeration was evident. Liaoning Coastal Urban Agglomeration and Central Liaoning Urban Agglomeration gradually developed into HSC hot spots, and the coordinated development ability of human settlements in urban agglomerations was satisfactory.
2) The relevance coefficient within urban agglomerations was higher than that between urban agglomerations. The density of the HSC relevance network showed an upward trend, reflecting that the relevance of the urban human settlements in northeastern cities was getting closer, and the network density was the highest in 2015 (0.569). Central Jilin Urban Agglomeration and Harbin-Daqing-Qiqihar Urban Agglomeration had significant intermediary capabilities, with betweenness centrality values of 21.23 and 22.49, respectively. Community detection showed that the association between HSC exists are obviously bounded by the borders of provinces or urban agglomerations
3) The difference coefficient within urban agglomerations was lower than that between urban agglomerations. The difference in network density showed a wavy downward trend. The lowest network density value of 0.441 was achieved in 2015 with the highest average value of HSC, reflecting the uncoordinated development of HSC in urban agglomerations. Central Jilin Urban Agglomeration and Central Liaoning Urban Agglomeration had significant intermediary ability with betweenness centrality values of 14.74 and 13.13, respectively. Community detection showed two main communities in the urban agglomerations: high-competitiveness and low-competitiveness communities.

This study believes that the Northeast urban agglomeration has not yet formed an effective HSC development path of co-opetition. In order to promote the sustainable development of the human settlement environment of the Northeast urban agglomerations, a coordination mechanism and a benefit distribution guarantee mechanism should be established among urban agglomerations to curb local protectionism, break down institutional barriers and promote regional dislocation development. Urban development gradient levels should be established within urban agglomerations to narrow the gap between HSCs within urban agglomerations, and at the same time, innovation and development should be taken as the core to promote industrial transformation and upgrading.

DATA AVAILABILITY STATEMENT

The raw data supporting the conclusion of this article will be made available by the authors, without undue reservation.

AUTHOR CONTRIBUTIONS

WY performed the data analyses and wrote the manuscript; JY contributed to the conception of the study; HY contributed significantly to analysis and manuscript preparation; DS and XX helped perform the analysis with constructive discussions. YY and JX reviewed the manuscript and provided valuable review comments.

FUNDING

This research study was supported by the National Natural Science Foundation of China (grant no's 41771178, 42030409, and 41671151), the Fundamental Research Funds for the Central Universities (grant no. N2111003), Basic Scientific Research Project (Key Project) of the Education Department of Liaoning Province (grant no. LJKZ0964), Natural Science Foundation of Guizhou Province (grant no. (2019)1150), the Second Tibetan Plateau Scientific Expedition and Research Program (STEP) (grant no. 2019QZKK1004).

ACKNOWLEDGMENTS

The authors would like to acknowledge all colleagues and friends who have voluntarily reviewed the translation of the survey and the manuscript of this study.

REFERENCES

Bell, G., and Gonzalez, A. (2011). Adaptation and Evolutionary Rescue in Metapopulations Experiencing Environmental Deterioration. *Science* 332, 1327–1330. doi:10.1126/science.1203105

Chen, W., Zhu, K., Wu, Q., Cai, Y., Lu, Y., and Wei, J. (2021). Adaptability Evaluation of Human Settlements in Chengdu Based on 3S Technology. *Environ. Sci. Pollut. Res.* 29, 5988–5999. doi:10.1007/s11356-021-15998-6

Chen, Y., and Zhang, D. (2021). Multiscale Assessment of the Coupling Coordination between Innovation and Economic Development in Resource-Based Cities: A Case Study of Northeast China. *J. Clean. Prod.* 318, 128597. doi:10.1016/j.jclepro.2021.128597

Cong, Y., Xia, B., and Zhang, J. (2010). Associated Evaluation of Subjective and Objective of Human Settlement on a City Scale: A Case Study of Guangzhou City. *Trop. Geogr.* 30, 183–187. doi:10.13284/j.cnki.rddl.001349

Derudder, B., and Taylor, P. (2016). Change in the World City Network, 2000-2012. *Prof. Geogr.* 68, 624–637. doi:10.1080/00330124.2016.1157500

Esmaeilpoorarabi, N., Yigitcanlar, T., and Guaralda, M. (2016). Place Quality and Urban Competitiveness Symbiosis? A Position Paper. *IJKBD* 7, 4–21. doi:10.1504/IJKBD.2016.075444

Esty, D., and Geradin, D. (2000). Regulatory Co-opetition. *J. Int. Econ. Law* 3, 235–255. doi:10.1093/jiel/3.2.235

Fan, Y., Zhang, S., He, Z., He, B., Yu, H., Ye, X., et al. (2018). Spatial Pattern and Evolution of Urban System Based on Gravity Model and Whole Network Analysis in the Huaihe River Basin of China. *Discrete Dyn. Nat. Soc.* 2018, 1–11. doi:10.1155/2018/3698071

Fu, J., Xiao, G., and Wu, C. (2020). Urban Green Transformation in Northeast China: A Comparative Study with Jiangsu, Zhejiang and Guangdong Provinces. *J. Clean. Prod.* 273, 122551. doi:10.1016/j.jclepro.2020.122551

Guo, A., Yang, J., Xiao, X., XiaJin, C., and Li, X. (2020). Influences of Urban Spatial Form on Urban Heat Island Effects at the Community Level in China. *Sust. Cities Soc.* 53, 101972. doi:10.1016/j.scs.2019.101972

Huang, Y., Hong, T., and Ma, T. (2020). Urban Network Externalities, Agglomeration Economies and Urban Economic Growth. *Cities* 107, 102882. doi:10.1016/j.cities.2020.102882

Jia, Z., and Gu, G. (2021). Is Local Government Intervention Effective in Promoting the tfp of an old Industrial Area? — a Spatial Econometric Analysis of Northeast China. *Singap. Econ. Rev.* 66, 933–951. doi:10.1142/S0217590820500319

Khorrami, Z., Ye, T., Sadatmoosavi, A., Mirzaee, M., Fadakar Davarani, M. M., and Khanjani, N. (2021). The Indicators and Methods Used for Measuring Urban Liveability: a Scoping Review. *Rev. Environ. Health* 36, 397–441. doi:10.1515/reveh-2020-0097

Li, F., Liu, X., Hu, D., Wang, R., Yang, W., Li, D., et al. (2009). Measurement Indicators and an Evaluation Approach for Assessing Urban Sustainable Development: A Case Study for China's Jining City. *Landsc. Urban Plan.* 90, 134–142. doi:10.1016/j.landurbplan.2008.10.022

Li, P., and Zhong, W. (2020). An Optimization Management Model for Countries with Mutually Competitive Regions. *Sustainability* 12, 2326. doi:10.3390/su12062326

Li, Q. (2019). *Research on the Spatial Correlation Structure of Urban Agglomeration Economic Growth and its Effects in Northeast China*. China: Northeast Normal University.

Li, X., Li, S., Gao, J., Zhao, P., and Li, H. (2018). Human Settlement Quality Evaluation Based on Air Quality in Major Cities of China. *Adv. Meteorology* 2018, 1–9. doi:10.1155/2018/4914760

Li, Z., Wang, J., Kong, X., Zhang, B., Liu, J., Ding, S., et al. (2021). Effects of Ecosystems Preservation on Economic Growth in China's Coastal Region: Multilevel Modelling and Exploration. *Ecol. Indic.* 132, 108224. doi:10.1016/j.ecolind.2021.108224

Lin, J.-J., and Yang, A.-T. (2006). Does the Compact-City Paradigm Foster Sustainability? an Empirical Study in Taiwan. *Environ. Plann B Plann Des.* 33, 365–380. doi:10.1068/b31174

Liu, D., Huang, A., Yang, D., Lin, J., and Liu, J. (2021). Niche-driven Socio-Environmental Linkages and Regional Sustainable Development. *Sustainability* 13, 1331. doi:10.3390/su13031331

Liu, R., Dong, X., Wang, X.-c., Zhang, P., Liu, M., and Zhang, Y. (2021). Study on the Relationship Among the Urbanization Process, Ecosystem Services and Human Well-Being in an Arid Region in the Context of Carbon Flow: Taking the Manas River Basin as an Example. *Ecol. Indic.* 132, 108248. doi:10.1016/j.ecolind.2021.108248

Liu, J., Nijkamp, P., Huang, X., and Lin, D. (2017). Urban Livability and Tourism Development in China: Analysis of Sustainable Development by Means of Spatial Panel Data. *Habitat Int.* 68, 99–107. doi:10.1016/j.habitatint.2017.02.005

Liu, K., and Wang, C. (2013). Progress and Prospect of Livable City Researches in China. *J. Landsc. Res.* 5, 2530–2626.

Liu, S., Li, W., and Wang, Q. (2018). Zoning Method for Environmental Engineering Geological Patterns in Underground Coal Mining Areas. *Sci. Total Environ.* 634, 1064–1076. doi:10.1016/j.scitotenv.2018.04.060

Luo, X., Yang, J., Sun, W., and He, B. (2021). Suitability of Human Settlements in Mountainous Areas from the Perspective of Ventilation: A Case Study of the Main Urban Area of Chongqing. *J. Clean. Prod.* 310, 127467. doi:10.1016/j.jclepro.2021.127467

Ma, J., Wang, J., and Szmedra, P. (2019). Economic Efficiency and its Influencing Factors on Urban Agglomeration-An Analysis Based on China's Top 10 Urban Agglomerations. *Sustainability* 11, 5380. doi:10.3390/su11195380

Ma, R., Wang, T., Zhang, W., Yu, J., Wang, D., Chen, L., et al. (2016). Overview and Progress of Chinese Geographical Human Settlement Research. *J. Geogr. Sci.* 26, 1159–1175. doi:10.1007/s11442-016-1320-1

Mamat, A. (2012). Evaluations of Living Environment Suitability of Hotan Prefecture in Xinjiang Based on GIS. *Arid. Land Geogr.* 35, 155–163. doi:10.13826/j.cnki.cn65-1103/x.2012.05.003

Meijers, E., and van der Wouw, D. (2019). Struggles and Strategies of Rural Regions in the Age of the 'urban Triumph'. *J. Rural Stud.* 66, 21–29. doi:10.1016/j.jrurstud.2019.01.027

Meng, Y., and Chen, L.-S. (2021). Evaluation of Urban Competitiveness in Environmental Protection Zones Based on Principal Component Analysis (Pca) and Entropy Method. *J. Environ. Prot. Ecol.* 22, 182–188.

Ni, P., Kamiya, M., and Ding, R. (2017). "Global Urban Competitiveness: Comparative Analysis from Different Perspectives," in *Cities Network along the Silk Road*. Singapore: Springer Singapore), 51–64. doi:10.1007/978-981-10-4834-0_4

Ni, P., Kresl, P., and Li, X. (2014). China Urban Competitiveness in Industrialization: Based on the Panel Data of 25 Cities in China from 1990 to 2009. *Urban Stud.* 51, 2787–2805. doi:10.1177/0042098013514461

Önsel, Ş., Ülengin, F., Ulusoy, G., Aktaş, E., Kabak, Ö., and Topcu, Y. İ. (2008). A New Perspective on the Competitiveness of Nations. *Socio-Economic Plan. Sci.* 42, 221–246. doi:10.1016/j.seps.2007.11.001

Portergoff, M. (1990). *The Competitive Advantage of Nations*. New York: Free Press.

Rogerson, R. J. (1999). Quality of Life and City Competitiveness. *Urban Stud.* 36, 969–985. doi:10.1080/0042098993303

Ren, J., Yang, J., Zhang, Y., Xiao, X., Li, X., Wang, S., et al. (2022). Exploring Thermal Comfort of Urban Buildings Based on Local Climate Zones. *J. Clean Prod.* 340, 130744. doi:10.1016/j.jclepro.2022.130744

Shi, H., and Gan, L. (2020). "Evaluation for Village Development Based on GRA-TOPSIS Method," in Proceedings of the 6th International Conference on Environmental Science and Civil Engineering, Bristol, 455, 012194. doi:10.1088/1755-1315/455/1/012194

Simis, M., Awang, A., and Arifin, K. (2016). From Ex-Landfill to Public Park: Impact on Local Community's Quality of Life and Living Environment. *Procedia - Soc. Behav. Sci.* 222, 763–771. doi:10.1016/j.sbspro.2016.05.157

Song, M., and Xie, Q. (2021). Evaluation of Urban Competitiveness of the Huaihe River Eco-Economic Belt Based on Dynamic Factor Analysis. *Comput. Econ.* 58, 615–639. doi:10.1007/s10614-019-09952-5

Sørensen, J. F. L., and Sørensen, L. (2015). The Impact of Residential Environment Reputation on Residential Environment Choices. *J Hous Built Environ* 30, 403–425. doi:10.1007/s10901-014-9419-0

Tang, L., Ruth, M., He, Q., and Mirzaee, S. (2017). Comprehensive Evaluation of Trends in Human Settlements Quality Changes and Spatial Differentiation Characteristics of 35 Chinese Major Cities. *Habitat Int.* 70, 81–90. doi:10.1016/j.habitatint.2017.10.001

Taylor, P. J., and Derudder, B. (2021). NY-LON 2020: The Changing Relations between London and New York in Corporate Globalisation. *Trans Inst Br. Geog* 47, 257–270. doi:10.1111/tran.12498

Tian, S., Li, X., Li, H., Zhang, Y., and Bao, T. (2016). Initial Evaluation of Provincial-Level Environmental Risks from the Perspective of Human Settlements. *Sustainability* 8, 1259. doi:10.3390/su8121259

Wang, J., Du, D., and Huang, J. (2020). Inter-city Connections in China: High-Speed Train vs. Inter-city Coach. *J. Transp. Geogr.* 82, 102619. doi:10.1016/j.jtrangeo.2019.102619

Wang, L., and Shen, J. (2017). Comparative Analysis of Urban Competitiveness in the Yangtze River Delta and Pearl River Delta Regions of China, 2000-2010. *Appl. Spat. Anal.* 10, 401–419. doi:10.1007/s12061-016-9210-6

Webster, D., and Muller, L. (2000). "Urban Competitiveness Assessment in Developing Country Urban Regions: The Road Forward," in *Paper Prepared for Urban Group, INFUD*. Washington D.C: The World Bank), 47.

Westerink, J., Haase, D., Bauer, A., Ravetz, J., Jarrige, F., and Aalbers, C. B. E. M. (2013). Dealing with Sustainability Trade-Offs of the Compact City in Peri-Urban Planning across European City Regions. *Eur. Plan. Stud.* 21, 473–497. doi:10.1080/09654313.2012.722927

Wu, L. (2001). *Introduction to Sciences of Human Settlements*. Beijing: China Architecture and Building Press.

Xu, Y., Sun, J., Zhang, J., Xu, Y., Zhang, M., and Liao, X. (2012). Combining AHP with GIS in Synthetic Evaluation of Environmental Suitability for Living in China's 35 Major Cities. *Int. J. Geogr. Inf. Sci.* 26, 1603–1623. doi:10.1080/13658816.2011.642800

Yang, J., Wang, Y., Xiu, C., Xiao, X., Xia, J., and Jin, C. (2020). Optimizing Local Climate Zones to Mitigate Urban Heat Island Effect in Human Settlements. *J. Clean Prod.* 275, 123767. doi:10.1016/j.jclepro.2020.123767

Yang, Z., Gao, W., Zhao, X., Hao, C., and Xie, X. (2020). Spatiotemporal Patterns of Population Mobility and its Determinants in Chinese Cities Based on Travel Big Data. *Sustainability* 12, 4012. doi:10.3390/su12104012

Yao, Y., Pan, H., Cui, X., and Wang, Z. (2022). Do compact Cities Have Higher Efficiencies of Agglomeration Economies? A Dynamic Panel Model with Compactness Indicators. *Land Use Policy* 115, 106005. doi:10.1016/j.landusepol.2022.106005

You, H., Yang, J., Xue, B., Xiao, X., Xia, J., Jin, C., et al. (2021). Spatial Evolution of Population Change in Northeast China during 1992-2018. *Sci. Total Environ.* 776, 146023. doi:10.1016/j.scitotenv.2021.146023

Yu, S., Liu, Y., Cui, C., and Xia, B. (2019). Influence of Outdoor Living Environment on Elders' Quality of Life in Old Residential Communities. *Sustainability* 11, 6638. doi:10.3390/su11236638

Yuan, Z., Zheng, X., Zhang, L., and Zhao, G. (2017). Urban Competitiveness Measurement of Chinese Cities Based on a Structural Equation Model. *Sustainability* 9, 666. doi:10.3390/su9040666

Zachary, N. (2012). *The Connected City: How Networks Are Shaping the Modern Metropolis*. New York: Routledge.

Zhang, H., Geng, Z., Yin, R., and Zhang, W. (2020). Regional Differences and Convergence Tendency of Green Development Competitiveness in China. *J. Clean. Prod.* 254, 119922. doi:10.1016/j.jclepro.2019.119922

Zhang, X., and Corrie, B. P. (2018). "Urban Competitive Analysis," in *Investing in China and Chinese Investment Abroad* (Singapore: Springer Singapore), 115–125. doi:10.1007/978-981-10-7983-2_10

Zhang, Y., and Fan, Q. (2020). The Application of the Fuzzy Analytic Hierarchy Process in the Assessment and Improvement of the Human Settlement Environment. *Sustainability* 12, 1563. doi:10.3390/su12041563

Zhao, H., Che, H., Zhang, X., Ma, Y., Wang, Y., Wang, X., et al. (2013). Aerosol Optical Properties over Urban and Industrial Region of Northeast China by Using Ground-Based Sun-Photometer Measurement. *Atmos. Environ.* 75, 270–278. doi:10.1016/j.atmosenv.2013.04.048

Zhao, H., Gui, K., Ma, Y., Wang, Y., Wang, Y., Wang, H., et al. (2021). Climatological Variations in Aerosol Optical Depth and Aerosol Type Identification in Liaoning of Northeast China Based on MODIS Data from 2002 to 2019. *Sci. Total Environ.* 781, 146810. doi:10.1016/j.scitotenv.2021.146810

Zhao, Z., Lao, X., Gu, H., Yu, H., and Lei, P. (2021). How Does Air Pollution Affect Urban Settlement of the Floating Population in China? New Evidence from a Push-Pull Migration Analysis. *BMC Public Health* 21, 1696. doi:10.1186/s12889-021-11711-x

Conflict of Interest: The authors declare that the research was conducted in the absence of any commercial or financial relationships that could be construed as a potential conflict of interest.

Publisher's Note: All claims expressed in this article are solely those of the authors and do not necessarily represent those of their affiliated organizations, or those of the publisher, the editors and the reviewers. Any product that may be evaluated in this article, or claim that may be made by its manufacturer, is not guaranteed or endorsed by the publisher.

Copyright © 2022 Yu, Yang, Sun, Yu, Yao, Xiao and Xia. This is an open-access article distributed under the terms of the Creative Commons Attribution License (CC BY). The use, distribution or reproduction in other forums is permitted, provided the original author(s) and the copyright owner(s) are credited and that the original publication in this journal is cited, in accordance with accepted academic practice. No use, distribution or reproduction is permitted which does not comply with these terms.

frontiers | Frontiers in Ecology and Evolution

ORIGINAL RESEARCH
published: 03 June 2022
doi: 10.3389/fevo.2022.918446

Research on the Regional Environmental Impact and Risk Assessment Affected by Mineral Resource Development: A Case Study of the Taojia River Watershed in Hunan

Hongying Cao[1,2], Ziwei Wang[1,2,3], Xiaoyong Liao[1,2], You Li[1,2] and Yongbing Zhu[4]*

[1] Key Laboratory of Land Surface Pattern and Simulation, Institute of Geographic Sciences and Natural Resources Research, Chinese Academy of Sciences, Beijing, China, [2] Beijing Key Laboratory of Environmental Damage Assessment and Remediation, Beijing, China, [3] University of Chinese Academy of Sciences, Beijing, China, [4] State Key Laboratory of Nuclear, Biological and Chemical (NBC) Protection for Civilian, Beijing, China

OPEN ACCESS

Edited by:
Jun Yang,
Northeastern University, China

Reviewed by:
Dongxue Zhao,
The University of Queensland, Australia
Shaohua Wang,
Aerospace Information Research Institute (CAS), China

***Correspondence:**
You Li
liyou@igsnrr.ac.cn

Specialty section:
This article was submitted to Environmental Informatics and Remote Sensing, a section of the journal Frontiers in Ecology and Evolution

Received: *12 April 2022*
Accepted: *02 May 2022*
Published: *03 June 2022*

Citation:
Cao H, Wang Z, Liao X, Li Y and Zhu Y (2022) Research on the Regional Environmental Impact and Risk Assessment Affected by Mineral Resource Development: A Case Study of the Taojia River Watershed in Hunan. Front. Ecol. Evol. 10:918446. doi: 10.3389/fevo.2022.918446

The mining and production of mineral resources can directly lead to soil and water pollution, posing a serious threat to human health. In this study, the Taojia River basin, a tributary of the Xiangjiang River, was selected as the study area. Based on the concentrations of heavy metals (As, Cd, Pb, and Zn) in 653 soil/substrate samples collected from 342 points in the study area in 2013 and 2021, the changes in soil heavy metal concentrations in the region were systematically analyzed to assess their environmental risks and impacts on regional environmental quality. The results showed that from 2013 to 2021, the As, Pb, and Zn pollution in regional soil, tailing sand, and surface water was reduced, while the Cd pollution increased. The average soil As, Pb, and Zn concentrations decreased from 3,750, 2,340, and 1,180 mg/kg to 457, 373, and 387 mg/kg, respectively, while the Cd concentration increased from 0.11to 1.91 mg/kg; additionally, the overall distribution trend of heavy metal concentrations was high in the south, low in the north, and gradually decreased from upstream to downstream. The single evaluation index of heavy metal pollution risk showed that the percentages of medium to heavy pollution points in the soil As, Pb, and Zn were 84, 57, and 28%, respectively, in 2013, and this index decreased to 38, 37, and 25%, respectively, in 2021. The regional environmental quality was closely related to the intensity of mineral resource development. From 2000 to 2010, frequent mining development activities led to an increase in the area of construction land and a continuous decrease in the area of arable land, grassland, and vegetation cover in the region. During 2010–2020, the area of construction land decreased, and the vegetation coverage increased. The comprehensive evaluation index showed that the overall soil pollution risk in the watershed decreased, and the proportion of heavily polluted points decreased from 80

to 65%. It was shown by principal component analysis and factor analysis that mining development activities were the largest source of heavy metal pollution, in addition to mixed sources of tailings, solid waste, agriculture, and traffic emission sources. The results provide a scientific basis for the management and risk control of heavy metal pollution in the Taojia River basin.

Keywords: mineral resource development, heavy metals, environmental quality, risk assessment, source analysis

INTRODUCTION

Heavy metal pollution and its environmental risks from mineral resource development activities are widely considered a global issue (Hudson-Edwards, 2016). The National Soil Pollution Survey Report (2014) reported that approximately 33.4% of soil samples around metal mines had excessive heavy metal contents (Li et al., 2019). Heavy metal elements (e.g., Pb, Zn, As, Cd, Ni, and Cu) are often discharged into the surrounding environment with media such as dust, tailings, slag, and acidic wastewater generated from mining activities, and these elements are continuously transported and dispersed through paths such as wind erosion, precipitation, surface runoff, groundwater, and artificial foul irrigation, leading to the deterioration of regional soil environmental quality (Ayrault et al., 2014; Liu et al., 2018; Wang P. et al., 2019; Zhao et al., 2020; Zhu et al., 2021). Heavy metals can enter plants and animals through inhalation, dermal contact, and ingestion, and they can accumulate along the food chain, posing serious threats to local ecological safety and human health (Cai et al., 2019; Timofeev et al., 2019; Wang S. et al., 2019).

Hunan is known as the "home of non-ferrous metals in China" and has large-scale mineral deposits in the watershed; the region has had a history of mining, processing, and smelting for over 400 years (Jiang et al., 2017; Liu et al., 2018). For a long time, pollution incidents in the basin have been frequent due to the irrational industrial structure, the sloppy development model, and the lack of supervision and management. Some studies have pointed out that Hunan has one of the highest enrichment rates of Pb, Cd, Zn, and As in the topsoil, with an average As concentration as high as 51.87 mg/kg (Cheng et al., 2015; Zhang et al., 2018). In the face of the increasing spread of soil pollution and the problem of food security under the threat of excessive heavy metal levels, local governments have introduced a series of pollution prevention and control action plans, actively promoted the remediation of legacy waste pollution and other problems in the Xiangjiang River basin, and strengthened the treatment and remediation of contaminated soil.

The exploitation of mineral resources in China is large in scale and intensity, and the accompanying environmental pollution is serious. Therefore, it is of strategic guidance to systematically study the impact of mineral resource development on regional environmental quality and its environmental risks and to resolve the pollution sources for regional soil pollution prevention and control. Pathak et al. (2015) studied the sources and spatial and temporal variations in Al, Fe, Mn, Ti, Ca, and Mg in topsoil collected from an industrial town in Haryana, India, in different seasons of the same year. Huang et al. (2021) studied the pollution around the Xiangjiang River and identified As, Cd, Pb, Cr, and Mg as the main influencing factors affecting human health. Xu Y. et al. (2021) analyzed the sources of heavy metals in the topsoil of Su Xian District, Chenzhou city, identifying four main sources of contamination, namely, dry and wet atmospheric deposition, natural sources, waste from extraction, and mixed industrial sources. However, most of the existing studies have focused on the spatial distribution and source analysis of regional soils under a single time, and few scholars have explored the impact of mineral resource development on heavy metal concentrations, environmental impacts, and their environmental risks in the Xiangjiang River basin under a long-term sequence scale.

Therefore, this study selected the Taojia River basin, a tributary of the Xiangjiang River in Hunan Province, as the study area; field surveys, sample collection, and analysis were carried out in 2013 and 2021 to systematically study the changes in the concentrations of heavy metals in soil, sediment, and surface water in the region. Additionally, the environmental impact affected by mineral resource development was evaluated by analyzing the changes in land use types, vegetation cover, and population density in the region. To assess the environmental risk of heavy metal pollution in the region, the study was carried out over a large sampling period and enabled a follow-up investigation and an analysis of the changes in the soil environment in the mineral resource development area. This research scientifically determined the evolution, the current situation, and the risk of heavy metal pollution in the Taojia River basin, providing a reference for ensuring the safety of people's production and living in the basin. It also provided a scientific basis and theoretical support for the prevention and management of heavy metal pollution in the Xiangjiang River, affected by industrial and mining development.

MATERIALS AND METHODS

Overview of the Study Area

The Taojia River is a secondary tributary of the Xiangjiang River and a primary tributary of Chunling River, which is the source of both, originating in the Xianghualing and thirty-six bay areas. The basin is located in southwestern Chenzhou city, Hunan Province, between 25°26′–25°46′ N and 112°2′–112°34′ E, with a total area of 602 km^2 (**Figure 1**). The region has a large concentration of non-ferrous metal mines. The Taojia River basin belongs to the subtropical monsoon humid climate zone, with an average annual rainfall of 1,404 mm, an average annual sunshine time of 1705 h, an average annual humidity of 80%, and

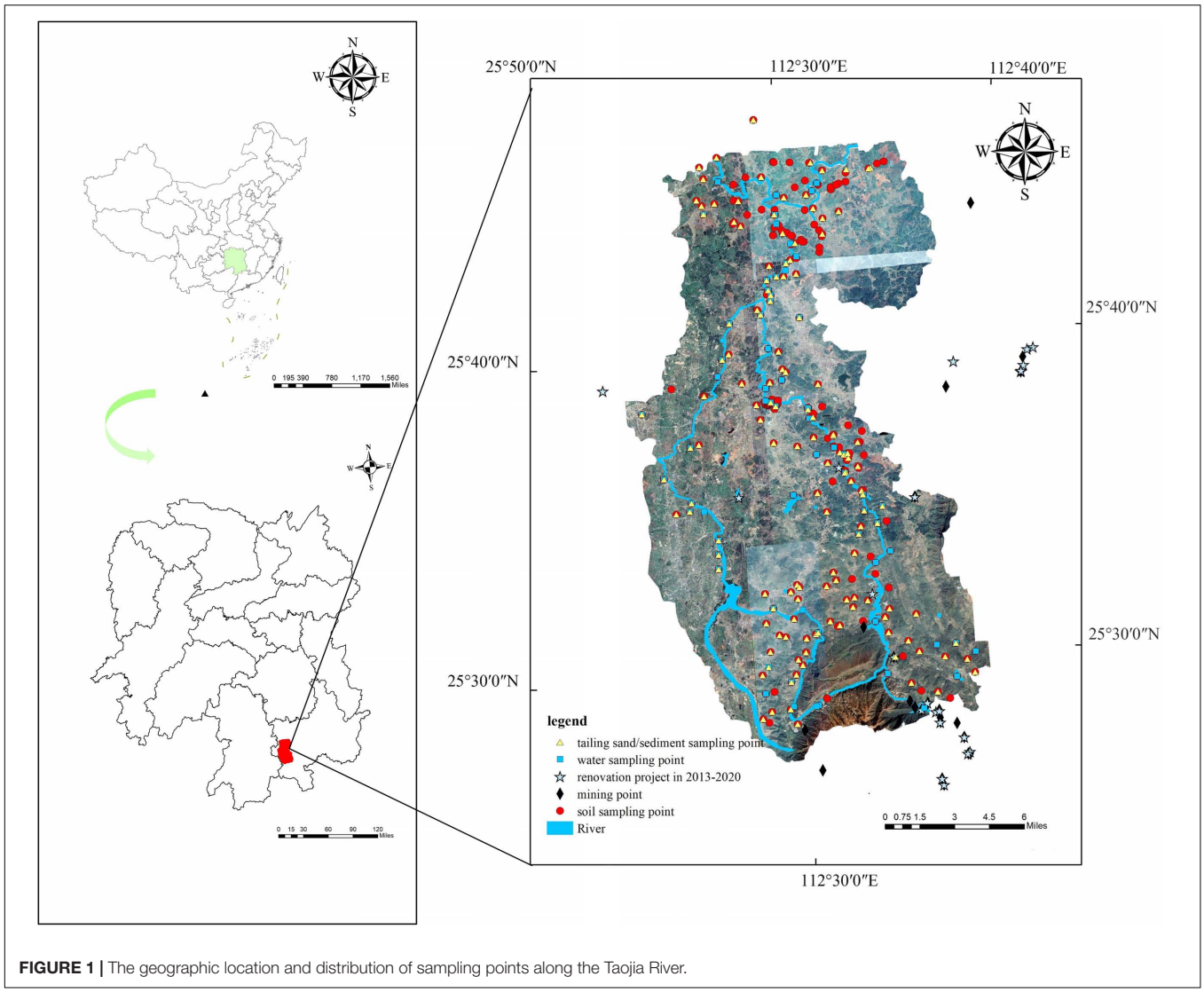

FIGURE 1 | The geographic location and distribution of sampling points along the Taojia River.

an average annual evaporation of 1,603 mm. The terrain of the basin is complex, mostly hilly, and a typical karst hilly landform.

Sample Collection and Analysis

Soil surface (0–30 cm) samples were collected from the study area, including tailings, sediments, farmland soil, and woodland soil (Boulet et al., 2020; Edori et al., 2021; Ekwere et al., 2021). Based on a 1 km × 1 km grid layout, points in the key areas and sensitive areas were encrypted, and points with an altitude greater than 1,000 m or a slope of more than 25° were discarded. In addition, obvious spots of pollution, rubbish heaps, and field ridges 100 m from main roads and railways were avoided. A total of 342 sampling points were arranged, with 643 soil supplies collected in 2013 and 2021 (in 2021, 41 sediment sample points located in the center of the river could not be sampled during the flood season). Depending on the field conditions, three sample squares (approximately 30–50 m apart) were selected near the sampling points to collect the soil mixture as the final sample to be tested.

The water samples were taken in a natural flow state without disturbing the water flow and bottom sediments, and 1,000 ml of water was taken from each sample site (2 × 500 ml water bottles). Before filling the water sample bottle, the bottle was washed three times with water from the location to prevent residue in the bottles from affecting assay results.

The collected soil samples were air-dried and demixed at room temperature, ground in a mortar, passed through a 100-mesh sieve, and stored in a refrigerator at 4°C in the dark until testing. Soil and water samples were digested by theHCl-HNO3-HF microwave airtight digestion method, and each sample was set up with 3 parallel samples. The total amount of As was determined by atomic fluorescence spectrometry (AFS), and the detection limit was 0.01 mg/kg. Inductively coupled plasma-mass spectrometry (ICP–MS) was used to determine the total amount of Cd, Pb, and Zn, and the detection limits were 0.01, 1.0, and

1.0 mg/kg, respectively. The calibration of the standard curve was carried out with heavy metal standard solutions to ensure that the measurement error of the instrument was less than 2%. The national standard soil sample GSS series was used for quality control to guarantee that the sample error range was less than 5%, and the standard addition recovery rate was more than 85%.

Evaluation Methods of Heavy Metal Pollution

The geo-accumulation index was used to evaluate the pollution characteristics of a single factor, and the Nemerow composite pollution index (NCP) method was used to assess the composite pollution in the basin (Hu et al., 2019). The limit selection was based on the "Soil Environmental Quality Agricultural Land Soil Pollution Risk Control Standard (GB15618-2018)," and the background value referred to the background value for soils in Hunan Province in "China Element Soil Background Value."

Data Collection and Analysis

To investigate the impact of mineral resource development on the regional ecological environment, in addition to analyzing and comparing the changes in the heavy metal concentrations of soil, sediment, and water samples, we screened indicators such as land use type, vegetation coverage, and population density for comparative analysis. The basic geographic data used in this study came from the China Resources and Environmental Science Data Center (CRESC), and data included administrative divisions, topography, road traffic, and land use data related to the Taojia River basin. The land use data were obtained from the ASTER GDEM 30 m resolution digital elevation model. The normalized difference vegetation index (NDVI) data came from the Fengyun Satellite Remote Sensing Data Service Network and LAADS WEB, and the data had a spatial resolution of 30 m × 30 m. Statistical values of population data were mainly from the county statistical yearbook and the statistical data provided by local departments. The data analysis and mapping software were OriginPro2020 and MATLAB 2014, and the remote sensing image processing and analysis software included ERDAS, ENVI5.0, and ArcGIS 10.4.

RESULTS AND DISCUSSION

Impact of Mineral Resource Development on Changes in Environmental Quality

Changes in Regional Soil Heavy Metal Concentrations

The regional soil heavy metal concentrations varied and are shown in **Figure 2**. The results showed that the mean concentrations of heavy metals in the soil all exceeded the soil environmental background values and environmental quality standards (except for Cd-2013), and there were significant differences within the 95% confidence interval. The mean values

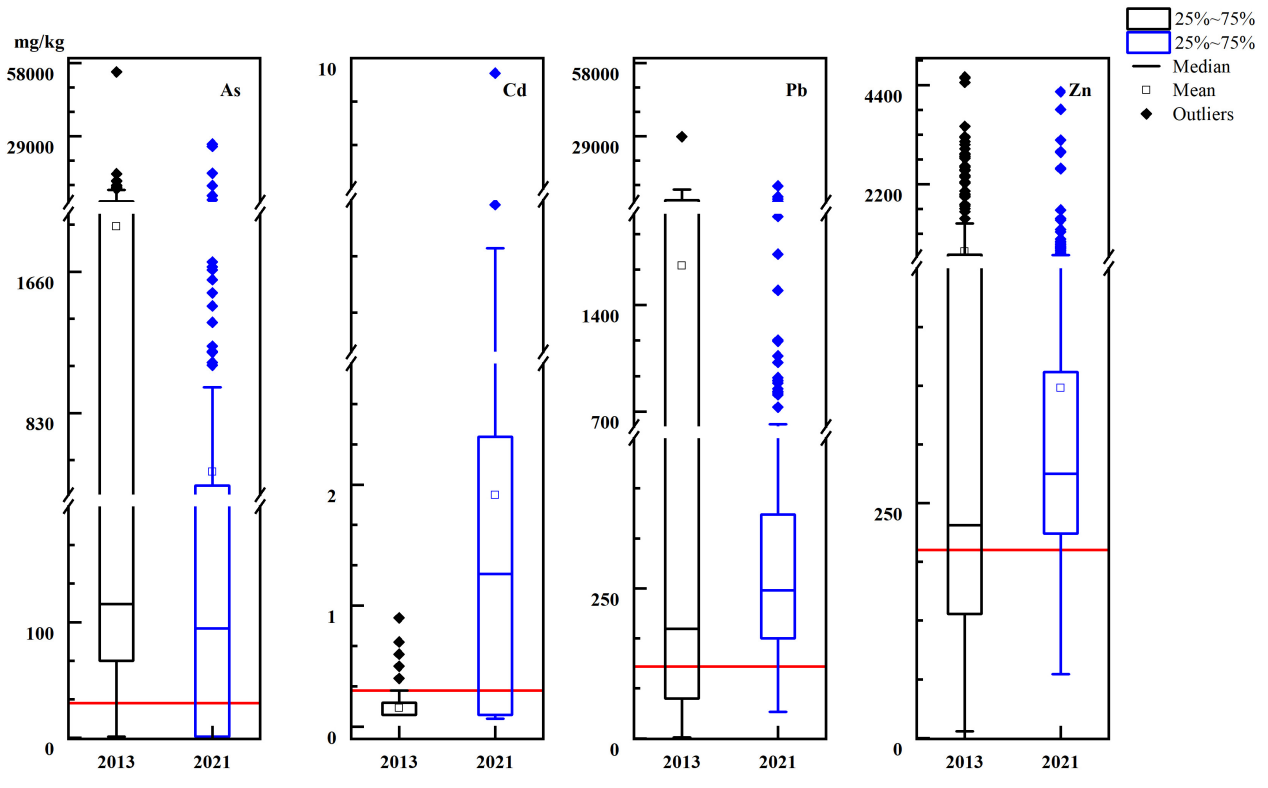

FIGURE 2 | Measured value of soil heavy metals in the study area.

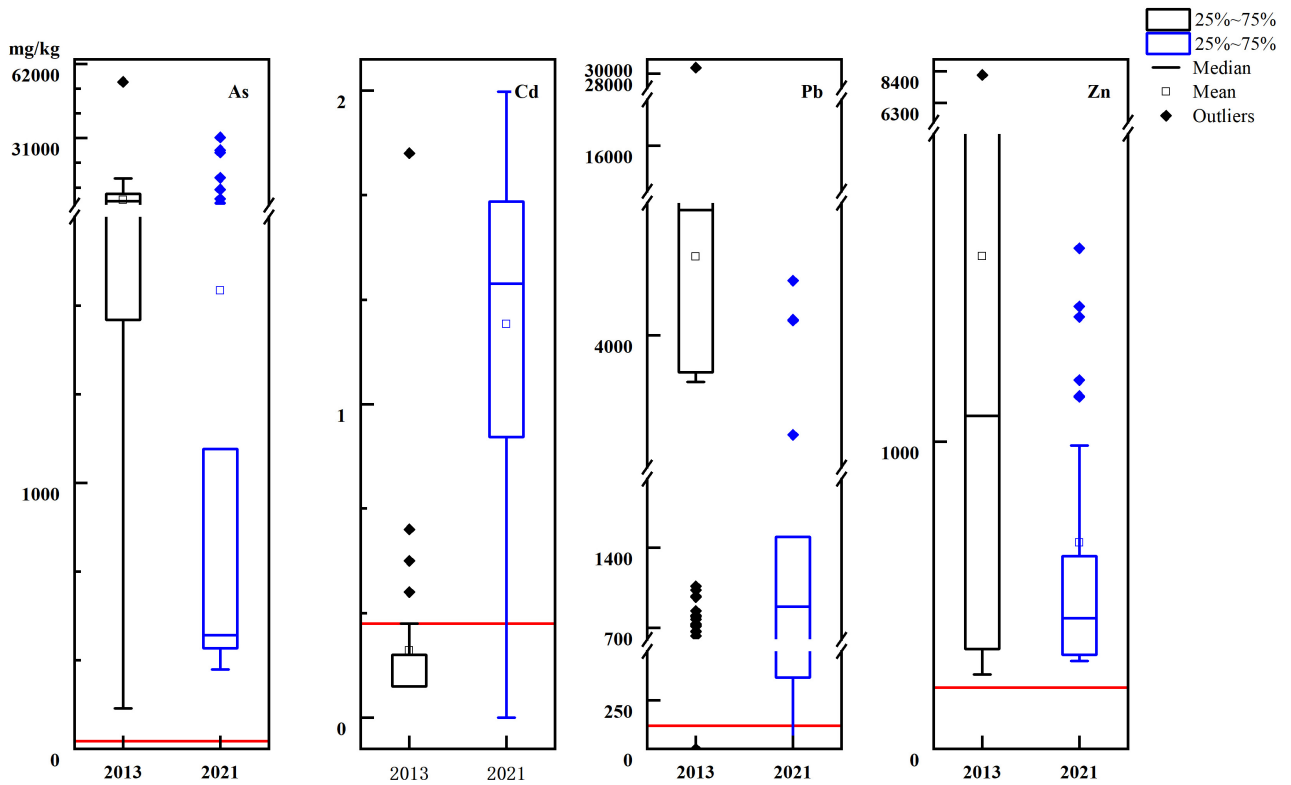

FIGURE 3 | Measured values of heavy metals in tailings sand in the study area.

of As, Pb, and Zn in the regional soil decreased from 3,750, 2,340, and 1,180 mg/kg to 457, 373, and 387 mg/kg, respectively, and the peak concentrations remained at high levels. Statistically, the exceedances of As, Pb, and Zn declined from 92, 85, and 68% to 73, 54, and 53%, respectively. It is worth noting that the average Cd concentration increased from 0.11to 1.91 mg/kg, and the exceedance rate increased significantly from 1.3 to 15%. In terms of the coefficient of variation of heavy metal contents, the coefficients of variation of As, Cd, Pb, and Zn in 2013 were 202.1, 162, 241.2, and 114.7%, respectively, while in 2021, the values were 196.9, 230.1, 176.6, and 145.2%, respectively, and the data showed extremely high variability, indicating that regional soil heavy metals have strong spatial heterogeneity.

In general, the improvement in regional soil heavy metal (As, Pb, and Zn) pollution between 2013 and 2021 was mainly attributed to a series of comprehensive heavy metal treatment projects and ecological restoration efforts carried out by the state and government within the Taojia River basin. The control engineering measures were mainly river dredging and lining, combined with measures to cover, isolate, and clean up river tailings; these efforts reduced ecological pollution and flooding hazards in the basin to a certain extent. The contents of heavy metals such as Pb and As in the watershed environment are mainly affected by the source input and are easily deposited in solid phases such as tailings and substrates during environmental transportation (Syed et al., 2017). This phenomenon was more pronounced in the regional environment affected by sulfidic mines. Therefore, the source control measures that have been implemented like dredging have been effective in mitigating regional As, Pb Zn, and other pollution. Unlike other heavy metals, the scope of Cd pollution in the region continued to expand, and the degree of pollution increased. This is because Cd mostly exists in the environment in a dissolved state. As a karst landform, the high Cd background value and acidic environmental conditions could further promote the migration, diffusion, and accumulation of Cd in the soils and water in the basin. This phenomenon was also confirmed in previous studies (Shao et al., 2016; Huang et al., 2018).

Variation in Heavy Metal Concentrations in River Sediment

As tailings/sediment in Class II are defined as general solid waste, referring to the Class III standard for surface water/groundwater, and the concentrations of As, Cd, Pb, and Zn all exceeded the limits. Based on the test results (**Figure 3**), the extreme values of As, Pb, and Zn in the tailings were significantly reduced from 54,500, 28,800, and 8,150 mg/kg, respectively, to 31,300, 4,410, and 3,420 mg/kg, respectively. The exceedance rates of As, Pb, and Zn in water decreased from 67, 65, and 48% to 44, 12, and 22%, respectively. The highest value of Cd in tailings was 1.8 mg/kg, and the exceedance rate of Cd in water increased from 65 to 86%. Concentrated tailings and other related projects, such as dredging, significantly reduced the levels of As, Pb, and Zn

contamination in tailings and sediments but did not affect the contamination of Cd (Migaszewski et al., 2022).

Changes in Heavy Metal Concentrations in the Waters of the Basin

Descriptive statistical analysis of heavy metal elements was conducted using 77 water samples collected in 2013 and 56 water samples collected in 2021 (**Figure 4**). In 2013, the concentrations of As, Cd, Pb, and Zn in the surface water of the basin were 1.87–1319, 0.03–84, 0.01–788, and 8.39–4,040 μg/L, respectively, with exceedance rates of 17, 10, 7.8, and 12%, respectively, indicating that the water of the basin was severely polluted. Among water samples from the Taojia River in 2021, the concentration ranges of As, Cd, Pb, and Zn were 0.16–105, 0.04–51.8, 0.06–49.57, and 0.15–220 μg/L, respectively. The concentrations of As, Cd, and Zn exceeded their standards, with exceedance rates of 7.12, 4.16, and 4.71%, respectively. Over time, the water contamination in the basin has improved, and the average concentrations of heavy metal elements have decreased significantly. In particular, none of the water body samples collected in 2021 exceeded the standard for Pb, and the highest reduction rate was observed for Zn, which reached 12.83%. The exceedance rates of Cd and As in the water bodies decreased by 7.29 and 0.68%, respectively.

Based on a comprehensive analysis of the sampling point concentrations and sampling locations, we found that the heavy metal pollution in the basin water was generally higher in the south and lower in the north, with a gradually decreasing distribution trend from upstream (Linwu) to midstream (Jiahe) to downstream (Guiyang). This phenomenon was mainly due to frequent mining activities that occur around the Thirty-Six Bay Mining Area in Linwu County, where the peak levels of As, Cd, Pb, and Zn were concentrated; these activities result in the severe pollution of surface waters, while the dilution effect of waters in the middle and downstream sections effectively reduced the concentrations of different heavy metals. In addition, there were obvious hot spots of heavy metal enrichment in the vicinity of industrial parks where industrial and mining industries are concentrated, with a few high-value areas scattered in the midstream section and the rest of the non-polluted areas. Moreover, the average pH value of the regional water body was 6.721, which was weakly acidic and accelerated the migration of metal elements to the middle and downstream sections.

Impact of Mineral Resource Development on the Regional Ecological Environment

Changes in Land Use Types

The changes in land use types in the region are shown in **Figure 5**, which indicates that the Taojia River basin is dominated by forestland, arable land, grassland, and construction land. The distribution of forestland in the basin was scattered and mainly included sparse woodland and shrub forest; arable land was scattered along the river, mainly in the mountainous areas located in the center and south, and grassland was mainly distributed in the mountainous areas where mining activities are prosperous

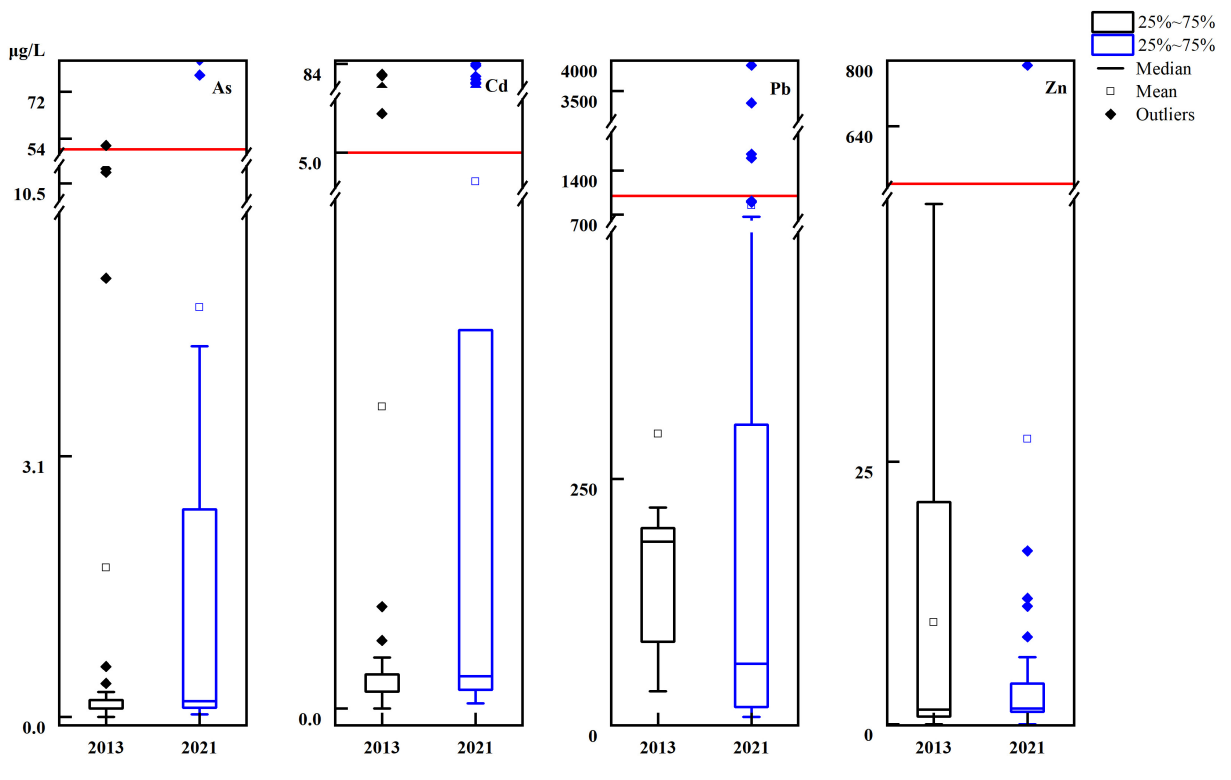

FIGURE 4 | Measured value of heavy metals in water in the study area.

in the department and the southern part. Apart from the Taojia River, there are few water sources in the region, including several small reservoirs. The area of industrial and mining land in the Taojia River basin increased rapidly in the first decade. The areas of industrial and mining, grassland, and other construction land far exceeded the areas of cultivated land and forestland in 2010. Among them, the area of industrial and mining land was 104.2 km^2, which was twice the area of arable land, and the construction land was scattered in the region.

The land use transfer matrices for the two periods 2000–2010 and 2010–2021 were calculated based on the land use data of the two phases, and the changes in the types and areas of land use transferred out/in for the two periods were counted separately, as shown in **Table 1**. During the period 2000–2021, the area of arable land continued to decrease, and the area of forestland continued to increase. According to calculations, compared to 2000, the area of cultivated land declined by more than 40% in the past 20 years. In the first decade, the area of construction land increased significantly, and the grassland area decreased, while the opposite trend was observed between 2010 and 2021. The areas of residential land and water area in the region were relatively stable, with small changes. Changes in land use types were closely related to factors such as topography, mineral resource development, and national policies. The continuous decrease in the area of arable land in the region was mainly attributed to frequent mining activities and the flooding of tailings. In addition, the study area is mostly mountainous and hilly, with scattered cultivated land, combined with a low level of mechanization and a low recultivation rate after abandonment. After 2010, the national government formulated a series of targeted environmental protection management efforts and implemented a regional environmental pollution comprehensive remediation action plan, and some of the waste gas mine sites were restored to grassland through comprehensive treatments.

Changes in Vegetation Coverage

Vegetation coverage is an essential indicator for measuring the ecological environment of a watershed. As a component of the ecological environment, vegetation can both directly characterize environmental change processes and interact with other drivers of the natural environment, such as hydrological conditions, soil conditions, and the climatic background. Therefore, the temporal and spatial changes in the correlation index with vegetation are clear indicators of environmental change in the study area. To

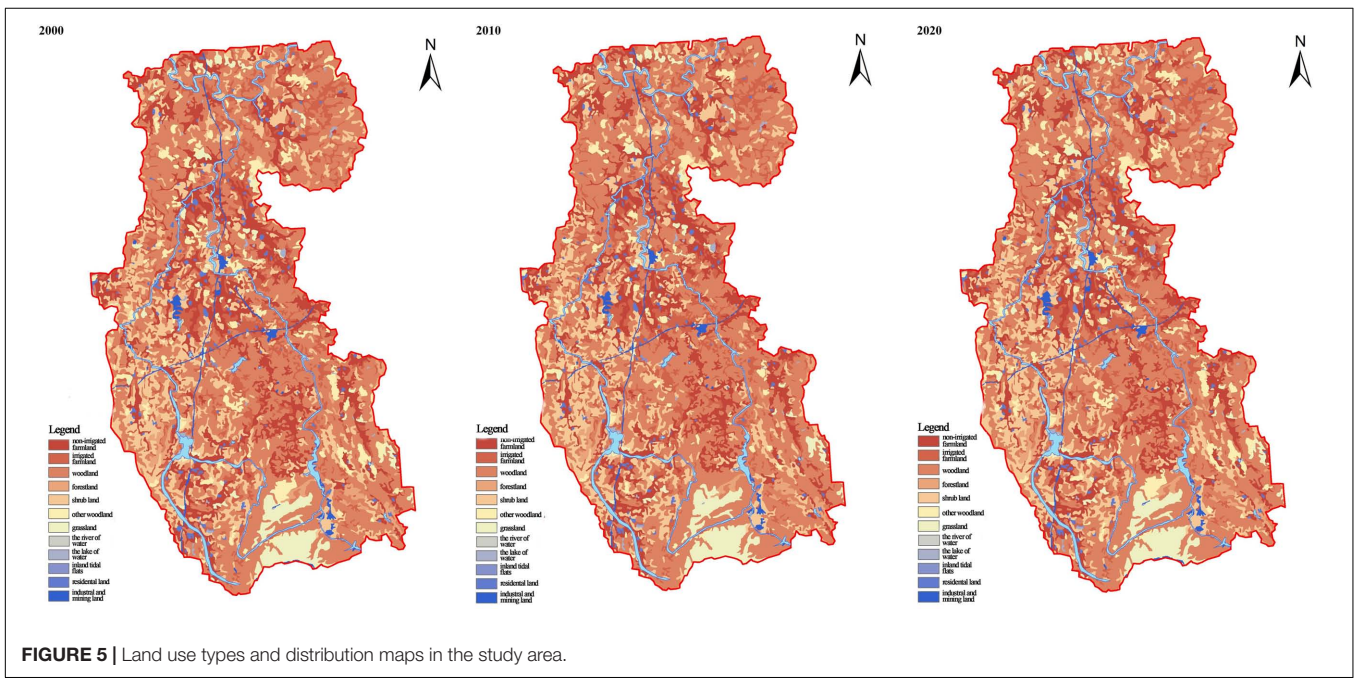

FIGURE 5 | Land use types and distribution maps in the study area.

TABLE 1 | The dynamic changes in land use in the study area.

	2000–2010		2010–2021	
	Area (km^2)	Proportion (%)	Area (km^2)	Proportion (%)
Farmland	−13.231	−34.60	−7.847	−23.325
Woodland	16.182	12.67	9.34	4.30
Grassland	−13.582	−18.45	2.353	1.22
Residential land	0.283	0.41	0.562	0.49
Industrial and mining land	12.391	7.69	−4.742	−2.33
River	0.445	0.52	−2.524	−3.45

further explore the spatial distribution of the vegetation coverage NDVI in the study area, the average annual NDVI values from 2001 to 2010 and 2010 to 2021 were calculated to reflect the vegetation growth in the basin. We classified the vegetation cover into the following five classes: 0–0.1 very low cover, 0.1–0.3 low cover, 0.3–0.5 medium cover, 0.5–0.7 medium-high cover, and >0.7 high cover, and the results are shown in **Figure 6**.

The NDVI distribution of vegetation coverage in the area varied greatly, mainly showing an increasing trend from north to the southeast (**Figure 6**). The highest NDVI value appeared at the border between Xiang Hua town and Guiyang County, where the main vegetation type was artificially reverted to subtropical deciduous forest, while the lowest value was found in Puman Township of Jiahe County. From 2000 to 2010, the average value of the NDVI was 0.375, and from 2010 to 2021, the average value of the NDVI was 0.483. In general, the area with low NDVI values decreased, and the area with high NDVI values increased, which indicated that the vegetation cover has been improving in the region. The proportion of low cover (0.1–0.3) showed a decreasing trend, with the proportion of very low cover (0–0.1) decreasing from 3.4% in 2000 to 0.2% in 2021. In the southern part of the study area, the vegetation cover in

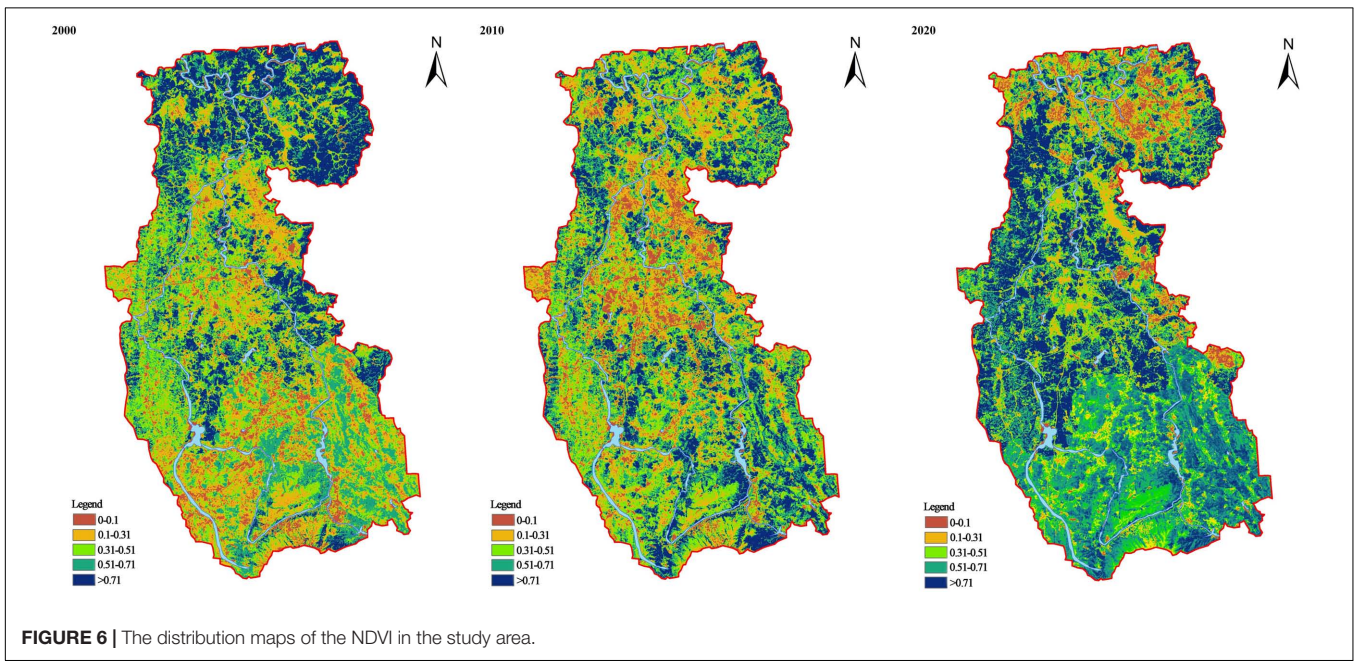

FIGURE 6 | The distribution maps of the NDVI in the study area.

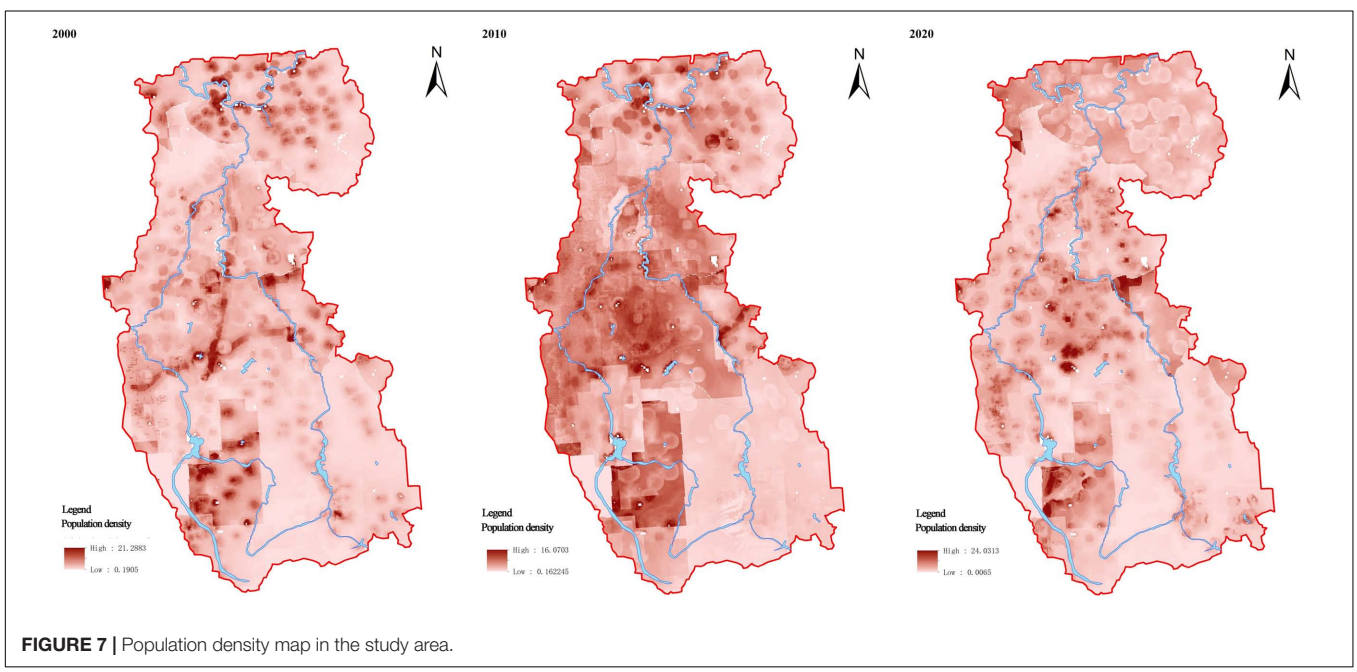

FIGURE 7 | Population density map in the study area.

Linwu County improved most significantly, with the proportion of medium or above cover increasing from 30.4 to 60.7%, indicating a significant improvement in vegetation cover in the area, which has had a significant positive effect on the ecological environment of the watershed. The north-eastern part of the study area has an agglomeration of non-ferrous polymetallic mines, and the vegetation coverage declined sharply from 2000 to 2010, while the average vegetation coverage in Guiyang County declined from 0.417 to 0.223. From 2010 to 2021, the vegetation coverage improved due to relevant policy controls and changes in land use types.

Changes in Population Density

The population density was calculated with 1 km × 1 km as the unit area, and inverse distance weighting was used for interpolation. Combined with the population density raster data map identified from the light data, a population density map was drawn (**Figure 7**). As seen from the figure, the population is mostly concentrated in the central and southern areas of the study area, where the elevation is lower and flatter. In addition, there are concentration hot spots around the sites where large deposits are mined and around hydroelectric power stations. This result is because the study area is mostly hilly and mountainous, with a low level of urbanization and a discrete distribution of administrative villages, and there are clusters of hot spots along rivers and in industrial and mining activities. Although the Xianghualing area of the Thirty-Six Bays has many mining industries, most are located in mountainous areas and have a relatively small population. In particular, the change in administrative planning of the townships in Jiahe County in 2009 and 2015 significantly affected the population density distribution in the central part of the study area.

TABLE 2 | Geo-accumulation index of heavy metals.

Geo-accumulation index	2013				2021			
	As	Cd	Pb	Zn	As	Cd	Pb	Zn
Maximum	11.34	2.58	9.47	5.25	10.27	7.67	7.84	5.15
Minimum	−1.83	−0.58	−4.57	−4.06	−4.39	−1.14	0.50	−0.64
Mean	3.99	−0.19	3.07	1.46	2.23	0.87	2.81	1.29

Evaluation of the Risk of Integrated Heavy Metal Contamination of Soil in the Taojia River Basin

The geo-accumulation index method was used to calculate the single-factor pollution indices of As, Cd, Pb, and Zn (**Table 2**), and the classification of pollution levels and their proportions (**Figure 8**). The results showed that the average values of the As, Pb, and Zn pollution indices in 2021 were lower than those in 2013, the point exceedance rate gradually decreased from upstream to downstream, and the proportion of uncontaminated to moderately contaminated ($igeo \leq 1$) increased significantly, indicating that the regional As, Pb, and Zn contamination risks had a decreasing trend. The rate of As exceedance of the standard

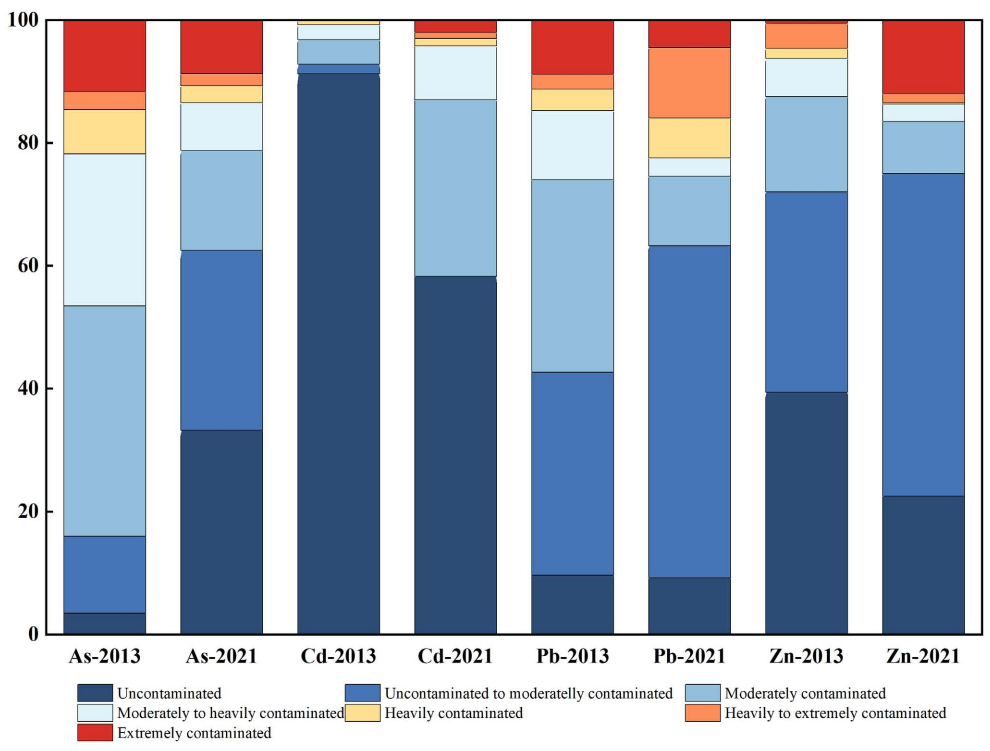

FIGURE 8 | Comparison of pollution results of the cumulative index in the study area.

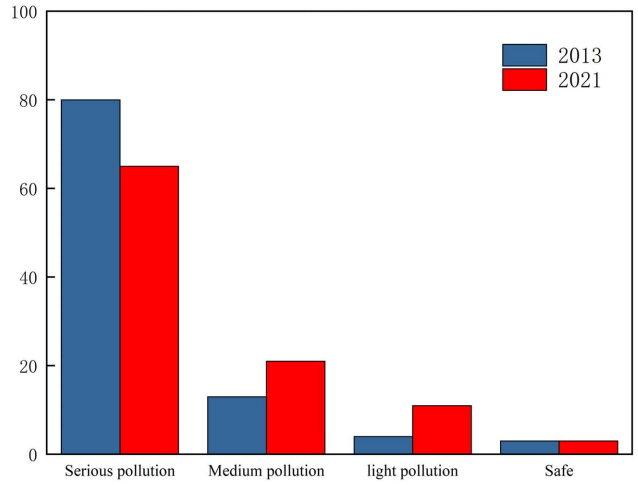

FIGURE 9 | Comparison of the pollution load index results in the study area.

rate declined significantly, from 97 to 67%. In 2013, the pollution of As (*igeo* > 1) accounted for 84.04%, and this indicator declined to 37.5% by 2021. At this stage, pollution was mainly mild to moderate (78.75%). The regional Pb exceedance rate was always approximately 90%, the proportion of extremely heavy pollution decreased, and the proportion of mild to moderate pollution increased by 21.02%. The exceedance rate of Zn increased slightly over time, and the proportions of uncontaminated to moderately contaminated ($0 < igeo \leq 1$) and extremely contaminated (*igeo* > 5) increased by 19.89 and 11.46%, respectively. It is worth noting that the Cd exceedance rate increased from 8.78% in 2013 to 41.75% in 2021, and the proportion of contamination (*igeo* > 0) increased significantly.

The Nemerow pollution integrated index method was used to calculate the regional pollution levels under the combined effect of multiple heavy metals. **Figure 9** shows the distribution of the integrated pollution index evaluation results, and specifically, the average value of the integrated pollution index in 2013 was 6.78 (0.46∼34.62), with safe points accounting for 4 and 13%, mainly distributed in the central and western parts of the study area. The proportion of serious pollution was as high as 80%, mainly distributed in the north-eastern part of the study area and the southern part of Xianghualing town, Thirty-Six Bay area. The average value of the composite index in 2021 was 4.53 (0.12∼41.66), the ranking of the safety rating remained unchanged, and the pattern of risk distribution was basically the same. The proportion of light pollution was 11 and 16%, and the proportion of serious pollution declined to 65%. Overall, the pollution level of the Taojia River basin improved overall, but it is still necessary to strengthen control and management.

Regional Pollution Source Identification and Analysis

The study area is located in the southern part of Hunan Province, where the background soil content is much higher than other local levels (Zhang et al., 2019; Zhao et al., 2020; Zhong et al., 2020), and the endogenous parent material and natural soil formation processes in karst limestone areas are one of the essential sources of regional heavy metal pollution (Zhang and Wang, 2020; Xu D. M. et al., 2021; Zhu et al., 2021). However, the heavy metal concentration data collected in this study were much higher than the soil background value, indicating that the input of human activities is the main cause of regional heavy metal pollution.

The first three principal components were extracted according to the principle that the eigenvalues of the matrix $\lambda > 1$, and they accounted for 95.1% of the total variance (**Figure 10**). The patterns of the factor loading values of heavy metal elements in 2013 and 2021 were similar, indicating that the year-to-year variation in each heavy metal element pollution source was small (**Figure 11**). The Exner function values for all factors were less than 0.1, and the cumulative contribution CV values were greater

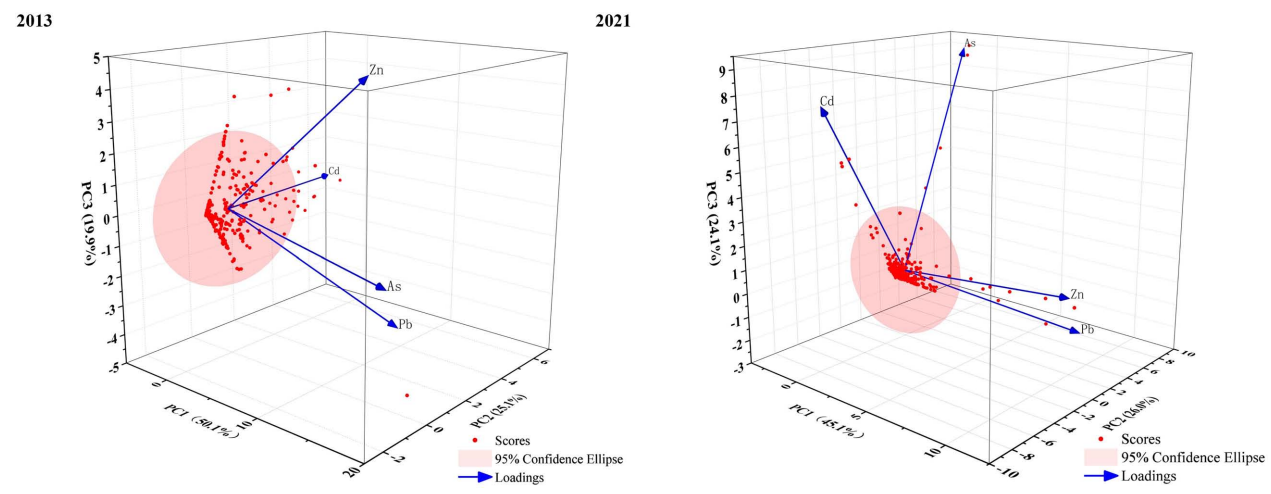

FIGURE 10 | Analysis results of PCA in the study area.

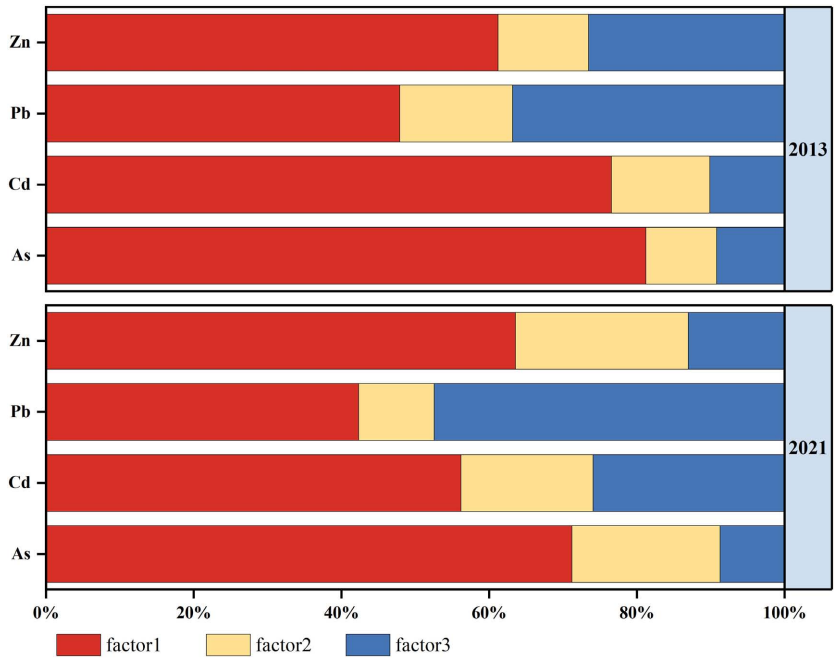

FIGURE 11 | Analysis results of FA-NNC in the study area.

than 95% for the three principal factors selected, indicating a strong correlation between the factors.

The first principal component (PC1) had a large factor loading value for Pb and Zn in 2013 and contributed a high proportion of pollution to As, Cd, Pb, and Zn, which had values of 71.21–81.21, 56.19–76.58, 42.33–47.88, and 61.02–63.54%, respectively. Based on the comprehensive judgment of factors such as the high pollution value and the location of sampling points, PC1 represented the input source of regional mining development activities and was the most important source of regional heavy metal pollution. Some studies have pointed out that the mining and smelting of non-ferrous metals accounts for approximately 40–73% of the anthropogenic emissions of heavy metals (such as Cd) in southwestern China (Wang and Zhao, 2017; Xiao et al., 2019; Wu et al., 2020). This result is generally consistent with the conclusion obtained in this study. In addition, the Taojia River basin in the study area is a karst landform with many caves, and the oxidation of sulfide minerals in mine tailings forms acidic mine wastewater, which promotes the migration and diffusion of metal elements in the environment and seriously endangers the regional environmental quality (Saby et al., 2009; Wang and Zhao, 2017; Salim et al., 2019).

The second principal component (PC2) had larger loading values for Pb and As in 2021, contributing, on average, 14.83, 15.60, 12.74, and 17.82% to the As, Cd, Pb, and Zn pollution, respectively. The sources of Zn and Pb in the environment had strong homology, mostly caused by wastewater, waste gas, and waste residue discharged from the non-ferrous metal smelting processes (Richard and Oliver, 2007; Xu D. M. et al., 2021). The mining and smelting of Pb-Zn-Tn-Cu polymetallic-associated ore in the Taojia River basin is an important source of Cd and As composite pollution. Elements are generally not precipitated as a concentrate product but are mostly found in tailings and other solid waste. Heavy metals in tailings are often diffused into the surrounding environment through wind and hydraulic transport in the form of wind erosion, dust, surface runoff, rainfall impact, and tailings diffusion (Qiu et al., 2016; Rafique and Tariq, 2016). This study found that regional soils and farmlands often experience mine tailing sand flooding during the flood season, and local residents mostly use water from nearby rivers to irrigate their farmlands. Therefore, pesticide and fertilizer inputs and sewage irrigation are additional main causes of heavy metal pollution in irrigated lands (Hu et al., 2020; Hossain Bhuiyan et al., 2021; Xu Y. et al., 2021). In a comprehensive analysis, the PC2 was categorized as a mixed input source of tailings sand, solid waste, and agriculture.

The third principal component (PC3) had the highest loading factor for Cd. The results of the FA-NNC two-period data model analysis showed that in 2013, the contributions of this factor to Pb and Zn were 36.85 and 26.44%, respectively. In 2021, the contributions of this factor to Cd and Pb were 25.92 and 47.46%, respectively. Cd and Zn are congeners, and in nature, Cd often cooccurs with Zn and Pb, and Cd and Zn are highly mobile. Dust from the friction of Zn containing petrochemical materials and exhaust fumes from the combustion of Pb rich gasoline are often interpreted as one of the main sources of Zn and Pb (Gan et al., 2019; Guan et al., 2019; Guo et al., 2019). Industrial waste gases and vehicle exhaust can pollute the surrounding environment through diffusion by atmospheric dry and wet deposition processes (Fei et al., 2019; Feng et al., 2019; Xu Y. et al., 2021). Therefore, the PC3 was identified as the input source of transportation emissions.

CONCLUSION

Based on the results of sampling and data research across long time scales, the tracking of pollution changes indicates that, in the last 10 years, the concentrations and pollution exceedance rate of As, Pb, and Zn in soil, tailings/substrate, and surface water all declined significantly, but the concentration of Cd increased and the pollution range expanded. While the spatial distribution of pollution maintains the same trend. The heavily polluted sites mainly gathered in the north-eastern part and the southern Thirty-Six Bay were active with industrial and mining activities.

The intensity of mineral resource development has impacted the regional environmental quality. In the first decade of this century, frequent mining development activities led to an increase in the area of construction land and a continuous decrease in the areas of cultivated land, grassland, and vegetation cover. Due to the implementation of environmental protection policies and industrial upgrading, the area of construction land declined, vegetation coverage increased, and the quality of the regional ecological environment improved significantly from 2010 to 2020.

The risk assessment results showed that the regional environmental risk levels of As, Pb, and Zn decreased, and the proportion of moderate and above pollution declined. The input sources of mining development activities; mixed sources of tailings sand, solid waste, and agriculture; and traffic emission sources were the main pollution sources of heavy metals. Among them, industrial and mining activities still remained the largest source of regional heavy metal pollution inputs. In general, the local historical pollution problems cannot be fully and effectively solved in a short period of time, and it is still necessary to strengthen source management and risk control.

DATA AVAILABILITY STATEMENT

The datasets presented in this study can be found in online repositories. The names of the repository/repositories and accession number(s) can be found in the article/supplementary material.

AUTHOR CONTRIBUTIONS

HC and XL: conceptualization. YL: methodology and formal analysis. ZW: software and validation. YZ: formal analysis. All authors agreed to be accountable for the content of the work, contributed to the article, and approved the submitted version.

FUNDING

This research was supported by the Major Project of the National Natural Science Foundation of China (71991483) and the Fund Program of State Key Laboratory of NBC Protection for Civilian (sklnbc2018-17).

REFERENCES

Ayrault, S., Pape, P. Le, Evrard, O., Priadi, C. R., Quantin, C., Bonte, P., et al. (2014). "Remanence of Lead Pollution in an Urban River System: a Multi-Scale Temporal and Spatial Study in the Seine River Basin, France.". *Environ. Sci. Pollut. Res.* 21, 4134–4148. doi: 10.1007/s11356-013-2240-6

Boulet, A. K., Veiga, A., Ferreira, C., and Ferreira, A. (2020). "Quantification of heavy metals in agricultural soils: the influence of sieving in standard analytical methods (No. EGU2020-1487)," in *Proceedings of the Copernicus Meetings, EGU General Assembly 2020, Online, 4–8 May 2020*. doi: 10.5194/egusphere-egu2020-1487

Cai, L. M., Wang, Q. S., Luo, J., Chen, L. G., Zhu, R. L., Wang, S., et al. (2019). Heavy Metal Contamination and Health Risk Assessment for Children near a Large Cu-Smelter in Central China. *Sci. Total Environ.* 650, 725–733. doi: 10.1016/j.scitotenv.2018.09.081

Cheng, J., Han, J. C., Wang, H. Y., and Tong, W. (2015). "Background of Land Development and Opportunity of Land Use Transition.". *Asian J. Agric. Res.* 7, 45–48.

Edori, E. S., Iyama, W. A., and Edori, O. S. (2021). Application of pollution assessment models in soil contaminated by heavy metals in two steel rods markets, Port Harcourt, Rivers State, Nigeria. *GSC Adv. Res. Rev.* 9, 025–035.

Ekwere, A. S., Kudamnya, E. A., and Osung, W. E. (2021). Assessment of potentially toxic metals and their mineral species in soils of arable farmlands in the southeastern Niger Delta basin, Nigeria. *Soil Environ.* 40, 119–126.

Fei, X. F., Xiao, R., Christakos, G., Langousis, A., Ren, Z. Q., Tian, Y., et al. (2019). "Comprehensive Assessment and Source Apportionment of Heavy Metals in Shanghai Agricultural Soils with Different Fertility Levels.". *Ecol. Indic.* 106, 105508–105517.

Feng, W., Guo, Z., Xiao, X., Peng, C., Shi, L., Ran, H., et al. (2019). "Atmospheric Deposition as a Source of Cadmium and Lead to Soil-Rice System and Associated Risk Assessment.". *Ecotoxicol. Environ. Saf.* 180, 160–167. doi: 10.1016/j.ecoenv.2019.04.090

Gan, Y. D., Huang, X. M., Li, S. S., Liu, N., Li, Y. C., Freidenreich, A., et al. (2019). "Source Quantification and Potential Risk of Mercury, Cadmium, Arsenic, Lead, and Chromium in Farmland Soils of Yellow River Delta.". *J. Clean. Prod.* 221, 98–107.

Guan, Q. Y., Zhao, R., Pan, N. H., Wang, F. F., Yang, Y. Y., and Luo, H. P. (2019). "Source Apportionment of Heavy Metals in Farmland Soil of Wuwei, China: comparison of Three Receptor Models.". *J. Clean. Prod.* 237, 117792–117802.

Guo, G., Zhang, D., and Wang, Y. (2019). "Probabilistic Human Health Risk Assessment of Heavy Metal Intake Via Vegetable Consumption around Pb/Zn Smelters in Southwest China.". *Int. J. Environ. Res. Public Health* 16, 3267–3284. doi: 10.3390/ijerph16183267

Hossain Bhuiyan, M. A., Chandra Karmaker, S., Bodrud-Doza, M., Rakib, M. A., and B. B. Saha. (2021). Enrichment, sources and ecological risk mapping of heavy metals in agricultural soils of dhaka district employing SOM, PMF and GIS methods. *Chemosphere* 263, 128339–128353. doi: 10.1016/j.chemosphere.2020.128339

Hu, B., Shao, S., Fu, Z., Li, Y., Ni, H., Chen, S., et al. (2019). "Identifying Heavy Metal Pollution Hot Spots in Soil-Rice Systems: a Case Study in South of Yangtze River Delta, China.". *Sci. Total Environ.* 658, 614–625. doi: 10.1016/j.scitotenv.2018.12.150

Hu, B., Zhou, Y., Jiang, Y., Ji, W., Fu, Z., Shao, S., et al. (2020). "Spatio-Temporal Variation and Source Changes of Potentially Toxic Elements in Soil on a Typical Plain of the Yangtze River Delta, China (2002-2012).". *J. Environ. Manage.* 271, 110943–110958. doi: 10.1016/j.jenvman.2020.110943

Huang, J., Guo, S., Zeng, G. M., Li, F., Gu, Y., Shi, Y., et al. (2018). "A New Exploration of Health Risk Assessment Quantification from Sources of Soil Heavy Metals under Different Land Use.". *Environ. Pollut.* 243, 49–58. doi: 10.1016/j.envpol.2018.08.038

Huang, Z. F., Zheng, S. S., Liu, Y., Zhao, X. R., Qiao, X. C., Liu, C. Y., et al. (2021). "Distribution, Toxicity Load, and Risk Assessment of Dissolved Metal in Surface

and Overlying Water at the Xiangjiang River in Southern China.". *Sci. Rep.* 11:109. doi: 10.1038/s41598-020-80403-0

Hudson-Edwards, K. (2016). Tackling Mine Wastes. *Science* 352, 288–290. doi: 10.1126/science.aaf3354

Jiang, Y., Xuefeng, H. U., Shu, Y., Jiang, Y., and Teng, Q. (2017). "Accumulation of Heavy Metals in the Soil-Rice System and Assessment of Dietary Safety of the Rice Produced in the Paddy Fields—a Case Study of a Town in the Northern Part of Hunan Province,China.". *Acta Pedol. Sin.* 54, 410–420.

Li, T. K., Liu, Y., Lin, S. J., Liu, Y. Z., and Xie, Y. F. (2019). "Soil Pollution Management in China: a Brief Introduction.". *Sustainability* 11, 556–571. doi: 10.13227/j.hjkx.201612068

Liu, F. Z., Hu, J. L., Liu, J. S., Zhao, Z. Q., Yang, X., Zhang, Y., et al. (2018). "Spatial Distribution and Risk Assessment of Heavy Metals in Soil in the Metal Mining Area of Paojinshan, Hunan, China.". *J. Agro-Environ. Sci.* 37, 86–95.

Migaszewski, Z. M., Galuszka, A., Dolegowska, S., and Michalik, A. (2022). "Abundance and Fate of Glass Microspheres in River Sediments and Roadside Soils: lessons from the Swietokrzyskie Region Case Study (South-Central Poland).". *Sci. Total Environ.* 821, 153410–153421. doi: 10.1016/j.scitotenv.2022.153410

Pathak, A. K., Kumar, R., Kumar, P., and Yadav, S. (2015). "Sources Apportionment and Spatio-Temporal Changes in Metal Pollution in Surface and Sub-Surface Soils of a Mixed Type Industrial Area in India.". *J. Geochem. Explor.* 159, 169–177.

Qiu, K. Y., Xing, W. Q., Scheckel, Kirk G., Cheng, Y. X., Zhao, Z. S., Ruan, X. L., et al. (2016). "Temporal and Seasonal Variations of as, Cd and Pb Atmospheric Deposition Flux in the Vicinity of Lead Smelters in Jiyuan, China.". *Atmos. Pollut. Res.* 7, 170–179.

Rafique, N., and Tariq, S. R. (2016). "Distribution and Source Apportionment Studies of Heavy Metals in Soil of Cotton/Wheat Fields.". *Environ. Monit. Assess.* 188, 309–319. doi: 10.1007/s10661-016-5309-0

Richard, W, and Oliver, M. A. (2007). *Geostatistics for Environmental Scientists*. Hoboken: John Wiley & Sons.

Saby, N. P., Thioulouse, J., Jolivet, C. C., Ratie, C., Boulonne, L., Bispo, A., et al. (2009). "Multivariate Analysis of the Spatial Patterns of 8 Trace Elements Using the French Soil Monitoring Network Data.". *Sci. Total Environ.* 407, 5644–5652. doi: 10.1016/j.scitotenv.2009.07.002

Salim, I., Sajjad, R. U., Paule-Mercado, M. C., Memon, S. A., Lee, B. Y., Sukhbaatar, C., et al. (2019). "Comparison of Two Receptor Models Pca-Mlr and Pmf for Source Identification and Apportionment of Pollution Carried by Runoff from Catchment and Sub-Watershed Areas with Mixed Land Cover in South Korea.". *Sci. Total Environ.* 663, 764–775. doi: 10.1016/j.scitotenv.2019.01.377

Shao, D., Zhan, Y., Zhou, W., and Zhu, L. (2016). "Current Status and Temporal Trend of Heavy Metals in Farmland Soil of the Yangtze River Delta Region: field Survey and Meta-Analysis.". *Environ. Pollut.* 219, 329–336. doi: 10.1016/j.envpol.2016.10.023

Syed, J. H., Iqbal, M., Zhong, G., Katsoyiannis, A., Yadav, I. C., Li, J., et al. (2017). "Polycyclic Aromatic Hydrocarbons (Pahs) in Chinese Forest Soils: profile Composition, Spatial Variations and Source Apportionment.". *Sci. Rep.* 7, 2692–2702. doi: 10.1038/s41598-017-02999-0

The National Soil Pollution Survey Report (2014). *The Report on the National General Survey of Soil Contamination*. Beijing: Ministry of Environmental Protection & Ministry of Land and Resources.

Timofeev, I., Kosheleva, N., and Kasimov, N. (2019). "Health Risk Assessment Based on the Contents of Potentially Toxic Elements in Urban Soils of Darkhan, Mongolia.". *J. Environ. Manage.* 242, 279–289. doi: 10.1016/j.jenvman.2019.04.090

Wang, J., and Zhao, T. (2017). "Regional Energy-Environmental Performance and Investment Strategy for China's Non-Ferrous Metals Industry: a Non-Radial Dea Based Analysis.". *J. Clean. Prod.* 163, 187–201.

Wang, P., Sun, Z., Hu, Y., and Cheng, H. (2019). "Leaching of Heavy Metals from Abandoned Mine Tailings Brought by Precipitation and the Associated Environmental Impact.". *Sci. Total Environ.* 695, 133893–133904. doi: 10.1016/j.scitotenv.2019.133893

Wang, S., Cai, L. M., Wen, H. H., Luo, J., Wang, Q. S., and Liu, X. (2019). "Spatial Distribution and Source Apportionment of Heavy Metals in Soil from a Typical County-Level City of Guangdong Province, China.". *Sci. Total Environ.* 655, 92–101. doi: 10.1016/j.scitotenv.2018.11.244

Wu, J. T., Margenot, A. J., Wei, X., Fan, M. M., Zhang, H., Best, J. L., et al. (2020). "Source Apportionment of Soil Heavy Metals in Fluvial Islands, Anhui Section of the Lower Yangtze River: comparison of Apcs–Mlr and Pmf.". *J. Soils Sediments* 20, 3380–3393.

Xiao, R., Guo, D., Ali, A., Mi, S., Liu, T., Ren, C., et al. (2019). "Accumulation, Ecological-Health Risks Assessment, and Source Apportionment of Heavy Metals in Paddy Soils: a Case Study in Hanzhong, Shaanxi, China.". *Environ. Pollut.* 248, 349–357. doi: 10.1016/j.envpol.2019.02.045

Xu, D. M., Fu, R. B., Liu, H. Q., and Guo, X. P. (2021). "Current Knowledge from Heavy Metal Pollution in Chinese Smelter Contaminated Soils, Health Risk Implications and Associated Remediation Progress in Recent Decades: a Critical Review.". *J. Clean. Prod.* 286, 124989–125048.

Xu, Y., Shi, H. D., Fei, Y., Wang, C., Mo, L., and Shu, M. (2021). "Identification of Soil Heavy Metal Sources in a Large-Scale Area Affected by Industry.". *Sustainability* 13:511.

Zhang, Q. C., and Wang, C. C. (2020). "Natural and Human Factors Affect the Distribution of Soil Heavy Metal Pollution: a Review.". *Water Air Soil Poll.* 231, 350–363.

Zhang, X., Wei, S., Sun, Q., Wadood, S. A., and Guo, B. (2018). "Source Identification and Spatial Distribution of Arsenic and Heavy Metals in Agricultural Soil around Hunan Industrial Estate by Positive Matrix Factorization Model, Principle Components Analysis and Geo Statistical Analysis.". *Ecotoxicol. Environ. Saf.* 159, 354–362. doi: 10.1016/j.ecoenv.2018.04.072

Zhang, Z. X., Zhang, N., Li, H. P., Lu, Y., Wang, Q. S., and Yang, Z. G. (2019). "Risk Assessment, Spatial Distribution, and Source Identification of Heavy Metal(Loid)S in Paddy Soils Along the Zijiang River Basin, in Hunan Province, China.". *J. Soils Sediments*19, 4042–4051.

Zhao, K. L., Zhang, L. Y., Dong, J. Q., Wu, J. S., Ye, Z. Q., Zhao, W. M., et al. (2020). "Risk Assessment, Spatial Patterns and Source Apportionment of Soil Heavy Metals in a Typical Chinese Hickory Plantation Region of Southeastern China.". *Geoderma* 360, 114011–114022.

Zhong, X., Chen, Z., Li, Y., Ding, K., Liu, W., Liu, Y., et al. (2020). "Factors Influencing Heavy Metal Availability and Risk Assessment of Soils at Typical Metal Mines in Eastern China.". *J. Hazard. Mater.* 400, 123289–123327.

Zhu, X., Yu, W., Li, F., Liu, C., Ma, J., Yan, J., et al. (2021). "Spatio-Temporal Distribution and Source Identification of Heavy Metals in Particle Size Fractions of Road Dust from a Typical Industrial District.". *Sci. Total Environ.* 780, 146357–146370. doi: 10.1016/j.scitotenv.2021.146357

Conflict of Interest: The authors declare that the research was conducted in the absence of any commercial or financial relationships that could be construed as a potential conflict of interest.

Publisher's Note: All claims expressed in this article are solely those of the authors and do not necessarily represent those of their affiliated organizations, or those of the publisher, the editors and the reviewers. Any product that may be evaluated in this article, or claim that may be made by its manufacturer, is not guaranteed or endorsed by the publisher.

Copyright © 2022 Cao, Wang, Liao, Li and Zhu. This is an open-access article distributed under the terms of the Creative Commons Attribution License (CC BY). The use, distribution or reproduction in other forums is permitted, provided the original author(s) and the copyright owner(s) are credited and that the original publication in this journal is cited, in accordance with accepted academic practice. No use, distribution or reproduction is permitted which does not comply with these terms.

frontiers | Frontiers in Earth Science

ORIGINAL RESEARCH
published: 15 June 2022
doi: 10.3389/feart.2022.920796

Impact of Rapid Transit Development on Urban Economic Growth: An Empirical Study of the Urban Agglomerations in China

Jinhuang Mao[1,2], *Qianwen Tian*[2] *and Chengpeng Lu*[1,2]*

[1]Institute of County Economic Development and Rural Revitalization Strategy, Lanzhou University, Lanzhou, China, [2]School of Economics, Lanzhou University, Lanzhou, China

Transportation infrastructure and market integration play an important role in building China's new development pattern of dual circulation. Taking 220 cities in 19 urban agglomerations in China as the study sample, this study analyzes the impact of rapid transit development on urban economic growth from 2008 to 2019 and examines the heterogeneity of the difference in market integration capability in promoting urban economic growth based on the two-way fixed effects model. The main conclusions are as follows: 1) the improvement of travel convenience brought about by the development of expressways and high-speed railways significantly promoted urban economic growth; 2) market integration has significantly restricted the promotion of the construction of expressways and high-speed railways to urban economic growth. In other words, cities with less market integration have greater economic benefits from expressway and high-speed railway construction; 3) there is a certain substitution of the role of expressways and high-speed railways in promoting urban economic growth, and for cities that already have a relatively complete expressway network, further construction of high-speed railways will inhibit the promotion effect of expressway development on urban economic growth; 4) expressway and market integration have a stronger role in promoting urban economic growth in the eastern region than in the central and western regions, while high-speed railway and market integration promote the economic growth in the eastern region, and the impact on economic growth in the central and western regions is not significant. The findings of this study have implications for optimizing the planning of expressway and high-speed railway construction and promoting high-quality regional development in China and other developing countries.

Keywords: rapid transit, economic growth, market integration, two-way fixed effects model, China

OPEN ACCESS

Edited by:
Jianhong Xia,
Curtin University, Australia

Reviewed by:
Qingsong He,
Huazhong University of Science and Technology, China
Dongxue Zhao,
The University of Queensland, Australia
Ye Wei,
Northeast Normal University, China

***Correspondence:**
Chengpeng Lu
lcp@lzu.edu.cn

Specialty section:
This article was submitted to Geoscience and Society, a section of the journal Frontiers in Earth Science

Received: *15 April 2022*
Accepted: *05 May 2022*
Published: *15 June 2022*

Citation:
Mao J, Tian Q and Lu C (2022) Impact of Rapid Transit Development on Urban Economic Growth: An Empirical Study of the Urban Agglomerations in China. Front. Earth Sci. 10:920796. doi: 10.3389/feart.2022.920796

1 INTRODUCTION

If you want to be rich, first build roads. This sentence has always been regarded as a *golden rule* of China's economic development; the government and ordinary people seem to believe that the construction of roads and railways can spread the economic resources of regional central cities to the surrounding small cities and drive the economic growth of the surrounding small cities (Zhang, 2017). Since the reform and opening up, China has carried out large-scale transportation

infrastructure construction, and various transportation modes represented by expressways and high-speed railways have achieved leapfrog development. In 2020, the total length of China's road and railway was 5.198 million kilometers and 146,000 km, which was 5.8 times and 2.8 times that in 1978, when the length of expressways and high-speed railways was 161,000 km and 37,900 km, creating a great feat of the length from scratch to the world's first (Ministry of Transport of the People's Republic of China, 2021).

Transportation infrastructure is often considered to be the key to promoting economic growth and development, as the organization of economic activity in geographic space depends crucially on the transportation of goods and people (Redding and Turner, 2015). Theoretically, the impact of transportation infrastructure on economic growth is accomplished through both direct and indirect effects. The direct effect means that the investment of transportation infrastructure, as a factor input, can not only directly drive the increase in total output but also affect capital accumulation through "multiplier effect," thereby driving the increase in social total demand and national income to be several times the investment (Li et al., 2011). Compared with the direct effect, the indirect effect of transportation infrastructure is more prominent (Wang and Ni, 2016). The essence of transportation infrastructure is to provide services for the public, and it has the basic attributes of public goods, that is, externalities, and it is easy to produce spatial spillover effect (Sun et al., 2020). On the one hand, the improvement of transportation infrastructure reduces transportation costs and time costs and improves the level of inter-regional accessibility, which accelerates the transfer of economic factors, such as capital and labor, from non-central cities to regional central cities, thus promoting economic agglomeration and growth in central cities and large cities (Qin et al.,. 2017; Banerjee et al., 2020). On the other hand, the improvement of transportation infrastructure connects the economic activities of different regions into a whole, which makes the boundaries of cities and urban agglomerations continue to overflow, breaking the limitation of knowledge spillover in geographical space and promoting economic growth in surrounding small cities through the diffusion of knowledge and technology in regional central cities and large cities (Baum-Snow et al., 2017; Miwa et al., 2022). It should be noted that although the improvement of transportation infrastructure can cause inter-regional spillover effect of regional economic growth, the economic decline of less developed areas is caused by the large concentration of production factors from surrounding small cities to central cities (Boarnet, 1998). The construction of transportation infrastructure may also increase environmental pollution, which is not conducive to economic growth (Li et al., 2021).

The impact of transportation infrastructure construction on economic growth has been empirically tested in a large number of literatures, but the conclusions are inconsistent. A large number of studies have shown that the construction of transportation infrastructure can reduce transaction costs and improve economic efficiency, promoting economic growth (Donaldson, 2018; Sun and Zhang, 2021). Some studies have found that the construction of transportation infrastructure has caused economic activities to agglomerate and transfer from non-central cities to central cities along the route, inhibiting the economic growth of non-central cities and leading to a polarized economic pattern between large cities and small cities (Yu F. et al., 2019). A few studies suggest that the impact of transportation infrastructure construction on economic growth may not be significant (Farhadi, 2015). Existing studies focus on the economic effects of the construction of roads (Coşar and Demir, 2016), railways (Forero et al., 2020), airports (Startz, 2016), and ports (Karimah and Yudhistira, 2020). With the rapid development of high-speed railways as a new mode of transportation, more and more research studies have begun to pay attention to the regional economic effects of high-speed railways in recent years (Li et al., 2018; Lu et al., 2022). High-speed railway refers to the passenger-dedicated railway with the design speed of the new line being 250 km/h (including reservation) and above, and the initial operating speed being not less than 200 km/h (Nation Railway Administration of the People's Republic of China, 2013). High-speed railway lines only undertake part of the passenger transport function. Due to the high fares of high-speed railways, the target audience is more business travelers (Tan et al., 2019); the importance of high-speed railways in the flow of medium- and long-distance people is becoming more and more prominent. However, from the perspective of short-distance transportation of people and goods, road transportation still occupies an absolutely dominant position. In 2020, the passenger volume and freight volume of China's road transport accounted for 71.3% and 73.8%, respectively. The most important in China's road transportation is expressway transportation. High-speed railway has the advantages of large passenger capacity, less time consumption, punctuality, low energy consumption, and little influence from weather, which makes it popular among people, while expressway has door-to-door flexibility to cover areas not accessible by high-speed railway (Jiang et al., 2015). Therefore, when analyzing the impact of rapid transportation on urban economic growth, expressways must be considered.

It is necessary to deeply analyze the influence of expressway and high-speed railway development on urban economic growth and further examine the mutual influence between expressway and high-speed railway. The mechanism of the impact of transportation infrastructure improvement on urban economic growth is complex, and the difference of the market integration level between regions will also affect urban economic growth. It is difficult for a fragmented and isolated market to play a positive role in the market mechanism. An integrated and unified market is not only conducive to expanding the market size and deepening the specialization of labor but also promoting full market competition, playing the role of scale economy and standardize market rules (Sheng and Mao, 2011). It allows labor, capital, and other factors of production to flow freely and eventually to the most efficient sectors and regions. Therefore, it is necessary to speed up the construction of a unified national market, break local protection and market segmentation, break through the key blocking points that restrict the economic cycle, and promote the smooth flow of commodity factor resources on a larger scale (Liu and Zhu, 2014).

The factors that lead to the fragmentation of the domestic market are diverse and can be roughly divided into three categories: natural factors, technical factors, and institutional factors (Fan et al., 2017). Natural market segmentation refers to two markets that are naturally formed and separated due to physical factors such as spatial distance; technical market segmentation refers to the formation of two technological markets characterized by horizontal differences; institutional market segmentation refers to the formation of two markets characterized by local protection under the influence of economic, political, and other human factors. As a result, we have obtained two effective ways to break the domestic market segmentation. One is to increase the investment in transportation infrastructure construction to improve the efficiency of market transactions, thereby reducing natural market segmentation and technical market segmentation. The second is to reduce institutional market segmentation by eliminating local protection and optimizing institutional design. However, by eliminating local protection and optimizing system design, it involves changes in laws and regulations and the economic system, which is more difficult (Pan and Ye, 2021). Therefore, only strengthening the construction of transportation infrastructure is the most effective way to break the segmentation of the domestic market. First, the "space-time compression effect" brought about by the improvement of transportation infrastructure can significantly improve the accessibility level of the city in which it is located, thus greatly alleviating the natural market segmentation caused by geographical distance barriers (Ye and Pan, 2020). Second, the improvement of transportation infrastructure can reduce the transaction cost of enterprises, promote the cross-regional flow of resources, and improve the efficiency of market transactions, thereby breaking the technical market segmentation (Ma et al., 2020). Third, transportation infrastructure improvement can expand the market scale and promote specialized division of labor, while the higher the degree of regional specialized division of labor, the more conducive it is to the comparative advantages of trade in different regions and promoting regional trade cooperation. In this context, local governments may face higher opportunity costs of market segmentation, which will motivate them to reduce local protection and market segmentation policies (Sun and Yin, 2021). It should also be noted that investment in transport infrastructure may increase the financial pressure on local governments and the competitive pressure on local enterprises, thereby incentivizing local governments to adopt market segmentation policies (Mao and Wang, 2018).

Market integration and market segmentation are two aspects of the same problem, and the existing research mostly analyzes it from the perspective of market segmentation. Some studies have found that market segmentation caused by local protection can distort the efficient allocation of resources, leading to the convergence of regional industrial structures and loss of efficiency of enterprises and industries, which can hinder economic growth (Jing and Zhang, 2019). There are also some views that the impact of market segmentation on economic growth is an inverted U-shaped curve (Sun and Lei, 2018). When the degree of market segmentation is low, local protection and market segmentation are beneficial to local economic growth, but when the degree of market segmentation exceeds a certain critical value, its effect on local economic growth will turn to inhibition. Market segmentation can be mediated by the highly isomorphic regional industrial structure, which can promote economic growth by promoting regional specialization and division of labor (Fu and Qiao, 2011). Some studies have also found that the impact of market segmentation on economic growth is uncertain; it may be inverted U-shaped or positive U-shaped, or it may not be significant (Song et al., 2014). In fact, the market segmentation that exists between regions in China is a "prisoner's dilemma" situation. When other local governments adopt local protection and market segmentation policies, the local government must also adopt a "beggar-thy-neighbor policy" in order to protect the local economy. This could lead to a market-segmentation race among local governments, which could improve the relative performance of the local economy by taking down rivals. If all local governments give up local protection and market segmentation, then all localities will benefit. However, this situation does not seem to occur in China. The fact is that some local governments are currently benefiting from market segmentation but at the cost of huge dis-economies of scale, which adversely affects China's overall economic growth (Lu and Chen, 2009).

The existence of market segmentation between regions will be detrimental to economic growth, while market integration can implement the free flow of commodities and factors between regions, give full play to the positive role of the market in allocating resources, and improve economic growth. The reduction of transaction costs and the improvement of transaction efficiency brought about by the improvement of transportation infrastructure can promote the cross-regional flow of commodities and production factors, reducing the degree of market segmentation between regions and improving the level of market integration. However, existing research seldom pays attention to the relationship between transportation infrastructure improvement, market integration, and economic growth and pays more attention to discussing and analyzing the relationship between the two. In 2020, *the fifth plenary session of the 19th Communist Party of China (CPC) Central Committee* proposed to accelerate "the new development paradigm featuring dual circulation, in which domestic and overseas markets reinforce each other, with the domestic market as the mainstay." From the perspective of regional coordinated development, the realization of the domestic circulation must break the market segmentation and realize the free flow of various elements between regions (Zhang and Yang, 2020; Liu et al., 2021). Based on the understanding of smoothing the domestic circulation and promoting coordinated regional development under the new situation, this study will take 220 cities in 19 urban agglomerations in China as research samples to empirically test the impact of the development of expressways and high-speed railways on urban economic growth and the heterogeneity of urban economic growth caused by different levels of market integration. This is of great significance for enriching existing research, optimizing

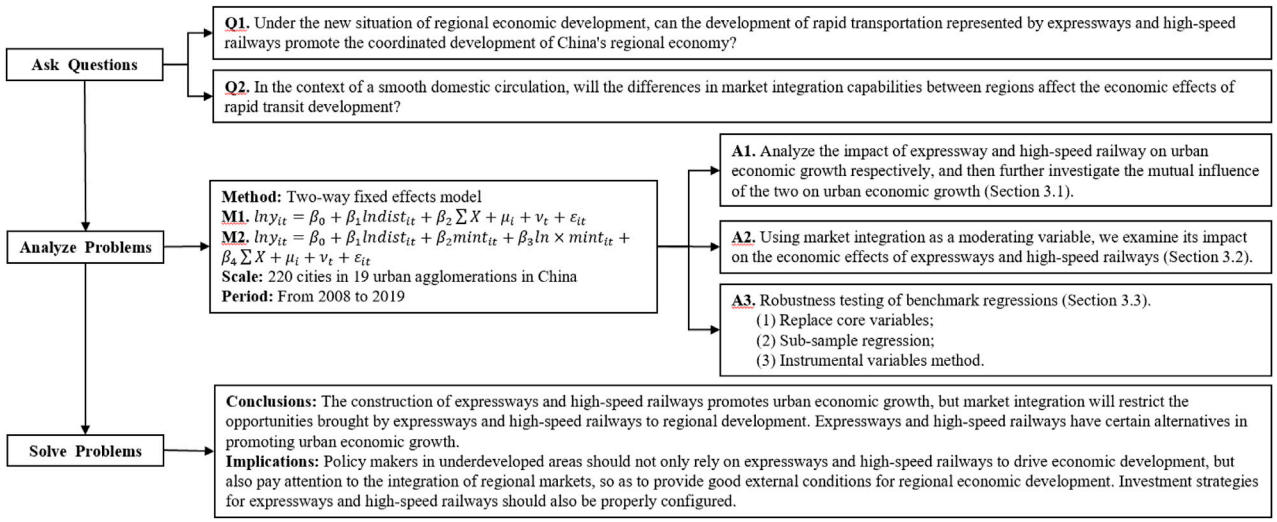

FIGURE 1 | Technical roadmap.

investment strategies for expressways and high-speed railways in China, and promoting regional high-quality development.

The possible marginal contributions of this study are mainly reflected in three aspects: 1) taking economic growth as the starting point, this study specifically examines the impact of the development of expressways and high-speed railways on economic activities and further explores the relationship between expressways and high-speed railways, supplementing the existing literature. Existing studies have discussed the respective economic growth effects of expressways (Liu et al., 2019) and high-speed railways (Yao and Wang, 2020), but there is little literature on the relationship between expressways and high-speed railways. 2) This study examines the heterogeneity of expressway and high-speed railway development affecting urban economic growth from the perspective of market integration, providing a new entry point and perspective for studying the impact of transportation infrastructure on economic activities. From the available studies, this study is closest to the study by Yao and Wang (2020), who discuss the heterogeneity of differences in market integration capacity with regard to the role of high-speed railroads in promoting high-quality development in Chinese counties from 2008 to 2013. Their study found that market integration reinforces the opportunities that high-speed railway brings to regional development, contrary to the findings of this study. Their explanation is that with the improvement of the travel convenience of high-speed railways, enterprises in the city will gain more development opportunities, and the improvement of market integration can reduce the transaction costs of enterprises, which ultimately leads to economic growth. Our interpretation is that more convenient rapid transportation infrastructure improves inter-regional accessibility, reduces transaction costs, and expands market size, thereby promoting urban economic growth; in cities with a low degree of market integration, the reduction of transaction costs and the expansion of market scale brought about by the development of expressways and high-speed railways will be more obvious, so that their role in promoting urban economic growth will be stronger. 3) This study provides a better identification strategy to address the endogeneity between transportation infrastructure and economic development by constructing instrumental variables of transportation infrastructure based on the geographical location of each city. The previous literature mostly used historical road (Baum-Snow et al., 2017; Zhang et al., 2018; Guo and Hu, 2021) or geographic slope (Bian et al., 2019) as instrumental variables of transportation infrastructure, which are not suitable for panel data because they do not change with time. **Figure 1** is the technical roadmap of this study.

2 METHOD AND DATA

2.1 Study Area

Urban agglomeration is a high-level organizational form of regional economic activities in the process of industrialization and urbanization, which can produce huge economic agglomeration effects, realize the rational allocation of resources in the region and the free flow of elements, and promote the process of regional integration (Sun and Zhou, 2022). Cities included in the urban agglomeration can fully obtain the radiation and driving role of the central city, driving the overall high-quality development of the region. Therefore, the study area of this study is determined according to the 19 urban agglomerations planned in the *Outline of the 14th Five-Year Plan (2021–2025) for National Economic and Social Development and Vision 2035 of the Peoples Republic of China*. In the process of collection, the content defined in the published planning text shall prevail, and the unpublished planning text shall be determined according to relevant planning and research literature. Considering the availability and comparability of data,

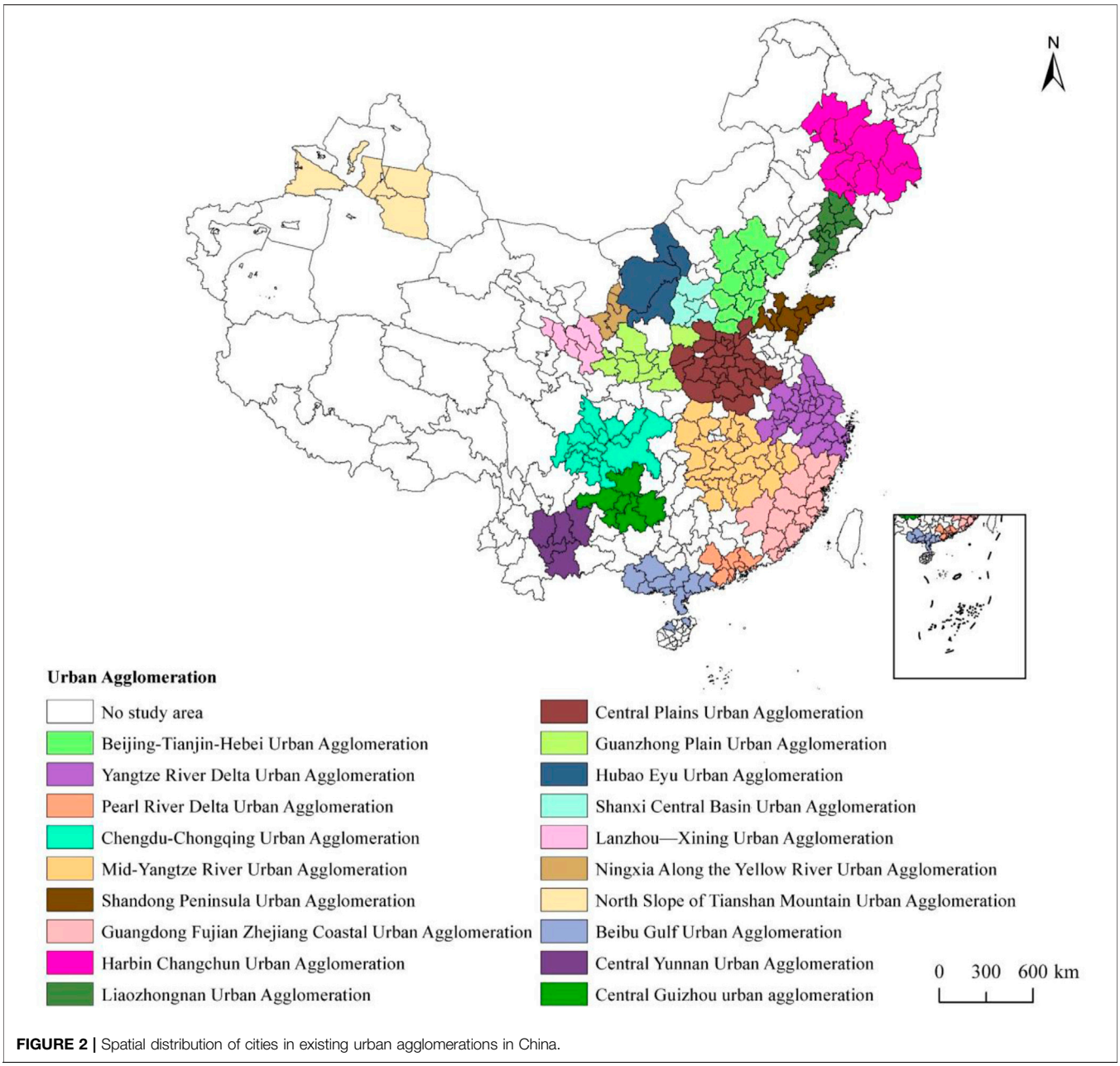

FIGURE 2 | Spatial distribution of cities in existing urban agglomerations in China.

the study area focuses on municipality- and prefecture-level cities (including autonomous prefectures), and 220 cities were finally determined **Figure 2**. In 2019, 220 cities in 19 urban agglomerations contributed 85,164.40 billion yuan to China's GDP, with a proportion of 86.33% of gross GDP, indicating that even if accounting errors are excluded, the 220 cities in 19 urban agglomerations have an absolute dominant position in China's economy. Therefore, the study area selected in this study can well reflect China's economic development.

2.2 Index Selection

The variables involved in this study include explained variables, core explanatory variables, moderator variables, and other control variables. This study uses real per capita GDP ($\boldsymbol{y}$) as the explained variable to measure urban economic growth. Specifically, the ratio of regional GDP to its resident population is used to measure urban economic growth. In order to eliminate the impact of price factors, the nominal GDP of each city is deflated at the constant price in 2007.

Regarding the core explanatory variables, referring to the practice of Faber (2014), the straight-line distance from the city center to the nearest expressway and high-speed railway station is used to measure the development level of expressways and high-speed railways in the city. Specifically, the mean of the straight-line distance between the city center and the nearest expressway and high-speed railway station of all counties under

the jurisdiction of each city is used. Considering that the built-up areas of many cities are not located in the center of the region, this study uses each regional government seat as the city center. First, manually sort out the construction and opening time of all expressways and high-speed railway stations, as well as the main control points and other information, using publicly available information on the Internet. Second, on the basis of the national expressways and high-speed railway stations opened before 2008, the information of newly built and opened expressways and high-speed railway stations was updated year by year, and finally, the rapid traffic database containing the distribution of expressways and high-speed railway stations from 2008 to 2019 was obtained. Then, the locations of the geographic centers of all cities were calculated by combining the 2007 county-level administrative boundaries of China. Finally, the straight-line distance from the city center to the nearest expressways and high-speed railway station was calculated based on the ArcGIS 10.8 for each year and each county-level administrative district.

For the market integration indicator, this study uses the inverse of the degree of market segmentation from 2008 to 2019 in China as measured using the "price method", considering the latest mainstream research directions. For the specific calculation methods, please refer to the study by Gui et al. (2006). The core idea of the "price method" comes from the "Model of Iceberg Cost" (Samuelson, 1964), which is a modification to the "Law of One Price." Due to transaction costs, some of the value of the commodity will melt like a glacier in the process of trade. Even if there is full arbitrage, the price of the same commodity in the two places will not be exactly equal but will fluctuate within a certain range. Take two places i and j as an example, assume that the price of a commodity in i is P_i and j is P_j, and the various losses caused by the transaction between the two places are a proportion of the price per unit c $(0 < c < 1)$. Only when $P_i(1-c) > P_j$ or $P_j(1-c) > P_i$, the two places can trade the commodity. When the above conditions are not satisfied, the relative price P_i/P_j between the two places will fluctuate within the no-arbitrage interval $[1-c, 1/1-c]$. In other words, if the relative price fluctuations of the same commodity between the two places tend to converge within a certain period of time, it means that the transaction cost and the degree of market segmentation between the two places is decreasing. When using the "price method" to calculate the level of market integration in each city, it is important to note the following: 1) regarding the price index, referring to the research of Lv and He (2020), the consumer price indices by category is adopted, including food; tobacco, liquor, and articles; clothing; household facilities, articles, and services; health care and personal articles; transportation and communication; recreation, education, and culture articles; and residence. 2) In previous studies, the mean of the relative price variance with neighboring cities was as the market segmentation index of the city. Since China's commodity market is being segmented from a regional market bounded by provincial boundaries to a regional market bounded by urban agglomeration segmentation evolution (Liu and Zhu, 2021), this study uses the mean of the relative price variance between each city and all cities in the urban agglomerations to represent the degree of market segmentation of the city. 3) Since market integration and market segmentation are two aspects of the same phenomenon, the reciprocal of each city's market segmentation is used to represent its level of market integration.

The factors affecting economic growth are quite complex, and the realization of regional economic growth may be the result of the spatial synergy of multidimensional factors (Zhang, 2012). In order to minimize the impact of other factors on urban economic growth, the following control variables were selected with reference to the research of Guo & Hu (2021) and Yu Y. Z. et al. (2019). 1) Human Capital Accumulation (***hum***). As an important variable in the new economic growth theory, its impact on urban economic growth has been increasingly emphasized by scholars, using the number of general higher-education schools enrolled per 10,000 people as a measure. 2) Government Intervention (***gov***). As an important participant in the market economy, the government plays a macro-control role in urban economic growth, which is measured by the proportion of fiscal expenditure in the local government budget to GDP. 3) Level of Urbanization (***urb***). Urbanization and industrialization have always been regarded as important drivers of China's economic growth, measured by the proportion of the population of municipal districts in the resident population. 4) Industry Structure (***is***). The upgrading of industrial structure can not only directly promote the increase in total output but, more importantly, it can promote economic growth by triggering technological progress and improving labor productivity, measured by the ratio of the added value of the secondary and tertiary industries in GDP. 5) Proportion of State-Owned Economy (***soe***). As an important part of the socialist public economy, the state-owned economy plays a dominant role in China's economic development, and it is measured by the proportion of employees in state-owned units in urban units. 6) Level of Opening Up (***ope***). Through foreign trade, new technologies and new systems can be introduced, which can drive urban economic growth, and it is measured by the proportion of total imports and exports to GDP. 7) Level of Informatization (***inf***). The extensive application of information technology enables information to play its role as an important production factor and strategic resource, which can improve labor productivity and social operation efficiency, and it is measured by the proportion of internet users in the resident population.

2.3 Methodology: Two-way Fixed Effects Model

Based on the travel convenience brought by the construction of expressways and high-speed railways from 2008 to 2019, this study aims to explore the impact of expressways and high-speed railways on urban economic growth and analyze the heterogeneity of the difference in market integration capability in promoting urban economic growth. First, analyze the impact of expressway and high-speed railway construction on urban economic growth without considering the impact of market consolidation. The regression equation is denoted as follows:

$$ln\,y_{it} = \beta_0 + \beta_1 lndist_{it} + \beta_2 \sum X + \mu_i + \nu_t + \varepsilon_{it} \quad (1)$$

where i represents the city, t represents the time, lny_{it} represents the logarithmic of the real GDP per capita of each city, $lndist_{it}$ represents the logarithmic of the straight-line distance from the city center to the nearest expressway and high-speed railway station, X represents the set of control variables, μ_i represents the individual fixed effect, ν_t represents the year fixed effect, and ε_{it} represents the random error term. Since the index $lndist_{it}$ is the straight-line distance from the city center to the nearest expressway and high-speed railway station, the smaller the value, the stronger the travel convenience in the area. This study expects that the coefficient β_1 is significantly negative, which reflects the promotion of the construction of expressways and high-speed railways to urban economic growth. The shorter the straight-line distance between the city center and the nearest expressway or high-speed railway station, the stronger the promotion effect on urban economic growth.

Then, on the basis of **Eq. 1**, the interaction terms of market integration with expressways and high-speed railways are added to investigate how different levels of market integration affect the economic growth effects of construction of expressways and high-speed railways. The regression equation is denoted as follows:

$$ln\,y_{it} = \beta_0 + \beta_1 lndist_{it} + \beta_2 min\,t_{it} + \beta_3 lndist_{it} \times min\,t_{it} + \beta_4 \sum X + \mu_i + \nu_t + \varepsilon_{it} \quad (2)$$

where $mint_{it}$ represents the level of market consolidation, and this study expects the coefficient β_2 to be significantly positive, indicating that market integration can promote urban economic growth. The interaction term $lndist_{it} \times mint_{it}$ is used to examine how market consolidation affects the economic growth effects of expressways and high-speed railways. If the coefficient β_3 of the interaction term is significantly positive, it is considered that market integration significantly weakens the promoting effect of development of expressways and high-speed railways on urban economic growth; if β_3 is significantly negative, it is considered that market integration significantly strengthens the promoting effect of development of expressways and high-speed railways on urban economic growth. Since the interaction term includes both the information of $lndist_{it}$ and the information of $mint_{it}$, in order to prevent multicollinearity, the interaction term is centralized.

2.4 Data Source

This study focused on 220 cities in 19 urban agglomerations in China from 2008 to 2019. The relevant data involved were mainly sourced from the *China city statistical yearbook*, China statistical yearbook for regional economy, and other statistical yearbooks and bulletins of various cities. Import and export data were obtained from the Wind database. The data such as the opening time and main control points of expressway lines and high-speed railway stations were derived from public information on the Internet. All latitude and longitude data for expressways, high-speed railways, and county-level administrative regions came from Baidu Electronic Maps. For some missing data, the linear interpolation method was used to complete the data. The results of descriptive statistics for all the above variables are shown in **Table 1**.

3 EMPIRICAL RESULTS

3.1 Rapid Transit Development and Urban Economic Growth

First, perform a multicollinearity test on the model before the regression analysis. The variance inflation factor (VIF) of all variables was less than 10, and the average variance inflation factor was 1.68, indicating that there was no serious multicollinearity among the variables. Second, according to the F test and Hausman test, the fixed effect (FE) result is the best, so the following regressions all use the fixed effect model. **Table 2** reports the regression results of the impact of expressway and high-speed railway development on urban economic growth. The results show that the coefficients of expressways (*ew_dist*) and high-speed railways (*hsr_dist*) are both negative regardless of whether control variables are added or not, indicating that the improvement of travel convenience brought about by the development of expressways and high-speed railways significantly promotes urban economic growth. From columns (5, 6), the coefficients of the interaction term between expressways and high-speed railways (*ew_hsr*) are significantly negative, indicating that there is a certain substitution of the role of expressways and high-speed railways in promoting urban economic growth. For cities that already have a relatively complete expressway network, further construction of high-speed railway will inhibit the promotion effect of development on urban economic growth.

Among the main control variables, human capital accumulation, government intervention, level of urbanization, and level of informatization are significantly positively correlated with urban economic growth, indicating that accelerating the accumulation of human capital, expanding the scale of government expenditure, and improving the level of urbanization and informatization significantly promote urban economic growth. The industrial structure is significantly negatively correlated with economic growth, indicating that China's current industrial structure upgrade is still in a period of deep adjustment. The coefficient of the proportion of the state-owned economy is significantly negative, indicating that increasing the proportion of state-owned economy in the national economy is not conducive to urban economic growth, and the ultimate goal of state-owned enterprise reform should be to improve the competitiveness of state-owned enterprises. The coefficient of the level of opening up is significantly negative, indicating that China's current foreign trade dependence is too high, and the domestic economy is subject to the world economy.

3.2 Rapid Transit Development, Market Integration, and Urban Economic Growth

Table 3 reports the impact of rapid transit development and market integration on urban economic growth. The regression results show that no matter whether the control variable is added

TABLE 1 | Descriptive statistics of variables.

Variable	Mean value	Standard deviation	Minimum value	Maximum value
lny	10.477	0.691	8.223	12.547
ew_dist	3.637	1.267	1.185	8.094
hsr_dist	4.353	1.345	1.409	8.177
mint	1.727	0.683	0.273	4.492
hum	0.189	0.219	0.000	1.276
gov	0.178	0.095	0.044	0.989
urb	0.373	0.248	0.044	1.000
is	0.072	0.450	1.000	0.899
soe	0.462	0.174	0.058	0.936
ope	0.217	0.343	0.001	3.231
inf	0.193	0.154	0.000	2.247

TABLE 2 | Rapid transit development and urban economic growth.

Variable	(1)	(2)	(3)	(4)	(5)	(6)
ew_dist	–0.253***	–0.095***			–0.122***	–0.059***
	(–21.35)	(–9.26)			(–9.75)	(–5.92)
hsr_dist			–0.241***	–0.106***	–0.171***	–0.083***
			(–27.39)	(–12.42)	(–20.50)	(–10.64)
ew_hsr					–0.018*	–0.021***
					(–1.62)	(–2.91)
hum		0.148***		0.130***		0.109***
		(5.23)		(4.60)		(4.51)
gov		0.014***		0.013***		0.011***
		(5.85)		(4.96)		(5.28)
urb		0.691***		0.509***		0.543***
		(6.26)		(3.97)		(4.77)
is		–0.083*		–0.107**		–0.091**
		(–1.92)		(–2.54)		(–2.28)
soe		–0.011***		–0.011***		–0.009***
		(–11.72)		(–12.37)		(–11.67)
ope		–0.139**		–0.057		–0.086*
		(–2.41)		(–1.09)		(–1.75)
inf		0.611***		0.546***		0.509***
		(5.58)		(5.43)		(5.21)
Constants	11.395***	10.084***	11.527***	10.336***	11.678***	10.523***
	(264.73)	(63.55)	(300.57)	(63.83)	(232.75)	(73.19)
Individual fixed effects	Yes	Yes	Yes	Yes	Yes	Yes
Year fixed Effects	Yes	Yes	Yes	Yes	Yes	Yes
N	2,640	2,640	2,640	2,640	2,640	2,640
R-square	0.488	0.787	0.600	0.805	0.672	0.823

*The value in small brackets are t statistics; *, ** and *** represent levels of significance at 10%, 5% and 1% respectively.*

or not, the estimated coefficient of market integration (*mint*) is significantly positive at the 1% level, indicating that the improvement of market integration level significantly promotes urban economic growth. The results in columns (1, 2) show that the coefficient of the interaction between expressway and market integration ($ew \times mint$) is significantly positive at the 1% level, indicating that market integration weakens the role of expressway construction in promoting urban economic growth under the condition of a given expressway development level. From columns (3, (4), the coefficient of the interaction between high-speed railway and market integration ($hsr \times mint$) is also significantly positive at the 1% level, indicating market integration also weakens the role of high-speed railway construction in promoting urban economic growth. Overall, given the level of rapid transportation development, market integration weakens the promotion of rapid transportation development to urban economic growth. In other words, in cities with a low level of market integration, the economic growth effect of rapid transit development is stronger, and in cities with a high level of market integration, the economic growth effect of rapid transit development is weaker. The possible explanation is that with the development of transportation infrastructure, inter-regional market integration is enhanced and businesses are given greater opportunities for market development, which will reduce their costs and boost their profits, thus promoting a thriving urban economy. However, for cities with high market integration capabilities, the "integration effect" brought about by the improvement of transportation

TABLE 3 | Rapid transit development, market integration, and urban economic growth.

Variable	(1)	(2)	(3)	(4)	(5)	(6)
ew_dist	−0.219***	-0.090***			−0.123***	−0.063***
	(−23.41)	(-9.28)			(−9.84)	(−6.20)
ew × mint	0.056***	0.037***			0.020	0.010
	(4.22)	(4.12)			(0.97)	(0.88)
hsr_dist			−0.214***	−0.096***	-0.147***	−0.075***
			(−27.11)	(−11.34)	(−19.56)	(−10.06)
hsr × mint			0.036***	0.027***	0.029**	0.017
			(2.69)	(2.90)	(2.04)	(1.51)
ew × hsr					−0.003	−0.014**
					(−0.38)	(−2.33)
ew × hsr × mint					−0.016	−0.008
					−0.74)	(−0.75)
mint	0.177***	0.078***	0.114***	0.053***	0.119***	0.059***
	(16.73)	(8.46)	(11.22)	(5.77)	(12.74)	(7.16)
hum		0.140***		0.129***		0.108***
		(5.28)		(4.76)		(4.41)
gov		0.012***		0.012***		0.010***
		(5.36)		(4.68)		(5.06)
urb		0.709***		0.540***		0.562***
		(6.54)		(4.22)		(5.00)
is		−0.082*		−0.107**		−0.087**
		(−1.86)		(−2.53)		(−2.17)
soe		−0.009***		−0.009***		−0.008***
		(−10.31)		(−11.02)		(−9.95)
ope		−0.140**		−0.057		−0.087*
		(−2.53)		(−1.12)		(−1.80)
inf		0.629***		0.565***		0.520***
		(5.56)		(5.44)		(5.20)
Constants	11.395***	9.906***	11.413***	10.158***	11.367***	10.365***
	(326.59)	(66.27)	(327.80)	(66.34)	(200.75)	(71.45)
Individual fixed effect	Yes	Yes	Yes	Yes	Yes	Yes
Year fixed effect	Yes	Yes	Yes	Yes	Yes	Yes
N	2,640	2,640	2,640	2,640	2,640	2,640
R-square	0.569	0.801	0.632	0.812	0.702	0.830

*The value in small brackets are t statistics; *, ** and *** represent levels of significance at 10%, 5% and 1% respectively.*

infrastructure is greatly reduced, resulting in a weakened "economic growth effect" of the transportation infrastructure. Because the market has been highly integrated, further integration is more difficult, which is not conducive to the further expansion of enterprises. For cities with a low level of market integration, the improvement of transportation infrastructure will further promote regional market integration, which will help companies obtain the transaction cost advantage brought about by the reduced degree of market segmentation, thereby further promoting urban economic development. The results in columns 5) and 6) show that the estimated coefficients of the interaction between expressway and high-speed railway and market integration (*ew* × *hsr* × *mint*) are not significant.

3.3 Robustness Test

3.3.1 Replace the Measurement Indicators of the Main Variables

In order to exclude the possible interference caused by the selection of variable measurement, this study replaces the measurement indicators of the main variables. First, after using real labor productivity calculated at constant prices in 2007 to replace real per capita GDP as a measure of urban economic growth, the results are reported in columns (1–3) of **Table 4**. The results show no significant changes in the sign and significance of the coefficients of the core explanatory variables, indicating that the above findings are robust.

Second, both expressways and high-speed railways are lagged by one period to replace the core explanatory variables, and the results are reported in columns (4–6) of **Table 4**. It can be seen from the results that the development of expressways and high-speed railways and the improvement of market integration level have significantly promoted urban economic growth, while market integration has significantly inhibited the promotion of expressway and high-speed railway development on urban economic growth, and there is a certain substitution of the role of expressways and high-speed railways in promoting urban economic growth. These results are consistent with the baseline regression, indicating that the baseline regression results are robust.

Third, drawing on the research of Ghani et al. (2016), the dummy variable of whether a city center is located within a certain distance of the nearest expressway and high-speed rail station is used to measure expressways and high-speed railways. Specifically, *ew_dist*1 indicates that the straight-line distance from the city center to the nearest expressway is less than or

TABLE 4 | Results of robustness tests 1

Variable	Labor productivity			Rapid traffic lag by one period		
	(1)	(2)	(3)	(4)	(5)	(6)
ew_dist	−0.091*** (−9.02)		−0.063*** (−6.24)	−0.086*** (−9.06)		−0.059*** (−6.65)
ew_mint	0.035*** (4.37)		0.009 (0.77)	0.038*** (3.01)		−0.005 (−0.36)
hsr_dist		−0.093*** (−10.87)	−0.071*** (−9.28)		−0.095*** (−12.47)	−0.077*** (−11.43)
hsr_mint		0.024*** (2.71)	0.015 (1.32)		0.033*** (3.77)	0.026*** (2.61)
ew × *hsr*			−0.013** (−2.10)			−0.019** (−2.34)
ew × *hsr* × *mint*			0.002 (0.15)			−0.003 (−0.39)
mint	0.063*** (6.59)	0.039*** (4.18)	0.046*** (4.55)	0.065*** (8.11)	0.037*** (4.25)	0.036*** (4.09)
Control variables	Yes	Yes	Yes	Yes	Yes	Yes
Individual fixed effect	Yes	Yes	Yes	Yes	Yes	Yes
Year fixed effect	Yes	Yes	Yes	Yes	Yes	Yes
N	2,640	2,640	2,640	2,420	2,420	2,420
R-square	0.488	0.787	0.802	0.767	0.789	0.809

*The value in small brackets are t statistics; *, ** and *** represent levels of significance at 10%, 5% and 1% respectively.*

TABLE 5 | Results of robustness tests 2

Variable	Expressway	High-speed railway
	(1)	(2)
*dist*1	0.112***	0.109***
	(3.85)	(4.72)
*dist*2	0.098***	0.093***
	(5.27)	(5.18)
*dist*1 × *mint*	−0.108***	−0.115***
	(−4.80)	(−5.94)
*dist*2 × *mint*	−0.038**	−0.081***
	(−2.39)	(−3.65)
Control variables	Yes	Yes
Individual fixed effect	Yes	Yes
Year fixed effect	Yes	Yes
N	2,640	2,640

*The value in small brackets are t statistics; *, ** and *** represent levels of significance at 10%, 5% and 1% respectively.*

equal to 10 km; *ew_dist*2 indicates that the straight-line distance from the city center to the nearest expressway is greater than 10 km and less than 50 km; *hsr_dist*1 indicates that the straight-line distance from the city center to the nearest high-speed rail station is less than or equal to 20 km; *hsr_dist*2 indicates that the straight-line distance from the city center to the nearest high-speed rail station is greater than 20 km and less than 50 km; and the regression results are shown in **Table 5**. The results show that the coefficients of the dummy variables of the straight-line distance from the city center to the nearest expressway and high-speed railway station are all significantly positive, and the estimated coefficients before *dist*1 are significantly larger than those before *dist*2, which indicates that the shorter the straight-line distance from the city center to the nearest expressway and high-speed railway station, the more prominent the role of expressway and high-speed railway development in promoting economic growth. It can also be seen that the coefficient of the interaction term of expressway and market integration (*ew* × *mint*) and the coefficient of the interaction term of high-speed railway and market integration (*hsr* × *mint*) are both significantly negative, and the absolute value of the coefficient before *dist*1 × *mint* is greater than the absolute value of the coefficient before *dist*2 × *mint*, which indicates that the decrease in the level of market integration has a stronger effect on promoting economic growth in cities that are closer to expressways and high-speed rail stations. Overall, the effects of expressways and high-speed railways on urban economic growth measured using dummy variables are consistent with the results when using continuous distance variables to measure expressways and high-speed railways.

3.3.2 Sub-Sample Regression

In general, provincial capitals and large cities tend to have better transportation infrastructure, excluding municipalities, provincial capitals, and sub-provincial cities can alleviate the endogeneity problem caused by reverse causality to a certain extent (Chandra and Thompson, 2000), and the regression results are shown in columns (1–3) of **Table 6**. The results show that after excluding municipalities, provincial capitals, and sub-provincial cities, the absolute value of the coefficient of the interaction between expressway and market integration and the coefficient of the interaction between high-speed railway and market integration have both decreased, but they are still significantly positive.

Considering China's vast territory, differences in geographical location and natural resource endowments lead to significant regional differences, and the level of transportation infrastructure and market integration as well as the level of economic and social development are also very different from place to place; this study further discusses the impact of expressway, high-speed railway, and market integration on urban economic growth in different regions. According to the classification standard published by the National Bureau of Statistics of the People's Republic of China, the research samples are divided into two regions, eastern region and central and western regions, and the regression results are shown in columns (4–9) of **Table 7**. From the results, the coefficients of expressway are significantly negative at the 1% level and the coefficients of its interaction term with market integration are significantly positive at the 5% level of significance, both in the eastern region and central and western regions. In terms of the absolute value of the coefficients, the eastern regions are significantly larger than the central and western regions, which indicates that the promotion effect of

TABLE 6 | Regression results of Sub-sample.

Variable	Non-provincial cities			Eastern region			Central and western regions		
	(1)	(2)	(3)	(4)	(5)	(6)	(7)	(8)	(9)
ew_dist	−0.086***		−0.055***	−0.091***		−0.065***	−0.087***		−0.059***
	(−7.57)		(−4.85)	(−6.94)		(−4.77)	(−6.51)		(−3.76)
ew × mint	0.037***		0.012	0.040**		−0.012	0.031**		0.023
	(3.64)		(0.93)	(2.50)		(−0.89)	(3.29)		(1.33)
hsr_dist		−0.095***	−0.076***		−0.099***	−0.071***		−0.093	−0.076***
		(−10.28)	(-9.53)		(−9.38)	(−6.55)		(−8.15)	(−7.73)
hsr × mint		0.022**	0.009		0.038***	0.044***		0.020	0.001
		(2.12)	(0.80)		(3.79)	(3.71)		(1.54)	(0.07)
ew × hsr			−0.018**			−0.011			−0.017**
			(−2.57)			(−1.21)			(-2.03)
ew × hsr × mint			−0.006			−0.005			−0.010
			(−0.59)			(−0.44)			(−0.56)
mint	0.080***	0.056***	0.059***	0.073***	0.080***	0.062***	0.055***	0.051***	0.055***
	(7.67)	(5.40)	−0.018**	(5.60)	(4.10)	(5.26)	(6.35)	(3.87)	(4.75)
Control variables	Yes	Yes	Yes	Yes	Yes	Yes	Yes	Yes	Yes
Individual fixed effect	Yes	Yes	Yes	Yes	Yes	Yes	Yes	Yes	Yes
Year fixed effect	Yes	Yes	Yes	Yes	Yes	Yes	Yes	Yes	Yes
N	2,220	2,220	2,220	2,220	2,220	972	1,668	1,668	1,668
R-square	0.791	0.807	0.822	0.805	0.817	0.835	0.807	0.818	0.835

*The value in small brackets are t statistics; *, ** and *** represent levels of significance at 10%, 5% and 1% respectively.*

TABLE 7 | The first stage regression results of instrumental variables.

Variable	Expressway			High-speed railway		
	(1)	(2)	(3)	(4)	(5)	(6)
	dist	***dist × mint***	***mint***	***dist***	***dist × mint***	***mint***
IV_dist	−1.804***			−0.746***		
	(−17.66)			(−8.80)		
IV_dist × mint		−0.964***			−0.941	
		(−9.97)			(−13.64)	
IV_mint			0.909***			0.915***
			(18.24)			(26.81)
Control variables	Yes	Yes	Yes	Yes	Yes	Yes
Individual fixed effect	Yes	Yes	Yes	Yes	Yes	Yes
Year fixed effect	Yes	Yes	Yes	Yes	Yes	Yes
N	2,640	2,640	2,640	2,640	2,640	2,640
R-square	0.709	0.314	0.807	0.553	0.247	0.807
Weak IV test	227.838 < 16.38>	80.646 < 16.38>				
IV identifiable test	144.232[0.000]	156.454[0.000]				

*The value in small brackets are t statistics; *, ** and *** represent levels of significance at 10%, 5% and 1% respectively; Weak instrumental variable test using Cragg-Donald Wald F statistic; The corresponding thresholds for tolerating 10% distortion provided by Stock and Yogo (2005) are reported in sharp brackets; Identifiable tests for instrumental variables were performed using the Kleibergen-Paap rk LM statistic and the corresponding p-values are reported in square brackets.*

expressway development and market integration on urban economic growth is stronger in the central and western regions. In the eastern region, the coefficient of the high-speed railway and the coefficient of the interaction between the high-speed railway and market integration are both significant at the 1% level, while in the central and western regions, the coefficient of the high-speed railway and the coefficient of the interaction between the high-speed railway and market integration are both not significant.

The possible explanation is that the construction of high-speed railways in the central and western regions started late, leading to few lines and low density, and even many cities in the central and western regions have not yet opened high-speed railways; thus, the economic growth effect of high-speed railway development in the central and western regions has not been played in a short time. Also, it is noted that the coefficient of the interaction term of expressway and high-speed railway is not significant in the eastern region, but it is significant in the central and western regions. This may be in the eastern region has formed a more complete network of expressways and high-speed railways, the new high-speed railway to the expressway replacement role is not obvious.

3.3.3 Instrumental Variables Method

Although the baseline regression controls as much as possible for factors that may affect both rapid transit development and urban

economic growth, the empirical results may still be influenced by some unobservable factors, and this omitted variable problem may lead to biased estimated coefficients for rapid transit development. At the same time, the higher the level of urban economic growth, the better the rapid transit development, and there may be a reverse causality between the two. In order to alleviate the endogeneity problem caused by omitted variables or reverse causality, this study further adopts the instrumental variable method to solve it. With regard to the selection of instrumental variables, we use the "least cost path spanning tree networks" method to connect the central cities with straight lines and use "whether the city is located on a straight line connecting the central cities" as an instrumental variable for "whether the city is connected to expressway or high-speed railway," following the ideas of Faber (2014) and Hornung (2015). The planning goal of China's expressways and high-speed railways is to connect to the central cities in each region of the country. Whether a non-central city is connected to an expressway or high-speed railroad depends to a large extent on whether the city is located in a straight line between the central cities in the expressway or high-speed railroad network. If the straight-line distance between a city and the central city is very far, to include the city in the expressway or high-speed railway network will make a substantial detour, which will greatly increase the construction cost of the expressway or high-speed railway, so the city will have a high probability of not being connected to the expressway or high-speed railway. Moreover, the distance between the city and the central city in a straight line is not related to its recent economic development level but is determined by its historical geographical location, so it has a strong exogenous nature.

The instrumental variables (*IV_ew* and *IV_hsr*) are constructed as follows: 1) use the expressways and high-speed railways that have been built before September 30 of the current year, find the central cities (municipalities, provincial capitals, and sub-provincial cities) that the completed lines pass through, and connect the central cities with straight lines according to the layout of the expressway and high-speed railway network. 2) Use ArcGIS 10.8 to calculate the straight-line distance from each city center to the nearest central city connection for each year, and if the straight-line distance is less than or equal to 100 km, the instrumental variable takes the value of 1 in the current year and subsequent years; otherwise, it takes the value of 0. Considering that market integration may also be endogenous, the average value of market integration in each urban agglomeration is used as an instrumental variable for market integration in all cities within the urban agglomeration.

Using the instrumental variables constructed above, the baseline regression was estimated using two-stage least squares (2SLS), and the regression results are presented in **Tables 7**, **8**. The Cragg–Donald Wald F-statistics of 227.838 and 80.646 in the first stage estimation, respectively, both passed the weak instrumental variables test, and the Kleibergen–Paaprk LM statistics of 144.232 and 156.454, respectively, also passed the instrumental variables identifiability test. The results of the second stage show that the coefficients of both expressways and high-speed railways are significantly negative, and the coefficients of the interaction term of expressway and high-speed railway with market integration, respectively, are all significantly positive, which are consistent with the baseline regression, indicating that the results of the baseline regression are still robust after addressing the endogeneity issue.

TABLE 8 | Second-stage regression results of instrumental variables.

Variable	(1)	(2)
ew_dist	–0.081***	
	(–10.78)	
ew × mint	0.096***	
	(12.45)	
hsr_dist		–0.212***
		(–10.82)
hsr × mint		0.147***
		(7.04)
mint	0.056***	0.013*
	(2.96)	(1.07)
Control variables	Yes	Yes
Individual fixed effect	Yes	Yes
Year fixed effect	Yes	Yes
N	2,640	2,640
R-square	0.800	0.686

*The value in small brackets are t statistics; *, ** and *** represent levels of significance at 10%, 5% and 1% respectively.*

4 DISCUSSION AND CONCLUSION

4.1 Discussion

When studying the impact of transportation infrastructure on economic activities, the most important thing is to deal with the endogeneity problem caused by causality (Liu and Zhou, 2014), which is addressed by two approaches in this study. The first method is to remove all municipalities, provincial capitals, and sub-provincial cities from the sample by referring to the study by Chandra and Thompson (2000). This is mainly because these cities tend to have better economic development than other cities, and the government tends to give priority to these cities when planning transportation infrastructure, so excluding these cities can suppress reverse causality to a certain extent. The second method is to draw on the work of Faber (2014) and Hornung (2015) to solve it by constructing instrumental variables for highways and high-speed railroads based on the geographical location of each city. The research conclusions of this study are still robust after dealing with endogeneity issues and a series of robustness tests.

The findings of this study help policy makers understand the contribution of transportation infrastructure to economic growth from the perspective of transportation infrastructure upgrading and market integration, especially for those in less developed regions. As a basic, leading and strategic industries and important service industries, transportation infrastructure is an important underpinning for sustainable development of urban economy (He et al., 2020). Thus, accelerating the construction of transportation infrastructure and striving to improve the coverage of transportation infrastructure in the country is the

basis of economic and social development. However, the construction of transportation infrastructure, especially high-grade transportation infrastructure, is characterized by large investment scale, long construction cycle, and low return on capital, which means that the government may induce a debt crisis if it recklessly makes large-scale transportation infrastructure construction investments (Fan et al., 2017). It is also important to be aware of the complexity of transportation infrastructure affecting economic activity. There is heterogeneity in the impact of different transportation infrastructures on urban economic growth, and differences in the level of market integration (Yao and Wang, 2020) and financial constraints (Liu et al., 2019) can also affect the economic effects of transportation infrastructure. Therefore, the government should reasonably guide the investment in transportation infrastructure and strive to maximize the economic effect of transportation infrastructure to narrow the regional economic development gap and achieve high-quality regional economic development.

However, there are some shortcomings in this study. First, this study only examines the impact of rapid transit development and market integration on urban economic growth at the macro-city level, but the micro-action mechanism of rapid transit development and market integration for urban economic growth is not discussed, which is the future research direction and focus of this study. Second, regarding the measurement index of expressways and high-speed railways, no unified standard has been formed in the academic community. This study uses the straight-line distance of the city center from the nearest expressways and high-speed railway stations, and since this distance varies little during the study period and there are several cities with no changes in consecutive years, there may be some bias in using this index to measure their economic effects, which requires further exploration of better measurement indexes in the future. Third, this study focuses only on the moderating effect of commodity market integration on rapid transit development, but differences in the degree of integration of factor markets, such as labor and capital, also affect the economic effects of rapid transit development, which also needs to be explored more in the future.

4.2 Conclusion

Taking 220 cities of 19 urban agglomerations in China as research samples, this study empirically tests the impact of rapid transportation development on urban economic growth from 2008 to 2019 and further analyzes the heterogeneity of urban economic growth due to different levels of market integration. The results show that 1) the shorter the straight-line distance from the city center to the nearest expressway and high-speed railway station, the higher the level of urban economic growth, indicating that the increased travel convenience brought by expressway and high-speed railway development significantly promotes urban economic growth. Simultaneously, there is a certain substitution between expressways and high-speed railways in promoting urban economic growth. For those cities that have already established a relatively well-developed expressway network, further development of high-speed railways will restrict the promotion of expressway development on urban economic growth. 2) Market integration significantly promotes urban economic growth, while different levels of market integration significantly restrict the promotion of expressway and high-speed railway on urban economic growth; the poorer the market integration, the greater the economic growth effect from the development of expressways and high-speed railways, while the stronger the market integration, the smaller the economic growth effect from the development of the development of expressways and high-speed railways. However, the impact of market integration on the substitution role between expressways and high-speed rail is not significant. 3) The development of expressways and market integration have a stronger role in promoting the economic growth in the eastern region than in the central and western regions, while the development of high-speed railways and market integration have only promoted the economic growth in the eastern region and do not have significant effects on economic growth in the central and western regions.

DATA AVAILABILITY STATEMENT

The original contributions presented in the study are included in the article/Supplementary Material; further inquiries can be directed to the corresponding author.

AUTHOR CONTRIBUTIONS

All authors listed have made a substantial, direct, and intellectual contribution to the work and approved it for publication.

FUNDING

This work was supported by the National Social Science Foundation Western Region Project (Grant No. 20XJL008) and the Fundamental Research Funds for the Central Universities (Grant No. 21lzujbkydx044).

REFERENCES

Banerjee, A., Duflo, E., and Qian, N. (2020). On the Road: Access to Transportation Infrastructure and Economic Growth in China. *J. Dev. Econ.* 11 (1), 1–53. doi:10.1016/j.jdeveco.2020.102442

Baum-Snow, N., Brandt, L., Henderson, J. V., Turner, M. A., and Zhang, Q. (2017). Roads, Railroads, and Decentralization of Chinese Cities. *Rev. Econ. Statistics* 99 (3), 435–448. doi:10.1162/rest_a_00660

Bian, Y. C., Wu, L. H., and Bai, J. H. (2019). Does High-Speed Rail Improve Regional Innovation in China? *J. Financial Res.* (06), 132–149.

Boarnet, M. G. (1998). Spillovers and the Locational Effects of Public Infrastructure. *J. regional Sci.* 38 (3), 381–400. doi:10.1111/0022-4146.00099

Chandra, A., and Thompson, E. (2000). Does Public Infrastructure Affect Economic Activity? *Regional Sci. urban Econ.* 30 (4), 457–490. doi:10.1016/s0166-0462(00)00040-5

Coşar, A. K., and Demir, B. (2016). Domestic Road Infrastructure and International Trade: Evidence from Turkey. *J. Dev. Econ.* 118, 232–244. doi:10.1016/j.jdeveco.2015.10.001

Donaldson, D. (2018). Railroads of the Raj: Estimating the Impact of Transportation Infrastructure. *Am. Econ. Rev.* 108 (4-5), 899–934. doi:10.1257/aer.20101199

Faber, B. (2014). Trade Integration, Market Size, and Industrialization: Evidence from China's National Trunk Highway System. *Rev. Econ. Stud.* 81 (3), 1046–1070. doi:10.1093/restud/rdu010

Fan, X., Song, D. L., and Zhang, X. Y. (2017). Does Infrastructure Construction Break up Domestic Market Segmentation? *Econ. Res. J.* 52 (02), 20–34.

Farhadi, M. (2015). Transport Infrastructure and Long-Run Economic Growth in OECD Countries. *Transp. Res. Part A Policy Pract.* 74, 73–90. doi:10.1016/j.tra.2015.02.006

Forero, A., Gallego, F. A., González, F., and Tapia, M. (2020). Railroads, Specialization, and Population Growth: Evidence from the First Globalization. *J. Popul. Econ.* 34 (3), 1027–1072. doi:10.1007/s00148-020-00804-3

Fu, Q., and Qiao, Y. (2011). How Government Competition Has Contributed to China's Rapid Economic Growth: A Re-examination of the Relationship between Market Segmentation and Economic Growth. *J. World Econ.* 34 (07), 43–63.

Ghani, E., Goswami, A. G., and Kerr, W. R. (2016). Highway to Success: The Impact of the Golden Quadrilateral Project for the Location and Performance of Indian Manufacturing. *Econ. J.* 126 (591), 317–357. doi:10.1111/ecoj.12207

Gui, Q. H., Chen, M., Lu, M., and Chen, Z. (2006). Segmentation or Consolidation in China's Domestic Commodity Markets: an Analysis Based on the Relative Price Approach. *J. World Econ.* (02), 20–30.

Guo, P. F., and Hu, X. Y. (2021). Infrastructure Investment, Market Integration and Regional Economic Growth. *Wuhan Univ. J. (Philosophy Soc. Sci.* 74 (06), 141–157. doi:10.14086/j.cnki.wujss.2021.06.013

He, G., Xie, Y., and Zhang, B. (2020). Expressways, GDP, and the Environment: the Case of China. *J. Dev. Econ.* 145, 102485. doi:10.1016/j.jdeveco.2020.102485

Hornung, E. (2015). Railroads and Growth in Prussia. *J. Eur. Econ. Assoc.* 13 (04), 699–736. doi:10.1111/jeea.12123

Jiang, H. B., Zhang, W. Z., Qi, Y., and Jiang, J. L. (2015). The Land Accessibility Influenced by China's High-Speed Rail Network and Travel Cost. *Geogr. Res.* 34 (06), 1015–1028. doi:10.11821/dlyj201506002

Jing, W. M., and Zhang, J. N. (2019). The Impact of Market Segmentation on Economic Growth: from the Perspective of Unbalanced Regional. *Reform* (09), 103–114.

Karimah, I. D., and Yudhistira, M. H. (2020). Does Small-Scale Port Investment Affect Local Economic Activity? Evidence from Small-Port Development in indonesia. *Econ. Transp.* 23, 100180. doi:10.1016/j.ecotra.2020.100180

Li, C., Lin, T., Zhang, Z., Xu, D., Huang, L., and Bai, W. (2021). Can Transportation Infrastructure Reduce Haze Pollution in China? *Environ. Sci. Pollut. Res.* 29 (11), 1–18. doi:10.1007/s11356-021-16902-y

Li, H., Strauss, J., Shunxiang, H., and Lui, L. (2018). Do high-speed Railways Lead to Urban Economic Growth in China? A Panel Data Study of China's Cities. *Q. Rev. Econ. finance* 69, 70–89. doi:10.1016/j.qref.2018.04.002

Li, P., Wang, C. H., and Yu, G. C. (2011). A Literature Review of Infrastructure and Economic Development. *J. World Econ.* 34 (05), 93–116.

Liu, C., Liu, C. R., and Sun, T. (2019). Transportation Infrastructure, Financial Constraint and County Industry Development: Evidence from China's National Trunk Highway System. *Manag. World* 35 (07), 78–88+203. doi:10.19744/j.cnki.11-1235/f.2019.0093

Liu, C., and Zhou, L. A. (2014). Expressway Construction and Regional Economic Development: Evidence from China's County Level. *Econ. Sci.* (02), 55–67. doi:10.19523/j.jjkx.2014.02.005

Liu, H., and Zhu, Z. Y. (2021). From Provincial Market to Regional Market—Based on the Calculation of Five Urban Agglomerations Market Segmentation. *Inq. into Econ. Issues* (01), 124–135.

Liu, R., Dai, W., and Li, Z. (2021). Reduce Trade Cost and Smoothen Domestic Economic Circulation. *Shanghai J. Econ.*, (02), 25–35. doi:10.19626/j.cnki.cn31-1163/f.2021.02.003

Lu, M., and Chen, Z. (2009). Fragmented Growth: Why Economic Opening May Worsen Domestic Market Segmentation? *Econ. Res. J.* 44 (03), 42–52.

Lu, Y., Yang, S., and Li, J. (2022). The Influence of High-Speed Rails on Urban Innovation and the Underlying Mechanism. *PloS One* 17 (3), e0264779. doi:10.1371/journal.pone.0264779

Lv, B. Y., and He, Y. (2020). On the Trend of Regional Market Integration: Measurement and Analysis on Chinese Commodity Market Segmentation Based on City Data. *Econ. Theory Bus. Manag.* (04), 13–25.

Ma, G. R., Cheng, X. M., and Yang, E. Y. (2020). How Does Transportation Infrastructure Affect Capital Fows: A Study from High-Speed Rail and Cross-Region Investment of Listed Companies. *China Ind. Econ.* (06), 5–23. doi:10.19581/j.cnki.ciejournal.2020.06.001

Mao, Q. L., and Wang, F. (2018). Transport Development, Market Segmentation and Regional Industrial Growth. *Finance Trade Res.* (08), 16–30. doi:10.19337/j.cnki.34-1093/f.2018.08.002

Ministry of Transport of the People's Republic of China (2021). China Sustainable Transport Development Report. Available at: https://xxgk.mot.gov.cn/2020/jigou/gjhzs/202112/t20211214_3631113.html.

Miwa, N., Bhatt, A., and Kato, H. (2022). High-speed Rail Development and Regional Inequalities: Evidence from japan. *Transp. Res. Rec. J. Transp. Res. Board*, 036119812210785. doi:10.1177/03611981221078566

Nation Railway Administration of the People's Republic of China. (2013). What Is High Speed Rail? Available at: http://www.nra.gov.cn/ztzl/hyjc/kjcxx/kp/201605/t20160526_24387.shtml.

Pan, S., and Ye, D. Z. (2021). Research on the Impact of Transport Infrastructure on Market Segmentation: Evidence from High-Speed Rail Opening and Cross-Districe M&A of Listed Companies. *Public Finance Res.* (03), 115–129. doi:10.19477/j.cnki.11-1077/f.2021.03.009

Qin, Y. (2017). 'No County Left behind?' the Distributional Impact of High-Speed Rail Upgrades in China. *J. Econ. Geogr.* 17 (3), 489–520. doi:10.1093/jeg/lbw013

Redding, S. J., and Turner, M. A. (2015). "Transportation Costs and the Spatial Organization of Economic Activity," in *Handbook of Regional and Urban Economics*, 5, 1339–1398.

Samuelson, P. A. (1964). Theoretical Notes on Trade Problems. *Rev. Econ. statistics* 46 (2), 145–154. doi:10.2307/1928178

Sheng, B., and Mao, Q. L. (2011). Trade Openness, Domestic Market Integration, and Interprovincial Economic Growth in China from 1985 to 2008. *J. World Econ.* (11), 44–66.

Song, D., Fan, X., and Zhao, X. (2014). Regional Development Strategy, Market Segmentation and Economic Growth. *Finance Trade Econ.* 35 (8), 115–126. doi:10.19795/j.cnki.cn11-1166/f.2014.08.012

Startz, M. (2016). The Value of Face-To-Face: Search and Contracting Problems in Nigerian Trade. *Available at SSRN 3096685*.

Stock, J. H., and Yogo, M. (2005). *Testing for Weak Instruments in Linear IV Regression*. Cambridge, MA: National Bureau of Economic Research, Inc. doi:10.3386/t0284

Sun, B. W., and Lei, M. (2018). Market Segmentation, Costs Reduction and High Quality Developmengt : an Analysis of a New Economic Geography Model. *Reform* (07), 53–63.

Sun, B. W., and Yin, J. (2021). How Can Transportation Investment Achieve High Quality Market Integration? A Perspective Based on Geographical and Institutional Market Segmentation. *J. Macro-quality Res.* (01), 113–128. doi:10.13948/j.cnki.hgzlyj.2021.01.009

Sun, J., and Zhou, L. (2022). Leading the Rise of Yangtze River Economic Belt with the Construction of Central Cities and City Clusters. *Journal of Jiangsu University (Social Science Edition)*, 24 (02), 91–102. doi:10.13317/j.cnki.jdskxb.2022.019

Sun, W. H., and Zhang, J. (2021). High-speed Rail Service and Urban Total Factor Productivity. *Shanghai J. Econ.* (01), 90–104. doi:10.19626/j.cnki.cn31-1163/f.2021.01.008

Sun, X. T., Li, Y., and Wang, Z. H. (2020). High-speed Rail Construction and Urban Economic Development: Industrial Heterogeneity and Spatial Spillover Effect. *J. Shanxi Univ. Finance Econ.* 42 (02), 58–71. doi:10.13781/j.cnki.1007-9556.2020.02.005

Tan, Y. H., Yu, F., Lin, F. Q., and Zheng, M. T. (2019). China's High-Speed Railway, Trade Cost and Firm Export. *Econ. Res. J.* 54 (07), 158–173.

Yao, B., and Wang, H. J. (2020). High Speed Rail, Market Integration and Regional High-Quality Development. *Industrial Econ. Res.* 29 (02), 1–14. doi:10.13269/j.cnki.ier.2020.06.001

Ye, D. S., and Pan, S. (2020). Distance, Accessibility and Innovation: A Study on the Optimal Working Radius of High-Speed Railway Openging for Urban

Innovation. *Finance Trade Econ.* 41 (02), 146–161. doi:10.19795/j.cnki.cn11-1166/f.20200211.004

Yu, F., Lin, F., Tang, Y., and Zhong, C. (2019a). High-speed Railway to Success? the Effects of High-speed Rail Connection on Regional Economic Development in China. *J. Reg. Sci.* 59 (4), 723–742. doi:10.1111/jors.12420

Yu, Y. Z., Zhuang, H. T., and Fu, Y. (2019b). Does the Opening of High-Speed Rail Accelerate the Spillover of Technological Innovation? Evidence from 230 Prefecture-Level Cities in China. *J. Finance Econ.* 45 (11), 20–31+111. doi:10.16538/j.cnki.jfe.2019.11.002

Zhang, J. (2017). High-speed Rail Construction and County Economic Development: the Research of Satellite Light Data. *China Econ. Q.* 16 (04), 1533–1562. doi:10.13821/j.cnki.ceq.2017.03.12

Zhang, X. L. (2012). Has Transport Infrastructure Promoted Regional Economic Growth? with an Analysis of the Spatial Spillover Effects of Transport Infrastructure. *Soc. Sci. China* (03), 60–77+206. doi:10.19626/j.cnki.cn31-1163/f.2021.02.003

Zhang, X. L., and Yang, C. Y. (2020). Accelerate the Formation of Domestic and International Dual Circulation of Mutual Promotion of the New Development Pattern. *Guaning Dly.* 07-07.

Zhang, X., Wang, X., Wan, G. H., and Sun, F. C. (2018). A Unified Framework of Road Infrastructure's Growth Effect. *Econ. Res. J.* 53 (01), 50–64.

Conflict of Interest: The authors declare that the research was conducted in the absence of any commercial or financial relationships that could be construed as a potential conflict of interest.

Publisher's Note: All claims expressed in this article are solely those of the authors and do not necessarily represent those of their affiliated organizations, or those of the publisher, the editors, and the reviewers. Any product that may be evaluated in this article, or claim that may be made by its manufacturer, is not guaranteed or endorsed by the publisher.

Copyright © 2022 Mao, Tian and Lu. This is an open-access article distributed under the terms of the Creative Commons Attribution License (CC BY). The use, distribution or reproduction in other forums is permitted, provided the original author(s) and the copyright owner(s) are credited and that the original publication in this journal is cited, in accordance with accepted academic practice. No use, distribution or reproduction is permitted which does not comply with these terms.

frontiers | Frontiers in Ecology and Evolution

ORIGINAL RESEARCH
published: 17 June 2022
doi: 10.3389/fevo.2022.912127

Spatio-Temporal Evolution and Quality Analysis of Construction Land in Urban Agglomerations in Central China

Qimeng Ning[1], Xiao Ouyang[2] and Shaobo Liu[3]**

[1] College of Architecture and Urban Planning, Hunan City University, Yiyang, China, [2] Hunan Institute of Economic Geography, Hunan University of Finance and Economics, Changsha, China, [3] School of Architecture and Art, Central South University, Changsha, China

OPEN ACCESS

Edited by:
Bing Xue,
Institute of Applied Ecology (CAS), China

Reviewed by:
Dongxue Zhao,
The University of Queensland, Australia
Ziqi Zhao,
China Meteorological Administration, China
Junsong Wang,
South China University of Technology, China

***Correspondence:**
Xiao Ouyang
xiao.ouyang@foxmail.com
Shaobo Liu
liushaobo@csu.edu.cn

Specialty section:
This article was submitted to Environmental Informatics and Remote Sensing, a section of the journal Frontiers in Ecology and Evolution

Received: *04 April 2022*
Accepted: *24 May 2022*
Published: *17 June 2022*

Citation:
Ning Q, Ouyang X and Liu S (2022) Spatio-Temporal Evolution and Quality Analysis of Construction Land in Urban Agglomerations in Central China. Front. Ecol. Evol. 10:912127. doi: 10.3389/fevo.2022.912127

Understanding the pattern and quality of construction land expansion in urban agglomerations is important for new urbanization and high-quality development of land spaces. Taking urban agglomeration in the middle reaches of the Yangtze River as the research object, this study analyzes the spatio-temporal pattern and quality level of construction land expansion at various scales using remote sensing images, the expansion intensity index, the coordination degree model, and the Tapio elastic decoupling model. The results show that from 2000 to 2020, (1) the construction land scale of urban agglomeration in the study area had expanded, with significant stage characteristics and spatial differentiation patterns. (2) The overall relationship between the construction land and the population in urban agglomerations was found to be uncoordinated, but the coordination degree had been improved. The optimization of human–land coordination was faster at the metropolitan scale than at the overall level and the sub-urban agglomerations. (3) The decoupling relationship between the overall construction land and the economy in urban agglomerations was weak and had improved. The coupling/decoupling relationship was found to be better at the metropolitan scale than at the overall level and sub-urban agglomerations.

Keywords: construction land, central region, urban agglomeration, human-land relationship, high-quality development

INTRODUCTION

Mainly due to urbanization and industrialization, the expansion of construction lands is a significant change in the earth's surface and is reflected in the transformation of natural and agricultural lands into non-agricultural lands (Lv and Huang, 2013). China has been experiencing rapid urbanization and construction land expansion since 1978, and the area of construction land in 2018 was 8.34 times the level in 1981 (Ministry of Housing and Urban-Rural Development, 2018). But the neglect of the quality of construction land expansion for a long time leads to a series of problems such as wild growth, environmental pollution, and low efficiency (Wang et al., 2018b). The quality of construction land expansion describes the comprehensive utilization and level of newly added construction land, and high-quality development is achieved by the resonance and coordination of people, land, and industry (Liu et al., 2021). In 2017, the Chinese government

put forward the concept of high-quality development and emphasized the coordination between regional people, land, and industry. In this context, seeking the path to improve the quality of construction land expansion has become an important issue of academic concern.

Urban agglomeration is the main form of urbanization and industrialization and is more crucial to China's participation in global competition and cooperation (Yao et al., 2016). In recent decades, China's urban agglomerations have developed rapidly. The spatial scope of some urban agglomerations has been greatly expanded and is characterized by rapid population agglomeration and economic growth (Fang, 2014), which contend with increasingly tense contradictions between people, land, and industry (Fang, 2018; Liu et al., 2019). How to promote the high-quality expansion of construction land in urban agglomerations and address the conflicts and contradicting demands of people, land, and industry has become an important research topic in China's urbanization development and territorial space development. The expansion of construction land has always been a key issue in academic circles, and previous research has mainly focused on space–time patterns (Li et al., 2020b), driving mechanisms (Wu et al., 2021), simulation prediction (Li et al., 2021), and expansion effect (Yang et al., 2020). As ecological, social, urban heat, and other problems become more serious during the expansion process (Zhao et al., 2018, 2021; Wei et al., 2021; He et al., 2022), and China's transition to high-quality development is accelerating, the quality of construction land expansion has become a prominent research topic in geographical science, land science, ecological science, and other disciplines. One of the primary research focuses has been on understanding the relationships between construction land expansion and economic development or the ecological environment (Li et al., 2020c; Chen et al., 2022; Yi et al., 2022). For example, Li et al. (2020c) used Liaoning Province to explore the relationship between construction land expansion and the population and the economy. But in general, most of the existing research studies still discuss the expansion of construction land, while the research on the expansion quality of construction land is still insufficient.

As the role of urban agglomeration in the new urbanization and regional spatial organization is growing increasingly, land expansion and quality research on urban agglomeration have gained the attention of scholars, and the related research results are mainly distributed in the efficiency of urban construction land expansion (Yu et al., 2019; Li et al., 2021), the relationship between population growth and economic growth (Li et al., 2018; Xiao et al., 2021), and the ecological function value changes (Ouyang et al., 2021a). Ouyang (Ouyang et al., 2021b) studied the relationship between the urban agglomeration construction space and the ecological function value in China. However, most of the current research studies are just based on a single aspect, and there is a lack of multi-scale comparative analysis on urban agglomerations.

Urban agglomeration in the middle reaches of the Yangtze River is an important part of the Yangtze River Economic Belt and an important growth pole of the central region in China. In the long process of urbanization and industrialization, it faces numerous problems, such as population imbalance and land pollution caused primarily by urban expansion, and its land ecology is fragile (Shen et al., 2019). Moreover, the development level of each sub-urban agglomeration varies significantly, with each having its unique characteristics in terms of construction land expansion and its connection with the economy and society. On March 30, 2021, the Political Bureau of the CPC Central Committee held a meeting to review "the Guideline on Promoting the High-Quality Development of the Country's Central Region in the New Era." The Bureau pointed out that it is crucial to promote the development of urban agglomeration in the middle reaches of the Yangtze River and the Central Plain urban agglomeration. Understanding the spatio-temporal changes and expansion quality levels of its construction land is crucial to help promote high-quality of urbanization and territorial space optimization.

Therefore, this study takes urban agglomeration in the middle reaches of the Yangtze River as an example, uses Landsat TM/ETM remote sensing data, and combines the expansion intensity index, coordination degree model, and Tapio elastic decoupling model to study the spatio-temporal process and quality level of urban agglomeration construction land expansion, to supplement and expand the existing literature. This study mainly aims to (1) explore the spatio-temporal pattern and characteristics of construction land expansion based on multi-scale comparative analyses and (2) evaluate the quality of construction land expansion in urban agglomerations from a human–land–industry coordination perspective and then provide a better understanding and support to the department about land planning and urban planning.

MATERIALS AND METHODS

Overview of the Study Area

Urban agglomeration in the middle reaches of the Yangtze River includes three regional urban agglomerations, Wuhan (WH), Poyang Lake (PY), and Changsha–Zhuzhou–Xiangtan (CZT), encompassing 13 cities in Hubei, eight cities in Hunan, and 10 cities in Jiangxi and covering a total area of 317,000 square kilometers (**Figure 1**). Setting the research scope to the metropolitan scale, we used documents from the "Wuhan Comprehensive Planning (2017–2035)," the "Changsha Comprehensive Planning (2017–2035)," and the "Greater Nanchang Metropolitan Area Development Planning (2019–2025)" for this study. The Wuhan metropolitan area is composed of 17 research units, including the Wuhan municipal area; the Changsha metropolitan area comprising 15 research units, including the Changsha municipal area; and the Nanchang metropolitan area, including the Nanchang municipal area. In total, there are 17 research units in 49 counties, cities, and urban areas.

Materials

We collected Landsat TM/ETM remote sensing images during the summer months for the years 2000, 2005, 2010, 2015, and 2020. We then adjusted and corrected the images, including band

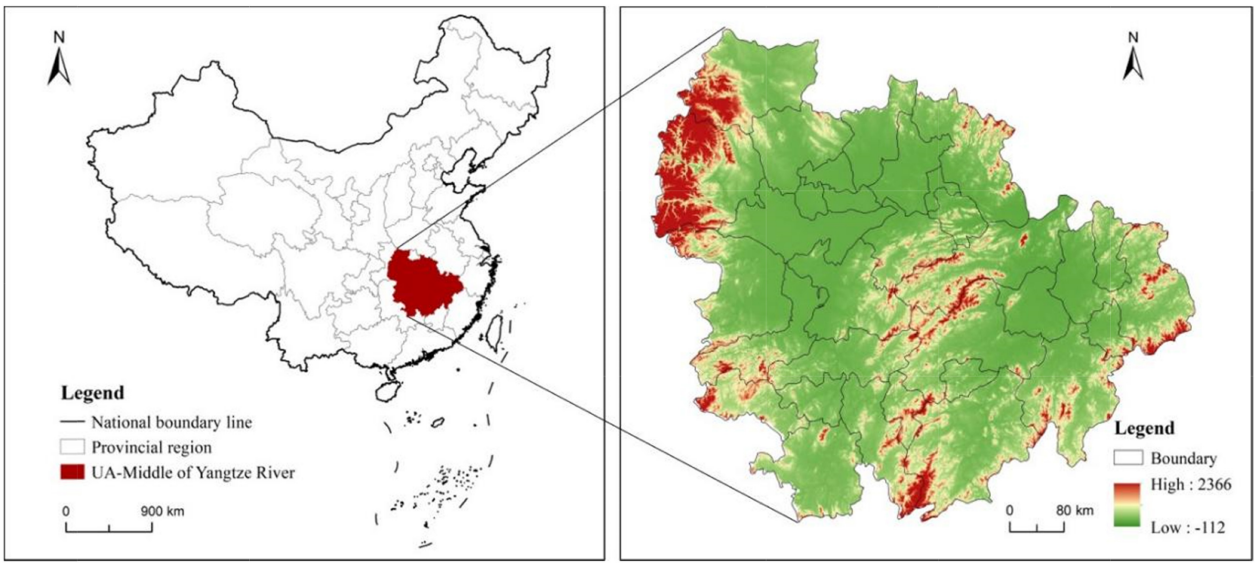

FIGURE 1 | Location of the study area and its basic geomorphology.

composition, geodetic datum correction, and ground control point calibration. The construction land included the urban land, rural residential land, and other construction lands. The population and GDP data were obtained from the "Hubei Statistical Yearbook," "Hunan Provincial Statistical Yearbook," "Jiangxi Provincial Statistical Yearbook," and the statistical bulletins of some prefectures and cities. Since some data from 2000 had been missing, we used relevant data from 2001 or 2002 and calculated the values using the change rate.

Methods

Urban Expansion Intensity Index

The expansion intensity index refers to the product of the newly added construction land, which can directly reflect the change rate of the construction land in a certain regional unit (Wang et al., 2018a). The expansion intensity index was used in this study to represent the time sequence state of urban agglomeration construction land expansion, given by the formula:

$$UEI_{\mathrm{n}} = \frac{A_n^{t_2} - A_n^{t_1}}{A_n^{t_1} \times \Delta t} \tag{1}$$

where UEI_{n} is the urban land expansion intensity index of the Nth urban agglomeration, $A_n^{t_1}$ is the urban land area of the Nth urban agglomeration in the t_1 time period, $A_n^{t_2}$ is the urban land area of the Nth urban agglomeration in the t_2 time period, and Δt is the interval year from t_1 to t_2.

Urban Expansion Intensity Differentiation Index

The urban land expansion intensity differentiation index is the ratio of the intensity of land use expansion for a particular urban agglomeration to the urban expansion intensity of all urban agglomerations, reflecting the heterogeneity in the expansion intensity among different urban areas agglomerations (Wang et al., 2018a). The index can be used in the horizontal comparative study of urban land expansion in urban agglomerations and to compare the variations in urban land expansion intensity of different urban agglomerations in the same period. In this study, we used the expansion intensity differentiation index to characterize the spatial patterns of construction land expansion in urban agglomeration. The formula used is as follows:

$$UEDI_n = \frac{\left|A_n^{t_2} - A_n^{t_1}\right| \times A^{t_1}}{\left|A^{t_2} - A^{t_1}\right| \times A_n^{t_1}} \tag{2}$$

where $UEDI_n$ is the urban land expansion intensity differentiation index of the Nth urban agglomeration.

Construction Land Expansion Quality

After the reform and its opening up, China has experienced rapid urbanization and industrialization. The rapid growth and the agglomeration of the population and economy have accelerated the outward expansion of construction lands. Due to the influence of the urban–rural dual structure system and the concept of extensive development, numerous problems have emerged, such as the indiscriminate proliferation of construction lands, increased environmental pollution, and inefficient and wasteful land use. These challenges are directly related to the incongruity of construction land expansion with population, economic, and ecological development. Therefore, quantifying the coordination between land, economy, and society is an important foundation for scientifically understanding the quality of construction land expansion and optimizing and coordinating the man–land relationship.

Coordination Model

The coordination degree model is a quantitative method to measure the degree of coordination between systems or

elements, which can be used to evaluate the consistency and coordination among various elements (Li et al., 2020a). In this study, the coordination degree model was used to explore the relationship between construction land expansion and population development, given by the following equations:

$$X = (P_t - P_{t1})/P_{t1}$$

$$Y = (L_t - L_{t1})/L_{t1}$$

$$C = (X + Y)/\sqrt{X^2 + Y^2} \quad (3)$$

where X and Y are the population growth rate and construction land growth rate, respectively; P_t and P_{t1} are the resident population at time t and time t_1, respectively; L_t and L_{t1} are the construction land area at time t and time t_1, respectively; and C is to the coordination degree ($-1.414 \leq C \leq 1.414$). The coordination types were divided into coordinated (C) ($1.40 \leq C$), relatively coordinated (RC) ($1.35 \leq C \leq 1.40$), relatively uncoordinated (RUC) ($1.30 \leq C \leq 1.35$), and uncoordinated (UC) ($C \leq 1.30$).

Tapio Elastic Decoupling Model

The Tapio elastic decoupling model was developed to study the relationship between European economic growth, traffic conditions, and carbon emissions (Tapio, 2005). This approach has been shown to effectively analyze the relationship between different systems or elements. This study used the Tapio model to explore the relationship between construction land expansion and economic growth. The calculation formula is as follows:

$$T = \frac{(L_t - L_{t1})/L_{t1}}{(GDP_t - GDP_{t1})/GDP_{t1}} \quad (4)$$

where T is the decoupling index, L_t and L_{t1} are the total construction land area of the geographical unit in years t, and GDP_t and GDP_{t1} are the gross domestic production (GDP) of the geographical unit in years t and t_1, respectively. From 2000 to 2020, the construction land and the GDP of all cities in the study area had increased. Both ΔL and ΔG were greater than 0, the Tapio index values ranged between 0.1 and 0.8, and the regional "construction land–economy" exhibited weak decoupling.

To further investigate the changes at different years and different internal units and also to consider the actual conditions in the study area, we subdivided the weak decoupling (WD) into three types according to the natural fracture point classification method: high WD (HWD, $\Delta L > 0, \Delta G > 0, 0 \leq T < 0.1$), moderate WD (MWD, $\Delta L > 0, \Delta G > 0, 0.1 \leq T < 0.5$), and low WD (LWD, $\Delta L > 0, \Delta G > 0, 0.5 \leq T < 0.8$).

RESULTS

Spatio-Temporal Evolution of Construction Lands

Temporal Series Characteristics

Based on the expansion intensity values computed at different scales and perspectives (see **Table 1**), the expansion intensity of the construction land in the study area exhibited distinct stage characteristics and pronounced differences. The expansion intensity indices for 2000–2005, 2005–2010, 2010–2015, and 2015–2020 were 2.32%, 1.26%, 5.29%, and 3.81%, respectively. Based on these values, the expansion can be divided into three stages. From 2000 to 2010, the first stage exhibited low-speed expansion, with an expansion intensity index lower than 2.5%. At this stage, the urban agglomeration was in the primary cultivation stage, presenting a relatively low regional development level and relatively weak expansion intensity. In the second stage, from 2010 to 2015, the expansion intensity index accelerated and reached its peak. Here, the urban agglomeration was in the stage of rapid development, with the regional economy and society quickly developing. Demands for industrial and residential lands had also increased significantly, causing the accelerated expansion of the construction land. The third stage covered the period 2015–2020, where the urban agglomeration was in a stable development stage, and the expansion rate had decreased. During this period, the focus was on the quality of construction land expansion, resulting in a decrease in expansion intensity.

TABLE 1 | Intensity index of construction land expansion from 2000 to 2020 (%).

Research unit	2000–2005	2005–2010	2010–2015	2015–2020	2000–2020
MYZ-UA	2.32	1.26	5.29	3.81	3.93
WH-UA	1.17	1.16	5.02	1.97	2.69
CZT-UA	2.77	1.83	6.65	6.05	5.78
PY-UA	4.19	1.04	4.75	5.19	4.92

At the sub-urban agglomeration scale, the temporal characteristics of construction land expansion were comparable to those of the entire research area. The first and third stages of the WH-UA had a low expansion intensity, with urban expansion intensity index (UEI) below 1.50%, while the second stage expanded rapidly, with a 5.02% UEI. The first stage of the CZT-UA had a comparatively low expansion intensity, with a UEI lower than 3.00%, whereas the second and third stages both exceeded 6.00%, with the second stage at 6.65%. The temporal change in the construction land expansion in the PY-UA was slightly different from the overall pattern. In the second half of the first stage, the expansion intensity dropped significantly, with the UEI decreasing from 4.19% to 1.04%. The third stage was slightly stronger than the second stage, with the UEI increasing from 4.75% to 5.19%.

The temporal characteristics of construction land expansion at the metropolitan scale were similar to those of the other two scales. The expansion intensity index showed a rising–falling–rising trend, while the growth in the different metropolitan areas exhibited significant differences. As shown in **Table 2**, the Wuhan metropolitan area had the lowest overall expansion intensity, decreasing slightly during the study period. Compared to 2000–2005, the UEI for 2015–2020 declined by 0.19%. In comparison, the overall expansion intensity was the highest in the Changsha metropolitan area. During this period, the overall expansion intensity increased, with the UEI rising by 1.04%. The overall expansion intensity of the Nanchang metropolitan area was weaker than that of Changsha, with its overall

TABLE 2 | Intensity index of construction land expansion in three metropolitan regions from 2000 to 2020 (%).

Research unit	2000–2005	2005–2010	2010–2015	2015–2020	2000–2020
The total	3.51	1.86	5.54	3.39	4.34
Wuhan metropolitan	2.55	1.68	3.49	2.36	2.86
Changsha metropolitan	3.95	2.61	6.51	4.99	5.81
Nanchang metropolitan	4.57	2.23	5.72	4.73	5.13

expansion intensity increasing only slightly and the UEI rising by 0.16% for 2000–2020.

Spatial Pattern Characteristics

There were distinct spatial differences in the construction land expansion in the study area (**Figure 2**). For the given study period, the high-value areas in expansion intensity were concentrated in the CZT-UA, mid-value regions were mainly in the PY-UA, and the low-value areas were situated primarily in the WH-UA. The results suggest that the CZT-UA had expanded most rapidly, followed by the PY-UA, and the WH-UA's expansion had been the slowest. The relatively low expansion rate was due to the large expanse of the construction land in the WH-UA. This is consistent with the analysis results of the expansion intensity index mentioned before. In comparison, the expansion in the CZT-UA had significantly accelerated due to the construction of numerous high-tech, economic development, and new national-level zones.

For the PY-UA, the development of the high-speed expansion areas and the area's rapid growth mainly occurred from 2000 to 2005. In particular, Nanchang and Pingxiang cities expanded the fastest, with urban expansion intensity differentiation index (UEDI) indexes reaching 6.37 and 8.14, respectively. Many medium- and low-speed expansion areas were found in the CZT-UA, while the WH-UA mainly had low-speed expansion areas. From 2005 to 2010, high-speed expansion areas were distributed throughout the three sub-urban agglomerations, but the number was small; only Changsha, Xianning, and Xinyu cities had high-speed expansion. Medium- and low-speed expansion areas were mostly found in WH-UA and CZT-UA, while slower expansion areas were mainly in the PY-UA.

From 2010 to 2015, Xiangtan, Loudi, Hengyang, Jiujiang, and Yingtan cities from the CZT-UA and the PY-UA experienced high-speed expansion. The medium-high expansion areas were found mainly in the WH-UA, while the medium-speed expansion area was distributed in many cities in all three urban agglomerations. The medium- to low-speed expansion areas were located primarily in the PY-UA, and the low-speed expansion areas were only found in the WH-UA. For 2015–2020, the high- and medium-speed expansion areas were concentrated in the PY-UA and the CZT-UA, while the medium- and low-speed expansion areas were mainly in the WH-UA.

There were also pronounced spatial differences in construction land expansion in the three major metropolitan regions (**Figure 3**). From 2000 to 2020, the UEDI for the Wuhan metropolitan area was generally low, and the expansion intensity was relatively weak. The UEDI for the Changsha and Nanchang metropolitan areas was not significantly different, but the expansion intensity of Changsha was slightly greater than that of Nanchang. From 2000 to 2005, the construction land in the Nanchang metropolitan area expanded rapidly, with a UEDI of 1.70, and the high-speed expansion areas were concentrated in the Nanchang municipal area, Xinjian district, Jing'an county, and Fengxin county. The expansion of the Wuhan metropolitan area was relatively slow, with low-speed expansion areas found mainly in Macheng, Tuanfeng, Ezhou, Xiantao, Hanchuan, and areas around the municipal area. From 2005 to 2010, the construction lands in the Changsha and Nanchang metropolitan areas expanded rapidly, with similar UEDI; the high-speed expansion areas were concentrated in Changsha county, Ningxiang city, Jing'an county, and Fengxin county.

From 2010 to 2015, the construction lands in the Changsha metropolitan area continued to expand, with a UEDI of 1.41; the high-speed expansion areas were mainly in Wangcheng district, Xiangtan county, and Zhuzhou county. From 2015 to 2020, the expansion intensities of the three metropolitan areas decreased, and there were no high-speed expansion areas. During this period, the expansion rate of the Changsha metropolitan area was relatively fast, with a UEDI of 1.36. Medium-high expansion areas were located in Changsha municipal district, Wangcheng district, Ningxiang city, Xiangtan city, Xiangtan county, Zhuzhou county, and Liling city and were distributed contiguously.

Expansion Quality Measurement

High-quality development is largely characterized by sustainable growth, which can address people's growing needs and tackle unbalanced and insufficient development. It encompasses various aspects of development, such as efficiency improvements, structural optimization, and coordination and order. High-quality development of construction lands is crucial to meet the spatial needs for production, living, and ecological activities; support the optimal allocation of resources; improve land-use efficiency; and help create a harmonious relationship between people and land.

While population and economy are important driving factors in construction land expansion, they are also major carriers of challenges and contradictions. The coupling and coordination of construction land, population, and economy can reflect the quality of urban expansion. In this study, we characterized the quality of construction land expansion by measuring the coordination degree of "construction land–population" and the coupling/decoupling degree of "construction land–economy."

Coordination Measure of "Construction Land—Population"

The "construction land–population" coordination degree was generally uncoordinated, varying at different periods but exhibiting a generally fluctuating upward trend (**Figure 4**). In 2000–2005, the coordination index between construction land and population was 1.212, and the coordination type was UC. For

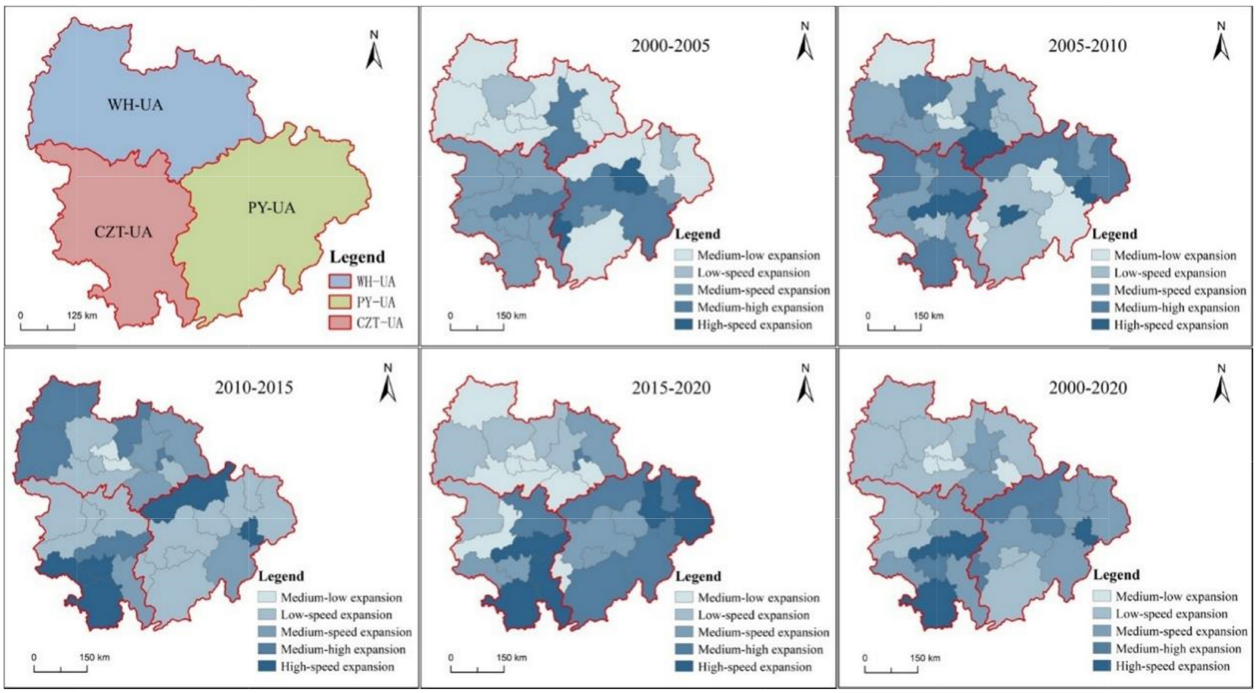

FIGURE 2 | Spatial pattern of difference of construction land expansion intensity from 2000 to 2020.

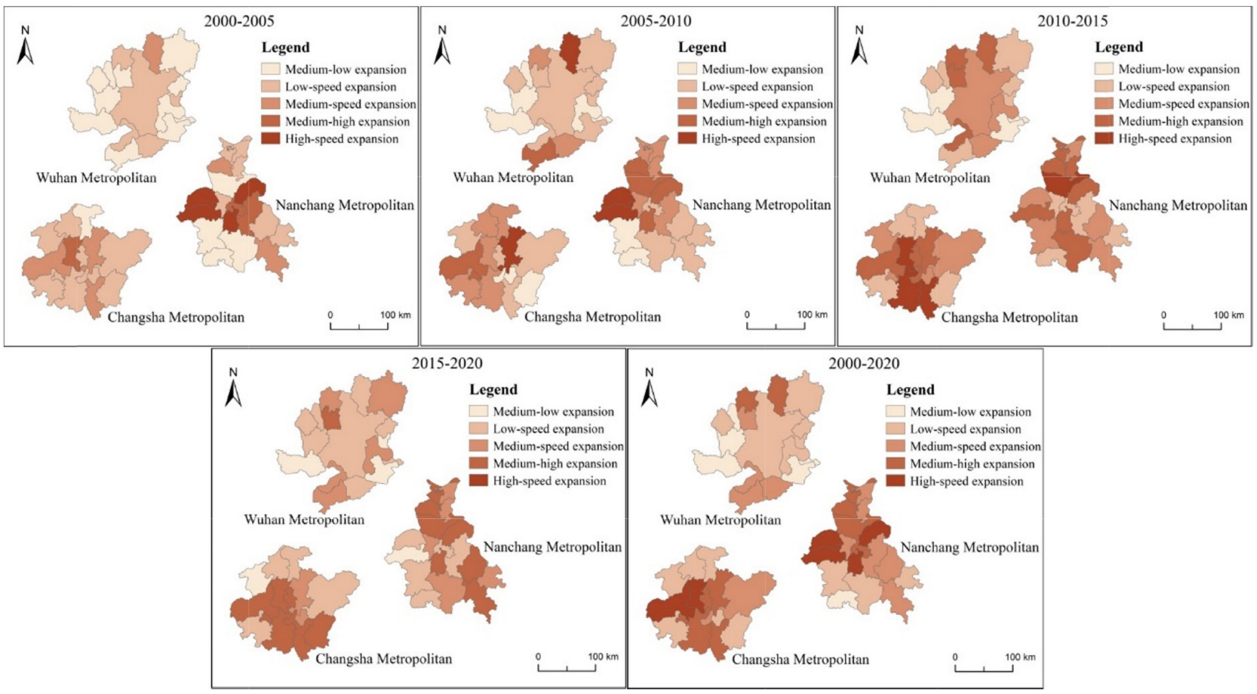

FIGURE 3 | Spatial pattern of difference of construction land expansion intensity in three metropolitan regions from 2000 to 2020.

2005–2010 and 2010–2015, the coordination type developed into RUC. In 2015–2020, the coordination index was 1.343, and the coordination type transitioned from RUC to RC.

Overall, the coordination state for "construction land–population" can be divided into three stages. The period 2000–2010 exhibited an uncoordinated stage dominated by

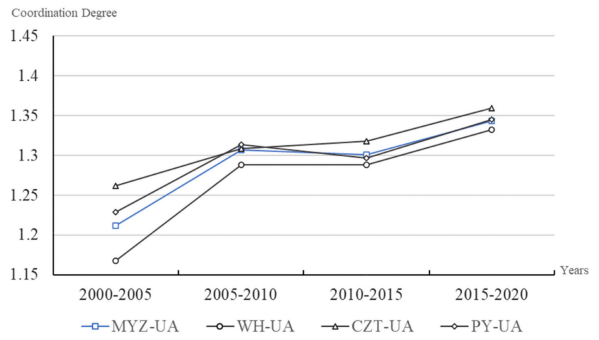

FIGURE 4 | Change of coordination degree of "construction land–population" from 2000 to 2020.

growth, 2010–2015 presented a relatively uncoordinated stage dominated by imbalance, and 2015–2020 displayed a more coordinated stage focusing on quality improvements. Since the start of the 21st century, China's regional development strategy has promoted the development of the central and western regions. Policies and measures focused on western development and major improvements in the central region have been proposed. However, due to the long-term lag in economic development and constraints in the industrial structure, the labor force in the central and western regions has been moving into the coastal areas. At the same time, the local government's fiscal and tax revenues have been overly dependent on land finance, causing land urbanization to significantly outpace population urbanization. This has resulted in a mismatch between population and construction land development in the central and western regions.

With the strengthening of the regional coordinated development strategy, the socio-economic progress in the urban agglomerations in the middle reaches of the Yangtze River has accelerated considerably. Construction lands have expanded rapidly, investments and industries have emerged in some large cities in the central region, and the population outflow has decelerated. The "construction land–population" coordination has improved, but the regional growth differences remain considerably large, leading to uneven development. After implementing new urbanization and encouraging high-quality development, the urbanization levels of many small and medium-sized cities in the study area have significantly improved. The influence of large cities has been further enhanced, the expansion of construction land has intensified, and the labor force has started to return. The "construction land–population" coordination has evolved toward a more coordinated state.

The "construction land–population" coordination in each of the sub-urban agglomerations was largely comparable to the overall urban agglomeration. While the coordination state generally exhibited an upward trend, there were slight variations at different time periods. The "construction land–population" coordination degree for the WH-UA was the lowest among the three urban agglomerations. The coordination relationship has improved significantly, from being in the UC state in 2000–2015 to the RUC state in 2015–2020. The coordination degree for the CZT-UA was in the UC state from 2000 to 2005, RUC from 2005 to 2015, and RC from 2015 to 2020. This means that its general coordination relationship has improved continuously. The PY-UA was in the UC state for 2000–2005, the RUC state for 2005–2010, slightly decreased in 2010–2015, and returned to the RUC for 2015–2020.

The overall "construction land–population" coordination degree in the three major metropolitan areas has been rising (**Figure 5**), developing from uncoordinated to relatively coordinated. However, the coordination degree and evolution process among the different metropolitan areas varied

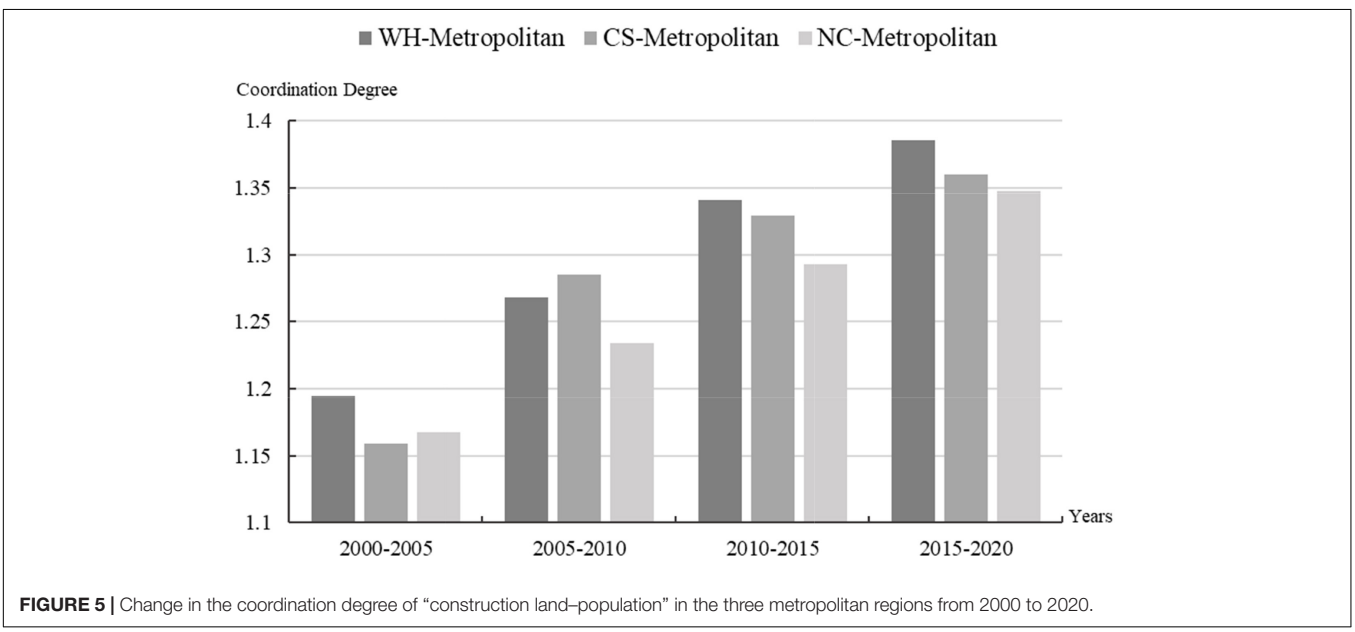

FIGURE 5 | Change in the coordination degree of "construction land–population" in the three metropolitan regions from 2000 to 2020.

considerably. The Wuhan metropolitan area had UC, RUC, and RC phases, with a 1.385 coordination degree in 2015–2020, the highest among the three metropolitan areas. The Changsha metropolitan area had similar coordination types as Wuhan, but the coordination was slightly lower at a 1.360 coordination degree for 2015–2020. The Nanchang metropolitan area had the lowest coordination degree and experienced three stages of coordination types: UC, UC, and RUC. Its coordination generally improved to relatively coordinated, with a coordination index of 1.347 in 2015–2020. The results suggest that the degree of "construction land–population" coordination in the three major metropolitan areas is better than the overall urban agglomeration and the different sub-urban agglomerations.

There are underlying reasons for the spatial differences between agglomerations in sub-urban and metropolitan areas. Due to its strategic location and policy advantages as a national central city, in one of the core nodes of the Yangtze River Economic Belt, many resources aggregate in Wuhan and the Wuhan metropolitan region. By contrast, other cities in the city group experience resource shortages and significant limitations. As a result, while the overall coordination degree for WH-UA is not high, the Wuhan metropolitan area exhibits a high degree of coordination. The CZT-UA has a comprehensive urban system with higher mobility and better linkages, so the overall level of man–land coordination tends to be higher than that in the other regions. For the PY-UA, however, because of its low development level, weak leadership, ineffective self-organization, and limited interactions with other cities, the overall coordination degree and the metropolitan's degree of coordination are generally low.

Decoupling of the "Construction Land–Economy"

The "construction land–economy" decoupling index of urban agglomerations in the middle reaches of the Yangtze River was calculated to be between 0 and 0.8, presenting a fluctuating downward trend from 0.409 in 2000–2005 to 0.335 in 2015–2020. The "construction land–economy" decoupling relationship is generally characterized as weak decoupling. Economic growth is notably faster than construction land expansion. The coupling/decoupling state is good, and the overall situation indicates further optimization (**Figure 6**). From 2000 to 2010, the regional expansion for construction lands did not exhibit a strong momentum, and the economic growth rate was much faster than construction land expansion. The results indicate that the decoupling index is relatively low and that the construction land expansion and economic development of urban agglomerations, as a whole, have low coordination levels.

In 2010–2015, delayed effects from economic growth began to appear, further accelerating urbanization. Numerous development policies and strategies for urban agglomerations in the middle reaches of the Yangtze River were also implemented to promote socio-economic growth. The construction land expanded more rapidly and grew slightly faster than economic growth. From 2015 to 2020, a national strategy and guiding principles were adopted to focus on high-quality development. The expansion of regional construction land was controlled and managed, causing the coupling/decoupling relationship between

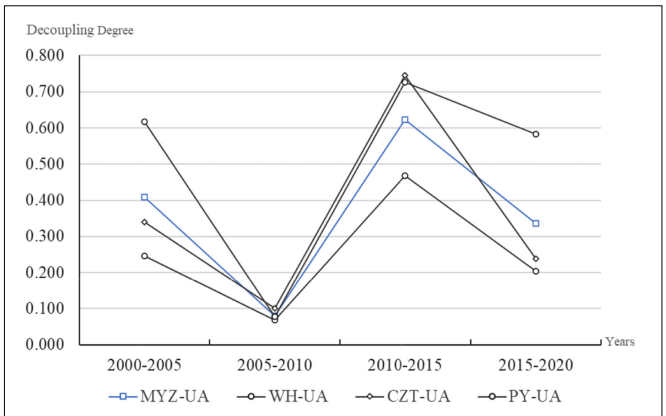

FIGURE 6 | Change in the decoupling degree of "construction land–economy" from 2000 to 2020.

"construction land and economy" to gradually enter a stage of quality-oriented optimization.

Among the sub-urban agglomerations, the WH-UA was mostly of the MWD type during the study period, except for 2005–2010, when it was of the HWD type. Its decoupling index at each time period was the lowest (all below 0.5) and slightly declined over time, indicating that it had the best coupling/decoupling relationship among the three and that the construction land expansion had entered the stage of quality growth (**Figure 6**). The CZT-UA was of the MWD type from 2000 to 2010, the LMD type from 2010 to 2015, and again of the MWD type from 2015 to 2020. The decoupling index value initially decreased, then increased, and then decreased again. Its overall value decreased, although its coupling/decoupling relationship was worse than that of the WH-UA. The PY-UA was of the HWD type from 2005 to 2010 and the LWD type in other periods. The construction land expansion and economic growth were generally coupled, although its decoupling index was the highest. There was a slight increase in decoupling over the research period, indicating that both economic growth and construction land expansion were in a rapid rising period and that the acceleration of construction land expansion was greater than economic growth.

The decoupling indices for the construction land and economy in the three major metropolitan areas were below 0.4 during the study period and exhibited a downward trend. The decoupling type was mostly MWD, with no LWD type. The coupling/decoupling relationship was generally better, indicating that the "construction land–economy" coupling at the metropolitan scale was significantly better than the overall urban agglomeration and the sub-urban scale (**Figure 7**). The "construction land–economy" coupling/decoupling relationship was best in the Wuhan metropolitan area. The overall decoupling index slightly decreased, indicating that the coupling/decoupling relationship was optimized. For the Changsha metropolitan area, the decoupling index dropped significantly. While the coupling/decoupling state was also optimized considerably, the overall coupling/decoupling degree differed slightly from that of Wuhan. The decoupling index of the Nanchang metropolitan

area, the highest among the three regions, increased slightly, and its coupling/decoupling relationship was slightly worse than the other two regions.

There are several explanations why the "construction land–economy" coupling at the metropolitan scale is better than the urban agglomeration. First, the foundation and development stages of the metropolitan area are higher than the overall urban agglomeration. Second, the development strategy focuses on catching up, and the role of leadership is inadequate. Third, as the urban agglomeration has a large spatial scope, the overall agglomeration effect is insufficient, and the spillover effect and leadership roles of core cities are not so strong.

DISCUSSION

Construction land expansion exhibited different expansion characteristics in different development periods and regions. The differences in expansion quality were also found to be closely linked to many elements in the regional spatial functional structure (Ouyang et al., 2022). The results of this study show that after the rapid expansion of the construction land in the study area, the expansion rate started to slow down, ushering in a new period focused on quality improvements. However, the level of coordination between the construction land and the population remains low. The increase in the construction land has neither supported the effective gathering and dispersal of the population nor improved the living environment. The spatio-temporal developments of the construction land and population have not yet reached a coordinated state.

While the coupling between the construction land and the economy in the study area can be characterized as generally good, there are still many places experiencing a shortage of construction lands. The lack of construction lands seems to be a significant problem restricting development (Li et al., 2020b). This problem implies that in the urban agglomerations of the middle reaches of the Yangtze River, the economic intensity of the construction land remains low and that unused lands can be commonly found in the cities. The coupling relationship between the two needs to be further enhanced.

Against the backdrop of high-quality development, new requirements are proposed for the coordinated symbiosis of productive, living, and ecological spaces (Li et al., 2021). These measures could make construction lands effectively support the agglomeration of the economy and population and satisfy the residents' needs and wellbeing. Haphazard expansion and the low utilization efficiency of land resources should be addressed to generate a more efficient development; achieve better coordination between land use and economy, society, and ecology; and promote coordination and balance among cities.

Several recommendations are proposed for the high-quality development of the study area. First, the government should ensure high-quality land resource planning and develop a rational plan to account for the various land-use types. The organic harmony of different land-use types in urban and rural areas should also be promoted. Second, reforms on the land system and land use policies should be explored and initiated, and the management of land resources should be further strengthened. An information database for land resources should also be developed to record changes in land use. Third, the effective renewal of cities must be continued by strengthening intensive and human-oriented urban land use and accelerating the withdrawal of rural homesteads. Rural hollowing should be reduced, promoting the development of new homesteads instead of demolishing old ones. Fourth, the radiation and driving role

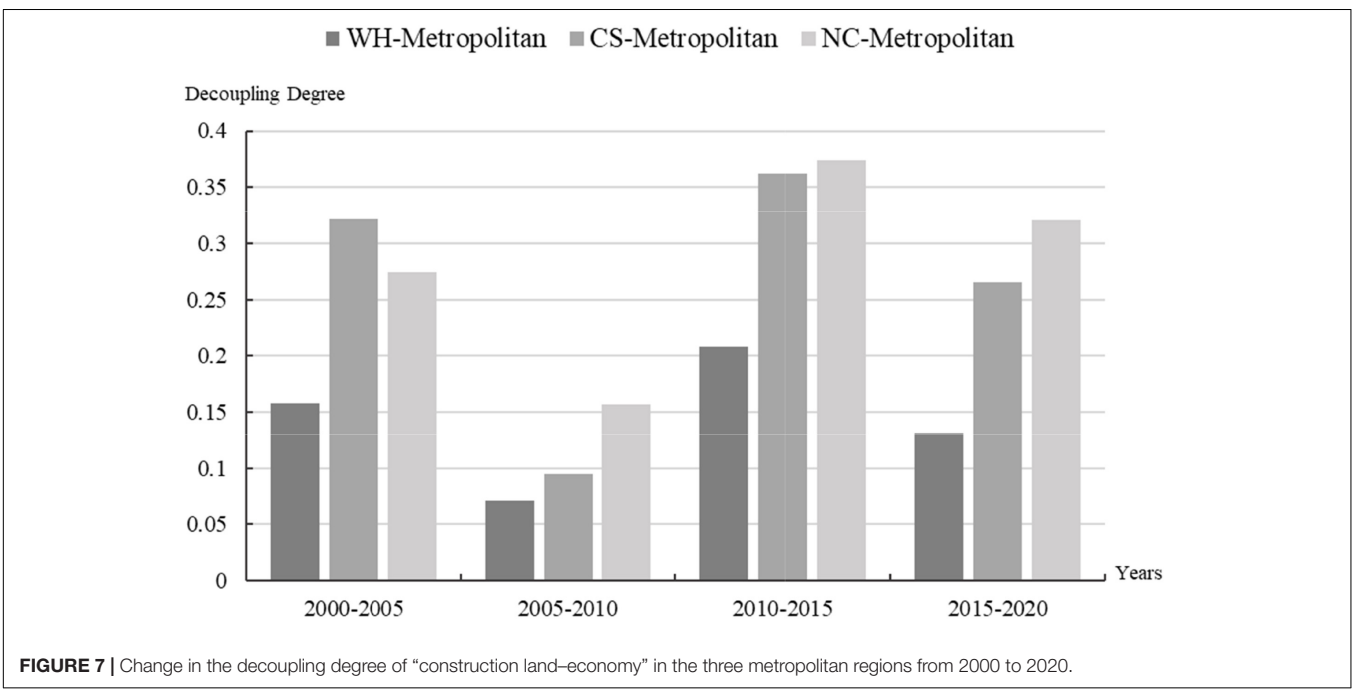

FIGURE 7 | Change in the decoupling degree of "construction land–economy" in the three metropolitan regions from 2000 to 2020.

of central cities should be strengthened, accelerating population agglomeration and socio-economic construction in small and medium-sized cities and towns. The government should aim to narrow the quality differences in the spatial development between cities and improve the coordination of high-quality development of the regional spatial structure.

Two issues that were not addressed in this study could be further explored in subsequent studies: The first is a comprehensive analysis of the spatial expansion quality of urban agglomerations based on the full perspective of economy, society, and ecology (Ren et al., 2022), and the second is establishing a scientific and systematic evaluation index system to quantitatively evaluate the quality of spatial development of urban agglomerations.

CONCLUSION

Using three scales (i.e., urban agglomeration, sub-urban agglomeration, and metropolitan), this study utilized the expansion intensity index to analyze the spatio-temporal evolution of construction lands in the urban agglomeration in the middle reaches of the Yangtze River. We used the coordination degree model, the Tapio elastic decoupling model, and the Theil index to explore the coordination and regional differences between the construction land, population, and economy. The main conclusions are as follows:

(1) The construction land in the research area continuously expanded during the study period. The expansion intensity varies at different periods and can be divided into three stages: slow expansion, accelerated expansion, and optimal expansion. In general, the expansion intensities of the CZT-UA and the Changsha metropolitan area were larger than those of the WH-UA and the Wuhan metropolitan area.

(2) Overall, the relationship between urban construction land expansion and the population has not been well-coordinated, but the coordination has gradually improved. Among the sub-urban agglomerations, the coordination degree was highest in the CZT-UA, while the Wuhan metropolitan area was highest at the metropolitan scale. Moreover, the optimization of the man–land coordination relationship was faster at the metropolitan scale than at the urban agglomeration scale.

(3) The decoupling relationship between the construction land expansion and the economy in the study area was found to be of the weak decoupling type. The coupling state was good and exhibited characteristics of further optimization. The coupling in the WH-UA and the Wuhan metropolitan area was the best among the sub-urban agglomerations and the metropolitan regions, while those in the PY-UA and the Nanchang metropolitan area were poor. In addition, the coupling/decoupling relationship at the metropolitan area scale was significantly better than that at the urban agglomeration scale.

DATA AVAILABILITY STATEMENT

The original contributions presented in this study are included in the article/supplementary material, further inquiries can be directed to the corresponding author/s.

AUTHOR CONTRIBUTIONS

QN conceived and designed the research. QN and XO drafted the manuscript, prepared figures, and revised the manuscript. SL discussed the results. All authors read and approved the final manuscript.

FUNDING

This research was funded by the Scientific Research Foundation of Hunan Provincial Education Department of China (No. 21A0506) and National Science Foundation of Hunan Province of China (No. 2021JJ40015).

REFERENCES

Chen, Y., Yang, J., Yang, R., Xiao, X., and Xia, J. C. (2022). Contribution of urban functional zones to the spatial distribution of urban thermal environment. *Build. Environ.* 216:109000. doi: 10.1016/j.buildenv.2022.109000

Fang, C. L. (2014). Progress and the future direction of research into urban agglomeration in China. *Acta Geogr. Sin.* 69, 1130–1144.

Fang, C. L. (2018). Important progress and prospects of China's urbanization and urban agglomeration in the past 40 years of reform and opening-up. *Econ. Geogr.* 38, 1–9.

He, B. J., Wang, J., Zhu, J., and Qi, J. (2022). Beating the urban heat: situation, background, impacts and the way forward in China. *Renew. Sustain. Energy Rev.* 161:112350. doi: 10.1016/j.rser.2022.112350

Li, G., Sun, S., and Fang, C. (2018). The varying driving forces of urban expansion in China: insights from a spatial-temporal analysis[J]. *Landsc. Urban Plan.* 174, 63–77. doi: 10.1016/j.landurbplan.2018.03.004

Li, J., Ouyang, X., and Zhu, X. (2021). Land space simulation of urban agglomerations from the perspective of the symbiosis of urban development and ecological protection: a case study of Changsha-Zhuzhou-Xiangtan urban agglomeration. *Ecol. Indic.* 126:107669. doi: 10.1016/j.ecolind.2021.107669

Li, Y. R., Li, Y., Karácsonyi, D., Yongsheng, W., Wang, J., and Zhengjia, L. (2020b). Spatio-temporal pattern and driving forces of construction land change in a poverty-stricken county of China and implications for poverty-alleviation-oriented land-use policies. *Land Use Policy* 91:104267. doi: 10.1016/j.landusepol.2019.104267

Li, Z. Y., Luan, W. X., Zhang, Z. C., and Su, M. (2020c). Relationship between urban construction land expansion and population/economic growth in Liaoning Province. China. *Land Use Policy* 99:105022. doi: 10.1016/j.landusepol.2020.105022

Li, Y. J., Kong, X. S., and Zhu, Z. Q. (2020a). Multi-scale analysis of the correlation patterns between the urban population and construction land in China. *Sustain. Cities Soc.* 61, 1–12. doi: 10.1016/j.scs.2020.102326

Liu, S., Zhang, H. X., and Cheng, W. Y. (2021). The quality of urban construction land expansion in Shandong Province: based on the analysis of different expansion patterns. *Urban Problems* 10, 76–84.

Liu, Y. Q., Song, W., and Deng, X. Z. (2019). Understanding the spatiotemporal variation of urban land expansion in oasis cities by integrating remote sensing and multi-dimensional DPSIR-based indicators. *Ecol. Indic.* 96, 23–37. doi: 10.1016/j.ecolind.2018.01.029

Lv, X., and Huang, X. J. (2013). Research progress and prospect of construction land expansion. *Geogr. Geo-Inf. Sci.* 29, 51–58.

Ministry of Housing and Urban-Rural Development, P. R. C. (2018). *China Urban-Rural Construction Statistical Yearbook*. Beijing: China Planning Press.

Ouyang, X., Tang, L., Wei, X., and Li, Y. (2021a). Spatial interaction between urbanization and ecosystem services in Chinese urban agglomerations. *Land Use Policy* 109:105587. doi: 10.1016/j.landusepol.2021.105587

Ouyang, X., Wei, X., Li, Y., Wang, X. C., and Klemeš, J. J. (2021b). Impacts of urban land morphology on PM2.5 concentration in the urban agglomerations of China. *Environ. Manage.* 283:112000. doi: 10.1016/j.jenvman.2021.112000

Ouyang, X., Xu, J., Li, J., Wei, X., and Li, Y. (2022). Land space optimization of urban-agriculture-ecological functions in the Changsha-Zhuzhou-Xiangtan urban agglomeration. China. *Land Use Policy* 117:106112. doi: 10.1016/j.landusepol.2022.106112

Ren, J., Yang, J., Zhang, Y., Xiao, X., Xia, J. C., Li, X., et al. (2022). Exploring thermal comfort of urban buildings based on local climate zones. *J. Clean. Prod.* 340:130744. doi: 10.1016/j.jclepro.2022.130744

Shen, W., Lu, F. X., and Qin, Y. C. (2019). Analysis of temporal- spatial patterns and influencing factors of urban ecosystem carrying capacity in urban agglomeration in the middle reaches of the Yangtze River. *Acta Ecologica Sinica* 39, 3937–3951.

Tapio, P. (2005). Towards a theory of decoupling: degrees of decoupling in the EU and the case of road traffic in Finland between 1970 and 2001. *Transp. Policy* 12, 137–151. doi: 10.1016/j.tranpol.2005.01.001

Wang, H. J., Zhang, B., Liu, Y. L., Yanfang, L., Shan, X., and Yu, D. (2018a). Multi-dimensional analysis of urban expansion patterns and driving forces based on the center of gravity-GTWR model: a case study of the Beijing-Tianjin-Hebei urban agglomeration. *Acta Geographica Sinica* 73, 1076–1092.

Wang, J., Wei, X., and Guo, Q. (2018b). A three-dimensional evaluation model for regional carrying capacity of ecological environment to social economic development: model development and a case study in China. *Ecol. Indic.* 89, 348–355. doi: 10.1016/j.ecolind.2018.02.005

Wei, G., Zhang, Z., Ouyang, X., Shen, Y., Jiang, S., Liu, B., et al. (2021). Delineating the spatial-temporal variation of air pollution with urbanization in the belt and road initiative area. *Environ. Impact Assess. Rev.* 91:106646. doi: 10.1016/j.eiar.2021.106646

Wu, R., Li, Z., and Wang, S. (2021). The varying driving forces of urban land expansion in China: insights from a spatial-temporal analysis. *Sci. Total Environ.* 766:142591. doi: 10.1016/j.scitotenv.2020.142591

Xiao, R., Yu, X. Y., Xiang, T., Zhang, Z., Wang, X., and Wu, J. (2021). Exploring the coordination between physical space expansion and social space growth of China's urban agglomerations based on hierarchical analysis. *Land Use Policy* 109:105700. doi: 10.1016/j.landusepol.2021.105700

Yang, Y. Y., Bao, W. K., Li, Y. H., Wang, Y., and Chen, Z. (2020). Land use transition and its eco-environmental effects in the Beijing–Tianjin–Hebei urban agglomeration: a production–living–ecological perspective. *Land* 9:285. doi: 10.3390/land9090285

Yao, S. M., Zhou, C. S., and Wang, D. (2016). New perspectives on urban agglomerations in China. *Beijing Sci. Press* 6, 150–155.

Yi, D., Guo, X., Han, Y., Guo, G., Ou, M., and Zhao, X. M. (2022). Coupling ecological security pattern establishment and construction land expansion simulation for urban growth boundary delineation: framework and application. *Land* 11:359. doi: 10.3390/land11030359

Yu, J. Q., Zhou, K. L., and Yang, S. L. (2019). Land use efficiency and influencing factors of urban agglomerations in China. *Land Use Policy* 88:104143. doi: 10.1016/j.landusepol.2019.104143

Zhao, D., Zhao, X., Khongnawang, T., Arshad, M., and Triantafilis, J. (2018). A Vis-NIR spectral library to predict clay in Australian cotton growing soil. *Soil Sci. Soc. Am. J.* 82, 1347–1357. doi: 10.2136/sssaj2018.03.0100

Zhao, Z., Sharifi, A., Dong, X., Shen, L., and He, B. J. (2021). Spatial variability and temporal heterogeneity of surface urban heat island patterns and the suitability of local climate zones for land surface temperature characterization. *Remote Sens.* 13:4338. doi: 10.3390/rs13214338

Conflict of Interest: The authors declare that the research was conducted in the absence of any commercial or financial relationships that could be construed as a potential conflict of interest.

Publisher's Note: All claims expressed in this article are solely those of the authors and do not necessarily represent those of their affiliated organizations, or those of the publisher, the editors and the reviewers. Any product that may be evaluated in this article, or claim that may be made by its manufacturer, is not guaranteed or endorsed by the publisher.

Copyright © 2022 Ning, Ouyang and Liu. This is an open-access article distributed under the terms of the Creative Commons Attribution License (CC BY). The use, distribution or reproduction in other forums is permitted, provided the original author(s) and the copyright owner(s) are credited and that the original publication in this journal is cited, in accordance with accepted academic practice. No use, distribution or reproduction is permitted which does not comply with these terms.

frontiers | Frontiers in Ecology and Evolution

ORIGINAL RESEARCH
published: 22 June 2022
doi: 10.3389/fevo.2022.922739

Dynamic Change of Vegetation Index and Its Influencing Factors in Alxa League in the Arid Area

Peng Zhou[1,2,3], Dongxue Zhao[4], Xiao Liu[5,6,7,8]*, Linghua Duo[9,10,11] and Bao-Jie He[2,8,12,13]*

[1] School of Surveying and Land Information Engineering, Henan Polytechnic University, Jiaozuo, China, [2] Smart City Research Institute of Chongqing University in Liyang, Chongqing University, Liyang, China, [3] State Environment Protection Key Laboratory of Satellite Remote Sensing, Aerospace Information Research Institute, Chinese Academy of Sciences, Beijing, China, [4] Centre for Crop Science, Queensland Alliance for Agriculture and Food Innovation, The University of Queensland, Gatton, QLD, Australia, [5] School of Architecture, South China University of Technology, Guangzhou, China, [6] Department of Urban Planning and Design, Faculty of Architecture, The University of Hong Kong, Pok Fu Lam, Hong Kong SAR, China, [7] Design and Research Institute Co., Ltd., South China University of Technology, Guangzhou, China, [8] State Key Laboratory of Subtropical Building Science, South China University of Technology, Guangzhou, China, [9] Jiangxi Ecological Civilization Construction System Research Center, East China University of Technology, Nanchang, China, [10] Faculty of Geomatics, East China University of Technology, Nanchang, China, [11] Key Laboratory of Mine Environmental Monitoring and Improving Around Poyang Lake, Ministry of Natural Resources, Nanchang, China, [12] Centre for Climate–Resilient and Low–Carbon Cities, School of Architecture and Urban Planning, Chongqing University, Chongqing, China, [13] Key Laboratory of New Technology for Construction of Cities in Mountain Area, Chongqing University, Ministry of Education, Chongqing, China

OPEN ACCESS

Edited by:
Bing Xue,
Institute of Applied Ecology (CAS), China

Reviewed by:
Yi Luo,
Yunnan Normal University, China
Chen Yang,
Peking University, China

***Correspondence:**
Dongxue Zhao
zhaodx08@gmail.com
Xiao Liu
xiaoliu@scut.edu.cn

Specialty section:
This article was submitted to Environmental Informatics and Remote Sensing, a section of the journal Frontiers in Ecology and Evolution

Received: *18 April 2022*
Accepted: *24 May 2022*
Published: *22 June 2022*

Citation:
Zhou P, Zhao D, Liu X, Duo L and He B-J (2022) Dynamic Change of Vegetation Index and Its Influencing Factors in Alxa League in the Arid Area. Front. Ecol. Evol. 10:922739. doi: 10.3389/fevo.2022.922739

While there have been various studies on global vegetation dynamics, limited studies have been conducted to understand vegetation changes in arid areas. Vegetation distribution patterns can be affected by multiple factors, so understanding their interactions can help improve the capability of predicting future vegetation dynamics. This study, therefore, analyzed the dynamic vegetation changes in Alxa League, China, using the Normalized Difference Vegetation Index (NDVI) dataset (2000–2019), with the consideration of land cover types, digital elevation model, air temperature, precipitation, soil moisture, total evaporation, and air quality. The results show that the NDVI in Alxa League is small. Before 2012, the NDVI value fluctuated, while after 2012, the NDVI value dropped sharply and then slowly recovered after 2015. High NDVI values were found in areas with high and frequent human activities (city centers). The NDVI in the northwest region showed a slight degradation trend, and the southeast showed a slight improvement trend. According to the land cover type analysis, the NDVI value was the largest when the land cover type was tree cover, and the NDVI value was the smallest when the land cover type was bare/sparse vegetation. Alxa League was dominated by a bare/sparse vegetation distribution. The terrain analysis indicates that when the height was between 1800 and 3492 m, the NDVI value was the highest, and high NDVI values were mainly distributed in the area with a slope $> 25°$. When the slope was flat, the NDVI value was the smallest. Considering climate factors, the NDVI was negatively correlated with air temperature, precipitation, soil moisture, and total evaporation in space, and only precipitation and soil moisture were positively correlated in time. Moreover, the population size has a strong positive correlation with the NDVI in this area. The monthly variation of the NDVI and absorbable particulate matter (PM_{10}) was

negatively correlated, i.e., strongly negatively correlated in spring, summer, and autumn, but only weakly positively correlated in winter. The seasonal variation of the NDVI was as follows: summer > autumn > spring > winter, and the seasonal variation of PM_{10} was spring > winter > summer > autumn. The interannual variation of the NDVI and PM_{10} was positively correlated. This suggests that the absorbable particulate matter (PM_{10}) may be an essential factor for the normalized vegetation index to underestimate the dynamic changes of vegetation in arid regions. This study provides a theoretical basis for the dynamic changes of vegetation in the dry Alxa League.

Keywords: drought, NDVI, topographical differentiation, climate factors, soil moisture, total evaporation, human activities, absorbable particulate matter

INTRODUCTION

Vegetation is important for global environmental changes (Latif et al., 2019), for it bridges the atmosphere, soil, water, and soil (Leanne et al., 2020). In particular, vegetation plays a pivotal role in water conservation, soil erosion prevention, wind and sand fixation, and ecosystem stability (Zhao et al., 2020; Kooch et al., 2022; Mor-Mussery et al., 2022). However, land degradation is aggravating, and especially arid ecosystems are being stressed by increasing demands on natural resources and increasing extreme weather. More frequent and severe droughts are expected to occur in the 21st century, especially in mid-latitudes (Sheffield and Wood, 2008; He et al., 2021, 2022). At the global and regional scales, complex climate changes and human activities significantly affect vegetation growth and development (Burrell et al., 2020; Jiao et al., 2021; Boulton et al., 2022), especially in arid regions. Furthermore, arid environments seriously affect plant growth and thereby pose a significant threat to human life, so it is urgent to address the ecological deterioration of arid regions under climate change and anthropogenic activities. Alxa League is a "severely critical ecological environment area" and a "natural protection barrier" in northern China. Timely, scientific, and accurate assessment of the dynamic vegetation changes in the dry Alxa League and the understanding of the spatial heterogeneity of vegetation changes and the interactions with extreme climates, human activities, and absorbable particulate matter are important.

The Normalized Difference Vegetation Index (NDVI) is closely related to vegetation coverage, leaf area index, biomass, and land use and can comprehensively reflect vegetation greenness, photosynthesis intensity, and vegetation metabolism intensity (Huang et al., 2019; Zhao D. et al., 2021). Therefore, the NDVI has been one of the critical indicators for desertification dynamics assessment and land cover classification, and it has been widely used in soil and water conservation and the ecological environment (Amano and Iwasaki, 2020; Bishnoi et al., 2021). For instance, Na et al. (2021) used AVHRR-GIMMS NDVI3g and the 1982–2015 climate reanalysis datasets to analyze the change of vegetation greenness and its response to climate change in the arid and semi-arid transition areas of the Inner Mongolia Plateau. Measho et al. (2021) used MODIS NDVI combined with evapotranspiration, air temperature, and precipitation datasets to assess vegetation dynamics and ecosystem resilience to climate change and drought in the Horn of Africa. Zhao et al. (2017) investigated the relationship between vegetation changes and extreme climates based on data from 52 meteorological observation stations on the Loess Plateau. Zhao M. et al. (2021) assessed the correlation between the NDVI, land-use dynamics, and water resources in the Mu Us Sandy land. Wu et al. (2020) analyzed the effects of human activities and climatic factors on the NDVI of the desert/steppe biome transition zone in the Sahel region of Africa.

Overall, previous studies focused on the vegetation changes in a region in the desertification degree, terrain, extreme climate, and human activities (Baniya et al., 2018; Nanzad et al., 2019). Among them, different elevations, slopes, and aspects in the topographic analysis could have effects on factors such as human activities, precipitation, and solar radiation in the regions, and climatic and anthropogenic factors have an impact on photosynthesis, transpiration, and growth environment of vegetation, making the results of the NDVI vary in different regions. Furthermore, many scholars have used these factors to conduct spatiotemporal analysis of the vegetation changes with the consideration of such factors. For instance, Ren et al. (2022) analyzed the correlation between air temperature, precipitation, human activities, and the NDVI in the Yellow River basin of China. Zhang et al. (2022) analyzed the spatial and temporal variations of the NDVI in the Qinba Mountains from 1985 to 2015 and combined elevation, air temperature, precipitation, soil type, and human activities to conduct the correlation analysis. However, these studies have not well explored the dynamic distribution of the NDVI and its influencing factors in the arid regions, and the analysis of NDVI dynamics and its relationship through the main component of sand and dust (PM_{10}) in dry areas have not been reported. Therefore, this study aimed to synthesize and analyze various factors, add the assessment of the impact in arid areas from the perspective of absorbable particulate matter (PM_{10}), and make a preliminary determination of whether absorbable particulate matter (PM_{10}) affects the NDVI. Accordingly, the primary objective of this study was to analyze the NDVI dynamic changes in the dry Alxa League, and the second one was to explore the relationship between the NDVI and many factors such as land cover types, digital elevation model (DEM), air temperature, precipitation, soil moisture, total evaporation, human activities (e.g., population size, engineering water supply, and total irrigation area), and air quality to

understand the characteristics of vegetation growth changes and the response to the driving factors. Overall, this study can provide a theoretical basis and new ideas for vegetation growth and ecological restoration in this area.

The remainder of this article is structured into four sections. Section "Materials and methods" describes the study area, the sources of all the data used, and the methods used. Section "Results" describes the study results on the temporal and spatial variations of the NDVI and its driving factors. Section "Discussion" discusses the causes of NDVI spatiotemporal variation and the specific responses of driving factors to NDVI spatiotemporal distribution. Conclusions are presented in Section "Conclusion."

MATERIALS AND METHODS

Study Area

Alxa League is located in the western part of the Inner Mongolia Autonomous Region, China, and it is divided into Ejin Jinna Banner, Alxa Right Banner, and Alxa Left Banner, with an administrative area of 2.7×10^5 km^2. The geographical coordinates are 97°10′∼106°53′E and 37°24′∼42°47′N. Alxa League has a significant air temperature difference between day and night, and the precipitation decreases from the southeast to the northwest. Its annual average air temperature is 8.25°C, and its annual rainfall is 10.64 mm. The landscape is mainly desert, has a Gobi climate, and is surrounder in mountainous hills, and the desertification area is as high as 2×10^5 km^2, accounting for 84% of the total land area. In addition, the natural vegetation in Alxa League is sparse, and the whole league presents steppe desert belt, typical desert belt, and arid desert belt from the southeast to the northwest. In particular, more than 0.88×10^5 km is covered by desert, accounting for one-third of the total area; the site is also one of the sandstorm outbreak sources in East Asia.

Data

Normalized Difference Vegetation Index Data

The NDVI data obtained were at the annual and quarter scales. Monthly 1 km vegetation (NDVI) spatial distribution datasets in China and the monthly NDVI datasets were generated based on SPOT/VEGETATION PROBA-V 1 KM PRODUCTS[1] (accessed on 17 January 2022), and decadal 1 km vegetation index data were generated based on the maximum synthesis method. Annual and quarterly NDVI data were generated using the same way based on monthly data. The annual NDVI data were selected from 2000 to 2019, and the monthly and seasonal NDVI data were chosen from 2015 to 2019. The reliability and accuracy of this dataset have been well demonstrated in studies related to spatial and temporal variations of the NDVI (Zhang Y. et al., 2021).

Vegetation-Type Data and Digital Elevation Model Data

ESA_WorldCover_10 land cover types were provided by the European space agency[2] (accessed on 17 January 2022) with a 10 m spatial resolution. With more than 74% overall accuracy, the ESA_WorldCover_10 data have been widely used for monitoring land use/land cover studies worldwide (Wang et al., 2022). The vegetation types of the region can be divided into eleven categories: tree cover, shrubland, grassland, cropland, built-up, bare/sparse vegetation, snow and ice, permanent water bodies, herbaceous wetland, mangroves, and moss and lichen (Zanaga et al., 2021). The areas with unchanged vegetation types from 2000 to 2019 were extracted here to represent the vegetation cover status of the study area in recent years. The DEM data at a spatial resolution of 90 m × 90 m in the TPRR were collected from the SRTM dataset[3] (accessed on 17 January 2022). The primary topographic features based on DEM data, such as elevation, slope, and aspect layers, were computed using the "Slope/Aspect Tool" in the ArcGIS 10.2 Spatial Analyst module. According to the Chinese classification standards for the potential hazard of soil erosion and some other relevant references (Jiang et al., 2014; He et al., 2020), four maps of land use type, elevation, slope, and aspect were generated (**Supplementary Figure 1**). In addition, spatial analysis tools were also used to overlay both the topographic factors layers and NDVI data to obtain the spatiotemporal distribution of the NDVI for each topographic factor over the past 20 years.

Other Data

The air temperature and precipitation applied were from the widely used and accepted climate dataset (CRU TS v. 4.05) produced by the Climatic Research Unit (CRU) (Harris et al., 2020). Soil moisture data were obtained from the NOAA Climate Prediction Center (van den Dool et al., 2003), a dataset describing global gridded monthly average soil moisture. The total evaporation data used in this study were obtained from the latest international climate reanalysis dataset (ERA5)[4] (accessed on 7 April 2022). Human activities data, including population size, engineering water supply, and total irrigation area, were derived from Alxa Statistical Yearbook[5] (accessed on 12 January 2022). Monthly and seasonal PM_{10} data were obtained from the National Real-time Air Quality Publishing Platform public website for air quality monitoring data maintained by the China National Environmental Monitoring Center (CMC) of the Ministry of Ecology and Environment of China[6] (accessed on 17 January 2022). The annual data of PM_{10} were from obtained from China HighPM_{10} (Wei et al., 2021). China HighPM_{10} is one of the series of long-term, full-coverage, high-resolution, and high-quality datasets of ground-level air pollutants of China (i.e., ChinaHighAirPollutants, CHAP). It is generated from the big data (e.g., ground-based measurements, satellite remote sensing products, atmospheric reanalysis, and model simulations) using artificial intelligence by considering the spatiotemporal heterogeneity of air pollution.

[1] http://www.vito-eodata.be

[2] https://viewer.esa-worldcover.org/worldcover

[3] https://srtm.csi.cgiar.org/srtmdata/

[4] https://cds.climate.copernicus.eu/cdsapp/search

[5] http://tjj.als.gov.cn/col/col4189/index.html

[6] http://www.mee.gov.cn/

Methods

Average Analyses of Normalized Difference Vegetation Index

The annual NDVI data were processed into 20-year overall NDVI mean data for analysis in time and space based on the maximum value synthesis method. In addition, annual, quarterly, and monthly data were analyzed temporally using NDVI mean values from raster images, and data on three different temporal metrics were used separately.

Spatial Trend Analysis Methods

Linear trend analysis can simulate the changing trend of the NDVI pixel by pixel and can be used to analyze the changing trend of the NDVI in the Alxa League region on the interannual scale. The regression slope is given as follows:

$$\text{Slope} = \frac{n \times \sum_{i=1}^{n} (i \times y_i) - (\sum_{i=1}^{n} i)(\sum_{i=1}^{n} y_i)}{n \times \sum_{i=1}^{n} i^2 - (\sum_{i=1}^{n} i)^2}, \quad (1)$$

where n is the study time 20, y_i is the NDVI of the year i, the slope is the slope of NDVI change, slope > 0 means an increase in the vegetation cover, and pitch < 0 means a decrease in the vegetation cover. To further analyze the significance of the vegetation cover change trend in Alxa League at the interannual scale, the *F*-test was conducted on the changing trend. The significance of NDVI trends in Alxa League was classified into four categories: nonsignificant degradation, nonsignificant improvement, significant degradation, and significant improvement.

Extraction and Classification of Land Cover Types and Terrain Factors

The land cover types were classified into eight categories: tree cover, shrubland, grassland, cropland, built-up, bare/sparse vegetation, permanent water bodies, and herbaceous wetland. In addition, this study used ArcGIS spatial analysis tools to extract elevation, slope, and aspect information from the DEM of the study area. According to the actual situation of the study area, the elevation was divided into seven grades: 651–800, 800–1000, 1000–1200, 1200–1400, 1400–1600, 1600–1800, and 1800–3492 m, and the slope of the study area was divided into eight grades: 0–2, 2–5, 5–15, 15–25, 25–35, 35–40, 40–45, and $> 45(°)$. According to the angle of 45° clockwise, the slope aspect was divided into nine grades: flat (-1°), N (0–22.5°) (337.5°–360°), NE (22.5°–67.5°), E (67.5°–112.5°), SE (112.5°–157.5°), S (157.5°–202.5°), SW (202.5°–247.5°), W (247.5°–292.5°), and NW (292.5°–337.5°).

Correlation Analysis

Correlation analysis was used to examine the correlation between the NDVI and air temperature, precipitation, soil moisture, and total evaporation. It then revealed the correlation between the interannual NDVI and air temperature, precipitation, soil moisture, and total evaporation in the Alxa League region from 2000 to 2019. It was calculated as follows:

$$R_{xy} = \frac{\sum_{i=1}^{n} (x_i - \bar{x})(y_i - \bar{y})}{\sqrt{\sum_{i=1}^{n} (x_i - \bar{x})^2 \sum_{i=1}^{n} (y_i - \bar{y})^2}}, \quad (2)$$

where Rxy is the correlation coefficient between x and y, the coefficient value is between -1 and 1; n is the study time; xi and yi are air temperature, precipitation, soil moisture, and total evaporation, and NDVI in the i year value; and $\bar{x}$ and $\bar{y}$ are the mean values of x and y, respectively; Rxy > 0 is a positive correlation; and Rxy ≤ 0 is a negative correlation. This study also analyzed the spatiotemporal changes of the NDVI and air temperature, precipitation, soil moisture, and total evaporation to explore the relationship between the NDVI and them.

We synthesized and selected three factors, population size, engineered water supply, and total irrigated area, to analyze human-induced impacts on the NDVI based on information from local statistical offices. The NDVI, which was correlated with the three factors, was analyzed using IBM SPSS Statistics. This study analyzed the correlation between the NDVI and PM_{10}, by the use of average daily 24-h PM_{10} data. In addition, the daily average data were then processed for monthly and seasonal averages to obtain the monthly and average seasonal data used in this study.

RESULTS

Spatiotemporal Variation of Normalized Difference Vegetation Index

Overall, the NDVI values in Alxa League were small, no more than 0.15 (**Figure 1**). From 2000, the NDVI values showed fluctuating changes until 2012, in which year the NDVI values peaked to 0.12131. From 2012 to 2015, the NDVI dropped sharply, with the lowest value of 0.08055 in 2015, while the NDVI rebounded slowly after 2015, with a trend of increase again.

The mean spatial distribution of the NDVI from 2000 to 2019 was calculated, as shown in **Figure 2**. The NDVI had a mean value of 0.098 during the 20 years. The spatial NDVI values in Alxa League were generally small, with smaller values in Alxa Right Banner and the smallest NDVI values in Ejin Jinna Banner,

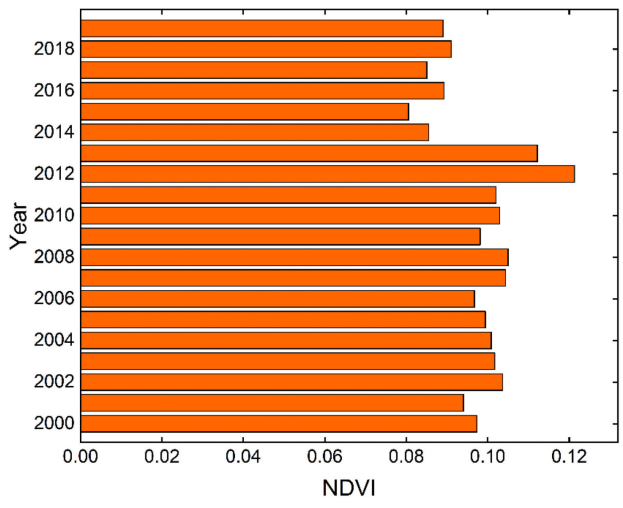

FIGURE 1 | Bar chart of interannual NDVI variation.

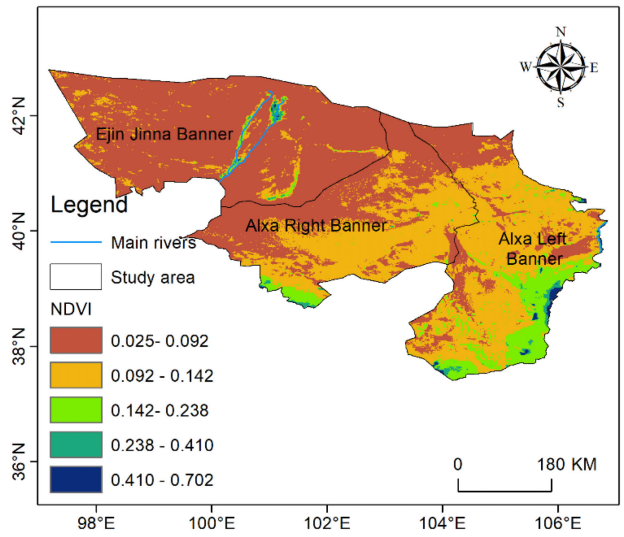

FIGURE 2 | Spatial distribution of 20-year overall NDVI mean values.

indicating only a small amount of vegetation cover in these areas. In comparison, the NDVI values in Alxa Left Banner were slightly larger, indicating a higher vegetation cover in these areas. The places with higher NDVI values in Ejin Jinna Banner, Alxa Right Banner, and Alxa Left Banner were mainly areas with high human activities (city centers), which means that human activities could be conducive to vegetation improvement in desert areas. The results further verified the gradually increasing NDVI values from northwest to southeast in spatial distribution, almost consistent with the description in Section "Study area".

Based on the trend analysis method, the pixel-by-pixel trend analysis of the NDVI of Alxa League in the past 20 years was carried out. The interannual variation trend and significance of the NDVI were judged based on the *F*-test (**Figure 3A**). The results indicated that the whole of Ejin Jinna Banner and part of Alxa Right Banner witnessed a slight trend of degradation (-0.005–0.001), while the vegetation in the Alxa Left Banner and some areas of the Alxa Right Banner was slightly improved (0.001–0.004), showing a slight improvement trend. The city center of Ejin Jinna Banner and some areas of Alxa Left Banner was highly enhanced (>0.004). Nevertheless, according to **Figure 3B**, the NDVI in most areas of Alxa League was nonsignificant. Significant changes were mainly found in the Alxa Left Banner. The general trend from the southeast to the northwest followed a rough trend of significant improvement, significant degradation, nonsignificant degradation, and nonsignificant improvement.

Figure 4 presents the proportion of the NDVI, NDVI trend, and significance of the spatial distribution. More than 90% of the interannual NDVI values were less than 0.142. The areas with the highest (0.410–0.702) and higher (0.238–0.410) NDVI only accounted for 0.31% and 0.93%, respectively. In **Figure 4B**, the NDVI trend was mainly slight degenerate and slight improved, with 58.98% and 38.13%, respectively. Fortunately, there was almost no severely degenerate (0.04%), and the severely improved (>0.004) accounted for 2.85% in this area. In **Figure 4C**, the significance of the NDVI trend was mainly nonsignificant improvement with a proportion of 52.91%, followed by nonsignificant degradation (25.52%), significant degradation (15.4%), and significant improvement (5.5%), which accounted for the smallest proportion.

Influence of Land Use Type, Elevation, Slope, and Aspect

Figure 5 is the overlay analysis of the NDVI by land use type, elevation, slope, and aspect. According to **Figure 5A**, when the

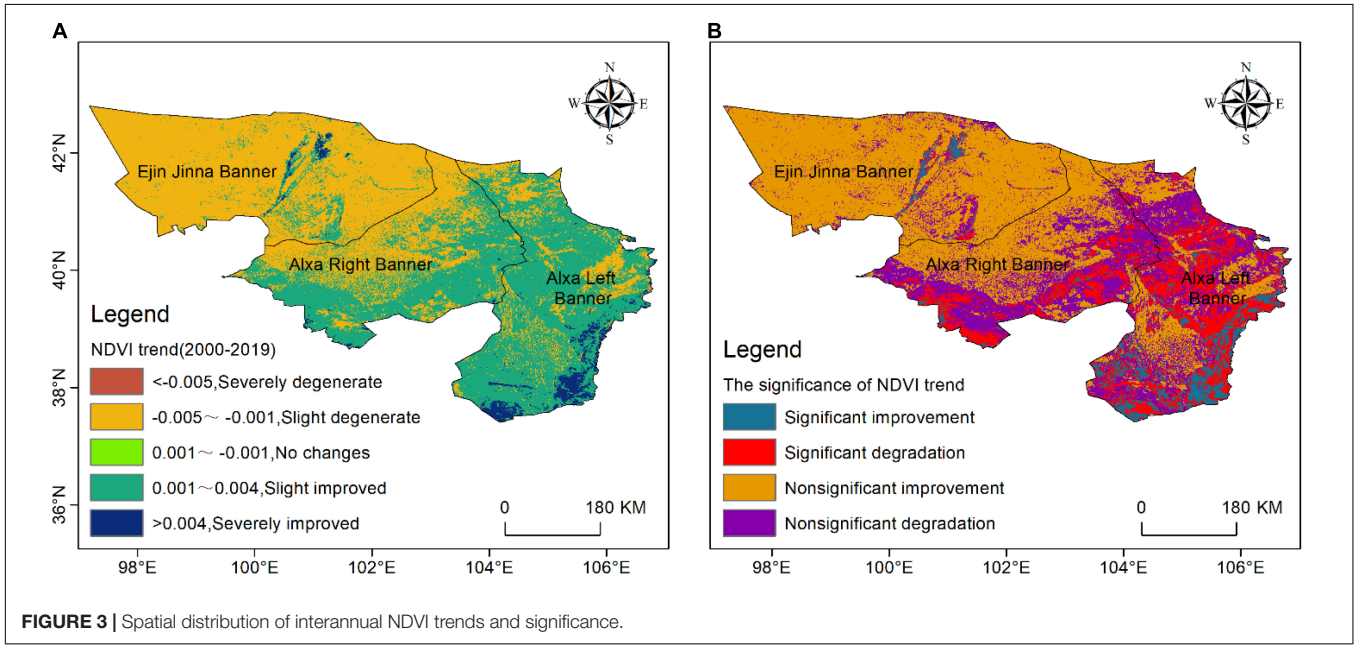

FIGURE 3 | Spatial distribution of interannual NDVI trends and significance.

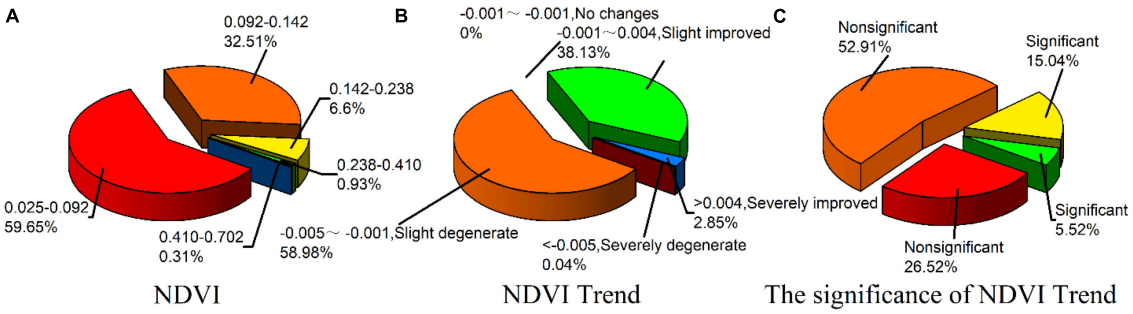

FIGURE 4 | Pie chart of NDVI value and its change trend and the proportion of significant spatial distribution change.

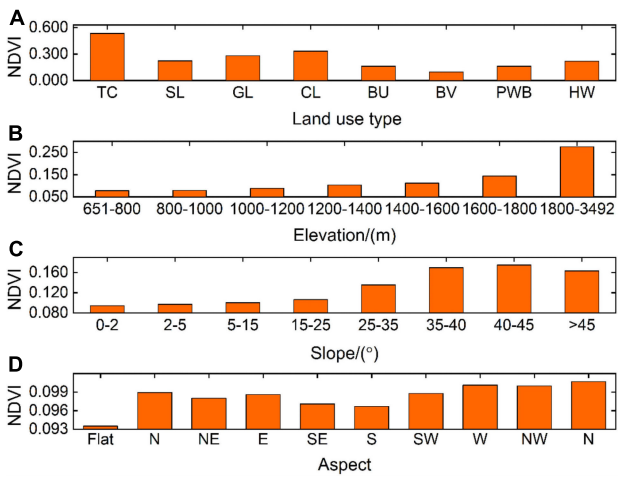

FIGURE 5 | Distribution characteristics of the average vegetation index in the range of different land use types, elevations, slopes, and aspects. Note: TC: tree cover, SL: shrubland, GL: grassland, CL: cropland, BU: built-up, BV: bare/sparse vegetation, PWB: permanent water bodies, HW: herbaceous wetland.

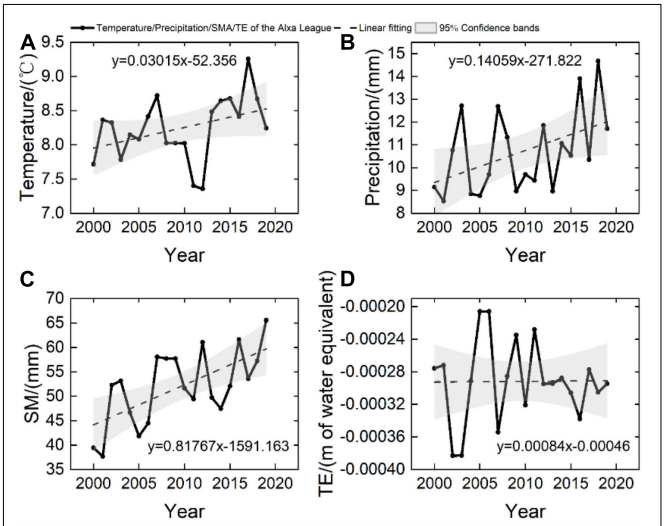

FIGURE 6 | Timeline chart of air temperature, precipitation, soil moisture, and total evaporation.

land use type was tree cover, the NDVI value was the largest. Moreover, the cropland and grassland were characterized by higher NDVI values. In comparison, the NDVI value was the smallest when the land use type was bare/sparse vegetation. **Figure 5B** indicates that the mean value of the NDVI increased with the elevation gradually, and the mean value of the NDVI reached the maximum at the elevation of 1800-3492 m and the minimum at 651–800m. In **Figure 5C**, the NDVI showed a trend of increase and then decrease with the slope, and the NDVI reached the maximum at 40–45° slope and the minimum at 0–2°. In **Figure 5D**, the NDVI fluctuated, and the NDVI was the largest when the aspect was north and the smallest when it was flat.

Impact of Air Temperature, Precipitation, Soil Moisture, and Total Evapotranspiration

This study further analyzed the effect of air temperature, precipitation, soil moisture, and total evaporation on vegetation growth. **Figure 6** presents the annual average changes in air temperature, precipitation, soil moisture, and total evaporation in Alxa League from 2000 to 2019. Overall, the air temperature showed an upward trend, with the lowest air temperature of 7.36°C in 2012 and the highest temperature of 9.26°C in 2017. The 20-year precipitation also showed an upward trend, and its fluctuation was also obvious. The typical years with a precipitation lower than the average were 2001 and 2005, and their precipitation values were 8.53 mm and 8.77 mm, respectively. The soil moisture content increased significantly. The soil moisture in 2000 was 39.48 mm, and the soil moisture increased to 51.94 mm by 2019, with an increase of 12.46 mm. The 20-year evaporation change was not apparent, but after 2012, the band amplitude decreased.

Figure 7 shows the spatial distribution of air temperature and precipitation and their correlations with the NDVI. Overall, the 20-year average air temperature was 8.25°C. The air temperature was higher in the central–eastern part of Alxa League and lower in the northwest and southwest areas (**Figure 7A**). The lowest air temperature was in the downtown area of the suitable banner

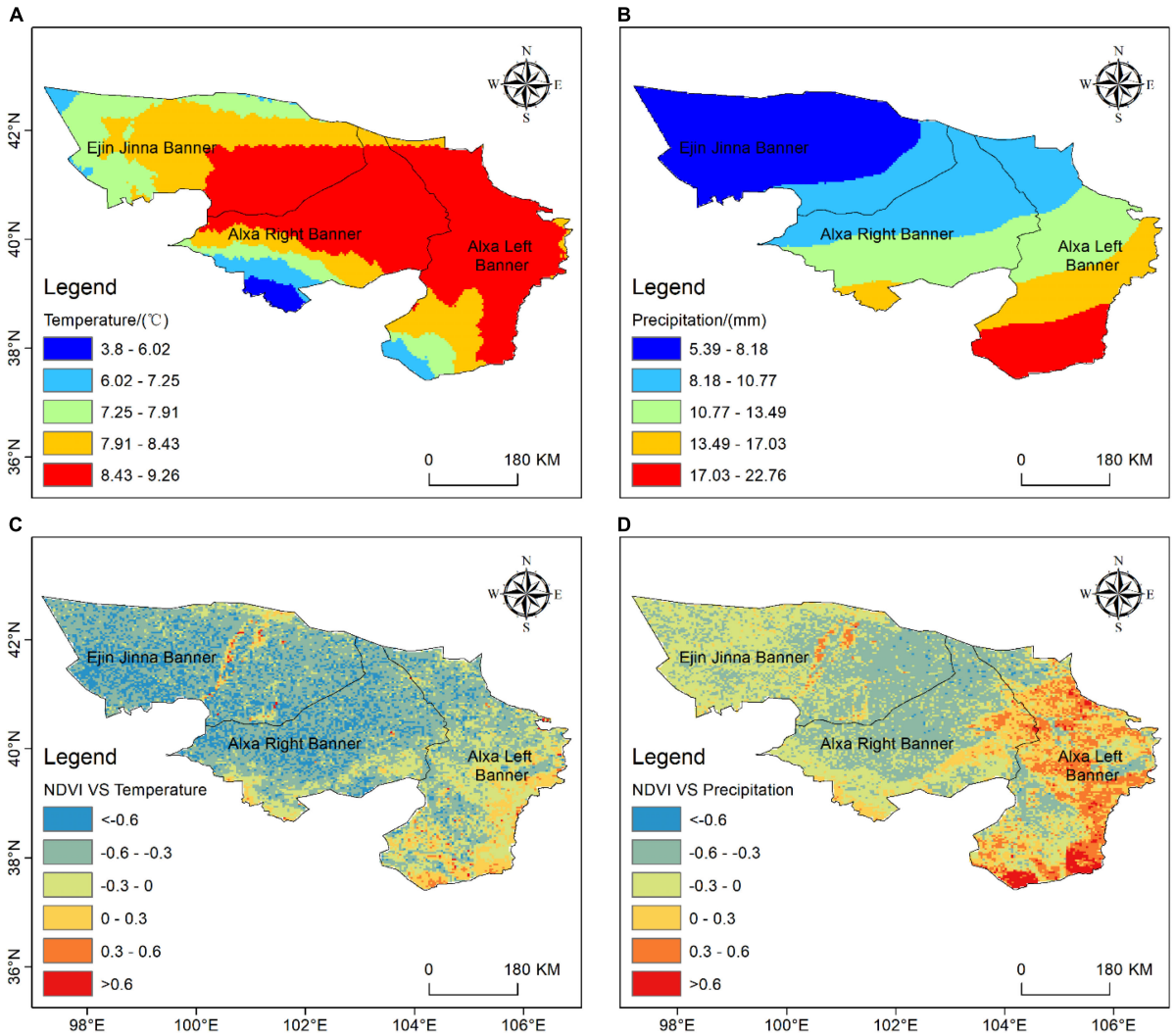

FIGURE 7 | Spatial distribution of mean air temperature and precipitation in Alxa League from 2000 to 2019 and their correlation with NDVI.

of Alxa League. The precipitation gradually increased from the northwest to the southeast, with the least rainfall in Ejin Jinna Banner and the most precipitation in the Left Banner of Alxa League (**Figure 7B**), and the 20-year average rainfall in the league area was 10.64 mm. The spatial distribution pattern of the NDVI was similar to that of rainfall, and there was a big difference in the spatial distribution of air temperature. In particular, according to **Figure 7C**, negative correlation was found in most areas of the league, especially in the central-western deserts and the Gobi region. The NDVI in the downtown, the eastern regions, mountain ranges, and river belts showed a weak positive correlation with the temperature. According to **Figure 7D**, the negative correlation was stronger in the central part, followed by the western part, the downtown, and the eastern part. The mountain and river zones showed a positive correlation. Overall, the spatial distribution shows a higher positive correlation of precipitation on the NDVI than the air temperature.

Figure 8 shows the spatial distribution pattern of soil moisture and total evaporation and their correlations with NDVI. The soil moisture gradually increased from the northwest to the southeast, and the soil moisture content in the northwestern and southeastern regions was quite different, with a minimum value of 21.15 mm and a maximum value of 135.09 mm (**Figure 8A**). **Figure 8B** shows that the total evapotranspiration decreased from northwest to southeast, but the spatial distribution appeared different in the center of Ejin Jinqi and some areas in the northeast of the Alxa League area. The NDVI and soil moisture were generally positively correlated in the central and the eastern part of the Alxa League, the Heihe River Basin, and the central area of Ejin Jinna Banner, while it was negatively correlated in the northwestern region. In **Figure 8D**, the NDVI and total evaporation showed a strong positive correlation in parts of the northern and southern areas and a negative correlation in the eastern and central regions.

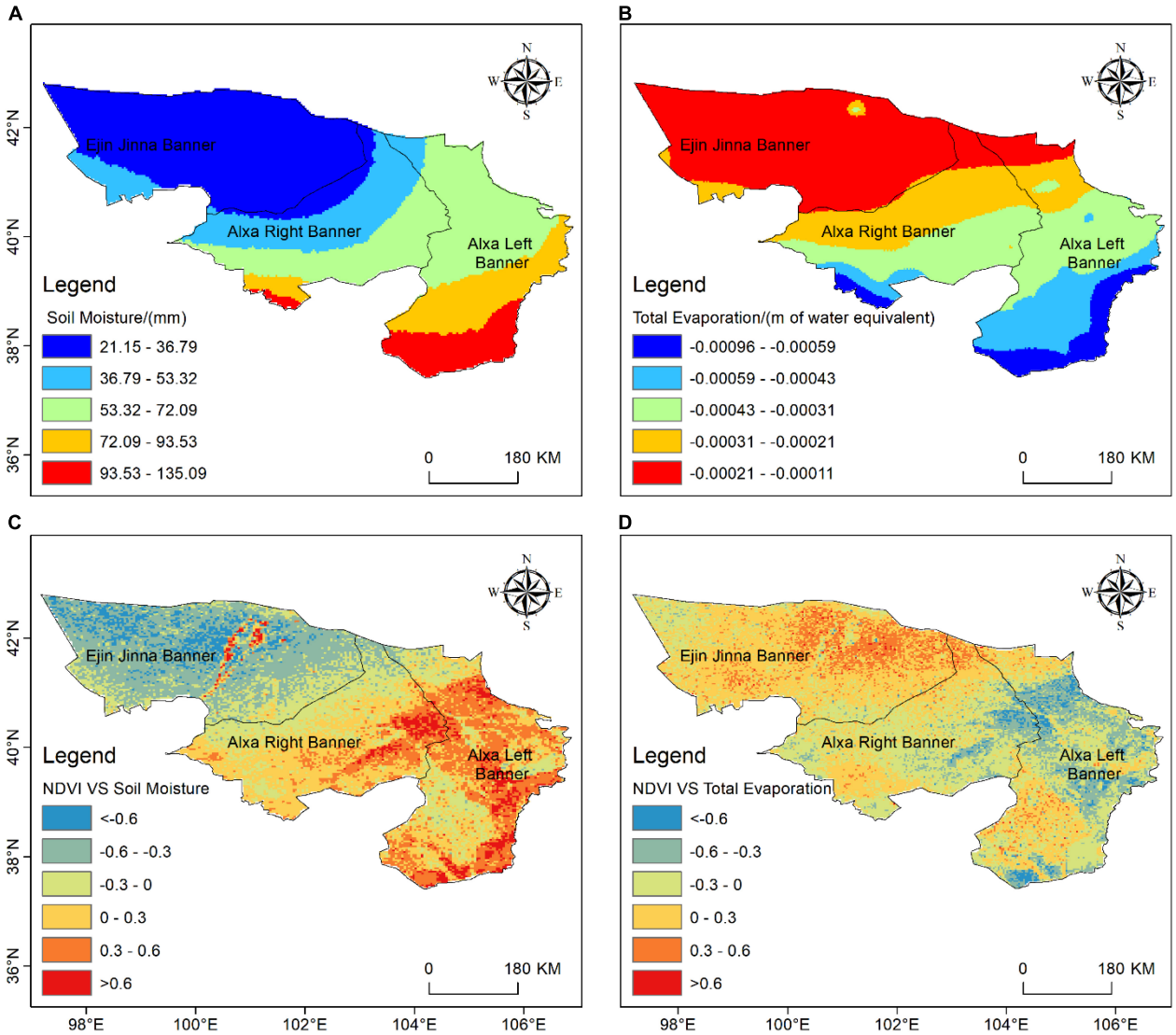

FIGURE 8 | Spatial distribution of mean soil moisture and total evaporation in Alxa League from 2000 to 2019 and their correlation with NDVI.

According to **Table 1**, furthermore, the NDVI and air temperature in Alxa League showed a strong negative correlation in both temporal and spatial scales. The NDVI negatively correlated with precipitation and soil moisture in space, and only soil moisture had a positive correlation in time. Moreover, the NDVI showed a weak negative correlation with total evaporation in both temporal and spatial correlations.

Impact of Human Activities

The population size, engineering water supply, and total irrigation area were human-related factors that could affect vegetation growth and development to a certain extent (Yang et al., 2020). The population of the arid area was mainly in the city center. The population data indicate that the Alxa League Left Banner had the largest population, followed by the Alxa League Right Banner, and the Ejina Banner had the smallest population. According to **Table 2**, the p-values of population size and engineering water supply in the analysis with the NDVI were less than 0.01, and the p-value of the NDVI and the total irrigated area was less than 0.05, indicating that three factors had significant correlations with the NDVI. The population size (R^2 = 0.982), engineering water supply (R^2 = 0.461), and total irrigation area (R^2 = 0.403) had significant positive correlations with the NDVI, and the population size has the strongest correlation, and the entire irrigation area had the weakest correlation.

Impact of Absorbable Particulate Matter

Figure 9 shows the inter-month variation of the NDVI and PM_{10} from 2015 to 2019. The results indicate that the NDVI reached the maximum in June, July, and August and reached the minimum in January, February, and March every year. However, the PM_{10} presented an opposite trend. In the past five years, there was

TABLE 1 | Correlation of interannual variation of the NDVI with air temperature, precipitation, soil moisture, and total evaporation.

	Air temperature	Precipitation	Soil moisture	Total evaporation
Correlation in temporal variation	−0.616	−0.127	0.066	−0.081
Correlation in spatial distribution	−0.417	−0.150	−0.034	−0.046

0.8 – 1.0 indicates extremely strong correlations; 0.6 – 0.8 indicates strong correlations; 0.4 – 0.6 indicates medium-level correlations; 0.2 – 0.4 indicates weak correlations; 0.0 – 0.2 indicates extremely weak or no correlations.

TABLE 2 | Correlation between NDVI and human factors in Alxa League from 2000 to 2019.

	Population size	Engineering water supply	Total irrigation area
NDVI	0.982**	0.461**	0.403*

*** is at the 0.01 level (two-tailed), with a significant correlation. * is at the 0.05 level (two-tailed), with a significant correlation.*

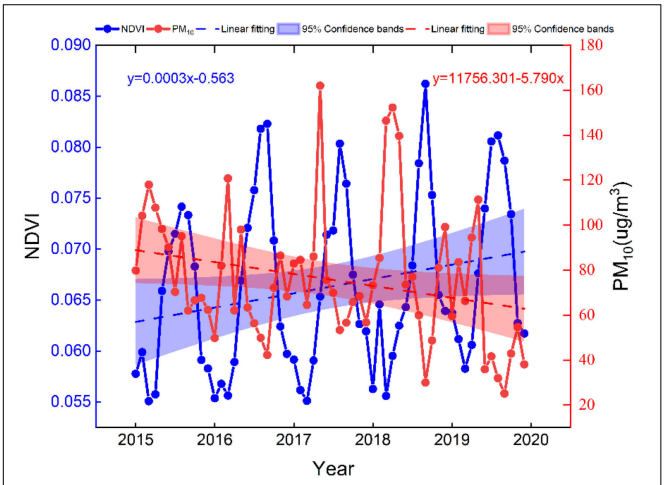

FIGURE 9 | Line chart of NDVI and PM_{10} of Alxa League from 2015 to 2019.

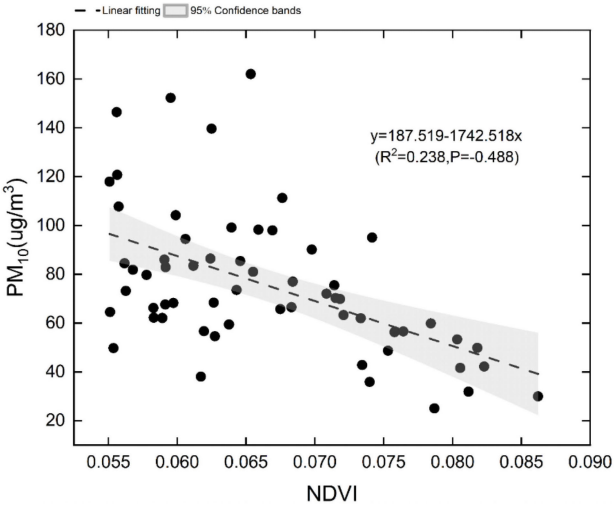

FIGURE 10 | A Scatter plot of NDVI and PM_{10} in Alxa League from 2015 to 2019.

a gradual increase in NDVI values and a gradual decrease in PM_{10}. **Figure 10** presents the correlation between NDVI and PM_{10}, which indicates that there could be a negative relationship between them, while the p-value was only 0.488, meaning that the relationship was not significant.

Figure 11 shows the spatial distribution of PM_{10} and its correlation with NDVI from 2000 to 2019. Overall, the average value of overall PM_{10} concentration in 20 years was 135.044ug/m^3. The high-concentration areas were mainly in the desert areas in the northwest and east parts, while the low-concentration areas were primarily in the mountain areas in the southeast part. The NDVI and PM_{10} were positively correlated in space, and the average correlation coefficient was 0.349. Moreover, there was a positive correlation with the desert area in the northwest part. In terms of time variation, the NDVI was positively correlated with PM_{10}, and the correlation coefficient was 0.522.

Table 3 shows the seasonal variations NDVI and PM_{10} from 2015 to 2019. The NDVI value in the winter of 2015 was the lowest at 0.059, and the PM_{10} in the spring of 2018 was the highest at 146.146 ug/m^3. In the five-year mean distribution, the NDVI and PM_{10} showed noticeable seasonal changes. The seasonal variation of NDVI was summer > autumn > spring > winter, and the seasonal variation of PM_{10} was spring > winter > summer > autumn. However, in these 5 years, when the PM_{10} concentration in spring increased, its NDVI value would decrease, making the case that the spring NDVI value was smaller than the winter NDVI value. Furthermore, **Figure 12** presents that NDVI was negatively correlated with PM_{10} in spring, summer, and autumn but was positively correlated with PM_{10} in winter. In addition, in summer, the negative correlation between the NDVI and PM_{10} was the strongest, with a correlation coefficient of -0.938. The correlation between NDVI and PM_{10} was weak in winter, with a correlation coefficient of 0.074.

DISCUSSION

Temporal and Spatial Distribution of Normalized Difference Vegetation Index

The NDVI value of Alxa League fluctuated before 2012, dropped sharply after 2012, and then slowly recovered after 2015. Our findings are consistent with those of other scholars who have studied vegetation in Alxa League or the entire Chinese region

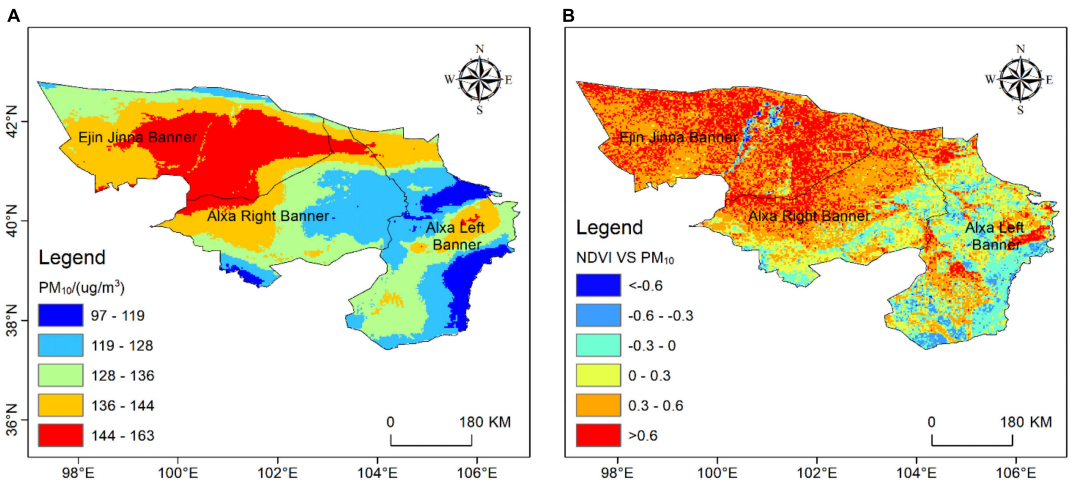

FIGURE 11 | Spatial distribution of overall PM_{10} and its correlation with NDVI for 20 years.

TABLE 3 | Seasonal and interannual dynamic changes of NDVI and PM_{10} in Alxa League from 2015 to 2019.

	Spring		Summer		Autumn		Winter	
	NDVI	**PM_{10}/(ug/m^3)**	**NDVI**	**PM_{10}/(ug/m^3)**	**NDVI**	**PM_{10}/(ug/m^3)**	**NDVI**	**PM_{10}/(ug/m^3)**
2015	0.065	108.009	0.076	85.177	0.073	65.402	0.059	64.657
2016	0.066	93.633	0.083	56.526	0.082	66.937	0.060	78.587
2017	0.064	104.197	0.081	66.272	0.076	63.601	0.064	71.789
2018	0.062	146.146	0.080	70.161	0.086	53.241	0.066	80.712
2019	0.068	90.687	0.084	36.503	0.079	40.875	0.064	51.755
Average	0.065	108.534	0.081	62.928	0.079	58.011	0.063	69.500

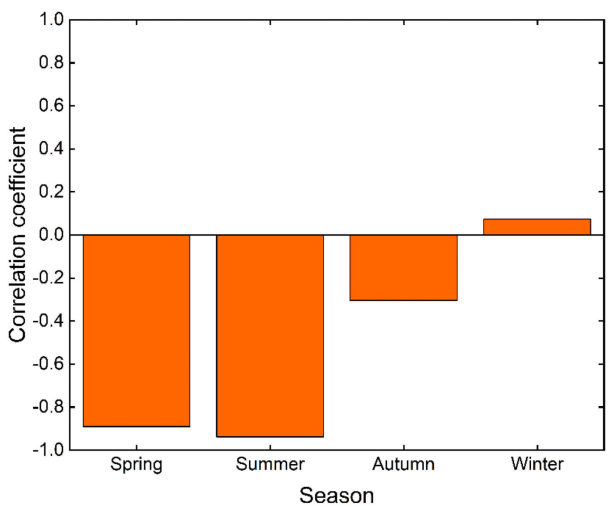

FIGURE 12 | Distribution of correlation coefficients between NDVI and PM10 seasonal changes.

(Xie et al., 2021). After 2012, the desertification situation of Alxa League worsened. Zhang and Huisingh (2018) and others found that warm and dry climates were the critical factor leading to the deterioration of the ecological environment, and the frequent occurrence of severe weather such as sand and dust weather was the driving factor for the decline of the environmental climate. In addition, in the Qinghai–Tibet Plateau, the warm and dry environment caused by the continuous uplift was the fundamental factor for the fragile ecological environment. In terms of spatial distribution, the overall NDVI value of Alxa League was low, which was the same as the change of the NDVI value in other arid regions (Suzuki et al., 2001; Shabanov et al., 2021). In areas with severe desertification, the vegetation was mainly in the city center, indicating that the population in the desert area was the most critical factor affecting the vegetation change. The higher NDVI values in the southern and southeastern regions were due to the extensive planting of trees and the distribution of mountains and rivers. In terms of the trend and significance of NDVI changes, the desertification in the northwestern part of the League intensified. The desertification in the southeastern region reduced, indicating that, although relevant measures and means to protect the ecological environment had been implemented, the desertification trend could not be solved in a short time. A series of policies and measures to improve the ecological environment implemented by the state, such as returning grazing land to grassland and planting artificial forests, indeed improved the environmental climate in arid areas. This

is also the one of most effective ways to improve the ecological environment in dry regions.

Spatial Heterogeneity of Land Use Type and Topographic Factors in Normalized Difference Vegetation Index

Topography controlled the distribution of vegetation patterns (Riihimäki et al., 2016). Our results show that elevation had the most significant impact on local vegetation patterns in the large-scale study range, followed by slope and aspect, consistent with previous studies (Wang et al., 2019; Xu et al., 2020). The average value of the NDVI was mainly concentrated in the area with a slope $> 25°$, which may be because the room with a higher pitch had suffered minor artificial damage, and the vegetation distribution in this area was mainly natural vegetation and abandoned farmland. A suitable slope aspect was conducive to the growth and survival of vegetation. The influence of the slope aspect on vegetation was reflected in the difference between solar radiation and sunshine hours. There were apparent differences in air temperature and vegetation between light-facing and back-lighting slopes. The solar radiation on the south slope was the strongest, followed by the southeast slope and the southwest slope. Again, the east and west slopes and the northeast and northwest slopes had the least solar radiation (Yirdaw et al., 2015). The north slope had the highest average NDVI in this study, and the flat had the lowest average NDVI. It might be because water-saving shrubs and semi-shrubs dominated the vegetation in this area. At the same time, the southern slope was a light-facing slope, with stronger solar radiation, higher air temperature, and faster water evaporation, resulting in a drier and hotter growth environment for vegetation. This negatively affected vegetation growth in the area, so the vegetation was concentrated on the northern slope with little solar radiation. However, our results show that the mean NDVI was the lowest when the slope aspect was flat because there were more deserts and Gobi regions in this area.

Effects of Air Temperature, Precipitation, Soil Moisture, Total Evaporation, and Human Activities on the Dynamic Changes of Normalized Difference Vegetation Index

Air temperature and precipitation indirectly affect the productivity of terrestrial ecosystems by changing nutrient availability (Vo and Johnson, 2001; Jobbágy et al., 2002), and these two climatic factors affect soil moisture and microbial activities in Alxa League, thereby affecting the photosynthesis and respiration in vegetation. In the study area, the air temperature negatively correlated with the NDVI in both time and space, consistent with the research results of related researchers in Iraq, also an arid region (Daham et al., 2018). This is because the air temperature will cause cell dehydration and affect plants' physiological and metabolic activities if it is too high. Precipitation had a weak positive correlation in both time and space. Still, areas with a positive correlation were relatively densely vegetated areas, which indicated that in most cases, precipitation was positively correlated with the NDVI. In addition, most of the negatively correlated areas were desert areas. Relevant studies have shown that the NDVI and precipitation in adjacent areas were also negatively correlated (Guan et al., 2018). The weather in the Alxa League area was cold and snowy and frozen, causing the water in the cells to freeze and rupture, especially in winter. The correlation coefficient between NDVI and soil moisture and the correlation coefficient between NDVI and precipitation were similar. Still, the soil moisture correlation was lower, and soil moisture was positively correlated in time. Similarly, the air temperature was identical to total evaporation. Still, total evaporation was less correlated, suggesting that the NDVI was more strongly associated with air temperature and precipitation among the four factors. This shows that a certain amount of soil moisture can promote the growth of vegetation. In addition, the NDVI was negatively correlated with total evaporation in space and time because an increase in total evaporation affected soil moisture and vegetation growth changes in the area. Around 2015, when the NDVI value dropped sharply, the air temperature increased and the fluctuation of total evaporation decreased, which may be the reason for its sharp decline. Alxa League NDVI and climatic factors were in such a state because the region was in a continental extreme arid climate zone, with hot summers and little rain, cold and windy winters, scarce precipitation, very scarce surface water resources, and intense evaporation. There was abundant wind and sand, and the power of human beings cannot withstand the harsh natural conditions. The NDVI has a strong positive correlation with population, indicating that, in other arid and semi-arid regions similar to arid climates, the impact of human habitation on ecological vegetation could dominate (Zhang Z. et al., 2021).

Influence of PM_{10} on the Dynamic Change of Normalized Difference Vegetation Index

Figures 9, **10** show the negative correlation between NDVI values and PM_{10}, which is consistent with previous studies (Xu et al., 2015). The NDVI values were the highest in June, July, and August in each year, and the PM_{10} concentrations were the highest in January, February, and March, which was in line with the maximum NDVI value in the growing season and the spring sandstorms in Alxa League area (Hao and Li, 2012; Lin et al., 2013). In addition, the results in **Figure 11** show that the NDVI and PM_{10} had a strong negative correlation in all three seasons and only a weak positive correlation in winter. The positive correlation in winter may be because the high pressure of Inner Mongolia influences the winter atmosphere in the Alxa League area, and the League area was windy in winter, making the sand particles on the vegetation surface to blow away. Moreover, the three deserts in the study area were the source of PM_{10} transported from many cities in China, transporting the absorbable particles in the area to other cities. **Table 3** shows that, in the 5-year average, the NDVI value reached the maximum value in every summer and the

minimum value in every winter, and the PM_{10} value showed an opposite pattern. However, in the years with high PM_{10} concentration, the NDVI value in spring was lower than that in winter, indicating that absorbable particulate matter did affect the observation accuracy of the Normalized Difference Vegetation Index. Although the overall spatial distribution of the NDVI and PM_{10} was positively correlated, in places with lush vegetation, the NDVI was significantly negatively correlated with PM_{10}. This indicates that the absorbable particulate matter may affect the observation accuracy of the NDVI, but when in the desert region of the League, the NDVI was positively correlated with PM_{10}. Overall, there is a need to conduct further field investigation and research reasons.

CONCLUSION

Using the NDVI, this study investigated the vegetation dynamic change in the arid Alxa League from 2000 to 2019 and analyzed the correlation between the NDVI and land cover types, topographic factors (elevation, slope, and aspect), climatic factors (air temperature and precipitation), soil moisture, total evaporation, human activity factors (population size, engineering water supply, and total irrigation area), and inhalable particulate matter (PM_{10}). The main conclusions drawn are presented as follows.

1. The NDVI across Alxa League was generally low, while high NDVI values were found in areas with frequent and high human activities (city centers, etc.). The highest NDVI of the region was found in 2012, while the NDVI has decreased significantly in recent years. The NDVI value in the northwest of the Alxa League area showed a slight degradation trend, and the NDVI value in the southeast showed a slight improvement trend.

2. The main land cover types in Alxa League are bare/sparse vegetation. When the land cover types were tree cover and bare/sparse vegetation, the NDVI values were the highest and lowest, respectively. The elevation, slope, and aspect made a difference in the spatial distribution pattern of the NDVI, and the impact of the elevation was the most significant.

3. The NDVI was negatively correlated with air temperature, precipitation, soil moisture, and total evaporation in space. In comparison, the NDVI was positively correlated with total evaporation in time, but the correlation was weak. There was also a strong positive correlation between the population and NDVI.

4. There was a negative correlation between the NDVI and PM_{10} in monthly changes. On the seasonal variations, there was a strong negative correlation between the NDVI and PM_{10} in spring, summer, and autumn but a weak positive correlation in winter. When the PM_{10} concentration was higher, the NDVI value in spring was lower than that in winter. In the interannual variation, the areas with high PM_{10} values were mainly desert areas. The NDVI showed a weak positive correlation with overall PM_{10} and a negative correlation in areas with lush vegetation. The interannual temporal variation also showed a positive correlation between the NDVI and PM_{10}.

DATA AVAILABILITY STATEMENT

The data analyzed in this study is subject to the following licenses/restrictions: The original contributions presented in the study are included in the article, further inquiries can be directed to PZ, 212104020091@home.hpu.edu.cn.

AUTHOR CONTRIBUTIONS

PZ, DZ, and XL: conceptualization, methodology, and visualization. PZ and XL: software and funding acquisition. DZ, LD, and B-JH: validation. PZ: formal analysis and investigation. DZ and XL: supervision. LD, DZ, and XL: writing—first draft. B-JH and XL: writing—review and editing. All authors contributed to the article and approved the submitted version.

FUNDING

This research was funded by the National Natural Science Foundation of China (Grant No. 52108011), China Postdoctoral Science Foundation (Grant No. 2021M701249), Guangzhou Philosophy and Social Science Planning 2022 Annual Project (Grant No. 2022GZQN14), the Department of Education of Guangdong Province (Grant No. 2021KTSCX004), Science and Technology Program of Guangzhou, China (Grant No. 202102020302), the Department of Housing and Urban–Rural Development of Guangdong Province (Grant No. 2021-K2-305243), and the State Key Laboratory of Subtropical Building Science, South China University of Technology (Grant No. 2021ZB16).

ACKNOWLEDGMENTS

We thank all individuals and organizations who provided data.

SUPPLEMENTARY MATERIAL

The Supplementary Material for this article can be found online at: https://www.frontiersin.org/articles/10.3389/fevo.2022.922739/full#supplementary-material

REFERENCES

Amano, H., and Iwasaki, Y. (2020). Land cover classification by integrating NDVI time series and gis data to evaluate water circulation in aso Caldera, Japan. *Int. J. Environ. Res. Public Health* 17:6605. doi: 10.3390/ijerph17186605

Baniya, B., Tang, Q., Huang, Z., Sun, S., and Techato, K. (2018). Spatial and temporal variation of NDVI in response to climate change and the implication for carbon dynamics in Nepal. *Forests* 9:329. doi: 10.3390/f9060329

Bishnoi, P., Sharma, P., and Kumar, E. M. (2021). Analyzing dynamics of degraded lands using NDVI time-series in a semi-arid region

of India. *Arab. J. Geosci.* 14:828. doi: 10.1007/s12517-021-07096-1

Boulton, C. A., Lenton, T. M., and Boers, N. (2022). Pronounced loss of Amazon rainforest resilience since the early 2000s. *Nat. Clim. Change* 12, 271–278. doi: 10.1038/s41558-022-01287-8

Burrell, A. L., Evans, J. P., and Kauwe, M. (2020). Anthropogenic climate change has driven over 5 million km2 of drylands towards desertification. *Nat. Commun.* 11:3853. doi: 10.1038/s41467-020-17710-7

Daham, A., Han, D., Rico-Ramirez, M., and Marsh, A. (2018). Analysis of NVDI variability in response to precipitation and air temperature in different regions of Iraq, using MODIS vegetation indices. *Environ. Earth Sci.* 77:389. doi: 10.1007/s12665-018-7560-x

Guan, Q., Yang, L., Guan, W., Wang, F., Liu, Z., and Xu, C. (2018). Assessing vegetation response to climatic variations and human activities: spatiotemporal NDVI variations in the hexi corridor and surrounding areas from 2000 to 2010. *Theor. Appl. Climatol.* 135, 1179–1193. doi: 10.1007/s00704-018-2437-1

Hao, Y., and Li, L. (2012). Study of the characteristics, disaster and prevention of sandstorm in the central and western regions of inner Mongolia. *Adv. Mat. Res.* 433-440, 1366–1371. doi: 10.4028/www.scientific.net/AMR.433-440.1366

Harris, I., Osborn, T. J., Jones, P., and Lister, D. (2020). Version 4 of the CRU TS monthly high-resolution gridded multivariate climate dataset. *Sci. Data* 7:109. doi: 10.1038/s41597-020-0453-3

He, B.-J., Wang, J., Liu, H., and Ulpiani, G. (2021). Localized synergies between heat waves and urban heat islands: implications on human thermal comfort and urban heat management. *Environ. Res.* 193:110584. doi: 10.1016/j.envres.2020.110584

He, B.-J., Wang, J., Zhu, J., and Qi, J. (2022). Beating the urban heat: situation, background, impacts and the way forward in China. *Renew. Sustain. Energy Rev.* 161:112350. doi: 10.1016/j.rser.2022.112350

He, W., Ye, C., Sun, J., Xiong, J., Wang, J., and Zhou, T. (2020). Dynamics and drivers of the alpine timberline on Gongga Mountain of tibetan plateau-adopted from the Otsu method on google earth engine. *Remote Sens.* 12:2651. doi: 10.3390/rs12162651

Huang, J., Gómez-Dans, J., Huang, H., Ma, H., and Xie, X. (2019). Assimilation of remote sensing into crop growth models: current status and perspectives. *Agric. For. Meteorol.* 276:107609. doi: 10.1016/j.agrformet.2019.06.008

Sheffield, J., and Wood, E. F. (2008). Projected changes in drought occurrence under future global warming from multi-model, multi-scenario, IPCC AR4 simulations. *Clim. Dyn.* 31, 79–105. doi: 10.1007/s00382-007-0340-z

Jiang, L., Liu, X., and Feng, Z. (2014). Remote sensing identification and spatial pattern analysis of the alpine timberline in the three parallel rivers region. *Res. Sci.* 36, 259–266. doi: <doi>

Jiao, W., Wang, L., Smith, W. K., Chang, Q., and D'Odorico, P. (2021). Observed increasing water constraint on vegetation growth over the last three decades. *Nat. Commun.* 12:3777. doi: 10.1038/s41467-021-24016-9

Jobbágy, E. G., Sala, O. E., and Paruelo, J. M. (2002). Patterns and controls of primary production in the patagonian steppe: a remote sensing. *Ecology* 83, 307–319. doi: 10.1890/0012-9658(2002)083[0307:PACOPP]2.0.CO;2

Kooch, Y., Amani, M., and Abedi, M. (2022). Vegetation degradation threatens soil health in a mountainous semi-arid region. *Sci. Total Environ.* 830:154827. doi: 10.1016/j.scitotenv.2022.154827

Latif, A., Sana, I., Zhang, Y., Xin, Y., Zhou, L., and Zhou, Q. (2019). Review on global change status and its impacts on the Tibetan Plateau environment. *J. Plant. Ecol.* 12, 917–930. doi: 10.1093/jpe/rtz038

Leanne, L. C., Guillermo, H. R., David, S. H., Isabel, C. B., Carol, M. F., Cristina, C. S., et al. (2020). A methane sink in the central American high elevation páramo: Topographic, soil moisture and vegetation effects. *Geoderma* 362:114092. doi: 10.1016/j.geoderma.2019.114092

Lin, Q., Sun, L., Wang, X., and Hu, L. (2013). Spatio-temporal variation of vegetation NDVI in China from 2001 to 2011. *Adv. Mat. Res.* 610-613, 3752–3755. doi: 10.4028/www.scientific.net/AMR.610-613.3752

Measho, S., Chen, B., Pellikka, P., Guo, L., Zhang, H., Cai, D., et al. (2021). Assessment of Vegetation dynamics and ecosystem resilience in the context of climate change and drought in the Horn of Africa. *Remote Sens* 13:1668. doi: 10.3390/rs13091668

Mor-Mussery, A., Ben-Eli, M., and Leu, S. (2022). Afforestation of gullies in arid regions, intensification of internal ecological functionality until rehabilitation of the whole area. Attir basin, the Northern Negev, Israel. *Catena* 213:106146. doi: 10.1016/j.catena.2022.106146

Na, R., Na, L., Du, H., He, H., Shan, Y., Zong, S., et al. (2021). Vegetation greenness variations and response to climate change in the arid and semi-arid transition zone of the mongo-Lian Plateau during 1982–2015. *Remote Sens* 13:4066. doi: 10.3390/rs13204066

Nanzad, L., Zhang, J., Tuvdendorj, B., Nabil, M., Zhang, S., and Yun, B. (2019). NDVI anomaly for drought monitoring and its correlation with climate factors over Mongolia from 2000 to 2016. *J. Arid Environ.* 164, 69–77. doi: 10.1016/j.jaridenv.2019.01.019

Ren, Z., Tian, Z., Wei, H., Liu, Y., and Yu, Y. (2022). Spatiotemporal evolution and driving mechanisms of vegetation in the yellow river basin, China during 2000–2020. *Ecol. Indic.* 138:108832. doi: 10.1016/j.ecolind.2022.108832

Riihimäki, H., Heiskanen, J., and Luoto, M. (2016). The effect of topography on arctic-alpine aboveground biomass and NDVI patterns. *Int. J. Appl. Earth Obs.* 56, 44–53. doi: 10.1016/j.jag.2016.11.005

Shabanov, R. M., Dedov, A. A., Vershinin, V. V., Khutorova, A. O., and Dedova, A. A. (2021). Geoecological estimate of grassland use in the desert and semi-desert zone of the Republic of Kalmykia. *IOP Conf. Ser. Earth Environ. Sci.* 867:012077. doi: 10.1088/1755-1315/867/1/012077

Suzuki, R., Nomaki, T., and Yasunari, T. (2001). Spatial distribution and its seasonality of satellite-derived vegetation index (NDVI) and climate in Siberia. *Int. J. Climatol.* 21, 1321–1335. doi: 10.1002/joc.653

van den Dool, C., Huang, J., and Fan, Y. (2003). Performance and analysis of the constructed analogue method applied to U.S. soil moisture over 1981–2001. *J. Geophys. Res. Atmos.* 108:8617. doi: 10.1029/2002JD003114

Vo, S. T. K., and Johnson, E. A. (2001). Alpine plant life: functional plant ecology of high mountain ecosystems. *Mt. Res. Dev.* 21:202. doi: 10.1659/0276-4741(2001)021[0202:APLFPE]2.0.CO;2

Wang, H., Qi, Y., Huang, C., Li, X., Deng, X., and Zhang, J. (2019). Analysis of vegetation changes and dominant factors on the Qinghai-Tibet Plateau. *China. Sci. Cold Arid. Reg.* 11, 62–70.

Wang, J., Yang, X., Wang, Z., Cheng, H., Kang, J., Tang, H., et al. (2022). Consistency analysis and accuracy assessment of three global ten-meter land cover products in rocky desertification Region&mdash: a case study of southwest China. *ISPRS Int. J. Geo. Inf.* 11:202. doi: 10.3390/ijgi11030202

Wei, J., Li, Z., Xue, W., Sun, L., Fan, T., Liu, L., et al. (2021). The ChinaHighPM10 dataset: generation, validation, and spatiotemporal variations from 2015 to 2019 across China. *Environ. Int.* 146:106290. doi: 10.1016/j.envint.2020.106290

Wu, S., Gao, X., Lei, J., Zhou, N., and Wang, Y. (2020). Spatial and temporal changes in the normalized difference vegetation index and their driving factors in the desert/grassland biome transition zone of the sahel region of Africa. *Remote Sens.* 12:119. doi: 10.3390/rs12244119

Xie, J., Lu, Z., Xiao, S., and Yan, C. (2021). Driving force and ecosystem service values estimation in the extreme arid region from 1975 to 2015: a case study of Alxa League. *China. Chin. Geogr. Sci.* 31, 1097–1107. doi: 10.1007/s11769-021-1244-2

Xu, H., Cheng, T., Gu, X., Yu, T., Xie, D., and Zheng, F. (2015). Spatiotemporal variability in dust observed over the Sinkiang and inner Mongolia regions of Northern China. *Atmos. Pollut. Res.* 6, 562–571. doi: 10.5094/APR.2015.063

Xu, M., Li, X., Liu, M., Shi, Y., Zhou, H., Zhang, B., et al. (2020). Spatial variation patterns of plant herbaceous community response to warming along latitudinal and altitudinal gradients in mountainous forests of the Loess Plateau, China. *Environ. Exp. Bot.* 172:103983. doi: 10.1016/j.envexpbot.2020.103983

Yang, L., Shen, F., Zhang, L., Cai, Y., Yi, F., and Zhou, C. (2020). Quantifying influences of natural and anthropogenic factors on vegetation changes using structural equation modeling: a case study in Jiangsu Province, China. *J. Clean. Prod.* 280:124330. doi: 10.1016/j.jclepro.2020.124330

Yirdaw, E., Starr, M., Negash, M., and Yimer, F. (2015). Influence of topographic aspect on floristic diversity, structure and treeline of afromontane cloud forests in the Bale Mountains, Ethiopia. *J. For. Res.* 26, 919–931. doi: 10.1007/s11676-015-0155-4

Zanaga, D., Van De Kerchove, R., De Keersmaecker, W., Souverijns, N., Brockmann, C., and Quast, R. (2021). *ESA WorldCover 10 m 2020 v100*. Wageningen: VITO Remote Sensing, Brockmann Consult, CS SI, Gamma Remote Sensing AG, IIASA and Wageningen University.

Zhang, Y., He, Y., Li, Y., and Jia, L. (2022). Spatiotemporal variation and driving forces of NDVI from 1982 to 2015 in the Qinba Mountains, China. *Environ. Sci. Pollut. Res*. doi: 10.1007/s11356-022-19502-6

Zhang, Y., Yu, W., Ji, R., Zhao, Y., Peng, R., Jia, Q., et al. (2021). Dynamic response of Phragmites australis and suaeda salsa to climate change in the Liaohe Delta wetland. *J. Meteor. Res.* 35, 157–171. doi: 10.1007/s13351-021-0016-3

Zhang, Z., and Huisingh, D. (2018). Combating desertification in China: monitoring, control, management and revegetation. *J. Clean. Prod.* 182, 765–775. doi: 10.1016/j.jclepro.2018.01.233

Zhang, Z., Xu, E., and Zhang, H. (2021). Complex network and redundancy analysis of spatial–temporal dynamic changes and driving forces behind changes in oases within the Tarim Basin in northwestern China. *Catena* 201:105216. doi: 10.1016/j.catena.2021.105216

Zhao, A., Zhang, A., Liu, X., and Cao, S. (2017). Spatiotemporal changes of normalized difference vegetation index (NDVI) and response to climate extremes and ecological restoration in the Loess Plateau, China. *Theor. Appl. Climatol.* 132, 555–567. doi: 10.1007/s00704-017-2107-8

Zhao, D., Arshad, M., Wang, J., and Triantafilis, J. (2021). Soil exchangeable cations estimation using Vis-NIR spectroscopy in different depths: effects of multiple calibration models and spiking. *Comput. Electron. Agric.* 182:105990. doi: 10.1016/j.compag.2021.105990

Zhao, D., Li, N., Zare, E., Wang, J., and Triantafilis, J. (2020). Mapping cation exchange capacity using a quasi-3d joint inversion of EM38 and EM31 data. *Soil Tillage Res.* 200:104618. doi: 10.1016/j.still.2020.104618

Zhao, M., Wang, Y., Liu, S., Zhong, P., and Li, R. (2021). Correlation assessment of NDVI and land use dynamics with water resources for the southern margin of Mu Us Sandy Land, China. *Environ. Sci. Pollut. R.* 29, 17049–17061. doi: 10.1007/s11356-021-16757-3

Conflict of Interest: XL was employed by Architectural Design & Research Institute Co., Ltd.

The remaining authors declare that the research was conducted in the absence of any commercial or financial relationships that could be construed as a potential conflict of interest.

Publisher's Note: All claims expressed in this article are solely those of the authors and do not necessarily represent those of their affiliated organizations, or those of the publisher, the editors and the reviewers. Any product that may be evaluated in this article, or claim that may be made by its manufacturer, is not guaranteed or endorsed by the publisher.

Copyright © 2022 Zhou, Zhao, Liu, Duo and He. This is an open-access article distributed under the terms of the Creative Commons Attribution License (CC BY). The use, distribution or reproduction in other forums is permitted, provided the original author(s) and the copyright owner(s) are credited and that the original publication in this journal is cited, in accordance with accepted academic practice. No use, distribution or reproduction is permitted which does not comply with these terms.

frontiers | Frontiers in Ecology and Evolution

ORIGINAL RESEARCH
published: 30 June 2022
doi: 10.3389/fevo.2022.943265

Evaluation of Cropland System Resilience to Climate Change at Municipal Scale Through Robustness, Adaptability, and Transformability: A Case Study of Hubei Province, China

Mingyan Yan[1], Bohan Yang[1,2], Siyu Sheng[1], Xiangyu Fan[1], Xiaoyun Li[3] and Xinhai Lu[1,2,4]*

[1] College of Public Administration, Central China Normal University, Wuhan, China, [2] Institute of Nature Resources Governance, Central China Normal University, Wuhan, China, [3] College of Economics and Management, Huazhong Agricultural University, Wuhan, China, [4] College of Public Administration, Huazhong University of Science and Technology, Wuhan, China

OPEN ACCESS

Edited by:
Jun Yang,
Northeastern University, China

Reviewed by:
Liye Wang,
Wuhan University, China
Qiushi Zhou,
Zhejiang University, China
Andong Guo,
Zhejiang University, China
Dongxue Zhao,
The University of Queensland, Australia
Chaohui Yin,
Henan Agricultural University, China

***Correspondence:**
Bohan Yang
bohan.yang@ccnu.edu.cn

Specialty section:
This article was submitted to Environmental Informatics and Remote Sensing, a section of the journal Frontiers in Ecology and Evolution

Received: *13 May 2022*
Accepted: *01 June 2022*
Published: *30 June 2022*

Citation:
Yan M, Yang B, Sheng S, Fan X, Li X and Lu X (2022) Evaluation of Cropland System Resilience to Climate Change at Municipal Scale Through Robustness, Adaptability, and Transformability: A Case Study of Hubei Province, China. Front. Ecol. Evol. 10:943265. doi: 10.3389/fevo.2022.943265

A cropland system is one of the most sensitive socio-ecological systems to climate change, such as drought and flood. Facing frequent extreme weather events worldwide, how to improve cropland system resilience to climate change (CSRCC) and thus ensure food production has been concerned. Although a small number of studies have attempted to evaluate CSRCC through single or multiple indicators, few studies have considered the perspective of the three basic capacities of resilience (i.e., robustness, adaptability, and transformability), which could ignore the dynamic characteristics of cropland system resilience against shocks within a certain period. Therefore, this study first constructs an evaluation index system from the three capacities of system resilience. Then, taking Hubei province, China, as a case and comprehensively using the methods of Delphi, AHP, and TOPSIS to assess the spatio-temporal characteristics of CSRCC at the municipal scale from 2011 to 2018. On this basis, the regional disparities of CSRCC are analyzed by using the Theil coefficient. The results show that the CSRCC of Hubei province fluctuates on a downward trend, with the lowest in 2017 and the highest in 2013. Most municipalities have witnessed a pattern of fluctuated decline, except for a few ones in the plains, such as Wuhan and Jingmen. Generally, municipalities in the plains have greater scores, while some municipalities in the southern and eastern hilly regions show higher adaptability and transformability. In addition, adaptability contributes the least to the CSRCC at the municipal scale. At last, indicator selection against different research objects, influencing mechanism of CSRCC, and policy implications are discussed. This study is expected to provide a reference for the practice in sustainable management and utilization of cropland systems.

Keywords: cropland system, resilience to climate change, regional disparity, spatio-temporal change, food security

INTRODUCTION

A cropland system is a socio-ecological system formed by the coupling interaction of cropland resources and human activities. Globally, the cropland system has been facing a series of environmental (Wang C. et al., 2021), socio-economic (Ullah and Uddin, 2021), and institutional (Niedertscheider et al., 2014) disturbances and shocks. For example, plant diseases (Gokulnath and Devi, 2021), insect pests (Gaur and Mogalapu, 2018), changes in market access (e.g., trade war and policy barriers) (He et al., 2019), land-use policies, and management measures (Mittenzwei and Øygarden, 2019) constantly affect agricultural production of the cropland system. Especially, extreme weather (such as drought, flood, and frost) caused by climate change has the most extensive and severe impacts on the cropland system (Kotzee and Reyers, 2016; Rey et al., 2017; Bombi, 2018; Yu and Wu, 2018). Between 1961 and 2010, two-thirds of the world's cropland systems were significantly affected by at least one large-scale climate oscillation (Heino et al., 2018). The measures taken on the cropland system to address these problems may exacerbate or buffer the impact of these challenges. The ability of the cropland system to cope with risks and maintain its stability during various disturbances and shocks is considered as cropland system resilience, which reflects the complex interaction between cropland resources and their utilizers in a specific socio-geographical environment.

Resilience emphasizes the variation, uncertainty, and ability of a system to adapt to the environment (Gunderson and Holling, 2002). The concept is multifaceted and should not be determined by a single indicator or by only observing the properties of a single system (Meuwissen et al., 2019). Previous studies indicate that the concept of robustness, adaptability, and transformability are the three core capacities of system resilience, which is more composite than other similar concepts, such as vulnerability, flexibility, or adaption (Buitenhuis et al., 2020). For a specific cropland system, its resilience to climate change should involve any or all of the following (**Figure 1**): *Robustness* is the capacity to withstand the transient shock to furthest maintain the original productivity (Urruty et al., 2016); *adaptability* is the capacity to make full use of the existing resources to restore the original productivity after the shock, without changing the internal structure and mechanism of the cropland system (Buitenhuis et al., 2020); and *transformability* is the capacity of a cropland system to improve itself to cope with climate change through structural and institutional changes, or collapse due to the failure to make changes in time (Meuwissen et al., 2019). It should be emphasized that among the three capacities of CSRCC, robustness can play a role in a short period, while adaptability and transformability may only be fully manifested for a long period after a disaster occurs.

Previous research studies on the evaluation of socio-ecological resilience mainly focus on the urban system (Bush and Doyon, 2019; Cariolet et al., 2019; Datola et al., 2022; Potapova et al., 2022; Wang et al., 2022), agricultural system (Gil et al., 2017), or food system (Tendall et al., 2015; Jacobi et al., 2018). Few studied CSRCC, which mainly centralized on the qualitative analysis of the definitions (Meyer, 2020) or connotations (Tendall et al., 2015). These studies discussed potential influential factors of CSRCC and how policies or measures can be developed to improve CSRCC (Egli et al., 2021; Javadinejad et al., 2021). Although less attention has been paid to the evaluation of CSRCC, we can refer to research on similar socio-ecological system resilience, such as farming system resilience and agricultural system resilience. Some evaluated socio-ecological resilience through a single indicator (Zampieri et al., 2021), fuzzy assessment based on an index system (Mutabazi et al., 2015; Zampieri et al., 2020), and decision behavior modeling (Badillo-Márquez et al., 2021; Herrera et al., 2022). Other studies attempted to innovate the theoretical framework for the evaluation (Altieri et al., 2015). For example, a recent study by Lyu et al. (2021) proposed an assessment framework based on cropland resource resilience, ecological resilience, production resilience, and scale structural resilience. Generally, previous research studies have evaluated cropland system resilience from various socio-ecological dimensions. However, few studies have considered the three capacities of system resilience, namely, robustness, adaptability, and transformability.

Climate change has substantially increased the frequency of extreme weather events, and it is considered one of the most serious threats to the cropland system around the world. In this context, improving CSRCC is crucial to realize the sustainable utilization of cropland, high-quality agricultural development, and regional food security. This study takes the Hubei province of China as an example and constructs the evaluation index system based on robustness, adaptability, and transformability. Methods of Delphi, AHP, and TOPSIS are used to measure the spatio-temporal characteristics of CSRCC in each municipality of Hubei province from 2011 to 2018. The regional disparities are analyzed by using the Theil coefficient.

METHODS AND DATA

Study Area

Hubei is located in central China and the middle reaches of the Yangtze River, between north latitude 29° 01′ 53 ″–33° 6′ 47″ and east longitude 108° 21′ 42 ″–116° 07′ 50″, which is roughly surrounded by mountains on three sides (east, west, and north) and is low and flat in the middle (**Figure 2**). Currently, Hubei has jurisdictions over 12 prefecture-level municipalities and three provincial governing county-level municipalities, with a total area of 1.86×10^5 km^2. It is rich in natural endowments and is an important agricultural commodity base of China. By the end of 2019, the cropland area of Hubei reached 4.77×10^4 km^2, which was mainly distributed in the central plain. Cropland with a slope above 25° accounted for 2.31% of the total cropland area. Among them, the sloping cultivated land in mountainous areas accounted for more than 85%. Meanwhile, drastic climate change has caused constant disasters of drought and flood in Hubei.

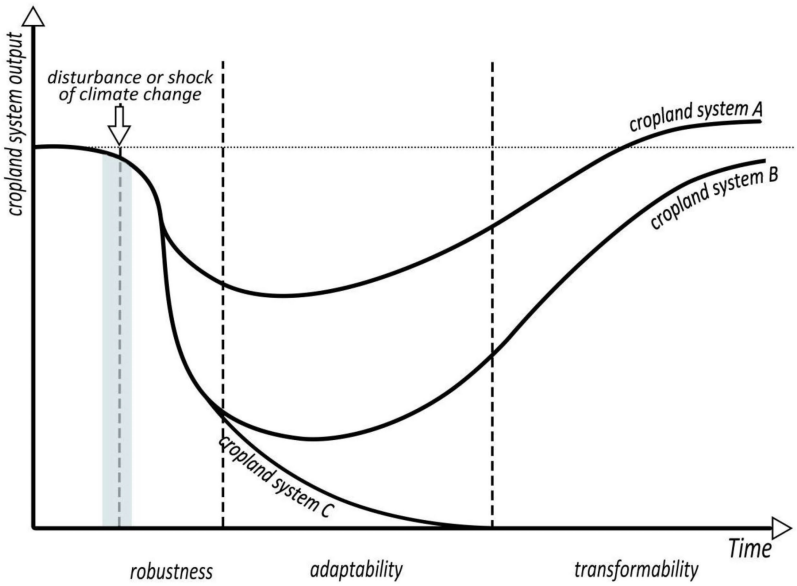

FIGURE 1 | Schematic diagram of the three capabilities of cropland system resilience. (Cropland system A has superior resilience, due to the less impact on the phases of robustness and adaptability and even higher output in the phase of transformability than the original level. Cropland system B has medium resilience, due to more significantly fluctuated output after the shock and longer recovery time than the original level. Cropland system C has the lowest resilience due to the collapse after the shock).

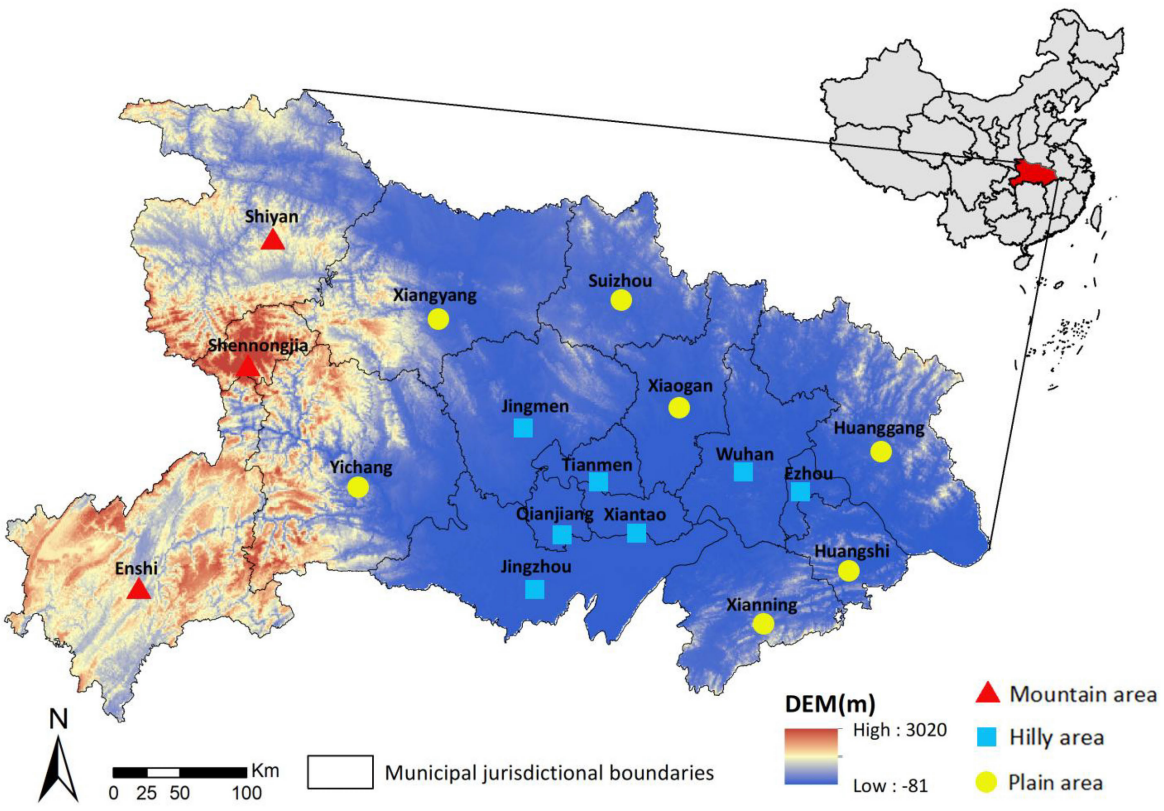

FIGURE 2 | Study area.

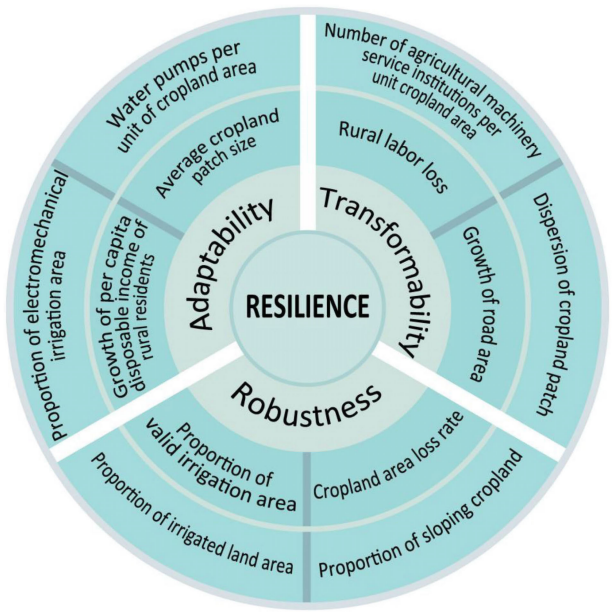

FIGURE 3 | Evaluation index system of cropland system resilience.

Methods

Evaluation Index System of Cropland System Resilience to Climate Change

Climate change, such as drought and flood, has been affecting Chinese cropland use and food production dramatically for a long time. To evaluate CSRCC, this study fully considers the impacts of droughts and floods caused by climate change on the cropland system, as well as the human–land coupling relation; takes the three capacities of socio-economic system resilience, namely, the robustness, adaptability, and transformability, as the criterion layer; and selects indicators that are directly or indirectly related to cropland system resilience against drought and flood (**Figure 3**).

Robustness is measured by four indicators: the proportion of irrigated land area, cropland area loss rate, proportion of the valid irrigation area, and proportion of sloping cropland. Specifically, (1) irrigated land refers to the cropland with water sources and irrigation facilities to protect against drought. Thus, when dealing with droughts, irrigated land can alleviate the disaster more quickly than other croplands (Meza et al., 2020). Crops can be irrigated in time, thereby ensuring the survival rate and growing environment (Ray et al., 2018). For a certain cropland system of an administration unit, the higher the proportion of irrigated land, the higher the robustness. (2) Cropland area loss will directly lead to a decline in the agricultural output regionally and a decrease in the production function of the cropland system (Chen et al., 2019). Cropland area loss caused by construction land occupation, abandonment, or non-plantation use results in local cropland system collapse (Deng et al., 2020; Vallés-Planells et al., 2020), thereby reducing the whole CSRCC. (3) The valid irrigation area is a relatively flat cropland area with certain water sources and supporting irrigation facilities (Liu et al., 2020), which provide cropland with the possibility of resisting drought. (4) Sloping cropland indicates the croplands with a slope above 25 degrees. Those lands are not conducive to soil growth, and the soil layer is weak. Moreover, soil erosion caused by disasters, such as flood, can easily damage the sloping cropland (Tuo et al., 2018; Peng et al., 2019). Thus, the higher the proportion of sloping cropland, the lower the robustness.

Adaptability is measured by considering water pumps per unit cropland area, the proportion of electromechanical irrigation area, the growth of per capita disposable income of rural residents, and the average cropland patch size. Specifically, (1) a water pump is an agricultural machine that increases the efficiency of drainage or irrigation. When floods or droughts occur, a cropland system with more pumps per unit area of cropland can restore production more quickly and the system can recover agricultural production rapidly, so the adaptability will be stronger (Amaranto et al., 2018). (2) The proportion of electromechanical irrigation area indicates the cropland irrigated by using diesel engines, gasoline engines, electric motors, or other power machinery in the effective irrigation area. Electromechanical irrigation, rather than traditional irrigation, can improve irrigation efficiency and relieve water stress in case of drought (Liu et al., 2021). (3) The growth of per capita disposable income of rural residents has a direct relation to fast production recovery after disasters. Increased income indicates more capital that can be reinvested in the restoration of agricultural production (Borychowski et al., 2020; Dixon et al.,2021), thereby increasing adaptability. (4) Average cropland patch size is related to the patch area and the number of patches. In large patches, cropland is more concentrated and generally flat, which is conducive to mechanical operation, labor force saving, and the speed of cropland recovery (Wang T. et al., 2021). A large number of plaques in a certain area will be unfavorable for large-scale mechanized farming.

Transformability is measured by the growth of road area, number of agricultural machinery service institutions per unit of cropland area, rural labor loss, and dispersion of cropland patch. Specifically, (1) the road area includes both urban and rural roads. The role of roads in enhancing the cropland system resilience is promoting the exchange of urban and rural means of production, including labor, agricultural facilities, and technology (Vishnu et al., 2021). From this point of view, the increase in the road area is conducive to the introduction of elements that can renew the cropland system after a disaster (Kasmalkar et al., 2020). (2) Mechanized service organizations can provide technical guidance to farmers. The improvement of agricultural production technology will be beneficial to the adjustment of cropland system structure, the improvement of production efficiency, and the guidance on disaster management, thereby maintaining or even improving the production capacity of the cropland system (Van Loon et al., 2020; Batung et al., 2022). (3) Rural labor loss could directly lead to the cropland abandonment and the reduction of the input of the cropland system. The shortage of rural labor will seriously affect the allocation of labor and reduce the efficiency of disaster relief (Zhou et al., 2021). Therefore, the greater the rural labor loss, the weaker the transformability of the cropland system.

(4) Dispersion of cropland patch measures the discreteness of cropland by calculating the weighted distance between the central points of each patch. The smaller the patch dispersion, the more the cropland conducive to the mechanical and human communication between the cropland patches and the higher the disaster relief efficiency and the transformability of the cropland system (Frei et al., 2020).

Index Weight Determination

The Delphi method is essentially a feedback anonymous inquiry method. Through repeated consultation with experts, a consensus is finally reached. The analytic hierarchy process (AHP) is a decision analysis method that combines qualitative and quantitative attributes. In this study, two methods are used comprehensively for the determination of index weights. Experts with relevant disciplinary backgrounds are invited to judge the importance of the criterion layer and the index layer and finally weighted. Thus, the thinking process is simple and clear, and the decision-making process is organized and more scientific.

In order to determine the weights of 12 indexes corresponding to robustness, adaptability, and transformability in the evaluation system of CSRCC, 16 experts in land resource management, environmental geography, public administration, and landscape ecology were invited for this study. In the case of no communication with each other, experts compared and scored the importance of each index relative to the higher level index to which it belongs. According to the pairwise judgment matrix constructed by expert scoring, the geometric mean is calculated and normalized. Through repeated scoring by experts, the matrix passes the consistency test, and finally, the weights of the primary and secondary indicators are obtained. The formula is as follows:

$$\mathrm{W} = \frac{\sqrt[n]{\prod_{i=1}^{n} \mathrm{A}}}{\sum_{1}^{n} \sqrt[n]{\prod_{i=1}^{n} \mathrm{A}}} \tag{1}$$

where A is the judgment matrix that passes the consistency test and n is the index number. Finally, the weights of each item in the criterion layer and the index layer are calculated (**Table 1**).

Calculation of Cropland System Resilience to Climate Change Based on TOPSIS

The Technique for Order Preference by Similarity to an Ideal Solution (TOPSIS) is a method that sorts evaluation objects by detecting the distance between the ideal solution and the anti-ideal solution. It can achieve the goal of replacing the optimal solution with a satisfactory solution by eliminating the poor solution and selecting a satisfactory solution (Wątróbski et al., 2022). For example, the evaluation object that is closest to the ideal solution is considered the ideal solution.

(1) Standardize panel data:

The standardized calculation formulas for the positive index and the negative index are as given as follows:

$$\mathrm{y(i,j)} = \frac{\mathrm{x(i,j)} - \mathrm{x_{min}(j)}}{\mathrm{x_{max}(j)} - \mathrm{x_{min}(j)}}, \mathrm{y(i,j)} = \frac{\mathrm{x_{max}(j)} - \mathrm{x(i,j)}}{\mathrm{x_{max}(j)} - \mathrm{x_{min}(j)}} \tag{2}$$

where $x_{max}(j)$ and $x_{min}(j)$ are the maximum and minimum values of the jth evaluation index, respectively, and i is the ith evaluation unit.

(2) Build a standardized decision matrix:

The X matrix is normalized to obtain the normalized matrix Y. The weight matrix W is obtained from the weight calculation result of the evaluation index. The normalization matrix Y and the weight matrix W calculate the weight normalization matrix V, namely, the comprehensive value of the resilience level of the cropland system. There are N municipalities, and each city has M evaluation indicators. The x_{ij} represents the jth index value of ith municipality. The initial decision matrix X, normalized matrix Y, weight matrix W, and decision value matrix V are expressed, respectively, as follows:

$$X = \begin{pmatrix} x_{11} & x_{12} & \cdots & x_{1M} \\ x_{21} & x_{22} & \cdots & x_{2M} \\ \vdots & \vdots & \ddots & \vdots \\ x_{N1} & x_{N2} & \cdots & x_{NM} \end{pmatrix} Y = \begin{pmatrix} y_{11} & y_{12} & \cdots & y_{1M} \\ y_{21} & y_{22} & \cdots & y_{2M} \\ \vdots & \vdots & \ddots & \vdots \\ y_{N1} & y_{N2} & \cdots & y_{NM} \end{pmatrix} W = \begin{pmatrix} w_1 \\ w_2 \\ \vdots \\ w_M \end{pmatrix}$$

$$V = YM = \begin{pmatrix} y_{11} & y_{12} & \cdots & y_{1M} \\ y_{21} & y_{22} & \cdots & y_{2M} \\ \vdots & \vdots & \ddots & \vdots \\ x_{N1} & x_{N2} & \cdots & y_{NM} \end{pmatrix} \begin{pmatrix} w_1 \\ w_2 \\ \vdots \\ w_M \end{pmatrix} = \begin{pmatrix} z_1 \\ z_2 \\ \vdots \\ z_N \end{pmatrix}^{T} \tag{3}$$

(3) Calculate the ideal solutions and the anti-ideal solutions:

The ideal solution A^+ and the anti-ideal solution A are determined by the weight normalization value ofv_{ij}:

$$A^+ = \left\{ \max_{1 \le i \le m} v_{ij} | j = 1, 2, \cdots, n \right\} = \left\{ v_1^+, v_2^+ \cdots, v_n^+ \right\}$$

$$A^- = \left\{ \max_{1 \le i \le m} v_{ij} | j = 1, 2, \cdots, n \right\} = \left\{ v_1^-, v_2^- \cdots, v_n^- \right\} \tag{4}$$

(4) Calculate the distance scale:

$$S^+ = \sqrt{\sum_{j=1}^{n} (v_{ij} - v_j^+)^2} \quad i = 1, 2, \ldots, m$$

$$S^- = \sqrt{\sum_{j=1}^{n} (v_{ij} - v_j^-)^2} \quad i = 1, 2, \ldots, m \tag{5}$$

where S^+ is the distance from the target to the ideal solution A^+; S^- is the distance to the anti-ideal solution A^-; $V^+$and V^- represent the distance between the jth target and the ideal solution and the anti-ideal solution, respectively; v_{ij} represents the normalized value of the ith target and the jth target; and S^+ indicates the proximity between the evaluation target and the optimal target; the smaller the S^+value, the better the results.

TABLE 1 | Weights of each index of cropland system resilience.

Criterion layer	Weights	Index layer	Attributes	Weights
Robustness	1/3	Proportion of irrigated land area	+	0.16
		Rate of cropland area loss	−	0.06
		Proportion of valid irrigation area	+	0.06
		Proportion of sloping cropland	−	0.05
Adaptability	1/3	Number of water pumps per unit cropland area	+	0.15
		Proportion of electromechanical irrigation area	+	0.08
		Growth of per capita disposable income of rural residents	+	0.05
		Average cropland patch size	+	0.05
Transformability	1/3	Growth of road area	+	0.13
		Number of agricultural machinery service institutions per unit cropland area	+	0.07
		Rural labor loss	−	0.07
		Dispersion of cropland patch	+	0.07

(5) Determine the ideal closeness:

$$C_i = \frac{S_i^-}{S_i^+ S_i^-} i = 1, 2, \ldots, m \quad (6)$$

In this way, the CSRCC and three capacities in Hubei province are obtained, respectively. By averaging the scores of each municipality for the same year, the overall resilience of Hubei province from 2011 to 2018 can be obtained.

Regional Disparity Analysis Based on Thiel Coefficient

The Thiel coefficient is mainly used to measure the level of regional disparities, including inter-group disparities and intra-group disparities, and it is able to decompose regional differences to clarify the source situation of the disparities. The calculation formula is as follows:

$$T = T_\omega + T_\beta = \frac{1}{n} \sum_{i=1}^{n} \frac{y_i}{\overline{y}} \ln \frac{y_i}{\overline{y}} \quad (7)$$

$$T_k = \frac{1}{n_k} \sum_{i} \frac{y_i}{\overline{y_k}} \ln \left(\frac{y_i}{\overline{y_k}} \right) \quad (8)$$

$$T_\omega = \sum_{k=1}^{K} y_k \ln \frac{y_k}{n_k / n} \quad (9)$$

$$T_\beta = \sum_{k=1}^{K} y_k \times \left[\sum_{k=1}^{K} \frac{y_i}{y_k} \ln \frac{y_i / y_k}{1 / n_k} \right] \quad (10)$$

where T is the Theil coefficient; T_ω and T_β are Theil coefficients of inter-group and intra-group disparities in mountain, hilly, and plain areas, respectively; k is the terrain area (k = 1, 2, 3 indicate mountain, hilly, and plain areas, respectively); y_i is the resilience value of the ith municipality; $\overline{y}$ is the average of all the municipality resilience values; y_k and $\overline{y_k}$ express the sum and average of the resilience values of the municipalities in the terrain area; and T_k is the Theil coefficient of the terrain area. The larger the T value, the greater the resilience disparities between the three terrain areas.

Data Source

The study data are the panel data of 16 prefecture-level municipalities of Hubei province (except for Shennongjia) from 2011 to 2018. The data of cropland, irrigated, and road areas (including urban roads and rural roads) are obtained from the Second National Land Resource Investigation of China. The data from land use and land cover change (LUCC) 30 m annual land cover datasets were obtained from Yang and Huang (2021), and then the data were processed using Fragstats 4.2 to obtain the number of patches, patch areas, patch dispersion degrees. We use DEM data from the Shuttle Radar Topography Mission (SRTM) to obtain the area of sloping cropland by ArcGIS. The data of other indexes are derived from the Hubei Rural Statistical Yearbook.

RESULTS

Evaluation of Three Capacities of Cropland System Resilience to Climate Change in Hubei Province

Robustness

From 2011 to 2018, the robustness of the cropland system in Hubei province has changed from 0.513 to 0.502, showing a fluctuating downward trend. The robustness value of each city mainly fluctuated around 0.5, and the fluctuation range did not exceed 0.2. The maximum robustness was 0.684 in Wuhan in 2011, which is much larger than that of other cities. The main reason is that the proportion of sloping cropland in Wuhan was extremely low, only 0.007% of the cropland area, and the comprehensive scores of other indicators were high. The robustness of most municipal scales declined in 2013 and returned to their original level in 2014, with Ezhou and Jingzhou having the largest fluctuations, and Ezhou reaching the lowest value of 0.392. The robustness of municipal scales, such as Wuhan, has undergone similar changes in the following year. Municipal scales, such as Ezhou, Jingzhou, and Shiyan, increased their robustness in 2016 and returned to their original levels in 2017. Wuhan is still producing similar changes a year later.

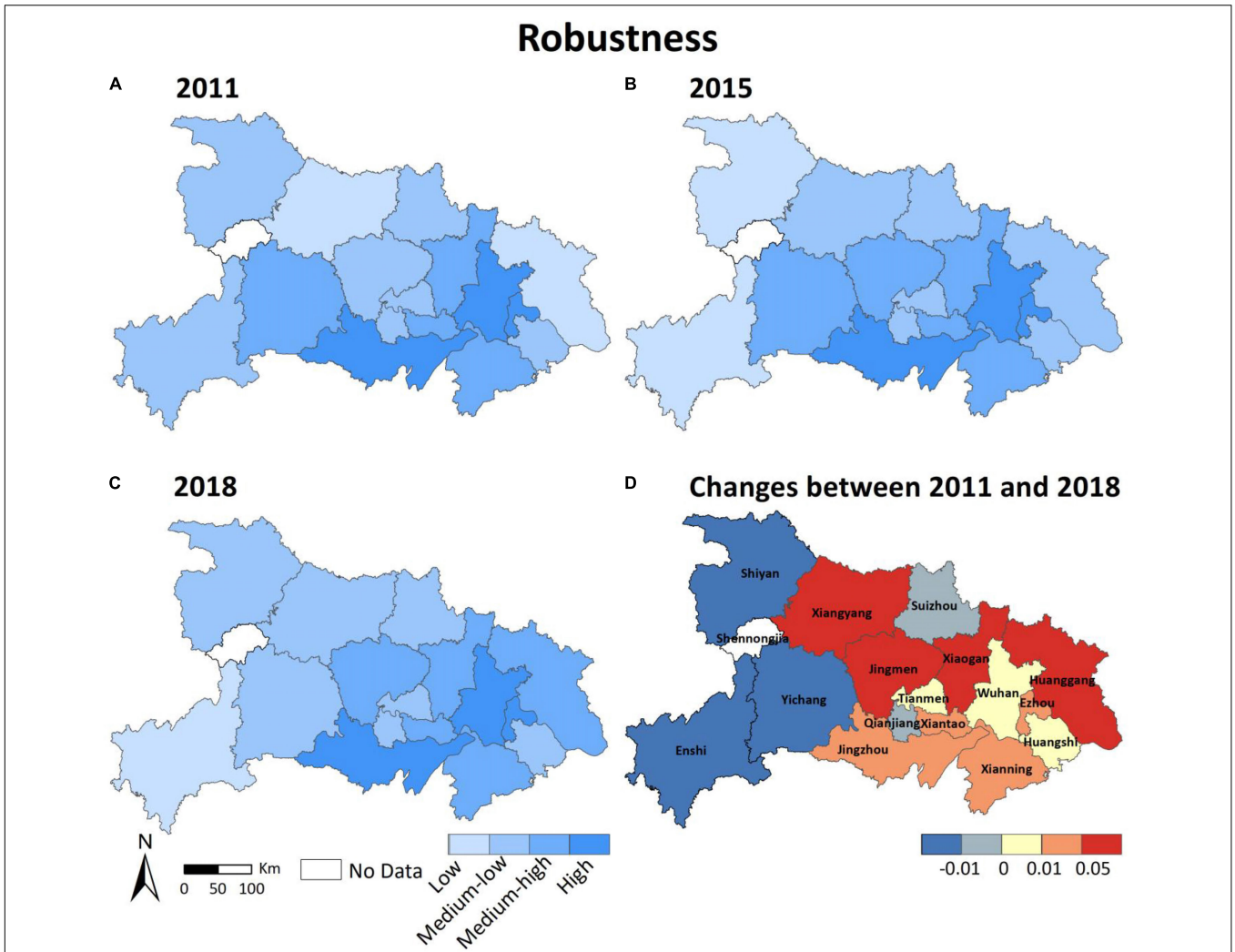

FIGURE 4 | Robustness level of CSRCC in Hubei Province **(A)** Robustness of CSRCC in 2011, **(B)** Robustness of CSRCC in 2015, **(C)** Robustness of CSRCC in 2018, **(D)** Changes of Robustness between 2011 and 2018.

Figures 4A–C reflect the spatial distribution of cropland system robustness in Hubei province in 2011, 2015, and 2018. It can be found that high robustness is mainly located in central and southern Hubei province, such as Wuhan, while northern Hubei province has low robustness, such as Xiangyang. By observing the spatial distribution of the cropland system robustness change in Hubei from 2011 to 2018 (**Figure 4D**), we found that from 2011 to 2018, the robustness of only five municipal scales decreased slightly, such as Wuhan (−0.185) and Huanggang (−0.042), while most municipalities showed an upward trend and the largest increase is Shiyan (0.243). In general, the robustness of the entire cropland system in Hubei province is not very different, and the inter-annual variation is relatively small.

Adaptability

From 2011 to 2018, the cropland system adaptability of Hubei province has changed from 0.241 to 0.173, showing a downward trend of fluctuation. During the study period, the regional disparities of the adaptability level of Hubei province were between 0.1 and 0.5. The cropland system adaptability of most municipal scales increased in 2011–2013 and then declined. Before 2014, the value of each municipal scale fluctuated considerably, and the change in adaptability was relatively stable from 2014 to 2018. **Figures 5A–C** show the spatial distribution of the cropland system adaptability of Hubei province in 2011, 2015, and 2018. It shows that high adaptability is mainly found in southern and eastern Hubei, such as Jingzhou, Wuhan, Ezhou, and Tianmen, and western and northern Hubei showed generally low adaptability, such as Enshi, Shiyan, and Suizhou. Moreover, most municipalities in Hubei province showed a downward trend (**Figure 5D**), among which Xiaogan, Yichang, Xiantao, and Huanggang decreased by 0.232, 0.157, 0.133, and 0.117, respectively. Only Huangshi in the southeast of Hubei province showed a fluctuating upward trend, whose adaptability improved by 0.003.

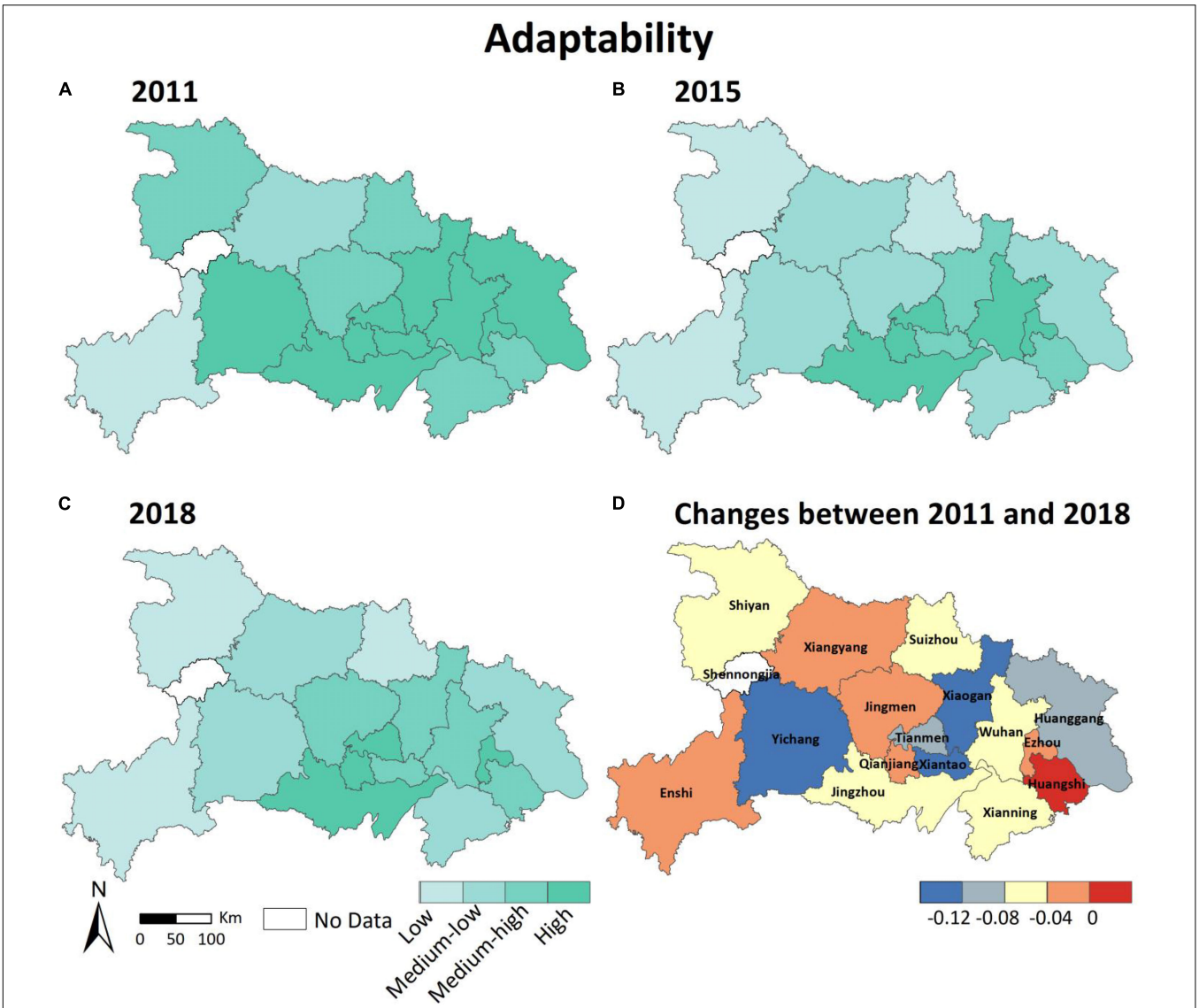

FIGURE 5 | Adaptability level of CSRCC in Hubei Province **(A)** Adaptability of CSRCC in 2011, **(B)** Adaptability of CSRCC in 2015, **(C)** Adaptability of CSRCC in 2018, **(D)** Changes of Adaptability between 2011 and 2018.

Transformability

From 2011 to 2018, the cropland system transformability in Hubei province fluctuated between 0.494 and 0.506 but remained at 0.500 in 2011 and 2018. The values of all municipal scales were also around 0.500, and the fluctuation range did not exceed 0.095. The maximum value was 0.542 in Wuhan in 2017, and the minimum value was 0.448 in Huanggang in 2016. **Figures 6A–C** shows the spatial distribution of the cropland system transformability of Hubei province in 2011, 2015, and 2018, and it can be found that high transformability is mainly found in the southern and eastern Hubei province, such as Wuhan and Jingzhou, while Xiaogan in central Hubei, Xiangyang in northern Hubei, and Huanggang in eastern Hubei have generally low cropland system transformability. In addition, most municipalities in Hubei province showed a downward trend (**Figure 6D**), which mainly concentrated in the southeast, north, and southwest Hubei province. The value of Xiaogan has been reduced the most (−0.023). On the contrary, other municipalities showed an increase, but not by much. Except for Jingzhou, which increased by 0.37, all other municipalities showed an increase by no more than 0.001.

Overall Evaluation of Cropland System Resilience to Climate Change in Hubei Province

The calculation results of the cropland system resilience in Hubei province from 2011 to 2018 are shown in **Table 2**. From 2011 to 2018, the cropland system resilience level in Hubei province generally showed a fluctuating downward trend,

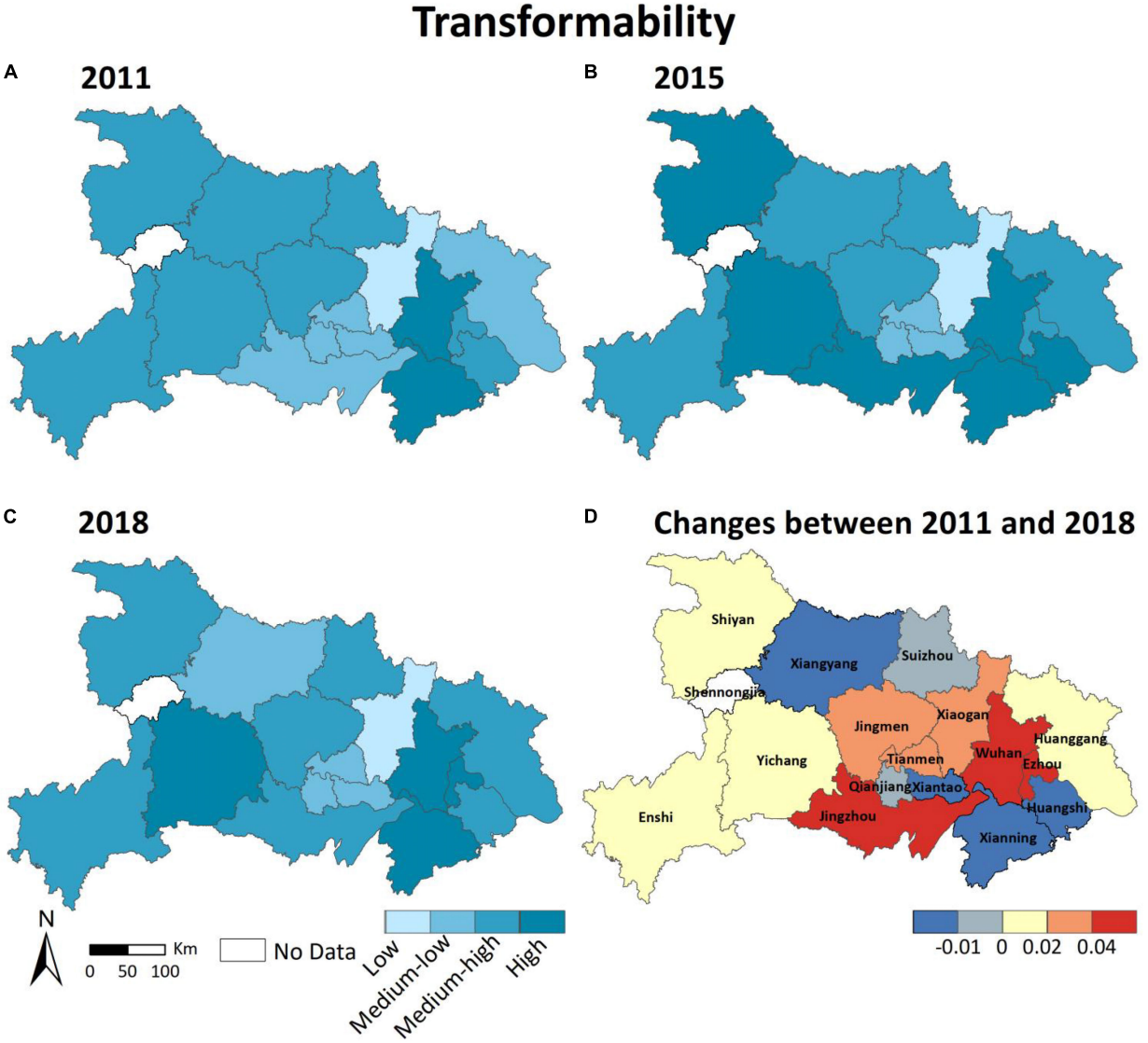

FIGURE 6 | Transformability level of CSRCC in Hubei Province **(A)** Transformability of CSRCC in 2011, **(B)** Transformability of CSRCC in 2015, **(C)** Transformability of CSRCC in 2018, **(D)** Changes of Transformability between 2011 and 2018.

decreasing from 0.340 to 0.320. During the study period, the cropland system resilience levels in most municipalities of Hubei province were concentrated at 0.2–0.4. The maximum value was 0.552 in Wuhan in 2013, and the minimum value was 0.226 in Jingmen in 2016. The fluctuations in each municipality from 2011 to 2018 were also small, not exceeding 0.057, and the inter-annual variation did not exceed 0.178. We obtained the spatial distribution of the cropland system resilience level of Hubei province for 2011, 2015, and 2018 (**Figures 7A–C**). Among them, the high resilience level was mainly concentrated in central and southern Hubei province, such as Wuhan, Jingzhou, and Ezhou. The low resilience level was mainly concentrated in the northwest Hubei province, such as Enshi and Shiyan. Moreover, during the study period, the cropland system resilience in Jingmen, Wuhan, and Jingzhou showed an upward trend, which increased by 0.006, 0.005, and 0.003, respectively, while other municipalities all showed a downward trend (**Figure 7D**). The performance of cropland system resilience in Xiantao was similar to its cropland system robustness, which indicate Xiantao's cropland system robustness has a greater impact on its cropland system resilience.

Regional Disparities of Cropland System Resilience to Climate Change

We measured the regional disparities and influence factors of the cropland system resilience in Hubei province. **Figure 8** shows the changes of resilience levels in different terrain areas in Hubei province during the study period. It can be found that from 2011 to 2018, the resilience values were highest in

TABLE 2 | CSRCC of each municipality in Hubei province from 2011 to 2018.

Terrain area	Region	2011	2012	2013	2014	2015	2016	2017	2018
Plain area	Wuhan	0.500	0.508	0.552	0.542	0.490	0.473	0.471	0.505
	Ezhou	0.485	0.499	0.496	0.451	0.470	0.459	0.428	0.481
	Jingmen	0.291	0.294	0.315	0.287	0.284	0.293	0.299	0.297
	Jingzhou	0.477	0.540	0.538	0.510	0.537	0.480	0.514	0.480
	Xiantao	0.328	0.454	0.482	0.305	0.287	0.290	0.295	0.302
	Qianjiang	0.315	0.322	0.302	0.311	0.297	0.275	0.300	0.300
	Tianmen	0.323	0.324	0.310	0.307	0.304	0.288	0.302	0.306
Hilly area	Huangshi	0.299	0.279	0.333	0.270	0.283	0.304	0.279	0.288
	Yichang	0.334	0.381	0.374	0.399	0.292	0.286	0.289	0.290
	Xiangyang	0.263	0.291	0.379	0.392	0.269	0.283	0.273	0.260
	Xiaogan	0.369	0.395	0.406	0.311	0.309	0.387	0.314	0.312
	Huanggang	0.292	0.287	0.428	0.327	0.280	0.262	0.283	0.273
	Xianning	0.375	0.365	0.397	0.390	0.324	0.315	0.323	0.322
	Suizhou	0.280	0.274	0.332	0.270	0.271	0.271	0.268	0.267
Mountain area	Shiyan	0.263	0.315	0.323	0.245	0.254	0.226	0.240	0.250
	Enshi	0.243	0.343	0.257	0.239	0.235	0.254	0.245	0.233

the plain area and lowest in the mountain area. The resilience change trends of the cropland system in three terrain areas were similar. The regional disparities increased first, then decreased to a minimum in 2017, eventually returned to the original gap level.

Table 3 indicates the Thiel coefficients and their decomposition of the resilience disparities in three terrain areas of Hubei province. Judging from the changing trend of the Theil coefficients in Hubei province, there were regional differences in the cropland system resilience in Hubei province during the study period, and the differences increased in an unstable manner. The Thiel coefficients of inter-group differences increased from 2011 to 2013 and reached a maximum of 11.418 in 2013, after which the volatility decreased. Coefficients of the intra-group difference fluctuated to a greater extent, but they returned to the original level in 2018. The Theil coefficients of the inter-group differences in Hubei province were much larger than those of the intra-group differences, indicating that the elastic differences within the three topographic regions were smaller than the elastic differences among the three topographic regions. The differences in the cropland system resilience in Hubei province were mainly due to inter-group differences, indicating that the differences in the resilience of cropland systems in Hubei province were mainly due to topographic differences.

From 2011 to 2018, the cropland system resilience in three areas generally decreased slightly. The Thiel coefficients in plain areas were relatively high, especially in 2015 (0.036), and showed an upward trend. The Thiel coefficients fluctuated considerably in the mountain area but returned to the original level. The Theil coefficients in the hilly regions decreased slightly, indicating that the regional disparities of cropland system resilience in hilly areas increased and decreased in plain areas. In addition, except for 2017, the Thiel coefficients in plain areas were always greater than those of hilly and mountain areas during the study period, indicating that the regional disparities of cropland system resilience in plain areas were more significant than those in hilly and mountain areas.

DISCUSSION

Index System for Evaluating Cropland System Resilience to Climate Change

Since the disturbances and shocks are from various aspects of social and environmental change, an undirected evaluation index system might have limited references for agricultural practice. A single indicator, such as grain output (Di Falco and Chavas, 2008; Birthal et al., 2015) or agricultural GDP (Hsiang and Jina, 2014), has been applied to indirectly reflect the resilience change. In addition, multi-dimension index systems are also constructed by previous studies (Allison and Hobbs, 2004; Tambo, 2016; Lyu et al., 2021; Nasr et al., 2021). However, few studies have focused on a specific disturbance or shock external to the system, which would be difficult to form a unified evaluation system or acknowledged indicators.

Moreover, the indicator selection may also differ considerably between the research objects. It is difficult to unify the evaluation system for both the household unit and the administrative unit. For example, research on the farmers usually considers the individual or family characteristics, the specific conditions of household cropland, and the intensity of utilization and management of cropland (Nyong et al., 2020; Thorsøe et al., 2020; Dixon et al., 2021), while research on administrative units focuses more on the regional cropland resource endowment and governance level (Meyer, 2020). Therefore, different research objects lead to differences in indicator selections. According to previous studies on the theoretical framework of social-ecological system resilience, we suggest that robustness, adaptability, and transformability could reasonably describe the dynamic characteristics of system resilience changing with time after the

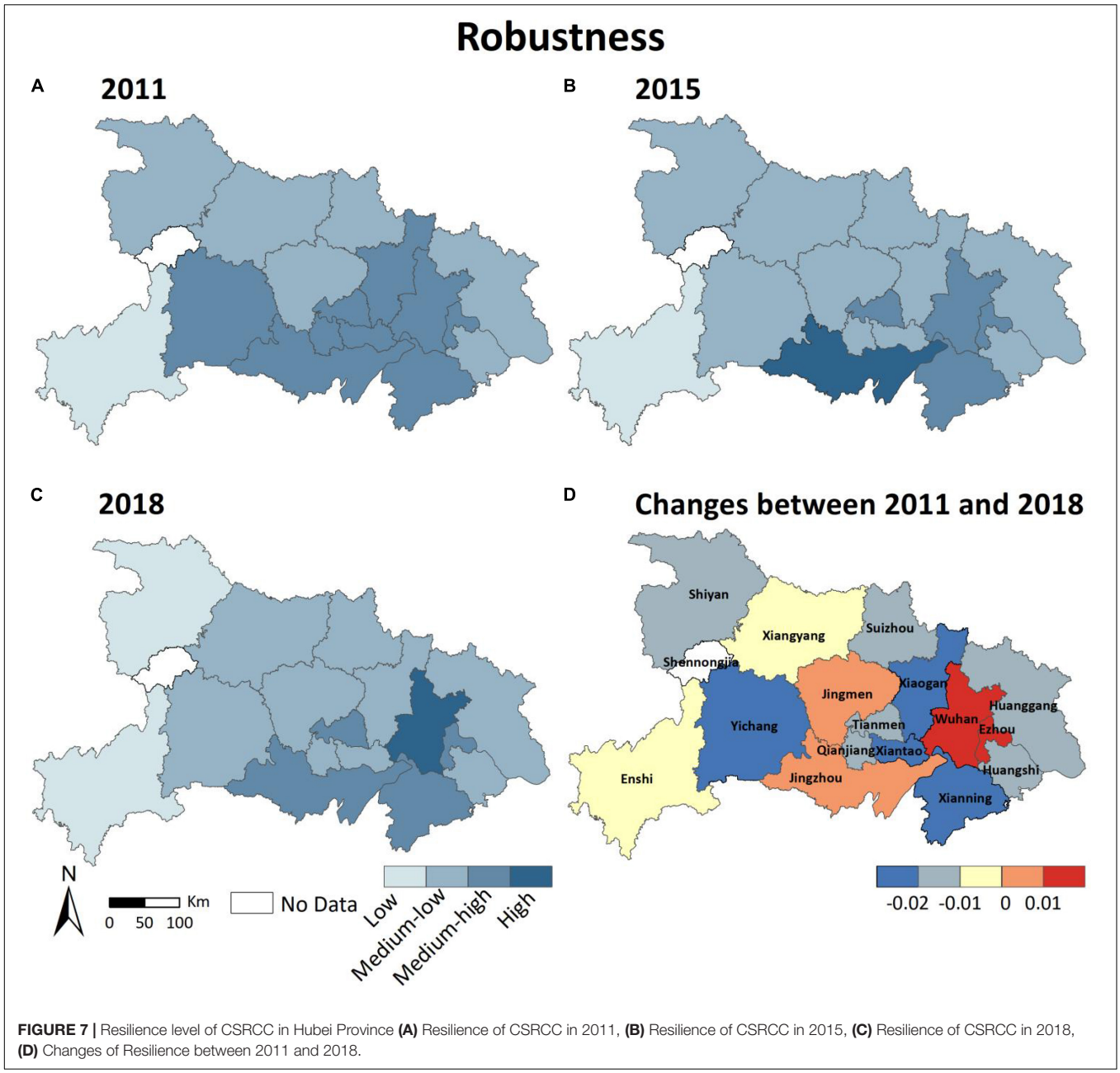

FIGURE 7 | Resilience level of CSRCC in Hubei Province **(A)** Resilience of CSRCC in 2011, **(B)** Resilience of CSRCC in 2015, **(C)** Resilience of CSRCC in 2018, **(D)** Changes of Resilience between 2011 and 2018.

disturbance. Therefore, this article proposes a new evaluation index system of CSRCC based on the impacts of climate change on the cropland system, the natural endowments, and utilization characteristics of the cropland system from the three dimensions of system resilience.

Influencing Mechanism of Cropland System Resilience to Climate Change

Since the cropland system is a socio-ecological system, the factors influencing CSRCC can be roughly divided into two categories: natural environmental factors and socio-economic factors. Natural environmental factors include climatic conditions, water resource distribution, topographic and geomorphic characteristics, soil properties, and landscape features. For example, Di Falco and Chavas (2008) argued that greater landscape heterogeneity supports higher species diversity and thus makes the agricultural system more resilient to future climate change. Lyu et al. (2021) believed that nature reserve area is an important factor affecting CSRCC because the establishment of nature reserves would hinder the large-scale sustainable management of cropland. In addition, geomorphic characteristics also deeply impact CSRCC because of weaker robustness to natural hazards and enormous difficulty in implementing agricultural mechanization in mountain or hilly areas (Li et al., 2018). In this study, natural endowment (cropland

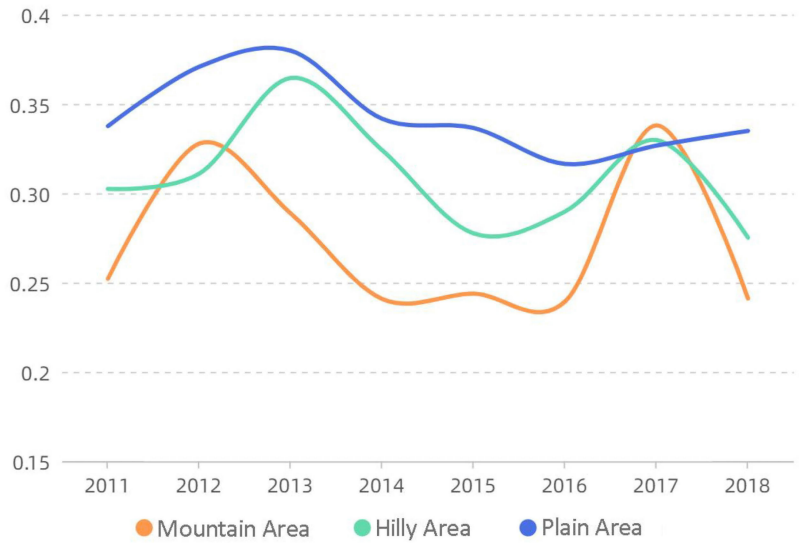

FIGURE 8 | Cropland system resilience in three terrain areas.

TABLE 3 | Thiel coefficient and decomposition.

Year	Theil coefficient	Mountain area	Hilly area	Plain area	Inter-group	Intra-group
2011	0.009	0.001	0.008	0.025	9.261	0.085
2012	0.012	0.001	0.011	0.026	10.434	0.104
2013	0.013	0.007	0.004	0.031	11.418	0.107
2014	0.018	0.000	0.012	0.033	9.579	0.120
2015	0.015	0.001	0.002	0.036	8.604	0.101
2016	0.010	0.002	0.008	0.031	8.478	0.096
2017	0.016	0.000	0.002	0.027	8.437	0.076
2018	0.012	0.001	0.003	0.029	8.558	0.084

area loss rate) and topographic (sloping cropland proportion) and landscape (average cropland patch size, dispersion of cropland patch) features are considered to have important influences on CSRCC.

From the perspective of socio-economic influences, farming profitability, labor force characteristics, regional economic development levels, agricultural market variation, cropland infrastructure, etc. could impact CSRCC distinctly. Holling (2001) noted that profitability simultaneously increases the resilience potential of the cropland system. Some argued that global market trade tends to decrease, rather than enhance, the adaptability of the cropland system (Milestad and Darnhofer, 2003; Cabell and Oelofse, 2012). In addition, regional economic development has weak adaptability of cropland (Yang et al., 2021). This study also suggests that agricultural technology and innovation could also be favorable to the improvement of CSRCC.

Implications for Chinese Cropland Protection Policies

Improving CSRCC is critical to averting large-scale future shortages and to ensuring food security, as well as good nutrition. China is a developing country with a large population but less available land. To ensure food security, the central government has proposed strict cropland protection policies to realize the "trinity" protection of quantity, quality, and ecology of cropland (Liang et al., 2015; Liu et al., 2017; Wu et al., 2017). In addition, China has also implemented "high-standard farmland construction" to improve cropland quality, agricultural infrastructure, and ecological maintenance, thus ensuring stable crop yields, despite various uncertain external disturbances. The implementation of the policies has objectively improved CSRCC but has not directly incorporated the resilience into the institutional system. Moreover, the weak agricultural infrastructure and risk resistance of the cropland system have not been fundamentally changed in China (Qin and Wu, 2021; Yu et al., 2022). This study suggests that the resilience-oriented policies should be proposed to cope with a range of future disturbances and shocks from environment and socio-economic changes. (1) Giving full play to the production advantages of different regions to optimize configuration of the cropland system; (2) effectively coordinating the resources of land, water, labor force, finance, etc., to improve the agricultural infrastructure to climate change, for increasing the robustness of the cropland system; (3) promoting agricultural diversity to improve the adaptability of the cropland system to climate change; and (4) increasing investment in agricultural technology innovation and cultivating agricultural talents to continuously strengthen the transformability of the cropland system are required.

Limitations and Prospect

This study constructed an evaluation index system of CSRCC at the municipal scale on the basis of the connotations of socio-ecological system resilience and used both of social statistic data and spatial data to explore the spatio-temporal characteristics of CSRCC. The research results could provide a reference

for comprehensively regulating the CSRCC and improving regional sustainable agricultural development. However, there are still some limitations: the robustness, adaptability, and transformability of CSRCC constitute a continuous process, and the order in which they occur is fixed. The interactions and conceptual boundaries are still blurry, which makes indicator selection confusing. Some important indicators have two or three attributes of the three capacities of CSRCC at the same time (Manevska-Tasevska et al., 2021; Nicholas-Davies et al., 2021). In our evaluation index system, for example, the cropland area loss rate is negative to the robustness and adaptability. The loss of rural labor force not only is not conducive to the transformation of the cropland system but also has a negative impact on the recovery of the cropland system after the disasters. The indicator selection is not specific enough and needs to be verified and continuously explored with mechanism analysis. Meanwhile, the accessibility and accuracy of data also limited the indicator selection. Specifically, cropland biodiversity, soil property, cropland infrastructure, etc. are the potential indicators of CSRCC, which are inaccessible.

On this basis, this study puts forward the following questions worthy of further research: (1) How to construct a systematic and integrated evaluation system for multi-scale CSRCC? (2) How to choose evaluation indicators by coupling the macro-level of socio-economic factors and the micro-level of natural environmental factors? (3) What are the important influence factors driving the regional disparity of CSRCC? (4) How do existing polices affect CSRCC, and how can specific policies be developed to improve CSRCC?

CONCLUSION

Based on the connotations of socio-ecological system resilience, we propose a new evaluation index system from robustness, adaptability, and transformability. Delphi, AHP, and TOPSIS methods are used to measure the CSRCC from 2011 to 2018 at the municipal scale in Hubei province, China. The regional disparities of CSRCC are analyzed by using the Theil coefficient. The results show that the CSRCC in Hubei province is generally low. There are a few municipalities whose CSRCC has been improved, while most have decreased. The cropland system resilience in Hubei province shows an increasing trend in the central south and a decreasing trend in the west. Specifically, CSRCC in the central and southern Hubei plains is high, such as Wuhan, Jingzhou, and Ezhou, while that in the western and northern Hubei mountain regions is low, such as Enshi and Shiyan. The construction of an evaluation index system at multi-scale, the influence mechanism of CSRCC change, and the policy implications are discussed. As a prospect, we aim to improve the evaluation system on the basis of the verification of the interactions between the three capacities of cropland system resilience, clarify the macro- and micro-mechanisms which affect CSRCC, and propose more practical policies in further studies.

DATA AVAILABILITY STATEMENT

Publicly available datasets were analyzed in this study. This data can be found here: https://zenodo.org/record/4417810#.YnksmfjP2Un.

AUTHOR CONTRIBUTIONS

MY collected the data, analyzed the data, wrote, and revised manuscripts. SS analyzed the data, wrote, and revised the manuscripts. XF provided data processing methods. XYL and XHL provided suggestions on research design and the manuscript. BY designed the study and revised the manuscript. All authors agreed to be accountable for the content of the work.

FUNDING

This work was funded by the National Natural Science Foundation of China (42101280), the Humanities and Social Science Fund of the Ministry of Education (20YJC630182, 19YJC790054), and the Key Project of Philosophy and Social Sciences Research, Ministry of Education (20JZD015).

ACKNOWLEDGMENTS

We acknowledge the contributions of specific colleagues, institutions, or agencies that aided the efforts of this research.

REFERENCES

Allison, H. E., and Hobbs, R. J. (2004). Resilience, adaptive capacity, and the "lock-in trap" of the Western Australian agricultural region. *Ecol. Soc.* 9:3. doi: 10.5751/ES-00641-090103

Altieri, M. A., Nicholls, C. I., Henao, A., and Lana, M. A. (2015). Agroecology and the design of climate change-resilient farming systems. *Agron. Sustain. Dev.* 35, 869–890. doi: 10.1007/s13593-015-0285-2

Amaranto, A., Munoz-Arriola, F., Corzo, G., Solomatine, D. P., and Meyer, G. (2018). Semi-seasonal groundwater forecast using multiple data-driven models in an irrigated cropland. *J. Hydroinf.* 20, 1227–1246. doi: 10.2166/hydro.2018.002

Badillo-Márquez, A. E., Aguilar-Lasserre, A. A., Miranda-Ackerman, M. A., Sandoval-González, O. O., Villanueva-Vásquez, D., and Posada-Gómez, R. (2021). An agent-based model-driven decision support system for assessment of agricultural vulnerability of sugarcane facing climatic change. *Mathematics* 9:3061. doi: 10.3390/math9233061

Batung, E. S., Mohammed, K., Kansanga, M. M., Nyantakyi-Frimpong, H., and Luginaah, I. (2022). Credit access and perceived climate change resilience of smallholder farmers in semi-arid northern Ghana. *Environ. Dev. Sustain.* 1–30. doi: 10.1007/s10668-021-02056-x

Birthal, P. S., Negi, D. S., Khan, M. T., and Agarwal, S. (2015). Is Indian agriculture becoming resilient to droughts? Evidence from rice production systems. *Food Policy* 56, 1–12. doi: 10.1016/j.foodpol.2015.07.005

Bombi, P. (2018). Potential impacts of climate change on Welwitschia mirabilis populations in the Namib Desert, *southern Africa. J. Arid Land* 10, 663–672. doi: 10.1007/s40333-018-0067-1

Borychowski, M., Stępień, S., Polcyn, J., Tošović-Stevanović, A., Ćalović, D., Lalić, G., et al. (2020). Socio-economic determinants of small family farms' resilience

in selected central and eastern european countries. *Sustainability* 12:10362. doi: 10.3390/su122410362

Buitenhuis, Y., Candel, J. J., Termeer, K. J., and Feindt, P. H. (2020). Does the Common Agricultural Policy enhance farming systems' resilience? Applying the Resilience Assessment Tool (ResAT) to a farming system case study in the Netherlands. *J. Rural Stud.* 80, 314–327. doi: 10.1016/j.jrurstud.2020.10.004

Bush, J., and Doyon, A. (2019). Building urban resilience with nature-based solutions: How can urban planning contribute? *Cities* 95:102483. doi: 10.1016/j.cities.2019.102483

Cabell, J. F., and Oelofse, M. (2012). An indicator framework for assessing agroecosystem resilience. *Ecol. Soc.* 17:18. doi: 10.5751/ES-04666-170118

Cariolet, J. M., Vuillet, M., and Diab, Y. (2019). Mapping urban resilience to disasters–A review. *Sustain. Cities Soc.* 51:101746. doi: 10.1016/j.scs.2019.101746

Chen, Y., Xie, W., and Xu, X. (2019). Changes of population, built-up land, and cropland exposure to natural hazards in China from 1995 to 2015. *Int. J. Disaster Risk Sci.* 10, 557–572. doi: 10.1007/s13753-019-00242-0

Datola, G., Bottero, M., De Angelis, E., and Romagnoli, F. (2022). Operationalising resilience: a methodological framework for assessing urban resilience through System Dynamics Model. *Ecol. Model.* 465:109851. doi: 10.1016/j.ecolmodel.2021.109851

Deng, C., Wang, H., Gong, S., Zhang, J., Yang, B., and Zhao, Z. (2020). Effects of urbanization on food-energy-water systems in mega-urban regions: a case study of the Bohai MUR, China. *Environ. Res. Lett.* 15:044014. doi: 10.1088/1748-9326/ab6fbb

Di Falco, S., and Chavas, J. P. (2008). Rainfall shocks, resilience, and the effects of crop biodiversity on agroecosystem productivity. *Land Econ.* 84, 83–96. doi: 10.3368/le.84.1.83

Dixon, J. M., Weerahewa, J., Hellin, J., Rola-Rubzen, M. F., Huang, J., Kumar, S., et al. (2021). Response and resilience of Asian agrifood systems to COVID-19: an assessment across twenty-five countries and four regional farming and food systems. *Agric. Syst.* 193:103168. doi: 10.1016/j.agsy.2021.103168

Egli, L., Schröter, M., Scherber, C., Tscharntke, T., and Seppelt, R. (2021). Crop diversity effects on temporal agricultural production stability across European regions. *Reg. Environ. Change* 21: 96. doi: 10.1007/s10113-021-01832-9

Frei, B., Queiroz, C., Chaplin-Kramer, B., Andersson, E., Renard, D., Rhemtulla, J. M., et al. (2020). A brighter future: complementary goals of diversity and multifunctionality to build resilient agricultural landscapes. *Glob. Food Secur.* 26:100407. doi: 10.1016/j.gfs.2020.100407

Gaur, N., and Mogalapu, S. (2018). "Pests of soybean," in *Pests and their Management*, ed. Omkar Singapore: Springer, 137–162. doi: 10.1007/978-981-10-8687-8_6

Gil, J. D., Cohn, A. S., Duncan, J., Newton, P., and Vermeulen, S. (2017). The resilience of integrated agricultural systems to climate change. *Wiley Interdiscip. Rev. Clim. Change* 8:e461. doi: 10.1002/wcc.461

Gokulnath, B. V., and Devi, G. U. (2021). Identifying and classifying plant disease using resilient LF-CNN. *Ecol. Inform.* 63:101283. doi: 10.1016/j.ecoinf.2021.101283

Gunderson, L. H., and Holling, C. S. (2002). *Panarchy: Understanding Transformations in Human and Natural Systems*. Washington, DC: Island Press.

He, R., Zhu, D., Chen, X., Cao, Y., Chen, Y., and Wang, X. (2019). How the trade barrier changes environmental costs of agricultural production: an implication derived from China's demand for soybean caused by the US-China trade war. *J. Clean. Prod.* 227, 578–588. doi: 10.1016/j.jclepro.2019.04.192

Heino, M., Puma, M. J., Ward, P. J., Gerten, D., Heck, V., Siebert, S., et al. (2018). Two-thirds of global cropland area impacted by climate oscillations. *Nat. Commun.* 9:1257. doi: 10.1038/s41467-017-02071-5

Herrera, H., Schütz, L., Paas, W., Reidsma, P., and Kopainsky, B. (2022). Understanding resilience of farming systems: insights from system dynamics modelling for an arable farming system in the Netherlands. *Ecol. Model.* 464:109848. doi: 10.1016/j.ecolmodel.2021.109848

Holling, C. S. (2001). Understanding the complexity of economic, ecological, and social systems. *Ecosystems* 4, 390–405. doi: 10.1007/s10021-001-0101-5

Hsiang, S. M., and Jina, A. S. (2014). "*The causal effect of environmental catastrophe on long-run economic growth: Evidence from 6,700 cyclones*."NBER Working Papers 20352. Cambridge, MA: National Bureau of Economic Research. doi: 10.3386/w20352

Jacobi, J., Mukhovi, S., Llanque, A., Augstburger, H., Käser, F., Pozo, C., et al. (2018). Operationalizing food system resilience: an indicator-based assessment in agroindustrial, smallholder farming, and agroecological contexts in Bolivia and Kenya. *Land Use Policy* 79, 433–446. doi: 10.1016/j.landusepol.2018.08.044

Javadinejad, S., Dara, R., and Jafary, F. (2021). Analysis and prioritization the effective factors on increasing farmers resilience under climate change and drought. *Agric. Res.* 10, 497–513. doi: 10.1007/s40003-020-00516-w

Kasmalkar, I. G., Serafin, K. A., Miao, Y., Bick, I. A., Ortolano, L., Ouyang, D., et al. (2020). When floods hit the road: resilience to flood-related traffic disruption in the San Francisco Bay Area and beyond. *Sci. Adv.* 6:eaba2423. doi: 10.1126/sciadv.aba2423

Kotzee, I., and Reyers, B. (2016). Piloting a social-ecological index for measuring flood resilience: a composite index approach. *Ecol. Indic.* 60, 45–53. doi: 10.1016/j.ecolind.2015.06.018

Li, W., Wei, X., Zhu, R., and Guo, K. (2018). Study on factors affecting the agricultural mechanization level in China based on structural equation modeling. *Sustainability* 11:51. doi: 10.3390/su11010051

Liang, C., Penghui, J., Manchun, L., Liyan, W., Yuan, G., Yuzhe, P., et al. (2015). Farmland protection policies and rapid urbanization in China: a case study for Changzhou City. *Land Use Policy* 48, 552–566. doi: 10.1016/j.landusepol.2015.06.014

Liu, D., Li, M., Ji, Y., Fu, Q., Li, M., Faiz, M. A., et al. (2021). Spatial-temporal characteristics analysis of water resource system resilience in irrigation areas based on a support vector machine model optimized by the modified gray wolf algorithm. *J. Hydrol.* 597:125758. doi: 10.1016/j.jhydrol.2020.125758

Liu, X., Zhao, C., and Song, W. (2017). Review of the evolution of cultivated land protection policies in the period following China's reform and liberalization. *Land Use Policy* 67, 660–669. doi: 10.1016/j.landusepol.2017.07.012

Liu, Y., Zou, L., and Wang, Y. (2020). Spatial-temporal characteristics and influencing factors of agricultural eco-efficiency in China in recent 40 years. *Land Use Policy* 97:104794. doi: 10.1016/j.landusepol.2020.104794

Lyu, X., Wang, Y., Niu, S., and Peng, W. (2021). Spatio-temporal pattern and influence mechanism of cultivated land system resilience: case from China. *Land* 11:11. doi: 10.3390/land11010011

Manevska-Tasevska, G., Petitt, A., Larsson, S., Bimbilovski, I., Meuwissen, M. P., Feindt, P. H., et al. (2021). Adaptive governance and resilience capacity of farms: the fit between farmers' decisions and agricultural policies. *Front. Environ. Sci.* 9:214. doi: 10.3389/fenvs.2021.668836

Meuwissen, M. P., Feindt, P. H., Spiegel, A., Termeer, C. J., Mathijs, E., de Mey, Y., et al. (2019). A framework to assess the resilience of farming systems. *Agric. Syst.* 176:102656. doi: 10.1016/j.agsy.2019.102656

Meyer, M. A. (2020). The role of resilience in food system studies in low-and middle-income countries. *Glob. Food Secur.* 24:100356. doi: 10.1016/j.gfs.2020.100356

Meza, I., Siebert, S., Döll, P., Kusche, J., Herbert, C., Eyshi Rezaei, E., et al. (2020). Global-scale drought risk assessment for agricultural systems. *Nat. Hazards Earth Syst. Sci.* 20, 695–712. doi: 10.5194/nhess-20-695-2020

Milestad, R., and Darnhofer, I. (2003). Building farm resilience: the prospects and challenges of organic farming. *J. Sustain. Agric.* 22, 81–97. doi: 10.1300/J064v22n03_09

Mittenzwei, K., and Øygarden, L. (2019). *The Increasing Impact of Environmental Policies on Agriculture: Perspectives from Norway 172nd EAAE Seminar*. Brussels: European Association of Agricultural Economists.

Mutabazi, K. D., Amjath-Babu, T. S., and Sieber, S. (2015). Influence of livelihood resources on adaptive strategies to enhance climatic resilience of farm households in Morogoro, Tanzania: an indicator-based analysis. *Reg. Environ. Change* 15, 1259–1268. doi: 10.1007/s10113-015-0800-7

Nasr, B. J., Chaar, H., Bouchiba, F., and Zaibet, L. (2021). Assessing and building climate change resilience of farming systems in Tunisian semi-arid areas. *Environ. Sci. Pollut. Res.* 28, 46797–46808. doi: 10.1007/s11356-021-13089-0

Nicholas-Davies, P., Fowler, S., Midmore, P., Coopmans, I., Draganova, M., Petitt, A., et al. (2021). Evidence of resilience capacity in farmers' narratives: accounts of robustness, adaptability and transformability across five different European farming systems. *J. Rural Stud.* 88, 388–399. doi: 10.1016/j.jrurstud.2021.07.027

Niedertscheider, M., Kuemmerle, T., Müller, D., and Erb, K. H. (2014). Exploring the effects of drastic institutional and socio-economic changes on land system

dynamics in Germany between 1883 and 2007. *Glob. Environ. Change* 28, 98–108. doi: 10.1016/j.gloenvcha.2014.06.006

Nyong, A. P., Ngankam, T. M., and Felicite, T. L. (2020). Enhancement of resilience to climate variability and change through agroforestry practices in smallholder farming systems in Cameroon. *Agrofor. Syst.* 94, 687–705. doi: 10.1007/s10457-019-00435-y

Peng, X., Tong, X., Hao, L., and Wu, F. (2019). Applicability of biochar for limiting interrill erosion and organic carbon export of sloping cropland in a semi-arid area of China. *Agric. Ecosyst. Environ.* 280, 68–76. doi: 10.1016/j.agee.2019.04.021

Potapova, E., Kruchina, E., Barkhatova, O., and Makarov, A. (2022). "Disasters and Resilient City," in *Proceedings of the IOP Conference Series: Earth and Environmental Science*, Bristol. doi: 10.1088/1755-1315/988/3/032007

Qin, X., and Wu, H. (2021). Rural Infrastructure and Poverty in China. *Paper Presented at the 31st International Conference of Agricultural Economists (ICAE)*, Noida.

Ray, R. L., Fares, A., and Risch, E. (2018). Effects of drought on crop production and cropping areas in Texas. *Agric. Environ. Lett.* 3:170037. doi: 10.2134/ael2017.11.0037

Rey, D., Holman, I. P., and Knox, J. W. (2017). Developing drought resilience in irrigated agriculture in the face of increasing water scarcity. *Reg. Environ. Change* 17, 1527–1540. doi: 10.1007/s10113-017-1116-6

Tambo, J. A. (2016). Adaptation and resilience to climate change and variability in north-east Ghana. *Int. J. Disaster Risk Reduct.* 17, 85–94. doi: 10.1016/j.ijdrr.2016.04.005

Tendall, D. M., Joerin, J., Kopainsky, B., Edwards, P., Shreck, A., Le, Q. B., et al. (2015). Food system resilience: defining the concept. *Glob. Food Secur.* 6, 17–23. doi: 10.1016/j.gfs.2015.08.001

Thorsøe, M., Noe, E., Maye, D., Vigani, M., Kirwan, J., Chiswell, H., et al. (2020). Responding to change: farming system resilience in a liberalized and volatile European dairy market. *Land Use Policy* 99:105029. doi: 10.1016/j.landusepol.2020.105029

Tuo, D., Xu, M., and Gao, G. (2018). Relative contributions of wind and water erosion to total soil loss and its effect on soil properties in sloping croplands of the Chinese Loess Plateau. *Sci. Total Environ.* 633, 1032–1040. doi: 10.1016/j.scitotenv.2018.03.237

Ullah, K. M., and Uddin, K. (2021). The relationships between economic growth and cropland changes in Bangladesh: an evidence based on annual land cover data. *Environ. Chall.* 5:100252. doi: 10.1016/j.envc.2021.100252

Urruty, N., Tailliez-Lefebvre, D., and Huyghe, C. (2016). Stability, robustness, vulnerability and resilience of agricultural systems. A review. *Agron. Sustain. Dev.* 36:15. doi: 10.1007/s13593-015-0347-5

Vallés-Planells, M., Galiana, F., and Díez Torrijos, I. (2020). Agricultural abandonment and resilience in a Mediterranean periurban traditional agroecosystem: a landscape approach. *Ecol. Soc.* 25:4845. doi: 10.5751/ES-11346-250105

Van Loon, J., Woltering, L., Krupnik, T. J., Baudron, F., Boa, M., and Govaerts, B. (2020). Scaling agricultural mechanization services in smallholder farming systems: case studies from sub-Saharan Africa. South Asia, and Latin America. *Agric. Syst.* 180:102792. doi: 10.1016/j.agsy.2020.102792

Vishnu, N., Kameshwar, S., and Padgett, J. E. (2021). Road transportation network hazard sustainability and resilience: correlations and comparisons. *Struct. Infrastruct. Eng.* 1–21. doi: 10.1080/15732479.2021.1945114

Wang, C., Wang, Z., Gao, Y., and Zhang, X. (2021). Planular-vertical distribution and pollution characteristics of cropland soil Hg and the estimated soil–air exchange fluxes of gaseous Hg over croplands in northern China. *Environ. Res.* 195:110810. doi: 10.1016/j.envres.2021.110810

Wang, M., Zhang, Y., Bakhshipour, A., Liu, M., Rao, Q., and Liu, Z. (2022). Designing coupled LID–GREI urban drainage systems: resilience assessment and decision-making framework. *Sci. Total Environ.* 834:155267. doi: 10.1016/j.scitotenv.2022.155267

Wang, T., Li, H., and Huang, Y. (2021). The complex ecological network's resilience of the Wuhan metropolitan area. *Ecol. Indic.* 130:108101. doi: 10.1016/j.ecolind.2021.108101

Wątróbski, J., Bączkiewicz, A., Ziemba, E., and Sałabun, W. (2022). Sustainable cities and communities assessment using the DARIA-TOPSIS method. *Sustain. Cities Soc.* 83:103926. doi: 10.1016/j.scs.2022.103926

Wu, Y., Shan, L., Guo, Z., and Peng, Y. (2017). Cultivated land protection policies in China facing 2030: dynamic balance system versus basic farmland zoning. *Habitat Int.* 69, 126–138. doi: 10.1016/j.habitatint.2017.09.002

Yang, J., and Huang, X. (2021). The 30 m annual land cover datasets and its dynamics in China from 1990 to 2020. *Earth Syst. Sci. Data* 13, 3907–3925. doi: 10.5194/essd-13-3907-2021

Yang, Y., Guo, H., Wang, D., Ke, X., Li, S., and Huang, S. (2021). Flood vulnerability and resilience assessment in China based on super-efficiency DEA and SBM-DEA methods. *J. Hydrol.* 600:126470. doi: 10.1016/j.jhydrol.2021.126470

Yu, J., and Wu, J. (2018). The sustainability of agricultural development in China: the agriculture–environment nexus. *Sustainability* 10:1776. doi: 10.3390/su10061776

Yu, T., Mahe, L., Li, Y., Wei, X., Deng, X., and Zhang, D. (2022). Benefits of crop rotation on climate resilience and its prospects in China. *Agronomy* 12:436. doi: 10.3390/agronomy12020436

Zampieri, M., Toreti, A., Ceglar, A., De Palma, P., Chatzopoulos, M., and Michetti, M. (2021). Analysing the resilience of agricultural production systems with ResiPy, the Python production resilience estimation package. *SoftwareX* 15:100738. doi: 10.1016/j.softx.2021.100738

Zampieri, M., Weissteiner, C. J., Grizzetti, B., Toreti, A., van den Berg, M., and Dentener, F. (2020). Estimating resilience of crop production systems: from theory to practice. *Sci. Total Environ.* 735:139378. doi: 10.1016/j.scitotenv.2020.139378

Zhou, W., Guo, S., Deng, X., and Xu, D. (2021). Livelihood resilience and strategies of rural residents of earthquake-threatened areas in Sichuan Province, China. *Natural Hazards* 106, 255–275. doi: 10.1007/s11069-020-04460-4

Conflict of Interest: The authors declare that the research was conducted in the absence of any commercial or financial relationships that could be construed as a potential conflict of interest.

Publisher's Note: All claims expressed in this article are solely those of the authors and do not necessarily represent those of their affiliated organizations, or those of the publisher, the editors and the reviewers. Any product that may be evaluated in this article, or claim that may be made by its manufacturer, is not guaranteed or endorsed by the publisher.

Copyright © 2022 Yan, Yang, Sheng, Fan, Li and Lu. This is an open-access article distributed under the terms of the Creative Commons Attribution License (CC BY). The use, distribution or reproduction in other forums is permitted, provided the original author(s) and the copyright owner(s) are credited and that the original publication in this journal is cited, in accordance with accepted academic practice. No use, distribution or reproduction is permitted which does not comply with these terms.

frontiers | Frontiers in Ecology and Evolution

ORIGINAL RESEARCH
published: 30 June 2022
doi: 10.3389/fevo.2022.927238

How Does Different Cropland Expansion Trajectories Affect Cropland Fragmentation? Insights From Three Urban Agglomerations in Yangtze River Economic Belt, China

*Liye Wang[1], Siyu Zhang[2], Yifan Xie[1], Yanfang Liu[1] and Yaolin Liu[1,3]**

[1] School of Resource and Environmental Sciences, Wuhan University, Wuhan, China, [2] College of Public Administration, Huazhong Agricultural University, Wuhan, China, [3] Collaborative Innovation Center of Geospatial Information Technology, Wuhan University, Wuhan, China

A clear understanding of cropland expansion dynamics and their effects is vital for cropland protection and food security. However, the trajectories of cropland expansion have been less discussed. This study referred to the modes of landscape expansion and assessed the cropland expansion trajectory in three urban agglomerations in the Yangtze River Economic Belt and its impact on cropland fragmentation. Specifically, we identified three cropland expansion trajectories using the landscape expansion index, namely, infilling, edge-expansion, and outlying. Moreover, the surface relief amplitude model was employed to characterize the relief amplitude effect on cropland expansion trajectories. By coupling landscape metrics (e.g., patch density, landscape shape index, the largest patch index, and aggregation index) and Spearman correlation analysis, the relationship between cropland expansion trajectories and cropland fragmentation was assessed. Results show that (1) three urban agglomerations experience cropland expansion, in which the edge-expansion trajectory is primary, followed by infilling and outlying trajectories; (2) the cumulative frequency curve indicates that infilling and edge-expansion trajectories are likely to be distributed in low topographic relief amplitude regions, while the outlying trajectory is located in relatively higher topographic relief amplitude regions; and (3) infilling and edge-expansion trajectories contribute to a significantly positive relationship with the decrease of cropland fragmentation, while the outlying trajectory has a negative relationship with cropland fragmentation. This research highlights that cropland protection policies should considerably focus on the trajectory of cropland expansion, not only request the total area of cropland in a dynamic balance.

Keywords: cropland expansion trajectory, land fragmentation, landscape metrics, topographic relief amplitude, correlation analysis, landscape expansion index

OPEN ACCESS

Edited by:
Jianhong Xia,
Curtin University, Australia

Reviewed by:
Qingsong He,
Huazhong University of Science and Technology, China
Hongyun Si,
Shandong University of Finance and Economics, China

***Correspondence:**
Yaolin Liu
yaolin610@163.com

Specialty section:
This article was submitted to Environmental Informatics and Remote Sensing, a section of the journal Frontiers in Ecology and Evolution

Received: *24 April 2022*
Accepted: *30 May 2022*
Published: *30 June 2022*

Citation:
Wang L, Zhang S, Xie Y, Liu Y and Liu Y (2022) How Does Different Cropland Expansion Trajectories Affect Cropland Fragmentation? Insights From Three Urban Agglomerations in Yangtze River Economic Belt, China. Front. Ecol. Evol. 10:927238. doi: 10.3389/fevo.2022.927238

INTRODUCTION

Agricultural activities have been consistently chosen by humans to cultivate the earth's surface for their needs in food, timber, and other living materials. In 2000, agricultural lands, including cropland and pasture, comprised at least 34% of the global land surface that is without ice (Ramankutty et al., 2008). Since the twenty-first century, the explosive population growth has

placed immense pressure on agricultural lands (Tscharntke et al., 2012). Due to increasing income and socioeconomic growth brought by urbanization and globalization, this pressure to satisfy human's increasing pursuit to improve their diet structure will keep on increasing in the foreseeable future (Phalan et al., 2011; Kastner et al., 2012; Dong et al., 2018). The requirement for food crops in 2050 is projected to increase by 100–110% compared with that in 2005, and the magnitude of land that will be cleared for agricultural expansion to meet this demand (Tilman et al., 2011).

Except for food use, crops are also used for animal feed, bioenergy, and industrial products, thereby affecting food availability for humans. Global research has shown that the allocation of crop yield for human food only accounts for 62% of the total cropland production (Foley et al., 2011). Cropland, as a vital producer of basic living materials, is one of the most important human-made landscapes on Earth and also a vital landscape for human society (Liu J. et al., 2014; van Vliet et al., 2017). A large number of policies have been implemented to maintain cropland to maintain food security (Liu et al., 2017). For example, the UK proposed the "Green Belt Policy" to restrict the loss of cropland and China implemented the "Basic Cropland Protection Policy" to prevent the disorderly urban sprawl (Cullingworth, 2014; Wang et al., 2022b). In the fields of land use science and landscape studies, cropland is consistently a popular issue for researchers (Sarparast et al., 2020; Zhou et al., 2021). Numerous cropland-related topics have been assessed by previous studies from the micro to macro scale, including cropland conversion encroaching with urban expansion and ecological land loss (Ke et al., 2018; Tu et al., 2021), interaction with ecosystem services (Ke et al., 2019; Wang et al., 2020), displacement (Yang et al., 2020), abandonment (Yan et al., 2009; Han and Song, 2020), driving forces (Prabhakar, 2021; Uisso and Tanrıvermiş, 2021), and expansion and intensification (Zabel et al., 2019; Nzabarinda et al., 2021).

Globally, cropland expansion has been considered as an important way to increase crop production (Zeng et al., 2018; van Vliet, 2019; Eigenbrod et al., 2020). By 2030, an estimated 7.3×10^6 km^2 of land globally will be additionally transformed into cropland (Zabel et al., 2019). Cropland expansion is a special topic because it increases food supply (Lambin and Meyfroidt, 2011; Cheng et al., 2021) and improves the income of farmers (He et al., 2021), but threatens biodiversity (Egli et al., 2018) and degrades ecosystem services (Ke et al., 2019). Given that China is the most populous developing country, ensuring food security, the strictest cropland protection policy has been promulgated by the Chinese government to protect the total area of cropland and promote cropland expansion (Song and Pijanowski, 2013; Wang et al., 2021). Tang et al. (2020b) explored the cropland expansion in Hubei Province, China and assessed its impact on carbon storage. They pointed out that the loss of carbon storage caused by cropland expansion is 3.89 times greater than that caused by urban expansion. Ma et al. (2019) mapped the cropland expansion in the Northwest of China and found the speed of cropland expansion in the Junggar Basin and Tarim Basin at 641.3 and 271.3 km^2/year, respectively. However, there is still a research gap in systematically understanding the rate and trajectory of cropland expansion, particularly in combining spatiotemporal data in the urban agglomerations. Besides, the spatiotemporal characteristics of cropland expansion and its consequences are particularly vital for cropland protection and future policy-making. Therefore, understanding the speed, expansion trajectory, and consequences of cropland expansion is an important issue for researchers.

Cropland fragmentation is another focus of the government and researchers due to its threat to cropland productivity and food security (Song and Liu, 2017; Liang et al., 2021a; Tian et al., 2021). Cropland fragmentation comprises two types of fragmentation, namely, cropland physical and ownership fragmentations (Farley et al., 2012; Su et al., 2014). Cropland physical fragmentation refers to an increase in cropland patch numbers and a decrease in patch size, which are closely related to land conversion processes (Qi et al., 2014), Ownership fragmentation represents the spatial dispersibility of cropland patches owned by one cropland owner (Tan et al., 2006). Existing research has mainly focused on cropland fragmentation brought by land use change such as urbanization (Tu et al., 2021), resulting from land protection strategies (Brabec and Smith, 2002), and spatiotemporal changes in cropland fragmentation (Cheng et al., 2015). Only a few researchers have explored the impact of cropland expansion on cropland fragmentation. Yu et al. (2018) explored the gross area change of cropland and its interaction with cropland fragmentation in China and found little net change in cropland area while there was greater cropland fragmentation due to the redistribution of cropland. A nuanced analysis of the interaction between cropland expansion and cropland fragmentation has yet to be conducted. The proposed modes of landscape expansion (i.e., infilling, edge-expansion, and outlying) have been widely employed to understand the landscape expansion process (Xu et al., 2007; Li et al., 2013; Jiao et al., 2015). The modes of landscape expansion can be used to understand cropland expansion.

The Yangtze River Economic Belt (YREB) program was launched by the central government of China in 2016, and aims to promote the economic development of the coastal areas along the Yangtze River by giving play to the leading roles of the urban agglomerations in the YREB (Yang et al., 2021; Wang et al., 2022b). The YREB is located in the central part of China and it spans the West, Middle, and East of China, experiencing large-scale elevation changes. A large amount of cropland and cropland expansion activities are detected in the YREB (Tang et al., 2021; Wang et al., 2022a,b). Studies related to cropland expansion in the YREB include several perspectives, such as ecosystem services or functions (Tang et al., 2020b; Zhang et al., 2021), ecological risks (Ran et al., 2022), driving factors of cropland expansion (Wang et al., 2022b), and interactions between cropland and construction land expansion (Wang et al., 2022a). It is important to understand the cropland expansion trajectories and their impacts on cropland fragmentation in such an area with large-scale elevation changes and active cropland expansion activities.

Thus, choosing the urban agglomerations in the YREB as the case areas, this study used the landscape expansion modes as the basis for defining the trajectory of cropland

expansion. Specifically, three cropland expansion trajectories were identified, namely, infilling, edge-expansion, and outlying trajectories. The research objectives of this study are to (1) identify the spatiotemporal heterogeneity of different cropland expansion trajectories; and (2) assess the interactions between cropland expansion trajectories and cropland fragmentation. In this study, cropland fragmentation refers to cropland physical fragmentation and cropland ownership fragmentation is not discussed.

STUDY AREA AND DATA

In total, three Chinese national urban agglomerations in the YREB were selected to identify the impact of cropland expansion trajectories on cropland fragmentation: Yangtze River Delta Urban Agglomeration (YRDUA), Middle Reaches of Yangtze River Urban Agglomeration (MRYRUA), and Cheng and Yu Urban Agglomeration (C&YUA) (**Figure 1**). YREB is one of the most important economic and agricultural development zones. According to statistical data from the National Bureau of Statistics of China,[1] YREB accounts for 44% of China's GDP. Among them, the GDP of the primary industry accounts for 42% of the country. YREB, as one of the most important grain yield bases, also has 3.08×10^7 ha of cropland, which contributes to 32.5% of grain yield, reflecting active agricultural activities. Therefore, frequent cropland transitions have been observed by recent studies (Cheng et al., 2020; Tang et al., 2021; Yang et al., 2021). With the exception of spontaneous cropland expansion activities, there are also some cropland expansion activities implemented under policy requirements, among which the Cropland Balance Policy is the most targeted policy (Song and Pijanowski, 2013; Liu et al., 2017). This policy regulates the activity of cropland compensation as a mitigation measure for cropland loss caused by urban land expansion, making cropland expansion activities considerably active in fast urbanization areas. Thus, YRDUA, MRYRUA, and C&YUA are superior regions for identifying cropland expansion trajectories.

The data chosen in this study consists of land use data from 2000 to 2015 (with a resolution of 30 m) from the Data Center of Resources and Environment, Chinese Academy of Sciences.[2] Due to data limits for landscape metric calculation, we reclassified land use types into cropland and other lands (not cropland) for further analysis and resampled the spatial resolution into 100 m.

MATERIALS AND METHODS

Identifying Cropland Expansion Trajectories

The three types of landscape expansion are infilling, edge-expansion, and outlying (Wilson et al., 2003; Li et al., 2013). All landscape expansion progress could be regarded as an integration of the three types (Forman, 1995; Ellman, 1997). Since Liu et al. (2010) proposed the landscape expansion index (LEI), numerous studies have used this index to identify the landscape expansion types in different regions, such as Wuhan and Beijing (Rao et al., 2021; Tu et al., 2021). By referencing studies related to landscape expansion, cropland expansion trajectories can also be subdivided into three trajectories, namely, infilling, edge-expansion, and outlying trajectories. The infilling trajectory specifically indicates the phenomenon that new expanded cropland is converted from the void area between or within the previous cropland. An edge-expansion trajectory represents a newly emerged cropland that spreads unidirectionally from the edge of the existing cropland. An outlying trajectory refers to a newly expanded area of cropland isolated from old patches.

The LEI is chosen to identify different cropland expansion trajectories. This index is calculated based on the interacted area between the buffer zone of newly expanded patches and old patches:

$$LEI_{i,j} = \frac{AO_{i,j}}{AO_{i,j} + AV_{i,j}} \times 100 \quad (1)$$

where $\mathrm{LEI}_{i,j}$ is the landscape expansion index; $AO_{i,j}$ is the interacted area between the buffer zone of new expanded patches and old patches; $AV_{i,j}$ denotes the interacted area between the buffer zone and vacant area, and i and j represent the study area and period, respectively.

The thresholds of LEI are defined by Liu et al. (2010): (1) For the infilling trajectory, the threshold is above 50 and below or equal to 100. (2) If LEI belongs to the range of (0, 50], then the new expanded path can be defined as an edge-expansion trajectory. (3) The threshold of the outlying trajectory is equal to 0. In addition, another key parameter for the LEI calculation is the buffer distance, which should be decided based on the spatial resolution of the land use data. Thus, this parameter is 100 m in the current study.

Topographic Relief Amplitude Extraction

Topographic factors, such as water and heat, can highly influence the spatial distribution of cropland and its expansion by affecting the distribution of farming conditions (Gao et al., 2019), thereby affecting the spatial distribution of different cropland expansion trajectories. The majority of the existing studies have explored the influence of DEM on cropland (Cheng et al., 2020; Folberth et al., 2020), and have disregarded the difference between the surface of relief amplitudes in different levels of DEM. For example, a district with a low DEM may have a higher relief amplitude than a district with a high DEM, thereby having limited cropland and cropland-related activities. Thus, the surface relief amplitude model was chosen to explore the characteristics of the distribution of different cropland expansion trajectories.

The surface relief amplitude model is an index to represent regional characteristics referring to the difference between the highest DEM and lowest DEM in a region. The related equation is shown as follows:

$$\mathrm{SRA}_i = \mathrm{DEM}_{i,max} - \mathrm{DEM}_{i,min} \quad (2)$$

where SRA_i represents the surface relief amplitude in the surface relief amplitude window i and $\mathrm{DEM}_{i,max}$ and $\mathrm{DEM}_{i,min}$ are the

[1] http://www.stats.gov.cn/

[2] http://www.resdc.cn/

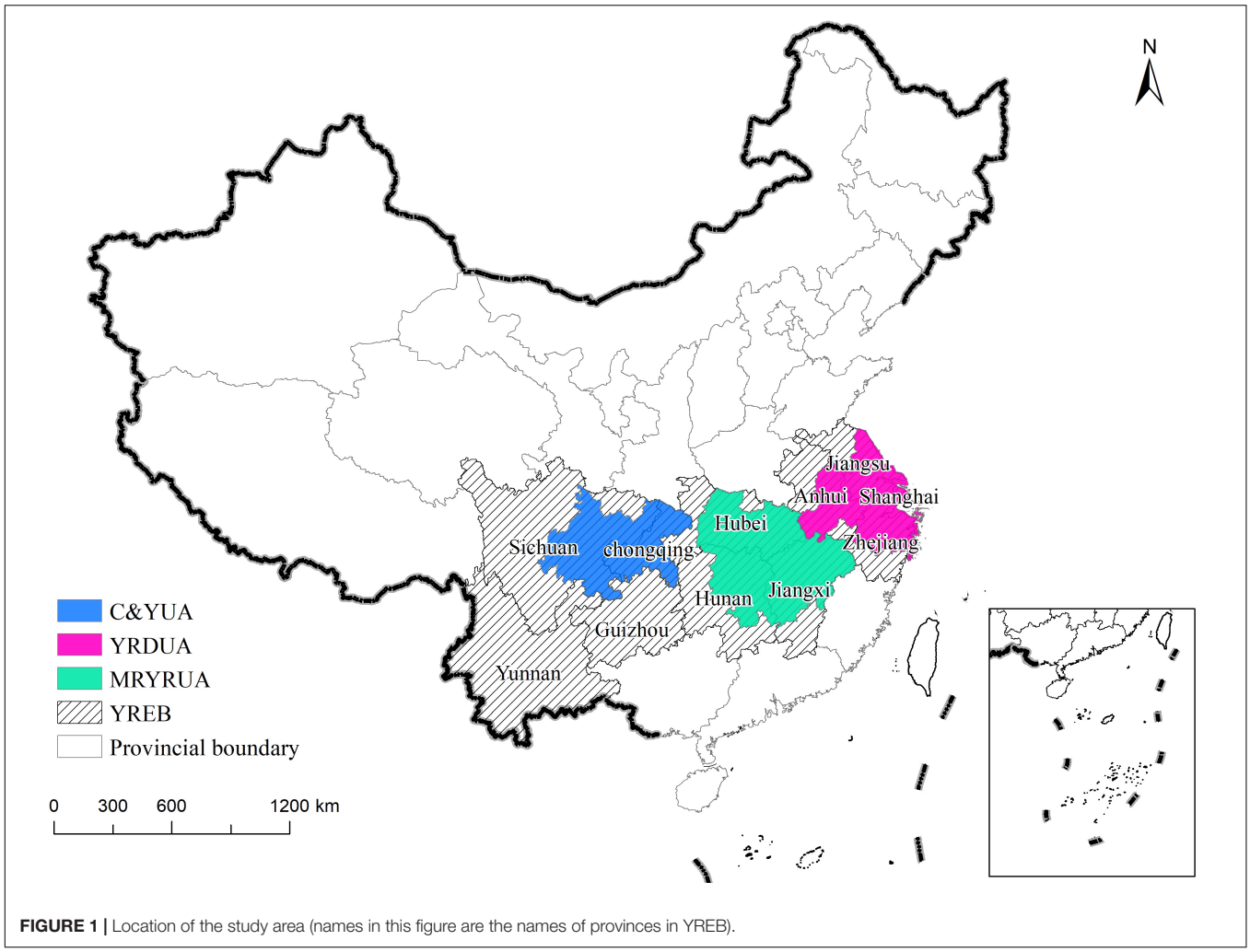

FIGURE 1 | Location of the study area (names in this figure are the names of provinces in YREB).

maximum and minimum, respectively, of DEM in the window i. The calculation results are scale-dependent, which means the spatial resolution of the surface relief amplitude window is the key factor to reflect the true situation of the surface relief amplitude (Liang et al., 2021b). Therefore, to determine the best scale of the window, the mean change point method is used to calculate the side length of the window.

First, we generate a series of surface relief amplitude windows with a side length of n ($n = 1, 2, 3,..., 20$) for the DEM data and calculate the surface relief amplitude by using Equation (2). Thereafter, we calculate the mean values of the surface relief amplitude in different side length windows and determine the surface relief amplitude per unit area. Lastly, we calculate the logarithm sequence $\{X_n\}$ according to Equation (3).

$$X_n = \ln UA_n \tag{3}$$

where UA_n is the surface relief amplitude per unit area in window n; n is the window's side length, with a value of 1, 2, ... 20. The variance of $\{X_n\}$ is labeled as T.

Second, we make $i = 2, 3,..., 19$, and each i places sequence $\{X_n\}$ into two sub-sequences: $\{X_1, X_2, ..., X_{i-1}\}$ and $\{X_i, X_{i+1}, ..., X_n\}$. The mean value of the two sub-sequences X_{i1} and X_{i2} are obtained separately. The statistic value T_i of each sequence is calculated by the following equation:

$$T_i = \sum_{t=1}^{i-1} (X_t - X_{i1})^2 + \sum_{t=i}^{19} (X_t - X_{i2})^2 \tag{4}$$

Last, we calculate the difference between T and T_i, and find the best side length of the surface relief amplitude window corresponding to the maximum value of $T-T_i$. **Figure 2** shows the statistical difference between T and T_i in three urban agglomerations. That is when $i = 5, 5, 4$, the difference between S and S_i reaches the maximum values in YRDUA, MRYRUA, and C&YUA, respectively. Thus, the most suitable spatial resolutions of the window side length are 6, 6, and 5 km in YRDUA, MRYRUA, and C&YUA, respectively.

Measurement of Cropland Fragmentation

Landscape metrics, which are the most widely used indexes in measuring landscape status, have been used in numerous studies to assess land fragmentation (Dewan et al., 2012; Su et al., 2012).

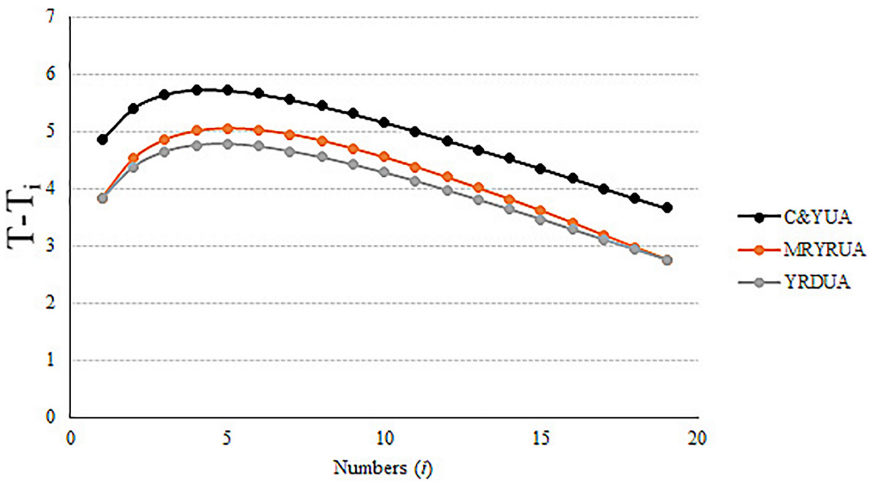

FIGURE 2 | Statistical differences corresponding to each number of *i*.

To measure cropland fragmentation, four indexes are chosen to represent the level of fragmentation and continuity at the class level according to previous research: patch density (PD), landscape shape index (LSI), the largest patch index (LPI), and aggregation index (AI) (Cabral and Costa, 2017; Qiu et al., 2019; Tu et al., 2021).

Patch density is used to represent the level of cropland fragmentation or subdivision. LSI adjusts the size of cropland through the measurement of the total edge length of cropland. LPI reports the ratio between the area of the largest cropland patch and the total cropland. Lastly, AI indicates the largest possible number of patch adjacencies of cropland. In the progress of cropland expansion, both the number of patches and the area of cropland are increasing. However, there is a mismatch between the speed of the patch increase and area increase under different cropland expansion trajectories. For example, a new expanded cropland in infilling and edge-expansion trajectories may only lead to an increase in cropland area, influence the largest patch area, and not affect the number of patches. Therefore, these landscape metrics can be used to reflect the impacts of cropland expansion trajectories on cropland fragmentation.

All landscape metrics are calculated in Fragstats 4.2.1 software with no sampling strategy at the class scale.

Identifying the Impact of Cropland Expansion Trajectory on Cropland Fragmentation

This study defined the impact of cropland expansion trajectories on cropland fragmentation as it assessed the impacts of a new expanded cropland in the infilling, edge-expansion, and outlying trajectories on the fragmentation of the total new expanded cropland. Thus, we calculated the landscape metrics for the total new expanded cropland and the expanded cropland in three cropland trajectories. We likewise used the Spearman correlation analysis to assess the correlation between cropland expansion trajectories and the total expanded cropland. A positive correlation coefficient indicates a promotional effect between cropland trajectory and cropland fragmentation and vice versa (Han and Song, 2020; Li et al., 2021).

RESULTS

Cropland Expansion Trajectories in 2000–2015

Given the scarcity of expanded cropland compared with the existing cropland and the readability of a figure, **Figure 3** only presents the spatial distribution of expanded cropland in different cropland expansion trajectories in a time period from 2000 to 2015, rather than the three-time intervals: 2000–2005, 2005–2010, and 2010–2015. And, **Table 1** shows the area of different cropland expansion trajectories in different periods.

The area of expanded cropland in different time intervals in each urban agglomeration varies with no rules to follow, while the area of cropland trajectories displays in a decreasing sequence of the edge-expansion, infilling, and outlying trajectories in each period (**Table 1**). From 2000 to 2005, YRDUA experienced the most cropland expansion, at 375,907 ha. Specifically, the areas of edge-expansion, infilling, and outlying trajectories are 234,955, 75,109, and 65,843 ha. In 2005–2010, the most active cropland expansion activity occurred in C&YUA, with 212,453, 14,783, and 10,858 ha of edge-expansion, infilling, and outlying trajectories. From 2010 to 2015, 7,053,360 ha of new expanded cropland occurred in MRYRUA, which is also the largest area of expanded cropland among all time intervals and regions. The detailed numbers are 5,596,801, 1,432,679, and 23,880 ha of edge-expansion, infilling, and outlying trajectories, respectively.

Figure 3 indicates the spatial distribution of different cropland expansion trajectories varies differently among urban agglomerations. As shown in **Figure 3A**, the infilling and edge-expansion trajectories exist throughout the study area in a scattered or aggregated status, while the outlying trajectory is

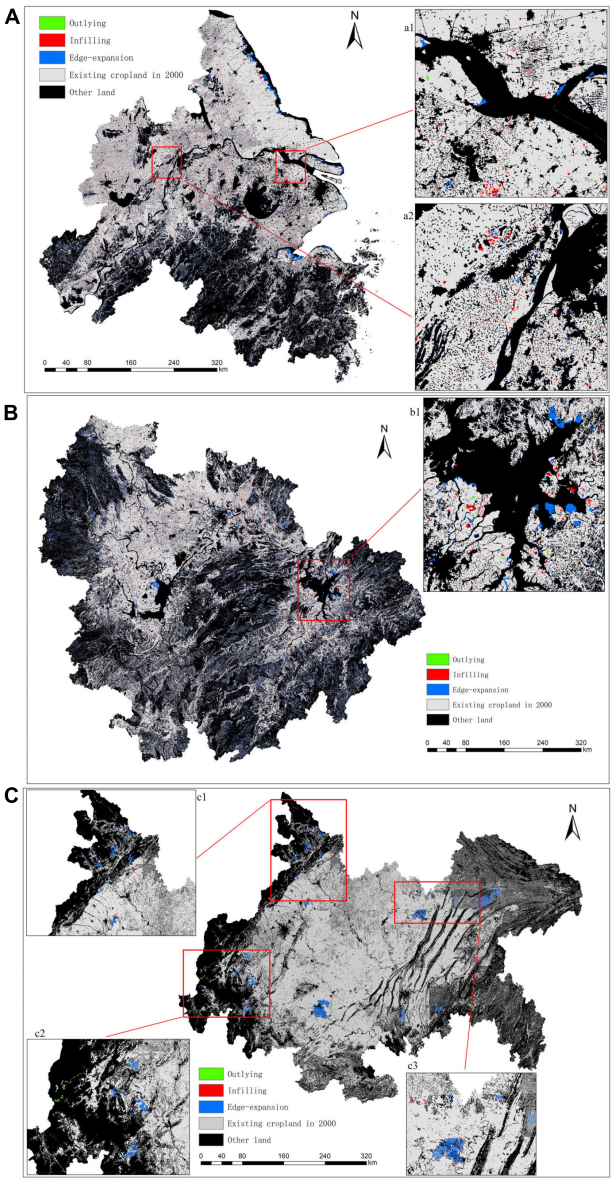

FIGURE 3 | Spatial distributions of different types of cropland expansion trajectories from 2000 to 2015 in **(A)** YRDUA, **(B)** MRYRUA, and **(C)** C&YUA.

minimally distributed, which can be detected in a few areas, such as in the middle (**Figure 3A2**) and eastern (**Figure 3A1**) of YRDUA. Some cropland in the edge-expansion trajectory were distributed in an aggregated status. This cropland is mainly clustered in the east, close to the eastern boundary of the existing cropland in 2000, and displayed in a belt distribution. In addition, a few cropland in the infilling trajectory also shows a centralized pattern, which is also shown in **Figures 3A1,A2**.

Figure 3B denotes the distribution of cropland expansion trajectories in MRYRUA. The distribution of the part that the infilling and edge-expansion trajectories are scattered located is similar to that in YRDUA, in which their existence is shown around the existing cropland. This figure shows that

TABLE 1 | Areas of different cropland expansion trajectories in 2000–2015 in YRDUA, MRYRUA, and C&YUA (ha).

Study area	Period	Infilling	Edge-expansion	Outlying	Cropland expansion
YRDUA	2000–2005	75,109	234,955	65,843	375,907
	2005–2010	13,835	24,309	3,525	41,669
	2010–2015	133,536	318,228	5,478	457,242
MRYRUA	2000–2005	11,123	12,166	3,577	26,866
	2005–2010	50,656	111,187	11,920	173,763
	2010–2015	1,432,679	5,596,801	23,880	7,053,360
C&YUA	2000–2005	6,218	7,796	1,946	15,960
	2005–2010	14,783	212,453	10,858	238,094
	2010–2015	1,457	8,812	94	10,363

the distribution of the parts concentrated in three cropland trajectories is aggregated around lakes. For example, lakes in the middle, north, and east are concentrated with an edge-expansion trajectory. In particular, the lake in the east (**Figure 3B1**) is surrounded by existing cropland in 2000 and expanded cropland in all trajectories.

Unlike the distributions of cropland expansion trajectories in YRDUA and MRYRUA, cropland expansion trajectories are displayed at a concentrated status in C&YUA (**Figure 3C**). Obviously, the edge-expansion trajectory shows the most concentrated status and largest distribution. The infilling trajectory mostly surrounds near the edge-expansion trajectory (**Figures 3C2,C3**) and a few of them are located in the north and northwest independently (**Figures 3C1,3**). In the west and northwest, a few of the outlying trajectories can be observed (**Figures 3C1,C2**).

Topographic Relief Effect of Cropland Expansion Trajectories

A significant difference in topographic relief amplitude exists in YRDUA, MRYRUA, and C&YUA at 1,571, 1,898, and 2,746 m, respectively, because they are located in the upper, middle, and lower reaches of the Yangtze River. Moreover, the variation range of the topographic relief amplitude of cropland expansion trajectories changes vastly over time and region.

In YRDUA, the infilling, edge-expansion, and outlying trajectory cumulative frequencies are up to at least 80% when the topographic reliefs are 91, 227, and 387 m in 2000–2005 (**Figure 4**). As time goes on, the topographic reliefs of the infilling and edge-expansion trajectories decrease to 25 and 168 m, respectively, while that of the outlying trajectory increases to 424 m in 2010–2015. From **Figure 4**, the distribution of the infilling and outlying trajectories is more concentrated with lower topographic relief amplitude, while the distribution of the outlying trajectory shows considerable dispersal.

In MRYRUA, the topographic relief amplitude of trajectories' cumulative frequency that reaches 80% shows an overall increase because of an increase in the topographic relief compared with that in YRDUA (**Figure 5**). Infilling and edge-expansion trajectories in 2010–2015 have the largest areas of cropland and display the most concentrated distribution, in which the

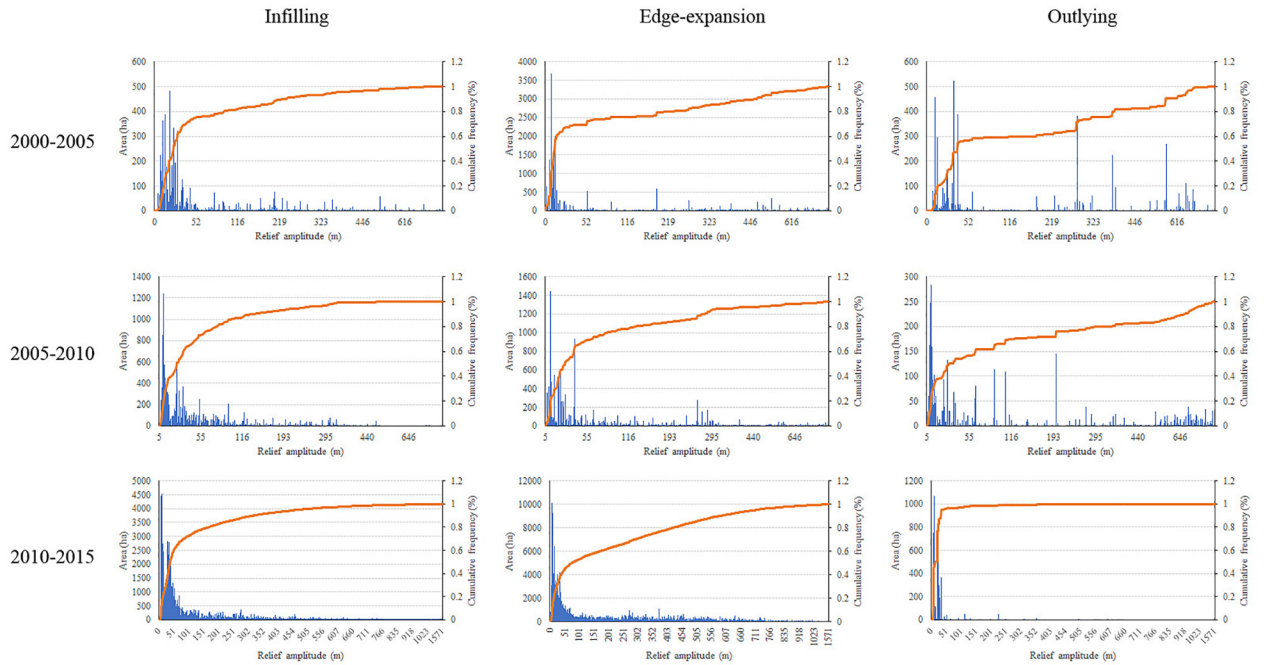

FIGURE 4 | Topographic relief effect in cropland expansion trajectories in YRDUA from 2000 to 2015.

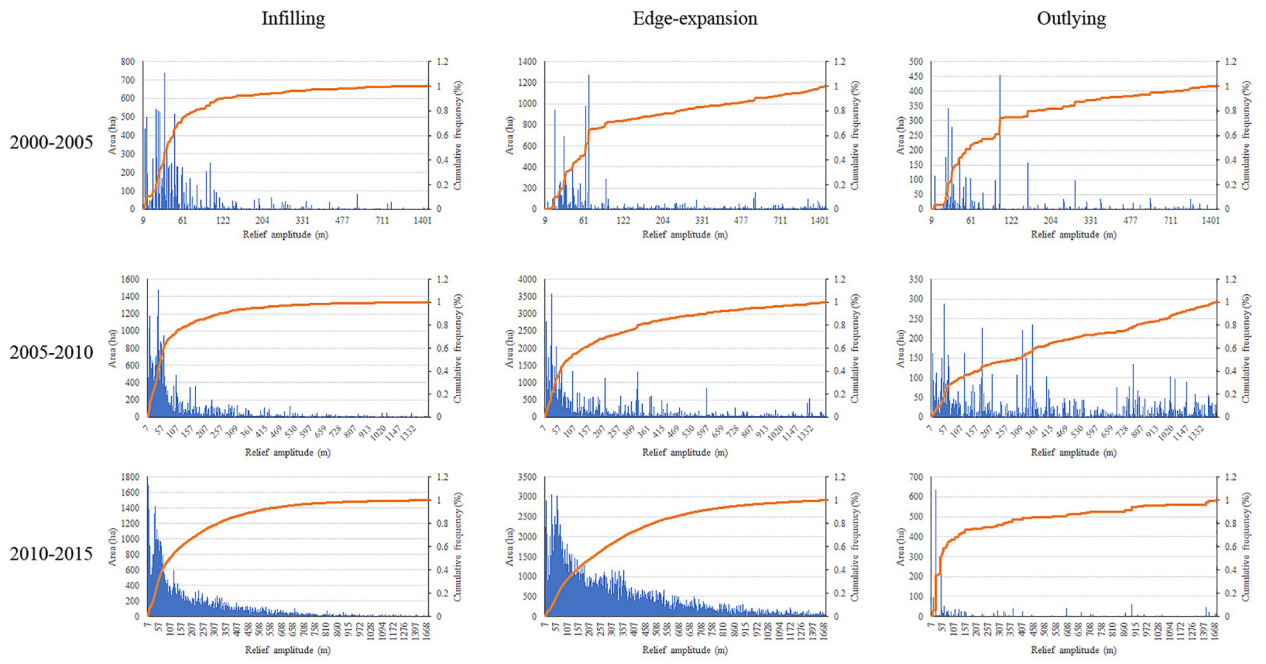

FIGURE 5 | Topographic relief effect in cropland expansion trajectories in MRYRUA from 2000 to 2015.

topographic relief amplitudes are 320 and 491 m, respectively, when the cumulative frequency is up to over 80%. For the outlying trajectory, at least 80% is distributed under the topographic relief amplitude of 781 m in 2005–2010, which is the highest distribution among those in the three-time intervals.

As the region with the highest degree of topographic relief amplitude, the distribution of different cropland expansion trajectories is located in a relatively higher topographic relief amplitude and is more dispersed (**Figure 6**). Different from those in YRDUA and MRYRUA, some of the cumulative frequency

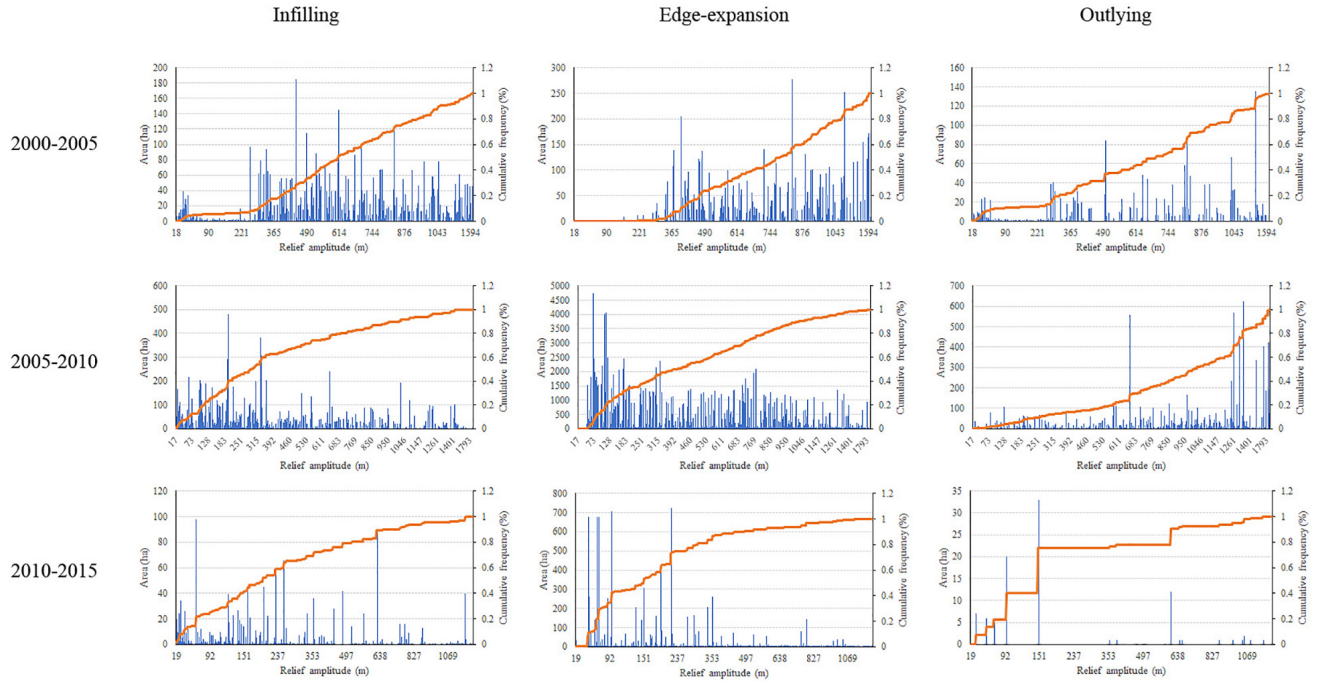

FIGURE 6 | Topographic relief effect in cropland expansion trajectories in C&YUA from 2000 to 2015.

curves of cropland expansion trajectories show a slight increase initially and a rapidly increasing pattern thereafter, such as the infilling, edge-expansion, and outlying trajectories in 2000–2005, and the outlying trajectory in 2005–2010. Meanwhile, the curves in 2010–2015 show a step-up trend. From 2010 to 2015, the cumulative frequency of the infilling, edge-expansion, and outlying trajectories is up to at least 80% at the topographic relief values of 522, 296, and 608 m, which is the lowest among the three-time intervals. These figures change to 933, 1,088, and 1,027 m, respectively, which are the highest among regions and periods.

The distribution of the accumulative frequency under different topographic relief amplitude shows the following trend: (1) Compared with that of the outlying trajectory, infilling and edge-expansion trajectories are distributed at lower topographic relief amplitude levels no matter in what DEM level. (2) As the time goes by, the distribution of different trajectories is more likely to occur in a lower topographic relief amplitude level, indicating a more scientific method of cropland expansion.

Effects of Cropland Expansion Trajectories on Cropland Metrics

Several steps have been taken to better understand the impact of different cropland expansion trajectories on cropland metrics. Several steps have been done: (1) Identify the no changed cropland (marked as NC) during the study period and calculate its landscape metrics; (2) distinguish the infilling, edge-expansion, and outlying trajectories; (3) overlie the no changed cropland and infilling trajectory (marked as infilling) and calculate its landscape metrics; (4) overlie the result of step 3 with the edge-expansion trajectory (marked as edge-expansion) and assess its landscape metrics; (5) the same calculation method is applied to the outlying trajectory (marked as outlying); and (6) a line chart is used to show the results (**Figure 7**).

As shown in **Figure 7**, the scores of PD, LPI, LSI, and AI change across times and regions. Although some of the landscape metrics have formed their own unique trend, the overall changes of landscape metrics show the following rules on the basis of the NC landscape metrics: (1) PD exhibits a continuously decreasing trend in the infilling and edge-expansion, while increasing in the outlying. (2) LPI and AI show a continuous increase in infilling and edge-expansion and a slight decrease in outlying. (3) LSI shows a pattern of decrease in infilling and increase in edge-expansion and outlying.

Moreover, we used Spearman correlation analysis and identified the correlation of landscape metric between the total new expanded cropland and different cropland expansion trajectories (**Figure 8A**) and their significant degree (**Figure 8B**). A significant positive correlation exists between the infilling and edge-expansion trajectories and total expanded cropland. Except for the LPI of the infilling trajectory and total expanded cropland, all the correlation coefficients range from 0.955 to 0.999 and are significant at the 0.01 level. The largest correlation coefficient is displayed in LSI between the edge-expansion trajectory and total expanded cropland, with a value of 0.999. The correlation coefficients in all landscape metrics between the outlying trajectory and total expanded cropland are both negative, with a score ranging from -0.539 to -0.337. They reflect the negative correlation between the outlying trajectory and landscape metrics.

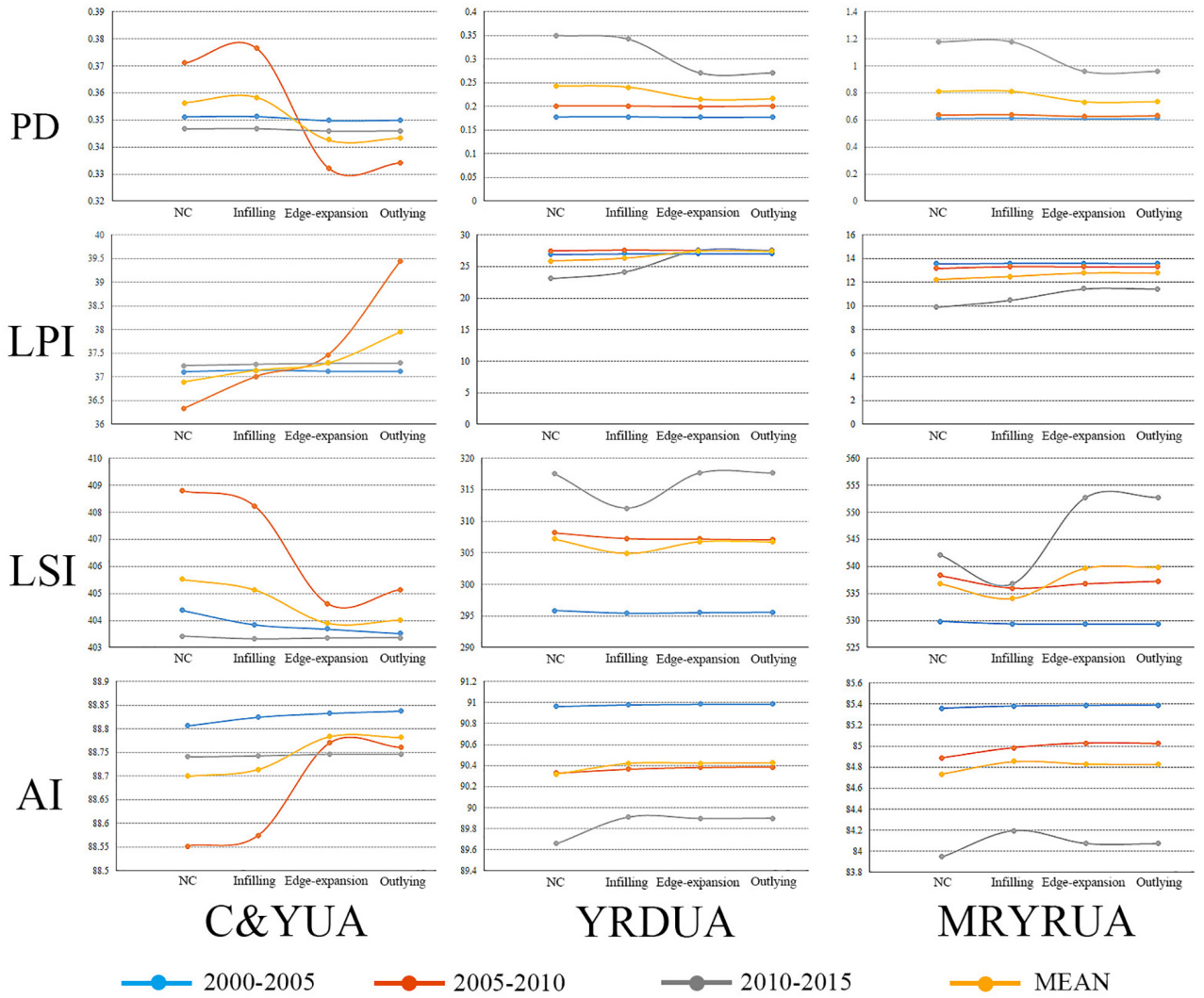

FIGURE 7 | Cropland metrics change in YRDUA, MRYRUA, and C&YUA from 2000 to 2015. NC represents the no changed cropland during the research period. Infilling includes the no change and infilling cropland. Edge-expansion consists of the cropland with no change, infilling, and edge-expansion. Outlying represents the cropland with no change, infilling, edge-expansion, and outlying.

DISCUSSION

Cropland expansion has become a popular issue for researchers. Existing research has studied the substantial sequences from various perspectives, such as natural habitat loss (van Vliet, 2019; Tang et al., 2021), deforestation (Ngoma et al., 2021), and changes in land productivity (Li et al., 2018; Yang et al., 2020). This study defines the three main cropland expansion trajectories, namely, infilling, edge-expansion, and outlying trajectories; and identifies their spatiotemporal distribution and their consequences on cropland fragmentation. The results show that cropland expansion will lead to an increase in cropland fragmentation, which is consistent with previous research (Brabec and Smith, 2002; Yu et al., 2018). Furthermore, we provided a nuanced analysis of the impact of different cropland expansion trajectories on cropland fragmentation through a step-by-step calculation of the fragmentation metrics of the expanded cropland in different cropland trajectories. We found that the increase in cropland fragmentation resulting from cropland expansion was mainly caused by the outlying trajectory, while infilling and edge-expansion trajectories in fact caused a decrease in fragmentation. The Spearman correlation analysis results showed a significantly positive correlation relationship between the infilling and edge-expansion trajectories and cropland fragmentation. Meanwhile, a negative correlation relationship was presented between the outlying trajectory and cropland fragmentation.

The LEI has been widely used to quantify the modes of urban expansion, which identifies that edge-expansion is the dominating mode followed by the infilling and outlying modes (Liu X. et al., 2014; Jiao et al., 2015; Rao et al., 2021). Our study demonstrated similar results for cropland expansion trajectories

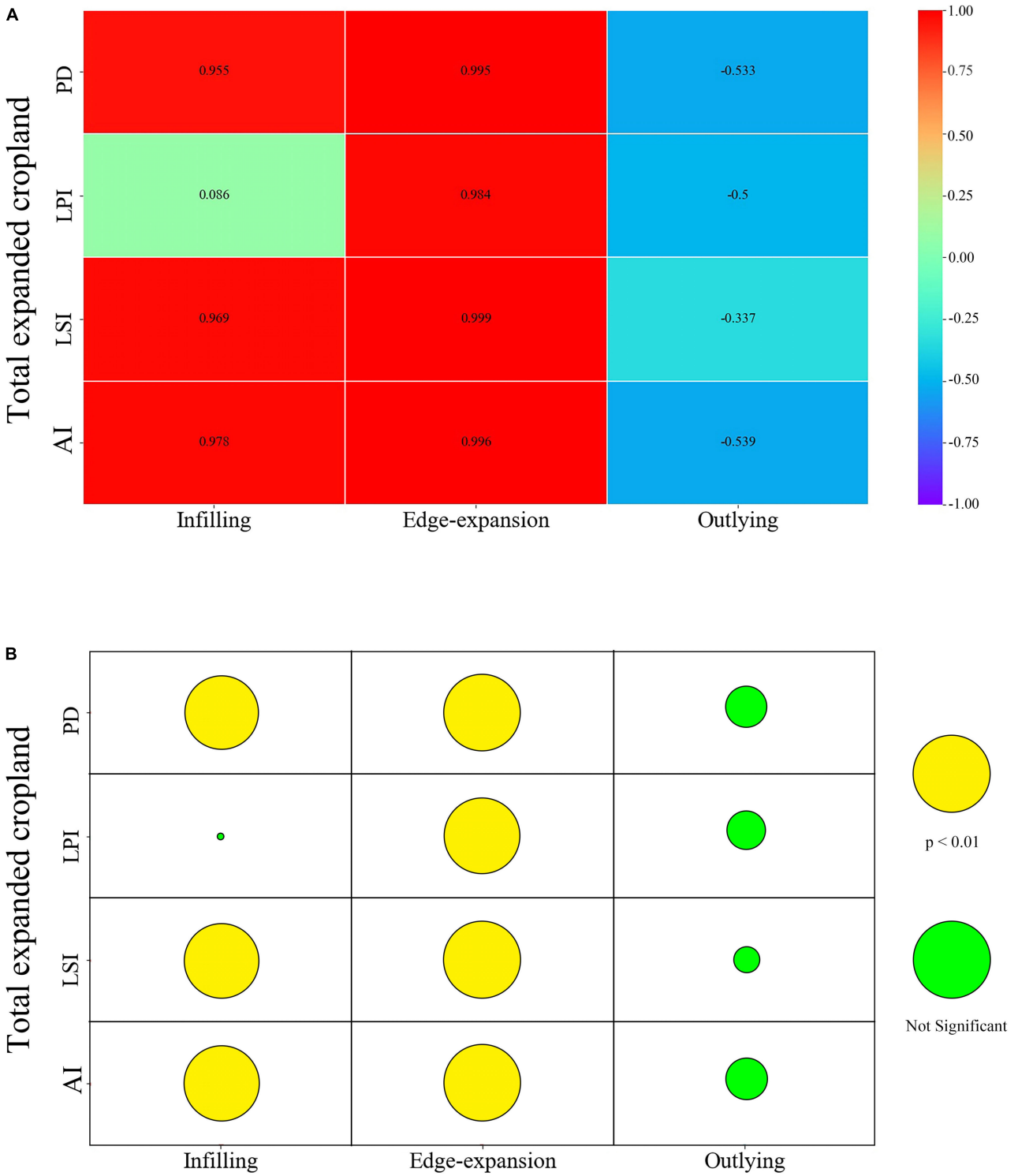

FIGURE 8 | Correlation coefficients of landscape metrics between the total expanded cropland and cropland trajectories **(A)** and significant degrees **(B)**. The size of circles represents the size of correlation coefficients.

with urban expansion modes: edge-expansion trajectory is primary over research areas and periods, and the decreasing sequence of cropland expansion trajectories is infilling trajectory and outlying trajectory. This result can be attributed to the following reasons: (1) The expansion of cropland is mainly from two aspects, namely, farmers' spontaneous agricultural activities

and requests of administrative policies (Lin and Ho, 2003; Tang et al., 2020a). (2) Despite spontaneous agricultural activities and requests of administrative policies prefer the land near or next to the existing cropland to develop new cropland, only where there is insufficient suitable land for cropland reclamation can reserve land resources be used to reclaim cropland to meet policy requirements (Song and Pijanowski, 2013; Xin and Li, 2018). Thus, edge-expansion and infilling trajectories are the two main forms of cropland expansion. In addition, our study demonstrated that the cropland expansion activities in China have become increasingly scientific in recent years: The proportion of edge-expansion trajectory continues to increase (62.50, 45.28, and 48.85% in 2000–2005 and 69.60, 79.35, and 85.03% in 2010–2015 in YRDUA, MRYRUA, and C&YUA, respectively), while that of outlying trajectory continuously decreases (17.52, 13.31, and 12.19% in 2000–2005 and 1.20, 0.34, and 0.91% in 2010–2015 in YRDUA, MRYRUA, and C&YUA, respectively).

Cropland fragmentation is an environment- and dimension-dependent issue. Different types of fragmentation are defined by different research foci. For example, physical fragmentation focuses on the connectivity and contiguity of cropland patches, while the main point of ownership fragmentation is the spatial connectivity of cropland owned by one owner (Su et al., 2014). Therefore, numerous methods measure different types of fragmentation. Based on remote sensing data, landscape metrics are the most used indexes to measure physical fragmentation, such as path density, edge density, mean patch size, and patch cohesion index (Li et al., 2013; He S. et al., 2020). Ownership fragmentation is considerably complex because it is highly connected with socioeconomic activities. Consequently, it is frequently measured based on cadastral survey and questionnaire investigation data (Tan et al., 2006; Rahman and Rahman, 2009; Deininger et al., 2012). In this study, we measured the cropland physical fragmentation in three urban agglomerations with landscape metrics, including PD, LSI, LPI, and AI, because of the convenience and reliability of this method in measuring landscape patterns at a large scale. The application of this method provides a convenient pathway to explore interactions between the environment and human-related activities in the following ways: (1) Quantitative measurement of changes in the environment coupled with human activities will provide a feedback on the impact of human actions on the environment, thereby correcting the wrong behaviors of humans; (2) defining the threshold of environmental changes, which can be used to promote the development of environmental protection policies.

Also, there are some limitations to this study. First, we only identified the topographic relief effect of the distribution of cropland expansion trajectories. While this method can only express a phenomenon that the edge-expansion and infilling trajectory are located at low topographic relief amplitude areas and the outlying trajectory is distributed at a higher level. However, the distribution of different cropland expansion trajectories is affected by multiple drivers, such as temperature, DEM, slope, and other socioeconomic factors (Ma et al., 2019; He Y. et al., 2020). Future studies should explore the driving forces behind the distribution of cropland expansion trajectories by integrating geographical and socioeconomic factors with the help of profound mechanism models. Secondly, we chose three urban agglomerations in YREB as our research area, while these regions are on a similar latitude. A larger-scale analysis should be conducted, such as on a national scale or through comparative analyses of cropland expansion trajectories in different latitudes. Lastly, LEI can only assess the cropland expansion trajectory in a period, while it cannot capture the information of multi-temporal landscape data for continuous landscape expansion (Jiao et al., 2015). Thus, future research can explore the multi-order landscape expansion index to capture information about the continuous cropland expansion.

CONCLUSION

This study focused on different cropland expansion trajectories and their impact on cropland fragmentation. To achieve this goal, we first quantified the spatiotemporal patterns of different cropland expansion trajectories with the surface relief amplitude model. Thereafter, we identified the impact of different cropland expansion trajectories on cropland fragmentation. The results indicate that the edge-expansion trajectory is primary for cropland expansion, followed by infilling and outlying trajectories and the proportion of the outlying trajectory is continuously decreasing. Additionally, the topographic relief amplitude analysis shows that the edge-expansion and infilling trajectory are distributed at a lower topographic relief amplitude than the outlying trajectory which is located at a high topographic relief amplitude region. Along with cropland expansion, cropland fragmentation presents an increasing trend. Specifically, edge-expansion and infilling trajectories have a significantly positive relationship with cropland fragmentation, while the outlying trajectory has a negative effect on cropland fragmentation. This study highlights the need to regulate the trajectory of cropland expansion from the point of protecting cropland fragmentation, rather than only requesting the area of cropland.

DATA AVAILABILITY STATEMENT

Publicly available datasets were analyzed in this study. This data can be found here: https://www.resdc.cn/data.aspx?DATAID=184.

AUTHOR CONTRIBUTIONS

LW: original draft preparation, methodology, and visualization. SZ: editing and conceptualization. YX: visualization and software. YfL: reviewing, editing, and methodology. YlL: editing and supervision. All authors contributed to the article and approved the submitted version.

FUNDING

This work was supported by the Key National Research and Development Project of China (Grant No. 2017YFB0503601).

REFERENCES

Brabec, E., and Smith, C. (2002). Agricultural land fragmentation: the spatial effects of three land protection strategies in the eastern United States. *Landsc. Urban Plan.* 58, 255–268. doi: 10.1016/S0169-2046(01)00225-0

Cabral, A. I. R., and Costa, F. L. (2017). Land cover changes and landscape pattern dynamics in Senegal and Guinea Bissau borderland. *Appl. Geogr.* 82, 115–128. doi: 10.1016/j.apgeog.2017.03.010

Cheng, C., Liu, Y., Liu, Y., Yang, R., Hong, Y., Lu, Y., et al. (2020). Cropland use sustainability in Cheng–Yu Urban agglomeration, China: evaluation framework, driving factors and development paths. *J. Clean. Prod.* 256:120692. doi: 10.1016/j.jclepro.2020.120692

Cheng, L., Xia, N., Jiang, P., Zhong, L., Pian, Y., Duan, Y., et al. (2015). Analysis of farmland fragmentation in China Modernization Demonstration Zone since " Reform and Openness": a case study of South Jiangsu Province. *Sci. Rep.* 5:11797. doi: 10.1038/srep11797

Cheng, P., Tang, H., Dong, Y., Liu, K., Jiang, P., and Liu, Y. (2021). Knowledge mapping of research on land use change and food security: a visual analysis using citespace and vosviewer. *Int. J. Environ. Res. Public Health* 18:13065. doi: 10.3390/ijerph182413065

Cullingworth, B. J. (2014). *Town and Country Planning in the UK*. Milton Park: Taylor and Francis.

Deininger, K., Savastano, S., and Carletto, C. (2012). Land Fragmentation, Cropland Abandonment, and Land Market Operation in Albania. *World Dev.* 40, 2108–2122. doi: 10.1016/j.worlddev.2012.05.010

Dewan, A. M., Yamaguchi, Y., and Rahman, M. Z. (2012). Dynamics of land use/cover changes and the analysis of landscape fragmentation in Dhaka Metropolitan, Bangladesh. *GeoJournal* 77, 315–330. doi: 10.1007/s10708-010-9399-x

Dong, C., Yin, Q., Lane, K. J., Yan, Z., Shi, T., Liu, Y., et al. (2018). Competition and transmission evolution of global food trade: a case study of wheat. *Phys. A Stat. Mech. Appl.* 509, 998–1008. doi: 10.1016/j.physa.2018.06.052

Egli, L., Meyer, C., Scherber, C., Kreft, H., and Tscharntke, T. (2018). Winners and losers of national and global efforts to reconcile agricultural intensification and biodiversity conservation. *Glob. Chang. Biol.* 24, 2212–2228. doi: 10.1111/gcb.14076

Eigenbrod, F., Beckmann, M., Dunnett, S., Graham, L., Holland, R. A., Meyfroidt, P., et al. (2020). Identifying agricultural frontiers for modfeling global cropland expansion. *One Earth* 3, 504–514. doi: 10.1016/j.oneear.2020.09.006

Ellman, T. (1997). *Infill: the Cure for Sprawl? Arizona Issue Analysis, No. 146.* Phoenix, AZ: The Goldwater Institute, 21.

Farley, K. A., Ojeda-Revah, L., Atkinson, E. E., and Eaton-González, B. R. (2012). Changes in land use, land tenure, and landscape fragmentation in the Tijuana River Watershed following reform of the ejido sector. *Land Use Policy* 29, 187–197. doi: 10.1016/j.landusepol.2011.06.006

Folberth, C., Khabarov, N., Balkovič, J., Skalský, R., Visconti, P., Ciais, P., et al. (2020). The global cropland-sparing potential of high-yield farming. *Nat. Sustain.* 3, 281–289. doi: 10.1038/s41893-020-0505-x

Foley, J. A., Ramankutty, N., Brauman, K. A., Cassidy, E. S., Gerber, J. S., Johnston, M., et al. (2011). Solutions for a cultivated planet. *Nature* 478, 337–342. doi: 10.1038/nature10452

Forman, R. T. (1995). *Land Mosaics: The Ecology of Landscapes and Regions.* Cambridge: Cambridge University Press.

Gao, X., Cheng, W., Wang, N., Liu, Q., Ma, T., Chen, Y., et al. (2019). Spatio-temporal distribution and transformation of cropland in geomorphologic regions of China during 1990–2015. *J. Geogr. Sci.* 29, 180–196. doi: 10.1007/s11442-019-1591-4

Han, Z., and Song, W. (2020). Abandoned cropland: patterns and determinants within the Guangxi Karst Mountainous Area, China. *Appl. Geogr.* 122:102245. doi: 10.1016/j.apgeog.2020.102245

He, S., Yu, S., Li, G., and Zhang, J. (2020). Exploring the influence of urban form on land-use efficiency from a spatiotemporal heterogeneity perspective: evidence from 336 Chinese cities. *Land Use Policy* 95, 104576. doi: 10.1016/j.landusepol.2020.104576

He, X., Yan, J., and Cheng, X. (2021). Household perspective on cropland expansion on the Tibetan Plateau. *Reg. Environ. Change* 21:21. doi: 10.1007/s10113-021-01752-8

He, Y., Lee, E., and Mankin, J. S. (2020). Seasonal tropospheric cooling in Northeast China associated with cropland expansion. *Environ. Res. Lett.* 15:034032. doi: 10.1088/1748-9326/ab6616

Jiao, L., Mao, L., and Liu, Y. (2015). Multi-order landscape expansion index: characterizing urban expansion dynamics. *Landsc. Urban Plan.* 137, 30–39. doi: 10.1016/j.landurbplan.2014.10.023

Kastner, T., Rivas, M. J. I., Koch, W., and Nonhebel, S. (2012). Global changes in diets and the consequences for land requirements for food. *Proc. Natl. Acad. Sci. U.S.A.* 109, 6868–6872. doi: 10.1073/pnas.1117054109

Ke, X., van Vliet, J., Zhou, T., Verburg, P. H., Zheng, W., and Liu, X. (2018). Direct and indirect loss of natural habitat due to built-up area expansion: a model-based analysis for the city of Wuhan, China. *Land Use Policy* 74, 231–239. doi: 10.1016/j.landusepol.2017.12.048

Ke, X., Wang, L., Ma, Y., Pu, K., Zhou, T., Xiao, B., et al. (2019). Impacts of strict cropland protection on water yield: a case study of Wuhan, China. *Sustainability* 11:184. doi: 10.3390/su11010184

Lambin, E. F., and Meyfroidt, P. (2011). Global land use change, economic globalization, and the looming land scarcity. *Proc. Natl. Acad. Sci. U.S.A.* 108, 3465–3472. doi: 10.1073/pnas.1100480108

Li, C., Li, J., and Wu, J. (2013). Quantifying the speed, growth modes, and landscape pattern changes of urbanization: a hierarchical patch dynamics approach. *Landsc. Ecol.* 28, 1875–1888. doi: 10.1007/s10980-013-9933-6

Li, J., Wang, Z., Lai, C., Wu, X., Zeng, Z., Chen, X., et al. (2018). Response of net primary production to land use and land cover change in mainland China since the late 1980s. *Sci. Total Environ.* 639, 237–247. doi: 10.1016/j.scitotenv.2018.05.155

Li, X., Yu, X., Wu, K., Feng, Z., Liu, Y., and Li, X. (2021). Land-use zoning management to protecting the regional key ecosystem services: a case study in the city belt along the Chaobai River, China. *Sci. Total Environ.* 762:143167. doi: 10.1016/j.scitotenv.2020.143167

Liang, X., Jin, X., Sun, R., Han, B., Liu, J., and Zhou, Y. (2021a). A typical phenomenon of cultivated land use in China's economically developed areas: anti-intensification in Jiangsu Province. *Land Use Policy* 102:105223. doi: 10.1016/j.landusepol.2020.105223

Liang, X., Jin, X., Yang, X., Xu, W., Lin, J., and Zhou, Y. (2021b). Exploring cultivated land evolution in mountainous areas of Southwest China, an empirical study of developments since the 1980s. *Land Degrad. Dev.* 32, 546–558. doi: 10.1002/ldr.3735

Lin, G. C. S., and Ho, S. P. S. (2003). China's land resources and land-use change: insights from the 1996 land survey. *Land Use Policy* 20, 87–107. doi: 10.1016/S0264-8377(03)00007-3

Liu, J., Kuang, W., Zhang, Z., Xu, X., Qin, Y., Ning, J., et al. (2014). Spatiotemporal characteristics, patterns, and causes of land-use changes in China since the late 1980s. *J. Geogr. Sci.* 24, 195–210. doi: 10.1007/s11442-014-1082-6

Liu, X., Li, X., Chen, Y., Tan, Z., Li, S., and Ai, B. (2010). A new landscape index for quantifying urban expansion using multi-temporal remotely sensed data. *Landsc. Ecol.* 25, 671–682. doi: 10.1007/s10980-010-9454-5

Liu, X., Ma, L., Li, X., Ai, B., Li, S., and He, Z. (2014). Simulating urban growth by integrating landscape expansion index (LEI) and cellular automata. *Int. J. Geogr. Inf. Sci.* 28, 148–163. doi: 10.1080/13658816.2013.831097

Liu, X., Zhao, C., and Song, W. (2017). Review of the evolution of cultivated land protection policies in the period following China's reform and liberalization. *Land Use Policy* 67, 660–669. doi: 10.1016/j.landusepol.2017.07.012

Ma, L., Yang, S., Gu, Q., Li, J., Yang, X., Wang, J., et al. (2019). Spatial and temporal mapping of cropland expansion in northwestern China with multisource remotely sensed data. *Catena* 183:104192. doi: 10.1016/j.catena.2019.104192

Ngoma, H., Pelletier, J., Mulenga, B. P., and Subakanya, M. (2021). Climate-smart agriculture, cropland expansion and deforestation in Zambia: linkages, processes and drivers. *Land Use Policy* 107, 105482. doi: 10.1016/j.landusepol.2021.105482

Nzabarinda, V., Bao, A., Xu, W., Uwamahoro, S., Huang, X., Gao, Z., et al. (2021). Impact of cropland development intensity and expansion on natural vegetation in different African countries. *Ecol. Inform.* 64:101359. doi: 10.1016/j.ecoinf.2021.101359

Phalan, B., Onial, M., Balmford, A., and Green, R. E. (2011). Reconciling food production and biodiversity conservation: land sharing and land sparing compared. *Science* 333, 1289–1291. doi: 10.1126/science.1208742

Prabhakar, S. V. R. K. (2021). A succinct review and analysis of drivers and impacts of agricultural land transformations in Asia. *Land Use Policy* 102, 105238. doi: 10.1016/j.landusepol.2020.105238

Qi, Z. F., Ye, X. Y., Zhang, H., and Yu, Z. L. (2014). Land fragmentation and variation of ecosystem services in the context of rapid urbanization: the case

of Taizhou city, China. *Stoch. Environ. Res. Risk Assess.* 28, 843–855. doi: 10.1007/s00477-013-0721-2

Qiu, L., Pan, Y., Zhu, J., Amable, G. S., and Xu, B. (2019). Integrated analysis of urbanization-triggered land use change trajectory and implications for ecological land management: a case study in Fuyang, China. *Sci. Total Environ.* 660, 209–217. doi: 10.1016/j.scitotenv.2018.12.320

Rahman, S., and Rahman, M. (2009). Impact of land fragmentation and resource ownership on productivity and efficiency: the case of rice producers in Bangladesh. *Land Use Policy* 26, 95–103. doi: 10.1016/j.landusepol.2008.01.003

Ramankutty, N., Evan, A. T., Monfreda, C., and Foley, J. A. (2008). Farming the planet: 1. Geographic distribution of global agricultural lands in the year 2000. *Glob. Biogeochem. Cycles* 22:GB1003. doi: 10.1029/2007GB002952

Ran, P., Hu, S., Frazier, A. E., Qu, S., Yu, D., and Tong, L. (2022). Exploring changes in landscape ecological risk in the Yangtze River Economic Belt from a spatiotemporal perspective. *Ecol. Indic.* 137:108744. doi: 10.1016/j.ecolind.2022.108744

Rao, Y., Yang, J., Dai, D., Wu, K., and He, Q. (2021). Urban growth pattern and commuting efficiency: empirical evidence from 100 Chinese cities. *J. Clean. Prod.* 302:126994. doi: 10.1016/j.jclepro.2021.126994

Sarparast, M., Ownegh, M., and Sepehr, A. (2020). Investigation the driving forces of land-use change in northeastern Iran: causes and effects. *Remote Sens. Appl. Soc. Environ.* 19:100348. doi: 10.1016/j.rsase.2020.100348

Song, W., and Liu, M. (2017). Farmland conversion decreases regional and national land quality in China. *L. Degrad. Dev.* 28, 459–471. doi: 10.1002/ldr.2518

Song, W., and Pijanowski, B. C. (2013). The effects of China's cultivated land balance program on potential land productivity at a national scale. *Appl. Geogr.* 46, 158–170. doi: 10.1016/j.apgeog.2013.11.009

Su, S., Hu, Y., Luo, F., Mai, G., and Wang, Y. (2014). Farmland fragmentation due to anthropogenic activity in rapidly developing region. *Agric. Syst.* 131, 87–93. doi: 10.1016/j.agsy.2014.08.005

Su, S., Xiao, R., Jiang, Z., and Zhang, Y. (2012). Characterizing landscape pattern and ecosystem service value changes for urbanization impacts at an eco-regional scale. *Appl. Geogr.* 34, 295–305. doi: 10.1016/j.apgeog.2011.12.001

Tan, S., Heerink, N., and Qu, F. (2006). Land fragmentation and its driving forces in China. *Land Use Policy* 23, 272–285. doi: 10.1016/j.landusepol.2004.12.001

Tang, L., Ke, X., Chen, Y., Wang, L., Zhou, Q., Zheng, W., et al. (2021). Which impacts more seriously on natural habitat loss and degradation? Cropland expansion or urban expansion? *Land Degrad. Dev.* 32, 946–964. doi: 10.1002/ldr.3768

Tang, L., Ke, X., Zhou, T., Zheng, W., and Wang, L. (2020b). Impacts of cropland expansion on carbon storage: a case study in Hubei, China. *J. Environ. Manage.* 265:110515. doi: 10.1016/j.jenvman.2020.110515

Tang, L., Ke, X., Zhou, Q., Wang, L., and Koomen, E. (2020a). Projecting future impacts of cropland reclamation policies on carbon storage. *Ecol. Indic.* 119:106835. doi: 10.1016/j.ecolind.2020.106835

Tian, G., Duan, J., and Yang, L. (2021). Spatio-temporal pattern and driving mechanisms of cropland circulation in China. *Land Use Policy* 100:105118. doi: 10.1016/j.landusepol.2020.105118

Tilman, D., Balzer, C., Hill, J., and Befort, B. L. (2011). Global food demand and the sustainable intensification of agriculture. *Proc. Natl. Acad. Sci. U.S.A.* 108, 20260–20264. doi: 10.1073/pnas.1116437108

Tscharntke, T., Clough, Y., Wanger, T. C., Jackson, L., Motzke, I., Perfecto, I., et al. (2012). Global food security, biodiversity conservation and the future of agricultural intensification. *Biol. Conserv.* 151, 53–59. doi: 10.1016/j.biocon.2012.01.068

Tu, Y., Chen, B., Yu, L., Xin, Q., Gong, P., and Xu, B. (2021). How does urban expansion interact with cropland loss? A comparison of 14 Chinese cities from 1980 to 2015. *Landsc. Ecol.* 36, 243–263. doi: 10.1007/s10980-020-01137-y

Uisso, A. M., and Tanrıvermiş, H. (2021). Driving factors and assessment of changes in the use of arable land in Tanzania. *Land Use Policy* 104:105359. doi: 10.1016/j.landusepol.2021.105359

van Vliet, J. (2019). Direct and indirect loss of natural area from urban expansion. *Nat. Sustain.* 2, 755–763. doi: 10.1038/s41893-019-0340-0

van Vliet, J., Eitelberg, D. A., and Verburg, P. H. (2017). A global analysis of land take in cropland areas and production displacement from urbanization. *Glob. Environ. Change* 43, 107–115. doi: 10.1016/j.gloenvcha.2017.02.001

Wang, L., Ke, X., and Hatab, A. A. (2020). Trade-offs between economic benefits and ecosystem services value under three cropland protection scenarios for Wuhan City in China. *Land* 9:117. doi: 10.3390/land9040117

Wang, L., Zhang, S., Xiong, Q., Liu, Y., Liu, Y., and Liu, Y. (2022b). Spatiotemporal dynamics of cropland expansion and its driving factors in the Yangtze River Economic Belt : a nuanced analysis at the county scale. *Land Use Policy* 119:106168. doi: 10.1016/j.landusepol.2022.106168

Wang, L., Zhang, S., Liu, Y., and Liu, Y. (2022a). Interaction between construction land expansion and cropland expansion and its socioeconomic determinants : evidence from urban agglomeration in the middle reaches of the Yangtze River, China. *Front. Environ. Sci.* 10:882582. doi: 10.3389/fenvs.2022.882582

Wang, L., Zheng, W., Tang, L., Zhang, S., Liu, Y., and Ke, X. (2021). Spatial optimization of urban land and cropland based on land production capacity to balance cropland protection and ecological conservation. *J. Environ. Manage.* 285:112054. doi: 10.1016/j.jenvman.2021.112054

Wilson, E. H., Hurd, J. D., Civco, D. L., Prisloe, M. P., and Arnold, C. (2003). Development of a geospatial model to quantify, describe and map urban growth. *Remote Sens. Environ.* 86, 275–285. doi: 10.1016/S0034-4257(03)00074-9

Xin, L., and Li, X. (2018). China should not massively reclaim new farmland. *Land Use Policy* 72, 12–15. doi: 10.1016/j.landusepol.2017.12.023

Xu, C., Liu, M., Zhang, C., An, S., Yu, W., and Chen, J. M. (2007). The spatiotemporal dynamics of rapid urban growth in the Nanjing metropolitan region of China. *Landsc. Ecol.* 22, 925–937. doi: 10.1007/s10980-007-9079-5

Yan, H., Liu, J., Huang, H. Q., Tao, B., and Cao, M. (2009). Assessing the consequence of land use change on agricultural productivity in China. *Glob. Planet. Change* 67, 13–19. doi: 10.1016/j.gloplacha.2008.12.012

Yang, B., Ke, X., van Vliet, J., Yu, Q., Zhou, T., and Verburg, P. H. (2020). Impact of cropland displacement on the potential crop production in China: a multi-scale analysis. *Reg. Environ. Change* 20:97. doi: 10.1007/s10113-020-01690-x

Yang, B., Wang, Z., Zou, L., Zou, L., and Zhang, H. (2021). Exploring the eco-efficiency of cultivated land utilization and its influencing factors in China's Yangtze River Economic Belt, 2001–2018. *J. Environ. Manage.* 294:112939. doi: 10.1016/j.jenvman.2021.112939

Yu, Q., Hu, Q., van Vliet, J., Verburg, P. H., and Wu, W. (2018). GlobeLand30 shows little cropland area loss but greater fragmentation in China. *Int. J. Appl. Earth Obs. Geoinf.* 66, 37–45. doi: 10.1016/j.jag.2017.11.002

Zabel, F., Delzeit, R., Schneider, J. M., Seppelt, R., Mauser, W., and Václavík, T. (2019). Global impacts of future cropland expansion and intensification on agricultural markets and biodiversity. *Nat. Commun.* 10:2844. doi: 10.1038/s41467-019-10775-z

Zeng, Z., Estes, L., Ziegler, A. D., Chen, A., Searchinger, T., Hua, F., et al. (2018). Highland cropland expansion and forest loss in Southeast Asia in the twenty-first century. *Nat. Geosci.* 11, 556–562. doi: 10.1038/s41561-018-0166-9

Zhang, S., Hu, W., Li, M., Guo, Z., Wang, L., and Wu, L. (2021). Multiscale research on spatial supply-demand mismatches and synergic strategies of multifunctional cultivated land. *J. Environ. Manage.* 299:113605. doi: 10.1016/j.jenvman.2021.113605

Zhou, B. B., Aggarwal, R., Wu, J., and Lv, L. (2021). Urbanization-associated farmland loss: a macro-micro comparative study in China. *Land Use Policy* 101:105228. doi: 10.1016/j.landusepol.2020.105228

Conflict of Interest: The authors declare that the research was conducted in the absence of any commercial or financial relationships that could be construed as a potential conflict of interest.

Publisher's Note: All claims expressed in this article are solely those of the authors and do not necessarily represent those of their affiliated organizations, or those of the publisher, the editors and the reviewers. Any product that may be evaluated in this article, or claim that may be made by its manufacturer, is not guaranteed or endorsed by the publisher.

Copyright © 2022 Wang, Zhang, Xie, Liu and Liu. This is an open-access article distributed under the terms of the Creative Commons Attribution License (CC BY). The use, distribution or reproduction in other forums is permitted, provided the original author(s) and the copyright owner(s) are credited and that the original publication in this journal is cited, in accordance with accepted academic practice. No use, distribution or reproduction is permitted which does not comply with these terms.

frontiers | Frontiers in Ecology and Evolution

ORIGINAL RESEARCH
published: 01 July 2022
doi: 10.3389/fevo.2022.960634

Spatiotemporal Variations of Human Pressure on Key Biodiversity Areas in the Qinghai–Tibet Plateau: A Comparative Analysis

Yuxi Zeng, Ling-en Wang and Linsheng Zhong*

Institute of Geographic Sciences and Natural Resources Research, Chinese Academy of Sciences, Beijing, China

A key biodiversity area (KBA) is one of the important emerging area-based conservation measures that is being implemented recently in China; however, the human pressure faced by a KBA is still unclear. This study analyzed the spatiotemporal variation of human pressure on KBAs from 1990 to 2017 and compared it with the human pressure on national natural reserves (NNRs) through a case study of the Qinghai–Tibet Plateau. In addition, changes in the trend of human pressure before and after 2010 were analyzed to examine the influence of conservation policies on human pressure. Results showed that human pressure on KBAs and NNRs gradually increased from 1990 to 2017. Furthermore, the growth rates and mean values of human pressure in KBAs were higher than those in NNRs. After the implementation of conservation policies in 2010, the growth rates of human pressure on both KBAs and NNRs have significantly slowed, and the areas with negative growth in both KBAs and NNRs have gradually expanded. In addition to providing an understanding of the changing spatiotemporal trends of human pressure on KBAs, this study can serve as a reference to formulate policies for the improvement of the effectiveness of conservation.

Keywords: human pressure, key biodiversity areas, spatiotemporal pattern, Qinghai-Tibet, national natural reserves

OPEN ACCESS

Edited by:
Jun Yang,
Northeastern University, China

Reviewed by:
Chenxi Li,
Xi'an University of Architecture and Technology, China
Huisheng Yu,
Northeastern University, China
Liguo Wang,
Jiangxi Agricultural University, China

****Correspondence:***
Ling-en Wang
wangle@igsnrr.ac.cn

Specialty section:
This article was submitted to Environmental Informatics and Remote Sensing, a section of the journal Frontiers in Ecology and Evolution

Received: *03 June 2022*
Accepted: *16 June 2022*
Published: *01 July 2022*

Citation:
Zeng YX, Wang L-e and Zhong LS (2022) Spatiotemporal Variations of Human Pressure on Key Biodiversity Areas in the Qinghai–Tibet Plateau: A Comparative Analysis. Front. Ecol. Evol. 10:960634. doi: 10.3389/fevo.2022.960634

INTRODUCTION

The negative effects of ecosystem degradation on social geographic sustainability have triggered ambitious targets for ecosystem conservation at the national, regional, and global levels (Strassburg et al., 2020). Protected areas (PAs), which are legally designated and managed for long-term nature conservation, have been widely adopted for ecosystem conservation by governments, policymakers, and many members of the conservation community (Maxwell et al., 2020). Although PAs have become the major means of area-based conservation, research shows that the existing global network of PAs is insufficient to prevent the continuing depletion of biodiversity (Pringle, 2017).

Key biodiversity areas (KBAs) were promoted as a type of "other effective area-based conservation measure" (Donald et al., 2019) by the International Union for Conservation of Nature (IUCN) since 2016, which acts as a means to identify "sites of importance for the global persistence of biodiversity" (International Union for Conservation of Nature [IUCN], 2016). Encompassing considerable populations of species and rich ecosystems of high conservation concern, KBAs not

only provide habitats for wildlife, but also various ecosystem services (Shrestha et al., 2021). Using KBAs to guide the effective expansion of the global PA network has become an important issue (Kullberg et al., 2019).

To date, over 15,000 KBAs have been identified (83.1% of which are important bird areas—the avian subset of KBAs; BirdLife International, 2019). However, the introduction of KBAs has been slow in the developing world (Shrestha et al., 2021). For example, only 25% of KBAs identified in Myanmar are legally protected (Wildlife Conservation Society, 2013). As a developing country, China introduced this measure in 2019 and it is in its initial stage of KBA identification and management (Li, 2021). Furthermore, China intends to reform its natural conservation system, which was formed in 1956 (Ma et al., 2019). This reform aims to transfer the core of natural conservation systems from natural reserves to national parks. This is expected to improve conservation effectiveness by adjusting the spatial scope of conservation areas and institutional mechanisms (General Office of the CPC Central Committee, and General Office of the State Council of China, 2019), which provides opportunities for KBAs to be incorporated into the Chinese official conservation plan.

Due to the lack of official guidance and long-term protective action, some KBAs have been exposed to high levels of human pressure (Jonas et al., 2014; Alves-Pinto et al., 2021). Donald et al. (2019) studied ten countries (Australia, Bolivia, Canada, Ecuador, India, Indonesia, Kazakhstan, Kenya, Philippines, and South Africa) and revealed that unprotected KBAs occur in areas with significantly higher human population density and on flatter land, where pressure on natural resources may be higher. The likelihood of the skies of a KBA experiencing skyglow tends to increase in countries with a higher gross domestic product (GDP), and in areas with a higher human population density (Garrett et al., 2020). Consequently, ongoing and accelerating threats (e.g., introduction of invasive species, habitat loss and fragmentation, and water abstraction) lead to rapid extirpation of species inside the KBAs (Nogueira et al., 2021). China has experienced rapid economic growth and urbanization over the past few decades. From 1990 to 2019, the urban built-up area of China increased from 12,200 to 60,300 km^2 (National Bureau of Statistics of China [NBSC], 2020), thereby exerting considerable stress on the ecosystem (Xie et al., 2021). Moreover, attempts to estimate human pressure on KBAs in China have been lacking, and urgent examination of the spatiotemporal pattern of human pressure on KBAs is necessary.

A case study of the Qinghai–Tibet Plateau was performed to analyze the spatiotemporal variations in human pressure on KBAs between 1990 and 2017. The Qinghai–Tibet Plateau is one of the national eco-safety barriers of China (National Development and Reform Commission of China [NDRC], and Ministry of Natural Resources of China [MNRC], 2020), and it has high ecological importance and vulnerability. Existing studies have found high-intensity human activities in national natural reserves (NNRs) in the Qinghai–Tibet Plateau (Hua et al., 2022), which emphasizes the urgency of adjusting area-based conservation management. The Chinese government put forward a series of policies around 2010 to protect the ecosystem of the Qinghai–Tibet Plateau. These include the Plan for Tibet Ecological Security Barrier Protection and Construction (2008–2030) and the Plan for Ecological Construction and Environmental Protection in the Qinghai–Tibet Plateau (2011–2030). Previous studies have shown that these conservation policies have had a positive effect on the ecological restoration of the Qinghai–Tibet Plateau (Li et al., 2021c). However, the effects of these policies on KBAs have not been reported. This study focuses on KBAs in the Qinghai–Tibet Plateau and compares them with NNRs, and aims to answer two questions: (i) Have KBAs suffered more human pressure than NNRs, and (ii) Have previous conservation policies led to changes in human pressure on KBAs and NNRs in the Qinghai–Tibet Plateau? What is the difference between these changes in KBAs and NNRs?

HUMAN PRESSURE ON THE QINGHAI–TIBET PLATEAU

In order to measure the pressure on ecosystems caused by human activities, it is necessary to understand the types of human activities that negatively affect ecosystems (Mu et al., 2022). According to existing studies, negative impacts of human activities on the Qinghai–Tibet Plateau ecosystems are mainly caused by population concentration, economic growth, agriculture and animal husbandry, urbanization, and construction of transportation facilities (Chen et al., 2015; Tian and Chen, 2022).

Population Density

In areas with large populations, the frequency and intensity of human disturbance to the ecosystem tends to be higher (Luo et al., 2021; Tian and Chen, 2022; Yu et al., 2022). From 1990 to 2015, the total population of the Qinghai–Tibet Plateau increased from 6.58 to 9.13 million (Bao and Liu, 2019). Increased human activity alters the natural succession direction of ecosystems by changing species richness, accelerating biodiversity loss, and discharging wastewater, gas, and solids into the environment, which has far-reaching impacts on ecosystems (Mottl et al., 2021; Pavlik et al., 2021). In this study, areas with a greater population density often suffered more pressure.

Economic Development

Following the environmental Kuznets curve, economic growth intensifies environmental pollution before the economic growth (indicated by per capita GDP) reaches a turning point (Zhao et al., 2021). Considering that environmental pollution is a major contributor to ecosystem degradation (Wang et al., 2021), it can be deduced that a high level of economic development will exert greater pressure on the ecosystem before the turning point. Yu et al. (2016) revealed that China will not approach the turning point until 2025, and the Qinghai–Tibet Plateau is still in the ascending stage of the Environmental Kuznets Curve. Therefore, areas with a high level of economic development in the Qinghai–Tibet Plateau are subjected to more human pressure.

Human-Managed Land Use

Land use is a typical form of human action on terrestrial surfaces, which affects ecosystems by disturbing the matter cycle and energy exchange between various layers of the Earth (de Queiroz et al., 2020). Land use affects the components of the atmosphere and underlying surfaces, changes soil texture, and disturbs water quality, quantity, and cycling (Trentman et al., 2022). Different land use types exert different pressures on ecosystems, with urbanized areas exerting the most. From 1990 to 2015, urban areas of the Qinghai–Tibet Plateau expanded largely, which led to an intensive heat island effect and increased virulent organic pollutants (Bao and Liu, 2019). Agricultural land also puts a large pressure on ecosystems, and agricultural activities cause soil erosion and desertification, which leads to reduction in biodiversity (Polazzo et al., 2022).

Animal Husbandry

Animal husbandry is one of the main sources of livelihood for residents living in the Qinghai–Tibet Plateau, and yaks and Tibetan sheep are the main livestock (Zhuang et al., 2019). The Qinghai–Tibet Plateau is dominated by dynamic and sensitive grassland ecosystems, and husbandry activities can easily cause ecological problems such as soil salinization, desertification, and deep soil drying (Li et al., 2021a,b). Therefore, intense animal husbandry leads to a greater pressure on the ecosystem.

Roads

During road construction, the excavation of roadbeds changes the geological landform, and pavements cause long-term damage to vegetation and aggravate desertification (Trombulak and Frissell, 2000). Road operations also affect animal migration, disturb animal habitat, and lead to changes in the number and structure of ecosystem components (Kroeger et al., 2022). Since 1989, the length and density of roads on the Qinghai–Tibet Plateau have increased considerably, which has resulted in intensified landscape fragmentation and increased ecological pressure (Zhao and Lu, 2017).

METHODOLOGY

Study Area

The Qinghai–Tibet Plateau is located in southwestern China (26–40° N, 73–105° E), and originates from the Yangtze, Yellow, and Mekong Rivers, and their water sustains cities and farms across Asia. The Qinghai–Tibet Plateau has a total area of 257×10^4 km^2, and accounts for 27% of the Chinese land area, with an average altitude of over 4,000 m.

For decades, 52 NNRs have acted as the cornerstone of conservation practice on the Qinghai–Tibet Plateau, and these have received substantial financial aid from the government (Fu et al., 2021; Liu et al., 2021). However, this plateau has recently been experiencing habitat fragmentation, alien invasion, and local ecosystem degradation (Fu et al., 2021), which indicates that merely protecting NNRs is not sufficient to maintain its ecological health. According to the KBA Partnership program, parts of the Qinghai–Tibet Plateau are covered by KBAs (**Figure 1**). These KBAs are partially inside NNRs (the overlapping areas occupy 61.86% of KBAs and 63.09% of NNRs), but some are outside NNRs and have no official identification or management.

Measuring Human Pressure

Previous studies have developed many composite indices to measure the anthropogenic pressure on ecosystems, such as human activity intensity (Chi et al., 2020; Gosselin and Callois, 2021) and human footprints (Sanderson et al., 2002; Venter et al., 2016; Duan and Luo, 2021). The human footprint index, a dimensionless metric that captures the extent of human influence on the terrestrial surface, is distinct from many land-use metrics in terms of its ability to singularly capture the total influence of human existence on a given location (Keys et al., 2021), and hence, it is widely applied in biodiversity conservation (Venter et al., 2016; Duan and Luo, 2021). This study draws on the method of Duan and Luo (2021) and uses the human footprint index to measure human pressure on each grid inside the KBAs and NNRs in the Qinghai–Tibet Plateau. Human pressure was calculated using the following formula:

$$HP_i = \sum_{j=1}^{5} HA_{ij} \quad (1)$$

where HP_i represents the human pressure on grid i, HA_{ij} refers to the intensity of a specific pressure type j in grid i, and includes the pressure from population density, economic development, animal husbandry, land use, and roads. According to the value of each pressure type (**Table 1**), the HP_i ranged from 0 (lowest) to 58 (highest).

Pressure From Population Density

According to Duan and Luo (2021), population density data were logarithmically calculated. The population density of 2017 was not available in the original datasets; therefore, this study used the average of 2015 and 2019 as the population density in 2017. According to the original data, the maximum population density is 32,866 people per km^2 (the maximum value of PD_i is 32,866). Therefore, the equation used for the calculation was constructed as follows:

$$PP_i = 2.21398 \times \log(PD_i + 1) \quad (2)$$

where PP_i represents the pressure intensity from the population density of grid i, which ranges from zero to 10. PD_i is the population density of grid i.

Pressure From Economic Development

Nighttime light data, which is considered a robust indicator of regional economic development, was used to reflect the economic development level of the Qinghai–Tibet Plateau (Chen and Zhang, 2020). Since the original nighttime light data only contains data from 1992 to 2013, this study replaced data of 1990 and 2017 with those of 1992 and 2013, respectively. In addition, the original data have discontinuities and oversaturation problems, which must be corrected after projection and cropping are completed. This study used a correction approach based on

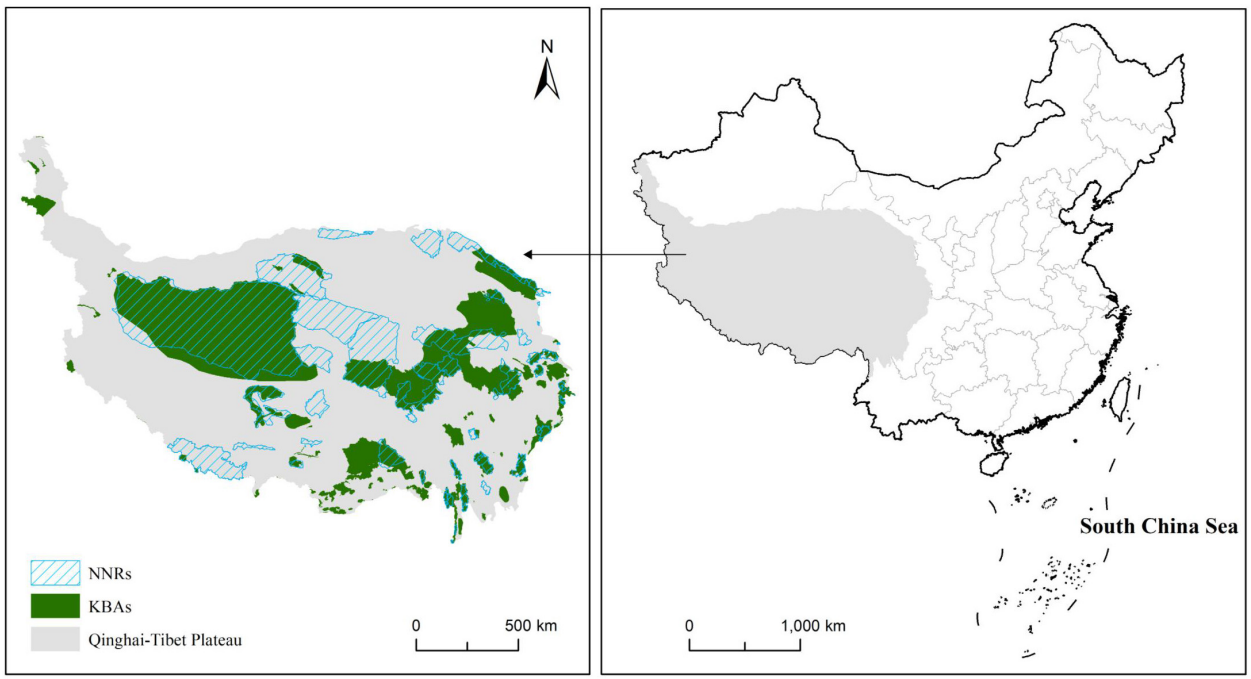

FIGURE 1 | KBAs and NNRs in the Qinghai–Tibet Plateau.

TABLE 1 | Evaluation of each type of pressure.

Indicators		Value range	Assignment approach
Pressure from population density		0–10	$PP_i = 2.21398 \times \log(PD_i + 1)$
Pressure from economic development		0–10	0, if digital number is 01–10, if digital number is greater than 0, valued according to the decile of 2017
Pressure from animal husbandry		0–10	AHP*i* 2.51531 × log(AHD*i* + 1)
Pressure from land use		0, 4, 7, and 10	10, Built-up areas7, Paddy fields and dry land4, Grassland0, The others
Pressure from roads	Railways	8	8, within 500 m on both sides
	Highways	4, 8, and 10	10, within 500 m on both sides8, within 500–1,500 m on both sides4, within 1,500–2,500 m on both sides

invariant target areas, which have been widely used in related studies (Zhang et al., 2020). Following Zhang et al. (2020), this study took Hegang City as the invariant target area, since its economic and social data have changed little over the past decades and the digital number of light images is widely distributed in it (Zhang et al., 2020). After forming the nightlight data for each year, values were assigned to each grid. First, 0 points were assigned to the grid, with a digital number equal to 0. Second, the grid was divided into 10 equal parts with a digital number value greater than 0 using the quantile method and assigned a value of 1–10 points in order from small to large (according to the 2017 data). For data of the remaining years, according to the 2017 decile, a grid with a digital number value greater than 0 was assigned a score of 1–10, and a digital number value of 0 was assigned a score of 0.

Pressure From Animal Husbandry

This study used the sum of cattle and sheep densities to represent the intensity of husbandry activities. Since the original spatial data were only in 2006, a trend extrapolation analysis was adopted to obtain a layer of husbandry density for each year (Duan and Luo, 2021). First, beef and mutton production in Qinghai and Tibet were collected in 1990, 2010, and 2017, and the change rates of beef and mutton production in different years relative to 2005 were calculated. Then, the cattle and sheep density layers in 2006 were multiplied by the change rates of each year to obtain the cattle and sheep density layers in different years. The density layers of cattle and sheep in the same year were superimposed to obtain the husbandry density. Husbandry density data were calculated logarithmically according to Duan and Luo (2021). The original data showed that the maximum grazing density was 9,454 head/km^2. Thus, the specific equation used for calculations was constructed as follows:

$$AHP_i = 2.51531 \times \log(AHD_i + 1) \quad (3)$$

where AHP*i* represents the pressure intensity from the animal husbandry of grid *i* ranging from 0 to 10. AHD*i* is the husbandry density value of grid *i*.

TABLE 2 | Datasets used in this study.

Original datasets	Period	Format	Data source
The spatial extent of the Qinghai–Tibet Plateau	2022	Shapefile	Resource and environment science and data center (http://www.resdc.cn/Default.aspx)
NNRs	2018	Shapefile	
Population density	1990, 2010, 2015, 2019	Raster, 1 km resolution	
Land use	1990, 2010, 2017	Raster, 1 km resolution	
KBAs	2018	Shapefile	Key Biodiversity Area Partnership (https://www.keybiodiversityareas.org/kba-data/request)
Cattle and sheep densities	2006	Raster, 10 km resolution	Food and Agriculture Organization of the United Nations (http://www.fao.org/geonetwork/srv/en/main.home)
Beef and mutton production	1990, 2010, 2017	Statistics	National Bureau of Statistics of China (http://www.stats.gov.cn/)
Nighttime light	1990–2013	Raster, 1 km resolution	National Oceanic and Atmospheric Administration (https://ngdc.noaa.gov/eog/dmsp/downloadV4composites.html)
Highways	1980–2010	Shapefile	National Aeronautics and Space Administration (https://sedac.ciesin.columbia.edu/data/set/groads-global-roads-open-access-v1/data-download)
	2018	Shapefile	Geographic Data Sharing Infrastructure, College of Urban and Environmental Science, Peking University (http://www.globio.info)
Railways	1990, 2010, 2017	Shapefile	Manual digitizing

Pressure From Land Use

This study used the type of land used to reflect ecological pressure from human-managed land. Specifically, built-up areas were assigned 10 points, paddy fields and dry land 7 points, and grasslands 4 points. The others were assigned 0 points (Duan and Luo, 2021).

Pressure From Roads

Railways and highways were used to reflect the pressure of roads on ecosystems. The construction of railways leads to ecosystem disturbance, while train operation has a relatively lower impact (Shen et al., 2004). Thus, only the area within 500 m on both sides of the railway was assigned 8 points. Highway construction and vehicle driving behaviors had a larger impact on both sides. Therefore, the areas within 500 m on both sides of highways were assigned 10 points, those within 500–1,500 m were assigned 8 points and those within 1,500–2,500 m were assigned 4 points. Limited by original data, this study replaced the highway data from 2017 with that from 2018.

Spatial Analysis of Human Pressure

We applied multiple spatial statistical approaches to compare the spatiotemporal changes in human pressure within KBAs and NNRs. First, we compared the mean value of the human footprint and its annual change rate of each unit in KBAs, NNRs, and their overlapping areas during 1990–2017. Second, we classified the area into seven levels according to human pressure: no human pressure (human pressure = 0) and areas with human pressure of $\in$ (0, 10), $\in$ (10, 20), $\in$ (20, 30), (30, 400), $\in$ (40, 50), and $\in$ (50). We analyzed the proportions of the seven levels in KBAs and NNRs from 1990 to 2017. Third, we used kernel density estimation (Parzen, 1962) to analyze the spatial scale and location changes of aggregation areas with a human pressure of above 10 and those areas under no human pressure from 1990 to 2017.

Analysis of Human Pressure Changes After the Implementation of Conservation Policies

As mentioned in section "Study Area," many ecological conservation policies have been implemented in the Qinghai–Tibet Plateau since 2010. Therefore, this study compared whether the human pressure within KBAs and NNRs before and after 2010 had a statistically significant variation through a Wilcoxon signed-rank test, which has been widely used in ecological conservation research (Lieb et al., 2021). The Wilcoxon signed-rank test is a nonparametric approach to test whether two groups of values are significantly different. It adds the rank of the absolute value of the difference between the observed value and center position of the null hypothesis according to different signs as its test statistic and does not require the difference between paired data to obey a normal distribution (Gibbons and Chakraborti, 2011).

The specific steps are as follows: first, we calculated the difference (d_i) of the average annual growth rate in human pressure between 1990–2010 and 2010–2017 for each grid in the KBAs and NNRs, respectively, and coded the absolute value of d_i in the order of magnitude to form a sequence. Then, we restored the positive and negative signs of the values in the sequence, summed the positive value (T+) and the negative value (T−), respectively, and selected the smaller one as the Wilcoxon test statistic T. Finally, we made judgments based on the significance level (Gibbons and Chakraborti, 2011).

Data Source

The datasets used in this study included the spatial extent of the Qinghai–Tibet Plateau, NNRs, KBAs, population density, land use, cattle and sheep densities, beef and mutton production, nighttime light, highway, and railway data (**Table 2**). Owing to

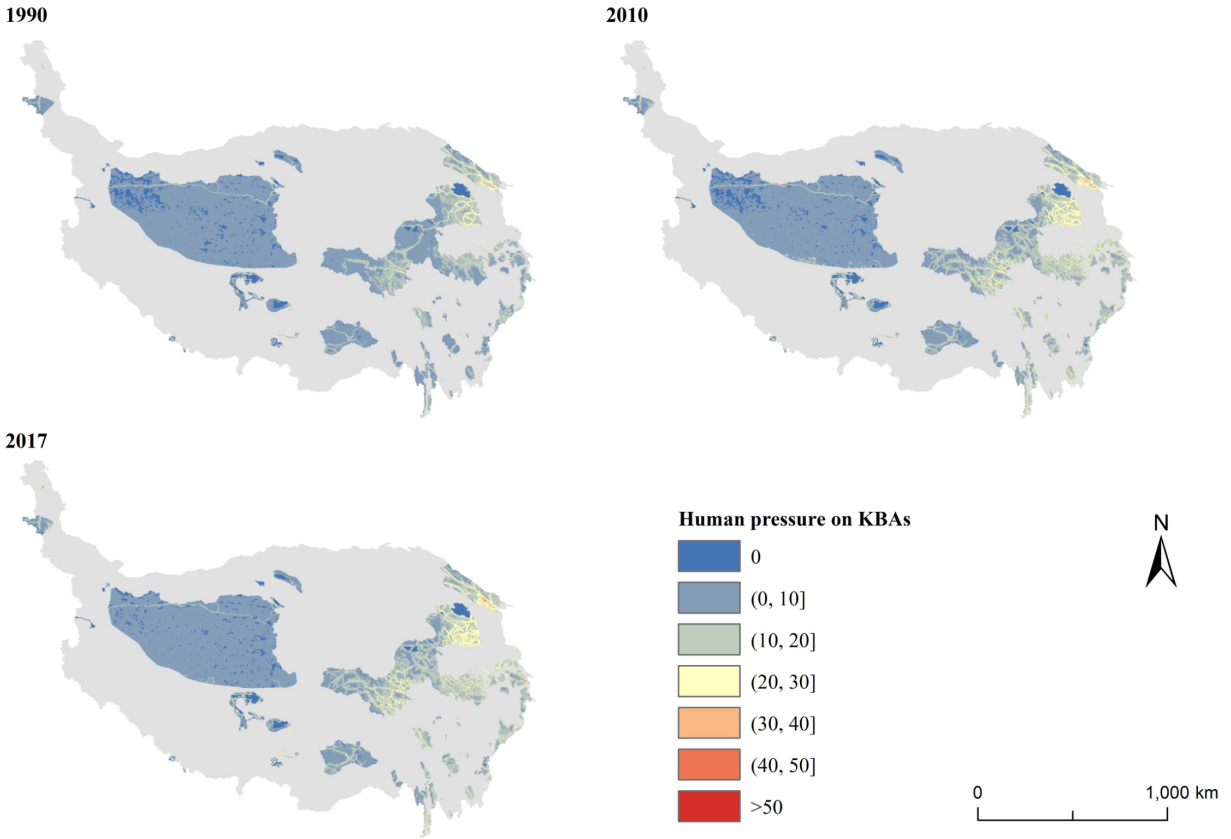

FIGURE 2 | Spatiotemporal pattern of human pressure in KBAs during 1990–2017.

inconsistencies in the projection, resolution, and spatial extent of data used, the original datasets must be preprocessed before data analysis. The projection coordinates were uniformly converted to an Albers equal-area projection suitable for China. The central meridian of the projection coordinate system parameter was set to 105° E, the two standard latitudes were 25° N and 47° N, and the spatial range was uniformly cut to the range of the Qinghai–Tibet Plateau. All raster data were resampled to a resolution of 1 km.

RESULTS

Spatiotemporal Variation of Human Pressure Within Key Biodiversity Areas and National Natural Reserves

The spatiotemporal patterns of human pressure within KBAs and NNRs from 1990 to 2017 are shown in **Figures 2**, **3**, respectively. The human pressure inside KBAs was higher than that inside NNRs and their overlapping areas, and the rising trend of human pressure was more obvious than that of NRRs and the overlapping areas. The mean value (**Figure 4**) revealed that human pressure within KBAs was higher than that within NNRs and the overlapping areas. From 1990 to 2017, the average annual increase in human pressure experienced by KBAs (0.84%) was higher than that experienced by NRRs (0.81%) and the overlapping areas (0.72%). From the perspective of the two periods, the average annual growth rate of human pressure in KBAs was higher than that in NNRs (1990–2010, 1.10% of KBAs > 1.07% of NNRs > 0.99% of the overlapping areas; 2010–2017, 0.18% of KBAs > 0.13% of NNRs > −0.001% of the overlapping areas).

In general, the high-pressure areas inside KBAs were more widely distributed than those inside NNRs (**Table 3**). There was no area with human pressure above 50 within NNRs, but 0.02% of KBAs in 2017 had human pressures above 50. The proportion of areas with human pressures above 10 within KBAs increased from 21.10% in 1990 to 34.41% in 2017, and within NNRs increased from 10.37% in 1990 to 16.07% in 2010 and subsequently decreased to 6.72% in 2017. The proportion of areas with human pressures above 20, 30, and 40 in KBAs and NNRs showed a continuously increasing trend from 1990 to 2017, but the expanded areas in KBAs were wider than those in NNRs. Only a small number of areas within KBAs were free from human pressure (human pressure = 0), and the proportion of this type of area continued to shrink from 7% in 1990 to 5.53% in 2017. Similarly, areas free from human pressure within NNRs also showed a downward trend from 11.57% in 1990 to 6.72% in 2017.

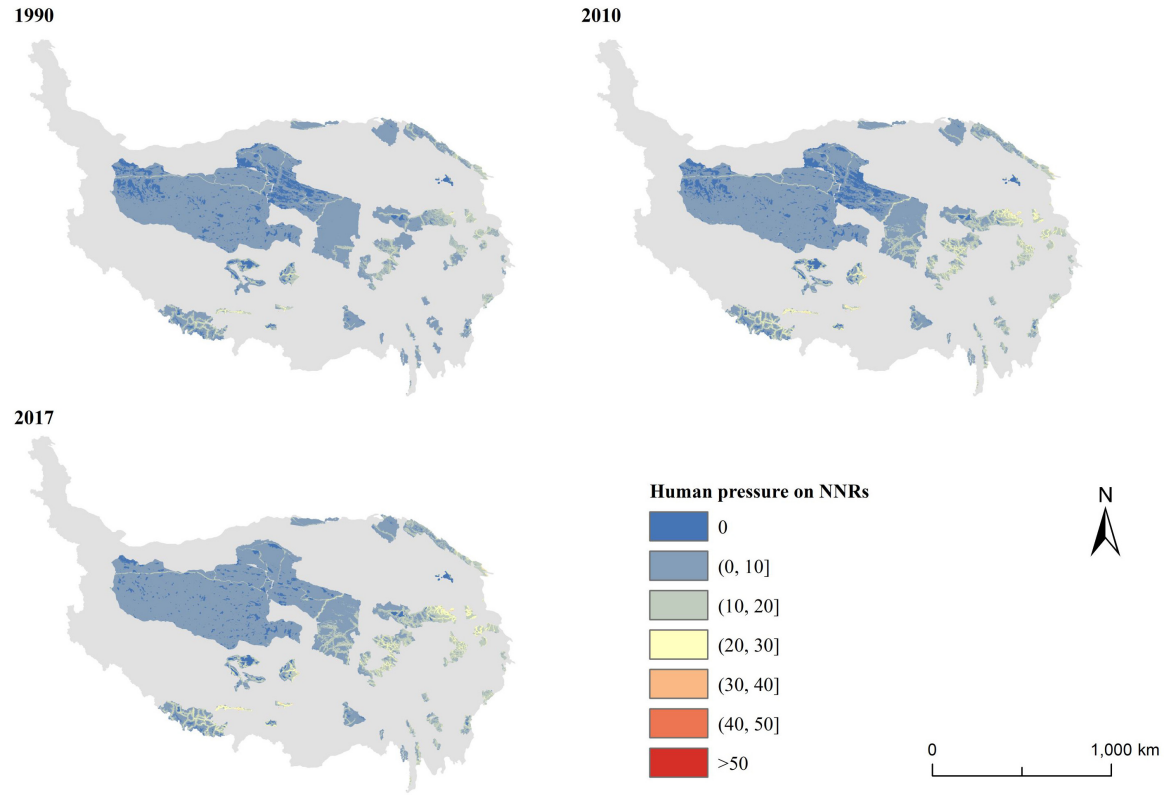

FIGURE 3 | Spatiotemporal pattern of human pressure in NNRs during 1990–2017.

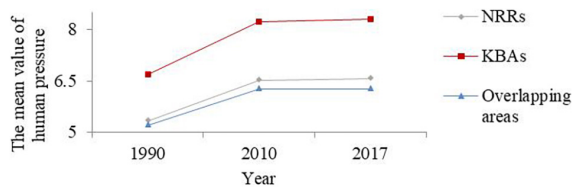

FIGURE 4 | Mean value of human pressure in NNRs and KBAs during 1990–2017.

TABLE 3 | Proportions of areas with various degree of human pressures in key biodiversity areas (KBAs) and national natural reserves (NNRs) during 1990–2017 (%).

	Year	0	(0, 10)	(10, 20)	(20, 30)	(30, 40)	(40, 50)	>50
KBAs	1990	7.00	71.90	19.26	1.79	0.05	0.00	0.00
	2010	6.99	59.13	28.08	5.55	0.24	0.01	0.00
	2017	5.53	60.06	28.05	6.03	0.30	0.02	0.02
NRRs	1990	11.57	78.07	9.78	0.58	0.00	0.00	0.00
	2010	11.55	72.38	14.07	1.93	0.00	0.07	0.00
	2017	6.72	76.92	14.28	2.01	0.00	0.07	0.00

Kernel density analysis results showed that the aggregation areas of KBAs with human pressure above 10 appeared inside the KBAs located in the eastern Qinghai–Tibet plateau (**Figure 5**). From 1990 to 2017, the agglomeration of human pressure above 10 gradually spread from east to west. The same trend also appears in the areas with human pressure above 10 of NNRs (**Figure 6**). Grids with high human pressure are mainly present in low-altitude areas that are highly accessible to humans. Over the past few years, increasing traffic and construction activities have occurred, and these areas have been greatly disturbed by humans. In KBAs, the areas under no human pressure are scattered. There were four agglomerations in 1990, and by 2017 the northwest agglomeration had disappeared. Among the NNRs, the accumulation area of under no human pressure area was larger, and mainly distributed in the northwest, the north of the central parts, and a few areas in the east. From 1990 to 2017, the range of the agglomeration areas in the northwest and central parts has reduced significantly, indicating that the influence of human activities has gradually increased. The accumulation area of the high pressure area has expanded, while the accumulation area of the no pressure area has gradually reduced.

Impact of Conservation Policy on Key Biodiversity Areas and National Natural Reserves

According to the Wilcoxon signed-rank test results, the average annual growth rate in human pressure of KBAs and NRRs significantly declined after the implementation of conservation policies in 2010 (**Table 4**). The average annual growth rate of

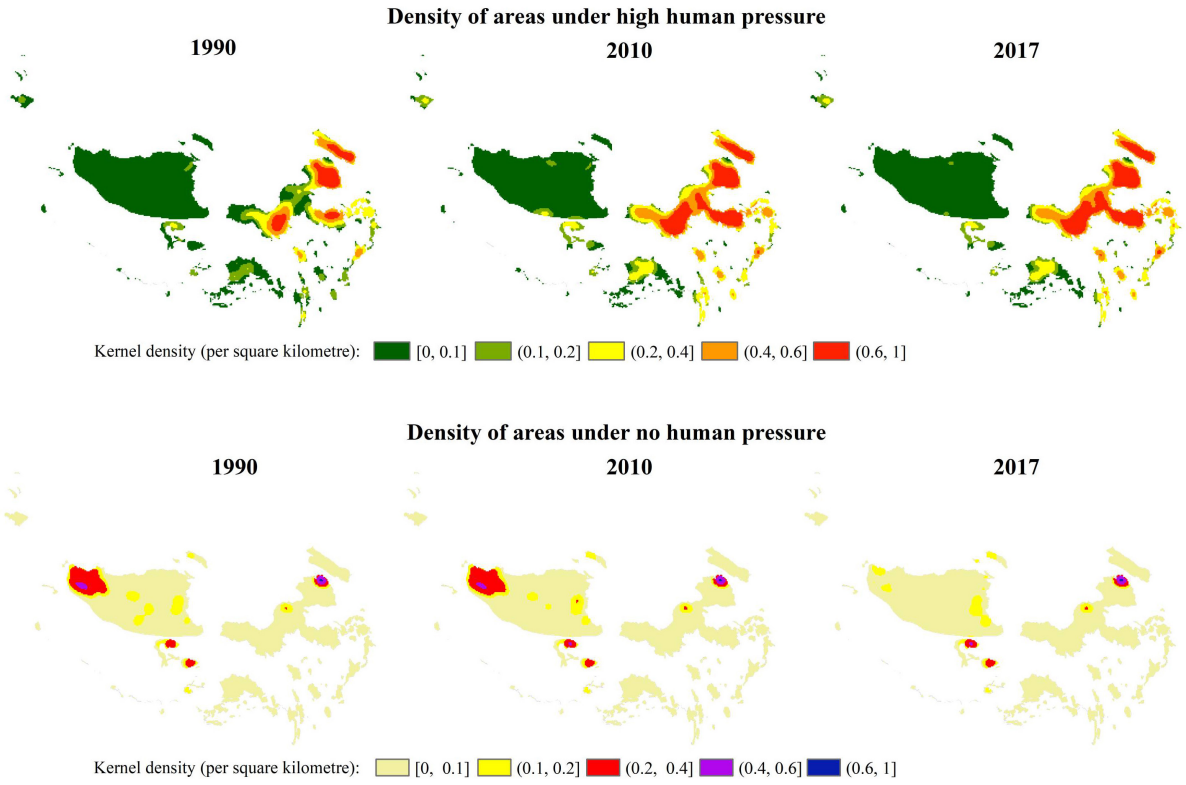

FIGURE 5 | Aggregation areas of KBAs with human pressure above 10 and under no human pressure in KBAs during 1990–2017.

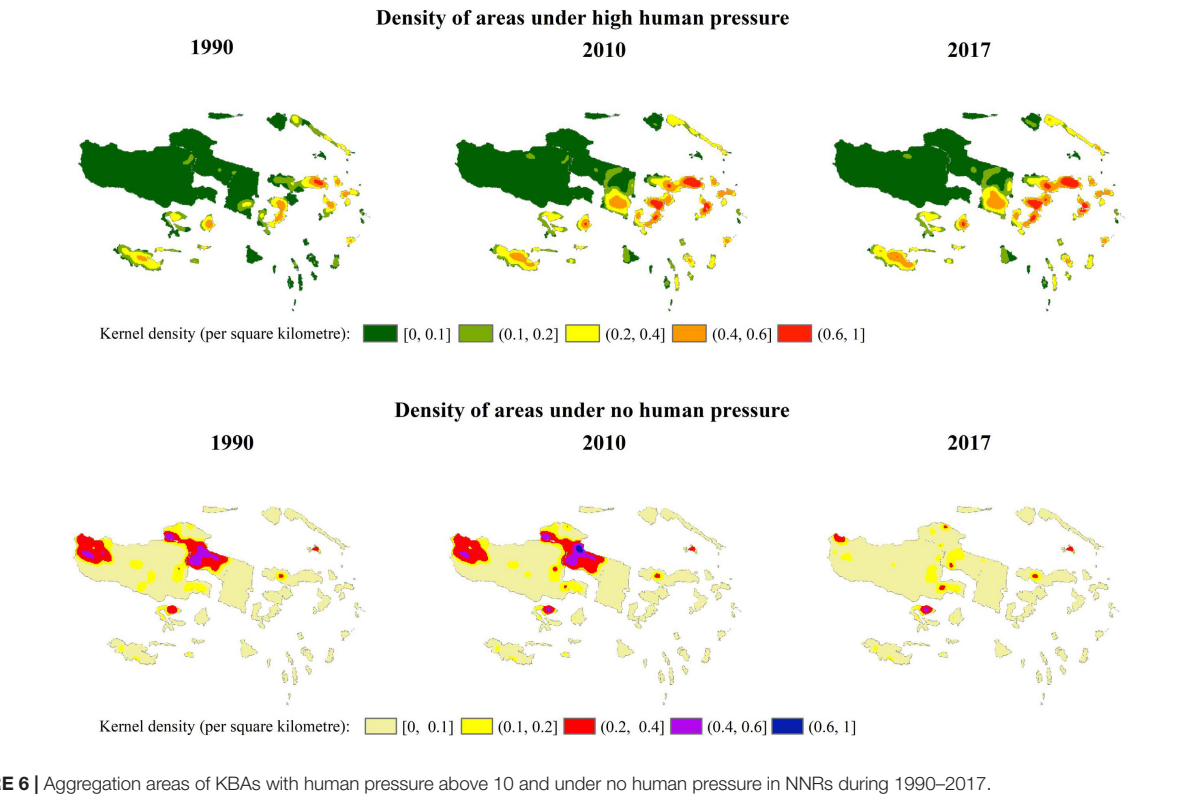

FIGURE 6 | Aggregation areas of KBAs with human pressure above 10 and under no human pressure in NNRs during 1990–2017.

TABLE 4 | The variation of average annual growth of human pressure between 1990–2010 and 2010–2017.

	Year	The average annual growth rate in grids (%)			Results of Wilcoxon signed-rank test
		Mean	Minimum	Maximum	
NRRs	1990–2010	0.059	1.369	−1.049	$z = -334.051$, $p = 0.000$, $n = 704{,}987$
	2010–2017	0.009	3.008	−3.183	
KBAs	1990–2010	0.078	1.305	−1.099	$z = -375.291$, $p = 0.000$, $n = 679{,}567$
	2010–2017	0.015	4.208	−3.908	

human pressure in KBAs declined from 0.078% before 2010 to 0.015% after 2010. Likewise, the average annual growth rate in human pressure within the NRRs was 0.059%, and it declined to 0.009% after 2010.

The implementation of conservation policies helps to expand areas with negative growth in human pressure (**Figure 7**). This effect was starker in NNRs. The area with negative growth in human pressure in the NRRs expanded from 18.31% in 1990–2020 to 31.74% in 2010–2017, and this type of area in KBAs expanded from 17.01% in 1990–2020 to 30.15% in 2010–2017.

DISCUSSION

Contribution and Implications

This study is the first to report the spatiotemporal variation of human pressure on KBAs in the Qinghai–Tibet Plateau. Thus, it improves our understanding of the pressure of human activities on the ecosystem. The Qinghai–Tibet Plateau is a developing area with relatively little human activity, but the findings suggest that areas with a higher human pressure exist in the plateau, which is similar to the findings of Hua et al. (2022), who observed that areas that are under high human pressure have appeared inside NNRs. However, this study found that such areas were distributed more widely within KBAs, and compared with NNRs, the scale of such areas in KBAs is continuously expanding. This study identified sites of high magnitude and rapid growth, and hence, it can provide clear spatial guidance for the management of human pressure on ecosystems.

The Qinghai–Tibet Plateau is of high ecological importance and it has received substantial conservation efforts; however,

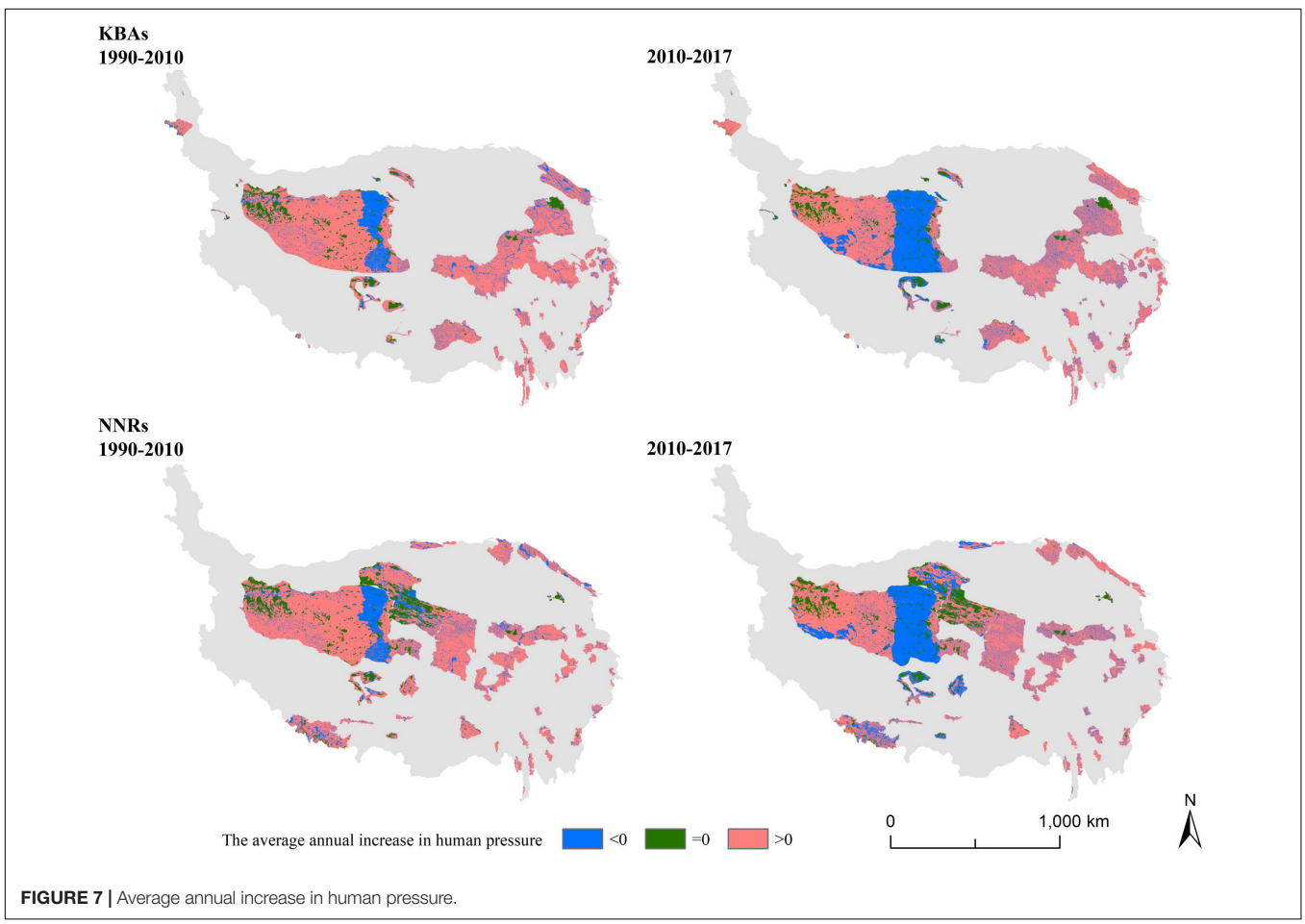

FIGURE 7 | Average annual increase in human pressure.

ecological problems appeared under the past NNRs-based protection scheme (Fu et al., 2021). This study found that human activities have enormous pressure on KBAs, indicating a theoretical variable for identifying the reasons for ecosystem problems on the Qinghai–Tibet Plateau. This study suggests that poor protection of KBAs and increased pressure from human activities on KBAs may be reasons for this dilemma. KBAs have many typical species (such as individual geographically restricted species) and threatened ecosystems, which contribute significantly to the global persistence of biodiversity at the genetic, species, and ecosystem levels (International Union for Conservation of Nature [IUCN], 2016). The effects of human pressure on these species and ecosystems are likely to be widespread. Therefore, increased human pressure on KBAs may be an important reason for the emergence of ecosystem problems in the Qinghai–Tibet Plateau.

Practically, this study helps focus policy attention on KBAs and provides a reference for the adjustment of the spatial scope of PAs. In fact, not only did KBAs go unnoticed in China, around 4,900 KBAs (33.0%) remained without official attention globally in 2019 (Maxwell et al., 2020). In the post-2020 conservation era, managers should pay more attention to KBAs (Maxwell et al., 2020). According to this study, managers should design tailored managerial policies for KBAs according to their ecological importance and human pressure. Furthermore, protection should be promptly strengthened in areas of high importance and severe human pressure. In contrast, areas with high human pressure and low ecological importance may be used for human economic development. This is an appropriate way for improving conservation efficiency from the overall perspective (Fuller et al., 2010). Considering the massive disappearance of the accumulation area under no human pressure, more ecologically dynamic monitoring on human activities in KBAs located in the northwest and in NNRs situated in the northwest and north of the central parts of the Qinghai–Tibet Plateau must be implemented.

Many developing countries worldwide, including China, are in the initial stage of acting on KBAs. This study found that KBAs were subjected to higher human pressures than NNRs, which has long been a focus for ecological conservation in China. This underscores the importance of focusing on KBAs. Further, KBAs play an important role in maintaining biodiversity (International Union for Conservation of Nature [IUCN], 2016). If KBAs are not under timely protection, the increase in human pressure will accelerate biodiversity loss and threaten the sustainability of socio-geographic systems. China is presently in the process of reforming its conservation system, which is characterized by the spatial adjustment of conservation areas. Therefore, it is necessary to incorporate KBAs into a new network of conservation areas and develop protection policies specific to them.

Limitations and Suggestions for Future Research

This study also had some limitations. First, it only considered the pressure of human activities and not the carrying capacity of the ecosystem. Different types of ecosystems have different adaptability to human pressure; therefore, measuring human pressure alone cannot directly reflect the degree of damage to the ecosystem. Future research should address this gap to reveal the actual state of the ecosystem. Second, this study did not directly consider the environmental pollution indicators caused by human beings. Future studies should examine the relationship between the human footprint and the real situation of environmental pollution to reveal the impacts of human activities in the ecosystem. Finally, this study did not consider dynamic traffic flow in human pressure assessments. The negative impacts of different traffic flows were different. For example, traffic flow has decreased significantly after COVID-19, which has played a positive role in ecosystem restoration. Therefore, future research should incorporate traffic flow analysis into the human pressure analysis.

CONCLUSION

This study compared the spatiotemporal patterns of human pressure on KBAs and NNRs during 1990–2017, and found that KBAs suffered more human pressure than NNRs. From 1990 to 2017, the human pressure on KBAs showed an upward trend, and the rate of increase of KBAs was greater than that of NNRs. Moreover, the average human pressure on KBAs was greater than that on NNRs. Areas of severe human pressure appeared within KBAs in 2017. Areas without human pressure are small within KBAs, and the proportion of this type of area continued to shrink during 1990–2017. Influenced by human activities, the accumulation area of the high pressure area expands, while the accumulation area of the no pressure area gradually shrinks, especially in KBAs. Furthermore, this study compared the effects of ecological conservation policies on the changing trend of human pressure in KBAs and NNRs. Results revealed that human pressure on both KBAs and NNRs significantly declined after the implementation of ecological conservation policies. After the implementation of ecological conservation policies (2010–2017), the average annual increase in human pressure in each grid of KBAs and NNRs was significantly lower than that before the implementation of ecological conservation policies (1990–2010), and the declining trend was more evident in NNRs than in KBAs. Our research provides novel insights on the spatiotemporal variation of human pressure on KBAs in the Qinghai–Tibet Plateau, thereby improving our understanding of the pressure of human activities on ecosystems and offering implications for post-2020 area-based conservation.

DATA AVAILABILITY STATEMENT

The original contributions presented in this study are included in the article/supplementary material; further inquiries can be directed to the corresponding author.

AUTHOR CONTRIBUTIONS

YZ and L-EW: methodology, software and validation, formal analysis, and original draft preparation. YZ, L-EW, and LZ: writing—review and editing. YZ and LZ: visualization. LZ: supervision. L-EW: funding acquisition. All authors have read and agreed to the published version of the manuscript.

FUNDING

This study was supported by the National Natural Science Foundation (4217011372), the Second Tibetan Plateau Scientific Expedition and Research Program (2019QZKK1002), Youth Innovation Promotion Association of Chinese Academy of Sciences, and China Postdoctoral Science Foundation (2020M680659).

REFERENCES

Alves-Pinto, H., Geldmann, J., Jonas, H., Maioli, V., Balmford, A., Latawiec, A. E., et al. (2021). Opportunities and challenges of other effective area-based conservation measures (OECMs) for biodiversity conservation. *Perspect. Ecol. Conserv.* 19, 115–120. doi: 10.1016/j.pecon.2021.01.004

Bao, C., and Liu, R. W. (2019). Spatiotemporal evolution of the urban system in the Tibetan Plateau. *J. Geo Inform. Sci.* 21, 1330–1340. doi: 10.12082/dqxxkx.2019.180681

BirdLife International (2019). *World Database of Key Biodiversity Areas*. Available online at: www.keybiodiversityareas.org (accessed June 20, 2019).

Chen, D. L., Xu, B. Q., Yao, T. D., Guo, Z. T., Cui, P., Chen, F. H., et al. (2015). Assessment of past, present and future environmental changes on the Tibetan Plateau. *Sci. Bull.* 60, 3025–3035. doi: 10.1360/N972014-013

Chen, M. G., and Zhang, S. (2020). Regional economic imbalance in China and the influence factors: based on night-time light data. *Stat. Res.* 37, 40–54. doi: 10.19343/j.cnki.11-1302/c.2020.06.004

Chi, Y., Liu, D., Wang, J., and Wang, E. (2020). Human negative, positive, and net influences on an estuarine area with intensive human activity based on land covers and ecological indices: an empirical study in Chongming Island, China. *Land Use Policy* 99:104846. doi: 10.1016/j.landusepol.2020.104846

de Queiroz, M. G., da Silva, T. G. F., Zolnier, S., Jardim, A. M. D. R. F., de Souza, C. A. A., Júnior, G. D. N. A., et al. (2020). Spatial and temporal dynamics of soil moisture for surfaces with a change in land use in the semi-arid region of Brazil. *Catena* 188:104457. doi: 10.1016/j.catena.2020.104457

Donald, P. F., Buchanan, G. M., Balmford, A., Bingham, H., Couturier, A. R., de la Rosa, G. E., et al. (2019). The prevalence, characteristics and effectiveness of Aichi Target 11's "other effective area-based conservation measures" (OECMs) in Key Biodiversity Areas. *Conserv. Lett.* 12:e12659. doi: 10.1111/conl.12659

Duan, Q., and Luo, L. (2021). *A Dataset of Human Footprint Over the Qinghai-Tibet Plateau During 1990–2017*. Beijing, National Tibetan Plateau Data Center.

Fu, B. J., Ouyang, Z. Y., Shi, P., Fan, J., Wang, X. D., Zheng, H., et al. (2021). Current condition and protection strategies of qinghai-tibet plateau ecological security barrier. *Bull. Chin. Acad. Sci.* 36, 1298–1306. doi: 10.16418/j.issn.1000-3045.20210919001

Fuller, R. A., McDonald-Madden, E., Wilson, K. A., Carwardine, J., Grantham, H. S., Watson, J. E., et al. (2010). Replacing underperforming protected areas achieves better conservation outcomes. *Nature* 466, 365–367. doi: 10.1038/nature09180

Garrett, J. K., Donald, P. F., and Gaston, K. J. (2020). Skyglow extends into the world's Key Biodiversity Areas. *Anim. Conserv.* 23, 153–159. doi: 10.1111/acv.12480

General Office of the CPC Central Committee, and General Office of the State Council of China (2019). *Guiding Opinions on Establishing a Natural Reserve System with National Parks as the Main Body*. Beijing. Available online at: http://www.gov.cn/zhengce/2019-06/26/content_5403497.htm (accessed June 26, 2019).

Gibbons, J. D., and Chakraborti, S. (2011). *Nonparametric Statistical Inference*. Boca Raton, FL: Chapman & Hall/CRC Press (Taylor & Francis).

Gosselin, F., and Callois, J. M. (2021). On the time lag between human activity and biodiversity in Europe at the national scale. *Anthropocene* 35:100303. doi: 10.1016/j.ancene.2021.100303

Hua, T., Zhao, W., Cherubini, F., Hu, X., and Pereira, P. (2022). Continuous growth of human footprint risks compromising the benefits of protected areas on the Qinghai-Tibet Plateau. *Glob. Ecol. Conserv.* 34:e02053. doi: 10.1016/j.gecco.2022.e02053

International Union for Conservation of Nature [IUCN] (2016). *A Global Standard for the Identification of Key Biodiversity Areas*. Gland: International Union for Conservation of Nature (IUCN).

Jonas, H. D., Barbuto, V., Jonas, H. C., Kothari, A., and Nelson, F. (2014). New steps of change: looking beyond protected areas to consider other effective area-based conservation measures. *Parks* 20, 111–128. doi: 10.2305/IUCN.CH.2014.PARKS-20-2.HDJ.en

Keys, P. W., Barnes, E. A., and Carter, N. H. (2021). A machine-learning approach to human footprint index estimation with applications to sustainable development. *Environ. Res. Lett.* 16:044061. doi: 10.1088/1748-9326/abe00a

Kroeger, S. B., Hanslin, H. M., Lennartsson, T., D'Amico, M., Kollmann, J., Fischer, C., et al. (2022). Impacts of roads on bird species richness: a meta-analysis considering road types, habitats and feeding guilds. *Sci. Tot. Environ.* 812:151478. doi: 10.1016/j.scitotenv.2021.151478

Kullberg, P., Di Minin, E., and Moilanen, A. (2019). Using key biodiversity areas to guide effective expansion of the global protected area network. *Glob. Ecol. Conserv.* 20:e00768. doi: 10.1016/j.gecco.2019.e00768

Li, J., Li, X., Gao, J., Ma, G., and Qi, X. (2021a). Micro-scale fragmentation of the alpine meadow landscape on the Qinghai-Tibet Plateau under external disturbances. *Catena* 201:105220. doi: 10.1016/j.catena.2021.105220

Li, J., Zhao, Y., Shao, X., Huang, D., Shang, J., Li, H., et al. (2021b). The Mixed Addition of Biochar and Nitrogen Improves Soil Properties and Microbial Structure of Moderate–Severe Degraded Alpine Grassland in Qinghai-Tibet Plateau. *Front. Plant Sci.* 12:765041. doi: 10.3389/fpls.2021.765041

Li, M., Wu, J., Feng, Y., Niu, B., He, Y., and Zhang, X. (2021c). Climate variability rather than livestock grazing dominates changes in alpine grassland productivity across Tibet. *Front. Ecol. Evol.* 9:631024. doi: 10.3389/fevo.2021.631024

Li, Y. (2021). Knowledge products of the International Union for Conservation of Nature (IUCN) and their domestic application status. *China Land* 2, 12–16. doi: 10.13816/j.cnki.ISSN1002-9729.2021.02.03

Lieb, Z., Tumurbaatar, B., Elfström, B., and Bull, J. (2021). Impact of livestock guardian dogs on livestock predation in rural Mongolia. *Conserv. Sci. Pract.* 3:e509. doi: 10.1111/csp2.509

Liu, F., Liu, F. G., Zhou, Q., Chen, Q., Wang, S. Z., Guo, R., et al. (2021). Ecological risk and regional differentiation in the Qinghai-Tibet Plateau. *J. Nat. Resour.* 36, 3232–3246. doi: 10.31497/zrzyxb.20211216

Luo, X., Yang, J., Sun, W., and He, B. (2021). Suitability of human settlements in mountainous areas from the perspective of ventilation: a case study of the main urban area of Chongqing. *J. Cleaner Prod.* 310:127467. doi: 10.1016/j.jclepro.2021.127467

Ma, Z., Chen, Y., Melville, D. S., Fan, J., Liu, J., Dong, J., et al. (2019). Changes in area and number of nature reserves in China. *Conserv. Biol.* 33, 1066–1075. doi: 10.1111/cobi.13285

Maxwell, S. L., Cazalis, V., Dudley, N., Hoffmann, M., Rodrigues, A. S., Stolton, S., et al. (2020). Area-based conservation in the twenty-first century. *Nature* 586, 217–227. doi: 10.1038/s41586-020-2773-z

Mottl, O., Flantua, S. G., Bhatta, K. P., Felde, V. A., Giesecke, T., Goring, S., et al. (2021). Global acceleration in rates of vegetation change over the past 18,000 years. *Science* 372, 860–864. doi: 10.1126/science.abg1685

Mu, H., Li, X., Wen, Y., Huang, J., Du, P., Su, W., et al. (2022). A global record of annual terrestrial Human Footprint dataset from 2000 to 2018. *Sci. Data* 9, 1–9. doi: 10.1038/s41597-022-01284-8

National Bureau of Statistics of China [NBSC] (2020). *China Statistical Yearbook*. Beijing: China Statistics Press.

National Development and Reform Commission of China [NDRC], and Ministry of Natural Resources of China [MNRC] (2020). *The Overall Plan for Major Projects in the Protection and Restoration of National Important Ecosystems (2021-2035)*. Beijing: National Development and Reform Commission of China.

Nogueira, J. G., Sousa, R., Benaissa, H., De Knijf, G., Ferreira, S., Ghamizi, M., et al. (2021). Alarming decline of freshwater trigger species in western Mediterranean key biodiversity areas. *Conserv. Biol.* 35, 1367–1379. doi: 10.1111/cobi.13810

Parzen, E. (1962). On estimation of a probability density function and mode. *Ann. Math. Stat.* 33, 1065–1076.

Pavlik, B. M., Louderback, L. A., Vernon, K. B., Yaworsky, P. M., Wilson, C., Clifford, A., et al. (2021). Plant species richness at archaeological sites suggests ecological legacy of Indigenous subsistence on the Colorado Plateau. *Proc. Natl. Acad. Sci. U.S.A.* 118:e2025047118. doi: 10.1073/pnas.2025047118

Polazzo, F., Dos Anjos, T. B. O., Arenas-Sánchez, A., Romo, S., Vighi, M., and Rico, A. (2022). Effect of multiple agricultural stressors on freshwater ecosystems: the role of community structure, trophic status, and biodiversity-functioning relationships on ecosystem responses. *Sci. Tot. Environ.* 807:151052. doi: 10.1016/j.scitotenv.2021.151052

Pringle, R. M. (2017). Upgrading protected areas to conserve wild biodiversity. *Nature* 546, 91–99. doi: 10.1038/nature22902

Sanderson, E. W., Jaiteh, M., Levy, M. A., Redford, K. H., Wannebo, A., and Woolmer, G. (2002). The human footprint and the last of the wild. *Bioscience* 52, 891–904.

Shen, W., Zhang, H., Zou, C., Cao, X., and Tang, X. (2004). Approaches to prediction of impact of Qinghai-Tibet Railway construction on alpine ecosystems alongside and its recovery. *Chin. Sci. Bull.* 49, 834–841. doi: 10.1360/03wd0376

Shrestha, M., Piman, T., and Grünbühel, C. (2021). Prioritizing key biodiversity areas for conservation based on threats and ecosystem services using participatory and GIS-based modeling in Chindwin River Basin, Myanmar. *Ecosyst. Serv.* 48:101244. doi: 10.1016/j.ecoser.2021.101244

Strassburg, B. B., Iribarrem, A., Beyer, H. L., Cordeiro, C. L., Crouzeilles, R., Jakovac, C. C., et al. (2020). Global priority areas for ecosystem restoration. *Nature* 586, 724–729. doi: 10.1038/s41586-020-2784-9

Tian, L., and Chen, J. (2022). Urban expansion inferenced by ecosystem production on the Qinghai-Tibet plateau. *Environ. Res. Lett.* 17:035001. doi: 10.1088/1748-9326/ac3178

Trentman, M. T., Tank, J. L., Davis, R. T., Hanrahan, B. R., Mahl, U. H., and Roley, S. S. (2022). Watershed-scale land use change increases ecosystem metabolism in an agricultural stream. *Ecosystems* 25, 441–456. doi: 10.1007/s10021-021-00664-2

Trombulak, S. C., and Frissell, C. A. (2000). Review of ecological effects of roads on terrestrial and aquatic communities. *Conserv. Biol.* 14, 18–30. doi: 10.1046/j.1523-1739.2000.99084.x

Venter, O., Sanderson, E. W., Magrach, A., Allan, J. R., Beher, J., Jones, K. R., et al. (2016). Sixteen years of change in the global terrestrial human footprint and implications for biodiversity conservation. *Nat. Commun.* 7, 1–11. doi: 10.1038/ncomms12558

Wang, L., Wu, W. M., Bolan, N. S., Tsang, D. C., Li, Y., Qin, M., et al. (2021). Environmental fate, toxicity and risk management strategies of nanoplastics in the environment: current status and future perspectives. *J. Hazardous Mater.* 401:123415. doi: 10.1016/j.jhazmat.2020.123415

Wildlife Conservation Society (2013). *Myanmar Biodiversity Conservation Investment Vision. Wildlife Conservation Society, Yangon, Myanmar*. New York, NY: Wildlife Conservation Society.

Xie, X., Fang, B., Xu, H., He, S., and Li, X. (2021). Study on the coordinated relationship between Urban Land use efficiency and ecosystem health in China. *Land Use Policy* 102:105235. doi: 10.1016/j.landusepol.2020.105235

Yu, H., Wang, Y., and Zhang, Y. L. (2016). *When Will the Turning Point of China's Environmental Kuznets Curve Come? Special Report on the Environmental Strategy and Policy*. 197. Beijing: Ministry of Ecology and Environment the People's Republic of China.

Yu, H., Yang, J., Sun, D., Li, T., and Liu, Y. (2022). Spatial responses of ecosystem service value during the development of urban agglomerations. *Land* 11:165.

Zhang, B. F., Miao, C. H., Song, Y. N., and Wang, J. J. (2020). Correction of DMSP/OLS stable night light images in China. *J. Geo inform. Sci.* 22, 1679–1691. doi: 10.12082/dqxxkx.2020.190397

Zhao, F., and Lu, T. (2017). Ecological effects of roads on land use and landscape pattern in Eastern Tibetan Plateau. *China. Ecol. Sci.* 36, 146–151. doi: 10.14108/j.cnki.1008-8873.2017.04.020

Zhao, J., Zhao, Z., and Zhang, H. (2021). The impact of growth, energy and financial development on environmental pollution in China: new evidence from a spatial econometric analysis. *Energy Econ.* 93:104506. doi: 10.1016/j.eneco.2019.104506

Zhuang, M., Zhang, J., and Li, W. (2019). Community-based seasonal movement grazing maintains lower greenhouse gas emission intensity on Qinghai-Tibet Plateau of China. *Land Use Policy* 85, 155–160. doi: 10.1016/j.landusepol.2019.03.032

Conflict of Interest: The authors declare that the research was conducted in the absence of any commercial or financial relationships that could be construed as a potential conflict of interest.

Publisher's Note: All claims expressed in this article are solely those of the authors and do not necessarily represent those of their affiliated organizations, or those of the publisher, the editors and the reviewers. Any product that may be evaluated in this article, or claim that may be made by its manufacturer, is not guaranteed or endorsed by the publisher.

Copyright © 2022 Zeng, Wang and Zhong. This is an open-access article distributed under the terms of the Creative Commons Attribution License (CC BY). The use, distribution or reproduction in other forums is permitted, provided the original author(s) and the copyright owner(s) are credited and that the original publication in this journal is cited, in accordance with accepted academic practice. No use, distribution or reproduction is permitted which does not comply with these terms.

frontiers | Frontiers in Environmental Science

ORIGINAL RESEARCH
published: 04 July 2022
doi: 10.3389/fenvs.2022.918621

Exploring Spatial Distributions and Formation Factors of Brownfields in China: From Macro-Scales

Xinjia Zhang[1], *Yang Song*[2,3]*, *Sitong Qian*[2], *Shijun Wang*[2,3] *and Donghang Wu*[4]

[1]School of Arts and Design, Yanshan University, Qinhuangdao, China, [2]School of Geographical Sciences, Northeast Normal University, Changchun, China, [3]Key Laboratory of Geographical Processes and Ecological Security of Changbai Mountains, Ministry of Education, Changchun, China, [4]School of Fine Arts, Northeast Normal University, Changchun, China

The spatial distribution pattern of brownfields can help governments at all levels, and investors have more detailed information on land resources, prioritize brownfield redevelopment, and guide urban spatial and strategic planning. Despite increasing global concern, yet knowledge of brownfield distribution patterns at the macro-scale remains limited, especially in China. Derived from the China National Knowledge Infrastructure (CNKI), Web of Science (WOS), and Chinese Industrial Heritage List published between 2001 and 2019, we present the first comprehensive dataset of known brownfield sites and their distributions in China. The results revealed that the dataset contains 816 georeferenced brownfield records from 255 cities. Brownfields were mainly distributed southeast of the "Heihe-Tengchong Line," with an overall spatial distribution pattern of "East-dense-West-sparse." In terms of brownfield type, industrial brownfields were the most numerous, followed by mining brownfields. Nearest neighbor indicator analysis suggested that brownfields in China present significant spatial agglomeration characteristics, and that the six types of brownfields manifest different scales of spatial agglomeration. The hot spots were mainly concentrated in the Yangtze River Delta, Beijing–Tianjin–Hebei, and Pearl River Delta urban agglomerations. Factors influencing brownfield formation were related to industrial structure adjustments, resource depletion, accelerated urbanization, and the orientation of national policies, with industrial structure adjustments being the leading cause. Mastering the spatial distribution of brownfields can coordinate land use transformation planning and guide brownfield redevelopment.

Keywords: brownfield, spatial distributions, formation factors, China, meta-analysis

OPEN ACCESS

Edited by:
Bing Xue,
Institute of Applied Ecology (CAS), China

Reviewed by:
Xiaohong Chen,
Harbin Normal University, China
Qingye Han,
Chongqing University, China

***Correspondence:**
Yang Song
song0317@nenu.edu.cn

Specialty section:
This article was submitted to Land Use Dynamics, a section of the journal Frontiers in Environmental Science

Received: *13 April 2022*
Accepted: *24 May 2022*
Published: *04 July 2022*

Citation:
Zhang X, Song Y, Qian S, Wang S and Wu D (2022) Exploring Spatial Distributions and Formation Factors of Brownfields in China: From Macro-Scales. Front. Environ. Sci. 10:918621. doi: 10.3389/fenvs.2022.918621

1 INTRODUCTION

The issue of brownfields remains one of the greatest challenges faced by urban planners and developers. In particular, in shrinking cities and old industrial areas, sites previously used for industrial, commercial, or mining purposes have been underutilized or abandoned (Hayek et al., 2010; Rall and Haase, 2011; Zhang et al., 2021). The existence of brownfields can lead to soil pollution and degraded quality of life, which adversely affects a city's economy, society, and the environment. Brownfield redevelopment can promote the creation of walkable neighborhoods, improve public transportation, control green field encroachment and urban sprawl, and revive local markets, in addition to the direct benefits of returning sites to productive use and increasing the tax base. The

rewards of brownfield redevelopment are vast and have the capability to last well into the future (Amekudzi et al., 2003; Chrysochoou et al., 2012).

Brownfields are common in both developed and developing countries (Howard and Olszewska, 2011; Loures and Vaz, 2018; Mahzouni, 2018). To better manage and update brownfield data, various countries have established national brownfield databases. For instance, in the United States, there are 500,000–1,000,000 registered brownfield sites (Hipel et al., 2010), while 21,000 contaminated sites have been identified in England (Longo and Campbell, 2017). In the Czech Republic, there are an estimated 8,500–11,700 brownfield sites (CzechInvest, 2021). The US Environmental Protection Agency (USEPA) established the first brownfield database with relatively complete information. The database is available to the public free of charge and shares the location of brownfield sites, addresses of units releasing toxic substances around them, and information on actions taken against contaminated plots for redevelopment and policy decisions (Leigh and Coffin, 2000; Coffin, 2003). The UK National Environment Agency, Transport, and Land Departments jointly established a National Land Use Database. The database was developed based on the need to monitor the supply of brownfields to provide adequate and strategic supply of land and buildings for housing and other economic activities. In the Czech Republic, an extensive database of brownfields is administered by the Ministry of Environment, the primary purpose of which is the protection of the environment (Osman et al., 2015).

The literature on brownfield spatial distributions and formation factors has grown considerably in the past few years, for example, the city of Minneapolis in the United States (Vaidya, 2015), Brno (Kunc et al., 2014; Frantál et al., 2015), Ostrava (Novosák et al., 2013), and Karvina in the Czech Republic (Martinat et al., 2016; Škrabal et al., 2021) and Changchun in China (Song et al., 2022). The research content of spatial distributions is mainly industrial brownfields (Smoļakova, 2017; Modica, 2019), which mostly guide local soil management (Bambra et al., 2014; Boente et al., 2018), land use policies (Page and Berger, 2006), and brownfield redevelopment (Filip and Cocean, 2012; Kramářová and Juhásová Šenitková, 2018; Bardos et al., 2020). Accurately determining macro-scale brownfield spatial distributions can provide a reference for formulating differentiated and regionalized redevelopment policies according to local conditions (Newell and McGreal, 2017). Previous studies have mainly analyzed the spatial characteristics, restoration methods, and redevelopment of brownfields from a micro perspective. Although they are highly targeted, the overall role of the macro-level has been ignored and has hindered the government from formulating reconstruction strategies. The research scale focuses on the spatial distribution of brownfields in a city or region. Moreover, the study of a single province and city cannot provide an overall grasp of the spatial distribution of macro-scale brownfields, which is limited by data collection. From the research content, they have most often been based on statistical classification of basic information, such as brownfield location, quantity, and area. The characteristics of such distributions have rarely been explored. The factors of brownfield formation are affected by the changes in the economic system, industrial structure adjustment, and accelerated urbanization. Some scholars have attributed the main causes of brownfield formation to deindustrialization and urbanization (Liu et al., 2014). The factors influencing the formation of brownfield sites in China contain both similarities and differences in relation to other countries. Deindustrialization and urbanization are the main factors in the production of global brownfields. Due to China's late industrialization process and its unique institutional environment, such as the dual land system, land ownership, spatial distribution, the mechanisms by which the sites are created, and the stakeholders involved, certain differences can be perceived compared to other countries.

As the largest developing country and second largest economy in the world, China plays an important role in the world economic system. It is also one of the countries with the largest brownfield stock. According to statistical data for 2015, more than 100,000 factories have closed since 2001, and over two million hectares of brownfield sites that had been seriously polluted have been left untreated in major cities (Liu et al., 2017). At present, China has not established a database of brownfields, and it is unclear how many exist, where they are concentrated, and to what types they belong. Second, due to the lack of open data on soil pollution across the country and the low degree of data availability, scientific research methods to identify brownfields have not been established, which poses a huge obstacle to mastering brownfield spatial distributions and redevelopment planning in China.

The contributions of this study are threefold. First, it established the first comprehensive dataset of known brownfields in China. Second, we analyzed the spatial distribution characteristics of these brownfields and identified the major factors in their formation. Third, this research can help governments at all levels and investors have more detailed information on land resources, prioritize brownfield redevelopment, and guide urban spatial and strategic planning.

The remainder of this article is organized as follows. An overview of the meta-analysis and spatial analysis utilized, with explanations for the main associated procedures is presented in **Section 2**. The overall spatial distributions of brownfields in China and of different types of brownfields based on the dataset are analyzed in **Section 3** and the main factors of brownfield formation are discussed. The results of and comparison with previous studies, as well as suggested policy responses are provided in **Section 4**. Finally, concluding remarks and discussion of future research directions are presented in **Section 5**.

2 MATERIALS AND METHODS

2.1 Meta-Analysis

As an important research method, meta-analysis refers to the systematic and comprehensive statistical analysis of the results of multiple experiments with the same research purpose and independent of each other (Brander et al., 2012; Chaikumbung

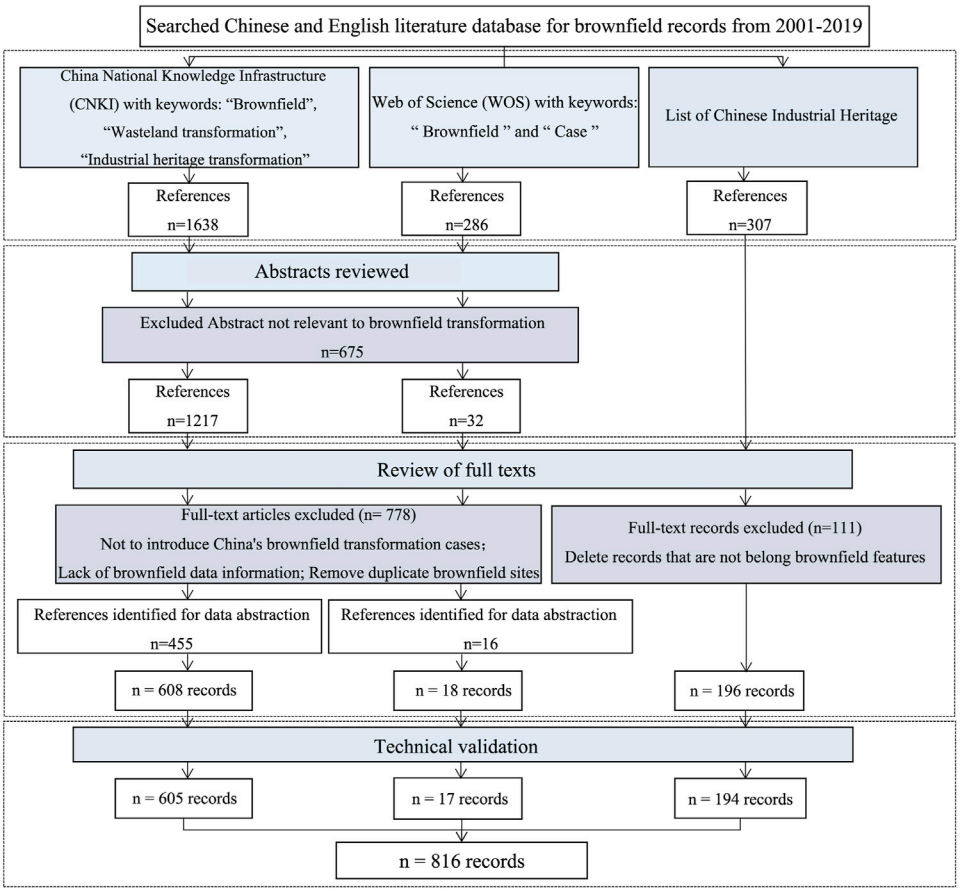

FIGURE 1 | Schematic overview of the literature search procedures and results.

et al., 2016). It was originally proposed as a research synthesis method by Glass (1976). Existing meta-analyses mainly use the induction, measurements, and conclusions of a research field, cases (Chen et al., 2019), and indicators to identify scientific consensus. Meta-analysis has been used in various fields, such as medicine, pedagogy, and psychology, and has gradually been applied to geography (van Zanten et al., 2014; Eötvös et al., 2018). Preferred Reporting Items for Systematic Reviews and Meta-Analyses (PRISMA) is an evidence-based minimum set of items for reporting in systematic reviews and meta-analyses (Moher et al., 2009). As a basic data source for China's brownfield spatial distributions, this study applies the PRISMA approach to collect brownfield case information from published literature and industrial heritage directories.

2.2 Data Collection

The literature review procedures are outlined in **Figure 1**. A literature search was performed following guidelines from PRISMA. Publications in both Chinese and English were collected by searching two major scientific citation indexing services, the China National Knowledge Infrastructure (CNKI) and Web of Science (WOS), respectively. Chinese brownfield-related literature is mainly published on CNKI. WOS is the most authoritative scientific and technological literature retrieval platform. The earliest Chinese literature on the theme of brownfields appeared in 2001 (Niu, 2001). Therefore, publication dates were limited to "2001.1.1–2019.12.31." We used the topics "brownfield" AND "China" with WOS. Since China has no official definition of brownfields, the following search terms were use in the CNKI: "brownfield," "industrial heritage AND transformation," "industrial heritage AND renovate," "industrial heritage AND regeneration," "abandoned land AND transformation," "abandoned land AND renovate," "abandoned land AND regeneration" in Chinese. We searched publications ranging from journal articles to conference proceedings or degree theses. We also searched the official list of China's industrial heritage sites and obtained 307 records.

A total of 1924 abstracts were retrieved for screening, 1,638 of which were from CNKI (in Chinese) and 286 from WOS (in English). 1) Abstracts that were not relevant to the brownfield transformation were excluded. This led to 1,217 Chinese and 32 English papers being selected for full-text review and further geo-information extraction. 2) Of the available full texts, publications that did not refer to China's brownfield cases, lacked brownfield data, or duplicate brownfield sites were deleted, leaving 455 Chinese and 16 English publications eligible for extraction. 3)

A total of 196 industrial heritage records were obtained by deleting records that did not meet brownfield requirements from 307 industrial heritage lists.

Location information was extracted from the records of the relevant primary papers. Following Zhang et al. (2019), the longitude and latitude of a location were determined using a combination of geospatial tools, including the Baidu Map, and Baidu Coordinate Picking System. We updated the place names to match the historical administrative names. We further classified all locations into four different levels according to their geographic scales and administrative levels (i.e., provincial, prefectural, county, and township and finer level). This helps potential users of this dataset extract appropriate sections for use. The locations of brownfields were then visualized using geographic information systems (GIS) software. In total, 608 Chinese, 18 English, and 196 industrial heritage records were identified.

After the data were entered, a second person thoroughly checked the dataset for validity, to avoid errors and duplication. A total of 816 records were identified, 605 of which were from CNKI, 17 from WOS, and 194 from China's industrial heritage list. Brownfield records include 23 provinces, 255 prefecture-level counties/cities, three autonomous regions, four municipalities directly under the central government, and two special administrative regions. The Xizang Autonomous Region and Ningxia Hui Autonomous Region did not have any brownfield sites.

In the dataset of distribution of brownfields in China, each row represents a single record. The columns in the dataset are as follows:

1) Brownfield location: the geographic scale of location (provincial, prefectural, county, township, or finer level)
2) Latitude and longitude coordinates: latitudinal and longitudinal coordinates (WGS1984 Datum)
3) Brownfield type: identifying brownfield types using brownfield definitions and "Code for Classification of Urban Land Use and Planning Standards of Development Land GB50137-2011"
4) Original use of brownfield information: CNKI, WOS, and list of China's industrial heritage
5) Brownfield formation factors: based on the literature

2.3 Spatial Distribution Analysis Method

2.3.1 Kernel Density Estimation

Kernel density estimation (KDE) is a non-parametric method used to estimate the probability density function of a random variable. When applied to geospatial analysis, the distribution of spatial variables is fitted as a smooth cone-shaped surface using the kernel function to illustrate its spatial distribution characteristics (Li W et al., 2019). We adopted the method to visually analyze brownfield spatial distributions in China. The formula is as follows:

$$f(x) = \frac{1}{nh^d}\sum_{i=1}^{n} K\left(\frac{x - X_i}{h}\right), \quad (1)$$

where $f(x)$ is the density value of the estimated point, h is the bandwidth, which indicates the spatial distance in the text. n is the number of known points in the bandwidth, and the number of brownfields within a given spatial distance in the text. d is the dimension of the data, in the text $d = 2$. $K(x)$ is the kernel function, and the quartic kernel function is used in ArcGIS software; it is the distance from the estimated point to the point i in the bandwidth range. $x - X_i$ is the distance from the estimated point to point i in the bandwidth range. $K(\frac{x-X_i}{h})$ represents the density value of the estimated point under the influence of point i.

2.3.2 Nearest Neighbor Indicator

Proposed by Clark and Evans (1954), the nearest neighbor indicator (*NNI*) is an index that indicates the proximity of the spatial distribution of point-like geographic elements. It can also determine the type of spatial distribution of point-like elements. The *NNI* calculation formula is as follows:

$$NNI = d(NN)/d(ran), \quad (2)$$

where $d\ (NN)$ is the nearest neighbor distance, $d\ (ran)$ is the expected average nearest neighbor distance, and its value can generally be expressed as

$$d(ran) = 0.5\sqrt{A/N}, \quad (3)$$

where N is the number of samples and A is the area of the study region. When *NNI* is less than 1, the sample points are distributed in an agglomeration. When *NNI* is greater than 1, the sample points are uniformly distributed, and when *NNI* is equal to 1, the sample points are randomly distributed. The Z test is generally used to test the reliability of the results.

3 RESULTS

3.1 Spatial Distribution Characteristics of Brownfields

Based on the results, brownfields are mainly concentrated in economically developed areas and near central urban areas. As shown in **Figure 2A**, the overall brownfield spatial distribution in China was basically consistent with the "Heihe-Tengchong Line" as the boundary, exhibiting a spatial pattern of "East-dense-West-sparse." There were 791 brownfield sites in the Southeast region of the "Heihe-Tengchong Line," accounting for 96.94% of the total, and 25 in the northwest region, accounting for 3.06% of the total. The "Heihe-Tengchong Line" is an important geographical boundary that reflects China's urbanization and economic development levels (Qi et al., 2015; Li et al., 2017). As shown in **Figure 2B**, the economically developed provinces of Jiangsu, Shandong, Guangdong, and Zhejiang have the largest number of brownfields, followed by resource-dependent regions such as Liaoning, Henan, Hebei, Hubei, and Hunan. The southern provinces have more brownfields than the North, followed by the northeastern provinces, with the lowest number in the Midwest. Brownfields have emerged as a result of the ongoing interaction between industrialization and urbanization, and their

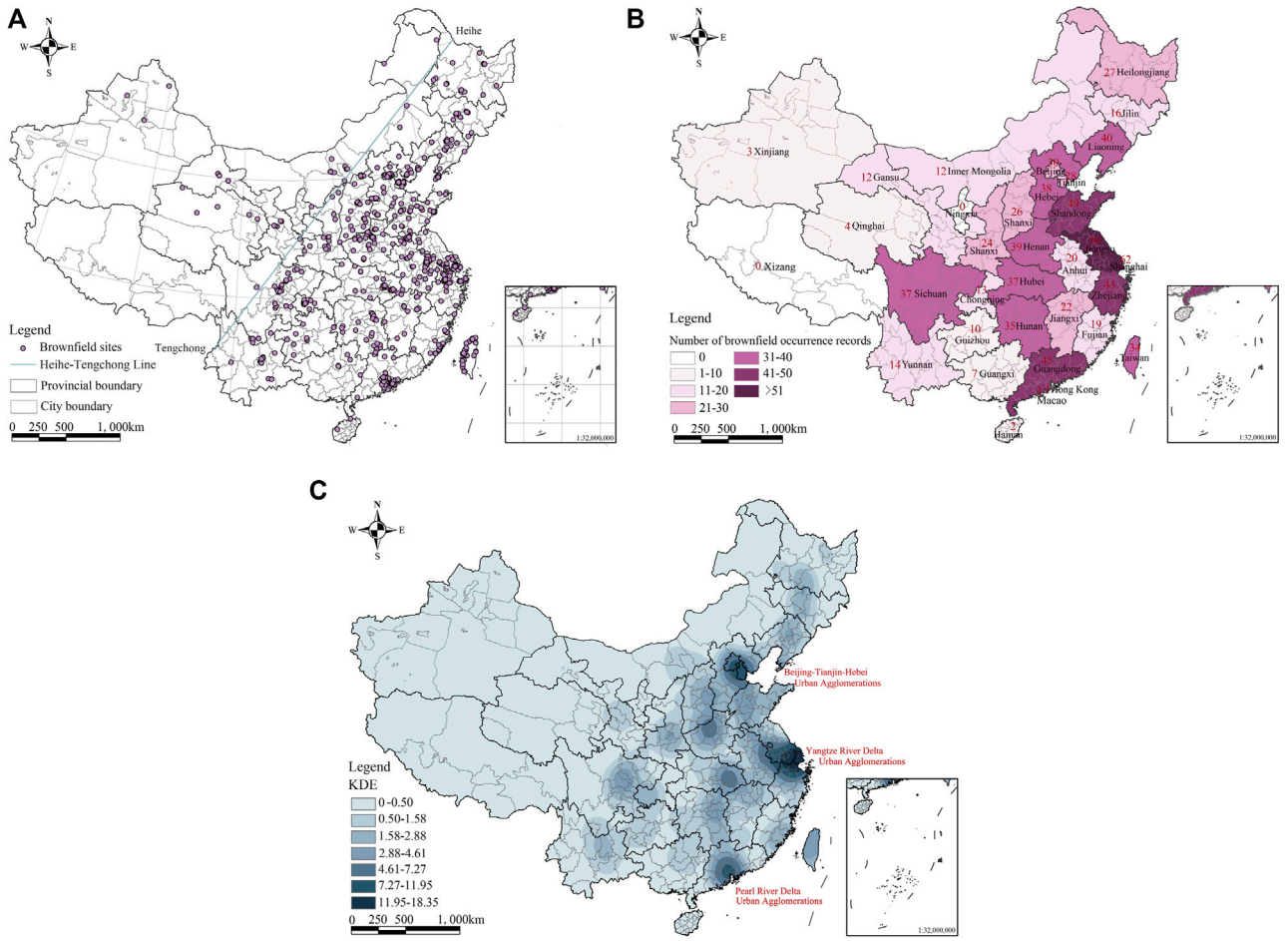

FIGURE 2 | Spatial distribution of brownfield occurrence records in China. **(A)** Locations of brownfield occurrence records in China. **(B)** Number of brownfield occurrence records by province-level divisions of China. **(C)** Kernel density estimation of brownfield occurrence records in China.

TABLE 1 | *NNI* of large-scale brownfield sites in China.

Type	Number of sites	Average nearest neighbor distance(m)	Expected average nearest neighbor distance(m)	Nearest neighbor indicator (*NNI*)	*Z* score	*p* value
Brownfields	816	21,498.14	53,965.20	0.40	−32.90	0
Industrial brownfields	459	18,155.44	71,953.61	0.25	−30.64	0
Transportation facilities brownfields	57	71,210.40	204,183.89	0.35	−9.41	0
Logistics and warehouse brownfields	33	120,213.15	268,350.21	0.45	−6.07	0
Public facilities brownfields	46	114,512.57	227,289.82	0.50	-6.44	0
Military brownfields	39	154,456.10	246,846.29	0.63	−4.47	0
Mining brownfields	182	75,094.27	114,267.63	0.66	−8.85	0

distribution is closely related to China's urbanization and economic development. We used the *NNI* module in ArcGIS to analyze the average nearest neighbor distance of each brownfield site. According to **Table 1**, the *NNI* for the overall spatial distribution of the 816 brownfield sites identified in the study was 0.4, and the *Z* score was −32.90, which passed the 1% significance level test, indicating that the spatial agglomeration characteristics of brownfields in China are highly significant. As shown in **Figure 2C**, the *KDE* method was used to analyze the spatial distribution. According to the natural break method, the kernel density values were divided into seven levels, from high to low. Regions with the highest kernel density values "7.27–18.35" were determined to be high-density areas, values from "1.58–7.27" represented medium-density areas, and those from

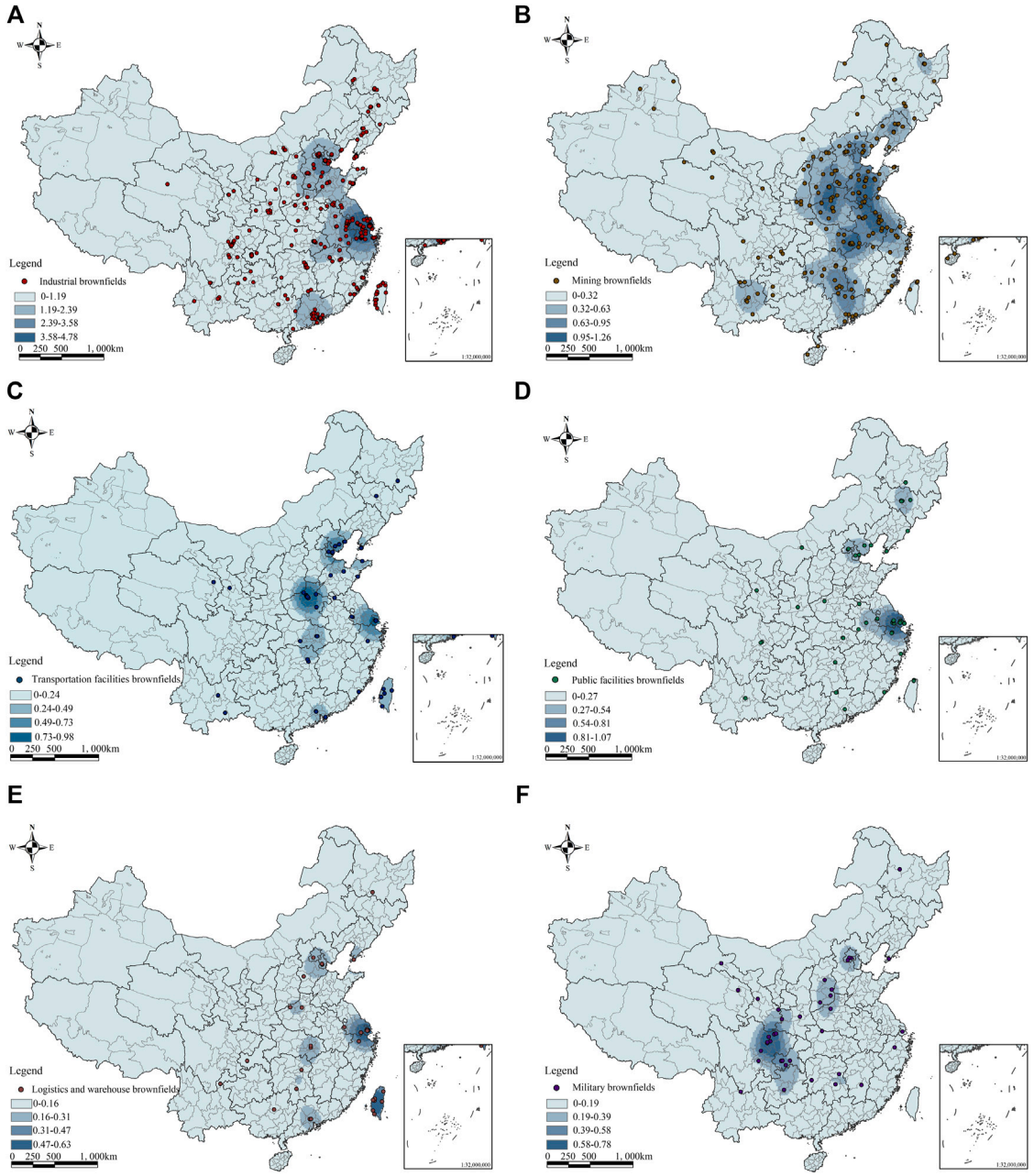

FIGURE 3 | Kernel density estimation of six brownfield types in China. **(A)** Industrial brownfields. **(B)** Mining brownfields. **(C)** Transportation facilities brownfields. **(D)** Public facilities brownfields. **(E)** Logistics and warehouse brownfields. **(F)** Military brownfields.

"0–1.58" represented low-density areas. China's brownfields were characterized by multi-center agglomerations, and high-density areas were found in the Yangtze River Delta, Beijing–Tianjin–Hebei, Pearl River Delta, and Central Plains urban agglomerations, as well as the urban agglomeration in the middle reaches of the Changjiang River with a strong industrial foundation and developed economy. Shanghai, Tianjin, Beijing, Guangzhou, Nanjing, and Wuhan had brownfield density clusters.

3.2 Spatial Distribution Characteristics of Different Brownfield Types

According to China's Code for Classification of Urban Land Use and Planning Standards of Development Land GB50137-2011, brownfield land use functions are classified as industrial, mining, military, commercial activities, storage, public facilities, and transportation facilities land. The brownfield information dataset divided brownfields into six types: industrial, mining, transportation facilities, public facilities, military, and logistics

and warehouse (Alker et al., 2000; Franz et al., 2006). Industrial brownfields accounted for the highest number, followed by mining brownfields. Transportation facilities, public facilities, military, and logistics and warehouse brownfields were less common.

NNI was used to test the agglomeration characteristics of the six types of brownfield spatial distribution (**Table 1**). The *NNI* of the six types of brownfields was less than 1 in all cases, which passed the 1% significance test and formed a part of a significant agglomeration model. The degree of agglomeration is in the following order: industrial brownfields > transportation facilities brownfields > logistics and warehouse brownfields > public facilities brownfields > military brownfields > mining brownfields.

Although the *NNI* reflects the overall distribution of brownfields in China, it cannot intuitively reflect the degree of agglomeration. Considering this, *KDE* was used to further measure six types of brownfield spatial agglomeration characteristics. As shown in **Figure 3A**, industrial brownfields were mainly concentrated in city clusters with strong industrial foundations, such as the Yangtze River Delta, Pearl River Delta, and Beijing-Tianjin-Hebei urban agglomerations, as well as other industrially developed provinces like Taiwan, Jiangsu, Guangdong, and Zhejiang. Industrial brownfields are widely distributed, regionally concentrated, and are characterized by a large abandoned area. Because deindustrialization and urbanization were higher than in other regions, they were found to be concentrated in the Eastern region. As shown in **Figure 3B**, high-density concentration areas of mining brownfields appeared in the Central Plains urban agglomerations, the Shandong Peninsula's urban agglomerations, the urban agglomeration in the middle reaches of the Changjiang River, and the Southern industrial zone. Cities with a large number of mining brownfields included Datong, Jiaozuo, Huangshi, Tongchuan, Xuzhou, Fushun, and other resource-based cities. As shown in **Figure 3C**, transportation facilities brownfields were concentrated in coastal cities along the Yellow River, Yangtze River, Bohai Bay, and transportation hub cities, such as Zhengzhou, Shanghai, Wuhan, and Tianjin. They mainly include the Shanghai Railway Station, Shanghai-Nanjing Railway, Shanghai Whampoa Dock, Lanzhou-Lianyungang Railway extension, and the Beijing-Guangzhou Railway. As shown in **Figure 3D** and **Figure 3E**, public facilities and logistics and warehouse brownfields belong to basic service land with a low degree of abandonment, so the quantity is relatively small. Jiangsu and Shanghai have more public facilities brownfields, and Taiwan and Shanghai have more logistics and warehouse brownfields. As shown in **Figure 3F**, military brownfields accounted for a small proportion and had a scattered distribution in Sichuan, Chongqing, Shanxi, Gansu, and other remote mountainous areas that are far from cities.

Industrial brownfields are more concentrated in industrially developed cities, mining brownfields are concentrated in areas with rich mineral resources, transportation facilities brownfields are concentrated in cities along the river and coastal and transportation hubs, public facilities brownfields and logistics and warehouse brownfields have no obvious agglomeration rule, and military brownfields are concentrated far from central cities.

TABLE 2 | Frequency of formation factors of brownfield occurrence records in China.

Causal factors of brownfields	Number	Frequency (%)
Industrial structure adjustment	158	62.70
Resource depletion	50	19.84
Acceleration urbanization	33	13.10
National policy orientation	11	4.37

3.3 Formation Factors of Brownfields in China

Among the 471 basic documents searched, 252 records from 219 articles summarized the formation factors of brownfields. The frequency counting method was used to count the formation factors mentioned in the articles' records. The factors can be classified into four categories: industrial structure adjustment, resource depletion, accelerated urbanization, and national policy orientation. Among the four types, industrial structure adjustment exhibits the highest frequency, followed by resource depletion, accelerated urbanization, and national policy orientation (see **Table 2**). Therefore, these four factors collaborate to produce brownfields, and their effects can be summarized as follows: industrial structure adjustment > resource depletion > urbanization process accelerated > national policy guidance.

To further demonstrate the correlation between brownfield spatial distributions and the factors that influence their formation, the distribution results were compared with the proportion of tertiary industries in China's provinces (Long et al., 2012), 262 resource-dependent cities (GOSCPRC. General Office of the State Council of the People's Republic of China, 2013; Feng et al., 2019), the level of urbanization in each province (Song et al., 2019), and the "Third-Front Movement" regions (Liu et al., 2014; Li H. C et al., 2019). **Figure 4A** compares brownfield locations with the proportion of tertiary industries in each province in 2018. Jiangsu, Guangdong, Zhejiang, Shandong, and Taiwan with a high proportion of tertiary industry also have a large number of brownfields. **Figure 4B** compares the brownfield locations of 262 resource-dependent cities. Mining brownfields were mostly located in resource-dependent cities, such as Huangshi, Tangshan, Jiaozuo, Fushun, Xuzhou, and Datong. **Figure 4C** compares those with provincial urbanization levels in 2018. Provinces with higher urbanization levels also had more brownfields. **Figure 4D** compares brownfield locations with the "Third-Front Movement" regions. Most military brownfields were concentrated in provinces with the "Third-Front Movement."

The production of brownfields in China is the result of a combination of many factors. A further comparison of formation factors and types revealed that the adjustment of the industrial structure and the acceleration of urbanization are common

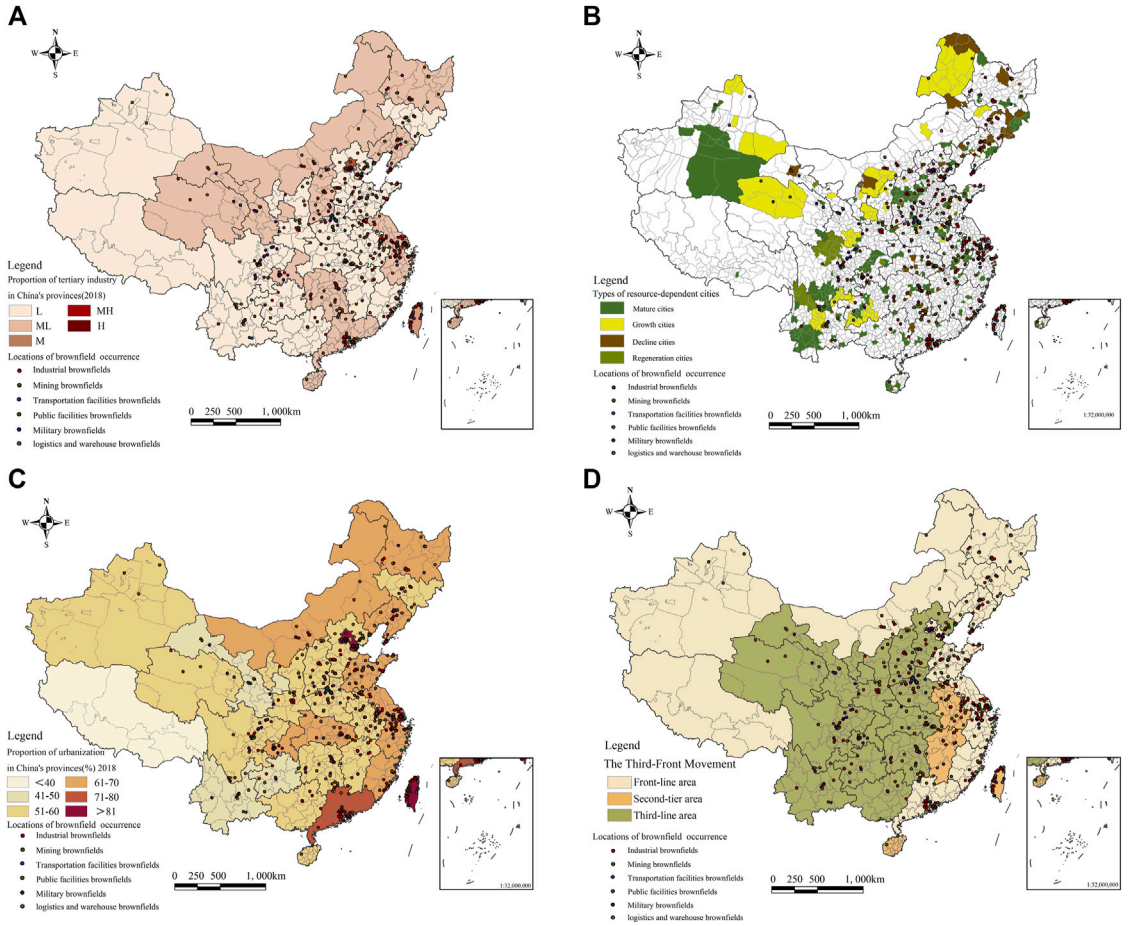

FIGURE 4 | Brownfield records in different zones. **(A)** Geo-locations of brownfield records on the industrial structure map of China. **(B)** Geo-locations of brownfield records on the resource-dependent cities map of China. **(C)** Geo-locations of brownfield records on the degree of urbanization map of China. **(D)** Geo-locations of brownfield records on the Third-Front Movement map of China.

factors, namely, those of industrial and mining, public facilities, transportation facilities, and logistics and storage land. The depletion of resources has tended to aggravate the formation of mining brownfields, while the "Third-Front Movement" policy has mainly promoted the formation of military brownfields.

The adjustment of China's industrial structure has constituted the dominant force in its economic growth over the past 40 years of reform and opening-up. With the acceleration of industrialization and the promotion of the policy of suppressing secondary industry and developing the tertiary sector, the latter occupies a dominant position in the industrial structure. The original urban land structure and industrial patterns are becoming increasingly less adaptable to the needs of China's economic development (Lai et al., 2020). To adapt to this change, enterprises have closed down or relocated, and leftover industrial and mining industries, logistics and storage industries, and transportation facilities have been abandoned, forming brownfields.

With the acceleration of urbanization and the expansion of urban areas, industrial, mining, public facilities, transportation facilities, and logistics and warehouse enterprises that originally belonged to the suburbs have become part of the city, forcing original industrial enterprises to relocate. This led to the formation of brownfields in China.

Resource depletion factors are key drivers behind the formation of mining brownfields. Due to the exhaustion of resources, the single industrial structure, and serious environmental pollution, the resource industry has shrunk, and industrial efficiency has declined. Resource-dependent industries face transformations and closures, resulting in more mining brownfields.

The "Third-Front Movement" was a major strategic decision made by President Mao Zedong in the mid-1960s. It was intended to strengthen wartime preparations under an increasingly tense international situation as a strategic shift from East to West to gradually change the distribution of China's productive forces. The emphasis was on construction in the Southwest and Northwest of the country (Naughton, 1988). Because most of the "Third-Front Movement" projects were "backed by the mountain, scattered, hidden," with the economic recession,

they had no advantageous location and difficulty in terms of access led to bankruptcy or relocation, forming military brownfields.

4 DISCUSSION

4.1 Current Research Results

The results of this study revealed that there were more brownfields in the South than North, Northeast, and Midwest. Possible reasons for this are as follows. First, the highest percentage of brownfields in southern provinces was related to the high level of local economic development. There was a greater degree of openness and rapid economic development in the South, coupled with high urbanization, dense population, urban land expansion, and high demand for land, which caused more attention to be paid to abandoned brownfield sites. Second, despite the gap in economic development between the South and North, the transformation of industrial structure and resource-dependent cities also produced a large number of brownfields, especially old industrial and resource-dependent cities in the North (Xie et al., 2022). Third, as the earliest developed old industrial base in the country, the Northeast should have more brownfields, but there were only 83 records in this region. This may be because the regional economy's relatively slow growth, transformation of its industrial structure, and large stock land resulted in a low demand for abandoned brownfield redevelopment. In addition, local scholars have done relatively little research on brownfields and the limited published documents may have led to a slight discrepancy between the recorded results and the actual situation in the Northeast. Fourth, there were fewer brownfield records in the Midwest provinces, mainly due to the small local population, relatively weak industrial foundation, and insufficient attention to brownfield research.

4.2 Comparison With Other Related Research Results

Compared to previous studies, brownfields in China are mainly concentrated in economically developed areas, near central urban areas, and along transportation routes such as railway hubs. This result is consistent with those of Lange and McNeil (2004), Longo and Campbell (2017), and Frantál et al. (2015), who analyzed the spatial distribution pattern of brownfields in the United States, the United Kingdom, and the Czech Republic, respectively. The brownfield spatial distributions of China were consistent with the results of the Survey Bulletin on Soil Pollution in China released by the State Council in 2014. The report highlighted that soil pollution is more serious in the South than in the North, and soil pollution problems in some regions, such as the Yangtze River Delta and the Pearl River Delta, are more prominent (MEP and MLR, 2014). The spatial distribution of soil pollution is consistent with the results of the current study. Aoki et al. (2018) established a database of known Chinese industrial heritage, and found that its distribution decreased from the Southeast coast to the West, mainly concentrated in the Yangtze River Delta Urban Agglomeration, Beijing-Tianjin-Hebei Urban Agglomeration, and Pearl River Delta Urban Agglomeration. In China, most industrial brownfields are rated industrial heritage due to their own value. The agglomeration results of industrial heritage were consistent with the concentrated industrial brownfield distribution pattern in this study. This study is not only consistent with the spatial distribution of soil pollution and industrial heritage; it is the first to describe the spatial distributions of brownfields in China. The methods and results lend credibility and practical significance to data and spatial distributions of brownfields in China and offer an effective empirical meta-analysis for brownfield studies.

4.3 Suggestions for the Government

China's urban development is gradually entering the adjustment and transformation period from the stage of rapid expansion, and traditional urban development based on incremental planning is gradually shifting toward inventory planning. Urban land optimization and improvement are important issues. This study proposes the following policy recommendations:

First, a database for China's brownfields should be established to enhance the openness and transparency of brownfield information. The availability of data is a major issue in China. It is necessary to construct a comprehensive database that includes the size, complexity, original use, ownership relations, and planned/allowed use of a site. To assist various levels of government, developers, research scholars, the public, and other groups of people in obtaining brownfield information, the government should establish a dedicated website for open brownfield databases.

Second, at the macro-level, it is necessary to formulate a targeted regional brownfield development direction strategy based on regional characteristics and brownfield types. The Eastern coastal areas, especially the Yangtze River Delta, Pearl River Delta, and Beijing-Tianjin-Hebei urban agglomerations, have more industrial brownfields, and there have been more successful transformation cases. In the future, the government should increase policies and preferential measures for brownfield redevelopment in these areas, and more attention should be paid to brownfield transformation models and later project supervision. Northern areas, especially Liaoning, Shanxi, Shandong, Henan, and other resource-dependent provinces, have more mining brownfields and are relatively far from urban areas. Brownfield reconstruction projects should be based on ecological restoration and prioritize the development of an ecological park model. A considerable amount of brownfield land remains in transition as an old industrial base in Northeast China. In the revitalization of the Northeast, emphasis should be placed on identifying and investigating existing industrial wastelands, encouraging investment in brownfield redevelopment, and academic research. There were relatively few brownfields in the Midwest. Attention should therefore be paid to their identification and restoration in this area. The Midwest is both densely and sparsely populated, and there is less demand for brownfield redevelopment. Restored brownfields can be used as reserve lands and will play a role in the new pattern of western development in the future. As different types of

brownfields vary in terms of their location, area, nature, pollution degree, heritage value, and redevelopment mode, the government should formulate guidelines for the redevelopment of different types of brownfields to guide practice.

Third, local governments should coordinate and prioritize brownfield redevelopment. The Chinese government controls the primary market for land and should be the first promoter of brownfield reuse. Brownfield locations, pollution degree, and stock land should be combined to evaluate the reuse potential and availability of brownfields, redevelopment priorities, and transformation directions, and identify brownfield resources to return them to the market.

5 CONCLUSION

The spatial distributions and formation factors of brownfields can reveal the characteristics of the times behind China's industrial development and the micro reconstruction process of industrial spaces within cities. It also helps coordinate land use conversion and guide redevelopment at the national level. We established a dataset of published brownfield records in China using a meta-analysis, which offered interesting conclusions despite their limited scope. Our results indicated that brownfield spatial distribution in China was basically consistent with the "Heihe-Tengchong Line" as the boundary, exhibiting a spatial pattern of "East-dense-West-sparse." Industrial structure adjustments were the main and direct causes of brownfield production, while resource depletion and accelerated urbanization were secondary and indirect factors. National policy orientation played a background role. This can supplement research on brownfield redevelopment and land renovation, as well as provide a reference for decision-making related to urban vitality enhancements. This is in line with important demands for urban renewal and sustainable development.

As China's central government attaches greater importance to brownfields, nationwide surveys of polluted land are gradually increasing. The state should increase investment in basic surveys, scientific research, funding, and development policies. Furthermore, brownfield sites should be identified using land contamination data, and land vacancy metrics and methods. In addition, the use of web crawler tools to supplement brownfield data retrieval from the internet, as well as an in-depth analysis of spatio-temporal dynamic features and landscape methods (Yang et al., 2016; Yang et al., 2019), will be the focus of further research. Although this study was conducted in the unique context of China, it is hoped that our research will also benefit other countries. For instance, in countries that have not established a brownfield database, existing brownfield-related data can be used to analyze spatial distributions to assist in the redevelopment of their brownfields.

DATA AVAILABILITY STATEMENT

The raw data supporting the conclusions of this article will be made available by the authors, without undue reservation.

AUTHOR CONTRIBUTIONS

Conceptualization, methodology, formal analysis, and writing—original draft preparation: XZ; software: XZ and SQ; validation: SQ and YS; investigation and visualization: SQ and DW; resources: SW and DW; data curation: SQ; writing—review and editing, and supervision: YS; and project administration and funding acquisition: YS and SW. All authors have read and agreed to the published version of the manuscript.

FUNDING

This research was funded by the National Social Science Fund of China (No. 17BJL051); the National Natural Science Foundation of China (No. 42171198); the Starting Research Fund of Yanshan University (No. 8190452); and the Innovation Development Strategy Research Project of Science and Technology Development Plan of Jilin Province.

ACKNOWLEDGMENTS

The authors sincerely thank the reviewers for their valuable comments and suggestions to improve the quality of this paper.

REFERENCES

Alker, S., Joy, V., Roberts, P., and Smith, N. (2000). The Definition of Brownfield. *J. Environ. Plan. Manag.* 43 (1), 49–69. doi:10.1080/09640560010766

Amekudzi, A., McNeil, S., and Koutsopoulos, H. N. (2003). Assessing Extrajurisdictional and Areawide Impacts of Clustered Brownfield Developments. *J. Urban Plann. Dev.* 129, 27–44. doi:10.1061/(asce)0733-9488(2003)129:1(27)

Aoki, N., Zhang, J. H., and Xu, S. (2018). Study on Construction and Application of Chinese Know Industrial Heritage Database. *Archit.* 4, 76–81. [in Chinese].

Bambra, C., Robertson, S., Kasim, A., Smith, J., Cairns-Nagi, J. M., Copeland, A., et al. (2014). Healthy Land? an Examination of the Area-Level Association between Brownfield Land and Morbidity and Mortality in England. *Environ. Plan. A* 46, 433–454. doi:10.1068/a46105

Bardos, P., Spencer, K. L., Ward, R. D., Maco, B. H., and Cundy, A. B. (2020). Integrated and Sustainable Management of Post-industrial Coasts. *Front. Environ. Sci.* 8, 1-14. doi:10.3389/fenvs.2020.00086

Boente, C., Albuquerque, M. T. D., Fernández-Braña, A., Gerassis, S., Sierra, C., and Gallego, J. R. (2018). Combining Raw and Compositional Data to Determine the Spatial Patterns of Potentially Toxic Elements in Soils. *Sci. Total Environ.* 631-632, 1117–1126. doi:10.1016/j.scitotenv.2018.03.048

Chaikumbung, M., Doucouliagos, H., and Scarborough, H. (2016). The Economic Value of Wetlands in Developing Countries: A Meta-Regression Analysis. *Ecol. Econ.* 124, 164–174. doi:10.1016/j.ecolecon.2016.01.022

Chen, W. Y., Li, X., and Hua, J. (2019). Environmental Amenities of Urban Rivers and Residential Property Values: A Global Meta-Analysis. *Sci. Total Environ.* 693, 133628. doi:10.1016/j.scitotenv.2019.133628

Chrysochoou, M., Brown, K., Dahal, G., Granda-Carvajal, C., Segerson, K., Garrick, N., et al. (2012). A GIS and Indexing Scheme to Screen Brownfields for Area-

wide Redevelopment Planning. *Landsc. Urban Plan.* 105, 187–198. doi:10.1016/j.landurbplan.2011.12.010

Clark, P. J., and Evans, F. C. (1954). Distance to Nearest Neighbor as a Measure of Spatial Relationships in Populations. *Ecology* 35, 445–453. doi:10.2307/1931034

Coffin, S. L. (2003). Closing the Brownfield Information Gap: Some Practical Methods for Identifying Brownfields. *Environ. Pract.* 5, 34–39. doi:10.1017/s1466046603030126

CzechInvest (2021). Investment and Business Development Agency. Available at: (Accessed 20 April, 2021).

Eötvös, C. B., Magura, T., and Lövei, G. L. (2018). A Meta-Analysis Indicates Reduced Predation Pressure with Increasing Urbanization. *Landsc. Urban Plan.* 180, 54–59. doi:10.1016/j.landurbplan.2018.08.010

Feng, S., Hou, W., and Chang, J. (2019). Changing Coal Mining Brownfields into Green Infrastructure Based on Ecological Potential Assessment in Xuzhou, Eastern China. *Sustainability* 11, 2252. doi:10.3390/su11082252

Filip, S., and Cocean, P. (2012). Urban Industrial Brownfields: Constraints and Opportunities in Romania. *Carpath. J. Earth. Env.* 7, 155–164.

Frantál, B., Greer-Wootten, B., Klusáček, P., Krejčí, T., Kunc, J., and Martinát, S. (2015). Exploring Spatial Patterns of Urban Brownfields Regeneration: The Case of Brno, Czech Republic. *Cities* 44, 9–18. doi:10.1016/j.cities.2014.12.007

Franz, M., Pahlen, G., Nathanail, P., Okuniek, N., and Koj, A. (2006). Sustainable Development and Brownfield Regeneration.what Defines the Quality of Derelict Land Recycling? *Environ. Sci.* 3, 135–151. doi:10.1080/15693430600800873

Glass, G. V. (1976). Primary, Secondary, and Meta-Analysis of Research. *Educ. Res.* 5, 3–8. doi:10.3102/0013189x005010003

GOSCPRC. General Office of the State Council of the People's Republic of China (2013-2020). The Sustainable Development Plan of Resource-dependent Cities Nationwide. Available at: http://www.gov.cn/zwgk/2013-12/03/content_2540070.htm (Accessed 13 March, 2021).

Hayek, M., Novak, M., Arku, G., and Gilliland, J. (2010). Mapping Industrial Legacies: Building a Comprehensive Brownfield Database in Geographic Information Systems. *Plan. Pract. Res.* 25, 461–475. doi:10.1080/02697459.2010.511018

Hipel, K. W., Hegazy, T., and Yousefi, S. (2010). Combined Strategic and Tactical Negotiation Methodology for Resolving Complex Brownfield Conflicts. *Pesqui. Oper.* 30, 281–304. doi:10.1590/S0101-74382010000200003

Howard, J. L., and Olszewska, D. (2011). Pedogenesis, Geochemical Forms of Heavy Metals, and Artifact Weathering in an Urban Soil Chronosequence, Detroit, Michigan. *Environ. Pollut.* 159, 754–761. doi:10.1016/j.envpol.2010.11.028

Kramářová, Z., and Juhásová Šenitková, I. (2018). Comparison of Informations from the Brownfield Catalog and the Data Needed to Evaluate Real Estate. EDP Sciences. *MATEC Web of Confer.* 146, 03016. doi:10.1051/matecconf/201814603016

Kunc, J., Martinát, S., Tonev, P., and Bohumil, F. (2014). Destiny of Urban Brownfields: Spatial Patterns Andperceived Consequences of Post-socialistic Deindustrialization. *Transylv. Rev. Adm. Sci.* 10, 109–128.

Lai, Y., Chen, K., Zhang, J., and Liu, F. (2020). Transformation of Industrial Land in Urban Renewal in Shenzhen, China. *Land* 9, 371. doi:10.3390/land9100371

Lange, D., and McNeil, S. (2004). Clean it and They Will Come? Defining Successful Brownfield Development. *J. Urban Plann. Dev.* 130, 101–108. doi:10.1061/(asce)0733-9488(2004)130:2(101)

Leigh, N. G., and Coffin, S. L. (2000). How Many Brownfields Are There? Building an Industrial Legacy Database. *J. Urban Technol.* 7, 1–18. doi:10.1080/10630730020021690

Li, H. C., Bai, W. L., Xiong, X., and Zhang, F. (2019). Exploration on "Ecological Restoration and Urban Renovation" in "Third-Front Movement" Industrial Cities—Take Jingmen of Hubei Province as an Example. *Chin. Landsc. Archit.* 35, 78–83. [in Chinese].

Li, J. M., Lu, D., Xu, C. D., Li, Y., and Chen, M. X. (2017). Spatial Heterogeneity and its Changes of Population on the Two Sides of Hu Line. *Acta Geogr. Sin.* 72, 148–160. [in Chinese]. doi:10.11821/dlxb201701012

Li, W., Wang, D., Li, H., Wang, J., Zhu, Y., and Yang, Y. (2019). Quantifying the Spatial Arrangement of Underutilized Land in a Rapidly Urbanized Rust Belt City: The Case of Changchun City-ScienceDirect. *Land Use Policy* 83, 113–123. doi:10.1016/j.landusepol.2019.01.032

Liu, C., Song, W., and Zhou, C. (2017). Unsuccessful Urban Governance of Brownfield Land Redevelopment: A Lesson from the Toxic Soil Event in Changzhou, China. *Sustainability* 9, 824. doi:10.3390/su9050824

Liu, Y., Van Oort, F., Geertman, S., and Lin, Y. (2014). Institutional Determinants of Brownfield Formation in Chinese Cities and Urban Villages. *Habitat Int.* 44, 72–78. doi:10.1016/j.habitatint.2014.05.005

Long, H., Li, Y., Liu, Y., Woods, M., and Zou, J. (2012). Accelerated Restructuring in Rural China Fueled by 'increasing vs. Decreasing Balance' Land-Use Policy for Dealing with Hollowed Villages. *Land Use Policy* 29, 11–22. doi:10.1016/j.landusepol.2011.04.003

Longo, A., and Campbell, D. (2017). The Determinants of Brownfields Redevelopment in England. *Environ. Resour. Econ.* 67, 261–283. doi:10.1007/s10640-015-9985-y

Loures, L., and Vaz, E. (2018). Exploring Expert Perception towards Brownfield Redevelopment Benefits According to Their Typology. *Habitat Int.* 72, 66–76. doi:10.1016/j.habitatint.2016.11.003

Mahzouni, A. (2018). Urban Brownfield Redevelopment and Energy Transition Pathways: A Review of Planning Policies and Practices in Freiburg. *J. Clean. Prod.* 195, 1476–1486. doi:10.1016/j.jclepro.2017.11.116

Martinat, S., Dvorak, P., Frantál, B., Klusacek, P., Kunc, J., Navratil, J., et al. (2016). Sustainable Urban Development in a City Affected by Heavy Industry and Mining? Case Study of Brownfields in Karvina, Czech Republic. *J. Clean. Prod.* 118, 78–87. doi:10.1016/j.jclepro.2016.01.029

M. Brander, L., J. Wagtendonk, A., S. Hussain, S., McVittie, A., Verburg, P. H., de Groot, R. S., et al. (2012). Ecosystem Service Values for Mangroves in Southeast Asia: A Meta-Analysis and Value Transfer Application. *Ecosyst. Serv.* 1, 62–69. doi:10.1016/j.ecoser.2012.06.003

MEP and MLR (2014). China Ministry of Environmental Protection, Ministry of Land and Resources.Survey Bulletin on Soil Pollution in China. Available at: http://www.gov.cn/foot/2014-04/17/content_2661768.htm (Accessed 21 December, 2021).

Modica, M. (2019). Industrial Brownfield Sites in the Alps. A First Quantitative Overview and Potential Implications for Regional Development. *Rev. Geogr. Alp.* 107, 1-17. doi:10.4000/rga.5274

Moher, D., Liberati, A., Tetzlaff, J., and Altman, D. G. (2009). Preferred Reporting Items for Systematic Reviews and Meta-Analyses: the PRISMA Statement. *BMJ* 339, b2535. doi:10.1136/bmj.b2535

Naughton, B. (1988). The Third Front: Defence Industrialization in the Chinese Interior. *China Q.* 115, 351–386. doi:10.1017/S030574100002748X

Newell, G., and McGreal, S. (2017). The Significance of Development Sites in Global Real Estate Transactions. *Habitat Int.* 66, 117–124. doi:10.1016/j.habitatint.2017.06.006

Niu, H. (2001). The Renovation and Redevelopment of 'Brownfield'in USA. *Urban Plan. Int.* 30, 26–48. [in Chinese].

Novosák, J., Hájek, O., Nekolová, J., and Bednář, P. (2013). The Spatial Pattern of Brownfields and Characteristics of Redeveloped Sites in the Ostrava Metropolitan Area (Czech Republic). *Morav. Geogr. Rep.* 21, 36–45. doi:10.2478/mgr-2013-0009

Osman, R., Frantál, B., Klusáček, P., Kunc, J., and Martinát, S. (2015). Factors Affecting Brownfield Regeneration in Post-socialist Space: The Case of the Czech Republic. *Land Use Policy* 48, 309–316. doi:10.1016/j.landusepol.2015.06.003

Page, G. W., and Berger, R. S. (2006). Characteristics and Land Use of Contaminated Brownfield Properties in Voluntary Cleanup Agreement Programs. *Land Use Policy* 23, 551–559. doi:10.1016/j.landusepol.2005.08.003

Qi, W., Liu, S. H., and Zhao, M. F. (2015). Study on the Stability of Hu Line and Different Spatial Patterns of Population Growth on its Both Sides. *Acta Geogr. Sin.* 70, 551–566. [in Chinese]. doi:10.11821/dlxb201504004

Rall, E. L., and Haase, D. (2011). Creative Intervention in a Dynamic City: A Sustainability Assessment of an Interim Use Strategy for Brownfields in Leipzig, Germany. *Landsc. Urban Plan.* 100, 189–201. doi:10.1016/j.landurbplan.2010.12.004

Škrabal, J., Turečková, K., and Nevima, J. (2021). Analysis of Brownfields Sites in the Villages and Towns in the Czech Republic. *Tras* 64E, 151–169. doi:10.24193/tras.64E.8

Smoļakova, A. (2017). "Exploring Spatial Patterns of Urban Brownfields: the Case of Daugavpils City," in Environment Technology Resources Proceedings of the

11th International Scientific and Practical Conference, Tomsk, Russia, 21-27 March 2005 1, 265–270. doi:10.17770/etr2017vol1.2589

Song, Y., Lyu, Y., Qian, S., Zhang, X., Lin, H., and Wang, S. (2022). Identifying Urban Candidate Brownfield Sites Using Multi-Source Data: The Case of Changchun City, China. *Land Use Policy* 117, 106084. doi:10.1016/j.landusepol.2022.106084

Song, Y., Zhang, X. J., Lyu, Y., Wang, S. J., and Lin, H. Y. (2019). Review and Prospects on Urban Brownfield Research from a Geographical Perspective. *Sci. Geogr. Sin.* 39, 886–897. [in Chinese]. doi:10.13249/j.cnki.sgs.2019.06.003

Vaidya, S. (2015). GIS Analysis of Brownfield Sites in the City of Minneapolis. Master's Thesis. Mankato,USA: The Minnesota State University.

van Zanten, B. T., Verburg, P. H., Koetse, M. J., and van Beukering, P. J. H. (2014). Preferences for European Agrarian Landscapes: A Meta-Analysis of Case Studies. *Landsc. Urban Plan.* 132, 89–101. doi:10.1016/j.landurbplan.2014.08.012

Xie, D., Bai, C., and Xiao, W. (2022). Institutional Environment, Development Model Transformation and North-South Economic Disparity in China. *Growth Change*. doi:10.1111/grow.12629

Yang, J., Guo, A., Li, Y., Zhang, Y., and Li, X. (2019). Simulation of Landscape Spatial Layout Evolution in Rural-Urban Fringe Areas: a Case Study of Ganjingzi District. *GIScience Remote Sens.* 56, 388–405. doi:10.1080/15481603.2018.1533680

Yang, J., Su, J., Chen, F., Xie, P., and Ge, Q. (2016). A Local Land Use Competition Cellular Automata Model and its Application. *Ijgi* 5, 106. doi:10.3390/ijgi5070106

Zhang, G., Zheng, D., Tian, Y. Q., and Li, S. (2019). A Dataset of Distribution and Diversity of Ticks in China. *Sci. Data* 6, 105. doi:10.1038/s41597-019-0115-5

Zhang, X., Song, Y., Wang, S., and Qian, S. (2021). Exploring Research Trends and Building a Multidisciplinary Framework Related to Brownfield: A Visual Analysis Using CiteSpace. *Complexity* 1-14, 8882415. doi:10.1155/2021/8882415

Conflict of Interest: The authors declare that the research was conducted in the absence of any commercial or financial relationships that could be construed as a potential conflict of interest.

Publisher's Note: All claims expressed in this article are solely those of the authors and do not necessarily represent those of their affiliated organizations, or those of the publisher, the editors, and the reviewers. Any product that may be evaluated in this article, or claim that may be made by its manufacturer, is not guaranteed or endorsed by the publisher.

Copyright © 2022 Zhang, Song, Qian, Wang and Wu. This is an open-access article distributed under the terms of the Creative Commons Attribution License (CC BY). The use, distribution or reproduction in other forums is permitted, provided the original author(s) and the copyright owner(s) are credited and that the original publication in this journal is cited, in accordance with accepted academic practice. No use, distribution or reproduction is permitted which does not comply with these terms.

frontiers | Frontiers in Ecology and Evolution

ORIGINAL RESEARCH
published: 06 July 2022
doi: 10.3389/fevo.2022.897574

Energy Consumption Connection of Industrial Sector Based on Industrial Link Theory: A Case Study of China

Jinwen Xia[1], Xiaojun Liu[1], Dongqi Sun[2], Chenxi Li[3,4]* and Zhaofei Wang[5]*

[1] School of Management, Xi'an University of Architecture and Technology, Xi'an, China, [2] Key Laboratory of Regional Sustainable Development Modeling, Institute of Geographic Sciences and Natural Resources Research, Chinese Academy of Sciences (CAS), Beijing, China, [3] School of Public Administration, Xi'an University of Architecture and Technology, Xi'an, China, [4] State Key Laboratory of Green Building in Western China, Xi'an University of Architecture and Technology, Xi'an, China, [5] College of Civil Engineering, Xi'an University of Architecture and Technology, Xi'an, China

OPEN ACCESS

Edited by:
Xinli Ke,
Huazhong Agricultural University, China

Reviewed by:
Ying Zhu,
Xi'an University of Architecture and Technology, China
Bao-Jie He,
Chongqing University, China
Bing Xue,
Institute of Applied Ecology (CAS), China

***Correspondence:**
Dongqi Sun
sundq@igsnrr.ac.cn
Chenxi Li
xywglcx@163.com

Specialty section:
This article was submitted to Environmental Informatics and Remote Sensing, a section of the journal Frontiers in Ecology and Evolution

Received: *16 March 2022*
Accepted: *23 May 2022*
Published: *06 July 2022*

Citation:
Xia J, Liu X, Sun D, Li C and Wang Z (2022) Energy Consumption Connection of Industrial Sector Based on Industrial Link Theory: A Case Study of China. Front. Ecol. Evol. 10:897574. doi: 10.3389/fevo.2022.897574

China's energy consumption and its growth trend determine the domestic energy production and supply pattern. The understanding of energy consumption and its changes will help to enhance urban resilience. Based on the improved input-output model and hypothesis extraction model, this paper aims at constructing the energy-industry connection model, analyzing the energy transfer implied in the economic activities of various industrial sectors, and examining the energy transfer effect between the supply-side (SS) and demand-side industry sectors of the Shaanxi Province. The results showed that, in 2017, the energy industrial sector was the most energy consumption industry in Shaanxi Province. The industrial energy sector belonged to the net energy output industrial sector, and the energy products were transferred to other industrial sectors. This paper can provide a scientific basis for the energy SS reform, adjusting the industrial layout of regions in the Yellow River Basin.

Keywords: supply side, demand-side, energy linkage, hypothetical extraction method, China

INTRODUCTION

Since the industrial revolution, greenhouse gas emissions have directly caused climate change and affected our daily lives (He et al., 2014a; Li et al., 2019a; Rahman et al., 2020; Wang F. et al., 2021; Yang et al., 2021b; Bherwani et al., 2022). The 2016 Paris Climate Change Agreement advised countries to take action to reduce greenhouse gas emissions and enhance their response to climate change (Seidler et al., 2020; Iraganaboina and Eluru, 2021). Achieving global temperature rise control and sustainable development goals requires rapid and far-reaching reforms in urban areas including land, energy, industry and building (He et al., 2014b; Li et al., 2019b; As et al., 2020; Estrella Guillen et al., 2021; Häring et al., 2021). In 2020, the United Nations developed the 17 Sustainable Development Goals (SDGs), but significant human infectious diseases represented by COVID-19 made it more challenging to achieve the goals (Christoforidis and Katrakilidis, 2021; Kousar and Shabbir, 2021; Shaikh, 2021). Due to the differences in development

stages and development capabilities of countries and regions, the implementation progress of SDGs is not ideal (Gao et al., 2021). We need to speed up the SDG progress since the SDGs are not at the right pace (He et al., 2022). China's energy consumption and its growth trend did not only determine the changes in the domestic energy production and supply pattern but also had a profound impact on the global energy production and supply (Xiao et al., 2019; Chen et al., 2020; Li J. et al., 2021; Wang R. et al., 2021). In 2020, China has proposed a development strategy for CO_2 emissions striving to peak before 2030 and striving to achieve carbon neutrality before 2060 (Xu et al., 2021). In the face of a new crisis arising in current and future human activities and climate change, a correct understanding of energy consumption and its growth changes helps to enhance urban resilience (Mensah et al., 2021; Qayyum et al., 2021; Salem, 2021).

The energy consumption of Shaanxi Province in the Yellow River Basin is still mainly fossil energy, especially coal consumption accounts for more than 80% of the overall primary energy consumption in 2016 (Cao et al., 2016; Yu et al., 2020). The imbalance of energy consumption structure objectively leads to low energy utilization efficiency and environmental pollution in Shaanxi Province. Since 2000, the overall urbanization rate of Shaanxi Province has increased from 24.0 to 56.8% (2017), the population density from 173 to 188 per km^2, the total resident population reached 38,640 (2018), and the annual gross regional product (GDP) has increased from 180.4 billion RMB to 2,443.8 billion RMB (2018) (Han and Cao, 2021). As the "One Belt and One Road" strategic location and one of the first national low-carbon pilot provinces, an in-depth exploration of energy consumption in Shaanxi Province will be conducive to improving energy utilization efficiency and realizing the sustainable development of energy resources (Mohammed et al., 2021).

According to the specific division of labor within the national economy, industrial sectors are the general term for enterprises and institutions specializing in similar economic activities (Li and Wu, 2022). The current relevant studies have explored the interaction between energy consumption and economic variables among industrial sectors (Cao et al., 2016; Bherwani et al., 2022). However, research on the complete measurement of energy demand from the perspectives of demand and supply is still insufficient. Measuring energy demand from the viewpoint of demand and supply has become a vital issue in this field. Therefore, based on the improved input-output model and hypothesis extraction model, this paper aims at constructing the energy-industry connection model, analyzing the energy transfer implied in the economic activities of various industrial sectors, and examining the energy transfer effect between the supply side (SS) and demand-side (DS) industry sectors of Shaanxi Province.

The remainder of this paper is structured as follows: Section 2 introduces the literature review Section 3 introduces the research idea, research methods, and data sources. Section 4 takes Shaanxi Province as an example and analyzes characteristics of energy demand, implied net energy transfer among industries and energy linkages between industry sectors. Section 5 discusses the applicability of the method and proposes policy suggestions to improve energy efficiency in this article. Section 6 provides the conclusion of this paper and suggests policy recommendations.

LITERATURE REVIEW

Industrial Connection Effect Based on Hypothetical Extraction Model

Input-output table, which can systematically reflect the input-output relationship among various sectors of the national economy, can provide a basis for the study of industrial structure, especially for the determination and verification of national economic plans and the development of various quantitative analyses (Xu et al., 2021). As a part of the national economic accounting system, input-output accounting reflects the economic flow of various sectors of the national economy in the form of an input-output table (Li and Wu, 2022). The hypothetical extraction method (HEM), based on the input-output table, assumes separating an industrial sector from the economic system to compare the changes in the total economic output before and after and to analyze the impact of the industrial sector on the economic system as a whole (Iqbal et al., 2021). The earliest research used the improved HEM for departmental water correlation impact effect calculation to measure the water correlation characteristics among industrial sectors (Duarte et al., 2002; Dyarto and Setyawan, 2021). The existing research mainly adopts a HEM to incorporate water resources, energy, carbon emissions, land use, and other elements into the accounting of economic activities and clarifies the correlation effect of various resources or environmental factors in various industrial sectors (Chen and Chen, 2013; Deng and Zhang, 2016; Chuai et al., 2020; Yang et al., 2021a). For example, Deng et al. (2016) expanded the HEM to the multiregional input-output model, and they studied the correlation effect of Chinese added value trade with other countries and regions and the international correlation effect of implied carbon trade, respectively. Based on the improved hypothetical extraction model, Chen and Xu (2017) explored the direct energy demand and implied energy demand for other sectors from the perspective of the SS and DS, thus analyzing the correlation effect of suggested energy consumption among various industries.

Energy Consumption Based on the Input-Output Model

The relevant research on input-output methods for energy problems is developed mainly from two spatial and temporal dimensions (Hao et al., 2021). Research on spatial dimensions focuses on energy problems at different spatial scales, including direct energy and implied energy accounting at different spatial scales, including international level, national level, regional level, energy transfer quantity calculation, energy efficiency calculation, etc. (Isik et al., 2021; Koondhar et al., 2021; Zafar et al., 2021). As for energy consumption calculation of import and export commodities, there are generally three models, namely, single-regional input-output model, bilateral-regional input-output

model, and multiregional input-output model, among which the multiregional input-output model is widely used (Mfb et al., 2021) because it can meet the needs of multiregional calculation (Mfb et al., 2021). For example, Han and Wang (2019) used the multiregional input-output model to measure the added value trade scale and the net value of China and the United States from 1995 to 2009. It used the energy consumption and carbon emission data in the environmental account to calculate the overall level of implied energy. It implied carbon emissions and its industrial structure. Research on the time scale mainly uses the input-output tables of different years to clarify the changing in energy consumption trends. For example, Cao et al. (2016) based the direct energy consumption coefficient and complete energy consumption coefficient in Shaanxi Province in 2002 and input-output tables in 2002, 2007, and 2012. They studied the economic energy efficiency in different years.

As the research deepened, more scholars focused on the energy consumption problem in the industrial dimension (Khan et al., 2021; Wang F. et al., 2021). The final use of the industrial sector and the final energy consumption caused by the intermediate use of the industrial sector are increasingly gaining attention from scholars (Zakari et al., 2021). Wang and Gao (2020) measured the energy consumption of the industrial sector from the perspective of implied energy. They found that there were significant differences in the implied energy intensity between the industrial sector, and 73.85% of the intermediate indicated energy is consumed by production in other industrial sectors downstream of the industrial chain. Yang et al. (2021c) analyzed the water and energy footprints of Heilongjiang based on the value-based input and output table, adding departmental water consumption and energy usage. The study found that the water industrial sector is also a high-energy consumption industrial sector. The top nine industrial sectors of the water resources of the national economic industrial sector of Heilongjiang Province and the total output are the same.

When establishing a model, there are generally two ways, namely, the method based on a value-based input-output equation and the method based on a hybrid input-output model. The value-type energy input-output model is more widely used in the existing literature (Ocal and Aslan, 2013; Qazi and Abushammala, 2021). The value-oriented input-output model is mainly used to analyze the implied energy volume of international trade and inter-regional trade, the energy consumption between different industrial sectors, the impact of household consumption on energy use, etc. (Hatice, 2021). Hybrid input-output models are also mainly used for implied energy calculation in residential consumption, influencing factor analysis of green productivity, energy consumption intensity, or energy consumption (Hatice, 2021; Iheonu et al., 2021). Zhang (2018) started with the energy balance equation and analyzed the essential characteristics and differences of the two models by obtaining the applicable scenarios. The results show that the hybrid energy input-output model can still guarantee the energy balance equation under the new final demand impact. Although the value energy input-output model uses the energy balance equation, it cannot be guaranteed under the new final demand impact. The above studies have explored the interaction between energy consumption and economic variables. The research on the complete measurement of energy demand from the perspectives of demand and supply is still insufficient. Therefore, this paper focuses on constructing the energy-industry connection model, analyzing the energy transfer implied in the economic activities of various industrial sectors, and examining the energy transfer effect between the SS and DS industry sectors.

STUDY MATERIALS

Study Context

In recent years, the Yellow River Basin has achieved rapid economic development and significant economic strength, which play an essential role in supporting China's future economic development (Demirtas, 2021; Li C. et al., 2021; Luo et al., 2021). The Yellow River basin is an important ecological function area in China and an ecological barrier in North China. Therefore, the ecological protection of the Yellow River basin is of great significance to ecological security in China (Li et al., 2020; Wu et al., 2020; Yang et al., 2021d). Energy conservation and emission reduction are essential links in realizing high-quality development, which is influenced by the energy structure and industrial structure of various provinces. Provinces in the Yellow River basin face great pressure on emission reduction, and the economic development of all provinces brings great pressure to the ecological environment. For example, the Yellow River basin ecological barrier is damaged, and carbon emissions continue to rise (Chen et al., 2020; Zhang et al., 2021). It is of great significance to the ecological protection and high-quality development of the Yellow River Basin to have a scientific understanding of the energy consumption status and characteristics of the typical areas of the Yellow River Basin. Therefore, Shaanxi Province is selected as the distinct study area of the Yellow River Basin (**Figure 1**).

Methods

Taking each industrial sector of the economic system of Shaanxi Province as the research object, this paper separates the energy sector, relies on the multiyear input-output table, analyzes the energy transfer between the sectoral economic activities implied in the economic activities of each sector, and compares the correlation effect of energy utilization.

Hypothetical Extraction Method

First, accounting for the energy input matrix of various industrial sectors q_i, it is the direct energy utilization coefficient line vector:

$$q_i = E_i / x_i \tag{1}$$

where *Ei* refers to the total sector energy consumption; *xi* refers to the total output of the corresponding sector; *i* refers to the industry sector; *-i* refers to excluding the remaining industrial

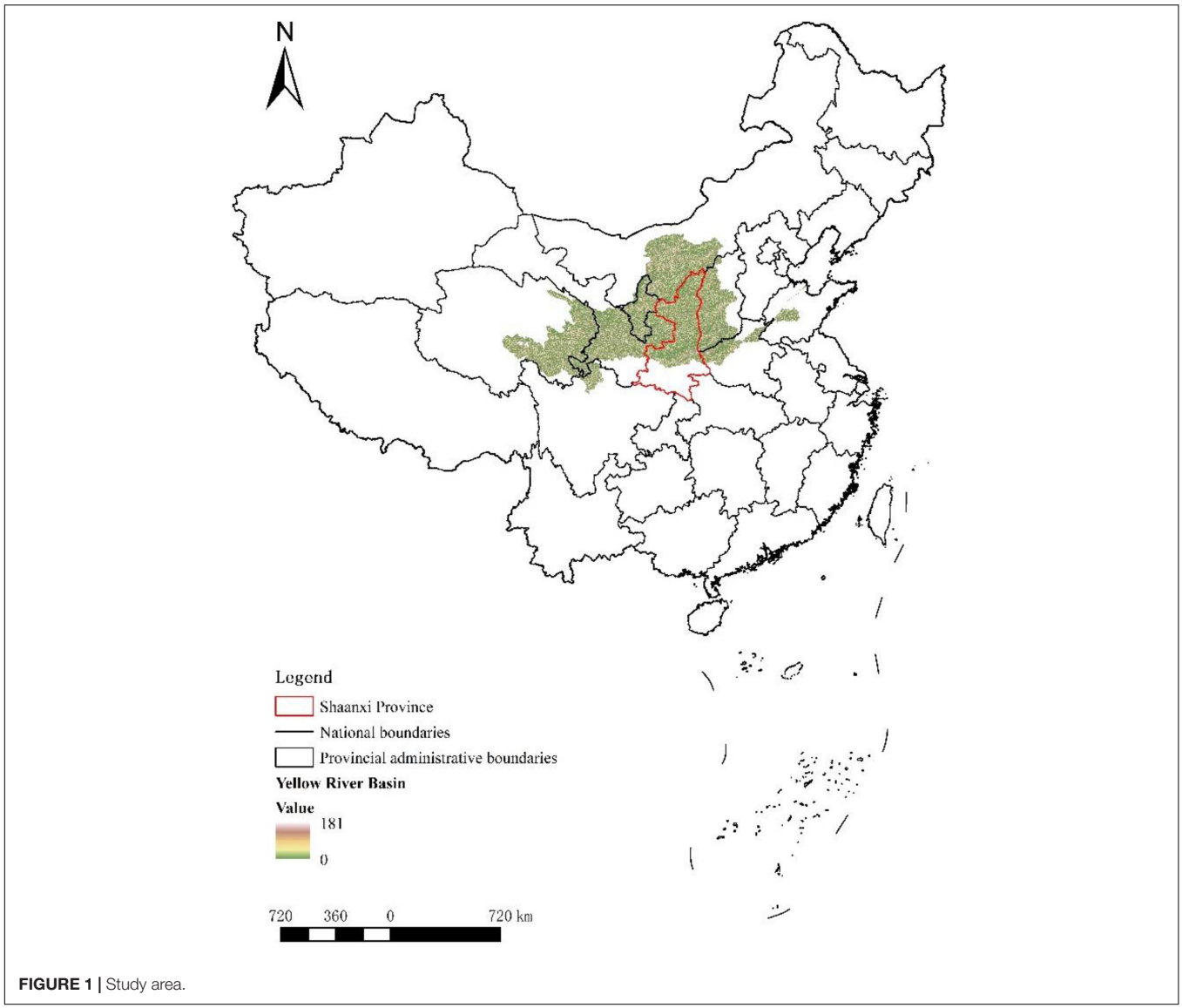

FIGURE 1 | Study area.

sector outside the *i*.

$$\begin{pmatrix} x_i \\ x_{-i} \end{pmatrix} = \begin{pmatrix} A_{i,i} & A_{i,-i} \\ A_{-i,i} & A_{-i,-i} \end{pmatrix} \begin{pmatrix} x_i \\ x_{-i} \end{pmatrix} + \begin{pmatrix} y_i \\ y_{-i} \end{pmatrix} = \begin{pmatrix} \Delta_{i,i} & \Delta_{i,-i} \\ \Delta_{-i,i} & \Delta_{-i,-i} \end{pmatrix} \begin{pmatrix} y_i \\ y_{-i} \end{pmatrix} \quad (2)$$

where $\begin{pmatrix} x_i \\ x_{-i} \end{pmatrix}$ refers to the total output matrix for the industrial sector; A refers to a direct consumption coefficient matrix; Ai,j refers to the amount of sector i products consumed by j manufacturing units; $L = (I - A)^{-1} = \begin{pmatrix} \Delta_{i,i} & \Delta_{i,-i} \\ \Delta_{-i,i} & \Delta_{-i,-i} \end{pmatrix}$ refers to the Leontief inverse matrix (Bherwani et al., 2022); $\Delta_{i,j}$ refers to the division j production unit final product complete demand for i division products; $\begin{pmatrix} y_i \\ y_{-i} \end{pmatrix}$ refers to the final demand matrix of each industrial sector, including total government consumption, total household consumption, capital, and exports.

Based on this research idea, the four connection effects of the energy connection of the industrial sectors are as follows:

(1) Internal effect (IE). The IE refers to the amount of energy consumed by the industry sector that does not connect with the outside world in the production process. The energy consumption of the means of production itself is provided within the industry sector.

$$IE_i = q_i \left(I - A_{i,i}\right)^{-1} y_i \quad (3)$$

(2) Mixed effect (ME). The ME is the energy consumed by part of the industry sector purchased by other industrial sectors as put into production and the final consumer goods purchased by the industry sector.

$$ME_i = q_i \left[\Delta_{i,i} - \left(I - A_{i,i}\right)^{-1}\right] y_i \quad (4)$$

(3) Net backward linkage (NBL). NBL means that the industry sector reflects the net energy input brought about to obtain the final demand by using intermediate products and services provided by other sectors.

$$NBL_i = q_{-i}\Delta_{-i,i}y_i \tag{5}$$

(4) Net forward linkage (NFL). NFL is the energy consumption of the industry sector products purchased by other sectors. It will not return to produce products, reflecting the net energy output of that sector.

$$NFL_i = q_i\Delta_{i,-i}y_{-i} \tag{6}$$

SS and DS Models

From the perspective of energy, the supply system mainly includes two aspects. First, the industrial energy sector itself directly supplies energy to the industrial sector, and second, the direct consumption or indirect consumption of energy in the process of economic activities of various industries. The former needs to be studied independently from the energy supply industrial sector, extraction, and processing of energy. In addition to the direct supply allocation of other industrial sectors, it also inevitably involves the further consumption of energy and the development of the economy and society in nonfossil energy ways such as power and heat. The latter needs to judge the implied trade energy transfer between industries. The implied indirect energy consumption of trade between producers in the economic sector is analyzed, the SS energy consumption and the DS energy consumption are analyzed, the energy input industrial sector and the energy output industrial sector are selected, and the internal connection between the economic system from the direct energy consumption and the indirect energy consumption is explored. Net energy transfer calculation of industrial sectors is as follows: calculate the energy transfer flow in the industrial production sector, clarify the dependence of the industrial sector and other industrial sectors, and identify the key industrial sectors in energy utilization (Cao et al., 2016).

$$NT_{st} = NFL_{\mathrm{st}} - NBL_{st} \tag{7}$$

where NT*st* refers to the net transfer of energy to the *t* sector for the *s* sector. If the value of NT*st* is positive, it indicates that *s* has net output to *t* and *s* is net output; The value of NT*st* is negative, which indicates that net energy input is from the *s* sector to the *t* sector and *s* is net input sector.

Energy connection between industrial sectors: through the research of energy connection between industrial sectors, we can explore the industrial sector energy demand from the supply and demand parts and scientifically analyze and define the carbon emission responsibility DS energy consumption of the industrial sector, also known as vertically integrated consumption. It is the sum of direct energy and indirect energy demands to meet the needs for productions and services in the industry sector, including IE, ME, NBL, and NFL of the industry sector. The SS consumption, also known as direct consumption, includes not only energy consumption in the production process that meets the final consumption of the industry sector but also energy consumption implied in goods purchased satisfying production and consumption activities. It is the sum of NFL, IE, and ME.

$$DS_i = IE_{\mathrm{i}} + ME_i + NBL_i \tag{8}$$

$$SS_i = IE_{\mathrm{i}} + ME_i + NFL_i \tag{9}$$

Data Collection

The input-output table can systematically reflect the input-output relationship between various sectors of the national economy, providing a basis for the study of industrial structure, especially for the determination and verification of national economic plans and various quantitative analyses. As an important part of the national economic accounting system, input-output accounting reflects the economic flow of various industrial sectors of the national economy in the form of the input-output table. The input-output table can be divided into regional tables (individual regions) and interregional tables (multiple regions). Since the domestic input-output table has been compiled once in the past 5 years, this paper only studies the transfer of energy demand industrial sectors among various industries in Shaanxi Province in 2007, 2012, and 2017 and then analyzes the energy correlation between industrial economic sectors from the perspective of SS and DS. Among them, the final demand of various industrial sectors, intermediate input, and total output is from Shaanxi Province in 2007, 2012, and 2017. With 2002 as the base period, various comprehensive energy utilization data came from Shaanxi Statistical Yearbook in 2008, 2013, and 2018. Due to some differences in the industry sector classification of the input-output table and statistical Yearbook, we need to form a unified industry classification. This paper divides industrial sectors into the energy sector and nonenergy industrial sector (China Input-Output Association, 2007). Industrial sector indicators will be unified according to caliber, classified into seven categories as follows: agriculture industry (AI), nonenergy industry (NEI), energy industry (EI), building industry (BI), transportation, warehousing, and postal industry (TWPI), wholesale and retail accommodation, catering industry (WRACI), and other service industry (OSI) (Chen and Xu, 2017; **Table 1**).

RESULTS

Energy Demand Characteristics in Shaanxi Province

By accounting for the energy consumption of the industrial economic sector of Shaanxi Province (**Table 2** and **Figure 2**), in 2017, the largest energy consumption industry in Shaanxi Province, the comprehensive energy consumption was 4,161.05 thousand tce, accounting for approximately 45% of the total consumption of the whole industry. Second, the nonenergy sector accounts for approximately 30% of the total consumption of the total industry. The construction industry is the industry with the most minor energy consumption in Shaanxi Province, with a comprehensive energy consumption of 175.76 million tce accounting for approximately 2% of the total consumption of

TABLE 1 | Industrial classification.

Industry	Input/Output table industrial sector classification
Agriculture Industry (AI)	Agriculture, Forestry, Pastoral and Fisheries Products and Services
Non-Energy Industry (NEI)	Metal mining and selection industry, Non-metallic mineral mining and selection industry, Food manufacturing industry, Textile Industry, Clothing Leather Down and its Products, Wood processing and furniture manufacturing industry, Paper printing and cultural and educational supplies manufacturing industry, The Chemical Industry, Non-metallic mineral products industry, Metal smelting and compression processing industry, The Metal Products Industry, General Equipment Manufacturing Industry, Special equipment manufacturing industry, Transportation Equipment manufacturing, Electrical, mechanical, and equipment manufacturing industries, Manufacturing industry of communications equipment, computers and other electronic equipment, Manufacturing industry of instruments and cultural office machinery, Other manufacturing industries, Metal Products, Mechanical, and Equipment Repair Services, Comprehensive utilization industry of waste resources, Water Production and Supply Industry
Energy Industry (EI)	Coal Mining and Washing, Oil and Gas Mining, Petroleum Processing, Coking and Nuclear Fuel Processing, Production and Supply of Power and Heat, and Industry of Gas Production and Supply
Building Industry (BI)	Building industry
Transportation, Warehousing and Postal Industry (TWPI)	Transportation, warehousing and postal industry
Wholesale and Retail Accommodation, Catering Industry (WRACI)	Wholesale and retail accommodation, catering industry
Other Services Industry (OSI)	Information Transmission, Software and Information Technology Services, Finance, Real Estate, Leasing and Business Services, Scientific Research and Technical Services, Water, Environmental and Public Facilities Management, Resident Services Repair and Other Services, Education Health and Social Work, Culture, Sports and Recreation, Public Administration, Social Security and Social Organizations

TABLE 2 | Energy consumption in 2007, 2012, and 2017.

Industry	Comprehensive energy consumption (Ten thousand tce)			Output value energy consumption (tce/Ten thousand)		
Agriculture industry	**2007**	**2012**	**2017**	**2007**	**2012**	**2017**
AI	51.69	187.81	227.32	0.10	0.19	0.04
NEI	1,609.27	1,702.97	2820.46	5.17	1.55	0.19
EI	1,021.43	5,730.96	4,161.05	12.02	1.05	0.61
BI	85.47	64.68	175.76	0.36	0.15	0.03
TWPI	176.89	579.33	1064.48	0.84	1.13	0.87
WRACI	47.10	339.61	359.97	0.35	0.19	0.31
OSI	44.49	160.13	442.67	0.20	4.70	0.23
Total Industry	3,036.34	8,765.49	9,251.71	2.72	1.28	0.33

the whole industry, followed by the agricultural industrial sector, accounting for approximately 3% of the total consumption of the entire industry. By analyzing the consumption of 10,000-yuan output value, the energy intensity of transportation, storage, and postal industry is 0.87tce/10,000 yuan, which is higher than the average energy consumption intensity of all industries by 0.33 tce/10,000 yuan, and the energy intensity of the energy sector is 0.61 tce/10,000 yuan. The energy intensity of wholesale and retail accommodation and catering, other service industries, nonenergy industrial sectors, and agricultural sectors is slightly lower than the average level. In comparison, the energy intensity of the construction industry is lower than 0.10 tce/10,000 yuan. Therefore, the high the energy intensity of transportation, warehousing, postal industry is, the high the industrial energy sectors are, directly leading to the increase in energy consumption in Shaanxi Province.

Based on the analysis of energy consumption in 2007, 2012, and 2017 (**Figure 3**), in the past 10 years, energy consumption in Shaanxi Province continued to grow, with energy intensity decreasing from 2.72 tce per 20,000 yuan to 0.33 tce per 10,000 yuan in 2017 by 88%, among which the energy sector has the most significant decline, reached 95%, the improvement of energy efficiency of the energy industry sector, thus promoting the energy intensity of the decline in Shaanxi Province in the past 10 years. Unlike the reduction of energy intensity in other industries, the energy intensity of other service industries is gradually increasing. Energy intensity increased from 0.20 tce per 10,000 in 2007 to 0.23 tce per 10,000 in 2017, indicating that the change rate of energy demand in other service industries increased the output value, while other service industries are in small energy consumption industrial sectors (approximately 5% of total energy consumption). The energy utilization intensity is small, reflecting the intensity of energy conservation and emission reduction in Shaanxi Province, and the energy use efficiency is increasing year by year.

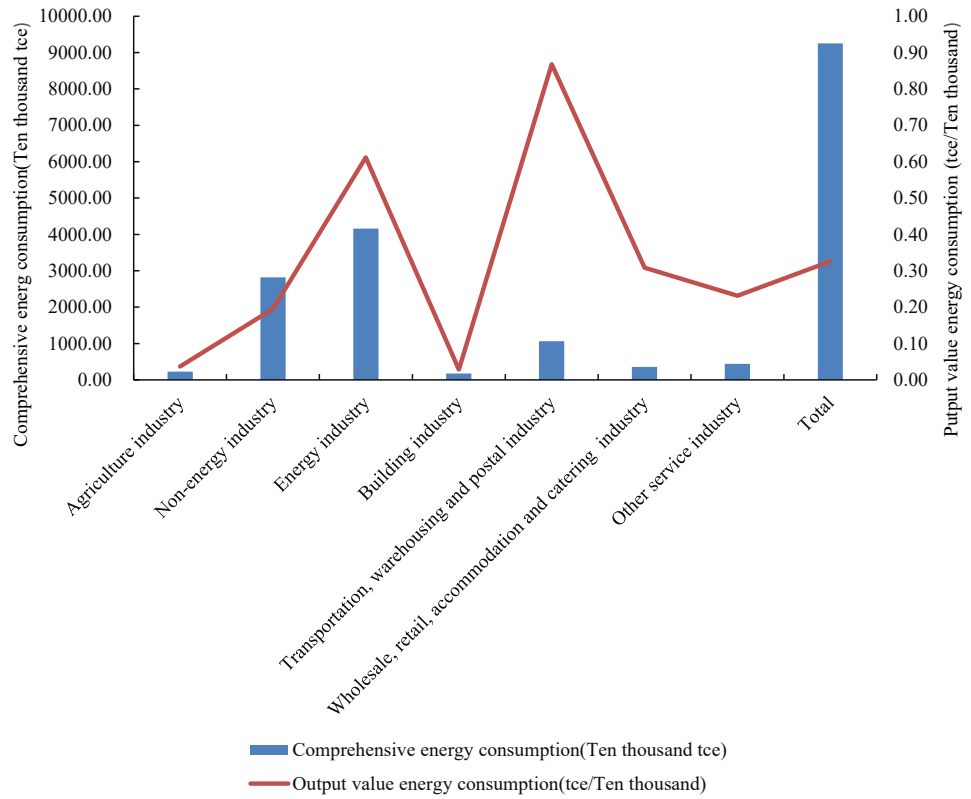

FIGURE 2 | Energy consumption analysis of various industries in Shaanxi Province in 2017.

Implicit Net Energy Transfer Among Industries in Shaanxi Province

According to Eq (14), taking data in 2017 as an example, it can indicate the quantity and specific direction of the implied net transfer of energy in Shaanxi Province among various industries (**Figure 4**). The energy sector is the net energy output sector with the most net transfer to the nonenergy industry sector, 35.751 million tce, followed by the net transfer to construction, 14.583 million tce. The construction industry is the energy net input industrial sector. In addition to the energy sector, the nonenergy sector transfer more implied energy transfer from the nonenergy industry sector to the transportation storage and postal industrial sector, 2.164 million tce.

Energy Connection of Industrial Sector in Shaanxi Province

According to Eq (10)–(16), IE, ME, NBL, and NFL in 2012 were calculated (**Figure 5**). Consumer energy in the agricultural sector IE is 129,600 tce. As for the raw material supply industrial sector, ME consumption energy accounts for 80% of the total DS energy consumption. It indicates that the agricultural sector is transferred to other industrial sectors, and the implied energy is 36,745.700 tce. Most of them transferred to other industrial sectors did not return. The nonenergy sector IE, as the direct energy supply sector, ranks first, with 26,973 million tce, accounting for approximately 10% of DS energy consumption. It indicates that most of the energy needed by the nonenergy industry sector to meet their final demand comes from product exchanges within the industry. The energy industry sector has the most NFL in all industries, ranking first at 66.94499 million tce, and the energy industry sector at 1,243,543 million tce, representing approximately 73% of DS energy consumption. It indicates that more energy implied by the energy industry is transferred to other sectors, and it has the most NBL of all industries. The construction industry, as the net energy input sector, has 82% of the total DS energy consumption for the exchange of 171,002 million tce, having an output of 72,900 tce, transferred to other sectors. In the transportation warehousing and postal industry, energy NFL accounts for the most minor proportion of SS energy consumption, at 8%. The transportation warehousing and postal industry have less implied energy transfer to the remaining industries. In wholesale and retail accommodation catering and agricultural sector, NBL is small compared with NFL, showing certain equilibrium. Net implied energy transfer in other services (net transfer energy volume minus net transferred energy volume) is −3.4554 million tce, which is the net input energy sector.

DISCUSSION

The HEM, based on the input-output table, assumes that an industrial sector is separated from the economic system,

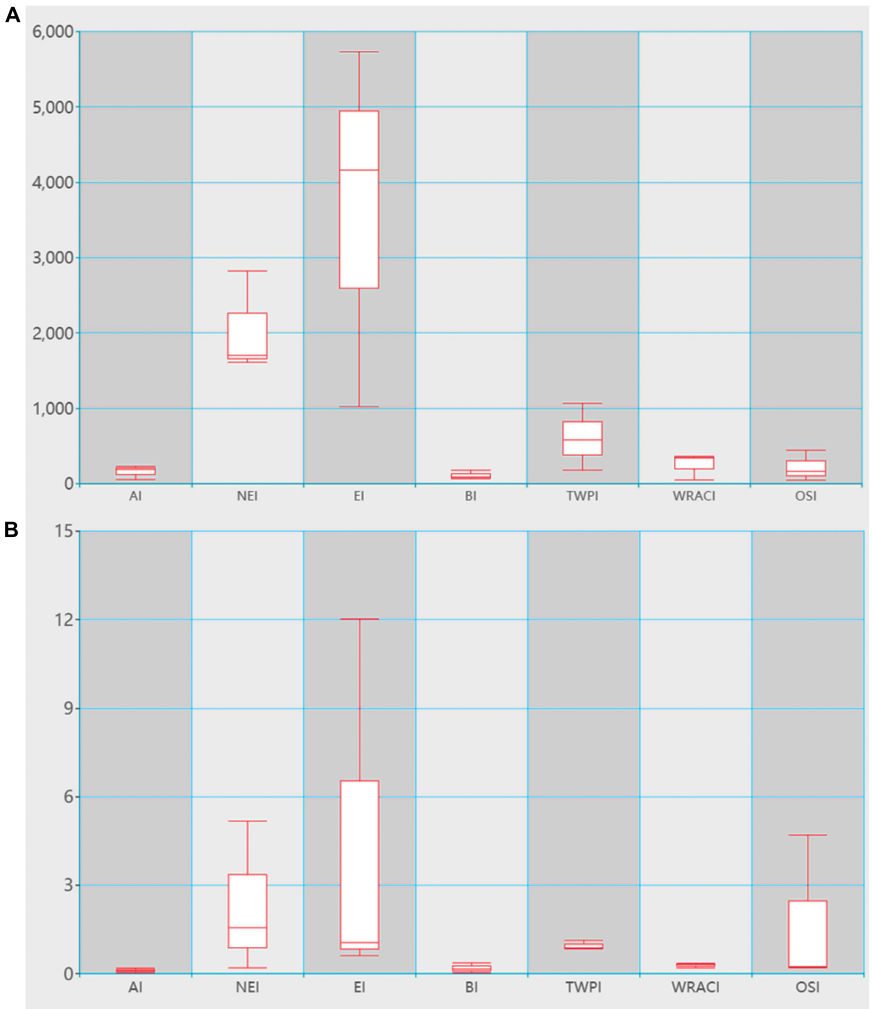

FIGURE 3 | (A) Comprehensive energy consumption of various industries in Shaanxi Province in 2007, 2012, and 2017; **(B)** energy consumption of 10,000 yuan in Shaanxi industries in 2007, 2012, and 2017.

compares the changes in the total output of the economic system, and analyzes the impact of the industrial sector on the whole economic system (Chen and Xu, 2017). However, the HEM cannot analyze IE, ME, NBL, and NFL. Based on the two methods of constructing the input-output model, the hybrid energy input-output model can still guarantee the establishment of the energy balance equation under the new final demand impact (Cao et al., 2016; Bherwani et al., 2022). Although the value-based energy input-output model uses the energy balance equation in the initial construction process, it cannot guarantee that the energy balance equation is established under the new final demand impact (Xu et al., 2021).

This paper analyzes the energy consumption inside and between industrial sectors from the economic system, explores the direct energy demand of other industries from the SS and DS, and analyzes the correlation effect of implied energy consumption (**Figure 6**). The method is applicable to identify the key industrial sectors in energy utilization and the implied energy flow law. It can be extended to other regions, clarifying the key energy consumption industrial sectors in the economic system. To speed up the SDG progress (He et al., 2022), it is not only to improve the supply efficiency of energy supply in the energy sector but also to solve the existing structural imbalance in the energy industry from the root cause. Besides, it is essential to address the characteristics of energy consumption, energy use efficiency, and social and economic conditions in various industries. It is also necessary to improve the energy utilization efficiency of various industries, especially the industrial industry, and coordinate the energy demand on the SS and the DS according to the characteristics of energy consumption, energy use efficiency, and social and economic conditions in various industries. Based on the above understandings, energy supply and economic, social, and environmental development should be planned in a coordinated manner.

Based on the above findings of this paper, we can formulate policy suggestions to improve energy efficiency from the aspects

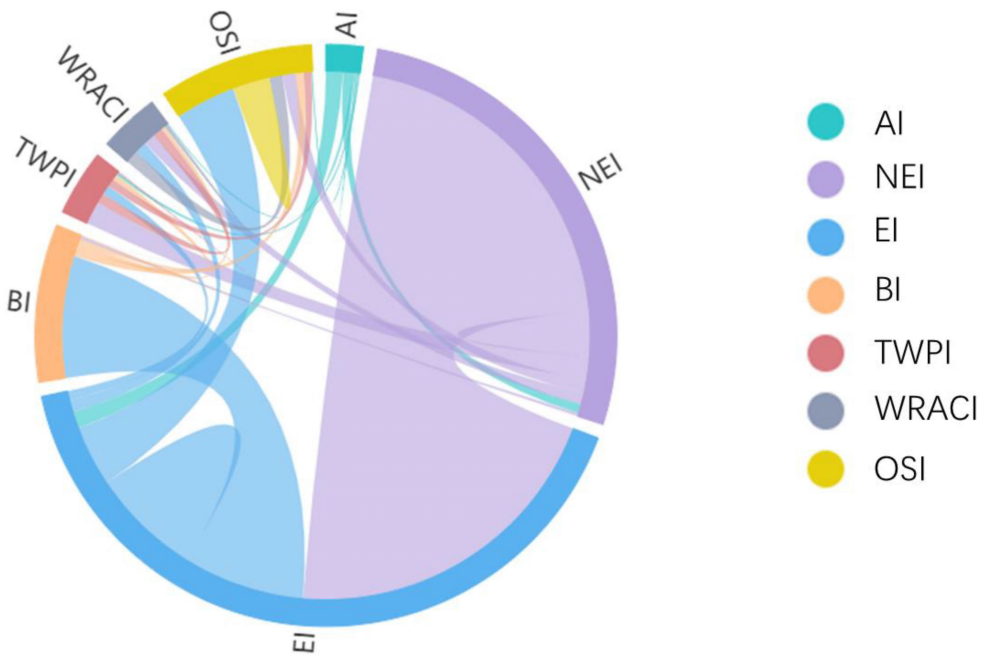

FIGURE 4 | Implicit net energy transfer between energy industries in Shaanxi Province in 2017.

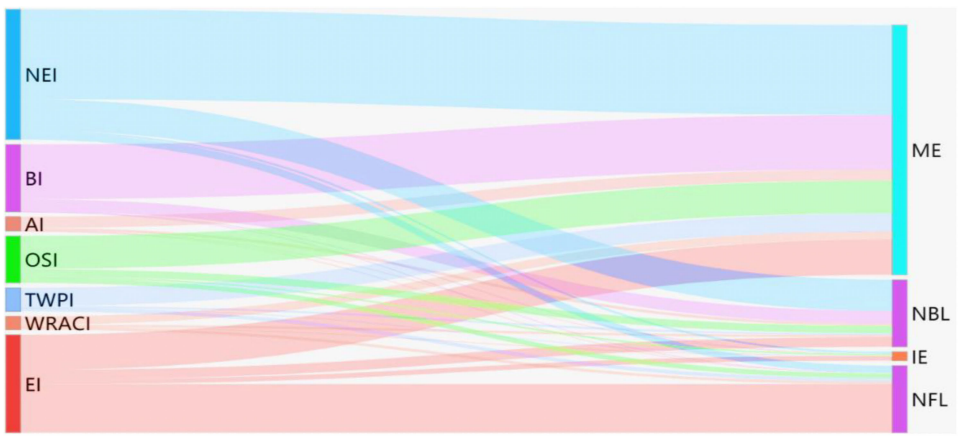

FIGURE 5 | Break decomposition of the energy industry in Shaanxi Province in 2017.

of industrial structure adjustment and technology improvement policy formulation. As a low energy consumption sector, the reduction of the full energy consumption intensity of the agricultural industry is mainly due to the improvement of energy production technology. Therefore, energy utilization could be improved by adjusting the energy consumption structure and the improvement of energy utilization technology. As a high-energy consumption department, the reduction of energy consumption intensity is mainly due to energy production technology. Energy efficiency could be improved by adjusting the energy consumption structure and energy utilization technology. In transportation, warehousing, and post-industry as a high-energy consumption department, the reduction of its full energy consumption intensity is mainly due to the net output structure effect and energy technology effect. While adjusting the energy consumption structure and improving energy utilization technology, we can pay attention to adjusting the input and output structures of its products, reduce the output scale of high energy consumption and low value-added products, and output more products with high value-added. As a low-energy sector, the reduction of total energy consumption intensity in the wholesale, retail, accommodation, and catering industries can be attributed to many reasons, such as the production technology effect, final demand structure effect, and energy technology effect, among which the consumption structure effect contributes to the most. As a low-energy sector, the reduction of full energy consumption

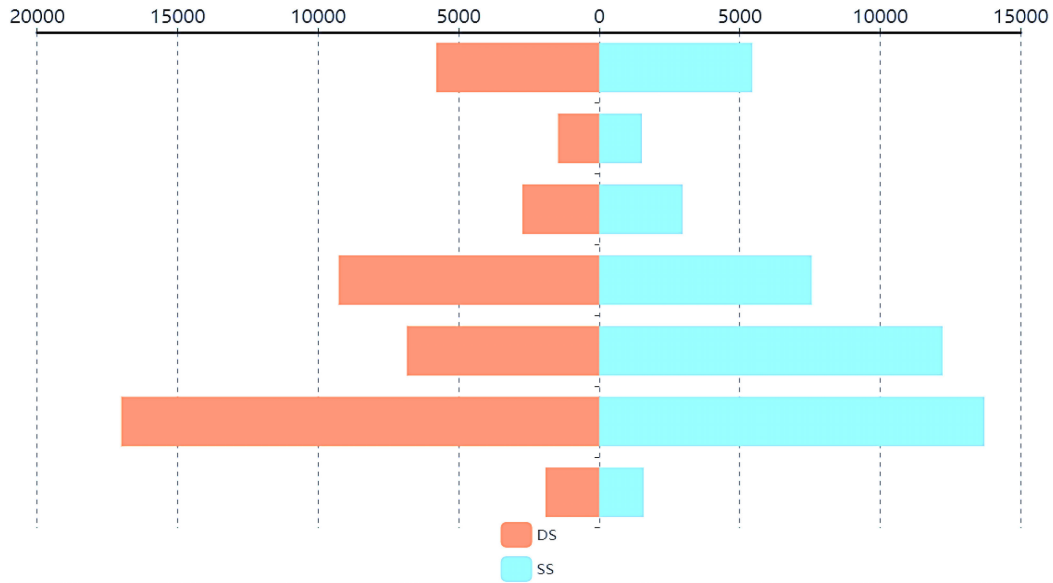

FIGURE 6 | Total energy industry supply and demand in Shaanxi Province in 2017.

intensity of other service industries mainly comes from the effect of energy technology and final demand structure. It can improve energy utilization efficiency from the aspects of introducing new energy technology, guiding rational public consumption and rational investment.

CONCLUSION

Based on the improved HEM, taking the industrial sectors of Shaanxi Province as the research object, relying on the multi-annual input-output table, this paper analyzes the energy transfer implied among industrial sectoral economic activities, compares the energy utilization correlation effect, and provides a scientific basis for the energy SS reform and adjusting the industrial layout of Shaanxi Province.

In 2017, the energy industrial sector was the most energy consumption industry in Shaanxi Province. The construction industry was the most minor energy consumption industry in Shaanxi Province, with high energy intensity in the transportation, warehousing, postal industry, and energy industrial sectors. The energy sector belongs to the net energy net output sector, followed by the net transfer of the energy sector to the construction industry is the net energy input sector. In addition to the energy sector and the nonenergy sector, there are more implied energy transfers from the nonenergy industry sector to the transportation, storage, and postal sector. The agricultural sector moved to other sectors, and recycled products implied more energy. Most of the energy needed by the nonenergy industry sector to meet their ultimate needs comes from product exchanges within the industry. The transfer of energy industry sectors to other sectors and recycling products implies more energy. Construction and other services belong to the net energy input sector. Transportation warehousing and postal industries have less indicated energy transfer to the remaining industries and return. Wholesale and retail accommodation, catering, and agricultural industrial sectors show a certain balance.

DATA AVAILABILITY STATEMENT

The original contributions presented in this study are included in the article/supplementary material, further inquiries can be directed to the corresponding author/s.

AUTHOR CONTRIBUTIONS

JX and XL contributed to the conception of this study. DS and CL performed the experiment. JX and CL contributed significantly to the analysis and manuscript preparation. JX and CL performed the data analyses and wrote the manuscript. XL and ZW helped perform the analysis with constructive discussions. All authors contributed to the article and approved the submitted version.

FUNDING

This study has been supported by the Shaanxi Province Soft Science Research Project (2020KRM197), Social Science Fund of Shaanxi Province (2020R051), Xi'an Social Science Planning Fund (22JX72), Shaanxi Province Soft Science Research Project (2021KRM093), Independent Research and Development project of State Key Laboratory of Green Building in Western China (LSZZ202215), and Joint Project of Major Theoretical and Practical Problems in the Social Sciences of Shaanxi Province (Grant no. 2022ND0429).

REFERENCES

As, A., Jmm, B., Bh, B., and Kba, B. (2020). Estimating residential building energy consumption using overhead imagery. *Appl. Energy* 280:116018. doi: 10.1016/j.apenergy.2020.116018

Bherwani, H., Nair, M., Niwalkar, A., Balachandran, D., and Kumar, R. (2022). Application of Circular Economy Framework for Reducing the Impacts of Climate Change: a Case Study from India on the Application of Carbon and Materials Footprint Nexus. *Energy Nexus* 5:100047. doi: 10.1016/j.nexus.2022.100047

Cao, D., Liu, J., and Zhang, S. (2016). Study on Energy Efficiency of Shaanxi Province Based on Input-output Technology. *J. Xidian University* 26, 36–44.

Chen, B., and Chen, S. (2013). Life cycle assessment of coupling household biogas production to agricultural industry: a case study of biogas-linked persimmon cultivation and processing system. *Energy Policy* 62, 707–716. doi: 10.1016/j.enpol.2013.07.084

Chen, C., Pinar, M., and Stengos, T. (2020). Renewable energy consumption and economic growth nexus: evidence from a threshold model. *Ener. Policy* 139:111295.

Chen, L., and Xu, L. (2017). Energy consumption of Guangdong based on the industry linkage analysis. *China Environ. Sci.* 37, 3972–3980.

China Input-Output Association. (2007). The Inter-Industrial Linkages of Energy Sectors in China-Study on the Improved Structural Coefficients by Using2002Input-Output Table of China. *Stat. Res.* 24, 3–6.

Christoforidis, T., and Katrakilidis, C. (2021). The dynamic role of institutional quality, renewable and non-renewable energy on the ecological footprint of OECD countries: do institutions and renewables function as leverage points for environmental sustainability? *Environ. Sci. Pollut. Res.* 28, 28038–28057. doi: 10.1007/s11356-021-13877-8

Chuai, X., Lu, Q., Huang, X., Gao, R., and Zhao, R. (2020). China's construction industry-linked economy-resources-environment flow in international trade. *J. Clean. Prod.* 278:123990. doi: 10.1016/j.jclepro.2020.123990

Demirtas, M. (2021). Evaluation of energy use and carbon dioxide emissions from the consumption of fossil fuels and agricultural chemicals for paste tomato cultivation in the Bursa region of Turkey. *Environ. Sci. Pollut. Res.* 28, 27132–27146. doi: 10.1007/s11356-021-12593-7

Deng, G., and Zhang, Z. (2016). A Study on the International Relating Effect of China's Embodied Carbon Trade: based on Generalized Hypothetical Extraction Method. *Mod. Finance Econ. J. Tianjin University Finance Econ.* 36, 102–113.

Deng, G., Zhang, Z., and Ren, S. (2016). Effect of the Value-added Trade of China in the Global Value Chains:Based on the Generalized Hypothetical Extraction Method. *Stat. Inf. Forum* 31, 46–51.

Duarte, R., Sanchez-Choliz, J., and Bielsa, J. (2002). Water use in the Spanish economy: an input-output approach. *Ecol. Econ.* 43, 71–85. doi: 10.1016/S0921-8009(02)00183-0

Dyarto, R., and Setyawan, D. (2021). Understanding the political challenges of introducing a carbon tax in Indonesia. *Int. J. Environ. Sci. Technol.* 18, 1479–1488. doi: 10.1007/s13762-020-02925-4

Estrella Guillen, E., Samuelson, H. W., and Vohringer, C. (2021). The impact of cultural assumptions on simulated energy, comfort, and investment returns of design decisions in two desert climates. *Build. Simul.* 14, 931–944. doi: 10.1007/s12273-020-0718-y

Gao, X., Zhang, X., and He, Z. (2021). Emergence of the urban goal and its practice: background and progress of the SDG11. *Chin. Popul. Resour. Environ.* 2021, 144–154.

Han, X., and Cao, T. (2021). Study on ecological environment quality evaluation of the energy consumption pollution treatment in industrial parks. *Environ. Sci. Pollut. Res.* 28, 28038–28057. doi: 10.1007/s11356-020-10147-x

Han, Z., and Wang, G. (2019). Estimation of embodied energy and carbon emissions in Sino-U.S.trade based on Multi-Region Input-Output Model. *Clim. Chang. Res.* 015, 416–426.

Hao, W., Rasul, F., Bhatti, Z., Hassan, M. S., Ahmed, I., and Asghar, N. (2021). A technological innovation and economic progress enhancement: an assessment of sustainable economic and environmental management. *Environ. Sci. Pollut. Res.* 28, 28585–28597. doi: 10.1007/s11356-021-12559-9

Häring, I., Fehling-Kaschek, M., Miller, N., Faist, K., Ganter, S., and Srivastava, K. (2021). A performance-based tabular approach for joint systematic improvement of risk control and resilience applied to telecommunication grid, gas network, and ultrasound localization system. *Environ. Syst. Decis.* 41, 286–329. doi: 10.1007/s10669-021-09811-5

Hatice, G. (2021). Renewable energy consumption policy in Turkey: an energy extended input-output analysis. *Renew. Energy* 175, 783–796. doi: 10.1016/j.renene.2021.05.025

He, B., Wang, J., Zhu, J., and Qi, J. (2022). Beating the urban heat: situation, background, impacts and the way forward in China. *Renew. Sustain. Energy Rev.* 161:112350. doi: 10.1016/j.rser.2022.112350

He, B. J., Yang, L., and Ye, M. (2014a). Building energy efficiency in China rural areas: situation, drawbacks, challenges, corresponding measures and policies. *Sustain. Cities Soc.* 11, 7–15. doi: 10.1016/j.scs.2013.11.005

He, B. J., Yang, L., Ye, M., Mou, B., and Zhou, Y. (2014b). Overview of rural building energy efficiency in China. *Energy Policy* 69, 385–396. doi: 10.1016/j.enpol.2014.03.018

Iheonu, C. O., Anyanwu, O. C., Odo, O. K., and Nathaniel, S. P. (2021). Does economic growth, international trade, and urbanization uphold environmental sustainability in sub-Saharan Africa? Insights from quantile and causality procedures. *Environ. Sci. Pollut. Res.* 28, 28222–28233. doi: 10.1007/s11356-021-12539-z

Iqbal, N., Sakhani, M. A., Khan, A. R., Atiq-Ur-Rehman, Ajmal, Z., and Khan, M. Z. (2021). Socioeconomic impacts of domestic biogas plants on rural households to strengthen energy security. *Environ. Sci. Pollut. Res.* 28, 27446–27456. doi: 10.1007/s11356-021-12633-2

Iraganaboina, N. C., and Eluru, N. (2021). An examination of factors affecting residential energy consumption using a multiple discrete continuous approach. *Energy Build.* 240:110934. doi: 10.1016/j.enbuild.2021.110934

Isik, C., Ongan, S., Ozdemir, D., Ahmad, M., and Ongan, A. (2021). The increases and decreases of the environment kuznets curve (ekc) for 8 OECD countries. *Environ. Sci. Pollut. Res.* 28, 28535–28543. doi: 10.1007/s11356-021-12637-y

Khan, I., Hou, F., Zakari, A., and Tawiah, V. (2021). The dynamic links among energy transitions, energy consumption, and sustainable economic growth: a novel framework for IEA countries. *Energy* 222:119935. doi: 10.1016/j.energy.2021.119935

Koondhar, M. A., Udemba, E. N., Cheng, Y., Khan, Z. A., and Kong, R. (2021). Asymmetric causality among carbon emission from agriculture, energy consumption, fertilizer, and cereal food production -a nonlinear analysis for Pakistan. *Sustain. Energy Technol. Assess.* 45:101099. doi: 10.1016/j.seta.2021.101099

Kousar, S., and Shabbir, A. (2021). Analysis of environmental degradation mechanism in the nexus among energy consumption and poverty in Pakistan. *Environ. Sci. Pollut. Res.* 28, 27528–27541. doi: 10.1007/s11356-020-12140-w

Li, C., Gao, X., He, B.-J., Wu, J., and Wu, K. (2019a). Coupling Coordination Relationships between Urban-industrial Land Use Efficiency and Accessibility of Highway Networks: evidence from Beijing-Tianjin-Hebei Urban Agglomeration, China. *Sustainability* 11:1446. doi: 10.3390/su11051446

Li, C., Gao, X., Wu, J., and Wu, K. (2019b). Demand prediction and regulation zoning of urban-industrial land: evidence from Beijing-Tianjin-Hebei Urban Agglomeration, China. *Environ. Monitor. Assess.* 191:412. doi: 10.1007/s10661-019-7547-4

Li, C., Hu, H., Deng, L., Liu, Y., and Wang, Z. (2021). Structural decoupling the sectoral growth from complete energy consumption in china. *Energy Strategy Rev.* 34:100634. doi: 10.1016/j.esr.2021.100634

Li, C., and Wu, K. (2022). An input–output analysis of transportation equipment manufacturing industrial transfer: evidence from Beijing-Tianjin-Hebei region, China. *Growth Change* 53, 91–111. doi: 10.1111/grow.12571

Li, G., Jiang, C., Zhang, Y., and Jiang, G. (2020). Whether land greening in different geomorphic units are beneficial to water yield in the yellow river basin? *Ecol. Indic.* 120:106926. doi: 10.1016/j.ecolind.2020.106926

Li, J., Sun, W., Li, M., and Meng, L. (2021). Coupling coordination degree of production, living and ecological spaces and its influencing factors in the yellow river basin. *J. Clean. Prod.* 298:126803. doi: 10.1016/j.jclepro.2021.126803

Luo, X., Yang, J., Sun, W., and He, B. (2021). Suitability of human settlements in mountainous areas from the perspective of ventilation: a case study of the main urban area of Chongqing. *J. Clean. Prod.* 310:127467. doi: 10.1016/j.jclepro.2021.127467

Mensah, H., Ahadzie, D. K., Takyi, S. A., and Amponsah, O. (2021). Climate change resilience: lessons from local climate-smart agricultural practices

in Ghana. *Energy Ecol. Environ.* 6, 271–284. doi: 10.1007/s40974-020-00181-3

Mfb, A., Mab, A., Msb, C., Us, D., and Xuan, V. (2021). Unveiling the heterogeneous impacts of environmental taxes on energy consumption and energy intensity: empirical evidence from OECD countries. *Energy* 226:120366. doi: 10.1016/j.energy.2021.120366

Mohammed, N. A. A., Xianhui, G., and Shah, S. A. A. (2021). Non-oil economic transition for economic and environmental sustainability in Saudi Arabia: a multi-factor analysis under fuzzy environment. *Environ. Sci. Pollut. Res.* 28, 56219–56233. doi: 10.1007/s11356-021-14304-8

Ocal, O., and Aslan, A. (2013). Renewable energy consumption–economic growth nexus in turkey. *Renew. Sustain. Energy Rev.* 28, 494–499. doi: 10.1016/j.rser.2013.08.036

Qayyum, M., Yu, Y., and Li, S. (2021). The impact of economic complexity on embodied carbon emission in trade: new empirical evidence from cross-country panel data. *Environ. Sci. Pollut. Res.* 28, 54015–54029. doi: 10.1007/s11356-021-14414-3

Qazi, W. A., and Abushammala, M. F. M. (2021). The analysis of electricity production and greenhouse-gas emission reduction from municipal solid waste sector in Oman. *Int. J. Environ. Sci. Technol.* 18, 1395–1406. doi: 10.1007/s13762-020-02871-1

Rahman, M. M., Hosan, S., Karmaker, S. C., Chapman, A. J., and Saha, B. B. (2020). The effect of remittance on energy consumption: panel cointegration and dynamic causality analysis for south asian countries. *Energy* 220:119684. doi: 10.3390/ijerph18094605 doi: 10.1016/j.energy.2020.119684

Salem, H. S. (2021). Evaluation of the stone and marble industry in palestine: environmental, geological, health, socioeconomic, cultural, and legal perspectives, in view of sustainable development. *Environ. Sci. Pollut. Res.* 28, 28058–28080. doi: 10.1007/s11356-021-12526-4

Seidler, J., Strugatchi, J., Grtner, T., and Waldvogel, S. R. (2020). Does electrifying organic synthesis pay off? The energy efficiency of electro-organic conversions. *MRS Energy Sustain.* 7:42. doi: 10.1557/mre.2020.42

Shaikh, I. (2021). Impact of covid-19 pandemic on the energy markets. *Econ. Change Restruct.* 55, 433–484. doi: 10.1007/s10644-021-09320-0

Wang, F., and Gao, C. (2020). Measurement,Decomposition,and Cross-Border Transfer of Embodied Energy of China's Industrial Sectors: based on the CRIO Model. *Inquiry Econ. Issues* 458, 5–15.

Wang, F., Xie, J., Wu, S., Li, J., and Zhang, L. (2021). Life cycle energy consumption by roads and associated interpretative analysis of sustainable policies. *Renew. Sustain. Energy Rev.* 141:110823. doi: 10.1016/j.rser.2021.110823

Wang, R., Lu, S., Feng, W., and Xu, B. (2021). Tradeoff between heating energy demand in winter and indoor overheating risk in summer constrained by building standards. *Build. Simul.* 14, 987–1003. doi: 10.1007/s12273-020-0719-x

Wu, J., Abban, O. J., Boadi, A. D., Haris, M., and Addo, A. A. (2020). Exploring the relationships among CO2 emissions, urbanization, economic growth, economic structure, energy consumption, and trade along the BRI based on income classification. *Energy Ecol. Environ.* 6, 213–231. doi: 10.1007/s40974-020-00176-0

Xiao, H., Ma, Z., Zhang, P., and Liu, M. (2019). Study of the impact of energy consumption structure on carbon emission intensity in China from the perspective of spatial effects. *Nat. Hazards* 99, 1365–1380. doi: 10.1007/s11356-021-16619-y

Xu, X., Zhang, N., Zhao, D., and Liu, C. (2021). The effect of trade openness on the relationship between agricultural technology inputs and carbon emissions: evidence from a panel threshold model. *Environ. Sci. Pollut. Res.* 28, 9991–10004. doi: 10.1007/s11356-020-11255-4

Yang, J., Wang, Y., Xue, B., Li, Y., Xiao, X., Xia, J., et al. (2021b). Contribution of urban ventilation to the thermal environment and urban energy demand: different climate background perspectives. *Sci. Total Environ.* 795:148791. doi: 10.1016/j.scitotenv.2021.148791

Yang, J., Ren, J., Sun, D., Xiao, X., and Li, X. (2021a). Understanding land surface temperature impact factors based on local climate zones. *Sustain. Cities Soc.* 69:102818. doi: 10.1016/j.scs.2021.102818

Yang, J., Yang, Y., Sun, D., Jin, C., and Xiao, X. (2021c). Influence of urban morphological characteristics on thermal environment. *Sustain. Cities Soc.* 72:103045. doi: 10.1016/j.scs.2021.103045

Yang, Y., Qiu, Y., Wang, X., Liu, H., Zhang, J., Li, H., et al. (2021d). Analysis of Water Resources and Energy Consumption Path in Heilongjiang Province. *Water Power* 47, 18–23.

Yu, C. A., Mz, A., Jl, B., Qian, Z. C., and Wm, D. (2020). Evaluation of ecological city and analysis of obstacle factors under the background of high-quality development: taking cities in the yellow river basin as examples. *Ecol. Indic.* 118:106771. doi: 10.1016/j.ecolind.2020.106771

Zafar, M. W., Sinha, A., Ahmed, Z., Qin, Q., and Zaidi, S. (2021). Effects of biomass energy consumption on environmental quality: the role of education and technology in asia-pacific economic cooperation countries. *Renew. Sustain. Energy Rev.* 142:110868. doi: 10.1016/j.rser.2021.110868

Zakari, A., Toplak, J., Ibtissem, M., Dagar, V., and Khan, M. K. (2021). Impact of nigeria's industrial sector on level of inefficiency for energy consumption: fisher ideal index decomposition analysis. *Heliyon* 7:e06952. doi: 10.1016/j.heliyon.2021.e06952

Zhang, H. (2018). Choosing energy input-output models: hybrid type or monetary type. *Econ. Theory Bus. Manag.* 334, 104–114.

Zhang, Y., Bai, H., Hou, H., Zhang, Y., and Zhang, Y. (2021). Exploring the consumption-based carbon emissions of industrial cities in china: a case study of tianjin. *Environ. Sci. Pollut. Res.* 28, 26948–26960. doi: 10.1007/s11356-021-12563-z

Conflict of Interest: The authors declare that the research was conducted in the absence of any commercial or financial relationships that could be construed as a potential conflict of interest.

The reviewer YZ declared a shared affiliation with the several authors JX, XL, CL, and ZW to the handling editor at the time of review.

Publisher's Note: All claims expressed in this article are solely those of the authors and do not necessarily represent those of their affiliated organizations, or those of the publisher, the editors and the reviewers. Any product that may be evaluated in this article, or claim that may be made by its manufacturer, is not guaranteed or endorsed by the publisher.

Copyright © 2022 Xia, Liu, Sun, Li and Wang. This is an open-access article distributed under the terms of the Creative Commons Attribution License (CC BY). The use, distribution or reproduction in other forums is permitted, provided the original author(s) and the copyright owner(s) are credited and that the original publication in this journal is cited, in accordance with accepted academic practice. No use, distribution or reproduction is permitted which does not comply with these terms.

frontiers | Frontiers in Earth Science

ORIGINAL RESEARCH
published: 08 July 2022
doi: 10.3389/feart.2022.944927

Exotic Food, Food Environment, and Geographical Patterns: Big Data Analytics From Japanese Cuisine in China

Chuang Tian, Weixin Luan and Hui Wang*

School of Maritime Economics and Management, Dalian Maritime University, Dalian, China

As urban amenity welfare, exotic food is related to consumers' equal access to diversified food and a healthy diet. This study uses big data provided by an online catering platform to explore Japanese cuisine in China. The field intensity model and spatial econometric model are used to analyze the place effect and its relationship with local socioeconomic factors. The results illustrate that 1) the spatial distribution of Japanese cuisine shows the characteristics of an unbalanced agglomeration distribution, with the coastal economically developed cities as the key layout area and gradually extending to inland cities. 2) Price characteristics indicate that the service target of Japanese cuisine is mainly the middle class. In addition, the spatial inequality of field intensity value indicates that wealthy Eastern cities have more opportunities to enjoy more kinds of and higher quality exotic food. 3) In the local socioeconomic environment, urbanization level, population size, and economic scale are significantly related to inequal access to Japanese cuisine. The essential mechanism of these circumstances is the internal needs of pricing characteristics and the negative externalities caused by unequal urban infrastructure.

Keywords: exotic food, spatial differentiation, local socioeconomic factors, spatial econometric model, POI (point of interest) data

OPEN ACCESS

Edited by:
Jianhong Xia,
Curtin University, Australia

Reviewed by:
Dahao Zhang,
Sun Yat-sen University, China
Chenxi Li,
Xi'an University of Architecture and Technology, China
Ling-en Wang,
Institute of Geographic Sciences and Natural Resources Research (CAS), China

****Correspondence:***
Weixin Luan
guanll2019@vip.163.com

Specialty section:
This article was submitted to Geoscience and Society, a section of the journal Frontiers in Earth Science

Received: *16 May 2022*
Accepted: *07 June 2022*
Published: *08 July 2022*

Citation:
Tian C, Luan W and Wang H (2022) Exotic Food, Food Environment, and Geographical Patterns: Big Data Analytics From Japanese Cuisine in China. Front. Earth Sci. 10:944927. doi: 10.3389/feart.2022.944927

1 INTRODUCTION

Love for variety is a common assumption of consumers in Modern Economics (Glaeser et al., 2001; Nathan, 2015). Rich and diverse diet not only can improve the supporting services of urbanization construction but also is a strong force to shape urban amenity welfare. With the increasing demand for food diversity and the advancement of globalization, more and more dietary choices are made for cross-local production (Willmott, 2007).

As a typical representative of space production, exotic food is a process of production of space, which constantly exceeds the limits of geographical space (Zeng and Liu, 2013). In different socio-economic environments, exotic food is providing differentiated services to meet people's diverse food preferences and needs (Armington, 1969; Clark et al., 2017). Its spatial distribution is related to whether consumers can have equal access to food and nutrients (Çanakçı and Birdir, 2020), and it affects the comfort and welfare level of cities (Glaeser et al., 2001). However, affected by spatial and non-spatial mediating factors (including geographical, economic, information, and cultural aspects), the distribution of food is often unbalanced, which leads to inequality of access to food and barriers to choice for consumers (Chen and Yang, 2014).

Most of the existing studies describe the spatial inequality of food by analyzing the differences of food environments in different places (An and Sturm, 2012; Caspi et al., 2012; Swinburn et al., 2015; An et al., 2020). Researchers usually describe food environment in terms of families, streets, and communities, such as

- Family food environment usually includes physical environment (e.g., family food supply) and socio-cultural environment (e.g., parenting styles, practices, and rules) (Adams et al., 2020; Jang et al., 2020);
- The street food environment was quantified as healthy food sources (chain stores and independent grocery stores, fruit and vegetable suppliers, and supermarkets) and unhealthy food sources (chain and independent convenience stores, fast food, and alcohol stores) (Lytle and Sokol, 2017; Anderson et al., 2020);
- The community food environment "comprises the foods available to people in their surroundings as they go about their everyday lives and the nutritional quality, safety, price, convenience, labeling, and promotion of these foods" (Black et al., 2014; Cobb et al., 2015; FAO-Food and Agriculture Organization of the United Nations, 2016; Luciene et al., 2020).

The abovementioned studies have found that regional differences in food environment will lead to food access inequalities in food clusters, eating patterns, and access routes in different spatial places, which will have many adverse effects on resident welfare and health status (Leslie et al., 2012; Chen and Yang, 2014; Eckert and Vojnovic, 2017; Garcia et al., 2020). However, the abovementioned research also has some limitations: 1) researchers mainly focus on the supply system and access of local food and interpret its relationship with the food environment of the community and street, but few researchers pay attention to exotic food; 2) by means of interviews and questionnaires, the research conclusion does not seem to be able to describe the food environment of urban units well.

The abovementioned findings confirm that urban food environment should include the sum of the effects of environment, opportunity, or living conditions on the health and eating behavior of individuals or people (Kwate and Loh, 2016; Osei-Kwasi et al., 2020). With the need for multiscale and three-dimensional research, it is more practical to measure the diversity of food environment at the urban level and its impact on food inequality. Especially with the acceleration of globalization and population flow, food from all over the world is part of the lives and social activities of residents in different cities in a variety of forms. To some extent, these foreign foods have affected the quality of life of urban residents and have become an important part of the local unique social landscape of the city. Social economic factors such as residential population, travel behavior, and mobility related to food environment have attracted more and more attention (Eckert and Vojnovic, 2017; Li and Kim, 2020).

The introduction of exotic food will bring about the remould and reframe of local food supply channels and supply structure. However, the local food environment with strong rooting will reverse the emergence of exotic food and form new service features (for example, deep-fried dough sticks and soybean milk appear on the menus of McDonald's and KFC in China) (Shen and Xiao, 2014; Rui et al., 2016). It is a city problem worthy of attention to analyze whether the influx and development of exotic food will improve the city's food access and purchase behavior.

As an important market for exotic food, China has a large consumer group, diverse dietary needs, unique food culture, and dramatic social and economic evolution. With the rise of e-commerce and online catering platforms, exotic food has formed a unique service characteristic and distribution status in China. It is more representative and typical to analyze the distribution characteristics of exotic foods and its relationship with the urban food environment. As one of the important forms of exotic food, Japanese cuisine is an important cooking school in the world. Compared with other exotic foods in China, the number of Japanese restaurants in 2019 is close to 70,000 (ranking first in the world), which has become the "leader" of exotic foods in China (data from dianping.com). According to the survey report of China's restaurant industry in 2019, China's catering revenue in 2018 was 4,271.6 billion yuan, 780 times that of 1978, while foreign catering accounted for 26.24% of that revenue, which has become an important part of China's catering industry. Taking Japanese restaurants as an example, our statistics show that the number of Japanese restaurants in China in 2022 increased by 13,678 compared with that in 2019.

Simultaneously, big data thinking has brought about a revolution in scientific research methods, and the data-intensive research paradigm has been widely recognized. An increasing number of scholars have obtained internet spatial–temporal data, such as the facility interest points of internet maps and social media check-in interest points, and analyzed and explored issues related to urban space through a new data-oriented research paradigm. In this study, Japanese cuisine in China is taken as a representative of exotic food, and the larger sample size of internet big data is used to describe the service characteristics and identify the internal relationship between the service characteristics and local food environment. The purpose of this study is to analyze whether the continuous influx of exotic food can alleviate the disadvantage of vulnerable group access to food diversity, meet the needs of theoretical development of dietary communication, and promote international dialogue on diet and explore the pricing strategy and distribution pattern of exotic food in consumption areas, which can also influence the diet structure, healthy diet concept, and nutrition intake of consumption areas. The approach provides evidence to promote the reproduction of traditional diet and healthy diet. The contribution of this study is as follows: It is the first time the data of online catering websites have been used to discuss the geographical pattern of Japanese restaurants in China and analyze the price differences of Japanese restaurants in 332 cities in China. In addition, we discuss the spatial distribution

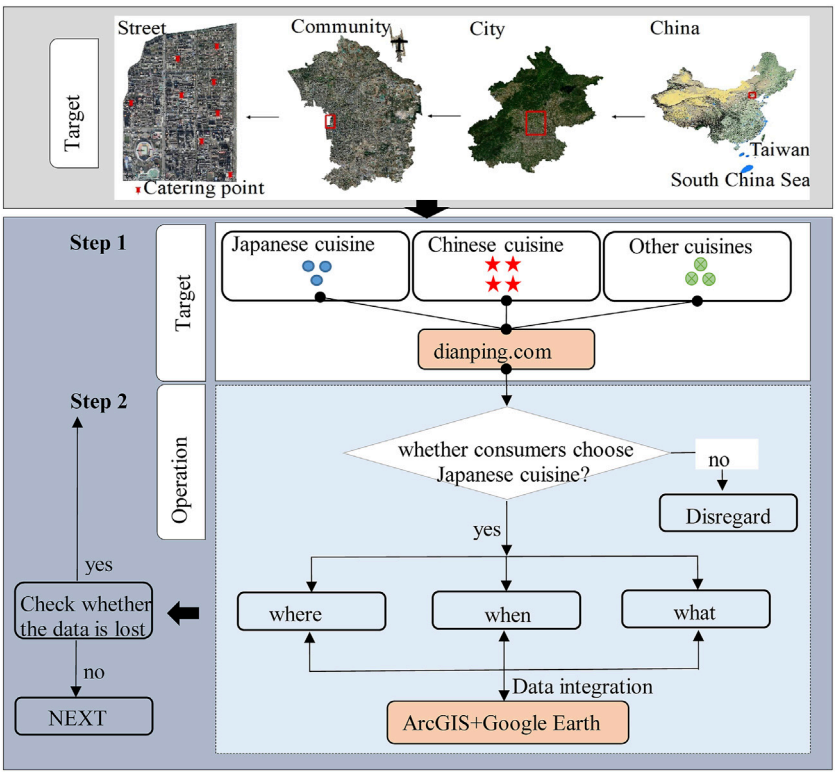

FIGURE 1 | Data acquisition and processing method.

differences of Japanese restaurants and the relationship between urban, social, and economic factors.

2 MATERIALS AND METHODS

2.1 Data

The traditional statistical data of the catering industry have some shortcomings, such as incomplete classification information and time lag. With the rapid development of internet technology, big data represented by mobile phone signaling data, GPS trajectory data, and POI (point of interest) data have been constantly enriched and improved. As a new spatial data source, POI data have the advantages of a large amount of data, wide coverage, and high recognition accuracy and is easy to obtain (Zhang et al., 2021b).

Figure 1 shows our data acquisition and processing method. We divide the target city into different regions to obtain the street locations of Japanese restaurants across different regions. Next, we aggregate these street data into the city data set and establish a database of Japanese restaurants in the city. We use dianping.com and map.baidu.com as our sources for Japanese restaurant data.

We use the key search term "Japanese cuisine" in dianping.com and map.baidu.com; meanwhile, our collection rule is "whether customers choose to eat Japanese cuisine" and the collection objects are from 332 cities in China. The data set was collected from 28 May to 30 May 2022. Then, the data set is checked and rechecked for data loss. Map matching and database establishment are performed *via* ArcGIS and Google Earth, respectively, (Qin et al., 2019; Tian et al., 2021).

In the process of data acquisition and cleaning, we obtain the text data of Japanese restaurants from dianping.com (including restaurants that provide sushi and other dishes). After eliminating duplicate data and data that did not meet the search requirements, a total of 82,687 restaurant text data were included as part of this study. We found that the obtained restaurant data could be queried through batch comparison with the restaurant location data provided by map.baidu.com. The data used met our subsequent research needs.

2.2 Methods

2.1.1 Field Intensity Model

The equations should be inserted in an editable format from the equation editor. The field intensity model is derived from a physical concept and is mostly used to determine the division of the radiation and development range of urban hinterlands (Wu et al., 2020; Wu et al., 2021). The field intensity model was selected to measure the service capacity of Japanese cuisine in different cities. The higher the field intensity value, the stronger the service capacity, and the wider the service range. City residents can also enjoy better Japanese cuisine and better services. The calculation formula is as follows:

$$E_{ij}^{k} = Z_k \Big/ \left(D_{ij}^{k}\right)^{b}, \tag{1}$$

where $[i, j]$ denotes the spatial position of the peripheral points, E_{ij}^{k} is the radiation field intensity of point $[i, j]$ affected by the central city k; Z_k is the nodule index of central city k, which is replaced by the product of the number of restaurants and dish styles; D_{ij}^{k} is the distance between k city and point $[i, j]$; and b is the coefficient of friction, which is generally taken as 2.

2.1.2 Multiple Linear Regression Model

Multiple linear regression models are usually used to study the relationship between a dependent variable and multiple independent variables. The spatial inequality of Japanese cuisine in China is not only affected by economic and social factors in the place of origin but also closely related to the external environment of the consumption location. If x1, x2, ... , xn socioeconomic factors are involved in the development of Japanese cuisine service characteristics in China, the regression model is as follows:

$$\begin{aligned} y_i = {} & \theta_0 + \theta_1 LNPGDP + \theta_2 LNUR + \theta_3 LNTIP + \theta_4 LNPOP \\ & + \theta_5 LNLR + \theta_6 LNIN + \theta_7 LNRND + \theta_8 LNDIS + \theta_9 LNTV \\ & + \theta_{10} LNWAR + \theta_{11} LNFL + \partial. \end{aligned} \tag{2}$$

2.1.3 Spatial Econometric Model

For model $y = \rho W_1 + X\beta_1 + W_1 X\beta_2 + \mu,\ \mu = \lambda W_2 \mu + \varepsilon,\ \varepsilon \sim (0, \sigma^2 I_n)$, when $\lambda = 0,\ \beta_2 = 0$, the model can be simplified as $Y = \rho W y + X\beta + \varepsilon$ (SLM, spatial lag model); when $\rho = 0,\ \beta_2 = 0$, the model can be simplified as $Y = X\beta + \varepsilon,\ \ \varepsilon = \lambda W \varepsilon + \mu$ (SEM, spatial error model).

Spatial econometric models can avoid the deviation of classical econometrics when analyzing spatial effects. The spatial econometric models used in this study are SLM (spatial lag model) and SEM (spatial error model). The spatial lag model is as follows:

$$Y = \rho W y + X\beta + \varepsilon \tag{3}$$

where Y is the dependent variable, X is the explanatory variable, W is the spatial weight matrix, Wy is the spatial lag variable, ρ is the spatial regression coefficient, reflecting the degree of diffusion or spillover between adjacent spatial units, β reflects the influence of X on Y, and ε is the random error term.

The spatial lag model mainly verifies the spatial spillover effect of dependent variables in a region and verifies that the influencing factors of dependent variables are applied to other regions through the spatial transmission mechanism. In contrast to the spatial lag model, the spatial error model verifies the spatial dependence existing in the disturbance error term and measures the impact of the error impact of the dependent variables in adjacent areas on the local dependent variables (Guo et al., 2020a). The spatial error model is as follows:

$$Y = X\beta + \varepsilon,\ \varepsilon = \lambda W \varepsilon + \mu, \tag{4}$$

where Y is the dependent variable, X is the explanatory variable, W is the spatial weight matrix, ε is the random error term, λ is the spatial error coefficient, μ is the random error term of the normal distribution, and β reflects the influence of X on Y.

2.3 The Choice of Socioeconomic Factors

In this study, the influencing factors are divided into economic factors, spatial factors, information factors, and humanistic factors (Yang et al., 2019; Guo et al., 2020b; Tian et al., 2021).

Economic factors: For the service industry, the pursuit of profit maximization is the factor preferred by producers for determining production location; that is, maximizing the difference between income and cost. Sufficient market demand is the first consideration in the spatial choice of the catering industry. Cities with large population size and high population density are the first choice for restaurant locations. Under sufficient market demand, the purchasing power level of the region is also an important factor in its location choice. The higher the disposable income of people in the region, the stronger the purchasing power, and the greater the possibility of the location will be. As an important part of the expansion cost of service enterprises, land rent is also one of the necessary conditions for location.

Spatial factors: Traffic accessibility is an important factor affecting the layout of the catering industry (Yang et al., 2018; Zhang et al., 2021a; Zhou et al., 2021). Good traffic accessibility is an important channel to communicate with consumers and retail facilities, and only areas with good accessibility can ensure that consumers can easily reach the retail business center. Simultaneously, smooth logistics distribution can save transportation costs for retail businesses, and good traffic accessibility can ensure the distribution of raw materials (Zhang et al., 2021b).

Information factors: Consumers often consider the place of origin of images and popularity of exotic foods, personal consumption concepts, eating habits, food quality, and impressions of a restaurant's decor and then reach a purchase intention and choice preferences. Of these criteria, consumer knowledge of exotic food mainly comes through public media such as Japanese variety shows, animation, film, and television (Thorogood, 2020).

Humanistic factors: War can expose people to exotic food and deepen the impression and association of exotic cultures (Wallin and Sandlin, 2020). To understand the influence of the War of Aggression against China on the spread and development of Japanese cuisine in China, the cities affected by the war were assigned a value of 1 and the cities not affected by the war were assigned a value of 0. Moreover, consumers can directly contact the origin of exotic food through travel, which also increases familiarity with specific exotic foods.

The socioeconomic factors screened in this study are shown in **Table 1**. Considering the integrity of urban, economic, and social data, we used data from the Statistical Yearbook of 2021 for analysis.

TABLE 1 | Socioeconomic factors and descriptions.

	Factors	Description	Meaning
Economic factors	Per capita GDP (LNPGDP)	Social and economic development level	Affects the size of the consumer market
	Urbanization rate (LNUR)	Land urbanization process	Provides activity location
	Tertiary industry proportion (LNTIP)	Development degree of service industry	Represents the vitality of the catering industry
	Population (LNPOP)	Urban population	Consumer size
	Land rent (LNLR)	Rent paid by the producer	Operating costs of merchants
	Income (LNIN)	Disposable income of urban residents	Consumer's ability to pay
Spatial factors	Road network density (LNRND)	Urban highway mileage/urban area	Accessibility of consumption locations
	Distance (LNDIS)	Geographical distance from Tokyo to Chinese cities	Distance from place of origin to place of consumption
Information factors	TV coverage (LNTV)	TV population coverage rate	Propaganda environment
Humanistic factors	War (LNWAR)	Japanese war of aggression against China	Reconstruction of urban socioeconomic environment
	Flight (LNFL)	Weekly direct flights to Japan	Convenience of access to place of origin

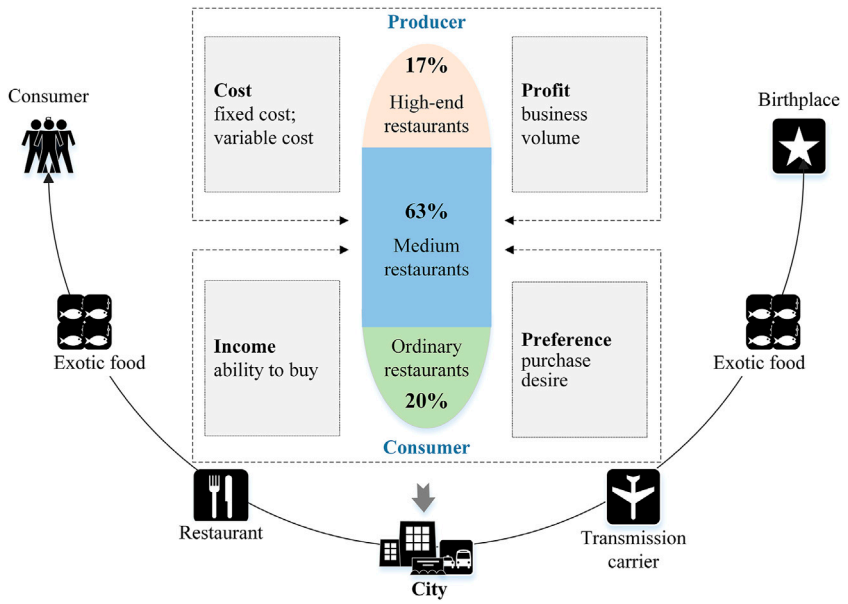

FIGURE 2 | Price characteristics of Japanese cuisine in China.

3 RESULTS

3.1 Price Characteristics: Middle-Income Group as Service Object

According to economics, consumer demand is the quantity of goods or services that consumers are willing and able to buy at a certain price level. There must be an effective demand with both purchasing desire and purchasing power. The main factors include the price of goods, consumer income levels, consumer preferences, and consumer expectations of the price of the goods. Studies conducted in different environments have indicated that price is one of the main barriers to consumer access to dietary diversity benefits (Herforth and Ahmed, 2015; Vittersø and Tangeland, 2015).

By analyzing the average price of Japanese restaurants, we found that 17% of restaurants have an average price lower than 50¥, 63% have an average price of 50–211¥, and 20% have an average price higher than 211¥. **Figure 2** shows that the pricing characteristic of Japanese cuisine is spindle-type, which signals that the main customers of Japanese cuisine are middle-income people, including the middle class and the "new middle class." Therefore, wealthier areas may have more opportunities to enjoy more diverse and higher quality foods, while small and medium-sized cities and their residents are at a disadvantage in this sense. The eastern cities of China, which are economically dominant, have more potential consumers and greater consumer demand. Therefore, these cities are more likely to have a spatial agglomeration of restaurants and dishes. This finding is in line with general knowledge that big cities often have greater quality of life and wellbeing.

3.2 Spatial Inequality of Geographical Distribution

The distribution of restaurant locations and the field intensity of Japanese restaurants is basically bounded by the Hu line (The Hu

TABLE 2 | Differences in restaurant dish styles and field intensity.

Distribution difference	Number of restaurants	Dish styles	Field intensity
80,212 (97%)	168 (0 ≤NR <100)	309 (4 ≤DS ≤7)	61 (0 ≤FI ≤0.08)
→ East	→ 51%	→ 93%	→ 18.4%
2,475 (3%)	164 (105 ≤NR <4,963)	23 (0 ≤DS <4)	271 (0.08 <FI <41)
→ West	→ 49%	→ 7%	→ 81.6%

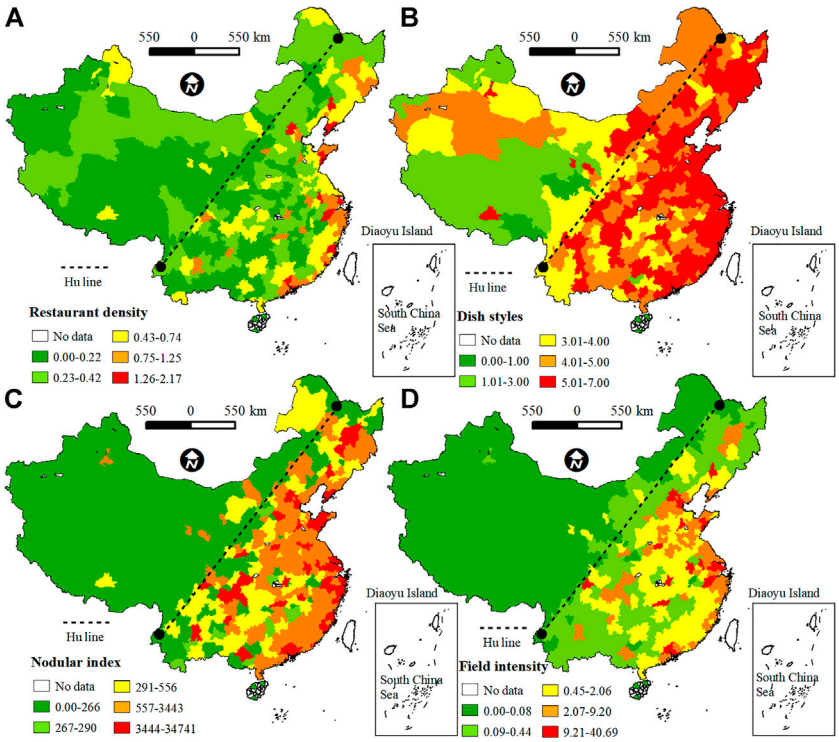

FIGURE 3 | Spatial inequality of Japanese cuisine distribution in China. **(A)** Shows the spatial imbalance of the restaurant density of Japanese cuisine between cities. **(B)** Shows the spatial imbalance of the dish styles of Japanese cuisine between cities. **(C)** Shows the spatial imbalance of the nodular index of Japanese cuisine between cities. **(D)** shows the spatial imbalance of the field intensity of Japanese cuisine between cities.

line is a line that divides China's population by density; it was proposed by Chinese geographer Hu Huanyong in 1935. According to the analysis of statistical data in 2000, the National Conditions group at the Chinese Academy of Sciences indicated that the southeast side of the Hu line accounts for 43.18% of China's total land area, with 93.77% of the population and 95.7% of the GDP, an area with an overwhelmingly high-density economic and social function), but its distribution characteristics are more significant than population density.

In addition, in cities east of the Hu line, the total number of restaurants is 80,212, accounting for 97% of the national total, whereas the total number of restaurants in western cities is 2,475, accounting for only 3% of the national total (**Table 2**). If NR represents the number of Japanese restaurants, 168 cities have 0 ≤NR <100 restaurants, accounting for 51% of all cities (**Table 2**), and these cities are mainly distributed in central and western regions; 164 cities with 100 ≤NR <4,963 restaurants, accounting for 49% of all cities, are mainly distributed in eastern coastal areas (**Figure 3A**).

Figure 3B shows that there are 309 cities with dish styles (DS) between 4 ≤DS ≤7, accounting for 93% of the total number of cities. There are only 23 cities with 0 ≤DS <4 styles, but 82 cities have seven kinds of dishes. In terms of dish styles, there is a significant two-level differentiation in the service characteristics of Japanese cuisine.

Figures 3C,D show the spatial imbalance of the service capacity of Japanese cuisine between cities. In cities east of the Hu line, the field intensity value is basically higher than 0.08, and the service ability is strong; in western cities, the field intensity (FI) value is basically lower than 0.08, and the service ability is weak. Overall, there are 61cities with 0 ≤FI ≤0.08, accounting for 18.4% of all cities, and these are concentrated in central and western regions; there are 271 cities with 0.09 <FI <41, accounting for 81.6% of all cities, and these are mainly distributed in the East.

TABLE 3 | Results of models 1, 2, and 3

	M1 = Restaurants			M2 = Dish styles			M3 = Field intensity		
	OLS	SLM	SEM	OLS	SLM	SEM	OLS	SLM	SEM
	Coef	Coef	Coef	Coef	Coef	Coef	Coef	Coef	Coef
LNPGDP	0.416a	0.335a	0.427a	0.087a	0.059b	0.076a	0.502a	0.369a	0.596a
LNUR	1.213a	1.113a	1.163a	0.339a	0.278a	0.290a	1.873a	1.553a	1.455a
LNTIP	1.106a	1.119a	1.047a	0.052	0.072	0.068	1.140a	1.256a	1.359a
LNPOP	1.01a	0.935a	1.014a	0.203a	0.172a	0.190a	1.338a	1.106a	1.128a
LNLR	0.366a	0.354a	0.188b	−0.018	0.009	−0.001	0.321c	0.399a	0.448a
LNIN	0.141	0.062	0.028	−0.081	−0.068	−0.053	0.296	0.130	0.009
LNRND	0.066b	−0.021	0.034	0.011	−0.009	0.013	0.463a	0.210a	0.182a
LNDIS	−0.09	−0.075	−0.071	−0.012	−0.008	−0.012	−0.157	−0.109	−0.125
LNTV	−1.471a	−1.467a	−1.123a	0.301c	0.144	0.233	−3.150a	−2.699a	−2.663a
LNWAR	0.295a	0.138c	0.126	0.082b	0.033	0.051	0.445a	0.140	0.186
LNFL	−0.047	−0.004	−0.009	−0.039b	−0.034b	−0.041b	−0.175b	−0.094	−0.131b
C	−0.006	−0.009	−0.011	−0.001	−0.002	−0.002	−0.002	−0.007	−0.009
ρ	—	0.231a	—	—	0.356a	—	—	0.338a	—
λ	—	—	0.631a	—	—	0.429a	—	—	0.678a
R^2	0.91	0.92	0.94	0.68	0.72	0.72	0.86	0.89	0.89
Adj-R^2	0.91	—	—	0.67	—	—	0.85	—	—
F	309.641	—	—	62.930	—	—	186.009	—	—
LIK	−194.227	−166.062	−147.656	70.699	88.916	85.017	−388.51	−344.413	−359.054
AIC	412.454	358.124	319.314	−117.399	−151.832	−146.035	801.019	714.826	742.109
SC	458.224	407.707	365.083	−71.629	−102.248	−100.265	846.789	764.409	787.879
Moran's I	10.818a			5.768a			5.989a		
LM lag	58.990a			36.620a			84.292a		
R-LM lag	15.132a			9.588a			55.144a		
LM err	106.642a			28.993a			31.369a		
R-LM err	62.784a			1.960			2.221		

Note: a, b, and c represent the 1%, 5%, and 10% significance levels, respectively.

3.3 The Relationship Between Spatial Imbalance and the Socioeconomic Factors

In the socioeconomic environment, the characteristics or identity of the media often determine the characteristics of catering services. The impact of non-equalization of the external environment, such as social economy, on producers and consumers became the main criteria for screening socio-economic environment factors in this study.

GeoDa is a free and open-source software tool that serves as an introduction to spatial data science; thus, we used GeoDa to solve the model. Before the establishment of the spatial econometric model, the spatial correlation of the sample data was tested. **Table 3** shows that Moran's I are 10.818, 5.768, and 5.989, and their significance levels are all lower than 0.001, indicating that the spatial distribution of restaurant locations, the formation of dish styles, and the consumption intensity of Japanese restaurants are not completely random, but have a certain spatial correlation. Therefore, the OLS regression results may be biased. It is necessary to use the spatial econometric model to for estimation.

From the perspective of variable coefficient and significance (**Table 3**), the results of the model calculation are consistently high, and the R^2 value increases after considering the spatial correlation (SLM = 0.92, 0.72, and 0.89 and SEM = 0.94, 0.72, 0.89, higher than the R^2 value of OLS). The SLM and SEM interpretation results are better than the OLS regression results. Combining the LM and R-LM values and their significance and comparing the fitting effects of SLM and SEM, the significance of SLM regression results and test results is better than SEM model results. Thus, this study selects SLM results for subsequent analysis.

Table 3 shows that urbanization level, population size, and economic scale are the key factors that lead to spatial distribution inequality and service imbalance of Japanese cuisine in China. Cities with a large economic scale can often gather more resources. This agglomeration enables economic activities to play a scale effect, which makes the price of products in big cities not only lower but also increases the variety available for selection (Handbury and Weinstein, 2015). Further research shows that in China, large cities have more products and lower prices (Feenstra et al., 2017). Therefore, larger economic-scale cities can gather more consumer demand and market of Japanese cuisine, and the scale of development of Japanese restaurants in these first-tier cities is significantly higher than in other cities.

Population size affects the quantity of food supply and the diversity of dishes. The main reason for this effect is that the size of a population increases the demand for food diversity at the consumption level, which leads to aggregation of various kinds of foods (including exotic foods) and finally results in greater diversity in a more densely populated city, giving the city stronger service ability and higher radiation field intensity. The larger the population, the more Japanese restaurants there are. For example, the top 25 Chinese cities for the number of restaurants accounts for 23% of the total population, but the number of restaurants accounts for 49% of the country

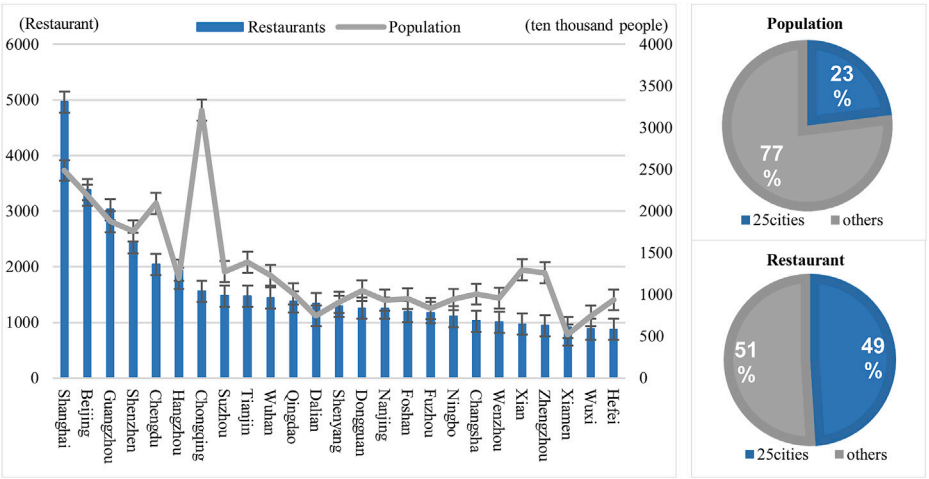

FIGURE 4 | Cities with top 25 restaurants.

(**Figure 4**). The number of restaurants in cities is basically consistent with the size of the urban population. In addition, the huge population size also entails a complex population structure and an ease in creating a complex heterogeneous demand set in a city, which produces high demand for food types in certain areas. The large coefficient also implies that there may be such a mechanism. The diversity of the population leads to integration of different cultures, making people more willing to try exotic foods (Glaeser et al., 2001).

Simultaneously, the degrees of effect of the elements in model 1 are the following: LNTV> LNTIP> LNUR> LNPOP> LNLR> LNPGDP> LNWAR. The degrees of the functions of the elements in model 2 are the following: LNUR> LNPOP> LNPGDP> LNFL. The degree of the functions of the elements in model 3 are the following: LNTV> LNUR> LNTIP> LNPOP> LNLR> LNPGDP> LNRND.

4 DISCUSSION AND CONCLUSION

4.1 Discussion

Consumer love for variety is a common assumption in modern economics (Glaeser et al., 2001). Due to the heterogeneity of cities and the non-equalization of service facilities, the spatial distribution of food and drink is often unbalanced and complex. Considering the necessity to promote food equality in different socioeconomic areas and the offsetting of the negative impact on the health of vulnerable groups, it is necessary to interpret the spatial equality of dietary distribution (Turner et al., 2018, Turner et al., 2020).

The global commodity network brings a systematic and interconnected consumption landscape. Considering that the socioeconomic environment of consumers is not consistent under different urbanization levels, the place effect should be considered when describing the characteristics of urban catering services; that is, different spatial locations of food, different degrees of realization of the same food, and different benefits. It is more comprehensive and objective to identify the service differences of Japanese cuisine in different regions and spaces with the help of a field intensity model.

This study also encourages and advocates the use of multiple geographic data, the use of data provided by other GeoWeb websites, and other Web2.0 online websites, actively exploring the connection and interaction between geosciences and socio-economic phenomena. In the era of mobile internet, the internet catering service platform has become an important channel for the majority of catering business operators to obtain business data and consumer evaluation information. This would largely change the impact of the competitive rent theory on the location choice of restaurants. These online catering websites can provide more positive and beneficial opportunities for researchers to pay attention to the urban food environment. Simultaneously, it is necessary to explore the application of big data in the field of geographical sustainability. The rise of big data provides new methods, new ideas, and new solutions to pressing urban issues (Xue et al., 2020; Liu et al., 2021; Yang et al., 2021). In contrast to questionnaire and interview approaches, we collected third-party big data provided by an online catering platform to analyze the spatial differences in the number of restaurants and dish styles of exotic food. The multifusion data and big data in this study also provided references for solutions to other urban problems (Shelestov et al., 2017; Haworth et al., 2018; Shirazi et al., 2021; Zhang et al., 2020).

Our results show that there are more Japanese restaurants and dish styles in Eastern China. This conclusion is consistent with the main findings of Tian et al. (2021) on the spatial distribution pattern of Chinese seafood restaurants. They found that seafood restaurants are concentrated in coastal cities. Our results also support the significant correlation between population size, economic development, and the distribution of different types of restaurants. However, this study does not confirm that the geographical distance proposed by Tian et al. (2022) has a significant impact on the distribution of restaurants. We believe that this may be related to consumers' eating habits and the pricing of Japanese restaurants. In addition to the socioeconomic factors in the socioeconomic environment, food similarity and cultural similarity may also have

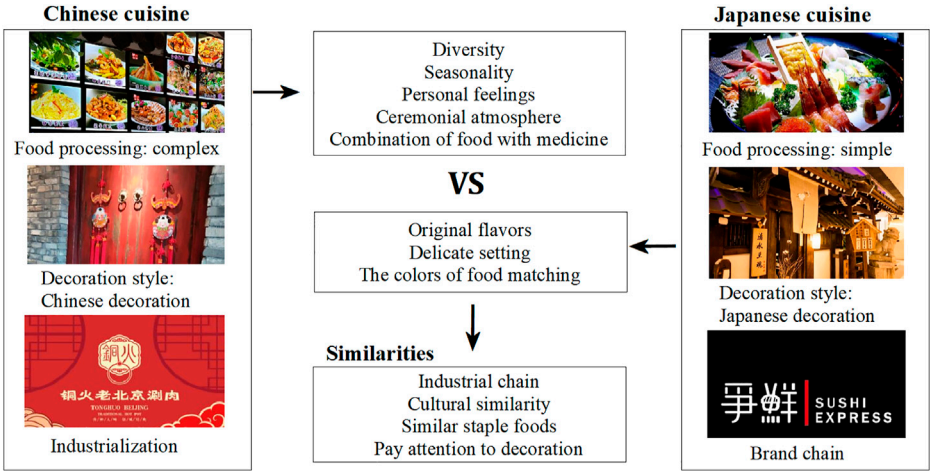

FIGURE 5 | Similarities between Japanese cuisine and a traditional Chinese cuisine.

a potential impact on the spatial inequality of dietary distribution (**Figure 5**). Rice is a staple of Japanese cuisine and so is very easily accepted by Chinese consumers. In addition, Japanese cuisine consists mainly of seafood, and the acceptability of seafood in China's coastal regions is very high. It is not difficult to understand that Eastern coastal cities become hot spots and regions where Japanese restaurants are found in higher concentrations. In inland cities, local consumers are not accustomed to eating seafood, and so, the acceptability of this cuisine is relatively low, making these cities cold spots of distribution. This also demonstrates the objectivity of our findings.

A limitation of this study is that the topographic division of urban space, such as by landscape patterns, hinders the spread and diffusion of Japanese cuisine in China, and the research results may contain some errors as a result. In addition, the distance friction coefficient in the field intensity model is usually between 1.0 and 3.0 (the distance attenuation curve varies with the coefficient). The difference in parameter values may lead to deviation from the actual situation, which, in turn, may lead to less accurate calculation.

4.2 Conclusion

By describing the place effect of Japanese cuisine on different spaces in China, we found that the number of restaurants, dish styles, and field intensity shows a gradual decline from eastern cities to western cities. Compared to the Hu line, which reflects the spatial difference in population, the number of restaurants in eastern cities is 32 times that in western cities.

The influx of Japanese cuisine has not alleviated inequality in the urban food environment. The pricing strategies of different grades of dishes show that Japanese cuisine mainly serves the middle class, which means that rich cities often enjoy higher quality food. For cities in a weak position, this undoubtedly damages the wellbeing and the diversity of comfort that food can provide.

Based on the analysis of the local socioeconomic factors, urbanization level, population size, and economic scale are significantly correlated with the maturity of Japanese cuisine. However, the degree of responsiveness of service ability to the socioeconomic environment changes with the location. This also implies that the positioning demand of Japanese cuisine and urban socioeconomic environment is intrinsically related to its price characteristics. The choice of restaurant location and the strength of service ability are the result of the interaction of external socioeconomic environment and internal price characteristics.

We also find that sushi (in 328 cities) and other culturally distinctive dishes have become the most accessible and most likely to be sampled. For certain dishes, the spatial imbalance may not be significant. In the future, it will be necessary to analyze consumer personal values and the relationship between their purchasing lines and specific food choices.

DATA AVAILABILITY STATEMENT

The original contributions presented in the study are included in the article/Supplementary Material; further inquiries can be directed to the corresponding author.

AUTHOR CONTRIBUTIONS

Methodology, WL; software and validation, CT and HW.; formal analysis, CT; writing—original draft preparation, CT; writing—review and editing, WL; visualization, HW; supervision, HW; funding acquisition, WL. All authors have read and agreed to the published version of the manuscript.

FUNDING

This research was funded by the Key Program of National Natural Science Foundation of China, Grant Number 42030409.

REFERENCES

Adams, E. L., Caccavale, L. J., Smith, D., and Bean, M. K. (2020). Food Insecurity, the Home Food Environment, and Parent Feeding Practices in the Era of COVID-19. *Obesity* 28 (11), 2056–2063. doi:10.1002/oby.22996

An, R., and Sturm, R. (2012). School and Residential Neighborhood Food Environment and Diet Among California Youth. *Am. J. Prev. Med.* 42 (2), 129–135. doi:10.1016/j.amepre.2011.10.012

An, R., He, L., and Shen, M. J. (2020). Impact of Neighbourhood Food Environment on Diet and Obesity in China: a Systematic Review. *Public Health Nutr.* 23 (3), 457–473. doi:10.1017/S1368980019002167

Anderson, C. E., Crespi, C. M., Wang, M. C., Whaley, S. E., and Chaparro, M. P. (2020). The Neighborhood Food Environment Modifies the Effect of the 2009 WIC Food Package Change on Childhood Obesity in Los Angeles County, California. *BMC Public Health* 20 (1), 678. doi:10.1186/s12889-020-08779-2

Armington, P. S. (1969). A Theory of Demand for Products Distinguished by Place of Production. *Staff Pap. - Int. Monet. Fund.* 16, 159–176. doi:10.2307/3866403

Black, C., Moon, G., and Baird, J. (2014). Dietary Inequalities: what Is the Evidence for the Effect of the Neighbourhood Food Environment? *Health Place* 27, 229–242. doi:10.1016/j.healthplace.2013.09.015

Çanakçı, S. D., and Birdir, K. (2020). The Relation Among Food Involvement, Food Variety Seeking and Food Neophobia: A Study on Foreign Tourists Visiting Turkey. *Curr. Issues Tour.* 23 (8), 917–928. doi:10.1080/13683500.2019.1602114

Caspi, C. E., Sorensen, G., Subramanian, S. V., and Kawachi, I. (2012). The Local Food Environment and Diet: a Systematic Review. *Health Place* 18 (5), 1172–1187. doi:10.1016/j.healthplace.2012.05.006

Chen, X., and Yang, X. (2014). Does Food Environment Influence Food Choices? A Geographical Analysis through "Tweets". *Appl. Geogr.* 51, 82–89. doi:10.1016/j.apgeog.2014.04.003

Clark, B., Stewart, G. B., Panzone, L. A., Kyriazakis, I., and Frewer, L. J. (2017). Citizens, Consumers and Farm Animal Welfare: a Meta-Analysis of Willingness-To-Pay Studies. *Food Policy* 68, 112–127. doi:10.1016/j.foodpol.2017.01.006

Cobb, L. K., Appel, L. J., Franco, M., Jones-Smith, J. C., Nur, A., and Anderson, C. A. M. (2015). The Relationship of the Local Food Environment with Obesity: a Systematic Review of Methods, Study Quality, and Results. *Obesity* 23 (7), 1331–1344. doi:10.1002/oby.21118

Eckert, J., and Vojnovic, I. (2017). Fast Food Landscapes: Exploring Restaurant Choice and Travel Behavior for Residents Living in Lower Eastside Detroit Neighborhoods. *Appl. Geogr.* 89, 41–51. doi:10.1016/j.apgeog.2017.09.011

FAO-Food and Agriculture Organization of the United Nations (2016). *Influencing Food Environments for Healthy Diets through Food Safety*. Rome: FAO.

Feenstra, R. C., Xu, M., and Antoniades, A. (2017). What Is the Price of Tea in China? towards the Relative Cost of Living in Chinese and U.S. Cities. *SSRN J.* (No. w23161). National Bureau of Economic Research. doi:10.2139/ssrn.2925530

Garcia, X., Garcia-Sierra, M., and Domene, E. (2020). Spatial Inequality and its Relationship with Local Food Environments: The Case of Barcelona. *Appl. Geogr.* 115, 102140. doi:10.1016/j.apgeog.2019.102140

Glaeser, E. L., Kolko, J., and Saiz, A. (2001). Consumer City. *J. Econ. Geogr.* 1 (1), 27–50. doi:10.1093/jeg/1.1.27

Guo, A., Yang, J., Sun, W., Xiao, X., Xia Cecilia, J., Jin, C., et al. (2020a). Impact of Urban Morphology and Landscape Characteristics on Spatiotemporal Heterogeneity of Land Surface Temperature. *Sustain. Cities Soc.* 63, 102443. doi:10.1016/j.scs.2020.102443

Guo, A., Yang, J., Xiao, X., Xia, J., Jin, C., and Li, X. (2020b). Influences of Urban Spatial Form on Urban Heat Island Effects at the Community Level in China. *Sustain. Cities Soc.* 53, 101972. doi:10.1016/j.scs.2019.101972

Handbury, J., and Weinstein, D. E. (2015). Goods Prices and Availability in Cities. *Rev. Econ. Stud.* 82 (1), 258–296. doi:10.1093/restud/rdu033

Haworth, B. T., Bruce, E., Whittaker, J., and Read, R. (2018). The Good, the Bad, and the Uncertain: Contributions of Volunteered Geographic Information to Community Disaster Resilience. *Front. Earth Sci.* 6, 183. doi:10.3389/feart.2018.00183

Herforth, A., and Ahmed, S. (2015). The Food Environment, its Effects on Dietary Consumption, and Potential for Measurement within Agriculture-Nutrition Interventions. *Food Sec.* 7 (3), 505–520. doi:10.1007/s12571-015-0455-8

Jang, M., Brown, R., and Vang, P. Y. (2020). The Relationships between Parental Stress, Home Food Environment, and Child Diet Patterns in Families of Preschool Children. *Am. J. Health Promot* 35, 131–139. doi:10.1177/0890117120929541

Kwate, N. O. A., and Loh, J. M. (2016). Fast Food and Liquor Store Density, Co-tenancy, and Turnover: Vice Store Operations in Chicago, 1995-2008. *Appl. Geogr.* 67, 1–13. doi:10.1016/j.apgeog.2015.11.021

Leslie, T. F., Frankenfeld, C. L., and Makara, M. A. (2012). The Spatial Food Environment of the DC Metropolitan Area: Clustering, Co-location, and Categorical Differentiation. *Appl. Geogr.* 35, 300–307. doi:10.1016/j.apgeog.2012.07.008

Li, J., and Kim, C. (2020). Exploring Relationships of Grocery Shopping Patterns and Healthy Food Accessibility in Residential Neighborhoods and Activity Space. *Appl. Geogr.* 116, 102169. doi:10.1016/j.apgeog.2020.102169

Liu, X., Fatoyinbo, T. E., Thomas, N. M., Guan, W. W., Zhan, Y., Mondal, P., et al. (2021). Large-Scale High-Resolution Coastal Mangrove Forests Mapping across West Africa with Machine Learning Ensemble and Satellite Big Data. *Front. Earth Sci.* 8. doi:10.3389/feart.2020.560933

Luciene, F. F. A., Taiane, G. N., Pessoa, M. C., Carmo, A. S. D., and Andréia, Q. R. (2020). Socioeconomic Disparities in the Community Food Environment of a Medium-Sized City of Brazil. *J. Am. Coll. Nutr.* 40 (2), 253–260. doi:10.1080/07315724.2020.1755911

Lytle, L. A., and Sokol, R. L. (2017). Measures of the Food Environment: A Systematic Review of the Field, 2007-2015. *Health Place* 44, 18–34. doi:10.1016/j.healthplace.2016.12.007

Osei-Kwasi, H., Mohindra, A., Booth, A., Laar, A., Wanjohi, M., Graham, F., et al. (2020). Factors Influencing Dietary Behaviours in Urban Food Environments in Africa: a Systematic Mapping Review. *Public Health Nutr.* 23, 2584–2601. doi:10.1017/S1368980019005305

Qin, X., Zhen, F., and Gong, Y. (2019). Combination of Big and Small Data: Empirical Study on the Distribution and Factors of Catering Space Popularity in Nanjing, China. *J. Urban Plann. Dev.* 145 (1), 05018022. doi:10.1061/(ASCE)UP.1943-5444.0000489

Rui, Y., Huang, H., Lu, M., Wang, B., and Wang, J. (2016). A Comparative Analysis of the Distributions of KFC and McDonald's Outlets in China. *ISPRS Int. J. Geo-Inf.* 5 (3), 27. doi:10.3390/ijgi5030027

Schiff, N. (2015). Cities and Product Variety: Evidence from Restaurants. *J. Econ. Geogr.* 15 (6), 1085–1123. doi:10.1093/jeg/lbu040

Shelestov, A., Lavreniuk, M., Kussul, N., Novikov, A., and Skakun, S. (2017). Exploring Google Earth Engine Platform for Big Data Processing: Classification of Multi-Temporal Satellite Imagery for Crop Mapping. *Front. Earth Sci.* 5, 17. doi:10.3389/feart.2017.00017

Shen, Q., and Xiao, P. (2014). McDonald's and KFC in China: Competitors or Companions? *Mark. Sci.* 33 (2), 287–307. doi:10.1287/mksc.2013.0824

Shirazi, Z., Wang, L., and Bondur, V. G. (2021). Modeling Conditions Appropriate for Wildfire in South East China-A Machine Learning Approach. *Front. Earth Sci.* 9, 361. doi:10.3389/feart.2021.622307

Swinburn, B., Kraak, V., Rutter, H., Vandevijvere, S., Lobstein, T., Sacks, G., et al. (2015). Strengthening of Accountability Systems to Create Healthy Food Environments and Reduce Global Obesity. *Lancet* 385 (9986), 2534–2545. doi:10.1016/s0140-6736(14)61747-5

Thorogood, J. (2020). Cartoon Controversies and Geopolitics: Archer, Animators and Audiences. *Soc. Cult. Geogr.* 21 (3), 357–379. doi:10.1080/14649365.2018.1497190

Tian, C., Luan, W., Li, S., Xue, Y., and Jin, X. (2021). Spatial Imbalance of Chinese Seafood Restaurants and its Relationship with Socioeconomic Factors. *Ocean Coast. Manag.* 211, 105764. doi:10.1016/j.ocecoaman.2021.105764

Tian, C., Luan, W., You, D., Su, M., and Jin, X. (2022). Seafood Availability and Geographical Distance: Evidence from Chinese Seafood Restaurants. *Ocean Coast. Manag.* 225, 106219. doi:10.1016/j.ocecoaman.2022.106219

Turner, C., Aggarwal, A., Walls, H., Herforth, A., Drewnowski, A., Coates, J., et al. (2018). Concepts and Critical Perspectives for Food Environment Research: A Global Framework with Implications for Action in Low-And Middle-Income Countries. *Glob. food Secur.* 18, 93–101. doi:10.1016/j.gfs.2018.08.003

Turner, C., Kalamatianou, S., Drewnowski, A., Kulkarni, B., Kinra, S., and Kadiyala, S. (2020). Food Environment Research in Low-And Middle-Income Countries: a Systematic Scoping Review. *Adv. Nutr.* 11 (2), 387–397. doi:10.1093/advances/nmz031

Vittersø, G., and Tangeland, T. (2015). The Role of Consumers in Transitions towards Sustainable Food Consumption. The Case of Organic Food in Norway. *J. Clean. Prod.* 92, 91–99. doi:10.1016/j.jclepro.2014.12.055

Wallin, J. J., and Sandlin, J. A. (2020). Plastic Fantasies: Globalization and the Japanese Cultural Imaginary. *Cult. Stud. ↔ Crit. Methodol.* 20 (6), 524–534. doi:10.1177/1532708620911407

Willmott, H. (2007). "Political Cultural Economy and the Financialization of Brand Equity," in ESRC Centre for Research on Socio-Cultural Change 3rd Annual Conference: Re-thinking Cultural Economy, Manchester, United Kingdom, September 5–7, 2007.

Wu, J., Feng, Z., Zhang, X., Xu, Y., and Peng, J. (2020). Delineating Urban Hinterland Boundaries in the Pearl River Delta: An Approach Integrating Toponym Co-occurrence with Field Strength Model. *Cities* 96, 102457. doi:10.1016/j.cities.2019.102457

Wu, M., Pei, T., Wang, W., Guo, S., Song, C., Chen, J., et al. (2021). Roles of Locational Factors in the Rise and Fall of Restaurants: A Case Study of Beijing with POI Data. *Cities* 113, 103185. doi:10.1016/j.cities.2021.103185

Xue, B., Xiao, X., and Li, J. (2020). Identification Method and Empirical Study of Urban Industrial Spatial Relationship Based on POI Big Data: a Case of Shenyang City, China. *Geogr. Sustain.* 1 (2), 152–162. doi:10.1016/j.geosus.2020.06.003

Yang, J., Guo, A., Li, X., and Huang, T. (2018). Study of the Impact of a High-Speed Railway Opening on China's Accessibility Pattern and Spatial Equality. *Sustainability* 10 (8), 2943. doi:10.3390/su10082943

Yang, J., Guo, A., Li, Y., Zhang, Y., and Li, X. (2019). Simulation of Landscape Spatial Layout Evolution in Rural-Urban Fringe Areas: a Case Study of Ganjingzi District. *GIScience remote Sens.* 56 (3), 388–405. doi:10.1080/15481603.2018.1533680

Yang, J., Ren, J., Sun, D., Xiao, X., Xia, J., Jin, C., et al. (2021). Understanding Land Surface Temperature Impact Factors Based on Local Climate Zones. *Sustain. Cities Soc.* 69, 102818. doi:10.1016/j.scs.2021.102818

Zeng, G. J., and Liu, M. (2013). Diet Geography and Translocal Restaurants' Cultural Production. *Tour. Trib.* 3, 9–11. doi:10.13284/j.cnki.rddl.002816

Zhang, D., Zhou, C., and Xu, W. (2020). Spatial-temporal Characteristics of Primary and Secondary Educational Resources for Relocated Children of Migrant Workers: The Case of Liaoning Province. *Complexity* 2020, 1–13. doi:10.1155/2020/7457109

Zhang, Z., Luan, W., Tian, C., Su, M., and Li, Z. (2021). Spatial Distribution Equilibrium and Relationship between Construction Land Expansion and Basic Education Schools in Shanghai Based on POI Data. *Land* 10 (10), 1059. doi:10.3390/land10101059

Zhang, D., Zhang, G., and Zhou, C. (2021a). Differences in Accessibility of Public Health Facilities in Hierarchical Municipalities and the Spatial Pattern Characteristics of Their Services in Doumen District, China. *Land* 10 (11), 1249. doi:10.3390/land10111249

Zhang, D., Zhou, C., Sun, D., and Qian, Y. (2021b). The Influence of the Spatial Pattern of Urban Road Networks on the Quality of Business Environments: the Case of Dalian City. *Environ. Dev. Sustain.*, 1–18. doi:10.1007/s10668-021-01832-z

Zhou, C., Zhang, D., and He, X. (2021). Transportation Accessibility Evaluation of Educational Institutions Conducting Field Environmental Education Activities in Ecological Protection Areas: A Case Study of Zhuhai City. *Sustainability* 13 (16), 9392. doi:10.3390/su13169392

Conflict of Interest: The authors declare that the research was conducted in the absence of any commercial or financial relationships that could be construed as a potential conflict of interest.

Publisher's Note: All claims expressed in this article are solely those of the authors and do not necessarily represent those of their affiliated organizations, or those of the publisher, the editors, and the reviewers. Any product that may be evaluated in this article, or claim that may be made by its manufacturer, is not guaranteed or endorsed by the publisher.

Copyright © 2022 Tian, Luan and Wang. This is an open-access article distributed under the terms of the Creative Commons Attribution License (CC BY). The use, distribution or reproduction in other forums is permitted, provided the original author(s) and the copyright owner(s) are credited and that the original publication in this journal is cited, in accordance with accepted academic practice. No use, distribution or reproduction is permitted which does not comply with these terms.

frontiers | Frontiers in Environmental Science

ORIGINAL RESEARCH
published: 14 July 2022
doi: 10.3389/fenvs.2022.940482

Impacts of Water Bodies on Microclimates and Outdoor Thermal Comfort: Implications for Sustainable Rural Revitalization

Yanyan Cheng[1†], Xiao Liu[2,3,4,5†], Zhi Zeng[1], Shengshuai Liu[1], Zhaoyu Wang[1], Xu Tang[3] and Bao-Jie He[5,6,7*]*

[1]North China University of Water Resources and Electric Power, Zhengzhou, China, [2]School of Architecture, South China University of Technology, Guangzhou, China, [3]Department of Urban Planning and Design, Faculty of Architecture, The University of Hong Kong, Hong Kong SAR, China, [4]Architectural Design & Research Institute Co., Ltd., South China University of Technology, Guangzhou, China, [5]State Key Laboratory of Subtropical Building Science, South China University of Technology, Guangzhou, China, [6]Centre for Climate-Resilient and Low-Carbon Cities, School of Architecture and Urban Planning, Chongqing University, Chongqing, China, [7]Key Laboratory of New Technology for Construction of Cities in Mountain Area, Ministry of Education, Chongqing University, Chongqing, China

OPEN ACCESS

Edited by:
Jianhong Xia,
Curtin University, Australia

Reviewed by:
Andong Guo,
Zhejiang University, China
Dahao Zhang,
Sun Yat-sen University, China
Decheng Zhou,
Nanjing University of Information Science and Technology, China

***Correspondence:**
Xiao Liu
xiaoliu@scut.edu.cn
Bao-Jie He
baojie.he@cqu.edu.cn

[†]These authors have contributed equally to this work and share first authorship

Specialty section:
This article was submitted to Environmental Informatics and Remote Sensing, a section of the journal Frontiers in Environmental Science

Received: 10 May 2022
Accepted: 15 June 2022
Published: 14 July 2022

Citation:
Cheng Y, Liu X, Zeng Z, Liu S, Wang Z, Tang X and He B-J (2022) Impacts of Water Bodies on Microclimates and Outdoor Thermal Comfort: Implications for Sustainable Rural Revitalization. Front. Environ. Sci. 10:940482. doi: 10.3389/fenvs.2022.940482

Water is the source of life and the fundamental element of ecology, and climate is inseparable from water. To evaluate the influence of water-adaptive space in a traditional Weizi (polder village) settlement on its microclimate, the authors analyzed the morphological characteristics of such a polder village and applied the ENVI-met model to simulate the impact of water bodies and village morphological elements on human thermal comfort. This paper demonstrates the positive impact of water bodies on improving the thermal environment of a village and regulating its microclimate by quantifying the impact of morphological elements of the settlement on microclimate. The results indicate that: 1) The simulation model fits the actual measurements well, and the simulation accurately reflects experimental results; 2) In summer, the cooling effect of water bodies is better in the afternoon than in the morning, especially from 12:00 to 15:00. The cooling effect is significantly correlated with the distance to water bodies, i.e., the closer, the better; 3) Building density and man-made underlying surface are negatively correlated with temperature, humidity, and Physiological Equivalent Temperature value, while greening rate and water body rate are positively correlated with microclimate. Overall, water bodies can improve outdoor comfort in summer and thus should be protected and developed in rural planning and design. Villages can be built around water bodies for a maximized cooling effect, and microclimate comfort can be effectively improved by increasing green plants near the village center, and reducing man-made underlying surface and building density. The results of this study will guide the improvement of the habitat environment in the process of rural revitalization, as well as the protection and re-development of traditional villages.

Keywords: water bodies, water-sensitive design, microclimate, thermal comfort, ENVI-met, rural revitalization

1 INTRODUCTION

Water plays a key role in ecosystem evolution (Zhang et al., 2009), and human intervention makes the impact of water on the ecological environment even more significant (Jewitt, 2002). Ecological revitalization is an important part of rural revitalization, and ecological stability directly affects the quality of human settlements (Li et al., 2020). Water-adaptive space in vernacular settlements reflects a dynamic relationship between human beings and water resources. The water-adaptive space presents ancestors' wisdom to adapt to and moderately transform the water environment and utilize water resources in a low-technology, low-cost, low-maintenance, and sustainable way. Early human settlements were always near the water, and people developed various methods to utilize water resources. A Weizi settlement or polder village is a typical example of human habitat that adapts to, transforms, and utilizes a water environment. It is a typical model of Chinese traditional human settlement that combines human habitat with farmland and water conservancy (Cheng and Guo, 2015). This type of traditional human habitat that coexists with water has exhibited a live model for current rural revitalization and sustainable development. Water meets the needs of agricultural production and daily life in the village and it also has a regulatory effect on microclimate, especially on thermal comfort (Jin et al., 2017; Zeng et al., 2017; Cruz et al., 2021; Zhou et al., 2021; He et al., 2022).

He et al. studied the relationship between urban heat island (UHI) and the ongoing sponge city (SPC) project in China (He et al., 2019). Paramita et al. used ENVI-met to simulate the outdoor Mean Radiation Temperature (Tmrt) and Physiological Equivalent Temperature (PET) to explore the outdoor thermal comfort surrounding low-rent housing in different layouts in Indonesia, finding that parallel plots of land with buildings facing north and south are the most favorable building forms and configurations (Paramita et al., 2018). Xu et al. took a plateau village (3,500 m above sea level) next to the Sichuan-Tibet Highway as a case and selected four typical courtyard layouts and outdoor reference points in the village to assess Tmrt and PET through field measurements. They confirmed that solar radiation and wind speed are the main factors affecting the courtyard thermal environment (Xu et al., 2022).

Moreover, PET has been widely mentioned and used as a criterion for microclimate evaluation. Sanusi et al. studied the thermal comfort of pedestrians on sidewalks, suggesting that the microclimate benefits increase with Plant Area Index (PAI), and PAI plays a decisive role in determining microclimate and PET benefits (Sanusi et al., 2017). Su et al. selected four typical blocks to simulate the microclimate with the ENVI-met model, showing that direct sunlight and wind speed are the key factors affecting people's thermal comfort. The outdoor thermal environment can be improved by adjusting the building orientation away from the traditional south direction, increasing the sunshine spacing coefficient, dislocating buildings, or adopting a peripheral-type building layout (Su et al., 2022). Ma et al. simulated and analyzed air temperature, wind speed, wind direction, and relative humidity of the Taihu "Dock Village", and examined the correlation between spatial characteristics and microclimate from four perspectives: plane space, cross-section space, vertical section space, and linear development space (Ma et al., 2019). Sayad et al. optimized outdoor thermal comfort through vegetation parameterization in a boulevard, finding that planting Washingtonia palm trees along the center of the boulevard can maximize the shaded area within the boulevard, with a maximum reduction of 1.8°C (air temperature) and 3.5°C (UTCI) at 16:00 (Sayad et al., 2021). Park et al. studied how to optimize plant types and vegetation coverage rate on green roof to reduce urban heat island effects. Their studies have shown that the green roof scenario with 70% grass and 30% trees is effective in closed areas, 50% shrubs and 50% trees are best in semi-open areas, and 70% grass with 30% trees, or 30% grass and 70% trees, is best in open areas (Park et al., 2022).

Based on the literature reviews, it is found that research on microclimate around traditional settlements mainly focuses on architectural forms, and plant ratios. However, studies on the relationship between the spatial form of water bodies and microclimate are still lacking. This paper analyzed the spatial-temporal variations of water-induced cooling effect in summer, with a case study of the Weizi settlement in China. The conclusions provide further technical guidance on designing and renovating Weizi settlements for better thermal comfort.

2 CASE STUDY AREA

Xufan is a typical Weizi settlement (**Figure 1**), in Guanweizi Village, Yanhe Town, Guangshan County, Xinyang, Henan, China. Xufan Village was enlisted as one of the traditional Chinese villages in 2017. The settlement site lies against the Fenghuang Mountain with Tasha River to its east and hills to its southwest. This village presents very distinctive water-sun-village characteristics. It was built on a lower hilly area to ensure sufficient sunlight. Ponds are dug around the village to facilitate drainage and help avoid flooding during the rainy season and provide other functions including irrigation, washing clothes, defense against enemies, and firefighting (See **Figure 2**, the village is surrounded by artificial water bodies).

The location and spatial layout of traditional settlements in southern Henan Province are subject to multiple factors, such as climatic conditions, land and water transportation, Fengshui concepts, war, and banditry, as well as farming culture (Gao et al., 2018). Typically, the layout of a traditional settlement site focuses on the following considerations:

1) Availability of surrounding resources. To meet the needs of production and daily life, the site selection should consider the availability of various surrounding resources such as water, terrain, and transportation.
2) Security. The site selection and layout of the settlement should be effectively protected against natural disasters, war, and banditry.
3) Amiable climatic conditions. Moderate temperature, sunlight, and precipitation, as well as a microclimate created by

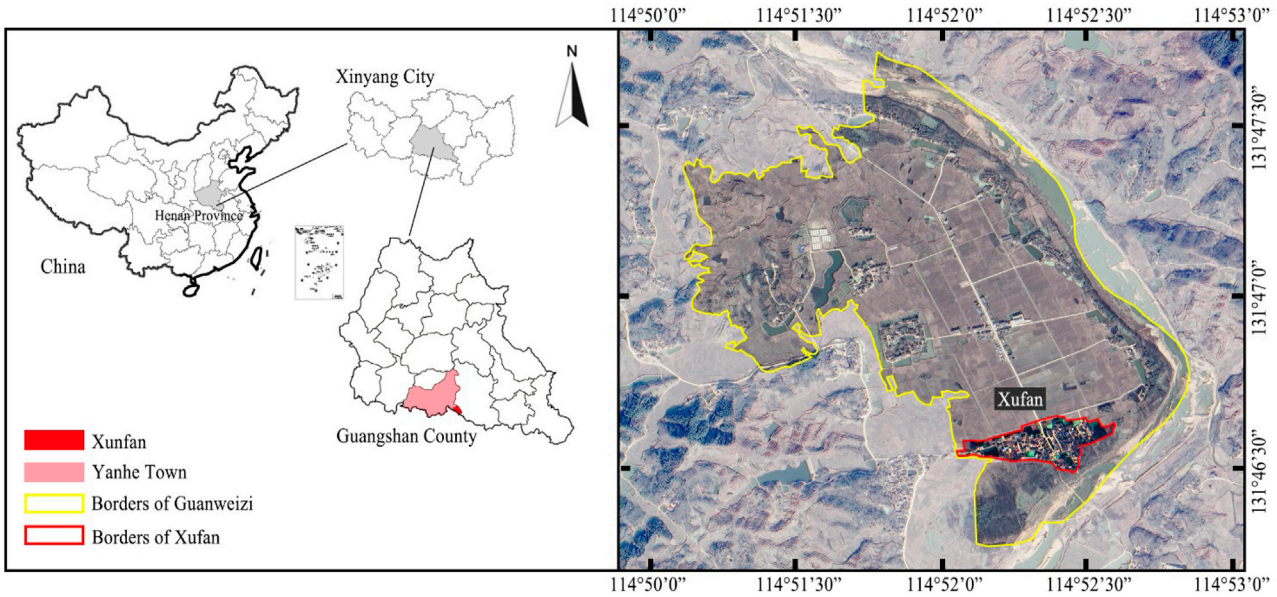

FIGURE 1 | Geographic location of the case study area.

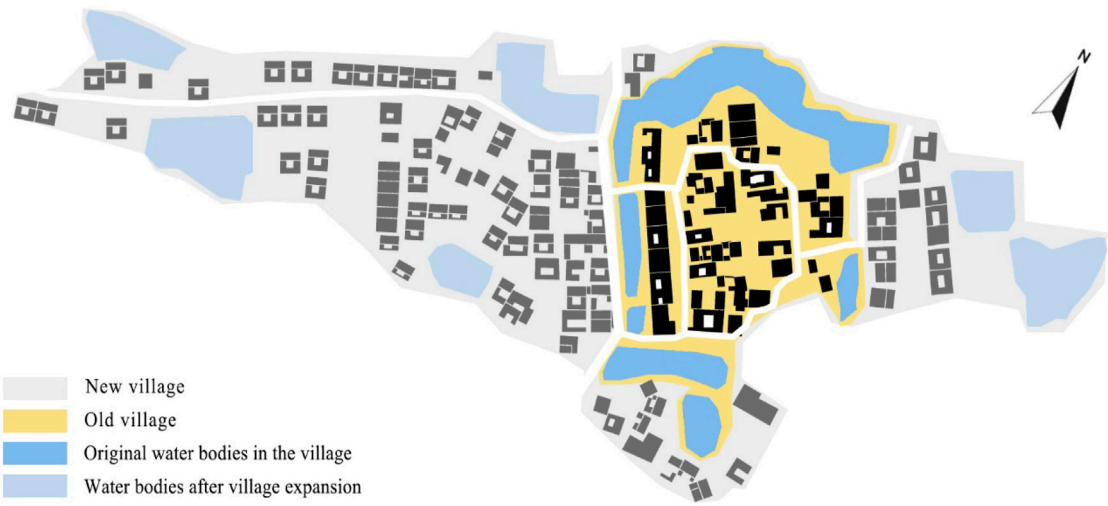

FIGURE 2 | Expansion from the old village to the new village with newly dug ponds.

surrounding rivers and mountains as a background, are also considerations in site selection and layout design.

Xinyang City is located in the transition zone from subtropical to warm temperate zones, exactly on the geographical dividing line of the two temperate zones (Qinling Mountains-Huaihe River), with the Huaihe River running through it. In China, it is generally understood as being divided by the mainstream of the Huaihe River. The southern part of the country has a humid subtropical monsoon climate and the northern part has a temperate monsoon semi-humid climate. Xinyang has sufficient sunlight, with an average annual sunshine of 1,990–2,173 h, an average annual air temperature of 15.1–15.3°C, an average annual soil temperature of 16.9°C, and an accumulated temperature of 5,250–5,383°C. It also has abundant rainfall with an annual average of 102–129 precipitation days, and an annual average rainfall of 900–1,400 mm. The air is humid, and the relative humidity is 75%–80% per year. Xinyang has four distinct seasons, which are controlled alternately by maritime tropical air masses and polar air masses in spring, summer, and autumn, and are mainly affected by continental polar air masses in winter. The salient

TABLE 1 | Dominant wind direction, and wind speed in summer in Xinyang City.

Wind direction, wind speed, and frequency	Average outdoor wind speed in summer (m/s)	2.4
	The most frequent wind direction in summer	SSW
	Frequency of the most frequent wind direction in summer (%)	10
	The average speed of the most frequent wind direction in summer (m/s)	3.2

characteristics of its climate are hot and humid summer, dry and cold winter, cool spring and autumn, four distinct seasons, rainy days with high temperature, and abundant precipitation. The dominant wind direction is south-southwest (SSW) in summer, and the average outdoor wind speed in summer is 3.2 m/s (**Table 1**) (Tsinghua University, 2018).

2.1 Spatial Forms of Weizi Settlements

The most prominent morphological feature of the Weizi settlement is its water bodies. The settlement space is composed of surrounding water bodies (i.e., the enclosing ditches), a water center island, dykes, enclosing walls, the gatehouse, and residential courtyards (Cheng, 2009). Weizi can be divided into a joint pattern and a continuous pattern in terms of form. A joint Weizi means several parallel Weizi connected via water bodies while a continuous Weizi is a cluster of Weizi connected via water bodies. Based on building purpose, Weizi can be divided into lake type, river type, and mountain torrent type. Based on the ownership in history, it can be divided into official type, civil type, and private type. Based on the location of residential dwellings, there are two types: residential houses built in the enclosure and residential houses built outside the enclosure (polder).

2.2 Adaptive Water Management in Weizi Settlements

Water is an indispensable part of the location selection of villages. Ponds were dug around Guanweizi Village to ensure drainage, water storage, and rainwater infiltration during the rainy season, and to provide irrigation, defensive, and firefighting functions. They also help improve the microclimate of the village together with other factors such as vegetation. Water bodies were retained during the expansion process of the new village and new water bodies were added to the area (**Figure 2**).

Water has a regulatory effect on climate. The water body absorbs and accumulates heat in summer, and through evaporation, it absorbs heat from the surrounding environment and keeps it cool. The unique natural environment, historical factors, and climate all contributed to the morphological characteristics of a Weizi settlement, which was born of water, built on the waterside, and made good use of water. In ancient times, people living in the settlement relied on water bodies around Weizi to defend against enemies. Gradually, the water bodies lost their defensive value and mainly provided irritation functions and helped improve living comfort.

This study focuses on the evaluation and improvement of thermal comfort in water-adaptive space in Weizi. Compared with urban space, the decay of outdoor open space in the rural area is mainly because of a lack of investment, weakened public function, and weak development theory (Li et al., 2019; Guo and Liu, 2021; Kan, 2021). In addition, the neglect of the comfort of rural outdoor spaces is also one of the factors. Human thermal perception depends not only on environmental conditions, but also on psychological, physiological, physical, and economic factors (Pacheco et al., 2012; Hsl et al., 2021). This study follows the guidelines of rural revitalization and takes thermal comfort in a rural area with water-adaptive space in the Weizi settlement as the major topic. It adopts computer fluid dynamics (CFD) technology in analyzing how a Weizi settlement can be better adapted to and integrated into the surrounding environment and how to build new countryside with rich ecological value. The water adaptability of Weizi settlements is manifested in the active and passive aspects of the relationship between people and water, that is, the utilization of water resources by the village and the impact of water bodies on the living environment of the settlement. From the perspective of thermal comfort assessment and improvement, this study explores the water adaptability characteristics of Xufan Weizi settlements.

3 METHODOLOGY

3.1 Field Measurement

Three locations are selected for field measurement (**Figure 3**), namely monitoring points 1, 2, and 3. Among them, Point 1 is located at the village entrance and near the water, Point 2 on the wide road, and point 3 at a road corner. The measurements were taken on 15 July 2021, the hottest period of the year. Air temperature (Ta), relative humidity (RH), and wind speed (Va) were measured and recorded at the same time at a pedestrian height of 1.5 m.

3.2 Data Simulation

This paper uses ENVI-met 5.0 to simulate the ambient microclimate of a traditional settlement. ENVI-met is derived from meteorological studies in Germany, and the accuracy of this model has been confirmed in a large number of studies of outdoor microclimate. In previous studies, ENVI-met has been proven to have some advantages in analyzing microclimate on a regional and local scale. In addition, ENVI-met performs well in small- and medium-scale urban microclimate simulations. ENVI-met can also incorporate air temperature, relative humidity, solar insolation, soil, vegetation, pollution, etc. into the simulated boundary conditions (Nikolova et al., 2011).

3.3 Assessment Indicators

3.3.1 Outdoor Thermal Environment

As a direct indicator of the thermal sensation experienced by the human body related to the environment, thermal comfort is a hot topic in studies of outdoor microclimate. The PET will be used in this paper to evaluate outdoor thermal comfort. It is based on the Munich

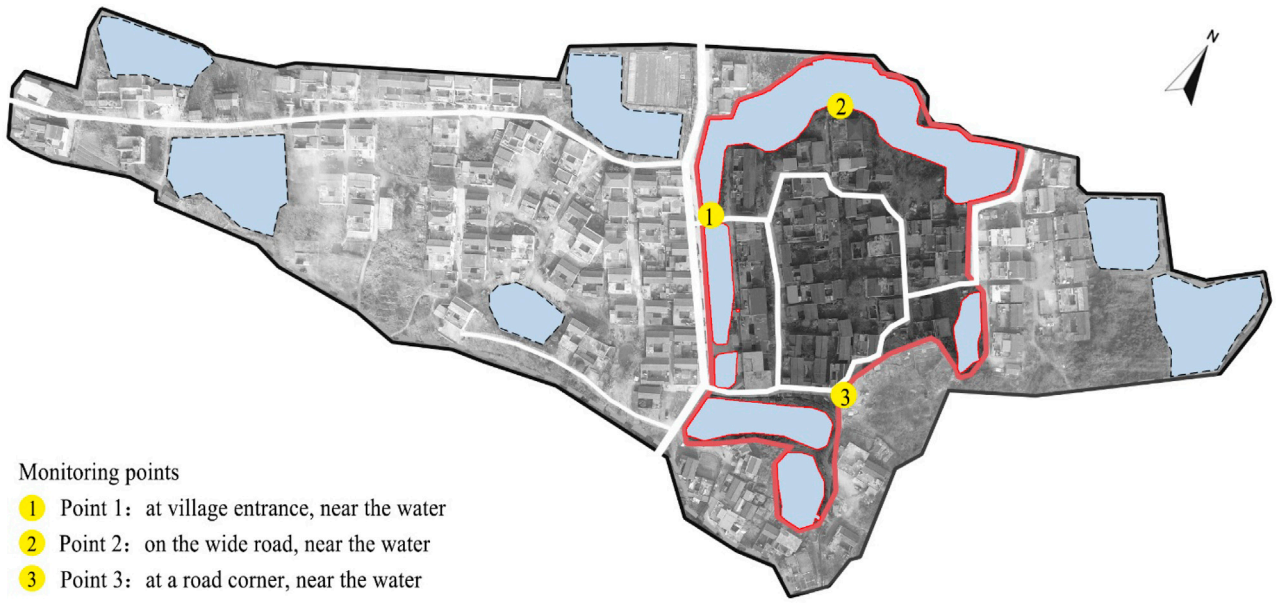

FIGURE 3 | Locations of monitoring points.

TABLE 2 | PET for different grades of thermal sensation.

PET (°C)	Thermal sensation	Physiological stress level
>41	Very hot	Extreme heat stress
35–41	Hot	Strong heat stress
29–35	Warm	Moderate heat stress
23–29	Slightly warm	Slight heat stress
18–23	Comfortable	No thermal stress
13–18	Slightly cool	Slight cold stress
8–13	Cool	Moderate cold stress
4–8	Cold	Strong cold stress
<4	Very cold	Extreme cold stress

Energy-balance Model for Individuals (MEMI) (Cheng et al., 2019). Based on the ranges of PET, human thermal sensation and physiological stress on human beings are divided into nine grades (**Table 2**) (Matzarakis and Mayer, 1997; Lin and Matzarakis, 2008).

3.3.2 Water Body Cooling Effect

Since the thermal environment at 1.5 m above the ground is most closely related to pedestrian activity and comfort, the water-cooling effect is calculated as per temperature at this height. The cooling effect of water bodies on air temperature can be calculated as follows:

$$\Delta T = T_w - T_n \quad (1)$$

where T_w and T_n refer to air temperature at 1.5 m height with or without water, respectively.

3.3.3 Village Morphological Indicators

The morphological indicators of villages and towns selected in this paper are as follows: 1) Water body morphological indicator includes water body rate and distance to a water body. Waterbody rate refers to the ratio of water body area to the case study area. Distance to the water body is the nearest distance between the monitoring point and the water body boundary. 2) The greening indicator, as represented by the greening rate, refers to the ratio of public greening area to the case study area. 3) The village spatial morphology indicator is indicated by building density and man-made underlying surface ratio. In the latter, the man-made underlying surface refers to hard pavement such as asphalt roads and cement.

As shown in **Figure 4**, data extraction points were selected every 21 m in the case study area, and 95 data points were available excluding useless ones on buildings. According to the satellite map of the villages and towns, a master plan was drawn in AutoCAD, and the area of each element was processed by a geographic information system (GIS). Buffer analysis in ArcGIS software was used to create a circular buffer around each monitoring point with a radius of 10, 20, 30, 40, and 50 m. The buffer layers were intersected with village building density, water bodies, greening, and man-made underlying surface to calculate the area proportion of each element. The nearest neighbor analysis tool in ArcGIS was used to calculate the nearest distance between each monitoring point and the water body boundary. Finally, Statistical Product Service Solutions (SPSS) software was used to conduct correlation analysis between various elements and temperature, humidity, and PET value, and finally confirmed their degree of impact on microclimate.

3.4 Modeling

The modeling grid is 204*146*10. The grid size is set to 3 × 3 × 3 m for more precise data (**Figure 5**). Most of the buildings are reinforced concrete buildings, the width of the road is between 3 and 6 m, surrounded by water, and the depth of water is about 2 m.

FIGURE 4 | Village configuration and data extraction points in ArcGIS.

FIGURE 5 | ENVI-met model of the case study area.

3.5 Meteorological Input Parameters

Meteorological data such as hourly temperature, relative humidity, wind speed, and wind direction are required for simulations. The average hourly temperature and relative humidity data measured at the three monitoring points are used as input meteorological data. Wind speed data at 10 m above the ground, and the most frequent daily wind direction data serve as wind environment boundary, while the wind environment data come from government weather stations. In addition, ENVI-met calculates incident solar radiation based on latitude/longitude, date, and time.

3.6 ENVI-met Model Evaluation

In this study, the accuracy of the model is evaluated by comparing the measured meteorological data with the simulated meteorological data. Commonly used evaluation metrics for predictive error analysis are Mean Bias Error (MBE), Mean Absolute Error (MAE), Root-Mean Square Error (RMSE), Mean Absolute Percentage Error (MAPE), and Theil's Inequality Coefficient (TIC) (Khan et al., 2021). Although MAE and RMSE can reflect the average error of the model, the use of RMSE is more common, but it does not reflect the relative magnitude of the average error (Willmott, 1982). Therefore, in addition to using RMSE and MAPE as evaluation indicators in this study, the Index of Agreement (d) developed by Willmott is also introduced to evaluate how the simulated data is close to the measured data, and the larger the d is, the closer the former is to the latter (Rosso et al., 2018).

$$\mathrm{RMSE} = \sqrt{\left[\sum_{i=1}^{n} (x_i - y_i)^2\right] \Big/ n} \tag{2}$$

$$\mathrm{MAPE} = (1/n)\sum_{i=1}^{n} \left[\left(\left|x_i - y_i\right|\right) / y_i \right] \times 100\% \tag{3}$$

$$d = 1 - \left[\sum_{i=1}^{n} (x_i - y_i)^2\right] \Big/ \left[\sum_{i=1}^{n} \left(\left|x_i - \bar{y}_i\right| + \left|y_i - \bar{y}_i\right|\right)^2\right] (0 \leqslant d \leqslant 1) \tag{4}$$

where x_i, y_i refer to the ith simulated value and the measured value. $\bar{y}_i$ is the average of the measured data. n is the number of measurements.

Figure 6 indicates that the measured and simulated air temperature and relative humidity of the three monitoring points have a high degree of coincidence. ENVI-met model is not able to simulate the impact of contingencies, such as heat waves from air conditioners in the afternoon that increase outdoor air temperature. Besides, cloud cover in the air is also an important factor affecting the ambient temperature.

Based on the measured and simulated data of each point, the accuracy of the ENVI-met simulation is analyzed, and the findings are that the temperature RMSEs of the three points are between 1.34–1.65°C, which fall in the generally accepted range of 0.52–4.30°C (**Table 3**). Humidity RMSEs are between 2.63%–2.94% and less than 5% (Rosso et al., 2018). The MAPEs of temperature and relative humidity are less than 10% (Chow et al., 2011; Salata et al., 2017). The Indexes of Agreement (d) are between 0.92–0.98, indicating that ENVI-met has a high simulation accuracy of outdoor temperature and relative humidity (Jiang et al., 2019).

4 RESULTS OF SIMULATION

4.1 Time-Space Variation of Water Body Cooling Effect

The minimum ΔT_{min} and the average ΔT_{ave} of ΔT were calculated (**Figure 7**). Meanwhile, the cooling values within the 12 h of study were divided into eight intervals, to calculate the space proportion corresponding to each cooling value interval (**Figure 8**). Water bodies can reduce the ambient air temperature in summer, but produce a different cooling effect at different times.

Figure 7 pointed out during the 12 h, ΔT_{min} reached the minimum value of −3.53°C at 14:00 and the maximum value of −0.53°C at 7:00. ΔT_{ave} reached the minimum value of −0.74°C at 14:00 and the maximum value of −0.11°C at 7:00. According to the spatial and temporal distribution of ΔT in **Figure 8**, the cooling effect of water bodies varies with temperature. ΔT in 46%–99% of the area is from −0.5 to 0°C, that in 10%–33% of the area from −1°C to −0.5°C, and that in 4%–20% of the area from −1.5°C to −1°C. In a very limited area, the cooling value can vary by over 3°C. During the 12 h of the day, the cooling value in the afternoon is higher than that in the morning, reaching the highest during 12:00 and 15:00, which is precisely the hottest time of the day. This indicates that water bodies can significantly improve local thermal environment and play a cooling effect in summer.

Figure 9 shows that the cooling effect of water bodies gradually weakens towards the village center. This is because an increase in wind speed can enhance the vapor-cooling effect of water bodies, and the convective heat transfer between water bodies and the surrounding air can also enhance the cooling intensity. Due to the shielding of buildings, wind speed gradually decreases towards the village center, and so does the cooling intensity. This indicates that wind speed and direction have an impact on the cooling effect and range of water bodies, and the shielding of buildings accounts for the main reason affecting wind speed, and eventually compromises the cooling effect of water bodies.

4.2 Impact of Village Morphological Elements on Microclimate

Overall, water bodies have a cooling effect. To further reveal factors influencing village microclimate, ArcGIS software was used to map village morphological elements and analyze their correlation with temperature, humidity, and PET value of each monitoring point.

Table 4 shows the Pearson correlation coefficient (r) between the distance of different monitoring points to a water body and simulated data. The distance of each monitoring point to the water body is significantly correlated with air temperature, relative humidity, and PET value. The distance of the monitoring point to the water body is positively, and very significantly, correlated with PET value and air temperature, but negatively, and also significantly, correlated with relative humidity.

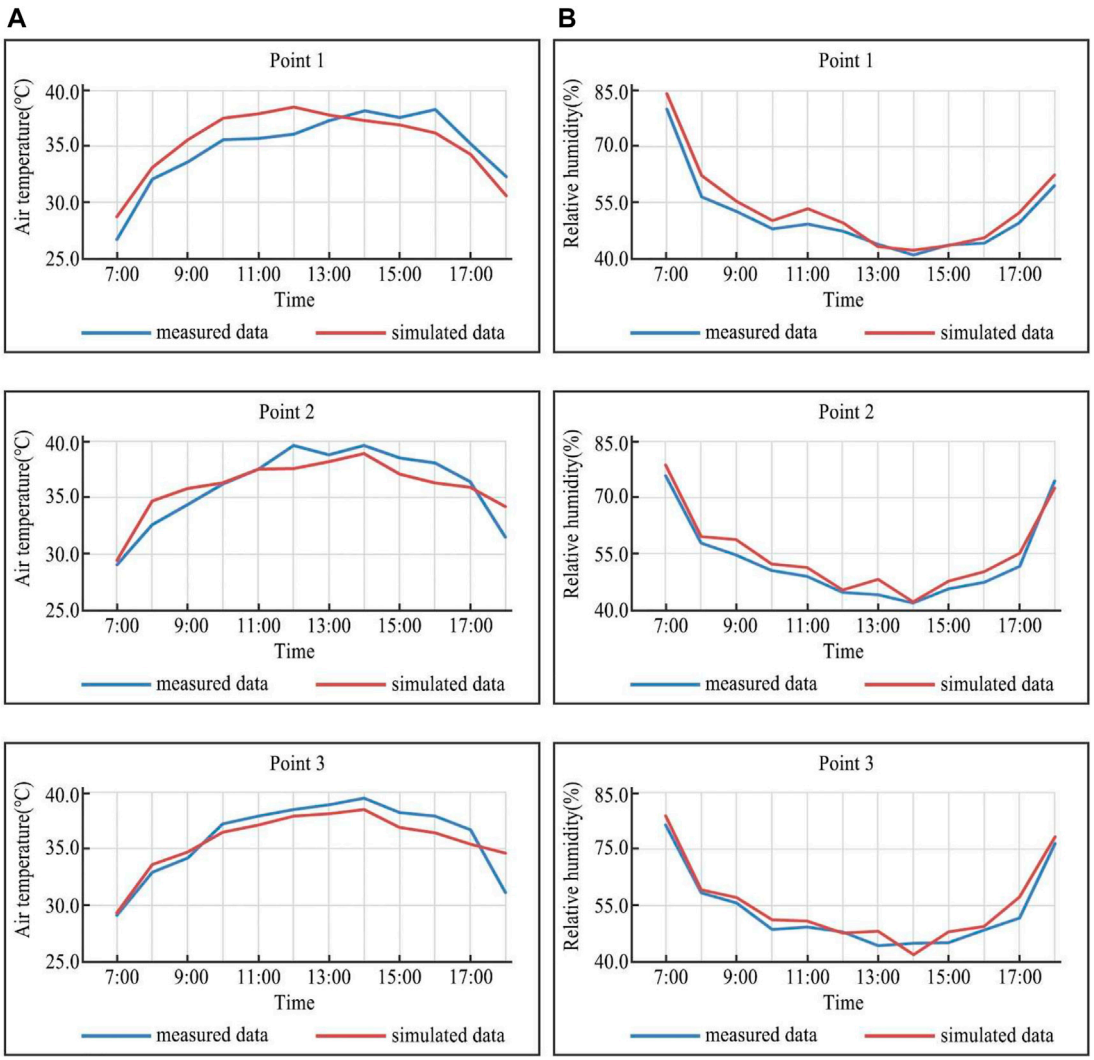

FIGURE 6 | Comparisons of data measured at 1.5 m above the ground from three monitoring points and simulated data are used to verify the effectiveness of the ENVI-met software. **(A)** air temperature. **(B)** relative humidity.

TABLE 3 | The goodness of fit analysis of measured data and simulated data.

Meteorological parameters	Evaluation indicators	Point 1	Point 2	Point 3
Ta	RMSE/°C	1.65	1.42	1.34
	MAPE/%	4.36	3.19	3
	d	0.92	0.93	0.94
RH	RMSE/%	2.94	2.63	2.63
	MAPE/%	4.49	4.68	4.68
	d	0.98	0.98	0.98

Table 5 shows the Pearson correlation coefficient (r) between greening rate and simulated data within different buffer radiuses. Within a radius of 10m, the greening rate is significantly correlated with PET value but has no significant correlation with air temperature or relative humidity. Within a radius of 20 m, the greening rate is significantly correlated with PET value and relative humidity but has no significant correlation with air temperature. There is no significant

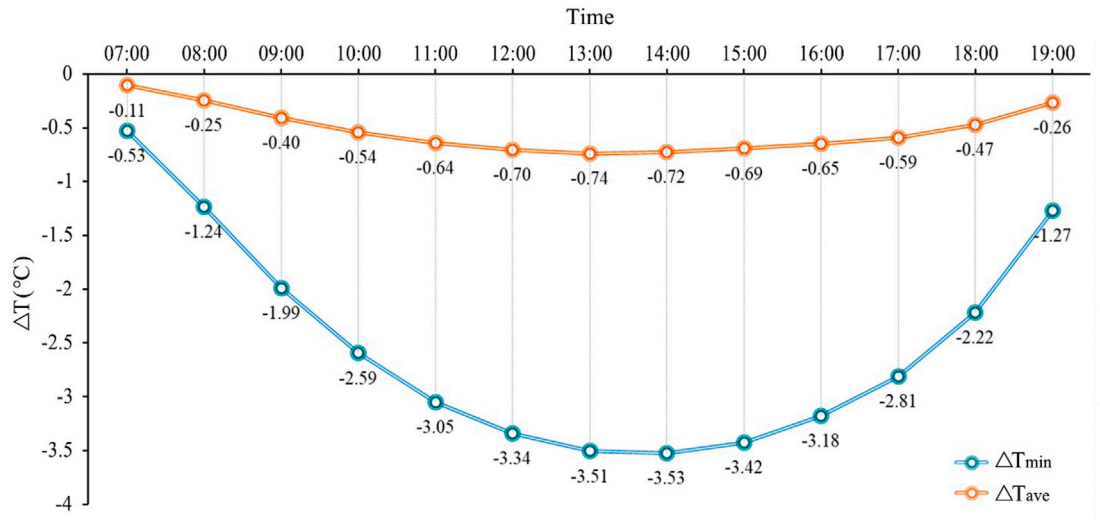

FIGURE 7 | Time-space distribution of minimum and maximum water body cooling effect.

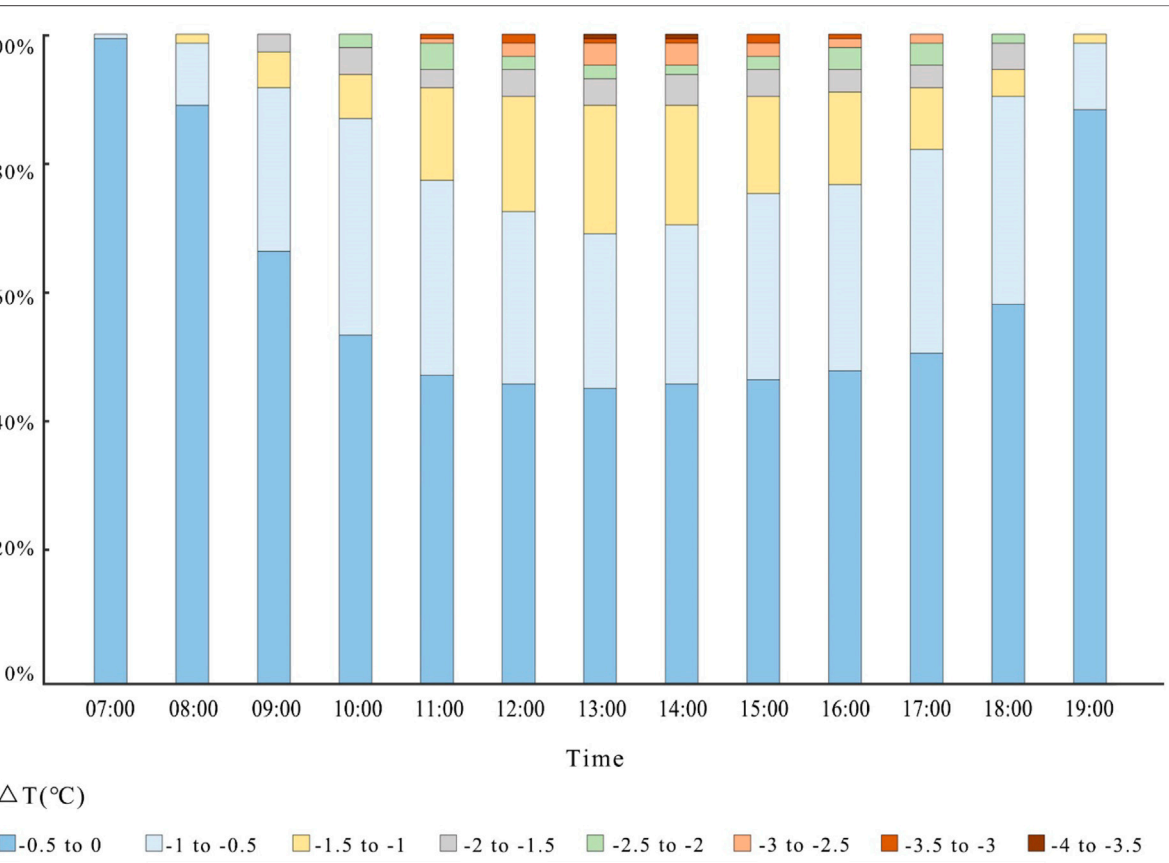

FIGURE 8 | Time-space proportion of water body cooling effect.

correlation between greening rate and simulated data within other buffer radiuses. This may be explained by the limited green areas in the village, which are mainly concentrated near the water bodies.

Table 6 shows the Pearson correlation coefficient (r) between building density and simulated data within different buffer radiuses. As can be seen from the table, building density is significantly positively correlated with PET value and air

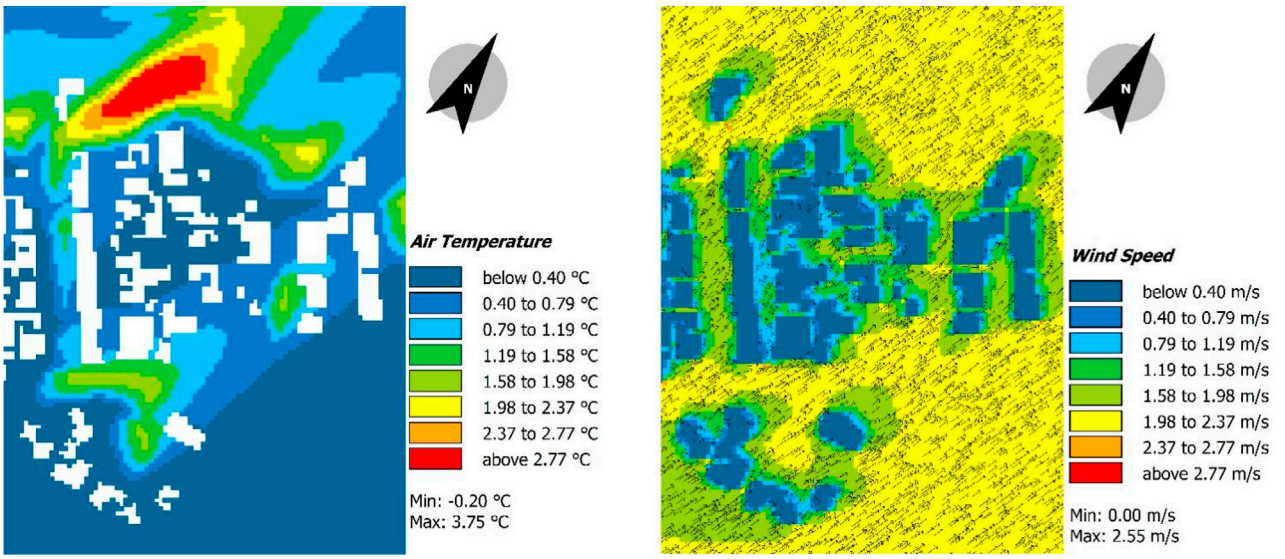

FIGURE 9 | Air temperature (left) and wind speed (right) within the case study area at 14:00 on July 15.

TABLE 4 | Correlation coefficients between distance to the water body and simulated data.

		PET	RH	Ta
Distance of monitoring point to water body	r	0.461[a]	−0.210[b]	0.443[a]
	Sig	0.000	0.042	0.000

[a]*Correlation significant at the 0.01 level (two-tailed).*
[b]*Correlation significant at the 0.05 level (two-tailed).*

TABLE 5 | Correlation coefficients between greening rate and simulated data within different buffer radiuses.

	Radius(m)		PET	RH	Ta
Greening rate	10	r	−0.236[b]	0.144	0.009
		Sig	0.021	0.164	0.933
	20	r	−0.209[b]	0.209[b]	−0.080
		Sig	0.042	0.042	0.441
	30	r	−0.027	0.152	−0.053
		Sig	0.793	0.142	0.612
	40	r	−0.027	0.152	−0.053
		Sig	0.793	0.142	0.612
	50	r	0.108	0.062	0.038
		Sig	0.295	0.549	0.717

[a]*Correlation significant at the 0.01 level (two-tailed).*
[b]*Correlation significant at the 0.05 level (two-tailed).*

temperature, and significantly negatively correlated with relative humidity. Among all, the r between building density and PET value reaches the highest within a radius of 20 m, which is 0.61. The r of building density with relative humidity and air temperature reaches the highest within a radius of 30 m, which is −0.594 and 0.702, respectively.

Table 7 shows the Pearson correlation coefficient (r) between water body rate and simulated data within different

TABLE 6 | Correlation coefficients between building density and simulated data within different buffer radiuses.

	Radius(m)		PET	RH	Ta
Building density	10	r	0.592[a]	−0.426[a]	0.491[a]
		Sig	0.000	0.000	0.000
	20	r	0.610[a]	−0.565[a]	0.698[a]
		Sig	0.000	0.000	0.000
	30	r	0.521[a]	−0.594[a]	0.702[a]
		Sig	0.000	0.000	0.000
	40	r	0.480[a]	−0.547[a]	0.644[a]
		Sig	0.000	0.000	0.000
	50	r	0.459[a]	−0.498[a]	0.587[a]
		Sig	0.000	0.000	0.000

[a]*Correlation significant at the 0.01 level (two-tailed).*
[b]*Correlation significant at the 0.05 level (two-tailed).*

buffer radiuses. Water body rate is significantly negatively correlated with PET value and air temperature, and significantly positively correlated with relative humidity. Among all, the r between water body rate and PET value reaches the highest within a radius of 40 m, which is −0.513. The r with relative humidity and air temperature reaches the highest within a radius of 20m, which is −0.75 and 0.388, respectively.

Table 8 shows the Pearson correlation coefficient (r) between man-made underlying surface ratio and simulated data within different buffer radiuses. Man-made underlying surface ratio is significantly positively correlated with PET value and air temperature, and significantly negatively correlated with relative humidity. Among all, the r of man-made underlying surface ratio with PET value reaches the highest within a radius of 40m, which is 0.269. The correlation of man-made underlying surface ratio with relative humidity and air temperature reaches the highest within a radius of 20 m, which is −0.56 and 0.502, respectively.

TABLE 7 | Correlation coefficients between water body rate and simulated data within different buffer radiuses.

	Radius(m)		PET	RH	Ta
Water body rate	10	r	–0.346[a]	0.354[a]	–0.685[a]
		Sig	0.001	0.000	0.000
	20	r	–0.413[a]	0.388[a]	–0.750[a]
		Sig	0.000	0.000	0.000
	30	r	–0.475[a]	0.341[a]	–0.733[a]
		Sig	0.000	0.001	0.000
	40	r	–0.513[a]	0.247[b]	–0.665[a]
		Sig	0.000	0.016	0.000
	50	r	–0.509[a]	0.130	–0.574[a]
		Sig	0.000	0.210	0.000

[a]*Correlation significant at the 0.01 level (two-tailed).*
[b]*Correlation significant at the 0.05 level (two-tailed).*

architectural space (Shi et al., 2020; Yang et al., 2021). In general, the appropriate placement of greening space helps lower temperature and cool the surrounding environment (Tsuyoshi et al., 1985; Safikhani et al., 2014). In a hot and humid climate, different vegetations can bring different cooling effects, and overall, they positively affect local temperature (Richards et al., 2020).

The impact of man-made underlying surfaces on microclimate should not be ignored either (Li et al., 2021). The study shows the man-made underlying surface ratio has a significantly positive correlation with PET value and air temperature and a significantly negative correlation with relative humidity. One of the impacts of urbanization on villages is the large area of hard pavement, but the increase of hard pavement also leads to temperature rise. Therefore, village development should never merely aim at the aesthetic appearance of hard pavement, but more importantly, should consider its impact on microclimate (He et al., 2021; Xie et al., 2021; Yang et al., 2022).

TABLE 8 | Correlation coefficients between man-made underlying surface ratio and simulated data within different buffer radiuses.

	Radius(m)		PET	RH	Ta
Man-made underlying surface ratio	10	r	0.208[b]	–0.553[a]	0.493[a]
		Sig	0.043	0.000	0.000
	20	r	0.203[b]	–0.560[a]	0.502[a]
		Sig	0.048	0.000	0.000
	30	r	0.249[b]	–0.540[a]	0.486[a]
		Sig	0.015	0.000	0.000
	40	r	0.269[a]	–0.517[a]	0.454[a]
		Sig	0.008	0.000	0.000
	50	r	0.243[b]	–0.499[a]	0.436[a]
		Sig	0.018	0.000	0.000

[a]*Correlation significant at the 0.01 level (two-tailed).*
[b]*Correlation significant at the 0.05 level (two-tailed).*

5 DISCUSSION

Analysis of the temporal and spatial variation of water body cooling effect shows that the cooling effect of water bodies in summer is stronger in the afternoon than in the morning, reaching the highest from 12:00 to 15:00. On the one hand, the cooling range and intensity decrease with the increase of distance; on the other hand, wind speed also constitutes an important factor influencing the cooling effect. The air temperature in the village center is generally higher than that outside, as increased building density will shield the wind, thus affecting the cooling effect of water bodies (Yang et al., 2020). Therefore, for developing and constructing Weizi settlements, living around the peripheral water sources is suggested for maximized cooling effect (Yang et al., 2019).

Analysis of building density, water body rate, greening rate, and man-made underlying surface shows less correlation between greening rate and microclimate than expected. This is probably because of the relatively small greening areas in Xufan Village, which are mainly concentrated on water banks, and the low greening rate in the village, where only a limited number of green plants grow on the roadside. At the same time, a significant correlation exists between water body rate and microclimate, which is consistent with the conclusion of Dachuan Shi et al. that greening and water body can co-produce a stronger cooling effect on microclimate than acting alone. Because greening space has less resistance to wind than

This paper studies the cooling effect of water bodies and the impact of village morphological elements on microclimate, but still lacks sufficient study on different forms of water bodies. As there are various enclosure forms of water bodies in Weizi settlements, the impact of different enclosure forms on microclimate will be the focus of our future studies.

6 CONCLUSION

For traditional villages, a combined approach of both protection and development is not only the primary principle of survival and development but also a major challenge in the context of modernization and urbanization (Zhao and Wang, 2018). This study explains the ecological wisdom of the water-adaptive space in Weizi settlements and applies software simulation method in the discussion of the impact of water bodies and settlement forms on local microclimate. This study provides new ideas for the development of traditional Weizi settlements:

1) Water bodies have a significant impact on the microclimate of a Weizi settlement, so they should not be directly filled but instead protected and utilized scientifically and rationally.

2) The distance to the water body is negatively correlated with the cooling effect, so villages can be constructed around water bodies to maximize the cooling effect.
3) Water body rate and greening rate are positively correlated with thermal comfort while building density and man-made underlying surface are negatively correlated with thermal comfort. Therefore, increasing green plants near the village center, while reducing man-made underlying surface and building density can effectively improve microclimate and thermal comfort.

There are essential differences between countryside and cities and in the process of countryside development, we should not follow the aesthetics of urbanization by increasing hard paving which harms human thermal comfort. On the contrary, we should build a comfortable, healthy, and livable rural habitat based on local conditions and actual needs.

DATA AVAILABILITY STATEMENT

The raw data supporting the conclusions of this article will be made available by the authors, without undue reservation.

AUTHOR CONTRIBUTIONS

All authors contributed to the development of the research and the elaboration of this article. Specifically, conceptualization, YC, BH, and XL; methodology, YC and XL; software, ZZ and XT; validation, SL and ZW; investigation, YC, ZW, and XL; data curation, ZZ, SL, and XL; writing—original draft preparation, YC, ZZ, SL, ZW, and XL; writing—review and editing, YC, XT, XL, and BH; supervision, XL and BH; funding acquisition, XL and BH. All authors have read and agreed to the published version of the manuscript.

FUNDING

This research is funded by the National Natural Science Foundation of China (Grant No. 52108011); Guangzhou Philosophy and Social Science Planning 2022 Annual Project (Grant No. 2022GZQN14); China Postdoctoral Science Foundation (Grant No. 2021M701249); Department of Education of Guangdong Province (Grant No. 2021KTSCX004); Science and Technology Program of Guangzhou, China (Grant No. 202102020302); Department of Housing and Urban-Rural Development of Guangdong Province (Grant No. 2021-K2-305243); State Key Laboratory of Subtropical Building Science, South China University of Technology (Grant No. 2021ZB16 and Grant No. 2022ZA01).

ACKNOWLEDGMENTS

The authors thank the editors and the reviewers for their helpful recommendations for improving this article.

REFERENCES

Cheng, B., Gou, Z., Zhang, F., Feng, Q., and Huang, Z. (2019). Thermal Comfort in Urban Mountain Parks in the Hot Summer and Cold Winter Climate. *Sustain. Cities Soc.* 51, 101756. doi:10.1016/j.scs.2019.101756

Cheng, Y., and Guo, W. (2015). An Analysis of the Principles that Create the Microclimate of Courtyards in Vernacular Houses Surrounded by Embankment (In Chinese). *Archit. J.* 70, 73.

Cheng, Y. (2009). Weizi Folk House in Western Anhui -- on the Construction Strategy of Traditional Architecture Adapting to the Climate (In Chinese). *Sichuan Build. Sci.* 35, 244–249. doi:10.3969/j.issn.1008-1933.2009.04.067

Chow, W. T. L., Pope, R. L., Martin, C. A., and Brazel, A. J. (2011). Observing and Modeling the Nocturnal Park Cool Island of an Arid City: Horizontal and Vertical Impacts. *Theor. Appl. Climatol.* 103, 197–211. doi:10.1007/s00704-010-0293-8

Cruz, J. A., Blanco, A. C., Garcia, J. J., Santos, J. A., and Moscoso, A. D. (2021). Evaluation of the Cooling Effect of Green and Blue Spaces on Urban Microclimate Through Numerical Simulation: A Case Study of Iloilo River Esplanade, Philippines. *Sustain. Cities Soc.* 74, 103184. doi:10.1016/j.scs.2021.103184

Gao, H., Wang, Y., Wang, S., Yi, L., and Fu, L. (2018). Studies on the Protection and Renewal of the Characteristics of Traditional Villages in the South of Henan Province——Take Xinyang Xihe Village as an Example (in Chinese). *J. Xinyang Norm. Univ. Sci. Ed.* 31, 687–692. doi:10.3969/j.issn.1003-0972.2018.04.033

Guo, Y., and Liu, Y. (2021). Poverty Alleviation Through Land Assetization and its Implications for Rural Revitalization in China. *Land Use Policy* 105, 105418. doi:10.1016/j.landusepol.2021.105418

He, B.-J., Wang, J., Zhu, J., and Qi, J. (2022). Beating the Urban Heat: Situation, Background, Impacts and the Way Forward in China. *Renew. Sustain. Energy Rev.* 161, 112350. doi:10.1016/j.rser.2022.112350

He, B.-J., Zhao, D., Xiong, K., Qi, J., Ulpiani, G., Pignatta, G., et al. (2021). A framework for Addressing Urban Heat Challenges and Associated Adaptive Behavior by the Public and the Issue of Willingness to Pay for Heat Resilient Infrastructure in Chongqing, China. *Sustain. Cities Soc.* 75, 103361. doi:10.1016/j.scs.2021.103361

He, B.-J., Zhu, J., Zhao, D.-X., Gou, Z.-H., Qi, J.-D., and Wang, J. (2019). Co-benefits approach: Opportunities for Implementing Sponge City and Urban Heat Island Mitigation. *Land Use Policy* 86, 147–157. doi:10.1016/j.landusepol.2019.05.003

Honjo, H., and Takakura, T. (1985). Analysis of Temperature Distribution of Urban Green Spaces Using Remote Sensing Data. *J. Jpn. Inst. Landsc. Archit.* 49, 299–304. doi:10.5632/jila1934.49.5_299

Jewitt, G. (2002). Can Integrated Water Resources Management Sustain the Provision of Ecosystem Goods and Services? *Phys. Chem. Earth, Parts A/B/C* 27, 887–895. doi:10.1016/S1474-7065(02)00091-8

Jiang, Y., Han, X., Shi, T., and Song, D. (2019). Microclimatic Impact Analysis of Multi-Dimensional Indicators of Streetscape Fabric in the Medium Spatial Zone. *Ijerph* 16, 952. doi:10.3390/ijerph16060952

Jin, H., Shao, T., and Zhang, R. (2017). Effect of Water Body Forms on Microclimate of Residential District. *Energy Procedia* 134, 256–265. doi:10.1016/j.egypro.2017.09.615

Kan, K. (2021). Creating Land Markets for Rural Revitalization: Land Transfer, Property Rights and Gentrification in China. *J. Rural Stud.* 81, 68–77. doi:10.1016/j.jrurstud.2020.08.006

Khan, A., Chatterjee, S., and Weng, Y. (2021). Simulating Microscale Thermal Interactions Using ENVI-met Climate Model. *Urban Heat. Isl. Model. Trop. Clim.* 2021, 179–213. doi:10.1016/B978-0-12-819669-4.00006-4

Li, B., Guo, W., Liu, X., Zhang, Y., Russell, P. J., and Schnabel, M. A. (2021). Sustainable Passive Design for Building Performance of Healthy Built Environment in the Lingnan Area. *Sustainability* 13, 9115. doi:10.3390/su13169115

Li, J., Yan, J., and Wang, J. (2019). Research Status of Rural Community Public Space in China and Related Reflections (In Chinese). *City Plan. Rev.* 43, 128–134. doi:10.11819/cpr20191115a

Li, Y., Zhang, X., Chen, Y., and Liu, Y. (2020). The Impact of Human Settlement Quality on Rural Development (In Chinese). *China Popul. Environ.* 30, 158–167. doi:10.12062/cpre.20200116

Lin, T.-P., and Matzarakis, A. (2008). Tourism Climate and Thermal Comfort in Sun Moon Lake, Taiwan. *Int. J. Biometeorol.* 52, 281–290. doi:10.1007/s00484-007-0122-7

Lopes, A., Remoaldo, B., Ribeiro, C., and Martín-Vide, D. (2021). Perceptions of Human Thermal Comfort in an Urban Tourism Destination - A Case Study of Porto (Portugal). *Build. Environ.* 205, 108246. doi:10.1016/j.buildenv.2021.108246

Ma, K., Tang, X., Ren, Y., and Wang, Y. (2019). Research on the Spatial Pattern Characteristics of the Taihu Lake "Dock Village" Based on Microclimate: A Case Study of Tangli Village. *Sustainability* 11, 368. doi:10.3390/su11020368

Matzarakis, A., and Mayer, H. (1997). Heat Stress in Greece. *Int. J. Biometeorology* 41, 34–39. doi:10.1007/s004840050051

Nikolova, I., Janssen, S., Vos, P., Vrancken, K., Mishra, V., and Berghmans, P. (2011). Dispersion Modelling of Traffic Induced Ultrafine Particles in a Street canyon in Antwerp, Belgium and Comparison with Observations. *Sci. Total Environ.* 412-413, 336–343. doi:10.1016/j.scitotenv.2011.09.081

Pacheco, R., Ordóñez, J., and Martínez, G. (2012). Energy Efficient Design of Building: A Review. *Renew. Sustain. Energy Rev.* 16, 3559–3573. doi:10.1016/j.rser.2012.03.045

Paramita, B., Fukuda, H., Perdana Khidmat, R., and Matzarakis, A. (2018). Building Configuration of Low-Cost Apartments in Bandung-Its Contribution to the Microclimate and Outdoor Thermal Comfort. *Buildings* 8, 123. doi:10.3390/buildings8090123

Park, J., Shin, Y., Kim, S., Lee, S.-W., and An, K. (2022). Efficient Plant Types and Coverage Rates for Optimal Green Roof to Reduce Urban Heat Island Effect. *Sustainability* 14, 2146. doi:10.3390/su14042146

Richards, D. R., Fung, T. K., Belcher, R. N., and Edwards, P. J. (2020). Differential Air Temperature Cooling Performance of Urban Vegetation Types in the Tropics. *Urban For. Urban Green.* 50, 126651. doi:10.1016/j.ufug.2020.126651

Rosso, F., Golasi, I., Castaldo, V. L., Piselli, C., Pisello, A. L., Salata, F., et al. (2018). On the Impact of Innovative Materials on Outdoor Thermal Comfort of Pedestrians in Historical Urban Canyons. *Renew. Energy* 118, 825–839. doi:10.1016/j.renene.2017.11.074

Safikhani, T., Abdullah, A. M., Ossen, D. R., and Baharvand, M. (2014). A Review of Energy Characteristic of Vertical Greenery Systems. *Renew. Sustain. Energy Rev.* 40, 450–462. doi:10.1016/j.rser.2014.07.166

Salata, F., Golasi, I., Petitti, D., de Lieto Vollaro, E., Coppi, M., and de Lieto Vollaro, A. (2017). Relating Microclimate, Human Thermal Comfort and Health During Heat Waves: An Analysis of Heat Island Mitigation Strategies Through a Case Study in an Urban Outdoor Environment. *Sustain. Cities Soc.* 30, 79–96. doi:10.1016/j.scs.2017.01.006

Sanusi, R., Johnstone, D., May, P., and Livesley, S. J. (2017). Microclimate benefits that Different Street Tree Species Provide to Sidewalk Pedestrians Relate to Differences in Plant Area Index. *Landsc. Urban Plan.* 157, 502–511. doi:10.1016/j.landurbplan.2016.08.010

Sayad, B., Alkama, D., Rebhi, R., Menni, Y., Ahmad, H., Inc, M., et al. (2021). Outdoor Thermal Comfort Optimization Through Vegetation Parameterization: Species and Tree Layout. *Sustainability* 13, 11791. doi:10.3390/su132111791

Shi, D., Song, J., Huang, J., Zhuang, C., Guo, R., and Gao, Y. (2020). Synergistic Cooling Effects (SCEs) of Urban Green-Blue Spaces on Local Thermal Environment: A Case Study in Chongqing, China. *Sustain. Cities Soc.* 55, 102065. doi:10.1016/j.scs.2020.102065

Su, Y., Zhao, Q., and Zhou, N. (2022). Improvement Strategies for Thermal Comfort of a City Block Based on PET Simulation- A case Study of Dalian, a Cold-Region City in China. *Energy Build.* 261, 111557. doi:10.1016/j.enbuild.2021.111557

Tsinghua University (2018). JGJ/T449-2018 Standard For Green Performance Calculation of Civil Buildings. (In Chinese) Beijing: China Construction Industry Press.

Willmott, C. J. (1982). Some Comments on the Evaluation of Model Performance. *Bull. Amer. Meteor. Soc.* 63, 1309–1313. doi:10.1175/1520-0477(1982)063<1309:scoteo>2.0.co;2

Xie, J., Sun, Y., Liu, X., Ding, Z., and Lu, M. (2021). Human Activities Introduced Degenerations of Wetlands (1975-2013) Across the Sanjiang Plain North of the Wandashan Mountain, China. *Land* 10, 1361. doi:10.3390/land10121361

Xu, S., Cheng, B., Huang, Z., and Shen, C. (2022). An Investigation on the Thermal Environment of Residential Courtyards in the Cold Area of Western Sichuan Plateau. *Buildings* 12, 49. doi:10.3390/buildings12010049

Yang, J., Ren, J., Sun, D., Xiao, X., Xia, J., Jin, C., et al. (2021). Understanding Land Surface Temperature Impact Factors Based on Local Climate Zones. *Sustain. Cities Soc.* 69, 102818. doi:10.1016/j.scs.2021.102818

Yang, J., Wang, Y., Xiao, X., Jin, C., Xia, J., and Li, X. (2019). Spatial Differentiation of Urban Wind and Thermal Environment in Different Grid Sizes. *Urban Clim.* 28, 100458. doi:10.1016/j.uclim.2019.100458

Yang, J., Wang, Y., Xiu, C., Xiao, X., Xia, J., and Jin, C. (2020). Optimizing Local Climate Zones to Mitigate Urban Heat Island Effect in Human Settlements. *J. Clean. Prod.* 275, 123767. doi:10.1016/j.jclepro.2020.123767

Yang, L., Liang, Y., He, B., Lu, Y., and Gou, Z. (2022). COVID-19Effects on Property Markets: The Pandemic Decreases the Implicit Price of Metro Accessibility. *Tunn. Undergr. Space Technol.* 125, 104528. doi:10.1016/j.tust.2022.104528

Zeng, Z., Zhou, X., and Li, L. (2017). The Impact of Water on Microclimate in Lingnan Area. *Procedia Eng.* 205, 2034–2040. doi:10.1016/j.proeng.2017.10.082

Zhang, S., Xiao, H., and Liu, Y. (2009). Analysis of the Relationship Between Ecological Environment and Water Environment (In Chinese). *Yellow River* 31, 3–4+7. doi:10.3969/j.issn.1000-1379.2009.08.002

Zhao, Y., and Wang, J. (2018). Research on the Traditional Rural Settlements Planning Based on Morphological Integration: The Application of Performance-Based Planning Techniques. (In Chinese) *City Plan. Rev.* 42, 33–40+53. doi:10.11819/cpr20181105a

Zhou, X., Zhang, S., and Zhu, D. (2021). Impact of Urban Water Networks on Microclimate and PM2.5 Distribution in Downtown Areas: A Case Study of Wuhan. *Build. Environ.* 203, 108073. doi:10.1016/j.buildenv.2021.108073

Conflict of Interest: Author XL was employed by Architectural Design & Research Institute Co., Ltd.

The remaining authors declare that the research was conducted in the absence of any commercial or financial relationships that could be construed as a potential conflict of interest.

Publisher's Note: All claims expressed in this article are solely those of the authors and do not necessarily represent those of their affiliated organizations, or those of the publisher, the editors and the reviewers. Any product that may be evaluated in this article, or claim that may be made by its manufacturer, is not guaranteed or endorsed by the publisher.

Copyright © 2022 Cheng, Liu, Zeng, Liu, Wang, Tang and He. This is an open-access article distributed under the terms of the Creative Commons Attribution License (CC BY). The use, distribution or reproduction in other forums is permitted, provided the original author(s) and the copyright owner(s) are credited and that the original publication in this journal is cited, in accordance with accepted academic practice. No use, distribution or reproduction is permitted which does not comply with these terms.

frontiers | Frontiers in Environmental Science

ORIGINAL RESEARCH
published: 14 July 2022
doi: 10.3389/fenvs.2022.927818

Quantifying the Temporal and Spatial Patterns of Ecosystem Services and Exploring the Spatial Differentiation of Driving Factors: a Case Study of Sichuan Basin, China

Chunguang Hu[1,2], *Ziyi Wang*[3], *Jiaming Li*[4]*, *Huan Liu*[5]* and *Dongqi Sun*[4]

[1]School of Architecture and Urban Planning, Huazhong University of Science and Technology, Wuhan, China, [2]Hubei Engineering and Technology Research Center of Urbanization, Wuhan, China, [3]School of Architecture and Urban Planning, Nanjing University, Nanjing, China, [4]Institute of Geographic Sciences and Natural Resources Research, Chinese Academy of Sciences (CAS), Beijing, China, [5]Disaster Prevention Research Institute, Kyoto University, Kyoto, Japan

OPEN ACCESS

Edited by:
Jianhong Xia,
Curtin University, Australia

Reviewed by:
Decheng Zhou,
Nanjing University of Information Science and Technology, China
Zhenhong Wang,
Guizhou University, China

***Correspondence:**
Jiaming Li
lijm@igsnrr.ac.cn
Huan Liu
huan.liu.b05@kyoto-u.jp

Specialty section:
This article was submitted to Environmental Informatics and Remote Sensing, a section of the journal Frontiers in Environmental Science

Received: 25 April 2022
Accepted: 09 June 2022
Published: 14 July 2022

Citation:
Hu C, Wang Z, Li J, Liu H and Sun D (2022) Quantifying the Temporal and Spatial Patterns of Ecosystem Services and Exploring the Spatial Differentiation of Driving Factors: a Case Study of Sichuan Basin, China. Front. Environ. Sci. 10:927818. doi: 10.3389/fenvs.2022.927818

Exploring the factors that drive the change of ecosystem services (ES) is very important for maintaining ES function and zoning ecological management, especially in the Sichuan Basin area with high spatial heterogeneity such as natural and socio-economic characteristics. Taking the Sichuan Basin in China as an example, the PCA-MGWR model was constructed to explore the temporal and spatial patterns of ES in the Sichuan Basin from 2000 to 2015. The potential driving factors including anthropogenic factors, geomorphological factors, climate factors, and vegetation factors would be analyzed by principal component analysis (PCA). To illustrate the impact of spatial dependence in the data, the multi-scale geographically weighted regression (MGWR) technology was selected to explore the spatial differentiation of the impact of these four dimensions on ES to reflect the local differences of ecosystem service driving mechanisms in more detail. The results showed that 1) from the perspective of time series evolution, carbon storage (CS) and soil conservation (SC) in ES in the Sichuan Basin showed an upward trend, while water yield (WY) showed a downward trend; from the perspective of spatial patterns, except the main urban areas of Chengdu and Chongqing, the CS service level of other regions was high; The spatial distribution characteristics of SC services were “low in the middle and high in the periphery”; the high value area of WY service was located in Northeast Sichuan. 2) Among natural factors, elevation (DEM), slope (SLO), NDVI, annual average temperature (TEM), and annual average precipitation (PRE) had a higher contribution rate to ES, while among socio-economic factors, GDP density (GDP), night light (LIG), and population density (POP) had a higher contribution rate to ES, while other factors had a lower contribution rate. 3) Combined with the PCA-MGWR model, we analyzed the comprehensive response and spatial differentiation of driving factors to ES in the Sichuan Basin and explained in detail the influence of anthropogenic factors, geomorphological factors, climatic factors, and vegetation factors and their spatial heterogeneity in ES. It is expected that the spatial differences in the impact degree of different indicators can be considered when formulating the countermeasures of ES in the

Sichuan Basin, to provide theoretical support for the implementation of regional ecological management and control.

Keywords: ecosystem services, PCA-MGWR model, driving factors, spatial heterogeneity, Sichuan Basin

1 INTRODUCTION

Ecosystem services (ES) are ecological characteristics, functions, or processes that contribute directly or indirectly to human well-being (Costanza et al., 1997; Yang et al., 2021a; Yu et al., 2022b). The United Nations Millennium Ecosystem Assessment divides ES into four categories: support services, regulation services, supply services, and cultural services. There are complex relationships between different services (Tallis and Kareiva, 2005; Luo et al., 2021). The concept of ES as a "bridge" between natural ecosystems and human social systems serves as a foundation for improving human well-being and achieving regional sustainable development. The integrated assessment of ES is an effective hybrid that has become a frontier and research hotspot in geography, ecology, and environmental science, and it is also central to the sustainable development of ecosystems and the management of ecological resources (Costanza et al., 2017; Castillo-Eguskitza et al., 2018; Yu et al., 2021; Chen et al., 2022; Hu et al., 2022).

It is generally accepted that ES can be influenced by both natural and human factors (Burkhard et al., 2012; Burkhard et al., 2015; Zhang et al., 2020; Yang et al., 2021b). First, climate change can directly change the capacity to supply services such as food production, freshwater supply, and net primary productivity by changing ecosystem properties. In addition to climate change, elevation, slope, soil, and vegetation also contribute to changes in ES (Wolff et al., 2015; Yang et al., 2020). Human activities have both direct and indirect impacts on the ecosystem, with both beneficial and detrimental impacts. For example, the human activities of urban construction, forest, and grassland into an impermeable surface, resulting in the decline of the ability to provide ES. Payments for Environmental Services (PES) practices around the world, such as China's "conversion of cropland to forest and grassland" and the South African government's Working for Water program, have improved soil conservation (SC) and water yield (WY) in the region (Wei et al., 2017; Wu et al., 2019; Bing et al., 2021).

Therefore, we not only need to fully understand the spatiotemporal patterns of ES but also need to explore the driving factors of ES to develop scientifically sound ES management approaches (Geijzendorffer et al., 2015; Wei et al., 2017). Several recent studies have shown this concern, including Chen et al. (2020) the need to consider different drivers and spatial spillovers in the formulation of strategies for integrated ecosystem management and sustainable land use in urban agglomerations (Chen et al., 2020). Peng et al. (2020) discussed the impact of urbanization on the ES budget through decoupling analysis (Peng et al., 2020). Hu et al. (2021) took the Shanxi province of China as an example; this study explored the spatial differentiation of five ES and captured the main driving factors of ES change from a geospatial perspective (Hu et al., 2021).

Existing studies have shown that ES often has certain spatial heterogeneity (Li et al., 2013; Song and Deng, 2017; Zhou et al., 2018; Licheng et al., 2019; Yang et al., 2019), which will be more obvious in regions with high spatial heterogeneity in geography, society, and economy. However, most of these studies are based on global regression, mainly considering a single driving factor, without considering the comprehensive effect. Less attention has been paid to the spatial non-stationary relationship between the leading factors affecting ES. Commonly used methods such as correlation analysis and overlay analysis can only clarify the relationship between individual factors and ES and cannot quantitatively derive significant impact factors and their intensity, nor can it reveal the spatial heterogeneity of factor interaction and the possible synergistic or antagonistic effects among the factors (Jiang et al., 2022), especially when exploring multivariate driver analysis, the problem of multicollinearity between drivers often occurs (Toutenburg, 2006; Yu et al., 2022a). When there is a multicollinearity problem, the variance of the parameter estimator will be too large, the accuracy will be reduced, the significance test of the variable will be meaningless, and the influence of the explanatory variable on the explained variable cannot be correctly judged, resulting in the unreasonable value of the parameter estimator (Yu et al., 2009). Therefore, based on the PCA-MGWR method, this study combines the advantages of principal component analysis (PCA) and MGWR. Before MGWR analysis, the PCA of independent variables is carried out, and several uncorrelated principal components extracted are used as independent input variables for MGWR to analyze the spatial impact distribution of each principal component. PCA-MGWR can not only eliminate the multicollinearity problem caused by the correlation of independent variables but also explain the spatial effects of different ecosystem service factors.

To sum up, although natural-human factors have a significant impact on ES, the current research on their comprehensive consideration is still insufficient. Therefore, this study hopes to make up for the current gap. Sichuan Basin is the ecological barrier to the upper reaches of the Yangtze River. The basin has a good natural resource endowment and is one of the regions with the largest supply of ES in China (Pan and Wang, 2021). Fully understanding the spatio-temporal pattern of ES in the Sichuan Basin, and exploring the natural-human multiple impact factors, is of great importance to ensure the ecological security of the upper reaches of the Yangtze River and even the ecological security of the country.

At present, more and more attention is focused on exploring the driving force of the impact on the ES (Zhong et al., 2019; Sannigrahi et al., 2020). Relevant studies have focused on the spatial-temporal pattern of ES in Sichuan Province and its various driving factors from a statistical perspective (Liu et al., 2020; Niu et al., 2022). However, these studies generally focus on the

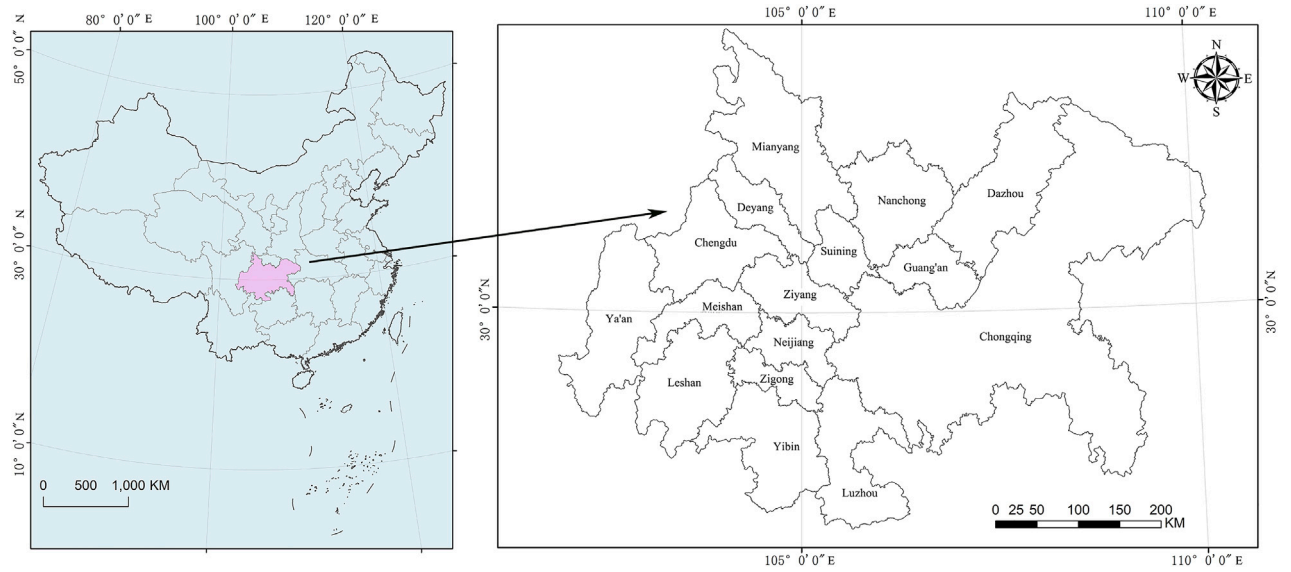

FIGURE 1 | Location and administrative division of the Sichuan Basin.

analysis of change patterns, paying less attention to the spatial change characteristics of driving forces, and often ignoring the scale differences of different driving factors. Therefore, some studies have used the spatial regression model to test the spatial non-stationary relationship between the four driving forces on SC and WY in Sichuan Province (Huang et al., 2022). This study not only adds the measurement indicators and driving factors of ES in the Sichuan Basin but also uses the MGWR model to explore the nature and intensity of the impact of various factors on ES in the Sichuan Basin. In view of the limitations and deficiencies of previous studies, this study has the following specific objectives: (I) evaluate the ES and their temporal and spatial changes in the Sichuan Basin; (II) quantitatively assess the driving factors of temporal and spatial changes of ES in Sichuan Basin; and (III) analyze the comprehensive response and spatial differentiation of various driving factors of ES in Sichuan Basin.

2 METHODOLOGY

2.1 Study Area

Sichuan Basin lies at the intersection of the Belt and Road and the Yangtze Economic Belt (27° 68′~ 32° 30′N, 101° 95′~ 108° 95 E, **Figure 1**). Influenced by the subtropical monsoon climate, the annual average temperature is 13–20°C, and the annual average precipitation is 1,000 mm. The scope of the study includes 15 cities, including Chengdu in Sichuan and 29 districts and counties in Chongqing, with a total area of about 185,000 km^2. There are many types of landforms in the region, forming various kinds of vertical climatic zones; the climatic differentiation is remarkable, the natural ecological environment is diverse, and the ecological resources are rich. In 2019, the Chengdu-Chongqing urban agglomeration had a resident population of 96 million and a regional GDP of nearly 6.3 trillion yuan. The 2021 outline for constructing the Double-City Economic Circle proposes that the Chengdu-Chongqing urban agglomeration should play an exemplary role in promoting the green development of the Yangtze River Economic Belt and the ecological protection of western China.

2.2 Data

This study refers to the methods of previous studies and the data requirements of the InVEST model to quantify the ES (Xie and Ng, 2013; Chen et al., 2020; Zhang X. et al., 2021; Huang et al., 2022). SC is an important indicator to measure the water and soil conservation of the ecosystem. Carbon storage (CS) can directly reflect the carbon absorption and storage capacity of the ecosystem. WY is the ability of the ecosystem to retain rainwater under the joint action of plants and soil. At the same time, considering that Sichuan Basin is an important water source and protected area of the Yangtze River and the Yellow River, soil erosion is an important factor in its flood disaster. Sichuan Basin is also rich in natural resources, including forests, meadows, wetlands, and snow mountains. It is a strategic area for ecological security in Western China. Therefore, combined with the natural landform and the regional characteristics of the social economy in the Sichuan Basin, these three ecosystems can be regarded as important ecosystems for the sustainable development of resources and the environment. It involves the use of multi-source data such as land use, digital elevation model, meteorological data, soil data, watershed boundary, and social and economic data. to comprehensively evaluate the ES in the Sichuan Basin. The data sources and their descriptions are shown in **Table 1**.

2.3 Quantification of Ecosystem Services

2.3.1 Carbon Storage (Carbon Storage)

Carbon sequestration services, also known as “Carbon Storage” services, are important regulatory services in ecosystems. The “carbon” module in the InVEST model is used to evaluate the CS

TABLE 1 | Data source and its detailed description.

Data	Data format	Data source	Data description
Land use maps	Raster (30 m)	Resource and Environmental Science Data Center of the Chinese Academy of Sciences (https://www.resdc.cn/, accessed on 1 February 2022)	Based on the Landsat TM image of the United States, it is generated through manual visual interpretation
Digital elevation model	Raster (30 m)	Geospatial Data Cloud (http://www.gscloud.cn, accessed on 3 February 2022)	Including elevation, slope, and aspect data
NDVI data	Raster (30 m)	National Earth System Science Data Center (http://www.geodata.cn/, accessed on 3 February 2022)	Vegetation is quantified by measuring the difference between near-infrared (vegetation strong reflection) and red light (vegetation absorption)
Climate data	Raster (1 km)	National Earth System Science Data Center (http://www.geodata.cn/, accessed on 3 February 2022); Terra Climate (http://www.climatologylab.org/terraclimate.html, accessed on 5 February 2022)	Including annual average precipitation, annual average temperature, and potential evapotranspiration
Soil data	Raster (1 km)	Harmonized World Soil Database (http://www.iiasa.ac.at/Research/LUC/External-World-soil-database/HTML/, accessed on 4 February 2022)	It includes soil texture, topsoil sand fraction, topsoil silt fraction, topsoil clay fraction, topsoil organic carbon, root limit depth, and plant available water content
Demographic and economic data	Raster (1 km)	Resource and Environmental Science Data Center of the Chinese Academy of Sciences (https://www.resdc.cn/, accessed on 1 February 2022); National Centers for Environmental Information (https://ngdc.noaa.gov/eog/dmsp.htm, accessed on 5 February 2022)	These include the GDP spatial distribution km grid data set, the population spatial distribution km grid data set; Suomi NPP VIIRS night light remote sensing data (2015)
Watershed boundary	Shapefile	HydroSHEDS (http://hydrosheds.org/, accessed on 4 February 2022)	Digital watershed atlas of natural resources

in Sichuan Basin as the supply of carbon sequestration services. The input carbon storage data refer to previous local studies (Liu et al., 2004; Tang et al., 2018; Liang et al., 2021). The formula is as follows:

$$C_{tot} = C_{above} + C_{below} + C_{soil} + C_{dead} \quad (1)$$

where C_{tot} is the total carbon storage $(t \cdot hm^{-2})$, C_{above} is aboveground biological carbon $(t \cdot hm^{-2})$, C_{below} is underground biological carbon $(t \cdot hm^{-2})$, C_{soil} is soil organic carbon $(t \cdot hm^{-2})$, and C_{dead} is dead organic matter. The details of each coefficient are shown in **Supplementary Table SA1** of the supplementary data.

2.3.2 Water Yield (Water Yield)

WY refers to the ability of ES to store water resources. The Sichuan Basin is located in the middle reaches of the Yangtze River, so it is vital to assess the WY for the storage and utilization of water resources. The "water yield" module is used to quantify the supply of WY in the Sichuan Basin. This module is defined as the part of precipitation minus evapotranspiration based on the principle of water balance (Sharp et al., 2014; Sun et al., 2018). The formula is as follows:

$$S_{wp} = \left(1 - \frac{AET_{xj}}{P_x}\right) \times P_x \quad (2)$$

$$\frac{AET_{(x)}}{P_{(x)}} = 1 + \frac{PET_{(x)}}{P_{(x)}} - \left[1 + \left(\frac{PET_{(x)}}{P_{(x)}}\right)^{w}\right]^{1/w} \quad (3)$$

$$PET_{(x)} = Kc_{(x)} \times ET_{o(x)} \quad (4)$$

$$W_{(x)} = \frac{AWC_{(x)} \times Z}{P_{(x)}} + 1.25 \quad (5)$$

where S_{wp} is the annual water yield (mm); $AET_{(x)}$ is the actual annual evapotranspiration (mm) of the grid unit; P_x is the annual precipitation (mm) of the grid unit; $PET_{(x)}$ is the potential evapotranspiration of the grid unit; $Kc_{(x)}$ is the crop evapotranspiration coefficient; $ET_{o(x)}$ is the reference crop scatter; $AWC_{(x)}$ is the plant available water content; $W_{(x)}$ is the empirical parameter; and Z is the Zhang coefficient (Zhang et al., 2004). The details of each coefficient are shown in **Supplementary Table SA2** of the supplementary data.

2.3.3 Soil Conservation (Soil Conservation)

In this study, the modified universal soil loss equation (USLE) is used to estimate regional soil conservation and soil erosion. In sediment retention, the model takes into account the important hydrological process of plant-induced soil erosion and sediment interception, which makes the simulation results more scientific and reasonable. We used the "sediment delivery ratio" module of the InVEST model to evaluate SC service. This module uses the revised universal soil loss equation (RUSLE) to express SC, according to the difference between potential soil loss and actual soil loss (Renard et al., 2017; Rao and Xiao, 2018). The calculation formula is as follows:

$$RKLS_i = R_i \times K_i \times LS_i \quad (6)$$

$$USLE_i = R_i \times K_i \times LS_i \times C_i \times P_i \quad (7)$$

$$SEDRET_i = RKLS_i - USLE_i + SEDR_i \quad (8)$$

where $RKLS_i$ grid I is based on geomorphology and climate calculation of potential soil erosion; R_i, K_i, LS_i, C_i, and P_i are the rainfall erosivity factor, soil erodibility factor, slope length factor, vegetation cover, and management factor, SC measure factor of the unit grid i; $USLE_i$ was the actual soil erosion amount of grid i, and $SEDRET_i$ was the SC amount of grid i; $C_i(P_i)$ is 0.05,0.03,0.04,0,0 (1,1,1,0,0) for cultivated land, woodland, grassland, water area, and construction land, respectively.

TABLE 2 | Selected potential factors.

Driving factor	Variable description	Abbreviation
Anthropogenic factors	Night light	LIG
	GDP density	GDP
	Population density	POP
Climatic factors	Annual average temperature	TEM
	Annual average precipitation	PRE
	Actual evapotranspiration	EVA
Vegetation factors	NDVI	NDVI
Geomorphological factors	Elevation	DEM
	Slope	SLO
	Aspect	ASP

Other factors are input based on the model recommendations. The details of each coefficient are shown in **Supplementary Table SA3** of the supplementary data.

2.4 Spatial Autocorrelation of Ecosystem Services

Spatial autocorrelation can reflect the degree of interdependence and aggregation between the attributes of a specific region and those of other regions (Hu et al., 2022). The calculation of the Moran'I equation in ArcGIS 10.5 can be used to examine spatial patterns of ES. The calculation formula is as follows:

$$Moran'I = \frac{\sum_{i=1}^{n}\sum_{j=1}^{n} W_{ij}\left(x_i - \bar{x}\right)\left(x_j - \bar{x}\right)}{S^2 \sum_{i=1}^{n}\sum_{j=1}^{n} W_{ij}}, \quad (9)$$

where n is the total number of each district (county) in Sichuan Basin; $S = 1/n\sum_{i=1}^{n}(x_i - \bar{x})^2$; x_i, x_j is the value of ES of each district (County); W_{ij} is the weight matrix of unit space; and x is the average of ES. When $Moran'I > 0$, the space is positively correlated, when $Moran'I < 0$, the space is negatively correlated, and when $Moran'I = 0$, the space is not correlated.

2.5 Spatial Differentiation of Driving Factors

2.5.1 Factor Identification and Data Dimensionality Reduction

First, we selected the factors associated with ES, including the four major factors: anthropogenic factors, climatic factors, vegetation factors, and geomorphological factors (Costanza et al., 2014; Zhou et al., 2018; Chen et al., 2019; Schirpke et al., 2019; Zhang Z. et al., 2021; Xu et al., 2022). To explore the overall correlation of ecosystem service impact factors, we conducted Spearman correlation research between CS, WY, and SC services and potential drivers based on SPSS 25. The final anthropogenic factors include night light, GDP density, and population density; climatic factors include annual average temperature, annual average precipitation, and actual evapotranspiration; vegetation factors include NDVI; and geomorphological factors include elevation, slope, and aspect (**Table 2**).

Second, to avoid the influence of multicollinearity of all variables, we mainly based on PCA to synthesize multiple related variables with the principle of as little information loss as possible and turn them into a few irrelevant variables to reduce the dimension of data, simplify the data structure and ensure that the VIF of explanatory variables is not greater than 7 (Plaza et al., 2005; Sannigrahi et al., 2020), thus to eliminate the possible influence of multicollinearity between variables (**Supplementary Table SB1**).

2.5.2 Local Regression Analysis

Geographically weighted regression (GWR) is a spatial regression method that can explain different local relationships among variables (Sun et al., 2020). Its greatest advantage is the ability to measure spatial variability accurately (Brunsdon et al., 1998). Although GWR captures the spatial heterogeneity of influencing factors to some extent, it is implemented under the assumption that all covariates change on the same spatial scale, and it is not enough to explain the spatial heterogeneity level of different urban landscape factors. MGWR relaxes the assumption of "same spatial scale" and allows optimization of covariate-specific bandwidths. The GWR and MGWR formulas are given in the equations:

$$y_i = \sum_{j=0}^{m} \beta_j(u_i, v_i) x_{ij} + \varepsilon_i, \quad (14)$$

$$y_i = \sum_{j=0}^{m} \beta_{bwj}(u_i, v_i) x_{ij} + \varepsilon_i, \quad (15)$$

where x_{ij} is the J prediction variable and (u_i, v_i) is the centroid coordinate of each region (county) i. β_{bwj} is the optimal bandwidth for calibrating the j condition relationship. By contrast, MGWR allows different processes to operate on different spatial scales by deriving the individual bandwidth of the conditional relationship between the response variables and the different predictive variables. MGWR uses the inverse fitting algorithm to calibrate and initializes the inverse fitting process by estimating the GWR parameters. Based on these initial values, the calibration process works iteratively, with all local parameter estimates and optimal bandwidth evaluated in each iteration. The iteration is terminated when the difference in the parameter estimates of the successive iterations converges to the specified threshold.

3 RESULTS

3.1 Temporal and Spatial Patterns of Ecosystem Services

From 2000 to 2015, the average values of CS and SC services increased from 5846835 t/ha and 6868780 t/ha to 5884678 t/ha and 7777234 t/ha, respectively, and the average WY decreased from 184656 m^3/ha to 174054 m^3/ha. The results showed that urbanization had a negative effect on the occupation of arable land, forest land, and carbon storage, and the implementation of ecological and water conservation projects had a positive effect on soil and water conservation. As far as the spatial distribution of ES was concerned (**Figure 2**), the CS service level was higher in all regions except Chengdu and Chongqing. The spatial distribution characteristics of SC services were "low in the middle and high in the periphery". The high-value area of WY service was located in the northeast of Sichuan

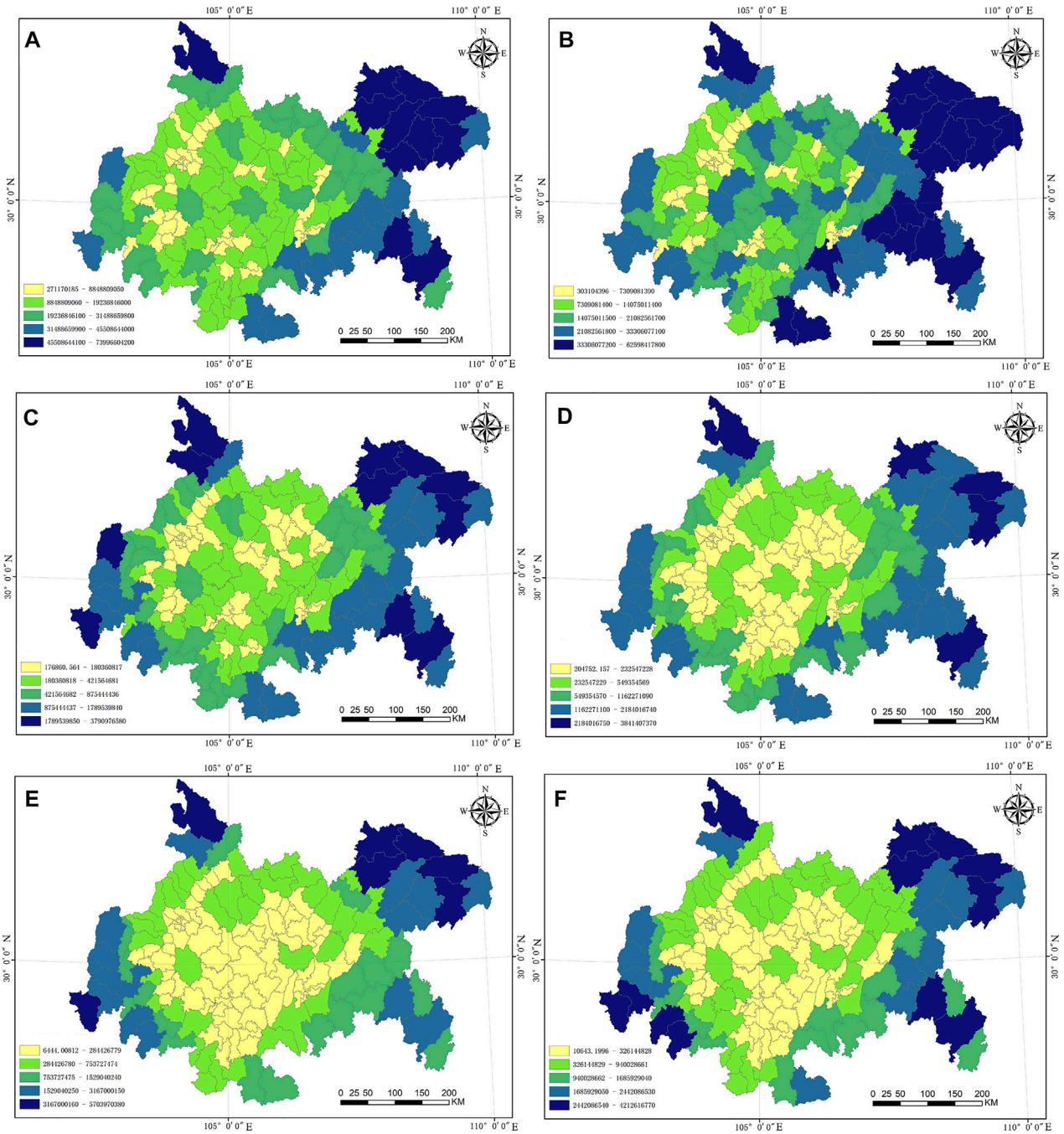

FIGURE 2 | Spatial distribution of ES from 2000 to 2015. **(A)** 2000 annual water yield (WY); **(B)** 2015 annual WY; **(C)** 2000 annual carbon storage (CS); **(D)** 2015 annual CS; **(E)** 2000 annual soil conservation (SC); and **(F)** 2015 annual SC.

Province. On the whole, the spatial distribution of various services was different, which was closely related to the regional geographical background. In terms of the spatial change of ES, most regions showed a decrease in CS services, especially in cities and towns and their surroundings. Except for some regions of Wushan County, Chongqing, Wuxi County, and Chengkou County, SC services showed a decreasing trend, the other regions showed an increasing trend, and the decrease of WY services was mainly located in the northeast of the study area.

3.2 Spatial Autocorrelation of Ecosystem Services

Spatial autocorrelation analysis of CS, WY, and SC ES in the Sichuan Basin was conducted from 2000 to 2015 (**Figure 3**), in

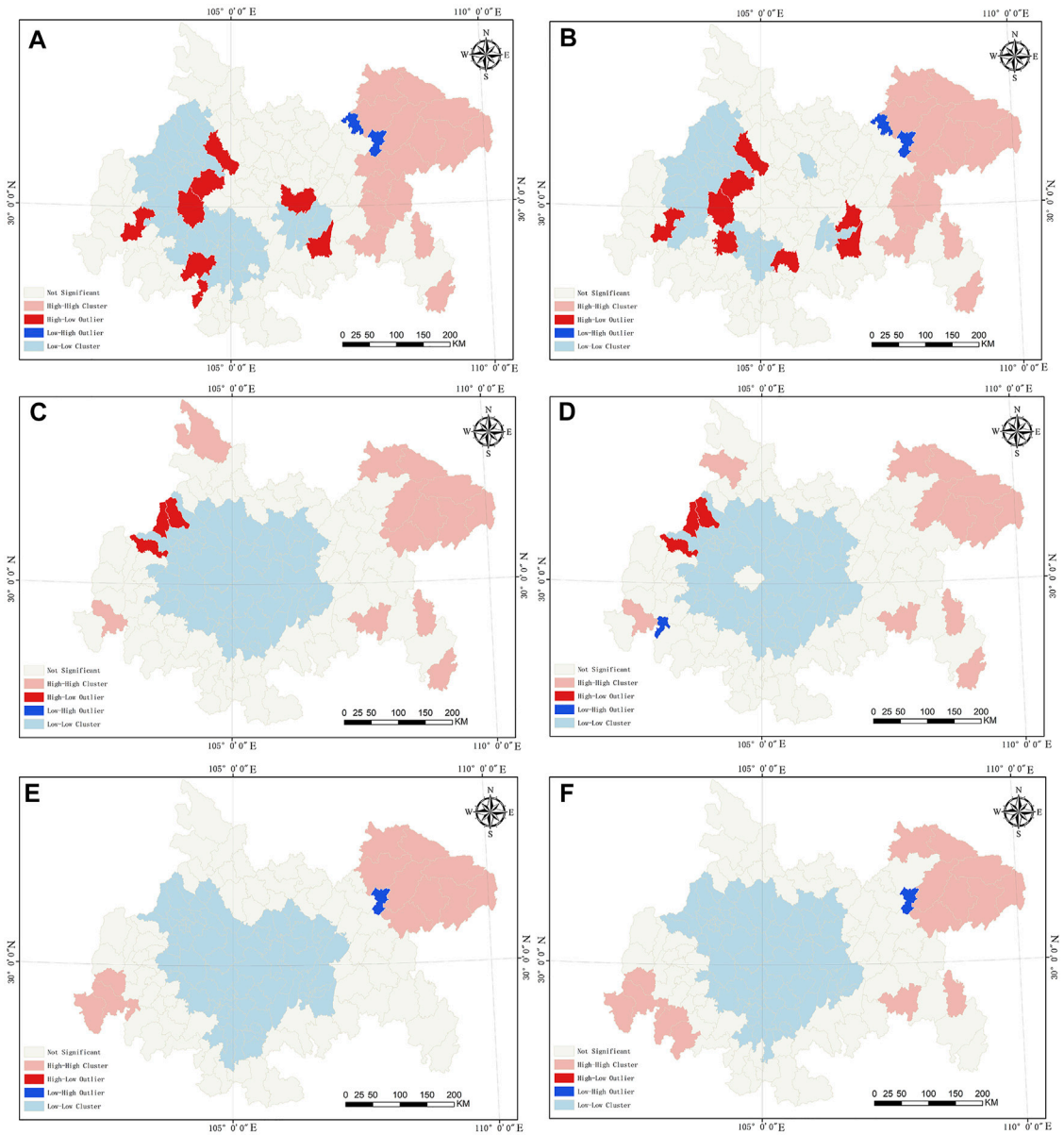

FIGURE 3 | LISA agglomeration distribution of ES from 2000 to 2015 **(A)** 2000 annual WY; **(B)** 2015 annual WY; **(C)** 2000 annual CS; **(D)** 2015 annual CS; **(E)** 2000 annual SC; and **(F)** 2015 annual SC.

which the 2000 CS Moran's I index was 0.359 and the standardized test Z (I) value was 10.073; in 2015, Moran ' s I index was 0.360 and Z (I) was 10.124, respectively, at the significance level of 0.05($p = 0$); the results showed that the spatial distribution of CS showed a significant positive autocorrelation, and the state of carbon accumulation was apparent.

Moran's I Index of WY in 2000 was 0.459, Z (I) value of the standardized test was 12.762, Moran's I Index of WY in 2015 was 0.470, Moran's I Index of WY in 2000 was 0.459, Moran's I value was 12.762, Moran's I value was 0.05, Moran's I Index of WY in 2015 was 0.470, the Z (I) value of the standardized test was 13.017, and it passed the test at the significance level of 0.05($p = 0$). The results showed that the spatial distribution of WY supply presented a significant positive autocorrelation and the aggregation was obvious.

In 2000, Moran's I index was 0.347, Z (I) of the standardized test was 9.819, and it passed the test at the significance level of 0.05($p = 0$) In 2015, Moran's I index was 0.409, and Z (I) of the standardized test was 11.399, which passed the test at the significance level of 0.05 ($p = 0$) The results showed that the spatial distribution of SC supply showed a significant positive autocorrelation and aggregation.

At the same time, the local spatial autocorrelation analysis of ES, such as CS, WY, and SC from 2000 to 2015, was carried out,

TABLE 3 | Statistical description of Spearman correlation between ES and various impact factors.

Correlation analysis	Carbon storage (CS)	Water yield (WY)	Soil conservation (SC)
LIG	–0.604**	–0.893**	–0.759**
GDP	–0.625**	–0.915**	–0.820**
POP	–0.727**	–1.000**	–0.840**
TEM	–0.397**	–0.617**	–0.748**
PRE	0.103	0.166*	0.229**
EVA	–0.065	–0.024	0.045
NDVI	0.649**	0.897**	0.892**
DEM	0.501**	0.609**	0.694**
SLO	0.564**	0.773**	0.917**
ASP	0.002	0.182*	0.171*

*In spearman correlation statistics, ** represents at the significant level of 0.01 (double tail). * represents at the significant level of 0.05 (two-tailed).*

and the distribution chart of local indicators for spatial autocorrelation (LISA) was drawn. As shown in **Figure 3**, from the results of local spatial autocorrelation analysis, the low-low aggregation types of ES were mainly distributed in the central part of the Sichuan Basin, including Ziyang, Suining, Neijiang, Deyang, eastern Chengdu, and western Chongqing, while high-concentration types were mainly distributed in the eastern and western border areas of Sichuan Basin, the northern part of Chongqing, the northern part of Dazhou, the southern part of Ya'an, and the southern part of Leshan, i.e., the northern part of Chengdu, the southern part of Deyang, the northern part of Ziyang and the eastern part of Meishan. The other places had not passed the local spatial autocorrelation significance test.

3.3 Influencing Factors

3.3.1 Correlation Analysis

To explore the overall correlation of the impact factors of ES in the Sichuan Basin from 2000 to 2015, the results of the Spearman correlation between services and factors (**Table 3**) found that, the spatial distribution of ES capacity in the Sichuan Basin was influenced by both natural and socio-economic factors, thus showing different spatial distribution characteristics. In general, terrain factors such as TEM and EVA contributed the most, while socio-economic factors such as GDP and POP contributed less, and the contribution rate of other factors was low. Among them, POP, GDP, and LIG had a significant negative correlation with these three services. NDVI, DEM, and SLO had a significant positive correlation with these three services.

3.3.2 Spatial Heterogeneity

SPSS 25 PCA was used to visualize the factors after 10 kinds of standardization, and the spatial pattern of coefficients was obtained (**Figure 4**), the spatial heterogeneity of different factors on WY, CS, and SC was further explored.

The spatial distribution of geomorphological factors in the Sichuan Basin had significant ring-shaped spatial features (**Figure 4A**). From the spatial distribution trend of influence intensity, with Ziyang, the central area of Sichuan Basin as the core, the negative driving force of topographic factors on the Sichuan Basin ecosystem was gradually increasing outwards and presented obvious ring-type distribution characteristics. The central part of the Sichuan Basin was affected by the surrounding mountainous terrain. The whole environment was closed and blocked, and the foundation of heat dissipation was poor.

The climate factors in Sichuan Basin had a negative correlation to the regional ES (**Figure 4B**) and had a significant gradient in the spatial distribution. In terms of the spatial distribution of the overall driving mechanism, except for the peripheral region of the Sichuan Basin, a few mountainous areas, and the central area of the Zhongliang mountain range in Jinyun, there was a strong positive correlation between driving characteristics, the climate of Chengdu-Chongqing urban agglomeration as a whole had an obvious positive effect on regional ES.

The anthropogenic factors in Sichuan Basin showed a significant negative correlation between the driving characteristics of regional ES and the spatial distribution of small patches (**Figure 4C**). The main driving force behind this phenomenon was that, on the one hand, the economic and industrial structure in Sichuan Basin was still in the stage of transition from primary production to secondary production and the basic demand for space and resources by industries such as industry and manufacturing led to the horizontal expansion of cities. On the other hand, the corridor of the Double-City Economic Circle in Chengdu and Chongqing was the main area of negative correlation, the spatial population density had a negative driving effect on the urban development, while a few marginal urban areas in the north showed a weak positive driving effect. From the perspective of the spatial distribution trend of driving intensity, the influence degree of the two core cities, Chengdu and Chongqing, gradually decreased outward.

The vegetation factors in Sichuan Basin showed a significant positive correlation to the regional ES and the patch spatial distribution trend (**Figure 4D**). As a whole, Sichuan Basin was dominated by farmland and grassland ecosystems and had prominent supply-type services. The increase in species diversity and community complexity would directly increase the stock of ES. At present, the stock of forest land ecological assets in each district of Chengdu-Chongqing urban agglomeration was insufficient, and the regulation, support, and cultural services in the core area of the central city were weak. Therefore, the enhancement and optimization of vegetation and other ecosystems had a significant effect on the enhancement of the Sichuan Basin's overall service functions.

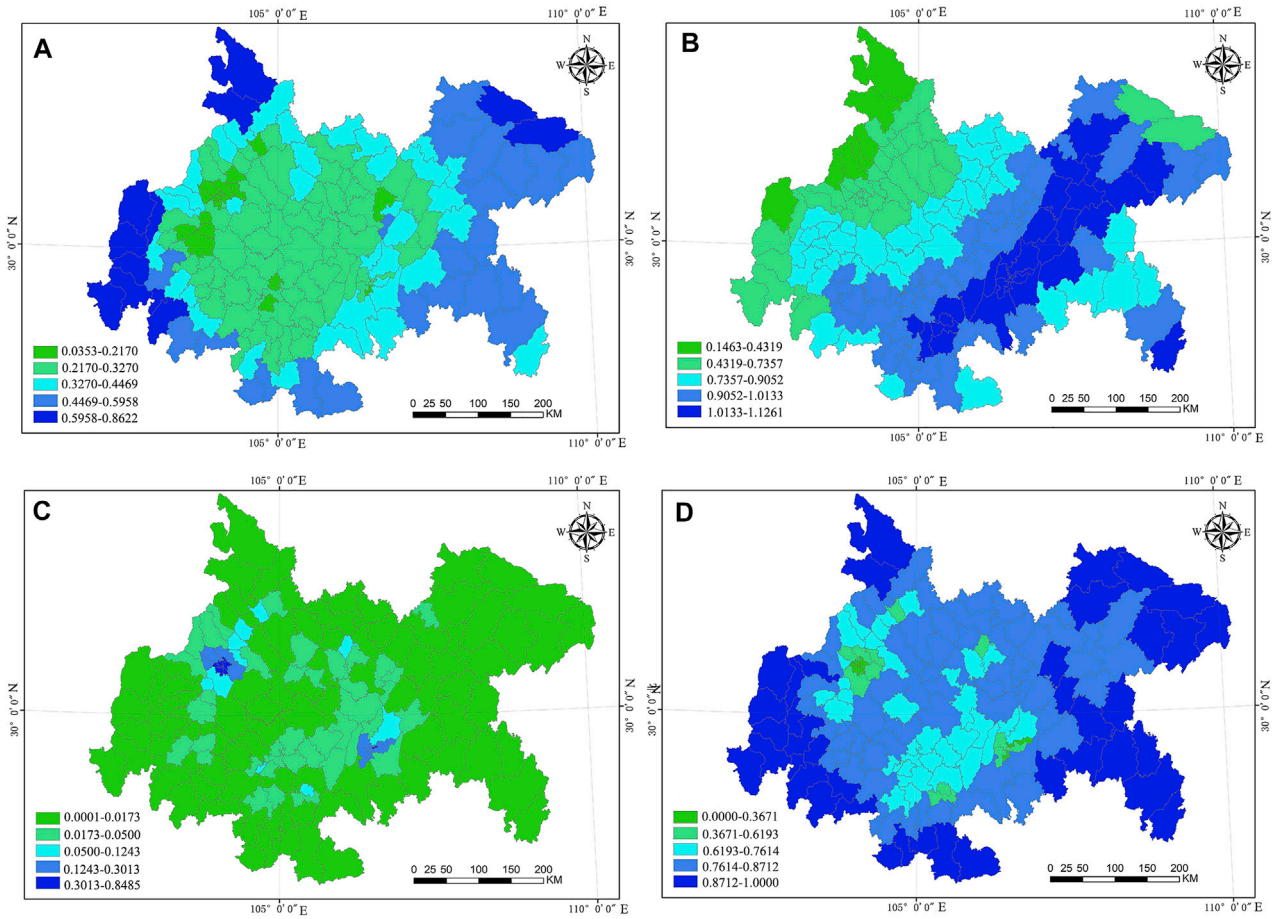

FIGURE 4 | Spatial effect of four kinds of influencing factors **(A)**. Geomorphological factors; **(B)** climatic factors; **(C)** anthropogenic factors; and **(D)** vegetation factors).

TABLE 4 | Comparison of the fitting results of OLS, GWR, and MGWR.

Model index	CS			WY			SC		
	OLS	GWR	MGWR	OLS	GWR	MGWR	OLS	GWR	MGWR
AICc	6645.997	291.141	186.472	7610.206	346.232	276.243	6700.948	242.548	168.989
R^2 (adjusted)	0.639	0.642	0.841	0.486	0.490	0.705	0.736	0.737	0.857

3.3.3 Multi-Scale Geographically Weighted Regression

The global model, GWR model, and MGWR model under the ordinary least squares method (OLS) were shown in **Table 4**. The result of OLS fitting showed that the VIF of all the factors was less than 7.5, which showed that there was no variable redundancy and there were no multiple linear relationships among the factors. At the same time, Jarque-Bera's result showed that the residuals did not obey the normal distribution, the model fitting was one-sided, and the GWR model should be combined to improve the fitting accuracy.

However, the local spatial regression model based on MGWR could better reflect the impact of the aforementioned influencing factors on WY services, CS services, and SC services in specific spaces, according to the results shown in **Figure 5**, which showed the local R^2 spatial distribution of the fitting results of the MGWR model. **Figure 5A** showed the impact of various factors on WY services, showing a vertical strip distribution in space, with the east being more intense, followed by the west, while the middle was less affected; **Figure 5B** showed the impact of various factors on CS services, showing a circular impact pattern opposite to WY services in space, that was, west > northeast > middle; **Figure 5C** showed the impact of various factors on SC services, showing local patches and overall axisymmetric distribution in space, and the northwest was the most affected.

From the descriptive statistical results of the coefficients of the MGWR Model (**Tables 5**, **6**, and **7**), it could be seen that the

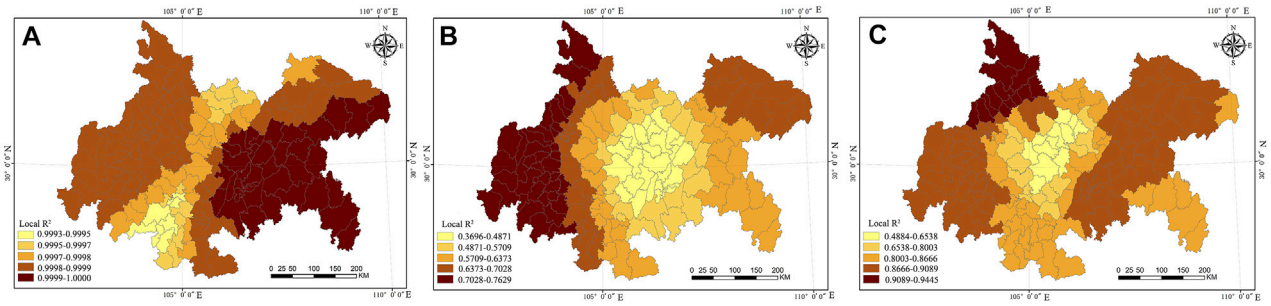

FIGURE 5 | Spatial heterogeneity distribution of ES under different factors **(A)**. WY; **(B)** CS; and **(C)** SC.

TABLE 5 | Statistical description of the MGWR coefficient of WY services.

Variable	Mean	STD	Min	Median	Max
Intercept	−0.001	0.000	−0.002	−0.001	−0.001
LIG	0.023	0.000	0.022	0.023	0.023
GDP	0.042	0.007	0.030	0.045	0.048
POP	−1.063	0.024	−1.098	−1.059	−1.037
TEM	0.002	0.001	0.001	0.002	0.003
PRE	−0.005	0.001	−0.007	−0.004	−0.003
NDVI	0.004	0.003	−0.001	0.002	0.007
DEM	0.001	0.001	−0.000	0.001	0.001
SLO	−0.003	0.001	−0.004	−0.003	−0.002
ASP	−0.002	0.000	−0.003	−0.002	−0.002

TABLE 6 | Statistical description of the MGWR coefficient of CS services.

Variable	Mean	STD	Min	Median	Max
Intercept	−0.097	0.277	−0.720	−0.026	0.382
LIG	−0.539	0.005	−0.545	−0.540	−0.528
GDP	0.460	0.224	0.109	0.594	0.690
POP	−0.200	0.292	−0.524	−0.244	0.208
TEM	0.547	0.229	−0.013	0.637	0.822
NDVI	−0.140	0.007	−0.154	−0.140	−0.116
DEM	1.157	0.024	1.128	1.147	1.223
SLO	0.108	0.015	0.077	0.105	0.166

TABLE 7 | Statistical description of the MGWR coefficient of SC services.

Variable	Mean	STD	Min	Median	Max
Intercept	−0.079	0.004	−0.085	−0.080	−0.068
LIG	0.002	0.003	−0.005	0.004	0.005
GDP	−0.019	0.001	−0.022	−0.019	−0.017
POP	0.057	0.068	−0.306	0.069	0.127
TEM	−0.271	0.054	−0.380	−0.285	−0.103
PRE	0.175	0.004	0.161	0.176	0.178
NDVI	0.176	0.003	0.171	0.177	0.184
DEM	0.196	0.089	0.004	0.229	0.330
SLO	0.326	0.260	0.047	0.247	0.890
ASP	−0.043	0.072	−0.292	−0.042	0.077

influence of different factors and their trend of action were quite different in-service spaces. DEM had the largest effect on CS, followed by POP on WY, while LIG had the least effect on SC and the temperature had the least effect on WY. From the ratio of positive and negative effects, the same factor had different effects on different services, which indicated that there was significant spatial heterogeneity of the factors, and the MGWR model could show the characteristics of local coefficients.

4 DISCUSSION

4.1 Spatio-Temporal Patterns of Ecosystem Services in the Sichuan Basin

In the Sichuan Basin, one of the major suppliers of ES in China (Pan and Wang, 2021), carbon sequestration services and SC services showed an upward trend, while water production services showed a downward trend. These results were mainly attributed to the great changes in land use types in the study area. The increase in vegetation coverage led to a significant increase in CS and SC, which was consistent with previous studies (Jiang et al., 2018; Luo et al., 2019). At the same time, large-scale planting led to a significant increase in water consumption and evapotranspiration, which is the main reason for the decline of WY(Feng et al., 2016). However, the *p*-value of the Moran index of the three ES is 0, indicating that there is a significant positive autocorrelation at the significance level of 0.05. L-L cluster areas are mainly concentrated in the central part of the Sichuan Basin, and H-H cluster areas are distributed in the northeast and the periphery of the cities. In general, the Chengdu Plain, basin hills, and mountain areas around the basin in the east are the concentrated areas for WY supply services, while the southwest Sichuan mountains, west Sichuan mountain valleys, and northwest Sichuan Plateau in the west are the concentrated areas for CS and SC supply services.

4.2 Quantitative Attribution of the Driving Factors of Ecosystem Services in the Sichuan Basin

Combined with the results of the impact of natural and socio-economic driving factors on the correlation of ecosystem services in the Sichuan Basin, it can be found that LIG, GDP, POP, and TEM have significant negative effects on ES, indicating that the rise of these indicators will make the state of ES tense to some

extent. NDVI, DEM, and SLO have significant positive effects on ES. These results are consistent with other studies but slightly different in the magnitude of the correlation coefficient (Lin et al., 2020), this is mainly due to the differences in research methods and scales, which provide a reference for enhancing ES in the Sichuan Basin research area (Sannigrahi et al., 2020; Huang et al., 2022). At the same time, according to the mean absolute value of regression coefficient of different factors, artificial factors such as LIG, GDP, and POP have a greater impact on WY services, the water production services are very sensitive to POP. CS services are sensitive to DEM and LIG. LIG, POP, and NDVI negatively affected CS services. SC services are sensitive to SLO and TEM, among which GDP, TEM, and SLO have negative effects on SC services, the rest were positive. The aforementioned results provide a basis for exploring the impact of different driving factors on ES in Sichuan Basin.

4.3 Comprehensive Response and Spatial Heterogeneity of Driving Factors to Ecosystem Services in the Sichuan Basin

Four comprehensive driving factors show different characteristics of the spatial pattern (**Figure 4**): geomorphological factors show the spatial characteristics of "centripetal trough", climatic factors show the spatial characteristics of "east high west low", anthropogenic factors show the spatial characteristics of "east-west dual-core", and vegetation factors show the spatial characteristics of "planarization". The contribution rate of geomorphological factors, TEM, and EVA to the three natural factors is higher, the contribution rate of GDP and POP to the three social-economic factors is higher, and the contribution rate of other factors is lower. POP, GDP, LIG, and other factors have a significant negative correlation with these three services, these variables are the main driving factors of ecosystem service changes, which are also consistent with previous relevant researchers (Wang et al., 2019; Yongxiu et al., 2020). It shows that the key to achieving coordinated development of regional ecosystems is to reduce the negative interference of human activities in the ecosystem.

Because of the regional and spatial differences in geological and meteorological conditions, the service and driving factors of CS, WY, and SC in the Sichuan Basin are characterized by spatial heterogeneity; the results of MGWR show that the AIC_C value of the MGWR model is smaller than that of OLS and GWR model, the adjusted R^2 is larger, and the bandwidth of variables is rich, which indicates that the fitting effect of MGWR is more reliable (Oshan et al., 2019; Li and Fotheringham, 2020), and can provide reference and guidance for regional units to adopt relevant policy regulation, according to local conditions.

Specifically, there is strong spatial heterogeneity in the driving factors of WY services in the Sichuan Basin (**Supplementary Figure SA1**), especially in Chongqing in the east and Chengdu in the west. It further explains that the eastern and western parts of the Sichuan Basin also have higher LIG and GDP, resulting in excessive demand for water in highly urbanized areas. At the same time, the altitude of surrounding areas leads to changes in precipitation, average temperature, and vegetation coverage, thus affecting WY services in external areas (Cao et al., 2020). To sum up, the Sichuan Basin River basin, which is composed of eastern Sichuan Ridge Valley, central Sichuan hilly area, and Chengdu Plain Lake area, has an uneven water production service space due to its special topography and spatial distribution of precipitation.

There is also a strong spatial heterogeneity in Sichuan Basin's CS services (**Supplementary Figure SA2**). The service capacity of CS in peripheral areas such as northern counties and western counties and cities is relatively large, the main reason is that the People's Government of Sichuan Province has taken the lead in setting up a natural forest resources protection project leading group to implement the system of chief responsibility and management by objectives responsibility for the natural forest resources protection projects within the areas under their jurisdiction, to prohibit the cutting of natural forests, and to close down the timber trading market in the project areas, and the logging ban was quickly extended to the entire province.

The SC services in Sichuan Basin still have spatial differences (**Supplementary Figure SA3**). The main reason is that the hilly area in the middle of Sichuan and the Chengdu Plain of Kawanishi is the most severe area of soil erosion in the upper reaches of the Yangtze River, accounting for 21.9% of the total area of soil erosion, the area is located in the middle and lower reaches of Min River, Tuo River, Jialing River, and the Yangtze River. The ground is cut and broken, the hills undulate and the west is plain. In most places in the region, the rainfall is about 1,000 mm, and most are heavy rain. The outcropping rock is mainly composed of purple-red sandstone and mudstone, which is easy to be weathered and eroded, resulting in severe hydraulic erosion in this area. However, the SC services in the mountainous areas around the basin are better, mainly due to the low, middle, and high mountains in the region, especially the widespread distribution of carbonate rocks and the intercalation of detrital rocks among them, as well as various human actions in recent years, such as the ecological protection of the red line, less population density distribution, and other comprehensive reasons, resulting in this area SC services steadily improved.

4.4 Limitations and Future Sustainable Development Measures

In this study, we used the InVEST model to estimate the value of CS, WY, and SC. However, the Sichuan Basin ecosystem is an integrated system with a wide variety of service functions (Kang et al., 2018; You et al., 2021). In addition to the three types of services considered in this study, food production, habitat quality, pollution control, entertainment, and culture are also important to service types, which are also important directions for follow-up research. On the other hand, the supply and demand of ecosystems together constitutes the flow of ES from natural systems to social systems (Burkhard et al., 2012; Burkhard et al., 2015). However, the current research focuses on the "supply" side analysis of ES, given the lack of research on the

"demand" side of ES, the synergy between supply and demand of ES should be quantified in the future.

5 CONCLUSION

The concept of ES has built a "bridge" between natural ecosystems and human social systems. This study evaluates the spatial and temporal patterns of ES in the Sichuan Basin from 2000 to 2015 and discusses the spatial heterogeneity of response of various driving factors to ES with the help of PCA-MGWR model. The results showed that the CS and SC services experienced an upward trend during the study period, while the WY services showed a downward trend. Especially from the perspective of spatial pattern, the carbon sequestration services in other regions except for the main urban areas of Chengdu and Chongqing were higher; the spatial distribution characteristics of SC services are "low in the middle and high in the periphery"; the high-value area of water production service is located in Northeast Sichuan. The results of the spatial regression model show that compared with the OLS model and GWR Model, the MGWR model has the best explanatory power, and there is a correlation between driving factors and ES change. In view of the differences in the driving factors on the geographical scale, this study helps to consider the spatial differences in the impact of different indicators when formulating the countermeasures for ES in the Sichuan Basin and provides more information for the refined management and zoning control of ES in the Sichuan Basin.

DATA AVAILABILITY STATEMENT

The original contributions presented in the study are included in the article/**Supplementary Material**; further inquiries can be directed to the corresponding authors.

AUTHOR CONTRIBUTIONS

CH: writing—original draft and data curation. ZW: data curation and software. JL: editing and supervision. HL: supervision and writing—review and editing. DS: supervision. All authors have read and agreed to the published version of the manuscript.

FUNDING

This work was supported by the Natural Science Foundation of China under the Grant 41971162 and the Second Scientific Investigation of the Tibetan Plateau (Grant no. 2019QZKK0406).

SUPPLEMENTARY MATERIAL

The Supplementary Material for this article can be found online at: https://www.frontiersin.org/articles/10.3389/fenvs.2022.927818/full#supplementary-material

REFERENCES

Bing, Z., Qiu, Y., Huang, H., Chen, T., Zhong, W., and Jiang, H. (2021). Spatial Distribution of Cultural Ecosystem Services Demand and Supply in Urban and Suburban Areas: A Case Study from Shanghai, China. *Ecol. Indic.* 127, 107720. doi:10.1016/j.ecolind.2021.107720

Brunsdon, C., Fotheringham, S., and Charlton, M. (1998). Geographically Weighted Regression. *J. R. Stat. Soc. D.* 47, 431–443. doi:10.1111/1467-9884.00145

Burkhard, B., Kroll, F., Nedkov, S., and Müller, F. (2012). Mapping Ecosystem Service Supply, Demand and Budgets. *Ecol. Indic.* 21, 17–29. doi:10.1016/j.ecolind.2011.06.019

Burkhard, B., Müller, A., Müller, F., Grescho, V., Anh, Q., Arida, G., et al. (2015). Land Cover-Based Ecosystem Service Assessment of Irrigated Rice Cropping Systems in Southeast Asia-An Explorative Study. *Ecosyst. Serv.* 14, 76–87. doi:10.1016/j.ecoser.2015.05.005

Cao, Y., Qiao, X., Hopke, P. K., Ying, Q., Zhang, Y., Zeng, Y., et al. (2020). Ozone Pollution in the West China Rain Zone and its Adjacent Regions, Southwestern China: Concentrations, Ecological Risk, and Sources. *Chemosphere* 256, 127008. doi:10.1016/j.chemosphere.2020.127008

Castillo-Eguskitza, N., Martín-López, B., and Onaindia, M. (2018). A Comprehensive Assessment of Ecosystem Services: Integrating Supply, Demand and Interest in the Urdaibai Biosphere Reserve. *Ecol. Indic.* 93, 1176–1189. doi:10.1016/j.ecolind.2018.06.004

Chen, J., Jiang, B., Bai, Y., Xu, X., and Alatalo, J. M. (2019). Quantifying Ecosystem Services Supply and Demand Shortfalls and Mismatches for Management Optimisation. *Sci. Total Environ.* 650, 1426–1439. doi:10.1016/j.scitotenv.2018.09.126

Chen, W., Chi, G., and Li, J. (2020). The Spatial Aspect of Ecosystem Services Balance and its Determinants. *Land Use Policy* 90, 104263. doi:10.1016/j.landusepol.2019.104263

Chen, Y., Yang, J., Yang, R., Xiao, X., and Xia, J. (2022). Contribution of Urban Functional Zones to the Spatial Distribution of Urban Thermal Environment. *Build. Environ.* 216, 109000. doi:10.1016/j.buildenv.2022.109000

Costanza, R., d'Arge, R., De Groot, R., Farber, S., Grasso, M., Hannon, B., et al. (1997). The Value of the World's Ecosystem Services and Natural Capital. *nature* 387, 253–260. doi:10.1038/387253a0

Costanza, R., De Groot, R., Braat, L., Kubiszewski, I., Fioramonti, L., Sutton, P., et al. (2017). Twenty Years of Ecosystem Services: How Far Have We Come and How Far Do We Still Need to Go? *Ecosyst. Serv.* 28, 1–16. doi:10.1016/j.ecoser.2017.09.008

Costanza, R., De Groot, R., Sutton, P., Van der Ploeg, S., Anderson, S. J., Kubiszewski, I., et al. (2014). Changes in the Global Value of Ecosystem Services. *Glob. Environ. Change* 26, 152–158. doi:10.1016/j.gloenvcha.2014.04.002

Feng, X., Fu, B., Piao, S., Wang, S., Ciais, P., Zeng, Z., et al. (2016). Revegetation in China's Loess Plateau Is Approaching Sustainable Water Resource Limits. *Nat. Clim. Change* 6, 1019–1022. doi:10.1038/nclimate3092

Geijzendorffer, I. R., Martín-López, B., and Roche, P. K. (2015). Improving the Identification of Mismatches in Ecosystem Services Assessments. *Ecol. Indic.* 52, 320–331. doi:10.1016/j.ecolind.2014.12.016

Hu, B., Kang, F., Han, H., Cheng, X., and Li, Z. (2021). Exploring Drivers of Ecosystem Services Variation from a Geospatial Perspective: Insights from China's Shanxi Province. *Ecol. Indic.* 131, 108188. doi:10.1016/j.ecolind.2021.108188

Hu, C., Wang, Z., Wang, Y., Sun, D., and Zhang, J. (2022). Combining MSPA-MCR Model to Evaluate the Ecological Network in Wuhan, China. *Land* 11, 213. doi:10.3390/land11020213

Huang, Y., Wu, Y., Niu, S., and Gan, X. (2022). Estimating the Effects of Driving Forces on Ecosystem Services and Their Responses to Environmental Conditions. *Environ. Sci. Pollut. Res.*, 1–13. doi:10.1007/s11356-022-20867-x

Jiang, C., Zhang, H., and Zhang, Z. (2018). Spatially Explicit Assessment of Ecosystem Services in China's Loess Plateau: Patterns, Interactions, Drivers, and Implications. *Glob. Planet. Change* 161, 41–52. doi:10.1016/j.gloplacha.2017.11.014

Jiang, M., Jiang, C., Huang, W., Chen, W., Gong, Q., Yang, J., et al. (2022). Quantifying the Supply-Demand Balance of Ecosystem Services and Identifying

its Spatial Determinants: A Case Study of Ecosystem Restoration Hotspot in Southwest China. *Ecol. Eng.* 174, 106472. doi:10.1016/j.ecoleng.2021.106472

Kang, P., Chen, W., Hou, Y., and Li, Y. (2018). Linking Ecosystem Services and Ecosystem Health to Ecological Risk Assessment: A Case Study of the Beijing-Tianjin-Hebei Urban Agglomeration. *Sci. Total Environ.* 636, 1442–1454. doi:10.1016/j.scitotenv.2018.04.427

Li, B., Shi, P., Jin, S., Wei, W. E. I., and Zhou, J. (2013). Theory and Quantitative Methodology of Spatial Heterogeneity Analysis of Ecosystem Service Value for the Shiyanghe River Basin, Gansu, China. *J. Desert Res.* 33, 943–951. doi:10.7522/j.issn.1000-694X.2013.00132

Li, Z., and Fotheringham, A. S. (2020). Computational Improvements to Multi-Scale Geographically Weighted Regression. *Int. J. Geogr. Inf. Sci.* 34, 1378–1397. doi:10.1080/13658816.2020.1720692

Liang, Y., Hashimoto, S., and Liu, L. (2021). Integrated Assessment of Land-Use/land-Cover Dynamics on Carbon Storage Services in the Loess Plateau of China from 1995 to 2050. *Ecol. Indic.* 120, 106939. doi:10.1016/j.ecolind.2020.106939

Licheng, L., Chunfang, L., Chuan, W., and Pengjie, L. (2019). Supply and Demand Matching of Ecosystem Services in Loess Hilly Region: A Case Study of Lanzhou. *Prog. Chem.* 74, 1921. doi:10.11821/dlxb201909016

Lin, Z. Y., Xiao, Y., Rao, E. M., Shi, X. W., and Zhang, P. (2020). Relationships Among Different Types of Ecosystem Service in Southwest China. *Ying Yong Sheng Tai Xue Bao* 31, 978–986. doi:10.13287/j.1001-9332.202003.015

Liu, J. Y., Wang, S. Q., Chen, J. M., Liu, M. L., and Zhuang, D. F. (2004). Storages of Soil Organic Carbon and Nitrogen and Land Use Changes in China: 1990–2000. *Acta Geogr. Sin.* 59, 483–496. doi:10.11821/xb200404001

Liu, Y., Yang, S., Han, C., Ni, W., and Zhu, Y. (2020). Variability in Regional Ecological Vulnerability: A Case Study of Sichuan Province, China. *Int. J. Disaster Risk Sci.* 11, 696–708. doi:10.1007/s13753-020-00295-6

Luo, X., Yang, J., Sun, W., and He, B. (2021). Suitability of Human Settlements in Mountainous Areas from the Perspective of Ventilation: A Case Study of the Main Urban Area of Chongqing. *J. Clean. Prod.* 310, 127467. doi:10.1016/j.jclepro.2021.127467

Luo, Y., Lü, Y., Fu, B., Zhang, Q., Li, T., Hu, W., et al. (2019). Half Century Change of Interactions Among Ecosystem Services Driven by Ecological Restoration: Quantification and Policy Implications at a Watershed Scale in the Chinese Loess Plateau. *Sci. Total Environ.* 651, 2546–2557. doi:10.1016/j.scitotenv.2018.10.116

Niu, L., Shao, Q., Ning, J., and Huang, H. (2022). Ecological Changes and the Tradeoff and Synergy of Ecosystem Services in Western China. *J. Geogr. Sci.* 32, 1059–1075. doi:10.1007/s11442-022-1985-6

Oshan, T., Li, Z., Kang, W., Wolf, L., and Fotheringham, A. (2019). Mgwr: A Python Implementation of Multiscale Geographically Weighted Regression for Investigating Process Spatial Heterogeneity and Scale. *ISPRS Int. J. Geo-Inf.* 8, 269. doi:10.3390/ijgi8060269

Pan, Z., and Wang, J. (2021). Spatially Heterogeneity Response of Ecosystem Services Supply and Demand to Urbanization in China. *Ecol. Eng.* 169, 106303. doi:10.1016/j.ecoleng.2021.106303

Peng, J., Wang, X., Liu, Y., Zhao, Y., Xu, Z., Zhao, M., et al. (2020). Urbanization Impact on the Supply-Demand Budget of Ecosystem Services: Decoupling Analysis. *Ecosyst. Serv.* 44, 101139. doi:10.1016/j.ecoser.2020.101139

Plaza, A., Martinez, P., Plaza, J., and Perez, R. (2005). Dimensionality Reduction and Classification of Hyperspectral Image Data Using Sequences of Extended Morphological Transformations. *IEEE Trans. Geosci. Remote Sens.* 43, 466–479. doi:10.1109/tgrs.2004.841417

Rao, E. M., and Xiao, Y. (2018). Spatial Characteristics and Effects of Soil Conservation Service in Sichuan Province. *Acta Ecol. Sin.* 38, 8741–8749. doi:10.5846/stxb201806011217

Renard, K. G., Laflen, J. M., Foster, G. R., and McCool, D. K. (2017). "The Revised Universal Soil Loss Equation," in *Soil Erosion Research Methods* (London: Routledge), 105–126. doi:10.1201/9780203739358-5

Sannigrahi, S., Zhang, Q., Pilla, F., Joshi, P. K., Basu, B., Keesstra, S., et al. (2020). Responses of Ecosystem Services to Natural and Anthropogenic Forcings: A Spatial Regression Based Assessment in the World's Largest Mangrove Ecosystem. *Sci. Total Environ.* 715, 137004. doi:10.1016/j.scitotenv.2020.137004

Schirpke, U., Candiago, S., Vigl, L. E., Jäger, H., Labadini, A., Marsoner, T., et al. (2019). Integrating Supply, Flow and Demand to Enhance the Understanding of Interactions Among Multiple Ecosystem Services. *Sci. Total Environ.* 651, 928–941. doi:10.1016/j.scitotenv.2018.09.235

Sharp, R., Tallis, H. T., Ricketts, T., Guerry, A. D., Wood, S. A., Chaplin-Kramer, R., et al. (2014). *InVEST User's Guide* (Palo Alto: The Natural Capital Project, Stanford University, University of Minnesota, The Nature Conservancy, World Wildlife Fund).

Song, W., and Deng, X. (2017). Land-use/land-cover Change and Ecosystem Service Provision in China. *Sci. Total Environ.* 576, 705–719. doi:10.1016/j.scitotenv.2016.07.078

Sun, X., Lu, Z., Li, F., and Crittenden, J. C. (2018). Analyzing Spatio-Temporal Changes and Trade-Offs to Support the Supply of Multiple Ecosystem Services in Beijing, China. *Ecol. Indic.* 94, 117–129. doi:10.1016/j.ecolind.2018.06.049

Sun, X., Tang, H., Yang, P., Hu, G., Liu, Z., and Wu, J. (2020). Spatiotemporal Patterns and Drivers of Ecosystem Service Supply and Demand across the Conterminous United States: A Multiscale Analysis. *Sci. Total Environ.* 703, 135005. doi:10.1016/j.scitotenv.2019.135005

Tallis, H., and Kareiva, P. (2005). Ecosystem Services. *Curr. Biol.* 15, R746–R748. doi:10.1016/j.cub.2005.09.007

Tang, X., Zhao, X., Bai, Y., Tang, Z., Wang, W., Zhao, Y., et al. (2018). Carbon Pools in China's Terrestrial Ecosystems: New Estimates Based on an Intensive Field Survey. *Proc. Natl. Acad. Sci. U.S.A.* 115, 4021–4026. doi:10.1073/pnas.1700291115

Toutenburg, H. (2006). in *Book Review: Regression Diagnostics–Identifying Influential Data and Sources of Collinearity*. Editors D. A. Belsley, E. Kuh, and R. E. Welsch (New York, NY: Wiley Online Library).

Wang, Y., Zhao, J., Fu, J., and Wei, W. (2019). Effects of the Grain for Green Program on the Water Ecosystem Services in an Arid Area of China-Using the Shiyang River Basin as an Example. *Ecol. Indic.* 104, 659–668. doi:10.1016/j.ecolind.2019.05.045

Wei, H., Fan, W., Wang, X., Lu, N., Dong, X., Zhao, Y., et al. (2017). Integrating Supply and Social Demand in Ecosystem Services Assessment: A Review. *Ecosyst. Serv.* 25, 15–27. doi:10.1016/j.ecoser.2017.03.017

Wolff, S., Schulp, C. J. E., and Verburg, P. H. (2015). Mapping Ecosystem Services Demand: A Review of Current Research and Future Perspectives. *Ecol. Indic.* 55, 159–171. doi:10.1016/j.ecolind.2015.03.016

Wu, X., Liu, S., Zhao, S., Hou, X., Xu, J., Dong, S., et al. (2019). Quantification and Driving Force Analysis of Ecosystem Services Supply, Demand and Balance in China. *Sci. Total Environ.* 652, 1375–1386. doi:10.1016/j.scitotenv.2018.10.329

Xie, Y. J., and Ng, C. N. (2013). Exploring Spatio-Temporal Variations of Habitat Loss and its Causal Factors in the Shenzhen River Cross-Border Watershed. *Appl. Geogr.* 39, 140–150. doi:10.1016/j.apgeog.2013.01.001

Xu, Z., Peng, J., Dong, J., Liu, Y., Liu, Q., Lyu, D., et al. (2022). Spatial Correlation between the Changes of Ecosystem Service Supply and Demand: An Ecological Zoning Approach. *Landsc. Urban Plan.* 217, 104258. doi:10.1016/j.landurbplan.2021.104258

Yang, J., Wang, Y., Xiu, C., Xiao, X., Xia, J., and Jin, C. (2020). Optimizing Local Climate Zones to Mitigate Urban Heat Island Effect in Human Settlements. *J. Clean. Prod.* 275, 123767. doi:10.1016/j.jclepro.2020.123767

Yang, J., Wang, Y., Xue, B., Li, Y., Xiao, X., Xia, J., et al. (2021a). Contribution of Urban Ventilation to the Thermal Environment and Urban Energy Demand: Different Climate Background Perspectives. *Sci. Total Environ.* 795, 148791. doi:10.1016/j.scitotenv.2021.148791

Yang, J., Yang, R., Chen, M.-H., Su, C.-H., Zhi, Y., and Xi, J. (2021b). Effects of Rural Revitalization on Rural Tourism. *J. Hosp. Tour. Manag.* 47, 35–45. doi:10.1016/j.jhtm.2021.02.008

Yang, M., Zhang, Y., and Wang, C. (2019). Spatial-temporal Variations in the Supply-demand Balance of Key Ecosystem Services in Hubei Province. *Resour. Env. Yangtze Basin* 28, 2080–2091.

Yongxiu, S., Shiliang, L., Fangning, S., Yi, A., Mingqi, L., and Yixuan, L. (2020). Spatio-temporal Variations and Coupling of Human Activity Intensity and Ecosystem Services Based on the Four-Quadrant Model on the Qinghai-Tibet Plateau. *Sci. Total Environ.* 743, 140721. doi:10.1016/j.scitotenv.2020.140721

You, H., Yang, J., Xue, B., Xiao, X., Xia, J., Jin, C., et al. (2021). Spatial Evolution of Population Change in Northeast China during 1992-2018. *Sci. Total Environ.* 776, 146023. doi:10.1016/j.scitotenv.2021.146023

Yu, D., Peterson, N. A., and Reid, R. J. (2009). Exploring the Impact of Non-normality on Spatial Non-stationarity in Geographically Weighted Regression Analyses: Tobacco Outlet Density in New Jersey. *GIScience Remote Sens.* 46, 329–346. doi:10.2747/1548-1603.46.3.329

Yu, H., Xie, W., Sun, L., and Wang, Y. (2021). Identifying the Regional Disparities of Ecosystem Services from a Supply-Demand Perspective. *Resour. Conservation Recycl.* 169, 105557. doi:10.1016/j.resconrec.2021.105557

Yu, H., Yang, J., Li, T., Jin, Y., and Sun, D. (2022a). Morphological and Functional Polycentric Structure Assessment of Megacity: An Integrated Approach with Spatial Distribution and Interaction. *Sustain. Cities Soc.* 80, 103800. doi:10.1016/j.scs.2022.103800

Yu, H., Yang, J., Sun, D., Li, T., and Liu, Y. (2022b). Spatial Responses of Ecosystem Service Value during the Development of Urban Agglomerations. *Land* 11, 165. doi:10.3390/land11020165

Zhang, H., Feng, J., Zhang, Z., Liu, K., Gao, X., and Wang, Z. (2020). Regional Spatial Management Based on Supply-Demand Risk of Ecosystem Services-A Case Study of the Fenghe River Watershed. *Int. J. Environ. Res. Public Health* 17, 4112. doi:10.3390/ijerph17114112

Zhang, L., Hickel, K., Dawes, W. R., Chiew, F. H., Western, A. W., and Briggs, P. R. (2004). A Rational Function Approach for Estimating Mean Annual Evapotranspiration. *Water Resour. Res.* 40, 89–97. doi:10.1029/2003wr002710

Zhang, X., Li, H., Xia, H., Tian, G., Yin, Y., Lei, Y., et al. (2021). The Ecosystem Services Value Change and its Driving Forces Responding to Spatio-Temporal Process of Landscape Pattern in the Co-urbanized Area. *Land* 10, 1043. doi:10.3390/land10101043

Zhang, Z., Peng, J., Xu, Z., Wang, X., and Meersmans, J. (2021). Ecosystem Services Supply and Demand Response to Urbanization: A Case Study of the Pearl River Delta, China. *Ecosyst. Serv.* 49, 101274. doi:10.1016/j.ecoser.2021.101274

Zhong, S., Geng, Y., Qian, Y., Chen, W., and Pan, H. (2019). Analyzing Ecosystem Services of Freshwater Lakes and Their Driving Forces: the Case of Erhai Lake, China. *Environ. Sci. Pollut. Res.* 26, 10219–10229. doi:10.1007/s11356-019-04476-9

Zhou, D., Tian, Y., and Jiang, G. (2018). Spatio-temporal Investigation of the Interactive Relationship between Urbanization and Ecosystem Services: Case Study of the Jingjinji Urban Agglomeration, China. *Ecol. Indic.* 95, 152–164. doi:10.1016/j.ecolind.2018.07.007

Conflict of Interest: The authors declare that the research was conducted in the absence of any commercial or financial relationships that could be construed as a potential conflict of interest.

Publisher's Note: All claims expressed in this article are solely those of the authors and do not necessarily represent those of their affiliated organizations, or those of the publisher, the editors, and the reviewers. Any product that may be evaluated in this article, or claim that may be made by its manufacturer, is not guaranteed or endorsed by the publisher.

Copyright © 2022 Hu, Wang, Li, Liu and Sun. This is an open-access article distributed under the terms of the Creative Commons Attribution License (CC BY). The use, distribution or reproduction in other forums is permitted, provided the original author(s) and the copyright owner(s) are credited and that the original publication in this journal is cited, in accordance with accepted academic practice. No use, distribution or reproduction is permitted which does not comply with these terms.

frontiers | Frontiers in Earth Science

ORIGINAL RESEARCH
published: 18 July 2022
doi: 10.3389/feart.2022.950853

Education Equality and Its Influencing Factors for Migrant Children in the Compulsory Education Stage Based on Multi-Source Data: A Case Study of Dalian, China

Zhenchao Zhang, Weixin Luan, Chuang Tian, Min Su and Zeyang Li*

School of Maritime Economics and Management, Dalian Maritime University, Dalian, China

Inequality in the admission of migrant children is an important manifestation of inequities at the compulsory education stage in China. Spatial differences in the allocation of educational resources and the factors affecting the number of enrolled migrant children led to the following conclusions: 1) the total number of migrant children in Dalian is growing situationally, with a total increase of 29,223 from 2008 to 2020. 2) The migrant children in Dalian in 2020 are distributed in a spatially uneven manner, with most of them concentrated in the periphery of the Ganjingzi District, south of the Jinzhou area (suburban areas), where very few of them were enrolled in high-quality junior high and primary schools. 3) The distribution of educational resources differed significantly between the central urban areas and suburban areas. 4) The internal factor of schools constraining the admission of migrant children is the teacher–student ratio. For every 1% increase in the teacher–student ratio, the number of migrant children decreases by 4.12%. The main external factors affecting the admission of migrant children were rental prices and the area occupied by construction, which increased by 1% for each 2,000 m buffer range of school and 0.25% for the number of migrant children and decreased by 0.29% for each 2,000 m buffer range of the school.

Keywords: migrant children, compulsory education, the spatial metrology model, influencing factors, multi-source data

OPEN ACCESS

Edited by:
Bing Xue,
Institute of Applied Ecology (CAS), China

Reviewed by:
Dahao Zhang,
Sun Yat-sen University, China
Chenxi Li,
Xi'an University of Architecture and Technology, China
Andong Guo,
Zhejiang University, China

****Correspondence:***
Weixin Luan
guanll2019@vip.163.com

Specialty section:
This article was submitted to Geoscience and Society, a section of the journal Frontiers in Earth Science

Received: *23 May 2022*
Accepted: *10 June 2022*
Published: *18 July 2022*

Citation:
Zhang Z, Luan W, Tian C, Su M and Li Z (2022) Education Equality and Its Influencing Factors for Migrant Children in the Compulsory Education Stage Based on Multi-Source Data: A Case Study of Dalian, China. Front. Earth Sci. 10:950853. doi: 10.3389/feart.2022.950853

1 INTRODUCTION

Since the economic reforms of the 1970s, China has been experiencing rapid industrialization and urbanization, which triggered the largest domestic urban–rural migration in the country's history (Wang and Holland, 2011). This has resulted in a large influx of migrant workers seeking better employment opportunities and living conditions (Fang et al., 2016). The children they bring with them are called migrant children (Yang, 2005). One of the challenges migrant workers and their children face during the migration process is the inequality of migrant children's access to educational resources, which is an important social problem in contemporary China (Ma and Wu, 2020). In 2020, there were 14,297,000 migrant children in China within the compulsory education stage, of which 85.8% went to public schools or had their tuition paid by government resources (National Bureau of Statistics, 2005). Particularly, large cities in China have seen many migrant children entering their public schools. Most migrant workers come from the inland

provinces and poor rural areas in the west, who migrated to the eastern coastal regions where economic development is more advanced (Goodburn, 2009). As a large coastal city with a rapidly developing economy, population, and education system, Dalian has attracted many migrant workers. In 2020, there were 123,030 migrant children at the compulsory education stage in Dalian, accounting for 47% of all children in the Liaoning Province and 23% of school children in junior high and primary schools in Dalian. As such, it is particularly important to solve the problem of education inequality for migrant children in Dalian.

With the increase of educational inequality in large cities, scholars have grown more concerned about the household registration system, an important factor in the inequality of migrant children's school admission (Qian and Walker, 2015; Wei and Gong, 2019). Theoretical concepts of isolation, assimilation, social mobility, social exclusion/integration, and citizenship have been widely used to study inequalities in education between urban and rural children and questioned whether migrant children could actually catch up with urban students. Because the government uses the household registration system to decide the configuration of educational resources, migrant children have poorer educational opportunities than their urban peers (Koo, 2012). Furthermore, Xiong (2015) suggested that the homogeneity of public schools under China's education system and the household registration system is reducing the opportunities of migrant children for upward social mobility. Although improvements in policies have benefited many migrant children, household barriers are not fully eliminated yet. In fact, Qian and Walker, (2015) showed that megacities such as Shanghai and Beijing have tightened immigration control by introducing new restrictive systems to replace the original household registration system.

The standard of permanent residence is so high that it is difficult for migrant workers and their families to obtain official certificates. However, although migrant children can enter urban public schools without local household registration, they can only apply for low-quality public schools that are usually located in urban–suburban areas (Qian and Walker, 2015). High-quality public schools are usually located in urban centers, but they are reserved for local students. Therefore, school quality (not school isolation) has become one of the most important factors affecting the education of migrant children. While earlier research provided rich background information on the educational issues of migrant children and discussed policy implications from different perspectives, most of these studies were qualitative in nature (Zhou, 2006). Furthermore, many of these studies only focused on one or two school students and cannot represent the education of all migrant children in the city (Chen and Feng, 2019). Research on the education of migrant children has gradually moved from a qualitative nature to a quantitative one (Goodburn, 2009; Xiong, 2015). Yet, the existing quantitative studies have either focused on institutional barriers (Lai et al., 2014; Guo and Zhao, 2019; Wei and Gong, 2019) or individual factors (Hu, 2018; Ma et al., 2018; Wang et al., 2018). They have not interpreted the overall school distribution of migrant children in the city and the reasons for this distribution.

Points of interest (POI) data, important geographic urban space big data (Liu K. et al., 2020; Zhang D. et al., 2020), can describe the spatial and attribute information of geographical entities in real-time, such as name, address, and coordinates. They have the advantage of larger sample sizes and more meticulous information coverage. POI-based research has been fruitful in areas such as business spatial distribution (Lan et al., 2018; Qiao et al., 2019; Zhang et al., 2021a; Xu et al., 2022), urban functional area identification (Zhai et al., 2019; Zhang et al., 2021b; Yu et al., 2022), urban built-up area identification (He, 2019; Yu et al., 2021; Zhang Z. et al., 2021), and spatial balance of basic education (Zhang et al., 2022). As such, the convergence of multi-source data such as school POI, internal data, and socio-economic data can provide a more comprehensive analysis of the specifics of migrant children's education.

In summary, the current studies on educational issues of migrant children have mainly been statistical analyses and economic measurements (Tang and Wang, 2021). Research on the analysis of migrant children's education using a geographic information system (GIS) spatial analysis and spatial econometric models is scant. In terms of data, research on migrant children's education has mainly used statistical data from a district or several schools in the city as samples. However, it is difficult to accurately reflect the internal relationships between the number of migrant children in the city, the internal factors of the school, and socioeconomic factors with small sample size. At the present stage of compulsory education, migrant children in China's big cities no longer have any problems attending public schools. To address educational inequality, what they need is to study in better public schools. As a megacity in China, Dalian is currently facing such a problem with migrant children in public schools. Therefore, in this study, our sample will comprise all junior middle schools and primary schools in Dalian in 2020, which will be combined with population, gross domestic product (GDP), and rental price data. Using ArcGIS 10.6, we will construct a geographic database and combine spatial analysis and measurement to analyze and interpret the educational equality of migrant children from the following three aspects: 1) change in the number of migrant children over time using districts and counties as units; 2) the distribution status of migrant children in junior high and primary schools in Dalian as well as the differences in the distribution of educational resources using schools as the unit; and 3) the influence of internal and external factors in school on the number of migrant children using the spatial metrology model and junior high/primary schools as samples. The innovation of this study lies in the richness of data types and the number of spatial measurement samples. It combines spatial visualization and spatial measurement to explore the education equality of migrant children and provide a new perspective for the research on education equality of migrant children in other cities.

2 METHODOLOGY

2.1 Study Area

Figure 1 show Dalian is an important hub and megacity along the northern coast of China covering a total area of 12,574 km^2. Like

most large cities in China, the development of compulsory education in Dalian is facing the problem of unequal allocation of educational spaces. Migrant children's education is particularly important for developing the equilibrium of compulsory education. In 2020, the number of migrant children in Dalian was 123,030, which was 47% of the total number of migrant children in Liaoning Province and 23% of the total number of students in junior high and primary schools in Dalian. Thus, studying the equilibrium of migrant children's education in Dalian is extremely representative. This study focuses on seven districts and one county under the Dalian jurisdiction. The main study area is the two county-level cities in the alternative tube, which provides us a sample size of 639 schools in the compulsory education stage. Out of these 639 schools, 411 are primary schools and 228 are junior middle schools, with 80,277 and 42,803 migrant children studying, respectively. We explored the spatial equitability of migrant children in the mandatory education stage and the influence of each factor on it, which can provide a valuable framework for studying the equality of migrant children's education in other cities in China.

2.2 Data Source and Processing

In this study, the number of migrant children attending junior high and primary schools in Dalian, China, was mainly derived from information provided by government agencies. The collected data included the number of school children in junior high and primary schools in Dalian in 2020, the number of dedicated teachers, the number of personnel with a professional technical title of intermediate and above, the construction area, the number of books, the number of computer stations, the value of teaching equipment, and other statistical information. We used the crawl Baidu Map API and Gaode Map API with Crawler software to get the longitude and latitude coordinates of the schools where the migrant children were located, so as to obtain the spatial attributes of the primary and secondary schools. The GDP data were obtained from the 2020 nighttime light imaging pass (https://ngdc.noaa.gov/) and are available for public download. Furthermore, Dalian 100 m * 100 m population raster data were primarily obtained from WorldPop (https://www.worldpop.org/), which is available for public download. The rental price data of Dalian were crawled using Python on the ANN dwelling website. Coordinate tangle, coordinate point counter inspection, and address information correction complement were performed to ensure data precision.

Furthermore, the whole and joint rental prices were uniformly adjusted to the whole rental price according to the housing estates, resulting in 2070 attributes with average rental price point coordinates. The data also included administrative divisions in the study area. Land under construction data were derived from the National Basic Geographic Information System Database. In this study, ArcGIS 10.6 was utilized after normalizing the aforementioned data to construct a geographic information database.

2.3 Methods

2.3.1 Spatial Interpolation

Spatial interpolation has been widely used in many fields, including deterministic, geodesic, and barrier-containing interpolation (Tian et al., 2021; Yang et al., 2021; Yu et al., 2021). The spatial data directly acquired in the research were based on point/face statistics or measured data of some monitoring points. The spatial precision of the data was lacking. Therefore, the correspondence with the space to produce high-precision full coverage was simulated by spatial interpolation to obtain continuous data surfaces. In this study, we used junior high and primary schools as basic points. The ArcGIS 10.6 software was used to construct a geographic database after processing the evaluation indicators of the impact factors on migrant children; the interpolation of inverse distance weight was used to transform each indicator into a data surface and spatially visualize it.

2.3.2 Correlation Analysis

Linear correlation analysis is commonly used to analyze the correlation between variables, and the index used to measure it is known as the linear correlation coefficient. There are three main correlation coefficients: Pearson, Spearman, and Kendall, which apply to different occasions. By calculating the correlation coefficient (mainly R-value), the value range of R is $[-1, 1]$. If there is a positive correlation, then $r > 0$; if the correlation is negative, then $r < 0$. Furthermore, the relationship strength is analyzed as follows: $|r| > 0.95$: significant correlation; $|r| \geq 0.8$: highly correlated; $0.5 \leq |r| < 0.8$: moderate correlation; $0.3 \leq |r| < 0.5$: low correlation, and $|r| < 0.3$: weak correlation.

Pearson's correlation coefficient:

$$\rho xy = \frac{\mathrm{cov}(X,Y)}{\sigma_X \sigma_Y}, \quad \mathrm{cov}(X,Y) = E\left[(X-\mu_X)(Y-\mu_Y)\right]. \tag{1}$$

Spearman's rank correlation:

$$\mathrm{r_s} = \rho \mathrm{r_{gX}} r_{gY} = \frac{cov(rgX, rgY)}{\sigma_{rgX}\sigma_{rgY}}, \quad r_s = 1 - \frac{6\sum_{i=1}^{n} d_i^2}{n(n^2-1)}. \tag{2}$$

Kendall:

$$\tau = \frac{numberofconcordantpairs - numberofdiscordantpairs}{n(n-1)/2}. \tag{3}$$

2.3.3 Spatial Econometric Model

The ordinary least squares (OLS) model is considered the standard analysis framework in econometric analysis. However, it may ignore spatial dependence, leading to biased or even invalid estimations. Many researchers who have attempted to solve this limitation have found that the most important analysis framework is actually the spatial econometric model.

Spatial econometric models can avoid the deviation of classical econometrics when analyzing spatial effects. The commonly used spatial econometric models include the spatial lag model (SLM)

and the spatial error model (SEM) (Kang, 2015; Chen et al., 2017). The SLM is as follows:

$$Y = \rho W y + X\beta + \varepsilon, \tag{4}$$

where Y is the dependent variable, X is the explanatory variable, W is the spatial weight matrix, Wy is the spatial lag variable, and ρ is the spatial regression coefficient, which reflects the degree of diffusion or spillover between adjacent spatial units as well as the influence of X on Y. It is also the random error term.

The SLM mainly verifies the spatial spillover effect of dependent variables in a region. It also ensures that the influencing factors of dependent variables are applied to other regions through the spatial transmission mechanism (Liu Y. et al., 2020). In contrast to the SLM, the SEM verifies the spatial dependence in the disturbance error term and measures the error impact of the dependent variables in adjacent areas on the local dependent variables. The SEM is as follows:

$$\begin{aligned} Y &= X\beta + \varepsilon, \\ \varepsilon &= \lambda W\varepsilon + \mu, \end{aligned} \tag{5}$$

where Y is the dependent variable, X is the explanatory variable, W is the spatial weight matrix, ε is the random error term, λ is the spatial error coefficient, μ is the random error term of the normal distribution, and β reflects the influence of X on Y.

2.3.4 Index Selection and Processing

Previous reviews on the influencing factors of equality in educational resource allocation have mainly focused on screening outside schools and screening the administrative unit with the smallest research scale being just to the streets (town) (Sajjad et al., 2022) or the regression analysis with some schools in the streets (town) as the sample; when the research scale is not fine enough, the study sample size is not enough (Omoeva et al., 2021). This study gives the indicators of geospatial attributes using ArcGIS software. Our sample included all the schools in Dalian that contained migrant children. This resulted in a large volume of data, which broke the administrative region's boundary limit. Considering the effect of educational resources on the number of migrant children from both inside and outside the school adds credibility to the study's results. The selected indicators are shown in **Table 1**.

Faculty is the core factor in the distribution of compulsory education resources, which has a decisive effect on the quality of compulsory education. Therefore, we measured the number of teachers using the student-to-teacher ratio to reflect the adequacy of the number of teachers. The proportion of primary (junior) teachers with higher (undergraduate) education and teachers with intermediate and above professional technical titles was also measured. The hardware resources include the campus area, books, computers, and teaching equipment. We also chose the area of school buildings with the students, the raw average number of books, and every hundred students having four secondary indicators of the number of computer stations.

Financial resources refer to compulsory educational funds mainly from government financial grants, which are mostly used to pay teacher salaries, acquire teaching equipment, and improve the campus environment. According to the principle of independence selected by the indicators, there is a causal relationship between educational funding and operational conditions. Therefore, this study focuses on two aspects: faculty strength and operational conditions.

Socio-economic factors can affect migrant workers' job choices and the admission choices for migrant children according to the service radius of junior high schools as prescribed by the country. Therefore, this study focuses on junior high and primary schools. We drew a buffer radius of 2,000 m around the schools and calculated the average GDP and population within this radius, which can reflect the quality of life and employment of migrant workers. This is important since the admission of migrant children is closely related to the cost of residence and the place of work of the migrant workers. Additionally, since most migrant workers in Dalian are likely to rent, the rental amount will affect the choice of schools for migrant children and subsequently the number of migrant children in school. Therefore, we used rental prices as an important indicator to calculate the average rental price within 2,000 m radius of junior high and primary schools.

The construction area reflects the development status of industries near the school. Large construction areas provide more employment opportunities for migrant workers. However, migrant workers working near the school will affect the number of migrant children in school. Therefore, we used the amount of construction going on within the school's 2,000 m buffer area as an important indicator.

3 RESULTS

3.1 Spatial–Temporal Evolution of Migrant Children

Figure 2 shows the total number of migrant children in various regions from 2008 to 2020: Ganjingzi District > Jinzhou District > Lvshunkou District > Shahekou District > Xigang District > Zhongshan District > Pulandian District > Wafangdian District > Zhuanghe District > Changhai District. Jinzhou District surpassed Ganjingzi District in 2019, and the total number of migrant children increased from 93,807 in 2008 to 123,030 in 2020. The number of migrant children in Ganjingzi, Jinzhou, and Lvshunkou districts showed an upward trend, while the number of migrant children in Changhai District showed a downward trend. There was no significant change in other regions. With rapid urbanization, more employment opportunities are available to migrant workers, especially in Ganjingzi, Jinzhou, and Lvshunkou districts. These opportunities are found in construction, machinery, smelting, textiles, clothing, aquatic work, catering, and other jobs. The quality of schools in the older urban areas of Zhongshan, Xigang, and Shahekou districts remains high. However, the number of schools and student capacity is about to reach saturation, which will make it difficult for migrant children to enter these areas in large numbers. Due to the geographical location of Changhai District, migrant children are now

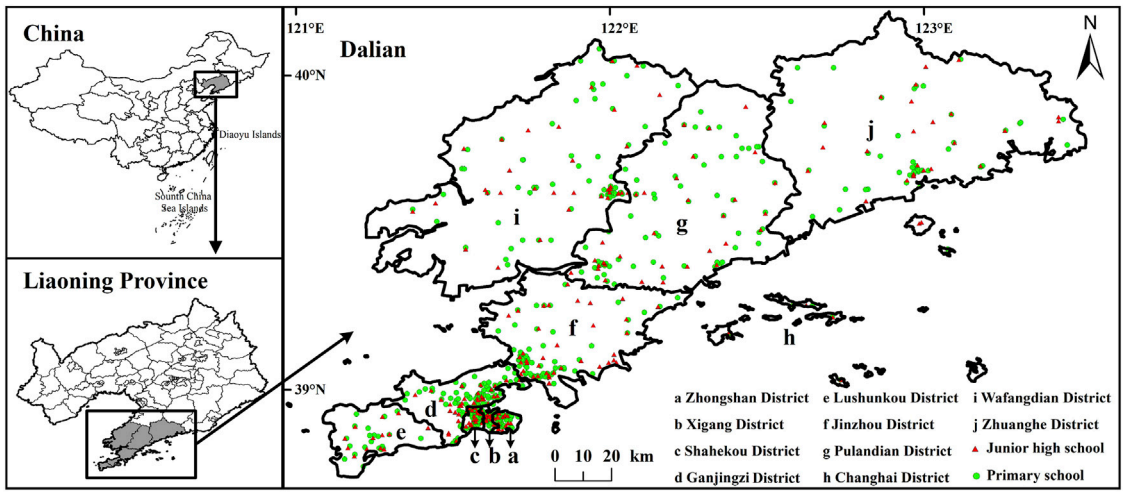

FIGURE 1 | Migrant children distribution in Dalian schools.

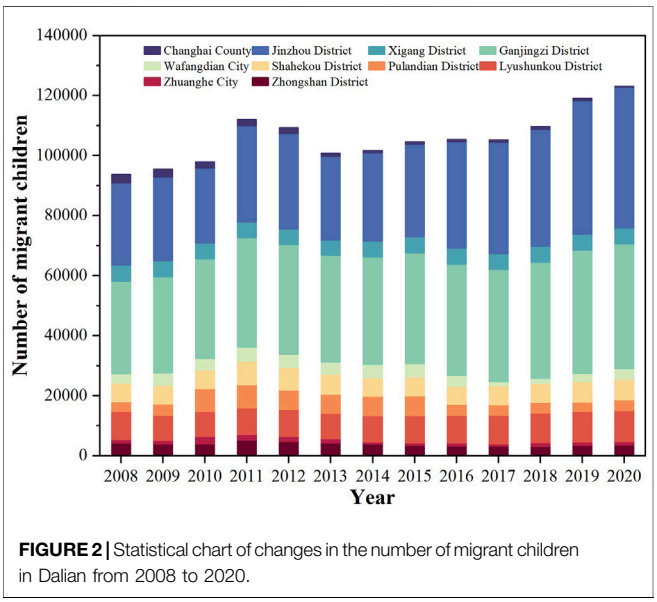

FIGURE 2 | Statistical chart of changes in the number of migrant children in Dalian from 2008 to 2020.

choosing to study in alternative areas with better educational development. To see the distribution of migrant children in different regions in detail, we used the school as a unit in ArcGIS 10.6 interpolation analysis, which visually expresses the spatial distribution of migrant children.

Figure 3A shows that schools with many migrant children are mainly located in the suburbs of Dalian, including the south of Jinzhou District and the periphery of Ganjingzi and Lvshunkou districts. From the ratio of the number of migrant children to the total number of school students in **Figure 3B**, we can see that migrant children are mostly located in Jinzhou, Ganjingzi, and Lvshunkov districts. Jinzhou District accounted for 38% of the migrant children, Ganjingzi District, 34%, and Lvshunkou District, 8%. The number and proportion of migrant children in Wafangdian (3%), Pulandian (3%), and Zhuanghe (1%) are much lower than those of Jinzhou, Ganjingzi, and Lvshunkov, which reflects the population flow from suburban to core areas during urbanization.

The survey data showed that high-quality primary and secondary schools in Dalian are mainly located in urban core areas such as Shahekou, Xigang, and Zhongshan districts. However, the number and proportion of migrant children are much lower in these core areas than those of the south of Jinzhou District and the peripheral areas of Ganjingzi and Lvshunkou districts. These districts show the uneven distribution of migrant children and the difficulties migrant children face in entering high-quality junior middle and primary schools at the compulsory education stage. It also reflects the unfairness to migrant children in terms of resource allocation at the compulsory stage. To further verify the aforementioned results statistically and analyze the changes in the number of migrant children in terms of socio-economics, teacher strength, school operating conditions, and other factors, we constructed a spatial econometric model. In this model, the number of migrant children is the dependent variable. Furthermore, teacher strength, school operating conditions, and socio-economic factors were set as the independent variables for subsequent spatial metrology studies.

The indicators of influencing factors after spatial interpolation are shown in **Figure 4**. As shown, there are significant differences in the distribution of educational resources between the central urban area and the suburbs. The distribution of resources as reflected by the teacher–student ratio, the construction area of school buildings per student, the number of books per student, computers per student, and teaching equipment per student are highly concentrated in Lvshunkou, Ganjingzi, and Wafangdian districts and other suburbs. Higher values of average GDP, population, rental price, and construction land area within the school's 2,000 m buffer zone were found in core areas such as Zhongshan, Shahekou, and Xigang districts and the south of Jinzhou District. The socio-economic development of suburbs

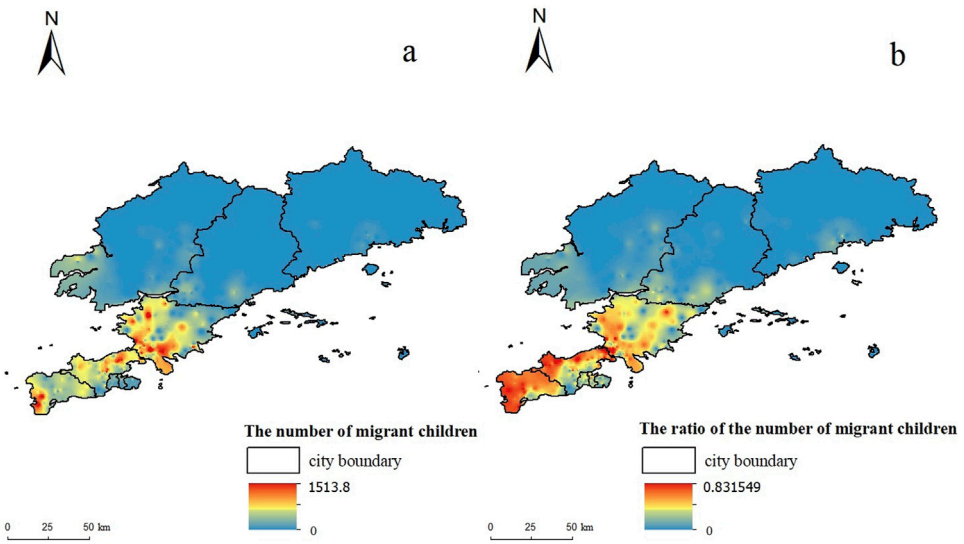

FIGURE 3 | Spatial distribution of the number **(A)** and proportion of migrant children **(B)** in Dalian from 2008 to 2020.

containing many migrant children was weaker than that of central urban areas. Compared to the central urban areas with relatively saturated educational resources, the suburbs still have a large room for development. We can improve the school attendance of migrant children in Jinzhou, Ganjingzi, and Lvshunkou districts by increasing educational investment and fairly reallocating existing resources to promote improved educational equality.

3.2 Analysis of Influencing Factors

Table 2 shows the analysis results of index correlation. The study found that LNUG and LNMPT failed the index correlation test, while other indices passed the correlation test. At the level of 0.01 (single tail), the correlation was significant.

This study used GeoDa software to calculate the regression results. Before establishing the spatial econometric model, a spatial correlation test was conducted on the sample data. **Table 3** shows that Moran's I value was 12.903. The significance level was lower than 0.001, indicating that the spatial distribution of migrant children's enrollment is not completely random but has a certain spatial correlation. Therefore, the regression results of OLS might deviate, so it is necessary to use the spatial econometric model while considering spatial effects for estimation. From the perspective of variable coefficient and significance, the calculation results of the model were consistent. This result indicated that the consistency of the results was high, and the R^2 value increased after considering the spatial correlation (SLM = 0.692 and SEM = 0.0.687), which were both higher than the R^2 value of OLS 0.592. The interpretation results of SLM and SEM were thus better than the OLS regression results.

However, the spatial lag coefficient was 0.749, and its significance level was lower than 0.001. Therefore, we can conclude that the number of migrant children in different schools is affected by the development of schools, socio-economic status, and other factors in the region. The spatial error coefficient was 0.971, and its significance level is lower than 0.001, which verifies that the number of migrant children in schools in each region is also affected by factors not considered in adjacent regions and random shocks. Combining the LM and R-LM values and comparing the fitting effects of SLM and SEM, the significance of the regression and test results of SLM was better than that of the model results of SEM. Therefore, SLM results were selected for subsequent analysis in this study.

Table 3 shows that in the regression results, LNSTR, LNPBA, LNPC, and LNHP showed significant negative effects, while LNPB, LNPTE, and LNCL showed significant positive effects. The effect degree of the significant factors also differed, and they are ranked as follows: LNSTR > LNPC > LNPTE > LNPB > LNPBA > LNHP > LNCL.

Among the internal influencing factors in schools, the most critical factor constraining the inequality in school children's admission at this stage was LNSTR. For every 1% increase in LNSTR, the number of migrant children decreased by 4.12%. Therefore, the greater the number of migrant children in junior high and primary schools, the fewer the teaching resources they get. Core area teachers and students were relatively low because the educational resources in the urban center were saturated, the universal source of students was fulminant, the supernumerary number of classes, and the operation of school overload, giving migrant children less access to quality public secondary and primary schools.

Therefore, the number of classes should be adjusted appropriately in the city's core area. Additionally, teachers should be allocated properly to schools with high numbers of migrant children to achieve a reasonable distribution of educational resources. From **Figure 3**, the higher LNSTR values were found in Wafangdian, Zhuanghe, and Pulandian districts, which was due to the low number of migrant children in

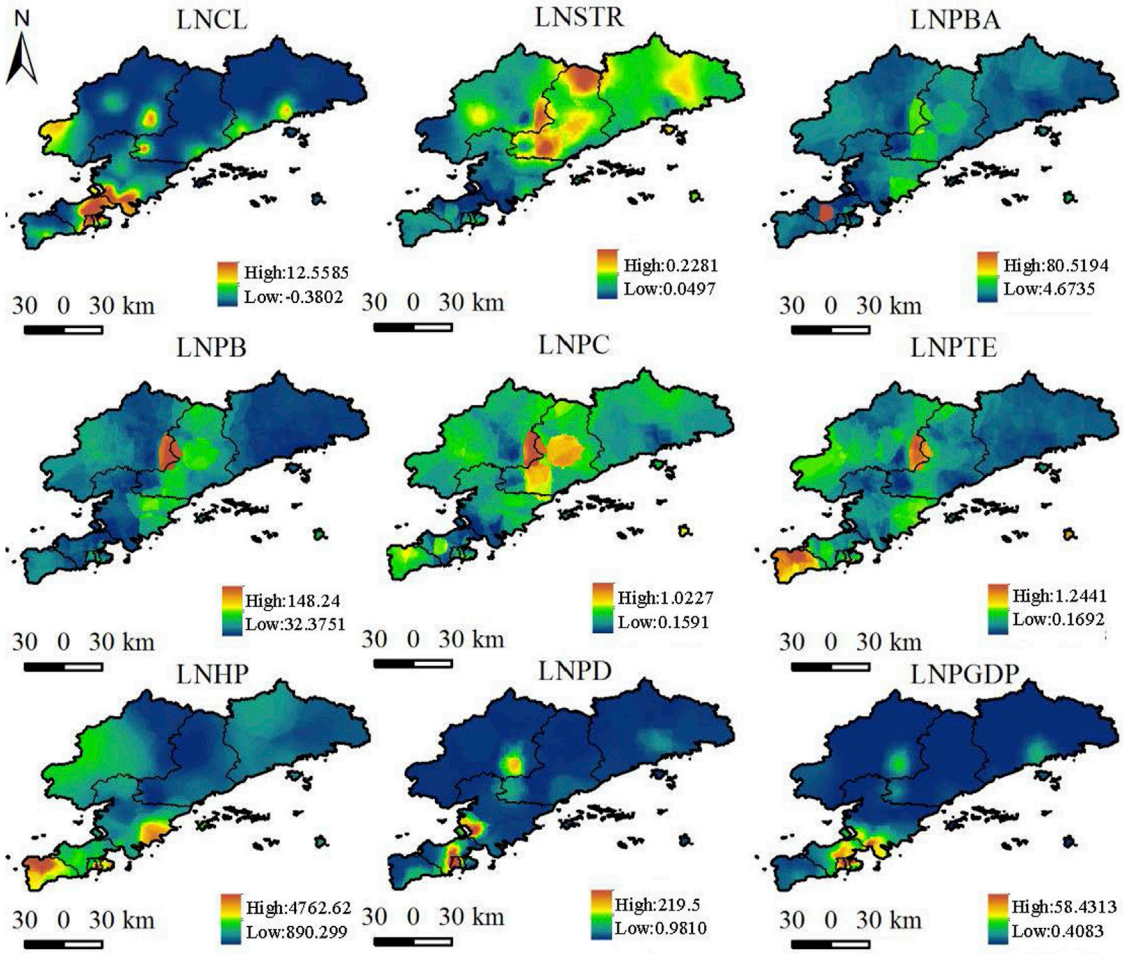

FIGURE 4 | Factors influencing the number of migrant children in the spatial distribution.

TABLE 1 | Selection of influencing factors and indicators.

Primary index	Symbol	Secondary index
Faculty	LNSTR	Teacher–student ratio
	LNUG	Proportion of primary school (junior middle school) teachers with higher than junior college (undergraduate) education
	LNMPT	Proportion of teachers with intermediate and above professional and technical titles
School operating conditions	LNPBA	Building area per student
	LNPB	Number of books per student
	LNPC	Number of computers per student
	LNPTE	Teaching equipment value per student
Socio-economic factors	LNHP	Average GDP of schools in the 2,000 m buffer zone
	LNPD	Average population of schools in 2,000 m buffer zone
	LNPGDP	Rental price in 2,000 m buffer zone
	LNCL	Construction land area of 2,000 m buffer zone

these areas. This shows that migrant children migrated from the edge to the center of the city and were mainly located in the developed subcenter area, which is the peripheral area of Ganjingzi District, the south area of Jinzhou District, and Lvshunkou District. In addition, the number of migrant children decreased by 0.51% for every 1% increase in LNPBA; for every 1% increase in LNPC, the number of migrant children decreased by 2.31%, which exacerbates the inequality of migrant children in schools to a certain extent. For every 1% increase in LNPB, the number of migrant children increased by 0.57%. For

TABLE 2 | Correlation analysis and test of indicators.

	LNSTR	LNUG	LNMPT	LNPBA	LNPB	LNPC	LNPTE	LNHP	LNPD	LNPGDP	LNCL
Pearson	−0.500**	0.003	−0.006	−0.371**	−0.161**	−0.365**	−0.067*	0.370**	0.524**	0.692**	0.702**
Kendall	−0.386**	0.013	−0.013	−0.271**	−0.146**	−0.290**	−0.018	0.217**	0.328**	0.421**	0.463**
Spearman	−0.563**	0.016	−0.016	−0.398**	−0.216**	−0.427**	−0.026	0.352**	0.485**	0.617**	0.634**

TABLE 3 | Regression results of the spatial econometric model.

	OLS			SLM			SEM	
	Coefficient	t-statistic	Probability	Coefficient	z-value	Probability	Coefficient	z-value	Probability
CONSTANT	−5.145***	−2.831	0.004	−0.396	−0.248	0.803	2.615	0.989	0.322
LNSTR	−10.213***	−4.850	0.000	−4.127**	−2.214	0.026	−4.204**	−2.215	0.026
LNPBA	−0.309**	−2.100	0.036	−0.507***	−3.986	0.000	−0.515***	−4.022	0.000
LNPB	0.64***	3.345	0.000	0.577***	3.457	0.000	0.522***	3.077	0.002
LNPC	−1.849**	−2.505	0.012	−2.311 ***	−3.627	0.000	−1.975***	−3.100	0.001
LNPTE	1.412***	2.886	0.004	0.851**	2.010	0.044	0.760*	1.766	0.077
LNHP	0.402**	2.000	0.045	−0.295*	−1.645	0.099	−0.454**	−2.298	0.021
LNPD	−0.129*	−1.751	0.080	−0.085	−1.342	0.179	−0.099	−1.565	0.117
LNPGDP	0.467***	3.826	0.000	−0.024	−0.224	0.822	0.068	0.578	0.562
LNCL	0.316***	7.097	0.000	0.255 ***	6.620	0.000	0.222***	5.730	0.000
ρ				0.749	15.419	0.000			
λ							0.971	54.638	0.000
R^2	0.592			0.692			0.687		
Adj-R^2	0.586								
F	101.540								
LIK	−1183.950			−1096.460			−1105.413		
AIC	2387.900			2214.920			2230.830		
SC	2432.500			2263.980			2275.430		
Moran's I	12.903		0.000						
LM lag	180.296		0.000						
R-LM lag	135.966		0.000						
LM err	74.582		0.000						
R-LM err	30.252		0.000						

****, **, and * represent 1%, 5%, and 10% significance levels, respectively.*

every 1% increase in LNPTE, the number of migrant children increased by 0.85%, which alleviates the inequality of migrant children in schools to a certain extent.

The study also found that LNPD and LNPGDP were negative and insignificant. Since the population in economically developed regions is relatively denser (Zhu and Chen, 2022), more children were enrolled in age-appropriate schools in the core areas, which leads to eventual saturation. Therefore, although more employment opportunities in economically developed areas may attract more exotic populations, the separation of employment from high rental prices and saturated competition among age-appropriate children make it harder for migrant children to attend schools in developed core areas.

4 DISCUSSION

This study mainly discusses the inequality that migrant children face in school admission. We focused on problems migrant children faced such as a difficult admission process and poor access to high-quality schools and educational resources. Then, we explored the effect of the internal school environment and external regional socio-economic factors on schools' admission of migrant children. Our study has made some unique contributions to the existing literature on education equality for Chinese migrant children. We confirmed that migrant students no longer had problems accessing schools. Instead, their problem lies in the difficulty of obtaining quality education resources. The starting point of the study is that migrant children and their families face many challenges in migration destinations, such as discrimination, economic insecurity, educational inequality, lack of access to health care, risk of being expelled back to rural areas, and social exclusion. However, educational inequality is currently the most concerning issue and social problem. Inequalities in school quality stem from economic, human, and socio-emotional factors, which exist in different types of school environments where migrant children live. Considering that school quality can significantly impact differences in achievement, this conclusion awaits wide acceptance among researchers (Ma and Wu, 2019; Zhang J. et al., 2020).

On the factors affecting the school admission of migrant children, we believe that in addition to the influence of the school's policies and governance, migrant children's admission

was also affected by the working and dwelling place of their migrant worker parents. Therefore, in this study, the average rent and construction land area within a 2,000 m buffer radius of the school were used as important indicators.

In terms of research data, we combined school POI data, socio-economic statistical data, and geographical data with the support of internal government data to examine 639 junior high and primary schools in Dalian with a total enrollment of 123,030 migrant children and endow them with spatial attributes. We then analyzed the spatial distribution status of the migrant children and the inequality of access to educational resources. Our results showed that migrant children were mostly concentrated in Ganjingzi District, Jinzhou Suburban, and Lvshunkov District. Only a few migrant children had access to high-quality schools with abundant educational resources within the core area, which is consistent with the findings of Chen et al. (2017). This study has several limitations. First, our study only covered the area of Dalian due to the limitation of data. Given that the equality of migrant children's education in all large cities of China must be addressed, it is necessary to conduct future studies on the distribution of educational resources for migrant children in other large cities in China. Second, due to the inconsistencies within the data sample, this study only used cross-sectional data from 2020. In the future, we will study the evolution of fairness in migrant children's education and further explore the different influencing factors.

5 CONCLUSION

In this study, spatial analysis and spatial measurement were combined to analyze the spatial fairness of the distribution of migrant children and the factors affecting the number of school staff children in Dalian. Our comprehensive interpretation of the educational equality issues facing migrant children provides a new perspective for similar research in other cities in China. The main conclusions are as follows: 1) the total number of migrant children in Dalian grew steadily between 2008 and 2020; 2) the migrant children in Dalian in 2020 are distributed in a spatially uneven manner, with most of them found in the suburban areas; 3) the distribution of educational resources differed significantly in central urban areas and suburban areas; and 4) the inequality in migrant children's school admission is closely related to rapid industrialization and urbanization in China. Therefore, regarding the inequality in migrant children's school admission, we further analyzed the association between the number of children, school housekeeping, school quality, and socio-economic factors. We found that the most prominent factor contributing to the inequality of school admission was LNSTR; however, infrastructure conditions such as teaching equipment in the school had a weak effect on the inequality of school admission for migrant children. The difference in land use and rent prices as external socio-economic factors also exacerbated inequality in the enrollment of migrant children. In contrast to urban residents, migrant children are mostly from disadvantaged, low-income families with low-educated parents, which means that the inequitable distribution of educational resources will only intensify without government intervention.

Furthermore, the government needs to introduce policies to ensure that migrant children are treated exactly the same as local students in all aspects of education and teaching activities and incorporate the admission of migrant children into the scope of social development planning and financial security. By treating them equally, migrant children can be better integrated into school life, which promotes the growth of their physical and mental health. This can help achieve educational equity for all.

DATA AVAILABILITY STATEMENT

The original contributions presented in the study are included in the article/Supplementary Material; further inquiries can be directed to the corresponding author.

AUTHOR CONTRIBUTIONS

Methodology, WL; software and validation, ZZ and CT; formal analysis, ZZ and MS; writing—original draft preparation, ZZ and ZL; writing—review and editing, WL; visualization, ZZ; funding acquisition, WL. All authors have read and agreed to the published version of the manuscript.

FUNDING

This work was supported by the Key Project of the National Natural Science Foundation of China (No. 42030409) and China Postdoctoral Science Foundation (No. 2021M702789).

REFERENCES

Chen, W. Y., Hu, F. Z. Y., Li, X., and Hua, J. (2017). Strategic Interaction in Municipal Governments' Provision of Public Green Spaces: A Dynamic Spatial Panel Data Analysis in Transitional China. *Cities* 71, 1–10. doi:10.1016/j.cities.2017.07.003

Chen, Y., and Feng, S. (2019). The Education of Migrant Children in China's Urban Public Elementary Schools: Evidence from Shanghai. *China Econ. Rev.* 54, 390–402. doi:10.1016/j.chieco.2019.02.002

Fang, L., Sun, R. C. F., and Yuen, M. (2016). Acculturation, Economic Stress, Social Relationships and School Satisfaction Among Migrant Children in Urban China. *J. Happiness Stud.* 17 (2), 507–531. doi:10.1007/s10902-014-9604-6

Goodburn, C. (2009). Learning from Migrant Education: a Case Study of the Schooling of Rural Migrant Children in Beijing. *Int. J. Educ. Dev.* 29 (5), 495–504. doi:10.1016/j.ijedudev.2009.04.005

Guo, Y., and Zhao, L. (2019). The Impact of Chinese Hukou Reforms on Migrant Students' Cognitive and Non-cognitive Outcomes. *Child. Youth Serv. Rev.* 101, 341–351. doi:10.1016/j.childyouth.2019.04.017

He, B.-J., et al. (2019). Towards the Next Generation of Green Building for Urban Heat Island Mitigation: Zero UHI Impact Building. *Sustain. Cities Soc.* 50, 101647. doi:10.1016/j.scs.2019.101647

He, Q., He, W., Song, Y., Wu, J., Yin, C., and Mou, Y. (2018). The Impact of Urban Growth Patterns on Urban Vitality in Newly Built-Up Areas Based on an Association Rules Analysis Using Geographical 'big Data'. *Land Use Policy* 78, 726–738. doi:10.1016/j.landusepol.2018.07.020

Hu, F. (2018). Migrant Peers in the Classroom: Is the Academic Performance of Local Students Negatively Affected? *J. Comp. Econ.* 46 (2), 582–597. doi:10.1016/j.jce.2017.11.001

Kang, C.-D. (2015). The Effects of Spatial Accessibility and Centrality to Land Use on Walking in Seoul, Korea. *Cities* 46, 94–103. doi:10.1016/j.cities.2015.05.006

Koo, A. (2012). Is There Any Chance to Get Ahead? Education Aspirations and Expectations of Migrant Families in China. *Br. J. Sociol. Educ.* 33 (4), 547–564. doi:10.1080/01425692.2012.678755

Lai, F., Liu, C., Luo, R., Zhang, L., Ma, X., Bai, Y., et al. (2014). The Education of China's Migrant Children: The Missing Link in China's Education System. *Int. J. Educ. Dev.* 37, 68–77. doi:10.1016/j.ijedudev.2013.11.006

Lan, T., Yu, M., Xu, Z., and Wu, Y. (2018). Temporal and Spatial Variation Characteristics of Catering Facilities Based on POI Data: a Case Study within 5th Ring Road in Beijing. *Procedia Comput. Sci.* 131, 1260–1268. doi:10.1016/j.procs.2018.04.343

Liu, K., Yin, L., Lu, F., and Mou, N. (2020a). Visualizing and Exploring POI Configurations of Urban Regions on POI-type Semantic Space. *Cities* 99, 102610. doi:10.1016/j.cities.2020.102610

Liu, Y., Zhang, X., Pan, X., Ma, X., and Tang, M. (2020b). The Spatial Integration and Coordinated Industrial Development of Urban Agglomerations in the Yangtze River Economic Belt, China. *Cities* 104, 102801. doi:10.1016/j.cities.2020.102801

Ma, G., and Wu, Q. (2020). Cultural Capital in Migration: Academic Achievements of Chinese Migrant Children in Urban Public Schools. *Child. Youth Serv. Rev.* 116, 105196. doi:10.1016/j.childyouth.2020.105196

Ma, G., and Wu, Q. (2019). Social Capital and Educational Inequality of Migrant Children in Contemporary China: a Multilevel Mediation Analysis. *Child. Youth Serv. Rev.* 99, 165–171. doi:10.1016/j.childyouth.2019.02.002

Ma, Y., Hou, X., Huang, J., Wang, W., Li, Y., Zhou, X., et al. (2018). Educational Inequality and Achievement Disparity: an Empirical Study of Migrant Children in China. *Child. Youth Serv. Rev.* 87, 145–153. doi:10.1016/j.childyouth.2018.02.026

National Bureau of Statistics (2005). *National Bureau of Statistics of China*. Beijing: State Council of the People's Republic of China.

Omoeva, C., Menezes Cunha, N., and Moussa, W. (2021). Measuring Equity of Education Resource Allocation: An Output-Based Approach. *Int. J. Educ. Dev.* 87, 102492. doi:10.1016/j.ijedudev.2021.102492

Qian, H., and Walker, A. (2015). The Education of Migrant Children in Shanghai: The Battle for Equity. *Int. J. Educ. Dev.* 44, 74–81. doi:10.1016/j.ijedudev.2015.07.009

Qiao, Z., Wu, C., Zhao, D., Xu, X., Yang, J., Feng, L., et al. (2019). Determining the Boundary and Probability of Surface Urban Heat Island Footprint Based on a Logistic Model. *Remote Sens.* 11 (11), 1368. doi:10.3390/rs11111368

Sajjad, M., Munir, H., Kanwal, S., and Naqvi, S. A. (2022). Spatial Inequalities in Education Status and its Determinants in Pakistan: a District-Level Modelling in the Context of Sustainable Development Goal-4. *Appl. Geogr.* 140, 102665. doi:10.1016/j.apgeog.2022.102665

Tang, Z., and Wang, N. (2021). School Disruption of Children in China: The Influence of Parents' Rural-Urban Migration. *Child. Youth Serv. Rev.* 129, 106167. doi:10.1016/j.childyouth.2021.106167

Tian, C., Luan, W., Li, S., Xue, Y., and Jin, X. (2021). Spatial Imbalance of Chinese Seafood Restaurants and its Relationship with Socioeconomic Factors. *Ocean Coast. Manag.* 211, 105764. doi:10.1016/j.ocecoaman.2021.105764

Wang, H., Cheng, Z., and Smyth, R. (2018). Do migrant Students Affect Local Students' Academic Achievements in Urban China? *Econ. Educ. Rev.* 63, 64–77. doi:10.1016/j.econedurev.2018.01.007

Wang, L., and Holland, T. (2011). In Search of Educational Equity for the Migrant Children of Shanghai. *Comp. Educ.* 47 (4), 471–487. doi:10.1080/03050068.2011.559701

Wei, Y., and Gong, Y. (2019). Understanding Chinese Rural-To-Urban Migrant Children's Education Predicament: A Dual System Perspective. *Int. J. Educ. Dev.* 69, 102066. doi:10.1016/j.ijedudev.2019.05.001

Xiong, Y. (2015). The Broken Ladder: Why Education Provides No Upward Mobility for Migrant Children in China. *China Q.* 221, 161–184. doi:10.1017/S0305741015000016

Xu, G., Jiang, Y., Wang, S., Qin, K., Ding, J., Liu, Y., et al. (2022). Spatial Disparities of Self-Reported COVID-19 Cases and Influencing Factors in Wuhan, China. *Sustain. Cities Soc.* 76, 103485. doi:10.1016/j.scs.2021.103485

Yang, J., Wang, Y., Xue, B., Li, Y., Xiao, X., Xia, J., et al. (2021). Contribution of Urban Ventilation to the Thermal Environment and Urban Energy Demand: Different Climate Background Perspectives. *Sci. Total Environ.* 795, 148791. doi:10.1016/j.scitotenv.2021.148791

Yang, Y. (2005). Migrant Workers in China: Spanning Rural and Urban Areas. *Popul. Res.*

Yu, H., Yang, J., Li, T., Jin, Y., and Sun, D. (2022). Morphological and Functional Polycentric Structure Assessment of Megacity: an Integrated Approach with Spatial Distribution and Interaction. *Sustain. Cities Soc.* 80, 103800. doi:10.1016/j.scs.2022.103800

Yu, Z., Song, Y., Song, D., and Liu, Y. (2021). Spatial Interpolation-Based Analysis Method Targeting Visualization of the Indoor Thermal Environment. *Build. Environ.* 188, 107484. doi:10.1016/j.buildenv.2020.107484

Zhai, W., Bai, X., Shi, Y., Han, Y., Peng, Z.-R., and Gu, C. (2019). Beyond Word2vec: an Approach for Urban Functional Region Extraction and Identification by Combining Place2vec and POIs. *Comput. Environ. Urban Syst.* 74, 1–12. doi:10.1016/j.compenvurbsys.2018.11.008

Zhang, D., Zhang, G., and Zhou, C. (2021a). Differences in Accessibility of Public Health Facilities in Hierarchical Municipalities and the Spatial Pattern Characteristics of Their Services in Doumen District, China. *Land* 10 (11), 1249. doi:10.3390/land10111249

Zhang, D., Zhou, C., Sun, D., and Qian, Y. (2021b). The Influence of the Spatial Pattern of Urban Road Networks on the Quality of Business Environments: the Case of Dalian City. *Environ. Dev. Sustain*. doi:10.1007/s10668-021-01832-z

Zhang, D., Zhou, C., and Xu, W. (2020a). Spatial-Temporal Characteristics of Primary and Secondary Educational Resources for Relocated Children of Migrant Workers: The Case of Liaoning Province. *Complexity* 2020, 1–13. doi:10.1155/2020/7457109

Zhang, J., Li, H., Lin, J., Zheng, W., Li, H., and Chen, Z. (2020b). Meta-analysis of the Relationship between High Quality Basic Education Resources and Housing Prices. *Land Use Policy* 99, 104843. doi:10.1016/j.landusepol.2020.104843

Zhang, N., Zhang, J., Chen, W., and Su, J. (2022). Block-based Variations in the Impact of Characteristics of Urban Functional Zones on the Urban Heat Island Effect: a Case Study of Beijing. *Sustain. Cities Soc.* 76, 103529. doi:10.1016/j.scs.2021.103529

Zhang, Z., Luan, W., Tian, C., Su, M., and Li, Z. (2021c). Spatial Distribution Equilibrium and Relationship between Construction Land Expansion and Basic Education Schools in Shanghai Based on POI Data. *Land* 10, 1059. doi:10.3390/land10101059

Zhou, C., Zhang, D., He, X., et al. (2021). Transportation Accessibility Evaluation of Educational Institutions Conducting Field Environmental Education Activities in Ecological Protection Areas: A Case Study of Zhuhai City. *Sustainability* 13 (16), 9392. doi:10.3390/su13169392

Zhou, H. (2006). Discussion and Policy Implication of Psychological Status of Migrant Children. *Inst. Popul. Econ.*

Zhu, W., and Chen, J. (2022). The Spatial Analysis of Digital Economy and Urban Development: a Case Study in Hangzhou, China. *Cities* 123, 103563. doi:10.1016/j.cities.2022.103563

Conflict of Interest: The authors declare that the research was conducted in the absence of any commercial or financial relationships that could be construed as a potential conflict of interest.

Publisher's Note: All claims expressed in this article are solely those of the authors and do not necessarily represent those of their affiliated organizations, or those of the publisher, the editors, and the reviewers. Any product that may be evaluated in this article, or claim that may be made by its manufacturer, is not guaranteed or endorsed by the publisher.

Copyright © 2022 Zhang, Luan, Tian, Su and Li. This is an open-access article distributed under the terms of the Creative Commons Attribution License (CC BY). The use, distribution or reproduction in other forums is permitted, provided the original author(s) and the copyright owner(s) are credited and that the original publication in this journal is cited, in accordance with accepted academic practice. No use, distribution or reproduction is permitted which does not comply with these terms.

frontiers | Frontiers in Earth Science

ORIGINAL RESEARCH
published: 05 August 2022
doi: 10.3389/feart.2022.921043

On the Contributions of the Northeast Cold Vortex to the Formation and Evolution of Backflow Blizzard

Qi Yan[1,2], *Jin Cui*[1], *Zhenghua Tan*[1,2] *and Bao-Jie He*[3,4,5]*

[1]*Key Opening Laboratory for Northeast China Cold Vortex Research, Institute of Atmospheric Environment, China Meteorological Administration, Shenyang, China,* [2]*Shenyang Central Meteorological Observatory, Liaoning Meteorological Bureau, Shenyang, China,* [3]*Smart City Research Institute of Chongqing University in Liyang, Chongqing University, Liyang, China,* [4]*Centre for Climate-Resilient and Low-Carbon Cities, School of Architecture and Urban Planning, Chongqing University, Chongqing, China,* [5]*Key Laboratory of New Technology for Construction of Cities in Mountain Area, Ministry of Education, Chongqing University, Chongqing, China*

Blizzard is a severe weather-related disaster with significant environmental, economic, and social impacts. What is worse, the blizzard is increasingly frequent along with climate change. To enhance resilience, it is important to accurately estimate the blizzards. While some studies have reported the blizzard formation and characteristics, limited studies have not well presented the backflow blizzard associated with the cold vortex in Northeast China. In order to overcome this research gap, this study aims to analyze the characteristics of a backflow blizzard in Liaoning, China, and reveal the reasons behind the spatial heterogeneity of snowstorm intensity and duration. With observation data and mesoscale numerical simulation, this study discovered that the northeast cold vortex was the combined results of airflows from the Sea of Japan transported by the easterly airflow, the East China Sea, and the Yellow Sea transported by the southeast airflow, and the low-level southwest airflow, and the vortex was an important driver to the blizzard. Results further indicate that the interactions of airflow movement, water vapor variation, and frontogenesis occurrence at different layers caused the differences in snowfall intensity, duration, and volume at Zhangwu and Huanren stations. In particular, at Zhangwu station, there was an interaction of warm-wet and cold-dry airflows, but low-layer water vapor content was small, under which background only the cold air pushed the warm air as the southwest wind did not increase significantly, leading warm-humid air to be forced to climb and resulting in frontogenesis at 700–925 hPa. Therefore, the situation of no frontogenesis and poor humidity conditions in the low-level cold air contributed to the weak and a short-duration of snowfall at Zhangwu Station. The water vapor content of warm-wet and cold-wet airflows over Huanren station was better than that at Zhangwu so that during cold and warm air interaction, there was frontogenesis at 500–925 hPa. Near the top of the inverted trough in the ground layer, there was a convergence of the southeasterly wind and the northeasterly winds, resulting in the occurrence of horizontal frontogenesis throughout the layer of 500 hPa and forming an upward movement column. Moreover, a deep near-saturated water vapor layer formed below 600 hPa due to the upward movement column. Overall, the abundant water vapor combined with the deep dynamic uplift led to the heavy and long duration of snowfall at the Huanren station. Overall, this study is an important

OPEN ACCESS

Edited by:
Xinli Ke,
Huazhong Agricultural University, China

Reviewed by:
Qian Cao,
China University of Geosciences Wuhan, China
Qingsong He,
Huazhong University of Science and Technology, China

***Correspondence:**
Bao-Jie He
baojie.unsw@gmail.com

Specialty section:
This article was submitted to Geoscience and Society, a section of the journal Frontiers in Earth Science

Received: *15 April 2022*
Accepted: *30 May 2022*
Published: *05 August 2022*

Citation:
Yan Q, Cui J, Tan Z and He B-J (2022) On the Contributions of the Northeast Cold Vortex to the Formation and Evolution of Backflow Blizzard. Front. Earth Sci. 10:921043. doi: 10.3389/feart.2022.921043

reference for understanding the backflow blizzard and its mechanism. Moreover, it is conducive to the accurate estimation of backflow blizzards in Northeast China and eastern China, the eastern coast of the Korean peninsula, and other similar areas where on the east part of the continent is the ocean.

Keywords: cold vortex, backflow blizzard, airflow movement, water vapor, frontogenesis occurrence

INTRODUCTION

Extensive greenhouse gas (GHG) emissions have brought significant challenges to the global climate (IPCC, 2018). The ever-changing climate leads to an increase in weather-related disasters such as heatwaves, drought, flooding, bushfire, and snowstorm, with serious environmental, social, and economic consequences (UNEP, 2021). Climate change mitigation and adaptation is a critical theme in the world, especially given the expectations that climate change will be a new normal in the coming decades (Solecki et al., 2018). There have been many international, national, and local frameworks and initiatives for curbing GHG emissions to limit global warming below 1.5°C and 2.0°C (Millar, 2017; Salvia et al., 2021). However, in the meantime of climate change mitigation, there is an urgent need for climate change adaptation through climate monitoring and forecasting to generate warning signals and response actions to protect people from climate-induced impacts (Rosenzweig et al., 2018). An accurate estimation of climate-related disasters is significant in supporting climate change adaptation (He et al., 2021).

Snowstorm or blizzard, one of the deadliest disasters, is increasingly frequent because of increasing vapor feeding into the atmosphere under warming conditions (Rawlins, 2022). It is reported that the blizzard in the United States in 2008–2018 increased to three times that in 1958–1968 (Rawlins, 2022). Moreover, blizzard severity in many cities hit the record frequently, such as Boston and New York, with intensifying consequences. The blizzard disasters are mainly in the mid- and high-latitude climates. Many northeast and northwest cities in China are also undergoing severe threats and risks of blizzards. In March 2007, a blizzard hit Northeast China, leading to the paralysis of urban road traffic and causing a direct economic loss of 14.59 billion RMB (Li et al., 2007). In March 2012, Liaoning province underwent severe, large-scale rain and snow weather, in which the blizzard in Zhuanghe, Dalian, caused the collapse of 122 agricultural greenhouses and many other facilities, covering an area of about 200,000 sqm. In November 2013, two historical snowstorms attacked Heilongjiang and Jilin provinces, causing serious impacts on civil aviation, railways, highway transportation, and agricultural facilities. In December 2017, a heavy snowstorm occurred in Urumqi, seriously affecting civil aviation transportation and urban traffic. Overall, mid- and high-latitude cities have already been and will be challenged by blizzards with significant consequences on urban traffic, highways, facility agriculture, and the safety of people's lives. It is important to improve the resilience to blizzards, and understanding the reasons behind snowstorm formation is meaningful.

Studies on blizzards started in the 1970s and are mainly contextualized in European and North American cities. Due to the heterogeneity of geographic characteristics (e.g., ocean, terrain, and latitude), the focus and findings on blizzards are diverse. For instance, early studies in Europe and the United States suggested that most blizzards are associated with the formation and development of extratropical cyclones (Braham, 1983; Pearce et al., 2001; Ulbrich et al., 2001). Studies in Japan exhibited that, under most conditions, the snowstorm is concurrent with the formation and evolution of low-pressure systems (Ninomiya, 1991; Shimizu & Uchida, 1974). A further understanding of the mechanism of blizzard formation has also been explored. With the combination of theoretical studies, numerical simulation, and observations based on Radar and Satellite, Bennetts and Hoskins suggested that the symmetric baroclinic instability in saturated air could contribute to the band characteristics of frontal cloud and precipitation (Bennetts & Hoskins, 1979). Based on the National Centers for Environmental Prediction (NCEP) reanalysis data on blizzards in North America in 2015, Cui and Qiao (2016) suggested that the occurrence of extra strong northerly wind and weakened westerly jet stream allowed the polar cold current and wet air to invade the North American continental area easily. Sanders and Bosart (1985) found an extensive snowstorm covering areas from Washington to Boston after a cyclone moved onshore in the northeast part of the United States in 1983 and explained that the frontogenesis forcing and symmetric instability might be the main drivers.

In comparison, within China context, most studies had focused on the fact and characteristics of heavy snow and blizzard when snowstorm studies emerged in the 1970s. Attention was gradually shifted to the blizzard cause analysis, where the diagnostic analysis of the blizzard process was particularly conducted on aspects of climate background, weather system evolution, and water vapor thermodynamic conditions (Duan et al., 2013; Zhao, 2007; Zhou et al., 2011). The blizzard characteristics and synoptic causes in different regions were classified. Based on daily and monthly average data from the NCEP, Gao et al. (2020) analyzed water vapor transport characteristics of regional snowstorms in Liaoning, finding that the water vapor was pumped by the Western Pacific, Sea of Japan, East China Sea, and the Yellow Sea, in which the East China Sea and the Yellow Sea were most direct vapor sources. Li et al. (2007) investigated the evolutions of three times of blizzards in Nanjing in the winter of 2018 and found that the snowflake spectrum exhibited a multimodal distribution and co-occurrence of frost growth and frost collision drove the

formation of heavy snowflakes. In particular, the mesoscale numerical simulation facilitated the analysis of the interactions among multi-scale weather systems and their impacts on snowfall, making up for the lack of observational data and low spatial resolution of reanalysis observational data (Ji et al., 2014; Miao et al., 2010; Wu et al., 2011). Based on the mesoscale numerical simulation, the studies on blizzards have achieved fruitful achievements as well (Fernández-González et al., 2015; Hamzeh et al., 2021).

Nevertheless, studies on blizzards in Northeast China are still limited, but it is important to conduct relevant studies because of its different blizzard characteristics from other regions. The mechanism behind the blizzards in Northeast China, particularly the backflow blizzards, is still unclear to support accurate forecasting. For instance, Wu et al. (2012) investigated factors driving the formation of backflow blizzards in Tianjin, pointing out that the backflow snowstorm resulted from the co-impacts of backflow cold high pressure and inverted low-pressure trough in North China. Cui and Su (2019) adopted observation data and NCEP reanalysis data to analyze the characteristics and causes of a heavy snowstorm in southern Henan in early 2018, suggesting that a low-level cold pad was conducive to the climb of southwest warm-humid air above the inversion layer, and the change of low-altitude vertical wind shear could indicate the change of snowfall intensity. Their interactions amplified the blizzard. Overall, previous studies have only explained that northeast airflow acted as a cold pad, causing the southwest warm-humid airflow near the height of 850 hPa to crawl, driving blizzard occurrence. However, limited studies have explained the heterogeneity of snowstorm intensity, namely, some areas undergoing heavy snowstorms but some areas undergoing light snowstorms, whereas these areas are under the same circulation conditions with warm-humid air crawl on the cold pad.

In order to overcome this research gap, this study aims to reveal the reasons behind snowstorm intensity heterogeneity. This study was conducted within the context of eastern Liaoning province, where an inverted snowstorm occurred under the background of a northeast cold vortex on 14–15 February 2020. The snowstorm exhibited a large spatial distribution gradient that the snowfall intensity in the east was about 15 times that in the west, whereas the distance between them was only about 300 km. Accordingly, the objectives of this study are as follows: 1) to investigate the characteristics of the northeast cold vortex and the associated sources and 2) to understand the cause of the backflow blizzard in aspects of snowfall environmental field evolution and the water vapor, thermodynamics, and low-level frontogenesis. Using mesoscale numerical simulation to explain snowstorm intensity heterogeneity is important because it reveals the interactions of airflows at different heights and with different properties. Moreover, this study will also address the gap in the snowstorm mechanism in Northeast China and even East and Northeast Asia to a certain extent.

MATERIALS AND METHODS

Case Study Area and Snowstorm Disaster

This study is conducted in the context of Liaoning province (118.835–125.787E, 38.723–43.491N), which is located on the east coast of Eurasia (**Figure 1**), and in the south part of Northeast China. Liaoning has a temperate continental monsoon climate. From 1961 to 2020, Liaoning underwent more than 10 episodes of snowstorm disasters with significant impacts, most of which happened in early winter and early spring. In comparison, only four episodes of snowstorms occurred in winters. Compared with winters, water vapors were better and conducive to snowstorm formation in early winter and early spring when cold and warm air movement was more active and frequent, and the temperature was higher.

Table 1 presents 18 snowfall episodes in winter (including December, January, and February) and their impacts from 2000 to 2020. The most significant blizzard was on 13 February 2009, with an economic loss of 36.52 million RMB, followed by the one on 25 February 2015, with an economic loss of 27.13 million RMB. The most recent one was on 15 February 2020, with an economic loss of 16.67 million RMB. In particular, Huanren Station witnessed the highest daily precipitation in 24 h snowfall, ranking fifth in its history from 1961 to 2020 (**Figure 1**). Dalian, Benxi, Dandong, and Yingkou were the four cities undergoing severe agricultural impacts, such as the greenhouses collapse and damage, livestock sheds damage, livestock death, and factory damage. The total impact areas were about 16,000 ha. Given its backflow characteristics and severe impacts, this snowstorm was selected for completing the study on snowstorm intensity heterogeneity.

Definition

The division of snowstorms is in alignment with the national standard of "Precipitation Grades" (GB/T 28592–2012) (**Table 2**). According to the definition of extreme winter snowstorm events, the wintertime period is from December to February of next year. There are 126 episodes with maximum daily precipitation of more than 10 mm per station during the winter period from 1961 to 2020. On 15 February 2022, the 24 h snowfall at Huanren station was 30.2 mm, also exceeding the 95th percentile of the historical snowfalls (27.4 mm). The precipitation phase was pure snow, so it is defined as an extreme blizzard episode. The northeast cold vortex is defined as having at least one closed contour in the range of 35–60°N, 105–145°E on the 500 hPa high-altitude synoptic map, and there is a cyclonic circulation with an obvious cold trough of a cold center. The same northeast cold vortex that could last for three or more consecutive days is defined as a continuous northeast cold vortex episode. Backflow snowfall refers to the snowfall that occurs after the surface cold front (east-northeast wind in this study) passes.

Data Sources

Data used for analyzing snowstorm evolution and its mechanism consists of field observation data, radar data (Liaoning Provincial Meteorological Information Center), and NCEP reanalysis data

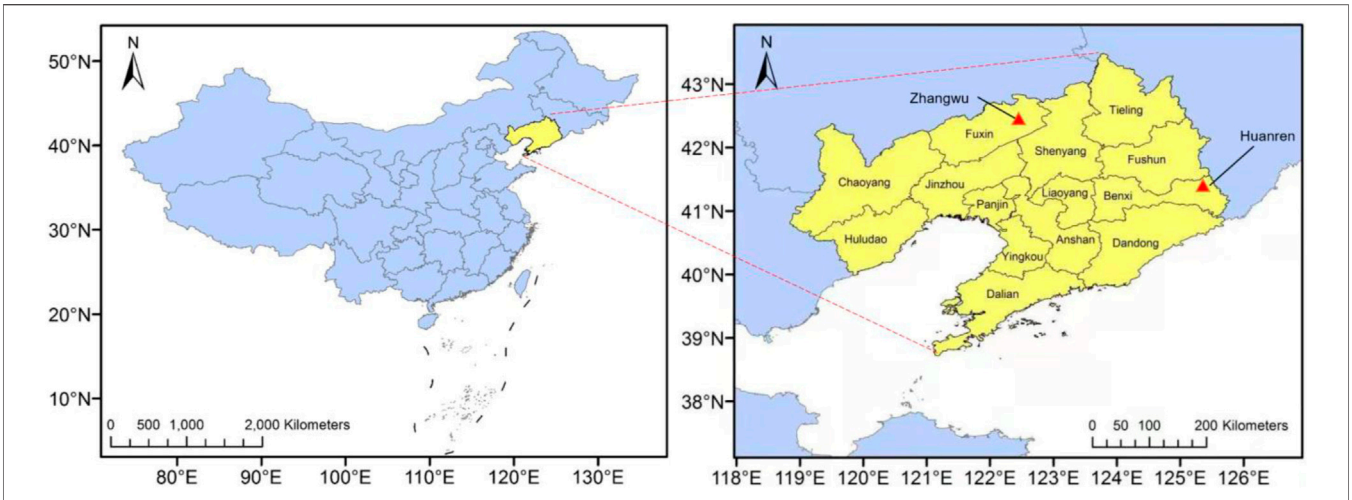

FIGURE 1 | Location and cities in Liaoning province, China.

TABLE 1 | The snowfall episodes and their impacts in 2000–2020.

Date	Maximum snowstorm intensity and the station (mm)	Economic loss (million RMB)
2020.02.15	Huanren (30.2)	16.67
2017.02.22	Shujiatun (14.2)	N/A
2017.01.26	Benxi (12.6)	N/A
2015.02.25	Dandong (18.3)	27.13
2013.02.01	Beizhen (12.0)	N/A
2012.12.03	Haicheng (25.4)	N/A
2010.02.25	Qingyuan (20.1)	N/A
2009.02.13	Huanren (34.9)	36.52
2009.01.22	Qingyuan (13.1)	N/A
2007.02.22	Benxixian (15.9)	N/A
2005.12.01	Liaozhong (19.7)	N/A
2005.01.28	Fushun (14.6)	N/A
2004.12.19	Tieling (16.3)	N/A
2004.12.12	Benxi (20.0)	N/A
2003.12.05	Huludao (16.4)	N/A
2002.01.06	Chaohekou (10.0)	N/A
2000.12.18	Kaiyuan (17.2)	N/A
2000.01.02	Yingkou (20.6)	N/A

(https://rda.ucar.edu/datasets/ds083.3/). The period of the data used ranged from 0:00 on 14 February (Day 1) to 24:00 on 15 February (Day 2) (universal time). The artificially encrypted hourly snowfall observation data were used to analyze the spatial distribution of snowfall amount and its hourly variation characteristics. Radar wind profile at Shenyang station with an hour interval was used to validate mesoscale numerical simulation of wind fields. The point-grid NCEP reanalysis data with a horizontal resolution of $1^{\circ} \times 1^{\circ}$ were adopted to understand the circulation background and the evolution of the large-scale influence system during the snowstorm. The vertical resolution was 25 hPa below 900 hPa and 50 hPa above 900 hPa, and the time step was 6 h.

The snowstorm started from 1:00 on Day 1 to 8:00 on 16 February 2020. The average provincial precipitation was 10.9 mm, where the blizzards occurred in the east of central Liaoning (**Figure 2A**), and it reached the maximum in the eastern part. The maximum snowfall was 36.2 mm at Huanren station, and the maximum snow depth was 29 cm at both Benxi station and Kuandian station. According to the observation at Huanren station, blizzards lasted for nearly 46 h. The snowfall became increasingly heavy from 8:00 to 14:00 on Day 2, whereas snow intensity generally was below 1.5 mm/h. The snowfall exhibited a spatial gradient with the highest in the east and smallest in the west (**Figure 2A**). Both Huanren and Zhangwu stations were selected for subsequent analysis due to their comparable snowfall volumes. The distance between them was about 320 km. The snowfall amount at Huanren station was about 15 times that at Zhangwu station, and the snowfall duration at Zhangwu Station was shorter than that at Huanren station (**Figure 2B**).

Mesoscale Numerical Simulation

Field data of the Global Forecasting System provided by the NCEP, with a spatial resolution of $0.5^{\circ} \times 0.5^{\circ}$ and a time interval of 6 h, were adopted as the initial field and lateral boundary conditions to drive the Weather Research and Forecast Model

TABLE 2 | Snow grade according to the national standard of "Precipitation Grades."

Grade	Light snowfall	Moderate snowfall	Heavy snowfall	Blizzard	Strong blizzard	Extreme blizzard
24 h snowfall	0.1–2.4	2.5–4.9	5.0–9.9	10.0–19.9	20.0–29.9	≥30.0
12 h snowfall	0.1–0.9	1.0–2.9	3.0–5.9	6.0–9.9	10.0–14.9	≥15.0

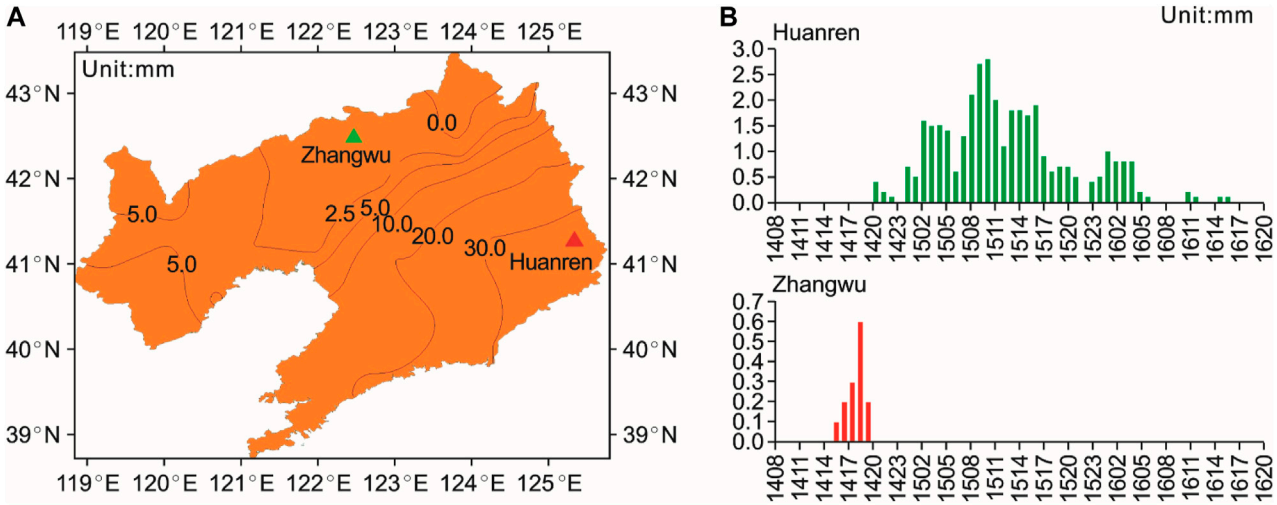

FIGURE 2 | Snowfall characteristics in Liaoning province **(A)** and the snowfall process at Huanren and Zhangwu stations **(B)**.

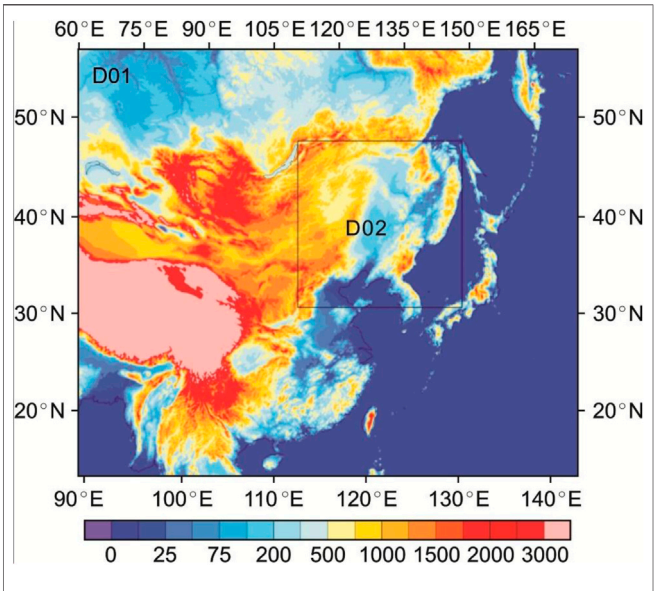

FIGURE 3 | The mesoscale simulation area and two-layer nested grid scheme in the WRF.

(WRF) (Version 4.1.2). The mesoscale simulation area is shown in **Figure 3**. The model adopted a two-layer nested grid scheme, in which the horizontal range was centered at (42°N, 116°E), the coarse grid spacing was 9 km with the grid number of 701 × 601, and the fine grid spacing was 3 km with the grid number of 691 × 703. The vertical direction was 50 layers, and the pressure at the top of the model was 10 hPa. The initial time of the model was 8:00 on Day 1, and the integration was 48 h until 8:00 on 16 February. In addition, the model adopted the WSM6 microphysics scheme, RRTM long-wave radiation scheme, the Dudhia short-wave radiation scheme, Noah land surface process scheme, YSU boundary layer parameterization scheme, cumulus convection parameterization 9 km based on the Kain–Fritsch (new Eta) scheme, and 3 km grid off cumulus parameterization scheme.

RESULTS AND DISCUSSION

This section presents results on the northeast cold vortex and the associated sources and the cause of the backflow blizzard in aspects of snowfall environmental field evolution and the water vapor, thermodynamics, and low-level frontogenesis.

Northeast Cold Vortex and Drivers

Figure 4 presents the air pressure at the 500 hPa and sea levels. Results indicate that at the 500 hPa level, there were two ridges and one trough, where the high-pressure ridges were around the Baikal Lake and the east coast of Asia. The meridional degree of atmospheric circulation in the mid and high latitudes increased, beneficial to a movement of cold air in the polar regions toward Northeast China. The southerly airflow in front of the high-altitude trough was also conducive to the warm-humid air transportation toward the northeast region. As a result, an intersection of cold and warm air occurred in the northeast region, promoting the development of strong northeast cold vortexes, as shown in **Figure 4B**. With the slow eastward movement of the northeast cold vortexes, the trough was enhanced between the two high-pressure ridges ranging from the central and southern regions to Northeast China. The southwest airflow front then transported the water vapors from southern China and the Bohai Sea areas to Liaoning province, as indicated by the red arrow in **Figure 4B**. Such long-distance and long-term water vapor transport were very scarce in the same season in Liaoning. At the 850 hPa level, in particular, the normalized outlier of specific humidity in the eastern part of Liaoning exceeded 2σ, reaching an extreme anomaly threshold, which can provide sufficient water vapor for the formation of this episode of the

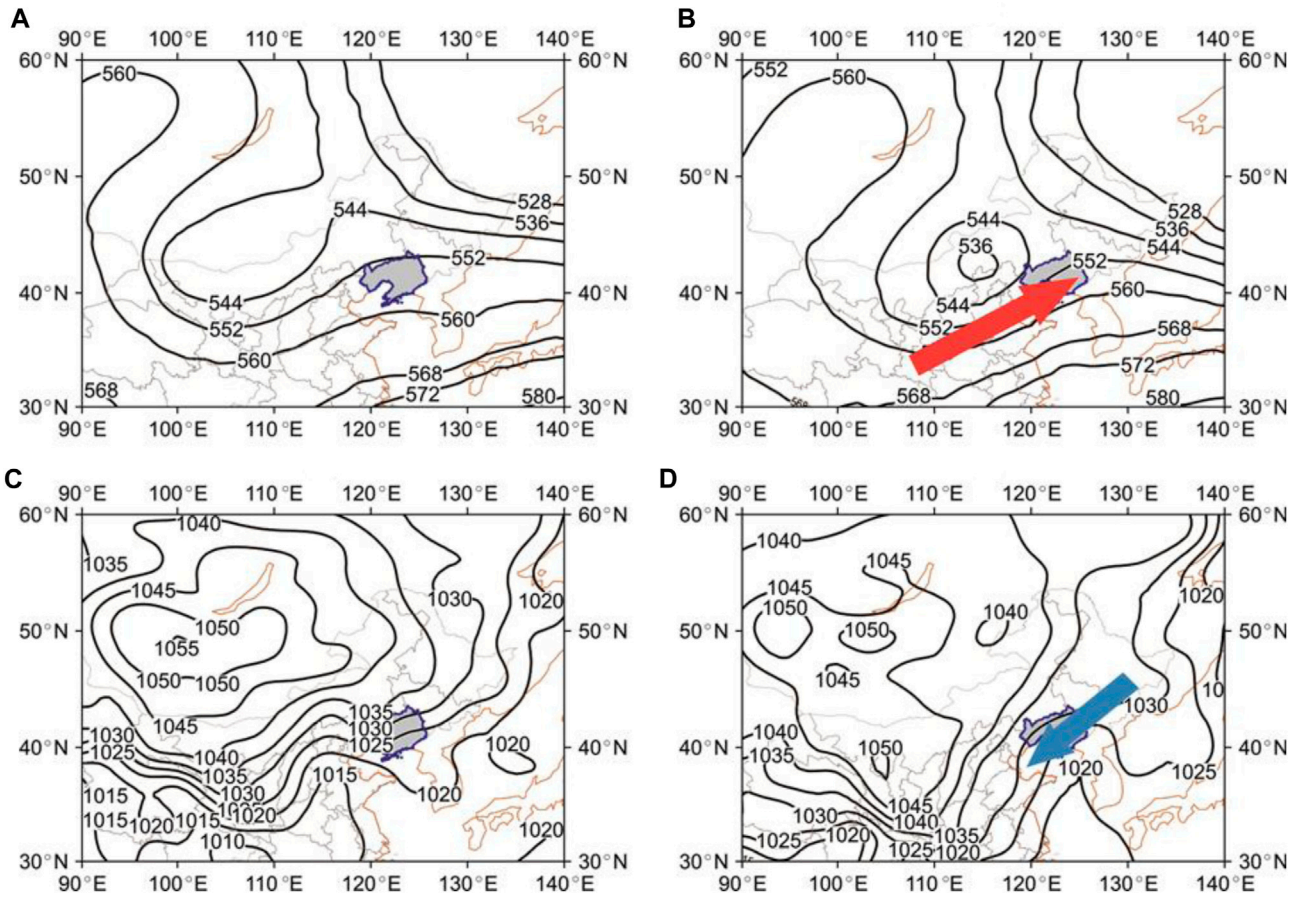

FIGURE 4 | Geopotential height at the 500 hPa level **(A)**, 0:00 on Day 1; **(B)**, 0:00 on Day 2) (unit: 10 gpm) and sea level **(C)**, 0:00 on Day 1; **(D)**, 0:00 on Day 2) (unit: hPa).

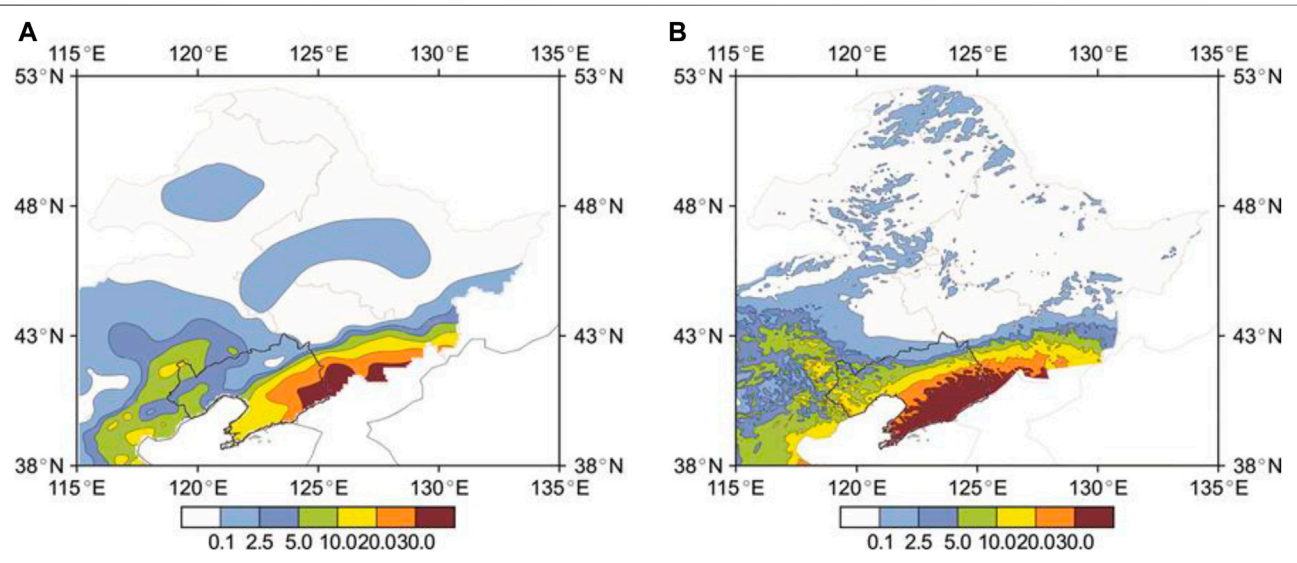

FIGURE 5 | Comparison of observed snowfall **(A)** and simulated snowfall **(B)** from 0:00 on Day 1 to 0:00 on Day 2.

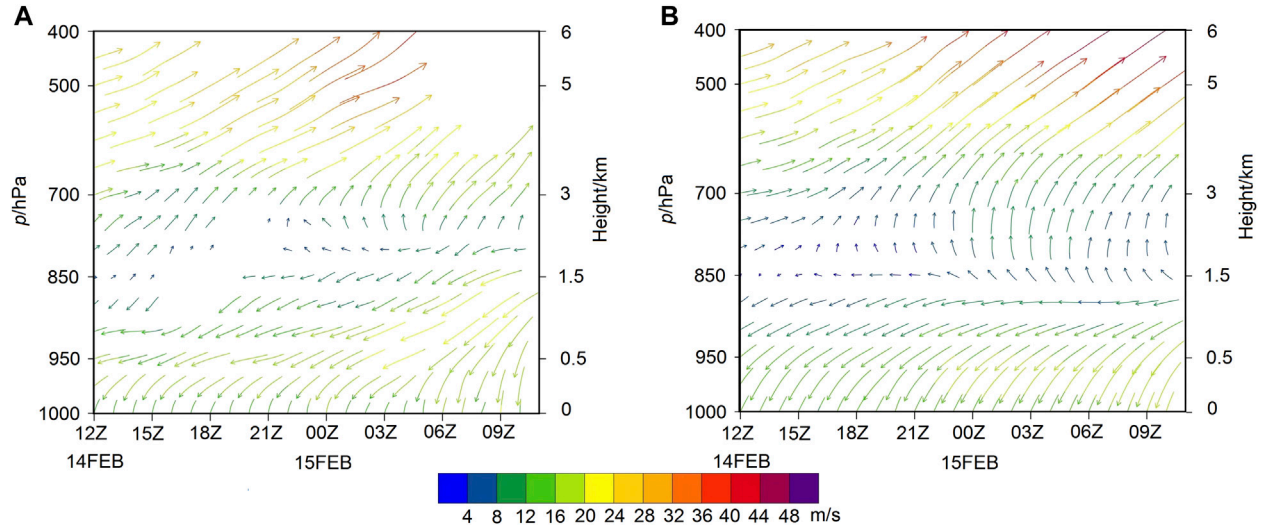

FIGURE 6 | Radar wind field **(A)** and simulated wind field **(B)** in Shenyang during the snowfall period from 0:00 on Day 1 to 0:00 on Day 2.

blizzard. According to **Figures 4C,D**, the Siberian continental high pressure at sea level was strong, so the cold air entered Liaoning from the northeast to southwest along with the easterly airflow (blue arrow). This fostered the cold air layer near the surface of Liaoning and pushed warm-humid air to climb over the cold air layer slowly. The interaction of cold and warm air in the mid and low layers could lead to a snowfall.

Validation of Mesoscale Numerical Simulation

According to **Figure 2**, there was a large difference in the snowfall volumes of the Huanren and Zhangwu stations. However, it is difficult to analyze the reasons behind it. In order to overcome this challenge, the mesoscale numerical simulation is expected to accurately compare the differences in water vapor and dynamic conditions. **Figure 5** compares the estimated heavy snowfall area and the actual situation. Results indicate that the southeastern part of Northeast China underwent heavy snowfall, and the snow distribution exhibited a belt pattern. Moreover, the snowfall intensity was above 30 mm at the center of the heavy snowfall area. Overall, the numerical results were accurate, regardless of the snowfall area or intensity. In addition, the simulated phase state was mainly snowfall, which is consistent with the observed snow phase in most areas, and the precipitation particles are mainly ice-phase particles.

Figure 6 compares wind fields obtained from radar observation and mesoscale numerical simulation. Overall, the simulated wind field was generally consistent with the observed field. In particular, at 8:00 in February, the intensifying southwest wind above the 850 hPa level and the northeast backflow below 850 hPa were well identified through simulation. The simulation results could well present the snowfall area, intensity, phase state, and wind field at each layer.

Wind, Humidity, and Temperature Field Variations

In Liaoning province, winter (including December, January, and February) is the dry season throughout the year. In this season, a specific humidity above 2 g/kg, a threshold to screen dry and wet air conditions, is a good water vapor content condition. Namely, air is defined as dry air when the specific humidity is below 2 g/kg and wet air when above 2 g/kg. Moreover, the airflow flowing from a low-temperature area to a high-temperature area is defined as cold airflow and vice versa. **Figure 7** and **Figure 8** present the variations of temperature, specific humidity, and wind at different altitudes, including 700, 850, 925, and 975 hPa. The bold black curve is the 2 g/kg iso-humidity line, and the blue solid line is the southerly and northerly wind shear lines. According to the hourly variations of the snowfall (**Figure 2B**), two moments 8:00 on Day 1 (**Figure 7**) and 01:00 on Day 2 (**Figure 8**), were selected for comparison. At 8:00 on Day 1, the snowfall was heavy at Zhangwu station, whereas the snowfall did not begin at Huanren station. At 01:00 on Day 2, the snowfall in Zhangwu ended, whereas the snowfall in Huanren peaked.

According to **Figure 7**, the warm-humid airflow covered the whole Liaoning province at 700 hPa. At 850 hPa, the center of the low-pressure vortex was around the point at 38°N and 117°E. The location of the southwesterly and northeasterly shear lines was at the top of the vortex, as shown by the blue solid line in **Figure 7B**. At this time, Zhangwu station was in a cold-wet northeasterly recirculation area. The convergence of the southwesterly warm-humid wind and the northeasterly cold-wet wind was conducive to the frontogenesis in the horizontal direction. Meanwhile, the warm-humid air near 700 hPa climbed on the cold pad of the northeasterly recirculation, resulting in frontogenesis in the vertical direction. Therefore, the frontogenesis in both horizontal and vertical directions strengthened the dynamic uplift effects at 700–850 hPa, associated with the humidity

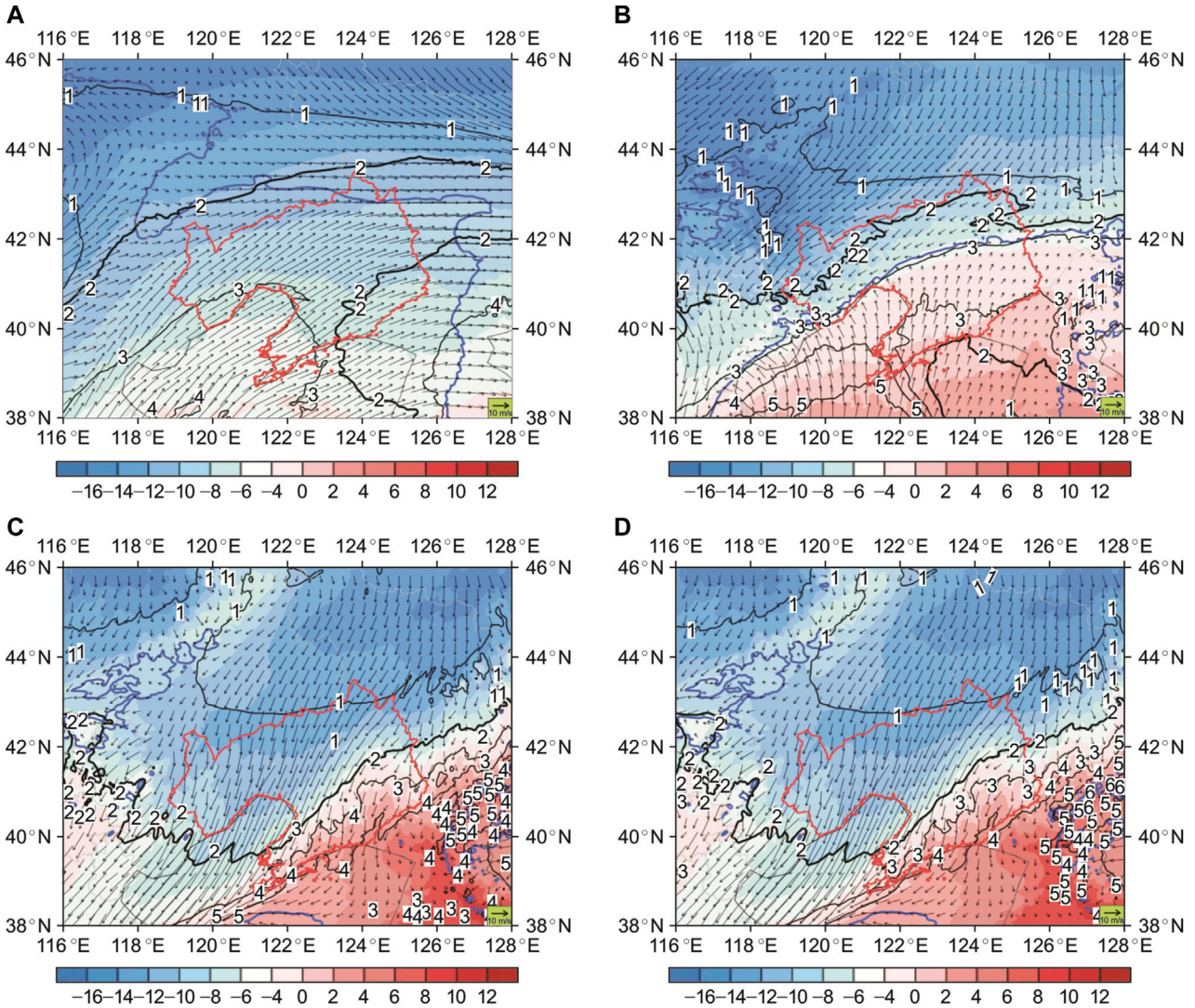

FIGURE 7 | Temperature, specific humidity, and wind at 700 **(A)**, 850 **(B)**, 925 **(C)**, and 975 **(D)** hPa at 8:00 on Day 1 (unit, temperature: °C, specific humidity: g/kg, wind speed: m/s, blue bold solid line: wind shear lines).

conditions, providing a favorable condition for snowfall formation at Zhangwu station. Below 925 hPa, Zhangwu station was in the domain of cold-dry northeast airflow, where the frontogenesis was not obvious in the horizontal and vertical directions, and the dynamic, uplifting effect of the lower layer was not strong. Moreover, the air was dry so that snowflakes formed between 700 and 850 hPa could fall to the cold-dry lower layers, leading to the occurrence of weak evaporation. All these processes contributed to a weak snowfall intensity at Zhangwu station. At this time, the Huanren station was in a wet environment, where it was in the control of warm-wet airflow above 850 hPa and cold-wet airflow below 850 hPa. The low-level shear was not obvious, which was not conducive to the formation of frontogenesis in the horizontal direction. In comparison, the southwest airflow near the 850 hPa was weak, and the wind speed near Huanren station ranged between 2 and 4 m/s. As a result, the warm-humid airflow was weak to climb along with the cold pad in the vertical direction. Meanwhile, while the water vapor at mid and low layers was good, the frontogenesis in the horizontal and vertical directions was not well coordinated. In particular, the frontogenesis in the vertical direction was weak, and the dynamic uplift conditions were poor, so there was no snowfall at the Huanren station.

At 01:00 on Day 2, the snowfall at Huanren station was the strongest, whereas the snowfall at Zhangwu station ended (**Figure 8**). At 700 hPa, the whole Liaoning was in the control of southwest warm-humid airflow. However, compared with **Figure 7A**, the southwesterly wind in the eastern Liaoning (Huanren station within this area) was significantly stronger, indicating that warm-humid airflow was identified in the eastern Liaoning. The vortex at 850 hPa moved toward the northeast (centered at 39.3°N and 112.5°E). The southwesterly and

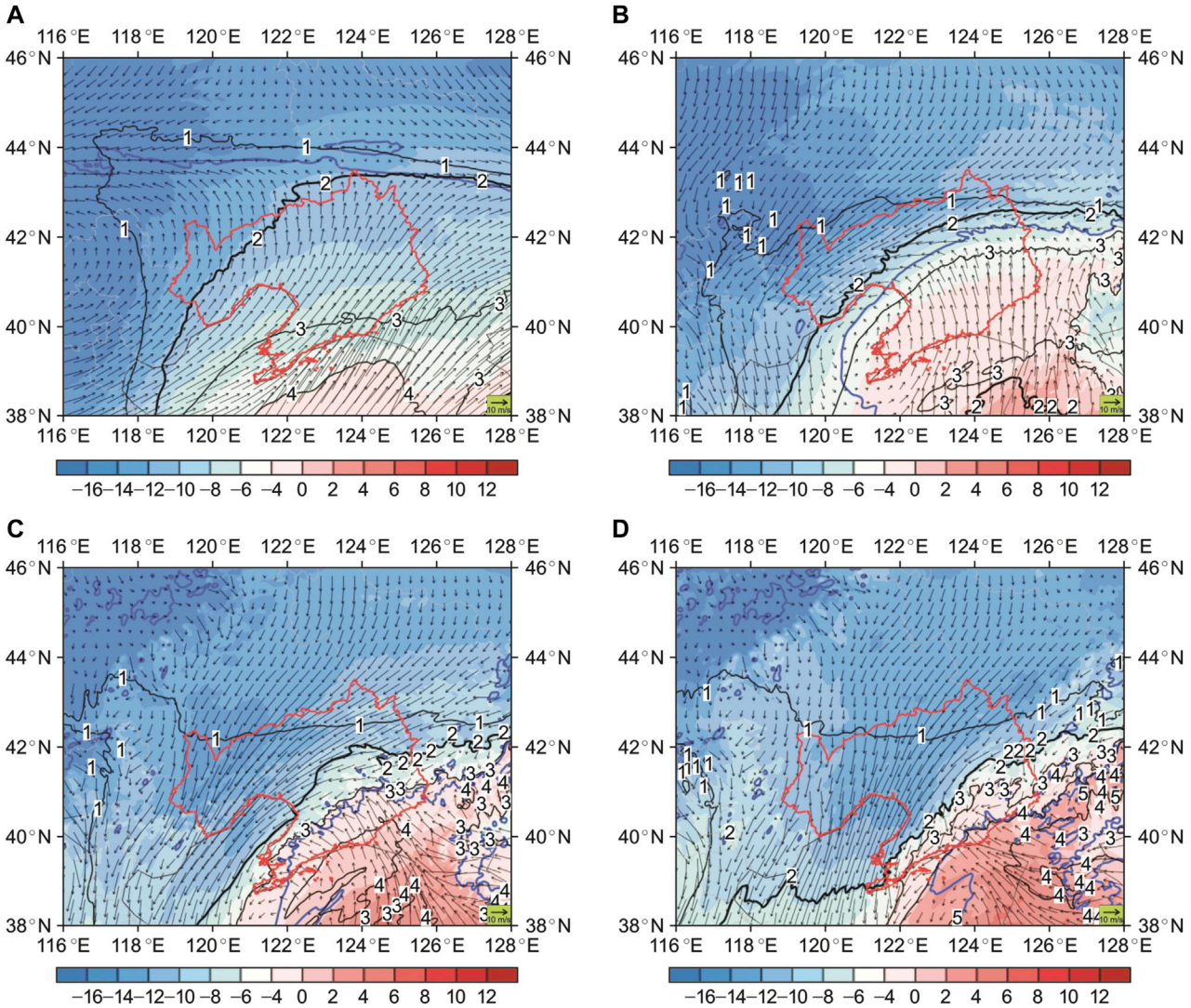

FIGURE 8 | Temperature, specific humidity, and wind at 700 **(A)**, 850 **(B)**, 925 **(C)**, and 975 **(D)** hPa at 1:00 on Day 2 (unit, temperature: °C, specific humidity: g/kg, wind speed: m/s, blue bold solid line: wind shear lines).

northeasterly wind shear lines at the top of the vortex moved slowly eastward and southward (**Figure 8B**), compared with the one in **Figure 7B**. In comparison, the Huanren station was in the control of warm-humid airflow. Wind speed was 6–8 m/s, about 4 m/s stronger than that at 8:00 on Day 1, and the warm-humid airflow intensity was significantly enhanced.

The convergence of southwesterly and northeasterly winds below 925 hPa strengthened (indicated by the blue lines in **Figure 8C** and **Figure 8D**, conducive to the frontogenesis in the horizontal direction. Meanwhile, the warm-humid airflow near 850 hPa climbed on the cold pad of the northeasterly backflow, conducive to the frontogenesis in the vertical direction. With the co-impacts of horizontal and vertical frontogenesis, the dynamic, uplifting effect below 700 hPa strengthened. Furthermore, the enhancement of the northeast cold vortex near 500 hPa fostered the formation of deep upward motion conditions. Overall, the lower layers of the Huanren station were under the control of cold-humid airflow, and its mid and upper layers were under the control of warm-humid airflow. The high humidity level and the deep upward movement were the main drivers for the heavy snowfall at Huanren station. However, the southwesterly wind around 700 hPa at Zhangwu station weakened obviously, and the cold-dry northeasterly backflow controlled the domain at 850 hPa. As a result, the snowfall ceased with the weakening frontogenesis and water vapor conditions.

Water Vapor, Thermodynamics, and Frontogenesis Variations

To further analyze the variation and differences of frontogenesis and water vapor at Zhangwu and Huanren stations in the vertical

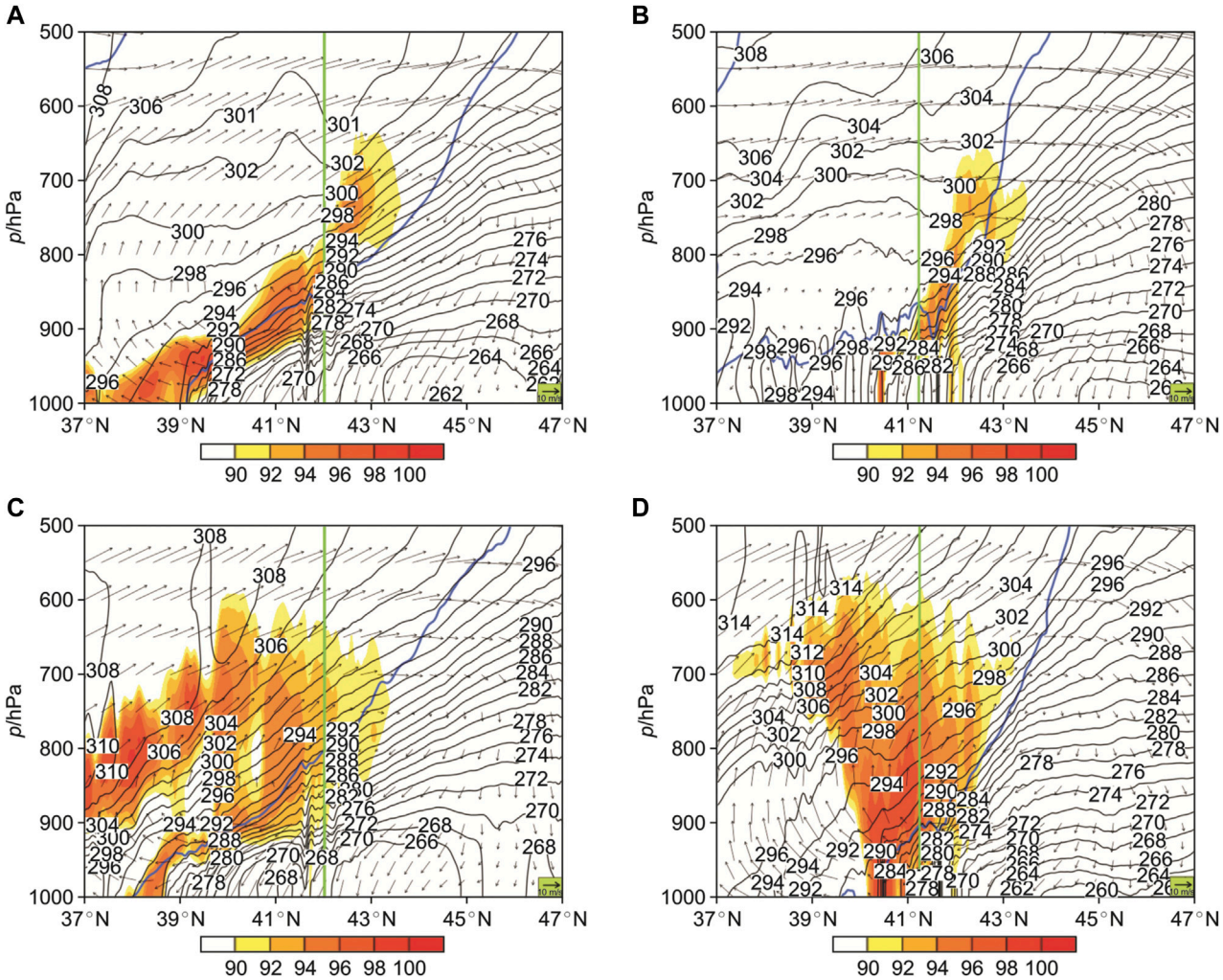

FIGURE 9 | Equivalent potential temperature (θse), relative humidity, and wind at the longitude positions of Zhangwu **(A)**, 1:00 on Day 1; **(C)**, 8:00 on Day 1 and Huanren **(B)**, 08:00 on Day 1; **(D)**, 1:00 on Day 2 stations (unit, temperature: K, relative humidity: %, and wind speed: m/s, green solid line: latitudes of Zhangwu and Huanren stations).

direction, the equivalent potential temperature (θse), relative humidity, and wind at the longitude where the two stations were located were screened, as shown in **Figure 9**. In **Figure 9**, the part with relative humidity above 90% was colored to represent a near-saturated water vapor state. The blue solid line was the shear line of southerly and northerly winds. The cold air was on the north side of the blue solid line, and warm air was on the south side of the solid line. The green straight line was the latitude of Zhangwu and Huanren stations. Before the snowfall at Zhangwu station (**Figure 9A**), the northeasterly cold air pad was around 850 hPa, so the iso-θse line was dense at 800–925 hPa with frontogenesis. However, only the water vapor at 800–850 hPa was above 90%, but that below 850 hPa was poor, resulting in a thin water vapor saturation layer and weak frontogenesis uplift (less than 0.2 hPa/s) (**Figure 10A**). The frontogenesis was not obvious below 925 hPa, not conducive to snowfall. At 8:00 on Day 1, the snowfall at Zhangwu station strengthened, as shown in **Figure 9C**. Compared with **Figure 9A**, the blue solid line moved southward, and the northeast cold air pad rose to 800 hPa, indicating that the cold air strongly pushed the warm air. The southwesterly wind at the south of 38°N was strengthened, the warm air crawled along with the cold air pad, and both the frontogenesis dynamic lifting effect between 700 and 925 hPa strengthened, as shown in **Figure 10A**. The upward movement between 600 and 800 hPa was above 0.2 hPa/s, with the highest speed of 0.4 hPa/s. By accompanying this, the near-saturated water vapor layer was thick at 700–900 hPa, beneficial for the snowfall formation at Zhangwu station. However, the space below 800 hPa was controlled by cold air with poor water vapor conditions, so the frontogenesis effect was not obvious and not conducive to snowfall. This explained the reason why the snowfall at Zhangwu station was weak, up only to 0.6 mm/h. The cold air advanced further to the southwest so that the cold air pad rose and the snowfall ended sooner with a small snowfall volume.

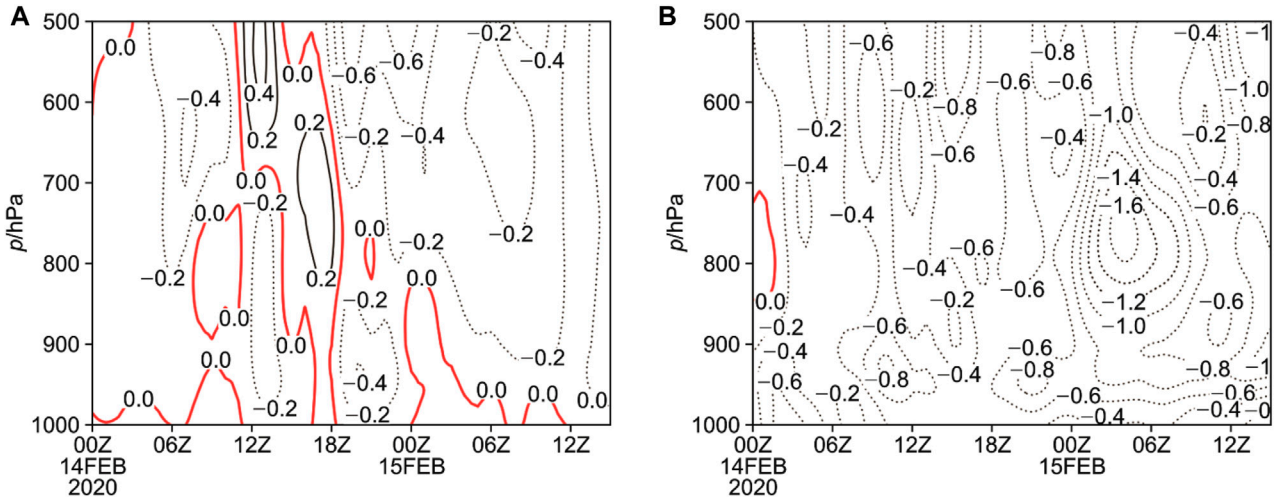

FIGURE 10 | Uplift movement at Zhangwu **(A)** and Huanren **(B)** stations with time and latitude (unit: hPa/s).

As shown in **Figure 9B**, before the snowfall at Huanren station, the northeasterly air pad was around 875 hPa, and the iso-θse lines were dense at 850–900 hPa with frontogenesis. In comparison, the frontogenesis below 900 hPa was not obvious. A water vapor above 90% was only found at 900–950 hPa, whereas the water vapor of cold air pad below 900 hPa was poor. In particular, the warm-humid air above 850 hPa was poor in air saturation due to the weak dynamic lift and weak rising condensation effect. Overall, the thin water vapor saturation layer and the weak frontogenesis dynamic uplift resulted in a lack of snowfall. At 1:00 on Day 2, as shown in **Figure 9D**, the snowfall at Huanren station gradually strengthened. The blue solid line moved northward, compared with **Figure 9B**, and the northeast cold air pad dropped below 900 hPa, indicating that the warm air pushed the cold air strongly. Meanwhile, southerly wind below 500 hPa strengthened, especially the weak northeasterly wind near the ground turning to the southerly wind and reaching an intensity of the ultra-low-level jet. The strong warm-humid air crawled on the cold air pad, causing the enhancement of interlayer frontogenesis at 500–925 hPa. The convergence of horizontal wind fields below 925 hPa was conducive to the formation of horizontal frontogenesis, resulting in the frontogenesis in the entire layer and deep dynamic uplift, as shown in **Figure 10B**.

At 1:00–9:00 on Day 2, there was an upward movement column from the ground to 500 hPa, in which the maximum upward movement was up to 1.4 hPa/s, significantly stronger than that of Zhangwu station. The warm-humid air and cold-humid air were superimposed in the vertical direction, leading to an enhanced dynamic uplift and thereby the formation of a deep wet layer. **Figure 9D** also indicated that a deep near-saturated water vapor layer appeared below 600 hPa. Overall, the deep and strong dynamic uplift and the near-saturated water vapor layer provided favorable environments for the strong snowfall at Huanren station, with a maximum snow intensity of 2.7 mm/h. When the warm air moved northward, the cold air pad persisted, acting as a barrier to the warm air, which resulted in lasting frontogenesis and long snowfall duration, and thereby a large snowfall volume.

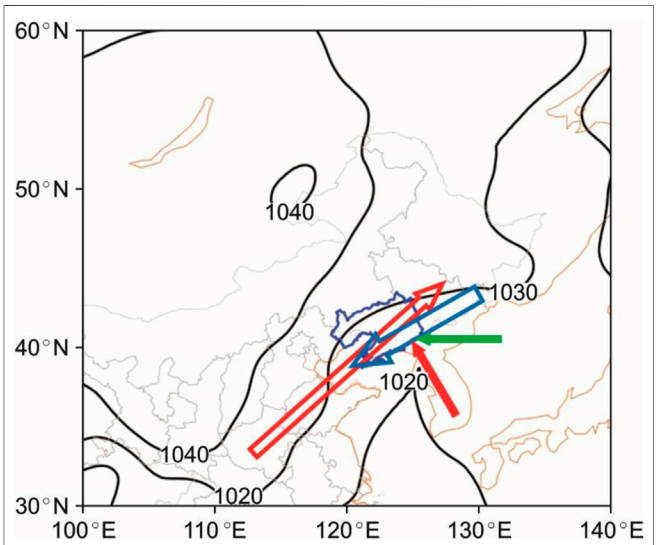

FIGURE 11 | Water vapor in Liaoning before the snowfall.

CONCLUSION

This study verified that the northeast cold vortex was an important driver of the blizzard in Liaoning on 14–15 February 2020. Overall, its strong development and movement eastward facilitated low-level low pressure, at which time the southwest jet stream developed in mid-layer, working simultaneously to transport warm-wet airflow toward Liaoning and guide ground low-pressure trough to move northeastward. In general, Liaoning is in the control of dry-cold air. However, the

northeast airflow front in the southeast quadrant of the high pressure was cold-wet (blue arrow in **Figure 11**) before this snowfall because of the interaction of three sources of water vapor, including the one from the sea of Japan transported by the easterly airflow (green arrow), the one from the East China Sea and the Yellow Sea transported by the southeast airflow (red solid arrow), and the one carried by the low-level southwest airflow (red hollow arrow). With the mesoscale numerical simulation, this study well revealed that the complex interactions of the strong northeast cold vortex, the movement of the ground low-pressure inverted trough, the northeasterly wind, and warm-humid airflow in the mid and low-layer were the main causes of significant snowfall differences in Zhangwu and Huanren stations.

The Zhangwu station first witnessed an interaction of warm-humid and cold-dry airs and small low-layer water vapor. Second, during snowfall enhancement, the southwest airflow did not intensify, and only the cold air pumped the rapid climb of warm air. Third, there was only frontogenesis at 700–925 hPa with the near-saturated water vapor at 700–900 hPa, whereas there was no frontogenesis in the low-layer cold-dry air, leading to a weak snowfall intensity at Zhangwu station. Fourth, the warm air kept advancing so that the cold-dry air pad rose rapidly, leading to a short snowfall duration and a small snowfall volume. For the Huanren station, first, the warm-humid and cold-humid air were superimposed to provide a favorable water vapor condition for snowfall formation. Second, during snowfall intensification, under the background of the northeast cold vortex, the southwest airflow strengthened, and the warm-humid air force increased, moving from the southwest to the northeast. On the one hand, the low-level warm-humid air pushed wet-cold air to move; on the other hand, the cold air force was also strong to enhance the climb of warm-humid air. As a result, there was obvious frontogenesis in the 500–925 hPa layer. Third, near the top of the inverted trough in the ground layer, there was a convergence of the southeasterly wind and the northeasterly winds, resulting in the occurrence of horizontal frontogenesis throughout the layer of 500 hPa and forming an upward movement column. Fourth, for the water vapor, the strong warm-humid airflow was superimposed on the cold-wet airflow so that a deep near-saturated water vapor layer formed below 600 hPa due to the upward movement column. In general, the abundant water vapor combined with the deep dynamic uplift led to the heavy snowfall at the Huanren station. The persisting cold air force and the slow movement of warm-humid air toward the north along with the cold air pad, provided a favorable condition for lasting snowfall and large snowfall volume.

Overall, by analyzing a blizzard in 2020 in Liaoning province, this study promotes the understanding of a typical backflow blizzard under the background of the northeast cold vortex. Moreover, with the adoption of the mesoscale numerical simulation, this study presented the formation, intensification, and termination of snowfall at Zhangwu and Huanren stations and revealed the contribution of airflow movement, water vapor variation, and frontogenesis occurrence to the snowfall intensity, duration, and volume. Therefore, this study provides a good reference for understanding snowfall heterogeneity and is conducive to the accurate prediction of backflow blizzards.

Overall, through the analysis of the heavy snowfall process under the northeast cold vortex, the heterogeneity of snowfall intensity and duration was revealed. This study has also generated some implications for the estimation of blizzards in Liaoning, a coastal area where the northeasterly wind may have different levels of water vapor. First, results are conducive to understanding such snowfall processes, which can further improve the numerical forecast and correction ability, thereby improving the accuracy and refined serviceability. Second, on the water vapor conditions, in this study, the northeasterly wind in the low-level coastal areas of eastern Liaoning carried ocean water vapor, which further transported and enhanced low-level water vapor. A similar situation might also be noticeable in the coastal areas in eastern China, the eastern coast of the Korean peninsula, and other similar areas where on the east part of the continent is the ocean. Third, the low-level northeasterly wind and the low-level wind that has an easterly wind component have the effect of transporting the water vapor on the ocean westward to the continent, which is beneficial to increasing water vapor in the lower layer. Such a process is not only applicable to the snowfall but also suitable for rainfall. Fourth, in the dynamic conditions, the low-level cold air in the northeast direction and the middle-level warm air in the southwest direction are superimposed in the vertical direction, where their forces are equivalent. Accordingly, this kind of weather situation and wind field could be a basis for analyzing the precipitation duration, which is also applicable in other regions.

DATA AVAILABILITY STATEMENT

The raw data supporting the conclusions of this article will be made available by the authors without undue reservation.

AUTHOR CONTRIBUTIONS

QY: conceptualization, methodology, formal analysis, investigation, writing—original draft. JC: formal analysis, software, review and editing, visualization. ZT: conceptualization, formal analysis, writing—review and editing, funding acquisition. B-JH: formal analysis, writing—original draft, supervision, project administration, writing—review and editing.

FUNDING

This project is financially sponsored by the National Key Research and Development Program (no. 2018YFC1507305) and the Special Project for Forecasters of China Meteorological Administration (no. CMAYBY 2019-024). Project NO. 2021CDJQY–004 supported by the Fundamental Research Funds for the Central Universities.

ACKNOWLEDGMENTS

The authors appreciate Miss Ziqi Zhao's help in preparing figures and tables.

REFERENCES

Bennetts, D. A., and Hoskins, B. J. (1979). Conditional Symmetric Instability - a Possible Explanation for Frontal Rainbands. *Q.J R. Met. Soc.* 105 (446), 945–962. doi:10.1002/qj.49710544615

Braham, R. R. (1983). The Midwest Snow Storm of 8-11 December 1977. *Mon. Wea. Rev.* 111 (2), 253–272. doi:10.1175/1520-0493(1983)111<0253:tmssod>2.0.co;2

Cui, H., and Su, A. (2019). Analysis on Characteristics and Causes of a Heavy Snowstorm Event in Southern Henan in the Beginning of January 2018. *Torrential Rain Disasters* 38 (2), 169–176. doi:10.3969/j.issn.1004-9045.2019.02.009

Cui, H.-Y., and Qiao, F.-L. (2016). Analysis of the Extremely Cold and Heavy Snowfall in North America in January 2015. *Atmos. Ocean. Sci. Lett.* 9 (2), 75–82. doi:10.1080/16742834.2016.1133057

Duan, Y., Wang, W., Tian, Z., and Zhang, N. (2013). Comparison of Two Rain-To-Blizzard Processes under Similar Conditions in Northern North China. *Arid. Meteorol.* 31 (4), 784–789. doi:10.11755/j.issn.1006-7639(2013)-04-0784

Fernández-González, S., Valero, F., Sánchez, J. L., Gascón, E., López, L., García-Ortega, E., et al. (2015). Numerical Simulations of Snowfall Events: Sensitivity Analysis of Physical Parameterizations. *J. Geophys. Res. Atmos.* 120 (19), 110130–110148. doi:10.1002/2015jd023793

Gao, S., Zhao, T., Song, L., Bai, H., Xu, L., Li, R., et al. (2020). Transporting Characteristics of Snowstorm Water Vapor over Liaoning Province in Winter. *J. Glaciol. Geocryol.* 42 (2), 439–446. doi:10.7522/j.issn.1000-0240.2020.0046

Hamzeh, N. H., Karami, S., Kaskaoutis, D. G., Tegen, I., Moradi, M., and Opp, C. (2021). Atmospheric Dynamics and Numerical Simulations of Six Frontal Dust Storms in the Middle East Region. *Atmosphere* 12 (1), 125. doi:10.3390/atmos12010125

He, B.-J., Zhao, D., Xiong, K., Qi, J., Ulpiani, G., Pignatta, G., et al. (2021). A Framework for Addressing Urban Heat Challenges and Associated Adaptive Behavior by the Public and the Issue of Willingness to Pay for Heat Resilient Infrastructure in Chongqing, China. *Sustain. Cities Soc.* 75, 103361. doi:10.1016/j.scs.2021.103361

IPCC (2018). "Global Warming of 1.5°C,". *An IPCC Special Report on the Impacts of Global Warming of 1.5°C above Pre-industrial Levels and Related Global Greenhouse Gas Emission Pathways, in the Context of Strengthening the Global Response to the Threat of Climate Change, Sustainable Development, and Efforts to Eradicate Poverty*. Editors V. Masson-Delmotte, P. Zhai, H.-O. Pörtner, D. Roberts, J. Skea, P. R. Shukla, et al. (Cambridge, United Kingdom and NewYork, NY: Cambridge University Press), 1, 3–24. doi:10.1017/9781009157940.001

Ji, L., Quan, Z., Song, L., Kong, X., and Zhang, J. (2014). Numerical Simulation and Analysis of a Snowstorm Event in East Gansu Province. *J. Arid Meteorology* 32 (5), 845–850. doi:10.11755/j.issn.1006-7639(2014)-05-0845

Li, X.-f., Zhu, J.-j., Jia, Y., Liu, J., Li, N., and Li, F. (2007). Formation Process of Extraordinarily Serious Snowstorm and its Induced Damage in 2007 in Liaoning Province. *Chin. J. Ecol.* 26, 1250–1258.

Miao, C.-S., Xie, J., Wang, J.-h., and Zhang, N. (2010). Numerical Simulation and Diagnostic Analysis of a Cold Airflow Snowstorm Process in Shandong Peninsula. *Journal of Nanjing Institute of Meteorology* 33 (3), 257–265.

Millar, R. J. (2017). IPCC Says Limiting Global Warming to 1.5 °C Will Require Drastic Action. *Nat. Geosci.* 10, 3031. doi:10.1038/ngeo3031

Ninomiya, K. (1991). Polar Low Development over the East Coast of the Asian Continent on 9-11 December 1985. *J. Meteorological Soc. Jpn.* 69 (6), 669–685. doi:10.2151/jmsj1965.69.6_669

Pearce, R., Lloyd, D., and McConnell, D. (2001). The Post-christmas 'French' Storms of 1999. *Weather* 56 (3), 81–91. doi:10.1002/j.1477-8696.2001.tb06541.x

Rawlins, M. (2022). *Why a Warming Climate Can Bring Bigger Snowstorms*. The Conversation. Available at: https://theconversation.com/why-a-warming-climate-can-bring-bigger-snowstorms-176201.

Rosenzweig, C., Solecki, W., Romero-Lankao, P., Mehrotra, S., Dhakal, S., and Ibrahim, S. A. (2018). "Pathways to Urban Transformation," in *Climate Change and Cities: Second Assessment Report of the Urban Climate Change Research Network* (New York: Cambridge University Press).

Salvia, M., Reckien, D., Pietrapertosa, F., Eckersley, P., Spyridaki, N.-A., Krook-Riekkola, A., et al. (2021). Will Climate Mitigation Ambitions Lead to Carbon Neutrality? an Analysis of the Local-Level Plans of 327 Cities in the EU. *Renew. Sustain. Energy Rev.* 135, 110253. doi:10.1016/j.rser.2020.110253

Sanders, F., and Bosart, L. F. (1985). Mesoscale Structure in the Megalopolitan Snowstorm of 11-12 February 1983. Part I: Frontogenetical Forcing and Symmetric Instability. *J. Atmos. Sci.* 42 (10), 1050–1061. doi:10.1175/1520-0469(1985)042<1050:msitms>2.0.co;2

Shimizu, N., and Uchida, A. (1974). An Observational Study of Organized Snow Echo over the Japan Sea. *J. Meteorological Soc. Jpn.* 52 (3), 289–299. doi:10.2151/jmsj1965.52.3_289

Solecki, W., Rosenzweig, C., Dhakal, S., Roberts, D., Barau, A. S., Schultz, S., et al. (2018). City Transformations in a 1.5 °C Warmer World. *Nat. Clim. Change* 8 (3), 177–181. doi:10.1038/s41558-018-0101-5

Ulbrich, U., Fink, A. H., Klawa, M., and Pinto, J. G. (2001). Three Extreme Storms over Europe in December 1999. *Weather* 56 (3), 70–80. doi:10.1002/j.1477-8696.2001.tb06540.x

UNEP (2021). "Facts about the Climate Emergency," in *Climate Actions* (United Nations Environment Programme). Available at: https://www.unep.org/explore-topics/climate-action/facts-about-climate-emergency.

Wu, W., Deng, L., and Wang, S. (2011). Numerical Simulation of the "0911" North China Snowstorm and Analysis of Cloud Microphysical Characteristics. *Meteorology* 37 (8), 991–998. doi:10.7519/j.issn.1000-0526.2011.8.011

Wu, Z., Wang, J., and Zhao, G. (2012). Diagnostic Analysis of a Heavy Snowstorm Process in Tianjin Area. *J. Meteorology Environ.* 28 (6), 8–13.

Zhao, G. (2007). Analysis of the Blizzard Weather Caused by the Combined Action of a Backflow and an Inverted Trough. *Meteorol. Mon.* 11, 41–48. doi:10.7519/j.issn.1000-0526.2007.11.00748

Zhou, Q., Cheng, Y., Zhou, G., Wang, S., Shang, K., and Yang, D. (2011). An Analysis of the Process and Climate Background of a Regional Snowstorm in the Eastern Part of the Qinghai-Tibet Plateau in October 2008. *Plateau Meteorol.* 30 (1), 22–29.

Conflict of Interest: The authors declare that the research was conducted in the absence of any commercial or financial relationships that could be construed as a potential conflict of interest.

Publisher's Note: All claims expressed in this article are solely those of the authors and do not necessarily represent those of their affiliated organizations or those of the publisher, the editors, and the reviewers. Any product that may be evaluated in this article, or claim that may be made by its manufacturer, is not guaranteed or endorsed by the publisher.

Copyright © 2022 Yan, Cui, Tan and He. This is an open-access article distributed under the terms of the Creative Commons Attribution License (CC BY). The use, distribution or reproduction in other forums is permitted, provided the original author(s) and the copyright owner(s) are credited and that the original publication in this journal is cited, in accordance with accepted academic practice. No use, distribution or reproduction is permitted which does not comply with these terms.

frontiers | Frontiers in Ecology and Evolution

TYPE Original Research
PUBLISHED 22 August 2022
DOI 10.3389/fevo.2022.973365

Check for updates

OPEN ACCESS

EDITED BY
Jun Yang,
Northeastern University, China

REVIEWED BY
Shaohua Wang,
Aerospace Information Research Institute (CAS), China
Xiaoping Zhang,
Shandong Jianzhu University, China

*CORRESPONDENCE
Lijian Ren
renlijian@126.com

†These authors have contributed equally to this work and share first authorship

SPECIALTY SECTION
This article was submitted to Environmental Informatics and Remote Sensing, a section of the journal Frontiers in Ecology and Evolution

RECEIVED 20 June 2022
ACCEPTED 26 July 2022
PUBLISHED 22 August 2022

CITATION
Huang H, Liu X and Ren L (2022) Analysis of the spatiotemporal mechanism of high temperature on residents' irritability in Beijing based on multiscale geographically weighted regression model.
Front. Ecol. Evol. 10:973365.
doi: 10.3389/fevo.2022.973365

COPYRIGHT
© 2022 Huang, Liu and Ren. This is an open-access article distributed under the terms of the Creative Commons Attribution License (CC BY). The use, distribution or reproduction in other forums is permitted, provided the original author(s) and the copyright owner(s) are credited and that the original publication in this journal is cited, in accordance with accepted academic practice. No use, distribution or reproduction is permitted which does not comply with these terms.

Analysis of the spatiotemporal mechanism of high temperature on residents' irritability in Beijing based on multiscale geographically weighted regression model

Huanchun Huang[1†], Xuan Liu[1†] and Lijian Ren[2*]

[1]College of Landscape Architecture, Nanjing Forestry University, Nanjing, China, [2]School of Architecture, Tianjin University, Tianjin, China

The emotional health of urban residents is increasingly threatened by high temperatures due to global heating. However, how high temperature affects residents' emotional health remains unknown. Therefore, this study investigated the spatiotemporal pattern of temperature's impact on residents' irritability using data from summer high-temperature measurement and emotional health survey in Beijing, combined with remote sensing images and statistical yearbooks. In detail, this study formulated a multiscale geographically weighted regression (MGWR) model, to study the differentiated and spatial influence of high-temperature factors on emotion. Results show: From 09:00 to 20:00, irritability level rose first then gradually dropped, with a pattern of "aggregation-fragmentation-aggregation." Irritability is very sensitive to intercept and building density (BD). Other variables all have spatial heterogeneity [except for fraction vegetation coverage (FVC) or road network density (RND) as they are global variables], including normalized difference vegetation index (NDVI), water surface rate (WSR), floor area ratio (FAR), and Modified Normalized Difference Water Index (MNDWI) (sorted from the smallest to the largest in scale). Irritability is negatively correlated with NDVI, WSR, and RND, while positively correlated with intercept, MNDWI, FVC, FAR, and BD. Influence on irritability: WSR < NDVI < BD < MNDWI < RND < intercept < FVC < FAR.

KEYWORDS

influencing factors of thermal environment, hourly temperature, emotional health, irritability, multiscale geographically weighted regression, Beijing

Introduction

Global heating and continued urbanization have aggravated the urban heat island (UHI) effect and created health challenges to the public. Oxford English Dictionary recently added a new phrase "global heating." According to the Oxford Monitor Corpus, the term "global heating" appeared nearly 15 times more frequently in the first half of 2021 than in the first half of 2018 (Simpson and Weiner, 1993). This word strengthens passive and mild terms such as "climate change" and "global warming" to express the seriousness of climate change caused by human activities and the urgency of solving such problem (World Meteorological Organization [WMO], 2021). In 2020, China's urbanization level has reached 63.89%, and more natural landscapes have been replaced by impervious surfaces, and highly concentrated human activities have been changing the urban thermal environment (Yang et al., 2019; Yin et al., 2022). This phenomenon occurs in nearly every urban area, no matter whether the city is small or large, or located in warm or cold climates. UHI effect, in turn, endangers residents' survival and wellbeing. UHI, in addition, is a major trigger of psychological issues like pain, anxiety, and fear (Fritze et al., 2008; Hayes and Poland, 2018).

The research on the influence of urban thermal environment on human health mainly focuses on physiological aspects, discussing the relationship between high temperature and heat-related diseases and mortality (Nitschke et al., 2011; Guo et al., 2018; Thompson et al., 2018; Yin et al., 2018), and paying less attention to emotional health. Studies have shown that there is a significant relationship between high temperature and mental illness. For example, according to a research in Australia, the number of patients hospitalized for mental illness increased by 7% during the heat waves (Hansen et al., 2008). A study of data during four heatwaves in Jinan also found that the number of daily medical visits for mental illness increased significantly during the heatwaves (Liu et al., 2012). Further, a study on the relationship between the daily average temperature and the hospitalization rate of mental disorders in Shanghai from 2008 to 2015 found that when the temperature reached 24.6°C and above, there was a significant positive correlation between the increase in temperature and the increase in the number of hospitalizations for schizophrenia. When the temperature was above 33.1°C, the risk of hospitalization for mental disorders was 1.266 times that of the mean (Peng et al., 2017). However, the analysis of the influence of thermal environment on the emotional health of the general population and its specific influencing factors is still lacking. Therefore, under the background of global heating, it is urgent to pay attention to the emotional health of residents in rapidly urbanized areas, carry out risk assessment of thermal environment on human emotional health, and explore the mechanism of urban thermal environment on emotional health.

The continuous rise of temperature, which concerns people' emotional health, is one of the major influences of UHI (Manning and Clayton, 2018). Compared to the comfortable temperature of 23°C, with every 1°C increase in temperature, the predictable psychological stress rises by 0.2% (Ding et al., 2016). And people may experience repression, rage, and pain when the temperature is too high (Vanos et al., 2012). Burke et al. (2018) discovered that the higher the monthly average temperature is, the more suppressed words are used on Twitter. In addition, climate change has exacerbated the social inequality faced by heat-vulnerable population, especially the middle-aged and elderly (McMichael, 2017) as they are more likely to develop mental health problems following natural disasters (Parker et al., 2016). When body temperature rises, the temperature of the central nervous system and brain rises as well, triggering the hypothalamus's selective cooling system to lower the brain temperature. However, for the middle-aged and elderly population, their physical functions and cooling system are not strong enough, thus being widely considered sensitive to extremely high temperature (Hames et al., 2016). To be more specific, heat-vulnerable population includes infants, children, and middle-aged and elderly people (Bielby, 2019). But, due to the insufficient cognitive ability of infants and children, they are not included in this study. Hence, based on Erikson Stages of Psychosocial Development (40–65 years old as Middle Adulthood), this study was targeted at middle-aged and elderly at and over 40 years old. Furthermore, our research team discovered that the negative emotions induced by thermal environment are mostly distress, irritability, nervousness, and hostility, with irritability the most obvious, thus this study decided on the negative emotion of irritability (Huang et al., 2020a).

The urban thermal environment is a complex physical phenomenon, and the influencing factors mainly include spatial structure features, land-use and land-cover change (LUCC), landscape pattern, artificial heat release, and wind environment (Yao et al., 2019; Yue et al., 2019; Xu et al., 2021). Research shows UHI is positively correlated with road network density (RND), while negatively correlated with fraction vegetation coverage (FVC) (Estoque et al., 2017). Moreover, water bodies are another identified source of reduced thermal load, at least during the day, due to a high thermic inertia (Liu and Weng, 2008). The cooling capacity of urban wetland is positively correlated with the wetland's area, shape, and degree, yet negatively correlated with the height and density of nearby buildings (Xue et al., 2019). Additionally, land surface temperature (LST) and near-surface temperature are two important parameters for studying the urban thermal field. Some scholars used temperature data to analyze the pattern characteristics of urban temperature field. For example, Shen et al. (2017) studied the spatiotemporal distribution of UHI in the center of Shanghai city based on hourly temperature. Heat island intensity and temperature differ in spatiotemporal

pattern, maybe because the "thermal hysteresis" of the large heat capacity of the underlying urban surface makes the change of heat island intensity lag behind that of temperature (Mao et al., 2021). Temperature is mainly influenced by each or the combination of LUCC indicators and human factors (Ren et al., 2005). Therefore, FAR, BD, RND, and other related indicators reflecting different human activities, as well as FVC, NDVI, WSR, MNDWI, and other LUCC-related indicators were selected in this study.

With the rapid development of urban thermal environment research, spatial non-stationarity becomes a new trend in studies on land surface index. Geographically weighted regression (GWR) algorithm is limited to a single optimal bandwidth and usually reflects the "average" of the optimal bandwidth of each process (Oshan et al., 2019). It is not suitable for changes in the urban thermal field, as different processes involve different spatial scales. In recent years, the development of MGWR (Fotheringham et al., 2017) has broken the limits. However, MGWR is still insufficient in estimating local parameters. In 2019, Yu et al. (2020) broke the limits of the MGWR model so that it can be widely used in empirical research. Shen et al. (2020) discussed how the MGWR model influences second-hand house price, and proved that it is helpful to studies on spatial variation; Chen and Deng (2021) and Li et al. (2021) used MGWR to analyze how urban landscape and form influence thermal environment.

This manuscript takes the Sixth Ring Road area of Beijing as the research object, and aims to study the spatial distribution characteristics and mechanism of the impact of urban thermal environment on residents' emotional health. Using Landsat remote sensing images, meteorological stations, and emotional health data to establish a theoretical relationship model between temperature and irritability; combined with ArcGIS, MATLAB, SPSS and other data analysis platforms to analyze the temporal and spatial effects of hourly temperature on irritability in summer from 09:00 to 20:00; based on the MGWR model to explore the spatial differentiation of residents' irritability affected by different thermal environmental factors. It provides a basis for optimizing the layout of urban green space, improving the urban thermal environment, and reducing the risk of emotional health.

The list of acronyms in this paper is shown in **Table 1**.

Material and methods

Overview of the study area

Beijing (39°24–41°36′ N, 115°42′–117°24′ E) is located in the northern part of North China Plain, adjacent to Bohai Bay, neighboring Liaodong Peninsula in the north and Shandong Peninsula in the south, belonging to a typical semi-humid continental monsoon climate in the north temperate zone. At the end of 2021, the permanent population of Beijing reached 21.886 million. The highly concentrated urbanized buildings, rapidly expanding special underlying surfaces, and frequent and intensive human activities in Beijing deteriorated the urban thermal environment and led to frequent heat waves. During 2011–2021, the average maximum temperature was more than 31°C, and the maximum temperature more than 35°C, seriously affecting the thermal comfort of residents. This study took the most densely populated area–the area within the Sixth Ring Road (Dongcheng District, Xicheng District, Chaoyang District, Haidian District, Fengtai District, Shijingshan District,

TABLE 1 List of acronyms.

Acronyms	Description
Intercept	The effect of different locations when other independent variables are determined
MGWR	Multiscale Geographically Weighted Regression
GWR	Geographically Weighted Regression
UHI	Urban Heat Island
LST	Land Surface Temperature
LUCC	Land-Use and Land-Cover Change
LCZ	Local Climate Zone
NDVI (Normalized Difference Vegetation Index)	Vegetation growth status, abundance, and coverage
FVC (Fraction Vegetation Coverage)	Regional vegetation coverage
MNDWI (Modified Normalized Difference Water Index)	Coverage of water bodies
WSR (Water Surface Ratio)	Regional water coverage
BD (Building Density)	Ratio of regional building area to the regional area
FAR (Floor Area Ratio)	Ratio of land development intensity, regional building area, and the product of floors to the regional area
RND (Road Network Density)	Road length per square kilometer of an urban built-up area or a certain urban area

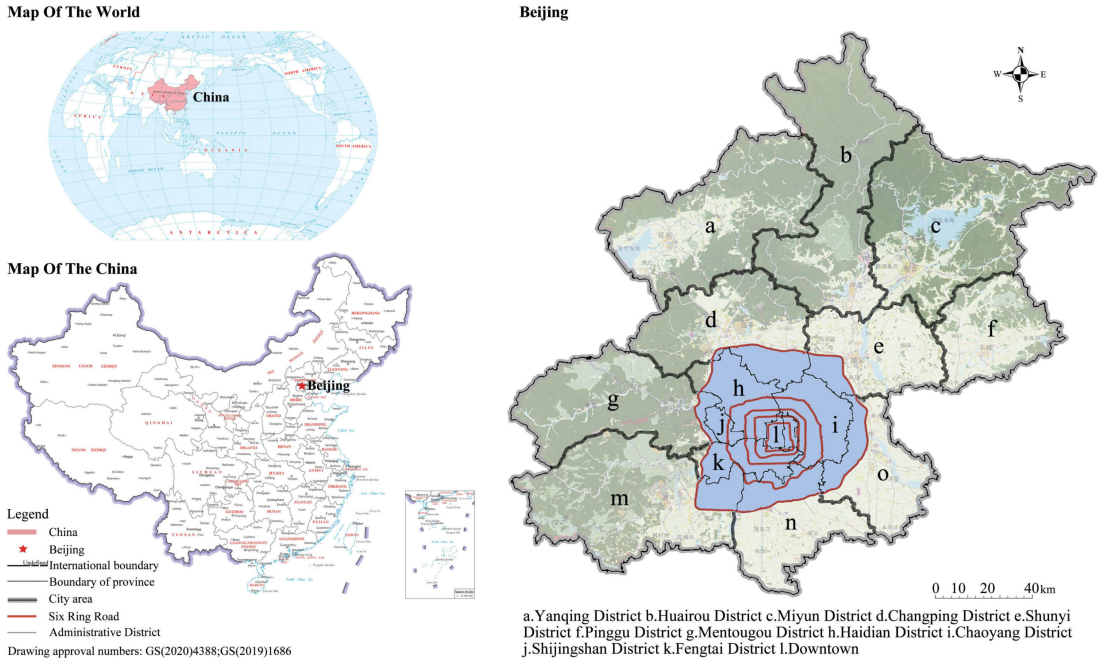

FIGURE 1
Overview of study areas. The map is the official map approved by the China's Ministry of Natural Resources and Beijing Municipal Planning Bureau.

etc.) as the study area, covering a total area of 2,257.01 km^2 (Figure 1).

Data sources

The data applied in this study include remote sensing images, meteorological data, and field survey questionnaires. The remote sensing image data is obtained by using the Landsat 8 satellite image provided by the United States Geological Survey (USGS) through the atmospheric correction method. The imaging time was 10:30 in August 2015, with a spatial resolution of 30 m, no precipitation on the imaging day, wind speed lower than 2 m/s, and no cloud coverage. So, the remote sensing images are high-quality, suitable for LST retrieval.

The temperature data was obtained from both fixed and hand-held weather stations. 380 fixed weather stations in different urban functional areas of Beijing, with little interference from the surrounding hard pavements, buildings, and artificial facilities, to guarantee scientific and reliable results. Meteorological data from the fixed weather stations was cleaned, to eliminate interference from cloud and rain and abnormal value, and eventually 183 meteorological stations were selected. The mobile weather station is aligned with the survey site. Combined with remote sensing satellite images, field investigation and related literature review, and according to the environmental characteristics and usage needs of local climate cells, 17 places were selected for microclimate measurement and emotional questionnaire survey.

The survey dates are July-August, the summer with the highest temperature in Beijing, to meet the high temperature requirements for the study. The experiment lasted for 14 days, and the daily maximum temperature was above 33°C. The survey was conducted from 08:00 to 17:00 every day, and the samples were distributed evenly in each time period. There was no rain or high winds for 1-2 days before the experiment. A small WS-30 handheld weather station 1.5m above the ground was used to collect temperature data. The equipment accuracy is ±0.3°C for temperature, ±3% for humidity, and ±0.3m/s for wind speed. After the data was stable, it was automatically recorded every 1min. The samples cover high temperature, medium temperature and low temperature areas in the urban area, and the temperature range is 23°–50°. The Positive and Negative Activation Scale (PANAS) for Chinese people was used in the questionnaire (Huang et al., 2003; Bao et al., 2020). Blank, incomplete and invalid questionnaires under the age of 40 were excluded, and 931 valid questionnaires were obtained. Moreover, in order to minimize the error of data analysis due to the influence of previous activities or unexpected events experienced by the subjects, this study initially screened the research subjects while ensuring the randomness of sampling, excluding those who are in indoor environment, going out of the car, doing outdoor strenuous exercise, or staying under shade for a long time.

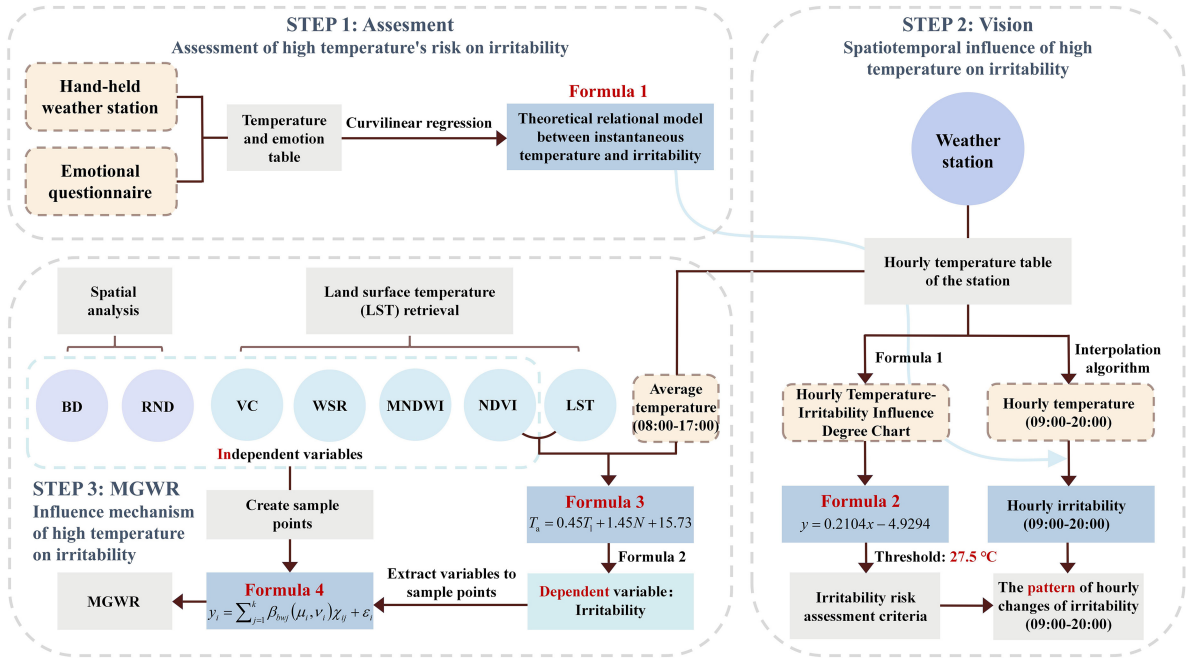

FIGURE 2
Analytical framework.

Data processing

The flow chart of the research method is shown in Figure 2.

Establishing a model of the relationship between average temperature and irritability in typical periods

First, according to the time and temperature data recorded by the handheld weather station and the time and emotion data collected by the questionnaire, matched temperature data with emotional data to set up a survey table of temperature and emotion. Multiple reviews ensure the correctness of the data. Temperature data collected from the hand-held weather stations was analyzed by plotting on the GraphPad platform (see Figure 3). Results show that the sample data covers 25.1–50.5°C with an excellent overall spatial distribution. The upper quartile is 42.9°C, median quartile 39.7°C, and lower quartile 35.2°C. Samples are concentrated during 35.2–42.9°C, enough to represent summer days above 35°C. A fundamental descriptive analysis suggests that the samples can be used to study urban heat's spatiotemporal effects on residents' irritability. Thereafter, based on the survey table of temperature and emotion, the influence degree index of irritability in each temperature range was obtained by cross-table analysis of SPSS. Next, smooth the data and standardize the impact index according to the maximum value.

The curve fitting toolbox Cftool of MATLAB software was used to analyze various curve regressions on questionnaire and temperature data, to establish a theoretical relational model between instantaneous temperature and irritability, and selected the most fitted equation as the practical relational model in this study (see Figure 4). The formula is as follows:

$$N_i = 6.1\sin(0.26t + 0.53) + 0.56\sin(3.28t - 0.74) + 0.43\sin(6.36t + 1.38) \quad (1)$$

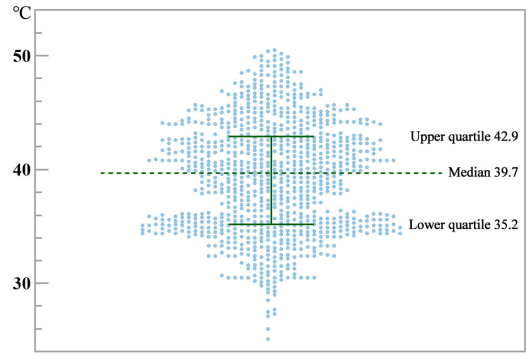

FIGURE 3
Sample temperature distribution.

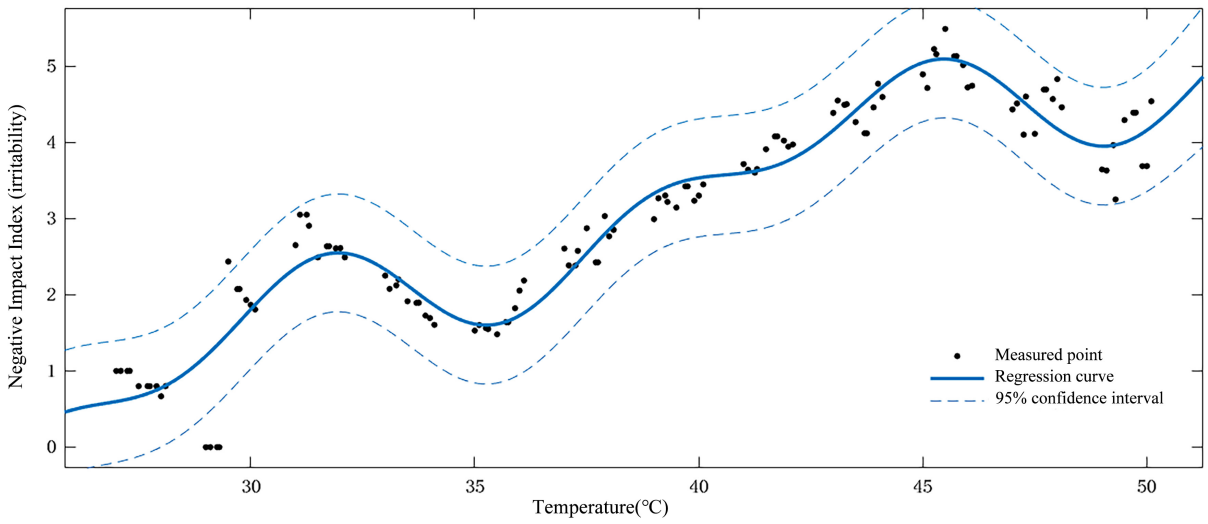

FIGURE 4
Relational model between instantaneous temperature and irritability.

where N_i is the irritability value, t is the instantaneous temperature. SSE: 15.85, $R^2 = 0.93$.

The fixed meteorological stations recorded the temperature every 30 min. 09:00–20:00 is the period when residents are intensively exposed to the outdoor environment, and when high temperature significantly influences their emotions. Therefore, the temperature data from 09:00 to 20:00 was extracted to form an hourly temperature table. Since the temperature field is a spatial variable that changes continuously, and the temperature captured by stations is an accurate value of a fixed point, in order to obtain both smooth and accurate interpolation results, this study used the spline function method to interpolate the stations, and attained the hourly temperature from 09:00 to 20:00. Then, hourly temperature was put into Eq. 1 to get hourly irritability value.

Finally, based on human body's reaction to high temperature (Li et al., 2017), the correlation curve between instantaneous temperature and irritability, and with the daily average temperature from 8:00 to 17:00 in the hourly temperature field data of the fixed meteorological station as the average temperature in the typical period, the relationship curve between the average temperature in the typical period and the irritability was established (**Figure 5**) (Formula 2), providing basic conditions for carrying out urban climate health risk assessment. The average daily temperature of 27.5°C calculated from the observation data of Beijing Meteorological Station was taken as the threshold temperature for the influence of high temperature on Irritability, and the impact of high temperature on Irritability was divided into ten grades (**Table 2**) as the standard for evaluating the risk of human Irritability (Denissen et al., 2008; Qi et al., 2015; Noelke et al., 2016).

$$\gamma = 0.2104x - 4.9294 \quad (2)$$

where γ is the average irritability value, and is the average temperature in the typical period. $R^2 = 0.93$, with good goodness of fit.

Constructing the multiscale geographically weighted regression model

First, based on the Landsat8 satellite image, LST was retrieved. This manuscript used the atmospheric correction method, with the influence of the atmosphere on the surface radiation excluded from the total amount of thermal radiation received by the satellite sensor, to obtain the surface brightness temperature value, and then the surface brightness temperature was converted into the corresponding LST (Yue and Liu, 2018).

The summer temperature field data measured by fixed meteorological stations were collected to form the hourly temperature data table of the station. The average hourly temperature from 8:00 to 17:00 every day was taken as the average temperature in typical periods, and regression analysis was performed on LST, NDVI, and the average temperature in typical periods, to formulate the linear regression equation of them (Eq. 3):

$$T_a = 0.45T_l + 1.45N + 15.73 \quad (3)$$

where T_a is the typical period average temperature, T_l is the land surface temperature (LST), and $N$is the NDVI. $R^2 = 0.58$.

Second, in order to obtain the average irritability value (dependent variable), the inversion of Beijing's 2015 summer

TABLE 2 Standard of evaluating risk of irritability.

Influence level	Instantaneous irritability value	Temperature/°C	Details
Level 1	≤0.2	<30	Comfortable
Level 2	0.2–0.6	30–31	Emotionally stable
Level 3	0.6–1.0	31–32	Fidgety
Level 4	1.0–1.5	32–33	Restless and irritable
Level 5	1.5–2.0	33–34	Panic with more negative emotions
Level 6	2.0–2.4	34–35	Irritable, agitated, and highly alert
Level 7	2.4–3.0	35–36	Painful and less energetic
Level 8	3.0–3.5	36–36.5	Persistently angry, inclined to be hostile
Level 9	3.5–4.5	36.5–37	Hostile, anxious, and nervous
Level 10	>4.5	>37	Intensively angry with brief behavioral outbursts

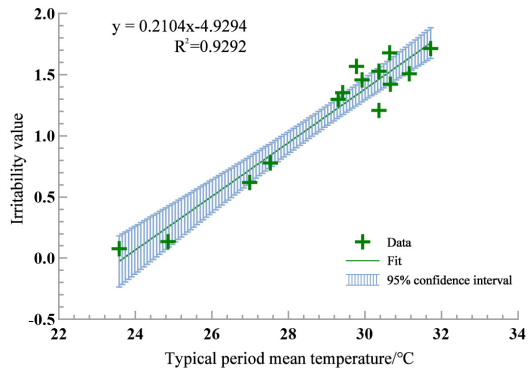

FIGURE 5
Relational model between average temperature and average irritability value in typical periods.

LST and NDVI are substituted into Formula 3 to obtain the average temperature in the corresponding typical period, and then the average temperature in the typical period is substituted into Formula 2 to obtain the corresponding average irritability value.

Further, *via* the ENVI software, the Landsat8 remote sensing images were preprocessed by radiometric calibration, atmospheric correction, and geometric correction, and NDVI (Tan et al., 2004) and MNDWI (Xu, 2006) were calculated, to exclude the parts where NDVI and MNDWI < 0, and obtain FVC and WSR. All the land-use indicators in the study area were counted, to attain BD, FAR, and RND to get the independent variables. Then, all factors were projected uniformly to ensure data consistency. Finally, the MGWR model was constructed. In the study area, based on the 1 km grid scale, 2,000 sample points were created, and variables were extracted to the sample points; 1,577 valid sample data were obtained after removing outliers. Independent variables, dependent variable, and intercept were imported to MGWR, and the quadratic kernel function of classical GWR and AICc was still utilized as the standard for choosing the kernel function and bandwidth. As a result, valid parameters: 1,577, covariates: 8, and iterations: 74. When the difference in parameter estimation of subsequent iterations converges to the specified threshold, the iteration is terminated, and the convergence threshold is 1.0e–05. The model formula is as follows (Formula 4):

$$y_i = \sum_{j=1}^{k} \beta_{bwj}(\mu_i, \nu_i)\, x_{ij} + \varepsilon_i \quad (4)$$

where y_i is the average irritability value of sample point i, β_{bwj} denotes the regression coefficients of different variables j at different bandwidth levels, x_{ij} is the observed value of variable j at location i, (μ_i, ν_i) denotes the geographical coordinates of variable i, and ε_i is the stochastic error term.

Results

Analysis of the spatiotemporal influence of high temperature on irritability

According to the risk evaluation standard of irritability, the spatial pattern of the impact of high temperature on irritability in the Sixth Ring Road area of Beijing in the summer of 2015 was evaluated (**Figure 6**).

During 09:00–20:00, the irritability level first increased then decreased. From 09:00 to 15:00, irritability rocketed; from 15:00 to 20:00, irritability declined slowly. Irritability peaked at Level 8 at 15:00. The influence pattern showed a trend of "aggregation-fragmentation-aggregation".

During 09:00–12:00 (A–C), water supply for plant transpiration decreased, drastically heating up the green area (Gill et al., 2007). High-level patches shifted from being scattered to a large matrix. After that, the temperature in urban and suburban areas continued to rise, temperature difference between urban areas and suburbs dwindled, urban cooling slowed down, a large number of artificial heat sources gathered

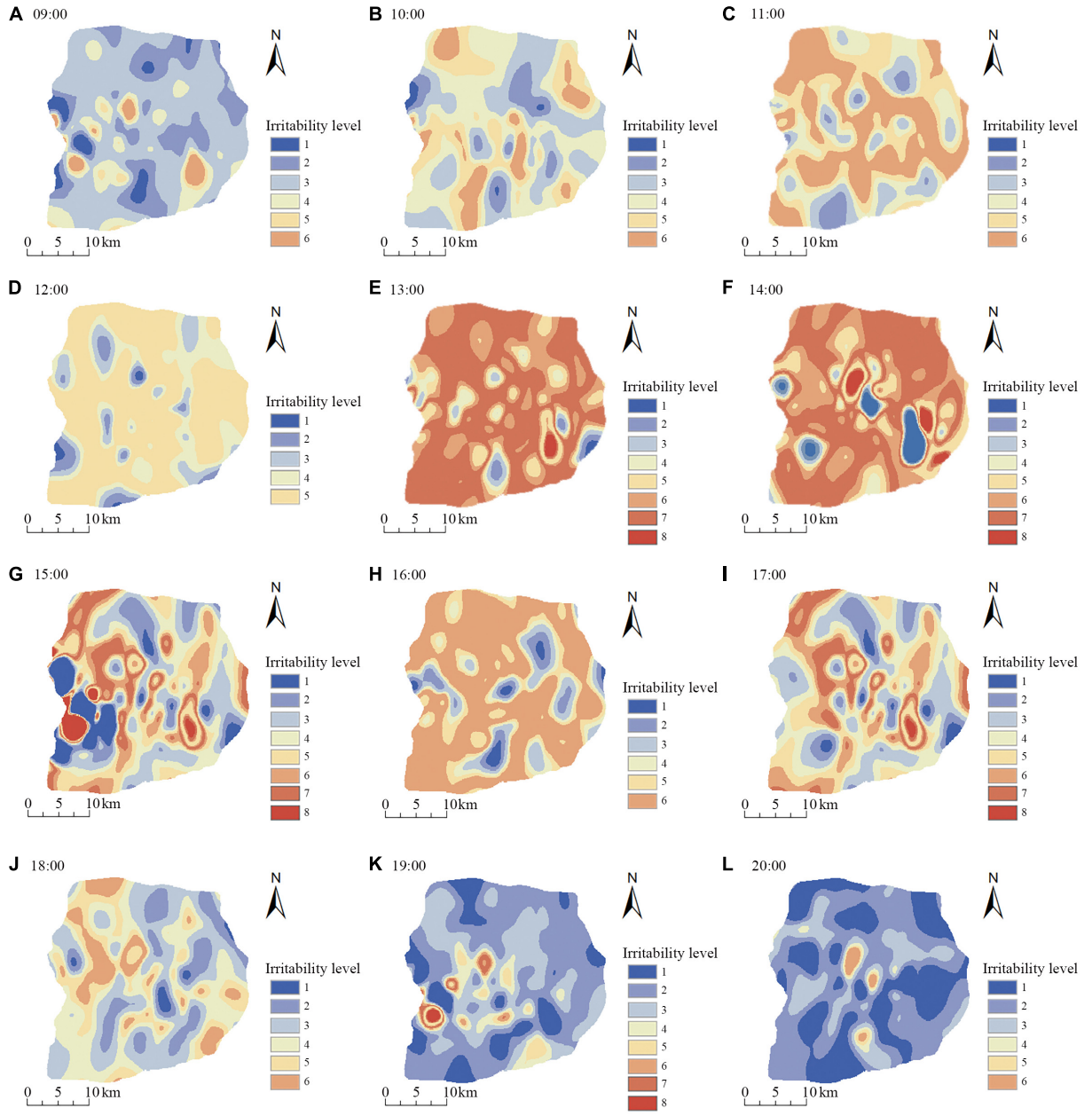

FIGURE 6
Evolution of spatiotemporal pattern of urban heat island (UHI)'s influence on irritability from 09:00 to 20:00.

TABLE 3 The correlation of thermal environmental factors influences irritability.

Variables	FVC	NDVI	WSR	MNDWI	FAR	BD	RND
Indicator	−0.410**	−0.496**	−0.427**	−0.007	0.402**	0.397**	0.344**

**, Significant correlation at the 0.01 level (two-tailed).

in the city center, and the irritability level increased toward the city center.

12:00–17:00 (D–I) is the high-temperature period. The temperature gradually rose, irritability rose to Level 8, and high temperature's influence on irritability became highly fragmented. After 14 o'clock, the increment of land surface heat storage dwindled, and at 15 o'clock, the heat continued to spread, and the cooling rate of green space and water bodies

accelerated. Large parks, especially Beijing Olympic Park, the Old Summer Palace, Fragrant Hills Park, and Century Forest Park, as well as large water systems in the north and south of the Sixth Ring Road cooled the surrounding areas by releasing latent heat and reducing the energy available for sensible heat (Peng et al., 2012), forming up large Level 1–3 patches, covering an area of about 579.88 km^2. At 16 o'clock, the cooling effect of the wedge-shaped green space around the city was the most obvious, and the irritability level decreased toward the city center along with the wedge-shaped green space.

During 17:00–20:00 (J–L), the temperature dropped, wind speed increased, and the intensity of human activities gradually decreased. Low-impact areas spread from the outskirts to the city center. The main reason is that the lower atmospheric layer of the city was under low pressure, while that of the suburbs under high pressure, pushing cold air flows into the city. At the same time, on the urban boundary layer, the cooling capacity was mainly attributed to the increased roughness of green surface which improved convection efficiency (Gunawardena et al., 2017).

Analysis of influence mechanism of high temperature on irritability

Correlation between regression coefficient and irritability

Results of correlation test using SPSS software show that (see **Table 3**): Except for MNDWI, all the other variables are significantly correlated with irritability at 0.01 level (two-tailed); The most significantly correlated one is NDVI—correlation coefficient around 0.5, followed by FVC and FAR—correlation coefficient above 0.4; FVC and NDVI are significantly negatively correlated with irritability, able to alleviate irritability; FAR, BD, and RND are significantly positively correlated with irritability—correlation coefficient above 0.3, indicating that the thermal environment effect of artificial surface is the main reason for intensified irritability. The correlation between MNDWI and irritability is not significant. Previous studies showed that MNDWI is negatively correlated with heat island in spring, summer, and autumn, and significantly negatively correlated in summer, indicating that increasing WSR alleviates heat island in summer (Chen and Deng, 2021).

TABLE 4 Comparison of regression model results.

Model index	MGWR	GWR
The goodness of fit R^2	0.879	0.875
AICc	1747.222	1876.036
Residual sum of squares	190.774	197.379
Number of valid parameters	251.884	277.827

Comparison of model accuracy

In this study, the precision results of classical GWR and MGWR models were compared. According to **Table 4**, the goodness of fit R^2 of MGWR is 0.879, higher than that of GWR, and the AICc is lower than that of GWR. Hence compared with classical GWR, MGWR produces more precise results. In addition, the number of effective parameters and the sum of residual squares of MGWR are both smaller than those of GWR, indicating that MGWR produces a more precise regression result with fewer parameters. In terms of the regression coefficient, all variables of MGWR are significant. Meanwhile, GWR cannot reflect the different functions of variables, resulting in a lot of noise and errors in the regression coefficient, causing instability (only intercept is the significant variable). Therefore, MGWR is superior to GWR in this study, more suitable for analyzing spatial heterogeneity of the thermal environment.

Scale analysis of regression coefficient

Results of model processing (see **Table 5**) show that classical GWR can only reflect the mean value of the function of each variable, while MGWR can directly reflect the different functions of each variable. The best-fitting bandwidth of each variable is (sorted from the largest to the smallest) VC, RND, MNDWI, FAR, WSR, NDVI, BD, and intercept. The bandwidths of different variables are significantly different:

1. Intercept, BD, and NDVI are close in bandwidth: 43, 49, and 77, respectively, far smaller than other variables, accounting for about 2.9, 2.9, and 4.9% of the total sample size, and covering 78, 78, and 130.7 km^2 of the study area, close to the street scale. When exceeding the function range, the regression coefficient alters dramatically. It proves that the thermal environment is very sensitive to the growth of vegetation and the distribution of buildings

TABLE 5 Comparison of bandwidth of classical geographically weighted regression (GWR) and multiscale geographically weighted regression (MGWR).

Variable	MGWR bandwidth	GWR bandwidth
Intercept	43	101
MNDWI	404	101
NDVI	77	101
VC	1576	101
WSR	148	101
FAR	231	101
BD	49	101
RND	1574	101

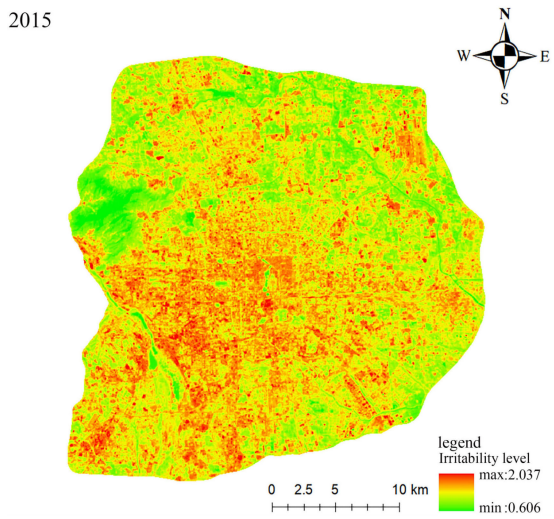

FIGURE 7
Risk pattern of irritability in the Sixth Ring Road in 2015.

on streets, so it is more effective to control the BD than to improve the cooling effect of greening (Han et al., 2016);

2. WSR and FAR are basically the same in bandwidth:148 and 231. This study selected a scale similar to the community scale in China's administrative division—different communities have large spatial heterogeneity between WSR and land development intensity. The function scale of MNDWI is 404, accounting for 25.6% of the total sample size, with great spatial heterogeneity. After exceeding the function range, the fitting effect changes considerably.
3. The bandwidths of FVC and RND are close to the total sample size, almost equal to that of global variables—stable in spatial influence without spatial heterogeneity.

Compared with the classical GWR, MGWR produces more accurate and actual regression results, revealing the spatial scale of driving factors, and directly affecting the spatial distribution of emotional health risk patterns.

Analysis of spatial pattern of irritability risk and regression coefficients

Due to the different heterogeneity and scale of different influencing factors, that is, within a certain range, the effect size is similar, but beyond this range, the effect size is significantly different. From Figure 7, it can be seen that the risk pattern of irritability in Beijing in 2015 had an obvious circle structure, which was expressed as follows: the center was high, the periphery was low, the southwest was high, and the northeast was low. The high-risk areas were mainly located in the city center, the West Fourth Ring Road, and along the expressway. Descriptive statistics of each coefficient are shown in Table 6. The degree of influence on irritability is WSR > NDVI > BD > MNDWI > RND > intercept > FVC > FAR. In particular, intercept, NDVI, BD, and FAR showed great difference in the spatial distribution of influence (see Figure 8).

Intercept

As shown in Figure 8A, the positive influence area is mainly concentrated in the southwestern part between the Second and Fifth Ring Roads, basically overlapping with the area of high irritability value. The intercept value ranges from −0.716 to 1.188, with an average value of 0.116, indicating that when the irritability value ranges from −0.716 to 1.188 per kilometer within the Sixth Ring Road, the influence of intercept on irritability is significantly different.

Normalized difference vegetation index

The negative ratio reaches 96.1%, critical in alleviating the thermal environment. The coefficient ranges from −0.572 to 0.284, with an average value of −0.254 and a standard deviation of 0.13, indicating that as NDVI increases by every unit, the average irritability value decreases by 0.254, and the area with the strongest negative effect can be reduced by 0.572. As shown in Figure 8B, the positive influence areas of NDVI are scattered in Haidian District and the boundary of the Eastern Fifth Ring Road. In contrast, the negative influence areas are scattered everywhere as a large mitigation matrix.

TABLE 6 Results of multiscale geographically weighted regression (MGWR) model operations.

Variable	Average value	Standard deviation	Minimum value	Median	Maximum value
Intercept	0.116	0.464	−0.716	0.071	1.188
MNDWI	0.185	0.070	0.053	0.182	0.316
NDVI	−0.254	0.130	−0.572	−0.263	0.284
VC	0.085	0.002	0.083	0.085	0.089
WSR	−0.349	0.092	−0.559	−0.341	−0.056
FAR	0.073	0.116	−0.123	0.084	0.304
BD	0.241	0.231	−0.296	0.193	1.340
RND	−0.132	0.006	−0.141	−0.133	−0.121

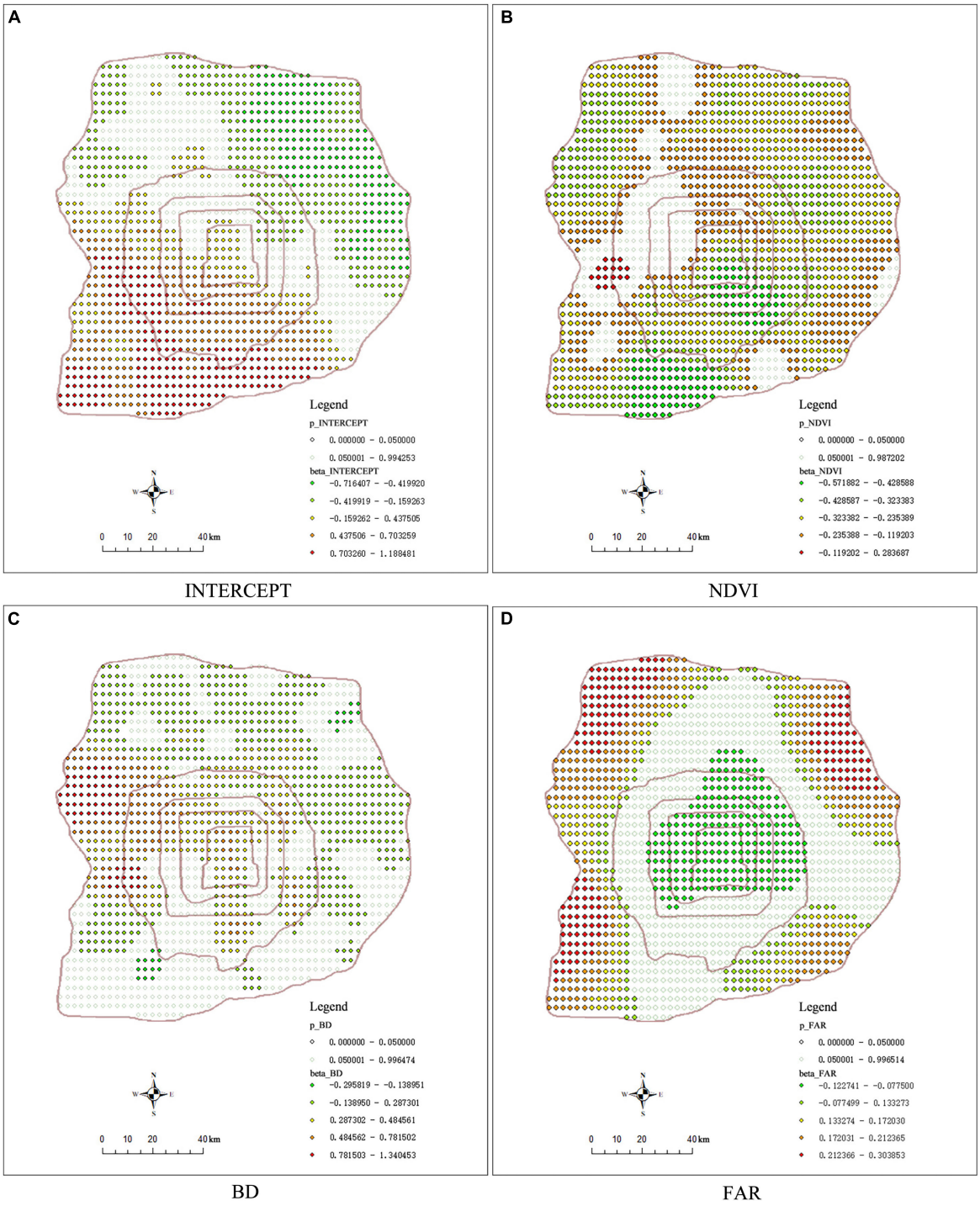

FIGURE 8
Spatial patterns of coefficients in the MGWR.

Building density

There is a circle structure similar to the irritability risk map. The value ranges from −0.296 to 1.340, with an average value of 0.241, a standard deviation of 0.231, and a positive ratio of 87.5. BD has an overall positive effect on irritability, and the area with the most substantial positive impact can increase the irritability value by 1.340 per unit. As shown in Figure 8C, the negative influence area is radially distributed between the Fourth and

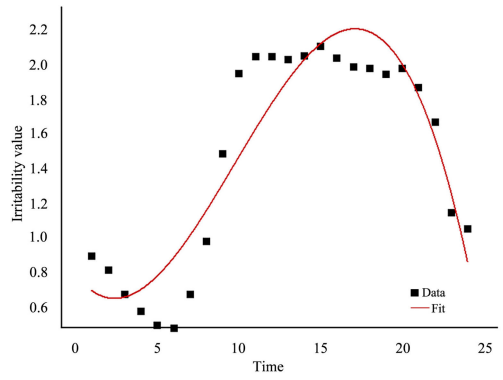

FIGURE 9
Irritability curve over time.

Fifth Ring Roads, with weak thermal effect; The positive value areas are mainly distributed in the south of Haidian District, north of Fengtai District, Dongcheng District, Xicheng District, and Shijingshan District, with dense building layout, large floor area, and strong thermal effect.

Floor area ratio

Floor area ratio yields a significant influence on irritability in the city and the outskirts, showing a trend of spreading outward from the center. The coefficient value ranges from –0.123 to 0.304, with an average value of 0.073. As shown in **Figure 8D**, the negative influence area of FAR is mainly concentrated in the city center, probably because of the large shadow area and low ground heat.

Discussion

First, different from other scholars' researches that focus on exploring the relationship between temperature and the morbidity and mortality of residents' physical or psychological diseases (Petitti et al., 2016; Ebi et al., 2021; Yang et al., 2021), this study focuses on the emotional health of the general population, especially the middle-aged and elderly, in an innovative way. The quantitative relationship between temperature and irritability was established, and based on this, the impact of urban high temperature on irritability was divided into 10 grades. Using the established irritability risk evaluation criteria, this manuscript analyzed the temporal and spatial pattern of irritable emotions in Beijing from 09:00 to 20:00 in summer. Consistent with the inverted "U-shaped" relationship between temperature and mental health (Mullins and White, 2019), there is a similar relationship between irritability and time (**Figure 9**). The difference is that this relationship further reflects the tolerance of the human body to high temperature in the environment and the time law of the emotional regulation mechanism, which provides an idea for further research on the impact of high temperature and human emotional health in the future. However, the impact of high temperature on human emotional health is the combined result of many factors. This manuscript ignored the influence of the subjects' own mental health level, education level, family status, economic status, race, etc., (Abbasi et al., 2019; Chang and Kajackaite, 2019) on their emotional status, as well as the interference of other environmental factors such as humidity and wind speed, resulting in biases in the validity and accuracy of the data.

Second, this manuscript also used MGWR to analyze the mechanism of high temperature on irritability, which is more conducive to the regulation of surface indicators in local high temperature areas and effectively reduces the risk of emotional health. Although they are not the same as the indicators selected for the thermal environment correlation research in recent years, they have obtained similar research results (Chen and Deng, 2021; Li et al., 2021). Yet, this paper only revealed the differential effect of a single land use type on temperature and irritability, but lacked the analysis of the joint effect of multiple land use types, and the effects of non-land-use type-related indicators such as regional climate, socio-demographics, local plant characteristics, albedo, and other environmental conditions were also ignored. For the analysis results, the increase of NDVI, WSR, and RND can alleviate irritability, but according to Li et al. (2011), the interspacing of urban green into other land use types seems to have a greater effect on mitigating the UHI effect than a large green area itself. Comparably, Dugord et al. (2014) found that forested green areas contribute better to thermal reduction when patches are more complex in shape and more distributed in space. Moreover, urban microclimate has prominent scale characteristics. MNDWI, NDVI, and other indicators would be quickly captured by satellite thermal sensors in a smaller spatial resolution, while the influence of human living, transportation, and commercial activities on the temperature field is difficult to be captured accurately (Huang et al., 2020b). The small sample size used for the MGWR model operation limits the statistical power, so that the analysis on the influence mechanism of thermal environment on irritability is imperfect, and open street maps and points of interest should be included in the future (Chen et al., 2022).

Conclusion

Based on the summer high-temperature measurement and emotional health survey in Beijing, ArcGIS, MATLAB, GraphPad and other platforms were used for data processing to construct a relationship model between temperature and

irritability, and to evaluate the time-space relationship between hourly temperature in summer and residents' irritability; the differential action scale and spatial action characteristics of high temperature driving factors on irritability risk were analyzed through the MGWR model. The conclusions are as follows:

1. During 09:00–20:00 in summer, irritability level increased then decreased. From 09:00 to 15:00, irritability value rocketed; From 15:00 to 20:00, irritability value declined slowly. Irritability reached the peak of Level 8 at 15:00. The influence pattern of high temperature on irritability showed a trend of "aggregation-fragmentation-aggregation".
2. Irritability is very sensitive to intercept and BD, with high spatial heterogeneity, close to the street scale. VC and RND are global variables without spatial heterogeneity. Other variables all have spatial heterogeneity (sorted by scale: NDVI < WSR < FAR < MNDWI).
3. The risk pattern of irritability in Beijing in 2015 had an obvious circle structure, which was expressed as follows: the center was high, the periphery was low, the southwest was high, and the northeast was low. The high-risk areas were mainly located in the city center, the West Fourth Ring Road, and along the expressway. NDVI, WSR, and RND have a negative impact on irritability, while intercept, MNDWI, VC, FAR, and BD have a positive effect on irritability. The degree of influence on irritability is WSR > NDVI > BD > MNDWI > RND > intercept > VC > FAR.
4. Compared with GWR, MGWR can avoid the noise and error caused by single-scale research methods, and can get more precise regression results with fewer parameters. It can be used for spatial analysis on a refined scale, serving as an excellent fitting model to study urban thermal environment, and providing a method for studying the spatial variation characteristics of other driving forces.
5. In future construction, green space and water bodies should be planned and laid out in areas with more land use types and more complex patches; building density and floor area ratio in high-risk areas of irritability should be controlled to maintain the cooling capacity of the water body, and at the same time, the density of the road network should be appropriately added to maximize the reduction of heat, to reduce the risk of emotional health.

Current research suggests that high temperatures in the context of global heating pose significant risks to the emotional health of the general population, and the magnitude of future risks will depend largely on planning and mitigation measures. Existing mental health resources are mostly concentrated on people with mental illnesses. For the general population and vulnerable groups with multiple physical comorbidities, it is suggested to identify areas where temperature-related emotional health risks are particularly increased, and clinically improve physical health may relieve heat stress. In the future, we will combine the regional changes of negative emotional risk in different years and the degree and scale of the effects of more high temperature drivers on emotional health risk to conduct regional emotional health risk assessment, providing reference for formulating regional planning and design strategies to reduce emotional health risk. Furthermore, temperature in different urban functional areas differs greatly—the average temperature difference between the center and the surrounding areas of Beijing can reach 268.6°C (Zhang et al., 2002). The complexity of the internal structure of human settlements should also be considered. To be specific, the local climate zone (LCZ) divides a city into built environment and natural environment, thus generating a classification system suitable for studying the thermal field changes in human settlements (Stewart and Oke, 2012; Yang et al., 2020). Therefore, this study will combine LCZ, crowd characteristics, and emotional health in the future, to make clear of how different climate layouts influence emotional health.

Data availability statement

The datasets for this study can be found the official website of NASA's landsat satellite (https://landsat.gsfc.nasa.gov/).

Author contributions

HH: conceptualization, methodology, data curation, formal analysis, writing—original draft preparation, review and editing, investigation, and visualization. XL: methodology, data curation, formal analysis, writing—original draft preparation, review and editing, investigation, and visualization. LR: conceptualization. All authors contributed critically to the manuscript and agreed to publication.

Funding

This work was supported by National Natural Science Foundation of China (NSFC), grant number 31971717 and Top-notch Academic Programs Project of Jiangsu, grant number PPZY2015A063.

Acknowledgments

We sincerely acknowledge Hao Cui for data provision and Yimin Zhao, Yang Li, and Shuying Zhang's help for investigation.

Conflict of interest

The authors declare that the research was conducted in the absence of any commercial or financial relationships that could be construed as a potential conflict of interest.

Publisher's note

All claims expressed in this article are solely those of the authors and do not necessarily represent those of their affiliated organizations, or those of the publisher, the editors and the reviewers. Any product that may be evaluated in this article, or claim that may be made by its manufacturer, is not guaranteed or endorsed by the publisher.

References

Abbasi, A. M., Motamedzade, M., Aliabadi, M., Golmohammadi, R., and Tapak, L. (2019). The impact of indoor air temperature on the executive functions of human brain and the physiological responses of body. *Health Promot. Perspect.* 9:55. doi: 10.15171/hpp.2019.07

Bao, L., Zhan, G., Li, C., and Wang, Y. (2020). Reliability and validity of the Chinese version of the positive negative emotion scale in the elderly. *China J. Health Psychol.* 28, 617–621. doi: 10.13342/j.cnki.cjhp.2020.04.029

Bielby, P. (2019). Not 'us' and 'them': towards a normative legal theory of mental health vulnerability. *Int. J. Law Context* 15, 51–67. doi: 10.1017/S1744552318000149

Burke, M., González, F., Baylis, P., Heft-Neal, S., Baysan, C., Basu, S., et al. (2018). Higher temperatures increase suicide rates in the United States and Mexico. *Nat. Climate Change* 8, 723–729. doi: 10.1038/s41558-018-0222-x

Chang, T. Y., and Kajackaite, A. (2019). Battle for the thermostat: Gender and the effect of temperature on cognitive performance. *PLoS One* 14:e0216362. doi: 10.1371/journal.pone.0216362

Chen, Y., Yang, J., Yang, R., Xiao, X., and Xia, J. C. (2022). Contribution of urban functional zones to the spatial distribution of urban thermal environment. *Build. Environ.* 216:109000. doi: 10.1016/j.buildenv.2022.109000

Chen, Z., and Deng, Z. (2021). Research on the relationship between block morphology and heat island intensity in Guangzhou's main urban area based on multi-scale geographically weighted regression. *Intellig. Build. Smart City* 10, 13–17. doi: 10.13655/j.cnki.ibci.2021.10.003

Denissen, J. J. A., Butalid, L., Penke, L., and van Aken, M. A. G. (2008). The effects of weather on daily mood: a multilevel approach. *Emotion* 8, 662–667. doi: 10.1037/a0013497

Ding, N., Berry, H. L., and Bennett, C. M. (2016). The importance of humidity in the relationship between heat and population mental health: evidence from Australia. *PLoS One* 11:e0164190. doi: 10.1371/journal.pone.0164190

Dugord, P. A., Lauf, S., Schuster, C., and Kleinschmit, B. (2014). Land use patterns, temperature distribution, and potential heat stress risk–the case study Berlin, Germany. *Comput. Environ. Urban Syst.* 48, 86–98. doi: 10.1016/j.compenvurbsys.2014.07.005

Ebi, K. L., Capon, A., Berry, P., BR257oderick, C., de Dear, R., Havenith, G., et al. (2021). Hot weather and heat extremes: Health risks. *Lancet* 398, 698–708. doi: 10.1016/S0140-6736(21)01208-3

Estoque, R. C., Murayama, Y., and Myint, S. W. (2017). Effects of landscape composition and pattern on land surface temperature: an urban heat island study in the megacities of Southeast Asia. *Sci. Total Environ.* 577, 349–359. doi: 10.1016/j.scitotenv.2016.10.195

Fotheringham, A. S., Yang, W., and Kang, W. (2017). Multiscale geographically weighted regression (MGWR). *Ann. Am. Assoc. Geogr.* 107, 1247–1265. doi: 10.1080/24694452.2017.1352480

Fritze, J. G., Blashki, G. A., Burke, S., and Wiseman, J. (2008). Hope, despair and transformation: climate change and the promotion of mental health and wellbeing. *Int. J. Ment. Health Syst.* 2, 1–10. doi: 10.1186/1752-4458-2-13

Gill, S. E., Handley, J. F., Ennos, A. R., and Pauleit, S. (2007). Adapting cities for climate change: the role of the green infrastructure. *Built Environ.* 33, 115–133. doi: 10.2148/benv.33.1.115

Gunawardena, K. R., Wells, M. J., and Kershaw, T. (2017). Utilising green and bluespace to mitigate urban heat island intensity. *Sci. Total Environ.* 584, 1040–1055. doi: 10.1016/j.scitotenv.2017.01.158

Guo, Y., Gasparrini, A., Li, S., Sera, F., Vicedo-Cabrera, A. M., de Sousa Zanotti Stagliorio Coelho, M., et al. (2018). Quantifying excess deaths related to heatwaves under climate change scenarios: A multicountry time series modelling study. *PLoS Med.* 15:e1002629. doi: 10.1371/journal.pmed.1002629

Hames, E., Stoler, J., Emrich, C. T., Tewary, S., and Pandya, N. (2016). A GIS approach to identifying socially and medically vulnerable older adult populations in south florida. *Gerontologist* 57, 1133–1141. doi: 10.1093/geront/gnw106

Han, G., Cai, Z., Xie, Y., and Zeng, W. (2016). Correlation between urban construction and urban heat island:A case study in Kaizhou District,Chongqing. *J. Civil Environ. Eng.* 38, 138–147. doi: 10.11835/j.issn.1674-4764.2016.05.018

Hansen, A., Bi, P., Nitschke, M., Ryan, P., Pisaniello, D., and Tucker, G. (2008). The effect of heat waves on mental health in a temperate Australian city. *Environ. Health Perspect.* 116, 1369–1375. doi: 10.1289/ehp.11339

Hayes, K., and Poland, B. (2018). Addressing mental health in a changing climate: incorporating mental health indicators into climate change and health vulnerability and adaptation assessments. *Int. J. Environ. Res. Public Health* 15:1806. doi: 10.3390/ijerph15091806

Huang, H., Deng, X., Yang, H., and Li, S. (2020a). Spatial evolution of the effects of urban heat island on residents' health. *Tehnički Vjesnik* 27, 1427–1435. doi: 10.17559/TV-20200503211912

Huang, H., Yang, H., Deng, X., Hao, C., Liu, Z., Liu, W., et al. (2020b). Analyzing the influencing factors of urban thermal field intensity using big-data-based GIS. *Sustain. Cities Soc.* 55:102024. doi: 10.1016/j.scs.2020.102024

Huang, L., Yang, T., and Li, Z. (2003). Applicability of the positive and negative affect scale in Chinese. *Chinese Ment. Health J.* 01, 54–56. doi: 10.3321/j.issn:1000-6729.2003.01.018

Li, B., Xing, H., and Liu, Y. (2021). Analysis of the relationship between urban landscape and thermal environment based on MGWR model. *J. Xian Univ. Technol.* 37, 517–525. doi: 10.19322/j.cnki.issn.1006-4710.2021.04.008

Li, J., Song, C., Cao, L., Zhu, F., Meng, X., and Wu, J. (2011). Impacts of landscape structure on surface urban heat islands: A case study of Shanghai, China. *Remote Sens. Environ.* 115, 3249–3263. doi: 10.1016/j.rse.2011.07.008

Li, J., Xu, X., Yang, J., Liu, Z., Xu, L., Gao, J., et al. (2017). Ambient high temperature and mortality in Jinan, China: a study of heat thresholds and vulnerable populations. *Environ. Res.* 156, 657–664. doi: 10.1016/j.envres.2017.04.020

Liu, H., and Weng, Q. (2008). Seasonal variations in the relationship between landscape pattern and land surface temperature in Indianapolis, USA. *Environ. Monit. Assess.* 144, 199–219. doi: 10.1007/s10661-007-9979-5

Liu, H., Zhan, Q., Gao, S., and Yang, C. (2019). Seasonal variation of the spatially non-stationary association between land surface temperature and urban landscape. *Remote Sens.* 11:1016. doi: 10.3390/rs11091016

Liu, X., Zhang, Y., Shan, X., Zhang, J., and Jiang, B. (2012). Association between heat waves and daily hospital visits for mental illness in Ji'nan: A case-crossover study. *J. Environ. Health* 29, 166–170. doi: 10.16241/j.cnki.1001-5914.2012.02.027

Manning, C., and Clayton, S. (2018). "Threats to mental health and wellbeing associated with climate change," in *Psychology and Climate Change*, eds S. Clayton and C. Manning (Cambridge, MA: Academic Press), 217–244.

Mao, C., Zhang, M., Liu, Y., Zhang, L., and Xiao, G. (2021). Analysis of urban heat island in yichang based on automatic weather station data. *Desert Oasis Meteorol.* 15, 103–110. doi: 10.12057/j.issn.1002-0799.2021.01.014

McMichael, A. (2017). *Climate Change and the Health of Nations: Famines, Fevers, and the Fate of Populations*. Oxford: Oxford University Press.

Mullins, J. T., and White, C. (2019). Temperature and mental health: Evidence from the spectrum of mental health outcomes. *J. Health Econ.* 68:102240. doi: 10.1016/j.jhealeco.2019.102240

Nitschke, M., Tucker, G. R., Hansen, A. L., Williams, S., Zhang, Y., and Bi, P. (2011). Impact of two recent extreme heat episodes on morbidity and mortality in Adelaide, South Australia: A case-series analysis. *Environ. Health* 10, 1–9. doi: 10.1186/1476-069X-10-42

Noelke, C., McGovern, M., Corsi, D. J., Jimenez, M. P., Stern, A., Wing, I. S., et al. (2016). Increasing ambient temperature reduces emotional well-being. *Environ. Res.* 151, 124–129. doi: 10.1016/j.envres.2016.06.045

Oshan, T. M., Li, Z., Kang, W., Wolf, L. J., and Fotheringham, A. S. (2019). mgwr: a Python implementation of multiscale geographically weighted regression for investigating process spatial heterogeneity and scale. *ISPRS Int. J. Geo Inform.* 8:269. doi: 10.3390/ijgi8060269

Parker, G., Lie, D., Siskind, D. J., Martin-Khan, M., Raphael, B., Crompton, D., et al. (2016). Mental health implications for older adults after natural disasters–a systematic review and meta-analysis. *Int. Psychogeriatr.* 28, 11–20. doi: 10.1017/S1041610215001210

Peng, S., Piao, S., Ciais, P., Friedlingstein, P., Ottle, C., Breìon, F. M., et al. (2012). Surface urban heat island across 419 global big cities. *Environ. Sci. Technol.* 46, 696–703. doi: 10.1021/es2030438

Peng, Z., Wang, Q., Kan, H., Chen, R., and Wang, W. (2017). Effects of ambient temperature on daily hospital admissions for mental disorders in Shanghai, China: A time-series analysis. *Sci. Total Environ.* 590, 281–286. doi: 10.1016/j.scitotenv.2017.02.237

Petitti, D. B., Hondula, D. M., Yang, S., Harlan, S. L., and Chowell, G. (2016). Multiple trigger points for quantifying heat-health impacts: New evidence from a hot climate. *Environ. Health Perspect.* 124, 176–183. doi: 10.1289/ehp.1409119

Qi, X., Hu, W. B., Page, A., and Tong, S. L. (2015). Associations between climate variability, unemployment and suicide in Australia: a multicity study. *BMC Psychiatry* 15:114. doi: 10.1186/s12888-015-0496-8

Ren, G., Chu, Z., Zhou, Y., Xu, M., Wang, Y., Tang, G., et al. (2005). Recent progresses in studies of regional temperature changes in China. *Clim. Environ. Res.* 10, 701–716. doi: 10.3969/j.issn.1006-9585.2005.04.001

Shen, T. Y., Yu, H. C., Zhou, L., Gu, H., and He, H. (2020). On hedonic price of second-hand houses in Beijing based on multi-scale geographically weighted regression: scale law of spatial heterogeneity. *Econ. Geogr.* 40, 75–83. doi: 10.15957/j.cnki.jjdl.2020.03.001

Shen, Z. P., Liang, P., and He, J. H. (2017). Analysis on the climatic characteristics of the fine structure of the urban heat island in Shanghai. *Trans. Atmos. Sci.* 40, 369–378. doi: 10.13878/j.cnki.dqkxxb.20160922001

Simpson, J. A., and Weiner, E. S. C. (1993). *Oxford English Dictionary–1989*. Oxford: Oxford University Press.

Stewart, I. D., and Oke, T. R. (2012). Local climate zones for urban temperature studies. *Bull. Am. Meteorol. Soc.* 93, 1879–1900. doi: 10.1175/BAMS-D-11-00019.1

Tan, Z., Li, W., Xu, B., Chen, Z., and Liu, J. (2004). The estimation of land surface emissivity for landsat TM6. *Remote Sens. Land Resour.* 28-32, 36–41. doi: 10.3969/j.issn.1001-070X.2004.03.007

Thompson, R., Hornigold, R., Page, L., and Waite, T. (2018). Associations between high ambient temperatures and heat waves with mental health outcomes: A systematic review. *Public Health* 161, 171–191. doi: 10.1016/j.puhe.2018.06.008

Vanos, J. K., Warland, J. S., Gillespie, T. J., and Kenny, N. A. (2012). Thermal comfort modelling of body temperature and psychological variations of a human exercising in an outdoor environment. *Int. J. Biometeorol.* 56, 21–32. doi: 10.1007/s00484-010-0393-2

World Meteorological Organization [WMO] (2021). *State of the Global Climate 2020*. Geneva: WMO.

Xu, H. (2006). Modification of normalised difference water index (NDWI) to enhance open water features in remotely sensed imagery. *Int. J. Remote Sens.* 27, 3025–3033. doi: 10.1080/01431160600589179

Xu, Q., Xu, Z., and Sun, C. (2021). Evaluation schoolyard wind comfort changes due to rapid developments: Case study of Nanjing, China. *Atmosphere* 13:43. doi: 10.3390/atmos13010043

Xue, Z., Hou, G., Zhang, Z., Lyu, X., Jiang, M., Zou, Y., et al. (2019). Quantifying the cooling-effects of urban and peri-urban wetlands using remote sensing data: case study of cities of Northeast China. *Landsc. Urban Plann.* 182, 92–100. doi: 10.1016/j.landurbplan.2018.10.015

Yang, B., Yang, X., Leung, L., Zhong, S., Qian, Y., Zhao, C., et al. (2019). Modeling the impacts of urbanization on summer thermal comfort: the role of urban land use and anthropogenic heat. *J. Geophys. Res. Atmos.* 124, 6681–6697. doi: 10.1029/2018JD029829

Yang, J., Wang, Y., Xiu, C., Xiao, X., Xia, J., and Jin, C. (2020). Optimizing local climate zones to mitigate urban heat island effect in human settlements. *J. Clean. Product.* 275:123767. doi: 10.1016/j.jclepro.2020.123767

Yang, J., Zhou, M., Ren, Z., Li, M., Wang, B., Liu, D. L., et al. (2021). Projecting heat-related excess mortality under climate change scenarios in China. *Nat. Commun.* 12, 1–11. doi: 10.1038/s41467-021-21305-1

Yao, L., Xu, Y., and Zhang, B. (2019). Effect of urban function and landscape structure on the urban heat island phenomenon in Beijing, China. *Landsc. Ecol. Eng.* 15, 379–390. doi: 10.1007/s11355-019-00388-5

Yin, P., Chen, R., Wang, L., Liu, C., Niu, Y., Wang, W., et al. (2018). The added effects of heatwaves on cause-specific mortality: A nationwide analysis in 272 Chinese cities. *Environ. Int.* 121, 898–905. doi: 10.1016/j.envint.2018.10.016

Yin, S., Gong, Z., Gu, L., Deng, Y., and Niu, Y. (2022). Driving forces of the efficiency of forest carbon sequestration production: spatial panel data from the national forest inventory in China. *J. Clean. Product.* 330:129776. doi: 10.1016/j.jclepro.2021.129776

Yu, H., Fotheringham, A. S., Li, Z., Oshan, T., Kang, W., and Wolf, L. J. (2020). Inference in multiscale geographically weighted regression. *Geogr. Anal.* 52, 87–106. doi: 10.1111/gean.12189

Yue, H., and Liu, Y. (2018). Comparison and analysis of land surface temperature retrieval algorithms based on Landsat 8 TIRS. *Sci. Technol. Eng.* 18, 200–205. doi: 10.3969/j.issn.1671-1815.2018.20.028

Yue, W., Qiu, S., Xu, H., Xu, L., and Zhang, L. (2019). Polycentric urban development and urban thermal environment: a case of Hangzhou, China. *Landsc. Urban Plann.* 189, 58–70. doi: 10.1016/j.landurbplan.2019.04.008

Zhang, G., Xu, X., Wang, J., and Yang, Y. (2002). A study of characteristics and evolution of urban heat island over Beijing and its surrounding area. *Q. J. Appl. Meteorl.* 13, 43–50. doi: 10.3969/j.issn.1001-7313.2002.z1.005

frontiers | Frontiers in Ecology and Evolution

TYPE Original Research
PUBLISHED 23 August 2022
DOI 10.3389/fevo.2022.953725

Check for updates

OPEN ACCESS

EDITED BY
Jianhong Xia,
Curtin University, Australia

REVIEWED BY
Xianheng Ouyang,
Zhejiang Agriculture and Forestry University, China
Andong Guo,
Zhejiang University, China
Yunchuan Dai,
Chongqing Academy of Social Sciences, China

*CORRESPONDENCE
Chunshan Zhou
zhoucs@mail.sysu.edu.cn

SPECIALTY SECTION
This article was submitted to Environmental Informatics and Remote Sensing, a section of the journal Frontiers in Ecology and Evolution

RECEIVED 26 May 2022
ACCEPTED 04 July 2022
PUBLISHED 23 August 2022

CITATION
Zhang D, Zhou C, Zhou Y and Zikirya B (2022) Spatiotemporal relationship characteristic of climate comfort of urban human settlement environment and population density in China.
Front. Ecol. Evol. 10:953725.
doi: 10.3389/fevo.2022.953725

COPYRIGHT
© 2022 Zhang, Zhou, Zhou and Zikirya. This is an open-access article distributed under the terms of the Creative Commons Attribution License (CC BY). The use, distribution or reproduction in other forums is permitted, provided the original author(s) and the copyright owner(s) are credited and that the original publication in this journal is cited, in accordance with accepted academic practice. No use, distribution or reproduction is permitted which does not comply with these terms.

Spatiotemporal relationship characteristic of climate comfort of urban human settlement environment and population density in China

Dahao Zhang[1], Chunshan Zhou[1]*, Yi Zhou[1] and Bahram Zikirya[2,3]

[1]School of Geography and Planning, Sun Yat-sen University, Guangzhou, China, [2]College of Tourism, Xinjiang University, Ürümqi, China, [3]Key Laboratory of the Sustainable Development of Xinjiang's Historical and Cultural Tourism, Xinjiang University, Ürümqi, China

Rapid urbanization in China has caused substantial changes in the urban climate, leading to accelerated shifts in the climate comfort of the human settlement environment. In addition, in certain regions of China, a glaring disproportion exists in the distribution of population to the available area. Therefore, the climate comfort of such areas needs to be improved to enhance their habitability. In this study, we explored the spatiotemporal evolution characteristics of the climate comfort of the urban human settlement environment in China from 2000 to 2015, based on a three-level time scale of year, month, and day using the temperature and humidity index and wind efficiency index. In addition, the population density in China was calculated by employing the population grid spatial calculation method. Subsequently, we compared and analyzed the spatiotemporal relationship characteristics between the climate comfort of the urban human settlement environment and population density. Our results indicated that (1) the extremely cold area was the largest, followed by the cold area, with the comfort area being the smallest. The area range of climate comfort and cold expanded northward, whereas the extremely cold area shrank from 2000 to 2015. (2) The duration of the comfort month and comfort day in southern China was higher than that in northern China. The climate comfort area of 3–4 months was the largest, and that of 7–12 months was the smallest, with the largest climate comfort area being 66–130 days and the smallest being 196–325 days. (3) The spatial difference in the climate comfort month was greater than that in the daily change, and the evolution process of various regions became relatively complex over time. The spatiotemporal evolution

of the climate comfort day showed minimal change in northwest, north, and northeast China, whereas it changed significantly in southwest, south, central, and east China. These results imply that the population density in the country is generally concentrated in the climate comfort areas.

KEYWORDS

human settlement environment, climate comfort, population density, spatiotemporal characteristics, China climate

Introduction

Since the 20th century, rapid advances in urbanization in China has led to a fundamental change in the urban climate, with the emergence of extreme weather accelerating shifts in the climate comfort of the human settlement environment (Yang et al., 2020; Yu et al., 2022). Climate change is an important element in the natural system of the human settlement environment and fundamentally affects the climate comfort of the environment. Climate comfort refers to the level of comfort—experienced by healthy humans—provided by climatic factors, such as temperature, humidity, wind speed, and sunshine, without the aid of temperature control devices or sunscreen. The habitability of an area increases with greater climate comfort. Along with continuous improvement in the quality of life, people have become more aware of the climate comfort of living in cities, implying that this aspect has become an important standard for choosing a place of residence (Stathopoulos et al., 2004; Dulal and Akbar, 2013).

Currently, research on the climate comfort of human settlement mainly includes the following aspects: (1) The spatial characteristics of the comfort degree of the tourism climate and the effects on tourism development; generally, such research includes analysis of temporal change in climate comfort based on the temperature and humidity index, wind chill, and dressing index of a tourism city (Li and Zhong, 2005; Ma et al., 2010, 2011; Cao et al., 2012); exploring the spatial layout characteristics of the tourism climate comfort degree by the tourism climate index (TCI) (Masoudi, 2021); applying geographic information system (GIS) technology to partition and evaluate the potential of ecotourism in the climate comfort area (Esmael et al., 2014); and evaluation of the influence of climate comfort on convalescence tourism and tourism activities (Amininia et al., 2020; Adiguzel et al., 2022). (2) The effect of natural elements and human activities on the climate comfort of the human settlement environment, including exploring the effects of the spatial layout of meteorology (Areti et al., 2010; Luo et al., 2021; Ren et al., 2022), river (Amorosi et al., 2013), vegetation (Maria et al., 2019; Du et al., 2020), and residential area (Liu et al., 2019). (3) Spatiotemporal analysis and evaluation of climate comfort of the human settlement environment, including measuring climate comfort by employing the climate comfort index and analyzing the spatial characteristics of climate comfort (Cao et al., 2019), as well as exploring the spatial difference characteristics of climate comfort in China based on the multiple phase scale (Kong, 2020). Furthermore, the thermal environment of rural areas has also been simulated using ArcGIS [environmental systems research institute (ESRI), United States] and the environment for visualizing images (ENVI) (L3Harris Geospatial, United States) software to evaluate climate comfort (Fan et al., 2021).

Related research on the effects of climate change on humans mainly includes (1) the effect of climate change on the spatial distribution of the population, such as exploring the dynamic relationship between climate change and population migration and conducting spatial modeling of this relationship (Alisson et al., 2010; Michael, 2018), for example, heavy rain to explore the effect of exposure to extreme weather on the spatial layout of human spaces (Liao et al., 2019). (2) The effects of climate change on human health by exploring such effects, for example, on the health of the elderly population through a literature survey (Chen et al., 2020), and analyzing the effect of increasing temperature on the number of diseases among the population (Pottier et al., 2021). (3) Human thermal perception of urban temperature, for example, by analyzing the thermal perception of the urban climate and the comfort levels of residents from both indoor and outdoor space dimensions (Cohen et al., 2013; Pantavou et al., 2013; Salata et al., 2016; Lai et al., 2021).

Current research on the climate comfort of the human settlement environment focuses on the spatiotemporal distribution and evaluation of climate comfort, influence of individual environmental factors on climate comfort, tourism climate comfort, and the number of tourists. Research on the correlation between climate and humans focuses on the effect of climate change on the distribution of the population, their health, and environmental heat perception. However, few studies have explored the relationship between climate comfort and population density.

In comparison with existing research, our study introduces improvements in terms of the research scale and research perspective. We consider investigation of the spatiotemporal relationship between climate comfort and population density

not only beneficial to improving resident perception of the climatic environment but also essential to reasonably predicting the spatial feature of population density (Smirnov et al., 2016). In view of the aforementioned discussion, with China as the study object and combining the temperature and humidity index with the wind efficiency index, we evaluated the climate comfort of the human settlement environment during 2000–2015, and we explored the spatiotemporal relationship between climate comfort and population density. This study not only enriches the related theory about the human settlement environment but also provides useful reference to improve the livability of the Chinese urban human settlement environment (Zhang et al., 2022).

Data sources and research methods

Overview of the study area

China has a vast territory, spanning multiple temperature zones and dry and wet areas, and is characterized by a complicated terrain between the east and west, leading to complex and diverse climate types. Moreover, China has a population of 1.4 billion in 2022, which makes it the most populous country in the world. Therefore, China is a good example to explore spatiotemporal relationship characteristics of the climate comfort of the human settlement environment and population density (**Figure 1**). We divided China into seven regions and explored the spatiotemporal relationship characteristic of climate comfort of the urban human settlement environment and population density based on the prefecture-level city regional scale (**Table 1**).

Data source and processing

The data employed in this study mainly include data derived from the China ground climate, that is, the daily value dataset (V3.0 processing and generation), China population spatial distribution kilometer grid dataset, digital elevation model (DEM), and administrative division information. The China ground climate dataset mainly includes daily data from 2000 to 2015 on the wind speed, humidity, precipitation, temperature, sunshine, station number, and longitude and latitude of 824 benchmark meteorological stations in China, and derives from the China Meteorological Data Service Center.[1] First, the data were cleaned, followed by the show point and projection, and the daily data were interpolated spatially by the inverse distance weight method. Finally, the data were divided and spliced according to administrative division to obtain the daily data for provinces and cities, as well as the average daily data of meteorological elements in different years and months to obtain the yearly and monthly data of the different regions.

The China population spatial distribution kilometer grid dataset reflects the detailed spatial distribution of population data in China. The dataset is based on county demographic

1 http://data.cma.cn/

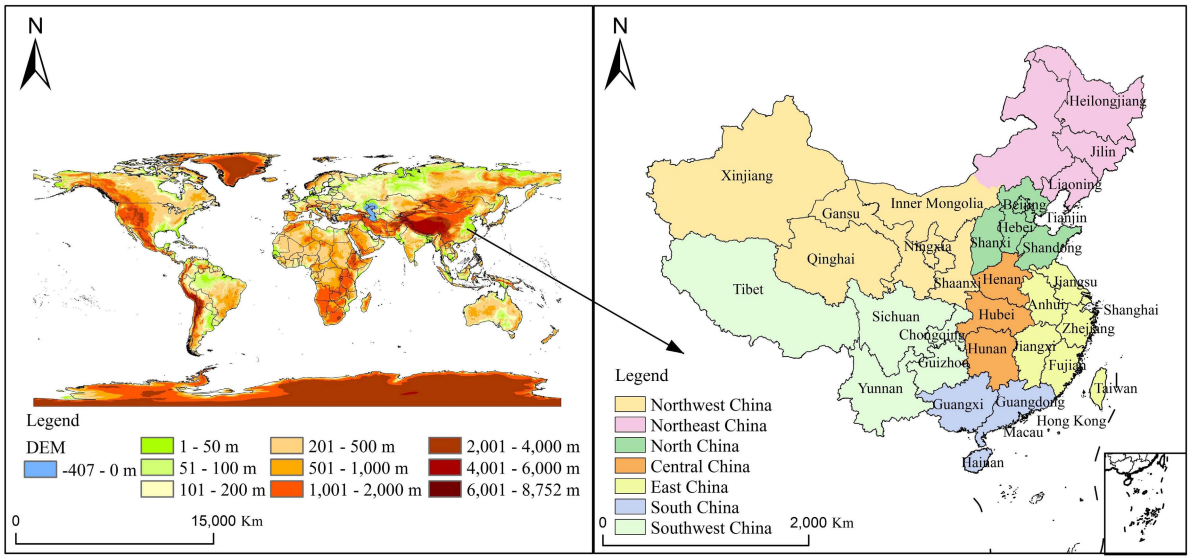

FIGURE 1
Location of study area.

TABLE 1 Regional classification of China.

Region	Province
East China	Jiangxi, Jiangsu, Anhui, Shanghai City, Zhejiang, Fujian, and Taiwan
Northeast China	Heilongjiang, Jilin, Liaoning, and eastern Inner Mongolia autonomous region
Central China	Henan, Hubei, and Hunan
North China	Beijing city, Tianjin city, Hebei, Shandong, and Shanxi
Northwest China	Xinjiang Uygur autonomous region, Qinghai, Gansu, Ningxia Hui autonomous region, Shaanxi, and western Inner Mongolia autonomous region
South China	Guangdong, Guangxi Zhuang autonomous region, Hong Kong special administrative region, Macau special administrative region, and Hainan
Southwest China	Yunnan, Guizhou, Sichuan, Chongqing city, and Tibet autonomous region

TABLE 2 Data sources and description.

Data category	Data description	Data type	Data source
China ground climate means daily value data	Wind speed, humidity, precipitation, temperature, sunshine, and others	Panel	China meteorological data service center
China population spatial distribution kilometer grid data	Population density	Grid	Resources and environment sciences and data center of the Chinese academy of sciences
DEM elevation data	Elevation data terrain	Grid	NOAA
Administrative territorial data	Administrative boundary	Vector	Resources and environment science and data center of the Chinese academy of sciences

data and comprehensively considers factors closely related to population, such as land-use type, night light brightness, residential density, and similar. The basic statistical unit is the administrative region, and the multi-factor weight allocation method is employed to spread the population data to the spatial grid, thereby achieving the spatialization of the population. The data format is grid data, with each grid representing the population within a grid range (1 km^2), with the unit being person/km^2. The data are based on the Krassovsky ellipsoid, and the projection function is Albers projection (Xu, 2017). The dataset derives from the Resource and Environment Sciences and Data Center of the Chinese Academy of Sciences[2] (DATA ID = 333). The global DEM elevation data at 1 km resolution are published by the U.S. National Oceanic and Atmospheric Administration (NOAA).[3] The administrative division data derive from the Resources and Environment Sciences and Data Center of the Chinese Academy of Sciences (see text footnote 2; DATA ID = 333) (**Table 2**).

Research methodology

Temperature and humidity index

The temperature and humidity index refers to an index of the human body's comprehensive perception of ambient temperature and humidity, calculated as follows (National Standardization Administration, 2012):

$$I = T - 0.55 \times (1 - RH) \times (T - 14.4) \quad (1)$$

where I is the temperature and humidity index, retain 1 decimal place; T is the average temperature of a certain evaluation period; unit is degree Celsius (°C); and RH is the average air relative humidity during an evaluation period (%).

Wind efficiency index

This refers to an index of comprehensively perceiving wind, temperature, and sunshine. The calculation formula of wind efficiency index K is as follows:

$$K = -\left(10\sqrt{V} + 10.45 - V\right)(33 - T) + 8.55S \quad (2)$$

where K is the wind efficiency index, taken as an integer; T is the average temperature of a certain evaluation period, measured in degree Celsius (°C); V is the average wind speed in meter per second (m/s); and S is the average sunshine hours during an evaluation period, measured in time per day (h/day).

Generally, an evaluation method combining the temperature and humidity index and the wind efficiency index is used to evaluate climate comfort. When the two indices are inconsistent, the wind efficiency index is used in the cold (winter) half-year, and the temperature and humidity index in the hot (summer) half-year. The wind efficiency index is used when the average wind speed exceeds 3 m/s during the evaluation period. March to May is considered as spring, June to August as summer, September to November as autumn, and December to February as winter. A high temperature and humidity index and wind efficiency index indicate a relatively sultry human settlement climate, whereas a low temperature and humidity index and wind efficiency index indicate an extremely cold human settlement climate. The only comfortable human settlement climate is a moderate temperature and humidity index and wind efficiency index (**Table 3**).

2 http://www.resdc.cn/data.aspx

3 https://www.noaa.gov/

TABLE 3 Classification of climate comfort degree of human settlement environment.

Rank	Feel extent	Temperature and humidity index	Wind efficiency index	Description of feeling of healthy people
1	Extremely cold	<14.0	<−400	Extremely cold, uncomfortable
2	Cold	14.0–16.9	−400 to 300	Relative cold, a little uncomfortable
3	Comfortable	17.0–25.4	−299 to 100	Comfortable
4	Hot	25.5–27.5	−99 to 10	Hot, a little uncomfortable
5	Sultry	>27.5	>−10	Sultry, uncomfortable

Population grid space calculation method

During data processing of the population spatial distribution kilometer grid, various factors were calculated first, namely, the weights of land-use type, night light brightness, and residential density of the population distribution. The total weight of each county-level administrative unit was calculated based on the effects of the weight standardization treatment of the aforementioned three aspects and, subsequently, based on the calculation of the proportion of population of each county-level administrative unit weight. Using grid space calculation, the population number on unit weight was combined with the total weight distribution map to spatialize the population. The calculation formula is as follows:

$$POP_{ij} = POP \times \left(Q_{ij}/Q\right) \quad (3)$$

where POP_{ij} is the steric grid cell value; POP is the population demographic value of the county-level administrative unit where the grid unit is located; Q_{ij} is the total weight of the land-use type, night light brightness, and the settlement density; and Q is the total weight of the land-use type, night light brightness, and settlement density of the county administrative unit where the grid unit is located. Finally, the population spatial distribution data of the 1-km grid were obtained employing the aforementioned method.

Results

Human settlement climate comfort yearly change

The annual climate comfort degrees of China are mainly extremely cold, cold, and comfortable, among which the area range of extremely cold was the largest, followed by cold, with comfortable being the smallest. From the perspective of the spatial layout characteristics of the annual human settlement climate comfort degree in 2015, the climate comfort areas were distributed mainly in south China and the southern part of east China; the eastern, central, and southern parts of southwest China; and southern central China. The areas with an annual cold human settlement climate were distributed mainly in the north of east China, central and north parts of central China, north and central parts of southwest China, the south of northwest China, and the south of north China. The areas with annual extremely cold human settlement climate were distributed mainly in northeast China; northwest China, except for the southern part of Shaanxi Province; the central and north parts of north China; and the western part of southwest China.

From the perspective of the annual change characteristics of the degree of human settlement climate comfort in China, the range of human settlement climate comfort and cold expanded northward from 2000 to 2015, whereas that of extremely cold shrank. The human settlement climate comfort area in southwest China (southwest of Guizhou Province and east of Sichuan Province) and central China (Hunan Province) apparently expanded northward, as well as the cold area in north China (Shandong Province) (**Figure 2**).

Human settlement climate comfort monthly change

From the perspective of the comfort month of the human settlement climate in China, the duration of the comfort month in southern China was generally longer than that in northern China. Using the equal interval method in ArcGIS 10.2, the duration of the comfort months was classified into six levels (0–2, 3–4, 5–6, 7–8, 9–10, and 11–12) based on the number of comfort months. The region representing 3–4 months of comfort was the largest, followed by regions representing 0–2 months and 5–6 months of comfort. The smallest region was that of 7–12 months of comfort. In 2015, the areas with long comfort months (7–12) of human settlement climate comfort were distributed mainly in the south and east of southwest China, south and west of south China, and the south of east China. Areas with short human settlement comfort months (0–2) were distributed mainly in the west of southwest China, central and southwest of northwest China, and north of northeast China.

From the perspective of the annual change characteristics of the comfort duration months, these characteristics differed from 2000 to 2015. The comfort duration months in the west and north of northwest China decreased, and those of northeast China decreased in the north and increased in the south, as well as those in central China. The comfort month duration in north China showed a trend of the east increasing first, then decreasing, and then increasing again, and the west increasing first and then decreasing. The comfort month in all provinces in east China showed a trend of decreasing first and then

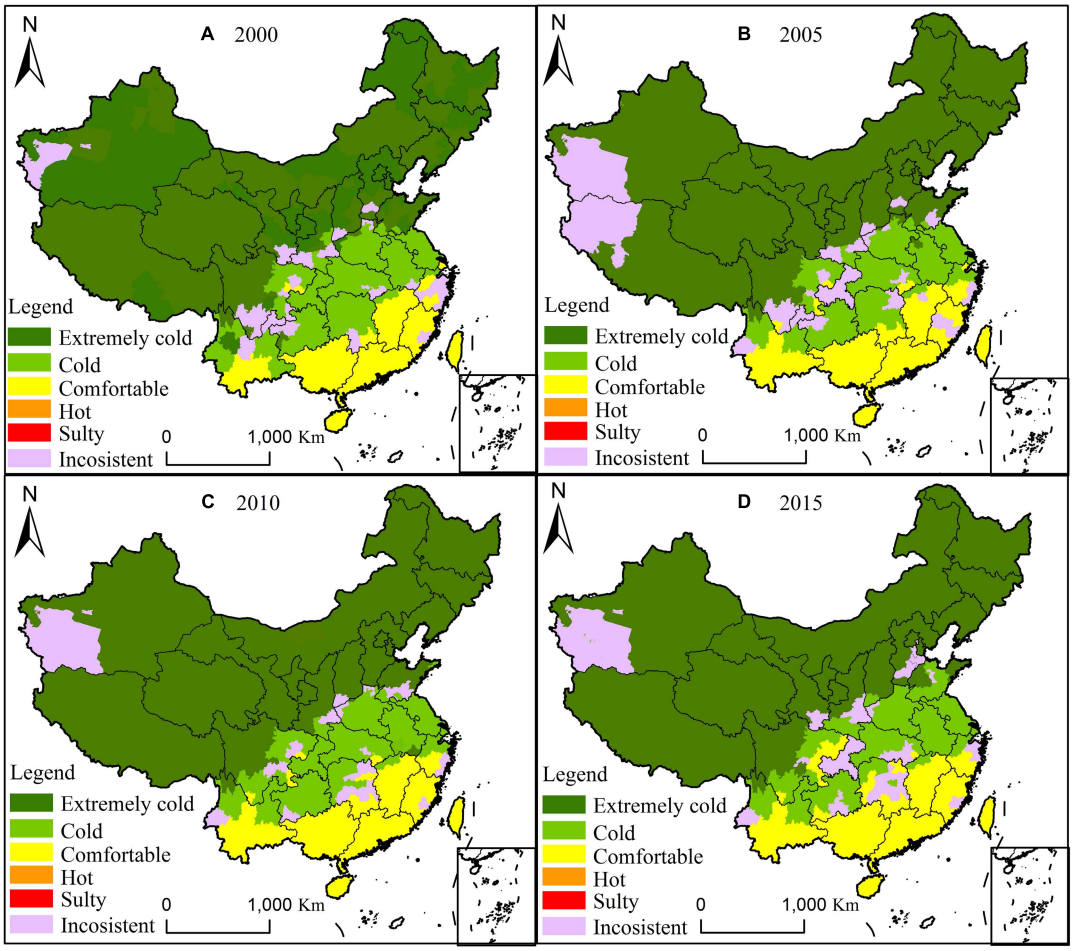

FIGURE 2
Annual change in climate comfort of human settlement environment in China from 2000 to 2015.

increasing, whereas that in the north of south China showed a trend of increasing first, then decreasing, and subsequently increasing. The southern part of south China was characterized by a trend of decreasing first and then increasing. The change in the comfort months in southwest China was relatively complex, but the comfort months of the human settlement climate in the west did not change significantly. In the east of southwest China, Chongqing city showed a trend of decreasing first and then increasing, whereas Guizhou Province showed a trend of increasing first and then decreasing. Yunnan Province in the southern part of southwest China showed characteristics of decreasing in the east and increasing in the west (Figure 3).

Human settlement climate comfort daily change

From the perspective of the daily change in the human settlement climate comfort, the comfort days in southern China were generally greater in number than those in the north. Using the equal interval method in ArcGIS 10.2, the duration of the comfort days was classified into five levels (i.e., 0–65, 66–130, 131–195, 196–260, and 261–325) based on the number of comfort days. The range area of 66–130 annual comfort days was the largest, followed by 0–65 and 131–195 days, with the range area of 196–325 annual comfort days being the smallest. In 2015, the areas with 261–325 comfort days and 196–260 comfort days were distributed mainly in the south of southwest China and the west of south China. Areas with a moderately comfortable daily duration (131–195 days) were distributed mainly in most parts of east China, south China, and central China, as well as the central and eastern regions of southwest China, the south of north China, and the south of northwest China. Areas with fewer human settlement climate comfort days (66–130 days) were distributed mainly in northeast China and most parts of northwest China and north China. The areas with the least human settlement climate comfort days (0–65 days) were distributed mainly in the west of southwest China and southwest of northwest China.

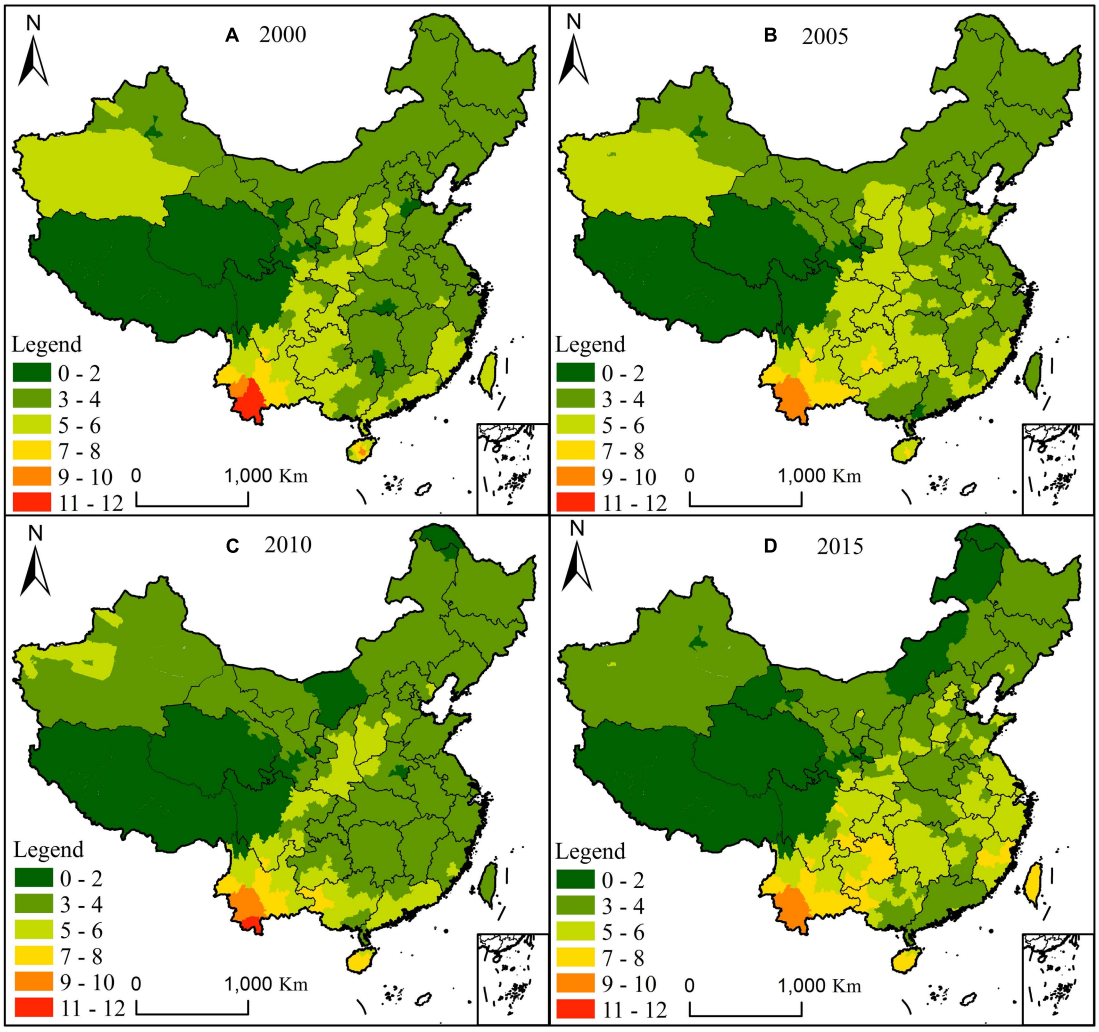

FIGURE 3
Monthly change in human settlement climate comfort in China from 2000 to 2015.

From the perspective of the annual change characteristics of comfort days from 2000 to 2015, comfort days varied in the different regions, being relatively minor in northwest, northeast, and north China, but substantial in central, southwest, south, and east China. The duration of comfort days in the Xinjiang Uygur Autonomous Region in northwest China first increased and then decreased, that in the north of northeast China increased, but in northwest and northeast China, the changes were not significant. The duration of comfort days in the west of the southwest region changed less, whereas that in the central, southern, and eastern parts of the southwest regions changed significantly. The comfort days increased in the south of the southwest regions, but those in the east of the southwest regions decreased first and then increased, whereas the comfort days first increased and then decreased in the center of the southwest regions. No significant change was observed in the northern part of north China, but the comfort days in the southern part of north China increased. The comfort days in the middle of south China showed a trend of first decreasing and then increasing, whereas those in the western region increased, but in the southern region, they first decreased and then increased. The trend in the south of Guangdong Province first showed a decreasing trend, followed by an increase and a subsequent decrease. In both east and central China, these days first decreased and then increased (Figure 4).

Spatial characteristics of population density

In 2015, the regions with high population density were located mainly in north China, the northern part of central China, the northern part of east China, the northeastern part of southwest China, and the eastern part of south China.

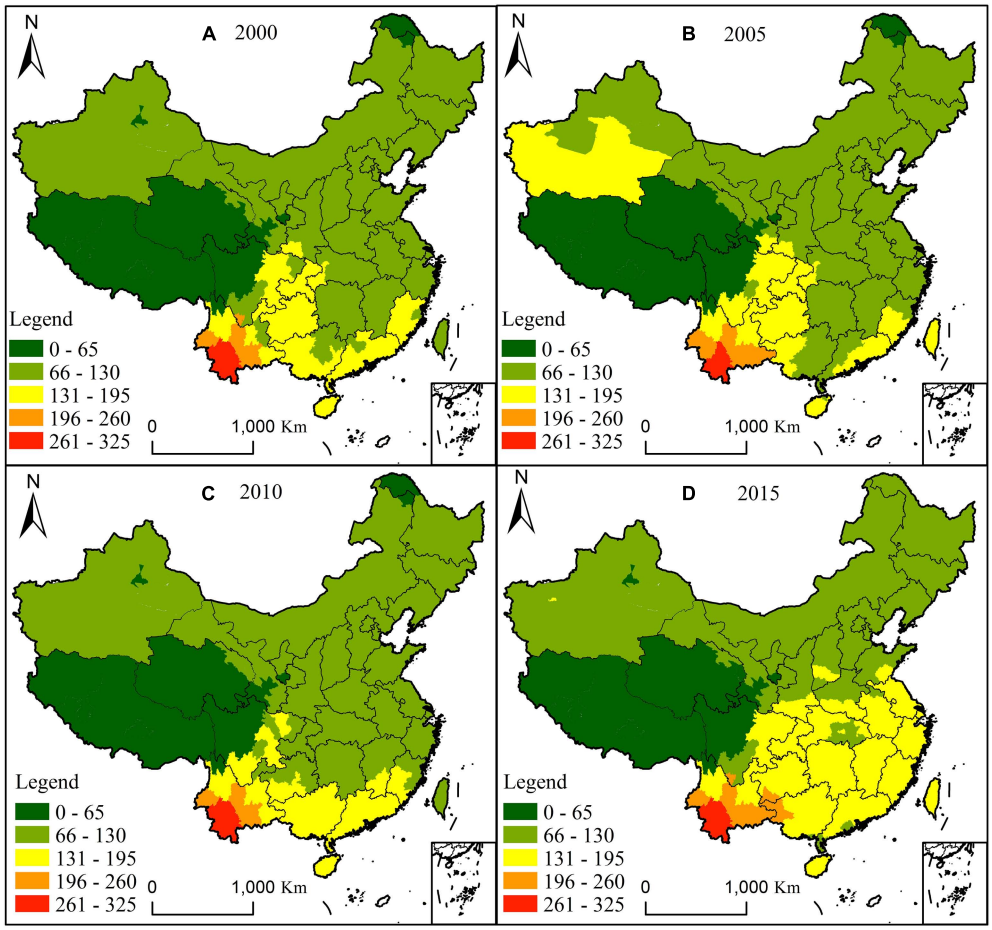

FIGURE 4
Daily change in human settlement climate comfort in China from 2000 to 2015.

Dotted population distribution was found in northeast China, northwest China, the southern part of southwest China, the southern part of central China, the southern part of east China, and the western part of south China. The population, here, was distributed mainly in the capitals of various provinces (autonomous regions).

From the perspective of the annual change characteristics of population density, the areas with an obvious increase in population density in China from 2000 to 2005 mainly included northeast, north, east, central, and southwest China, whereas the areas with decreased population density were mainly in south China. The regional concentration of population density increased mainly in the northern part of north China, and east, south, and southwest China. The areas with a significant decrease in population density were concentrated mainly in the northeast, south of north China, northern part of central China, and northern part of east China.

From the perspective of the annual change characteristics of human settlement climate comfort, the population density concentration areas in 2015 mainly included the annual climate extremely cold zone, cold zone, and the transition zone between comfort and cold zones. From 2000 to 2015, the population density was concentrated from climate comfort extremely cold areas to cold and comfort areas. From the characteristics of the comfort month duration during the annual human settlement climate, the high population density area in 2015 was concentrated mainly in the annual 3- to 6-month comfort duration zone, followed by 7–10 and 11–12, with 0–2 having the lowest population density value. From 2000 to 2015, the population density was concentrated from the area of annual human settlement climate comfort month duration 3–4 months to the area of comfort month duration 5–6 months. From the characteristics of the comfort day length of the annual human settlement climate, the high population density in 2015 was concentrated mainly in the 66–195 comfort day zone, followed by the 196–260 comfort day zone, with the lowest population density value in the human settlement climate comfort day zones 261–325 and 0–65. During this period, the population density was concentrated from the area of 66–130 comfort days to the area of 131–195 comfort days (Figure 5).

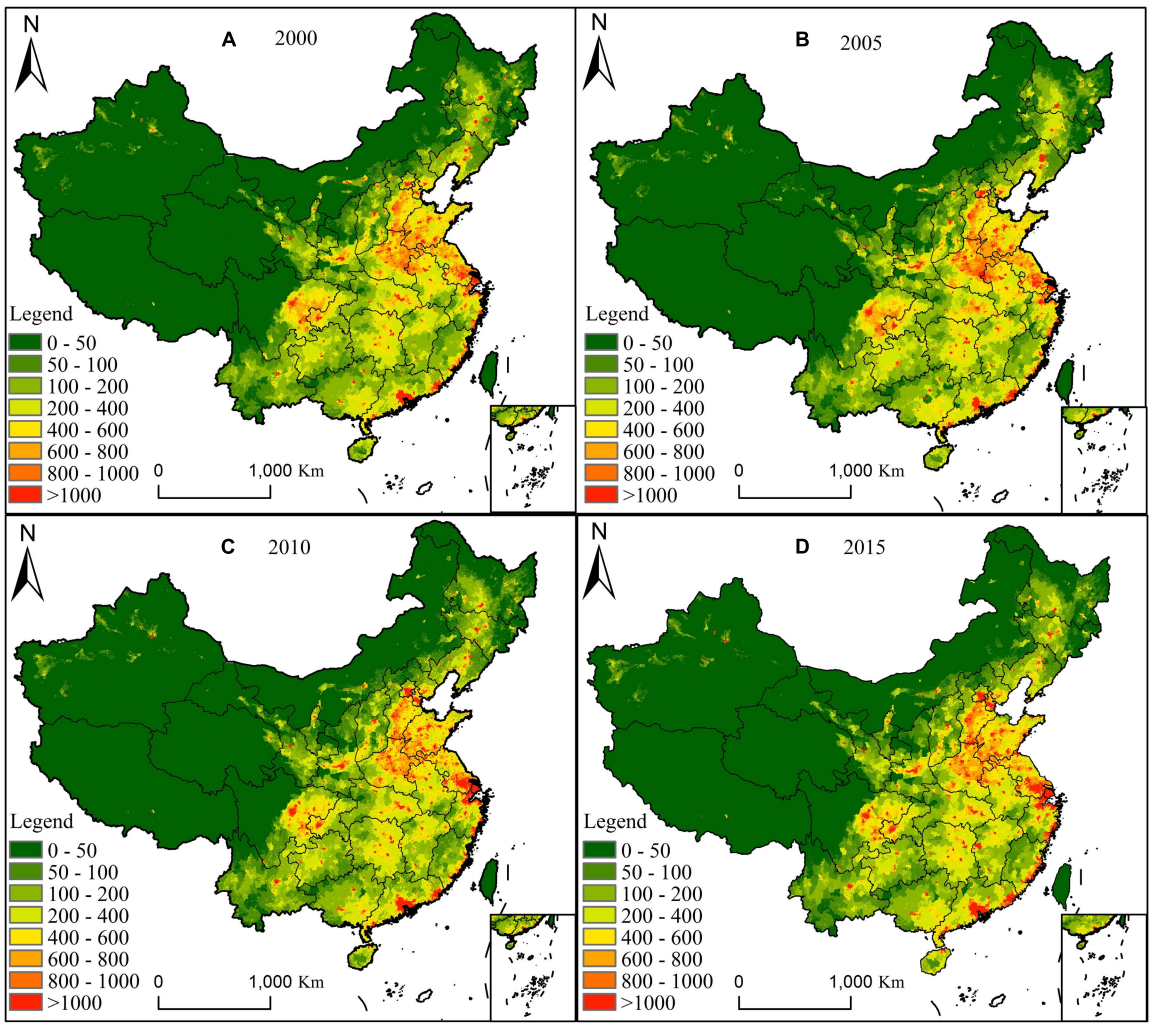

FIGURE 5
Spatial distribution of population density in China from 2000 to 2015.

Discussion

This study analyzed the spatial and temporal evolution characteristics of human settlement climate comfort in China through the temperature and humidity index and wind efficiency index and, subsequently, analyzed the spatial relationship of human settlement climate comfort and population density in China. Improving the climate comfort of the human settlement environment in China is important for guiding an orderly flow of population, thereby optimizing the regional population structure.

Compared with existing research, our study presents improvements in the research scale and the research perspective. With respect to the research scale, existing research on urban climate comfort evaluation is based mainly on the single year, month, and day time scale (Lyu and Chen, 2021; Xiong and Zhang, 2021), with a lack of comparative analysis of the spatial characteristics of urban climate comfort based on the three time dimensions (year, month, and day). With respect to the research perspective, existing research mainly focuses on summarizing the spatial and temporal change characteristics of regional human settlement climate comfort (Camila et al., 2021; Lin et al., 2021), but it does not explore the effect of change in human settlement climate comfort on the spatial layout of population density.

In view of the spatiotemporal evolution of human settlement climate comfort, our study presents the following suggestions.

(1) Improve the comfort level of the human settlement climate by changing meteorological elements, for example, by making full use of the natural landscape for regulating temperature, humidity, and other climatic elements. Various cities have adopted the principle of adjusting measures to local conditions and choosing appropriate

natural landscapes to adjust their comfort levels. Humidity and temperature in cities could also be improved by artificial water bodies and topography.

(2) Attract people by planning cities with a comfortable climate. For instance, the territory occupied by northwest and northeast China and the Yunnan–Guizhou region in southwest China is vast, but the population density is low. Therefore, the climate comfort in northwest and northeast China should be improved, and habitable cities should be planned for areas of relative comfort. In addition, the advantages of the human settlement climate in the Yunnan–Guizhou region should be used to the maximum, and a habitable urban agglomeration should be constructed.

The limitations of our study are as follows:

(1) The population density data reflect only relevant changes between different years, but as shifts at monthly scale are not reflected, the effect of changes in human settlement climate comfort on population density in different months could not be analyzed.

(2) When the temperature and humidity index and the wind efficiency index were inconsistent, the wind efficiency index was used in winter and the temperature and humidity index in summer. This approach solved the problem of two exponential inconsistencies in the monthly and daily time scales but could not solve this problem at an annual scale. It appears that people are often inclined to follow the example of bird migration, that is, migrating to warmer climes when it is cold and back to cooler climes when it is hot. Therefore, follow-up studies should explore the spatial flow characteristics of the population at the monthly scale by, for example, mobile phone signaling data. Such research would facilitate analyses of the effects of seasonal changes in human settlement climate comfort on population migration. Furthermore, a reasonable method should be explored to evaluate human settlement climate comfort when the temperature and humidity index and wind efficiency index are inconsistent at the annual scale.

Conclusion

Based on the China ground climate (mean daily value data) and China population spatial distribution kilometer grid dataset, the temperature and humidity climate index and population grid space calculation were employed to determine human settlement climate comfort and population density, respectively, in China. The spatiotemporal relationship between the human settlement climate comfort and population density was also analyzed. Our conclusions are as follows:

(1) From the perspective of the annual human settlement climate comfort range in China, the area range of annual human settlement climate extremely cold was the largest, followed by the cold range, while the comfort climate range was the smallest. In 2015, human settlement climate comfort areas were distributed mainly in the south of east China, south China, the central-south, and the east of southwest China, and the south of central China. The cold human settlement climate was distributed mainly in the north of east China, middle and north of central China, middle and north of southwest China, south of northwest China, and south of north China. The extremely cold human settlement climate was distributed mainly in northeast China, most areas of northwest China, the middle and north of north China, and the west of southwest China. From 2000 to 2015, the annual range of human settlement climate comfort area and cold area showed a trend of northward expansion, and the range of extremely cold human settlement climate shrank. At present, most regions of the human settlement climate in China have poor climate comfort, and there are relatively few human settlement climate comfort areas. However, over time, the human settlement climate comfort area and sub-comfort area will expand gradually.

(2) The comfort month duration of the human settlement climate in southern China was generally higher than that in northern China. The regional range was the largest in comfort monthly duration of 3–4, followed by 0–2 and 5–6, and was the smallest in comfort monthly length of 7–12. From 2000 to 2015, the comfort monthly length of human settlement climate in the west and north of northwest China showed a decreasing trend, whereas northeast and central China showed the spatial characteristics of a decrease in the north and increase in the south. In north China, the east increased first, then decreased, and subsequently increased, and the west increased first and then decreased. East China showed a trend of decrease first and then increase; the north of south China increased first and then decreased and, subsequently, increased; whereas the southern part of south China decreased first and then increased. The human settlement climate change in southwest China was relatively complex, with significant differences in the comfort month length in southwest China.

(3) The comfort day length of the human settlement climate in southern China was generally higher than that in northern China. The area range of comfort day length of 66–130 was the largest, followed by 0–65 and 131–195, with that of 196–325 being the smallest. From 2000 to 2015, the human settlement climate in northwest, north,

and northeast China changed less, whereas the human settlement climate in southwest, south, central, and east China changed significantly.

(4) High population density in 2015 was concentrated mainly in the area of annual climate comfort extremely cold, cold, and the transition area between comfort and cold, as well as the area of comfort monthly length 3–6 and the area of comfort day length 66–195. From 2000 to 2015, the population density migrated from extremely cold human settlement climate areas to cold and comfort areas, from the area of comfort month length 3–4 to 5–6, and from the area of comfort days 66–130 to 131–195. Our results show that population density has a certain trend relevant to the duration of comfort months and days, and people prefer to live in an area with a comfort month duration of 5–6 and 131–195 days. In general, population migration and settlement in China are expected to gradually show the spatial characteristics of agglomeration from north to south.

Data availability statement

The original contributions presented in the study are included in the article/supplementary material, further inquiries can be directed to the corresponding author.

Author contributions

CZ and DZ: conceptualization. DZ and YZ: methodology, software, and data curation. CZ: validation and formal analysis. DZ: writing—original draft. CZ and BZ: writing—review and editing. All authors have read and agreed to the published version of the manuscript.

Conflict of interest

The authors declare that the research was conducted in the absence of any commercial or financial relationships that could be construed as a potential conflict of interest.

Publisher's note

All claims expressed in this article are solely those of the authors and do not necessarily represent those of their affiliated organizations, or those of the publisher, the editors and the reviewers. Any product that may be evaluated in this article, or claim that may be made by its manufacturer, is not guaranteed or endorsed by the publisher.

References

Adiguzel, F., Sert, E. B., Dinc, Y., Cetin, M., Gungor, S., Yuka, P., et al. (2022). Determining the relationships between climatic elements and thermal comfort and tourism activities using the tourism climate index for urban planning: A case study of Izmir Province. *Theor. Appl. Climatol.* 147, 1105–1120. doi: 10.1007/s00704-021-03874-9

Alisson, F., Edson, D., Bernardo, L., Queiroz, R., José, I., José, A., et al. (2010). Climate change and population migration in Brazil's Northeast: Scenarios for 2025-2050. *Popul. Environ.* 31, 344–370. doi: 10.1007/s11111-010-0105-1

Amininia, K., Abad, B., Safarianzengir, V., GhaffariGilandeh, A., and Sobhani, B. (2020). Investigation and analysis of climate comfort on people health tourism in Ardabil province, Iran. *Air Qual. Atmos. Health* 13, 1293–1303. doi: 10.1007/s11869-020-00883-x

Amorosi, A., Bini, M., Giacomelli, S., Pappalardo, M., Ribecai, C., Rossi, V., et al. (2013). Middle to late Holocene environmental evolution of the Pisa coastal plain (Tuscany, Italy) and early human settlements. *Quat. Int.* 303, 93–106. doi: 10.1016/j.quaint.2013.03.030

Areti, T., Ioannis, X., Tsiros, S. L., and Marialena, N. (2010). An evaluation of three biometeorological indices for human thermal comfort in urban outdoor areas under real climatic conditions. *Build. Environ.* 45, 1346–1352. doi: 10.1016/j.buildenv.2009.11.009

Camila, T. P., Érico, M., and Vandoir, B. (2021). Socio-spatial inequality and its relationship to thermal (dis)comfort in two major Local Climate Zones in a tropical coastal city. *Int. J. Biometeorol.* 65, 1177–1187. doi: 10.1007/s00484-021-02099-9

Cao, W., He, Y., Li, Z., Wang, S., and Wang, C. (2012). Evaluation of the tourism climate comfort index in Lijiang City, Yunnan. *J. Glaciol. Geocryol.* 34, 201–206.

Cao, Y., Sun, Y., and Wu, M. (2019). Spatial and temporal characteristics of the periods of climate comfort in the Beijing-Tianjin-Hebei region from 1966 to 2015. *Acta Ecol. Sin.* 39, 7567–7582. doi: 10.5846/stxb201805181096

Chen, K., Cabrera, A., and Dubrow, R. (2020). Projections of ambient temperature- and air pollution-related mortality burden under combined climate change and population aging scenarios: A review. *Curr. Environ. Health Rep.* 7, 243–255. doi: 10.1007/s40572-020-00281-6

Cohen, P., Potchter, O., and Matzarakis, A. (2013). Human thermal perception of Coastal Mediterranean outdoor urban environments. *Appl. Geogr.* 37, 1–10. doi: 10.1016/j.apgeog.2012.11.001

Du, J., Liu, L., Chen, X., and Liu, J. (2020). Field assessment of neighboring building and tree shading effects on the 3D radiant environment and human thermal comfort in summer within urban settlements in Northeast China. *Adv. Meteorol.* 2020:8843676. doi: 10.1155/2020/8843676

Dulal, H. B., and Akbar, S. (2013). Greenhouse gas emission reduction options for cities:Finding the "Coincidence of Agendas" between local priorities and climate change mitigation objectives. *Habitat Int.* 38, 100–105. doi: 10.1016/j.habitatint.2012.05.001

Esmael, N., Zahraei, A., Ghadiri, H., and Komasi, H. (2014). Zoning evaluation of Eco-Touristic potentials of bio-climatic comfortability in the province of Fars, using Geographical information system (GIS). *Int. J. Adv. Res.* 2, 768–776.

Fan, Q., Du, F., Li, H., and Zhang, C. (2021). Thermal-comfort evaluation of and plan for public space of Maling Village, Henan, China. *PLoS One* 16:e0256439. doi: 10.1371/journal.pone.0256439

Kong, F. (2020). Multi-temporal scale assessment of climate comfort of habitat environment and spatial differences in China. *J. Arid Land Resour. Environ.* 34, 102–111. doi: 10.13448/j.cnki.jalre.2020.72

Lai, D., Liu, J., Wu, Z., Pei, J., Qi, Y., Zhang, H., et al. (2021). Thermal comfort diversity in Chinese urban residential buildings across various climates. *Energy Build.* 231:110632. doi: 10.1016/j.enbuild.2020.110632

Li, Q., and Zhong, G. (2005). Evaluation on climate resource for tourism in the region around Bohai. *J. Arid Land Resour. Environ.* 19, 149–153. doi: 10.13448/j.cnki.jalre.2005.02.029

Liao, X., Xu, W., Zhang, J., Li, Y., and Tian, Y. (2019). Global exposure to rainstorms and the contribution rates of climate change and population change. *Sci. Total Environ.* 663, 644–653. doi: 10.1016/j.scitotenv.2019.01.290

Lin, Y., Li, P., Feng, Z., Yang, Y., Zhen, Y., and Zhu, F. (2021). Climate suitability assessment of human settlements for regions along the belt and road. *Chin. Geogr. Sci.* 31, 996–1010. doi: 10.1007/s11769-021-1241-5

Liu, Z., Jin, Y., and Jin, H. (2019). The effects of different space forms in residential areas on outdoor thermal comfort in severe cold regions of China. *Int. J. Environ. Res. Public Health* 16:3960. doi: 10.3390/ijerph16203960

Luo, X., Yang, J., Sun, W., and He, B. (2021). Suitability of human settlements in mountainous areas from the perspective of ventilation: A case study of the main urban area of Chongqing. *J. Clean. Prod.* 310:127467. doi: 10.1016/j.jclepro.2021.127467

Lyu, L., and Chen, D. (2021). Impact of climate comfort of urban human settlements on urban innovation. *Areal Res. Dev.* 40, 45–49. doi: 10.3969/j.issn.1003-2363.2021.02.008

Ma, L., Sun, G., Ma, Y., Cai, X., and Hou, K. (2011). Variation of tourism climate comfort degree in Beijing in the last years. *J. Arid Land Resour. Environ.* 25, 161–166. doi: 10.13448/j.cnki.jalre.2011.10.021

Ma, L., Sun, G., Xie, Y., and Long, M. (2010). A study on variations of the tourism climate comfort degree in five typical cities in Eastern China during the last 50 years. *Resour. Sci.* 32, 1963–1970.

Maria, C., Célia, M., Raquel, C., Beatriz, D. A. B., and João, P. A. G. (2019). Preliminary approach to the analysis of climate perception and human thermal comfort for riverside dwellings the Brazilian Amazon. *J. Build. Eng.* 23, 77–89. doi: 10.1016/j.jobe.2019.01.019

Masoudi, M. (2021). Estimation of the spatial climate comfort distribution using tourism climate index (TCI) and inverse distance weighting (IDW) (case study: Fars Province, Iran). *Arab. J. Geosci.* 14:363. doi: 10.1007/s12517-021-06605-6

Michael, P. (2018). Climate change, internal migration, and the future spatial distribution of population: A case study of New Zealand. *Popul. Environ.* 39, 239–260. doi: 10.1007/s11111-017-0289-8

National Standardization Administration (2012). *National standard of the People's Republic of China GB/T 27963-2011: Climatic suitability evaluating on human settlement*. Beijing: Standards Press of China.

Pantavou, K., Theoharatos, G., Santamouris, M., and Asimakopoulos, D. (2013). Outdoor thermal sensation of pedestrians in a Mediterranean climate and a comparison with UTCI. *Build. Environ.* 66, 82–95. doi: 10.1016/j.buildenv.2013.02.014

Pottier, A., Fleurbaey, M., Méjean, A., and Zuber, S. (2021). Climate change and population: An assessment of mortality due to health impacts. *Ecol. Econ.* 183:106967. doi: 10.1016/j.ecolecon.2021.106967

Ren, J., Yang, J., Zhang, Y., Xiao, X., Xia, J., Li, X., et al. (2022). Exploring thermal comfort of urban buildings based on local climate zones. *J. Clean. Prod.* 340:130744.

Salata, F., Golasi, I., Roberto, V., and Andrea, V. (2016). Outdoor thermal comfort in the Mediterranean area. A transversal study in Rome, Italy. *Build. Environ.* 96, 46–61. doi: 10.1016/j.buildenv.2015.11.023

Smirnov, O., Zhang, M., Xiao, T., Orbell, J., Lobben, A., and Gordon, J. (2016). The relative importance of climate change and population growth for exposure to future extreme droughts. *Clim. Change* 138, 41–53. doi: 10.1007/s10584-016-1716-z

Stathopoulos, T., Wu, H., and Zacharias, J. (2004). Outdoor human comfort in an urban climate. *Build. Environ.* 39, 297–305. doi: 10.1016/j.buildenv.2003.09.001

Xiong, Y., and Zhang, F. (2021). Effect of human settlements on urban thermal environment and factor analysis based on multi-source data: A case study of Changsha city. *J. Geogr. Sci.* 31, 819–838. doi: 10.1007/s11442-021-1873-5

Xu, X. (2017). *Data registration and publishing system of resources and environmental science data center. China population spatial distribution 1 km grid dataset*. Beijing: Chinese Academy of Sciences, doi: 10.12078/2017121101

Yang, J., Wang, Y., Xiu, C., Xiao, X., Xia, J., and Jin, C. (2020). Optimizing local climate zones to mitigate urban heat island effect in human settlements. *J. Clean. Prod.* 275:123767. doi: 10.1016/j.jclepro.2020.123767

Yu, H., Yang, J., Li, T., Jin, Y., and Sun, D. (2022). Morphological and functional polycentric structure assessment of megacity: An integrated approach with spatial distribution and interaction. *Sustain. Cities Soc.* 80:103800. doi: 10.1016/j.scs.2022.103800

Zhang, D., Zhou, C., Sun, D., and Qian, Y. (2022). The influence of the spatial pattern of urban road networks on the quality of business environments: The case of Dalian City. *Environ. Dev. Sustain.* 24, 9429–9446. doi: 10.1007/s10668-021-01832-z

frontiers | Frontiers in Environmental Science

TYPE Original Research
PUBLISHED 29 August 2022
DOI 10.3389/fenvs.2022.991502

Check for updates

OPEN ACCESS

EDITED BY
Jun Yang,
Northeastern University, China

REVIEWED BY
Bao-Jie He,
Chongqing University, China
Liang Zhou,
Lanzhou Jiaotong University, China

*CORRESPONDENCE
Yi Luo,
lysist@ynnu.edu.cn

†These authors have contributed equally to this work and share first authorship

SPECIALTY SECTION
This article was submitted to Environmental Informatics and Remote Sensing,
a section of the journal
Frontiers in Environmental Science

RECEIVED 11 July 2022
ACCEPTED 05 August 2022
PUBLISHED 29 August 2022

CITATION
Tang L, Yang K, Shang C, Peng Z and Luo Y (2022), Spatial impact of urban expansion on lake surface water temperature based on the perspective of watershed scale.
Front. Environ. Sci. 10:991502.
doi: 10.3389/fenvs.2022.991502

COPYRIGHT
© 2022 Tang, Yang, Shang, Peng and Luo. This is an open-access article distributed under the terms of the Creative Commons Attribution License (CC BY). The use, distribution or reproduction in other forums is permitted, provided the original author(s) and the copyright owner(s) are credited and that the original publication in this journal is cited, in accordance with accepted academic practice. No use, distribution or reproduction is permitted which does not comply with these terms.

Spatial impact of urban expansion on lake surface water temperature based on the perspective of watershed scale

Linfeng Tang[1,2†], Kun Yang[1,2†], Chunxue Shang[3], Zongqi Peng[1,2] and Yi Luo[1,2*]

[1]Faculty of Geography, Yunnan Normal University, Kunming, Yunnan, China, [2]GIS Technology Research Center of Resource and Environment in Western China, Ministry of Education, Yunnan Normal University, Kunming, Yunnan, China, [3]Dean's Office, Yunnan Normal University, Kunming, Yunnan, China

As an important ecological environmental factor, the lake water surface temperature (LSWT) has an important impact on the ecological diversity of lakes and watersheds. With the acceleration of urbanization in China, the impact of urban expansion on LSWT can not be ignored. In this study, we introduced the spatial influence(G) equation, selected MOD11A2, impervious surface (IS), digital elevation model (DEM) and Landsat series remote sensing images as data sources, and took six lakes with rapid urban expansion in China as the empirical research object to explore the variation characteristics of urban expansion and LSWT in six lake watersheds and the spatial influence of urban expansion on LSWT. Finally, the following conclusions can be drawn: The results show that 1) The IS in the six watersheds all experienced significant expansion, with an increase of 1.80–3.91 times. 2) From the annual average LSWT from 2001 to 2018, only Poyang Lake's LSWT-night shows a cooling trend, while other lakes, whether LSWT-day or LSWT-night, show a warming trend. 3) G is used to comprehensively consider the area change of IS in the watershed, the influence of distance and the change of lake area, which can quantify the impact of IS on LSWT, so as to further explain and describe the spatial influence process and characteristics of IS expansion on LSWT.

KEYWORDS

impervious surface, lake surface water temperature, urban expansion, spatial influence, watershed

1 Introduction

As an important factor affecting the lake ecological environment (Woolway et al., 2016; Huang et al., 2021; Yu et al., 2021), lake surface water temperature (LSWT) directly reflects material and energy exchange processes at the water-air interface (Woolway et al., 2016; Huang et al., 2021). Previous studies have shown that the LSWT in most regions of the world has shown a warming trend in recent decades, and the warming trend is different in different regions (Sharma et al., 2015; Kainz et al., 2017). O'Reilly et al. (2015) conducted a

statistical analysis of global lake ecological environmental factors from 1985 to 2009 and found that the average rate of temperature increase of the global LSWT in summer reached 0.34 °C/decade. Other authors have made similar findings regarding the lakes on the Qinghai-Tibet Plateau and the Great Lakes and have concluded that the LSWT of the Great Lakes will rise significantly (Trumpickas et al., 2009; Wan et al., 2018). Changes in LSWT will affect lake ecology, biogeochemical processes and lake biological communities. For example, the research results of Oglu et al. (2020) on fourth largest lake in Europe show that the continuous warming of LSWT in winter and the change of ice cover phenology are expected to be crucial to the function of the lake ecosystem and its impact on the lake biota, especially for temperature sensitive fish. The research results of Mushtaq et al. (2021) show that the LSWT are important reasons for the outbreak of water blooms. In addition, the research results of Yang et al. (2018) on Dianchi Lake also show that the LSWT was closely related to several water quality parameters, and the LSWT was highly related to the characteristics of the ecosystem and the level of biodiversity in the watershed. Compared with other environmental factors, the LSWT is affected by many factors. First, the LSWT is sensitive to climate change (Woolway and Merchant, 2018; Huang et al., 2021), so the changes of temperature, pressure, solar radiation, cloud cover, and wind speed will affect the LSWT (Yang et al., 2020b; Woolway et al., 2020). Moreover, the number of people, IS and the morphological characteristics, water color and transparency of the lake itself will also affect the LSWT (Houser, 2006; Ptak et al., 2018; Yang et al., 2019b; Yu et al., 2020).

Because of the importance of LSWT, many authors have been attracted to study it, and the data used are also different, mainly including measured data, simulation through models and remote sensing data retrieval. Most *in situ* measured data at this stage are used to verify the datasets of remote sensing retrieval or the datasets of model simulation. From the point of view of model simulation, authors have developed several simulation models of LSWT or have improved the original model to simulate LSWT (Ngai et al., 2013; Piccolroaz et al., 2013; Layden et al., 2016), some of which can achieve better results in simulating and predicting LSWT (Heddam et al., 2020; Zhu et al., 2020; Huang et al., 2021). For the retrieval of remote sensing data, different remote sensing sensors are used, including the advanced very high-resolution radiometer (AVHRR) (Riffler et al., 2015; Lieberherr and Wunderle, 2018) and medium-imaging spectral radiometer, and the retrieved LSWT has a long-term robustness in different scenarios. MODIS surface temperature data products have become a more commonly used data source because of their high-temporal and spatial resolution, which can also meet the monitoring of spatiotemporal characteristics of large and mesoscale LSWT (Liu et al., 2015; Pareeth et al., 2016; Liu et al., 2019; Luo et al., 2019b; Yang et al., 2021b).

As we mentioned in the first paragraph, the IS is one of the factors affecting the LSWT, and the change of the IS in the watershed will have an important impact on the LSWT (Yang et al., 2019). With the acceleration of urbanization in China, as the main manifestation of urbanization (Luo et al., 2018), the impact of the expansion of IS on the LSWT cannot be ignored. According to data from China's seventh census, the number of people living in urban areas in regard to the country's population reached 902 million, accounting for 63.9% of the total population (https://data.stats.gov.cn/easyquery.htm?cn=C01&zb=A0301&sj=2020). Moreover, from 1981 to 2018, the average growth rate of China's construction land area reached 5.90% (Zhou et al., 2021). At the same time, predictions from related studies have indicated that China's urbanization rate will reach approximately 75% by 2050 (Gu et al., 2017). In the world, it is estimated that 68% of the world's population will live in cities by 2050 (Zhao et al., 2021). The massive influx of people into cities will aggravate the urban heat island effect and the negative impact of the thermal environment (Yang et al., 2019; He et al., 2021; Xie et al., 2022; Yu et al., 2022), and urban heat island is a common problem in almost all Chinese cities (He et al., 2022). Therefore, urban expansion has gradually become a topic of increasing concern among the factors affecting the LSWT. Previous studies have shown that there are significant differences in land surface temperature between green surface and IS. The land surface temperature of IS is 5–10°C higher than that of green surface (Soydan, 2020). The research results of other authors also show that the impact of public service facilities and residential land on urban thermal environment is greater than that of green space (Chen et al., 2022). The land surface temperature in the built-up area is also significantly higher than the natural surface temperature (Ren et al., 2022), and the land surface temperature is positively correlated with the building area (Yang et al., 2021). Moreover, the research results of Zhou et al. (2022) also show that with the increase in the spatial level of the urban thermal environment and the contribution from is IS is also increasing, and the landscape indicators related to is at the regional level of the entire urban heat island contribute the most to the surface temperature. Urban expansion mainly affects the LSWT by increasing the near surface temperature and through thermal runoff. In the absence of precipitation, IS will have a positive impact on urban near surface air temperature, He et al. (2013) taking the urban expansion around the meteorological station as the research object, it was found that every 10% increase in the cities within 1 km around the meteorological station would lead to an increase of 0.13°C in the air temperature record. When a precipitation event occurs, the underlying surface of the city will transfer heat to the runoff in the form of convection, which will increase the temperature of the runoff (Thompson et al., 2008; Li et al., 2019; Luo et al., 2019). If the impervious surface area coverage rate (ISACR) in the catchment area increases from 20% to 50%, the runoff temperature will increase by 3°C (Sabouri et al., 2013). Every 1% increase in the proportion of IS in the watershed

in summer will cause the runoff temperature to rise by 0.09°C (Galli, 1990; Janke et al., 2009; Sabouri et al., 2013). Therefore, in the process of urbanization, whether the warming of near surface temperature or the warming of runoff will ultimately directly or indirectly affect the LSWT. However, as far as the current research is concerned, because the spatial relationship between IS and lake is different from other influencing factors of LSWT, which makes it difficult to study the impact of urban expansion on IS. Taking air temperature as an example, the lake surface is in direct contact with the air, resulting in energy exchange, which directly affects LSWT. However, in most cases, there is a certain distance between IS and the lake, so the impact of IS on the LSWT is more indirect. For example, urban expansion leads to the warming of near surface air, and then transfers heat to the lake. Another effect is that the thermal runoff generated by is during rainfall eventually converges into the lake, thus affecting the LSWT. This indirect effect makes it more difficult to study the impact of urban expansion on the LSWT. According to our understanding, the existing studies do not consider the characteristics that the impact of is on LSWT decreases with the increase of distance, nor the impact of the spatial distribution of is in the watershed on LSWT. Therefore, at present, no scholar has comprehensively considered the impact of urban expansion on LSWT from the perspective of the spatial distribution of is, the distance between IS and the lake, and the lake area. In addition, in the existing studies, some authors only put the IS and other influencing factors together to study the impact of these factors on LSWT (Yang et al., 2019), rarely analyze the impact of urban IS expansion on LSWT alone, and most of the analysis methods are simple correlation analysis (Yang et al., 2021c). Therefore, in order to explore the impact mechanism of IS expansion on LSWT in the watershed, we selected Dianchi Lake (DCL), Poyanghu Lake (PYHL), Chaohu Lake (CHL), Dongtinghu Lake (DTHL), Hongzehu Lake (HZHL) and Taihu Lake (THL) as the study area, and used G to quantify the impact of IS expansion on LSWT in the watershed, the spatial impacts of IS characteristics on LSWT in six lake watersheds were discussed.

Previous studies have proved that the IS is an important factor affecting the LSWT. Therefore, our research purpose is not to prove that the IS will affect LSWT again, nor to calculate the specific temperature increase value of the IS to LSWT. The purpose of this paper is to take six lakes with rapid urban expansion in China as the object of empirical research. By discussing the spatial impact of urban expansion on LSWT in these six lake watersheds, it is proved that G can be used to measure the impact of urban expansion on LSWT in the watershed, so as to further provide reference for ecological environment protection, watershed governance and urban planning. The final results show that based on the sub-watershed scale, the spatial influence equation considering the impervious surface area (ISA), distance and Lake area can better quantify the impact of urban expansion on LSWT in the watershed, and explain the inconsistency between the growth rate of IS and that of LSWT.

The remainder of this paper is organized as follows. Section 2 introduces the study area, data sources, methods of calculating spatial influence and data processing methods. Section 3 introduces the change characteristics of IS, the change characteristics of LSWT, the spatial impact of IS on LSWT, and the correlation between G and LSWT. Section 4 discusses the impact of urban expansion in the watershed on the LSWT, the inconsistency between the expansion rate of IS and the change rate of LSWT, and the availability of G to quantify the impact of urban expansion on the LSWT. Section 5 provides conclusions.

2 Materials and methods

2.1 Study area

This study selected six lakes with rapid urbanization in the watershed as the study area, and the locations of the six lakes and the watershed are shown in Figure 1. With the rapid development of China's economy, the ISA of these lake watersheds has increased rapidly in recent decades. According to our statistics, from 2001 to 2018, the ISA in the six lake watersheds increased by at least 1.80 times, and the ISA in the THL watershed increased by 3.91 times (See Figure 2 and Supplementary Appendix Table SA2 for details). Studying the changes in IS in these lake watersheds and their effects on LSWT is of great significance to the protection of the aquatic ecological environment of these lakes and the planning of cities in the watershed.

2.2 Data source

The data used in this study include the LSWT, watershed boundary, lake boundary of six lakes, and IS data in the six watersheds. Watershed boundaries and sub-watershed boundaries are directly extracted from the SWAT model based on DEM data. LSWT is an 8-days synthetic product with a resolution of 1 km, extracted from MODIS/Terra LST level 3 MOD11A2 images. We downloaded all images from 2001 to 2018 from NASA's Earth Observation System Data and Information System (EOSDIS, https://earthdata.nasa.gov). The lake boundary used to clip the LSWT is extracted from the Landsat series of remote sensing images, which are downloaded from the official website of the United States Geological Survey (USGS, https://earthexplorer.usgs.gov/).For the selection of remote sensing image time, we try to choose the remote sensing image of the current year. If there is an image missing, we choose the remote sensing image of the latest year. At the

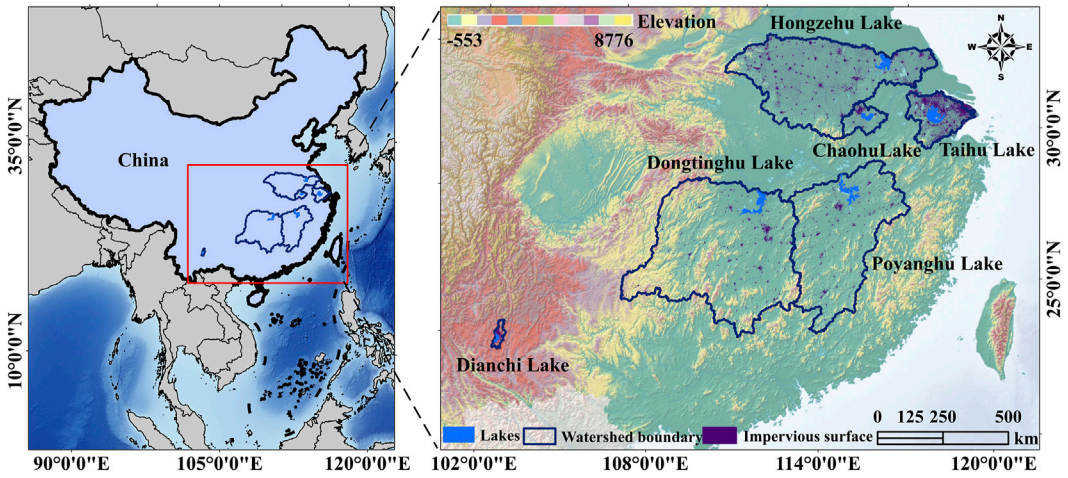

FIGURE 1
Location of the study area.

same time, in order to avoid the extraction error of LSWT caused by the lake boundary as much as possible, we try to choose remote sensing images of the same or similar months in a year. IS data is a data set established by Gong Peng's team at Tsinghua University. This data set provides China's IS data from 1985 to 2018 years by year, and the spatial resolution of this data is 30 m. We downloaded the data from 2001 to 2018 from http://data.ess.tshughua.edu.cn. DEM data are downloaded from the geospatial data cloud platform (https://www.gscloud.cn/).

2.3 Research methods

2.3.1 Spatial influence analysis

G is used to measure the strength or influence of interaction between two geographic areas that are not adjacent to each other (Fotheringham, 1981; Yang et al., 2020a). Among them, the distance-decay model is a multidisciplinary research topic that both natural sciences and social sciences utilize, and it is also a research hotspot in environmental sciences (Osth et al., 2016; Clark et al., 2021). To quantify the impact of the IS in the lake watershed on LSWT, we introduce the spatial influence equation.

$$G_{i,j} = k \times w_i \times w_j \times f\left(d_{i,j}\right) \quad (1)$$

In Eq. 1, $G_{i,j}$ represents the interaction strength between two geographic objects that are not adjacent to each other and G is dimensionless, k is a constant term, w_i and w_j are the volume of geographic objects, and $f(d)$ represents the distance-decay function. At present, the most commonly used distance decay functions are the exponential decay function, power-law decay function and Gaussian decay function. Among them, the power-law decay function is scale-free, which is more suitable for large-scale interaction problems and at the same time conforms to the first law of geography (Yang et al., 2020a). Eq. 1 is simplified to get the following Equation:

$$G_i = w_i \times w_j \times d^{-2} \quad (2)$$

$$G_r = \sum G_i \quad (3)$$

In Eq. 2, G_i represents the spatial influence of the IS in the sub-watershed, w_i represents the ISA in the sub-watershed, w_j represents the area of the lake (In this paper, in order to facilitate the comparison between six lakes, we standardize the area of six lakes to less than 10), and d represents the shortest distance from the sub-watershed to the lake, where we calculate the shortest distance from the centroid of the sub-watershed to the lake. In Eq. 3, G_r represents the sum of the G of the sub-watershed.

2.3.2 Lake boundary extraction

In order to ensure the accuracy of extracting the LSWT using the lake boundary as much as possible, we select Landsat series remote sensing data with high spatial-temporal resolution as the data source (see Supplementary Appendix Table SA1 in the Appendix for the details of the selected remote sensing images). The normalized water index (NDWI), revised normalized water body index (RNDWI), and enhanced water index (EWI) are used to extract the lake boundary. Finally, the lake boundary results with the highest accuracy are selected according to different lakes.

2.3.3 Lake water surface temperature extraction and missing value interpolation method

The selected lakes are all located in the subtropical monsoon region, and the summer is a rainy season. Therefore, the data of LSWT is inevitably polluted by clouds, resulting in the lack of data. Therefore, for the downloaded MOD11A2 images, we first perform batch projection on the data and convert them to Geo Tiff format and then use the lake boundary to batch clip them to obtain the LSWT data of each lake. Then, we set a threshold of 10% for the preprocessed data, eliminate the images with a missing ratio greater than 10%, use the 8 days before and after image interpolation instead. In this paper, the research scale of LSWT includes six Lake seasonal and annual scale data. Since MOD11A2 data is 8-days resolution LSWT data, it is necessary to synthesize the data. Therefore, for the 8-days resolution MOD11A2 data that has been pretreated by interpolation, We use the raster calculator in the ArcGIS 5.2 platform to add them one by one, and finally calculate the seasonal and annual average. Finally, the brightness temperature of the MOD11A2 image is converted into degrees Celsius (°C).

2.3.4 Watershed boundary extraction

The DEM data with 30-m resolution in China were used to extract the sub-watersheds of six lakes using SWAT model after preprocessing. Total watershed boundaries are obtained by merging sub-watershed boundaries (See Supplementary Appendix results and Supplementary Appendix Figure SA15 for sub-watershed extraction results).

2.3.5 Trend analysis and correlation analysis

The variation trend of IS and LSWT in the watershed is calculated with a linear regression equation, and the significance test is carried out. In addition, the Pearson correlation coefficient is used for the correlation test in this paper.

3 Results

3.1 Expansion characteristics of impervious surface

From 2001 to 2018, the ISA in the six lake watersheds has increased significantly, as shown in Figure 2 and Supplementary Appendix Table SA2. In the watersheds of the six lakes, THL (3.91 times) had the highest growth multiple of IS from 2001 to 2018, followed by DTHL (3.59 times), PYHL (3.48 times), DCL (2.5 times), CHL (2.16 times) and HZHL (1.80 times). In terms of growth rate, HZHL (5,192.73 km^2/decade) has the fastest growth rate, followed by THL (4,945.96 km^2/decade), DTHL (1,668.55 km^2/decade), PYHL (1,382.26 km^2/decade), CHL (473.34 km^2/decade) and DCL (237.29 km^2/decade). From Supplementary Appendix Figures SA1–6 in the Appendix, it can be seen that the IS in the six lake watersheds changes year by year. Before 2001, the IS in the DCL watershed was mainly distributed in the main urban area of Kunming on the North Bank of DCL. Over time, it mainly expanded outward from the main urban area of Kunming and southward along the east bank of DCL. The IS in PYHL, DTHL and HZHL watersheds is scattered, and it has expanded outward in the original IS distribution area since 2001. The IS of CHL watershed is mainly distributed in Hefei City on the northwest bank of CHL. It has expanded from the center of Hefei since 2001 to the northwest coast of CHL by 2018. The THL watershed experienced significant growth in the whole watershed from 2001 to 2018.

3.2 The characteristics of lake surface water temperature changes.

3.2.1 Annual variation characteristics of lake surface water temperature

From Figure 3 and Supplementary Appendix Table SA3, we can see the annual changes of LSWT from 2001 to 2018, the LSWT of the six lakes showed an overall warming trend, but the warming rate of each lake was different, and the LSWT-day of all lakes showed a warming trend, with an average warming rate of 0.24 °C/decade. At night, only PYHL showed a cooling trend (−0.03°C/decade), and the other lakes showed a warming trend, with an average warming rate of 0.35°C/decade.

According to the warming rate of the LSWT-day of the six lakes, the fastest warming rate was in CHL (0.41°C/decade), and the slowest warming rate was in PYHL (0.10°C/decade). From the LSWT-night of the six lakes, HZHL (0.55°C/decade) had the fastest warming rate, and DTHL (0.25°C/decade) had the slowest warming rate.

3.2.1 The seasonal variation characteristics of lake surface water temperature

From Figure 3 and Supplementary Appendix Table SA3, we can see the seasonal variation of LSWT from 2001 to 2018, the LSWT-day of the six lakes showed a warming trend in spring, the fastest warming rate was in THL (0.72°C/decade), and the slowest was in PYHL (0.15°C/decade), and the average warming rate of the six lakes in spring was 0.40°C/decade. Judging from the LSWT-day of the six lakes in summer, only DCL had a cooling trend (−0.24°C/decade), and the fastest warming rate among the other five lakes was in THL (0.48°C/decade), while the slowest warming rate was in HZHL (0.22°C/decade), and the average warming rate of these five lakes was 0.39°C/decade. Judging from the LSWT-day of the six lakes in autumn, there were three lakes showing a warming trend, namely, DCL (0.51°C/decade), PYHL (0.31°C/decade) and CHL (0.09°C/decade), while DTHL (-0.08°C/decade), HZHL (-0.24°C/decade), and THL (−0.07°C/decade) showed a cooling trend. Judging from the variation characteristics of the LSWT-day of the six lakes in winter, only PYHL showed a cooling trend (−0.32°C/decade), and the other five lakes showed a warming trend, of which the fastest warming rate was DTHL (0.51°C/

decade), the slowest warming rate was DCL (0.03°C/decade), and the average warming rate of these lakes was 0.27°C/decade.

From the variation characteristics of the LSWT-night of six lakes in spring, only PYHL showed a cooling trend (−0.54°C/decade), and the other five lakes showed a warming trend. Among the five lakes, HZHL had the fastest warming rate (0.98°C/decade), and DCL had the slowest warming rate (0.24°C/decade), while the average warming rate of the five lakes was 0.56°C/decade. Judging from the LSWT-night of the six lakes in summer, all six lakes showed a warming trend; the fastest warming rate was in THL (0.58°C/decade), and the slowest warming rate was in DCL (0.06°C/decade). The average warming rate of these lakes was 0.27°C/decade. Judging from the changing characteristics of the LSWT-night of the six lakes in autumn, only PYHL showed a cooling trend (−0.29°C/decade), and the other five lakes showed a warming trend, of which the fastest warming rate was in DCL (0.64°C/decade), the slowest warming rate was in THL (0.01°C/decade), and the average warming rate of these five lakes was 0.24°C/decade. Judging from the changing characteristics of the LSWT-night of the six lakes in winter, the six lakes all showed a warming trend; the fastest warming rate was in HZHL (0.60°C/decade), and the slowest warming rate was in CHL (0.04°C/decade). The average warming rate of the six lakes was 0.28°C/decade.

3.3 Spatial influence of impervious surface on lake surface water temperature.

Figure 4 shows the change of G value of IS on LSWT over time in six lake watersheds. It can be seen from the figure that the G value of the six lakes generally shows an upward trend, which is similar to the growth of ISA. The growth rate of the G value of the six lakes accelerated after 2011 and began to slow down in 2016. The decrease of G value of HZHL and DTHL after 2017 is due to the change of lake boundary. See Supplementary Appendix Figures SA7–12 in the Appendix for details of spatio-temporal changes of G value of the six Lake sub-watersheds.

3.4 Correlation between G and lake surface water temperature.

Figure 5 shows the correlation of G with the annual average LSWT and seasonal LSWT. From the perspective of the correlation between the average annual LSWT-day and G, the highest correlation was in CHL (0.47), and the lowest correlation was in HZHL (-0.02). According to the correlation between the annual average LSWT-night and the G, the highest was in DCL (0.56), and the lowest was in PYHL (-0.07).

From the perspective of LSWT-day and G in each season, the highest correlation between LSWT-day and G in spring was in THL (0.46), and the lowest was in DTHL (-0.06). From the perspective of summer, the highest correlation was in THL (0.44), and the lowest correlation was in DTHL (−0.26). From the perspective of autumn, the highest correlation was in DCL (0.40), and the lowest correlation was in HZHL (−0.18). From the perspective of winter, the highest correlation was in DCL (0.45), and the lowest correlation was in HZHL (−0.23).

From the perspective of LSWT-night and G in each season, the highest correlation between LSWT-night and G in spring was in HZHL (0.47), and the lowest was in PYHL (−0.37). From the perspective of summer, the highest correlation was in THL (0.36), and the lowest correlation was in DTHL (−0.12). From the perspective of autumn, the highest correlation was in DCL (0.66), and the lowest correlation was in PYHL (−0.17). From the perspective of winter, the highest correlation was in DTHL (0.27), and the lowest correlation was in CHL (0.04).

4 Discussion

4.1 The impact of impervious surface expansion in the watersheds on lake surface water temperature

The expansion of IS in the watersheds will have an important impact on the aquatic ecological environment of the lakes (Yang et al., 2018). In the introduction, we have mentioned that every 10% increase in cities within 1 km around the meteorological station will lead to a 0.13°C increase in temperature records (He et al., 2013). In addition, when the ISACR increased from 20% to 50%, the surface runoff temperature increased by 3°C, which could have had a direct warming effect on LSWT (Sabouri et al., 2013). Every 1% increase in the proportion of IS in the watershed in summer will cause the runoff temperature to rise by 0.09°C (Galli, 1990; Janke et al., 2009; Sabouri et al., 2013). The increase of near surface temperature and thermal runoff of IS will eventually act on the lake, making LSWT rise. Therefore, we have made statistics on the ISACR in each sub-watershed (see Supplementary Appendix Table SA4 for details). By 2018, the ISACR of 15 sub-watersheds of DCL, 1 of PYHL, 6 of CHL and 58 sub-watersheds of THL has exceeded 20%. Among the sub-watersheds with ISACR of more than 50%, there are 4 in DCL and 16 in THL. Except for PYHL, DTHL and HZHL watersheds, the ISACR of their sub-watersheds has increased slowly due to their large watershed area, most sub-watersheds of the other three lakes have experienced significant growth. The increase of IS in these watersheds will eventually have a warming effect on LSWT of the lake directly or indirectly. In addition, it can be seen from Supplementary Appendix Figure SA14 of the Appendix that the increment of IS in each year shows an upward trend in the increment of ISA of all lakes before 2015, but the increment of ISA has decreased since 2016, especially in 2017 and 2018, the increment of its area has remained at a low level. Such a situation will slow down the warming rate of the LSWT to a certain extent,

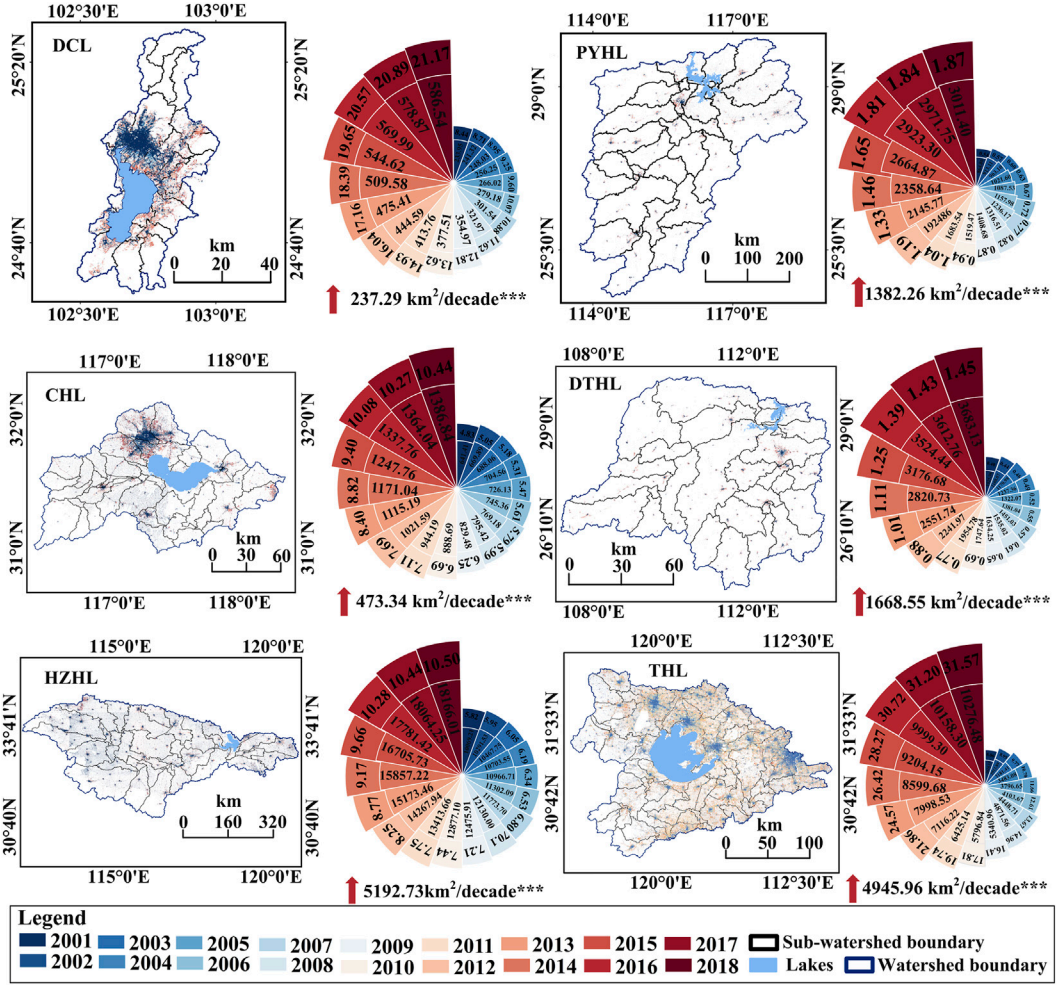

FIGURE 2
Temporal and spatial changes in IS in the watersheds. Note: In the above picture, the left picture represents the temporal and spatial changes in IS in the six lake watersheds, and the fan-shaped values on the right represent the ISA and ISACR in the corresponding year. The inner side is the ISA, in square kilometers (km^2), and the outer side is the ISACR, in %. The arrows and numbers at the bottom of the pie chart indicate the growth rate of IS. The change in the size of the sector also shows the rate of change of the ISA. Significance level: $p < 0.001$ (***).

and will also be beneficial to the protection of the aquatic ecological environment of the lake.

4.2 The influence of watershed characteristics and impervious surface distribution characteristics on lake surface water temperature

We have made statistics on the changes of ISA and ISACR of six lakes, as shown in Figure 2; Supplementary Appendix Table SA2. After comparing the growth rate of ISA and ISACR of the six lakes with the warming rate of LSWT of the six lakes, it was found that the growth of ISA or ISACR was not completely consistent with the warming rate of LSWT. From the perspective of CHL, the growth rate of ISA in CHL watershed is only 473.34 km^2/decade, and the ISACR has only increased from 4.83% to 10.44%. However, from the perspective of the warming rate of LSWT, the LSWT of CHL has a high warming rate, especially in spring, the warming rates during the day and at night are 0.69°C/decade and 0.78°C/decade respectively. In contrast, the growth rate of ISA in THL watershed is 4,945.56 km^2/decade, while the ISA increases from 8.06% to 31.57%, but the warming rate of LSWT of the two lakes is similar. In addition, although the ISA of DTHL and PYHL has a growth rate of 1,668.55 km^2/decade and 1,382.26 km^2/decade, respectively, the LSWT of PYHL and DTHL is not as fast as that of CHL, while the ISA of HZHL has the fastest growth rate of 5,192.73 km^2/decade, but LSWT of HZHL is not significantly higher than that of the other five lakes,

It also shows that only considering the change of ISA in the watershed will enlarge or reduce the impact of urban expansion on LSWT. This phenomenon can be explained by quantifying the impact of urban expansion on LSWT through G and combining the watershed characteristics of each lake, the distribution of IS in the watershed and the lake area.

As for CHL, it can be seen from Supplementary Appendix Figure SA10; Supplementary Appendix Table SA5 the two sub-watersheds with the largest G value for CHL are located on the north bank and south bank of CHL respectively. The sub-watershed on the north bank is the area with the most dense IS distribution in CHL watershed. Although the ISA of the sub-watershed on the south bank is small, the centroid of the sub-watershed is close to the lake, making its G value to CHL larger. According to the statistics of ISA in the sub-watershed on the north bank, from 2001 to 2018, the ISA in the watershed increased from 64.82 to 175.6 km^2, and the proportion of ISA in the total ISA increased from 10.11% to 12.66%. In addition, previous studies have shown that the temperature of surface thermal runoff will decrease with the increase of distance (Hathaway et al., 2016). This sub-watershed is directly adjacent to CHL. The heat runoff with increased temperature due to IS is discharged into CHL without too much heat consumption. The warming of near surface temperature will also significantly warm CHL, making the ISA in CHL watershed grow slower than that of other lakes, However, the LSWT of CHL increased rapidly.

For THL, it can be seen from Supplementary Appendix Figure SA12; Supplementary Appendix Table SA5 that the sub-watersheds with large G values are located along the THL. According to the statistics of the IS of the coastal sub-watersheds, from 2001 to 2018, the ISA increased from 373.75 to 1,425.64 km^2, the proportion in the total ISA ranges from 14.24 to 13.87%. Therefore, it has a great impact on LSWT of THL. However, there are two main reasons why the LSWT of THL is not significantly higher than that of CHL. The first reason is that THL has a large lake area (as can be seen in Supplementary Appendix Table SA1), because larger lakes have a better ability to regulate the water temperature (Song et al., 2016). Second, the IS in the THL watershed is mainly distributed in the downstream of THL (as can be seen from Supplementary Appendix Figure SA6; Supplementary Appendix Figure SA13). By 2018, the ISA in these watersheds has reached 6,659.21 km^2, accounting for 64.80% of the total ISA. This part of IS only affects LSWT of the lake by increasing the near surface temperature.

For HZHL, the growth rate of ISA in the watershed is the fastest among the six lakes. The G value of each sub-watershed can be seen from Supplementary Appendix Figure SA11; Supplementary Appendix Table SA5. We have made statistics on the ISA in the three sub-watersheds with the largest G value. As of 2018, its area is 1,047.49 km^2, accounting for only 5.77% of the total ISA. The IS of other sub-watersheds has little impact on the LSWT due to the long distance. Therefore, despite the rapid growth of ISA, the warming of LSWT is not significantly higher than that of lake.

For PYHL and DTHL, the G values of each sub-watershed of PYHL and DTHL can be seen from Supplementary Appendix Figures SA8,9 of the Supplementary Appendix Table SA5 of the Appendix. According to the statistics of the three sub-watersheds with the largest G value, as of 2018, the ISA of the three sub-watershed of PYHL was 663.4 km^2, accounting for 22.3% of the total ISA. The ISA of the three sub-watersheds of DTHL is 1,048.2 km^2, accounting for 28.46% of the total ISA. However, the water area of the two lakes has a large seasonal change, among which the area of DTHL has a seasonal change of 730–2000 km^2 (Ding and Li, 2011). Supplementary Appendix Table SA1 of the Appendix also shows the change of the water area of the two lakes in different time periods. Previous studies have proved that the impact of summer air temperature on LSWT is the most important (O'Reilly et al., 2015). One of the ways that IS affects LSWT is to increase the temperature near the surface. In addition, the IS can store more heat in summer, and the thermal runoff generated during precipitation becomes another way for IS to affect the LSWT, while the rapidly increasing Lake area of the two lakes in summer weakens the warming of LSWT.

The watershed area of DCL is small, so the ISA and the growth rate of ISA of DCL are smaller than other lakes (see Figure 2 and Supplementary Appendix Table SA2 for details). We can see from Supplementary Appendix Figures SA1,7 the spatial distribution of IS in DCL watershed and the size of G value in each sub-watershed. From the two figures, we can see that the sub-watersheds with large G value are located along DCL, which is more consistent with the spatial distribution of IS in DCL watershed. Due to the close distance between IS and lake and the small lake area of DCL, the warming rate of LSWT of DCL is similar to that of PYHL and DTHL, and even higher in some seasons.

4.3 Availability of using spatial influence to quantify the impact of impervious surface expansion on lake surface water temperature

It can be seen from Figure 4 that the G values of THL and CHL are significantly higher than those of the other four lakes. It can be seen from Figure 3 that the LSWT increase rate of CHL and THL is significantly higher than that of the other four lakes. The warming rate of LSWT of the six lakes shows strong consistency with the size of G value. However, we can see from Figure 4 that the G values of HZHL, DTHL and CHL have not been in the same growth state as the IS. In some years, the G values of these three lakes have decreased, mainly because the change of the lake boundary leads to the change of the distance between the IS and the lake, which affects the G value. Therefore, for lakes with large changes in Lake boundaries, its availability should be considered when using spatial impact equation to guide urban planning.

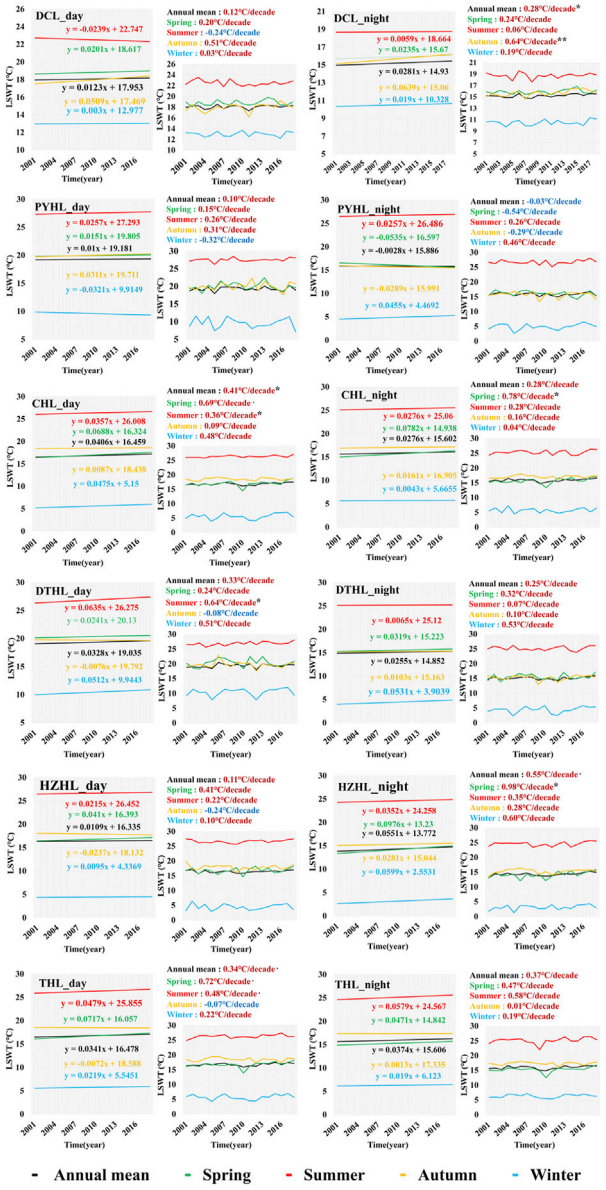

FIGURE 3
The changing trend of lake surface water temperature. Note: The *X*-axis represents time, and the *Y*-axis represents LSWT in degrees Celsius (°C). The left graph represents the changing trend line of LSWT, the right lower corner line graph represents the actual change in LSWT, the black line represents the annual average LSWT, the green line represents LSWT in spring, the red line represents LSWT in summer, the orange line represents LSWT in autumn, and the blue line represents LSWT in winter. The upper right corner number indicates that LSWT becomes cold or warm, the deep red font indicates that LSWT presents a warming trend, and the deep blue font indicates that LSWT presents a cooling trend. Significance level: $p < 0.01$ (**), $p < 0.05$ (*) and $p < 0.1$ (·).

It can be seen from Figure 5 that the correlation between LSWT of DCL, CHL and THL and G is greater than that of PYHL, DTHL and HZHL in most cases. By comparing the watershed area, it can be seen that the watershed areas of HZHL, DTHL and PYHL are relatively large. Among them, the largest DTHL has an area of 253,357.88 km^2, HZHL has an area of 161,406.77 km^2 and PYHL has an area of 161406 km^2. Compared with these three lakes, the watershed areas of THL (32,553.96 km^2), CHL (13,277.80 km^2) and DCL (2,771.15 km^2) are much smaller, Larger watershed area means that it is affected by more factors in energy transmission, which makes it more difficult to quantify the impact of IS expansion on LSWT.

In addition, although the correlation between LSWT and G in DCL, DCL and THL is higher than that in other lakes, the highest correlation between LSWT and G in these three lakes is only 0.66. Previous studies have proved that for the LSWT of most lakes, air temperature is the most important factor affecting LSWT. O'Reilly et al. (2015) after analyzing LSWT of global lakes, it is concluded that the impact of temperature and landform on LSWT is greater than that of other factors. The results of the selected research area of Schmid and Koster (2016) show that the contribution rate of near surface temperature to LSWT of lakes reaches 60%. Compared with the temperature, the influence of IS on LSWT is much smaller. Yang et al. (2020b) taking the main lakes in the Yunnan Guizhou Plateau as the research object, the driving factors of LSWT are discussed. The results show that there is a strong correlation between LSWT and air temperature (the correlation between LSWT and near surface air temperature in the daytime is 0.83, and that at night is 0.81). The relationship between other influencing factors and LSWT is relatively low. Therefore, it can be explained that the correlation between G value and LSWT is not very high.

To sum up, this research can provide decision-making basis for urban development in the watershed, so as to minimize the impact of IS expansion on LSWT and realize green and sustainable urban development.

5 Conclusion

Based on the IS and LSWT data, a spatial influence equation is introduced to quantitatively analyze the spatial influence of IS expansion in the watershed on LSWT. Our research conclusion shows that:

(1) IS of the six lakes in the watershed experienced significant expansion from 2001 to 2018, and the ISA and ISACR of each lake had different growth rates. From the growth rate of ISA, the growth rate of ISA is between 237.29 km^2/decade −5,192.73 km^2/decade. From the perspective of the growth of ISACR, the growth of ISACR is between 1.05%–23.51%, and the urban expansion in the watershed of these lakes will directly or indirectly affect the surface water temperature of the lakes.

(2) Through a comparative analysis of the growth rate of ISA or ISACR and the warming rate of LSWT in six lake watersheds, we found that the warming rate of

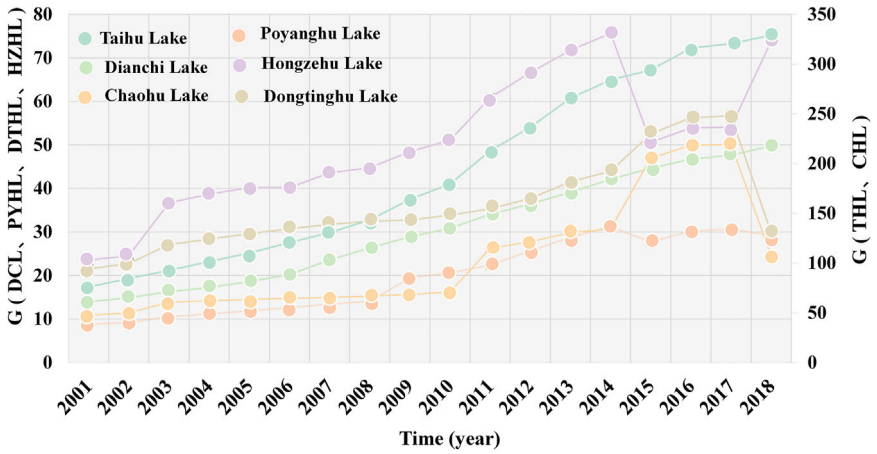

FIGURE 4
Spatial influence of impervious surface on lake surface water temperature. Note: G is dimensionless.

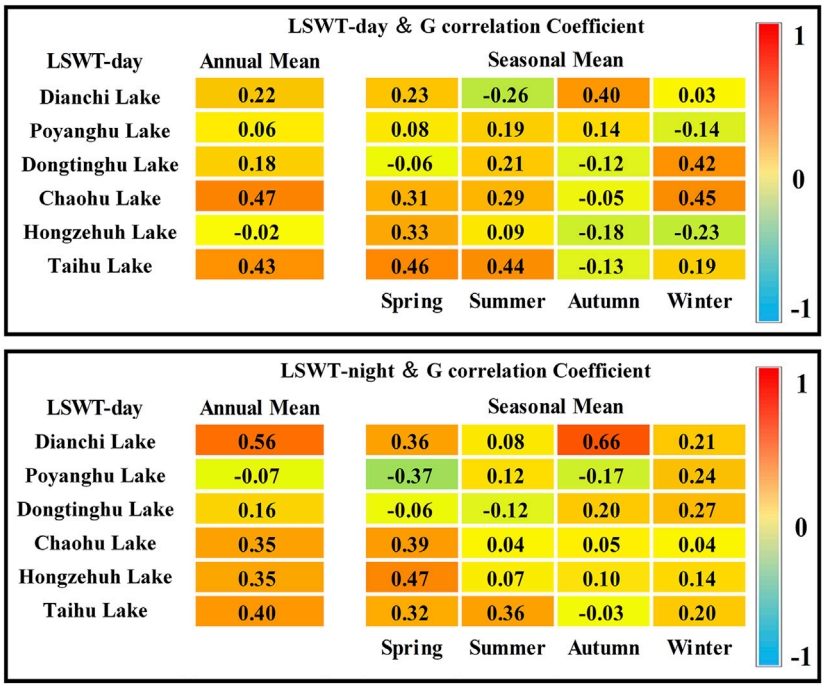

FIGURE 5
Correlation between lake surface water temperature and G. Note: Two decimal places are reserved for the correlation in the figure.

LSWT was not absolutely consistent with the growth rate of ISA or ISACR. Among them, the growth rate of ISA in CHL is only 473.34 km^2/decade, and ISACR increases from 4.83% to 10.44%. However, the annual average temperature rise rate of LSWT in daytime and night in CHL has reached 0.41°C/decade and 0.28°C/decade respectively. Therefore, without considering distance attenuation, only considering the growth rate of ISA or ISACR to analyze the impact of IS expansion on LSWT may amplify or reduce the impact of IS on LSWT.

(3) The introduction of the spatial influence equation can solve the problem in which the discretization of the spatial distribution of IS and the lake makes it difficult to study the impact of IS on LSWT. Furthermore, by quantifying the impact of IS on LSWT in the watershed, combined with the spatial distribution of IS in the watershed, the lake area and distance, the phenomenon of the inconsistency between the IS warming rate and the ISA or ISACR growth rate can be further explained. At the same time, by comparing the correlation between the LSWT of the six lakes during the day and at night and G, it can be seen that DCL (0.22 and 0.56), CHL (0.47 and 0.35) and THL (0.43 and 0.40) with smaller watershed areas have higher correlation than PYHL (0.06 and −0.07), THHL (0.18 and 0.16) and HZHL (−0.02 and 0.35), which have larger watershed areas, indicating that compared with lakes with large watershed area, the spatial influence equation can better quantify the impact of urban expansion on LSWT in a small-scale watershed.

Data availability statement

The datasets presented in this study can be found in online repositories. The names of the repository/repositories and accession number(s) can be found below: https://doi.org/10.5281/zenodo.6818189.

Author contributions

Linfeng Tang: Methodology, Validation, Writing—original draft. **Kun Yang:** Conceptualization, Resources. **Chunxue Shang:** Writing—review and editing. **Zongqi Peng:** Data processing. **Yi Luo:** Conceptualization, Resources, Funding acquisition, Writing—review and editing.

Funding

This work was supported by the National Natural Science Foundation of China [41761084]. LT and KY contributed equally to this work and should be considered co-first authors.

Conflict of interest

The authors declare that the research was conducted in the absence of any commercial or financial relationships that could be construed as a potential conflict of interest.

Publisher's note

All claims expressed in this article are solely those of the authors and do not necessarily represent those of their affiliated organizations, or those of the publisher, the editors and the reviewers. Any product that may be evaluated in this article, or claim that may be made by its manufacturer, is not guaranteed or endorsed by the publisher.

Supplementary material

The Supplementary Material for this article can be found online at: https://www.frontiersin.org/articles/10.3389/fenvs.2022.991502/full#supplementary-material

References

Chen, Y., Yang, J., Yang, R. X., Xiao, X. M., and Xia, J. H. (2022). Contribution of urban functional zones to the spatial distribution of urban thermal environment. *Build. Environ.* 216, 109000. doi:10.1016/j.buildenv.2022.109000

Clark, D. R., Underwood, G. J. C., McGenity, T. J., and Dumbrell, A. J. (2021). What drives study-dependent differences in distance-decay relationships of microbial communities? *Glob. Ecol. Biogeogr.* 30 (4), 811–825. doi:10.1111/geb.13266

Ding, X. W., and Li, X. F. (2011). Monitoring of the water-area variations of Lake Dongting in China with ENVISAT ASAR images. *Int. J. Appl. Earth Observation Geoinformation* 13 (6), 894–901. doi:10.1016/j.jag.2011.06.009

Fotheringham, A. S. (1981). Spatial structure and distance-decay parameters. *Ann. Assoc. Am. Geogr.* 71 (3), 425–436. doi:10.1111/j.1467-8306.1981.tb01367.x

Galli, J. (1990). *Thermal impacts associated with urbanization and stormwater best management practices*. Washington, DC: Metropolitan Washington Council of Governments, 188.

Gu, C. L., Guan, W. H., and Liu, H. L. (2017). Chinese urbanization 2050: SD modeling and process simulation. *Sci. China Earth Sci.* 60 (6), 1067–1082. doi:10.1007/s11430-016-9022-2

Hathaway, J. M., Winston, R. J., Brown, R. A., Hunt, W. F., and McCarthy, D. T. (2016). Temperature dynamics of stormwater runoff in Australia and the USA. *Sci. Total Environ.* 559, 141–150. doi:10.1016/j.scitotenv.2016.03.155

He, B. J., Wang, J. S., Zhu, J., and Qi, J. D. (2022). Beating the urban heat: Situation, background, impacts and the way forward in China. *Renew. Sustain. Energy Rev.* 161, 112350. doi:10.1016/j.rser.2022.112350

He, B. J., Zhao, D. X., Xiong, K., Qi, J. D., Ulpiani, G., Pignatta, G., et al. (2021). A framework for addressing urban heat challenges and associated adaptive behavior by the public and the issue of willingness to pay for heat resilient infrastructure in Chongqing, China. *Sustain. Cities Soc.* 75, 103361. doi:10.1016/j.scs.2021.103361

He, Y. T., Jia, G. S., Hu, Y. H., and Zhou, Z. J. (2013). Detecting urban warming signals in climate records. *Adv. Atmos. Sci.* 30 (4), 1143–1153. doi:10.1007/s00376-012-2135-3

Heddam, S., Ptak, M., and Zhu, S. L. (2020). Modelling of daily lake surface water temperature from air temperature: Extremely randomized trees (ERT) versus Air2Water, MARS, M5Tree, RF and MLPNN. *J. Hydrology* 588, 125130. doi:10.1016/j.jhydrol.2020.125130

Houser, J. N. (2006). Water color affects the stratification, surface temperature, heat content, and mean epilimnetic irradiance of small lakes. *Can. J. Fish. Aquat. Sci.* 63 (11), 2447–2455. doi:10.1139/f06-131

Huang, L., Wang, X. H., Sang, Y. X., Tang, S. C., Jin, L., Yang, H., et al. (2021). Optimizing lake surface water temperature simulations over large lakes in China with FLake model. *Earth Space Sci.* 8 (8), 21. doi:10.1029/2021ea001737

Janke, B. D., Herb, W. R., Mohseni, O., and Stefan, H. G. (2009). Simulation of heat export by rainfall-runoff from a paved surface. *J. Hydrology* 365 (3-4), 195–212. doi:10.1016/j.jhydrol.2008.11.019

Kainz, M. J., Ptacnik, R., Rasconi, S., and Hager, H. H. (2017). Irregular changes in lake surface water temperature and ice cover in subalpine Lake Lunz, Austria. *Inland Waters* 7 (1), 27–33. doi:10.1080/20442041.2017.1294332

Layden, A., MacCallum, S. N., and Merchant, C. J. (2016). Determining lake surface water temperatures worldwide using a tuned one-dimensional lake model (<i> FLake</i>, v1). *Geosci. Model Dev.* 9 (6), 2167–2189. doi:10.5194/gmd-9-2167-2016

Li, J. Q., Gong, Y. W., Li, X. J., Yin, D. K., and Shi, H. H. (2019). Urban stormwater runoff thermal characteristics and mitigation effect of low impact development measures. *J. Water Clim. Chang.* 10 (1), 53–62. doi:10.2166/wcc.2018.145

Lieberherr, G., and Wunderle, S. (2018). lake surface water temperature derived from 35 Years of AVHRR sensor data for European lakes. *Remote Sens.* 10 (7), 990. doi:10.3390/rs10070990

Liu, B. J., Wan, W., Xie, H. J., Li, H., Zhu, S. Y., Zhang, G. Q., et al. (2019). A long-term dataset of lake surface water temperature over the Tibetan Plateau derived from AVHRR 1981-2015. *Sci. Data* 6, 48. doi:10.1038/s41597-019-0040-7

Liu, G., Ou, W. X., Zhang, Y. L., Wu, T. F., Zhu, G. W., Shi, K., et al. (2015). Validating and mapping surface water temperatures in lake Taihu: Results from MODIS land surface temperature products. *IEEE J. Sel. Top. Appl. Earth Obs. Remote Sens.* 8 (3), 1230–1244. doi:10.1109/jstars.2014.2386333

Luo, Y., Li, Q. L., Yang, K., Xie, W. Q., Zhou, X. L., Shang, C. X., et al. (2019a). Thermodynamic analysis of air-ground and water-ground energy exchange process in urban space at micro scale. *Sci. Total Environ.* 694. doi:10.1016/j.scitotenv.2019.133612

Luo, Y., Zhang, Y. Y., Yang, K., Yu, Z. Y., and Zhu, Y. (2019b). Spatiotemporal Variations in Dianchi Lake's Surface Water Temperature From 2001 to 2017 Under the Influence of Climate Warming. *Ieee Access* 7, 115378–115387. doi:10.1109/access.2019.2935767

Luo, Y., Zhao, Y. S., Yang, K., Chen, K. X., Pan, M. E., and Zhou, X. L. (2018). Dianchi Lake watershed impervious surface area dynamics and their impact on lake water quality from 1988 to 2017. *Environ. Sci. Poll. Res.* 25 (29), 29643–29653. doi:10.1007/s11356-018-2967-1

Mushtaq, F., Ahmed, P., and Lala, M. G. N. (2021). Spatiotemporal change in the surface temperature of Himalayan lake and its inter-relation with water quality and growth in aquatic vegetation. *Geocarto Int.* 36 (3), 241–261. doi:10.1080/10106049.2019.1590467

Ngai, K. L. C., Shuter, B. J., Jackson, D. A., and Chandra, S. (2013). Projecting impacts of climate change on surface water temperatures of a large subalpine lake: Lake Tahoe, USA. *Clim. Change* 118 (3-4), 841–855. doi:10.1007/s10584-013-0695-6

O'Reilly, C. M., Sharma, S., Gray, D. K., Hampton, S. E., Read, J. S., Rowley, R. J., et al. (2015). Rapid and highly variable warming of lake surface waters around the globe. *Geophys. Res. Lett.* 42 (24), 10773–10781. doi:10.1002/2015gl066235

Oglu, B., Mols, T., Kaart, T., Cremona, F., and Kangur, K. (2020). Parameterization of surface water temperature and long-term trends in Europe's fourth largest lake shows recent and rapid warming in winter. *Limnologica* 82, 125777. doi:10.1016/j.limno.2020.125777

Osth, J., Lyhagen, J., and Reggiani, A. (2016). A new way of determining distance decay parameters in spatial interaction models with application to job accessibility analysis in Sweden. *Eur. J. Transp. Infrastructure Res.* 16 (2), 344–362. doi:10.18757/ejtir.2016.16.2.3142

Pareeth, S., Salmaso, N., Adrian, R., and Neteler, M. (2016). Homogenised daily lake surface water temperature data generated from multiple satellite sensors: A long-term case study of a large sub-alpine lake. *Sci. Rep.* 6, 31251. doi:10.1038/srep31251

Piccolroaz, S., Toffolon, M., and Majone, B. (2013). A simple lumped model to convert air temperature into surface water temperature in lakes. *Hydrol. Earth Syst. Sci.* 17 (8), 3323–3338. doi:10.5194/hess-17-3323-2013

Ptak, M., Sojka, M., Choinski, A., and Nowak, B. (2018). Effect of environmental conditions and morphometric parameters on surface water temperature in polish lakes. *Water* 10 (5), 580. doi:10.3390/w10050580

Ren, J. Y., Yang, J., Zhang, Y. Q., Xiao, X. M., Li, X. M., Wang, S. H., et al. (2022). Exploring thermal comfort of urban buildings based on local climate zones. *J. Clean. Prod.* 340, 130744. doi:10.1016/j.jclepro.2022.130744

Riffler, M., Lieberherr, G., and Wunderle, S. (2015). Lake surface water temperatures of European Alpine lakes (1989-2013) based on the Advanced Very High Resolution Radiometer (AVHRR) 1 km data set. *Earth Syst. Sci. Data* 7 (1), 1–17. doi:10.5194/essd-7-1-2015

Sabouri, F., Gharabaghi, B., Mahboubi, A. A., and McBean, E. A. (2013). Impervious surfaces and sewer pipe effects on stormwater runoff temperature. *J. Hydrology* 502, 10–17. doi:10.1016/j.jhydrol.2013.08.016

Schmid, M., and Koster, O. (2016). Excess warming of a Central European lake driven by solar brightening. *Water Resour. Res.* 52 (10), 8103–8116. doi:10.1002/2016wr018651

Sharma, S., Gray, D. K., Read, J. S., O'Reilly, C. M., Schneider, P., Qudrat, A., et al. (2015). A global database of lake surface temperatures collected by *in situ* and satellite methods from 1985-2009. *Sci. Data* 2, 150008. doi:10.1038/sdata.2015.8

Song, K. S., Wang, M., Du, J., Yuan, Y., Ma, J. H., Wang, M., et al. (2016). Spatiotemporal variations of lake surface temperature across the Tibetan plateau using MODIS LST product. *Remote Sens.* 8 (10), 854. doi:10.3390/rs8100854

Soydan, O. (2020). Effects of landscape composition and patterns on land surface temperature: Urban heat island case study for Nigde, Turkey. *Urban Clim.* 34, 100688. doi:10.1016/j.uclim.2020.100688

Thompson, A. M., Vandermuss, A. J., Norman, J. M., and Roa-Espinosa, A. (2008). Modeling the effect of a rock crib on reducing stormwater runoff temperature. *Trans. Asabe* 51 (3), 947–960. doi:10.13031/2013.24533

Trumpickas, J., Shuter, B. J., and Minns, C. K. (2009). Forecasting impacts of climate change on Great Lakes surface water temperatures. *J. Gt. Lakes. Res.* 35 (3), 454–463. doi:10.1016/j.jglr.2009.04.005

Wan, W., Zhao, L., Xie, H., Liu, B., Li, H., Cui, Y., et al. (2018). lake surface water temperature change over the Tibetan plateau from 2001 to 2015: A sensitive indicator of the warming climate. *Geophys. Res. Lett.* 45 (20), 11177–11186. doi:10.1029/2018gl078601

Woolway, R. I., Jennings, E., and Carrea, L. (2020). Impact of the 2018 European heatwave on lake surface water temperature. *Inland Waters* 10 (3), 322–332. doi:10.1080/20442041.2020.1712180

Woolway, R. I., Jones, I. D., Maberly, S. C., French, J. R., Livingstone, D. M., Monteith, D. T., et al. (2016). Diel surface temperature range scales with lake size. *Plos One* 11 (3), e0152466. doi:10.1371/journal.pone.0152466

Woolway, R. I., and Merchant, C. J. (2018). Intralake heterogeneity of thermal responses to climate change: A study of large northern hemisphere lakes. *J. Geophys. Res. Atmos.* 123 (6), 3087–3098. doi:10.1002/2017jd027661

Xie, P., Yang, J., Sun, W., Xiao, X. M., and Xia, J. C. (2022). Urban scale ventilation analysis based on neighborhood normalized current model. *Sustain. Cities Soc.* 80, 103746. doi:10.1016/j.scs.2022.103746

Yang, J., Wang, Y. C., Xiao, X. M., Jin, C., Xia, J. H., and Li, X. M. (2019a). Spatial differentiation of urban wind and thermal environment in different grid sizes. *Urban Clim.* 28, 100458. doi:10.1016/j.uclim.2019.100458

Yang, J., Yang, Y. X., Sun, D. Q., Jin, C., and Xiao, X. M. (2021a). Influence of urban morphological characteristics on thermal environment. *Sustain. Cities Soc.* 72, 103045. doi:10.1016/j.scs.2021.103045

Yang, K., Luo, Y., Chen, K. X., Yang, Y., Shang, C. X., Yu, Z. Y., et al. (2020a). Spatial-temporal variations in urbanization in Kunming and their impact on urban lake water quality. *Land Degrad. Dev.* 31 (11), 1392–1407. doi:10.1002/ldr.3543

Yang, K., Yu, Z. Y., and Luo, Y. (2020b). Analysis on driving factors of lake surface water temperature for major lakes in Yunnan-Guizhou Plateau. *Water Res.* 184, 116018. doi:10.1016/j.watres.2020.116018

Yang, K., Yu, Z. Y., Luo, Y., Yang, Y., Zhao, L., and Zhou, X. L. (2018). Spatial and temporal variations in the relationship between lake water surface temperatures and water quality - a case study of Dianchi Lake. *Sci. Total Environ.* 624, 859–871. doi:10.1016/j.scitotenv.2017.12.119

Yang, K., Yu, Z. Y., Luo, Y., Zhou, X. L., and Shang, C. X. (2019b). Spatial-temporal variation of lake surface water temperature and its driving factors in yunnan-Guizhou Plateau. *Water Resour. Res.* 55 (6), 4688–4703. doi:10.1029/2019wr025316

Yang, K., Zhang, Y., Luo, Y., and Shang, C. X. (2021c). Precipitation events impact on urban lake surface water temperature under the perspective of macroscopic scale. *Environ. Sci. Pollut. Res.* 28 (13), 16767–16780. doi:10.1007/s11356-020-12093-0

Yang, K., Peng, Z. Q., Luo, Y., and Shang, C. X. (2021b). The heat exchange process between surface water and near-surface atmosphere in the front of the Three Gorges Dam. *Internat. J. Appl. Earth Observ. Geoinform.* 102, 12. doi:10.1016/j.jag.2021.102372

Yu, Z. Y., Yang, K., Luo, Y., Wang, P., and Yang, Z. (2021). Research on the lake surface water temperature downscaling based on deep learning. *Ieee J. Sel. Top. Appl. Earth Observ. Remote Sens.* 14, 5550–5558. doi:10.1109/jstars.2021.3079357

Yu, Z. Y., Yang, K., Luo, Y., Shang, C. X., and Zhu, Y. (2020). Lake surface water temperature prediction and changing characteristics analysis–A case study of 11 natural lakes in Yunnan-Guizhou Plateau. *J. Clean. Produc.* 276, 17. doi:10.1016/j.jclepro.2020.122689

Yu, H. S., Yang, J., Li, T., Jin, Y., and Sun, D. Q. (2022). Morphological and functional polycentric structure assessment of megacity: An integrated approach with spatial distribution and interaction. *Sustain. Cities Soc.* 80, 103800. doi:10.1016/j.scs.2022.103800

Zhao, Z. Q., Sharifi, A., Dong, X., Shen, L. D., and He, B. J. (2021). Spatial variability and temporal heterogeneity of surface urban heat island patterns and the suitability of local climate zones for land surface temperature characterization. *Remote Sens.* 13 (21), 4338. doi:10.3390/rs13214338

Zhou, L., Dang, X., Mu, H., Wang, B., and Wang, S. (2021). Cities are going uphill: Slope gradient analysis of urban expansion and its driving factors in China. *Sci. Total Environ.* 775, 145836. doi:10.1016/j.scitotenv.2021.145836

Zhou, L., Hu, F. N., Wang, B., Wei, C. Z., Sun, D. Q., and Wang, S. H. (2022). Relationship between urban landscape structure and land surface temperature: Spatial hierarchy and interaction effects. *Sustain. Cities Soc.* 80, 103795. doi:10.1016/j.scs.2022.103795

Zhu, S. L., Ptak, M., Yaseen, Z. M., Dai, J. Y., and Sivakumar, B. (2020). Forecasting surface water temperature in lakes: A comparison of approaches. *J. Hydrology* 585, 124809. doi:10.1016/j.jhydrol.2020.124809

frontiers | Frontiers in Environmental Science

TYPE Original Research
PUBLISHED 30 August 2022
DOI 10.3389/fenvs.2022.988346

Check for updates

OPEN ACCESS

EDITED BY
Bing Xue,
Institute of Applied Ecology (CAS), China

REVIEWED BY
Dahao Zhang,
Sun Yat-sen University, China
Asish Saha,
University of Burdwan, India

*CORRESPONDENCE
Yanhua Fu,
fuyanhua@mail.neu.edu.cn
Yalin Zhang,
2001428@stu.neu.edu.cn

SPECIALTY SECTION
This article was submitted to Environmental Informatics and Remote Sensing,
a section of the journal
Frontiers in Environmental Science

RECEIVED 07 July 2022
ACCEPTED 05 August 2022
PUBLISHED 30 August 2022

CITATION
Fu Y and Zhang Y (2022), Research on temporal and spatial evolution of land use and landscape pattern in Anshan City based on GEE.
Front. Environ. Sci. 10:988346.
doi: 10.3389/fenvs.2022.988346

COPYRIGHT
© 2022 Fu and Zhang. This is an open-access article distributed under the terms of the Creative Commons Attribution License (CC BY). The use, distribution or reproduction in other forums is permitted, provided the original author(s) and the copyright owner(s) are credited and that the original publication in this journal is cited, in accordance with accepted academic practice. No use, distribution or reproduction is permitted which does not comply with these terms.

Research on temporal and spatial evolution of land use and landscape pattern in Anshan City based on GEE

Yanhua Fu* and Yalin Zhang*

Jangho Architecture College, Northeastern University, Shenyang, China

Frequent mining activities can bring about problems such as soil erosion and environmental pollution, which are detrimental to the efficient use of land and the sustainable development of cities. Existing studies have paid little attention to mining areas and lack comparative analysis of landscape changes in multiple mining pits. In this paper, the main urban area of Anshan City, where the mining areas are concentrated, was used as the research area, and the Landsat TM/OLI surface reflectance (SR) data of the Google Earth Engine (GEE) platform and the random forest algorithm were used to map the land use in 2008, 2014, and 2020. On this basis, land use dynamics and landscape pattern indices were used to analyze the changes in land use and landscape patterns in the Anshan City area. In addition, a moving window method was combined to further analyze and compare the landscape changes between different pits. The results show that:1. From 2008 to 2020, the construction land in Anshan urban area continued to decline, the forest land continued to expand, and the construction land was shifted to the forest land and cultivated land. Mining land increased before 2014 and remained almost unchanged after 2014, which is in line with the actual situation. 2. During the study period, the landscape fragmentation degree and landscape heterogeneity in the urban area of Anshan kept increasing. The high value areas of landscape fragmentation were the urban-rural combination areas and the mining areas. Among them, the reclamation of Dagushan and Donganshan is better, while the reclamation of Anqian, Yanqianshan and Xiaolingzi mines needs to be strengthened. 3. The random forest algorithm based on GEE shows a high degree of accuracy for land use classification. The overall classification accuracy in 3 years exceeds 90% and the kappa coefficient exceeds 0.85. The study results can be used as an essential reference for optimizing the urban ecological environment and provide technical backing for the urbanization construction and rational use of land in Anshan City.

KEYWORDS

GEE, random forest, moving window, land use, landscape pattern, temporal and spatial evolution, anshan City

1 Introduction

Land use change is driven by human behavior and affects the structure and function of landscape ecosystems (Schmitt et al., 2010; Bajocco et al., 2012). Since the 1990s, land use change research has become one of the central issues in global environmental change research (Peng et al., 2008; Liu and Deng, 2010; Chang et al., 2018). Landscape pattern is the spatial distribution and arrangement of landscape elements (Liu et al., 2010), which represents the effects of different ecological processes acting at different spatial scales, and is the embodiment of landscape heterogeneity (Cheung et al., 2016; Feng et al., 2018). Changes in landscape patterns are an integrated reflection of the regional ecosystem as a result of a combination of human activities, natural and biological factors (Turner, 1990; Bürgi et al., 2004). Therefore, monitoring and analyzing the spatial and temporal evolutionary characteristics of land use and landscape patterns can help reveal the links between land use and landscape patterns, regulate the direction and speed of human activities, and provide important references for the rational use of land resources and the coordinated development of landscape types.

With the continuous advancement of RS and GIS, the application of RS and GIS to analyze the changing characteristics of landscape pattern and land use has become a research hotspot in geography, environmental science and other disciplines (Tekle and Hedlund, 2000; Groom et al., 2006; Shao and Wu, 2008; Du et al., 2012). The research includes the use of RS and machine learning methods to obtain long time series remote sensing to monitor the spatial and temporal evolution characteristics of land use and its driving factors (Gao et al., 2015; Thakkar et al., 2017), the use of Fragstats software and landscape pattern index to analyze landscape pattern changes (Huang et al., 2008; Liu et al., 2012) and the impact of land use and landscape pattern on the ecological environment (Singh et al., 2010; Jazouli et al., 2019; Tian et al., 2020). Tang et al. (2020) linked land use, landscape pattern and ecosystem service values and used Pearson correlation coefficients to explore the extent to which changes in land use and landscape pattern are associated with ecosystem services, finding that high intensity land use leads to degradation of ecosystem services. These studies have focused on ecologically important areas (Wang et al., 2009; Wan et al., 2015; Liu et al., 2018; Li et al., 2021a) and rapidly urbanizing areas (Deng et al., 2009; Hassan, 2017; Dadashpoor et al., 2019), but less on ecologically fragile urbanized areas such as mining areas and resource-based cities.

The exploitation of mineral resources has become the backbone of China's sustained and stable economic and social development (Wang et al., 2016; Zhai et al., 2021). Frequent mining activities have changed the surface characteristics (Wu et al., 2021b), the integrity of the original landscape pattern has been damaged under human interference, and the landscape spatial structure has undergone dramatic changes, breaking the local ecological balance and damaging the regional ecological environment. At the same time, this has led to the degradation of urban ecology and aggravated environmental pollution (Xu et al., 2019; Takam Tiamgne et al., 2021; Wang et al., 2021; Yu et al., 2022), which has seriously affected the human settlement environment and restricted the green, healthy and sustainable development of cities (Yang et al., 2021). At present, environmental monitoring in mining areas mainly focuses on studies of vegetation cover changes in traditional mining areas (Lei et al., 2010; Liu et al., 2016b; Fang et al., 2019; Li et al., 2021b) and the characteristics of landscape use changes before and after mine reclamation (Townsend et al., 2009; Ge et al., 2010; Yang et al., 2018). Kuzevic et al. (2022) analyzed the vegetation cover of the Slovakian mining area containing four deposits using NDVI and further compared the vegetation changes in the four deposits using Forest Spatial Division Unit data. Zhang et al. (2020b) used multi-temporal remote sensing images and landscape pattern indexes to study the change characteristics of landscape pattern and land use in the Pingshuo mining area containing three open pits, and constructed a complex network to analyze the correlation between indexes, but did not further compare the landscape changes of the three open pits. Most mining and mineral resource cities have more than one pit, often multiple pits clustered together, and there are differences in landscape pattern changes between individual pits, so using the landscape pattern index to analyze overall trends does not reflect the changes in individual open pits. The moving window method produces a quantitative, spatially distributed metric. Raster mapping through moving windows allows specific changes in the landscape to be monitored both spatially and quantitatively (Hayes and Robeson, 2013).

However, when multi-temporal remote sensing images are used for land use mapping, it often takes a lot of time to download and process remote sensing images. The emergence of Google Earth Engine (GEE) has greatly promoted the research on land use by remote sensing. GEE not only provides massive satellite image datasets and geographic datasets (Kumar and Mutanga, 2018) but also provides API interfaces (Prasai et al., 2021), analysis algorithms and tools based on JavaScript and Python languages (Gorelick et al., 2017; Amani et al., 2020). Programming languages are directly used to analyze and process remote sensing data in GEE (Chang et al., 2018; Mutanga and Kumar, 2019), which avoids the tedious processes of data download, preprocessing, and image classification brought about by traditional remote sensing analysis models. Ang (Ang et al., 2021) and Pericak (Pericak et al., 2018) used GEE to draw land use maps for the Didipio mine and the Appalachian open-pit coal mine respectively. It was found that GEE can not only quickly and efficiently process remote sensing images of large areas over many years but also quantify land use change.

As a typical mineral resource city, Anshan City has abundant iron ore resources, and its iron ore reserves account for 52% of China's total iron ore resources. Anshan iron ore is concentrated in the main urban area of Anshan City. According to statistics,

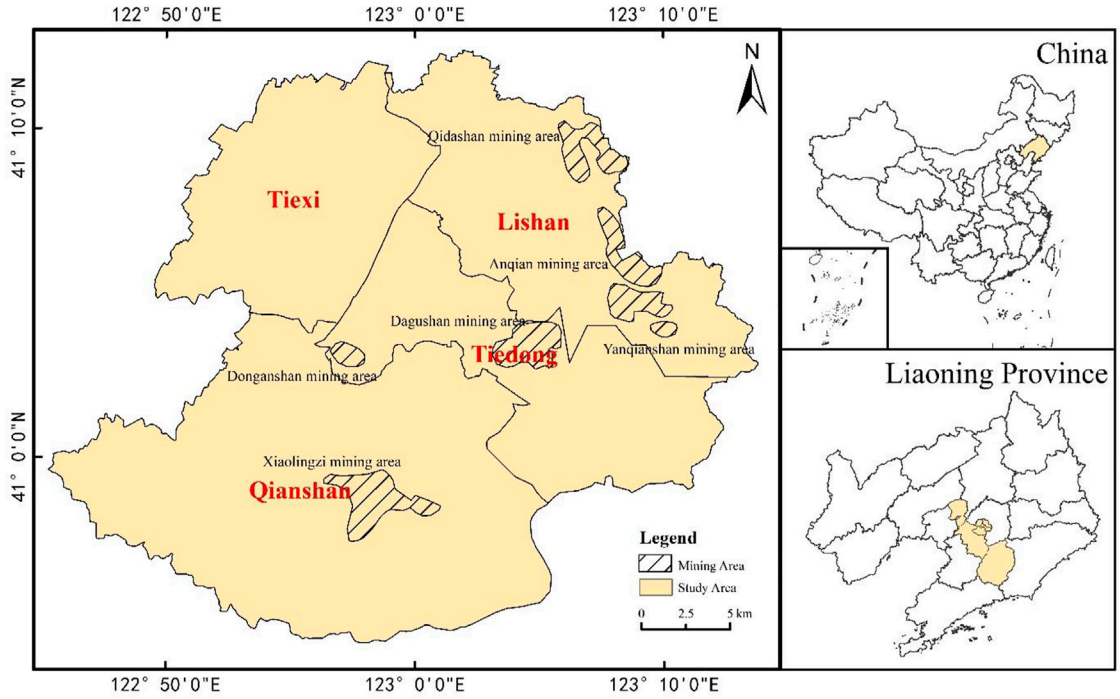

FIGURE 1
Location of study area and mining areas.

the total area of the mining area in Anshan is about 50 km^2 and the mining area in the main urban area of Anshan alone exceeds 30 km^2, which means 60% of the iron ore in Anshan City is concentrated in the main urban area of Anshan. With the uninterrupted mining for a hundred years, a large area of dumps and tailings ponds have been formed in the main urban area of Anshan City, which not only wastes land resources, destroys geological landforms, but also brings many negative impacts to the urban and rural living environment of Anshan. Therefore, this paper uses GEE-based multi-temporal Landsat remote sensing data, combined with the moving window method and the landscape pattern index, to explore 1) the spatial and temporal evolutionary characteristics of land use and landscape patterns in the main urban area of Anshan. 2) Further analysis of landscape changes between different pits in Anshan. 3) The driving factors causing the changes. To provide reference for mine reclamation, rational land use and comprehensive environmental management in Anshan.

2 Data and methods

2.1 Study area

Anshan's main urban area is the study area (122°4′-123°1′E, 40°5′-41°1′N), situated in the central part of Anshan City, Liaoning Province, bordering Liaoyang City, including Tiexi District, Tiedong District, Lishan District and Qianshan District. The urban area of Anshan is 796 km^2. The population of Anshan reaches 1.45 million in 2020. Six major mining areas surround the main urban area of Anshan City. It can be seen from Figure 1 that they are the Qidashan mining area, Anqian mining area, Yanqianshan mining area, Dagushan mining area, Donganshan mining area and Xiaolingzi mining area. The Qidashan, Dagushan, Donganshan and Xiaolingzi mining areas are all composed of mining areas and tailings ponds. The Anqian mining area is composed of several small iron ore stopes, and the Yanqianshan is an independent mining area. These iron mines are concentrated in Anshan's main urban area. The mining area in the urban area is about 34 km^2, or 4.2% of the overall area of the main urban area. Continuous and uninterrupted mining activities have resulted in deepening mines, increasing the height of dumps, expanding tailings ponds and bringing mines closer to urban areas in Anshan, damaging the ecological environment of the city and restricting the sustainable development of the city.

2.2 Data source and processing

Data for the study are Landsat TM/OLI surface reflectance (SR) data, administrative division data and digital elevation data.

TABLE 1 Data source and description.

Data types	Resolution (m)	Year	Data sources
LANDSAT-5 (TM) SR	30	2008	https://developers.google.com/earth-engine/datasets/catalog/LANDSAT_LT05_C02_T1_L2?hl=en
LANDSAT-8(OLI) SR	30	2014, 2020	https://developers.google.com/earth-engine/datasets/catalog/LANDSAT_LC08_C02_T1_L2?hl=en
NASA DEM	30	2000	https://developers.google.com/earth-engine/datasets/catalog/NASA_NASADEM_HGT_001?hl=en
Administrative division		2015	http://www.resdc.cn/

TABLE 2 Land use classification.

Category	Describe
Construction land	Land transformed by human activities, including urban residences, commercial areas, industrial areas, road traffic
Cultivated land	Land capable of growing crops, including vegetable fields, paddy fields and dry land
Forest land	Covered by woods, including forests, woodlands and meadows, and urban parkland
Mining land	Areas used for mining activities, including stopes, tailings ponds, dumps
Water	Includes standing water in rivers, lakes, cisterns, land reservoirs, fish ponds, and mining subsidence

Table 1 provides details of these data. On the basis of GEE platform, we obtained and processed: 1) Landsat TM/OLI surface reflectance (SR) data with a resolution of 30 m provided by USGS. Among them, the images in 2008 were Landsat five TM SR data, and those in 2014 and 2020 were Landsat eight OLI SR data. The SR data was preprocessed by geometric correction and atmospheric correction, and the data contained the image quality assessment (QA) band obtained by the FMASK algorithm (Qiu et al., 2018). The composite algorithm was used to stitch the SR data from January to December of the current year, and the median value was selected to synthesize the image with the smallest annual cloud cover. The QA band was then used to automatically mask clouds, snow and cloud shadows to remove clouds from images (Wahap and Shafri, 2020). The vector data of the study area was uploaded to GEE to crop the three-phase remote sensing images. The cloud-free images of the study area in 2008, 2014, and 2020 were obtained respectively. 2) NASA DEM data with a resolution of 30 m released by NASA LP DAAC. NASA DEM serves as an approach to reprocessing STRM data, improving its accuracy by incorporating auxiliary data from datasets such as STER GDEM.

2.3 Sample selection

Based on the Classification of Current Land Use Status (GB/T21010-2017) and with the land cover and landscape conditions of Anshan City taken into account, the land use types in the study area were categorized into five categories: mining land, construction land, forest land, water and cultivated land (Table 2). The training samples were selected on the basis of the features of five types of land use. This study used the hyperspectral satellite Sentinel-2A data with a resolution of 10 m, combined with the 2020 Landsat-8 OLI image, to select samples in 2020. The 2008 and 2014 samples were obtained by examining Google Earth Pro historical images and Landsat TM/OLI images. The number of sample points in 2008, 2014, and 2020 were 753, 601, and 906, respectively. 70% of the samples were randomly selected as training data and the rest as test data for accuracy evaluation.

In order to obtain classification results of higher accuracy, it is necessary to introduce feature variables. This study not only selected five spectral bands of blue, green, red, near-infrared, and short-wave infrared (SWIR 1) in the Landsat image, but also used the GEE platform to calculate with the normalized difference vegetation index (NDVI), enhanced vegetation index (EVI), bare soil index (BSI), normalized difference water index (NDWI) and index-based built-up index (IBI) (Kupidura, 2019; Cui et al., 2022; Fathololoumi et al., 2022). At the same time, DEM was introduced to account for the apparent variance related to topographical factors. The above 11 feature variables were selected and introduced to the original image to improve the accuracy of image classification.

2.4 Processes and methods

2.4.1 Land use classification based on random forest

Random forest is a machine learning algorithm consisting of multiple decision trees (Ghimire et al., 2013; Zhang and Yang, 2020). It uses the bootstrap resampling technique

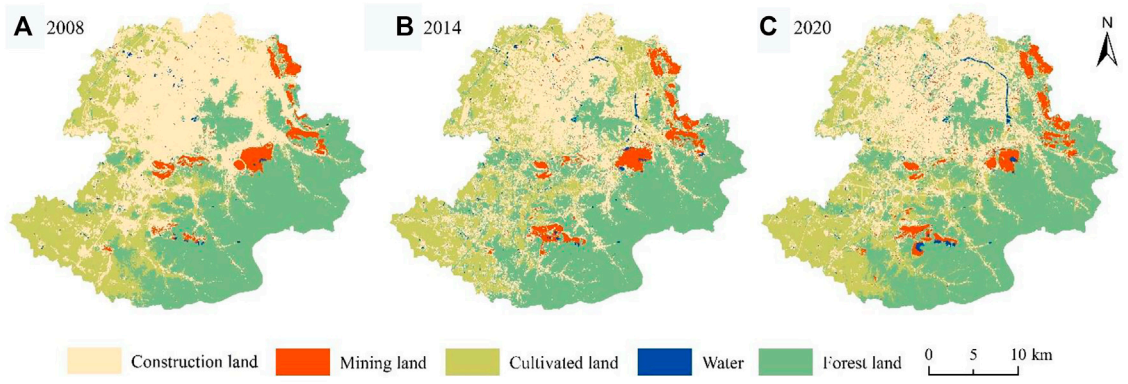

FIGURE 2
The land use map of Anshan urban area. **(A)** 2008; **(B)** 2014; **(C)** 2020.

(Breiman, 2001b) to randomly choose n samples from the original dataset D to form a sub-data set (Wu et al., 2021a), and then uses the sub-data set to build a single decision tree. After each sample has been drawn, the drawn sample needs to be put back into data set D again. Repeat the above steps to produce m decision trees to form a random forest. Decision trees are independent and parallel to each other, and each decision tree outputs a result. Finally, the classification result of the new data is derived from the joint voting of m decision trees (He et al., 2022b). The specific classification process is described below: 1) Randomly choose n samples from the data set and then put them back into the data set. 2) Randomly select k features for the selected samples to generate a decision tree (Magidi et al., 2021). 3) Repeat the above steps m times to obtain m decision trees, resulting in a random forest. 4) For the input new data, m decision trees are used to classify it respectively. Count the votes of these m classification results. The category with the most votes is the result of the classification of the new data.

The construction of the decision tree in the random forest algorithm selects some samples and features randomly, which enhances the anti-noise performance of the method and avoids overfitting to a certain extent (Breiman, 2001a; Belgiu and Drăguț, 2016). Moreover, the random forest adopts the bagging ensemble algorithm, and multiple independent decision trees make common decisions, which not only has high accuracy but also saves time (Schmidt et al., 2019). Classification using random forests in GEE requires setting five variables: the number of decision trees, the maximum number of leaf nodes in each tree, the randomization seed, the fraction of input to bag per tree, and the number of variables per split. In this study, the amount of feature variables for each split was the square root of the total amount of feature variables, the amount of decision trees was set to 100, the fraction of input to bag per tree was 0.8, and the rest of the parameters were default values. After the above parameters in GEE had been set, the land use map of Anshan urban area in 2008, 2014, and 2020 was obtained through random forest classification (Figure 2).

Random forest classification accuracy was evaluated by confusion matrix in GEE. Through the evaluation, overall classification accuracy and Kappa coefficient were educed. Among them, the Kappa coefficient is considered to be the most representative and comprehensive calculation accuracy index. If the Kappa coefficient exceeds 0.8, it means that the simulation is almost completely consistent (He et al., 2022a). Through the confusion matrix, the overall classification accuracy in 2008, 2014, and 2020 was 90.15%, 90.74%, and 91.94% respectively, and the Kappa coefficients were all above 0.85, indicating that the classification was efficient and of high accuracy.

2.4.2 Land use dynamic degree

The dynamic degree of land use is the rate of change of the area between various land use types over a certain period and reflects the degree of change in different land-use types over the study period. It is expressed as follows (Yang et al., 2022):

$$K = \frac{S_b - S_a}{S_a} \times \frac{1}{T} \times 100\%$$

Where K is the degree of dynamic change in a certain land use type within the study time T; S_a and S_b indicate the area of this land use type at the beginning and end of the study respectively. When T is a year, K represents the annual change rate of land use.

2.4.3 Landscape pattern based on landscape pattern index

Landscape pattern index is commonly used to quantify landscape changes and it allows quantitative monitoring and

TABLE 3 Formula and significance of landscape pattern index.

Formula	Meaning
$PD = \frac{n_i}{A}$	Indicates the number of patches of a certain landscape type per unit area, reflecting the fragmentation degree of the patch type and the complexity of the spatial structure
$LPI = \frac{Max(a_{ij})}{A} \times 100$	Reflect the dominant type of landscape
$LSI = \frac{25\sum_{k=1}^{m} e_{ik}}{\sqrt{A}}$	Indicates the complexity of the shape of the patch, the larger the value, the more complex the shape and the narrower the geometry
$PAFRAC = \frac{2}{\frac{[n_i \sum_{j=1}^{n} (\ln p_{ij} \times \ln a_{ij})] - [\sum_{j=1}^{n} \ln p_{ij} \times \sum_{j=1}^{n} \ln a_{ij}]}{(n_i \sum_{j=1}^{n} \ln p_{ij}^2) - (\sum_{j=1}^{n} \ln p_{ij})^2}}$	Reflects the complexity of the shape of the landscape. The higher the value, the more complex the shape and the more irregular the boundary
$CONTAG = [1 + \frac{\sum_{i=1}^{m}\sum_{k=1}^{m} (p_i \times \frac{g_{ik}}{\sum_{k=1}^{m} g_{ik}}) \times [\ln(p_i \times \frac{g_{ik}}{\sum_{k=1}^{m} g_{ik}})]}{2 \ln m}] \times 100$	Reflects spatial information and describes the degree of aggregation and trends in the extension of different patch types in the landscape
$SHDI = -\sum_{i=1}^{m} (p_i \ln p_i)$	Reflects landscape heterogeneity, the larger the value, the richer the landscape types
$SHEI = \frac{-\sum_{i=1}^{m} (p_i \ln p_i)}{\ln m}$	Describe how evenly distributed among different landscape types

Note: $i = 1 \ldots$ m patch types; $j = 1 \ldots$ n patches; $k = 1 \ldots$ m patch types; n_i = total number of patches for patch type i; A = total landscape area; a_{ij} = area of patch ij; e_{ik} = total length of edge in landscape between patch types i and k; p_{ij} = perimeter of patch ij; p_i = proportion of the landscape occupied by patch type i; g_{ik} = number of neighbouring patches of patch type i and k.

analysis of evolution in the spatial structure of the landscape (Bai et al., 2008; Fan and Ding, 2016). Landscape pattern index can reflect landscape characteristics from three levels: landscape, class and patch. Based on the landscape conditions of Anshan City, the study chose to research the landscape pattern from the two levels of landscape and class. And Fragstats4.2 was used to compute the landscape index in 2008, 2014, and 2020 respectively.

Regarding the selection of the index, in view of the morphological complexity, fragmentation, agglomeration and diversity of the landscape pattern, seven indexes including patch density (PD), perimeter-area fractal dimension (PAFRAC), landscape shape index (LSI), largest patch index (LPI), Shannon's diversity index (SHDI), contagion (CONTAG), and Shannon's evenness index (SHEI) were chosen to quantify the landscape pattern of Anshan urban area. The specific calculation formula and meaning of each index are given in Table 3.

2.4.4 Landscape pattern based on moving window

Using a moving window to generate a raster map can be a better way to analyze the landscape pattern from a spatial perspective. A moving window is a window with a fixed radius. It starts to move from the upper left corner. Each time it moves by one grid, the landscape index value within the window range is calculated, and the value is assigned to the center grid of the window. Finally, a raster map that can reflect the landscape pattern is formed (Hagen-Zanker, 2016). In this method, the size of the window radius may affect the landscape pattern directly. When the window radius is too small, the landscape pattern index between adjacent pixels will have a significant difference, which will easily lead to distortion of the results. When the window radius is too large, some small areas with changes will be ignored, which is not conducive to research and analysis. Therefore, in this study, 500, 800, 1000, 1200, and 1500 m were set as the window radius in Fragstats4.2. It was found that when the window radius was 1000 m, the result was the most consistent with the landscape pattern of the area. So 1000 m was used as the moving window radius to generate the raster map.

3 Result analysis

3.1 Land use

3.1.1 Land use changes

Forest land, construction land and cultivated land are the main types of land use in the urban areas of Anshan, with the sum of the three areas exceeding 95% of the total land area. Construction land is mainly in the northern plains, namely Tiexi District, Tiedong District and Lishan District. The forest land is located in the southeast of the urban area, cultivated land in the southwest and northwest of it and mining land in the east and south of it. The proportion of water is small, mainly consisting of rivers, lakes and mining subsidence stagnant water.

The transfer direction and transfer quantity of various types of land in Anshan urban area were analyzed on the basis of Figure 3. Between 2008 and 2014, cultivated land and construction land declined, while forest land, mining land, and water increased (Table 4). Cultivated land was converted to construction land and forest land, of which 5.66% was converted to construction land and 3.44% to forest land. Construction land was converted to cultivated land, forest land and mining land, of which 8.44% was converted to cultivated land, 3.64% to forest land, and 0.87% to mining land. The increased area of forest land came from construction land and cultivated land. 0.87% of construction land and 0.75% of forest land were transformed to mining land,

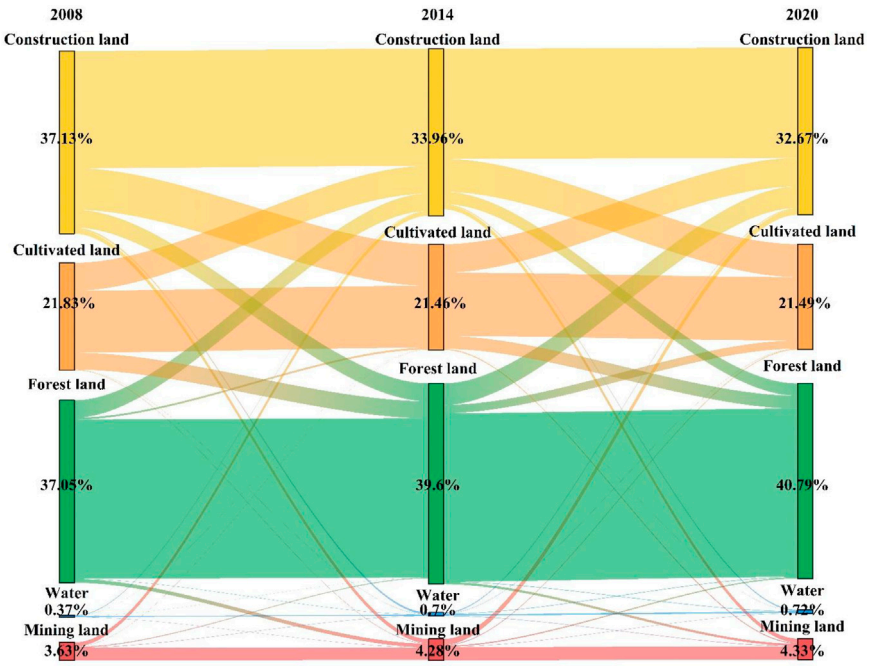

FIGURE 3
The transfer situation of various land use types in urban area of Anshan.

TABLE 4 Land use transfer matrix in Anshan urban area from 2008 to 2014.

2008	2014					Total (%)
	Cultivated land (%)	Construction land (%)	Mining land (%)	Water (%)	Forest land (%)	
Cultivated land	12.59	5.66	0.08	0.05	3.44	21.83
Construction land	8.44	23.81	0.87	0.37	3.64	37.13
Mining land	0.03	0.85	2.53	0.07	0.15	3.63
Water	0.02	0.12	0.05	0.16	0.02	0.37
Forest land	0.37	3.53	0.75	0.06	32.35	37.05
Total	21.46	33.96	4.28	0.70	39.60	100.00

and the mining land increased. 0.37% of the construction land was converted into water, and the water area increased. From 2014 to 2020, construction land area decreased, forest land area grew, and cultivated land, mining land and water area remained almost unchanged (Table 5). Construction land was transformed to cultivated land and forest land, of which 6.7% was converted to cultivated land and 2.49% to forest land. The increased forest land area came from construction land and 2.61% of cultivated land.

In short, from 2008 to 2020, construction land area continued to decrease, and forest land area continued to increase, with a transfer of construction land to forest land and cultivated land. Water area increased significantly from 2008 to 2014 and remained unchanged from 2014 to 2020. Mining land area grew first and then remained almost unchanged, while cultivated land area decreased first and then remained unchanged.

3.1.2 Changes in land use dynamic degree

From Figure 4, it can be noticed that the annual change rate of cultivated land from 2008 to 2020 was −0.13%, indicating that there was nearly no change. The dynamic attitude of forest land, mining land and water were 0.84%, 1.61%, and 8.1% respectively, among which only the construction land was negative. The

TABLE 5 Land use transfer matrix in Anshan urban area from 2014 to 2020.

2014	2020					Total (%)
	Cultivated land (%)	Construction land (%)	Mining land (%)	Water (%)	Forest land (%)	
Cultivated land	12.88	5.78	0.19	0.03	2.61	21.49
Construction land	6.70	22.40	0.85	0.23	2.49	32.67
Mining land	0.14	1.20	2.69	0.06	0.23	4.33
Water	0.06	0.19	0.09	0.29	0.10	0.72
Forest land	1.66	4.39	0.46	0.09	34.18	40.79
Total	21.45	33.97	4.28	0.70	39.61	100.00

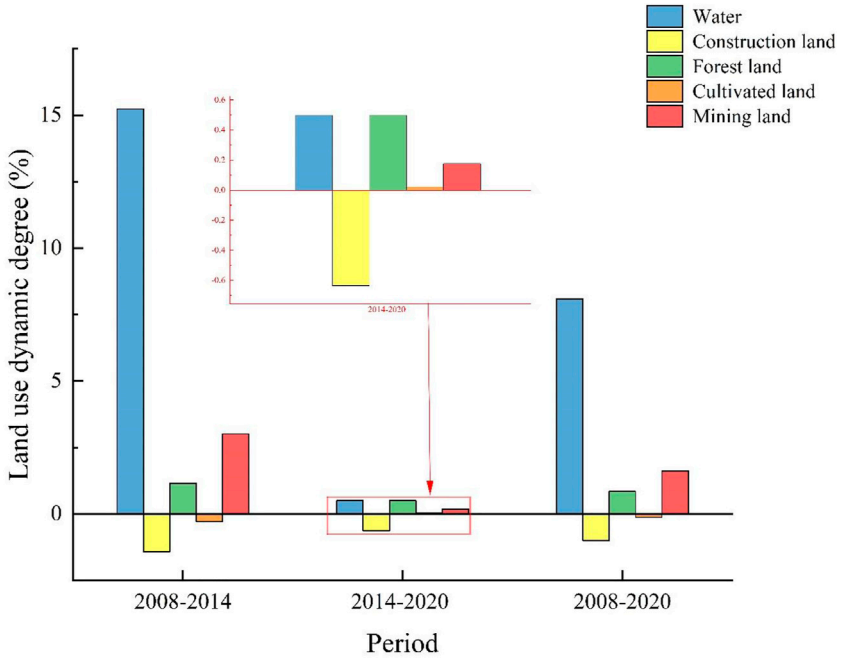

FIGURE 4
Dynamic degree of land use in Anshan urban area from 2008 to 2020.

annual change rate of water is 8.1 times that of construction land, and water is the type with the most volatile degree of change. Comparing the degree of annual change of each land use type over different periods, it is found that the dynamics from 2008 to 2014 were relatively variable, with the rate of change for each land use type from 2014 to 2020 not exceeding 1%. Among them, the dynamic degree of construction land was negative, but the values for the first 6 years are approximately 2.2 times higher than those for the last 6 years. The annual change rate of forest land in the first 6 years was 1.15%, which was about 2.3 times that in the next 6 years. The dynamic degree of mining land in the first 6 years was 3.01%, which was approximately 16.7 times that in the following 6 years. The dynamic degree of water in 2008–2014 was 15.24%, while that in 2014–2020 was only 0.5%. The dynamic degree of the water in the first 6 years was about 30.5 times that of the latter years. The change of cultivated land was the least severe. The annual change rate of cultivated land was −0.28% from 2008 to 2014 and 0.02% from 2014 to 2020.

In conclusion, the dynamics of each land use type changed markedly during the first 6 years of the research period, with flat changes in the second 6 years. From 2008 to 2020, the most significant change was in water, followed by mining land, and cultivated land almost remained unchanged. The annual change rate of construction land remained negative.

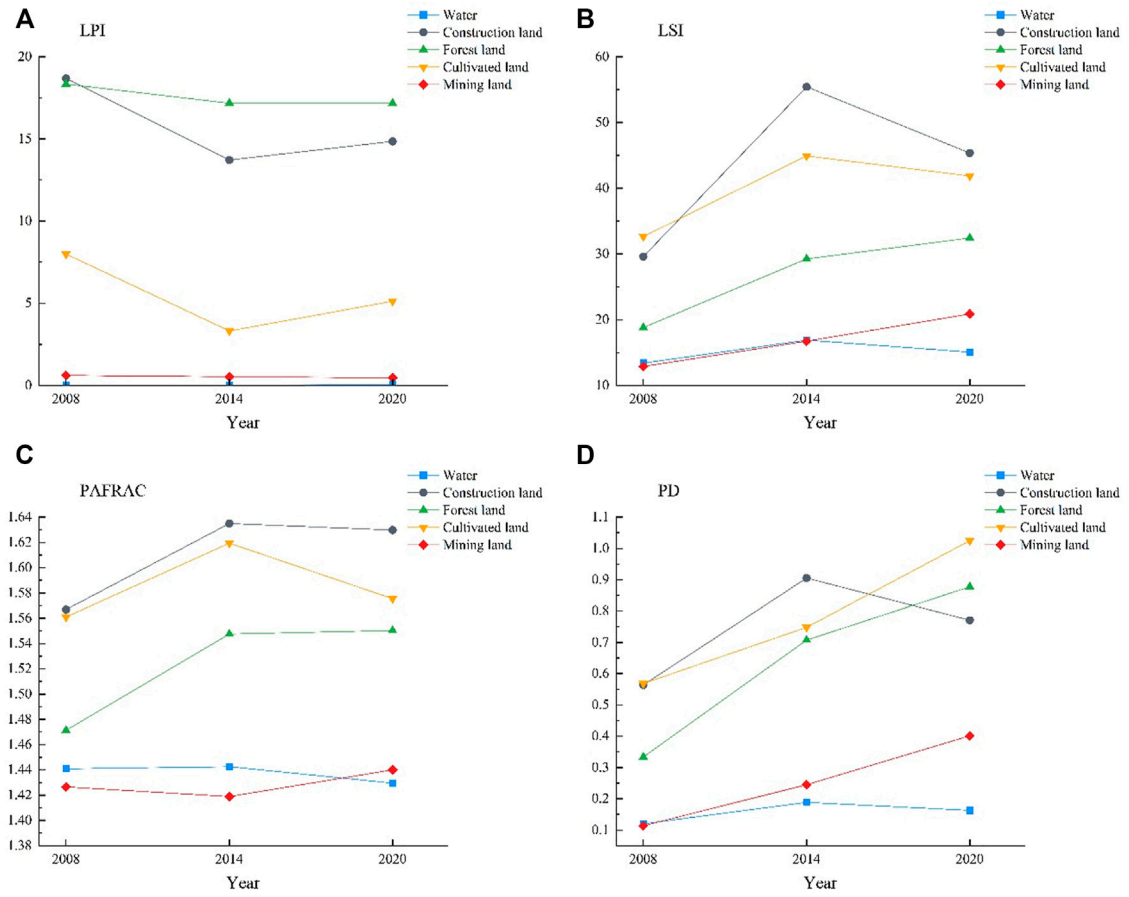

FIGURE 5
Landscape pattern index at class level. **(A)** change in largest patch index; **(B)** change in landscape shape index; **(C)** change in perimeter-area fractal dimension; **(D)** change in patch density.

3.2 Landscape pattern analysis

3.2.1 Comprehensive analysis at the class level

For the chosen seven landscape pattern indices, considered from the class level, the indices with similar results or high overlap were excluded, and PD, LSI, LPI, and PAFRAC were chosen to identify the landscape pattern characteristics of the study area at the class level (Figure 5).

1. From 2008 to 2014, the PD and LSI of water increased, but the PAFRAC remained almost unchanged. At this stage, the management of the Nansha River has achieved remarkable results, and the previously unconnected Nansha River is gradually being connected. At the same time, the development of mining activities has caused an increase in the accumulation of water in the subsidence. Secondly, with the urban construction and agricultural development, the number of ornamental lakes and rural reservoirs in the study area has increased. Water area increased and dispersed, and the agglomeration level decreased. At the same time, the fragmentation of water has increased under the impact of human activity. From 2014 to 2020, PD, LSI, and PAFRAC of water all decreased. During this period, the scattered rural reservoirs were gradually replaced by construction land, and with the continuous reconstruction of the Nansha River, the length of the Nansha River increased. The agglomeration degree of water rose, the degree of fragmentation declined, and the shape tended to be regular.
2. PD, LSI, and PAFRAC for construction land increased from 2008 to 2014. This period saw an increase in the fragmentation degree of construction land, a tendency for fragmented patches to become more complex in shape and a decrease in overall agglomeration. The reason is that the urbanization process of Anshan City was accelerating. According to the 2011 "Anshan City Master Plan," the new urban land would expand in conformity with the development direction of the central urban area and spread mainly to the western Dadaowan New City and the southern Tanggang

New City. The construction land has continued to expand to the west and south, not only in the central urban area, but also in the scattered townships and villages in the Qianshan Mountains. From 2014 to 2020, the PD and LSI of construction land decreased, and PAFRAC remained almost unchanged. During this period, the construction land expanded outwards, constantly encroaching on other surrounding lands. The original scattered construction land was connected into large pieces with the development of the city. At this time, the agglomeration of construction land increased and the degree of fragmentation decreased. In 2008, the LSI of construction land was the highest. At this time, construction land was the dominant type in the area. With the continuous reduction of construction land, forest land became the dominant type in Anshan urban area. The LSI and PAFRAC of construction land have always been the highest over the study period, indicating that construction land is the type with the lowest degree of aggregation and the most complex patch shape among the land types.

3. The LPI of forest land did not change much. From 2008 to 2020, the forest land continued to grow and gradually became the dominant type in this area. During the study period, PD, LSI, and PAFRAC of the woodland increased continuously. Due to the increase of park green space in urban construction as well as the policy of returning farmland to forest and mining area reclamation policy, part of the arable land and construction land have been converted to forest land and its area has increased. The forest land was less clustered, more fragmented and tended to be more complex in shape.
4. From 2008 to 2014, LSI, and PAFRAC of cultivated land increased, while LPI decreased. During this period, urbanization accelerated, the original cultivated land was replaced by construction land, and the degree of dominance of cultivated land was reduced. The concentrated cultivated land was divided by built-up land, the degree of agglomeration of cultivated land was reduced, and the shape and boundary became complex and irregular. Between 2014 and 2020, LSI and PAFRAC decreased and LPI rebounded. As a result of the policy, part of the cultivated land has been restored to forest land, and the cultivated land has been concentrated into pieces under the influence of agricultural activities, showing a state of agglomeration and distribution as a whole. The agglomeration degree has increased, and the boundaries have become regularized. The patch density of arable land continued to grow over the study period, indicating that fragmentation of arable land continued to rise.
5. The PD and LSI of mining land continued to increase over the study period. PAFRAC remained almost unchanged from 2008 to 2014 and increased from 2014 to 2020, demonstrating that the fragmentation of industrial and mining land was continuously increased due to human activities during the study period. After the implementation of closed-pit mine ecological management in Anshan City in 2014, some mining areas were reclaimed and converted into forest land, the degree of agglomeration was reduced, and the shape became complex and irregular.

TABLE 6 Landscape pattern index at landscape level.

Year	PD	CONTAG	SHDI	SHEI
2008	1.706	49.8409	1.4011	0.782
2014	2.8	46.1504	1.4153	0.7899
2020	3.2443	45.9326	1.4178	0.7913

3.2.2 Comprehensive analysis at the landscape level

From the landscape level, indexes that can reflect the characteristics of landscape aggregation, fragmentation and diversity were selected to study the landscape pattern of Anshan urban area (Table 6). From 2008 to 2020, PD, SHEI, and SHDI in Anshan urban area continued to increase, while CONTAG continued to decrease. In terms of the degree of change, each indicator changed more from 2008 to 2014, and slightly changed from 2014 to 2020. It is indicated that the degree of fragmentation and heterogeneity of landscape in Anshan urban area kept increasing over the study period. In particular, the degree of fragmentation and landscape heterogeneity increased significantly from 2008 to 2014.

3.2.3 Spatial level comparative analysis

The index calculation reveals that the overall fragmentation degree and landscape heterogeneity of Anshan urban area have been increased. However, due to the agglomeration of mines in the study area, it is impossible to compare the landscape pattern changes of different mining areas. Therefore, a raster map was drawn with a moving window to reflect landscape fragmentation and landscape heterogeneity in space and to compare the landscape pattern characteristics of different regions.

PD indicates the fragmentation degree of the landscape. The higher the value, the greater the degree of fragmentation. As can be seen from Figure 6, the areas with high PD values in 2008 are mainly the mining areas of Qidashan and Xiaolingzi, as well as the urban-rural areas in the southern part of the main city. Moreover, the high value areas are scattered and not connected to each other. Compared with 2008, the number of PD high-value areas increased significantly in 2014. The high-value areas are mainly divided into three areas: the urban-rural integration area in the western part of Qianshan District, the urban-rural integration area in the western part of Tiexi District, and areas where mining areas such as Anqian and Yanqianshan are concentrated. Anshan City expands to the west and the south. Both of these urban-rural areas are major areas of urban development with a fragmented distribution of

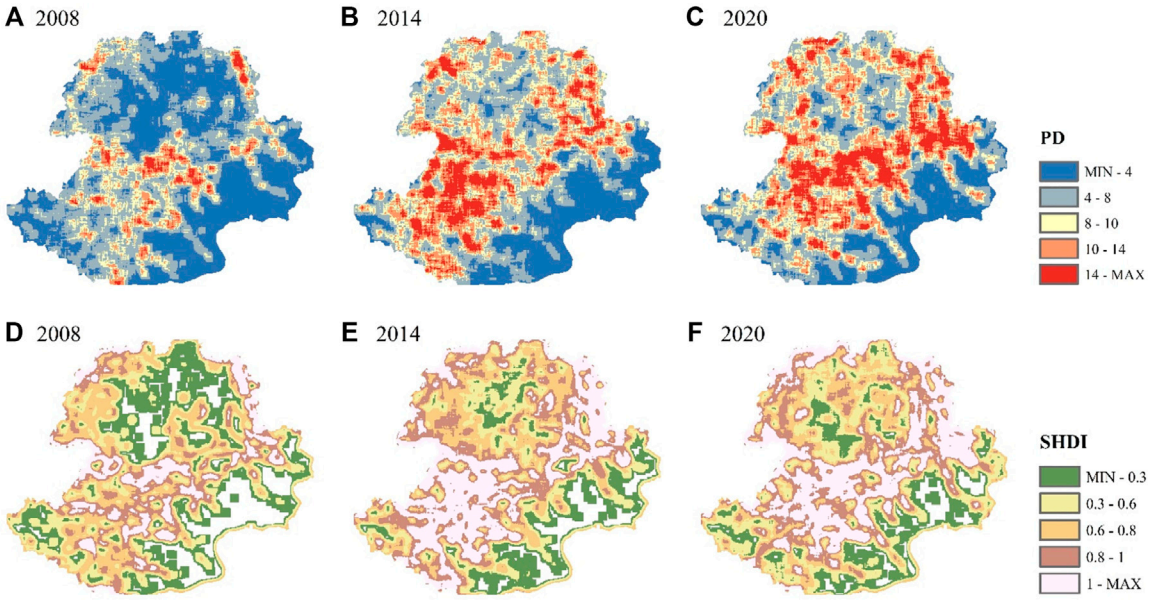

FIGURE 6
Raster map of landscape pattern in urban area of Anshan. **(A)** Patch density in 2008; **(B)** Patch density in 2014; **(C)** Patch density in 2020; **(D)** 2008 Shannon's diversity index; **(E)** 2014 Shannon's diversity Index; **(F)** 2020 Shannon's diversity Index.

arable land and building land. There is a high degree of fragmentation in both areas. With the development of mining activities, the degree of fragmentation in the Anqian mining area and the Yanqianshan mining area increased significantly, while the relative decline in the Qidashan and the Donganshan mining areas. The PD high-value areas in 2020 are similar to those in 2014, but they have expanded again compared to 2014. The high-value area surrounded the main urban area, and the original three high-value areas were connected into a ring. The reason is that Anshan City expanded from the central city to the surrounding areas and the landscape fragmentation degree around the main urban area increased during this period.

SHDI indicates landscape heterogeneity. The higher the value, the greater the heterogeneity. The high-value area of SHDI is nearly the same as the high-value area of PD. In 2008, the areas with high heterogeneity were mainly mining areas. In 2014, the areas with high SHDI values consisted of two parts: the urban-rural integration area in the west of Qianshan District and the mining agglomeration area in the east. With the constant development of Anshan City to the south and west, the original cultivated land and forest land have been replaced by construction land and water due to anthropogenic interventions. The landscape heterogeneity in the urban-rural integration area in the western part of Qianshan District has increased, the landscape richness has been improved, and the types have become diversified. Under the influence of mining activities, the mining area expanded and some workers built houses and farmland around the mining area, leading to the increase of landscape heterogeneity of the mining area. The high value areas in 2020 are similar to those in 2014, with increased landscape heterogeneity near the Dagushan mine, due to the implementation of mine reclamation in Anshan and the conversion of some industrial and mining land to forest land and construction land.

4 Discussion

4.1 Random forest classification optimization

With the continuous advancement of computer technology, machine learning technology is widely applied in remote sensing land use classification and mapping (Hansen et al., 2007; Liu et al., 2016a). Common classification methods include support vector machine (SVM), decision tree (DT), maximum likelihood classification (MLC), random forest (RF), etc. Yu et al. (2014) found that MLC is the most commonly used remote sensing classification method. Pal and Mather. (2006) compared the three methods of support vector machine, maximum likelihood classification and neural network and found that support vector machine accuracy is higher. Then Pal (2007) compared the support vector machine and the random forest,

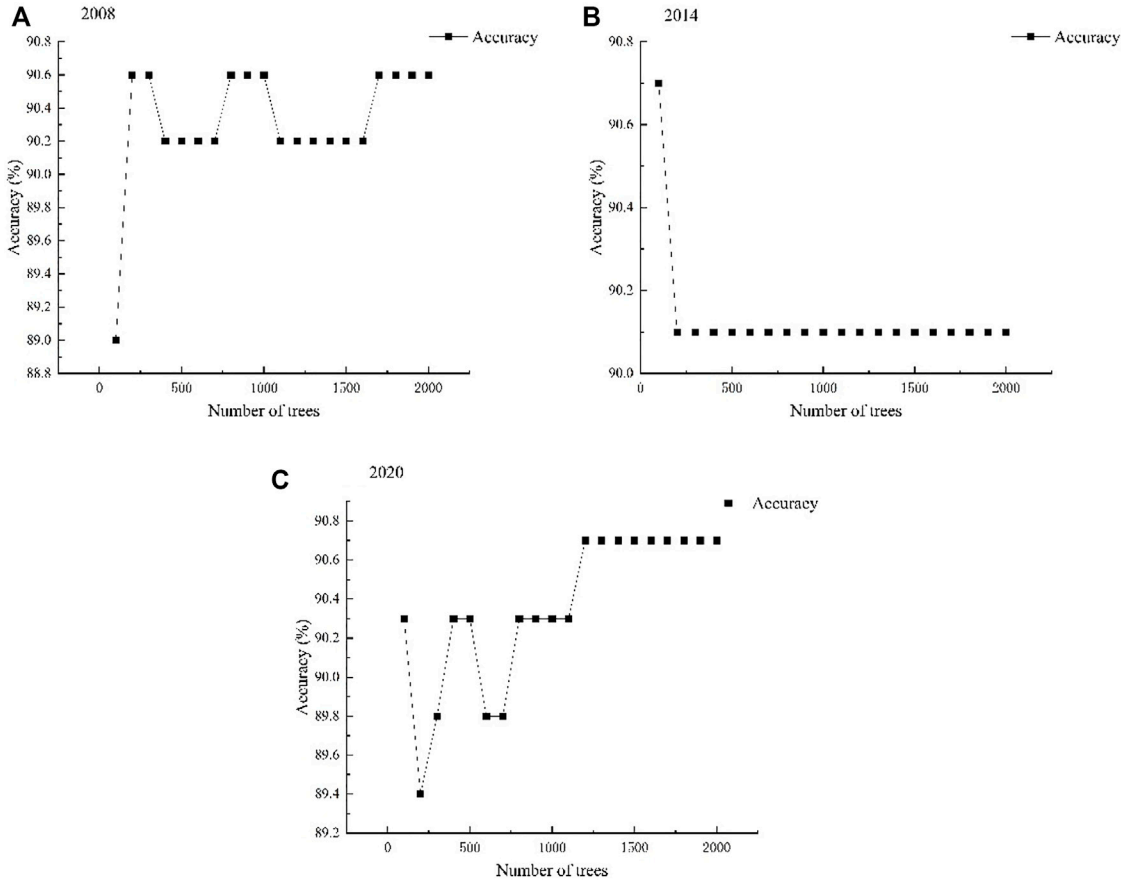

FIGURE 7
The effect of the number of decision trees on classification accuracy. **(A)** 2008; **(B)** 2014; **(C)** 2020.

and found that the classification accuracy of the two methods is not much different, but the random forest needs to set fewer parameters. Lawrence and Moran (2015) compared SVM, RF, DT, and other six classification methods, and found that the classification accuracy of RF is higher than other classification methods.

Random forest has high classification accuracy. At the same time, in contrast to classification methods such as NN and SVM, this classification method can help to achieve the optimization of classification results by defining two parameters, the number of input feature variables and the number of decision trees (Rodriguez-Galiano et al., 2012; Phan et al., 2020). In this study, through the GEE platform, the random forest classifier was applied to classify remote sensing images, and the number of decision trees was adjusted in GEE to improve the classification accuracy. From 100 to 2000, 20 tests were carried out at intervals of 100 trees to observe the test accuracy (Figure 7). It is found that the test accuracy leveled off when the number of decision trees was 1700 in 2008, 200 in 2014, and 1,200 in 2020. In 2008, when the number of decision trees was changed from the initial 100 trees to 1700 trees, the classification accuracy increased by 1.6%. The optimized parameters were respectively input into the random forest classifier to improve the classification accuracy.

4.2 Comparison of landscape changes in different pits

There are six large pits in the study area, and the extent of reclamation varies from mine to mine due to different mining and management patterns. Based on the spatial and temporal characteristics of the land use and landscape patterns of the six pits, it was found that the Donganshan and Dagushan mines were the most effective in terms of reclamation. These two mines have been significantly reduced in size. The Donganshan mine follows the principle of "greening while mining" and reclaims the open pit and tailings ponds, and the Yuemingshan tailings pond in the northeast of the mine and the Shannan tailings pond in the south have been effectively treated. The greening of the discharge

site at the Dagushan mine has been effective and the mine area has been significantly reduced. The Donganshan and Dagushan mines have the lowest PD and SHDI values and the lowest degree of landscape fragmentation and landscape heterogeneity compared to the other mines. Reclamation of the Qidashan mine is generally effective, with no significant change in the size of the mine and consistently high PD and SHDI values, which have remained largely unchanged over the course of the study. The reclamation of the Yanqianshan, Anqian and Xiaolingzi mines is not satisfactory, as the size of these pits has increased to varying degrees due to ongoing mining activities, and PD and SHDI values have increased over time.

Based on the effectiveness of reclamation and changes in the landscape pattern, these pits are divided into three categories: 1. Mine areas with significant reclamation and low landscape fragmentation (Donganshan and Dagushan mines); 2. Mine areas with average reclamation and no increase in landscape fragmentation and heterogeneity (Qidashan mines); 3. Mine areas with unsatisfactory reclamation and increasing landscape fragmentation and heterogeneity (Yanqianshan, Anqian and Xiaolingzi mines). In the future management of mining areas in Anshan, there is an urgent need to strengthen the intensity of reclamation of Category three mining areas and improve the mining environment. Attention should be paid to changes in the landscape pattern of Category two mining areas to prevent an increase in landscape fragmentation. Continue to increase the area of greening and expand the scope of reclamation for Category one mining areas.

4.3 Factors affecting changes in land use and landscape patterns

Urbanization is one of the main drivers contributing to changes in land use and landscape patterns (Lambin et al., 2001; Deng et al., 2009; Wu et al., 2010). After the reform and opening up, urbanization in China has accelerated and a large number of people have flowed from rural areas to cities, leading to a rapid decrease in arable land and an increasing amount of land for construction (Deng et al., 2015; Zhang et al., 2020a). As Liaoyang City lies to the north of Anshan City, the urban development direction of Anshan City is mainly to the south, east and west. In 2008, Anshan City developed mainly to the south, hence the high PD value of the urban-rural area between the Donganshan and Dagushan mining areas. Urban roads are also the core areas of urban construction (Zhang et al., 2021). From 2008 to 2014, Anshan City continued to expand to the southwest along the Heida Line, and the PD value in the southwest area of Qianshan was relatively high. Between 2014 and 2020, the main city of Anshan expanded in all directions, with construction along the Anshan Ring Road, dominated by construction in the south and east. The main urban area of Anshan was surrounded by high value areas of PD and SHDI.

The evolution of land use and landscape patterns in Anshan City are obviously affected by policies. In 2007, Anshan City began to renovate the Nansha River, repairing bridge decks, building embankments and dams, regulating river water, and widening the river surface. Under the influence of river governance policies, the Nansha River basin has been connected and the water area increased. In 2014, Anshan City implemented the closed mine ecological management plan. Before 2014, with the development of mining activities, the fragmentation degree and landscape heterogeneity of the mining area increased. After 2014, mining activities in Anshan City were restricted, some mines were shifted from open pit to underground mining, and open-pit mines were gradually restored and managed. Among them, the belt rock dumping fields in the northern and central parts of the Qidashan mining area have been reclaimed, and some of them have been turned into forest land. The Dagushan and Donganshan mining areas have achieved remarkable results in reclamation, and the rock dumping fields and slopes have been treated. In 2015, Anshan City fully implemented the project of returning arable land to forest, and carried out afforestation in a planned way, and some cultivated land was changed into forest land from 2014 to 2020.

Mining activities affect land use and landscape patterns. Mining activities destroy land use and landscape structure, leading to landscape fragmentation and increased heterogeneity. At the same time, the mining industry attracts large numbers of people to the mining areas. Workers developed urban activities in the vicinity of the mines, and commercial facilities, housing, and public amenities near the mines increased.

Population also affects changes in land use and landscape patterns. According to the Anshan City Statistical Yearbook, the population of Anshan City was 1.473 million in 2008, 1.511 million in 2014, and 1.45 million in 2020. From 2008 to 2014, due to the urbanization of Anshan City and the development of mineral resources, a large number of people flowed into Anshan City, arable land decreased, and industrial and mining land increased. From 2014 to 2020, due to the transformation of the economic development model, Anshan City lost its population, the urban development slowed down, and the changes in various land use types were not obvious.

4.4 Limitations

This study has certain limitations. First, the analysis of land use and landscape pattern changes relies on the results of random forest classification. The study used Landsat data at a

resolution of 30 m for land classification. At 30 m resolution, it is impossible to distinguish precisely various types of land use and then differentiate collapsed land, stope and dump in the mining area. In future research, high-resolution sentinel data can be used for land use classification, which may improve the accuracy of analysis and comparison studies on changes in subsidence, dumps and slopes in different mining areas. At the same time, this study selected 11 characteristic variables for random forest classification, which would generate a certain amount of data redundancy. In future research, characteristic variables with high correlation can be selected for training to improve classification efficiency. Secondly, the causes of variations in land use and landscape patterns are complex and diverse. The study only analyzed the impact of anthropogenic factors such as urbanization, policy, mining and population on change, and did not consider the impact of natural factors such as climate and soil on change, nor did it conduct a correlation analysis. The next step will be to conduct a principal components analysis of the drivers to clarify the main causes of change in both. Future research should focus on the evolution of land use and landscape patterns in mineral resource-based cities and areas where mining areas are concentrated, and further analyze the impact of change on regional ecosystems.

5 Conclusion

Building on the GEE platform, the study selected multi-temporal Landsat images and random forest classification algorithm to draw the land use map of Anshan urban area in 2008, 2014, and 2020. Using confusion matrices to verify the accuracy of classification. The results show that the overall classification accuracy in 3 years is more than 90% and the Kappa coefficient is more than 0.8. The classification accuracy is high. The dynamic land use attitude and the moving window method combined with the landscape pattern index were applied to analyze the spatial and temporal characteristics of land use and landscape patterns in Anshan City. The results of the study are as follows.

From 2008 to 2020, the change in land use in Anshan City District shows a continuous decline in construction land and a continuous growth in forest land, with a shift from construction land to forest land and cultivated land. The area of mining areas grew before 2014 but remained largely unchanged after mine management was carried out in Anshan City in 2014. During the study period, changes in the landscape pattern of the Anshan city area were characterized by increasing landscape fragmentation and landscape heterogeneity. The areas with high values of landscape fragmentation and heterogeneity in 2008 were the Qidashan mining area and the urban-rural combination area in the southern part of the main city. With urbanization and mining activities, the areas with high values of landscape fragmentation and landscape heterogeneity increased significantly. 2014 saw the development of Anshan City to the southwest, and the areas with severe landscape fragmentation were the urban-rural combination areas in the Qianshan District. During this phase, mining activities are frequent and landscape fragmentation is severe in the mining areas of Anshan Qian and the immediate mountain area. 2014–2020 sees little change in the landscape pattern of Anshan, but the city develops to the east, west and south, with the areas of severe landscape fragmentation being the combined urban-rural areas around the main urban area.

The six mining sites in the study area vary in their reclamation effectiveness. The best reclamation results were found at the Dagushan and Donganshan mines, where the mine area was significantly reduced and the landscape fragmentation was low. There is a need to continue to expand the greening area. The relatively good results of reclamation are in Qidashan, where the area of the mine and the degree of landscape fragmentation remain largely unchanged, but the degree of fragmentation is still high and the rate of reclamation needs to be accelerated. The least satisfactory results are found in the mining areas of Yanqianshan, Anqian and Xiaolingzi, where the size of the mining area is still increasing and the degree of landscape fragmentation continues to increase, requiring increased reclamation efforts.

Land use and landscape pattern changes in Anshan are influenced by urbanization, policies, population and mining activities. Between 2008 and 2014, Anshan experienced rapid urbanization, increased population, reduced arable land, increased industrial and mining land use, and a significant increase in landscape fragmentation. Since 2014, Anshan City has paid attention to environmental governance. Due to policies on returning farmland to forests, mining area restoration and watershed management, Anshan City set about planting trees, reclaiming mining areas and making rivers circulate. The landscape pattern and land use changes in Anshan City have slowed significantly since 2014.

Data availability statement

The original contributions presented in the study are included in the article/Supplementary Material, further inquiries can be directed to the corresponding authors.

Author contributions

YZ performed the data analysis and wrote the manuscript; YF and YZ contributed to the idea of the study; YF helped with the

analysis through constructive discussions and provided valuable reviewer comments.

Funding

This work was supported by the National Natural Science Foundation of China under Grand 52074064.

Conflict of interest

The authors declare that the research was conducted in the absence of any commercial or financial relationships that could be construed as a potential conflict of interest.

Publisher's note

All claims expressed in this article are solely those of the authors and do not necessarily represent those of their affiliated organizations, or those of the publisher, the editors and the reviewers. Any product that may be evaluated in this article, or claim that may be made by its manufacturer, is not guaranteed or endorsed by the publisher.

Supplementary material

The Supplementary Material for this article can be found online at: https://www.frontiersin.org/articles/10.3389/fenvs.2022.988346/full#supplementary-material

References

Amani, M., Ghorbanian, A., Ahmadi, S. A., Kakooei, M., Moghimi, A., Mirmazloumi, S. M., et al. (2020). Google earth engine cloud computing platform for remote sensing big data applications: A comprehensive review. *IEEE J. Sel. Top. Appl. Earth Obs. Remote Sens.* 13, 5326–5350. doi:10.1109/jstars.2020.3021052

Ang, M. L. E., Arts, D., Crawford, D., Labatos, B. V., Jr, Ngo, K. D., Owen, J. R., et al. (2021). Socio-environmental land cover time-series analysis of mining landscapes using Google Earth Engine and web-based mapping. *Remote Sens. Appl. Soc. Environ.* 21, 100458. doi:10.1016/j.rsase.2020.100458

Bai, J., Ouyang, H., Cui, B., Wang, Q., and Chen, H. (2008). Changes in landscape pattern of alpine wetlands on the Zoige Plateau in the past four decades. *Acta Ecol. Sin.* 28 (5), 2245–2252. doi:10.1016/s1872-2032(08)60046-3

Bajocco, S., De Angelis, A., Perini, L., Ferrara, A., and Salvati, L. (2012). The impact of land use/land cover changes on land degradation dynamics: A mediterranean case study. *Environ. Manage.* 49 (5), 980–989. doi:10.1007/s00267-012-9831-8

Belgiu, M., and Drăguţ, L. (2016). Random forest in remote sensing: A review of applications and future directions. *ISPRS J. Photogrammetry Remote Sens.* 114, 24–31. doi:10.1016/j.isprsjprs.2016.01.011

Breiman, L. (2001a). Random forests. *Mach. Learn.* 45 (1), 5–32. doi:10.1023/a:1010933404324

Breiman, L. (2001b). Using iterated bagging to debias regressions. *Mach. Learn.* 45 (3), 5–32. doi:10.1023/a:1010933404324

Bürgi, M., Hersperger, A. M., and Schneeberger, N. (2004). Driving forces of landscape change - current and new directions. *Landsc. Ecol.* 19 (8), 857–868. doi:10.1007/s10980-004-0245-8

Chang, Y., Hou, K., Li, X., Zhang, Y., and Chen, P. (2018). Review of land use and land cover change research progress. *IOP Conf. Ser. Earth Environ. Sci.* 113, 012087. doi:10.1088/1755-1315/113/1/012087

Cheung, A. K. L., Brierley, G., and O'Sullivan, D. (2016). Landscape structure and dynamics on the qinghai-Tibetan plateau. *Ecol. Model.* 339, 7–22. doi:10.1016/j.ecolmodel.2016.07.015

Cui, J., Zhu, M., Liang, Y., Qin, G., Li, J., and Liu, Y. (2022). Land use/land cover change and their driving factors in the yellow River basin of shandong Province based on Google earth engine from 2000 to 2020. *ISPRS Int. J. Geoinf.* 11 (3), 163. doi:10.3390/ijgi11030163

Dadashpoor, H., Azizi, P., and Moghadasi, M. (2019). Land use change, urbanization, and change in landscape pattern in a metropolitan area. *Sci. Total Environ.* 655, 707–719. doi:10.1016/j.scitotenv.2018.11.267

Deng, J. S., Wang, K., Hong, Y., and Qi, J. G. (2009). Spatio-temporal dynamics and evolution of land use change and landscape pattern in response to rapid urbanization. *Landsc. Urban Plan.* 92 (3-4), 187–198. doi:10.1016/j.landurbplan.2009.05.001

Deng, X., Huang, J., Rozelle, S., Zhang, J., and Li, Z. (2015). Impact of urbanization on cultivated land changes in China. *Land Use Policy* 45, 1–7. doi:10.1016/j.landusepol.2015.01.007

Du, P., Xia, J., Zhang, W., Tan, K., Liu, Y., and Liu, S. (2012). Multiple classifier system for remote sensing image classification: A review. *Sensors (Basel)* 12 (4), 4764–4792. doi:10.3390/s120404764

Fan, Q., and Ding, S. (2016). Landscape pattern changes at a county scale: A case study in fengqiu, henan Province, China from 1990 to 2013. *Catena* 137, 152–160. doi:10.1016/j.catena.2015.09.012

Fang, A., Dong, J., Cao, Z., Zhang, F., and Li, Y. (2019). Tempo-spatial variation of vegetation coverage and influencing factors of large-scale mining areas in eastern inner Mongolia, China. *Int. J. Environ. Res. Public Health* 17 (1), 47. doi:10.3390/ijerph17010047

Fathololoumi, S., Firozjaei, M. K., Li, H., and Biswas, A. (2022). Surface biophysical features fusion in remote sensing for improving land crop/cover classification accuracy. *Sci. Total Environ.* 156520, 156520. doi:10.1016/j.scitotenv.2022.156520

Feng, Y., Liu, Y., and Tong, X. (2018). Spatiotemporal variation of landscape patterns and their spatial determinants in Shanghai, China. *Ecol. Indic.* 87, 22–32. doi:10.1016/j.ecolind.2017.12.034

Gao, P., Niu, X., Wang, B., and Zheng, Y. (2015). Land use changes and its driving forces in hilly ecological restoration area based on gis and RS of northern China. *Sci. Rep.* 5, 11038. doi:10.1038/srep11038

Ge, H., Yi, Y., Yang, X., Yang, L., Su, D., and Ma, L. (2010). Study on ecological characteristic and reclamation in Xiangshui coal mining area, Guizhou, China. *Int. J. Min. Reclam. Environ.* 24 (1), 18–33. doi:10.1080/17480930903474774

Ghimire, B., Rogan, J., Galiano, V. R., Panday, P., and Neeti, N. (2013). An evaluation of bagging, boosting, and random forests for land-cover classification in cape cod, Massachusetts, USA. *GIScience Remote Sens.* 49 (5), 623–643. doi:10.2747/1548-1603.49.5.623

Gorelick, N., Hancher, M., Dixon, M., Ilyushchenko, S., Thau, D., and Moore, R. (2017). Google earth engine: Planetary-scale geospatial analysis for everyone. *Remote Sens. Environ.* 202, 18–27. doi:10.1016/j.rse.2017.06.031

Groom, G., Mücher, C. A., Ihse, M., and Wrbka, T. (2006). Remote sensing in landscape ecology: Experiences and perspectives in a European context. *Landsc. Ecol.* 21 (3), 391–408. doi:10.1007/s10980-004-4212-1

Hagen-Zanker, A. (2016). A computational framework for generalized moving windows and its application to landscape pattern analysis. *Int. J. Appl. Earth Observation Geoinformation* 44, 205–216. doi:10.1016/j.jag.2015.09.010

Hansen, M., Dubayah, R., and Defries, R. (2007). Classification trees: An alternative to traditional land cover classifiers. *Int. J. Remote Sens.* 17 (5), 1075–1081. doi:10.1080/01431169608949069

Hassan, M. M. (2017). Monitoring land use/land cover change, urban growth dynamics and landscape pattern analysis in five fastest urbanized cities in Bangladesh. *Remote Sens. Appl. Soc. Environ.* 7, 69–83. doi:10.1016/j.rsase.2017.07.001

Hayes, J. J., and Robeson, S. M. (2013). Spatial variability of landscape pattern change following a ponderosa pine wildfire in northeastern New Mexico, USA. *Phys. Geogr.* 30 (5), 410–429. doi:10.2747/0272-3646.30.5.410

He, F., Yang, J., Zhang, Y., Sun, D., Wang, L., Xiao, X., et al. (2022a). Offshore island connection line: A new perspective of coastal urban development boundary simulation and multi-scenario prediction. *GIScience Remote Sens.* 59 (1), 801–821. doi:10.1080/15481603.2022.2071056

He, Y., Oh, J., Lee, E., and Kim, Y. (2022b). Land cover and land use mapping of the east asian summer monsoon region from 1982 to 2015. *Land* 11 (3), 391. doi:10.3390/land11030391

Huang, J., Lin, J., and Tu, Z. (2008). Detecting spatiotemporal change of land use and landscape pattern in a coastal gulf region, southeast of China. *Environ. Dev. Sustain.* 12 (1), 35–48. doi:10.1007/s10668-008-9178-8

Jazouli, A. E., Barakat, A., Khellouk, R., Rais, J., and Baghdadi, M. E. (2019). Remote sensing and GIS techniques for prediction of land use land cover change effects on soil erosion in the high basin of the Oum Er Rbia River (Morocco). *Remote Sens. Appl. Soc. Environ.* 13, 361–374. doi:10.1016/j.rsase.2018.12.004

Kumar, L., and Mutanga, O. (2018). Google earth engine applications since inception: Usage, trends, and potential. *Remote Sens.* 10 (10), 1509. doi:10.3390/rs10101509

Kupidura, P. (2019). The comparison of different methods of texture analysis for their efficacy for land use classification in satellite imagery. *Remote Sens.* 11 (10), 1233. doi:10.3390/rs11101233

Kuzevic, S., Bobikova, D., and Kuzevicova, Z. (2022). Land cover and vegetation coverage changes in the mining area—a case study from Slovakia. *Sustainability* 14 (3), 1180. doi:10.3390/su14031180

Lambin, E. F., Turner, B. L., Geist, H. J., Agbola, S. B., Angelsen, A., Bruce, J. W., et al. (2001). The causes of land-use and land-cover change: Moving beyond the myths. *Glob. Environ. Change* 11 (4), 261–269. doi:10.1016/s0959-3780(01)00007-3

Lawrence, R. L., and Moran, C. J. (2015). The AmericaView classification methods accuracy comparison project: A rigorous approach for model selection. *Remote Sens. Environ.* 170, 115–120. doi:10.1016/j.rse.2015.09.008

Lei, S., Bian, Z., Daniels, J. L., and He, X. (2010). Spatio-temporal variation of vegetation in an arid and vulnerable coal mining region. *Min. Sci. Technol. (China)* 20 (3), 485–490. doi:10.1016/s1674-5264(09)60230-1

Li, P., Zuo, D., Xu, Z., Zhang, R., Han, Y., Sun, W., et al. (2021a). Dynamic changes of land use/cover and landscape pattern in a typical alpine river basin of the Qinghai-Tibet Plateau, China. *Land Degrad. Dev.* 32 (15), 4327–4339. doi:10.1002/ldr.4039

Li, S., Wang, J., Zhang, M., and Tang, Q. (2021b). Characterizing and attributing the vegetation coverage changes in North Shanxi coal base of China from 1987 to 2020. *Resour. Policy* 74, 102331. doi:10.1016/j.resourpol.2021.102331

Liu, D., Hao, S., Liu, X., Li, B., He, S., and Warrington, D. N. (2012). Effects of land use classification on landscape metrics based on remote sensing and GIS. *Environ. Earth Sci.* 68 (8), 2229–2237. doi:10.1007/s12665-012-1905-7

Liu, J., and Deng, X. (2010). Progress of the research methodologies on the temporal and spatial process of LUCC. *Chin. Sci. Bull.* 55 (14), 1354–1362. doi:10.1007/s11434-009-0733-y

Liu, X., Li, X., Chen, Y., Tan, Z., Li, S., and Ai, B. (2010). A new landscape index for quantifying urban expansion using multi-temporal remotely sensed data. *Landsc. Ecol.* 25 (5), 671–682. doi:10.1007/s10980-010-9454-5

Liu, P., Choo, K.-K. R., Wang, L., and Huang, F. (2016a). SVM or deep learning? A comparative study on remote sensing image classification. *Soft Comput.* 21 (23), 7053–7065. doi:10.1007/s00500-016-2247-2

Liu, X., Zhou, W., and Bai, Z. (2016b). Vegetation coverage change and stability in large open-pit coal mine dumps in China during 1990–2015. *Ecol. Eng.* 95, 447–451. doi:10.1016/j.ecoleng.2016.06.051

Liu, X., An, Y., Dong, G., and Jiang, M. (2018). Land use and landscape pattern changes in the sanjiang plain, northeast China. *Forests* 9 (10), 637. doi:10.3390/f9100637

Magidi, J., Nhamo, L., Mpandeli, S., and Mabhaudhi, T. (2021). Application of the random forest classifier to map irrigated areas using Google earth engine. *Remote Sens.* 13 (5), 876. doi:10.3390/rs13050876

Mutanga, O., and Kumar, L. (2019). Google earth engine applications. *Remote Sens.* 11 (5), 591. doi:10.3390/rs11050591

Pal, M., and Mather, P. M. (2006). Support vector machines for classification in remote sensing. *Int. J. Remote Sens.* 26 (5), 1007–1011. doi:10.1080/01431160512331314083

Pal, M. (2007). Random forest classifier for remote sensing classification. *Int. J. Remote Sens.* 26 (1), 217–222. doi:10.1080/01431160412331269698

Peng, J., Wu, J., Yin, H., Li, Z., Chang, Q., and Mu, T. (2008). Rural land use change during 1986-2002 in lijiang, China, based on remote sensing and GIS data. *Sensors (Basel)* 8 (12), 8201–8223. doi:10.3390/s8128201

Pericak, A. A., Thomas, C. J., Kroodsma, D. A., Wasson, M. F., Ross, M. R. V., Clinton, N. E., et al. (2018). Mapping the yearly extent of surface coal mining in central appalachia using Landsat and Google earth engine. *PLoS One* 13 (7), e0197758. doi:10.1371/journal.pone.0197758

Phan, T. N., Kuch, V., and Lehnert, L. W. (2020). Land cover classification using Google earth engine and random forest classifier—the role of image composition. *Remote Sens.* 12 (15), 2411. doi:10.3390/rs12152411

Prasai, R., Schwertner, T. W., Mainali, K., Mathewson, H., Kafley, H., Thapa, S., et al. (2021). Application of Google earth engine python API and naip imagery for land use and land cover classification: A case study in Florida, USA. *Ecol. Inf.* 66, 101474. doi:10.1016/j.ecoinf.2021.101474

Qiu, S., Lin, Y., Shang, R., Zhang, J., Ma, L., and Zhu, Z. (2018). Making Landsat time series consistent: Evaluating and improving Landsat analysis ready data. *Remote Sens.* 11 (1), 51. doi:10.3390/rs11010051

Rodriguez-Galiano, V. F., Ghimire, B., Rogan, J., Chica-Olmo, M., and Rigol-Sanchez, J. P. (2012). An assessment of the effectiveness of a random forest classifier for land-cover classification. *ISPRS J. Photogrammetry Remote Sens.* 67, 93–104. doi:10.1016/j.isprsjprs.2011.11.002

Schmidt, J., Marques, M. R. G., Botti, S., and Marques, M. A. L. (2019). Recent advances and applications of machine learning in solid-state materials science. *npj Comput. Mat.* 5 (1), 83. doi:10.1038/s41524-019-0221-0

Schmitt, M., Bahn, M., Wohlfahrt, G., Tappeiner, U., and Cernusca, A. (2010). Land use affects the net ecosystem CO₂ exchange and its components in mountain grasslands. *Biogeosciences* 7 (8), 2297–2309. doi:10.5194/bg-7-2297-2010

Shao, G., and Wu, J. (2008). On the accuracy of landscape pattern analysis using remote sensing data. *Landsc. Ecol.* 23 (5), 505–511. doi:10.1007/s10980-008-9215-x

Singh, S., Singh, C., and Mukherjee, S. (2010). Impact of land-use and land-cover change on groundwater quality in the lower shiwalik hills: A remote sensing and GIS based approach. *Open Geosci.* 2 (2), 124–131. doi:10.2478/v10085-010-0003-x

Takam Tiamgne, X., Kalaba, F. K., and Nyirenda, V. R. (2021). Land use and cover change dynamics in Zambia's Solwezi copper mining district. *Sci. Afr.* 14, e01007. doi:10.1016/j.sciaf.2021.e01007

Tang, J., Li, Y., Cui, S., Xu, L., Ding, S., and Nie, W. (2020). Linking land-use change, landscape patterns, and ecosystem services in a coastal watershed of southeastern China. *Glob. Ecol. Conservation* 23, e01177. doi:10.1016/j.gecco.2020.e01177

Tekle, K., and Hedlund, L. (2000). Land cover changes between 1958 and 1986 in kalu district, southern wello, Ethiopia. *Mt. Res. Dev.* 20 (1), 42–51. doi:10.1659/0276-4741(2000)020[0042:Lccbai]2.0.Co;2

Thakkar, A. K., Desai, V. R., Patel, A., and Potdar, M. B. (2017). Post-classification corrections in improving the classification of Land Use/Land Cover of arid region using RS and GIS: The case of Arjuni watershed, Gujarat, India. *Egypt. J. Remote Sens. Space Sci.* 20 (1), 79–89. doi:10.1016/j.ejrs.2016.11.006

Tian, Y., Liu, B., Hu, Y., Xu, Q., Qu, M., and Xu, D. (2020). Spatio-temporal land-use changes and the response in landscape pattern to hemeroby in a resource-based city. *ISPRS Int. J. Geoinf.* 9 (1), 20. doi:10.3390/ijgi9010020

Townsend, P. A., Helmers, D. P., Kingdon, C. C., McNeil, B. E., de Beurs, K. M., and Eshleman, K. N. (2009). Changes in the extent of surface mining and reclamation in the Central Appalachians detected using a 1976–2006 Landsat time series. *Remote Sens. Environ.* 113 (1), 62–72. doi:10.1016/j.rse.2008.08.012

Turner, M. G. (1990). Spatial and temporal analysis of landscape patterns. *Landsc. Ecol.* 4 (1), 21–30. doi:10.1007/bf02573948

Wahap, N. A., and Shafri, H. Z. M. (2020). Utilization of Google earth engine (GEE) for land cover monitoring over klang valley, Malaysia. *IOP Conf. Ser. Earth Environ. Sci.* 540 (1), 012003. doi:10.1088/1755-1315/540/1/012003

Wan, L., Zhang, Y., Zhang, X., Qi, S., and Na, X. (2015). Comparison of land use/land cover change and landscape patterns in Honghe National Nature Reserve and the surrounding Jiansanjiang Region, China. *Ecol. Indic.* 51, 205–214. doi:10.1016/j.ecolind.2014.11.025

Wang, S., Zhao, Y., Yin, X. a., Yu, L., and Xu, F. (2009). Land use and landscape pattern changes in Nenjiang River basin during 1988–2002. *Front. Earth Sci. China* 4 (1), 33–41. doi:10.1007/s11707-010-0006-8

Wang, R., Cheng, J., Zhu, Y., and Xiong, W. (2016). Research on diversity of mineral resources carrying capacity in Chinese mining cities. *Resour. Policy* 47, 108–114. doi:10.1016/j.resourpol.2015.12.003

Wang, D., Huang, Z., Wang, Y., and Mao, J. (2021). Ecological security of mineral resource-based cities in China: Multidimensional measurements, spatiotemporal evolution, and comparisons of classifications. *Ecol. Indic.* 132, 108269. doi:10.1016/j.ecolind.2021.108269

Wu, Y., Zhang, X., and Shen, L. (2010). The impact of urbanization policy on land use change: A scenario analysis. *Cities* 28 (2), 147–159. doi:10.1016/j.cities.2010.11.002

Wu, H., Lin, A., Xing, X., Song, D., and Li, Y. (2021a). Identifying core driving factors of urban land use change from global land cover products and POI data using the random forest method. *Int. J. Appl. Earth Observation Geoinformation* 103, 102475. doi:10.1016/j.jag.2021.102475

Wu, J., Zhu, Q., Qiao, N., Wang, Z., Sha, W., Luo, K., et al. (2021b). Ecological risk assessment of coal mine area based on "source-sink" landscape theory – a case study of Pingshuo mining area. *J. Clean. Prod.* 295, 126371. doi:10.1016/j.jclepro.2021.126371

Xu, J., Zhao, H., Yin, P., Wu, L., and Li, G. (2019). Landscape ecological quality assessment and its dynamic change in coal mining area: A case study of peixian. *Environ. Earth Sci.* 78 (24), 708. doi:10.1007/s12665-019-8747-5

Yang, Y., Erskine, P. D., Lechner, A. M., Mulligan, D., Zhang, S., and Wang, Z. (2018). Detecting the dynamics of vegetation disturbance and recovery in surface mining area via Landsat imagery and LandTrendr algorithm. *J. Clean. Prod.* 178, 353–362. doi:10.1016/j.jclepro.2018.01.050

Yang, J., Yang, R., Chen, M.-H., Su, C.-H., Zhi, Y., and Xi, J. (2021). Effects of rural revitalization on rural tourism. *J. Hosp. Tour. Manag.* 47, 35–45. doi:10.1016/j.jhtm.2021.02.008

Yang, H., Zhong, X., Deng, S., and Nie, S. (2022). Impact of LUCC on landscape pattern in the yangtze River basin during 2001–2019. *Ecol. Inf.* 69, 101631. doi:10.1016/j.ecoinf.2022.101631

Yu, L., Liang, L., Wang, J., Zhao, Y., Cheng, Q., Hu, L., et al. (2014). Meta-discoveries from a synthesis of satellite-based land-cover mapping research. *Int. J. Remote Sens.* 35 (13), 4573–4588. doi:10.1080/01431161.2014.930206

Yu, H., Yang, J., Sun, D., Li, T., and Liu, Y. (2022). Spatial responses of ecosystem service value during the development of urban agglomerations. *Land* 11 (2), 165. doi:10.3390/land11020165

Zhai, M., Hu, R., Wang, Y., Jiang, S., Wang, R., Li, J., et al. (2021). Mineral resource science in China: Review and perspective. *Geogr. Sustain.* 2 (2), 107–114. doi:10.1016/j.geosus.2021.05.002

Zhang, F., and Yang, X. (2020). Improving land cover classification in an urbanized coastal area by random forests: The role of variable selection. *Remote Sens. Environ.* 251, 112105. doi:10.1016/j.rse.2020.112105

Zhang, D., Zhou, C., and Xu, W. (2020a). Spatial-temporal characteristics of primary and secondary educational resources for relocated children of migrant workers: The case of liaoning Province. *Complexity* 2020, 1–13. doi:10.1155/2020/7457109

Zhang, M., Wang, J., Li, S., Feng, D., and Cao, E. (2020b). Dynamic changes in landscape pattern in a large-scale opencast coal mine area from 1986 to 2015: A complex network approach. *Catena* 194, 104738. doi:10.1016/j.catena.2020.104738

Zhang, D., Zhou, C., Sun, D., and Qian, Y. (2021). The influence of the spatial pattern of urban road networks on the quality of business environments: The case of dalian city. *Environ. Dev. Sustain.* 24 (7), 9429–9446. doi:10.1007/s10668-021-01832-z

frontiers | Frontiers in Environmental Science

TYPE Original Research
PUBLISHED 30 August 2022
DOI 10.3389/fenvs.2022.992092

Check for updates

OPEN ACCESS

EDITED BY
Jianhong Xia,
Curtin University, Australia

REVIEWED BY
Xiang Li,
Xiamen University, China
Xiao Qin,
Nanjing University, China

*CORRESPONDENCE
Linchuan Yang,
yanglc0125@swjtu.edu.cn

SPECIALTY SECTION
This article was submitted to Land Use Dynamics,
a section of the journal
Frontiers in Environmental Science

RECEIVED 12 July 2022
ACCEPTED 01 August 2022
PUBLISHED 30 August 2022

CITATION
Yang Q, Liu Y and Yang L (2022), Commercial gentrification in China and its distribution, development, and correlates: The case of Chengdu.
Front. Environ. Sci. 10:992092.
doi: 10.3389/fenvs.2022.992092

COPYRIGHT
© 2022 Yang, Liu and Yang. This is an open-access article distributed under the terms of the Creative Commons Attribution License (CC BY). The use, distribution or reproduction in other forums is permitted, provided the original author(s) and the copyright owner(s) are credited and that the original publication in this journal is cited, in accordance with accepted academic practice. No use, distribution or reproduction is permitted which does not comply with these terms.

Commercial gentrification in China and its distribution, development, and correlates: The case of Chengdu

Qinran Yang, Yang Liu and Linchuan Yang*

Department of Urban and Rural Planning, School of Architecture, Southwest Jiaotong University, Chengdu, China

Within the Anglo-American literature, commercial, along with residential, gentrification has often been treated as an attendant neighborhood phenomenon. This study aims to uncover the distribution of areas for emerging consumption that indicate the occurrence of commercial gentrification, as well as to explain the development process and spatial correlations of commercial gentrification in Chengdu, a large Chinese city. With the data of points of interest (POIs), the study categorizes new retail places for commercial gentrification and conducts spatial and statistical analyses. The following findings are revealed: First, the distribution of new retail places changed from a monocentric to a polycentric structure in the main urban areas of Chengdu from 2010 to 2020, wherein high-density areas were partially overlapped with traditional commercial centers. Second, commercial gentrification in Chengdu was presented by the fastest growth of the entertainment services in the 2010s. Third, commercial gentrification in Chengdu shifted from a centripetal to a centrifugal development pattern from 2010 to 2020. The geographies of development were variegated, connected with multiple location attributes and impacted by local governments' urban development strategies. Fourth, commercial gentrification was positively correlated with the growth of knowledge-intensive industries but negatively related to the change in both traditionally secondary and tertiary sectors in the past decade. Finally, changes in housing prices showed no connection with commercial gentrification during the studied period. The study suggests that commercial gentrification should be treated as a phenomenon of industrial gentrification, independent of residential gentrification. The commercial spatial planning in the city should play close attention to the synergic and exclusive relations between new retail industries and the evolution of industrial spaces in the emerging post-industrial city economy.

KEYWORDS

commercial gentrification, space for emerging consumption, knowledge-intensive industry, development characteristic, residential gentrification, spatial correlation, Chengdu, China

1 Introduction

Gentrification has been extensively studied on a global scale since 2000 (Atkinson et al., 2004; Lees et al., 2016). The connotations surrounding this concept range from early-stage residential substitution to the upward filtering of urban socio-spatial structures. The literature on gentrification has developed various analytical concepts, including school-district gentrification, rural gentrification, and commercial gentrification (Huang and Yang, 2012). Commercial gentrification is the transformation of residential, commercial, or industrial spaces into spaces with higher-value retail businesses; this process often entails the displacement of original residents and business owners (Gonzalez and Waley, 2003; Zukin et al., 2009).

In general, commercial gentrification entails emerging consumption activities and the advancement of retail industries within a city. Without a precise definition, the existing literature refers to emerging consumption as those activities cultivated in the formation of new consumer culture and consumption patterns (Bird and Macedo, 2021). However, while traditional consumption meets the necessary material and service demands of residents in daily life, emerging consumption creates and satisfies their higher-level demands, such as those for cultural capital and social status (Zhu, 2020; Areiza-Padilla and Manzi-Puertas, 2021). Moreover, the application of new technologies (e.g., internet technology and social media platforms) in transactions further distinguishes emerging from traditional consumption (Sun and Wang, 2021; Xiang et al., 2021). Emerging consumption gives rise to new consumption spaces and brings about the evolution of urban space. In particular, both commercial and residential gentrification can be contextualized in the emerging consumption of the new middle class, who, in Western cities, denotes a particular segment of the service classes with greater access to cultural and economic capital in post-industrial society (Zukin et al., 2009; Sun et al., 2018).

In China, commercial gentrification emerged amid unique social and political dynamics. Since the founding of the People's Republic of China, urban society in the country has been production-oriented, with individual consumption substituted by collective consumption. Since the country's process of reform and opening-up, its market economy grew dramatically, leading to sharp increases in citizens' average income; and Chinese society has gradually shifted from a production-oriented society to a consumption-oriented society (Davis, 2000; Tomba, 2004). The 2010s witnessed a significant acceleration in the post-industrial social transformation of large Chinese cities and, in turn, in the growth of the Chinese middle class through the development of new tech-heavy industries. International urban development strategies have encouraged intercity labor competition, boosting human capital development. However, given the lack of equitable development across China's regions, many major cities still struggle to use high-skilled workers (Yang and Zhou, 2018).

Furthermore, China's central and local governments have played a significant role in the development of a consumption-oriented society and economy. In 2015, the State Council released *Guidelines on Accelerated Cultivation of New Supply Power by Actively Exerting the Leading Effect of Emerging Consumption* (hereafter, the 2015 policy of *Guidelines on Emerging Consumption*) to accelerate the development of emerging consumption styles. *The 14th Five-Year Plan*, released on 11 March 2021, proclaimed the promotion of domestic consumption to be the main objective of social and economic development. The plan includes a series of national strategies, such as upgrading traditional consumption, encouraging new consumption types, and developing international central cities of consumption.

Hence, research into commercial gentrification is theoretically important for explaining the spatial characteristics of emerging consumption and their effects on urban transformation in the unique context of major Chinese cities. Furthermore, it can enrich comparative analyses between commercial and residential gentrification. In more practical terms, it generates implications for the optimization of commercial spatial planning. In this paper, Chengdu—a representative consumption-oriented city in southwest China—is used as a case study to assess the spatial evolution of commercial gentrification in Chinese cities, especially concerning the relevant spatial correlations and effects of commercial gentrification.

2 Emerging consumption, commercial gentrification, and urban change

In the Western literature on this subject, commercial gentrification is considered an accompanying neighborhood phenomenon to residential gentrification (Sun and Song, 2021). Residential gentrification results from the housing choices of the emerging middle class in inner cities (Yang et al., 2019a; Yang et al., 2019b). These housing choices then influence the resource-allocation decisions of business owners, leading to commercial gentrification as a second-hand phenomenon (Davidson and Loretta, 2010; Pastak et al., 2019). Therefore, the forces of commercial gentrification have been explained by two traditional theories of residential gentrification focusing on the demand side or the supply side. On the one hand, humanist scholars represented by David Ley (Ley, 1996) assert that gentrification in Western cities since the 1980s has mainly stemmed from a dramatic increase in high-skilled, middle-class individuals and their consumption patterns (Zukin, 1982; Hamnett, 2003). The new middle-class residents may also accelerate the restructuring of the community retail

industries through local marketing strategies (Keatinge and Deborah, 2016). On the other hand, scholars like Neil Smith (Smith, 1996) argue that both residential and commercial gentrification are the result of basic capitalist economic dynamics (i.e., the deprivation and agglomeration of surplus values). From this perspective, gentrification essentially comprises the plundering of rent gaps by reinvesting in recession-affected inner-city areas with high economic potential. A few studies in urban China emphasize that the pursuit of rent gaps of commercial land by local governments and capitalists is the main reason for commercial gentrification in large cities (Wang, 2011; Liu and Chen, 2018; Song et al., 2020).

On this basis, the spatial characteristics of commercial gentrification have largely been investigated by focusing on individual cases, lacking proper assessments of city-level laws (Liu et al., 2019). For instance, the literature has spatially characterized commercial gentrification in Western cities with the following three aspects: 1) increasing "boutiques" featuring leisure experiences and cultural attributes; 2) growing large corporate chain; and 3) the declining of localized retail formats (Zukin et al., 2009; Pastak et al., 2019; Sun and Song, 2021). Still, commercial gentrification generally occurs in inner-city areas and on certain historically or culturally significant blocks (Pratt, 2009). Song et al. (2020) creatively characterize the commercial gentrification of Nanjing from 2008 to 2018, proposing a corresponding development pattern: leaping-type diffusion from traditional business centers to surrounding emerging business districts. This development pattern comprises three spatial types: overall implantation type, invasive succession type, and transformation and upgrading type.

In addition to research explicitly focusing on commercial gentrification, research on spaces for emerging consumption in Chinese cities is gaining prominence with a particular focus on e-commerce spaces and web celebrity shops. More specifically, researchers have proposed that the distribution of e-commerce spaces has a macro-agglomerated and multi-core structure (Sun and Wang, 2021). Web celebrity shops also present a structure of multi-core agglomeration, and they have developed from central areas to the urban periphery (Xiang et al., 2021; Zhou et al., 2021). While these new retail places have distribution laws identical to traditional retail places (i.e., invisible consumption spaces still present a mode of large-scale development and are greatly affected by traditional urban commercial centers), they also present unique characteristics (e.g., the distribution of online celebrity spaces is more even, and invisible consumption spaces harbor more low-rent commercial and residential buildings in central areas). Furthermore, new consumption types have boosted the development of rural consumption economies, bridging the divide between urban and rural areas (Xu et al., 2021). In summary, the literature has largely focused on spaces for the individual type of consumption; but it lacks systematic research on spaces for emerging consumption.

The social influence of gentrification—a major research topic in critical geography—has risen greatly in recent years. Increasingly, research has begun to focus on how gentrification excludes ethnic minority groups and other disadvantaged groups (Sakzlolu and Lees, 2020; Huang and Liu, 2022). Both commercial gentrification and residential gentrification are generally seen as squeezing the survival space for original residents and traditional industries by driving retail shop/house prices higher, forcing outward migration (Gonzalez and Waley, 2003; Zukin, 2008; Ferm, 2016; Song et al., 2020), and destroying the authenticity of the city (Martinez, 2016). Startlingly, the effect of commercial gentrification on urban spatial evolution has scarcely been explored. According to some studies, commercial gentrification can revitalize the economies, improve built environments, and stimulate new employment opportunities in inner-city areas (Bridge and Dowling, 2001; Meltzer, 2016; Sun et al., 2018). Creative industries and historical streets generally interact with the spaces for emerging consumption in a bidirectional causal relationship (Wang et al., 2019). Furthermore, commercial gentrification boosts the globalization of consumer culture (Mermet, 2017).

Based on the insight provided by the studies detailed above, this study screens out the sorts of retail places that signify the advent of commercial gentrification. It then quantitatively analyzes the spatial distribution of these new retail places in 2010, 2015, and 2020 in the sub-districts of Chengdu, which is called Street (*jiedao*) in China. Street (*Jiedao*) refers to the lowest level of administrative units in Chinese cities. Next, this study measures the development levels of commercial gentrification in different Streets using the location quotient (LQ) index. Then, it reveals the correlations between commercial gentrification and urban spatial evolution from five major perspectives: knowledge-intensive industrial space, manufacturing space, ordinary office space, commercial space, and residential space. In this way, the study depicts the characteristics of commercial gentrification at a city level against the context of urban China and offers a comparison between the commercial gentrification of Chengdu with that of Western cities.

3 Retail places representing commercial gentrification

Residential gentrification has been traditionally measured by socioeconomic and housing indicators. However, retail industry indicators for measuring commercial gentrification have not yet been established (Kosta, 2019). This study proposes categories of retail places representing commercial gentrification by considering areas for emerging consumption in general, and the consumer culture of China's new middle class in particular. In the 2015 policy of *Guidelines on Emerging Consumption*, the types of emerging consumption were defined as service

TABLE 1 Categories of retail places representing emerging consumption.

Category	Sub-category
Catering Service	Western restaurant
	Hong Kong-style tea restaurant
	Other foreign restaurants
	Leisure catering
	Coffee house
Cultural and Educational Service	Exhibition hall
	Art museum
	Concert hall
	Theater
	Theme cultural museum
Sports Service	Emerging sport stadium
	Fitness center
	Natatorium
	Taekwondo stadium
	Equestrian club
	Racecourse
	Golf course
Entertainment Service	Bar
	E-sports facility
	Escape room
	Entertainment hall
	Nightclub

consumption, information consumption, green consumption, fashion consumption, quality consumption, and rural consumption, all of which respond to the changing consumer culture that values meaningful experience, health, knowledge, individualization, quality, and environmental protection (Yin, 2005).

The new middle class relevant to gentrification research in Western literature generally comprises professional and managerial personnel workers—members of the professional and managerial class (PMC)—in the service industry aged 30–45 years. Relative to that in the West, China's new middle class is both smaller and younger (Li, 2010). Additionally, personal consumption has only recently begun to be promoted in Chinese cities, meaning that the consumer culture of the new middle class is forming and has a low internal homogeneity (Wang and Lau, 2009). Given these dynamics, China's emerging middle class often engages in consumption with the aim of achieving greater social distinction and status. Therefore, its consumption pattern is characterized by "international brand consumption, hedonic consumption and conspicuous consumption" (Yu, 2005). Given the rapid growth of the new middle class in recent years, branding-oriented material consumption patterns are increasingly being overshadowed by rational and personalized consumption patterns. Middle-class consumers tend to appreciate the quality, experience, and pursuit of knowledge through consumption (Zhu, 2020).

In their investigation of Nanjing's commercial gentrification, Song et al. (2020) considered six classes of high-end commercial places, including exotic cuisine, coffee and tea, cosmetology and body care, yoga and fitness, business clubs, and bars. Wang and Gao (2008) divided businesses targeting the middle class into experience-type entertainment places (e.g., golf, coffee and tea, and cultural shows) and stimulant entertainment places (e.g., nightclubs and bars).

The above research has shown that the new middle class is drawn to medium- and high-end individual consumption with a focus on high-quality, entertaining experiences as well as cultural consumption that effectively indicates social status. Based on the classification of the point of interest (POI) data in Chengdu, this study identified four categories (and 22 sub-categories) of retail places targeting the new middle-class consumers in China: 1) catering services, 2) cultural and educational services, 3) sports services, and 4) entertainment services (Table 1).

4 Research area, data, and methods

4.1 Research area

Chengdu, a major city in the west of China and the capital city of Sichuan Province, has recently begun to undergo rapid development (Yang et al., 2022). Chengdu has been a pilot city for the national strategy of "developing China's west" since 2000. In 2013, the Belt and Road Initiative was promoted by President Xi Jinping. Cities in west China such as Chengdu started to play an increasingly important role in the development of the export-oriented economy. New state-led urban strategies have been devised, converting the city from a battleground of investments and industries to an agglomeration of talented people. Moreover, Chengdu is a transportation junction to China's external areas and an administrative and cultural center in Western China. Located on the Chengdu Plain for over a thousand years, Chengdu is largely flat, with a warm, humid climate. The city is known for its livability, comfortability, and leisure. Following the prosperous development of its consumption culture, the 14th Party Congress of Chengdu in 2022 highlighted the city as a site planned to be transformed into a hub of international consumption. Numerous ambitious plans that followed made Chengdu a suitable site for this research. As the emerging retail industry tends to develop in dense urban areas, this study considers the five main urban areas (*wu chengqu*) in Chengdu, which include Qingyang District, Jinniu District, Wuhou District, Chenghua District, and Jinjiang District (Figure 1). Given that

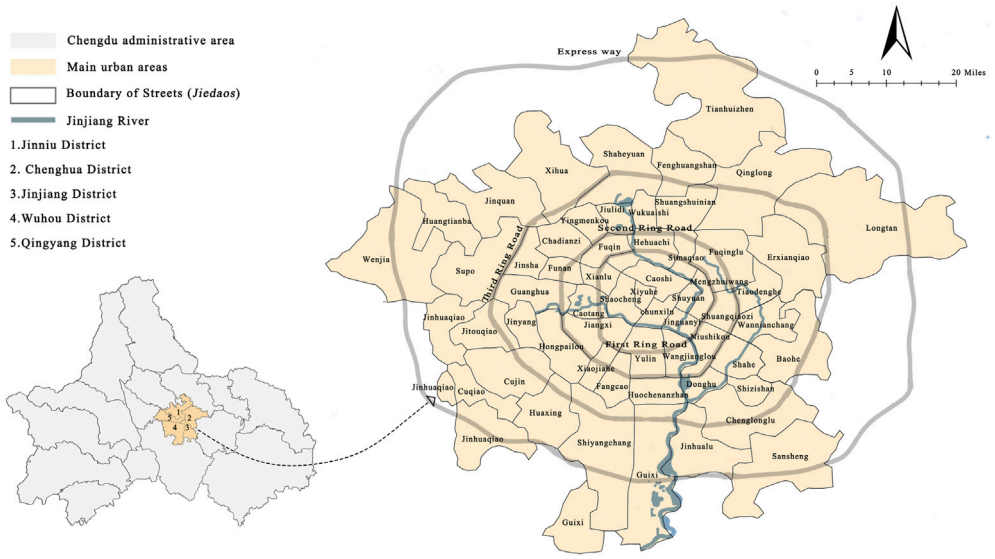

FIGURE 1
The five main urban districts and the Streets (*jiedaos*) of Chengdu.

emerging consumption is still developing in Chinese cities, the sum of the corresponding retail places remains limited. Commercial gentrification is expected to become a prominent feature in areas larger than individual communities, at least. The study thus chooses Street (*jiedao*), for which the geographical area is larger than that of a community but smaller than that of an urban district, as a basic unit for the analysis of commercial gentrification.

4.2 Data

We used the POI data, the second-hand housing prices of Chengdu's main urban area in 2010, 2015, and 2020, and government policies as the study's main data.[1] We employed 184,838, 314,508, and 724,536 POIs for the main urban areas of Chengdu in 2010, 2015, and 2020, respectively. The POI data were screened, cleaned, and classified as one of the abovementioned four classes. Ultimately, we used 2,054, 5,360, and 10,477 POIs for the four categories of retail industries in 2010, 2015, and 2020, respectively.

1 The POIs data is obtained from the Resource and Environmental Science and Data Center in China. This data is obtained by applying the key in the Autonavi map and using *Python* to crawl the real-time map of the year. The housing price data come from the HomeLink Real estate data platform. HomeLink is one of the top 100 real estate brokerage enterprises and the largest second-hand real estate trading platform in China.

4.3 Methods

We combined three methods to analyze commercial gentrification in Chengdu. First, We selected Kernel density estimation (KDE) to detect the spatial distribution of the four categories of new retail places. Kernel density is a non-parametric method of estimation, which does not assume the potential structure of the variable, but rather estimates the probability density function based on the data of a random variable (Parzen, 1962). It fits into the exploration of the distribution of a finite data sample in an area. Second, the changing location quotient (LQ) of the new retail places in a Street was used to measure the developmental level of commercial gentrification. The development level of a segment of retail industries in a Street is impacted by the Street scale and the scale of commercial land use in the Street. The LQ indicator can reduce the impact of regional scale and can be used to calculate the relative level of specialization with reference to the average level of the city. Finally, industrial distribution in different sections of the city tends not to follow the rules of normal distribution due to the aggregation effect of industries, the bias of some industries to particular geographical positions, and the influence of urban planning on the display of urban industries. Accordingly, we selected Spearman's rank correlation coefficient to assess the connections between commercial gentrification and urban spatial change.

4.3.1 Kernel density estimation

The KDE of the new retail places from 2010 to 2020 was made in ArcGIS (version 10.6). The density maps of traditional

retail places were also constructed for the purpose of comparison. The study defines 1 km × 1 km square, roughly equal to the size of a daily living area, as the bandwidth of the kernel density estimation. In order to facilitate comparison, we have unified the classification of kernel density levels over the 3 years. The formula is as follows:

$$f_n(x) = \frac{1}{nh}\sum_{i=1}^{n} k\left(\frac{x - x_i}{h}\right)$$

where $f_n(x)$ is the density value of the estimated point, k (.) is the kernel function, h is the bandwidth, n is the number of known points in the bandwidth (in this study, the places for the emerging consumption), and $x - x_i$ is the distance from the estimated point to point i.

4.3.2 LQ analysis

We calculated the LQs of the four retail industry categories for the 58 Streets. Each Street gains five LQ values for 2010, 2015, 2020, and the changes every 5 years. The changing index marks the developmental level of commercial gentrification during the 5 years. The calculation formula is as follows:

$$Q_i = S_i / P$$

Where i stands for the index of a Street, Q_i represents the LQ of the *i*th Street, S_i denotes the ratio of the number of emerging commercial units to the total number of commercial units in Street i, and P is the ratio of the number of emerging commercial units to the total number of commercial units in the research area (the main urban area of Chengdu). If $Q_i > 1$, the commercial gentrification level in the Street is higher than the average level—and vice versa if $Q_i < 1$.

4.3.3 Spearman's rank correlation coefficient analysis

The five major Street-level functions correlated with commercial gentrification are the development level of knowledge-intensive industries, the development level of manufacturing, the development level of ordinary companies and enterprises, the degree of retail mixing, and housing price. Knowledge-intensive industries include financial, high-tech, cultural, and creative industries. The first three indicators were calculated through LQ, while housing price was denoted by the growth rate. Using Spearman's correlation coefficient, three models for 2010, 2020, and 2010–2020 were established to explain the correlations between commercial gentrification and the five variables. Spearman's correlation coefficient (ρ) was calculated using the following formula:

$$\rho = 1 - \frac{6\sum d_i^2}{n(n^2 - 1)}$$

Where $d_i = x_i - y_i$ indicates the difference between the two rankings x_i and y_i, and *n* represents the sample size.

5 Results

5.1 The distribution of new retail places representing commercial gentrification

5.1.1 From monocentric to polycentric structure

Figure 2 shows the kernel density maps of places for the new and traditional consumption in 2010, 2015, and 2020 in the main urban areas of Chengdu. The distribution of these new retail places has changed from a monocentric to a polycentric structure from 2010 to 2020. The difference in densities between the core and the surrounding areas has greatly enlarged. In 2010, spaces for emerging consumption formed only one dense area of Chunxilu Street, where the city-level commercial center is located. In 2015, high-density areas developed outside the center. The Chunxilu core was expanded in scale, and its density was further enhanced. From 2015 to 2020, the number of new consumption cores and the unevenness of density distribution continued to enlarge. Further still, the new consumption cores in 2020 have overlapped with some of the traditional commercial centers, such as those of Chunxilu, Shaocheng, Jinsha, Shuangnan, Shupo, Jinyang, Donghu, and Fuqinglu Streets (Figures 2C, F). However, the density levels could be divergent between the overlapped two centers, such as those in Yulin, Donghu, Jinsha, Shuangnan, and Jiulidi Streets. Furthermore, a few new centers, namely Sansheng, Tiaodenghe, and Wangjianglu Streets, have grown outside of the traditional ones.

5.1.2 Diffusion from the center to inner suburbs and high-tech zone

From 2010 to 2020, the new retailing spread from the inner city to the inner suburbs and grew rapidly in the south part of the city, where the high-tech south zone is located. The high-tech south zone is affiliated with the Chengdu High-Tech Industrial Development Zone (CHTIDZ), which was designated by the national government in 1990. From 2010 to 2020, the development of the high-tech south zone reached a high point. In 2016, the Ministry of Science and Technology ranked the comprehensive strength of the CHTIDZ the third of the national zones, right below Zhongguancun Science Park in Beijing and ZhangJiang high-tech Park in Shanghai. In comparison, traditional retail industries experienced rapid development in various directions of inner suburbs and outskirts during the decade, with a comparative advantage over the new retail industries in the north and southwest suburbs.

5.2 The development characteristics of commercial gentrification

5.2.1 A growing total number but a stable proportion

The total number of the four categories of retail places grew significantly between 2010 and 2020, rising from 2,054 in 2010 to

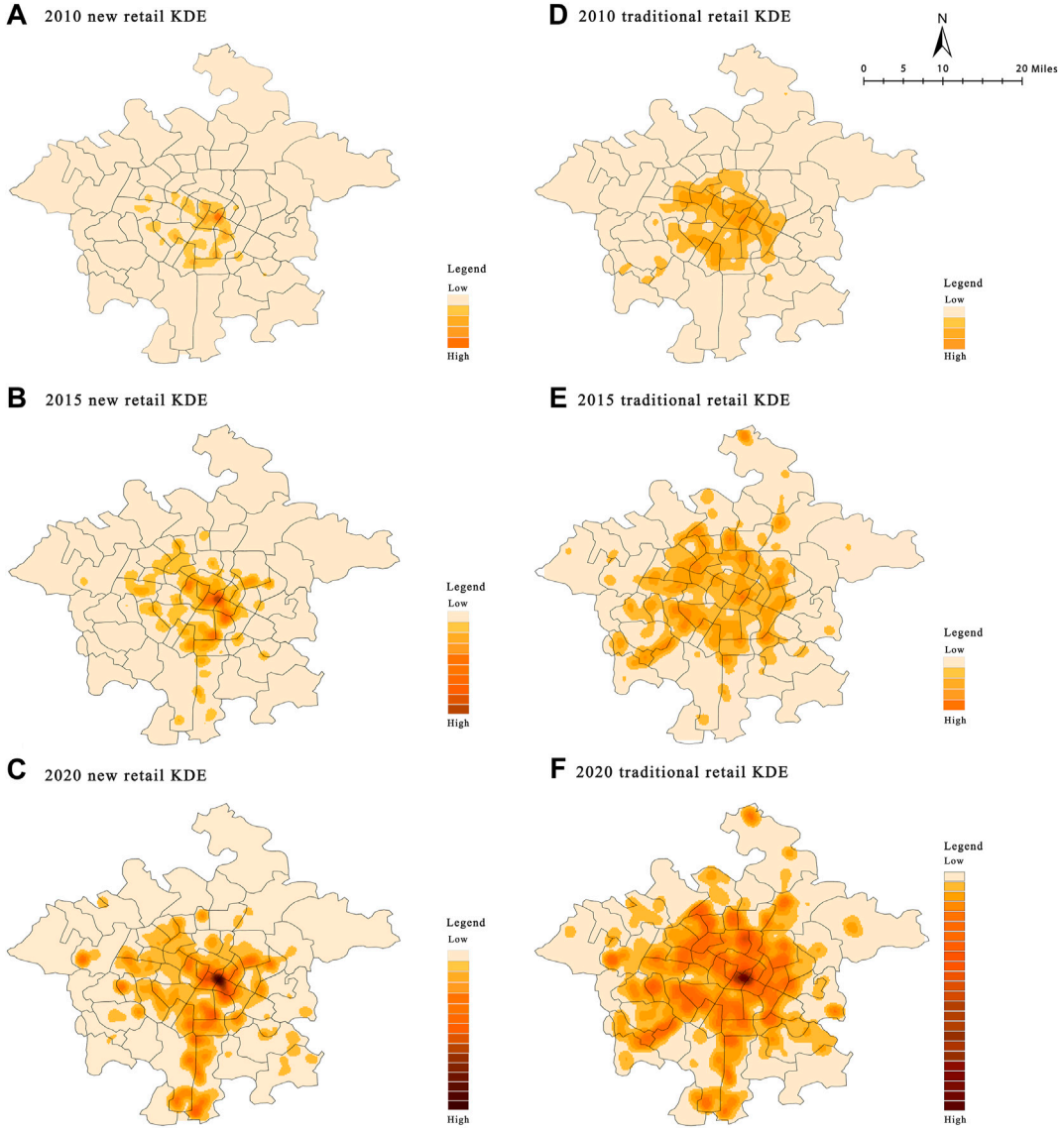

FIGURE 2
Kernel density map of the new and traditional retail places in Chengdu from 2010 to 2020.

5,360 in 2015 and 10,477 in 2020. Despite this growth, however, the proportion of these places for emerging consumption across the overall retail places remained constant, which accounted for only 2.2%, 3.0%, and 2.8% in 2010, 2015, and 2020, respectively. The result indicates that the retail industries for emerging consumption were developing at a steady pace in line with the rest of the Chengdu retail industries.

5.2.2 Rapid development of spaces for entertainment service consumption

Among the four classes of emerging consumption, catering services constituted the dominant type in Chengdu, accounting for about 40% of the total from 2010 to 2020 (Table 2). In terms of growth speed, however, entertainment service consumption grew the fastest from 2010 to 2020 with a sustained, steady pace, followed by catering consumption with the second-fastest growth rate. The proportion of sports service consumption was 35.15% in 2010, though this figure declined over the course of the next decade, ultimately falling below that of entertainment service consumption in 2020. In 2020, places for cultural and educational services were the least prominent in Chengdu, with the figure declining despite some initial growth.

TABLE 2 The numbers, proportions, and growth rates of the four categories of new retail places.

	Catering Services			Cultural and educational Services			Sports Services			Entertainment Services			Total	
	No	Proportion (%)	Growth rate (%)	No	Proportion (%)	Growth rate (%)	No	Proportion (%)	Growth rate (%)	No	Proportion (%)	Growth rate (%)	No	Growth rate (%)
2010	785	38.22	—	114	5.55	—	722	35.15	—	433	21.08	—	2054	—
2015	2052	38.28	161.4	456	8.51	300	1,330	24.81	84.21	1,522	28.4	251.5	5,360	160.95
2020	4,596	43.87	123.98	649	6.19	42.32	2036	19.44	53.08	3,196	30.5	110	10,477	95.47

5.2.3 Transition from centripetal development to centrifugal development

(1) 2010–2015

Table 3 shows the LQs of the new retail places at the Street level. Figure 3 maps the geography of commercial gentrification from 2010 to 2020. In 2010, Streets with high levels of new retail industries emerged in different parts of the city, including Chunxilu (with the commercial center) in the middle, Jinsha (with historical sites) in the west, Fuqinglu (with industrial sites) in the east and Guixi (in the high-tech zone) in the South. Generally, the west of the city affiliated with Qinqyang district (see Figure 1) was at the head of the development during the 2000s of the new retail industries in 2010. Qingyang District is famous for its abundant educational and cultural resources. It has a strong advantage in urban renewal and tourism development during the 2000s, as it hosts numerous important historical and cultural sites, such as Wide and Narrow Alley, the Du Fu Thatched Cottage, Qingyang Temple, Huanhuaxi Park, and the Jinsha archaeological site.

From 2010 to 2015, Streets in the central areas witnessed a rapid increase in the LQs of the places for emerging consumption. The condition could be attributed to the disinvestment of traditional retail sectors and then the initiation of commercial regeneration by the district government in the city center at this stage. In the Outline of the Twelfth Five-Year Plan for National Economic and Social Development of Jinjiang District (2011–2015), a plan of industrial agglomeration in the city core was made, positioning Chunxilu Street as a business and trade agglomeration area, Jinguanyi Street as a business, cultural and leisure industry agglomeration area, and the eastward Niushikou as a financial services agglomeration area and Shahe Streets as an international business and commerce agglomeration area. The city center regeneration was formally set off. The iconic spaces for consumption, such as International Financial Square, Taikoo Li, and Lan Kwai Fong in Jinguanyi Street, were all developed by Hongkong-based developers at this stage.

Shaocheng historical area on the west side of the city center and Wangjianglu on the southeast side were also developing fast from 2010 to 2015. Located in Shaocheng Street, a historic area called Wide and Narrow Alleys experienced commercial redevelopment in 2008. The 12th Five-Year Plan of Qingyang District of Chengdu (2011–2015) positioned Shaocheng Street to advance high-end financial and commercial services, which generated new opportunities for Shaocheng in the growth of offices and consumption spaces. The remarkable development of Wangjianglu, on the other hand, took advantage of the environmental governance of Jinjiang River, the development of riverside leisure industries, and the regeneration of university areas.

Finally, in 2015, an area with concentrated places for emerging consumption took shape on the belt of Xiyuhe,

TABLE 3 The levels of commercial gentrification in the Streets of Chengdu 2010–2020.

NO.	Street Name	2010	2015	2020	2010–2015	2015–2020	2010–2020
1	Sansheng	1.045	1.683	3.207	0.638	1.524	2.162
2	Shiyangchang	0.698	0.953	1.711	0.255	0.758	1.013
3	Shuyuan	1.313	2.576	2.280	1.262	−0.296	0.966
4	Shahe	0.916	1.641	1.632	0.725	−0.008	0.716
5	Tiaodenghe	1.423	2.495	2.101	1.072	−0.394	0.678
6	Longtan	0.100	0.276	0.733	0.177	0.456	0.633
7	Fangcaojie	1.292	1.929	1.882	0.637	−0.047	0.590
8	Jinguanyi	2.130	4.318	2.669	2.188	−1.649	0.539
9	Jinhualu	0.315	0.256	0.793	−0.059	0.537	0.478
10	Wannianchang	0.489	0.470	0.924	−0.020	0.455	0.435
11	Cujin	0.497	0.374	0.919	−0.123	0.545	0.422
12	Yinmenkou	0.381	1.145	0.777	0.764	−0.368	0.396
13	Shuangshuinian	0.331	0.338	0.646	0.007	0.308	0.316
14	Simaqiao	0.200	0.588	0.514	0.388	−0.074	0.314
15	Wukuaishi	0.253	0.572	0.551	0.319	−0.021	0.298
16	Caotang	0.968	1.420	1.235	0.451	−0.185	0.267
17	Shuangqiaozi	0.458	0.592	0.709	0.134	0.117	0.252
18	Mengzhuiwan	0.537	0.785	0.784	0.247	−0.001	0.246
19	Niushikou	0.744	1.156	0.923	0.413	−0.233	0.179
20	Jinquan	0.927	0.699	1.080	−0.228	0.382	0.154
21	Shizishan	0.436	0.140	0.589	−0.296	0.449	0.153
22	Wangjianglu	2.334	3.946	2.440	1.612	−1.506	0.105
23	Qinglong	0.291	0.209	0.386	−0.082	0.177	0.095
24	Yulin	0.976	1.247	0.993	0.271	−0.254	0.017
25	Wenjia	0.559	0.681	0.553	0.122	−0.128	−0.006
26	Xiaojiahe	1.166	1.021	1.158	−0.145	0.137	−0.008
27	Xiyuhe	2.093	4.161	2.070	2.068	−2.090	−0.022
28	Jinyang	0.866	0.501	0.833	−0.365	0.332	−0.033
29	Jitouqiao	0.420	0.309	0.357	−0.110	0.048	−0.063
30	Shaheyuan	0.201	0.050	0.135	−0.151	0.085	−0.066
31	Shupo	1.088	0.752	1.020	−0.336	0.268	−0.067
32	Caoshi	0.633	1.419	0.561	0.787	−0.858	−0.071
33	Cuqiao	0.317	0.260	0.234	−0.057	−0.026	−0.082
34	Funan	0.623	0.674	0.539	0.051	−0.135	−0.084
35	Chenglonglu	1.063	0.753	0.976	−0.310	0.223	−0.087
36	Fuqin	0.586	0.783	0.496	0.197	−0.288	−0.090
37	Erxianqiao	1.037	0.430	0.941	−0.607	0.511	−0.096
38	Huangtianba	0.493	0.393	0.387	−0.100	−0.006	−0.106
39	Shaocheng	1.689	3.135	1.553	1.446	−1.582	−0.135
40	Hehuachi	0.573	0.764	0.434	0.191	−0.330	−0.140
41	Xianlu	1.197	1.133	1.033	−0.064	−0.100	−0.164
42	Fenghuangshan	0.520	0.091	0.355	−0.429	0.264	−0.165
43	Tianhuizhen	0.529	0.128	0.324	−0.401	0.196	−0.205
44	Jinhuaqiao	0.640	0.238	0.398	−0.402	0.160	−0.242
45	Jiulidi	0.701	0.632	0.442	−0.068	−0.191	−0.259
46	Hongpailou	1.122	0.930	0.858	−0.193	−0.072	−0.265
47	Guanghua	1.676	1.343	1.309	−0.333	−0.034	−0.367
48	Baohe	1.078	0.500	0.638	−0.578	0.138	−0.440

(Continued on following page)

TABLE 3 (*Continued*) The levels of commercial gentrification in the Streets of Chengdu 2010–2020.

NO.	Street Name	2010	2015	2020	2010–2015	2015–2020	2010–2020
49	Huaxing	0.629	0.184	0.175	−0.445	−0.009	−0.455
50	Chadianzi	1.363	0.995	0.828	−0.369	−0.166	−0.535
51	Xihua	1.093	0.540	0.553	−0.553	0.014	−0.540
52	Donghu	1.593	1.004	1.047	−0.588	0.042	−0.546
53	Huochenanzhan	2.483	1.899	1.893	−0.584	−0.006	−0.590
54	Jiangxi	1.580	0.931	0.922	−0.649	−0.009	−0.658
55	Chunxilu	2.429	3.600	1.526	1.171	−2.074	−0.903
56	Guixi	2.947	1.536	1.869	−1.411	0.333	−1.078
57	Fuqinglu	1.971	1.013	0.827	−0.958	−0.186	−1.144
58	Jinsha	2.786	1.232	1.157	−1.555	−0.075	−1.630

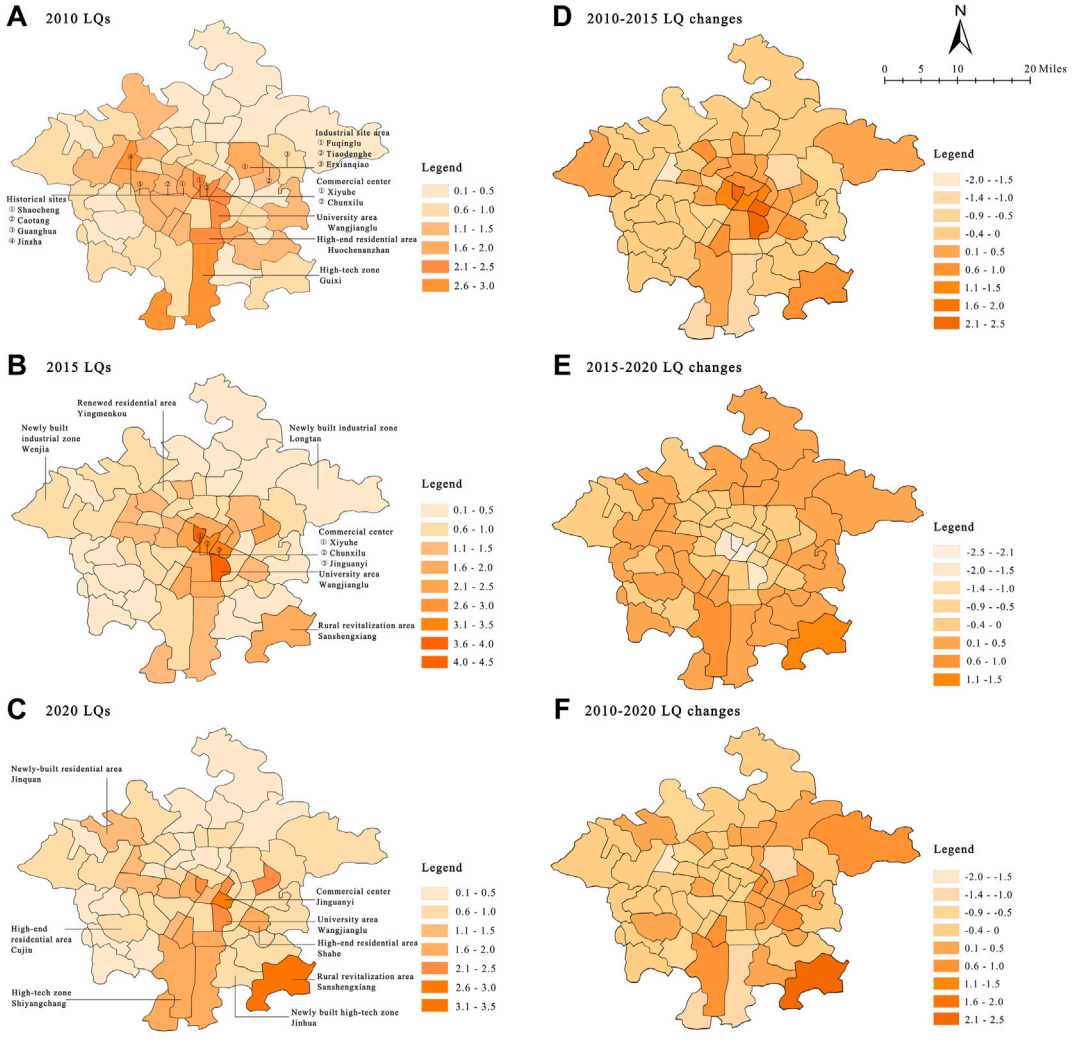

FIGURE 3
The LQs of spaces for emerging consumption in Chengdu from 2010 to 2020.

Chunxilu, Jinguanyi, and Wangjianglu Streets, reversing the westward trend of commercial gentrification and pushing the east toward greater development. The concentration of the new retail industries in the southern CHTIDZ (Guixi Street) was slightly slowed down during the 5 years as a result of the comprehensive improvement of various types of retail industries in the southern high-tech zone. Sansheng Street (previously Sansheng Township), an area representative of rural revitalization in Chengdu, achieved early development in 2015, exhibiting fast growth in emerging consumption.

(2) 2015–2020

From 2015 to 2020, the advantage of the city center, especially Shaocheng, Chunxilu, Xiyuhe, and Jinguangyu Streets, in developing new retail industries was weakened, although these Streets still had agglomeration degree higher than the average level of the city stemming from LQs in 2020. The agglomeration degree for Chunxilu Street, the city-level commercial center, declined from 3.6 in 2015 to 1.5 in 2020. This was likely due to the fact that, with the commercial revitalization of the city center, the scale of the traditional retail industry grew substantially, and the proportion of emerging retail places declined.

On the contrary, the inner suburbs and urban peripheries began to lead the advancement of commercial gentrification, with high growth rates most evident around Shiyangchang Street in the high-tech zone, two newly built residential areas of Cujin and Jinhualu Streets and Sansheng Street. Shiyangchang Street was a demonstration area of creative industries designated by the government in the Chengdu High-tech Zone Innovation and Entrepreneurship Development Plan (2016–2020). In addition, Chengdu's rural revitalization strategy is another policy that has had an important impact on commercial gentrification. Sansheng Street is a showcase of rural tourism in Chengdu. The first plan was made in 2003, focusing on the development of traditionally rural tourist industries. Later, foreign catering, cultural, and leisure industries increasingly assembled here and made Sansheng into an era of rural gentrification. In 2016, following the concept of building Chengdu as "a pilot of Park City" put forward by President Xi Jinping, Sansheng welcomed a new stage of development in ecological tourism. In 2020, the top-three Streets in Chengdu in terms of the agglomeration of places for emerging consumption were Sanshengxiang, Jinguanyi, and Wangjianglu Streets.

In 2020, Chengdu's new retail places presented two developmental belts. One runs from the west to the southeast, and the other from the center to the south. Generally, from 2010 to 2020, the geography of commercial gentrification showed a trend of multi-directional development. The fast-growing Streets were located in different areas of the city, with the most concentrated being in the southeast of the city center. The city center, finally, has entered into a period of slow development.

5.3 Correlations between commercial gentrification and urban spatial change

To determine the correlations between commercial gentrification and urban spatial evolution, the study relies on five sets of indicators to describe the spatial attributes of a Street in the main urban areas: LQ of knowledge-intensive industries, LQ of manufacturing, LQ of ordinary companies and enterprises, mixing degree of retail, average housing price. Three variables were assigned for each indicator, indicating the attribute of a Street in 2010, in 2020, and the value changes over the decade. Three sets of coefficients were then calculated by correlating the three sets of variables with commercial gentrification indicators separately (Table 4). Table 5 presents the results of this descriptive analysis.

Commercial gentrification showed the highest correlation with the concentration of knowledge-intensive industries in 2010, 2020, or 2010–2020. On the contrary, the advancement of the four categories of new retailing did not significantly associate with the growth rate of housing prices from 2010 to 2020, although the indicators of commercial gentrification in 2010 and 2020 were both positively related to housing prices. Then, the development of the new retailing was positively correlated with the degree of retail mixing, verifying the positive effect of gentrification on local vitality. Even with the new retail places excluded, commercial gentrification was found to exert a positive effect on the diversity of retail industries, especially in the life-services field and cultural and educational fields. Finally, the development of commercial gentrification was negatively correlated with the development of manufacturing and companies not under the umbrella of the finance, high-tech, and cultural and creative industries from 2010 to 2020, but the correlation coefficients and significance are both relatively low. It is also worth noting that commercial gentrification has already been shown to elevate shop prices and repel traditional retail stores (Pratt, 2009; Liu et al., 2019).

6 Discussion

The above study sought to understand the distribution, development characteristics, and spatial correlations of commercial gentrification in a major Chinese city. Following its analysis, the three sets of distinctions of commercial gentrification in the city can be drawn.

6.1 A moderate development of commercial gentrification in Chengdu

As the number of retail places for emerging consumption is increasing at a rate of doubling every 5 years, its share across the overall retail places is relatively constant. Moreover, the new

TABLE 4 Spearman correlations for 2000, 2010, and 2000–2010 change against the commercial gentrification index in Chengdu (N = 58).

Variable	Correlation Coefficient (p-value)		
	2010	2020	2010–2020 Changes
LQ of knowledge-intensive industries	0.548 (0.000**)	0.774 (0.000**)	0.479 (0.000**)
LQ of manufacturing	−0.461 (0.000**)	−0.507 (0.000**)	−0.265 (0.059*)
LQ of ordinary companies and enterprises	0.181 (0.175)	−0.752 (0.000**)	−0.264 (0.053*)
Mixing degree of retail	0.294 (0.025**)	0.731 (0.000**)	0.356 (0.006**)
Average housing price	0.578 (0.000**)	0.560 (0.000**)	0.046 (0.732)

Note: Knowledge-intensive industries include finance, high-tech, and cultural and creative industries. ** and * represent the significance level of 1 and 10%, respectively.

TABLE 5 Descriptive analysis of variables.

Variables	Max	Min	Mean	Std
Commercial gentrification (2010)	2.947	0.1	1.014	0.692
LQ of knowledge-intensive industries (2010)	2.009	0.088	0.876	0.426
LQ of manufacturing (2010)	3.472	0.084	1.288	0.883
LQ of other companies and enterprises (2010)	1.286	0.56	0.979	0.129
Mixing degree of retail (2010)	0.68	0.309	0.548	0.058
Average housing price (yuan/m^2) (2010)	10,193.38	6,393.88	8,079.10	964.31
Commercial gentrification (2020)	3.207	0.135	1.015	0.5664
LQ of knowledge-intensive industries (2020)	1.546	0.244	0.952	0.298
LQ of manufacturing (2020)	6.342	0	1.121	1.492
LQ of other companies and enterprises (2020)	1.202	0.819	1.009	0.084
Mixing degree of retail (2020)	0.647	0.307	0.542	0.056
Average housing price (yuan/m^2) (2020)	22,636.77	11,106.032	15,268.616	3,182.53
Commercial gentrification (2010–2020)	2.162	−1.63	0.001	0.57
Change of knowledge-intensive industries (2010–2020)	0.706	−0.735	0.065	0.251
Change of manufacturing (2010–2020)	3.652	−3.19	−0.167	1.034
Change of other companies and enterprises (2010–2020)	0.554	−0.228	0.03	0.175
Change of the mixing degree of retail (2010–2020)	0.109	−0.159	−0.006	0.056
Change of housing price (2010–2020)	1.531	0.458	0.891	0.312

retail industries are still in a transitional phase from sports services to the stimulating of entertainment experiences; they have yet to develop into a generalized cultural-consumption phase. The results suggest that Chengdu's consumption-oriented approach to development has not resulted in the new retail industries pushing significantly ahead of other types of retail industries. This could be a result of the limitations of the demand-side of commercial gentrification in Chengdu. As Yang (2022) has revealed that the employees in producer services took only 11.52% of all employed population in 2010 in Chengdu. Moreover, Chengdu, as the capital city of Sichuan province, has constantly attracted immigrants from the less-developed areas in the province. According to the population census, the city accommodated 4.71 million intra-provincial immigrants in 2020, while the highest proportion of these immigrants were those with secondary education. The demographic structure of the city could have hindered the rapid development of the emerging consumption industries.

6.2 Variegated geographies of commercial gentrification

Based on the KDE and LQ results, commercial gentrification in Chengdu is consistent with that in Western cities, primarily emerging in inner-city areas and, in particular, city-level commercial centers. Moreover, the multiple nuclei of new retail places seems partially consistent with traditional commercial centers. However, the density levels could be varied between the traditional and new retailing cores, and

high-density new retailing can also develop in non-traditional commercial centers. Based on the developmental process of commercial gentrification from 2010 to 2020—which was significantly oriented by the government's urban strategies—the frontiers of commercial gentrification possess mutable location attributes, including historical blocks, waterfront areas, urban commercial centers, universities, high-end residences, and rural landscapes.

The results illustrate that, although the emergence of commercial gentrification relies on traditional retail centers, its development may hinge on multiple factors. The findings further enrich our academic understanding of commercial geography. In the existing literature, the essential function of retail commerce is to meet residents' daily material and service needs. Research in commercial geography has thus emphasized the completeness of functional levels of commercial centers, the relative locations between commercial centers and residential areas, and the extent to which the distribution of retailing optimizes consumer travel (Chai et al., 2008; Wand et al., 2013). The significance of retail industries for emerging consumption has been divorced from the daily necessities of residents to the higher level of individual demands. Most importantly, boosting emerging consumption has become the main tool with which city governors can help sustain economic vitality, which corresponds to Neil Smith's viewpoint of gentrification as a globalized neoliberal urban strategy (Smith, 2002). Consequently, the development of new retailing would welcome greater creativity in location advantages than simply limited by service scope. Accordingly, the geographies of commercial gentrification tend to be both more variegated and selective by local governments and entrepreneurs, especially when compared to residential gentrification in Chinese cities, which usually occurs in areas with superior living resources—especially in terms of transport, the environment, and education (Huang and Yang, 2017).

6.3 Commercial gentrification as a type of industrial gentrification

As commercial gentrification may develop in different types of locations, it is nonetheless significantly correlated with the spatial evolution of knowledge-intensive industries. More notably, commercial gentrification is likely to emerge in areas already characterized by high housing prices. However, the development of commercial gentrification does not necessarily accompany the increase in housing prices. For example, between 2010 and 2015, retail sectors for emerging consumption shrunk in the commercial centers of Chunxilu, Xiyuhe, Jinsha, and Guixi Streets due to the expansion of the other retail sectors (Figure 3C). The housing prices of these Streets, nevertheless, witnessed a stabilized growth due to their location advantages. Some other Streets located at the fringe of the main urban areas, such as Baohe and Jitouqiao, saw a sharp rise in housing prices due to large-scale housing construction, but experienced a slower development of commercial gentrification in recent years. Therefore, commercial gentrification seems to have been cultivated in some high-end residential areas that also accommodated a large share of knowledge-intensive industries, but its temporal and spatial synchronization with residential gentrification was lower than that with the spatial evolution of knowledge-intensive industries.

The findings of the current study suggest broadening the scholarship of commercial gentrification to become a type of industrial gentrification in the Chinese context. As Pratt (2019, p. 1057) has claimed, "the gentrification approach was found to be partial...industrial gentrification may have a different set of dynamics." The development of commercial gentrification exerts a greater influence on urban industrial spatial change than residential spatial upgrading and displacement. It is an indicator of the post-industrial transformation of the city. However, it is worth bearing in mind that it also generates indirectly negative effects on traditional manufacturing industries and ordinary office spaces in addition to their direct negative effects on traditional retail industries.

7 Conclusion

Through unfolding the conditions of commercial gentrification in Chengdu, the current study provides certain theoretical and practical implications for commercial gentrification and spatial planning for new retail industries. First, commercial gentrification is representative of industrial gentrification in major Chinese cities. Its developmental path and spatial effects differ from those of residential gentrification. On the one hand, commercial gentrification is characterized by variegated geographies. It is compatible with diverse locational conditions and may develop away from traditional commercial centers. On the other hand, the phenomenon accompanies urban industrial spatial change—especially post-industrial transformation. Second, the study also sheds light on the developmental characteristics of new retail industries for emerging consumption in large Chinese cities. As far as Chengdu is concerned, the development of emerging consumption remains moderate. The main types of emerging consumption are sports and entertainment (which satisfy sensory stimulation), whereas cultural consumption that meets consumers' spiritual and knowledge demands is immature.

This study has implications for the layout of emerging commercial spaces. Since 2011, the rate of urbanization in China has been over 50%. Policies of urban renewal at the national and sub-national levels have shifted their focus to the quality improvement of built environments and the economic revitalization of old city areas. The mode of large-scale urban

redevelopment—a strategy widely used by municipal governments in the 2000s, and which triggered the wave of newly-built residential gentrification—has been intensively criticized. In this case, commercial gentrification is expected to receive even more overt state intervention. Planning for emerging commercial spaces would do well to more thoroughly investigate the diversified location advantages in the city, break the spatial limits of existing commercial spaces, coordinate with financial, high-tech, and cultural industries, and minimize the unreasonable the exclusion of traditionally secondary and tertiary industries. At the same time, local governments should encourage retailing development in cultural and educational services both prudently and gradually in order to reach an active interaction between the supply and demand side of the consumer market.

Data availability statement

The original contributions presented in the study are included in the article/Supplementary Material, further inquiries can be directed to the corresponding author.

Author contributions

QY: conceptualization, methodology, funding acquisition, supervision, and writing–original draft. YL: formal analysis, methodology, writing—review and editing. LY: conceptualization, methodology, supervision, and writing–original draft. All authors contributed to the article and approved the submitted version.

Funding

This study was supported by the National Natural Science Foundation of China (No. 51808452) and the General Program of the Sichuan Federation of Social Science Associations (No. SC20B113).

Conflict of interest

The authors declare that the research was conducted in the absence of any commercial or financial relationships that could be construed as a potential conflict of interest.

Publisher's note

All claims expressed in this article are solely those of the authors and do not necessarily represent those of their affiliated organizations, or those of the publisher, the editors and the reviewers. Any product that may be evaluated in this article, or claim that may be made by its manufacturer, is not guaranteed or endorsed by the publisher.

References

Areiza-Padilla, J. A., and Manzi-Puertas, M. A. (2021). Conspicuous consumption in emerging markets: the case of Starbucks in Colombia as a global and sustainable brand. *Front. Psychol.* 12, 662950. doi:10.3389/fpsyg.2021.662950

Atkinson, R., and Bridge, G. (2004). "Introduction," in *Gentrification in a global context: the new urban colonialism*. Editors R. Atkinson and G. Bridge (London: Routledge), 1–17.

Bird, D., and Macedo, P. (2021). *Seeking growth in emerging markets exploring consumer trends*. (Boca Raton, FL: Polen Capital).

Bridge, G., and Dowling, R. (2001). Microgeographies of retailing and gentrification. *Aust. Geogr.* 32 (1), 93–107. doi:10.1080/00049180020036259

Chai, Y., Weng, G., and Shen, J. (2008). A study on commercial structure of Shanghai based on residents' shopping behavior. *Geogr. Res.* (4), 897–906. doi:10.3321/j.issn:1000-0585.2008.04.018

Davidson, M., and Loretta, L. (2010). New-build gentrification: its histories, trajectories, and critical geographies. *Popul. Space Place* 16 (5), 395–411. doi:10.1002/psp.584

Davis, D. (2000). *The consumer revolution in urban China*. Berkeley: University of California Press.

Ferm, J. (2016). Preventing the displacement of small businesses through commercial gentrification: are affordable workspace. *Plan. Pract. Res.* 31 (4), 402–419. doi:10.1080/02697459.2016.1198546

Gonzalez, S., and Waley, P. (2003). Traditional retail markets: the new gentrification frontier? *Antipode* 45 (4), 965–983. doi:10.1111/j.1467-8330.2012.01040.x

Hamnett, C. (2003). Gentrification and the middle-class remaking of inner London, 1961-2001. *Urban Stud.* 40 (12), 2401–2426. doi:10.1080/0042098032000136138

Huang, X., and Liu, Y. (2022). Worse life, psychological suffering, but 'better' housing: the post-gentrification experiences of displaced residents from Xuanwumen, Beijing. *Popul. Space Place* 28 (4), 2523. doi:10.1002/psp.2523

Huang, X., and Yang, Y. C. (2012). The research progress of gentrification in western countries and China with the implications for China's urban planning. *Urban Plan. Int.* (02), 54–60. doi:10.3969/j.issn.1673-9493.2012.02.008

Huang, X., and Yang, Y. (2017). Urban redevelopment, gentrification and gentrifiers in post-reform inland China: a case study of Chengdu, China. *Chin. Geogr. Sci.* 27 (1), 151–164. doi:10.1007/s11769-017-0852-3

Keatinge, B., and Deborah, G. M. (2016). A'Bedford Falls'kind of place: neighbourhood branding and commercial revitalisation in processes of gentrification in Toronto, Ontario. *Urban Stud.* 53 (5), 867–883. doi:10.1177/0042098015569681

Kosta, E. B. (2019). Commercial gentrification indexes: using business directories to map urban change at the street level. *City Community* 18 (4), 1101–1122. doi:10.1111/cico.12468

Lees, L., Shin, H. B., and López-Morales, E. (2016). *Planetary gentrification*. Cambridge, Malden, MA: Polity Press.

Ley, D. (1996). *The new middle class and the remaking of the central city*. Oxford: Oxford University Press.

Li, C. (2010). *Introduction: The rise of the middle class in the middle kingdom. in Li, Chen (Ed.), China's Emerging Middle Class: Beyond Economic Transformation,* 3–31. Washington, DC: Brookings Institution Press.

Liu, B., and Chen, Z. N. P. (2018). Power, capital and space-production of urban consumption space based on the transformation of historical street area: a case study of sino-ocean Taikoo Li in Chengdu. *Urban Plan. Int.* 33 (1), 75–80. doi:10.22217/upi.2016.265

Liu, F., Zhu, X., Li, J., and Huang, Q. (2019). Progress of gentrification research in China: a bibliometric review. *Sustainability* 11 (2), 367–395. doi:10.3390/su11020367

Martinez, G. P. (2016). Authenticity as a challenge in the transformation of Beijing's urban heritage: the commercial gentrification of the Guozijian Historic Area. *Cities* 59, 48–56. doi:10.1016/j.cities.2016.05.026

Meltzer, R. (2016). Gentrification and small business: threat or opportunity? *Cityscape* 18 (3), 57–86. Available at: https://www.jstor.org/stable/26328273.

Mermet, A. C. (2017). Global retail capital and the city: towards an intensification of gentrification. *Urban Geogr.* 38 (8), 1158–1181. doi:10.1080/02723638.2016.1200328

Parzen, E. (1962). On estimation of a probability density function and mode. *Ann. Math. Stat.* 33 (3), 1065–1076. doi:10.1214/aoms/1177704472

Pastak, I., Eneli, K., Tiit, T., Reinout, K., and Maarten, V. H. (2019). Commercial gentrification in post-industrial neighbourhoods: a dynamic view from an entrepreneur's perspective. *Tijds. Econ. Soc. Geog.* 110 (5), 588–604. doi:10.1111/tesg.12377

Pratt, A. (2009). Urban regeneration: From the arts 'Feel good' factor to the cultural economy: a case study of hoxton, London. *Urban Stud.* 46 (5/6), 1041–1061. doi:10.1177/0042098009103854

Sakzlolu, B., and Lees, L. (2020). Commercial gentrification, ethnicity, and social mixedness: the case of javastraat, indische buurt, amsterdam. *City Community* 19 (4), 870–889. doi:10.1111/cico.12451

Smith, N. (2002). New globalism, new urbanism: gentrification as global urban strategy. *Antipode* 34 (3), 427–450. doi:10.1111/1467-8330.00249

Smith, N. (1996). *The new urban frontier: Gentrification and the revanchist city*. New York: Rutledge.

Song, W. X., Sun, J., Chen, Y. R., Yin, S. G., and Cheng, P. Y. (2020). Commercial gentrification in the inner city of Nanjing, China. *Acta Geogr. Sin.* 75 (2), 426–442. doi:10.11821/dlxb202002015

Sun, J., and Song, W. X. (2021). Literature review of foreign research on commercial gentrification and the enlightenment for Chinese studies. *World Reg. Stud.* 30 (5), 1096–1105. doi:10.3969/j.issn.1004-9479.2021.05.2019592

Sun, J., Zhu, X. G., Song, W. X., and Ma, G. Q. (2018). Commercial gentrification driven by cultural consumption in neighborhoods around university campuses: a case study of the original campuses of nanjing university and angina normal university. *Urban Plan.* 42 (07), 25–32. doi:10.11819/cpr20180705a

Sun, S. J., and Wang, J. Y. (2021). Distributional characteristics and influencing factors of invisible consumption space: a case study of Nanjing old city. *Urban Plan.* 261 (1), 97–103. doi:10.16361/j.upf.202100012

Tomba, L. (2004). Creating an urban middle class: social engineering in Beijing. *China J.* 51, 1–26. doi:10.2307/3182144

Wang, D., Duan, W., and Ma, L. (2013). Spatial impact analysis on the development of large business center—The case of wujiaochang area in shangha. *Urban Plan. Forum* 207 (2), 79–86. doi:10.3969/j.issn.1000-3363.2013

Wang, J., and Lau, S. Y. (2009). Gentrification and Shanghai's new middle-class: another reflection on the cultural consumption thesis. *Cities* 26 (2), 57–66. doi:10.1016/j.cities.2009.01.004

Wang, L., Qiu, S., and Liao, S. W. (2019). Gentrification of the surrounding area of creative industry cluster: an empirical study based on Shanghai cases. *Morden Urban Res.* (02), 69–77. doi:10.3969/j.issn.1009-6000.2019.02.010

Wang, W. H. (2011). Commercial gentrification and entrepreneurial governance in shanghai: a case study of taikang road creative cluster. *Urban Policy Res.* 29 (4), 363–380. doi:10.1080/08111146.2011.598226

Wang, X. Z., and Gao, L. (2008). Gentrification and the spatial structure of recreational places in big cities. *Hum. Geogr.* 23 (2), 49–55. doi:10.13959/j.issn.1003-2398.2008.02.005

Xiang, J. Y., Luo, Z. D., Zhang, J. Y., and Cheng, L. (2021). Research on the distribution characteristics of "net celebrity space" in the mobile internet era: A case study in main area of Hangzhou, China. *Mod. Urban Res.* 36 (9), 20–27. doi:10.3969/j.issn.1009-6000.2021.09.002

Xu, Y., Zhang, M., and Xiao, H. (2021). New urban-rural connection brought by food consumption: a case study of organic food and organic farm. *Mod. Urban Res.* 36 (9), 2–10. doi:10.3969/j.issn.1009-6000.2021.09.001

Yang, L., Chau, K. W., and Chu, X. (2019). Accessibility-based premiums and proximity-induced discounts stemming from bus rapid transit in China: empirical evidence and policy implications. *Sustain. Cities Soc.* 48, 101561. doi:10.1016/j.scs.2019.101561

Yang, L., Chau, K. W., and Wang, X. (2019). Are low-end housing purchasers more willing to pay for access to public services? Evidence from China. *Res. Transp. Econ.* 76, 100734. doi:10.1016/j.retrec.2019.06.001

Yang, L., Liang, Y., He, B., Lu, Y., and Gou, Z. (2022). COVID-19 effects on property markets: the pandemic decreases the implicit price of metro accessibility. *Tunn. Undergr. Space Technol.* 125, 104528. doi:10.1016/j.tust.2022.104528

Yang, Q. (2022). "Gentrification in Chinese cities," in *Urban sustainability* (Singapore: Springer). doi:10.1007/978-981-19-2286-2_5

Yang, Q., and Zhou, M. (2018). Interpreting gentrification in Chengdu in the post-socialist transition of China: a sociocultural perspective. *Geoforum* 93, 120–132. doi:10.1016/j.geoforum.2018.05.014

Yin, X. (2005). New Trends of leisure consumption in China. *J. Fam. Econ. Issues* 26 (1), 175–182. doi:10.1007/s10834-004-1419-x

Yu, F. (2005). The Change and characteristics of China's middle-class consumer culture since the end of the 19th century. *Acad. Res.* 2005 (7), 13–19. doi:10.3969/j.issn

Zhou, K., Zhang, H. T., Xia, Y, N., and Liu, C. (2021). New urban consumption space shaped by social media: a case study of the geo-tagging places of changsha on xiaohongshu. *Mod. Urban Res.* 36 (9), 11–19. doi:10.3969/j.issn.1009-6000.2021.09.003

Zhu, D. (2020). *The new middle class and the new consumption: Class structure transition and lifestyle changes against the background of internet development*. Beijing: Social Sciences Academic Press.

Zukin, S. (2008). Consuming authenticity: from outposts of difference to means of exclusion. *Cult. Stud.* 22 (5), 724–748. doi:10.1080/09502380802245985

Zukin, S. (1982). *Loft living: culture and capital in urban change*. Baltimore: The Johns Hopskins University Press.

Zukin, S., Trujillo, V., Frase, P., Jackson, D., Recuber, T., and Walker, A. (2009). New retail capital and neighborhood change: boutiques and gentrification in New York city. *City Community* 8 (1), 47–64. doi:10.1111/j.1540-6040.2009.01269.x

frontiers | Frontiers in Environmental Science

TYPE Original Research
PUBLISHED 01 September 2022
DOI 10.3389/fenvs.2022.1002014

Check for updates

OPEN ACCESS

EDITED BY
Jun Yang,
Northeastern University, China

REVIEWED BY
Huisheng Yu,
Northeastern University, China
Dongrui Han,
Shandong Academy of Agricultural Sciences, China

*CORRESPONDENCE
Debin Ma,
2235419204@qq.com
Jiaming Li,
lijm@igsnrr.ac.cn

SPECIALTY SECTION
This article was submitted to Environmental Informatics and Remote Sensing,
a section of the journal
Frontiers in Environmental Science

RECEIVED 24 July 2022
ACCEPTED 09 August 2022
PUBLISHED 01 September 2022

CITATION
Wang Z, Wang Y, Zhou Z, Yu F, Ma D and Li J (2022), Combining spatial planning and ecosystem services value to assist ecological compensation decision-making—A case study of Yangtze River Delta ecological barrier, China.
Front. Environ. Sci. 10:1002014.
doi: 10.3389/fenvs.2022.1002014

COPYRIGHT
© 2022 Wang, Wang, Zhou, Yu, Ma and Li. This is an open-access article distributed under the terms of the Creative Commons Attribution License (CC BY). The use, distribution or reproduction in other forums is permitted, provided the original author(s) and the copyright owner(s) are credited and that the original publication in this journal is cited, in accordance with accepted academic practice. No use, distribution or reproduction is permitted which does not comply with these terms.

Combining spatial planning and ecosystem services value to assist ecological compensation decision-making—A case study of Yangtze River Delta ecological barrier, China

Ziyi Wang[1], Yu Wang[2], Zihang Zhou[3], Fan Yu[1], Debin Ma[4]* and Jiaming Li[5]*

[1]School of Architecture and Urban Planning, Nanjing University, Nanjing, China, [2]School of Architecture, Tsinghua University, Beijing, China, [3]Department of Geography and Resource Management, The Chinese University of Hong Kong, Shatin, Hong Kong SAR, China, [4]School of Business, Nanjing Normal University, Nanjing, China, [5]Institute of Geographic Sciences and Natural Resources Research, Chinese Academy of Sciences, Beijing, China

China's ecological compensation (EC) is based on the property rights structure of public ownership of natural resources, which should be based on the spatial planning, which is defined by local government as the boundary of property right management and the distribution of development power. This study combined spatial planning and ecosystem service value (ESV) accounting to design a decision-making framework of EC, which includes "Subject choice, Value accounting, Priority evaluation, Policy supply". We selected 32 counties (districts) in the Yangtze River Delta region as the research object with the consideration of spatial planning and expert advice, and found that the implementation of EC slowed down the urbanization process and promoted the increase of ecological space. We conducted an accounting and sensitivity analysis on the spatial and temporal changes of ESV in the region from 2000 to 2019, and finally determined the amount and priority of accepting EC. The research results show that the ESV in the study area shows a general trend of increasing and then decreasing in time, and a spatial pattern of high in the south and low in the north and high in the east and low in the west. Forestland and water area are the main providers of ESV in the study area. The sensitivity coefficients of each type of ESV do not change much in each period, but the coefficients between the types have large differences. The total amount of EC in the Yangtze River Delta ecological barrier (YRDEB) is RMB 38,098.11 billion, and Shitai County is the area with the highest priority for compensation. We believe that this decision-making framework has the potential to be applied to the implementation of EC in other regions of China. At the same time, it can also be used to enrich the international views on EC research.

KEYWORDS

spatial planning, ecosystem services value, ecological compensation, compensation priority, main function area

1 Introduction

Since the industrial revolution, the world has been paying a heavy price for the growth way of extensive economy, and the problems of global warming, biodiversity decrease and heat island effect have become increasingly serious (Banks-Leite et al., 2014; Burke et al., 2015; Huang et al., 2020; Wang et al., 2022). In response to these growing global environmental problems, the Millennium Ecosystem Assessment promoted the concept of ecosystem services (ESs) and argued that maintaining ESs plays an important role in the sustainable development of human beings (MEA, 2005; Chan et al., 2012; Schrter et al., 2014). With the integration of ESs into mainstream environmental policy and planning management research frameworks (Gómez-Baggethun et al., 2010; Soh and Cho, 2019), paying for ESs to ease the contradiction between ecosystem and economic and social development has become a hot international topic (Muradian et al., 2013; Bremer et al., 2014; Ouyang et al., 2020). Many scholars have debated over the concept of payment for ecosystem services (PES) (Muradian et al., 2010; Wunder, 2015), value goals (Muradian et al., 2013), and implementation procedures (Wunder et al., 2018). Combining a number of views, Wunder put forward a revised concept of PES which is widely accepted, the concept is: "Voluntary transactions between users based on agreed natural resource management rules for generating offsite services." At the same time, many PES practices have been carried out in different countries, such as China's Grain-to-Green Program (GTGP) (Xie et al., 2022), Costa Rica's forest EC (Tafoya et al., 2020), Ecuador's SocioParamo Program (Bremer et al., 2014), etc. According to statistics, there were more than 552 PES programs in 2017 (Salzman et al., 2018).

The ecosystem valuation proposed by Costanza and Daily's is a ground-breaking and controversial study, which changed the past perception that ESs are "Free" (Costanza et al., 1997; Daily, 1997; Costanza et al., 2017). While there is much support for incorporating ESV into the PES implementation framework, it is still difficult to see cases where payments are made entirely in accordance with the market model in practice (Wunder, 2007; Fletcher and Büscher, 2017), more cases are made through negotiations or government action (Van Hecken et al., 2015). Some scholars regard EC in China as the equivalence of the PES (Shang et al., 2018; Yu et al., 2020). China has provided EC to China's key ecological function areas and restricted development areas through financial transfer payments since 2008. By 2022, more than 800 counties in China have received ecological transfer payments, with total transfer payments exceeding 600 billion yuan (Cao et al., 2022). Most of the money is used to protect and rehabilitate key ecological functional areas and compensate for the sacrifices for ecosystem protection made by the administrative units in such areas.

The selection of the subjects and the order of compensation are the basis for the implementation of EC. The subject of EC is essentially the issue of property rights (Engel et al., 2008). The private property rights system in Western countries provides the preconditions for PES. But they ignore that the property rights of natural resources in China are owned by the whole people and executed by different local administrative bodies. If we cannot understand this logic, we cannot understand the practice of EC in China for more than 20 years, and even cause some scholars "Misjudge" the effect of EC (He and Sikor, 2015; Shang et al., 2018). The priority of the allocation of EC funds is related to how to allocate the limited budget more efficiently, which directly affects the effectiveness and fairness of compensation (Li et al., 2021). It needs to consider the supply of ESs and the stage of economic and social development of the main body of EC. Because the main body of EC often has the characteristics of an underdeveloped economy and a high supply of ESs. The motive for judging this priority is not the effect of environmental protection actions, but the right of different regions to pursue development.

With the advancement of the theory and practice of EC, the combination of EC and spatial planning has attracted more and more attention (Chen et al., 2022; Yu et al., 2022a). Because of the difference of natural resources and ecological endowment in different regions, the development level of different regions is different (Moran et al., 2007). As an important public policy, spatial planning has a natural "Referee" role. For example, spatial planning can make overall arrangements for the development of different regions from a macro perspective, and alleviate the extreme imbalance of regional development caused by capital concentration (Wünscher and Engel, 2012; Fagan et al., 2016; Moreira et al., 2018; Yu et al., 2022b). Cuperus regarded spatial planning as an important factor in promoting the implementation of EC for infrastructure in the Netherlands (Cuperus et al., 1999). The combination of spatial planning and ecological compensation can help the spatial identification of ecological compensation, and find out the most effective ecological suppliers (Areas accepting EC), so as to improve the efficiency and accuracy of EC (Grêt-Regamey et al., 2017; Zulian et al., 2018; Huang et al., 2021).Wunder found that the principle of spatial positioning is beneficial to the practice of PES through the research on the global social science literature data set (Wunder et al., 2018). Fan constructed a quantitative estimation model of EC based on village, which provides a feasible way to reconcile the conflicts of interests among

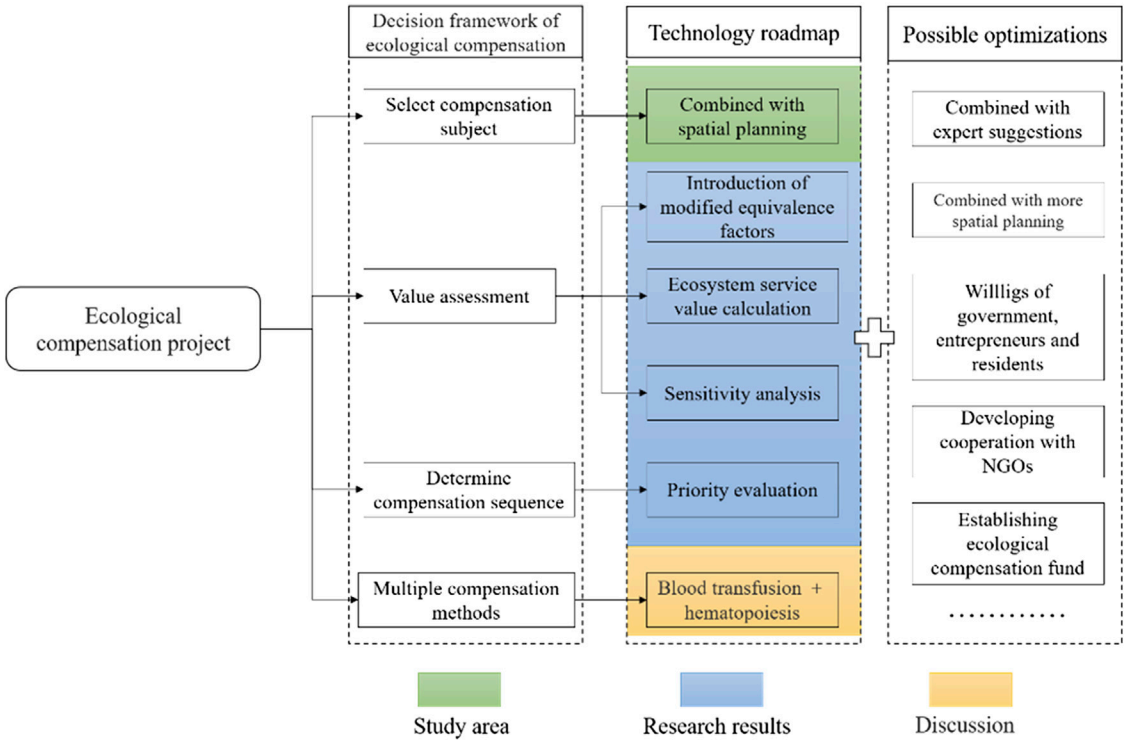

FIGURE 1
Decision framework of EC.

regional economy, society and ecology (Fan et al., 2019). Taking the Middle Route of South-to-North Water Diversion Project as an example, Su conducted an in-depth analysis of how EC can be implemented in spatial planning, which is conducive to promoting regional water resources protection and ecological sustainability (Su et al., 2022).However, there are few studies on the selection of EC subjects and the determination of compensation order in combination with spatial planning.

Based on the background of China's territorial spatial planning, this study analyzes China's EC decisions from a spatial perspective, in order to design a new framework to respond to the problems of the subject selection and compensation order of EC. It can be used to assist the decision-making of EC in China and enrich the theory and practice of international EC. We choose YRDEB as a case. On the one hand, this area is an important ecological function area in China and an ecological security barrier for the Yangtze River Delta urban agglomeration. On the other hand, it has made huge sacrifices for the green development of the Yangtze River Delta region and has been regarded as the key object of EC by the Chinese government. In Section 2, the paper describes in detail about the decision-making framework of EC on the basis of spatial planning and ecosystem service accounting. In Section 3, we introduce methods and data sources. In Section 4, we give a brief description of the empirical results. Finally, we reiterate our main points and research uncertainties in the discussion.

2 Design a decision framework

We designed a decision-making framework for EC combining spatial planning and ESs accounting (Figure 1):

1) The implementation of EC through spatial planning is determined by China's special property rights structure. Unlike the private ownership of property rights in Western countries, China takes state ownership of natural resources, so the state is normally both a provider of ESs and a beneficiary. It is the governments at all levels that exercise natural resource management rights and income rights. Therefore, they may become both payers and recipients of EC under different scenarios. In China, individuals may become payers of EC only in a few instances, such as farmland where individuals have quasi-private property rights. In most instances they will only become payees of EC. Under the background of departing from the logic of Neoclassical and Neoliberalism market behavior (Fletcher and Büscher, 2017; Van Hecken

et al., 2018), what has driven China's two-decade-long practice of EC? We believe that the following three points are central to China's promotion of EC practices: ①The setting of macro-objectives reflects the will of the state. ②The creation of inter-regional supply and demand through the regulation of factors and uses. ③Through the establishment of the right to development to endow the rights and responsibilities of different administrative subjects. As we can see, all of these initiatives need to be implemented through spatial planning. Spatial planning, as the main means of space development, protection and management of administrative units at all levels, is the most unquestionable tool to achieve EC in China. Moreover, spatial planning plays an active role in the rational use of resources, environmental protection and coordinated regional development in developed countries (Mascarenhas et al., 2012).

2) After clarifying the subject of EC, the theoretical amount and priority should be determined. We evaluated ESV in these areas. At present, the methods of EC amount evaluation mainly include the direct cost method (Li, 2011), conditional value method (Chu et al., 2020), opportunity cost method (Adhikari et al., 2017), ESV method, etc (Costanza et al., 1997). The direct cost method is less common in concrete practice. The opportunity cost method requires high accuracy and completeness of data. The conditional value method mainly determines compensation between interest subjects and is highly influenced by subjective will. Ecosystem service valuation applies spatially explicit integrated ecological and economic models to account for costs and benefits that are not taken into account by the market and incorporated into economic decisions (Ouyang et al., 2020). Constanza's first assessment of the ESV on a global scale, using the value equivalent factor approach, has been widely discussed (Costanza et al., 1997).
3) Furthermore, we evaluate the priority of EC with the theoretical compensation amount. Since the resources for EC are limited, we must prioritize the allocation of limited resources to areas of greater need (Ceballos et al., 2015). Although this distribution is not done in a full market, it cannot achieve the "Ideal kingdom" of Pareto efficiency, the design of the "Complex" decision-making framework for EC implies the pursuit of spatial positioning, differentiated payment and supervision-regulation (Wunder et al., 2018). In the end, this distribution method may achieve a better EC effect.
4) We put forward multiple EC methods. We do not think that ESV is the true amount of EC. Since the nature of EC is not only the economic means to adjust the interests of stakeholders, but also many participants to affect the supply and demand of ESs decision-making process (Metzger et al., 2020), which should be reflected in a variety of ways. Therefore, compared with the "Blood-transfusion" EC model, which is directly subsidy, the "Blood-making" EC model may have a longer lasting vitality (Liu et al., 2020).
5) Finally, we propose possible ways to optimize our framework. It includes demonstrating the spatial selection of EC with the suggestions of experts; optimizing the distribution of development rights through more scientific planning methods; determining the amount of EC based on the wishes of the government, enterprises and individuals, not just by the ESV evaluation; introducing NGOs to participate in the practice of EC and establishing EC funds.

3 Methods and data sources

3.1 Selection of EC subjects

According to the research framework, we have to select out the EC area according to China's important spatial planning document "National Major Functional Area Planning". In the main functional zoning, different functional areas take different responsibilities, among which urban areas can promote economic development and lead China's modernization process, major agricultural production areas can ensure food security and sustainable human survival (Yu et al., 2022), while key ecological function areas can ensure ecological security and ecological sustainability (Du et al., 2021). Our criteria for selecting study areas are as follows: 1) According to the "Yangtze River Delta regional integration development plan outline", which pointed out to build the Yangtze River Delta green ecological barrier in the 'West Anhui Dabie Mountains and South Anhui-Zhejiang West-South Zhejiang mountainous area', it determines the region is an important ecological protection area in the Yangtze River Delta region. 2) Based on "Zhejiang Province Main Function Area Planning" and "Anhui Province Main Function Area Planning", restricted development areas and prohibited development areas are selected as EC areas. 3) According to the experts' suggestion, we should consider other major agricultural production areas, eco-economy areas, and administrative areas where world-class natural and cultural heritage and national cultural relics protection units are located. 4) To ensure the integrity of administrative subject's business and financial rights, and to implement EC action (Table 1).

We selected 32 counties (cities and districts) as the YRDEB, which is also the research area of this paper. In general, the YRDEB spans 115°–120° degrees east and 27°–32° degrees north, and is located in the lower reaches of the Yangtze River, southwest of Anhui Province and southwest of Zhejiang province. it covers Hangzhou, Wenzhou, Quzhou, Lishui, Lu'an, Xuancheng, Chizhou, Anqing and Huangshan City, covering a total area of 57,558.19 km^2. This area is an important ecological reserve and food security area in China (Figure 2.).

TABLE 1 Selection basis of the study area.

Province	County	Selection basis	Province	County	Selection basis
Anhui	Jinzhai	National key ecological function area	Anhui	Tunxi	World Cultural and Natural Heritage
	Huoshan			Huizhou	
	Taihu		Zhejiang	Qujiang	National major agricultural product producing areas
	Yuexi			Longyou	
	Qianshan			Jiangshan	
	Shitai			Chun'an	Provincial key ecological functional areas
	Shexian	Provincial key ecological functional areas		Wencheng	
	Yixian			Taishun	
	Qimen			Suichang	
	Xiuning			Yunhe	
	Huangshan			Qingyuan	
	Qingyang			Jingning She	
	Jing			Longquan	
	Jingde			Kaihua	
	Jixi			Changshan	Provincial Ecological and Economic Region
	Ningguo			Kecheng	Provincial Ecological Civilization Construction Demonstration Zone

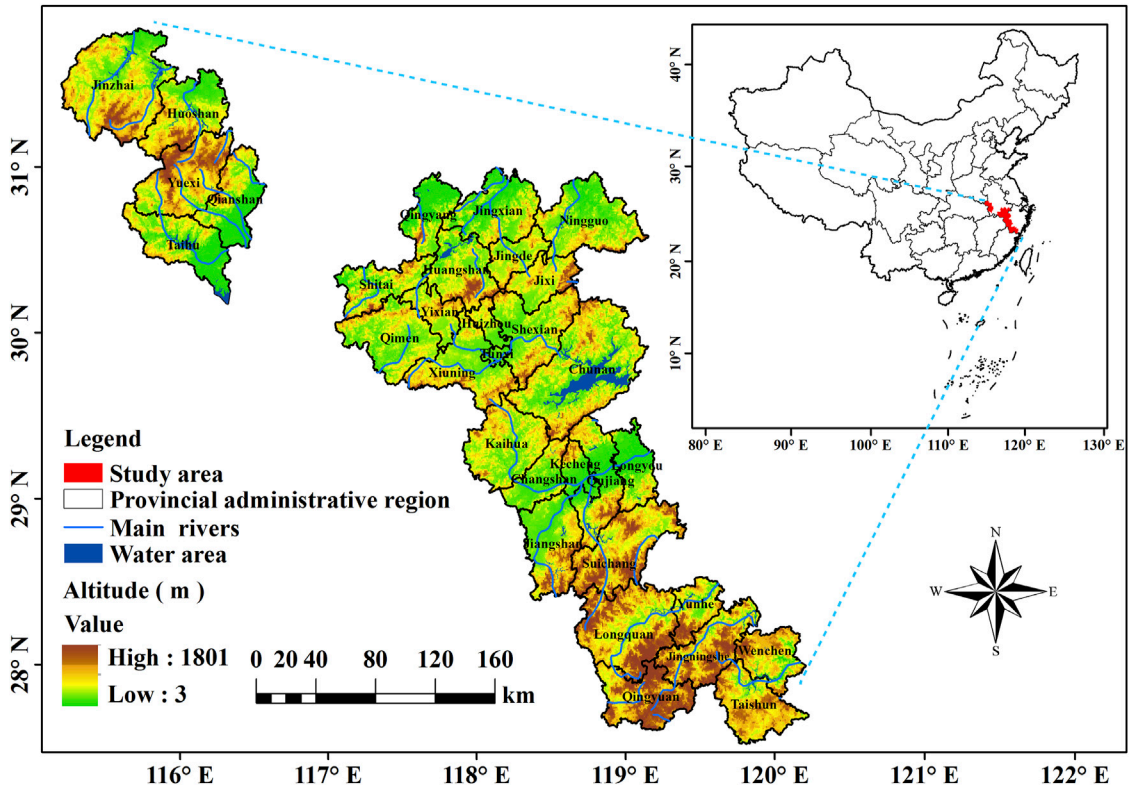

FIGURE 2
The research area.

TABLE 2 Ecological service value per unit area of different ecosystems in the YRDEB.

Primary classification		Secondary classification	Farmland	Forest land	Grassland	Water area	Urban area	Unused land
Market value	Supply service	Food production	4,796.98	1,096.14	1,012.94	3,472.93	0	0
		Raw material production	1,063.58	2,517.87	1,490.46	998.47	0	0
		Water supply	−5,665.21	1,302.35	824.82	35,988.20	0	0
Non-market value	Regulatory service	Gas regulation	3,863.63	8,280.76	5,238.33	3,342.69	0	86.82
		Climate regulation	2018.64	24,777.16	13,848.29	9,941.25	0	0
		Environmental purification	586.06	7,260.59	4,572.69	24,093.43	0	434.12
		Water regulation	6,490.03	16,214.23	10,143.84	443,840.02	0	130.23
	Support service	Soil conservation	2,257.40	10,082.34	6,381.50	4,037.28	0	86.82
		Maintaining nutrient cycle	672.88	770.56	492.00	303.88	0	0.00
		Maintaining biodiversity	738.00	9,181.55	5,802.68	11,069.95	0	86.82
	Cultural service	Provide aesthetic landscape	325.59	4,026.42	2,561.28	8,204.79	0	43.41
Sum			17,147.58	85,509.97	52,368.84	545,292.89	0	868.23

3.2 Accounting of ESV

3.2.1 Correction of equivalence factor

The precondition of using the equivalent factor method to evaluate ESV is to construct an objective and accurate equivalent factor table. In this paper, based on the ESV calculation method proposed by Costanza et al. (1997), referring to the research results of Chinese ESV equivalent scale published by Xie et al. (2015), the ESs are divided into 11 categories. Meanwhile, combined with the research results proposed by Wang et al. (2010) the ESV is divided into market value and non-market value. We made a localized correction to the unit ecological service value equivalent factor, combined with the actual production capacity of Anhui and Zhejiang and the availability of data considerations, and selected wheat, cotton and rapeseed as the main grain crop species. By consulting the "National Compilation of Agricultural Product Cost-benefit Data in 2019" and the yearbooks of each region, the average grain yield was 5,686.484 kg/hm^2 in the study area from 2000 to 2019. According to the economic value of one ESV equivalent factor is 1/7 of the average grain yield market value of the study area in 2019, the average grain price of the study area is 2.225 yuan/kg, and the economic value of natural grain yield of farmland was about 1807.095 yuan/hm^2. Also, since ESV is susceptible to different factors, including physical geographic factors, willingness-to-pay and ability-to-pay, the coefficients need to be corrected when calculating ESV at the regional scale to further calculate the adjustment coefficient C. As has been mentioned above, ESV per unit area of different ecosystems in the study area is calculated (Table 2). The formulas are as follows:

$$D_n = 1 \Big/ 7 \sum_{i=1}^{n} \frac{q_i p_i}{M} \tag{1}$$

$$C = A \times W \times N \tag{2}$$

$$A = \frac{GDP_{st}}{GDP_{CN}} \tag{3}$$

$$W = \frac{2}{1 + e^{-s}} \tag{4}$$

$$s = \frac{1}{En} - 2.5 \tag{5}$$

$$En = En_t \times U + En_c \times R \tag{6}$$

$$N = \frac{NPP_{st}}{NPP_{CN}} \tag{7}$$

$$NPP = 3000\left[1 - e^{-0.0009695\,(E-20)}\right] \tag{8}$$

$$E = \frac{1.05P}{\sqrt{1 + (1 + 1.05P/L)^2}} \tag{9}$$

$$Em = 3000 + 25T + 0.05T^3 \tag{10}$$

Where D_n refers to the economic value of food production services provided per unit area of farmland ecosystem in the study area (Yuan/ha), n refers to the main food crop species in the study area, q_i refers to the price of the crop i (Yuan/kg), p_i refers to the total yield of the crop i (kg), and M refers to the total area of n food crops (hm^2), C represents the adjustment coefficient, A represents the ability to pay ESV, W represents the willingness to pay ESV, and N represents the ratio of net primary productivity (NPP) in the study areas to the national average NPP. GDP_{st} andGDP_{CN} represent the 2019 GDP per capita ($/person) for the study areas and China, respectively. s represents Engel coefficient; En_t andEn_c represent the urban and rural Engel coefficients, respectively. U refers to the proportion of urban population in 2019 and R refers to the proportion of rural population in 2019. NPP_{st} and NPP_{CN} represent the 2019 NPP (t/km^2/a) for the study area and the national average, respectively. E represents actual annual evaporation(mm), P,

Em and *T* represent the annual precipitation (mm), average evaporation(mm) and temperature (°C) in 2019, respectively.

3.2.2 Calculation of ESV

This study corresponded the land use types to those close to the ecosystem types in the study by Xie et al. (2003, 2015). We have classified farmland, forestland and unused land corresponding to each other with farmland, forest and desert respectively, and residential, industrial, mining land and transportation land as urban area, and the ESV of urban area is taken as 0. The calculation formulas of ESV and individual ESV (ESV_f) are as follows:

$$ESV = \sum (A_k \times VC_k) \tag{11}$$

$$ESV_f = \sum \left(A_k \times VC_{kf}\right) \tag{12}$$

Where A_k refers to the area of the k th land use type in the study area; VC_k refers to the ESV per unit area of land use type k, and VC_{kf} is the ESV per unit area of land use type k.

3.3 Calculation of priority and standard of EC

3.3.1 The priority of EC

This study proposed an EC priority index, which provides a basis for objectively reflecting the supply and demand of regional ESs and measuring the urgency of EC. The prioritization in this study was determined by two variables: the level of economic development and ESV. Since the market value (food production, raw material production and water supply values) has been converted into currency in the market mechanism and is reflected in the regional economic development, only non-market value is considered when estimating the ESV. The specific relation is as follows:

$$ECPS = \frac{N_ESV}{GDP} \tag{13}$$

Where ECPS refers to the priority index of EC;N_ESV represents the non-market service value of the ESV of each county (city, district) except the value of food production, raw material production and water supply; GDP represents the gross national economic product of the county (city, district). The higher the ECPS value, the greater the impact on the economic situation of the region after payment of EC, EC support should take the lead. On the contrary, it shows that the payment of EC has little influence on the economic situation of the region and should be the first to pay the EC funds.

3.3.2 Estimation of EC standard

This paper introduced the intensity of EC demand (the urgency of EC in different regions) and the conversion coefficient of non-market ESV (converted by regional actual non-market ESV) to reflect the regional differences in the amount of EC (Wang et al., 2010). The demand intensity coefficient of EC was characterized by the normalized result of EC priority. The specific expressions are as follows:

$$V_i = k \times N_ESV_i \times T_i \tag{14}$$

$$T_i = 2 \times arctan\, ECPS_i/\pi \tag{15}$$

Where V_i refers to the total amount of EC in region i; N_ESV_i refers to non-market ESV in region i; k refers to the discount factor for the non-market ESV, select 15% based on existing studies; T_i refers to the EC demand intensity; $ECPS_i$ refer to the EC priority index of region i; π refers to the circumference rate; i refers to different counties (cities and districts) in the study area.

3.4 Ecosystem sensitivity analysis

The coefficient of sensitivity (CS) was introduced to verify the representativeness of ecosystem types for various land cover types and the accuracy of the selected ecological value coefficients, which is calculated as:

$$CS = \left| \frac{\left(ESV_j - ESV_i\right)}{ESV_i} \Big/ \frac{\left(VC_{jk} - VC_{ik}\right)}{VC_{ik}} \right| \tag{16}$$

Where ESV、 VC、 k have the same meaning as before; i and j refer to the initial value and the ecological value factor adjusted value. When CS < 1, it shows that ESV is inelastic to ecological value coefficient; When CS >1, it shows that ESV is elastic to ecological value coefficient.

3.5 Data sources

The data used in this paper mainly includes land use, vegetation classification, socio-economic, main functional zoning and administrative data of Zhejiang and Anhui provinces. Among them, the land use and vegetation classification data were downloaded from the Resource and Environmental Science Data Center of the Chinese Academy of Sciences (https://www.resdc.cn/). The data was generated by manual visual interpretation based on Landsat TM imagery from the United States Landsat satellite (He et al., 2022). The land use types include six categories: farmland, forestland, grassland, urban area, water area and unused land. Socio-economic data were obtained from the statistical yearbooks and government website bulletins of cities and counties in the study area (Obtained on 28 November 2020). The "National Main Functional Area Planning," "Zhejiang Provincial Main Functional Area Planning" and "Anhui Provincial Main Functional Area Planning" referenced in the division of the main functional area of each county (city and district) in the study area were from the documents published by the government. The administrative data

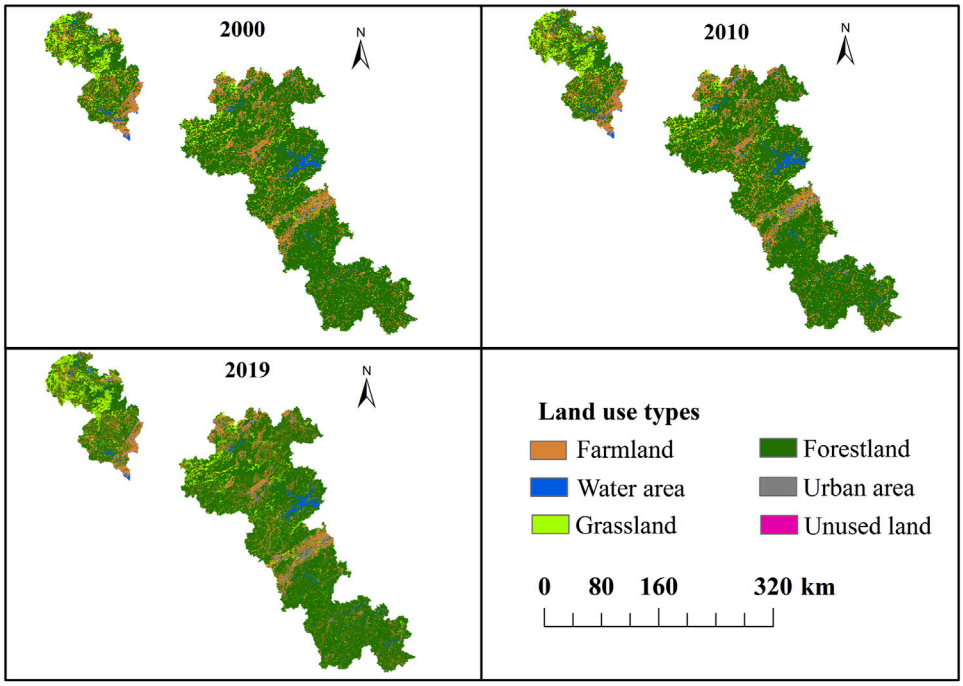

FIGURE 3
Spatial distribution of land use types in YRDEB from 2000 to 2019.

was provided by the National Geographic Information Center on a scale of 1:4 million.

4 Results analysis

4.1 Spatial distribution and changes of land use types

By using ArcGIS, the spatial distribution maps of three stages of various land areas, types of land use (Figure 3) and types of land use transfer were obtained (Figure 4). The area and proportion of land types in each period were calculated based on the classification of land use, as well as the absolute amount and rate of change of area for each land use type from 2000 to 2019. The results showed that forest, farmland and grassland were the main land use types in the YRDEB (Figure 3). The total area of these three types accounted for more than 95% of the total area. Among them, the proportion of forestland was the largest, which was 74.44%, 74.01% and 73.70% in the three stages. In terms of the amount of change, the land use change in the study area from 2000 to 2019 showed that urban area, water area, and grassland increased, while forestland, farmland, and unused land decreased. The urban area increased the most, which was 76,589.55 hm^2, the proportion increased from 0.69% in 2000 to 2.02% in 2019. Forestland decreased the most with a decrease of 42,022.89 hm^2, followed by farmland with a decrease of 42,022.89 hm^2 and the rest of the land with a little change. The spatial distribution of different land use types of transfer was explored from 2000–2019, and it was found that the maximum amount of farmland-forestland transfer was 440.73 hm^2, farmland-grassland transfer was 42.57 hm^2, and farmland-water area transfer was 15.66 hm^2, the forestland-farmland conversion was 436.32 hm^2, and forestland-grassland transfer was 209.25 hm^2, while the urban area-farmland shifted 10.8 hm^2.

4.2 Changes of ESV and sensitivity test

As we can see from Figure 5, the ESV such as climate regulation, hydrological regulation and soil conservation was more prominent. With the change of land area, the total ESV in the study area increased first and then decreased from 2000 to 2019, and the total ESV decreased by 0.75 billion CNY. Specifically, forestland and water area were the main providers of ESV of the YRDEB, accounting for more than 90% in the three periods. In terms of the absolute value, from 2000 to 2019, the total value of forestland decreased the most, the change rate of farmland was -4.71%, which decreased by 720 million CNY. The ESV in water area increased year by year, with a cumulative increase of 4.309 billion CNY and a growth rate of 7.29%.

From the perspective of every single ESV (Supplementary Appendix Figure S1), the proportion of the same ESV was

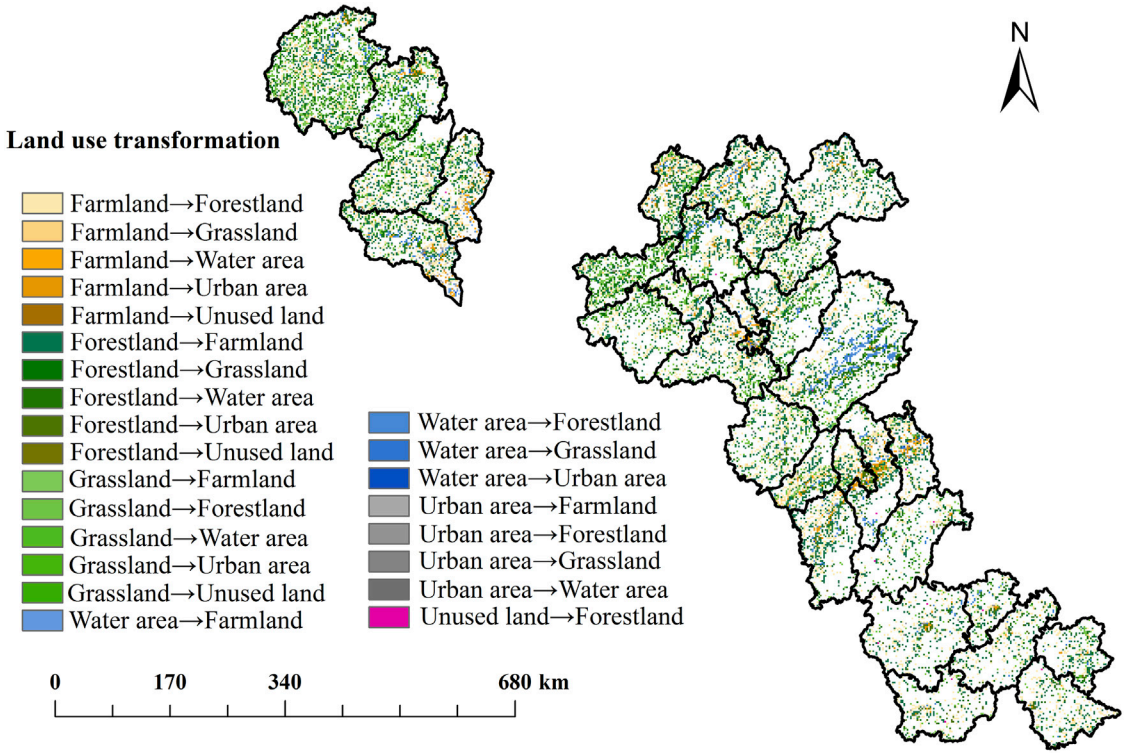

FIGURE 4
Spatial distribution map of land use type transfer in YRDEB from 2000 to 2019. Changes of ESV and sensitivity test.

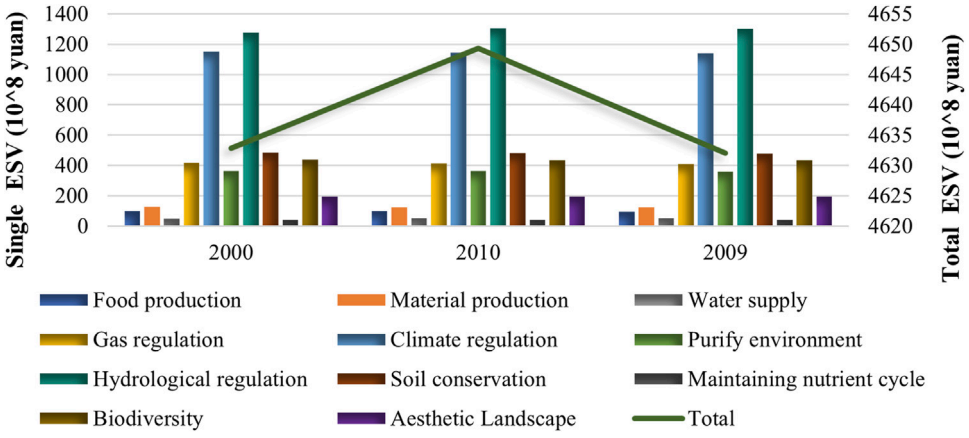

FIGURE 5
The single service value and the total value of ecosystem in YRDEB in 2000, 2010, 2019.

relatively stable from 2000 to 2019, but there were significant differences in the proportion of each ESV during the same period. Among them, the value of hydrologic adjustment and climate regulation accounted for more than 50% of the total value, followed by soil conservation and gas regulation, accounting for more than 19% of the total value, the smallest was to maintain the nutrient cycle, accounting for less than 1%. From the dynamic point of view, the overall growth of

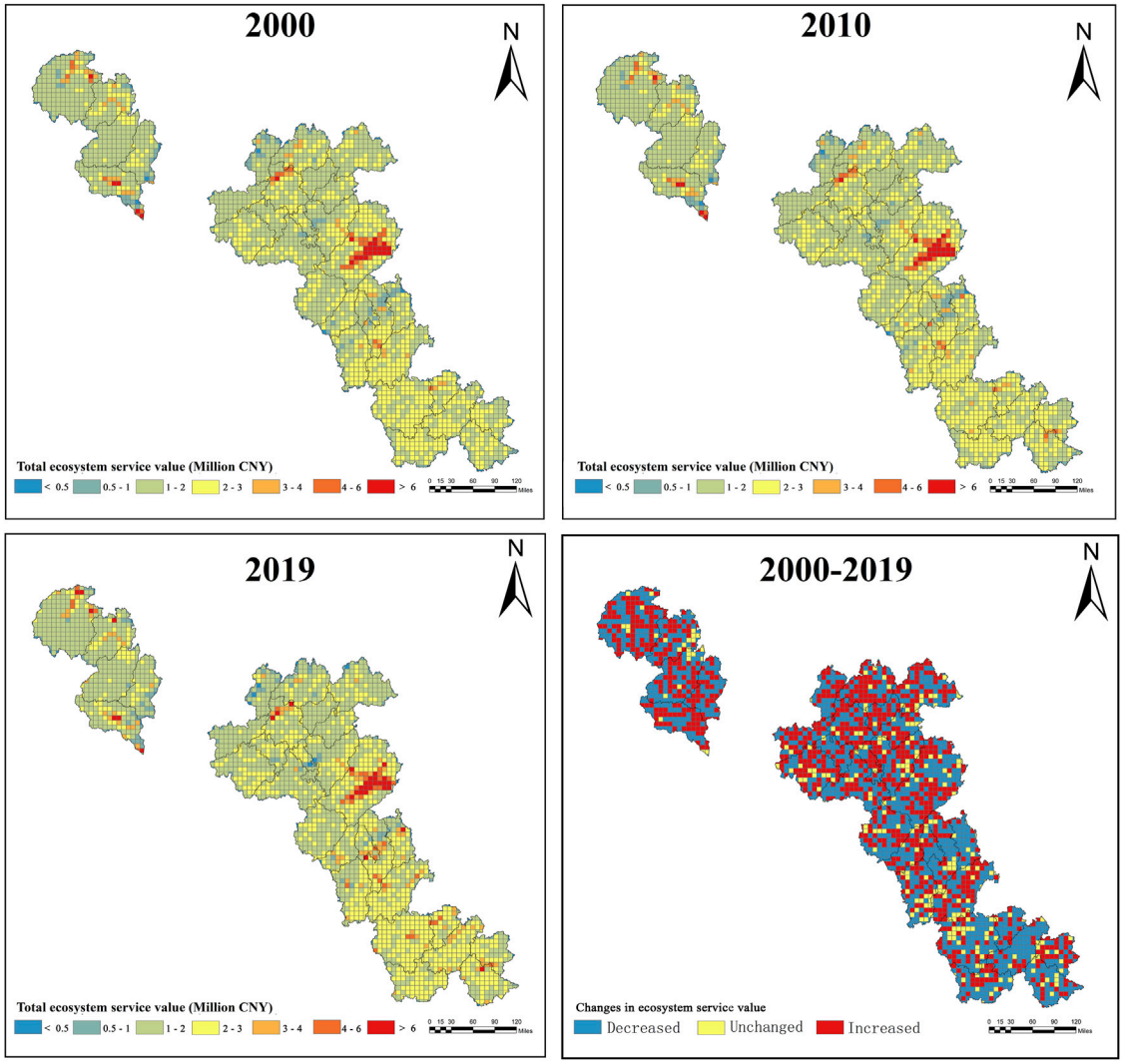

FIGURE 6
Spatial distribution of ESV in the YRDEB from 2000 to 2019.

hydrological regulation services from 2000–2019 was 1.99%, and ESV decreased steadily.

From the spatial point of view (Figure 6), the areas with high ESV in the study area were mainly located in central Chun'an County, northern Huangshan District, and northeastern Jinzhai County. The EVS increased significantly in the northern and southern areas of the study area, including parts of Huangshan District, Huoshan County, Longyou County, Longquan City, Suichang County, and Yunhe County. According to Figure 3, forestland and water areas were the main land use types in the above-mentioned areas. The areas with an ESV less than 1 million CNY in the unit grid showed a decreasing trend from 2000 to 2019, mainly in the northern part of Jinzhai County, the northeastern part of Huoshan County, and the southeastern part of Qianshan County, and the southern part of Taihu County. Overall, the ESV of the grid units in the YRDEB showed spatial variability of high in the south and low in the north, and high in the east and low in the west.

According to the above formula, the VC of 5 land use types were adjusted by 50% up and down to calculate the sensitivity index, to reflect the sensitivity of the ESV to the value coefficient in the YRDEB. As we can see from Table 3, the ESV sensitivity coefficients for each land use type were less than 1, indicating that the chosen ecological value coefficients were suitable for the study of the YRDEB and were inelastic. Horizontally, the sensitivity coefficients of each type of ESV did not change much in each period, among which farmland, forestland, and unused land decreased year by year, grassland showed a decrease and then an increase, and the sensitivity coefficient of water area increased year by year from 0.12 in 2000 to 0.13 in 2019, reflecting its continuous contribution to ESV.

TABLE 3 Sensitivity index of ESs value in YRDEB from 2000 to 2019.

Land use types	ESV (hundred million RMB)			2000–2019 variation	2000–2019 change rate	CS		
	2000	2010	2019			2000	2010	2019
FarmlandVC+50%	229.52	222.64	218.71	−10.81	−4.71%	0.033	0.032	0.031
FarmlandVC-50%	76.51	74.21	72.90	−3.60	−4.71%			
ForestlandVC+50%	5,496.59	5,465.09	5,441.42	−55.18	−1.00%	0.791	0.784	0.783
ForestlandVC-50%	1832.20	1821.70	1813.81	−18.39	−1.00%			
GrasslandVC+50%	336.55	337.13	336.76	0.22	0.06%	0.048	0.048	0.049
GrasslandVC-50%	112.18	112.38	112.25	0.07	0.06%			
Water areaVC+50%	886.51	949.08	951.15	64.64	7.29%	0.128	0.136	0.137
Water areaVC-50%	295.50	316.36	317.05	21.55	7.29%			
Unused landVC+50%	0.0221	0.0196	0.0195	−0.0026	−11.76%	0.000	0.000	0.00
Unused landVC-50%	0.0074	0.0065	0.0065	−0.0009	−11.76%			

4.3 EC amount and spatial selection

In 2019, the theoretical EC of the YRDEB was 38.098 billion CNY (Supplementary Appendix Table S1). Among the 32 compensation areas, Chun'an County received the highest compensation, reaching 5.668 billion CNY, accounting for 14.9% of the total compensation; followed by Jinzhai County with 2.987 billion CNY, accounting for 7.8%. Ke Cheng District and Tunxi District received a smaller amount of ecological compensation, accounting for only 0.18% of the total amount of compensation (Supplementary Appendix Table S2). In terms of the proportion of the compensation amount to GDP, the EC amount of each county (city and district) in the study area was smaller than the local GDP of that year, but the proportion difference among the different regions was large, the extreme difference was 0.43, and there were 14 counties, accounting for 44% of the total area, whose total compensation was less than 0.09% of the total GDP. From the priority index distribution (Figure 7), Shitai County has the highest priority, and Jingning County, Qimen County, Jinzhai County and Chun'an County are also located in high-value areas, indicating that the output capacity of ecological value was strong, and the regional economic level was relatively backward. Regional ecological protection bore great development pressure and should be paid for first.

5 Discussion and prospect

5.1 Taking spatial planning as a logical starting point for EC

The origin of this research is to try to design a frame that accords with the Chinese system characteristic to explain the EC practice in China. The Chinese government regards ecological civilization as the development strategy of the whole country, and the EC project is an important part of this strategy (Liu et al., 2021). Government action is not constrained by economic rationality. It is motivated by multiple political goals that are "bundled" (Lv et al., 2015), such as alleviating poverty through EC (Fan et al., 2020). In China, EC entails not only the monetized expression of ESs, but also includes a range of policies and institutions (Li et al., 2016; Hagedoorn et al., 2021). The implementation of EC is based on China's main functional area planning, which takes the development, protection and utilization of natural resources into account (Zhang and Zong, 2010). The main functional areas set up 'key development zone, optimized development zone, restricted development zone and prohibited development zone' with the county as an administrative unit. The starting point of the plan is not only space development based on the carrying capacity of natural resources, but also defines the development rights of different regions by means of government intervention. EC can be regarded as compensation for areas that have sacrificed the right to develop.

We believe that ecological compensation under the guidance of spatial planning mitigates the extensive development behavior in the past. The period 2000–2019 is a 20-year period of rapid urbanization in China. The growth rate of urban area in the Yangtze River Delta area is 6.21%. In contrast, the growth rate of urban area in the study area is only 1.33%. One of the reasons is that China has limited the urbanization and industrialization of the YRDEB through the main function area planning (Yang et al., 2018). At the same time, we found that 498.96 hm^2 of farmland was transferred to the forestland, grassland and water area, which was benefited from the biggest ecological space construction project in China - The conversion of farmland to the forestland (Yang et al., 2020). At present, the government has

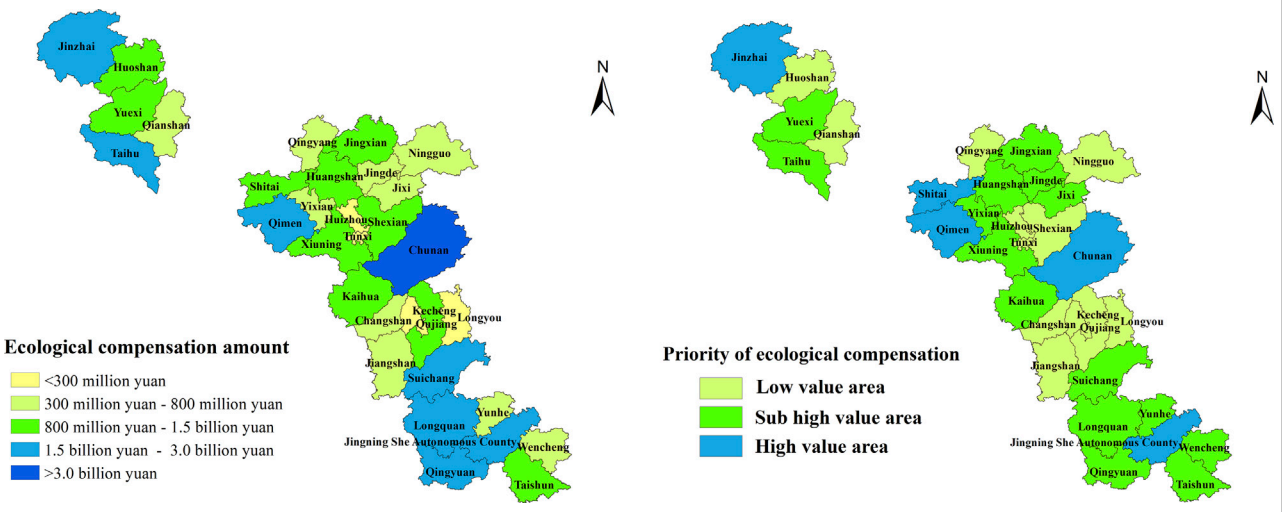

FIGURE 7
EC amount and priority level of counties (districts) in YRDEB.

invested over $51.95 billion in this project. The conversion of farmland to the forestland was introduced to the world as a typical case of EC (Bennett, 2008; He and Sikor, 2015).

5.2 ESV is an important reference for EC

The evaluation of ESV has been carried out on a global scale for more than 20 years, but we rarely see cases where payments are made according to this logic (Li et al., 2022). We do not deny the need for price assessment, because a clearer understanding of ESV can help to connect nature with society and make better decisions (Braat and De Groot, 2012). Without "prices" it is impossible to solve a series of problems arising from the neoliberal economy under the logic of neoliberalism (Jia and Zhao, 2006). In order to obtain a more reasonable compensation amount, we did not use ESV directly as the criterion for compensation proposal but used GDP for correction. The results show that in 2019, the theoretical EC of the YRDEB is 38.098 billion CNY, accounting for 9% of the region's GDP. However, we think that this value is still just a reference value. Since "price" do not come from evaluation, "price" should be internalized in the value and supply-demand, and reflected in the market exchange.

We proposed a priority proposal of accepting EC as a further application after ESV. This means that this value can be transferred into feasible actions, such as the prioritization of EC to determine a "right of access to funds". EC is not necessarily a "monetary" compensation, but can also be a policy compensation, a development right compensation. In part 4.3, five counties were given priority to receive compensation, namely Shitai County, jingning, Qimen County, Jinzhai County and Chun'an County. The meaning of this study is that we can jump out the debate of whether it makes sense of monetary compensation, and move on to applying value assessment to the prioritization of development authority, it may provide a solution to the current difficult situation of PES and EC implementation on a global scale.

5.3 EC action should consider not only currency but also system and policy

EC should consider not only monetary compensation, but also system and policy (He B. J. et al., 2022). Because the nature of ecological compensation is not only an economic means to regulate the interests of stakeholders, but also a series of participants to affect the supply and demand of ESs decision-making process (Metzger et al., 2020). Direct financial support to receiving EC areas is model of "Blood-transfusion," which is consider to be an inefficient way of compensation (Li et al., 2020). The "blood-making" EC emphasizes multiple policy supplies. In Section 4.3, we identified the priority levels of EC for different regions. We should design a more diverse approach to EC in the context of current Chinese national policies. For example, we should expand market-based green finance in these regions and develop financing tools based on water rights, emission rights, carbon emission rights, and other types of resource and environmental rights. As far as we know, Chun'an County and Chizhou City have already formulated relevant policies. The EC project of Xin'an River in Chun'an County is also taken as a typical case of government-led EC in China (Ren et al., 2021). We can moderately guide the population in ecologically important areas with high environmental carrying

pressure to gradually and orderly move outward and reduce human disturbance to the natural ecosystem. China's "EC for immigration" policy is an important part of China's poverty alleviation strategy. Since 2011, China's Ningxia Hui Autonomous Region has been home to nearly 1.3 million eco-migrants. From 2016 to 2020,1.42 million people were relocated in Guizhou, China. In addition, other ways include industrial transfer, personnel training, and park co-construction.

6 Conclusion and deficiencies

We developed a decision-making framework of "Subject choice, Value accounting, Priority evaluation, Policy supply" for EC in the context of China's current system. Taking the YRDEB as a case study, the spatio-temporal changes of its ESV were calculated and analyzed by using relevant data and methods from the spatial perspective, the spatial subject selection and compensation order of EC space were studied. The results show that the ESV in the study area increases first and then decreases. Forestland and water area are the main providers of ecosystem services value in the study area, the proportion of individual ESs was relatively stable. The spatial pattern of ESV showed a high in the south and a low in the north, and a high in the east and a low in the west. The theoretical amount of EC in the YRDEB is RMB 38,098.11 billion, accounting for a relatively low proportion of GDP. Chun'an County should receive the largest amount of compensation, and Shitai County is the highest priority area for compensation. We determine the priority of EC based on the spatial planning and ESV, and put forward the corresponding countermeasures. We hope that this study will optimize future EC practice.

Although this paper has designed a complete framework and carried out empirical studies, there are still many deficiencies: First, although this study has made localized corrections of the "ESV equivalent per unit area in China" proposed by Xie et al. (2015), the problem of spatial heterogeneity of the ecological service value of different valuation objects cannot be completely solved due to the limitation of data information. Second, for the reason that most of the county-level and even city-level ecological environment statistics are lagging behind, the depth of the study has been hindered. Third, the dynamic evaluation of priority is very important. However, these problems do not affect the reference significance of this paper in methodologies and conclusions.

Data availability statement

The datasets presented in this study can be found in online repositories. The names of the repository/repositories and accession number(s) can be found in the article/ Supplementary Material.

Author contributions

ZW: Conceptualization, Formal analysis, Writing—original draft. DM: Methodology, Visualization, Writing–original draft. JL: Validation, Supervision, Writing—review and editing. YW: Conceptualization, Writing—review and editing. ZZ: Conceptualization, Writing—review and editing. FY: Writing—review and editing. All authors have read and agreed to the published version of the manuscript.

Funding

This research was funded by the National Natural Science Foundation of China, grant numbers 42171178.

Conflict of interest

The authors declare that the research was conducted in the absence of any commercial or financial relationships that could be construed as a potential conflict of interest.

Publisher's note

All claims expressed in this article are solely those of the authors and do not necessarily represent those of their affiliated organizations, or those of the publisher, the editors and the reviewers. Any product that may be evaluated in this article, or claim that may be made by its manufacturer, is not guaranteed or endorsed by the publisher.

Supplementary material

The Supplementary Material for this article can be found online at: https://www.frontiersin.org/articles/10.3389/fenvs.2022.1002014/full#supplementary-material

References

Adhikari, R. K., Kindu, M., Pokharel, R., Castro, L. M., and Knoke, T. (2017). Financial compensation for biodiversity conservation in Ba Be national park of northern vietnam. *J. Nat. Conserv.* 35, 92–100. doi:10.1016/j.jnc.2016.12.003

Banks-Leite, C., Pardini, R., Tambosi, L. R., Pearse, W. D., Bueno, A. A., Bruscagin, R. T., et al. (2014). Using ecological thresholds to evaluate the costs and benefits of set-asides in a biodiversity hotspot. *Science* 345, 1041–1045. doi:10.1126/science.1255768

Bennett, M. T. (2008). China's sloping land conversion program: institutional innovation or business as usual? *Ecol. Econ.* 65, 699–711. doi:10.1016/j.ecolecon.2007.09.017

Braat, L. C., and De Groot, R. (2012). The ecosystem services agenda: bridging the worlds of natural science and economics, conservation and development, and public and private policy. *Ecosyst. Serv.* 1, 4–15. doi:10.1016/j.ecoser.2012.07.011

Bremer, L. L., Farley, K. A., and Lopez-Carr, D. (2014). What factors influence participation in payment for ecosystem services programs? An evaluation of Ecuador's SocioPáramo program. *Land use policy* 36, 122–133. doi:10.1016/j.landusepol.2013.08.002

Burke, M., Hsiang, S. M., and Miguel, E. (2015). Global non-linear effect of temperature on economic production. *Nature* 527, 235–239. doi:10.1038/nature15725

Cao, H., Li, M., Qin, F., Xu, Y., Zhang, L., and Zhang, Z. (2022). Economic development, fiscal ecological compensation, and ecological environment quality. *Int. J. Environ. Res. Public Health* 19, 4725. doi:10.3390/ijerph19084725

Ceballos, G., Ehrlich, P. R., Barnosky, A. D., García, A., Pringle, R. M., and Palmer, T. M. (2015). Accelerated modern human–induced species losses: Entering the sixth mass extinction. *Sci. Adv.* 1, e1400253. doi:10.1126/sciadv.1400253

Chan, K., Satterfield, T., and Goldstein, J. (2012). Rethinking ecosystem services to better address and navigate cultural values. *Ecol. Econ.* 74, 8–18. doi:10.1016/j.ecolecon.2011.11.011

Chen, Y., Yang, J., Yang, R., Xiao, X., and Xia, J. (2022). Contribution of urban functional zones to the spatial distribution of urban thermal environment. *Build. Environ.* 216, 109000. doi:10.1016/j.buildenv.2022.109000

Chu, X., Zhan, J., Wang, C., Hameeda, S., and Wang, X. (2020). Households' willingness to accept improved ecosystem services and influencing factors: Application of contingent valuation method in Bashang Plateau, Hebei Province, China. *J. Environ. Manage.* 255, 109925. doi:10.1016/j.jenvman.2019.109925

Costanza, R., D'Arge, R., De Groot, R., Farber, S., Grasso, M., Hannon, B., et al. (1997). The value of the world's ecosystem services and natural capital. *Nature* 387, 253–260. doi:10.1038/387253a0

Costanza, R., De Groot, R., Braat, L., Kubiszewski, I., Fioramonti, L., Sutton, P., et al. (2017). Twenty years of ecosystem services: How far have we come and how far do we still need to go? *Ecosyst. Serv.* 28, 1–16. doi:10.1016/j.ecoser.2017.09.008

Cuperus, R., Canters, K. J., de Haes, H. A. U., and Friedman, D. S. (1999). Guidelines for ecological compensation associated with highways. *Biol. Conserv.* 90, 41–51. doi:10.1016/S0006-3207(99)00007-5

Daily, G. C. (1997). *Nature's services: Societal dependence on natural ecosystems*. Washington D.C: Island Press.

Du, W., Yan, H., Feng, Z., Yang, Y., and Liu, F. (2021). The supply-consumption relationship of ecological resources under ecological civilization construction in China. *Resour. Conserv. Recycl.* 172, 105679. doi:10.1016/j.resconrec.2021.105679

Engel, S., Pagiola, S., and Wunder, S. (2008). Designing payments for environmental services in theory and practice: An overview of the issues. *Ecol. Econ.* 65, 663–674. doi:10.1016/j.ecolecon.2008.03.011

Fagan, M. E., DeFries, R. S., Sesnie, S. E., Arroyo-Mora, J. P., and Chazdon, R. L. (2016). Targeted reforestation could reverse declines in connectivity for understory birds in a tropical habitat corridor. *Ecol. Appl.* 26, 1456–1474. doi:10.1890/14-2188

Fan, M., Chen, L., and Wang, Q. (2019). Assessing the high impacts of land use change: Spatial characteristics of land uses and ecological compensation based on payment for ecosystem services model in a mountainous area, China. *Mitig. Adapt. Strateg. Glob. Chang.* 24, 1431–1460. doi:10.1007/s11027-019-09858-5

Fan, J., Zhou, K., and Wu, J. (2020). Typical study on sustainable development in relative poverty areas and policy outlook of China. *Bull. Chin. Acad. Sci.* 35, 1249–1263. doi:10.16418/j.issn.1000-3045.20201008001

Fletcher, R., and Büscher, B. (2017). The PES conceit: Revisiting the relationship between payments for environmental services and neoliberal conservation. *Ecol. Econ.* 132, 224–231. doi:10.1016/j.ecolecon.2016.11.002

Gómez-Baggethun, E., De Groot, R., Lomas, P. L., and Montes, C. (2010). The history of ecosystem services in economic theory and practice: From early notions to markets and payment schemes. *Ecol. Econ.* 69, 1209–1218. doi:10.1016/j.ecolecon.2009.11.007

Grêt-Regamey, A., Altwegg, J., Sirén, E. A., Van Strien, M. J., and Weibel, B. (2017). Integrating ecosystem services into spatial planning—a spatial decision support tool. *Landsc. Urban Plan.* 165, 206–219. doi:10.1016/j.landurbplan.2016.05.003

Hagedoorn, L. C., Koetse, M. J., and van Beukering, P. J. (2021). Estimating benefits of nature-based solutions: Diverging values from choice experiments with time or money payments. *Front. Environ. Sci.* 275. doi:10.3389/fenvs.2021.686077

He, J., and Sikor, T. (2015). Notions of justice in payments for ecosystem services: Insights from China's sloping land conversion program in yunnan province. *Land Use Policy* 43, 207–216. doi:10.1016/j.landusepol.2014.11.011

He, B. J., Wang, J., Zhu, J., and Qi, J. (2022). Beating the urban heat: Situation, background, impacts and the way forward in China. *Renew. Sustain. Energy Rev.* 161, 112350. doi:10.1016/j.rser.2022.112350

He, F., Yang, J., Zhang, Y., Sun, D., Wang, L., Xiao, X., et al. (2022). Offshore island connection line: A new perspective of coastal urban development boundary simulation and multi-scenario prediction. *Gisci. Remote Sens.* 59, 801–821. doi:10.1080/15481603.2022.2071056

Huang, H., Yang, H., Deng, X., Hao, C., Liu, Z., Liu, W., et al. (2020). Analyzing the influencing factors of urban thermal field intensity using big-data-based GIS. *Sustain. Cities Soc.* 55, 102024. doi:10.1016/j.scs.2020.102024

Huang, H., Yang, H., Chen, Y., Chen, T., Bai, L., and Peng, Z. R. (2021). Urban green space optimization based on a climate health risk appraisal–A case study of Beijing city, China. *Urban For. Urban Green.* 62, 127154. doi:10.1016/j.ufug.2021.127154

Jia, G., and Zhao, K. (2006). Evolutionary economics and Neo - liberalism are totally different economic policy views. *Comp. Econ. Soc. Syst.* 2, 137–143. doi:10.3969/j.issn.1003-3947.2006.02.025

Li, G., Fang, C., and Wang, S. (2016). Exploring spatiotemporal changes in ecosystem-service values and hotspots in China. *Sci. Total Environ.* 545, 609–620. doi:10.1016/j.scitotenv.2015.12.067

Li, J., Deng, X., Zhang, F., and Cai, C. (2020). The effects of ecological forest compensation on farmers' income from the perspective of incentive compatibility theory: An empirical study in Sanming, Fujian. *J. Nat. Resour.* 35, 2942–2955. doi:10.31497/zrzyxb.20201210

Li, J., Li, L., Wang, J., Zhou, C., Niu, Q., Zhang, C., et al. (2021). Priority areas recognition of ecological compensation for soil and water conservation: Taking Dongting Lake Eco-economic Zone as an example. *J. Ecol. Rural. Environ.* 37, 474–483. doi:10.19741/j.issn.1673-4831.2020.0848

Li, H., Ren, J., Li, N., Fu, B., Song, Y., and Xu, H. (2022). Research hotspot and case analysis of ecological compensation based on bibliometrics. *Ecol. Sci.* 41, 171–180. doi:10.14108/j.cnki.1008-8873.2022.04.020

Li, Y. (2011). Study on construction method and implementation approaches of ecological compensation mechanism for China's nature reserves. *Ecol. Environ. Sci.* 20, 1957–1965. doi:10.16258/j.cnki.1674-5906.2011.12.034

Liu, M., Bai, Y., Ma, N., Rao, D., Yang, L., and Min, Q. (2020). Blood transfusion or hematopoiesis? How to select between the subsidy mode and the long-term mode of eco-compensation. *Environ. Res. Lett.* 15, 094059. doi:10.1088/1748-9326/ab9793

Liu, Z., Wu, R., Chen, Y., Fang, C., and Wang, S. (2021). Factors of ecosystem service values in a fast-developing region in China: Insights from the joint impacts of human activities and natural conditions. *J. Clean. Prod.* 297, 126588. doi:10.1016/j.jclepro.2021.126588

Lv, Y., Liu, X., Liu, Y., and Zeng, Y. (2015). *Lee kuan yew: How can Singapore govern effectively*. Beijing: Beijing Book Co. Inc.

Mascarenhas, A., Ramos, T. B., and Nunes, L. (2012). Developing an integrated approach for the strategic monitoring of regional spatial plans. *Land Use Policy* 29, 641–651. doi:10.1016/j.landusepol.2011.10.006

Metzger, J. P., Fidelman, P., Sattler, C., Schroter, B., Maron, M., Eigenbrod, F., et al. (2020). Connecting governance interventions to ecosystem services provision: A social-ecological network approach. *People Nat. Hob.* 3, 266–280. doi:10.1002/pan3.10172

Millennium_Ecosystem_Assessment (2005). *Ecosystems and human well-being: General synthesis*. Washington, D.C: Island Press.

Moran, D., McVittie, A., Allcroft, D. J., and Elston, D. A. (2007). Quantifying public preferences for agri-environmental policy in scotland: A comparison of methods. *Ecol. Econ.* 63, 42–53. doi:10.1016/j.ecolecon.2006.09.018

Moreira, M., Fonseca, C., Vergílio, M., Calado, H., and Gil, A. (2018). Spatial assessment of habitat conservation status in a macaronesian island based on the InVEST model: A case study of pico island (azores, Portugal). *Land Use Policy* 78, 637–649. doi:10.1016/j.landusepol.2018.07.015

Muradian, R., Corbera, E., Pascual, U., Kosoy, N., and May, P. H. (2010). Reconciling theory and practice: An alternative conceptual framework for understanding payments for environmental services. *Ecol. Econ.* 69, 1202–1208. doi:10.1016/j.ecolecon.2009.11.006

Muradian, R., Arsel, M., Pellegrini, L., Adaman, F., Aguilar, B., Agarwal, B., et al. (2013). Payments for ecosystem services and the fatal attraction of win-win solutions. *Conserv. Lett.* 6, 274–279. doi:10.1111/j.1755-263X.2012.00309.x

Ouyang, Z., Song, C., Zheng, H., Polasky, S., Xiao, Y., Bateman, I. J., et al. (2020). Using gross ecosystem product (GEP) to value nature in decision making. *Proc. Natl. Acad. Sci. U. S. A.* 117, 14593–14601. doi:10.1073/pnas.1911439117

Ren, Y., Lu, L., Yu, H., and Zhu, D. (2021). Game strategies in government-led eco-compensation in the Xin'an River Basin from the perspective of the politics of scale. *J. Geogr. Sci.* 31, 1205–1221. doi:10.1007/s11442-021-1893-1

Salzman, J., Bennett, G., Carroll, N., Goldstein, A., and Jenkins, M. (2018). The global status and trends of payments for ecosystem services. *Nat. Sustain.* 1, 136–144. doi:10.1038/s41893-018-0033-0

Schrter, M., Zanden, E., Oudenhoven, A., Remme, R. P., Serna-Chavez, H. M., Groot, R., et al. (2014). Ecosystem services as a contested concept: A synthesis of critique and counter-arguments. *Conserv. Lett.* 7, 514–523. doi:10.1111/conl.12091

Shang, W., Gong, Y., Wang, Z., and Stewardson, M. J. (2018). Eco-compensation in China: Theory, practices and suggestions for the future. *J. Environ. Manage.* 210, 162–170. doi:10.1016/j.jenvman.2017.12.077

Soh, M., and Cho, S. (2019). Spatial targeting of payments for ecosystem services to achieve conservation goals and promote social equity and economic impact. *Nat. Resour. Model.* 32, e12219. doi:10.1111/nrm.12219

Su, Z., Wang, Z., and Zhang, L. (2022). Spatial-temporal characteristics of ecosystem service values of watershed and ecological compensation scheme considering its realization in spatial planning. *Sustainability* 14, 8204. doi:10.3390/su14138204

Tafoya, K. A., Brondizio, E. S., Johnson, C. E., Beck, P., Wallace, M., Quirós, R., et al. (2020). Effectiveness of Costa Rica's conservation portfolio to lower deforestation, protect primates, and increase community participation. *Front. Environ. Sci.* 8, 580724. doi:10.3389/fenvs.2020.580724

Van Hecken, G., Bastiaensen, J., and Huybrechs, F. (2015). What's in a name? epistemic perspectives and payments for ecosystem services policies in Nicaragua. *Geoforum* 63, 55–66. doi:10.1016/j.geoforum.2015.05.020

Van Hecken, G., Kolinjivadi, V., Windey, C., McElwee, P., Shapiro-Garza, E., Huybrechs, F., et al. (2018). Silencing agency in payments for ecosystem services (PES) by essentializing a neoliberal 'monster'into being: a response to fletcher & büscher's 'PES conceit. *Ecol. Econ.* 144, 314–318. doi:10.1016/j.ecolecon.2017.10.023

Wang, N., Liu, J., Daqian, W. U., Gao, S., and Wang, R. (2010). Regional eco-compensation based on ecosystem service assessment: a case study of Shandong province. *Acta Ecol. Sin.* 30, 66466653. doi:10.1016/S1872-5813(11)60001-7

Wang, Z., Sun, D., Hu, C., Wang, Y., and Zhang, J. (2022). Seasonal contrast and interactive effects of potential drivers on land surface temperature in the Sichuan Basin, China. *Remote Sens. (Basel).* 14 (5), 1292. doi:10.3390/rs14051292

Wunder, S., Brouwer, R., Engel, S., Ezzine-de-Blas, D., Muradian, R., Pascual, U., et al. (2018). From principles to practice in paying for nature's services. *Nat. Sustain.* 1, 145–150. doi:10.1038/s41893-018-0036-x

Wunder, S. (2007). The efficiency of payments for environmental services in tropical conservation. *Conserv. Biol.* 21, 48–58. doi:10.1111/j.1523-1739.2006.00559.x

Wunder, S. (2015). Revisiting the concept of payments for environmental services. *Ecol. Econ.* 117, 234–243. doi:10.1016/j.ecolecon.2014.08.016

Wünscher, T., and Engel, S. (2012). International payments for biodiversity services: Review and evaluation of conservation targeting approaches. *Biol. Conserv.* 152, 222–230. doi:10.1016/j.biocon.2012.04.003

Xie, G., Lu, C., Leng, Y., Zheng, D., and Li, S. (2003). Ecological assets valuation of the Tibetan Plateau. *J. Nat. Resour.* 18, 189–196. doi:10.11849/zrzyxb.2003.02.010

Xie, G., Zhang, C., Zhang, L., Chen, W., and Li, S. (2015). Improvement of the evaluation method for ecosystem service value based on per unit area. *J. Nat. Resour.* 30, 1243–1254. doi:10.11849/zrzyxb.2015.08.001

Xie, Y., Wang, L., An, R., Luo, X., Lu, Y., Liu, Y., et al. (2022). The effect of sloping land conversion program on soil erosion in shaanxi province, China: A spatial panel approach. *Front. Environ. Sci.* 10, 913712. doi:10.3389/fenvs.2022.913712

Yang, J., Guan, Y., Xia, J. C., Jin, C., and Li, X. (2018). Spatiotemporal variation characteristics of green space ecosystem service value at urban fringes: A case study on ganjingzi district in dalian, China. *Sci. Total Environ.* 639, 1453–1461. doi:10.1016/j.scitotenv.2018.05.253

Yang, Y., Yao, C., and Xu, D. (2020). Ecological compensation standards of national scenic spots in western China: A case study of taibai mountain. *Tour. Manag.* 76, 103950–103950.17. doi:10.1016/j.tourman.2019.103950

Yu, H., Xie, W., Yang, L., Du, A., Almeida, C. M., and Wang, Y. (2020). From payments for ecosystem services to eco-compensation: Conceptual change or paradigm shift? *Sci. Total Environ.* 700, 134627. doi:10.1016/j.scitotenv.2019.134627

Yu, H., Yang, J., Li, T., J., and Sun, D. (2022a). Morphological and functional polycentric structure assessment of megacity: An integrated approach with spatial distribution and interaction. *Sustain. Cities Soc.* 80, 103800. doi:10.1016/j.scs.2022.103800

Yu, H., Yang, J., Sun, D., Li, T., and Liu, Y. (2022b). Spatial responses of ecosystem service value during the development of urban agglomerations. *Land* 11, 165. doi:10.3390/land11020165

Zhang, X., and Zong, Y. (2010). Application of model and method in the planning of region major functional zones—a case study of beijing–tianjin region, China. *Sci. Geog. Sin.* 30, 728–734. doi:10.1097/ICO.0b013e3182000add

Zulian, G., Stange, E., Woods, H., Carvalho, L., Dick, J., Andrews, C., et al. (2018). Practical application of spatial ecosystem service models to aid decision support. *Ecosyst. Serv.* 29, 465–480. doi:10.1016/j.ecoser.2017.11.005

frontiers | Frontiers in Earth Science

TYPE Original Research
PUBLISHED 06 September 2022
DOI 10.3389/feart.2022.929927

Check for updates

OPEN ACCESS

EDITED BY
Bing Xue,
Institute of Applied Ecology (CAS), China

REVIEWED BY
Chengpeng Lu,
Lanzhou University, China
Xiaoping Zhang,
Shandong Jianzhu University, China
Bao-Jie He,
Chongqing University, China

*CORRESPONDENCE
Jiaming Li,
lijm@igsnrr.ac.cn

SPECIALTY SECTION
This article was submitted to Environmental Informatics and Remote Sensing,
a section of the journal
Frontiers in Earth Science

RECEIVED 27 April 2022
ACCEPTED 08 August 2022
PUBLISHED 06 September 2022

CITATION
Lu S, Zhang W, Li J and Wang S (2022), Resource-based cities: Spatial structure and evolutionary identification based on nighttime light images.
Front. Earth Sci. 10:929927.
doi: 10.3389/feart.2022.929927

COPYRIGHT
© 2022 Lu, Zhang, Li and Wang. This is an open-access article distributed under the terms of the Creative Commons Attribution License (CC BY). The use, distribution or reproduction in other forums is permitted, provided the original author(s) and the copyright owner(s) are credited and that the original publication in this journal is cited, in accordance with accepted academic practice. No use, distribution or reproduction is permitted which does not comply with these terms.

Resource-based cities: Spatial structure and evolutionary identification based on nighttime light images

Shuo Lu[1,2], Wenzhong Zhang[1,2], Jiaming Li[1]* and Shaohua Wang[3]

[1]Key Laboratory of Regional Sustainable Development Modeling, Institute of Geographic Sciences and Natural Resources Research, Chinese Academy of Sciences, Beijing, China, [2]College of Resources and Environment, University of Chinese Academy of Sciences, Beijing, China, [3]Aerospace Information Research Institute, Chinese Academy of Sciences, Beijing, China

Dividing the development stage and grasping the best time to transition are significant for resource-based cities (RBCs). However, there is still a lack of research on how to judge the developmental stage of RBCs through objective indicators of urban development. Identifying the developmental stage of RBCs relies heavily on the researcher's subjective judgment. Based on nighttime light data, this study utilizes the urban center primacy ratio as a unique indication of the growth stage of RBCs. This method is more detailed and objective than studies that define stages of development based on socio-economic indicators. It provides a fresh viewpoint on the stages of urban life cycle development. Based on the mining economy's development cycle, the proportion of mining employees at 3.9% and 44.9% can be used to divide RBCs into growth, maturity, recession, and regeneration periods, with 3.9% serving as the dividing line between RBCs and non-RBCs. In addition, when an RBC reaches maturity, a particular range of the urban center primacy ratio has a positive correlation with the GDP growth rate and is negatively correlated outside of that range. This indicates that this period is crucial for the shift from agglomeration diseconomy to agglomeration economy. The government and social institutions can use this period to drive the economic transformation of RBCs through various policies and actions.

KEYWORDS

light image data, spatial structure, urban transformation, resource-based cities, China

1 Introduction

Resource-based cities (RBCs) are those cities where the mining and primary processing of mineral resources dominate economic activities. The main economic activity of these cities is resource extraction, which is concentrated in the suburbs (Deacon et al., 2018; Udelsmann Rodrigues et al., 2021). This paper focuses on objectively and precisely detecting the spatial structural evolution trend of RBCs. The urban spatial structure expresses the interaction between the physical environment,

functional activities, and other city components (Anas et al., 1998). Unlike urban planning, which focuses on the spatial pattern of cities, this study highlights the spatial representation of human behavior and economic and social activities from a geographical perspective. Currently, the identification of the urban spatial structure focuses mostly on three facets: first, a model analysis and statistical testing approach are used to incorporate location information and spatial distance into the research framework of spatial structure identification based on statistical indicators such as population size and employment-population density (Li, 2020; Veneri, 2018; Garcia–Lopez et al., 2020; Luo et al., 2021). Second, identifying urban spatial information based on the multisource remote sensing data, including Landsat, MODIS, SPOT, DMSP-OLS, and other remote sensing data (Yang et al., 2022), is performed to help researchers identify urban boundaries and structures more objectively and accurately (Yang et al., 2021a; Dembski et al., 2021; He et al., 2021; Hajrasouliha and Hamidi, 2017). Third, real-time monitoring of urban spatial dynamics is performed through spatio-temporal big data. This includes mobile location data, Twitter or Weibo data, public transportation card data, and so on. (Kim, 2019; Chen et al., 2019; Chaix et al., 2012; Hu et al., 2018). This research paper uses remote sensing data to examine the spatial structural evolution of RBCs over a lengthy period because of the presence of statistical flaws in statistical data and the difficulty of accessing spatio-temporal big data.

The evolution of the spatial structure of RBCs has its specificities. One of the main reasons is that RBCs significantly differ from the general urban development model. Generally, spatial agglomeration is helpful to the growth of cities (Williamson, 1965; Morrison Paul and Siegel, 1999; Matlaba et al., 2012; Du and Vanino, 2021). However, there is a different story in RBCs: the extractive industry, the economic backbone of RBCs, relies heavily on mineral resources, and mineral resources are randomly and scattered distributed in geographic space. Therefore, the extractive industry also presents the characteristic of decentralization in space. The decentralized extractive industry supports forming several isolated mining areas and mining towns in RBCs. The rise of mining towns reduces the concentration of economic activities in the urban center of RBCs and begins a looser urban spatial structure (Waddington et al., 2001;Dale, 2002; Graulau, 2008). Marais et al. studied the evolution trend of residential density in five mining towns in South Africa. The results showed that mining towns had sustained low-density development due to path dependence (Marais et al., 2020). Sołtysik conducted a comprehensive review of European resource cities, and the results displayed that the distribution of resources strongly influences the spatial structure of RBCs, showing a distinctly loose character (Sołtysik and Mazur-Belzyt, 2020). Since, in developing countries, some RBCs are established only to obtain mineral resources, the service industry in urban centers is generally underdeveloped, further weakening the agglomeration capacity of urban centers (Yakovleva and Alabaster, 2003; Kotsadam and Tolonen, 2015; Farahani and Shadi, 2017). This shows that the pattern of spatial structure evolution of RBCs is decentralized. However, few studies have explored the specificities of the evolution of the spatial structure in RBCs, which limits scholars' exploration of the life cycle theory of RBCs.

The evolution of the spatial structure of RBCs is mainly influenced by the rise and fall of resource-based industries. For example, when the resources of RBCs are depleted, the evolution of the urban spatial structure will change fundamentally. Therefore, RBCs' spatial structure change trend is closely related to the development stage. Because of the apparent differences in the spatial agglomeration and dispersion characteristics between non-RBCs and RBCs, the spatial structure is a suitable indicator light to objectively evaluate the development stage of RBCs (Yang et al., 2021b; Guo et al., 2020). There is a long history of research on the classification of RBC development stages (Batty, 2006; Czamanski and Broitman, 2018). The model first appeared when reflecting Canada's mature mining economic system in 1971 (Lucas, 2019). Based on this, the life cycle theory and stage division of RBCs have been continuously improved (Bradbury and St- Martin, 1983; Yu et al., 2018). In general, scholars believe that the development of RBCs can be divided into five stages (Figure 1): Rise, growth, maturity, recession, and regeneration (Bruce et al., 2004; Prideaux and Timothy, 2011). However, the main problem is that there is no consensus on the signs of the division of stages. For example, Wilson took 20% as the criterion of resource-dependent communities (Wilson, 2004), while Bruce and Clemenson thought that the criterion should be 25% and 30%, respectively (Bruce et al., 2004; Clemenson, 1992). It can be found that the current classification of RBCs' development stages is mainly based on subjective judgments made by socio-economic data (Halseth and Sullivan, 2002; Jia et al., 2004). One of the most straightforward approaches, comparing the population or economic size of the central and peripheral areas, reflects the degree of urban agglomeration or dispersion (He et al., 2019). However, intracity statistics is not easily accessible, even for common indicators like population or economic size (Dong et al., 2021). In particular, for the long-timescale data needed to study the evolution of RBCs, these data are time-consuming and not very accurate to obtain. In summary, through the analysis of the current studies related to the division of urban development stages, few studies have classified the development stages of RBCs from the perspective of the urban spatial structure, and it is innovative to explore the evolution of the spatial structure of RBCs by using nighttime light data. This research differs from previous analyses of urban spatial evolution based on light data in two ways. First, unlike studies based on DMSP-OLS nighttime light image data only, this study constructs long time-series image data from 2000 to 2017 by integrating two nighttime light image data sets derived from DMSP-OLS and NPP-VIIRS, respectively.

	Exploration period	Rise period	Growth period	Mature period	Recession period	Regenerative period
Lucas 1971						
Riffel 1975						
Bradbury et al.1984						
Bone 1998						
Halseth 1999						
Halseth et al.2002						
Bruce 2005						
Jia 2004						
Prideaux et al.2011						
Yu et al. 2018						

FIGURE 1
RBC development stage division.

Second, the research of urban space based on the light image is mainly the identification of space form. This study combines image and statistical data to identify the key parameters that cause spatial structural transformation and thus objectively identify the development stages of RBCs.

This study aims to divide the development stages of RBCs from the perspective of the spatial structure, and the results support exploring the optimal time window for the implementation of transformation policies in RBCs. First, the degree of aggregation of RBCs in central cities was measured by using nighttime light data. The threshold model was used to analyze the non-linear relationship between the industry and spatial structure in the complete life cycle of RBCs and classify the development stages from the perspective of the urban spatial structure; finally, the relationship between spatial agglomeration and economic growth at different development periods is explored to point out the optimal period for the implementation of transformation policies in RBCs.

This study is organized into five sections. The second section briefly describes the study area, data sets, and methodologies. The third section integrates the two data sets of DMSP-OLS and NPP-VIIRS and identifies the key parameters that trigger the spatial structure and developmental stage transition. The fourth section investigates the correlation between agglomeration and growth in different stages of development and determines the optimal stage of policy intervention. Finally, the fifth section concludes the study with some remarks.

2 Materials and methods

2.1 Study area

As mentioned earlier, there is still no widely recognized standard definition for RBCs. The National Sustainable Development Plan for RBCs (2013–2020) classifies 126 RBCs

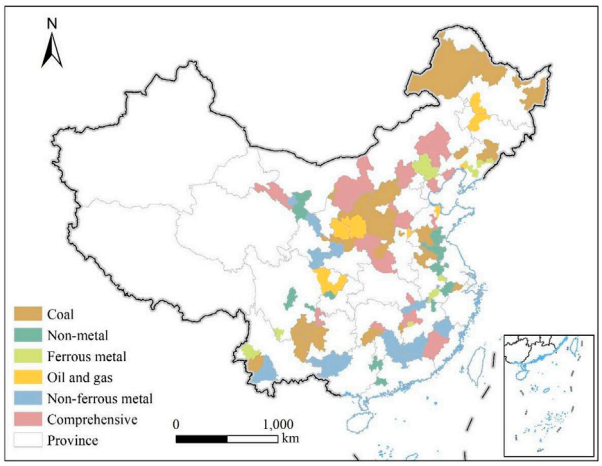

FIGURE 2
Resource-based cities in China.

based on three key indicators: Intensity of extractive functions, output scale factor, and degree of resource contribution. Based on the accessibility of data, 110 RBCs were identified as the research subjects, and these 110 RBCs are scattered in 23 provinces in mainland China (Figure 2). Regarding resource types, coal-based cities have the most significant number of 43, accounting for 40%, followed by comprehensive-based cities with 23. The number of ferrous metal and oil and gas cities is relatively similar, 8 and 10, respectively. The number of non-metal and non-ferrous cities is 12 and 14, respectively.

Notably, although the government regards these cities as RBCs, resource-based industries or communities are not the only factors considered in identifying them. As preferential policies and transfer payments are involved, factors such as regional balance also have a particular impact. Therefore, from an objective point of view, some cities may only be in the early

stage of RBCs or may no longer be RBCs. However, because these cities are at different stages, our research has a comprehensive examination of the various stages of the life cycle of RBCs.

2.2 Data

The measurement of the urban spatial structure is mainly based on remote sensing data (Zhao et al., 2021). Light image data are a good proxy for urban spatial structure and expansion studies. Croft has been using light data to identify built-up areas of cities since the 1970s (Croft, 1978). Since then, many scholars have applied light data to studying urban spatial expansion and different types of urban spatial structures at long time scales (Milesi et al., 2003; Henderson et al., 2003; Yang et al., 2020). Especially in developing countries where statistical data are not perfect, light data are undoubtedly a reliable means to analyze the spatial structure of mining towns and their evolutionary processes.

Light image data are used to measure RBCs' spatial structure and evolution. The study of the urban spatial structure usually uses demographic or economic data from different areas within the city (Champion, 2001; Kim, 2007; Wu et al., 2022). However, it is difficult to obtain statistical data in different areas within the city, especially continuous socio-economic statistics over a more extended period. Therefore, the study uses continuous nighttime stable light image data as the primary data for measuring the urban spatial structure. Plenty of studies have shown a significant positive correlation between light and the intensity of economic activity (Mellander et al., 2015; Henderson et al., 2012). Nighttime light data serve as objective data to capture the faint light on the earth's surface in real time, and it can obtain information that is unavailable from remote sensing during the daytime. Because the vast majority of stable nighttime lighting comes from artificial light sources in cities, it is widely used in areas such as economic vitality estimation, urban built-up area identification, urbanization monitoring, and carbon emissions (Zhao et al., 2014; Zhang et al., 2017; Bagan et al., 2019). To further verify the relationship between DN (DN stands for brightness level) and human activity intensity, several scholars have carried out calibration work and found that the DN values fit linearly well with other data sources characterizing the intensity of economic activity, such as urban GDP and total electricity consumption works well (Cui et al., 2020; Zhao et al., 2019). This shows that the nighttime light data can meet the requirements of my research and can reflect the spatial structural differences in the intensity of economic activities between the central city and the suburban areas.

The light image data used in this study are DMSP-OLS and NPP-VIIRS. DMSP-OLS nighttime light image data are nighttime remote sensing data captured by the National Oceanic and Atmospheric Administration's Operational Linescan System (OLS) sensor carried by the Defense Meteorological Satellite Program (DMSP), a dedicated weather satellite. In 2013, with the decay and expiration of DMSP/OLS, the Visible Infrared Imaging Radiometer Suite (VIIRS) nighttime light band on board the Suomi National Polar-Orbiting Partnership (Suomi-NPP) became the successor to DMSP/OLS. Compared to DMSP/OLS, NPP/VIIRS has higher subsatellite spatial resolution and better detection capability for nighttime lights. Therefore, the nighttime lighting used in this study is the 2000–2013 DMSP/OLS (Version 4) and NPP/VIIRS DNB for the 2012–2017 monthly synthetic product data sets (Levin and Zhang, 2017). The study differs from the existing analysis of urban spatial evolution based on light data in two aspects: 1) unlike studies based on DMSP-OLS nighttime light image data only, this study constructs long time-series image data from 2000 to 2017 by integrating two nighttime light image data sets derived from DMSP-OLS and NPP-VIIRS, respectively; 2) the research of urban space based on the light image is mainly the identification of space form. This study combines image and statistical data to identify the key parameters that cause spatial structural transformation and thus objectively identify the development stages of RBCs. Indeed, statistics is also essential. Hence, socio-economic data such as the proportion of employees in extractive industries and GDP growth rate are derived from the China Urban Statistical Yearbook 2001–2018 and the Statistical Yearbook of provinces and cities.

2.3 Methods

2.3.1 Urban center primacy ratio estimated center

The urban spatial structure focuses on the degree of agglomeration of economic activities in the urban center, draws on measurement methods such as industry concentration, and constructs an RBC center urban spatial concentration based on light data to characterize the spatial structure of the resource-based city. To avoid the deviation of the measurement results due to the incomparable light image data of consecutive years, it is first necessary to use the constant target area method to perform regression correction and saturation correction on the image data (Huang et al., 2014). Elvidge et al. (2009) inter-corrected the DMSP/OLS nighttime light image data set for a long time series by extracting the presence of relatively stable image elements in the remote sensing image as an invariant target region. Therefore, He-gang City in the Heilongjiang province study selected the same image as the target region for the quadratic regression calibration model:

$$DN_{cal} = a \times DN_{hg}^2 + b \times DN_{hg} + c, \quad (1)$$

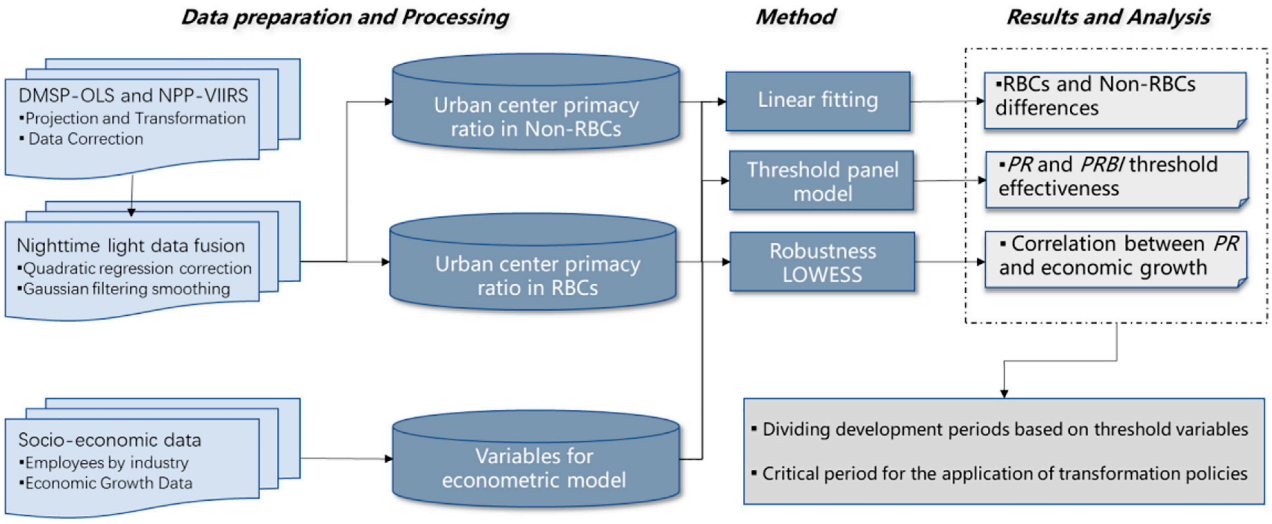

FIGURE 3
Research framework for this study.

where DN_{cal} is the *DN* value of the image pixel after correction in Hegang City; DN_{hg} is the *DN* value of the image pixel to be corrected in Hegang City; and a, b, and c are all parameters obtained in the fitting process.

Saturation correction for the whole country is carried out by using the parameters of each expected correction image and the reference image correction model regression:

$$DN' = a \times DN^2 + b \times DN + c, \tag{2}$$

where *DN*' is the *DN* value of the image pixel after correction in the national area, and *DN* is the *DN* value of the original image pixel in the national area.

Since the available years of DMSP-OLS nighttime light image data are 2000–2013, this study uses the 2013–2017 NPP-VIIRS nighttime light data to make up for the lack of DMSP-OLS nighttime light image data. The integration of the two data types is based on the data cross-correction method proposed by Li in his study of nighttime light dynamics in Syria. There are four main steps: 1) the spatial resolution resampling of all image data of NPP-VIIRS synthesis data and DMSP-OLS was reduced to 1 KM in December 2013, achieving the spatial resolution of the two kinds of data; 2) using the DMSP-OLS data *DN* value in the range of 0–50 as a mask, the average of the pre-processed NPP-VIIRS data is counted, and the data simulation is achieved by fitting; 3) the NPP-VIIRS data for 2013 and December 2017 were fitted with fitted parameters, and then the fitted image was smoothed with a Gaussian low-pass filter by Matlab; and 4) using the continuity correction method, conditions are set by comparing the *DN* values of the data with the DN value of the previous period and thus correct the *DN* values of the later period.

The specific method for measuring the spatial concentration of the urban center area is as follows:

$$PR = \frac{N_1}{\sum_{i=1}^{n} N_i}, \tag{3}$$

where *PR* is the urban center primacy ratio, N_1 is the total amount of lights in the urban center, and $\sum_{i=1}^{n} N_i$ is the total amount of lights of all i districts and counties in the resource-based city.

2.3.2 Threshold panel model

Compared with the linear model, the threshold effect model, developed by Hansen (1999), can more accurately explore the relationship between the dependent variable and the independent variable. The threshold effect model is designed to capture the inflection point formed by a significant change in the marginal effect of the independent variable y with a change in the dependent variable x. The regression equation does not need to be set as nonlinear in advance but only needs to be set in the linear form for regression, which is a process that effectively circumvents *a priori* errors. The accurate identification of nonlinear relationships and inflection points among variables makes this model widely used in policy analysis and research (AbdulahiShu and Khan, 2019; Vinayagathasan, 2013). Our research hopes to identify the different development stages of RBCs by confirming the nonlinear impact of resource-based economic development on the urban spatial structure and determining turning points. Therefore, the threshold panel model is the right method to test the impact of a resource-based economy on the urban spatial structure. The former is represented by the proportion of employees in the extractive industry, and the urban center primacy represents the latter.

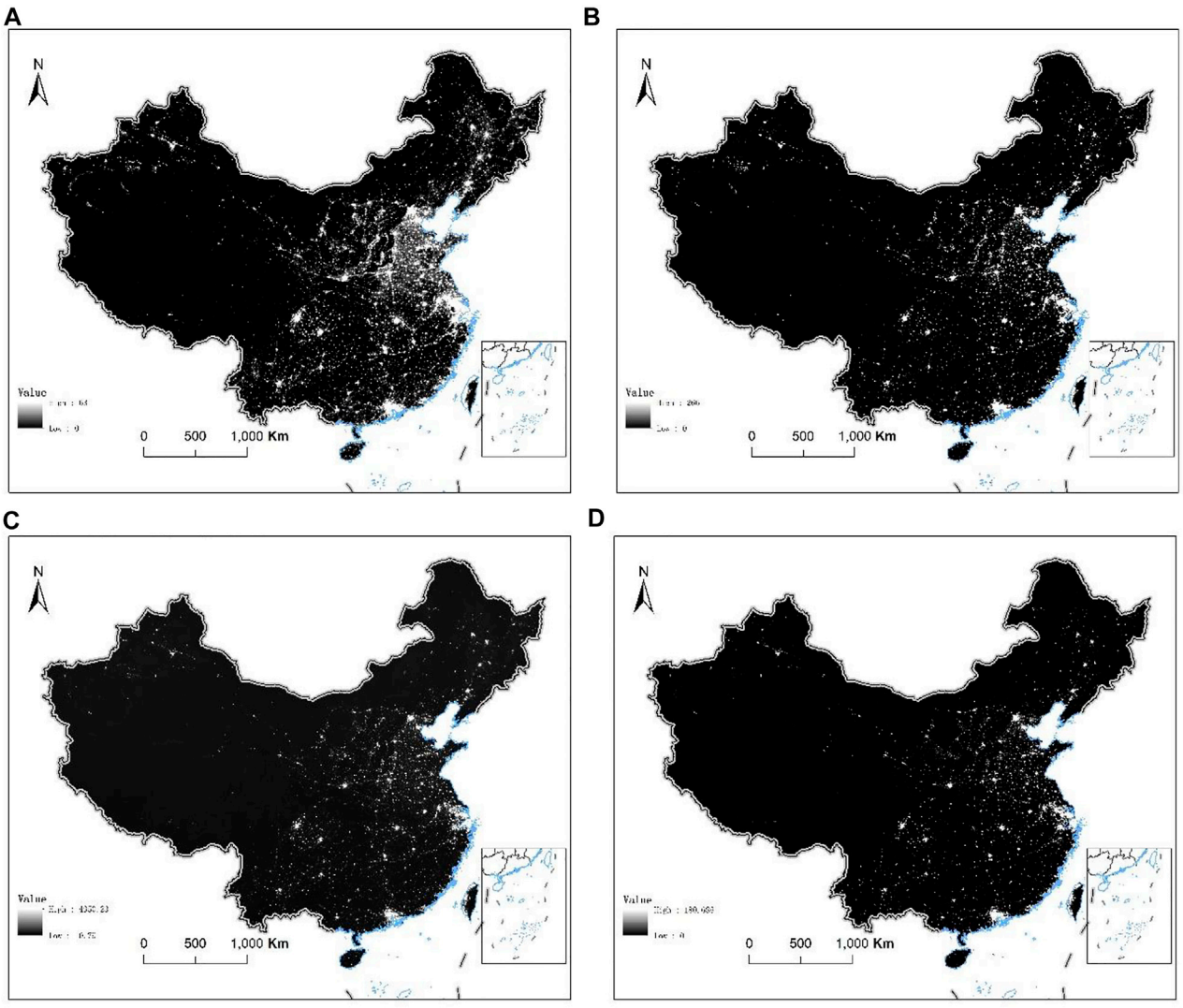

FIGURE 4
DMSP-OLS and NPP-VIIRS nighttime light data before and after processing in 2013. **(A)** and **(B)** are raw and processed DMSP/OLS in 2013; **(C)** and **(D)** are raw and processed NPP/VIIRS in 2013.

Existing studies have shown that the urban spatial structure is also affected by economic development and city-scale factors (Meijers and Burger, 2010; Paulsen, 2012). Therefore, such factors should be added to the regression model as control variables. This study refers to the research of Clarke et al. (2006) to construct a threshold regression model.

$$PR_{it} = \mu_{it} + \beta_1 PRBI_{it} I(g_{it} \le \gamma_1) + \beta_2 PRBI_{it} I(\gamma_1 \le g_{it} < \gamma_2) + \beta_n PRBI_{it} I(\gamma_{n-1} \le g_{it} < \gamma_n) + \theta_1 TNE_{it} + \theta_2 RGDP_{it} + \epsilon_{it}, \quad (4)$$

Here, *PR* is the urban center primacy; *PRBI* is the proportion of employees in resource-based industries, reflecting the proportion of resource-based industries in the economic structure. Other control variables that affect the spatial concentration of urban center areas include the level of economic development expressed in terms of per capita *GDP* (*RGDP*), and the city size is expressed in terms of the total number of employees (*TNE*). The meanings of g_{it}, μ_{it}, I, γ_n, and ϵ_{it} are the same as above. In addition, i represents the city, t represents the year, y_{it} and x_{it} are the explained variable and the explanatory variable, respectively, and β is the corresponding coefficient vector. g_{it} is the threshold variable; γ is the specific threshold value; I is an index function (I is 1 when the conditions in parentheses are met and 0 otherwise); μ_{it} is used to reflect the individual effects of the city, and ϵ_{it} is a random interference item. According to the panel threshold model estimation method

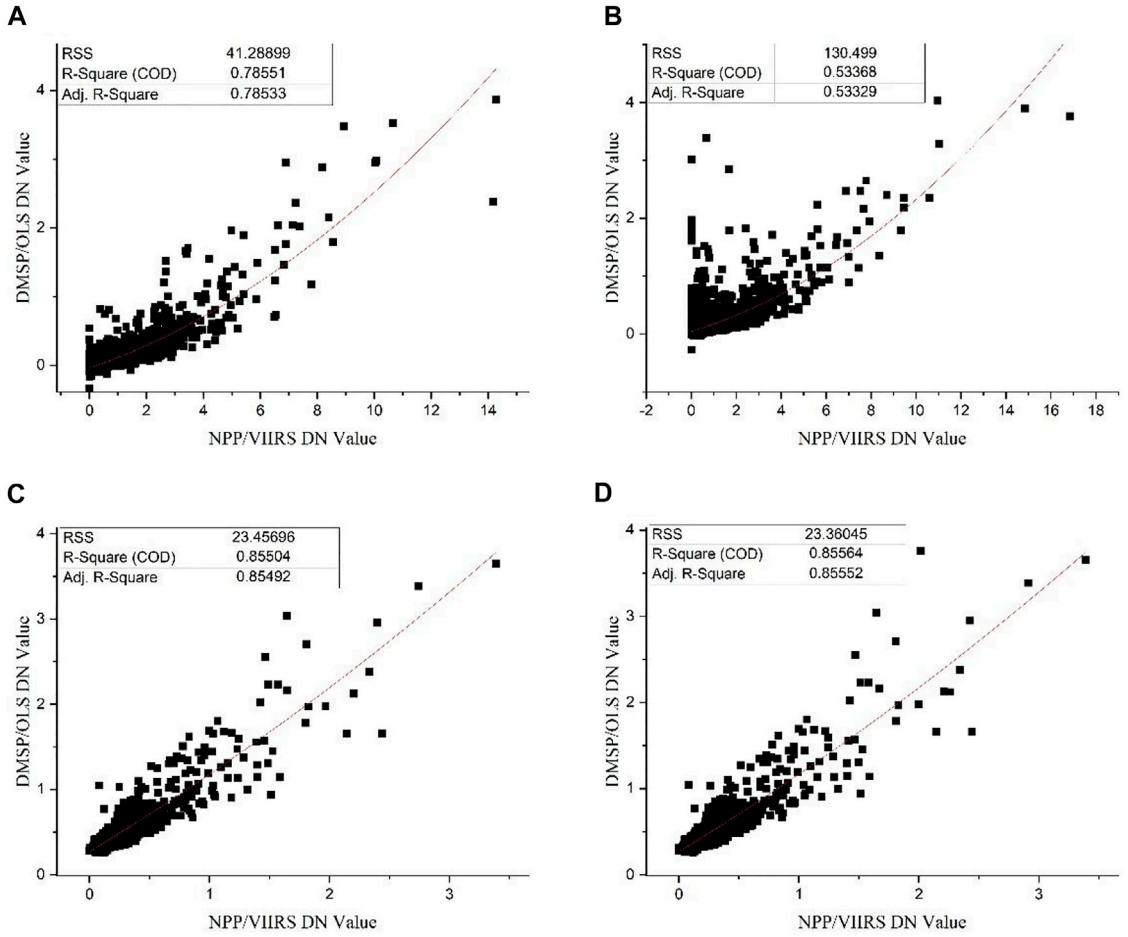

FIGURE 5
Comparison of data integration effects in 2012 and 2013. **(A)** and **(B)** are the raw DMSP and NPP lighting data fits in 2012 and 2013; **(C)** and **(D)** are the processed DMSP and NPP lighting data fits in 2012 and 2013.

proposed by Hansen, this study first assigned any g_{it} as the initial value to γ and performed OLS estimation to obtain the corresponding residual sum of squares, then determined the optimal threshold value according to the principle of minimizing the residual sum of squares, and then obtained the estimated value of each slope coefficient (Figure 3).

3 Spatial structure and development stages of RBCs

3.1 Measurement of the spatial structure based on nightlight image data

The nighttime light data are used to measure the urban spatial structure from 2000 to 2017, but there is a lack of continuous comparable light data, and the information needs to be integrated and processed. The nighttime light image data have the characteristics of timeliness, wide coverage, and practicality, so they can better meet the demand for the study of the urban spatial structure. Since the available years of DMSP-OLS image data are 2000–2013 and the data after 2013 are not available, this study uses the NPP-VIIRS nighttime light data from 2013 to 2017 to make up for the shortage of DMSP-OLS nighttime light image data. However, there are apparent differences between the two satellite image data: different sensor parameters, spatial resolutions, and spectral response modes. In this study, the two nighttime light data are processed concerning the data correction method proposed by Li in the study of nighttime light dynamics in the Syrian region (Li et al., 2017).

To verify the rationality of the processing method, the differences between the raw and processed data are compared based on the overlay of DMSP/OLS and NPP/VIIRS data in 2012 and 2013 (Figure 4). The overall integration effect of the nighttime light image data was evaluated by comparing the

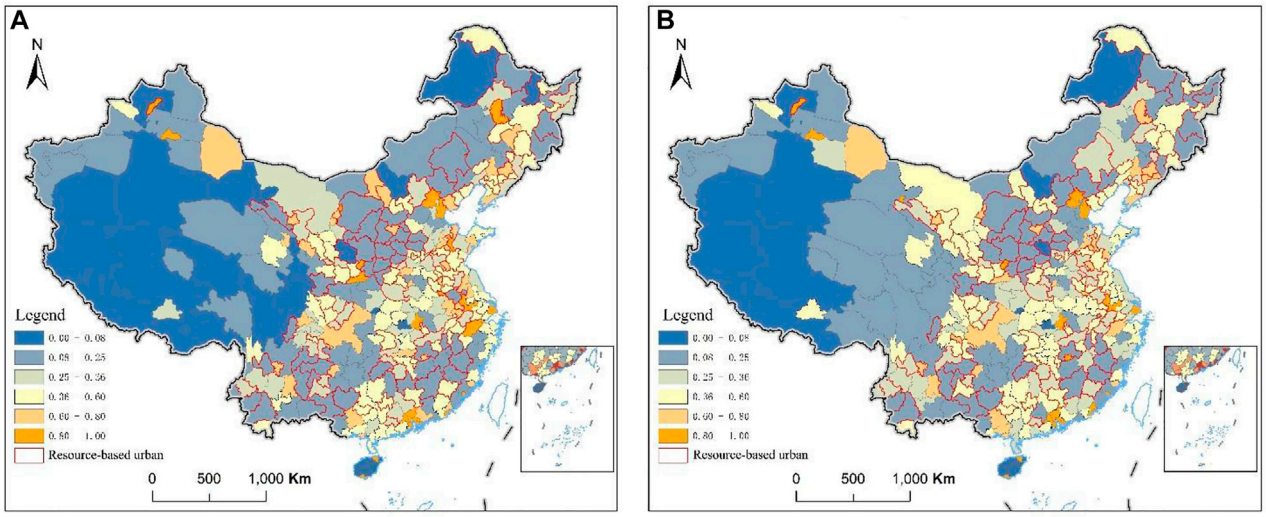

FIGURE 6
Spatial concentration of central urban areas in China. **(A)** 2000; **(B)** 2017.

differences between the raw DMSP/OLS and NPP/VIIRS data and the processed NPP/VIIRS and DMSP/OLS data. The results showed that compared with the raw data, the correlation between the NPP/VIIRS and the DMSP/OLS of the processed data obtained by this research method was significantly enhanced, and the standard error was reduced considerably. R^2 reached 0.85 and 0.85, respectively, and RSS was only 23.46 and 23.36 after excluding outliers (Figure 5). The simulation parameters obtained from the 2013 data are still stable when applied to the 2012 data, so the overall integration of the data is considered well and this processing method is feasible.

3.2 Urban spatial structure of RBCs

Compared with non-RBCs, RBCs have a significantly lower urban center primacy (*PR*) and a continuous widening gap. Figure 6 shows that RBCs are mostly light blue in color, and the PR of RBCs in other regions is below the 0.25 horizontal line, except for those in the central region. In 2017, the average *PR* of RBCs was 0.328, while the average of non-RBCs was 0.421, significantly higher than that of RBCs. From the perspective of changing trends, the *PR* of Chinese cities from 2000 to 2017 rose first and then declined, and compared to 2000, the overall decrease was 0.0021. The orange area in the figure is significantly less in 2017 compared to 2000. This may be due to the multi-center development trend of some large cities in China. For example, the overall planning of Hangzhou proposes a multi-center urban spatial structure of "one master, three assistants, and six groups." During this period, the *PR* of RBCs decreased by 0.0008, reflecting the trend of narrowing the gap between RBCs and non-RBCs. However, the degree of spatial agglomeration of RBCs is still significantly low, indicating that the relatively scattered spatial structure remains.

Furthermore, we have also analyzed the spatial structure of cities with different resource types, and the results showed that there are also differences among these cities. The *PR* of ferrous metal RBCs is higher than the average level in Chinese cities. The urban center area of ferrous metal cities has the highest *PR*, with an average of 0.392. The figure even exceeds the average level of Chinese cities. However, the levels of coal, oil and gas, non-metallic and non-ferrous metals, and *PR* are significantly lower. The average *PR* is 0.346, 0.345, 0.337, and 0.289, respectively. Generally, the *PR* of RBCs is lower than the city's overall level.

In addition, there is a significant difference between RBCs and non-RBCs in the correlation between the spatial structure and the scale of employees. In non-RBCs, with the expansion of urban employment, urban center *PR* generally shows an increasing trend, while the two variables of RBCs show a decreasing trend (Figure 7). Comparing with non-RBCs proves that RBCs are primarily concentrated in mining areas on the periphery of the central city. The differentiated results further confirmed that the spatial structure is a good indicator for identifying RBCs and non-RBCs.

3.3 Development stages of RBCs

There is a strong correlation between the spatial concentration of resource-based urban centers and the proportion of resource-based industries such as extractive industries (Li and Zhang, 2001; Li et al., 2013). The higher

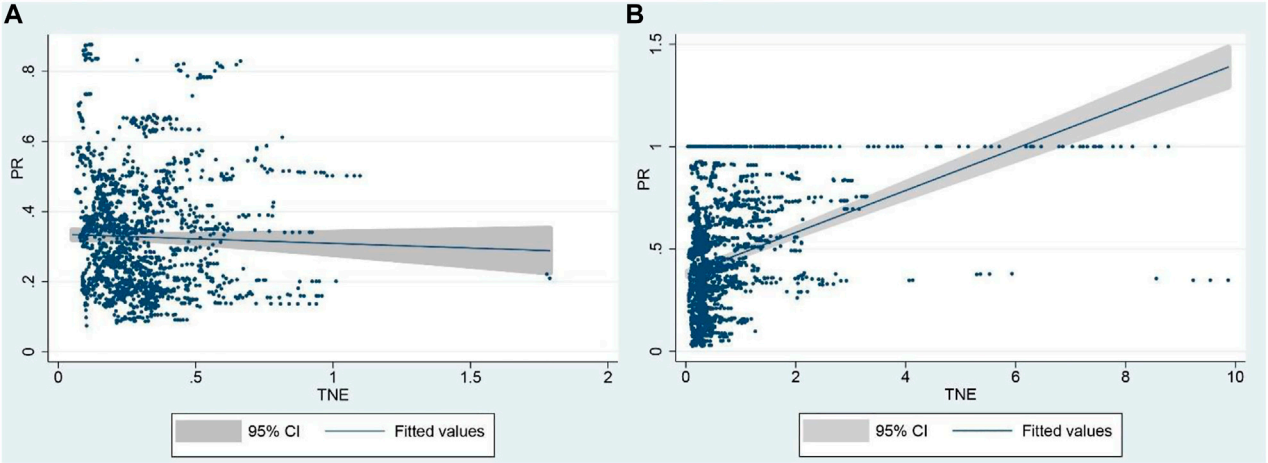

FIGURE 7
The difference in the correlation between the spatial structure and the scale of employees in RBCs and non-RBCs. **(A)** RBCs; **(B)** non-RBCs.

TABLE 1 Double threshold estimate and confidence interval.

Threshold value	Estimated value	95% confidence interval
γ_1'	0.039	[0.016, 0.359]
γ_2'	0.449	[0.449, 0.449]

TABLE 2 Threshold effect test results.

Threshold test	Critical value				
	F Value	*p*-value	1%	5%	10%
Single threshold	37.929***	0.007	35.517	22.259	18.411
Double threshold	151.539***	0.000	−16.109	−28.120	−33.993
Triple threshold	0.000	0.080	0.000	0.000	0.000

***, **, * indicate significant at 1%, 5%, 10% statistical level.

the ratio of the extractive industry in the urban economy, the more developed mining towns that rely on extractive industry activities. Mining towns' rapid economic growth and population growth have reduced the degree of agglomeration in the urban center. Therefore, the high proportion of the extractive industry in the urban economy leads to a low level of spatial concentration in urban center areas.

Empirical analysis has been done using the proportion of employees in the extractive industry as the threshold variable. The results showed that the dual-threshold test of the balance of employees in the extractive industry had the highest significance at the 1% level (Table 1), and the *p*-value was less than 0.01, so there were two thresholds of 0.039 and 0.449 (Table 2). The test result and *p*-value are obtained through repeated sampling 300 times by the self-sampling method.

The results demonstrated that the increase in the share of resource-based industries has a significant impact on the urban spatial structure, and the threshold test result reached a significance level of 1%. Importantly, the impact of the proportion of resource-based industries (*PRBI*) on the urban spatial structure is not linear. Two obvious mutation thresholds have been found (Table 3). The first threshold is that the *PRBI* reaches 3.9%. When the *PRBI* is less than 3.9%, there is a positive correlation between urban spatial concentration and the *PRBI*, and the correlation coefficient is 1.870. This means that the urban spatial concentration increases as the *PRBI* increases. When the *PRBI* is higher than 3.9%, the two variables are still positively correlated. The difference is that the correlation coefficient is significantly reduced to 0.435 from 1.870. The findings show that when the share of resource-based industries is more than 3.9%, its role in promoting the agglomeration capacity of urban center begins to decrease.

The most significant turning point comes from the second threshold when resource-based industries account for 44.9%. After this value is exceeded, the concentration of urban center areas decreases as the proportion of resource-based industries increases. In other words, the development of resource-based industries has weakened the agglomeration capacity of urban centers. This differs from the spatial agglomeration of economic activities usually caused by industrial externalities.

According to the two thresholds, the interaction between *PRBI* and *PR* is further sorted out. *PRBI* accounts for only 3.9%, indicating a relatively low proportion of the mining economy and relatively few industrial workers. It is difficult for these workers to support a mining town, so they prefer to live in the urban center. Finally, mining and economic development strengthen the agglomeration capacity of the urban center. This is the reason

TABLE 3 Double threshold estimate and confidence interval.

Variables	Coef	Std.Err	T	P>|t|	95% Conf. Interval
$x_{it}I(g_{it} < 0.039)$	1.870	0.342	5.47	0.000	[1.120, 2.540]
$x_{it}I(0.039 < g_{it} < 0.449)$	0.435	0.044	9.95	0.000	[0.350, 0.521]
$x_{it}I(g_{it} > 0.449)$	−0.265	0.054	−4.92	0.000	[−0.370, −0.159]
ln*RGDP*	0.023	0.003	7.17	0.001	[0.017, 0.029]
ln*TNE*	−0.072	0.009	−7.88	0.000	[−0.090, −0.054]
_cons	0.948	0.110	8.62	0.000	[0.732, 1.164]

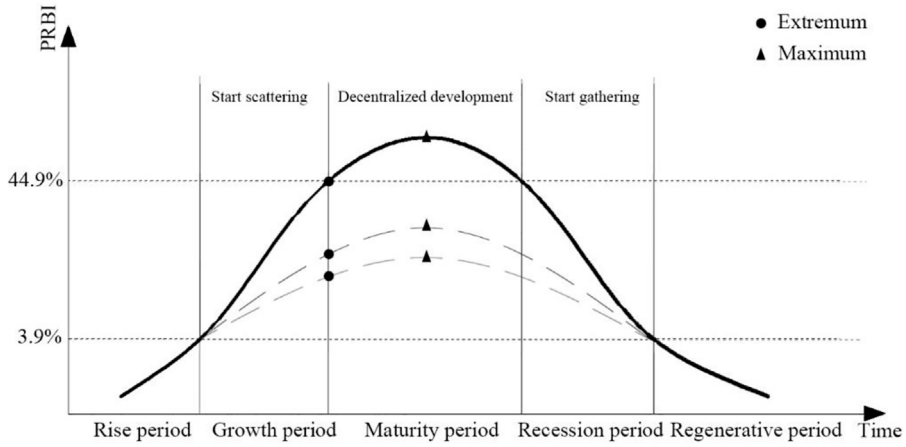

FIGURE 8
The identification of the resource-based urban development stage. Each line in the figure represents the life cycle trajectory of different RBCs, and the dotted line indicates that some cities cannot exceed a PRBI of 44.9% during their life cycle.

why when the mining economy was at a relatively low level, the degree of agglomeration in the urban center continuously increased as the mining economy grew. This also shows that when the *PRBI* is less than 3.9%, there is no diffusion effect on the urban spatial structure, and the characteristics of RBCs are not obvious. In adddition, the proportion of 3.9% of resource-based industry employees is also significantly higher than the national urban average of 1.07%. Therefore, this value can be used as an important node for the transformation of ordinary cities to RBCs or RBCs to regenerative cities. Meanwhile, the results of the control variables are consistent with theoretical expectations, and the coefficient of the *RGDP* variable is significantly positive, indicating that the increase in the level of economic development has promoted the increasing degree of agglomeration in the urban center. There is a significant negative correlation between *TNE* and *PR*, demonstrating that the larger the scale of employees, the more dispersed the urban spatial structure.

The proportion of employees in the resource-based industry reached 44.9%; nearly one-half of the labor force is employed in the mining sector. The mining economy has dominated the urban economy (Figure 8). After exceeding this level, the further growth of the mining economy has led to the decentralized development of urban space. This indicates that mining towns surrounding RBCs are built under the support of the mining economy, and their dependence on urban centers is also significantly reduced. The effect of decentralization in peripheral mining towns is the same or surpasses the impact of economic agglomeration in the urban centers. Therefore, 44.9% of *PRBI* can be used as an essential indicator that RBC is entering the decentralized development stage. At this stage, the urban spatial structure of these RBCs showed prominent decentralization characteristics. However, not all RBCs will stage spatial dispersion. In other words, although each mining town's development will weaken the urban center's agglomeration power, not all RBCs have sufficiently developed mining towns that can completely offset or even exceed the agglomeration power of urban centers. In the case of China, from 2000 to 2017, there were only four cities with more than 44% of employees in the extractive industry.

The abovementioned is the first half of the life cycle of RBCs. The first threshold value of 3.9% can be taken as a turning point for RBCs from the resource-based stage to the non-resource-based stage, and the second threshold is a sign that RBCs shift from agglomeration development to decentralized development. Correspondingly in the latter half of the life cycle of a resource-based city, the values of the first and second thresholds become the demarcation point between recession and regeneration as well as decentralization and agglomeration.

The first threshold is a sign of a rise or regenerative period, while whether the spatial structure is scattered or not is not suitable as a marker for a maturity or recession period. The changing trend of the proportion of employees in resource-based industries is still an important indicator of the development stage of RBCs. According to the change in the percentage of employees in extractive industries from 2000 to 2017, RBCs can be further divided into three types: cities in a period of growth, recession, and maturity. It is clear that those cities where the proportion of employees in the extractive industry continues to increase are in the growth period; those where the proportion of extractive industry employees continues to decrease are recession cities. Defining maturity cities is a tricky issue. RBCs have two important characteristics: one is that the proportion of employees in resource-based industries has experienced a process of growth first and then decline, and the other is that the development is relatively stable. Therefore, the maturity period of RBCs is defined as the range between Time1 and Time2 (Figure 8), where Time1 and Time2 are the first years to the left and right of the year in which the global maximum is located, respectively, satisfying y=f(x)=90% of global maximum y'. If there is no extreme point or the gap between the extreme point and the maximum point is greater than 1%, the year in which the maximum point is located is identified as the maturity period.

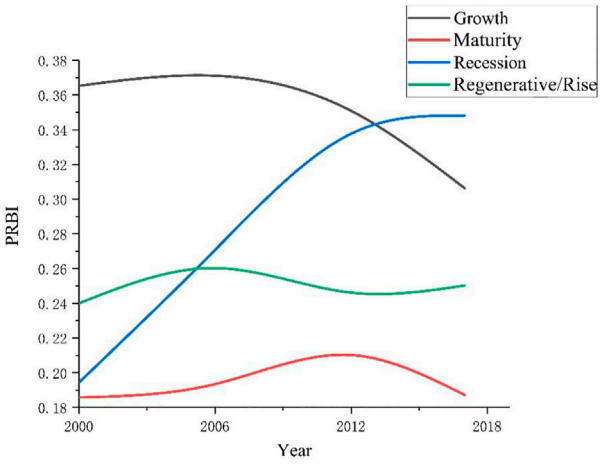

FIGURE 9
Trends in the spatial concentration of the urban central area of RBCs at different periods of development.

4 Spatial agglomeration and economic growth of RBCs at different development stages

4.1 Evolution trend of the spatial structure of RBCs at different development stages

According to the criteria of resource-based urban development, 110 RBCs in China were divided into four stages, growth, maturity, recession, and regeneration periods, between 2000 and 2017. The median of the *PRBI* of the four types of cities from 2000 to 2017 was calculated to characterize the changing trend of the spatial structure of RBCs at different stages. The results are basically in line with our expectations. RBCs in the development stage have continued to decline in spatial agglomeration, while those cities in the recession stage have a significant increase in the agglomeration of economic activities in the urban center. The degree of agglomeration of cities in the maturity stage and regeneration stage tends to decrease and increase, respectively, in the process of fluctuating development (Figure 9).

Differences in the *PRBI* trends reflect the significant impact of resource-based industries on the urban spatial structure during the evolution of RBCs' life cycle. In the emerging stage of RBCs, resource extraction is an important pillar of urban economic development, and socio-economic activities are basically organized and arranged around the resource extraction industry. Ultimately, the scattered distribution of mineral resources leads to the decentralization of the urban spatial structure. When an RBC is in a recession stage, the situation is completely different. Due to the exhaustion of resources, the mining economy cannot support the development of the entire economy alone. The gradual development of non-resource-based industries has prompted cities to present the characteristics of non-RBCs, that is, the rapid concentration of economic activities in the urban center.

4.2 Spatial structure and economic growth of RBCs at the different stages

The abovementioned analysis has suggested that there are obvious differences in the spatial structure of RBCs at different stages, and we also want to know whether such a spatial structure is conducive to the economic growth of cities or not. For non-RBCs, spatial agglomeration tends to be beneficial to the economic efficiency and growth of the city (Fujita et al., 1999; Krugman, 1991). However, some important questions need to be answered for RBCs, such as whether agglomeration is also

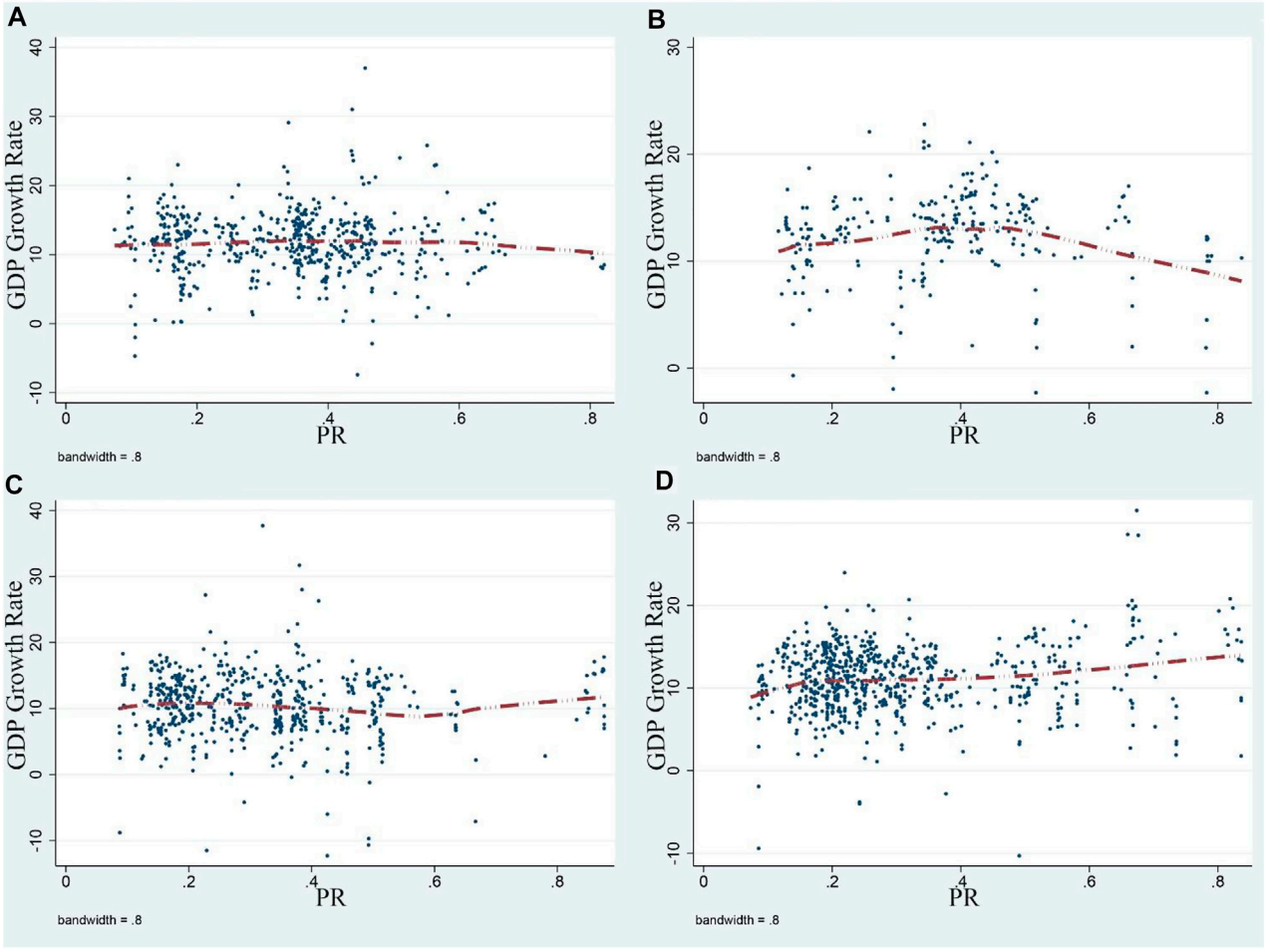

FIGURE 10
Correlation analysis between the spatial concentration and economic growth of regional central cities at **(A)** growth period, **(B)** maturity period, **(C)** recession period, **(D)** regenerative period.

beneficial to urban development in the transformation process of RBC development or not and whether policy measures should be adopted to limit urban decentralization at the beginning of RBCs or not. These answers are an essential basis for the focus and timing of sustainable development intervention policies for RBCs.

There is no doubt that before resources are exhausted, the government should intervene in RBCs to promote their transformation, but when is it appropriate? As early as 1983, Bradbury used the coal resource town of Quebec-Labrador to propose a work strategy for establishing early warning, financial assistance, transfer training, and relocation, taking into account the pattern of the development cycle of the extractive industry and changes in jobs (Bradbury and St- Martin, 1983). Lu et al. (2007) also compared the differences in the transformation of RBCs in China and Western countries and argued that the main reason for the decline of RBCs in Western countries was a change in comparative advantage, while in China, it is mainly resource depletion and the lack of compensation mechanisms. There is no shortage of resource-based towns that have paid a significant cost or even disappeared due to missing the best time for transformation (Cao et al., 2015; Chen et al., 2018; Martinez-Fernandez et al., 2012). Therefore, it is essential to determine the direction of the transformation policy and the timing of intervention.

To accurately understand the development pattern of RBCs, it is necessary to distinguish RBCs in different stages of development. After classifying RBCs according to the classification criteria proposed above, the results of Robustness LOWESS confirmed the above theoretical expectations (Figure 10). The concentration of economic activity in the urban center area is not significantly correlated with urban economic growth when the mining economy in RBCs proliferates and dominates the urban economy. However, there is a significant negative correlation when the concentration in the urban center area is too high. When the

mining economy is in maturity stage, there is an inverted "U" relationship between the concentration of economic activities in the urban center area and the city's economic growth. With the decline of the mining economy, the concentration of economic activities and economic growth shows a more apparent positive correlation.

In general, during the period of the rapid growth of the mining economy, the high concentration of socio-economic factors in the urban center area was not conducive to the economic development of RBCs and showed the characteristic of agglomeration diseconomy. In the maturity period, the agglomeration diseconomy began to shift to the agglomeration economy gradually, and the positive externality of the agglomeration economy began to emerge. When the mining economy entered a period of recession and regeneration, the rapid concentration of economic factors in the urban center area significantly boosted the economic growth of RBCs, showing apparent characteristics of an agglomeration economy.

Moreover, the characteristics of agglomeration economies and agglomeration diseconomy exhibited by RBCs are also present in non-RBCs. Still, the processes and reasons for transforming the two types of cities are significantly different. RBCs are transforming from agglomeration economy to agglomeration diseconomy, while non-RBCs are the opposite. Moreover, cost-saving and efficiency improvement are the common reasons for the agglomeration economy in RBCs and non-RBCs. Still, the reasons for the agglomeration diseconomy of the two types of cities are entirely different. The agglomeration diseconomy in the early stage of RBCs is determined by the industrial characteristics of the basic material-oriented layout of the mining economy, while the agglomeration diseconomy in the later stage of non-RBCs is due to the excessive concentration of factors in the space that makes the city appear with traffic congestion and labor cost increase.

Finally, the mature RBCs have a distinct agglomeration economy characteristic that indicates the important timing and overall policy direction for policy interventions related to urban transformation. The diseconomy of agglomeration makes it inappropriate for the government to adopt policies that promote the spatial concentration of economic factors during the growth period of rapid development of RBCs. Still, it is necessary to clarify this period's short-term and transitional features, and the construction of large-scale, permanent urban facilities is inappropriate. When the city enters a maturity stage, especially when it is in recession, the government should promote the gathering of population, industry, and other socio-economic factors to the urban center area through comprehensive measures such as land supply, industrial guidance, and allocation of public services and facilities and constantly strengthen the urban center agglomeration capacity. It should be emphasized that industrial guidance is not to concentrate heavy industries such as electricity and raw material industry to the metropolitan center area but to attract high-tech and manufacturing industries that can promote industrial transformation and upgrade the city and at the same time focus on the development of manufacturing and service industries that have a solid ability to absorb employment to attract the population to the urban center area through a large number of jobs and promote the smooth transformation of RBCs into generic cities.

5 Discussion

As shown by the estimated results, the degree of agglomeration in the central city of RBCs is much lower than that of non-RBCs, and the performance of spatial agglomeration development in RBCs is closely related to the development stage. PRBI acts as a signal indicator in response to the RBC stage and determines the current stage of RBC development.

On the one hand, when RBCs are in the growth period, decentralized development patterns dominate urban spatial development. This is when the mining economy is booming and the suburbs and mining towns around the central city are developing better. Land and infrastructure policies should focus on infrastructure development and public services for residents in areas outside the central city, including the economic and transport links between the central city and the surrounding towns. On the other hand, as RBCs enter a maturity stage, city government managers need to realize that this stage is a critical period in the transformation of agglomeration diseconomy to agglomeration economy and therefore need to make advance deployment and planning for urban change and start to focus on building the economy of the central city. The central city is the core area of the city's economy and a significant growth pole of the city economy. The central town strengthens the city's industrial agglomeration function by attracting the agglomeration of production factors such as talents, information, and capital. For RBCs whose urban spatial structure is still at the stage of scattered development, the government should not only further improve the urban infrastructure to enhance the regional radiation capacity of the central city but also expand the industrial space to the transportation system and broaden the scale of investment attraction. At the same time, efforts should be made to attract or cultivate several key enterprises with advanced technology, apparent advantages, and sustainable profitability to create conditions for a smooth transition from the maturity period to the recession period.

There are limitations in the current study: 1) the formulation of the spatial structure of RBCs is relatively broad, and there is a lack of specific description and analysis of the urban spatial structure of typical RBCs at long time scales; 2) the research object of this paper is 110 resource-based prefecture-level cities, and there is a lack of attention to the development of the urban

spatial structure at more minor scales, such as county-level cities or districts, leading to the lack of comprehensive results of the relevant research.

6 Conclusion

RBCs transform from a particular type of city that relies on the decentralized development of mineral resources to a general city driven by an agglomeration economy to realize the city's sustainable development. Therefore, reunderstanding the development stage of RBCs from the perspective of spatial structure transformation is meaningful for promoting the sustainable development of RBCs and determining the timing of intervention in transitional policies. The results show that when the proportion of employees in the mining industry reaches 3.9% and 44.9%, it will significantly impact the urban spatial structure. The former indicates that the decentralized resource-based economy began to have a significant impact, and the role of agglomeration on economic development has weakened; the latter suggests that the surrounding mining towns are more attractive than the central city, and the city has begun to decentralize development. Combining with the changing trend of the proportion of employees in the mining industry, the four development stages of growth, maturity, recession, and regeneration are quantitatively identified.

Generally, the spatial concentration of RBCs in the growth and maturity periods tends to decrease. In contrast, the overall *PR* in the recession period shows an increasing trend, and the *PR* in the regeneration period is relatively stable. Significant differences exist in the correlation between the economic growth of RBCs and the degree of urban spatial agglomeration in the four development stages of RBCs. In a set of rapid development of resource-based industries, spatial aggregation and economic growth are negatively related; in the maturity stage of stable development, there is an inverted "U"-shaped relationship, and a high degree of agglomeration in urban centers is not conducive to economic growth; when resource-based industries enter a period of recession, spatial aggregation and economic growth show a positive correlation as a whole; for regenerative cities, where the extractive industry accounts for less than 3.9%, agglomeration and growth also show a positive correlation.

To a large extent, the transformation of RBCs from agglomeration diseconomy in the rapid growth stage to agglomeration economy in the background of maturity and recession is also the process of transforming RBCs to non-RBCs. The maturity stage is when the correlation between RBCs' GDP growth rate and spatial structure has changed significantly. Therefore, the maturity stage has become a critical period for the economic transformation of RBCs. When RBCs develop to a maturity stage, land, industry, and infrastructure policies should gradually change from decentralized development to cluster development oriented toward the central city. Measures to promote the concentration of social and economic factors in the urban center will benefit RBCs' economic sustainability in the later period.

Data availability statement

Publicly available data sets were analyzed in this study. This data can be found here: https://eogdata.mines.edu/products/dmsp/#v4_dmsp_download.

Author contributions

Conceptualization, SL and JL; methodology, SL; validation, SL, JL, and WZ; formal analysis, JL; investigation, SL; resources, JL; data curation, SL and SH; writing—original draft preparation, SL; writing—review and editing, JL and WZ; visualization, SL and SH; supervision, JL and WZ. All authors have read and agreed to the published version of the manuscript.

Funding

This research was funded by the Second Tibetan Plateau Scientific Expedition and Research, Grant No. 2019QZKK0406.

Conflict of interest

The authors declare that the research was conducted without any commercial or financial relationships construed as a potential conflict of interest.

Publisher's note

All claims expressed in this article are solely those of the authors and do not necessarily represent those of their affiliated organizations or those of the publisher, the editors, and the reviewers. Any product that may be evaluated in this article or claim that may be made by its manufacturer is not guaranteed or endorsed by the publisher.

References

Abdulahi, M. E., Shu, Y., and Khan, M. A. (2019). Resource rents, economic growth, and the role of institutional quality: A panel threshold analysis. *Resour. Policy*, 61, 293–303, doi:10.1016/j.resourpol.2019.02.011

Anas, A., Arnott, R., and Small, K. A. (1998). Urban spatial structure. *J. Econ. literature* 36 (3), 1426–1464.

Bagan, H., Borjigin, H., and Yamagata, Y. (2019). Assessing nighttime lights for mapping the urban areas of 50 cities across the globe. *Environ. Plan. B Urban Anal. City Sci.* 46 (6), 1097–1114. doi:10.1177/2399808317752926

Batty, M. (2006). Rank clocks. *Nature* 444 (7119), 592–596. doi:10.1038/nature05302

Bradbury, J. H., and St- Martin, I. (1983). Winding down in a Quebec mining town: A case study of schefferville. *Can. Geogr.* 27 (2), 128–144. doi:10.1111/j.1541-0064.1983.tb01468.x

Bruce, D., Ryser, L., Halseth, G., and Giesbrecht, K. (2004). *Economic development framework of small communities in Canada: Phase two: Economic clustering approaches for small communities*. Ottawa, Canada: Canada Mortgage and Housing Corporation.

Cao, Z., Wu, Z., Kuang, Y., and Huang, N. (2015). Correction and application of DMSP/OLS night light image in China. *J. Geo-Information Sci.* 17 (9), 1092–1102. doi:10.3724/SP.J.1047.2015.01092

Champion, A. G. (2001). A changing demographic regime and evolving poly centric urban regions: Consequences for the size, Composition and Distribution of City Populations. *Urban Stud.* 38 (4), 657–677. doi:10.1080/00420980120035277

Chaix, B., Kestens, Y., Perchoux, C., Karusisi, N., Merlo, J., and Labadi, K. (2012). An interactive mapping tool to assess individual mobility patterns in neighborhood studies. *Am. J. Prev. Med.* 43 (4), 440–450.

Chen, T., Hui, E. C., Wu, J., Lang, W., and Li, X. (2019). Identifying urban spatial structure and urban vibrancy in highly dense cities using georeferenced social media data. *Habitat Int.* 89, 102005. doi:10.1016/j.habitatint.2019.102005

Chen, W., Shen, Y., and Wang, Y. (2018). Evaluation of economic transformation and upgrading of resource-based cities in Shaanxi province based on an improved TOPSIS method. *Sustain. Cities Soc.* 37, 232–240. doi:10.1016/j.scs.2017.11.019

Clarke, G. R., Xu, L. C., and Zou, H. F. (2006). Finance and income inequality: What do the data tell us? *South. Econ. J.* 72 (3), 578–596. doi:10.2307/20111834

Clemenson, H. (1992). "Are single industry towns diversifying? An examination of fishing, forestry and mining towns," in *Rural and small town Canada*. Editor R. Bollman (Toronto, Canada: Thompson Educational Publishing Inc.), 151–166.

Croft, T. A. (1978). Night time images of the earth from space. *Sci. Am.* 239, 86–98. doi:10.1038/scientificamerican0778-86

Cui, Y., Shi, K., Jiang, L., Qiu, L., and Wu, S. (2020). Identifying and evaluating the nighttime economy in China using multisource data. *IEEE Geosci. Remote Sens. Lett.* 18 (11), 1906–1910. doi:10.1109/lgrs.2020.3010936

Czamanski, D., and Broitman, D. (2018). The life cycle of cities. *Habitat Int.* 72, 100–108. doi:10.1016/j.habitatint.2016.09.002

Dale, B. (2002). An institutionalist approach to local restructuring: The case of four Norwegian mining towns. *Eur. Urban Regional Stud.* 9 (1), 5–20. doi:10.1177/096977640200900101

Deacon, L., Van Assche, K., Papineau, J., and Gruezmacher, M. (2018). Speculation, planning, and resilience: Case studies from resource-based communities in Western Canada. *Futures* 104, 37–46.

Dembski, S., Sykes, O., Couch, C., Desjardins, X., Evers, D., Osterhage, F., et al. (2021). Reurbanisation and suburbia in northwest europe: A comparative perspective on spatial trends and policy approaches. *Prog. Plan.* 150, 100462. doi:10.1016/j.progress.2019.100462

Dong, L., Longwu, L., Zhenbo, W., Liangkan, C., and Faming, Z. (2021). Exploration of coupling effects in the economy–society–environment system in urban areas: Case study of the yangtze river delta urban agglomeration. *Ecol. Indic.* 128, 107858. doi:10.1016/j.ecolind.2021.107858

Du, J., and Vanino, E. (2021). Agglomeration externalities of fast-growth firms. *Reg. Stud.* 55 (2), 167–181. doi:10.1080/00343404.2020.1760234

Elvidge, C. D., Daniel, Z., Baugh, K. E., Tuttle, B. T., Mikhail, Z., Pack, D., et al. (2009). A fifteen year record of global natural gas flaring derived from satellite data. *Energies* 2 (3), 595–622. doi:10.3390/en20300595

Farahani, H., and Shadi, B. (2017). Modeling the assessment of socio-economical and environmental impacts of sand mining on local communities: A case study of villages tatao river bank in north-western part of Iran. *Resour. Policy* 55, 87–95. doi:10.1016/j.resourpol.2017.11.001

Fujita, M., Krugman, P. R., and Venables, A. (1999). *The spatial economy: Cities, regions, and international trade*. Cambridge: MIT Press.

Garcia–Lopez, M. À., Nicolini, R., and Roig, J. L. (2020). Segregation and urban spatial structure in Barcelona. *Pap. Reg. Sci.* 99 (3), 749–772. doi:10.1111/pirs.12484

Graulau, J. (2008). 'Is mining good for development?' the intellectual history of an unsettled question. *Prog. Dev. Stud.* 8 (2), 129–162. doi:10.1177/146499340700800201

Guo, A., Yang, J., Sun, W., Xiao, X., Cecilia, J. X., Jin, C., et al. (2020). Impact of urban morphology and landscape characteristics on spatiotemporal heterogeneity of land surface temperature. *Sustain. Cities Soc.* 63, 102443. doi:10.1016/j.scs.2020.102443

Hajrasouliha, A. H., and Hamidi, S. (2017). The typology of the American metropolis: Monocentricity, polycentricity, or generalized dispersion? *Urban Geogr.* 38 (3), 420–444. doi:10.1080/02723638.2016.1165386

Halseth, G., and Sullivan, L. (2002). *Building community in an instant town: A social geography of mackenzie and tumbler ridge, B.C.* Prince George, BC: University of Northern British Columbia Press.

Hansen, B. E. (1999). Threshold effects in non-dynamic panels: Estimation, testing and inference. *J. Econ.* 93 (2), 345–368. doi:10.1016/s0304-4076(99)00025-1

He, B. J., Ding, L., and Prasad, D. (2019). Enhancing urban ventilation performance through the development of precinct ventilation zones: A case study based on the greater sydney, Australia. *Sustain. Cities Soc.* 47, 101472. doi:10.1016/j.scs.2019.101472

He, X., Cao, Y., and Zhou, C. (2021). Evaluation of polycentric spatial structure in the urban agglomeration of the pearl river delta (PRD) based on multi-source big data fusion. *Remote Sens.* 13 (18), 3639. doi:10.3390/rs13183639

Henderson, J. V., Storeygard, A., and Weil, D. N. (2012). Measuring economic growth from outer space. *Am. Econ. Rev.* 102 (2), 994–1028. doi:10.1257/aer.102.2.994

Henderson, M., Yeh, E. T., Gong, P., Elvidge, C., and Baugh, K. (2003). Validation of urban boundaries derived from global night-time satellite imagery. *Int. J. Remote Sens.* 24 (3), 595–609. doi:10.1080/01431160304982

Hu, L., Sun, T., and Wang, L. (2018). Evolving urban spatial structure and commuting patterns: A case study of Beijing, China. *Transp. Res. Part D Transp. Environ.* 59, 11–22.

Huang, Q., Yang, X., Gao, B., Yang, Y., and Zhao, Y. (2014). Application of DMSP/OLS nighttime light images: A meta-analysis and a systematic literature review. *Remote Sens.* 6 (8), 6844–6866.

Jia, J., Huang, Q., and Xu, M. (2004). *Research on China's resource (Mining) exhausted city economic transformation technology strategy*. Beijing, China: China Agricultural Science and Technology Press.

Kim, K. (2019). Identifying the structure of cities by clustering using a new similarity measure based on smart card data. *IEEE Trans. Intell. Transp. Syst.* 21 (5), 2002–2011. doi:10.1109/tits.2019.2910548

Kim, S. (2007). Changes in the nature of urban spatial structure in the United States, 1890–2000. *J. Regional Sci.* 47 (2), 273–287. doi:10.1111/j.1467-9787.2007.00509.x

Kotsadam, A., and Tolonen, A. (2015). African mining, gender, and local employment. *World Dev.* 83 (83), 325–339. doi:10.1016/j.worlddev.2016.01.007

Krugman, P. (1991). Increasing returns and economic geography. *J. Political Econ.* 99 (3), 483–499. doi:10.1086/261763

Levin, N., and Zhang, Q. (2017). A global analysis of factors controlling VIIRS nighttime light levels from densely populated areas. *Remote Sens. Environ.* 190, 366–382. doi:10.1016/j.rse.2017.01.006

Li, G., and Zhang, Y. (2001). Industrialization and urban morphology and structural evolution of Fushun coalfield area. *Sci. Geogr. Sin.* 6 (6), 511–518.

Li, H., Long, R., and Chen, H. (2013). Economic transition policies in Chinese resource-based cities: An overview of government efforts. *Energy Policy* 55, 251–260. doi:10.1016/j.enpol.2012.12.007

Li, X., Li, D., Xu, H., and Wu, C. (2017). Intercalibration between DMSP/OLS and VIIRS nighttime light images to evaluate city light dynamics of Syria's major human settlement during Syrian Civil War. *Int. J. Remote Sens.* 38 (21), 5934–5951. doi:10.1080/01431161.2017.1331476

Li, Y. (2020). Towards concentration and decentralization: The evolution of urban spatial structure of Chinese cities, 2001–2016. *Comput. Environ. Urban Syst.* 80, 101425. doi:10.1016/j.compenvurbsys.2019.101425

Lu, Z., Hu, G., and Luo, H. (2007). Comparison of resource-based urban recession and economic transformation in China and foreign countries. *Macroeconomics* 11, 32–37. doi:10.16304/j.cnki.11-3952/f.2007.11.010

Lucas, R. (2019). *Minetown, milltown, railtown*. Toronto, Canada: University of Toronto Press.

Luo, X., Yang, J., Sun, W., and He, B. (2021). Suitability of human settlements in mountainous areas from the perspective of ventilation: A case study of the main urban area of chongqing. *J. Clean. Prod.* 310, 127467. doi:10.1016/j.jclepro.2021.127467

Marais, L., Denoon-Stevens, S., and Cloete, J. (2020). Mining towns and urban sprawl in South Africa. *Land Use Policy* 93, 103953. doi:10.1016/j.landusepol.2019.04.014

Martinez-Fernandez, C., Wu, C. T., Schatz, L. K., Taira, N., and Vargas-Hernández, J. G. (2012). The shrinking mining city: Urban dynamics and contested territory. *Int. J. Urban Regional Res.* 36 (2), 245–260. doi:10.1111/j.1468-2427.2011.01094.x

Matlaba, V. J., Holmes, M., McCann, P., and Poot, J. (2012). Agglomeration externalities and 1981-2006 regional growth in Brazil. *Chiikigaku. Kenkyu.* 42 (1), 145–161. doi:10.2457/srs.42.145

Meijers, E. J., and Burger, M. J. (2010). Spatial structure and productivity in US metropolitan areas. *Environ. Plan. A* 42 (6), 1383–1402. doi:10.1068/a42151

Mellander, C., Lobo, J., Stolarick, K., and Matheson, Z. (2015). Night-time light data: A good proxy measure for economic activity? *Plos One* 10 (10), e0139779–18. doi:10.1371/journal.pone.0139779

Milesi, C., Elvidge, C. D., Nemani, R. R., and Running, S. W. (2003). Assessing the impact of urban land development on net primary productivity in the southeastern United States. *Remote Sens. Environ.* 86 (3), 401–410. doi:10.1016/S0034-4257(03)00081-6

Morrison Paul, C. J., and Siegel, D. S. (1999). Scale economies and industry agglomeration externalities: A dynamic cost function approach. *Am. Econ. Rev.* 89 (1), 272–290. doi:10.1257/aer.89.1.272

Paulsen, K. (2012). Yet even more evidence on the spatial size of cities: Urban spatial expansion in the US, 1980-2000. *Regional Sci. Urban Econ.* 42 (4), 561–568. doi:10.1016/j.regsciurbeco.2012.02.002

Prideaux, B., and Timothy, D. J. (2011). "From mining boom towns to tourist haunts: The ghost town life cycle," in *Mining heritage tourism*. Editors M. V. Conlin and L. Jolliffe (London, UK: Routledge), 327–338.

Sołtysik, M., and Mazur-Belzyt, K. (2020)., 960. Bristol, United Kingdom: IOP Publishing, 042016.City space recycling: The example of Brownfield redevelopment. in IOP Conference Series: Materials Science and Engineering.

Udelsmann Rodrigues, C., Mususa, P., Büscher, K., and Cuvelier, J. (2021). Boomtown urbanization and rural-urban transformation in mining and conflict regions in Angola, the DRC and Zambia. *Sustainability* 13 (4), 2285. doi:10.3390/su13042285

Veneri, P. (2018). Urban spatial structure in OECD cities: Is urban population decentralising or clustering? *Pap. Regional Sci.* 97 (4), 1355–1374. doi:10.1111/pirs.12300

Vinayagathasan, T. (2013). Inflation and economic growth: A dynamic panel threshold analysis for asian economies. *J. Asian Econ.* 26, 31–41. doi:10.1016/j.asieco.2013.04.001

Waddington, D., Critcher, C., and Dicks, B. (2001). *Out of the ashes? The social impact of industrial contraction and regeneration on britain's mining communities*. London: The Stationery Office.

Williamson, J. G. (1965). Regional inequality and the process of national development: A description of the patterns. *Econ. Dev. Cult. Change* 13 (4), 1–84. doi:10.1086/450136

Wilson, L. (2004). Riding the resource roller coaster: Understanding socioeconomic differences between mining communities. *Rural. Sociol.* 69 (2), 261–281. doi:10.1526/003601104323087606

Wu, C., Zhao, M., and Ye, Y. (2022). Measuring urban nighttime vitality and its relationship with urban spatial structure: A data-driven approach. *Environ. Plan. B Urban Anal. City Sci.* 23998083221108191, 239980832211081. doi:10.1177/23998083221108191

Yakovleva, N., and Alabaster, T. (2003). Tri-sector partnership for community development in mining: A case study of the SAPI foundation and target fund in the republic of sakha (yakutia). *Resour. Policy* 29 (3-4), 83–98. doi:10.1016/j.resourpol.2004.06.003

Yang, J., Wang, Y., Xiu, C., Xiao, X., Xia, J., and Jin, C. (2020). Optimizing local climate zones to mitigate urban heat island effect in human settlements. *J. Clean. Prod.* 275, 123767. doi:10.1016/j.jclepro.2020.123767

Yang, J., Wang, Y., Xue, B., Li, Y., Xiao, X., Xia, J. C., et al. (2021a). Contribution of urban ventilation to the thermal environment and urban energy demand: Different climate background perspectives. *Sci. Total Environ.* 795, 148791. doi:10.1016/j.scitotenv.2021.148791

Yang, J., Xin, J., Zhang, Y., Xiao, X., and Xia, J. C. (2022). Contributions of sea–land breeze and local climate zones to daytime and nighttime heat island intensity. *npj Urban Sustain.* 2 (1), 12–11. doi:10.1038/s42949-022-00055-z

Yang, J., Yang, Y., Sun, D., Jin, C., and Xiao, X. (2021b). Influence of urban morphological characteristics on thermal environment. *Sustain. Cities Soc.* 72, 103045. doi:10.1016/j.scs.2021.103045

Yu, J., Li, J., and Zhang, W. (2018). Identification and comprehensive type classification of resource-based cities in China. *Acta Geogr. Sin.*, 73(4), 677–687, (in Chinese). doi:10.11821/dlxb201804007

Zhang, X., Wu, J., Peng, J., and Cao, Q. (2017). The uncertainty of nighttime light data in estimating carbon dioxide emissions in China: A comparison between DMSP-OLS and NPP-VIIRS. *Remote Sens.* 9 (8), 797. doi:10.3390/rs9080797

Zhao, M., Zhou, Y., Li, X., Cao, W., He, C., Yu, B., et al. (2019). Applications of satellite remote sensing of nighttime light observations: Advances, challenges, and perspectives. *Remote Sens.* 11 (17), 1971. doi:10.3390/rs11171971

Zhao, N., Zhou, Y., and Samson, E. L. (2014). Correcting incompatible DN values and geometric errors in nighttime lights time-series images. *IEEE Trans. Geosci. Remote Sens.* 53 (4), 2039–2049. doi:10.1109/tgrs.2014.2352598

Zhao, Z., Sharifi, A., Dong, X., Shen, L., and He, B. J. (2021). Spatial variability and temporal heterogeneity of surface urban heat island patterns and the suitability of local climate zones for land surface temperature characterization. *Remote Sens.* 13 (21), 4338. doi:10.3390/rs13214338

frontiers | Frontiers in Environmental Science

TYPE Original Research
PUBLISHED 06 September 2022
DOI 10.3389/fenvs.2022.989747

Check for updates

OPEN ACCESS

EDITED BY
Jun Yang,
Northeastern University, China

REVIEWED BY
Yuanyuan Guo,
Tianjin University, China
Longzhu Xiao,
Xiamen University, China

*CORRESPONDENCE
Ran Wu,
wuran@swjtu.edu.cn

SPECIALTY SECTION
This article was submitted to Land Use Dynamics,
a section of the journal
Frontiers in Environmental Science

RECEIVED 08 July 2022
ACCEPTED 26 July 2022
PUBLISHED 06 September 2022

CITATION
Wu R, Lan H, Cao Y and Li P (2022), Optimization of low-carbon land use in Chengdu based on multi-objective linear programming and the future land use simulation model.
Front. Environ. Sci. 10:989747.
doi: 10.3389/fenvs.2022.989747

COPYRIGHT
© 2022 Wu, Lan, Cao and Li. This is an open-access article distributed under the terms of the Creative Commons Attribution License (CC BY). The use, distribution or reproduction in other forums is permitted, provided the original author(s) and the copyright owner(s) are credited and that the original publication in this journal is cited, in accordance with accepted academic practice. No use, distribution or reproduction is permitted which does not comply with these terms.

Optimization of low-carbon land use in Chengdu based on multi-objective linear programming and the future land use simulation model

Ran Wu[1]*, Haifeng Lan[2], Yuxin Cao[1] and Pingyi Li[3]

[1]School of Architecture, Southwest Jiaotong University, Chengdu, China, [2]Department of Building Environment and Energy Engineering, The Hong Kong Polytechnic University, Kowloon, Hong Kong SAR, China, [3]Chair of Renewable and Sustainable Energy Systems, TUM School of Engineering and Design, Technical University of Munich, Munich, Germany

Optimizing the structure of land use is essential to the low-carbon sustainable development of a region. This article takes Chengdu, a typical western China city, as the case study. First, carbon emission coefficients of land use are used to calculate the carbon emissions. Then, based on multi-objective linear programming (MOP), economic development priority scenario (S1), low-carbon economic development scenario (S2), and strengthening low-carbon economic scenario (S3) are proposed. Finally, the future land use simulation (FLUS) model is used to predict the spatial layout of land use under the three scenarios. The result shows that from 1990 to 2020, the carbon emissions increased by 7,617.61 thousand tons, with an annual growth rate of 3.75%. The main difference among the three scenarios is the occupied degree of farmland caused by the expansion of construction land, and the potential carbon reduction is 969.72 (5.2%), 2414.31 (13.1%), and 3878.89 tons (21.0%) in S1, S2, and S3, respectively. The FLUS model shows that conversion mainly occurs around the urban built-up area of Chengdu. This research can provide planning suggestions for the low-carbon development of Chengdu and a reference for other regions.

KEYWORDS

low-carbon land use, multi-objective linear programming, FLUS model, scenario analysis, land use and cover changes

1 Introduction

The focus on global warming caused by carbon emissions from human activities is growing (Wei et al., 2022). In response to climate change, in 2016, 197 countries signed the "Paris agreement." It aspires to drastically decrease global greenhouse gas emissions and limit global temperature rise to less than 2°C this century, while pursuing further steps to limit temperature rise to less than 1.5°C (United Nations 2015). At present, more than 75% of the earth's land surface has been affected by human development because of the

rapid development of urbanization (Ellis and Ramankutty 2008). Among them, land use/cover changes (LUCCs) caused by human activities are the most direct influencing factors of terrestrial and atmospheric carbon cycles, and the impact of land use on carbon storage in terrestrial ecosystems depends on changes in ecosystem types and land use patterns (Chang et al., 2022). The IPCC report states that from 2007–2016, land use and related activities account for about 13% of CO_2 emissions, 44% of methane (CH_4) emissions, 81% of nitrous oxide (N_2O) emissions, and 23% of the total net anthropogenic GHG emissions (IPCC 2019).

A low-carbon economic land use model is advocated to achieve harmonious growth and a win–win situation for the environment, society, and economy. (Dale 1997; Popp et al., 2014). There are two main relationships between land use and the carbon cycle. Land use can be regarded as the carbon source or carbon sink, depending on whether there is net carbon emission or net carbon absorption (Mendelsohn and Dinar 2009; Kaplan et al., 2012; Chang et al., 2022). The research on land use carbon emissions and land use structure optimization has achieved many remarkable research results, and relevant cases have also proved that the transformation of land use can effectively achieve carbon emission reduction (Han et al., 2019; Wei and Duan. 2021). However, there are still some limitation in relevant studies. First, many previous studies focused on the analysis and calculation of the effect of land carbon emissions and had considered how to make optimized land use structure to meet carbon emission reduction goals, but less to ensure the economic benefits of land use. Second, in terms of introducing the concept of low-carbon land to optimize the land use structure, the majority of studies only adjust and optimize the quantitative structure of land use in the study area for some time in the future, and lack of discussion on the regional spatial layout of the adjusted land use structure.

Therefore, according to the requirements of low-carbon economic development, this article has two main objectives: 1) To establish a multi-objective land use optimization model that integrates carbon emission reduction and economic benefits. 2) Using the land use simulation model to simulate the spatial optimization of regional land use spatial layout (He Fei et al., 2022) and then provide ideas and directions for the low-carbon regulation of regional land use. This study has an important theoretical and practical significance in exploring the potential of carbon emission reduction in optimizing the quantitative structure and spatial layout of regional land use.

2 Literature review

The effect of LUCC on carbon emissions was widely explored (Mendelsohn and Dinar 2009; Kaplan et al., 2012; Popp et al., 2014). Houghton and Hackler (1999) did a study on carbon emissions from land use change in tropical Asia. They found that approximately 75% of the region's total carbon are from LUCC in the 1980s. Forest and grassland are generally thought of as the source of carbon sinks in a region (Yang Linchuan et al., 2021). One of the evidence is from Asner et al., (2010). The authors studied the carbon emissions and carbon absorption in Amazon Rainforest and found that from 1999 to 2009, forest degradation alone increased regional carbon emissions by 47%, with secondary forest growth offsetting 18% of total emissions. Grassland covers approximately 25% of the earth's land surface and contains roughly 12% of the terrestrial carbon stocks. Unlike forests, grasslands are dominated by herbaceous plants, and the carbon of aboveground vegetation accounts for only a small part of the carbon pool of the whole ecosystem (Adams et al., 1990; Ojima et al., 1993). While construction land and farmland are regarded as the main carbon source of land use (Sullivan 2010), carbon emission intensity of construction land is hundreds of times that of farmland (Lai et al., 2016).

Previous research mainly focused on the impact of LUCC on the carbon cycle. With the increasingly serious environmental problems such as global warming, many scholars have turned to optimizing the structural and spatial layout of land use to achieve low-carbon land use. For example, Han et al. (2019) predicted the optimization structure of land use in Shenzhen in 2020 and 2025 under different carbon emission goals, based on a multi-objective linear programming (MOP) model. Mohammady et al. (2018). predicted the low-carbon land use structure of the Bagsariya Basin in Iran in 2030 based on the CLUE-S model. In addition, some scholars conducted spatial structure simulations of low-carbon land use based on other models such as the GeoSUS-FLUS model (Cao et al., 2019), the GEOMOD model (Pontius et al., 2001), and the AGENT model (Millington et al., 2011).

China's economy has grown significantly over the last several decades, and it is now the world's biggest developing country and second-largest economy. (Wang and Cao 2021; Dotsey et al., 2022). Environmental issues exacerbated by China's fast urbanization and industrialization have garnered increasing attention (Zhang et al., 2020; Zhang et al., 2022). China is attempting to strike a balance between ecological environment protection and economic expansion (Wang and Jiang 2019; Wu et al., 2019; Yang et al., 2020a; Yang et al., 2020b). Recently, land use-related carbon emissions has become a research hotspot. For large developed cities in eastern China, such as Beijing, Shanghai, and Shenzhen, as well as for particular economically developed regions, such as the Beijing–Tianjin–Hebei, the Pearl River Delta, and the Yangtze River Delta urban agglomeration, many previous studies have examined carbon emissions linked to LUCC, and the result shows that optimizing land use structure is an effective means to reduce carbon emissions (Li et al., 2013; Fang and Zhao 2018; Han et al., 2019; Yu et al., 2021). However, there has been little

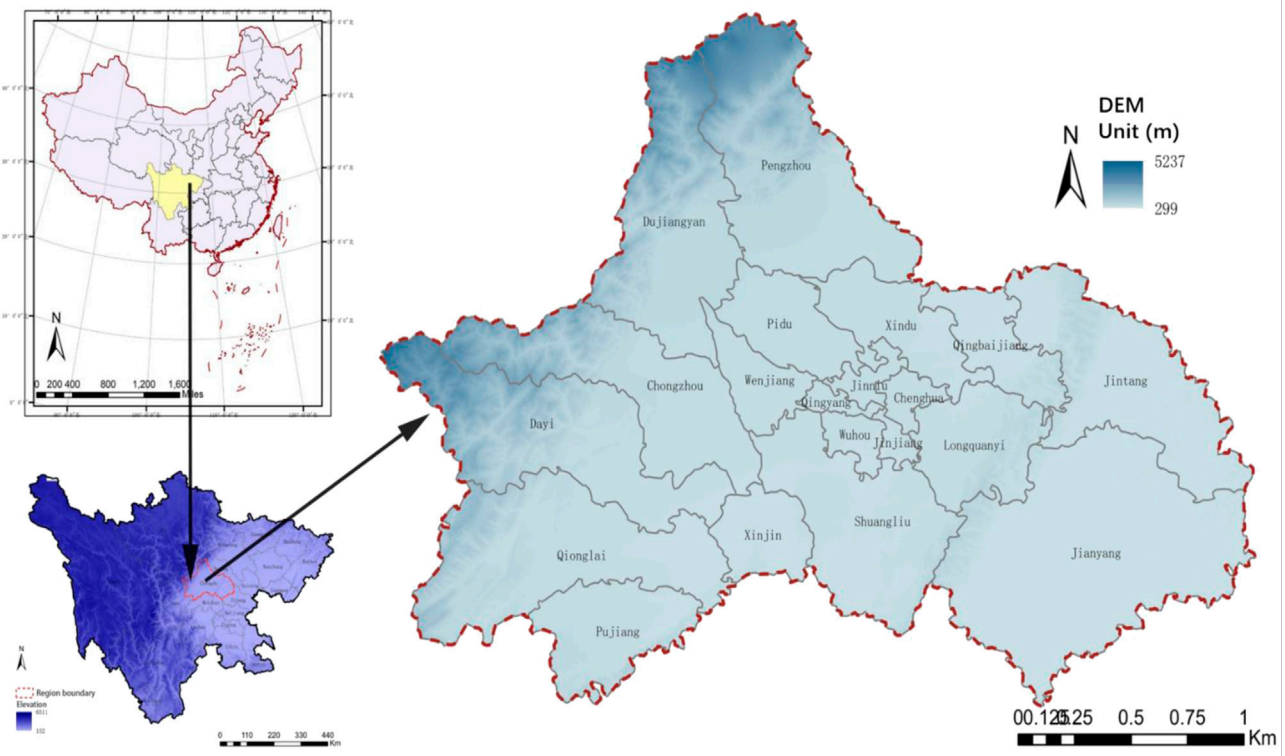

FIGURE 1
Location of Chengdu.

study on western China's developing and relatively undeveloped cities and areas, where there are significant differences from eastern cities and areas in terms of landform, climate, and social and economic background (Yang et al., 2019; Nie et al., 2021).

It is necessary to carry out more studies associated with the carbon emissions of LUCC in these western cities (Nie et al., 2021). This article takes Chengdu, the largest metropolis in western China and the capital of Sichuan province, as a case study. The city is in a period of fast industrialization and urbanization, and the land use pattern is changing substantially (Wei, X., Duan, L. 2021; Yang et al., 2022a; Yang et al., 2022b). As the first proposed park city and a low-carbon pilot city approved by the state, Chengdu is taking the lead in laying out low-carbon industries and carrying out carbon reduction actions in order to achieve the goal of carbon peak and carbon neutrality. Therefore, this study focuses on carbon emissions associated with LUCC in Chengdu to optimize and regulate the structure and spatial layout of low-carbon land use. This study is anticipated to offer planning recommendations for Chengdu's low-carbon development that will support the achievement of carbon peak and carbon neutrality, as well as a reference for the low-carbon planning of other regions.

3 Methodology

3.1 Research area and data

3.1.1 Research area

As the provincial capital of Sichuan, Chengdu is situated in southwest China's lowlands of the Sichuan Basin, between 102°54′ and 104°53′E and 30°05′ and 31°26′N, as shown in Figure 1. In the east and west, the terrain is high and low, respectively. The city has an area of 14,335 square kilometers, with a permanent population of 21.192 million. By 2021, about 79.48% of permanent populations live in 931.58 square kilometers of urban built-up area (Zhang et al., 2020). In the last decade, with the rapid economic and urbanization development, Chengdu became the first in Sichuan province and the seventh in China in terms of gross regional product (GDP). In 2020, Chengdu achieved a GDP of 1,771.67 billion Yuan, and the GDP per capita reached 94,622 Yuan.

However, with the rapid development of urbanization and economy, carbon emissions in Chengdu increase promptly, which is not beneficial to sustainable development (Chen et al., 2020). Therefore, it is urgent for Chengdu to find a reasonable balance between low-carbon land use and economic development (Cui et al., 2022). Meanwhile, taking

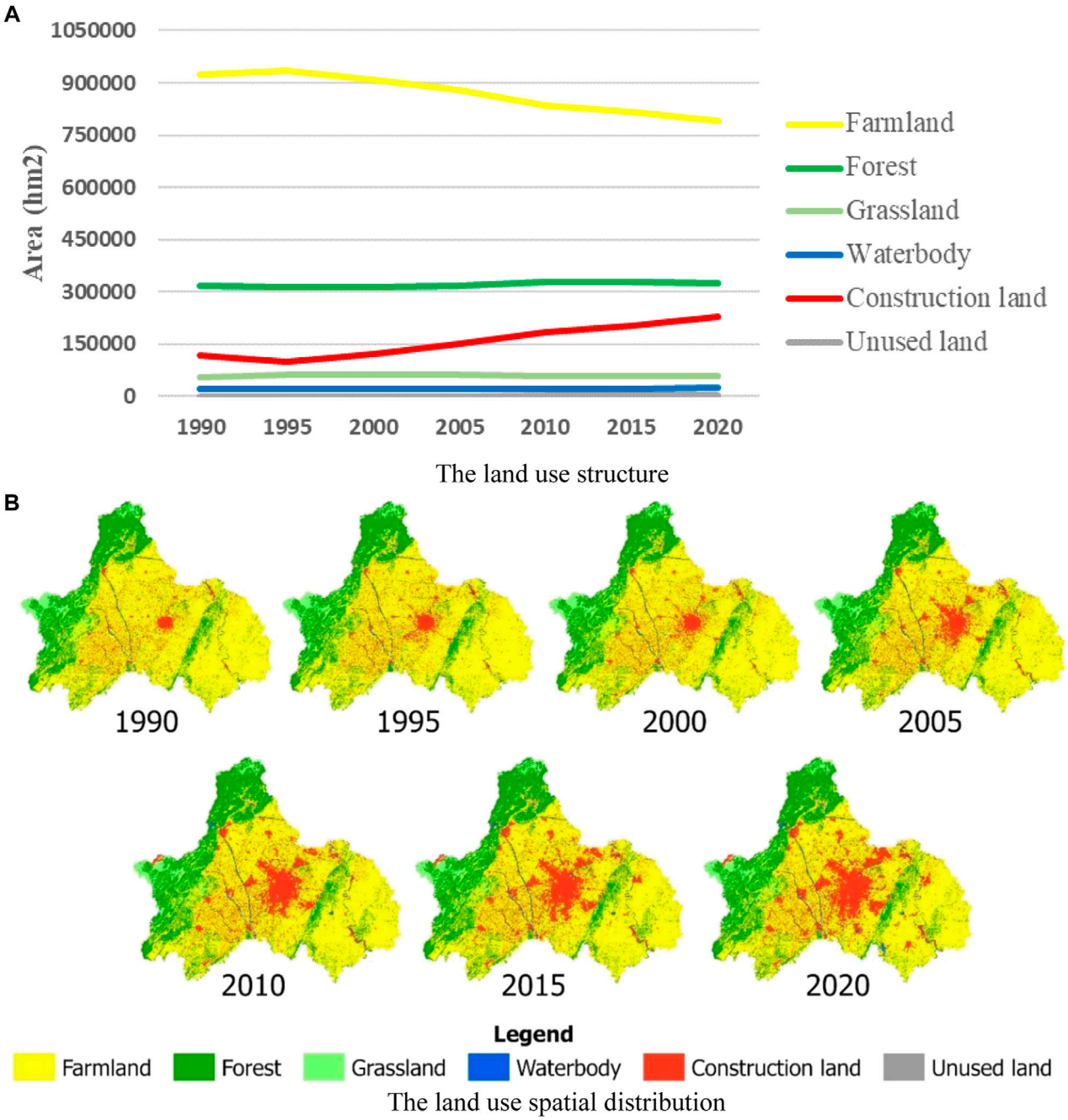

FIGURE 2
Spatiotemporal change of land use in Chengdu from 1990 to 2020.

Chengdu as an example can not only provide a basis for sustainable development and low-carbon city pilot in Sichuan Province but also play a leading and demonstration role for other cities in western China.

Figure 2 demonstrates the spatiotemporal change in land use in Chengdu from 1990 to 2020. From Figure 2A, it can be seen that farmland and construction land have an obvious change, while other types of land use are relatively steady. The area of farmland showed a continuous decline, whereas construction land had constantly increased. In 1990, farmland accounted for 64.34% of the total land area and construction land accounted 8.26%. In 2020, farmland occupied a proportion of 55.30% and construction land occupied 15.99%. Although farmland still has the largest area among Chengdu's land use types, construction

land is gradually encroaching on farmland. Figure 2B shows that urban construction land mainly extends radially outward from the central built-up area of Chengdu, and the surrounding farmland is gradually occupied by the construction land. Forest and grassland are mainly distributed in mountainous areas with large elevation and fluctuation, and waterbody is mainly distributed in the river network.

3.1.2 Data source

The land use data of this research are from the land use database of Resource and Environment Sciences and Data Center (RESDC 2022), and the classification of land use refers to (GB/T 21010-2017 2022). The socioeconomic data and energy consumption data are extracted from the "Sichuan Statistical Yearbook" (CBS 2022) and "China Energy Statistical Yearbook" (NBS 2022). The carbon emission factors of fossil fuels come from the IPCC Guidelines for National Greenhouse Gas Inventories (Yona et al., 2020). Land use policies and requirements refer to the Chengdu Land Use Master Plan (2020–2035), issued by the Chengdu Municipal Bureau of Planning and Natural Recourses (CMBPNR 2022).

3.2 Estimation of carbon emissions from land use

Direct and indirect carbon emissions are both a part of the carbon footprint of land use. Direct emissions refer to five nonconstruction land's individual direct carbon emissions (farmland, forestland, grassland, waterbody, and unused land). Indirect carbon emissions refer to the indirect carbon emission generated by fossil fuel consumption on construction land. For the convenience of calculation, this article adopts the carbon emission coefficient of land use multiplied by the area of the corresponding land use type to represent the carbon emissions of the corresponding land uses. The carbon emission coefficient of nonconstruction land can be obtained from the previous relevant research carried out in a similar study area. The carbon emission coefficient of construction land can be calculated by dividing the total carbon emissions from fossil fuel consumption (natural gas, diesel oil, kerosene oil, gasoline, fuel oil, crude oil, coke, and coal) by the area of construction land. The calculation is described in Eq 1,2, and the carbon emission coefficients for Chengdu's six different land use categories are listed in Table 1.

$$C_T = \sum_{i=1}^{6} A_i \times E_i = A_i^{con} \times E_i^{con} + \sum_{i=1}^{5} A_i^{non} \times E_i^{non}, \quad (1)$$

$$E_i^{con} = \frac{\sum_{j=1}^{8} m_j \times \beta_j \times r_j}{A_i^{con}}, \quad (2)$$

where C_T is the total quantity of carbon emitted by land use; A_i is the area of the land use type i; E_i is the carbon emission coefficient of land use type i; A_i^{con} represents the area of the construction land; E_i^{con} represents the carbon emission coefficient of construction land; A_i^{non} represents the area of the nonconstruction land use type i; E_i^{non} represents the carbon emission coefficient of nonconstruction land use type i; m_j represents the consumption of fossil fuels; β_j represents the standard coal conversion coefficient; and r_j represents the carbon emission factor of fossil fuels.

3.3 Multi-objective linear programming

The optimization of land use structure is a process of allocating the best proportion of each land type according to the regional development goals (Dong and Wan 2019). This article adopts multi-objective linear programming (MOP) as the optimization model of land use structure. The principle of the model is to set the objective function and constraints conditions, and based on this, the optimal value of decision variables can be calculated. In this article, six types of land use areas are used as decision variables to build the model: farmland (X1), forest land (X2), grassland (X3), water area (X4), construction land (X5), and unused land (X6), and LINGO11.0, a software package for solving mathematical problems or equations, is used to calculate those optimal value of decision variables.

3.3.1 Objective functions

The optimization of land use structure under low-carbon orientation should not only consider the realization of land carbon emission reduction but also consider whether the land use structure can meet the needs of social and economic development. Therefore, this article sets up two objective functions: minimizing land use emissions (Eq 3,4) and maximizing land use economic benefits (Eq 5,6).

$$Minf(x)_1 = \sum_{i=1}^{6} E_i X_i, \quad (3)$$

$$f(x)_1 = 0.4595X_1 - 0.5706X_2 - 0.0205X_3 + 0.0253X_4 + 58.5423X_5 - 0.005X_6, \quad (4)$$

where $f(x)_1$ is the total carbon emission function, X_i is the optimal area of land use type i, and E_i is the carbon emission coefficient of land use type i, adopting the average value of relevant studies.

$$Maxf(x)_2 = \sum_{i=1}^{6} P_i X_i, \quad (5)$$

$$f(x)_2 = 0.0538 + 0.055X_2 + 0.3216X_3 + 0.0848X_4 + 7.3571X_5 + 0.0000X_6, \quad (6)$$

where $f(x)_2$ is the total economic output value; X_i is the optimal area of land use type i; p_i is the economic output coefficient of land use type i; p_i (100 Million Yuan/hm2) means the economic

TABLE 1 Carbon emission coefficient of construction land in Chengdu.

Land use type	Carbon emission coefficient (kg/hm2)	References	Average value (kg/hm2)
Farmland	0.422–0.497	(Zhou et al., 2017; Cai et al., 2005; Chinesestandard, 2022; Li et al., 2008; Su and Zhang 2011)	0.4595
Forest	−0.538~−0.644	(Wang et al., 2016; Zhang et al., 2020; Li et al., 2008; Su and Zhang 2011)	−0.5706
Grassland	−0.021~−0.0205	(Li et al., 2008; Su and Zhang 2011; Wang et al., 2016; Zhang et al., 2020)	−0.0205
Waterbody	−0.0248~−0.0253	Zhang et al. (2020)	−0.0253
Unused land	−0.005	Sun et al	−0.005
Construction land	52.603–64.731	Calculated from 1990–2020	58.5423

output per hectare value of the corresponding land use types i. The economic output value of the farmland corresponds to agriculture industry; the economic output value of the grassland corresponds to animal husbandry; the economic output value of the forest land corresponds to forestry; the economic output value of the waterbody corresponds to the fishery; and the construction land corresponds to the economic output value of the secondary and tertiary industries.

The optimization of land use structure under low-carbon orientation should not only consider the realization of land carbon emission reduction but also consider whether the land use structure can meet the needs of social and economic development.

To comprehensively balance the carbon emission reduction of regional economic development, this article sets up three scenarios according to the land use decision variables: economic development priority scenario (S1, α = 0.2), low-carbon economic development (S2, α = 0.5), and strengthening low-carbon economic scenario (S3, α = 0.8).

$$\boldsymbol{X_i = \alpha\left(X_i \middle| Minf\,(x)_1\right) + (1-\alpha)\left(X_i \middle| Maxf\,(x)_2\right).} \quad (7)$$

3.3.2 Constraint conditions

The value of each constraint condition is determined according to the current land use situation and future development trend of Chengdu, as well as the requirements of the overall land and space planning of Chengdu (2020–2035). The restrictions of six land use types are summarized in Table 2, and the constraint condition functions are listed as follows:

$$\begin{cases} \boldsymbol{X_1 + X_2 + X_3 + X_4 + X_5 + X_6 = 1433499.92} \\ \boldsymbol{645074.96 \le X_1 \le 792565.92} \\ \boldsymbol{325084.14 \le X_2 \le 377533.21} \\ \boldsymbol{59504.31 \le X_3 \le 69104.73} \\ \boldsymbol{22747.02 \le X_4 \le 26417.03} \\ \boldsymbol{231905.82 \le X_5 \le 315369.98} \\ \boldsymbol{0 \le X_6 \le 1692.71} \\ \boldsymbol{X_2 + X_3 + X_4 \ge 473054.97} \end{cases}, \quad (8)$$

where X_1 is the optimal area of farmland, X_2 is the optimal area of forest land , X_3 is the optimal area of grassland , X_4 is the optimal area of waterbody , X_5 is the optimal area of construction land , and X_6 is the optimal area of unused land.

3.4 Future land use simulation model

Based on the improved CA model (Cellular automata), Liu et al. (2017) and Cao et al. (2019) proposed the FLUS (future land use simulation) model. The implementation of CA allocation in the FLUS model is divided into two steps. First, artificial neural networks (ANN) are used to train drivers such as topography, population distribution, and road network, to assess the probability of occurrence of land use on a specific grid cell (Liang et al., 2018). Second, the designed adaptive inertia and competition mechanism can reflect the competition and interaction among various land use types, so it can simulate transformation land uses (Liu et al., 2017). The model can better solve the uncertainty and complexity problems caused by the mutual transformation of land use types under the joint action of natural and human activities and can more accurately meet the actual simulation requirements and results (Cao et al., 2019).

3.4.1 Probability-of-occurrence estimation using ANN

The ANN is used to predict the probability-of-occurrence estimation in the FLUS model, which needs the land use data and driving factors data (such as elevation, slope, aspect, soil erosion, traffic map, urban distribution map, GDP, and population density) for model training. After model training, the relationship between the occurrence probability of different land types and the driving factors is established, which means that the probability of occurrence of different land use type on each spatial grid cell can be predicted according to the driving factors (Liu et al., 2017; Wang et al., 2021). The calculation principle of ANN is shown in Figure 3 and the following equations:

TABLE 2 Restrictions of six land use types.

Land use type	Variables	Land use planning policy requirements	Upper limit (hm2)	Lower limit (hm2)
Farmland	X1	The basic farmland shall be strictly protected, no less than 45% of the total area of the city	792565.92	645074.96
Forestland	X2	Maintain the existing ecological pattern, give priority to protecting ecological space, no less than 33% of the total area of the city	377533.21	325084.14
Grassland	X3		69104.73	59504.31
Waterbody	X4		26417.03	22747.02
Construction land	X5	The reasonable intensity of development, no more than more than 22% of the total area of the city	315369.98	231905.82
Unused land	X6		1692.71	

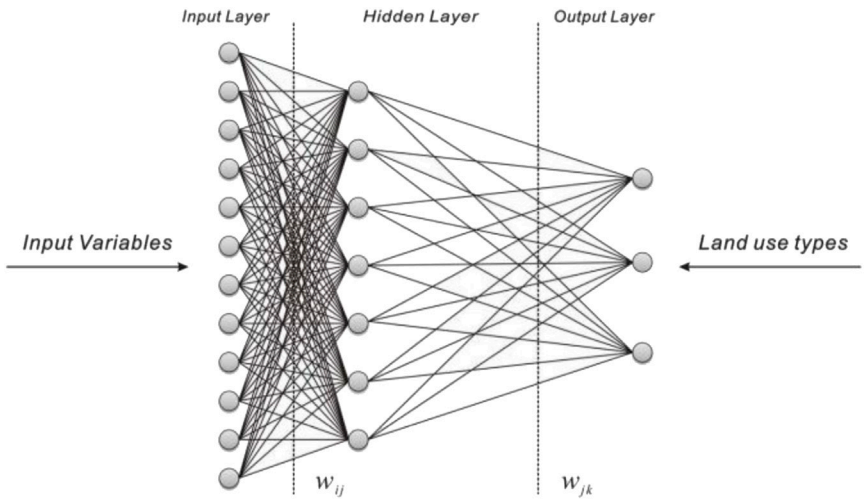

FIGURE 3
Basic structure of neural network in the FLUS model.

TABLE 3 Conversion cost of land use pairs.

Land use type	Farmland	Forestland	Grassland	Waterbody	Construction land	Unused land
Farmland	0	0.9	0.1	0.8	0.1	0.4
Forestland	0.7	0.7	0	0.3	0.99	0.8
Grassland	0.5	0.8	0	0.4	0.3	0.1
Waterbody	0.9	0.9	0.9	0	0.99	0.8
Urban land	1	1	1	1	0	1
Unused land	0.9	0.99	0.5	0.8	0.3	0

$$net_j(c,t) = \sum_i w_{i,j} x_i(c,t), \tag{9}$$

$$P(c,k,t) = \sum_j w_{j,k} \frac{1}{1+e^{-net_j(c,t)}}, \tag{10}$$

where $net_j(c,t)$ is the signal received by neuron j in the hidden layer; $w_{i,j}$ is an adaptive weight between the input layer and the hidden layer; $x_i(c,t)$ is the variable associated with the input neuron i on grid cell c at training time t; $w_{j,k}$ is an adaptive weight

between the hidden layer and the outer layer; and P (c, k, t) is the probability-of-occurrence of land use type k on grid cell c at training time t.

3.4.2 Self-adaptive inertia and competition mechanism

In addition to the P (c,k, and t) (probability-of-occurrence) of different land use types, the FLUS model adds self-adaptive inertia and competition mechanism. Specifically, it adds the neighborhood effect, inertia coefficient, and conversion cost for land use in the model (Liu et al., 2017; Liang et al., 2018; Wang et al., 2021). The total probability ($TProb^t_{c,k}$) that grid cell c changes form the original land use type j to the target type k at time t can be expressed as

$$\boldsymbol{TProb^t_{c,k}} = \boldsymbol{P(c,k,t)} \times \boldsymbol{\Omega^t_{c,k}} \times \boldsymbol{Intertia^t_k} \times \left(1 - \boldsymbol{SC_{j\to k}}\right). \quad (11)$$

1) Neighborhood effects:

$$\boldsymbol{\Omega^t_{c,k}} = \frac{\sum_{N\times N} \boldsymbol{con}\left(\boldsymbol{C^{t-1}_c} = \boldsymbol{k}\right)}{\boldsymbol{N}*\boldsymbol{N} - 1} \times \boldsymbol{w_k}. \quad (12)$$

In this equation, $\sum_{N\times N} con(C^{t-1}_c = k)$ indicates an N × N window, counting the total number of grid cells occupied by the land use type k at the last iteration time t −1. w_k is the variable weight among the different land use types. Because the land use types in different regions have different neighborhood effects due to climate, terrain, and other factors, the neighborhood weight value of land use types in this article is set with reference to the humid and hot regions in southern China.

2) Inertia coefficient:

$$\boldsymbol{Intertia^t_k} \begin{cases} \boldsymbol{Intertia^{t-1}_k}, & \boldsymbol{if}\ |\boldsymbol{C_k}| \le |\boldsymbol{D_k}| \\ \boldsymbol{Intertia^{t-1}_k} \times \dfrac{\boldsymbol{D_k}}{\boldsymbol{C_k}}, & \boldsymbol{if}\ \boldsymbol{C_k} < \boldsymbol{D_k} < \boldsymbol{0} \\ \boldsymbol{Intertia^{t-1}_k} \times \dfrac{\boldsymbol{C_k}}{\boldsymbol{D_k}}, & \boldsymbol{if}\ \boldsymbol{0} < \boldsymbol{D_k} < \boldsymbol{C_k} \end{cases}, \quad (13)$$

where $Intertia^t_k$ is the inertia coefficient of land use type k at iteration time t, $Intertia^{t-1}_k$ is the inertia coefficient of land use type k at iteration time t-1, D^{t-2}_k D_k is the macro demand of land use type k; and C_k is the current allocation amount of land use type k.

3) Conversion cost:

Conversion cost $SC_{j\to k}$ refers to the difficulty of converting the existing land use type j to the target land type k. In this study, the conversion cost of each land use pair refers to the research results of Professor Li Xia and Professor Liu Xiaoping of Sun Yat-sen University and their team on the FLUS model (Liu et al., 2017), as shown in Table 3.

4 Result

4.1 Optimization of the structure of low-carbon land use

4.1.1 Low-carbon land use structure

According to objective function and constraints, the optimal solution for the corresponding land use area can be obtained, and then the results are compared with the existing land use structure and the land use structure set in the land use planning (Table 4 and Figure 4A). In general, the area of farmland and unused land in the three scenarios is lower than the base year of 2020, but higher than the planning scheme of 2020–2035. The construction land presents an opposite tendency that is higher than the base year of 2020 but lowers the planning scheme of 2020–2035. While the area of forest (3775,33 km^2), grassland (691.05 km^2), and waterbody (264.17 km^2) is the same as 2020–2035 planning scheme which is higher than the base year of 2020. The main changes in land use in the three scenarios are demonstrated as follows.

1) Economic development priority scenario (α = 0.2)

The area of farmland in the economic development priority scenario is 6,614.29 km^2, about 1,311.37 km^2 less than the base year of 2020 but 166.93 km^2 higher than the planning scheme of 2020–2035. The area of the construction land is 2,986.77km^2, 667.71 km^2 more than the 2020 base year but 166.93 km^2 lower than the 2020–2035 planning scheme.

2) Low-carbon economic development scenario (α = 0.5)

The area of farmland in low-carbon economic development scenario (6859.61 km^2) was reduced by 1,066.06 km^2, about 408.86 km^2 higher than the 2020–2035 planning scheme. The area of the construction land is 2,736.38, 417.32 km^2 more than the 2020 base year and 417.32 km^2 higher than the 2020–2035 planning scheme.

3) Strengthening low-carbon economic scenario (α = 0.8)

Compared to 2020 base year, the area of farmland (7,104.92 km^2) in the strengthening low-carbon economic scenario was reduced by 820.74 km^2, which is 635.25 km^2 higher than the 2020–2035 planning scheme. The area of the construction land (2485.99) increased by 166.93, 660.71 km^2 lower than the 2020–2035 planning scheme.

4.1.2 The potential carbon emission reduction of land use

Due to carbon emissions and carbon sink of each land use type being different, the potential carbon emission reduction of the three scenarios is different. Although there are no significant

TABLE 4 Optimization results of land use structure.

	Economic development priority scenario (α = 0.2)		Low-carbon economic development (α = 0.5)		Strengthening low-carbon economic scenario (α = 0.8)		2020 base year		2020–2035 planning scheme	
	Area (km2)	Carbon emission (thousand ton)	Area (km2)	Carbon emission (thousand ton)	Area (km2)	Carbon emission (thousand ton)	Area (km2)	Carbon emission (thousand ton)	Area (hm2)	Carbon emission (thousand ton)
Farmland	6614.29	303.93	6859.61	315.20	7,104.92	326.47	7,925.66	364.18	6450.75	296.41
Forest	3775.33	−215.42	3775.33	−215.42	3775.33	−215.42	3250.84	−185.49	3775.33	−215.42
Grassland	691.05	−1.42	691.05	−1.42	691.05	−1.42	595.04	−1.22	691.05	−1.42
Waterbody	264.17	−0.67	264.17	−0.67	264.17	−0.67	227.47	−0.58	264.17	−0.67
Construction land	2986.77	17485.25	2736.38	16019.39	2485.99	14553.54	2319.06	13576.30	3153.70	18462.48
Unused land	3.39	0.00	8.46	0.00	13.54	-0.01	16.93	-0.01	0.00	0.00
Total	14335.00	17571.67	14335.00	16117.08	14335.00	14662.50	14335.00	13753.19	14335.00	18541.39

variations in the area of forest, grassland, waterbody, and unused land, the area of farmland and construction land has changed a lot in the three scenarios. Therefore, there are differences in carbon emissions under the three scenarios.

The carbon emission of land use in the three scenarios and the 2020–2035 planning scheme are shown in Figure 4B. Overall, total carbon emissions from the three scenarios are less than the 2020–2035 planning scheme. In the economic development priority scenario, the carbon emission is 17,571.67 tons, which is 969.39 tons (5.2%) less than the 2020–2035 planning scheme. In the low-carbon economic development scenario, the carbon emission is 16,117.08 tons, which is 2,428.39 tons (13.1%) less than the 2020–2035 planning scheme. In strengthening the low-carbon economic development scenario, the carbon emission is 14,662.50 tons, which is 3,879.39 tons (21.3%) less than the 2020–2035 planning scheme.

4.2 Optimization of the spatial layout of low-carbon land use

Multi-objective linear programming can optimize the structure of low-carbon land use, but it cannot provide an optimal spatial layout scheme. In this article, the FLUS model was introduced to simulate and forecast the optimal layout of land use structures predicted by multi-objective linear programming. This article first takes the 2005 land use data of Chengdu as the initial research data to simulate the spatial layout of regional land use in 2020. Then, the simulation accuracy of the model is verified by comparing the actual land use data in 2020. Finally, the FLUS model is used to stimulate the spatial layout of land use in Chengdu in 2035 under the three scenarios.

4.2.1 Model verification

Although the FLUS model has been successfully applied widely, it is still necessary to tune the parameters and verify the simulation result in different study areas. Only after verification is successful, the model can be used to simulate and predict future land use change. Comprehensively considering the characteristics of the spatial layout of land use in Chengdu and the accuracy and accessibility of spatial data, this article selected 11 driving factors (elevation, slope, slope aspect, distance from the nearest river, distance from the nearest highway, distance from the nearest railway, distance from the nearest subway, distance from the nearest main road, population density, per capita GDP, and night-time light), as shown in Figure 5, which are used in ANN module training of the FLUS model.

1) ANN-based suitability probability calculation and evaluation

Using the land use data of Chengdu in 2005 and the 11 driving factors affecting land use change for ANN training, the spatial occurrence probability map of various land use types in Chengdu can be generated (Figure 6). The root mean square error (RMSE) of model training is 0.236203, which indicates that the training accuracy is high. However, the accuracy of the occurrence probability of each land use type generated by the ANN training needs to be further evaluated. Furthermore, the generated occurrence probability maps and the binary attribute data of land use are randomly sampled using ArcGIS. Then, those data are input into the ROC (receiver operating characteristic) curve tool under the analyze module of SPSS software for AUC (area under the curve) calculation. In Figure 7, the ROC curve and AUC value of each land use occurrence probability and corresponding actual land use types in 2005 are compared. The closer the curve is to the top left corner

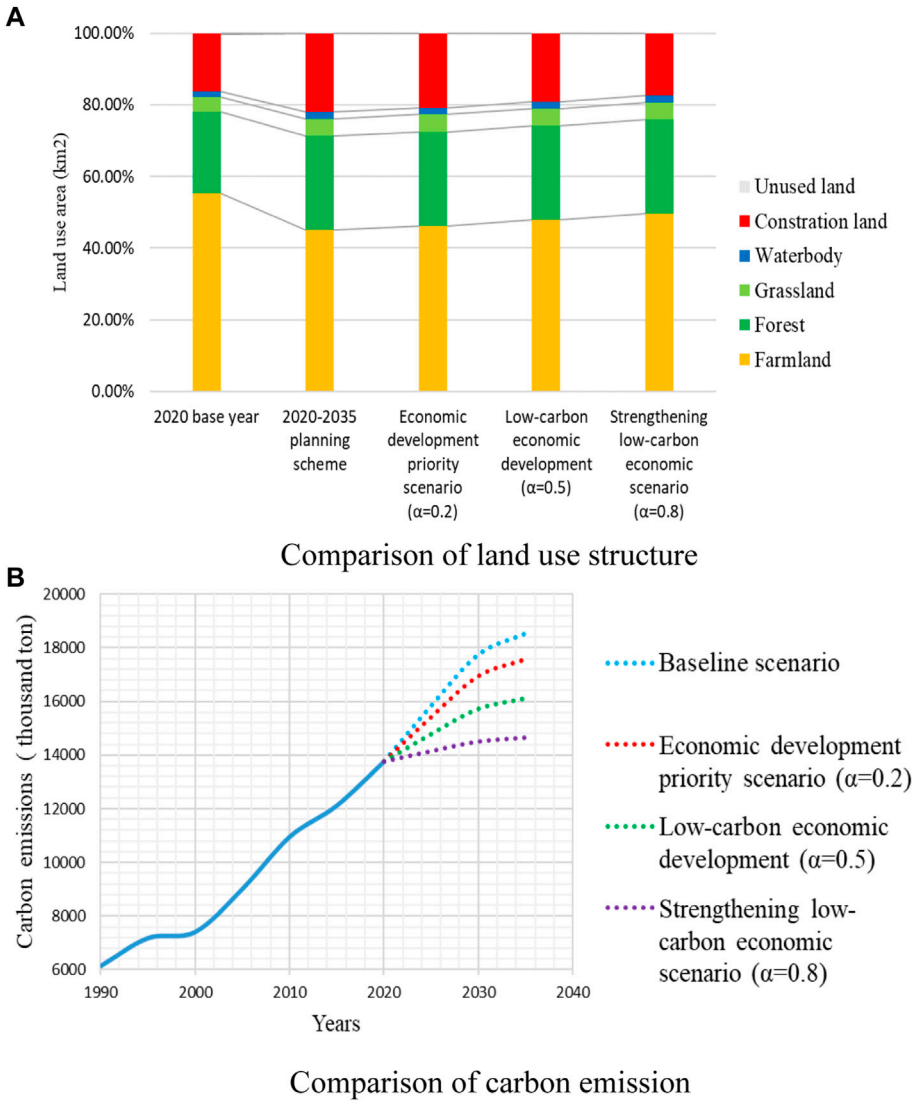

FIGURE 4
Optimize the land use structure and carbon emission reduction potential of the scenarios.

(the smaller the X, the larger the Y), the greater the prediction accuracy. The ROC curve represents the relationship between sensitivity and specificity. The area under the curve (AUC) is a measure of the prediction accuracy. The greater the AUC number, the more accurate the forecast.

The results show that the ROC curve of the construction land and farmland is closer to the left (higher accuracy), and the following is forest, grassland, and waterbody (medium accuracy). The ROC curve of the unused land is closer to diagonal (lower accuracy). Also, the AUC values also confirmed the result, that is, except for the unused land, the AUC values of all land use types are greater than 0.6. In general, the selected driving factors have the good explanatory ability for all land use types except the unused land. But the proportion of the unused land area is very small (0.023%), and it has small impact on the overall prediction accuracy of the model, so this deviation can be ignored.

2) Parameter setting and model accuracy verification

In this article, the basic data required for the cellular automatic simulation of adaptive inertia mechanism mainly include the land use data of the initial year and the input suitability probability data. After many experiments and referring to relevant research, the specific parameter settings of simulation are shown in Table 5. The actual area of six land types in 2020 is set as the area simulation target of land uses. Then, the basic data and model parameters are input into the model for simulation, and the simulated spatial land use distribution map in 2020 can be obtained, as shown in Figure 8.

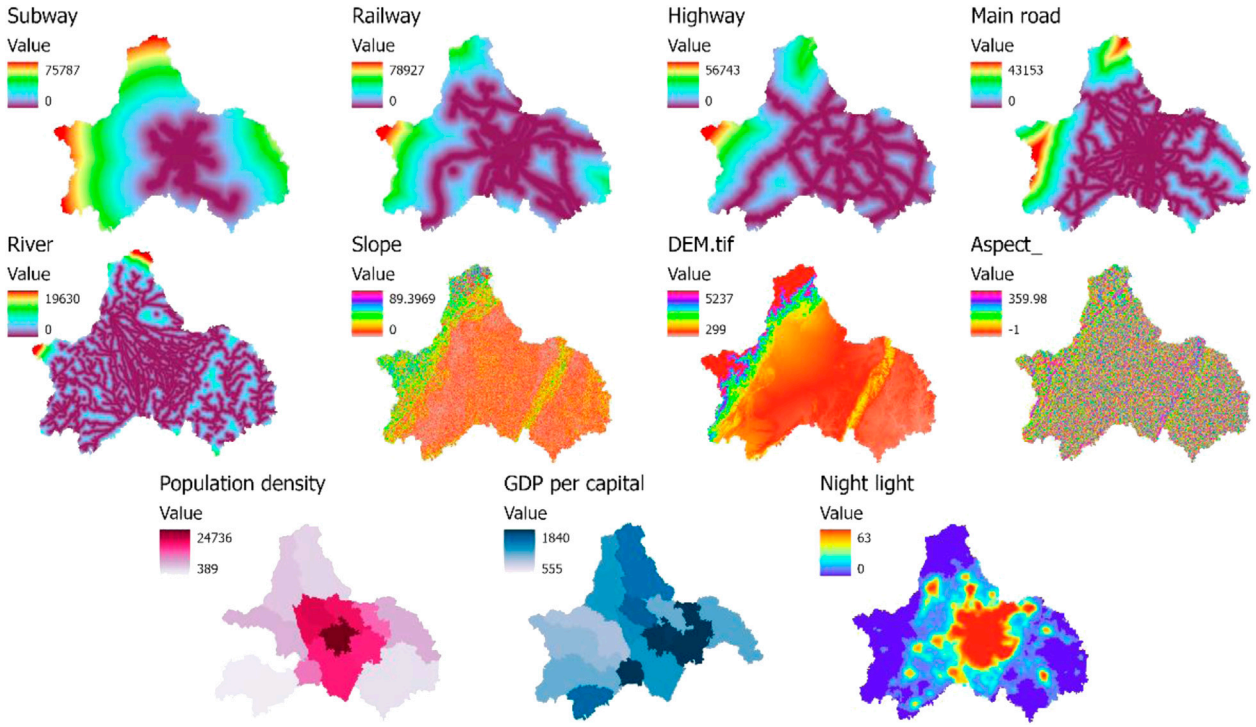

FIGURE 5
Driving factor for ANN-based Probability-of-occurrence estimation.

After the cellular automatic simulation based on the adaptive inertia mechanism is completed, random sampling and uniform sampling provided by the Precision Validation module in the FLUS model are used to conduct accuracy tests on simulation results. It was found that the Kappa index of the two test methods was greater than 0.82, and the simulation effect was ideal, which met the test standard. The results indicate that the FLUS model can be used to simulate the future land use change in Chengdu and can be used to simulate the future land use change in Chengdu city under different land use scenarios.

4.2.2 Model application

Taking the land use data in 2020 as the base period and setting the six land use types demand of the three scenarios calculated from the multi-objective linear programming, the verified FLUS model is used to optimize the land use spatial distribution of the three scenarios. The spatial optimization results are shown in Figure 9. As expected, in the three scenarios, the spatial patterns of forest land, grassland, and water body are basically consistent and relatively stable, while the spatial distribution of farmland and construction land is quite different. Specifically, in the economic development priority scenario, the growth trend of the construction land is the most obvious. The construction land spreads outward along the existing scope, constantly eroding the surrounding cultivated land, so the cultivated land is evidently reduced. In the low-carbon economic development scenario, especially in the strengthening low-carbon economic scenario, the expansion range of the construction land is smaller and restricted. The extended scope of the construction land is mainly concentrated around the main urban area of Chengdu due to convenient transportation and flat terrain and sufficient water resources.

Furthermore, the main transfer distribution of land use types under the three scenarios is compared with the land use situation of Chengdu in 2020 as a reference. The results are shown in Figure 10. The transfer of land use types mainly include conversion of farmland to construction land, conversion of farmland to woodland, conversion of farmland to grassland, conversion of farmland to water body, conversion of forest to farmland, and conversion of construction land to farmland. Among them, in terms of the degree of conversing farmland to construction land, the economic development priority scenario is higher than the low-carbon economic development scenario and higher than the strengthening low-carbon economic scenario. While the degree of converting farmland into forest, grassland, and water body present the opposite result, that is, the strengthening low-carbon economic scenario is higher than the low-carbon economic development scenario, and higher than the economic development priority scenario. In addition, the conversion of forests to farmland mainly occurs in the flat

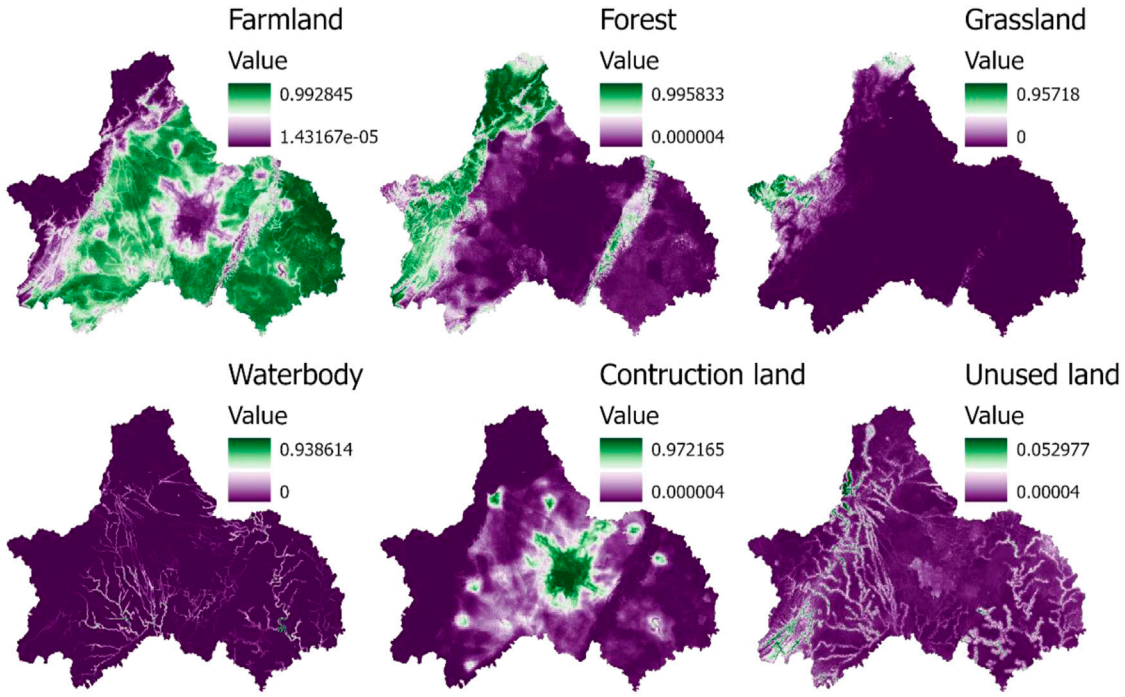

FIGURE 6
Occurrence probability map of land use.

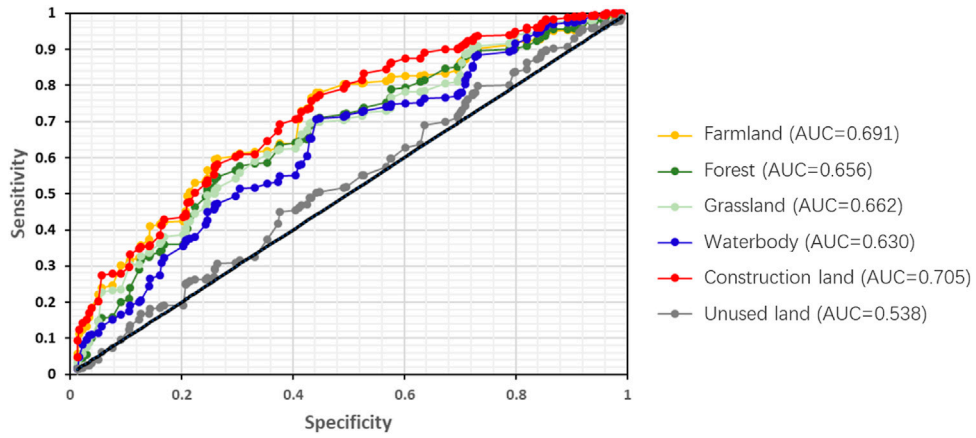

FIGURE 7
ROC curve and AUC value of land use after the ANN training.

areas in the southeast of the country, and the places where construction land is converted to cultivated land are scattered and far away from the existing cities and towns. In addition, the conversion of forests to farmland mainly occurs in the flat areas in the southeast of Chengdu, and the conversion of construction land to farmland mainly occurs in the scattered construction land areas that are far away from the existing large cities and towns.

5 Discussion

The carbon emission coefficient used in this article refers to the report of IPCC and relevant research results. Although the current accounting technical standards of carbon emissions have been preliminarily agreed upon, there is no unified understanding of the carbon emission coefficient of land use

TABLE 5 Parameter settings in the CA module.

No.	Configuration items	Parameter setting
1	Initial data	Land use in 2005
	Validated data	Land use in 2020
2	ANN-based probability-of-occurrence estimation	P (c, k, t)
3	Interactions	300
4	Cellular neighborhood size	3 × 3
6	Weight of neighborhood	Farmland = 0.7, grassland = 0.5, forest = 0.3, waterbody = 0.2, construction land = 1, unused land = 1
7	Cost matrix	Natural development scenario
8	Accelerated factor	0.1
9	Land use demand	Economic development priority scenario (α = 0.2) Low-carbon economic development scenario (α = 0.5) Strengthening low-carbon economic scenario (α = 0.8)

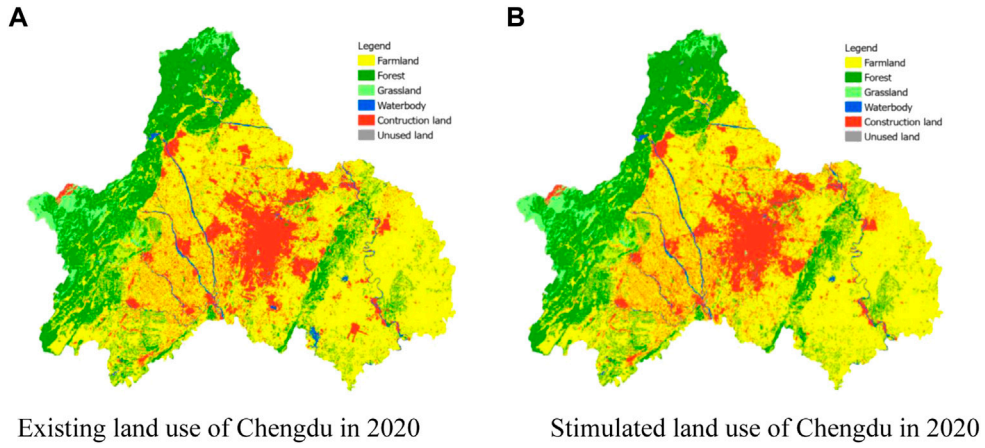

FIGURE 8
Actual land use map and simulated land use map of Chengdu in 2020.

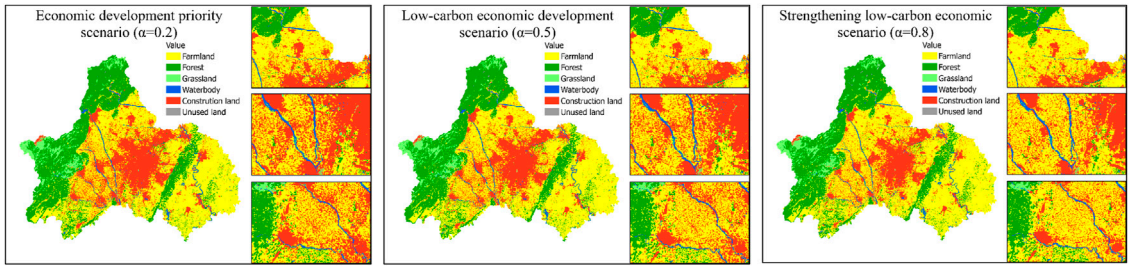

FIGURE 9
Simulated distribution of land use types under three scenarios.

(Rong et al., 2020). The majority of the existing carbon emission coefficient of land use is the estimated results by studying a wide range of research areas, such as a state, a country, and a climate zone (Li et al., 2013; Fang and Zhao 2018; Han et al., 2019; Yu et al., 2021). But in fact, the carbon emission coefficient of land use is affected by climate, vegetation, soil, and other factors,

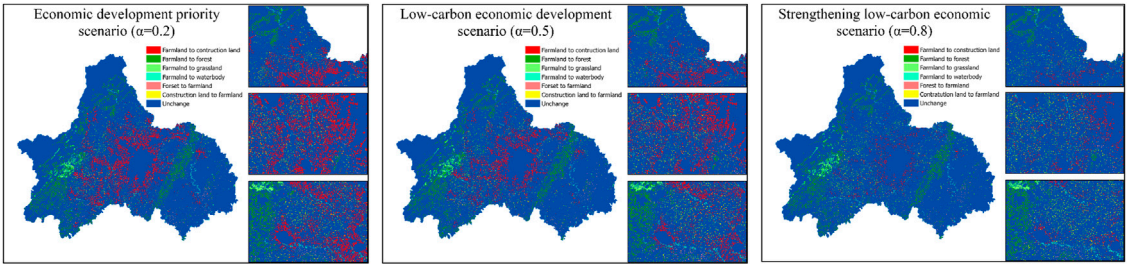

FIGURE 10
Distribution of main transfer in land use types under three scenarios.

which differ from region to region (Chen et al., 2020; Wei, X., Duan, L. 2021). This article adopts the average value from the existing studies in similar locations, although the actual carbon emissions of various types of land may not be estimated accurately. The results in this article are basically consistent with the relevant studies on the net change trend of carbon emissions, and the research results still have a certain reference value. This study found that carbon emissions from land use in Chengdu continue to increase from 1990 to 2020, because the growth rate of carbon sources was much faster than that of carbon sinks. Forest land, grassland, and garden land, as the main force of carbon sink in the ecosystem, and their carbon sink capacity has not changed significantly in the last 30 years. The construction land, as a major contributor to carbon sources, has been expanding in the past 30 years, resulting in a continuous increase in total carbon emissions.

Based on the multi-objective linear programming and FLUS model, this article simulates the land use structure, spatial distribution pattern, and transfer of land use of Chengdu under three scenarios, taking the land use planning scheme as constraint conditions. It is worth noting that when using the FLUS model, due to the limitations of available data in the selected research area and some model parameters set subjectively, the simulated future land use distribution may be biased (Liu et al., 2017; Cao et al., 2019; He F. et al., 2022). Therefore, considering the driving factors and setting model parameters more objectively to improve the accuracy of prediction still needs further exploration.

The main differences in land use patterns in the three scenarios proposed in this article are reflected in the differences between farmland and construction land. By comparing and analyzing these three scenarios, it can be found that there are two main strategies to realize low-carbon land use in Chengdu. One is to reasonably control urban expansion by limiting the erosion of construction land on farmland. The other is, within the red line of farmland, to transform as much farmland as possible into other land use types with a stronger carbon sink effect, such as forest land, grassland, and water body. However, such low-carbon land use may have a negative impact on the economic development. For the sustainable development of Chengdu in the future, efforts can be devoted to the following aspects.

First of all, it is necessary to increase the economic output value of the construction land per unit rather than blindly increasing the amount of construction land. Adjusting the industrial structure by increasing the proportion of high-tech industries and service industries is beneficial to a sustainable green economy because those industries has high economic benefits but low pollution (Sun et al., 2015). Second, improving energy efficiency and increasing the usage of new and clean energy is vital to reduce the intensity of carbon emissions from the construction land (Sullivan 2010; Zhou, Y., He, Z., Ma, Li., Yang, Y., Zhang, T., Chen, L. 2017; Zhang et al., 2019). Third, for the nonconstruction land, such as forest, grassland, and water body, exploring new development models for the combination of forestry, husbandry, fishing, and tourism will enhance the economic added value of those kinds of land use, which is conducive to the win–win of economic and ecological benefits (Dale 1997; Rong et al., 2020; Yang et al., 2021). Finally, adopting more modern and advanced agricultural technology on farmland to increase the total grain output and ensure that more farmland can be returned to forests (West 2003; Schulp et al., 2008).

6 Conclusion

This article studies the change characteristics of carbon emissions from land use in Chengdu from 1990 to 2020, and uses the MOP model to propose the optimal structure of land use under three scenarios: economic development priority scenario, low-carbon economic development scenario, and strengthening low-carbon economic scenario. Then, a FLUS model is adopted to simulate the spatial layout of land use under three scenarios in Chengdu in 2035. The research results of this article are expected to provide suggestions for the future optimization of land use structure in Chengdu and provide a reference for the construction and sustainable development of low-carbon cities

in Chengdu. The specific research results are summarized as follows:

From 1990 to 2020, the net carbon emissions from land use in Chengdu showed an overall increasing trend, and the carbon source increased by 7,617.603 thousand tons, with an average annual increase of 243.901 thousand tons (with an annual growth rate of 3.75%), of which construction land contributes the most to carbon sources, followed by farmland. Forest land contributes the most to carbon sink, followed by grassland and water area. The high carbon emissions are mainly concentrated in the plain areas in the center of Chengdu, and low-carbon emissions are mainly distributed in the northwest and southwest mountainous areas of Chengdu.

In the three scenarios of land structure optimization based on the MOP model, the areas of forests (3775,33 km^2), grasslands (691.05 km^2), and water bodies (264.17 km^2) are consistent with the targets set in the planning scheme for 2020–2035 in Chengdu. However, construction land has different degrees of erosion from farmland, so these two show opposite trend in these three scenarios. In terms of the degree of farmland erosion caused by construction land, the economic development priority scenario (667.71 km^2) is stronger than the low-carbon economic development scenario (417.32 km^2) and stronger than the strengthening low-carbon economic scenario (166.93 km^2). Compared with the planning scheme of 2020–2035 in Chengdu, the carbon emission of the economic development priority scenario was reduced by 969.72 tons (5.2%), the economic development priority scenario reduced carbon emissions by 2,414.31 tons (13.1%), and stronger than strengthening low-carbon economic scenario reduced carbon emissions by 3,878.89 tons (21.0%).

The spatial optimization results of land use predicted by the FLUS model under the three scenarios show that the pattern of the forest, grassland, and water body is basically consistent and relatively stable, while the spatial distribution of farmland and construction land changes greatly. The construction land mainly occupied the farmland area that was originally around the built-up area of Chengdu with sufficient water resources, convenient transportation, and flat terrain. In the stronger low-carbon economic development scenario, especially the strengthening low-carbon economic scenario, the continuous expansion of construction land was significantly restrained.

As the park city and the national approval of low-carbon pilot city, Chengdu is playing an increasingly prominent role in the field of "carbon neutrality and carbon peak", especially in western China. This article, considering the economic benefits carbon reducing potential, takes Chengdu as a case study to demonstrate how to realize the low carbonization of land use by optimizing and regulating the structure and spatial layout of land use. This research fills the gap in western China. The research can provide planning suggestions for the low-carbon development of Chengdu and other regions in western China. More importantly, the research method proposed in this article can provide a reference for similar research in other cities.

Data availability statement

The original contributions presented in the study are included in the article/Supplementary Material. Further inquiries can be directed to the corresponding author.

Author contributions

RW conceived the overall framework of the study and wrote the main content of the manuscript. HL provided technical guidance. YC and PL were responsible for data collection and analysis.

Funding

This study was supported by the National Natural Science Foundation of China (No. 52008346).

Acknowledgments

The authors thank the Resources and Environmental Science and Data Center, China, for providing land for use and relevant geospatial data.

Conflict of interest

The authors declare that the research was conducted in the absence of any commercial or financial relationships that could be construed as a potential conflict of interest.

Publisher's note

All claims expressed in this article are solely those of the authors and do not necessarily represent those of their affiliated organizations, or those of the publisher, the editors, and the reviewers. Any product that may be evaluated in this article, or claim that may be made by its manufacturer, is not guaranteed or endorsed by the publisher.

References

Adams, J. M., Faure, H., Faure-Denard, L., McGlade, J. M., and Woodward, F. I. (1990). Increases in terrestrial carbon storage from the Last Glacial Maximum to the present. *Nature* 348 (6303), 711–714. doi:10.1038/348711a0

Asner, Gregory P., Powell, George V. N., Mascaro, Joseph, Knapp, David E., Clark, John K., Jacobson, James, et al. (2010). High-resolution forest carbon stocks and emissions in the Amazon. *Proc. Natl. Acad. Sci. U. S. A.* 107 (38), 16738–16742. doi:10.1073/pnas.1004875107

Cao, Shuai, Jin, Xiao-bin, Yang, Xu-hong, Sun, Rui, Liu, Jing, Han, Bo, et al. (2019). Coupled MOP and GeoSOS-FLUS models research on optimization of land use structure and layout in Jintan district. *J. Nat. Resour.* 34 (6), 1171. doi:10.31497/zrzyxb.20190604

CBS (2022). Available at http://cdstats.chengdu.gov.cn/tjgzxxw/c112708/tjxx_listTime1.shtml?0205.

Chang, Xiaoqing, Xing, Yanqiu, Wang, Jiaqi, Yang, Hong, and Gong, Weishu (2022). Effects of land use and cover change (LUCC) on terrestrial carbon stocks in China between 2000 and 2018. *Resour. Conservation Recycl.* 182, 106333. doi:10.1016/j.resconrec.2022.106333

Chen, Yizhong, Lu, Hongwei, Li, Jing, and Xia, Jun (2020). Effects of land use cover change on carbon emissions and ecosystem services in Chengyu urban agglomeration, China. *Stoch. Environ. Res. Risk Assess.* 34 (8), 1197–1215. doi:10.1007/s00477-020-01819-8

chinesestandard (2022). GB/T 21010-2017. Available atupdated on 7/7/2022, checked on 7/7/2022 https://www.chinesestandard.net/PDF/English.aspx/GBT21010-2017.

CMBPNR (2022). Chengdu city land use master plan (2020-2035). Available atupdated on 7/7/2022checked on http://mpnr.chengdu.gov.cn/ghhzrzyj/tzgg/2021-07/09/content_6ad6e63b21c542b5bd6548ca06ad7f5f.shtml 77, 2022).

Cui, Yong, Lan, Haifeng, Zhang, Xinshuo, and He, Ying (2022). Confirmatory analysis of the effect of socioeconomic factors on ecosystem service value variation based on the structural equation model—a case study in sichuan province. *Land* 11 (4), 483. doi:10.3390/land11040483

Dale, Virginia H. (1997). The relationship between land-use change and climate change. *Ecol. Appl.* 7 (3), 753–769. (1997)007[0753:TRBLUC]2.0.CO;2. doi:10.1890/1051-0761

Dong, Jiuying, and Wan, Shuping (2019). A new method for solving fuzzy multi-objective linear programming problems. *Iran. J. Fuzzy Syst.* 16 (3), 145–159. doi:10.22111/ijfs.2019.4651

Dotsey, Micheal, Li, Wenli, and Yang, Fang (2022). *Demographic Transition, Industrial Policies, and Chinese Economic Growth*. Rochester, NY: FRB of Philadelphia Working Paper No. 22-17. Available at SSRN: https://ssrn.com/abstract=4148112 or http://dx.doi.org/10.21799/frbp.wp.2022.17.

Ellis, Erle C., and Ramankutty, Navin (2008). Putting people in the map: Anthropogenic biomes of the world. *Front. Ecol. Environ.* 6 (8), 439–447. doi:10.1890/070062

Fang, Chenyu, and Zhao, Shuqing (2018). A comparative study of spatiotemporal patterns of urban expansion in six major cities of the Yangtze River Delta from 1980 to 2015. *Ecosyst. Health Sustain.* 4 (4), 95–114. doi:10.1080/20964129.2018.1469960

Han, Dang, Qiao, Ruilin, and Ma, Xiaoming (2019). Optimization of land-use structure based on the trade-off between carbon emission targets and economic development in shenzhen, China. *Sustainability* 11 (1), 11. doi:10.3390/su11010011

He, Fei, Yang, Jun, Zhang, Yuqing, Sun, Dongqi, Wang, Li, Xiao, Xiangming, et al. (2022a). Offshore island connection line: A new perspective of coastal urban development boundary simulation and multi-scenario prediction. *GIScience Remote Sens.* 59 (1), 801–821. doi:10.1080/15481603.2022.2071056

He, F., Yang, J., Zhang, Y., Sun, D., Wang, L., Xiao, X., et al. (2022b). Offshore island connection line: A new perspective of coastal urban development boundary simulation and multi-scenario prediction. *GIScience Remote Sens.* 59 (1), 801–821. doi:10.1080/15481603.2022.2071056

Houghton, R. A., and Hackler, J. L. (1999). Emissions of carbon from forestry and land-use change in tropical Asia. *Glob. Change Biol.* 5 (4), 481–492. doi:10.1046/j.1365-2486.1999.00244.x

Kaplan, J. O., Krumhardt, K. M., and Zimmermann, N. E. (2012). The effects of land use and climate change on the carbon cycle of E urope over the past 500 years. *Glob. Chang. Biol.* 18 (3), 902–914. doi:10.1111/j.1365-2486.2011.02580.x

Lai, Li, Huang, Xianjin, Yang, Hong, Chuai, Xiaowei, Zhang, Mei, Zhong, Taiyang, et al. (2016). Carbon emissions from land-use change and management in China between 1990 and 2010. *Sci. Adv.* 2 (11), e1601063. doi:10.1126/sciadv.1601063

Li, Junxiang, Li, Cheng, Zhu, Feige, Song, Conghe, and Wu, Jianguo (2013). Spatiotemporal pattern of urbanization in Shanghai, China between 1989 and 2005. *Landsc. Ecol.* 28 (8), 1545–1565. doi:10.1007/s10980-013-9901-1

Liang, Xun, Liu, Xiaoping, Li, Dan, Zhao, Hui, and Chen, Guangzhao (2018). Urban growth simulation by incorporating planning policies into a CA-based future land-use simulation model. *Int. J. Geogr. Inf. Sci.* 32 (11), 2294–2316. doi:10.1080/13658816.2018.1502441

Liu, Xiaoping, Liang, Xun, Li, Xia, Xu, Xiaocong, Ou, Jinpei, Chen, Yimin, et al. (2017). A future land use simulation model (FLUS) for simulating multiple land use scenarios by coupling human and natural effects. *Landsc. Urban Plan.* 168, 94–116. doi:10.1016/j.landurbplan.2017.09.019

Mendelsohn, R., and Dinar, A. (2009). Land use and climate change interactions. *Annu. Rev. Resour. Econ.* 1 (1), 309–332. doi:10.1146/annurev.resource.050708.144246

Millington, James D. A., Demeritt, David, and Romero-Calcerrada, R. (2011). Participatory evaluation of agent-based land-use models. *J. Land Use Sci.* 6 (2-3), 195–210. doi:10.1080/1747423X.2011.558595

Mohammady, Majid, Moradi, Hamid Reza, Zeinivand, Hossein, Temme, A. J. A. M., YazdaniMohammad, Reza, and Pourghasemi, Hamid Reza (2018). Modeling and assessing the effects of land use changes on runoff generation with the CLUE-s and WetSpa models. *Theor. Appl. Climatol.* 133 (1-2), 459–471. doi:10.1007/s00704-017-2190-x

NBS (2022). Available atupdated on 6/30/2022, checked on 7/7/2022 http://www.stats.gov.cn/tjsj/tjcbw/201909/t20190924_1699094.html.

Nie, Xin, Wu, Jianxian, Zhang, Wei, Zhang, Jun, Wang, Wenhuan, Wang, Yinghui, et al. (2021). Can environmental regulation promote urban innovation in the underdeveloped coastal regions of western China? *Mar. Policy* 133, 104709. doi:10.1016/j.marpol.2021.104709

Ojima, Dennis S., Dirks, Bjrn O. M., Glenn, Edward P., Owensby, Clenton E., and Scurlock, Jonathan O. (1993). Assessment of C budget for grasslands and drylands of the world. *Water Air Soil Pollut.* 70 (1-4), 95–109. doi:10.1007/BF01104990

Pontius, R. Gil, Cornell, Joseph D., and Hall, Charles A. S. (2001). Modeling the spatial pattern of land-use change with GEOMOD2: Application and validation for Costa Rica. *Agric. Ecosyst. Environ.* 85 (1-3), 191–203. doi:10.1016/S0167-8809(01)00183-9

Popp, Alexander, Humpenöder, Florian, Weindl, Isabelle, Bodirsky, Benjamin Leon, Bonsch, Markus, Lotze-Campen, H., et al. (2014). Land-use protection for climate change mitigation. *Nat. Clim. Chang.* 4 (12), 1095–1098. doi:10.1038/nclimate2444

RESDC (2022). Resource and environment Sciences and data center. Available atupdated on 7/7/2022, checked on 7/7/2022 https://www.resdc.cn/lds.aspx.

Rong, Tianqi, Zhang, Pengyan, Jing, Wenlong, Zhang, Yu, Li, Yanyan, Yang, Dan, et al. (2020). Carbon dioxide emissions and their driving forces of land use change based on economic contributive coefficient (ECC) and ecological support coefficient (ESC) in the lower yellow river region (1995–2018). *Energies* 13 (10), 2600. doi:10.3390/en13102600

Schulp, Catharina J. E., Nabuurs, Gert-Jan, and Verburg, Peter H. (2008). Future carbon sequestration in europe—effects of land use change. *Agric. Ecosyst. Environ.* 127 (3-4), 251–264. doi:10.1016/j.agee.2008.04.010

IPCC (2019). "Climate change and land: An IPCC special report on climate change, desertification, land degradation, sustainable land management," in *Food security, and greenhouse gas fluxes in terrestrial ecosystems. With assistance of P.* Editors R. Shukla, J. Skea, E. Calvo Buendia, V. Masson-Delmotte, H.-O. Pörtner, D. C. Roberts, et al. (Geneva: In press. IPCC).

Sullivan, Paul (2010). Energetic cities: Energy, environment and strategic thinking. *World Policy J.* 27 (4), 11–13. doi:10.1162/wopj.2011.27.4.11

Sun, He, Liang, Hongmei, Chang, Xueli, Cui, Qingchun, and Tao, Yun (2015). Land use patterns on carbon emission and spatial association in China. *Econ. Geogr.* 35 (3), 154–162. doi:10.15957/j.cnki.jjdl.2015.03.023

United Nations (2015). Support sustainable development and climate action. Available atupdated on 12/22/2021, checked on 7/5/2022 https://www.un.org/en/our-work/support-sustainable-development-and-climate-action.

Wang, Changrong, and Cao, Yun (2021). Forecasting Chinese economic growth, energy consumption, and urbanization using two novel grey multivariable forecasting models. *J. Clean. Prod.* 299, 126863. doi:10.1016/j.jclepro.2021.126863

Wang, Qiang, and Jiang, Rui (2019). Is China's economic growth decoupled from carbon emissions? *J. Clean. Prod.* 225, 1194–1208. doi:10.1016/j.jclepro.2019.03.301

Wang, Qingzheng, Guan, Qingyu, Lin, Jinkuo, Luo, Haiping, Tan, Zhe, and Ma, Yunrui (2021). Simulating land use/land cover change in an arid region with the coupling models. *Ecol. Indic.* 122, 107231. doi:10.1016/j.ecolind.2020.107231

Wei, Dong, Yang, Linchuan, Bao, Zhikang, Lu, Yi, and Yang, Hongtai (2022). Variations in outdoor thermal comfort in an urban park in the hot-summer and cold-winter region of China. *Sustain. Cities Soc.* 77, 103535. doi:10.1016/j.scs.2021.103535

Wei, X., and Duan, L. (2021). Study on spatial and temporal structure change of land use in Chengdu. *J. Sichuan For. Sci. Technol.* 44 (2), 77–81. doi:10.12172/202008120001

West, T. O. (2003). Net carbon flux from agriculture: Carbon emissions, carbon sequestration, crop yield, and land-use change. *Biogeochemistry* 63 (1), 73–83. doi:10.1023/A:1023394024790

Wu, Ya, Tam, Vivian W. Y., Shuai, Chenyang, Shen, Liyin, Zhang, Yu, and Liao, Shiju (2019). Decoupling China's economic growth from carbon emissions: Empirical studies from 30 Chinese provinces (2001-2015). *Sci. Total Environ.* 656, 576–588. doi:10.1016/j.scitotenv.2018.11.384

Yang, Jun, Yang, Ruxin, Chen, Ming-Hsiang, Su, Ching-Hui, Joan; Zhi, Yin, and Xi, Jianchao (2021). Jianchao (2021a): Effects of rural revitalization on rural tourism. *J. Hosp. Tour. Manag.* 47, 35–45. doi:10.1016/j.jhtm.2021.02.008

Yang, Linchuan, Chau, K. W., Szeto, W. Y., Cui, Xu, and Wang, Xu (2020a). Accessibility to transit, by transit, and property prices: Spatially varying relationships. *Transp. Res. Part D Transp. Environ.* 85, 102387. doi:10.1016/j.trd.2020.102387

Yang, Linchuan, Chu, Xiaoling, Gou, Zhonghua, Yang, Hongtai, Lu, Yi, and Huang, Wencheng (2020b). Accessibility and proximity effects of bus rapid transit on housing prices: Heterogeneity across price quantiles and space. *J. Transp. Geogr.* 88, 102850. doi:10.1016/j.jtrangeo.2020.102850

Yang, Linchuan, Liang, Yuan, He, Baojie, Lu, Yi, and Gou, Zhonghua (2022a). COVID-19 effects on property markets: The pandemic decreases the implicit price of metro accessibility. *Tunn. Undergr. Space Technol.* 125, 104528. doi:10.1016/j.tust.2022.10452810.1016/j.tust.2022.104528

Yang, Linchuan, Liu, Jixiang, Liang, Yuan, Lu, Yi, and Yang, Hongtai (2021b). Spatially varying effects of street greenery on walking time of older adults. *ISPRS Int. J. Geoinf.* 10 (9), 596. doi:10.3390/ijgi10090596

Yang, Linchuan, Yu, Bingjie, Liang, Pengpeng, Tang, Xianglong, and Li, Ji (2022b). Crowdsourced data for physical activity-built environment research: Applying strava data in Chengdu, China. *Front. Public Health* 10, 883177. doi:10.3389/fpubh.2022.883177

Yang, Ye, Lan, Haifeng, and Li, Jing (2019). Spatial econometric analysis of the impact of socioeconomic factors on PM2.5 concentration in China's inland cities: A case study from Chengdu plain economic zone. *Int. J. Environ. Res. Public Health* 17 (1), 74. doi:10.3390/ijerph17010074

Yona, Leehi, Cashore, Benjamin, Jackson, Robert B., Ometto, Jean, and Bradford, Mark A. (2020). Refining national greenhouse gas inventories. *Ambio* 49 (10), 1581–1586. doi:10.1007/s13280-019-01312-9

Yu, Xiaohong, Liang, Zifen, Fan, Jiajia, Zhang, Jialing, Luo, Yihang, and Zhu, Xiaoyuan (2021). Spatial decomposition of city-level CO2 emission changes in Beijing-Tianjin-Hebei. *J. Clean. Prod.* 296, 126613. doi:10.1016/j.jclepro.2021.126613

Zhang, Lili, Liu, Haoru, Wei, Dong, Liu, Fei, Li, Yanru, Li, Haolin, et al. (2022). Impacts of spatial components on outdoor thermal comfort in traditional linpan settlements. *Int. J. Environ. Res. Public Health* 19 (11), 6421. doi:10.3390/ijerph19116421

Zhang, Lili, Liu, Zu'an, Hou, Chaoping, Hou, Jiawen, Wei, Dong, and Hou, Yuyao (2019). Optimization analysis of thermal insulation layer attributes of building envelope exterior wall based on DeST and life cycle economic evaluation. *Case Stud. Therm. Eng.* 14, 100410. doi:10.1016/j.csite.2019.100410

Zhang, Lili, Wei, Dong, Hou, Yuyao, Du, Junfei, Liu, Zu'an, Zhang, Guomin, et al. (2020). Outdoor thermal comfort of urban park—A case study. *Sustainability* 12 (5), 1961. doi:10.3390/su12051961

Zhou, Y., He, Z., Ma, Li., Yang, Y., Zhang, T., and Chen, L. (2017). Spatial and temporal differentiation of China's provincial scale energy consumption structure. *Resour. Sci.* 39 (12), 2247–2257. doi:10.18402/resci.2017.12.04

frontiers | Frontiers in Earth Science

TYPE Original Research
PUBLISHED 07 September 2022
DOI 10.3389/feart.2022.988608

Check for updates

OPEN ACCESS

EDITED BY
Jianhong Xia,
Curtin University, Australia

REVIEWED BY
Huisheng Yu,
Northeastern University, China
Yangyang Xia,
The University of Hong Kong, Hong Kong, SAR China
Zhenchao Zhang,
University of Toronto, Canada

*CORRESPONDENCE
Dahao Zhang,
zhangdh27@mail2.sysu.edu.cn

SPECIALTY SECTION
This article was submitted to Geoscience and Society, a section of the journal Frontiers in Earth Science

RECEIVED 07 July 2022
ACCEPTED 10 August 2022
PUBLISHED 07 September 2022

CITATION
Zhou C, Zhang D and Chen Y (2022), Theoretical framework and research prospect of the impact of China's digital economic development on population. *Front. Earth Sci.* 10:988608. doi: 10.3389/feart.2022.988608

COPYRIGHT
© 2022 Zhou, Zhang and Chen. This is an open-access article distributed under the terms of the Creative Commons Attribution License (CC BY). The use, distribution or reproduction in other forums is permitted, provided the original author(s) and the copyright owner(s) are credited and that the original publication in this journal is cited, in accordance with accepted academic practice. No use, distribution or reproduction is permitted which does not comply with these terms.

Theoretical framework and research prospect of the impact of China's digital economic development on population

Chunshan Zhou, Dahao Zhang* and Yu Chen

School of Geography and Planning, Sun Yat-sen University, Guangzhou, China

Against the background of social digitalization, networking, and intelligent development, the relationship between China's digital economy and regional factors is increasingly close. This study systematically cards the relevant references of the digital economy, regional factors, and population based on the six perspectives of industry, residents' income, urban human settlement environment, infrastructure, the real economy, and government management level to explore the influence of the digital economy on regional factors and regional factors on population. The results show that: 1) the digital economy has a bidirectional influence on the population. Digital economy can both attract population and lead to population outflow through relevant regional factors. 2) Digital economy can indirectly affect the spatial layout of population attributes by giving digital connotations to regional elements. We analyze the influence of China's digital economic development on the population, build the influence of the digital economy on the population research framework, and put forward the research prospect of the impact of the digital economy on the population to provide a new research perspective on digital economic geography and population, as well as provide significant reference to guide the reasonable population flow and narrow the digital divide gap.

KEYWORDS

digital economy, population, digital divide, digital technology, China

1 Introduction

With the continuous development of technology, the new economy represented by the digital economy will not only reshape the world economic development pattern but also guide a new direction for the global technological revolution. At present, the development of information technology has continuously expanded the breadth and depth of the integration of the digital economy and elements of different regions and plays a vital role in stimulating consumption, driving investment, and creating jobs (Zhao et al., 2020). Due to the $PM_{2.5}$, residents' income; number of per capita non-agricultural employment, per capita medical staff, and per capita primary and secondary school teachers; and other factors, China's population spatial pattern changed significantly (Liu B. et al., 2022). The population of middle and west urban China presents single

centralization, while the populations of eastern coastal cities present decentralization. The population scale of the provincial capital is expanding, while that of small and medium-sized cities is shrinking (Sun et al., 2021), and the development of the digital economy plays a positive role in urban economic growth and improvement of public service quality. Therefore, cities with rapid digital economic growth have a certain siphoning effect on the population.

Research on the digital economy domestically and abroad is still in its primary stage. It mainly includes the following aspects. First, there is an imbalance in digital economic development, based on the overall structure of economic geography, exploring the limitations of the digital economy and the imbalance in two aspects of gender and space from the social and spatial perspective (Perrons, 2004). Using the Digital Economy and Social Index (DESI) data, the time series and cluster analysis method are applied to explore the dynamic evolution and spatial agglomeration characteristics of the digital economy and social index in EU countries and to explore the polarization degree of the index from the four dimensions of connectivity, human capital, Internet services, and digital economy public services (Ryszard et al., 2021). Second, research has undertaken a dynamic evaluation of the digital economy by connecting economic growth and the construction function of information technology to reasonably predict the development trajectory of the digital economy in the information age (Akaev & Sadovnichii, 2019). The nearly 50 years of data on digital facilities, multilateral digital platforms, and users and enterprises were obtained, and the development of future companies in digital platform economics through the data were evaluated (Acs et al., 2021). Based on the World Bank's pilot evaluation program, the overall development of the digital economy in different countries was evaluated, and the current challenges of the digital economy were put forward, which mainly include the priority sequence of digital diagnostics and the need for new technology problems, to provide advice to developing countries and relevant institutions (Nagy, 2020). Third, the impact of the digital economy on other regional factors was measured by exploring the impact of the digital economy on industry (Litvinenko, 2020), environment (Sui & Rejeski, 2002), public services (Adeyinka et al., 2020), innovation and entrepreneurship (Molina-Lopez et al., 2021), infrastructure (Adriaens and Ajami, 2021), government services (Banhidi et al., 2020), the real economy (Zhang et al., 2022), residents' income (Chen et al., 2020), employment (Sun et al., 2019), and so on.

In sum, the current research domestically and abroad on the digital economy mainly focuses on its spatial characteristics and dynamic evaluation and its impact on the industry, environment, and other regional factors; however, there is a lack of research on the impact of digital economic development on population factors. The logical framework of exploring the impact of digital economic development on the population can enrich not only the relevant theories on digital economy but also guide the orderly flow of population. Therefore, this study analyzes the logical relationship of the impact of the digital economy on population attributes from a multi-dimensional perspective by the references carding and logical inference methods, which is of great significance for the reasonable prediction of population movements, and provides a useful reference for improving the science and rationality of regional planning and reducing the digital divide gap between different regions. This manuscript comprises six sections. Section 1 is the introduction. Section 2 is the logic analysis of the impact of the digital economy on population. Section 3 is the logic analysis of the impact of the digital economy on regional factors. Section 4 is the logic analysis of the impact of regional factors on population. Section 5 is the discussion. Finally, Section 6 concludes this study. Sections 3 and 4 are used to provide evidence for the rationality of the logic of Section 2.

2 Logical analysis of the impact of digital economy on population

From the perspective of industrial development, the development of the digital economy is conducive to increasing the population scale and improving the structure of the population's educational level. First, the development of the digital economy promotes the digital development of industry, not only in traditional industries, but also in intelligent industries, which is conducive to increasing jobs and has a certain attraction to the surrounding population. Although the development of intelligence and digitalization makes some repetitive primary work replaceable, advanced management and other related work will not be completely replaced by artificial intelligence in a short time. Second, the development of digital technology urgently requires relevant professionals. To some extent, the introduction of high-level talents not only increases the population scale but also improves the educational level of the urban population. In addition, development of the information technology industry provides more opportunities and convenience for workers to participate in the labor market and is especially favorable for improving the employment participation rate of vulnerable workers, such as female, elderly, and rural workers. However, it is not only that the digital divide needs to be removed so that vulnerable workers can master the relevant information technology skills. According to Marxist economic theory, the mechanization of factories reduces labor intensity, includes women and children in the employment force, and expands the scope of employed and exploited groups. Under China's population aging trend, industrial digitalization (represented by the Internet of Things and artificial intelligence) lags behind the digital development of the service industry (represented by the information channel and business digital upgrading). It includes promoting the transformation of the employment of middle and low-skilled workers from the

industry to the service industry, and from the traditional industry to industries of the new economy. The mechanism consists of two parts, push and pull, as follows: Under push, industrial digitalization with high input and slow benefits faces the dual dilemma of population aging, which reduces the effective labor force, and lagging digital transformation. This means that the division of labor is not complete within the industry, and the cost transfer leads to low-quality employment and a severe loss of low-skilled industrial labor. Under pull, the degree of integration of service industry digitalization and development is high, and the profit growth of the service industry relaxes the tightness of the labor market, creates jobs in the new economy industries, and improves the quality of employment, thus promoting the employment transformation of middle and low-skilled workers to the service and new economy industries.

From the perspective of residents' income, the development of the digital economy has bidirectional characteristics for population growth. On the one hand, the development of the digital economy is conducive to further increasing the income of the residents in the local region, thus attracting a large number of people to settle and work there. On the other hand, the development of the digital economy is conducive to eliminating the digital divide gap and further narrowing the development gap between different regions. In addition, the development of information technology and networking makes online stores popular, the emergence of online shops makes practitioners' work inflexible, and some merchants move to regions with lower operating costs, which can result in the loss of population.

From the perspective of the urban human settlement environment, the development of the digital economy is conducive to optimizing the industrial structure, and digital technology can reduce the environmental pollution of enterprises. In addition, the digital economy can reduce regional carbon emissions and alleviate the urban heat island effect, thus creating a cool human settlement environment. In terms of the market environment, the digital economy can strengthen the supervision of the market environment and establish an orderly and unified market order. A comfortable and livable natural environment and a good market environment can attract population settlement, especially technological innovation talents and older adults, thus changing the educational level and age structure of the population in the region.

From the perspective of urban infrastructure, the digital economy can promote the digital development of medical, educational, and transportation facilities, and other infrastructure. Furthermore, the deep integration and development of infrastructure and digital platforms bring great convenience to residents' lives. Efficient and high-quality living conditions have a strong attraction to the population, especially older adults and school-age children, who have a strong demand for high-quality medical facilities and educational resources. This demand often leads to family-style migration, thus changing the age structure of the regional population to a certain extent. In addition, the extensive application of digital infrastructure is also conducive to improving the digital literacy of residents.

From the perspective of the real economy, the development of the digital economy is conducive to stimulating regional production and consumption and driving the development of the digital financial industry. Regions with rapid economic development also have relatively high wages; hence, they not only have good employment prospects but also have many development opportunities. Therefore, they attract a large number of migrant workers who take their families with them to work in areas with rapid economic development, thereby increasing the population in such areas.

From the perspective of the government management level, the digital economy is conducive to promoting the digital office of local government affairs, thus reducing the procedures for residents and enterprises to handle affairs. The development of the office network platform can better meet the needs of residents to handle affairs without leaving home. Efficient digital government management can not only save residents' time and improve residents' happiness but also attract the establishment of foreign enterprises. The improvement of residents' happiness and enterprise settlement can also attract a large number of migrants (Figure 1).

3 Logical analysis of the impact of digital economy on regional factors

3.1 Impact of digital economy on industry

The digital economy includes the data industry and also new products, industries, business forms, and models shaped by integrating the data industry with the economy and society. The new economic form created by the integrated development of the data industry and the first, second, third, and fourth industries has gradually become a new driving force for China's economic transformation and upgrading. The development of the digital economy promotes the upgrading of industrial structures and can provide a new development path for China's industry (Su et al., 2021). The impact of the digital economy on different industries includes the following aspects. First is the impact of the digital economy on industry. Against the backdrop of the fourth Industrial Revolution, the development of the digital economy has great potential for strengthening cooperation, data sharing, efficiency improvement, and sustainable development in the construction industry (Teisserenc & Sepasgozar, 2021). Meanwhile, the digital economy can also promote the internal and external practices of the construction industry (Li et al., 2019). The development of the digital economy is also constantly injecting new vitality into

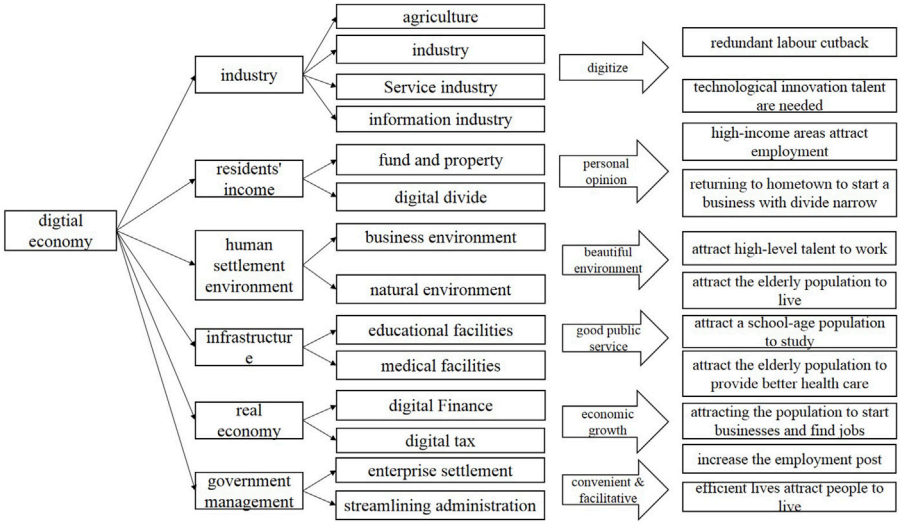

FIGURE 1
Logical diagram of the impact of the digital economy on the population.

traditional manufacturing industries, which can increase the added value of manufacturing exports and imports, and the domestic value-added rate of intermediate-product exports. Increasing investment in the digital economy has a significant positive effect on the capital-intensive and knowledge-intensive manufacturing industries (Ding et al., 2021). Additionally, the application of the digital economy to the industrial manufacturing industry is not only conducive to promoting coordination and cooperation between government, enterprise, universities, and research (Pozdneev et al., 2019) but can also extend the industrial chain of enterprises and integrate them into the world's factories (Andrea, 2020). Second is the impact of the digital economy on the leisure and entertainment industry. The application of digital technology in the hotel industry can significantly improve the network agglomeration of the population and the accessibility of digital services and expand the category of related services provided by hotels to guests (Dzhandzhugazova et al., 2018). Digital technology can also influence people's experience of enjoying music, prompting the restructuring of the music industry (Lee, 2009). From the perspective of tourism, the digital economy can continuously meet the changes in the tourism market and the personalized needs of tourists, promote the deep integration of culture and tourism, and attract professional staff engaged in the tourism industry, thus creating a large number of jobs (Samira & Alireza, 2011; Li et al., 2022). Digital technology can not only expand the physical market but also the virtual market and promote the development of the game industry (Nieborg et al., 2019). Third is the impact of the digital economy on high-tech industries. Digital economy can promote the optimization of high-tech industrial structures and the spatial agglomeration of high-tech enterprises and can form different sizes of high-tech industrial clusters according to the development of the regional digital economy (Trofimov et al., 2021). Furthermore, the development of the digital economy has created labor demand in service industries, such as express delivery, fast-food takeout, and homemaking, creating informal jobs and improving employment structure and quality.

3.2 Impact of digital economy on residents' income

The "digital divide" phenomenon not only exists between regions and countries but also between different social groups and strata. The digital divide reveals the unbalanced development of digital information technology, which may cause the differentiation of residents' income levels among regions (Liu & Zhang, 2019). Strengthening the construction of the digital economy can enhance the sustainability of farmers' income generation (Sun & Liu, 2022). The Internet can connect villages and cities, achieve the information development of the industrial chain, help farmers to improve productivity, reduce costs, and increase farmers' income. In addition, the development of block chain technology also provides opportunities for "digital poverty reduction" and innovation of agricultural development, to narrow the development gap between urban and rural residents. Therefore, the digital economy can give full play to its universality and sharing, narrow the unbalanced development between urban and rural areas, and reduce the income gap between urban and rural residents (Wang & Xiao, 2021). Sometimes workers' incomes

may reduce after changes in jobs. If the management of enterprises involving dangerous occupations and heavy physical labor can replace labor with machines and artificial intelligence, these jobs will no longer need a wage supplement, and the wage gap between occupations will narrow. However, the replaced workforce needs to be reemployed, or the income gap will widen. If work supervision can be achieved using information technology, then enterprises do not need to use performance wages to motivate workers, and the wage gap will narrow, which will also help to clear the labor market and achieve full employment at the social level. The characteristic gaps between different types of work are narrowing. The learning effect of the Internet reduces the skill distance of each occupation, which is conducive to narrowing the wage gap through the mobility of the labor force between occupations.

3.3 Impact of digital economy on urban human settlement environment

From the perspective of urban green development, the agglomeration of the digital economy can not only alleviate regional energy consumption and environmental pollution but also optimize the industrial structure and human capital, thereby promoting the green development of the regional environment (Ren et al., 2022). In addition, the digital economy can significantly improve the regional green total factor energy efficiency by improving the level of economic growth, urbanization, and research and development (R&D) (Zhang W. et al., 2021). From the perspective of urban carbon emission, industrial, financial, and innovative digitalization are important factors for the digital economy to influence and significantly reduce urban carbon emissions, effectively alleviate the urban heat island effect, and improve the comfort of the living climate (Yang et al., 2019; Xu et al., 2022). From the perspective of the business environment, the digital economy provides a basic guarantee for the development of the business environment, and it can optimize the market business environment by improving market service levels and strengthening market supervision. In addition, the digital transformation and coordinated development of physical enterprises and e-commerce platforms are conducive to promoting the orderly flow of market factors, thus optimizing the digital business environment (Zhang S. et al., 2021).

3.4 Impact of digital economy on urban infrastructure

The Internet, as an important catalyst in the digital economy, aids the development of urban infrastructure transfer to the digital direction. The digital economy has broadened the number and scope of Internet users and strengthened the integration of business, education, and health infrastructure into a network infrastructure (Qin & Liu., 2022). It can not only promote the digital transformation of living infrastructure and improve the convenience of residents' lives but also strengthen the application of handicraft industries and other industries in digital infrastructure, thus improving the operation scale and efficiency of regional industries (Kim, 2006).

3.5 Impact of digital economy on real economy

As one of the main components of the digital economy, the development of digital finance can stimulate regional innovation potential and indirectly promote the development of the real economy. This phenomenon is especially significant in the central and western cities with low urbanization rates and low material capital levels (Jiang et al., 2021). The direct and spillover effects of the digital economy on the sustainable development of China's real economy are positive, and the direct effect is greater than the spillover effect (Jiao & Sun, 2021). The digital economy also has a significant spatial spillover effect on the high-quality development of the real economy; however, the influence of the spillover effect differs for each urban real economy (Ding et al., 2022). In addition, the digital economy can remotely control the operation of the production and transportation process on e-commerce platforms. Even if the city where the e-commerce platform headquarters is located does not participate in the process of production and transportation, the digital tax generated during the operation process remains in the city where the headquarters is located, thus increasing economic development.

3.6 Impact of digital economy on government management level

The development of the digital economy connecting enterprises, residents, and the government through the network makes government management a network and a platform (Wilson & Mergel, 2022). With the further promotion of digital government affairs, government agencies have come to conduct all kinds of business processing online. The development of the digital economy has the greatest convenience for urban residents to handle various businesses, and also reduces the cumbersome procedures required of foreign enterprises to settle and apply for a license, to meet the needs of society and enterprises (Rytova et al., 2020), and is conducive to the digital development and transfer of the government office system. During the COVID-19 pandemic, the development of the digital economy made great contributions to the government's prevention and management of the pandemic, population travel restrictions, pandemic situation statistics, and material

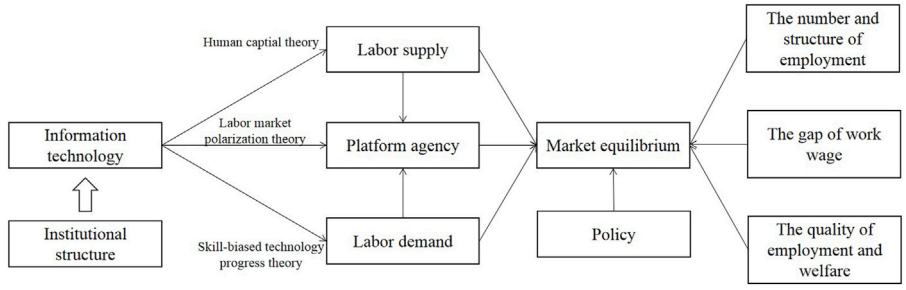

FIGURE 2
The impact of information technology development on labor supply and demand.

transportation. To some extent, the development of the digital economy represents the administrative level of cities (Wu et al., 2022).

4 Logical analysis of the impact of regional factors on population

4.1 Impact of industry on population

In the process of continuous upgrading and high-end development, the industrial structure will lead to population changes in the region. The adjustment of the urban industrial structure will attract a large number of migrants, and cross-regional flow of the labor force is particularly common. Aside from the natural flow of the labor force, many cities have promulgated various preferential policies to strengthen the introduction of professionals. The essence of this phenomenon is also a measure for local governments to deal with the pressure of industrial transformation. However, with the development of urban industries to high-end, industrial upgrading has an inhibitory effect on the scale of the urban population (Tong et al., 2021). Moreover, the spatial agglomeration characteristics of the industry and urban population have converged, and the spatial coupling relationship between the industry and population presents a gradient spatial evolution pattern (Liu et al., 2021). The development of information technology will also have an impact on human capital investment and the quality of labor supply. Some learning resources can be shared for free on the Internet, reducing the cost of human capital investment, which is conducive to improving the quality of labor supply. It is easier for workers to move and change occupations, but if labor is flowing too frequently, it is not conducive to forming long-term talented human capital in enterprises. Generally speaking, if information technology is used to replace workers, the demand for labor will decline. From the perspective of labor demand structure, the skill-biased technology progress theory posits that demand for highly skilled labor has increased, and the demand for low-skilled labor, which is easily replaced by information technology, will decrease. The labor market polarization theory suggests that with increased demand for unconventional tasks, the demand for highly skilled and low-skilled labor increases, the demand for moderately skilled workers who engage in routine tasks is reduced (Figure 2). Therefore, it can be seen that industry is the core of population competitiveness.

4.2 Impact of residents' income on population

Population migration is an important stage in the mobile population, and the population's willingness to settle plays a vital role in the degree of development of the regional population. The influence factors of the mobile population's willingness to settle include individual, economic, and social characteristics; economic characteristics are the core factors affecting the urban population. Income is an important component of economic characteristics; it directly affects the quality of life of residents in the city, and people with a higher quality of life will have a stronger willingness to settle (Zhu & Chen, 2010). Income inequality and the reduction in the rural population are related (Butler et al., 2020), and this correlation is increasingly evident as cities expand (Rattso & Stokke, 2014). The impact of population migration caused by income inequality is much greater than that caused by natural mobility. Population migration caused by income inequality has the most obvious influence on the middle-class population (Laskiene et al., 2020).

4.3 Impact of urban human settlement environment on population

The distribution of population is uneven in space; this phenomenon is formed by the interaction of various factors,

such as a good settlement environment (Kummu et al., 2016), and the suitability of the settlement environment has a strong correlation with the population (Li & Cao, 2013). Natural factors such as air quality, vegetation coverage rate, and land use are important indicators to evaluate the urban human settlement environment, which can not only evaluate the livability of the urban natural human settlement environment but also the activities and quantity of the population (Henderson & Xia, 1997). The quality of the natural environment has an important impact on the willingness of people to settle. Studies show that for every increasing unit of the annual average $PM_{2.5}$ concentration in the air, the possibility of immigrant settlement decreases by 8.7% (Zhao et al., 2021).

4.4 Impact of urban infrastructure on population

The coverage and accessibility of urban infrastructure services have an important impact on spatial migration between different regions (Roldán et al., 2017). Public service facilities also show a significant positive correlation with population (Shi et al., 2020); this correlation is mainly present in the influence of transportation, environment, energy, and other infrastructure on a population scale and employment structure (Lu et al., 2021). Transportation facilities determine urban residents' commuting capacity; environmental facilities and energy facilities determine the urban population carrying capacity (Kasu & Chi, 2018); medical and education facilities have a strong attraction for the older and school-age population (Buckeridge et al., 2012). Therefore, improving the quality, accessibility, and equalization of medical care and education infrastructure is important for improving the population's willingness to settle (Liu T. et al., 2022).

4.5 Impact of real economy on population

The development of the urban economy can not only promote the development of industries but also increase employment opportunities and labor wages. Cities with a high level of economic development are more attractive to the population, resulting in the siphoning effect. Relevant studies show that there is an interdependent relationship between China's real economy and population, and there are spatial agglomeration characteristics between them. The eastern region of the Hu Huan Yong Line has a rapid economic development, and the population is relatively concentrated, while the western region of the Hu Huan Yong Line has slow economic development and the population is relatively dispersed (Deng et al., 2022).

4.6 Impact of government management level on population

Government reforms such as streamlining administration and delegating power and the reform separating permits from business licenses not only makes it convenient for residents to handle related living matters but also simplifies the cumbersome process of enterprise establishment. Therefore, an efficient government service environment is conducive to creating a good urban business environment and attracting enterprises to settle and set up factories. A large number of businesses can create more jobs and thus attract the population of the surrounding areas. In addition, the government service hotline is an important support for construction of the smart government platform, and the public hotline can not only satisfy the residents for government service complaints but also solve the cut-throat market competition. A good government management level can improve the life efficiency of residents and the happiness index. Furthermore, the impact of information technology on government labor market supervision can protect the interests and efficiency of network workers. The high-quality government management and public service level can also be attractive to the population (Schmitt et al., 2006).

5 Discussion

5.1 Study innovations and significance

Based on the qualitative perspective of analyzing the relationship between digital economy, regional factors, and population, and then exploring the impact of digital economic development on regional population, this study not only enriches the relevant theories of the digital economy and population but can also reasonably guide the orderly flow of different population elements by changing the development of regional factors.

This research contributes to the literature through the following two points of innovation: 1) The innovation of research thinking: there exists an inverse two-direction relation among digital economy, regional elements, and population. Digital economy can indirectly affect the population through industry, and the agglomeration of the population can also indirectly affect digital economy development through industry. At present, most studies take single factors as study objects, such as medical care (Zhang et al., 2022), education (Zhang et al., 2020; Zhang Z. et al., 2021; Zhou et al., 2021), population (Yang et al., 2021), and the environment (Yang et al., 2020; Yu et al., 2022a; Chen et al., 2022; Yang et al., 2022), or only analyze the unilateral impact of population on regional factors. There is a lack of an indirect exploration of the impact of the digital economy on population based on the digital thinking mode. 2) The innovation of research vision: existing studies mainly explore the influence of the digital economy on

the environment, economy, and other factors, and lack exploration of the impact of the digital economy on the population.

5.2 Countermeasures and suggestions

According to the impact of the digital economy on the population, this study proposes the following development strategies. First, improving the digital management of the regional population. This would coordinate the regional human resources efficiently and in an orderly fashion and strengthen the cross-regional government management of the mobile population. The government should establish digital population files, carry out scientific demographic statistical studies of the population, dynamically monitor the age structure of urban population and talent flow in real-time, and strengthen the coordinated management of epidemic prevention of regional population flow. In addition, the service attitude and professional quality of government hotline telephone operators should be improved, and a digital operation system of human–machine collaboration should be built to encourage the interaction between government and people and carry out services benefiting enterprises. Second, establishing a digital supervision platform for humans in a settlement environment. This would provide a basic guarantee for the construction of a high-quality human settlement environment through the launch of a digital platform for urban human settlement environment governance. It would also give full play to the digital regulation ability, inspire residents to discuss communication and make recommendations on the platform, and urge the environmental protection department to curb environmental pollution in time to improve residents for human settlement environment supervision enthusiasm and participation, achieve the "Internet + human settlement environment" digital environment management way. In addition, relying on a good ecological environment to build a livable city attracts a large number of scientific and technological talents and high-tech enterprises to the city. Third, strengthen the deep integration of digital technology and public service facilities. This would involve improving the application of digital technology in the medical service system, comprehensively promoting the "Internet + medical service," establishing population health digital files interconnected at the national, provincial, city, and county levels, and completely preserving the digital medical footprints of residents, to ensure the refinement and convenience of residents' medical treatment. At the same time, it should promote "Internet + education service," strengthen the establishment of students' digital files for personal learning, achieve the interconnection of digital files from compulsory education to higher education, and make students' study footprints traceable, to formulate scientific and personalized teaching plans for each student.

5.3 Outlook

This study explores the impact of the digital economy on the population from a qualitative perspective, but it also has some limitations. First, since the quality of urban infrastructure, government management, and other elements are difficult to quantify, this study does not analyze the correlation coefficient between the digital economy and population quantitatively, or build network model methods (Yu et al., 2022b). Second, the digital economy is a huge and complex system constituting many systems, and each system contains a large number of subsystems. Therefore, this study cannot further analyze the impact of the digital economy on the population through communication infrastructure, industrial digitalization, and other subsystems. In future, the subsystem of the digital economy will be further refined to explore the correlation coefficient of digital economy and population through quantitative ways, and then analyze the impact of the digital economy on the distribution of population.

6 Conclusion

This study analyzes the impact of digital economic development on the population from the six dimensions of industry, residents' income, human settlement environment, infrastructure, the real economy, and government management, and also analyzes the relationship between digital economic development and population from a qualitative perspective. The study results are as follows:

1) The impact of the digital economy on the population is bidirectional. Digital economy can not only attract population inflow through the advantages of diverse industries, high income, good human settlement environment, convenient facilities and services, rapid economic development, and efficient government management but also cause population outflow in the region due to the elimination of repetitive workers. Overall, the digital economy attracts more people than encouraging population outflows.
2) The digital economy can indirectly affect the spatial layout of the population by giving digital connotations to regional elements. The digital economy can have an impact on population elements such as permanent population, population density, registered population, the age structure

and educational level of the population, and the number of employees in different industries. The spatial migration of the population caused by the different degrees of digital economic development in various regions results in the differences in population elements between different regions.

Data availability statement

The original contributions presented in the study are included in the article/Supplementary Material, further inquiries can be directed to the corresponding author.

Author contributions

Conceptualization, CZ and DZ; methodology, DZ and YC; software, DZ and YC; validation, CZ; formal analysis, CZ; writing-original draft, CZ and DZ; writing-review and editing, YC All authors have read and agreed to the published version of the manuscript.

Acknowledgments

The authors are grateful to the editor and reviewers for their valuable comments and suggestions.

Conflict of interest

The authors declare that the research was conducted in the absence of any commercial or financial relationships that could be construed as a potential conflict of interest.

Publisher's note

All claims expressed in this article are solely those of the authors and do not necessarily represent those of their affiliated organizations, or those of the publisher, the editors and the reviewers. Any product that may be evaluated in this article, or claim that may be made by its manufacturer, is not guaranteed or endorsed by the publisher.

References

Acs, Z., Song, A., Szerb, L., Audretsch, D., and Komlósi, É. (2021). The evolution of the global digital platform economy:1971-2021. *Small Bus. Econ.* 57, 1629–1659. doi:10.1007/s11187-021-00561-x

Adeyinka, S., Lee, S., Abdullah, S., and Teo, J. (2020) Hospitality and tourism education in an emerging digital economy. *Worldw. Hosp. Tour. Themes*.12(2): 113–125. doi:10.1108/WHATT-12-2019-0075

Adriaens, P., and Ajami, N. (2021). Infrastructure and the digital economy: Reinventing our role in the design, financing, and governance of essential services for society. *J. Environ. Eng.* 147 (5), 02521001. doi:10.1061/(ASCE)EE.1943-7870.0001866

Akaev, A., and Sadovnichii, V. (2019). On the choice of mathematical models for describing the dynamics of digital economy. *Diff. Equat.* 55 (5), 729–738. doi:10.1134/S0012266119050136

Andrea, S. (2020). Digital transformation-enabling factory economy actors' entrepreneurial integration in global value chains? *Post-Communist Econ.* 32 (6), 771–792. doi:10.1080/14631377.2020.1722588

Banhidi, Z., Dobos, I., and Nemeslaki, A. (2020). What the overall digital economy and society index reveals: A statistical analysis of the DESI EU28 dimensions. *Reg. Stat.* 10 (2), 46–62. doi:10.15196/RS100209

Buckeridge, D., Izadi, M., Shaban-Nejad, A., Mondor, L., Jauvin, C., Dube, L., et al. (2012). An infrastructure for real-time population health assessment and monitoring. *IBM J. Res. Dev.* 56 (5), 1–2. doi:10.1147/JRD.2012.2197132

Butler, J., Wildermuth, G., Thiede, B., and Brown, D. (2020). Population change and income inequality in rural America. *Popul. Res. Policy Rev.* 39, 889–911. doi:10.1007/s11113-020-09606-7

Chen, B., Liu, T., Guo, L., and Xie, Z. (2020). The disembedded digital economy: Social protection for new economy employment in China. *Soc. Policy Adm.* 54, 1246–1260. doi:10.1111/spol.12603

Chen, Y., Yang, J., Yang, R., Xiao, X., and Xia, J. (2022). Contribution of urban functional zones to the spatial distribution of urban thermal environment. *Build. Environ.* 216, 109000. doi:10.1016/j.buildenv.2022.109000

Deng, W., Cheng, Y., Yu, H., Peng, L., Kong, B., and Hou, Y. (2022). Spatio-temporal characteristics of population and economy in transitional geographic space at the southern end of "Hu Huan-yong Line". *J. Mt. Sci.* 19 (2), 350–364. doi:10.1007/s11629-021-6846-8

Ding, C., Liu, C., Zheng, C., and Li, F. (2022). Digital economy, technological innovation and high-quality economic development: Based on spatial effect and mediation effect. *Sustainability* 14, 216. doi:10.3390/su14010216

Ding, Y., Zhang, H., and Tang, S. (2021). How does the digital economy affect the domestic value-added rate of Chinese exports? *J. Glob. Inf. Manag.* 29 (5), 71–85. doi:10.4018/JGIM.20210901.oa5

Dzhandzhugazova, E., Dusenko, S., Kabelkaite-Vaitkiene, J., Morozova, M., and Avilova, N. (2018). Hotel industry in the context of Russia's emerging digital economy. *Mod. J. Lang. Teach. Methods* 8 (6), 224–232.

Henderson, F., and Xia, Z. (1997). SAR applications in human settlement detection, population estimation and urban land use pattern analysis: A status report. *IEEE Trans. Geosci. Remote Sens.* 35 (1), 79–85. doi:10.1109/36.551936

Jiang, X., Wang, X., Ren, J., and Xie, Z. (2021). The nexus between digital finance and economic development: Evidence from China. *Sustainability* 13, 7289. doi:10.3390/su13137289

Jiao, S., and Sun, Q. (2021). Digital economic development and its impact on econimic growth in China: Research based on the prespective of sustainability. *Sustainability* 13, 10245. doi:10.3390/su131810245

Kasu, B., and Chi, G. (2018). The evolving and complementary impacts of transportation infrastructures on population and employment change in the United States, 1970-2010. *Popul. Res. Policy Rev.* 37, 1003–1029. doi:10.1007/s11113-018-9491-3

Kim, J. (2006). Infrastructure of the digital economy: Some empirical findings with the case of Korea. *Technol. Forecast. Soc. Change* 73, 377–389. doi:10.1016/j.techfore.2004.09.003

Kummu, M., De Moel, H., Salvucci, G., Viviroli, D., Ward, P., and Varis, O. (2016). Over the hills and further away from coast: Global geospatial patterns of human and environment over the 20th-21st centuries. *Environ. Res. Lett.* 11, 034010. doi:10.1088/1748-9326/11/3/034010

Laskiene, D., Zykiene, I., and Verdnikovaite, P. (2020). Assessment of the impact of income inequality on population's migration. *Inzinerine Ekonomika-Engineering Econ.* 31 (5), 547–557. doi:10.5755/j01.ee.31.5.25193

Lee, J. (2009). Contesting the digital economy and culture: Digital technologies and the transformation of popular music in korea. *Inter-Asia Cult. Stud.* 10 (4), 489–506. doi:10.1080/14649370903166143

Li, B., and Cao, D. (2013). Regionalization on the suitability of human settlement environment and its relationship with population distribution based on gis—A case of human province. *J. Huazhong Normal University(Nat.Sci.).* 47 (1), 110–116. doi:10.19603/j.cnki.1000-1190.2013.01.025

Li, X., Liang, X., Yu, T., Ruan, S., and Fan, R. (2022). Research on the integration of cultural tourism industry driven by digital economy in the context of COVID-19-

based on the data of 31 Chinese provinces. *Front. Public Health* 10, Article780476. doi:10.3389/fpubh.2022.780476

Li, Y., Ding, R., Cui, L., Lei, Z., and Mou, J. (2019). The impact of sharing economy practices on sustainability performance in the Chinese construction industry. *Resour. Conserv. Recycl.* 150, 104409. doi:10.1016/j.resconrec.2019.104409

Litvinenko, V. (2020). Digital economy as a factor in the technological development of the mineral sector. *Nat. Resour. Res.* 29, 1521–1541. doi:10.1007/s11053-019-09568-4

Liu, B., Li, W., and Ma, H. (2022). The effect of educational public service on the residence willingness of urban floating population: Take taiyuan city as an example. *Econ. Problems* 4, 116–123. doi:10.16011/j.cnki.jjwt.2022.04.010

Liu, G., and Zhang, X. (2019). Research on the dynamics and mechanism of digital economy development in underdeveloped areas—take guizhou digital economy development as an example. *Econ. Rev. J.* 6, 88–100. doi:10.16528/j.cnki.22-1054/f.201906088

Liu, T., Peng, R., Zhuo, Y., and Cao, G. (2022). China's changing population distribution and influencing factors: Insights from the 2020 census data. *Acta Geogr. Sin.* 77 (2), 381–394. doi:10.11821/dlxb202202008

Liu, Y., Li, D., Yu, Z., Zhang, H., Wang, Z., and Liu, D. (2021). Multidimensional mechanism of spatial coordination between urban population and service industry: A case of fujian province. *Sci. Geogr. Sin.* 41 (8), 1354–1363. doi:10.13249/j.cnki.sgs.2021.08.006

Lu, C., Hong, W., Wang, Y., and Zhao, D. (2021). Study on the coupling coordination of urban infrastructure and population in the perspective of urban integration. *IEEE Access* 9, 124070–124086. doi:10.1109/Access.2021.3110368

Molina-Lopez, M., Koller, M., Rubio-Andres, M., and Gonzalez-Perez, S. (2021). Never too late to learn: How education helps female entrepreneurs at overcoming barriers in the digital economy. *Sustainability* 13, 11037. doi:10.3390/su131911037

Nagy, K. (2020). Assessing the digital economy: Aims, frameworks, pilots, results, and lessons. *J. Innov. Entrep.* 9, 16. doi:10.1186/s13731-020-00129-1

Nieborg, D., Young, C., and Joseph, D. (2019). Lost in the app store: The state of the Canadian game app economy. *Can. J. Commun.* 44, PP57–PP62. doi:10.22230/cjc.2019v44n2a3505

Perrons, D. (2004). Understanding social and spatial divisions in the new economy: New media clusters and the digital divide. *Econ. Geogr.* 80 (1), 45–61. doi:10.1111/j.1944-8287.2004.tb00228.x

Pozdneev, B., Levchenko, A., Ovchinnikov, P., and Sharovatov, V. (2019). Integration of the automated control systems at a manufacturing enterprise. *Russ. Engin. Res.* 39 (12), 1057–1060. doi:10.3103/S1068798X19120165

Qin, W., and Liu, X. (2022). Research on the impact of network infrastructure construction on the digital economy's development——a quasi-natural experiment of the "broadband China" pilot policy. *Inq. into Econ. Issues* 3, 15–30.

Rattso, J., and Stokke, H. (2014). Population divergence and income convergence: Regional distribution dynamics for Norway. *Reg. Stud.* 48 (11), 1884–1895. doi:10.1080/00343404.2013.799842

Ren, S., Li, L., Han, Y., Hao, Y., and Wu, H. (2022). The emerging driving force of inclusive green growth: Does digital economy agglomeration work? *Bus. Strategy Environ.* 31 (4), 1656–1678. doi:10.1002/bse.2975

Roldán, J., Álvarez, M., Carrasco, M., Guarneros, N., Ledesma, J., Cuchillo-Hilario, M., et al. (2017). Marginalization and health service coverage among indigenous, rural, and urban populations: A public health problem in Mexico. *Rural. Remote Health* 17, 3948. doi:10.22605/RRH3948

Ryszard, B., Barbara, S., Jolanta, M., Marcin, S., Agnieszka, T., and Katarzyna, Ż. (2021). Developing digital economy and society in the light of the issue of digital convergence of the markets in the European union countries. *Energies* 14, 2717. doi:10.3390/en14092717

Rytova, E., Verevka, T., Gutman, S., and Kuznetsov, S. (2020). Assessing the maturity level of saint petersburg's digital government. *IJTech.* 11 (6), 1081–1090. doi:10.14716/ijtech.v11i6.4440

Samira, B., and Alireza, N. (2011). Digital economy and tourism impacts, influences and challenges. *Procedia - Soc. Behav. Sci.* 19, 308–316. doi:10.1016/j.sbspro.2011.05.136

Schmitt, B., Henry, M., Piguet, V., and Hilal, M. (2006). Urban growth effects on rural population, export and service employment: Evidence from eastern France. *Ann. Reg. Sci.* 40, 779–801. doi:10.1007/s00168-006-0069-3

Shi, Y., Yang, J., and Shen, P. (2020). Revealing the correlation between population density and the spatial distribution of urban public service facilities with mobile phone data. *ISPRS Int. J. Geoinf.* 9, 38. doi:10.3390/ijgi9010038

Su, J., Su, K., and Wang, S. (2021). Does the digital economy promote industrial structural upgrading?—a test of mediating effects based on heterogeneous technological innovation. *Sustainability* 13, 10105. doi:10.3390/su131810105

Sui, D., and Rejeski, D. (2002). Environmental impacts of the emerging digital economy: The E-for-environment E-commerce? *Environ. Manage.* 29 (2), 155–163. doi:10.1007/s00267-001-0027-X

Sun, B., Zhang, Z., and Li, W. (2021). Characteristics and impact of population spatial structure on economic performance in China based on spatial identification of physical cities. *Sci. Geogr. Sin.* 41 (11), 1884–1896. doi:10.13249/j.cnki.sgs.2021.11.002

Sun, J., Miao, Z., and Chen, X. (2019) The impact of China's information technology gap on regional income difference economic geography. 39(12): 31–38. doi:10.15957/j.cnki.jjdl.2019.12.004

Sun, W., and Liu, Z. (2022). Digital economy, urbanization and the increase of farmers' income——an empirical analysis based on cities in the yangtze river economic belt. *Inq. into Econ. Issues* 3, 1–14.

Teisserenc, B., and Sepasgozar, S. (2021). Project data categorization, adoption factors, and non-functional requirements for blockchain based digital twins in the construction industry 4.0. *Buildings* 11, 626. doi:10.3390/buildings11120626

Tong, Y., Zhou, M., and Zhou, W. (2021). The impact of industrial structure upgrade in beijing on the changes in population size. *Labor Econ. Rev.* 2, 1–12. doi:10.19744/j.cnki.11-1235/f.2021.0156

Trofimov, O., Frolov, V., Klimova, E., Ilyicheva, N., and Kislinskaya, M. (2021). Assessment and analysis of innovative activities of high-tech industries in the digital economy based on the cluster approach. *Nexo Rev. Cient.* 34, 1344–1354. doi:10.5377/nexo.v34i04.12669

Wang, J., and Xiao, H. (2021). Has the development of digital economy narrowed the income gap between urban and rural residents? *Reform Econ. Syst.* 6, 56–61.

Wilson, C., and Mergel, I. (2022). Overcoming barriers to digital government: Mapping the strategies of digital champions. *Gov. Inf. Q.* 39, 101681. doi:10.1016/j.giq.2022.101681

Wu, X., Shi, L., Lu, X., Li, X., and Ma, L. (2022). Government dissemination of epidemic information as a policy instrument during COVID-19 pandemic: Evidence from Chinese cities. *Cities* 125, 103658. doi:10.1016/j.cities.2022.103658

Xu, W., Zhou, J., and Liu, C. (2022). The impact of digital economy on urban carbon emissions: Based on the analysis of spatial effects. *Geogr. Res.* 41 (1), 111–129. doi:10.11821/dlyj020210459

Yang, J., Jin, S., Xiao, X., Jin, C., Xia, J., Li, X., et al. (2019). Local climate zone ventilation and urban land surface temperatures: Towards a performance based and wind-sensitive planning proposal in megacities. *Sustain. Cities Soc.* 47, 101487. doi:10.1016/j.scs.2019.101487

Yang, J., Wang, Y., Xiu, C., Xiao, X., Xia, J., and Jin, C. (2020). Optimizing local climate zones to mitigate urban heat island effect in human settlements. *J. Clean. Prod.* 275, 123767. doi:10.1016/j.jclepro.2020.123767

Yang, J., Xin, J., Zhang, Y., Xiao, X., and Xia, J. (2022). Contributions of sea-land breeze and local climate zones to daytime and nighttime heat island intensity. *npj Urban Sustain.* 2, 12. doi:10.1038/s42949-022-00055-z

You, H., Yang, J., Xue, B., Xiao, X., Xia, J., Jin, C., et al. (2021). Spatial evolution of population change in Northeast China during 1992-2018. *Sci. Total Environ.* 776, 146023. doi:10.1016/j.scitotenv.2021.146023

Yu, H., Yang, J., Li, T., Jin, Y., and Sun, D. (2022b). Morphological and functional polycentric structure assessment of megacity: An integrated approach with spatial distribution and interaction. *Sustain. Cities Soc.* 80, 103800. doi:10.1016/j.scs.2022.103800

Yu, H., Yang, J., Sun, D., Li, T., and Liu, Y. (2022a). Spatial responses of ecosystem service value during the development of urban agglomerations. *Land* 11, 165. doi:10.3390/land11020165

Zhang, D., Zhang, G., and Zhou, C. (2021). Differences in accessibility of public health facilities in hierarchical municipalities and the spatial pattern characteristics of their services in doumen district, China. *Land* 10, 1249. doi:10.3390/land10111249

Zhang, D., Zhou, C., Sun, D., and Qian, Y. (2022). The influence of the spatial pattern of urban road networks on the quality of business environments: The case of dalian city. *Environ. Dev. Sustain.* 24, 9429–9446. doi:10.1007/s10668-021-01832-z

Zhang, D., Zhou, C., and Xu, W. (2020). Spatial-Temporal characteristics of primary and secondary educational resources for relocated children of migrant workers: The case of liaoning province. *Complexity* 2020, 7457109. doi:10.1155/2020/7457109

Zhang, S., Ma, X., and Cui, Q. (2021). Assessing the impact of the digital economy on green total factor energy efficiency in the post-COVID-19 era. *Front. Energy Res.* 9, 798922. doi:10.3389/fenrg.2021.798922, ,

Zhang, W., Zhao, S., Wan, X., and Yao, Y. (2021). Study on the effect of digital economy on high-quality economic development in China. *PLoS One* 16 (9), e0257365. doi:10.1371/journal.pone.0257365

Zhang, Z., Luan, W., Tian, C., Su, M., and Li, Z. (2021). Spatial distribution equilibrium and relationship between construction land expansion and basic education schools in shanghai based on POI data. *Land* 10, 1059. doi:10.3390/land10101059

Zhao, T., Zhang, Z., and Liang, S. (2020). Digital economy, entrepreneurship, and high-quality economic development: Empirical evidence from urban China. *J. Manag. World* 10, 65–75. doi:10.19744/j.cnki.11-1235/f.2020.0154

Zhao, Z., Lao, X., Gu, H., Yu, H., and Lei, P. (2021). How does air pollution affect urban settlement of the floating population in China? New evidence from a push-pull migration analysis. *BMC Public Health* 21, 1696. doi:10.1186/s12889-021-11711-x

Zhou, C., Zhang, D., and He, X. (2021). Transportation accessibility evaluation of educational institutions conducting field environmental education activities in ecological protection areas: A case study of zhuhai city. *Sustainability* 13, 9392. doi:10.3390/su13169392

Zhu, Y., and Chen, W. (2010). The settlement intention of China's floating population in the cities: Recent changes and multifaceted individual-level determinants. *Popul. Space Place* 16, 253–267. doi:10.1002/psp.544

frontiers | Frontiers in Environmental Science

TYPE Original Research
PUBLISHED 09 September 2022
DOI 10.3389/fenvs.2022.974811

Check for updates

OPEN ACCESS

EDITED BY
Christos H. Halios,
Public Health England, United Kingdom

REVIEWED BY
Decheng Zhou,
Nanjing University of Information Science and Technology, China
Miaomiao Xie,
China University of Geosciences, China

*CORRESPONDENCE
Jun Yang,
yangjun8@mail.neu.edu.cn
Ling-en Wang,
wangle@igsnrr.ac.cn
Cui Jin,
jincui@lnnu.edu.cn

SPECIALTY SECTION
This article was submitted to Environmental Informatics and Remote Sensing,
a section of the journal
Frontiers in Environmental Science

RECEIVED 21 June 2022
ACCEPTED 24 August 2022
PUBLISHED 09 September 2022

CITATION
Xin J, Yang J, Wang L-e, Jin C, Xiao X and Xia JC (2022), Seasonal differences in the dominant factors of surface urban heat islands along the urban-rural gradient.
Front. Environ. Sci. 10:974811.
doi: 10.3389/fenvs.2022.974811

COPYRIGHT
© 2022 Xin, Yang, Wang, Jin, Xiao and Xia. This is an open-access article distributed under the terms of the Creative Commons Attribution License (CC BY). The use, distribution or reproduction in other forums is permitted, provided the original author(s) and the copyright owner(s) are credited and that the original publication in this journal is cited, in accordance with accepted academic practice. No use, distribution or reproduction is permitted which does not comply with these terms.

Seasonal differences in the dominant factors of surface urban heat islands along the urban-rural gradient

Jiaxing Xin[1], Jun Yang[1,2,3]*, Ling-en Wang[4]*, Cui Jin[1]*, Xiangming Xiao[5] and Jianhong (Cecilia) Xia[6]

[1]Human Settlements Research Center, Liaoning Normal University, Dalian, China, [2]School of Humanities and Law, Northeastern University, Shenyang, China, [3]Jangho Architecture College, Northeastern University, Shenyang, China, [4]Institute of Geographic Sciences and Natural Resources Research, Chinese Academy of Sciences, Beijing, China, [5]Department of Microbiology and Plant Biology, Center for Earth Observation and Modeling, University of Oklahoma, Norman, OK, United States, [6]School of Earth and Planetary Sciences (EPS), Curtin University, Perth, WA, Australia

Urbanization has been accelerating; hence the effect of urban heat island (UHI) has increased. There has been extensive research on spatiotemporal UHI changes and drivers, however, data on the dominant seasonal factors of UHIs and the differences along urban-rural gradients remain limited. Based on Luojia-1A, Landsat 8, and moderate resolution imaging spectroradiometer (MODIS) data, we assessed the seasonal differences in surface UHI (SUHI), normalized differences in vegetation index (NDVI), built-up index (NDBI), and water index (NDWI) and their relationships in the Dalian City, Northeast China. We found that in the urban built-up area, the mean SUHI intensity (SUHII) decreased from that in summer (2.74°C) > autumn (1.65°C) > winter (0.28°C) > spring (−0.79°C). SUHII was more strongly affected by NDWI and NDBI than NDVI, and NDBI and NDWI showed positive and negative correlations with SUHII in different seasons, while NDVI and SUHII were positively correlated in spring and negatively correlated in the other seasons. When analyzing the dominant factors of SUHII, the importance results showed that, in spring, NDBI > NDVI > NDWI, in autumn, NDVI > NDWI > NDBI, in summer and winter, NDWI > NDVI > NDBI. In addition, SUHII changed the most in summer along the urban-rural gradient, decreasing from 2.74°C to −2.74°C. Among these indicators, except for spring NDVI which increased from 0.09 to 0.59 with distance from built-up areas, there was minimal change in NDVI, NDBI, and NDWI along the urban-rural gradient in other seasons (i.e., all were within 0.2). In this study, the difference analysis of SUHI and remote sensing indices along the urban-rural gradient can help to facilitate the rational layout of cities.

KEYWORDS

surface urban heat island, urban-rural gradient, normalized difference vegetation index, normalized difference build-up index, normalized difference water body index, dalian city

Introduction

Under rapid global urbanization, the population has shown a surging trend accompanied with the expansion of urban areas, thereby causing a series of ecological environment and climate problems such as urban heat islands (UHIs), extreme climate and heat waves (Manoli et al., 2019; Wang et al., 2021a; Ma et al., 2021b; Smith et al., 2021; Koç et al., 2022; Shi et al., 2022), severely threating human life, health, and safety (Chang et al., 2021; Yao et al., 2021; Yang et al., 2022). UHI refers to a phenomenon whereby the temperature in the suburbs is lower than that in the city center, and has been extensively studied (Wu et al., 2017; Yang et al., 2021b). UHI includes two categories: atmospheric UHI (AUHI) (Tran et al., 2006) and surface UHI (SUHI) (Imhoff et al., 2010; Peng et al., 2012). AUHI is obtained through observation of meteorological stations, whereas SUHI is mainly obtained through remote sensing images obtained *via* satellite sensors (Zhou et al., 2014a). Compared with the AUHI, SUHI is widely used due to its advantages of easy data acquisition and spatial continuity (Kim and Brown, 2021).

A key in SUHI research is the calculation of land surface temperature (LST). At present, the LST calculations are mainly obtained by inversion of the thermal infrared band of satellites; common data sources include Landsat (Yang et al., 2021c; Kamali Maskooni et al., 2021; Najafzadeh et al., 2021; Carrillo-Niquete et al., 2022) and moderate resolution imaging spectroradiometer (MODIS) (Li et al., 2020; Mohammad and Goswami, 2021a; Niu et al., 2021). The lower resolution of MODIS data is more suitable for mesoscale research, whereas the resolution of Landsat data is 30 m, more suitable for urban scale research. Therefore, this study calculated LST based on Landsat 8 data. SUHI intensity (SUHII) refers to the temperature difference between urban and rural areas, and the definition of urban-rural boundaries is the key to SUHI research. At present, there is no unified standard for the definition of the urban-rural boundary, hence new SUHII calculation methods are constantly being proposed of which the most commonly used are the urban-rural dichotomy, mean—standard deviation, positive planning, and normalization methods (Shastri et al., 2017; Liu et al., 2021b; Hsu et al., 2021; Morabito et al., 2021). When calculating SUHII using the urban-rural dichotomy, urban area mainly refers to the area covered by actual urban construction land. The built-up area extraction methods are roughly divided into three types: One is to extract built-up areas by classifying the spectral features of high-resolution satellite images; the second is to use night light data as the data source to obtain the best threshold through a series of methods and extract the built-up area by binarization according to the threshold; the third is to combine night light and high-resolution remote sensing data to extract built-up areas. The most widely used data source is night light data, from which the best threshold is obtained, following which the urban built-up area is then extracted. Night light data are mainly Defense Meteorological Satellite Program/Operational Linescan System DMSP/OLS and National Polar-orbiting Partnership/Visible Infrared Imaging Radiometer NPP-VIIRS (Zhou et al., 2014b; Yang et al., 2021a; Li et al., 2021); however, their spatial resolutions are low, i.e., 1,000 m and 500 m, respectively. The Luojia-1 satellite (Luojia-1A) launched by China in 2018 has efficiently addressed this problem (Jun et al., 2021), where its spatial resolution reaches 130 m; therefore, this study extracted built-up areas based on the Luojia-1A satellite. However, the definition of suburban backgrounds remains controversial. Most scholars have obtained suburbs by establishing buffer zones with built-up areas as boundaries. The buffer zone can be the same area or 150% of the urban area calculated according to the size of the city (Peng et al., 2012; Meng et al., 2018; Feng et al., 2021), and can be a buffer distance of approximately 0–25 km from the urban built-up area (Dewan et al., 2021; Yao et al., 2021; Li et al., 2022). In the selection of the suburban background, this study referred to the definition method based on the buffer zone of Yao et al. (2021), Yao et al. (2018), and Li et al. (2022), by establishing a buffer zone with the built-up area as the boundary to determine the suburban background. Due to the unique shape of the administrative boundary of the Dalian City, in this study, we selected the 10-km range as the suburb.

In SUHI research, in addition to the spatiotemporal evolution of SUHI, research on the influencing factors has been the primary focus of several studies (Wang et al., 2021b; Erdem et al., 2021; Niu et al., 2021; Zhang et al., 2021; Ren et al., 2022). Blue-green space, building roof materials, building density, building height, vegetation coverage, and urban ventilation are all driving factors of SUHI (Guo et al., 2020; Yang et al., 2020; Hu et al., 2021b; Deliry et al., 2021; Luo et al., 2021; Ma and Peng, 2022). The research angle is divided into several aspects, such as land-use type, surface biophysical conditions, landscape pattern, human activities, meteorological conditions and geographical location, and policy elements. In addition, there may be differences in the dominance of SUHI by different influencing factors in different seasons. For example, Mohammad and Goswami (2021a) quantified the daily, seasonal, and inter-annual SUHII of 150 major Indian cities located in different climate zones based on MODIS data. The study found differences in SUHI, in addition to the leading roles of different influencing factors in winter and summer. However, studies have been conducted on the dominant drivers of seasonal SUHI, which showed differences in different gradients between urban and rural areas (Ma et al., 2021a; Mohammad and Goswami, 2021b; Ma and Peng, 2022), but this has received little attention. Therefore, this study not only assessed the seasonal differences of SUHII and its dominant factors, but also analyzed the differences of the dominant factors of SUHII along the urban-rural gradient.

We considered the Dalian City, Northeast China, as a case study and extracted urban built-up areas based on Landsat 8, digital elevation model (DEM), Luojia-1A night light, and other data. We established a buffer zone within 10 km outside the built-up area (defined as suburbs), and calculated SUHII, normalized differences in vegetation index (NDVI), built-up index (NDBI), and water index (NDWI), and the difference in SUHI, NDVI,

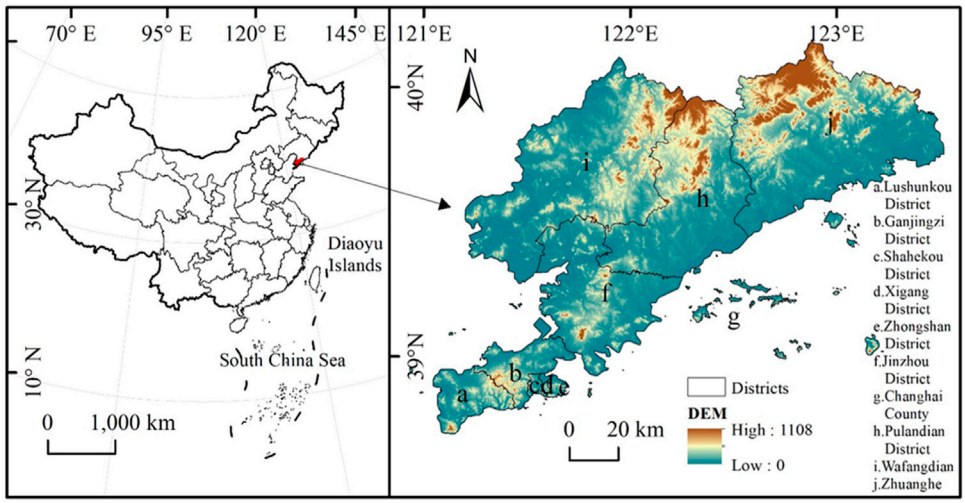

FIGURE 1
Study area location. DEM—digital elevation model.

NDBI, and NDWI along –the urban-rural gradient. Meanwhile, we analyzed the differences in SUHII by the dominant factors in different seasons. This study investigated the seasonal differences in SUHI and various remote sensing indices and the dominant factors of SUHI. The differences in SUHI along the urban-rural gradient were also studied, which provides an important reference for SUHI mitigation strategies and rational urban layout.

Materials and methods

Study area

The Dalian City is located in the southern area of the Liaodong Peninsula, Northeast China, between 38°43′–40°12′N and 120°58′–123°31′E, and has jurisdiction over seven municipal districts and one county and manages two county-level cities. The terrain is high and wide in the north, and low and narrow in the south (Figure 1). The total land area of the city is approximately 12,574 km^2, of which the urban area is approximately 2,414.96 km^2, and the counties (cities) under its jurisdiction cover an area of approximately 10,158.89 km^2.

Data sources

The data used in this study included Landsat eight OLI/TIRS, Luojia-1A night light, statistical yearbook, MODIS, and administrative division data. Table 1 lists data sources, preprocessing process, and detailed descriptions.

Remote sensing indices

Development of urbanization leads to the conversion of a large amount of natural land to anthropogenic land, thereby changing urban surface cover, such as reductions in vegetation and increases in urban impervious surfaces, thus changes urban surface heat absorption, ultimately leadings to the UHI effect. To study the seasonal variation of SUHI and its relationship with vegetation cover, water body, bare soil, and impervious surfaces (Koko et al., 2021), we used NDVI, NDBI, and NDWI, the specific calculation formulas for which are as follows:

$$NDVI = \frac{NIR - Red}{NIR + Red} \quad (1)$$

$$NDWI = \frac{NIR - SWIR}{NIR + SWIR} \quad (2)$$

$$NDBI = \frac{SWIR - NIR}{SWIR + NIR} \quad (3)$$

Where, NIR, Red, and SWIR represent the near-infrared band, the red band, and the mid-infrared band, respectively, corresponding to the fourth, fifth, and sixth bands of the Landsat eight OLI data, respectively.

land surface temperature retrieval

The better the quality of remote sensing images, the higher the accuracy of LST inversion results. Therefore, in this study, images with minimal precipitation, sunny and minimal cloudy (<5% cloud cover) weather were selected in the corresponding time range. We then referred to the single-window algorithm

TABLE 1 Data sources and descriptions.

Data type	Data	Time/Year	Resolution	Sources	Data processing
Remote sensing image	Landsat 8 OLI/TIRS	2018 (Acquisition time: Spring: 2018/4/19 and 2018/4/28. Summer: 2018/8/2 and 2018/8/9. Autumn: 2018/9/10 & 2018/10/5. Winter: 2018/1/6 and 2018/1/13)	30 m (Multispectral) 100 m (Thermal)	https://earthexplorer.usgs.gov/	Radiometric calibration, atmospheric correction
Nightlight	Luojia-1A	2018 (Acquisition time: 2018/9/9)	130 m	http://59.175.109.173:8,888/index.html	Radiance conversion
China City Statistical Yearbook	Urban built-up area	2018	—	National Bureau of Statistics of China	—
Land surface temperature	MOD11B3	2018	—	https://ladsweb.modaps.eosdis.nasa.gov/search/	Projection and format conversion
Administrative divisions	—	2021	—	National Catalogue Service for Geographic Information	Extract administrative divisions

proposed by Qin et al. (2001), and to Hu et al. (2015) to calculate LST using Landsat eight band10 data, the formulas are as follows:

$$T_s = (a(1 - C - D) + (b(1 - C - D) + C + D)T_{10} - DT_a) \times / (C - 273.15) \quad (4)$$

$$C = \varepsilon\tau \quad (5)$$

$$D = (1 - \tau)[1 + (1 - \varepsilon)\tau] \quad (6)$$

Where,T_s is LST (K); T_{10} is the brightness temperature (K); T_a is the average temperature of the atmosphere (K); a and b are reference coefficients (a =−67.355,351 and b = 0.458,606 when LST is in the range from 0 to 70°C); ε is the land surface emissivity ofT_{10}; τ is the atmospheric transmittance of T_{10}. Finally, the LST inversion results were clipped based on the extraction tool by mask of ArcGIS, taking the administrative boundary of Dalian City as the boundary.

Surface urban heat island

The LST difference between the urban and rural is defined as the SUHII (Zhao et al., 2021), Urban areas were obtained based on night light data, while rural areas were obtained after buffer zones for urban areas have been established.

In researching the extraction of built-up areas, the determination of the optimal threshold for nighttime light data has been challenging. Various methods have been proposed such as mutation detection, empirical threshold, and higher-resolution data comparison methods (Jun et al., 2021; Zhang et al., 2022), each of which has its own limitations. The mutation detection method does not consider the regional differences in urban development; the empirical threshold and higher-resolution data comparison methods are highly subjective and the results obtained by different studies often differ. To this end, this study referred to the extraction method of Liu et al. (2021c), combined the brightness and texture information of night lights to perform object-oriented segmentation, and comprehensively extracted the built-up area.

First, we performed object-oriented multi-scale segmentation on the night light data after reprojection and resampling. On the premise of ensuring the minimum mean heterogeneity between objects and the maximum homogeneity between pixels within the object, image segmentation was performed based on the region merging technology using the brightness and texture features of the image. We then calculated the mean brightness value and area of each object following segmentation. Zhou et al. (2014b) comprehensively considered and verified the influence of the area and mean brightness of different areas on the extraction threshold of built-up areas during their study on the extraction of built-up areas from night light data. We used the area and mean brightness of different objects to construct the built-up area index X of night lights as a standard to measure the probability of each object being a built-up area. The formula for X is:

$$X = \text{Area}^{0.2} * NTL_{\text{mean}} \quad (7)$$

Where, Area is the area size of each object and NTL_{mean} refers the mean value of night light brightness of each object. We sorted the X value of each object and accumulated and summed the area of each object according to the X value from large to small until it was the closest to the total built-up area (henceforth UA) in the same period in the statistical data of the region, which was derived from the China City Statistical Yearbook. The specific conditions are as shown in Eq. 2:

$$\left|UA - \sum_{i-1}^{\max} X_i\right| \geq \left|UA - \sum_{i}^{\max} X_i\right| \leq \left|UA - \sum_{i+1}^{\max} X_i\right| \quad (8)$$

Where, the X value X_i of object i was used as the threshold value T for extracting the built-up area from night light data, and objects with X value > T were extracted as built-up areas. The built-up area extraction results can reflect the approximate range and overall shape of the built-up area distribution.

We consulted relevant literature and found that the accuracy verification of built-up area extraction is mainly through the method of creating random points, based on the Google Earth high-definition map combined with visual interpretation to determine the proportion of valid points (correct division) (He et al., 2021). Therefore, we adopted ArcGIS Create Random Point Tool, created 200 random points, counted the number of valid points, and calculated the proportion of valid points as the overall accuracy.

We also considered 10 km outside the built-up area as the suburban boundary, combined with the unique geographical location of Dalian City and the LST results obtained from Landsat eight data inversion, and used the ArcGIS 10.4 raster calculator tool to determine the difference between the LST of the study area and the mean LST of the suburbs to obtain SUHII. The calculation formula is as follows:

$$SUHII = T_{urban} - Mean\,T_{rural} \tag{9}$$

Where, T represents the LST value of each pixel in the study area, and $Mean\,T_{rural}$ is the mean LST value in the rural.

In this study, a multi-level buffer zone was established with the urban area as the boundary (Implemented with Multiple Ring Buffers tool of ArcGIS), and a total of 10 multi-level buffer zones were established as the urban-rural gradient with an interval of 1 km, which was how we calculated the urban-rural gradient.

Correlation analysis

Bivariate correlation analysis involves two or more variables. Since the data here do not obey the normal distribution, we used SPSS 24.0 software to select the Spearman correlation coefficient to study the responses of SUHII to various remote sensing indices. The calculation formula is as follows:

$$r_s = 1 - \frac{6\sum d_i^2}{N(N^2 - 1)} \tag{10}$$

Where, $d_i = X_i^{'} - Y_i^{'}$ is the difference between each pair of the ranked variables and N is the total number of the samples.

To further analyze the importance of each influencing factor of SUHII, we used the Random Tree model in IBM SPSS Modeler 18.0 software for modeling (Joloudari et al., 2020; Nhu et al., 2020), using default parameters for modeling, taking SUHII as the target value, and obtained the importance of predictor variables of NDVI, NDBI, and NDWI.

Results

Built-up area extraction

We calculated the built-up area extracted from the night light data and compared it with the statistical yearbook. Since the total calculated area of the built-up area was infinite approximation to built-up area values recorded in statistical yearbook when the light threshold was set for the extraction of the built-up area, the mean deviation and the standard deviation were 0.0054 and 0.0076, respectively. In order to verify the accuracy of the spatial distribution, we adopted ArcGIS Create Random Point Tool, created 200 random points, using Google Earth historical image, we found that 186 random points were correctly classified, and the overall accuracy reached 0.93. The visualization of the extraction results of built-up areas through ArcGIS is shown in Figure 2. Built-up areas were mainly gathered in the Zhongshan, Xigang, Shahekou, Ganjingzi, and Jinzhou districts, and they were less distributed in the Lushunkou District, Pulandian District, Wafangdian City, and Zhuanghe City.

Seasonal variations of surface urban heat island

In this study, the LST inversion results were verified before calculation of SUHII. Due to the lack of public weather station data in Dalian City, we referred to Arabi Aliabad et al. (2021) and Jiang and Lin. (2021) using MODIS data for verification. Since this study investigated seasonal differences, we selected the monthly mean LST data (MOD11B3) and 1,000 random points through ArcGIS software (MOD11B3 was resampled to 30 m), tested the LST results of the Landsat thermal infrared inversion after the α = 0.05 level of confidence test, and calculated the mean deviation (bias), standard deviation (STD), and root mean square error (RMSE). The spring LST inversion results were the best, with bias, STD, and RMSE all ~2°C (Table 2). Except for the RMSE = 9.35°C in autumn, the other results were all around 5°C.Therefore, SUHII was calculated using the LST value obtained by inversion, and as shown in Figure 3 and Table 3. Overall (the entire study area), the mean SUHII decreased from that in spring (1.41°C) > winter (0.13°C) > autumn (−0.80°C) > summer (−1.54°C). However, within the urban built-up area, the mean SUHII decreased from that in summer (2.74°C) > autumn (1.65°C) > winter (0.28°C) > spring (−0.79°C). Overall, the maximum SUHII value decreased from that in autumn (25.34°C) > summer (19.64°C) > winter (17.59°C) > spring (15.26°C); whereas, the minimum value decreased from that in winter (−20.52°C) > summer (−22.37°C) > spring (−23.73°C) > autumn (−25.31°C). In the built-up area, the maximum SUHII value decreased from that in autumn (25.34°C) > summer (18.95°C) > spring (10.27°C) > winter (9.77°C); the minimum value decreased from that in winter (−9.25°C) > autumn (−10.63°C) > summer (−16.24°C) > spring (−19.73°C).

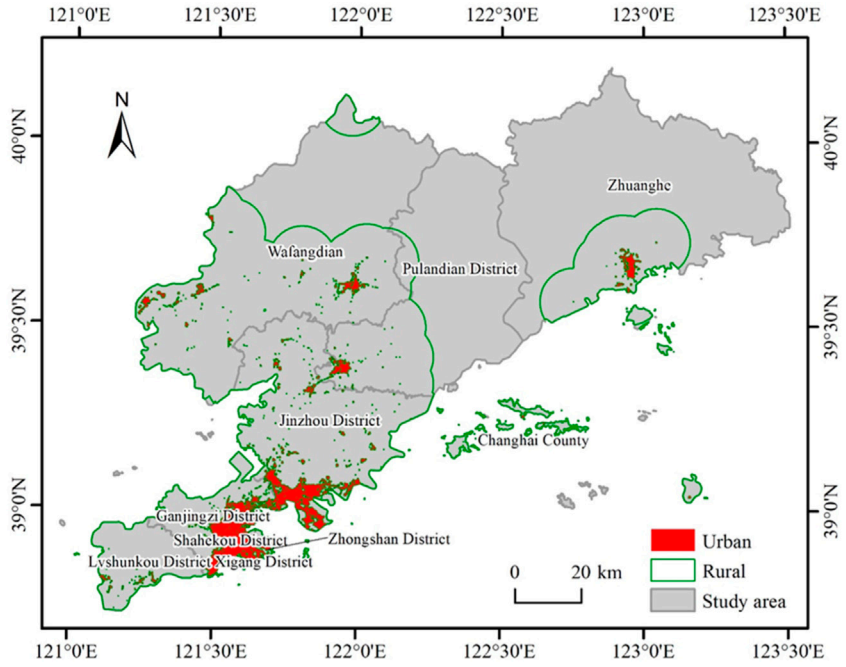

FIGURE 2
Extraction result of built-up area.

TABLE 2 Comparison of LST accuracy with α = 0.05 level confidence test (°C).

	spring	Summer	Autumn	Winter
Bias	1.70	3.17	5.10	3.80
STD	2.090	4.81	6.55	4.48
RMSE	2.57	6.04	9.35	7.04

Seasonal responses of surface urban heat island to different drivers.

Table 4 shows that, overall, NDBI and SUHII positively correlated with NDWI, while SUHII showed negative correlations in all four seasons, whereas NDVI showed positive correlation in spring but negative correlations in summer, autumn and winter. Buildings enhanced UHI and water weakened UHI, whereas vegetation enhanced UHI in spring and weakened UHI in summer, autumn and winter. Specifically, in spring, the correlation coefficients of NDVI, NDBI, NDWI, and SUHII were 0.42, 0.43, and −0.60, respectively, indicating that in spring, SUHII was more affected by water, followed by buildings and vegetation. In summer, the correlation coefficients of NDVI, NDBI, NDWI, and SUHII were −0.18, 0.44, and −0.56, respectively, indicating that in summer, SUHII was also more affected by water, followed by buildings, and that vegetation had the smallest effect. In autumn, the correlation coefficients of NDVI, NDBI, NDWI, and SUHII were −0.25, 0.59, and −0.59, respectively, indicating that in autumn, SUHII was more affected by water and buildings, and less affected by vegetation. In winter, the correlation coefficients of NDVI, NDBI, NDWI, and SUHII were −0.02, 0.33, and −0.33, respectively, indicating that in winter, SUHII was also more affected by water and buildings, and less by vegetation.

The importance of each predictor variable is shown in Figure 4. In spring, the contribution of NDBI was the largest, followed by NDVI, and the smallest was NDWI; while in summer and winter, the contribution of NDWI was the largest, followed by NDVI; in autumn, NDVI contributed the most, followed by NDWI.

Variation trends of SUHII, NDVI, NDBI, and NDWI along the urban-rural gradient in different seasons.

The mean SUHI, NDVI, NDBI, and NDWI outside the built-up area 0–10 km range (1 km interval, The distance map from the built-up area was shown in Figure 5) were calculated separately *via* ArcGIS; the results are shown in Figure 6. SUHII decreased along the urban-rural gradient in summer and autumn. The change was the largest in summer (2.74 to −2.74°C) and that in spring was relatively small (−1 to 1°C); whereas, in winter, along the urban-rural gradient, SUHII showed a trend of first decreasing and then increasing, with an overall increase of 0.50°C. When far from the built-up area, NDVI showed an increasing trend in spring,

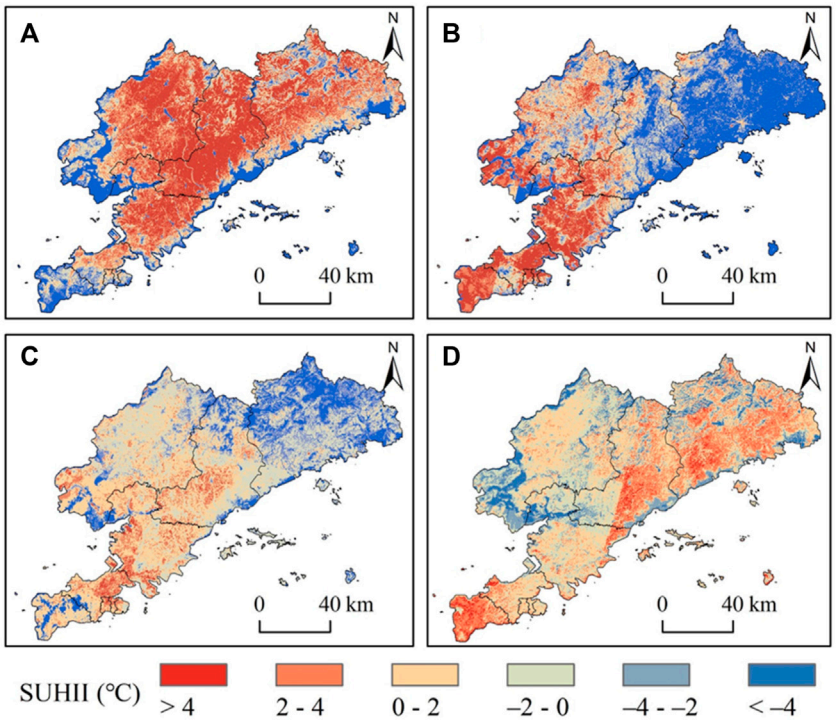

FIGURE 3
Surface urban heat island (SUHII) intensity spatial distribution map in: **(A)** spring, **(B)** summer, **(C)** autumn, and **(D)** winter.

TABLE 3 SUHII varies in different seasons.

SUHII (°C)	spring			Summer			Autumn			Winter		
	Mean	Max	Min	Mean	Max	Min	Mean	Max	Min	Mean	Max	Min
All	1.41	15.26	−23.73	−1.54	19.64	−22.37	−0.80	25.34	−25.31	0.13	17.59	−17.09
Urban	−1.77	10.27	−19.73	2.74	18.95	−16.24	1.65	25.34	−10.63	0.28	9.77	−9.25

TABLE 4 Correlation between NDVI, NDBI, NDWI, and SUHII in different seasons.

	Spearman's correlation coefficient			
	Season	NDVI	NDBI	NDWI
SUHII	Spring	0.42*	0.43*	−0.60*
	Summer	−0.18*	0.44*	−0.56*
	Autumn	−0.25**	0.59*	−0.59*
	Winter	−0.02	0.33*	−0.33*

*The correlation is significant at the 0.01 level (two-tailed).
**The correlation is significant at the 0.05 level (two-tailed).

summer, and autumn (0.09–0.59, 0.32 to 0.59, and 0.29 to 0.44, respectively), and decreased in winter, with a small decrease from 0.24 to 0.20. When far from the built-up area, NDBI showed an increasing trend in winter, while NDBI in summer showed a decreasing trend along the urban-rural gradient, but the variation range was not large (around 0.1), and there was minimal change in NDBI along the urban-rural gradient in spring and autumn. For NDWI, there was little change in spring and autumn, a large change in summer (an increase from 0.12 to 0.26 along the urban-rural gradient), and the change in winter was relatively small and decreased when far from the built-up area (from 0.09 to −0.05).

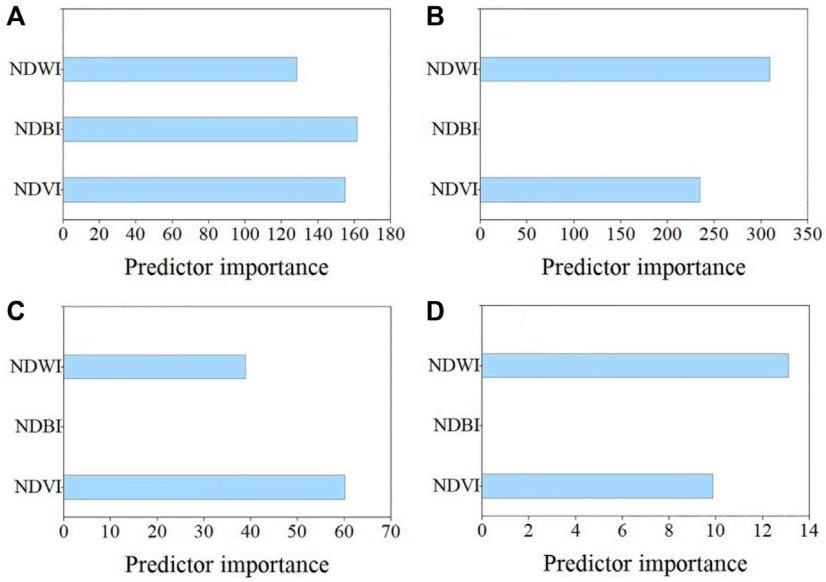

FIGURE 4
The importance of each predictor variable in: **(A)** spring, **(B)** summer, **(C)** autumn, and **(D)** winter. The predictor values refers to the importance and contribution of NDVI, NDBI, and NDWI.

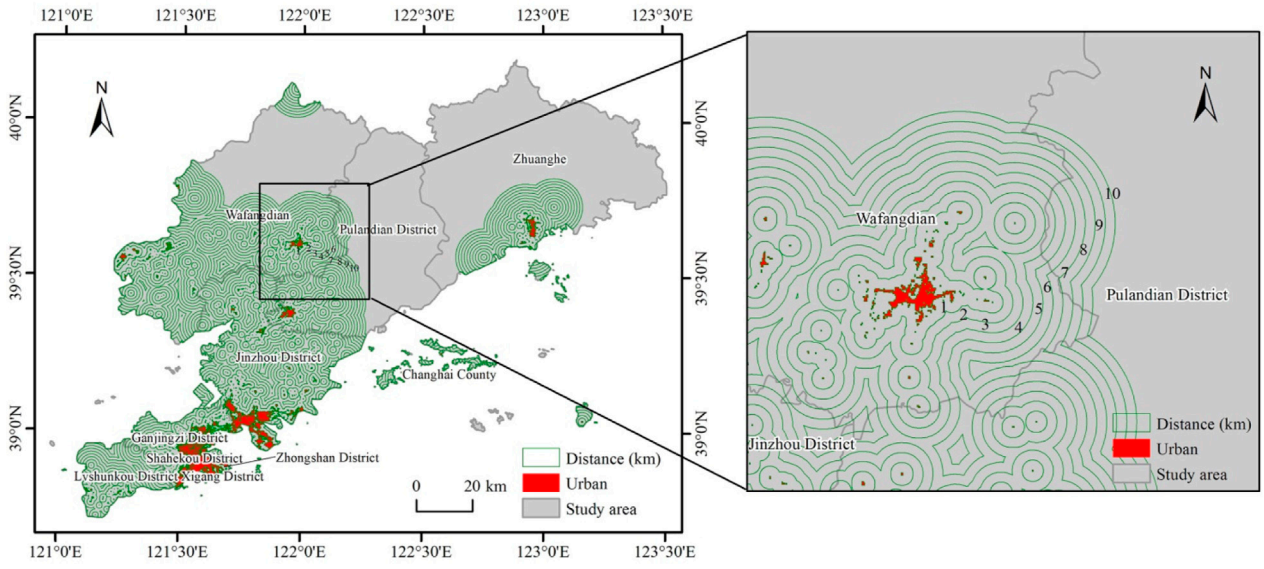

FIGURE 5
Buffer map of distance from built-up area. Distance represents that from the built-up area, in km.

To further study the changes of SUHII, NDVI, NDBI, and NDWI along the urban-rural gradient, we calculated ΔSUHII, ΔNDVI, ΔNDBI, and ΔNDWI (The mean SUHII, NDVI, NDBI, and NDWI in built-up area minus the mean SUHII, NDVI, NDBI, and NDWI values of different urban-rural gradient zones), the change values of SUHII, NDVI, NDBI, and NDWI, and the relationship between ΔSUHII, ΔNDVI, ΔNDBI, and ΔNDWI with the urban-rural gradient (Figure 7). The results showed that for ΔSUHII, in summer and autumn, ΔSUHII is positively correlated with the urban-

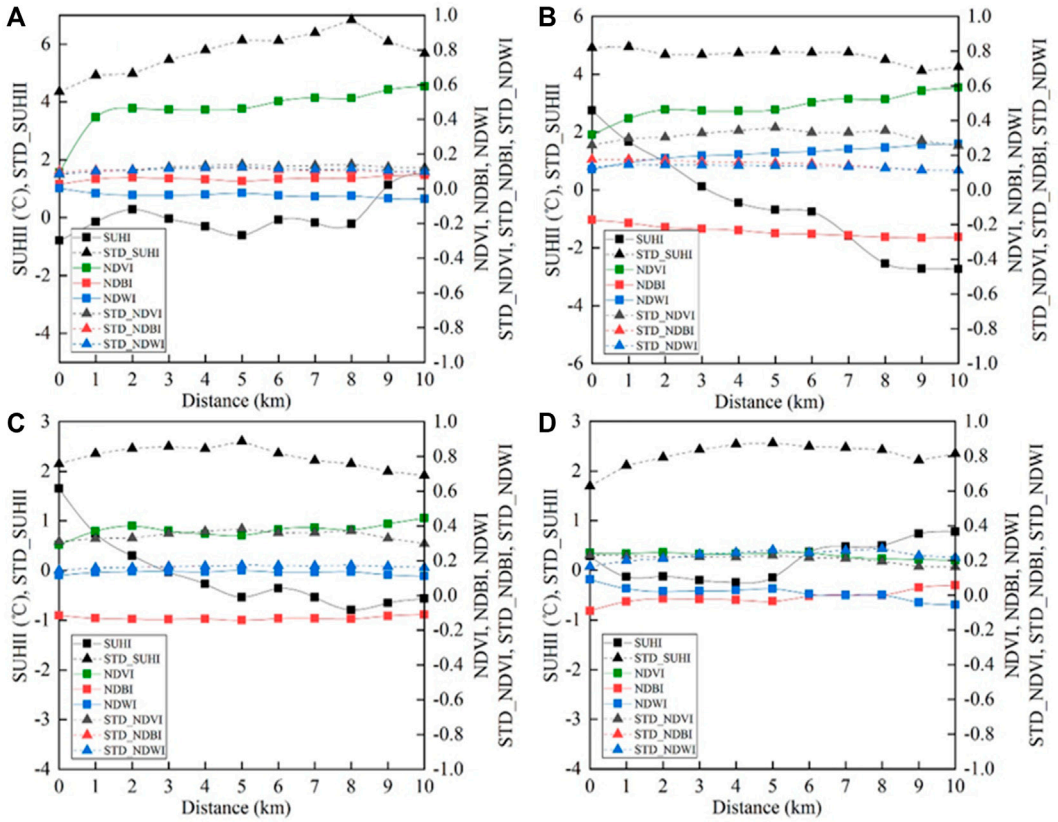

FIGURE 6
Variations of surface urban heat island (SUHII), normalized difference vegetation index (NDVI), normalized difference built-up index (NDBI), and normalized difference water index (NDWI) along the urban-rural gradient in: **(A)** spring, **(B)** summer, **(C)** autumn, and **(D)** winter. Distance represents that from the built-up area, in km.

rural gradient, with correlation coefficients of 0.498 and 0.139, respectively, indicating that the greater the distance from the built-up area, the greater the ΔSUHII, while in spring and winter, ΔSUHII was negatively correlated with the urban-rural gradient, with correlation coefficients of −0.128 and −0.124, respectively, indicating that the greater the distance from the built-up area, the smaller the ΔSUHII. For ΔNDVI, in spring, summer and autumn, ΔNDVI was negatively correlated with the urban-rural gradient, with correlation coefficients of−0.018, −0.080, and −0.006, respectively, indicating that the greater the distance from the built-up area, the smaller the ΔNDVI, but the change trend was not large, while in winter, there was a positive correlation between ΔNDVI and the urban-rural gradient, and the correlation coefficient was 0.005, which also showed that the variation trend of ΔNDVI along the urban-rural gradient was small. For ΔNDBI, in spring, autumn and winter, ΔNDBI had a negative correlation with the urban-rural gradient, and the correlation coefficients were all very small, which were −0.001, −0.002, and −0.009, respectively, while in winter, there was a positive correlation between ΔNDBI and the urban-rural gradient, with correlation coefficient of 0.023, indicating that the variation of ΔNDBI along the urban-rural gradient was still small. For ΔNDWI, in spring, autumn and winter, ΔNDWI had a positive correlation with the urban-rural gradient, and the correlation coefficient was very small, 0.003, 0.002, and 0.009, respectively, while in summer, ΔNDWI was negatively correlated with the urban-rural gradient, and the correlation coefficient was −0.038, indicating that ΔNDWI also changed little along the urban-rural gradient.

Discussion

Urban built-up area extraction

At present, most night light data selected for the extraction of built-up areas are DMSP/OLS and NPP-VIIRS (Yu et al., 2021; Zheng et al., 2021), which have low spatial resolution. However, the Luojia-1A data used in this study had a spatial resolution of 130 m, and studies have showed that Luojia-1A data was more

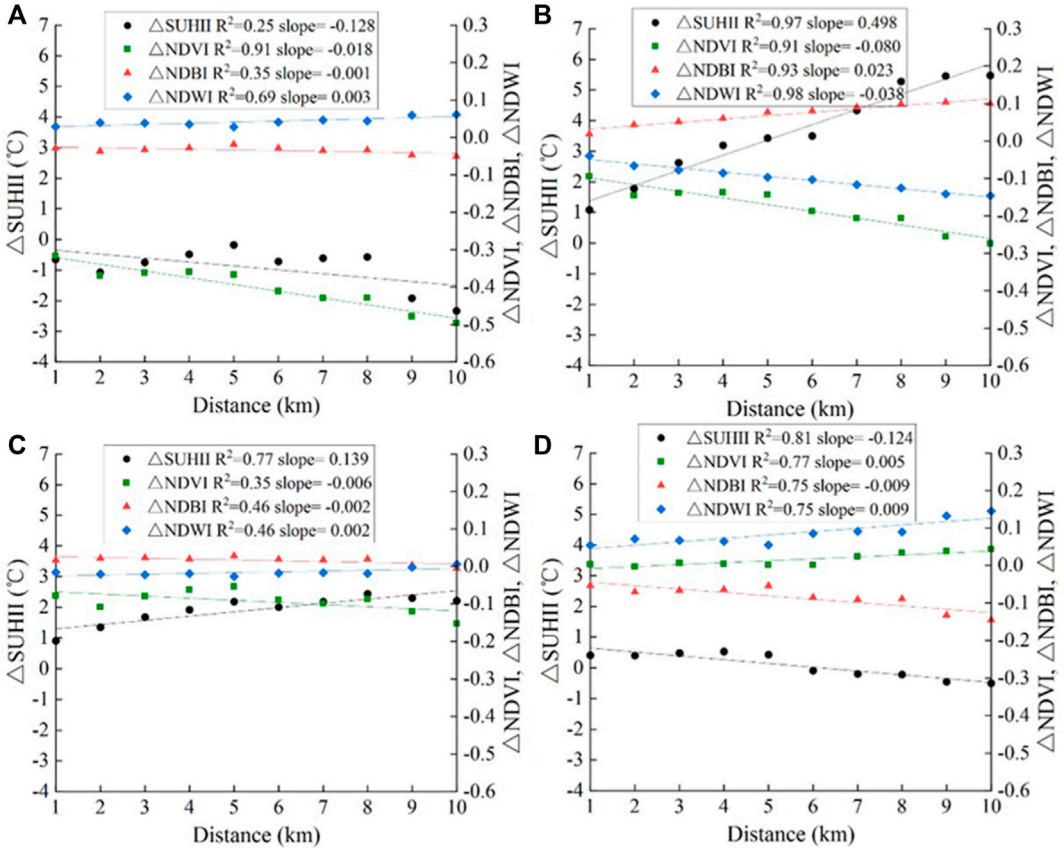

FIGURE 7
Correlation between ΔSUHII, ΔNDVI, ΔNDBI, and ΔNDWI, and the distance from the built-up area in: **(A)** spring, **(B)** summer, **(C)** autumn, and **(D)** winter. Distance represents that from the built-up area, in km.

sensitive in detecting new emerging urban built-up areas, which can better reflect the spatial structure of urban system and achieve a higher extraction accuracy (Li et al., 2018; Hu et al., 2021b; Wang and Shen, 2021). In addition, this study adopted an object-oriented segmentation method for determining the optimal threshold. Comparing the built-up area data in the statistical yearbook, the mean deviation and standard deviation of the two were 0.0054 and 0.0076, respectively, which greatly improved the accuracy of the built-up area extraction.

Correlations between surface urban heat island and normalized differences in vegetation index, built-up index, and normalized differences in water index

Recently, the UHI effect has attracted much attention with the acceleration of urbanization. With the continuous improvement of remote sensing technology, many scholars have begun to explore the spatiotemporal changes, impact mechanisms, and mitigation strategies of SUHI (Cosgrove and Berkelhammer, 2018; Zhang, 2020;Liu et al., 2021a; Schwaab et al., 2021). To explore the relationship between SUHI and vegetation, water, bare soil, and impervious surface, three indices (NDVI, NDBI, and NDWI) were selected to analyze the seasonal differences in SUHII and the relationships among them. To further study the differences of dominant role of SUHII along the urban-rural gradient, this study used ArcGIS software to create fishnet (the rectangular cells) of 300 m, intersected the fishnet with the urban-rural gradient, and counted the values of SUHII, NDVI, NDBI, and NDWI corresponding to each fishnet, Finally, each fishnet was selected according to the urban-rural gradient, and the correlation between SUHII and NDVI, NDBI, and NDWI was calculated by SPSS 24.0 software. The correlations between SUHII and NDVI, NDBI, and NDWI at different distances were shown in Table 5. Overall, the correlations between NDBI, NDWI, and SUHII were significant, and NDBI and SUHII showed a positive correlation regardless of

TABLE 5 The correlation between SUHII and NDVI, NDBI, and NDWI on the urban-rural gradient in different seasons.

	Distance (km)	Season	Spearman's correlation coefficient		
			NDVI	NDBI	NDWI
SUHII	0	Spring	.26*	49**	−55**
		Summer	−26**	57**	−63**
		Autumn	−30**	66**	−66**
		Winter	06**	05**	−05**
	1	Spring	42**	52**	−63**
		Summer	−.06**	45**	−50**
		Autumn	−04**	58**	−58**
		Winter	15**	02**	−02**
	2	Spring	54**	59**	−69**
		Summer	01	50**	−50**
		Autumn	04*	62**	−62**
		Winter	12**	20**	−20**
	3	SSpring	51**	56**	−66**
		Summer	−10**	49**	−52**
		Autumn	−01	60**	−60**
		Winter	04**	37**	−37**
	4	Spring	45**	59**	−62**
		Summer	−06*	47**	−45**
		Autumn	03	63**	−63**
		Winter	−02**	46**	−46**
	5	Spring	46**	62**	−66**
		Summer	05	53**	−45**
		Autumn	05	67**	−67**
		Winter	−03**	43**	−43**
	6	Spring	44**	60**	−60**
		Summer	−08*	51**	−46**
		Autumn	37**	28**	−28**
		Winter	04	68**	−68**
	7	Spring	29**	46**	−46**
		Summer	−14*	48**	−52**
		Autumn	−13**	72**	−72**
		Winter	01	39**	−39**
	8	Spring	39**	38**	−42**
		Summer	−4**	47**	−60**
		Autumn	−22**	63**	−63**
		Winter	−01	50**	−50**
	9	Spring	46**	39**	−43**
		Summer	−12	37**	−61**
		Autumn	−11	64**	−64**
		Winter	−13**	57**	−57**
	10	Spring	−27	53*	−86**
		Summer	−62**	08	−80**
		Autumn	−46*	61**	−61**
		Winter	−14**	58**	−58**

*The correlation is significant at the 0.05 level (two-tailed).

**The correlation is significant at the 0.01 level (two-tailed).

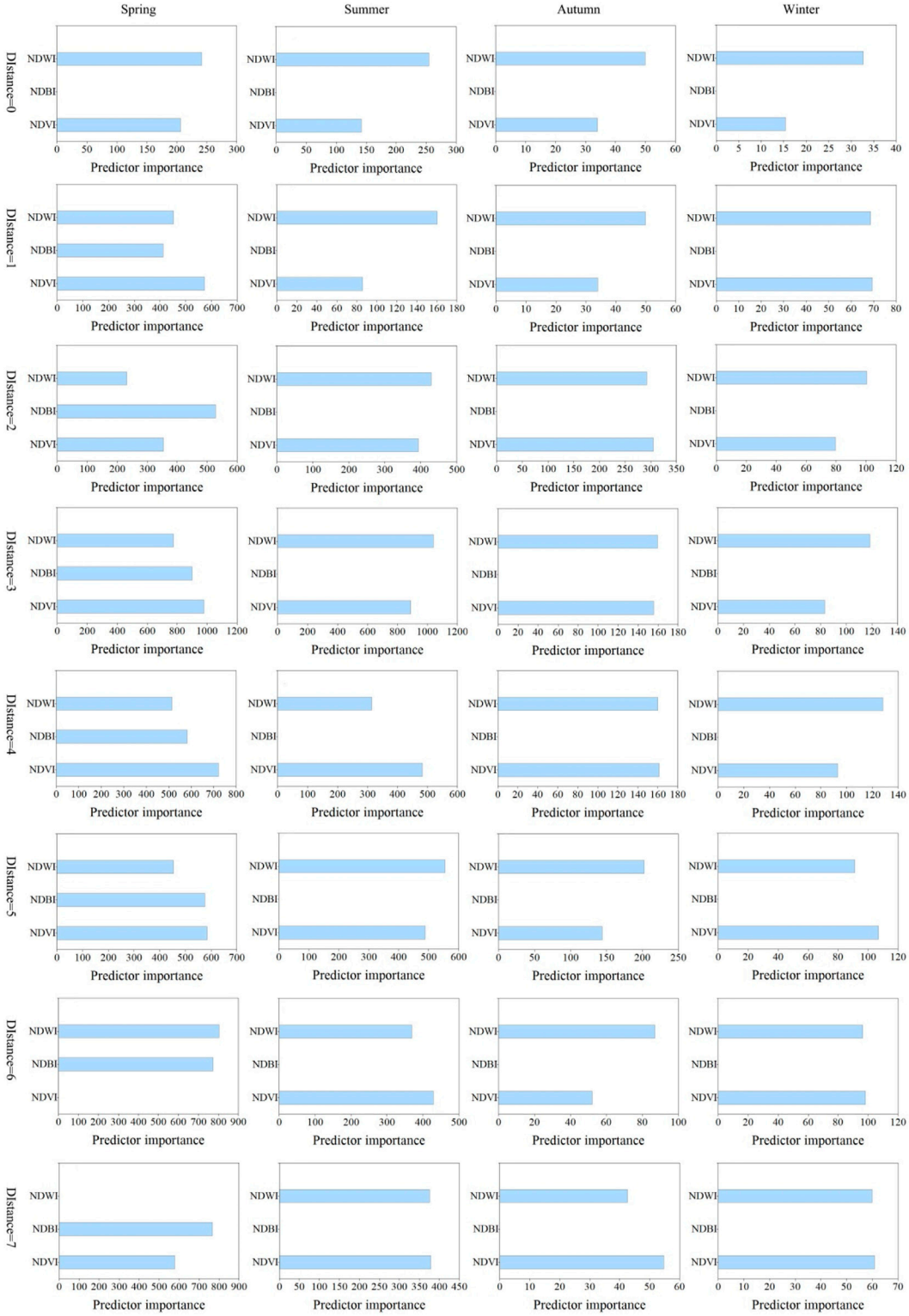

FIGURE 8
The importance of each predictor variable in different seasons. Distance represents that from the built-up area, in km. The predictor values refers to the importance and contribution of NDVI, NDBI, and NDWI.

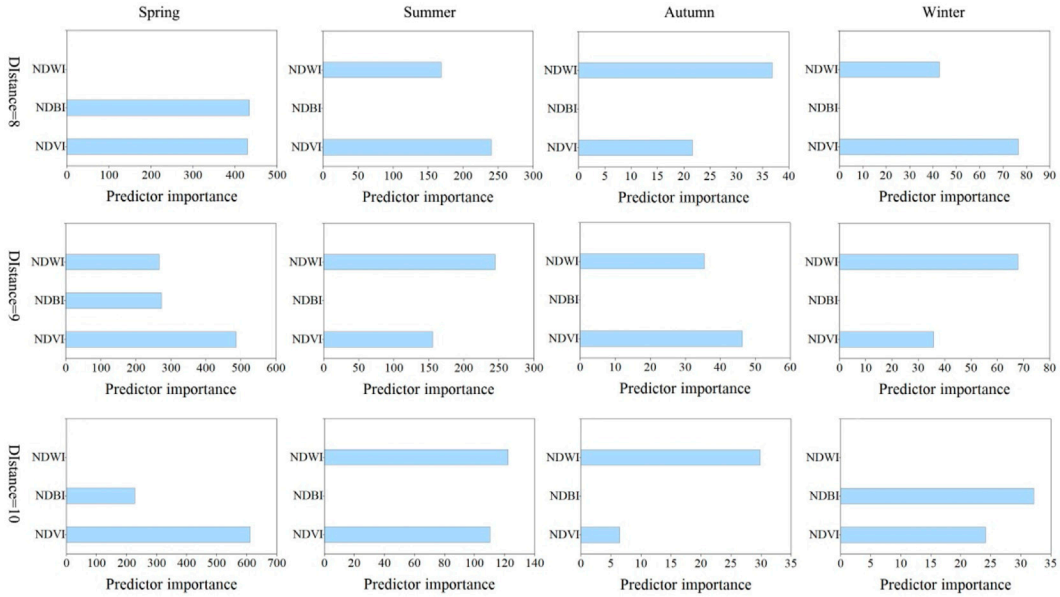

FIGURE 9
The importance of each predictor variable in different seasons. Distance represents that from the built-up area, in km. The predictor values refers to the importance and contribution of NDVI, NDBI, and NDWI.

the season. NDWI and SUHII showed a negative correlation; whereas, for NDVI, 52.4% showed a negative correlation with SUHII, most of which occurred in summer and autumn, 47.6% showed a positive correlation, and 25% showed a non-significant correlation. Specifically, most within the range of 0–10 km from the built-up area, the dominant factor of SUHII changes was partially consistent with the analysis results. That is, in spring and summer, SUHII was more affected by water, followed by buildings, and less affected by vegetation; whereas, in autumn and winter, SUHII was more affected by water and building, and less affected by vegetation. However, in summer within 4 and 5 km and in spring within 6 km from the built-up area, SUHII was more affected by buildings (−0.47, −0.53, and 0.60 respectively) than water and vegetation, and the effect of water (−0.45, −0.45, and −0.60, respectively) was higher than that of vegetation (−0.06, 0.05, and 0.44, respectively). In autumn within 7 km from the built-up area, SUHII was mostly affected by vegetation (correlation coefficient of 0.37) followed by water and buildings (correlation coefficients of 0.28 and −0.28, respectively). In spring within 8 and 9 km and in summer within 10 km, from the built-up area, the correlations between vegetation and SUHII were higher than those between buildings and water. In other urban-rural gradients in different seasons, the dominant factors of SUHII changes were consistent with the overall conclusions in the results analysis. In addition, NDVI correlation with SUHII showed a trend of first increasing and then decreasing along the urban-rural gradient in spring, while in summer showed a trend of first decreasing and then increasing, in autumn, except for 0, 6 and 10 km from the built-up area, the absolute value of the correlation coefficient was basically stable between 0 and 0.2, and in winter, the correlation coefficient was basically stable between 0 and 0.2. For NDBI, its correlation with SUHII showed a trend of first increasing and then decreasing in spring along the urban-rural gradient and the inflection point was within 5 km from the built-up area, in summer, there was a trend of fluctuation and decline, and the inflection point was also within 5 km from the built-up area, in autumn, the correlation coefficient with SUHII was basically stable at approximately 0.6, except for the significantly low value within 6 km from the built-up area, and in winter, there was a fluctuating upward trend, and the maximum correlation coefficient appeared within 6 km from the built-up area. NDWI correlation with SUHII along the urban-rural gradient showed a minimum value in spring except for 6 km away from the built-up area, and the absolute value of the remaining correlation coefficients was stable between 0.5 and 0.7, while in summer showed a trend of rising after fluctuation and decline and the inflection point was 6 km away from the built-up area, and in autumn and winter, its changing trend was the same as that of NDBI. Therefore, the correlations between NDVI, NDBI, and NDWI and SUHII showed significant differences along the urban-rural gradient, and the main inflection point was within 5–6 km from the built-up area. Hence, for future urbanization construction, the urban layout can be reasonably planned with reference to the role of different

land use types on SUHI. However, our study have not conducted in-depth research on the reasons for this difference, and the effects of other factors such as land cover and landscape pattern should also be considered in future studies.

In Distance, 0 represents the built-up area, 1–10 represent the distance from the built-up area, and in km.

The results of the importance of each variable (Figures 8, 9) showed that: in spring, within 0, and 6 km from the built-up area, NDWI was more important, followed by NDVI; at 7 and 8 km, NDBI was more important, followed by NDVI, at 10 km, NDBI contributed more, followed by NDVI, at 3, 4, 5, and 9 km, the importance result was NDVI > NDBI > NDWI, at 1 km, the importance result was NDVI > NDWI > NDBI, at 2 km, the importance result was NDBI > NDVI > NDWI. In summer and autumn, NDWI and NDVI contribute greatly, and in 63.6% of cases, NDWI contributed more; in winter, only at 10 km, the influence of NDBI was greater, followed by NDVI, while the rest of the gradients were mainly contributed by NDVI and NDWI. The cases where NDVI and NDWI were the most contributing variables accounted for 50% each.

Although many studies have assessed the influencing factors of SUHI, most have focused more on the simple correlation between SUHI and various factors (Li and Zhou, 2019; Varentsov et al., 2021; Liu et al., 2022), and have not conducted in-depth research on the contribution of each factor (Xiong et al., 2022). NDVI, NDBI, and NDWI do not always show strong importance in different seasons and different gradients in this paper, which has important reference significance for understanding the influencing factors of SUHI.

Limitations

This study analyzed the seasonal differences of SUHII and its dominant factors in different seasons. In addition, the changes in SUHII, NDVI, NDBI, and NDWI in different urban–rural gradients were analyzed, which provided an important insights into mechanism of SUHII and identifying appropriate mitigation strategies. However, this study has some limitations. In the extraction of built-up areas, we used Luojia-1A data, and the resolution was increased to 130 m. However, the resolution was still not sufficiently high, hence higher-precision data should be considered for cross-extraction in the future. Secondly, due to the long-term revisit period of the Landsat data, only one period of seasonal data in the study area could be selected for analysis, and data with higher temporal resolution should be considered for research in the future. Finally, since the Landsat data were only from the daytime, this study only considered seasonal differences, and hence diurnal differences should be considered in the future.

Conclusion

Since the beginning of the 21st century, China's urbanization process has accelerated, especially in coastal cities. As a typical coastal city in the Liaoning Province, Dalian City has experienced a surge in urban population and a significant UHI effect. Based on Luojia-1A, statistical yearbook, and Landsat eight remote sensing image data, this study analyzed the seasonal differences in SUHI and remote sensing indices along the urban-rural gradient. The conclusions were as follows:

The SUHII differed among seasons. In the urban built-up area, the mean SUHI intensity (SUHII) decreased from that in summer (2.74°C) > autumn (1.65°C) > winter (0.28°C) > spring (−0.79°C), while the maximum (25.34°C) and minimum (−19.73°C) SUHII values appeared in autumn and spring, respectively.

Overall, NDBI and SUHII showed positive correlations, while NDWI and SUHII showed negative correlations in all seasons. Whereas, NDVI showed positive correlations in spring, but negative correlations in summer, autumn and winter. In all seasons, buildings enhanced UHI, while water weakened UHI, whereas vegetation enhanced UHI in winter and spring and weakened UHI in summer and autumn.

SUHII, NDVI, NDBI, and NDWI showed differences along the urban-rural gradient. In summer and autumn, SUHII decreased along the urban-rural gradient, with the largest change in summer (2.74°C to −2.74°C), while that in spring was lower (−1 and 1°C). In winter, SUHII showed a trend of first decreasing and then increasing with an increase along the urban-rural gradient, with an overall increase of 0.50°C. Except in spring, NDVI increased from 0.09 to 0.59 with an increase in the distance from built-up areas. In other seasons, NDVI, NDBI, and NDWI remote sensing indices changed little along the urban-rural gradient and were all within 0.2.

Data availability statement

The original contributions presented in the study are included in the article/supplementary material, further inquiries can be directed to the corresponding authors.

Author contributions

JY contributed to all aspects of this work, JX wrote the main manuscript text. L-EW, CJ, XX, and JX conducted the experiment and analyzed the data. All authors reviewed the manuscript.

Funding

This research study was supported by the National Natural Science Foundation of China (Grant Nos

41771178, 42030409), the Fundamental Research Funds for the Central Universities (Grant No. N2111003), Basic Scientific Research Project (Key Project) of the Education Department of Liaoning Province (Grant No. LJKZ0964), the Second Tibetan Plateau Scientific Expedition and Research Program (STEP) (Grant No. 2019QZKK1004), and Innovative Talents Support Program of Liaoning Province (Grant No. LR2017017).

Acknowledgments

The authors would like to acknowledge all colleagues and friends who have voluntarily reviewed the translation of the survey and the manuscript of this study.

Conflict of interest

The authors declare that the research was conducted in the absence of any commercial or financial relationships that could be construed as a potential conflict of interest.

Publisher's note

All claims expressed in this article are solely those of the authors and do not necessarily represent those of their affiliated organizations, or those of the publisher, the editors and the reviewers. Any product that may be evaluated in this article, or claim that may be made by its manufacturer, is not guaranteed or endorsed by the publisher.

References

Arabi Aliabad, F., Zare, M., and Ghafarian Malamiri, H. (2021). Comparison of the accuracy of daytime land surface temperature retrieval methods using Landsat 8 images in arid regions. *Infrared Phys. Technol.* 115, 103692. doi:10.1016/j.infrared.2021.103692

Carrillo-Niquete, G. A., Andrade, J. L., Valdez-Lazalde, J. R., Reyes-García, C., and Hernández-Stefanoni, J. L. (2022). Characterizing spatial and temporal deforestation and its effects on surface urban heat islands in a tropical city using Landsat time series. *Landsc. Urban Plan.* 217, 104280. doi:10.1016/j.landurbplan.2021.104280

Chang, Y., Xiao, J., Li, X., Frolking, S., Zhou, D., Schneider, A., et al. (2021). Exploring diurnal cycles of surface urban heat island intensity in Boston with land surface temperature data derived from GOES-R geostationary satellites. *Sci. Total Environ.* 763, 144224. doi:10.1016/j.scitotenv.2020.144224

Cosgrove, A., and Berkelhammer, M. (2018). Downwind footprint of an urban heat island on air and lake temperatures. *npj Clim. Atmos. Sci.* 1, 1–10. doi:10.1038/s41612-018-0055-3

Deliry, S. I., Avdan, Z. Y., and Avdan, U. (2021). Extracting urban impervious surfaces from Sentinel-2 and Landsat-8 satellite data for urban planning and environmental management. *Environ. Sci. Pollut. Res.* 28, 6572–6586. doi:10.1007/s11356-020-11007-4

Dewan, A., Kiselev, G., Botje, D., Mahmud, G. I., Bhuian, Md. H., and Hassan, Q. K. (2021). Surface urban heat island intensity in five major cities of Bangladesh: Patterns, drivers and trends. *Sustain. Cities Soc.* 71, 102926. doi:10.1016/j.scs.2021.102926

Erdem, U., Cubukcu, K. M., and Sharifi, A. (2021). An analysis of urban form factors driving urban heat island: The case of izmir. *Environ. Dev. Sustain* 23, 7835–7859. doi:10.1007/s10668-020-00950-4

Feng, R., Wang, F., Wang, K., Wang, H., and Li, L. (2021). Urban ecological land and natural-anthropogenic environment interactively drive surface urban heat island: An urban agglomeration-level study in China. *Environ. Int.* 157, 106857. doi:10.1016/j.envint.2021.106857

Guo, A., Yang, J., Xiao, X., Xia (Cecilia), J., Jin, C., and Li, X. (2020). Influences of urban spatial form on urban heat island effects at the community level in China. *Sustain. Cities Soc.* 53, 101972. doi:10.1016/j.scs.2019.101972

He, X., Zhang, Z., and Yang, Z. (2021). Extraction of urban built-up area based on the fusion of night-time light data and point of interest data. *R. Soc. Open Sci.* 8, 210838. doi:10.1098/rsos.210838

Hsu, A., Sheriff, G., Chakraborty, T., and Manya, D. (2021). Disproportionate exposure to urban heat island intensity across major US cities. *Nat. Commun.* 12, 1–11. doi:10.1038/s41467-021-22799-5

Hu, D., Qiao, K., Wang, X., Zhao, L., and Ji, G. (2015). Land surface temperature retrieval from Landsat 8 thermal infrared data using mono-window algorithm. *J. Remote Sens.* 19, 964–976. https://kns.cnki.net/kcms/detail/11.3841.tp.20150929.1027.022.html.

Hu, T., Jin, S., Yan, Q., and Guo, X. (2021a). "Built-up areas mapping from Luojia 1-01 nighttime light imagery with considering observation number," in *2021 photonics & electromagnetics research symposium* (Hangzhou, China: IEEE), 2254–2259. doi:10.1109/PIERS53385.2021.9694698

Hu, Y., Dai, Z., and Guldmann, J.-M. (2021b). Greenspace configuration impact on the urban heat island in the Olympic Area of Beijing. *Environ. Sci. Pollut. Res.* 28, 33096–33107. doi:10.1007/s11356-020-12086-z

Imhoff, M. L., Zhang, P., Wolfe, R. E., and Bounoua, L. (2010). Remote sensing of the urban heat island effect across biomes in the continental USA. *Remote Sens. Environ.* 114, 504–513. doi:10.1016/j.rse.2009.10.008

Jiang, Y., and Lin, W. (2021). A comparative analysis of retrieval algorithms of land surface temperature from landsat-8 data: A case study of shanghai, China. *Int. J. Environ. Res. Public Health* 18, 5659. doi:10.3390/ijerph18115659

Joloudari, J. H., Hassannataj Joloudari, E., Saadatfar, H., Ghasemigol, M., Razavi, S. M., Mosavi, A., et al. (2020). Coronary artery disease diagnosis; ranking the significant features using a random trees model. *Int. J. Environ. Res. Public Health* 17, 731. doi:10.3390/ijerph17030731

Jun, Z., Xiao-Die, Y., and Han, L. (2021). The extraction of urban built-up areas by integrating night-time light and POI data—a case study of kunming, China. *IEEE Access* 9, 22417–22429. doi:10.1109/ACCESS.2021.3054169

Kamali Maskooni, E., Hashemi, H., Berndtsson, R., Daneshkar Arasteh, P., and Kazemi, M. (2021). Impact of spatiotemporal land-use and land-cover changes on surface urban heat islands in a semiarid region using Landsat data. *null* 14, 250–270. doi:10.1080/17538947.2020.1813210

Kim, S. W., and Brown, R. D. (2021). Urban heat island (UHI) intensity and magnitude estimations: A systematic literature review. *Sci. Total Environ.* 779, 146389. doi:10.1016/j.scitotenv.2021.146389

Koç, A., Caf, A., Koç, C., and Kejanli, D. T. (2022). Examining the temporal and spatial distribution of potential urban heat island formations. *Environ. Sci. Pollut. Res.* 29, 11455–11468. doi:10.1007/s11356-021-16422-9

Koko, A. F., Yue, W., Abubakar, G. A., Alabsi, A. A. N., and Hamed, R. (2021). Spatiotemporal influence of land use/land cover change dynamics on surface urban heat island: A case study of abuja metropolis, Nigeria. *ISPRS Int. J. Geo-Information* 10, 272. doi:10.3390/ijgi10050272

Li, C., Duan, P., Wang, M., Li, J., and Zhang, B. (2021). The extraction of built-up areas in Chinese mainland cities based on the local optimal threshold method using NPP-viirs images. *J. Indian Soc. Remote Sens.* 49, 233–248. doi:10.1007/s12524-020-01209-1

Li, H., Zhou, Y., Jia, G., Zhao, K., and Dong, J. (2022). Quantifying the response of surface urban heat island to urbanization using the annual temperature cycle model. *Geosci. Front.* 13, 101141. doi:10.1016/j.gsf.2021.101141

Li, L., Zha, Y., and Zhang, J. (2020). Spatially non-stationary effect of underlying driving factors on surface urban heat islands in global major cities. *Int. J. Appl. Earth Observation Geoinformation* 90, 102131. doi:10.1016/j.jag.2020.102131

Li, X., Zhao, L., Li, D., and Xu, H. (2018). Mapping urban extent using Luojia 1-01 nighttime light imagery. *Sensors* 18, 3665. doi:10.3390/s18113665

Li, X., and Zhou, W. (2019). Spatial patterns and driving factors of surface urban heat island intensity: A comparative study for two agriculture-dominated regions in China and the USA. *Sustain. Cities Soc.* 48, 101518. doi:10.1016/j.scs.2019.101518

Liu, H., Huang, B., Zhan, Q., Gao, S., Li, R., and Fan, Z. (2021a). The influence of urban form on surface urban heat island and its planning implications: Evidence from 1288 urban clusters in China. *Sustain. Cities Soc.* 71, 102987. doi:10.1016/j.scs.2021.102987

Liu, J., Zhang, L., Zhang, Q., Zhang, G., and Teng, J. (2021b). Predicting the surface urban heat island intensity of future urban green space development using a multi-scenario simulation. *Sustain. Cities Soc.* 66, 102698. doi:10.1016/j.scs.2020.102698

Liu, Q., Zhan, Q., Li, J., Yang, C., and Liu, W. (2021c). Extracting built-up areas using luojia-1A nighttime light imageries in wuhan, China. *WHDXXBXXKXB* 46, 30–39. doi:10.13203/j.whugis20190376

Liu, W., Zhao, H., Sun, S., Xu, X., Huang, T., and Zhu, J. (2022). Green space cooling effect and contribution to mitigate heat island effect of surrounding communities in beijing metropolitan area. *Front. Public Health* 10, 870403. doi:10.3389/fpubh.2022.870403

Luo, X., Yang, J., Sun, W., and He, B. (2021). Suitability of human settlements in mountainous areas from the perspective of ventilation: A case study of the main urban area of chongqing. *J. Clean. Prod.* 310, 127467. doi:10.1016/j.jclepro.2021.127467

Ma, L., Wang, Y., Liang, Z., Ding, J., Shen, J., Wei, F., et al. (2021a). Changing effect of urban form on the seasonal and diurnal variations of surface urban heat island intensities (SUHIIs) in more than 3000 cities in China. *Sustainability* 13, 2877. doi:10.3390/su13052877

Ma, X., and Peng, S. (2022). Research on the spatiotemporal coupling relationships between land use/land cover compositions or patterns and the surface urban heat island effect. *Environ. Sci. Pollut. Res.* 29, 39723–39742. doi:10.1007/s11356-022-18838-3

Ma, X., Zhang, L., Guo, M., and Zhao, J. (2021b). The effect of various urban design parameter in alleviating urban heat island and improving thermal health—A case study in a built pedestrianized block of China. *Environ. Sci. Pollut. Res.* 28, 38406–38425. doi:10.1007/s11356-021-13179-z

Manoli, G., Fatichi, S., Schläpfer, M., Yu, K., Crowther, T. W., Meili, N., et al. (2019). Magnitude of urban heat islands largely explained by climate and population. *Nature* 573, 55–60. doi:10.1038/s41586-019-1512-9

Meng, Q., Zhang, L., Sun, Z., Meng, F., Wang, L., and Sun, Y. (2018). Characterizing spatial and temporal trends of surface urban heat island effect in an urban main built-up area: A 12-year case study in beijing, China. *Remote Sens. Environ.* 204, 826–837. doi:10.1016/j.rse.2017.09.019

Mohammad, P., and Goswami, A. (2021a). Quantifying diurnal and seasonal variation of surface urban heat island intensity and its associated determinants across different climatic zones over Indian cities. *null* 58, 955–981. doi:10.1080/15481603.2021.1940739

Mohammad, P., and Goswami, A. (2021b). Spatial variation of surface urban heat island magnitude along the urban-rural gradient of four rapidly growing Indian cities. *null* 1, 23. doi:10.1080/10106049.2021.1886338

Morabito, M., Crisci, A., Guerri, G., Messeri, A., Congedo, L., and Munafò, M. (2021). Surface urban heat islands in Italian metropolitan cities: Tree cover and impervious surface influences. *Sci. Total Environ.* 751, 142334. doi:10.1016/j.scitotenv.2020.142334

Najafzadeh, F., Mohammadzadeh, A., Ghorbanian, A., and Jamali, S. (2021). Spatial and temporal analysis of surface urban heat island and thermal comfort using Landsat satellite images between 1989 and 2019: A case study in tehran. *Remote Sens.* 13, 4469. doi:10.3390/rs13214469

Nhu, V.-H., Shahabi, H., Nohani, E., Shirzadi, A., Al-Ansari, N., Bahrami, S., et al. (2020). Daily water level prediction of zrebar lake (Iran): A comparison between M5P, random forest, random tree and reduced error pruning trees algorithms. *ISPRS Int. J. Geo-Information* 9, 479. doi:10.3390/ijgi9080479

Niu, L., Zhang, Z., Peng, Z., Liang, Y., Liu, M., Jiang, Y., et al. (2021). Identifying surface urban heat island drivers and their spatial heterogeneity in China's 281 cities: An empirical study based on multiscale geographically weighted regression. *Remote Sens.* 13, 4428. doi:10.3390/rs13214428

Peng, S., Piao, S., Ciais, P., Friedlingstein, P., Ottle, C., Bréon, F.-M., et al. (2012). Surface urban heat island across 419 global big cities. *Environ. Sci. Technol.* 46, 696–703. doi:10.1021/es2030438

Qin, Z. H., Zhang, M. H., Karnieli, A., and Berliner, P. (2001). Mono-window algorithm for retrieving land surface temperature from Landsat TM6 data. *Acta Geogr. Sin.* 56, 456–466. doi:10.11821/xb200104009

Ren, J., Yang, J., Zhang, Y., Xiao, X., Xia, J. C., Li, X., et al. (2022). Exploring thermal comfort of urban buildings based on local climate zones. *J. Clean. Prod.* 340, 130744. doi:10.1016/j.jclepro.2022.130744

Schwaab, J., Meier, R., Mussetti, G., Seneviratne, S., Bürgi, C., and Davin, E. L. (2021). The role of urban trees in reducing land surface temperatures in European cities. *Nat. Commun.* 12, 1–11. doi:10.1038/s41467-021-26768-w

Shastri, H., Barik, B., Ghosh, S., Venkataraman, C., and Sadavarte, P. (2017). Flip flop of day-night and summer-winter surface urban heat island intensity in India. *Sci. Rep.* 7, 1–8. doi:10.1038/srep40178

Shi, Z., Yang, J., Zhang, Y., Xiao, X., and Xia, J. C. (2022). Urban ventilation corridors and spatiotemporal divergence patterns of urban heat island intensity: A local climate zone perspective. *Environ. Sci. Pollut. Res.* 1, 13. doi:10.1007/s11356-022-21037-9

Smith, I. A., Winbourne, J. B., Tieskens, K. F., Jones, T. S., Bromley, F. L., Li, D., et al. (2021). A satellite-based model for estimating latent heat flux from urban vegetation. *Front. Ecol. Evol.* 9, 695995. doi:10.3389/fevo.2021.695995

Tran, H., Uchihama, D., Ochi, S., and Yasuoka, Y. (2006). Assessment with satellite data of the urban heat island effects in Asian mega cities. *Int. J. Appl. Earth Observation Geoinformation* 8, 34–48. doi:10.1016/j.jag.2005.05.003

Varentsov, M., Fenner, D., Meier, F., Samsonov, T., and Demuzere, M. (2021). Quantifying local and mesoscale drivers of the urban heat island of moscow with reference and crowdsourced observations. *Front. Environ. Sci.* 9, 716968. doi:10.3389/fenvs.2021.716968

Wang, J., Chen, Y., Liao, W., He, G., Tett, S. F. B., Yan, Z., et al. (2021a). Anthropogenic emissions and urbanization increase risk of compound hot extremes in cities. *Nat. Clim. Chang.* 11, 1084–1089. doi:10.1038/s41558-021-01196-2

Wang, Y., and Shen, Z. (2021). Comparing Luojia 1-01 and VIIRS nighttime light data in detecting urban spatial structure using a threshold-based kernel density estimation. *Remote Sens.* 13, 1574. doi:10.3390/rs13081574

Wang, Z., Meng, Q., Allam, M., Hu, D., Zhang, L., and Menenti, M. (2021b). Environmental and anthropogenic drivers of surface urban heat island intensity: A case-study in the yangtze river delta, China. *Ecol. Indic.* 128, 107845. doi:10.1016/j.ecolind.2021.107845

Wu, H., Wang, T., Riemer, N., Chen, P., Li, M., and Li, S. (2017). Urban heat island impacted by fine particles in Nanjing, China. *Sci. Rep.* 7, 1–11. doi:10.1038/s41598-017-11705-z

Xiong, L., Li, S., Zou, B., Peng, F., Fang, X., and Xue, Y. (2022). Long time-series urban heat island monitoring and driving factors analysis using remote sensing and geodetector. *Front. Environ. Sci.* 9, 828230. doi:10.3389/fenvs.2021.828230

Yang, G., Ma, Y., and Hu, J. (2021a). A fused variable by night light images and MODIS products for improving urban built-up area extraction. *Technologies* 9, 40. doi:10.3390/technologies9020040

Yang, J., Ren, J., Sun, D., Xiao, X., Xia, J., Cecilia), et al. (2021b). Understanding land surface temperature impact factors based on local climate zones. *Sustain. Cities Soc.* 69, 102818. doi:10.1016/j.scs.2021.102818

Yang, J., Wang, Y., Xiu, C., Xiao, X., Xia, J., and Jin, C. (2020). Optimizing local climate zones to mitigate urban heat island effect in human settlements. *J. Clean. Prod.* 275, 123767. doi:10.1016/j.jclepro.2020.123767

Yang, J., Xin, J., Zhang, Y., Xiao, X., and Xia, J. C. (2022). Contributions of sea–land breeze and local climate zones to daytime and nighttime heat island intensity. *npj Urban Sustain* 2, 1–11. doi:10.1038/s42949-022-00055-z

Yang, J., Yang, Y., Sun, D., Jin, C., and Xiao, X. (2021c). Influence of urban morphological characteristics on thermal environment. *Sustain. Cities Soc.* 72, 103045. doi:10.1016/j.scs.2021.103045

Yao, R., Wang, L., Huang, X., Liu, Y., Niu, Z., Wang, S., et al. (2021). Long-term trends of surface and canopy layer urban heat island intensity in 272 cities in the mainland of China. *Sci. Total Environ.* 772, 145607. doi:10.1016/j.scitotenv.2021.145607

Yao, R., Wang, L., Huang, X., Zhang, W., Li, J., and Niu, Z. (2018). Interannual variations in surface urban heat island intensity and associated drivers in China. *J. Environ. Manag.* 222, 86–94. doi:10.1016/j.jenvman.2018.05.024

Yu, M., Guo, S., Guan, Y., Cai, D., Zhang, C., Fraedrich, K., et al. (2021). Spatiotemporal heterogeneity analysis of yangtze river delta urban agglomeration: Evidence from nighttime light data (2001–2019). *Remote Sens.* 13, 1235. doi:10.3390/rs13071235

Zhang, H., Liang, C., and Pan, Y. (2022). Spatial expansion of built-up areas in the beijing–tianjin–hebei urban agglomeration based on nighttime light data: 1992–2020. *Int. J. Environ. Res. Public Health* 19, 3760. doi:10.3390/ijerph19073760

Zhang, R. (2020). Cooling effect and control factors of common shrubs on the urban heat island effect in a southern city in China. *Sci. Rep.* 10, 1–8. doi:10.1038/s41598-020-74559-y

Zhang, Y., Li, D., Liu, L., Liang, Z., Shen, J., Wei, F., et al. (2021). Spatiotemporal characteristics of the surface urban heat island and its driving factors based on local climate zones and population in beijing, China. *Atmosphere* 12, 1271. doi:10.3390/atmos12101271

Zhao, Z., Sharifi, A., Dong, X., Shen, L., and He, B.-J. (2021). Spatial variability and temporal heterogeneity of surface urban heat island patterns and the suitability of local climate zones for land surface temperature characterization. *Remote Sens.* 13, 4338. doi:10.3390/rs13214338

Zheng, Y., Tang, L., and Wang, H. (2021). An improved approach for monitoring urban built-up areas by combining NPP-VIIRS nighttime light, NDVI, NDWI, and NDBI. *J. Clean. Prod.* 328, 129488. doi:10.1016/j.jclepro.2021.129488

Zhou, D., Zhao, S., Liu, S., Zhang, L., and Zhu, C. (2014a). Surface urban heat island in China's 32 major cities: Spatial patterns and drivers. *Remote Sens. Environ.* 152, 51–61. doi:10.1016/j.rse.2014.05.017

Zhou, Y., Smith, S. J., Elvidge, C. D., Zhao, K., Thomson, A., and Imhoff, M. (2014b). A cluster-based method to map urban area from DMSP/OLS nightlights. *Remote Sens. Environ.* 147, 173–185. doi:10.1016/j.rse.2014.03.004

frontiers | Frontiers in Environmental Science

TYPE Original Research
PUBLISHED 09 September 2022
DOI 10.3389/fenvs.2022.1001064

Check for updates

OPEN ACCESS

EDITED BY
Bing Xue,
Institute of Applied Ecology, (CAS), China

REVIEWED BY
Xiao Liu,
South China University of Technology, China
An Liu,
Shenzhen University, China

*CORRESPONDENCE
Guojun Zhang,
guojunz@gdufe.edu.cn

SPECIALTY SECTION
This article was submitted to Environmental Informatics and Remote Sensing,
a section of the journal
Frontiers in Environmental Science

RECEIVED 22 July 2022
ACCEPTED 15 August 2022
PUBLISHED 09 September 2022

CITATION
Zhou C, Zhang D, Cao Y, Wang Y and Zhang G (2022), Spatio–temporal evolution and factors of climate comfort for urban human settlements in the Guangdong–Hong Kong–Macau Greater Bay Area.
Front. Environ. Sci. 10:1001064.
doi: 10.3389/fenvs.2022.1001064

COPYRIGHT
© 2022 Zhou, Zhang, Cao, Wang and Zhang. This is an open-access article distributed under the terms of the Creative Commons Attribution License (CC BY). The use, distribution or reproduction in other forums is permitted, provided the original author(s) and the copyright owner(s) are credited and that the original publication in this journal is cited, in accordance with accepted academic practice. No use, distribution or reproduction is permitted which does not comply with these terms.

Spatio–temporal evolution and factors of climate comfort for urban human settlements in the Guangdong–Hong Kong–Macau Greater Bay Area

Chunshan Zhou[1], Dahao Zhang[1], Yongwang Cao[1], Yunzhe Wang[2] and Guojun Zhang[3]*

[1]School of Geography and Planning, Sun Yat-sen University, Guangzhou, China, [2]School of Civil Engineering and Architecture, Jishou University, Zhangjiajie, China, [3]School of Finance, Guangdong University of Finance and Economics, Guangzhou, China

This study used both temperature-humidity and wind efficiency indices at three time-scale resolutions (year, season, and month) for the first time, to analyze the spatio–temporal evolution of urban climate comfort in the Guangdong–Hong Kong–Macau Greater Bay Area (GBA). The main factors affecting human-settlement climate comfort were elucidated and the annual changes in both indices used in the study area exhibited fluctuating growth from 2005 to 2020. Moreover, the annual growth of the temperature-humidity and wind efficiency indices in the southern cities of the GBA was relatively fast. In contrast, the annual growth of these indices in the northern cities of the GBA was relatively slow. Overall, the climate of the human-settlement environments in the GBA was the most comfortable in spring and autumn, and summer and winter were characterized by hot and cold climate conditions, respectively. We did not identify any prominent change in the climate comfort of spring and autumn from 2005 to 2020; however, the climate comfort degree deteriorated in summer and ameliorated in winter. On a monthly scale, the human-settlement environments in the GBA were the coldest in December and the hottest in July. The urban human settlements were cold in January and February, hot in May, June, August, and September, and the most comfortable in March, April, October, and November in 2020. We analyzed the factors affecting the climate comfort of human-settlement environments in the study area and found that elevation, gross industrial production, population scale, and construction land area were the most influential parameters. Notably, the impact of natural factors on the climate comfort of human-settlement environments was more significant than that of anthropogenic factors. Moreover, the related factors affected the temperature-humidity index more strongly than the wind efficiency index. Overall, our results provide data-driven guidelines for improving the climate comfort of urban human settlements in the GBA.

KEYWORDS

urban human settlement environment, climate comfort, temporal and spatial evolution, influencing factor, Guangdong-Hong Kong-Macau Greater Bay Area

1 Introduction

The "Outline Development Plan for the Guangdong–Hong Kong–Macau Greater Bay Area (GBA)" is becoming a national strategy in China; thus, it is increasingly important to understand how a vibrant and internationally competitive first-class bay area and world-class city agglomeration can be developed for the society, industry, and government. The objective "to develop a high-quality living circle for living, working, and traveling," mentioned among the five key aspects of this endeavor not only reflects the governance philosophy of "the people center" but also facilitates the attraction of innovative talents. In this context, climate comfort is one of the most important factors to study for the development of the bay area toward more comfortable ways of living, working, and traveling. In general, urban human-settlement environments are residences in which people live and engage in production, thereby reflecting the economic development level of a region and the quality of life of residents (Li et al., 2021). Structurally, a human-settlement environment is a complex system, which mainly consists of natural, human, living, support, and social systems (Tian et al., 2022; Yang et al., 2020). Of these, the natural system is the foundation, and its overall development and state largely determine the quality of the human-settlement environment (Yang et al., 2022). In this context, climate change is an important element in the natural system and plays a crucial role in controlling the climate comfort of human-settlement environments. Climate comfort generally reflects the level of comfort experienced by healthy human beings without the aid of temperature control devices and is determined by meteorological factors, such as temperature, humidity, wind speed, and sunshine. Fundamentally, it represents a bio-meteorological index, which can be used to evaluate the comfort state of a human body under different climate conditions. In the context of global warming, the recently accelerated urbanization has substantially affected regional climates. Moreover, many people seriously consider the livability standards of a location before choosing their place of residence (Dulal and Akbar, 2013; Wang et al., 2021). Thus, understanding and improving the comfort level of human-settlement climates can improve the quality of human settlements, while uniquely unraveling the fundamental needs of social sustainable development (Zhang et al., 2022).

To date, the research on the climate comfort of human-settlement environments has mainly focused on a narrow scope of topics. First, some studies have examined the spatial characteristics of tourism climate comfort, assessing its impact on tourism potential and development. Specifically, scholars have explored spatial layout characteristics of tourism climate comfort using the tourism climate index (TCI) (Masoudi, 2021). Moreover, a geographic information system (GIS) can be applied to partition and evaluate the ecotourism potential of climate comfort areas (Nasirihendkhaleh et al., 2014). In this way, the impact of climate comfort on health tourism has been elucidated (Amininia et al., 2020). Furthermore, some other studies used the TCI, temperature-humidity, and holiday climate indices to evaluate the influence of climate comfort on tourist visitation patterns for world heritage sites (Hasanah et al., 2020). These studies utilized daily climate data to quantify the comfort climate of national 5A scenic spots (Lei et al., 2020). A comprehensive TCI can be used to evaluate the spatio–temporal evolution of climate comfort for tourists and predict its future development trend (Zhao and Wang., 2021). A previous study used the Grand Shangri-La region as a case study and investigated the change in tourism climate from 1980 to 2016 under intensifying global warming (Cheng and Zhong., 2019). As a result, the spatial distribution of the TCI was analyzed and quantified, thereby covering the areas with different TCI classes in Iran (Bakhtiari et al., 2018). Another study applied the Mediterranean outdoor comfort index and the predicted the mean vote for international tourism to examine the climatic conditions and outdoor thermal comfort in Venice, Rome, and Palermo, located in the north, center, and south of Italy, respectively (Salata et al., 2017).

The second aspect of climate comfort has been addressed by other studies, which examined the influence of natural factors on the climate comfort of the human-settlement environments. These studies explored the impact of natural elements such as elevation (Li and Chi, 2014), meteorology (Tseliou et al., 2010; Eludoyin et al., 2014; Müller et al., 2014; Orosa et al., 2014), rivers (Amorosi et al., 2013; Giannakis et al., 2016), vegetation (Celuppi et al., 2019), air movement acceptability (Cândido et al., 2010), and CO_2 concentration (Yüksel et al., 2020), on the climate comfort of human-settlement environments. The third aspect was addressed by some scholars who investigated the influence of human factors on the climate comfort of human-settlement environments; they elucidated the influence of human factors, such as architectural design (Gonzalez-Longo and Sahabuddin, 2019) and land use in an urban area (Cetin, 2020), on the climate comfort of human-settlement environments. The fourth aspect of the climate comfort of human settlements was covered by studies that reported the spatio–temporal characteristics of the climate comfort of human-settlement environments. Such studies quantified the climate comfort of urban human-settlement environments using the climate comfort index and by examining the spatial characteristics of climate comfort (Cao et al., 2019). As a result, the spatio–temporal and seasonal evolutions of the climate comfort of human-settlement environments in China were explored using data from the ground-based meteorological observation station (Yin et al., 2018).

Currently, most studies focusing on the climate comfort of the human-settlement environments address the spatio–temporal distribution of climate comfort, tourism climate comfort, and the influence of individual natural and human factors on climate comfort. However, our knowledge on

the climate comfort of human-settlement environments is incomplete at country (e.g., China) (Kong et al., 2019; Kambezidis et al., 2021; Katavoutas et al., 2021; Zhang et al., 2022), economic corridor (e.g., the China-Pakistan Economic Corridor) (Zeng et al., 2020), regional (e.g., northwest China) (Yao et al., 2021), urban agglomeration (e.g., Beijing-Tianjin-Hebei Area) (Liu et al., 2020), provincial (e.g., Liaoning) (Cheung and Hart, 2014; Cao et al., 2016), city (Urumqi) (Li et al., 2014), county (district) (e.g. Changsha county) (Liu et al., 2013), and township scales (e.g., Qiankou town) (Yu et al., 2021). Moreover, studies on the spatio–temporal changes in the climate comfort of human-settlement environments at the bay area scale are very scarce. The Guangdong–Hong Kong–Macau GBA is located at the frontier coastal opening of China, with the Pan-Pearl River Delta region as its vast development hinterland. Guangdong, Hong Kong, and Macau all stand out with prominent development in science and technology, thereby attracting residents, businesses, and investments to the area. By elucidating the climate comfort of the human-settlement environments in the GBA, the quality of life of residents can be improved, while the attraction of talents can lead to the formation of an international science and technology innovation center in the GBA.

To this end, our study used the GBA as the study region, where we combined the temperature-humidity and wind efficiency indices to evaluate the climate comfort of the human-settlement environment from 2005 to 2020. The objectives of this study are 1) to conduct a spatio–temporal analysis of the climate comfort of human-settlement environments using GIS technology and 2) explore the factors that impact the climate comfort of human-settlement environments by multiple logistic regression methods. By elucidating the climate comfort of the human-settlement environments in the GBA, this study provides a scientific reference for attracting innovative talents and improving the quality of life of residents, in addition to providing a useful reference for enabling rational urban regional planning, such as the formation of an international science and technology innovation center in the GBA.

2 Data sources and research methods

2.1 Overview of the study area

The GBA (China) consists of the Hong Kong and Macau special administrative regions, and nine cities in Guangdong Province. The total area of GBA is 5.6 km^2. This area has the highest degree of openness and strongest economic vitality compared to that of other regions in China and also has an important strategic position (Figure 1).

2.2 Data source and processing

This study used data from near-ground-based climatology databases in China. We used a daily-scale value dataset (v3.0 processing and generation), statistical yearbook data, PM2.5 data, land cover data, vegetation coverage data, digital elevation model (DEM) data, and administrative division data. The China ground climate dataset mainly includes the daily data from 2005 to 2020, containing the following parameters: wind speed, humidity, precipitation, temperature, sunshine, station number, and coordinates (longitude and latitude). The dataset was originally composed based on observations from 824 benchmark meteorological stations in China and provided by the China Meteorological Data Service Center (http://data.cma.cn/).

From a data processing perspective, the data were first collected and sorted, then projected at specific points to overlap with the base map, and daily data were spatially interpolated by the inverse-distance weighting method. Finally, the data were divided and split according to the administrative divisions. By doing this we obtained the final daily data for provinces and cities, as well as the average daily data of meteorological elements in different years and months as the basis for the yearly and monthly data for the different regions.

We used the following socioeconomic data: the permanent population, gross domestic product (GDP), gross industrial production (%), and construction land area. These data were obtained from the China City Statistical Yearbook (http://www.stats.gov.cn/tjsj/), Guangdong Statistical Yearbook (http://stats.gd.gov.cn/), Hong Kong Annual Digest of Statistics (https://www.censtatd.gov.hk/sc/), and Anuário Estatístico Yearbook of Statistics (https://www.dsec.gov.mo/zh-MO/) from 2005 to 2021. The $PM_{2.5}$ concentrations of cities in the GBA were obtained from the Atmospheric Composition Analysis Group of Dalhousie University (http://fizz.phys.dal.ca/~atmos/martin/?page_id=140). The $PM_{2.5}$ data were first rasterized and spatially optimized to the boundaries of the analyzed cities to derive the $PM_{2.5}$ concentration annual mean data. The land cover data included estimates of arable land, forests, grassland, and artificial ground. The land cover-related data were obtained from the National Catalogue Service for Geographic information (https://www.webmap.cn/main.do?method=index). The GBA DEM elevation, vegetation coverage, and administrative division data were acquired from the Resources and Environment Sciences and Data Center of the Chinese Academy of Sciences (http://www.resdc.cn/data.aspx; DATA ID = 333) (Table 1).

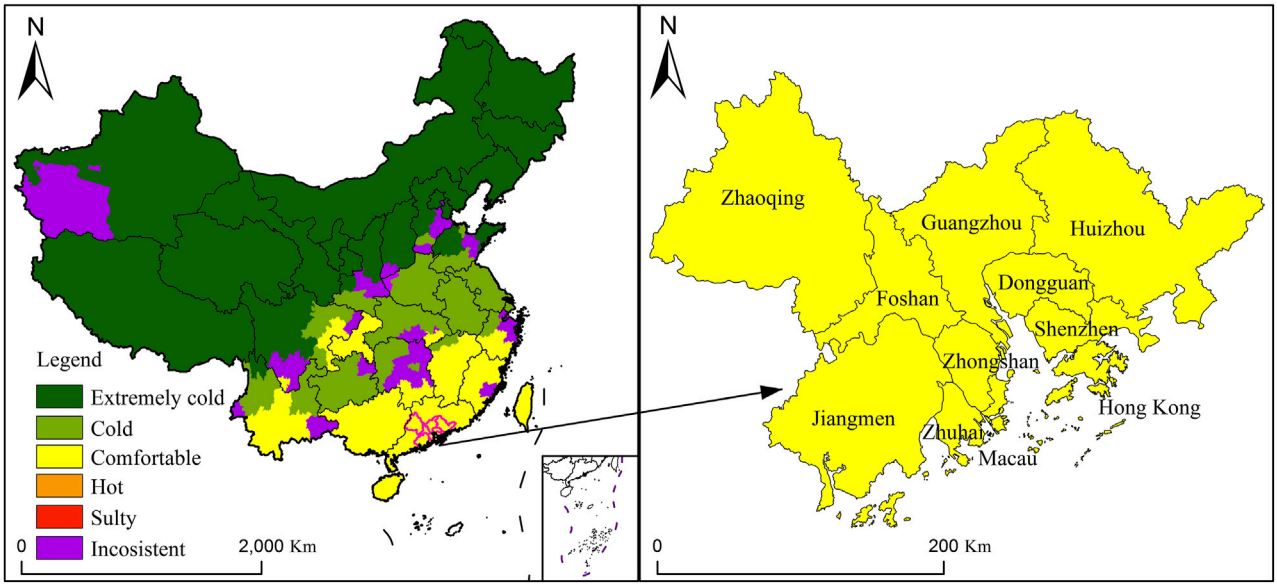

FIGURE 1
The average annual residential climate comfort chart in China from 2005 to 2020 (Map Content Approval Number: GS (2019)1822).

TABLE 1 Data sources and description.

Data Category	Data description	Data type	Data source
China ground climate means daily value data	Wind speed, humidity, precipitation, temperature, sunshine, and others	Panel	China Meteorological Data Service Center
Statistical yearbook data	Permanent population, gross domestic product (GDP), the percentage of gross industrial production and construction land area	Panel	China City Statistical Yearbook, Guangdong Statistical Yearbook, Hong Kong Annual Digest of Statistics and Anuário Estatístico Yearbook of Statistics
Land cover data	Arable land, forest, grassland, artificial ground etc.	Grid	National Catalogue Service for Geographic information
DEM elevation data	Elevation data terrain	Grid	Resources and Environment Science and Data Center of the Chinese Academy of Sciences
Normalized Difference Vegetation Index data	Vegetation coverage	Grid	Resources and Environment Science and Data Center of the Chinese Academy of Sciences
Administrative territorial data	Administrative boundary	Vector	Resources and Environment Science and Data Center of the Chinese Academy of Sciences

2.3 Research methodology

2.3.1 Temperature-humidity index

The temperature-humidity index refers to an index of the comprehensive perception of ambient temperature and humidity of the human body, calculated using Eq. 1:

$$I = T - 0.55 \times (1 - RH) \times (T - 14.4) \quad (1)$$

where I is the temperature-humidity index, retaining 1 decimal place; T is the average temperature of a certain evaluation period (°C); and RH is the average air relative humidity during an evaluation period (%).

2.3.2 Wind efficiency index

This refers to an index of comprehensively perceiving wind, temperature, and sunshine, calculated using Eq. 2:

$$K = -\left(10\sqrt{V} + 10.45 - V\right)(33 - T) + 8.55S \quad (2)$$

where K is the wind efficiency index, taken as an integer; T is the average temperature of a certain evaluation period (°C); V is the average wind speed (m/s); and S is the average hours of sunshine during an evaluation period, measured in hours per day (h/d).

Generally, an evaluation method combining the temperature-humidity and wind efficiency indices is used to

TABLE 2 Classification of climate comfort degree of human-settlement environments.

Rank	Feel extent	Temperature and humidity index	Wind efficiency index	Description of feeling of healthy people
1	Extremely cold	<14.0	<-400	Extremely cold, uncomfortable
2	Cold	14.0–16.9	−400–300	Relative cold, a little uncomfortable
3	Comfortable	17.0–25.4	−299–100	Comfortable
4	Hot	25.5–27.5	−99–10	Hot, a little uncomfortable
5	Sultry	>27.5	>-10	Sultry, uncomfortable

evaluate climate comfort. When the two indices are inconsistent, the wind efficiency index is used in the cold (winter) half-year, and the temperature-humidity index in the hot (summer) half-year. The wind efficiency index is used when the average wind speed exceeds 3 m/s during the evaluation period. The March–May period is regarded as spring, June–August as summer, September–November as autumn, and December–February as winter. High temperature-humidity and wind efficiency indices values indicate a relatively sultry human-settlement climate, whereas low values indicate an extremely cold human settlement climate. The only comfortable human-settlement climate is a moderate temperature-humidity and wind efficiency indices value (Table 2).

3 Results

3.1 Spatio–temporal evolution characteristics of climate comfort of human-settlement environments

3.1.1 Spatio–temporal evolution characteristics of the temperature-humidity index

We analyzed the temporal evolution characteristics of the temperature-humidity index and found that the index values of the 11 cities in the GBA increased with various intermittent fluctuations from 2005 to 2020 (Figure 2). From a spatial perspective, the temperature-humidity index values of the GBA exhibited gradual increases from north to south in 2020. We found that Macau was among the regions with the highest temperature-humidity index values, while the lowest value was found in Zhaoqing. We further ranked the regions according to the descending order of their temperature-humidity indices values. This analysis revealed the spatial evolution of the northern cities in the GBA (Zhaoqing, Guangzhou, and Huizhou) and most of the southern cities in the GBA (Jiangmen, Dongguan, Shenzhen, Zhuhai, Hong Kong, and Macau), which generally showed an overall growth trend. However, the spatial evolution of the central cities in the GBA (Foshan and Dongguan) and a single southern city in the GBA (Zhongshan) experienced decreases at first but then increased (exhibited growth). We also analyzed the growth range of the temperature-humidity index. It was found that the southern cities in the GBA with relatively large areas exhibited growth of the temperature-humidity index values by 0.8–1. The growth range of the temperature-humidity index values of the northern cities in the GBA was lower (0.6–0.7) (Figure 3).

3.1.2 Spatio–temporal evolution characteristics of wind efficiency index

Furthermore, we analyzed the temporal evolution characteristics of the wind efficiency index. It was found that the rank of the wind index interval range values in the GBA from 2005 to 2020 generally exhibited a decreasing trend first, and then changed to an increasing trend (Figure 4). From a spatial perspective, the wind efficiency index values of the GBA decreased from the central areas in the GBA to the periphery in 2020. Hong Kong exhibited the highest wind efficiency index value, while Zhaoqing exhibited the lowest. Compared with the temperature-humidity index, the spatial differences in wind efficiency in the different cities were more prominent. Moreover, the wind efficiency index values of the southern cities in the GBA demonstrated a growth range of 20–28, indicating relatively strong growth. However, the wind efficiency index values of the northern cities in the GBA exhibited weaker increases, with a growth range of 2–15 (Figure 5).

3.2 Seasonal and monthly evolution characteristics of climate comfort of human-settlement environments

3.2.1 Seasonal evolution characteristics of climate comfort of human-settlement environments

The seasonal evolution characteristics of the climate comfort of human-settlement environments in the GBA were analyzed from 2005 to 2020. No prominent change in the climate comfort of human-settlement environments was discerned in spring and autumn, but the climate comfort in summer and winter exhibited significant changes. We identified an increase in regional temperature in July–August, compared with that in previous years (2005, 2010, and 2015). However, the regional precipitation

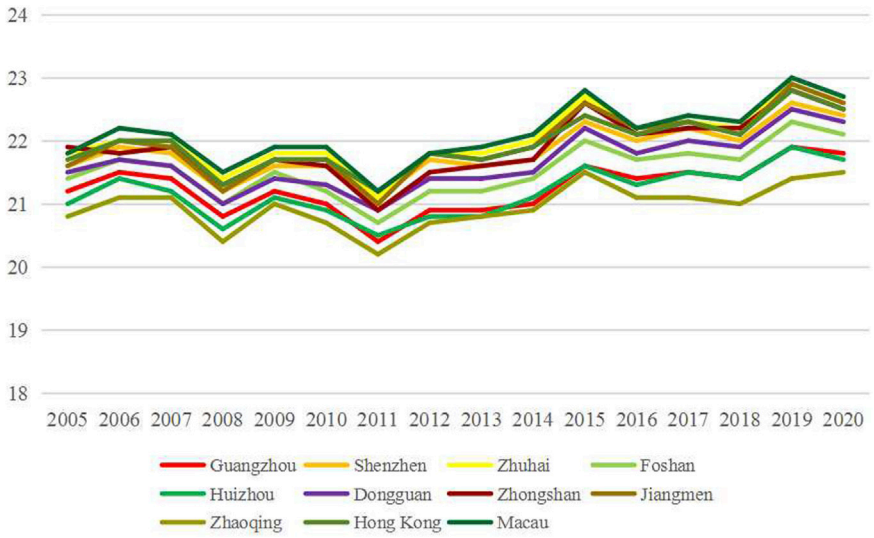

FIGURE 2
Temporal evolution diagram of the temperature-humidity index from 2005 to 2020.

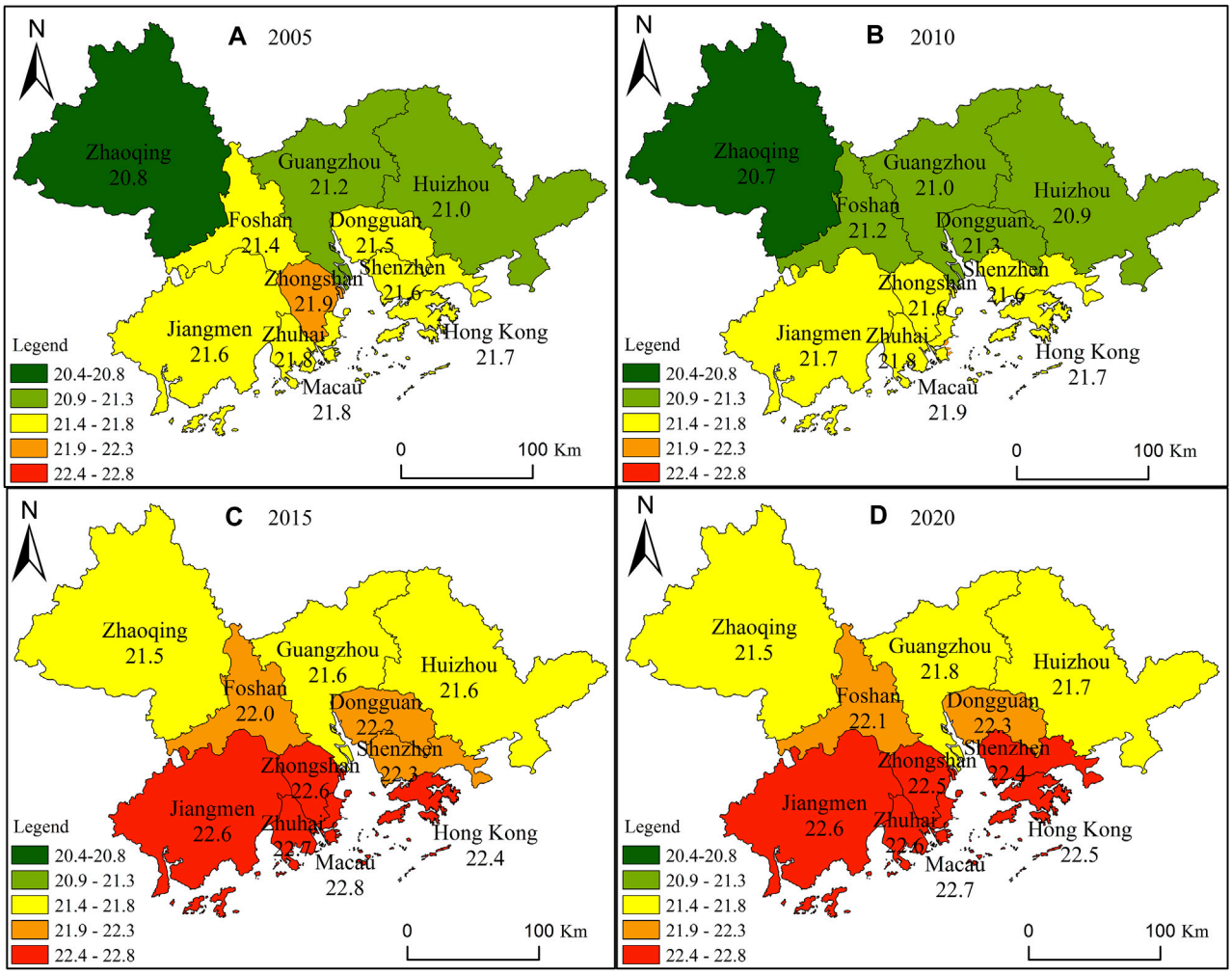

FIGURE 3
The annual change of temperature-humidity index in the Guangdong–Hong Kong–Macau Greater Bay Area in **(A)** 2005, **(B)** 2010, **(C)** 2015, and **(D)** 2020.

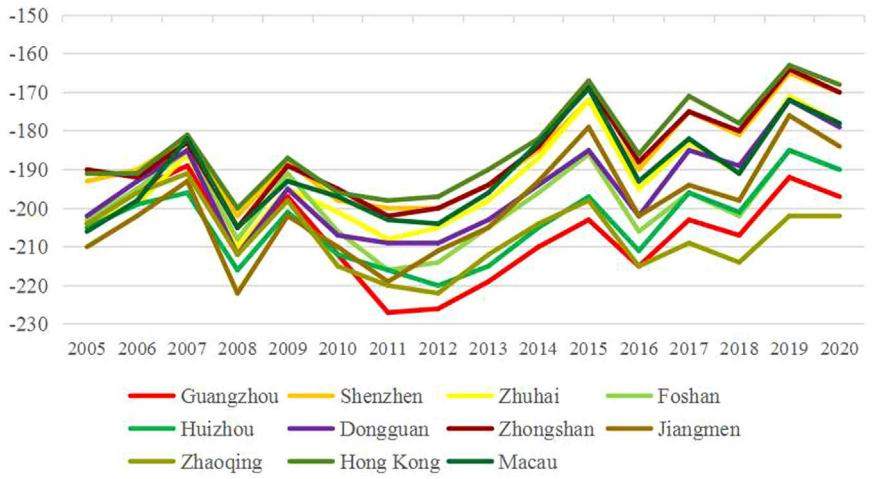

FIGURE 4
Temporal evolution diagram of the wind efficiency index from 2005 to 2020.

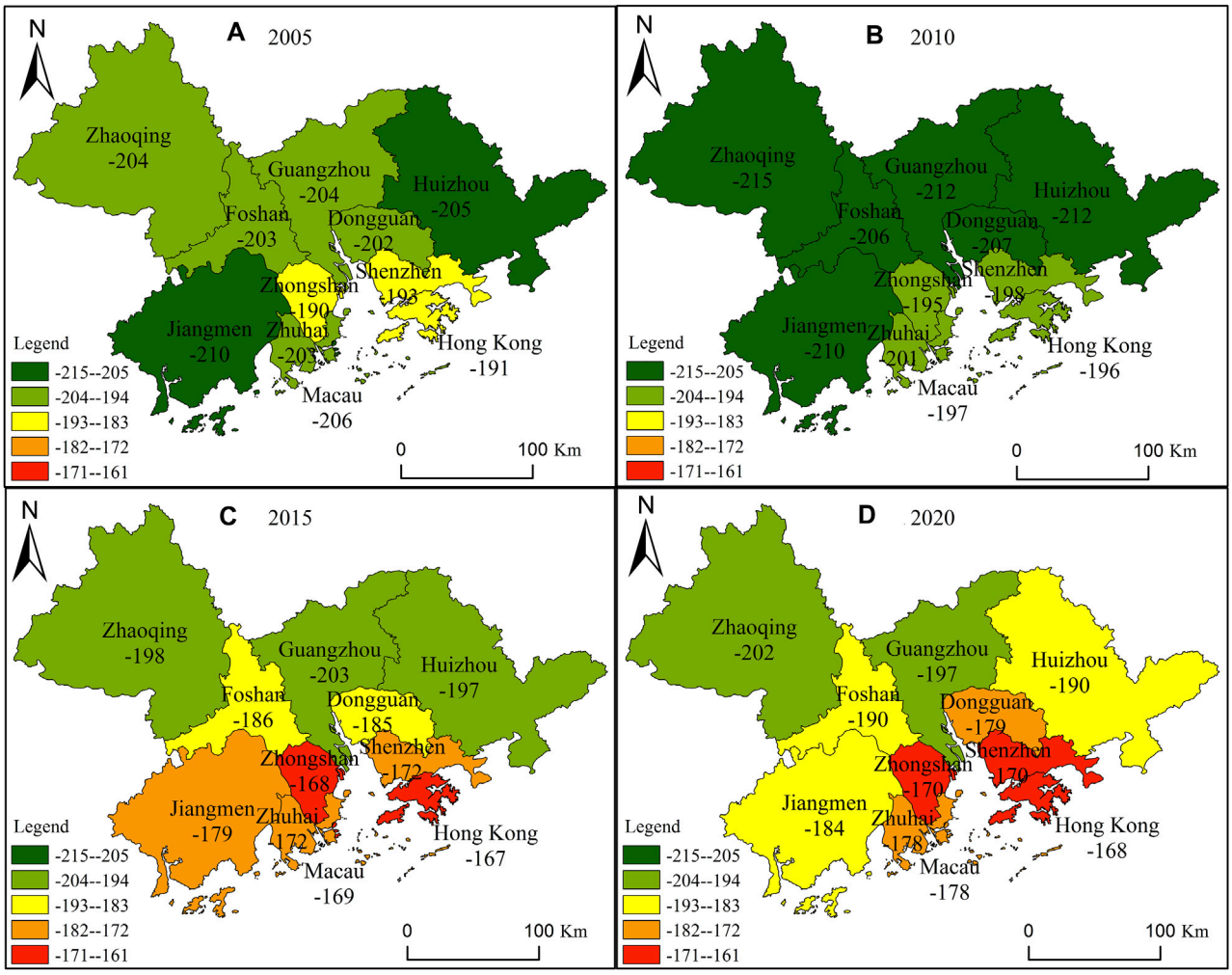

FIGURE 5
Annual change of wind efficiency index in Guangdong–Hong Kong–Macau Greater Bay Area in 2005, 2010, 2015, and 2020. Seasonal and monthly evolution characteristics of climate comfort of human-settlement environments.

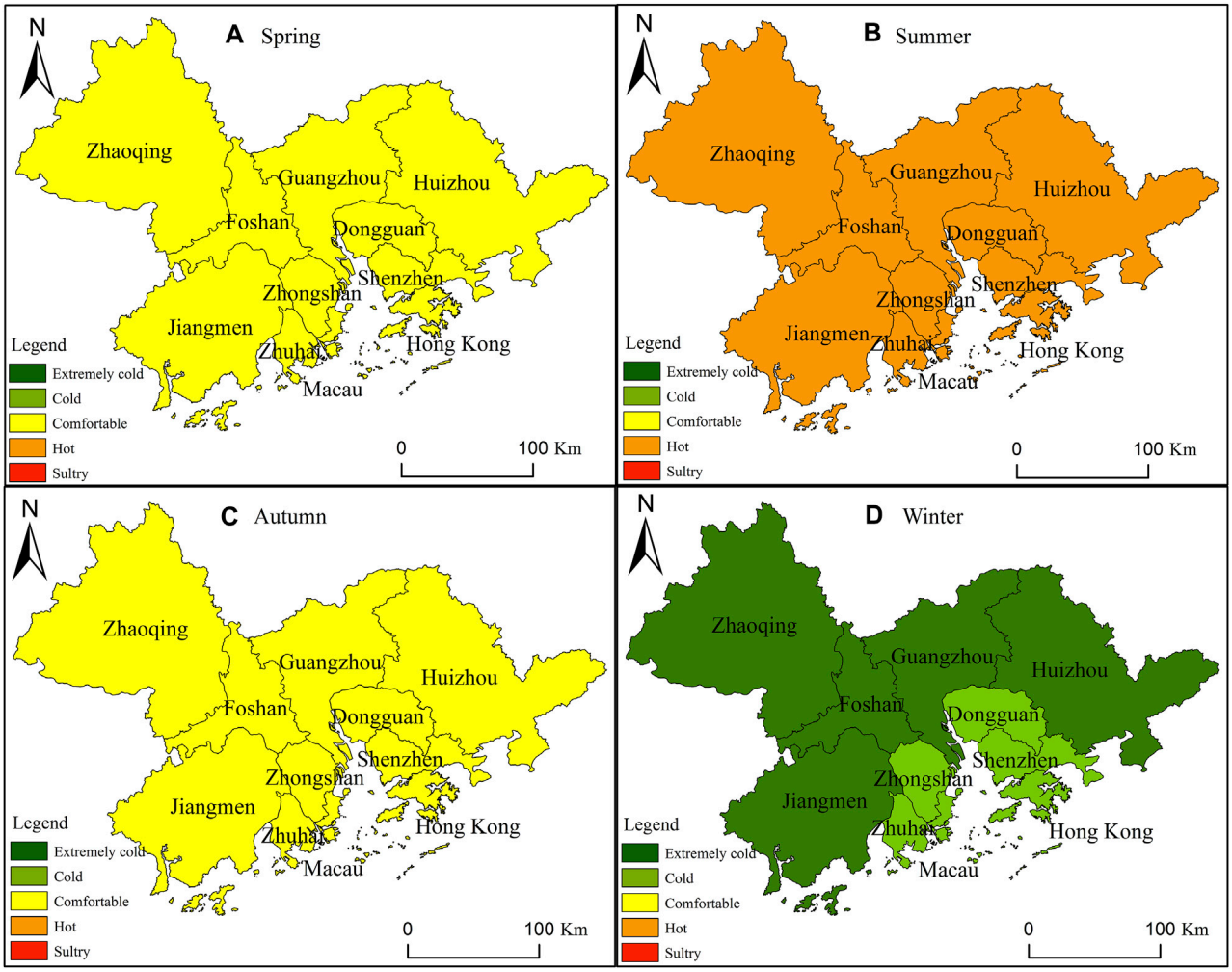

FIGURE 6
Seasonal change of climate comfort of human settlements in the Guangdong–Hong Kong–Macau Greater Bay Area in 2005.

decreased compared with that in previous years, and precipitation increased in the eastern regions in the GBA because of typhoons (Zhang et al., 2020). Moreover, the temperature in November–December increased and precipitation decreased (Li et al., 2021), compared with that in previous years. Thus, the climate comfort of human-settlement environments in the western cities in the GBA changed from "heat" to "sultry" gradually in the summer, while no prominent change was found in the summer for other cities. The climate comfort of human-settlement environments for peripheral cities in the GBA changed from "extremely cold" to "cold" in winter, while the climate comfort for the central cities in the GBA exhibited no significant change. Note that gas emissions, driven by the industrial transformation of different cities and anthropogenic activities during the process of urbanization also theoretically affect the climate comfort of human-settlement environments. The detected change in the climate comfort of human-settlement environments (from "heat" to "sultry") worsened the livability in the GBA in the summer, but the change in the climate comfort from "extremely cold" to "cold" ameliorated the livability in the GBA in winter.

The spatial evolution of the seasonal climate comfort of human-settlement environments was also analyzed in the GBA. It was found that all cities were somewhat comfortable in spring in 2020 (Figure 9). As the temperature increased in the summer, the climate comfort in the cities gradually worsened. Moreover, spatial heterogeneity of the climate comfort was discerned in the GBA. Overall, the western cities (Zhuhai, Jiangmen, Foshan, Zhongshan, and Macau) in the GBA were found to have a sultry climate, while the eastern cities (Guangzhou, Dongguan, Shenzhen, Huizhou, and Hong Kong) and a single northern city (Zhaoqing) had

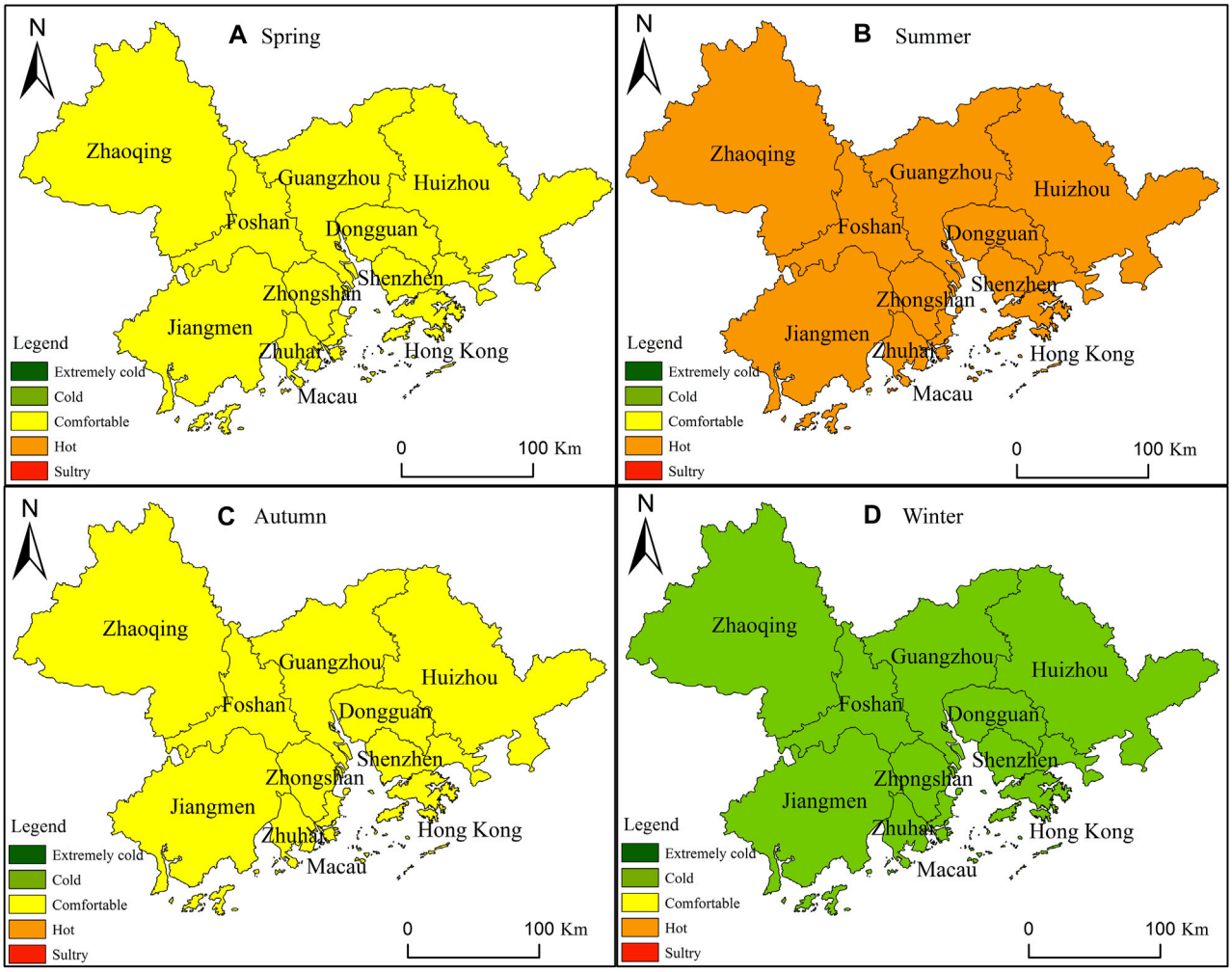

FIGURE 7
Seasonal change of climate comfort of human settlements in the Guangdong–Hong Kong–Macau Greater Bay Area in 2010.

comparatively better climate comfort. However, the climate comfort of human-settlement environments was still relatively hot. The human-settlement environments in different cities in the GBA were found to be comfortable in autumn, while the climate of all cities was reportedly relatively cold in winter. In 2005, the climate comfort of human-settlement environments in all cities was found to be comfortable in spring and autumn. However, the cities were found to be relatively hot in summer, with the peripheral cities in the GBA experiencing an extremely cold climate in winter (Figure 6). In 2010, the climate comfort of human settlement environments in spring, summer, and autumn was found to be the same as that in 2005, while the climate comfort of human-settlement environments for all cities was deemed cold in winter (Figure 7). In 2015, the climate comfort of human settlement environments for all cities in the GBA was somewhat high in spring and autumn, but the comfort for west-central cities in the bay (Zhongshan, Zhuhai, and Macao) was deemed "sultry" (Figures 8, 9).

All cities in the Beijing–Tianjin–Hebei region during the March–June and September–October periods were the most comfortable from a climate perspective (Cao and Wang, 2017). The comprehensive synthesis comfort period of the Hohhot–Baotou–Ordos region was mainly April–October (Zhao, 2022), while the months with a higher comfort level in the three northeastern provinces (Liaoning, Jilin, and Heilongjiang) were June–August (Bai, 2020). Although the GBA is hot and the climate comfort is worse than that in northern China in summer, the region is comfortable in both spring and autumn, compared with northern China. Moreover, the climate of human-settlement environments was cold in winter, but compared with that in northern

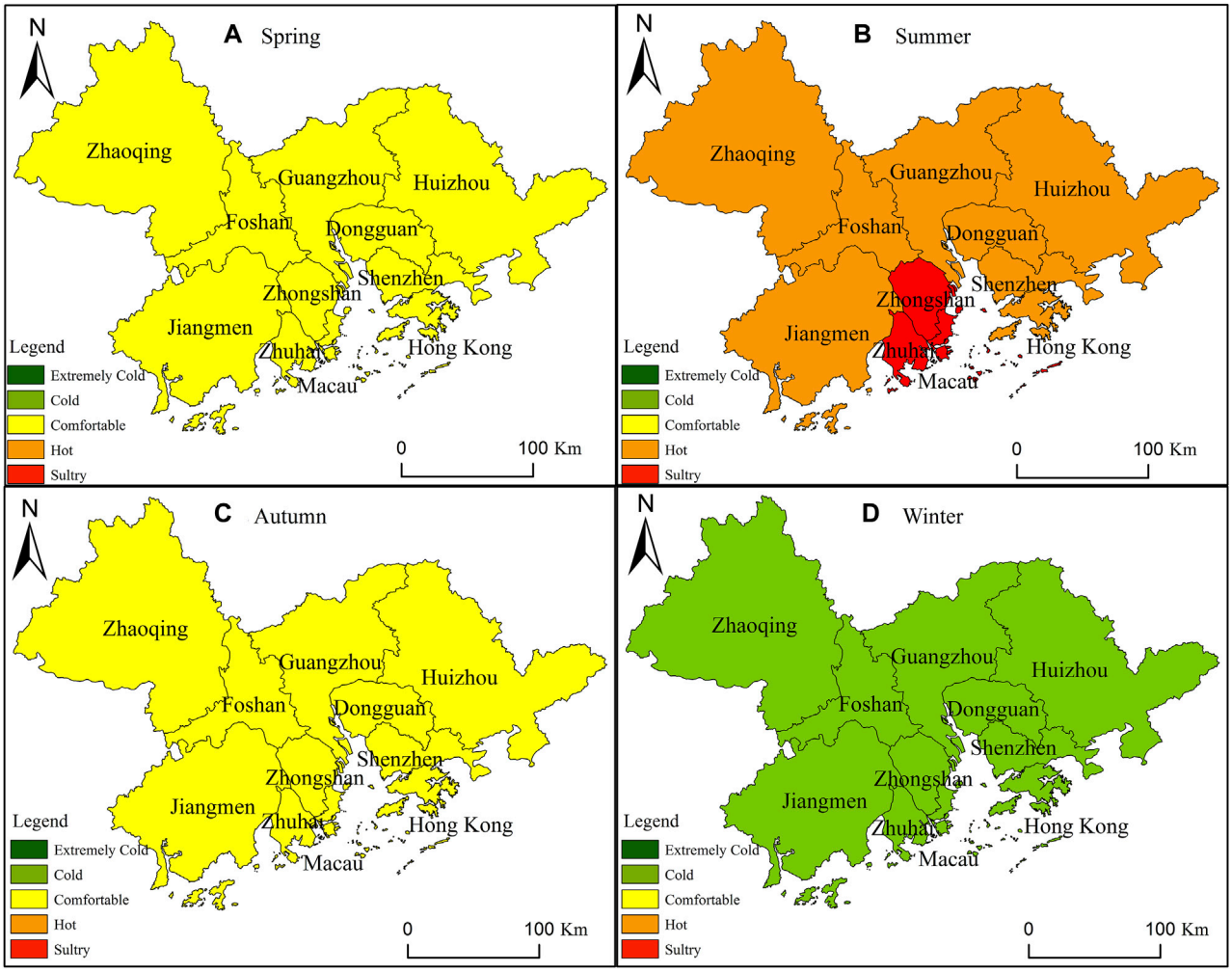

FIGURE 8
Seasonal change of climate comfort of human settlements in the Guangdong–Hong Kong–Macau Greater Bay Area in 2015.

China, which is extremely cold in winter, the GBA was evidently more comfortable.

3.2.2 Monthly evolution characteristics of climate comfort of human-settlement environments

The monthly changes in the climate comfort of human-settlement environments in the GBA were analyzed. As January and February represent winter months, the climate comfort of human-settlement environments is correspondingly cold in the GBA. Our results showed that the climate comfort changes from "cold" to "comfortable" in March and April, when the GBA experiences spring. May and June represent the transitional season for the GBA (from spring to summer), when the climate comfort gradually changes from "comfortable" to "hot." Overall, the climate comfort of human-settlement environments in the GBA can be characterized as "hot" in May, and the southwestern cities (Jiangmen, Zhongshan, Zhuhai, and Hong Kong) start experiencing extremely high temperatures in June. Thus, the climate comfort of human-settlement environments shifts to "sultry" in these cities, while the climate comfort of other cities in the area becomes "hot." In July, the GBA typically enters midsummer, and the climate comfort of human-settlement environments in all cities becomes "sultry." In August and September, the GBA experiences a transition from summer to autumn. In August, the climate comfort of human-settlement environments in all cities in the GBA becomes "hot." In September, besides the "comfortable" level of the climate comfort in Zhaoqing, the climate comfort of other cities was "hot." In October and November, the GBA enters the late autumn period, and the climate comfort of human-settlement environments in all cities can be deemed

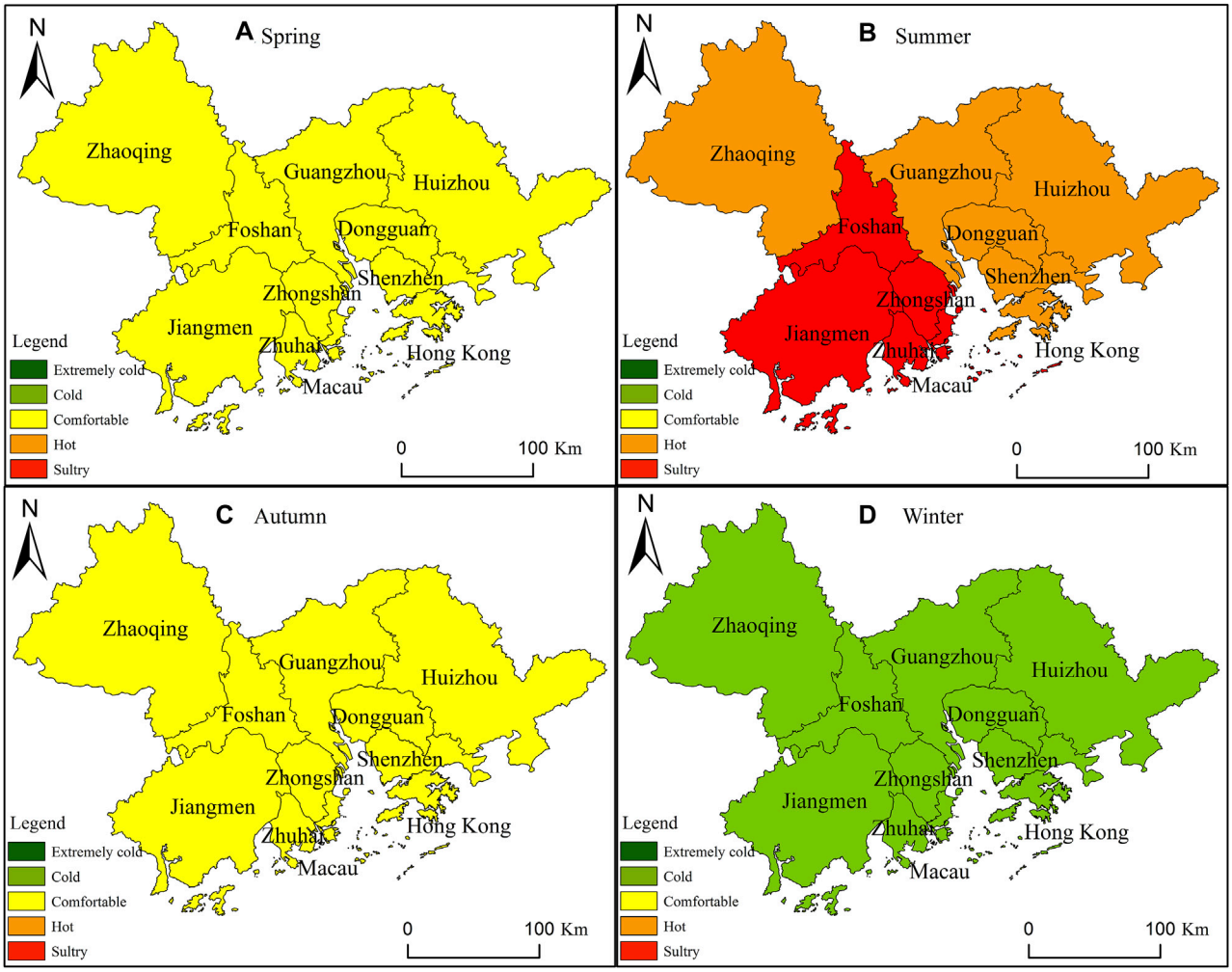

FIGURE 9
Seasonal change of climate comfort of human settlements in the Guangdong–Hong Kong–Macau Greater Bay Area in 2020.

as "comfortable." In December, the GBA experiences a seasonal change from autumn to winter, when the climate comfort of human-settlement environments in all cities tends to cool down; overall, the climate comfort level of human-settlement environments in Zhaoqing and Guangzhou prominently changed to "extremely cold," whereas the climate comfort level of human-settlement environments for all other cities was "cold," with their climate comfort experiencing a minor change (Figure 10). Notably, elucidating the seasonal and monthly evolution characteristics of climate comfort of human-settlement environments allows us to unravel the spatial characteristics of the "migratory" elderly population and it also allows us to determine the most comfortable period for tourism. Finally, our findings could provide data-driven guidelines for planning the migration of the elderly, while also establishing an innovative and livable highland.

4 Analysis of influencing factors

Human settlements represent a relationship between the five basic elements of ekistics: nature, human, society, buildings, and networks. Of these elements, natural environments play a basic function in human settlement. From the perspective of metropolises, urban groups, and large urban agglomerations, an urban area scale can be used to explore the relationship between various elements in human settlements for building a good livable environment. As global warming is intensifying, the GBA is experiencing

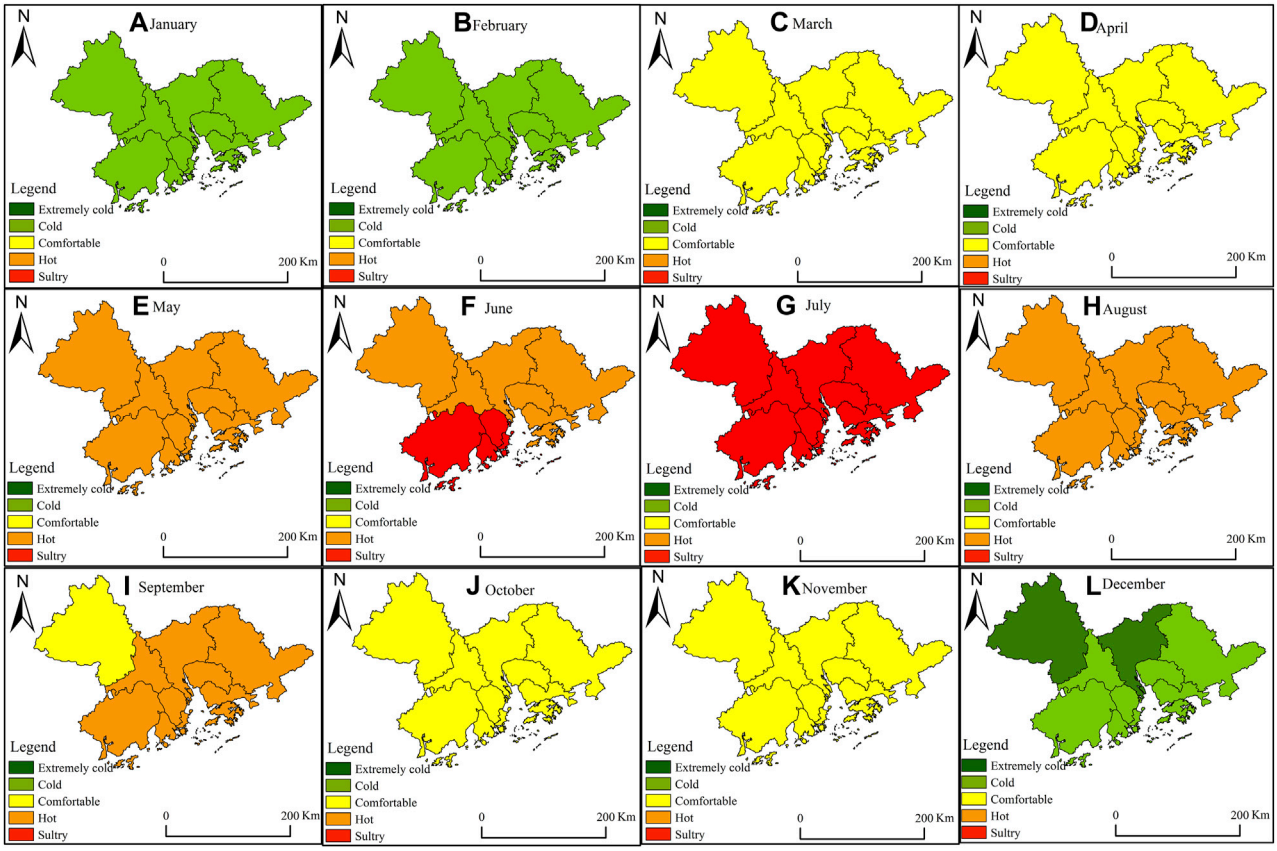

FIGURE 10
The monthly variation of the climate comfort of human settlements in the Guangdong–Hong Kong–Macau Greater Bay Area in 2020.

TABLE 3 Correlation of factors affecting climate comfort of human-settlement in 2005, 2010, 2015, and 2020.

	Temperature and humidity index				Wind efficiency index			
	Temperature and humidity index in 2005	Wind efficiency index in 2005	Temperature and humidity index in 2010	Wind efficiency index in 2010	Temperature and humidity index in 2015	Wind efficiency index in 2015	Temperature and humidity index in 2020	Wind efficiency index in 2020
Population size (ten thousand people)	0.000***	0.07*	0.004***	0.000***	0.001***	0.049**	0.000***	0.000***
Elevation (m)	0.000***	0.000***	0.000***	0.000***	0.000***	0.000***	0.002***	0.048**
Percentage of gross industrial production (%)	0.000***	0.003***	0.001***	0.082*	0.160	0.000***	0.000***	0.003***
Construction land area (Km^2)	0.000***	0.009***	0.452	0.000***	0.000***	0.001***	0.000***	0.072*

*Correlation is significant at the 0.1 level (2-tailed).
**Correlation is significant at the 0.05 level (2-tailed).
***Correlation is significant at the 0.01 level (2-tailed).

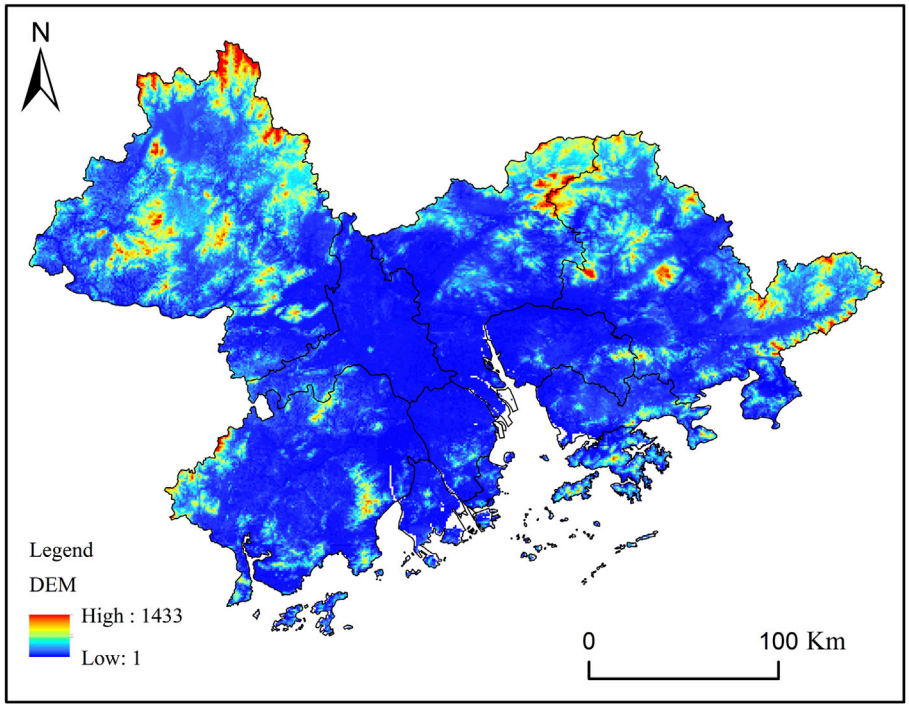

FIGURE 11
Digital elevation model (DEM) of the Guangdong–Hong Kong–Macau Greater Bay Area.

extreme temperatures more often (Huang et al., 2012). Thus, climate change crucially affects the climate comfort of human settlements in the area. Given the novelty of this research domain and the data availability, we selected six key indicators that could potentially affect the climate comfort of urban settlements: elevation (Wei and Wang, 2022), vegetation coverage (Hu et al., 2011), haze (Cai et al., 2017), population scale (Nwankwo et al., 2021), gross industrial production (%) (Streimikiene et al., 2012), and construction land area (Wang et al., 2020). Based on this, we performed a diagnosis of multicollinearity to select the required indices. Overall, the elevation, construction land area, population scale, and gross industrial production (%) passed the collinearity test. The correlation of the four elements with the temperature-humidity and wind efficiency indices was quantified using multiple logistic regression. The correlation analysis revealed some related factors, exhibiting a relationship with the temperature-humidity and wind efficiency indices in 2005, 2010, 2015, and 2020. However, there were significant differences in the indices as the influence of related factors on the temperature-humidity index was more important than that on the wind efficiency index. Additionally, the influence of natural factors on climate comfort was greater than that of anthropogenic activities (Table 3). Overall, this study elucidated that the factors influencing climate comfort were elevation, construction land, population scale, and the percentage of gross industrial production.

4.1 Effect of elevation on climate comfort of human-settlement environments

The topography of the GBA is mainly characterized by low mountains and hills. In general, different elevation levels fundamentally control regional meteorological elements such as temperature and wind speed, thereby affecting the climate comfort of human-settlement environments (Yan et al., 2022). Specifically, higher elevations lead to lower temperatures. The lower elevation (310 m) site is warmer (28.5°C average monthly maximum air temperature) and drier (224 mm yr^{-1}) than the upper elevation (844 m) site (23.5°C average monthly maximum air temperature; 272 mm yr^{-1}) (Link et al., 2003). Areas with high elevation are mainly distributed in the northern regions in the GBA, while areas in the southern regions have relatively low elevation (Figure 11). Thus, in the summer, the northern cities in the GBA enter the sultry period later than the southern cities. However, the shift to the comfortable period occurs earlier in the southern cities in the GBA in autumn, and this phenomenon is also affected by elevation. Moreover, the climate comfort of human-settlement

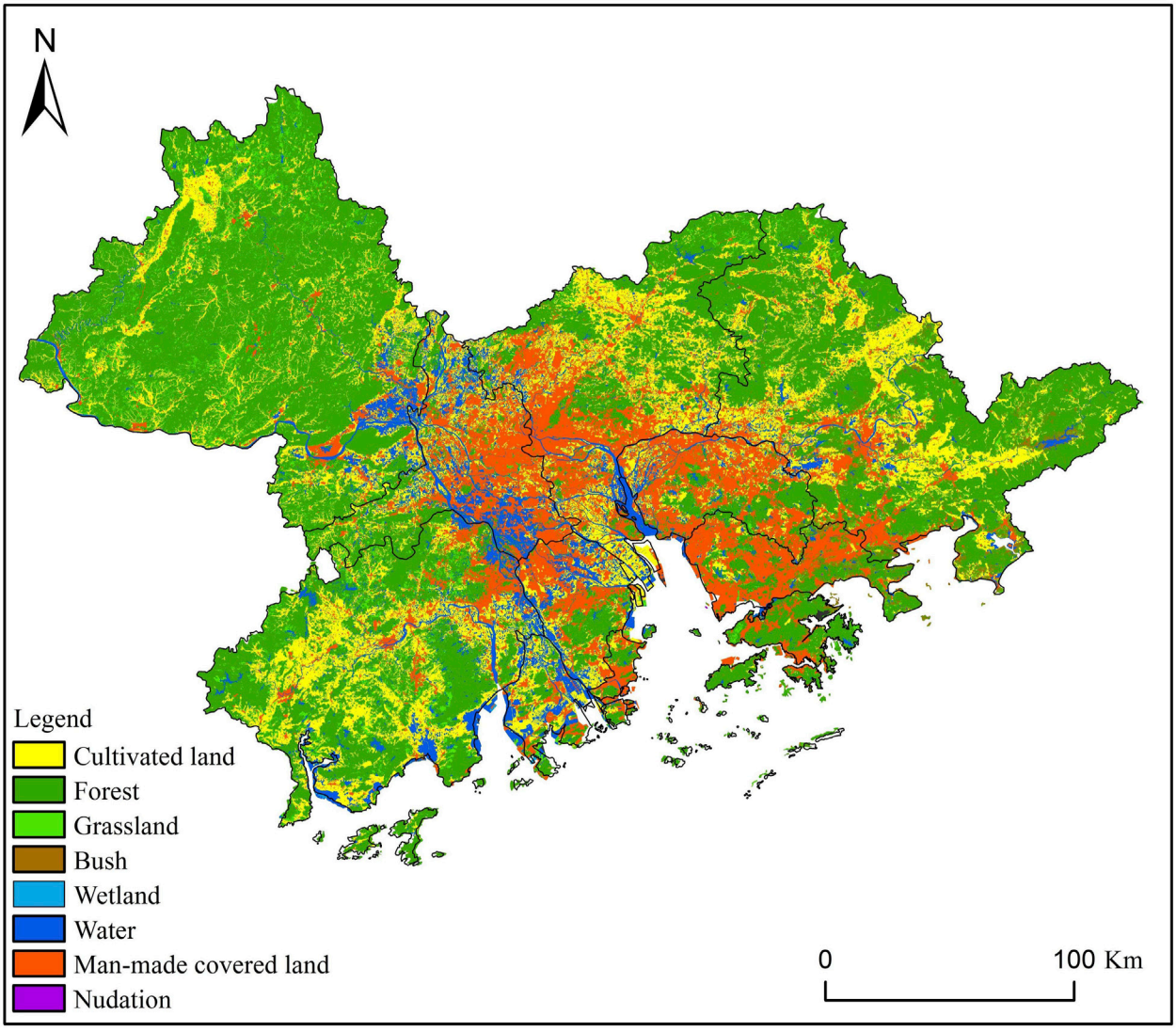

FIGURE 12
Surface cover map of the Guangdong–Hong Kong–Macau Greater Bay Area in 2020.

environments in the northern cities in the GBA is deemed extremely cold in the winter, while that of the southern cities is cold, which is also affected by the elevation.

4.2 Effect of construction land area on the climate comfort of human-settlement environments

The construction land area reflects the carrying and storage capacity of natural elements and the degree of land use change in a region of interest. This is an important factor that affects regional urban construction and development (Zhao et al., 2021). The various types of urban land have different contributions to the urban thermal environment. Among the various types of urban land, public service-facility land contributed the most to the urban thermal environment with an impact of 21.65%, followed by residential, industrial, and commercial service-facility lands, with impacts of 19.89, 18.44, and 17.58%, respectively. Additionally, the impact of road traffic land was 14.92%, whereas that of green square land was the lowest at 7.51%, 14.14% lower than that of public-service facility land (Chen et al., 2022). In general, cities with widespread construction land areas are characterized by higher development intensity, high pollution, and low vegetation coverage and, thus, experience a substantial heat island effect. Continuous urban development (building up) promotes the urban heat island effect. The magnitude of the

urban heat island ranged from 0.2 to 4.7°C, subject to seasonal variations and weather conditions (Weng and Yang., 2004). In contrast, cities with low construction land areas have less development intensity, less pollution, relatively high vegetation coverage, and thus, a relatively cooler climate (Ren et al., 2022). Urban land is mainly concentrated in the central cities in the GBA, while forests, grassland, and cultivated land are mainly concentrated in the peripheral cities. The concentration of urban land considerably exacerbates the heat island effect. Thus, the temperature of central cities in the GBA is generally higher than that of the peripheral cities (Figure 12). In addition, the southern areas of the GBA are adjacent to the ocean. The ocean has a large specific heat capacity, which affects the climate factors such as humidity and wind speed; it changes the annual evolution of climate comfort of human-settlement environments slightly or greatly, depending on the season. The average water-cooling island intensity ranges from 1.19 °C to 5.02°C in the four seasons, and the WCI (Wind Chill Index) intensity of all water bodies exhibits the largest fluctuation in summer (Wu et al., 2020).

4.3 Influence of the population scale on the climate comfort of human-settlement environments

Population growth can potentially promote the progress of scientific and technological innovation (Chen et al., 2018), thereby moving the region toward economic growth. However, economic development can trigger a sizeable growth in energy consumption, inducing a sharp increase in carbon emissions (Wang et al., 2021). Therefore, population growth and carbon emissions exhibit a positive correlation. In addition, population density and migration are also strongly correlated with carbon emissions. An increase in population density is unfavorable to the reduction of carbon emissions (Minx et al., 2013), and population migration from rural to urban areas will increase the carbon footprint; the apparent carbon emission difference between rural residents and migrants is about 1.5-ton CO_2 per capita (Zhang et al., 2016). Anthropogenic CO_2 emissions, driven by fossil fuel use, are the main driver of global warming. Thus, an increase in population can considerably alter the regional climate temperature, further affecting the climate comfort of human settlement environments.

4.4 Effect of gross industrial production change on the climate comfort of human-settlement environments

A reduction in gross industrial production can help reduce energy consumption, ameliorate energy utilization efficiency, and facilitate the optimization of the energy structure, thereby enhancing land carbon sinks. Such phenomena, in turn, alter the climate comfort of human-settlement environments. Furthermore, intensive gross industrial production can potentially attract high-polluting industries; thus, inducing a significant increase in energy consumption and greenhouse gas emissions and as an indirect effect, the urban heat island effect would be exacerbated in the case of increased production.

5 Discussion and conclusion

5.1 Discussion

This study elucidated unique aspects of climate comfort in the GBA. We estimated the climate comfort at unprecedented scales (national, urban agglomeration, provincial, and municipal scales) by analyzing the spatio–temporal evolution characteristics of climate comfort, on which few studies have been done. Thus, our study deepened the knowledge on the evolution of the climate comfort of human-settlement environments in the GBA. Moreover, we elucidated the factors influencing the studied phenomenon for the first time. In particular, we explored the influence of the related factors on the climate comfort of human-settlement environments by analyzing elevation, population scale, gross industrial production, and construction land area.

Despite these promising findings, our study had the following limitations: 1) because the statistical measurements between Guangdong, Hong Kong, and Macau were inconsistent, the interpretation of the impact of greenhouse gases and other related indicators on the climate comfort of human-settlement environments were critically hindered; 2) when the temperature-humidity and wind efficiency indices were inconsistent, the wind efficiency index was used to analyze the cold (winter) season, and the temperature-humidity index was used to analyze the hot (summer) season. Thus, the evaluation of the climate comfort of human-settlement environments was slightly asymmetric. In particular, the evaluation did not consider the intensity of interactions between these two indices and the comfortable threshold. Future studies should further refine the value range of the climate comfort of human-settlement environments. Moreover, the complex interplay between the two indices (temperature-humidity and wind efficiency indices) used for analysis should be quantified in future studies to improve the evaluation accuracy of the climate comfort of human-settlement environments.

5.2 Conclusion

This study used multiple datasets including ground-based climate (mean daily-value data) and land cover data in China, and the temperature-humidity and wind efficiency indices. These data were used to explore the spatio–temporal evolution of the climate comfort of human-settlement environments in the GBA. Furthermore, we elucidated the main factors affecting climate comfort and the following conclusions were drawn: 1) The annual changes in the climate comfort of human settlement environments were analyzed and this revealed that the values of the temperature-humidity index of the GBA decreased from north to south, and that of the wind

efficiency index decreased from the center to the periphery in 2020. From 2005 to 2020, the temperature-humidity index values of the northern cities and most southern cities in the GBA exhibited increases, while the central cities and some southern cities first exhibited a decrease and then an increase. Moreover, the wind efficiency index values of the GBA first exhibited a decreasing trend, but then an increasing trend from 2005 to 2020. Overall, the climate comfort of human-settlement environments in the GBA experienced a significant change in spring and summer; the summer conditions changed from "hot" to "sultry" and the winter conditions changed from "extremely cold" to "cold."

2) The spatio–temporal heterogeneity of the climate comfort of human-settlement environments in the GBA was mainly affected by the elevation, gross industrial production, population scale, and construction land area. Of these factors, elevation had the most significant effect on climate comfort. The impact of the population scale on climate comfort was secondary, followed by gross industrial production and construction land area.

3) The spatial characteristics of the climate comfort of human-settlement environments in the GBA were characterized by an asymmetric pattern. Moreover, the area experiences a comfortable climate in spring, autumn, and winter, thereby agreeing with existing studies (Li et al., 2016). Additionally, we compared the influence of natural factors with that of anthropogenic activities on the climate comfort of human settlement environments. This comparison demonstrated that the correlation between natural factors and the climate comfort of human-settlement environments was more important than that of anthropogenic activities.

Data availability statement

The original contributions presented in the study are included in the article/Supplementary Material, further inquiries can be directed to the corresponding author.

Author contributions

Conceptualization, CZ, and DZ; methodology, DZ, and YC; software, YC, and YW; Validation, CZ, and GZ; formal analysis, CZ, and GZ; data curation, DZ, and YC; writing-original draft, GZ, and DZ; writing-review and editing, CZ, and GZ. All authors have read and agreed to the published version of the manuscript.

Funding

This research was supported by the Major Program of the National Social Science Foundation of China (Grant No. 21&ZD107).

Conflict of interest

The authors declare that the research was conducted in the absence of any commercial or financial relationships that could be construed as a potential conflict of interest.

Publisher's note

All claims expressed in this article are solely those of the authors and do not necessarily represent those of their affiliated organizations, or those of the publisher, the editors and the reviewers. Any product that may be evaluated in this article, or claim that may be made by its manufacturer, is not guaranteed or endorsed by the publisher.

Supplementary material

The Supplementary Material for this article can be found online at: https://www.frontiersin.org/articles/10.3389/fenvs.2022.1001064/full#supplementary-material

References

Amininia, K., Abad, B., Safarianzengir, V., GhaffariGilandeh, A., and Sobhani, B. (2020). Investigation and analysis of climate comfort on people health tourism in Ardabil province, Iran. *Air Qual. Atmos. Health* 13, 1293–1303. doi:10.1007/s11869-020-00883-x

Amorosi, A., Bini, M., Giacomelli, S., Pappalardo, M., Ribecai, C., Rossi, V., et al. (2013). Middle to late Holocene environmental evolution of the Pisa coastal plain(Tuscany, Italy) and early human settlements. *Quat. Int.* 303, 93–106. doi:10.1016/j.quaint.2013.03.030

Bai, Z. (2020). Spatio-temporal differences in climate comfort of human settlements in the three provinces of Northeast China and influencing factor. Dalian: Liaoning Normal University.

Bakhtiari, B., Bakhtiari, A., and Gorouh, Z. (2018). Investigation of climate change impacts on tourism climate comfort in Iran. *Glob. Nest J.* 20 (2), 291–303. doi:10.30955/gnj.002435

Cai, W., Li, K., Liao, H., Wang, H., and Wu, L. (2017). Weather conditions conducive to Beijing severe haze more frequent under climate change. *Nat. Clim. Chang.* 7, 257–262. doi:10.1038/NCLIMATE3249

Cândido, C., de Dear, R., Lamberts, R., and Bittencourt, L. (2010). Air movement acceptability limits and thermal comfort in Brazil's hot humid climate zone. *Build. Environ.* 45, 222–229. doi:10.1016/j.buildenv.2009.06.005

Cao, W., and Wang, S. (2017). Evaluation of climate suitability for urban human settlement in Beijing-Tianjin-Hebei region. *J. Glaciol. Geocryol.* 39 (2), 435–442. doi:10.7522/j.issn.1000-0240.2017.0050

Cao, Y., Gao, L., and Wang, X. (2016). Regional characteristics of climate comfort in summer in Liaoning during past 30 years. *Sci. Geogr. Sin.* 36 (8), 1205–1211. doi:10.13249/j.cnki.sgs.2016.08.011

Cao, Y., Sun, Y., and Wu, M. (2019). Spatial and temporal characteristics of the periods of climate comfort in the Beijing-Tianjin-Hebei region from 1966 to 2015. *Acta Ecol. Sin.* 39 (20), 7567–7582. doi:10.105846/stxb201805181096

Celuppi, M., Meirelles, C., Cymrot, R., Borst, B., and Gobo, J. (2019). Preliminary approach to the analysis of climate perception and human thermal comfort for riverside dwellings the Brazilian Amazon. *J. Build. Eng.* 23, 77–89. doi:10.1016/j.jobe.2019.01.019

Cetin, M. (2020). Climate comfort depending on different altitudes and land use in the urban areas in Kahramanmaras City. *Air Qual. Atmos. Health* 13, 991–999. doi:10.1007/s11869-020-00858-y

Chen, L., Li, X., Yao, Y., and Chen, D. (2018). Effect of population agglomeration on urban economic growth in China. *Acta Geogr. Sin.* 73 (6), 1107–1120. doi:10.11821/dlxb201806009

Chen, Y., Yang, J., Yang, R., Xiao, X., and Xia, J. (2022). Contribution of urban functional zones to the spatial distribution of urban thermal environment. *Build. Environ.* 216, 109000. doi:10.1016/j.buildenv.2022.109000

Cheng, Q., and Zhong, F. (2019). Evaluation of tourism climate comfort in the Grand Shangri-La region. *J. Mt. Sci.* 16 (6), 1452–1469. doi:10.1007/s11629-018-5081-4

Cheung, C., and Hart, M. (2014). Climate change and thermal comfort in Hong Kong. *Int. J. Biometeorol.* 58, 137–148. doi:10.1007/s00484-012-0608-9

Dulal, H., and Akbar, S. (2013). Greenhouse gas emission reduction options for cities: Finding the "Coincidence of Agendas" between local priorities and climate change mitigation objectives. *Habitat Int.* 38, 100–105. doi:10.1016/j.habitatint.2012.05.001

Eludoyin, O., Adelekan, I., Webster, R., and Eludoyin, A. (2014). Air temperature, relative humidity, climate regionalization and thermal comfort of Nigeria. *Int. J. Climatol.* 34, 2000–2018. doi:10.1002/joc.3817

Giannakis, E., Bruggeman, A., Poulou, D., Zoumides, C., and Eliades, M. (2016). Linear parks along urban rivers: Perceptions of thermal comfort and climate change adaptation in Cyprus. *Sustainability* 8, 1023. doi:10.3390/su8101023

Gonzalez-Longo, C., and Sahabuddin, M. (2019). High-rise social housing in hot-humid climates: Towards an 'airhouse' standard for comfort. *Appl. Sci. (Basel).* 9, 4985. doi:10.3390/app9234985

Hasanah, N., Maryetnowati, D., Edelweis, F., Indriyani, F., and Nugrahayu, Q. (2020). The climate comfort assessment for tourism purposes in Borobudur Temple Indonesia. *Heliyon* 6, e05828. doi:10.1016/j.heliyon.2020.e05828

Hu, M., Mao, F., Sun, H., and Hou, Y. (2011). Study of normalized difference vegetation index variation and its correlation with climate factors in the three-river-source region. *Int. J. Appl. Earth Observation Geoinformation* 13, 24–33. doi:10.1016/j.jag.2010.06.003

Huang, Q., Chen, Z., and Liu, Z. (2012). Temporal and spatial variations of extreme temperature in Guangdong over the last 60 years in the background of global warming. *Trop. Geogr.* 32 (3), 246–251. doi:10.13284/j.cnki.rddl.001618

Kambezidis, H., Psiloglou, B., Varotsos, K., and Giannakopoulos, C. (2021). Climate change and thermal comfort in Greece. *Climate* 9, 10. doi:10.3390/cli9010010

Katavoutas, G., Founda, D., Kitsara, G., and Giannakopoulos, C. (2021). Climate change and thermal comfort in top tourist destinations—the case of santorini(Greece). *Sustainability* 13, 9107. doi:10.3390/su13169107

Kong, Q., Zheng, J., Fowler, H., Ge, Q., and Xi, J. (2019). Climate change and summer thermal comfort in China. *Theor. Appl. Climatol.* 137, 1077–1088. doi:10.1007/s00704-018-2648-5

Lei, H., Zhang, H., Liu, X., Yang, X., Duan, H., Wu, T., et al. (2020). Climate comfort evaluation of national 5A tourist attractions in the mainland of China based on universal thermal climate index. *Adv. Meteorology*, 1. 4256164. doi:10.1155/2020/4256164

Li, D., Yang, Z., Shi, H., Luan, F., and Wang, Z. (2014). Tourism climate and its comfort degree in Urumqi. *Arid Zone Res.* 31 (3), 404–409. doi:10.13866/j.azr.2014.03.008

Li, R., and Chi, X. (2014). Thermal comfort and tourism climate changes in the Qinghai-Tibet Plateau in the last 50 years. *Theor. Appl. Climatol.* 117, 613–624. doi:10.1007/s00704-013-1027-5

Li, S., Sun, M., Zhang, W., Tan, L., Zhu, N., and Wang, Y. (2016). Spatial patterns and evolving characteristics of climate comfortable period in the mainland of China: 1961-2010. *Geogr. Res.* 35 (11), 2053–2070. doi:10.11821/dlyj201611005

Li, W., Du, Y., Liu, W., and Pang, G. (2021). Comments on the characteristics and its impact of weather and climate in Guangdong province from November to December in 2020. *Guangdong meteorol.* Inside front cover, inside back cover, 43. doi:10.3969/j.issn.1007-6190.2021.01.020

Li, X., Li, S., Tian, S., Guan, Y., and Liu, H. (2021) Air quality and the spatial-temporal differentiation of mechanisms underlying Chinese urban human settlements. *Land*, 10:1207. doi:10.3390/land10111207

Link, S., Smith, J., Halvorson, J., and Bolton, H. (2003). A reciprocal transplant experiment within a climatic gradient in a semiarid shrub-steppe ecosystem: Effects on bunchgrass growth and reproduction, soil carbon, and soil nitrogen. *Glob. Chang. Biol.* 9, 1097–1105. doi:10.1046/j.1365-2486.2003.00647.x

Liu, P., Liao, L., and Liu, C. (2013). Urban residential amenity index and its composition factors: The case of Changsha County in Hunan Province. *Prog. Geogr.* 32 (5), 769–776. doi:10.11820/dlkxjz.2013.05.008

Liu, S., Long, B., Pan, Z., Lun, F., Song, Y., Yuan, W., et al. (2020). Evaluation of climatic comfort of living environment based on age differentials in Beijing-Tianjin-Hebei Area. *Ecosyst. Health Sustain.* 6 (1), 1843371. doi:10.1080/20964129.2020.1843371

Masoudi, M. (2021). Estimation of the spatial climate comfort distribution using tourism climate index(TCI)and inverse distance weighting(IDW) (case study:Fars Province, Iran). *Arab. J. Geosci.* 14, 363. doi:10.1007/s12517-021-06605-6

Minx, J., Baiocchi, G., Wiedmann, T., Barrett, J., Creutzig, F., Feng, K. S., et al. (2013). Carbon footprints of cities and other human settlements in the UK. *Environ. Res. Lett.* 8, 035039. doi:10.1088/1748-9326/8/3/035039

Müller, N., Wilhelm, K., and Barlag, A. (2014). Counteracting urban climate change: Adaptation measures and their effect on thermal comfort. *Theor. Appl. Climatol.* 115, 243–257. doi:10.1007/s00704-013-0890-4

Nasirihendkhaleh, E., Zahraei, A., Ghadiri, H., and Komasi, H. (2014). Zoning evaluation of Eco-Touristic potentials of bio-climatic comfortability in the province of Fars, using Geographical information system(GIS). *Int. J. Adv. Res.* 2 (4), 768–776.

Nwankwo, C., Ossai, O., Ayadiuno, R., and Ikeogu, C. (2021). Spatial dimension of climate change vulnerability and urbanization relationship in Nigeria. *Int. J. Urban Sci.*, 1–22. doi:10.1080/12265934.2021.1956365

Orosa, J., Costa, A., Rodríguez-Fernández, A., and Roshan, G. (2014). Effect of climate change on outdoor thermal comfort in humid climates. *J. Environ. Health Sci. Eng.* 12, 46. doi:10.1186/2052-336X-12-46

Ren, J., Yang, J., Zhang, Y., Xiao, X., Xia, J., Li, X., et al. (2022). Exploring thermal comfort of urban buildings based on local climate zones. *J. Clean. Prod.* 340, 130744. doi:10.1016/j.jclepro.2022.130744

Salata, F., Golasi, I., Proietti, R., and Vollaro, A. (2017). Implications of climate and outdoor thermal comfort on tourism: The case of Italy. *Int. J. Biometeorol.* 61, 2229–2244. doi:10.1007/s00484-017-1430-1

Streimikiene, D., Balezentis, T., and Krisciukaitiene, I. (2012). Promoting interactions between local climate change mitigation, sustainable energy development, and rural development policies in Lithuania. *Energy policy* 50, 699–710. doi:10.1016/j.enpol.2012.08.015

Tian, S., Qi, A., Li, Z., Pan, X., Liu, Y., and Li, X. (2022). Urban "three states" human settlements high-quality coordinated development. *Buildings* 12, 178. doi:10.3390/buildings12020178

Tseliou, A., Tsiros, I., Lykoudis, S., and Nikolopoulou, M. (2010). An evaluation of three biometeorological indices for human thermal comfort in urban outdoor areas under real climatic conditions. *Build. Environ.* 45, 1346–1352. doi:10.1016/j.buildenv.2009.11.009

Wang, R., Zhang, H., Qiang, W., Li, F., and Peng, J. (2021). Spatial characteristics and influencing factors of carbon emissions in county-level cities of China based on urbanization. *Prog. Geogr.* 40 (12), 1999–2010. doi:10.18306/dlkxjz.2021.12.002

Wang, S., Liu, Y., Gao, Q., Li, H., Yu, Y., and Yang, L. (2021). Applicability of passive design strategies in China promoted under global warming in past half century. *Build. Environ.* 195, 107777. doi:10.1016/j.buildenv.2021.107777

Wang, Y., Song, L., Han, Z., Liao, Y., Xu, H., Zhai, J., et al. (2020). Climate-related risks in the construction of xiongan new area, China. *Theor. Appl. Climatol.* 141, 1301–1311. doi:10.1007/s00704-020-03277-2

Wei, X., and Wang, X. (2022). Analyzing the spatial distribution of LST and its relationship with underlying surfaces in different months by classification and intersection. *Front. Environ. Sci.* 10, 872282. doi:10.3389/fenvs.2022.872282

Weng, Q., and Yang, S. (2004). Managing the adverse thermal effects of urban development in a densely populated Chinese city. *J. Environ. Manag.* 70, 145–156. doi:10.1016/j.jenvman.2003.11.006

Wu, J., Li, C., Zhang, X., Zhao, Y., Liang, J., and Wang, Z. (2020). Seasonal variations and main influencing factors of the water cooling islands effect in Shenzhen. *Ecol. Indic.* 117, 106699. doi:10.1016/j.ecolind.2020.106699

Yan, W., He, Y., and Qu, X. (2022). Elevation gradient dependence of extreme climate indices on Yunnan Plateau, China. *Int. J. Climatol.*, 1–20. doi:10.1002/joc.7578

Yang, J., Wang, Y., Xiu, C., Xiao, X., Xia, J., and Jin, C. (2020). Optimizing local climate zones to mitigate urban heat island effect in human settlements. *J. Clean. Prod.* 275, 123767. doi:10.1016/j.jclepro.2020.123767

Yang, J., Xin, J., Zhang, Y., Xiao, X., and Xia, J. (2022). Contributions of sea-land breeze and local climate zones to daytime and nighttime heat island intensity. *npj Urban Sustain.* 2, 12. doi:10.1038/s42949-022-00055-z

Yao, X., Zhang, M., Zhang, Y., Xiao, H., and Wang, J. (2021). Research on evaluation of climate comfort in northwest China under climate change. *Sustainability* 13, 10111. doi:10.3390/su131810111

Yin, W., Pan, Z., Pan, Y., Han, G., Wang, J., Huang, N., et al. (2018). The temporal and spatial characteristics of climatic comfortability on human settlement in mainland China. *China Popul. Resour. Environ.* 28 (7), 5–8.

Yu, Q., Shen, T., Wang, S., and Zhang, Y. (2021). Natural suitability evaluation of human settlement environment in the town of Huangshan City based on GIS. *Environ. Pollut. Control* 43 (7), 880–885. doi:10.15985/j.cnki.1001-3865.2021.07.015

Yüksel, A., Arici, M., Krajčík, M., and Karabay, H. (2020). Experimental investigation of thermal comfort and CO(2) concentration in mosques: A case study in warm temperate climate of yalova, Turkey. *Sustain. Cities Soc.* 52, 101809. doi:10.1016/j.scs.2019.101809

Zeng, D., Wu, J., Mu, Y., Li, H., Deng, M., Wei, Y., et al. (2020). An assessment of tourism climate comfort in the China-Pakistan economic corridor. *Sustainability* 12, 6981. doi:10.3390/su12176981

Zhang, C., Cao, X., and Ramaswami, A. (2016). A novel analysis of consumption-based carbon footprints in China: Unpacking the effects of urban settlement and rural-to-urban migration. *Glob. Environ. Change* 39, 285–293. doi:10.1016/j.gloenvcha.2016.06.003

Zhang, D., Zhou, C., Sun, D., and Qian, Y. (2022). The influence of the spatial pattern of urban road networks on the quality of business environments: The case of dalian city. *Environ. Dev. Sustain.* 24, 9429–9446. doi:10.1007/s10668-021-01832-z

Zhang, D., Zhou, C., Zhou, Y., and Zikirya, B. (2022). Spatiotemporal relationship characteristic of climate comfort of urban human settlement environment and population density in China. *Front. Ecol. Evol.* 10, 953725. doi:10.3389/fevo.2022.953725

Zhang, L., Guo, X ., Du, Y., and Li, W. (2020). Comments on the characteristics and its impact of weather and climate in Guangdong province from July to August in 2020. *Guangdong meteorol.* Inside front cover, inside back cover, 42. doi:10.3969/j.issn.1007-6190.2020.05.0205

Zhao, F., Lan, X., Li, W., Zhu, W., and Li, T. (2021). Influence of land use change on the Surface albedo and climate change in the qinling-daba mountains. *Sustainability* 13, 10153. doi:10.3390/su131810153

Zhao, J., and Wang, S. (2021). Spatio-temporal evolution and prediction of tourism comprehensive climate comfort in henan province, China. *Atmosphere* 12, 823. doi:10.3390/atmos12070823

Zhao, J., Wu, Y., Liang, S., and Piao, X. (2022). Activation of SSAT1/ALOX15 Axis Aggravates cerebral ischemia/reperfusion injury via triggering neuronal ferroptosis. *Neuroscience* 38 (2), 78–90. doi:10.1016/j.neuroscience.2022.01.017

frontiers | Frontiers in Ecology and Evolution

TYPE Systematic Review
PUBLISHED 14 September 2022
DOI 10.3389/fevo.2022.975426

Check for updates

OPEN ACCESS

EDITED BY
Bing Xue,
Institute of Applied Ecology (CAS), China

REVIEWED BY
Bo Fu,
Chinese Academy of Sciences (CAS), China
Bao-Jie He,
Chongqing University, China

*CORRESPONDENCE
Chunyao Guo
2001424 @stu.neu.edu.cn

SPECIALTY SECTION
This article was submitted to Environmental Informatics and Remote Sensing, a section of the journal Frontiers in Ecology and Evolution

RECEIVED 22 June 2022
ACCEPTED 25 August 2022
PUBLISHED 14 September 2022

CITATION
Gao Y, Guo C and Wei Y (2022) Study on the dynamic evolution and synergistic relationship between urbanization and eco-efficiency through the selection of 76 agricultural counties and districts in Liaoning province as research units. *Front. Ecol. Evol.* 10:975426. doi: 10.3389/fevo.2022.975426

COPYRIGHT
© 2022 Gao, Guo and Wei. This is an open-access article distributed under the terms of the Creative Commons Attribution License (CC BY). The use, distribution or reproduction in other forums is permitted, provided the original author(s) and the copyright owner(s) are credited and that the original publication in this journal is cited, in accordance with accepted academic practice. No use, distribution or reproduction is permitted which does not comply with these terms.

Study on the dynamic evolution and synergistic relationship between urbanization and eco-efficiency through the selection of 76 agricultural counties and districts in Liaoning province as research units

Yanpeng Gao[1], Chunyao Guo[1]* and Ye Wei[2]

[1]Jangho Architecture College, Northeastern University, Shenyang, China, [2]School of Geographical Sciences, Northeast Normal University, Changchun, China

Coordination and interaction among urbanization processes, efficient resource utilization, and ecological protection have emerged as key challenges for spatial development and protection of a territory. In this paper, we quantitatively determined the urbanization level and eco-efficiency by utilizing the entropy evaluation method and the SBM model with undesirable outputs, and then employed kernel density estimation, center movement method, and bivariate Moran's I index method to examine the spatial-temporal pattern as well as the interaction between the above two factors. This study provides a new framework for the measurement of urbanization and eco-efficiency and their interaction. The results of the study in the research area demonstrate that: (1) From 2013 to 2017, the urbanization level exhibited a steady increase from 0.2468 to 0.2789, while eco-efficiency depicted an N-shaped development trend before suffering an overall decline from 0.4364 to 0.3117; (2) the low-level units of urbanization level illustrated a strong convergence trend, and each unit possessed low eco-efficiency with weak spatial matching in general; (3) an ambiguous symbiosis exists between the center of gravity of movements of the two factors within each region; and (4) a global positive correlation was found between the urbanization level and eco-efficiency in Liaoning Province. The global Moran's I index first increased and then decreased.

KEYWORDS

interaction and synergy, spatial-temporal evolution, urbanization, Liaoning Province in China, eco-efficiency

Introduction

Rapid urbanization has become a global phenomenon in recent decades, leading to several environmental problems such as the heat island effect, habitat degradation, congestion, and other challenges to human life (Ochoa et al., 2018). Against this backdrop, sustainable management, considering multiple aspects such as technology,

economy, society, and environment, is on the agenda (Sheikhipour et al., 2018; Cohen-Shacham et al., 2019; United Nations, 2020). As an important indicator to measure the input-output mode of factors, the concept of eco-efficiency was first introduced by Schaltegger and Sturm (Schaltegger and Sturm, 1990), and since then, its connotation has been enriched by numerous international organizations and scholars (Weizsäcker et al., 1997; Schaltegger and Synnestvedt, 2002; Reith and Guirdy, 2003). Eco-efficiency is considered an important basis for measuring the quality of urban resource utilization and sustainable development capability from the perspective of resource and environmental input and economic output, to minimize the environmental impact and maximize the value impact (Prothero, 1999; Jollands et al., 2004). There is a complex interaction mechanism between eco-efficiency and urbanization (Wei and Ye, 2014; Luederitz et al., 2015; Hak et al., 2016). The urbanization process provides new input factors for urban production activities, and the efficient and reasonable utilization of input factors determines the urban eco-efficiency. At the same time, the level of eco-efficiency has positive feedback on the sustainability and efficiency of urbanization. At present, the urbanization process in China is in a transitional stage (Yang et al., 2019; He et al., 2022). Being a vital old industrial base in China, Liaoning Province faces several developmental challenges such as low-density spatial expansion and the contradiction between the supply and demand of resources, in tackling the dual pressure of socio-economic development and resources and environment (Yu et al., 2022). Counties are an integral component of the urban system in China and provide key support for the integrated development of urban and rural areas. Agricultural counties and districts are currently in a critical period of transformation and development and face problems such as insufficient urbanization development capacity and low long-term resource utilization. The conventional development model featuring high investment, high consumption, and high emission is unsustainable, and urbanization development where there is a fusion of optimal utilization of energy resources and effective protection of the ecological environment has become a necessary trend. Therefore, scientific measurement and an effective balance between the urbanization level and eco-efficiency of counties are of immense significance in achieving sustainable high-quality regional development and in optimizing the spatial development pattern of the country. The purpose of this study is to demonstrate a method to balance coordinated county urbanization development and ecological protection by analyzing the dynamic evolution process of urbanization and eco-efficiency and the time-space exchange relationship.

The term "urbanization" was first proposed by Serda in 1867 in "Introduction to Urbanization," wherein urbanization was defined as the process of gathering rural populations in cities and towns. Subsequently, urbanization is generally defined as the process of growth in the proportion of a country's population living in urban areas, whereas, economists consider urbanization as a process of transformation from a rural economy to an urban economy (Fuchs and Pernia, 1987). In recent years, scholars have increasingly suggested that urbanization is not just a simple problem of population and economic agglomeration, but a comprehensive concept (He et al., 2017; Chen et al., 2022). In this context, a new type of urbanization that focuses on the coordinated development of population, land, economy, society and environment has attracted the attention of Chinese scholars (Zhang et al., 2022). Eco-efficiency was formally proposed by the World Business Council for Sustainable Development (WBCSD) (WBCSD, 1996), which is defined as the goods and services provided by enterprises that can meet the needs of human life and reduce the impact on ecology and resources. The Organization for Economic Cooperation and Development (Duggett, 1998) further expanded the scope of the concept of eco-efficiency, extending the subject to other organizations other than enterprises. Huppes et al. raised the eco-efficiency to the macro-level economic activities on the empirical relationship between environmental costs and environmental impacts (Huppes and Ishikawa, 2005). Research on eco-efficiency has gradually shifted from focusing on a certain industry to the macro level, that is, the research on the evolution of EE's cross-regional spatiotemporal patterns, mainly involving the national (Kounetas et al., 2021) and state scale (Grossman and Krueger, 1991).

The British scholar, Howard (2003), put forward the concept of an "idyllic city," and pioneered research on the connection between urbanization and the environment. Since then, scholars around the world have conducted extensive research on this issue. Current studies on urbanization and eco-efficiency mainly focus on the following three aspects: Firstly, to characterize the relationship between urbanization and eco-efficiency, some scholars used an empirical approach, proposing that urbanization and eco-efficiency present a U-shape based on econometric theory, that is, the environmental Kuznets curve (EKC curve) (Grossman and Krueger, 1991), or N-shaped relationship (Bai et al., 2018). Secondly, scholars focused on the interaction between urbanization and eco-efficiency. Yao et al. (2021) analyzed the impact mechanisms of urbanization dimensions and the internal structure effect of each dimension on eco-efficiency using the Spatial Durbin model based on panel data from 30 provinces of China, from 2008 to 2017. The results demonstrate that local eco-efficiency exhibits a negative spatial effect on the surrounding areas, and population and ecological urbanization have significant positive impacts on local eco-efficiency, while social and spatial urbanization had significant negative impacts. Yue et al. (2020) constructed a spatial model to empirically analyze the effects of urbanization on eco-efficiency at the national level, and

at four regional levels, observing an effect of spatial spillover in eco-efficiency, which was significant and positive for the whole country, except for the western region. The influence of urbanization on China's eco-efficiency exhibits a U-shaped curve. However, the trend exhibited an inverted U-shaped curve in the northeastern region. Thirdly, scholars conducted research on the coupling relationship between urbanization and eco-efficiency. Liu et al. (2021) evaluated and analyzed the spatial-temporal change trends of comprehensive urbanization level, energy eco-efficiency and their coupling coordination degree in 281 prefecture-level cities in China, from 2006 to 2016, showing that the coupling coordination degree manifested an increasing trend, which enabled China to move toward a high coordination level. Ren et al. (2022) analyzed the spatial correlation between urbanization efficiency and eco-efficiency by applying the spatial association model. Based on the relative development and spatial coupling models, the spatiotemporal coupling relationship was estimated, and it was found that the coupling relationship between the two is an N-type relationship. These studies mainly focus on macro-scales such as countries and urban agglomerations, but do not pay enough attention to micro-scales. When revealing the evolution law of urbanization and eco-efficiency, the dynamic migration of the two in space was ignored. When characterizing the spatial autocorrelation relationship between the two, the influence of one system on another system in space cannot be fully measured.

Although previous studies have described the time-series characteristics, impact mechanism, and coupling coordination relationship between urbanization and eco-efficiency, the research at the county scale is still insufficient, and the spatiotemporal synergistic relationship model between urbanization and eco-efficiency has not been established. Analysis of ecological macro issues from a micro perspective can help consider the particularity of eco-efficiency formation in different regions and conduct more rigorous exploration of spatial heterogeneity. Research on the temporal and spatial evolution trends and interactive synergies between eco-efficiency and urbanization can provide theoretical and policy references for balancing the two processes, transforming the development model of urbanization, and improving eco-efficiency utilization. To alleviate the predicament of county development, we first constructed an urbanization evaluation system and an eco-efficiency evaluation system suitable for agricultural counties utilizing available data, and second, we built a time-space interaction model for the dynamic evolution of urbanization and eco-efficiency, to demonstrate the sustainable development path of agricultural counties under the dual pressures of urbanization and eco-efficiency, in this paper. This study can also provide reference for the development of other regions and counties.

Research methods and data

Research region and data source

Located in the southern part of Northeast China, Liaoning Province has 14 provincial cities and 100 counties (county-level cities and districts) under its jurisdiction. By the end of 2021, the rate of urbanization of the province was 72.81%. In the process of long-term urbanization development, Liaoning Province is faced with problems such as high structural pollution pressure, unstable improvement of ecological environment quality, and a large number of arrears in environmental infrastructure. In 2016, the Implementation Opinions on Deepening the Construction of New Urbanization proposed to strengthen the weak links of counties and towns, promote the optimization of the province's urban structure, focus on the control of "urban diseases" and promote harmony between people and city development. After that, the 14th Five-Year Plan for Ecological Economic Development of Liaoning Province proposed that the structural, root and trend pressures of ecological environmental protection will generally remain in the 14th Five-Year Plan period, making it particularly important to quantify the level of urbanization development and the quality and stability of ecosystems in Liaoning Province. There are 81 agricultural counties and districts in Liaoning listed in the Liaoning Statistical Yearbook; considering the continuity, comparability, and availability of data as well as the adjustment of administrative area divisions, Yuanbao District, Zhenxing District, Wensheng District, Hongwei District, and Qianshan District were excluded in this study. Finally, the remaining 76 agricultural counties and districts in Liaoning Province were selected as the research units, with data from 2013 to 2017.

County-level administrative units (divided into municipal districts, counties, county-level cities, banners, forest districts, and special zones) are the most basic comprehensive administrative unit in China (referred to as "counties and districts" in this paper) connecting urban and rural areas and are important spatial carriers for coordinating the implementation of new urbanization and rural revitalization strategies. So far, there is no consensus in academic circles with respect to the concept of agricultural counties and districts. The agricultural counties and districts mentioned in this paper are selected from the list of agricultural counties and districts listed in the Statistical Yearbook of Liaoning Province, which includes 35 districts, 16 county-level cities, and 25 counties. In general, the level of economic development, pace of urbanization, and population density of a district is greater than that of a county-level city and that of a county. The economic base of agricultural counties and districts is dominated by agriculture, and the foundation of urbanization is relatively weak. In recent years, with the development of *in-situ* urbanization in agricultural counties and districts, the economic and social

TABLE 1 Index system for measuring county urbanization level.

Target layer	Criterion layer	Indicator layer	Information entropy	Weight
Urbanization	A Population urbanization	A1 Proportion of Urban Population (100%)	0.9652	0.0666
		A2 Proportion of Non-agricultural Industry Employees (100%)	0.9877	0.0235
		A3 Population Density (person/km^2)	0.8841	0.2218
	B Economic urbanization	B1 GDP Per Capita (RMB 10,000/person)	0.9485	0.0986
		B2 Per Capita Disposable Income of Urban Residents (RMB)	0.9752	0.0474
		B3 Proportion of Added Value of Secondary and Tertiary Industries in GDP (100%)	0.9938	0.0118
	C Land urbanization	C1 Proportion of Construction Land (100%)	0.9328	0.1285
		C2 Road Area Per Capita (m^2)	0.9655	0.0659
	D Social urbanization	D1 Public Expenditure on Science and Education as a Percentage of GDP (100%)	0.9627	0.0713
		D2 Technical Staff in Medical and Health Institutions Per Thousand People (people/1,000 persons)	0.9678	0.0616
		D3 Number of Beds Per Thousand People in Medical and Health Institutions (units/1,000 persons)	0.9594	0.0778
		D4 Urban and Rural Endowment Insurance Coverage (100%)	0.9835	0.0315
		D5 Internet Broadband Penetration Rate (100%)	0.9531	0.0896
	E Ecological urbanization	E1 Domestic Sewage Treatment Rate (100%)	0.9979	0.0041

growth and ecological utilization of counties and districts have shown significant differences, and it is imperative to study the process and synergistic relationship between urbanization and eco-efficiency in agricultural counties and districts to explore the enhancement path of counties, to cope with ecological problems.

The statistical data used in this paper were derived from the Liaoning Statistical Yearbook (http://tjj.ln.gov.cn/tjsj/sjcx/ndsj/). In case of data missing for some years or regions, the statistical yearbook of each city in the corresponding year was used to supplement the same. If certain data were still missing, they were processed using the moving average method. The land use data were obtained from Landsat's China Land Cover Annual Dataset (CLCD) from 2013 to 2017, with a resolution of 30 m (http://doi.org/10.5281/zenodo.4417809).

Establishment of evaluation index system

Establishment of urbanization level index system

Urbanization measurement needs to be considered holistically. Towns and cities have many components or "urban ingredients"— facilities, systems, and utilities, and the attributes that are desirable for an urban area to possess (Thomas, 2009; Van der Bruggen et al., 2010). Therefore, measuring the level of urbanization requires in-depth consideration, comprehension and balance of all urban elements, and appreciation for the local environment (Drakakis-Smith and Dixon, 1997; Enserink and Koppenjan, 2007; Liu et al., 2016). Based on the evaluation index system of the National New Urbanization Plan (2014–2020) and existing studies, we established an urbanization level measurement index system in this paper composed of the following five aspects: population, economy, land, society, and ecology (Table 1). The convergence of population to cities is the most typical process and result of urbanization. We choose proportion of urban population, proportion of non-agricultural industry employees and population density to represent the level of population urbanization. Urbanization is an inevitable result of economic development and the economic development level is a direct indicator that reflects the urbanization rate. The sub-system of economic urbanization mainly focuses on economic scale, residents' income level and industrial structure, in which the main indicators include GDP/capita and per capita disposable income of urban residents and proportion of added value of secondary and tertiary industries in GDP. Land elements are the carrier and basic conditions for promoting urbanization. The proportion of construction land and per capita road area are used to characterize land urbanization in this paper. The new urbanization adheres to the people-oriented approach, emphasizing the transformation of residents' lifestyles, the improvement of life quality, the acquisition of social recognition, and the full coverage and equalization of basic public services in the process of population citizenization. This paper uses public expenditure on science and education as a percentage of GDP, technical

TABLE 2 County-level eco-efficiency evaluation index.

Index	Category	First-level indicator	Specific indicators
Input indicators		Power consumption	Electricity Consumption of the Whole Society (10,000 kWh)
		Capital investment	Total Investment in Fixed Assets of the Whole Society (RMB 10,000)
		Land resource consumption	Construction Land Area (km^2)
			Cultivated Area (km^2)
		Labor resource consumption	Industry Practitioners (persons)
Output indicator	Expected output	Economic output	General Budgetary Revenue of Local Finance (RMB 10,000)
			Gross Regional Product (RMB 10,000)
	Unexpected output	Environmental output	Industrial Sulfur Dioxide Emissions (ton)
			Nitrogen Oxide Emissions (ton)
			Smoke (Powder) Dust Emission (ton)

staff in medical and health institutions per thousand people, number of beds per thousand people in medical and health institutions, urban and rural endowment insurance coverage and internet broadband penetration rate to measure the impact of social development. Urbanization is increasingly emphasizing the concept of ecological civilization, advocating reducing disturbance and damage to nature during urban development. We choose domestic sewage treatment rate to measure ecological urbanization.

Establishment of eco-efficiency index system

Eco-efficiency focuses on maximizing the economic value output by minimizing resource consumption and environmental pollution (Sadorsky, 2021). To ensure proper measurement of concurrent progress toward environmental sustainability and inclusive economic growth, eco-efficiency indicators should be assessed by combining indicators from two or more dimensions (Kuosmanen, 2005; Mickwitz et al., 2005). Referring to relevant literature, we comprehensively describe eco-efficiency from the perspective of input, expected output, and undesired output. Relevant indicators of social capital, energy and labor consumption, and natural resource are selected for the inputs. Social and economic output are mainly considered for the expected output, and the problem of environmental pollution is mainly considered for the undesired output, with pollutant discharge selected as the evaluation index. The combination of these three systems in one score satisfies the question of assessing the social development and environmental use trade-offs between domains of sustainability (Wursthorn et al., 2011; Bianchi et al., 2020; Kounetas et al., 2021). Furthermore, we established a county-level eco-efficiency evaluation index system that complies with scientific principles while keeping in mind efficacy (Table 2). When selecting resource input indicators, we selected social and natural resource indicators that are closely related to human production and life. Specifically, power input is measured by electricity consumption of the whole society, capital input is measured by total investment in fixed assets of the whole society, and land resource input is measured by construction land area and cultivated area, labor resource input is measured by industry practitioners. Regarding expected output indicators, consistent with the majority of scholars, general budgetary revenue of local finance and gross regional product were selected for measurement. Pollutant emissions are used to measure unexpected outputs, including industrial sulfur dioxide emissions, nitrogen oxide emissions and smoke (powder) dust emission.

Research methods

In this study, we scientifically measure and evaluate the dynamic evolution and synergistic relationship between urbanization and eco-efficiency in 76 agricultural counties and districts in Liaoning Province through the following methods and steps: (1) Construct an evaluation system for the urbanization level and eco-efficiency using the entropy evaluation method and the SBM model with undesirable outputs and complete the measurement calculation. (2) Measure the spatial-temporal evolution trend of urbanization and eco-efficiency using kernel density estimation curve and the gravity center transfer model to effectively measure the threshold distribution characteristics and direction characteristics. (3) Adopt bivariate Moran's I index to portray spatial-temporal interaction between county-level urbanization and eco-efficiency, describe the spatial aggregation and correlation of the two, and effectively resolve the endogeneity of variable data. Through the above methods, we clarify the development and evolution characteristics of county urbanization and eco-efficiency, as well as the dynamic and synergistic development ability of the two, to provide a theoretical basis to further balance the level of urban construction and eco-efficiency in the study area.

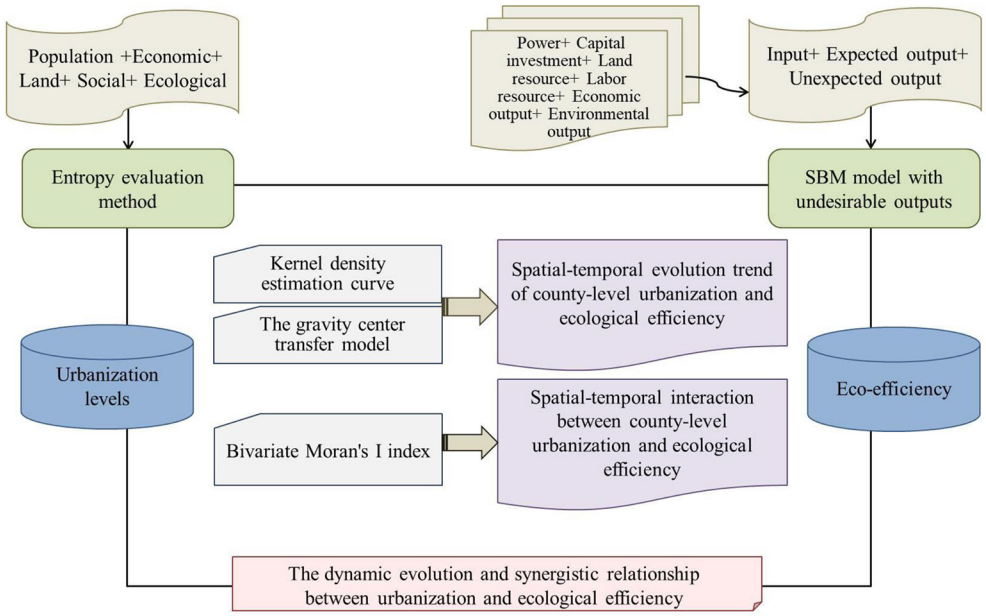

FIGURE 1
Method flow chart of the article.

The research methods and main contents are shown in Figure 1.

Entropy evaluation method

The entropy method can profoundly reflect the utility value of the entropy value of the index information, and the index weight determined by it can effectively overcome subjectivity and has high reliability (Polesie et al., 2020). The entropy evaluation method deals with the utilization of information entropy to effectively transfer the information in accordance with the degree of discreteness of each indicator, which in turn helps to determine the weight of each indicator (Zhou and Zhou, 2015). Herein, we adopted the entropy evaluation method to measure the urbanization level; the calculation formula is as follows:

1. Data standardization

$$\text{Positive indicators}: X'_{ij} = \frac{X_{ij} - X_{min}}{X_{max} - X_{min}}, \quad i = 1, 2, \ldots, m; j = 1, 2, \ldots, n \quad (1)$$

$$\text{Negative indicators}: X'_{ij} = \frac{X_{max} - X_{ij}}{X_{max} - X_{min}}, \quad i = 1, 2, \ldots, m; j = 1, 2, \ldots, n \quad (2)$$

2. Calculating information entropy

$$e_j = -K^* \sum_{i=1}^{n} P_{ij} \ \ln P_{ij}, K = \frac{1}{\ln m}, e \in [0, 1], \ P_{ij} = \frac{X'_{ij}}{\sum_{i=1}^{n} X'_{ij}} \quad (3)$$

3. Calculating the difference coefficient (information utility)

$$g_j = 1 - e_j \quad (4)$$

4. Calculating the weight of each indicator

$$W_j = g_j / \sum_{j=1}^{m} g_j \quad (5)$$

5. Calculating comprehensive indicators

$$S_i = \sum_{j=1}^{n} W_j * X'_{ij} \quad (6)$$

SBM model with undesirable outputs

Most eco-efficiency measurement models choose "input + expected output + undesired output," and the measurement methods mainly include data envelopment analysis including DEA model (Picazo-Tadeo et al., 2011; Yasmeen et al., 2020; Moutinho and Madaleno, 2021) and SBM mode (Li and Shi, 2014; Cecchini et al., 2018; Xu et al., 2020), and life cycle assessments (Avadí et al., 2014; Lorenzo-Toja et al., 2015; Beltrán-Estevea et al., 2017). As a systematic analysis method used to evaluate the relative efficiency of the same type of decision-making units based on various inputs and outputs, the data envelopment analysis is widely used to measure eco-efficiency. To solve the long-standing traditional issue of the DEA model being prone to relaxation of variables, Tone

(Tone and Tsutsui, 2010, 2013) proposed a non-radial non-angular-based SBM model, which could effectively circumvent the deviation caused by the selection of radial and angular outputs and could also overcome the problem of input-output relaxation. Since multiple inputs and outputs need to be entered into the evaluation system when measuring the efficiency, Tone also upgraded the SBM model by considering the negative externalities of the environment, so that the relationship between the inputs and the outputs could be estimated meticulously. In this paper, the eco-efficiency was measured by employing the SBM model with unexpected output, non-orientation, and constant payoff to scale. The model is as follows:

$$\beta_j^* = \min \frac{1 - \frac{1}{m}\sum_{i=1}^{m} \frac{s_{ij}^-}{x_{ik}}}{1 + \frac{1}{u1+u2}\left(\sum_{r=1}^{u1} \frac{s_{rj}^y}{y_{rj}} + \sum_{r=1}^{u2} \frac{s_{rj}^-}{b_{rj}}\right)} \tag{7}$$

$$s.t. \begin{cases} x_j = X\lambda + s_j^- \\ y_j = Y\lambda - s_j^y \\ b_j = D\lambda + s_j^b \\ s_j^- \geq 0, s_j^y \geq 0, s_j^b \geq 0, \lambda \geq 0 \end{cases}$$

In the formula: s_j^- and s_j^b stand for the redundant value of input and undesired output, respectively; the vector s_j^y indicates the state of the desired output, which does not reach the maximum; the subscript j represents the jth DMU (Decision Making Unit). At the time of $0 < \beta^* < 1$, the DMU is in an inefficient state, while an efficient state can be achieved by further optimizing the input or output. At the time of $\beta^* = 1$, the DMU is in a relatively effective state and at that time, $s_j^- = s_j^b = s_j^y = 0$.

Kernel density estimation curve

Kernel density estimation is a non-parametric estimation method that can describe the distribution state and distribution characteristics of random variables with a continuous probability density curve under the null hypothesis of a parametric model, as it can objectively and truly reflect the estimation; it is widely employed in measuring the regional differences of spatial elements (Minoiu and Reddy, 2014). In this paper, we employed kernel density estimation to describe the distribution state and distribution characteristics of random variables (Van Kerm, 2003). The calculation formula is as follows:

$$f(x) = \sum_{i=1}^{n} \frac{1}{\pi h^2} K\left(\frac{x - x_i}{h}\right) \tag{8}$$

In the formula, h stands for the bandwidth, K represents the kernel function, and n is the number of elements covered in the circle, with point x as the center and bandwidth h as the radius. The nearest neighbor distance method was adopted to determine the bandwidth:

$$h = \frac{\left(\sum_{i=1}^{n} \sum_{j=1}^{k} d_{ij}\right)}{k \times n} \tag{9}$$

In the formula, d_{ij} stands for the distance between the points i and j, n is the total number of interest points, and k denotes the number of adjacent points around the interest point i.

The center of gravity transfer model

The center of gravity model is an important analytical tool to study the spatial variation of factors in the process of regional development. The regional center of gravity is an index to measure the overall distribution of a certain attribute in the region and the movement of the center of gravity reflects the spatial trajectory of regional development (Zhao et al., 2020). In this paper, the center of gravity transfer model was adopted to determine the overall variation trend of the spatial distribution of variables (Liang et al., 2021). The formula of the barycentric coordinate solution model is as follows:

$$X = \frac{\sum_{i=1}^{n} M_i X_i}{\sum_{i=1}^{n} M_i}, Y = \frac{\sum_{i=1}^{n} M_i Y_i}{\sum_{i=1}^{n} M_i} \tag{10}$$

In the formula: x and y stand for the center of gravity longitude and latitude of a certain index for the total area, respectively; X_i and Y_i represent the coordinates of the geographic center of gravity in the sub-area, respectively; i stands for the ith research unit, n stands for the total number of research units, and M_i for the weight of an index in the area.

The formula for solving the moving distance of the regional center is as follows:

$$D_{s-k} = C \times \left[(Y_s - Y_k)^2 + (X_s - X_k)^2\right]^{0.5} \tag{11}$$

In the formula: D_{s-k} stands for the moving distance of the center in two different years; and s and k represent the 2 years, respectively; X_s, X_s, X_k, Y_k denote the longitude and latitude coordinates of the geographic location of the regional center in the sth year and the kth year, respectively; C represents the conversion rate between geographic coordinates and plane projection coordinates, which is generally a constant, $1^\circ \approx 111.111$ km; $C \times (X_s - X_k)$ and $C \times (Y_s - Y_k)$ stand for the absolute distance that the center of a certain element moves in terms of longitude and latitude from the kth year to the sth year, respectively.

Bivariate Moran's I index

Spatial autocorrelation analysis is commonly used to reveal whether the distribution of spatial variables and their

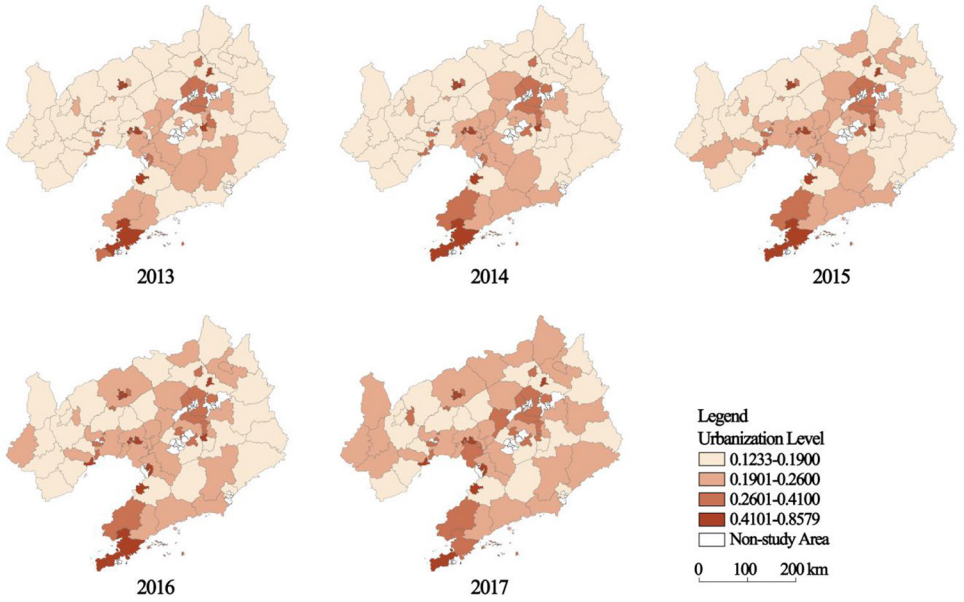

FIGURE 2
Spatial pattern of urbanization in agricultural counties and districts of Liaoning province (2013–2017).

adjacent regions have agglomeration. It includes two aspects—global spatial autocorrelation and local spatial autocorrelation (Wartenberg, 1985), which are represented by Moran's I and Local Moran's I indices (Batlle and van der Hoek, 2018). The bivariate Moran's I index is an improved version of the traditional Moran's I index (Kruger et al., 2017; Antczak, 2020). The global bivariate Moran's I index is used in this paper to test whether any spatial clustering and discrete features are present in the global range of the variable. The formula is as shown in Equation (12):

$$I_{kl} = \frac{\sum_{i=1}^{n}\sum_{j=1}^{n} w_{ij}\,(x_k^i - \bar{x}_l)}{S^2 \sum_{i=1}^{n}\sum_{j=1}^{n} w_{ij}} \tag{12}$$

The local bivariate Moran's I index was adopted to examine the local anomalies and spatial agglomeration triggered by the spatial stagnation effect amongst the research units. The formula is as shown in Equation (13):

$$I'_{kl} = \frac{x_k^i - \bar{x}_k}{S_k^2} \sum_{j=1}^{n} w_{ij} \frac{x_l^j - \bar{x}_l}{S_l^2} \tag{13}$$

In the formula: x_k^i stands for the observation value of the variable k on the space unit i, x_l^j is the observation value of the variable l on the space unit j, $\bar{x}_k$ and $\bar{x}_l$ are the average observation values for the variables k and l, respectively, w_{ij} stands for the spatial weight matrix, and S_k^2 and S_l^2 stand for the variances of the observation values for the variables k and l, respectively.

Result analysis

Spatial-temporal pattern of county-level urbanization and eco-efficiency

In this paper, the natural discontinuity method was employed to divide the measured urbanization levels and eco-efficiency results into four grades, ranging from low to high. As shown in Figure 2, the urbanization level of agricultural counties and districts in Liaoning Province exhibited an overall upward trend from 2013 to 2017, while the average index rose from 0.2468 in 2013 to 0.2789 in 2017. In terms of the variation range, the level of urbanization first increased and then decreased, with 2014 being the turning point, and subsequently the urbanization process became stable. The highest value of urbanization was observed at the centers of Fuxin City and Tieling City, demonstrating a unique and prominent "siphon effect." Furthermore, the two high-value centers came into being in Dalian City and Shenyang City, from where they diffused from inwards to outwards, thus forming high-value agglomeration areas with a striking driving effect of urbanization. In terms of spatial-temporal evolution characteristics, the urbanization level of the agricultural counties and districts in Liaoning Province depicted a positive shift from exclusively northeast–southwest strip development to overall regional development.

The measurement results of eco-efficiency (Figure 3) show that the eco-efficiency of agricultural counties and districts in Liaoning Province demonstrates an N-shaped development

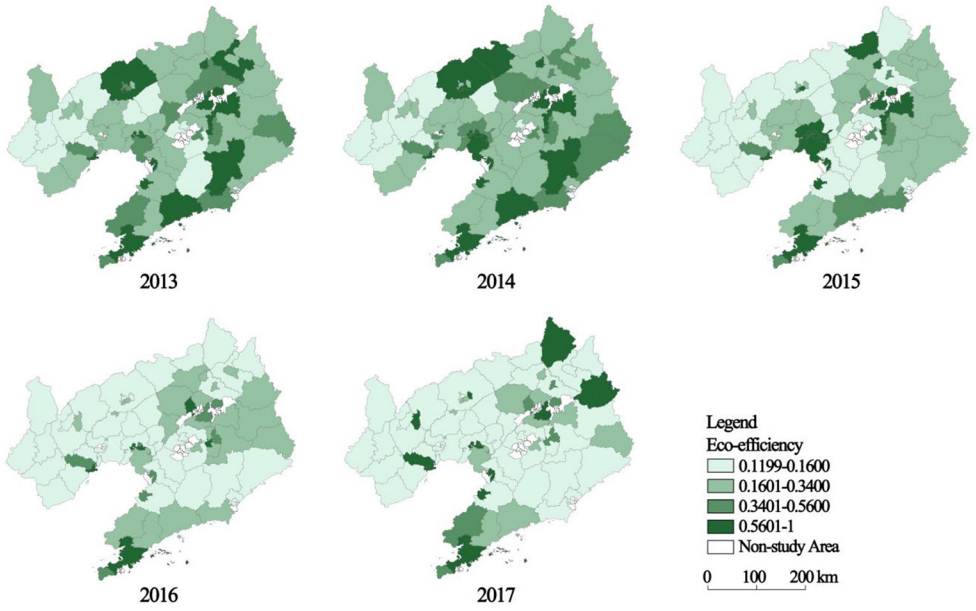

FIGURE 3
Spatial pattern of eco-efficiency in agricultural counties and districts of Liaoning province (2013–2017).

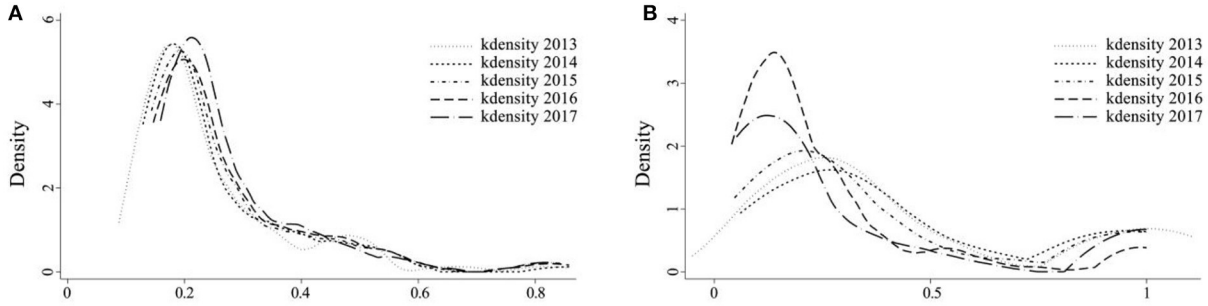

FIGURE 4
Kernel density curve of urbanization level and eco-efficiency of agricultural counties and districts in Liaoning province (2013–2017). **(A)** Urbanization levels. **(B)** Eco-efficiency.

curve (Kuznets curve), with the years 2014 and 2016 being the inflection points and subsequently undergoing an overall reduction. The average value declined from 0.4364 in 2013 to 0.3117 in 2017, reflecting poor stability of eco-efficiency. The southern Liaoning region presented relatively better eco-efficiency, but still endured depletion to some extent owing to urbanization development. The eco-efficiency of the western Liaoning region fell behind. The eco-efficiency of the central, eastern, and northern parts of Liaoning thrived during the initial period, but then suffered a declining trend with each year, with only certain regions recuperating. In a nutshell, the urbanization level and eco-efficiency of Liaoning Province portrayed a reverse development trend in terms of time, and even the spatial pattern of the two was characterized by an identical imbalance.

Spatial-temporal evolution trend of county-level urbanization and eco-efficiency

Time series evolution characteristics of county-level urbanization and eco-efficiency

In this paper, the kernel density estimation curve was implemented to evaluate the quantitative change characteristics

TABLE 3 Movement distance and rate of urbanization (U) and eco-efficiency (EE) of centers of agricultural counties and districts in Liaoning province (2013–2017).

		Liaoning province	Eastern Liaoning	Western Liaoning	Central Liaoning	Northern Liaoning	Southern Liaoning
Center movement distance (km)	U	13.66	6.67	8.64	5.14	9.52	4.42
	EE	49.14	18.98	56.14	10.67	39.67	32.80
Center movement rate (km/a)	U	3.41	1.67	2.16	1.29	2.38	1.10
	EE	12.28	4.74	14.04	2.67	9.92	8.20

of the values of the two factors on the time scale (Figure 4); the results reveal that: (1) During the research period, the urbanization level distribution curve of the agricultural counties and districts in Liaoning Province shifted to the right on the whole, indicating that the urbanization level was on the rise; the wave crest was sharp and the height first decreased and then increased, suggesting that no decline occurred in the difference in the urbanization level between counties and districts; a prominent diffusion phenomenon followed by striking agglomerated development was observed within the region. All the curves over the years exhibited the characteristics of right-trailing, indicating that the number of units with higher urbanization level were still small, whereas the low-value units possessed a remarkable convergence trend. (2) The increase and decrease in the eco-efficiency distribution curve varied considerably, and the peak shape and tailing of the curve also differed greatly, signifying that the eco-efficiency of each unit failed to assume a highly correlated spatial matching; the distribution curve showed a "right-left-right" movement trend, with the year 2016 as the node. The eco-efficiency of agricultural counties and districts in Liaoning province first increased, then decreased, and then increased again. The ecological utilization level first decreased and then increased slightly, but it still failed to reach the previous level. The eco-efficiency curve over the years presented characteristics of double peaks, and the two peaks were at both the ends, which implied severe polarization of eco-efficiency. The highest peak on the left side shows that the eco-efficiency of each unit was still lower, by and large. The peak location showed an "upward-downward" trend, and the curve transformed from a wide front to a sharp peak and then mitigated, suggesting that the difference in county-level eco-efficiency was constantly widening, before being curbed to some extent.

Spatial evolution characteristics of county-level urbanization and eco-efficiency

To manifest the varying trends of urbanization and eco-efficiency at different spatial scales, the center transfer model was adopted to characterize the spatial evolution trajectories of urbanization and eco-efficiency. The calculation results are shown in Table 3 and Figure 5. The center of county-level urbanization in Liaoning Province demonstrated a relatively smooth movement, and the center of eco-efficiency presented a substantial movement, with a larger difference in the moving trend between various regions. At the provincial level, the urbanization development of Liaoning Province portrayed a "southwest–northeast" movement during the study period, and the center was positioned in Tai'an County and Panshan County in the central part of Liaoning. The total distance covered by the movement was 13.65 km, with an average movement rate of 3.41 km/a. The eco-efficiency presented a "southwest–northwest" movement, with the center positioned in Liaoyang County, and gradually shifting to Haicheng City. The total distance covered by the movement was 49.14 km, with an average movement rate of 12.28 km/a, and the variation rate depicted an overall increasing trend. No remarkable synergy was observed between the variation rate and the direction of the two centers.

The center change characteristics of urbanization level and eco-efficiency in different regions are as follows: (1) The urbanization center of the eastern Liaoning region moved along the "southeast–northeast" direction, with slight fluctuations and a stable moving rate; the eco-efficiency center moved southwards on the whole, and the movement rate tended to be stable after a considerable change in 2014. The two behaved relatively similarly in terms of the center location, movement rate, and movement direction. (2) Urbanization in the western Liaoning region occurred at a steady pace and the movement rate declined with each year, whereas, there was a slight change in the location of the center. The center of eco-efficiency moved southwards, with weak stability of the moving rate. A significant spatial change was observed in the development of eco-efficiency. In addition, an increase was witnessed in the spatial difference of the development center between the two factors. (3) The center location of urbanization and eco-efficiency in central Liaoning suffered a slight change, but both the factors illustrated prominent spatial stability during the development phase. (4) The urbanization center of the northern Liaoning region moved northwards overall, undergoing stable changes; the center of eco-efficiency first moved southwards and then shifted northwards, with the variation speed accelerating constantly. (5)

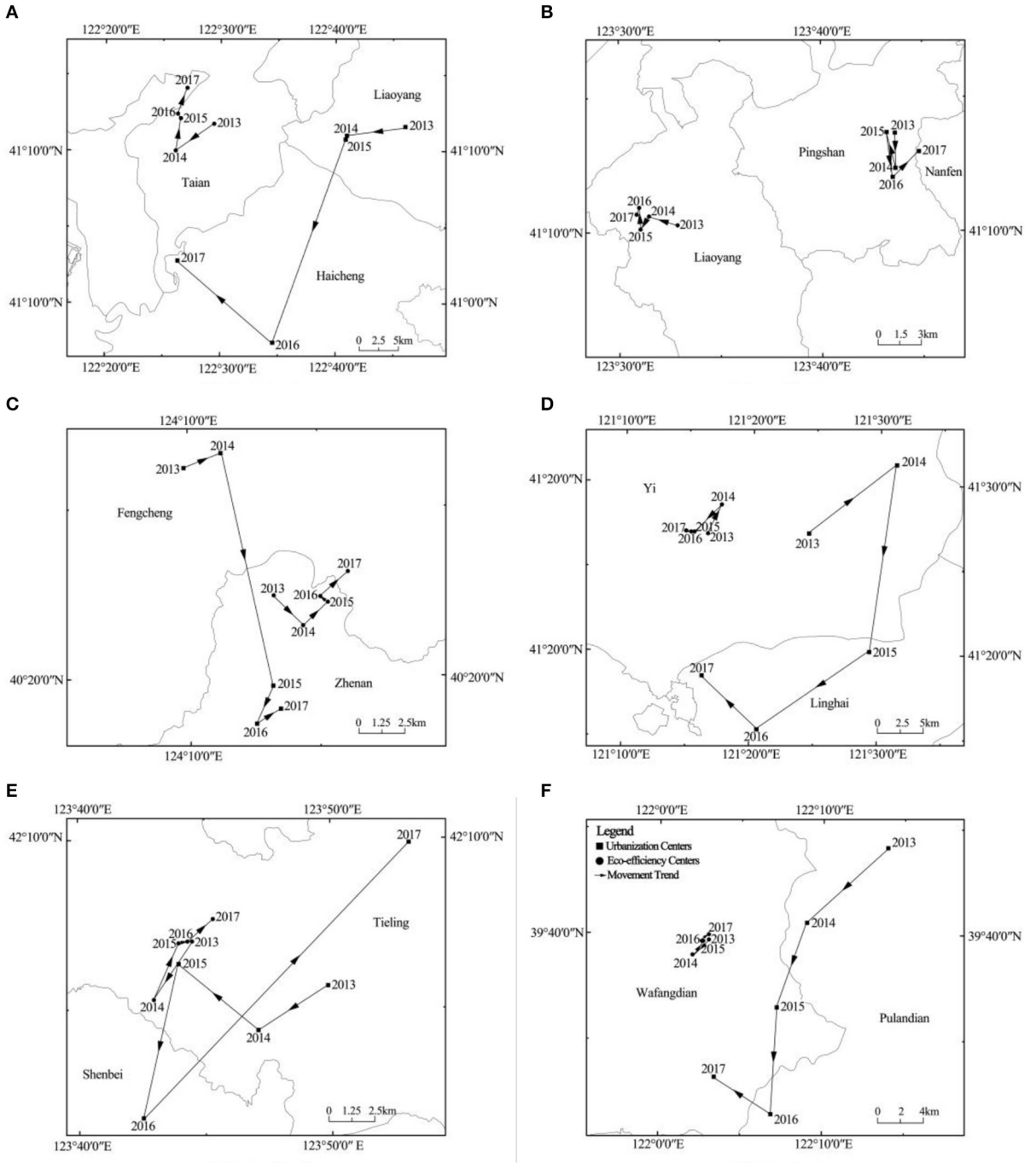

FIGURE 5
Movement trend of urbanization and eco-efficiency centers of agricultural counties and districts in Liaoning province (2013–2017). **(A)** Liaoning province. **(B)** Central Liaoning. **(C)** Eastern Liaoning. **(D)** Western Liaoning. **(E)** Northern Liaoning. **(F)** Southern Liaoning.

The urbanization center of the southern Liaoning region moved slightly around the same place but mostly remained fixed. The center of eco-efficiency moved southwards overall, and enjoyed considerable changes in 2014, with only stable changes in all the other years.

By and large, at the provincial and the regional level, Liaoning Province exhibited a relatively stable urbanization process and a relatively robust urbanization spatial pattern. No remarkable trend was observed in the movement of the urbanization center in each region. The urbanization

TABLE 4 Changes in bivariate Moran's I index of agricultural counties and districts in Liaoning province over the years.

	2013	2014	2015	2016	2017
Urbanization-eco-efficiency	0.152	0.289	0.170	0.141	0.109
Eco-efficiency-urbanization	0.117	0.219	0.170	0.172	0.133

migration distance and rate ranking of the different regions are attributable to the regional urbanization construction base. The better the foundation of urbanization development, the more stable is the movement trend. The eco-efficiency presented significant movement changes, with an unbalanced movement direction and rate among the regions. Except for the eastern and the central Liaoning regions, the center of eco-efficiency showed significant dynamic changes in all the other regions of the province. Generally, Liaoning was labeled with poor stability in eco-efficiency development, weak trend of agglomeration development across the province, shortage of proper guidance and specifications for eco-efficiency development, and prominent development randomness and variability. In terms of the coordinated development of urbanization and eco-efficiency, there was some insufficient correlation between the variations in the center of the two within specific regions, and insignificant overlapping and synchronization of the variations in the center of the two, within specific regions.

Spatial-temporal interaction between county-level urbanization and eco-efficiency

In this paper, urbanization is considered as the first variable and eco-efficiency as the second variable (urbanization-eco-efficiency), while it is the vice-versa (eco-efficiency-urbanization) when calculating the two-variable global Moran's I index. The calculation results are shown in Table 4. The results reveal that a positive spatial correlation exists between the urbanization level and eco-efficiency of Liaoning Province, which indicates that a positive correlation exists between the urbanization level and the eco-efficiency of the surrounding areas as well as between the eco-efficiency and the urbanization of the surrounding areas. The Moran's I index of "urbanization-eco-efficiency" exceeded the Moran's I index of "eco-efficiency-urbanization" in 2014, signifying that the impact of eco-efficiency on the urbanization of the surrounding areas was eventually greater than the impact of urbanization on the eco-efficiency of the surrounding areas. Both the Moran indices demonstrated an "up-down" trend, suggesting that the cluster development or stagnant development capability of the two factors first increased and then decreased.

The calculation results of the local Moran's I index of urbanization-eco-efficiency (Figure 6A) reveal that: (1) On the whole, the research units presented a certain number of abnormal agglomeration characteristics, with the LL agglomeration forming the primary type. (2) In terms of space, LL agglomeration areas emerged adjacent to each other in the western Liaoning region, which was characterized with backward urbanization development, relatively extensive and inefficient development of the surrounding areas, and inadequate emphasis on eco-efficiency utilization; furthermore, small-scale HH agglomeration areas formed in the central and southern Liaoning regions, which focused on input-output efficiency and interaction between urbanization level and eco-efficiency of the surrounding areas during the course of rapid urbanization; HL agglomeration areas emerged in the western, central, and southern Liaoning regions, which were labeled with prominent urbanization agglomeration effect and negative development externalities. In the process of urban development, such areas are likely to capture development resources of surrounding areas. The LH agglomeration areas emerged in the central and eastern part of the province, which were characterized with relatively backward urbanization development and refined ecological protection in the development process. (3) From the perspective of time series variations, the number and distribution pattern of each abnormal agglomeration type of urbanization-eco-efficiency remained stable overall. LL type gradually moved from the western Liaoning region along the southeastern direction, and HH type shifted from the central Liaoning region to the southern part, while the number of HL and LH areas reduced.

The calculation results of local Moran's I index of eco-efficiency-urbanization suggest that (Figure 6B): (1) The impact of eco-efficiency in Liaoning Province on the urbanization level of the surrounding areas was predominantly generated by the LL and HL agglomeration types. (2) From the perspective of space, the LL agglomeration areas were basically distributed in the western, northern, and eastern parts of Liaoning Province along the topographical characteristics, featuring low input-output ratio of economic and ecological development, and the relatively backward urbanization development of their surrounding areas; local HL agglomeration areas emerged in the eastern and the northern parts of Liaoning Province, which enjoyed a superior level of eco-efficiency than the urbanization development level of their surrounding areas; the concentrated HH and LH areas were formed adjacent to each other in

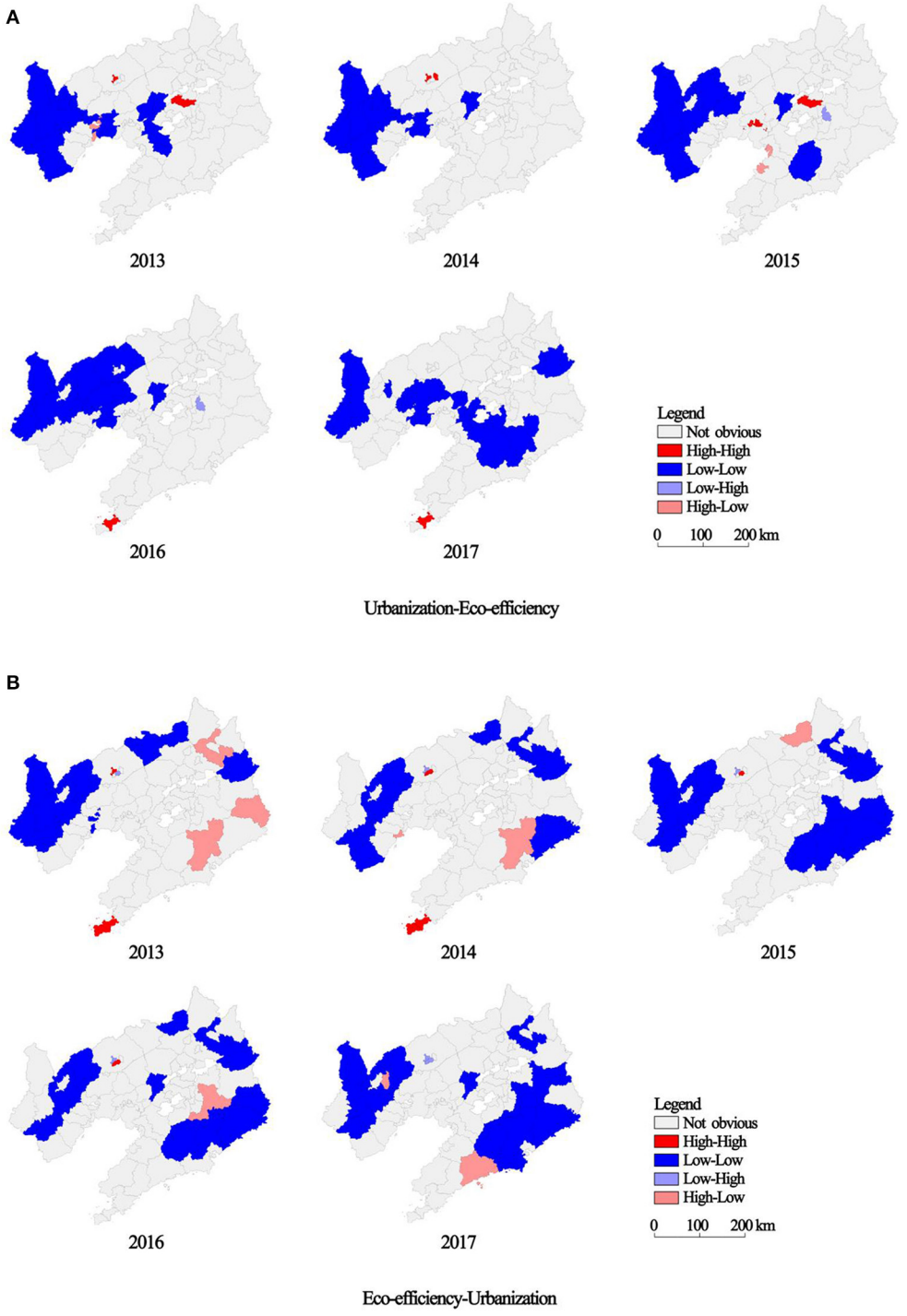

FIGURE 6
LISA agglomerations of urbanization and eco-efficiency of agricultural counties and districts in Liaoning province (2013–2017). **(A)** Urbanization-eco-efficiency. **(B)** Eco-efficiency-urbanization.

the northwest Liaoning region, and eventually transformed into the LH type, demonstrating that these areas experienced higher agglomerated urbanization development, and were likely to deplete eco-efficiency in exchange for the urbanization development of their surrounding areas; HH agglomeration areas formed in the southern Liaoning region and subsequently

exhibited poor development performance, establishing that the high level of eco-efficiency in such areas weakened the urbanization development of their surrounding areas. (3) From the perspective of time series variations, the spatial pattern of the LL areas remained stable; a drop was witnessed in the number of HH and HL types of research units, and high eco-efficiency promoted weaker urbanization development in the surrounding areas. An increase was observed in the number of LH-type areas, where the situation of promoting urbanization development of the surrounding areas while ignoring eco-efficiency grew increasingly severe during the study period.

Discussions

Spatial-temporal evolution trend of urbanization and eco-efficiency

The level of urbanization in agricultural counties and districts in Liaoning Province during the study period has been increasing and gradually moving toward region-wide development, which coincides with China's acceleration into a new stage of urbanization transformation and development that focuses on improving quality after the issuance of the National New Urbanization Plan (2014–2020) by the State Council and the Central Committee of the Communist Party of China in 2014. This has caused the agglomeration capacity of central cities to become increasingly prominent and surrounding counties and districts have gradually formed a new growth pole for coordinated regional development. Eco-efficiency has generally decreased and become less stable during the study period. Urbanization has promoted the non-agricultural transformation of industries and resources, but the new economic and social development model has brought about "urban diseases" such as environmental pollution and imbalance in the input and output of energy flow. Eco-efficiency has an N-shaped structure with inflection points in 2014 and 2016, which may be a response to the strategic decision of "vigorously promoting the construction of ecological civilization" proposed at the 18th National Congress of the Communist Party of China in 2012 and the *General Plan for the Reform of the Ecological Civilization System* issued by the State Council and the Central Committee of the Communist Party of China in 2015. However, due to the immaturity of China's internal structural system and operational processes, as well as environmental debt, the positive impact of ecological use transformation in counties and regions is still not obvious (Yao et al., 2021).

Interactive relationship between urbanization and eco-efficiency

Different from the results of previous studies, in this paper, we propose that the temporal development of eco-efficiency and urbanization in the study area is not synchronized, and the coupling coordination between the two is in the shape of an inverted U, suggesting that coordinated development of urbanization and eco-efficiency has not yet occurred in the study area. And there is a disconnect between the pursuit of urban construction and ecological protection in the development of agricultural counties and districts. The spatial heterogeneity of urbanization and eco-efficiency agglomeration development in the counties and districts is strong, but generally speaking, the low-urbanization level and eco-efficiency development areas under the dual pressure of the two are obvious. The development of urbanization has a positive impact on the eco-efficiency of the surrounding areas, and the optimization of eco-efficiency has an overall positive impact on the improvement of urbanization in the surrounding areas. However, the negative effects of urbanization spread to neighboring counties, forming a "pollution refuge effect," and the phenomenon of maintaining eco-efficiency at the expense of surrounding urbanization development still exists. The ability to coordinate and integrate regional urbanization development and eco-efficiency still needs to be further strengthened.

Limitations

Owing to the limitation of some objective factors, this study still has some shortcomings. Firstly, the social statistical data used in this paper may contain certain arbitrary fluctuations attributable to different statistical calibers, which may lead to certain errors in the calculation results. Secondly, in view of the limited availability and continuity of the data, this paper may lack a certain level of accuracy and comprehensiveness in determining the evaluation years and indicators. The inclusion of the panel data into longer time series and broader indicator system may also be challenging for subsequent studies.

Conclusions

Based on the panel data of 76 county-level units in Liaoning Province, we describe the spatial-temporal evolution trends and interaction characteristics of the urbanization level and eco-efficiency of agricultural counties and districts in Liaoning Province, in this paper. The main conclusions drawn are as follows:

(1) From 2013 to 2017, the average value of urbanization of agricultural counties and districts in Liaoning Province gradually climbed from 0.2468 to 0.2789, and the urbanization process switched from strip development to regional development, entirely. The eco-efficiency of agricultural counties and districts in Liaoning Province exhibited an N-shaped development trend and declined from 0.4364 to 0.3117. Eco-efficiency was relatively better in the southern Liaoning

region but was underdeveloped in the western Liaoning region. Eco-efficiency of the other regions in the province had a good foundation but was badly deteriorated due to urbanization development. Overall, the urbanization level and eco-efficiency of agricultural counties and districts in Liaoning Province portrayed a reverse development trend, and the spatial pattern of the two also showed similar unbalanced characteristics.

(2) From 2013 to 2017, no reduction was seen in the urbanization difference among the agricultural counties and districts in Liaoning Province. There were certain diffusion characteristics, followed by the evident agglomerated development within the region. Most of the research units were low-level units and demonstrated a remarkable convergence trend. After experiencing a fluctuating decrease, the eco-efficiency slightly increased but failed to reach the previous elevated level. Severe polarization of eco-efficiency was observed, and the value of each unit was generally low. The difference in the county-level eco-efficiency was curtailed to some extent before it continued to increase again.

(3) From 2013 to 2017, the center of urbanization in Liaoning Province moved in the "southwest–northeast" direction, with an average movement rate of 3.41 km/a, and the moving trend was stable. The center of eco-efficiency moved in the "southwest–northwest" direction, with an average movement rate of 12.28 km/a, and the overall variation rate increased. There was insufficient correlation between the changes in the center of the two factors in various regions, and insignificant synchronization in changes in the movement of the center of the two, within each region.

(4) From 2013 to 2017, there was a global positive correlation between the urbanization level and eco-efficiency in Liaoning Province, which exhibited an inverted "U" shaped development trend, with the year 2014 as the inflection point. The global Moran's I index of "urbanization-eco-efficiency" rose from 0.152 in 2013 to 0.289 in 2014 and then continued to drop to 0.109 in 2017. The global Moran's I index of "eco-efficiency-urbanization" increased from 0.117 in 2013 to 0.219 in 2014, and then reduced to 0.133 in 2017. The local autocorrelation of "urbanization-eco-efficiency" was dominated by the LL agglomeration type, which was adjacently distributed in the western region and subsequently shifted to the southeastern region. The southern region gradually replaced the central region to form the HH agglomeration areas, and the HL and LH agglomeration areas were minimal in number and declined gradually. "Eco-efficiency-urbanization" agglomeration areas primarily belonged to the LL and HL types. LL agglomeration areas were distributed in the western, northern, and eastern parts of Liaoning Province with a stable spatial pattern. A gradual decrease was observed in the number of HL and HH agglomeration areas, while a surge was witnessed in the number of LH agglomeration areas.

The results herein have important reference values for ecological construction and sustainable development and can effectively help guide regional managers in regional planning and policy formulation, as well as provide reference for other regions to conduct interactive research on urbanization and eco-efficiency. This paper draws the following inspirations for the development of the county: (1) Establish a comprehensive evaluation system for the urbanization level and ecological environment, and dynamically monitor the process of urbanization and eco-efficiency. (2) Continue to follow the path of sustainable development, optimize resource allocation, and improve the coordination and interaction between regional construction and ecological utilization. (3) Fully consider the spatial spillover effects of urbanization and eco-efficiency, and build regional integration, planning docking, and policy coordination mechanisms, and cross-regional ecological compensation mechanisms.

Data availability statement

The raw data supporting the conclusions of this article will be made available by the authors, without undue reservation.

Author contributions

YG: data curation and investigation. CG: data curation, writing—original draft, and writing—review and editing. YW: conceptualization, formal analysis, and supervision. All authors contributed to the article and approved the submitted version.

Conflict of interest

The authors declare that the research was conducted in the absence of any commercial or financial relationships that could be construed as a potential conflict of interest.

Publisher's note

All claims expressed in this article are solely those of the authors and do not necessarily represent those of their affiliated organizations, or those of the publisher, the editors and the reviewers. Any product that may be evaluated in this article, or claim that may be made by its manufacturer, is not guaranteed or endorsed by the publisher.

References

Antczak, E. (2020). Regional patterns in dumping sites in poland - analysis in context of the new "sustainable" waste policy. *Polish J. Environ. Stud.* 29, 1037–1049. doi: 10.15244/pjoes/108484

Avadí, Á., Vázquez-Rowe, I., and Fréon, P. (2014). Eco-efficiency assessment of the peruvian anchoveta steel and wooden fleets using the LCA+DEA framework. *J. Clean. Prod.* 70, 118–131. doi: 10.1016/j.jclepro.2014.01.047

Bai, Y., Deng, X., Jiang, S., Zhang, Q., and Wang, Z. (2018). Exploring the relationship between urbanization and urban eco-efficiency, evidence from prefecture-level cities in China. *J. Clean. Prod.* 195, 487–1496. doi: 10.1016/j.jclepro.2017.11.115

Batlle, J. R. M., and van der Hoek, Y. (2018). Clusters of high abundance of plants detected from local indicators of spatial association (LISA) in a semi-deciduous tropical forest. *PLoS ONE* 13, e208780. doi: 10.1371/journal.pone.0208780

Beltrán-Estevea, M., Reig-Martínez, E., and Estruch-Guitart, V. (2017). Assessing eco efficiency, a metafrontier directional distance function approach using life cycle analysis. *Environ. Impact Assess. Rev.* 63, 116–127. doi: 10.1016/j.eiar.2017.01.001

Bianchi, M., del Valle, I., and Tapia, C. (2020). Measuring eco-efficiency in European regions, evidence from a territorial perspective. *J. Clean. Prod.* 276, 123246. doi: 10.1016/j.jclepro.2020.123246

Cecchini, L., Venanzi, S., Pierri, A., and Chiorri, M. (2018). Environmental efficiency analysis and estimation of CO2 abatement costs in dairy cattle farms in Umbria (Italy), a SBM-DEA model with undesirable output. *J. Clean. Prod.* 197, 895–907. doi: 10.1016/j.jclepro.2018.06.165

Chen, Y., Yang, J., Yang, R., Xiao, X., and Xia, J. (2022). Contribution of urban functional zones to the spatial distribution of urban thermal environment. *Build. Environ.* 216, 109000. doi: 10.1016/j.buildenv.2022.109000

Cohen-Shacham, E., Andrade, A., Dalton, J., Dudley, N., Jones, M., Kumar, C., et al. (2019). Core principles for successfully implementing and upscaling nature-based solutions. *Environ. Sci. Policy* 98, 20–29. doi: 10.1016/j.envsci.2019.04.014

Drakakis-Smith, D., and Dixon, C. (1997). Sustainable uribanization in Vietnam. *Geoforum* 28, 21–38. doi: 10.1016/S0016-7185(97)85525-X

Duggett, M. (1998). Organisation for economic cooperation and development. *Piblic Administr.* 76, 189–190.

Enserink, B., and Koppenjan, J. (2007). Public participation in China, sustainable urbanization and governance. *Manage. Environ. Q.* 18, 459–474. doi: 10.1108/14777830710753848

Fuchs, R. J., and Pernia, E. M. (1987). *Urbanization and Urban Policies in Pacific Asia*. Boulder; London, Westview Press.

Grossman, G. M., and Krueger, A. B. (1991). Environmental impacts of a North American free trade agreement. *National Bureau of Economic Research Working Paper*, Cambridge, Vol. 3914, 1–57.

Hak, T., Janoušková, S., and Moldan, B. (2016). Sustainable development goals, a need for relevant indicators. *Ecol. Indic.* 60, 565–573. doi: 10.1016/j.ecolind.2015.08.003

He, F., Yang, J., Zhang, Y., Sun, D., Wang, L., Xiao, X., et al. (2022). Offshore Island Connection Line, a new perspective of coastal urban development boundary simulation and multi-scenario prediction. *GIScience Remote Sens.* 59, 801–821. doi: 10.1080/15481603.2022.2071056

He, J., Wang, S., Liu, Y., Ma, H., and Liu, Q. (2017). Examining the relationship between urbanization and the eco-environment using a coupling analysis, case study of Shanghai, China. *Ecol. Ind.* 77, 185–193. doi: 10.1016/j.ecolind.2017.01.017

Howard, E. (2003). Garden cities of to-morrow. *Organ. Environ.* 16, 98–107. doi: 10.1177/1086026602250259

Huppes, G., and Ishikawa, M. (2005). A framework for quantified eco-efficiency analysis. *J. Indus. Ecol.* 9, 25–41. doi: 10.1162/108819805775247882

Jollands, N., Lermit, J., and Patterson, M. (2004). Aggregate eco-efficiency indices for New Zealand-a principal components analysis. *J. Environ. Manage.* 73, 293–305. doi: 10.1016/j.jenvman.2004.07.002

Kounetas, K. E., Polemis, M. L., and Tzeremes, N. G. (2021). Measurement of eco-efficiency and convergence, evidence from a non-parametric frontier analysis. *Eur. J. Oper. Res.* 291, 365–378. doi: 10.1016/j.ejor.2020.09.024

Kruger, R. V., Nunes, P. A., and Bourscheidt, D. M. (2017). Programa Bolsa Família e o mercado de trabalho no Paraná em 2010. *Econ. Sociedad Territorio* 17, 777–808. doi: 10.22136/est2017926

Kuosmanen, T. (2005). Measurement and analysis of eco-efficiency, an economist's perspective. *J. Ind. Ecol.* 9, 15–18. doi: 10.1162/108819805775248025

Li, H., and Shi, J. (2014). Energy efficiency analysis on Chinese industrial sectors, an improved Super-SBM model with undesirable outputs. *J. Clean. Prod.* 65, 97–107. doi: 10.1016/j.jclepro.2013.09.035

Liang, L., Chen, M., Luo, X., Xian, Y. (2021). Changes pattern in the population and economic gravity centers since the Reform and Opening up in China: The widening gaps between the South and North. *J. Clean. Prod.* 310:127379. doi: 10.1016/j.jclepro.2021.127379

Liu, S., Zhang, P., Wang, Z., Liu, W., and Tan, J. (2016). Measuring the sustainable urbanization potential of cities in Northeast China. *J. Geogr. Sci.* 26, 549–567. doi: 10.1007/s11442-016-1285-0

Liu, W., Zhan, J. Y., Zhao, F., Wei, X. Q., and Zhang, F. (2021). Exploring the coupling relationship between urbanization and energy eco-efficiency, a case study of 281 prefecture-level cities in China. *Sustain. Cities Soc.*64, 102563. doi: 10.1016/j.scs.2020.102563

Lorenzo-Toja, Y., Vázquez-Rowe, I., Chenel, S., Marín-Navarro, D., Moreira, M. T., and Feijoo, G. (2015). Eco-efficiency analysis of Spanish WWTPs using the LCA + DEA method. *Water Res.* 68, 651–666. doi: 10.1016/j.watres.2014.10.040

Luederitz, C., Brink, E., Gralla, F., Hermelingmeier, V., Meyer, M., Niven, L., et al. (2015). A review of urban ecosystem services, six key challenges for future research. *Ecosyst. Serv.* 14, 98–112. doi: 10.1016/j.ecoser.2015.05.001

Mickwitz, P., Melanen, M., Rosenström, U., and Seppala, J. (2005). Regional eco-efficiency indicators - a participatory approach. *J. Clean. Prod.* 14, 1603–1611. doi: 10.1016/j.jclepro.2005.05.025

Minoiu, C., and Reddy, S. G. (2014). Kernel density estimation on grouped data, the case of poverty assessment. *J. Econ. Inequal.* 12, 163–189. doi: 10.1007/s10888-012-9220-9

Moutinho, V., and Madaleno, M. (2021). A two-stage DEA model to evaluate the technical eco-efficiency indicator in the EU countries. *Int. J. Environ. Res. Public Health.* 18, 3038. doi: 10.3390/ijerph18063038

Ochoa, J. J., Tan, Y., Qian, Q. K., Shen, L., and Moreno, E. L. (2018). Learning from best practices in sustainable urbanization. *Habitat Int.* 78, 83–95. doi: 10.1016/j.habitatint.2018.05.013

Picazo-Tadeo, A. J., Gómez-Limón, J. A., and Reig-Martínez, E. (2011). Assessing farming eco-efficiency, a data envelopment analysis approach. *J. Environ. Manage.* 92, 1154–1164. doi: 10.1016/j.jenvman.2010.11.025

Polesie, S., Gillstedt, M., Kittler, H., Lallas, A., Tschandl, P., Zalaudek, I., and Paoli, J. (2020). Attitudes towards artificial intelligence within dermatology, an international online survey. *Br. J. Dermatol.* 7, 160–161. doi: 10.1111/bjd.18875

Prothero, A. (1999). *Eco-efficiency, The Business Link to Sustainable Development*, Emerald Group Publishing Limited, Vol. 8, 119–120.

Reith, C., and Guirdy, M. (2003). Eco-efficiency analysis of an agricultural research complex. *J. Environ. Manage.* 68, 219–229. doi: 10.1016/S0301-4797(02)00161-5

Ren, Y., Bai, Y., Liu, Y., Wang, J., Zhang, F., and Wang, Z. (2022). Conflict or coordination? Analysis of spatio-temporal coupling relationship between urbanization and eco-efficiency, a case study of urban Agglomerations in the Yellow River Basin, China. *Land* 11, 882. doi: 10.3390/land11060882

Sadorsky, P. (2021). Eco-efficiency for the G18, trends and future outlook. *Sustainability* 13, 11196. doi: 10.3390/su132011196

Schaltegger, S., and Sturm, A. (1990). Okologische rationalitat. *Die Unternehmung* 44, 273–290.

Schaltegger, S., and Synnestvedt, T. (2002). The link between 'green' and economic success, environmental management as the crucial trigger between environmental and economic performance. *J. Environ. Manage.* 65, 339–346. doi: 10.1006/jema.2002.0555

Sheikhipour, B., Javadi, S., and Banihabib, M. E. (2018). A hybrid multiple criteria decision-making model for the sustainable management of aquifers. *Environ. Earth Sci.* 77, 1–16. doi: 10.1007/s12665-018-7894-4

Thomas, S. (2009). Urbanization as a driver of change. In, Gospodini A, Brebbia CA, editors. *Sustainable City V, Urban Regeneration and Sustainability. WIT Transactions On Ecology and the Environment*, WIT PRESS/COMPUTATIONAL MECHANICS PUBLICATIONS, Vol. 117, 95–104.

Tone, K., and Tsutsui, M. (2010). Dynamic DEA, a slacks-based measure approach. *Omega* 38, 145–156. doi: 10.1016/j.omega.2009.07.003

Tone, K., and Tsutsui, M. (2013). Dynamic DEA with network structure, a slacks-based measure approach. *Omega* 42, 124–131. doi: 10.1016/j.omega.2013.04.002

United Nations (2020). *The Sustainable Development Goals Report 2020*. New York, NY, United Nations.

Van der Bruggen, B., Borghgraef, K., and Vinckier, C. (2010). Causes of water supply problems in urbanised regions in developing countries. *Water Resour Manage*. 24, 1885–1902. doi: 10.1007/s11269-009-9529-8

Van Kerm, P. (2003). Adaptive kernel density estimation. *Stata J.* 3, 148–156. doi: 10.1177/1536867X0300300204

Wartenberg, D. (1985). Multivariate spatial correlation, a method for exploratory geographical analysis. *Geogr. Anal.* 17, 263–283. doi: 10.1111/j.1538-4632.1985.tb00849.x

WBCSD (1996). *Eco-Efficient Leadership for Improved Economic and Environmental Performance*, Geneva, 3–16.

Wei, Y. D., and Ye, X. (2014). Urbanization, urban land expansion and environmental change in China. *Stoch. Environ. Res. Risk Assess.* 28, 757–765. doi: 10.1007/s00477-013-0840-9

Weizsäcker, v. E. U., Lovins, A., and Lovins, H. (1997). *Factor Four, Doubling Wealth - Halving Resource Use*. London, Earthscan.

Wursthorn, S., Poganietz, W. R., and Schebek, L. (2011). Economic-environmental monitoring indicators for European countries, a disaggregated sector-based approach for monitoring eco-efficiency. *Ecol. Econ.* 70, 487–496. doi: 10.1016/j.ecolecon.2010.09.033

Xu, K., Bossink, B., and Chen, Q. (2020). Efficiency evaluation of regional sustainable innovation in China, a slack-based measure (SBM) model with undesirable outputs. *Sustainability* 12, 31. doi: 10.3390/su12010031

Yang, J., Guo, A., Li, Y., Zhang, Y., and Li, X. (2019). Simulation of landscape spatial layout evolution in rural-urban fringe areas, a case study of Ganjingzi District. *GIScience Remote Sens.* 56, 388–405. doi: 10.1080/15481603.2018.1533680

Yao, J., Xu, P., and Huang, Z. (2021). Impact of urbanization on ecological efficiency in China, an empirical analysis based on provincial panel data. *Ecol. Indic.* 129, 107827. doi: 10.1016/j.ecolind.2021.107827

Yasmeen, H., Tan, Q., Zameer, H., Tan, J., and Nawaz, K. (2020). Exploring the impact of technological innovation, environmental regulations and urbanization on ecological efficiency of China in the context of COP21. *J. Environ. Manage.* 274, 111210. doi: 10.1016/j.jenvman.2020.111210

Yu, W., Yang, J., Sun, D., Yu, H., Yao, Y., Xiao, X., et al. (2022). Spatial-temporal patterns of network structure of human settlements competitiveness in resource-based urban agglomerations. *Front. Environ. Sci.* 10, 893876. doi: 10.3389/fenvs.2022.893876

Yue, L., Xue, D., Draz, M. U., Ahmad, F., Li, J., Shahzad, F., and Ali, S. (2020). The double-edged sword of urbanization and its nexus with eco-efficiency in China. *Int. J. Environ. Res. Public Health* 17, 446. doi: 10.3390/ijerph17020446

Zhang, H., Chen, M., and Liang, C. (2022). Urbanization of county in China, spatial patterns and influencing factors. *J. Geograph. Sci.* 32, 1241–1260. doi: 10.1007/s11442-022-1995-4

Zhao, H., Liu, Y., and Lindley, S. (2020). Change, mechanism, and response of pollutant discharge pattern resulting from manufacturing industrial transfer, a case study of the Pan-Yangtze River Delta, China. *J. Clean. Prod.* 224, 118587. doi: 10.1016/j.jclepro.2019.118587

Zhou, T., and Zhou, Y. (2015). Fuzzy comprehensive evaluation of urban regeneration decision-making based on entropy weight method, case study of Yuzhong Peninsula, China. *J. Intelligent Fuzzy Syst.* 29, 2661–2668. doi: 10.3233/IFS-151969

frontiers | Frontiers in Earth Science

TYPE Original Research
PUBLISHED 19 September 2022
DOI 10.3389/feart.2022.974219

Check for updates

OPEN ACCESS

EDITED BY
Bing Xue,
Institute of Applied Ecology (CAS), China

REVIEWED BY
Chenxi Li,
Xi'an University of Architecture and Technology, China
Jun Yang,
Northeastern University, China

*CORRESPONDENCE
Haitao Ma,
maht@igsnrr.ac.cn

SPECIALTY SECTION
This article was submitted to Geoscience and Society, a section of the journal Frontiers in Earth Science

RECEIVED 21 June 2022
ACCEPTED 29 August 2022
PUBLISHED 19 September 2022

CITATION
Ma H, Xu X, Li X and Liu J (2022), Towards innovation resilience through urban networks of co-invention: A case study of cities in China.
Front. Earth Sci. 10:974219.
doi: 10.3389/feart.2022.974219

COPYRIGHT
© 2022 Ma, Xu, Li and Liu. This is an open-access article distributed under the terms of the Creative Commons Attribution License (CC BY). The use, distribution or reproduction in other forums is permitted, provided the original author(s) and the copyright owner(s) are credited and that the original publication in this journal is cited, in accordance with accepted academic practice. No use, distribution or reproduction is permitted which does not comply with these terms.

Towards innovation resilience through urban networks of co-invention: A case study of cities in China

Haitao Ma[1]*, Xuanfang Xu[1], Xiaozhen Li[2] and Jingyu Liu[2]

[1]Key Laboratory of Regional Sustainable Development Modeling, Institute of Geographic Sciences and Natural Resources Research, Chinese Academy of Sciences, Beijing, China, [2]Research Center of Regional Development and Planning, Key Laboratory of Geospatial Technology for the Middle and Lower Yellow River Region, College of Geography and Environmental Science, Henan University, Kaifeng, China

The intensified competition for innovation among countries and the various risks that come with it have made innovation resilience a central concern of the international community in recent years. The concepts of resilience and innovation are inextricably intertwined; however, both theoretical discussions and case studies on innovation resilience are in the "embryonic" stage. This article attempts to integrate the system and nodes of network resilience, the potential and connectivity of city resilience, and the hierarchy and assortativity of urban network resilience to construct a theoretical analysis framework of intercity innovation network resilience and conduct a case study on the resilience of a patent cooperation network among 338 prefecture-level cities in China during 2017–2019. The results show that the systemic resilience of Chinese urban innovation networks exhibits relatively low hierarchical and yearly decreasing disassortative characteristics, and the node resilience shows a spatial pattern of being high in the southeast and low in the northwest, as well as higher innovation resilience in cities with higher administrative levels. The results provide insights into the overall systemic and internal structural characteristics of innovation resilience in Chinese urban networks and also expand the application of resilience concepts in the field of innovation research from the perspective of urban networks.

KEYWORDS

innovation resilience, network resilience, urban network, co-invention, patent, China

1 Introduction

Resilience and innovation are both regarded as central aspects of UN's sustainable development goals (Berkes et al., 2003; Lv et al., 2018; Van Wellen, 2019). In the process of scientific and technological innovation and interaction, uncertainty and unknown risks such as technology blockade, talent monopoly, and the impact of major public health emergencies are rising constantly (Lee, 2018); many countries even find themselves squeezed out of their former technology marketplaces in recent years (Cooke et al., 2012).

The US promulgated the Innovation and Competition Act of 2021 (Sun and Luo, 2021), which has triggered a new round of discussions on innovation competition among countries, and brought more risks and challenges to China's innovation and development. Innovation collaboration is increasingly affected and restricted by national borders. Therefore, improving national innovation resilience has become an important issue. Resilience is connected with vulnerability which implies risk, meaning the capacity to tackle "shocks" and "stresses." Shocks are inevitable and come in many forms whose impact depends on activity types and their traits in terms of uncertainty, riskiness, and resistance. The concept "resilience" originated from engineering mechanics, and was later applied to the field of ecology (Holling, 1973). Nowadays, it has been widely applied in many fields of economy and society (Liu et al., 2007) where policy discussions of regional development have recently shifted from a focus on growth and competitiveness to the analysis of the relative resilience of regional economies in response to rapid transitions in technologies, markets, and exogenous economic shocks (Clark et al., 2010). Resilience is a highly multidisciplinary concept, and there are different meanings and approaches within different disciplines (Vogus and Sutcliffe, 2003; Ponis and Koronis, 2012; Hosseini et al., 2016; Linnenluecke, 2017; Sanchez et al., 2017). It is possible to identify a sequence of resilience concepts: from systemic equilibrium toward a more open, non-static, ongoing, co-evolutionary, non-linear, complex, and socio-ecological-technological systems (Fastenrath et al., 2019). There have been multiple positive conceptualizations of resilience (Pike et al., 2010), along with some skepticism, questioning the value of the concept, especially by the followers of evolutionary economic geography (Hassink, 2010; Pike et al., 2010). This "evolutionary" perspective of resilience (Davoudi et al., 2013) is a criticism of the static understanding of resilience, which is an important turning point in conceptualizing and understanding resilience, inspiring researchers to explore more aspects of resilience.

Resilience is the basis for the continuity of innovative activities and for entering a new development path which is crucial in determining aptitude for sustained innovative output (Balland et al., 2015). Therefore, sustained evolutionary performance for regional innovation systems necessitates the capacity for those regions to reconfigure themselves effectively and rapidly to adapt to new or altered surroundings generated by these shocks (Lee, 2018). Innovation plays a key role in the renewal and reorientation of development (Athey et al., 2008), which is the driving force of long-term economic transformation and change (Schumpeter, 1939, 1942). However, innovation involves a high level of uncertainty, idiosyncrasy, risk, and sensitivity to turbulence; and the innovative outcomes are uncertain (Freeman and Soete, 1997; Fleming, 2007). By its nature, resilience of innovation considerably differs from other types of resilience due to the specifics, and the essence of innovation is knowledge (Pavit, 2006; Popadiuk and Choo, 2006; Salter and Alexy, 2014; Dost et al., 2019), which is a unique, cumulative, and peculiar economic good, whose resources, features, continuing cumulatively immuring to further turbulences is the key element of the resilience of innovation (Antonelli, 2019). Meanwhile, learning of emerging types of knowledge and the absorption of external knowledge is also based on the constant combination and complementarity with existing types of knowledge (Wang, 2007), creating unlimited opportunities and potentials for innovation. As for a country or region, the agglomeration and diffusion of knowledge will accelerate the cumulative effect of knowledge and thus enhance the overall innovation capacity; this ability of agglomeration and diffusion will affect the continuity of regional innovation and the ability to adapt to environmental changes, which involves the issue of innovation resilience.

The role of innovation and knowledge has also been highlighted in relation to the concept of regional resilience (Lawson, 1999; Amin and Cohendet, 2004; Simmie and Martin, 2010). Following the concept of resilience, innovation resilience was viewed as the capability to cope with uncertainties associated with innovation through effectively integrating stability and adaptability (Lv et al., 2018; Pinto et al., 2018). However, these concepts are too general and do not demonstrate the essential characteristics of knowledge and innovation. Innovation resilience is generated in the process of knowledge aggregation and diffusion, so innovation resilience should highlight the ability of innovation entities to create, reorganize, reconstruct, and apply various types of knowledge within the territory they belong to, as well as the ability to generate new synergies and complementarities in shocks, and thus show stronger adaptation (variations within predetermined paths) and adaptability (departing or altering from the present path) under external shocks.

Resilience theory (Gunderson and Holling, 2002) and the diffusion of innovations theory (Rogers, 2003) are two interdisciplinary routes of inquiry that explore the interaction between human decision-making and the process of change (R.C. Atwell et al., 2008; Euchner, 2019). Resilience theory is in its theoretical adolescence and is favored by scientists and practitioners in different fields (Liu et al., 2007); but, it is also criticized for its weak integration and application of social science theories and complex network approaches (Janssen et al., 2006). In contrast, innovation diffusion theory has evolved more maturely over half a century of research. However, over the past 2 decades, the field of innovation diffusion research has also changed to focus on the sort of multilevel and ecological system drivers, which are the core topics of concern for resilience theory (Rogers, 2003).

Innovation resilience has received international attention, but it is particularly important to explore the issue of innovation resilience at the national scale due to the growing competition for innovation between countries, which has made innovation diffusion increasingly influenced by national governments or

national borders. In addition, as agglomerations of innovative resources and elements, cities are the basic nodes of national innovation development (Ma et al., 2015). The network pattern of knowledge flows within and between cities, becoming a reflection of national innovation capacity and profoundly affects the national innovation resilience (Clark et al., 2010). We explore the innovation resilience of national-scale urban networks from the perspective of knowledge flow and technological innovation cooperation, expecting to establish a method to evaluate national innovation resilience and aim to find a way to improve the national innovation resilience from the perspective of urban networks of co-invention.

The remainder of this article is arranged as follows. Section 2 discusses how innovation and knowledge networks are influential in the framework of the abounding literature on regional resilience. Section 3 introduces the research methodology and data, which is followed by five structural properties to measure the innovation network resilience. The research results related to the systemic structural and nodal characteristics of urban innovation network resilience using Chinese cities as an example are demonstrated in Section 4. The article concludes in Section 5 by making summaries and giving new insights for future studies.

2 Literature review and theoretical foundations

2.1 The concept of resilience in regional innovation

Research studies on resilience are nowadays indicate a growing interest as the macroeconomic context is characterized by chronic instability, as financial crisis, rapid technological cycles, environmental considerations, and new growing consumption paradigms challenge global but also regional policies (Crespo et al., 2013). In an increasingly interconnected world, challenges in one part may have a strong impact on other parts. The uncertainty associated with complex urban systems and networks calls for more attention to resilience. The development of the resilience theory has evolved through three stages: engineering resilience, ecological resilience, and evolutionary resilience (Modica and Reggiani, 2015). The first definition of resilience in the social and ecology domain dates back to 1973 (Holling, 1973) for understanding how some performing regions can decline at a given moment in time, while others are able to renew and sustain their growth in a disturbed economic environment.

There are two main perspectives of the meaning of resilience: as a double capacity, that of resisting a shock or limiting its effects but also that of anticipating and thus adapting to the shock or to a rapid evolution in the economic context by creating new systems (Gilly et al., 2014). The first one as a static property, namely, as engineering resilience, refers to stability and resistance capacity to pre-shock structure and function or stable equilibrium when subject to change (McDonald, 2006; Burnard and Bhamra, 2011; Lengnick-Hall et al., 2011). The second perspective has a dynamic character. It corresponds to the recovery ability of an equilibrium state to restore damaged components and redistribute flows, as well as create a new opportunity to change structure and function in response to a shock, which means forging a new pathway rather than continuing with an established path dependence (Reggiani et al., 2002; Allenby and Fink, 2005; Folke, 2006; Brede and de Vries, 2009; Schweitzer et al., 2009).

From the duality view, the concept of innovation resilience can be divided into two primary dimensions: stability and adaptability, which are integral parts of resilience and provide implications for constructing and measuring innovation resilience (Jackson, 1999; Eisenhardt et al., 2010; Farjoun, 2010; Sonenshein, 2016). Stability means reducing the vulnerabilities and absorbing shocks (Lengnick-Hall and Beck, 2005), which involves standardization, modularization, institutionalization, systematic planning, and focuses on the efficiency of innovation in a low-changing and predictable context. Adaptability is targeted at flexibility of taking advantage of opportunities and creating a fundamentally new system in high-variation and unpredictable environments. Nevertheless, behind this large consensus on regional resilience and its links with innovation and knowledge networks (Lawson, 1999; Amin and Cohendet, 2004; Simmie and Martin, 2010), we have found that few research studies have pursued the question of the elements of resilience in the innovation and the long-run evolution of regional innovative structures (Crespo et al., 2013). Overlooking the role that resilience plays in the long-term prosperity of a regional innovation system restricts a holistic understanding of the factors comprising such a dynamic structure.

Mainly dedicated to innovative cities and technological collaborations, this research is part of a more general wave of research on regional resilience. We emphasize the dynamic nature of resilience in an innovation network and consider it an ongoing process to create and use the accumulation of knowledge. Following the concept of regional resilience, we view innovation resilience as the capability to cope with the uncertainties associated with innovation, perform innovation continuously in turbulent environments, increase knowledge accumulation persistently, and create reinforcement mechanisms in innovation that translate into new capabilities. The differing spatial dynamics of innovation activities suggests that networks can be of either a local or regional nature (Clark et al., 2010), of which regional innovation resilience studies should rely on the structural and topological properties as key factors (Andergassen et al., 2014).

Using the structural properties of networks to evaluate regional resilience has been adopted by many scholars

(Crespo et al., 2013; Suire and Vicente, 2014; Kurth et al., 2020), but research studies on the knowledge network were mainly conducted from a micro perspective based on a local firm or industrial level, and it has been challenging to investigate the spatial characteristics of regional resilience. Although the emergence of network properties is commonly founded on micro-economic behaviors, these innovation entities and their behaviors are constrained by their local space. The aggregation of knowledge flows between actors or organizations in the micro scale into spatial flows between cities in the macro scale, constituting an appropriate measure to reflect spatial knowledge diffusion and spillover (Ma et al., 2018). In other words, the resilience of an intercity network structure can essentially be seen as the spatial performance of regional resilience (Newman, 2003; Crespo et al., 2013; Boschma, 2015). In this study, an intercity co-invention network was built from a macro perspective for better analyzing spatial characteristics of regional innovation resilience. When we take a city as the study area, these networks include both internal parts established within the city and external connections existing outside the city.

2.2 Innovation network resilience on the system level

In most of the definitions found in the literature, resilience is identified as an inherent attribute of a system (Holling, 1973; Hollnagel et al., 2006; Erol et al., 2010), the resilience of which relates to the functioning and interaction rather than to the stability of their components or the ability to maintain or return to some equilibrium state. Regions that are capable of taking advantage of new opportunities logically achieve higher resilience to potential shocks (Dabson et al., 2012). These extra-regional competencies serve to diversify a region's risk or decrease its vulnerability to internal or external perturbations (Asheim and Isaksen, 2002; Bathelt et al., 2004; Moodysson, 2008; Fitjar and Rodriguez-Pose, 2011). In the knowledge-based view, resources are the result of the creation and development of knowledge, whose accumulation plays a critical role in innovation resilience. Along the same line, Lundvall (Lundvall, 1992) formulated an understanding of regional innovation systems as the actors and exchanges that jointly participate in the development, diffusion, and subsequent use of new and useful knowledge. It is through these interactions underpinning the regional innovation system that cities access knowledge that cannot be generated internally, making regions inclined to exhibit less rigidity and more flexibility to outside influences.

As cities typically no longer innovate in isolation but through a complex set of intra or intercity interactions, networks have been recognized as a crucial ingredient in regional innovation resilience (Watts and Strogatz., 1998; Nooteboom and Gilsing, 2004; Christopherson et al., 2010; Pike et al., 2010). Structural properties of a network can provide insights about how the network is structured and the most important nodes and connections (Reggiani, 2013). The literature acknowledges two categories that shape social network structures: closure and bridging network strategies. Triadic closure implies that a node associates with two other nodes will increase the probability for these two nodes to have a tie between them. The higher the degree of a node, the more the node is attractive for receiving new ties, so that the network grows through an increasing core-component hierarchy (Albert and Barabasi, 2001). Since the low connectivity between the core nodes and the peripheral ones limits the reorganization of knowledge flows, closure favors network assortativity. Bridging ties is more entrepreneurial than the former, meaning that one node finds an opportunity to connect disconnected nodes, which has implications on the overall structure since they can enable better circulation of knowledge between the core and the periphery of nodes (Cattani and Ferriani, 2008).

The level of hierarchy of the node degree and the level of assortativity therefore appear as two simple statistical signatures of the ability of the regional innovation system to perform through their endogenous resilient capabilities. The hierarchy exemplifies the level of heterogeneity in terms of actual relational capacities and positions, which reveals a pattern that the network dynamics is being driven by a process of self-organization determining a hierarchical connectivity structure (Carrington et al., 2005; Reggiani and Nijkamp, 2006). A network with a rather flat hierarchy displays high resistance to external shock regardless of whatever node is removed, but the absence of a core group weakens the control of the collective behaviors (Crespo et al., 2013). On the other hand, a network with a rather sloped hierarchy remains sufficiently linked to fresh and new ideas coming from peripheral nodes for future collaborations. But when closure strategies of core groups exceed a certain threshold, then the redundancy of knowledge flows and conformity effects prevail and the possibilities for regional resilience fall unavoidably. That is to say, the hierarchy in the appropriate interval is helpful to improve the resilience of the regional innovation system.

Based on the extent of whether the node degree displays a positive or negative correlation, networks can be characterized as assortative or disassortative (Crespo et al., 2013). A network structure is assortative when high-degree nodes are connected disproportionately to other high-degree nodes, and low-degree nodes are preferentially connected to low-degree nodes, which gives a formal representation of the way knowledge flows between central and more peripheral nodes. The emergence of such structures is mainly due to the preferential attachment process (Newman, 2003; Dorogovtsev et al., 2008). Generally, highly connected nodes are tied predominantly with other highly connected nodes in the core, and peripheral nodes remain connected between themselves. Networks have to develop bridging strategies in order to open more disruptive relations

between the core and peripheral nodes, so as to enable the system as a whole to facilitate a collective process of knowledge integration between complementary cities along the knowledge value chain than for the entirely assortative one.

2.3 Innovation network resilience on the node level

As cities are well-connected by knowledge networks, even a moderate shock in a city may cause unpredictable changes in the entire innovation network system. Cities' resilience is based on both absorption of external knowledge through networking and creation of new knowledge. More diversified regions, especially those able to rely more heavily on outside influences are structured in a more resilient manner (Simmie and Martin, 2010; Balland et al., 2015). The generation of new knowledge builds upon previously learned information which extend knowledge stocks, reduces resource constraints, and increases the probability of subsequent innovation (Duguet and Monjon, 2002; Clausen et al., 2012). In this way, the transformation of accumulated knowledge conceivably enables the region to better prepare for unforeseen shocks and better recover from shocks by rapidly adapting to new conditions. This involves assessing the quality and strength of two key features of the innovation system at the node level: innovative potential and connectivity which together represent their degrees of resilience (Sunley, 2013). These two in combination allow for the capacity of a node/city to face destabilizing shocks, manage processes of creative destruction through innovation, and recovery.

First is its potential, measured in terms of the variety of innovation resources and achievements present from the interaction among diverse local entities. A region that is technologically capable must include local entities featuring an autonomous innovative capacity owing to learning, searching, and gathering of information ultimately leading to innovation. Innovative activities initially take place in the active interaction between innovative subjects in the city, as geographic proximity reduces uncertainty and resolves coordination problems in balancing risks and costs of innovation (Boschma, 2005; Ma et al., 2021). Regional innovation system theorists such as Cooke (Cooke, 2001) pointed out that the richer the local innovation resources and the closer the internal connections, the healthier the network innovation system and the stronger the competitiveness (Ma and Xu, 2022). The unintended spillover effects generated by the linkage of innovation agents within cities cannot be ignored on the overall regional resilience.

The second is connectedness, the degree to which it has interlocking systems assisting its governance. For physical networks, efficiency and resilience are incompatible, that is, the more efficient the network is in minimizing ties and maximizing reachability, the more sensitive it is to external shocks and the more it exhibits fragility properties (Brede and de Vries, 2009). But for innovation network as one type of socio-economic networks, because of the ability of nodes to build and maintain ties for overlapping explorative and exploitative ties, performing networks are not necessarily incompatible with regional resilience. Erhardt et al. (2007) studied the relationship between connectivity and social network resilience and showed that sharp transitions, hysteresis, and equilibrium multiplicity of connectivity are salient characteristics of social dynamics. More diversified regions, especially those able to rely more heavily on outside influences are structured in a more resilient manner (Simmie and Martin, 2010; Balland et al., 2015). A node with high transitivity means that it can quickly exchange knowledge and technology with others in the network, promote learning and innovation in the whole system, and enhance the resilience to withstand shocks (Dabson et al., 2012; Rose and Krausmann, 2013).

Equally important to the high transitivity of a node in a regional innovation system as the interaction of innovation-focused actors is the assurance that the external links of the nodes are of made up of many diverse paths. In an evolutionary framework, adaptability and adaptation are two critical concepts (Hassink, 2010). Adaptability means to develop a new path while regions with adaptation typically might be locked into historical path dependence. Resilient regions usually are able to overcome a trade-off between adaptation and adaptability (Pike et al., 2010). In other words, a resilient network should be redundant (Ouyang et al., 2012). It has been proven that cities with a knowledge base that has a high degree of relatedness to technologies that are not yet present in the city are better able to avoid technological crises. Therefore, diversified innovation systems, presenting openness to a variety of extra local links would be able to redirect their development paths to adapt to changing conditions, and would be less susceptible to lock-in effects (Dabson et al., 2012; Balland et al., 2015). Regardless, if the node is removed, the knowledge flow will still find paths to irrigate the whole network. Such a network displays a strong potential for knowledge flow reorganization and diffusion since the nodes are linked by many paths.

3 Materials and methods

3.1 Study area and data source

This study takes 338 cities in China as examples, including 289 prefecture-level cities, 26 autonomous prefectures, 4 municipalities, 6 prefectures, 3 leagues, and 10 counties administrated by the province (excluding Taiwan, Macao, and Hong Kong). Patent co-invention is a manifestation of knowledge spillover, which is an important achievement of scientific and technological achievement, and a major indicator of regional innovation capabilities. Using the

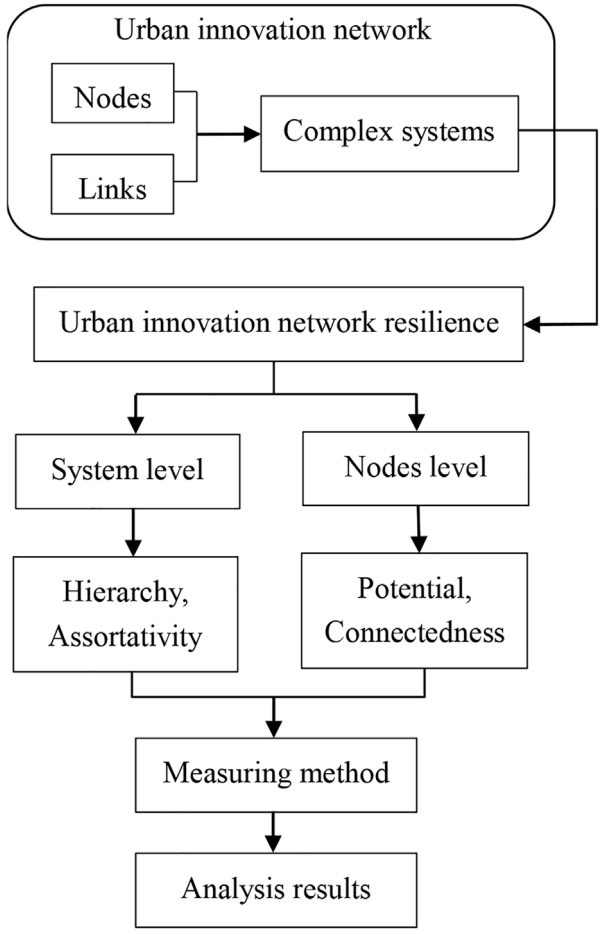

FIGURE 1
Assessment process of the urban innovation network resilience.

information of China's patent co-invention number as the original data from 2017 to 2019, we analyzed the resilience of China's urban innovation network based on the structural and topological properties. Vector files of administrative boundaries and urban administrative centers at a scale of 1:1,000,000 were provided by the basic geographical database of the National Geomatics Center of China.

3.2 Conceptual framework

Network is a simple but useful method to analyze resilience from an evolutionary perspective (Boschma, 2015). Drawing on the conceptual framework of the transportation infrastructure proposed by Wang et al. (2020) and the previous theoretical analysis of innovation resilience and network structure; the analytical framework of urban innovation network resilience is shown in Figure 1.

The first step is defining and constructing urban innovation network resilience. As a complex system, an urban innovation network consists of nodes and links, where nodes represent different cities and links manifest the relational innovation connections and interactions among cities. Next, urban innovation network resilience is identified from the system level and node level. Systemic resilience represents the comprehensive ability of the urban innovation network against technological ricks, which can be quantitatively measured by two simple statistical signatures: hierarchy and assortativity. Resilience of innovation on the node level represents the capacity of a city to face destabilizing shocks, manage processes of creative destruction through innovation, and recover, which can be measured by potential and connectivity. The following is a detailed description of measurement methods and the final is calculations and a result analysis of the urban innovation network resilience.

3.3 Measuring methods

3.3.1 System resilience: hierarchy and assortativity

3.3.1.1 Hierarchy

Hierarchy represents the ranking of nodes in a network (Ye and Qian, 2021). Crespo (Crespo et al., 2013) proposed that the measure of hierarchy can be reflected by the network degree distribution exponent, and the greater the slope of the degree distribution, the more significant the degree of hierarchy between nodes. The degree distribution is the probability distribution of degrees, where K* is the probability that a node chosen randomly from the network has degree K. We calculated the probability of each degree and then draw the distribution on a log–log scale, such that:

$$K_i = C\left(K_i^{*a}\right) \quad (1)$$

$$\mathrm{Log}\left(\mathrm{K_i^*}\right) = \log\left(\mathrm{C}\right) + \mathrm{a}\log\left(\mathrm{K_i}\right). \quad (2)$$

with K_i^* being the probability of random city i with degree K in the degree distribution, C being a constant, and a <0 the slope of the distribution.

3.3.1.2 Assortativity

The measure of assortativity can be reflected by the network degree correlation index (Crespo et al., 2013; Wei and Pan, 2021; Ye and Qian, 2021). The mean degree of the relevant neighborhood (V_j) for each node *i* can be calculated from following equations:

$$\overline{K_i} = \sum_{j\in v} K_j / K_i. \quad (3)$$

where K_j is the degree of node *j* belonging to the interaction neighborhood of node *i*.

Then, we estimate a linear relationship between $\bar{K}_i$ and K_i:

$$\overline{K_i} = D + bK_i, \quad (4)$$

with D as a constant and b as a coefficient capturing the degree correlation. If b>0, the network N exhibits assortativity with a positive-degree correlation, whereas if b<0, the network N is disassortative with a negative-degree correlation.

The "core/periphery and resilient network" exhibits another high-sloped degree distribution, but the degree correlation is now negative (b<0), so that the network presents a certain level of disassortativity. The larger |a| of the degree distribution coefficient, the higher its structural hierarchy, enabling it to be cohesive and competitive; the larger the |b| of the degree correlation coefficient, the more the disassortative patterns of relations increase regional resilience capabilities (Crespo et al., 2013). It can be used as the basis for judging the system resilience of the urban innovation network.

3.3.2 Node resilience: potential and connectivity

Network node resilience reflects the ability of a node to maintain its original innovation and connection strength when it is attacked (Wang et al., 2020), that is potential and connectivity.

3.3.2.1 Potential

Potential is measured by self-organization, which can be represented by the number of intracity patent co-inventions. In order to avoid the effect of numerical magnitude differences on the results, the data are normalized as:

$$y_i = \frac{x_i - \min(x_i)}{\max(x_i) - \min(x_i)}. \quad (5)$$

x_i is the number of intracity patent co-inventions in city *i*, min (x_i) is the minimum number of intracity patent co-inventions, and max (x_i) is the maximum number of intracity patent co-inventions.

3.3.2.2 Connectivity

We use two indicators—transitivity and diversity to measure the connectedness of nodes. Betweenness is used to quantitatively evaluate the transitivity of cities in the network, which is defined as the ratio of the number of shortest paths between any two cities in the network that pass through the city to the total number of shortest paths, representing the city's mediation effect and connection function in the innovation network. The betweenness of cities are calculated by the following equations:

$$K_i = \sum_{m \neq i \neq n} \frac{P^i_{mn}}{T_{mn}}, \quad (6)$$

where T_{mn} is the number of shortest paths from city *m* to city *n*, and P_{mn}^{i} is the number of shortest paths from city *m* to city *n* passing through city *i*.

The diversity of the urban innovation network between two cities depends on whether there are other by-pass paths apart from the normal path. We draw on the concept of independent path proposed by Ip and Wang (2011) to measure diversity. If a path set includes the path-connected nodes i and j without any common edges with other paths between nodes i and j, the set is defined as an independent passageway set of nodes i and j. The element of the set is called as a path (Ip and Wang, 2011). Diversity is quantified by the average number of independent paths, which is defined as the ratio of the number of independent paths between any two cities in the network to the total number of possible paths between cities. Here, an interruption scenario is set up, assuming that the city is attacked, the change of the average number of independent paths in the network reflects the city's diversity. The overall network diversity can be calculated as:

$$V(G) = \frac{\sum_{i \neq j \in G} N_{ij}}{n(n-1)}, \quad (7)$$

$$N_{ij} = \min\{Di, Dj\}. \quad (8)$$

V(G) is the average number of independent paths. N_{ij} represents the number of independent paths of cities *i* and *j*, which can be approximately replaced by the smaller of the two city degrees. Since the N_{ij} +1 paths have no common edges, they certainly have N_{ij} +1 edges to depart from city i or j. N_{ij} +1 > N_{ij} =Di or Dj, which conflicts with the definition of node degree. N_{ij} is the upper bound of the passageway number of an independent passageway set between the city pair i and j (Ip and Wang, 2011).

The diversity for each city is calculated as:

$$V_i = |V(G) - V(G)'|, \quad (9)$$

where V(G)' represents the network diversity after removing the connection between city *i* and its neighboring cities.

4 Results and discussion

Using the network theory and adopting a network structural analysis, our study attempts to assess the resilience of the urban innovation network based on endogenous mechanisms. As a network can be represented by two basic elements including the nodes and the ties that connect the nodes (Crespo et al., 2013), the correlation between relational behavior and individual node features has to be captured in parallel. Next, we introduce system resilience and node resilience separately from different dimensions of network structural properties.

4.1 System resilience

System resilience is measured by the "Hierarchy" and the "Assortativity," that by collaborating across different hierarchies and with complementary cities, scientists, and researchers can combine their techniques and complementary skills through

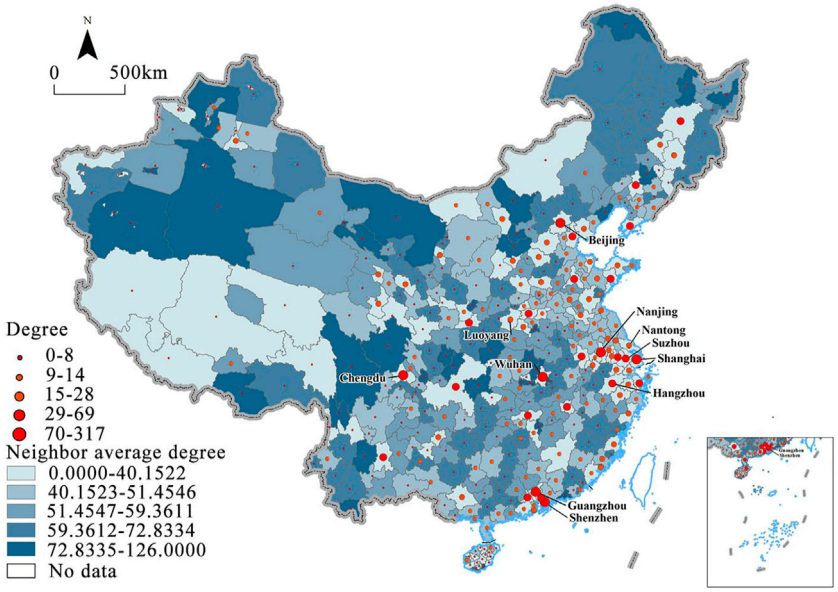

FIGURE 2
Spatial distribution of the degree and neighbor average degree of China's urban innovation network (average value from 2017 to 2019).

perceptions and opinions in pursuit of corporate goals and providing better fertile ground for long-term knowledge creation. The hierarchy characteristic is quantitatively calculated using the index of degree distribution and degree correlation mirrors the assortativity characteristic of innovation network resilience.

4.1.1 Hierarchy

There are 10,178 edges in China's urban innovation network, with an average degree of 30.11. Figure 2 shows the spatial distribution of 338 cities whose node degrees are divided into five levels. The number of the cities with the node degree at the first level is only 34 and the top nine cities are, respectively, Beijing, Shanghai, Shenzhen, Nanjing, Wuhan, Chengdu, Guangzhou, Suzhou, and Hangzhou. Among them, there are seven cities in the eastern region, one city in the central region, and one city in the western region, which shows the huge spatial differentiation at the national scale and reflects the simultaneous characteristics of innovation as unique and non-reproducibility. The cities at the second and third levels include sub-provincial cities, province capital cities, and cities within the innovation radiation sphere of the cities at the first level, such as Nantong and Luoyang, engaging with innovative cities actively by taking advantage of geographic proximity. Cities at the fourth and fifth levels are mostly distributed at the edge of the innovation network, with the maximum degree value being 14, only 1/23 of Beijing, indicates that the spatial differences of the degree distribution of innovation networks in Chinese cities are significant.

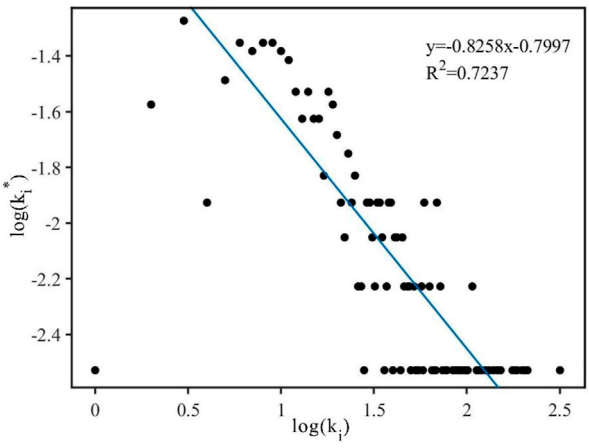

FIGURE 3
Degree distribution of urban innovation networks average from 2017 to 2019.

We calculated the probability of each degree in the innovation network and drew the degree distribution on a log–log scale to analyze the overall hierarchy by using Matlab software (Figure 3). The fitted curve appears as a straight line with a negative slope of a power exponent on a log–log scale and the R^2 of the degree distribution regression is 0.7237, indicating that the power–law distribution is suitable for fitting. We would expect that China's urban innovation network presents a power–law degree distribution and is a

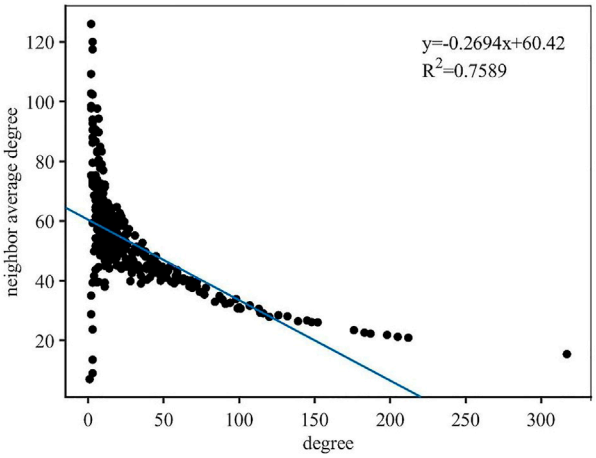

FIGURE 4
Degree correlation of urban innovation networks average from 2017 to 2019.

scale-free network (Barabási and Albert, 1999; Barabasi et al., 2000), indicating that it has certain cohesion and competitiveness, providing resistance and robustness to resist scientific and technological risks and shocks. In theory, the power exponent of a scale-free network is usually between 2 and 3 (Barabási and Albert, 1999; Barabasi et al., 2000). The slope |a| of the curve is 0.8258, which is relatively low compared with the hierarchical coefficient of the resilience of information networks and economic networks studied by Wei and Pan (2021), respectively, 1.229 and 1.727, and the result of the resilient network studied by Crespo et al. (2013) which was 1.063. The low coefficient indicates that the innovation network may exhibit an insufficient level of cohesiveness into the core in some fields. In that case, leading cities may not succeed in maintaining a high level of knowledge integration. Thus, few but important fields should be focused on improving the cohesive force of the core to strengthen network resilience further.

4.1.2 Assortativity

The assortativity of the network reflects the preference attachment of cities. Using NAD, the degree correlation is measured based on average data from 2017 to 2019 and the coefficients are negative with a value of −0.2694 (Figure 4), indicating that the Chinese urban innovation network is disassortative. In Figure 2, we can find that cities in the innovation network with high-degree/low-degree values are usually neighbored by cities with low/high average values, which confirms the existence of disassortative innovation links in the urban

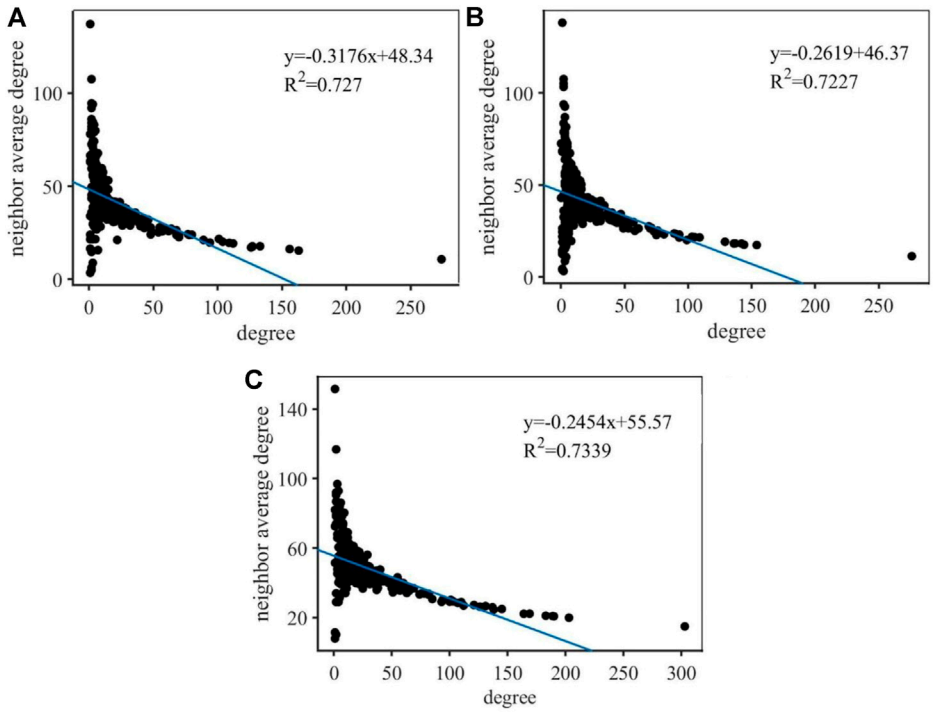

FIGURE 5
Degree correlation of urban innovation networks: **(A)** 2017; **(B)** 2018; and **(C)** 2019.

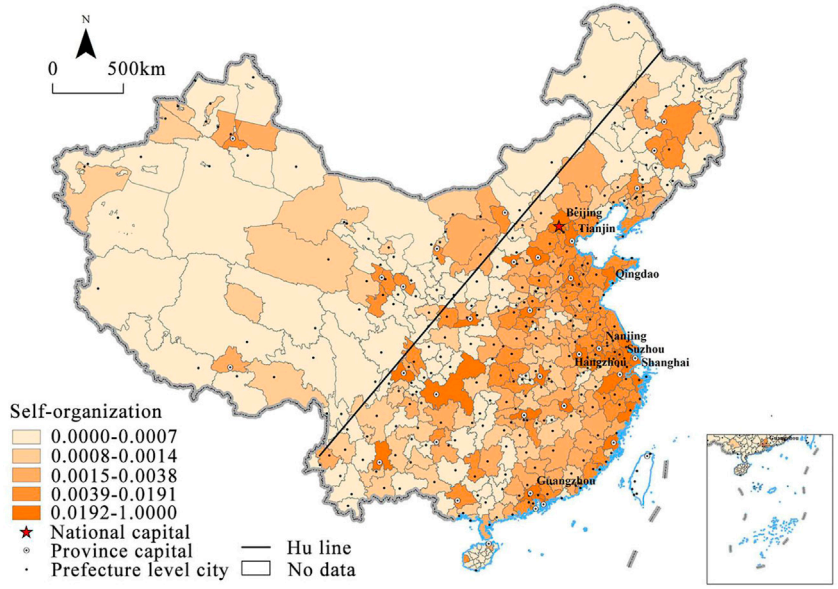

FIGURE 6
Spatial distribution of the self-organization of China's urban innovation network.

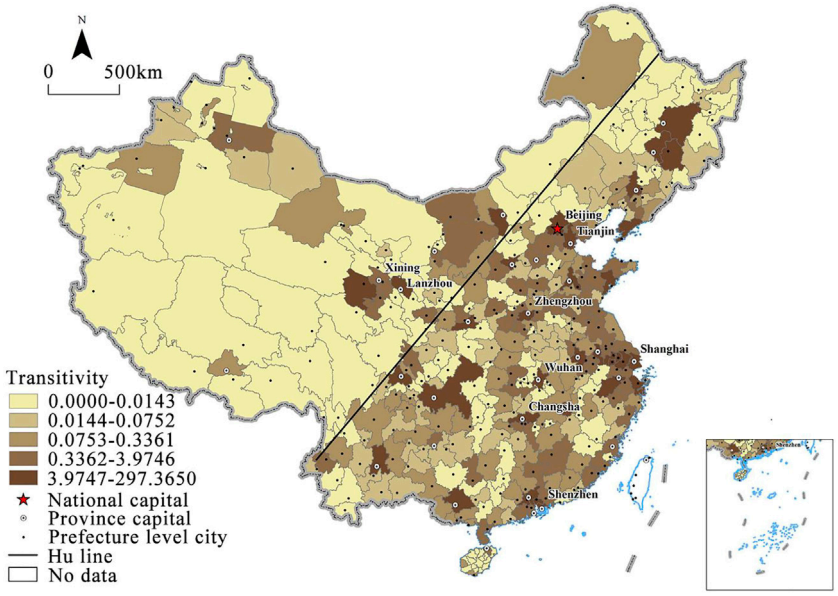

FIGURE 7
Spatial distribution of the transitivity of China's urban innovation network.

innovation network. As if cities with high-degree values build innovative connections and cooperation with cities at the lower level, knowledge and technology can circulate through many structural bridges between the core and the periphery, making the structural resilience of the network become stronger.

Figure 5 displays the degree correlation, respectively, in 2017, 2018, and 2019. Specifically, the absolute values of the coefficient in 3 years are 0.3176, 0.2619, and 0.2454. The decreasing trend indicates that the network disassortativity is weakening year by year, as the assortative relationships are

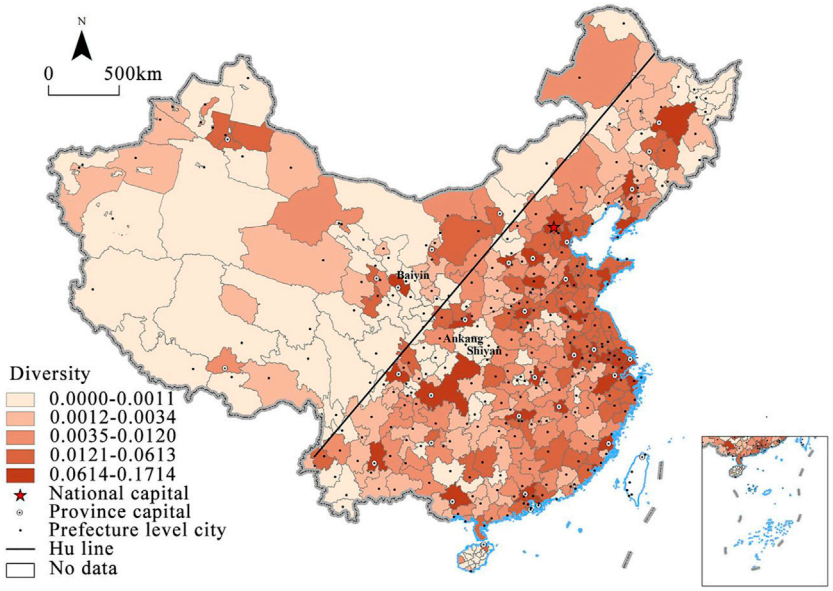

FIGURE 8
Spatial distribution of the diversity of China's urban innovation network.

growing stronger and quicker than the disassortative relationships. The enhancement of assortative linkages may lead to potential crises such as path dependence and regional lock-in, reducing the probability of innovative activities and the infiltration of external information.

4.2 Node resilience

Node resilience consists of two parts: potential and connectivity. Potential is measured by the self-organization, which relates to the ability to learn, create, restructure, recombine, adopt various types of knowledge, and develop generalized responses to foreseen or unforeseen events (Walker et al., 2002); connectivity is measured by transitivity and diversity. The transitivity of the nodes concerns the closeness with which contributing actors in a region collaborate in ways that lead directly or indirectly to innovation-spawning activities; and a diverse regional innovation system structure often provides greater resistance to shocks since different cities have different sensitivities to external downturns.

4.2.1 Potential: Self-organization

Figure 6 displays the spatial patterns of a self-organization level in the urban innovation network. Specifically, cities with self-organization at the first level are mainly national central cities and national science and technology innovation cities, such as Beijing, Tianjin, Shanghai, Guangzhou, Nanjing, Hangzhou, Qingdao, and Suzhou, surrounded by cities at the lower level which are able to receive technological radiation. Cities at the fourth and fifth levels are mostly located in the northeast, northwest, and southwest areas of China. Due to single path dependence and weak innovation capabilities, they have a low status in the self-organization hierarchy and lack development momentum. This result is roughly consistent with the spatial distribution of the urban degree (Figure 2), indicating that cities with higher internal innovation potential also have higher external connection strength.

4.2.2 Connectivity: Transitivity and diversity

The spatial pattern of transitivity is that the southeast is strong and the northwest is weak (Figure 7). There is a strip-shaped spatial distribution pattern of cities with high transitivity along the eastern coast. Cities with high transitivity in the central area are distributed roughly consistently with the main railway trunk lines, for example, Zhengzhou, Wuhan, and Changsha connect the middle of the Beijing–Guangzhou Railway, showing that the transportation infrastructure brings convenience to the flow of innovation elements, and is beneficial to the diffusion and dissemination of knowledge and technology between cities. The high transitivity areas in the west are mainly the core and sub-core cities within the urban agglomerations, such as Lanzhou and Xining in the Lan–Xi urban agglomeration. Core cities such as

Beijing, Tianjin, Shanghai, and Shenzhen have a good mediation effect and connection function in the network, acting as bridges to build connections with other cities through knowledge spillovers, and promote the rapid flow of technology. The speed and breadth of the transitivity of innovative elements should be strengthened in cities in the western areas to better buffer technological risks and impacts in the future.

When different cities are removed, the average number of independent paths in the network decreases to different degrees, which reflects the diversity of cities (Figure 8). Specifically, the eastern coastal cities, provincial capital cities in central and western areas have strong diversity and appropriate redundant paths, which has stronger resilience in the face of technological risks. The non-core cities have little impact on the resilience of the overall innovation network and the decrease of the network resilience can be ignored when they are attacked, such as Shiyan, Ankang, and Baiyin. However, considering the improvement of the overall network resilience, it is of great significance to increase the abundance of connections in non-core cities, which could limit serious downturns in patent productivity and ensure a speedy recovery from crises through a complex overlapping process between a mature market domain and a new emerging related one.

5 Conclusion

The concept of resilience originating from engineering mechanics is originally clear and unambiguous, but the expansion of the applications of resilience, especially in the socio-economic field, has increased the complexity of understanding resilience; of course, this complexity is also closely related to the complexity of the object of study, that is, the socio-economic system. The urban innovation network studied in this article is inherently characterized by complexity, making it difficult to provide a comprehensive and quantitative understanding of its resilience.

The main contribution of this article is to establish an analytical framework for exploring the innovative resilience of urban networks, which integrates systematic and nodal thinking on resilience research in network science (Wang et al., 2020) with the potential and connectivity concepts of resilience research in urban science (Philip Cooke et al., 2012), as well as the hierarchical and assortativity characteristics of recent research on urban network resilience (Wei and Pan, 2021). This framework contributes to a comprehensive perception of stability and adaptability issues in the development of innovation (characterized by uncertainty and sensitivity) and strives to promote the expanded application of the concept of resilience in the field of innovation.

Using this framework, this article analyses the resilience characteristics of Chinese urban technology cooperation innovation networks. From a systemic perspective, Chinese urban innovation networks exhibit relatively low hierarchical and yearly decreasing heterogeneity characteristics. Compared with intercity transportation network, information network, and economic network, the innovation network in China has a lower hierarchy (Wei and Pan, 2021), indicating that China still lacks cities with stronger innovation-leading ability. The disassortativity indicates that Chinese cities are characterized by "preferential attachment" in the innovation process (Wei and Pan, 2021), but the continuous decline in the past 3 years reflects that the cooperative innovation of cities at the same level has increased. From a nodal perspective, both the potential and connectivity of urban innovation show a spatial pattern of high in the southeast and low in the northwest, and cities with higher administrative level have higher innovation resilience. These patterns are basically consistent with other studies, confirming the spatial differentiation characteristics divided by the Hu line in China (Wei and Pan, 2021) and the spatial political bias of urban development. Although this article only explores the national innovation resilience from the perspective of urban networks of co-invention, it is also closely related to the national natural, cultural, and social landscape, which can be confirmed by the Hu Line reflecting China's spatial differentiation due to its comprehensive nature. These results are more representative of the internal structure of the innovation resilience of urban networks than the resilience values calculated by a formula and contribute to a deeper understanding of the current status of innovation resilience in China.

Resilience has become a highly elusive concept (Veloz et al., 2022), and its application in the field of innovation is just beginning. There are also some shortcomings in the measurement of urban innovation network resilience, for example, what is the optimal interval range of hierarchy? And whether the assortativity is better or disassortativity is better, which have not been solved in this article. We have to say, these problems are difficult to solve in one article. This is a question we are committed to address in our future research. Due to practical difficulties such as data acquisition and processing, the impact of COVID-19 on the national innovation resilience network is not discussed in this article, which will be further explored in future research. Referring to the division of industrial space clusters (Li et al., 2019), we can further divide resilience space clusters on the basis of resilience measurement and propose more targeted policy suggestions to improve regional innovation resilience. This article is only an exploration of the innovation resilience at the national scale from the perspective of urban networks, while a true understanding of innovation resilience requires more extensive research on different scales, different subjects, and different knowledge flows. Only in this way can the concept of resilience be better applied to innovation development, both theoretically and practically.

Data availability statement

The original contributions presented in the study are included in the article/supplementary material; further inquiries can be directed to the corresponding author.

Author contributions

HM and XL contributed to the conception and design of the study. XL and JL organized the database. XL, JL, and HM performed the statistical analysis. HM, XX, and XL wrote the first draft of the manuscript. HM, XX, XL, and JL wrote sections of the manuscript. All authors contributed to manuscript revision, read, and approved the submitted version.

Funding

The author(s) disclosed receipt of the following financial support for the research, authorship and/or publication of this article: This work is supported by the National Natural Science Foundation of China (grant no. 41971209), the Third Xinjiang Scientific Expedition Program (grant no. 2021xjkk0900), and the Second Tibetan Plateau Scientific Expedition and Research Program (STEP) (grant no. 2019QZKK1005).

Conflict of interest

The authors declare that the research was conducted in the absence of any commercial or financial relationships that could be construed as a potential conflict of interest.

Publisher's note

All claims expressed in this article are solely those of the authors and do not necessarily represent those of their affiliated organizations, or those of the publisher, the editors, and the reviewers. Any product that may be evaluated in this article, or claim that may be made by its manufacturer, is not guaranteed or endorsed by the publisher.

References

Albert, R., and Barabasi, A.-L. (2001). Statistical mechanics of complex networks. *Rev. Mod. Phys.* 74, 47–97. doi:10.1103/RevModPhys.74.47

Allenby, B., and Fink, J. (2005). Toward inherently secure and resilient societies. *Science* 309 (5737), 1034–1036. doi:10.1126/science.1111534

Amin, A., and Cohendet, P. (2004). *Architectures of knowledge, companies, capabilities, and communities*. Oxford: Oxford University Press.

Andergassen, R., Nardini, F., and Ricottilli, M. (2014). Emergence and resilience in a model of innovation and network formation. *Netw. Spat. Econ.* 15 (2), 293–311. doi:10.1007/s11067-014-9262-6

Antonelli, C. (2019). *The knowledge growth regime: A schumpeterian approach*. Cambridge.

Asheim, B. T., and Isaksen, A. (2002). Regional innovation systems: The integration of local 'sticky' and global 'ubiquitous' knowledge. *J. Technol. Transf.* 27 (1), 77–86. doi:10.1023/a:1013100704794

Athey, G., Nathan, M., Webber, C., and Mahroum, S. (2008). Innovation and the city. *Innov. (Camb).* 10(2-3), 156–169. doi:10.5172/impp.453.10.2-3.156

Atwell, R. C., Schulte, L. A., and Westphal, L. M. (2008). Linking resilience theory and diffusion of innovations theory to understand the potential for perennials in the U.S. Corn belt. *Ecol. Soc.* 14 (1), 30. doi:10.5751/es-02787-140130

Balland, P. A., Rigby, D., and Boschma, R. (2015). The technological resilience of US cities. *Camb. J. Regions Econ. Soc.* 8 (2), 167–184. doi:10.1093/cjres/rsv007

Barabási, A.-L., and Albert, R. (1999). Emergence of scaling in random networks. *Science* 286 (5439), 509–512. doi:10.1126/science.286.5439.509

Barabasi, A. L., Albert, R., and Jeong, H. (2000). Scale-free characteristics of random networks: The topology of the world-wide web. *Phys. A Stat. Mech. its Appl.* 281 (1-4), 69–77. doi:10.1016/s0378-4371(00)00018-2

Bathelt, H., Malmberg, A., and Maskell, P. (2004). Clusters and knowledge: Local buzz, global pipelines and the process of knowledge creation. *Prog. Hum. Geogr.* 28 (1), 31–56. doi:10.1191/0309132504ph469oa

Berkes, F., Colding, J., and Folke, C. (2003). *Navigating social-ecological systems: Building resilience for complexity and change*. Cambridge, UK: Cambridge University Press.

Boschma, R. (2005). Proximity and innovation: A critical assessment. *Reg. Stud.* 39, 61–74. doi:10.1080/0034340052000320887

Boschma, R. (2015). Towards an evolutionary perspective on regional resilience. *Reg. Stud.* 49 (5), 733–751. doi:10.1080/00343404.2014.959481

Brede, M., and de Vries, B. J. M. (2009). in *Networks that optimize a trade-off between efficiency and dynamical ResilienceComplex sciences*. Editor J. Zhou (Berlin, Heidelberg: Springer Berlin Heidelberg).

Burnard, K., and Bhamra, R. (2011). Organisational resilience: Development of a conceptual framework for organisational responses. *Int. J. Prod. Res.* 49, 5581–5599. doi:10.1080/00207543.2011.563827

Carrington, P. J., Scott, J., and Wasserman, S. (2005). *Models and methods in social network analysis*. Cambridge: Cambridge University Press.

Cattani, G., and Ferriani, S. (2008). A core/periphery perspective on individual creative performance: Social networks and cinematic achievements in the hollywood film industry. *Organ. Sci.* 19 (6), 824–844. doi:10.1287/orsc.1070.0350

Christopherson, S., Michie, J., and Tyler, P. (2010). Regional resilience: Theoretical and empirical perspectives. *Camb. J. Regions Econ. Soc.* 3 (1), 3–10. doi:10.1093/cjres/rsq004

Clark, J., Huang, H. I., and Walsh, J. P. (2010). A typology of 'innovation districts': What it means for regional resilience. *Camb. J. Regions, Econ. Soc.* 3 (1), 121–137. doi:10.1093/cjres/rsp034

Clausen, T., Pohjola, M., Sapprasert, K., and Verspagen, B. (2012). Innovation strategies as a source of persistent innovation. *Industrial Corp. Change* 21 (3), 553–585. doi:10.1093/icc/dtr051

Cooke, P., Parrilli, M. D., and Curbelo, J. L. (2012). *Innovation, global change and territorial resilience*. Cheltenham: Edward Elgar.

Cooke, P. (2001). Regional innovation systems, clusters, and the knowledge economy. *Industrial Corp. Change* 10, 945–974. doi:10.1093/icc/10.4.945

Crespo, J., Suire, R., and Vicente, J. (2013). Lock-in or lock-out? How structural properties of knowledge networks affect regional resilience. *J. Econ. Geogr.* 14 (1), 199–219. doi:10.1093/jeg/lbt006

Dabson, B., Heflin, C., and Miller, K. (2012). *Regional resilience.* Research and policy brief, RUPRI, rural futures lab, harry S. Truman School of public affairs. Missouri: University of Missouri.

Davoudi, S., Brooks, E., and Mehmood, A. (2013). Evolutionary resilience and strategies for climate adaptation. *Plan. Pract. Res.* 28 (3), 307–322. doi:10.1080/02697459.2013.787695

Dorogovtsev, S. N., Goltsev, A. V., and Mendes, J. F. F. (2008). Critical phenomena in complex networks. *Rev. Mod. Phys.* 80 (4), 1275–1335. doi:10.1103/RevModPhys.80.1275

Dost, M., Pahi, M. H., Magsi, H. B., and Umrani, W. A. (2019). Effects of sources of knowledge on frugal innovation: Moderating role of environmental turbulence. *J. Knowl. Manag.* 23 (7), 1245–1259. doi:10.1108/JKM-01-2019-0035

Duguet, E., and Monjon, S. (2002). *Creative destruction and the innovative core: Is innovation persistent at the firm level?* Discussion paper. London: University College.

Eisenhardt, K. M., Furr, N. R., and Bingham, C. B. (2010). CROSSROADS—microfoundations of performance: Balancing efficiency and flexibility in dynamic environments. *Organ. Sci.* 21 (6), 1263–1273. doi:10.1287/orsc.1100.0564

Erhardt, G., Marsili, M., and Vega-Redondo, F. (2007). *Emergence and resilience of social networks: A general theoretical framework*. Switzerland: Annales d'Economie et de Statistique, 1–14.

Erol, O., Sauser, B. J., and Mansouri, M. (2010). A framework for investigation into extended enterprise resilience. *Enterp. Inf. Syst.* 4 (2), 111–136. doi:10.1080/17517570903474304

Euchner, J. (2019). Innovation and resilience. *Research-Technology Manag.* 62 (4), 10–11. doi:10.1080/08956308.2019.1613113

Farjoun, M. (2010). Beyond dualism: Stability and change as a duality. *Acad. Manage. Rev.* 35(2), 202–225. doi:10.5465/Amr.2010.48463331

Fastenrath, S., Coenen, L., and Davidson, K. (2019). Urban resilience in action: The resilient melbourne strategy as transformative urban innovation policy? *Sustainability* 11 (3), 693. doi:10.3390/su11030693

Fitjar, R. D., and Rodriguez-Pose, A. (2011). When local interaction does not suffice: Sources of firm innovation in urban Norway. *Environ. Plan. A* 43, 1248–1267. doi:10.1068/a43516

Fleming, L. (2007). Breakthroughs and the "Long tail" of innovation. *Mit Sloan Manag. Rev.* 49 (1), 69.

Folke, C. (2006). Resilience: The emergence of a perspective for social-ecological systems analyses. *Glob. Environ. Change* 16 (3), 253–267. doi:10.1016/j.gloenvcha.2006.04.002

Freeman, C., and Soete, L. (1997). *The economics of industrial innovation*. Cambridge: The MIT Press.

Gilly, J. P., Kechidi, M., and Talbot, D. (2014). Resilience of organisations and territories: The role of pivot firms. *Eur. Manag. J.* 32 (4), 596–602. doi:10.1016/j.emj.2013.09.004

Gunderson, L. H., and Holling, C. S. (2002). *Panarchy: Understanding transformations in human and natural systems*. Washington, D.C., USA: Island Press.

Hassink, R. (2010). Regional resilience: A promising concept to explain differences in regional economic adaptability? *Camb. J. Regions Econ. Soc.* 3 (1), 45–58. doi:10.1093/cjres/rsp033

Holling, C. S. (1973). Resilience and stability of ecological systems. *Annu. Rev. Ecol. Syst.* 4, 1–23. doi:10.1146/annurev.es.04.110173.000245

Hollnagel, E., Woods, D. D., and Leveson, N. G. (2006). *Resilience engineering : Concepts and precepts*.

Hosseini, S., Barker, K., and Ramirez-Marquez, J. E. (2016). A review of definitions and measures of system resilience. *Reliab. Eng. Syst. Saf.* 145, 47–61. doi:10.1016/j.ress.2015.08.006

Ip, W. H., and Wang, D. (2011). Resilience and friability of transportation networks: Evaluation, analysis and optimization. *IEEE Syst. J.* 5 (2), 189–198. doi:10.1109/jsyst.2010.2096670

Jackson, W. A. (1999). Dualism, duality and the complexity of economic institutions. *Int. J. Soc. Econ.* 26 (4), 545–558. doi:10.1108/03068299910215997

Janssen, M. A., Schoon, M. L., Ke, W. M., and Borner, K. (2006). Scholarly networks on resilience, vulnerability and adaptation within the human dimensions of global environmental change. *Glob. Environ. Change* 16 (3), 240–252. doi:10.1016/j.gloenvcha.2006.04.001

Kurth, M., Kozlowski, W., Ganin, A., Mersky, A., Leung, B., Dykes, J., et al. (2020). Lack of resilience in transportation networks: Economic implications. *Transp. Res. Part D-Transport Environ.* 86, 102419. doi:10.1016/j.trd.2020.102419

Lawson, C. (1999). Towards a competence theory of the region. *Camb. J. Econ.* 23, 151–166. doi:10.1093/cje/23.2.151

Lee, D.-S. (2018). Towards urban resilience through inter-city networks of Co-invention: A case study of U.S. Cities. *Sustainability* 10 (2), 289. doi:10.3390/su10020289

Lengnick-Hall, C. A., and Beck, T. E. (2005). Adaptive fit versus robust transformation: How organizations respond to environmental change. *J. Manag.* 31 (5), 738–757. doi:10.1177/0149206305279367

Lengnick-Hall, C. A., Beck, T. E., and Lengnick-Hall, M. L. (2011). Developing a capacity for organizational resilience through strategic human resource management. *Hum. Resour. Manag. Rev.* 21 (3), 243–255. doi:10.1016/j.hrmr.2010.07.001

Li, C., Wu, K., and Gao, X. (2019). Manufacturing industry agglomeration and spatial clustering: Evidence from Hebei Province, China. *Environ. Dev. Sustain.* 22 (4), 2941–2965. doi:10.1007/s10668-019-00328-1

Linnenluecke, M. K. (2017). Resilience in business and management research: A review of influential publications and a research agenda. *Int. J. Manag. Rev.* 19 (1), 4–30. doi:10.1111/ijmr.12076

Liu, J. G., Dietz, T., Carpenter, S. R., Alberti, M., Folke, C., Moran, E., et al. (2007). Complexity of coupled human and natural systems. *Science* 317 (5844), 1513–1516. doi:10.1126/science.1144004

Lundvall, B. Å. (1992). *National systems of innovation: Toward a theory of innovation and interactive learning*. London: Anthem Press.

Lv, W.-D., Tian, D., Wei, Y., and Xi, R.-X. (2018). Innovation resilience: A new approach for managing uncertainties concerned with sustainable innovation. *Sustainability* 10 (10), 3641. doi:10.3390/su10103641

Ma, H. T., Fang, C. L., Lin, S. N., Huang, X. D., and Xu, C. D. (2018). Hierarchy, clusters, and spatial differences in Chinese inter-city networks constructed by scientific collaborators. *J. Geogr. Sci.*, 1793–1809. doi:10.1007/s11442-018-1579-5

Ma, H. T., Fang, C. L., Pang, B., and Wang, S. J. (2015). Structure of Chinese city network as driven by technological knowledge flows. *Chin. Geogr. Sci.* 25 (4), 498–510. doi:10.1007/s11769-014-0731-0

Ma, H. T., Li, Y. C., and Huang, X. D. (2021). Proximity and the evolving knowledge polycentricity of megalopolitan science: Evidence from China's Guangdong-Hong Kong-Macao Greater Bay Area, 1990–2016. *Urban Stud.* 58 (12), 2405–2423. doi:10.1177/0042098020942665

Ma, H. T., and Xu, X. F. (2022). Knowledge polycentricity of China's urban agglomerations. *J. Urban Plan. Dev.* 148 (2), 04022014. doi:10.1061/(ASCE)UP.1943-5444.0000828

McDonald, N. (2006). *Organisational resilience and industrial risk*. USA: Ashgate publishing company.

Modica, M., and Reggiani, A. (2015). Spatial economic resilience: Overview and perspectives. *Netw. Spat. Econ.* 15 (2), 211–233. doi:10.1007/s11067-014-9261-7

Moodysson, J. (2008). Principles and practices of knowledge creation: On the organization of "buzz" and "pipelines" in life science communities. *Econ. Geogr.* 84 (4), 449–469. doi:10.1111/j.1944-8287.2008.00004.x

Newman, M. E. J. (2003). Mixing patterns in networks. *Phys. Rev. E* 67 (2), 026126. doi:10.1103/physreve.67.026126

Nooteboom, B., and Gilsing, V. A. (2004). *Density and strength of ties in innovation networks: A competence and governance view*. Rotterdam: Erasmus Research Institute of Management (ERIM).

Ouyang, M., Dueñas-Osorio, L., and Min, X. (2012). A three-stage resilience analysis framework for urban infrastructure systems. *Struct. Saf.* 36-37, 23–31. doi:10.1016/j.strusafe.2011.12.004

Pavit, K. (2006). *Innovation processes*. Oxford: Oxford University Press.

Pike, A., Dawley, S., and Tomaney, J. (2010). Resilience, adaptation and adaptability. *Camb. J. Regions Econ. Soc.* 3 (1), 59–70. doi:10.1093/cjres/rsq001

Pinto, H., Noronha, T., and Vaz, E. (2018). Economic crisis, turbulence and the resilince in innovation: Insights from the atlantic martime cluster. *Resil. Regional Dyn. Int. Approach a New Res. Agenda*, E1. doi:10.1007/978-3-319-95135-5_14

Ponis, S. T., and Koronis, E. (2012). Supply chain resilience: Definition of concept and its formative elements. *J. Appl. Bus. Res.* 28 (5), 921. doi:10.19030/jabr.v28i5.7234

Popadiuk, S., and Choo, C. W. (2006). Innovation and knowledge creation: How are these concepts related? *Int. J. Inf. Manag.* 26 (4), 302–312. doi:10.1016/j.ijinfomgt.2006.03.011

Reggiani, A., De Graaff, T., and Nijkamp, P. (2002). Resilience: An evolutionary approach to spatial economic systems. *Netw. Spat. Econ.* 2 (2), 211–229. doi:10.1023/A:1015377515690

Reggiani, A. (2013). Network resilience for transport security: Some methodological considerations. *Transp. Policy* 28, 63–68. doi:10.1016/j.tranpol.2012.09.007

Reggiani, A., and Nijkamp, P. (2006). *Spatial dynamics, networks and modelling*. Cheltenham, UK: Edward Elgar Publishing.

Rogers, E. M. (2003). *Diffusion of innovations*. New York, USA: Free Press.

Rose, A., and Krausmann, E. (2013). An economic framework for the development of a resilience index for business recovery. *Int. J. Disaster Risk Reduct.* 5, 73–83. doi:10.1016/j.ijdrr.2013.08.003

Salter, A., and Alexy, O. (2014). *The nature of innovation*. United Kingdom: Oxford University Clarendon street.

Sanchez, A. X., Osmond, P., and van der Heijden, J. (2017). Are some forms of resilience more sustainable than others? *Procedia Eng.* 180, 881–889. doi:10.1016/j.proeng.2017.04.249

Schumpeter, J. A. (1939). *Business cycles: A theoretical, historical and statistical analysis of the capitalist process*. New York: McGraw-Hill.

Schumpeter, J. A. (1942). *Capitalism, socialism and democracy*. New York: McGraw-Hill.

Schweitzer, F., Fagiolo, G., Sornette, D., Vega-Redondo, F., Vespignani, A., and White, D. R. (2009). Economic networks: The new challenges. *Science* 325 (1095-9203), 422–425. (Electronic)). doi:10.1126/science.1173644

Simmie, J., and Martin, R. (2010). The economic resilience of regions: Towards an evolutionary approach. *Camb. J. Regions Econ. Soc.* 3 (1), 27–43. doi:10.1093/cjres/rsp029

Sonenshein, S. (2016). Routines and creativity: From dualism to duality. *Organ. Sci.* 27 (3), 739–758. doi:10.1287/orsc.2016.1044

Suire, R., and Vicente, J. (2014). Clusters for life or life cycles of clusters: In search of the critical factors of clusters' resilience. *Entrepreneursh. Regional Dev.* 26 (1-2), 142–164. doi:10.1080/08985626.2013.877985

Sun, Y., and Luo, M. (2021). Development and enlightenment of American intelligent manufacturing. *Bull. Chin. Acad. Sci.* 36 (11), 1316–1325.

Sunley, P. (2013). Innovation, global change and territorial resilience. *Reg. Stud.* 47 (4), 644–645. doi:10.1080/00343404.2013.781754

Van Wellen, E. (2019). Global engineering congress (GEC): Notes and goals from the 2018 conference. *J. Coast. Res.* 35 (3), 485–488. doi:10.2112/JCOASTRES-D-19A-00004.1

Veloz, T., Maldonado, P., Busssenіers, E., Bassi, A., Beigi, S., Lenartowicz, M., et al. (2022). Towards an analytic framework for system resilience based on reaction networks. *Complexity* 2022, 1. doi:10.1155/2022/9944562

Vogus, T. J., and Sutcliffe, K. M. (2003). *Organizing for resilience*. San Francisco: Berrett-Koehler.

Walker, B., Carpenter, S., Anderies, J., Abel, N., Cumming, G., Janssen, M., et al. (2002). Resilience management in social-ecological systems: A working hypothesis for a participatory approach. *Conserv. Ecol.* 6 (1), art14. doi:10.5751/es-00356-060114

Wang, L., Xue, X., and Zhou, X. (2020). A new approach for measuring the resilience of transport infrastructure networks. *Complexity* 2020, 1–16. doi:10.1155/2020/7952309

Wang, Z. (2007). Technological innovation and market turbulence: The dot-com experience. *Rev. Econ. Dyn.* 10 (1), 78–105. doi:10.1016/j.red.2006.10.001

Watts, D. J., and Strogatz, S. H. (1998). Collective dynamics of 'smallworld'networks. *nature* 393 (6684), 440–442. doi:10.1038/30918

Wei, S. M., and Pan, J. H. (2021). Resilience of urban network structure in China: The perspective of disruption. *ISPRS Int. J. Geoinf.* 10 (12), 796. doi:10.3390/ijgi10120796

Ye, S. S., and Qian, Z. (2021). The economic network resilience of the guanzhong plain city cluster, China: A network analysis from the evolutionary perspective. *Growth Change* 52 (4), 2391–2411. doi:10.1111/grow.12530

frontiers | Frontiers in Environmental Science

TYPE Original Research
PUBLISHED 19 September 2022
DOI 10.3389/fenvs.2022.990416

Check for updates

OPEN ACCESS

EDITED BY
Jun Yang,
Northeastern University, China

REVIEWED BY
Yibin Ao,
Chengdu University of Technology, China
Jixiang Liu,
Xiamen University, China

*CORRESPONDENCE
Zhongwei Shen,
szwpaper@163.com

SPECIALTY SECTION
This article was submitted to Land Use Dynamics,
a section of the journal
Frontiers in Environmental Science

RECEIVED 10 July 2022
ACCEPTED 12 August 2022
PUBLISHED 19 September 2022

CITATION
Ma J, Shen Z, Xie Y, Liang P, Yu B and Chen L (2022), Node-place model extended by system support: Evaluation and classification of metro station areas in Tianfu new area of Chengdu.
Front. Environ. Sci. 10:990416.
doi: 10.3389/fenvs.2022.990416

COPYRIGHT
© 2022 Ma, Shen, Xie, Liang, Yu and Chen. This is an open-access article distributed under the terms of the Creative Commons Attribution License (CC BY). The use, distribution or reproduction in other forums is permitted, provided the original author(s) and the copyright owner(s) are credited and that the original publication in this journal is cited, in accordance with accepted academic practice. No use, distribution or reproduction is permitted which does not comply with these terms.

Node-place model extended by system support: Evaluation and classification of metro station areas in Tianfu new area of Chengdu

Jiexi Ma[1], Zhongwei Shen[1]*, Yi Xie[1], Pengpeng Liang[1], Bingjie Yu[1] and Li Chen[2]

[1]School of Architecture, Southwest Jiaotong University, Chengdu, China, [2]College of Civil Engineering and Architecture, Zhejiang University, Hangzhou, China

The construction of new urban areas has become one of the important ways for urban regeneration throughout the process of polycentric urban development. New urban area construction following transit-oriented development (TOD) conception advocates development around the public transportation stations. To gain more benefits around the stations, it is necessary to conduct an ex-ante evaluation of TOD projects in the new urban area. The Node-place (NP) model is a commonly used method for TOD evaluation and classification, which essentially designs an analytical framework for assessing station areas in both transport (node) and land use (place) aspects. The objective of our study is twofold. First, based on the original NP model, we propose the node-place-system support (NPS) model by introducing a novel evaluation dimension—system support—which quantitatively describes the relationship between local stations and the overall urban system. Second, taking advantage of multi-sourced data and Geographical Information System (GIS) techniques, we employ the proposed NPS model to evaluate and classify the metro stations in the Tianfu New Area of Chengdu, China. The results show that most stations present a balanced relationship between transport and land use performances. However, for a fraction of these balanced stations, we observe a mismatch between the system support and NP performances. Accordingly, we identify the system-mismatched stations and provide targeted improvement strategies for urban design.

KEYWORDS

node-place model, metro station, TOD, urban planning, Tianfu new area

Introduction

In recent years, there has been rapid urbanization worldwide. Cities will become the main carriers of human living, resulting in both benefits and problems. Sustainable urbanization has become an important aspect of promoting sustainable development (Shen et al., 2012; Wang et al., 2019). To improve urban capacity and upgrade infrastructure structure, urban expansion has become a distinctive characteristic of urban development and regeneration (Leichenko and Solecki, 2005; Wang et al., 2012). The urbanization rate of China reached 63.9% in 2020 (Ma and Gao, 2021). A large number of new urban areas (including 19 state-level new areas so far) have been approved and built to respond to population growth and industrial expansion. In this situation, transport-oriented development (TOD) has been adopted as a commonly followed urban planning strategy for connecting the whole city (Ibraeva et al., 2020; Yang et al., 2022a). TOD has become well known by urban planners after being introduced by Calthorpe in his book "The Next American Metropolis" (Calthorpe, 1993). It advocates group development, which plans a pattern of dense, diverse, pedestrian-friendly land uses near public transportation stations that, under the right conditions, translate into higher patronage (Bertolini, 1998). It also plays an important role in reducing traffic pollution, alleviating congestion, and improving commuting efficiency, as well as providing opportunities for urban regeneration. The relevant literature shows that TOD seems to be seen above all as a strategy to help channel mega-city growth in mass rapid transit corridors in Asian countries especially (Yang and Lew, 2009).

At present, various researchers have attempted to establish comparable TOD typologies for better strategic planning, investment guidance, and station quantification (Zemp et al., 2011; Papagiannakis et al., 2021; Qiang et al., 2022). One of the widely used theories of TOD typology is the node-place model (NP model) proposed by Bertolini (1996; 1999). It is a conceptual framework that contains both the transport (node) supply and land use (place) characteristics of the station area simultaneously. Its basic idea is that improving the transport provision of a location, by improving accessibility, creates favorable conditions for the further development of land. In turn, the development of a location, because of a growing demand for transport, creates conditions favorable to the further development of the transport system (Yang et al., 2020a; Yang et al., 2020b). Hence the potential relationship between the node and place is of great significance to the development planning and policy formulation of TOD areas. The NP model, as a quantitative method, is widely used to evaluate the coordination between transportation and land use.

In the current planning of the TOD area, despite the benefits of the NP model (or the extended NP model) for evaluating the built environment, pre-evaluating and correcting in advance is a more effective preventive measure against unreasonable urban planning. However, the current methods are not completely suitable for pre-evaluation because: on the one hand, the new areas lack some precise measurements from the built environment because it has not been fully built or in use. On the other hand, the benefit of the station area in the new area is affected by the urban structure salience and the policy priorities because the new and old areas still belong to an organic and holistic system in the process of urban renewal. In other words, the TOD concept should not only remain in station catchment areas at a local scale but extends to a broader geographical level (Zhang et al., 2019).

To address the above research gaps, we extended the traditional NP model to an NPS model by introducing a novel evaluation dimension named system support that is used to quantitatively describe the significance of a station in the entire city and set up a set of predictable indicators. The NPS model put forward a kind of pre-evaluation method which is suitable for new urban areas or urban planning schemes. Then we applied it to the new metro stations in the Tianfu New Area of Chengdu. The three-pronged approach combined local and system levels, which help us better identify the specific categories in advance and provide guidance for Chengdu's subsequent urban planning policy and design work. It should be added that the reason why Chengdu city is chosen as the TOD empirical case is that Chengdu's urban area has expanded rapidly in recent years. The metro-dominated public transportation is widely used as a means to activate the expanded areas. Chengdu ranks third in the length of metro lines, only after Beijing and Shanghai (Han et al., 2022). And the government has issued policies to clarify the development concept of comprehensive land development around the metro station (TOD) in the city. In addition, some evidence shows that second-class and third-class cities probably have greater potential to achieve large urban form impacts from TOD strategies than the first-class cities in China nowadays (Xu et al., 2017). Chengdu, as a typical second-class city, is a suitable sample for TOD studying in recent years, which can provide a good model for similar cities.

The rest of the paper is organized as follows: the second section reviews the node-place model and its extensions in existing research and introduces the extended node-place model combined with system structure indicators. The third and fourth sections present the study areas, data sources, index calculations, and classification methods. The NPS model is then applied to new metro stations in Tianfu New Area, Chengdu, to evaluate its node and place performance and degree of system support, classify the station areas, summarize problems in different categories, and give corresponding improvement suggestions. Last, we summarized the research in the fifth section.

Literature review

The node-place model

Bertolini (1996; 1999) defined the NP model as a regional organization model based on the interaction between

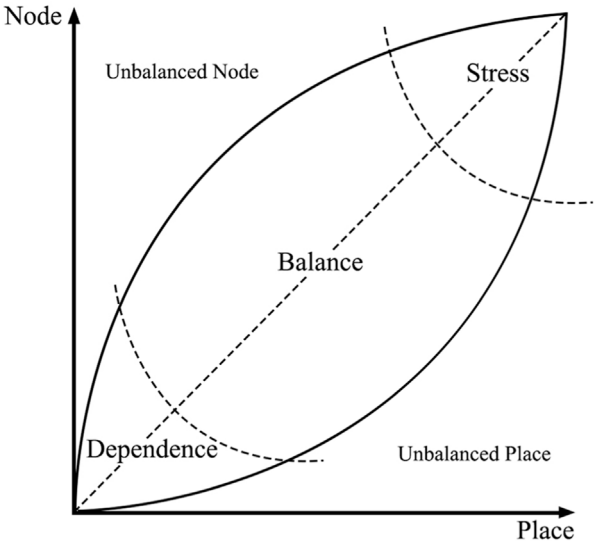

FIGURE 1
The node-place model by Bertolini (1999).

transportation and land use oriented under public transportation. The TOD catchment area is set as both a node of the transport network and a place in the city in a frame-like concept provided by the NP model, which allows it to stimulate the intensity and diversity of land development by improving regional transportation support and *vice versa* (Bertolini, 2008). The value of node dimension and place dimension are decomposed into indexes that express node and place performances, respectively, in the model, and different variables are then combined through multi-criteria analysis. The node and place indexes are expressed on the Y- and *X*-axis of a two-dimensional graph, respectively, and the site of points in the coordinates express the synergy between node and place. Five typical categories can be identified. In Figure 1, the points along the intermediate line mean that the performances of transportation and land use are equal to each other. We, therefore, define points on the line or floating in a small range up and down as "balance". The upper part of the balanced area is "stress", indicating that both node and place values have reached the upper limit, where competition between transportation and land use is fierce. Contrary to the stress is "dependence", which is the area located in the lower part of the balanced area. Its transportation supply and degree of land use are low, and here space competition is also small. In addition, two types of unbalanced categories can also be identified, the first is "unbalanced node", in which traffic performance is much higher than that of land utilization, and the second is "unbalanced place", which has the opposite situation. In the long term, most unbalanced stations tend to approach the balanced state (Reusser et al., 2008).

The application of the node-place model to a specific case study has two main advantages. First, it allows us to classify the overall transport and land use equilibrium of a region based on the interpretation of the mean value of the node and place indexes of all station areas, therefore allowing us to compare different stations to each other. Second, it allows us to identify categories of stations, either the original five categories or even other categories based on the land use and transport features of the station areas (Vale, 2015). With the introduction of urban design indicators, the NP model has been widely used in the field of urban planning. For example, Vale et al. (2018) extended the NP model to include a design index, reflecting the urban design conditions that influence pedestrian accessibility of station areas, and Lyu et al. (2016) used indicators about urban design details such as intersection density and average block size and added them into a new evaluation dimension named "oriented".

Expansion of the NP model from an urban perspective.

In the traditional NP model, the exploration of an index itself or new dimension has always been focused on local areas, with little attention paid to development driving force distribution brought by the whole urban system structure. There is an obvious synergy between urban form and metro network planning (Wang et al., 2008). Therefore, by analyzing the structure of subway line networks, stations can be examined from a broader urban perspective. Network centrality is a modeling method based on network graphics and has been used widely to model pairwise relations between objects in the systems. In this approach, measures are applied to estimate the importance or contribution amount of each component in a system (Zadeh and Rajabi, 2013). Zhong et al. (2014) applied the method of network analysis to spatial analysis to find the spatial structure of an urban hub, center, and boundary through people's activity network and found that the urban development pattern was consistent with the results of network centrality analysis. Freke et al. (2018) added the network centrality index as an indicator to measure the node value of Brussels railway stations using the NP model, and Cao et al. (2020) constructed a node-place-ridership model in which node indicators included accessibility opportunities and network centrality.

The first in-depth interpretation of the role of network centrality and its independent evaluation dimension was conducted by Zhang et al. (2019), who emphasized the addition of criteria of different scales in evaluation. From the perspective of entire cities, strategic network (criticality) component indicators were used to measure the relationship between urban network structure and node, place, and design performance. Thus, the authors were able to estimate whether an area was in line with expectations of its future development direction. In addition, Kim and Shin (2021) also proposed two

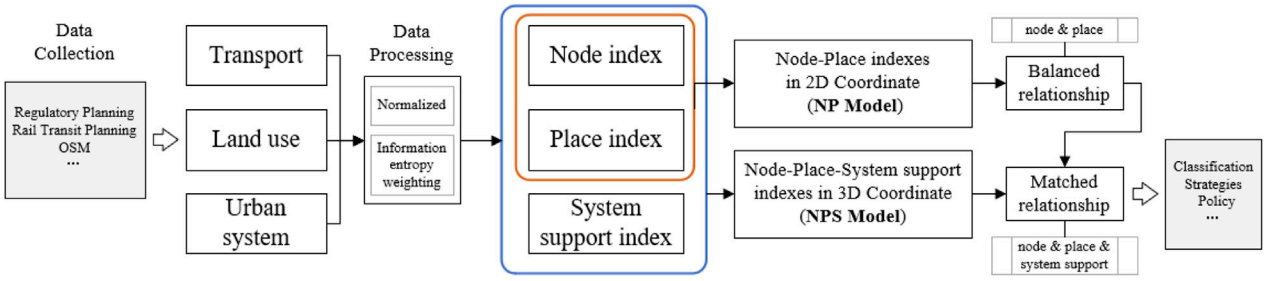

FIGURE 2
Research process.

decision-making perspectives, local performance, and network performance, and the corresponding evaluation methods for these are the NP model and network centrality evaluation. Dou et al. (2021) introduced a travel network as the index for the third dimension, compared the research results of the NP model and NP-Network (NPN) model, and demonstrated the effectiveness of the NPN model. Many empirical studies show that complex network theory can be used to measure the structure support strength for each point in a network and capture location advantages.(Roth et al., 2011; Wang et al., 2014).

Method and data

In this section, we first introduced the research scope and data sources, then we introduced the extended NPS model in detail, including indicators selection, data processing, and classification. Taking Shanghai as an empirical case, Our research process has been depicted in Figure 2.

Study scope and data sources

We chose the Tianfu New Area of Chengdu as the research object, which is a state-level new area established in 2014. It is located in the south of the main urban area of Chengdu and has 13 municipal metro lines planned in the long term. We conducted a study of the 38 metro stations currently built or under construction (whose schemes have been decided), involving 6 subway lines. The walking radius of this TOD comprehensive development zone is 400–800 m generally, which corresponds to a 5–10-min walk (Calthorpe, 1993). To continue, we first need to explore the most suitable scope for this study due to the presence of the modifiable areal unit problem (MAUP) (Dark and Bram, 2007). We calculated the straight-line distance between the nearest entrances of each station, and the average distance was about 524 m. Therefore, it is reasonable to adopt 500 m as the radius of the catchment area for this study. The data we used in this study are from OpenStreetMap, the Regulatory Planning of Tianfu New Area, Chengdu Urban Planning Management Technical Regulations, and Chengdu Urban Rail Transit Planning of Chengdu.

Node-place-system support model

The traditional NP model can be used to predict the degree of coordination between transport and land use in the local scope. But for the new area, we need to assess not only the relationship of NP performance but also whether the NP values in the ideal planning conditions can be realized as expected.

In other words, the support of the urban system gives largely determines the innate conditions for the development of each area. Therefore, we extended the NP model to an NPS model by introducing a novel dimension of system support (Figure 3) to further test the NP results' compatibility with the urban overall planning under the conditions of the metro network and policy. Different from node and place indicators, system support is calculated based on the overall planning of an entire city rather than the scope of the catchment area.

Indicator selection and calculation methods

There have been many detailed indicators to define NP performances in previous research. Improving the quantity and coverage of indicators can help to evaluate the catchment area more comprehensively. However, the new areas lack some precise measurements from the built environment, such as the transfer bus of the transport system, and the POI of land use, because it has not been fully built or in use (Yang et al., 2021; Yang et al., 2022b). Therefore, after selecting indicators based on references and expert opinions, availability should also be considered for screening indicators. For measuring the maximum potential value of the catchment area, the

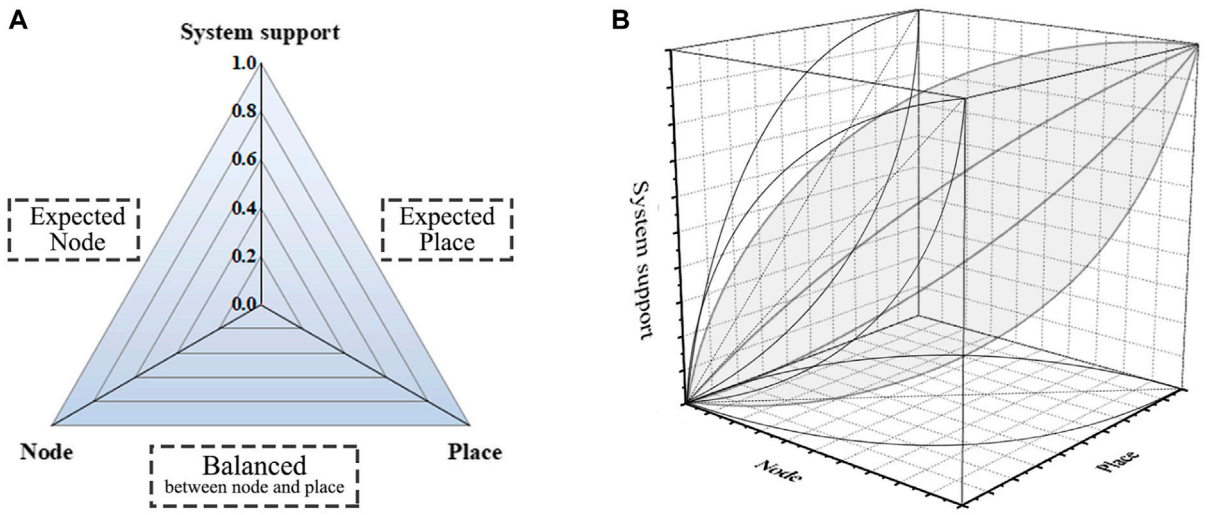

FIGURE 3
Illustrations of the node-place-system support model. **(A)** overall structure **(B)** model illustration.

TABLE 1 Indicators of the node, place, and system support dimensions.

Dimension	Indicator		Description	References
Node	Transfer	Road network accessibility	N1 = maximum road accessibility potential within 500 m	Monajem and Nosratian, (2015)
		Directions served by metro	N2 = number of subway service directions of subway stations	(Bertolini, 1999; Chorus and Bertolini, 2011; Song and Deguchi, 2013)
	Station design	Station entrances	N3 = number of station entrances	Monajem and Nosratian, (2015)
		Station capacity	N4 = area of the station building	
Place	Intensity	—	P1 = Average plot ratio within 500 m	Cervero and Murakami, (2009)
	Land use mix	—	P2 = Mixing entropy of land use within 500 m	(Kamruzzaman et al., 2014; Singh et al., 2014)
	Population	Residential capacity	P3 = Area of the resident within 500 m	—
		Commercial capacity	P4 = Area of commerce building within 500 m	—
System support	Centricity	Betweenness	S1 = Number of shortest paths through the node in the vision subway plan	(Zhang et al., 2019; Cao et al., 2020; Dou et al., 2021; Kim and Shin, 2021)
		Coseness	S2 = Reciprocal of the average distance from the site to others in the vision subway plan	Cao et al. (2020)
	Core plot of land	—	S3 = Percentage of core land parcel area in the total catchment area	—

indicators are calculated by the maximum value within the range of the planning conditions.

We screened a total of 11 indicators to form a comprehensive evaluation set of node, place, and system support. We define the node value as composed of two parts: the capacity of transfer and the construction of the station design. Place value is composed of three parts: density of construction, degree of functional mixing, and population size. Since the population in the new area is not reliably measurable, we use the maximum permanent population capacity to represent the potential of carrying population size. The indicators for system support are divided into two parts: network centrality and core plot of land. Based on network analysis, we convert the entire planning metro lines of Chengdu into a network graph, G = (V, E), in which the vertex set V represents stations and the edge set E represents the connections between stations. The importance of each point (metro station) in the city is quantified by using the analysis method of network centrality. For our purposes, we selected

closeness and betweenness indicators of centrality. Another indicator of system support is the core plot of land, which is the pre-positioning of land level in urban planning. The core plot of land implies the probability of having beneficial development policies and commercial resources, which means a higher development ceiling. Table 1 is a complete description of the NPS model indicators.

Road network accessibility (N1): Road network accessibility reflects the connectivity and flexibility of road design in the region (Jin et al., 2022). sDNA (Chiaradia et al., 2014; Cooper et al., 2018) under the GIS platform we use can more objectively and accurately calculate the potential of people's through-movement within the catchment area.

Directions served by metro (N2): Directions served by metro are an indicator to measure the capability of subway transfers, and more directions mean the higher the support of the subway. Following Chengdu Vision Subway Planning, we count the number of subway service directions that are provided in each station plan.

Station entrances (N3): The entrances of subway stations are used to reflect the rationality of absorbing people from different directions and streets. We count the number of entrances according to the subway station design scheme, including both current entrances and reserved entrances.

Station capacity (N4): The station area reflects the capacity limit of the station for commuters, especially the coping ability and degree of comfort during peak passenger flow. The station area is counted according to the subway station design scheme, including both the current and reserved area.

Intensity (P1): Development intensity reflects the economic benefits that the land can produce to a certain extent. The upper limit of the plot ratio is given according to the construction land within the catchment area, and the maximum value of its average plot ratio is also calculated for intensity.

Land use mix (P2): The degree of functional mixing reflects the richness of land use. We divided land use into 6 categories according to Chengdu Urban Planning Management Technical Regulations (34). Calculating the functional mixing degree of catchment area by the information entropy in Eq. 1:

$$H(\mathrm{x}) = -\sum_{i=1}^{n} Pi \log Pi \tag{1}$$

where $\sigma_{kt}(i)$ is the number of shortest paths through i between any two stations k and t, and σ_{kt} is the total number of paths between k and t.

Betweenness (S1): Betweenness reflects the transit capacity of stations, which can better identify the most critical stations compared to other centrality algorithms. The stronger the intermediary centrality of the station, the more routes passing through the shortest path of the point, and the more obvious the hub role of the road node in the whole road network. We calculate the betweenness index in Eq. (2):

$$C_{\text{betweeness}}(\mathrm{i}) = \sum_{\mathrm{kt}} \frac{\sigma_{\mathrm{kt}}(\mathrm{i})}{\sigma_{\mathrm{kt}}} \tag{2}$$

where $\sigma_{kt}(i)$ is the number of shortest paths through i between any two stations k and t, and σ_{kt} is the total number of paths between k and t.

Closeness (S2): Closeness centrality reflects a node's proximity and reachability within the network. By definition, a node that is closer to the geographic center has a higher index of closeness. However, in reality, geographical location is not the only influencing factor due to the multi-directional connections or cross-station running. Therefore, this index is of great significance to our model. We calculate the closeness index in Eq. 3:

$$C_{\text{closeness}}(\mathrm{k}) = \frac{1}{\sum_{t=1}^{n} \mathrm{d}_{\mathrm{kt}}(\mathrm{k} \neq t)} \tag{3}$$

where d_{kt} represents the shortest transfer distance between site k and site t.

Core land (S3): We calculate the proportion of core land in the catchment area according to the Urban Form Zoning Map (34) published by the planning management department.

Information entropy weighting

We use the information entropy weighting method (Shannon, 1997) to combine three dimensions indicators. This method overcomes the subjectivity of artificial weighting and has a strong adaptive ability (Xing and Yang, 2022). Taking the node value as an example, the calculation steps are as follows:

Step 1. Constructing the decision matrix in Eq. 4. X consists of m stations and n indicators of node value, and X_{pq} is the value of indicator q at station p:

$$\mathrm{X} = \{X_{\mathrm{pq}}\}\mathrm{m} \times \mathrm{n} \tag{4}$$

Step 2. All indicators are positive indicators, so normalizing the decision matrix among m stations in Eq. 5:

$$X'_{\mathrm{pq}} = \left(X_{\mathrm{pq}} - \min\{X_{\mathrm{q}}\}\right) \Big/ \left(\max\{X_{\mathrm{q}}\} - \min\{X_{\mathrm{q}}\}\right) + 0.00001 \tag{5}$$

Step 3. Calculating the proportion R'pq of station p for indicator q in Eq. 6

$$R'_{\mathrm{pq}} = X'_{\mathrm{pq}} \Big/ \sum_{\mathrm{p}=1}^{\mathrm{m}} X'_{\mathrm{pq}} \tag{6}$$

Step 4. Calculating the entropy value eq of indicator q in Eq. 7:

$$\mathrm{e_q} = \frac{1}{-\ln^{m}} \times \sum\nolimits_{\mathrm{p}=1}^{\mathrm{m}} R'_{\mathrm{pq}} \cdot \ln\left(R'_{\mathrm{pq}}\right)\left(\text{If } \mathrm{R}' = 0,\ \ln R'_{\mathrm{pq}} = 0\right) \tag{7}$$

Step 5. Calculating the imbalance coefficient g_q of indicator q. Since most e_q of indicator q in this study is very close to 1, We

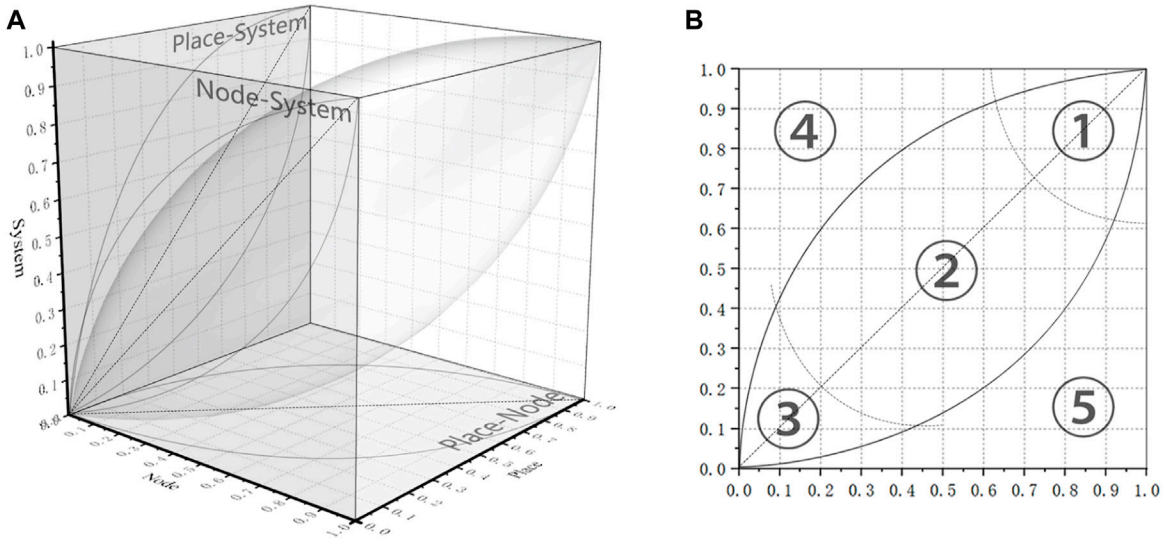

FIGURE 4
Method of classification **(A)** Coordinate system combination of three dimensions **(B)** position in the coordinate system.

TABLE 2 Position and corresponding category in the NPS model.

Classify by the NP model

Coordinates	Place-node	Type	The specific category
Area	1,2,3	Balance (B)	Balance, Press, Dependence
	4,5	Unbalance (UB)	UB-Node, UB-Place
Classify by the Extend NPS Model			
Coordinates	**Node-System**	**Place-System**	**Type**
Area	1,2,3	1,2,3	NP
	4	1,2,3	N-
	5	1,2,3	N+
	1,2,3	4	P-
	1,2,3	5	P+
	4	4	N-P-
	5	5	N + P+

refer to the method of Cao et al. (2020), which uses the inverse of eq to calculate g_q in Eq. 8 for enhancing the evenness.

$$g_q = \frac{1}{e_q} \tag{8}$$

Step 6. Calculating the weight Wq of indicator q in Eq. 9:

$$W_q = g_q \Big/ \sum_{q=1}^{n} g_q \tag{9}$$

Step 7. Calculating the composite node value index Np for station p in Eq. 10

$$N_p^{'} = \sum_{q=1}^{n} W_q \times X_{pq}^{'} \tag{10}$$

Step 8. Normalizing station p's node value index between 0 and 1 among m stations in Eq. 11, wherein N is the array of node value index of m stations:

$$N_p^{'} = \left(N_p - \min\{N\}\right) \Big/ \left(\max\{N\} - \min\{N\}\right) \tag{11}$$

TABLE 3 Correlation between the indicators.

	P1	P2	P3	P4	N1	N2	N3	N4	S1	S2	S3
P1	1	.326*	.518**	.380*	0.259	0.228	0.210	−0.043	0.146	0.223	.396*
P2	.326*	1	−0.161	.422**	0.082	0.286	0.309	0.266	.340*	0.031	0.207
P3	.518**	−0.161	1	−.543**	−0.293	−0.053	0.113	−0.284	−0.127	0.198	-0.292
P4	.380*	.422**	−.543**	1	.522**	0.278	0.249	.330*	.328*	0.154	.669**
N1	0.259	0.082	−0.293	.522**	1	0.049	0.039	0.067	0.040	0.116	.523**
N2	0.228	0.286	−0.053	0.278	0.049	1	−0.010	.435**	.498**	.398*	0.158
N3	0.210	0.309	0.113	0.249	0.039	−0.010	1	0.197	0.083	0.314	0.025
N4	−0.043	0.266	−0.284	.330*	0.067	.435**	0.197	1	.568**	0.311	0.184
C1	0.146	.340*	−0.127	.328*	0.040	.498**	0.083	.568**	1	.598**	0.245
C2	0.223	0.031	0.198	0.154	0.116	.398*	0.314	0.311	.598**	1	0.106
C3	.396*	0.207	−0.292	.669**	.523**	0.158	0.025	0.184	0.245	0.106	1

Note: **p < 0.05; *p < 0.1.

Likewise, place and system support value indexes are calculated in the same steps.

Classification

Figure 4 and Table 2 show that the NPS model provides two levels of classification paths. By observing the position of a calculated point in the three-dimensional coordinate system, we can estimate whether the node and place performances are balanced relative to each other (NP model) and then whether the corresponding system support can be matched (NPS model). In the node-place coordinate system, the stations are divided into the balanced (type B) type and the unbalanced (type UB) type as introduced in *The Node-Place Model Section*. The two categories can be further subdivided into 5 categories: balance, balanced stress, balanced dependence, unbalanced node, and unbalanced place.

By comparing the system support index with node and place indexes in node-system (N-S) and place-system (P-S) coordinate systems (Figure 4), seven categories can be identified (Table 2). When the node and place indexes are both close to the system support index, it means that the potential performances of transport and land use of the planning are matched with the orientation in the entire city, and the urban system is sufficient to support the expected development (type NP). When the node index is significantly lower than the system support index, it indicates that the transport development is lower than expected (type N-). Otherwise, it indicates that the transport development is higher than expected (type N+). The comparison between the place and system support indexes shows another two similar categories (type P- and type P+). When both node and place indexes are significantly higher than the system support index, it means that the city system cannot support the current plan of transportation and land use (type N + P+). When both node and place indexes are much lower than the system support index (type N-P-), it indicates that the plan cannot meet the motive force of development provided by the system. Although theoretically there should also be cases of type N + P- or type N-P+, the reality is that the construction of TOD is based on the simultaneous consideration of transport and land use, and there is a certain positive correlation between the two. We, therefore, do not discuss these two extreme cases.

Results and discussion

Variables

Using Pearson's correlation coefficient (Table 3), we found that the correlations of most indexes are not high, which speaks to the independence of our chosen indicators. However, a fraction of the results show a high correlation between some variables because the planning itself is systematic. For example, there is a significant and positive correlation between the proportion of core plots of land and commercial area. This is because more commercial land is usually planned in each city sub-center to provide more jobs, and the proportion of core land is also usually improved to raise the upper limit of various development indicators. We do not consider these variables that show a significant correlation to be problematic because they are given different weights in different dimensions before finally being integrated into a comprehensive indicator set.

The relative importance of each variable is shown in Table 4. The weight distribution of each variable in node and place indicators is relatively homogeneous, which indicates that their influence is similar. Among the indicators for system support, the core plot of land is the most influential one, followed by betweenness and closeness.

After analyzing the correlation of the quantitative results of stations (Table 5), we can see there is a significant positive

TABLE 4 The weight of each indicator.

Dimension	Variables	Relative importance	Rank
Node	Directions served by metro	0.26	1
	Road network accessibility	0.25	2
	Station capacity	0.25	3
	Station entrances	0.24	4
Place	Residential capacity	0.26	1
	Residential capacity	0.25	2
	Land use mix	0.25	3
	Intensity	0.24	4
System Support	Core plot of land	0.38	1
	Betweenness	0.33	2
	Closeness	0.28	3

TABLE 5 Correlation between the node, place, and system support results.

	Place	Node	System support
Place	1	.407*	.39 9*
Node	.407*	1	.609**
System support	.399*	.609**	1

Note: $^{**}p < 0.05$; $^{*}p < 0.1$.

TABLE 6 Descriptive statistics of the node, place, and system support indexes.

Index	Min	Max	Mean	Std.Deviation
Node	0.0563	0.7923	0.3424	0.1658
Place	0.0750	0.7844	0.4503	0.1667
System support	0.0335	0.7406	0.2121	0.1529

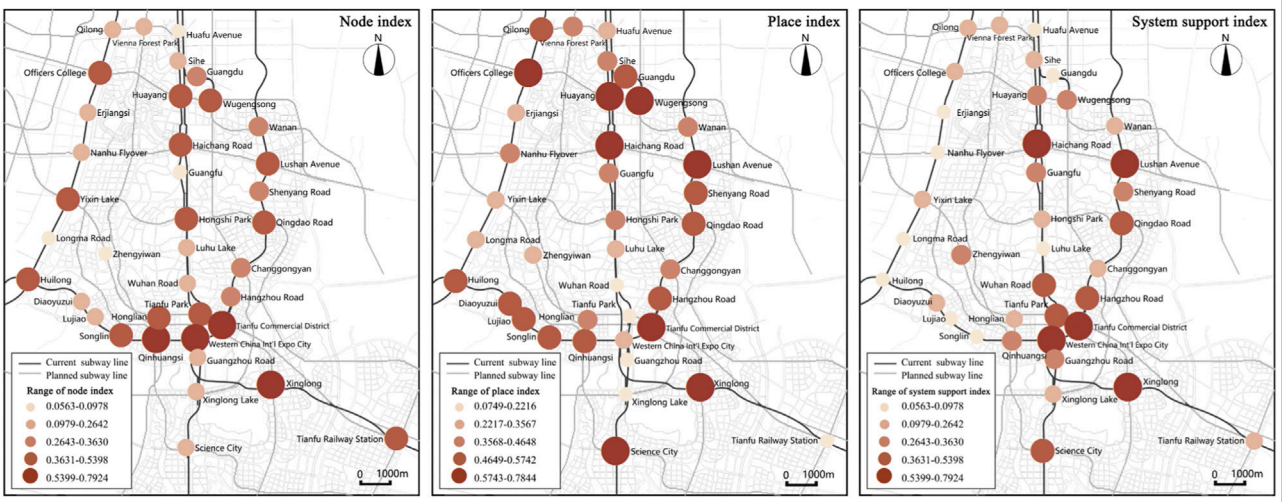

FIGURE 5
Node, place, and system support indexes of the metro stations.

correlation between the node, place, and system support indexes. That is, there is a matching relationship between transport, land use, and urban system when the quantity of data is significant. The result is the same as the initial setting of this study, which also agrees with the effectiveness of the NPS model quantitatively.

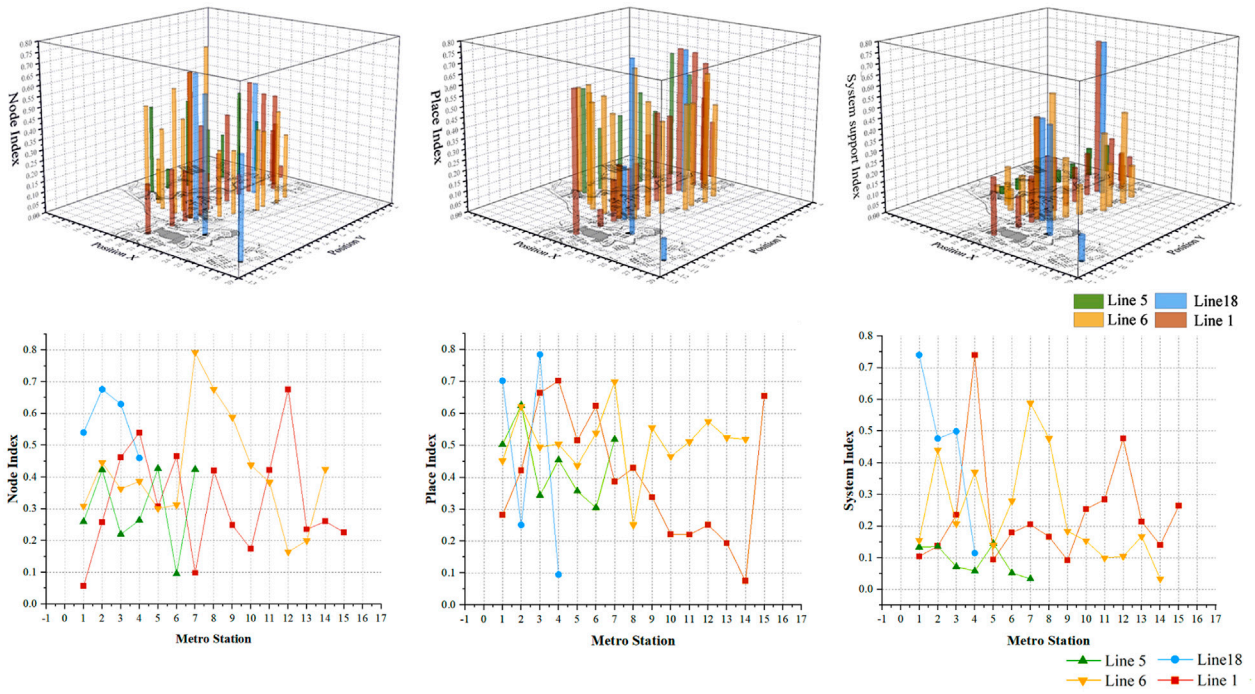

FIGURE 6
Node, Place, and System Support Indexes for each subway line.

TABLE 7 Descriptive statistics of the node, place, and system support indexes of each metro line.

	1			18			5			6		
	Node	Place	System	Node	Place	System	Node	Place	System	Node	Place	System
Min	0.0563	0.0750	0.0927	0.4595	0.0952	0.1148	0.0956	0.3051	0.0335	0.1645	0.2508	0.0335
Max	0.6760	0.7021	0.7406	0.6760	0.7844	0.7406	0.4270	0.6250	0.1452	0.7923	0.6990	0.5882
Mean	0.3232	0.3983	0.2393	0.5762	0.4581	0.4578	0.3020	0.4437	0.0901	0.4129	0.5102	0.2428
Std.D	0.1644	0.1902	0.1637	0.0833	0.2918	0.2234	0.1181	0.1061	0.0431	0.1669	0.0977	0.1582

Figure 5 shows the quantization level of node, place, and system support values for each station. Haichang Road and Tianfu Commercial District show a high performance in the three aspects, so they are more likely to be the sub-centers of the area. By comparing the system support value with node and place values, we find that the degree of system support is generally low (Table 6). Among them, the centrality index is generally low, which is similar to the character of the station cluster on the edge of the city in the previous studies (Zhang et al., 2019; Dou et al., 2021). In addition, the core plot of land proportion is low because Tianfu New Area was defined as a park city, with a large number of ecological green spaces and low-density plots, which restricts the upper limit of land development.

Metro lines

Metro lines are the driving force for development through the combination of traffic points and traffic axes to help planners realize regional development projects (Lu, 1986; Zhu et al., 2021). Therefore, by comparing the results in different metro lines, we can observe the development status and degree of equilibrium for different drive axes, which can assist in setting the departure frequency and carriage capacity for different lines. For those lines with high load pressure and system importance, cross-station parallel subway lines can be added. The stations we evaluated involve metro Lines 1, 5, 6, 15, 18, and 19. Lines 1, 5, and 8 are parallel to the main north-south axis of Chengdu. Line 6 connects Lines 1, 5, and 18 in the east-west direction. Most sections of Line

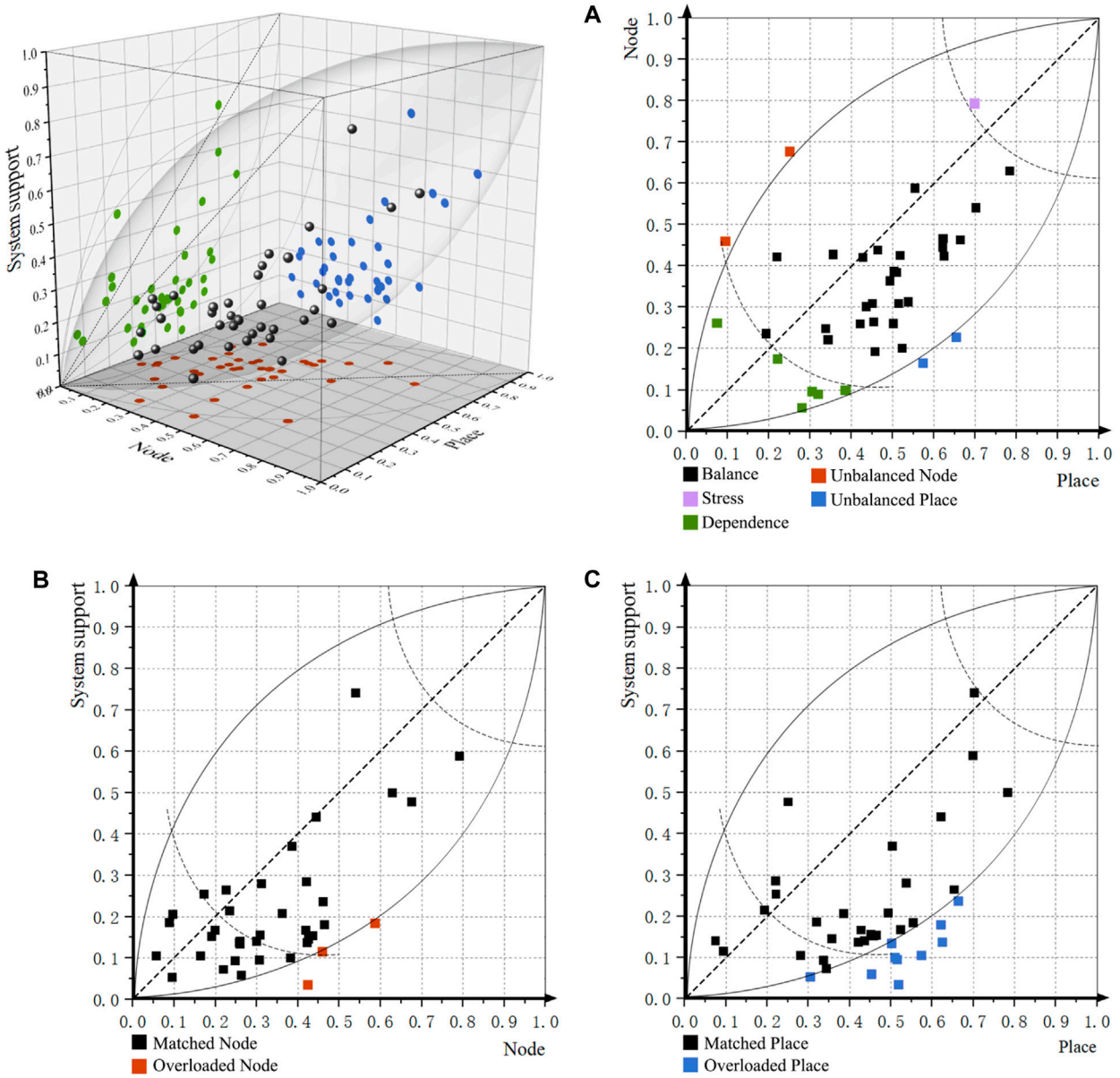

FIGURE 7
Scatter plot of node, place, and system support indexes of the metro stations in the NPS model. **(A)** Node-place coordinate **(B)** System support-node coordinate **(C)** System support-place coordinate.

18 are cross-station crossing lines of Line 1 (built to relieve the transportation pressure on Line 1). We did not discuss Lines 15 and 19 due to the small number of involved samples.

Figure 6 shows the performance and fluctuation of each line on node, place, and system support values and their corresponding geographical locations. Table 7 shows the overall data description of each line. Lines 1 and 18 show a balanced state in node and place value, and a matched relationship with system support. The index of Line 1 fluctuates greatly, reaching a high value at the intersections with Line 18. The place value of Line 1 shows a general downward trend with its southward extension, reaching a low value near Tianfu Park and Xinglong Lake because ecological protection requires a low-intensity development. Line 18 is similar to that of Line 1, but its node and place values are significantly higher, and the mean system index is almost twice as high as that of Line 1. That's because the planners have chosen important points in Line 1 to set stations for Line 18, which reduces the pressure of the flow and promotes the benefit for Line 1. This also further explains why Line 1 shows a strong fluctuation in the node

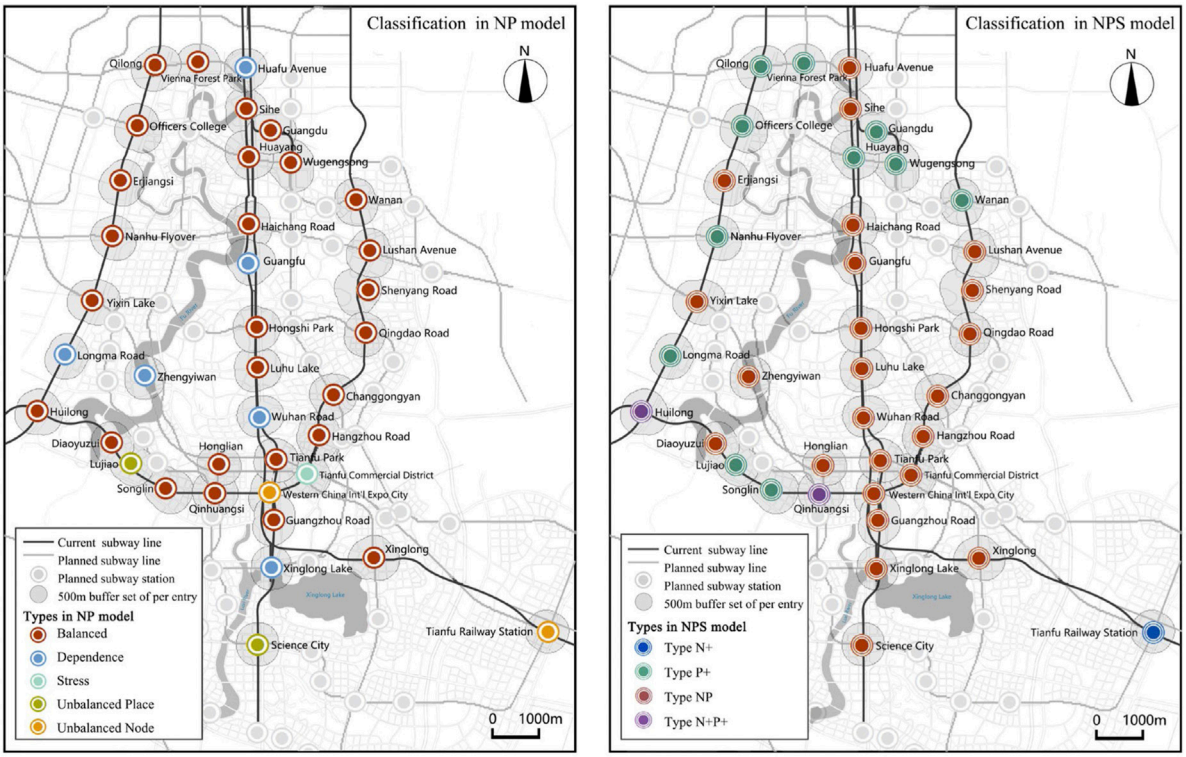

FIGURE 8
Results of metro stations in the NP model and the NPS model.

value. Both Line 5 and 6 show a low value of system support because they are located on the fringes of Tianfu New Area while they still have high and mismatched values of node and place, which means the development of the areas along them may not be as good as expected.

Typologies and suggestions.

We classified the stations by the position in the NPS model in Figure 7, and Figure 8 shows the results of distribution by the NP model and NPS model.

As shown in Figure 7A, the relationship between node and place for most metro stations is in a balanced state. However, Western China International Expo City Station and Tianfu Railway Station are unbalanced nodes (type UB-N). The land development is limited due to the large buildings within the area, which is one of their common features. Taking Western China International Expo City St\\tnation as an example, as seen in Figure 5, its area is positioned as a sub-center with high system support and node indexes. However, the building of Western China International Expo City with low plot ratios is the main reason for limiting the place value. Improving the place index is therefore a logical direction for future development. The place value can be improved by setting special catchment area shuttle buses to expand the catchment area of the station artificially, or by improving the functional richness of the interior of the building and improving the intensity of the rest of the land. Lujiao Station and Science City Station are unbalanced places (type UB-P). Taking Lujiao Station as an example, the development intensity and degree of mixing of the catchment area are both high, but the design of the station cannot meet the requirements, which is manifested by too few entrances and a small area. The site is located on the urban fringe. Combined with the system support indicators, we suggest that the development intensity and degree of land use mix of the station's area can be appropriately lowered to reduce costs.

In the above two examples, we suggest adjusting the place performance in the face of different types of unbalanced states, but in the traditional NP model, two separate correction methods are usually recommended (adjust node or place performances). Based on the NPS model, we can propose more specific strategies to calibrate the relationship between node and place.

We consider cluster 1 (type NP) to be reasonably planned, balanced in NP performance, and matched with the urban system. For a typical station such as Tianfu Business District Station (N = 0.79, p = 0.67, S = 0.59) (Figures 9, 10), the indexes of node and place indicate that the station is under stress, but the comparisons with system support show that they are still in

10.3389/fenvs.2022.990416

FIGURE 9
Typical Case Analysis **(A)** values of node, place, and design indexes for each typical case; **(B)** comparison of indexes of each typical case with average indexes; **(C)** road accessibility; **(D)** land use in the regulatory plan; **(E)** station design.

matched states, reflecting that the transport and land use of the station is in line with the expectation. The station area is oriented as one of the main centers of Tianfu New Area, the result of the NPS model shows that the planning meets the preliminary positioning. However, this area may face some problems like mixed traffic and traffic congestion in the future because its high accessibility index indicates that the block division scale is very small, and the land-use intensity related to population capacity is very high. This catchment area can be considered for the construction of underground passages to divert foot traffic, or for increasing the proportion of public transfer transportation to reduce the number of private cars.

Cluster 2 (type P+) is the overloaded place, where land use performance exceeds system support. One representative station of this type is Wugensong (N = 0.42, $p = 0.62$, S = 0.14) (Figures 9, 10), here, there is land for the subway operation company and several large-scale old residential areas with high intensity in the catchment area. Although it shows good performance on centrality, its proportion of core plots of land is very low. In addition, the distance from this station to the recent CBD is approximately 1.2 km, so it also makes sense for it to act as an ancillary area. However, the Xinchuan Road Station of Line 6 is significantly closer to the CBD, so the follow-up development of Wugensong relies too much on the overflow population of the

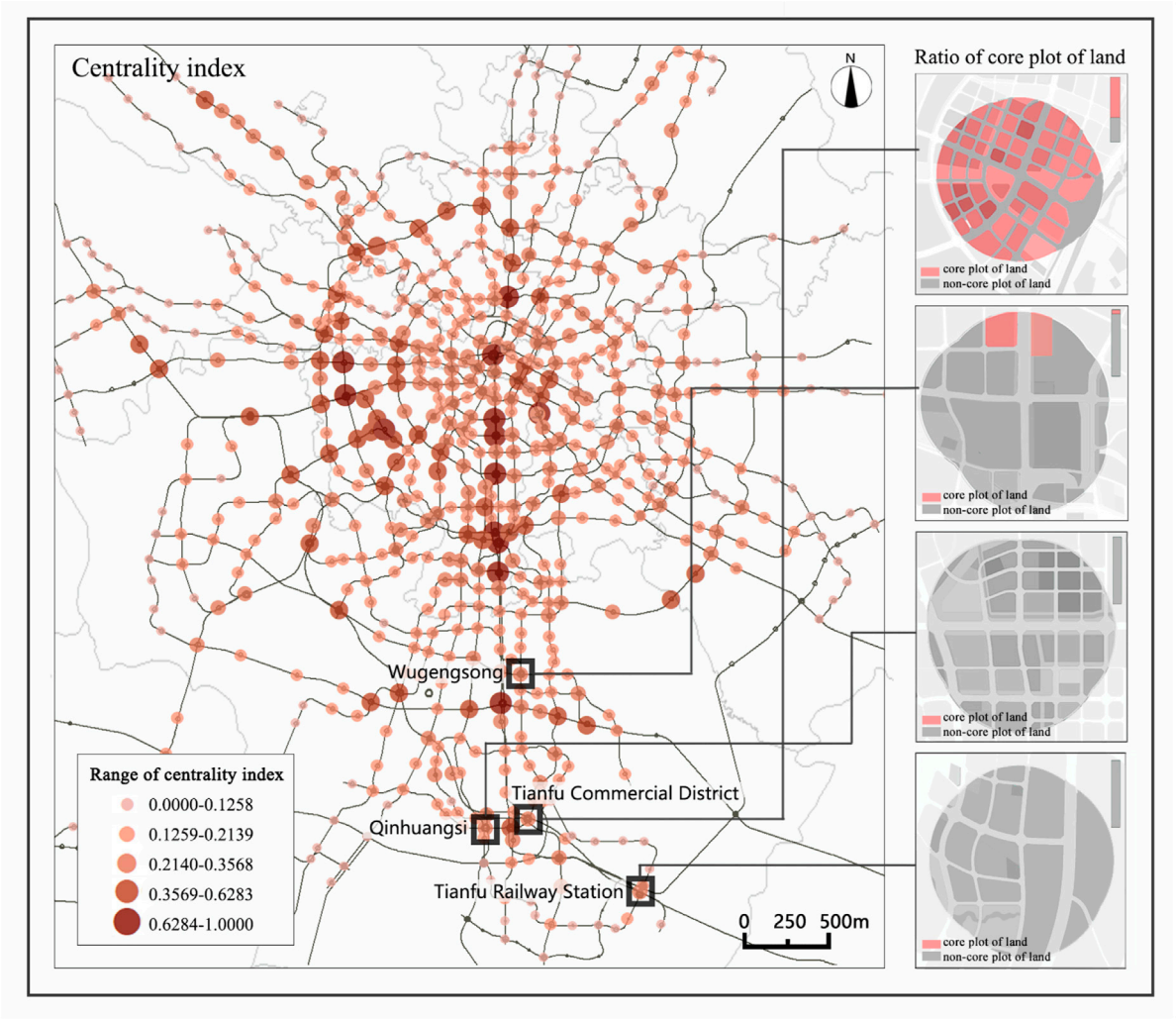

FIGURE 10
Centrality index of all metro stations in Chengdu City and core plot of land of four typical Cases.

CBD and Xinchuan Road Station, and the development is relatively passive.

Cluster 3 (type N+) is the overloaded node, which means that the planned node performance exceeds system support. Tianfu New Station (N = 0.46, p = 0.10, S = 0.11) (Figures 9, 10 shows such characteristics. Its reserved building area is sufficient, but its functions in the area are relatively singular. As a result, this station's land use development and system support index are very low. However, even though we classified it as type N+ only base on the Chengdu area traffic within the network structure, in reality, Tianfu New Station serves as the high-speed rail hub at the inter-city level and should therefore have higher system support and transport design index.

Cluster 4 (type N + P+) is the overload nodes and places, indicating that the performance of both traffic and land use exceeds expectations and that the urban system is unable to support their development. Qinhuangsi Station (N = 0.59, p = 0.57, S = 0.18) (Figures 9, 10) is one such station. Qinhuangsi Station is on the fringe of the entire urban metro network, and not any core plot of land is planned within the catchment area, leading to a lower degree of system support. Additionally, its node and place indexes are very high. This station shows excellent balance in transportation and land use planning, but it is likely to be short of development in the future. For this example, planners may want to expand the size of blocks (reduce the number of intersections), reduce the intensity of commercial and residential buildings, and

increase the area of ecological green space to improve environmental quality.

In general, although most of the stations in the Tianfu New Area are in a balanced state of node and place, more than 80% of the points are still below the model's 45-degree line (the best-expected state) in the NPS model. This reflects, to some extent, that the planning of most catchment areas in Tianfu New Area can not be supported enough by the urban system. For this reason, in a future implementation, the development speed may be relatively slow, and even after being fully built and put into use, the value of transport and land use may still be lower than expected.

Conclusion

This paper is about the predictive evaluation of the potential development collaboration of metro TOD areas in the new urban area by applying the extended NPS model. Then we conducted an empirical study in the newly built metro station areas of Tianfu New District, Chengdu.

Bertolini (Bertolini, 1996) illustrated that there exist dual performances of transport and land use in the catchment area of TOD stations, and the two should be in a dynamically balanced relationship to achieve developmental sustainability. The traditional NP model can be used to recognize the balance on the local scale. But for the development of the new urban area, the inbuilt advantages provided by the conditions of position and policy, which are not included in the original NP indicators, are important. Therefore, we extended the classic NP model by proposing a new concept of system support and introducing it as a new evaluation dimension aligned with the node and place dimensions. By comparing the three scores, we can assess the balance of NP performance and further whether the balanced relationship can be recognized at the broader urban system level. This viewpoint was echoed by Vale et al. (Vale et al., 2018) and Zhang et al. (2019). Based on the multi-sourced data, we apply the NPS model to the station areas in Tianfu New Area for evaluation and classification. There are three key findings:

- Traffic supply, land use, and system support degree are considered as a whole in advance in the planning of Tianfu New Area, and the results of the above three show a positive correlation.
- The stations belong to different metro lines, which results in different lines generally showing different performances and fluctuations. Line 18 is a cross-station line of Line 1, the common stations of Line 18 and 1 show high values both in node and place aspects, and they are relatively balanced and in line with expectations of the urban system. Lines 5 and 6, which run parallel to the north-south axis, have generally exceeded expectations.
- Compare the node index with the place index, most of the stations are balanced of NP, but after adding the system support indicator, some balanced stations still have a mismatch between the system support and NP performances. And most of the mismatch types are concentrated in the range of overload node (type N+), overload place (type P+), and overload node & place (type N + P+), which reflects that the planning of transport and land use in Tianfu New Area is generally beyond the support of the system to some extend.

Our empirical results provide some policy implications. We suggest policymakers and planners consider the pre-assessment for the newly planned or built stations in advance with the two-tier perspective of local and system. The system support score of the NPS model can be used as a reference for assessing the rank and orientation of a station. Stations with a high system support index (such as Tianfu Commercial District and Haichang Road) could be worthy of attention as potential sub-centers for encouraging densification, diversification, and accessibility to increase transport and land use efficiency to accommodate urban growth. On the contrary, the stations with a low system support index could be reduced investment. In addition, the unbalanced or mismatched stations are needed to pay attention to. Firstly, modify the dynamic coordination of the NP performance according to the important reference provided by the system support. For instance, Lujiao is an unbalanced-place station, it is suggested to reduce densification and diversification because the place index exceeds the system support index. Secondly, comparing the NP and system support index and estimating whether the balanced NP performance can be recognized by system support. Some stations, such as stations in Cluster 2(N+), Cluster 3(P+), and Cluster 4(N + P+), did not get sufficient system support. Maybe it is easier to achieve the ideal balance in the future by appropriately reducing the development expected in the planning scheme.

However, there is still room for improvement. First, our evaluation is based on inner-city traffic, but the performance of some stations which involve inter-city transport cannot be objectively assessed. Referring to the greater London area studied by Zhang et al. (2019), we can expand the study area to the greater Chengdu area in subsequent research. Second, the centricity index calculation is based on the entire urban metro network structure, which is a part of the system support. However, experience shows that the range of people's daily activities no longer expands when the urban expansion reaches a certain extent. For example, people tend to work and shop daily nearby rather than somewhere too far from their homes, so the boundaries of the study area should also be redefined in terms of the majority of people's activity areas. Therefore, a variety of scopes of perspective and novel evaluation indicators are recommended for subsequent research.

Data availability statement

The original contributions presented in the study are included in the article/Supplementary material, further inquiries can be directed to the corresponding author.

Author contributions

JM: methodology, software, data curation, writing original draft; ZS: conceptualization, funding acquisition, writing review; YX: data curation, review, and editing; PL: investigation, validation, writing review; BY: investigation, validation, writing review; LC: data curation, and editing. All authors have read and agreed to the published version of the manuscript. All authors contributed to the article and approved the submitted version.

Funding

This research was supported by the Projects of the National Natural Science Foundation of China (grant number 51978573).

Acknowledgments

The authors would like to thank all the editors and reviewers for their valuable insights and suggestions.

Conflict of interest

The authors declare that the research was conducted in the absence of any commercial or financial relationships that could be construed as a potential conflict of interest.

Publisher's note

All claims expressed in this article are solely those of the authors and do not necessarily represent those of their affiliated organizations, or those of the publisher, the editors, and the reviewers. Any product that may be evaluated in this article, or claim that may be made by its manufacturer, is not guaranteed or endorsed by the publisher.

References

Bertolini, L. (1998). *Cities on rails: The redevelopment of railway station areas*. London: Routledge.

Bertolini, L. (1996). Nodes and places: Complexities of railway station redevelopment. *Eur. Plan. Stud.* 4 (3), 331–345. doi:10.1080/09654319608720349

Bertolini, L. (1999). Spatial development patterns and public transport: The application of an analytical model in The Netherlands. *Plan. Pract. Res.* 14 (2), 199–210. doi:10.1080/02697459915724

Bertolini, L. (2008). *Station areas as nodes and places in urban networks: An analytical tool and alternative development strategies*. Physica-Verlag HD.

Calthorpe, P. (1993). *The Next American Metropolis: Ecology, community, and the American dream*. New York: Princeton Architectural Press.

Cao, Z., Asakura, Y. S., and Tan, Z. (2020), Coordination between node, place, and ridership: Comparing three transit operators in Tokyo. *Transportation Research Part D-Transport and Environment*. 87, 1–19. doi:10.1016/j.trd.2020.102518

Cervero, R., and Murakami, J. (2009). Rail and property development in Hong Kong: Experiences and extensions. *Urban Stud.* 46 (10), 2019–2043. doi:10.1177/0042098009339431

Chiaradia, A., Crispin, C., and Webster, C. (2014). sDNA a software for spatial design networt analysis. [Online] Available at: https://sdna.cardiff.ac.uk/sdna/.

Chorus, P., and Bertolini, L. (2011). An application of the node-place model to explore the spatial development dynamics of station areas in Tokyo. *J. Transp. Land Use* 4 (1), 45–58. doi:10.5198/JTLU.V4I1.145

Cooper, C., Chiaradia, A., and Webster, C.sDNA2. (2018). *Spatial design network analysis software*. Cardiff, England: Cardiff University.Available at: https://sdna.cardiff.ac.uk/sdna/.

Dark, S. J., and Bram, D. (2007). The modifiable areal unit problem (MAUP) in physical geography. *Prog. Phys. Geogr. Earth Environ.* 31 (5), 471–479. doi:10.1177/0309133307083294

Dou, M., Wang, Y., and Dong, S. (2021). Integrating network centrality and node-place model to evaluate and classify station areas in Shanghai. *ISPRS Int. J. Geoinf.* 10 (6), 414. doi:10.3390/ijgi10060414

Freke, C., Vale, D. S., and Viana, C. M. (2018). Correction to: Measuring the accessibility of railway stations in the Brussels regional express network: A node-place modeling approach. *Netw. Spatial Econ.* 18, 495–530. doi:10.1007/s11067-018-9420-3

Han, B., Li, Y., Lu, F., Yang, Z., Yang, R., Chen, Y., et al. (2022). Statistical analysis of urban rail transit operations in the world in 2021: A review. *Urban Rapid Rail Transit* 35 (1), 5.

Ibraeva, A., Correia, G. H. D., Silva, C., and Antunes, A. P. (2020). Transit-oriented development: A review of research achievements and challenges. *Transp. Res. Part A Policy Pract.* 132, 110–130. doi:10.1016/j.tra.2019.10.018

Jin, L., Lu, W., and Sun, P. (2022). Effect of the street environment on walking behavior: A case study using the route choice model in the chunliu community of dalian. *Front. Public Health* 10, 874788. doi:10.3389/fpubh.2022.874788

Kamruzzaman, M., Baker, D., Washington, S., and Turrell, G. (2014). Advance transit oriented development typology: Case study in brisbane, Australia. *J. Transp. Geogr.* 34, 54–70. doi:10.1016/j.jtrangeo.2013.11.002

Kim, J. S., and Shin, N. (2021). Planning for railway station network sustainability based on node-place analysis of local stations. *Sustainability* 13 (9), 4778. doi:10.3390/su13094778

Leichenko, R. M., and Solecki, W. D. (2005). Exporting the American dream: The globalization of suburban consumption landscapes. *Reg. Stud.* 39 (2), 241–253. doi:10.1080/0034340052000600080

Lu, D. (1986). Scientific basis of the general layout of China's industrial productivity in 2000 [In Chinses]. *Sci. Geogr. Sin.* 6 (2), 110.

Lyu, G., Bertolini, L., and Pfeffer, K. (2016). Developing a TOD typology for Beijing metro station areas. *J. Transp. Geogr.* 55, 40–50. doi:10.1016/j.jtrangeo.2016.07.002

Ma, T., and Gao, B. (2021). The association of social capital and self-rated health between urban residents and urbanized rural residents in southwest China. *Front. Public Health* 9, 718793. doi:10.3389/fpubh.2021.718793

Monajem, S., and Nosratian, F. E. (2015). The evaluation of the spatial integration of station areas *via* the node place model; an application to subway station areas in Tehran. *Transp. Res. Part D Transp. Environ.* 40, 14–27. doi:10.1016/j.trd.2015.07.009

Papagiannakis, A., Vitopoulou, A., and Yiannakou, A. (2021). Transit-oriented development in the southern European city of thessaloniki introducing urban railway: Typology and implementation issues. *Eur. Plan. Stud.* 29 (1), 117–141. doi:10.1080/09654313.2020.1724267

Qiang, D., Zhang, L., and Huang, X. (2022). Quantitative evaluation of TOD performance based on multi-source data: A case study of Shanghai. *Front. Public Health* 10, 820694. doi:10.3389/fpubh.2022.820694

Reusser, D. E., Loukopoulos, P., Stauffacher, M., and Scholz, R. W. (2008). Classifying railway stations for sustainable transitions - balancing node and place functions. *J. Transp. Geogr.* 16 (3), 191–202. doi:10.1016/j.jtrangeo.2007.05.004

Roth, C., Kang, S. M., Batty, M., and Barthelemy, M. (2011). Structure of urban movements: Polycentric activity and entangled hierarchical flows. *Plos One* 6 (1), e15923. doi:10.1371/journal.pone.0015923

Shannon, C. E. (1997). The mathematical theory of communication. 1963. *Md. Comput.* 14 (4), 306.

Shen, L., Peng, Y., Zhang, X., and Wu, Y. (2012). An alternative model for evaluating sustainable urbanization. *Cities* 29 (1), 32–39. doi:10.1016/j.cities.2011.06.008

Singh, Y. J., Fard, P., Zuidgeest, M., Brussel, M., and Maarseveen, M. V. (2014). Measuring transit oriented development: A spatial multi criteria assessment approach for the city region arnhem and nijmegen. *J. Transp. Geogr.* 35, 130–143. doi:10.1016/j.jtrangeo.2014.01.014

Song, J., and Deguchi, A. (2013). Evaluation and typology of railway station areas in a 30km circumference surrounding central Tokyo from view of transit-oriented development [In Japenese]. *Trans. AIJ.* 78 (648), 413–420. doi:10.3130/aija.78.413

Vale, D. S. (2015). Transit-oriented development, integration of land use and transport, and pedestrian accessibility: Combining node-place model with pedestrian shed ratio to evaluate and classify station areas in Lisbon. *J. Transp. Geogr.* 45, 70–80. doi:10.1016/j.jtrangeo.2015.04.009

Vale, D. S., Viana, C. M., and Pereira, M. (2018). The extended node-place model at the local scale: Evaluating the integration of land use and transport for Lisbon's subway network. *J. Transp. Geogr.* 69, 282–293. doi:10.1016/j.jtrangeo.2018.05.004

Wang, F., Chen, C., Xiu, C., and Zhang, P. (2014). Location analysis of retail stores in changchun, China: A street centrality perspective. *Cities* 41, 54–63. doi:10.1016/j.cities.2014.05.005

Wang, L., Li, C., Ying, Q., Cheng, X., Wang, X., Li, X., et al. (2012). China's urban expansion from 1990 to 2010 determined with satellite remote sensing. *Chin. Sci. Bull.* 57 (22), 2802–2812. doi:10.1007/s11434-012-5235-7

Wang, X., Tong, D., Gao, J., and Chen, Y. (2019). The reshaping of land development density through rail transit: The stories of central areas vs. suburbs in Shenzhen, China. *Cities* 89, 35–45. doi:10.1016/j.cities.2019.01.013

Wang, Y., Chen, K., and Chao-Qun, M. A. (2008). Quantitative analysis of coordination between rail transit network configuration and urban form. *J. Railw. Eng. Soc* 11, 11–15.

Xing, Q., and Yang, Z. (2022). Assessment of the coordination of low-carbon development and socio-economic development based on a comprehensive model: A case study of anhui province (China). *Front. Public Health* 10, 884342. doi:10.3389/fpubh.2022.884342

Xu, W., Guthrie, A., Fan, Y., and Li, Y. (2017). Transit-oriented development: Literature review and evaluation of TOD potential across 50 Chinese cities. *J. Transp. Land Use* 10 (1), 743–762. doi:10.5198/jtlu.2017.922

Yang, L., Chau, K. W., Szeto, W. Y., Cui, X., and Wang, X. (2020a). Accessibility to transit, by transit, and property prices: Spatially varying relationships. *Transp. Res. Part D Transp. Environ.* 85, 102387. doi:10.1016/j.trd.2020.102387

Yang, L., Chu, X., Gou, Z., Yang, H., Lu, Y., and Huang, W. (2020b). Accessibility and proximity effects of bus rapid transit on housing prices: Heterogeneity across price quantiles and space. *J. Transp. Geogr.* 88, 102850. doi:10.1016/j.jtrangeo.2020.102850

Yang, L., Liang, Y., He, B. J., Lu, Y., and Gou, Z. H. (2022a). COVID-19 effects on property markets: The pandemic decreases the implicit price of metro accessibility. *Tunn. Undergr. Space Technol.* 125, 104528. doi:10.1016/j.tust.2022.104528

Yang, L., Liu, J., Liang, Y., Lu, Y., and Yang, H. (2021). Spatially varying effects of street greenery on walking time of older adults. *ISPRS Int. J. Geoinf.* 10 (9), 596. doi:10.3390/ijgi10090596

Yang, L., Tang, X., Yang, H., Meng, F., and Liu, J. (2022b). Using a system of equations to assess the determinants of the walking behavior of older adults. *Trans. GIS* 26 (4), 1339–1354. doi:10.1111/tgis.12916

Yang, P., and Lew, S. (2009). *An Asian model of TOD: The planning integration in Singapore*. Hampshire: Ashgate Publishing Ltd.

Zadeh, A. S. M., and Rajabi, M. A. (2013). Analyzing the effect of the street network configuration on the efficiency of an urban transportation system. *Cities* 31, 285–297. doi:10.1016/j.cities.2012.08.008

Zemp, S., Stauffacher, M., Lang, D. J., and Scholz, R. W. (2011). Classifying railway stations for strategic transport and land use planning: Context matters. *J. Transp. Geogr.* 19 (4), 670–679. doi:10.1016/j.jtrangeo.2010.08.008

Zhang, Y., Marshall, S., and Manley, E. (2019). Network criticality and the node-place-design model: Classifying metro station areas in Greater London. *J. Transp. Geogr.* 79, 102485. doi:10.1016/j.jtrangeo.2019.102485

Zhong, C., Arisona, S. M., Huang, X., Batty, M., and Schmitt, G. (2014). Detecting the dynamics of urban structure through spatial network analysis. *Int. J. Geogr. Inf. Sci.* 28 (11), 2178–2199. doi:10.1080/13658816.2014.914521

Zhu, R., Wang, Y., Lin, D., Jendryke, M., Xie, M., Guo, J., et al. (2021). Exploring the rich-club characteristic in internal migration: Evidence from Chinese Chunyun migration. *Cities* 114, 103198. doi:10.1016/j.cities.2021.103198

frontiers | Frontiers in Ecology and Evolution

TYPE Original Research
PUBLISHED 20 September 2022
DOI 10.3389/fevo.2022.978145

Check for updates

OPEN ACCESS

EDITED BY
Jun Yang,
Northeastern University, China

REVIEWED BY
Likai Zhu,
East China Normal University, China
Decheng Zhou,
Nanjing University of Information Science and Technology, China

*CORRESPONDENCE
Wei Chen
chenwei@iae.ac.cn

SPECIALTY SECTION
This article was submitted to Environmental Informatics and Remote Sensing, a section of the journal Frontiers in Ecology and Evolution

RECEIVED 25 June 2022
ACCEPTED 23 August 2022
PUBLISHED 20 September 2022

CITATION
Jia G, Dong Y, Zhang S, He X, Zheng H, Guo Y, Shen G and Chen W (2022) Spatiotemporal changes of ecosystem service trade-offs under the influence of forest conservation project in Northeast China.
Front. Ecol. Evol. 10:978145.
doi: 10.3389/fevo.2022.978145

COPYRIGHT
© 2022 Jia, Dong, Zhang, He, Zheng, Guo, Shen and Chen. This is an open-access article distributed under the terms of the Creative Commons Attribution License (CC BY). The use, distribution or reproduction in other forums is permitted, provided the original author(s) and the copyright owner(s) are credited and that the original publication in this journal is cited, in accordance with accepted academic practice. No use, distribution or reproduction is permitted which does not comply with these terms.

Spatiotemporal changes of ecosystem service trade-offs under the influence of forest conservation project in Northeast China

Guangliang Jia[1,2], Yulin Dong[2,3], Siyu Zhang[2,3,4], Xingyuan He[1,2], Haifeng Zheng[2,3], Yujie Guo[2,3], Guoqiang Shen[2,3] and Wei Chen[1,2]*

[1]Key Laboratory of Forest Ecology and Management, Institute of Applied Ecology, Chinese Academy of Sciences, Shenyang, China, [2]University of Chinese Academy of Sciences, Beijing, China, [3]Key Laboratory of Wetland Ecology and Management, Northeast Institute of Geography and Agroecology, Chinese Academy of Sciences, Changchun, China, [4]Guizhou Provincial Key Laboratory of Geographic State Monitoring of Watershed, Guizhou Education University, Guiyang, China

Trade-offs between ecosystem services are measures of the degree to which the changing differences between the individual ecosystem services. Although changes in ecosystem service trade-offs are critical for forest ecosystem management, spatiotemporal changes in trade-offs are currently less studied, especially under the influence of ecological engineering implementation. Therefore this study explored the spatiotemporal changes and drivers of ecosystem service trade-offs in various forest types following the implementation of the natural forest conservation project (NFCP), with the example of the Greater Khingan Mountains. Spatial analyses, and root mean square error (RMSE) were applied to investigate spatiotemporal changes in trade-offs, and geodetector was employed to assess their driving factors. The results indicated that among all ecosystem service pairs from 1990 to 2020, the trade-offs between habitat quality and net primary productivity (NPP), NPP and soil conservation showed a growing trend. However, the trade-offs between habitat quality and water conservation, NPP and water conservation, and soil conservation and water conservation showed a declining trend. The ecosystem service trade-offs of coniferous (0.47) were higher than either broad-leaved (0.37) or shrubs (0.28). Moreover, changes in the ecosystem service trade-offs of all kinds of forests were spatially heterogeneous. The drivers with the greatest explanatory power in coniferous, broad-leaved, and shrubs were land use (22.68%), land use (15.19%), and NDVI (20.63%), respectively. Environmental factors contributed great mean explanatory power (62.27–71.67%) to the trade-offs than anthropogenic

activity factors. Therefore, spatiotemporal changes and drivers of trade-offs in different forests should be contemplated when conducting subsequent ecological restoration programs in the future.

KEYWORDS

natural forest conservation project, forest ecosystem service, trade-off, spatiotemporal changes, driving factors

Introduction

Forests are the largest natural ecosystems on Earth (FAO, 2020). They provide natural environment for humans by delivering numerous ecosystem services (Nkem et al., 2007; Mbow et al., 2014). Global climate change and increased human activities have resulted in environmental devastation and forest deterioration, such as soil erosion, water shortage, and habitat degradation (Foley et al., 2005). Habitat degradation and supply decreases in ecosystem services threaten ecosystem balance and thus human welfare (Wang et al., 2017). To tackle this issue and ensure the sustainable development of forest ecosystems, China has implemented several successively ecological projects, for instance, the natural forest conservation project (NFCP) since 2000 (Mao et al., 2019). Restoration programs have greatly improved habitat quality and ecosystem services in forest ecosystems (Benayas et al., 2009). Assessing forest ecosystem services after restoration can provide insights into future ecological projects' implementation to maximize ecosystem service benefits (Tallis et al., 2008).

Trade-offs between ecosystem services measure the degree to which the changing differences between the individual ecosystem services (Bennett et al., 2009; Qiu et al., 2021). Trade-off interactions between forest ecosystem services may enhance or weaken by spatiotemporal changes in ecosystem services (Bennett et al., 2009). They are closely connected with spatiotemporal dynamics of ecological processes, and are spatiotemporally heterogeneous (Liu et al., 2019; Qiao J. M. et al., 2019; Qiu et al., 2021; Zhao et al., 2021). With global warming and human activities increasing, the spatiotemporal dynamic property of trade-offs makes their management more unsure and challenging (Gonzalez-Ollauri and Mickovski, 2017; Dong et al., 2020). However, most related studies were mainly focused on spatiotemporal changes in forest ecosystem services. For instance, ecosystem services provided by different forest types were significantly improved after dam construction in the Three Gorges reservoir area (Chu et al., 2019). The spatial variations of forest ecosystem services were closely connected with land use patterns (Aznar-Sánchez et al., 2018). Spatiotemporal changes in trade-offs among different forest ecosystem services can affect the increase or decrease of different ecosystem services, and thus change the ecosystem overall benefits. Comprehending the spatiotemporal disparities in trade-offs among different forest ecosystem services is relatively limited, especially the spatiotemporal changes after the ecological project implementation. Therefore, a greater comprehension of the spatiotemporal changes in forest ecosystem service trade-offs is necessary to provide an effective policy basis for forest ecosystem management.

Explicating the drivers of trade-offs is crucial for confirming corresponding solutions to alleviate trade-offs and improve ecosystem services (Power, 2010). Numerous studies indicated that the spatiotemporal dynamics of trade-offs between forest ecosystem services depended on natural factors (i.e., precipitation, elevation, slope, etc.) and anthropogenic activity factors (i.e., land use, population distribution, etc.) (Lyu et al., 2019; Peng et al., 2019). Although these studies focused on the effects of environmental factors and anthropogenic activity factors, there is still a lack of comprehensive comparison of driving factors. In addition, most of these studies used traditional correlation or regression analysis that focused on driver effects from a numerical perspective, but ignored the spatial heterogeneity of drivers themselves. Geodetector is a new tool for geographic research that can effectively analyze spatial differentiation in geographic phenomena and assess how the factors influence spatial differentiation (Han et al., 2015). The core assumption of geodetector is that if the independent variable X and the dependent variable Y have a virtual spatial correlation, they are linked (Wang et al., 2010). This approach has been progressively applied to identify the spatially stratified characteristics of land use and landscape patterns. It detects spatial differences and principal causes efficiently in geographic phenomena and can be applied to analyze the driving factors of trade-offs.

As the mainstay of the natural ecosystem in northern China, forests play a critical part in maintaining regional climate and environmental protection. The Greater Khingan Mountains are boreal forests and are necessary ecological barriers in northern China. They also play an essential role in net primary productivity (NPP), soil conservation, water conservation, and habitat quality (Mao et al., 2019; Zhang et al., 2022). To protect the ecological environment, the Chinese government has implemented the NFCP since 2000. The first phase of the NFCP ended in 2010, and the second round of the NFCP started

in 2011. The effect of the NFCP on ecosystem services could guide subsequent ecological engineering. The Greater Khingan Mountains were the main area for NFCP implementation in Northeast China. Therefore, taking the Greater Khingan Mountains as an example, this paper aims to: (1) evaluate the spatiotemporal changes of forest ecosystem services in the Greater Khingan Mountains from 1990 to 2020; (2) investigate the spatiotemporal changes in ecosystem service trade-offs and their differences among various forest types; (3) measure the influence of drivers on forest ecosystem service trade-offs among various forest types using geodetector.

Materials and methods

Study area

The Greater Khingan Mountains are located at 118°14′∼127°44′E, 45°13′∼53°56′N (**Figure 1**). Their administrative scope includes the Hinggan League of Inner Mongolia Autonomous Region, Hulunbuir City, and the Greater Khingan Mountains area of Heilongjiang Province, with an area of about 260,000 km^2. It has a temperate continental climate characterized by long, cold winters and short, rainy summers. It is rich in solar radiation resources, with a mean average temperature of –2.5 to 6.8°C and a mean annual rainfall of 310–750 mm. The vegetation types in this region are mainly coniferous, coniferous and broad-leaved mixed, broad-leaved, and shrubs. Since the areas of coniferous and broad-leaved mixed were too small, three types of forest types including coniferous, broad-leaved, and shrubs were selected in this study. The spatial patterns of the forests were digitized using the Vegetation Atlas of China (Editorial Committee for Vegetation Atlas of China, 2001).

Data sources and processing

The datasets employed incorporated land use, NDVI, meteorological, elevation, soil data, GDP per land area and,

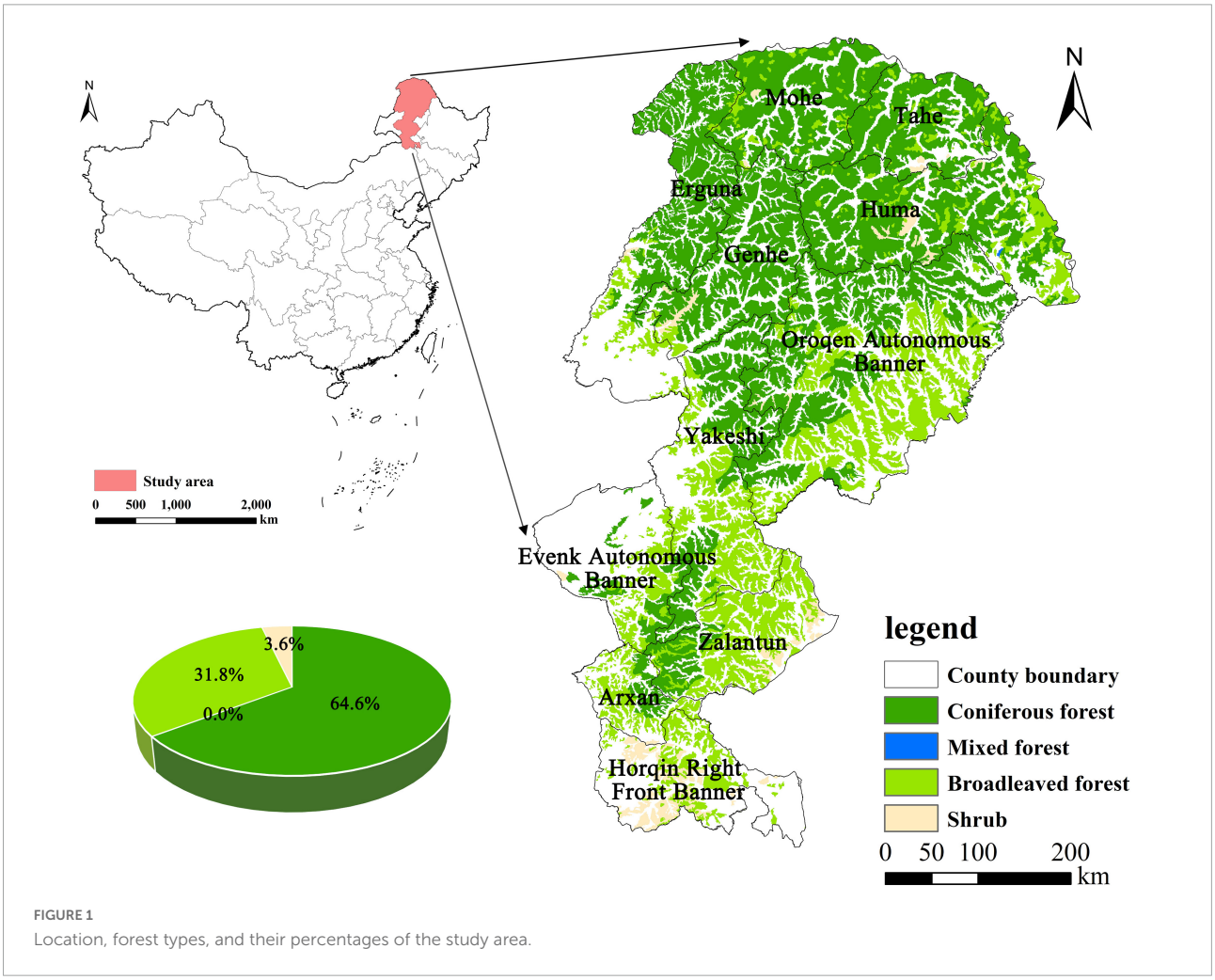

FIGURE 1
Location, forest types, and their percentages of the study area.

population density in this paper. The specifics were shown in Table 1. Land use was used to estimate habitat quality. NDVI was used to retrieve the absorbed photosynthetic active radiation (APAR) when estimating NPP. Rainfall data were used to estimate the rainfall erosion factor. Slope, slope length, and topography factor were calculated using the elevation. Soil data were used to estimate the soil erodibility factor. All data were rescaled to 300 m to satisfy the calculation requirements.

Quantification of forest ecosystem services

In recent decades, many ecological problems have been arisen in the Greater Khingan Mountains, such as soil erosion, water shortage, and habitat degradation (Mao et al., 2014). Based on previous studies and field research, we chose 4 key forest ecosystem services: NPP, soil conservation, water conservation, and habitat quality, which are highly relevant to the stakeholders in this area (Mao et al., 2019; Zhang et al., 2022).

Net primary productivity

We adopted the Carnegie-Ames-Stanford-Approach (CASA) model to estimate NPP at the grid cell scale (Potter et al., 1993). The specific calculation was as follows:

$$\mathbf{N}PP\,(\mathbf{x},\mathbf{t}) \;=\; \mathbf{A}PAR(\mathbf{x},\mathbf{t}) \;\times\; \varepsilon(\mathbf{x},\mathbf{t})$$

where net primary productivity (x, t) denotes the net primary productivity at points x and t, APAR (x, t) denotes the incident solar radiation received by the canopy at a particular time period ($MJ{\cdot}m^{-2}$), and ε(x, t) denotes the light energy utilization rate ($gC{\cdot}MJ^{-1}$). More information about the model can be available in the Supplementary Table 1.

Soil conservation

We employed the RUSLE model to simulate the soil conservation amount. Soil conservation was the discrepancy between potential and actual soil erosion in an ecosystem process (Ausseil et al., 2013). It was calculated using the following equation:

$$\mathbf{S}C \;=\; \mathbf{R} \;\times\; \mathbf{K} \;\times\; \mathbf{L}S \;\times\; (\mathbf{1}-\mathbf{P} \;\times\; \mathbf{C})$$

where SC denotes the soil conservation amount, and unit is $t/(km^2{\cdot}a)$, R denotes the rainfall erosion force factor $[MJ{\cdot}mm/(km^2{\cdot}h{\cdot}a)]$ (Fournier, 1960), K denotes the soil erodibility factor $[t{\cdot}km^2{\cdot}h/(km^2{\cdot}MJ{\cdot}mm)]$ (Williams et al., 1983), LS denotes the topography factor, C denotes the cropping management factor (Cai et al., 2000), and P denotes the engineering measure factor (You and Li, 1999). More details about the model can be available in the Supplementary Table 1.

Water conservation

The water conservation module in InVEST model is grounded on the Budyko hydrothermal coupling water balance hypothesis (Budyko, 1974; Donohue et al., 2012). Taking into account the average annual rainfall and actual evapotranspiration (Zhang et al., 2001), the water yield was calculated as follows:

$$\mathbf{Y}(\mathbf{x}) \;=\; \left(\mathbf{1}-\frac{\mathbf{A}ET(\mathbf{x})}{\mathbf{P}\,(\mathbf{x})}\right) \;\times\; \mathbf{P}(\mathbf{x})$$

where Y(x) denotes the water yield in grid cell x (mm), AET(x) denotes the practical evapotranspiration in grid cell x, and P(x) denotes the annual rainfall in grid cell x (mm). More details about the model can be available in Supplementary Table 1.

Habitat quality

Habitat quality was considered as an indicator of biodiversity (Feng et al., 2018), and it was calculated as follows:

$$\mathbf{Q}_{\mathbf{x}j} \;=\; \mathbf{H}_{\mathbf{j}}\left[\mathbf{1}-\left(\frac{\mathbf{D}_{\mathbf{x}y}^{\mathbf{z}}}{\mathbf{D}_{\mathbf{x}y}^{\mathbf{z}}+\mathbf{k}^{\mathbf{z}}}\right)\right]$$

where Q_{xj} denotes the habitat quality at grid cell x of land use type j. D_{xy} and H_j are overall threat degree and habitat

TABLE 1 Data sources used in this paper.

Data set	Data sources and descriptions	Resolution
Land use	Land use data in 1990, 2000, 2010, and 2020 were taken from Copernicus Climate Change Service (https://cds.climate.copernicus.eu/).	300 m
NDVI	Data for 1990 were obtained from GIMMS-NDVI dataset (https://climatedataguide.ucar.edu/climate-data/ndvi-normalized-difference-vegetation-index-3rd-generation-nasagfsc-gimms), Data for 2000, 2010, and 2020 were derived from MOD13A3 NDVI dataset (https://search.earthdata.nasa.gov/).	8,000 m, 1,000 m
Meteorological	The meteorological data, including month temperature and precipitation, were obtained from the China Meteorological Data Service Center (http://www.cma.gov.cn/)	1,000 m
DEM	NASA/USGS published of SRTM Global DEM (https://lpdaac.usgs.gov/)	90 m
Soil data	The soil data, including clay content, silt content, sand content, and organic matter content, were derived from the Chinese soil dataset based on the Harmonized World Soil Database (HWSD) (v1.1) (http://bdc.casnw.net/)	1,000 m
GDP per land area	Acquired from the Resource and Environment Science and Data Center (http://www.resdc.cn/).	1,000 m
Population density	Acquired from the Resource and Environment Science and Data Center (http://www.resdc.cn/).	1,000 m

suitability, respectively. z is set as 2.5, and k is the half-saturation constant, which has been set as 0.5. In this paper, we took farmland, urban land and highways as threats sources. More details about the model can be available in the **Supplementary Table 1**.

Measurement of the forest ecosystem service trade-offs

Root mean square error (RMSE) was used to quantify the trade-offs between each two ecosystem services (Bradford and D'Amato, 2012; Feng et al., 2017). It calculates trade-offs as the distance from point to line (**Figure 2**). The further the distance is, the greater the trade-off is. Whereas, the shorter the distance is, the more it tended to be synergistic. RMSE is a simplistic and efficient approach to express the extent of trade-offs between any two ecosystem services, regardless of their correlation. Data normalization was conducted to remove the impacts of grid cells on each ecosystem service before RMSE calculation as follows:

$$ES_{std} = \frac{(ES_{obs} - ES_{min})}{(ES_{max} - ES_{min})}$$

where ES_{std} denotes the normalized value of ecosystem services, ES_{obs} denotes the observed value of ecosystem services, ES_{min} and ES_{max} are the minimum and maximum observed value of ecosystem services, correspondingly. The value range of ES_{std} is 0–1.

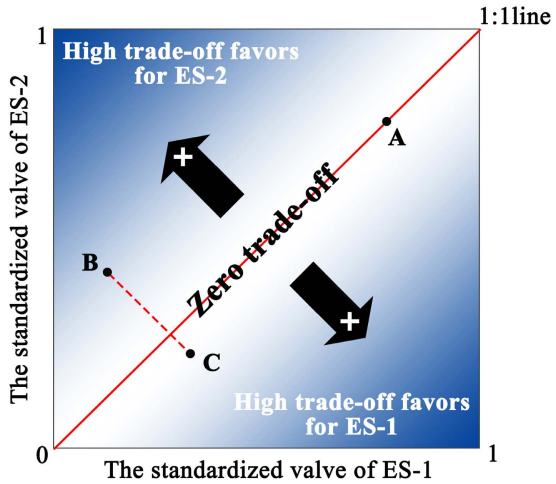

FIGURE 2
Illustration and example of the trade-offs between two ecosystem services. The RMSE is the distance between an ecosystem service pair's coordinates and line 1:1, where the two ecosystem services are equal. Take **Figure 2** as an example, the trade-off value at point A is 0; the trade-off value at point B is higher than that at C. Moreover, at point B the trade-off favors ES2, but at point C the trade-off favors ES1. The graph was revised based on previous studies (Bradford and D'Amato, 2012; Lu et al., 2014).

Then, RMSE was calculated as follows:

$$RMSE = \sqrt{\frac{1}{n-1} \times \sum_{i=1}^{n} (ES_i - \widehat{ES})^2}$$

where ES_i denotes the normalized value of ecosystem services i, and $\widehat{ES}$ denotes the expected value of the i number of ecosystem services, n denotes the number of ecosystem service types. $\widehat{ES}$ is the mean value of the i number of ES_i (Bradford and D'Amato, 2012). The RMSE denotes the mean disparity between each ES_{std} and mean ES_{std}, and it characterizes the amplitude of scattering from the mean (Feng et al., 2017; Han et al., 2020; Xu et al., 2020). The RMSE value is between 0 and 1.

Identification of the key drivers

Nine driving factors were chosen from published studies (Lyu et al., 2019; Peng et al., 2019; Qiu et al., 2021), and they were categorized into environmental factors and anthropogenic activity factors. Environmental factors include NDVI, temperature, precipitation, elevation, slope, and soil types. Anthropogenic activity factors include land use, population density, and GDP density.

GeoDetector has particular benefit in the treatment of spatially stratified heterogeneity and categorical variables (Wang et al., 2010; Chen et al., 2020). Geodetector was applied to quantitatively identify the explanatory power of drivers for forest ecosystem service trade-offs, the value was measured by the *q*-value. The calculation equation is as follows:

$$q = 1 - \frac{1}{n\sigma^2} \sum_{h=1}^{L} n_h \sigma_h^2$$

where q denotes the explanatory power of the driving factor, n denotes the sum of sample points, σ^2 denotes the sum regional variance, h = 1,2,3...L denotes the layer of factor X, n_h and σ_h^2 denote the number of sample points and variance of layer h. The q-statistic is between 0 and 1. The larger the q-statistic, the greater the explanation of ecosystem services by the influencing factors.

Results

Spatiotemporal changes in forest ecosystem services after natural forest conservation project implementation

From 1990 to 2020, all NPP, soil conservation, water conservation, and habitat quality in the Greater Khingan Mountains gradually increased. The spatial distribution of the four ecosystem services decreased from northern to southern in

the Greater Khingan Mountains (Figure 3 and Table 2). Habitat quality was relatively uniform across the area. The mean value of habitat quality fluctuated between 0.57 and 0.58. The mean values of different forest types were significantly different, with values of 0.73, 0.58, and 0.42 for coniferous, broad-leaved, and shrubs, respectively. In 2000, the highest habitat quality was

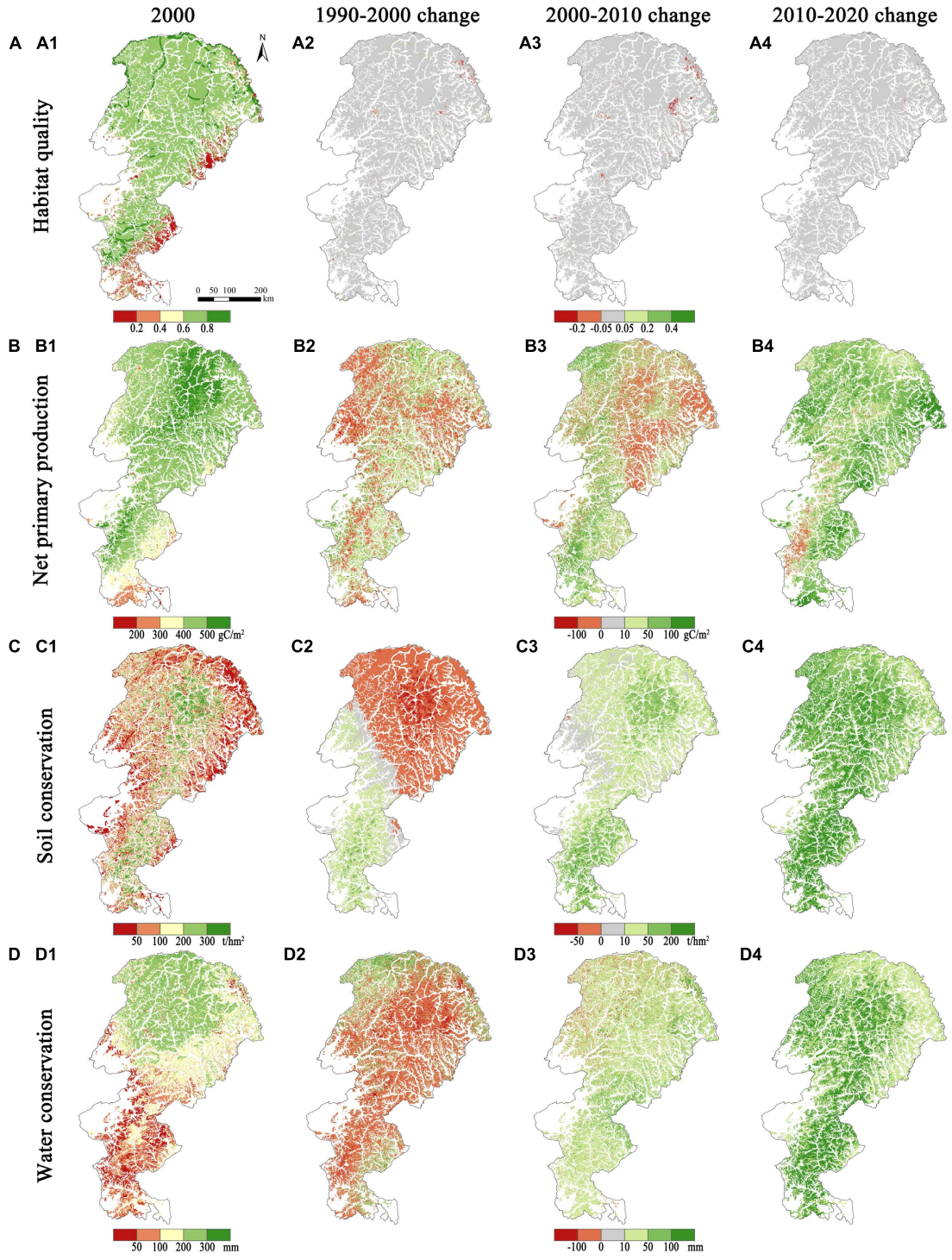

FIGURE 3
Changes of forest ecosystem services in the Greater Khingan Mountains from 1990 to 2020. **(A)** Habitat quality, **(B)** net primary production, **(C)** soil conservation, and **(D)** water conservation.

TABLE 2 Temporal changes of forest ecosystem services in the Greater Khingan Mountains from 1990 to 2020.

	NPP (gC/m^2)			Soil conservation (t/hm^2)			Water conservation (mm)			Habitat quality		
	CF	BF	SH	CF	BF	SH	CF	BF	SH	CF	BF	SH
1990	460.25	407.997	338.212	141.293	106.319	95.706	208.921	124.745	135.377	0.739	0.576	0.408
2000	465.297	421.755	345.482	129.141	114.19	104.195	187.053	106.104	121.714	0.742	0.581	0.423
2010	485.521	448.41	381.733	161.322	156.638	152.413	245.926	178.67	180.26	0.73	0.584	0.426
2020	546.474	512.918	457.726	310.28	325.507	288.577	394.884	347.539	316.424	0.725	0.589	0.427
1990–2000	5.047	13.758	7.27	−12.152	7.871	8.489	−21.868	−18.641	−13.663	0.003	0.005	0.015
2000–2010	20.224	26.655	36.251	32.181	42.448	48.218	58.873	72.566	58.546	−0.012	0.003	0.003
2010–2020	60.953	64.508	75.993	148.958	168.869	136.164	148.958	168.869	136.164	−0.005	0.005	0.001

CF, BF, and SH represent coniferous forest, broad–leaved forest and shrub.

in the northwestern portion, and the lowest mainly focused on the southeast (Figure 3A1). In terms of temporal variation, habitat quality was relatively stable from 1990 to 2020, with small interannual variation. The mean value of habitat quality in coniferous showed a small downward trend, but small increased trends in both broad-leaved and shrubs. The stable zone (i.e., variations between −0.05 and 0.05) of habitat quality accounted for 93–98% (Figures 3A2–4). Habitat quality changed in a very small space and was less influenced by land use and threatened source changes.

The NPP showed a gradually increasing trend under various forest types. The average NPP in 1990, 2000, 2010, and 2020 were 402.15, 410.84, 438.55, and 505.71 gC/m^2, respectively. The average NPP increased by 67.15 gC/m^2 in 2010–2020, which was significantly higher than that in 1990–2000 (8.69 gC/m^2) and 2000–2010 (27.71 gC/m^2). Moreover, the increased NPP of shrubs (75.99 gC/m^2) was significantly higher than that of coniferous (60.95 gC/m^2) and broad-leaved (64.50 gC/m^2) in 2010–2020. The average NPP of coniferous was higher than that of broad-leaved, higher than that of shrubs between 1990 and 2020. For spatial distribution, NPP gradually decreased from northeastern to southwestern in 2000. Compared with 1990–2000, the NPP in 2010–2020 increased more in the northwestern and southeastern Greater Khingan Mountains, with an increasing percentage of 48–76%, respectively.

In terms of temporal variation, soil conservation decreased and then increased from 1990 to 2020. It slightly decreased in 1990–2000, slightly increased in 2000–2010, but significantly increased in 2010–2020. The soil conservation in various forest types changed different showed different trends. Soil conservation of coniferous decreased and then increased, while soil conservation of broad-leaved and shrubs constantly increased from 1990 to 2020. In terms of spatial distribution, the highest soil conservation was in the northwestern Greater Khingan Mountains, and the lowest primarily focused on the peripheral areas in 2000. From 1990 to 2000, the proportions of the area where the soil conservation increased and decreased were 62 and 38%, respectively. The increased areas of soil conservation during 2000–2010 and 2010–2020 accounted for 83 and 92%, respectively. The increased soil conservation was associated with the NFCP implementation.

Water conservation significantly decreased and increased from 1990 to 2020 (Figure 3D). The mean value of water conservation slightly decreased from 1990 to 2000, gradually increased from 2000 to 2010, and significantly increased from 2010 to 2020. Water conservation under different forest types showed consistent temporal variations from 1990 to 2020. Among them, water conservation of coniferous had the highest average value. Water conservation of broad-leaved had the fastest growth. The highest water conservation was found in the coniferous in the northern Greater Khingan Mountains, whereas the lowest water conservation was found in the shrubs in the southwest. From 1990 to 2000, the area of decreased water conservation accounted for 68% of the region, while in 2000–2010 and 2010–2020, the area of increased water conservation accounted for 82 and 86%, respectively.

Spatiotemporal changes in forest ecosystem service trade-offs after natural forest conservation project implementation

In this paper, we used the forest ecosystem service trade-offs in 2000 as a reference to compare the trade-off changes after NFCP implementation (Figure 4). From 1990 to 2020, the trade-offs between habitat quality and NPP, NPP and soil conservation, and soil conservation and water conservation increased, while the trade-offs between habitat quality and water conservation, NPP and water conservation decreased. The trade-off between habitat quality and soil conservation were relatively stable before and after NFCP implementation. Moreover, all the trade-offs of three forest types showed clear stratifications. The RMSE of coniferous (0.47) was higher than that of broad-leaved (0.37), was higher than that of shrub (0.28). The trade-off between habitat quality and soil conservation in coniferous and broad-leaved decreased by 0.06 and 0.07 from

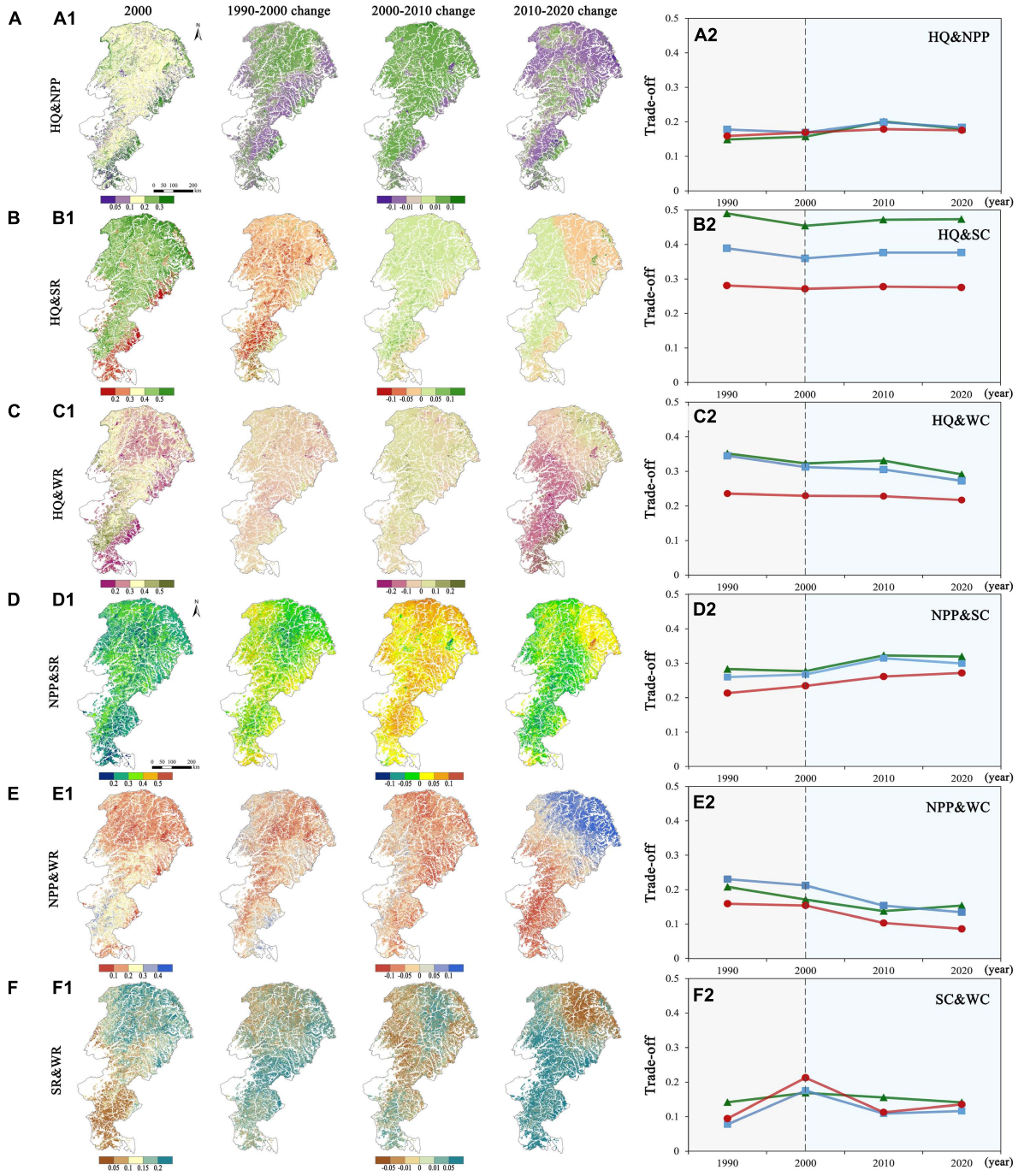

FIGURE 4
Spatial variations of forest ecosystem service trade-offs in the Greater Khingan Mountains from 1990 to 2020, and temporal variations in trade-offs of different forest types from 1990 to 2020. **(A)** HQ and NPP, **(B)** HQ and SC, **(C)** HQ and WC, **(D)** NPP and SC, **(E)** NPP and WC, **(F)** SC and WC. HQ, SC, and WC represent habitat quality, soil conservation, and water conservation.

1990 to 2020, respectively. While the trade-off between habitat quality and soil conservation in shrubs remained essentially unchanged. Both the NPP and soil conservation trade-offs in 1990–2000 and in 2000–2020 increased. The trade-off between NPP and soil conservation in shrubs increased by 0.06 over 30 years, which was higher than in coniferous and broad-leaved. The soil conservation and water conservation trade-offs increased and then decreased from 1990 to 2020. The trade-offs between soil conservation and water conservation decreased after NFCP implementation.

In terms of spatial distribution, the trade-offs between pairs of ecosystem services showed significant spatial heterogeneity in the three forest types. From 2000 to 2010, the trade-off between habitat quality and NPP increased in the 84% areas of the Greater Khingan Mountains. The trade-off between habitat quality and soil conservation in 2000 decreased from northern to southern. The highest values were found in northern coniferous, while the lowest values were in the southeastern shrubs. The trade-off between habitat quality and water conservation decreased in the 71% areas of the region from 2010 to 2020. The trade-offs between NPP and soil conservation increased in 64, 92, and 53% areas of the region during 1990–2000, 2000–2010, and 2010–2020, respectively. The spatial heterogeneity trade-offs between soil conservation and water conservation from 1990 to 2020 were higher than that between any other two ecosystem services. It suggested that the trade-offs between soil conservation and water conservation were more affected by the NFCP than between other ecosystem services.

The trade-offs between each two ecosystem services were considerably different among the three forest types (**Figure 5A**). In the histogram, the trade-offs in coniferous were significantly higher than either in broad-leaved or in shrubs (**Figure 5B**). The points in the soil conservation-water conservation scatter plot mostly fell on the 1:1 line, indicating a slight trade-off between soil conservation and water conservation (0.13). Moreover, the points in the soil conservation-water conservation scatter plot of shrubs were relatively far away from the 1:1 line, showing high trade-offs between soil conservation and water conservation in shrubs. In addition, the trade-offs between NPP and water conservation were low (0.15). The points in the NPP-soil conservation, and habitat quality-water conservation scatter plot were somewhat away from line 1:1, suggesting appropriate trade-offs (0.28 and 0.29, respectively). The trade-offs between habitat quality and soil conservation (0.37) were significantly higher than the trade-offs between any other two ecosystem services. RMSE between habitat quality and soil conservation in coniferous and broad-leaved exceeded 0.4.

Influence of drivers on forest ecosystem service trade-offs

Overall, the effects of the drivers differed significantly among the three forest types (**Figure 6**). In coniferous, the explanatory power of temperature and land use on habitat quality and soil conservation trade-offs were significantly higher than other factors (52 and 55%, respectively). In broad-leaved, land use influenced habitat quality-soil conservation trade-offs most (54%). In shrubs, land use and NDVI influenced habitat quality-soil conservation tradeoffs more than the other factors (44 and 34%, respectively). The explanatory power of land use on habitat quality-soil conservation trade-offs (45%), habitat quality-water conservation trade-offs (32%), NPP-soil conservation trade-offs (29%), and NPP water conservation trade-offs (31%) were higher than the other factors. Precipitation could explain 15, 30, and 26% of habitat quality-soil conservation, NPP-soil conservation, and soil conservation-water conservation trade-offs, respectively. It was noteworthy that habitat quality-NPP trade-offs were less influenced by the drivers. It might be related to the low trade-offs between them.

The average explanatory power of anthropogenic activities factors on ecosystem service trade-offs was 10%. This indicated a low influence of anthropogenic activities on forest ecosystem services. For environmental factors, the explanatory power of NDVI on trade-offs differed significantly among coniferous (9%), broad-leaved (8%), and shrubs (20%). The explanatory power of temperature on habitat quality-soil conservation trade-offs (52%) was considerably higher than on any other two ecosystem services. Moreover, soil type was of little importance to trade-offs. The result indicated that the influence of environmental factors on forest ecosystem service tradeoffs was regular and high variation from 1990 to 2020.

Discussion

Generally, ecosystem services in the Greater Khingan Mountains increased after NFCP implementation. This result was in line with the published research, which also indicated a crucial increase in forest ecosystems after the implementation of the NFCP (Wang et al., 2017; Mao et al., 2019). But soil conservation and water conservation decreased and then increased from 1990 to 2020. These two ecosystem services were more affected by rainfall factors (Wang and Dai, 2020). The rainfall instability exacerbated the change magnitude in these two ecosystem services before and after the NFCP implementation. The ecosystem services of the three forest types showed different degrees of increase after the NFCP implementation in this study. It increased more in broad-leaved than in the other two forest types, which may be related to spatial distribution and area of broad-leaved. The spatial distribution, interrelationships and, drivers of ecosystem services were impacted by spatial scale nature (He et al., 2019; Sun et al., 2020). It was notable that the trade-offs during the second phase of the NFCP increased more than during the first phase. The forest ecosystem gradually entered a period of rapid growth after the first decade of recovery, which was in line with the trend of secondary ecosystem evolution. In addition, the Chinese government paid more attention to forest protection in recent years. It launched several ecological restoration programs, for instance, the grain to green project, the three north shelter forest system project, and the national nature reserves (Mao et al., 2019). Moreover, great promotions of ecological civilization and increased public awareness of environmental protection were also important in promoting

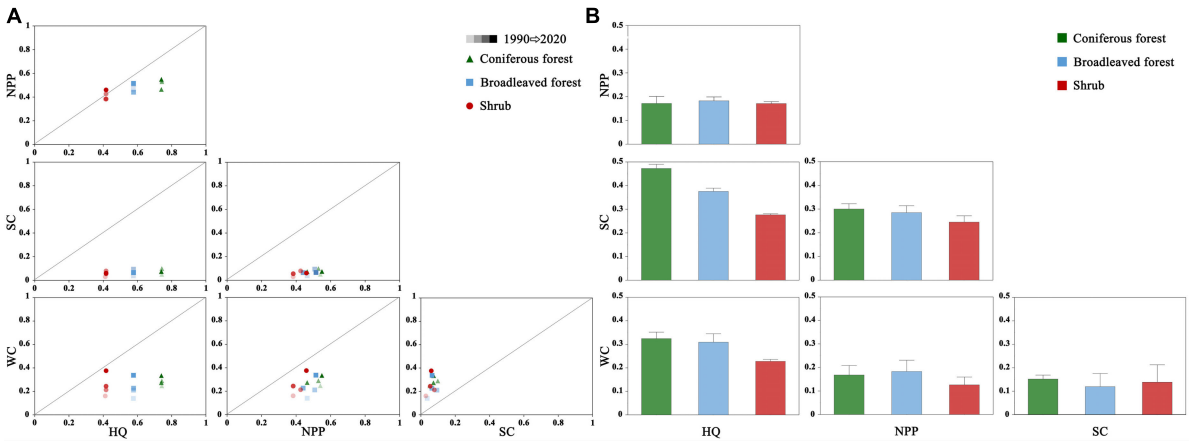

FIGURE 5
(A) Scatter plots and **(B)** trade-off values of pairwise forest ecosystem services under different forest types. HQ, SC, and WC represent habitat quality, soil conservation, and water conservation.

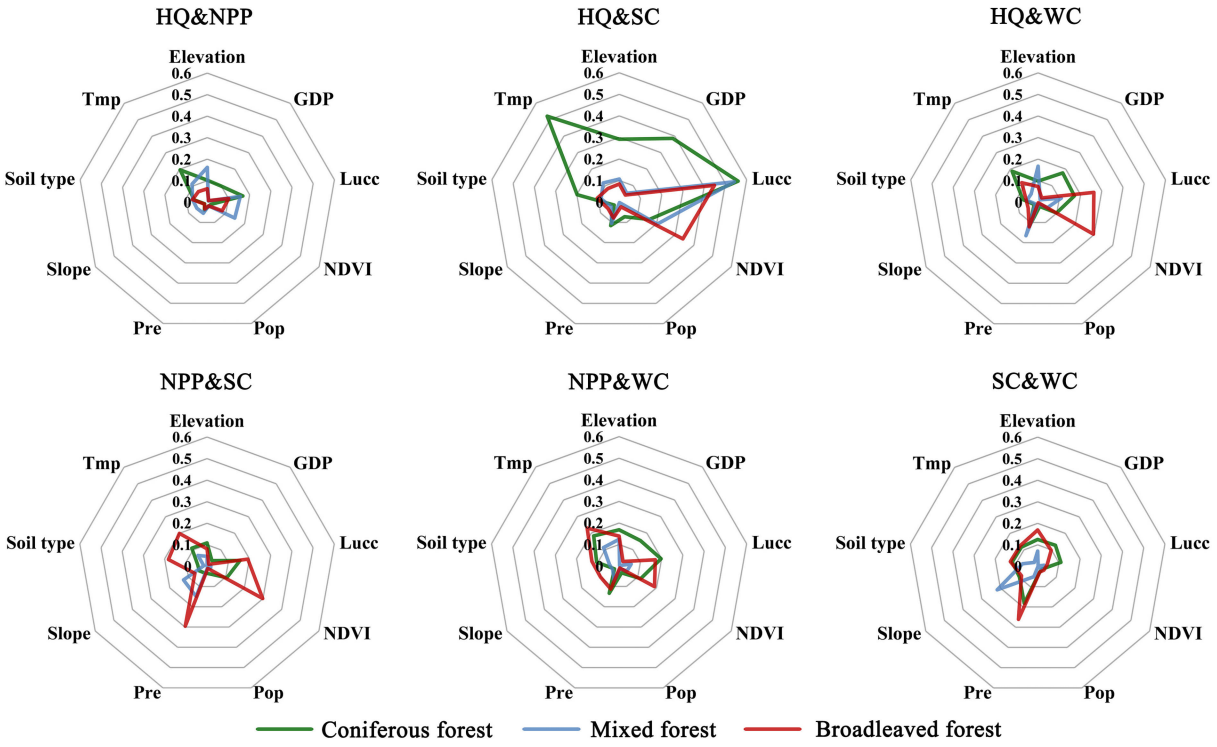

FIGURE 6
Influence of drivers on forest ecosystem service trade-offs. GDP, Gross Domestic Product; Lucc, land use type; Pop, population density; Pre, precipitation, and Tmp, temperature.

the continuous improvement of forest ecosystems during the second phase (Zhao et al., 2017; Dong et al., 2021; Yang et al., 2021).

The forest ecosystem service trade-offs in coniferous and broad-leaved was higher than in shrubs. Published research has explored the ecosystem service's interrelationships in terms of spatiotemporal variations (Qiao X. et al., 2019; Qiu et al., 2021). Nevertheless, few research investigated their discrepancies among different forest types. The results of this study indicated that the trade-offs in coniferous were higher than both in broad-leaved and shrubs. It may be due to their large distribution area and relatively low intensity of anthropogenic activities in coniferous. Coniferous was the highest total of ecosystem services than broad-leaved and shrubs. The high trade-offs in

coniferous were detrimental to the sustainability of ecosystem benefits (Bradford and D'Amato, 2012).

Ecosystem service trade-offs in various regions changed spatiotemporally after the ecological project implemented (Li et al., 2018; Qiao X. et al., 2019). The trade-offs between different ecosystem services were different in the Greater Khingan Mountains during 1990–2020. The trade-off relationships involving NPP increased, while the trade-offs related to water conservation decreased from 1990 to 2020. It has shown that understanding trade-off mechanisms requires an integrated consideration of multiple ecosystem services in one ecosystem (Bradford and D'Amato, 2012; Lu et al., 2014). The change rates of ecosystem services were not the same between 1990–2000 and 2000–2020 (**Figure 3**). Similar findings were reported for the spatiotemporal variances in other ecosystem services after ecological projects (Wang et al., 2021). Uneven changes in forest ecosystem services at different project phases might be the main reason for spatiotemporal variations of trade-offs.

The ecosystem service trade-offs were closely related to climatic factors (Runting et al., 2017; Qiu et al., 2021). Topographical and soil type factors also affected trade-offs to some extent (Feng et al., 2017). This study showed that the influence of environmental factors on trade-offs were more than anthropogenic activities in the Greater Khingan Mountains. This might be related to the different sensitivity of ecosystem service trade-offs to drivers in the Greater Khingan Mountains. The result was in line with published research (Wang et al., 2021; Chen et al., 2022). Generally, changes in forest ecosystems after the project were mainly influenced by environmental factors, rather than anthropogenic activities. However, certain anthropogenic activity factors had a crucial influence on trade-offs. For instance, land use was the most important factor on the trade-offs from 1990 to 2020. It was owing to the prominent effects of land use on four ecological services. The rapid spread of urbanization was an important reason for forest ecosystem destruction, and the transformation of land use types was closely connected with the rapid urbanization (Yang et al., 2020; Han et al., 2021). In addition, population density and GDP density were also significant driving factors in the trade-offs, which was consistent with previously published studies (Yang et al., 2017; Zhang et al., 2020).

Several limits ought to be recognized in this study. Firstly, although NPP, soil conservation, water conservation, and habitat quality were considered as the forest ecosystem services in the Greater Khingan Mountains, wood production was not involved. Because of corresponding data missing and inconsistent statistical calibration standards across provinces. There are some challenges to the rasterization of statistical data because the study area was not a complete administrative region. Secondly, due to the constraints of data collection, it is not possible to simulate ecosystem services with high accuracy due to the constraints of data collection. Finally, the RMSE approach could not accommodate the issue of non-linear interactions and thresholds between forest ecosystem services (Qiao J. M. et al., 2019; Wang et al., 2021). Thus, inflection points and thresholds of ecosystem trade-offs should be investigated for the guidance of ecosystem management in the future.

Conclusion

The study evaluated the spatiotemporal changes of forest ecosystem service trade-offs and their drivers in the Greater Khingan Mountains after NFCP implementation. All of the ecosystem services in the three forest types increased after the project. The trade-offs between habitat quality and NPP, NPP and soil conservation increased, while the trade-offs between habitat quality and water conservation, NPP and water conservation, and soil conservation and water conservation decreased after the project. The ecosystem service trade-offs in coniferous was higher than in broad-leaved and shrubs. The explanatory power of the drivers (except for soil type) was significant different among the three forest types. The most important drivers for the trade-offs in coniferous and broad-leaved regions were land use, while the most important drivers were NDVI and precipitation in shrubs. Environmental factors affected the ecosystem service trade-offs more than anthropogenic activities in the Greater Khingan Mountains. Among all anthropogenic activity factors, land use was the most important one. Overall, exploring the ecosystem service trade-off changes after NFCP provides valuable insights for future policy development and subsequent ecological project implementation.

Data availability statement

The original contributions presented in this study are included in the article/**Supplementary material**, further inquiries can be directed to the corresponding author.

Author contributions

WC conceived the article. GJ and YD wrote the first draft. WC and SZ edited subsequent drafts. All authors contributed to the manuscript and approved the submitted version.

Funding

This study was funded by the Major Science and Technology Projects in Jilin Province (Grant No. 20200503001SF) and the National Natural Science Foundation of China (Grant No. 32130068).

Conflict of interest

The authors declare that the research was conducted in the absence of any commercial or financial relationships that could be construed as a potential conflict of interest.

Publisher's note

All claims expressed in this article are solely those of the authors and do not necessarily represent those of their affiliated organizations, or those of the publisher, the editors and the reviewers. Any product that may be evaluated in this article, or claim that may be made by its manufacturer, is not guaranteed or endorsed by the publisher.

Supplementary material

The Supplementary Material for this article can be found online at: https://www.frontiersin.org/articles/10.3389/fevo.2022.978145/full#supplementary-material

References

Ausseil, A. E., Dymond, J. R., Kirschbaum, M., Andrew, R. M., and Parfitt, R. L. (2013). Assessment of multiple ecosystem services in New Zealand at the catchment scale. *Environ. Model. Softw.* 43, 37–48. doi: 10.1016/j.envsoft.2013.01.006

Aznar-Sánchez, J. A., Belmonte-Ureña, L. J., López-Serrano, M. J., and Velasco-Muñoz, J. F. (2018). Forest ecosystem services: An analysis of worldwide research. *Forests* 9:453. doi: 10.3390/f9080453

Benayas, J., Newton, A. C., Diaz, A., and Bullock, J. M. (2009). Enhancement of biodiversity and ecosystem services by ecological restoration: A meta-analysis. *Science* 325, 1121–1124. doi: 10.1126/science.1172460

Bennett, E. M., Peterson, G. D., and Gordon, L. J. (2009). Understanding relationships among multiple ecosystem services. *Ecol. Lett.* 12, 1394–1404. doi: 10.1111/j.1461-0248.2009.01387.x

Bradford, J. B., and D'Amato, A. W. (2012). Recognizing trade-offs in multi-objective land management. *Front. Ecol. Environ.* 10, 210–216. doi: 10.1890/110031

Budyko, M. I. (1974). *Climate and life*. SanDiego, CA: Academic.

Cai, C. F., Ding, S. W., Shi, Z. H., Huang, L., and Zhang, G. Y. (2000). Study of applying USLE and geographical information system IDRISI to predict soil erosion in small watershed. *J. Soil Water Conserv.* 14, 19–24.

Chen, T., Feng, Z., Zhao, H., and Wu, K. (2020). Identification of ecosystem service bundles and driving factors in Beijing and its surrounding areas. *Sci. Total Environ.* 711:134687. doi: 10.1016/j.scitotenv.2019.134687

Chen, T., Peng, L., and Wang, Q. (2022). Response and multiscenario simulation of trade-offs/synergies among ecosystem services to the Grain to Green Program: A case study of the Chengdu-Chongqing urban agglomeration, China. *Environ. Sci. Pollut. Res. Int.* 29, 33572–33586. doi: 10.1007/s11356-021-18336-y

Chu, X. L., Li, L., Zeng, L. X., Huang, Z. L., Liu, C. F., and Xiao, W. F. (2019). Dynamics of forest ecosystem services before and after dam construction in the three gorges reservoir area. *Resour. Environ. Yangtze Basin* 28:8.

Dong, Y. L., Ren, Z. B., Fu, Y., Yang, R., Sun, H. C., and He, X. Y. (2021). Land use/cover change and its policy implications in typical agriculture-forest ecotone of Central Jilin Province, China. *Chin. Geogr. Sci.* 31, 261–275. doi: 10.1007/s11769-021-1189-5

Dong, Y. L., Ren, Z. B., Wang, Z. M., Yu, Q. Y., Zhu, L., Yu, H., et al. (2020). Spatiotemporal patterns of forest changes in Korean Peninsula using landsat images during 1990–2015: A comparative study of two neighboring countries. *IEEE Access* 8, 73623–73633. doi: 10.1109/access.2020.2988122

Donohue, R. J., Roderick, M. L., and McVicar, T. R. (2012). Roots, storms and soil pores: Incorporating key ecohydrological processes into Budyko's hydrological model. *J. Hydrol.* 436–437, 35–50. doi: 10.1016/j.jhydrol.2012.02.033

Editorial Committee for Vegetation Atlas of China (2001). *Vegetation atlas of China*. Beijing: China Science Press.

FAO (2020). *Global forest resources assessment 2020: Main report*. Rome: Food & Agriculture Org, 164.

Feng, Q., Zhao, W., Fu, B., Ding, J., and Wang, S. (2017). Ecosystem service trade-offs and their influencing factors: A case study in the Loess Plateau of China. *Sci. Total Environ.* 607–608, 1250–1263. doi: 10.1016/j.scitotenv.2017.07.079

Feng, S., Sun, R., and Chen, L. (2018). Spatio-temporal variability of habitat quality based on land use pattern change in Beijing. *Acta. Ecol.* 38, 4167–4179.

Foley, J. A., DeFries, R., Asner, G. P., Barford, C., Bonan, G., Carpenter, S. R., et al. (2005). Global consequences of land use. *Science* 309, 570–574. doi: 10.1126/science.1111772

Fournier, F. (1960). *Climate and erosion*. Paris: Presses Universitaires de France.

Gonzalez-Ollauri, A., and Mickovski, S. B. (2017). Providing ecosystem services in a challenging environment by dealing with bundles, trade-offs, and synergies. *Ecosyst. Serv.* 28, 261–263. doi: 10.1016/j.ecoser.2017.10.004

Han, H. Q., Liu, Y., Gao, H. J., Zhang, Y. J., Wang, Z., and Chen, X. Q. (2020). Tradeoffs and synergies between ecosystem services: A comparison of the karst and non-karst area. *J. Mt. Sci.* 17, 1221–1234. doi: 10.1007/s11629-019-5667-5

Han, J., Liu, Y., and Zhang, Y. (2015). Sand stabilization effect of feldspathic sandstone during the fallow period in Mu Us Sandy Land. *J. Geogr. Sci.* 25, 428–436. doi: 10.1007/s11442-015-1178-7

Han, J. H., Dong, Y. L., Ren, Z. B., Du, Y. X., Wang, C. C., Jia, G. L., et al. (2021). Remarkable effects of urbanization on forest landscape multifunctionality in urban peripheries: Evidence from Liaoyuan City in Northeast China. *Forests* 12:1779. doi: 10.3390/f12121779

He, B. J., Zhao, Z. Q., Shen, L. D., Wang, H. B., and Li, L. G. (2019). An approach to examining performances of cool/hot sources in mitigating/enhancing land surface temperature under different temperature backgrounds based on landsat 8 image. *Sustain. Cities Soc.* 44, 416–427. doi: 10.1016/j.scs.2018.10.049

Li, B. Y., Chen, N. C., Wang, Y. C., and Wang, W. (2018). Spatio-temporal quantification of the trade-offs and synergies among ecosystem services based on grid-cells: A case study of Guanzhong Basin, NW China. *Ecol. Indic.* 94, 246–253. doi: 10.1016/j.ecolind.2018.06.069

Liu, L. B., Wang, Z., Wang, Y., Zhang, Y. T., Shen, J. S., Qin, D. H., et al. (2019). Trade-off analyses of multiple mountain ecosystem services along elevation, vegetation cover and precipitation gradients: A case study in the Taihang Mountains. *Ecol. Indic.* 103, 94–104. doi: 10.1016/j.ecolind.2019.03.034

Lu, N., Fu, B. J., Jin, T. T., and Chang, R. Y. (2014). Trade-off analyses of multiple ecosystem services by plantations along a precipitation gradient across Loess Plateau landscapes. *Landsc. Ecol.* 29, 1697–1708. doi: 10.1007/s10980-014-0101-4

Lyu, R. F., Clarke, K. C., Zhang, J. M., Feng, J. L., Jia, X. H., and Li, J. J. (2019). Spatial correlations among ecosystem services and their socio-ecological driving factors: A case study in the city belt along the Yellow River in Ningxia, China. *Appl. Geogr.* 108, 64–73. doi: 10.1016/j.apgeog.2019.05.003

Mao, D. H., He, X. Y., Wang, Z. M., Tian, Y. L., Xiang, H. X., Yu, H., et al. (2019). Diverse policies leading to contrasting impacts on land cover and ecosystem services in Northeast China. *J. Clean. Prod.* 240:117961. doi: 10.1016/j.jclepro.2019.117961

Mao, D. H., Wang, Z. M., Wu, C. S., Song, K. S., and Ren, C. Y. (2014). Examining forest net primary productivity dynamics and driving forces in northeastern China during 1982–2010. *Chin. Geogr. Sci.* 24, 631–646. doi: 10.1007/s11769-014-0662-9

Mbow, C., Noordwijk, M. V., Luedeling, E., Neufeldt, H., Minang, P. A., and Kowero, G. (2014). Agroforestry solutions to address food security and climate change challenges in Africa. *Curr. Opin. Environ. Sustain.* 6, 61–67. doi: 10.1016/j.cosust.2013.10.014

Nkem, J., Santoso, H., Murdiyarso, D., Brockhaus, M., and Kanninen, M. (2007). Using tropical forest ecosystem goods and services for planning climate change adaptation with implications for food security and poverty reduction. *J. Semi. Arid Trop. Agric. Res.* 4, 1–23.

Peng, J., Hu, X. X., Wang, X. Y., Meersmans, J., Liu, Y. X., and Qiu, S. J. (2019). Simulating the impact of Grain-for-Green Programme on ecosystem services trade-offs in Northwestern Yunnan, China. *Ecosyst. Serv.* 39:100998. doi: 10.1016/j.ecoser.2019.100998

Potter, C. S., Randerson, J. T., Field, C. B., Matson, P. A., Vitousek, P. M., Mooney, H. A., et al. (1993). Terrestrial ecosystem production: A process model based on global satellite and surface data. *Glob. Biogeochem. Cycle* 7, 811–841. doi: 10.1029/93gb02725

Power, A. G. (2010). Ecosystem services and agriculture: Tradeoffs and synergies. *Philos. Trans. R. Soc. Lond. B Biol. Sci.* 365, 2959–2971. doi: 10.1098/rstb.2010.0143

Qiao, J. M., Yu, D. Y., Cao, Q., and Hao, R. F. (2019). Identifying the relationships and drivers of agro-ecosystem services using a constraint line approach in the agro-pastoral transitional zone of China. *Ecol. Indic.* 106:105439. doi: 10.1016/j.ecolind.2019.105439

Qiao, X., Gu, Y., Zou, C., Xu, D., Wang, L., Ye, X., et al. (2019). Temporal variation and spatial scale dependency of the trade-offs and synergies among multiple ecosystem services in the Taihu Lake Basin of China. *Sci. Total Environ.* 651, 218–229. doi: 10.1016/j.scitotenv.2018.09.135

Qiu, M. L., Voorde, T. V., Li, T., Yuan, C. C., and Yin, G. Y. (2021). Spatiotemporal variation of agroecosystem service trade-offs and its driving factors across different climate zones. *Ecol. Indic.* 130:108154. doi: 10.1016/j.ecolind.2021.108154

Runting, R. K., Bryan, B. A., Dee, L. E., Maseyk, F. J., Mandle, L., Hamel, P., et al. (2017). Incorporating climate change into ecosystem service assessments and decisions: A review. *Glob. Change Biol.* 23, 28–41. doi: 10.1111/gcb.13457

Sun, X. Y., Shan, R. F., and Liu, F. (2020). Spatio-temporal quantification of patterns, trade-offs and synergies among multiple hydrological ecosystem services in different topographic basins. *J. Clean. Prod.* 268:122338. doi: 10.1016/j.jclepro.2020.122338

Tallis, H., Kareiva, P., Marvier, M., and Chang, A. (2008). An ecosystem services framework to support both practical conservation and economic development. *Proc. Natl. Acad. Sci. U.S.A.* 105, 9457–9464.

Wang, J., Peng, J., Zhao, M., Liu, Y., and Chen, Y. (2017). Significant trade-off for the impact of Grain-for-Green Programme on ecosystem services in Northwestern Yunnan, China. *Sci. Total Environ.* 574, 57–64. doi: 10.1016/j.scitotenv.2016.09.026

Wang, J. F., Li, X. H., Christakos, G., Liao, Y. L., Zhang, T., Gu, X., et al. (2010). Geographical detectors-based health risk assessment and its application in the neural tube defects study of the Heshun Region, China. *Int. J. Geogr. Inf. Sci.* 24, 107–127. doi: 10.1080/13658810802443457

Wang, Y. H., and Dai, E. (2020). Spatial-temporal changes in ecosystem services and the trade-off relationship in mountain regions: A case study of Hengduan Mountain region in Southwest China. *J. Clean. Prod.* 264:121573. doi: 10.1016/j.jclepro.2020.121573

Wang, Y. H., Dai, E. F., Ge, Q. S., Zhang, X. Z., and Yu, C. Q. (2021). Spatial heterogeneity of ecosystem services and their trade-offs in the Hengduan Mountain region, Southwest China. *Catena* 207:105632. doi: 10.1016/j.catena.2021.105632

Williams, J. R., Renard, K. G., and Dyke, P. T. (1983). EPIC: A new method for assessing erosion's effect on soil productivity. *J. Soil Water Conserv.* 38, 381–383.

Xu, J. Y., Chen, J. X., and Liu, Y. X. (2020). Partitioned responses of ecosystem services and their tradeoffs to human activities in the Belt and Road region. *J. Clean. Prod.* 276:123205. doi: 10.1016/j.jclepro.2020.123205

Yang, J., Ren, J. Y., Sun, D. Q., Xiao, X. M., Xia, J. H., Jin, C., et al. (2021). Understanding land surface temperature impact factors based on local climate zones. *Sustain. Cities Soc.* 69:102818. doi: 10.1016/j.scs.2021.102818

Yang, J., Sun, J., Ge, Q. S., and Li, X. (2017). Assessing the impacts of urbanization-associated green space on urban land surface temperature: A case study of Dalian, China. *Urban For. Urban Green.* 22, 1–10. doi: 10.1016/j.ufug.2017.01.002

Yang, J., Wang, Y. C., Xiu, C. L., Xiao, X. M., Xia, J. H., and Jin, C. (2020). Optimizing local climate zones to mitigate urban heat island effect in human settlements. *J. Cleaner Prod.* 275:123767. doi: 10.1016/j.jclepro.2020.123767

You, S. C., and Li, W. Q. (1999). Estimation of soil erosion supported by GIS a case study in Guanji township, Taihe, Jiangxi. *J. Nat. Resour.* 14, 62–68.

Zhang, L., Dawes, W. R., and Walker, G. R. (2001). Response of mean annual evapotranspiration to vegetation changes at catchment scale. *Water Resour. Res.* 37, 701–708. doi: 10.1029/2000WR900325

Zhang, T., Lyu, X., Zou, Y., Liu, J., Jiang, M., and Xu, C. (2022). Value assessment of wetland ecosystem services in the Da Hinggan Mountains, China. *Chin. Geogr. Sci.* 32, 302–311. doi: 10.1007/s11769-022-1268-2

Zhang, Z. Y., Liu, Y. F., Wang, Y. H., Liu, Y. L., Zhang, Y., and Zhang, Y. (2020). What factors affect the synergy and tradeoff between ecosystem services, and how, from a geospatial perspective? *J. Clean. Prod.* 257:120454. doi: 10.1016/j.jclepro.2020.120454

Zhao, Z., Sharifi, A., Dong, X., Shen, L., and He, B. J. (2021). Spatial variability and temporal heterogeneity of surface urban heat island patterns and the suitability of local climate zones for land surface temperature characterization. *Remote Sens.* 13:4338. doi: 10.3390/rs13214338

Zhao, Z. Q., He, B. J., Li, L. G., Wang, H. B., and Darko, A. (2017). Profile and concentric zonal analysis of relationships between land use/land cover and land surface temperature: Case study of Shenyang, China. *Energy Build.* 155, 282–295. doi: 10.1016/j.enbuild.2017.09.046

frontiers | Frontiers in Ecology and Evolution

TYPE Original Research
PUBLISHED 23 September 2022
DOI 10.3389/fevo.2022.1010400

Check for updates

OPEN ACCESS

EDITED BY
Jun Yang,
Northeastern University, China

REVIEWED BY
Chao Yang,
Shenzhen University, China
Dongrui Han,
Shandong Academy of Agricultural Sciences, China

*CORRESPONDENCE
Tongtong Liu
fjyl503@163.com

SPECIALTY SECTION
This article was submitted to Environmental Informatics and Remote Sensing, a section of the journal Frontiers in Ecology and Evolution

RECEIVED 03 August 2022
ACCEPTED 29 August 2022
PUBLISHED 23 September 2022

CITATION
Dai Y and Liu T (2022) Spatiotemporal mechanism of urban heat island effects on human health—Evidence from Tianjin city of China. *Front. Ecol. Evol.* 10:1010400. doi: 10.3389/fevo.2022.1010400

COPYRIGHT
© 2022 Dai and Liu. This is an open-access article distributed under the terms of the Creative Commons Attribution License (CC BY). The use, distribution or reproduction in other forums is permitted, provided the original author(s) and the copyright owner(s) are credited and that the original publication in this journal is cited, in accordance with accepted academic practice. No use, distribution or reproduction is permitted which does not comply with these terms.

Spatiotemporal mechanism of urban heat island effects on human health—Evidence from Tianjin city of China

Yifang Dai and Tongtong Liu*

School of Architecture, Tianjin University, Tianjin, China

The increasingly intensifying global warming and urban heat island (UHIs) are seriously damaging the physical and mental health of urban residents. However, the spatiotemporal evolution of how high temperatures affect human health in megacities remains unclear. Therefore, in this study, with Tianjin during 2006–2020 as an example, and based on data from meteorological stations, Landsat remote sensing images, and point of interest big data, this study applied hot- and cold-spot statistics and remote sensing retrieval in numerical modeling and established an appraisal system to assess how and to what extent UHIs affect resident health. The results showed that the overall influence of UHIs on respiratory and cardiovascular diseases and mental health increased to 373 km^2 in area and two levels in intensity; the influence was mainly concentrated in the downtown area, with a rising influence level. Owing to the dual-core structure of the city, the influence was distributed along the main traffic lines in Binhai New District, having a strong influence in the area mainly concentrated in the southeastern part. Many cold spots clustered in the central urban area to cool the thermal environment: the cooled area was 6.5 times larger than the area of intense cooling influence. Our study provides a method for identifying health risks in urban spaces, lays a theoretical foundation to improve the planning of urban green space systems, and offers some decision-making guidance for the planning of healthy cities.

KEYWORDS

urban heat island, health damage, mechanism features, spatiotemporal, residents health

Introduction

Recent years have witnessed serious global warming, frequent extreme weather conditions, and heatwaves (Huang et al., 2022). Accelerating urbanization exacerbates the effects of urban heat islands (UHIs), causing higher summer temperatures and seriously damaging the physical and mental health of residents (Ebi et al., 2021). By 2050, 6.252 billion people will live in cities, accounting for 68% of the world population

(United Nations, 2018). Against the backdrop of global climate change, the high summer temperatures in China and the health risks they pose have become increasingly serious (Wang et al., 2020; Ren et al., 2022). The temperature in cities, which are highly intensive spaces for production and living, changes faster than that in the countryside. In China, a country where urbanization is accelerating and the urban thermal environment continues to change, urban residents suffer from the combined effects of global warming and UHIs (Huanchun et al., 2020). Therefore, UHIs must be managed to address problems related to the environmental health of cities.

In recent years, heat waves have occurred in cities, mainly due to two factors: global warming and UHIs (Silva et al., 2022). Urban areas with a crowded population and a serious thermal environment also suffer from high brightness (Chen et al., 2022), and the thermal environment is related to the spatial structure and ventilation corridor of a city (Luo et al., 2021; You et al., 2021). UHIs mainly form through the following processes: underlying surfaces absorb more solar radiation in urban areas, human production and living activities release more heat, less heat evaporates from cities, and the average wind speed in cities is lower, transmitting less heat outward (Niu et al., 2021; Fu et al., 2022). The main measure implemented to alleviate the health risks in urban thermal environments is to optimize the functional spaces in a city based on land, such as by building cooling and ventilation corridors (Yang et al., 2020; Song et al., 2022). UHIs are a typical environmental result of urban microclimates, which are high spatial heterogeneity [14]. Hence, the spatial layout of the heat islands must be examined. Huang et al. (2021) identified the spatial features and patterns of UHIs and proposed planning and design strategies to reduce the health risks posed by UHIs (Wang et al., 2019). The macro exposure–response mechanism between the human body and temperature was identified, and policy suggestions were provided for public health and safeguards for different groups of people.

At high temperatures, humans struggle to adjust to their environment. Once the temperature exceeds the upper tolerance limit, heat waves may directly affect human health, leading to a higher incidence and mortality for certain diseases (Tian et al., 2021). However, as people in different cities or regions vary in adaptability and vulnerability, and they widely vary in background information (age, sex, geographical location, socioeconomic status, health condition, and medical level), different researchers have applied different methods of analyzing the effects of heat waves. In terms of deaths caused by heat waves, the elderly face the highest risk (Conti et al., 2004). Older people and patients suffer from the highest mortality during heat waves, which is usually related to cardiovascular, cerebrovascular, and respiratory diseases (Tan and Wang, 2004). In addition, during heat waves, patients with chronic diseases, such as mental disorders, diabetes, and lung, cardiovascular, and cerebrovascular diseases, are at a higher risk (Kovats and Hajat, 2008). A meta-analysis showed that patients with lung diseases or diabetes have a higher mortality risk during heatwaves (Bunker et al., 2016; Moon, 2021). In addition, on heat wave days in 2003, the mortality of patients with cardiovascular diseases in Europe rose by 30% (Kenny et al., 2010). Liu and Zhang (2010) examined daily non-accidental deaths and deaths due to respiratory diseases in Beijing and found that heat waves take 2–3 days to affect non-accidental deaths and 2–5 days to affect deaths due to respiratory diseases. In particular, with higher temperature and humidity, heat waves more strongly influence deaths due to respiratory diseases. Studies on the mortality of different diseases in 272 Chinese cities during 2013-2015 found that the attributed risks of respiratory diseases (J00-J99) and cardiovascular diseases (I00-I99) caused by temperature were 10.57% and 17.48%, respectively (Chen et al., 2018). Meanwhile, more studies are needed to analyze the spatiotemporal pattern of high-temperature health risks to reduce such risks.

High temperatures not only affect those with cardiovascular, cerebrovascular, and respiratory diseases (Linares and Díaz, 2008), but also increase the incidence and mortality of those with mental disorders. Ambient temperature is positively correlated with the admission rate of people with mental or behavioral disorders, including those with symptoms, dementia, affective disorders, neurosis, stress-related diseases, somatoform disorders, and psychological development disorders (Mullins and White, 2019). As heat waves become more frequent, patients with mental disorders will require increased care to prevent the incidence of mortality from increasing (Bando et al., 2017). To this end, epidemiologic studies focusing on the relationship between climate change and human health risk must be conducted to better understand how climate change affects our health and induces diseases, and to lay a theoretical foundation for assessing the health risk posed by high temperatures in different urban spaces.

The World Health Organization (WHO) stated that a healthy environment is part of a healthy city. Europe also treats urban planning and evaluation as an integral part of healthy cities (Barboza et al., 2021). In other words, the health risks posed by high temperatures can be mitigated through environmental engineering, urban planning, and landscape architecture (Daniel et al., 2018; Lee and Mayer, 2021). In detail, we can identify people vulnerable to heat waves, provide warnings or precautions, and prepare effective and targeted countermeasures to protect residents' health, publicize healthcare knowledge, and reduce the medical burden due to heat waves (Kotharkar and Ghosh, 2022). In 1993, the National Health Commission of China (former Ministry of Health) attended a bidirectional meeting on urban health development convened by the WHO in

Manila and initiated the planning of healthy cities. In 1995, based on the science of human settlements, Wu (1995) proposed buildings and cities that achieve environmental balance and pose zero harm to the physical and mental health of residents. Currently, researchers are focusing on improving the urban thermal environment through intelligent and data-driven analysis (Zheng et al., 2016; Shi et al., 2022).

The effect of global climate change, especially high temperatures, on human health has become an emerging research direction. However, studies are lacking on the spatiotemporal evolution of UHIs and the mechanism through which climate influences public health, hindering the development of reliable measures to improve ecological engineering. Specifically, further studies are required to explore the inner spaces in coastal cities. Therefore, in this study, we selected Tianjin, a typical city in south Asia, as an example; applied data from Landsat satellite imaging and electronic maps; and employed technologies such as ArcGIS, remote sensing, and spatial hotspots to analyze the influence of UHIs on residents' health during 2006–2020 and the health risks they pose. The remainder of this paper is structured as follows: Section "Data and methods" describes the methods we used to assess the health risks posed by high temperatures, detect thermal fields, and identify hot and cold spots. Section "Results" describes the mechanism we used to evaluate the health risks posed by high temperatures in cities and our analyses of the driving factors and patterns of such risks. Sections "Discussion" and "Conclusion" present the discussion and conclusions, respectively.

Data and methods

Health risk assessment and study area

Assessing health risks posed by high temperatures

Based on how temperature affects human physical and mental health and disease incidence and mortality, we drew upon the study of Huang et al. (2021) and chose to focus on respiratory diseases (J00–J99), cardiovascular diseases (I00–I99), and mental disorders (Huang et al., 2021). We selected emotional health, a factor relevant to the general public, as a factor influencing mental disorders. Regarding the influence of high temperatures on human health, we applied the grading standard of the Chinese Centers for Disease Control and Prevention in our data analysis to guarantee accuracy. Specifically, the weights in the assessment method were 0.5 for mental health and 0.5 for physical health (0.25 for respiratory diseases and 0.25 for cardiovascular disease; **Table 1**).

TABLE 1 Standards for assessing influence of high temperature on resident health.

Influence level	Respiratory disease		Cardiovascular disease		Mental health	Grading standard
	Temperature (°C)	Increase in mortality (%)	Temperature (°C)	Increase in mortality (%)	Emotional temperature (°C)	
Level 1	28–30	–	26–28	–	28–30	Curve and threshold temperatures of how high temperature affects negative emotion factors
Level 2	30–31	–	28–29	0–7.2	30–31	
Level 3	31–32	0–25.3	29–30	7.2–14.4	31–32	
Level 4	32–33	25.3–50.6	30–31	14.4–21.6	32–33	
Level 5	33–34.5	50.6–88.55	31–32	21.6–28.8	33–34.5	
Level 6	34.5–35	88.55–126.5	32–33	28.8–36	34.5–35	
Level 7	35–35.5	126.5–164.45	33–34	36–43.2	35–35.5	
Level 8	35.5–36	164.45–177.1	34–35	43.2–50.4	35.5–36	
Level 9	36–36.5	177.1–189.75	35–36	50.4–57.6	36–36.5	
Level 10	>36.5	>189.75	36–37	57.6–64.8	>36.5	

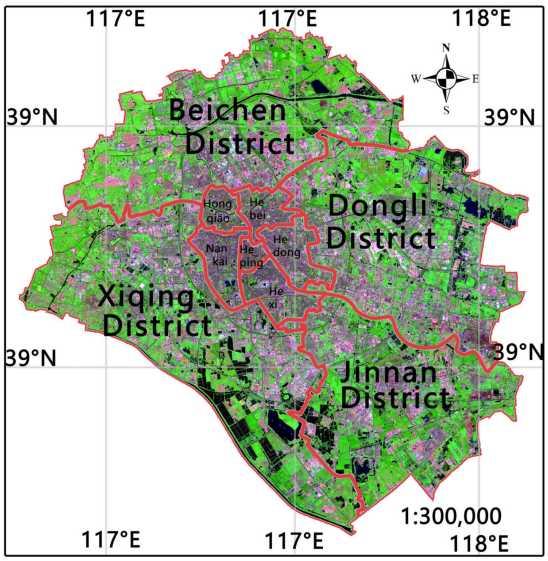

FIGURE 1
Overview of study area.

Overview of study area

The study area was downtown Tianjin (Figure 1), located at 117°13′45″–117°18′50″ and 39°4′25″–39°10′4″. Tianjin has an Asian monsoon climate and is located in the semihumid continental warm temperate zone. In the summer, the city experiences a subtropical high, mainly south wind, high temperatures (28°C on average in July), and heavy precipitation. In addition, Tianjin suffers from UHIs in summer, seriously affecting the comfort of residents as well as their respiratory, circulatory, and mental health.

As a pillar metropolitan area in the center of the Asia-Pacific region, Tianjin has a population of approximately 13.73 million. Along with rapid urbanization, the urban area sprawls in a typical manner. Specifically, after the new *Tianjin City Master Plan (2005–2020)* was implemented in 2005, its urban area rapidly expanded, population density increased, industries clustered, and old low-rise buildings (one to two stories) were replaced by high-rise buildings, resulting in the typical UHI effects and changes in urban health space.

Optimizing hot spot analysis

Spatial autocorrelation is an effective method used for probing the changes in spatial patterns. The key to the method lies in analyzing the correlation among spatial data, finding observed singular values, and revealing the spatial correlation and changes in spatial heterogeneity. Driving factors can be identified and extracted by examining the spatial patterns and time variation. Therefore, we employed the Getis-Ord G_i^* to identify the spatial hot spots where UHIs affect human health during urbanization and to understand the spatial evolution of such effects (Formula 1).

$$G_i^* = \frac{\sum_{j=1}^{n} w_{i,j}x_j - \frac{\sum_{j=1}^{n} x_j}{n}\sum_{j=1}^{n} w_{i,j}}{\sqrt{\frac{\sum_{j=1}^{n} x_j^2 - (\bar{X})^2}{n}}\sqrt{\frac{n\sum_{j=1}^{n} w_{i,j}^2 - \left(\sum_{j=1}^{n} w_{ij}\right)}{n-1}}} \quad (1)$$

where x_j is the attribute value of factor j, w_{ij} is the spatial weight between factors i and j, and n is the sum of the factors. We calculated the spatial correlation of the Getis-Ord G_i^* with $|z| > 1.96$, a significance level of $p < 0.05$, and a confidence level of 95% to identify whether spatial agglomeration existed and the spatial structure, and to determine if certain basic spatial processes exerted an influence.

Retrieving urban temperature field

We retrieved the urban temperature field to effectively assess the health risks posed by high temperatures, so we considered the baseline temperature, land surface temperature (LST), air temperature, and UHI intensity. The LST changes with the air temperature above the surface. Therefore, we selected 20 typical villages in the suburbs and recorded their average temperatures.

First, we used ENVI for LST then near-surface air temperature (NSAT) retrieval. Finally, we measured the UHI intensity based on the baseline temperature. Then, in accordance with the data from the meteorological stations and satellite images, we established a linear relationship between LST and daily average temperature using MATLAB.

Second, during LST retrieval, we obtained the 10th thermal waveband of the Landsat 8 satellite, along with ENVI and atmospheric correction. We performed radiometric calibration according to the NASA manual.[1] We then calculated the normalized difference vegetation index (NDVI), vegetation coverage, and land surface emissivity (based on the formula proposed by Qin). Third, we calculated the LST. Finally, we used the linear relationship between LST and daily average temperature to obtain Equation (2):

$$TA = T1 + \lambda T\rho ln\varepsilon - 273.15 \times 0.85 + 1.4 \quad (2)$$

where T_A is the temperature of the UHI (°C), T is the temperature (°C), λ is the central wavelength of the TM6 band (11.5 μm), $\rho = h \times \frac{c}{\sigma} = 1.438 \times 10^{-2}K$ (where the Stefan-Boltzmann constant σ is 1.38×10^{-23} J/K), Planck's constant h is 6.626×10^{-34} Js, the speed of light c is 2.998×10^{-8} m/s, and ε is the land surface emissivity.

In addition, we combined baseline temperature and UHI warming to comprehensively assess different factors influencing high urban temperatures. Specifically, we set the baseline

1 www.usgs.gov/landsat

temperature as 28.6°C, which is the average minimum temperature between 10:00 and18:00 in Tianjin from July 7 to August 7 (summer) in multiple years. After that, the heat island warming in different locations was added, to eliminate the influence of occasional rainy days, and to effectively assess the minimum influence of UHI on residents' health, as well as the overall influence of temperature on human health.

Results

Temperature field

We used Landsat 5 and 8 satellite images for UHI temperature retrieval and combined the baseline temperature between 10:00 and18:00 in the summer to identify the spatiotemporal patterns and layout of the urban thermal field during 2006–2020 in Tianjin (Figure 2). We divided the temperature field into five levels: low-temperature (<30°C), low–medium-temperature (30–31°C), medium-temperature (31–32°C), high-temperature (32–33°C), and extremely high-temperature (>33°C) zones.

The results showed that in 2006, the low-temperature zone accounted for the largest proportion of the temperature zones, and the high-temperature zone was mainly concentrated in the six districts in central Tianjin: Heping, Hongqiao, Hebei, Nankai, Hexi, and Hedong Districts. Additionally, many urban heating elements weaken the cooling capacity of the city. In 2020, the medium- and high-temperature zones expanded from the downtown areas to the surroundings, with high-temperature zones scattered as small, yet high-density, patches. Tianjin has been rapidly urbanizing, and urban construction has expanded outward, breaking the original single-center pattern. Simultaneously, the green spaces were evenly distributed in the downtown area, mitigating the heating of the environment to some extent. In addition, the increases in high-temperature patches and artificial landscapes, and the lack of blue and green infrastructure have weakened the ability of the city to mitigate the effects of UHI, posing a threat to the emotional health of residents.

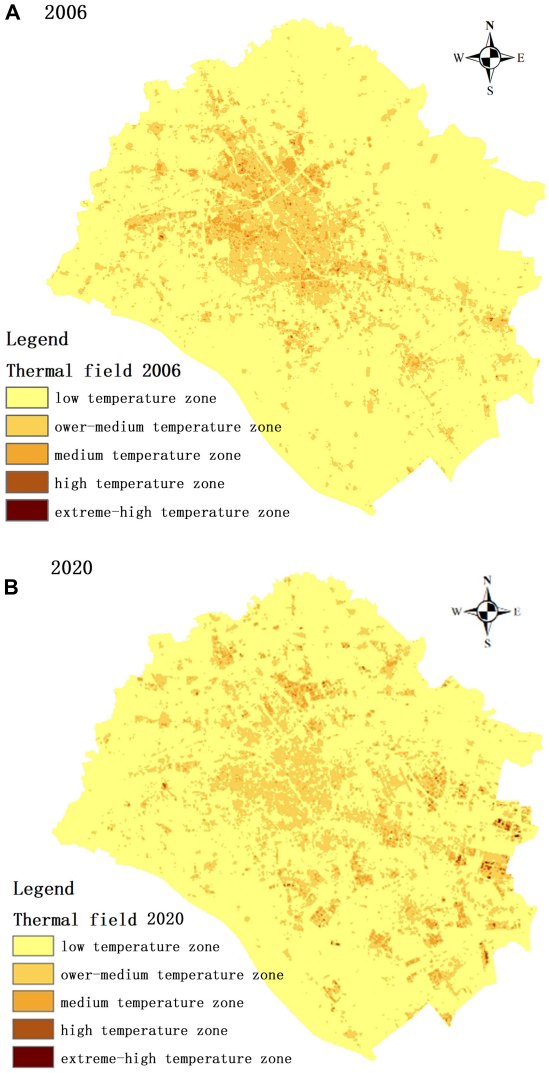

FIGURE 2
Changes in thermal field distribution from **(A)** 2006 to **(B)** 2020.

Spatial distribution of high-temperature influence on health

In this study, we combined the incidence and mortality of three typical diseases caused by high temperatures into a map of the UHIs to identify their influence on health during 2006–2020 (Figure 3). The results showed that the influence of UHIs on health gradually increased, with the level of influence increasing from mainly Levels 1 and 2 to Levels 2 and 3, expanding from the downtown area to the surroundings, and the areas of Level 3 and 4 zones increased 7 and 74 times, respectively. In addition, the areas with a low health influence were concentrated in the suburbs, while the medium- and high-level areas were divided into large patches by rivers, lakes, and belt-shaped green spaces and were distributed as circles around the downtown. In 2020, the downtown area changed from large single-level patches to scattered and fragmented patches. Meanwhile, in the suburbs, areas, where the influence on health was high, were clustered as groups, mainly concentrated on industrial land, large-area waterproof hardened surfaces, high-density building complexes, and business centers. The main reason is that in these areas, the hardened surface area is larger and green space is limited, so the area easily absorb heats and the temperature increases. Industrial heat

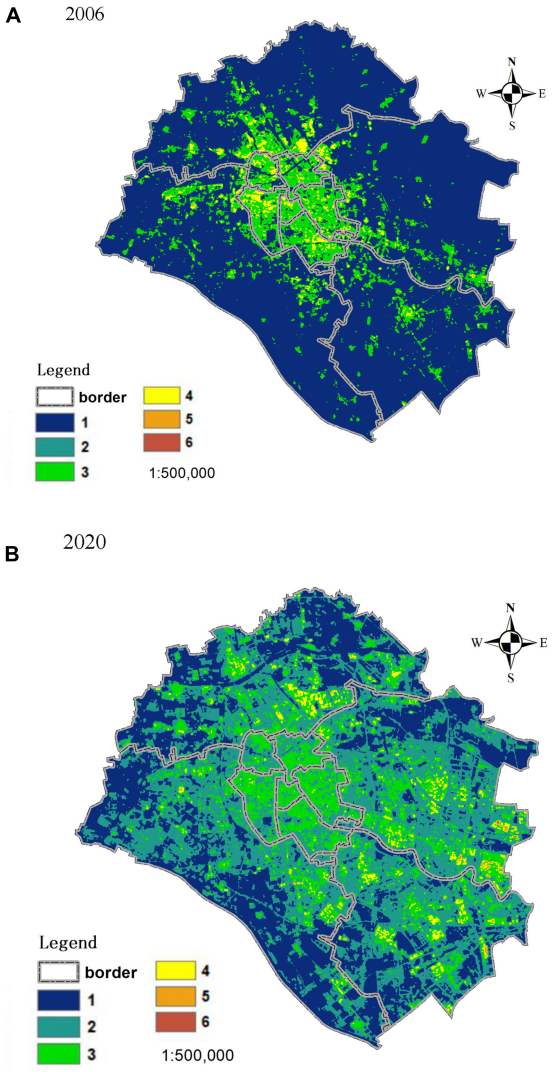

FIGURE 3
Spatial distribution of the influence of urban heat islands (UHIs) on health in **(A)** 2006 and **(B)** 2020.

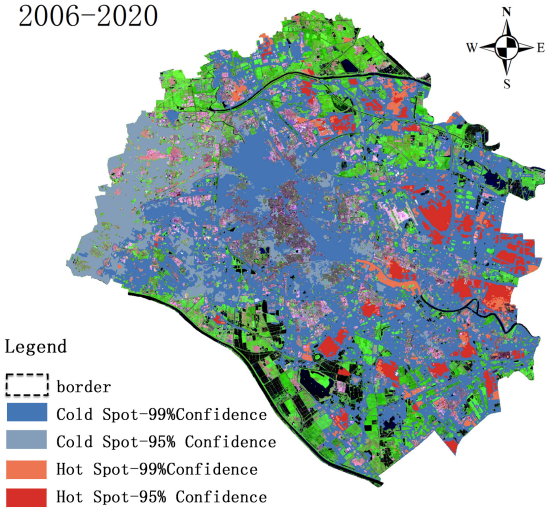

FIGURE 4
Distribution of cold and hot spots of health risk posed by high temperatures during 2006–2020.

sources release heat and raise the temperature in summer, and the lack of green space cannot mitigate the effects on UHIs.

Hot spots of spatiotemporal urban heat island influence on health

Using ArcGIS, we explored and analyzed the cold and hot spots of the influence of UHIs on resident health during 2006–2020. Figure 4 shows that areas of severe health risk due to high temperatures mainly concentrated in the southeastern part of Binhai New District, covering the Tianjin Airport Economic Area, Dasi Industrial Park, and Tianjin Haihe Education Park, which the central area for the dual-core development in Tianjin. Therefore, the areas where health was seriously influenced by UHI distributed along the main traffic lines, with hot spots concentrated in the core of traffic lines. Cold spots separated the hot spots in the downtown area. This has mainly occurred owing to the progress in urban construction, urban planning, and development strategies and policies on urban spaces. After the *Tianjin City Master Plan (2005–2020)* was implemented, human health in developed areas was highly influenced, especially in areas where industries were clustered.

The zones where health was less influenced were concentrated on the outskirts of downtown Tianjin, covering a relatively large area. The main reason for this finding that as the city services and the economic center have been improved and perfected, Tianjin has become less involved in production, and large enterprises and industries gradually moved away, thus reducing the effects of local UHIs; however, the influence of temperature on health has been exacerbated in the margins of the downtown areas. The land use in these areas is mostly low-rise buildings, composed of metals and stones, and the vegetation coverage is low. In addition, such areas discharge artificial heat, posing serious health risks.

The large areas of cold spots in downtown Tianjin helped to mitigate the influence of the high-temperature environment on the health of residents for the following main reasons: high-rise buildings protect the surface from solar radiation; local climate zones with high-rise buildings provide more open, ventilated green spaces; high-density low-rise buildings in the downtown area were upgraded and refurbished. Green space structures along the seashores

and river banks separated the different levels of thermal environmental influence on health.

Discussion

Contributions

The influence of summer UHIs on the health of residents is mainly reflected in respiratory and cardiovascular diseases, and mental health issues, and this influence spatially varies (Huang et al., 2020). In Beijing, areas of higher health risk caused by UHIs were concentrated within the Third Ring Road; due to insufficient cooling facilities and green spaces, residents in the suburbs were also exposed to increased health risks (Huang et al., 2021). These results are in line with ours: hotspots of urban health risk were distributed in concentrated industrial districts and areas of high-intensity urban construction in the suburbs.

In this study, we obtained temperature data from remote sensing images and meteorological stations to assess the health risk posed by high temperatures to residents. This method produced more accurate results than LST retrieval using only remote sensing images. Currently, researchers have mostly retrieved LST from Landsat and MODIS data. Landsat data have a resolution of 100 m, so are suitable for analyzing mixed pixels in microurban studies. MODIS data have a resolution of 1 km, so are more suitable for regional-scale studies.

Researchers have mostly analyzed the relationship between temperature and mental health in the form of summaries (Arbuthnott and Hajat, 2017) or statistics; we instead focused on the spatial distribution of mental health risks in cities. Due to the complex evolution of and forces driving urban form (Ren et al., 2022), assessing the health influence of UHIs requires the combination of various theories with many practical cases. The findings of our study on Tianjin city revealed the features of spatial transfer in the influence of UHIs on urban resident health, from clusters to scattered groups. Therefore, we propose adding more green spaces and water areas in high-risk areas and taking full advantage of the cooling benefits provided by large wetlands and water bodies around Tianjin to improve urban ventilation.

Limitations

With Tianjin as the case study, we explored the characteristics of the spatial evolution of the health risks posed by high temperature to residents during urbanization. However, further temporal analysis of these changes is required. We study selected Landsat remote sensing images covering nearly 15 years to analyze the changes in how summer UHIs influence the health of residents, without comparing how different seasons or temperatures at different times affect such influences. Moreover, limited by the scale of the data, we could not further refine the time scale to further analyze the changes in how the thermal environment affects the health of residents, so our results cannot serve as a reference for implementing management policies in real time.

We analyzed the differences in the spatial distribution of the influence of UHIs on resident health in a city. However, our spatial scale was not sufficiently refined. In the future, we will conduct refined empirical studies on the differences in the emotional health of residents in different inner-urban landscapes such as parks and squares. In addition, we will optimize the landscape index by including indicators applicable to the planning of healthy cities to offer references for urban planning and construction. Additionally, because of the lack of meteorological data for the years of the corresponding remote sensing images, we only employed remote sensing images to analyze changes in the UHIs, without performing a verification analysis using high-resolution spatiotemporal data.

Conclusion

Based on data from multiple sources, such as meteorological stations, satellite images, and points of interest, in this study, we analyzed the spatial patterns and processes of the influence of UHIs on health, and the spatial changes in hot spots of climate-related health impacts in Tianjin during 2006–2020. Our conclusions were as follows:

(1) With increasing UHI area in summer, both the high- and extreme-high-temperature areas expanded. The influence of UHIs on resident health increased by two levels in intensity and 373 km^2 in area, with areas of high-level influence moving from the downtown area to the suburbs.
(2) The locations where the thermal environment influenced health notably shifted toward the eastern part of Tianjin, along the major traffic lines in the dual-core structure in Tianjin; the concentrated high-level influence area transformed into scattered and fragmented patches, and the properties and landscapes of the transferred spaces also contributed to this influence.
(3) The distribution of cold and hot spots of health risk due to high temperature showed that, affected by the changes in the layout of the urban function of Tianjin and with a confidence coefficient surpassing 95%, the zones where the influence was lessened (963 km^2) were located within the outer ring road, around the downtown area. The hot spots (135 km^2) were expanding in areas concentrated in the key development areas of Tianjin.

Data availability statement

The original contributions presented in this study are included in the article/supplementary material, further inquiries can be directed to the corresponding author.

Author contributions

YD: conceptualization, methodology, data curation, formal analysis, writing—original draft preparation, review and editing, investigation, and visualization. TL: methodology, data curation, formal analysis, writing—original draft preparation, review and editing, investigation, and visualization. Both authors contributed to the article and approved the submitted version.

Conflict of interest

The authors declare that the research was conducted in the absence of any commercial or financial relationships that could be construed as a potential conflict of interest.

Publisher's note

All claims expressed in this article are solely those of the authors and do not necessarily represent those of their affiliated organizations, or those of the publisher, the editors and the reviewers. Any product that may be evaluated in this article, or claim that may be made by its manufacturer, is not guaranteed or endorsed by the publisher.

References

Arbuthnott, K. G., and Hajat, S. (2017). The health effects of hotter summers and heat waves in the population of the United Kingdom: a review of the evidence. *Environ. Health* 16:119. doi: 10.1186/s12940-017-0322-5

Bando, D. H., Teng, C. T., Volpe, F. M., de Masi, E., Pereira, L. A., and Braga, A. L. (2017). Suicide and meteorological factors in São Paulo, Brazil, 1996–2011: a time-series analysis. *Braz. J. Psychiatry* 39, 220–227. doi: 10.1590/1516-4446-2016-2057

Barboza, E. P., Cirach, M., Khomenko, S., Iungman, T., Mueller, N., Barrera-Gómez, J., et al. (2021). Green space and mortality in European cities: a health impact assessment study. *Lancet Planet. Health* 5, e718–e730. doi: 10.1016/S2542-5196(21)00229-1

Bunker, A., Wildenhain, J., Vandenbergh, A., Henschke, N., Rocklöv, J., Hajat, S., et al. (2016). Effects of air temperature on climate-sensitive mortality and morbidity outcomes in the elderly: a systematic review and meta-analysis of epidemiological evidence. *EBiomedicine* 6, 258–268. doi: 10.1016/j.ebiom.2016.02.034

Chen, R. J., Yin, P., Wang, L. J., Liu, C., Niu, Y., Wang, W. D., et al. (2018). Association between ambient temperature and mortality risk and burden: a time series study in 272 main Chinese cities. *BMJ* 363:k4306. doi: 10.1136/bmj.k4306

Chen, Y., Yang, J., Yang, R. X., Xiao, X. M., and Xia, J. H. (2022). Contribution of urban functional zones to spatial distribution of urban thermal environments. *Build. Environ.* 216:109000. doi: 10.1016/j.buildenv.2022.109000

Conti, S., Meli, P., Minelli, G., Solimini, R., Toccaceli, V., Vichi, M., et al. (2004). "Epidemiological study of mortality during summer 2003 in Italian regional capitals: results of a rapid survey," in *Proceedings of the 4th Ministerial Conference on Environment and Health*, Budapest, 109–120.

Daniel, M., Lemonsu, A., and Viguié, V. (2018). The role of watering practices in large-scale urban planning strategies to face heat wave risks in future climates. *Urban Clim.* 23, 287–308. doi: 10.1016/j.uclim.2016.11.001

Ebi, K. L., Capon, A., Berry, P., Broderick, C., de Dear, R., Havenith, G., et al. (2021). Hot weather and heat extremes: health risks. *Lancet* 398, 698–708. doi: 10.1016/S0140-6736(21)01208-3

Fu, X. C., Yao, L., Xu, W. T., Wang, Y. X., and Sun, S. (2022). Exploring the multitemporal surface urban heat island effect and its driving relationship in the Beijing-Tianjin-Hebei urban agglomeration. *Appl. Geogr.* 144:102714. doi: 10.1016/j.apgeog.2022.102714

Huanchun, H., Hailin, Y., Xin, D., Cui, H., Liu, Z., Wei, L., et al. (2020). The factors influencingfactors urban thermal field intensity were analyzed using big data-based GIS. *Sustain. Cities Soc.* 55:102024. doi: 10.1016/j.scs.2020.102024

Huang, H. C., Deng, X., Yang, H. L., Zhou, X. H., and Jia, Q. (2020). Spatio-temporal mechanism underlying the effect of urban heat Island on cardiovascular diseases. *Iran. J. Pub. Health* 49, 1455–1466. doi: 10.18502/ijph.v49i8.3889

Huang, H. C., Yang, H. L., Chen, Y. L., Chen, T. N., Bai, L., and Peng, Z. R. (2021). Urban green space optimization based on a climate health risk appraisal: a case study of Beijing City, China. *Urban For. Urban Greening* 62:127154. doi: 10.1016/j.ufug.2021.127154

Huang, H. C., Zhou, X. H., Qu, Y. C., and Zhang, H. (2022). Spatial effects of climate warming on health risks due to urban heat exposure: a case study of China. *DYNA* 97, 162–168. doi: 10.6036/10426

Kenny, G. P., Yardley, J., Brown, C., Sigal, R. J., and Jay, O. (2010). Heat stress in older individuals and patients with common chronic diseases. *CMAJ* 182, 1053–1060. doi: 10.1503/cmaj.081050

Kotharkar, R., and Ghosh, A. (2022). Progress in extreme heat management and warning systems: a systematic review of heat health action plans (1995–2020). *Sustain. Cities Soc.* 76:103487. doi: 10.1016/j.scs.2021.103487

Kovats, R. S., and Hajat, S. (2008). Heat stress and public health: a critical review. *Annu. Rev. Public Health* 29, 41–55. doi: 10.1146/annurev.publhealth.29.020907.090843

Lee, H., and Mayer, H. (2021). Solar elevation impacts the heat stress mitigation of pedestrians on tree-lined sidewalks of E-W street canyons under Central European heat wave conditions. *Urban For. Urban Greening* 58:126905. doi: 10.1016/j.ufug.2020.126905

Linares, C., and Díaz, J. (2008). Impact of high temperatures on hospital admissions: comparative analysis with previous studies on mortality (Madrid). *Eur. J. Public Health.* 18, 317–322. doi: 10.1093/eurpub/ckm108

Liu, L., and Zhang, J. L. (2010). Relationship between heatwaves and daily death from non-accidental death and respiratory disease: a case-crossover study. *J. Environ. Health.* 02, 95–99. doi: 10.16241/j.cnki.1001-5914.2010.02.010

Luo, X., Yang, J., Sun, W., and He, B. J. (2021). Suitability of human settlements in mountainous areas from the perspective of ventilation: a case study of the main urban area of Chongqing. *J. Cleaner Prod.* 310:127467. doi: 10.1016/j.jclepro.2021.127467

Moon, J. (2021). The effect of the heatwave on the morbidity and mortality of diabetes patients: a meta-analysis of the era of the climate crisis. *Environ. Res.* 195:110762. doi: 10.1016/j.envres.2021.110762

Mullins, J. T., and White, C. (2019). Temperature and mental health: evidence from the spectrum of mental health outcomes. *J. Health Econ.* 68:102240. doi: 10.1016/j.jhealeco.2019.102240

Niu, L., Zhang, Z. F., Peng, Z., Liang, Y. Z., Liu, M., Jiang, Y. Z., et al. (2021). Identifying surface urban heat island drivers and their spatial heterogeneity in China's 281 cities in China: an empirical study based on multiscale geographically weighted regression. *Remote Sens.* 13:4428. doi: 10.3390/rs13214428

Ren, J., Yang, J., Zhang, Y., Xiao, X., Xia, J. C., Li, X., et al. (2022). Exploring the thermal comfort of urban buildings based on climate zones. *J. Cleaner Prod.* 340:130744. doi: 10.1016/j.jclepro.2022.130744

Shi, Z., Yang, J., Zhang, Y., Xiao, X., and Xia, J. C. (2022). Urban ventilation corridors and spatiotemporal divergence patterns of urban heat island intensity: a local climate zone perspective. *Environ. Sci. Pollut. Res. Int*. 1–13. doi: 10.1007/s11356-022-21037-9

Silva, R., Carvalho, A. C., Pereira, S. C., Carvalho, D., and Rocha, A. (2022). Lisbon urban heat island in future urban and climate scenarios. *Urban Clim.* 44:101218. doi: 10.1016/j.uclim.2022.101218

Song, J. L., Lu, Y., Zhao, Q., Zhang, Y. Q., Yang, X. C., Chen, Q., et al. (2022). Effect modifications of green space and blue space on heat-mortality association in Hong Kong, 2008–2017. *Sci. Total Environ.* 838:156127. doi: 10.1016/j.scitotenv.2022.156127

Tan, J. G., and Wang, J. X. (2004). The impacts of heat waves on human health and its research methods. *Clim. Environ. Res.* 04, 680–686.

Tian, L., Lu, J., Li, Y. C., Bu, D., Liao, Y., and Wang, J. (2021). Temporal characteristics of urban heat island and its response to heat waves and energy consumption in the mountainous Chongqing, China. *Sustain. Cities Soc.* 75:103260. doi: 10.1016/j.scs.2021.103260

United Nations (2018). *Revision of World Urbanization Prospects*. New York, NY: United Nations.

Wang, J., Feng, J. M., Yan, Z. W., and Chen, Y. (2020). Future risks of unprecedented compound heat waves over three vast urban agglomerations in China. *Earths Future* 8:e2020EF001716. doi: 10.1029/2020EF001716

Wang, S. Z., Huang, H. C., Hao, C., Cao, L., and Liu, T. (2019). Sensitivity microscale of urban heat island reduction by green space. *Open House Int.* 44, 147–151. doi: 10.1108/OHI-03-2019-B0034

Wu, L. Y. (1995). Concluding speech at the "Human Gathering Environment and the 21st century Chinese Architecture Symposium" on the development of human settlements facing the new century. *Hua Zhong Archit.* 02, 1–9.

Yang, J., Wang, Y. C., Xiu, C. L., Xiao, X. M., Xia, J. H., and Jin, C. (2020). Optimizing local climate zones to mitigate urban heat island effect in human settlements. *J. Cleaner Prod.* 275:123767. doi: 10.1016/j.jclepro.2020.123767

You, H. L., Yang, J., Xue, B., Xiao, X. M., Xia, J., Jin, C., et al. (2021). Spatial evolution of population change in Northeast China during 1992–2018. *Sci. Total Environ.* 776:146023. doi: 10.1016/j.scitotenv.2021.146023

Zheng, S., Zhao, L., and Li, Q. (2016). Numerical simulation of the impact of different vegetation species on the outdoor thermal environment. *Urban Forest. Urban Green.* 18, 138–150. doi: 10.1016/j.ufug.2016.05.008

frontiers | Frontiers in Earth Science

TYPE Original Research
PUBLISHED 27 September 2022
DOI 10.3389/feart.2022.1014490

Check for updates

OPEN ACCESS

EDITED BY
Bing Xue,
Institute for Advanced Sustainability Studies (IASS), Germany

REVIEWED BY
Huisheng Yu,
Northeastern University, China
Xiaoping Zhang,
Shandong Jianzhu University, China

*CORRESPONDENCE
Zhenghui Zhu,
zzh@lnnu.edu.cn

SPECIALTY SECTION
This article was submitted to Geoscience and Society, a section of the journal Frontiers in Earth Science

RECEIVED 08 August 2022
ACCEPTED 12 September 2022
PUBLISHED 27 September 2022

CITATION
Liu W, Zhu Z and Wang L (2022), Spatiotemporal heterogeneity of primary and secondary school student distribution in Liaoning Province, China from 2010 to 2020.
Front. Earth Sci. 10:1014490.
doi: 10.3389/feart.2022.1014490

COPYRIGHT
© 2022 Liu, Zhu and Wang. This is an open-access article distributed under the terms of the Creative Commons Attribution License (CC BY). The use, distribution or reproduction in other forums is permitted, provided the original author(s) and the copyright owner(s) are credited and that the original publication in this journal is cited, in accordance with accepted academic practice. No use, distribution or reproduction is permitted which does not comply with these terms.

Spatiotemporal heterogeneity of primary and secondary school student distribution in Liaoning Province, China from 2010 to 2020

Wanbo Liu[1], Zhenghui Zhu[1,2]* and Ling-en Wang[3]

[1]School of Geography, Liaoning Normal University, Dalian, China, [2]School of Government, Liaoning Normal University, Dalian, China, [3]Department of Resource Ecology and Biological Resources, Institute of Geographic Sciences and Natural Resources Research, Chinese Academy of Sciences, Beijing, China

Data mining student information helps to understand the compulsory education population size, structure, distribution and flow characteristics. Here, the spatial evolution, regional disparity, and emerging spatiotemporal distribution patterns are analyzed based on statistical data of primary and secondary education in Liaoning Province from 2010 to 2020. Demographic and spatial analysis methods, population size and structural changes were used in the assessments. The scale of primary and secondary school students in Liaoning Province declined, the gender imbalance was alleviated, and the proportion of migrant students increased. The distribution of students in primary and secondary schools is clearly unbalanced, and an increasingly evident central direction of flow from the countryside to the city exists. The overall difference in distribution of primary and secondary school students in Liaoning Province exhibits a trend of narrowing and then expanding, which is largely due to the uneven distribution among the non-agricultural municipal district, agriculture-related municipal district, and agriculture-related county. The emerging hot spot analysis patterns were dominated by consecutive and intensifying cold spots, spatiotemporal persistent and intensifying hot spots. Overall, these educational statistics and spatial analysis results provide important insights into population and educational geography.

KEYWORDS

compulsory education, school student size, population distribution, education urbanization, spatial pattern evolution, regional disparity, urban-rural disparity

1 Introduction

With the rapid development of industrialization and urbanization, population size and demographic structure have undergone major changes (Wu et al., 2021; Liu T et al., 2022). This has manifested as a decline in birth rate and number of births, resulting in a shortage of students. In addition to the large-scale migration and flow of population, the population has moved from

villages to towns, and from small and medium cities to large cities (Wu, et al., 2019; Liu Z et al., 2022). Education urbanization is the result of population urbanization and the dualization of urban and rural education, which is reflected in the transfer of rural students to urban schools (Fowler and Walberg, 1991; Mei et al., 2015; Ye et al., 2019; Xu et al., 2021). This has a profound impact on the size and structure of the compulsory education school-age population in big cities (Ding et al., 2018). On one hand, school-ready children either move with their migrant worker parents to study in another place or they transfer to a central school with higher teaching quality and become local left-behind children (Han and Yu, 2020). On the other hand, the cross-scale flow of students from rural to urban areas in the compulsory education stage has led to the continuous adjustment of the number, scale and layout of schools (Kenny, 1982; Zhao et al., 2022), and promoted changes in the distribution system, method and scope of compulsory education schools (Zhao et al., 2012; Hamnett and Butler, 2013). The spatiotemporal distribution of the educational population forms the basic feature of educational development level of a region or country (Zhao et al., 2020). Further, the increase or decrease in the number of students in primary and secondary schools is an important indicator of expansion or shrinkage of compulsory education schools (Zhao et al., 2016). Therefore, scientifically understanding the temporal and spatial evolution pattern of the compulsory education population is important for promoting the optimal allocation of educational resources and for sustainable economic and social development.

Previous studies have measured the distribution characteristics of the number of students in compulsory education and the changes in the scope of school services based on school size (Yang et al., 2018; Liu et al., 2020; Zhang et al., 2020; Sajjad et al., 2022). Liu and Chen (2019) determined that the number of students in individual schools can affect the number of students in other schools through inter-school interactions. Some studies selected big cities or villages as case studies of typical regions, with interesting results. For example, Yin et al. (2016) found that the proportion of non-Beijing students in compulsory education in Beijing increased rapidly between 2001 and 2015. Liu and Liu (2017) conducted an empirical study in Biyang County, Henan Province from 2004 to 2016, and determined that the development in the county center had a strong radiation effect on the surrounding towns, resulting in a sharp decline in the number of primary and secondary school students in rural areas, and a concentration in the county center. In addition, some studies have been based on a nationwide provincial scale. Among these, based on the 1987–2014 "China Education Statistical Yearbook", Wu et al. (2018) selected the number of urban and rural students in compulsory education, and investigated the temporal changes and inter-provincial differences of China's education urbanization.

To summarize, extensive research has been conducted on temporal changes and spatial differences in the number of students in compulsory education in different regions, urban and rural areas, and between schools. However, the geographic interpretation of educational activities in existing research remains limited and misunderstood (Hones and Ryba, 1972) and analysis beyond the study area and across scales is lacking (Zhang et al., 2022). Further, trend research based on large research samples, a large research scope, and long-term time-series distribution patterns is rare, which is highly important to study the evolution law of population distribution. Geography focuses on spatial distribution patterns, regional differences, and scale correlations. It has a tradition of spatial analysis and map language, which helps to understand the spatiotemporal evolution of characteristics, such as population and cities, and to fully comprehend the concept of regional development differences and cross-spatial correlations; advancing civil society and government decision-making (Yu et al., 2022a; Yu et al., 2022b). For instance, Liaoning Province, a province with significant changes in population structure and a relatively high level of educational development, is undergoing a rapid urbanization process. Thus, to a degree, Liaoning Province represents the epitome of demographic changes and social structural transformation in China. Therefore, the current study is based on the statistical data of the development of compulsory education in Liaoning Province. Here, we construct a geographic database and combine mathematical statistics and spatial analysis methods using different spatial scales such as cities, counties, and towns, to analyze the regional and urban-rural differences in the distribution of students in compulsory education schools in Liaoning Province. In addition, the temporal change characteristics and spatial clustering and dispersion characteristics are investigated. The innovation of this study is based on vast research samples and rich research scales, and combining temporal information, spatial information and attribute information of school data to explore the evolution characteristics of the temporal and spatial distribution of compulsory education students. This study provides a new perspective for investigating the spatial distribution of students in schools to help provide additional case areas worldwide.

2 Materials and methods

2.1 Study area

Liaoning Province is located in the southern part of northeast China (Figure 1). As an important old industrial base in China, Liaoning Province has recently faced a profound economic and social transformation, and its population structure has undergone drastic changes. From 2010 to 2020, the regional and per capita GDP increased from 1,389.6 billion yuan to 2,511.5 billion yuan and from 31,888 yuan to 57,713 yuan, respectively. Liaoning Province has entered a stage of negative population growth to become a society with fewer births and an

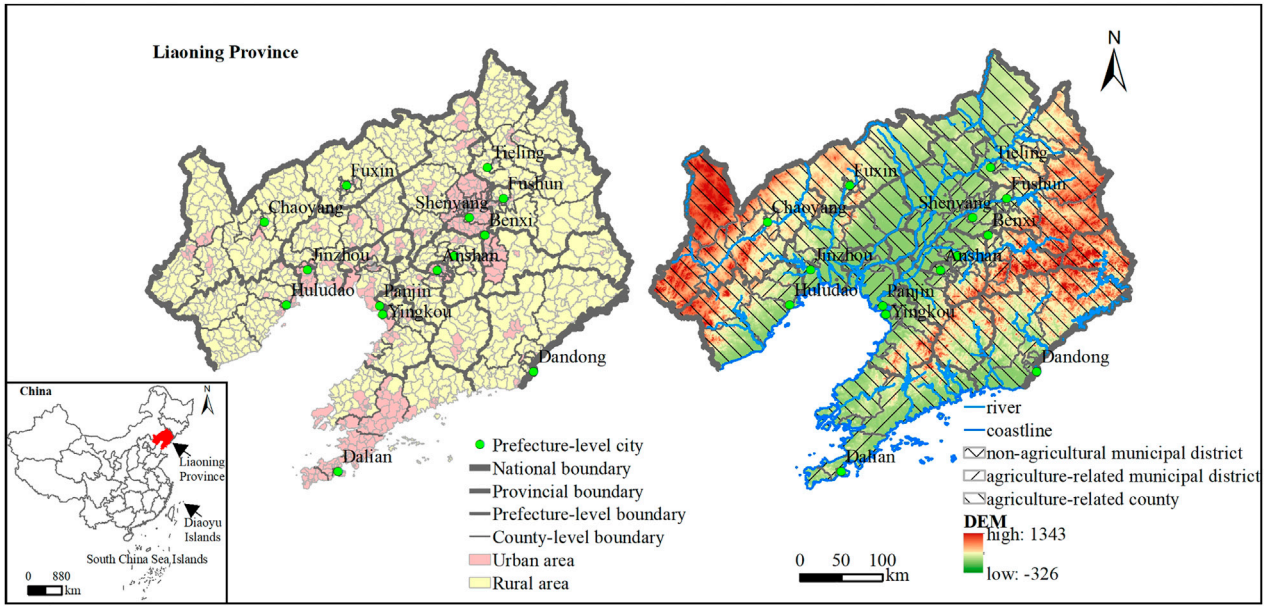

FIGURE 1
Location of Liaoning Province, China.

aging population, and the population has demonstrated a historical trend of change. The main contradiction in population development has shifted from population number to population structure. The 2010 and 2020 census data showed that the permanent population of Liaoning Province declined from 4,374.63 ten thousand to 4,259.14 ten thousand, whereas the urbanization rate increased from 62.10% to 72.14%. The number of students in compulsory education in Liaoning Province decreased from 345.48 ten thousand in 2010 to 296.84 ten thousand in 2020. Due to the regional and urban-rural differences in the level of social and economic development, the population flow has exhibited a trend from villages to towns, and from small towns to large cities. The number of students studying in different locations during the compulsory education stage has increased from 22.95 ten thousand in 2010 to 26.26 ten thousand in 2020. By the end of 2020, Liaoning Province had jurisdiction over 14 prefecture-level cities including Shenyang and Dalian, 100 county-level administrative districts, and 1,350 township-level districts. Based on the administrative divisions of Liaoning Province by the end of 2020 and the "Liaoning Provincial Statistical Yearbook 2021", this study delineated 23 non-agricultural municipal districts, 36 agricultural municipal districts, 41 counties (Figure 1). Among these, non-agricultural municipal districts refer to municipal districts that do not involve agriculture, rural areas and farmers. Agriculture-related districts and counties refer to municipal districts or counties that involve agriculture, rural areas, and farmers. According to the "Regulations on Statistical Division of Urban and Rural Areas" approved by the State Council of People's Republic of China and the "China Counties Statistical Yearbook (2021)," we delineated Chengguan towns and agricultural towns to delineate urban and rural areas at the town scale. Among them, Chengguan towns and subdistricts were generally urban areas with a relatively developed economy and agglomerated population, and a high level of urbanization in the county, whereas agricultural towns and streets were primarily rural areas with relatively important primary industries.

2.2 Data source

The data acquired in this study included basic geospatial data and socioeconomic statistics of Liaoning Province (Table 1). Data preprocessing included determining school lists and school coordinates as well as the extraction of student information. The school list was determined according to the research scope of compulsory education schools, and the reserved school type codes were 211 (primary school), 218 primary school teaching points, 219 (primary school classes attached), 311 (junior middle school), 312 (nine-year consistent system school), 319 (with ordinary junior high school classes), and 345 (twelve-year consistent schools). To determine school coordinates, we first compared and analyzed information from the Baidu map (https://map.baidu.com/), Baidu search engine (https://map.baidu.com/), and Google Earth satellite images to confirm the

TABLE 1 Data sources and descriptions.

Data box	Data name	Data description	Data source
Education statistics	School information statistics	School name, school identification code, school type code	Education department of Liaoning Province
	Student information statistics	Number of students (including the number of boys, the number of girls, the number of students in the primary school, the number of students in the junior high school, and the number of children of migrant workers who moved to cities)	
Administrative division data	Administrative division data	Administrative division name and code, administrative division adjustment document, prefecture-level city government resident	Liaoning Provincial geographic information public service platform (https://liaoning.tianditu.gov.cn/), Ministry of civil affairs of the People's Republic of China (http://www.mca.gov.cn/), "Brief book of administrative divisions of the People's Republic of China" over the years
Digital line map (DLG) data	1:1 million vector map data	River, coastline	China national geographic information center (http://www.webmap.cn/)
Digital elevation model (DEM) data	ASTER GDEM V02	30 m*30 m DEM data	US national geological survey website (https://www.usgs.gov/)

geographic location of each school. Then, we obtained the BD-09 geographic coordinates of each school using the Baidu Map Coordinate Picking System (https://api.map.baidu.com/). Finally, we used the Baidu Map APIs (forward and reverse geocoding function) provided by the Baidu Map Open Platform (https://lbsyun.baidu.com/) to convert the BD-09 geographic coordinates into WGS1984 geographic coordinates. To extract student information, we used 2020 as the standard year to identify 14 prefecture-level cities, 100 county-level administrative units, and 1,530 town-level administrative units in Liaoning Province. Then, we used Microsoft Excel 2019 and ArcGIS 10.7, according to the gender, source and education stage of the students, to summarize the number of students in each school into their respective research unit.

2.3 Research methods

We used data from Liaoning Province between 2010 and 2020 in this study. First, a multi-dimensional analysis of the population, gender structure, student source composition, and education stage of primary and secondary school students was performed based on educational statistics and geospatial data, and using demographic methods. Next, using standard deviational ellipse and the center of gravity transfer method, the spatial evolution characteristics of primary and secondary school students at the municipal scale were analyzed. Third, using the one-stage decomposition method of Theil indices, the regional difference characteristics of primary and secondary school students at the county level were analyzed. Finally, using the emerging spatiotemporal hotspot analysis method, the emerging spatiotemporal distribution pattern of primary and secondary school students at the township level was analyzed. The technical route of this study is shown in Figure 2.

2.3.1 Standard deviational ellipse

Standard deviational ellipse, a classical method to analyze the directional characteristics of spatial distribution, primarily uses the center, long, and short axes as the basic parameters to quantitatively describe geographical elements and was first proposed by Lefever (Lefever, 1926). In physics, the "center of gravity" refers to the point of action where the force exerted on each point in the object produces a resultant force. The direction of the deviation of the center of gravity indicates the "high-density" part of the distribution of students in the school, while the migration of the center of gravity reflects the aggregation and displacement law of students in the study area. The size and declination angle (major semi-axis) of the standard deviation ellipse reflects the concentration and dominant direction of the spatial distribution pattern of school students, respectively. Using the spatial difference of the standard deviation ellipse and the center of gravity of students in Liaoning Province reflects the distribution characteristics of students in the two-dimensional space and identifies the core gathering area of students. This study used an ellipse with one standard deviation, which covered approximately 68% of the study element amount. The formula used is as follows (Bai et al., 2021):

$$\bar{x} = \sum_{i=1}^{n} w_i x_i \Big/ \sum_{i=1}^{n} w_i, \bar{y} = \sum_{i=1}^{n} w_i y_i \Big/ \sum_{i=1}^{n} w_i \tag{1}$$

$$\tan\theta = \left[\left(\sum_{i=1}^{n} w_i^2 y_i^2 - \sum_{i=1}^{n} w_i^2 y_i^2 \right) + \sqrt{\left(\sum_{i=1}^{n} w_i^2 y_i^2 - \sum_{i=1}^{n} w_i^2 y_i^2 \right)^2 + 4 \sum_{i=1}^{n} w_i^2 x_i^2 y_i^2} \right] \Big/ 2 \sum_{i=1}^{n} w_i^2 x_i y_i \tag{2}$$

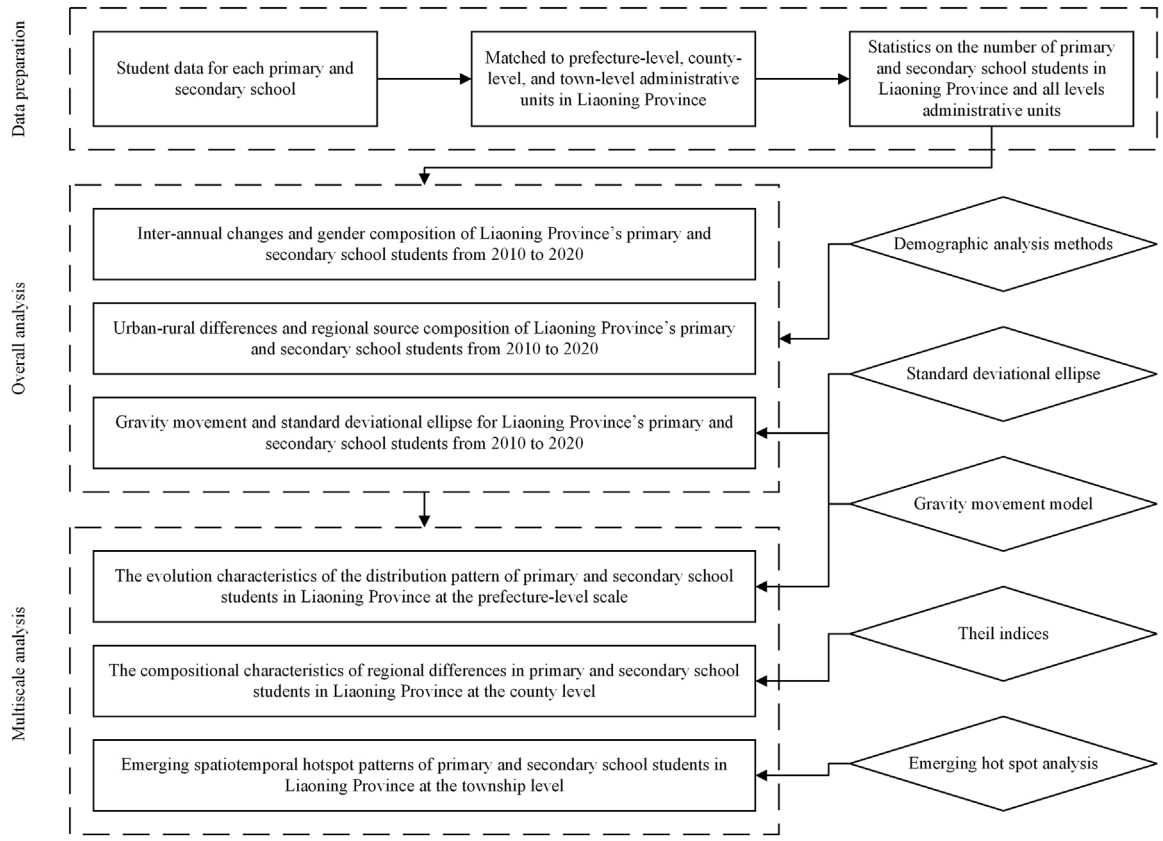

FIGURE 2
Flow diagram of this study.

$$\sigma_x = \sqrt{2\sum_{i=1}^{n}\left(w_i\tilde{x}_i\cos\theta - w_i\tilde{y}_i\sin\theta\right)^2 \Big/ \sum_{i=1}^{n} w_i^2} \tag{3}$$

$$\sigma_y = \sqrt{2\sum_{i=1}^{n}\left(w_i\tilde{x}_i\sin\theta + w_i\tilde{y}_i\cos\theta\right)^2 \Big/ \sum_{i=1}^{n} w_i^2} \tag{4}$$

$$\tilde{x}_i = x_i - \bar{x}, \tilde{y}_i = y_i - \bar{y} \tag{5}$$

$$S = \pi\varphi_x\varphi_y \tag{6}$$

$$o = (\alpha - \beta)/\alpha \tag{7}$$

In the formula, n is the number of units; $(\bar{x}, \bar{y})$ is the barycentric coordinate of the area; (x_i, y_i) is the latitude and longitude coordinates of the unit; w_i is the weight value of the unit i; θ is the azimuth angle of the ellipse; σ_x, σ_y are the standard deviation of the ellipse axis x and axis y, respectively; $\tilde{x}$, $\tilde{y}$ are the coordinate deviation of each unit to the center of gravity; S is the area of the ellipse; O is the oblateness of the ellipse that reflects how flat the ellipse is. The size of O is determined by the major semi-axis α and the minor semi-axis β of the ellipse, with a value between 0 and 1. When $\alpha = \beta$, the ellipse becomes a circle; when β decreases and α increases, the ellipse becomes flat; when $\beta = 0$, $\alpha = 1$, the ellipse becomes a line.

2.3.2 Theil indices

Theil indices can be broken down into independent inter-group and intra-group gaps and are widely used to measure relative differences in phenomena such as economic development, income distribution, and population distribution (Xu et al., 2005; Yan and Bian., 2008). The expression is as follows:

$$T = \sum_{i=1}^{m}\left(\frac{p_i}{p}\right) \times \log\left(\frac{p_i/p}{s_i/s}\right) \tag{8}$$

where, m is the number of county-level administrative units, and the value of is 100; p is the number of students in Liaoning Province; p_i is the number of students enrolled in the sub-region i; s is the area of Liaoning Province; s_i is the area of the sub-region i. The larger the value of Theil indices T, the greater the difference in the distribution of students in different regions; on the

contrary, the smaller the value of Theil indices T, the smaller the difference in the distribution of students in different regions.

If the sub-region is used as the basic space unit, Theil indices T can be decomposed in one stage. Therefore, the overall differences in Liaoning Province are broken down into the differences between three sub-regions (non-agricultural municipal districts, agricultural-related municipal districts, and agricultural-related counties) and the differences between county-level administrative units within the three sub-regions. Then, the formula for calculating T_{province}, which represents the overall difference in the distribution of students in Liaoning Province, is as follows:

$$\boldsymbol{T}_{\mathbf{province}} = \sum_{i=1}^{m}\sum_{j=1}^{n}\left(\frac{\boldsymbol{p}_{ij}}{\boldsymbol{p}}\right) \times \mathbf{log}\left(\frac{\boldsymbol{p}_{ij}/\boldsymbol{p}}{\boldsymbol{s}_{ij}/\boldsymbol{s}}\right) \tag{9}$$

where: p_{ij} is the number of students in county-level administrative unit j of sub-region i; s_{ij} is the area of county-level administrative unit j of sub-region i; n is the number of sub-regions, and the value of n is 3.

If the interregional difference of the sub-region i is defined as:

$$\boldsymbol{T}_{\mathbf{area}} = \sum_{j=1}^{n}\left(\frac{\boldsymbol{p}_{ij}}{\boldsymbol{p}_{i}}\right) \times \mathbf{log}\left(\frac{\boldsymbol{p}_{ij}/\boldsymbol{p}_{i}}{\boldsymbol{s}_{ij}/\boldsymbol{s}_{i}}\right) \tag{10}$$

Then the Theil indices T_{province} in Eq. 9 can be decomposed as:

$$\begin{aligned}\boldsymbol{T}_{\mathbf{province}} &= \sum_{i=1}^{m}\left(\frac{\boldsymbol{p}_{i}}{\boldsymbol{p}}\right)\boldsymbol{T}_{\mathbf{area}} + \sum_{i=1}^{m}\left(\frac{\boldsymbol{p}_{i}}{\boldsymbol{p}}\right) \times \mathbf{log}\left(\frac{\boldsymbol{p}_{i}/\boldsymbol{p}}{\boldsymbol{s}_{i}/\boldsymbol{s}}\right)\\ &= \sum_{i=1}^{m}\left(\frac{\boldsymbol{p}_{i}}{\boldsymbol{p}}\right)\boldsymbol{T}_{\mathbf{area}} + \boldsymbol{T}_{\mathbf{zone}} = \boldsymbol{T}_{\mathbf{county}} + \boldsymbol{T}_{\mathbf{zone}}\end{aligned} \tag{11}$$

where: p_i is the number of students in the sub-region i; s_i is the area of the sub-region i; T_{zone} is the difference in the distribution of students between the 3 sub-regions; T_{county} is the difference in the distribution of students in each county-level administrative unit within the three sub-regions. The essence of T_{county} is the weighted average of the absolute differences in the distribution of students in each county-level administrative unit in the three sub-regions, and the weight is the proportion of each sub-region in the number of students in Liaoning Province.

2.3.3 Emerging hot spot analysis

Emerging hot spot analysis refers to the generation of a space-time cube of time and space NetCDF as input by specifying neighborhood distance and time step to perform Getis-Ord G_i^* hotspot analysis on sequence data in spatiotemporal data one-by-one, and use Mann-Kendall trend analysis to evaluate hot and cold spot trends in spatiotemporal data. The space-time cube model employs a two-dimensional coordinate axis to represent the spatial position of geographic elements, a one-dimensional time axis represents the change of geographic elements with the change of time step and uses the geometric features of the time dimension to express the process of geographic phenomena changing with time. The space and one-dimensional time are then combined into a three-dimensional space-time cube (Langran, 1989; Huang et al., 2015).

Hot spot analysis is often used to reveal the spatial agglomeration features of a local area and identify statistically significant spatial clusters of high values (hot spots) and low values (cold spots). The calculation formula of Getis-Ord G_i^* is as follows (Getis and Ord, 1992):

$$\boldsymbol{G}_{\boldsymbol{i}}(\boldsymbol{d}) = \sum_{j=1}^{n}\boldsymbol{w}_{\boldsymbol{ij}}(\boldsymbol{d})\boldsymbol{x}_{\boldsymbol{j}} \Big/ \sum_{j=1}^{n}\boldsymbol{x}_{\boldsymbol{j}} \tag{12}$$

In the formula: $w_{ij}(d)$ is the spatial weight matrix, $i \neq j$. $G_i(d)$ is the degree of correlation between the statistic of the research unit i and the adjacent research unit j. The formula for normalization of $G_i(d)$ is:

$$\boldsymbol{Z}(\boldsymbol{G}_{\boldsymbol{i}}) = \frac{[\boldsymbol{G}_{\boldsymbol{i}}(\boldsymbol{d})] - \boldsymbol{E}(\boldsymbol{G}_{\boldsymbol{i}})}{\sqrt{\boldsymbol{VAR}(\boldsymbol{G}_{\boldsymbol{i}})}} \tag{13}$$

where: $E(G_i)$ and $VAR(G_i)$ represent the mathematical expectation and theoretical variance of G_i, respectively. When $Z(G_i)$ is positive and significant, it indicates that the attribute values of the units around the research unit i are relatively high, and the research unit i belongs to the hotspot area; when $Z(G_i)$ is negative and significant, it means that the attribute values of the units around the research unit i are low, and the research unit i belongs to the cold spot area.

The Mann-Kendall trend analysis method is a nonparametric statistical test method for testing independent space-time column series. For a time series with a sample size of n, the trend test statistic is as follows (Zhu et al., 2019):

$$\boldsymbol{S} = \sum_{i=1}^{n-1}\sum_{j=i+1}^{n}\mathbf{sgn}\left(\boldsymbol{x}_{\boldsymbol{j}} - \boldsymbol{x}_{\boldsymbol{i}}\right) \tag{14}$$

$$\mathbf{sgn}\left(\boldsymbol{x}_{\boldsymbol{j}} - \boldsymbol{x}_{\boldsymbol{i}}\right) = \begin{cases} 1 & \boldsymbol{x}_{\boldsymbol{j}} > \boldsymbol{x}_{\boldsymbol{i}} \\ 0 & \boldsymbol{x}_{\boldsymbol{j}} = \boldsymbol{x}_{\boldsymbol{i}} \\ -1 & \boldsymbol{x}_{\boldsymbol{j}} < \boldsymbol{x}_{\boldsymbol{i}} \end{cases} \tag{15}$$

When the statistic follows a normal distribution, the variance is as follows:

$$\mathbf{Var}(\boldsymbol{S}) = [\boldsymbol{n}(\boldsymbol{n}-1)(2\boldsymbol{n}+5)]/18 \tag{16}$$

$$\mathbf{sgn}\left(\boldsymbol{x}_{\boldsymbol{j}} - \boldsymbol{x}_{\boldsymbol{i}}\right) = \begin{cases} (\boldsymbol{S}-1)/\sqrt{\mathbf{Var}(\boldsymbol{S})} & \boldsymbol{S} > 0 \\ 0 & \boldsymbol{S} = 0 \\ (\boldsymbol{S}-1)/\sqrt{\mathbf{Var}(\boldsymbol{S})} & \boldsymbol{S} < 0 \end{cases} \tag{17}$$

Corresponding z-scores and p-values were obtained using Mann-Kendall trend analysis. If the z-score was greater than 1.65, it indicates that the time series was in an upward trend, that is, the number of primary and secondary school students increased annually; if the z-score was less than −1.65, it infers that the time series was in a downward trend, that is, the number of primary and secondary school students decreased annually; if the z-score is greater than 1.65, it indicates that there was no significant

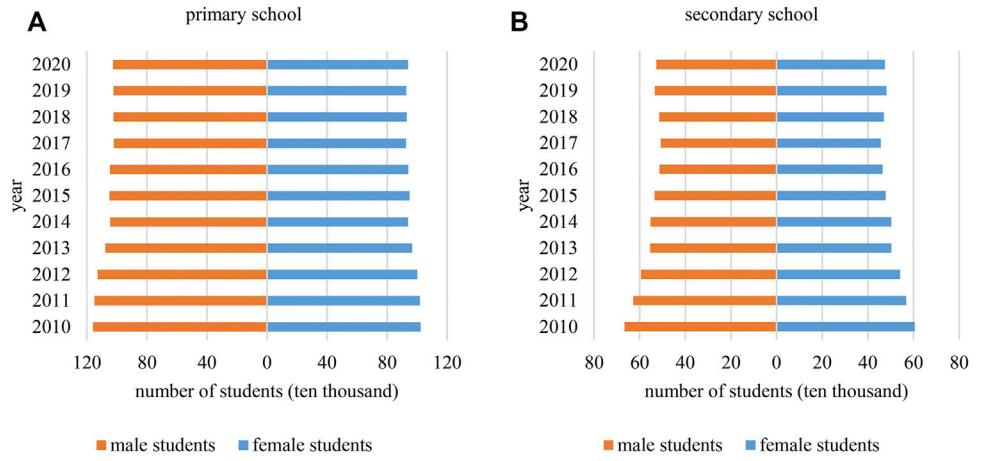

FIGURE 3
Inter-annual changes and gender composition of Liaoning Province's primary and secondary school students from 2010 to 2020.

change in the number of primary and secondary school students with time series. The significance level was determined according to the range of the *p*-value. According to *z*-scores and *p*-values, the significance of cold and hot trends in the number of primary and secondary school students was classified into several categories such as new, consecutive, intensifying, persistent, diminishing, sporadic, oscillating, historical, 16 hot and cold patterns, and no pattern detected (Li et al., 2021).

3 Results

3.1 Changes in overall characteristics of Liaoning Province

Figure 3A shows that the number of primary school students in Liaoning Province decreased from 218.25 ten thousand to 196.61 ten thousand, representing a decrease of 9.99%, and was accompanied by a decline in the sex ratio from 113.42 to 109.24 between 2010 and 2020. Figure 3B demonstrates that the number of junior high school students in Liaoning Province decreased by 21.22% from 127.23 ten thousand to 100.23 ten thousand, and was accompanied by an increase in the sex ratio from 110.07 to 111.11. We observed that the number of students in primary and junior high schools experienced an initial fluctuation followed by a slight increase. We determined that the ratio of primary to junior high school students rose from 1.72 to 1.96. In general, a reducing trend in the scale of primary and secondary school students in Liaoning Province occurred. In recent years, the number of students in school has remained stable, and the downward trend has been curbed. In addition, the imbalance between males and females has been alleviated to a certain extent.

Figure 4A shows that from 2010 to 2020, the number of local primary school students in Liaoning Province decreased from 201.48 ten thousand to 178.64 ten thousand, a decrease of 11.34%, accompanied by a decline in the sex ratio from 111.69 to 108.32. Figure 4B shows that the number of local students in junior high schools in Liaoning Province decreased by 23.38% from 62.92 ten thousand to 48.21 ten thousand, accompanied by an increase in sex ratio from 108.25 to 110.25 during the study period. We determined that the number of local students in primary and junior high schools initially fluctuated and decreased before becoming stabilized. The ratio of number of local students in primary schools to that in junior high schools rose from 1.66 to 1.94, suggesting that Liaoning Province has faced the increasing issue of low birthrate which has impacted compulsory education since the beginning of the 21st century.

Figure 5A shows that from 2010 to 2020, the number of migrant students in primary schools in Liaoning Province increased by 7.22% from 16.77 ten thousand to 17.98 ten thousand, accompanied by a decrease in the sex ratio from 136.70 to 118.74. Figure 5B shows that the number of migrant students in junior high schools increased from 6.18 ten thousand to 8.28 ten thousand, an increase of 34.02%, with a decrease in the sex ratio from 153.42 to 121.09. We observed fluctuation in both the number of migrant students in primary and junior high schools. The ratio of migrant students in primary schools to those in junior high schools declined from 2.71 to 2.17. This finding indicates a trend of increasing population mobility in Liaoning Province, with more children attending nearby schools, and more girls given this opportunity. Moreover, this suggests that the schooling needs of children of migrant workers have been met, and more children, especially girls, are no longer excluded. These further highlights that in addition to the exclusion issue of

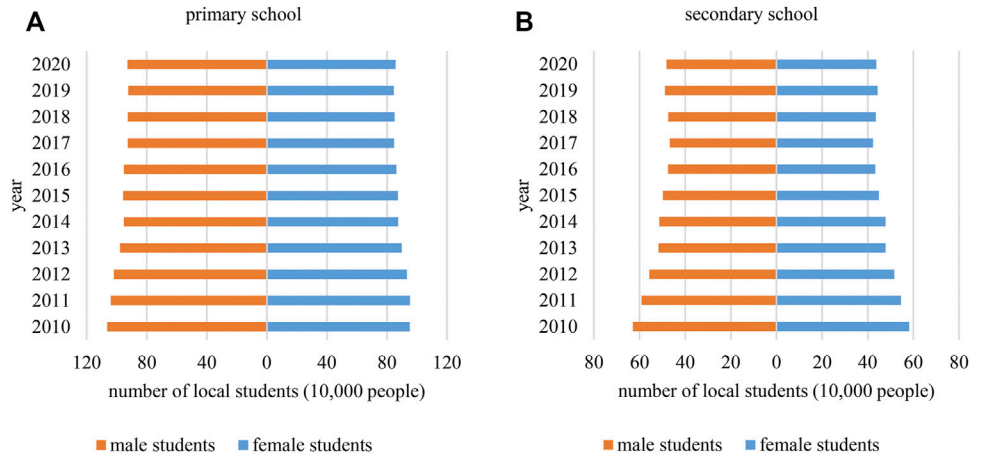

FIGURE 4
Inter-annual changes and gender composition of Liaoning Province's primary and secondary school local students from 2010 to 2020.

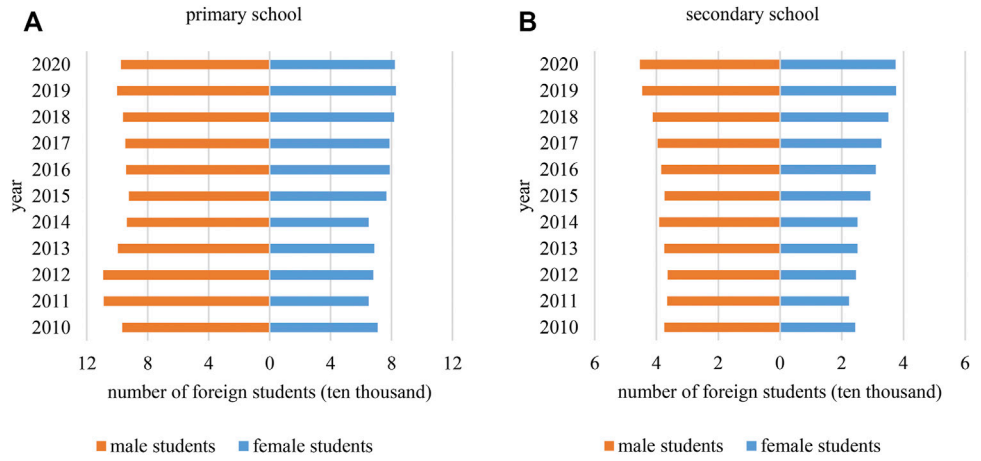

FIGURE 5
Inter-annual changes and gender composition of Liaoning Province's primary and secondary school foreign students from 2010 to 2020.

children in rural areas, the issue of urban migrant children requires attention.

As shown in Figure 6, the number of local students in urban areas was slightly higher than in rural areas in 2010, with the absolute scale being almost double that of rural areas in 2020. Over the past 10 years, the vast majority of students from different areas have been concentrated in urban areas, and this trend is becoming increasingly evident. We found that the number of local students in urban areas declined slightly before 2017 and then remained stable. After 2017, the number of urban and rural students exhibited an increase of 8.77% over the 10 years. However, the number of local students in rural areas continued to decline, with a 41.97% decrease over the 10 years. Similarly, we observed a fluctuating upward trend in the number of migrant students in urban areas, whereas in rural areas a fluctuating downward trend occurred, with an increase of 15.93% and a decrease of 21.25%, respectively. Overall, a gap between urban and rural areas appears to be growing as urban areas have been attracting the school-age population, leading to the continuous loss of students in rural areas. This is becoming an increasingly serious issue.

As shown in Table 2 and Figure 7, the rotation angle of the standard deviational ellipse of primary and secondary school students fluctuated within the range of 41–52° for a long period of

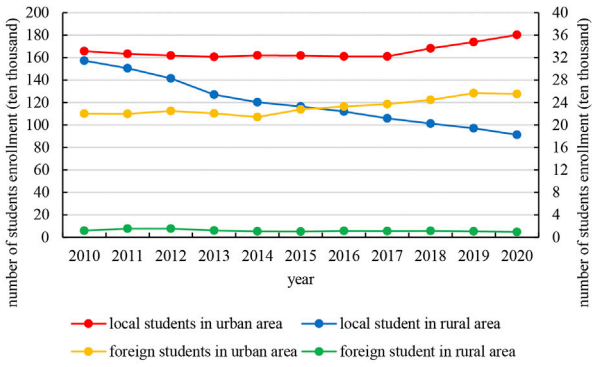

FIGURE 6
Urban-rural differences and regional source composition of Liaoning Province's primary and secondary school students from 2010 to 2020.

time, indicating that the distribution of primary and secondary school students mainly follows the northeast-southwest direction. In particular, the rotation angle of the standard deviation ellipse exhibited a decreasing trend, from 51.152° in 2010 to 41.657° in 2020. We also recorded an area of the standard deviational ellipse that was slightly changed, whereas the size of the ellipse remained stable. The aggregation area of primary and secondary school students exhibited a tendency of moving towards coastal areas. In addition, the influence of Dalian and Shenyang on the distribution of primary and secondary school students in Liaoning Province gradually increased. We determined that the major semi-axis primarily fluctuated in the range of 181–186 km, indicating an expansion trend. Whereas, the short semi-axis fluctuated in the range of 131–136 km, showing a shrinking trend. Based on the changes of the long and short semi-axes, we found that the distribution of primary and secondary school students exhibited a continuous expansion trend in the north-south direction and a continuous contraction trend in the east-west direction. Moreover, the flat rate exhibited a continuously increasing trend from 2010 to 2020, indicating that the distribution area of primary and secondary school students in Liaoning Province was approximately circular, with a flattening trend.

Judging from the movement trajectory of the center of gravity (Table 2; Figure 7) from 2010 to 2020, the distribution center of gravity of primary and secondary school students in Liaoning Province shifted by a total of 12.022 km, with an apparent trend of moving south to west. More specifically, from 2010 to 2012, we determined that this moved 1.049 km in a west–south direction, from 2013 to 2017 it moved 7.172 km in a west-southwest direction, and from 2018 to 2020 it moved 3.802 km in a south-east direction. In conclusion, from 2010 to 2012, the center of gravity showed a westward dominant moving direction, with a shorter moving distance, whereas from 2013 to 2020, the center of gravity demonstrated a southward dominant moving direction, with a longer moving distance. This southward moving trend of the center of gravity became increasingly obvious with time.

3.2 Variation characteristics of prefecture-level division scale

Table 3 shows that in 2010 and 2020, Shenyang and Dalian ranked as the top two for the number of students; moreover, these were the only two cities with an increase in student numbers. We observed that the number of students in the remaining 12 prefecture-level cities decreased by 10%. This finding demonstrated the obvious siphon effect of Shenyang and Dalian, highlighting the significant differences and serious imbalance between cities. In 2020, except for Shenyang, Dalian, and Yingkou, the proportion of primary school students in the remaining 11 prefecture-level cities was lower than the average of Liaoning Province. This suggests that the number of students in these 11 prefecture-level cities will be insufficient in follow-up supply and is facing huge pressure from the weak natural growth of the school-age population. In 2020, Dalian had the highest proportion (almost 25%) of migrant students. Moreover, the number of migrant students in Dalian was nearly half of that in Liaoning Province, indicating that Dalian, as the most economically developed city in Liaoning Province, has great advantage in attracting population. However, it also experiences the pressure of migrant children attending school. In addition, we determined that the scale of migrant students in Shenyang was relatively large and associated with a high proportion. Whereas, the other 12 prefecture-level cities are experiencing enormous pressure from the loss of school-age population. In 2020, the number of female students was significantly lower than that of male students, and the gender ratio was severely unbalanced. Among them, Chaoyang City had the highest gender ratio, which is related to the low level of local economic and social development and the prevailing ideology of "prefer sons to daughters." Conclusively, Dalian and Shenyang are facing the pressures associated with the supply to primary and secondary schools, whereas the remaining 12 prefecture-level cities are suffering with a reduced number of students enrolled in school.

In order to effectively observe the changes in the distribution centers of primary and secondary school students in various prefecture-level cities in Liaoning Province, as well as the relative positions of the centers of gravity and administrative centers which are represented by the prefecture-level city governments in different years, we calculated the coordinates of the center of gravity of the distribution of students in primary and secondary schools in prefecture-level cities in 2010 and 2020 and their distance from the administrative center (Table 4). According to Figure 7 and Table 4, the distance between the distribution center

TABLE 2 Inter-city differences in the number of Liaoning's primary and secondary school students in 2010 and 2020.

Prefecture-level city	Students in 2010	Students in 2020		Primary school students in 2020		Migrant school students in 2020		Male students in 2020	Female students in 2020	Sex ratio (female = 100)
	Number of people (10,000 people)	Number of people (10,000 people)	Increase from 2010 (%)	Number of people (10,000 people)	Proportion (%)	Number of people (10,000 people)	Proportion (%)	Number of people (10,000 people)	Number of people (10,000 people)	
Shenyang	52.07	61.18	17.49	42.22	69.01	5.99	9.79	32.14	29.04	111.65
Dalian	46.31	51.80	11.87	36.67	70.79	12.30	23.75	27.04	24.76	109.22
Anshan	28.95	23.05	−20.37	15.00	65.08	0.77	3.34	11.98	11.07	108.29
Fushun	14.01	10.89	−22.25	7.15	65.68	0.49	4.47	5.65	5.24	107.89
Benxi	10.81	7.64	−28.02	5.00	65.42	0.37	4.82	3.99	3.65	109.17
Dandong	20.52	13.11	−36.09	8.59	65.53	0.43	3.27	6.74	6.38	105.66
Jinzhou	25.39	16.76	−33.98	10.68	63.74	0.69	4.13	8.67	8.09	107.13
Yingkou	19.91	17.23	−13.47	11.61	67.38	0.92	5.34	8.99	8.24	109.06
Fuxin	15.81	11.08	−29.92	6.94	62.67	0.48	4.33	5.83	5.25	110.89
Liaoyang	15.90	10.07	−36.65	6.40	63.55	0.46	4.55	5.22	4.85	107.80
Panjin	12.09	10.72	−11.37	6.62	61.73	0.71	6.60	5.63	5.09	110.42
Tieling	24.82	15.83	−35.69	9.63	60.85	0.75	4.73	8.25	7.58	108.74
Chaoyang	32.88	26.60	−19.11	16.93	63.64	0.95	3.56	14.28	12.32	115.83
Huludao	26.42	20.88	−20.95	13.17	63.06	0.96	4.60	11.01	9.88	111.42
Total	345.48	296.84	−14.08	196.61	66.24	26.26	8.85	155.40	141.45	109.86

10.3389/feart.2022.1014490

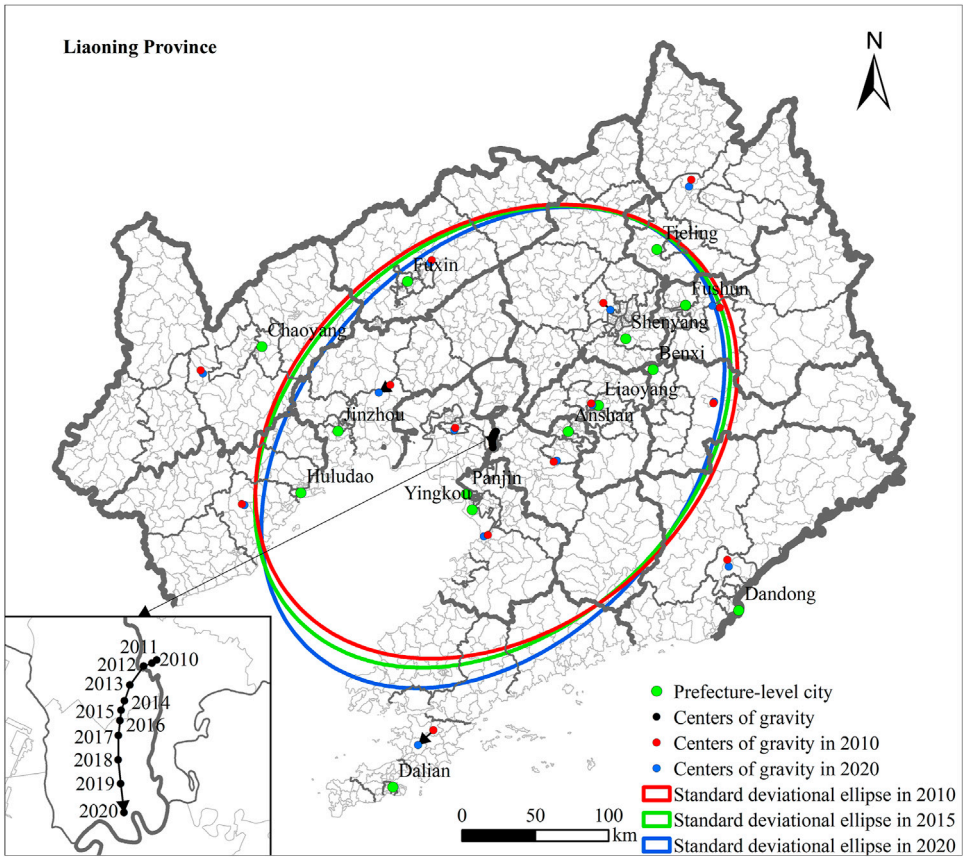

FIGURE 7
Gravity movement and standard deviational ellipse for Liaoning Province's primary and secondary school students from 2010 to 2020.

TABLE 3 Standard deviational ellipse parameters for Liaoning's primary and secondary school students from 2010 to 2020.

Year	Longitude/°	Latitude/°	Migration distance (km)	Major semi-axis (km)	Minor semi-axis (km)	Flattening	Rotation angle/°	Ellipse area (10,000 km^2)
2010	122.410	41.108	Null	180.191	135.854	0.246	51.152	7.690
2011	122.406	41.106	0.415	180.342	135.462	0.249	50.991	7.674
2012	122.399	41.104	0.634	180.506	135.288	0.251	50.992	7.671
2013	122.388	41.092	1.678	180.826	134.186	0.258	49.403	7.622
2014	122.383	41.082	1.195	181.572	133.906	0.263	48.344	7.638
2015	122.381	41.076	0.725	182.098	133.746	0.266	47.782	7.651
2016	122.380	41.069	0.751	182.877	133.543	0.270	47.034	7.672
2017	122.379	41.060	1.064	183.581	133.262	0.274	46.131	7.685
2018	122.379	41.044	1.759	184.283	132.509	0.281	44.461	7.671
2019	122.381	41.029	1.725	184.964	132.021	0.286	43.173	7.671
2020	122.385	41.010	2.076	185.861	131.315	0.293	41.657	7.667

of primary and secondary school students in 14 prefecture-level cities in Liaoning Province (2010–2020) and the administrative center narrowed, with all shifting in the direction of the urban administrative center. The administrative center is often an economic and cultural center and this finding reveals that the center orientation of the distribution of students in schools was

TABLE 4 Gravity parameters of the number of primary and secondary school students in 14 prefecture-level cities in Liaoning Province from 2010 to 2020.

Prefecture-level city	Center of gravity in 2010			Center of gravity in 2020					Migration distance (km)
	Longitude/°	Latitude/°	Distance from administrative center (km)	Longitude/°	Latitude/°	Distance from administrative center (km)	Where: distance change (km)	Where: distance increase (%)	
Shenyang	123.277	41.895	28.701	123.333	41.852	22.242	−6.458	−22.503	6.660
Dalian	121.923	39.267	47.646	121.804	39.175	33.551	−14.096	−29.584	14.431
Anshan	122.872	40.920	22.932	122.896	40.927	21.380	−1.552	−6.766	2.184
Fushun	124.233	41.860	23.452	124.173	41.872	18.405	−5.048	−21.523	5.144
Benxi	124.169	41.274	47.144	124.175	41.283	47.130	−0.014	−0.030	1.114
Dandong	124.265	40.311	35.321	124.275	40.270	30.686	−4.635	−13.122	4.635
Jinzhou	121.538	41.383	47.430	121.446	41.335	38.196	−9.235	−19.470	9.344
Yingkou	122.343	40.469	20.334	122.310	40.460	19.892	−0.441	−2.171	3.019
Fuxin	121.863	42.153	22.107	121.850	42.137	20.119	−1.988	−8.993	2.081
Liaoyang	123.175	41.279	5.142	123.185	41.269	4.140	−1.002	−19.493	1.331
Panjin	122.071	41.126	45.962	122.065	41.111	44.506	−1.455	−3.167	1.680
Tieling	124.011	42.649	53.129	123.992	42.606	48.146	−4.983	−9.379	5.049
Chaoyang	119.991	41.443	44.570	120.010	41.424	44.055	−0.516	−1.157	2.576
Huludao	120.360	40.630	40.833	120.380	40.625	39.297	−1.536	−3.761	1.766

10.3389/feart.2022.1014490

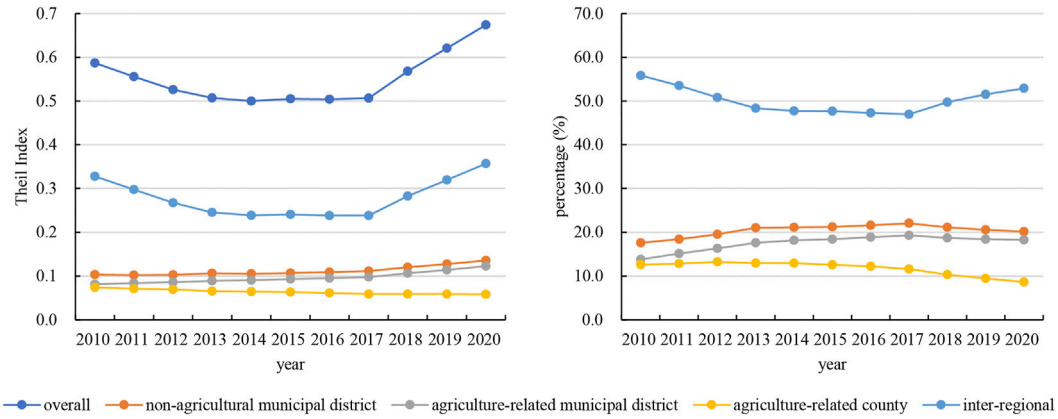

FIGURE 8
One-stage nested decomposition of Theil index of the distribution of students in primary and secondary schools of Liaoning Province from 2010 to 2020.

strengthened, with the students in primary and secondary schools showing a trend of flowing out from the edge and into the center. We detected that the center of gravity migration distance was the longest in Dalian, reaching 14.431 km, followed by Jinzhou (9.344 km) and Shenyang (6.660 km). This indicates that the distribution of primary and secondary school students in these cities has undergone a relatively drastic change in the centripetal direction, revealing clear educational urbanization in which rural students are first concentrated in urban schools.

3.3 Variation characteristics of county-level division scale

Theil indices T between Liaoning Province, non-agricultural municipal districts, agricultural municipal districts, agricultural counties, and the Theil indices T between the three major regions from 2010 to 2020 were calculated by taking the county-level administrative unit as the research unit and using the one-stage decomposition method of Theil indices. Figure 8 reveals the regional composition of the relative differences in the distribution of primary and secondary school students in Liaoning Province on a county-level division scale, as well as the changing process of differences between the three major regions and within each region. The results demonstrate that when 2013 and 2017 are set as the boundary, the difference in the distribution of primary and secondary school students in Liaoning Province as a whole exhibited a trend of shrinking in the early stage, stability in the mid-term, and expanding in the later stage. The change trend of the distribution difference of primary and secondary school students between the three regions was almost the same as Liaoning Province, while the change trend of the distribution difference within the three regions presented different trends. Specifically, from 2010 to 2020, the relative differences in the distribution of primary and secondary school students in non-agricultural municipal districts and agricultural-related municipal districts showed an expanding trend, while the relative differences in the distribution of primary and secondary school students in agricultural counties exhibited a narrowing trend. In order to reveal the correlation of their changing trends, we further calculated the Kendall correlation between the Theil indices T between Liaoning Province, non-agricultural municipal districts, agricultural municipal districts, agricultural counties, and the Theil indices T between the three major regions from 2010 to 2020. A two-sided test was performed at the significance level $\alpha = 0.05$. The results showed that Liaoning Province and the three regions were highly significant, while Liaoning Province and non-agricultural municipal districts, agricultural-related municipal districts, and agricultural-related counties were not significant. This indicates that the relative trend of the distribution of primary and secondary school students in Liaoning Province and the three major regions were essentially equal.

The contribution of regions to the overall difference in Liaoning Province first decreased from 55.87% (2010) to 46.99% (2017) and then increased to 52.92% in 2020 (Figure 8). The contribution of non-agricultural municipal districts and agricultural municipal districts increased from 17.63% to 13.84% in 2010, respectively, to 22.07% and 19.31% in 2017, and then decreased to 20.17% and 18.27% in 2020, respectively. The contribution of agricultural counties to the overall difference in Liaoning Province first increased from 12.66% (2010) to 13.25% (2012), and then decreased to 8.64% in 2020. Therefore, from 2010 to 2020, the contribution of the differences between the three major regions to the changes in the

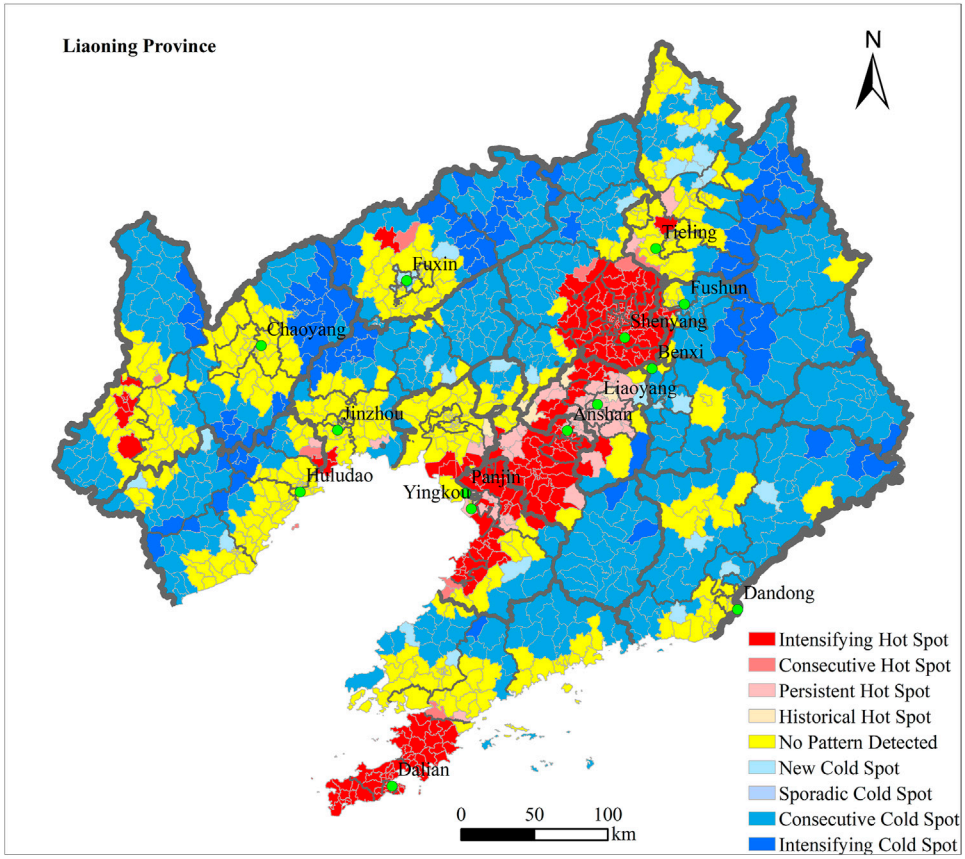

FIGURE 9
Emerging hot spot analysis of Liaoning Province's primary and secondary school students from 2010 to 2020.

overall differences in Liaoning Province first declined and then increased, remaining at approximately 50%. This indicates that the expansion of the overall difference change in Liaoning Province was largely due to the uneven distribution among the three regions. The distribution of primary and secondary school students is unbalanced among the county-level administrative units in non-agricultural municipal districts and agricultural-related municipal districts, and there are large differences between county-level administrative units. However, the distribution of students in primary and secondary schools among the county-level administrative units in the agriculture-related counties and districts is relatively balanced, and the differences between the county-level administrative units are relatively small.

3.4 Variation characteristics of town-level division scale

Using the Space-Time Pattern Mining (STPM) toolbox of ArcGIS Pro2.5 with the "Create Space Time Cube From Defined Locations" tool, and setting the time step interval to 1 year, we created the space time cube of the number of primary and secondary school students. This represented the changes in the number of primary and secondary school students in each township and street over time. Subsequently, we used emerging hot spot analysis to analyze the emerging spatiotemporal hot spot patterns. Based on Mann-Kendall trend analysis, we calculated a z-score of −2.647 and a p-value of 0.008, which indicated that with time, the overall change trend in the number of primary and secondary school students in Liaoning Province was decreasing.

According to analysis of the emerging spatiotemporal hotspots (Figure 9), we determined that the number of cold spots (595) for the primary and secondary school students in Liaoning Province from 2010 to 2020 was higher than the number of hot spots (362). In particular, hot spots were concentrated in the areas along the line from Shenyang to Dalian in central Liaoning Province. Conversely, cold-spot areas were concentrated in the eastern and western regions of Liaoning Province. Interestingly, hot and cold spot areas were separated by areas with no cold-spot pattern. Specifically, we identified 287 intensifying hot spots, with characteristics of

aggregation distribution. Intensifying hot spots were mainly distributed in municipal districts of Shenyang City, municipal districts of Dalian City (except Pulandian district), Anshan City, Yingkou City and its surrounding areas, and a small number in Tieling City, Fuxin City, Chaoyang City, Jinzhou City, and Huludao City. This finding showed that in the past 11 years, significant hot spots were detected in at least 10 of the years, accompanied by a significant increase in the number of primary and secondary school students. We identified 60 persistent hot spots, mainly in Liaoyang City, Anshan City, and Yingkou City. These areas maintained a large number of primary and secondary school students for a long time, retaining an unaltered intensity of hot spots over time. We also detected 10 consecutive hot spots scattered in Gaizhou county-level city under Yingkou City, and Pulandian District under Dalian City, indicating that the number of primary and secondary school students in these areas had always been high. Historical hot spots were detected in a total of five township-level administrative units, which are located in Liaozhong District under Shenyang City, Panshan County under Panjin City, Wensheng District and Liaoyang County under Liaoyang City, and Liaoyang County under the jurisdiction of Liaoyang City. These five township-level administrative units were not significant hotspots in recent years, but have been hotspots for a long time previously. We also identified 463 consecutive cold spots, which were widely distributed in the eastern and western regions of Liaoning Province, indicating that the number of primary and secondary school students in these regions had always been small. In particular, we detected 99 intensifying cold spots, mainly located in Chaoyang City, Huludao City, Fuxin City, Jinzhou City, Tieling City, and Fushun City. This finding demonstrates that in the past 11 years, significant cold spots in urban and rural areas were present for at least the last 10 years, and accompanied by a significant increase in the number of primary and secondary school students. We further detected 32 new cold spots, which were widely distributed and scattered in Tieling, Dandong, Fuxin, and other prefecture-level cities. The number of students in primary and secondary schools in these areas was low for the first time in 2020, and no area exhibited a new high value for the number of students in primary and secondary schools. Liushan subdistrict, Xinfu District, and Fushun City were the only sporadic cold spots. This finding indicated that in the past 11 years, the number of primary and secondary school students was high for most of the years.

4 Discussion

This study explores the spatial distribution characteristics of compulsory education students at different scales over time, as well as regional and urban-rural differences. Although the trend of population concentration in compulsory education helps to achieve the agglomeration effect, it has caused unfair allocation of compulsory education resources (Zheng et al., 2011), and aggravated the social and economic development between different regions and urban and rural areas. Differences strengthen the phenomenon of educational grouping, hindering the mobility of social classes (Song et al., 2021), and pose an important challenge to the quality and balanced development of urban and rural compulsory education. First, the population facing compulsory education is constantly flowing from rural areas to concentrate in urban areas. In order to allow more school-age children to receive equal education, reasonable plans and supporting measures should be given for the decommissioning of rural schools, and compulsory education schools in central urban areas should be added or expanded. Secondly, the uneven distribution of the population in compulsory education is an inevitable phenomenon in the process of social and economic development. The new-type urbanization construction must adhere to the concept of "people-oriented" and "serving the family", and accelerate the process of urbanization of the floating population. Finally, due to the impact of low fertility and low birthrate, the number of students in primary and secondary schools has been reduced, the number of students in school has declined significantly, and the risk of population structure imbalance in compulsory education has increased. Thus, it is necessary to continuously improve the safety awareness of population development, build a fertility-friendly society, and achieve a long-term balanced development of the population with compulsory education.

This study surveyed thousands of compulsory education schools and millions of students in Liaoning Province and assigned them spatial attributes. Spatial panel data was formed and a geographic database was established through combinations with administrative division data in 2020. Next, we analyzed the spatiotemporal distribution characteristics of primary and secondary school students in Liaoning Province from 2010 to 2020, and identified emerging local characteristics based on the overall characteristics. Our findings were compared with the traditional hotspot analysis method, such as local indictor of spatial association (Local Moran's *I*, LISA), Getis-Ord G_i^*, and SatScan. The emerging hotspot analysis technology has the advantages of dynamic analysis and improved refinement, and can show the evolution process of student distribution hotspots in both time and space dimensions. This study inevitably had some limitations. First, due to data limitations, our study only covers Liaoning Province. In view of China's complex geographical environment and obvious regional differences, it is necessary to investigate the distribution of compulsory education students in other regions of China in the future, and to further analyze the influencing factors and driving mechanisms behind the changes in the distribution of compulsory education students. Secondly, our study did not compare or analyze other data, such as permanent population data provided by the statistics department, household

registration population data provided by the public security department or mobile phone data provided by telecom operators (Wu et al., 2020; You et al., 2021; Zhuo et al., 2022). Finally, it did not consider the sensitivity of methodology parameters. Thus, the correlations and differences in the distribution of different groups should be analyzed in the future.

5 Conclusion

Based on the theory and methods of spatial statistics, including emerging spatiotemporal hotspot analysis and the standard deviational ellipse method, as well as other methods such as Theil indices, the temporal and spatial variation characteristics and trends of the distribution of primary and secondary school students, and regional and urban-rural differences, in Liaoning Province from 2010 to 2020 were investigated. Our main findings were as follows:

(1) The number of students in primary and secondary schools in Liaoning Province has declined but stabilized in recent years, and the gender imbalance has been alleviated to a certain extent. The reduction in the scale of students in secondary schools was greater than that in primary schools. The number of migrant students has also grown rapidly, whereas the gender ratio has dropped.

(2) The distribution of primary and secondary school students in Liaoning Province mainly followed a northeast-southwest distribution, exhibiting a trend of spatial shrinkage. The distribution center of primary and secondary school students in Liaoning Province primarily moved to the south, with the agglomeration area showing a tendency to move to coastal areas. From 2010 to 2020, the distance between the distribution center of primary and secondary school students in 14 prefecture-level cities in Liaoning Province and the administrative center were narrowed, and the directivity of the center was strengthened, demonstrating the characteristics of outflow from the edge and inflow to the center. Among them, the most typical prefecture-level cities for education urbanization were Dalian and Shenyang.

(3) There was evident inter-city, regional and urban-rural differences in the scale of primary and secondary school students and their changing trends in Liaoning Province. Shenyang and Dalian exhibited a large-scale, rapid growth, and a high proportion of migrant students. The number of primary and secondary school students in other cities, most of which are local, has decreased, and this decline has been relatively intense. There were obvious regional differences among non-agricultural municipal districts, agricultural-related municipal districts, and agricultural-related counties. Urban areas have absorbed a large number of primary and secondary school students, and there is a serious loss of primary and secondary school students in rural areas.

(4) Consecutive cold spots and intensifying cold spots were the main emerging spatiotemporal hot spot patterns of primary and secondary school students in Liaoning Province, with the cold spot areas being mainly located in the eastern and west-ern regions of Liaoning Province. Hot spots were mainly located in the dual-core with their axis area consisting of central urban areas of Shenyang prefecture-level city and central urban areas of Dalian prefecture-level city in Liaoning Province, and were mainly manifested as emerging spatiotemporal persistent and intensifying hot spots.

Data availability statement

The raw data supporting the conclusions of this article will be made available by the authors, without undue reservation.

Author contributions

Methodology, WL; software and validation, WL; formal analysis, WL and LW; writing—original draft preparation, WL and ZZ; writing—review and editing, WL; visualization, WL; funding acquisition, ZZ. All authors contributed to the article and approved the submitted version.

Funding

This work was supported by the Humanities and Social Sciences Research Project of Liaoning Provincial Department of Education (Grant no. LJKQR2021046), the National Social Science Foundation of China (Grant no. 18BRK037), and Youth Innovation Promotion Association of Chinese Academy of Sciences.

Conflict of interest

The authors declare that the research was conducted in the absence of any commercial or financial relationships that could be construed as a potential conflict of interest.

Publisher's note

All claims expressed in this article are solely those of the authors and do not necessarily represent those of their affiliated organizations, or those of the publisher, the editors and the reviewers. Any product that may be evaluated in this article, or claim that may be made by its manufacturer, is not guaranteed or endorsed by the publisher.

References

Bai, B., Xue, Z. Q., Zhao, P., and Zhang, Z. (2021). Functionalizations of boron nitride nanostructures. *Sci. China Technol. Sci.Geogr* 64, 1–10. doi:10.15957/j.cnki.jjdl.2021.02.00110.1007/s11431-020-1559-2

Ding, X. S., Wu, Z. H., and Xia, B. S. (2018). An analysis of the scale and structure of the school-age population of compulsory education in big cities under the background of urbanization. *J. Educ. Sci. HNNU.* 17, 66–74. doi:10.19503/j.cnki.1671-6124.2018.04.009

Fowler, W. J., and Walberg, H. J. (1991). School size, characteristics, and outcomes. *Educ. Eval. Policy Analysis* 13, 189–202. doi:10.3102/01623737013002189

Getis, A., and Ord, J. K. (1992). The analysis of spatial association by use of distance statistics. *Geogr. Anal.* 24, 189–206. doi:10.1111/j.1538-4632.1992.tb00261.x

Hamnett, C., and Butler, T. (2013). Distance, education and inequality. *Comp. Educ.* 49, 317–330. doi:10.1080/03050068.2013.807165

Han, J. L., and Yu, J. Q. (2020). Children's educational choices by the new generation migrant workers' families in the trend of new-type urbanization. *Soc. Sci. B* 35, 4–13. doi:10.13262/j.bjsshkxy.bjshkx.200601

Hones, G. H., and Ryba, R. H. (1972). Why not a geography of education? *J. Geogr.* 71, 135–139. doi:10.1080/00221347208981469

Huang, J. X., Wang, J. F., Li, Z. J., Wang, Y., Lai, S. J., and Yang, W. Z. (2015). Visualized exploratory spatiotemporal analysis of Hand-Foot-Mouth disease in Southern China. *PloS One* 10, e0143411. doi:10.1371/journal.pone.0143411

Kenny, L. W. (1982). Economies of scale in schooling. *Econ. Educ. Rev.* 2, 1–24. doi:10.1016/0272-7757(82)90046-2

Langran, G. (1989). A review of temporal database research and its use in GIS applications. *Int. J. Geogr. Inf. Syst.* 3, 215–232. doi:10.1080/02693798908941509

Lefever, D. W. (1926). Measuring geographic concentration by means of the standard deviational ellipse. *Am. J. Sociol.* 32, 88–94. doi:10.1086/214027

Li, J., Zheng, B. Y., and Wang, J. F. (2021). Spatial-temporal heterogeneity of hand, foot and mouth disease in China from 2008 to 2018. *Int. J. Geogr. Inf. Sci.* 23, 419–430. doi:10.12082/dqxxkx.2021.190778

Liu, H. Y., Chen, W., and Li, S. (2019). Random loose packings of polydisperse adhesive microparticles with Gaussian size distribution. *Powder Technol.* 357, 64–73. doi:10.7523/j.issn.2095-6134.2019.01.01010.1016/j.powtec.2019.08.092

Liu, K., Liu, R. Z., Chen, T. T., and Nie, G. G. (2020). Scale and accessibility of school system and its spatial differentiation of elementary schools in Henan province. *Sci. Geogr. Sin.* 40, 1698–1709. doi:10.13249/j.cnki.sgs.2020.10.014

Liu, K., and Liu, R. Z. (2017). Spatial concentration tendency and unbalanced development of elementary and middle schools under the background of urbanization in central rural area: A case study of Biyang county in henan province. *Geogr. Res.* 36, 1680–1696. doi:10.11821/dlyj201709007

Liu, T., Peng, R. X., Zhuo, Y. X., and Cao, G. Z. (2022). China's changing population distribution and influencing factors: Insights from the 2020 census data. *Acta Geogr. Sin.* 77, 381–394. doi:10.11821/dlxb202202008

Liu, Z., Qi, H. G., and Liu, S. H. (2022). Labor shrinkage and its driving forces in China from 1990 to 2015: A geographical analysis. *Appl. Spat. Anal.* 15, 339–364. doi:10.1007/s12061-021-09414-2

Mei, H., Jiang, Q. B., Xiang, Y. Y., and Song, X. P. (2015). School consolidation: Whither China's rural education? *Asian Soc. Work Pol. Rev.* 9, 138–150. doi:10.1111/aswp.12053

Sajjad, M., Munir, H., Kanwal, S., and Asad Naqvi, S. A. (2022). Spatial inequalities in education status and its determinants in Pakistan: A district-level modelling in the context of sustainable development goal-4. *Appl. Geogr.* 140, 102665. doi:10.1016/j.apgeog.2022.102665

Song, Z. N., Hua, F. L., and Liu, S. L. (2021). Research progress and review of capitalization of compulsory educational resources. *Prog. Geogr.* 40, 1771–1787. doi:10.18306/dlkxjz.2021.10.013

Wu, J. W., Yu, Z., Wei, Y. H. D., and Yang, L. Q. (2019). Changing distribution of migrant population and its influencing factors in urban China: Economic transition, public policy, and amenities. *Habitat Int.* 94, 102063. doi:10.1016/j.habitatint.2019.102063

Wu, L., Jiao, H. F., Ye, L., and Tang, P. (2018). Temporal and spatial characteristics of provincial education urbanization in China and its influencing factors. *Sci. Geogr. Sin.* 38, 58–66. doi:10.13249/j.cnki.sgs.2018.01.007

Wu, L. X., Huang, Z. Y., and Pan, Z. H. (2021). The spatiality and driving forces of population ageing in China. *PloS One* 16, e0243559. doi:10.1371/journal.pone.0243559

Wu, Y. M., Wang, L., Fan, L. H., Yang, M., Zhang, Y., and Feng, Y. H. (2020). Comparison of the spatiotemporal mobility patterns among typical subgroups of the actual population with mobile phone data: A case study of beijing. *Cities* 100, 102670. doi:10.1016/j.cities.2020.102670

Xu, J. H., Lu, F., Su, F. L., and Lu, Y. (2005). Spatial and temporal scale analysis on the regional economic disparities in China. *Geogr. Res.* 24, 57–68. doi:10.11821/yj2005010007

Xu, W. W., Song, C. R., Sun, D. Q., and Yu, B. C. (2021). Spatiotemporal differentiation of the school-age migrant population in liaoning province, China, and its driving factors. *Land* 10, 1036. doi:10.3390/land10101036

Yan, Q. W., and Bian, Z. F. (2008). Study on population distribution inequalities based on the two-stage nested Theil decomposition method. *Northwest Pop. J.* 29, 103–106+110. doi:10.3969/j.issn.1007-0672.2008.05.005

Yang, H. M., Zhang, X. L., Li, L., Li, X. J., and Wang, B. (2018). Changing spatial pattern and accessibility of primary and secondary schools in a poor mountainous county: A case study of song county, henan province. *Prog. Geog.* 37, 556–566. doi:10.18306/dlkxjz.2018.04.011

Ye, L., Zeng, G., and Wang, Y. (2019). The influence of population urbanization and urban-rural development gap on education urbanization. *Econ. Surv.* 36, 9–15. doi:10.15931/j.cnki.1006-1096.20190521.002

Yin, D. T., Hu, Y. P., and Hao, W. Y. (2016). Interaction research between educational resources allocation and population development trend in Beijing. *Popul. Econ.* 37, 62–70. doi:10.3969/j.issn.1000-4149.2016.04.007

You, H. L., Yang, J., Xue, B., Xiao, X. M., Xia, J. H., Jin, C., et al. (2021). Spatial evolution of population change in Northeast China during 1992-2018. *Sci. Total Environ.* 776, 146023. doi:10.1016/j.scitotenv.2021.146023

Yu, H. S., Yang, J., Li, T., Jin, Y., and Sun, D. Q. (2022a). Morphological and functional polycentric structure assessment of megacity: An integrated approach with spatial distribution and interaction. *Sustain. Cities Soc.* 80, 103800. doi:10.1016/j.scs.2022.103800

Yu, H. S., Yang, J., Sun, D. Q., Li, T., and Liu, Y. J. (2022b). Spatial responses of ecosystem service value during the development of urban agglomerations. *Land* 11, 165. doi:10.3390/land11020165

Zhang, D. H., Zhou, C. S., and Xu, W. W. (2020). Spatial-temporal characteristics of primary and secondary educational resources for relocated children of migrant workers: The case of liaoning province. *Complexity* 2020, 1–13. doi:10.1155/2020/7457109

Zhang, Z. C., Luan, W. X., Tian, C., Su, M., and Li, Z. Y. (2022). Education equality and its influencing factors for migrant children in the compulsory education stage based on multi-source data: A case study of dalian, China. *Front. Earth Sci.* 10, 950853. doi:10.3389/feart.2022.950853

Zhao, C. X., Shao, J. A., Guo, Y., and Xu, X. L. (2016). Spatial pattern evolvement characteristics of rural schools and their development level in the mountainous area. *Geogr. Res.* 35, 455–470. doi:10.11821/dlyj201603005

Zhao, D., Wu, H. C., and Bruno, P. (2012). The impact of school closure on students' schooling distance in rural areas: Based on GIS and ordinal logit model analysis. *J. Educ.* 8, 62–73. doi:10.3969/j.issn.1673-1298.2012.03.009

Zhao, Q. D., Huang, Y. H., and Liu, Y. S. (2020). Spatiotemporal evolution pattern and driving factors of higher-education population in China. *Complexity* 2020, 1–11. doi:10.1155/2020/1927364

Zhao, S. M., Rui, Y., and Yang, Y. H. (2022). The cross scale flow of students in the pre-school and compulsory education stages in the rural areas: A case study in chunhua county, shaanxi province. *Geogr. Res.* 41, 810–829. doi:10.11821/dlyj020210062

Zheng, T., Lv, B., and Zhang, C. (2011). Research on the inequity of compulsory education infrastructure for migrant children in beijing: A case study of fengtai district. *Urban Dev. Res.* 18, 115–123. doi:10.3969/j.issn.1006-3862.2011.10.019

Zhu, Y. L., Jing, C. F., Fu, J. Y., Du, M. Y., and Zhou, L. (2019). Analysis of space-time pattern of robbery crime based on space-time cube. *Sci. Surv. Mapp.* 44, 132–138. doi:10.16251/j.cnki.1009-2307.2019.09.019

Zhuo, L., Chen, Z., Wu, C. Z., Shi, Q. L., Gu, Z. H., Tao, H. Y., et al. (2022). Deriving intercity human flow pattern and mechanism based on cell phone location data: Case study of guangdong province, China. *Comput.Urban Sci.* 2, 4. doi:10.1007/s43762-022-00033-2

frontiers | Frontiers in Environmental Science

TYPE Original Research
PUBLISHED 27 September 2022
DOI 10.3389/fenvs.2022.1004343

Check for updates

OPEN ACCESS

EDITED BY
Bing Xue,
Institute of Applied Ecology (CAS), China

REVIEWED BY
Qiang Yu,
Beijing Forestry University, China
Tao Ding,
Hefei University of Technology, China
Miao Li,
Tongji University, China
Jinhua Li,
Inner Mongolia University, China

*CORRESPONDENCE
Ye Duan,
dydl@lnnu.edu.cn

SPECIALTY SECTION
This article was submitted to Environmental Informatics and Remote Sensing,
a section of the journal
Frontiers in Environmental Science

RECEIVED 27 July 2022
ACCEPTED 30 August 2022
PUBLISHED 27 September 2022

CITATION
Qin Y, Zhang H, Zhao H, Li D, Duan Y and Han Z (2022), Research on the spatial correlation and drivers of industrial agglomeration and pollution discharge in the Yellow River Basin.
Front. Environ. Sci. 10:1004343.
doi: 10.3389/fenvs.2022.1004343

COPYRIGHT
© 2022 Qin, Zhang, Zhao, Li, Duan and Han. This is an open-access article distributed under the terms of the Creative Commons Attribution License (CC BY). The use, distribution or reproduction in other forums is permitted, provided the original author(s) and the copyright owner(s) are credited and that the original publication in this journal is cited, in accordance with accepted academic practice. No use, distribution or reproduction is permitted which does not comply with these terms.

Research on the spatial correlation and drivers of industrial agglomeration and pollution discharge in the Yellow River Basin

Yuming Qin[1], Hao Zhang[1], Huimin Zhao[1], Di Li[1], Ye Duan[1]* and Zenglin Han[2]

[1]School of Geography, Liaoning Normal University, Dalian, China, [2]Center for Studies of Marine Economy and Sustainable Development, Liaoning Normal University, Dalian, China

The spatial auto-correlation analysis approach is used to examine the agglomeration features and geographical correlation of industrial agglomeration and pollutant discharge using 91 prefecture-level cities in the Yellow River Basin from 2005 to 2020 as the research target. The Yellow River Basin and the upper, middle, and lower reaches were investigated for the effects of industrial agglomeration on industrial pollution emissions. The Dubin model of the spatial panel is used to investigate the drivers of industrial pollution from both indirect effects and direct effects. The findings indicated that ① the spatial pattern of industrial pollution agglomeration and industrial agglomeration in the Yellow River Basin has spatial convergence; ② the global clustering characteristics of industrial pollution in the Yellow River Basin are apparent. The global correlations of the three pollutants are industrial wastewater > industrial smoke and dust > industrial SO_2; there is a spatial association between industrial agglomeration and pollution agglomeration, and there are differences in the spatial interconnection between industrial agglomeration and the accumulation of different pollutants; ③ from the overall point of view of the Yellow River Basin, industrial agglomeration will reduce the pollution levels of industrial wastewater, industrial SO_2, and industrial smoke and dust. From the perspective of different regions, industrial agglomeration in the upper, middle, and lower reaches is conducive to the decline of industrial pollution, and the role is in the middle, downstream, and upstream in order from large to small; and ④ the Yellow River Basin's industrial pollution is primarily caused by population agglomeration, industrial structure, environmental regulation, opening to the outside world, and economic development. Their effects on industrial wastewater, industrial SO_2, industrial smoke, and dust pollution vary.

KEYWORDS

industrial agglomeration, industrial pollution, spatial correlation, the Yellow River Basin, regional heterogeneity, spatial Dubin model

1 Introduction

Since the reform and opening up, China's industrial development has reached a stage of rapid development. It has effectively facilitated the rapid economic growth of the country. However, fostering economic growth, the long-term extended industrial development model has also produced a significant amount of industrial pollutants, causing serious damage to the ecological environment (Ji and Zhou, 2020). Under severe pressure, this industrial development model obviously does not conform to the ecological development concept of "lucid waters and lush mountains are invaluable assets" in the context of the new era (Lu and Sun, 2019). Some existing studies on the link between industrial pollution and health status show that industrial pollution will not only produce bronchitis and kidney disease, potentially jeopardizing the occupants' physical and mental well-being (Rahman et al., 2021; You, 2022), but also hinder economic augmentation and social steadiness (Yan and Cao, 2020). As a result, in an effort to address the serious issue of industrial pollution, the Chinese government has put in place a number of strict policies to limit environmental pollution (CPGPRC, 2013; Xinhua, 2015). The Yellow River Basin (YRB) is a crucial ecological protective screen and economic zone in China, and it is also a crucial location to win the war against poverty (Lu et al., 2021). It is a highly vital region for China's economic, social, and ecological development (Xi, 2019). Industrial agglomeration effectively promotes the YRB's flourishing social and economic environment and also leads to pollution agglomeration (Yang et al., 2020). In order to establish a scientific foundation for industrial pollution control in the YRB, it is vital to investigate the spatial correlation between industrial agglomeration and pollution discharge in the YRB and its affecting elements.

The YRB stretches across the three strategic regions of China's east, west, and middle (Song and Zhang, 2020). It is an essential ecological protection district in China and a crucial spatial carrier for China's economic and social progress (Lu et al., 2021). In October 2021, General Secretary Xi Jinping presided over the "symposium on in-depth promotion of ecological protection and high-quality development in the Yellow River Basin" in Jinan and delivered a great speech (Xinhua, 2021), pointing out that environmental preservation and superior development are neither separate from each other, nor are they confrontational and conflicting. Still, they are inherently unified and mutually reinforcing (Xinhua, 2021). However, the ecology of the YRB is vulnerable, the quality of development needs to be improved, and it faces serious environmental pollution problems (Jin, 2019). At present, the research on environmental pollution in the YRB chiefly focuses on water pollution, air pollution, and soil pollution. Bai believes that the distribution of water pollutant emissions is consistent with the pattern of economic development. The stepped distribution pattern is particularly prominent in the upstream, midstream, and downstream regions, and the primary water pollutant emissions show a pronounced spatial agglomeration influence. The characteristics of pollution agglomeration in the lower and middle reaches of the basin are particularly obvious (Bai et al., 2020). Teng described the spatial evolution pattern of two types of typical air pollutants, industrial SO_2 and $PM_{2.5}$ in the YRB, and realized that the air pollution in the YRB has significant agglomeration and correlation characteristics, showing a gradient of decreasing agglomeration pattern from southeast to northwest. Compared with SO_2 pollution, $PM_{2.5}$ pollution has a broader distribution and stronger spatial correlation (Teng et al., 2021). Liu believes that the quality of the soil environment in the YRB is generally good, but the soil environment in some areas is not optimistic. It is suggested that in view of the fact that the soil pollution risk prevention and control system in the YRB is not perfect and the management foundation is weak, which comprehensively improve the ability of soil environmental supervision and implement soil pollution risk zoning control (Liu et al., 2021). From the 1990s to the present, numerous studies have supported the hypothesis that the "Kuznets curve" shows an inverted "U" link between environmental quality and economic development (Liang et al., 2019; Du and Xie, 2020). With the rapid economic growth, environmental pollution has gradually increased, and industrial pollution has become the focus of domestic and foreign scholars (Grossman and Kreuger, 1995). Numerous research projects have been conducted on the spatio-temporal pattern of industrial pollution (Wu et al., 2020), influencing factors (Li et al., 2019), industrial pollution and economic growth (Zhou et al., 2020), industrial pollution and environmental regulation (Jia and Zhao, 2012), industrial pollution and industrial agglomeration (Yang, 2018). The research methods include geographically weighted regression (Feng et al., 2020), spatial econometric models (Hu et al., 2016), spatial auto-correlation (Li et al., 2019), and barycentric shift curves (Zhao et al., 2014), the STIRPAT model (Liu et al., 2015), and the Log-Mean Divisia Index (LMDI) diesel decomposition model (Geng et al., 2014). At present, there are few studies on industrial pollution in the YRB. Li found that industrial pollution presents a "high in the east and low in the west" spatial distribution pattern, and from west to east, the basin is divided into highly low-value areas, low-value areas, high-value areas, and extremely high-value areas of pollution emissions (Li, 2021). Previous studies have fully explained the spatial and temporal distribution and contributing factors of various pollutants in the YRB (Ding et al., 2022); however, most of them have only analyzed the pollution problem alone, and there are fewer studies consider industrial agglomeration and pollution emissions.

At present, there has not been much research done on the connection between industrial clusters and pollution emissions, and the academic community has not yet formed a consensus on the link between the two. The following are three representative views: first, industrial encroachment increases local pollutant

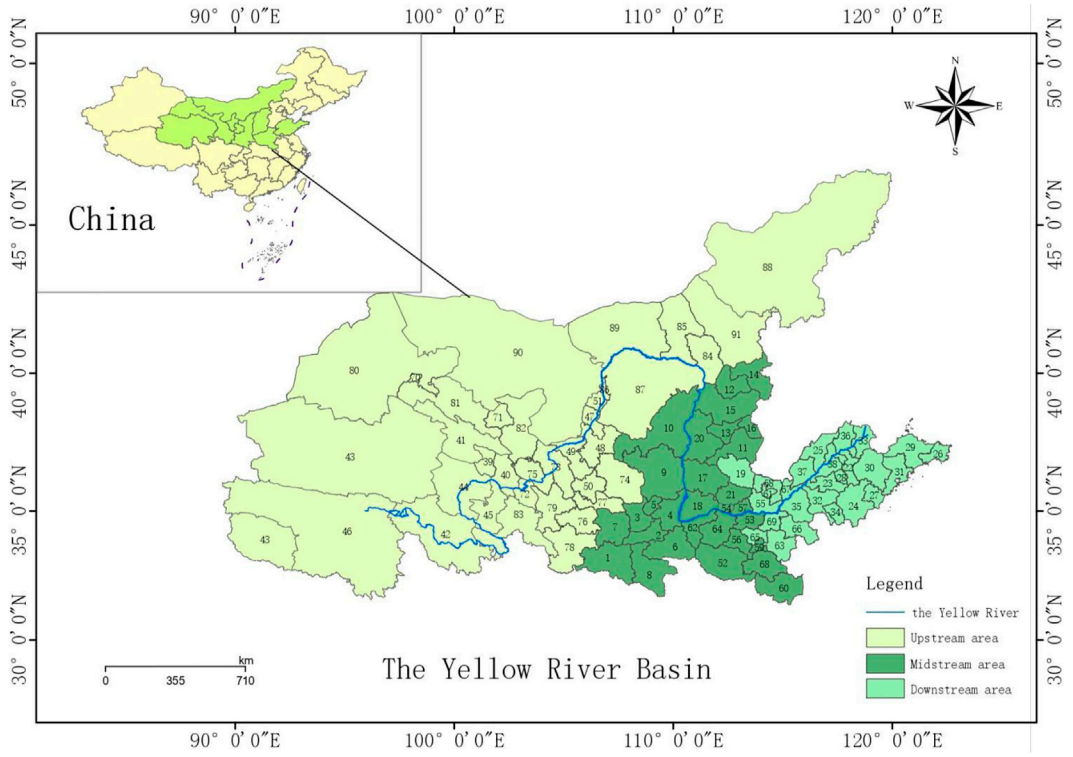

FIGURE 1
Location map of the study area.

emissions (Chen C. et al., 2020); second, industrial agglomeration reduces regional pollution emissions (Fang et al., 2020); third, the connection between industrial clusters and emissions of industrial pollution is uncertain (He et al., 2014; Shen and Peng, 2021). In addition, prior research focused on the relationship between industrial agglomeration and individual pollutants (Li B. G. et al., 2021; Li and Han, 2022), and a few scholars from the whole country (Hu et al., 2018), urban agglomerations (Jia et al., 2020), and other administrative divisions conducted a comprehensive study of the geographical association between industrial clusters and different pollutants, but there are still gaps in the literature for the study of the YRB. So, for the YRB, where industrialization is currently accelerating, is there spatial convergence between industrial agglomeration and pollution agglomeration? Whether the two have a spatial correlation at the municipal scale? What are the different influences of industrial agglomeration on the discharge of different types of industrial pollutants? The study of the spatial relationship between industrial agglomeration and industrial pollution emissions in the YRB is helpful to clarify the spatial link between industrial agglomeration and pollution emissions here (Wu et al., 2021). It is really important for the logical formulation of regional emission reduction measures, the reduction of industrial pollution emissions, and the promotion of green and excellent development in the YRB (Ma and Xu, 2020).

In addition, considering that the YRB spans a large area, the degree of socioeconomic development, as well as the biological and topographical factors, vary by region, it is yet unclear how industrial agglomeration would affect the levels of industrial pollution in those areas. Divide the YRB into parts and study the correlation between industrial agglomeration and industrial pollution in the middle, lower, and upper reaches of the YRB, so as to fully understand whether the current YRB environmental management policy is reasonable. Policies should be enacted according to local circumstances (Wang et al., 2022), and accurate identification of the economic and social causes of industrial pollution in the YRB is the premise for rationally formulating and effectively implementing pollution control policies.

The novelty of this study is primarily seen in the following: first, under the YRB's setting of environmental protection and high-quality advancement (Xinhua, 2021), there has been a lot of interest in the studies on environmental pollution in the YRB. At present, most of the existing studies only analyze pollution problems alone, while there are still few studies considering industrial agglomeration and pollution agglomeration. This article conducts a comprehensive study on the spatial

relationship between industrial agglomeration and various pollutants in the YRB, which is not available in previous studies. Second, considering that the YRB spans a large area, we analyze the link between industrial agglomeration and industrial wastewater, industrial SO_2, and industrial smoke and dust pollution in the upper, lower, and middle reaches of the YRB. Further regional heterogeneity analysis is helpful for the government to take into account the variations in the key elements affecting industrial pollution in various regions when formulating and implementing pollution control measures and implementing policies based on regional circumstances.

The main goal of this research is: to use the YRB as the study subject from 2005 to 2020, using the spatial auto-correlation analysis method to explore the agglomeration features and spatial correlation of industrial agglomeration and pollution emissions, and using the space panel Dubin model to analyze the contributing factors of industrial pollution from the two aspects of direct influence and indirect effect, and how industrial agglomeration affects the discharge of industrial pollutants at different scales in the YRB as a whole and the upper, lower, and middle reaches are, respectively, explored. It offers the theoretical underpinnings and a decision-making guide for the coordinated industrial growth of the YRB, as well as cooperative pollution prevention and control.

The frame of the rest of this article is as follows: part two is the study method and data source; the third and fourth parts are the results of the empirical study, and the third part is the space of agglomeration analysis and spatial correlation analysis of industrial agglomeration and pollution by three industrial pollutants in the YRB; the fourth part is the impact of industrial agglomeration on industrial pollution discharge at different scales in the YRB as an integral and in the upper, lower, and middle reaches; and in the fifth part, the article ends with conclusions and suggestions.

2 Research design

2.1 Study area and data source

The YRB is a key area for China's national land ecological security. It is not only the core area of the sand control belt in northern China, the ecological barrier of the Qinghai-Tibet Plateau, and the "two screens and three belts" ecological barrier pattern of the Loess Plateau, but also the birthplace of important rivers such as the Yangtze River, the Yellow River, and the Lancang River, and an important supply area for China's freshwater resources (Jin et al., 2020). The YRB is located at 36° 45′ 14.08″ N and 117° 01′ 32.72″ E. From east to west, it is about 1900 km long, and from north to south, it is 1,100 km wide. On the premise of maintaining the integrity of provincial administrative divisions and the availability of data, this article sets the scope of the study object to be eight provinces (autonomous regions): Qinghai, Gansu, Ningxia, Inner Mongolia, Shaanxi, Shanxi, Henan, and Shandong (Li Z. J. et al., 2021). Further considering the availability of data, this article finally selects 91 prefecture-level units as the research objects and divides the study area into three major areas: the upper, lower, and middle reaches. At present, there are various ways to divide the YRB. According to the "Flood Control Plan for the Yellow River Basin" approved by the State Council in 2008 (CPGPRC, 2008), the dividing points between the upper and middle reaches of the YRB are Hekou Town, Tuoke Country, Inner Mongolia Autonomous Region; the dividing point between the lower and middle reaches is Taohuayu Town, Xingyang City, Henan Province. The Qinghai-Tibet Plateau, Inner Mongolia Plateau, Loess Plateau, and Huaihai Plain are the four geomorphic units that make up the YRB's landscape, which gradually declines from west to east (Ma and Xu, 2020). Since the YRB is expressed as a plane rather than a line in geographical space, and considering historical, cultural, and geographical factors and the feasibility of research, the upper, lower, and middle reaches of the YRB are divided as follows: The upstream area includes 36 cities including Lanzhou, Baiyin, Zhongwei, and Hohhot; the midstream region includes 29 cities including Taiyuan, Luliang, Xi'an, Yan'an, and Zhengzhou; and the downstream region includes 26 cities including Kaifeng, Xinxiang, Jinan, Zibo, etc. (Figure 1). It is worth noting that these three sub-basins are different in terms of economic space and ecological resources. The upstream water resources are sufficient, the ecological environment is good, the population is small, and the level of economic and social development is relatively backward; the middle reaches are rich in energy resources, the ecological environment is relatively fragile, and soil erosion is more serious; the lower reaches have fertile land, developed agriculture, and a high level of social and economic development, but development is greatly restricted by the lack of water resources (Chen Y. et al., 2020).

The three major pollutant discharge data, industrial data, and data on the population, land area, GDP, the comprehensive utilization rate of industrial solid waste, and actual foreign investment in each city and state used in this article are derived from the 2005–2021 "China Urban Statistical Yearbook" (NBS, 2005-2021a), the "China Regional Economic Statistical Yearbook" (NBS, 2005-2021b), and the statistical yearbooks and statistical bulletins of relevant provinces (autonomous regions, municipalities) and prefecture-level cities.

2.2 Research methods

2.2.1 Agglomeration indicators

Herfindahl index, Gini coefficient, location entropy, etc., are usually used to characterize the degree of agglomeration, but these

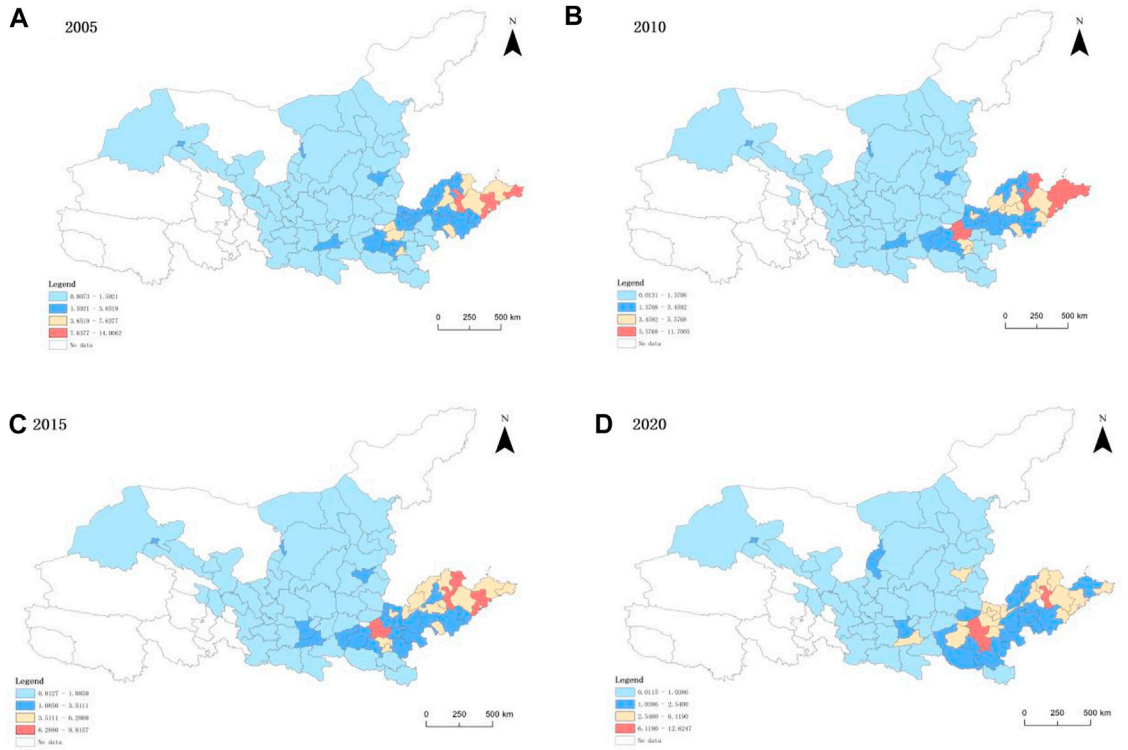

FIGURE 2
Spatial pattern of industrial agglomeration in the Yellow River Basin in 2005, 2010, 2015, 2020.

indicators do not effectively consider spatial bias, while the geographical concentration index is considered to be an effective tool to describe industrial agglomeration and pollution agglomeration. Therefore, the geographical concentration index is used to calculate industrial agglomeration and pollution agglomeration separately:

$$R_{it} = \frac{\left(x_{it} \Big/ \sum_{i=1}^{n} x_{it}\right)}{\left(TER_i \Big/ \sum_{i=1}^{n} TER_i\right)}. \quad (1)$$

In Eq. 1, recognizing that the manner in which interactions occur may vary between industrial agglomeration and pollutants in different physical forms, industrial wastewater, industrial SO_2, and industrial smoke and dust are used to represent three physical forms of industrial pollutants; *R*it indicates the *t* year of industrial agglomeration and pollution agglomeration in a city *i*; X_{it} is the industrial added value and pollution discharge of city *i* *in* the *t* year; *TERi* it represents the administrative area of the city *i*; *n* it is the 91 cities in the YRB.

2.2.2 Spatial statistical methods

The geographical dependency of industrial agglomeration and pollution agglomeration was examined using the univariate global Moran's *I* in 91 prefecture-level cities in the YRB (Chen, 2009). The univariate Moran's *I* is between -1 and 1, and the significance value is tested with a *p* value.

The relationship between industrial and pollution agglomerations in space in 91 prefecture-level cities in the YRB was analyzed using bivariate global Moran's *I*. The bivariate global Moran's *I* is between -1 and 1, and the *p* value is used to test the significance:

$$I_{ab} = \frac{n\sum_{i=1}^{n}\sum_{j\neq 1}^{n} W_{ij} Z_i^a Z_j^b}{(n-1)\sum_{i=1}^{n}\sum_{j\neq 1}^{n} W_{ij}}. \quad (2)$$

In Eq. 2, I_{ab} is the bivariate global Moran's *I*; *n*is the 91 prefecture-level cities in the YRB; W_{ij} is the geospatial weight matrix based on Queen's principle; $Z_i^a$is the industrial agglomeration of the prefecture-level city *i*; and Z_j^b*is* the pollution agglomeration of the prefecture-level city *j*.

2.2.3 Space panel Dubin model

The formation of the industrial pollution agglomeration pattern between prefecture-level cities in the YRB has a strong spatial interaction effect. If the spatial correlation between its contributing factors is ignored, the model estimation result will have a large error compared to the actual situation. The spatial lag model, the spatial error

model, and the spatial Dubin model are common spatial econometric models, and the differences in the models are mainly due to the interaction terms of the spatial matrix and variables. Among the three models, the spatial Dubin model is the most standard because it not only fully accounts for the spatial correlation issues brought on by the explanatory and explained variables as well as their interactions but also has the ability to capture the spatial spillover effects of various variables. Therefore, for the sake of solving the problems of spatial dependence of spatial data, the spatial Dubin model is used in this work to analyze the data by regression, and its general formula is as follows:

$$\boldsymbol{Y}_{it} = \boldsymbol{\alpha}_{it} + \boldsymbol{\rho}\boldsymbol{W}_{ij}\boldsymbol{Y}_{it} + \boldsymbol{\beta}\boldsymbol{X}_{it} + \boldsymbol{\delta}\boldsymbol{W}_{ij}\boldsymbol{X}_{it} + \boldsymbol{u}_{i} + \boldsymbol{\delta}_{i} + \boldsymbol{\varepsilon}_{it}. \quad (3)$$

In Eq. 3, i and j both represent urban individuals; t represents the year; ρ represents the estimable spatial auto-regressive relationship coefficient to assess how the dependent variable Y affects nearby spatial observations; X represents all explanatory variables; W is a geospatial weights matrix based on Queen's principles; WY is the spatial lag variable of the dependent variable; βrepresents the influence of the independent variable on the dependent variable (Shen and Peng, 2021); $\delta$is the coefficient of the spatial lag term WX of the independent variable; ui, δi are individual fixation and time fixation, respectively; and ε is a normal-distributed random error term.

3 Spatial pattern and correlation of industrial agglomeration and industrial pollution

3.1 Spatial characteristics of the industrial agglomeration level

ArcGIS 10.8 was used to visualize the industrial agglomeration of 91 prefecture-level cities in the YRB in 2005, 2010, 2015, and 2020, respectively, (Figure 2). Using the natural fracture method, in this study, the value of an urban industrial cluster is divided into four categories, which are defined as an extremely low-value area, a low-value area, a high-value area, and an extremely high-value area, from low to high.

From the perspective of changing trends, the agglomeration of industrial level in the lower reaches of the YRB showed a slow downward trend from 2005 to 2020, the middle reaches expanded annually, and the upper reaches grew steadily. The high-value regions of industrial agglomeration in the YRB are chiefly concentrated in Qingdao, Zibo, and Zaozhuang in the downstream area, followed by Jinan and Weihai, etc.; the high-value regions of industrial agglomeration are chiefly distributed in Taiyuan and Zhengzhou in the middle reaches; the low-value regions of industrial agglomeration are chiefly distributed in Baiyin and Yinchuan in the upper reaches of the YRB. It is evident that the spatial pattern of industrial agglomeration in the YRB shows non-equilibrium because there are striking differences in growth policies, infrastructure, location conditions, and industrial foundations between the YRB's high-value industrial agglomeration areas and low-value industrial agglomeration areas, causing elements such as population, funds, and technology to continuously flow from the low-value areas of industrial agglomeration to the high-value areas of industrial agglomeration (Pierson, 2000).

3.2 Spatial aggregation characteristics of the three major industrial pollutants

ArcGIS 10.8 was used to spatially visualize the three major industrial pollutants (industrial wastewater, industrial SO_2, and industrial smoke and dust) and pollution agglomeration in 91 prefecture-level cities in the YRB in 2005, 2010, 2015, and 2020, respectively. As shown in the figure: there is spatial convergence in the spatial pattern of pollution agglomeration and industrial agglomeration . The areas with extremely high pollution concentrations are chiefly concentrated in Zibo and Zaozhuang in the downstream areas, and the pollution agglomeration high-value regions are around the extremely high pollution accumulation areas. Baiyin, Yinchuan, and Haidong in the upper reaches of the YRB have formed contiguous low-value areas of pollution agglomeration. The spatial distribution patterns of pollution agglomeration of the three major industrial pollutants have strong similarities with slight differences, as follows:

3.2.1 Industrial wastewater

According to the geographical distribution pattern, the industrial wastewater pollution agglomeration level in the YRB is typically high in the lower and middle reaches and low in the upper reaches (Figure 3). The extremely high-value regions are chiefly concentrated in Kaifeng, Zibo, and Zaozhuang in the downstream area, and the high-value areas are chiefly distributed in Xi'an and Taiyuan in the midstream area; the low-value areas and extremely low-value areas where industrial wastewater pollution is concentrated are chiefly distributed in Baotou City, Baiyin City, and Haidong City in the upstream region.

3.2.2 Industrial SO_2

The level of industrial SO_2 pollution agglomeration in the YRB generally shows a spatial distribution pattern of low agglomeration levels in addition to the high levels of individual cities in the lower and middle reaches of the YRB (Figure 4). The majority of high-value locations are found in Rizhao, Zibo, and Luliang in the lower and middle reaches; the majority of the highly low-value zones with industrial SO_2 pollution are dispersed in Ordos, Baiyin, and Tianshui in the upstream areas; low-value areas are chiefly concentrated and distributed in Lanzhou, Haidong, and Yinchuan.

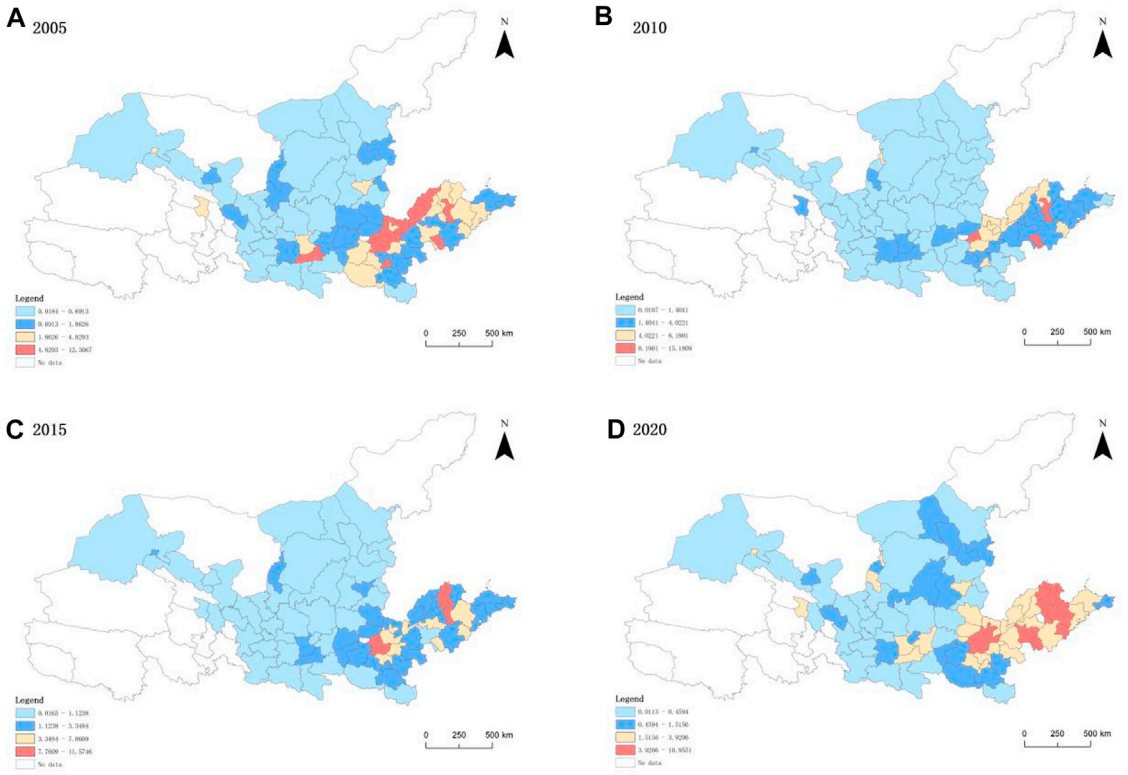

FIGURE 3
Spatial pattern of industrial wastewater discharge agglomeration in the Yellow River Basin in 2005, 2010, 2015, 2020.

3.2.3 Industrial smoke and dust

According to the spatial distribution pattern, the level of industrial smoke and dust pollution accumulation in the YRB is typically higher in the downstream area and lower in the upper and middle reaches (Figure 5). The extremely high-value regions are chiefly distributed in Rizhao City, Zibo City, and Binzhou City in the downstream area, and also in Shizuishan, Xining, and Jiayuguan in the upstream area; the high-value regions are chiefly located in Taiyuan, Zhengzhou, and Jinan in the lower and middle reaches; the extremely low-value areas and low-value areas of industrial smoke and dust pollution are chiefly dispersed in Lanzhou City, Baiyin City, and Haidong City in the upstream area.

3.3 Spatial correlation characteristics of industrial agglomeration and pollution agglomeration

Geoda 1.18.0 was used to calculate the univariate global Moran's *I* and its significance for industrial agglomeration and pollution agglomeration in the YRB from 2005 to 2020 (Table 1). The results show that the univariate global Moran's *I* of industrial agglomeration and the three major industrial pollutants' agglomeration are all positive and pass the significance test. It can be proved that the spatial distribution of industrial agglomeration and pollution agglomeration in the YRB has a positive spatial correlation, and the phenomenon of spatial agglomeration is evident, but there are differences in the spatial dependence of different pollutants. It can be proved that the pollution of the three major industrial pollutants in the cities in the research area is not merely affected by their emissions but also by the cities nearby. Industrial wastewater agglomeration's fluctuations of Moran's *I* from 2005 to 2020 revealed a changing rising tendency, and the changes of Moran's *I* of industrial agglomeration, industrial SO_2 agglomeration, and industrial smoke and dust agglomeration showed a fluctuating downward tendency. The spatial correlation with pollution agglomeration is still strong.

The bivariate global Moran's *I* of industrial agglomeration and agglomeration of three major industrial pollutants in the YRB from 2005 to 2020 were calculated and their significance. The findings demonstrated that the industrial agglomeration and pollution agglomeration interact spatially. The three bivariate global Moran's *I* all passed the significance test, in which the results of industrial agglomeration and industrial smoke and dust pollution agglomeration were negative values, and the other two were positive values, which can be obtained, that there is spatial relativity between industrial agglomeration and pollution agglomeration, and there are

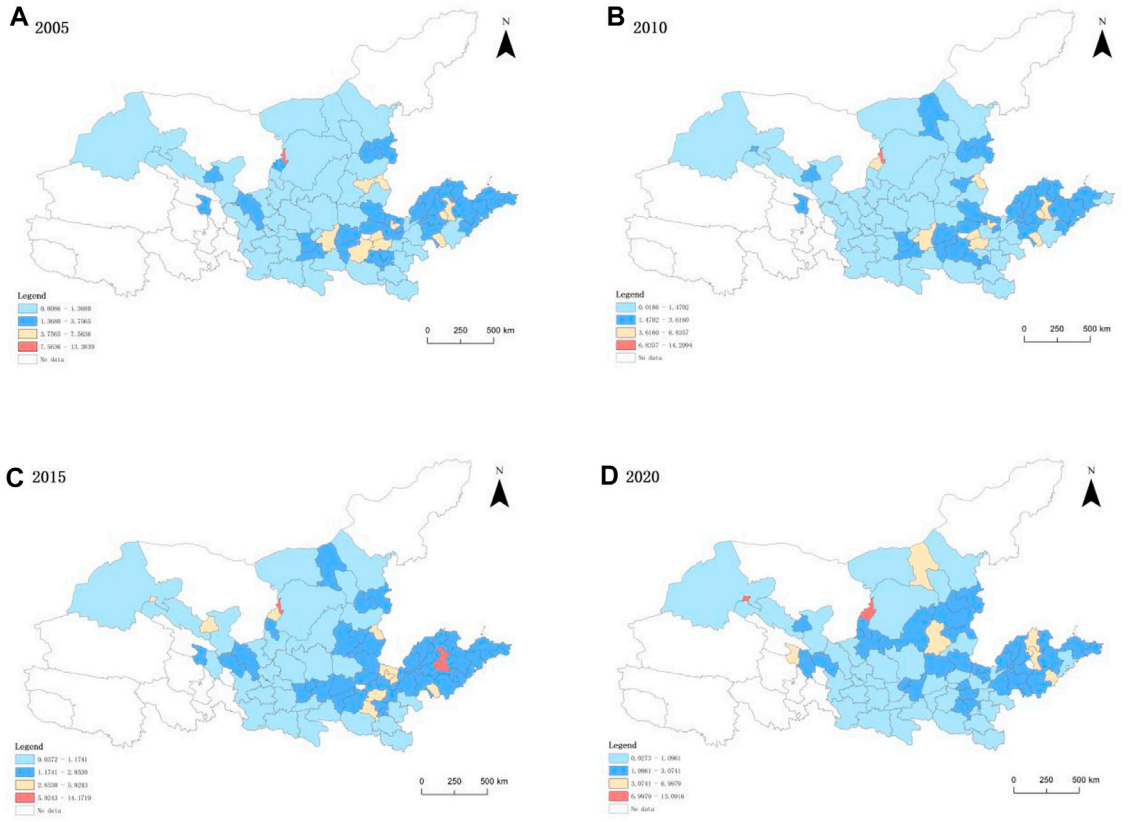

FIGURE 4
Spatial pattern of industrial SO_2 emission agglomeration in the Yellow River Basin in 2005, 2010, 2015, 2020.

discrepancies in the spatial interaction influences of industrial agglomeration and different pollutant agglomerations. According to the index value, consequently, industrial wastewater has the largest spatial association with industrial agglomeration, followed by industrial SO_2, and industrial smoke and dust has the lowest correlation.

4 An empirical analysis of the influencing factors of industrial agglomeration on industrial pollution in the Yellow River Basin

4.1 Indicator selection and model construction

Considering the quantifiability, representativeness, and availability of indicators, industrial pollution is used as the elucidated variable, industrial agglomeration is used as the explanatory variable, and population agglomeration, industrial structure, opening to the outside world, economic development, and environmental regulation are used as control variables. The connection between industrial agglomeration and pollution from industry is investigated by constructing an econometric model. The specific indicators are shown in Table 2.

① Population agglomeration: the expansion of the density of the population can bring about an increase in consumption needs, thereby increasing the consumption of resources such as energy (Sheng and Tang, 2020; Yuan et al., 2020), and the higher the density of the population, the larger the production scale, and the more serious the environmental pollution (Xiao et al., 2021). This article expresses the population agglomeration based on the total population of the region at the years'end rather than the administrative area of the region. ② Industrial structure: modernizing the industrial infrastructure can stop the spread of industrial pollution (Ma and Cao, 2021). The production value of the secondary industry is used in this work as a proportion of GDP to characterize the industrial structure. ③ Environmental control: it is generally accepted that environmental regulation plays a vital part in reducing air pollution (Hao et al., 2018; Zhang et al., 2020), and this study describes environmental regulation using the industrial solid waste's total use rate. ④ Open to the outside world: foreign direct investment can play a technological spillover effect, thereby improving the environmental pollution in the region where it is located; at the same time, it may also increase air pollution in less

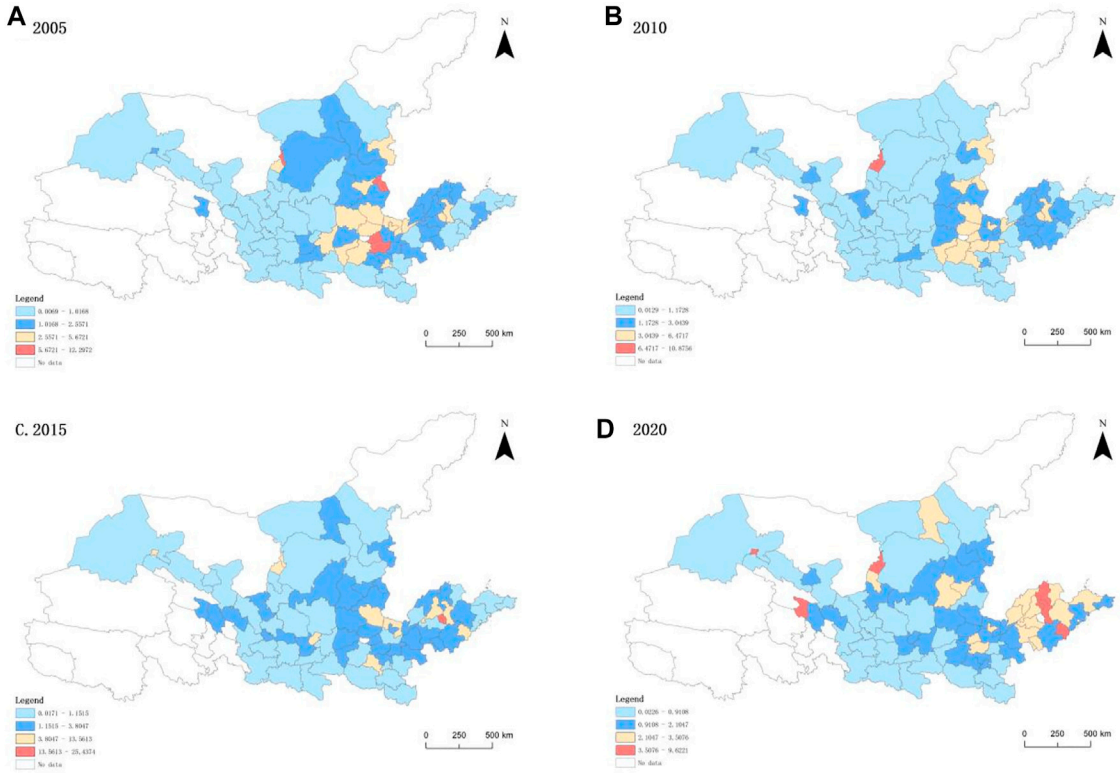

FIGURE 5
Spatial pattern of industrial smoke and dust emission concentration in the Yellow River Basin in 2005, 2010, 2015, 2020.

developed regions (Huang and Zhou, 2019). This article expresses the dependence on foreign capital in terms of the actual amount of foreign capital utilized each year. ⑤ The level of economic development: the environmental Kuznets curve theory deems that the degree of economic progress and pollution are closely correlated, and generally have an inverted "U" shape relationship (Grossman and Kreuger, 1995). In this study, the GDP per capita is a measure of economic growth (Dai and Lin, 2021). ⑥ Industrial agglomeration: pollution agglomeration is a derivative of industrial agglomeration . The pollution effect of industrial agglomeration encourages pollution agglomeration and results in a rise in pollution emissions; on the other side, the self-purification effect of industrial agglomeration brings out the reduction in pollution emissions and inhibits pollution agglomeration (Jia et al., 2020). This study uses the geographical concentration of the industrial added value to represent industrial agglomeration.

This study first performs the appropriate tests on the model and indicators to assure the reliability of the regression results: to ensure data stationarity and weaken the influence of the collinearity and heteroscedasticity of the series on the estimated results, take the logarithm of some indicators of the model; use the Hausman test to measure the feasibility of the random effect model. If the chi-square p value of the model is less than 0.1, it means the fixed effect should be chosen as the model's estimate approach; otherwise, the random effect should be selected as the estimation method.

4.2 Regression results

Before performing the spatial econometric estimation, and after successfully passing the Lagrangian multiplier (LM), the robust Lagrangian multiplier (Robust LM), the likelihood ratio (LR), and the Hausman test, this article finally chooses the city and time to be double fixed; the effect SPDM was used for regression estimation.

LeSage et al. believed that using the sum WX of the spatial lag terms directly WY to describe the spatial interaction may generate wrong results. Therefore, it is necessary to decompose the direct influence and the indirect influence in the form of partial derivatives. The area's industrial pollution discharge is directly impacted by changes in many social and economic aspects, as shown by the direct influence. In contrast, the region's shifting social and economic conditions have an impact on the release of industrial pollutants into nearby areas, which is what the indirect effect indicates (Zhuang et al., 2021).

TABLE 1 Moran's *I* statistics on industrial agglomeration and pollution agglomeration in the Yellow River Basin in 2005–2020.

Year	Univariate Moran's *I*				Bivariate Moran's *I*		
	Industrial agglomeration	Industrial wastewater agglomeration	Industrial SO_2 agglomeration	Industrial smoke and dust collection	Industrial agglomeration and industrial wastewater aggregation	Industrial agglomeration and industrial SO_2 agglomeration	Industrial agglomeration and industrial smoke and dust aggregation
2005	0.716***	0.337***	0.197***	0.349***	0.325***	0.117***	-0.106***
2006	0.725***	0.375***	0.200***	0.366***	0.338***	0.106***	-0.119***
2007	0.723***	0.404***	0.184***	0.388***	0.382***	0.094***	-0.092***
2008	0.724***	0.399***	0.229***	0.355***	0.410***	0.086***	-0.053***
2009	0.721***	0.445***	0.188***	0.341***	0.441***	0.088***	-0.026***
2010	0.684***	0.453***	0.199***	0.261***	0.484***	0.094***	-0.006***
2011	0.655***	0.477***	0.184***	0.158***	0.566***	0.104***	-0.055***
2012	0.639***	0.541***	0.248***	0.005***	0.611***	0.140***	-0.065***
2013	0.648***	0.581***	0.334***	0.020***	0.667***	0.138***	-0.057***
2014	0.637***	0.524***	0.251***	0.176***	0.626***	0.105***	-0.076***
2015	0.641***	0.465***	0.262***	0.191***	0.622***	0.100***	-0.063***
2016	0.633***	0.245***	0.246***	0.285***	0.466***	0.228***	-0.130***
2017	0.622***	0.476***	0.104***	0.285***	0.479***	0.080***	-0.039***
2018	0.567***	0.545***	0.134***	0.197***	0.387***	0.078***	-0.071***
2019	0.723***	0.563***	0.216***	0.284***	0.544***	0.019***	-0.064***
2020	0.518***	0.536***	0.144***	0.220***	0.461***	0.026***	-0.191***

***fnlowast** indicates that the statistical value is significant at the 1% level.

TABLE 2 Definition and explanation of variables.

Variable type	Variable	Index	Variable code
Explained variable	Industrial pollution	Industrial wastewater discharge (10,000 tons)	Wastewater
		Industrial SO_2 emissions (t)	SO_2
		Industrial smoke and dust emissions (t)	Smoke and dust
Explanatory variables	Industrial agglomeration	Gross industrial output value (ten thousand yuan)	aggl
Control variable	Population agglomeration	Population density (person/km^2)	Pop
	Industrial structure	Proportion of secondary industry (%)	str
	environmental regulation	Comprehensive utilization rate of industrial solid waste (%)	er
	open to the outside world	Amount of foreign capital actually utilized (10,000 yuan)	Open
	economic development	GDP per capita (yuan)	GDP

Therefore, this study analyzes the indirect influence, direct influence, and total influence of the SPDM model to further evaluate the geographical interaction of the influencing elements of industrial pollution (Table 3).

4.2.1 Industrial wastewater

Negative is the agglomeration of the industrial regression coefficient with respect to industrial wastewater discharge; however, it does not pass the significance test, proving that industrial agglomeration reduces the intensity of wastewater discharge to a certain extent, but the effect is not significant. This may be due to the higher demands of residents for local environmental quality, which forces the government to adopt stricter environmental regulations, increase investment in pollution prevention and control, and curb pollution accumulation. Population concentration and industrial wastewater pollution have a 0.3616 correlation coefficient, which is positive and has passed the significance test. That

TABLE 3 Regression results of the impact of industrial agglomeration on industrial pollution in the Yellow River Basin.

Explanatory variable	Industrial waste			Industrial SO_2			Industrial smoke and dust		
	Direct effect	Indirect effect	Total effect	Direct effect	Indirect effect	Total effect	Direct effect	Indirect effect	Total effect
aggl	−0.0047	−0.0787	−0.0834	−0.0949**	−0.5002***	−0.5951***	−0.3032***	−0.1244	−0.4276***
	(0.0397)	(0.0678)	(0.0684)	(0.0456)	(0.0903)	(0.0963)	(0.0551)	(0.1027)	(0.1078)
pop	0.3616*	0.1346	0.4962	−0.0556	0.5266	0.4710	−0.1005	1.2478**	1.1473*
	(0.1898)	(0.3706)	(0.4163)	(0.2238)	(0.5057)	(0.5879)	(0.2675)	(0.5700)	(0.6567)
str	0.0016	−0.0042	−0.0026	0.0024	0.0125	0.0150 *	0.0073 *	0.0011	0.0084
	(0.0029)	(0.0057)	(0.0061)	(0.0034)	(0.0077)	(0.0086)	(0.0040)	(0.0087)	(0.0096)
er	0.0006	−0.0000	0.0005	−0.0044***	0.0017	−0.0027	−0.0020 *	−0.0057 **	−0.0076 **
	(0.0008)	(0.0017)	(0.0019)	(0.0010)	(0.0023)	(0.0027)	(0.0012)	(0.0026)	(0.0030)
open	0.0035	−0.0337	−0.0302	−0.015	0.0752**	0.0602	−0.0701***	0.0363	−0.0338
	(0.0140)	(0.0254)	(0.0271)	(0.0162)	(0.0345)	(0.0384)	(0.0195)	(0.0389)	(0.0429)
GDP	−0.2207**	−0.1894	−0.4100**	0.4808***	0.1078	0.5886**	0.3397**	−0.1106	0.2291
	(0.0989)	(0.1745)	(0.1848)	(0.1148)	(0.2315)	(0.2582)	(0.1379)	(0.2642)	(0.2898)

*** stands for $p < 0.01$, **fnlowast* stands for $p < 0.05$, and *fnlowast stands for $p < 0.1$. Robust standard errors are reported in parentheses.

is, the increase in population size significantly exacerbates local industrial wastewater pollution, and the rising levels of population agglomeration often mean an increase in the scale of production, which can cause the intensity of industrial wastewater outflow to increase. The regression coefficients of industrial structure, environmental regulation, and opening to the outside world on industrial wastewater discharge are positive, yet none of them have been shown to be significant. It may be that the degree of openness and supervision is not strong enough, so their effect on the intensity of discharge is not significant. The influence coefficient of economic development on industrial wastewater is −0.2207, and it has passed the significance test at the level of 5%, illustrating that economic growth is helpful in reducing the intensity of wastewater discharge.

4.2.2 Industrial SO_2

The four factors of industrial agglomeration, environmental control, economic growth level, and opening up to the outside world, are important reasons affecting urban industrial SO_2 pollution. From the perspective of direct effects, industrial SO_2 pollution is negatively correlated with industrial agglomeration and environmental control; that is, the increase in industrial agglomeration and environmental management and control has significantly reduced local industrial SO_2 pollution, playing a restraining role. The main reason is that most cities in the YRB are dominated by industrial development at the present stage, and China emphasizes green growth as the orientation and has issued a number of policies (Xinhua, 2021), thereby restraining industrial SO_2 emissions. From the perspective of indirect effects, the greater a city's level of industrial agglomeration , the more it will inhibit the industrial SO_2 pollution of surrounding municipalities, while the direction of the city's opening to the outside world is just the opposite. Positive spillover effects from growth in the urban industrial agglomeration may benefit the nearby cities, while the expansion of the openness of the city to the outside world will promote an increase in the production volume, resulting in an increase in pollution emissions and spreading to the surrounding towns. In addition, population concentration and industrial organization do not significantly affect industrial SO_2 pollution.

4.2.3 Industrial smoke and dust

A total of six factors, including industrial agglomeration, population agglomeration, industrial structure, environmental control, opening to the outside world, and economic development, have an important impact on urban industrial smoke and dust pollution. The impact coefficients of industrial agglomeration, environmental control, and exposure to the outside world on regional industrial smoke and dust pollution are, in terms of direct consequences, −0.3032, −0.002, and −0.0701, respectively. This shows that industrial agglomeration, environmental control, and opening up have a significant inhibitory effect on local industrial smoke and dust pollution and can be used as a key factor in controlling industrial smoke and dust pollution in the YRB. Next, the degree of industrial structure and economic growth has increased, which has intensified the industrial smoke and dust pollution in the area. As a result, the proportion of the secondary industry has increased, and the purpose of enterprises engaged in economic activities is to make profits, and in the process of profitability, some enterprises may cause environmental pollution. The effective coefficient

TABLE 4 Regression results of the impact of industrial agglomeration on industrial pollution in the upper, middle, and lower reaches of the Yellow River Basin.

Explanatory variable	Industrial waste			Industrial SO_2			Industrial smoke and dust		
	Upstream	Midstream	Downstream	Upstream	Midstream	Downstream	Upstream	Midstream	Downstream
aggl	−0.2253*	−1.0296***	−0.4012***	−0.2024	−0.6638***	−0.2200*	−0.0715	−0.5494**	−0.4735***
	(0.1355)	(0.1879)	(0.1160)	(0.1793)	(0.1827)	(0.1301)	(0.1908)	(0.2723)	(0.1434)
pop	0.0063*	−0.0009	0.0001	0.0056	−0.0005	−0.0007	0.0079	−0.0019	−0.0021*
	(0.0036)	(0.0008)	(0.0009)	(0.0048)	(0.0008)	(0.0010)	(0.0051)	(0.0012)	(0.0011)
str	−0.013	0.0232***	0.0266**	−0.0233	0.0168*	0.0439***	−0.0077	-0.0174	0.0789***
	(0.0108)	(0.0089)	(0.0113)	(0.0145)	(0.0086)	(0.0125)	(0.0153)	(0.0130)	(0.0142)
er	−0.000 1	−0.0047*	−0.0021	−0.0058	−0.0060**	−0.0060	−0.0109**	-0.0088 **	−0.0051
	(0.003)	(0.0025)	(0.0048)	(0.0040)	(0.0024)	(0.0054)	(0.0043)	(0.0036)	(0.0060)
open	−0.0377	-0.0349	−0.0216	0.0117	−0.0673	−0.0958	−0.0789	−0.1032	−0.4493***
	(0.0523)	(0.0454)	(0.0581)	(0.0699)	(0.0440)	(0.0645)	(0.0747)	(0.0653)	(0.0725)
GDP	−0.8938**	0.4787	−0.6404*	1.8246***	0.7377**	−0.4837	1.0692**	2.3169***	1.0928**
	(0.3619)	(0.3040)	(0.3444)	(0.5072)	(0.2962)	(0.3869)	(0.5300)	(0.4438)	(0.4250)

*** stands for $p < 0.01$, ** stands for $p < 0.05$, and *stands for $p < 0.1$. Robust standard errors are reported in parentheses.

10.3389/fenvs.2022.1004343

of environmental regulation on industrial smoke and dust pollution in surrounding areas is −0.0057 when looking at indirect effects, and it has passed the significance test at a level of 5%; it demonstrates how the region's tight environmental regulations not only limit local pollution but also slow down the spread of industrial smoke and dust pollution to nearby cities. Environmental laws, both statutory and informal, directly control how industrial firms discharge pollutants, and this regulatory constraint sends a signal of emission reduction to neighboring areas through the demonstration warning effect, and there is no nearby transfer of pollution under environmental regulations (Shen et al., 2017); similarly, due to the increase of the municipal population, the pollution emissions of the city will increase. For industrial smoke and dust, a pollutant with spatial mobility, the degree of industrial smoke and dust pollution in the surrounding neighboring cities will increase as a result of the city's pollution level having an effect on the pollution levels of its bordering cities.

4.3 Upper, middle, and lower sections of the Yellow River Basin heterogeneity analysis

The YRB is further divided into three sections in this article: upstream, midstream, and downstream which investigate the influences of industrial agglomeration on industrial pollution in various regions and conduct regression analysis on the link between industrial agglomeration and three major industrial pollutants (Table 4).

The regression results demonstrate that, at the scale of the YRB, the regression coefficients of industrial agglomeration on three major industrial pollutant emissions are all negative, indicating that, from a broad perspective, an increase in industrial agglomeration will result in a reduction in the level of industrial pollution. The magnitude of the coefficient shows that industrial agglomeration has a more obvious effect on industrial SO_2 emission reduction. From a regional perspective, industrial agglomeration has a significantly detrimental impact on the amount of three major industrial pollutants that is emitted in the middle, lower, and upper reaches, and the regression coefficients from large to small are in the middle, downstream, and upstream, indicating that industrial agglomeration of all the three regions will be beneficial to the reduction of industrial pollution; and the regional differences are more obvious, and the effect on the reduction of industrial pollution in the lower and middle reaches is more obvious than that in the upstream. Possible causes are as follows: recently, the lower and middle reaches of the YRB began to develop earlier than the upstream areas, and with the improvement of industrial agglomeration, the features of high added value, low energy consumption, and low pollution of industries in the region are particularly prominent; the level of environmental protection technology in the lower and middle reaches is relatively high, and industrial agglomeration is helpful for centralized pollution control and disposal, so industrial agglomeration brings positive externalities that benefit the environment within the region. Due to geographical and historical reasons, the upstream region's industrial development is comparatively slow, and the overall technical level of the industry is relatively low. The upstream region's production efficiency has increased as a result of the technological diffusion effect, and as the industrial agglomeration occurs, pollution emissions become less intense, although there are still gaps as compared to the region's lower and middle reaches.

Second, the regression results demonstrate that the industrial structure in the lower and middle reaches significantly aggravates industrial pollution. In the context of industrialization promoting urban development, an important factor causing pollution agglomeration is the rise in the share of secondary industry in the national economic structure. The YRB's high, lower, and middle reaches all have negative environmental control coefficients that are affected differently by industrial pollution, and the reason is that the regional environmental management and control efforts are different, which indicates that the upper, lower, and middle reaches of the YRB should continue to strengthen the control of industrial pollution; the local industrial smoke and dust pollution is significantly hampered by the opening of the downstream areas to the outside world. Foreign capital has introduced a higher degree of technology, and as technology spreads, the production process will be improved to some extent, lowering the overall amount of pollutant emissions, the less pronounced pollution in the upstream and midstream areas may be due to the low level of openness to the outside world and the difficulty of obtaining trade opportunities. From the significant values in the data obtained from economic development, economic growth has a similar impact on industrial pollution in the middle, lower, and upper reaches as it has on the entire YRB.

5 Conclusion and policy implications

5.1 Conclusion

This research uses the spatial auto-correlation analysis approach to thoroughly examine the distribution characteristics and geographical correlation of industrial agglomeration and pollution from the YRB's industrial statistics from 2005 to 2020, and on this basis, utilizing the spatial econometric model to explore the critical variables influencing industrial pollution in the YRB, the principal findings are as follows:

1) The YRB's industrial pollution agglomeration and agglomeration of industrial spatial patterns are spatially converging. The high-value areas of pollution agglomeration and industrial agglomeration are chiefly concentrated in Zibo, Zaozhuang, Zhengzhou, and Taiyuan in the lower and middle reaches. The agglomerated low-value regions are chiefly concentrated in Baiyin City, Yinchuan City, and Haidong City in the upper reaches.
2) Moran's *I* of industrial agglomeration, industrial wastewater, industrial SO_2, and industrial smoke and dust are all obviously positive, manifesting that the global clustering characteristics of industrial pollution in the YRB are obvious, and the global correlations of the three pollutants are industrial wastewater > industrial smoke and dust > industrial SO_2. The spatial correlation intensity varied and altered over the study period, exhibiting a trend toward a gradual waning.
3) There is a spatial association between agglomeration of industrial and pollution agglomeration, on the basis of the bivariate global spatial auto-correlation test. Additionally, there are variations in the spatial interaction impacts of various pollution agglomerations and agglomeration of industrial. From the correlation index value, it can draw a conclusion that the largest spatial association exists between industrial wastewater and agglomerations of industries, followed by industrial SO_2, and industrial smoke and dust is the lowest.
4) Industrial agglomeration, population agglomeration, industrial structure, environmental control, opening to the outside world, and economic development are the primary determinants of industrial pollution in the YRB, and there are differences in their impact on three major industrial pollutants. In terms of immediate effects, the population growth exacerbates local industrial wastewater pollution, while economic development is beneficial to reduce the intensity of wastewater discharge. Additionally, the degree of industrial agglomeration can be increased, and environmental regulation can lower local industrial SO_2 emissions, and the development of the economic level will aggravate the local industrial SO_2 pollution. Industrial agglomeration, environmental regulation, and opening to the outside world have a significant inhibitory effect on local industrial smoke and dust pollution, and the improvement of industrial structure and economic development level has exacerbated the industrial smoke and dust pollution in the region.
5) Industrial agglomeration, population agglomeration, environmental management and control, and opening to the outside world can affect industrial pollution in adjacent areas through indirect effects, and there are differences in their impact on three major industrial pollutants in adjacent cities. Industrial SO_2 pollution in neighboring cities was more severely restricted and the more agglomeration of industrial there was. However, the higher the degree of opening up of the city, the more it will promote industrial SO_2 pollution in surrounding cities. In addition, the contributing factors of industrial smoke and dust pollution are more complex and diverse, the enhancement of environmental control has a very obvious inhibitory effect on industrial smoke and dust pollution in surrounding cities, and one of the primary causes of industrial smoke and dust pollution is the growth of the population.
6) Industrial agglomeration will lower the pollution levels of three major industrial pollutants from a broad perspective of the YRB. From the standpoint of different regions, industrial agglomeration in the middle, lower, and upper reaches is beneficial to the reduction of industrial pollution, and the impact is in the middle, lower, and upper reaches in descending order. In addition, due to differences in industrial structure, opening to the outside world, environmental control, and economic development levels in the middle, lower, and upper reaches, the pollution levels of industrial wastewater, industrial SO_2, and industrial smoke and dust differ between regions.

5.2 Policy implications

1) The YRB's ecological environment quality, sustainable economic and social growth, and influence on the nation as a whole are crucial, and it is also a key area for comprehensive environmental pollution control, and there is a problem of unbalanced regional development (Xinhua, 2021). Although the natural resource endowments and economic development conditions are different in each region of the YRB, the YRB may achieve high-quality development by sticking to the environmental bottom line of economic growth and encouraging the green transformation of industry.
2) Industrial agglomeration and pollution agglomeration are spatially interconnected, indicating that pollution agglomeration in the YRB is both an environmental issue and a development issue. The YRB frequently struggles with the conflict between coordinating industrial expansion and environmental prevention. Industrial agglomeration, pollution agglomeration, and the surrounding areas are closely related as a result of the spatial effects of these phenomena. Therefore, when formulating industrial development policies and environmental governance policies, to eliminate local "policy islands," a joint cross-provincial and cross-regional prevention and control system should be implemented through government power, enterprise power, market power, and social power to jointly promote green industrial transformation and improve quality and efficiency (Zhou et al., 2022).

3) The YRB must fundamentally restructure its economic development model and adhere to the idea of green development in order to effectively control industrial pollution and organize the promotion of the development of an ecological society. which improve the degree of agglomeration of industries, lower the production costs for businesses, and accelerate the flow of factors and technology spillovers. Furthermore, implement stricter pollution control policies and put in place an environmentally friendly development path that is innately compatible with the objectives and methods of ecological and environmental protection governance.
4) To control industrial pollution in the YRB, we must continue to take the road of industrial agglomeration development. At the same time, coordination of the overall situation is required, and efforts should be made to implement actions in accordance with regional conditions. Given the regional variations in industrial pollution output, actions should be performed in accordance with local circumstances, and the management and control of high industrial pollution discharge areas should be strengthened. A combined preventive and control mechanism for industrial pollution emissions must first be established, along with ongoing efforts to promote regional exchanges and collaboration. ① It should be considered the primary location for industrial pollution control in the entire YRB for areas with a relatively established economy and substantial pollution in the lower parts of the basin, and the policy strength and capital arrangement should be arranged. ② The natural setting in the middle reaches of the YRB has been impacted by the industrial firms' fast expansion, where industrial pollution is gradually transported. Environmental concerns should be given more attention, inspection and oversight should be increased, the economic structure should be transformed and upgraded, and green growth should be pursued. ③ For the YRB's upper reaches, where the degree of industrial pollution is low when shifting sectors, it is important to avoid the phenomenon of pollution transfer and fully follow the developmental principle that "clear streams and green mountains are priceless assets."

Based on the research purpose of how to develop industrial agglomeration while ensuring environmental quality, this article analyzes the spatial correlation between industrial agglomeration and industrial pollution in the YRB, studies the impact of industrial agglomeration on environmental pollution, and provides support for ecological protection and high-quality development in the YRB. Since the upper YRB involves many ethnic autonomous regions, some of its data have not been made public. The authors tried their best to supplement it through various methods during the research process, but there are still some missing data to a certain extent. At the same time, due to data limitations, six indicators were selected as the factors affecting industrial pollution in the YRB, and there are still some omissions of variables, which need to be further explored.

Data availability statement

The datasets presented in this study can be found in online repositories. The names of the repository/repositories and accession number(s) can be found in the article/ Supplementary Material.

Author contributions

Several authors made the most widely varied contributions. In particular, YQ had original ideas for this study and conceived and designed the methodology. The manuscript was written, processed, and analyzed by YQ and revised and reviewed by YD, HaZ, HMZ, DL, and ZH, and YD provided financial support. All authors read and agree to the published version of the manuscript.

Funding

This research was funded by the Social Science Foundation of Liaoning Province (L19CJY006).

Acknowledgments

The authors of this article thank the School of Geography of Liaoning Normal University for assistance in developing this research.

Conflict of interest

The authors declare that the research was conducted in the absence of any commercial or financial relationships that could be construed as a potential conflict of interest.

Publisher's note

All claims expressed in this article are solely those of the authors and do not necessarily represent those of their affiliated organizations, or those of the publisher, the editors, and the reviewers. Any product that may be evaluated in this article, or claim that may be made by its manufacturer, is not guaranteed or endorsed by the publisher.

Supplementary material

The Supplementary Material for this article can be found online at: https://www.frontiersin.org/articles/10.3389/fenvs.2022.1004343/full#supplementary-material

References

Bai, L., Sun, Y. Y., Zhao, X. T., Qiao, Q., Li, X. Y., and Zhou, X. Y. (2020). Analysis of water pollution discharge characteristics and pollution agglomeration patterns in the Yellow River Basin. *Environ. Sci. Res.* 33 (12), 2683–2694. doi:10.13198/j.issn.1001-6929.2020.10.23

Chen, C., Sun, Y., Lan, Q., and Jiang, F. (2020a). Impacts of industrial agglomeration on pollution and ecological efficiency-A spatial econometric analysis based on a big panel data set of China's 259 cities. *J. Clean. Prod.* 258, 120721. doi:10.1016/j.jclepro.2020.120721

Chen, Y. G. (2009). Development of spatial autocorrelation theory and method improvement based on moran statistics. *Geogr. Res.* 28 (06), 1449–1463. doi:10.11821/yj2009060002

Chen, Y., Zhu, M. K., Lu, J. L., Zhou, Q., and Ma, W. B. (2020b). Evaluation of ecological city and analysis of obstacle factors under the background of high-quality development: Taking cities in the Yellow River Basin as examples. *Ecol. Indic.* 118, 106771. doi:10.1016/j.ecolind.2020.106771

CPGPRC (2013). A circular on "action plan on prevention and control of air pollution" issued by the state Council in China. Available At: http://www.gov.cn/zwgk/2013-09/12/content_2486773.htm (accessed on July 21, 2022).

CPGPRC (2008). The central committee of the communist party of China and the state Council issued the "flood control plan for the Yellow River basin. Available At: http://www.gov.cn/zwgk/2008-07/28/content_1057822.htm (accessed on July 21, 2022).

Dai, P., and Lin, Y. (2021). Should there Be industrial agglomeration in sustainable cities? A perspective based on haze pollution. *Sustainability* 13 (12), 6609. doi:10.3390/su13126609

Ding, J. S., Deng, Y. Y., and Ma, L. (2022). Spatio-temporal characteristics of haze pollution in the Yellow River Basin and its influencing factors. *Statistics decision-making* 38 (06), 60–64. doi:10.13546/j.cnki.tjyjc.2022.06.012

Du, X. Y., and Xie, Z. X. (2020). Occurrence of turning point on environmental Kuznets curve in the process of (de)industrialization. *Struct. Change Econ. Dyn.* 53, 359–369. doi:10.1016/j.strueco.2019.06.003

Fang, J., Tang, X., Xie, R., and Han, F. (2020). The effect of manufacturing agglomerations on smog pollution. *Struct. Change Econ. Dyn.* 54, 92–101. doi:10.1016/j.strueco.2020.04.003

Feng, D., Wang, Y., Zheng, L., Li, J. Y., and Xie, S. X. (2020). Can industrial agglomeration promote pollution agglomeration? Evidence from China. *J. Clean. Prod.* 246 (C), 118960. doi:10.1016/j.jclepro.2019.118960

Geng, Y., Wang, M., Sarkis, J., Xue, B., Zhang, L., Fujita, T., et al. (2014). Spatial-temporal patterns and driving factors for industrial wastewater emission in China. *J. Clean. Prod.* 76, 116–124. doi:10.1016/j.jclepro.2014.04.047

Grossman, G., and Kreuger, A. (1995). Economic growth and the environment. *Q. J. Econ.* 110 (2), 353–377. doi:10.2307/2118443

Hao, Y., Deng, Y., Lu, Z. N., and Chen, H. (2018). Is environmental regulation effective in China? Evidence from city-level panel data. *J. Clean. Prod.* 188, 966–976. doi:10.1016/j.jclepro.2018.04.003

He, C., Huang, Z., and Ye, X. (2014). Spatial heterogeneity of economic development and industrial pollution in urban China. *Stoch. Environ. Res. Risk Assess.* 28 (4), 767–781. doi:10.1007/s00477-013-0736-8

Hu, Z. Q., Miao, J. M., and Miao, C. H. (2016). Agglomeration characteristics and influencing factors of industrial pollution at the prefecture-level in China. *Geogr. Res.* 35 (08), 1470–1482. doi:10.11821/dlyj201608006

Hu, Z. Q., Miao, J. M., and Miao, C. H. (2018). Spatial characteristics and measurement and inspection of industrial agglomeration and pollution emissions in China's prefectures and cities. *Geogr. Sci.* 38 (02), 168–176. doi:10.13249/j.cnki.sgs.02.002

Huang, R. Y., and Zhou, Q. J. (2019). Will FDI lead to environmental pollution in the host country? Empirical evidence from the Yangtze River economic belt. *Contemp. Financial Res.* 5, 41–53.

Ji, D. J., and Zhou, P. (2020). Marginal abatement cost, air pollution and economic growth: Evidence from Chinese cities. *Energy Econ.* 86, 104658. doi:10.1016/j.eneco.2019.104658

Jia, R. Y., and Zhao, D. T. (2012). Performance evaluation model of industrial pollution control: An empirical study based on the perspective of environmental regulation. *Syst. Eng.* 30 (06), 1–9.

Jia, Z., Qing, W. L., Wang, Y. J., Li, E. L., and Chen, X. P. (2020). The pattern of industrial pollution agglomeration and its spatial effects in Lanzhou-Xining urban agglomeration. *Econ. Geogr.* 40 (01), 68–75+84. doi:10.15957/j.cnki.jjdl.2020.01.008

Jin, F. J. (2019). Coordinated promotion strategies for ecological protection and high-quality development in the Yellow River Basin. *Reform* 11, 33–39.

Jin, F. J., Ma, L., and Xu, D. (2020). Environmental stress and optimized path of industrial development in the Yellow River Basin. *Resour. Sci.* 42 (1), 127–136. doi:10.18402/resci.2020.01.13

Li, B. G., Hu, Z. Q., Miao, C. H., Zhang, B. F., and Kang, W. (2021a). Spatial differentiation characteristics and influencing factors of industrial ecological efficiency in the Yellow River Basin. *Geogr. study* 40 (08), 2156–2169. doi:10.11821/dlyj020200516

Li, H., and Han, Y. (2022). Analysis of spatio-temporal evolution characteristics and influencing factors of PM $_{(2.5)}$ in the Yellow River basin. *World Geogr. Res.* 31 (01), 130–141. doi:10.3969/j.issn.1004-9479.2022.01.2020212

Li, H., Zhao, X. Y., Wang, W. J., and Xue, B. (2019). Spatial-temporal differentiation and influencing factors of urban industrial pollution in China based on multi-scale. *Geogr. Res.* 38 (08), 1993–2007. doi:10.11821/dlyj020180480

Li, S. (2021). Study on the Spatio-temporal pattern and influencing factors of industrial pollution in the Yellow River Basin. China (Gansu Province): Lanzhou University. [master's thesis]. doi:10.27204/d.cnki.glzhu.2021.002401

Li, Z. J., Hu, M. J., Zhang, A. P., and Nian, X. (2021b). The impact of industrial eco-efficiency on pollution of PM $_{(2.5)}$ and its spillover effect. *J. Nat. Resour.* 36 (03), 737–751. doi:10.31497/zrzyxb.20210315

Liang, L. W., Wang, Z. B., and Li, J. X. (2019). The effect of urbanization on environmental pollution in rapidly developing urban agglomerations. *J. Clean. Prod.* 237, 117649–126526. doi:10.1016/j.jclepro.2019.117649

Liu, R. P., Wei, N., Song, Z. X., and Wang, X. H. (2021). Strategic study on soil pollution control in the Yellow River Basin. *Environ. Sci. Manag.* 46 (09), 45–49. doi:10.3969/j.issn.1673-1212.2021.09.012

Liu, Y. S., Zhou, Y., and Wu, W. X. (2015). Assessing the impact of population, income and technology on energy consumption and industrial pollutant emissions in China. *Appl. Energy* 155, 904–917. doi:10.1016/j.apenergy.2015.06.051

Lu, C. P., Hou, M. C., Liu, Z. L., Li, H. Z., and Lu, C. Y. (2021). Variation characteristic of NDVI and its response to climate change in the middle and upper reaches of Yellow River basin, China. *IEEE J. Sel. Top. Appl. Earth Obs. Remote Sens.* 14, 8484–8496. doi:10.1109/JSTARS.2021.3105897

Lu, D. D., and Sun, D. Q. (2019). Comprehensive management and sustainable development of the Yellow River basin. *Acta Geogr. Sin.* 74 (12), 2431–2436. doi:10.11821/dlxb201912001

Ma, H. T., and Xu, Y. Y. (2020). Differentiation between high-quality development assessment and spatial pattern of urban agglomerations in the Yellow River Basin. *Econ. Geogr.* 40 (04), 11–18. doi:10.15957/j.cnki.jjdl.2020.04.002

Ma, T., and Cao, X. X. (2021). The effect of the industrial structure and haze pollution: Spatial evidence for China. *Environ. Sci. Pollut. Res.* 29 (16), 23578–23594. doi:10.1007/s11356-021-17477-4

NBS (20052021b). *China regional economic statistics yearbook*. Beijing: China Statistics Press.

NBS (2005-2021a). *Yearbook of Chinese urban statistics*. Beijing: China Statistics Press.

Pierson, P. (2000). Increasing returns, path dependence, and the study of politics. *Am. Polit. Sci. Rev.* 94 (2), 251–267. doi:10.2307/2586011

Rahman, M. M., Alam, K., and Velayutham, E. (2021). Is industrial pollution detrimental to public health? Evidence from the world's most industrialized countries. *BMC Public Health* 21, 1175. doi:10.1186/s12889-021-11217-6

Shen, K. R., King, K., and Fang, X. (2017). Does environmental regulation cause pollution to transfer nearby? *Econ. Res.* 52 (05), 44–59.

Shen, N., and Peng, H. (2021). Can industrial agglomeration achieve the emission-reduction effect? *Socio-Economic Plan. Sci.* 75, 100867–110121. doi:10.1016/j.seps.2020.100867

Sheng, J. C., and Tang, W. Z. (2020). Spatio-temporal variation patterns of water pollution drivers: The case of China's south-north water transfer project. *Sci. Total Environ.* 761, 143190–149697. doi:10.1016/j.scitotenv.2020.143190

Song, H. Q., and Zhang, M. (2020). "Investigation of regional gap in the Yellow River Basin and analysis of high-quality development strategies," in 2020 International Conference on Urban Engineering and Management Science (ICUEMS), Zhuhai, China, 24-26 April 2020 (IEEE), 105–111. doi:10.1109/ICUEMS50872.2020.00033

Teng, T. W., Chen, D. H., and Hu, L. L. (2021). Spatial pattern evolution and influencing factors of air pollution in the Yellow River Basin. *Geogr. Sci.* 41 (10), 1852–1861. doi:10.13249/j.cnki.sgs.2021.10.017

Wang, Y. Z., Duan, X. J., Wang, L. Q., and Zou, H. (2022). Spatial-temporal patterns and driving factors of industrial pollution and structures in the Yangtze River Economic Belt. *Chemosphere* 303, 134996–136535. doi:10.1016/j.chemosphere.2022.134996

Wu, J. W., Chen, W., Geng, P., and Yang, L. Q. (2020). Study on the evolution of industrial pollution and its driving factors under the background of economic transformation: A case study of Yangtze River delta region. *Resour. Environ. Yangtze River Basin* 29 (03), 535–546. doi:10.11870/cjlyzyyhj202003001

Wu, J. X., Xu, H., and Tang, K. (2021). Industrial agglomeration, CO_2 emissions, and regional development programs: A decomposition analysis based on 286 Chinese cities. *Energy* 225, 120239–125442. doi:10.1016/j.energy.2021.120239

Xi, J. P. (2019). Speech at a symposium on ecological protection and quality development in the Yellow River Basin. *Qiushi* 20, 1–5.

Xiao, Z. Y., Li, H. H., and Sun, L. (2021). Does population and industrial agglomeration exacerbate China's pollution? *J. Environ. Plan. Manag.* 9, 711033. doi:10.1080/09640568.2021.1978059

Xinhua, H. (2015). The state Council issued the "water pollution prevention and control action plan. Available At: http://www.gov.cn/xinwen/2015-04/16/content_2847709.htm (Accessed on July 21, 2022).

Xinhua, H. (2021). Xi Jinping presided over a symposium on the in-depth promotion of ecological protection and high-quality development of the Yellow River Basin. Available At: http://www.gov.cn/xinwen/2021-10/22/content_5644385.htm#1 (accessed on July 21, 2022).

Yan, S., and Cao, Y. M. (2020). The impact of environmental pollution on China's economic growth: Based on the perspective of environmental pollution control expenditure. *Environ. Sci. Manag.* 45 (03), 15–20+83. doi:10.3969/j.issn.1673-1212.2020.03.004

Yang, M. (2018). An empirical study on the impact of industrial agglomeration on industrial pollution emissions—based on the comparison of manufacturing agglomeration and service industry agglomeration. *Qiushi* 2, 59–74+111. doi:10.3969/j.issn.1007-8487.2018.02.006

Yang, Y. C., Mu, Y. J., and Zhang, W. (2020). Basic conditions and core strategies of high-quality development in the Yellow River Basin. *Resour. Sci.* 42 (3), 409–423. doi:10.18402/resci.2020.03.01

You, J. H. (2022). Research on the impact of industrial pollution on residents' health. China (Hebei Province): The Hebei University of Geosciences. [master's thesis].

Yuan, H. X., Feng, Y. D., Lee, C. C., and Cen, Y. (2020). How does manufacturing agglomeration affect green economic efficiency? *Energy Econ.* 92, 104944. doi:10.1016/j.eneco.2020.104944

Zhang, Z., Zhang, G., Song, S., and Su, B. (2020). Spatial heterogeneity influences of environmental control and informal regulation on air pollutant emissions in China. *Int. J. Environ. Res. Public Health* 17, 4857. doi:10.3390/ijerph17134857

Zhao, H. X., Jiang, X. W., and Cui, J. X. (2014). [Shifting path of industrial pollution gravity centers and its driving mechanism in Pan-Yangtze River Delta]. *Environ. Sci.* 35 (11), 4387–4394. doi:10.13227/j.hjkx.2014.11.048

Zhou, D., Zhong, Z. X., Chen, L. B., Gao, W. X., and Wang, M. Z. (2022). Can the joint regional air pollution control policy achieve a win-win outcome for the environment and economy? Evidence from China. *Econ. Analysis Policy* 74, 0313–0333. doi:10.1016/j.eap.2022.01.011

Zhou, Z. Z., Liu, Q. B., and Wang, Y. Y. (2020). Environmental Kuznets curve test on the relationship between economic growth and industrial environmental pollution—panel econometric model based on provinces in the Yangtze River economic belt. *J. Nanjing Univ. Technol. Soc. Sci. Ed.* 19 (02), 64–72+112. doi:10.3969/j.issn.1671-7287.2020.02.008

Zhuang, R., Mi, K., and Feng, Z. (2021). Industrial Co-agglomeration and air pollution reduction: An empirical evidence based on provincial panel data. *Int. J. Environ. Res. Public Health* 18 (22), 12097. doi:10.3390/ijerph182212097

frontiers | Frontiers in Ecology and Evolution

TYPE Original Research
PUBLISHED 29 September 2022
DOI 10.3389/fevo.2022.1016774

Check for updates

OPEN ACCESS

EDITED BY
Jun Yang,
Northeastern University, China

REVIEWED BY
Liang Jiao,
Northwest Normal University, China
Tiange Shi,
Xinjiang University of Finance and Economics, China
Huabin Xiao,
Shandong Jianzhu University, China

*CORRESPONDENCE
Haitao Ma
maht@igsnrr.ac.cn

SPECIALTY SECTION
This article was submitted to Environmental Informatics and Remote Sensing, a section of the journal Frontiers in Ecology and Evolution

RECEIVED 11 August 2022
ACCEPTED 12 September 2022
PUBLISHED 29 September 2022

CITATION
Ma H (2022) Spatiotemporal analysis of land use changes and their trade-offs on the northern slope of the Tianshan Mountains, China. *Front. Ecol. Evol.* 10:1016774. doi: 10.3389/fevo.2022.1016774

COPYRIGHT
© 2022 Ma. This is an open-access article distributed under the terms of the Creative Commons Attribution License (CC BY). The use, distribution or reproduction in other forums is permitted, provided the original author(s) and the copyright owner(s) are credited and that the original publication in this journal is cited, in accordance with accepted academic practice. No use, distribution or reproduction is permitted which does not comply with these terms.

Spatiotemporal analysis of land use changes and their trade-offs on the northern slope of the Tianshan Mountains, China

Haitao Ma*

Key Laboratory of Regional Sustainable Development Modeling, Institute of Geographic Sciences and Natural Resources Research, Chinese Academy of Sciences, Beijing, China

The unprecedented urbanization recently has inevitably intensified the changes in land use morphology. However, current studies on land use primarily analyze a single morphology, ignoring the relationships between different land use morphologies. Taking the northern slope of the Tianshan Mountains (NSTM) as the study area, this article quantifies the spatiotemporal pattern of land use change, and estimates trade-offs and synergies between dominant (patch density, largest patch index, and landscape shape index) and recessive (land use efficiency, land use intensity, and agricultural non-point source pollution) morphologies to fully understand the dynamic characteristics of land use. Results showed bare areas and grassland were always predominant land use types, and land use change from 1990 to 2020 was characterized by the increase of impervious surfaces and the decrease of bare areas. The strongest trade-off was found between largest patch index and land use intensity, while the synergy between landscape shape index and land use intensity was strongest. There are significant disparities in terms of temporal and spatial patterns of trade-offs/synergies. The correlation coefficients in different study periods were much smaller than their estimations in the whole region, and the trade-offs/synergies in the eastern NSTM were basically identical with the whole relationships. The findings reveal the interactions among various land use characteristics, and provide significant references for coordinated land management and regional high-quality development.

KEYWORDS

land use change, trade-off and synergy, landscape pattern, dominant and recessive morphologies, the northern slope of the Tianshan Mountains (NSTM)

Introduction

Land systems are not only the surface covered by natural and artificial elements, but also the utilization of land by human beings. Land systems are complex and highly associated with climate change, food security, and regional inequality in the 2030 Agenda for Sustainable Development Goals (SDGs) (Fujimori et al., 2022; Meyfroidt et al., 2022; van Marle et al., 2022). This indicates that the efficient management and sustainable development of land systems will be of utmost importance to achieving SDGs in the following years. Recently, China has experienced unprecedented urbanization with increasing population, which inevitably intensifies the evolution of land systems (Zuo et al., 2018; Liu et al., 2021; He et al., 2022). Land use change refers to the transformation of land use morphology in a region during a certain period driven by human activities (Long et al., 2014). The concept of land use morphology was firstly proposed by Grainger (1995), who defined it as the overall pattern of actual land cover in a region at a given time. With the continuous social and economic changes, Long and Li (2012) enriched the connotation of the traditional quantity and distribution of land use morphology, and argued that land use morphology could be represented by dominant and recessive morphologies. Specifically, land use dominant morphology represents the directly visible features of land use, such as areas and spatial patterns, which is highly connected with the landscape patterns of land use. While land use recessive morphology refers to quality embodied in land use, such as property rights, functions, management mode, input, and output (Qu et al., 2021).

At present, studies of land use dominant morphology mainly focus on land use transition research (Long et al., 2021). Much attention had paid to the evolution of land use structure and the changes in the proportion of various land use categories (Ouedraogo et al., 2016; Buckley Biggs, 2022). They found that the proportions and areas of artificial land, especially urban construction land, gradually increased during the process of urbanization and industrialization, while those of natural land, such as forest, grassland, and unused land, displayed significant decreasing trends simultaneously. Some indices, such as gross gain, gross loss, and change rate, were also calculated to evaluate the temporal characteristics of land use during a certain period (Sumari et al., 2020; Duan et al., 2021; Chen et al., 2022). Recent empirical analysis validated the spatiotemporal differentiation of certain land use categories, primarily including cropland and impervious areas (Cai et al., 2020; Yang et al., 2021; Ray et al., 2022), and further discovered the hotspot characteristics of land use on the regional scale or explored the driving forces of land-use spatial distribution (Zhu et al., 2021). In terms of the studies of land use recessive morphology, scholars mainly concentrated on the changes in land use function (Schiavina et al., 2022). It was defined as goods and services provided by different land use categories in order to meet the demands of human activities. Considerable progress had identified land use function from the aspects of production, living, and ecology, by establishing a comprehensive index system (Meng et al., 2022). Besides, some literatures measured the degree of human activities on land use (Howison et al., 2018; Yin et al., 2020; Zhou et al., 2022), and captured the changes in fixed input or economic output efficiency per unit of land in a certain administrative region (Guo and Shen, 2015; Jiang et al., 2021).

Overall, most of the current studies on land use morphology primarily analyze a single morphology, but ignore the interactions between land use dominant and recessive morphologies. The loss of natural land not only reshapes the dominant landscape patterns of land use but also intensifies its recessive input and output. Natural land has consistently transferred into artificial land with the increasing human activities. The landscape patterns of land use became fragmented and dispersed over time. Simultaneously, the input and output embodied in land use increased sharply. There normally exists a positive correlation between dominant landscape patterns and recessive intensity of land use. In some certain cases, the dominant and recessive morphologies of land use do not present a positive correlation theoretically. For example, extensive management of land use has altered its dominant landscape patterns, but it does not bring corresponding economic benefits. Besides, some nature reserves take advantage of their abundant ecologic resources to attract sightseers without altering the dominant morphology of land use. It achieves a better combination of economic development and land protection. In summary, dominant and recessive morphologies of land use are concurrent, and it is of great importance to investigate their relationships to fully understand the dynamic characteristics of land use.

Nowadays, trade-off analysis has become an important method to manifest the relationships of multiple systems (Bradford and D'Amato, 2012). The trade-off is generally described as the status where a specific system benefits at the cost of others (Hamilton et al., 2019). A wealth of studies investigated the links and interactions among multiple natural ecosystem services (Howe et al., 2014; Cord et al., 2017; Geng et al., 2022), and some scholars recently explored the trade-offs/synergies between natural and artificial ecosystems such as multiple land use functions (Fan et al., 2021; Zhu et al., 2021; Meng et al., 2022), but it is relatively scarce to quantify the trade-offs and synergies of different land use characteristics. To fill this research gap, this article focused on the relationships between land use dominant and recessive morphologies. Taking the northern slope of the Tianshan Mountains (NSTM), an important developing area with a fragile environment in China, as the study area, we investigated the changes in land use and its landscape metrics based on land use data in 1990, 1995, 2000, 2005, 2010, 2015, and 2020. Next, the spatiotemporal characteristics of land use change in the NSTM from 1990 to 2020 were examined. Finally, land use dominant and recessive morphologies at the whole and county

scales were estimated by incorporating land use and socio-economic datasets. On this basis, their trade-offs and synergies between land use morphology were qualified through Pearson correlation analysis. The findings contribute to revealing the interactions among various land use morphologies, and provide significant references for coordinated land management and regional high-quality development.

Materials and methods

Study area and data source

The northern slope of the Tianshan Mountains (NSTM) is located in the inland center of the Eurasian continent (Figure 1). It covers 79°53′E-96°23′E and 40°52′N-47°14′N with an area of three hundred and ninety-six thousand square kilometers, accounting for 23.8% of the total area of Xinjiang Uygur Autonomous Region. The terrain, ranging from −192 to 5,166 m, is high in the Tianshan Mountains and low in the surrounding basins. The NSTM includes areas of Urumqi City, Karamay City, Bortala Mongol Autonomous Prefecture, Changji Hui Autonomous Prefecture, Hami City, Tacheng Administrative Office, Turpan City, Kuytun City, and four county-level cities (i.e., Shuanghe City, Wujiaqu City, Huyanghe City, and Shihezi City). The NSTM is the main area of urbanization and economic development in the autonomous region, whose GDP accounts for more than 60% of that in Xinjiang. The NSTM has a typical continental climate with hot-dry summer and cold-long winter, and the temperature

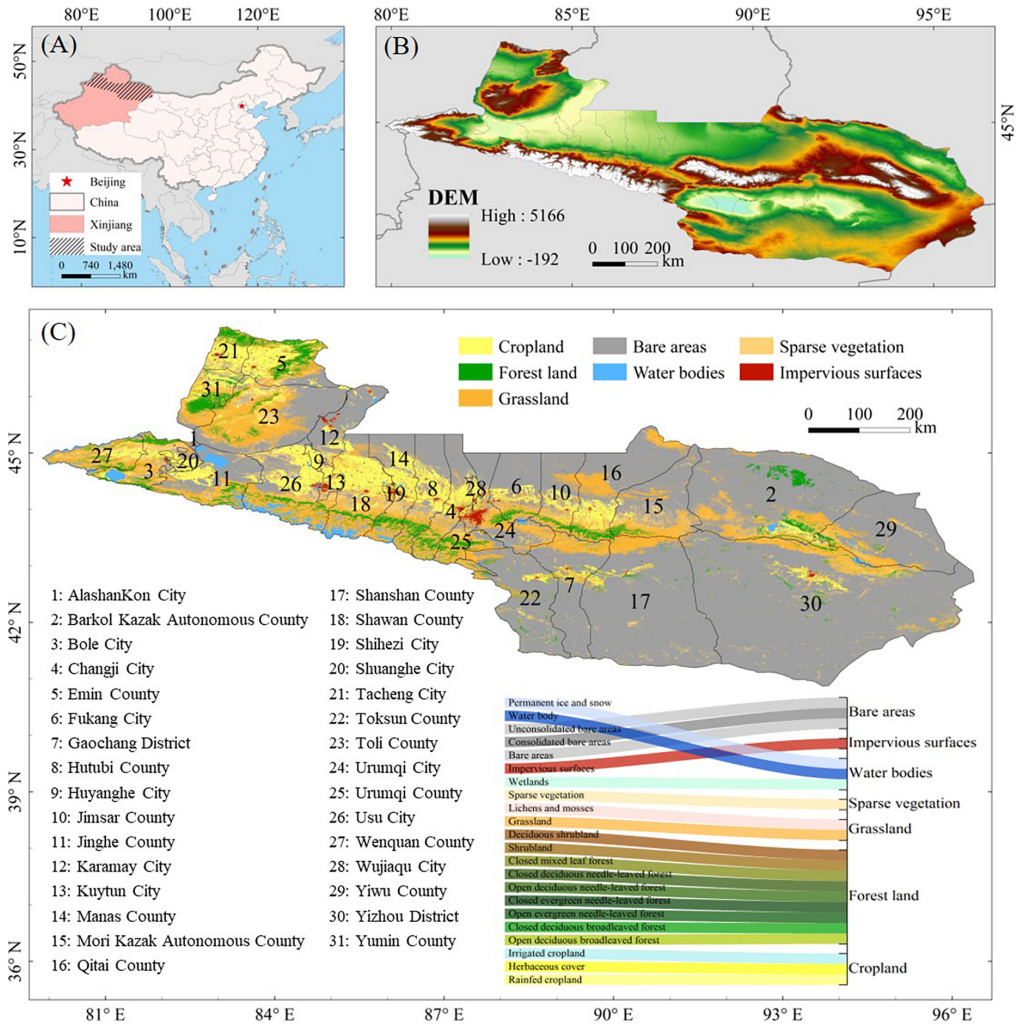

FIGURE 1
(A) The location of the NSTM. **(B)** The elevation of the NSTM derived from the ASTER Global Digital Elevation Model at 30 m, and downloaded from the Geospatial Data Cloud of China. **(C)** The spatial patterns of land use of the NSTM in 2020 derived from GLC_FCS30. The corresponding relationships between the land use classification used in this study and the original system of the dataset are also depicted.

changes greatly from morning to night, and its annual average temperature is 6–7.2°C. The annual average precipitation ranges from 20 to 400 mm, but the annual evaporation amount reaches 1,817 mm. Geological feature is mainly characterized by limestone, sedimentary rock, carbonate, and silicate rock in the NSTM. There are various soil types in the NSTM, including gray brown desert, brown soil, chestnut, chernozem, gray cinnamon, and meadow soil.

Data used in this study are primarily obtained in two ways. Firstly, the Global land-cover product with fine classification system at 30 m (GLC_FCS30) is employed in the study due to its high spatial resolution and long time series, which is freely available at https://doi.org/10.5281/zenodo.3986872. Validation results have shown the overall accuracy and kappa coefficient of this product are 0.825 and 0.784 in terms of nine major land-cover types, which is higher than GlobaLand30 and FROM_GLC products. This dataset, extracted from Landsat remote sensing images and high-quality training data from Global Spatial Temporal Spectra Library, provides a detailed classification system containing 29 land cover types (Zhang X. et al., 2021). Considering the land use structure of the study area, a new classification system is established by reclassing land use types into seven groups: cropland, forest land, grassland, water bodies, bare areas, sparse vegetation, and impervious surfaces. The data processing of land use was implemented using ENVI 5.3 and ArcGIS 10.8 software platform. The land use data every 5-year interval (i.e., 1990, 1995, 2000, 2005, 2010, 2015, and 2020) are employed to identify the changes in land use morphology. According to the land cover of the NSTM in 2020, land cover type displayed obvious divergence in the study area. Specifically, cropland was mainly distributed in the north of the study area, while forest land, grassland, and sparse vegetation were roughly distributed along the Tianshan Mountains due to elevation gradients. Bare areas were the largest land surface cover, accounting for 61.2% of the total area, which was distributed in the eastern study area. The distributions of water bodies were scattered, including Sayram Lake, Ebinur Lake, and Kashgar River Basin. Impervious surfaces were mainly distributed in the center of Urumqi City, Shihezi City, Kuytun City, Karamay City, and other cities. Secondly, socio-economic data are collected from the Xinjiang Uygur Autonomous Region[1] and their affiliated districts and counties.

Land use change indices

Land use change indices have been used to quantify the characteristics of land use change during a certain period (Sumari et al., 2020; Duan et al., 2021). The gross gain and gross loss are the most basic components at the category level. They are calculated as follows:

$$G_i = P_{+i} - P_{ii} \quad (1)$$

$$L_i = P_{i+} - P_{ii} \quad (2)$$

where G_i denotes the gross gain of category i during a certain period, which is given by P_{+i} minus P_{ii}. L_i denotes the gross loss of category i during a certain period, which is given by P_{i+} minus P_{ii}. P_{+i} and P_{i+} are the percentage of the area in category i at the final time and the initial time of a certain period, respectively. P_{ii} represents the area that shows the persistence of category i.

Based on the above two basic components, other components of land use change can be estimated: net change, swap change, total change, and change rate (Chen et al., 2022). The net change shows the change percentage of a certain land use type during the study period, which is given by the gross gain minus the gross loss. The calculation formula is:

$$N_i = G_i - L_i = P_{+i} - P_{i+} \quad (3)$$

where N_i is the net change of category i during a certain period.

The swap change is quantitatively calculated by twice the minimum of the gross gain and the gross loss, which is expressed as follows:

$$S_i = 2 \times \min(G_i, L_i) \quad (4)$$

where S_i is the swap change of category i during a certain period.

The total change reflects the sum of changed areas of a certain land use type during the study period. The calculation formula is as follows:

$$T_i = G_i + L_i \quad (5)$$

where T_i is the total change of category i during a certain period.

The change rate represents the changing trend of a certain land use type during the study, which is expressed as follows:

$$R_i = \frac{N_i}{P_{i+}} \quad (6)$$

where R_i is the change rate of category i during a certain period.

Land use morphology indices

Land use change refers to the spatiotemporal changes in land use morphology driven by social and economic development. It is acknowledged that there are two formats to describe land use morphology, i.e., dominant morphology and recessive morphology (Long and Li, 2012).

Dominant morphology

Landscape pattern indicators have been widely used to analyze landscape composition and spatial structure among

1 http://tjj.xinjiang.gov.cn/

patches within a category or region level (Lausch et al., 2015; Li et al., 2017; Yang et al., 2019; Sumari et al., 2020; Müller et al., 2022). Land use change is always accompanied by changes in landscape characteristics, which has directly transformed the landscape fragmentation, concentration, and connectivity. Therefore, the dominant morphology is quantitatively estimated by landscape pattern indicators in this study. In accordance with previous studies (Ma et al., 2019; Wu and Lu, 2021; Fu et al., 2022), patch density (PD), largest patch index (LPI), and landscape shape index (LSI) are selected and calculated using the Fragstats 4.2 software. Kubacka et al. (2022) have also proved there are no strong relationships among PD, LPI, and LSI, which can overcome multivariable multicollinearity in terms of different indicators and provide reliable information to explore the land use dominant morphology. The definitions and calculation formulas of the selected landscape metrics are listed in **Table 1**.

Recessive morphology

Studies of land use recessive morphology mainly concentrated on the changes in land use efficiency (Jiang et al., 2021; Schiavina et al., 2022), land use intensity (Tan et al., 2022; Zhou et al., 2022), and its environmental effects (Searchinger et al., 2018; Hong et al., 2021; DeFries et al., 2022; van Marle et al., 2022). The efficiency of land use directly reflects the level of socio-economic development (Yu et al., 2019). Compared with the primary industry, manufacturing and service industries are more efficient and productive obtained from land use. Land use efficiency (LUE) is expressed as the economic output per unit of land in this study. Land use intensity (LUI) is employed to evaluate the status of land development within a region. Referring to Xu et al. (2020), a specific weight value is assigned to each basic land use type by considering the extent of human activities and fixed inputs. Seven land use types are reclassed into five new groups: high-use-intensity artificial land, low-use-intensity artificial land, high-use-intensity natural land, mid-use-intensity natural land, and low-use-intensity natural land. The LUI index is calculated by the weighted sum of each reclassed group. Agricultural system, accounting for about 30% of global greenhouse gasses, is a major source of climate change (Clark et al., 2020; Foong et al., 2022; Wang et al., 2022). Agricultural non-point source pollution (ANSP) caused by intensive chemical fertilizer consumption greatly contributes to the decline of ecological environment, and further threatens food security in the country (Zhang Y. et al., 2021; Plunge et al., 2022). Therefore, the chemical fertilizer consumption per cropland area is employed to represent the environmental effects of land use. The definitions and calculation formulas of the selected variables are listed in **Table 2**.

Trade-off/synergy analysis

Based on the long-time series data from 1990 to 2020, the relationships between land use dominant and recessive morphologies are evaluated using correlation analysis. Compared with other methods, like Spearman correlation analysis, Pearson correlation analysis is capable of capturing information embedded in the sample data, and has been widely used in the relationships between two variables (Zhu et al., 2021; Bai et al., 2022; Ren et al., 2022). Pearson correlation analysis is employed and the calculation formula is as follows:

$$r\left(X_i, Y_i\right) = \frac{\sum_{i=1}^{N}\left(X_i-\overline{X}\right)\left(Y_i-\overline{Y}\right)}{\sqrt{\sum_{i=1}^{N}\left(X_i-\overline{X}\right)^2\sum_{i=1}^{N}\left(Y_i-\overline{Y}\right)^2}} \quad (7)$$

where $r\left(X_i, Y_i\right)$ represents the Pearson correlation analysis between X and Y. X_i and Y_i are the estimated value of land use dominant and recessive morphologies in region i. $\overline{X}$ and $\overline{Y}$ are their average values, respectively. N is the number of regions.

We used the Stata 16 software to estimate the correlation coefficients (r) and significance tests (P). The positive coefficient represents a trade-off relationship between different indicators, meaning both land use morphologies increase or decrease simultaneously. Otherwise, a synergy relationship occurs when the coefficient is negative, indicating an increase in one land use morphology leads to the decrease in another. In this regard, the relationships between land use dominant and recessive morphologies are classified into seven types: high synergy ($r > 0$, $P < 0.01$), middle synergy ($r > 0$, $0.01 < P < 0.05$), low synergy ($r < 0$, $0.05 < P < 0.1$), high trade-off ($r < 0$,$P < 0.01$),

TABLE 1 Description of land-use dominant morphology index.

Index	Significance	Formula
PD	PD reflects the degree of landscape fragmentation. It is calculated by the number of patches involving the corresponding patch type divided by the total landscape area.	$PD = \frac{n_i}{A_i}$
LPI	LPI reflects the concentration degree of patches. It is calculated by the largest patch of the corresponding patch type divided by the total landscape area.	$LPI = \frac{maxa_{ij}}{A_i}$
LSI	LSI reflects the degree of shape complexity. It is calculated by 0.25 times the total length of edge divided by the square root of the total landscape area.	$LSI = \frac{0.25E_i}{\sqrt{A_i}}$

n_i is the number of patches of category/region i. A_i is the total landscape area of category/region i. a_{ij} is the area of patch j of category/region i. E_i is the total length of the edge of category/region i.

TABLE 2 Description of land-use recessive morphology index.

Index	Significance	Formula
LUE	LUE reflects the economic output of land use, which is accompanied by the level of socio-economic development. It is calculated by the output of GDP in a certain region divided by its corresponding impervious area.	$LUE = \frac{GDP_i}{A_{iI}}$
LUI	LUI reflects the degree of human activities on land use. It is calculated by the sum of each land-use group multiplied by its weight value.	$LUI = \sum_{j=1}^{5} \frac{A_{ij}}{A_i} \cdot W_j$
ANSP	ANSP reflects the environmental effects of land use. It is calculated by the chemical fertilizer consumption per cropland area, that is, the consumption of chemical fertilizer in a certain region divided by its corresponding farmland area.	$ANSP = \frac{CFC_i}{A_{iF}}$

GDP_i is the output of GDP of region i. A_{iI} and A_{iF} are the impervious area and farmland area of region i, respectively. A_i is the total area of region i. A_{ij} is the area of group j in region i. W_j is the weight value of group j. The weight values of high-use-intensity artificial land (i.e., impervious surfaces), low-use-intensity artificial land (i.e., cropland), high-use-intensity natural land (including forest land, grassland, and water bodies), mid-use-intensity natural land (i.e., sparse vegetation), and low-use-intensity natural land (i.e., bare areas) are set to 5, 4, 3, 2, and 1, respectively. CFC_i is the chemical fertilizer consumption of region i.

middle trade-off ($r < 0$, $0.01 < P < 0.05$), low trade-off ($r < 0$, $0.05 < P < 0.1$), and insignificance ($P > 0.1$).

Results

Land use and landscape characteristics in the northern slope of the Tianshan Mountains

The proportions of land use types and their changes from 1990 to 2020 are shown in Figure 2. Overall, though the proportion of each land use type changed over time, the order of their proportions approximately remained the same. Bare areas and grassland were always predominant land use types from 1990 to 2020 in the NSTM, and their proportions both showed downward trends over time. The proportions of impervious surfaces and water bodies always were in the last two land use types in the NSTM, and their values both displayed upward trends over time. Specifically, bare areas decreased from 64.89 to 61.20% from 1990 to 2020, while impervious surfaces gradually and consistently increased from 0.33 to 0.77%. The trends of cropland, sparse vegetation, and forest land increased in fluctuation.

The landscape patterns of each land use type from 1990 to 2020 were obtained (Figure 3). The PD of sparse vegetation and grassland were largest, and their values exhibited increasing trends over time. Water bodies and impervious surfaces had lower PD than other land use categories, and they were basically unchanged during the study period. According to the results of LPI, bare areas had the largest values mainly due to their vast areas, and their values were 10 times more than others. There existed substantial differences in LPI among different land use types. As for the LSI at the category level, sparse vegetation and grassland ranked as the top two among various land use types, while water bodies and impervious surfaces were low. The values of six categories (except cropland) displayed increasing trends from 1990 to 2020. Overall, the LPI of various land use types were roughly proportional to their areas. The PD and LSI of cropland showed a decreasing trend, while the values of LPI increased over time, indicating the cropland in the NSTM gradually became concentrated and integrated in the past three decades. The values of water bodies and impervious surfaces were low in terms of three landscape metrics, mainly due to their small areas. But impervious surfaces had larger PD and LSI, and smaller LPI than water bodies, indicating that impervious surfaces were more dispersed and fragmented in the NSTM.

Temporal and spatial patterns of land use change in the northern slope of the Tianshan Mountains

Four variables, i.e., net change, swap change, total change, and change rate, were evaluated to identify the land use change at the category level during the 5-year intervals (Figure 4). Land use categories with larger proportions, such as bare areas and grassland experienced the net losses during all intervals. The areas of forest land and cropland experienced a slight net loss in the last decade. The net changes of impervious surfaces from 1990 to 2020 were always positive, indicating the areas of impervious surfaces increased consistently. As for the swap change index, bare areas, grassland, and sparse vegetation experienced the largest values, followed by cropland, then forest land and water bodies. It should be noticed that the swap changes of impervious surfaces were nearly zero because impervious surfaces were hardly transferred out. The larger the land use category areas, the larger their total changes. The total change of bare areas was largest among various land use types. Land use categories with small proportions, such as water bodies and impervious surfaces, and experienced very small total changes. The change rates of impervious surfaces were above 10% during all intervals, and the fastest period was from 2000 to 2005, of which the value was 25.18%. The change rates of bare areas and grassland were negative from 1990 to 2000. Though the net loss of bare areas was greater than those of

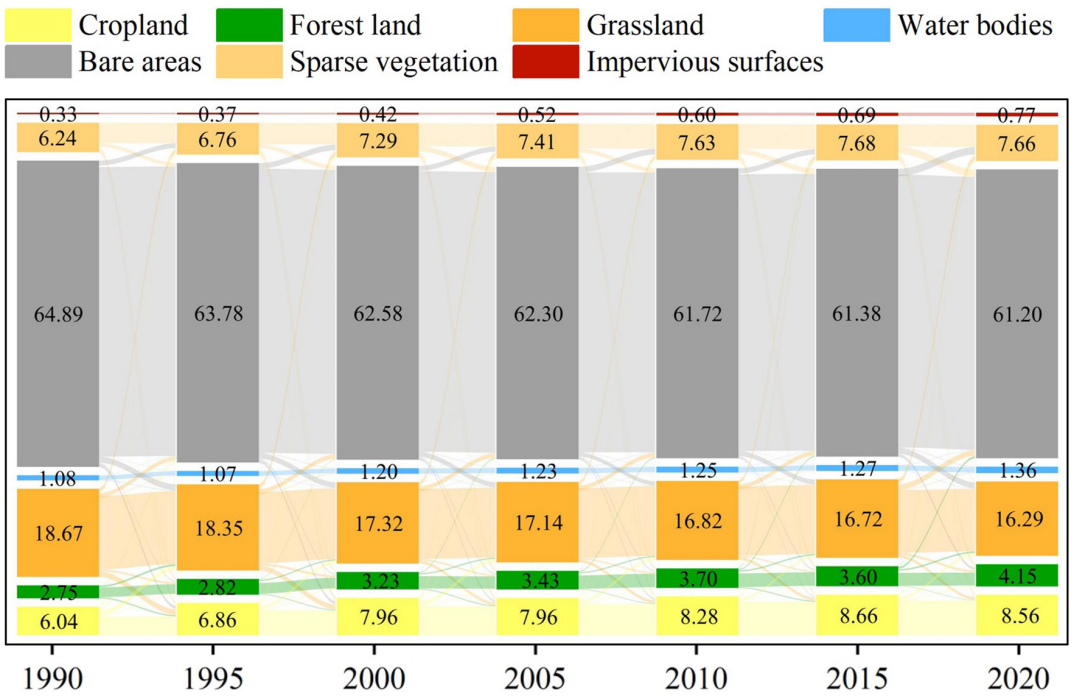

FIGURE 2
Sankey plot of land use change in the NSTM. Stacked vertical bars represent the proportions of various land use types from 1990 to 2020. Lines between each pair of bars visualize the changes of each land use type in the 5-year interval. The thickness of each line represents the proportion of the corresponding land-use area that experiences the persistence or transition.

grassland, the change rates of bare areas were smaller due to their high proportion and vast areas.

To clearly understand the general condition of land use change in the NSTM, temporal and spatial patterns of land use change from 1990 to 2020 were depicted. According to the estimated results in **Figures 5A,C**, more than 20% of the total area in the NSTM experienced land use change, and the transformations of bare areas, grassland, and sparse vegetation were predominant during the past three decades.

From the perspective of outflow based on land use structure in 1990 (**Figures 5A,B**), 41.51% of cropland had transformed into other land use categories in 2020, primarily including grassland, sparse vegetation, and bare areas, which mainly covered Jimsar County, Urumqi City, Urumqi County, Changji City, and so on. 25.60% of forest land had transformed into other land use categories, primarily including grassland, cropland, and bare areas, which mainly covered Yumin County, Tacheng City, Jinghe County, Shuanghe City, and so on. 35.41% of grassland had transformed into other land use categories, primarily including cropland, sparse vegetation, and bare areas, which mainly covered Toli County, Emin County, Usu City, Wenquan County, and so on. 54.51% of sparse vegetation had transformed into other land use categories, primarily including bare areas, cropland, and grassland, which mainly covered Mori Kazak Autonomous County, Qitai County, Hutubi County, Shihezi City, and so on. 11.30% of bare areas had transformed into other land use categories, primarily including sparse vegetation, grassland, and cropland, which mainly covered Yizhou District, Barkol Kazak Autonomous County, Gaochang District, Usu City, Kuytun City, and so on. 19.03% of water bodies had transformed into other land use categories, primarily including grassland, and bare areas, mainly covering Ebinur Lake Watershed in Jinghe County. Only 0.07% of impervious surfaces in 1990 had transferred into other land use categories in 2020.

From the perspective of inflow based on land use structure in 2020 (**Figures 5C,D**), 58.76% of cropland had been transferred from other land use categories in 1990, primarily including grassland (22.23%), bare areas (20.61%), and sparse vegetation (13.69%), which mainly covered Tacheng City, Emin County, Shawan County, Usu City, and so on. 50.71% of forest land had been transferred from other land use categories, primarily including grassland, and bare areas, which mainly covered Changji City, Hutubi County, Urumqi County, Barkol Kazak Autonomous County, and so on. 25.95% of grassland had been transferred from other land use categories, primarily including bare areas, cropland, and sparse vegetation, which mainly covered Toli County, Urumqi County, Jimsar County, Shawan County, and so on. 62.95% of sparse vegetation had been transferred from other land use categories, primarily including

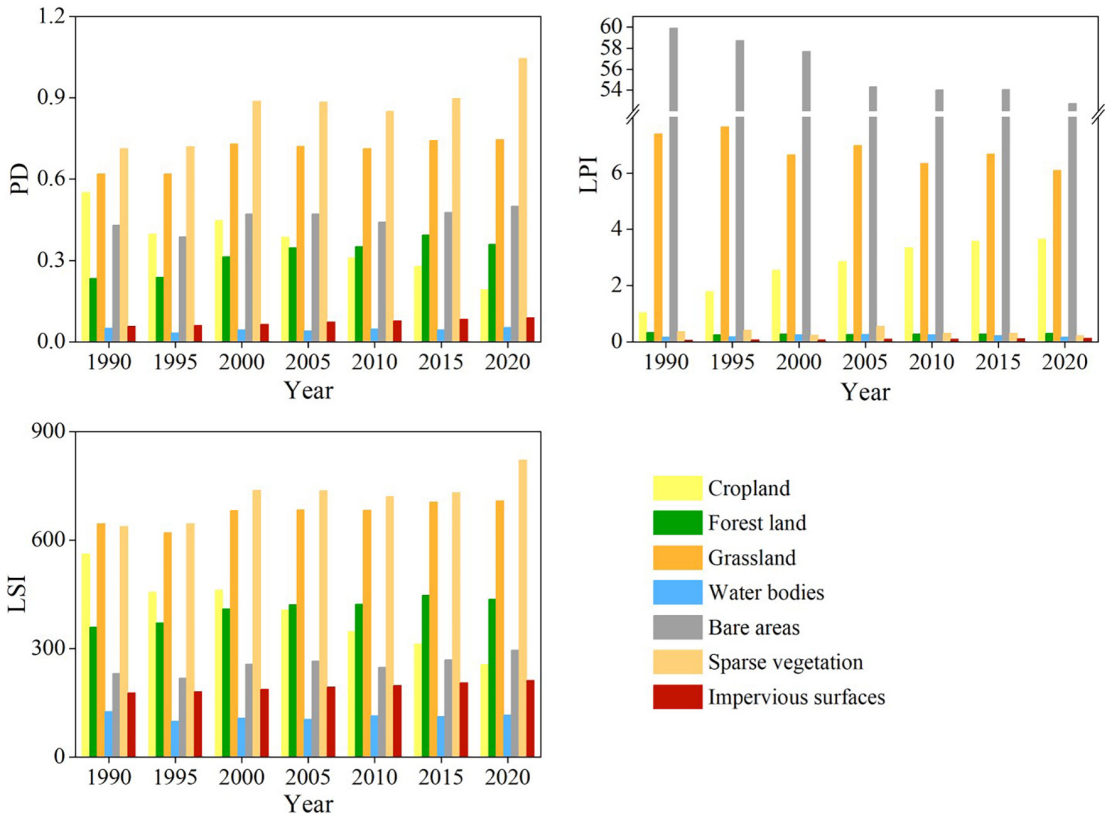

FIGURE 3
The changes in landscape metrics at the category level from 1990 to 2020.

bare areas, grassland, and cropland, which mainly covered Yizhou District, Shanshan County, Wenquan County, Yumin County, and so on. 5.97% of bare areas had been transferred from other land use categories, primarily including grassland and sparse vegetation, which mainly covered Jinghe County, Bole City, Mori Kazak Autonomous County, Urumqi City, and so on. 35.59% of water bodies had been transferred from other land use categories, primarily including grassland, and bare areas, mainly covering Barkol Kazak Autonomous County and the Kashgar River Basin. 57.09% of impervious surfaces had been transferred from other land use categories, primarily including cropland, bare areas, and grassland, which mainly covered Urumqi City, Changji City, Yiwu County, Kuytun City, and so on.

Trade-off and synergy of land use morphology

Trade-off and synergy analysis in the whole region

We quantified the temporal patterns of land use dominant and recessive morphologies from 1990 to 2020 in the NSTM using land use and socio-economic datasets. On this basis, the trade-offs and synergies between land use morphology in the whole region were estimated. Figure 6 shows the temporal changes in land use dominant and recessive morphologies in the NSTM. The whole PD decreased from 2.65 in 1990 to 2.45 in 1995, and fluctuated from 2.79 to 2.98 after 2000. The whole LPI displayed a consistent downward trend, decreasing from 59.90 in 1990 to 52.71 in 2020. The temporal trend of LSI was more complicated than PD and LPI. LPI reached its lowest value in 1995, which was similar to that of PD. It decreased in the first decade of the new century and increased in the following decade, whose largest value occurred in 2020. As for land use recessive morphology, the whole LUE displayed an increasing trend during the past three decades, meaning land use in the NSTM became more efficient and productive. It increased from 0.91 in 1990 to 21.33 in 2020, and this upward trend gradually increased in strength over time. The whole LUI also showed an upward trend over time, increasing from 1.71 in 1990 to 1.80 in 2020. The whole ANSP increased significantly from 1990 to 2005, and fluctuated between 248.89 and 386.03 during the following years.

The trade-offs and synergies between land use morphology in the whole region are presented in Figure 7. The strongest

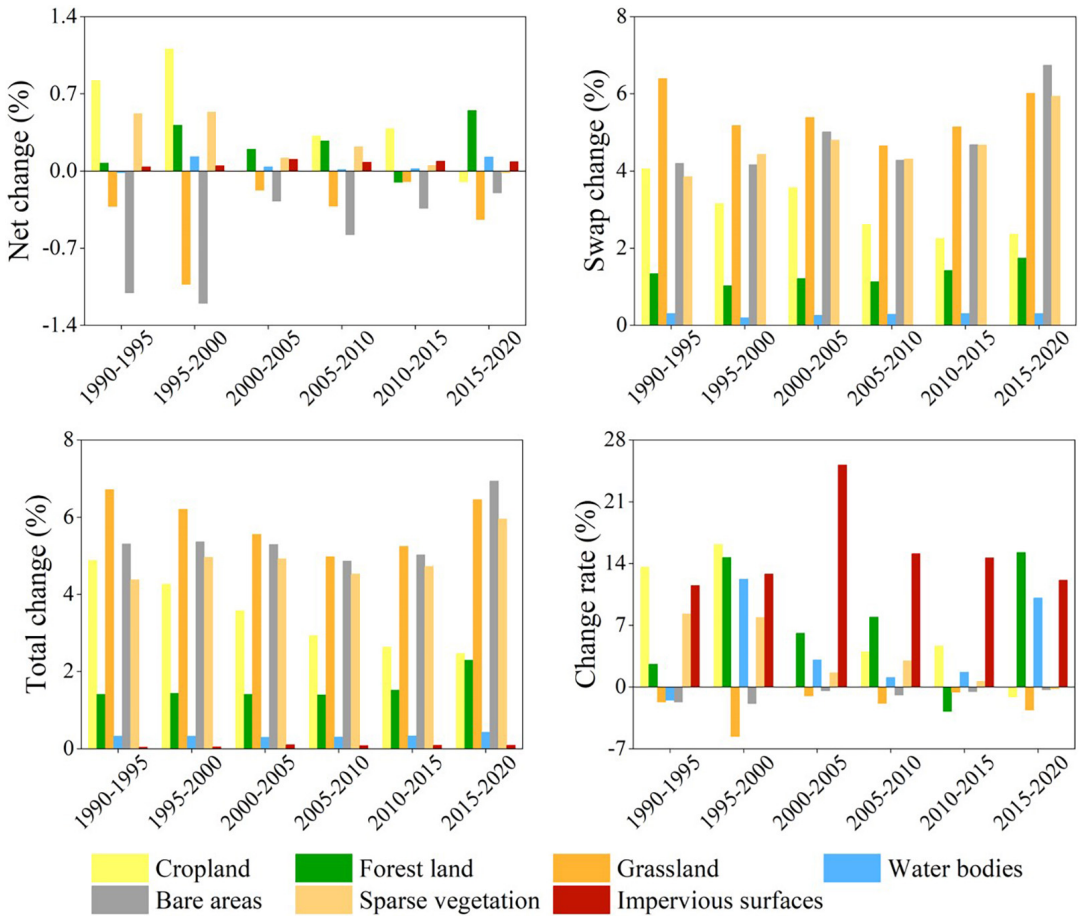

FIGURE 4
The land use change indices at the category level of the NSTM during the 5-year intervals.

trade-off relationship occurred between LSI and LUI, while the synergetic relationship between LPI and LUI was strongest, indicating the degree of human activities on land use was highly connected with land use dominant morphology index. The correlation coefficient between PD and LUE was positive and insignificant, indicating there was no significant synergetic relationship between landscape fragmentation and economic output of land use in the NSTM. The correlation coefficients between LPI and LUE as well as ANSP were significantly negative at the 5% level, which meant the degree of shape complexity displayed the strong trade-off relationships with the economic output and environmental effects of land use. The correlation coefficients between PD and LUI as well as ANSP were significantly positive at the 10% level, indicating the degree of landscape fragmentation had synergetic relationships with human activities and environmental effects of land use. The correlation coefficients between LSI and LUE as well as ANSP were also significantly positive at the 10% level, meaning the concentration degree of patches had synergetic relationships with the economic output and environmental effects of land use.

Trade-off and synergy analysis at the county level

In this section, we firstly explored their trade-off and synergetic relationships in 1990, 1995, 2000, 2005, 2010, 2015, and 2020 using land use morphology estimations at the county level, as presented in Figure 8. The relationships between dominant and recessive morphologies of land use exhibited significant disparities over time, and the correlation coefficients in different study periods were much smaller than their estimations in the whole region. The relationships between LSI and LUE were consistently negative in all periods, indicating a county with a high degree of shape complexity was inclined to decrease its economic output of land use. The correlation coefficients of PD and LUI were negative, while LPI and LUI displayed positive relationships from 1990 to 2020. It meant the counties with lower fragmentation and higher concentration of patches were prone to experiencing high-intensity human activities, which contributed to the improvement of labor productivity under large-scale and intensive production. However, the trade-off and synergetic

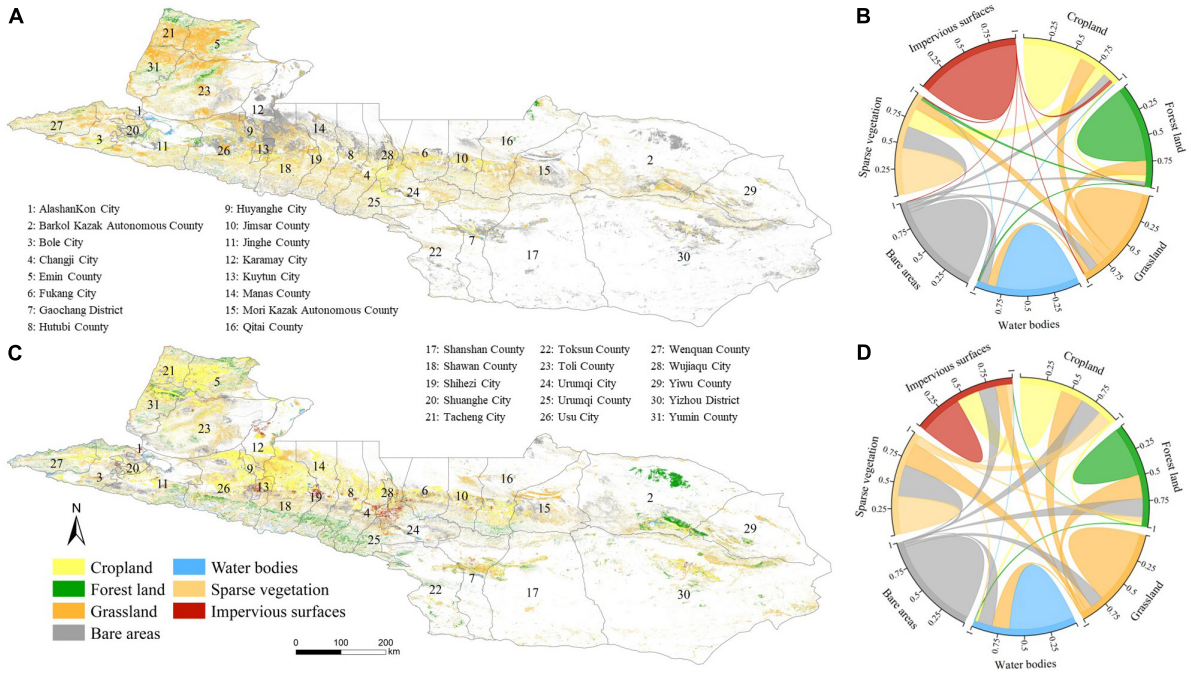

FIGURE 5
Land use change from 1990 to 2020 in the NSTM. The spatial distribution **(A)** and its outflow proportion **(B)** of each category to other categories based on land use structure in 1990. The spatial distribution **(C)** and its inflow proportion **(D)** of each category from other categories based on land use structure in 2020.

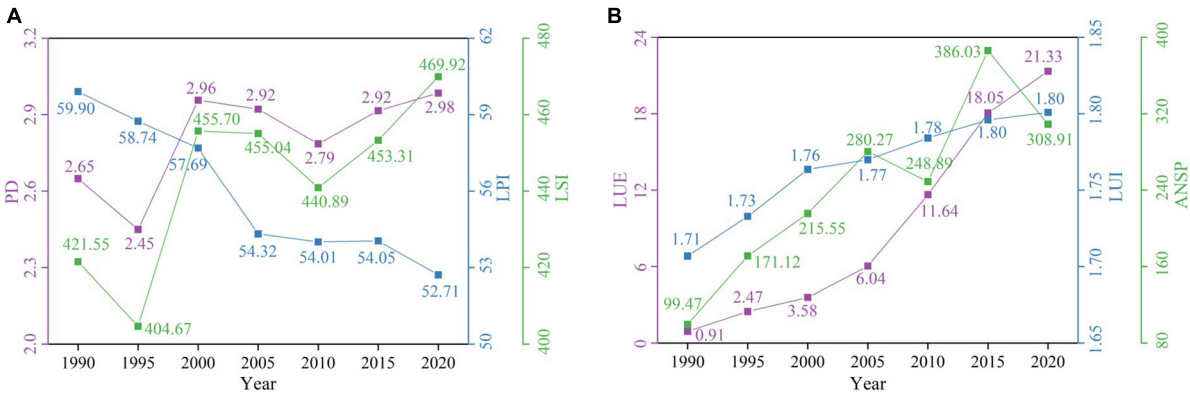

FIGURE 6
(A) The changes in global land use dominant morphology from 1990 to 2020 in the NSTM. **(B)** The changes in global land use recessive morphology from 1990 to 2020 in the NSTM.

relationships of other land use morphology indicators were up and down over time, which means different counties in the NSTM exhibited their individual characteristics, so there was no fixed relationship between land use dominant and recessive morphologies.

Moreover, distinct spatial patterns of various counties were identified through the trade-off analysis, as shown in Figure 9. There are significant disparities in terms of spatial patterns of trade-offs/synergies. The relationships in the east of the NSTM were basically identical with the whole region. A possible reason was that eastern counties, including Yizhou District, Shanshan County, Barkol Kazak Autonomous County, and Mori Kazak Autonomous County, are located at the Turpan Hami basin with vast desert and Gobi, and their proportion of bare areas was 20% higher than the average value according to the land cover in 2020. The supply of artificial land was insufficient for the demand of increasing population, so natural land had transformed into impervious surfaces to

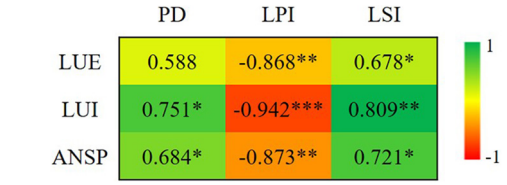

FIGURE 7
The global trade-offs/synergies between dominant and recessive morphologies of land use in the NSTM. *, **, and *** denote the significance level of 0.1, 0.05, and 0.01, respectively.

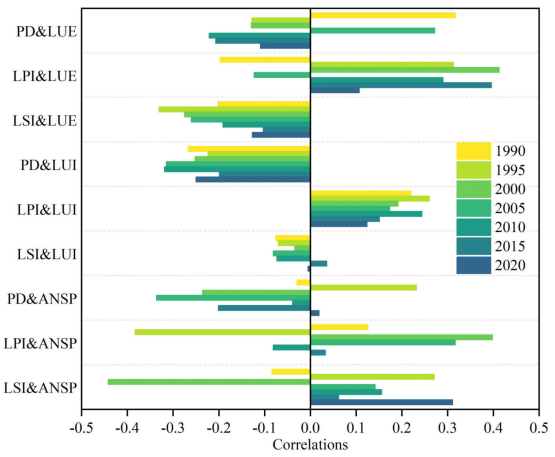

FIGURE 8
The temporal patterns of trade-offs/synergies between land use dominant and recessive morphologies.

promote economic development, which was consistent with the characteristics of land use in the whole region. However, the middle-south regions, including Huyanghe City, Kuytun City, Shawan County, and Usu City, displayed the opposite relationships with the NSTM. It was found that the infilling type of land use was dominant in these counties, representing the newly added patches were filled into or spread along the edge of the old land patches. The temporal patterns of PD and LSI decreased over time, while LPI increased. One explanation for this phenomenon could lie in the geographical conditions of these counties. They are located at the foot of Tianshan Mountains with smooth terrain, and there are sufficient water resources provided by rivers and streams, which is instrumental in mechanized operations, so their land use morphology became compact and integrated over time. Besides, some counties, including Bole City, Fukang City, Jinghe County, Manas County, Qitai County, and Wenquan County, showed insignificant relationships between land use dominant and recessive morphologies. Though the economic output and fertilizer input of land use significantly increased in the past three decades, their land use structure changed slightly, and land use dominant landscape patterns experienced minor changes within a small range. Therefore, the correlation coefficients between land use morphology in these counties were insignificant.

Discussion

This study explored the spatiotemporal patterns of land use and landscape changes, and the trade-offs of land use morphology. The NSTM has experienced rapid economic development over the past decades, leading to extensive land use and insufficient land supply. The proportion of cropland increased in fluctuation, and its change rate was much lower than that of impervious surfaces. One reason for this phenomenon was that the improvement of agricultural technology greatly increased crop production efficiency, and less cropland was required to achieve the food demand brought by the increasing population (Coomes et al., 2019). Another reason could lie in the extensive utilization of construction land. It is acknowledged that the pace of land-oriented urbanization is faster than that of demographic urbanization (Long et al., 2021). The areas of forest land increased recently mainly due to the implementation of environmental protection policies, and the ecological function of land use has gained more and more attention nowadays (Ma et al., 2019; An et al., 2022). It should be noticed that the land use in the NSTM became more fragmented over time according to the changes in landscape patterns, which pose serious threats to the efficient utilization and sustainable development of land systems.

The changes in land use dominant morphology presented the landscape complexity increased in the NSTM, and land use became more fragmented and dispersed over time. The whole LPI was determined by the largest patch of bare areas. Vast bare areas transformed into other land use categories in the context of agricultural development, thus decreasing its patch areas. Besides, in the initial stages of economic development before 1995, the old land use type was primarily filled up with new patches, and land use morphology became compact. Then the outlying type became predominant during the period of 1995–2000, and the degree of landscape fragmentation and shape complexity in the NSTM greatly increased. After the implementation of China's western development strategy in 2000, the landscape patterns of land use showed a volatile trend over time. The whole LUE and LUI increased due to the consistent transformation from natural land to artificial land and its GDP increased from 16.63 billion yuan in 1990 to 903.47 billion yuan in 2020. Compared with the trend of LUE, the upward trend of LUI gradually became slight over time. It was mainly because technological innovations and management practices had significantly promoted the quality of land use with fewer land resource utilization (Tan et al., 2021). The change in ANSP lied in the fact modern agricultural mechanization with high fixed costs was less effective in smallholder farms. Previous

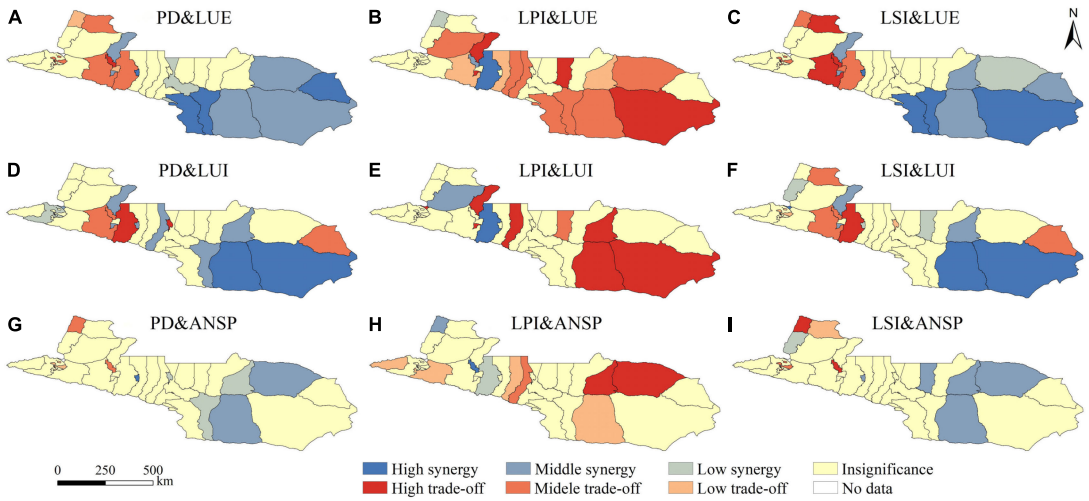

FIGURE 9
The spatial patterns of trade-offs/synergies between each pair of land use dominant and recessive morphology indices. Alashankou City was set in 2012, so the indices based on statistical data (LUE and ANSP) before its establishment is unavailable, which is denoted using blank space.

study has also shown that Chinese cropland was featured by smaller farm size and more agricultural chemicals than others (Wu et al., 2018). Besides, China has implemented the cultivated land occupation-supplement policy balance to ensure food security since 1997. Cultivated land was compensated by land exploitation, and the quantity balance was met. But urban expansion occupied highly productive cropland, and the quality had decreased sharply (Cai et al., 2020). Therefore, farmers were inclined to use more chemical fertilizers to increase crop yields. In recent years, some advanced technologies, such as soil testing, have been adopted to control agricultural pollution under China's ecological civilization construction.

Based on the trade-offs and synergies of land use morphology, several implications are proposed for high-quality development in the NSTM. Turpan Hami basin in the south of the NSTM, including Gaochang District, Toksun County, Shanshan County, Barkol Kazak Autonomous County, Mori Kazak Autonomous County, and Yizhou District, exhibits a synergetic relationship between PD and LSI and three recessive morphology indices, are key ecological zones. These regions are mainly covered by bare areas with fragile ecological environments and scarce water resources, and are vulnerable to land desertification, so their primary goals are to protect biodiversity, conserve water, and prevent desertification (An et al., 2022). County-level cities are relatively scattered in the NSTM through establish cities in the Gobi. Landscape fragmentation displayed a consistently increasing trend in Shihezi City during the past three decades, and land use morphology became more complex with the expansion of construction land boosted by industrial structure optimization. The role of these regions is to maintain the stability of the border regions. Urumqi City, the economic center of the NSTM, should take full advantage of its economy and location strength to form the innovation-oriented development mode and strengthen its spillover effect on surrounding regions. Overall, being an important location of the Belt and Road Initiative, infrastructure construction in the NSTM should be improved to strengthen commercial and cultural links with other regions, and take advantage of their cultural and tourism resources.

There are three prospective directions for this study that could be further explored in the future. First, this study identified the patterns of land use changes and their trade-offs, but it ignores the driving mechanism of land use by integrating geographical features and socio-economic indicators, which requires further exploration in future research by considering quantifiable influencing forces to enhance its accuracy and reliability. Second, it is meaningful to establish a systematic evaluation index system through an in-depth exploration of the relationship between land use dominant and recessive morphologies, which is helpful to explore various land use modes for regional high-quality development. Finally, the historical land use change in the past three decades was evaluated. Future studies should predict the land use changes in the following years under various development scenarios, and further understand its effects on climate change, biological diversity, and so on (Bukovsky et al., 2021; Huang et al., 2022; Li et al., 2022).

Conclusion

Taking the NSTM, an important developing area with a vulnerable environment in China, as the study area, this study investigated the changes in land use and its landscape metrics

based on land use data in 1990, 1995, 2000, 2005, 2010, 2015, and 2020. Next, land use dominant and recessive morphologies at the whole and county levels were estimated by incorporating land use and socio-economic datasets. On this basis, their trade-offs and synergies were qualified through Pearson correlation analysis. The main conclusions are presented as follows:

(1) Bare areas were always the largest land surface cover in the NSTM, and the proportion showed a downward trend over time. The proportion of impervious surfaces gradually and consistently increased from 0.33% in 1990 to 0.77% in 2020. Landscape metrics showed land use structure became more dispersed and fragmented in the past three decades.
(2) More than 20% of the total area in the NSTM experienced land use change from 1990 to 2020. Typically, impervious surfaces were primarily transformed from cropland, bare areas, and grassland, but they were hardly transferred into other land use categories. Bare areas and grassland experienced the large net losses, swap changes, and total changes, while the change rates of impervious surfaces were highest.
(3) Among three land use dominant morphology indices, PD and LSI increased in fluctuation. LPI decreased mainly because vast bare areas transformed into other land use categories. As for land use recessive morphology, LUE, LUI, and ANSP displayed an increasing trend during the past three decades, and this upward trend gradually increased in strength over time.
(4) The strongest trade-off occurred between LSI and LUI, while the synergy between LPI and LUI was strongest. There are significant disparities in terms of spatiotemporal patterns of trade-off and synergetic relationships. The correlation coefficients in different study periods were much smaller than their whole estimations, and the relationships in the eastern NSTM were basically identical with the whole region.

Data availability statement

The original contributions presented in this study are included in the article/supplementary material, further inquiries can be directed to the corresponding author.

Author contributions

HM: conceptualization, methodology, software, validation, formal analysis, investigation, resources, data curation, writing—original draft, review and editing, visualization, and funding acquisition.

Funding

This work was supported by the Third Xinjiang Scientific Expedition Program under Grant 2021xjkk0905.

Acknowledgments

The author grateful to the editor and reviewers for their valuable comments and suggestions.

Conflict of interest

The author declares that the research was conducted in the absence of any commercial or financial relationships that could be construed as a potential conflict of interest.

Publisher's note

All claims expressed in this article are solely those of the authors and do not necessarily represent those of their affiliated organizations, or those of the publisher, the editors and the reviewers. Any product that may be evaluated in this article, or claim that may be made by its manufacturer, is not guaranteed or endorsed by the publisher.

References

An, M., Xie, P., He, W., Wang, B., Huang, J., and Khanal, R. (2022). Spatiotemporal change of ecologic environment quality and human interaction factors in three gorges ecologic economic corridor, based on RSEI. *Ecol. Indic.* 141:109090. doi: 10.1016/j.ecolind.2022.109090

Bai, Y., Li, S., Liu, M., and Guo, Q. (2022). Assessment of vegetation change on the Mongolian Plateau over three decades using different remote sensing products. *J. Environ. Manag.* 317:115509. doi: 10.1016/j.jenvman.2022.115509

Bradford, J. B., and D'Amato, A. W. (2012). Recognizing trade-offs in multi-objective land management. *Front. Ecol. Environ.* 10, 210–216. doi: 10.1890/110031

Buckley Biggs, N. (2022). Drivers and constraints of land use transitions on Western grasslands: insights from a California mountain ranching community. *Landsc. Ecol.* 37, 1185–1205. doi: 10.1007/s10980-021-01385-6

Bukovsky, M. S., Gao, J., Mearns, L. O., and O'Neill, B. C. (2021). SSP-Based Land-Use Change Scenarios: A Critical Uncertainty in Future Regional Climate Change Projections. *Earth Fut.* 9:82. doi: 10.1029/2020EF001782

Cai, E., Liu, Y., Li, J., and Chen, W. (2020). Spatiotemporal Characteristics of Urban–Rural Construction Land Transition and Rural–Urban Migrants in Rapid-Urbanization Areas of Central China. *J. Urban Plann. Dev.* 146:05019023. doi: 10.1061/(ASCE)UP.1943-5444.0000551

Chen, A., Yang, X., Guo, J., Zhang, M., Xing, X., Yang, D., et al. (2022). Dynamic of land use, landscape, and their impact on ecological quality in the northern sand-prevention belt of China. *J. Environ. Manage.* 317:115351. doi: 10.1016/j.jenvman.2022.115351

Clark, M. A., Domingo, N. G. G., Colgan, K., Thakrar, S. K., Tilman, D., Lynch, J., et al. (2020). Global food system emissions could preclude achieving the 1.5° and 2°C climate change targets. *Science* 370, 705–708. doi: 10.1126/science.aba7357

Coomes, O. T., Barham, B. L., MacDonald, G. K., Ramankutty, N., and Chavas, J.-P. (2019). Leveraging total factor productivity growth for sustainable and resilient farming. *Nat. Sustain.* 2, 22–28. doi: 10.1038/s41893-018-0200-3

Cord, A. F., Bartkowski, B., Beckmann, M., Dittrich, A., Hermans-Neumann, K., Kaim, A., et al. (2017). Towards systematic analyses of ecosystem service trade-offs and synergies: Main concepts, methods and the road ahead. *Ecosyst. Serv.* 28, 264–272. doi: 10.1016/j.ecoser.2017.07.012

DeFries, R., Ahuja, R., Friedman, J., Gordon, D. R., Hamburg, S. P., Kerr, S., et al. (2022). Land management can contribute to net zero. *Science* 376, 1163–1165. doi: 10.1126/science.abo0613

Duan, H., Xie, Y., Du, T., and Wang, X. (2021). Random and systematic change analysis in land use change at the category level—A case study on Mu Us area of China. *Sci. Total Environ.* 777:145920. doi: 10.1016/j.scitotenv.2021.145920

Fan, Y., Gan, L., Hong, C., Jessup, L. H., Jin, X., Pijanowski, B. C., et al. (2021). Spatial identification and determinants of trade-offs among multiple land use functions in Jiangsu Province, China. *Sci. Tot. Environ.* 772:145022. doi: 10.1016/j.scitotenv.2021.145022

Foong, A., Pradhan, P., Frör, O., and Kropp, J. P. (2022). Adjusting agricultural emissions for trade matters for climate change mitigation. *Nat. Commun.* 13:3024. doi: 10.1038/s41467-022-30607-x

Fu, F., Deng, S., Wu, D., Liu, W., and Bai, Z. (2022). Research on the spatiotemporal evolution of land use landscape pattern in a county area based on CA-Markov model. *Sustainab. Cities Soc.* 80:103760. doi: 10.1016/j.scs.2022.103760

Fujimori, S., Wu, W., Doelman, J., Frank, S., Hristov, J., Kyle, P., et al. (2022). Land-based climate change mitigation measures can affect agricultural markets and food security. *Nat. Food.* 3, 110–121. doi: 10.1038/s43016-022-00464-4

Geng, W., Li, Y., Zhang, P., Yang, D., Jing, W., and Rong, T. (2022). Analyzing spatio-temporal changes and trade-offs/synergies among ecosystem services in the Yellow River Basin China. *Ecol. Indic.* 138:108825. doi: 10.1016/j.ecolind.2022.108825

Grainger, A. (1995). National Land Use Morphology: Patterns and Possibilities. *Geogr.* 80, 235–245. doi: 10.2307/40572668

Guo, S., and Shen, G. Q. (2015). Multiregional Input–Output Model for China's Farm Land and Water Use. *Environ. Sci. Technol.* 49, 403–414. doi: 10.1021/es503637f

Hamilton, M., Salerno, J., and Fischer, A. P. (2019). Cognition of complexity and trade-offs in a wildfire-prone social-ecological system. *Environ. Res. Lett.* 14:125017. doi: 10.1088/1748-9326/ab59c1

He, F., Yang, J., Zhang, Y., Sun, D., Wang, L., Xiao, X., et al. (2022). Offshore Island Connection Line: A new perspective of coastal urban development boundary simulation and multi-scenario prediction. *GISci. Remote Sens.* 59, 801–821. doi: 10.1080/15481603.2022.2071056

Hong, C., Burney, J. A., Pongratz, J., Nabel, J. E. M. S., Mueller, N. D., Jackson, R. B., et al. (2021). Global and regional drivers of land-use emissions in 1961–2017. *Nature* 589, 554–561. doi: 10.1038/s41586-020-03138-y

Howe, C., Suich, H., Vira, B., and Mace, G. M. (2014). Creating win-wins from trade-offs? Ecosystem services for human well-being: A meta-analysis of ecosystem service trade-offs and synergies in the real world. *Glob. Environ. Change* 28, 263–275. doi: 10.1016/j.gloenvcha.2014.07.005

Howison, R. A., Piersma, T., Kentie, R., Hooijmeijer, J. C. E. W., and Olff, H. (2018). Quantifying landscape-level land-use intensity patterns through radar-based remote sensing. *J. Appl. Ecol.* 55, 1276–1287. doi: 10.1111/1365-2664.13077

Huang, M., Wang, Z., Pan, X., Gong, B., Tu, M., and Liu, Z. (2022). Delimiting China's Urban Growth Boundaries Under Localized Shared Socioeconomic Pathways and Various Urban Expansion Modes. *Earth Fut.* 10:e2021EF002572. doi: 10.1029/2021EF002572

Jiang, H., Sun, Z., Guo, H., Weng, Q., Du, W., Xing, Q., et al. (2021). An assessment of urbanization sustainability in China between 1990 and 2015 using land use efficiency indicators. *NPJ Urban Sustain* 1:34. doi: 10.1038/s42949-021-00032-y

Kubacka, M., Żywica, P., Vila Subirós, J., Bródka, S., and Macias, A. (2022). How do the surrounding areas of national parks work in the context of landscape fragmentation? A case study of 159 protected areas selected in 11 EU countries. *Land Use Policy* 113:105910. doi: 10.1016/j.landusepol.2021.105910

Lausch, A., Blaschke, T., Haase, D., Herzog, F., Syrbe, R.-U., Tischendorf, L., et al. (2015). Understanding and quantifying landscape structure – A review on relevant process characteristics, data models and landscape metrics. *Ecol. Model.* 295, 31–41. doi: 10.1016/j.ecolmodel.2014.08.018

Li, G., Fang, C., Li, Y., Wang, Z., Sun, S., He, S., et al. (2022). Global impacts of future urban expansion on terrestrial vertebrate diversity. *Nat. Commun.* 13:1628. doi: 10.1038/s41467-022-29324-2

Li, H., Peng, J., Liu, Y., and Hu, Y. (2017). Urbanization impact on landscape patterns in Beijing City, China: A spatial heterogeneity perspective. *Ecol. Indic.* 82, 50–60. doi: 10.1016/j.ecolind.2017.06.032

Liu, M., Ma, H., and Bai, Y. (2021). Understanding the Drivers of Land Surface Temperature Based on Multisource Data: A Spatial Econometric Perspective. *IEEE J. Sel. Top. Appl. Earth Observ. Remote Sens.* 14, 12263–12272. doi: 10.1109/JSTARS.2021.3129842

Long, H., and Li, T. (2012). The coupling characteristics and mechanism of farmland and rural housing land transition in China. *J. Geogr. Sci.* 22, 548–562. doi: 10.1007/s11442-012-0946-x

Long, H., Liu, Y., Hou, X., Li, T., and Li, Y. (2014). Effects of land use transitions due to rapid urbanization on ecosystem services: Implications for urban planning in the new developing area of China. *Habitat Int.* 44, 536–544. doi: 10.1016/j.habitatint.2014.10.011

Long, H., Zhang, Y., Ma, L., and Tu, S. (2021). Land Use Transitions: Progress. *Challeng. Prospects. Land* 10:903. doi: 10.3390/land10090903

Ma, L., Bo, J., Li, X., Fang, F., and Cheng, W. (2019). Identifying key landscape pattern indices influencing the ecological security of inland river basin: The middle and lower reaches of Shule River Basin as an example. *Sci. Total Environ.* 674, 424–438. doi: 10.1016/j.scitotenv.2019.04.107

Meng, J., Cheng, H., Li, F., Han, Z., Wei, C., Wu, Y., et al. (2022). Spatial-temporal trade-offs of land multi-functionality and function zoning at finer township scale in the middle reaches of the Heihe River. *Land Use Policy* 115:106019. doi: 10.1016/j.landusepol.2022.106019

Meyfroidt, P., de Bremond, A., Ryan, C. M., Archer, E., Aspinall, R., Chhabra, A., et al. (2022). Ten facts about land systems for sustainability. *Proc. Natl. Acad. Sci. U.S.A.* 119:e2109217118. doi: 10.1073/pnas.2109217118

Müller, S., Gossner, M. M., Penone, C., Jung, K., Renner, S. C., Farina, A., et al. (2022). Land-use intensity and landscape structure drive the acoustic composition of grasslands. *Agricult. Ecosyst. Environ.* 328:107845. doi: 10.1016/j.agee.2021.107845

Ouedraogo, I., Barron, J., Tumbo, S. D., and Kahimba, F. C. (2016). Land Cover Transition in Northern Tanzania. *Land Degrad. Develop.* 27, 682–692. doi: 10.1002/ldr.2461

Plunge, S., Gudas, M., and Povilaitis, A. (2022). Effectiveness of best management practices for non-point source agricultural water pollution control with changing climate – Lithuania's case. *Agricult. Water Manag.* 267:107635. doi: 10.1016/j.agwat.2022.107635

Qu, Y., Shu, Y., Zong, H., Si, H., Yang, Z., and Liu, T. (2021). Understanding the Characteristics and Realization Path of Urban Land Use Transition in the Bohai Economic Rim: An Analytical Framework of "Dominant–Recessive" Morphology Coupling. *Land* 10:493. doi: 10.3390/land10050493

Ray, D. K., Sloat, L. L., Garcia, A. S., Davis, K. F., Ali, T., and Xie, W. (2022). Crop harvests for direct food use insufficient to meet the UN's food security goal. *Nat. Food* 3, 367–374. doi: 10.1038/s43016-022-00504-z

Ren, J., Yang, J., Zhang, Y., Xiao, X., Xia, J. C., Li, X., et al. (2022). Exploring thermal comfort of urban buildings based on local climate zones. *J. Clean. Product.* 340:130744. doi: 10.1016/j.jclepro.2022.130744

Schiavina, M., Melchiorri, M., Freire, S., Florio, P., Ehrlich, D., Tommasi, P., et al. (2022). Land use efficiency of functional urban areas: Global pattern and evolution of development trajectories. *Habitat Int.* 123:02543. doi: 10.1016/j.habitatint.2022.102543

Searchinger, T. D., Wirsenius, S., Beringer, T., and Dumas, P. (2018). Assessing the efficiency of changes in land use for mitigating climate change. *Nature* 564, 249–253. doi: 10.1038/s41586-018-0757-z

Sumari, N. S., Cobbinah, P. B., Ujoh, F., and Xu, G. (2020). On the absurdity of rapid urbanization: Spatio-temporal analysis of land-use changes in Morogoro, Tanzania. *Cities* 107:102876. doi: 10.1016/j.cities.2020.102876

Tan, L. M., Arbabi, H., Densley Tingley, D., Brockway, P. E., and Mayfield, M. (2021). Mapping resource effectiveness across urban systems. *NPJ Urban Sustain* 1, 1–14. doi: 10.1038/s42949-020-00009-3

Tan, S., Liu, Q., and Han, S. (2022). Spatial-temporal evolution of coupling relationship between land development intensity and resources environment carrying capacity in China. *J. Environ. Manag.* 301:113778. doi: 10.1016/j.jenvman.2021.113778

van Marle, M. J. E., van Wees, D., Houghton, R. A., Field, R. D., Verbesselt, J., and van der Werf, G. R. (2022). New land-use-change emissions indicate a declining CO2 airborne fraction. *Nature* 603, 450–454. doi: 10.1038/s41586-021-04376-4

Wang, R., Bai, Z., Chang, J., Li, Q., Hristov, A. N., Smith, P., et al. (2022). China's low-emission pathways toward climate-neutral livestock production for animal-derived foods. *Innovation* 3:100220. doi: 10.1016/j.xinn.2022.100220

Wu, J., and Lu, J. (2021). Spatial scale effects of landscape metrics on stream water quality and their seasonal changes. *Water Res.* 191:116811. doi: 10.1016/j.watres.2021.116811

Wu, Y., Xi, X., Tang, X., Luo, D., Gu, B., Lam, S. K., et al. (2018). Policy distortions, farm size, and the overuse of agricultural chemicals in China. *Proc. Natl. Acad. Sci.U.S.A.* 115, 7010–7015. doi: 10.1073/pnas.1806645115

Xu, F., Wang, Z., Chi, G., and Zhang, Z. (2020). The impacts of population and agglomeration development on land use intensity: New evidence behind urbanization in China. *Land Use Policy* 95:104639. doi: 10.1016/j.landusepol.2020.104639

Yang, J., Guo, A., Li, Y., Zhang, Y., and Li, X. (2019). Simulation of landscape spatial layout evolution in rural-urban fringe areas: a case study of Ganjingzi District. *GISci. Remote Sens.* 56, 388–405. doi: 10.1080/15481603.2018.1533680

Yang, J., Yang, R., Chen, M.-H., Su, C.-H., Zhi, Y., and Xi, J. (2021). Effects of rural revitalization on rural tourism. *J. Hospital. Tourism Manag.* 47, 35–45. doi: 10.1016/j.jhtm.2021.02.008

Yin, G., Lin, Z., Jiang, X., Qiu, M., and Sun, J. (2020). How do the industrial land use intensity and dominant industries guide the urban land use? Evidences from 19 industrial land categories in ten cities of China. *Sustainab. Cities Soc.* 53:101978. doi: 10.1016/j.scs.2019.101978

Yu, J., Zhou, K., and Yang, S. (2019). Land use efficiency and influencing factors of urban agglomerations in China. *Land Use Policy* 88:104143. doi: 10.1016/j.landusepol.2019.104143

Zhang, X., Liu, L., Chen, X., Gao, Y., Xie, S., and Mi, J. (2021). GLC_FCS30: global land-cover product with fine classification system at 30 m using time-series Landsat imagery. *Earth Syst. Sci. Data* 13, 2753–2776. doi: 10.5194/essd-13-2753-2021

Zhang, Y., Long, H., Li, Y., Tu, S., and Jiang, T. (2021). Non-point source pollution in response to rural transformation development: A comprehensive analysis of China's traditional farming area. *J. Rural Stud.* 83, 165–176. doi: 10.1016/j.jrurstud.2020.10.010

Zhou, Q., Zhang, Y., Tao, J., Ye, L., Wang, H., Shan, K., et al. (2022). Water depth and land-use intensity indirectly determine phytoplankton functional diversity and further regulate resource use efficiency at a multi-lake scale. *Sci. Total Environ.* 834:155303. doi: 10.1016/j.scitotenv.2022.155303

Zhu, C., Dong, B., Li, S., Lin, Y., Shahtahmassebi, A., You, S., et al. (2021). Identifying the trade-offs and synergies among land use functions and their influencing factors from a geospatial perspective: A case study in Hangzhou, China. *J. Clean. Product.* 314:128026. doi: 10.1016/j.jclepro.2021.128026

Zuo, L., Zhang, Z., Carlson, K. M., MacDonald, G. K., Brauman, K. A., Liu, Y., et al. (2018). Progress towards sustainable intensification in China challenged by land-use change. *Nat. Sustain* 1, 304–313. doi: 10.1038/s41893-018-0076-2

frontiers | Frontiers in Environmental Science

TYPE Original Research
PUBLISHED 29 September 2022
DOI 10.3389/fenvs.2022.1009094

Check for updates

OPEN ACCESS

EDITED BY
Jun Yang,
Northeastern University, China

REVIEWED BY
John Renne,
Florida Atlantic University, United States
Yang Chen,
The University of Hong Kong, Hong Kong SAR, China
Yu Ye,
Tongji University, China

*CORRESPONDENCE
Xu Cui,
cuixu@home.swjtu.edu.cn

SPECIALTY SECTION
This article was submitted to Land Use Dynamics,
a section of the journal
Frontiers in Environmental Science

RECEIVED 01 August 2022
ACCEPTED 29 August 2022
PUBLISHED 29 September 2022

CITATION
Yu B, Cui X, Li H, Luo P, Liu R and Yang T (2022), TOD and vibrancy: The spatio-temporal impacts of the built environment on vibrancy.
Front. Environ. Sci. 10:1009094.
doi: 10.3389/fenvs.2022.1009094

COPYRIGHT
© 2022 Yu, Cui, Li, Luo, Liu and Yang. This is an open-access article distributed under the terms of the Creative Commons Attribution License (CC BY). The use, distribution or reproduction in other forums is permitted, provided the original author(s) and the copyright owner(s) are credited and that the original publication in this journal is cited, in accordance with accepted academic practice. No use, distribution or reproduction is permitted which does not comply with these terms.

TOD and vibrancy: The spatio-temporal impacts of the built environment on vibrancy

Bingjie Yu[1], Xu Cui[1]*, Hong Li[2], Pinyang Luo[1], Runze Liu[1] and Tian Yang[1]

[1]School of architecture, Southwest Jiaotong University, Chengdu, China, [2]Changsha Planning and Design Institute Co., Ltd., Changsha, China

Urban vibrancy is described by the activities of residents and their spatio-temporal dynamics. The metro station area (MSA) is one of the densest and most populous areas of the city. Thus, creating a vibrant and diverse urban environment becomes an important goal of transit-oriented development (TOD). Existing studies indicate that the built environment decisively determines MSA-level urban vibrancy. Meanwhile, the spatio-temporal heterogeneity of such effects requires thoroughly exploration and justification. In this study, we first apply mobile signaling data to quantify and decipher the spatio-temporal distribution characteristics of the MSA-level urban vibrancy in Chengdu, China. Then, we measure the built environment of the MSA by using multi-source big data. Finally, we employ geographically and temporally weighted regression (GTWR) models to examine the spatio-temporal non-stationarity of the impact of the MSA-level built environment on urban vibrancy. The results show that: 1) The high-vibrant MSAs concentrate in the commercial center and the employment center. 2) Indicators such as residential density, overpasses, road density, road network integration index, enterprise density, and restaurant density are significantly and positively associated with urban vibrancy, while indicators such as housing price and bus stop density are negatively associated with urban vibrancy. 3) The GTWR model better fits the data than the stepwise regression model. The impact of the MSA-level built environment on urban vibrancy shows a strong non-stationarity in both spatial and temporal dimensions, which matches with the spatio-temporal dynamic patterns of the residents' daily work, leisure, and consumption activities. The findings can provide references for planners and city managers on how to frame vibrant TOD communities.

KEYWORDS

spatial-temporally non-stationary, built environment, urban vibrancy, TOD, GTWR, Chengdu, mobile phone signaling data

1 Introduction

Urban vibrancy has constantly been a hot topic in the research field of urban geography and urban planning (Yue et al., 2017; Niu et al., 2022). Many cities regard the construction of a vibrant urban environment as the leading objective during the development process (Zhang et al., 2021). The conception of urban vibrancy originated from Jacobs' idea of urban diversity and Gehl's theory of street space vibrancy. Jacobs (1961) considers that "liveliness and variety attract more liveliness; deadness and monotony repel life". Gehl (2011) divides human activities into three categories: necessary activities, optional activities, and social activities. He also points out that optional activities and social activities are the keys to the public space vibrancy. In general, the spatial distribution of people and their activities act as the core of urban vibrancy, which reflects the quality of space and the vibrancy of the city (Montgomery, 1998). A vibrant city is able to promote residents' life qualities, stimulate the consciousness of communities, and enhance the city's attractiveness (Xiao et al., 2021). In this regard, the research on urban vibrancy will help urban planners to understand the spatial structure of cities, recognize the pattern of citizens' activities, and optimize the layout of facilities.

Since the 21st century, with rapid urbanization and urban rail transit construction, TOD has become an important concept that guides urban development and enhances urban vibrancy in China (Yang et al., 2022a; Qiang et al., 2022). TOD transit nodes are generally located in developed areas with multiple functions such as transportation, commerce, resident, and office. These also are areas with the most advanced urban transportation network and the most intensive travel activities. Also, relevant studies reveal that the proximity to metro stations and corridors exerts significant positive effects on urban vibrancy (Long and Huang, 2019; Xiao et al., 2021). Meanwhile, due to the differences in development intensity and geography location (e.g., city center versus suburban area), the vibrancy of some neighborhoods around the metro stations is still at a low level and constantly attenuated. Thus, urban planners need to have an in-depth understanding of the spatio-temporal distribution patterns and influencing factors of the TOD vibrancy.

Urban built environment, as the carriers of various human activities (Chen et al., 2022a; Chen et al., 2022b), determines the evolution and spread of urban vibrancy. Previous studies (Tu et al., 2020; Peng et al., 2021) have explored the impact of the built environment (using the 3Ds and 5Ds frameworks) (Cervero and Kockelman, 1997; Ewing and Cervero, 2010) on urban vibrancy at the city scale, but few of them scrutinize such interplay from a TOD scope. Furthermore, there is a lack of human-scale built environment indicators research, especially the refine spatial indicators such as the pedestrian system of TOD and the environmental quality of streets. In addition, most existing studies use linear (Tu et al., 2022) or nonlinear (Yang et al., 2021a; Xiao et al., 2021) models to analyze the effects of the built environment on urban vibrancy. However, the above two types of models and their extensions ignore the typical time-varying tidal characteristics of human activities in the MSA. Hence, these models fail to characterize the spatio-temporal non-stationarity of the built environment impact on urban vibrancy.

To address these gaps, we use multi-source big data to measure the built environment of MSA in Chengdu, China (with the fourth largest rail transit system in China). Then, we leverage mobile phone signaling data to capture the intensity of human activities (urban vibrancy) around the metro stations for 18 separate hours (from 6:00 to 23:00). Finally, we analyze the spatio-temporal non-stationarity of the impact of the MSA-level built environment on urban vibrancy based on a geographically temporally weighted regression model (GTWR). The empirical findings can provide theoretical support and policy implications for the people-oriented built environment design of TOD and the creation of vibrant cities.

The remainder of this paper is structured as follows: Section 2 reviews and analyzes previous studies. Section 3 introduces the study area, data sources, and methodology. Section 4 analyzes and discusses the model results. Section 5 concludes and provides evidence-based policy implications.

2 Literature review

2.1 Urban vibrancy

The exploration of urban vibrancy started in the 1950s and 1960s. Jacobs and Gehl analyzed the connotation of urban vibrancy from multidimensional perspectives, including sociology, urban space, and even anthropology (Jacobs, 1961; Gehl, 2011). Since then, the definition of urban vibrancy has been widely discussed by scholars. For example, Ravenscroft (2000) argued that urban vibrancy reflects how busy neighborhoods are in different spatial and temporal dimensions. Mehta (2007) pointed out that a vibrant space requires a high density of continuous pedestrian flow and activity participation. Montgomery (1998) stated that urban vibrancy can be measured by the amount of foot traffic, use frequency of facilities, and density of activities. Dougal et al. (2015) defined urban vibrancy as the spillover effect generated from the interactions of city residents.

There is always a debate on the selection of suitable metrics that quantify urban vibrancy or the intensity of human activities. Early studies mostly used traditional methods such as manual counts and population censuses to measure urban vibrancy (Harvey, 2001; Xu and Chen, 2021). Even containing detailed information about the population and types of activities, these quantitative measures still suffer from disadvantages such as small survey sample sizes, discontinuity in time, and the

subjectivity of the interviewees. In recent years, with the rapid spread of smart phones as well as the advances in location aware device (LAD) and location based service (LBS), burgeoning technologies have brought new data sources and research tools for urban vibrancy studies (Wu et al., 2022). Multiple-source spatio-temporal big data, with its characteristics of massive scale, rapid flow, and diversity (Zhou et al., 2020), enriches the human social activities and urban spatial information. Thus, urban researchers can carry out refined spatio-temporal behavior analysis of the population through multiple sources of big data. Some studies quantify the urban vibrancy through the distribution of people and activities which is obtained from big data such as the distribution and density of commercial facilities (POI, etc.) (Xia et al., 2020), social media check-in (Facebook, Twitter, Weibo, etc.) (Wu et al., 2018a), GDP (Wang et al., 2022a), heat map of mobile applications (mobile phone signaling, Baidu heat map, etc.) (Yang et al., 2021a), and traffic flow (shared bicycle, smartcard, cab GPS, etc.) (Sulis et al., 2018). For instance, Niu et al. (2022) used data from Tencent, Easygo, and Sina Weibo to assess the distribution of the community vibrancy index in Guangzhou. Li et al. (2021) used urban sensor data to detect street vibrancy in historic districts (Baitasi Area) in Beijing. Sulis et al. (2018) leveraged bus smartcard data from a mobility perspective to reveal the characteristics of London's urban vibrancy distribution. Gómez-Varo et al. (2022), based on Jacobs' urban vibrancy framework, added another two dimensions of indicators including accessibility and distance to border vacuums, and then integrated the urban vibrancy index of the Nou Barris district in Barcelona. Kim (2018) used Wi-Fi data, mobile phone signaling data, and bank card transactions to measure virtual, social, and economic vibrancy in Seoul, and then analyzed the interplay between these three types of urban vibrancy.

2.2 The relationship between the built environment and urban vibrancy

The built environment has a significant impact on the generation and persistence of urban vibrancy. In Jacobs (1961) seminal text, *The Death and Life of America's Great Cities*, she highlighted the crucial role of the physical spatial built environment on urban vibrancy in terms of diversity, neighborhood scale, building form, and density. Previous research launches extensive analysis of the interplay between the built environment and urban vibrancy. Wu et al. (2018b) found a significant contribution of high-density development to neighborhood vibrancy in Beijing. Meanwhile, excessive population density may exert a negative impact on urban vibrancy. Simmel (2012) pointed out that the high concentration of population in industrial cities may inhibit urban vibrancy and lead to negative life attitudes of residents. Moreover, the land-use mix implies a diversity of urban forms and functions. Theories such as New Urbanism, Compact Cities, and Smart Growth all see land-use mix as an important means of urban vibrancy creation. For example, the research of Jacobs-Crisioni et al. (2014), Yue et al. (2017), and Ye et al. (2018) showed that neighborhoods with higher land-use diversity are more vibrant, for land-use mix provides abundant functions for residents' daily activities, employment, and consumption, thus meets their diverse needs. In addition, the design of street space form is also important to urban vibrancy. Relevant studies analyze the impact of the built environment on urban vibrancy in dimensions including density, scale, order, and connectivity of street networks. They argue that topographic, cultural, and socioeconomic conditions combine to shape the spatial structure and geometric order of urban street networks (Kostof, 1991), which in turn affect the intensity of human travel activities (Rose-Redwood and Bigon, 2018). Natural movement theory also suggests that the density of pedestrian flow on a street is influenced primarily by the spatial structure and accessibility to this area (Hillier et al., 1987). For instance, Huang et al. (2020) found that spatial accessibility of the road network contributes to the human activity intensity. The work of Li et al. (2022) revealed that the proportion of sidewalks, the number of streetlights, and the proximity of public transit exert a positive effect on urban vibrancy.

2.3 The relationship between the transit-oriented development and urban vibrancy

The founder of TOD, Calthorpe, aimed to create vibrant, equitable, and station-centered communities through high-density, land-use mix, walkable development patterns (Ibraeva et al., 2020; Sun et al., 2022). In recent years, with the rapid construction of urban rail transit all over the world and the comprehensive promotion of the TOD concept, some scholars have started to delve from macro-scale vibrancy (city-level) research to micro-scale vibrancy (MSA-level) research. Previous studies mostly considered ridership as the manifestation of TOD vibrancy, and analyzed the impact of MSA-level built environment on ridership to guide the built environment construction and low-carbon travel of residents. Some scholars have studied the interactions between the built environment and metro ridership in mega-cities such as Shanghai (An et al., 2019), Shenzhen (Taylor and Morris, 2015; Shao et al., 2020), Guangzhou (Li et al., 2020a), Hong Kong (Loo et al., 2010), Seoul (Choi et al., 2012), Washington, D.C. (Ding et al., 2019), and Chicago (Yang et al., 2020a). However, recent research has shown that ridership only represents the "T" (Transportation) in "TOD", but ignores the "D" (Development) which represents the TOD vibrancy

(Yang et al., 2021a). Thus, several scholars start to shift from "point-based" metro ridership to "area-based" MSA-level human activities. They leverage burgeoning datasets such as social media, heat map of mobile applications, and POI to analyze the impact of the built environment on the MSA-level human activities intensity (Tu et al., 2022). For example, Xiao et al. (2021) and Yang et al. (2021a) both investigated the non-linear relationship between TOD and MSA-level vibrancy in Shenzhen based on the Gradient Boosted Decision Tree (GBDT) model, and their study revealed that indicators such as transportation accessibility, building density, and land-use mix are non-linearly positively correlated with vibrancy around the MSA. Tu et al. (2022) explored the interplay between MSA built environment and urban vibrancy using a spatial lag model and found that the differences of land-use mix, road network density, and commercial land area affect urban vibrancy. Xu and Chen (2021) characterized the population density and activities of MSA underground spaces and found that the human activities in the underground spaces are affected by the combination of spatial comprehensibility, accessibility, functional mix, business organization, and entrance/exit layouts.

Although the above studies analyze the interplay between built environment indicators (population density, FAR, road density, land-use mix, etc.) and MSA-level vibrancy from the macroscopic scale of cities and the microscopic scale of MSAs, little has been done on the microscopic scale from the human-scale perspective. For example, pedestrian system indicators including the three-dimensional indicators such as metro entrances/exits number and overpass facilities, and visual perception indicators of street space such as green view rate and sky rate are usually ignored (Yang et al., 2021b). In addition, the traditional linear models (OLS, SEM, etc.) and the burgeoning nonlinear models (GBDT, RF) employed in relevant studies are all global models. These models fail to explain the local spatial effects of the built environment on vibrancy. Some previous studies employed GWR models to reveal the spatial heterogeneity of built environment effects on vibrancy. While due to the time-varying tidal characteristics of MSA-level human activities with typical morning and evening peak fluctuations, this phenomena lead to significant spatio-temporal heterogeneity of the influencing factors. Hence, the GWR model fails to explain the spatio-temporal non-stationarity of the impact factors. For the above reasons, there is a need to establish a modeling approach that considers both spatial and temporal effects.

3 Study area and data

3.1 Study area

Chengdu, located in southwest China and as one of the largest cities in the west of the country, is selected as the case study in this work. With a population of 21,192,000, Chengdu becomes the fourth largest city in China, only after Chongqing, Shanghai, and Beijing. Chengdu currently has one of the fast-developed metro systems in the world, with the rail network has grown to 518.5 km in 2021 since the opening of the 1st subway line (Line 1, Phase 1, 18.5 km) in 2010. Considering the dramatic impact of the Covid-19 epidemic on the city's human activities, we chose November 2019 as the time point of this study. As of November 2019, the length of the Chengdu metro lines in service is 226 km, and the average daily ridership reaches 3.834 million. A total of 6 lines are opened, namely metro lines 1, 2, 3, 4, 7, and 10, with 156 metro stations in all (Figure 1). In recent years, Chengdu has released development strategies such as "TOD City", TOD has become an important mean to achieve low-carbon city development and cultivate urban vibrancy. In this study, we use an 800 m buffer zone outward from the core of the station as the scale of MSA.

3.2 Data sources

According to the definition of urban vibrancy by previous studies of Jacobs (1961) and Montgomery (1998), we consider the intensity of human activities in a certain area, or the total number of vibrant populations at different times periods through the day, as the concentrated expression of this area's vibrancy. Mobile Signaling Data (MSD) has the advantages of large sample size, wide coverage, and real-time continuity and serves as an important data basis for travel trajectory identification and spatio-temporal behavior calculation (Shi et al., 2020). In order to ensure the continuity and smoothness of mobile phone signals, cellular networks have been recording the real-time location of users at the mobile station (MS). Therefore, the mobile phone signaling data contains information related to the cell phone base stations which are associated with the subscribers (where the location area code (LAC) is located) and also contain rich information on crowd attributes. Compared with other emerging big data such as social media, POI, and business reviews, mobile phone signaling data can continuously record people's activity trajectories and activity time (Tu et al., 2020). Hence, the human activity information recorded by mobile phone signaling is more abundant and more accurate.

Moreover, since most of the metro stations are built underground, a large number of human activities in MSA are in the city's underground spaces. It is worth noting that most of the big data is unable to record the pedestrian flow in underground spaces. Given that mobile operators such as China Mobile, China Unicom, and China Telecom, have built a large number of underground base stations in China's major cities to secure mobile communication networks, the mobile signaling data not only records the MSA ground-level pedestrian flow but also the underground-level pedestrian flow. Thus, the

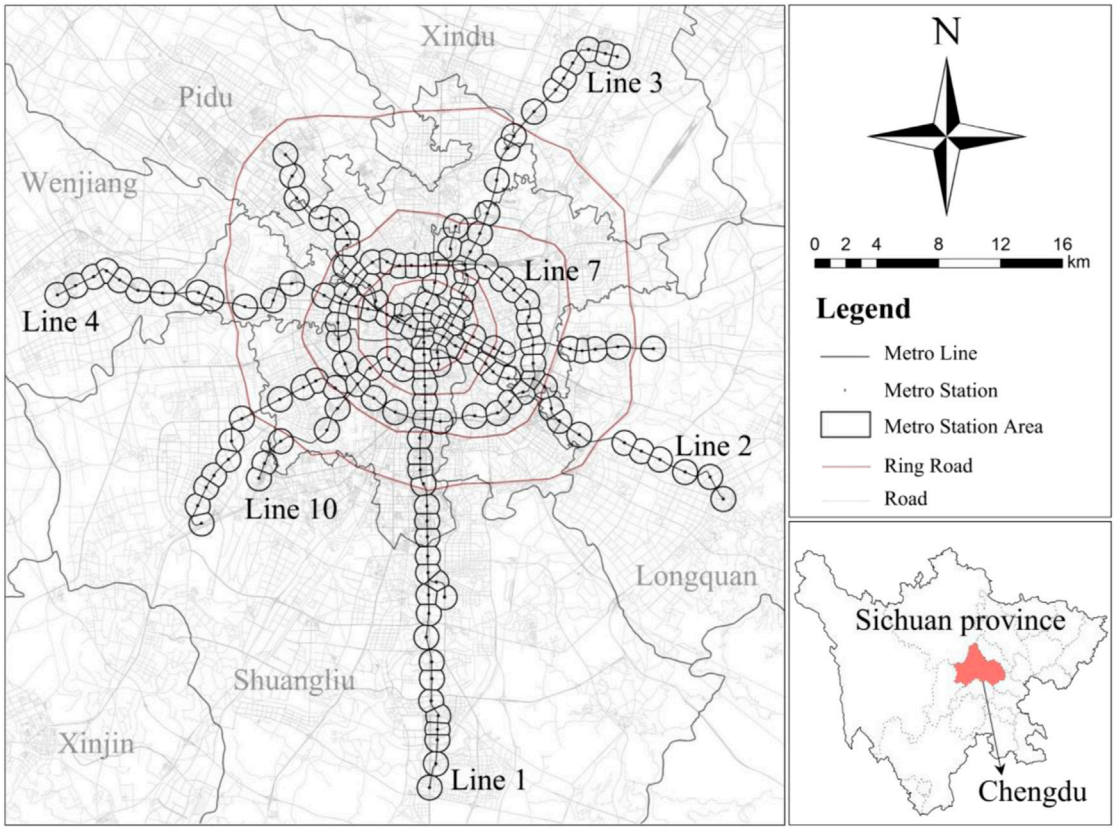

FIGURE 1
Study area of Chengdu.

mobile signaling data can further ensure the accuracy of the human activity intensity recorded.

For the above reasons, in this study we use mobile phone signaling data dating from 11–17 November 2019 in Chengdu as the data basis of urban vibrancy characterization. The mobile phone signaling data are obtained from DASS platform of SmartSteps, which is owned by China Unicom (one of the three major communication companies in China). We consider that the pedestrian flow which generates staying activities (leisure, consumption or employment, etc.) is the real vibrancy of the MSAs (Figure 2). Therefore, we use the time periods kept by the mobile phone signaling data to record the vibrant populations that stay within 800 m of the MSA for more than 30 min as the manifestation of urban vibrancy. Also, according to the daily routines of city residents and the operating hours of the metro system, we only record the MSA-level vibrant populations of each hour from 6:00 to 23:00. Then we divide the number of vibrant populations by the area of each MSA to obtain its density, and treat it as an indicator of urban vibrancy.

In the past few years, multi-source big data has greatly enriched the set of built environment elements and promoted the refinement and three-dimensionality of built environment indicator calculation (Li et al., 2021). For the selection of built environment indicators, we use Jacobs' four conditions for the built environment that influence the diversity of urban activities as theory basis. Then we refer to the "5D" model of the built environment from Ewing and Cervero (2010). Finally, combined with the situations of the study area, we select six dimensions including density, diversity, pedestrian system, function, transportation accessibility, and economic attributes as the MSA-level built environment indicators. The data of the built environment in this study are mainly obtained from open online maps, mobile phone signaling data, and the official website of Chengdu Metro. The sources of indicators and data are as follows:

(1) Density: The density indicators of the MSAs are mainly measured using building footprint data (https://www.baidu.com/) and mobile phone signaling data (provided by SmartSteps). Based on these data we calculate the floor area ratio and resident population density of the MSAs respectively. In addition, we correct the resident population data using *the seventh census* data.

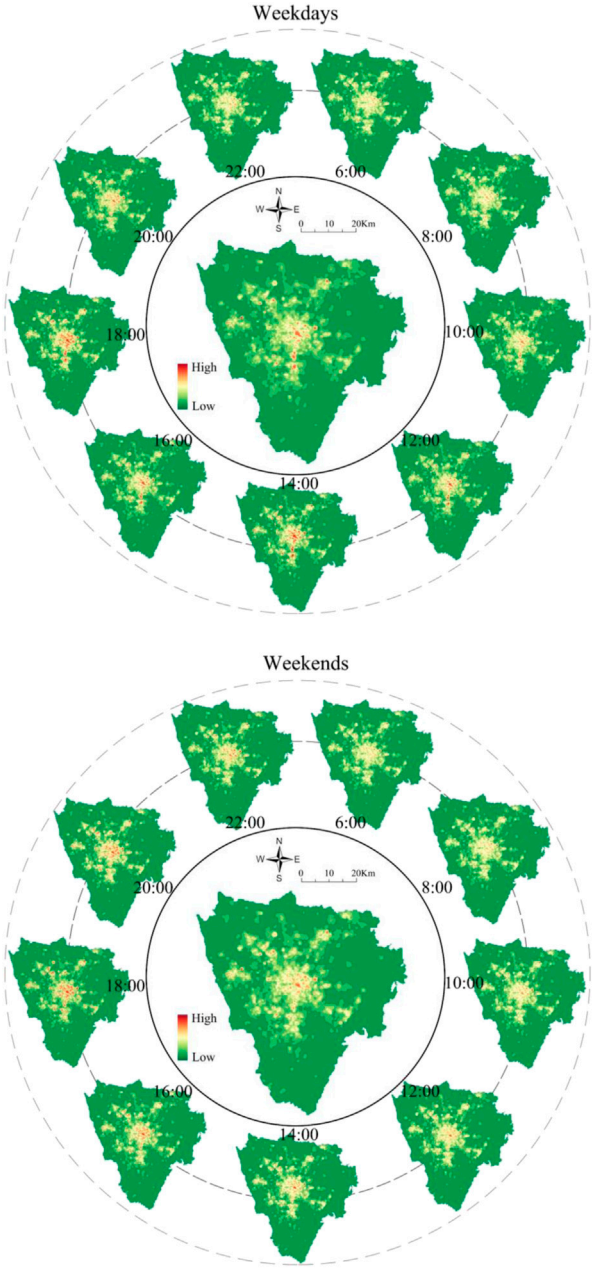

FIGURE 2
The results of the vibrant populations for 18 h at different times.

(2) Pedestrian system: We use Gaode Map (https://www.amap.com/), the structure of Chengdu metro stations(https://www.chengdurail.com), Baidu Street View (http://quanjing.baidu.com), road network data of OSM, *Chengdu transport development annual report (2019),* and field investigation to calculate the number of entrances/exits, road density, green view index (Yang et al., 2021c), and the overpass facilities around the MSA. These data are considered as the indicators of the MSA-level pedestrian system. The green view index is calculated by

$$VGI = \frac{\sum_{i=1}^{4} Green\ pixels_i}{\sum_{i=1}^{4} Total\ pixels_i}$$

We selected four orientations for each point. In this equation, where "VGI" is the average green view index of each point. We use the semantic segmentation method to recognize the green space in each image, and the recognition effect is shown in Figure 3.

(3) Diversity: We calculate the land-use mix (obtained from POI) of the MSAs based on the land mix calculation method of relevant research (Yue et al., 2017).
(4) Function: According to the POI data, seven categories of facilities such as density of commercial facilities, parks, restaurant facilities, financial facilities, enterprises, educational facilities, and medical facilities in the MSA are calculated separately. Then we treat these data as the function indicators.
(5) Transportation accessibility: In this work, the bus stop density of the MSA, which is calculated based on the bus stop distribution and route data provided by the map service provider, serves as the MSA-level transportation accessibility indicators.
(6) Economic attributes: Using the points of housing price data on the internet, we calculate the average housing price around MSAs and treat it as the economic attributes indicator (Yang et al., 2020b). The descriptive statistics of all indicators are shown in Table 1.

3.3 Methodology

We use the stepwise regression method (Li et al., 2020b) to filter the 18 built environment variables. However, stepwise regression models fail to reflect the spatio-temporal non-stationarity and spatio-temporal dynamics of variables. Therefore, to reveal the spatio-temporal impact of MSA-level built environment factors on urban vibrancy, we employ the GTWR model formulating weekdays (14 independent variables) and weekends (15 independent variables) separately to investigate their effects on urban vibrancy. The overall research framework is shown in Figure 4. The GTWR model incorporates the spatio-temporal structure into the regression analysis (Huang et al., 2010), and its regression coefficients serve as the function of spatio-temporal coordinates. The coordinates of spatio-temporal location "i" are denoted as (u_i, v_i, t_i) in the spatio-temporal coordinate system. There is strong randomness and rhythm in urban residents' activities, so GTWR is more

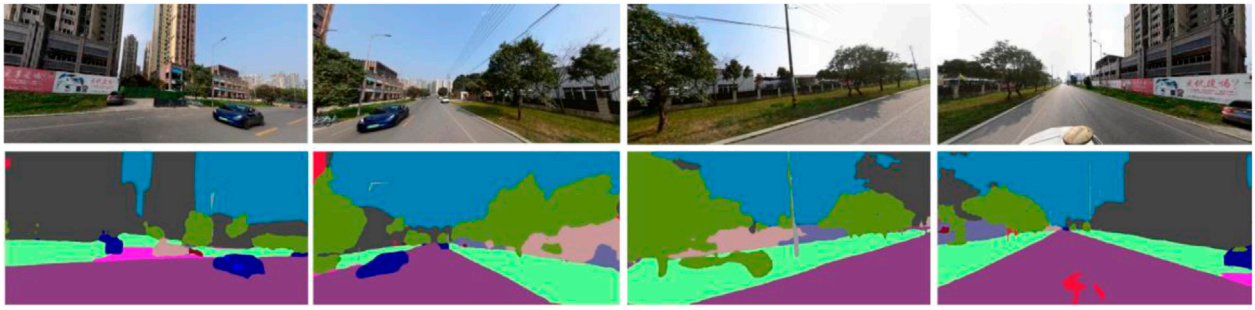

FIGURE 3
The recognition effect of green space in MSA.

TABLE 1 Descriptive statistics.

	Variables	Std	Mean	Min	Max
Density	Residential density (10^4/km^2)	2.865	4	0.096	12.834
	FAR (floor area ratio)	0.612	1.219	0.031	2.928
Pedestrian system	Road density (km/km^2)	4.589	13.648	3.758	28.728
	Number of entrances	1.821	4.699	2	13
	Overpass	1.198	0.974	0	7
	Road network integration index	0.186	0.642	0.078	1.227
	Green view index (%)	0.048	0.187	0.05	0.324
Diversity	Land-use mix	0.083	0.76	0.271	0.893
Function	Enterprise density (1/km^2)	106.45	90.526	0.569	612.112
	Financial facility density (1/km^2)	24.289	19.579	0	138.335
	Educational facility density (1/km^2)	53.148	56.183	0	242.086
	Medical facility density (1/km^2)	38.126	40.148	0	291.303
	Restaurant density (1/km^2)	186.256	193.649	0	1518.053
	Park density (1/km^2)	3.46	2.32	0	21.484
	Distance to CBD (km)	6.77	9.518	0	28.698
	Commercial facility density (1/km^2)	490.068	335.317	0	4258.328
Transportation accessibility	Bus stop density (1/km^2)	4.726	8.514	0.572	27.362
Economic attribute	Housing price (10^4 yuan/m^2)	0.492	1.556	0.38	3.54

suitable for analyzing the impact of built environment characteristics on urban vibrancy (Chen et al., 2022c), and the model expression is

$$Y_i = \beta_0(u_i, v_i, t_i) + \sum_k \beta_k(u_i, v_i, t_i) X_{ik} + \varepsilon_i$$
$$i = 1, 2, \cdots, n$$

Where Y_i is the vibrancy (intensity of human activities) of the station i; n is the number of observations; u_i is the longitude coordinate of the station i; v_i is the latitude coordinate of the station i; t_i is the temporal coordinate of the station i; $\beta_0(u_i, v_i, t_i)$ denotes the spatio-temporal intercept term of the station i; X_{ik} denotes the value of the kth explanatory variable of the station i; $\beta_k(u_i, v_i, t_i)$ denotes the regression coefficient of the kth

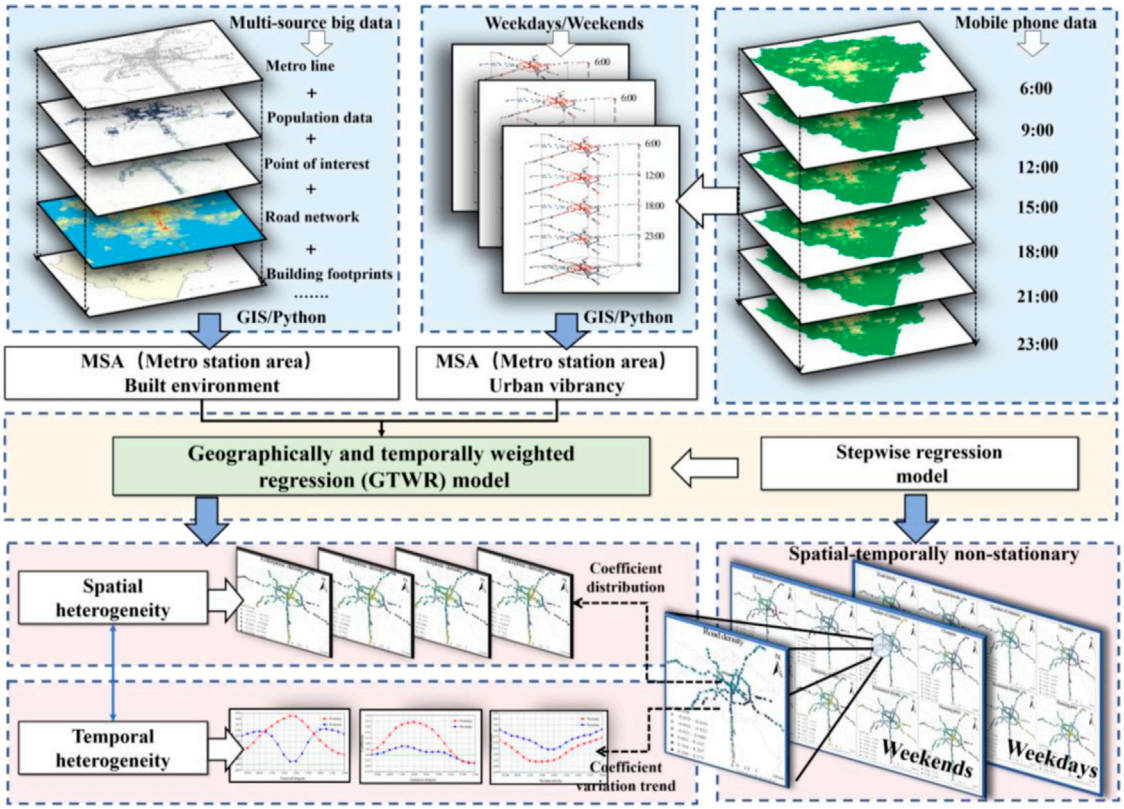

FIGURE 4
Research framework of the spatio-temporal analysis for urban MSA-level vibrancy.

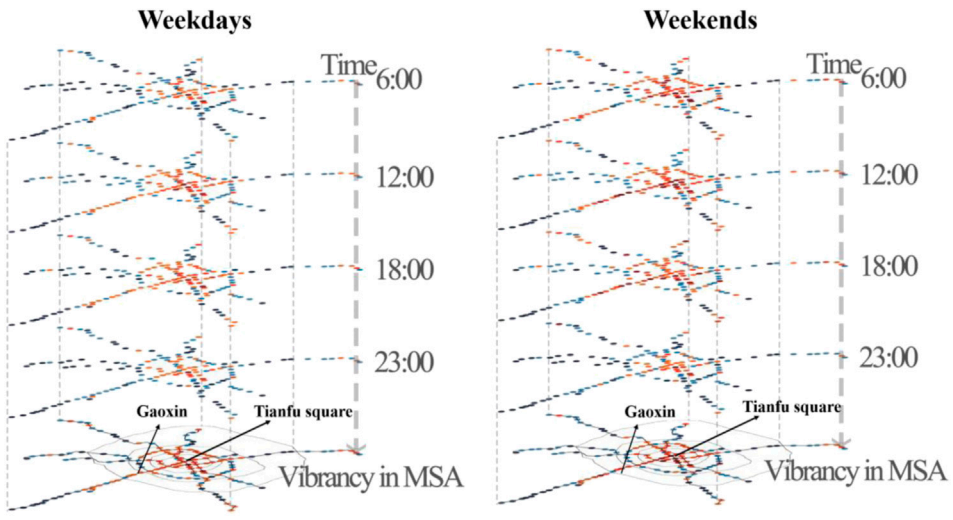

FIGURE 5
The spatio-temporal distribution of the MSA-level vibrancy.

TABLE 2 Stepwise regression model and GTWR model summary results for weekdays.

	Stepwise regression Model		GTWR Model				
	Coef.	Std.Err	Mean	Min.	1st Q	3rd Q	Max.
Residential density	0.540***	0.015	0.499	0.113	0.404	0.616	1.095
Road density	0.148***	0.012	0.100	−0.115	0.016	0.180	0.365
Number of entrances	0.039***	0.010	0.027	−0.125	−0.006	0.066	0.169
Overpass	0.042***	0.011	0.094	−0.055	0.034	0.154	0.276
Road network integration index	0.024**	0.009	0.025	−0.134	−0.016	0.062	0.181
Green view index	0.048***	0.010	−0.017	−0.423	−0.062	0.035	0.288
Enterprise density	0.203***	0.015	0.103	−0.256	−0.041	0.208	1.182
Financial facility density	0.187***	0.018	0.256	−0.108	0.110	0.314	4.221
Educational facility density	−0.133***	0.020	−0.125	−1.755	−0.146	−0.032	0.523
Medical facility density	0.050***	0.013	0.010	−1.053	−0.057	0.117	0.588
Restaurant density	0.147***	0.018	0.199	−2.582	0.045	0.331	1.759
Distance to CBD	0.074***	0.011	0.002	−1.080	−0.149	0.167	0.903
Bus stop density	−0.023**	0.012	−0.030	−0.416	−0.087	0.016	0.170
Housing price	−0.094***	0.010	−0.037	−0.272	−0.100	0.011	0.314
R^2	0.808		0.941				
AIC	3365.124		582.444				

***$p < 0.01$, **$p < 0.05$, *$p < 0.1$.

explanatory variable of the station i, which serve as the function of spatio-temporal coordinates; ε_i is the error term.

4 Results and discussion

4.1 The spatio-temporal distribution of the metro station area-level vibrancy

Figure 5 shows the spatio-temporal distribution of the MSA-level vibrancy based on mobile phone signaling data (Yue et al., 2017). The spatio-temporal distribution of vibrancy on weekdays possesses obvious dynamic characteristics of "dispersion and agglomeration". The most vibrant MSAs are mainly concentrated in two areas which are located within the "1st Ring Road" and in "Gaoxinnan", reflecting the "dual-core" spatial structure of Chengdu. The stations with high vibrancy during the morning peak are mainly Xipu, Guangfu, Shenxianshu, and others. These stations are mostly surrounded by large scale of residential districts, with typical characteristics of "commuter towns". During the afternoon and evening peak, the stations with high vibrancy are mainly Tianfu Sanjie, Century City, and Gaoxin station, which are surrounded by abundant employment facilities and commercial facilities. Stations such as Chunxi Road, Tianfu Square, and Huaxiba in the central part of the city maintain a consistently high level of vibrancy throughout the day. The main reasons for this are that these stations possess strong attractiveness and influence due to their location and comprehensive service functions. In addition, some of the stations at the southern end of the city and outside the 3rd Ring Road are generally less vibrant, possibly since these stations' development is still in its infancy.

Compared with weekdays, residents have more flexible schedule of travel and activities on weekends, and spare more time for daily leisure activities such as shopping, sports, and visiting friends. Therefore, the spatial distribution of the MSA-level vibrancy on weekends is relatively homogeneous. MSAs with high vibrancy are mainly located in the traditional central areas of the city (within the 2nd Ring Road) where commercial facilities are concentrated and transportation facilities are developed. The vibrancy around these stations shows a continuous increase from 8:00 to 14:00 and keeps at a high level from 14:00 to 23:00, which is closely related to the vibrant nightlife and thriving food culture in Chengdu. As can be seen, the distribution of the MSA-level vibrancy basically reflects the dynamic patterns of residents' rail commuting on weekdays and consumption habits on weekends.

4.2 Results of stepwise regression and geographically temporally weighted regression model

Table 2 shows the model results of the stepwise regression and GTWR model on weekdays, and the R^2 of the two models are 0.808 and 0.941, respectively. The R^2 of the GTWR model is

TABLE 3 Stepwise regression model and GTWR model summary results for weekends.

	Stepwise regression Model		GTWR Model				
	Coef.	Std.Err	Mean	Min.	1st Q	3rd Q	Max.
Residential density	0.620***	0.013	0.559	−0.692	0.428	0.747	1.678
Road density	0.080***	0.010	0.019	−1.056	−0.070	0.146	1.088
Number of entrances	0.042***	0.009	0.049	−0.664	−0.033	0.097	0.708
Overpass	0.051***	0.011	0.101	−0.092	0.021	0.175	0.588
Road network integration index	0.025***	0.008	−0.010	−1.334	−0.041	0.078	0.855
Green view index	0.023***	0.008	−0.033	−0.927	−0.060	0.054	0.181
Enterprise density	−0.071***	0.014	0.010	−0.673	−0.234	0.098	2.623
Financial facility density	0.114***	0.017	0.221	−4.899	0.041	0.380	6.149
Educational facility density	−0.090***	0.018	0.155	−1.673	−0.162	0.068	7.649
Medical facility density	−0.021*	0.011	−0.327	−8.436	−0.238	0.064	1.924
Restaurant density	0.309***	0.019	0.347	−3.771	−0.067	0.421	7.405
Park density	0.042***	0.010	0.013	−2.242	−0.022	0.128	0.733
Distance to CBD	0.049***	0.010	0.058	−1.219	−0.142	0.274	1.730
Commercial facility density	0.067***	0.014	0.559	−2.797	0.012	0.309	15.226
Housing price	−0.107***	0.009	−0.058	−1.029	−0.132	0.020	0.378
R^2	0.852		0.959				
AIC	2627.598		−524.473				

***$p < 0.01$, **$p < 0.05$, *$p < 0.1$.

significantly higher, which indicates that the GTWR model is suitable for the spatio-temporal data structure of this study. The results of the stepwise regression method on weekdays show that density indicators (residential density) and pedestrian system indicators (road density, number of entrances, overpass, road network integration index, and green view index) are positively correlated with vibrancy. Function indicators including distance to CBD, enterprise density, financial facility density, restaurant density, and medical facility density are also positively correlated with the MSA-level vibrancy. However, housing price, bus stop density, and educational facility density are negatively correlated with the MSA-level vibrancy. Notably, the commercial facility density and park density indicators are not significantly related to vibrancy, suggesting that people traveling on weekdays are more interested in work-related facilities such as companies in MSAs, but less interested in leisure activities such as shopping and hanging out. It is believed that these findings are reasonable. The results are consistent with the research of Huang et al. (2020), Tu et al. (2022), and Xiao et al. (2021).

Table 3 shows the model results of the stepwise regression method and GTWR model on the weekends. It can be seen that the R^2 of the GTWR model (0.959) is still larger compared to the R^2 of the stepwise regression model (0.852). We find that the results of the stepwise regression method are mostly relatively similar for weekdays and weekends. The difference is that both commercial facility density and park density are significantly and positively correlated with the MSA-level vibrancy on weekends. In addition, enterprise density is negatively correlated with vibrancy. This is more identical to the travel and activities routines of residents on weekends. Surprisingly, there is no significant relationship between the vibrancy and two important indicators, FAR and land-use mix, for both weekends and weekdays. The same results are obtained in the study of De Nadai et al. (2016) and Tang et al. (2018). The study of Lu et al. (2019a) based in Chengdu indicates that excessive spatial development leads to a decrease in the neighborhood vibrancy. However, in this study, we suggest that maybe the vibrancy of multiple time periods dilutes the effect of FAR and Land-use mix.

4.3 Analysis of the spatio-temporal variation

4.3.1 Temporal heterogeneity of average coefficients

The temporal variation trend of the influence coefficient for the MSA-level built environment indicators on vibrancy is shown in Figure 6. The red and blue lines represent variables on weekdays and weekends, respectively. It can be seen that the impact of built environment indicators on the MSA-level vibrancy has typical time-varying characteristics, and there are differences in the coefficient fluctuations between weekdays and weekends. The temporal variation of the coefficients has a strong

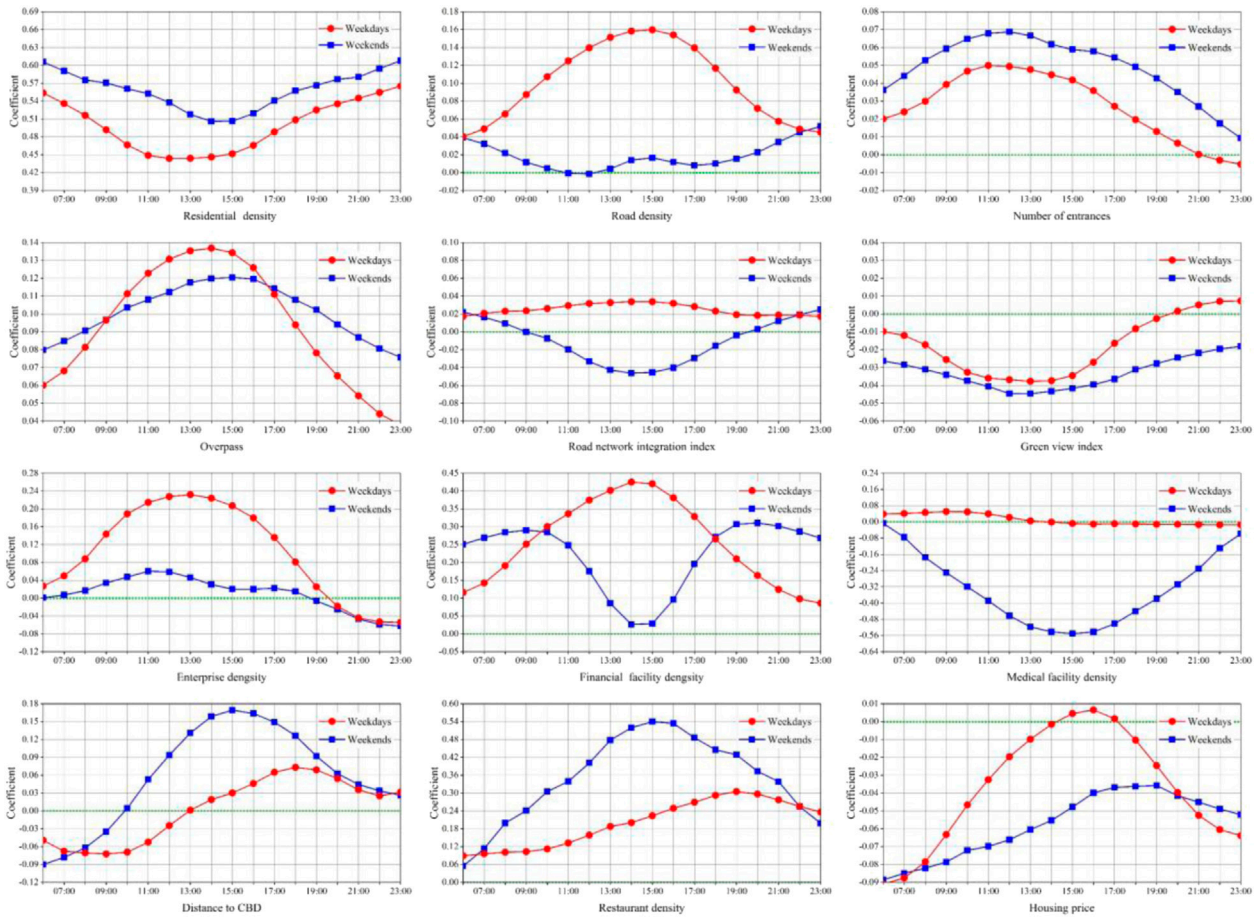

FIGURE 6
Temporal average coefficients of the built environment factors.

relationship with the life patterns of Chinese urban residents (Li et al., 2019; Wang et al., 2022b). For example, we find that the coefficients generate time-varying inflection points at 9:00, 13:00, and 17:00, which are the time points for going to work, taking a lunch break, and getting off work, respectively.

Firstly, residential population density possesses the largest average coefficient of all indicators (Tables 2, 3), and it has a positive influence coefficient on MSA-level vibrancy both on weekdays and weekends. A high-density residential population tends to create a scale effect and provides more social contacts, which is important for the creation of vibrancy in TOD communities. In addition, the coefficient is generally higher on weekends than on weekdays. The coefficient of residential density has a "U-shaped" characteristic, which decreases from 6: 00–11:00, stays the same from 11:00–17:00, and increases after 17:00. This time pattern is significantly consistent with the "go out early and come back at dusk" travel habits of communities (Wu et al., 2018a; Huang et al., 2019). As shown in Figure 6, the separation of work and residential spaces leads to less attractive of MSAs during the daytime, despite the high accessibility provided by the TOD (Wu et al., 2018a; Li et al., 2020a).

Secondly, compared with the residential density, the variation trends of enterprise density are opposite, with a positive correlation before 19:00 and a negative correlation after 19:00. The variation trend of the coefficient on weekends basically remains flat. While, on weekdays, there is an inverted U-shaped characteristic that maintains a high coefficient value from 11:00 to 17:00. This is the time period with the highest employment population density around the TOD of the day. It can be seen that there is a certain lag in the dissipation of work-related activities in MSAs due to the "Nine-nine-six work system" (Xiao et al., 2020) working overtime culture (the usual clocking out time in China is around 17:30). The variation trends of the restaurant density coefficient are very interesting, with positive coefficient for both weekends and weekdays throughout the day. Meanwhile, the variation trend of coefficient peaks at around 16:00 on weekends and at 19:00 on weekdays, respectively. Chengdu owns a well-developed food

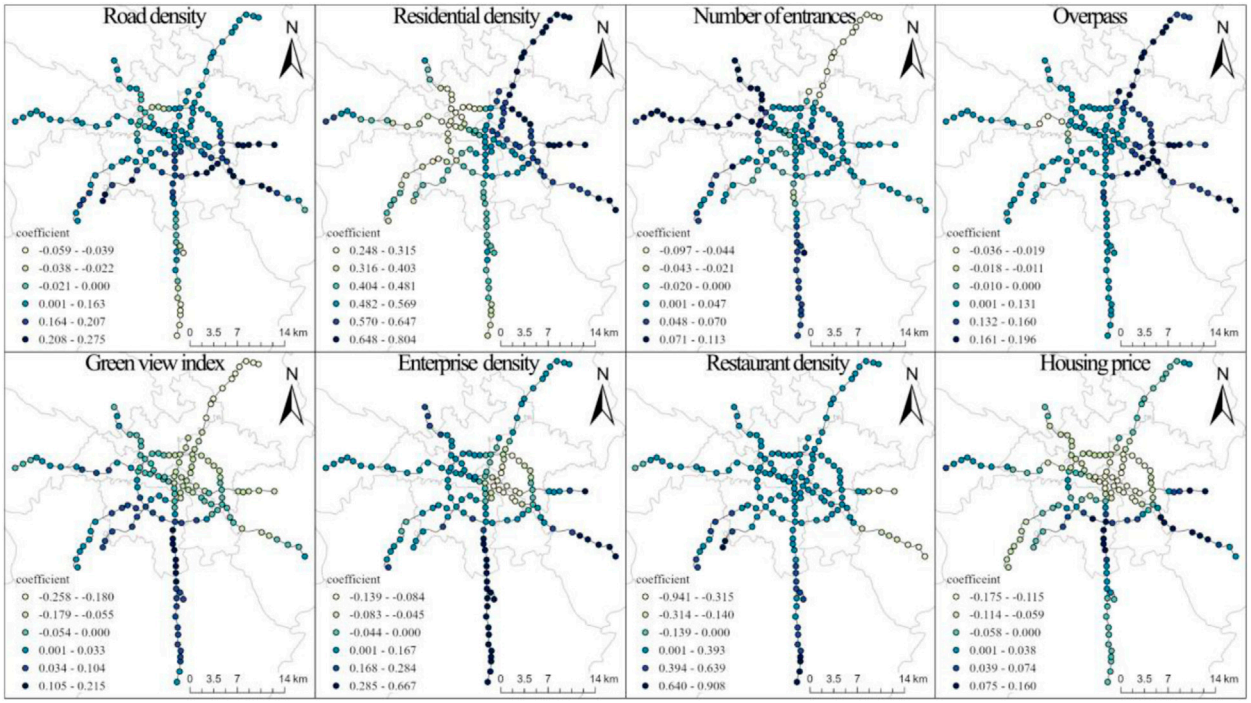

FIGURE 7
Spatial heterogeneity of average coefficients for the built environment factors on weekdays.

culture and is known as the "Gastronomic Capital and City of the Night" in China. The MSAs are at core locations with high concentration of restaurants in Chengdu. Residents often choose to start lining up for dinner at around 16:00 or 17:00 on weekends due to a large number of consumers. On weekdays, the time of getting off work is usually 17:30, and those who choose to dine out usually arrive at the nearby restaurant at around 19:00.

Thirdly, in terms of pedestrian system design, the average influence coefficients of road density, number of entrances, and overpass facilities on vibrancy are positive, as is the coefficient of road network integration, on weekdays. MSA is a highly spatialized and populated neighborhood in the city, and it is also a "fast-paced area" of urban life, where people work, live, and consume with more emphasis on the efficiency of walking. Therefore, people are more focused on the spatial accessibility of the pedestrian system in MSAs. Interestingly, the coefficients of road density and integration are higher on weekdays than on weekends. Oppositely, the coefficients of the entrance number and overpass facilities are higher on weekends than on weekdays. This indicates that commuting traffic is more concerned with the plane accessibility in the MSA, while leisure and consumption traffic on weekends is more concerned with the three-dimensional accessibility of the pedestrian system. As a result, commercial complexes in MSAs generally use three-dimensional pedestrian systems to connect ground-level spaces for the introduction of pedestrian flow (Yang et al., 2021b). In the studies of Lu et al. (2019b), the positive impact of the green view index on urban vibrancy has been confirmed. In this study, however, we find that the coefficient of green view index on MSA-level vibrancy is always negative with time-varying. The possible reason is that, unlike other zones in the city, the high-density development of TOD generates the need to evacuate people quickly, and the larger volume of greenery may affect sight as well as the mobility of people to some extent. Some studies are similar to our findings: Meng and Xing (2019) pointed out that the area of ecology spaces, such as water bodies and green spaces, have a negative impact on urban vibrancy. Chen et al. (2022c) also point out that green space is not significantly related to urban vibrancy.

Fourthly, the average coefficient of housing price is negative and the negative effect of weekends is stronger than that of weekdays. The possible reason is that there exists a relationship between housing prices and floor area ratio in China's major cities. The houses with higher prices usually have smaller floor area ratios and residential density, which means a higher quality of living space and lower population density. Also, the housing prices are higher in MSAs than in other parts of the city due to the excellent location and transportation resources. However, high housing prices are often accompanied by gentrification, which can cause the lower- and middle-income classes to relocate and thus affect the vibrancy of the community. A study by Tu et al. (2022) on

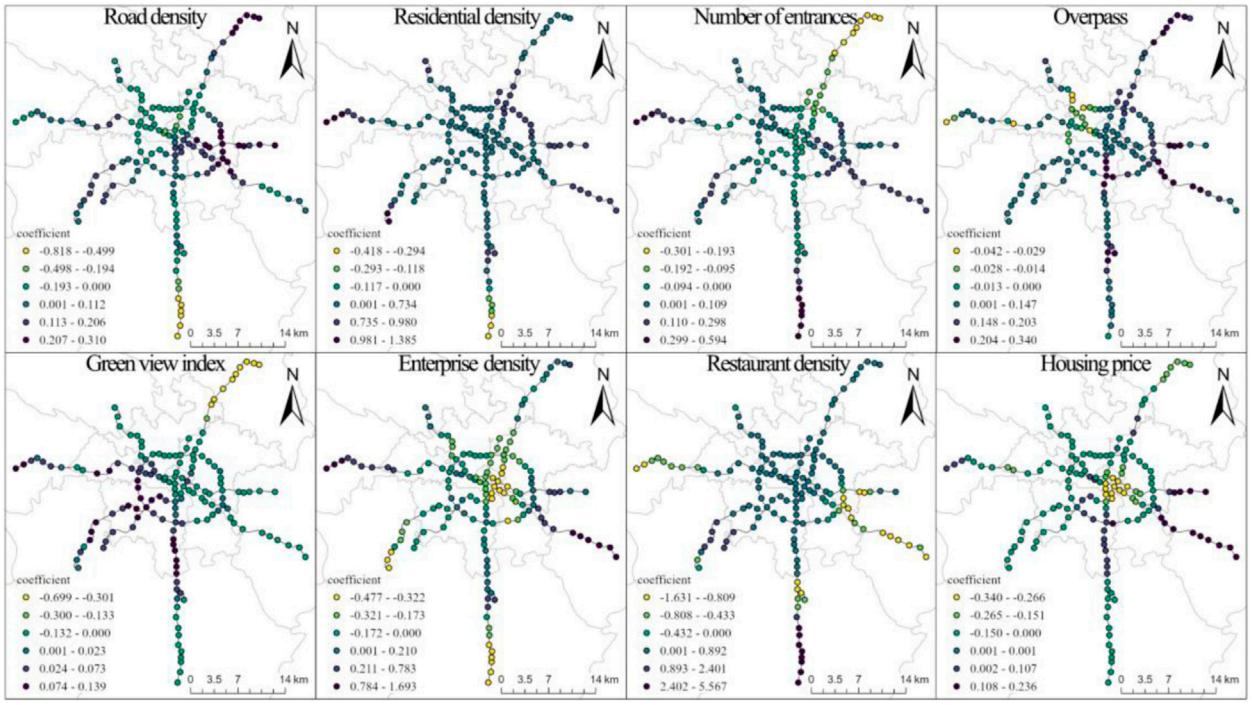

FIGURE 8
Spatial heterogeneity of average coefficients for the built environment factors on weekends.

TOD in Singapore reveals that high income negatively affects MSA-level vibrancy. Jia et al. (2021) also find that high housing prices have an inhibiting effect on urban vibrancy.

4.3.2 Spatial heterogeneity of average coefficients

The spatial distribution of average influence coefficients for the MSA-level built environment indicators on vibrancy is shown in Figure 7 (weekdays) and Figure 8 (weekends), respectively. Moreover, we classify the coefficients into six categories based on the natural breakpoint method (Wu et al., 2018a). In order to distinguish the positive and negative effects of the coefficients, we manually grade the values of the coefficients.

4.3.2.1 Density

As Jacobs (1961) argues, we find that high-density development is closely related to the maintenance of urban vibrancy. The findings also show that the spatial distribution of the coefficient for the residential density on vibrancy is generally positive on both weekdays and weekends. The negative values only exist in a few undeveloped sites in the southern end of the city with relatively few residential population. Similarly, as Glaeser (2013) proposes in the "Triumph of the city", spatial agglomeration contributes to the creation of urban vibrancy.

4.3.2.2 Pedestrian system

The spatial distribution of the coefficient for the number of entrances and overpasses is generally positive, with the highest values in areas near the "3rd Ring Road" and the expressway at the southern end of the city. The roads around MSAs in these districts are relatively wider with larger traffic flow, which is not suitable for walking. Therefore, the provision of overpass facilities and the reasonable layout of metro entrances in these areas can significantly enhance the spatial accessibility, thus meeting people's demand for travel as well as other activities. On the contrary, the coefficients of road density at the southern end of the city, such as Science City, Xinglong Lake, and Guangzhou Road, exert a significantly negative effect on vibrancy. This may be due to the typical ring-radial city structure of Chengdu, and the road network structure here is "dense inside and sparse outside". Furthermore, the construction of new areas in Chinese cities is usually "the road first, then the city". Thus, the road density and the building construction around these new district sites, which are far from the city center, are at a low level and cannot attract enough people in a short time. It is worth noting that the spatial distribution of the coefficient for the green view index shows a negative correlation between the central region and the northeastern region, and the average coefficient is also negative, which is different from the previous studies (Lu et al., 2019b).

4.3.2.3 Function

The spatial distribution of the coefficient for the enterprise density is negative in the central part of the city. While the coefficient is positive in the southern part (Gaoxin and Tianfu New District) and southeastern part (Longquan) of the city. This spatially divergent feature is more obvious on weekdays. The main reason is that the development strategy of Chengdu is guiding the city to grow toward the east and south, which was enacted in the overall plan in 2016. Currently, the MSAs in the south, as well as the east of the city, are urban high-tech industrial clusters (Century City, Financial City, Tianfu Sanjie, and other sites), while the MSAs in the traditional employment centers (South Taisheng Road, Qianfeng Road, and Luomashi) are dominated by retail business and service-oriented businesses. In recent years, the vibrancy of employment clusters in urban centers has declined due to the continued impact of the burgeoning online shopping and the outward shift of high-tech industries. The spatial distribution of coefficient for restaurant density is positive in most areas on weekdays, but the coefficient on weekends shows an "inside positive and outside negative" spatial characteristic. This may be related to the difference in the demand orientation of restaurants in different locations. On the one hand, most catering service facilities in the city center are chains or well-known brands, they tend to choose these hot areas in order to attract more consumers, and generally the peak consumption periods of these restaurants occur on weekends. On the other hand, most of the catering service facilities in the urban periphery are small in scale that rely heavily on residential and employment populations, so these restaurants usually have more stable consumption during weekdays. Moreover, after comparing the spatial distribution of coefficient for the enterprise density and restaurant density on working days, we can obviously find that the spatial distribution of these two variables is basically the same in most regions, except for some sites in the central areas.

4.3.2.4 Housing price

The distribution of coefficient for housing price on the MSA-level vibrancy is also strongly spatially heterogeneous. The study by Fan and Khattak (2008) shows that higher income groups have more travel activity options. Thus, they are more likely to engage in non-work activities in the city center than in the urban periphery. However, we find the opposite result. The housing prices of MSA in the city center are negatively associated with vibrancy, both on weekdays and weekends, while the high housing prices in new areas such as Gaoxinnan have a positive impact on urban vibrancy. This is because settlements of the MSAs within the 2nd Ring Road in Chengdu have been built for a long time and there are a large number of old neighborhoods with poor environmental quality. These old neighborhoods are close to the city center and metro stations, so housing prices here are generally higher, contributing to the difficulties of urban renewal (Demolition costs are high). As a result, a large number of local people move to the suburban areas to improve their living quality, leading to the "inner city decay" (Farjam and Motlaq, 2019) and the decline of vibrancy. Conversely, new areas such as Gaoxinan are emerging as another core of Chengdu, where the government has promoted the rapid development through the TOD strategy and constructed a number of high-quality TOD communities with developed infrastructure and complete services. These areas become the new vibrant hotspots of the city. With the rapid urbanization and urban expansion in China over the past three decades, this shift of vibrant hotspots (inner city decline) has occurred in cities of many regions, including the northeast and north. Since then, urban renewal policies for inner city revitalization are being advocated in major cities.

5 Conclusion

In this study, we first use the mobile signaling data (based on staying time and mobile trajectories of cellular users) to quantify the spatio-temporal distribution of the metro station areas' (MSA) vibrancy in Chengdu. Then, we measure the 18 built environment indicators of MSA based on Jacobs' four conditions of vibrancy and the 5Ds built environment framework. Finally, we employ the stepwise regression model and the geographically temporal weighted regression model (GTWR) to analyze the effect that the MSA-level built environment exerts on urban vibrancy. The results show that: 1) Chengdu's highly vibrant MSAs are concentrated in two districts: the traditional city center and the Gaoxinnan District, which are consistent with the city's "dual core" spatial structure. 2) Density indicators (residential density), pedestrian system indicators (road density, number of entrances, overpass, road network integration index, and green view index), and function indicators (enterprise density, restaurant density) are positively associated with the MSA-level vibrancy. However, economic attributes (housing price) and transportation accessibility (bus stop density) are negatively correlated with the MSA-level vibrancy. 3) The associations between built environment factors and the MSA-level vibrancy exhibit strong spatio-temporal non-stationarity patterns. This is in line with the spatio-temporal patterns of residents' daily work, leisure, and consumption activities in TOD communities. For example, the spatial distribution of the influence coefficients for enterprise density, housing price, and restaurant density has the characteristic of "low within the city center and high outside the city center". The temporal variation of the influence coefficients of enterprise density and residential density embraces the symmetrical characteristics of "U-shaped" and "inverted U-shaped", respectively. The temporal variation of the coefficients for the plane pedestrian system indicators (road density and road network integration index) and the three-dimensional indicators (overpass facilities and green view index) differ significantly between weekdays and weekends.

These findings provide theoretical support for the creation of MSA-level vibrancy. Urban planners should recognize the spatio-temporal impacts of MSA-level built environment characteristics on urban vibrancy at the micro-scale, and develop differentiated planning interventions for different types of metro stations. Based on this, we propose the following planning suggestions: First, the creation of vibrant TOD communities should not only consider the design of the built environment but also the spatio-temporal heterogeneity of its influence on vibrancy. For example, the allocation of dining service facilities needs to match the distribution of urban vibrancy and the different activity patterns (work and leisure activities) of urban residents. Secondly, appropriate neighborhood-scale and street-space design are of great importance for the enhancement of TOD vibrancy. MSA in urban peripheral areas should also be accompanied by the development of small-scale neighborhoods and complex road networks to promote sufficient spatial accessibility and attract more pedestrian flows. Thirdly, in the dense and populous MSAs of city centers, planners should establish three-dimensional pedestrian systems to connect crucial spatial nodes such as subway entrances and exits, office buildings, and commercial complexes to increase the efficiency of pedestrian flow (Yang et al., 2022b). Fourthly, this study shows that the green view index exerts a negative effect on the vibrancy of MSAs in CBD. We argue that the applicability of the ultra-high green view index in MSAs still requires further justification. Small green plants or flat green spaces (lawns, potted plants, etc.) may be more suitable for high-dense TOD neighborhoods. Considering the need for large-scale pedestrian evacuation and visual accessibility, planners may need to be cautious about the utilization of tall greenery in high-density MSAs.

The main contributions of this study are as follows: 1) providing the method that measures the urban vibrancy considering the staying time of crowd, which is oriented from human activity perspective, and analyzing the spatio-temporary distribution of MSA-level vibrancy. 2) revealing the spatio-temporary non-stationarity of the effect that the MSA-level built environment exerts on TOD vibrancy based on the plane dimension and human scale. 3) providing insights for urban planners and management departments when proceeding community plan and design of TOD.

This study has several limitations. Firstly, although the mobile phone signaling data has the advantages of wide coverage and large sample size. While, due to the different market shares of mobile operators, and the low-frequency usage of cell phones by some age groups (children and senior citizens), the study is unlikely to cover all ages. Secondly, this study only uses the mobile phone signaling data in November, while several studies have pointed out that climatic factors such as season and temperature can affect human activeness. This important factor is ignored in our study due to the difficulty of data acquisition. In this regard, the next study should add multiple months of mobile phone signaling data to explore the spatio-temporal distribution characteristics of urban vibrancy in different seasons.

Data availability statement

The original contributions presented in the study are included in the article/Supplementary Material, further inquiries can be directed to the corresponding author.

Author contributions

BY: conceptualization, funding acquisition, supervision, and writing—original draft. XC: conceptualization, funding acquisition, methodology, and writing—review and editing. HL: conceptualization, methodology, formal analysis, validation, and writing—review and editing. PL: validation and writing—review and editing. RL: formal analysis and writing—review and editing. TY: validation and writing—review and editing. All authors contributed to the article and approved the submitted version.

Funding

This study was supported by the Doctoral Innovation Fund Program of Southwest Jiaotong University (No. 2017310253) and the National Natural Science Foundation of China (No. U20A20330).

Conflict of interest

Author HL was employed by Changsha Planning and Design Institute Co., Ltd.

The remaining authors declare that the research was conducted in the absence of any commercial or financial relationships that could be construed as a potential conflict of interest.

Publisher's note

All claims expressed in this article are solely those of the authors and do not necessarily represent those of their affiliated organizations, or those of the publisher, the editors and the reviewers. Any product that may be evaluated in this article, or claim that may be made by its manufacturer, is not guaranteed or endorsed by the publisher.

References

An, D., Tong, X., Liu, K., and Chan, E. H. (2019). Understanding the impact of built environment on metro ridership using open source in Shanghai. *Cities* 93, 177–187. doi:10.1016/j.cities.2019.05.013

Cervero, R., and Kockelman, K. (1997). Travel demand and the 3Ds: Density, diversity, and design. *Transp. Res. part D Transp. Environ.* 2 (3), 199–219. doi:10.1016/s1361-9209(97)00009-6

Chen, L., Zhao, L., Xiao, Y., and Lu, Y. (2022). Investigating the spatiotemporal pattern between the built environment and urban vibrancy using big data in Shenzhen, China. *Comput. Environ. Urban Syst.* 95, 101827. doi:10.1016/j.compenvurbsys.2022.101827

Chen, S., Bao, Z., and Lou, V. (2022). Assessing the impact of the built environment on healthy aging: A gender-oriented Hong Kong study. *Environ. Impact Assess. Rev.* 95, 106812. doi:10.1016/j.eiar.2022.106812

Chen, S., Wang, T., Bao, Z., and Lou, V. (2022). A path analysis of the effect of neighborhood built environment on public health of older adults: A Hong Kong study. *Front. Public Health* 10, 861836. doi:10.3389/fpubh.2022.861836

Choi, J., Lee, Y. J., Kim, T., and Sohn, K. (2012). An analysis of Metro ridership at the station-to-station level in Seoul. *Transportation* 39 (3), 705–722. doi:10.1007/s11116-011-9368-3

M. De Nadai, J. Staiano, R. Larcher, N. Sebe, D. Quercia, and B. Lepri (Editors) (2016). "The death and life of great Italian cities: A mobile phone data perspective," in *Proceedings of the 25th international conference on world wide web* (Québec, Canada: Montréal).

Ding, C., Cao, X., and Liu, C. (2019). How does the station-area built environment influence metrorail ridership? Using gradient boosting decision trees to identify non-linear thresholds. *J. Transp. Geogr.* 77, 70–78. doi:10.1016/j.jtrangeo.2019.04.011

Dougal, C., Parsons, C. A., and Titman, S. (2015). Urban vibrancy and corporate growth. *J. Finance* 70 (1), 163–210. doi:10.1111/jofi.12215

Ewing, R., and Cervero, R. (2010). Travel and the built environment: A meta-analysis. *J. Am. Plan. Assoc.* 76 (3), 265–294. doi:10.1080/01944361003766766

Fan, Y., and Khattak, A. J. (2008). Urban form, individual spatial footprints, and travel: Examination of space-use behavior. *Transp. Res. Rec.* 2082 (1), 98–106. doi:10.3141/2082-12

Farjam, R., and Motlaq, S. M. H. (2019). Does urban mixed use development approach explain spatial analysis of inner city decay? *J. Urban Manag.* 8 (2), 245–260. doi:10.1016/j.jum.2019.01.003

Gehl, J. (2011). *Life between buildings: Using public space*. Washington, Covelo, London: Island PressGehl J.

Glaeser, E. L. (2013). Triumph of the city: How our greatest invention makes us richer, smarter, greener, healthier, and happier (an excerpt)(translated by inna kushnareva). *J. Econ. Sociol.* 14 (4), 75–94. doi:10.17323/1726-3247-2013-4-75-94

Gómez-Varo, I., Delclòs-Alió, X., and Jane Jacobs reloaded, Miralles-Guasch C. (2022). Jane Jacobs reloaded: A contemporary operationalization of urban vitality in a district in barcelona. *Cities* 123, 103565. doi:10.1016/j.cities.2022.103565

Harvey, L. (2001). Defining and measuring employability. *Qual. High. Educ.* 7 (2), 97–109. doi:10.1080/13538320120059990

Hillier, B., Hanson, J., and Graham, H. (1987). Ideas are in things: An application of the space syntax method to discovering house genotypes. *Environ. Plann. B* 14 (4), 363–385. doi:10.1068/b140363

Huang, B., Wu, B., and Barry, M. (2010). Geographically and temporally weighted regression for modeling spatio-temporal variation in house prices. *Int. J. Geogr. Inf. Sci.* 24 (3), 383–401. doi:10.1080/13658810802672469

Huang, B., Zhou, Y., Li, Z., Song, Y., Cai, J., and Tu, W. (2020). Evaluating and characterizing urban vibrancy using spatial big data: Shanghai as a case study. *Environ. Plan. B Urban Anal. City Sci.* 47 (9), 1543–1559. doi:10.1177/2399808319828730

Huang, J., Levinson, D., Wang, J., and Jin, H. (2019). Job-worker spatial dynamics in Beijing: Insights from smart card data. *Cities* 86, 83–93. doi:10.1016/j.cities.2018.11.021

Ibraeva, A., de Almeida Correia, G. H., Silva, C., and Antunes, A. P. (2020). Transit-oriented development: A review of research achievements and challenges. *Transp. Res. Part A Policy Pract.* 132, 110–130. doi:10.1016/j.tra.2019.10.018

Jacobs, J. (1961). *The death and life of great American cities*. New York: Random House.

Jacobs-Crisioni, C., Rietveld, P., Koomen, E., and Tranos, E. (2014). Evaluating the impact of land-use density and mix on spatiotemporal urban activity patterns: An exploratory study using mobile phone data. *Environ. Plan. A* 46 (11), 2769–2785. doi:10.1068/a130309p

Jia, C., Liu, Y., Du, Y., Huang, J., and Fei, T. (2021). Evaluation of urban vibrancy and its relationship with the economic landscape: A case study of beijing. *ISPRS Int. J. Geoinf.* 10 (2), 72. doi:10.3390/ijgi10020072

Kim, Y-L. (2018). Seoul's Wi-Fi hotspots: Wi-Fi access points as an indicator of urban vitality. *Comput. Environ. Urban Syst.* 72, 13–24. doi:10.1016/j.compenvurbsys.2018.06.004

Kostof, S. (1991). *The city shaped: Urban patterns and meanings through history*. New York: Thames & Hudson, P52.

Li, J., Li, J., Yuan, Y., and Li, G. (2019). Spatiotemporal distribution characteristics and mechanism analysis of urban population density: A case of xi'an, shaanxi, China. *Cities* 86, 62–70. doi:10.1016/j.cities.2018.12.008

Li, M., Liu, J., Lin, Y., Xiao, L., and Zhou, J. (2021). Revitalizing historic districts: Identifying built environment predictors for street vibrancy based on urban sensor data. *Cities* 117, 103305. doi:10.1016/j.cities.2021.103305

Li, S., Lyu, D., Huang, G., Zhang, X., Gao, F., Chen, Y., et al. (2020). Spatially varying impacts of built environment factors on rail transit ridership at station level: A case study in Guangzhou, China. *J. Transp. Geogr.* 82, 102631. doi:10.1016/j.jtrangeo.2019.102631

Li, S., Lyu, D., Liu, X., Tan, Z., Gao, F., Huang, G., et al. (2020). The varying patterns of rail transit ridership and their relationships with fine-scale built environment factors: Big data analytics from Guangzhou. *Cities* 99, 102580. doi:10.1016/j.cities.2019.102580

Li, X., Li, Y., Jia, T., Zhou, L., and Hijazi, I. H. (2022). The six dimensions of built environment on urban vitality: Fusion evidence from multi-source data. *Cities* 121, 103482. doi:10.1016/j.cities.2021.103482

Long, Y., and Huang, C. (2019). Does block size matter? The impact of urban design on economic vitality for Chinese cities. *Environ. Plan. B Urban Anal. City Sci.* 46 (3), 406–422. doi:10.1177/2399808317715640

Loo, B. P., Chen, C., and Chan, E. T. (2010). Rail-based transit-oriented development: Lessons from New York city and Hong Kong. *Landsc. urban Plan.* 97 (3), 202–212. doi:10.1016/j.landurbplan.2010.06.002

Lu, S., Huang, Y., Shi, C., and Yang, X. (2019). Exploring the associations between urban form and neighborhood vibrancy: A case study of Chengdu, China. *ISPRS Int. J. Geoinf.* 8 (4), 165. doi:10.3390/ijgi8040165

Lu, Y., Yang, Y., Sun, G., and Gou, Z. (2019). Associations between overhead-view and eye-level urban greenness and cycling behaviors. *Cities* 88, 10–18. doi:10.1016/j.cities.2019.01.003

Mehta, V. (2007). Lively streets: Determining environmental characteristics to support social behavior. *J. Plan. Educ. Res.* 27 (2), 165–187. doi:10.1177/0739456x07307947

Meng, Y., and Xing, H. (2019). Exploring the relationship between landscape characteristics and urban vibrancy: A case study using morphology and review data. *Cities* 95, 102389. doi:10.1016/j.cities.2019.102389

Montgomery, J. (1998). Making a city: Urbanity, vitality and urban design. *J. urban Des.* 3 (1), 93–116. doi:10.1080/13574809808724418

Niu, N., Li, L., Li, X., and He, J. (2022). The structural dimensions and community vibrancy: An exploratory analysis in Guangzhou, China. *Cities* 127, 103771. doi:10.1016/j.cities.2022.103771

Peng, Y., Liu, J., Zhang, T., and Li, X. (2021). The relationship between urban population density distribution and land use in Guangzhou, China: A spatial spillover perspective. *Int. J. Environ. Res. Public Health* 18 (22), 12160. doi:10.3390/ijerph182212160

Qiang, D., Zhang, L., and Huang, X. (2022). Quantitative evaluation of TOD performance based on multi-source data: A case study of Shanghai. *Front. Public Health* 10, 820694. doi:10.3389/fpubh.2022.820694

Ravenscroft, N. (2000). The vitality and viability of town centres. *Urban Stud.* 37 (13), 2533–2549. doi:10.1080/00420980020080681

Rose-Redwood, R., and Bigon, L. (2018). *Gridded worlds: An urban anthology*. Berlin: Springer.

Shao, Q., Zhang, W., Cao, X., Yang, J., and Yin, J. (2020). Threshold and moderating effects of land use on metro ridership in Shenzhen: Implications for TOD planning. *J. Transp. Geogr.* 89, 102878. doi:10.1016/j.jtrangeo.2020.102878

Shi, Y., Yang, J., and Shen, P. (2020). Revealing the correlation between population density and the spatial distribution of urban public service facilities with mobile phone data. *ISPRS Int. J. Geoinf.* 9 (1), 38. doi:10.3390/ijgi9010038

Simmel, G. (2012). *The metropolis and mental life. The urban sociology reader*. London: Routledge, 37

Sulis, P., Manley, E., Zhong, C., and Batty, M. (2018). Using mobility data as proxy for measuring urban vitality. *J. Spatial Inf. Sci.* 16, 137–162. doi:10.5311/josis.2018.16.384

Sun, Z., Allan, A., Zou, X., and Scrafton, D. (2022). Scientometric analysis and mapping of transit-oriented development studies. *Plan. Pract. Res.* 37 (1), 35–60. doi:10.1080/02697459.2021.1920724

Tang, L., Lin, Y., Li, S., Li, S., Li, J., Ren, F., et al. (2018). Exploring the influence of urban form on urban vibrancy in shenzhen based on mobile phone data. *Sustainability* 10 (12), 4565. doi:10.3390/su10124565

Taylor, B. D., and Morris, E. A. (2015). Public transportation objectives and rider demographics: Are transit's priorities poor public policy? *Transportation* 42 (2), 347–367. doi:10.1007/s11116-014-9547-0

Tu, W., Zhu, T., Xia, J., Zhou, Y., Lai, Y., Jiang, J., et al. (2020). Portraying the spatial dynamics of urban vibrancy using multisource urban big data. *Comput. Environ. Urban Syst.* 80, 101428. doi:10.1016/j.compenvurbsys.2019.101428

Tu, W., Zhu, T., Zhong, C., Zhang, X., Xu, Y., and Li, Q. (2022). Exploring metro vibrancy and its relationship with built environment: A cross-city comparison using multi-source urban data. *Geo-spatial Inf. Sci.* 25, 182–196. doi:10.1080/10095020.2021.1996212

Wang, B., Lei, Y., Xue, D., Liu, J., and Wei, C. (2022). Elaborating spatiotemporal associations between the built environment and urban vibrancy: A case of Guangzhou city, China. *Chin. Geogr. Sci.* 32, 480–492. doi:10.1007/s11769-022-1272-6

Wang, X., Zhang, Y., Yu, D., Qi, J., and Li, S. (2022). Investigating the spatiotemporal pattern of urban vibrancy and its determinants: Spatial big data analyses in Beijing, China. *Land Use Policy* 119, 106162. doi:10.1016/j.landusepol.2022.106162

Wu, C., Ye, X., Ren, F., and Du, Q. (2018). Check-in behaviour and spatio-temporal vibrancy: An exploratory analysis in Shenzhen, China. *Cities* 77, 104–116. doi:10.1016/j.cities.2018.01.017

Wu, C., Zhao, M., and Ye, Y. (2022). Measuring urban nighttime vitality and its relationship with urban spatial structure: A data-driven approach. *Environ. Plan. B Urban Anal. City Sci.*, 239980832211081. doi:10.1177/23998083221108191

Wu, J., Ta, N., Song, Y., Lin, J., and Chai, Y. (2018). Urban form breeds neighborhood vibrancy: A case study using a GPS-based activity survey in suburban beijing. *Cities* 74, 100–108. doi:10.1016/j.cities.2017.11.008

Xia, C., Yeh, A. G-O., and Zhang, A. (2020). Analyzing spatial relationships between urban land use intensity and urban vitality at street block level: A case study of five Chinese megacities. *Landsc. Urban Plan.* 193, 103669. doi:10.1016/j.landurbplan.2019.103669

Xiao, C., Silva, E. A., and Zhang, C. (2020). Nine-nine-six work system and people's movement patterns: Using big data sets to analyse overtime working in Shanghai. *Land Use Policy* 90, 104340. doi:10.1016/j.landusepol.2019.104340

Xiao, L., Lo, S., Liu, J., Zhou, J., and Li, Q. (2021). Nonlinear and synergistic effects of TOD on urban vibrancy: Applying local explanations for gradient boosting decision tree. *Sustain. Cities Soc.* 72, 103063. doi:10.1016/j.scs.2021.103063

Xu, Y., and Chen, X. (2021). Quantitative analysis of spatial vitality and spatial characteristics of urban underground space (UUS) in metro area. *Tunn. Undergr. Space Technol.* 111, 103875. doi:10.1016/j.tust.2021.103875

Yang, H., Xu, T., Chen, D., Yang, H., and Pu, L. (2020). Direct modeling of subway ridership at the station level: A study based on mixed geographically weighted regression. *Can. J. Civ. Eng.* 47 (5), 534–545. doi:10.1139/cjce-2018-0727

Yang, J., Cao, J., and Zhou, Y. (2021). Elaborating non-linear associations and synergies of subway access and land uses with urban vitality in Shenzhen. *Transp. Res. Part A Policy Pract.* 144, 74–88. doi:10.1016/j.tra.2020.11.014

Yang, L., Ao, Y., Ke, J., Lu, Y., and Liang, Y. (2021). To walk or not to walk? Examining non-linear effects of streetscape greenery on walking propensity of older adults. *J. Transp. Geogr.* 94, 103099. doi:10.1016/j.jtrangeo.2021.103099

Yang, L., Chau, K., Szeto, W., Cui, X., and Wang, X. (2020). Accessibility to transit, by transit, and property prices: Spatially varying relationships. *Transp. Res. Part D Transp. Environ.* 85, 102387. doi:10.1016/j.trd.2020.102387

Yang, L., Liang, Y., He, B., Lu, Y., and Gou, Z. (2022). COVID-19 effects on property markets: The pandemic decreases the implicit price of metro accessibility. *Tunn. Undergr. Space Technol.* 125, 104528. doi:10.1016/j.tust.2022.104528

Yang, L., Liu, J., Liang, Y., Lu, Y., and Yang, H. (2021). Spatially varying effects of street greenery on walking time of older adults. *ISPRS Int. J. Geoinf.* 10 (9), 596. doi:10.3390/ijgi10090596

Yang, L., Tang, X., Yang, H., Meng, F., and Liu, J. (2022). Using a system of equations to assess the determinants of the walking behavior of older adults. *Trans. GIS* 26 (3), 1339–1354. doi:10.1111/tgis.12916

Ye, Y., Li, D., and Liu, X. (2018). How block density and typology affect urban vitality: An exploratory analysis in Shenzhen, China. *Urban Geogr.* 39 (4), 631–652. doi:10.1080/02723638.2017.1381536

Yue, Y., Zhuang, Y., Yeh, A. G., Xie, J-Y., Ma, C-L., and Li, Q-Q. (2017). Measurements of POI-based mixed use and their relationships with neighbourhood vibrancy. *Int. J. Geogr. Inf. Sci.* 31 (4), 658–675. doi:10.1080/13658816.2016.1220561

Zhang, A., Li, W., Wu, J., Lin, J., Chu, J., and Xia, C. (2021). How can the urban landscape affect urban vitality at the street block level? A case study of 15 metropolises in China. *Environ. Plan. B Urban Anal. City Sci.* 48 (5), 1245–1262. doi:10.1177/2399808320924425

Zhou, J., Yang, Y., and Webster, C. (2020). Using big and open data to analyze transit-oriented development: New outcomes and improved attributes. *J. Am. Plan. Assoc.* 86 (3), 364–376. doi:10.1080/01944363.2020.1737182

frontiers | Frontiers in Environmental Science

TYPE Original Research
PUBLISHED 05 October 2022
DOI 10.3389/fenvs.2022.1029917

Check for updates

OPEN ACCESS

EDITED BY
Bing Xue,
Institute for Advanced Sustainability Studies (IASS), Germany

REVIEWED BY
Dewei Yang,
Southwest University, China
Dafang Wu,
Guangzhou University, China

*CORRESPONDENCE
Binggeng Xie,
xbgyb1961@163.com
Jingzhong Li,
lijingzhong@xcu.edu.cn

SPECIALTY SECTION
This article was submitted to Environmental Informatics and Remote Sensing, a section of the journal Frontiers in Environmental Science

RECEIVED 28 August 2022
ACCEPTED 16 September 2022
PUBLISHED 05 October 2022

CITATION
Wu L, Zhou J, Xie B, Yang S and Li J (2022), Spatiotemporal differences of land use pattern between mountainous areas and basin areas at township scale: A case study of Yuxi City. *Front. Environ. Sci.* 10:1029917. doi: 10.3389/fenvs.2022.1029917

COPYRIGHT
© 2022 Wu, Zhou, Xie, Yang and Li. This is an open-access article distributed under the terms of the Creative Commons Attribution License (CC BY). The use, distribution or reproduction in other forums is permitted, provided the original author(s) and the copyright owner(s) are credited and that the original publication in this journal is cited, in accordance with accepted academic practice. No use, distribution or reproduction is permitted which does not comply with these terms.

Spatiotemporal differences of land use pattern between mountainous areas and basin areas at township scale: A case study of Yuxi City

Li Wu[1], Jing Zhou[1], Binggeng Xie[2]*, Sizhong Yang[3] and Jingzhong Li[4]*

[1]College of Geography and Land Engineering, Yuxi Normal University, Yuxi, China, [2]School of Geographic Sciences, Hunan Normal University, Changsha, China, [3]German Research Center for Geosciences (GfZ), Potsdam, Germany, [4]College of Urban Planning and Architecture, Xuchang University, Xuchang, China

Land use/land cover change is an important carrier for the study of human-land relationship. Yuxi City is a typical area of with alternating mountain and basin landforms, forming a special human-land system with "mountains" and "basins" as the core elements. Taking 75 towns in Yuxi City, Yunnan Province as a case study, this paper uses a comprehensive evaluation model of land use/land cover change and related analysis methods to analyze the changes of land use pattern in mountainous areas and basin areas respectively from 1995 to 2018, and to reveal their spatial differences and its influencing factors. The results show that: 1) The dynamic evolution of land use in the mountainous area and the basin area presented obvious stage characteristics. From 1995 to 2005, the average comprehensive dynamic degree of land use in the mountainous area was 1.7861, which was significantly higher than the 1.7033 in the basin area. The average comprehensive dynamic degree of land use in mountainous areas from 2005 to 2018 was 1.1284, which was significantly lower than 1.9427 in the basin area. 2) From 1995 to 2018, the land use degree and the comprehensive dynamic degree of land use continued to rise in the basin area, while the mountainous area showed a trend of rising first and then falling. The overall change trend of land use depletion in the mountainous area was consistent with that in the basin area, but the mountainous area was always higher than that in the basin area. 3) The land use change in mountainous areas and basin areas was mainly reflected in the difference of natural factors and socio-economic fators. The radiation and agglomeration functions of the basin area have always attracted people to migrate from the mountains to the basin, which was beneficial to the ecological restoration of the vegetation in the mountains. Since the mountainous area and the basin area are geographically adjacent, the coupling and coordination of the two is the premise and foundation for the sustainable development of the region. This causal relationship of land use changes provides a reliable basis for the regulation of mountain-basin human-land coupling relationship.

KEYWORDS
land use change, mountainous areas, basin areas, township scale, Yuxi city

1 Introduction

As an important carrier of social and economic development and human activities (Smiraglia et al., 2015), land resources utilization change can not only reflect the spatio-temporal change characteristics of regional land use, but also reflect the influence of natural and human factors on its long-term effects, representing the spatio-temporal change of natural and human factors and reflecting the coupling relationship between human and land (Gondwe et al., 2019; Olorunfemi et al., 2020). With the increase of human activities and climate change, the land use/land cover has undergone great changes and become a core issue of major international research projects (Xie et al., 2021). Land use/land cover change is an important source of information for understanding the complex interactions between human activities and the ecological environment, which helps to protect and manage related resources, solve the dilemma of current decision-making among land, water, energy and food sectors, and improve human well-being and ecological security (Wolde et al., 2021; Parven et al., 2022). At present, the dynamic change analysis of land use mainly uses the land use/land cover data interpreted by remote sensing images, and they have been used to analyze the temporal and spatial evolution process and pattern of land use/land cover (Kumar et al., 2021; Matlhodi et al., 2021), and to understand and analyze the driving force, change speed and pattern of land use/land cover change from different research scales (Isufi and Berila, 2021; Twongyirwe et al., 2022). In recent years, with the continuous improvement of urbanization level and the change of population quantity and spatial distribution structure, the problems of resource environment and ecological security brought by land use change have become increasingly prominent (Hou et al., 2022; Siddik et al., 2022). At present, discussing the dynamic change process of land use from the perspective of coupling between human activities and the natural environment, and the dynamic change law of land use (Solomon et al., 2020) as well as its impact on the environment and ecology (Meer and Mishra, 2020; Msofe et al., 2020; Yang et al., 2022) from different levels is the focus of many scholars. However, it should be pointed out that, this kind of research results mainly came from the sociallly and economically developed areas (Guo et al., 2009; Lu et al., 2019), the ecologically environment fragile zones (Zhou et al., 2016; Zhao et al., 2018), and the urban fringe areas (Yang et al., 2011; Cui et al., 2013; Li et al., 2018). But there are relatively few studies on mountainous areas, especially from the perspectives of "mountain" and "basin" sub-regions, which have not attracted enough attention and formed a significant research system.

The sustainable management of mountainous areas has aroused considerable interest in recent decades and occupied a prominent space in the international debates on regional sustainable development. Mountainous areas are an important carrier for ecosystem services and biodiversity maintenance (Schild, 2008), as well as an ecological barrier for regional socio-economic development (Scheurer and Jost, 2012). However, with the advancement of urbanization, mountainous areas have gradually become marginal and conflicting areas of economic development (Schild and Sharma, 2011). The conflicts between the fragility characteristics of mountain ecosystems and high-intensity human activities have led to problems such as ecological degradation, economic backwardness, and population poverty (Kohler and von Dach, 2015; Ma et al., 2018; Zhang et al., 2020), confronting the sustainable development of mountainous areas great challenges. The unsustainability faced by mountainous areas is mainly due to the land use against the natural laws. With the growth of the population, when the output of plain farmland cannot meet the food demand, human beings have no choice but to go to the mountains to reclaim the relatively barren land (Zhang et al., 2016; Buchner et al., 2020). However, the over-exploitation of mountain land will bring a series of negative ecological effects such as soil erosion (Feng et al., 2010; Nguyen et al., 2022). From another perspective, the current urbanization development strategy has accelerated the labor migration and flow from mountainous areas to the basin areas, which reduces the human disturbance of the mountain land, and further drives the significant transformation of land use. For example, the cultivated land in the mountainous area is transformed into forest and grassland, and the conversion of the cultivated land in the basin area is further accelerated, resulting in a series of socio-economic and ecological environmental responses (Zhang et al., 2018; Zhang et al., 2020).

In the terrestrial landscape system of China, the generalized mountain landscape accounts for two-thirds. Due to the invasion and influence of human activities, the characteristic human-earth system with "mountain" and "basin" as the core elements has been formed, and then constitutes an important and unique natural-human geography unit, which has become an important content of the scientific research of the human-earth system. However, for a long time, comprehensive geographical studies on mountainous/basin areas have mainly focused on natural landscape differentiation (e.g., macroscopic classification or vertical differentiation rules of mountain-basin, etc.) (Fang et al., 2021) or the development of medium-macro scale planning (e.g., territorial space development at provincial and municipal scales, etc.) (Song et al., 2021). The results have played an important role in supporting the precise spatial governance and the decisions correlation of regional sustainable development. With the refinement of regional development policies and the development of nature-human geography,

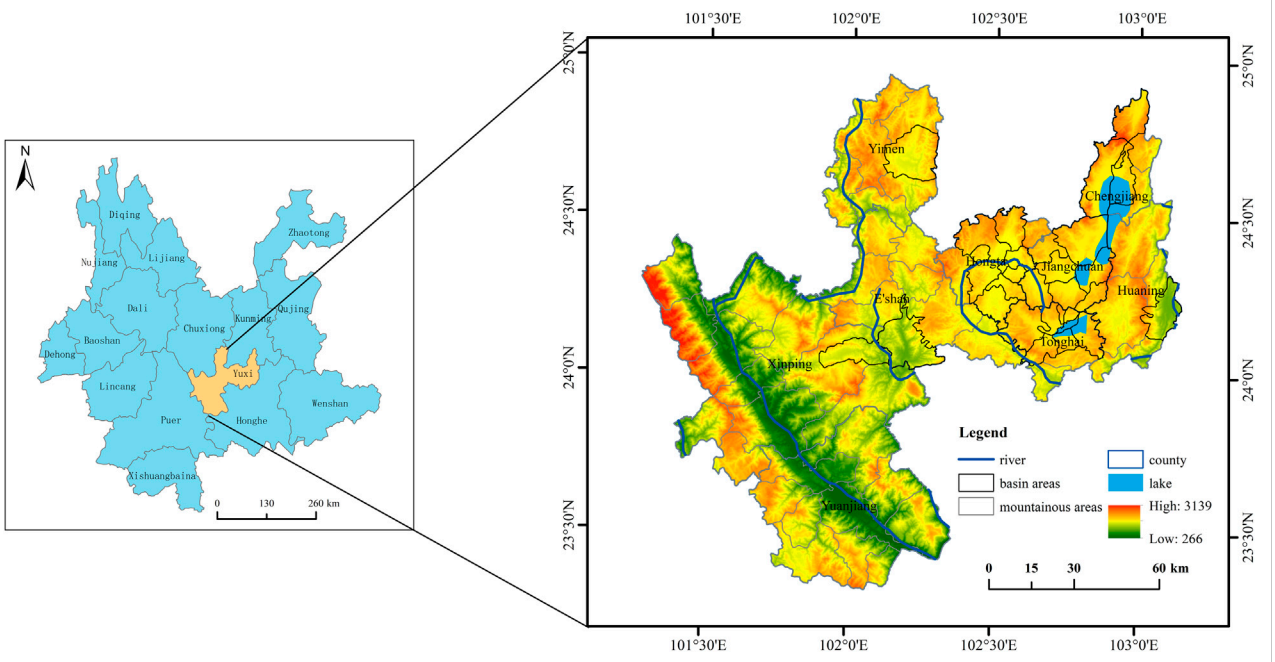

FIGURE 1
Location of study area.

there is an urgent need to strengthen the micro-scale refinement research, especially the research on the variation of factors between "mountains" and "basins" and the coupling evolution of land use in a broad sense. Thus, more scientific and precise strategies will be provided for the rural revitalization, mountainous area development, spatial governance, and ecosystem service maintenance and improvement.

Yuxi City is located in the mountainous area of southwest China, with typical mountain-basin landform characteristics (Wu and Xie, 2019). The basin area is flat, suitable for farming and construction, and is an important carrier of human economic activities, while the natural conditions in the mountainous area are complex and difficult to use (Meybeck et al., 2001; Li et al., 2014; Liu and Li, 2020). However, the mountainous area and the basin area are adjacent in the region, which makes the coupling relationship between them exist in the land use evolution. Therefore, based on the divided mountain-basin types in Yuxi City at the township scale (Wu et al., 2020a), the differences in land use changes between mountainous areas and basin areas in Yuxi City at different time periods were discussed to reveal the differential laws of land use changes. According to the correlation analysis method, the influencing factors of land use difference changes were analyzed respectively, so as to provide some references for the difference analysis on the land use coupling evolution relationship between mountainous areas and basin areas.

2 Materials and methods

2.1 Materials

2.1.1 Regional overview

Yuxi City is located at the central part of Yunnan Province, on the Yunnan Plateau at low latitudes, with a subtropical plateau monsoon climate, ranging from 23°19′ to 24°53′ north latitude and 101°16′ to 103°09′ east longitude (Figure 1). Yuxi is located at the core position of Yunnan Province, connecting the east to the west and the north to the south. It is not only an important hub of an "international channel", but also a strategic "hinterland" of Yunnan Province facing Southeast Asia and South Asia. The city has a land area of 15,285 km^2 and has jurisdiction over 75 townships (towns and streets) in seven counties and two districts. The main landform in the west is the deep-cut high mountain and valley landform, the central and eastern part belongs to the mountainous area of central Yunnan, and is dominated by the mid-mountain landform, the eastern region is mainly composed of the plateau lake basin landforms, and the terrain in the basin is flat and open. At the end of 2018, the total permanent population of Yuxi City was 2.386 million, of which the urban population was 1.238 million and the rural population was 1.148 million, with an urbanization rate of 51.9%.

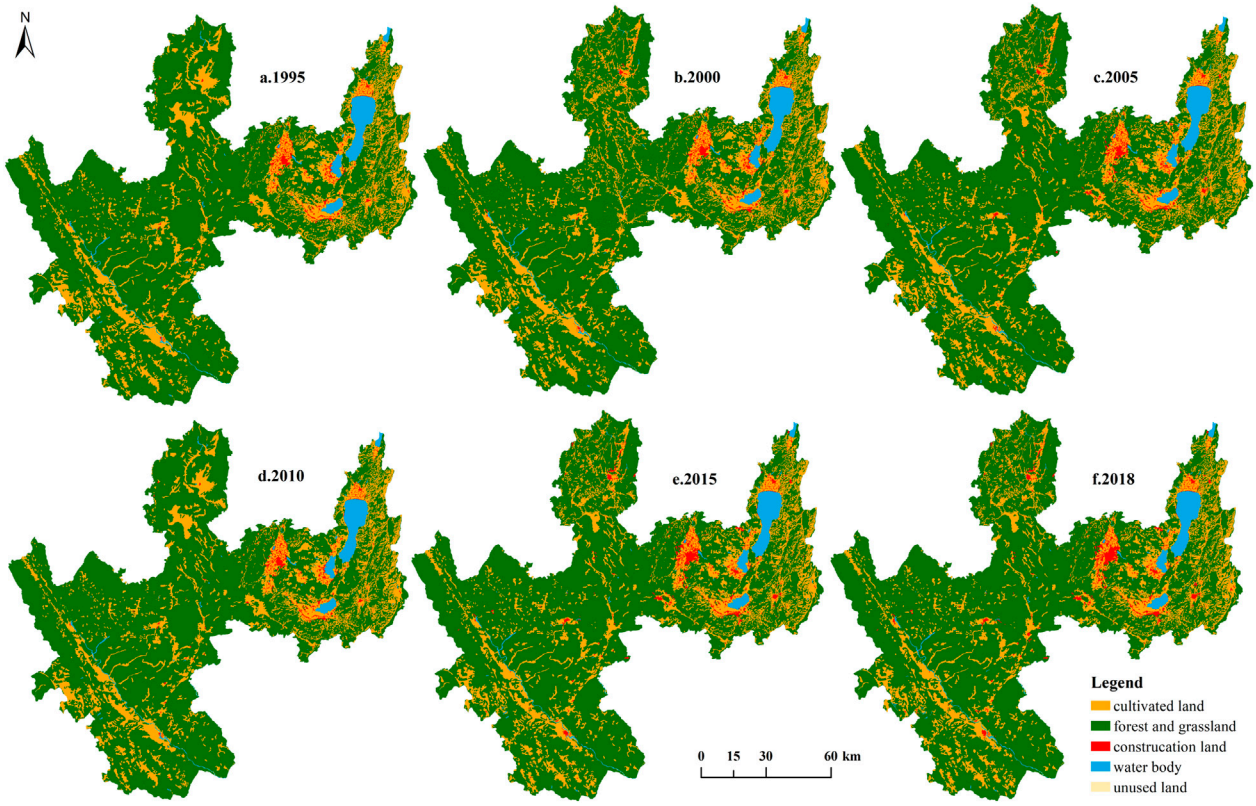

FIGURE 2
Interpretation of land use type in Yuxi City from 1995 to 2018.

2.1.2 Data sources

The data of land use/land cover used in the study consists of two parts. The first part is the research data of dynamic change in land use, which is mainly obtained by interpretating six Landsat remote sensing images in Yuxi City from 1995 to 2018. It mainly includes Landsat five TM images, Landsat seven ETM + images and Landsat eight OLI images, which are obtained from the geospatial data cloud website (www.gscloud.cn). Based on ArcGIS 10.8 software, the maximum likelihood classification method was used to classify land use/land cover (Richards, 1995), which was divided into six categories: cultivated land, forest land, grassland, water body, construction land and unused land. According to the research needs, forest land and grassland were combined into forest and grassland. A total of six periods of land use/land cover data of Yuxi City from 1995 to 2018 were obtained (Figure 2). The second part is the driving force analysis data of land use change, including land use survey data and social and economic data. The land use survey data came from the survey data of Yuxi City over the years. The socio-economic data were obtained from the Statistical Yearbook of Yunnan Province from 1996 to 2019, the Statistical Yearbook of Yuxi City from 1995 to 2018, and the statistical yearbook of each county and district of Yuxi City from 1995 to 2018.

2.2 Methods

2.2.1 Land use degree

The land use degree can reflect the breadth and depth of land use (Zhuang and Liu, 1997). In this study, the comprehensive index of land use degree was used as an index to measure the land use degree, and its calculation formula is as follows:

$$L_a = 100 \times \sum_{i=1}^{n} A_i \times C_i \quad (1)$$

Where, *La* is the comprehensive index of land use degree, *Ai* is the grading index of the *i*th land use type, *Ci* is the area percentage of the *i*th land use type, and *n* is the number of land use types. In this paper, the natural and humanistic attributes of land are comprehensively considered, and the land use types are combined and reorganized into four categories, which are further divided into four levels according

TABLE 1 Land use degree classification index.

	Unused land	Forset, grass, water	Agricultural land	Land for urban settlement
Land use types	Unused land or unable land	Woodland, grassland, water body	Cultivated land	Urban land, residential land, land for mining and industry, land for transportaion
Grading index	1	2	3	4

to the land use degree and endowed with corresponding grading indexes (Table 1).

2.2.2 Land use change speed

The speed of land use change can be reflected by the model of comprehensive dynamic degree of land use (Wu et al., 2014). Comprehensive dynamic degree of land use refers to the overall speed of land use change in a region, and its calculation formula is as follows:

$$LC = \left[\frac{\sum_{i=1}^{n}\Delta LU_{i-j}}{\sum_{i=1}^{n}LU_i}\right] \times \frac{1}{T} \times 100\% \quad (2)$$

Where, LC is the comprehensive dynamic degree of land use, LU_i is the area of class i land use type at the beginning of the study period, $\Delta LU_{i\text{-}j}$ is the area of transformation from class i to class j at the end of the study period, and T is the study duration.

2.2.3 Land use consumption degree

Land use consumption degree represents the actual consumption degree of a certain land use type per unit time (Lu et al., 2007), and its calculation formula is as follows:

$$LCU = \frac{C_{ab}}{U_a} \times \frac{1}{T} \times 100\% \quad (3)$$

Where, LCU is the reduction degree of a certain land use type during the study period, C_{ab} is the total area of a certain land use type that transformed into other land use types from time a to time b, U_a is the area of this land use type at time a, and T is the study duration.

2.2.4 Land use transfer matrix

The changes in the transfer and outflow of various land classes during the study period can be reflected by the land use transfer matrix, and the transfer direction at the beginning of maturity and the transfer source at the end of the term can also be understood (Lu et al., 2007). Its mathematical model is as follows:

$$S_{ij} = \begin{bmatrix} S_{11} & S_{11} & \cdots & S_{1n} \\ S_{21} & S_{22} & \cdots & S2n \\ \cdots & \cdots & \cdots & \cdots \\ S_{n1} & S_{n2} & \cdots & S_{nn} \end{bmatrix} \quad (4)$$

Where, S is the area of the land class, n is the number of land use types, i and j are the land use types at the beginning and end of the study period respectively.

3 Land use dynamic differences between mountainous and basin areas

3.1 Land use structure and degree change

The land use in the mountainous area and basin area of Yuxi City is dominated by forest, grassland and cultivated land, but the cultivated land, construction land and water body in the basin area are significantly more than those in the mountainous area. The cultivated land accounts for 15–16% in the mountainous area while 20–23% in the basin area. The total water area, construction land and unused land do not exceed 30% of the total area of the mountainous area or basin area. The proportion of the cultivated land, water area and construction land in the basin area is more than 20, 10 and 6% respectively, which are significantly higher than that in the mountainous area (15, 1.5 and 2%). From 1995 to 2018, the proportion of the construction land in mountainous areas was 2–3%, and that in basin areas increased from 5.00 to 9.43%. The proportion of the cultivated land in the mountainous area was 15–16%, while the proportion of the cultivated land in the basin area is decreased significantly from 23.80 to 20.75%. The comprehensive index of land use degree in the basin area increased from 227.25 to 233.78, and that in the mountainous area increased from 213.67 to 214.49, and then decreased continuously to 214.09 in 2018. That is, the land use degree in the basin area continued to rise, while in the mountainous area, it increased first and then decreased, with a small change range (Figure 3A). From 1995 to 2018, the urbanization level of the basin area increased from 15.65 to 58.26%. The increase of urban population led to the continuous expansion of construction land, and the occupation of the unused land, forest and grassland, and cultivated land, which improved the land use degree continuously. On the contrary, in mountainous areas, although the area of construction land increased to some extent, the abandonment of arable land and the natural restoration of forest and grassland contributed to a large

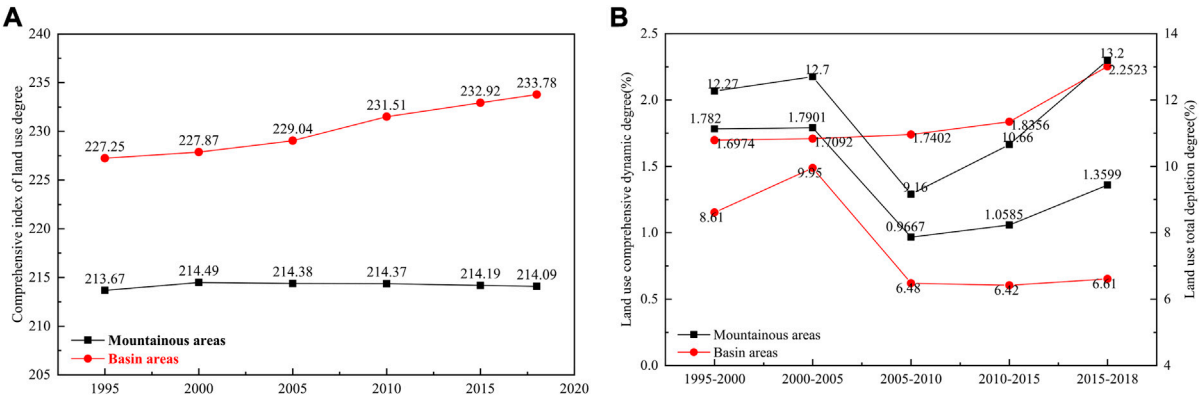

FIGURE 3
Land use dynamic changes in mountainous areas and basin areas of Yuxi City from 1995 to 2018.

amount of natural ecological space and reduced the land use degree.

3.2 Land use comprehensive dynamic degree change

The comprehensive dynamic degree of land use in the basin area rose from 1.6974 in 1995 to 2.2523 in 2018, with an increase of 33%. The comprehensive dynamic degree change of the land use in mountainous areas showed a characteristics of stage change. During the study period, the comprehensive dynamic degree decreased from 1.782 to 1.3599, but the overall trend was in the shape of an "*S*" (Figure 3B), including three stages, the slight rise stage (1995–2005), the sharp decline stage (2005–2010) and the continuous rise stage (2010–2018). The comprehensive dynamic degree of the land use in the slight rise stage was higher than that in the basin area, while in the latter two stages, the dynamic degree of the land use in the basin area was higher than that in the mountainous area. In comparison, the land use change in the mountainous area was more severe than that in the basin area from 1995 to 2005, while the change in the land use of the basin area from 2005 to 2018 was more severe than that in the mountainous area. The main reason was that with the continuous improvement of urbanization level, the population in the mountainous area migrated to the basin area, and the intensity of human activities weakened in the mountainous area while increased in the basin area.

3.3 Land use consumption change

From 1995 to 2018, the overall consumption of land use in mountainous areas first increased from 12.27 to 12.70, then decreased to the lowest, with the value of 9.16, and then continued to rise. From 2015 to 2018, it significantly increased to a peak value of 13.20, with an increase of 44.10% (Figure 3B). The change range of land use consumption in the basin area is small, with a peak of 9.95 from 2000 to 2005, and then a slow decline. Compared with the mountainous area in the same period, the increase range was only 2.01%. In general, there was an obvious trend of stage change of the overall land use reduction degree in mountainous areas and basin areas, with a change pattern of "rise-down-rise". The construction land consumption degree in the mountainous area in the last three stages reached 3.79, 6.97 and 19.00 times of that in the basin area, respectively, and the gap showed a trend of further widening trend. The main reason was that the increase of population density and urbanization level in the basin area increased the demand of land. Due to the difference of natural conditions, the large area of water in Yuxi City is mainly located in the basin area, mainly three lakes, the water area is large and the variation is small, while the area of water in the mountainous area is small and varies greatly under the influence of annual precipitation. The migration of population from mountainous areas to the basin area, the consolidation of the rural residential areas, demolition and so on greatly reduced the amount of construction land.

3.4 Land use transfer change

From 1995 to 2018, land transfer in mountainous areas mainly occurred between the cultivated land and the forest and grassland, and the transfer amount of other land types was relatively small (Figure 4). The main direction of the cultivated land transfer in and out in each stage was forest and grassland. From 1995 to 2018, the area of the cultivated land converted to forest and grassland was 86,800 hm^2, accounting for 90.78% of the total area of cultivated land

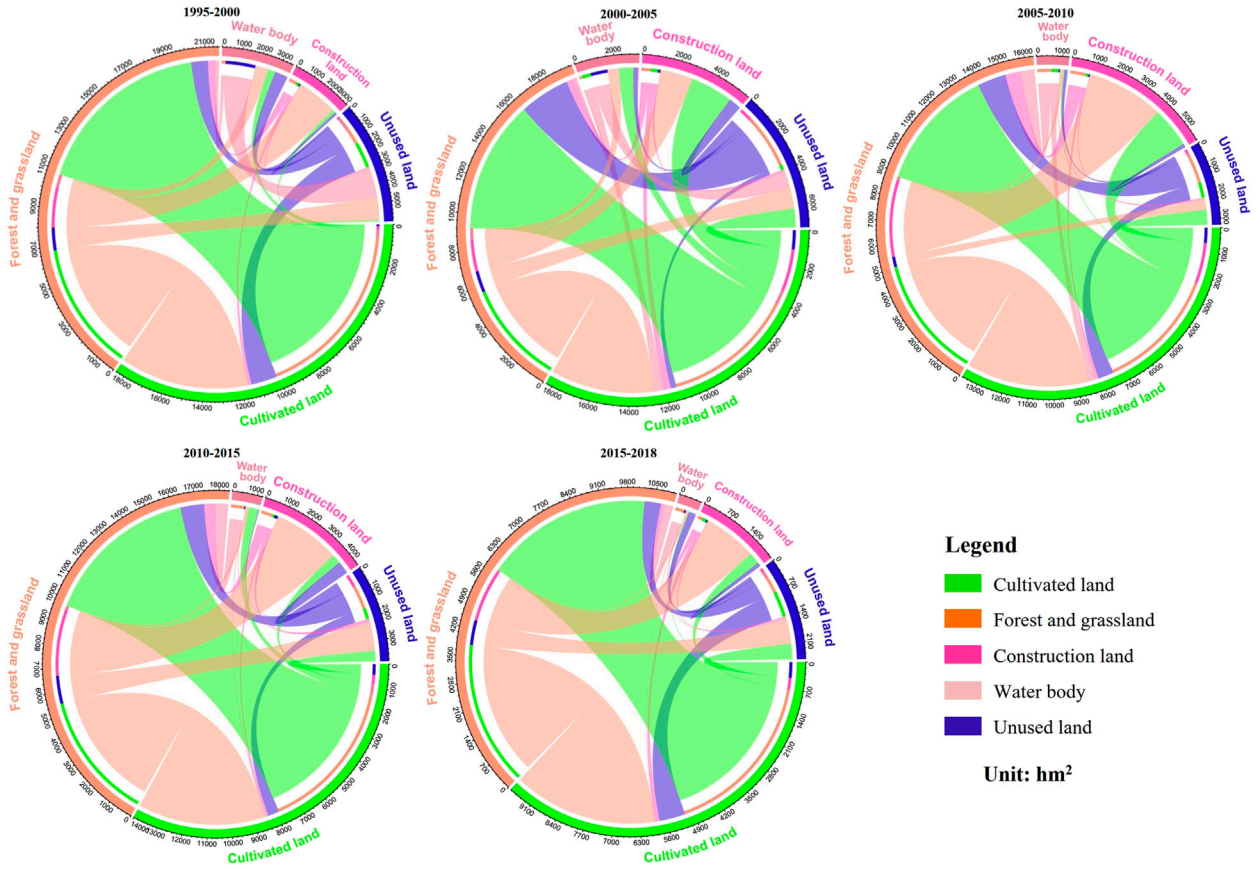

FIGURE 4
Land use types transfer in the mountainous area of Yuxi City from 1995 to 2018.

transferred out. The area of the forest and grassland which was converted to the cultivated land was 79,881 hm^2, accounting for 47.37% of the total area of forest and grassland transferred out. The transfer-in and transfer-out directions of the construction land are the cultivated land and the forest and grassland, and the transfer amount in the latter two stages was significantly higher than that in the first three stages. From 2010 to 2015 and from 2015 to 2018, the total area of the cultivated land converted to the construction land was 5,838 hm^2, accounting for 72.48% of the total amount of the cultivated land which was converted to construction land during the study period. In the same period, the conversion amount from construction land to forest, grassland and cultivated land reached 9,112 hm^2, accounting for 53.23% of the total amount of conversion from construction land to forest, grassland and arable land during the study period. The main transfer sources and destinations of the unused land were the forest and grassland and cultivated land, but the conversion of unused land to forest and grassland and cultivated land continued to decline. From 1995 to 2000, the area of the unused land converted to the cultivated land and forest and grassland reached an average of 1,611 hm^2, while from 2015 to 2018, it reached an annual average of 881 hm^2, with a decrease of 45.28%.

In general, the land type change in mountainous areas was mainly the mutual transfer between the cultivated land and the forest-grassland. During 1995–2000, it was mainly the transformation from the forest-grassland into the cultivated land, but after 2000, it was mainly the transformation from the cultivated land and unused land into the forest-grassland. The transfer intensity of construction land after 2010 was greater than that before 2010, and the transfer intensity of other land types before 2005 was greater than that after 2005.

From 1995 to 2018, the land type transfer in the basin area changed drastically, mainly among the cultivated land, the forest and grassland, and the construction land (Figure 5). During the study period, the accumulated transfer-out and transfer-in amount of forest and grassland were the largest, and the transfer-out direction was mainly cultivated land and construction land. Among them, the conversion of forest and grassland to cultivated land reached an area of 26,809 hm^2,

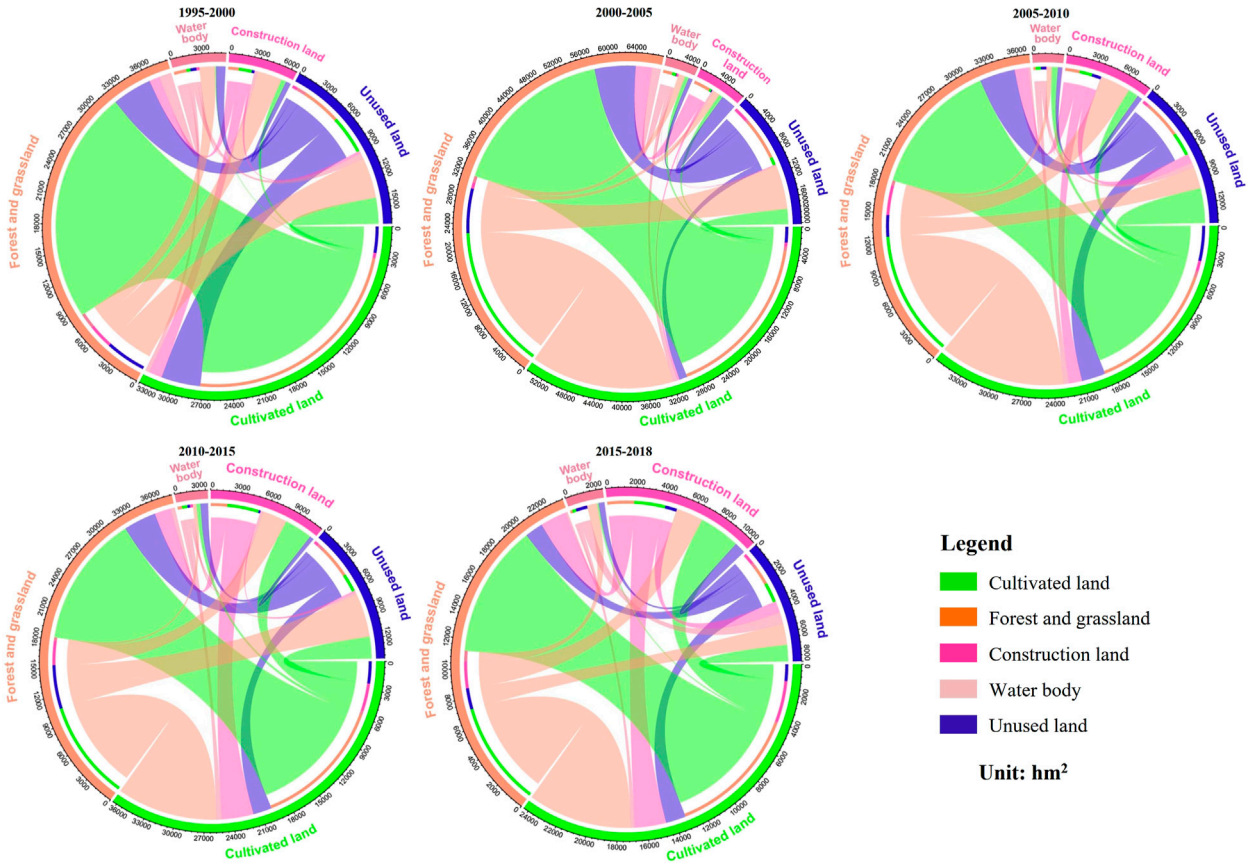

FIGURE 5
Land use types transfer in the basin area of Yuxi City from 1995 to 2018.

accounting for 83.56% of the cumulative amount of transferred in construction land. The conversion of forest and grassland to construction land reached 11,354 hm^2, accounting for 63.45% of the accumulative amount of construction land transferred in. The cultivated land was transferred to forest and grassland and construction land. Among them, the conversion of cultivated land to forest and grassland reached 32,792 hm^2, accounting for 76.64% of the cumulative transfer of forest and grassland. The cultivated land was converted to construction land with an area of 4,903 hm^2, accounting for 27.41% of the total amount of construction land which was transferred in. The transfer direction of unused land was the cultivated land and forest and grassland, and the total amount of the unused land to cultivated land and the forest and grassland was 9,739 hm^2, accounting for 95.04% of the total amount of the unused land transferred out.

In general, the main changes of land types in the basin area occurred in the mutual transfer of the cultivated land, forest-grassland and the construction land, mainly manifested as the transformation from the forest-grassland to the cultivated land and construction land, and the transformation from the cultivated land to the forest-grassland and the construction land. The average annual transfer volume of the first two stages was 5,356 hm^2, and the average annual transfer volume of the last three stages was 4,181 hm^2. The transfer intensity showed a downward trend.

4 Causative differentiation of land use change between mountainous areas and basin areas

4.1 Analysis framework and factor selection

As internal factors, the natural factors determine the basic pattern of the large-scale land use, with a cumulative effect in time. In the short term, social and economic factors are the main external driving force for land use change (Wu et al., 2022). As the secondary core of the urban agglomeration in central Yunnan, Yuxi City has obvious advantages in location. In mountainous areas and basin areas, there are differences in

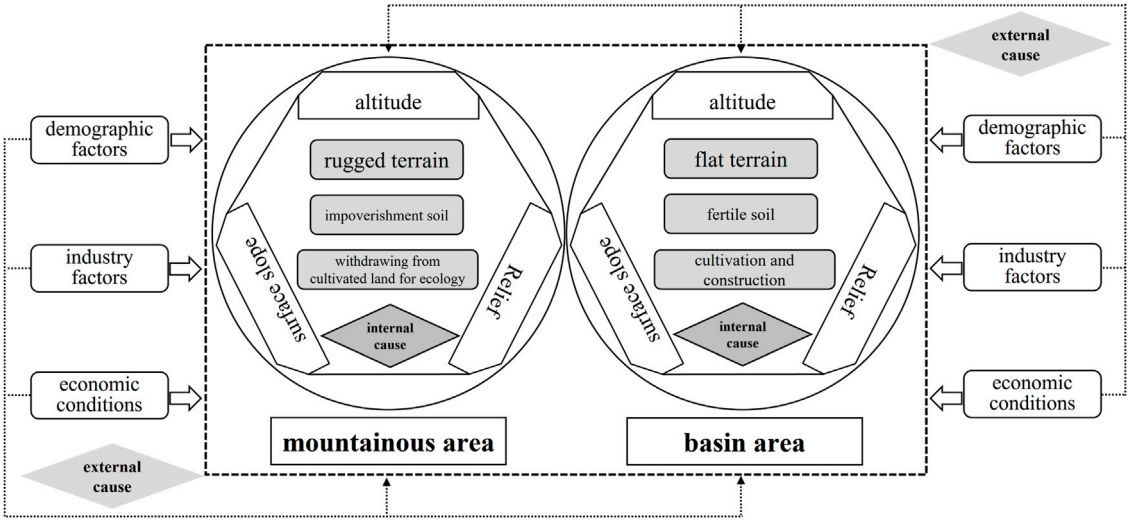

FIGURE 6
Motivation analysis of land use change in moutain-basin of Yuxi City.

social and economic development, as well as in land use pattern and its changes due to the different ecological environment differences laid by topography and landform (Figure 6).

According to the actual situation of Yuxi City and the availability of data, the social and economic factors were selected from three aspects: population factors, industrial factors and the economic situation. The influencing factors reflecting the population factors in the study area include the total population (X_1), the urbanization rate (X_2) and the rural population (X_3). The influencing factors characterizing regional industrial factors include the added value of primary industry (X_4), the added value of secondary industry (X_5), the added value of tertiary industry (X_6), the total agricultural output value (X_7) and the total industrial output value (X_8). The influencing factors reflecting regional economic conditions include the gross regional product (X_9), the fixed asset investment (X_{10}), the local fiscal revenue (X_{11}) and the total retail sales of consumer goods (X_{12}).

4.2 Analysis on influencing factors

Due to the difficulty in obtaining partial data of natural factors and their temporal and spatial fixity, Pearson correlation analysis was only used in this study to explore the relationships between socio-economic factors and land use changes. In order to eliminate the possible influences caused by the difference of the data dimension of different indicators, the data was first normalized. Pearson correlation analysis was then conducted on the normalized land area and land use degree of the mountainous area and basin area, and the selected influencing factors, and SPSS 25.0 software was employed to obtain the correlation between the socio-economic factors and the change of land area (Figures 7, 8). (Note: ** indicates that the correlation is significant at the 0.01 level and * indicates that the correlation is significant at the 0.05 level). No matter in the basin area or mountainous area, the correlation between land use change and the socio-economic factors is relatively significant, but there are still obvious regional differences for each type.

Among the various types of mountainous areas, cultivated land is most significantly affected by industrial factors, and each factor has a significant negative correlation with the area of cultivated land, and the highest correlation coefficient was found for total industrial output value, followed by economic status. The forest and grassland area is more significantly affected by industrial factors, and each factor has a significant positive correlation with it. Besides, the correlation coefficient of the added value of the primary industry is the highest. The area of construction land has a significant positive correlation with industrial factors and economic conditions, also has the largest correlation coefficient with the total population. Except for the total population, there is no significant correlation between the area of water body and unused land and socioeconomic factors. The mountain water area is positively correlated with the total population, and the unused land area is negatively correlated with the total population, and the correlation degrees are all low. In addition to being significantly positively correlated with the total population, the degree of land use has no significant correlations with other factors (Figure 7). Therefore, the total population of the

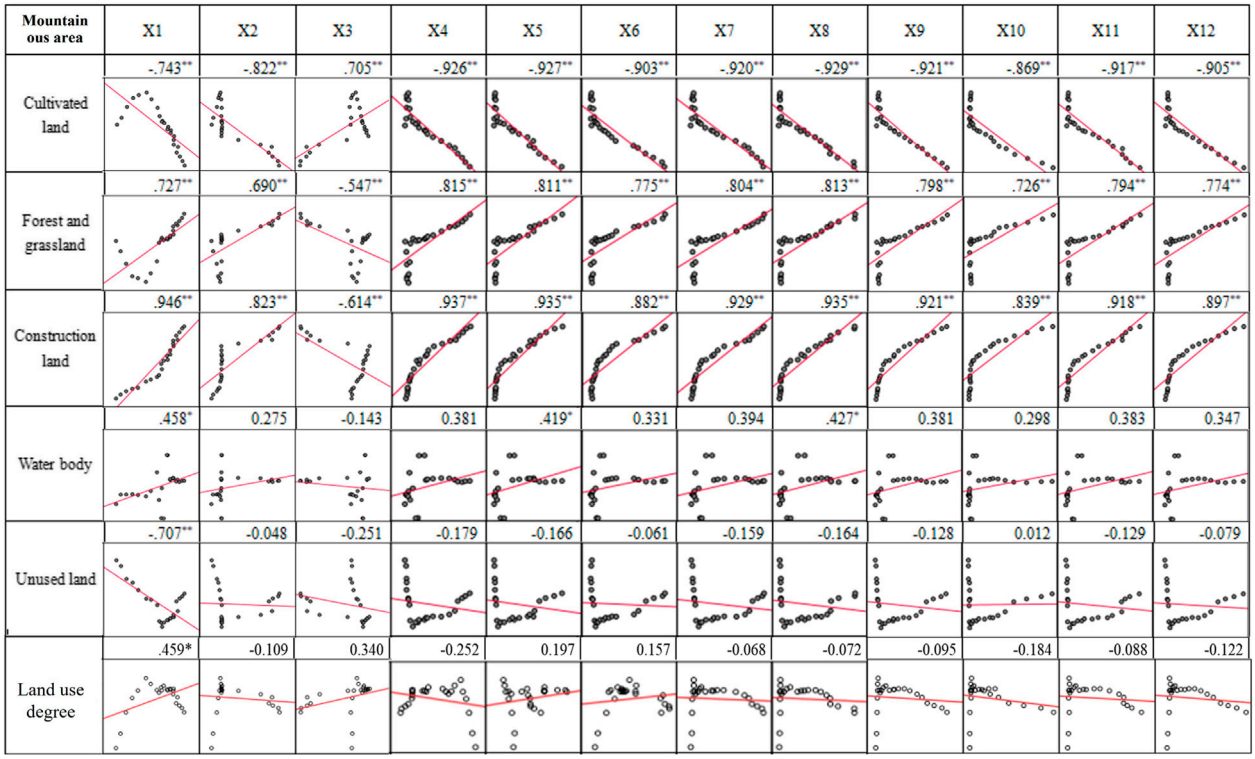

FIGURE 7
Correlation between land use types, land use degree and influencing factors in the mountainous area.

mountainous areas has the most significant impact on the area of the built-up land. Secondly, the cultivated land, forest and grassland and built-up land in mountainous areas are significantly affected by the added value of primary and secondary industries and the total industrial output value.

Except for the rural population, the cultivated land in the basin area is significantly negatively correlated with other socio-economic factors, among which the correlation coefficient between the total population and the cultivated land area is the largest, and the cultivated land is more affected by industrial factors than other factors. The correlation direction between the forest and grassland and the social and economic factors is similar to that of cultivated land, but the correlation degree is significantly lower, and the correlation coefficient between the completed investment of fixed assets and the area of forest and grassland is the highest. Except for the rural population, the construction land has a significant positive correlation with other factors, and the industrial factor has the most significant influence, and the total population and the added value of the primary industry have the highest correlation degree. Except for the rural population, the area of water body and the area of unused land are significantly negatively correlated with other socioeconomic factors. The correlation coefficient between the area of water body and the added value of the secondary industry is the highest, while the correlation coefficient between the unused land area and the total population is also the highest. The land use degree is significantly correlated with all factors, except for the rural population and the added value of the secondary industry, which are significantly negatively correlated, and the rest are significantly positively correlated (Figure 8). Therefore, the cultivated land and unused land in the basin area are most significantly affected by the total population. The construction land is most significantly affected by the total population and the added value of the primary industry. What follows by the construction land is more obviously affected by the total agricultural output value and industrial output value, and the land use degree is obviously affected by the socio-economic effect.

5 Discussion

With the increasing impact of human activities and climate change on the Earth's surface system, the natural and human elements as well as the natural-socio-economic complex system are also undergoing dramatic changes. It reflects the complex spatial pattern and process mechanism of physical geography and human geography, and the understanding of this pattern,

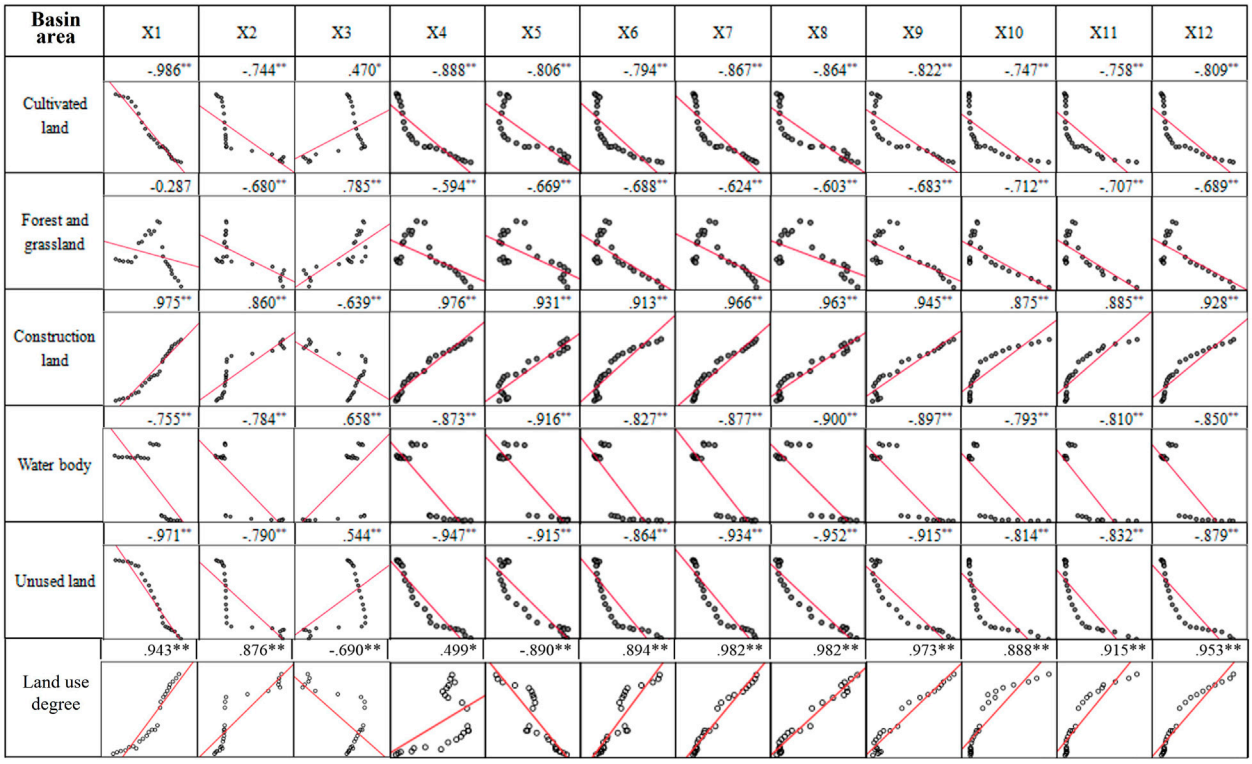

FIGURE 8
Correlation between land use types, land use degree and influencing factors in the basin area.

process and mechanism is inseparable from the analysis technology of information geography. In this study, mountainous areas and basin areas are regarded as two different spatial types of human-land system, and the research results show that the dynamic change process of land use is significantly different. This study believes that this is not only the result of the formation of different geographical patterns, but also the driving factors for further development of geographical pattern differences. At the same time, the different land use structure and change characteristics of the mountainous area and the basin area are closely related to the local natural environment, social and economic factors (Wu and Xie, 2019). One of the biggest inspirations of this research process is that geography, on the basis of being divided into three branches: physical geography, human geography and information geography, has once again moved towards synthesis in the field of human-earth system research (Fan, 2018). Thus, to some extent, it effectively responds to and corroborates the thinking of Chen Fahu, chairman of the Geographical Society of China, on the establishment of a new research branch of "Comprehensive Geography," based on the system of geographical science. He believes that "regional synthesis is the basis for the existence of geographic science, the greatest feature of geographic science, and also the biggest difficulty of geographic science". Therefore, comprehensive geography should be "guided by the methods and theories of geographic science, to solve all kinds of practical application problems closely related to the development of nature and human society and economy". That is to say, "the regionality of geography is based on the human-land relationship, using the new means of information geography to integrate the process of physical geography and human geography to understand the regional spatial process, forming a second-level discipline of comprehensive geography" (Chen et al., 2021).

Previous studies have found that the land use pattern in mountainous areas of southwest China is affected by the landform of mountains and river valleys, which is mainly dominated by forest and grassland (Zhang et al., 2021), followed by cultivated land. Forest and grass land and a large number of sloping farmland are mainly distributed in mountainous areas, and high-quality farmland is mainly continuously distributed in flat basin area, trough valley area and low mountain valley area (Li et al., 2020; Liang et al., 2021; Ma et al., 2021; Zhang et al., 2021). Before 2000, mountain forests were largely cut down (Li et al., 2019), and the area of arable land increased, and it was mainly transferred from woodland and grassland (Yang et al., 2017). Since 2000, with the acceleration of urbanization and industrialization in the mountainous areas of Southwest China, the land use types have changed greatly. A large

number of high-quality cultivated land has been occupied in the basin area, and the construction land has increased significantly (Ma et al., 2021). The conversion of the land use types mainly occurred between cultivated land, woodland and grassland (Li et al., 2019). With the implementation of the national policy of "returning farmland to forest" and the government's emphasis on ecological environment protection, the cultivated land in mountainous areas was transferred to woodland and grassland (Yang et al., 2017), and the expansion intensity of urban construction land in basin areas was significantly higher than that in mountainous areas (Wang et al., 2021). Yuxi City is located in Yunnan Province, a mountainous area in the southwest of China. It is a typical area with alternating mountains and basins. The natural ecological conditions are fragile, the land use conversion is dynamic, and at the same time, it is disturbed by high-intensity human activities and affected by governance policies. In addition to the three major characteristics of regionality, space and complexity under the traditional geographical concept, there are also two emerging characteristics of conflict and dynamicity. In the real world, Yuxi City and other mountainous areas are similar to a certain extent, that is, there are more mountains and fewer basins. The conflicts between the economic and the social development and ecological environmental protection are inevitably transformed into a conflict between the land use of regional human activities and the land use of biodiversity protection, which is manifested as the conflict between land resources and their natural ecological function and human development function. Before 2000, due to the growth of population and the livelihood characteristics of relying on farming output, farmers in mountainous areas reclaimed a large number of cultivated land, and the overdevelopment of land brought serious soil erosion and other problems (Zhang et al., 2018). After 2000, it entered the stage of rapid urbanization. Although the high-quality cultivated land in the basin area was largely occupied due to urban construction and industrial development, the rapid economic development also created a large number of employment opportunities, which provided conditions for the large-scale migration of farmers in mountainous areas to the basin area. The transfer of rural labor force in mountainous areas mitigated the human disturbance of mountainous land (Tian et al., 2010), resulting in farmland abandonment and marginalization (Shao et al., 2015), idle and abandoned homesteads (Liu et al., 2009), forest expansion and restoration of grassland natural vegetation (Li and Zhao, 2011).

With the accelerated development of urbanization in the basin area, population migration has a significant impact on the land use in the area of population outflow and inflow. The migration of population from mountainous areas to basin areas leads to the difference and correlation between the two geographical spaces in the spatio-temporal dynamic changes of land use (Zhang and Li, 2021). With the enhancement of productivity and economic radiation capacity, the intensity of construction land expansion increases accordingly, thus promoting the intensive use of land. However, the situation of the cultivated land protection is severe, and part of natural ecological space is occupied. In mountainous areas, because of labor output, reduction in human activity intensity, and changes in livelihood patterns, farmers gradually abandoned their arable land, and cultivated land gradually evolved into forest and grassland, showing the phenomenon of shrinking cultivated land and expansion of forest and grassland areas. The natural restoration of vegetation reduces the vulnerability of land ecosystem and significantly improves the function of ecological security barrier (Wu et al., 2020b). Due to the differences of the natural environment itself, many factors driving land use/land cover change in the basin area not only act in the internal system of the basin area, but also have an impact on land use/land cover change in the mountainous area. Conversely, the driving factors of land use/land cover change in the mountainous area are also the same. Thus, between the two different geographical spaces of the mountainous area and the basin area, there is not only the interaction within the system, that is, the internal coupling, but also the interaction with the adjacent exterior, that is, the peripheral coupling. According to the dynamic mechanism of different coupling evolution of mountain-basin land use, H. Zhang divided the coupling evolution modes of mountain-basin land use landscape into three categories: strong synergy, moderate synergy and weak synergy (Zhang and Li, 2021), and pointed out that there were different evolution characteristics of land use in southwest mountain and basin land at different stages. From this perspective, land use change should be regarded as a dynamic interaction across spatial and temporal scales within the socio-ecological coupling system (Liu et al., 2013), and the optimal allocation of mountain-basin land use provides a practical grip for the "landing" of mountain-basin land use coupling relationship regulation.

In addition, according to the availability of data, this study selected three factors of population, industry and economy to analyze the factors which would influence land use change. The land use data mainly came from the survey data of land use change in the past years, and the social and economic data mainly came from the statistical yearbook and the statistical bulletin of national economic and social development in the past years. Some data showed a sudden change due to the inconsistency of the statistical caliber before and after, which may have a certain impact on the magnitude of the Pearson correlation coefficient, but did not affect its significance and correlation direction. At the same time, the mountain-basin system is complex and comprehensive. In addition to the factors selected in this paper, the influencing factors of land use change should also consider the differential effects of the special regional policies, such as nearby urbanization, relocation of impoverished residents, rural revitalization,

plateau characteristic agriculture development, and ecological protection on the coupled evolution of mountain-basin land use.

6 Conclusion

Based on the types of mountains and basins in Yuxi City, the spatial and temporal changes of land use and its influencing factors in mountainous areas and basin areas from 1995 to 2018 were analyzed at the township scale by integrating the methods of land use degree, land use change rate, comprehensive dynamic degree of land use, land use consumption degree and land use transfer matrix.

As is shown in the study, the land use change in the mountain-basin system shows a phased character, but the intensity is slowing. The comprehensive dynamic attitude of land use in the mountainous area is significantly higher than that in the basin area from 1995 to 2005, and significantly lower than that in the basin area from 2005 to 2018. The trend of land use reduction in the mountainous area is consistent with that in the basin area, but it was always higher in the mountainous area than in the basin area. There is a significant difference in land type change between mountainous areas and basin areas. The construction land in the basin area increases rapidly, while the cultivated land, forest and grassland and unused land continue to decrease, while the construction land in the mountainous area increases slowly, with the cultivated land increasing first and then decreasing, and the forest and grassland and unused land decreasing first and then increasing. Social and economic development are the main driving factors of land use difference between mountainous areas and basin areas. The radiative agglomeration of the basin area attracts the population to migrate from the mountainous area to the basin area, and promotes the ecological restoration of the vegetation in the mountainous area. The increase of construction land and economic development in the basin area increases non-agricultural employment opportunities, promotes population migration, and reduces the cultivated land in the mountainous area, increases the forest and grass land, and continues to improve the ecology.

There are obvious differences in the characteristics of land use change in the mountainous area and the basin area at different time periods. When the urbanization level is low, the land use change in the mountainous area is more drastic than that in the basin area. However, with the rapid improvement of the urbanization level, the population in the mountainous area migrates to the basin area, and the intensity of land use change in the basin area is significantly higher than that in the mountainous area. The non-agricultural construction land in the basin area is rapidly increasing, the protection of cultivated land is severe, and part of the natural ecological space is occupied. In the mountainous area, arable land is abandoned, and the phenomenon of empty villages is serious. The natural restoration of vegetation reduces the vulnerability of land ecosystem, and the function of ecological security barrier is significantly improved. Influenced by the difference of social and economic development, a mutual “driving” and “linkage” relationship between the mountainous area and the basin area exist, which brings the difference of coupling evolution of the land use, so that the urban expansion and the increase of construction land in the basin area are mutually causal with the decline of the mountainous area, the decrease of cultivated land and the increase of forest and grassland.

Data availability statement

Publicly available datasets were analyzed in this study. This data can be found here: www.gscloud.cn. The datasets presented in this study are from the interpretation data of remote sensing images and statistical yearbooks of counties and districts.

Author contributions

LW and BX contributed to the conception of this study. JZ and SY carried out the design and production of some diagrams. LW, BX, and JL contributed significantly to the analysis and manuscript preparation. LW performed the data analyses and wrote the manuscript. BX and JL helped perform the analysis with constructive discussions. All authors contributed to the article and approved the submitted version.

Funding

This study was supported by the National Natural Science Foundation of China (Grant no. 42161041).

Conflict of interest

The authors declare that the research was conducted in the absence of any commercial or financial relationships that could be construed as a potential conflict of interest.

Publisher’s note

All claims expressed in this article are solely those of the authors and do not necessarily represent those of their affiliated organizations, or those of the publisher, the editors and the reviewers. Any product that may be evaluated in this article, or claim that may be made by its manufacturer, is not guaranteed or endorsed by the publisher.

References

Buchner, J., Yin, H., Frantz, D., Kuemmerle, T., Askerov, E., Bakuradze, T., et al. (2020). Land-cover change in the Caucasus Mountains since 1987 based on the topographic correction of multi-temporal Landsat composites. *Remote Sens. Environ.* 248 (2020), 111967. doi:10.1016/j.rse.2020.111967

Chen, F. H., Li, X., Wu, S. H., Fan, J., Xiong, J. H., and Zhang, G. Y. (2021). Disciplinary structure of geographic science in China. *Acta Geogr. Sin.* 76 (9), 2069–2073. doi:10.11821/dlxb202109001

Cui, X. L., Bai, H. Y., Wang, T., Guo, L., and Zhang, J. L. (2013). Land use change and driving factors for Jingbian County in farming-pasturing ecotone of North China. *Bull. Soil Water Conservation* 33 (1), 34–43. doi:10.13961/j.cnki.stbctb.2013.01.040

Fan, J. (2018). Territorial system of human-environment interaction": A theoretical cornerstone for comprehensive research on formation and evolution of the geographical pattern. *Acta Geogr. Sin.* 73 (4), 597–607. doi:10.11821/dlxb201804001

Fang, Y. Y., Zhao, Y. L., Xue, C. L., and Wei, X. F. (2021). Differentiation characteristics and optimization of mountain basin lands suitable for contrstructions: A case study of guiyang city. *J. Nat. Sci. Hunan Normal Univ.* 44 (1), 21–29. doi:10.7612/j.issn.2096-5281.2021.01.003

Feng, X. M., Wang, Y. F., Chen, L. D., Fu, B. J., and Bai, G. S. (2010). Modeling soil erosion and its response to land-use change in hilly catchments of the Chinese Loess Plateau. *Geomorphology* 118 (3-4), 239–248. doi:10.1016/j.geomorph.2010.01.004

Gondwe, M. F., Cho, M. A., Chirwa, P. W., and Geldenhuys, C. J. (2019). Land use/land cover change and the comparative impact of co-management and government-management on the forest cover in Malawi (1999-2018). *J. Land Use Sci.* 14 (4-6), 281–305. doi:10.1080/1747423x.2019.1706654

Guo, L. Y., Wang, D. L., Qiu, J. J., Wang, L. G., and Liu, Y. (2009). Spatio-temporal patterns of land use change along the Bohai Rim in China during 1985-2005. *J. Geogr. Sci.* 19 (5), 568–576. doi:10.1007/s11442-009-0568-0

Hou, Y. F., Chen, Y. N., Ding, J. L., Li, Z., Li, Y. P., and Sun, F. (2022). Ecological impacts of land use change in the arid tarim river basin of China. *Remote Sens.* 14 (8), 1894–1909. doi:10.3390/rs14081894

Isufi, F., and Berila, A. (2021). Using geospatial technology to analyse land use/cover changes in Prishtina, Kosovo (2000-2020). *GeoJournal* 2021 (2021), 1–15. doi:10.1007/s10708-021-10452-z

Kohler, T., and von Dach, S. W. (2015). CDE links regional research and global efforts for sustainable mountain development. *Mt. Res. Dev.* 35 (2), 203–207. doi:10.1659/mrd-journal-d-15-00028.1

Kumar, P., Dobriyal, M., Kale, A., and Pandey, A. K. (2021). Temporal dynamics change of land use/land cover in Jhansi district of Uttar Pradesh over past 20 years using LANDSAT TM, ETM+ and OLI sensors. *Remote Sens. Appl. Soc. Environ.* 23 (2021), 100579. doi:10.1016/j.rsase.2021.100579

Li, J., Liao, H. P., Jin, C., Li, T., and Zhang, T. (2018). Distribution characteristic on terrain gradient of land use pattern and change in the fringe of mountainous cities: A case study of banan district in chongqing. *Resour. Environ. Yangtze Basin* 27 (2), 296–305. doi:10.11870/cjlyzyyhj201802008

Li, X. B., and Zhao, Y. L. (2011). Forest transition, agricultural land marginalization and ecological restoration. *China Popul. Resour. amd Environ.* 21 (10), 91–95. doi:10.3969/j.issn.1002-2104.2011.10.014

Li, X. N., Deng, Z. J., Wang, Q. H., Wang, Y. H., and Wan, S. R. (2019). Temporal and spatial dynamics of the land-use types in the Northwest Yunnan from 1986 to 2015. *J. Southwest For. Univ.* 39 (6), 137–145. doi:10.11929/j.swfu.201903116

Li, Y. J., Yang, X. H., Cai, H. Y., Xiao, L. L., Xu, X. L., and Liu, L. (2014). Topographical characteristics of agricultural potential productivity during cropland transformation in China. *Sustainability* 7 (1), 96–110. doi:10.3390/su7010096

Li, Y. M., Wang, D. C., Yuan, J., and Liu, X. Z. (2020). Temporal and spatial pattern and functional zoning of land use in Alpine Canyon Region based on terrain gradient. *Bull. Soil Water Conservation* 40 (6), 303–311.

Liang, J. T., Deng, Y., Cao, J. H., Jin, Z. J., and Li, X. Y. (2021). Temporal and spatial differentiation of the ecosystem service value in typical fault-depression basins. *Carsologica Sin.* 40 (3), 476–486. doi:10.11932/karst2021y28

Liu, J. G., Hull, V., Batistella, M., DeFries, R., Dietz, T., Fu, F., et al. (2013). Framing sustainability in a telecoupled world. *Ecol. Soc.* 18 (2), art26. doi:10.5751/es-05873-180226

Liu, Y. S., Liu, Y., and Zhai, R. X. (2009). Geographical research and optimizing practice of rural hollowing in China. *Acta Geogr. Sin.* 64 (10), 1193–1202.

Liu, Y. X., and Li, Y. B. (2020). Spatial evolution of land use production function in the basin of Guizhou Province under the background of rural transformation. *Geogr. Res.* 39 (2), 430–446. doi:10.11821/dlyj020180650

Lu, C. Y., Qi, L. G., and Sang, C. J. (2007). Analysis on mathematic model of land-use changes. *Resour. Dev. Mark.* 23 (1), 25–27.

Lu, H. Y., Wei, Y. Q., Yang, S. C., and Liu, Y. W. (2019). Regional spatial patterns and influencing factors of environmental auditing for sustainable development: Summaries and illuminations from international experiences. *Environ. Dev. Sustain.* 22 (2019), 3577–3597. doi:10.1007/s10668-019-00357-w

Ma, H. Y., Zhang, L. L., Wei, X. Q., Shi, T. T., and Chen, T. X. (2021). Spatial and temporal variations of land use and vegetation cover in Southwest China from 2000 to 2015. *Chin. J. Appl. Ecol.* 32 (2), 618–628. doi:10.13287/j.1001-9332.202102.017

Ma, Z. B., Chen, X. P., and Chen, H. (2018). Multi-scale spatial patterns and influencing factors of rural poverty: A case study in the liupan mountain region, gansu province, China. *Chin. Geogr. Sci.* 28 (2), 296–312. doi:10.1007/s11769-018-0943-9

Matlhodi, B., Kenabatho, P. K., Parida, B. P., and Maphanyane, J. G. (2021). Analysis of the future land use land cover changes in the gaborone dam catchment using CA-markov model: Implications on water resources. *Remote Sens.* 13 (13), 2427–2446. doi:10.3390/rs13132427

Meer, M. S., and Mishra, A. K. (2020). Land use/land cover changes over a district in Northern India using remote sensing and GIS and their impact on society and environment. *J. Geol. Soc. India* 95 (2), 179–182. doi:10.1007/s12594-020-1407-2

Meybeck, M., Green, P., and Vörösmarty, C. (2001). A new typology for mountains and other relief classes. *Mt. Res. Dev.* 21 (1), 34–45. doi:10.1659/0276-4741(2001)021[0034:Antfma]2.0.Co;2

Msofe, N. K., Sheng, L. X., Li, Z. X., and James, L. (2020). Impact of land use/cover change on ecosystem service values in the Kilombero Valley Floodplain, Southeastern Tanzania. *Forests* 11 (1), 109. doi:10.3390/f11010109

Nguyen, T. C., Whelan, M., and Nichols, J. D. (2022). Soil erosion response to land use change in a mountainous rural area of Son La Province of Vietnam. *Environ. Monit. Assess.* 194 (3), 149. doi:10.1007/s10661-022-09844-6

Olorunfemi, I. E., Fasinmirin, J. T., Olufayo, A. A., and Komolafe, A. A. (2020). GIS and remote sensing-based analysis of the impacts of land use/land cover change (LULCC) on the environmental sustainability of Ekiti State, southwestern Nigeria. *Environ. Dev. Sustain.* 22 (2), 661–692. doi:10.1007/s10668-018-0214-z

Parven, A., Pal, I., Witayangkurn, A., Pramanik, M., Nagai, M., Miyazaki, H., et al. (2022). Impacts of disaster and land-use change on food security and adaptation: Evidence from the delta community in Bangladesh. *Int. J. Disaster Risk Reduct.* 78 (2022), 103119. doi:10.1016/j.ijdrr.2022.103119

Richards, J. A. (1995). Remote sensing digital image analysis. an introduction. *Geol. Mag.* 132 (4), 453–457.

Scheurer, T., and Jost, S. (2012). Sustainable mountain development beyond Rio+20: Regional and national perspectives. *Mt. Res. Dev.* 32 (1), 92–95. doi:10.1659/mrd-journal-d-12-00004.1

Schild, A. (2008). ICIMOD's position on climate change and mountain systems. *Mt. Res. Dev.* 28 (3-4), 328–331. doi:10.1659/mrd.mp009

Schild, A., and Sharma, E. (2011). Sustainable mountain development revisited. *Mt. Res. Dev.* 31 (3), 237–241. doi:10.1659/mrd-journal-d-11-00069.1

Shao, J. A., Zhang, S. C., and Li, X. B. (2015). Farmland marginalization in the mountainous areas: Characteristics, influencing factors and policy implications. *J. Geogr. Sci.* 25 (6), 701–722. doi:10.1007/s11442-015-1197-4

Siddik, M. S., Tulip, S. S., Rahman, A., Islam, M. N., Haghighi, A. T., and Mustafa, S. M. T. (2022). The impact of land use and land cover change on groundwater recharge in Northwestern Bangladesh. *J. Environ. Manag.* 315 (2022), 115130. doi:10.1016/j.jenvman.2022.115130

Smiraglia, D., Ceccarelli, T., Bajocco, S., Perini, L., and Salvati, L. (2015). Unraveling landscape complexity: Land use/land cover changes and landscape pattern dynamics (1954-2008) in contrasting peri-urban and agro-forest regions of northern Italy. *Environ. Manag.* 56 (4), 916–932. doi:10.1007/s00267-015-0533-x

Solomon, H., Bewket, W., Nyssen, J., and James, L. (2020). Analysing past land use land cover change and CA-Markov-based future modelling in the Middle Suluh Valley, Northern Ethiopia. *Geocarto Int.* 35 (3), 225–255. doi:10.1080/10106049.2018.1516241

Song, Z., Han, J. X., Ni, H. Y., Wang, D. H., and Huang, T. J. (2021). Research on development and protection planning of land space for Chengdu-German-Mei-Zizhi urban construction in Sichuan Province Geology in China. 2021, 1–18.

Tian, Y. J., Li, X. B., Ma, G. X., and Hao, H. G. (2010). Influences of labor emigration from agriculture on the production abandonment of cultivated land in ecological sensitive areas. *China Land Sci.* 24 (7), 4–9. doi:10.13708/j.cnki.cn11-2640.2010.07.004

Twongyirwe, R., Fisher, E., Karungi, C., and Ndugu, N. (2022). Projected land use change in an oil-rich landscape in Uganda: A participatory modelling approach. *Extr. Industries Soc.* 10 (2022), 101071. doi:10.1016/j.exis.2022.101071

Wang, X. X., Peng, L., Liu, S. J., and Wei, Y. Y. (2021). Characteristics and the driving mechanism of urban construction land expansion in mountainous areas of southwest China. *Chin. J. Ecol.* 40 (9), 2895–2903. doi:10.13292/j.1000-4890.202109.017

Wolde, Z., Wu, W., Likessa, D., Omari, R., and Ketema, H. (2021). Understanding the impact of land use and land cover change on water–energy–food nexus in the Gidabo Watershed, East African Rift Valley. *Nat. Resour. Res.* 30 (3), 2687–2702. doi:10.1007/s11053-021-09819-3

Wu, F. Q., Mo, C. J., and Dai, X. J. (2022). Analysis of the driving force of land use change based on geographic detection and simulation of future land use scenarios. *Sustainability* 14 (9), 5254–5270. doi:10.3390/su14095254

Wu, L. N., Yang, S. T., Liu, X. Y., Luo, Y., Zhou, X., and Zhao, H. G. (2014). Response analysis of land use change to the degree of human activities in Beiluo River basin since 1976. *Acta Geogr. Sin.* 69 (1), 54–63. doi:10.11821/dlxb201401005

Wu, L., and Xie, B. G. (2019). The variation differences of cultivated land ecological security between flatland and mountainous areas based on LUCC. *PLoS One* 14 (8), e0220747. doi:10.1371/journal.pone.0220747

Wu, L., Xie, B. G., Xiao, X., Xue, B., and Li, J. Z. (2020a). Classification method and determination of mountainous area types at township scales: A case study of Yuxi city, yunnan province. *Complexity* 2020, 1–13. doi:10.1155/2020/3484568

Wu, L., Zhou, J., and Li, Z. H. (2020b). Applying of GA-BP neural network in the land ecological security evaluation. *Int. J. Comput. Sci.* 47 (1), 1–8.

Xie, F. D., Wu, X., Liu, L. S., Zhang, Y. L., and Paudel, B. (2021). Land use and land cover change within the Koshi River Basin of the central Himalayas since 1990. *J. Mt. Sci.* 18 (1), 159–177. doi:10.1007/s11629-019-5944-3

Yang, M., Zhang, G. L., and Hou, Y. P. (2011). Advances and prospects of the driving force of regional land use change researches. *Geogr. Geo-Information Sci.* 27 (1), 95–100.

Yang, Y. L., Ma, M. G., and Zhou, Z. Y. (2017). Research on land use patterns and temporal and spatial evolution in mountainous watershed based on topographic gradient. *Eng. Surv. Mapp.* 26 (12), 8–16. doi:10.19349/j.cnki.issn1006-7949.2017.12.002

Yang, Y. W., Tian, Y. C., Zhang, Q., Tao, J., Huang, Y. J., Gao, C. P., et al. (2022). Impact of current and future land use change on biodiversity in nanliu river basin, beibu gulf of south China. *Ecol. Indic.* 141 (2022), 109093. doi:10.1016/j.ecolind.2022.109093

Zhang, B. L., Cai, W. M., Zhang, F. R., Feng, T., and Zhang, L. (2016). Spatio-temporal evolution of rural settlements and its driving forces in Yishui County, Shandong Province from Sui dynasty to 1949. *Geogr. Res.* 35 (6), 1141–1150. doi:10.11821/dlyj201606011

Zhang, B. L., Gao, J. B., Ggo, Y., Cai, W. M., and Zhang, F. R. (2018). Land use transition of mountainous rural areas in China. *Acta Geogr. Sin.* 73 (3), 503–517. doi:10.11821/dlxb201803009

Zhang, H., and Li, Y. B. (2021). Coupling and coordinated evolution between land-use and landscape in mountain-basin system in the context of rural transformation: A case study of six mountain-basin systems in guizhou province, China. *Mt. Res.* 39 (2), 248–261. doi:10.16089/j.cnki.1008-2786.000592

Zhang, Y. X., Halder, P., Zhang, X. N., and Qu, M. (2020). Analyzing the deviation between farmers' land transfer intention and behavior in China's impoverished mountainous area: A logistic-ISM model approach. *Land Use Policy* 94 (2020), 104534. doi:10.1016/j.landusepol.2020.104534

Zhang, Y. Y., Sun, M. Y., Yang, R. J., and Zhang, L. (2021). Impact of land-use change on ecosystem service value in Southwest China. *J. Environ. Eng. Technol.* 12 (1), 207–214. doi:10.12153/j.issn.1674-991X.20210159

Zhao, H. F., He, H. M., Bai, C. Y., and Zhang, C. J. (2018). Spatial-temporal characteristics of land use change in the Loess Plateau and its environmental effects. *China Land Sci.* 32 (7), 49–57. doi:10.11994/zgtdkx.20180622.104942

Zhou, S. G., Shao, Q. Q., and Cao, W. (2016). Characteristics of land use and land cover change in the Loess Plateau over the past 20 years. *J. Geo-information Sci.* 18 (2), 190–199. doi:10.3724/SP.J.1047.2016.00190

Zhuang, D. F., and Liu, J. Y. (1997). Study on the model of regional differentiation of land use degree in China. *J. Nat. Resour.* 12 (2), 10–16.

frontiers | Frontiers in Environmental Science

TYPE Original Research
PUBLISHED 05 October 2022
DOI 10.3389/fenvs.2022.1021081

Check for updates

OPEN ACCESS

EDITED BY
Jun Yang,
Northeastern University, China

REVIEWED BY
Hao Zhu,
Chengdu University of Technology, China
Jingxiong Huang,
Tsinghua University, China

*CORRESPONDENCE
Bingjie Yu,
270433051@qq.com

SPECIALTY SECTION
This article was submitted to Environmental Informatics and Remote Sensing, a section of the journal Frontiers in Environmental Science

RECEIVED 17 August 2022
ACCEPTED 15 September 2022
PUBLISHED 05 October 2022

CITATION
Luo P, Yu B, Li P and Liang P (2022), Spatially varying impacts of the built environment on physical activity from a human-scale view: Using street view data.
Front. Environ. Sci. 10:1021081.
doi: 10.3389/fenvs.2022.1021081

COPYRIGHT
© 2022 Luo, Yu, Li and Liang. This is an open-access article distributed under the terms of the Creative Commons Attribution License (CC BY). The use, distribution or reproduction in other forums is permitted, provided the original author(s) and the copyright owner(s) are credited and that the original publication in this journal is cited, in accordance with accepted academic practice. No use, distribution or reproduction is permitted which does not comply with these terms.

Spatially varying impacts of the built environment on physical activity from a human-scale view: Using street view data

Pinyang Luo[1], Bingjie Yu[1]*, Pengfei Li[2] and Pengpeng Liang[1]

[1]School of Architecture, Southwest Jiaotong University, Chengdu, China, [2]School of Civil Engineering and Architecture, Southwest University of Science and Technology, Mianyang, China

Developing evidence-based planning interventions for promoting physical activity (PA) is considered an effective way to address urban public health issues. However, previous studies exploring how the built environment affects PA over-relied on small-sample survey data, lacked human-centered measurements of the built environment, and overlooked spatially-varying relationships. To fill these gaps, we use cycling and running activity trajectories derived from the Strava crowdsourcing data to comprehensively measure PA in the central city area of Chengdu, China. Meanwhile, we introduce a set of human-scale, eye-level built environment factors such as green, sky, and road view indexes by extracting streetscape characteristics from the Baidu street-view map using the fully Convolutional Neural Network (CNN). Based on these data, we utilize the geographically weighted regression (GWR) model to scrutinize the spatially heterogeneous impact of the built environment on PA. The results are summarized as follows: First, model comparisons show that GWR models outperform global models in terms of the goodness-of-fit, and most built environment factors have spatially varying impacts on cycling and running activities. Second, the green view index restrains cycling activities in general. In contrast, it has a wide-ranging and positive impact on running activities while hampers them in the PA-unfriendly old town. Third, the sky view index stimulates cycling activities in most areas. However, it has a mixed influence on running activities. Fourth, the road view index widely promotes cycling and running activities but hinders them in some areas of the old town dominated by automobiles and under construction. Finally, according to these empirical findings, we propose several recommendations for PA-informed planning initiatives.

KEYWORDS

physical activity, the built environment, the geographically weighted regression model, Strava, street view data, street greenery

Introduction

Urban public health issues have become a global obstacle to sustainable human development (Haskell et al., 2007; Beaglehole et al., 2011). For instance, the rampant communicable diseases and the harsh urban environment severely hamper the physical activity (PA) of urban residents and thus lead to non-communicable diseases (NCDs), such as obesity, hypertension, and anxiety (Haskell et al., 2007; Biddle and Asare, 2011; Bauman et al., 2012; Koohsari et al., 2013). Numerous studies have shown that PA, as a crucial determinant of the physical health of the population, is widely influenced by the built environment (e.g., road density and green space area) (Sarmiento et al., 2010; Wang et al., 2019). Therefore, many scholars are starting to or have already called for public health-oriented urban planning, that is, leveraging planning interventions to address public health issues (Corburn, 2004). To this end, we must have sufficient knowledge of the relationship between PA and the built environment.

The World Health Organization defines PA as all movements, including running, cycling, sports, active recreation, and play. It is considered an effective way to alleviate urban public health issues (Haskell et al., 2007; Beaglehole et al., 2011; Koohsari et al., 2013). Because the right amount of PA can prevent and reduce NCDs and thus helps improve health and well-being, as evidenced by The World Health Organization and The American Disease Control and Prevention.

The built environment refers to the man-made environment with physical characteristics created by human activities. Existing research has extensively explored the relationship between PA and the built environment and reached mixed conclusions (Ewing and Cervero, 2001; An et al., 2019). For instance, some scholars reveal that built environment factors such as sidewalks, bike paths, land-use mix, and low residential densities promote PA and prevent childhood comorbidity, whereas transit stops and high FAR hinder PA (Salvo et al., 2014; Ma and Dill, 2015; Mertens et al., 2017; Chen et al., 2022a). However, these studies largely suffer from the small sample size, given they over-rely on self-reported questionnaires and telephone surveys (Wang et al., 2019; Zhao and Wan, 2020; Chen et al., 2022b). Besides, researchers widely adopt the traditionally built environment factors (e.g., density and diversity), which only reflect the amount and layout of facilities (Lu et al., 2018a; Zhang et al., 2022). In contrast, little attention has been paid to human-scale measurements (Lu et al., 2019). In addition, many studies explored the relationship between the built environment and PA from a global perspective, i.e., examining the "average" correlation across the space (Handy et al., 2002; Ma and Dill, 2015). But it remains uncertain whether such correlation is spatially varying and how.

To bridge these gaps, this study uses the GWR model to scrutinize the relationship between PA and the built environment and its spatial heterogeneity in Chengdu, China. To be specific, we first use the Strava crowdsourcing data (a web platform that people can upload and share their PA trajectories) to measure the cycling and running activities at a grid cell level. Second, we enrich the built environment evaluating system by introducing novel human-scale streetscape indicators, such as the green view index and sky view index (Lu et al., 2019; Koo et al., 2022). The streetscape indicators can capture and reflect the scene seen by pedestrians at eye level, which has more advantages than the traditionally built environment, such as widely spatial distribution and low data bias (Lu et al., 2018b; Du and Huang, 2022). Finally, beyond the global modeling approaches (e.g., the ordinary least square model and the binary logit model), we utilize the geographically weighted regression (GWR) model to decipher the heterogeneity and complexity of the impact of the built environment on PA across space.

The remaining of this paper is organized as follows. *Literature review* Section reviews the literature on the relationship between PA and the built environment. *Methodology* Section and *Result* Section show data sources and the research methods. *Discussion* Section presents the results of the OLS and GWR model. These results are discussed in *Conclusion* Section. *Data availability statement* Section summarizes the findings, puts forward some suggestions for policymakers and urban planners, and discusses the limitations of this study.

Literature review

The built environment has a wide and direct impact on the PA of the inhabitants. Numerous scholars have researched PA and the built environment and have demonstrated a high correlation between them (Ewing and Handy, 2009; Sarmiento et al., 2010; Ying et al., 2015; Yang et al., 2022a). The existing studies focus on North America (e.g., Kansas, Massachusetts, Cuernavaca, and Alabama), Oceania (e.g., Adelaide), and Asia (e.g., Beijing, Shanghai, Nanning, and Hongkong). The research scales mainly include city level, neighborhood level (Zhao and Wan, 2020), and street level (Lu et al., 2018a). Table 1 summarizes some of the research on the relationship between PA and the built environment.

However, previous studies have the following gaps. Most research data on PA are generally derived from questionnaires, telephone surveys, and travel trajectories of sports participants (Forsyth et al., 2009; Sarmiento et al., 2010). But these suffer from a small sample size, and thus existing studies describe PA without using data from a larger spatial scale. Moreover, numerous studies have reached inconsistent conclusions on the impact of the built environment on PA due to the different data samples and built environment factors. Remarkably, researchers have used the traditionally built environment measurement to extract the built environment factors from

TABLE 1 Review of the research on PA and the built environment.

Reference	Context	Modeling approach	Physical activity data sources	Built environment measures	Findings
Handy et al. (2002)	Gainesville, Florida	Simple econometric model	Regional travel diary survey	Land use patterns, transportation systems, etc.	Land use patterns and transportation systems help increase PA.
Ma and Dill (2015)	Kansas, the U. S	Binary logit linear regression model	A random phone survey	Bicycle paths, bicycle lanes, minor streets, etc.	Bicycle paths and minor streets stimulate bicycling activities
Zhang et al. (2022)	Beijing, China	Spatial analysis	Questionnaires in three typical neighborhoods	Sidewalks, street safety, low-rise housing type, etc.	Sidewalk quality and street safety promote physical activity
Wang et al. (2019)	Nanning, China	Order Probity regression model	The physical activity of 513 residents in urban green open space	Accessibility, infrastruct-ures, green space, etc.	Infrastructure, green space, and recrea-tional facilities are significantly associated with PA.
Troped et al. (2010)	Massachusetts, the U. S	Multiple regression model	PA trajectories of 148 adults over 4 days	Intersection density, land-use mix, etc.	Intersection density and land-use mix increase PA.
Sarmiento et al. (2010)	Bogotá, Colombia	Logistic regression multilevel model	The International Physical Activity Questionnaire	Land-use heterogeneity; park density, etc.	Land-use heterogeneity and park density promote physical activity, but transit stops hinder physical activity
Heinrich et al. (2007)	Kansas, the USA	Multilevel regression model	The survey from residents residing in 12 public housing developments and section 8 housing	Physical activity resources; street connectivity, etc.	More activity resources, less incivility, and greater street connectivity increase physical activity
Ying et al. (2015)	Shanghai, China	Hierarchical linear model	From1100 residents aged 46 to 80 from 80 neighborhoods of 13 selected communities	Street connectivity; River proximity, land-use mix, etc.	Street connectivity, river proximity, garden, and land-use mix have a positive correlation with physical activity
Yang et al. (2021b)	Hong Kong, China	Linear regression and GWR model	The Travel Characteristic Survey 2011 of Hong Kong	Street greenery, access to recreational facilities, etc.	Street greenery has spatially varying effects on seniors' walking time
Yang et al. (2021a)	Hong Kong, China	Machine technique, (random forest)	The travel Characteristic Survey 2011 of Hong Kong	Green view index, population density, etc.	The green view index stimulates walking activities, but in a non-linear way
Salvo et al. (2014)	Cuernavaca, Mexico	Linear regression model	Activity traces of partici-pants wearing Actigraph GT3X accelerometers	Distance to park, bus routes, etc.	Bus routes and parks are not significantly associated with physical activity
Zhao and Wan (2020)	Beijing, China	Multilevel regression model	3,748 questionnaires	High density; land use diversity; walking-friendly street design, etc.	High-density development, land use diversity, and friendly street design promote walking behavior
Duncan et al. (2010)	Adelaide, Australia	Generalized Linear Model	Physical activity behaviors of 2,506 adults in 154 Census Collection Districts	Land-use mix, etc.	Land use mix is related to pedestrian traffic
Lu et al. (2018a)	Hongkong, China	Multilevel mixed model	The International Physical Activity Questionnaire	Street network design, land-use diversity, density, etc.	Land use mix restrains walking, but positive impact on bus stops and MTR.
Li et al. (2022)	Bunkyo Ward, Tokyo	The SW score predict-ion model and the logistic regression analysis	A questionnaire of the walking time source data	Vegetation, sky, and building are calculated by the deep learning model, etc.	Vegetation and sky harm walking, and building promotes walking

various data such as Geographic Information System (GIS) data, POI, and satellite imagery data (Ding and Gebel, 2012; Yu et al., 2022a). Using data in these studies are effectively reflective of the number and spatial distribution of facilities (e.g., parks and enterprises) and neglect the impact of the human-oriented street on PA. In addition, previous studies have commonly used global analysis models, such as the simple econometric model, binary logit model, and multiple regression model, to explore the impact of the built environment on PA (Handy et al., 2002; Troped et al., 2010; Ma and Dill, 2015). These studies enriched the researches on the relationship between the built environment and PA, but ignored the factors of spatial variation.

With the development of information and communication technology, crowdsourcing data such as Strava data emerged, which provides technical support for measuring the spatial distribution of PA on large sample sizes (Yang et al., 2022b). Moreover, many researchers have found

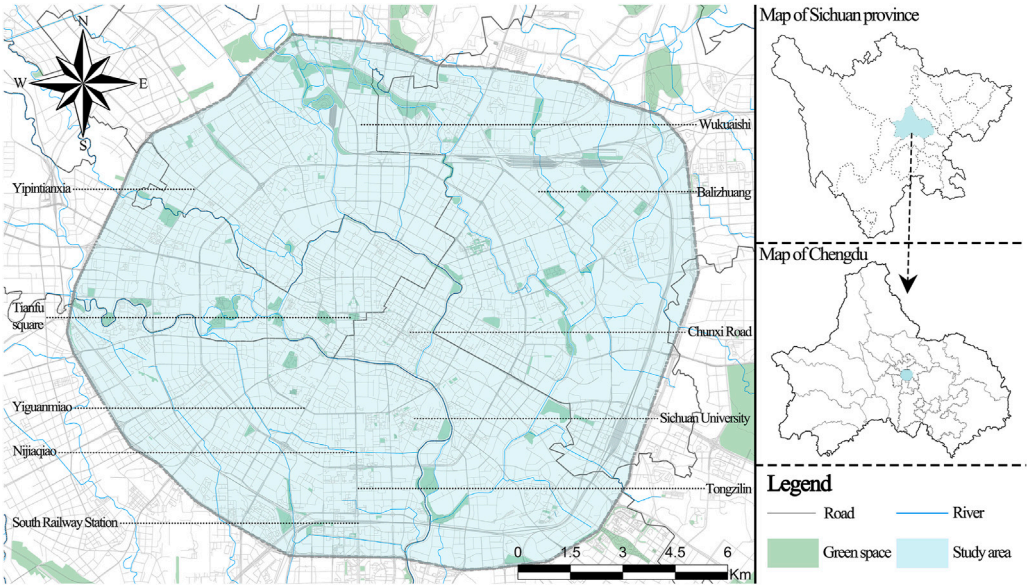

FIGURE 1
The study area.

that streets play an important role in the promotion of physical activities such as running and cycling (Lu et al., 2018b; Yang et al., 2021a). One study reported that streets with rich vegetation create an ecological running environment and hence promote the PA of old people (Du and Huang, 2022). Another study reported that eye-level street greenery stimulates physical activity and thus improves the health of residents (Lu et al., 2018a). These researches use street view data which provide a large and objective record of the streetscape. Therefore, we can use semantic segmentation techniques to identify the street view data and measure the streetscape attribute factors from the human-scale view, which enriches the traditionally built environment evaluating system (Yang et al., 2021b). Furthermore, existing research on the correlation between PA and the built environment focuses on the global analysis of spatial elements, but many scholars in other research directions of urban space have used the GWR model to describe the local impact effects of spatial elements (Yang et al., 2017).

Therefore, this study makes the following innovations to fill these gaps. First, we measure the spatial distribution trajectory of PA on a large sample size with the Strava crowdsourcing data. Second, we increase the streetscape attribute factors from the human-scale view calculated by semantic segmentation techniques based on the traditionally built environment evaluating system. Third, we use the GWR model to scrutinize the spatial heterogeneity in the impact of the built environment on PA.

Methodology

Study area

Chengdu is a mega-city gathering economy, politics, culture, and ecology in western China. It is located in the middle of Sichuan Province, with 102°54′–104°53′ East and 30°05′–31°26′ North. By the end of 2021, it has a total area of 14,335 km^2 and 21.19 million people. Currently, it is pursuing the Park City and building 476 parks and 150 km of greenways to ameliorate the living environment of residents and increase their motivation for outdoor activities. Moreover, the urban spatial structure of Chengdu is divided by ring roads such as the Third Ring Road. PA of central urban residents is mainly concentrated in the areas within the Third Ring Road. Therefore, this study chooses the area within the Third Ring Road as the study area to scrutinize the correlation between the built environment and PA (Figure 1).

Methods

Tobler's first law reveals that most things are correlated in space; especially, the closer things have the high spatial autocorrelation (Tobler, 1970). Currently, models such as the OLS model and binary logit models can only study the relationship between independent variables and dependent variables from a global perspective, which overlooks the mutual spatially varying impacts of elements. Therefore, to improve the accuracy of the model and obtain more "real" results, Brunsdon et al. (1996) proposed the GWR model to

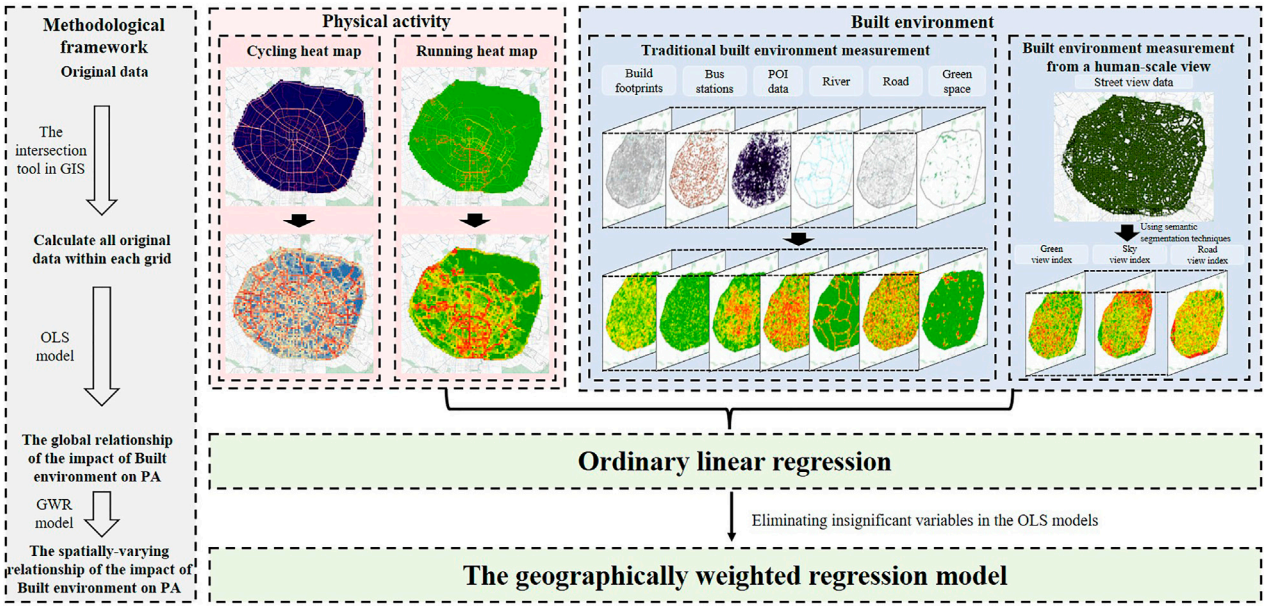

FIGURE 2
Research framework.

explore the changes in elements in different spatial locations. GWR model is the local analysis model, which mainly analyzes the spatial heterogeneity of elements (Yang et al., 2020a; Yang et al., 2020b; Yu et al., 2022b). It gives higher weight to adjacent elements at a certain location and constructs different equations for elements at different spatial locations. In this way, variables can be better fitted, and more accurate results can be obtained (Yang et al., 2018; Liu et al., 2022). The specific formula is as follows.

$$y_i = \sum_k \beta_k (u_i, v_i) x_{k,i} + \varepsilon_i \quad (1)$$

where y_i is the i-th variable of the dependent variable; k denotes the number of independent variables; $\beta_k (u_i,v_i)$ is the geolocation coordinates of the k-th point; and $x_{k,i}$ is the k-th independent variable and the Gaussian error at location i. Figure 2 shows the research framework of this paper.

Strava data

Strava, as a professional sports logging software, is compatible with GPS logging devices such as sports watches and mobile phones and can record people's activity trajectories in real-time. Moreover, it shares people's monthly activity trajectories as a heat map on its website (https://www.strava.com/heatmap), which enables people to choose their routes when traveling for sport. The Strava data have specific advantages, such as highly accurate and large-scale data, over traditional questionnaires and telephone surveys.

We collect cycling and running activity trajectories from the heat map in Chengdu in December 2021. Moreover, the Chinese Ministry of Housing and Urban-Rural Construction released an annual report on road network density and traffic operation in major Chinese cities in 2022, which stated that the average road density in Chengdu is 8.4 km/km^2 and the street spacing is 250 m. Therefore, we divide the study area into 250 m × 250 m grids using the GIS tools. Meanwhile, we use the raster to polygon tool in GIS to convert the heat map of cycling and running (raster data), into feature data, with the value of each feature representing the intensity of walking or cycling use. Then, we use the intersection tool in GIS to link the cycling and running heat map (feature data) to 250 m × 250 m grids of the study area. Finally, we calculate the average value of the cycling index and running index within each grid, for presenting residents' activity trajectories at the street level. Figure 3 illustrates the calculation of the cycling and running index. The specific formulae used to calculate them are as follows.

$$y_k = \frac{\sum_{i=1}^{n} X_i}{n} \quad (2)$$

Where y_k is the cycling index and running index within the k-th grid, X_i is the value of the i-th heat map feature within k-th grid, n is the count of all heat map features in the k-th grid.

Figure 4 summarizes the different spatial distributions of the running index and cycling index. The cycling index is mainly distributed along the ring road, and it is lower in the center and the northeast of the city. The running index is mainly concentrated in the city center and the south of the

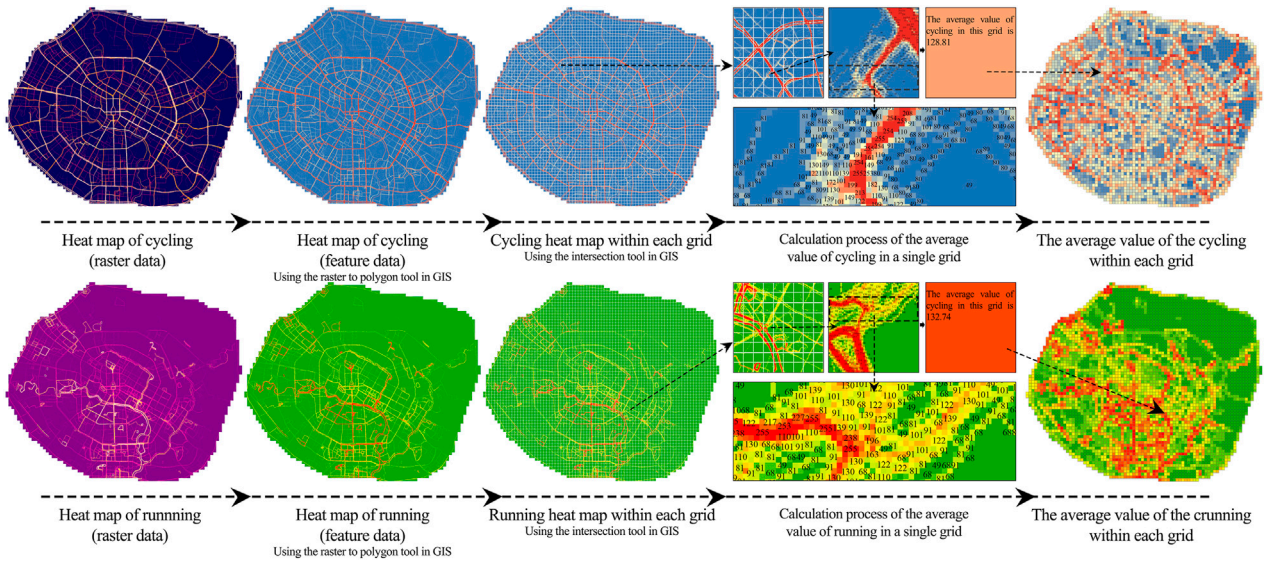

FIGURE 3
Illustration of the calculation of the cycling and running index in each grid.

city, while the northeast of the city has a lower running index.

Street view data

The street-view map records the 360°streetscape provided by the Baidu map (Li et al., 2022). It simulates human eye-level vision and converts the landscape environment felt by them from planar digital images to three-dimensional images, which restores the street space of human-level travel. The street view data are collected by street visits from cars equipped with GPS systems and panoramic cameras, and four images will be collected for each street view point (i.e., divide 360°street view image of a street view point into 4 images according to 0–90°, 90–180°, 180–270°,270–360°). We collect Baidu map street view data of Chengdu mostly in March 2020, which covers the whole study area. Figure 5 shows the distribution of these 11622 street view data points.

Currently, numerous studies based on street view data use semantic segmentation techniques (a deep learning technique based on the fully Convolutional Neural Network (CNN)) (Ewing and Handy, 2009; Yin and Wang, 2016; Nagata et al., 2020). After the operation of image pixels as required, it extracts specific streetscape attributes (e.g., green view index, sky view index, and road view index). In this study, these streetscape attribute variables representing streetscape attributes are mainly selected. Figure 6 reveals the calculation method of these variables based on CNN.

Among them, the green view index and sky view index respectively refer to the proportion of greenery pixels and sky pixels in the 360°street-view map. These proportions represent the green landscape or sky landscape felt by pedestrians during street travel, which reflects the corresponding streetscape level. Moreover, the road view index refers to the proportion of road pixels in the 360°street-view map, which represents the road space for pedestrian travel and reflects the road construction level. The specific calculation methods of the three variables above are as follows, where i is the i-th images of this streetscape point.

$$Green\ view\ index = \frac{\sum_{i=1}^{4} Greenery\ Pixels_i}{\sum_{i=1}^{4} Total\ Pixels_i} \quad (3)$$

$$Sky\ view\ index = \frac{\sum_{i=1}^{4} Sky\ Pixels_i}{\sum_{i=1}^{4} Total\ Pixels_i} \quad (4)$$

$$Road\ view\ index = \frac{\sum_{i=1}^{4} Road\ Pixels_i}{\sum_{i=1}^{4} Total\ Pixels_i} \quad (5)$$

Variables

Table 2 describes the statistics of the independent and dependent variables. We use the cycling index and running index as the dependent variables and select 10 independent variables composed of control and explanatory variables. The control variables are underpinned by the traditionally built

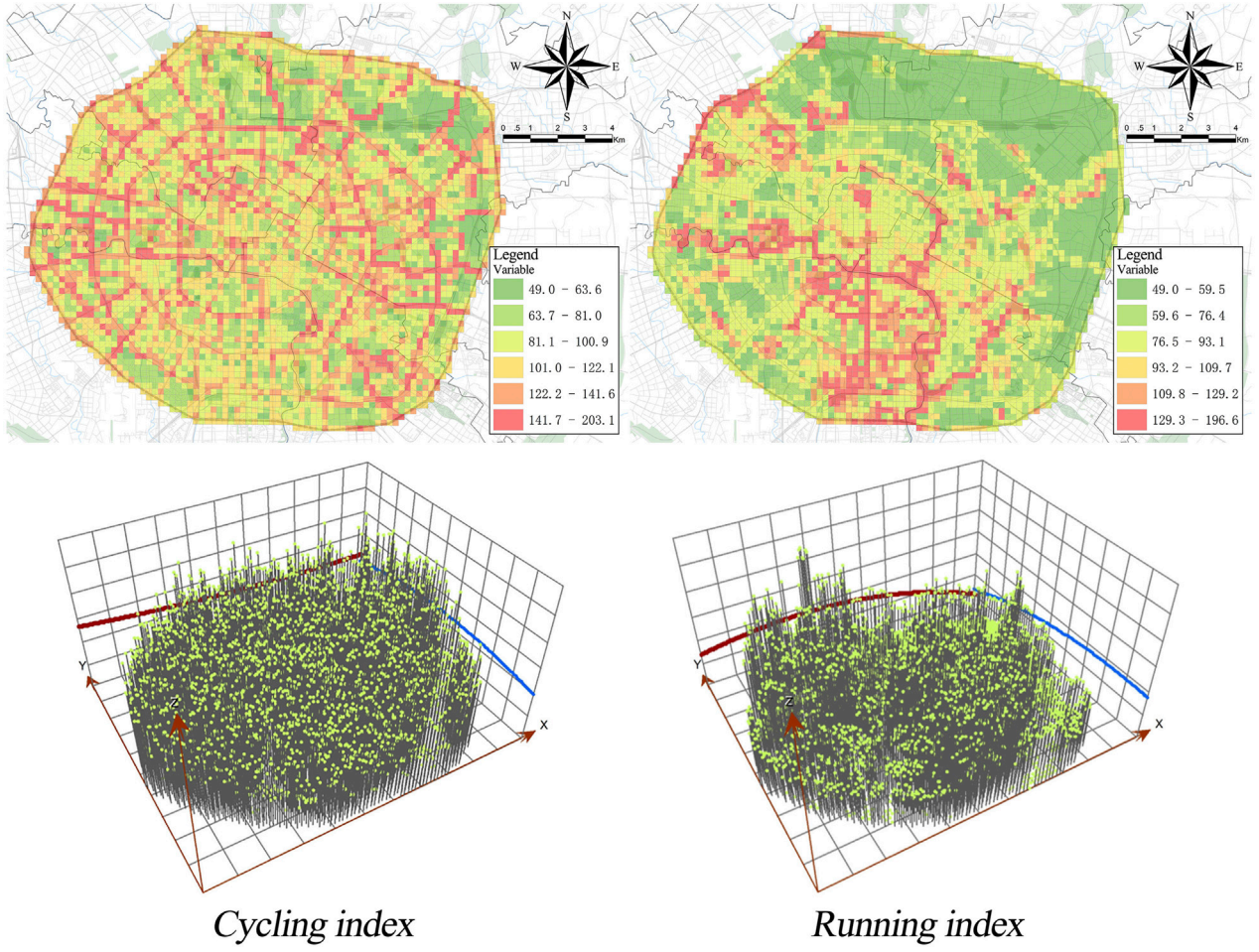

FIGURE 4
Spatial distribution of the cycling index and running index from Strava data.

environment factors, and the explanatory variables consist of streetscape factors from the human-scale view.

To scrutinize these independent variables, we use Python to crawl POI data and river data from the Baidu map and then connect them to the 250 m × 250 m grid using the spatial connection tool in GIS. Thereafter, we calculate the land-use mix, the number of companies, and the river line length in the grid. Moreover, we crawl the building outline, building height, and the spatial position of the bus station from the Gaode map, and count the number of bus stations, road density, and FAR in the grid. Finally, we utilize semantic segmentation techniques to calculate the streetscape attribute variables (green view index, sky view index, and road view index) for each street view data point. Then, we calculate the average value of the streetscape attribute variables for all street view data points in each raster, which is taken as the value of the streetscape variables corresponding to this raster.

Result

First, we analyze the pair-wise correlation of all independent variables to detect the multicollinearity of variables. Figure 7 reveals that the variables have no multicollinearity (correlation <0.7). Then, we use the OLS models to scrutinize the global relationship between the variables and the running index and cycling index. Table 3 presents the OLS model results. The results indicate that most of the variables are significantly correlated with the running index and cycling index at the 0.1% level.

OLS modeling results

The following describes the control variables in the running OLS model and the cycling OLS model. The OLS

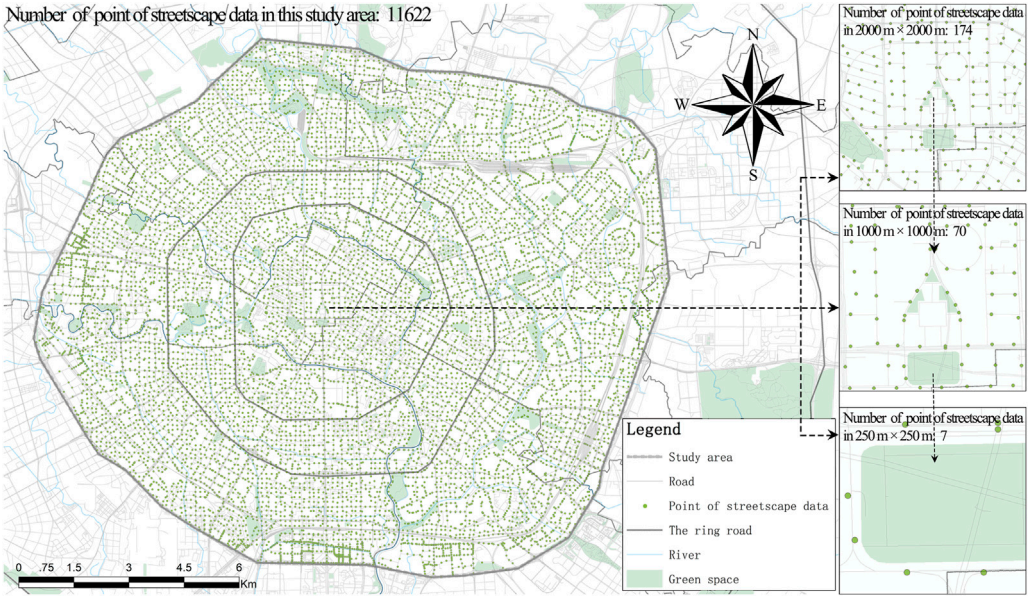

FIGURE 5
Distribution of 11622 points of street view data.

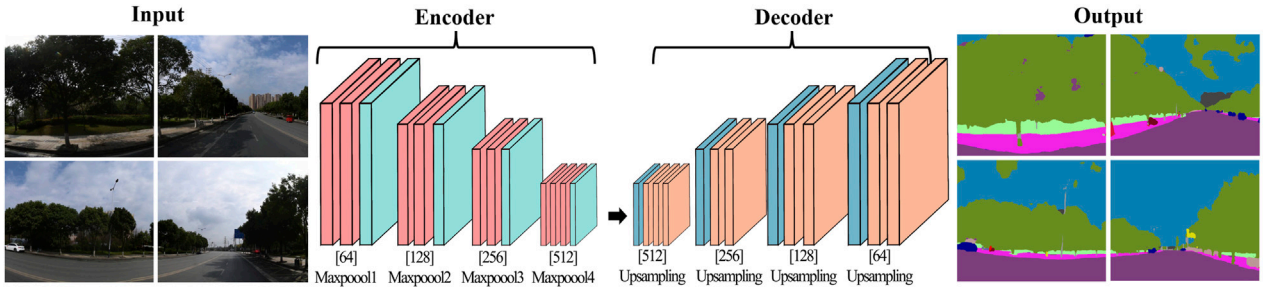

FIGURE 6
Illustration of semantic segmentation techniques-based streetscape attribute variables calculation method.

model results of the cycling index demonstrate that FAR, land-use mix, river line length, road density, and the number of bus stations are significantly related to the cycling index (most variables' p-value < 0.01). However, green space areas and the number of enterprises are insignificantly related to it. Remarkably, only FAR is negatively associated with the cycling index, and the other control variables are positively associated with the cycling index (Duncan et al., 2010). Moreover, the OLS model results of the running index indicate that land-use mix, river line length, green space area, number of bus stations, and number of enterprises are significantly related to the running index (p-value < 0.01). However, FAR and road density are insignificantly related to the running index. Incredibly, all of the control variables positively impact the running index.

It is most important to describe the explanatory variables. The results of both OLS models are shown that the green view index, sky view index, and road view index are significantly correlated with the cycling index and running index, and it is consistent with the results of previous research (Lu et al., 2018b; Lu et al., 2019; Du and Huang, 2022). Specifically, the green view index is significantly related to the running index at the 1% level, and the other variables are significantly related to the cycling and running index at the 0.1% level. The abovementioned results show that explanatory variables play a prominent role in the PA of cycling and running, which enhances the rationality of this

TABLE 2 Descriptive statistics of the variables.

Variables		Before Z-score normalization				After Z-score normalization	
		Std	Mean	Min	Max	Min	Max
Dependent variables							
	Cycling index	105.498	29.709	49	203.074	−1.902	3.284
	Running index	82.928	29.764	49	196.555	−1.14	3.818
Independent variables							
Control variables	FAR	0.808	0.646	0	18.803	−1.252	27.865
	Land-use mix	0.697	0.275	0	1.087	−2.532	1.414
	River line length (km)	0.043	0.096	0	0.626	−0.442	6.054
	Road density (km/km^2)	1.915	1.194	0	6.632	−1.604	3.949
	Green space area (ha)	0.248	0.866	0	6.25	−0.286	6.93
	Number of bus stations	0.392	0.609	0	4	−0.643	5.927
	Number of enterprises	3.294	4.124	0	31	−0.799	6.719
Explanatory variables	Green view index	0.217	0.159	0	0.882	−1.359	4.175
	Sky view index	0.298	0.159	0	0.681	−1.875	2.417
	Road view index	0.161	0.065	0	0.452	−2.474	4.498

study. Interestingly, the different explanatory variables have a different impact on the running index and cycling index. The green view index has a negative impact on the cycling index and a positive impact on the running index. The sky view index is positively associated with the cycling index and negatively associated with the running index. The road view index promotes the cycling index and the running index.

Thereafter, we use Moran's index to analyze the spatial autocorrelation of the residual of the OLS models. The results indicate that the Moran's index values of the running index and cycling index are 0.831 and 0.894, the Z-values are 234.773 and 259.446, and the *p*-value is less than 0.1% (Figure 8). It shows that variables have a high spatial autocorrelation, but the OLS model overlooks the spatially-varying relationships of variables. Thus, the GWR model needs to be used to scrutinize the spatial heterogeneity in the impact of the built environment on PA.

GWR modeling results

On the basis of the abovementioned analysis, we eliminate insignificant variables in the OLS models and use the GWR software (4.0) to analyze the impact of surplus variables on the cycling and running index. Table 4 presents the GWR modeling results. The results of the comparison between the OLS models and the GWR models show that the Adj R-squared of the GWR model is higher than the OLS models and the AIC index of the GWR models is lower than the OLS models. In a word, the GWR models outperform the OLS models in terms of the goodness-of-fit, and this result agrees with our expectations.

The evidence-based result of both GWR modeling indicates that the built environment has spatial heterogeneity in the impact of the built environment on PA. In other words, all variables have a different effect (i.e., positive or negative) on the cycling and running index at different spatial locations.

Figure 9 shows the spatial distribution of the coefficient of FAR, road density, green space area, and the number of enterprises in the GWR models using GIS tools. First, a negative correlation is found between FAR and the cycling index, which is mainly distributed in the urban center. Notably, in some areas near the Third Ring Road, the FAR is a positive impact on the cycling index. In addition, road density promotes the cycling index in the west, northeast, and southeast of the city, but it harms the cycling index in the east-central region of the city. Then, the green space area stimulates the running index in the central, eastern, and southwestern parts of the city. However, it inhibits the running index in a few parts of the city, such as the south of the city. Moreover, the number of enterprises restrains the running index in most areas of the third Ring Road and has a positive effect in only a few areas.

Figure 10 shows the spatial distribution of the coefficient of river line length, number of bus stations, and land-use mix in the GWR models using GIS tools. River line length is positively correlated with the running index in the central and eastern parts of the city, but it is negatively correlated with the running index in the northwest, south, and eastern edge of the city. Most areas of the river line length are positively correlated with the cycling index, but the river line length in some regions harms the cycling index. Moreover, most bus stations have a positive impact on the cycling index, and only a few areas in the northwest, southwest,

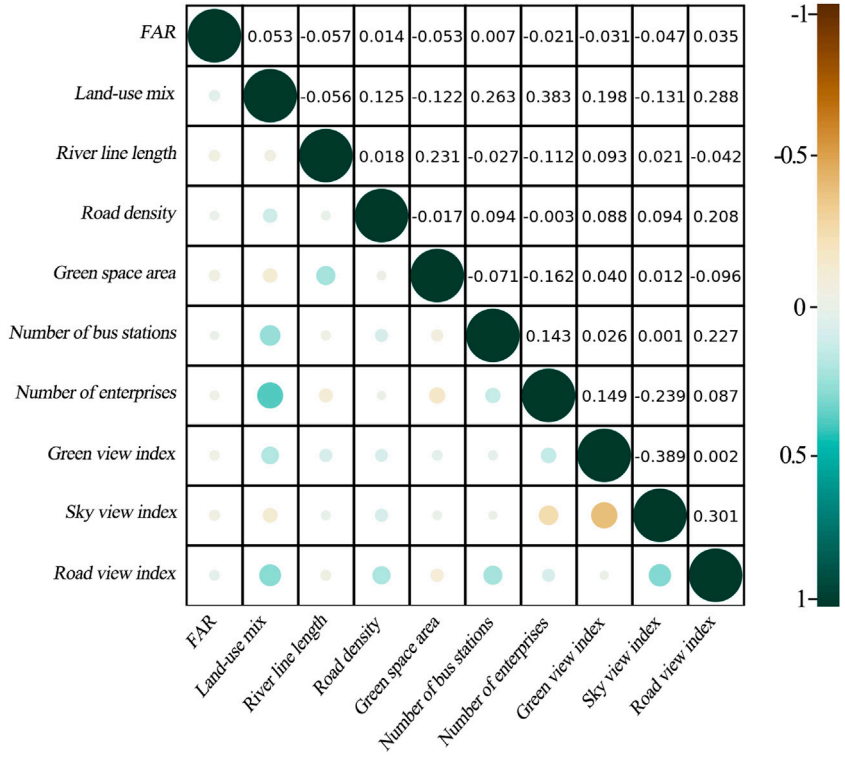

FIGURE 7
Pair-wise Correlation analysis results.

TABLE 3 OLS modeling results.

Variables	Cycling index				Running index			
	Coef	St.Er	t-statistic	p-value	Coef	St.Er	t-statistic	p- value
FAR	−0.031**	0.014	−2.21	0.027	0.003	0.015	0.22	0.826
Land-use mix	0.2***	0.016	12.21	0.000	0.175***	0.017	10.38	0.000
River line length	0.074***	0.015	5.07	0.000	0.122***	0.015	8.15	0.000
Road density	0.064***	0.014	4.39	0.000	0.000	0.015	0.02	0.987
Green space area	0.022	0.015	1.53	0.126	0.113***	0.015	7.50	0.000
Number of bus stations	0.12***	0.015	8.12	0.000	0.052***	0.015	3.40	0.001
Number of enterprises	0.006	0.016	0.38	0.701	0.073***	0.016	4.49	0.000
Green view index	−0.138***	0.016	−8.76	0.000	0.028*	0.016	1.70	0.089
Sky view index	0.062***	0.017	3.70	0.000	−0.082***	0.017	−4.74	0.000
Road view index	0.167***	0.016	10.34	0.000	0.081***	0.017	4.90	0.000
R-squared	0.1563				0.1050			
Adj R-squared	0.1544				0.1029			
Akaike crit	11554.267				11809.725			
Number of Obs	4,323							

***$p < 0.01$, **$p < 0.05$, *$p < 0.1$.

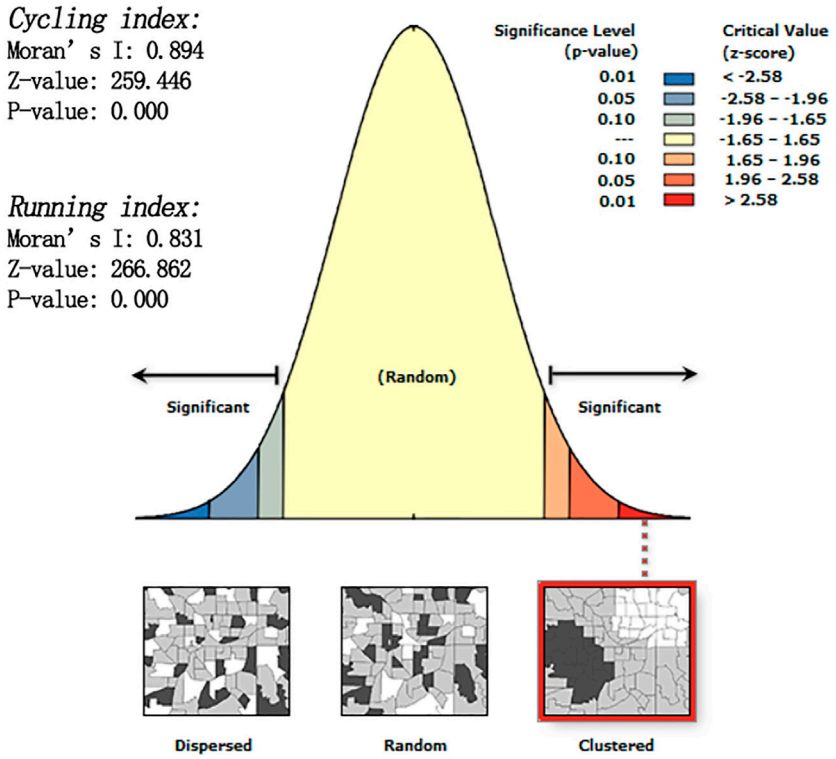

FIGURE 8
Moran's index results.

TABLE 4 GWR modeling results.

Variables	Cycling index					Running index				
	Mean	Std	Min	Median	Max	Mean	Std	Min	Median	Max
FAR	−0.049	0.098	−0.413	−0.040	0.205	—	—	—	—	—
Land-use mix	0.137	0.139	−0.214	0.126	0.569	0.035	0.181	−0.745	0.024	0.650
River line length	0.076	0.086	-0.323	0.071	0.306	0.111	0.216	−0.449	0.074	0.800
Road density	0.044	0.100	−0.214	0.048	0.350	—	—	—	—	—
Green space area	—	—	—	—	—	0.118	0.259	-0.687	0.090	2.099
Number of bus stations	0.132	0.088	-0.074	0.128	0.383	0.041	0.114	-0.293	0.035	0.811
Number of enterprises	—	—	—	—	—	−0.094	0.232	−1.499	−0.090	1.477
Green view index	−0.125	0.087	−0.344	−0.129	0.136	−0.005	0.147	−0.868	−0.002	0.590
Sky view index	0.069	0.118	−0.204	0.072	0.357	0.045	0.182	−0.468	0.011	1.115
Road view index	0.208	0.154	-0.074	0.183	0.642	0.055	0.152	−0.870	0.050	0.613
R-squared	0.353					0.690				
Adj R-squared	0.296					0.623				
Akaike crit	11081.715					8738.663				

and northeast of the city have a negative effect. However, it promotes the running index, especially in urban centers such as Tianfu square, and harms it in the northwest and northeast of the city. Furthermore, land-use mix stimulates the running index in the urban center (Duncan et al., 2010), especially Chunxi Road and other urban consumption centers. It inhibits the running index in the areas under reconstruction in the south and the old town in the northwest of the city. By contrast, land-use mix

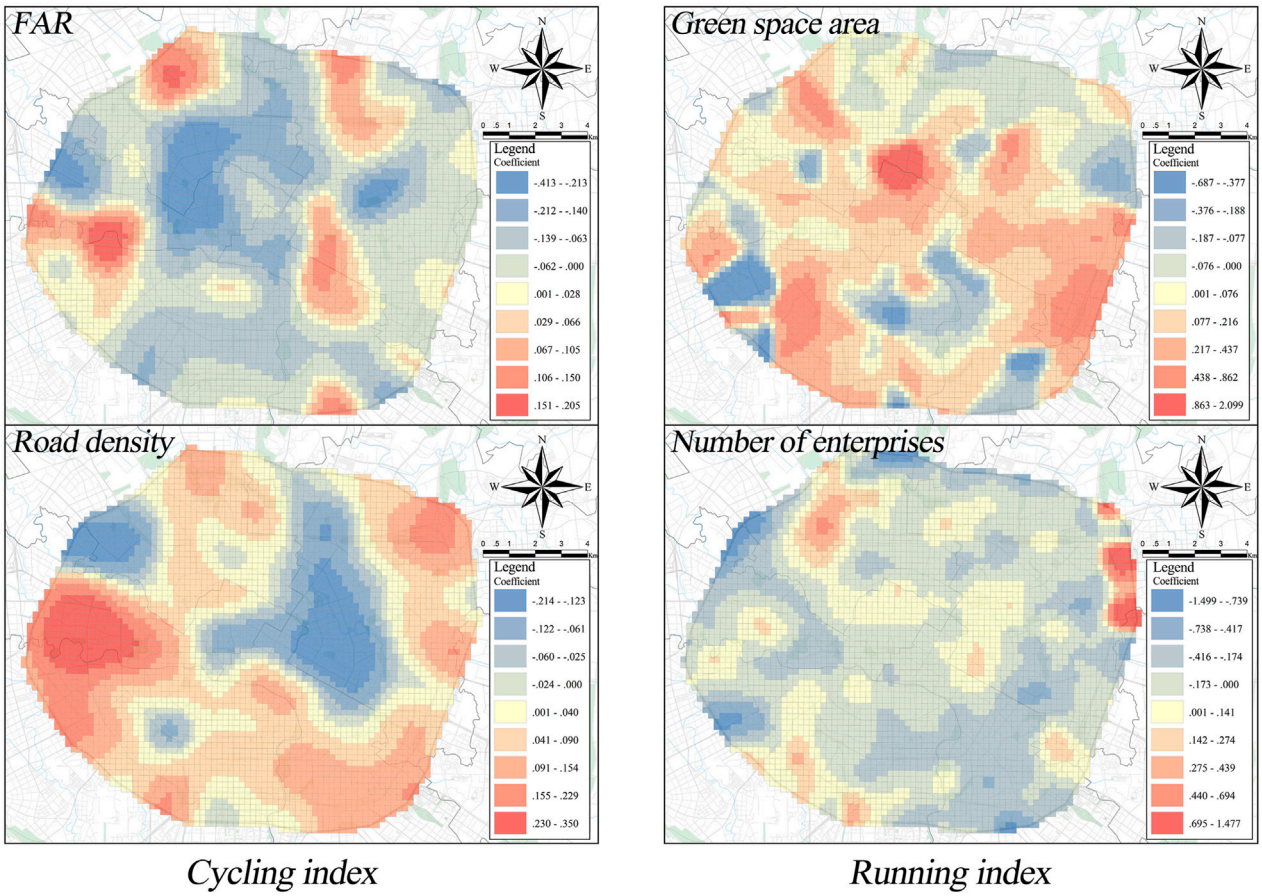

FIGURE 9
The spatial distribution of the coefficient of FAR, road density, green space. Area, and the number of enterprises in the GWR models.

stimulates the cycling index in most regions and restrains it only in central and southern cities.

Figure 11 shows the spatial distribution of the coefficient of green view index, sky view index, and road view index in the GWR models using GIS tools. First, the green view index harms the cycling index in most regions. It promotes the cycling index in only a few areas, such as the urban center and some point areas in the eastern part of the city. Remarkably, it facilitates running index in the central, southern, and southeastern parts of the city, while it restrains running index in the northwestern and south-central parts of the city. Second, the sky view index is positively correlated with the cycling index in the central, western, and southern areas of the city. It is negatively correlated with the cycling index in the north and northeast of the city. Meanwhile, it stimulates the running index in the western and central areas of the city and harms the running index in most areas in the eastern part of the city. Third, the road view index has a positive impact on the cycling index except for a few areas. It is also positively correlated with the running index in the eastern and southwestern parts of the city.

These results indicate that different built environment variables have spatially varying influences on the cycling and running index, especially the green view index, sky view index, and road view index. Therefore, compared with the global analysis results of the OLS model, the GWR model can more accurately identify the positive or negative effects of the built environment on PA in different spatial locations. Thus, it will provide support for policymakers and urban planners to put forward more accurate recommendations. This aspect is the practical significance of this study.

Discussion

Control variables in the cycling index GWR model

First, in terms of FAR, it inhibits the PA of cycling in most areas, such as Fuqing and Nijiaqiao. This contradicts the results of previous studies. Compared to the living habits of residents in

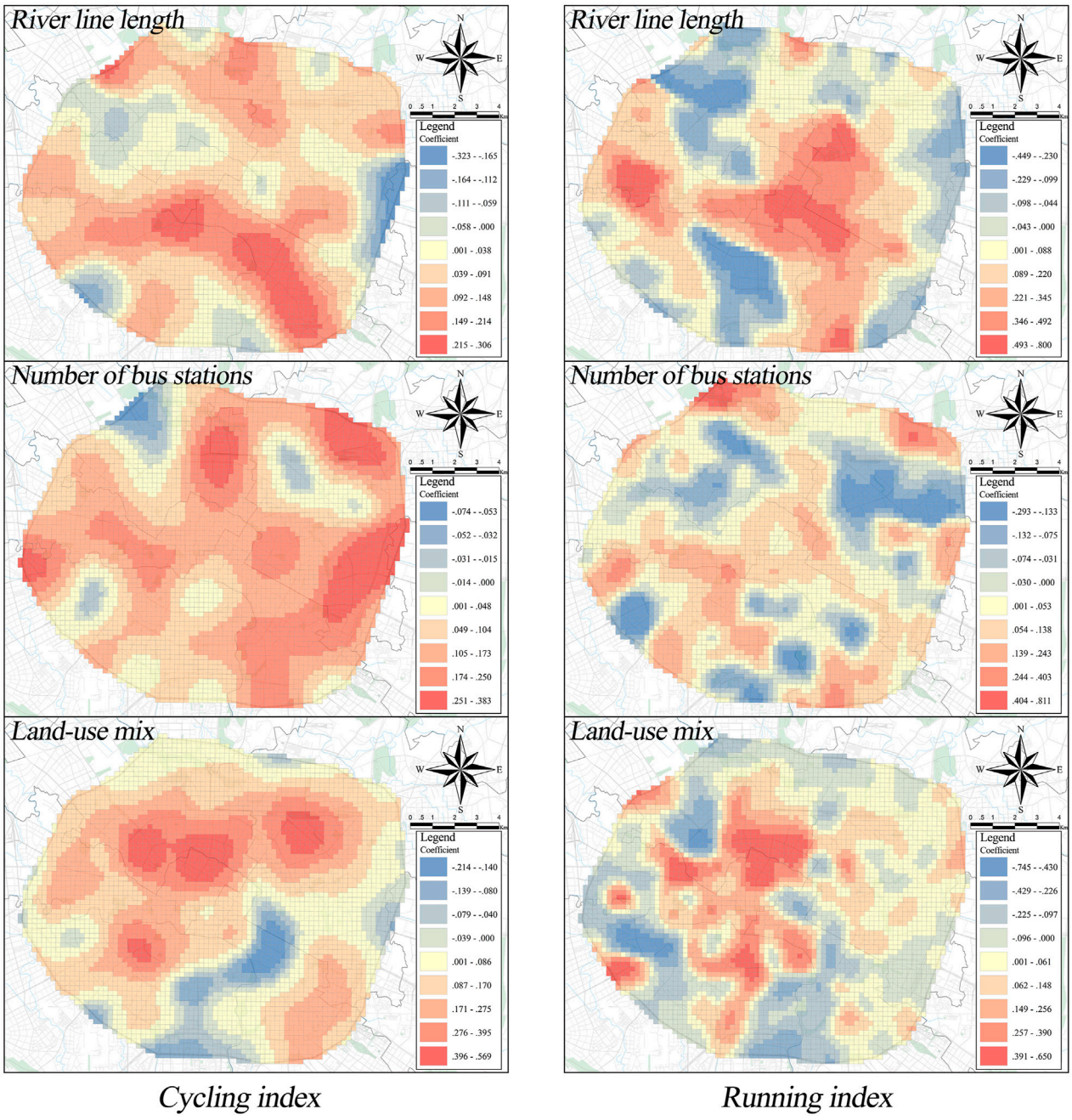

FIGURE 10
The spatial distribution of the coefficient of river line length, the number of bus stations, and land-use mix in the GWR models.

Europe and the United States, people have different feelings in Chengdu about high-density development. The reason is that residents in Chengdu have a laid-back attitude to life, but a high FAR produces a relatively crowded environment, which leads to a decrease in cycling activities.

Second, the land-use mix greatly promotes the generation of cycling activities in the northern and central areas of the city. This finding may be ascribed to the diverse characteristics of these areas, such as commercial, public service, residential and other facilities. This conclusion is supported by New Urbanism, i.e., the land-use mix stimulates the physical activities of residents (Newman and Kenworthy, 1996). However, in areas such as Tongzilin and Sichuan University, there are obstacles to the PA of cycling, due to

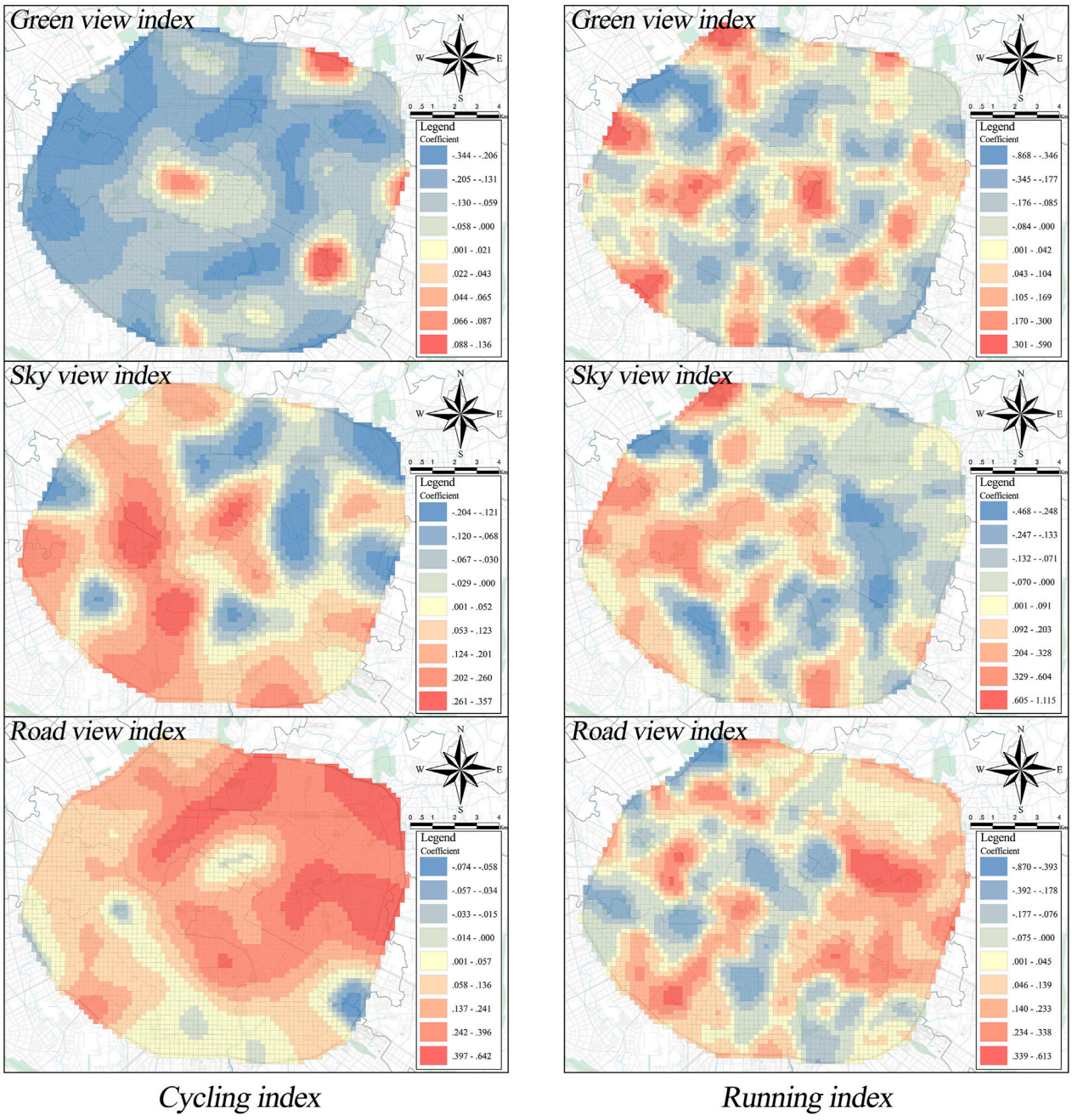

FIGURE 11
The spatial distribution of the coefficient of green view index, sky view index, and road view index in the GWR models.

the closed space and inability to communicate with the outside world.

Third, existing studies have shown that road density has a positive correlation with cycling activities. However, our finding diverges from this conclusion. While road density facilitates cycling activities in most areas, it has a dampening effect in some areas. The evidence-based result indicates that there are serious problems of mixed traffic between motor vehicles and non-motor vehicles and low road quality in some old towns of Chengdu (e.g., Xinhong community and Jianshe Road). These issues may lead to traffic accidents and thus reduce the enthusiasm for cycling activities.

Fourth, the river line length in some areas hinders cycling activities, such as Yipintianxia and Taipingyuan. We think this

situation is due to the absence of suitable cycling paths built along the river, while the bicycle paths in Chengdu are mainly distributed along the greenway.

Fifth, bus stations in most regions have a positive impact on the PA of cycling, such as Wannianchang and Qingyanggong, which contradicts the conclusion of Zhao (2013) and Salvo et al. (2014). This difference may be related to the widespread use of shared bikes in China. About 1.85 million rides are taken on shared bikes a day in Chengdu, according to *the Regulations on Operation and Service of The City's Internet Bike Rental Industry*. During work, weekends, or holidays, residents usually ride shared bikes to reach their travel destinations after taking the bus.

Control variables in the running index GWR model

First, many studies have revealed from a global perspective that land use mixing either only promotes or inhibits running activities (Handy et al., 2002; Troped et al., 2010; Lu et al., 2018a). However, unlike the above studies, we found that those have mixed, that is, positive and negative, both impacts at different spatial locations. Although the areas with a high land-use mix have diversified facilities, the facilities and surrounding environment may be polarized due to the government's different governance policy, old-fashioned design, and loopholes in maintenance policies. These factors have mixed impacts on running activities.

Second, river line length can significantly promote the PA of running in most areas, which is consistent with (Ying et al., 2015). However, compared with other cities that have a relatively complete blue and green infrastructure, the Park City implemented by Chengdu is still under construction. As a result, the effect may be hindered in some areas with a poor running environment along the river, such as Yiguanmiao, Huazhaobi, and Shizishan.

Third, most green space areas stimulate running activities. However, some areas with rich green space resources harm running activities, such as closed universities and large public activity places (i.e., Sichuan University and Sichuan Gymnasium), which block the connection between green space and surrounding residents. This partially differs from the findings of many researchers who found that green space area facilitates running activities (Wang et al., 2019). This is because most of them use global analysis models to explore and lack local analysis. In contrast, the GWR model can more accurately identify the relationship between the effects of spatially varying. It makes this study more reasonable.

Fourth, compared to the conclusion of Sarmiento et al. (2010), there is a negative correlation between bus stations and running activities. This study found a mixed effect between the two, which may be related to the living habits of Chinese residents. They often use running as a way to connect with buses, and it improves the enthusiasm for running activities.

Fifth, contrary to the results of some studies that enterprises promote running activities (Yang et al., 2022b), in most areas, such as Shuhan Road and Balizhuang, enterprises harm running activities. It may be attributed to the job-housing imbalances among Chengdu residents. The long commutes caused by this imbalance cause difficulty for residents to reach the office directly on foot. As a result, they generally choose some other means of transportation.

Explanatory variables in the cycling index GWR model

First, the green view index generally restrains the PA of cycling. But previous studies have shown that the green view index plays an important role in increasing residents' cycling activities (Lu et al., 2019). We believe that this difference is related to the characteristics of each study area. Compared to some other studies, a large number of old towns exist in the Third Ring Road of Chengdu. It has a high green view index but blocks the view and sunlight, thus leading to an unsuitable cycling environment. In addition, the green view index also stimulates cycling activities in some areas (e. g., Kuanzhaixiangzi Alleys and Chengdu Bus terminal). Through the field survey of positive correlation areas, we find that the level of street greenery in these areas is too low, which may mean that basic green plants also are required to create a comfortable cycling environment. In other words, if the standard of basic street greenery is met, then a further increase in the green view index will hinder cycling activities.

Second, the sky view index in most areas has a positive correlation with the PA of cycling. This finding resonates with conclusions in color psychology that blue is thought to be associated with comfort and security, giving people a sense of safety (Wexner, 1954; Ballast, 2002). The sky view index has to do with the need for broad vision and sun exposure for cycling, which can make cyclists feel free, comfortable, and secure. However, we also find that some areas are obstructing cycling activities, especially in the north and northeast of the city (e.g., North Railway Station and Jianshe Road). Through specific investigation and analysis, we discover that these areas belong to the area to be demolished. There are problems such as empty streets, dilapidated facades, and a poor overall environment, thus hindering cycling activities.

Third, the road view index stimulates the PA of cycling in most areas. This may be because the calculation using the semantic segmentation techniques can only contain all the paths (including bicycle paths) in the area in the road view index, which leads to a significant positive correlation between the road view index and cycling activities. However, a few areas restrain cycling activities with unequal distribution of road rights. In other words, the unreasonable allocation of road rights and low sharing squeeze the cycling space (Lubitow and Miller, 2013;

Colville-Andersen, 2018). These areas are mainly located near Daguan Station and East Chengdu Railway Station. A field survey of the streets in this area reveals that large-scale construction is taking place in it, and the road is not demarcated for bicycle paths. This makes it impossible for people to cycle safely and also suffer from noise and construction waste in this process.

On the whole, the GWR model results of the cycling index reveal the spatial mismatch problem in the Third Ring Road of Chengdu. This is highly correlated with the rapid development of new urban areas leading to neglect in the management of old towns. Chengdu has been expanding outward at a high rate of speed for the past 10 years but has overlooked the renewal and maintenance of the old towns. We discover the areas where the green view index, sky view index, and road view index restrain cycling activities are mainly concentrated in the north and northeast. These are mostly PA-unfriendly areas to be demolished or old urban areas, such as North Railway Station and Chengdu Bus Terminal.

Explanatory variables in the running index GWR model

First, the results indicate that the green view index is positively correlated with the PA of running in some areas (e.g., Dufu Thatched Cottage, Wukuaishi), and this conclusion resonates with the findings of Koo et al. (2022) and Du and Huang (2022). The reason is that the tree shade can give people a sense of security and thus stimulate the resident' travel. However, although green is generally regarded as an important indicator for arousing activities (Kaya and Epps, 2004; Bell et al., 2008; Nagata et al., 2020), a different result is found in this study, in which the green view index inhibited running activities in other areas. A field survey of the negatively related areas (e.g., Chadianzi, Shuangqiao community, and Simaqiao community) reveals that these areas are PA-unfriendly old town areas. These areas have more greenery, but it lacks overall maintenance (e.g., trees grow indiscriminately without not being pruned). This situation results in the formation of street spaces in the area that is not suitable for running activities.

Second, the sky view index inhibits running activities in most areas, such as Wannianchang and Dongjiao Memory, and this result resonates with numerous studies (Ewing and Handy, 2009; Yin and Wang, 2016; Nagata et al., 2020). The reason may be that a higher sky view index results in stronger solar exposure and those open areas can be unsuitable for PA. On the contrary, in some areas, the sky view index promotes running activities, and we believe that it is seasonally and weather-related. Specifically, the Strava data were collected during the winter of 2021 in Chengdu. It had only 5 sunny days in December 2021 compared with the relatively long winter sunshine hours in major cities such as Beijing, New York, and Washington. Therefore, areas with a basic sky view index in Chengdu during lack of sunshine bring comfortable sun exposure on sunny days in winter, which stimulates running activities among residents.

Third, on the whole, the road view index is a positive impact on the running index in most areas. In our opinion, the road view index represents the construction level of the street, and streets with a higher construction level will be equipped with more suitable walking paths. In addition, a field survey of negatively related areas (e.g., Wenshu Monastery and Huaxiba) reveals that these areas with a high road view index are designed by the car-oriented. But they ignore that urban design should pay more attention to people-oriented design and the equity of walking rights (Jacobs, 1961; Bevan et al., 2007). In general, the space allocation for walking, cycling, and driving in these areas is not reasonable, and the design method of street space is not well used to enhance the rights and interests of pedestrians. This situation, as well as the lack of management of roadside facilities in the old town, inhibits running activities.

Overall, the running index of the GWR model result reveals a similar spatial mismatch problem as the results of the cycling index of it. We discover that most of the areas where the green view index, sky view index, and road view index restrain running activities are old towns or areas under construction, such as Shuangqiao Community, Shengxian Lake, Qianfang Road, and Lijiatuo.

Conclusion

Planning intervention is considered an effective way to solve urban public health issues. Optimizing the built environment through planning intervention can tremendously promote PA. Therefore, it is necessary to scrutinize the relationship between the built environment and PA to inform the public health-oriented urban planning process. However, previous studies over-rely on data derived from questionnaires and surveys, which suffer from small sample sizes. And researchers focus predominantly on the traditionally built environment factors and seldomly measure them from the human-scale view. Meanwhile, existing studies neglect the spatial heterogeneity in the impact of the built environment on PA. To address these gaps, we use the novel PA crowdsourced data, i.e., the Strava, to decipher the spatially-varying relationships between the built environment and PA. Specifically, we examine how human-scale streetscape attributes affect PA across different areas after controlling for traditionally built environment variables. The empirical findings are conducive to providing guidance for optimizing the urban built environment, promoting PA of residents, and thus addressing the urban public health issues.

The core findings of this study are as follows. First, most built environment factors have spatial heterogeneity, and the GWR model can help better explain the spatial heterogeneity in the impacts of the built environment on PA. In other words, control variables (e.g., land-use mix, river line length, and road density)

and explanatory variables (e.g., green view index, sky view index, and road view index) have wide and mixed impacts on PA across different areas.

More importantly, this study focuses on the impacts of human-scale streetscape factors (explanatory variables) and draws the following findings. 1) In general, the green view index restrains cycling activities. But in the area with a low green view index, appropriately increasing the green view index will promote cycling activities. By contrast, it stimulates running activities. However, there are exceptions in some areas of the old town, of which the street space has low-level streetscape greenery and lacks renewal and maintenance. 2) The sky view index is positively correlated with cycling activities. A high sky view index represents a broad vision for cycling, which improves safety. In addition, the sky view index has mixed impacts on running activities. 3) The road view index stimulates cycling and running activities, given a high road view index means a higher level of road construction. However, it restrains PA in the old towns dominated by cars and slated for demolition. According to the above, we identify the spatial mismatch issue in the study area. The sky view index and road view index in the north and northeast of the city, in which the demolished old towns locate, hinder cycling activities. Meanwhile, most of the areas with negative impacts of human-scale streetscape factors on running activities belong to old towns or areas under urban construction (e.g., Shuangqiao Community, Shengxian Lake, Qianfeng Road, and Lijiatuo).

Therefore, according to the above findings, this study puts forward policy suggestions and planning intervention measures as follows.

First, while building a Healthy City and Park City, the government should vigorously develop blue and green infrastructure and rationally allocate urban green space and water landscape. At the same time, the greenways (e.g., cycling paths and walking paths) of the riverside area and the green space system should be ameliorated to promote the PA of residents and improve their physical health.

Secondly, for the old town with a high land-use mix but unfriendly to PA (e.g., Chadianzi and Tongzilin), the planning agencies should promote the update of the active travel facilities and the fine-scale design to shape the active travel-friendly community.

Third, street space is the major place for the PA of residents. Planning agencies should put forward active intervention measures for the built environment based on the actual situation of community streets. Above all, for the old town with high demand for running activities, the level of street greening should be promoted, and more walkable green plants should be configured to improve the comfort and interest of residents. Moreover, in communities with more cycling activities, relevant administrative departments should timely repair street landscapes, provide enough broad vision for cyclists, and promote the safety of cycling activities.

Fourthly, in terms of road and public transport construction, planning agencies should optimize street space design, appropriately increase road density, and rationally allocate bus facilities according to the location and current characteristics of the community. In the old town with a high road view index but non-suitable for PA, the reasonable distribution and moderate sharing of the three road rights of walking, cycling, and driving, should be strengthened. For instance, the cross-section design of street space is necessary to realize the benign adaptation of street space and residents' activities. In addition, in communities with high demand for PA, relevant planning departments should build more branch roads and walking roads to perfect the basic road network structure to improve the density and accessibility of the community road networks. This contributes to creating a continuous and complete environment for active travel.

However, this study also has some limitations. First, due to difficulties in data acquisition, built environment factors such as bike paths and sidewalks cannot be included in this study. Secondly, explanatory variables measured by semantic segmentation techniques at the human scale view can be further explored, such as aspect ratio and sidewalk index. Finally, the explanatory variables measure streetscape attributes from the objective perspective. However, just like Kang et al. (2020), a questionnaire survey can be appropriately conducted to analyze the subjective perception of people on different streetscape maps. And then, more reasonable streetscape variables can be obtained by combining subjective perception with objective perception.

Data availability statement

The raw data supporting the conclusions of this article will be made available by the authors, without undue reservation.

Author contributions

PiL: conceptualization, funding acquisition, supervision, and writing—original draft. BY: conceptualization, funding acquisition, methodology, and writing—review and editing. PeL: formal analysis and writing—review and editing. PpL: validation and writing—review and editing. All authors have read and agreed to the published version of the manuscript.

Funding

This study was supported by the Key Program of the Center on Child Protection and Development, Sichuan (No. ETBH2021-ZD001), the Sichuan Science and Technology Program (No.

2022JDR0178), and the National Natural Science Foundation of China (No. 52278080).

Conflict of interest

The authors declare that the research was conducted in the absence of any commercial or financial relationships that could be construed as a potential conflict of interest.

Publisher's note

All claims expressed in this article are solely those of the authors and do not necessarily represent those of their affiliated organizations, or those of the publisher, the editors and the reviewers. Any product that may be evaluated in this article, or claim that may be made by its manufacturer, is not guaranteed or endorsed by the publisher.

References

An, R., Shen, J., Yang, Q., and Yang, Y. (2019). Impact of built environment on physical activity and obesity among children and adolescents in China: A narrative systematic review. *J. sport health Sci.* 8 (2), 153–169. doi:10.1016/j.jshs.2018.11.003

Ballast, D. (2002). *Interior design reference manual*. Belmont, CA: Professional Pub. Inc.

Bauman, A. E., Reis, R. S., Sallis, J. F., Wells, J. C., Loos, R. J. F., and Martin, B. W. (2012). Correlates of physical activity: Why are some people physically active and others not? *Lancet* 380 (9838), 258–271. doi:10.1016/s0140-6736(12)60735-1

Beaglehole, R., Bonita, R., Horton, R., Adams, C., Alleyne, G., Asaria, P., et al. (2011). Priority actions for the non-communicable disease crisis. *lancet* 377 (9775), 1438–1447. doi:10.1016/s0140-6736(11)60393-0

Bell, J. F., Wilson, J. S., and Liu, G. C. (2008). Neighborhood greenness and 2-year changes in body mass index of children and youth. *Am. J. Prev. Med.* 35 (6), 547–553. doi:10.1016/j.amepre.2008.07.006

Bevan, T. A., Sklenar, O., McKenzie, J. A., and Derry, W. E. (2007). "Sustainable urban street design and assessment," in *3rd urban street symposium: Citeseer)*.

Biddle, S. J., and Asare, M. (2011). Physical activity and mental health in children and adolescents: A review of reviews. *Br. J. Sports Med.* 45 (11), 886–895. doi:10.1136/bjsports-2011-090185

Brunsdon, C., Fotheringham, A. S., and Charlton, M. E. (1996). Geographically weighted regression: A method for exploring spatial nonstationarity. *Geogr. Anal.* 28 (4), 281–298. doi:10.1111/j.1538-4632.1996.tb00936.x

Chen, S., Bao, Z., and Lou, V. (2022a). Assessing the impact of the built environment on healthy aging: A gender-oriented Hong Kong study. *Environ. Impact Assess. Rev.* 95, 106812. doi:10.1016/j.eiar.2022.106812

Chen, S., Wang, T., Bao, Z., and Lou, V. (2022b). A path analysis of the effect of neighborhood built environment on public health of older adults: A Hong Kong study. *Front. Public Health* 10, 861836. doi:10.3389/fpubh.2022.861836

Colville-Andersen, M. (2018). *Copenhagenize: The definitive guide to global bicycle urbanism*. Island Press.

Corburn, J. (2004). Confronting the challenges in reconnecting urban planning and public health. *Am. J. Public Health* 94 (4), 541–546. doi:10.2105/ajph.94.4.541

Ding, D., and Gebel, K. (2012). Built environment, physical activity, and obesity: What have we learned from reviewing the literature? *Health Place* 18 (1), 100–105. doi:10.1016/j.healthplace.2011.08.021

Du, Y., and Huang, W. (2022). Evaluation of street space quality using streetscape data: Perspective from recreational physical activity of the elderly. *ISPRS Int. J. Geoinf.* 11 (4), 241. doi:10.3390/ijgi11040241

Duncan, M. J., Winkler, E., Sugiyama, T., Cerin, E., Dutoit, L., Leslie, E., et al. (2010). Relationships of land use mix with walking for transport: Do land uses and geographical scale matter? *J. Urban Health* 87 (5), 782–795. doi:10.1007/s11524-010-9488-7

Ewing, R., and Cervero, R. (2001). Travel and the built environment: A synthesis. *Transp. Res. Rec.* 1780 (1), 87–114. doi:10.3141/1780-10

Ewing, R., and Handy, S. (2009). Measuring the unmeasurable: Urban design qualities related to walkability. *J. Urban Des.* 14 (1), 65–84. doi:10.1080/13574800802451155

Forsyth, A., Michael Oakes, J., Lee, B., and Schmitz, K. H. (2009). The built environment, walking, and physical activity: Is the environment more important to some people than others? *Transp. Res. Part D Transp. Environ.* 14 (1), 42–49. doi:10.1016/j.trd.2008.10.003

Handy, S. L., Boarnet, M. G., Ewing, R., and Killingsworth, R. E. (2002). How the built environment affects physical activity: Views from urban planning. *Am. J. Prev. Med.* 23 (2), 64–73. doi:10.1016/s0749-3797(02)00475-0

Haskell, W. L., Lee, I.-M., Pate, R. R., Powell, K. E., Blair, S. N., Franklin, B. A., et al. (2007). Physical activity and public health: Updated recommendation for adults from the American college of sports medicine and the American heart association. *Circulation* 116 (9), 1081–1093. doi:10.1161/CIRCULATIONAHA.107.185649

Heinrich, K. M., Lee, R. E., Suminski, R. R., Regan, G. R., Reese-Smith, J. Y., Howard, H. H., et al. (2007). Associations between the built environment and physical activity in public housing residents. *Int. J. Behav. Nutr. Phys. Act.* 4 (1), 56–59. doi:10.1186/1479-5868-4-56

Jacobs, J. (1961). *The life and death of great American Cities*. New York, NY: Random House.

Kang, Y., Zhang, F., Gao, S., Lin, H., and Liu, Y. (2020). A review of urban physical environment sensing using street view imagery in public health studies. *Ann. GIS* 26 (3), 261–275. doi:10.1080/19475683.2020.1791954

Kaya, N., and Epps, H. H. (2004). Relationship between color and emotion: A study of college students. *Coll. student J.* 38 (3), 396

Koo, B. W., Guhathakurta, S., and Botchwey, N. (2022). How are neighborhood and street-level walkability factors associated with walking behaviors? A big data approach using street view images. *Environ. Behav.* 54 (1), 211–241. doi:10.1177/00139165211014609

Koohsari, M. J., Badland, H., and Giles-Corti, B. (2013). Re) Designing the built environment to support physical activity: Bringing public health back into urban design and planning. *Cities* 35, 294–298. doi:10.1016/j.cities.2013.07.001

Li, S., Ma, S., Tong, D., Jia, Z., Li, P., and Long, Y. (2022). Associations between the quality of street space and the attributes of the built environment using large volumes of street view pictures. *Environ. Plan. B Urban Anal. City Sci.* 49 (4), 1197–1211. doi:10.1177/23998083211056341

Liu, Q., Zhao, P., Xiao, Y., Zhou, X., and Yang, J. (2022). Walking accessibility to the bus stop: Does it affect residential rents? The case of jinan, China. *Land* 11 (6), 860. doi:10.3390/land11060860

Lu, Y., Chen, L., Yang, Y., and Gou, Z. (2018a). The association of built environment and physical activity in older adults: Using a citywide public housing scheme to reduce residential self-selection bias. *Int. J. Environ. Res. Public Health* 15 (9), 1973. doi:10.3390/ijerph15091973

Lu, Y., Sarkar, C., and Xiao, Y. (2018b). The effect of street-level greenery on walking behavior: Evidence from Hong Kong. *Soc. Sci. Med.* 208, 41–49. doi:10.1016/j.socscimed.2018.05.022

Lu, Y., Yang, Y., Sun, G., and Gou, Z. (2019). Associations between overhead-view and eye-level urban greenness and cycling behaviors. *Cities* 88, 10–18. doi:10.1016/j.cities.2019.01.003

Lubitow, A., and Miller, T. R. (2013). Contesting sustainability: Bikes, race, and politics in Portlandia. *Environ. Justice* 6 (4), 121–126. doi:10.1089/env.2013.0018

Ma, L., and Dill, J. (2015). Associations between the objective and perceived built environment and bicycling for transportation. *J. Transp. Health* 2 (2), 248–255. doi:10.1016/j.jth.2015.03.002

Mertens, L., Compernolle, S., Deforche, B., Mackenbach, J. D., Lakerveld, J., Brug, J., et al. (2017). Built environmental correlates of cycling for transport across Europe. *Health Place* 44, 35–42. doi:10.1016/j.healthplace.2017.01.007

Nagata, S., Nakaya, T., Hanibuchi, T., Amagasa, S., Kikuchi, H., and Inoue, S. (2020). Objective scoring of streetscape walkability related to leisure walking: Statistical modeling approach with semantic segmentation of Google Street View images. *Health. Place* 66, 102428. doi:10.1016/j.healthplace.2020.102428

Newman, P. W., and Kenworthy, J. R. (1996). The land use—Transport connection: An overview. *Land use policy* 13 (1), 1–22. doi:10.1016/0264-8377(95)00027-5

Salvo, D., Reis, R. S., Stein, A. D., Rivera, J., Martorell, R., and Pratt, M. (2014). Characteristics of the built environment in relation to objectively measured physical activity among Mexican adults, 2011. *Prev. Chronic Dis.* 11, 140047. doi:10.5888/pcd11.140047

Sarmiento, O. L., Schmid, T. L., Parra, D. C., Díaz-del-Castillo, A., Gómez, L. F., Pratt, M., et al. (2010). Quality of life, physical activity, and built environment characteristics among colombian adults. *J. Phys. Activity Health* 7 (2), S181–S195. doi:10.1123/jpah.7.s2.s181

Tobler, W. R. (1970). A computer movie simulating urban growth in the Detroit region. *Econ. Geogr.* 46 (1), 234–240. doi:10.2307/143141

Troped, P. J., Wilson, J. S., Matthews, C. E., Cromley, E. K., and Melly, S. J. (2010). The built environment and location-based physical activity. *Am. J. Prev. Med.* 38 (4), 429–438. doi:10.1016/j.amepre.2009.12.032

Wang, H., Dai, X., Wu, J., Wu, X., and Nie, X. (2019). Influence of urban green open space on residents' physical activity in China. *BMC public health* 19 (1), 1093–1112. doi:10.1186/s12889-019-7416-7

Wexner, L. B. (1954). The degree to which colors (hues) are associated with mood-tones. *J. Appl. Psychol.* 38 (6), 432–435. doi:10.1037/h0062181

Yang, H., Lu, X., Cherry, C., Liu, X., and Li, Y. (2017). Spatial variations in active mode trip volume at intersections: A local analysis utilizing geographically weighted regression. *J. Transp. Geogr.* 64, 184–194. doi:10.1016/j.jtrangeo.2017.09.007

Yang, J., Bao, Y., Zhang, Y., Li, X., and Ge, Q. (2018). Impact of accessibility on housing prices in Dalian city of China based on a geographically weighted regression model. *Chin. Geogr. Sci.* 28 (3), 505–515. doi:10.1007/s11769-018-0954-6

Yang, L., Ao, Y., Ke, J., Lu, Y., and Liang, Y. (2021a). To walk or not to walk? Examining non-linear effects of streetscape greenery on walking propensity of older adults. *J. Transp. Geogr.* 94, 103099. doi:10.1016/j.jtrangeo.2021.103099

Yang, L., Chau, K. W., Szeto, W. Y., Cui, X., and Wang, X. (2020a). Accessibility to transit, by transit, and property prices: Spatially varying relationships. *Transp. Res. Part D Transp. Environ.* 85, 102387. doi:10.1016/j.trd.2020.102387

Yang, L., Chu, X., Gou, Z., Yang, H., Lu, Y., and Huang, W. (2020b). Accessibility and proximity effects of bus rapid transit on housing prices: Heterogeneity across price quantiles and space. *J. Transp. Geogr.* 88, 102850. doi:10.1016/j.jtrangeo.2020.102850

Yang, L., Liu, J., Liang, Y., Lu, Y., and Yang, H. (2021b). Spatially varying effects of street greenery on walking time of older adults. *ISPRS Int. J. Geoinf.* 10 (9), 596. doi:10.3390/ijgi10090596

Yang, L., Tang, X., Yang, H., Meng, F., and Liu, J. (2022a). Using a system of equations to assess the determinants of the walking behavior of older adults. *Trans. GIS* 26 (4), 1339–1354. doi:10.1111/tgis.12916

Yang, L., Yu, B., Liang, P., Tang, X., and Li, J. (2022b). Crowdsourced data for physical activity-built environment research: Applying Strava data in Chengdu, China. *Front. Public Health* 10, 883177. doi:10.3389/fpubh.2022.883177

Yin, L., and Wang, Z. (2016). Measuring visual enclosure for street walkability: Using machine learning algorithms and Google Street View imagery. *Appl. Geogr.* 76, 147–153. doi:10.1016/j.apgeog.2016.09.024

Ying, Z., Ning, L. D., and Xin, L. (2015). Relationship between built environment, physical activity, adiposity, and health in adults aged 46-80 in Shanghai, China. *J. Phys. Act. Health* 12 (4), 569–578. doi:10.1123/jpah.2013-0126

Yu, H., Yang, J., Li, T., Jin, Y., and Sun, D. (2022a). Morphological and functional polycentric structure assessment of megacity: An integrated approach with spatial distribution and interaction. *Sustain. Cities Soc.* 80, 103800. doi:10.1016/j.scs.2022.103800

Yu, H., Yang, J., Sun, D., Li, T., and Liu, Y. (2022b). Spatial responses of ecosystem service value during the development of urban agglomerations. *Land* 11 (2), 165. doi:10.3390/land11020165

Zhang, Y., van Dijk, T., and Wagenaar, C. (2022). How the built environment promotes residents' physical activity: The importance of a holistic people-centered perspective. *Int. J. Environ. Res. Public Health* 19 (9), 5595. doi:10.3390/ijerph19095595

Zhao, P. (2013). The impact of the built environment on bicycle commuting: Evidence from beijing. *Urban Stud.* 51 (5), 1019–1037. doi:10.1177/0042098013494423

Zhao, P., and Wan, J. (2020). Examining the effects of neighbourhood design on walking in growing megacity. *Transp. Res. part D Transp. Environ.* 86, 102417. doi:10.1016/j.trd.2020.102417

frontiers | Frontiers in Ecology and Evolution

TYPE Original Research
PUBLISHED 10 October 2022
DOI 10.3389/fevo.2022.1031517

Check for updates

OPEN ACCESS

EDITED BY
Bing Xue,
Institute for Advanced Sustainability Studies (IASS), Germany

REVIEWED BY
Lei Wang,
Shandong Normal University, China
Kun Jia,
Shandong Jianzhu University, China
Wenhao Li,
Nanjing Tech University, China
Bao-Jie He,
Chongqing University, China

*CORRESPONDENCE
Hongmin An
anhm@sdu.edu.cn
Dongrui Han
handr@lreis.ac.cn

SPECIALTY SECTION
This article was submitted to Environmental Informatics and Remote Sensing, a section of the journal Frontiers in Ecology and Evolution

RECEIVED 30 August 2022
ACCEPTED 20 September 2022
PUBLISHED 10 October 2022

CITATION
Liu Y, Xu X, Wang F, Qiao Z, An H, Han D and Luo J (2022) Exploring the cooling effect of urban parks based on the ECOSTRESS land surface temperature.
Front. Ecol. Evol. 10:1031517.
doi: 10.3389/fevo.2022.1031517

COPYRIGHT
© 2022 Liu, Xu, Wang, Qiao, An, Han and Luo. This is an open-access article distributed under the terms of the Creative Commons Attribution License (CC BY). The use, distribution or reproduction in other forums is permitted, provided the original author(s) and the copyright owner(s) are credited and that the original publication in this journal is cited, in accordance with accepted academic practice. No use, distribution or reproduction is permitted which does not comply with these terms.

Exploring the cooling effect of urban parks based on the ECOSTRESS land surface temperature

Yihui Liu[1,2], Xinliang Xu[3], Fei Wang[4], Zhi Qiao[5], Hongmin An[6]*, Dongrui Han[4]* and Jie Luo[7]

[1]Urban and Rural Planning Research Center, Linyi Bureau of Natural Resources and Planning, Linyi, China, [2]School of Civil and Architectural Engineering, Linyi University, Linyi, China, [3]State Key Laboratory of Resources and Environmental Information System, Institute of Geographic Sciences and Natural Resources Research, Chinese Academy of Sciences, Beijing, China, [4]Institute of Agricultural Information and Economics, Shandong Academy of Agricultural Sciences, Jinan, China, [5]School of Environmental Science and Engineering, Tianjin University, Tianjin, China, [6]School of Management, Shandong University, Jinan, China, [7]School of Remote Sensing and Information Engineering, Wuhan University, Wuhan, China

Understanding the cooling effect (CE) of urban parks is vital to mitigate the urban heat islands. ECOsystem Spaceborne Thermal Radiometer Experiment on Space Station (ECOSTRESS) land surface temperature data (LST) data were used to construct diurnal thermal variations to explore the CE of urban parks in the fifth ring regions of Beijing. Local climate zone (LCZ) classification was used to distinguish different parks for examining the internal CE of parks. New subclasses of LCZ (e.g., LCZAG, LCZBG, LCZCG) were created based on the basic subclasses, such as LCZA (mainly consist of dense trees), LCZB (scattered tress with dense bush), LCZC (scattered bush), and LCZG (water). The external CE of parks was evaluated in different directions, and the impacts of buildings around parks on the external CE were also analyzed. The results showed that urban parks tended to heat up slower than the whole urban regions during the daytime, and water releasing energy dominated the mean LST of parks at night. Large parks meeting the minimum area (40,000 m^2) of LCZ had better CE inside each park during the daytime. Three hundred thirty four large parks were divided into six types of LCZ. The strength of the CE decrease with the increases of distance, and seemed to exist at a distance of up to 150–200 m. Such impacts of parks were insignificant at night. In addition, parks containing

certain dense trees and water had better CE inside and out. The height and density of buildings had a relatively obvious impact on the CE of parks. This study can provide insight into the impacts of urban parks on the urban thermal environment and promote the CE of urban parks in future urban planning.

KEYWORDS

cooling effect, urban park, local climate zone, thermal variation, diurnal cycling

Introduction

Rapid urbanization, landscapes changing, growth of urban residents, and anthropogenic activities increased, have a significant influence on the local climate, leading to urban heat islands (UHI) effects (Oke, 1982; Mackey et al., 2012; Buo et al., 2021). Inevitably, the effects seriously threaten the quality and health of residents, and the negative effects will be exacerbated in the future under the context of urbanization and global warming (Yang et al., 2021b; You et al., 2021). It is provided that there is localized interplay between heat waves and UHI (He et al., 2020). The urban heat wave has become an important issue in China for environmental, ecosystem, social, health consequences, and economic impacts (He et al., 2022). Therefore, how to mitigate the UHI effects and provide a comfortable living environment for residents has drawn the attention of urban planners (Qiao et al., 2019; Maharjan et al., 2021).

Urban parks, which consist of forests, grasslands, and water bodies, have been regarded as a promising method to mitigate the UHI effects with 1∼7°C lower temperature distributed in and around parks (Xu et al., 2017; Yan et al., 2018; Yao et al., 2022). Many previous studies have investigated the cooling effect (CE) of parks, and noted that the size and shape of the park can effectively affect the CE of parks (Chang and Li, 2014; Cheng et al., 2015, 2019; Dai et al., 2018). Importantly, the CE of parks is influenced by landscape compositions and configurations inside and around parks (Xu et al., 2018; Han et al., 2020; Gao et al., 2022). For interior conditions, it is widely accepted that landscapes of parks, such as forests and grasslands, can take away some heat because of their evaporation and evapotranspiration (Li et al., 2021; Lin et al., 2021; Yang et al., 2021a). A series of landscape composition and configuration metrics, such as percentage of landscape (PLAND), landscape shape index (LSI), and aggregation index (AI), were widely used to investigate the relationship between landscapes and land surface temperature (LST) (Peng et al., 2021; Qin et al., 2021; Yu et al., 2022). Furthermore, the characteristics of the area around the park, such as impervious surface and road, had a significant influence on the CE of parks (Feng and Myint, 2016; Lin et al., 2021; Luo et al., 2021).

However, there are only a few studies evaluating the CE among different urban parks. Previous studies considered the parks as a whole, or analyzed UHI based on urban green space containing urban parks as a whole (Chang et al., 2021). It's important to note that the characteristics of different vegetation (e.g., tree and bush) and water have a huge difference (e.g., heat capacity and reflectivity) (Chen et al., 2015; Kong et al., 2021; Yang et al., 2020, 2021c). It is necessary to consider the types of parks in the research of the CE (Zhu et al., 2021). LCZ derived from logical division of the landscape (Stewart, 2011), can be used to overcome the limitations of the "urban-rural" dichotomy and to further investigate the impacts of park forms on the CE at local scales (Stewart and Oke, 2012; Yang et al., 2019; Wu et al., 2020). The urban landscapes can be divided into seven basic land cover types with considering their interior and external landscape composition and configuration metrics (Stewart and Oke, 2012). Furthermore, LCZ can divide landscapes into new types based on the surface cover, structure, material, and human activity, which provides a possibility for exploring the different spatial formation of urban landscapes at smaller scales (Stewart and Oke, 2012). To quickly and precisely determine types of parks, a machine learning algorithm based on the deep residual network, which has been widely used for classification, will be applied to this study (He et al., 2016). Additionally, the surrounding conditions of the parks are complicated, and the impacts of surrounding buildings (two- and three-dimensional perspectives) on the CE of parks are still less understood (Qiao et al., 2020; Amani-Beni et al., 2021; Chen et al., 2022). The precise building data, including building footprints and height, make it possible to explore the impacts of surrounding buildings on the CE of parks (Yang et al., 2018). LCZ is not used to classify the regions around urban parks in this study. Because the thermal climate is spatially continuous (Stewart and Oke, 2012), the buildings closer to the parks are possible to have stronger impacts on the CE of parks.

The study aims to investigate the CE of parks and the impacts of surrounding buildings on them. The objects of this study were (1) to determine park types using basic LCZ subclasses and new subcalsses created with considering the impacts of water (e.g., LCZ-A, AG, B, BG, C, and CG); (2) to investigate the CE of parks at different times among different types of parks; and (3) to explore the impacts of surrounding buildings on CE of different types of parks. This

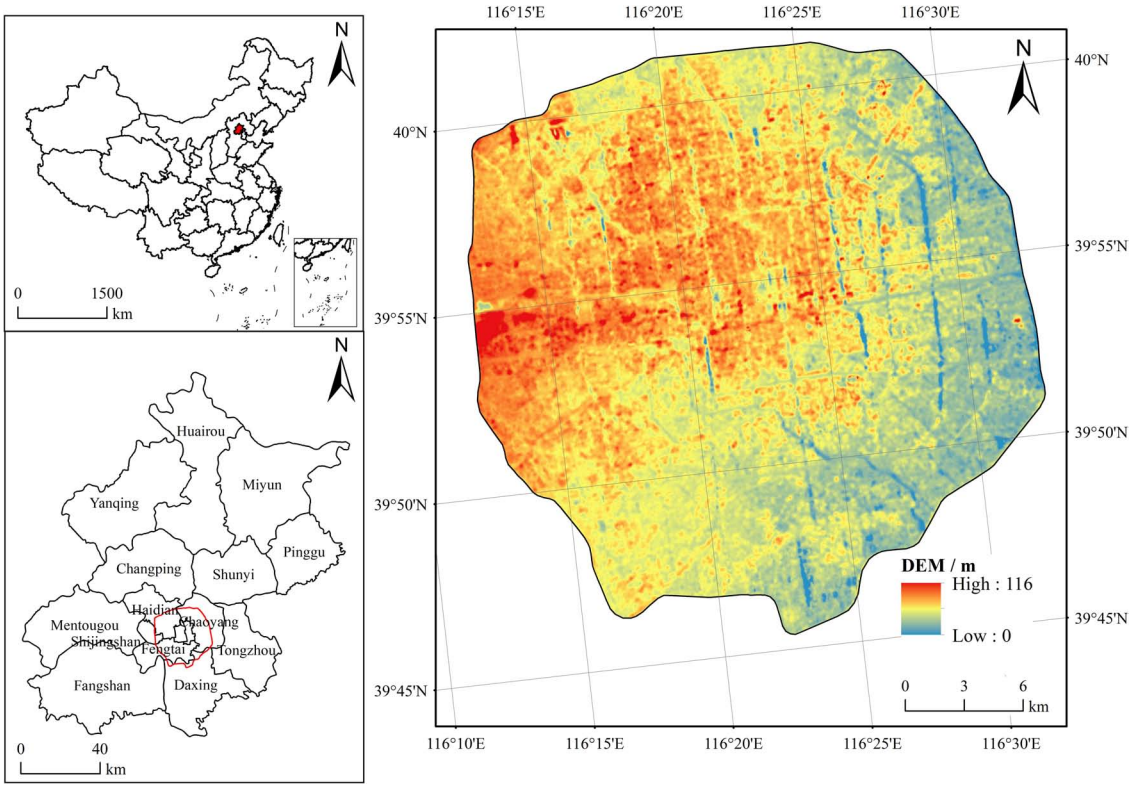

FIGURE 1
Location and digital elevation model of the study area.

study provides scientific guidance to urban planners on how to optimize the design of parks and provides a basis for improving the CE of parks.

Materials and methods

Study area

Beijing, the capital of China, is located in the north of China (39°26'-41°03'N, 115°25'-117°30'E) (Figure 1). It has a warm-temperate, semi-humid continental monsoon climate. It is the political, cultural, and international communication center, as well as the highest urbanization level city in China. The study area is located within the fifth ring road, which covers an area of approximately 668 km^2. Residents are dense and buildings are diverse in this region, leading to a severe UHI effect. According to the China National Bureau of Statistics, the urban green coverage (48.5%) of Beijing is the highest in China.[1] The urban parks are the vital part of urban greening system, and play a key role in mitigating UHI effects. Therefore, this region was chosen as the study area to investigate the CE of parks and the impacts of surrounding buildings on them.

Data source

ECOSTRESS LST data, park boundary data, Map World images, and building datasets were used in this study, and the details are as follows.

TABLE 1 The time of ECOSTRESS 2B-LST data, and their corresponding weather condition.

Data	Time	Max-Min air temperature (°C)	Wind speed (m/s)	Weather condition
20220617	7:11	30–21	≤3.3	Partly cloudy
20220602	13:37	35–20	≤3.3	Partly cloudy
20220529	15:13	28–14	≤1.5	Fine
20220521	18:24	34–19	≤3.3	Fine
20220606	18:30	28–16	≤3.3	Fine
20220602	20:07	35–20	≤3.3	Fine
20220529	21:43	28–14	≤1.5	Fine
20220522	0:54	34–20	≤3.3	Fine

1 http://www.stats.gov.cn/

TABLE 2 LCZ classification of urban park.

LCZ type	Park type	Percentage of green coverage*	Percentage of water coverage	Images
A	Dense tress	>70	<10	
AG	A with water	>70	>10	
B	Scattered tress with dense bush	>40	<10	
BG	B with water	>40	>10	
C	Scattered bush	<40	<10	
CG	C with water	<40	> 10	

*Water coverage is not included in the total area.

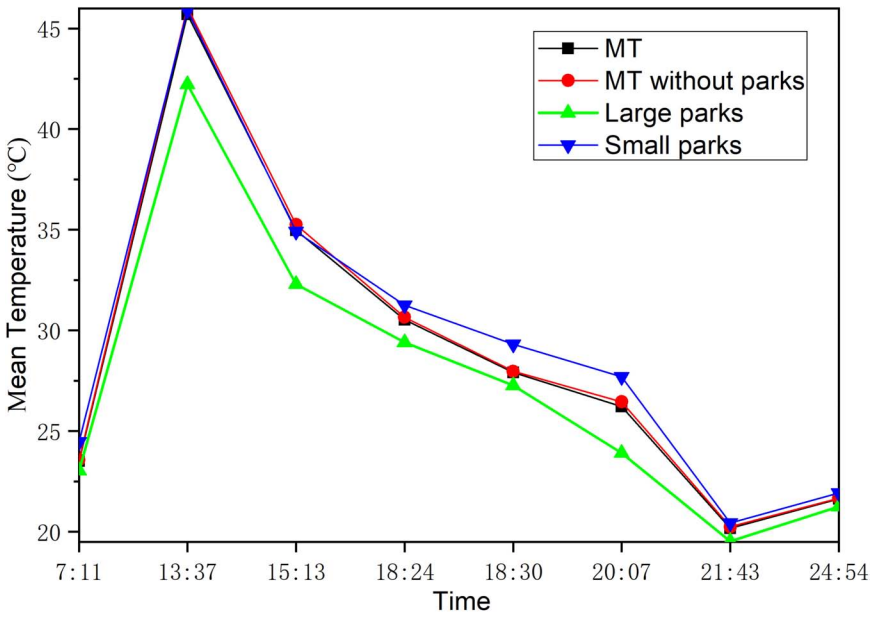

FIGURE 2
Mean LST at different time in fifth ring. Mean temperature (MT) in fifth ring is shown in black line, in fifth ring without parks is in red line, in large parks (>40,000 m^2) is in green line and in small parks is in blue line.

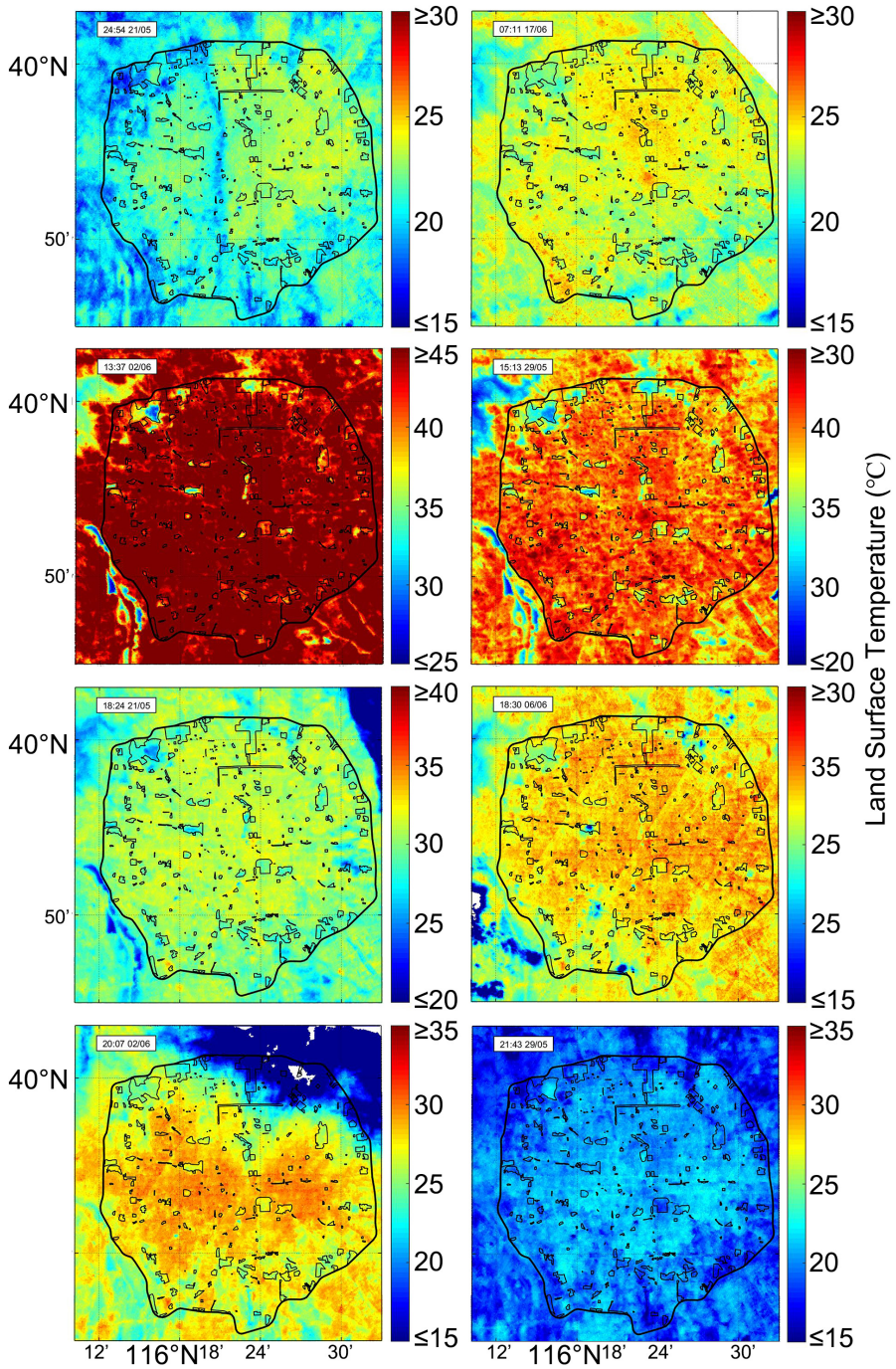

FIGURE 3
The distribution of LST at different time in fifth ring, and the measuring time is shown on the left top of each figures. The time is Beijing time (UTC + 8).

LST data are provided by the ECOsystem Spaceborne Thermal Radiometer Experiment on Space Station (ECOSTRESS), which is aimed at measuring the temperature of the earth and estimating the water requirement of plants. The ECOSTRESS mission is operated by the National Aeronautics and Space Administration Land Processes Distributed Active Archive Center[2] started on June 29, 2018. The Prototype HyspIRI Thermal Infrared Radiometer placed on the satellite can measure middle and lower latitude regions (53°N-53°S)

2 https://lpdaac.usgs.gov/

with a measuring resolution of $\leq$ 0.3 K and horizontal resolution of 70 m (Hook et al., 2020). The Level-2 LST data is retrieved by the physics-based Temperature Emissivity Separation algorithm based on the five thermal infrared bands (8–12.5 μm).

The satellite uses a processing orbit rather than a sun synchronous orbit, and can cross over the same region at different times of the day compared with Landsat and MODIS. Thus, it provides a feasible way to construct the diurnal variation LST in some regions (Chang et al., 2021). Although the influence of daily weather variations cannot be ignored (Hu et al., 2016), it is widely acknowledged that the CE of parks does indeed exist in different temperatures and regions. In addition, the urban form will maintain stable for a relatively short time. Therefore, the ECOSTRESS data from different days are used to analyze the CE of parks. Because the temperature in Beijing is more than 30°C lasting for 1 week since May 18, and rainy weather occurred after June 22, to better estimate the CE of the urban parks during the warmest months, eight ECOSTRESS 2B-LST data during a month are used in this study (**Table 1**).

The urban parks are the important part of urban green system, and provide relaxed and entertainment places for citizens. The parks which have these functions and clear names have been estimated in this study, and parks covering more than 400 m^2 have been classified into different LCZs. The park boundary data are acquired using Baidu Map API.[3] The park boundary data are revised by high-resolution images (<0.6 m) provided by Map World of the China State Bureau of Surveying and Mapping.[4] Three hundred and fifty six urban parks have been investigated, and the larger parks are mainly distributed in the north of the fifth ring.

Building datasets are derived from the Resources and Environmental Scientific Data Center (RESDC), Chinese Academy of Sciences (CAS).[5] Several parameters of buildings, such as building outline, the number of floors, and the height of buildings, are included in this dataset. It provides fundamental data for analysis of impacts of neighboring buildings on the CE of parks.

Methodology

Local climate zone classifications of parks

The park forms are not exactly the same. Parks are possibly formed by dense tress, scattered tress, bush, or water. To better understand the CE of different parks, the method of LCZ classification is used in this study. The LCZ classification has been widely used to investigate the impacts of urban form on LST, and has seven land cover types including dense trees, scattered trees, bush, low plants, bare rock, bare soil, and water (from A to G) (Stewart and Oke, 2012). Since none of these parks are only formed with grass, we use three types of LCZ (LCZA, LCZB, and LCZC) and create new subclasses for those parks containing water (LCZAG, LCZBG, and LCZCG) (**Table 2**). In addition, previous studies point out that LCZ region should have a minimum radius of 200 m (Stewart and Oke, 2012). Thus, only the parks covering more than 400 m^2 have been used.

Then, a deep residual network (ResNet) is used for artificial intelligence automatic classification of parks on the basis of high-resolution images provided by Map World. This method uses a residual learning framework to ease the training of networks and solve the degradation problem (He et al., 2016). At last, the artificial visual interpretation method is used to correct the classification results.

Cooling effect of parks

Inside and outside CE of parks were investigated in this study. For inside CE of park, the average temperature of each type of park at different times were compared. For outside CE of park, buffer analysis was adopted to analyze LST differences of different types of parks within a certain buffer distance (e.g., 30, 60, and 90 m). Furthermore, the CE of parks is different in different directions. Therefore, the CE of parks is averagely distributed at eight orientations, including north (N), northeast (NE), east (E), southeast (SE), south (S), southwest (SW), west (W), and northwest (NW).

Impacts of buildings on cooling effect of parks

To better understand the impacts of surrounding buildings on the CE of parks, a building dataset with outline and height was used in this study. In this study, three perspectives, including average height, density, and shape of buildings, will be adopted to investigate the impacts of buildings on the CE of parks. Particularly, the density and shape of a building can be calculated by building height (BH), building density (BD), and landscape shape index (LSI), respectively. Then, these indicators in eight directions can be calculated within a certain buffer distance. Finally, the impacts of buildings will be analyzed from the above perspectives.

Results

The diurnal variations of land surface temperature

The diurnal variations of mean LST in the fifth ring are showed in **Figure 2** with the time coverage from 24:54 to 21:43. It was obvious that LST during the daytime was higher than it during the night. LST in the morning (7:11) was about 3.34°C higher than at night (21:43), and LST at noon (13:37) was almost 2 times higher than at night. It indicated that urban landscapes would be quickly heated by solar radiation. LST in the large

3 https://lbsyun.baidu.com/
4 http://lbs.tianditu.gov.cn/
5 www.resdc.cn

parks was about 3.49°C lower than in the whole urban regions, but in the small parks was similar to other urban regions. As expected, the CE was better inside the large parks. The weak influence of small parks was possible due to the limited area and vegetation coverage, and LST in small parks was influenced easily by the surrounding environment. The difference (2.63°C) in the mean temperature of LST at 18:24 (21 May) and 18:30 (6 June) was mainly caused by the day-to-day variations. The release of the remained energy from buildings and waters, and human activities led to the increase of LST at midnight (Chan and Chau, 2021).

LST in the different regions of the fifth ring showed similar trends between day and night (Figure 3). The regions close to the fifth ring showed lower LST all day owing to the low-rise buildings (e.g., factories) were generally located in the suburbs. LST in the urban parks, especially in the large parks (e.g., Beihai park, Tiantan park, Chaoyang park, and so on) was obviously low during daytime. However, the CE of parks had limited impacts on the surrounding environment with extremely high temperatures, e.g., at 13:37. At night, the parks containing a mass of water (e.g., the Summer Palace located in the northwest) released energy rising local temperature, but the rise of LST was mainly distributed in the urban built-up area, e.g., in the northeast region. In addition, there was a low temperature corridor running through the south and north of the fifth ring at 24:54, which was consistent with ventilation corridors found in a previous study (Qiao et al., 2017).

The local climate zone classification of urban parks

The urban parks in the fifth ring have been classified into six zones based on the main vegetation types: dense trees with water or not (LCZAG or LCZA), scattered stress and dense bush with water or not (LCZBG or LCZB), scattered bush with water or not (LCZCG and LCZC). The spatial distributions of parks was imbalanced as showed in Figure 4. LCZAG was mainly distributed in the middle and northwest, and LCZA and LCZBG were concentrated in the north of the fifth ring. LCZB was the major form of urban parks widely distributed in urban regions. LCZC with less vegetation coverage and a large bare area was located in the south.

Figure 5 shows the number and mean area of different parks. LCZB had 143 urban parks with a mean area of 0.127 km^2 accounting for 42.5% of all large parks. The mean area of LCZC was similar to LCZB, but LCZC had obvious open spaces. The number of LCZA was less than LCZB and LCZC, because dense trees within a large area would weaken the service function of urban parks for cultural activities and entertainments. The source of water had restricted the presence of LCZAG, LCZBG, and LCZCG, and water also resulted in the larger area of these parks.

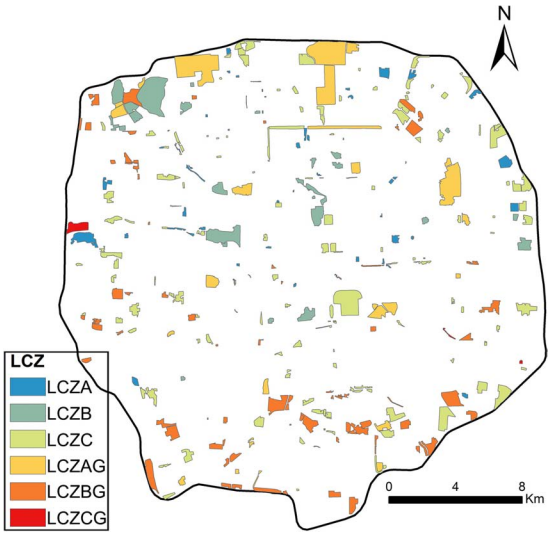

FIGURE 4
The distribution of different types of urban parks.

The cooling effect of urban parks

The CE existed in and out of the urban parks. Figure 6 shows the mean temperature inside different parks, which had a similar trend to the whole urban area (Figure 2). All parks had the highest LST at noon and the lowest LST at midnight. It is suggested that strong solar radiation was the dominant reason for the rise in urban temperature. The vegetation coverage and density of trees led to the different CE of parks with few water during daytime. Mean LST in LCZAG was the lowest during the daytime, and LCZC was the opposite. The parks with water were cooler than LCZA, LCZB, and LCZC. The difference in CE between the parks with water or not was larger with higher air temperature possibly caused by the specific heat capacity of water. LCZBG and LCZCG showed similar LST at daytime, e.g., about 41.02°–40.29°C at 13:37, and 31.77°–32.29°C. It should be noted that LCZCG was mainly located in the south with lower LST. After nightfall, LCZBG and LCZA could provide a more comfortable environment for rest and entertainment with lower LST (20.86° and 23.14°C, respectively).

Mean LST around parks at different distances and times was showed in Figure 7. The closer to parks, the stronger CE existed during daytime (e.g., 13:37 and 15:13) especially at a distance of 50 m. LST had an obvious increase at a distance of 100 m, and increases gradually with the increase of distance. LCZAG showed the best CE in the daytime compared with other types of parks. Different from CE inside parks, LST around LCZA was lower than LCZBG and LCZCG (e.g., at 15:13). However, CE of LCZBG was similar to LCZA within the range of 100 m under hotter conditions (e.g., at 13:37). It is suggested that water can play a bigger role in such conditions. At night, a relatively low

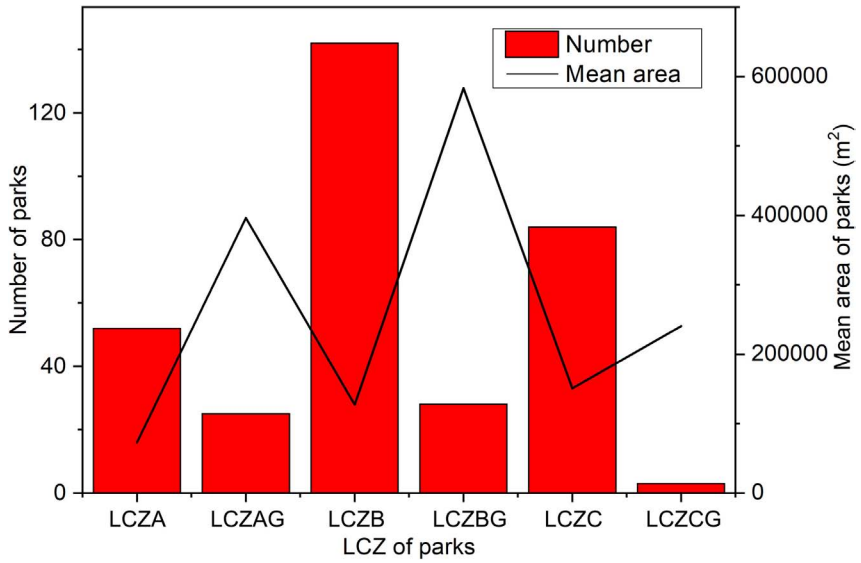

FIGURE 5
The number of parks (Number) and mean area of parks (Mean area).

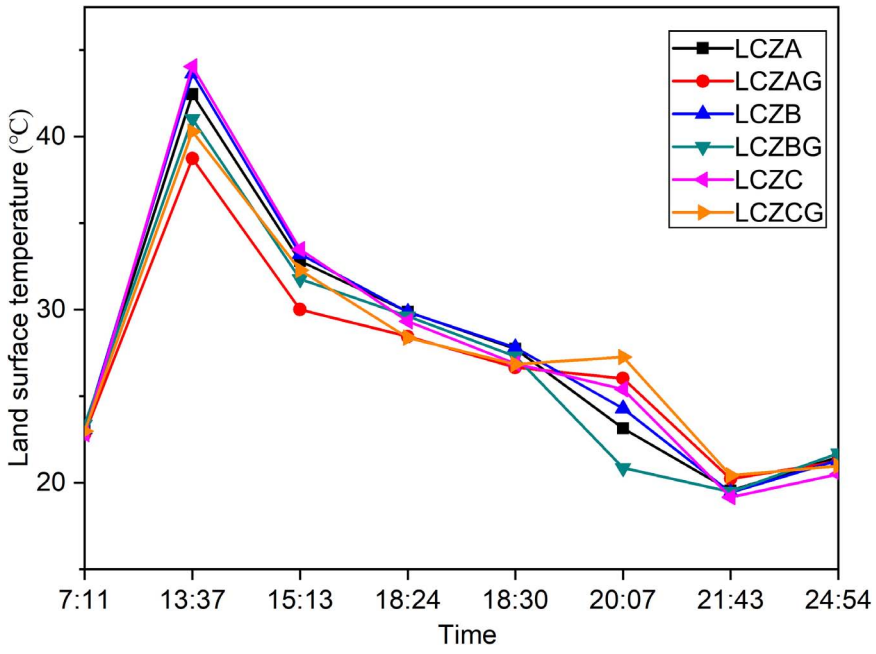

FIGURE 6
The mean land surface temperature of parks at different time.

LST was around LCZC probably due to its open space. LCZAG, LCZBG, LCZA, and LCZB had less open space likely resulting in the reduction of airflow and higher LST around them.

The spatial distribution of LST around different parks have been examined at the hottest time (13:37). The LST around LCZC and LCZCG had not been showed in Figure 8 due to the weaker CE in the daytime and the number of parks, respectively. The areas of all parks in the radar map were increasing with the increase of distance to parks, and have few increases for a distance of after 200 m. It indicated the same result as Figure 7 that the potential CE of parks could influence the outer regions of parks within a radius of 200 m. LST around LCZA was high in the south which was similar to LCZB, on the contrary, LST around LCZAG was relatively low, especially in the north and

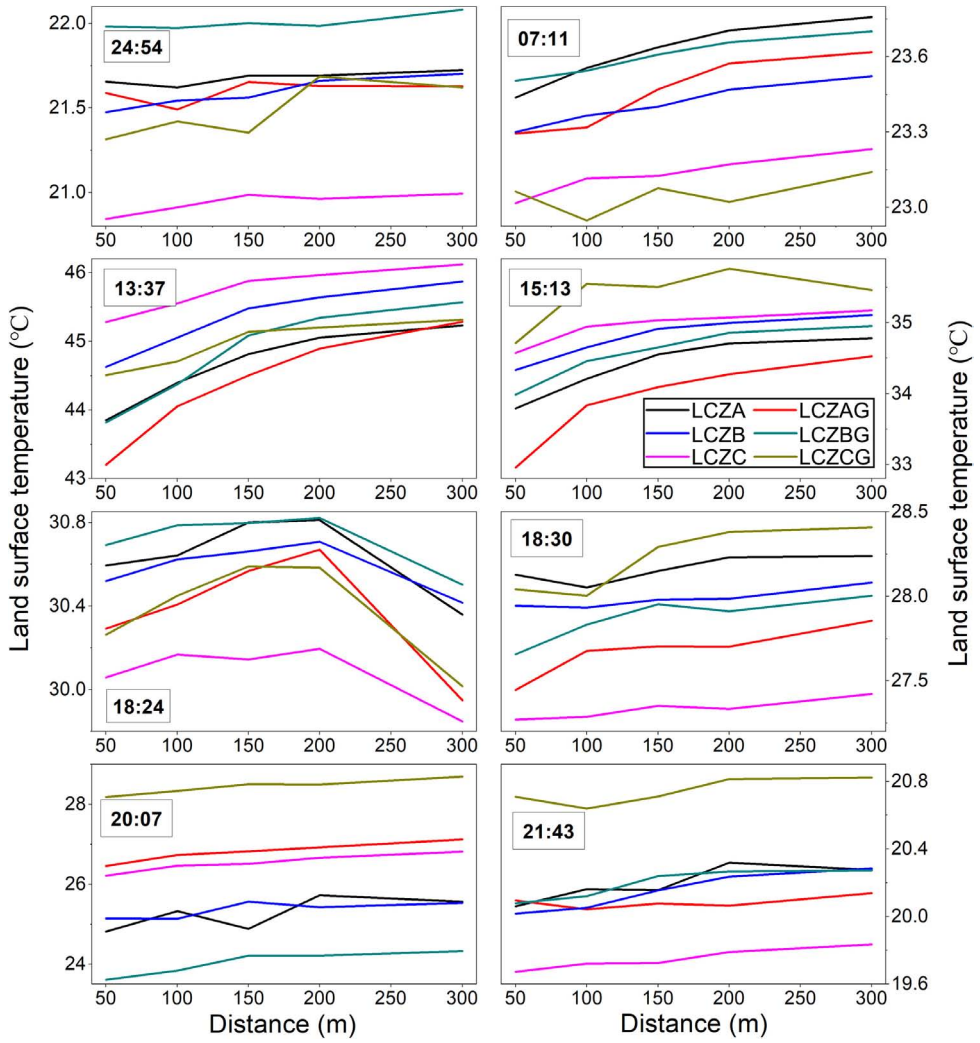

FIGURE 7
The mean land surface temperature round each park at different distances. The x axes present the distance from the regions to parks, e.g., 50 presents 0–50 m, 100 presents 50–100 m.

northwest. The CE of LCZBG was obviously weak in the west and southwest.

The impacts of building form on urban parks

To make a further insight into the CE of urban parks, the building form around parks has been investigated as showed in Figure 9. The mean BH was lower at a distance of 50 m to parks mainly caused by the neighboring parks instead of buildings. It was seemed that higher buildings located in the north show few impacts on the LST, probably due to the direction of the summer monsoon breezing from the southeast. LCZAG showed better CE (Figure 7), but the effect was probably reduced by higher buildings in the east and west. Such an impact of buildings also occurred for LCZBG in the southwest. Higher buildings located around LCZA may be the reason that made the CE of LCZA similar to LCZB (Figure 8). The distribution of BH around LCZBG and LCZB showed few changes. In response to this, the distribution of LST around LCZBG and LCZB had insignificant changes at 50 m or 100 m. In addition, the distribution changes of BH at a further distance (e.g., 200 or 300 m) made less impact on the LST around parks. It is also suggested that the range of the CE of parks was limited.

Figure 10 shows LCZBD indexes in eight directions around four types of urban parks. The closer to parks, the indexes were lower, and the indexes distributed on the north-south of parks were relatively low. The regions around LCZAG showed the highest indexes at different distances, especially on the east and southeast of parks, which probably led to weak CE of LCZAG in

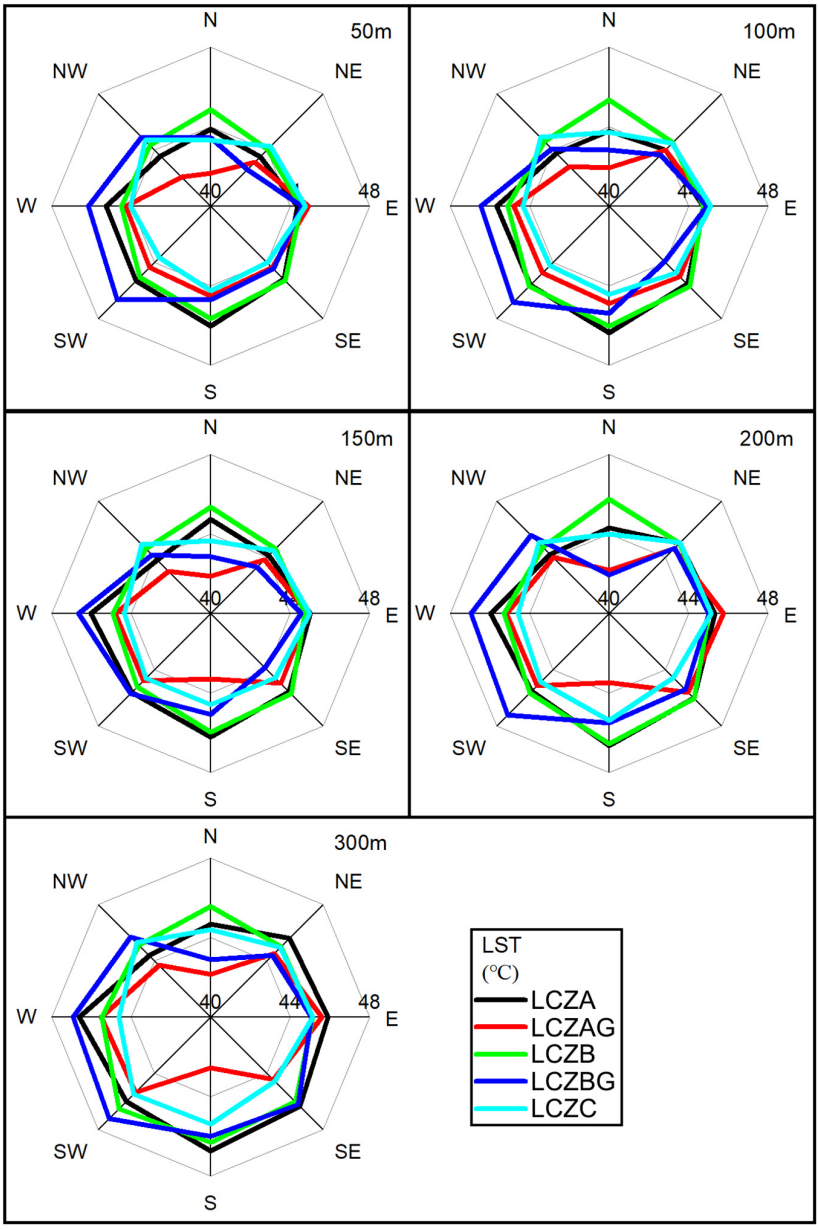

FIGURE 8
The distribution of LST around parks. Eight axes present the LST located around parks in eight direction.

this direction as showed in Figure 8. LCZA and LCZB showed similar indexes, and this similarity occurred in the distribution of LST. Higher indexes were located in the southwest of LCZBG which was not consistent with the distribution of LST.

LSI of buildings around urban parks was showed in Figure 11. The indexes increased rapidly with distance to parks. The shape of buildings around LCZB was the most complicate in all directions. Higher indexes were located in the southeast of LCZA, and in other directions LCZAG, LCZA, and LCZBG showed similar indexes. However, the rapidly growing trend and the distribution of LSI showed insignificant relationships with LST around parks. It probably indicated the shape of buildings had weak impact on the CE of parks to a certain extent.

Discussion

Construction of land surface temperature diurnal variations data

Diurnal variations data of LST are constructed based on the data measured at different times when the satellite passed

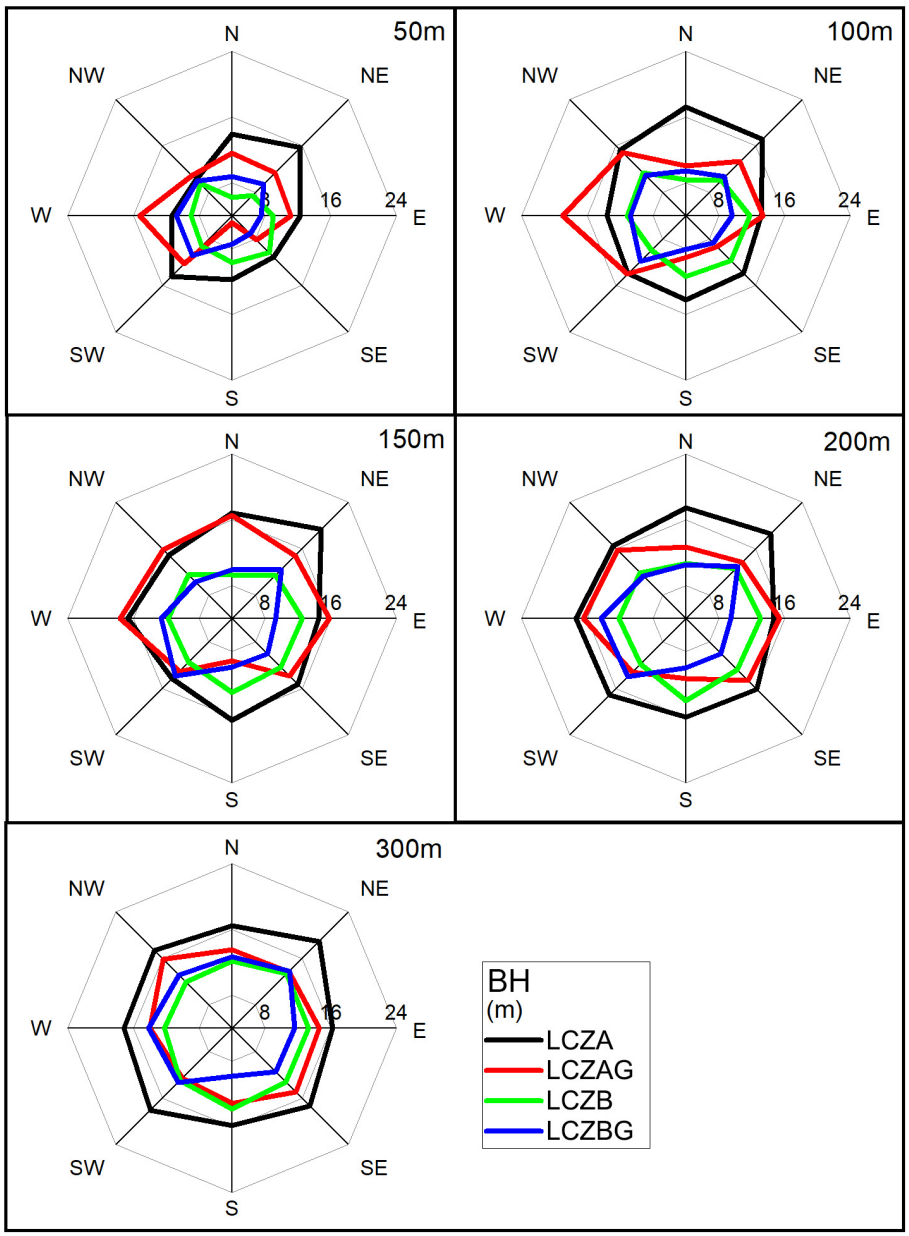

FIGURE 9
The distribution of BH around parks, and eight axes present the height of buildings located around parks in eight direction.

over the study area during a summer month with fine weather conditions. Although day-to-day variations exist in LST on different days, such variations show limited influence on the daily changing rule of LST (Hu et al., 2016; Chang et al., 2021). We also examine LST data during other summer months which are not used in this study due to data quality or similar measuring time, and the available parts of those data show the same daily changing rule of LST. Therefore, ECOSTRESS LST data can be used to analyze diurnal thermal impacts of other urban landscapes in different regions of the world. It is worth noting that rainfall has an obvious impact on the ECOSTRESS data, especially during summer rains, and the time interval of revisit could last up to 10 days in different regions, e.g., pass over Chengdu (30.67°N, 104.06°E) in the southwest of China at June 6 and 17, 2022. In addition, LST is influenced by meteorological factors, such as wind speed, air temperature, and relative humidity. However, hourly and daily meteorological data are not easily obtained due to data availability. The impacts of these factors on LST should be taken into account in future research.

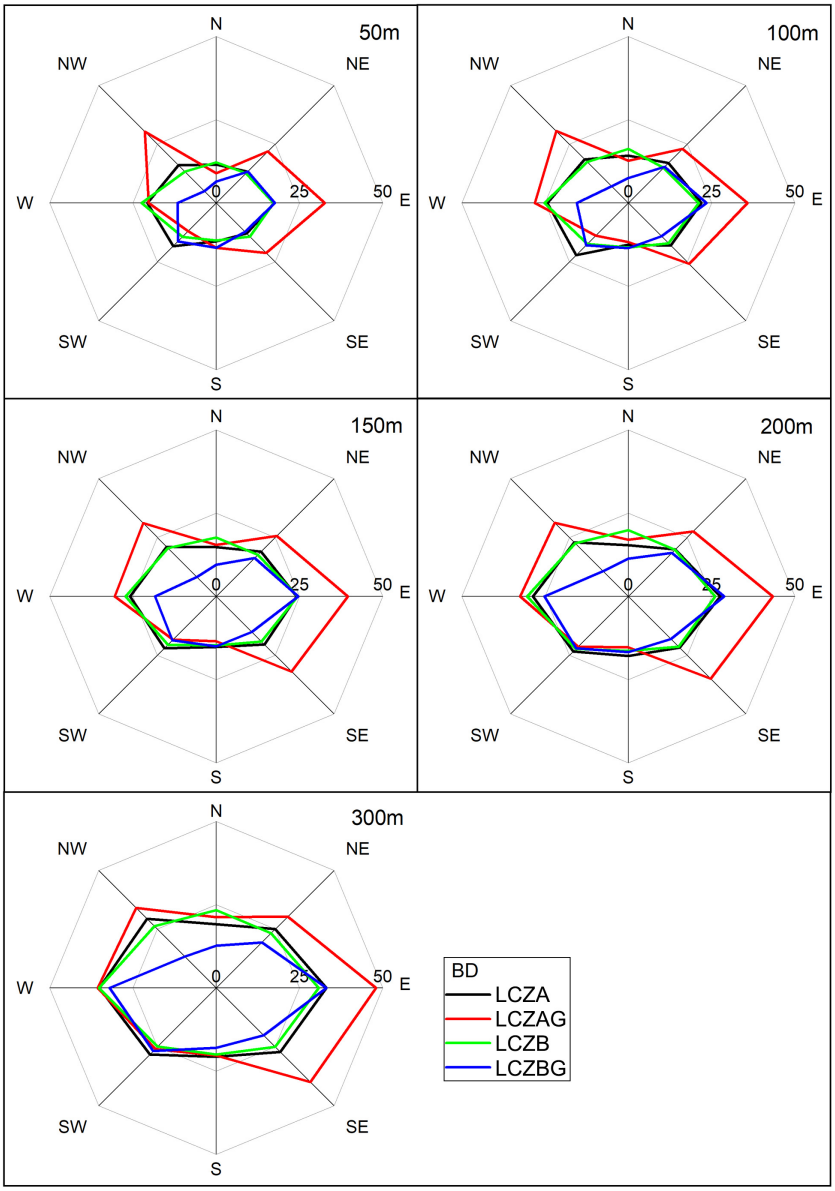

FIGURE 10
The BD at eight directions around different urban parks.

Differences in cooling effect of parks

Large parks heat up slowly compared with the whole urban regions during the daytime and show a relatively lower mean LST at the hottest time. But LST in small parks shows an insignificant difference with peripheral regions suggesting that the CE of these parks is weakened by the surrounding environment. The result agrees with previous studies that the region should have a minimum radius of 200 m to avoid the influence of the surrounding environment (Oke and Cleugh, 1987; Stewart and Oke, 2012). The impacts between different area and shape of different LCZ should be studied in the future.

To further evaluate the CE of urban parks, they have been divided into six LCZs. In the large parks, the higher vegetation coverage is corresponding the better CE (e.g., LCZAG and LCZA), and a certain amount of water can obviously strengthen the CE of parks with lower vegetation coverage (e.g., LCZBG and LCZCG). It is mainly due to the high specific heat capacity of water. It is also suggested that there should be more parks containing water to help mitigate UHI during daytime, and open spaces inside parks should belong to the water. The CE around parks is stronger within the distance of 150 m during daytime, and dominated by the vegetation coverage and types. The parks mainly composed of dense trees have better external

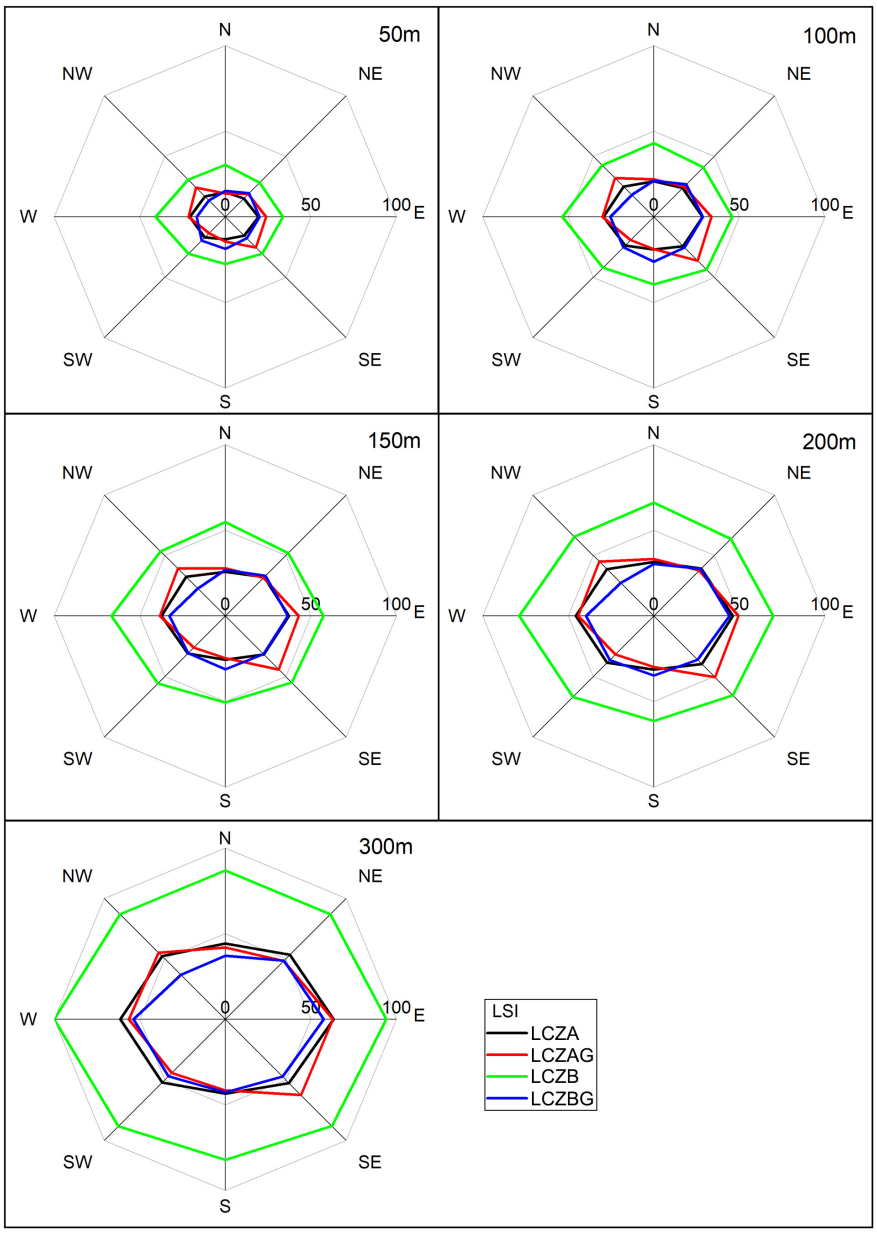

FIGURE 11
The LSI of buildings at eight directions around different urban parks.

CE (e.g., LCZAG and LCZA), and the water inside parks can magnify external CE to a certain extent. It should be noted that the external CE of different types of parks is not same in different directions. Furthermore, LCZBG shows better CE in the southeast compared with LCZAG, and all types of parks show similar CE in the east. It indicates that the external CE produced by the vegetation inside parks is significantly influenced by the external environment. Besides, water will make a warmer and damp environment inside parks at night, which will reduce the comfort of citizens. Therefore, further research is needed to explore heat exchange between parks and external environment, and to enhance the CE of different parks.

Spatial distribution optimization of parks

Urban landscapes would influence the thermal transitions between parks and their neighboring zones (Oke, 2006). Buildings are the dominant urban landscapes around the parks, and their heights impact the distribution of LST around Parks.

The CE of parks seemed to be limited to a distance of 150–200 m on the basis of types of parks. Thus, in order to bring the parks' CE into full play, it should build more parks containing certainly vegetation cover, water, and open space with a lower building located in the south. The height and density of buildings around parks in different directions were consistent with the distribution of LST in a specific direction for different parks. For example, higher buildings and more intensive buildings were corresponding to the higher LST on the west and southeast of LCZA, respectively, at a distance of 50 m. Furthermore, the influence factors on the CE of parks are comprehensive including the distance between buildings, dense, volumetric fraction, vegetation structure, and other open spaces. Therefore, it is necessary to evaluate the CE of each urban parks considering as many factors as possible in regions with different scales, and to quantify the impacts of building characteristics on the CE of different parks in further study. These studies are important to mitigate the urban heat island effects.

Conclusion

ECOSTRESS LST data can provide vital data to improve our understanding of the diurnal variations of LST in urban regions. This study aimed to construct synoptic LST data in the fifth ring of Beijing to investigate the CE of different urban parks, which is important for the research on urban heat mitigation strategies. An artificial intelligence method was used to help classify parks into six LCZs based on the park form. The CE of urban parks was obvious in the daytime, especially during the hottest time, and the heating effect occurred inside parks with certain water. The CE of all parks was stronger within 150 m and sharply reduced with the distance increased. The combination of vegetation and water was advantageous to enhance the CE. The impacts of the height, density, and shape of building distributed in different parks and different directions have been examined. The CE of urban parks were obviously influenced by higher and denser buildings.

Data availability statement

The original contributions presented in this study are included in the article/supplementary material, further inquiries can be directed to the corresponding author/s.

Author contributions

YL: conceptualization, methodology, and writing the original draft. XX: data curation and analysis. FW: investigation and formal analysis. ZQ: software and formal analysis. HA: analysis, supervision, and revising the manuscript. DH: conceptualization, supervision, and revising the manuscript. JL: software. All authors contributed to the article and approved the submitted version.

Funding

This research was funded by the National Natural Science Foundation of China (No. 41971389), Strategic Priority Research Program of the Chinese Academy of Sciences (No. XDA20010302), and Agricultural Science and Technology Innovation Project of Shandong Academy of Agricultural Sciences (No. CXGC2022E07).

Acknowledgments

We are grateful to the editor and reviewers for their valuable comments and suggestions.

Conflict of interest

The authors declare that the research was conducted in the absence of any commercial or financial relationships that could be construed as a potential conflict of interest.

Publisher's note

All claims expressed in this article are solely those of the authors and do not necessarily represent those of their affiliated organizations, or those of the publisher, the editors and the reviewers. Any product that may be evaluated in this article, or claim that may be made by its manufacturer, is not guaranteed or endorsed by the publisher.

References

Amani-Beni, M., Zhang, B., Xie, G.-D., and Odgaard, A. J. (2021). Impacts of the microclimate of a large urban park on its surrounding built environment in the summertime. *Remote Sens.* 13:4703. doi: 10.3390/rs13224703

Buo, I., Sagris, V., Burdun, I., and Uuemaa, E. (2021). Estimating the expansion of urban areas and urban heat islands (UHI) in Ghana: A case study. *Nat. Hazards* 105, 1299–1321. doi: 10.1007/s11069-020-04355-4

Chan, S. Y., and Chau, C. K. (2021). On the study of the effects of microclimate and park and surrounding building configuration on thermal comfort in urban parks. *Sustain. Cities Soc.* 64:102512. doi: 10.1016/j.scs.2020.102512

Chang, C.-R., and Li, M.-H. (2014). Effects of urban parks on the local urban thermal environment. *Urban For. Urban Greening* 13, 672–681. doi: 10.1016/j.ufug.2014.08.001

Chang, Y., Xiao, J., Li, X., Middel, A., and He, S. (2021). Exploring diurnal thermal variations in urban local climate zones with ECOSTRESS land surface temperature data. *Remote Sens. Environ.* 263:112544.

Chen, L., Wen, Y., Zhang, L., and Xiang, W.-N. (2015). Studies of thermal comfort and space use in an urban park square in cool and cold seasons in Shanghai. *Build. Environ.* 94, 644–653. doi: 10.1016/j.buildenv.2015.10.020

Chen, Y., Yang, J., Yang, R., Xiao, X., and Xia, J. (2022). Contribution of urban functional zones to the spatial distribution of urban thermal environment. *Build. Environ.* 216:109000. doi: 10.1016/j.buildenv.2022.109000

Cheng, B., Gou, Z., Zhang, F., Feng, Q., and Huang, Z. (2019). Thermal comfort in urban mountain parks in the hot summer and cold winter climate. *Sustain. Cities Soc.* 51:101756. doi: 10.1016/j.scs.2019.101756

Cheng, X., Wei, B., Chen, G., Li, J., and Song, C. (2015). Influence of Park Size and Its Surrounding Urban Landscape Patterns on the Park Cooling Effect. *J. Urban Planning Dev.* 141:A4014002. doi: 10.1061/(asce)up.1943-5444.0000256

Dai, Z. X., Guldmann, J. M., and Hu, Y. F. (2018). Spatial regression models of park and land-use impacts on the urban heat island in central Beijing. *Sci. Total Environ.* 626, 1136–1147. doi: 10.1016/j.scitotenv.2018.01.165

Feng, X., and Myint, S. W. (2016). Exploring the effect of neighboring land cover pattern on land surface temperature of central building objects. *Build. Environ.* 95, 346–354. doi: 10.1016/j.buildenv.2015.09.019

Gao, Z., Zaitchik, B. F., Hou, Y., and Chen, W. (2022). Toward park design optimization to mitigate the urban heat Island: Assessment of the cooling effect in five US cities. *Sustain. Cities Soc.* 81:103870. doi: 10.1016/j.scs.2022.103870

Han, D., Yang, X., Cai, H., and Xu, X. (2020). Impacts of neighboring buildings on the cold island effect of central parks: A case study of beijing. *China. Sustain.* 12:9499.

He, B. J., Wang, J., Liu, H., and Ulpiani, G. (2020). Localized synergies between heat waves and urban heat islands: Implications on human thermal comfort and urban heat management. *Environ. Res.* 193:110584. doi: 10.1016/j.envres.2020.110584

He, B.-J., Wang, J., Zhu, J., and Qi, J. (2022). Beating the urban heat: Situation, background, impacts and the way forward in China. *Renew. Sustain. Energy Rev.* 161:112350. doi: 10.1016/j.rser.2022.112350

He, K., Zhang, X., Ren, S., and Sun, J. (2016). Deep Residual Learning for Image Recognition. *arXiv* [Preprint]. doi: 10.48550/arXiv.1512.03385

Hook, S. J., Cawse-Nicholson, K., Barsi, J., Radocinski, R., Hulley, G. C., Johnson, W. R., et al. (2020). In-Flight validation of the ecostress, landsats 7 and 8 thermal infrared spectral channels using the lake tahoe ca/nv and salton sea ca automated validation sites. *IEEE Trans. Geosci. Remote Sens.* 58, 1294–1302.

Hu, L., Monaghan, A., Voogt, J., and Barlage, M. (2016). A first satellite-based observational assessment of urban thermal anisotropy. *Remote Sens. Environ.* 181, 111–121. doi: 10.1016/j.rse.2016.03.043

Kong, H., Choi, N., and Park, S. (2021). Thermal environment analysis of landscape parameters of an urban park in summer-A case study in Suwon, Republic of Korea. *Urban For. Urban Greening* 65:127377. doi: 10.1016/j.ufug.2021.127377

Li, Y. L., Fan, S. X., Li, K., Zhang, Y., Kong, L. X., Xie, Y. F., et al. (2021). Large urban parks summertime cool and wet island intensity and its influencing factors in Beijing, China. *Urban For. Urban Greening* 65:127375.

Lin, P., Song, D., and Qin, H. (2021). Impact of parking and greening design strategies on summertime outdoor thermal condition in old mid-rise residential estates. *Urban For. Urban Greening* 63:127200. doi: 10.1016/j.ufug.2021.127200

Luo, X., Yang, J., Sun, W., and He, B. (2021). Suitability of human settlements in mountainous areas from the perspective of ventilation: A case study of the main urban area of Chongqing. *J. Clean. Produc.* 310:127467. doi: 10.1016/j.jclepro.2021.127467

Mackey, C., Lee, X., and Smith, R. (2012). Remotely sensing the cooling effects of city scale efforts to reduce urban heat island. *Fuel Energy Abstr.* 49, 348–358. doi: 10.1016/j.buildenv.2011.08.004

Maharjan, M., Aryal, A., Shakya, B., Talchabhadel, R., and Thapa, B. (2021). Evaluation of urban heat island (uhi) using satellite images in densely populated cities of south asia. *Earth* 2021, 86–110. doi: 10.3390/earth2010006

Oke, T. R. (1982). The energetic basis of the urban heat island. *Quart. J. R. Meteorol. Soc.* 108, 1–24. doi: 10.1002/qj.49710845502

Oke, T., and Cleugh, H. (1987). Urban heat storage derived as energy residuals. *Bound. Lay. Meteorol.* 39, 233–245. doi: 10.1007/BF00116120

Oke, T. R. (2006). Towards better scientific communication in urban climate. *Theor. Appl. Climatol.* 84, 179–190.

Peng, J., Dan, Y., Qiao, R., Liu, Y., Dong, J., and Wu, J. (2021). How to quantify the cooling effect of urban parks? Linking maximum and accumulation perspectives. *Remote Sens. Environ.* 252:112135. doi: 10.1016/j.rse.2020.112135

Qiao, Z., Han, X., Wu, C., Luo, L., Xu, X., Sun, Z., et al. (2020). Scale effects of the relationships between 3d building morphology and urban heat island: A case study of provincial capital cities of mainland china. *Complexity* 2020, 1–12. doi: 10.1155/2020/9326793

Qiao, Z., Wu, C., Zhao, D., Xu, X., Yang, J., Feng, L., et al. (2019). Determining the boundary and probability of surface urban heat island footprint based on a logistic model. *Remote Sens.* 11:1368. doi: 10.3390/rs11111368

Qiao, Z., Xu, X., Luo, W., Wang, F., Luo, L., and Sun, Z. (2017). Urban ventilation network model: A case study of the core zone of capital function in Beijing metropolitan area. *J. Clean. Produc.* 168, 526–535. doi: 10.1016/j.jclepro.2017.09.006

Qin, H., Cheng, X., Han, G., Wang, Y., Deng, J., and Yang, Y. (2021). How thermal conditions affect the spatial-temporal distribution of visitors in urban parks: A case study in Chongqing, China. *Urban For. Urban Greening* 66:127393. doi: 10.1016/j.ufug.2021.127393

Stewart, I. D. (2011). *Redefining the Urban Heat Island*, Ph D. thesis. Vancouver, BC: University of British Columbia

Stewart, I. D., and Oke, T. (2012). Local climate zones for urban temperature studies. *Bull. Am. Meteorol. Soc.* 93, 1879–1900.

Wu, Z., Yao, L., and Ren, Y. (2020). Characterizing the spatial heterogeneity and controlling factors of land surface temperature clusters: A case study in Beijing. *Build. Environ.* 169:106598.

Xu, M., Hong, B., Mi, J., and Yan, S. (2018). Outdoor thermal comfort in an urban park during winter in cold regions of China. *Sustain. Cities Soc.* 43, 208–220. doi: 10.1016/j.scs.2018.08.034

Xu, X. L., Cai, H. Y., Qiao, Z., Wang, L., Jin, C., Ge, Y. N., et al. (2017). Impacts of park landscape structure on thermal environment using QuickBird and Landsat images. *Chin. Geographical. Sci.* 27, 818–826. doi: 10.1007/s11769-017-0910-x

Yan, H., Wu, F., and Dong, L. (2018). Influence of a large urban park on the local urban thermal environment. *Sci. Total Environ.* 622, 882–891. doi: 10.1016/j.scitotenv.2017.11.327

Yang, J., Wang, Y., Xue, B., Li, Y., Xiao, X., Xia, J., et al. (2021b). Contribution of urban ventilation to the thermal environment and urban energy demand: Different climate background perspectives. *Sci. Total Environ.* 795:148791. doi: 10.1016/j.scitotenv.2021.148791

Yang, J., Hu, X., Feng, H., and Marvin, S. (2021a). Verifying an ENVI-met simulation of the thermal environment of Yanzhong Square Park in Shanghai. *Urban For. Urban Greening* 66:127384. doi: 10.1016/j.ufug.2021.127384

Yang, J., Yang, Y., Sun, D., Jin, C., and Xiao, X. (2021c). Influence of urban morphological characteristics on thermal environment. *Sustain. Cities Soc.* 72:103045. doi: 10.1016/j.scs.2021.103045

Yang, J., Su, J., Xia, J., Jin, C., Li, X., and Ge, Q. (2018). The impact of spatial form of urban architecture on the urban thermal environment: A case study of the zhongshan district, dalian, china. *IEEE J. Sel. Topics Appl. Earth Obs. Remote Sens.* 11, 2709–2716. doi: 10.1109/JSTARS.2018.2808469

Yang, J., Wang, Y., Xiao, X., Jin, C., Xia, J., and Li, X. (2019). Spatial differentiation of urban wind and thermal environment in different grid sizes. *Urban Climate* 28:100458. doi: 10.1016/j.uclim.2019.100458

Yang, J., Wang, Y., Xiu, C., Xiao, X., Xia, J., and Jin, C. (2020). Optimizing local climate zones to mitigate urban heat island effect in human settlements. *J. Clean. Produc.* 275:123767. doi: 10.1016/j.jclepro.2020.123767

Yao, X., Yu, K., Zeng, X., Lin, Y., Ye, B., Shen, X., et al. (2022). How can urban parks be planned to mitigate urban heat island effect in "Furnace cities" ? An accumulation perspective. *J. Clean. Produc.* 330:129852. doi: 10.1016/j.jclepro.2021.129852

You, H., Yang, J., Xue, B., Xiao, X., Xia, J., Jin, C., et al. (2021). Spatial evolution of population change in Northeast China during 1992–2018. *Sci. Total Environ.* 776:146023. doi: 10.1016/j.scitotenv.2021.146023

Yu, H., Yang, J., Li, T., Jin, Y., and Sun, D. (2022). Morphological and functional polycentric structure assessment of megacity: An integrated approach with spatial distribution and interaction. *Sustain. Cities Soc.* 80:103800. doi: 10.1016/j.scs.2022.103800

Zhu, W., Sun, J., Yang, C., Liu, M., Xu, X., and Ji, C. (2021). How to measure the urban park cooling island? A perspective of absolute and relative indicators using remote sensing and buffer analysis. *Remote Sens.* 13:3154. doi: 10.3390/rs13163154

frontiers | Frontiers in Environmental Science

TYPE Original Research
PUBLISHED 21 October 2022
DOI 10.3389/fenvs.2022.1044837

Check for updates

OPEN ACCESS

EDITED BY
Jun Yang,
Northeastern University, China

REVIEWED BY
Xiao Liu,
South China University of Technology, China
Liang Zhou,
Lanzhou Jiaotong University, China

*CORRESPONDENCE
Yuanshan Gong,
403988252@qq.com

SPECIALTY SECTION
This article was submitted to Environmental Informatics and Remote Sensing, a section of the journal Frontiers in Environmental Science

RECEIVED 15 September 2022
ACCEPTED 10 October 2022
PUBLISHED 21 October 2022

CITATION
Gong Y (2022), Spatio-temporal distribution characteristics and influencing factors of drought in the Liaohe river basin, China.
Front. Environ. Sci. 10:1044837.
doi: 10.3389/fenvs.2022.1044837

COPYRIGHT
© 2022 Gong. This is an open-access article distributed under the terms of the Creative Commons Attribution License (CC BY). The use, distribution or reproduction in other forums is permitted, provided the original author(s) and the copyright owner(s) are credited and that the original publication in this journal is cited, in accordance with accepted academic practice. No use, distribution or reproduction is permitted which does not comply with these terms.

Spatio-temporal distribution characteristics and influencing factors of drought in the Liaohe river basin, China

Yuanshan Gong[1,2]*

[1]School of Architecture, Tianjin University, Tianjin, China, [2]Shenyang Urban Planning and Design Institute Co, Ltd., Shenyang, China

Effective identification of drought-related events and quantitative analysis of the spatio-temporal evolution of drought are essential for regional disaster prevention and mitigation and sustainable development. Based on monthly precipitation and average temperature data from 113 grid points in the Liaohe River Basin (LRB) from 1961 to 2018, this study evaluated the standardized precipitation evapotranspiration index (SPEI) on monthly, quarterly, 6-monthly, and annual scales. Run-length theory was used to extract three characteristic variables of drought—frequency, severity, and duration—for different grades of drought. Linear regressions, Manner–Kendall mutation tests, correlations, and other methods were used to analyze the spatio-temporal distribution characteristics of the different levels of drought and their influencing factors. Results from this research can provide a scientific reference for disaster prevention and mitigation, water conservancy project planning and construction, land space ecological restoration, and development and protection in the LRB. Our results indicated the following: 1) overall, from 1961 to 2018, the short-term SPEI (monthly, quarterly) showed an upward trend (0.06/103a, 0.01/103a), while the long-term SPEI (6-monthly, annual) showed a downward trend (–0.01/103a, –0.3/103a), and the overall change occurred in three stages, specifically stable–decline–increase. From a seasonal point of view, the SPEI in spring, summer, and autumn showed an upward trend, and although the SPEI showed multiple mutations during all seasons, they were not significant ($p > 0.05$). 2) Moderate drought occurred the most frequently (32 times) and was concentrated in the northern and western parts of the LRB. The severity of extreme drought in the upper reaches of the Chagan Mulun River was low, with a minimum SPEI of –7.07, and the durations of mild, moderate, severe, and extreme drought were 2, 2-2.5, 2–3, and 3–4 months, respectively. 3) SPEI-1 (monthly) showed the strongest correlation with precipitation and air temperature, which decreased with increasing time frames, such that SPEI-12 (annual) showed the weakest correlation. The correlations between SPEI and precipitation at different time scales were all highly significant ($p < 0.01$), and the correlation strength was much greater than that for air temperature, indicating that precipitation had the most significant impact on drought conditions in the LRB.

KEYWORDS

SPEI, run theory, spatio-temporal distribution, correlation, Liaohe river basin

1 Introduction

Since the 1990s, the frequency and intensity of extreme climate events have been increasing globally under the combined effects of changing climate, environmental conditions, and human activities (Omer et al., 2020). Drought is an extreme and common natural disaster (Hao et al., 2014; Spinoni et al., 2014). Unlike other climate events, droughts develop slowly and severely impact human life, the ecological environment, and socio-economic development (Xu et al., 2019; Mondol et al., 2021). Economic losses caused by droughts account for more than half of all meteorological disasters worldwide. From 1983 to 2009, production from approximately 454 million hectares of arable land was lost owing to droughts, resulting in economic losses of US$166 billion (Kim et al., 2019). In China, disaster areas and food losses caused by droughts are increasing, and the average annual direct economic losses are estimated to be as high as 25 billion yuan (Qin, 2015). Increased temperature and precipitation variations have led to increased uncertainty in drought studies. Therefore, effective identification of drought events and quantitative analysis of their temporal and spatial evolution is needed to enable disaster prevention and mitigation and to ensure sustainable regional development.

Currently, drought monitoring is conducted mainly using the time series of drought indicators to identify and characterize the occurrence and development of regional droughts. The Palmer Drought Severity Index (PDSI) and the Standardized Precipitation Index (SPI) are widely used drought indicators. The PDSI evaluates drought based on regional rainfall, evapotranspiration (ET), runoff, soil moisture, and other parameters at a fixed time scale. Therefore, the complexity of drought is considered, but calculating the PDSI is complex and requires extensive data (Palmer, 1965; Alley, 1984; Yang et al., 2018). The SPI assesses regional drought based on only precipitation data, with a flexible time scale (Kumar et al., 2021). The standardized precipitation evapotranspiration index (SPEI) is more flexible because it is based on the SPI calculation but combines precipitation and evapotranspiration, thus, making up for the shortcomings of PDSI's fixed time scale and numerous required parameters (Stagge et al., 2015; Tan et al., 2015). Drought studies in Northeast China and the Qaidam Basin have shown that compared with the SPI and PDSI, the SPEI is more usable and flexible, more sensitive to temperature, and more accurately captures drought characteristics (Zhao et al., 2017; Pei et al., 2020). Ullah et al. (2021) pointed out in the assessment of meteorological drought in Iran that the SPEI could capture more drought events than the SPI. Therefore, the SPEI was selected in the present study to monitor and identify drought events in the Liaohe River Basin (LRB) in China.

The LRB is an important agricultural production base in Northeastern China, associated with a high demand for water (Wang et al., 2020) despite the serious shortage of water resources. The per capita water resource of this area is only 530 m^3, less than half of the national level (Liu et al., 2012). The rapid industrial development has further exacerbated the water resource shortage (Song et al., 2015; Wang et al., 2020). Water shortages combined with droughts pose a serious threat to regional food security and economic development. Therefore, this study used the precipitation and temperature data of 113 grid points in the LRB to calculate its SPEI. Run-length theory was used to extract characteristic variables, such as drought frequency, severity, and duration. Methods such as linear regressions, M-K mutation tests, and correlations were used to analyze the spatial and temporal distributions of drought. The study aimed to provide a basis for disaster prevention and mitigation, enable the rational allocation of water resources and optimize ecological and environmental protection policies in the basin.

2 Study area and data

2.1 Study area

The Liaohe River (40°30′ N, 117°00′ E–45°10′ N, 127°30′ E) originates from Guangtou Mountain in the Qilaotu Mountains in Pingquan, Hebei Province, flows through Hebei Province, Inner Mongolia Autonomous Region, Jilin Province, and Liaoning Province, and finally enters the Bohai Sea from Panshan County, Liaoning Province. In total it is 1,345 km long and has a drainage area of 219,000 km^2 (Zhao et al., 2018; Figure 1). Its tributaries, the Taizi, Hun, Dongliao, West Liaohe, Laoha, Xilamulun, and Chagan Mulun Rivers, are distributed in a dendritic shape (Li et al., 2012). The southern part of the LRB is adjacent to the Bohai and Yellow Seas, the southwestern part is adjacent to the Inland and Hailuan Rivers in Inner Mongolia, and the northern part is adjacent to the Songhua River. The basin has a typical temperate continental monsoon climate, with cold and dry winters and hot and humid summers. The average annual temperature and precipitation range from 4 to 9°C and 400 to 1,100 mm, respectively. There are significant seasonal differences in precipitation, which is concentrated in July, August, and September, mainly as heavy rain, with a small amount of snowmelt in winter (He et al., 2015; Gao et al., 2017). The terrain of the basin is high in the north and low in the south, with slopes from the east and west to the Liaohe Plain in the middle (Jiang and Wang, 2016). The climate–ecological environment of the LRB is complex, with diverse vegetation types. However, the ecological environment of the basin has been

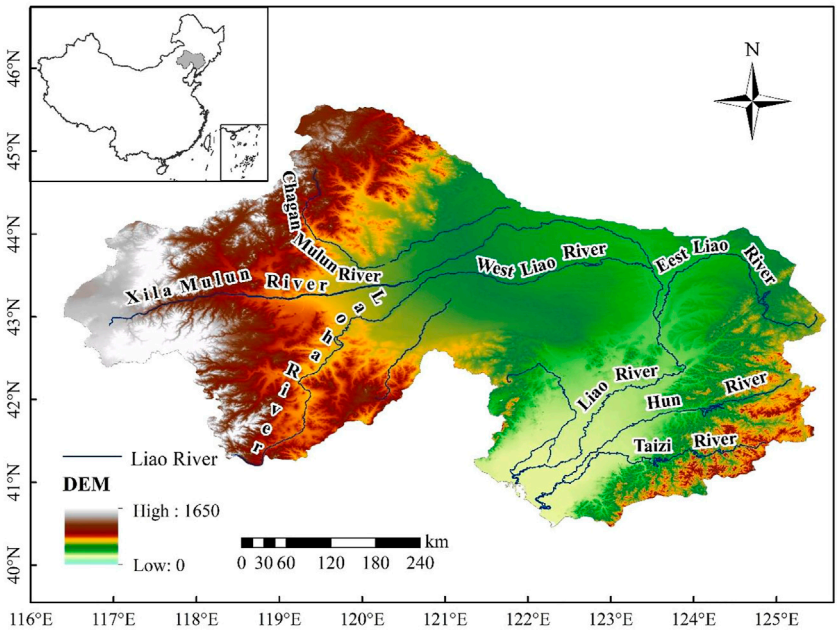

FIGURE 1
Geographical location and DEM of LRB.

disrupted in recent years owing to anthropogenic influences, which have even caused the river to stop flowing at times.

2.2 Data sources

The monthly precipitation and average temperature data used in this study were obtained from grid data with a spatial resolution of 0.5° provided by the China Meteorological Data Service Centre, with a time range from 1961 to 2018. There are 113 grid points in the LRB. Elevation data were a digital elevation product of SRTMDEM 90M resolution obtained from Geospatial Data Cloud. The DEM of the LRB was extracted using ArcGIS software.

3 Research methods

3.1 Drought index

Drought indices are basic tools that can be used to monitor drought conditions quantitatively. For example, the SPEI, proposed by Vicente-Serranosm et al., in 2010, is a commonly used index for evaluating meteorological drought (Xu et al., 2020). Potential evapotranspiration (PET) was calculated using the Thornthwaite method.

SPEI-1, SPEI-3, SPEI-6, and SPEI-12 were used to characterize the monthly, quarterly, 6-monthly, and annual drought conditions in the LRB, respectively. According to the national standard of Grades of Meteorological Drought (GB/T 20,481-2017) of the People's Republic of China (National Standardization Management Committee of China, drought can be divided into five grades: normal conditions and mild, moderate, severe, and extreme drought (Table 1).

TABLE 1 Range of SPEI values corresponding to different drought grades.

SPEI value	Drought grade
SPEI > −0.5	normal condition
(−1, −0.5)	mild drought
(−1.5, −1)	moderate drought
(−2, −1.5)	severe drought
SPEI ≤ −2	extreme drought

3.2 Identification of drought characteristic elements

The run-length theory was used to identify drought events and judge drought and flood conditions (Zhang et al., 2022). Any SPEI value less than the threshold, X_1 (Figure 2), was recorded as a drought event. A total of five drought events occurred during the time period, t, which were recorded as events a, b, c, d, and e. If the drought duration was confined to only one period (such as

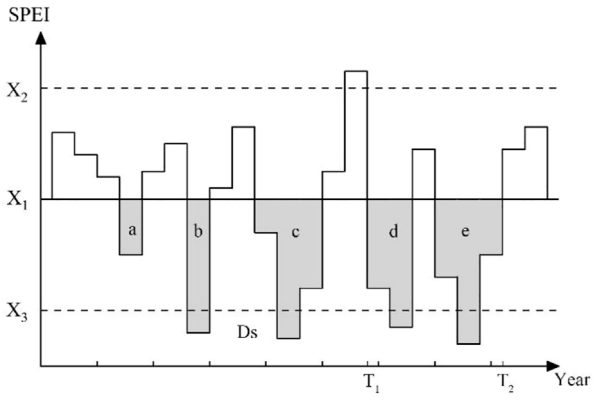

FIGURE 2
Schematic diagram of extracting drought characteristic elements by run-length theory.

a and b), and its SPEI value was less than X_3 (such as b), it was recorded as a drought event, but otherwise (such as for a), it was not. If the SPEI value of the interval between two adjacent drought events, such as d and e, was less than X_2, the two adjacent droughts were regarded as a single drought event, with the combined drought duration $T = T_2\text{-}T_1+1$, and drought severity $S=SPEI_c + SPEI_d$; otherwise, it was recorded as two independent drought events. According to this definition of drought events, there were three drought events, namely b, c, and d + e (Figure 2). As the SPEI value is negative, the severity of drought increases with a decrease in the index's value.

The thresholds were selected based on the SPEI values associated with the different drought grades (Table 1). Based on the SPEI-1, run-length theory was used to identify and analyze the frequency, severity, and duration of different drought grades and to quantify the drought characteristics.

3.3 Analysis method of drought spatio-temporal characteristics

Univariate linear regression analyses were used to assess the variation trends in SPEI at different time scales. Linear regression is commonly used to analyze the linear relationship between independent (x) and dependent variables (y). The calculation formula was based on Uyanık's method (Uyanık and Güler, 2013).

The Mann-Kendall (M-K) method is typically used to test randomly distributed time series data. This test has a low sensitivity to outliers. In this paper, the MK test was used to assess the change trend of SPEI-3 and -12, and ±1.96 was selected as the significance level to judge whether the change in the SPEI-3 and -12 sequence was significant. The calculation formula was derived from Zhang et al. (2021).

The Pearson product-moment correlation coefficient is usually used to reflect the degree of linear correlation between two meteorological elements. The value of P ranges between −1 and 1. The closer |P| is to 1, the stronger the correlation between the two meteorological elements. The formula for the calculation of the coefficient was derived from Jain et al. (2015). Correlation analyses of SPEI-1, SPEI-3, SPEI-6, and SPEI-12 with precipitation and air temperature were carried out using Pearson's correlation coefficient.

Inverse distance weighting (IDW) is a commonly used spatial interpolation method in regional drought analysis. It is a deterministic spatial interpolation method based on the principle of similarity and proximity (Chen et al., 2017). In ArcGIS, IDW was used to spatially interpolate the drought characteristics of the LRB from 1961 to 2018 to analyze spatial distribution characteristics.

4 Results

4.1 Temporal variation characteristics of drought

Annual (SPEI-12) and quarterly (SPEI-3) SPEI in the LRB from 1961 to 2018 were subjected to trend analyses and the M-K mutation test. SPEI-12 decreased at a rate of 0.0514/10a, and presented four periods of normal–wet–dry–wet, corresponding to 1961–1983, 1984–1996, 1996–2010, and 2011–2018, respectively (Figure 3A). Post 1995, the severity and frequency of droughts and floods in the LRB have increased. A prolonged severe drought occurred from 1996 to 2010, with SPEI values of −1.56 and −1.6 in 2000 and 2009, respectively. From 2011 to 2018, a wet period was observed. Based on the UF values, the SPEI showed a significant downward trend from 1997 to 2001 ($p < 0.05$; Figure 3A).

In spring, the SPEI increased at a rate of 0.0518/10a and presented four periods of dry–wet–dry–wet (Figure 3B). A prolonged dry period was noted during 1998–2013, and the lowest spring SPEI value in nearly 60 years (−2.07) was identified in 2002. Additionally, the SPEI value experienced several sudden changes from 1985 to 1998, indicating that the dry and wet conditions were unstable. The abrupt changes in 1968 and 2014 changed the conditions in the LRB from dry to wet.

The SPEI increased at a rate of 0.0737/10a in summer but fluctuated greatly, with frequent changes between wet and dry; three abrupt changes, in 1962, 1991, and 1999, were noted (Figure 3C).

The SPEI in autumn decreased at a rate of 0.0368/10a, with a severe drought event in 1991, when the SPEI was -1.76. A total of five mutations occurred during the study period, and the UF values in 1969–1989 and 1996–2018 were all above 0, indicating that SPEI showed an overall upward trend (Figure 3D).

The winter SPEI, which increased at a rate of 0.0324/10a, was divided into three stages of dry–wet–dry, corresponding to

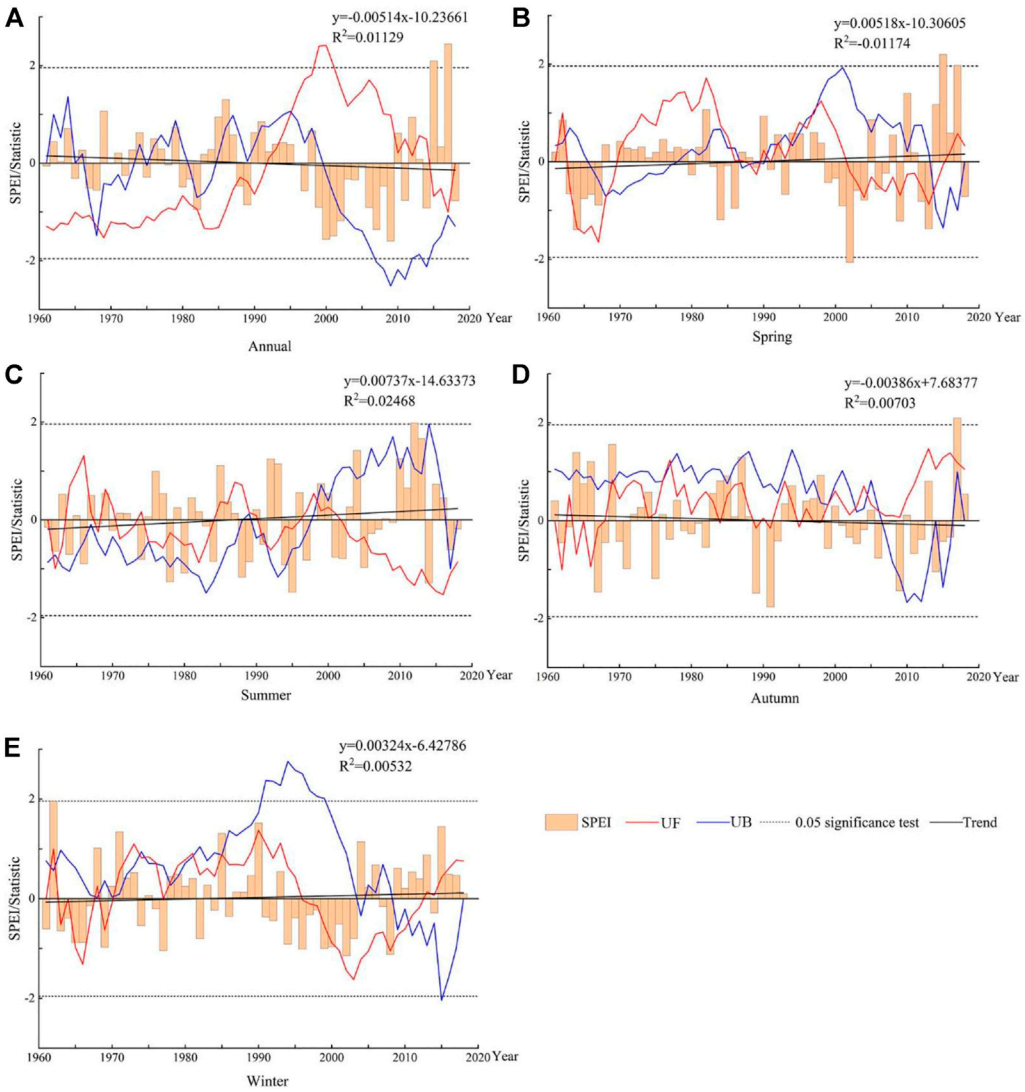

FIGURE 3
SPEI changes and M-K mutation test in the LRB from 1961 to 2018. **(A)** is the annual change trend and M-K mutation test of SPEI. **(B–E)** are the spring, summer, autumn and winter changes and M-K mutation test of SPEI, respectively.

1961–1970, 1971–1995, and 1996–2018, respectively (Figure 3E). The SPEI in winter had multiple mutations. The mutation years mainly occurred before 1985. No significant mutations in SPEI were found across all four seasons ($p > 0.05$).

4.2 Spatial variation of drought characteristics

4.2.1 Drought frequency

The frequency of different grades of drought in the LRB varied substantially in space (Figure 4). Overall, the frequency of mild drought was relatively high (Figure 4A). The frequency of mild droughts in the East Liaohe River Basin, the lower reaches of the West Liaohe River Basin, and the Chagan Mulun River Basin was relatively high, with the highest frequency of 29 noted in the middle reaches of the East Liaohe River during the study period. The drought frequency in the Hunhe and Taizi River Basins and the headwaters of the Xilamulun River was relatively low, with the lowest being 8 in the northern Liaohe River Basin. Moderate droughts occurred the most frequently (slightly more often than mild droughts), with relatively little spatial variability (Figure 4B). The western and northern parts of the LRB had a higher frequency of moderate droughts, with the middle reaches of the Xilamulun River having the highest frequency (32), and the East Liaohe River Basin a

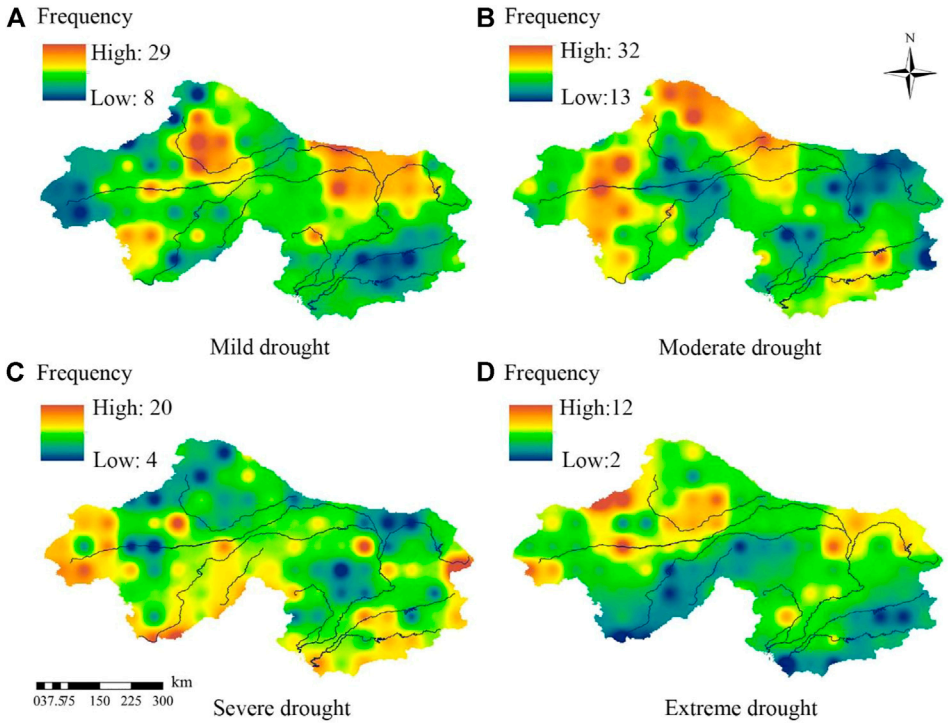

FIGURE 4
Spatial frequency distribution of different grades of droughts from 1962 to 2019. **(A)** is mild drought, **(B)** is moderate drought, **(C)** is severe drought, **(D)** is extreme drought.

comparatively lower frequency (13). Severe droughts were most frequent (20) in the south and least frequent (4) in the north (Figure 4C). The frequency of extreme droughts was higher in the East Liaohe River Basin and the northwest of the LRB, occurring up to 12 times. In the Liaohe and Laoha River estuaries, extreme droughts were the least frequent, occurring a minimum of two times (Figure 4D).

4.2.2 Drought severity

A decreasing trend in the SPEI value represents an increasing trend in drought severity. Overall, mild droughts in the LRB were more severe in the east, less severe in the west, and most severe in the middle reaches of the Laoha River (SPEI = −1.79; Figure 5A). Moderate droughts were less severe in the north and more so in the south, while drought severity in the Hunhe and Laoha River Basins was high (SPEI = −2.58; Figure 5B). Severe droughts were most severe in the upper reaches of the Xilamulun River and the lower reaches of the Xiliao River, with the lowest SPEI value being −5.24 (Figure 5C). However, regions with an SPEI value below −2.5 accounted for only 2.65% of the study area. Extreme droughts were quite severe in the northwest of the LRB, with the lowest SPEI value being −7.07 (Figure 5D), but this was quite localized, with only 4% of the total area of the LRB having an SPEI value of less than −6.

4.2.3 Drought duration

Drought duration has a direct impact on regional drought status. When the drought grade is low but the duration is very long, the impact becomes more serious. Therefore, studying drought duration is essential for evaluating the drought status in a given area. For the LRB, the drought level and duration were positively related, such that the more severe the drought level was, the longer the duration of each drought was. The duration of mild droughts remained stable at 2–2.11 months. There was little spatial heterogeneity (Figure 6A). The duration of moderate droughts ranged from 2 months (in the eastern LRB) to 3.5 months (in the southern LRB and southern Chaganmulun River Basin; Figure 6B). The duration of severe droughts ranged from 2 months (in the northeastern Liao River Basin) to 5 months (in the Xilamulun and West Liao River Basins; Figure 6C). The shortest extreme droughts occurred in the Xilamulun and southern Taizi River Basins (3 months) while the longest ones occurred in the northwest of the LRB and in the lower reaches of the West Liaohe River (up to 6.22 mo; Figure 6D).

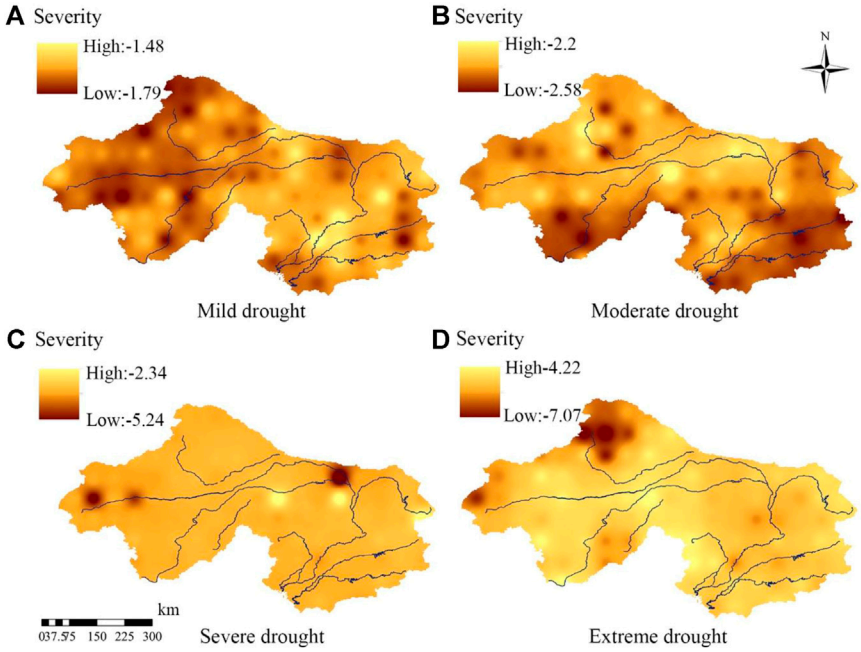

FIGURE 5
Spatial distribution of drought severity at different levels in the LRB from 1962 to 2019. **(A)** is mild drought, **(B)** is moderate drought, **(C)** is severe drought, **(D)** is extreme drought.

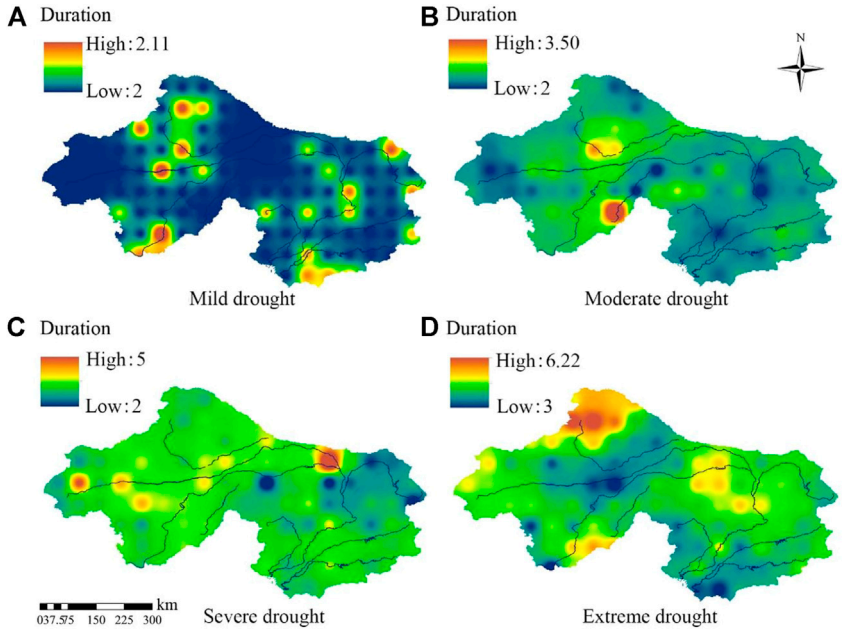

FIGURE 6
Spatial distribution of drought duration at different drought levels from 1961 to 2018. **(A)** is mild drought, **(B)** is moderate drought, **(C)** is severe drought, **(D)** is extreme drought. (Numerical unit: month).

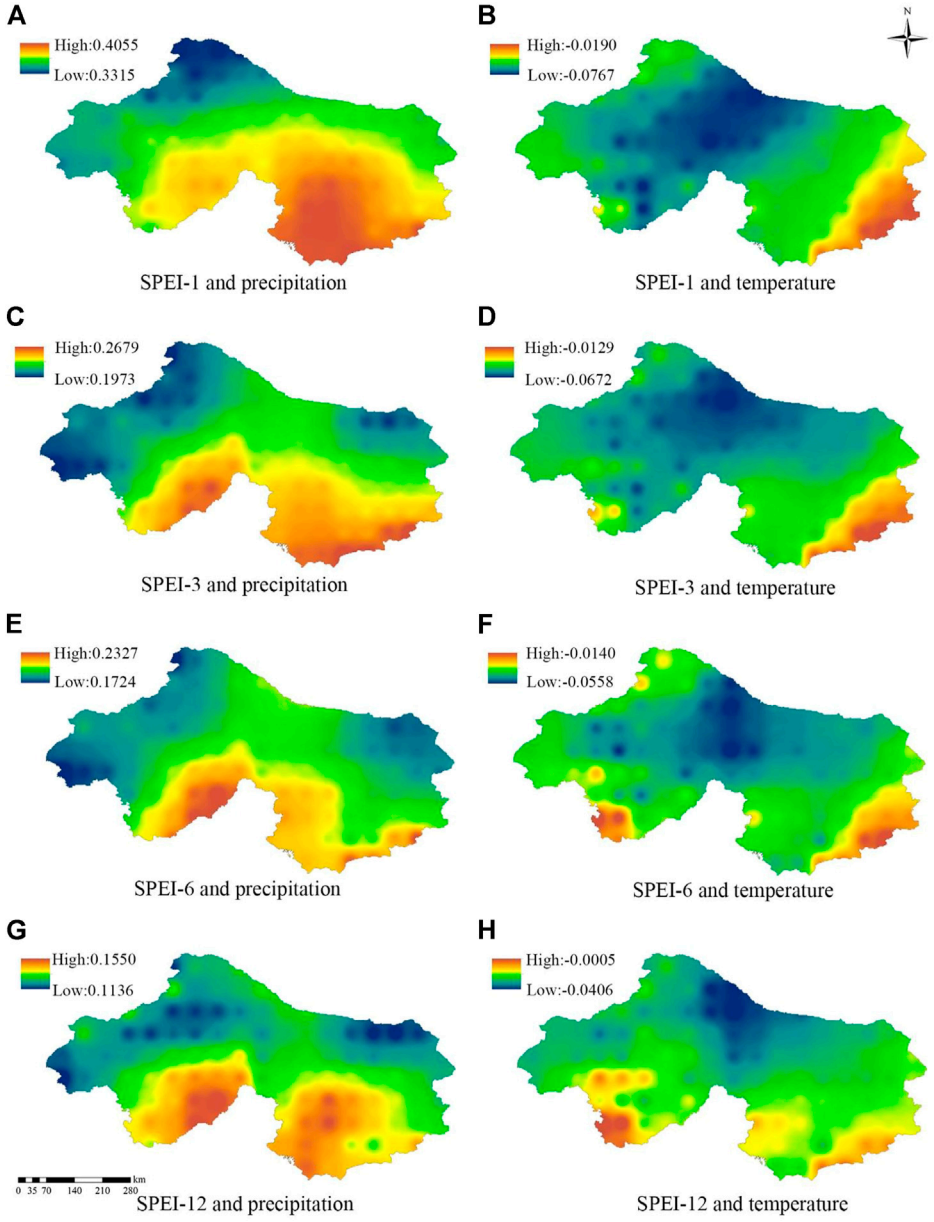

FIGURE 7
Spatial distribution of the Pearsons correlation between SPEI and precipitation and air temperature at different time scales from 1961 to 2018. **(A, C, E, G)** are the Pearson correlations between SPEI-1, SPEI-3, SPEI-6, SPEI-12 and precipitation respectively; **(B, D, F, H)** are the Pearson correlations between SPEI-1, SPEI-3, SPEI-6, SPEI-12 and temperature respectively.

4.3 Correlation between multi-scale drought index and climatic factors

The spatial distribution of the correlations between SPEI and temperature and precipitation at different time scales is shown in Figure 7. The SPEI was positively correlated with precipitation and negatively correlated with air temperature across all the time scales. SPEI correlated more strongly with precipitation than air temperature, and the level of correlation with both meteorological elements varied spatially. SPEI-1 had the strongest correlation with precipitation and air temperature, but increased time frames made this relationship progressively weaker. Across all time frames, the correlation between SPEI and precipitation presented a decreasing trend from southeast to northwest (Figures 7A,C,E,G). The correlation between SPEI-1 and precipitation in the southeast of the LRB was the strongest,

reaching 0.4055 (Figure 7A). The correlation between SPEI and air temperature across all the time frames was high in the middle and low on both sides (Figures 7B,D,F,H). Among them, SPEI-1 had the strongest correlation (−0.0767) with air temperature in the middle of the LRB (Figure 7B). Across all time frames, the SPEI correlated significantly with precipitation ($p < 0.01$), but SPEI-1 correlated significantly with temperature ($p < 0.05$) for only some areas (accounting for 7% of the LRB).

5 Discussion

In a natural state, meteorological drought is the only external factor that drives hydrological and agricultural drought. Therefore, the quantitative analysis of temporal and spatial variations in meteorological drought forms the basis for understanding regional drought conditions. Some studies have indicated that China may be undergoing a drying trend as a whole, wherein the drought trend in the northeast has intensified, and the center of drought intensity in the northeast is gradually shifting to the Liaoning region (Shao et al., 2018; Zhao et al., 2020). Therefore, based on the multi-time-scale SPEI, this study explored the spatial and temporal distribution characteristics and influencing factors of drought in the LRB during the past 60 years. The results showed that the LRB as a whole is becoming more arid, which is consistent with other research results.

The present study showed that the higher the level of drought, the less frequent and severe they are, and the longer they persist. That is, extreme droughts occurred the least, had the lowest severity (within that level of drought), and continued the longest. Cavus and Aksoy (2020) constructed a drought severity/intensity–duration–frequency curve (S/IDF) and found that the higher the grade of drought in the Seyhan River basin, the lower the frequency, the longer the duration, and the lower the severity. Wang et al. (2015) proposed that in the Huang Huai Hai Plain, severe droughts were most commonly long-term events, as a long-term water deficit reduces the severity of drought but eventually leads to an increase in the level of drought, which is consistent with the results of this study. However, Han et al. (2021) and Zhang et al. (2015) pointed out that drought in the west of China has a higher frequency, longer duration, and lower severity than drought in eastern China. In the analysis of drought characteristics, this study only divided drought grades based on drought severity to analyze the spatial distribution of drought frequency, severity, and duration. Therefore, the relationship between drought characteristics still needs to be elucidated.

The evolution of drought is influenced largely by changes in precipitation and temperature. Quantitative analysis of the relationship of SPEI with precipitation and temperature indicated that the drought conditions in the LRB were highly dependent on regional precipitation, which showed a significant negative correlation with the drought index. This may be attributed to the temperate continental monsoon climate and the significant seasonal variation in precipitation in the LRB (Yuan et al., 2021), which means that the climatic conditions of the basin are very much determined by changes in precipitation. Guo et al. (2020) showed that variations in droughts are significantly correlated with the temporal and spatial distribution of precipitation and that areas with excessive precipitation have a significantly negative correlation with drought indicators, agreeing with the results of the present study. Because the causes of drought are extremely complex, the effects of different meteorological factors on the drought conditions affecting the LRB need further investigation. Although the current study only discusses the influence of precipitation and temperature on drought conditions in the LRB, droughts can be induced by various meteorological factors. Their formation mechanisms are complex, with different factors exerting different degrees of influence on drought characteristics. Therefore, future research should consider other influencing factors, such as relative humidity, sunshine hours, and average wind speed, to improve the research content (Shen et al., 2017; Zhang et al., 2020). At present, climate warming and the impact of human activities lead to more complex drought formation mechanisms. Therefore, moving forward, the impact of underlying surface changes and human activities on drought should be considered (Xie et al., 2021).

As climate warming and drying trends intensify, extreme drought events are likely to continue increasing. Thus, emergency response and management plans for droughts may play an important role in regional development. As foundational research, the outcomes of this research have value in the following contexts: 1) The LRB, especially the West Liaohe River Basin, is an important sand-control and sand-fixing area for shelter forests in North China and Northeast China. Due to the causal relationship between drought, wind erosion, organic matter removal, and desertification, this work supports the formulation of sand control and sand fixation policies. 2) Highlighting the need for the protection and responsible utilization of water resources, the planning and construction of water conservancy projects, and the formulation of water safety policies in the LRB. 3) Promoting the territorial and spatial planning of the LRB, which highlights "the whole area, the whole element, and the whole process" concept. This is especially important for ecological restoration and management, construction of the ecological security pattern, and the rational layout of the ecological, production and living spaces. The LRB is located in a semi-humid to humid area, where public awareness of disaster prevention and mitigation and drought early-warning forecasting, emergency response, and management capabilities are poor. If not improved in time, these will seriously affect agriculture and the social economy (Chen et al., 2018). Therefore, relevant departments should raise awareness and attach great importance to issues such as crop drought resistance and water resource management and

allocation in order to reduce the damage associated with droughts.

6 Conclusion

This study used the monthly precipitation and monthly average temperature grid point data (0.5° × 0.5°) in the LRB from 1961 to 2018 to calculate the multi-time-scale SPEI, and analyze the spatial and temporal distribution characteristics and influencing factors of drought. The following conclusions were reached:

(1) From 1961 to 2018, the annual SPEI decreased at 0.0514/10a. This trend was significant from 1997 to 2001. Seasonally, the SPEI in spring (0.0518/10a), summer (0.0737/10a), and winter (0.0324/10a) showed an upward trend; multiple mutations occurred, but no significant trends were observed.
(2) Concerning the frequency of droughts, the frequency of mild droughts in the northern LRB was relatively high, with a maximum of 29 occurrences. The frequency of extreme droughts was similar to that of mild droughts; the highest frequency was 12. In the northern and western parts of the LRB, the frequency of moderate droughts was the highest, with a maximum of 32 occurrences. In the southern part of the LRB, the frequency of severe droughts was the highest, with a maximum of 20 occurrences.
(3) Regarding drought severity, mild and moderate droughts gradually increased from west to east and from south to north, respectively. Severe droughts in the north of the Xilamulun and Xiliao River Basins were comparatively more severe, with an SPEI value as low as −5.24. Also, the upper reaches of the Chagan Mulun River experienced extreme drought, with the lowest SPEI value being −7.07.
(4) Concerning the drought duration, 79% of the regions experienced a mild drought that lasted for 2°months, with the longest duration of mild droughts being 2.11 months. In 96% of the regions, the duration of moderate droughts was 2–2.5 months, while the longest duration was 3.5 months. Severe droughts lasted for 2–3 months in 65% of the regions, while the longest duration was 5 months. The duration of extreme drought in 88% of the regions was 3–4 months, while the longest duration was 6.22 months.
(5) The SPEI of different time scales showed a positive correlation with precipitation and a negative correlation with air temperature. The correlation between the SPEI and precipitation was significant and stronger than that between the SPEI and air temperature. Only the correlation between SPEI-1 and the temperature of 7% of the regions was significant, indicating that precipitation exerts a more pronounced and significant effect on drought.

Data availability statement

The raw data supporting the conclusion of this article will be made available by the authors, without undue reservation.

Author contributions

YG is solely responsible for the development of the manuscript, including but not limited to, data collection and analysis, creating graphics, and writing.

Acknowledgments

The author thanks the editor and reviewers for their valuable comments and suggestions.

Conflict of interest

Author YG was employed by Shenyang Urban Planning and Design Institute Co, Ltd.

Publisher's note

All claims expressed in this article are solely those of the authors and do not necessarily represent those of their affiliated organizations, or those of the publisher, the editors and the reviewers. Any product that may be evaluated in this article, or claim that may be made by its manufacturer, is not guaranteed or endorsed by the publisher.

References

Alley, W. M. (1984). The palmer drought severity index: Limitations and assumptions. *J. Clim. Appl. Meteor.* 23, 1100–1109. doi:10.1175/1520-0450(1984)023<1100:tpdsil>2.0.co;2

Cavus, Y., and Aksoy, H. (2020). Critical drought severity/intensity-duration-frequency curves based on precipitation deficit. *J. Hydrol. X.* 584, 124312. doi:10.1016/j.jhydrol.2019.124312

Chen, H., Fan, L., Wu, W., and Liu, H. (2017). Comparison of spatial interpolation methods for soil moisture and its application for monitoring drought. *Environ. Monit. Assess.* 189 (10), 525–613. doi:10.1007/s10661-017-6244-4

Chen, X., Jiang, J., and Li, H. (2018). Drought and flood monitoring of the Liao River Basin in Northeast China using extended GRACE data. *Remote Sens.* 10 (8), 1168. doi:10.3390/rs10081168

Gao, Z., He, J., Dong, K., and Li, X. (2017). Trends in reference evapotranspiration and their causative factors in the West Liao River basin, China. *Agric. For. Meteorol.* 232, 106–117. doi:10.1016/j.agrformet.2016.08.006

Guo, E., Wang, Y., Jirigala, B., and Jin, E. (2020). Spatiotemporal variations of precipitation concentration and their potential links to drought in mainland China. *J. Clean. Prod.* 267, 122004. doi:10.1016/j.jclepro.2020.122004

Han, L., Zhang, Q., Zhang, Z., Jia, J., Wang, Y., Huang, T., et al. (2021). Drought area, intensity and frequency changes in China under climate warming, 1961–2014. *J. Arid Environ.* 193, 104596. doi:10.1016/j.jaridenv.2021.104596

Hao, Z., AghaKouchak, A., Nakhjiri, N., and Farahmand, A. (2014). Global integrated drought monitoring and prediction system. *Sci. Data* 1 (1), 140001–140010. doi:10.1038/sdata.2014.1

He, C., Tian, J., Gao, B., and Zhao, Y. (2015). Differentiating climate-and human-induced drivers of grassland degradation in the Liao River Basin, China. *Environ. Monit. Assess.* 187 (1), 4199–4214. doi:10.1007/s10661-014-4199-2

Jain, V. K., Pandey, R. P., Jain, M. K., and Byun, H. (2015). Comparison of drought indices for appraisal of drought characteristics in the Ken River Basin. *Weather Clim. Extrem.* 8, 1–11. doi:10.1016/j.wace.2015.05.002

Jiang, C., and Wang, F. (2016). Temporal changes of streamflow and its causes in the Liao River Basin over the period of 1953-2011, northeastern China. *Catena* 145, 227–238. doi:10.1016/j.catena.2016.06.015

Kim, W., Iizumi, T., and Nishimori, M. (2019). Global patterns of crop production losses associated with droughts from 1983 to 2009. *J. Appl. Meteorol. Climatol.* 58 (6), 1233–1244. doi:10.1175/JAMC-D-18-0174.1

Kumar, U., Singh, S., Bisht, J. K., and Kant, L. (2021). Use of meteorological data for identification of agricultural drought in Kumaon region of Uttarakhand. *J. Earth Syst. Sci.* 130 (3), 121–213. doi:10.1007/s12040-021-01622-1

Li, Y., Liu, K., Li, L., and Xu, Z. (2012). Relationship of land use/cover on water quality in the Liao River basin, China. *Procedia Environ. Sci.* 13, 1484–1493. doi:10.1016/j.proenv.2012.01.140

Liu, X., Xu, Z., and Yu, R. (2012). Spatiotemporal variability of drought and the potential climatological driving factors in the Liao River basin. *Hydrol. Process.* 26 (1), 1–14. doi:10.1002/hyp.8104

Mondol, M. A. H., Zhu, X., Dunkerley, D., and Henley, B. J. (2021). Observed meteorological drought trends in Bangladesh identified with the Effective Drought Index (EDI). *Agric. Water Manag.* 255, 107001. doi:10.1016/j.agwat.2021.107001

Omer, A., Ma, Z., Zheng, Z., and Saleem, F. (2020). Natural and anthropogenic influences on the recent droughts in Yellow River Basin, China. *Sci. Total Environ.* 704, 135428. doi:10.1016/j.scitotenv.2019.135428

Palmer, W. C. (1965). *Meteorological drought*. Washington, D.C. US Department of Commerce, Weather Bureau.

Pei, Z., Fang, S., Wang, L., and Yang, W. (2020). Comparative analysis of drought indicated by the SPI and SPEI at various timescales in inner Mongolia, China. *Water* 12 (7), 1925. doi:10.3390/w12071925

Qin, D. (2015). *China national assessment report on risk management and adaptation of climate extremes and disasters*. Beijing: Science Press.

Shao, D., Chen, S., Tan, X., and Gu, W. (2018). Drought characteristics over China during 1980-2015. *Int. J. Climatol.* 38 (9), 3532–3545. doi:10.1002/joc.5515

Shen, Q., Liang, L., Luo, X., Li, Y., and Zhang, L. (2017). Analysis of the spatial-temporal variation characteristics of vegetative drought and its relationship with meteorological factors in China from 1982 to 2010. *Environ. Monit. Assess.* 189 (9), 471–514. doi:10.1007/s10661-017-6187-9

Song, Y., Liu, R., Sun, Y., Lei, K., and Kolditz, O. (2015). Waste water treatment and pollution control in the Liao River Basin. *Environ. Earth Sci.* 73 (9), 4875–4880. doi:10.1007/s12665-015-4333-7

Spinoni, J., Naumann, G., Carrao, H., Barbosa, P., and Vogt, J. (2014). World drought frequency, duration, and severity for 1951-2010. *Int. J. Climatol.* 34 (8), 2792–2804. doi:10.1002/joc.3875

Stagge, J. H., Tallaksen, L. M., Gudmundsson, L., Van Loon, A. F., and Stahl, K. (2015). Candidate distributions for climatological drought indices (SPI and SPEI). *Int. J. Climatol.* 35 (13), 4027–4040. doi:10.1002/joc.4267

Tan, C., Yang, J., and Li, M. (2015). Temporal-spatial variation of drought indicated by SPI and SPEI in ningxia hui autonomous region, China. *Atmosphere* 6 (10), 1399–1421. doi:10.3390/atmos6101399

Ullah, I., Ma, X., Yin, J., Asfaw, T. G., Azam, K., Syed, S., et al. (2021). Evaluating the meteorological drought characteristics over Pakistan using *in situ* observations and reanalysis products. *Int. J. Climatol.* 41 (9), joc.7063–4459. doi:10.1002/joc.7063

Uyanık, G. K., and Güler, N. (2013). A study on multiple linear regression analysis. *Procedia - Soc. Behav. Sci.* 106, 234–240. doi:10.1016/j.sbspro.2013.12.027

Wang, Q., Shi, P., Lei, T., Geng, G., Liu, J., Mo, X., et al. (2015). The alleviating trend of drought in the Huang-Huai-Hai Plain of China based on the daily SPEI. *Int. J. Climatol.* 35 (13), 3760–3769. doi:10.1002/joc.4244

Wang, X., Li, J., Chen, J., Cui, L., Li, W., Gao, X., et al. (2020). Water quality criteria of total ammonia nitrogen (TAN) and un-ionized ammonia (NH3-N) and their ecological risk in the Liao River, China. *Chemosphere* 243, 125328. doi:10.1016/j.chemosphere.2019.125328

Xie, J., Sun, Y., Liu, X., Ding, Z., and Lu, M. (2021). Human activities introduced degenerations of wetlands (1975–2013) across the sanjiang plain north of the wandashan mountain, China. *Land* 10 (12), 1361. doi:10.3390/land10121361

Xu, L., Abbaszadeh, P., Moradkhani, H., Chen, N., and Zhang, X. (2020). Continental drought monitoring using satellite soil moisture, data assimilation and an integrated drought index. *Remote Sens. Environ.* 250, 112028. doi:10.1016/j.rse.2020.112028

Xu, Y., Zhang, X., Wang, X., Hao, Z., Singh, V. P., and Hao, F. (2019). Propagation from meteorological drought to hydrological drought under the impact of human activities: A case study in northern China. *J. Hydrol. X.* 579, 124147. doi:10.1016/j.jhydrol.2019.124147

Yang, P., Xia, J., Zhang, Y., Zhan, C., and Qiao, Y. (2018). Comprehensive assessment of drought risk in the arid region of Northwest China based on the global palmer drought severity index gridded data. *Sci. Total Environ.* 627, 951–962. doi:10.1016/j.scitotenv.2018.01.234

Yuan, Z., Xu, Q., Song, Y., Wei, J., Duan, L., and Gao, Y. (2021). Practice and enlightenment of water ecological integrity restoration in Liaohe River Basin of Liaoning Province[J]. *Journal of Environmental Engineering Technology* 11 (1), 48–55. doi:10.12153/j.issn.1674-991X.20200113

Zhang, Q., Qi, T., Singh, V. P., Chen, Y. D., and Xiao, M. (2015). Regional frequency analysis of droughts in China: A multivariate perspective. *Water Resour. manage.* 29 (6), 1767–1787. doi:10.1007/s11269-014-0910-x

Zhang, Q., Yao, Y., Li, Y., Huang, J., Ma, Z., Wang, Z., et al. (2020). Causes and changes of drought in China: Research progress and prospects. *J. Meteorol. Res.* 34 (3), 460–481. doi:10.1007/s13351-020-9829-8

Zhang, R., Wu, X., Zhou, X., Ren, B., Zeng, J., and Wang, Q. (2022). Investigating the effect of improved drought events extraction method on spatiotemporal characteristics of drought. *Theor. Appl. Climatol.* 147 (1), 395–408. doi:10.1007/s00704-021-03838-z

Zhang, Y., Luo, Y., and Su, H. (2021). Study on land use and precipitation changes in the main urban area of kunming in the past 40 years. *IOP Conf. Ser. Earth Environ. Sci.* 658 (1), 012008. doi:10.1088/1755-1315/658/1/012008

Zhao, C., Wang, C., Yan, Y., Shan, P., Li, J., and Chen, J. (2018). Ecological security patterns assessment of liao River basin. *Sustainability* 10 (7), 2401. doi:10.3390/su10072401

Zhao, P., Lu, H., Fu, G., Zhu, Y., Su, J., and Wang, J. (2017). Uncertainty of hydrological drought characteristics with copula functions and probability distributions: A case study of weihe river, China. *Water* 9 (5), 334. doi:10.3390/w9050334

Zhao, Z., Wang, H., Yu, C., Deng, C., Liu, C., Wu, Y., et al. (2020). Changes in spatiotemporal drought characteristics over northeast China from 1960 to 2018 based on the modified nested Copula model. *Sci. Total Environ.* 739, 140328. doi:10.1016/j.scitotenv.2020.140328

frontiers | Frontiers in Environmental Science

TYPE Original Research
PUBLISHED 24 October 2022
DOI 10.3389/fenvs.2022.1032584

Check for updates

OPEN ACCESS

EDITED BY
Bing Xue,
Institute for Advanced Sustainability Studies (IASS), Germany

REVIEWED BY
Dahao Zhang,
Sun Yat-sen University, China
Xiaoping Zhang,
Shandong Jianzhu University, China

*CORRESPONDENCE
Xin Liu,
306541493@qq.com
Jiajia Yang,
haixianxiaomei@163.com

SPECIALTY SECTION
This article was submitted to Environmental Informatics and Remote Sensing,
a section of the journal
Frontiers in Environmental Science

RECEIVED 31 August 2022
ACCEPTED 10 October 2022
PUBLISHED 24 October 2022

CITATION
Jin S, Liu X, Yang J, Lv J, Gu Y, Yan J, Yuan R and Shi Y (2022), Spatial-temporal changes of land use/cover change and habitat quality in Sanjiang plain from 1985 to 2017.
Front. Environ. Sci. 10:1032584.
doi: 10.3389/fenvs.2022.1032584

COPYRIGHT
© 2022 Jin, Liu, Yang, Lv, Gu, Yan, Yuan and Shi. This is an open-access article distributed under the terms of the Creative Commons Attribution License (CC BY). The use, distribution or reproduction in other forums is permitted, provided the original author(s) and the copyright owner(s) are credited and that the original publication in this journal is cited, in accordance with accepted academic practice. No use, distribution or reproduction is permitted which does not comply with these terms.

Spatial-temporal changes of land use/cover change and habitat quality in Sanjiang plain from 1985 to 2017

Shanhe Jin[1], Xin Liu[1]*, Jiajia Yang[1]*, Junchao Lv[1], Yuchao Gu[1], Jishun Yan[2], Ruiyang Yuan[3] and Yudi Shi[4]

[1]Shenyang Center of China Geological Survey, Shenyang, China, [2]National Marine Environmental Monitoring Center, Dalian, China, [3]CCTEG Shenyang Research Institute, Shenyang, China, [4]Eco-Meteorology and Satellite Remote Sensing Center of Liaoning Province, Shenyang, China

Land use/Land cover (LULC) change seriously affects ecosystem services and ecosystem functions. In order to maintain ecological security and orderly social development, habitat quality assessment based on Land use/Land cover change is worth exploring. Based on multi-source land use data and Google remote sensing data from 1985 to 2017, land use transfer matrix and habitat quality index were used to study land use change, spatial-temporal evolution of habitat quality, and driving factors influencing habitat quality change in Sanjiang Plain. The results showed that Land use/Land cover changed significantly from 1985 to 2017, especially paddy land increased by 22,184.92 km^2, while unutilized land decreased by 11,533.53 km^2. The increase of construction land was mainly at the expense of dry land. There was a polarization in habitat quality, and the high intensity of land use utilization and development resulted in a significant decrease in habitat quality. From 1985 to 2017, the largest change in habitat quality was grassland, which decreased from 0.99 to 0.91.

KEYWORDS

land use transfer, habitat Quality, inVEST model, Sanjiang plain, land use/cover change (LUCC)

1 Introduction

With the rapid development of cities, there have been negative effects on the global climate, living environment, and ecological environment (Yang et al., 2019b; Guo et al., 2020; Chen Y. et al., 2022; Zhang et al., 2022b; Ren et al., 2022; Yu et al., 2022), The CPC Central Committee has given prominence to the construction of ecological civilization, comprehensively strengthened the construction of ecological civilization, and carried out a series of efforts to control mountains, rivers, forests, fields, lakes, grass and sand in an integrated manner (Du et al., 2021; Meng et al., 2021). Therefore, understanding the changes of habitat quality caused by land use transformation is of great significance for the construction of ecological civilization.

Land is the spatial carrier of human economic and social activities, and the huge transformation of land use/land cover (LULC) has brought about a series of environmental problems (Shan et al., 2019; Wang et al., 2019). The development and utilization of land resources not only affects the ecological structure and ecosystem services, but also directly affects habitat quality and biodiversity (Duo et al., 2022; He et al., 2022), Rational land development can achieve a win-win situation between human resource demand and sustainable ecosystem development (Tan et al., 2020). Land use is the main driving factor of urban landscape pattern change (Feng et al., 2016; Yang et al., 2019a), and land use type is the determinant of ecological service value, population growth and changes in farming methods, is the main driving force of LULC changes (Liyew et al., 2019), and in the simulation of different ecological restoration and land reclamation, returning farmland to forest increases all the Ecosystem services, among which the scenario of returning farmland to grassland has the greatest impact on ecosystem services, and the natural succession scenario of shrub land has the least impact on ecosystem services (Yang et al., 2018). The occupation of cultivated land and grassland for construction land leads to serious losses of ESV(Chuai et al., 2016; Yang et al., 2022), some studies have also shown that at the economic level, the expansion of cultivated land will lead to an increase in the value of ecosystem services, and the loss of services such as climate, water and air regulation in natural ecosystems may lead to economic losses, thereby reducing the value of ecological services (Arowolo et al., 2018). Land development and use restrictions are conducive to maintaining the stability and sustainability of ecosystem services (Hu et al., 2019).

Habitat quality refers to the ability of an ecosystem to provide suitable living conditions for the sustainable development of individuals and populations, which can reflect ecosystem service functions and ecosystem health to a certain extent (Hall et al., 1997). Habitat quality models are used to assess overlaps and trade-offs between biodiversity conservation, ecosystem service provision and land use patterns (Terrado et al., 2016; Han et al., 2019). In recent years, with the continuous development of computer technology, GIS, and remote sensing technology, and the continuous updating of data acquisition methods, ecosystem service assessment models have been widely used to quantitatively assess habitat quality. There are many factors that affect habitat quality, and changes such as urban growth, socioeconomic development, and climate can degrade and lose large amounts of habitat quality, thereby threatening biodiversity. The natural environment determines the overall distribution pattern of habitats, while human activities play a leading role in habitat changes (Bai et al., 2019; Huang et al., 2020; Song et al., 2020; Zhang H et al., 2020), and nighttime lighting and land urbanization rates are negatively correlated with habitat quality. From the perspective of landscape pattern, landscape aggregation index was positively correlated with habitat quality (Zhu et al., 2020). At present, the commonly used methods for studying ecological services at home and abroad include the Integrated Valuation of Ecosystem Services and Trade-offs (InVEST) model, the Ecological Suitability model, and the artificial intelligence ecosystem assessment model (Artificial Intelligence for Ecosystem Services (ARIES) model and Social Values for Ecosystem Services (SolVES) model (Costa et al., 2010; Bagstad et al., 2013; Open-File Report, 2015; Moreira et al., 2018), of which the InVEST model is the most widely used. A set of model systems for assessing the capacity and economic value of ecosystem services, supporting ecosystem management and decision-making, including three types of ecosystem service assessment models: terrestrial, freshwater and marine (Richard et al., 2018; Tang et al., 2020; Zhang X et al., 2020), the InVEST model is now widely used in Ecological assessment (Claudia et al., 2020; Hu et al., 2020).

This paper takes the Sanjiang Plain as the research area, explores the impact of LULC on the habitat quality of the Sanjiang Plain from 1985 to 2017, quantitatively assessed habitat quality in Sanjiang Plain, and explored the relationship between habitat quality and natural and social influencing factors, so as to provide valuable reference for ecological civilization construction.

2 Data and methods

2.1 Study area

Sanjiang Plain is located in the northeast of Heilongjiang Province (45°01′05″N~48°27′56″N, 130°12′01″E~135°05′26″E), “Sanjiang” refers to Heilongjiang, Wusuli River, Songhua River, the three rivers alluvial formed this piece of flat fertile soil. Including Jiamusi City, Hegang City, Shuangyashan City, Qitaihe City, 21 counties (cities) under Jixi City and Yilan County under Harbin City (Figure 1). The climate type is a mid-temperate continental monsoon climate, with an average temperature of 2.5–3.6°C, an accumulated temperature of ≥10°C of 2,200–2,500°C, and an annual precipitation of 500–600 mm. Influenced by comprehensive factors such as topography and landform, land property differences and social economy, Sanjiang Plain mainly develops agriculture, with relatively high land use intensification and serious population loss. These changes have been accompanied by massive biodiversity loss and habitat degradation.

2.2 Data sources and pre-processing

Land use data in this paper comes from the project of the Shenyang Center of China Geological Survey (Table 1). The

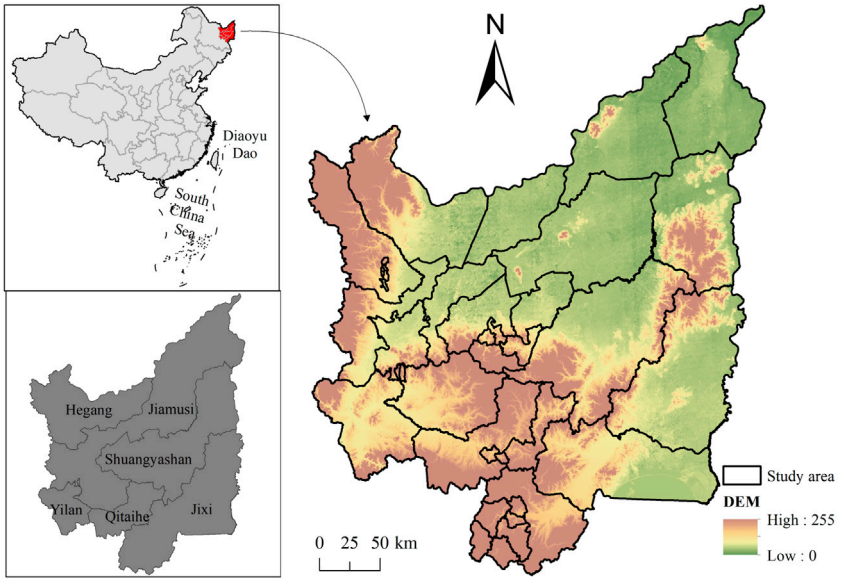

FIGURE 1
The location of the study area.

TABLE 1 Data sources and descriptions.

Data type	Time	Resolution (m)	Data sources	Explanation
Landsat5	1985	30	USGS	Obtain the original medium and high resolution original image
Landsat7	2000	30	USGS	Obtain the original medium and high resolution original image
GF-1	2017	8	Program application	Obtain the original medium and high resolution original image
Google Map	1985–2017	6	http://www.rivermap.cn/	Obtain the original high resolution original image
LULC	1985–2017	6	Shenyang Center of China Geological Survey	Obtain LULC

original remote sensing images of landsat5 and landsat7 in 1985 and 2000 were downloaded by USGS, and the GF-1 image in 2017 was obtained through project application. Data preprocessing is to perform radiometric calibration, atmospheric correction and image enhancement on the original image, and destrip the original Landsat7 TM data.

In order to extract LULC data in the research area, remote sensing images were initially classified by the supervised classification method in ENVI. Secondly, Google historical remote sensing images with a scale of 1:1 million and a spatial resolution of 6 m were downloaded from water micromaps, and the supervised classification results were corrected by manual visual interpretation and interpretation. In addition, 300 points were randomly selected for field verification and field verification, and the LULC data of Sanjiang Plain in 1985, 2000 and 2017 were finally obtained (Figure 2, Figure 3).

2.3 Methodology

2.1.1 Land use transfer change

Land use transition matrix is a quantitative description of the system state and state transition in the system analysis, which can reflect the transition of land use types in two periods. The calculation formula is as follows:

$$S_{ij} = \begin{bmatrix} S_{11} & \cdots & S_{1n} \\ \vdots & \ddots & \vdots \\ S_{n1} & \cdots & S_{nn} \end{bmatrix} \quad (1)$$

S is the land type area, n is the land use type, i, j are the land types at the initial and final stages, respectively.

2.1.2 InVEST model habitat quality

The habitat degradation index is used to describe the negative impact of threat sources on habitats. The habitat quality is mainly

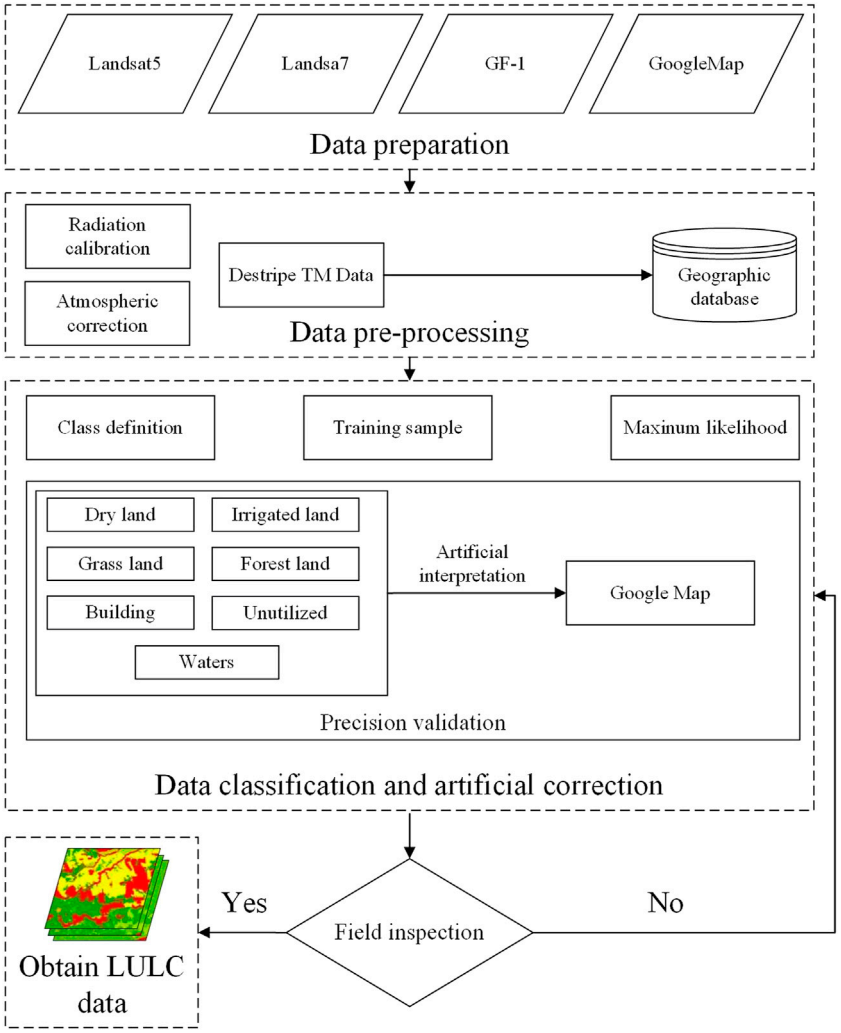

FIGURE 2
Data pre-processing process.

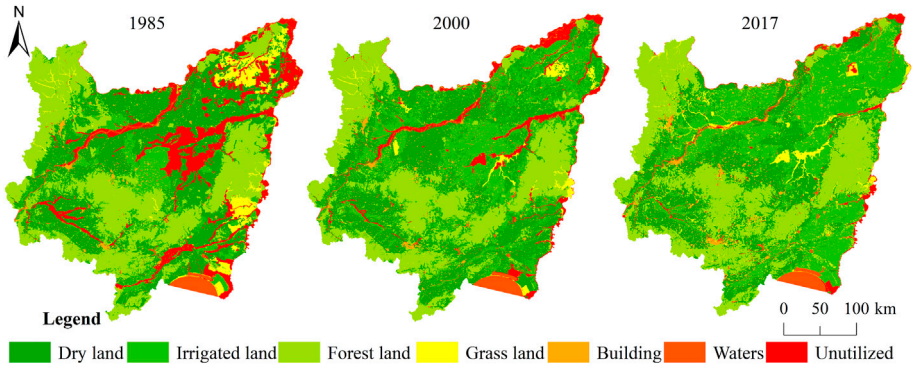

FIGURE 3
1985–2017 Land use/Land cover.

TABLE 2 Weight and maximum influence distance of threat sources.

Threat source	Maximum influence distance	Weight	Regression linear correlation
Irrigated land	1.0	0.2	linear
Dry land	1.0	0.2	linear
Building	10.0	1.0	exponent

TABLE 3 Habitat suitability of land use types and their sensitivity to various threat sources.

LULC types	Habitat suitability	Dry land	Irrigated land	Building
Grass land	1.0	0.5	0.5	0.6
Forest land	1.0	0.9	0.9	1.0
Waters	1.0	0.7	0.7	0.8
Unutilized	1.0	0.4	0.4	0.4
Dry land	0.0	0.0	0.0	0.0
Irrigated land	0.0	0.0	0.0	0.0
Building	0.0	0.0	0.0	0.0

affected by four factors: the relative impact of each threat, the relative sensitivity of each habitat to each threat factor, the distance between the habitat and the threat source, and the level of legal protection of land. The higher the sensitivity of the habitat to the threat factor, the greater the habitat degradation index will be. The calculation formula is as follows:

$$D_{xj} = \sum_{r=1}^{R} \sum_{y=1}^{Y_r} \left(\frac{\omega_r}{\sum_{r=1}^{R} \omega_r} \right) r_y i_{rxy} \beta_x S_{jr} \tag{2}$$

$$i_{rxy} = \begin{cases} 1 - \left(\frac{d_{xy}}{d_{r\,max}} \right) & \text{(linear)} \\ exp\left(- \left(\frac{2.99}{d_{r\,max}} \right) d_{xy} \right) & \text{(exponent)} \end{cases} \tag{3}$$

D_{xj} is the degree of habitat degradation, R is the total amount of threat factors, Y_r is the sum of the grids in the threat factor r layer, ω_r is the normalized threat weight, and r_y is used to determine whether the grid y is the source of the threat factor r, i_{rxy} is the distance function between the habitat and the threat factor, β_x represents the accessibility level of the threat source to the grid x under social and legal protection status, and S_{jr} represents the sensitivity of the land type j to the threat factor r.

The habitat quality is calculated based on the habitat degradation index, and the calculation formula is as follows:

$$Q_{xj} = H_j \left[1 - \left(\frac{D_{xj}^z}{D_{xj}^z + K^z} \right) \right] \tag{4}$$

Q_{xj} is the habitat quality index of the grid x in the land category j, H_j is the habitat suitability of the land category j, D_{xj} is the stress level of the grid x in the land category j, z is a normalized constant, usually 2.5, K is the half-saturation constant, usually 0.5.

2.3.3 Habitat quality threats

Each habitat quality type is affected by its own habitat suitability and sensitivity to threat sources, the higher the habitat suitability, the better the habitat quality, and the stronger the sensitivity to threat sources, indicating the lower the anti-disturbance ability and the worse the habitat quality. Since the Sanjiang Plain is mainly agricultural and animal husbandry, this study divides the cultivated land into irrigated land and dry land. There are three types of threat sources, namely irrigated land, dry land and construction land (Table 2). Refer to the InVest User Guide for the maximum impact distance, first set to 0.5 and adjusted by the degradation index data, the facility is 0.095. The spatial impact of threat was mainly affected by the distance between threat factor and habitat and the attenuation mode. The decay mode is composed of linear decay and exponential decay (Table 2, Table 3).

3 Results

3.1 Spatial-temporal evolution of land use

By calculating the area change of each LULC type and the proportion of each type of LULC from 1985 to 2017

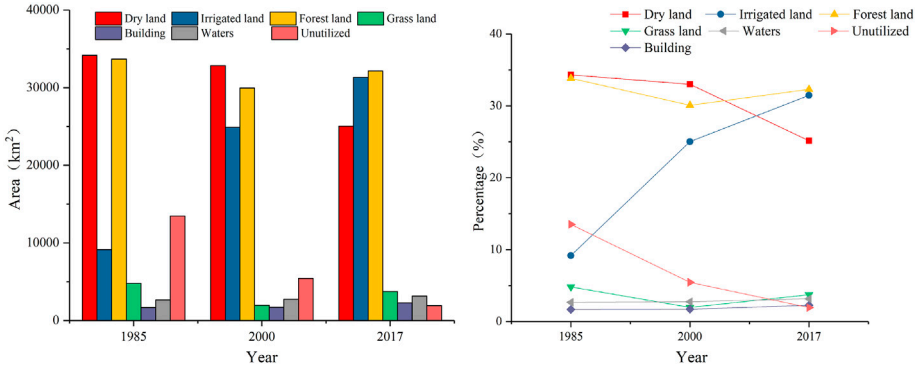

FIGURE 4
Land use/Land cover change.

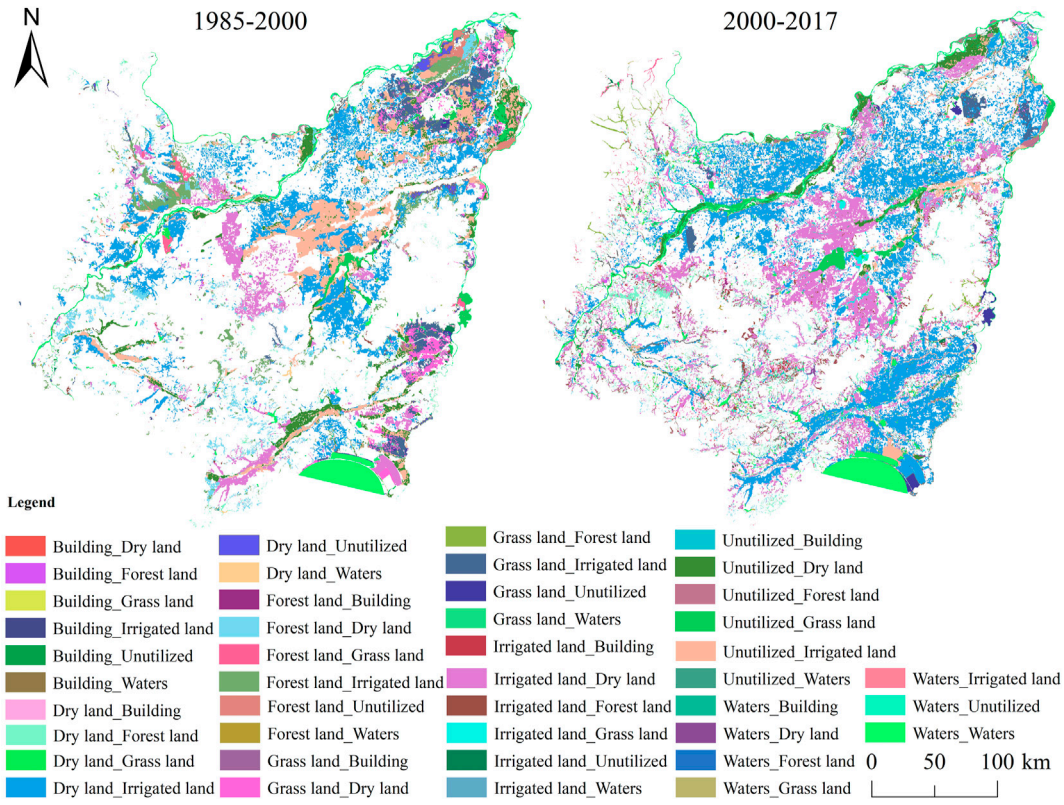

FIGURE 5
Land use/cover transfer from 1985 to 2017.

(Figure 4), it can be seen that land use has undergone huge changes. In 1985, the Sanjiang Plain occupied the largest area of cultivated land, including dry land and irrigated land, covering an area of 34,157.88 km^2 and 9,141.66 km^2, respectively. Dry land accounted for 34.3%, forest land accounted for 33.8%, and construction land area was at least 1,659.53 km^2, accounting for 1.7%. In 2000, the irrigated land area doubled to 24,908.22 km^2, accounting for 25.02%, and unutilized land was greatly reduced. In 2017, dry land continued to decrease, covering an area of

TABLE 4 Land use transition matrixes between 1985 and 2000.

1985	2000				(km$^{2)}$			
	Grass land	Dry land	Building	Forest land	Irrigated land	Waters	Unutilized	Total
Grass land	875.97	1,333.64	2.37	137.63	2,277.25	25.45	132.40	4,784.73
Dry land	80.71	23,535.69	67.23	581.41	9,390.36	91.60	410.87	34,157.88
Building	0.52	24.30	1,607.04	15.69	11.17	0.59	0.22	1,659.53
Forest land	212.83	1845.84	12.32	28,915.46	2,165.21	24.19	508.87	33,684.73
Irrigated land	6.61	3,121.84	10.51	79.23	5,797.87	51.97	73.63	9,141.66
Waters	11.61	36.78	2.48	18.93	33.96	2,337.73	211.22	2,652.71
Unutilized	766.76	2,947.85	7.06	204.51	5,232.40	204.75	4,090.90	13,454.24
Total	1955.01	32,845.95	1709.01	29,952.87	24,908.22	2,736.29	5,428.11	99,535.47

TABLE 5 Land use transition matrixes between 2000 and 2000.

2000	2017				(km^2)			
	Grass land	Dry land	Building	Forest land	Irrigated land	Waters	Unutilized	Total
Grass land	596.61	99.41	1.88	292.06	641.51	17.46	306.08	1955.01
Dry land	759.95	13,687.65	511.77	1786.66	15,842.88	128.52	128.53	32,845.95
Building	31.15	102.12	1,430.90	42.52	86.83	7.09	8.41	1709.01
Forest land	365.77	734.76	44.68	28,343.06	365.04	46.30	53.28	29,952.88
Irrigated land	841.15	9,036.90	250.64	1,292.55	13,245.17	111.58	131.01	24,909.00
Waters	37.94	62.78	1.62	27.91	65.02	2,465.70	75.33	2,736.29
Unutilized	1,088.35	1,308.58	7.98	353.21	1,080.14	371.78	1,218.07	5,428.11
Total	3,720.91	25,032.21	2,249.45	32,137.97	31,326.58	3,148.42	1920.71	99,536.26

25,032.21 km^2, while irrigated land continued to increase, increasing to 31,326.58 km^2, accounting for 31.47% From 1985 to 2017, irrigated land continued to grow, dry land and unutilized land continued to decrease, forest land first decreased and then increased, and other land types did not change significantly. In 1985 and 2000, dry land accounted for the largest proportion of land types, but irrigated land accounted for the largest proportion of land types in 2017.

It can be seen that the Sanjiang Plain is rich in black soil resources and water resources, mainly for agricultural production, so the conversion of LULC shows the continuous increase of irrigated land. In addition, the growth rate of construction land is very small, mainly in the west. The accelerated urbanization process and the continuous growth of population have led to the growth of construction land. However, urban expansion is not obvious, and industrial development is slow.

From the land use matrix (Figure 5), it can be seen that from 1985 to 2000, the conversion of unutilizedland into irrigated land and dry land was the most obvious, especially in the middle of the study area, followed by the conversion of grassland into irrigated land, mainly in the northeast. From 2000 to 2017, it was mainly the mutual conversion between dry land and irrigated land, which was distributed in the north and southeast of the study area, followed by the conversion of dry land to forest land, which was distributed in the southwest. In addition, it can be seen that the increase in construction land is mainly due to the conversion of dry land to construction land. Quantitative analysis of land use transfer changes (Table 4, Table 5) shows that from 1985 to 2000, irrigated land increased by 15,766.56 km^2 and unutilized land decreased by 8,026.13 km^2. From 2000 to 2017, irrigated land increased by 6,417.58 km^2, dry landdecreased by 7,813.74 km^2, and unused land decreased by 8,026.13 km^2. Reduced by 3,507.40 km^2. This paper analyzes and organizes the information of LULC in the study area in the past 30 years, and it is of great significance to grasp the changing law and direction of LULC in the study area.

TABLE 6 Average habitat quality of different LULC types.

LULC types	1985	2000	2017
Grass land	0.99	0.98	0.91
Dry land	0.00	0.00	0.00
Building	0.00	0.00	0.00
Forest land	0.94	0.92	0.92
Irrigated land	0.00	0.00	0.00
Waters	0.96	0.94	0.91
Unutilized	0.99	0.98	0.97

3.2 Spatial-temporal evolution of habitat quality

The habitat quality ranges from 0 to 1, and the closer it is to 1, the higher the habitat quality. From 1985 to 2017, the habitat quality of the Sanjiang Plain showed a phenomenon of polarization, and the habitat quality decreased year by year. Among them, the habitat quality decreased significantly from 1985 to 2000, mainly in the northeast and southeast of the study area, and the habitat quality from 2000 to 2017. The quality change is not obvious, but it can be seen that the habitat quality in the northeastern part of the study area is significantly reduced, showing a circular shape and gradually spreading inward, and the habitat quality in the southwestern part is significantly increased (Figure 6).

Quantitative analysis shows that in 1985, the habitat quality was good, and the habitat quality value was above 0.8, reaching 30%. However, in 2000 and 2017, the habitat quality value was below 0.2, reaching more than 90%. Due to the high-intensity development and utilization of land, resulting in a sharp decline in habitat quality.

The assessment of habitat quality by the InVest model includes many aspects, and the degree of degradation reflects the degree of habitat quality decline. From 1985 to 2017, the degree of habitat degradation increased year by year, and the areas with the highest degree of degradation occurred in the west and northwest of the study area, near towns, industrial and mining, residential land, and near various watersheds (Figure 7). The damage is the worst. The areas with a high degree of degradation are irrigated land and dry land, and human activities have had a negative impact on the ecological environment. The places with low degree of degradation are forest land and grass land, and the vegetation cover has a positive impact on the ecological environment.

3.3 Effects of land use change on habitat quality

Land use change will have positive and negative impacts on habitat quality, and the area with obvious changes in habitat quality is the concentrated area of land use change. Statistical analysis of the average habitat quality from 1985 to 2017 shows that the habitat quality of dry land, irrigated land and construction land is 0, and the habitat quality of grassland, forest land and unutilized land is above 0.90 (Table 6). In recent years, due to the development of unutilized land by agricultural production, the increase of construction land and the loss of grassland, the habitat quality has been reduced.

Analyzing the changes of habitat quality during different LULC conversions, it was found that when the land was converted to urban and rural, industrial and mining, and residential land, the habitat quality decreased the most, especially when the unutilized land was converted to construction land, the habitat quality decreased the fastest,

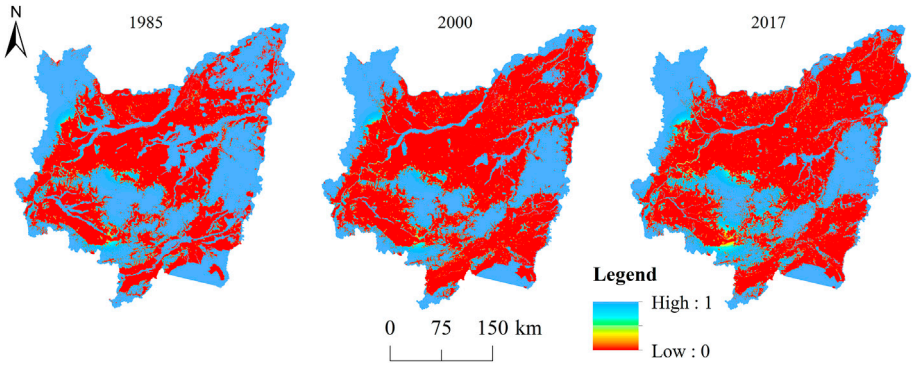

FIGURE 6
Spatial-temporal changes in habitat quality from 1985 to 2017.

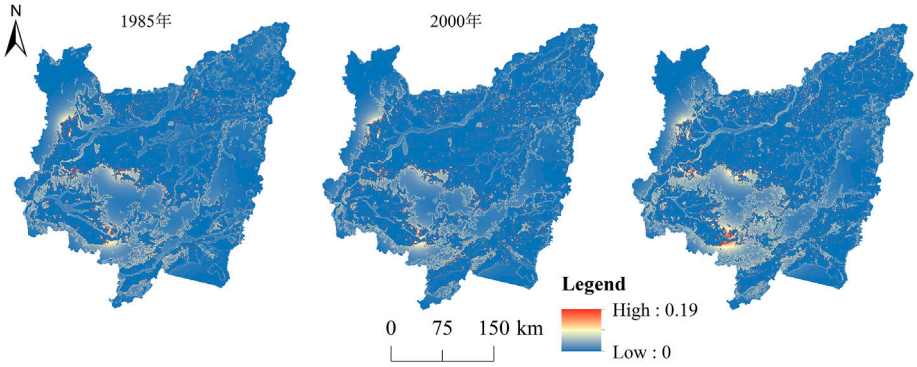

FIGURE 7
Spatial-temporal changes of degradation dgree.

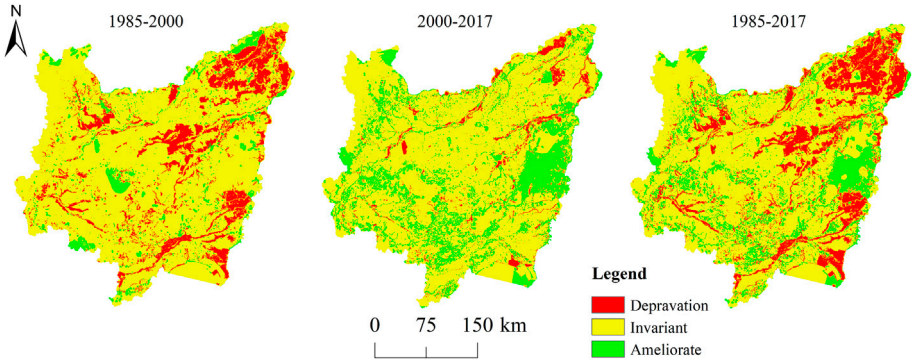

FIGURE 8
Changes in habitat quality.

followed by the conversion of forest land to construction land. The habitat quality of irrigated land and dry land also decreased, and the habitat quality of irrigated land decreased more than that of dry land. The habitat quality increased when converted to grassland, unutilized land and forest land, and the grassland habitat quality increased the most.

In order to further study the effect of LULC change on habitat quality change, the results of habitat quality from 1985 to 2017 were superimposed and analyzed to obtain the habitat quality change (Figure 8). From 1985 to 2017, most of the habitat quality remained unchanged, while a small part of the habitat quality improved, and more areas of the habitat quality deteriorated than improved. In the first 15 years, the habitat quality became worse, and in the last 17 years, the habitat quality became better. Combined with Figure 4, it can be seen that the deterioration of habitat quality from 1985 to 2000 was due to the reduction of grass land and forest land, and the improvement of habitat quality from 2000 to 2017 was due to the conversion of other land to forest land.

4 Discussion

4.1 Land use/cover and habitat quality change driving mechanisms

This paper obtains LULC types in the study area through remote sensing technology and field verification, which improves the accuracy of data compared with traditional classification methods (Xie and Wang, 2015), studies land use transfer and habitat quality change, quantitatively analyzes the driving mechanism of habitat quality change, and provides scientific reference for ecological environment construction in the Sanjiang Plain. Analyzing the impact of land use change on habitat quality could provide meaningful reference for

optimizing habitat quality in the Sanjiang Plain. The LULC variation in Sanjiang Plain is affected by topography, climate, social and economic factors (Wang et al., 2015; Chen H. et al., 2022). In the late 1985s, the domestic industry was transformed, and the demand for cultivated land increased significantly, which led to the transformation of LULC type to cultivated land (Yang et al., 2013, 2000–2009), so irrigated land were gradually increasing. With China's emphasis on the ecological environment (Jiang et al., 2021; Hu et al., 2022), grass land and forest land have also increased since 2000. The uncertainty of LULC type data leads to great differences in ecological environment results, and this uncertainty also shows great differences between different biological communities and soil types (Ouyang et al., 2013; Song, 2018; Wang et al., 2022). Therefore, LULC change is a direct factor affecting ecosystem services. LULC change is closely related to national policies and social and economic development (Yang et al., 2021). In order to further strengthen the control of LULC spatial conversion, the speed of LULC conversion should be slowed down, the conversion of land with good habitat quality should be reduced, and the degree of landscape fragmentation should be reduced.

Habitat quality change is affected by many aspects and is a complex process. LULC change is one of the main driving factors leading to the change of habitat quality. We found that construction land was the most threatening to habitat quality, and human activities seriously damaged urban climate and ecological environment (Zhang et al., 2022a). Agricultural activities pose a greater threat due to the effects of fertilizers and pesticides, mechanical activities during harvest or human trampling on the land (Yang et al., 2012), but farming is not entirely negative for the ecological environment (Zhang et al., 2012). In order to promote the ecological environment, on the premise of ensuring food security, the use of fallow irrigated land can protect the ecological environment (Luo et al., 2020). In order to slow down the degradation of habitat quality, it is necessary to make reasonable planning for urban expansion and strive for greater ecological benefits.

With the change of land use pattern, habitat quality also changed. In the future planning of land use pattern in Sanjiang Plain, we should pay attention to the protection of grassland and woodland, rationally control the amount of cultivated land and construction land, optimize the landscape pattern of woodland, grassland, cultivated land and construction land, and pay attention to ecological benefits while pursuing economic benefits, so as to achieve the coordinated development of human-land system.

4.2 Limitation

This paper only analyzes the habitat quality from the perspective of land use, and draws some conclusions that are beneficial to the construction of regional ecological civilization. There are differences in the impact of LULC types on habitat quality. Due to the aggregation of agricultural production in the Sanjiang Plain, this paper divides the cultivated land types into irrigated land and dry land. However, subdividing LULC types can explore LULC changes more microscopically (Yan and Zhang, 2019; Luo et al., 2022). In addition, the source of habitat quality threat is not only the impact of human economic activities, but also natural disasters under unstable factors.

5 Conclusion

Sanjiang Plain plays an important role in regional and national food security. This paper integrates the land use/cover situation of the Sanjiang Plain in the past 30 years through remote sensing data, and uses the Invest model to calculate the habitat quality of the study area and evaluate the impact of LULC change on the habitat quality, and provide a scientific basis for ecological protection in the study area. The conclusion is as follows: 1) From 1985 to 2017, the most obvious land use changes were irrigated land and unutilized land. The Sanjiang Plain is rich in black soil resources. With the breakthrough of rice technology, a large number of farmers have opened up wasteland and the area of irrigated land has continued to grow. Due to serious population loss and slow economic development in Northeast China, although construction land have increased, they are extremely slow. After 2000, China has attached great importance to ecological protection, and the forest land and grassland have decreased first and then increased. 2) From 1985 to 2017, the habitat quality showed a downward trend year by year, and the increase of urban, industrial and mining, residential land and agricultural land was the main reason for the change of habitat quality. 3) Land use change and land development intensity, along with the change of habitat quality, the habitat quality of the Sanjiang Plain is getting worse and worse, indicating that agricultural production has a negative impact on the habitat quality. LULC and habitat quality were significantly correlated in Sanjiang Plain. When LULC types were forest land and grass land, the habitat quality was significantly improved, and with the social development, the habitat quality was significantly worse when irrigated land increased.

Data availability statement

The original contributions presented in the study are included in the article/supplementary material, further inquiries can be directed to the corresponding authors.

Author contributions

SJ contributed to all aspects of this work and wrote the main manuscript text; XL and JY wrote the data analysis section, JL, YG, JY, RY, and YS conducted the experiment and analyzed the data. All authors reviewed the manuscript.

Funding

This research study was supported by the Shenyang Center of China Geological Survey (Grant No.DD20211389-2).

Acknowledgments

The authors would like to acknowledge all colleagues and friends who have voluntarily reviewed the translation of the survey and the manuscript of this study.

Conflict of interest

The authors declare that the research was conducted in the absence of any commercial or financial relationships that could be construed as a potential conflict of interest.

Publisher's note

All claims expressed in this article are solely those of the authors and do not necessarily represent those of their affiliated organizations, or those of the publisher, the editors and the reviewers. Any product that may be evaluated in this article, or claim that may be made by its manufacturer, is not guaranteed or endorsed by the publisher.

References

Arowolo, A. O., Deng, X., Olatunji, O. A., and Obayelu, A. E. (2018). Assessing changes in the value of ecosystem services in response to land-use/land-cover dynamics in Nigeria. *Sci. Total Environ.* 636, 597–609. doi:10.1016/j.scitotenv.2018.04.277

Bagstad, K. J., Johnson, G. W., Voigt, B., and Villa, F. (2013). Spatial dynamics of ecosystem service flows: A comprehensive approach to quantifying actual services. *Ecosyst. Serv.* 4, 117–125. doi:10.1016/j.ecoser.2012.07.012

Bai, L., Xiu, C., Feng, X., and Liu, D. (2019). Influence of urbanization on regional habitat quality:a case study of Changchun City. *Habitat Int.* 93, 102042. doi:10.1016/j.habitatint.2019.102042

Chen, H., Meng, F., Yu, Z., and Tan, Y. (2022a). Spatial–temporal characteristics and influencing factors of farmland expansion in different agricultural regions of Heilongjiang Province, China. *Land Use Policy* 115, 106007. doi:10.1016/j.landusepol.2022.106007

Chen, Y., Yang, J., Yang, R., Xiao, X., Xia, J., and Cecilia) (2022b). Contribution of urban functional zones to the spatial distribution of urban thermal environment. *Build. Environ.* 216, 109000. doi:10.1016/j.buildenv.2022.109000

Chuai, X., Huang, X., Wu, C., Li, J., Lu, Q., Qi, X., et al. (2016). Land use and ecosystems services value changes and ecological land management in coastal Jiangsu, China. *Habitat Int.* 57, 164–174. doi:10.1016/j.habitatint.2016.07.004

Claudia, C., Carlos, M. J., Cunha Pedro, P., and Teixeira, Z. (2020). Ecosystem services as a resilience descriptor in habitat risk assessment using the InVEST model. *Ecol. Indic.* 115, 106426. doi:10.1016/j.ecolind.2020.106426

Costa, G. C., Nogueira, C., Machado, R. B., and Colli, G. R. (2010). Sampling bias and the use of ecological niche modeling in conservation planning: A field evaluation in a biodiversity hotspot. *Biodivers. Conserv.* 19, 883–899. doi:10.1007/s10531-009-9746-8

Du, W., Yan, H., Feng, Z., Yang, Y., and Liu, F. (2021). The supply-consumption relationship of ecological resources under ecological civilization construction in China. *Resour. Conservation Recycl.* 172, 105679. doi:10.1016/j.resconrec.2021.105679

Duo, L., Li, Y., Zhang, M., Zhao, Y., Wu, Z., and Zhao, D. (2022). Spatiotemporal pattern evolution of urban ecosystem resilience based on "resistance-adaptation-vitality": A case study of nanchang city. *Front. Earth Sci.* 10, 902444. doi:10.3389/feart.2022.902444

Feng, Y., Yang, J., and Wu, M. (2016). Land cover transition in the shuanghe natural reserve area, Heilongjiang province:A study based on landscape transfer matrix. *Geol. Resour.* 25, 500–504. doi:10.13686/j.cnki.dzyzy.2016.05.014

Guo, A., Yang, J., Sun, W., Xiao, X., Xia Cecilia, J., Jin, C., et al. (2020). Impact of urban morphology and landscape characteristics on spatiotemporal heterogeneity of land surface temperature. *Sustain. Cities Soc.* 63, 102443. doi:10.1016/j.scs.2020.102443

Hall, L. S., Krausman, P. R., and Morrison, M. L. (1997). The habitat concept and a plea for standard terminology. *Wildlife Society Bulletin*. 25, 173–182.

Han, Y., Kang, W., Thorne, J., and Song, Y. (2019). Modeling the effects of landscape patterns of current forests on the habitat quality of historical remnants in a highly urbanized area. *Urban For. Urban Green.* 41, 354–363. doi:10.1016/j.ufug.2019.04.015

He, F., Yang, J., Zhang, Y., Sun, D., Wang, L., Xiao, X., et al. (2022). Offshore island connection line: A new perspective of coastal urban development boundary simulation and multi-scenario prediction. *GIScience Remote Sens.* 59, 801–821. doi:10.1080/15481603.2022.2071056

Hu, M., Li, Z., Wang, Y., Jiao, M., Li, M., and Xia, B. (2019). Spatio-temporal changes in ecosystem service value in response to land-use/cover changes in the Pearl River Delta. *Resour. Conservation Recycl.* 149, 106–114. doi:10.1016/j.resconrec.2019.05.032

Hu, P., Zhou, Y., Zhou, J., Wang, G., and Zhu, G. (2022). Uncovering the willingness to pay for ecological red lines protection: Evidence from China. *Ecol. Indic.* 134, 108458. doi:10.1016/j.ecolind.2021.108458

Hu, W., Li, G., Gao, Z., Jia, G., Wang, Z., and Li, Y. (2020). Assessment of the impact of the Poplar Ecological Retreat Project on water conservation in the Dongting Lake wetland region using the InVEST model. *Sci. Total Environ.* 733, 139423. doi:10.1016/j.scitotenv.2020.139423

Huang, J., Tang, Z., Liu, D., and He, J. (2020). Ecological response to urban development in a changing socio-economic and climate context: Policy implications for balancing regional development and habitat conservation. *Land Use Policy* 97, 104772. doi:10.1016/j.landusepol.2020.104772

Jiang, L., Liu, Y., Wu, S., and Yang, C. (2021). Analyzing ecological environment change and associated driving factors in China based on NDVI time series data. *Ecol. Indic.* 129, 107933. doi:10.1016/j.ecolind.2021.107933

Liyew, B. M., Atsushi, T., Nigussie, H., Tsegaye, M. D., Enyew, A., Mitsuru, T., et al. (2019). Exploring land use/land cover changes, drivers and their implications in contrasting agro-ecological environments of Ethiopia. *Land Use Policy* 87, 104052. doi:10.1016/j.landusepol.2019.104052

Luo, C., Fu, X., Zeng, X., Cao, H., Wang, J., Ni, H., et al. (2022). Responses of remnant wetlands in the Sanjiang Plain to farming-landscape patterns. *Ecol. Indic.* 135, 108542. doi:10.1016/j.ecolind.2022.108542

Luo, C., Liu, H., Fu, Q., Guan, H., Ye, Q., Zhang, X., et al. (2020). Mapping the fallowed area of paddy fields on Sanjiang Plain of Northeast China to assist water security assessments. *J. Integr. Agric.* 19, 1885–1896. doi:10.1016/S2095-3119(19)62871-6

Meng, F., Guo, J., Guo, Z., Lee, J. C. K., Liu, G., and Wang, N. (2021). Urban ecological transition: The practice of ecological civilization construction in China. *Sci. Total Environ.* 755, 142633. doi:10.1016/j.scitotenv.2020.142633

Moreira, M., Fonseca, C., Marta, V., Helena, C., and Gil, A. (2018). Spatial assessment of habitat conservation status in a macaronesian island based on the InVEST model: A case study of pico island (azores, Portugal). *Land Use Policy* 78, 637–649. doi:10.1016/j.landusepol.2018.07.015

Open-File Report (2015). *Open-file Report*. United States: U.S. Department of the Interior, U.S. Geological Survey.

Ouyang, W., Xu, Y., Hao, F., Wang, X., Siyang, C., and Lin, C. (2013). Effect of long-term agricultural cultivation and land use conversion on soil nutrient contents in the Sanjiang Plain. *CATENA* 104, 243–250. doi:10.1016/j.catena.2012.12.002

Ren, J., Yang, J., Zhang, Y., Xiao, X., Xia, J. C., Li, X., et al. (2022). Exploring thermal comfort of urban buildings based on local climate zones. *J. Clean. Prod.* 340, 130744. doi:10.1016/j.jclepro.2022.130744

Richard, S., Rebecca, C.-K., Spencer, W., Anne, G., Heather, T., Taylor, R., et al. (2018). *InVEST user's Guide*. United States: The Natural Capital Project, Stanford University, University of Minnesota. doi:10.13140/RG.2.2.32693.78567

Shan, W., Jin, X., Ren, J., Wang, Y., Xu, Z., Fan, Y., et al. (2019). Ecological environment quality assessment based on remote sensing data for land consolidation. *J. Clean. Prod.* 239, 118126. doi:10.1016/j.jclepro.2019.118126

Song, S., Liu, Z., He, C., and Lu, W. (2020). Evaluating the effects of urban expansion on natural habitat quality by coupling localized shared socioeconomic pathways and the land use scenario dynamics-urban model. *Ecol. Indic.* 112, 106071. doi:10.1016/j.ecolind.2020.106071

Song, X.-P. (2018). Global estimates of ecosystem service value and change: Taking into account uncertainties in satellite-based land cover data. *Ecol. Econ.* 143, 227–235. doi:10.1016/j.ecolecon.2017.07.019

Tan, Z., Guan, Q., Lin, J., Yang, L., Luo, H., Ma, Y., et al. (2020). The response and simulation of ecosystem services value to land use/land cover in an oasis, Northwest China. *Ecol. Indic.* 118, 106711. doi:10.1016/j.ecolind.2020.106711

Tang, F., Fu, M., Li, W., and Zhang, P. (2020). Land-use change in Changli County, China: Predicting its spatio-temporal evolution in habitat quality. *Ecol. Indic.* 117, 106719. doi:10.1016/j.ecolind.2020.106719

Terrado, M., Sabater, S., Chaplin-Kramer, B., Mandle, L., Ziv, G., and Acuña, V. (2016). Model development for the assessment of terrestrial and aquatic habitat quality in conservation planning. *Sci. Total Environ.* 540, 63–70. doi:10.1016/j.scitotenv.2015.03.064

Wang, C., Jiang, Q., Shao, Y., Sun, S., Xiao, L., and Guo, J. (2019). Ecological environment assessment based on land use simulation: A case study in the heihe river basin. *Sci. Total Environ.* 697, 133928. doi:10.1016/j.scitotenv.2019.133928

Wang, Q., Kang, Q., Zhao, B., Li, H., Lu, H., Liu, J., et al. (2022). Effect of land-use and land-cover change on mangrove soil carbon fraction and metal pollution risk in Zhangjiang Estuary, China. *Sci. Total Environ.* 807, 150973. doi:10.1016/j.scitotenv.2021.150973

Wang, Z., Mao, D., Li, L., Jia, M., Dong, Z., Miao, Z., et al. (2015). Quantifying changes in multiple ecosystem services during 1992–2012 in the Sanjiang Plain of China. *Sci. Total Environ.* 514, 119–130. doi:10.1016/j.scitotenv.2015.01.007

Xie, S., and Wang, Z. (2015). Study on the dynamic change of land use in Shenyang based on Object-oriented classification technology. *Geol. Resour.* 24, 255–260. doi:10.13686/j.cnki.dzyzy.2015.03.015

Yan, F., and Zhang, S. (2019). Ecosystem service decline in response to wetland loss in the Sanjiang Plain, Northeast China. *Ecol. Eng.* 130, 117–121. doi:10.1016/j.ecoleng.2019.02.009

Yang, D., Lou, Y., Zhang, P., and Jiang, L. (2022). Spillover effects of built-up land expansion under ecological security constraint at multiple spatial scales. *Front. Ecol. Evol.* 10, 907691. doi:10.3389/fevo.2022.907691

Yang, J., Guo, A., Li, Y., Zhang, Y., and Li, X. (2019a). Simulation of landscape spatial layout evolution in rural-urban fringe areas: A case study of ganjingzi district. *GIScience Remote Sens.* 56, 388–405. doi:10.1080/15481603.2018.1533680

Yang, J., Wang, Y., Xiao, X., Jin, C., Xia, J., Cecilia)and Li, X. (2019b). Spatial differentiation of urban wind and thermal environment in different grid sizes. *Urban Clim.* 28, 100458. doi:10.1016/j.uclim.2019.100458

Yang, J., Yang, R., Chen, M.-H., Su, C.-H., Joan)Zhi, Y., and Xi, J. (2021). Effects of rural revitalization on rural tourism. *J. Hosp. Tour. Manag.* 47, 35–45. doi:10.1016/j.jhtm.2021.02.008

Yang, S., Bai, Y., Wang, S., and Feng, N. (2013). Evaluating the transformation of China's industrial development mode during 2000–2009. *Renew. Sustain. Energy Rev.* 20, 585–594. doi:10.1016/j.rser.2012.12.034

Yang, S., Zhao, W., Liu, Y., Wang, S., Wang, J., and Zhai, R. (2018). Influence of land use change on the ecosystem service trade-offs in the ecological restoration area: Dynamics and scenarios in the Yanhe watershed, China. *Sci. Total Environ.* 644, 556–566. doi:10.1016/j.scitotenv.2018.06.348

Yang, W., Cheng, H., Hao, F., Ouyang, W., Liu, S., and Lin, C. (2012). The influence of land-use change on the forms of phosphorus in soil profiles from the Sanjiang Plain of China. *Geoderma* 189–190, 207–214. doi:10.1016/j.geoderma.2012.06.025

Yu, W., Yang, J., Sun, D., Yu, H., Yao, Y., Xiao, X., et al. (2022). Spatial-temporal patterns of network structure of human settlements competitiveness in resource-based urban agglomerations. *Front. Environ. Sci.* 10, 893876. doi:10.3389/fenvs.2022.893876

Zhang, D., Min, Q., Liu, M., and Cheng, S. (2012). Ecosystem service tradeoff between traditional and modern agriculture: A case study in congjiang county, guizhou province, China. *Front. Environ. Sci. Eng.* 6, 743–752. doi:10.1007/s11783-011-0385-4

Zhang, D., Zhou, C., and He, B.-J. (2022a). Spatial and temporal heterogeneity of urban land area and PM2.5 concentration in China. *Urban Clim.* 45, 101268. doi:10.1016/j.uclim.2022.101268

Zhang, D., Zhou, C., Zhou, Y., and Zikirya, B. (2022b). Spatiotemporal relationship characteristic of climate comfort of urban human settlement environment and population density in China. *Front. Ecol. Evol.* 10, 953725. doi:10.3389/fevo.2022.953725

Zhang H, H., Zhang, C., Hu, T., Zhang, M., Ren, X., and Hou, L. (2020). Exploration of roadway factors and habitat quality using InVEST. *Transp. Res. Part D Transp. Environ.* 87, 102551. doi:10.1016/j.trd.2020.102551

Zhang X, X., Song, W., Lang, Y., Xiaomiao, F., Yuan, Q., and Wang, J. (2020). Land use changes in the coastal zone of China's Hebei Province and the corresponding impacts on habitat quality. *Land Use Policy* 99, 104957. doi:10.1016/j.landusepol.2020.104957

Zhu, C., Zhang, X., Zhou, M., He, S., Gan, M., Yang, L., et al. (2020). Impacts of urbanization and landscape pattern on habitat quality using OLS and GWR models in Hangzhou, China. *Ecol. Indic.* 117, 106654. doi:10.1016/j.ecolind.2020.106654

frontiers | Frontiers in Earth Science

TYPE Original Research
PUBLISHED 27 October 2022
DOI 10.3389/feart.2022.1016491

Check for updates

OPEN ACCESS

EDITED BY
Jun Yang,
Northeastern University, China

REVIEWED BY
Jie Dong,
Wuhan University, China
Saygin Abdikan,
Hacettepe University, Turkey

*CORRESPONDENCE
Ruiqi Zhao,
zrq@mails.cqjtu.edu.cn

†These authors have contributed equally to this work and share first authorship

SPECIALTY SECTION
This article was submitted to Environmental Informatics and Remote Sensing, a section of the journal Frontiers in Earth Science

RECEIVED 11 August 2022
ACCEPTED 20 September 2022
PUBLISHED 27 October 2022

CITATION
Pan J, Zhao R, Xu Z, Cai Z and Yuan Y (2022), Quantitative estimation of sentinel-1A interferometric decorrelation using vegetation index. *Front. Earth Sci.* 10:1016491. doi: 10.3389/feart.2022.1016491

COPYRIGHT
© 2022 Pan, Zhao, Xu, Cai and Yuan. This is an open-access article distributed under the terms of the Creative Commons Attribution License (CC BY). The use, distribution or reproduction in other forums is permitted, provided the original author(s) and the copyright owner(s) are credited and that the original publication in this journal is cited, in accordance with accepted academic practice. No use, distribution or reproduction is permitted which does not comply with these terms.

Quantitative estimation of sentinel-1A interferometric decorrelation using vegetation index

Jianping Pan[1†], Ruiqi Zhao[1†*], Zhengxuan Xu[2], Zhuoyan Cai[1] and Yuxin Yuan[1]

[1]School of Smart City, Chongqing Jiaotong University, Chongqing, China, [2]Geological Survey Institute, China Railway Eryuan Engineering Group CO.LTD, Chengdu, China

Sentinel-1A data are widely used in interferometric synthetic aperture radar (InSAR) studies due to the free and open access policy. However, the short wavelength (C-band) of Sentinal-1A data leads to decorrelation in numerous applications, especially in vegetated areas. Phase blurring and reduced monitoring accuracy can occur owing to changes in the physical and chemical characteristics of vegetation during the satellite revisit period, which essentially makes poor use of SAR data and increases the time and economic costs for researchers. Interferometric coherence is a commonly used index to measure the interference quality of two single-look complex (SLC) images, and its value can be used to characterize the decorrelation degree. The normalized difference vegetation index (NDVI) is obtained from optical images, and its value can be used to characterize the surface vegetation coverage. In order to solve the problem that Sentinel-1A decorrelation in the vegetated area is difficult to estimate prior to single-look complex interference, this paper selects a vegetated area in Sichuan Province, China as the study area and establishes two two-order linear quantitative models between Landsat8-derived normalized difference vegetation index and Sentinel-1A interferometric coherence in co- and cross-polarization: When NDVI at extremely high and low levels, coherence is close to zero, while NDVI and coherence show two different linear relationships in co- and cross-polarization in terms of NDVI at the middle level. The models global error basically obeys the normal distribution with the mean value of −0.037 and −0.045, and the standard deviation of 0.205 and 0.201 at the VV and VH channels. The two models are then validated in two validation areas, and the results confirm the reliability of the models and reveal the relationships between Sentinel-1A InSAR decorrelation and vegetation coverage in co- and cross-polarization, thus demonstrating that the NDVI can be applied to quantitatively estimate the InSAR decorrelation in vegetated area of Sentinel-1A data in both polarization modes prior to SLC interference.

KEYWORDS

quantitative models, Sentinel-1A, NDVI, decorrelation, linear relationship

1 Introduction

Sentinel-1A data were made available to users worldwide on 3 October 2014 (Potin et al., 2016). Since the time, Sentinel-1A data have been widely used in seismic and geological structure monitoring (Suresh and Yarrakula, 2020; Han et al., 2022), volcano monitoring (Guo et al., 2019; Bato et al., 2021; Corsa et al., 2022), glacier monitoring (Liang et al., 2021a; Zhang et al., 2021a; Manjula et al., 2022), agricultural monitoring and mapping (Diniz et al., 2022; Guo et al., 2022; Wuyun et al., 2022), other deformation mapping fields (Dai et al., 2016; He et al., 2020; Zhao et al., 2020), and are also an important C-band (wavelength = 5.5 cm) data source in the field of interferometric synthetic aperture radar (InSAR) and agriculture. However, the short-wavelength characteristics bring a range of limitations to its application, especially in vegetated areas, because C-band signals normally do not penetrate the surface or top layer of the forest (i.e., leaves and twigs) (Anh and Hang, 2019). Phenological changes to vegetation—or even leaf and branch movement—can lead to decorrelation (Merchant et al., 2022), which is a primary error source that limits the capability of InSAR for deformation mapping in areas with low coherence (Liang et al., 2021b) and what's more, its data handing, processing, and interpretation are barriers preventing a rapid uptake of SAR data by application specialists and non-expert domain users in the field of agricultural monitoring (Kumar et al., 2022).

Previous studies have shown that decorrelation in vegetated areas must be estimated using interferometric coherence (hereinafter referred to as coherence) or other indicators after the interference of two single-look complex (SLC) images (Sedze et al., 2012; Jiang et al., 2014). This inevitably leads to blind spots in the data selection, which makes it difficult for researchers to select the most effective interferometric pairs, thus reducing the efficiency of InSAR surface deformation monitoring, making poor use of SAR data, and increasing the time and economic costs for researchers. An accurate estimate of the decorrelation prior to SLC interference would therefore be very helpful to overcome the weaknesses of post-interference estimations, especially for the short-wavelength C-band Sentinel-1A data.

Coherence refers to the complex correlation between two complex SAR images and consists of a phase and a magnitude component (Abdel-Hamid et al., 2021). Coherence can be used to measure the quality of interference fringes and quantify the amplitude and phase changes of image pixels in a complex cross-correlated InSAR image pair (Tampuu et al., 2021). The composition principle of coherence, which was proposed by Wang et al. (Wang et al., 2010). and discussed in several studies (Pinto et al., 2013; Wang et al., 2015b, 2015a), essentially states that correlation in pass-to-pass, interferometric radar can be degraded by thermal noise, a lack of parallelism between radar flight tracks, spatial baseline noise, and surficial changes (Zebker and Villasenor, 1992). The total coherence is accordingly considered to represent the contribution of thermal noise decorrelation, spatial decorrelation, and temporal decorrelation.

Thermal noise decorrelation is determined by thermal noise in the interferometric instrument (Jung et al., 2016) and can generally be ignored. Spatial decorrelation can be directly estimated by a formulation given in the literature (Lee and Liu, 2001). However, the mechanism of temporal decorrelation is most complicated, which is difficult to model (Zhang et al., 2021b). Temporal decorrelation is a mixture of natural changes and changes possibly associated with major events (Jung et al., 2016). Decorrelation in vegetation coverage areas is mainly caused by changes in the physical and chemical characteristics of the vegetation. The most effective way to estimate the decorrelation in vegetated areas is therefore to establish a quantitative relationship between vegetation coverage and coherence. Chen et al. (Chen et al., 2021) developed a quantitative model between the Landsat5-derived normalized difference vegetation index (NDVI) and long-wavelength band (L-band, wavelength = 23.6 cm) ALOS-1/PALSAR-1 coherence in co-polarization. The radar wave emitted by the long-wavelength SAR satellite has a strong penetrating power and can penetrate the vegetation canopy or even directly reach the surface; its vegetation decorrelation is therefore not particularly severe. However, the application scenarios of this model have certain limitations and do not account for the decorrelation differences between co-polarization and cross-polarization. Other previous studies have focused on qualitatively illustrating the relationship between coherence and vegetation coverage (Santoro et al., 2010; Arab-Sedze et al., 2014; Bai et al., 2020; Amani et al., 2021), retrieving vegetation parameters (Engdahl et al., 2001; Flynn et al., 2002; Blaes and Defourny, 2003) and vegetation classifications (Hall-Atkinson et al., 2001; Canisius et al., 2019; Nikaein et al., 2021) using SAR coherence.

The first vegetation index (VI) was proposed in 1969, and there are now more than 100 developed Vis. Among them, the NDVI stands out as the most widely used (Yang et al., 2020b, Yang et al., 2020a, 2021b, 19, Yang et al., 2021a; Wang et al., 2022). The satellite-based NDVI has been shown to be closely related to vegetation coverage and is reliable for monitoring the vegetation dynamics of land surfaces. The NDVI's reliable characterization of surface vegetation coverage allows its quantitative relationship with interferometric decorrelation to be established. This paper proposes two second-order linear models between the NDVI and Sentinel-1A coherence (interferometric decorrelation) in both VV-polarization and VH-polarization in a study area in Sichuan Province, China. The two models are validated in two validation areas. The remainder of this paper is organized as follows. Section 2 provides an overview of the study and validation areas, data processing methods, and how the models were established. Section 3 discusses the results and potential future work. The final section provides the conclusion of this study.

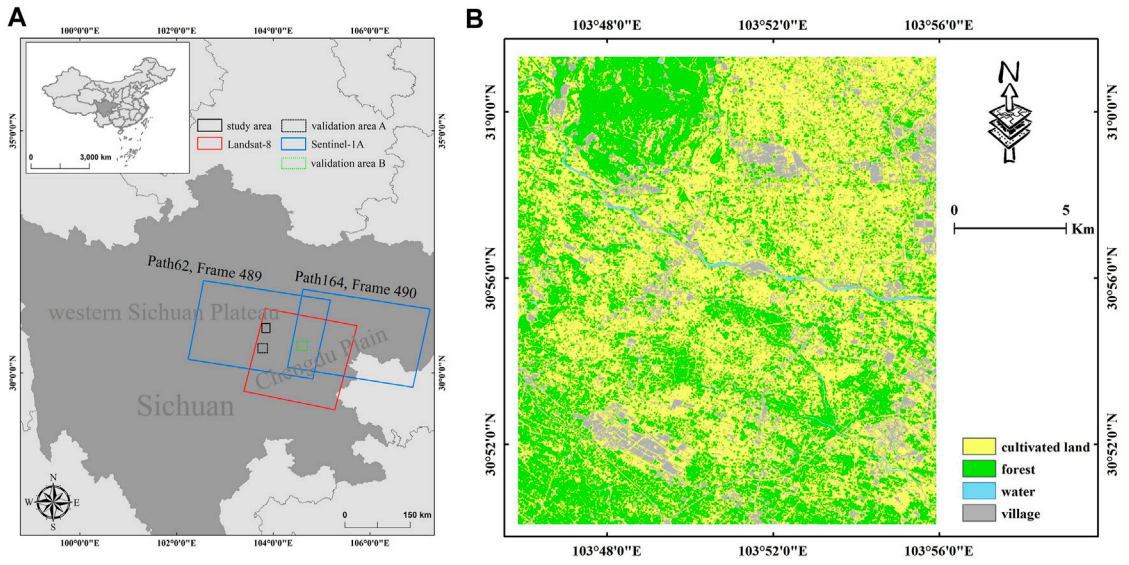

FIGURE 1
The study area and validation areas **(A)** Location of the study area and validation areas **(B)** Land cover map of the study area.

2 Material and methods

2.1 Study area and validation areas

The study area is located in Sichuan Province, China, adjacent to the western Sichuan Plateau to the west and the Chengdu Plain to the east (Figure 1A), and covers an area of approximately 340 km^2. This region was selected based on the following considerations. Although the formulation given in the literature (31) is used to remove the contribution of spatial decorrelation, the relatively flat terrain (average slope angle <15°) of the study area minimizes the influence of spatial decorrelation. The study area is densely covered with vegetation, including cultivated land (mostly rice fields) and forest, and there are few villages (Figure 1B). This area is therefore not in the "comfort zone" of Sentinel-1A InSAR deformation monitoring (i.e., cities, sparsely vegetated areas, and other high coherent areas) and is easily affected by decorrelation caused by vegetation, thus strengthening the application value of the established models in this area.

The validation area A is adjacent to the study area (Figure 1A), with similar terrain (average slope angle <13°) and surface vegetation coverage, and also does not belong to the "comfort zone" of Sentinel-1A InSAR deformation monitoring. The reliability of the established models were validated in this area.

The validation area B is located in the southeast of the study area (Figure 1A), with larger average slope angle and more lush vegetation cover, and the land surface type is mainly forest. The established models were validated in this area based on SAR data from different imaging perspectives to verify the reliability and universality of the models.

2.2 Data and data preprocessing

We collected an approximately cloud-free Landsat-8 Operational Land Imager (OLI) image (Table 1) taken in the summer to calculate the NDVI. The atmospheric correction and radiometric correction were first performed on the Landsat8 OLI image, and the image was cropped based on the vector boundaries of the study area and validation areas, then we calculated the NDVI (Figure 2) based on the following equation:

$$NDVI = \frac{P_{NIR} - P_{RED}}{P_{NIR} + P_{RED}} \quad (1)$$

where P_{NIR} and P_{RED} represent the reflection of the near-infrared band and red band, corresponding to band-5 and band-4 of Landsat8 OLI, respectively. The NDVI varies between [−1, 1]: it is negative when the cloud cover is exceedingly high or the surface is covered with water or snow; zero when the surface is covered with rocks or bare soil; and positive when the surface is covered with vegetation, where increasing positive values are associated with increasing vegetation coverage.

For the SAR data, we collected descending Sentinel-1A images (Table 2) covering the study area and validation area A, and the data from different imaging perspective covering validation area B (Table 3), footprints of Sentinel-1A data we used are displayed in blue rectangle in Figure 1A. The following three preprocessing steps were performed. (1) Interferometric

TABLE 1 Landsat-8 image.

Sensor	Path	Acquisition data	Cloud cover	Resolution
Landsat-8 OLI	129	August11, 2019	0.89%	30 m

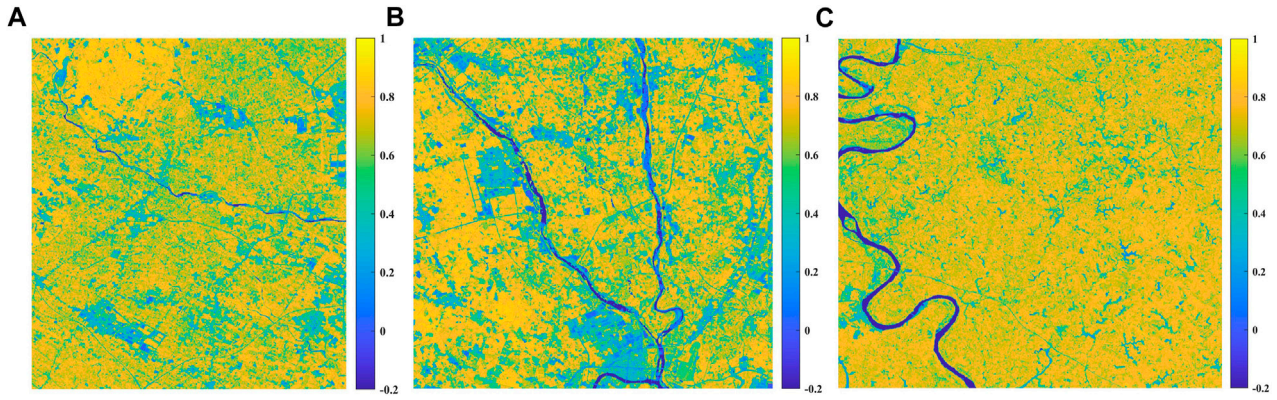

FIGURE 2
NDVI images **(A)** Study area **(B)** Validation area A **(C)** Validation area B.

TABLE 2 Sentinel-1A images covering the study area and validation area A.

	Path	Frame	Acquisition date	Temporal baseline	Polarization mode
Master	62	489	3 July 2019	48 days	VV/VH
Slave	62	489	20 August 2019		VV/VH

TABLE 3 Sentinel-1A images covering the validation area B.

	Path	Frame	Acquisition date	Temporal baseline	Polarization mode
Master	164	490	3 August 2019	12 days	VV/VH
Slave	164	490	15 August 2019		VV/VH

pair SLC interference was performed using double-pass differential interferometry, and precise orbit ephemerides and shuttle radar topography mission (SRTM) DEM (30 m) were used to correct the orbit errors and simulate the terrain phase, respectively. (2) Multi-look processing was performed to suppress speckle noise and ensure that the SAR images maintained the same resolution as the Landsat8 image. (3) The coherence was calculated and the contribution of the spatial decorrelation was removed according to the theoretical formula given in the literature (Lee and Liu, 2001). The theoretical model (Nasirzadehdizaji et al., 2021) of coherence is:

$$\gamma = \frac{E[\mu_1 \mu_2^*]}{\sqrt{E[|\mu_1|^2]E[|\mu_2|^2]}} \quad (2)$$

Where γ indicates coherence, $E[\cdot]$ is the mathematical expectation and μ^* is the conjugate complex of the SLC image. However, thermal noise and other factors of the radar system can easily generate a jump in the calculation result. This causes the coherence to present a strong spatial fluctuation, which compromises the calculation

accuracy. The coherence calculation scheme based on the amplitude data of the SAR. image can better resolve this problem.

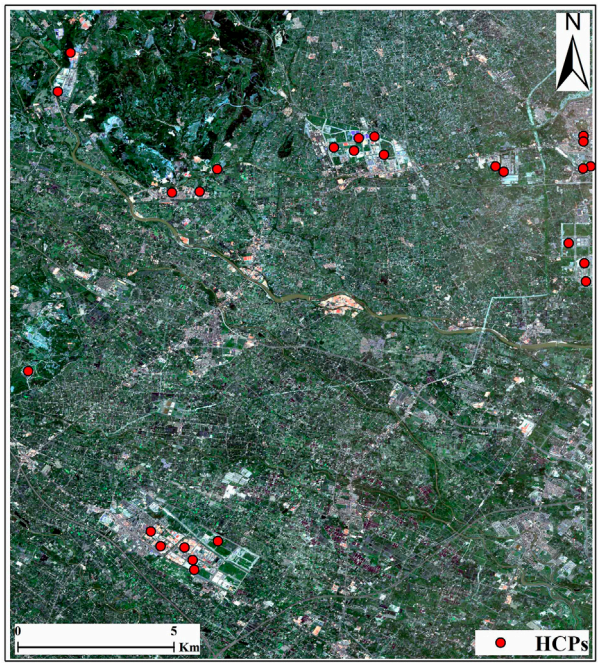

FIGURE 3
Distribution of ground highly coherent points (HCPs) in the study area. The background is 10-m resolution Sentinel-2 true-color image.

Although thermal noise decorrelation is generally ignored, this calculation strategy is still applied to minimize the ambiguity of the thermal noise on the coherence calculation results. The formulation is given as:

$$\gamma = \frac{\sum_{n=1}^{N}\sum_{m=1}^{M}\left|\mu_1(n,m)\right|\left|\mu_2(n,m)\right|}{\sqrt{\sum_{n=1}^{N}\sum_{m=1}^{M}\left|\mu_1(n,m)\right|^2\sum_{n=1}^{N}\sum_{m=1}^{M}\left|\mu_2(n,m)\right|^2}} \quad (3)$$

where M and N are the sizes of the data blocks for calculating coherence, n and m are the row and column numbers in the data windows, $\mu_1(n,m)$ and $\mu_2(n,m)$ represent the complex values at the image coordinates (n, m) in the master and slave image data blocks, respectively, $|\cdot|$ is the absolute value of the complex, and $|\cdot|^2$ is the second-order norm of the data.

The coherence ranges from zero in the case of complete decorrelation (i.e., the interferometric phase is only noise) to one if the two signals are fully correlated (i.e., complete absence of phase noise). The coherence reaches the maximum value when the scatterer position and physical properties within the averaging window are the same for the two observations. In contrast, any differences in the scatterer position or properties in the interval between the two observations introduce a phase difference of two backscattered signals and accordingly cause the coherence value to decrease (Nasirzadehdizaji et al., 2021). After completing the coherence calculation, the coherence images were geocoded and co-registered with the NDVI image by SRTM DEM (30 m) and ground highly coherent points (HCPs), which displayed in Figure 3. The data preprocessing work flow is shown in Figure 4.

2.3 Contribution of temporal decorrelation to coherence

The coherence obtained in Section 2.2 removed the contribution of the spatial decorrelation, but the contribution of the temporal decorrelation should also be considered. Rocca et al. (Rocca, 2007) proposed an exponential decay function between the coherence and temporal baseline for C-band ERS-1 data, and assigned an exponential decay constant to the model to represent the decay rate of coherence with an increasing temporal baseline. A decay function of surface reflectors was thereafter proposed, which still maintains the correlation under a long-term temporal baseline (Parizzi et al., 2009). Other time-coherence decay functions have also been discussed (Krieger et al., 2007; Sica et al., 2019). The study area in this paper has dense vegetation and few highly coherent surface reflectors, thus the time-coherence decay function does not need to account for highly coherent ground objects. Multiple interferometric pairs were generated under the multi-master image strategy, the Sentinel-1A data used are displayed in Table 4. The results show that when the temporal baseline is less than 216 days, the VV-polarization coherence decays exponentially with increasing temporal baseline, whereas the VV-polarization coherence shows no notable decay trend when the temporal baseline exceeds 216 days and fluctuates around a stable value (Figure 5A). Figure 5B shows that the VH-polarization coherence also decays exponentially with increasing temporal baseline when it is less than 168 days. If the temporal baseline exceeds 168 days, the VH-polarization coherence fluctuates around another stable value, and also exhibits no clear decay trend. We therefore define 216 and 168 days as the critical exponent decay temporal baselines for this study. The coefficients $A1$, $t1$, $A2$, and $t2$ shown in Figure 5 were obtained as 0.743, 206 days, 0.560, and 222 days, respectively. The two stable values around which the coherence fluctuated are 0.370 and 0.325, respectively.

2.4 Model building based on the absolute value of the Pearson correlation coefficient

All of the pixels in the NDVI image and coherence images were initially involved in the analysis; however, we found that large global errors were introduced and reliable relationships could not be established. We therefore applied the window sampling method proposed in the literature (Chen et al., 2021) to account for the coherence value is related with the

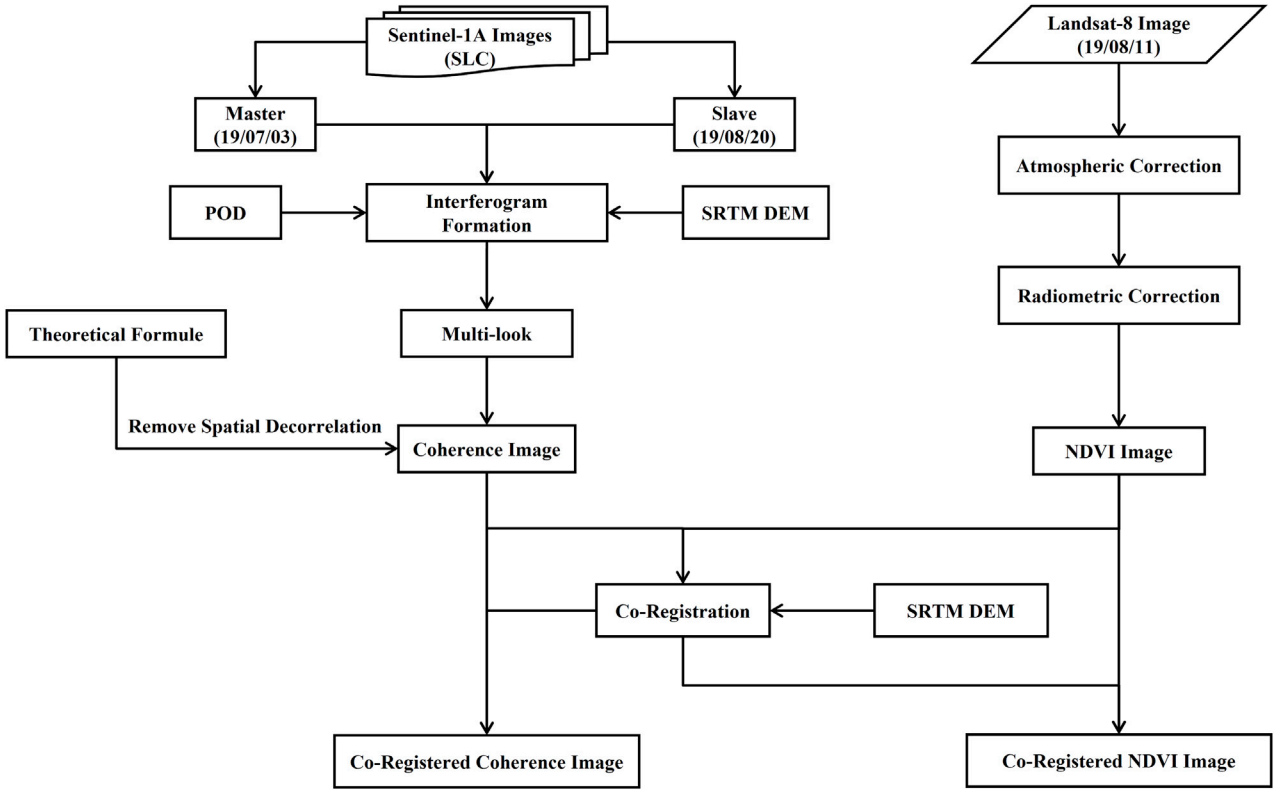

FIGURE 4
Data preprocessing work flow.

window size (Zhang et al., 2018). The steps of this method are as follows. (1) Set a moving window to sample the NDVI image, and a second moving window of the same size to simultaneously sample the coherence image until the two windows traverse the two images, respectively. (2) Calculate the Pearson correlation coefficient (Pearson, 1895) between the NDVI pixels and coherence pixels in the two windows based on Eq. 4.

$$\rho(X,Y) = \frac{\sum_{i=1}^{n}(X_i-\bar{X})(Y_i-\bar{Y})}{\sqrt{\sum_{i=1}^{n}(X_i-\bar{X})^2}\sqrt{\sum_{i=1}^{n}(Y_i-\bar{Y})^2}} \quad (4)$$

where $\rho(X,Y)$ represents the Pearson correlation coefficient, X_i represents the elements in a dataset, $\bar{X}$ is the mean value of the elements in this dataset, and Y_i and $\bar{Y}$ are the elements and mean value of another dataset, respectively. (3) Set a threshold: if the Pearson correlation coefficient between the two windows meet the preset threshold, the pixels in the two windows are retained for subsequent analysis; otherwise, all pixels in the two windows are abandoned. The above method was used to build a quantitative model between the NDVI and L-band ALOS-1/PALSAR-1 coherence. For the C-band Sentinel-1A data, the strong negative linear correlation between the NDVI and coherence was revealed in preliminary experiments, showing a linear decrease of the coherence with increasing surface vegetation coverage. This method thus directly ignores numerous pixels with a negative linear correlation and significantly reduces the accuracy of the established models.

We therefore improved the correlation measurement of the two windows using the above method by calculating the absolute value of the Pearson correlation coefficient (marked as T) of the pixels in the two windows to account for the large number of pixels with a negative linear correlation. When the T value of the pixels in the two windows is greater than or equal to the preset threshold (marked as T0), these pixels are retained and participate in the subsequent analysis; otherwise, they are abandoned and not included in the analysis. Numerous experiments revealed that this window sampling method with the improved correlation measurement can significantly increase the accuracy of the quantitative relationship between the Landsat8-derived NDVI and Sentinel-1A coherence. The ideal sampling window size and threshold for VV- and VH-polarization were also obtained. The window sampling method with the improved correlation measurement is shown in Figure 6, the top and bottom pictures represent the NDVI and coherence image, respectively. T is the absolute value of the Pearson correlation coefficient, and T0 is the preset threshold.

TABLE 4 Sentinel-1A images used in the multi-master image strategy.

Path	Frame	Acquisition date	Polarization mode
62	489	4 January 2019	VV/VH
62	489	16 January 2019	VV/VH
62	489	28 January 2019	VV/VH
62	489	09 February 2019	VV/VH
62	489	21 February 2019	VV/VH
62	489	29 March 2019	VV/VH
62	489	22 April 2019	VV/VH
62	489	28 May 2019	VV/VH
62	489	21 June 2019	VV/VH
62	489	3 July 2019	VV/VH
62	489	15 July2019	VV/VH
62	489	20 August2019	VV/VH
62	489	25 September2019	VV/VH
62	489	31 October 2019	VV/VH
62	489	6 December 2019	VV/VH
62	489	11 January 2020	VV/VH
62	489	16 February 2020	VV/VH
62	489	23 March 2020	VV/VH
62	489	28 April 2020	VV/VH
62	489	03 June 2020	VV/VH
62	489	09 July 2020	VV/VH
62	489	14 August 2020	VV/VH

We have found that the size of the sampling window is positively proportional to the amount of data that meet the threshold. when the sampling window size is small (less than 5×5), there is a significant linear relationship between the two variables, however, the global error of the models obtained after fitting are significant. The amount of data that meet the threshold are numerous in terms of the sampling window size are large (more than 10×10), and there is no obvious functional relationship between the two variables. Tables 5, 6 respectively display the determination coefficient (R2) and root mean square error (RMSE) of the optimal fitting function corresponding to each threshold when the sampling window is between 5×5 and 9×9 at VV and VH channels, then we obtain the optimal sampling window size and threshold at two polarization channels considering the accuracy of the fitting function and the global error of the models after fitting. The optimal sampling window size is 5×5 for VV-polarization and the threshold is 0.7, whereas the optimal values for VH-polarization are 9×9 and 0.6, respectively. All of the pixels that met the preset threshold were retained, and then some abnormal pixels are artificially abandoned.

Then we get the relationships between the Landsat8-derived NDVI and Sentinel-1A coherence of the retained pixels, as shown in Figure 7.

Section 2.3 discussed the relationship between the coherence and temporal baseline. The results indicate an exponential decay effect of the temporal decorrelation on the coherence, and that the critical temporal baseline of the VV- and VH-polarization coherences are 216 and 168 days, respectively. The temporal baseline of the interferometric pair used in this study is 48 days (Table 2). In this study, inspired by the work of Chen et al. (Chen et al., 2021), it is necessary to add a temporal decay factor to the models to improve their reliability. We then obtained a second-order linear model between the Landsat8-derived NDVI and Sentinel-1A coherence (VV) as follows:

$$\gamma 1 = \begin{cases} 0, -1 < NDVI < 0.15, NDVI > 0.87 \\ a1 \cdot exp\left(-\frac{x}{t1}\right) \cdot NDVI + b1, \ 0.15 \le NDVI \le 0.87 \end{cases} \tag{5}$$

where $\gamma 1$ and x represent the coherence (VV) and temporal baseline of the interferometric pair, respectively, $exp(-x/t1)$ and $t1$ represent the temporal decay factor and exponential decay speed factor of the coherence (VV), respectively, and $a1$ and $b1$ are parameters to be estimated. In this study, x = 48 days (Table 2) and $t1$ = 206 days (Section 2.3).

A significant negative linear relationship was also observed between the Landsat8-derived NDVI and Sentinel-1A coherence (VH). The coherence (VH) was found to linearly decrease with increasing NDVI at a slightly lower rate than that of the coherence (VV). The second-order linear model between the Landsat8-derived NDVI and Sentinel-1A coherence (VH) is given as:

$$\gamma 2 = \begin{cases} 0, -1 < NDVI < 0.14, NDVI > 0.89 \\ a2 \cdot \exp\left(-\frac{x}{t2}\right) \cdot NDVI + b2, \ 0.14 \le NDVI \le 0.89 \end{cases} \tag{6}$$

where $\gamma 2$ and x represent the coherence (VH) and temporal baseline of the interferometric pair, respectively, $exp(-x/t2)$ and $t1$ represent the temporal decay factor and exponential decay speed factor of the coherence (VH), respectively, and $a2$ and $b2$ are parameters to be estimated.

The least squares method is used to fit the two formulas to improve the robustness, thus yielding two quantitative models between the Landsat8-derived NDVI and Sentinel-1A coherence. The obtained parameters are $a1$ = −1.168, $b1$ = 0.992, $a2$ = −1.086, and $b2$ = 0.905.

3 Results and discussion

3.1 Results and error analysis

Eq. 3 was used to calculate the true VV-polarization coherence image (Figure 8A) of the study area according to the amplitude information, and Eq. 5 was applied to estimate the VV-polarization coherence image (Figure 8B) using the

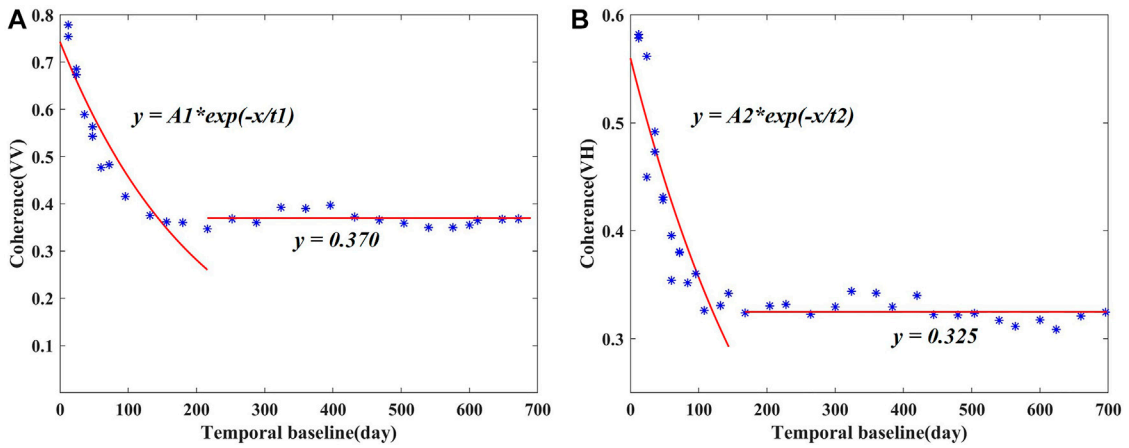

FIGURE 5
Relationship between the temporal baseline and coherence **(A)** VV channel **(B)** VH channel.

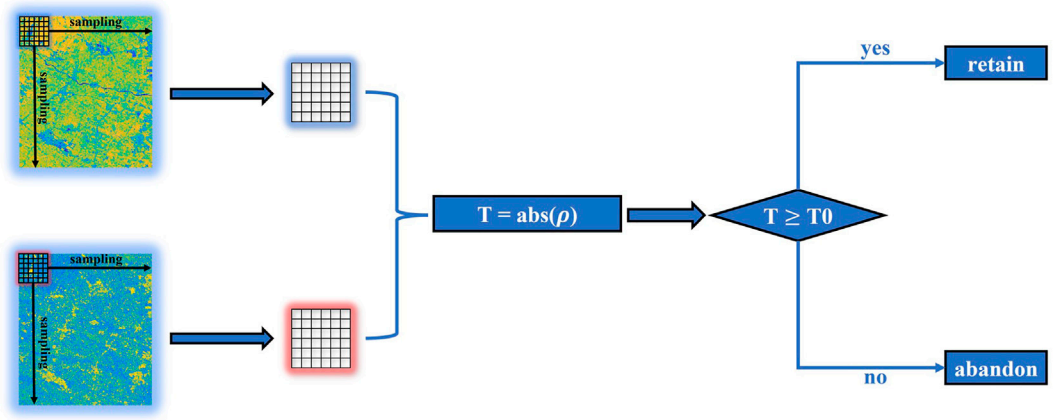

FIGURE 6
Window sampling method with improved correlation measurement.

Landsat8-derived NDVI. For VH-polarization coherence, Eq. 3 was used to calculate the true coherence image (Figure 8C) and estimate the coherence (Figure 8D) based on the model given in Eq. 6 of the study area. The differences distribution obtained by subtracting the estimated coherence from the true coherence in VV-polarization and VH-polarization are displayed in Figures 8E, F, respectively. It can be found that the differences distribution in VV-polarization are uniformly distributed without significant concentrated error, whereas those in VH-polarization are mainly concentrated in the red circle (village distribution area) of Figure 8F.

As shown in Figure 9A, the mean error in VV-polarization is -0.037 with a standard deviation of 0.205. Most of the errors distribute between −0.3 and 0.3, and the global errors obey a normal distribution. Figure 9B shows that the mean error in VH-polarization is −0.045 with a standard deviation of 0.201, and the global errors still obey the normal distribution.

3.2 Models validation

3.2.1 Performance of established models in validation area A

We performed the same experiments in the validation area A to consider the model reliability using consistent data and data processing methods as those in the study area We then obtained the true VV-polarization coherence image (Figure 10A) and estimated the VV-polarization coherence

TABLE 5 performance of different sampling window size and threshold at VV channel.

Threshold/Window size	5×5		6 × 6		7 × 7		8 × 8		9 × 9	
\	R^2	RMSE	R^2	RMSE	R^2	RMSE	R^2	RMSE	R^2	RMSE
0.5	0.259	40.480	0.320	34.040	0.365	30.960	0.380	29.270	0.381	28.410
0.6	0.349	26.730	0.406	22.090	0.429	19.900	0.443	18.150	0.459	17.760
0.7	0.616	12.570	0.481	12.750	0.483	12.320	0.560	9.721	0.552	7.846
0.8	0.514	8.048	0.581	5.025	0.647	4.737	0.581	3.240	0.696	2.856

TABLE 6 performance of different sampling window size and threshold at VH channel.

Threshold/Window size	5×5		6 × 6		7 × 7		8 × 8		9 × 9	
\	R^2	RMSE	R^2	RMSE	R^2	RMSE	R^2	RMSE	R^2	RMSE
0.5	0.233	34.790	0.276	30.390	0.302	27.810	0.356	25.150	0.368	23.790
0.6	0.336	22.320	0.369	19.810	0.423	17.100	0.432	16.230	0.6347	11.990
0.7	0.411	13.000	0.516	10.750	0.571	8.949	0.495	8.877	0.6302	7.278
0.8	0.622	5.528	0.668	3.871	0.670	4.153	0.718	3.099	0.719	3.233

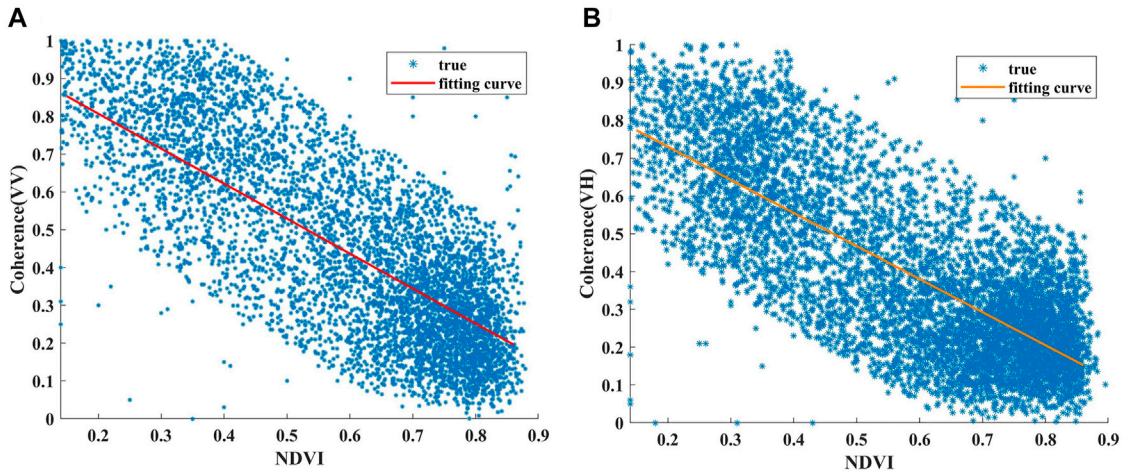

FIGURE 7
Relationship between the Landsat8-derived NDVI and Sentinel-1A coherence **(A)** VV channel **(B)** VH channel.

image (Figure 10B) of the validation area. Those in VH-polarization are displayed in Figures 10C, D, respectively. Figures 10E, F give the differences distribution in validation area were obtained by subtracting the estimated coherence from the true coherence. It can be found that relatively large errors are concentrated in villages and river distribution areas, as shown in the red circle in Figures 10E, F. Figure 11A shows that the mean error in VV-polarization is -0.067 with a standard deviation of 0.256, most of the errors distribute between −0.4 and 0.4 and basically obey a normal distribution. As shown in Figure 11B, the mean error in VH-polarization is −0.065 with a standard deviation of 0.230, these errors are larger and more discrete than those in the study area on the whole, but still roughly obey a normal

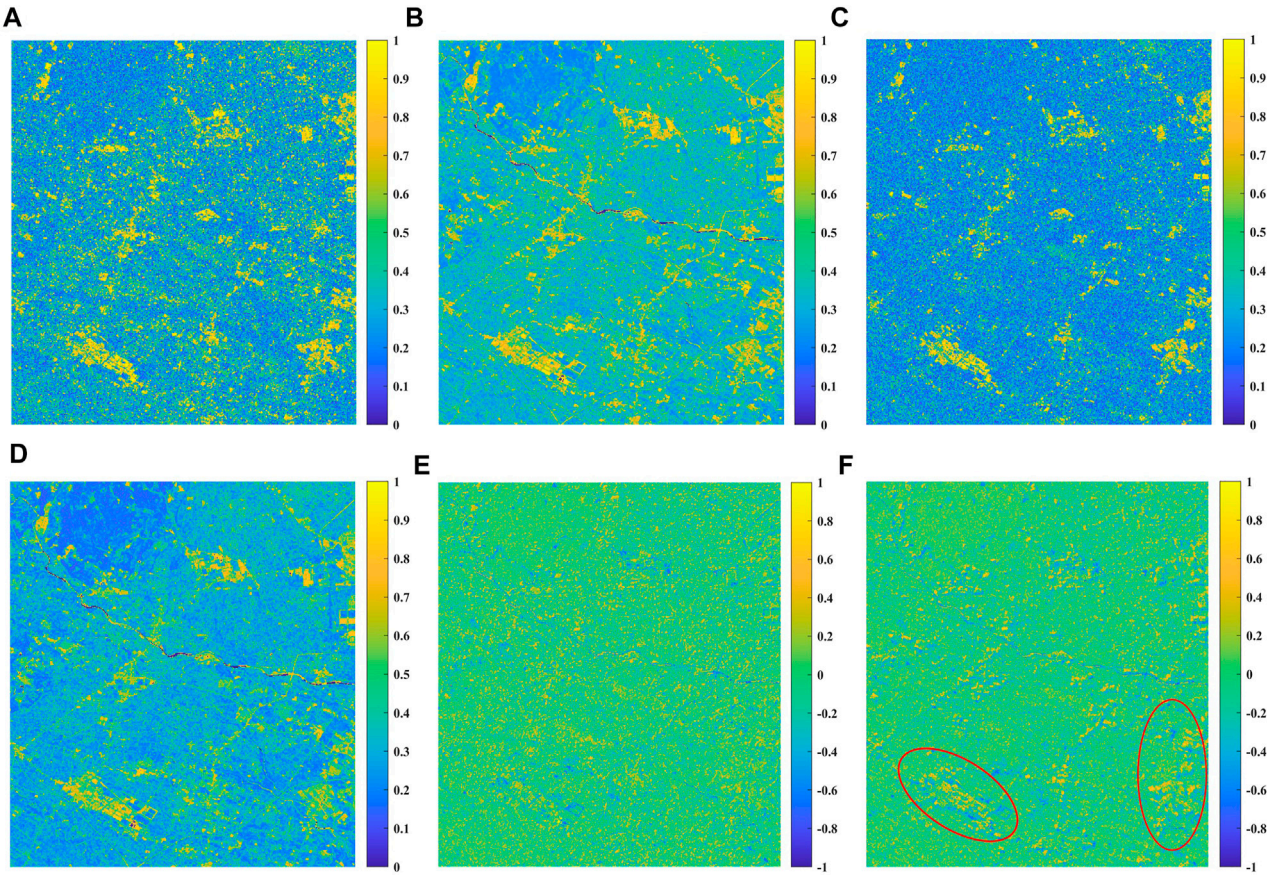

FIGURE 8
Coherence images of the study area **(A)** True at VV channel **(B)** Estimation at VV channel **(C)** True at VH channel **(D)** Estimation at VH channel **(E)** Differences distribution at VV channel **(F)** Differences distribution at VH channel.

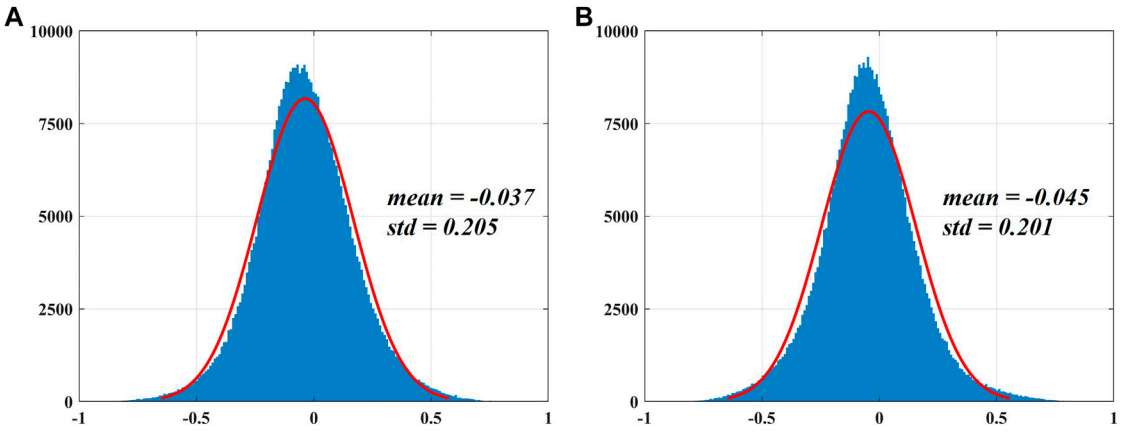

FIGURE 9
The error histogram of the study area **(A)** VV channel **(B)** VH channel.

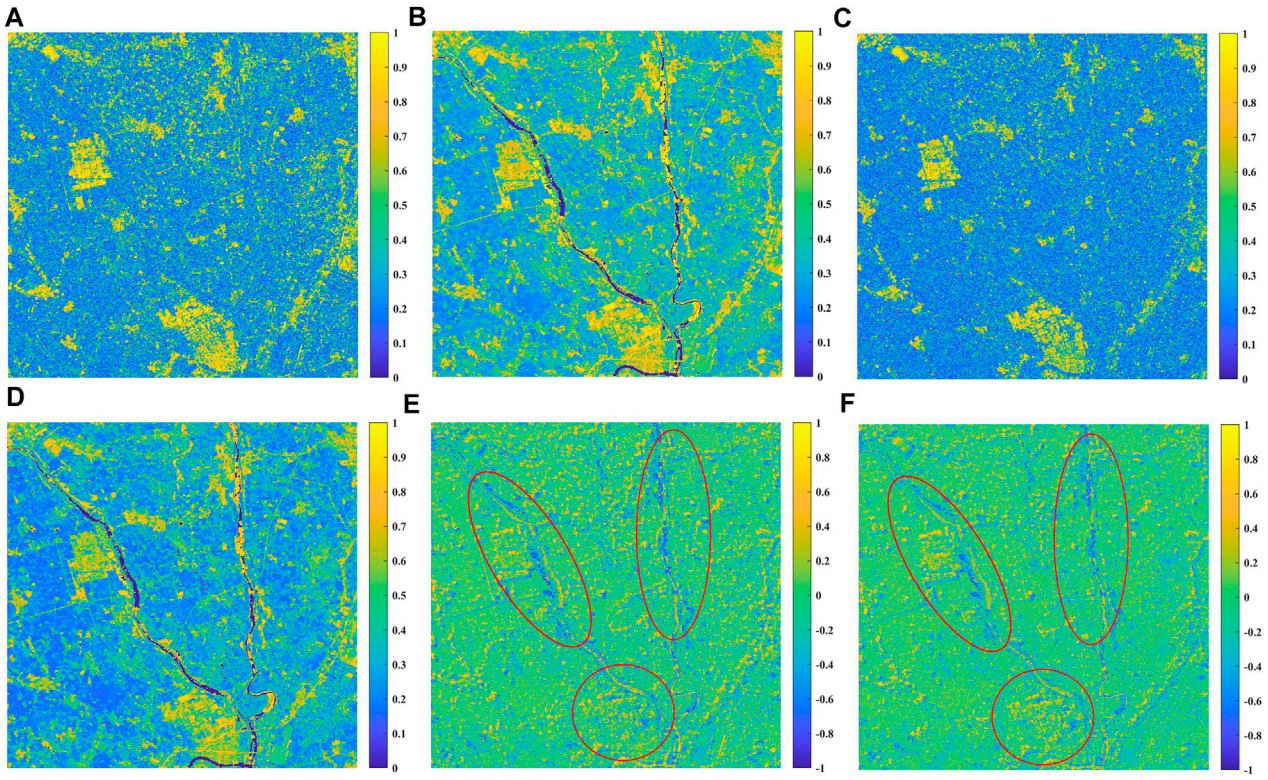

FIGURE 10
Coherence images of the validation A **(A)** True at VV channel **(B)** Estimation at VV channel **(C)** True at VH channel **(D)** Estimation at VH channel **(E)** Differences distribution at VV channel **(F)** Differences distribution at VH channel.

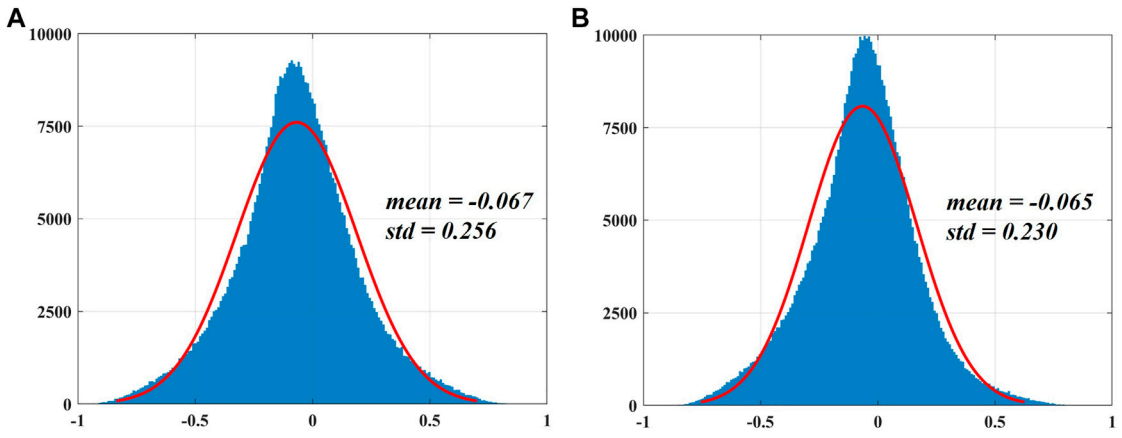

FIGURE 11
The error histogram of the validation area A **(A)** VV channel **(B)** VH channel.

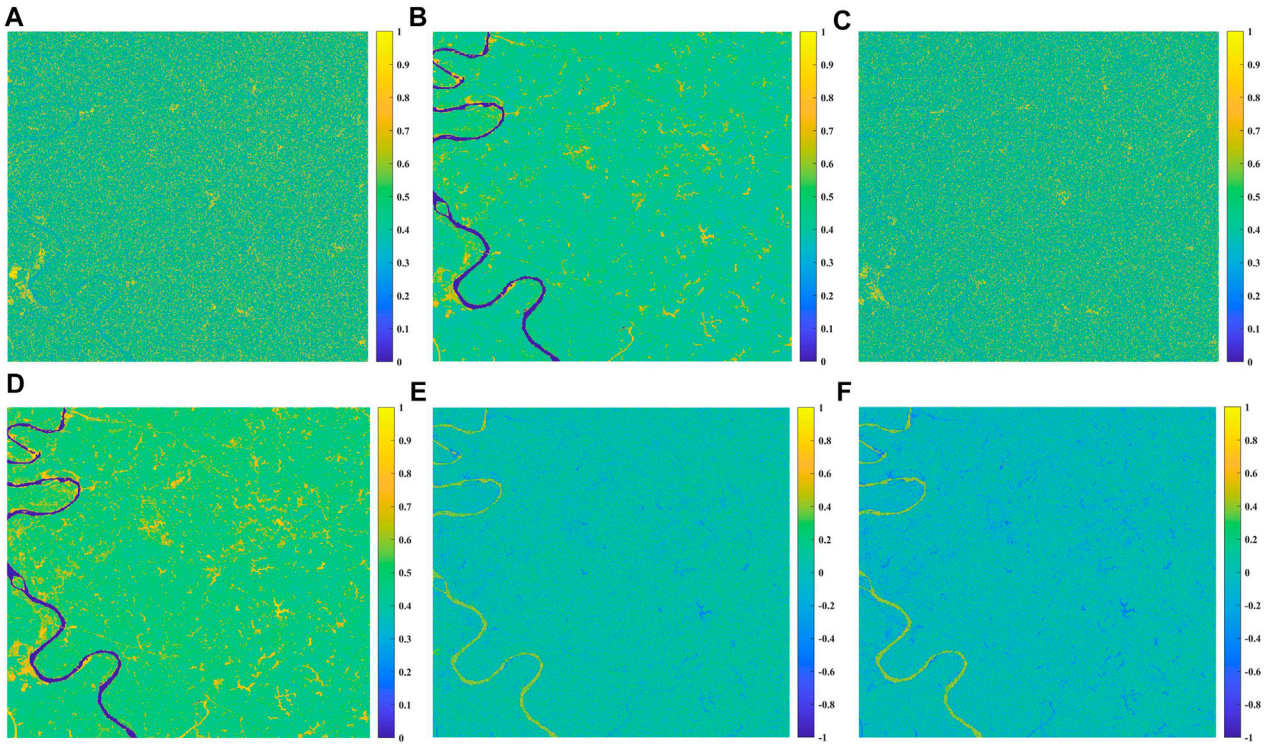

FIGURE 12
Coherence images of the validation area B **(A)** True at VV channel **(B)** Estimation at VV channel **(C)** True at VH channel **(D)** Estimation at VH channel **(E)** Differences distribution at VV channel **(F)** Differences distribution at VH channel.

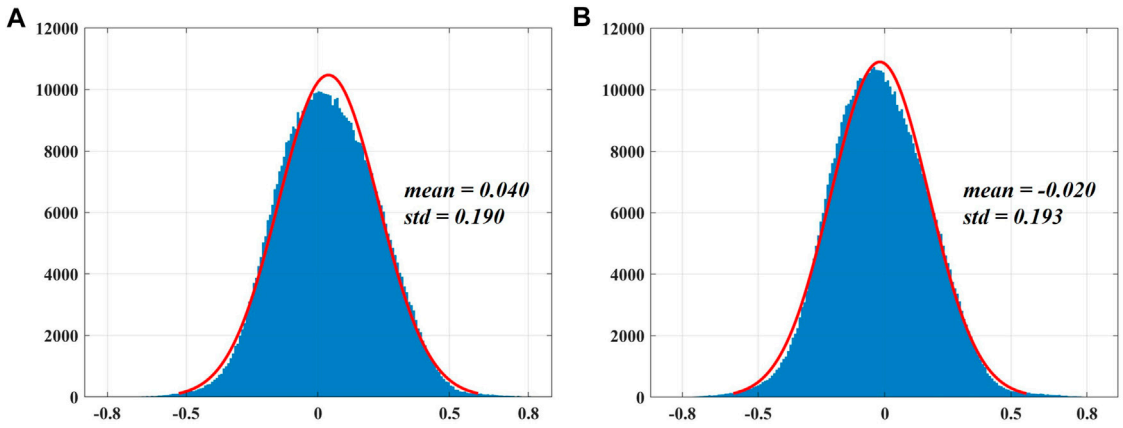

FIGURE 13
The error histogram of the validation area B **(A)** VV channel **(B)** VH channel.

distribution and mostly distribute between −0.35 and 0.35. Based on the error distribution in the study area and validation area A, it is confirmed that the models given in Eq. 5–6 are reliable without significant trend and random error.

3.2.2 Performance of established models in validation area B

We used Sentinel-1A images from different imaging perspectives covering validation area B that were

independent from the study area and validation area A regard of the reliability and universality of the models, the data processing method is consistent with the study area and validation area A. As observed in Figure 12, the true coherence images at the two polarization channels are similar to the estimated coherence images, and the errors are mainly distributed in the river region, even though these areas are generally not included in the scope of InSAR ground deformation monitoring. Consistent with the study area and validation area A, we counted the error distribution of the validation area B. For errors statistics, Figure 13A shows that the errors of the validation area B at the VV channel are concentrated between -0.4 and 0.4 with the mean value and standard deviation are 0.040 and 0.190, respectively. The error distribution basically follows a normal distribution and no obvious random error existing. Those in VH-polarization are displayed in Figure 13B, most of the errors at VH channel distribute between -0.35 and 0.35 with the mean value and standard deviation are −0.020 and 0.193, respectively, and the global error still basically obeys the normal distribution. Based on the above distribution of differences and errors statistics, it allows us to confirm that the established models perform well in validation area B, and indicates the universality and dataset independence of the models to a certain extent.

3.3 Discussion

Figures 8A,C indicate that the VV-polarization coherence of the study area is higher than that of the VH-polarization on the whole owing to its high sensitivity to volume scattering, which strongly depends on the geometrical alignment and vegetation characteristics (Gao et al., 2017). The surface coverage of the study area is also mainly cultivated lands, followed by woodlands. The main crop of the cultivated lands is rice, for which the biophysical parameters have been shown to have a stronger relationship with VH-polarization than with VV-polarization (Wali et al., 2020). The VH-polarization radar signal is therefore more sensitive to rice than the VV-polarization radar signal. The decorrelation of the VH-polarization radar signal is accordingly more severe and the overall coherence is lower for the same temporal baseline.

The accuracy of the models in the study area is found to be higher than that in the validation area A, owing to the smaller and more concentrated global errors, for both VV-polarization and VH-polarization. However, the same interferometric pairs are used in the study area and validation area A, thus the differences of the spatial decorrelation and temporal decorrelation caused by different imaging geometry and temporal baselines of the interferometric pair are excluded. We interpret there to be two reasons for the higher model accuracy in the study area. (1) Although the topography of the study area is similar to the validation area A, slight differences still remain. The terrain fluctuation and average slope (average slope angle <13°) in the validation area are slightly gentler than those in the study area, thus the spatial decorrelation errors caused by slight terrain differences may reduce the model accuracy in the validation area, even if the contribution of the spatial decorrelation is removed from the models. (2) The estimated coherence of water system areas are zero based on the established models. There are two rivers in the validation area A where the true coherence is almost zero. Thus, owing to the limited number of samples within the coherence estimation window, the underestimation bias in the low coherence area leads to a random distribution of pixels within the completely decorrelated areas. Apart from this, although the optimal sampling window size and threshold for the two polarization modes were obtained experimentally, the number of pixels participating in the VH-polarization model fitting analysis was still more than that in the VV-polarization model and the distribution was more discrete, resulting in a lower model accuracy. The VV-polarization model accuracy is therefore better than that of the VH channel in both the study area and the validation area A.

The performance of the established models in the validation area B shows their universality and dataset independence under different imaging geometry. Like the validation area A, the estimated coherence errors at the two polarization channels are still mainly concentrated in the river distribution area, and there is no obvious error trend and random error in other areas within the validation area B, however, in a broader context, the established models need to be verified in wider areas and richer dataset under different imaging geometry to further illustrate their robustness and universality.

The established models still have some weaknesses in terms of the different abovementioned perspectives. We suggest that the following improvements be made in subsequent study. (1) Although the contribution of spatial decorrelation was removed in the models, slight topographic differences between the different areas can still introduce spatial decorrelation errors into the models. A method to completely remove the contribution of spatial decorrelation must therefore be considered to improve the model universality. (2) We defined the exponent decay critical temporal baseline as 216 and 168 days for Sentinel-1A VV- and VH-polarization coherence, respectively. These two critical values are greater than 48 and 12 days of the temporal baseline for the interferometric pairs used in this study. It is thus reasonable to add a temporal decay factor to the models. On the contrary, if the temporal baseline exceeds the exponential decay critical temporal baseline, (i.e., when the

coherence decays to a low level with no notable decay trend), it is unreasonable to add such a decay factor. It is therefore important to establish a more reliable relationship between the coherence and interferometric pair temporal baseline in the case of a long-term application to improve the model accuracy, even if such a long-term baseline is not suitable for traditional InSAR surface deformation monitoring in vegetated area of C-band sentinel-1A data. (3) Rivers inevitably exist in some vegetated areas, thus a quantitative relationship between the water indexes and coherence must be established and incorporated into the models to improve their robustness. Other factors should also be considered to improve the models. For example, the weather conditions in the study area leads to refractivity of the atmosphere through which a traveling radar wave imparts a phase delay (or advance) that can vary in both space and time owing to the dependence of refractivity on various atmospheric properties (Wadge et al., 2010). These induced propagation delays (or advances) affect the quality of the interference fringe and coherence calculation. Furthermore, different response characteristics of the different vegetation types to the SAR echo signals will also lead to differing coherence and decorrelation (Zhang et al., 2016), which will be constructed in future models.

4 Conclusion

This study establishes two second-order linear models between the Landsat8-derived NDVI and Sentinel-1A coherence in co- and cross-polarization that reveal the relationship between InSAR decorrelation and vegetation coverage. Coherence is found to linearly decrease with increasing vegetation coverage, and the linear trend differs depending on the co-polarization and cross-polarization mode. The two models were validated simultaneously using similar data in the validation area A and independent imaging geometry data in the validation area B. The NDVI obtained from free optical satellites can therefore be used to estimate the coherence prior to performing InSAR processing on vegetated areas to monitor the surface deformation (i.e., prior to the interferometric pair's SLC interference) to quantitatively estimate the decorrelation of these areas. The SAR data selection can be determined using quantitative models prior to interference, thereby increasing the research productivity and reducing the time and economic costs. This study fills the gap of the above models in C-band SAR data, in addition to the C-band Sentinel-1A data, the quantitative relationship between the NDVI and L-band co-polarization ALOS-1/PALSAR-1 coherence has been established (29), and other quantitative models should be constructed for the L-band and X-band SAR data at different polarization channels in the future.

Data availability statement

The raw data supporting the conclusions of this article will be made available by the authors, without undue reservation.

Author contributions

RZ: Conceptualization; Methodology; Formal analysis; Data curation; Writing–original draft, review, and editing. JP: Formal analysis; Funding acquisition; Supervision. ZX: Funding acquisition. ZC: Conceptualization; Methodology. YY: Writing–original draft, review, and editing.

Funding

This work was supported by Key R&D Program of Ningxia Autonomous Region: Ecological environment monitoring and platform development of ecological barrier protection system for Helan Mountain (ID: 2022CMG02014) and Scientific research project managed by Guizhou bureau of Geology and mineral resources in 2019: key technology and application of ecological environment monitoring of mountains, rivers, forests, fields, lakes and grasses - Taking Bailidujuan as an example (ID: 201909).

Acknowledgments

Thanks to Yaogang Chen of Central South University for his helpful and efficient guidance. The Sentinel-1A data and Landsat-8 data were provided by ESA and USGS, respectively.

Conflict of interest

Author ZX was employed by the company China Railway Eryuan Engineering Group CO.LTD.

The remaining authors declare that the research was conducted in the absence of any commercial or financial relationships that could be construed as a potential conflict of interest.

Publisher's note

All claims expressed in this article are solely those of the authors and do not necessarily represent those of their affiliated organizations, or those of the publisher, the editors and the reviewers. Any product that may be evaluated in this article, or claim that may be made by its manufacturer, is not guaranteed or endorsed by the publisher.

Reference

Abdel-Hamid, A., Dubovyk, O., and Greve, K. (2021). The potential of sentinel-1 InSAR coherence for grasslands monitoring in Eastern Cape, South Africa. *International Journal of Applied Earth Observation and Geoinformation* 98, 102306. doi:10.1016/j.jag.2021.102306

Amani, M., Poncos, V., Brisco, B., Foroughnia, F., DeLancey, E. R., and Ranjbar, S. (2021). InSAR Coherence Analysis for Wetlands in Alberta, Canada Using Time-Series Sentinel-1 Data. *Remote Sensing* 13, 3315. doi:10.3390/rs13163315

Anh, N., and Hang, N. (2019). Deforestation Detection Using Sentinel-1 Time-Series Case Study In Quang Son -Dak Glong District. *Dak Nong Province*. doi:10.13140/RG.2.2.28003.09761

Arab-Sedze, M., Heggy, E., Bretar, F., Berveiller, D., and Jacquemoud, S. (2014). Quantification of L-band InSAR coherence over volcanic areas using LiDAR and *in situ* measurements. *Remote Sensing of Environment* 152, 202–216. doi:10.1016/j.rse.2014.06.011

Bai, Z., Fang, S., Gao, J., Zhang, Y., Jin, G., Wang, S., et al. (2020). Could Vegetation Index be Derive from Synthetic Aperture Radar? – The Linear Relationship between Interferometric Coherence and NDVI. *Sci. Rep.* 10, 6749. doi:10.1038/s41598-020-63560-0

Bato, M. G., Lundgren, P., Pinel, V., Solidum, R., Daag, A., and Cahulogan, M. (2021). The 2020 Eruption and Large Lateral Dike Emplacement at Taal Volcano, Philippines: Insights From Satellite Radar Data. *Geophys. Res. Lett.* 48. doi:10.1029/2021GL092803

Blaes, X., and Defourny, P. (2003). Retrieving crop parameters based on tandem ERS 1/2 interferometric coherence images. *Remote Sensing of Environment* 88, 374–385. doi:10.1016/j.rse.2003.08.008

Canisius, F., Brisco, B., Murnaghan, K., Van Der Kooij, M., and Keizer, E. (2019). SAR Backscatter and InSAR Coherence for Monitoring Wetland Extent, Flood Pulse and Vegetation: A Study of the Amazon Lowland. *Remote Sensing* 11, 720. doi:10.3390/rs11060720

Chen, Y., Sun, Q., and Hu, J. (2021). Quantitatively Estimating of InSAR Decorrelation Based on Landsat-Derived NDVI. *Remote Sensing* 13, 2440. doi:10.3390/rs13132440

Corsa, B., Barba-Sevilla, M., Tiampo, K., and Meertens, C. (2022). Integration of DInSAR Time Series and GNSS Data for Continuous Volcanic Deformation Monitoring and Eruption Early Warning Applications. *Remote Sensing* 14, 784. doi:10.3390/rs14030784

Xu, X., Sandwell, D. T., and Smith-Konter, B. (2020). Coseismic Displacements and Surface Fractures from Sentinel-1 InSAR: 2019 Ridgecrest Earthquakes. *Seismological Research Letters* 91, 1979–1985. doi:10.1785/0220190275

Dai, K., Li, Z., Tomás, R., Liu, G., Yu, B., Wang, X., et al. (2016). Monitoring activity at the Daguangbao mega-landslide (China) using Sentinel-1 TOPS time series interferometry. *Remote Sensing of Environment* 186, 501–513. doi:10.1016/j.rse.2016.09.009

Diniz, J. M. F. de S., Gama, F. F., and Adami, M. (2022). Evaluation of polarimetry and interferometry of sentinel-1A SAR data for land use and land cover of the Brazilian Amazon Region. *Geocarto International* 37, 1482–1500. doi:10.1080/10106049.2020.1773544

Engdahl, M. E., Borgeaud, M., and Rast, M. (2001). The use of ERS-1/2 Tandem interferometric coherence in the estimation of agricultural crop heights. *IEEE Trans. Geosci. Remote Sens.* 39, 1799–1806. doi:10.1109/36.942558

Flynn, T., Tabb, M., and Carande, R. (2002). Coherence region shape extraction for vegetation parameter estimation in polarimetric SAR interferometry. *IEEE International Geoscience and Remote Sensing Symposium* 5, 2596–2598.

Gao, Q., Zribi, M., Escorihuela, M. J., and Baghdadi, N. (2017). Synergetic Use of Sentinel-1 and Sentinel-2 Data for Soil Moisture Mapping at 100 m Resolution. *Sensors* 17, 1966. doi:10.3390/s17091966

Guo, Q., Xu, C., Wen, Y., Liu, Y., and Xu, G. (2019). The 2017 Noneruptive Unrest at the Caldera of Cerro Azul Volcano (Galápagos Islands) Revealed by InSAR Observations and Geodetic Modelling. *Remote Sensing* 11, 1992. doi:10.3390/rs11171992

Guo, Z., Qi, W., Huang, Y., Zhao, J., Yang, H., Koo, V.-C., et al. (2022). Identification of Crop Type Based on C-AENN Using Time Series Sentinel-1A SAR Data. *Remote Sensing* 14, 1379.

Hall-Atkinson, C., Smith, L. C., and Mackenzie (2001). *Delineation of delta ecozones using interferometric SAR phase coherence*, 78, 229–238. doi:10.1016/S0034-4257(01)00221-8River Delta, N.W.T., Canada*Remote Sensing of Environment*

Han, B., Yang, C., Li, Z., Yu, C., Zhao, C., and Zhang, Q. (2022). Coseismic and postseismic deformation of the 2016 Mw 6.0 Petermann ranges earthquake from satellite radar observations. *Advances in Space Research* 69, 376–385.

He, Y., Wang, W., Yan, H., Zhang, L., Chen, Y., and Yang, S. (2020). Characteristics of Surface Deformation in Lanzhou with Sentinel-1A TOPS. *Geosciences* 10, 99. doi:10.3390/geosciences10030099

Jiang, M., Ding, X., Li, Z., Tian, X., Wang, C., and Zhu, W. (2014). InSAR Coherence Estimation for Small Data Sets and Its Impact on Temporal Decorrelation Extraction. *IEEE Trans. Geosci. Remote Sens.* 52, 6584–6596. doi:10.1109/TGRS.2014.2298408

Jung, J., Kim, D., Lavalle, M., and Yun, S.-H. (2016). Coherent Change Detection Using InSAR Temporal Decorrelation Model: A Case Study for Volcanic Ash Detection. *IEEE Trans. Geosci. Remote Sens.* 54, 5765–5775. doi:10.1109/TGRS.2016.2572166

Krieger, G., Moreira, A., Fiedler, H., Hajnsek, I., Werner, M., Younis, M., et al. (2007). TanDEM-X: A Satellite Formation for High-Resolution SAR Interferometry. *IEEE Trans. Geosci. Remote Sens.* 45, 3317–3341.

Kumar, V., Huber, M., Rommen, B., and Steele-Dunne, S. C. (2022). Agricultural SandboxNL: A national-scale database of parcel-level processed Sentinel-1 SAR data. *Sci. Data* 9, 402. doi:10.1038/s41597-022-01474-4

Lee, H., and Liu, J. G. (2001). Analysis of topographic decorrelation in SAR interferometry using ratio coherence imagery. *IEEE Trans. Geosci. Remote Sens.* 39, 223–232. doi:10.1109/36.905230

Liang, D., Guo, H., Zhang, L., Cheng, Y., Zhu, Q., and Liu, X. (2021a). Time-series snowmelt detection over the Antarctic using Sentinel-1 SAR images on Google Earth Engine. *Remote Sensing of Environment* 256, 112318. doi:10.1016/j.rse.2021.112318

Liang, H., Zhang, L., Ding, X., Lu, Z., Li, X., Hu, J., et al. (2021b). Suppression of Coherence Matrix Bias for Phase Linking and Ambiguity Detection in MTInSAR. *IEEE Trans. Geosci. Remote Sensing* 59, 1263–1274. doi:10.1109/TGRS.2020.3000991

Manjula, T. R., Ramesh, A., Unnikrishnan, L., Reddy, V. C., Sethia, G., Nagarjan, N., et al. (2022). "Temporal Variation of Glacier Melting Rate of Helheim and Gangotri Glaciers Using Sentinel 1A Images," in *Advanced Computational Paradigms and Hybrid Intelligent Computing Advances in Intelligent Systems and Computing*. Editors T. K. Gandhi, D. Konar, B. Sen, and K. Sharma (Singapore: Springer), 231–239. doi:10.1007/978-981-16-4369-9_24

Merchant, M. A., Obadia, M., Brisco, B., DeVries, B., and Berg, A. (2022). Applying Machine Learning and Time-Series Analysis on Sentinel-1A SAR/InSAR for Characterizing Arctic Tundra Hydro-Ecological Conditions. *Remote Sensing* 14, 1123. doi:10.3390/rs14051123

Nasirzadehdizaji, R., Cakir, Z., Balik Sanli, F., Abdikan, S., Pepe, A., and Calò, F. (2021). Sentinel-1 interferometric coherence and backscattering analysis for crop monitoring. *Computers and Electronics in Agriculture* 185, 106118. doi:10.1016/j.compag.2021.106118

Nikaein, T., Iannini, L., Molijn, R. A., and Lopez-Dekker, P. (2021). On the Value of Sentinel-1 InSAR Coherence Time-Series for Vegetation Classification. *Remote Sensing* 13, 3300. doi:10.3390/rs13163300

Parizzi, A., Cong, X., and Eineder, M. (2009). *First Results from Multifrequency Interferometry. A comparison of different decorrelation time constants at L, C, and X Band*. ESA Scientific Publications Frascati, 1. –5.

Pearson, K. (1895). *Correlation coefficient*. Royal Society Proceedings, 214.

Pinto, N., Simard, M., and Dubayah, R. (2013). Using InSAR Coherence to Map Stand Age in a Boreal Forest. *Remote Sensing* 5, 42–56. doi:10.3390/rs5010042

Potin, P., Rosich, B., Grimont, P., Miranda, N., Shurmer, I., O'Connell, A., et al. (2016). Sentinel-1 Mission Status. Proceedings of EUSAR 2016: 11th European Conference on Synthetic Aperture Radar. 1–6.

Rocca, F. (2007). Modeling Interferogram Stacks. *IEEE Trans. Geosci. Remote Sens.* 45, 3289–3299. doi:10.1109/TGRS.2007.902286

Santoro, M., Wegmuller, U., and Askne, J. I. H. (2010). Signatures of ERS–Envisat Interferometric SAR Coherence and Phase of Short Vegetation: An Analysis in the Case of Maize Fields. *IEEE Trans. Geosci. Remote Sens.* 48, 1702–1713. doi:10.1109/TGRS.2009.2034257

Sedze, M., Heggy, E., Bretar, F., Berveiller, D., and Jacquemoud, S. (2012). L-band InSAR decorrelation analysis in volcanic terrains using airborne LiDAR data and *in situ* measurements: The case of the Piton de la Fournaise volcano, France. *IEEE International Geoscience and Remote Sensing Symposium*, 3907–3910. doi:10.1109/IGARSS.2012.6350558

Sica, F., Pulella, A., Nannini, M., Pinheiro, M., and Rizzoli, P. (2019). Repeat-pass SAR interferometry for land cover classification: A methodology using Sentinel-1 Short-Time-Series. *Remote Sensing of Environment* 232, 111277. doi:10.1016/j.rse.2019.111277

Suresh, D., and Yarrakula, K. (2020). InSAR based deformation mapping of earthquake using Sentinel 1A imagery. *Geocarto International* 35, 559–568. doi:10.1080/10106049.2018.1544289

Tampuu, T., Praks, J., Kull, A., Uiboupin, R., Tamm, T., and Voormansik, K. (2021). Detecting peat extraction related activity with multi-temporal Sentinel-1 InSAR coherence time series. *International Journal of Applied Earth Observation and Geoinformation* 98, 102309. doi:10.1016/j.jag.2021.102309

Wadge, G., Zhu, M., Holley, R. J., James, I. N., Clark, P. A., Wang, C., et al. (2010). Correction of atmospheric delay effects in radar interferometry using a nested mesoscale atmospheric model. *Journal of Applied Geophysics* 72, 141–149. doi:10.1016/j.jappgeo.2010.08.005

Wali, E., Tasumi, M., and Moriyama, M. (2020). Combination of Linear Regression Lines to Understand the Response of Sentinel-1 Dual Polarization SAR Data with Crop Phenology—Case Study in Miyazaki, Japan. *Remote Sensing* 12, 189. doi:10.3390/rs12010189

Wang, R., Dong, P., Dong, G., Xiao, X., Huang, J., Yang, L., et al. (2022). Exploring the impacts of street-level greenspace on stroke and cardiovascular diseases in Chinese adults. *Ecotoxicology and Environmental Safety* 243, 113974. doi:10.1016/j.ecoenv.2022.113974

Wang, T., Liao, M., and Perissin, D. (2010). InSAR Coherence-Decomposition Analysis. *IEEE Geosci. Remote Sens. Lett.* 7, 156–160. doi:10.1109/LGRS.2009.2029126

Wang, Y., Wang, L., Li, H., Yang, Y., and Yang, T. (2015a). Assessment of Snow Status Changes Using L-HH Temporal-Coherence Components at Mt. Dagu, China. *Remote Sensing* 7, 11602–11620. doi:10.3390/rs70911602

Wang, Y., Wang, L., Zhang, Y., and Yang, T. (2015b). Investigation of snow cover change using multi-temporal PALSAR InSAR data at Dagu Glacier, China. IEEE International Geoscience and Remote Sensing Symposium. 26-31 July 2015. Milan, Italy. IGARSS, 747–750. doi:10.1109/IGARSS.2015.7325872

Wuyun, D., Sun, L., Sun, Z., Chen, Z., Hou, A., Teixeira Crusiol, L. G., et al. (2022). Mapping fallow fields using Sentinel-1 and Sentinel-2 archives over farming-pastoral ecotone of Northern China with Google Earth Engine. *GIScience & Remote Sensing* 59, 333–353. doi:10.1080/15481603.2022.2026638

Yang, L., Liu, J., Liang, Y., Lu, Y., and Yang, H. (2021a). Spatially Varying Effects of Street Greenery on Walking Time of Older Adults. *ISPRS Int. J. Geoinf.* 10, 596. doi:10.3390/ijgi10090596

Yang, L., Liu, J., Lu, Y., Ao, Y., Guo, Y., Huang, W., et al. (2020a). Global and local associations between urban greenery and travel propensity of older adults in Hong Kong. *Sustainable Cities and Society* 63, 102442. doi:10.1016/j.scs.2020.102442

Yang, Y., Lu, Y., Yang, L., Gou, Z., and Liu, Y. (2021b). Urban greenery cushions the decrease in leisure-time physical activity during the COVID-19 pandemic: A natural experimental study. *Urban Forestry & Urban Greening* 62, 127136. doi:10.1016/j.ufug.2021.127136

Yang, Y., Lu, Y., Yang, L., Gou, Z., and Zhang, X. (2020b). Urban greenery, active school transport, and body weight among Hong Kong children. *Travel Behaviour and Society* 20, 104–113. doi:10.1016/j.tbs.2020.03.001

Zebker, H. A., and Villasenor, J. (1992). Decorrelation in interferometric radar echoes. *IEEE Trans. Geosci. Remote Sens.* 30, 950–959. doi:10.1109/36.175330

Zhang, B., Liu, G., Zhang, R., Fu, Y., Liu, Q., Cai, J., et al. (2021a2021). Monitoring Dynamic Evolution of the Glacial Lakes by Using Time Series of Sentinel-1A SAR Images. *Remote Sens. (Basel).* 13, 1313. doi:10.3390/rs13071313

Zhang, M., Li, Z., Tian, B., Zhou, J., and Tang, P. (2016). The backscattering characteristics of wetland vegetation and water-level changes detection using multi-mode SAR: A case study. *International Journal of Applied Earth Observation and Geoinformation* 45, 1–13. doi:10.1016/j.jag.2015.10.001

Zhang, Q., Wang, T., Pei, Y., and Shi, X. (2021b). Selective Kernel Res-Attention UNet: Deep Learning for Generating Decorrelation Mask With Applications to TanDEM-X Interferograms. *IEEE J. Sel. Top. Appl. Earth Obs. Remote Sens.* 14, 8537–8551. doi:10.1109/JSTARS.2021.3105703

Zhang, Z., Wang, C., Zhang, H., Tang, Y., and Liu, X. (2018). Analysis of Permafrost Region Coherence Variation in the Qinghai–Tibet Plateau with a High-Resolution TerraSAR-X Image. *Remote Sensing* 10, 298. doi:10.3390/rs10020298

Zhao, B., Xiang, Y., Yao, W., Shi, Y., Huang, Y., Zheng, J., et al. (2020). Monitoring surface subsidence in the Binchang mining area using small baseline subset differential interferometric synthetic aperture radar with Sentinel-1A data. *J. Appl. Remote Sens.* 14, 044507. doi:10.1117/1.JRS.14.044507

frontiers | Frontiers in Ecology and Evolution

TYPE Original Research
PUBLISHED 03 November 2022
DOI 10.3389/fevo.2022.1017728

Check for updates

OPEN ACCESS

EDITED BY
Bing Xue,
Institute for Advanced Sustainability Studies (IASS), Germany

REVIEWED BY
Zaijun Li,
Yangzhou University, China
Sanwei He,
Zhongnan University of Economics and Law, China

*CORRESPONDENCE
Wei Sun
wsun@niglas.ac.cn

SPECIALTY SECTION
This article was submitted to Environmental Informatics and Remote Sensing, a section of the journal Frontiers in Ecology and Evolution

RECEIVED 12 August 2022
ACCEPTED 12 October 2022
PUBLISHED 03 November 2022

CITATION
Wu J, Liu C and Sun W (2022) Eco-environmental constraints, economic incentives, and spatiotemporal variations of construction land use efficiency in regional China.
Front. Ecol. Evol. 10:1017728.
doi: 10.3389/fevo.2022.1017728

COPYRIGHT
© 2022 Wu, Liu and Sun. This is an open-access article distributed under the terms of the Creative Commons Attribution License (CC BY). The use, distribution or reproduction in other forums is permitted, provided the original author(s) and the copyright owner(s) are credited and that the original publication in this journal is cited, in accordance with accepted academic practice. No use, distribution or reproduction is permitted which does not comply with these terms.

Eco-environmental constraints, economic incentives, and spatiotemporal variations of construction land use efficiency in regional China

Jiawei Wu[1], Chonggang Liu[1,2] and Wei Sun[1]*

[1]Key Laboratory of Watershed Geographic Sciences, Nanjing Institute of Geography and Limnology, Chinese Academy of Sciences, Nanjing, China, [2]University of Chinese Academy of Sciences, Beijing, China

Construction land expansion and use efficiency are tied to the promotion of sustainable cities and communities. This article explores how and why the spatiotemporal variation of construction land use efficiency (CLUE) evolved in the Yangtze River Delta (YRD), China between 2000 and 2020. Our descriptive results show that county-level regions with higher CLUE are concentrated in major cities in the core YRD, as well as ecologically sensitive regions in the peripheral YRD. Although CLUE improvement in peripheral regions has been more remarkable since the early 2010s, the efficiency gap in construction land use between the core YRD (central cities) and the peripheral YRD (suburban counties) has doubled. The modeling results indicate the temporally and spatially heterogeneous impacts of various factors related to economic incentives and eco-environmental constraints on the uneven CLUE. Economic level and ecological sensitivity are positively associated with regional CLUE. The continuing growth of service industries and the spatial agglomeration of knowledge-intensive and foreign-invested firms are increasingly vital for CLUE improvement in the core YRD, while the prosperity of manufacturing industries is more important for the peripheral YRD. The "crowding out effect" of environmental pollution on CLUE could be proved in the peripheral rather than the core YRD. Our findings suggest that proper policies should be tailored to specific places to coordinate construction land use, economic growth, and eco-environmental sustainability.

KEYWORDS

land use transition, economic transition, eco-environmental system, regional sustainable development, regional inequality, China

Introduction

Global construction land (i.e., built-up area) has experienced a rapid increase in the last century, largely resulting from population urbanization and economic agglomeration (Lambin and Meyfroidt, 2011; Liu et al., 2020; Mahtta et al., 2022). Unordered land sprawl and inefficient land use, meanwhile, generated various negative impacts including eco-environmental degradation and cultivated land shrinking at multiple spatial scales (Estoque et al., 2021). An increasingly intensive contradiction between land shortage and inefficient use was observed worldwide, especially in the Global South and developing economies (Liu et al., 2014; Fetzel et al., 2016). Rational and efficient land use become the key to achieving sustainable cities and communities (UN-Habitat, 2016; Akuraju et al., 2020; Rahman and Szabó, 2021). The spatiotemporal variations and determinants of construction land-use efficiency (CLUE) have attracted much attention from scholars and policy-makers.

A large body of literature has focused on the driving forces of uneven CLUE from the perspective of locally socioeconomic and institutional contexts (Wu et al., 2017; Masini et al., 2019). The impacts of economic incentives, such as income growth, technical progress, and industrial upgrading, on CLUE have been well-studied empirically (Koroso et al., 2020; Yue et al., 2022; Zhang et al., 2022). To our knowledge, the aggregate movements of the economy at the macro-level are mainly driven by firm-specific changes (Capasso et al., 2015). However, attempts to address the influences of firm heterogeneities, including firm size, industrial attribute, and ownership structure, at the micro-level on CLUE are thin on the ground. In addition, following the social-ecological systems framework, land-use practices should be viewed as the feedback of changes in ecosystem goods and services (Lambin and Meyfroidt, 2010). There is a vast literature focusing on the implications of land-use transition (e.g., efficiency improvement) for global and regional eco-environmental status (Lambin and Meyfroidt, 2010; Searchinger et al., 2018). In contrast, with few exceptions (Peng et al., 2017; Wang K. et al., 2021), researches on the driving mechanisms of eco-environmental constraints behind land-use efficiency are quite limited.

China's rapid urbanization and industrialization provide a rich context. The high-growth and resource-intensive developmental trajectory that China pursued has led to a series of eco-environmental issues related to the irrational use of construction land (Liu et al., 2014; Dong et al., 2020), especially in socioeconomically developed metropolises and urban agglomerations (Gao et al., 2020; Ning et al., 2022). This forces the Chinese government to further strengthen natural resource supervision and pay more attention to sustainable use. Therefore, construction land expansion has been increasingly restricted by local eco-environment and relevant regulations (Xie et al., 2021). Promoting industrial agglomeration and upgrading has become an important measure for the intensive use of construction land (Liu J. et al., 2021; Zhang et al., 2022). The investigation and interpretation of geographically uneven CLUE in China need to take local eco-environmental constraints and industrial dynamics into account, however, the number of empirical researches on relevant issues, particularly at finer spatial scales, is still small.

To fill the aforementioned research gaps, this article aims to examine the spatiotemporal variation of CLUE and its driving forces in regional China, with particular attention given to local eco-environmental constraints and economic incentives. Taking the Yangtze River Delta (YRD), one of the emerging global city-region in China, as a case study, we focus on two interrelated research questions: (1) How have the spatiotemporal patterns of CLUE changed between 2000 and 2020? (2) What factors drive the changes in CLUE, and how has the relative importance of driving forces differed across regions and changed over time? Regional corporate demography, namely the range, structure, and diversity of corporate organizations in a specific place (Carroll and Hannan, 2000), and spatial dynamics of firms are used to measure economic incentives at the micro-level in this study. Empirical results will advance our understanding of the uneven CLUE under different eco-environmental systems and socioeconomic contexts at regional or local scale. Our findings on the changes in the economic performance of construction land use in regional China can generate policy implications for sustainable land use and urbanization in other emerging economies.

Literature review and conceptual framework

Given the importance of CLUE improvement in achieving sustainable cities and communities, the definition and measurement of CLUE have been profoundly discussed in the literature from the perspective of "input-output system" (Chen et al., 2019; Masini et al., 2019; Zhu et al., 2019). CLUE is usually defined as the economic output or population carried by built-up areas (Wu et al., 2017; He et al., 2020; Koroso et al., 2020; Estoque et al., 2021). Inputs (e.g., labor and capital) in addition to land, as well as unexpected outputs including environmental pollution and ecological degradation, have been increasingly considered in the calculation of CLUE (Yu et al., 2019; Liu S. et al., 2021; Zhang et al., 2021). Previous studies demonstrated that construction land use practices and efficiency significantly differ across continents, countries, regions, and cities (He et al., 2020; Jiao et al., 2020; Estoque et al., 2021; Schiavina et al., 2022). Scholars largely attributed this phenomenon to place-specific disparities in socioeconomic contexts and eco-environmental conditions. Based on seminal works and the Chinese contexts, we develop a conceptual framework to explain spatiotemporal variations of CLUE at a finer geographical scale, with particular attention given to

the effects of microeconomic incentives, eco-environmental constraints, and relevant regulations (see **Figure 1**).

Socioeconomic contexts, corporate demography, and land use efficiency

A large body of literature has examined the impacts of socioeconomic contexts on changing spatial patterns of CLUE across places (Masini et al., 2019; He et al., 2020; Zhang et al., 2022). There is a consensus that regional differences in construction land use performance are tightly associated with economic incentives, such as population agglomeration, industrial structure optimization, and technological progress (Chen et al., 2018; Mahtta et al., 2022). Better economic performance of construction land use tends to be observed in places with higher income level and stronger innovative capability (Masini et al., 2019). Industrial transformation and relocation, especially the exit of traditional manufacturing and the entry of high-tech industries, play a vital role in improving CLUE (Liu J. et al., 2021; Yue et al., 2022). Existing studies mainly examined the effects of economic incentives at the macro-level, however, the relationship between microeconomic incentives (e.g., firm-specific changes) and CLUE has been largely ignored in the literature.

The unique transitional contexts, including globalization, marketization, decentralization, and urbanization (Gao et al., 2014; Wu et al., 2017), should be taken into account to understand better China's construction land use. Particularly, China's developmental model has been gradually shifting from high-growth and resource-intensive to high-quality oriented and innovation-driven (Chen et al., 2016; Wu et al., 2016). China tends to be more active in promoting efficient and intensive utilization of land resources. For instance, policy instruments related to technical innovation and industrial upgrading have been issued by Chinese central and local governments to improve CLUE, and relevant research largely confirmed the positive effects of these policies (Peng et al., 2017; Wu et al., 2017; Li J. et al., 2021). To our knowledge, economic transition, industrial restructuring, and technical progress largely result from firm-specific changes (Capasso et al., 2015). Research on the relationship between economic incentives and uneven CLUE should consider regional corporate demography or spatial dynamics of firms.

To be specific, the spatial agglomeration of corporate organizations and their businesses is tightly associated with economic density and land use efficiency, and variegated features such as size, industrial attribute, and ownership structure of firms matter. Compared with middle and small-sized enterprises (SMEs), large firms with advanced technologies and value-added businesses are capable of using resources efficiently. Land use performance of the "new economy," especially producer service and knowledge-intensive industries, may be better than that of traditional manufacturing. Moreover, foreign-invested enterprises (FIEs) are more likely to show superior performance in land use than domestic enterprises in China due to their advanced technologies and management experiences (Yue et al., 2022).

Eco-environmental conditions, regulations, and land use efficiency

Seminal works based on the social-ecological system framework indicated that regional eco-environmental systems and regulatory policies are important for understanding land-use transition (Lambin and Meyfroidt, 2010, 2011). Land use practices, especially urban land expansion, are severely confined by natural resources endowment, and eco-environmental capacity at regional or local scale (Bryan et al., 2015; Liu et al., 2017; Yang et al., 2022). Relationships between eco-environmental constraints and CLUE have received particular attention in the literature (Lu et al., 2018; Tang et al., 2021; Zhang et al., 2021). Environmental pollution and deterioration may have a significant "crowding out effect" on CLUE (Peng et al., 2017), and CLUE improvement would contribute to pollution reduction (Dong et al., 2020; Li et al., 2021). Relevant institutional settings and policies also matter (Tu et al., 2014; Wang Q. et al., 2021). The implementation of more strict natural resources supervision and environmental regulation would improve CLUE (Wang K. et al., 2021; Zhang et al., 2021). However, attempts to examine the potential impacts of regional eco-environmental conditions and regulations, by contrast with socioeconomic variables, on CLUE are quite limited.

Eco-environmental carrying capacity, territorial exploiting suitability, and regulatory policies significantly vary across the Chinese regions. This largely leads to regional disparities in construction land expansion and use efficiency. On the one hand, land resources available for industrialization and urbanization are even scarcer in China. By implementing rigid zoning plans and regulations, the protection of natural cover and ecological space has taken priority over urban and industrial expansion, especially in ecologically sensitive regions. This enforces local governments to pay more attention to facilitating efficient use of existing construction land to stabilize economic growth. On the other hand, environmental pollution and degeneration in China partly attribute to rapid expansion and inefficient use of construction land. In addition to environmental laws and regulations, optimizing land use practice and performance is also an effective means to solve pollution problems under China's low-carbon or sustainable developmental strategies. It should be noted that the demand for CLUE improvement in metropolises or developed regions where eco-environmental constraints and agglomeration diseconomies presented earlier is more urgent. In contrast, socioeconomic development in lower-tier cities or less-developed regions relies more on cheaper productive elements and looser environmental regulations, probably resulting in inefficient use of land resources.

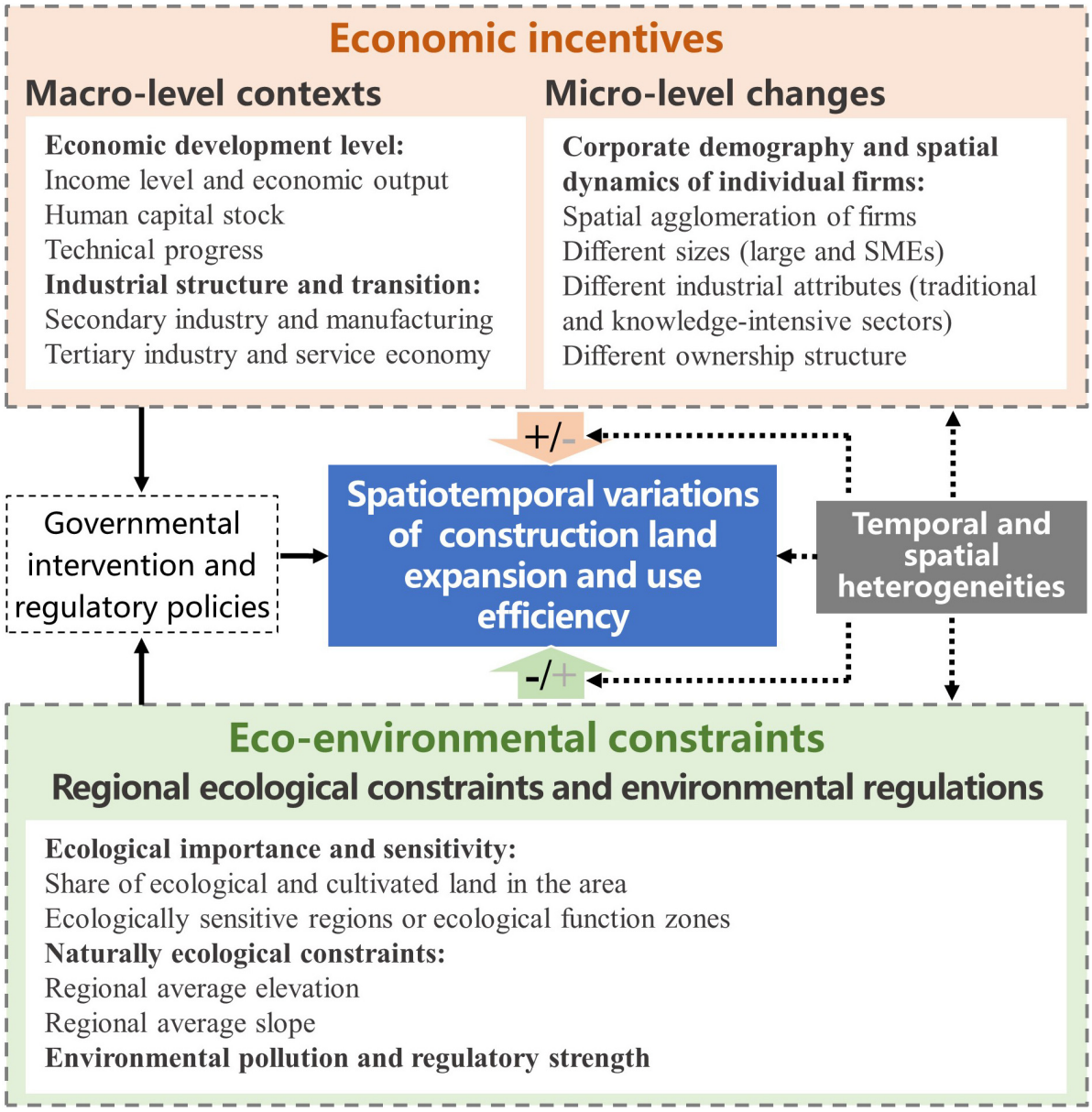

FIGURE 1
Conceptual framework of construction land expansion and use efficiency in China.

Research materials and methodologies

Study area: The Yangtze River Delta

Located in eastern coastal China, the YRD is an emerging global city-region around the world. With only 3.7% of China's territory, the YRD carries 16.7% of China's population and 24.1% of China's gross domestic product (GDP) in 2020. The YRD is selected as the study area according to the following considerations: First, as the epitome of China's industrialization and urbanization, the YRD has been experiencing an unpredictable process of economic growth and urban expansion, which resulted in serious eco-environmental deterioration, since the start of Reform and Opening-Up. The YRD accounts for 11.7% of COD emissions and 8.7% of SO2 emissions in China in 2020. The contradiction between urbanization, economic development, and eco-environmental protection is more prominent in the YRD, forcing local governments to become more active in promoting sustainable and efficient utilization of natural resources (e.g., land). Second, although the YRD has advantages in population, GDP, and urban size, it still lags far behind the recognized global-city-regions in the USA and Europe in terms of economic

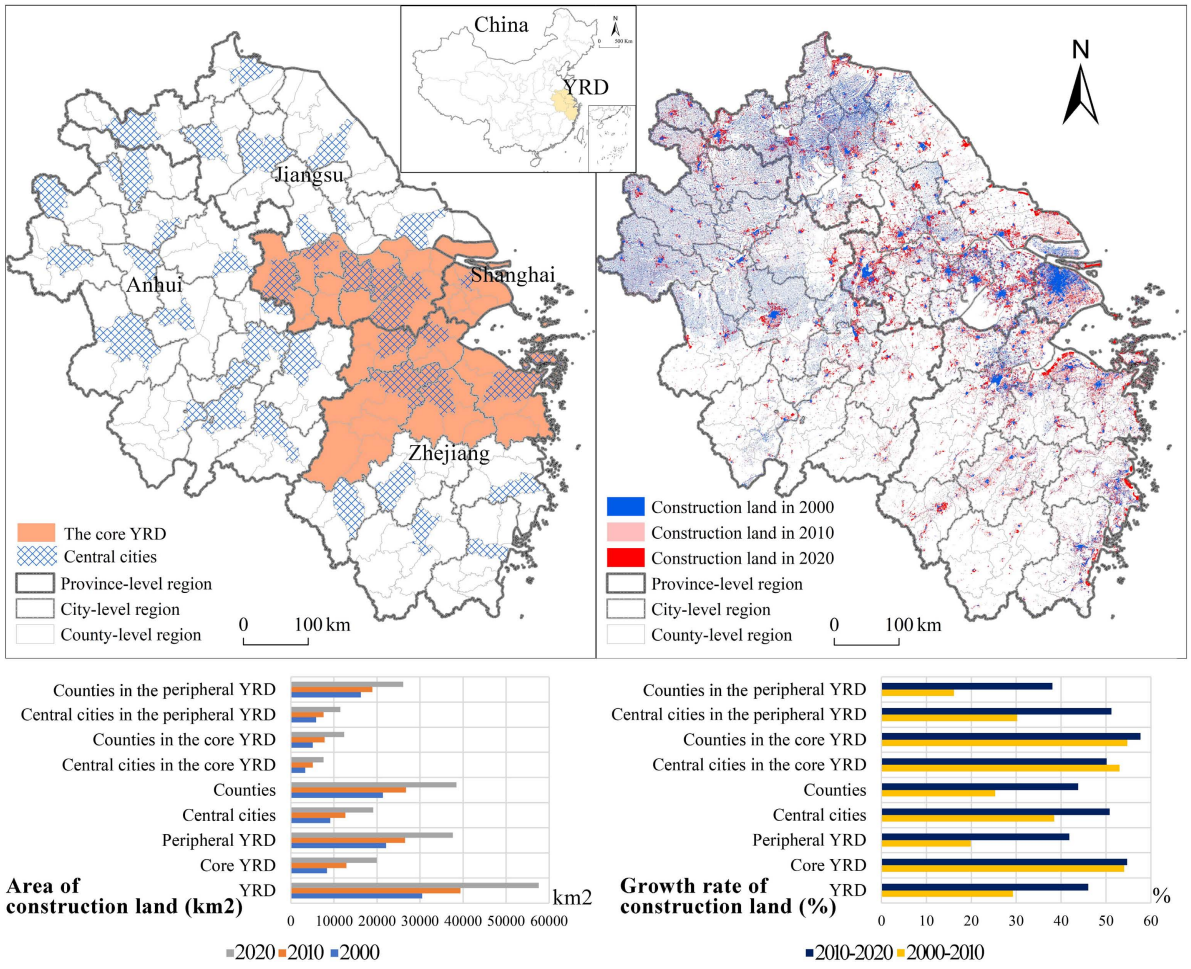

FIGURE 2
Location and construction land expansion of the study area.

efficiency and innovative capability. The growth trajectories and predicaments of the YRD are more similar to those of emerging economies. Third, the regional difference in eco-environmental condition and socioeconomic development level is a vital feature of the YRD, as in most emerging economies. Land use practice and performance are no exception to that feature. Therefore, we believe that the evidence from the YRD can serve as a strong reference for China and a large number of emerging economies (or global-city regions).

Figure 2 presents the location of the YRD, as well as the spatial pattern of construction land expansion. The YRD includes four province-level regions, namely Shanghai, Jiangsu, Zhejiang, and Anhui. To examine the spatiotemporal variation of CLUE at a finer geographical scale, we group the YRD into core (central city) or peripheral (suburban) subregions according to their administrative affiliations, eco-environmental conditions, and socioeconomic levels. Urban districts are merged and defined as the central city areas to distinguish them from suburban counties. We find that the total area of construction land in the YRD has increased from 30,498.8 km^2 in 2000 to 39,425.8 km^2 and 57,586.7 km^2 in 2010 and 2020, respectively. The expansion of construction land significantly differed across regions and changed over time. The growth rate of construction land area in the core YRD was higher than that in the peripheral YRD during 2000–2010 and 2010–2020. However, this gap has been narrowed due to the rapid expansion of construction land in the peripheral YRD. The growth rates of construction land area in the central cities and counties of the peripheral YRD, respectively increased from 30.22 and 16.17% during 2000–2010 to 51.23 and 38.08% during 2010–2020.

Data source and processing

Construction land and natural cover data for analysis are drawn from Chinese 30 m GlobalLand30 datasets (2000, 2010, and 2020). GlobalLand30 comprises datasets collected at 30-m resolution, which are valuable for monitoring environmental (or land use) changes and for resource management at multiple spatial scales (Jun et al., 2014). GlobalLand30 is the first global

geo-information public product provided by China to the United Nations with extensive use[1], and it can be obtained online for free. Based on ten types of land cover in the GlobalLand30 datasets, the artificial surface is regarded as construction land or built-up area in this study.

In addition, the datasets of fine particulate matter (PM2.5) originated from the Atmospheric Composition Analysis Group (van Donkelaar et al., 2021). We acquire socioeconomic developmental statistics, especially the total output value of the secondary and tertiary industries, from the China City Statistical Yearbook (CCSY) and published statistical materials of relevant provinces or cities. The data relating to industrial output value are calculated based on the year 2000 constant price to eliminate the influences of currency inflation. We collect the data on the size, industrial attributes, and ownership structures of individual firms in a specific place from *Qichacha*, which is one of the authoritative inquiry systems of corporate credit and information in China.

Methodologies

Measurement of construction land-use efficiency

According to the existing literature, economic output per unit of land is an effective or comparable indicator that can directly estimates land-use performance (Wu et al., 2017; Chen et al., 2018; Masini et al., 2019). Considering the non-agricultural socioeconomic activities carried by built-up area, we apply the total output value of secondary and tertiary industries per hectare of construction land to measure CLUE:

$$CLUE_{it} = \frac{IOV_{it}}{CLA_{it}} \tag{1}$$

where, IOV_{it} is the total output value of secondary and tertiary industries of research unit i in year t.CLA_{it} is the total construction land area of research unit i in year t.

Spatial autocorrelation and clustering analysis

The Global Moran's I (GMI) and the Local Moran's I (LMI_i), which are used to investigate the spatial autocorrelation of CLUE in the YRD, can be defined as equations (2) and (3), respectively.

$$GMI = \frac{n\sum_{i=1}^{n}\sum_{j=1}^{n} w_{i,j}\left(X_i-\overline{X}\right)\left(X_j-\overline{X}\right)}{\sum_{i=1}^{n}\sum_{j=1}^{n} w_{i,j}\sum_{i=1}^{n}\left(X_i-\overline{X}\right)^2} \tag{2}$$

$$LMI_i = \frac{\left(X_i-\overline{X}\right)}{\sum_{i=1}^{n}\left(X_i-\overline{X}\right)^2}\sum_{j=1}^{n} w_{ij}\left(X_i-\overline{X}\right) \tag{3}$$

where, X_i and X_j are CLUE of research units i and j, respectively. $\overline{X}$ stands for the average CLUE by research units in the YRD. n is the number of research units. w_{ij} represents the spatial adjacency matrix. According to the result of LMI_i, the spatial pattern of CLUE can be described by four types of research units, namely high-high (H-H), high-low (H-L), low-high (L-H), and low-low (L-L). For instance, the H-H indicates that the CLUE of regions surrounding regions with high CLUE is relatively high.

In addition, the Hot Spot analysis tool (Getis-Ord Gi* statistic) is applied to explore the spatial clustering dynamics of CLUE changes. The standardized G_i^* can be calculated as:

$$Z\left(G_i^*\right) = \frac{\sum_{j=1}^{n} w_{i,j}C_X_j - \overline{C_X}\sum_{j=1}^{n} w_{i,j}}{S\sqrt{\frac{\left[n\sum_{j=1}^{n} w_{i,j}^2-\left(\sum_{j=1}^{n} w_{i,j}\right)^2\right]}{n-1}}} \tag{4}$$

where, C_X_j is the increase or decrease of CLUE of research unit j from year t to year $t+1$. $\overline{C_X}$ and S, respectively stand for the average increase/decrease and standard deviation of CLUE by research units. The research unit, which has a high (low) C_X value and is surrounded by other units with relatively high (low) C_X values, can be grouped as a statistically significant hot (cold) spot.

Regression model and variable specification

OLS and spatial regression models are applied to uncover the driving forces of the spatiotemporal variation of CLUE. OLS regression model can be estimated as:

$$y_i = \beta_0 + \sum_{k=1}^{m}\beta_k x_{ik} + \varepsilon_i \tag{5}$$

where, y_i represents the dependent variable ($CLUE_i$). x_{ik} and β_k stand for the observed value of independent variable k and its regression coefficient. m is the number of independent variables. β_0 and ε_i are the constant term and the error term, respectively.

The spatial lag model (SLM) and spatial error model (SEM), which are used to avoid the potential deviation of estimation based on the OLS model, can be built as follows:

$$y = \alpha + \rho wy + \beta_k x_k + \varepsilon \tag{6}$$

$$\begin{cases} y = \alpha + \beta_k x_k + \varepsilon \\ \varepsilon = \gamma w_\varepsilon + \mu \end{cases} \tag{7}$$

where, y and x_k represent the dependent variable and independent variable, respectively. β_k is the estimated coefficient of the independent variable. ε and μ are error terms. ρ and γ stand for the estimated coefficients of the spatial lag term of dependent variable and spatial autocorrelation error term (ε). w and w_ε are the spatial matrix of the dependent variable and residual error, respectively. Lagrange Multiplier (LM) test and Robust LM test of OLS regression residuals are taken to check the suitability of SLM and SEM.

Furthermore, we apply the geographically weighted regression (GWR) model to uncover the spatial effects of influential factors on CLUE in different research units. The GWR model can be built as follows:

$$y_i = \sum_{k}\beta_k\left(u_i, v_i\right)x_{ik} + \varepsilon_i \tag{8}$$

1 www.globallandcover.com

TABLE 1 The definitions of independent variables.

Category		Variables	Definition and calculation (abbreviation)
Economic incentives	Economic development level	Per capita GDP	The ratio of the GDP in each research unit and the average level of the YRD (PGDP)
	Industrial structure and transition	industrial economy	The ratio of the share of the output value of secondary industry in each research unit and the average level of the YRD (IND)
		service economy	The ratio of the share of the output value of tertiary industry in each research unit and the average level of the YRD (SERV)
	Corporate demography and spatial dynamics of firms	Firm density	The ratio of the number of corporate organizations per km^2 (administrative area) in each research unit and the average level of the YRD (FIRM)
		Firm size	Quotient index of the number of corporate organizations with paid-in capital of more than 50 million yuan for each research unit (SCALE)
		Corporate industrial attribute	Quotient index of the number of corporate organizations in knowledge-intensive industries for each research unit (KNOW)
		Corporate ownership structure	Quotient index of the number of the foreign-invested corporate organizations for each research unit (OWN)
Eco-environmental constraints	Ecological importance and sensitivity	Ecological land area	The ratio of the share of ecological and cultivated land and the average level of the YRD (ECO)
		Regional elevation	The ratio of regional average elevation of each research unit and the average level of the YRD (DEM)
		Regional slope	The ratio of regional average slope in each research unit and the average level of the YRD (SLOP)
	Environmental pollution and regulatory strength	Air pollution	The ratio of regional annual average PM2.5 concentration in each research unit and the average level of the YRD (PM2.5)

We calculate the quotient index as follows: $Q_i = \left(x_i/\sum_{i=1}^{n} x_i\right)/\left(X_i/\sum_{i=1}^{n} X_i\right)$, where x_i represents the number of large, knowledge-intensive, and foreign-invested corporate organizations in research unit i, X_i stands for all corporate organizations in research unit i. Knowledge-intensive industries include: Medical and pharmaceutical products, chemical fiber, general and special-purpose equipment, automobiles, transport equipment, electrical machinery and apparatus, electronic equipment, transport, storage, information transmission, software and information technology, financial intermediation, leasing and business services, and scientific research and technical services.

where, y_i and x_{ik} are dependent variable and independent variable k of research unit i. (u_i, v_i) indicates the spatial location of research unit i, and ε_i stands for error term.

According to our conceptual framework and previous studies, we model the CLUE as the function of variables related to economic incentives and eco-environmental constraints. Per capita GDP, which is positively correlated with regional advantages in economic output, human capital stock, and technological progress (Cheung and Ping, 2004; Tahir et al., 2020), is used to measure economic development level. We use the share of the output value of secondary/tertiary industry to GDP to represent the transition of regional industrial structure. The effects of regional corporate demography and spatial dynamics of firms are measured by firm density, as well as a set of location quotient indexes related to the amount of large, knowledge-intensive, and foreign-invested enterprises. Place-specific ecological importance and sensitivity are measured by the share of ecological land (e.g., forest, grassland, shrubland, wetland, and tundra) and cultivated land in the area. The effects of ecological constraints on construction land expansion and use efficiency are modeled by regional average elevation and slope. The regional annual average PM2.5 concentration is applied to measure the level of environmental pollution and regulatory strength. The definitions and descriptions of independent variables are presented in Table 1.

Empirical results and interpretation

Spatiotemporal variations of construction land use efficiency in the Yangtze River Delta

Spatiotemporal characteristics of construction land use efficiency

Figure 3 shows the overall changing trends of CLUE in the YRD. The CLUE of the YRD increased from 0.65 million RMB per hectare in 2000 to 1.92 million and 2.60 million RMB per hectare in 2010 and 2020, respectively. The annual growth rate of CLUE (7.1%) was higher than that of the construction land area (3.2%). More than 95% of research units have experienced CLUE growth. These results indicate that the economic performance of construction land use in the YRD has been significantly improved since the early 2000s. However, the upper quartile of CLUE by county-level regions and the number of places with CLUE greater than five million RMB per hectare decreased from 2010 to 2020. Moreover, the standard deviation of CLUE by county-level regions increased from 0.89 in 2000 to 1.93 and 2.10 in 2010 and 2020, respectively. These results imply

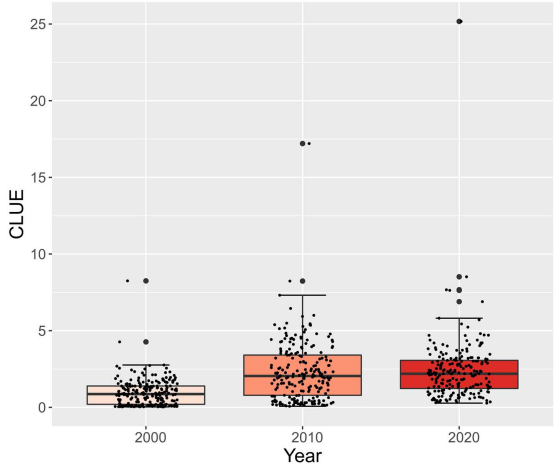

FIGURE 3
Boxplot of the changing trends of CLUE (million RMB per hectare) in the YRD in 2000, 2010, and 2020.

that the economic performance of construction land use might vary across regions in the YRD.

As Figure 4 illustrates, the spatial pattern of CLUE significantly changed over time in the YRD. Except for the central city of Shanghai and a few counties in Southern Zhejiang, CLUE of county-level regions in the YRD was relatively low in 2000. Particularly, CLUE in 50% of counties located in Anhui province and central and Northern Jiangsu was less than 0.3 million RMB per hectare. We observed a markable improvement of county-specific CLUE in 2010. CLUE improvements in central cities and counties in Shanghai, Southern Jiangsu, and Northern and Southwestern Zhejiang were the most prominent, while that of county-level regions in Northern Jiangsu and Northern Anhui was not obvious. In 2020, central cities of metropolises presented better performance of construction land use. CLUE of the central cities of Shanghai, Nanjing, Hangzhou, Hefei, Suzhou, and Wuxi all exceeded 5 million RMB per hectare. Figure 4 also shows that the GMI indexes were significantly positive and kept rising from 2000 to 2020. Moreover, the H-H county-level regions of CLUE were largely distributed in Shanghai, Southern Jiangsu, and Southwestern Zhejiang, while the L-L county-level regions were mainly located in Northern Jiangsu and Northern Anhui. These results signify that places with relatively higher or lower CLUE tended to spatially agglomerate in the YRD, which is largely associated with the spatial autocorrelation and spillover effect of land use practice at the regional scale.

Spatial clustering of construction land use efficiency changes

Figure 5 shows the results of the Hot Spot analysis based on CLUE increase or decrease by county-level regions in the YRD. Between 2000 and 2010, hot spots were largely located in Shanghai, Southern Jiangsu, and Southwestern Zhejiang, while cold spots were in Northern Jiangsu and Northern Anhui; CLUE of county-level regions located in Shanghai and Southern Jiangsu has increased by an average of 2 million RMB per hectare. Between 2010 and 2020, hot spots were mainly distributed in Shanghai, Hefei, and their surrounding regions, while cold spots were transferred to Southwestern Zhejiang and Southern Anhui; It is noteworthy that CLUE of some counties located in Southwestern YRD, which is an ecologically important and sensitive region, experienced a significant decline.

Comparing the increase or decrease of CLUE by county-level regions during 2000–2010 and 2010–2020, Figure 5C presents the spatial restructuring of CLUE changing clusters in the YRD. On the one hand, hot spots were mainly in the peripheral regions, especially Hefei, Northern Anhui, and Northern Jiangsu, signifying that CLUE improvement in the peripheral YRD was more markable during 2010–2020. On the other hand, cold spots were largely located in Southern Jiangsu, and Southern and Western Zhejiang, indicating that the growth rate of CLUE in suburban counties of major cities and ecologically sensitive regions was relatively low during 2010–2020. Some suburban counties of major cities (e.g., Nanjing, Suzhou, Hangzhou, and Ningbo) even experienced a decline in CLUE from 2010 to 2020, probably because industrial and population agglomeration in relevant suburbs were lower than expected under the rapid expansion of construction land. These results suggest that the hot spots of CLUE growth tend to shift from the core YRD and ecologically sensitive regions to central cities in the peripheral YRD since the early 2010s.

Regional group differences in construction land use efficiency

Figure 6 reports the differences in CLUE among eight groups, which are divided by the core YRD (central cities) and peripheral YRD (counties). The median, upper quartile, and lower quartile of CLUE in groups related to central cities showed a trend of continuing increase from 2000 to 2020. In contrast, the upper quartile of CLUE in other groups, especially the counties in the core YRD, underwent a significant decline from 2010 to 2020. Moreover, the average CLUE of the central cities in the core YRD was the highest, followed by that of the counties in the core YRD, while that of the counties in the peripheral YRD was the lowest. Although the average CLUE of the core and peripheral YRD has increased significantly, the gap in CLUE between the core and peripheral YRD doubled during 2000–2020. A similar result can be drawn from the comparison of CLUE between the central cities and counties. These results indicate that construction land use in the central cities shows better economic performance than that in the suburbs and peripheral counties, even more, this gap has been widening in the YRD since the early 2010s.

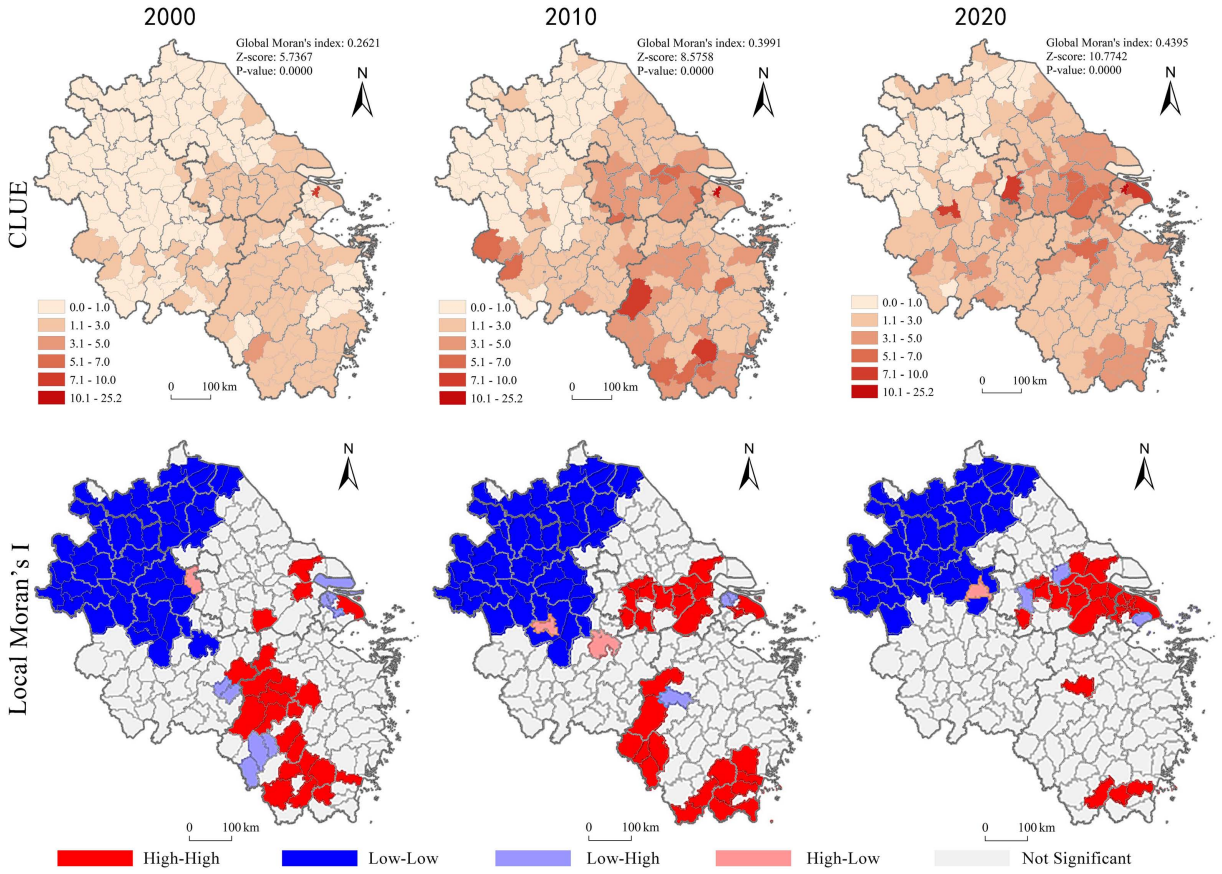

FIGURE 4
The spatial patterns of CLUE (million RMB per hectare) in the YRD in 2000, 2010, and 2020.

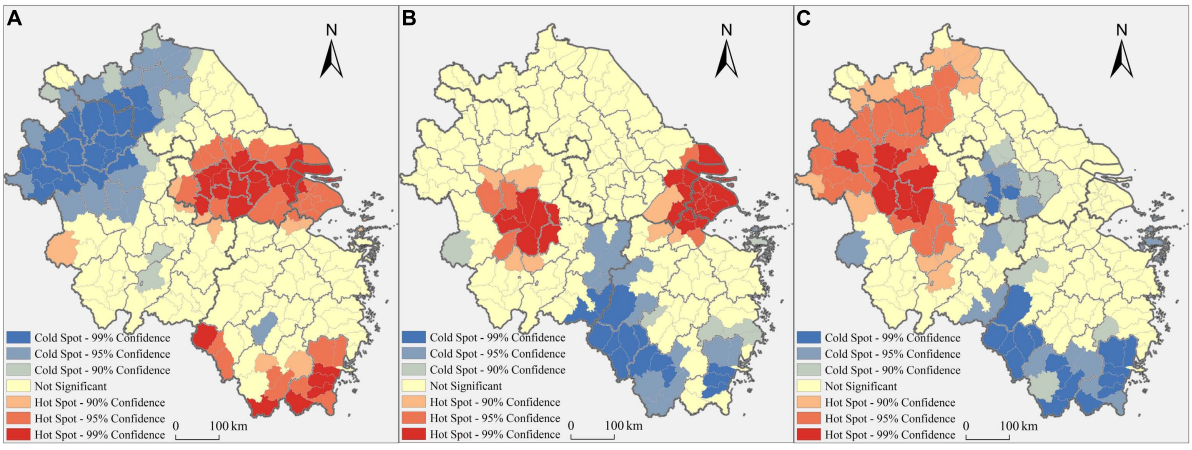

FIGURE 5
The spatial clusters of CLUE changes in the YRD from 2000 to 2020. **(A)** During 2000–2010. **(B)** During 2010–2020. **(C)** Annual changing differentials between the two periods.

With regard to the standard deviation of CLUE by research units, a trend of continuing growth can be found in the groups of the core YRD and the central cities, while the groups of the peripheral YRD and counties presented a rising trend at first and then fell from 2000 to 2020. Moreover, regional differences in CLUE between the central cities and counties within the core

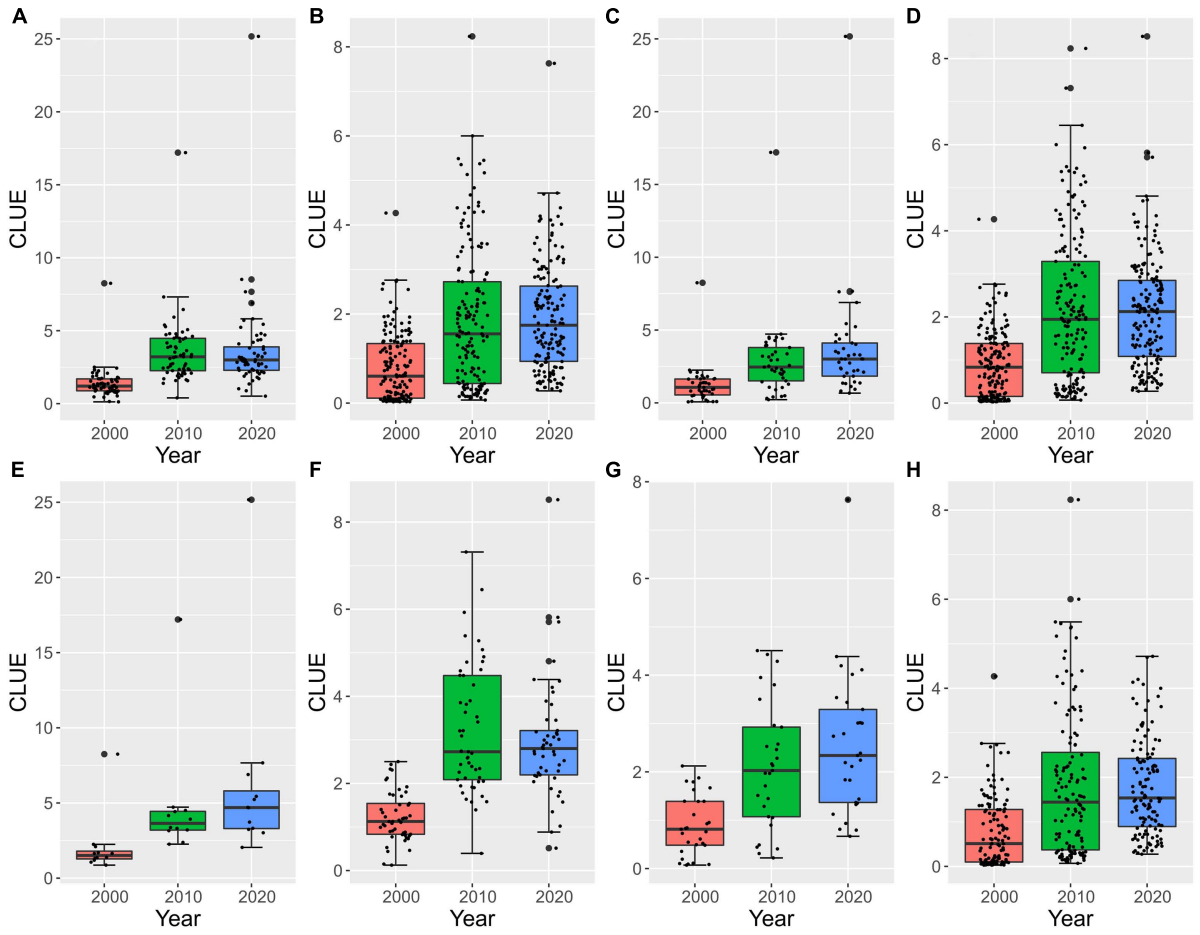

FIGURE 6
Regional group differences in CLUE (million RMB per hectare) in the YRD between 2000 and 2020. **(A)** The core YRD; **(B)** the peripheral YRD; **(C)** all central cities; **(D)** all counties; **(E)** all central cities in the core YRD; **(F)** all counties in the core YRD; **(G)** all central cities in the peripheral YRD; **(H)** all counties in the peripheral YRD.

YRD were more significant than that within the peripheral YRD during 2000–2020. These results indicate that interregional gaps of CLUE within the core YRD or the central cities have been widening, while that within the groups of the peripheral YRD or counties was the opposite since the early 2010s.

Driving forces of uneven construction land use efficiency in the Yangtze River Delta

Land use efficiency is largely affected by various exogenous factors (Lambin and Meyfroidt, 2011; Wang Q. et al., 2021; Zhang et al., 2022), indicating that spatial dependence of the error term should be taken in modeling. Insignificant coefficients for LM-lag or Robust LM-lag confirm that the estimated models of SEM have a higher fitting degree than that of SLM (see **Appendix A**). According to the results of the variance inflation factor (VIF), DEM and SLOP are put into the models separately to avoid the potential problems of multicollinearity. The regression results of OLS, SEM, and GWR models are presented in **Table 2**. On the one hand, the estimated coefficients and their signs of most variables changed over time, implying that the driving forces of CLUE are temporally heterogeneous. On the other hand, the median, maximum and minimum values of coefficients for each variable are different in GWR models (see **Appendix B**), signifying that the determinants of CLUE have significantly spatial heterogeneities.

Impacts of regional economic incentives and firm dynamics

The estimated results imply that regional disparities in economic development level and industrial structure play a vital role in the spatiotemporal variation of CLUE, which is in line with the findings documented by previous studies (Peng et al., 2017; Chen et al., 2019; Yu et al., 2019). The coefficients for PGDP are positive and significant in all models, indicating that construction land use in economically developed regions (e.g., central cities in the core YRD) might show better economic performance. Particularly, regional innovative milieu

TABLE 2 Regression results of OLS, SEM, and GWR models.

	2000			2010			2020		
	OLS	**SEM**	**GWR**	**OLS**	**SEM**	**GWR**	**OLS**	**SEM**	**GWR**
Constant/ intercept	−0.086 (−0.304)	0.531 (0.176)	−0.374 (−0.400)	−2.070 (−2.400*)	−0.532 (−0.599)	−0.625 (−0.908)	−6.800*** (−7.439***)	−6.287*** (−6.500***)	−3.265 (−3.754)
PGDP	0.334*** (0.325***)	0.318*** (0.316***)	2.284 (2.033)	1.797*** (1.781***)	1.727*** (1.734***)	6.150 (6.100)	1.829*** (1.855***)	1.749*** (1.764***)	3.595 (3.796)
IND	0.364* (0.345*)	0.414** (0.399**)	0.502 (0.468)	−0.325 (−0.368)	−0.238 (−0.313)	−0.353 (−0.333)	0.357 (0.348)	0.578 (0.446)	1.535 (1.562)
SERV	0.292 (0.275)	0.192 (0.190)	0.231 (0.170)	0.460 (0.413)	0.266 (0.185)	0.546 (0.484)	2.591*** (2.477***)	1.758** (1.676**)	2.840 (2.764)
FIRM	0.113*** (0.111***)	0.125*** (0.121***)	1.383 (3.894)	0.254*** (0.255***)	0.268*** (0.264***)	7.511 (10.876)	0.484*** (0.483***)	0.605*** (0.597***)	17.094 (17.097)
SCALE	0.337*** (0.342***)	0.328*** (0.332***)	1.053 (1.170)	0.385* (0.380)	0.208 (0.200)	1.238 (1.403)	0.104 (0.100)	0.032 (0.040)	0.724 (0.908)
KNOW	−0.166 (−0.168)	−0.315** (−0.301**)	−0.542 (−0.512)	0.255 (0.246)	0.001 (−0.019)	0.136 (0.071)	0.272 (0.259)	0.129 (0.121)	0.284 (0.055)
OWN	−0.046 (−0.018)	0.075 (0.078)	0.086 (0.048)	−0.278 (−0.279)	0.240 (0.234)	−0.771 (−1.131)	0.663*** (0.698***)	1.327*** (1.296***)	0.090 (−0.231)
ECO	0.986*** (0.727**)	0.622* (0.447)	0.916 (0.631)	1.858*** (1.693**)	1.105* (0.973)	1.719 (1.325)	2.558*** (2.253***)	2.295*** (2.242***)	1.911 (1.279)
DEM	0.063	0.051	0.350	0.423***	0.372***	1.866	0.251***	0.276**	−0.569
SLOP	(0.198***)	(0.186***)	(1.981)	(0.682***)	(0.581**)	(1.828)	(0.594***)	(0.471**)	(1.829)
ENV	−1.220*** (−0.853***)	−1.378*** (−0.976**)	−0.752 (−0.484)	−0.470 (−0.117)	−0.966 (−0.789)	−1.582 (−0.812)	0.390 (1.082**)	0.575 (0.867)	0.050 (1.843)
λ	/	0.458*** (0.438***)	/	/	0.559*** (0.559***)	/	/	0.748*** (0.728***)	/
R^2	0.655 (0.671)	0.694 (0.706)	0.773 (0.774)	0.668 (0.664)	0.725 (0.723)	0.806 (0.797)	0.785 0.791	0.854 0.852	0.912 (0.902)
F	39.27*** (42.23***)	/	/	41.61*** (40.95***)	/	/	75.70*** (78.25***)	/	/

***, **, *denote statistical significance at 1, 5, and 10% level, respectively. Regression results of models including the variable SLOP are presented in the parentheses. Regression coefficients for independent variables of GWR models are presented as the mean value in this table.

and technical progress are positively associated with place-specific CLUE (Chen et al., 2019). The effects of industrial structure and transition are mixed. The coefficients for IND and SERV are, respectively significantly and insignificantly positive in models for 2000, however, the results are opposite in models for 2020. This suggests that, concerning CLUE improvement, regional advantages in the service economy are more influential than the spatial agglomeration of the industrial economy in recent YRD. This is probably because industrial upgrading that local governments pursued has facilitated the transition of economic structure from industry-led to service-led, especially in central cities with relatively high CLUE, in the YRD since the early 2010s. Our finding tallies with the existing studies that highlighted the impacts of industrial agglomeration and transformation on land use efficiency (Chen et al., 2018; Liu J. et al., 2021).

Corporate demography, as well as spatial dynamics of individual firms, are valuable in explaining the spatiotemporal variation of CLUE at the regional scale. The coefficients for FIRM are significantly positive in all models, signifying that the spatial agglomeration of corporate organizations, activities, and functions is positively associated with relatively higher CLUE. The coefficients for SCALE are positive and significant in models for 2000, but insignificant in models for 2010 and 2020. This indicates that the spatial agglomeration of large firms could notably improve CLUE in the early 2000s, however, this relationship has become unclear since the early 2010s. This is partly because some counties, especially in ecologically sensitive regions, with few larger firms show relatively higher CLUE in the YRD. The coefficients for KNOW show positive signs in models for 2010 and 2020. This is partly because the spatial agglomeration of knowledge-intensive enterprises, which largely represents a stronger regional innovative capability, plays an increasingly important role in improving local CLUE. Therefore, a series of regulations related to pollution control and energy conservation have been carried out by local governments to facilitate the relocation of traditional manufacturers and inefficient firms, and then provide space for high-tech firms.

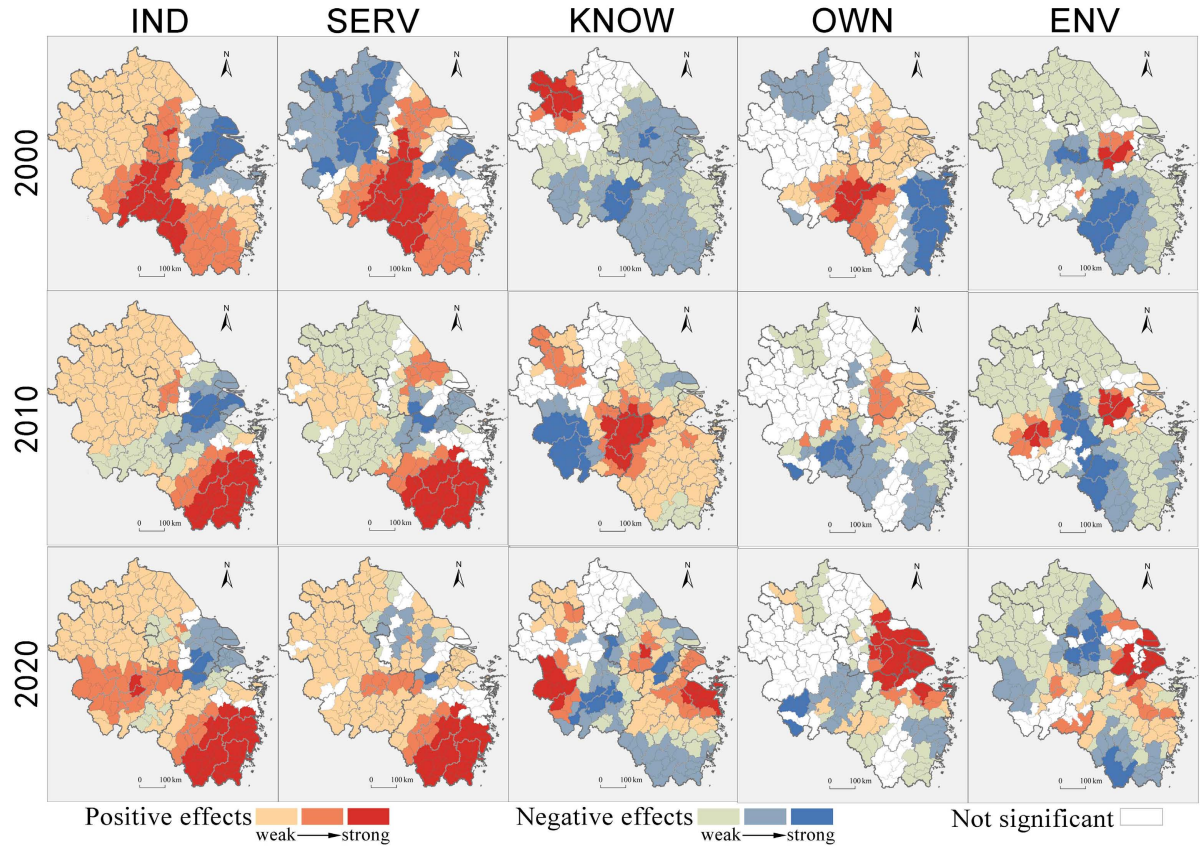

FIGURE 7
GWR estimated coefficients for independent variables in 2000, 2010, and 2020 (the estimated coefficients with *p*-values less than 0.1 are considered significant).

Furthermore, the coefficients for OWN are ambiguous in models for 2000 and 2010, but significantly positive in models for 2020. This may suggest that the spatial agglomeration of FIEs, which is closely related to the continuing opening up and export-oriented economic growth, will contribute to the improvement of CLUE in the YRD.

Impacts of regional ecological constraints and environmental regulations

The regression results suggest that regional ecological sensitivity and constraints are positively associated with the economic performance of construction land use in the YRD. The coefficients for ECO, DEM, and SLOP are significantly positive in most models, indicating that county-level regions with a larger proportion of ecological and cultivated land, as well as higher elevation and steeper slope, tend to have higher CLUE than other regions. It is acknowledged that, by prioritizing ecological benefits and green development, the Chinese government has issued a series of policies for pollution prevention, ecological restoration, and economic transition since the early 2010s. According to the national major function-oriented zoning, ecologically sensitive counties located in Southwestern YRD have been zoned for eco-environmental conservation and food production. Economic activities, especially those with negative impacts on the eco-environmental system, are limited or even prohibited in the planned ecological function and restricted development zones. Regional ecological constraints and strict regulations restrain urban sprawl and land expansion on one hand, and force local governments to efficiently use the limited construction land resources on the other hand. This is partly because, in addition to eco-environmental benefits, regional economic development and social welfare improvement still play an important role in the evaluation and promotion of local officials in China.

The coefficients for ENV are negative and significant in OLS and SEM models for the year 2000, indicating that the poor regional environmental quality is not conducive to improving CLUE. This result is consistent with the finding of Peng et al. (2017), who suggested that environmental pollution has a "crowding out effect" on urban land use efficiency. However, ENV's coefficients are insignificant in models for the years 2010 and 2020 and even appear positive signs. With the

aggravation of environmental deterioration, Chinese central and local governments have devoted substantial efforts to pursuing cleaner production and to reducing pollution since the early 2010s. A series of regulations related to resource conservation and intensive utilization have therefore been implemented, resulting in an increasing level of natural resources supervision and environmental stringency (Zhu et al., 2014; Wang K. et al., 2021). Our results indicate that rising environmental standards and regulations, particularly in developed regions and major cities, might weaken the "crowding out effect" of pollution on land use efficiency at the regional scale.

Spatial heterogeneity of influential factors and driving mechanisms

Considering the spatial clustering and spillover of uneven CLUE in the YRD, it is essential to examine the spatially heterogeneous effects of influential factors. **Figure 7** shows the changing spatial patterns of the estimated coefficients for independent variables, such as IND, SERV, KNOW, OWN, and ENV, in GWR models.

Expect for Shanghai and its neighboring regions, the local coefficients for IND are positive and significant. This implies that a larger proportion of the industrial economy in GDP would be positively associated with higher CLUE, especially in the peripheral YRD. Our findings suggest that promoting manufacturing agglomeration, as well as the undertaking of industrial transfer from developed regions, should be an important way for less-developed regions to improve land use efficiency. In contrast, the positive influence of SERV on CLUE has been increasingly strengthening across the YRD, particularly in Shanghai and its neighboring regions, since the early 2010s. This signifies that the higher CLUE in major cities is largely dependent on place-specific advantages in producer and consumer services. With the rapid expansion of urban residential and commercial land, local governments in major cities are concerned more about the critical role played by the service economy in improving CLUE. We can conclude that the impacts of economic structure on CLUE differ between developed and less-developed regions, which is related to their respective industrial restructuring paths.

Figure 7 presents that the negative coefficients for KNOW and the positive coefficients for OWN played a leading role in the YRD in 2000. At the early stage of industrialization in the YRD, traditional manufacturing, township industries, and low-value production dominated regional economic development, and advanced technologies and management experiences were mainly introduced or controlled by FIEs. The spatial agglomeration of FIEs might be positively associated with higher CLUE. Since the early 2010s, the number of county-level regions with positive coefficients for KNOW has increased significantly, especially in the core YRD. With the continuing industrial upgrading, the Chinese government has issued a series of incentive policies to support the promotion of strategic emerging industries and technical innovation. In addition to the service economy, the spatial agglomeration of knowledge-intensive industries is increasingly vital to CLUE improvement in the YRD. However, negative coefficients for KNOW and OWN can still be found in some peripheral counties, this is partly because the attraction of high-tech industries and high-quality FIEs in less-developed regions is largely limited by their location, agglomeration economies, and doing business environment.

Figure 7 shows that the negative effect of ENV on CLUE played a leading role in the peripheral YRD, especially in Northern Jiangsu, Southern Zhejiang, and Anhui province. This may indicate that environmental pollution has a stronger "crowding out effect" on the economic performance of construction land use in less-developed regions. Our findings suggest that promoting economic development and improving CLUE in less-developed regions cannot be at the expense of ecosystem and environmental quality. "Left behind" regions should avoid becoming pollution heavens when undertaking industrial transfer from developed regions. In contrast, the positive effect of ENV played a leading role in the core YRD, especially in cities (e.g., Suzhou, Wuxi, and Shanghai) with relatively higher CLUE. The increasing pollution problems in major cities enforce environmental regulations and standards more stringent, which could effectively facilitate technical innovation, clean production, and intensive utilization of natural resources at the firm- and regional level.

Discussion and conclusion

Discussion

Construction land expansion and use efficiency are tied to the promotion of sustainable cities and communities around the world (UN-Habitat, 2016; Akuraju et al., 2020; Estoque et al., 2021). Although there is a large body of literature on the driving forces and implications of the spatiotemporal variation of CLUE, however, we know little about how socioeconomic contexts and eco-environmental constraints work together for CLUE at a finer geographical scale. Particularly, previous studies paid insufficient attention to the impacts of economic incentives at the micro-level, such as the spatial dynamics of individual firms, on local land use efficiency. Urbanization, economic development, and corporate strategy in emerging economies (e.g., China) will predict a substantial transition in the near future (Zhu et al., 2014; Chen et al., 2016; Tang et al., 2021), and how changes in economic dynamics and eco-environmental regulations affect land use practice and performance in relevant countries or regions will deserve more scholarly investigation.

Focusing on the aforementioned research gaps, this study will contribute to the literature on land use efficiency in the following aspects. First, a conceptual framework of

the spatiotemporal variation of construction land expansion and use efficiency in transitional China is developed, with particular attention to regional eco-environmental constraints and regulations, as well as economic incentives driven by firm-specific changes. By highlighting the direct influences of regional corporate demography and the spatial dynamics of firms on CLUE, this study will advance our understanding of the microcosmic dynamics underlying the relationships between economic incentives and land use efficiency. Our conceptual framework can provide an alternative and effective theoretical perspective for relevant research, especially on land use transition in emerging economies. Second, this study examines the changing "core-periphery" pattern of CLUE at the sub-national scale through distinguishing the central city and suburban county. Uncovering the spatiotemporal variation of CLUE at a finer geographical scale, this study might be an important supplement to the existing studies that focus on global, national, provincial, and urban scales. Third, taking the YRD, one of the emerging global city-regions in the Global South, as a case, this article discusses the changes in construction land use practice and performance under new-type urbanization and economic transition during the past three decades. Such empirical research and related evidence can assist in uncovering the driving forces of uneven CLUE in places within extensive emerging economies or global city-regions, which calls for more attention from scholars and policy-makers.

Our findings can also generate several policy implications for improving CLUE under sustainable urbanization in China and other emerging economies. First, the central cities of metropolises, as well as developed regions, should promote urban renewal and stock construction land vitalization to provide sufficient space for the "new economy" and knowledge-intensive firms. Second, with the rapid expansion of construction land, urban suburbs should actively facilitate population and industrial agglomeration to avoid the inefficient sprawl of built-up areas. Third, in the process of improving CLUE, the peripheral and less-developed regions should not only promote the spatial agglomeration of manufacturing industries but also control pollution resulting from undertaking industrial transfer through implementing proper regulations. Additionally, incentive policies to encourage the development of pollution-free and low-carbon industries should be issued by ecologically sensitive regions to improve the economic performance of construction land use.

This article has twofold limitations. On the one hand, this article only examines the effects of eco-spatial area, elevation, and slope, a few facets of the regional ecological system, on uneven CLUE. The role played by other facets that can embody regional ecological importance and sensitivity need more research attention. Regional disparities in the strength of resources supervision and environmental regulation are difficult to quantify, and their influences on uneven CLUE have not been investigated in this study. On the other hand, our analysis did not distinguish the difference in use efficiency between construction land in urbanized areas, small towns, and villages due to data availability. The regression models did not include variables that directly measure technological progress due to the lack of relevant data (e.g., patent and R&D) at the county-level in 2000. Data constraints also force us to measure regional corporate demography only by the number of corporate organizations rather than output value. We leave these issues for future studies.

Conclusion

This article examines the spatiotemporal variation of CLUE and its driving forces in the YRD, China. We depicted the changing spatial pattern, including spatial clustering and regional group differences, of CLUE between 2000 and 2020. Then, temporal and spatial heterogeneities of the impacts of economic incentives and eco-environmental constraints on uneven CLUE have been measured in the YRD.

The descriptive results indicate that, with rapid industrialization and urbanization, CLUE in the YRD has increased significantly since the early 2000s. It should be noted that the CLUE and its changing trends and magnitudes differ across county-level regions. The CLUE in the central cities, especially those located in the core YRD, is higher than that in peripheral counties, indicating a significant "core-periphery" spatial pattern. County-level regions with remarkable improvement of CLUE have been increasingly concentrated in the central cities of major cities. The efficiency gap in construction land use between the core and peripheral YRD, as well as the central cities and suburban counties, has widened since the early 2010s. It is also found that the economic performance of construction land use in some counties located in Southwestern Zhejiang and Southwestern Anhui, which are ecologically sensitive regions, is relatively better. Furthermore, the improvement of CLUE in peripheral regions such as Northern Jiangsu and Northern Anhui from 2010 to 2020 was more markable than that during 2000–2010, but it was the opposite in Southwestern Zhejiang. To some extent, these trends will restructure the "core-periphery" pattern of CLUE in the YRD.

The regression results signify that uneven CLUE is closely associated with spatiotemporal heterogeneities in socioeconomic contexts and eco-environmental constraints across the YRD. On the one hand, regional disparities in economic incentives, such as economic level, industrial transformation, and firm-specific dynamics, are the main drivers of the spatiotemporal variation of CLUE. The spatial agglomeration of the "new economy" and capable corporations, especially service industries, knowledge-intensive firms, and FIEs, have been playing an increasingly important role in improving CLUE since the early 2010s. On the other hand, factors related to regional ecological constraints show positive

effects on CLUE. We can conclude that regional ecological constraints (e.g., large eco-spatial area, high elevation, and steep slope) severely restrict the expansion of the urban built-up area, but this forces local governments and market entities to make efficient use of the limited construction land resources. Furthermore, the modeling results imply that the influences of driving forces, such as industrial structure and environmental quality, vary across regions. The positive effects of service and knowledge-intensive industries, as well as FIEs, on CLUE are strengthening in the core YRD, while CLUE improvement in the peripheral YRD will rely more on the continuing growth of manufacturing industries. We also find a stronger "crowding out effect" of environmental pollution on CLUE in the peripheral YRD, however, this relationship does not exist in most county-level regions located in the core YRD.

Data availability statement

The raw data supporting the conclusions of this article will be made available by the authors, without undue reservation.

Author contributions

JW and WS designed the research. JW drafted and revised the manuscript. JW and CL analyzed the data and prepared figures. WS discussed the results and revised the manuscript. All authors contributed to the article and approved the submitted version.

Funding

This research was funded by the National Natural Science Foundation of China (grant number: 41871119), and Jiangsu R&D Special Fund for Carbon Peaking and Carbon Neutrality (grant number: BK20220014).

Conflict of interest

The authors declare that the research was conducted in the absence of any commercial or financial relationships that could be construed as a potential conflict of interest.

Publisher's note

All claims expressed in this article are solely those of the authors and do not necessarily represent those of their affiliated organizations, or those of the publisher, the editors and the reviewers. Any product that may be evaluated in this article, or claim that may be made by its manufacturer, is not guaranteed or endorsed by the publisher.

References

Akuraju, V., Pradhan, P., Haase, D., Kropp, J. P., and Rybski, D. (2020). Relating SDG11 indicators and urban scaling – An exploratory study. *Sustain. Cities Soc.* 52:101853. doi: 10.1016/j.scs.2019.101853

Bryan, B. A., Crossman, N. D., Nolan, M., Li, J., Navarro, J., Connor, J. D., et al. (2015). Land use efficiency: Anticipating future demand for land-sector greenhouse gas emissions abatement and managing trade-offs with agriculture, water, and biodiversity. *Glob. Change Biol.* 21, 4098–4114. doi: 10.1111/gcb.13020

Capasso, M., Stam, E., and Cefis, E. (2015). Industrial dynamics and economic geography. *Region. Stud.* 49, 5–9. doi: 10.1080/00343404.2014.982440

Carroll, G. R., and Hannan, M. T. (2000). Why corporate demography matters: Policy implications of organizational diversity. *Calif. Manag. Rev.* 42, 148–163. doi: 10.2307/41166046

Chen, M., Liu, W., and Lu, D. (2016). Challenges and the way forward in China's new-type urbanization. *Land Use Policy* 55, 334–339. doi: 10.1016/j.landusepol.2015.07.025

Chen, W., Chen, W., and Ning, S. (2019). Exploring the industrial land use efficiency of China's resource-based cities. *Cities* 93, 215–223. doi: 10.1016/j.cities.2019.05.009

Chen, W., Shen, Y., Wang, Y., and Wu, Q. (2018). The effect of industrial relocation on industrial land use efficiency in China: A spatial econometrics approach. *J. Clean. Product.* 205, 525–535. doi: 10.1016/j.jclepro.2018.09.106

Cheung, K., and Ping, L. (2004). Spillover effects of FDI on innovation in China: Evidence from the provincial data. *China Econ. Rev.* 15, 25–44. doi: 10.1016/S1043-951X(03)00027-0

Dong, Y., Jin, G., and Deng, X. (2020). Dynamic interactive effects of urban land-use efficiency, industrial transformation, and carbon emissions. *J. Clean. Product.* 270:122547. doi: 10.1016/j.jclepro.2020.122547

Estoque, R. C., Ooba, M., Togawa, T., and Hijioka, Y. (2021). Monitoring global land-use efficiency in the context of the UN 2030 agenda for sustainable development. *Habitat Int.* 115:102403. doi: 10.1016/j.habitatint.2021.102403

Fetzel, T., Niedertscheider, M., and Haberl, H. (2016). Patterns and changes of land use and land-use efficiency in Africa 1980–2005: An analysis based on the human appropriation of net primary production framework. *Region. Environ. Change* 16, 1507–1520. doi: 10.1007/s10113-015-0891-1

Gao, J., Wei, Y. D., and Chen, W. (2014). Economic transition and urban land expansion in provincial China. *Habitat Int.* 44, 461–473. doi: 10.1016/j.habitatint.2014.09.002

Gao, X., Zhang, A., and Sun, Z. (2020). How regional economic integration influence on urban land use efficiency? A case study of Wuhan metropolitan area, China. *Land Use Policy* 90:104329. doi: 10.1016/j.landusepol.2019.104329

He, S., Yu, S., and Li, G. (2020). Exploring the influence of urban form on land-use efficiency from a spatiotemporal heterogeneity perspective: Evidence from 336 Chinese citie. *Land Use Policy* 95:104576. doi: 10.1016/j.landusepol.2020.104576

Jiao, L., Xu, Z., and Xu, G. (2020). Assessment of urban land use efficiency in China: A perspective of scaling law. *Habitat Int.* 99:102172. doi: 10.1016/j.habitatint.2020.102172

Jun, C., Ban, Y., and Li, S. (2014). Open access to earth land-cover map. *Nature* 514, 434–434. doi: 10.1038/514434c

Koroso, N. H., Zevenbergen, J. A., and Lengoiboni, M. (2020). Urban land use efficiency in Ethiopia: An assessment of urban land use sustainability in Addis Ababa. *Land Use Policy* 99:105081. doi: 10.1016/j.landusepol.2020.105081

Lambin, E. F., and Meyfroidt, P. (2010). Land use transitions: Socio-ecological feedback versus socio-economic change. *Land Use Policy* 27, 108–118. doi: 10.1016/j.landusepol.2009.09.003

Lambin, E. F., and Meyfroidt, P. (2011). Global land use change, economic globalization, and the looming land scarcity. *Proc. Natl. Acad. Sci. U.S.A.* 108, 3465–3472. doi: 10.1073/pnas.1100480108

Li, Q., Wang, Y., and Chen, W. (2021). Does improvement of industrial land use efficiency reduce PM2. 5 pollution? Evidence from a spatiotemporal analysis of China. *Ecol. Indic.* 132:108333. doi: 10.1016/j.ecolind.2021.108333

Liu, J., Hou, X., and Wang, Z. (2021). Study the effect of industrial structure optimization on urban land-use efficiency in China. *Land Use Policy* 105:105390. doi: 10.1016/j.landusepol.2021.105390

Liu, J., Li, J., and Qin, K. (2017). Changes in land-uses and ecosystem services under multi-scenarios simulation. *Sci. Total Environ.* 586, 522–526. doi: 10.1016/j.scitotenv.2017.02.005

Liu, S., Lin, Y., and Ye, Y. (2021). Spatial-temporal characteristics of industrial land use efficiency in provincial China based on a stochastic frontier production function approach. *J. Clean. Product.* 295:126432. doi: 10.1016/j.jclepro.2021.126432

Liu, X., Huang, Y., and Xu, X. (2020). High-spatiotemporal-resolution mapping of global urban change from 1985 to 2015. *Nat. Sustain.* 3, 564–570. doi: 10.1038/s41893-020-0521-x

Liu, Y., Fang, F., and Li, Y. (2014). Key issues of land use in China and implications for policy making. *Land Use Policy* 40, 6–12. doi: 10.1016/j.landusepol.2013.03.013

Lu, X., Kuang, B., and Li, J. (2018). Regional difference decomposition and policy implications of China's urban land use efficiency under the environmental restriction. *Habitat Int.* 77, 32–39. doi: 10.1016/j.habitatint.2017.11.016

Mahtta, R., Fragkias, M., Güneralp, B., Mahendra, A., Reba, M., Wentz, E. A., et al. (2022). Urban land expansion: the role of population and economic growth for 300+ cities. *NPJ Urban Sustain.* 2:5. doi: 10.1038/s42949-022-00048-y

Masini, E., Tomao, A., Barbati, A., Corona, P., Serra, P., Salvati, L., et al. (2019). Urban Growth, Land-use Efficiency and Local Socioeconomic Context: A comparative analysis of 417 Metropolitan Regions in Europe. *Environ. Manag.* 63, 322–337. doi: 10.1007/s00267-018-1119-1

Ning, Q., Ouyang, X., and Liu, S. (2022). Spatio-temporal evolution and quality analysis of construction land in urban agglomerations in central China. *Front. Ecol. Evolut.* 10:912127. doi: 10.3389/fevo.2022.912127

Peng, C., Xiao, H., Liu, Y., and Zhang, J. (2017). Economic structure and environmental quality and their impact on changing land use efficiency in China. *Front. Earth Sci.* 11, 372–384. doi: 10.1007/s11707-016-0596-x

Rahman, M. M., and Szabó, G. (2021). Multi-objective urban land use optimization using spatial data: A systematic review. *Sustain. Cities Soc.* 74:103214. doi: 10.1016/j.scs.2021.103214

Schiavina, M., Melchiorri, M., Freire, S., Florio, P., Ehrlich, D., Tommasi, P., et al. (2022). Land use efficiency of functional urban areas: Global pattern and evolution of development trajectories. *Habitat Int.* 123:102543. doi: 10.1016/j.habitatint.2022.102543

Searchinger, T. D., Wirsenius, S., Beringer, T., and Dumas, P. (2018). Assessing the efficiency of changes in land use for mitigating climate change. *Nature* 564, 249–253. doi: 10.1038/s41586-018-0757-z

Tahir, M., Hayat, A., Rashid, K., Afridi, M. A., and Tariq, Y. B. (2020). Human capital and economic growth in OECD countries: some new insights. *J. Econ. Administ. Sci.* 36, 367–380. doi: 10.1108/JEAS-07-2019-0073

Tang, Y., Wang, K., Ji, X., Xu, H., and Xiao, Y. (2021). Assessment and spatial-temporal evolution analysis of urban land use efficiency under green development orientation: Case of the Yangtze River Delta Urban Agglomerations. *Land* 10:715. doi: 10.3390/land10070715

Tu, F., Yu, X., and Ruan, J. (2014). Industrial land use efficiency under government intervention: Evidence from Hangzhou, China. *Habitat Int.* 43, 1–10. doi: 10.1016/j.habitatint.2014.01.017

UN-Habitat (2016). *Indicator 11.3.1: Ratio of land consumption rate to population growth rate*. Kenya: UN-Habitat.

van Donkelaar, A., Hammer, M. S., Bindle, L., Brauer, M., Brook, J. R., Garay, M. J., et al. (2021). Monthly global estimates of fine particulate matter and their uncertainty. *Environ. Sci. Technol.* 55, 15287–15300. doi: 10.1021/acs.est.1c05309

Wang, K., Li, G., and Liu, H. (2021). Does natural resources supervision improve construction land use efficiency: Evidence from China. *J. Environ. Manag.* 297:113317. doi: 10.1016/j.jenvman.2021.113317

Wang, Q., Wang, Y., Chen, W., Zhou, X., and Zhao, M. (2021). Factors affecting industrial land use efficiency in China: Analysis from government and land market. *Environ. Devel. Sustain.* 23, 10973–10993. doi: 10.1007/s10668-020-01100-6

Wu, C., Wei, Y. D., Huang, X., and Chen, B. (2017). Economic transition, spatial development and urban land use efficiency in the Yangtze River Delta China. *Habitat Int.* 63, 67–78. doi: 10.1016/j.habitatint.2017.03.012

Wu, Y., Luo, J., Zhang, X., and Skitmore, M. (2016). Urban growth dilemmas and solutions in China: Looking forward to 2030. *Habitat Int.* 56, 42–51. doi: 10.1016/j.habitatint.2016.04.004

Xie, X., Fang, B., Xu, H., He, S., and Li, X. (2021). Study on the coordinated relationship between Urban Land use efficiency and ecosystem health in China. *Land Use Policy* 102:105235. doi: 10.1016/j.landusepol.2020.105235

Yang, D., Lou, Y., Zhang, P., and Jiang, L. (2022). Spillover effects of built-up land expansion under ecological security constraint at multiple spatial scales. *Front. Ecol. Evolut.* 10:907691. doi: 10.3389/fevo.2022.907691

Yu, J., Zhou, K., and Yang, S. (2019). Land use efficiency and influencing factors of urban agglomerations in China. *Land Use Policy* 88:104143. doi: 10.1016/j.landusepol.2019.104143

Yue, L., Miao, J., Ahmad, F., Draz, M. U., Guan, H., Chandio, A. A., et al. (2022). Investigating the role of international industrial transfer and technology spillovers on industrial land production efficiency: Fresh evidence based on directional distance functions for Chinese provinces. *J. Clean. Product.* 340:130814. doi: 10.1016/j.jclepro.2022.130814

Zhang, W., Wang, B., Wang, J., Wu, Q., and Dennis Wei, Y. (2022). How does industrial agglomeration affect urban land use efficiency? A spatial analysis of Chinese cities. *Land Use Policy* 119:106178. doi: 10.1016/j.landusepol.2022.106178

Zhang, X., Lu, X., Chen, D., Zhang, C., Ge, K., Kuang, B., et al. (2021). Is environmental regulation a blessing or a curse for China's urban land use efficiency? Evidence from a threshold effect model. *Growth Change* 52, 265–282. doi: 10.1111/grow.12465

Zhu, S., He, C., and Liu, Y. (2014). Going green or going away: Environmental regulation, economic geography and firms' strategies in China's pollution-intensive industries. *Geoforum* 55, 53–65. doi: 10.1016/j.geoforum.2014.05.004

Zhu, X., Li, Y., and Zhang, P. (2019). Temporal–spatial characteristics of urban land use efficiency of China's 35mega cities based on DEA: Decomposing technology and scale efficiency. *Land Use Policy* 88:104083. doi: 10.1016/j.landusepol.2019.104083

10.3389/fevo.2022.1017728

Appendix

Appendix A Results of lagrange multiplier test.

	2000		2010		2020	
	Model 1	Model 2	Model 1	Model 2	Model 1	Model 2
Lagrange multiplier (lag)	2.170	1.874	5.279**	7.519***	2.349	1.176
Robust LM (lag)	1.802	1.667	1.107	0.403	33.478***	27.405***
Lagrange multiplier (error)	10.581***	9.619***	16.245***	17.347***	26.791***	25.386***
Robust LM (error)	10.213***	9.412***	12.073***	10.231***	57.918***	51.615***

*** and ** denote statistical significance at 1 and 5% level, respectively. Model 1 includes the variable DEM, and Model 2 includes the variable SLOP.

Appendix B Descriptive statistics of the estimated coefficients for variables in GWR.

Variable	2000			2010			2020		
	Max	Min	Med	Max	Min	Med	Max	Min	Med
Intercept	1.930 (0.761)	−4.718 (−4.540)	−0.541 (−0.406)	11.623 (10.049)	−5.171 (−5.063)	−1.589 (−1.796)	19.082 (4.875)	−7.743 (−7.855)	−2.912 (−3.128)
PGDP	4.927 (3.616)	0.300 (0.347)	2.143 (2.064)	9.752 (9.476)	2.596 (3.808)	5.971 (5.981)	7.389 (6.553)	0.629 (1.740)	3.604 (3.841)
IND	2.058 (1.903)	−1.963 (−1.370)	0.506 (0.412)	6.029 (5.170)	−16.753 (−15.21)	0.537 (0.419)	7.441 (5.886)	−21.443 (−8.070)	1.595 (1.497)
SERV	1.587 (1.475)	−0.530 (−0.616)	0.105 (0.082)	7.685 (7.129)	−12.346 (−11.32)	−0.078 (−0.328)	10.621 (9.414)	−19.446 (−4.162)	1.812 (1.707)
FIRM	13.361 (15.251)	−21.727 (−17.60)	1.182 (5.135)	28.389 (38.844)	−40.600 (−34.84)	10.971 (11.112)	32.955 (31.582)	0.886 (1.875)	16.833 (15.281)
SCALE	2.575 (2.572)	−0.574 (−0.369)	1.205 (1.272)	5.07 1 (6.163)	−3.449 (−2.897)	1.081 (1.365)	8.084 (5.754)	−5.064 (−2.846)	0.625 (0.621)
KNOW	0.617 (0.527)	−2.043 (−1.854)	−0.634 (−0.652)	3.170 (2.950)	−4.366 (−4.178)	0.247 (0.083)	3.914 (1.847)	−1.365 (−1.615)	0.142 (0.170)
OWN	2.458 (1.608)	−1.630 (−1.175)	0.097 (−0.021)	2.592 (1.466)	−6.815 (−9.522)	−0.741 (−0.851)	6.731 (5.498)	−9.520 (−10.68)	−0.503 (−0.764)
ECO	4.068 (3.428)	−1.927 (−2.397)	1.199 (0.974)	6.085 (6.014)	−6.100 (−4.207)	1.831 (1.950)	5.538 (5.054)	−0.957 (−2.363)	2.046 (1.899)
DEM	7.115	−5.509	0.871	20.433	−13.494	2.455	18.431	−57.254	1.461
SLOP	(4.471)	(0.276)	(1.435)	(6.266)	(−4.062)	(1.576)	(6.375)	(−6.722)	(2.221)
ENV	0.951 (1.273)	−3.260 (−2.095)	−0.488 (−0.511)	3.610 (3.815)	−9.852 (−5.762)	−1.235 (−0.647)	7.350 (7.205)	−5.599 (−3.470)	−0.579 (1.398)
RSS	39.030 (38.869)			158.014 (165.717)			84.728 (94.887)		
Sigma	0.423 (0.423)			0.851 (0.872)			0.623 (0.660)		
CV	356.066 (221.106)			413.789 (399.741)			428.736 (399.066)		
R^2	0.773 (0.774)			0.806 (0.797)			0.912 (0.902)		

Estimated coefficients of models including the variable SLOP are presented in the parentheses.

frontiers | Frontiers in Ecology and Evolution

TYPE Review
PUBLISHED 04 November 2022
DOI 10.3389/fevo.2022.1018581

Check for updates

OPEN ACCESS

EDITED BY
Jun Yang,
Northeastern University, China

REVIEWED BY
Wei Zhang,
Sichuan University, China
Bingjie Yu,
Southwest Jiaotong University, China

*CORRESPONDENCE
Yan Wang
wangyan@scac.edu.cn

SPECIALTY SECTION
This article was submitted to Environmental Informatics and Remote Sensing, a section of the journal Frontiers in Ecology and Evolution

RECEIVED 13 August 2022
ACCEPTED 06 October 2022
PUBLISHED 04 November 2022

CITATION
Ao Y, Li M, Ding X, Zheng J, Xiao S, Deng S, Zhang Z, Wang Y, Wang T and Martek I (2022) Built environment and travel behavior in rural areas: A scientometric literature review. *Front. Ecol. Evol.* 10:1018581. doi: 10.3389/fevo.2022.1018581

COPYRIGHT
© 2022 Ao, Li, Ding, Zheng, Xiao, Deng, Zhang, Wang, Wang and Martek. This is an open-access article distributed under the terms of the Creative Commons Attribution License (CC BY). The use, distribution or reproduction in other forums is permitted, provided the original author(s) and the copyright owner(s) are credited and that the original publication in this journal is cited, in accordance with accepted academic practice. No use, distribution or reproduction is permitted which does not comply with these terms.

Built environment and travel behavior in rural areas: A scientometric literature review

Yibin Ao[1,2], Mingyang Li[2], Xuan Ding[1], Junjie Zheng[1], Shan Xiao[1], Shulin Deng[1], Zijun Zhang[1], Yan Wang[3]*, Tong Wang[4] and Igor Martek[5]

[1]College of Environment and Civil Engineering, Chengdu University of Technology, Chengdu, China, [2]College of Management Science, Chengdu University of Technology, Chengdu, China, [3]Department of Engineering Management, Sichuan College of Architectural Technology, Chengdu, China, [4]Delft University of Technology, Delft, Netherlands, [5]School of Architecture and Built Environment, Faculty of Science, Engineering and Built Environment, Deakin University, Geelong, VIC, Australia

With the rise of global urbanization, the rural built environment has undergone tremendous changes. As such, the rural built environment impacts on residents' daily travel behavior is getting more researchers' attention. To date, most of the research focuses on urban areas in developed countries. To understand the state-of-the-art of interplay between the rural built environment and travel behaviors and to identify future research directions, this study adopts a science mapping approach to identify the relevant topics, authors, journals, and countries of the research done. This study proceeds through bibliometric retrieval of articles from 2005, followed by scientometric analysis and qualitative discussion. 37 documents are found to compare urban and rural domains, with 28 on the rural built environment. Research gaps and the research trends are discussed, of which the main themes are multi-dimensional correlation comparison of rural transportation service systems and emerging transportation modes, the influence of rural social and cultural factors on travel behavior, and low-carbon sustainable transportation. This review provides empirical foundation for current state-of-the-art and identifies the future research directions, specifically for rural built environment impact on travel behavior.

KEYWORDS

rural built environment, travel behavior, science mapping, scientometric analysis, literature review

Introduction

In recent years, with the incessant improvement of people's living standards and the extensive diversification of lifestyles, the travel behavior of residents, along with the traffic problems, attract researchers' attention (Sun et al., 2017). Though studies of urban travel behavior have been performed (Chen and Gan, 2014; Wang and Zhou, 2017; Yang et al., 2021a,b, 2022b), rural areas remain often neglected (Wang et al., 2019; Ao et al., 2020). In the

context of global urbanization, rural conditions have undergone tremendous changes, profoundly affecting the 3.4 billion rural residents worldwide (Doloi et al., 2018; Ao et al., 2021). Therefore, it is necessary to conduct a comprehensive review of the research on the rural built environment and residents' daily travel behavior from relevant authors, topics, and countries' perspectives, to provide a complete and systematic understanding of the studied and emerging topics such that future research can be formulated to support stakeholders in their decision-making processes.

Literature reviews are a good approach to getting a deeper understanding of a research field (He et al., 2017). As such, this study attempts to find out and analyze the relevant research focusing on the rural built environment and residents' travel behavior, to provide a comprehensive and systematic description of research trends. The science mapping approach will be applied which aims to establish bibliometric maps of specific disciplines and research fields (Cobo et al., 2011), including bibliometric literature search and scientometric analysis (Hosseini et al., 2018). Based on the extracted data, the emerging research topics, the most influential journals, scholars, and countries in the domain of rural built environment and residents' travel behavior are presented in the form of a visual network diagram, which reduces subjective bias and makes the analysis objective, and explicit.

The contributions of this study to the research field of the rural built environment and residents' travel behavior are as follows: (1) High-frequency keywords related to the rural built environment and travel behavior are extracted and analyzed from literature samples. (2) High-impact articles and scholars related to the rural built environment and travel behavior are presented. (3) This paper points out the shortcomings and gaps of the existing research and proposes future research trends.

The remainder of this article is organized as follows. Section "Methodology" describes a holistic review approach. Section "Results of scientometric analysis" presents the preliminary findings from science mapping. Section "Discussion" expands the science mapping approach to reason the factors affecting the travel behavior of rural residents, as well as the research gaps and trends in this field. Section "Conclusion" summarizes this study.

Methodology

This study proceeds through bibliometric retrieval of articles from 2005, followed by scientometric analysis and qualitative discussion The overall workflow is illustrated in Figure 1, which shows the whole science mapping approach.

Bibliometric search

The literature in the domain of rural built environment and travel behavior is retrieved from the Web of Science. It is known that the Web of Science combines a traditional citation index with advanced web technology, along with multiple and unique functions which accurately retrieve targeted literature. This study conducted two rounds of literature searches using the Web of Science. The rule for the first round is TS = ("built environment" OR "physical environment" OR infrastructure OR neighborhood) AND TS = (rural OR village) And TS = ("travel behavior" OR mobility OR "travel behavior") NOT TS = ("urban village"). As this review aims to serve the planning and travel behavior field, some irrelevant directions such as Agriculture, Physiology, and Biodiversity were excluded. After that, 455 records were selected. Generally speaking, the first round of search is enough, but considering the comprehensiveness of the search results, TS = ("travel behavior" OR mobility OR "travel behavior") NOT TS = ("urban village") was changed to TS = (travel) and then the second round of search was conducted. So The rule for the second round is TS = ("built environment" OR "physical environment" OR infrastructure OR neighborhood) AND TS = (rural OR village) AND TS = (travel), excluding the research directions of Food Science Technology, Geology, Pharmacology and so on, and 398 records were retrieved. The researchers imported the twice search results into Endnote software and screened out 100 duplicate records, thus the duplication rate was about 13.28%. So using the Web of Science search engine, 753 journal articles were identified by a two keyword-based bibliometric search, with duplicate journal articles being removed. A further detailed reading of the titles and abstracts of the articles resulted in the exclusion of 570 other articles. For example, although two studies by Jiao et al. (2017) and Gieling et al. (2019) focus on rural areas, the former was a study on the livelihood strategies of rural families (Jiao et al., 2017), while the latter explored the influence of different forms of rural attachment on local volunteer services (Gieling et al., 2019). Similarly, while Wolny et al. (2019) and Balestrieri and Congiu (2017) both explored the impact of rural road accessibility on the rural economy, they do so without reference to rural residents' travel behavior (Balestrieri and Congiu, 2017; Wolny et al., 2019). Finally, reading the remaining literature in full resulted in some further eliminations for the theme mainly on the spatial reconstruction of rural areas, the integration of land resources, or utilization efficiency (Wang et al., 2016; Bu et al., 2020), and no reference was made to the rural built environment and travel behavior. Thus, another 118 journal articles were excluded. Ultimately, the final number of journal articles that formed the database for this review study settled at 65.

Science mapping

VOSviewer is a text-mining tool developed by Van Eck and Waltman for analyzing and visualizing the bibliometric network in this study (Van Eck, 2010). This was done to reach the following goals: (1) Loading the literature samples downloaded from the Web of Science; (2) Visualizing, calculating, and analyzing the influence of core journals, scholars, and countries in the field of the rural built environment and residents' travel behavior research; (3) Researching the mainstream research keywords and their inter-relationships.

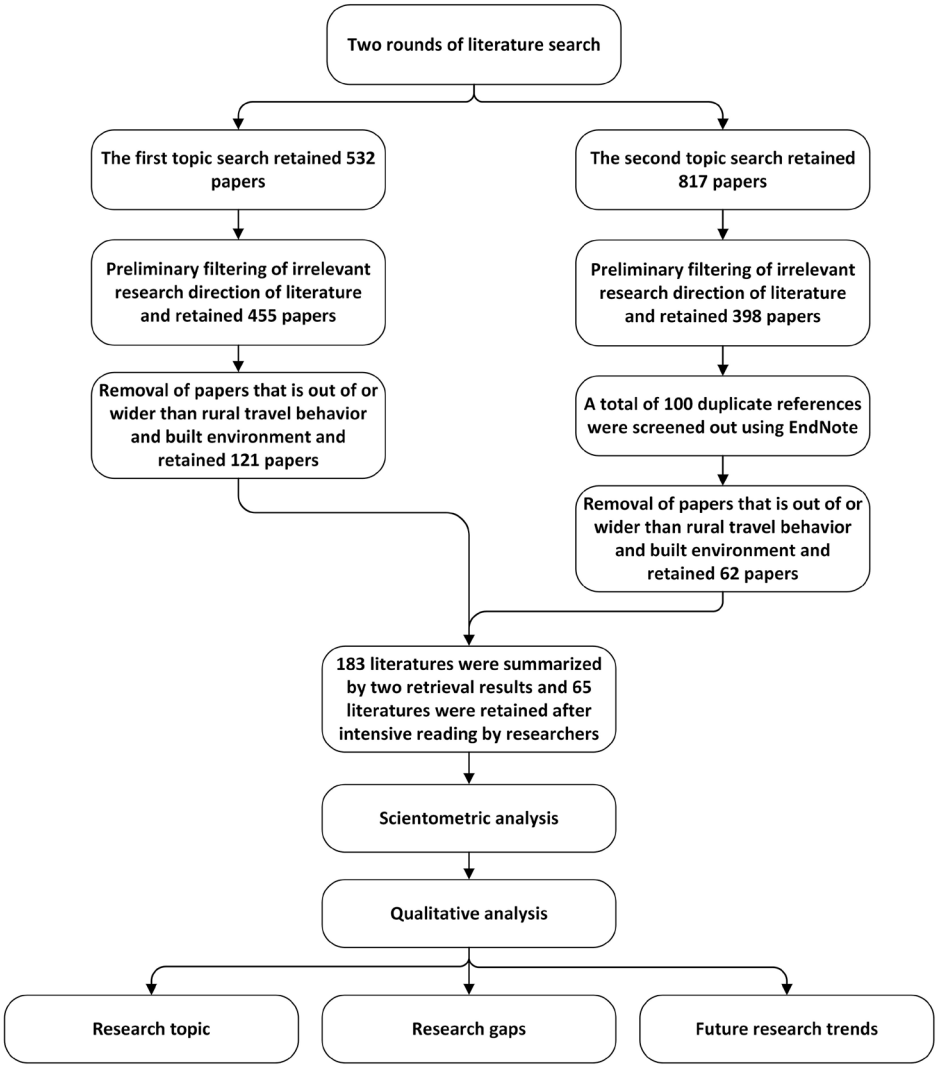

FIGURE 1
Flow chart of scientific analysis of literature on this research topic.

Qualitative discussion

The last step comprised qualitative discussion. As shown in Figure 1, there are three main objectives to be achieved through the in-depth qualitative discussion. This paper summarizes the main research results in the field of the rural built environment and residents' travel behavior, points out the gaps in the research and puts forward proposals for future research.

Results of scientometric analysis

An overview of the literature sample

Overall, scholars pay limited attention to the built environment and travel behavior in rural areas, especially in developing countries. Before 2011, as shown in Figure 2, we find only a few articles published on the theme of the rural built environment and travel behavior. Research in this area has only gradually increased in the last decade. Since 2010, several articles have appeared every year. Though the volume of publications fluctuates significantly, the trend as a whole is on the rise. (The point of literature retrieval in this study was November 21st, 2021, so the final output for the year can be expected to exceed the previous 6). Compared with previous years, the past 10 years have been the most productive in this research realm.

Science mapping of journal sources

This study systematically analyzed the source journals of 65 research articles on rural built environment and travel behavior, and the analysis results are shown in Figure 3. In VOSviewer, both the

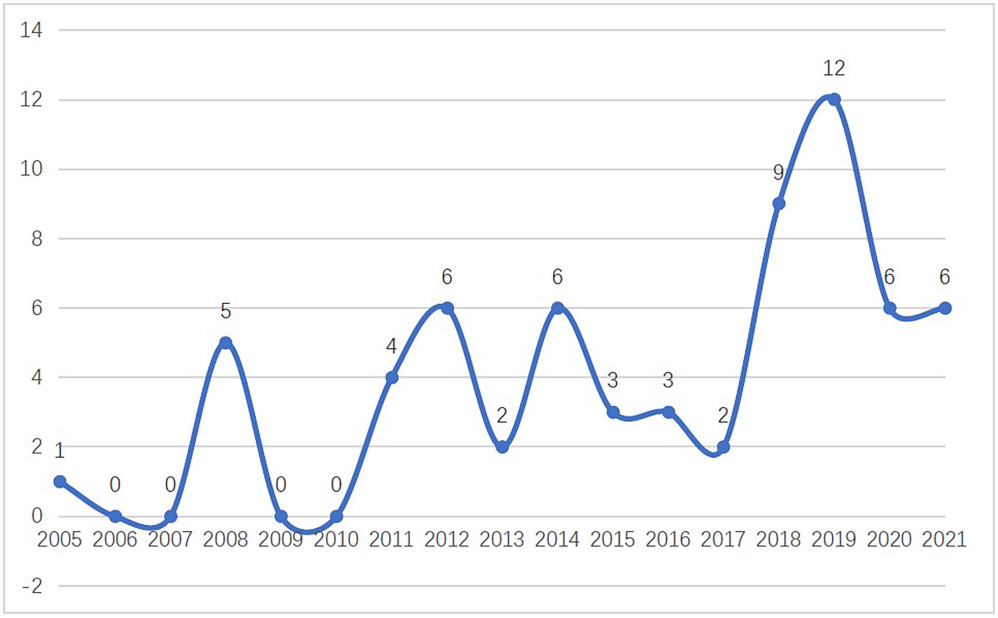

FIGURE 2
Annual publications from 2005 to 2021 in the research field.

minimum number of published papers and the minimum number of citations were set to 1, resulting in 12 of the 28 journals meeting this threshold. Figure 3 shows the clusters of journal sources and their inter-relationships through connection lines. In Figure 3, the number of publications of a given journal is represented by the font and node size visually, while different colors and connecting lines show the proximity of journals in terms of mutual citations. Citation is the major measure of the influence of academic works, and the use of direct citation is a recognized standard to identify influential research in a certain field (Van Eck and Waltman, 2014). The most influential journals are: *Journal of Transport Geography* has the highest literature output, while *Transport and Journal of Rural Studies* has relatively high literature output and average citation times, indicating the high influence on literature output and research significance. From the perspective of average standardized citations, journals such as *Gender Place and Culture*, *Transportation,* and *Journal of Rural Studies* all share the highest annual average influence. Although the highest number of publications and total citation rate belongs to *Journal of transportation geography*, its average citation rate and average standardized citation rate are not the highest. Appendix 1 summarizes the number of publications, total citations received, average citation per publication and average normalized citations.

Co-occurrence of keywords

Keywords spotlight the main topics of the research and describe the focused themes in a given domain (Su and Lee, 2010). The knowledge inter-relationship and intellectual organization of the research themes are shown by the keyword network (Van Eck and Waltman, 2014). In VOSviewer analysis, the minimum occurrence of a keyword was set to 3, using "All keywords" and "Fractional counting." At first, 44 of the 406 keywords reached the threshold. By combining some keywords sharing the same semantic meaning, such as "neighborhood type" and "neighborhood," "travel behaviour," and "travel behavior," "auto ownership" and "car ownership," and "impact" and "Impact," a final body of 40 keywords was selected, as shown in Figure 4.

VOSviewer divides 40 keywords into five clusters with different colors: red green blue purple and yellow according to the connection strength between these keywords. It can be seen that health and walking are closely related and both belong to the red cluster representing aspects related to mobility. Similarly keywords in different clusters are closely related such as gender accessibility and mobility. Generally speaking the main research keywords of rural travel behavior can be classified according to the built environment accessibility mobility and other influencing factors.

Further keywords of quantitative nature are summarized in Appendix 2. In the research domain of rural built environment and travel behavior, the keyword "Self-selection" has been cited as the highest on average. Thus, it may be surmised that this research theme has received the most attention since 2005. The average normalized citation value is calculated by dividing the total number of references by the average number of references published each year. This normalization corrects the misconception that the holder's literature has more time to be cited than the more recent publications (Van Eck and Waltman, 2014). After eliminating the time error, the average normalized

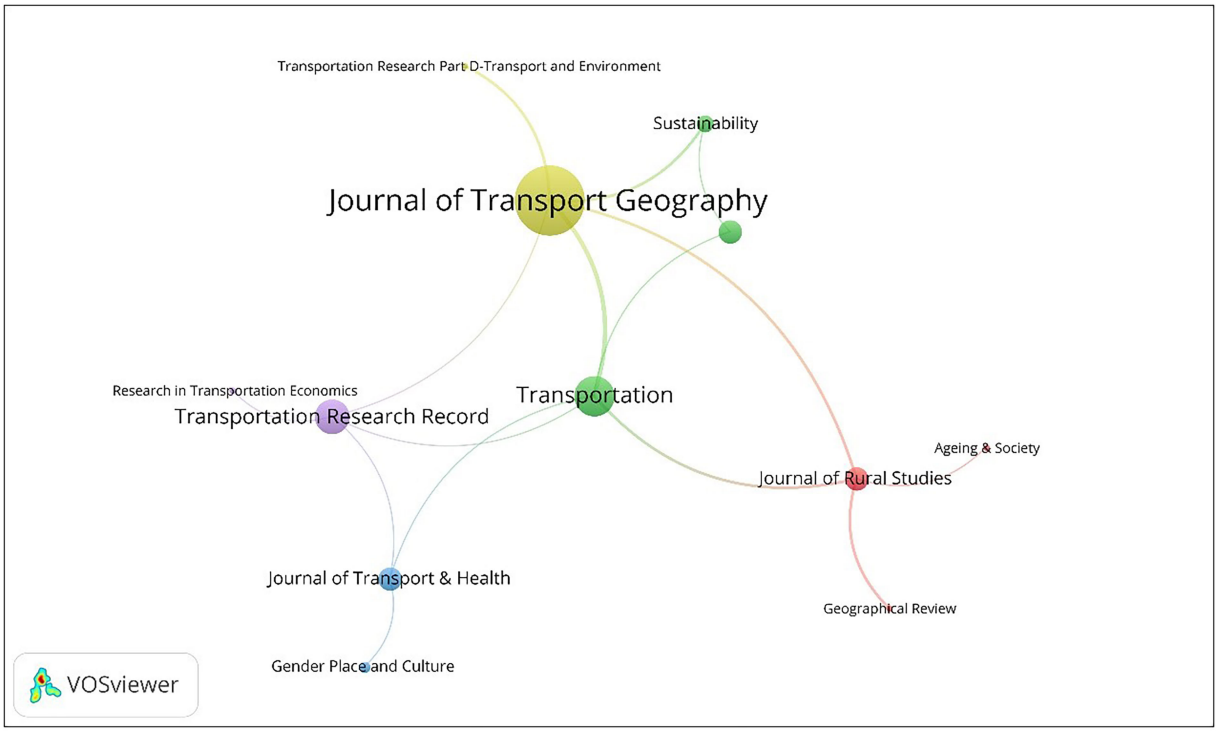

FIGURE 3
Map of mainstream journals in the field of rural travel behavior.

citation value of the word "Children" is higher than any other keyword, which reveals that rural children's travel has emerged as a topic of great interest.

Co-authorship analysis

In VOSviewer, this study screened 65 publications whose authors published two or more papers, with corresponding citations. Literature influence was assessed using Norm. Citations. The visualization is shown in Figure 5. In this field, the series of studies by Ao's research team are shown to have made important contributions.

The literature with the highest value of Norm. Citations belong to Ao and Wang (Ao et al., 2018, 2019a,b, 2020; Wang et al., 2019). They explored the influence of the rural built environment in Sichuan, China in regards to the vehicle ownership of rural households. Among them, Ao et al. (2019b) highlighted recent shifts in car ownership in rural areas, analyzing the factors affecting car ownership, and offering a discussion of the characteristics and changes of rural travel behavior. They further expounded on the relationship between travel behavior variables and carbon dioxide emissions, providing a reference for the formulation of transportation policies in rural regions (Ao et al., 2019a). De Vos et al. (2012) explored the relationship between attitude and lifestyle with travel behavior and travel mode choices regarding "soft variables" (De Vos et al., 2012). These researches analyze the impact on travel behavior from the degree of matching between subjective perception and objective environment and generally conclude that spatial matching has influenced rural residents, especially those residing in built-up settings (Van Acker et al., 2013). Appendix 3 lists further details of these scholars.

Countries active in rural built environment and travel behavior research

In the chart analysis of countries, this study identified countries pursuing active indagation on the rural built environment and residents' travel behavior. VOSviewer was used to further identify and evaluate the contribution of these countries to the field. Due to the small number of related journal articles in this study, the thresholds for the minimum number of documents and the cited number were both set to 1 when constructing the national cooperation map of cited documents, with 14 of the 23 countries meeting the requirements. Figure 6 displays the countries that have been actively engaged in research on the rural built environment and travel behavior in the last decade.

It clears that the scholars studying the United States, the Netherlands, Britain, and Canada have published a large number of documents, while a growing number of developing countries have also become active in the research of the rural built environment and travel behavior, such as China, India, Ecuador,

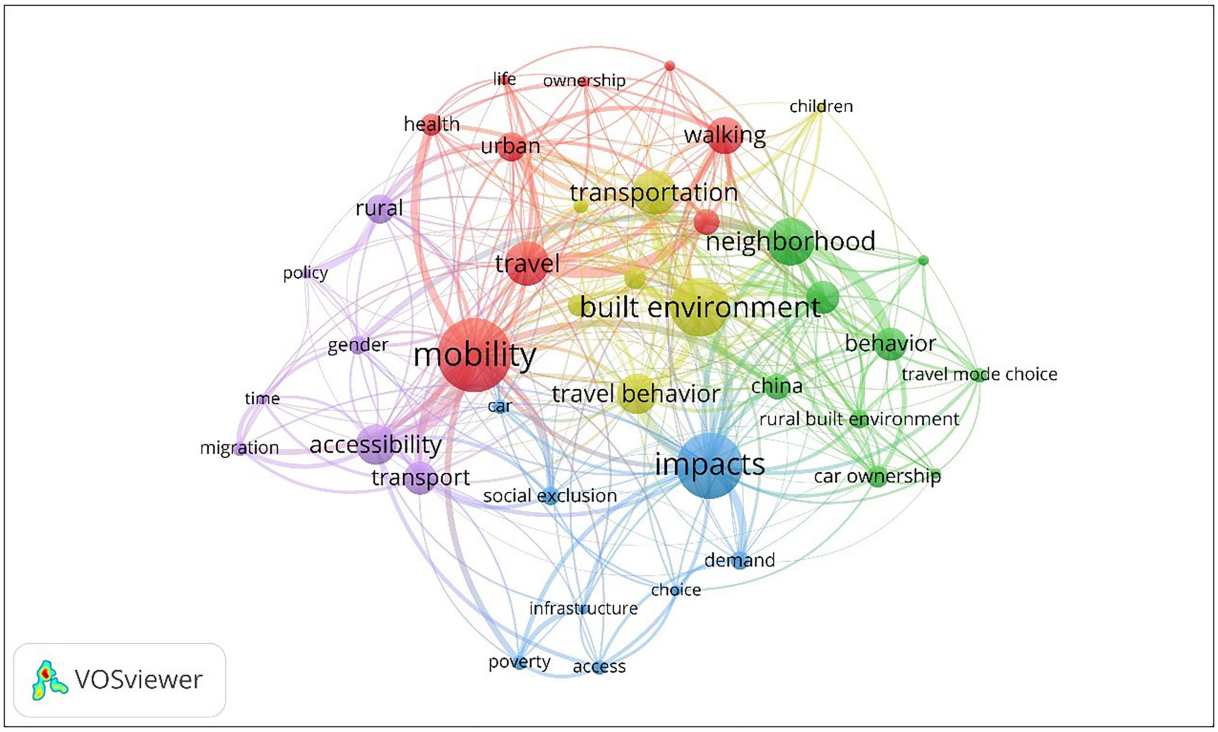

FIGURE 4
Map of co-occurrence of keywords.

and Ethiopia. Appendix 4 further provides relevant quantitative measurement data, including the number of publications, the average publication year, the number of citations, the average citations, and the average normalized citations. As shown in Appendix 4, it is evident that studies for the United States, China, and the Netherlands have the largest number of publications. From the point of total cited times, American, British and Australian literature were cited the most frequently. According to the average normalized citations, China, Britain, Canada, and Australia are the most studied countries in this research field.

Discussion

Comparative study of urban and rural areas

Of the 65 papers studied, 37 have drawn conclusions based on comparative studies between urban and rural areas, while the other 28 have carried out more in-depth research on rural areas.

Overall, the relevant conclusions of the urban–rural comparative study on the relationship between the built environment and travel behavior are more macroscopic. For instance, a study in the Netherlands discovered that the difference in travel behavior between urban and rural areas was determined by the location and the accessibility of transport infrastructure (Kasraian et al., 2018). Zhou and Kockelman (2008) also attributed the changes in household Vehicle Miles Traveled (VMT) of families moving between cities and rural areas to differences in the built environment (Zhou and Kockelman, 2008). Certain scholars have proposed incentivizing residents to use active travel modes (such as cycling and walking) through improvements to the built environment (Stewart et al., 2016; Tribby and Tharp, 2019). In urban areas, the existence of bicycle-friendly streets seems to be important in promoting active transportation, while in rural areas, access to trails is significantly associated with active travel (Grabow et al., 2019). Kamargianni and Polydoropoulou (2014) also drew a similar conclusion that the presence of wide sidewalks significantly affects rural residents' choice of active travel modes (Kamargianni and Polydoropoulou, 2014). In addition, evidence from the Household Mobility Survey in the Baltimore–Washington area of Maryland, United States, shows that increasing the number of retail and recreational locations increases bicycle use among urban residents, while in rural areas, improving traffic accessibility may increase residents' bicycle use (Cui et al., 2014). In China, people living in rural areas are more likely to choose public transportation when commuting to workplaces located in dense commercial zones, while urban residents with shorter commuting distances tend to walk to work (Hu et al., 2021). Another study on the influence of the built environment on the use of public transportation by the elderly in urban and rural China indicates that the location of rural bus stops should be optimized while the density of rural bus stops should be increased in urban and rural developments. This would

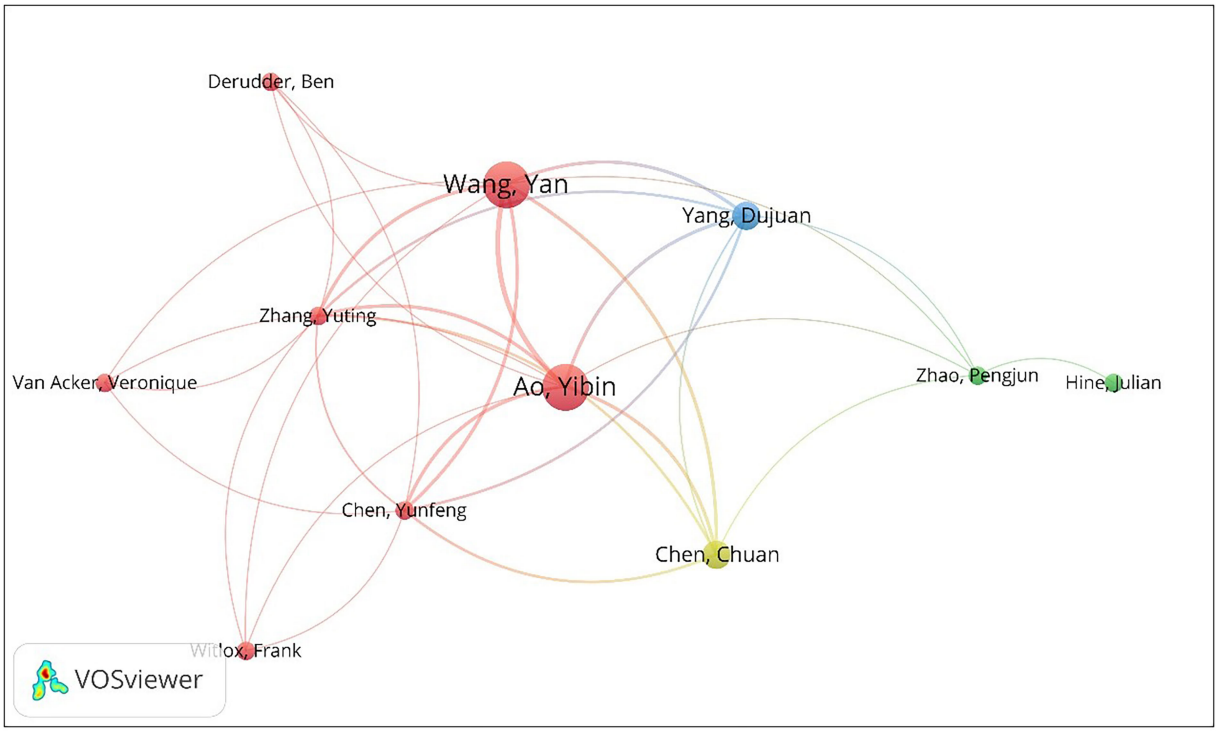

FIGURE 5
Map of co-authorship in the field of rural travel behavior.

encourage the elderly in rural areas to use public transportation (Zhang et al., 2018).

It is clear from these studies that compared with urban areas, the destinations of daily activities in rural areas are highly dispersed, while rural residents have to travel further to get the services they need, such as for medical care, education, and postal services (Shergold and Parkhurst, 2012). It is for this reason that they rely more on cars and convenient transportation.

Research in rural areas

The influence of the five recognized factors of the built environment, such as density (Cui et al., 2014; Ralph et al., 2016), diversity (Kamruzzaman and Hine, 2013), design (Hu et al., 2021), destination accessibility (Hough et al., 2008), and traffic accessibility (Zhang et al., 2018) on residents' travel behavior has been consistently demonstrated across many urban studies in various countries. In recent years, research on rural areas has gained more interest. Scholars' research on rural areas is more microscopic and specific. Subjective and objective aspects of the built environment in rural areas are known to have a prominent impact on the daily travel behavior of rural residents.

In terms of density, rural residents living in high-density areas experience shorter travel distances (Ao et al., 2019a). Rural building density and road density have a meaningful impact on the incidence of car ownership across rural residents' families (Ao et al., 2019b). Households located in higher building and road density areas prefer to own high-carbon cars (Ao et al., 2018). At the same time, an increase in road density can stimulate the travel frequency of electric bicycles and motor vehicles used by rural residents (Wang et al., 2019).

In terms of diversity, the land use in rural regions is relatively uniform (Ao et al., 2019b), leading to problems such as fewer opportunities for residents to work along with poor access to medical care. For this reason, rural residents choose long-distance travel more often, which makes the mobility level in rural regions usually higher than that in urban places (Pucher and Renne, 2005).

In terms of destination accessibility, existing research shows that individuals living in rural areas with higher accessibility are more likely to integrate into local communities (Hine et al., 2011). As an important place for rural residents' daily activities, rural residents can sell crops and get daily necessities at the market. Studies have shown that the time it takes for rural residents to get to the market or downtown is negatively correlated with their travel frequency (Shilpi and Umali-Deininger, 2008; Yu and Zhao, 2021). Thus, it is important to improve market accessibility. In addition, medical facilities are closely related to the healthy travel of residents (Hine et al., 2011). In a study on the effects of distance from personal residence to medical facilities on the choice of medical treatment, researchers found that people tend to prefer immediate emergency care nearby rather than high-quality medical care much farther away

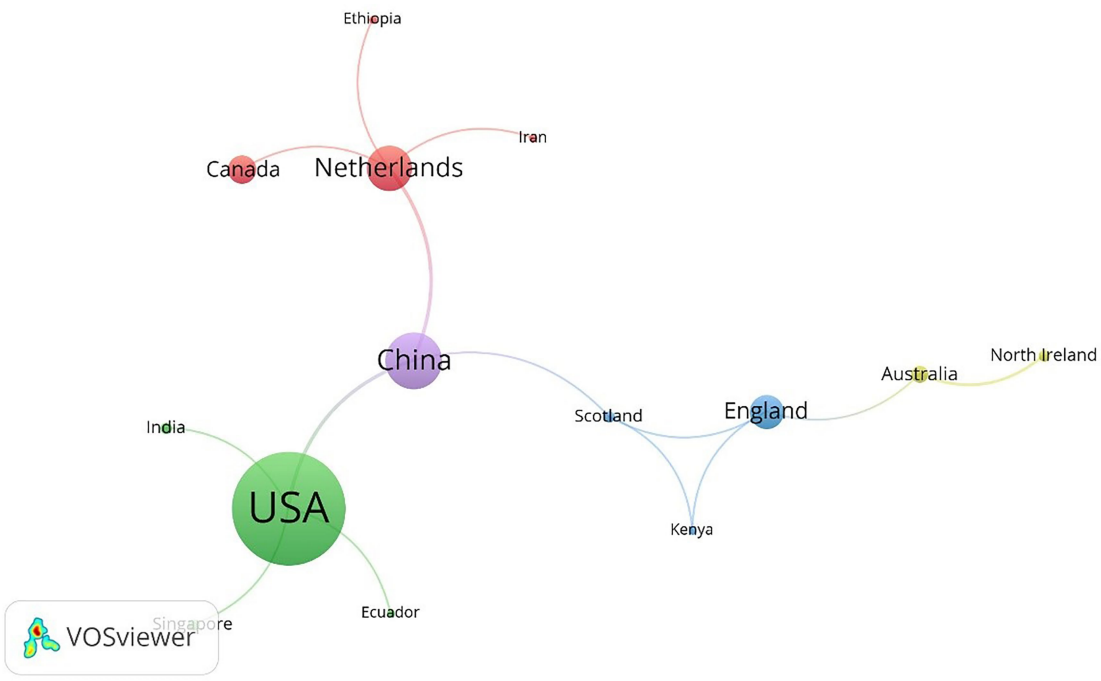

FIGURE 6
Map of countries actively engaged in this research topic.

(Idei and Kato, 2019). Generally speaking, the space available for rural activities is limited (Chen and Akar, 2016), while proximity to the destination promotes more walking (Nathan et al., 2012). The farther away the service distance is, the more residents are likely to own cars or other means of transportation (Wiersma et al., 2017; Zhao and Bai, 2019). Especially nowadays, the elderly in rural regions rely more on cars to meet their travel needs (Hanson and Hildebrand, 2011). However, unfortunate economic conditions combined with poor road facilities in rural areas combine to restrict rural residents from owning cars, resulting in burdensome inconveniences.

In terms of transportation accessibility, transportation infrastructure construction is considered to play a crucial role in the development of residential areas (Dalkmann et al., 2008; Yang et al., 2020, 2022a). For rural residents, their daily travel destinations are limited and scattered, and the corresponding transportation services lag due to the dearth of bus stops and scheduled bus travel frequencies in rural regions (Abhishek et al., 2020). At present, the accessibility of daily activities of residents in rural areas is generally poor and inconvenient (Van Acker et al., 2013). Studies have shown that the distance to the public transportation stations directly correlates with the mobility of rural residents (Yu and Zhao, 2021), especially for rural non-agricultural women (Ranković Plazinić and Jović, 2014). Rural women cannot drive motor vehicles or electric cars often, and they rely almost solely on walking to get to places (Miralles-Guasch et al., 2015). Where the distance to destinations is too great to walk, public transportation is left as the only alternative mode of transportation.

In terms of design, the barrier-free performance of roads in rural areas increases the probability of residents using cars. At the same time, better road connectivity can promote residents' inclination to walk (Nathan et al., 2012; Shergold and Parkhurst, 2012). Yu and Zhao (2021) considered that residents in small rural towns with limited local services, residing far away from transportation infrastructure, have relatively more travel needs. Thus, rural towns with inadequate local services and less transportation infrastructure are the priority recipients of investment in road infrastructure optimization that would be needed to support such peoples' travel needs (Yu and Zhao, 2021).

Regarding the subjective built environment or rural residents' perception and evaluation of the rural built environment, existing research found that perceived accessibility had a positive influence on residents' walking habits (Shergold and Parkhurst, 2012). When rural residents perceive that the rural roads are in good condition, the accident rate in residential areas is low, the degree of security is high, and the road infrastructure such as sidewalks and traffic lights is complete, the probability of rural residents choosing to travel by walking or cycling will increase significantly (Nathan et al., 2012; Wang et al., 2019). In addition, rural residents living in a harmonious neighborhood, all else being equal, are more probably to choose to walk (Wang et al., 2019). Therefore, improving rural residents' feelings about the accessibility of

destinations, travel safety, neighborhood environments, and road infrastructure can promote more active travel.

Research gaps and trends

The body of indagation literature on rural built environment and travel behavior is limited. Nevertheless, broad research gaps can be identified, pointing to key research priorities in subsequent research endeavors.Based on the discussion of mainstream research topics and gaps, the framework of near-future directions on rural built environment and travel behavior is proposed and shown in Figure 7.

Comparative research can tease out similarities and differences

In comparative studies between developed countries and developing countries, some scholars have explored the differences in the relationship between the rural built environment and travel behavior in terms of family income (Zhou and Kockelman, 2008) and transportation choice (Delclòs-alió and Miralles-guasch, 2019), yet these comparisons remain limited. In urban–rural comparison studies, the main problem is that indicators used in making comparisons between the urban and rural contexts should remain consistent (Ao et al., 2019b). Studies of different groups such as children, women, young people, and the elderly are relatively common (Ryser and Halseth, 2012), but other demographics remain neglected, such as those with disabilities, the critically ill, and those who have lost their ability to care for themselves. Thus, a more comprehensive and in-depth comparative study investigating these deficiencies is called for, and certainly needed so as to develop a profound theoretical understanding regarding the development of rural infrastructure.

Forward-looking attention to rural transportation service systems and emerging transportation modes

Compared with urban areas, the rural public transport system has much scope for improvement (Ao et al., 2020). This would include research on public transportation accessibility, types of public transportation facilities, public transportation route planning, station setting, and similar concerns (Zhou et al., 2019). The development of innovative transportation modes, such as shared cars (Illgen and Höck, 2018), shared (electric) bicycles, and carpooling services, also require more attention. Further research in these two directions would directly and effectively help improve rural residents' travel accessibility, providing faster and more convenient travel modes and, consequently, improved quality of life.

Rural local culture and residents' subjective experiences cannot be overlooked

Rural regions cover a large area, and there are great cultural differences between jurisdictions (Farmer et al., 2012). Rural residents' feelings of belongingness to the local community, neighborhood relations, and other locationally associated emotions vary widely (Jain et al., 2018; Blondin, 2020). Considerations of local culture and rural residents' subjective experiences are therefore necessary to be taken into account when researching the rural built environment and residents' travel behavior. Such subjective considerations are an effective mechanism by which to maintain local characteristics associated with village life (Yu and Zhao, 2021), while also preserving cultural heritage and diversity through the inclusion of diverse stakeholder views.

Low-carbon travel-oriented rural planning

Nowadays, the energy consumption of rural transportation is extremely high and rising (Zhou et al., 2021). Thus, it needs to pay attention to the sustainable development of rural transportation planning and rural residents' travel. Green transportation modes, such as active transportation (walking, cycling; Wang et al., 2019), more private transportation utilizing low energy consumption (public transportation, 'green energy' vehicles), are beneficial to the rural residents' physical and mental health as well as in favor of the sustainable development (Hiselius and Rosqvist, 2018).

Conclusion

This research explores the influence of the built environment on travel behavior by a holistic bibliometric search, scientometric analysis, and qualitative analysis. In considering the number of studies published each year, it is only relatively recently that the field has gained traction, coming into its own around the years 2018 and 2019. The results of the quantitative analysis are as follows: (1) The influential journals that publish research results on the rural built environment and travel behavior include *Journal of Transport Geography*, *Transportation* and *Journal of Rural Studies*. (2) The keyword analysis reveals the main keywords related to the built environment, which are transportation, accessibility, infrastructure. In regards to travel behavior, the keywords are travel behavior, walking, and travel mode choice. In respect of vehicle ownership, the keyword is car ownership; while for regional studies, the keywords are: rural, urban, and China. (3) Citation analysis reflects the most frequently cited articles, among which Ao et al. deliver the highest Norm. Citations value, with research content mainly discussing the relationship between the rural built environment and travel behavior in China. (4) The countries that have been actively and consistently researched in rural built environment and travel behavior are principally the United States, China, and the Netherlands.

Beyond the results of the scientometric analysis, this study further identifies research deficiencies in this field and puts forward a systematic framework and outlook for further research. The future research outlooked notes the following: (1)

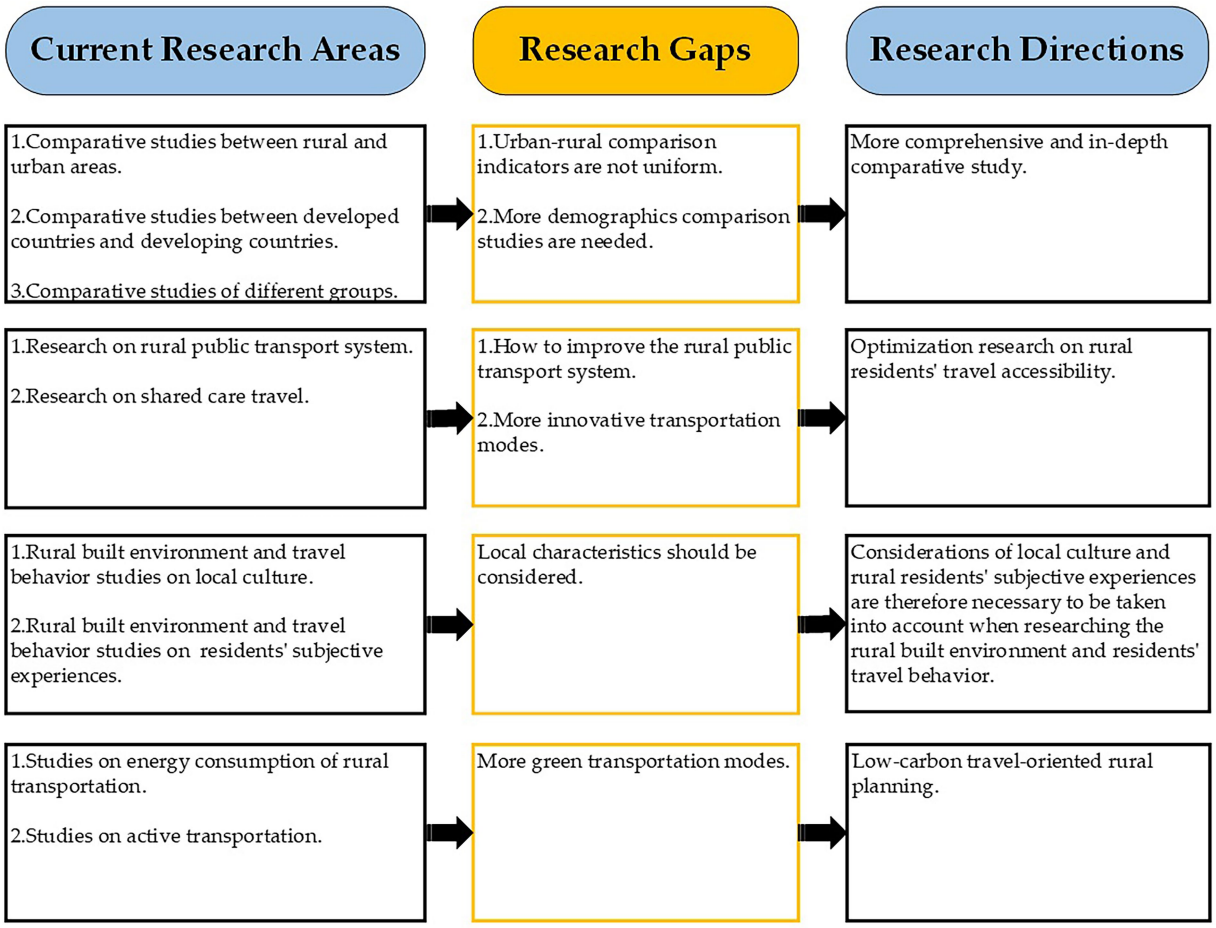

FIGURE 7
Framework linking current research topics to future research directions.

there are few multi-dimensional comparative studies, and more attention should be paid to comparisons between developed countries and developing countries, between urban built environment indicators and rural built environment indicators, and between special groups such as the disabled; (2) Compared to urban transportation systems, rural transportation has much more room for development and improvement, and both the government and private enterprise should actively encourage innovative research on rural transportation; (3) Rural local culture is a factor that cannot be ignored in conducting research in the field of the built environment and travel behavior, requiring an emphasis on empirical research that takes into account local characteristics; (4) Low-carbon travel is a global priority and research related to urban transportation is needed, yet such studies are lacking in the rural context, being limited by such factors as the poorer economy and environmental conditions.

This study focuses on the research progress made to date regarding the rural built environment and travel behavior. The results are, however, limited by the research literature samples: (1) The samples used in this study were sourced from the Web of Science only; (2) In the literature selection stage, only journal articles were selected, excluding documents in the form of conference proceedings, which may have additional pertinent findings; (3) Finally, this literature review's samples only English language literature, and does not analyze the research output published in other languages. Again, this may result in the omission of additional insightful findings. Notwithstanding, the findings are robust and substantially summarize the state of play regarding research within the domain of the rural built environment and travel behavior.

Author contributions

YA: supervision, methodology, and draft writing. ML: methodology, formal analysis, draft writing, and visualizaion. XD, JZ, SX, DS, and ZZ: methodology, formal analysis, and draft writing. YW: supervision and revision. TW: draft writing, supervision, resource, and revision. IM: draft writing and revision. All authors contributed to the article and approved the submitted version.

Funding

This study is jointly supported by the National Natural Science Foundation of China (72171028), China Postdoctoral Science Foundation (2022T150077 and 2022M710496), Sichuan Provincial Social Science Planning Project (22GL086), Development Research Center of Sichuan Old Revolutionary Base Area (SLQ2022SB-23), The article processing costs are funded by Delft University of Technology.

Conflict of interest

The authors declare that the research was conducted in the absence of any commercial or financial relationships that could be construed as a potential conflict of interest.

Publisher's note

All claims expressed in this article are solely those of the authors and do not necessarily represent those of their affiliated organizations, or those of the publisher, the editors and the reviewers. Any product that may be evaluated in this article, or claim that may be made by its manufacturer, is not guaranteed or endorsed by the publisher.

Supplementary material

The Supplementary material for this article can be found online at: https://www.frontiersin.org/articles/10.3389/fevo.2022.1018581/full#supplementary-material

References

Abhishek, A., Borgia, C., Manjur, K., van Steenbergen, F., and Vera, L. F. (2020). Gender mainstreaming in rural road construction/usage in Ethiopia: impact and implications. *Proceed. Institut. Civil Eng. Trans.* 173, 122–131. doi: 10.1680/jtran.18.00154

Ao, Y., Chen, C., Yang, D., and Wang, Y. (2018). Relationship between rural built environment and household vehicle ownership: an empirical analysis in rural Sichuan, China. *Sustainability* 10:1566. doi: 10.3390/su10051566

Ao, Y., Yang, D., Chen, C., and Wang, Y. (2019a). Effects of rural built environment on travel-related CO2 emissions considering travel attitudes. *Transp. Res. Part D: Transp. Environ.* 73, 187–204. doi: 10.1016/j.trd.2019.07.004

Ao, Y., Yang, D., Chen, C., and Wang, Y. (2019b). Exploring the effects of the rural built environment on household car ownership after controlling for preference and attitude: evidence from Sichuan, China. *J. Transp. Geogr.* 74, 24–36. doi: 10.1016/j.jtrangeo.2018.11.002

Ao, Y., Zhang, Y., Wang, Y., Chen, Y., and Yang, L. (2020). Influences of rural built environment on travel mode choice of rural residents: the case of rural Sichuan. *J. Transp. Geogr.* 85:102708. doi: 10.1016/j.jtrangeo.2020.102708

Ao, Y., Zhang, H., Yang, L., Wang, Y., Martek, I., and Wang, G. (2021). Impacts of earthquake knowledge and risk perception on earthquake preparedness of rural residents. *Nat. Hazards* 107, 1287–1310. doi: 10.1007/s11069-021-04632-w

Balestrieri, M., and Congiu, T. (2017). Rediscovering rural territories by means of religious route planning. *Sustainability* 9:363. doi: 10.3390/su9030363

Blondin, S. (2020). Understanding involuntary immobility in the Bartang Valley of Tajikistan through the prism of motility. *Mobilities* 15, 543–558. doi: 10.1080/17450101.2020.1746146

Bu, X., Pu, L., Shen, C., Xie, X., and Xu, C. (2020). Study on the spatial restructuring of the village system at the county level oriented toward the rural revitalization strategy: a case of Jintan District, Jiangsu Province. *Land* 9:478. doi: 10.3390/land9120478

Chen, N., and Akar, G. (2016). Effects of neighborhood types & socio-demographics on activity space. *J. Transp. Geogr.* 54, 112–121. doi: 10.1016/j.jtrangeo.2016.05.017

Chen, J., and Gan, M. (2014). A review of latent variable on urban travel behavior. *J. Transporat. Syst. Eng. Informat. Technol.* 14, 21–29. doi: 10.1016/S1570-6672(13)60144-0

Cobo, M. J., López-Herrera, A. G., Herrera-Viedma, E., and Herrera, F. (2011). Science mapping software tools: review, analysis, and cooperative study among tools. *J. Am. Soc. Inf. Sci. Technol.* 62, 1382–1402. doi: 10.1002/asi.21525

Cui, Y., Mishra, S., and Welch, T. F. (2014). Land use effects on bicycle ridership: a framework for state planning agencies. *J. Transp. Geogr.* 41, 220–228. doi: 10.1016/j.jtrangeo.2014.10.004

Dalkmann, H., Hutfilter, S., Vogelpohl, K., and Schnabel, P. (2008). Sustainable mobility in rural China. *J. Environ. Manag.* 87, 249–261. doi: 10.1016/j.jenvman.2007.03.049

De Vos, J., Derudder, B., Van Acker, V., and Witlox, F. (2012). Reducing car use: changing attitudes or relocating? The influence of residential dissonance on travel behavior. *J. Transp. Geogr.* 22, 1–9. doi: 10.1016/j.jtrangeo.2011.11.005

Delclòs-alió, X., and Miralles-guasch, C. (2019). Youth mobility and territorial disparities: an analysis of urban and rural Barcelona. *Geogr. Rev.* 109, 399–415. doi: 10.1111/gere.12321

Doloi, H., Green, R., and Donovan, S. (2018). *Planning, Housing and Infrastructure for Smart Villages*. London: Routledge.

Farmer, J., Bourke, L., Taylor, J., Marley, J. V., Reid, J., Bracksley, S., et al. (2012). Culture and rural health. *Aust. J. Rural Health* 20, 243–247. doi: 10.1111/j.1440-1584.2012.01304.x

Gieling, J., Haartsen, T., Vermeij, L., and Strijker, D. (2019). Out of love for the village? How general and selective forms of attachment to the village explain volunteering in Dutch community life. *J. Rural. Stud.* 71, 181–188. doi: 10.1016/j.jrurstud.2018.06.008

Grabow, M. L., Bernardinello, M., Bersch, A. J., Engelman, C. D., Martinez-Donate, A., Patz, J. A., et al. (2019). What moves us: subjective and objective predictors of active transportation. *J. Transp. Health* 15:100625. doi: 10.1016/j.jth.2019.100625

Hanson, T. R., and Hildebrand, E. D. (2011). Can rural older drivers meet their needs without a car? Stated adaptation responses from a GPS travel diary survey. *Transportation* 38, 975–992. doi: 10.1007/s11116-011-9323-3

He, Q., Wang, G., Luo, L., Shi, Q., Xie, J., and Meng, X. (2017). Mapping the managerial areas of building information modeling (BIM) using scientometric analysis. *Int. J. Proj. Manag.* 35, 670–685. doi: 10.1016/j.ijproman.2016.08.001

Hine, J., Kamruzzaman, M., and Blair, N. (2011). Weekly activity-travel behaviour in rural Northern Ireland: differences by context and socio-demographic. *Transportation* 39, 175–195. doi: 10.1007/s11116-011-9322-4

Hiselius, L. W., and Rosqvist, L. S. (2018). Segmentation of the current levels of passenger mileage by car in the light of sustainability targets – the Swedish case. *J. Clean. Prod.* 182, 331–337. doi: 10.1016/j.jclepro.2018.02.072

Hosseini, M. R., Martek, I., Zavadskas, E. K., Aibinu, A. A., Arashpour, M., and Chileshe, N. (2018). Critical evaluation of off-site construction research: a Scientometric analysis. *Autom. Constr.* 87, 235–247. doi: 10.1016/j.autcon.2017.12.002

Hough, J. A., Cao, X., and Handy, S. L. (2008). Exploring travel behavior of elderly women in rural and small urban North Dakota. *Transp. Res. Rec.* 2082, 125–131. doi: 10.3141/2082-15

Hu, Y., Sobhani, A., and Ettema, D. (2021). To e-bike or not to e-bike? A study of the impact of the built environment on commute mode choice in small Chinese city. *J. Transp. Land Use* 14, 479–497. doi: 10.5198/jtlu.2021.1807

Idei, R., and Kato, H. (2019). Medical-purposed travel behaviors in rural areas in developing countries: a case study in rural Cambodia. *Transportation* 47, 1415–1438. doi: 10.1007/s11116-018-9971-7

Illgen, S., and Höck, M. (2018). Establishing car sharing services in rural areas: a simulation-based fleet operations analysis. *Transportation* 47, 811–826. doi: 10.1007/s11116-018-9920-5

Jain, M., Korzhenevych, A., and Hecht, R. (2018). Determinants of commuting patterns in a rural-urban megaregion of India. *Transp. Policy* 68, 98–106. doi: 10.1016/j.tranpol.2018.04.018

Jiao, X., Pouliot, M., and Walelign, S. Z. (2017). Livelihood strategies and dynamics in rural Cambodia. *World Dev.* 97, 266–278. doi: 10.1016/j.worlddev.2017.04.019

Kamargianni, M., and Polydoropoulou, A. (2014). Generation Y's travel behavior and perceptions of walkability constraints. *Transp. Res. Rec.* 2430, 59–71. doi: 10.3141/2430-07

Kamruzzaman, M., and Hine, J. (2013). Self-proxy agreement and weekly school travel behaviour in a sectarian divided society. *J. Transp. Geogr.* 29, 74–85. doi: 10.1016/j.jtrangeo.2013.01.002

Kasraian, D., Maat, K., and van Wee, B. (2018). Urban developments and daily travel distances: fixed, random and hybrid effects models using a Dutch pseudo-panel over three decades. *J. Transp. Geogr.* 72, 228–236. doi: 10.1016/j.jtrangeo.2018.09.006

Miralles-Guasch, C., Melo, M. M., and Marquet, O. (2015). A gender analysis of everyday mobility in urban and rural territories: from challenges to sustainability. *Gend. Place Cult.* 23, 398–417. doi: 10.1080/0966369X.2015.1013448

Nathan, A., Wood, L., and Giles-Corti, B. (2012). Perceptions of the built environment and associations with walking among retirement village residents. *Environ. Behav.* 46, 46–69. doi: 10.1177/0013916512450173

Pucher, J., and Renne, J. L. (2005). Rural mobility and mode choice: evidence from the 2001 National Household Travel Survey. *Transportation* 32, 165–186. doi: 10.1007/s11116-004-5508-3

Ralph, K., Voulgaris, C. T., Taylor, B. D., Blumenberg, E., and Brown, A. E. (2016). Millennials, built form, and travel insights from a nationwide typology of U.S. neighborhoods. *J. Transp. Geogr.* 57, 218–226. doi: 10.1016/j.jtrangeo.2016.10.007

Ranković Plazinić, B., and Jović, J. (2014). Women and transportation demands in rural Serbia. *J. Rural. Stud.* 36, 207–218. doi: 10.1016/j.jrurstud.2014.08.002

Ryser, L., and Halseth, G. (2012). Resolving mobility constraints impeding rural seniors' access to regionalized services. *J. Aging Soc. Policy* 24, 328–344. doi: 10.1080/08959420.2012.683329

Shergold, I., and Parkhurst, G. (2012). Transport-related social exclusion amongst older people in rural Southwest England and Wales. *J. Rural. Stud.* 28, 412–421. doi: 10.1016/j.jrurstud.2012.01.010

Shilpi, F., and Umali-Deininger, D. (2008). Market facilities and agricultural marketing: evidence from Tamil Nadu, India. *Agric. Econ.* 39, 281–294. doi: 10.1111/j.1574-0862.2008.00333.x

Stewart, O. T., Vernez Moudon, A., Saelens, B. E., Lee, C., Kang, B., and Doescher, M. P. (2016). Comparing associations between the built environment and walking in rural small towns and a large metropolitan area. *Environ. Behav.* 48, 13–36. doi: 10.1177/0013916515612253

Su, H.-N., and Lee, P.-C. (2010). Mapping knowledge structure by keyword co-occurrence: a first look at journal papers in technology foresight. *Scientometrics* 85, 65–79. doi: 10.1007/s11192-010-0259-8

Sun, X., Han, X., Yan, X., Wang, W., Jiang, R., and Jia, B. (2017). Review of laboratory experiments on travel choice behavior. *Complex Syst. Complex. Sci.* 14, 1–7. doi: 10.13306/j.1672-3813.2017.03.001

Tribby, C. P., and Tharp, D. S. (2019). Examining urban and rural bicycling in the United States: early findings from the 2017 National Household Travel Survey. *J. Transp. Health* 13, 143–149. doi: 10.1016/j.jth.2019.03.015

Van Acker, V., Derudder, B., and Witlox, F. (2013). Why people use their cars while the built environment imposes cycling. *J. Transp. Land Use* 6, 53–62. doi: 10.5198/jtlu.v6i1.288

Van Eck, N. J., and Waltman, L. (2010). Software survey: VOSviewer, a computer program for bibliometric mapping. *Scientometrics* 84, 523–538. doi: 10.1007/s11192-009-0146-3

Van Eck, N., and Waltman, L. (2014). "Visualizing bibliometric networks," in *Measuring Scholarly Impact: Methods and Practice*. eds. Y. Ding, R. Rousseau and D. Wolfram (Cham: Springer), 285–320.

Wang, Y., Ao, Y., Zhang, Y., Liu, Y., Zhao, L., and Chen, Y. (2019). Impact of the built environment and bicycling psychological factors on the acceptable bicycling distance of rural residents. *Sustainability* 11:4404. doi: 10.3390/su11164404

Wang, C., Huang, B., Deng, C., Wan, Q., Zhang, L., Fei, Z., et al. (2016). Rural settlement restructuring based on analysis of the peasant household symbiotic system at village level: a case study of Fengsi Village in Chongqing, China. *J. Rural. Stud.* 47, 485–495. doi: 10.1016/j.jrurstud.2016.07.002

Wang, D., and Zhou, M. (2017). The built environment and travel behavior in urban China: a literature review. *Transp. Res. Part D: Transp. Environ.* 52, 574–585. doi: 10.1016/j.trd.2016.10.031

Wiersma, J., Bertolini, L., and Straatemeier, T. (2017). Adapting spatial conditions to reduce car dependency in mid-sized 'post growth' European city regions: the case of South Limburg, Netherlands. *Transp. Policy* 55, 62–69. doi: 10.1016/j.tranpol.2016.12.004

Wolny, A., Ogryzek, M., and Źróbek, R. (2019). Towards sustainable development and preventing exclusions—determining road accessibility at the sub-regional and local level in rural areas of Poland. *Sustainability* 11, 1–21. doi: 10.3390/su11184880

Yang, L., Ao, Y., Ke, J., Lu, Y., and Liang, Y. (2021a). To walk or not to walk? Examining non-linear effects of streetscape greenery on walking propensity of older adults. *J. Transp. Geogr.* 94:103099. doi: 10.1016/j.jtrangeo.2021.103099

Yang, L., Chau, K. W., Szeto, W. Y., Cui, X., and Wang, X. (2020). Accessibility to transit, by transit, and property prices: spatially varying relationships. *Transp. Res. Part D: Transp. Environ.* 85:102387. doi: 10.1016/j.trd.2020.102387

Yang, L., Liang, Y., He, B., Lu, Y., and Gou, Z. (2022a). COVID-19 effects on property markets: the pandemic decreases the implicit price of metro accessibility. *Tunn. Undergr. Space Technol.* 125:104528. doi: 10.1016/j.tust.2022.104528

Yang, L., Liu, J., Liang, Y., Lu, Y., and Yang, H. (2021b). Spatially varying effects of street greenery on walking time of older adults. *ISPRS Int. J. Geo Inf.* 10:596. doi: 10.3390/ijgi10090596

Yang, L., Tang, X., Yang, H., Meng, F., and Liu, J. (2022b). Using a system of equations to assess the determinants of the walking behavior of older adults. *Trans. GIS* 26, 1339–1354. doi: 10.1111/tgis.12916

Yu, Z., and Zhao, P. (2021). The factors in residents' mobility in rural towns of China: car ownership, road infrastructure and public transport services. *J. Transp. Geogr.* 91:102950. doi: 10.1016/j.jtrangeo.2021.102950

Zhang, Y., Wu, W., He, Q., and Li, C. (2018). Public transport use among the urban and rural elderly in China: effects of personal, attitudinal, household, social-environment and built-environment factors. *J. Transp. Land Use* 11, 701–719. doi: 10.5198/jtlu.2018.978

Zhao, P., and Bai, Y. (2019). The gap between and determinants of growth in car ownership in urban and rural areas of China: a longitudinal data case study. *J. Transp. Geogr.* 79:102487. doi: 10.1016/j.jtrangeo.2019.102487

Zhou, Y., Aeschliman, S., and Gohlke, D. (2021). Household transportation energy affordability by region and socioeconomic factors. *Transp. Res. Rec.* 2675, 81–95. doi: 10.1177/03611981211010186

Zhou, B., and Kockelman, K. M. (2008). Self-selection in home choice. *Transp. Res. Rec.* 2077, 54–61. doi: 10.3141/2077-08

Zhou, X., Liang, J., Ji, X., and Cottrill, C. (2019). The influence of information services on public transport behavior of urban and rural residents. *Sustainability* 11:5454. doi: 10.3390/su11195454

frontiers | Frontiers in Ecology and Evolution

TYPE Original Research
PUBLISHED 07 November 2022
DOI 10.3389/fevo.2022.1031008

Check for updates

OPEN ACCESS

EDITED BY
Jun Yang,
Northeastern University,
China

REVIEWED BY
Hao Zhang,
Institute of Mountain Hazards and Environment (CAS), China
Zhi Qiao,
Tianjin University,
China

*CORRESPONDENCE
Yanhong Zhang
giswork@163.com

SPECIALTY SECTION
This article was submitted to Environmental Informatics and Remote Sensing, a section of the journal Frontiers in Ecology and Evolution

RECEIVED 29 August 2022
ACCEPTED 17 October 2022
PUBLISHED 07 November 2022

CITATION
Chen Z, Liu Z, Hou G, Dong K, Zhang Y and Yang C (2022) Period-oriented spatial comparative evaluation of biodiversity conservation effectiveness in China. *Front. Ecol. Evol.* 10:1031008. doi: 10.3389/fevo.2022.1031008

COPYRIGHT
© 2022 Chen, Liu, Hou, Dong, Zhang and Yang. This is an open-access article distributed under the terms of the Creative Commons Attribution License (CC BY). The use, distribution or reproduction in other forums is permitted, provided the original author(s) and the copyright owner(s) are credited and that the original publication in this journal is cited, in accordance with accepted academic practice. No use, distribution or reproduction is permitted which does not comply with these terms.

Period-oriented spatial comparative evaluation of biodiversity conservation effectiveness in China

Ziqi Chen[1,2], Zhaoli Liu[2], Guanglei Hou[2], Kaikai Dong[2,3], Yanhong Zhang[1]* and Changbao Yang[1]

[1]College of Geo-Exploration Science and Technology, Jilin University, Changchun, China, [2]Northeast Institute of Geography and Agriculture, Chinese Academy of Science, Changchun, China, [3]Shandong Key Laboratory of Eco-Environmental for the Yellow River Delta, Binzhou University, Binzhou, China

The period-oriented comparative evaluation of biodiversity conservation effectiveness is the main basis for implementing the transfer payment policy of ecological compensation. In response to the lack of such a spatial comparative assessment system, the paper proposes a method to construct the period conservation effectiveness index (PCEI) and applies it to the spatial comparative assessment of Chinese biodiversity conservation effectiveness in three periods from 1990 to 2015, while validating the rationality of the reference. The results show that (1) spatially, the biodiversity conservation effectiveness of key ecological function areas (KEFAs) in Central China and South China is better, while Southwest and Northwest are in the middle, and East China and Northeast are worse; (2) temporally, the biodiversity conservation effectiveness of KEFAs as a whole is worse from 1990 to 2000, best from 2000 to 2010, and middle from 2010 to 2015; (3) The existing reference establishment methods can reflect the spatial differences of natural environment background, which effectively support the spatial comparison assessment of biodiversity conservation effectiveness. This study constructs a spatial comparison assessment system of biodiversity conservation effectiveness within periods, which can provide a scientific basis for national and even global large-scale ecological compensation and other fund allocation methods.

KEYWORDS

biodiversity, conservation effectiveness, spatial comparison, reference, transfer payment

Introduction

In the past decades, the establishment of various protected areas has played an important role in improving the ecological environment (Gaston and Cruz-Piñón, 2008; Brooks et al., 2009; Hou et al., 2017; Xu et al., 2017). To promote and encourage ecological protection, the state invests a lot of money in the construction and

restoration of protected areas (Gantioler et al., 2014). As an important basis for fund allocation, a set of time-oriented, reasonable, and spatially comparable methods for assessing biodiversity conservation effectiveness is particularly important.

Currently, Zheng et al. (2012) carried out the conservation effectiveness assessment of national wetland nature reserves, but the essence is to assess the biodiversity conservation function rather than the biodiversity conservation effectiveness. Conservation effectiveness focuses on the changes in biodiversity conservation function under human influence, and the comparison of biodiversity conservation function inside and outside protected areas is commonly used to measure conservation effectiveness, thus realizing the spatial comparison of conservation effectiveness at a large scale (Ren et al., 2015; Gray et al., 2016; Feng et al., 2021). The above methods cannot achieve effective spatial comparative assessment of conservation effectiveness, because they do not take into account the differences in the natural environment background conditions of each region. In response to the above problems, Xu et al. (2018) used the construction of reference to exclude the influence of differences in natural environmental backgrounds, and initially developed a set of spatial comparative assessment methods for biodiversity conservation effectiveness. However, the above studies only addressed spatial differences in the biodiversity conservation effectiveness in wetland ecosystem types, and Dong et al. (2018) extended them to the assessment of different ecosystem types such as wetlands and forests. Although the above methods can achieve spatial comparison of biodiversity conservation effectiveness, they are limited to the examination of assessment methods. Chen et al. (2022) then applied the methods to the whole Chinese region and comparatively assessed the spatial differences of biodiversity conservation effectiveness among several KEFAs. Nevertheless, the allocation of transfer funds is based on the temporal changes of conservation effectiveness (He et al., 2014), while the above method reflects the biodiversity conservation effectiveness from the original state to the assessment moment, and cannot provide the comparative results of conservation effectiveness at a certain time, so the above method still has some limitations. In addition, the reference is the basis of the spatial comparative assessment method, and there is still a lack of effective scientific tests on whether the existing reference can reflect the differences in natural environment background between different assessment areas.

Against this background, on the one hand, we aim to develop a set of spatial comparison assessment methods that can reflect the biodiversity conservation effectiveness at a certain period, and on the other hand, to analyze whether the reference obtained can effectively reflect the spatial differences in ecological background, and thus provide a scientific basis for the allocation of transfer payments.

Materials and methods

Study area

The revised version of the National Ecological Function Zoning released by the Ministry of Environmental Protection in 2015 delineates 63 KEFAs on a national scale from the types of biodiversity protection, water conservation, soil and water conservation, wind and sand control, and flood storage. Among them, there are 24 KEFAs mainly for biodiversity protection, with a total area of 2.208 million km^2, which cover 23.1% of the land area, and their codes and locations are shown in Figure 1. China contains seven geographic regions, except for North China, biodiversity KEFAs are distributed in other six administrative regions, and the proportion of KEFAs in each administrative geographic division are Southwest (57.25%), East China (7.45%), South China (3.02%), Northwest (15.12%), Northeast (7.31%), and Central China (9.85%).

SN, LH, and SJ in the Northeast are mainly for wetland biodiversity conservation, and the objects of conservation are mainly rare waterfowl such as the Red crown crane; XXAL is mainly for forest biodiversity conservation, and the objects of conservation are mainly endangered forest vegetation such as broad-leaved red pine forests and large rare animals such as the Siberian tiger. HH and SB in East China also focus on wetland biodiversity conservation, which are the wintering grounds of the Red crown crane and other rare waterfowl; Ginkgo, Tsuga Chinensis, and other rare relict plants are distributed in WY-DY in East China; QL-DB at the junction of Northwest and Central China is the main habitat of national protected animals such as Panda, Golden Monkey, and Takin; WL in Central China protects rare and endangered plants such as dove trees and leopards. In South China, DY protects precious animals such as crocodilians, while HN protects plant species such as Cycas taiwaniana and animal species such as Varanus salvator in tropical rainforest ecosystems. In the eastern part of Southwest, M-QL-L borders QL-DB and protects rare animal species similar to QL-DB; in the southern part of the region, DXB, DX, DN, and WL-AL are distributed with endangered animals such as Yunnan snub-nosed monkeys, Stump-tailed macaques, and black Concolor gibbons, and rare plants such as different types of Taxus Chinensis; in the central part of the region, ZDN is distributed with all plant species from tropical to boreal zones and rare animal species such as Entellus. The highest terrain in the world, the ZMLMF is located in the southwest and has unique and rare wildlife such as Assamese macaque, while the ZXB in the northwest is a unique distribution area for large ungulates such as the Tibetan antelope in the alpine ecosystem. The AEJ in the southwestern part of the Northwest shares similar biodiversity with ZXB in the Southwest; ZD and ZX in the northwestern part are located in the arid desert zone in the interior of Asia and Europe, and their unique climatic

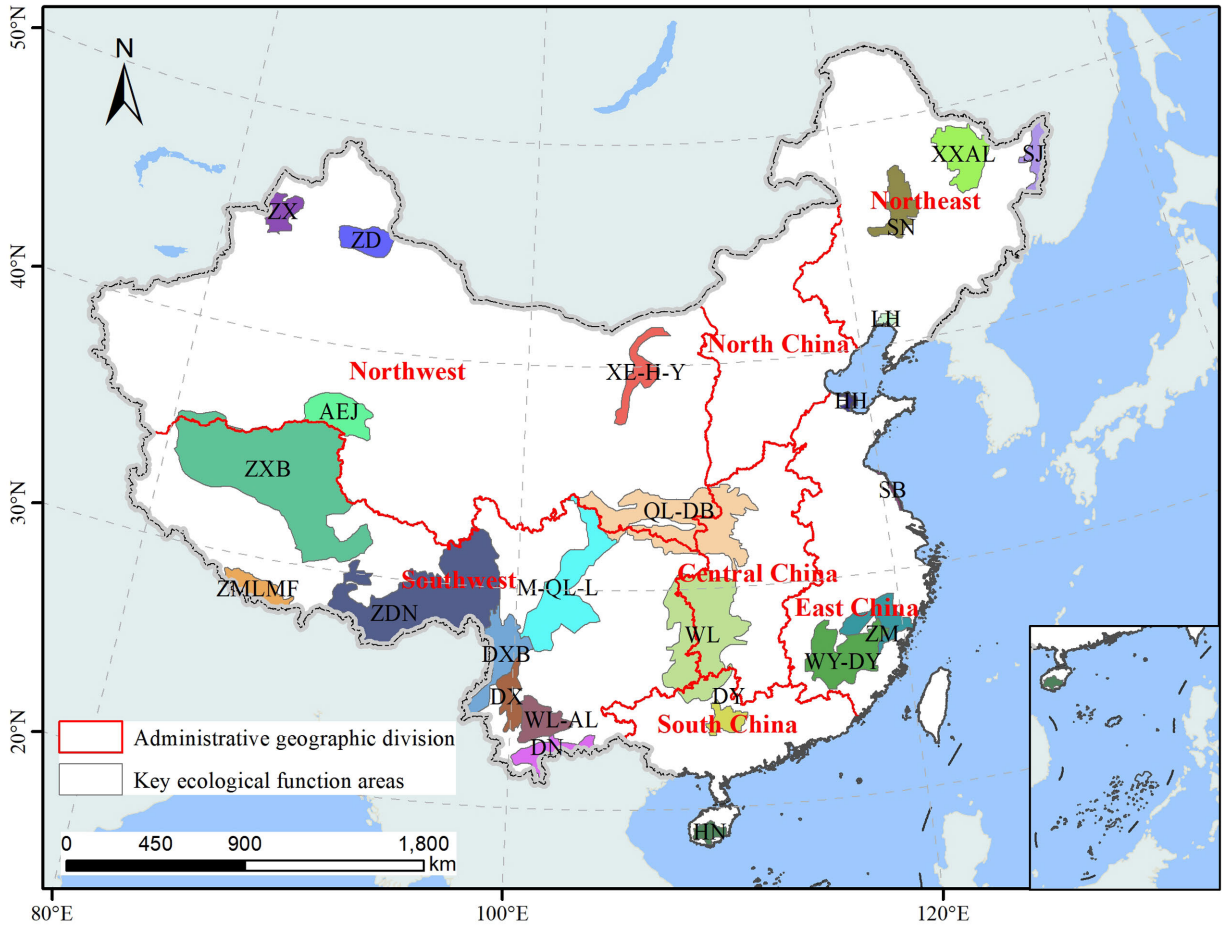

FIGURE 1
Distribution of KEFAs for biodiversity conservation in China.

environment has nurtured endemic animals with significant desert characteristics, such as Equus Przewalskii, Aspiorhynchus laticeps, Ranodon sibiricus, Testudo horsfieldii and other precious animal species; XE-H-Y in the eastern part has national protected plants such as Ammopiptanthus mongolicus and rare animal species such as red deer and Musk deer.

Data and processing

The land cover dataset is provided by Project 1 of the National Key R&D Program "Ecosystem assessment technology based on multi-source data fusion and its application research," which uses the domestic environmental disaster satellite (HJ-1A/B) and the Landsat data as information sources. The land cover dataset for 1990, 2000, 2010, and 2015 with a spatial resolution of 1 km, was obtained using a 40-class classification system and an object-oriented multi-scale segmentation and change detection classification method.

China administrative region boundary data is obtained by combining the administrative division scheme and the regional merging operation of China provincial boundary vector data. The vector boundary data of KEFAs were obtained from the revised version of the National Ecological Function Zoning in 2015 by scanning and digitizing and extracting by manual visual tracking. The national-level nature reserve boundary vector data were obtained from the Resource and Environment Science Data Center of the Chinese Academy of Sciences.[1]

The DEM data were downloaded from USGS GMTED2010 with a resolution of 30 arc seconds, and the Chinese digital elevation model was obtained by overlaying with the national provincial boundary vector data. The climate zones are derived from the important geographic boundaries of China, which are obtained by scanning digitization and manual visual tracking extraction.

1 http://www.resdc.cn/

Methods

Indicators for spatial comparative evaluation of conservation effectiveness period-oriented

The existing Conservation Effectiveness Comparison Index (CECI) is setting the maximum value of the Habitat Quality Index (HQI) of the nature reserve in previous years as the Habitat Quality Reference (HQR) of the assessment area, then constructed by comparing the habitat quality of the assessment area at the time of assessment with the reference (Xu et al., 2018), with the following formula:

$$CECI = HQI - HQR$$

where, CECI is the conservation effectiveness comparison index, HQI is the habitat quality index of KEFAs, and HQR is the habitat quality reference of KEFAs.

In fact, the above index expresses the original state of habitat quality in the assessment area assuming the maximum habitat quality of nature reserves, and the distance of habitat quality in the assessment area from the reference at the time of assessment reflects the temporal change of habitat quality under human influence, i.e., the conservation effectiveness of biodiversity maintenance function. However, the spatial comparison assessment of biodiversity conservation effectiveness for transfer payment is for a certain assessment period, while the existing CECI reflects the effectiveness of biodiversity conservation from the original state to the assessment time, therefore, it is difficult to apply this method system to the reasonable allocation of ecological compensation funds.

The assessment period is the time interval between two different assessment moments before and after, and the corresponding CECI exist before and after the assessment moments, respectively. Accordingly, the quantitative difference between the CECI of the two assessment moments is used to reflect the biodiversity conservation effectiveness in the assessment area during the assessment period, and the specific formula is as follows:

$$PCEI_{i-j} = CECI_j - CECI_i$$

where, $CECI_i$ and $CECI_j$ are the conservation effectiveness comparison index in the year i and year j, respectively. If $PCEI_{i-j}$ is positive, it indicates that the biodiversity conservation effect is good from i to j, and the habitat quality of KEFAs is approaching the reference; if $PCEI_{i-j}$ is negative, it indicates that the biodiversity conservation effect of KEFAs is deteriorating from i to j, and the habitat quality of KEFAs is moving away from the reference.

Procedures for spatial comparative evaluation of conservation effectiveness period-oriented

1. Habitat quality index calculation for the assessment area.

Based on previous habitat quality assessment studies (Shui et al., 2018; Gong et al., 2019; Sun et al., 2019; Liu and Xu, 2020; Tang et al., 2020; Wang et al., 2020; Zhu et al., 2020), the habitat suitability of the ecological land types in the assessment area was taken into account, and a parameter weighting table was established (Chen et al., 2022). Secondly, 1990, 2000, 2010, and 2015 land use data and the parameter weight tables were input into the InVEST model to generate habitat quality raster data; finally, based on the vector boundaries of KEFAs, the habitat quality raster data were regionally averaged to obtain the HQI of the four-year assessment area.

2. Assessment area reference construction.

Based on the vector range of the KEFAs and nature reserves, the nature reserves within or near the KEFAs are extracted as the reference areas; based on the vector boundary of the nature reserves, the habitat quality raster data of each of the above years are averaged to obtain the HQI of the four-year reference areas; the maximum value is selected as the reference of the assessment areas.

3. Conservation Effectiveness Comparison Index acquisition.

Based on the HQI of the assessment areas in 1990, 2000, 2010, and 2015 calculated above and the constructed HQR, the CECI at the four assessment moments were obtained by subtracting the HQI of the assessment areas in each period from the reference, respectively.

4. Period Conservation Effectiveness Index generation.

The biodiversity conservation effectiveness in a certain period is mainly reflected in the change of the CECI of KEFAs in a fixed time interval. By subtracting the CECI in the later period of the assessment period from the earlier period, a PCEI is generated, which illustrates the biodiversity conservation effectiveness in KEFAs between 2 years, the index was magnified 100 times in this study.

5. Period-oriented spatial comparative evaluation of biodiversity conservation effectiveness.

Based on the PCEI of KEFAs in China from 1990 to 2000, 2000 to 2010, 2010 to 2015, and the whole assessment period of 1990–2015, spatial comparative assessment of biodiversity conservation effectiveness in KEFAs can be realized. Further, the spatial differences in the biodiversity conservation effectiveness in China can be analyzed by counting the PCEI of the geo-administrative divisions in which the KEFAs are located, based on the weighting of the area of the KEFAs into the seven geo-administrative divisions in China.

Results and analysis

Regional comparative evaluation of biodiversity conservation effectiveness

The PCEI of KEFAs during 1990–2015 are shown in Figure 2. As you can see from the space the Northeast and East China KEFAs fall into the negative area of PCEI, which indicates that the

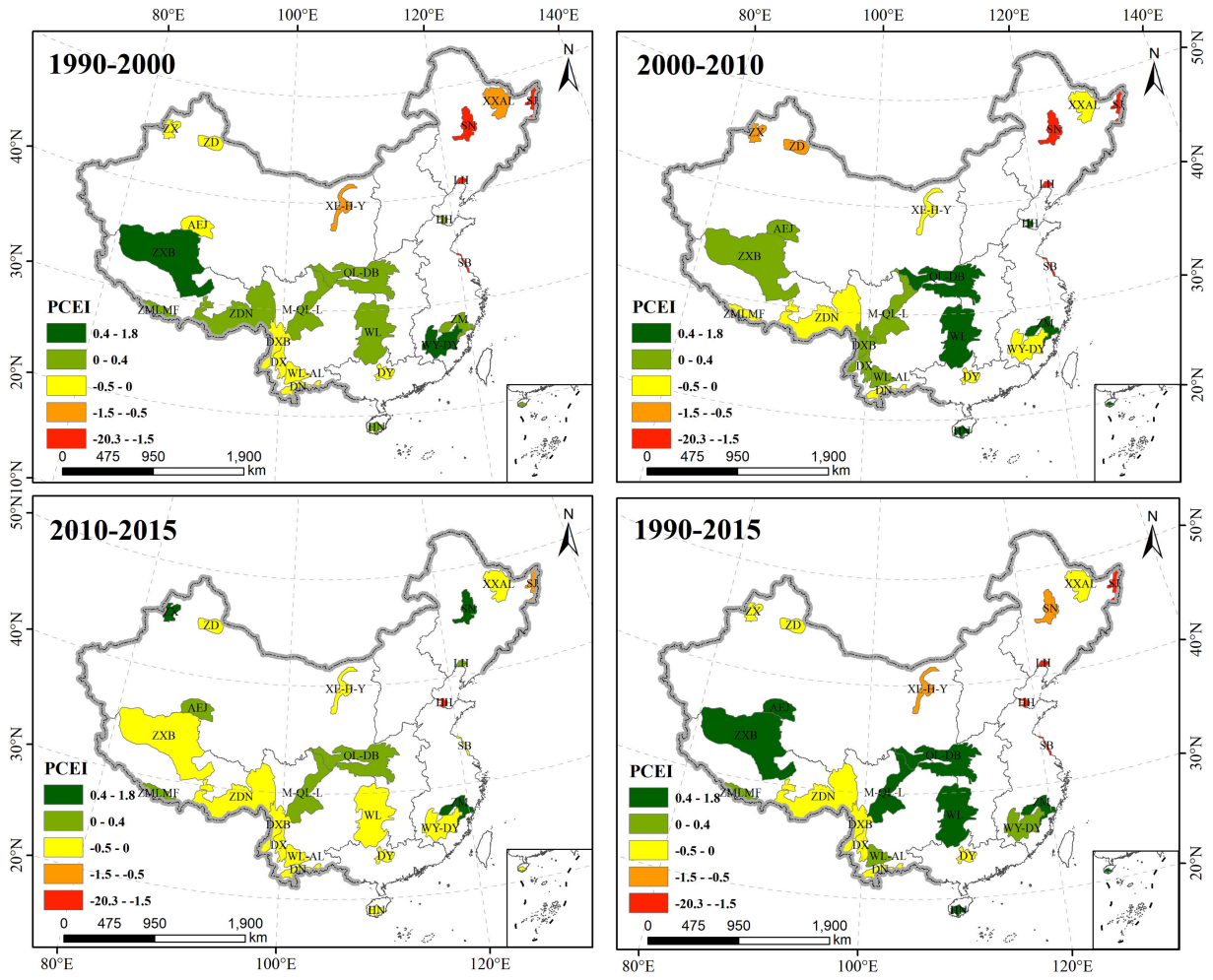

FIGURE 2
The PCEI of KEFAs during 1990–2015.

HQI is generally deteriorating in each period and the biodiversity conservation effectiveness is relatively poor; the Central China and South China KEFAs fall into the small positive type of PCEI, which indicates that the HQI is developing in the good direction in each period and the biodiversity conservation effectiveness is good; the PCEI of KEFAs in the Southwest and Northwest fluctuate up and down around the value of 0, indicating the HQI of KEFAs is unchanged and the biodiversity conservation effectiveness is in the middle. Among them, the PCEI of SJ, which is located within the Northeast, has a large negative value (−20.2), and has the worst biodiversity conservation effectiveness; the PCEI of XXAL belongs to the upper level of the region, and the conservation effectiveness is relatively good (−1.48). The PCEI of ZM and WY-DY, which are mainly forest ecosystems in East China, showed positive values, while SB and HH, which are mainly wetland ecosystems, had negative values. Only the HQI of DY in Central China and South China showed a decreasing trend and a small magnitude ($PCEI_{1990\text{-}2015} = -0.38$), while the PCEI of the rest of the KEFAs showed positive values, reflecting the good effect of biodiversity conservation. The KEFAs in the Northwest showed a small decrease in general, and the Southwest showed a small increase.

In terms of time, the results of the biodiversity conservation effectiveness assessment include three time periods: 1990–2000, 2000–2010, and 2010–2015. The differences in the direction and magnitude of changes in HQI reflect the differences in the biodiversity conservation effectiveness among the KEFAs and show a certain spatial divergence pattern in general. The HQI of KEFAs showed a significant decrease during 1990–2000, and the biodiversity conservation effectiveness was poor. The biodiversity conservation effectiveness was in the upper reaches from 2000 to 2010, and the period of 2010–2015 was in the middle of the whole assessment period. Among them, the HQI of the KEFAs in the Northeast declined significantly from 1990 to 2000, with the PCEI reaching −3.5. In addition, the biodiversity conservation effectiveness of the KEFAs in South China was poor. During 2000–2010, only the HQI of KEFAs in the Northeast continued to decline, but improved compared with the previous period. From

2010 to 2015, the HQI of KEFAs in the Northwest increased, and the biodiversity conservation effectiveness was better, while the biodiversity conservation function in the rest of the regions decreased.

Reasonableness test of the reference

The HQR is a prerequisite and basis for the implementation of the spatial comparative assessment of biodiversity conservation effectiveness, whether it can effectively reflect the spatial variation of China's natural geography will determine the quality of regional comparative assessment at the national scale. Therefore, the validation and analysis of the HQR are essential.

The pattern of spatial differentiation of climatic and topographic conditions in China necessarily constrains the spatial distribution of plant and animal species and determines the spatial differences in the natural geographic environmental context. The climatic zoning is shown in Figure 3A, the eastern part of China is divided into monsoon climate of medium latitudes, subtropical and tropical monsoon climate zones from north to south, while the northwestern part is the temperate continental climate zone and the southwestern part is the plateau climate zone. They are based on latitudinal and longitudinal zonation patterns, and the combination of Chinese terrain (Figure 3B) leads to vertical zonation. In comparison with Figure 3C, East China and South China are close to the coast, with sufficient moisture and high temperatures throughout the year, and have the best ecological environment in the country; Northeast and Central China are flat, inland, and have obvious seasonal alternation, and their natural environment background is in the middle of the country; The ecological conditions in the Northwest and Southwest are slightly inferior. The deep interior of the Northwest and the natural conditions of aridity and low rainfall results in poor biodiversity levels, while the temperature conditions in the Southwest are slightly better than those in the Northwest, but its unique vertical geographical differentiation is obvious, resulting in large differences in ecological environments within the same region. In addition, Chinese geographer Hu Huanyong discovered in 1935 that a straight line from Heihe in the Northeast to Tengchong in the Southwest could effectively distinguish the spatial distribution of population density in China, the so-called Hu Huanyong line, which is densely populated in the southeast and sparsely populated in the northwest. In essence, it also reflects the spatial differentiation of China's physical geography. There is a significant difference between the HQR of KEFAs on both sides of the Hu Huanyong line, and the HQR on the southeast side of the line (0.92) is significantly better than that on the northwest side (0.74). Therefore, the HQR can initially reflect the spatial differences in the natural environmental background of China.

The spatial variation of temperature and precipitation due to different climatic zones, the regional statistics of annual mean temperature and annual precipitation raster data using the vector boundary of the reference area, respectively, and the scatter plot are generated to quantitatively verify the rationality of the reference. As can be seen from Figure 4 and Table 1, the Northwest is in the middle to lower level, but it is the driest region in China, and under such drought conditions, its HQR presents a correspondingly low value (0.68); the HQR of the Southwest shows a positive correlation with climate elements, and the core areas of the nature reserves are distributed in both warm and humid climate zones and alpine and arid climate zones, reflecting the extreme diversity of the ecological environment due to the vertical; Although the annual mean temperature and the annual precipitation of the Northeast are low, the precipitation was higher than evaporation, this causes the HQR of the region to be at the middle to the upper level (0.93); the HQR of South China and East China is the highest because of the high annual mean temperature and high precipitation climatic conditions due to their latitude and proximity to the coast; the latitude of Central China is similar to that of East China, the average annual temperature is above the middle level, however, due to its inland location, the average annual precipitation is slightly lower than that of South China, and under these climatic conditions, the HQR of this region is in the middle to upper state (0.94). Thus, the HQR of KEFAs shows good consistency with the corresponding climatic environment elements, i.e., the better the matching of water and heat conditions, the higher their HQR.

The above analysis indicates that the HQR can better reflect the spatial differences in the ecological background of China, thus laying a good foundation for the implementation of the regional comparative assessment of biodiversity conservation effectiveness in KEFAs.

Discussion and conclusion

Discussion

The spatial variation of the HQR is reflected in the area share of ecological land in nature reserves in pristine condition, and the higher the share of ecological land, the greater the HQI. The nature reserves in South China and East China have the best climatic conditions, are close to the coast, have sufficient moisture, and have the best temperature conditions due to their lower latitude. With these two main factors, the soil is fertile and vegetation grows luxuriantly, resulting in the highest percentage of ecological land area in nature reserves. The nature reserves in Northeast and Central China have superior ecological conditions and larger ecological land areas, but the hydrothermal conditions in these regions are slightly worse than those in East China and South China, so the HQR is in the middle. The Northwest is far from the coast and has a dry climate with little rainfall, resulting in a lower percentage of ecological land area in nature reserves. Although the vegetation growth conditions in the Southwest are better than those in the Northwest, the ecological land area is still at the downstream level because of

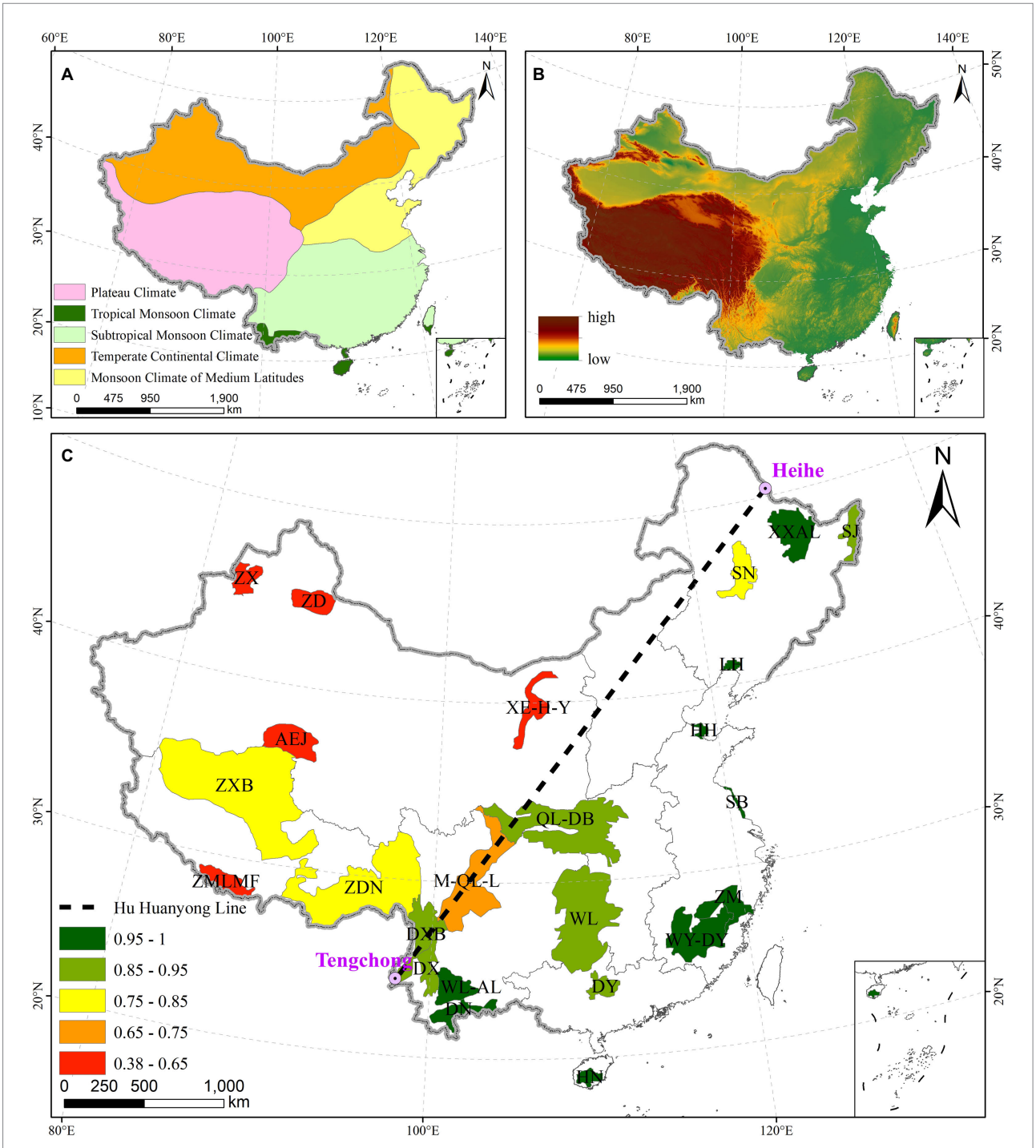

FIGURE 3
(A) China climate zone map. **(B)** China terrain map. **(C)** The HQR.

its significant vertical divergence and lower temperatures in areas located at higher elevations.

Spatially, the biodiversity conservation effectiveness is poor in the KEFAs of Northeast and East China, intermediate in Northwest and Southwest, and best in Central China and South China. Northeast has the largest plain area, which is easy for agricultural development, resulting in an increased demand for land due to rapid economic development and population growth, which substantially occupies ecological land. East China has more mountains and hills, and the land area available for development is limited, so the biodiversity conservation effectiveness is better than that of the Northeast. Northwest is arid and has little rainfall, and its unique climatic conditions lead to poor soil quality and less ecological land area, and at the same time, considering the poor

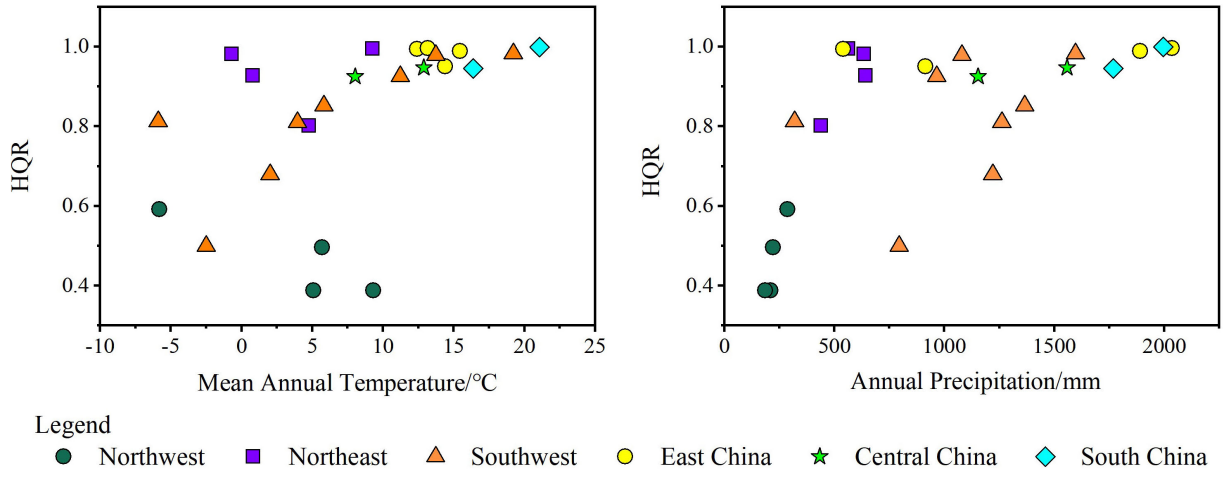

FIGURE 4
The HQR and mean annual temperature – annual precipitation scattered map.

TABLE 1 The HQR and mean annual temperature – annual precipitation.

Administrative divisions	Mean annual temperature/°C	Annual precipitation/mm	HQR
East China	13.85	1345.06	0.98
South China	18.72	1881.94	0.97
Central China	10.46	1355.90	0.94
Northeast	3.52	569.21	0.93
Southwest	5.95	1075.58	0.82
Northwest	3.56	225.61	0.47

economic benefits of the developed land, human interference is less intense; The Southwest is rich in terrain, its biodiversity has been gradually paid attention to, and the effect of carrying out conservation work has shown positive feedback, so the biodiversity conservation effectiveness in the above two regions is at the middle level of the country. Central China and South China are located in the high-quality economic development areas of China, and the ecological environment is at the forefront. Therefore, the biodiversity conservation effectiveness is at the upper level.

Temporally, the biodiversity conservation effectiveness is poor during 1990–2000, and from 2010 to 2015 is in the middle, 2000–2010 has the best conservation effectiveness. The total area of cultivated land in China is increasing from 1990 to 2000, mainly due to the reclamation of grassland and forest land in the north (Liu et al., 2003). Subsequently, biodiversity conservation functions in the Northeast and Northwest continue to decline, especially in the Northeast where intense cultivation of arable land, increased population and regional economic development, and accelerated urbanization are important driving factors (Li et al., 2010). Among them, the reclamation of arable land in the Sanjiang Plain is extremely serious, mainly from wetlands (Li et al., 2018). Compared with 1990–2000, the biodiversity conservation function in the Northeast improved slightly between 2000 and 2010 but still showed a decreasing trend, while other KEFAs increased. After 2000, the degree of human disturbance in East China showed a decreasing trend due to the implementation of the project of returning farmland to forests and grasses (Zhao et al., 2014). As a result, the biodiversity conservation function has been moderated. During 2000–2010, East China, Central China, South China, and Southwest presented better biodiversity conservation work in the project of returning farmland to forest, grass, wetland, and natural forest protection projects, respectively. Only the biodiversity conservation function of KEFAs in the Northwest increased slightly after 2010. Especially, the vegetation cover in the Northeast has improved (Shao et al., 2022), and the biodiversity conservation function has rebounded, but the ecological land was consumed too much in the early stage, and the effectiveness of biodiversity conservation is still at a low level in the national scale.

The Period-oriented spatial comparison assessment of biodiversity conservation effectiveness can effectively realize the reasonable allocation of ecological environment subsidy funds. Based on the results of this study, the number of subsidy funds can be increased for areas with better biodiversity conservation effectiveness and reduced for areas with poorer conservation effectiveness based on the PCEI. The weight of fund distribution is obtained by extracting the minimum value of PCEI of all assessment areas, taking the value downward as x, calculating the absolute value after subtracting x from the PCEI of assessment areas, and then calculating the absolute value of each area as the weight of all assessment areas, which is the fund distribution ratio (FDR), and the formula is as follows:

$$FDR = \frac{|x - PCEI_i|}{\sum_1^n |x - PCEI_i|} \times 100\%$$

where, x is a set fixed value, PCEI is the period conservation effectiveness index.

Conclusion

In this study, a PCEI was established and used to achieve a spatially comparative assessment of the biodiversity conservation effectiveness in China's KEFAs in different ecosystem types under different ecological backgrounds in three periods from 1990 to 2015, and at the same time, the scientific validity of the reference to reflect the differences in the natural environmental background was further verified.

The main conclusions are as follows:

1. Spatially, the KEFAs in Central China and South China have reached saturation level of development and have begun to focus on rational land use, with better biodiversity conservation effectiveness. Southwest and Northwest have less development potential and less intensive human interference, so the biodiversity conservation effectiveness is medium. East China and the Northeast have fertile soil and are conducive to reclamation, so the biodiversity conservation effectiveness is poor.

2. In terms of time, the biodiversity conservation effectiveness was poor from 1990 to 2000, and the intensity of land development was the highest in this period, which turned better from 2000 to 2010 and the biodiversity conservation effectiveness was the best in this period, during 2010–2015 was in the middle.

3. The reference can better reflect the differences in the natural environment background of China, and can effectively support the spatial comparison assessment of the biodiversity conservation effectiveness. Based on the results of this study, can provide a scientific basis for the transfer payment policy in China and the implementation of ecological compensation in other countries.

Data availability statement

The original contributions presented in the study are included in the article/supplementary material, further inquiries can be directed to the corresponding author.

Author contributions

ZC designed and completed the manuscript. ZL and YZ reviewed and revised the manuscript. GH, KD and CY contributed to data collection. All authors have read and agreed to the published version of the manuscript.

Funding

This research was funded by the National Key Research and Development Program of China (Project Nos. 2021YFD1500104-3 and 2016YFC0500204).

Conflict of interest

The authors declare that the research was conducted in the absence of any commercial or financial relationships that could be construed as a potential conflict of interest.

The handling editor HZ declared a shared affiliation with the authors ZL and GH at the time of review.

Publisher's note

All claims expressed in this article are solely those of the authors and do not necessarily represent those of their affiliated organizations, or those of the publisher, the editors and the reviewers. Any product that may be evaluated in this article, or claim that may be made by its manufacturer, is not guaranteed or endorsed by the publisher.

References

Brooks, T. M., Wright, S. J., and Sheil, D. (2009). Evaluating the success of conservation actions in safeguarding tropical forest biodiversity. *Conserv. Biol.* 23, 1448–1457. doi: 10.1111/j.1523-1739.2009.01334.x

Chen, Z. Q., Dong, K. K., Zhang, Y. H., Hou, G. L., and Liu, Z. L. (2022). Regional comparative assessment of biodiversity conservation effectiveness in national important ecological function areas. *J. Ecol.* 42, 5264–5274. doi: 10.5846/stxb202105081205

Dong, K. K., Hou, G. L., Xu, D. D., He, H. L., and Liu, Z. L. (2018). A method to compare the biodiversity conservation effectiveness between regions based on a reference condition. *Sustainability* 10:3694. doi: 10.3390/su10103694

Feng, C., Cao, M., Wang, W., Wang, H., Liu, F., Zhang, L., et al. (2021). Which management measures lead to better performance of China's protected areas in reducing forest loss? *Sci. Total Environ.* 764:142895. doi: 10.1016/j.scitotenv.2020.142895

Gantioler, S., Rayment, M., ten Brink, P., McConville, A., Kettunen, M., and Bassi, S. (2014). The costs and socio-economic benefits associated with the Natura 2000 network. *Int. J. Sustain. Soc.* 6:135. doi: 10.1504/IJSSOC.2014.057894

Gaston, K. J., and Cruz-Piñón, G. (2008). The ecological performance of protected areas. *Annu. Rev. Ecol. Evol. Syst.* 39, 93–113. doi: 10.1146/annurev.ecolsys.39.110707.173529

Gong, J., Xie, Y., Cao, E., Huang, Q., and Li, H. (2019). Integration of InVEST-habitat quality model with landscape pattern indexes to assess mountain plant biodiversity change: a case study of Bailongjiang watershed in Gansu Province. *J. Geogr. Sci.* 29, 1193–1210. doi: 10.1007/s11442-019-1653-7

Gray, C. L., Hill, S. L., Newbold, T., Hudson, L. N., Börger, L., Contu, S., et al. (2016). Local biodiversity is higher inside than outside terrestrial protected areas worldwide. *Nat. Commun.* 7, 1–7. doi: 10.1038/ncomms12306

He, L. H., Liu, H. J., Li, B. L., and Wang, Y. Y. (2014). Design and application practice of ecological environment quality assessment index system for counties in national key ecological function areas. *Environ. Prot.* 42, 42–45. doi: 10.14026/j.cnki.0253-9705.2014.12.011

Hou, P., Yang, M., Zhai, J., Liu, X., Wan, H., Li, J., et al. (2017). On nature reserves and the construction of national ecological security pattern. *Geogr. Res.* 36, 420–428. doi: 10.11821/dlyj201703002

Li, Y. Y., Tan, M. H., and Zhang, H. Q. (2018). The impact of changing spatial patterns of cropland on grain production in China. *China Eng. Sci.* 20, 90–95. doi: 10.15302/J-SSCAE-2018.05.014

Li, X. Y., Zhao, G. M., and Li, B. Y. (2010). Analysis of land resource change trends in Northeast China. *Soil Water Conserv. Res.* 17, 68–74.

Liu, F. T., and Xu, E. Q. (2020). Comparison of spatial and temporal evolution of habitat quality between Xinjiang corps and non-corps based on land use. *J. Appl. Ecol.* 31, 2341–2351. doi: 10.13287/j.1001-9332.202007.014

Liu, J. Y., Zhang, Z. X., Zhuang, D. F., Wang, Y. M., Zhou, W. C., Zhang, S. W., et al. (2003). Spatial and temporal characteristics of land use change in China in the 1990s and its causes. *Geogr. Res.* 01, 1–12. doi: 10.11821/yj2003010001

Ren, G., Young, S. S., Wang, L., Wang, W., Long, Y., Wu, R., et al. (2015). Effectiveness of China's national forest protection program and nature reserves. *Conserv. Biol.* 29, 1368–1377. doi: 10.1111/cobi.12561

Shao, Q. Q., Liu, S. C., Ning, J., Liu, G. B., Yang, F., Zhang, X. Y., et al. (2022). Remote sensing assessment of ecological benefits of major ecological projects in China from 2000 to 2019. *J. Geogr.* 77, 2133–2153. doi: 10.11821/dlxb202209001

Shui, Y. P., Lu, H. T., Wang, H. F., Yan, Y., and Wu, G. (2018). Habitat quality assessment of the Lhasa River basin based on land cover and NDVI changes. *J. Ecol.* 38, 8946–8954.

Sun, X., Jiang, Z., Liu, F., and Zhang, D. (2019). Monitoring spatio-temporal dynamics of habitat quality in Nansihu Lake basin, eastern China, from 1980 to 2015. *Ecol. Indic.* 102, 716–723. doi: 10.1016/j.ecolind.2019.03.041

Tang, F., Fu, M., Wang, L., and Zhang, P. (2020). Land-use change in Changli County, China: predicting its spatio-temporal evolution in habitat quality. *Ecol. Indic.* 117:106719. doi: 10.1016/j.ecolind.2020.106719

Wang, H., Tang, L., Qiu, Q., and Chen, H. (2020). Assessing the impacts of urban expansion on habitat quality by combining the concepts of land use, landscape, and habitat in two urban agglomerations in China. *Sustainability* 12:4346. doi: 10.3390/su12114346

Xu, D. D., Hou, G. L., Dong, K. K., He, H. L., and Liu, Z. L. (2018). Regional comparative assessment of the effectiveness of wetland biodiversity conservation based on reference. *Wetland Sci.* 16, 120–129.

Xu, W. H., Xiao, Y., Zhang, J. J., Yang, W., Zhang, L., Hull, V., et al. (2017). Strengthening protected areas for biodiversity and ecosystem services in China. *PNAS* 114, 1601–1606. doi: 10.1073/pnas.1620503114

Zhao, G. S., Liu, J. Y., Kuang, W. H., and Ouyang, Z. Y. (2014). Land use change perturbation in priority areas for biodiversity conservation in China from 1990 to 2010. *J. Geogr.* 69, 1640–1650. doi: 10.11821/dlxb201411005

Zheng, Y. M., Zhang, H. Y., Niu, Z. G., and Gong, P. (2012). Preliminary assessment of the conservation effectiveness of national wetland nature reserves in China. *Sci. Bull.* 57, 207–230. doi: 10.1007/s11434-011-4942-9

Zhu, C., Zhang, X., Zhou, M., He, S., Gan, M., Yang, L., et al. (2020). Impacts of urbanization and landscape pattern on habitat quality using OLS and GWR models in Hangzhou, China. *Ecol. Indic.* 117:106654. doi: 10.1016/j.ecolind.2020.106654

10.3389/fevo.2022.1031008

Appendix

The following abbreviations are used in this manuscript:
Abbreviations

XXAL - Xiaoxing'an Ling ecological function area

SJ - Sanjiang Plain Wetland ecological function area

SN - The Songnen Plain ecological function area

LH - Liaohe Delta Wetland ecological function area

HH - Yellow River Delta Wetland ecological function area

SB - Coastal SuBei Delta Wetland ecological function area

ZM - ZheMin mountains ecological function area

WY-DY - WuYI-DaiYun mountains ecological function area

QL-DB - QinLing-DaBa mountains ecological function area

WL - WuLing mountains ecological function area

DY - DaYao mountains ecological function area

HN - Central HaiNan ecological function area

DN - Southern Yunnan ecological function area

WL-AL - WuLiang-AiLao mountains ecological function area

DX - West YunNan mountains ecological function area

DXB - Northwest YunNan Plateau ecological function area

M-QL-L - Min -Qionglai-Liang mountains ecological function area

ZDN - Southeast Tibet ecological function area

ZMLMF - Mount Everest ecological function area

ZXB - Qiangtang Plateau, Northwest Tibet ecological function area

AEJ - Southern foothills of altun mountain ecological function area

XE-H-Y - West Ordos-Helan-Yin Mountains ecological function area

ZD - Eastern Junggar Basin ecological function area

ZX - Western Junggar Basin ecological function area

frontiers | Frontiers in Environmental Science

TYPE Original Research
PUBLISHED 10 November 2022
DOI 10.3389/fenvs.2022.1014856

Check for updates

OPEN ACCESS

EDITED BY
Bing Xue,
Institute for Advanced Sustainability Studies (IASS), Germany

REVIEWED BY
Dongrui Han,
Shandong Academy of Agricultural Sciences, China
Bao-Jie He,
Chongqing University, China

*CORRESPONDENCE
Jilin Gu,
gujilin@lnnu.edu.cn
Ling-en Wang,
wangle@igsnrr.ac.cn

SPECIALTY SECTION
This article was submitted to Environmental Informatics and Remote Sensing,
a section of the journal
Frontiers in Environmental Science

RECEIVED 09 August 2022
ACCEPTED 14 October 2022
PUBLISHED 10 November 2022

CITATION
Meng F, Gu J, Wang L-e, Qin Z, Gao M, Chen J and Li X (2022), A quantitative model based on grey theory for sea surface temperature prediction. *Front. Environ. Sci.* 10:1014856. doi: 10.3389/fenvs.2022.1014856

COPYRIGHT
© 2022 Meng, Gu, Wang, Qin, Gao, Chen and Li. This is an open-access article distributed under the terms of the Creative Commons Attribution License (CC BY). The use, distribution or reproduction in other forums is permitted, provided the original author(s) and the copyright owner(s) are credited and that the original publication in this journal is cited, in accordance with accepted academic practice. No use, distribution or reproduction is permitted which does not comply with these terms.

A quantitative model based on grey theory for sea surface temperature prediction

Fanyu Meng[1], Jilin Gu[1,2]*, Ling-en Wang[3]*, Zhibin Qin[1], Mingyao Gao[4], Junhong Chen[1] and Xueming Li[2]

[1]School of Physics and Electronic Technology, Liaoning Normal University, Dalian, China, [2]School of Geography, Liaoning Normal University, Dalian, China, [3]Institute of Geographic Sciences and Natural Resources Research, Chinese Academy of Sciences, Beijing, China, [4]School of Foreign Languages, Liaoning Normal University, Dalian, China

In order to predict sea surface temperature (SST), combined with the genetic algorithm and the least-squares method, a GM(1,1|sin) power model prediction method based on similarity deviation is proposed. We first combined the data of two consecutive years into a new time series, analyzed the similarity of the data of the previous year, and obtained the most similar year and the corresponding new time series. Then, we established a GM(1,1|sin) power model to predict SST. In model validation, we predicted the monthly average SST from 2016 to 2020 with the data from 1985 to 2015, 2016, 2017, 2018, and 2019. The validation results showed that the maximum mean relative error (MRE) was 13.28%, the minimum MRE was 5.54%, and the average MRE and the root mean square error (RMSE) were 9.81% and 1.0627, respectively. All of evaluation metrics of Lin's concordance correlation coefficient (LCCC) and the ratio of performance to deviation (RPD) were excellent. We iteratively predicted the monthly average SST from 2016 to 2020 with the data from 1985 to 2015, the maximum MRE was 13.91%, the minimum was 7.80%, and the average MRE, RMSE, LCCC and RPD are 11.07% 1.0603, 0.9894, and 7.497, respectively. Compared with GM(1,1), GM(1,1|sin + cos), and GM(1,1|sin) models, the proposed model outperformed these models with at least 50% in the MRE. It proves that the proposed model can be regarded as a better solution to predicting SST.

KEYWORDS

sea surface temperature, grey theory, GM(1,1|sin) power model, genetic algorithm, prediction

1 Introduction

SST prediction is closely related to the daily life of human beings, and understanding the changes of SST in advance plays an important leading role in the school of fish swimming, deep sea exploration, cold wave warning, and even military defense (Shi et al., 2018).SST is one of the most important parameters in the study of global oceanic and atmospheric interactions. The prediction of SST is to predict the sea temperature field, especially the SST changes with time. Accurate prediction of SST can provide effective

support for coping with marine disasters such as storms and typhoons and prevent red tide (Sun et al., 2020).

Today, more than a dozen countries have made outstanding contributions to sea water temperature prediction services. Among them, the United States, the former Soviet Union, and Japan publicly provide the largest number of sea water temperature analysis and prediction products (Wang et al., 2021). Sea water temperature prediction in China began in the early 1960s. At first, Shandong Ocean University, Shandong Marine and Fishery Research Institute, and Yantai Meteorological Institute cooperated to explore the single-station water temperature prediction method in the offshore area of Yantai. With the need of the development of marine economy, the daily average SST prediction of a single station in coastal cities and the water temperature prediction of coastal bathing beaches have been successively carried out (Zhang, 2004).

There have been many studies on the prediction of sea water temperature in recent years. Dong et al. (2008) reconstructed the time series in phase space and used a fuzzy neural network. The relative error of the predicted value was controlled within 10%, and the fitting correlation coefficient was 0.98. Jin et al. (1999) using a threshold autoregressive model selected sea surface temperature data from 1963 to May 1994 in Dalian's Tiger Beach. The number of threshold intervals and the search range of threshold values were found by global optimization combined with a genetic algorithm. The predicted value in May 1995 was 0.58°C which was different from the measured value. Lu et al. (2009) selected CTD data of the East China Sea and the non-stationary time series were stabilized by the EMD method, and the correlation coefficient reached 0.94. He et al. (2020) selected remote-sensing data from the AVHRR satellite and adopted the periodic trend decomposition method of locally weighted regression, combined with the neural network, and the root mean square error reached 0.79°C. Kim et al. (2020) proposed a HWT prediction method based on a recursive neural network (RNN). The correlation coefficient range of prediction was from 0.9936 to 0.959, and the root mean square error range was from 0.5076°C to 1.3238°C. Wang et al. (2021) established a multi-variable artificial neural network model. The RMSE achieved based on the training results of SST was 0.348°C. Zhang et al. (2020) designed a recursive unit (GRU) neural network algorithm on the basis of gating for medium and long-term SST prediction, and its average absolute error was within the range of 0–2.5°C. Zhang et al. (2019) using EEMD obtained the eigenmode function, which solved the problem of the high signal-to-noise ratio of the results of the EMD algorithm and further improved the prediction accuracy, and the agreement degree between the predicted value and the measured value reached 99.61%. Qu et al. (2021) used the multi-scale fusion method to predict the daily mean temperature of sea water with a root mean square error of 0.996°C and also made a prediction on an hourly scale with a root mean square error of 1.06°C. Li et al. (2020) used the deep neural network based on long and short memory to achieve a root mean square error of 0.5°C in 1 month and 0.66°C in 12 months. Lu et al. (2021) used the CMIP5 model to predict the next 100 years, and the results showed that SST would increase significantly by 2100: SST would increase by about 1.55°C per decade, while seasonal SST would increase by 1.03–1.95°C. Sung et al. (2021) used the CMIP6 model to calculate the temperature around the Korean Peninsula which will increase from 0.49°C to 0.59°C every 10 years.

How to improve the accuracy of grey prediction theory in the oscillation sequence has become a topic for mathematicians. The research achievements that have made breakthroughs are mainly divided into two aspects in recent years: on the one hand, the processing of the original sequence is improved. Zhao and Wu (2010) carried out translation transformation and geometric average transformation operation on the original data sequence. Li and Liu (2020) proposed the grey interval GM(1,1) model by the upper bound sequence and the lower bound sequence of the original sequence was taken. Zeng et al. (2020) used a new-structure grey Verhulst model for predicting China's tight gas production and the comprehensive error was 2.07%. Qian and Dang (2009) carried out accelerated translation transformation and weighted mean generation transformation of the original sequence. Cui and Liu (2012) proposed to carry out accelerated exponential transformation and geometric average generation transformation of the original sequence. On the other hand, the bleaching equation in grey prediction theory is improved, Wang and Luo (2017) used a fractional discrete GM(1,1) power model based on the GM(1,1) power model. Wang et al. (2013) carried out the power function optimization of the GM(1,1) power model, and five derived models are proposed, including the oscillating GM(1,1) power model with time-varying parameters and considering the system delay. The residual error is also predicted by using the Fourier series, which improves the grey prediction theory to certain extent. Zeng and Li (2021) introduced a new action quantity k^2d and r-order was introduced into the traditional three-parameter discrete grey forecasting model. The results show that the comprehensive mean relative percentage error of the new model was 0.4765%. In this study, the GM(1,1|sin) power model is selected to estimate the SST.

To minimize the impact of the cold snap on the SST prediction, we used data from 1985 to 2020 to predict the SST for the next 50 years. However, these 35 years of data are not sufficient to predict temperature trends over the next 50 years. In view of the current situation, we designed a grey prediction model to obtain more reliable data to successfully overcome the problem resulting from insufficient data. Grey prediction theory is a kind of the dynamic model which uses discrete data to establish a differential equation based on the concepts of correlation space, smooth discrete functions, and so on. The equation is named as the grey model (GM) that generates discrete random numbers into numbers whose randomness is significantly weakened and more regular, so

that it is convenient to study and describe the process of its change. The GM has a strict theoretical foundation and advantage of practicality. Therefore, the results of the grey prediction model are relatively stable, which is not only applicable to the prediction of large data amount, but also accurate when the data amount is small (Zeng et al., 2020).The GM is a powerful method for the problems characterized by samples with uncertainty. By identifying different degrees of development trends among system factors, the GM generates strong regularity of data sequences and then establishes the corresponding differential equation model to predict the future trend. The GM holds that the behaviors of systems are in order for the purpose of the implementation of a certain function, although they seem hazy and complex (Yin, 2017). The traditional GM(1,1) prediction curve is approximate to a straight line, so it can only be predicted for some monotonic increasing or decreasing sequences. The prediction of the sea water temperature with strong fluctuation of vibration is not suitable for GM(1,1) (Tang et al., 2008). Zeng, 2019 established a GM(1,1|sin) power model based on the GM(1,1|sin) model to solve the compound oscillation sequence with different periods.

The purpose of this study was to use the experience predict method to establish a prediction model of SST which can be easily implemented and applied, a GM(1,1|sin) power model prediction method based on similarity deviation was proposed. We first combined the data of two consecutive years into a new time series, analyzed the similarity of the data of the previous year, and obtained the most similar year and the corresponding new time series. Then, we established a GM(1,1|sin) power model to predict SST. Based on the MATLAB simulation, this method used data from 1985 to 2015, a total of 372 monthly average SST to predict data of 2016–2020, and compared with the measured data, then predicted the SST of the 50 years after 2020, and drew conclusions.

2. Materials and methods

2.1 Data sources

The SST series is a kind of a time series. A time series refers to the sequence formed by arranging the values of a variable at different times in time sequence, and its time scale can be a day, month, year, hour, etc. The time series model is a mathematical model established by using the time series. It is mainly used for short-term prediction of the future and belongs to the trend predicting method. In reality, the vast majority of phenomena are rapidly changing. With the passage of time, the internal and external influencing factors change greatly, which reduces the prediction accuracy gradually. The method of time series analysis and prediction predicts the future according to the development trends and change rules of past and present, which can only make effective predictions in a relatively short period of time.

The SST data used in this study are reanalysis data and measured data from the National Data Center for Marine Science. The data are from the Northwest Pacific Ocean Reanalysis Product (CORA V1.0). The product elements include sea surface height, temperature, salinity, and currents. The sea area ranges from 99°E to 150°E and 10°S to 52°N, the spatial horizontal grid resolution is 0.5° × 0.5°, and the number of the vertical layer is 35. The length of time is 60 years from January 1958 to December 2018, and the time resolution is the monthly average of the past years. The spatial horizontal grid resolution of the measured data is 0.125° × 0.125°, which is the same as that of the reanalyzed data. The time span is 5 years from 2016 to 2020, and the time resolution is the daily average. If there is a null value in the data set, the cubic spline interpolation method is used for complement.

The product was developed based on the ocean reanalysis system of the Northwest Pacific Ocean, and the ocean dynamic model of the system was the Princeton Ocean Model with the Generalized Coordinate System (POMGCS). The meteorological driving field is the NCEP meteorological reanalysis field. The ocean data assimilation method used is the multi-grid three-dimensional variational ocean data assimilation method. The assimilated ocean observations include *in situ* temperature and salinity observations, satellite remote sensing sea surface height anomaly (SSHA), and sea surface temperature (Reynolds SST) data. National Marine Science data in the heart of the reanalysis data format for.nc database files is more than 67 Giga bytes, at the same time, the original file format in the actual use process is relatively complex, so it must be prepared in advance according to the requirements that will be appropriate for waters of the sea surface temperature extracted and stored as .mat format, and the read load can be used on MATLAB. This study takes the Bohai Sea as the research object and obtains the surface temperature of the Bohai Sea on a certain day, as shown in Figure 1.

As shown in Figure 2A, the observation of the SST series shows that the Bohai Sea area presents a single peak shape in the process of changing with month, that is, the maximum and minimum temperature values only appear once in every 12 months in a year. Along with the number of days in a month to promote the process of SST rendering multiple peak shapes, as shown in Figure 2B, that is, the trend of rising and falling will appear multiple times in a month. It can be seen that the variation characteristics of SST in different time scales are also different. If we observe

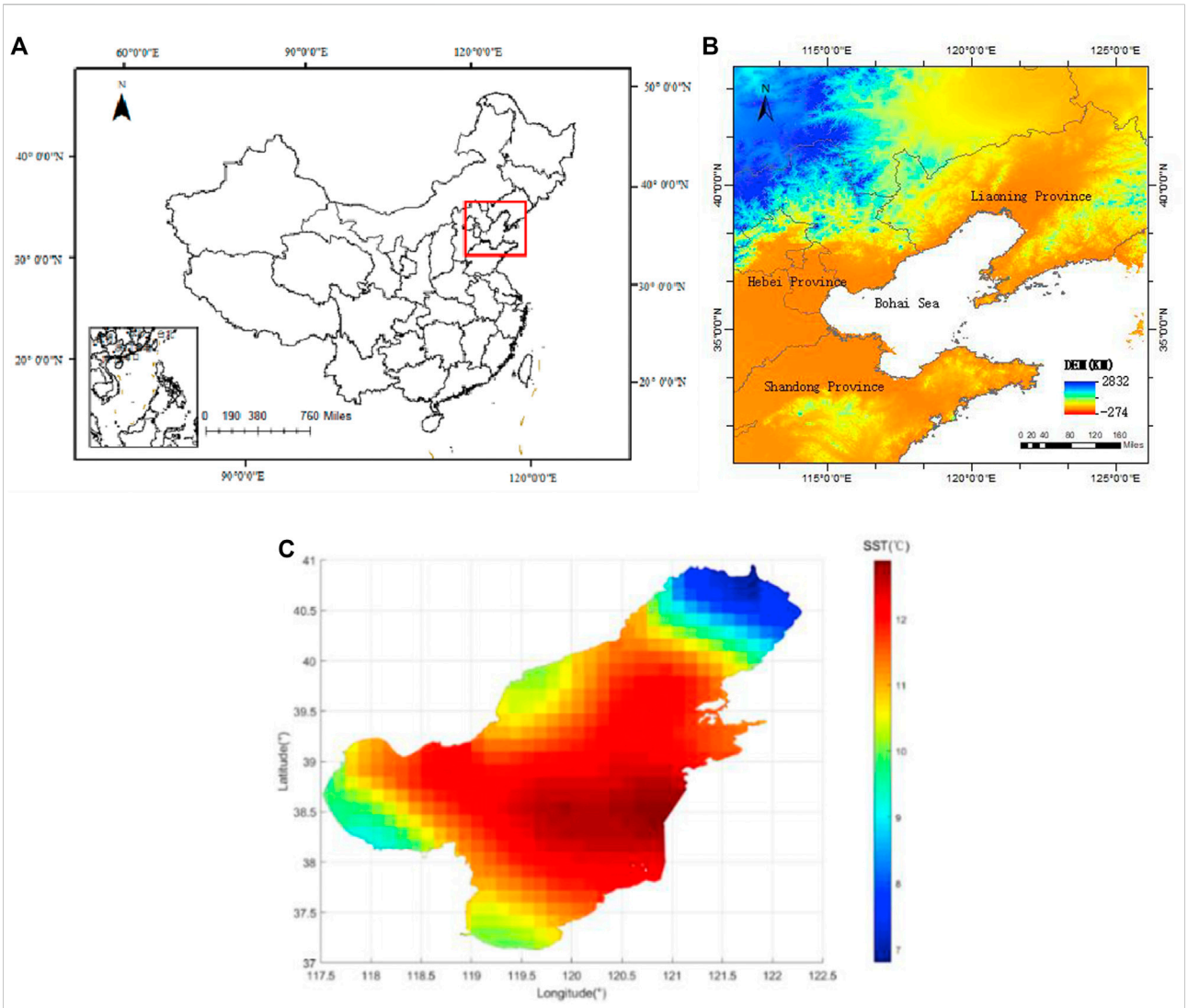

FIGURE 1
Map of China **(A)**. Elevation map of the Bohai Sea **(B)**. SST of the Bohai Sea **(C)**.

SST on a daily scale, we can find that the change in SST is very dissimilar. If we observe SST on a monthly scale, it can be found that the SST has high similarity and obvious periodicity in different years. The similarity and periodicity of SST are conducive to the prediction of future temperature.

2.2 The evaluation metrics of sea surface temperature

In the process of predicting the future monthly average SST, we can make use of the similarity of the data over the past years to conduct the appropriate comparison. Therefore, the metrics of similarity assessment directly determine the accuracy of SST prediction results. There are many metrics to evaluate the similarity between two samples. The similarity deviation is introduced in this study. The mean relative error (MRE), the posterior difference ratio (PDR), and the probability of small error (PSE) are the metrics to evaluate whether the prediction sequence is suitable for the real sequence and sufficient to predict in the future.

If we have two samples, A(1) is the value of the first sample, B(1) is the value of the second sample, and the total number of both samples is N. Then, the mean relative error is as follows:

$$\mathrm{MRE} = \frac{1}{N}\sum_{i=1}^{N}\left|\frac{A(i) - B(i)}{A(i)}\right| \times 100\%. \quad (1)$$

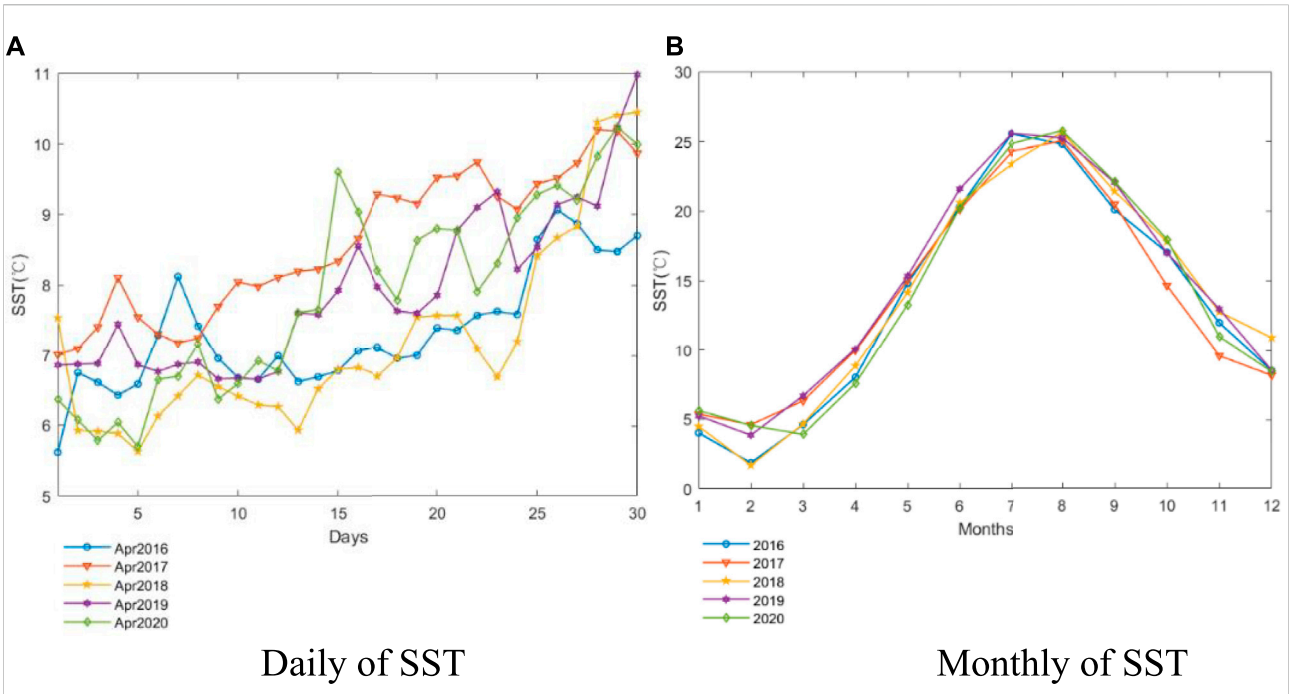

FIGURE 2
Change trend of SST in recent 5 years.

TABLE 1 Predictive model test criteria.

Level	MRE	PDR	PSE
I level	<0.01	<0.35	>0.95
II level	<0.05	<0.50	<0.80
III level	<0.10	<0.65	<0.70
IV level	>0.20	>0.80	<0.60

The residuals between two samples $e(i)$ and the mean values of the residuals $\overline{e(i)}$:

$$e(i) = A(i) - B(i), \tag{2}$$

$$\overline{e(i)} = \frac{\sum_{i=1}^{N} e(i)}{N}. \tag{3}$$

Posterior difference ratio:

$$PDR = \frac{S_2}{S_1}, \tag{4}$$

where

$$S_1 = \frac{\sum_{i=1}^{N} \left[A(i) - \overline{A(i)}\right]^2}{N}, \tag{5}$$

$$S_2 = \frac{\sum_{i=1}^{N} \left[e(i) - \overline{e(i)}\right]^2}{N}. \tag{6}$$

The S_1 is the variance of sample one, and S_2 is the variance of the residual between the first and second samples.

The calculation formula of the probability of small error (PSE) is defined in Eq. 7. Table 1 shows the relationship between the aforementioned parameters and the grey model accuracy.

$$PSE = P\{|e(i)| < 0.6745S_1\}. \tag{7}$$

In addition, the root mean square error (RMSE) and MRE are selected as the evaluation parameters of prediction accuracy. The formula for RMSE is as follows:

$$RMSE = \sqrt{\frac{\sum_{i=1}^{N} (A(i) - B(i))^2}{N}}. \tag{8}$$

Similarity deviation is the parameter to reflect the difference between the "shape" and "value" of two samples. The similarity deviation of these two samples can be defined as S_{AB}.

$$S_{AB} = \frac{D_{AB} + E_{AB}}{2}, \tag{9}$$

where

$$D_{AB} = \frac{\sum_{i=1}^{N} |A(i) - B(i)|}{N}, \tag{10}$$

$$E_{AB} = \frac{\sum_{i=1}^{N} \left|e(i) - \overline{e(i)}\right|}{N}. \tag{11}$$

TABLE 2 Result of similarity deviation.

Sample	I						D_{AB}	E_{AB}	S_{AB}
	1	2	3	4	5	6			
$A(i)$	4.0181	1.8664	3.6023	6.9999	11.7975	17.3094	—	—	—
$B(i)$	5.3615	3.6011	4.3084	7.9513	13.0270	18.1010	1.126	0.309	0.718
$C(i)$	5.6174	3.5502	3.9109	7.9562	11.2700	19.2323	1.166	0.745	0.956

TABLE 3 Result of similarity deviation.

Evaluation	LCCC	RPD
Excellent	>0.9	>2.5
Very good	0.8–0.9	2–2.5
Good	0.65–0.8	1.8–2
Poor	<0.65	<1.8

In Eq. 10, D_{AB} reflects the coefficient of "value." In Eq. 11, E_{AB} reflects the coefficient of "shape." The default similarity deviation is the average value of the two metrics. The smaller the similarity deviation is, the higher the similarity between the two samples is. The monthly average temperature of the first two quarters of 3 years at a point in the Bohai Sea is defined as three samples. Based on the first sample as the benchmark, Table 2 shows the data points of the last two samples, as well as the calculated "value" coefficient, "shape" coefficient, and similar deviation. The results show that the second sample is more similar to the first sample. In other words, the use of this similarity criterion can provide some reference in the subsequent prediction.

The Lin's concordance correlation coefficient (LCCC) was used to evaluate the prediction model performance, because it measures the "agreement" between predicted and measured values (Zhao et al., 2021a,b).

$$LCCC = \frac{2s_{AB}}{s_A^2 + s_B^2 + \left(\bar{A} - \bar{B}\right)^2}, \tag{12}$$

where $\bar{A}$ and $\bar{B}$ are the means for the real and predicted values, and s_A^2 and s_B^2 are the corresponding variances.

$$s_{AB} = \frac{1}{N}\sum_{i=1}^{N}\left(A(i) - \bar{A}\right)\left(B(i) - \bar{B}\right). \tag{13}$$

Prediction accuracy was also assessed using the ratio of performance to deviation (RPD), which is calculated as the ratio of standard deviation (SD) to RMSE.

$$RPD = \frac{SD}{RMSE}. \tag{14}$$

These two indexes divide the accuracy of the prediction model into four levels, as shown in Table 3.

2.3 The SST prediction model

2.3.1 Data preprocessing

$X^{(0)}$ is defined as the sea surface temperature (SST) sequence.

$$X^{(0)} = \{X_1^{(0)}, X_2^{(0)}, X_3^{(0)}, \ldots, X_n^{(0)}\}. \tag{15}$$

The original data were cumulated to get the cumulative sequence, so as to weaken the volatility and randomness of the original sequence. The new data sequence is defined as $X^{(1)}$.

$$X^{(1)} = \{X_1^{(1)}, X_2^{(1)}, X_3^{(1)}, \ldots, X_n^{(1)}\}, \tag{16}$$

$$X_t^{(1)} = \sum_{k=1}^{t} X_k^{(0)}. \tag{17}$$

According to the smoothness ratio test theory, the grade ratio and smoothness ratio test of SST can be defined as

$$\sigma(i) = \frac{X_i^{(1)}}{X_{i-1}^{(1)}} \quad i = 2, 3, 4, \ldots, n, \tag{18}$$

$$\rho(i) = \frac{X_i^{(0)}}{X_{i-1}^{(1)}} \quad i = 2, 3, 4, \ldots, n. \tag{19}$$

When $i > 3$, if $\sigma(i) < 2$ and $\rho(i) < 0.5$, the data follow the exponential law and meet the smoothness requirements, so the grey prediction model for the sequence can be established (Wang, 2017). Table 4 shows the grade ratio and smoothness ratio of the monthly average SST in the recent 5 years. According to the corresponding data, it can be found that when $i > 3$, the maximum grade ratio of the monthly average SST series of 2020 is 1.613, and the maximum smoothness ratio is 0.380, which meets the data index law and smoothness requirements.

2.3.2 Modeling

For the cumulative sequence $X^{(1)}$ set up GM(1,1|sin) power model, the corresponding bleaching equation is define

$$\frac{dX^{(1)}}{dt} + aX^{(1)} = b(\sin \omega t)^{\beta} + u, \tag{20}$$

TABLE 4 Original sequence grade ratio and smoothness ratio test.

Month i	2016		2017		2018		2019		2020	
	$\sigma(i)$	$\rho(i)$	$\sigma(i)$	$\rho(i)$	$\sigma(i)$	$\rho(i)$	$\sigma(i)$	$\rho(i)$	$\sigma(i)$	$\rho(i)$
2	1.464	0.317	1.858	0.462	1.378	0.274	1.738	0.424	1.810	0.448
3	1.782	0.439	1.633	0.388	1.754	0.430	1.734	0.423	1.385	0.278
4	1.763	0.433	1.612	0.379	1.815	0.449	1.638	0.389	1.537	0.349
5	1.800	0.445	1.573	0.364	1.720	0.419	1.594	0.373	1.613	0.380
6	1.610	0.379	1.487	0.328	1.609	0.379	1.525	0.344	1.580	0.367
7	1.477	0.323	1.395	0.283	1.429	0.300	1.408	0.290	1.450	0.310
8	1.313	0.239	1.293	0.226	1.330	0.248	1.286	0.222	1.322	0.244
9	1.193	0.162	1.185	0.156	1.207	0.171	1.194	0.163	1.209	0.173
10	1.137	0.121	1.112	0.100	1.143	0.125	1.125	0.111	1.140	0.123
11	1.085	0.078	1.066	0.062	1.089	0.082	1.085	0.078	1.075	0.070
12	1.056	0.053	1.053	0.050	1.070	0.065	1.052	0.049	1.054	0.051

where a, b is called the development coefficient, u is called the grey action, and ω and β are constant. When $\omega = 0$, this model is converted into the traditional GM(1,1) model, when the $\beta = 1$, this model is converted into the GM(1,1|sin) model. After the values of ω and β are determined, the column matrix composed of a, b , and u is denoted as $\hat{a}$.

$$\hat{a} = \begin{pmatrix} a \\ b \\ u \end{pmatrix}. \tag{21}$$

According to the cumulative sequence $X^{(1)}$, the mean generator matrix B and the constant term vector Y_n are defined as follows:

$$B = \begin{pmatrix} -0.5\left(X^{(1)}(1) + X^{(1)}(2)\right)(\sin 2\omega)^{\beta} & 1 \\ -0.5\left(X^{(1)}(2) + X^{(1)}(3)\right)(\sin 3\omega)^{\beta} & 1 \\ \cdots & \cdots \quad \cdots \\ -0.5\left(X^{(1)}(n-1) + X^{(1)}(n)\right)(\sin n\omega)^{\beta} & 1 \end{pmatrix}, \tag{22}$$

$$Y_n = \begin{pmatrix} X^{(0)}(2) \\ X^{(0)}(3) \\ \cdots \\ X^{0}(n) \end{pmatrix}. \tag{23}$$

The least-squares method is used to obtain the grey parameter $\hat{a}$ shown in .

$$\hat{a} = \begin{pmatrix} a \\ b \\ u \end{pmatrix} = \left(B^T B\right)^{-1} B^T Y_n. \tag{24}$$

By putting the grey parameter $\hat{a}$ into the linear equation, we obtain the following value:

$$\hat{X}^{(1)}(t+1) = be^{-a(t+1)}\left\{\int_1^{t+1} (sin\,\omega\varepsilon)^{\beta} e^{a\varepsilon} d\varepsilon + \frac{1}{b}\left[\hat{X}^{(0)}(1) - \frac{u}{a}\right]e^{a}\right\} + \frac{u}{a}. \tag{25}$$

The 3/8 Simpson integral formula turns the integral into an interval sum (Shen and Zhang, 2016), and then, an approximate solution is obtained. Then, the integral is converted into

$$\int_1^{t+1} (sinkx)^n e^{ax} dx = \int_1^{t+1} f(x) dx$$
$$= \frac{1}{8m}\left\{f(1) + \sum_{i=1}^{t}\sum_{j=1}^{m}\left[3f\left(i + \frac{3j-2}{3m}\right) + 3f\left(i + \frac{3j-1}{3m}\right) + 2f\left(i + \frac{j}{m}\right) - f(t+1)\right]\right\}. \tag{26}$$

The final solution of the bleaching equation is shown as follows:

$$\hat{X}^{(1)}(t+1) = \frac{u}{a} + \frac{b}{8m}e^{-a(t+1)}\left\{(sin\,\omega)^{\beta}e^{a} + \sum_{i=1}^{t}\sum_{j=1}^{m}\left[3\left[sin\,\omega\left(i + \frac{3j-2}{3m}\right)\right]^{\beta} e^{a\left(i+\frac{3j-2}{3m}\right)} + \right.\right.$$
$$\left.\left. 3\left[sin\,\omega\left(i + \frac{3j-1}{3m}\right)\right]^{\beta} e^{a\left(i+\frac{3j-1}{3m}\right)} + 2\left[sin\,\omega\left(i + \frac{j}{m}\right)\right]^{\beta} e^{a\left(i+\frac{j}{m}\right)}\right]\right\} + \left[\hat{X}^{(0)}(1) - \frac{u}{a}\right]e^{-at}. \tag{27}$$

$\hat{a}$ is an approximate value obtained by the least-squares method, so $\hat{X}^{(1)}(t+1)$ is just an approximate result. In order to distinguish it from the cumulative sequence $X^{(1)}$, it is written as $\hat{X}^{(1)}$. The function expression $\hat{X}^{(1)}(t+1)$ subtracts $\hat{X}^{(1)}(t)$ in order to restore the original sequence, and then the approximate original sequence $\hat{X}^{(0)}(t+1)$ was obtained.That is,

$$\hat{X}^{(0)}(t+1) = \hat{X}^{(1)}(t+1) - \hat{X}^{(1)}(t). \tag{28}$$

Given ω and β, the least-squares method can be used to solve the remaining parameters, and then the prediction curve is obtained. The least-squares method is a given algorithm that takes the sum of squares of errors as the objective function to find its minimum value, and the result has a unique output value. In the whole process of solving the model, the two parameters ω and β directly determine the quality of the predicted results, so the reasonable choice of these two parameters is particularly

TABLE 5 Similarity deviation between all years and 2019.

Years	**1985**	**1986**	**1987**	**1988**	**1989**
Similarity deviation	2.773	2.481	2.771	2.801	2.266
Years	**1990**	**1991**	**1992**	**1993**	**1994**
Similarity deviation	2.727	2.556	2.315	2.473	2.546
Years	**1995**	**1996**	**1997**	**1998**	**1999**
Similarity deviation	2.368	2.446	2.249	2.389	2.453
Years	**2000**	**2001**	**2002**	**2003**	**2004**
Similarity deviation	2.501	2.375	1.840	2.367	2.573
Years	**2005**	**2006**	**2007**	**2008**	**2009**
Similarity deviation	2.697	2.760	2.464	2.473	1.367
Years	**2010**	**2011**	**2012**	**2013**	**2014**
Similarity deviation	1.663	1.369	1.160	3.105	2.659
Years	**2015**	**2016**	**2017**	**2018**	**2019**
Similarity deviation	1.482	**0.883***	0.984	1.118	0.000

The bold values represent that the results of the model of our paper compared with other models. The results of our paper are the best.

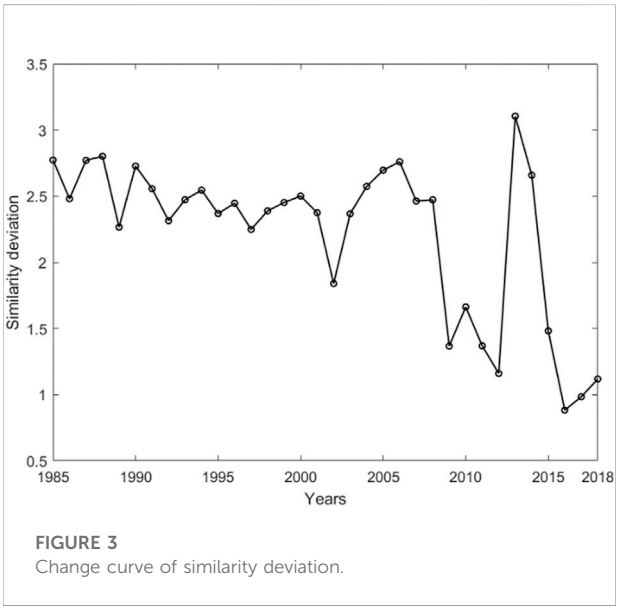

FIGURE 3
Change curve of similarity deviation.

important in the whole solution. The MRE of the prediction model is taken as the objective function, and the global search is carried out by using the genetic algorithm to calculate the minimum value of the average relative error.

3 Results

3.1 The similarity deviation

With a similar predict method, the GM(1,1|sin) power model realizes the SST prediction. Therefore, this study puts forward a new method, the GM(1,1|sin) power model based on the similarity deviation. This method takes two successive years as an original sequence, combined with the similarity of the SST changes and determines the appropriate original sequence on the basis of similarity deviation, in order to solve the model parameters, then solves the grey prediction model to predict. The unknown SST of 2020 can be assumed and predicted. The data of two consecutive years (2019–2020) are first combined, and the similarity of SST changes can be used to calculate the similarity deviation between each year and 2019 according to Eq. 9. The year with the highest similarity to 2019 was found and combined with the data of the next year to form the original sequence composed of 24 data for the module to determine the model parameters, and then the prediction curve was obtained.

Table 5 shows the data of similarity deviation of each year and 2019. The changing trend is shown in Figure 3. According to the calculation results, 2016 is the year most similar to 2019.

TABLE 6 Prediction results in 2020.

Month	**Real value**	**GM(1,1|sin) power model prediction value ω =-0.251 β =3.103**
1	5.6174	3.8666
2	4.5502	3.8743
3	3.9109	3.4965
4	7.5562	6.1501
5	13.2700	12.5664
6	20.2323	19.4237
7	24.8172	23.8727
8	25.7587	24.2542
9	22.1002	20.7817
10	17.9540	15.3944
11	10.9540	10.7021
12	8.4831	8.3704

TABLE 7 Evaluation metrics of SST prediction results in 2020.

Evaluation metrics of SST	**MRE (%)**	**RMSE**	**LCCC**	**RPD**
Value	9.84	1.2363	0.9870	6.0996

3.2 Monthly scale prediction

By combining the monthly average SST from 2016 to 2017 and bringing them into the model, the bleaching equation and the evaluation metrics are obtained. The prediction model is shown in Eq. 26. The specific data are shown in Table 6 and Table 7. The average values of MRE, RMSE, LCCC, and RPD are 9.84%, 1.2363, 0.9870, and 6.0996,

TABLE 8 Prediction models in 5 years.

Year	GM(1,1|sin) power model	MRE (%)	RMSE	LCCC	RPD
2016	$\frac{dX^{(1)}}{dt} - 0.0249X^{(1)} = 20.4053(-\sin 0.248t)^{3.175} + 4.0113$	11.84	0.8793	0.9936	8.6965
2017	$\frac{dX^{(1)}}{dt} - 0.0103X^{(1)} = 20.5796(-\sin 0.246t)^{3.182} + 4.6621$	8.52	1.3285	0.9835	5.3129
2018	$\frac{dX^{(1)}}{dt} - 0.0605X^{(1)} = 21.1477(-\sin 0.252t)^{3.036} + 4.6785$	13.28	1.2174	0.9885	6.8892
2019	$\frac{dX^{(1)}}{dt} - 0.0120X^{(1)} = 19.5911(-\sin 0.247t)^{3.012} + 5.1279$	5.54	0.6522	0.9961	11.0875
2020	$\frac{dX^{(1)}}{dt} - 0.0558X^{(1)} = 23.6333(-\sin 0.251t)^{3.103} + 3.4206$	9.84	1.2363	0.9870	6.0995

respectively. The evaluation metrics of LCCC and RPD were excellent based on Table 3.

$$\frac{dX^{(1)}}{dt} - 0.0558X^{(1)} = 23.6333(-\sin 0.251t)^{3.103} + 3.4206. \quad (29)$$

In order to eliminate the particularity of some years, the GM(1,1|sin) power model based on similarity deviation is used to predict the monthly average SST in the recent 5 years. The specific steps will not be repeated. Table 8 shows each predict year and its corresponding model. The maximum MRE is 13.28%, and the minimum is 5.54%. The 5-year MRE is 9.81%. In addition, the maximum RMSE is 1.3285, and the minimum is 0.6522. The 5-year RMSE is 1.0627, which indicates that the 5-year forecast deviated from the real value by about 1°C. All of evaluation metrics of LCCC and RPD were excellent. The specific contrast between prediction and reality is shown in Figure 4.

In the recent 5 years, there are 2 years in which the MRE is more than 10%, which are 2016 and 2018. Comparing the real value of these 2 years with the value of other years, the lowest temperature on record occurred in February 2018 and February 2016, and the highest temperature in 2016 occurred in July, and there was a sudden temperature change from June to August in 2018. Because the grey prediction model belongs to an autoregressive model, these abnormal temperature phenomena will directly affect the prediction results, resulting in deviation of the prediction results from the real value. In the other 3 years, due to the relatively stable temperature change, the prediction value all obtained good results. It can be seen that the factors affecting the quality of the grey prediction model are not only related to the established parameters in the model, but also related to the data of the original sequence.

3.3 Spatial distribution map of the monthly scale

We have verified the suitability of the prediction model based on the results of the monthly scale prediction. The Bohai Sea is the only inland sea in China, and it is connected to the Yellow Sea in the southeast. There are many factors influencing SST variation in this area near the land margin. In winter, due to the cold current, the temperature in the central and southeastern areas of the Bohai Sea was lower than that in other areas. Accordingly, the temperature in these areas was higher under the influence of the summer warm current.

The spatial distribution of the Bohai Sea area is represented according to the data of the monthly scale prediction in 2020, as shown in Figure 5. In January and February, the SST in the center was low and around the coastline was almost the same. The lowest was 3.88°C in the area connected with the Yellow Sea. In March, the SST was further reduced, and the temperature range was between 3.768 and 3.786. This is because the land temperature in January and February is the lowest in the year. The spatial distribution of the SST was roughly the same from April to December. The temperature rose first and then decreased, and the highest was about 25.5°C in August.

4 Discussions

4.1 Comparison of the prediction models

This study selects a central Bohai Sea area (120°E-120.125°E and 38.5°N-38.625°N) as the research object. The monthly average SST of 2020 is selected as an original sequence. Table 9 shows the established GM(1,1|sin) power model ($\omega = 0.676$; $\beta = 1.094$).Using the least-squares method, $a = -0.0282$, $b = -10.2337$, and $u = 13.8242$ were determined. The MRE of the GM(1,1|sin) power model is 4.20%, which is better than that of the GM(1,1|sin) model with 12.8%. The RMSE, LCCC, and RPD of GM(1,1|sin) power model are 0.5783, 0.9972, and 13.1378, respectively, which are better than other model results. The traditional GM(1,1) model and GM(1,1|sin + cos) model fail to describe the trend of the SST. Figure 6 shows the SST by four different models.

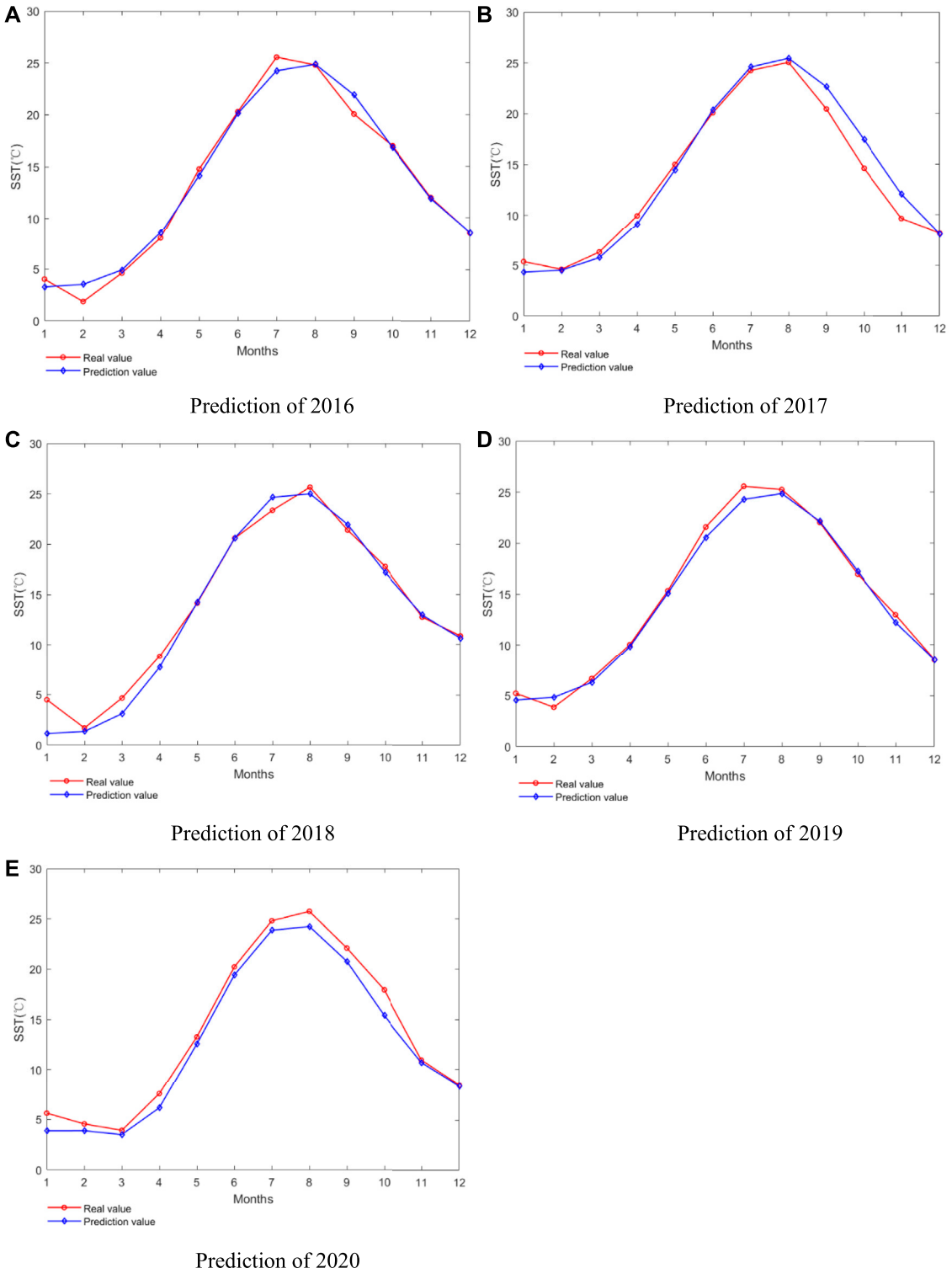

FIGURE 4
Respective prediction of the recent 5 years.

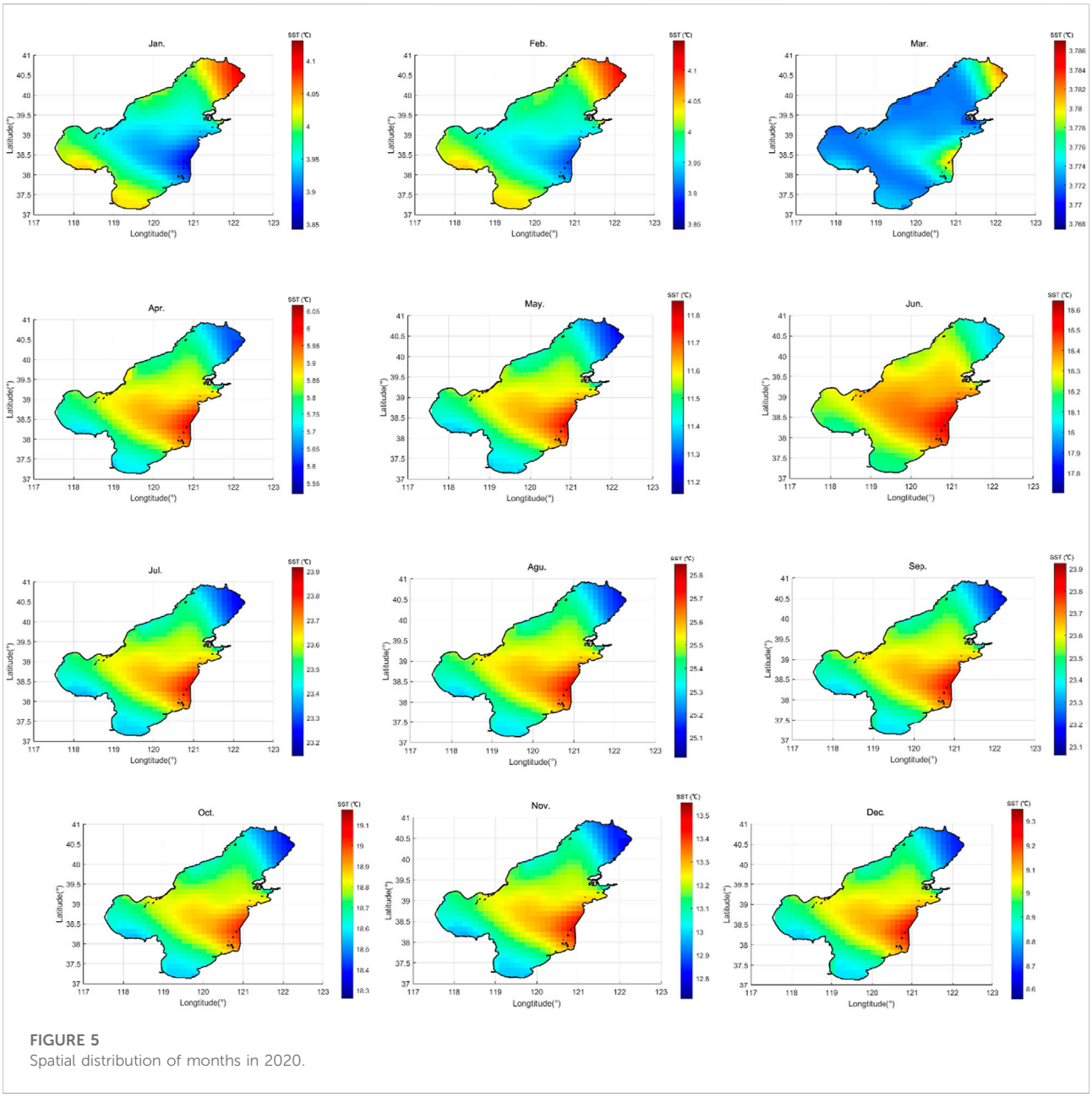

FIGURE 5
Spatial distribution of months in 2020.

The metrics of the four models were also obtained as shown in Table 10. The optimal model, GM(1,1|sin) power model achieves II level accuracy standard. Each model corresponding to the relative error is shown in Figure 7A, the GM(11|sin) power model of relative error is shown in Figure 7B. The maximum and minimum relative error of GM(1,1) model are 2.01 and 0.00557, respectively. The GM(1,1|sin + cos) model corresponding relative error maximum value is 1.53, and the minimum value is 0.0042. The GM(1,1|sin) model corresponding relative error maximum value is 0.45, and the minimum value is 0.00163. The GM(1,1|sin) power model corresponding relative error maximum value is 0.25, and the minimum value is 0.00026. According to the relevant metrics PDR and PSE based on Table 1, the results proved that the GM(1,1|sin) power model can approximately reflect the monthly changes in SST.

4.2 Comparison of respective prediction and consecutive prediction

Considering that the monthly average SST from 2016 to 2020 is to be predicted, the prediction value of 2016 will be taken as the real value after obtained, and the data will be predicted for

TABLE 9 Different models data of months average SST in 2020.

Month	Real value of SST (°C)	GM(1,1) model prediction value (°C)	GM(1,1|sin + cos) model prediction value (°C) p = -2.393 q = 0.237	GM(1,1|sin) model prediction value (°C) p = -0.787	GM(1,1|sin) power model prediction value (°C) ω =0.676 β =1.094
1	5.6174	5.6174	5.6174	5.6174	5.6174
2	4.5502	11.1317	4.5692	4.7592	5.6896
3	3.9109	11.7812	9.8852	5.0414	4.2765
4	7.5562	12.4685	12.8207	5.2994	7.5564
5	13.2700	13.1960	15.2564	10.7893	13.7744
6	20.2323	13.9659	14.9172	18.7113	20.3134
7	24.8172	14.7807	17.2497	24.8576	25.2506
8	25.7587	15.6430	15.8132	26.0877	25.8409
9	22.1002	16.5557	14.2823	22.1762	22.0370
10	17.9540	17.5216	13.6845	15.9472	16.5014
11	10.9540	18.5438	9.03279	11.6142	11.0398
12	8.4831	19.6257	6.98089	12.3042	8.4228
MRE		62.52%	35.63%	12.8%	**4.20%***
RMSE		6.9786	5.3000	1.6848	**0.5783**
LCCC		0.3365	0.6537	0.9757	**0.9972**
RPD		0.5237	0.7762	4.4858	**13.1378**

The bold values represent that the results of the model of our paper compared with other models. The results of our paper are the best.

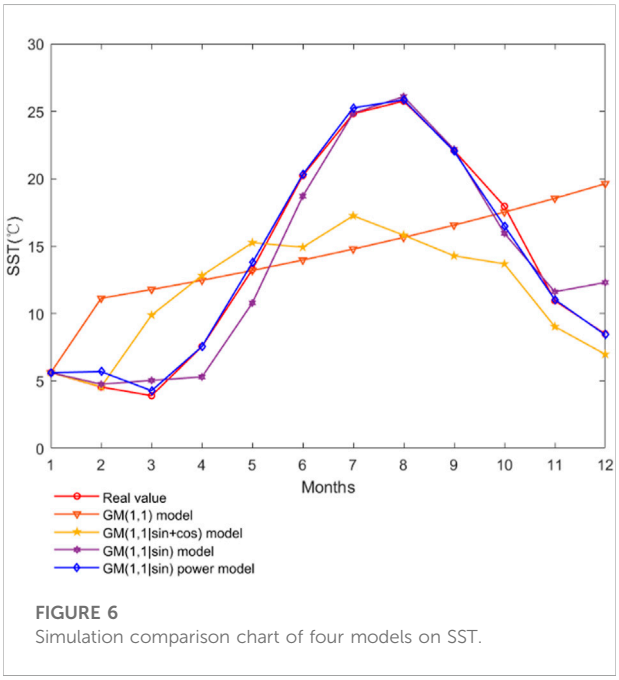

FIGURE 6
Simulation comparison chart of four models on SST.

five consecutive years by using the cycle prediction method. The results of the monthly SST prediction from 2016 to 2020 with the data from 1985 to 2015, 2016, 2017, 2018, and 2019 are shown in Table 8. The maximum MRE is 13.28%, and the minimum is

TABLE 10 Evaluation metrics of grey models in SST.

Model	MRE	PDR	PSE
GM(1,1) model	0.6252	0.8104	1
GM(1,1|sin + cos) model	0.3563	0.3965	1
GM(1,1|sin)model	0.1280	0.0470	1
GM(1,1|sin) power model*	0.0420	0.0056	1

5.54%. The 5-year MRE is 9.81%. The average RMSE, LCCC, and RPD are 1.0627, 0.9897, and 7.617, respectively. The annual prediction model is shown in Table 11. The maximum value of the MRE is 13.91%, the minimum is 7.80%, and the average value is 11.07%. The average RMSE, LCCC, and RPD are 1.0603, 0.9894, and 7.497, respectively. All of evaluation metrics of LCCC and RPD were excellent. It can be seen that the prediction performance of the GM(1,1|sin) power model is stable because the deviation between the predicted value and the real value is very close in the respective prediction and consecutive prediction. The specific contrast between prediction and real is shown in Figure 8.

The overall prediction trend and real condition in recent 5 years are shown in Figure 9. The overall data trend of the two predictions is the same, and the MRE of all of the respective prediction is larger. The MRE of the prediction value is 9.84%. Using the same method to predict from 2016 to 2019, the MRE is

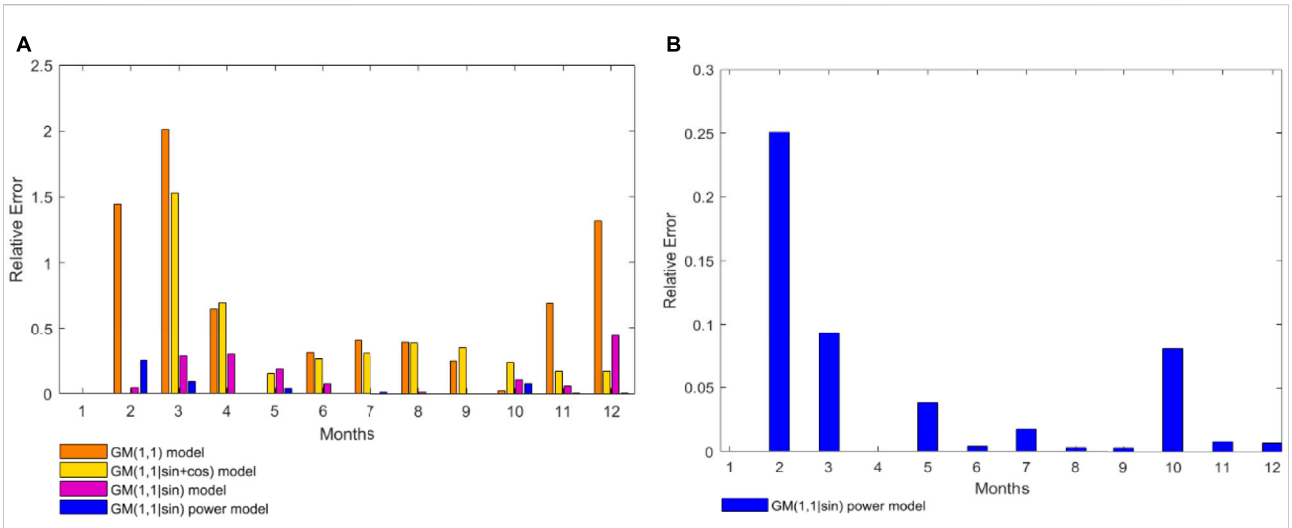

FIGURE 7
Relative error diagram.

TABLE 11 Adjusted prediction models in 5 years.

Year	GM(1,1|sin) power model	MRE (%)	RMSE	LCCC	RPD
2016	$\frac{dX^{(1)}}{dt} - 0.0249X^{(1)} = 20.4053(-\sin 0.248t)^{3.175} + 4.0113$	11.84	0.8793	0.9925	8.6965
2017	$\frac{dX^{(1)}}{dt} - 0.0214X^{(1)} = 19.0090(-\sin 0.247t)^{3.455} + 3.7930$	9.92	1.5314	0.9768	4.6402
2018	$\frac{dX^{(1)}}{dt} - 0.0507X^{(1)} = 21.9562(-\sin 0.251t)^{3.135} + 4.0025$	13.91	0.9371	0.9928	8.4634
2019	$\frac{dX^{(1)}}{dt} - 0.0419X^{(1)} = 19.8794(-\sin 0.252t)^{3.277} + 3.7394$	7.80	0.8833	0.9936	8.1988
2020	$\frac{dX^{(1)}}{dt} - 0.0162X^{(1)} = 20.8246(-\sin 0.247t)^{3.164} + 4.2683$	11.90	1.0706	0.9908	7.4863

11.84%, 8.52%, 13.28%, and 5.54%. Compared with the real value, the prediction value obtained using this method in the continuous prediction of the past 5 years has a maximum MRE of 13.91%, a minimum of 7.80%, and an average of 11.07%. The average values of RMSE, LCCC, and RPD are 1.0603, 0.9894, and 7.497, respectively. The average monthly SST from 1985 to 2020 is selected to predict the SST in the next 50 years, and the obtained results are given in Figure 10. It also predicted the daily average SST in each month.

4.3 Limitations

Due to the limitation of time and data, there are still more work conducted in future study. For example,

(1) In the process of predicting sea surface temperature, only the temperature itself is considered for analysis and prediction. Actually, SST is related to a set of factors such as atmospheric temperature, sea water salinity, ocean current movement, and so on. These factors should be considered comprehensively in the model, and the factors should be weighted to rank the influencing factors to find out the physical theories that really affect the SST.
(2) Because the effective time interval of time series prediction is short, the longer the prediction time is, the greater the error will be. In addition, since many countries have been aware of the impact of global warming, they will take more green and sustainable measures to mitigate the adverse trend in the future.

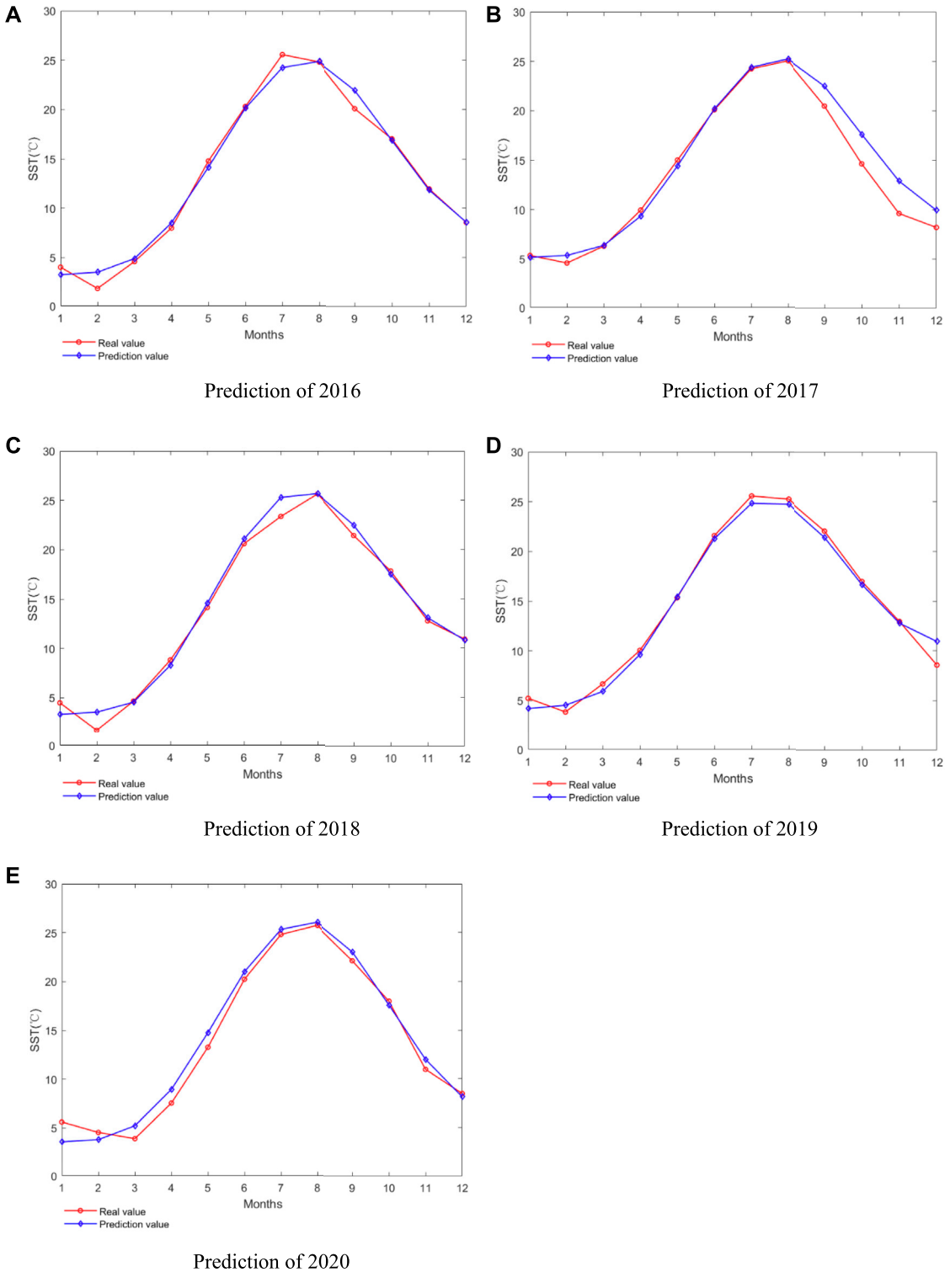

FIGURE 8
Consecutive prediction of the recent 5 years.

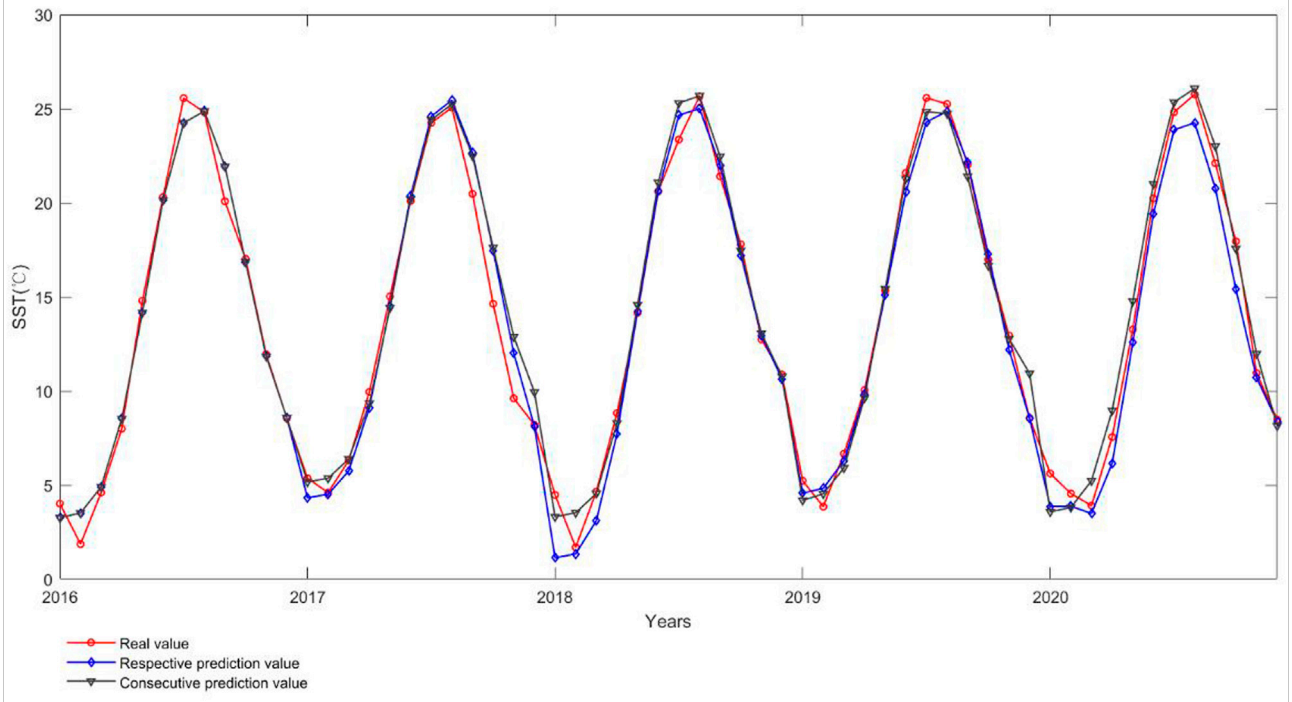

FIGURE 9
Respective prediction vs. consecutive prediction.

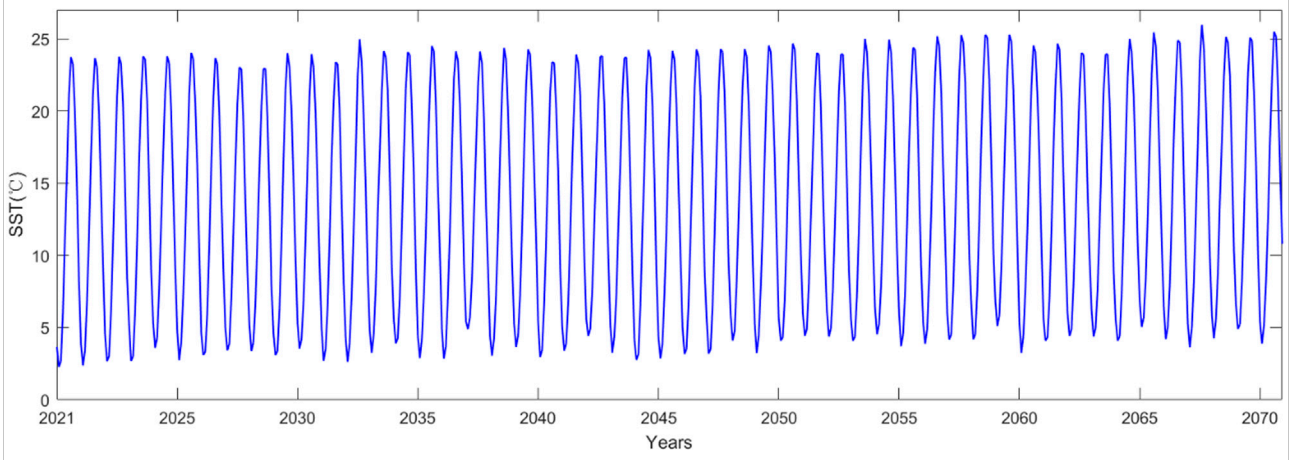

FIGURE 10
Change trend of SST from 2021 to 2070.

Therefore, the prediction results of this study after 50 years are believed to have certain deviation from the measured results.

(3) We used the cubic spline interpolation method to fill the null values, which will definitely cause deviation from the real value. In the selection of data points, only the data near the center of the Bohai Sea were collected, and the data from other areas were ignored. The model established on the data set may not be completely applicable universally.

5 Conclusion

In this study, based on the empirical prediction method, the grey prediction method is used to analyze the sea surface temperature changing trend and create the prediction model. The prediction models are validated by the mean relative error and the similarity deviation metrics. The main work and achievements of this study are summarized as follows:

(1) The study carried out the analysis by experience prediction methods, considering that the SST has certain periodicity and the sustainability of change, similarity, and correlation with other marine elements, to make a qualitative or quantitative prediction. The method is simple and easy to construct, the predict effect is satisfactory. The MRE of this model is 4.20% when describing the monthly average SST in 2020.
(2) According to the constructed grey prediction model, a validation experiment was conducted from January to December 2020. The experiment combined the similarity deviation in statistics, establishing a model by selecting appropriate similar years, and then predicting the target year. The MRE of the prediction value is 9.84%. Using the same method to predict from 2016 to 2019, the MRE values are 11.84%, 8.52%, 13.28%, and 5.54%. Compared with the real value, the prediction value obtained using this method in the continuous predict of the past 5 years has a maximum MRE of 13.91%, a minimum of 7.80%, and the average values of MRE RMSE, LCCC, and RPD are 11.07% 1.0603, 0.9894, and 7.497, respectively. It also predicted the daily average SST in each month of 2020. The MRE is between 1.49% and 9.89%. The lowest result appears in December and the highest occurs in March.

Data availability statement

We appreciate the data provided by National Science and Technology Resource Sharing Service Platform - National Marine Science Data Center (http://mds.nmdis.org.cn/ accessed on 10 January 2021). Information about the data accessed can be found in the article, further inquiries can be directed to the corresponding authors.

Author contributions

Conceptualization: JG, FM, and XL; methodology, data curation, formal analysis, investigation, and writing—original draft preparation: FM, ZQ, MG, and JC; and writing—review andediting and supervision: JG, LW-e, and FM. All authors have read and agreed to the published version of the manuscript.

Funding

This research was funded by the National Natural Science Foundation of China, grant number 41671158, supported by the Foundation of Liaoning Educational Committee (LJKZ0979), supported by the College Students' Innovative Entrepreneurial Training Plan Program (S202110165051), and supported by Youth Innovation Promotion Association of Chinese Academy of Sciences to LW-e.

Acknowledgments

The authors would like to thank Liaoning Normal University for the laboratory facilities and the necessary technical support. They also thank the National Science and Technology Resource Sharing Service Platform (China National Marine Science Data Center) for data support.

Conflict of interest

The authors declare that the research was conducted in the absence of any commercial or financial relationships that could be construed as a potential conflict of interest.

Publisher's note

All claims expressed in this article are solely those of the authors and do not necessarily represent those of their affiliated organizations, or those of the publisher, the editors, and the reviewers. Any product that may be evaluated in this article, or claim that may be made by its manufacturer, is not guaranteed or endorsed by the publisher.

References

Cui, L., and Liu, S. (2012). Characteristics and application on GM(1,1) model based on sequence of random vibration. *Math. Pract. Knowl.* 42 (11), 160–165. 10.3969j.issn.1000-0984.2012.11.021

Dong, Z., Teng, J., and Wang, J. (2008). Application of phase space reconstruction and ANFIS model in SST forecasting. *J. Trop. Oceanogr.* 27 (4), 73–76. doi:10.3969/j.issn.1009-5470.2008.04.011

He, Q., Cheng, Z., Song, W., Qi, F., Hao, Z., and Huang, D. (2020). Sea surface temperature prediction algorithm based on STL model. *Mar. Environ. Sci.* 39 (6), 918–925. doi:10.13634/j.cnki.mes.2020.06.015

Jin, J., Ding, J., and Wei, Y. (1999). Application of threshold auto-regressive model based on genetic algorithm in sea surface temperature prediction. *Mar. Environ. Sci. Technol.* 18 (3), 1–6. doi:10.3969/j.issn.1007-6336.1999.03.001

Kim, M., Yang, H., and Kim, J. (2020). sea surface temperature and high water temperature occurrence prediction using a long short-term memory model. *Remote Sens. (Basel).* 12, 3654. doi:10.3390/rs12213654

Li, W., Lei, G., Qu, L., and Guo, D. (2020). Prediction of sea surface temperature in the China seas based on long short-term memory neural networks. *Remote Sens. (Basel).* 12, 2697. doi:10.3390/rs12172697

Li, Z., and Liu, S. (2020). Oscillation sequence prediction based on the gray interval GM(1, 1) model: Taking Shanghai Consumer Confidence Index as an example. *Statistics Decis.* 36 (14), 145–148. doi:10.13546/j.cnki.tjyjc.2020.14.032

Lu, H., Xie, C., Zhang, C., and Zhai, J. (2021). CMIP5-Based projection of decadal and seasonal sea surface temperature variations in East China shelf seas. *J. Mar. Sci. Eng.* 9, 367. doi:10.3390/jmse9040367

Lu, X., Sun, Y., and Da, L. (2009). Prediction of seawater temperature time series based on EMD. *Mar. Technol.* 28 (3), 79–82. doi:10.3969/j.issn.1003-2029.2009.03.021

Qian, W., and Dang, Y. (2009). GM(1, 1) model based on oscillation sequence. *Syst. Eng. Theory Pract.* 29 (03), 149–154. doi:10.3321/j.issn:1000-6788.2009.03.021

Qu, P., Wang, W., Liu, Z., Gong, X., Shi, C., and Xu, B. (2021). Assessment of a fusion sea surface temperature product for numerical weather predictions in China: A case study. *Atmosphere* 12, 604. doi:10.3390/atmos12050604

Shen, Y., Zhang, L., Zhou, X. Q., Fang, Y. M., Liu, Y., and Ma, L. Q. (2016). Photosynthetic electron-transfer reactions in the gametophyte of Pteris multifida reveal the presence of allelopathic interference from the invasive plant species Bidens pilos. *J. Photochem. Photobiol. B* 43 (04), 81–88. doi:10.1016/j.jphotobiol.2016.02.026

Shi, W., Zhu, B., and Zhang, C. (2018). Analysis and prediction of China's Marine industrial structure based on grey model. *J. Zhejiang Ocean Univ. Humanit. Ed.* 35 (04), 1–8. doi:10.3969/j.issn.1008-8318.2018.04.001

Sun, D., Song, J., Ren, K., Li, X., and Wang, G. (2020). A survey on the relationship between ocean subsurface temperature and tropical cyclone over the western north pacific. *Adv. Meteorology* 2020, 1–14. doi:10.1155/2020/9290837

Sung, H. M., Kim, J., Lee, J.-H., Shim, S., Boo, K.-O., Ha, J.-C., et al. (2021). Future changes in the global and regional sea level rise and sea surface temperature based on CMIP6 models. *Atmosphere* 12, 90. doi:10.3390/atmos12010090

Tang, L., Jia, D., and Meng, Q. (2008). To accomplish gray forecasting GM(1,1) model using the MATLAB. *J. Cangzhou Teach. Coll.* 24 (02), 35–37. doi:10.3969/j.issn.1008-4762.2008.02.017

Wang, H., Song, T., Zhu, S., Yang, S., and Feng, L. (2021). Subsurface temperature estimation from sea surface data using neural network models in the western Pacific ocean. *Mathematics* 9, 852. doi:10.3390/math9080852

Wang, J. (2017). *Study on the influence of high speed railway on regional economy in Beijing Tianjin Hebei region*. Beijing: Capital University of Economics and Business. doi:10.7666/d.D01197223

Wang, J., and Luo, D. (2017). Fractional discrete GM(1, 1) power model of oscillating sequence and its application. *Control Decis.* 32 (01), 176–180. doi:10.13195/j.kzyjc.2015.1233

Wang, Y., Chen, P., and Chen, X. (2013). Characteristics of sea surface temperature for major ecosystems in the Northwest Pacific under climate change. *J. Shanghai Ocean Univ.* 38 (6), 1–14. doi:10.12024/jsou.20200603074

Wang, Z. (2013). Models derived GM(1,1) power model. *Syst. Eng. Theory Pract.* 33 (11), 2894–2902. doi:10.12011/1000-6788(2013)11-2894

Yin, P. (2017). Grey predicting system GM(1, 1) model and its realization in Matlab. *Heilongjiang Water Conservancy Sci. Technol.* 45 (07), 16–18. doi:10.3969/j.issn.1007-7596.2017.07.005

Zeng, B., and Li, H. (2021). Prediction of coalbed methane production in China based on an optimized grey system model. *Energy fuels.* 35 (5), 4333–4344. doi:10.1021/acs.energyfuels.0c04195

Zeng, B., Tong, M., and Ma, X. (2020). A new-structure grey Verhulst model: Development and performance comparison. *Appl. Math. Model.* 81, 522–537. doi:10.1016/j.apm.2020.01.014

Zeng, L. (2019). Grey GM(1,1|sin) power model based on oscillation sequences and its application. *J. Zhejiang Univ. Sci. Ed.* 46 (06), 697–704. doi:10.3785/j.issn.1008-9497.2019.06.010

Zhang, J. (2004). Lectures on sea temperature predicting knowledge. *Ocean. Predict* 21 (1), 85–90. doi:10.3969/j.issn.1003-0239.2004.01.013

Zhang, Y., Tan, Y., and Peng, F. (2019). Study on time series prediction model of sea surface temperature based on Ensemble Empirical Mode Decomposition and Autoregressive Integrated Moving Average. *J. Mar. Sci.* 37 (1), 9–14. doi:10.3969/j.issn.1001-909X.2019.01.002

Zhang, Z., Pan, X., Jiang, T., Sui, B., Liu, C., and Sun, W. (2020). Monthly and quarterly sea surface temperature prediction based on gated recurrent unit neural network. *J. Mar. Sci. Eng.* 8, 249. doi:10.3390/jmse8040249

Zhao, D., Arshad, M., Li, N., and Triantafilis, J. (2021b). Predicting soil physical and chemical properties using vis-NIR in Australian cotton areas. *Catena* 196, 104938. doi:10.1016/j.catena.2020.104938

Zhao, D., Arshad, M., Wang, J., and Triantafilis, J. (2021a). Soil exchangeable cations estimation using Vis-NIR spectroscopy in different depths: Effects of multiple calibration models and spiking. *Comput. Electron. Agric* 182, 105990. doi:10.1016/j.compag.2021.105990

Zhao, Y., Wu, C., Wang, J. N., and Wang, L. (2010). Factors associated with occupational stress among Chinese doctors: A cross-sectional survey. *Int. Arch. Occup. Environ. Health* 19 (05), 155–164. doi:10.1007/s00420-009-0456-z

frontiers | Frontiers in Environmental Science

TYPE Original Research
PUBLISHED 24 November 2022
DOI 10.3389/fenvs.2022.1049333

Check for updates

OPEN ACCESS

EDITED BY
Jun Yang,
Northeastern University, China

REVIEWED BY
Jixiang Liu,
Xiamen University, China
Hao Zhu,
Chengdu University of Technology, China

*CORRESPONDENCE
Bo Shu,
shubo@swjtu.edu.cn,
shubo@mail.xhu.edu.cn

SPECIALTY SECTION
This article was submitted to Land Use Dynamics, a section of the journal Frontiers in Environmental Science

RECEIVED 20 September 2022
ACCEPTED 09 November 2022
PUBLISHED 24 November 2022

CITATION
Shu B, Chen Y, Amani-Beni M and Zhang R (2022), Spatial distribution and influencing factors of mountainous geological disasters in southwest China: A fine-scale multi-type assessment. *Front. Environ. Sci.* 10:1049333. doi: 10.3389/fenvs.2022.1049333

COPYRIGHT
© 2022 Shu, Chen, Amani-Beni and Zhang. This is an open-access article distributed under the terms of the Creative Commons Attribution License (CC BY). The use, distribution or reproduction in other forums is permitted, provided the original author(s) and the copyright owner(s) are credited and that the original publication in this journal is cited, in accordance with accepted academic practice. No use, distribution or reproduction is permitted which does not comply with these terms.

Spatial distribution and influencing factors of mountainous geological disasters in southwest China: A fine-scale multi-type assessment

Bo Shu[1,2]*, Yang Chen[2], Majid Amani-Beni[2] and Ruizhi Zhang[2]

[1]School of Architecture and Civil Engineering, Xihua University, Chengdu, China, [2]School of Architecture, Southwest Jiaotong University, Chengdu, China

Abstract: Geological disasters have long been a constant threat to socioeconomic development and human life and property. Many studies focus on the occurred geological disasters and ignore the potential risk events. Fine-scale multi-type analysis of Potential Geological Disasters Spots (PGDSs) is a necessary but insufficiently explored research field in China's mountainous areas. Taking Meigu County (Sichuan Province, Southwest China), a typical disaster-prone region, as the study area. Average nearest neighbor (ANN), standard deviational ellipse (SDE), kernel density estimation (KDE), and ordinary least squares (OLS) regression are used to assess the spatial distribution of potential geological disasters spots and their influencing factors. The findings show that: potential geological disasters spots have a significant spatial heterogeneity and exhibited a prominent clustering characteristic. They were distributed in an elevation range of 1,500–2000 m, which receives an average monthly rainfall of more than 240 mm, as well as in highly foliated (0.6 < Normalized Difference Vegetation Index (NDVI) < 0.8), west-facing (247.5–292.5°), and slopes of 10–20°. In addition, slope, aspect, population density, and rainfall were found as the main influencing factors. The results provide practical rural development measures with support for potential geological disasters spots avoidance and preparedness.

KEYWORDS

potential geological disasters spots, spatial distribution, mountainous rural areas, rainfall, disaster-prone region

1 Introduction

In recent years, frequent climate change and geological disasters seriously obstructed socioeconomic development and posed a serious threat to achieving sustainable development goals worldwide (Fedeski and Gwilliam, 2007; Zhuang et al., 2020; Wan et al., 2021; Wang et al., 2021). China is one of the countries with the highest incidence and frequency of geological disasters in the world (Li et al., 2015; Hou et al., 2016; Xiao et al., 2022). Geological disasters have long been a persistent threat to the development of urban

and rural construction in China (Bulte et al., 2018; Ao et al., 2021; Zhao Z. et al., 2021; Zeng et al., 2021; Zhou et al., 2021; Pu et al., 2022), especially in mountainous rural areas that are more disaster-prone (Xu et al., 2020; Lin J et al., 2021; Qing et al., 2021; Gan et al., 2022). According to a report released by the Ministry of Natural Resources of China, a total of 7,840 geological disasters occurred in China in 2020, resulting in 139 deaths (missing), 58 injuries, and direct economic losses of 50.2 billion yuan (http://vod.mnr.gov.cn/). Over the past decades, China's rural society and economy have developed rapidly (Li K. et al., 2021). All the rural villages were lifted out of extreme poverty at the end of 2020. However, in the vast mountainous regions of China, people's lives and properties are still under serious threat due to frequent geological disasters, accompanied by the risk of returning to poverty due to disasters, and the sustainable development of the rural areas is seriously hindered. In addition, with rapid urbanization, the land use cover of the mountainous rural areas has changed dramatically. Many infrastructures, such as roads and gas engineering, have been put into construction, which means that human activities are disturbing the ecological environment more and more. The risk of geological disasters will gradually increase (Jiang et al., 2016). Therefore, research on the risk of geological disasters in mountainous rural areas must be addressed.

The concept of "Potential Geological Disaster Spots (PGDSs)" refers to a broad range of point and partial non-point events (Gan et al., 2022), which are potentially dangerous to occur or have already occurred but still are unstable. There are many PGDSs, including landslides, debris flows, unstable slopes, avalanches, ground subsidence, *etc.* The different causes of different types of geological disasters lead to significant variability in their spatial distribution and time of occurrence. In addition, the PGDSs are widely distributed, sudden, and temporally erratic, resulting in severe threats to people's lives and property (Xu D. et al., 2018; Lin J et al., 2021; Wang et al., 2021; Yao et al., 2022). Most studies on geological disasters mainly focus on the spatiotemporal characteristics of different types of geological disasters (Zuo et al., 2009; Pu et al., 2022), assessment of severity and susceptibility (Chang et al., 2022; Kim et al., 2022), impact on human lives and production (Wu et al., 2022), *etc.* However, few studies focus on potential geological disasters. Related studies have confirmed that PGDSs are more hidden and sudden than those that have occurred or have been managed. Therefore, in the prevention of geological disasters, special attention needs to be paid to identifying PGDSs where no disaster has occurred. According to a notice issued by the Sichuan provincial government on a geological disaster prevention program, by the end of 2020, there are about 36,000 geological disaster potential sites in Sichuan, posing varying degrees of threat to the lives of nearly 1.5 million people and 850 billion yuan of property (https://www.sc.gov.cn/). In addition, the abovementioned studies primarily focus on the macro scale, such as city level, province level, and river basin level, ignoring the fine-scale analysis at the county or town level. Notably, China's mountainous rural areas, often geological disaster-prone areas, have faced increasing risk from PGDSs caused by global climate change and increasing human engineering activities (Qing et al., 2021). The residents in mountainous rural areas are more profoundly affected by PGDSs due to impaired transportation and delayed rescue operations compared to the plain areas (Pan, 2016). Therefore, to better characterize the risk and undertake precautionary measures, scientific insight into pre-disaster preparedness is required by identifying the spatial distribution characteristics, patterns, and influencing factors of PGDSs.

Meigu County, the case study area of this research, is increasingly affected by a variety of homogeneously distributed PGDSs in Sichuan Province, Southwest China. We select Meigu County as the case study for two reasons: 1) The case representation. Meigu County is one of the specific areas in China most prone to geological disasters, with a large number and widely distributed PGDSs. 2) The urgency of studies. Due to the unique topographical complexity, rainfall regime, and intensive human engineering activities, the PGDSs have been remarkable and have shown an increasing trend in recent years. As a result, most local communities are constantly affected by PGDSs, and people's living and production are seriously threatened. Thus, Meigu County is an ideal case to assess the PGDSs spatial distribution and influencing factors in China's mountainous rural areas.

The contributions of this paper are as follows: 1) analyzed the spatial distribution characteristics and fine-scale spatial heterogeneity mapping of PGDSs; 2) Identified the main PGDSs contributing factors using the ordinary least squares (OLS) model; and 3) tailored PGDSs-based planning recommendations for better pre-disaster planning and preparedness.

The remainder of this paper is structured as follows: Section 2 reviews the existing literature on the PGDS spatial distribution and the influencing factors. Section 3 introduces the study area, methods, and datasets. Section 4 shows the results. Section 5 discusses the results and highlights recommendations for disaster avoidance in mountainous rural areas. Finally, Section 6 provides the conclusion drawn from the findings.

2 Literature review

2.1 Spatial distribution of geological disasters in China

China has a wide distribution of geological disasters due to its many mountainous areas and complex terrain, and different types of geological disasters cover almost all areas of inland China. The spatiotemporal distribution pattern of geological disasters is influenced by the natural geographical

environment and human activities. In the beginning, scholars have spared no effort to study disaster risk zoning and visualization maps (van Westen et al., 2000). Geological disaster risk zones are divided into different classes according to their susceptibility and hazardousness, which is a method to reveal the spatial distribution characteristics of geological disasters. Then, more and more scholars realize that the distribution of geological disasters is closely related to their causes, so the spatial distribution characteristics of different types of geological disasters have significant differences (Jiang et al., 2016). In recent years, many related studies have further confirmed that the spatial distribution of different types of geological disasters varies in China. For instance, landslide disasters are mainly gathered in North and Southern China, while debris flow disasters are often distributed in Southeastern China (Liu et al., 2012). Regarding distribution, the vulnerability to geological disasters in China is generally the lowest in eastern China, the highest in western China, and gradually decreasing from western to eastern (Li et al., 2015).

However, on a fine scale, the distribution of geological disasters is closely related to their elevation, slope, rainfall, and other natural environmental features (Lin J et al., 2021; Chang et al., 2022). For instance, a study in the Fujian delta region, South China, showed that the incidence of geological disasters is higher at an altitude of 600–800 m, a slope of 6–15°, a southwest orientation, and a distance of 200 m from the river than other regions (Lin J et al., 2021). But another study showed that 90.2% of the total geological disasters are distributed at altitudes over 1,000 m in mountainous rural areas (Jiang et al., 2016). The abovementioned studies indicate that the subdivision of the spatial distribution of geological disasters is determined by local topographic features. Furthermore, some scholars argue that the disturbance of human activities is essential in inducing geological disasters. Therefore, the geological disaster-prone areas are primarily distributed in areas with dense populations and economic activities (Zhao D. et al., 2021; Wang et al., 2021). In mountainous rural areas, due to the disturbance of the rapid construction of engineering infrastructure, geological disasters are often distributed in a linear pattern along traffic arteries, and in a cluster pattern along townships and settlements (Qin et al., 2021). In addition, the distribution of geological disasters spots is also related to other influencing factors. For instance, geological disasters are often distributed in areas with low vegetation coverage because the root system of vegetation can improve soil stability.

In summary, the spatial distribution of geological disasters is essential to disaster prevention research. A clear understanding of the distribution pattern of geological disasters is of great significance for formulating effective countermeasures. Previous studies have established a cognitive system of the spatial distribution characteristics of geological disasters in China, revealing the heterogeneity of the spatial distribution of geological disasters and enabling us to have a macroscopic understanding of the distribution of geological disasters. However, as mentioned above, the distribution of geological disasters is closely related to the local geographical and natural environment and human activities, and micro-scale research can help to fine-grained knowledge of the distribution characteristics of regional geological disasters, which in turn can help in disaster prevention and mitigation planning, resource allocation optimization, *etc.*

2.2 Influencing factors of geological disasters

The influencing factors of geological disasters are divided into two categories, natural environment and human activities (Lin J et al., 2021). In recent years, geological risk assessment has attracted increasing scholarly attention, especially regarding the factors influencing geological disasters. Numerous studies have shown that a complex interaction of global and functionally region-specific factors governs geological disasters (Li et al., 2016; Wang et al., 2020; Tang et al., 2021), such as elevation, slope, rainfall, population density, distance from faults, *etc.* (Youssef et al., 2012; Li et al., 2013; Wang et al., 2021; Siddique et al., 2022; Wang et al., 2022). For instance, Qin et al. (2010) examined the relationship between landslides and the topography in Wenchuan County, which showed that the number of landslides is positively correlated with the slope and elevation, while negatively associated with aspect. Another study also in the mountainous areas in southern China showed that elevation, distance from faults and slope are the main influencing factors causing geological disasters (Lin J et al., 2021). Furthermore, according to the time of high frequency of geological disasters, debris flows and landslides primarily occur in the summer months of June to August, when there is very heavy and prolonged rainfall. Therefore, the water system and rainfall are crucial factors inducing geological disasters.

The abovementioned studies provide the basis for a deeper understanding of geological disasters. However, most studies focused on single-type disasters such as debris flow (Chiou et al., 2015), landslides (Bai et al., 2010; Chen et al., 2017; Li et al., 2017; Deng et al., 2022; Lv et al., 2022), rockfall (Chiessi et al., 2010), flood hazard (Wang et al., 2015), *etc.*, or adopted macro-regional scale investigations such as coastal areas (China) (Pan, 2016), Pearl River Delta (China) (Li H. et al., 2021), urban agglomerations (Lin J et al., 2021), and river basin (Chiou et al., 2015; Dong et al., 2021; Lv et al., 2022). Most micro-scale studies at the county level also lacked multi-type disaster investigations (Zhao Z. et al., 2021). In summary, to have a more precise view of geological disasters in China's mountainous rural areas, fine-scale multi-type disaster analysis procedures are needed to provide a more robust interpretation and analysis regarding the distribution, preparedness, and avoidance of geological disasters.

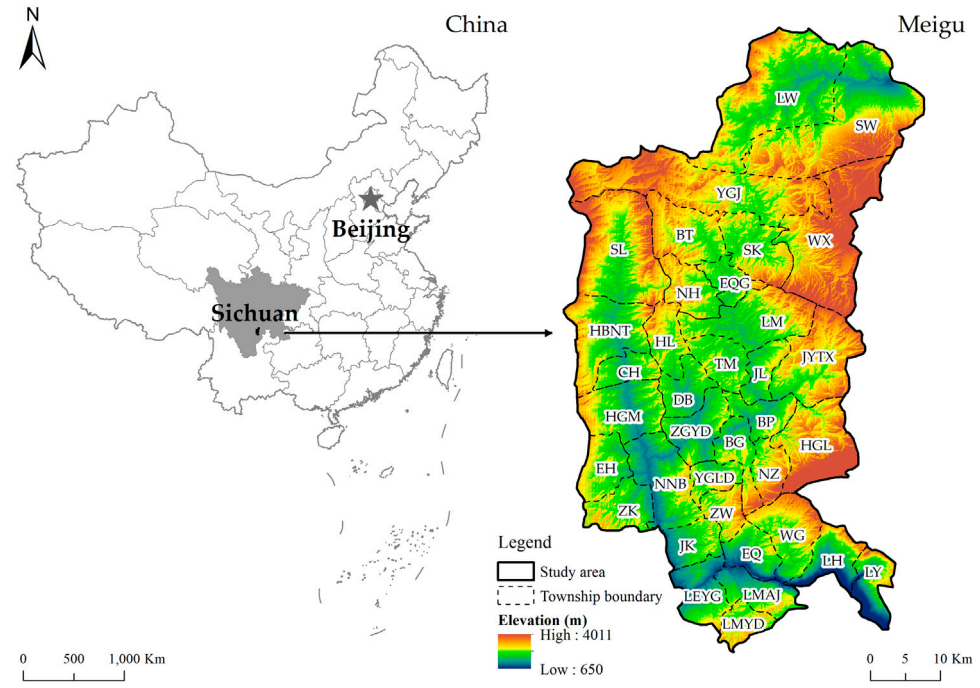

FIGURE 1
Geographic location of Meigu County.

3 Materials and methods

3.1 Study area

Meigu County, located in Southwestern China (102°53′-103°21′E, 28°02′-28°54′N), covers a total area of approximately 2,573 km^2. At the end of 2020, the county had a population of 0.26 million distributed in one town and 35 townships according to official statistics (Figure 1) (http://www.meigu.gov.cn/). The region is geologically or geomorphologically complex and is characterized by a typical four-season pattern with an annual temperature of 11.4°C (Song et al., 2020). The rainy season with a mean yearly rainfall of approximately 814.6 mm, stretches between June and September, with heavy rainstorms occurring in the summer. The complex geological, geomorphological, and climatic characteristics of the region trigger an increasing occurrence of geological human-affecting disasters (Tang et al., 2020), which primarily include landslides, desire flows, and collapse (Figure 2). Xinhua News Agency reported that a continuous heavy rainfall turned into severe debris flow in Meigu County on 26 June 2016, resulting in 79 people injured, six missing, 20 ha of arable lands and 16 houses damaged, including ten partially affected, five collapsed and one buried house (www.xinhuanet.com). In addition, according to the statistics of the Megu County government, 75 PGDSs were identified from 2016–2020, resulting in 722 rural households and 68.21 million yuan in the property at serious risk (http://www.meigu.gov.cn/). In recent years, with increasing extreme weather conditions and continuous progress of human engineering activities, the region's rural settlements have faced heightened challenges and threats of geological disasters.

3.2 Methods

We analyzed the PGDSs spatial distribution characteristics using Average Nearest Neighbor Ratio (ANN), Kernel Density Estimation (KDE) and Standard Deviational Ellipse (SDE) models. Then, we constructed OLS regression models to identify the main influencing factors to PGDSs. The analytical framework is shown in Figure 3.

3.2.1 Spatial distribution analysis of potential geological disasters spots

3.2.1.1 Standard deviational ellipse

SDE explores the spatial distribution direction and trend characteristics of point elements (Xu F. et al., 2018; Yang et al., 2021). Its standard basic parameters include the center, long axis, short axis and azimuth of the ellipse. The center indicates the

FIGURE 2
Geological disasters in the study area. (Photo source: China Weather, http://www.weather.com.cn/).

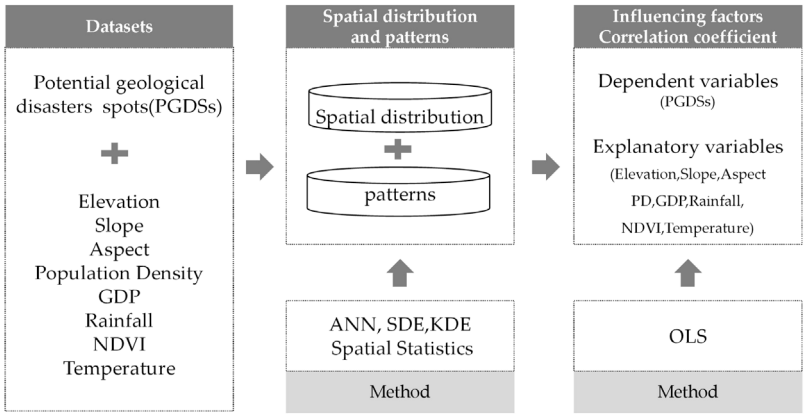

FIGURE 3
Analytical framework.

relative position of its distribution, the long axis characterizes its dispersion in the direction of the primary trend, and the azimuth reflects the direction of the primary distribution trend (Zhang et al., 2022).

$$\sigma_x = \sqrt{\frac{\sum_{i=1}^{n}\left(w_i\hat{x}_i\cos\theta - w_i\hat{y}_i\sin\theta\right)^2}{\sum_{i=1}^{n}w_i^2}} \quad (1)$$

$$\sigma_y = \sqrt{\frac{\sum_{i=1}^{n}\left(w_i\hat{x}_i\sin\theta - w_i\hat{y}_i\cos\theta\right)^2}{\sum_{i=1}^{n}w_i^2}} \quad (2)$$

$$\tan\theta = \frac{\left(\sum_{i=1}^{n}w_i^2\hat{x}_i^2 - \sum_{i=1}^{n}w_i^2\hat{y}_i^2\right) + \sqrt{\left(\sum_{i=1}^{n}w_i^2\hat{x}_i^2 - \sum_{i=1}^{n}w_i^2\hat{y}_i^2\right)^2 + 4\left(\sum_{i=1}^{n}w_i^2\hat{x}_i\hat{y}_i\right)^2}}{2\sum_{i=1}^{n}w_i^2\hat{x}_i\hat{y}_i} \quad (3)$$

Where θ refers to the azimuth of the ellipse and the standard deviation along the major axis x and minor axis y of the SDE. $\hat{x}_i$ and $\hat{y}_i$ are the coordinate deviations from each point to the mean center, respectively (Kong et al., 2022).

3.2.1.2 Average nearest neighbor

ANN measures the spatial distribution characteristics of point-like elements by using a criterion.

$$R = \frac{D_0}{D} \tag{4}$$

$$D = \sum_{i=1}^{N} \frac{d_i}{N} \tag{5}$$

$$D_0 = \frac{1}{2}\sqrt{\frac{A}{N}} \tag{6}$$

Where R is the ratio, D0 is the actual nearest neighbor distance, and D is the theoretical closest neighbor distance. A is the area of the study area, and N is the number of point-like elements. The spatial distribution characteristics of PGDSs are evaluated according to the value of R: R = 1 indicates random distribution, R < 1 indicates agglomerative distribution, R > 1 indicates discrete distribution.

3.2.1.3 kernel density estimation

KDE is a common spatial analysis method (Dong et al., 2020; Song and Li, 2020; Xu et al., 2022), used to visualize the spatial clustering status of PGDSs.

$$f_n(x) = \frac{1}{nh^2}\sum_{i=1}^{n} k\left(\frac{d_i}{n}\right) \tag{7}$$

Where, k is the kernel function, h is the bandwidth with a value greater than 0, n is the number of spots within the bandwidth, di is the distance of the location from the *i*th observed location, and a fixed bandwidth value is used in this study.

3.2.2 Ordinary least squares regression model

3.2.2.1 Ordinary least squares model

The OLS method involves a global linear regression model and is a multivariate linear function between the dependent and independent variables (Yang L et al., 2020a; Yang L et al., 2020b; Guo et al., 2020; Yang et al., 2022).

$$Y_i = \beta_0 + \sum_k \beta_k \chi_k + \varepsilon \tag{8}$$

Where Y_i is the dependent variable, β_0, β_k and ε represent a constant, the regression coefficient, and a random error term, respectively.

3.2.2.2 Dependent and explanatory variables

The identification of influencing factors is critical for the construction of the regression model. We selected the density of PGDSs in each unit as the dependent variable. As described, the natural environment and human activities are the two main influencing factors inducing geological disasters. Therefore, for the explanatory variables, we divided the eight variables into four groups based on the previous studies and field investigation: terrain, human activities, climate, and ecology. Steep terrain and slopes are more likely to form landslides and debris flows, so the terrain category must represent the complex and variable terrain conditions. Elevation, slope, and aspect are selected by referencing relevant studies. For the human activities category, we choose population density and GDP as the variables representing the density of populations and economic activities. Furthermore, frequent climate change affects the distribution of rainfall and vegetation growth, to a certain extent, can lead to the potential occurrence of geological disasters. Thus, rainfall and temperature are selected as the proxy of the climate category. The event of geological disasters is usually concentrated in the summer months of June to October in the study area; therefore, rainfall and temperature data are collected for the same periods and are averaged. Previous studies have shown that vegetation coverage is an essential factor induce geological disaster. High vegetation coverage can enhance soil stability, reduce erosion, and prevent landslides and debris flow geological disasters. Previously, we tried to use the biological abundance index and soil erosion intensity to reflect the ecological environment. But in the remote mountainous rural areas of China, it is difficult to obtain fine data to support micro-scale studies. Therefore, we attempt to represent the fragile ecological environment of Meigu County using NDVI. Compared with the relevant studies, we did not select the variables such as stratigraphic lithology, distance from water, or distance from fault (Xi et al., 2021; Wang et al., 2022), because the topography of the study area is highly undulating and significantly different from the two-dimensional planar analysis, and the above factors can hardly reflect the variability of the variables in the vertical dimension. Finally, the explanatory variables include elevation, slope, aspect, normalized difference vegetation index (NDVI), gross domestic product (GDP), population density, rainfall, and temperature (Table 1; Figure 4).

3.3 Data

The data source used in this research are summarized as follows:

(1) The PGDSs data, including 137 spots, were obtained from the geospatial data cloud (China, http://www.gscloud.cn/).
(2) The vector data were obtained from the national 1:1 million public versions topographic data (2021) provided by the National Catalogue Service for Geographic Information in China (https://www.webmap.cn/main.do?method=index).
(3) Digital elevation model (DEM) data was obtained from a geospatial data cloud (China, http://www.gscloud.cn/) and used to calculate elevation, aspect, and slope; population density data were obtained from World POP (https://www.worldpop.org/). GDP, rainfall data, and NDVI data were obtained from resource and environmental science and data

TABLE 1 Explanatory variables in the study.

Description	Explanatory variables	Sources
Terrain	Elevation Slope Aspect	Wang et al. (2022), Oliveira et al. (2014), Qi et al. (2010), Lv et al. (2022), Xi et al. (2021), Zhao Z. et al., 2021, Lin J et al., 2021, Wang et al. (2020)
Human activities	Population density GDP	Oliveira et al. (2014), Zhao Z. et al., (2021)
Climate	Rainfall Temperature	Oliveira et al. (2014), Wang et al. (2022), Zhao Z. et al., 2021, Lin J et al., 2021, Wang et al. (2020)
Ecology	NDVI	Wang et al. (2022), Lv et al. (2022), Xi et al. (2021), Lin J et al., 2021

center (China, https://www.resdc.cn/Default.aspx). The data of rainfall and temperature were averaged over July-September data.

The study area was divided into 36 units consisting of one town and 35 townships. Descriptive statistics of the explanatory variables are given in Table 2.

4 Results

4.1 Spatial distribution of potential geological disasters spots

As seen in Figure 5, Meigu county suffers from a multitude of PGDSs, among which debris flow is the primary type of disaster, with a number of 69, accounting for 50.36% of the total; followed by landslide, with a number of 61 and a proportion of 44.53%. These two PGDSs are densely distributed along the Meigu river. The number of unstable slopes is only 7, accounting for 5.11% of the total, mainly distributed in Jiukou Township and Erqi Township in the south of the study area.

Combined with the SDE result (Figure 6), PGDSs present a north-to-south direction distribution pattern except for unstable slopes and landslides which were unevenly distributed across the study area.

The results of the ANN model showed that the spatial distribution of geological disasters has a significant accumulation characteristic except for collapses (Table 3). Regarding accumulation, desire flows were the highest, with an R of 0.512, followed by landslides (R = 0.3854). Only the collapse reflected a dispersed distribution characteristic (R = 1.60).

The kernel density map was divided into five levels using the natural break-point method in ArcGIS (version 10.5): low, medium-low, medium, medium-high, and high (Figure 7). The results showed that: (i)The spatial distribution of landslides formed four agglomeration areas, in which Caihong (CH) township, Equgu (EQG) township, Jingyetexi Township (JYTX) and Bapu (BP) Township were categorized as core areas (Figure 7A). 2) The spatial distribution of mudslides formed two belt-like shapes (Figure 7B). (3) The collapse was mainly concentrated in Jiukou Township (JK), and the junction of the Lamuajue Township (LMQJ) and Erqi Township (EQ) (Figure 7C). In summary, the spatial distribution of PGDSs has a significant heterogeneity with cluster formations (Figure 7D).

4.2 Patterns of potential geological disasters spots incorporating explanatory variables

(1) The elevation of the study area ranged from 650 to 4100 m and was divided into 500 m interval classes referencing the previous studies (Li et al., 2013), then we superimposed PGDSs. Through the statistical analysis, we found that approximately 95.65% of the PGDSs distribute below 2500m, and the largest percentage of PGDSs distribute between 1500m and 2000m (Figure 8A).

(2) The slope ranges from 0–69.5° and can also be divided into seven grades at 10°intervals. It is shown that 92.70% of the population density occur below the slope of 30°. The largest percentage of PGDSs distribute between 10° and 20°; the ratio was 48.91% (Figure 8B).

(3) The aspect is divided into eight grades at 45° intervals, which represent eight common directions, namely north (0–22.5°,337.5–360°), northeast (22.5–67.5°), east (67.5–112.5°), southeast (112.5–157.5°), south (157.5–202.5°), southwest (202.5–247.5°), west (247.5–292.5°), northwest (292.5–337.5°). We found that most PGDSs distribute in the west direction (accounting for 25.55% of the total) (Figure 8C).

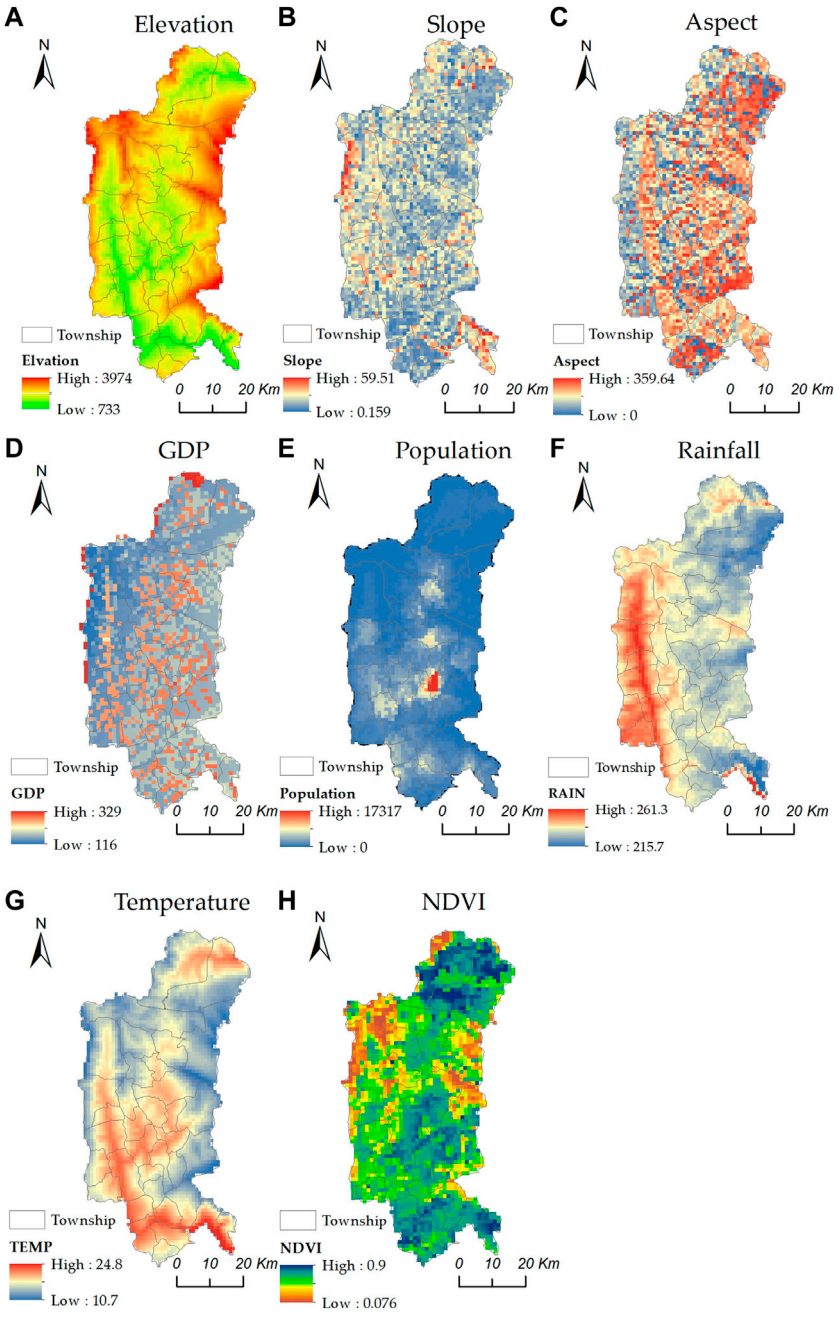

FIGURE 4
Spatial distribution of explanatory variables.

(4) The population density was divided into five grades at 500 pcs/km^2 intervals. Most PGDSs distribute in the 500–1,000 pcs/km^2; the ratio is 29.20% (Figure 8D).

(5) The GDP was also divided into five grades at 20 thousand CNY/1 km^2 intervals. Most PGDSs distribute in the 1.20–1.40 million CNY/km^2; the ratio is 27.74% (Figure 8E).

(6) The NDVI was also divided into five grades at 0.2 intervals. Most PGDSs distribute in the range of 0.6–0.8; the ratio is 60.85% (Figure 8F).

(7) The rainfall was divided into five grades at 20 mm intervals. Most PGDSs distribute in the range of over 240 mm; the ratio is 41.61% (Figure 8G).

TABLE 2 Descriptive statistics of explanatory variables.

Explanatory variables (units)	Min	Mean	Max	St.D
Elevation (m)	650.00	2,544.95	4,011.00	513.98
Slope (°)	0.00	17.21	69.00	8.44
Aspect	−1.00	189.61	360.00	103.32
GDP (10^4 CNY/1 km^2)	116.00	145.02	329.00	23.25
Population density (pcs/10^4m^2)	0.00	621.80	28,710.00	900.90
Rainfall (mm)	216.00	233.34	261.00	6.05
Temperature (°C)	11.00	16.70	25.00	2.59
NDVI	0.00	0.59	1.00	0.20

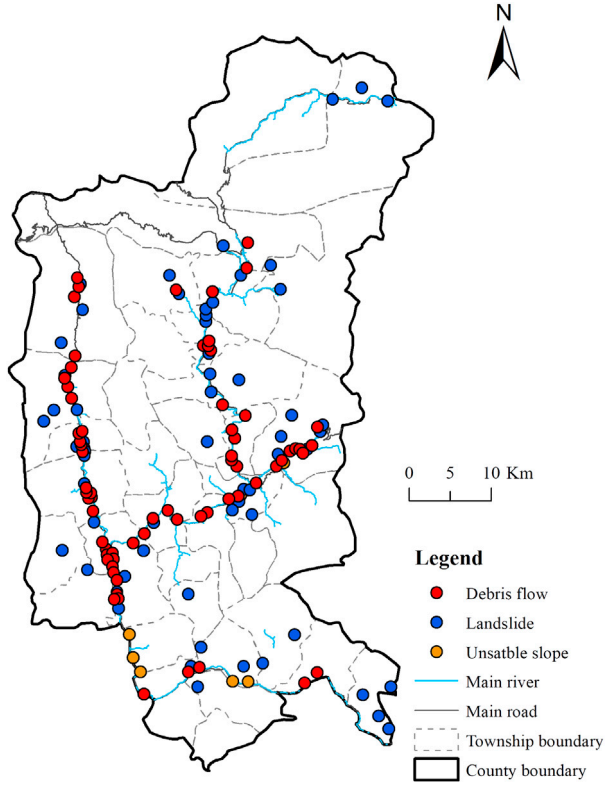

FIGURE 5
Location of PGDSs.

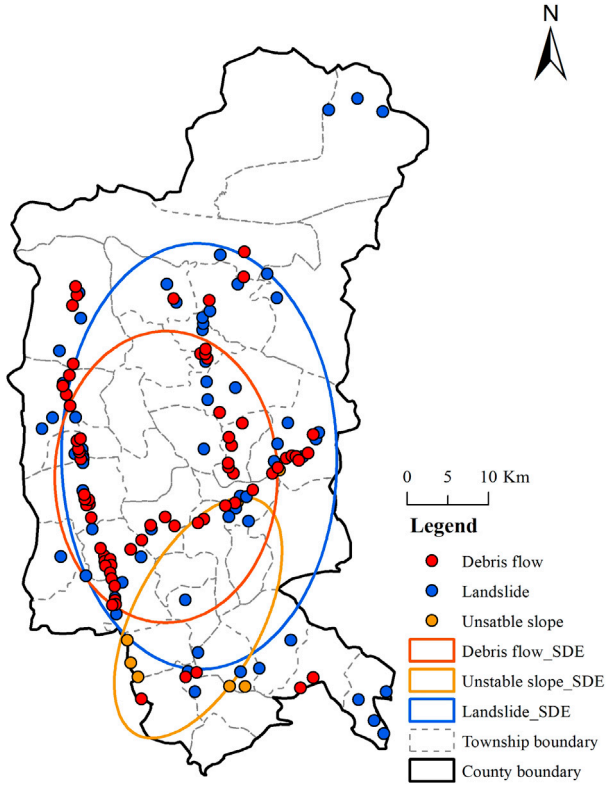

FIGURE 6
SDE distribution of PGDSs.

(8) The temperature was divided into five grades at 2°C. We found most PGDSs distribute in the range of 19–21°C; the ratio is 40.88% (Figure 8H).

4.3 Correlation coefficient and the impacts of determinants

Table 4 shows the results of the OLS model. The VIF of the explanatory variables are all lower than the threshold of 10 except for temperature (the variable will be removed in the OLS model), indicating no obvious collinearity. It can be seen in Table 4 that the PGDSs are significantly correlated with slope, aspect, population density, and rainfall. The coefficient values are 1.398, 0.137, 0.010, and 1.979, respectively ($p < 0.05$). The adjusted R-squared is 0.5493, which means the model has a good explanatory. The model could be shown as follows: $Y_{PGDSs} = -439.318 + 1.398\ X_1 + 0.1367\ X_2 + 0.010\ X_3 + 1.979\ X_4$, where Y_{PGDSs} was the density of PGDSs in each unit, X_1 is slope, X_2 is aspect, X_3 is population density, and X_4 is rainfall.

TABLE 3 Spatial characteristics of PGDSs distribution using the ANN.

Category	Observed mean Distance(m)	Expected mean Distance(m)	Ratio	Z-score	*p*-value	Distributed pattern
Landslide	769.33	1996.19	0.39	−16.96	0	Clustered
Desire flows	1,618.0538	3,154.21	0.51	−7.57	0	Clustered
Collapse	10,951.56	6,849.25	1.60	2.81	0.0050	Dispersed
All spots	506.40	1758.42	0.29	−22.79	0	Clustered

5 Discussion

This study attempts to identify the PGDSs spatial distribution characteristics and its influencing factors in the geological disaster-prone mountainous rural areas, the results reveal that rainfall and slope are the main contributing factors to PGDSs occurrence.

5.1 Spatial distribution of potential geological disasters spots in mountainous rural areas

Due to their remote location and sparse population, mountainous rural areas have received little scholarly attention (Klein et al., 2003; Chen et al., 2008). We emphasize the importance of conducting research on mountainous rural areas for two reasons: First, most mountainous rural areas are always geologically disaster-prone in China, thus hindering its development (Xu et al., 2017), where Geological Disaster Induced Poverty (GDIP; *yin zai zhi pin*) is a frequent problem (Xu et al., 2020). Second, there is an essential need to investigate the spatial distribution and influencing factors of PGDSs on a fine scale (Wang et al., 2020). We found that PGDSs are distributed westwardly (247.5–292.5°) in an elevation range of 1,500–2000 m, the surface slope of 10–20°, high vegetation cover of 0.6 < NDVI <0.8, and high average monthly rainfall of >240 mm which is approximately in agreement with the findings of Lin J et al., 2021 who showed that PGDSs are distributed in areas with low elevation (200–400 m), gentle slopes (5–15°), and high rainfall (annual average 1500–1600 mm). The results, however, contradict those of previous studies (Chiessi et al., 2010; Li et al., 2013; Lin J et al., 2021), probably due to differences in topographical attributes and highlight the importance of geographical differences when analyzing the PGDSs spatial distribution and its influencing factors.

Some unexpected findings are obtained. First, the density of PGDSs is a surrogate for its susceptibility in mountainous areas, consistent with the findings of Jiang et al. (2016). More clearly, the spatial distribution of PGDSs is a simpler and more efficient path to identifying PGDSs susceptibility than constructing a causal relationship with topographical and climatic explanatory variables. Second, in this research, we found that the spatial distribution of landslide and debris flow seems to have possible correlations that merit further investigation.

5.2 Geographical differentiation of influencing factors

In comparison with previous studies, we found that rainfall and slope are the main factors affecting PGDSs incidence (Table 4), which differs from those of Wang et al. (2021). Furthermore, another study suggested that human activities and rainfall are the most prominent factors in similar mountainous areas (Wang et al., 2020). Aiming to characterize the magnitude effect of these factors, we found that rainfall and slope have a stronger correlation with PGDS occurrence than other factors. Consistent with these findings, Smyth & Royle (2000) confirmed that heavy rainfall and natural environment features are the primary triggers of PGDS incidence. Consistent with the findings, natural factors had a more profound impact on PGDSs in mountainous areas than human activities, possibly because of the low population density and their insignificant effects in mountainous rural areas. Overall, it can be concluded that there exist similarities in the forming mechanism of micro-scale PGDSs in mountainous rural areas. We also found a non-strong correlation between NDVI and PGDS; however, PGDSs are mainly distributed in high vegetation areas, primarily in steep slope regions.

5.3 Recommendation for potential geological disasters spots avoidance

Arguably, based on most previous studies, human engineering activities are always the main but unavoidable influencing factors increasing the susceptibility of PGDSs in mountainous rural areas (Tselios and Tompkins, 2020; Tan et al., 2021; Khan et al., 2022). These factors are a consequence of rural development and can potentially be used for PGDS prevention. Additionally, although settlement relocation policies have proven to be an effective strategy for PGDSs prevention in disaster-proven areas (Xu et al., 2020), these strategies have limited practical effectiveness

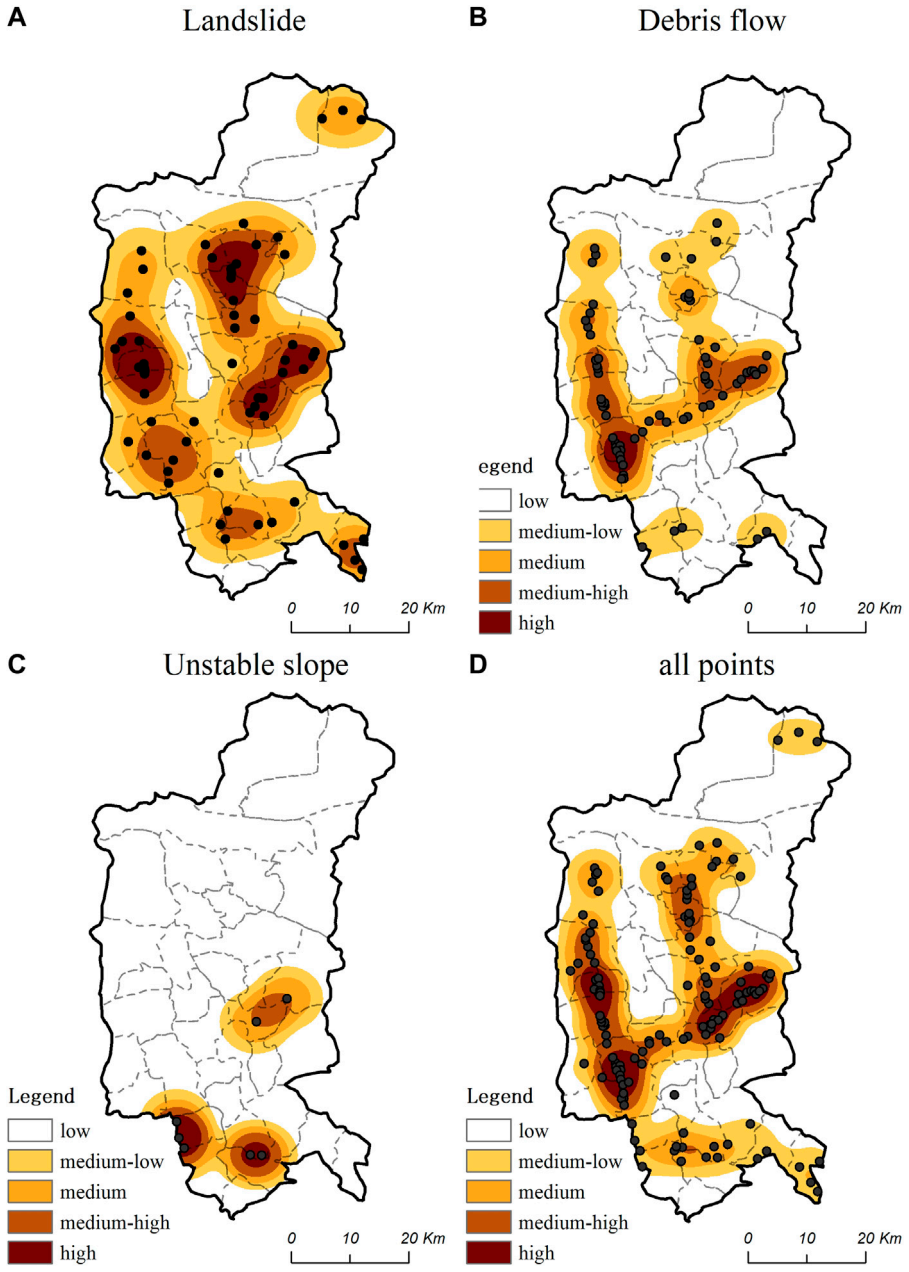

FIGURE 7
Maps of Kernel density of PGDSs.

in mountainous rural areas which suffer from widespread low development suitability (Liu et al., 2022). Under these conditions, a good understanding of the PGDSs spatial distribution and influencing factors is essential in PGDS preparedness.

As concluding recommendations, a careful suitability analysis and planning considering topographical and climatic features are needed to identify low PGDSs affected areas for settlement relocation and future developments. Second, a meteorological risk warning system can be established for the region's rural communities against ubiquitous and recurrent PGDSs, such as continuous heavy rainfalls, which is a critical factor that induces PGDS in mountainous areas. Finally, a combination of prevention and preparedness strategies and practical planning measures, such as the engineering of unfavorable terrains or relocation, should be constructed to avoid high-risk PGDSs (Li H. et al., 2021).

10.3389/fenvs.2022.1049333

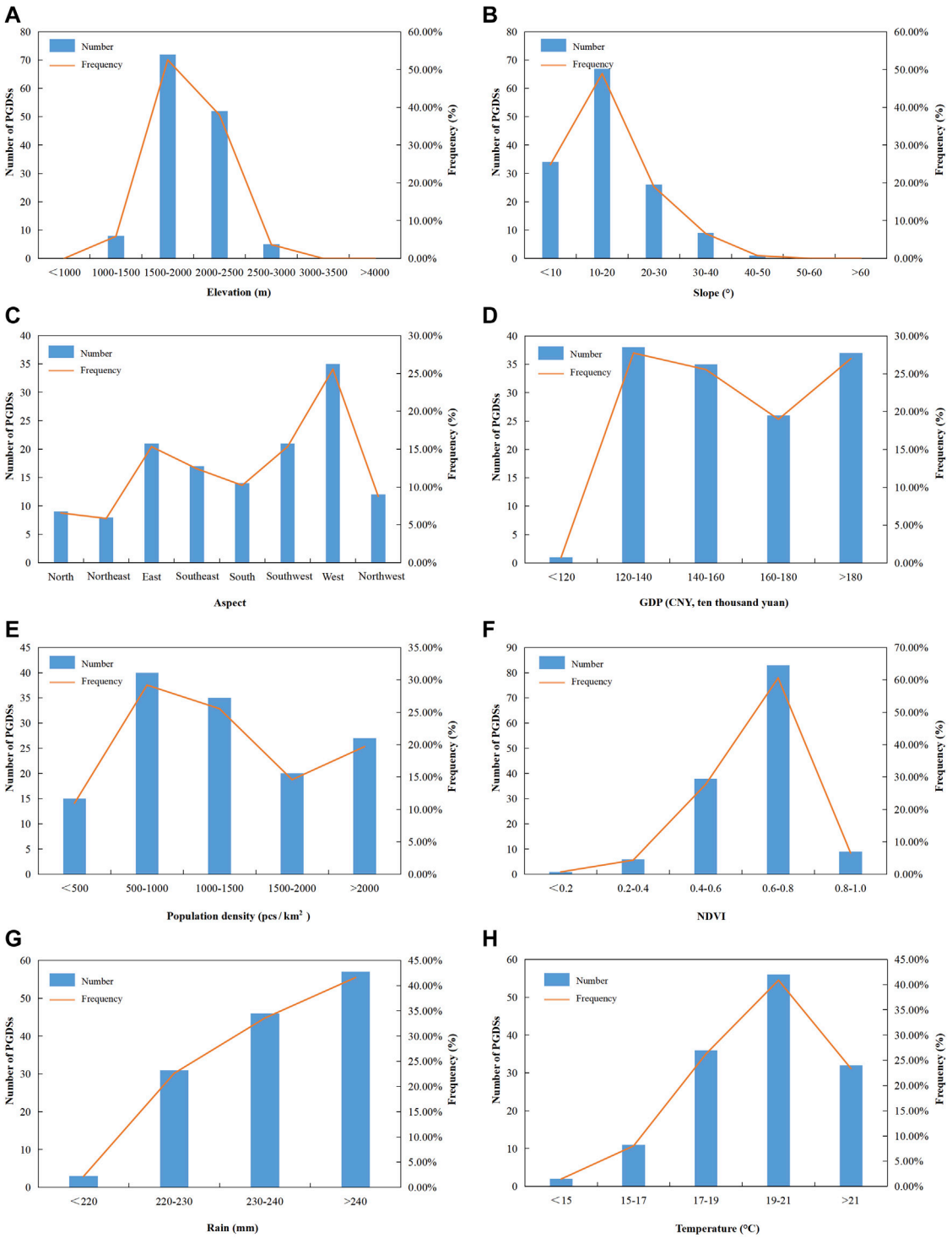

FIGURE 8
Statistics analysis of PGDS.

TABLE 4 Summary of OLS results and diagnostics.

Variable	Coefficient	Stderr	t-Statistic	Probability	VIF
Intercept	−439.318	156.952	2.799	−0.009*	–
Elevation	0.083	0.061	1.354	0.186	3.246
Slope	1.398	0.406	3.446	0.001*	1.341
Aspect	0.137	0.052	2.613	0.014*	1.833
Population density	0.010	0.002	4.581	0.000*	1.617
Rainfall	1.979	0.625	3.166	0.003*	2.675
NDVI	−0.120	0.380	−0.316	0.754	2.323
Performance statistics					
Joint F-Statistic		7.095	Akaike's Information Criterion (AICc)		255.160
Multiple R-Squared		0.639	Adjusted R-Squared		0.549
Number of observations		36			

Note: * significant at 0.05 level.

5.4 Research limitations

In this research, we analyzed the PGDSs spatial pattern and influencing factors to reflect on the PGDSs distribution characteristics and possible planning recommendations. However, due to limited data accuracy, this study neglected to include the PGDSs extent (e.g., large, medium, small) and level (e.g., minor, moderate, severe). Furthermore, this study only explored the PGDSs potentialities in the region and suggested holistic susceptibility and vulnerability assessments and the construction of evaluation indicator systems to gain practical insights. Moreover, the study area is a mountainous rural area, while the soil geological map is two-dimensional that does not truly reflect the current situation. Therefore, we did not consider the influence of soil properties on PGDSs. In the future, we will combine field surveys to obtain more fine-grained data.

6 Conclusion

Taking Meigu County as the study case, the paper analyzed the spatial distribution characteristics, patterns, and influencing factors of PGDS using GIS technology. Compared with the previous studies, we focused on mountainous rural areas to perform a fine-scale multi-type PGDS analysis using multiple analysis methods (e.g., ANN, KDE, SDE, *etc.*). We found PGDSs are distributed in an elevation range of 1,500–2000 m which receives a mean monthly rainfall of more than 240 mm and in highly foliated (0.6 < NDVI <0.8) west-facing slopes. We also found that PGDSs significantly correlate with slope, aspect, population density, and rainfall. The results can provide important implications for land use planning of resource allocation for disaster prediction and prevention.

Data availability statement

The original contributions presented in the study are included in the article/Supplementary Material, further inquiries can be directed to the corresponding author.

Author contributions

BS: conceptualization, funding acquisition, supervision, and writing—original draft. YC: formal analysis and writing—review and editing. MA: writing—review and editing. RZ: writing—review and editing.

Funding

This work was supported by the Science and Technology Department of Sichuan Province (No. 2020YFS0309), Si Chuan Research Center of Yi Culture (No. w202311).

Conflict of interest

The authors declare that the research was conducted in the absence of any commercial or financial relationships that could be construed as a potential conflict of interest.

Publisher's note

All claims expressed in this article are solely those of the authors and do not necessarily represent those of their affiliated organizations, or those of the publisher, the editors and the reviewers. Any product that may be evaluated in this article, or claim that may be made by its manufacturer, is not guaranteed or endorsed by the publisher.

References

Ao, Y., Zhang, H., Yang, L., Wang, Y., Martek, I., and Wang, G. (2021). Impacts of earthquake knowledge and risk perception on earthquake preparedness of rural residents. *Nat. Hazards (Dordr)* 107 (2), 1287–1310. doi:10.1007/s11069-021-04632-w

Bai, S., Wang, J., Lu, G., Zhou, P., Hou, S., and Xu, S. (2010). GIS-based logistic regression for landslide susceptibility mapping of the Zhongxian segment in the Three Gorges area, China. *Geomorphology* 115 (1-2), 23–31. doi:10.1016/j.geomorph.2009.09.025

Bulte, E., Xu, L., and Zhang, X. (2018). Post-disaster aid and development of the manufacturing sector: Lessons from a natural experiment in China. *Eur. Econ. Rev* 101, 441–458. doi:10.1016/j.euroecorev.2017.10.019

Chang, M., Dou, X., Tang, L., and Xu, H. (2022). Risk assessment of multi-disaster in mining area of guizhou, China. *Int. J. Disaster Risk Reduct* 78, 103128. doi:10.1016/j.ijdrr.2022.103128

Chen, S., Ferng, J., Wang, Y., Wu, T., and Wang, J. (2008). Assessment of disaster resilience capacity of hillslope communities with high risk for geological hazards. *Eng. Geol* 98 (3-4), 86–101. doi:10.1016/j.enggeo.2008.01.008

Chen, W., Xie, X., Wang, J., Pradhan, B., Hong, H., Bui, D., et al. (2017). A comparative study of logistic model tree, random forest, and classification and regression tree models for spatial prediction of landslide susceptibility. *Catena* 151, 147–160. doi:10.1016/j.catena.2016.11.032

Chiessi, V., D'Orefice, M., Mugnozza, G. S., Vitale, V., and Cannese, C. (2010). Geological, geomechanical and geostatistical assessment of rockfall hazard in San Quirico Village (Abruzzo, Italy). *Geomorphology* 119 (3-4), 147–161. doi:10.1016/j.geomorph.2010.03.010

Chiou, I., Chen, C., Liu, W., Huang, S., and Chang, Y. (2015). Methodology of disaster risk assessment for debris flows in a river basin. *Stoch. Environ. Res. Risk Assess* 29 (3), 775–792. doi:10.1007/s00477-014-0932-1

Deng, N., Li, Y., Ma, J., Shahabi, H., Hashim, M., de Oliveira, G., et al. (2022). A comparative study for landslide susceptibility assessment using machine learning algorithms based on grid unit and slope unit. *Front. Environ. Sci* 10. doi:10.3389/fenvs.2022.1009433

Dong, J., Peng, J., Liu, Y., Qiu, S., and Han, Y. (2020). Integrating spatial continuous wavelet transform and kernel density estimation to identify ecological corridors in megacities. *Landsc. Urban Plan* 199, 103815. doi:10.1016/j.landurbplan.2020.103815

Dong, Z., Wang, G., Amankwah, S. O. Y., Wei, X., Hu, Y., and Feng, A. (2021). Monitoring the summer flooding in the Poyang Lake area of China in 2020 based on Sentinel-1 data and multiple convolutional neural networks. *Int. J. Appl. Earth Observation Geoinformation* 102, 102400. doi:10.1016/j.jag.2021.102400

Fedeski, M., and Gwilliam, J. (2007). Urban sustainability in the presence of flood and geological hazards: The development of a GIS-based vulnerability and risk assessment methodology. *Landsc. Urban Plan.* 83 (1), 50–61. doi:10.1016/j.landurbplan.2007.05.012

Gan, L., Wang, L., Hu, Z., Lev, B., Gang, J., and Lan, H. (2022). Do geologic hazards affect the sustainability of rural development? Evidence from rural areas in China. *J. Clean. Prod* 339, 130693. doi:10.1016/j.jclepro.2022.130693

Guo, A., Yang, J., Sun, W., Xiao, X., Cecilia, J., Jin, C., et al. (2020). Impact of urban morphology and landscape characteristics on spatiotemporal heterogeneity of land surface temperature. *Sustain. Cities Soc* 63, 102443. doi:10.1016/j.scs.2020.102443

Hou, J., Lv, J., Chen, X., and Yu, S. (2016). China's regional social vulnerability to geological disasters: Evaluation and spatial characteristics analysis. *Nat. Hazards (Dordr).* 84 (1), 97–111. doi:10.1007/s11069-015-1931-3

Jiang, W., Deng, Y., Tang, Z., Cao, R., Chen, Z., and Jia, K. (2016). Adaptive capacity of mountainous rural communities under restructuring to geological disasters: The case of Yunnan Province. *J. Rural Stud.* 47, 622–629. doi:10.1016/j.jrurstud.2016.05.002

Khan, I., Ali, A., Waqas, T., Ullah, S., Ullah, S., Shah, A. A., et al. (2022). Investing in disaster relief and recovery: A reactive approach of disaster management in Pakistan. *Int. J. Disaster Risk Reduct.* 75, 102975. doi:10.1016/j.ijdrr.2022.102975

Kim, D., Won, J., Lee, E., Park, K. R., Kim, J., Park, S., et al. (2022). Disaster assessment using computer vision and satellite imagery: Applications in detecting water-related building damages. *Front. Environ. Sci* 10. doi:10.3389/fenvs.2022.969758

Klein, R. J. T., Nicholls, R. J., and Thomalla, F. (2003). Resilience to natural hazards: How useful is this concept? *Environ. Hazards* 5 (1), 35–45. doi:10.1016/j.hazards.2004.02.001

Kong, Y., He, W., Zhang, Z., Shen, J., Yuan, L., Gao, X., et al. (2022). Spatial-temporal variation and driving factors decomposition of agricultural grey water footprint in China. *J. Environ. Manag* 318, 115601. doi:10.1016/j.jenvman.2022.115601

Li, H., Xu, E., and Zhang, H. (2021). Examining the coupling relationship between urbanization and natural disasters: A case study of the Pearl River delta, China. *Int. J. Disaster Risk Reduct* 55, 102057. doi:10.1016/j.ijdrr.2021.102057

Li, K., Geng, H., Yue, L., Li, K., and Huang, L. (2021). Spatial differentiation characteristics and driving mechanism of rural settlements transformation in the metropolis: A case study of pudong district, shanghai. *Front. Environ. Sci.* 9. doi:10.3389/fenvs.2021.755207

Li, L., Lan, H., Guo, C., Zhang, Y., Li, Q., and Wu, Y. (2017). A modified frequency ratio method for landslide susceptibility assessment. *Landslides* 14 (2), 727–741. doi:10.1007/s10346-016-0771-x

Li, M., Lv, J., Chen, X., and Jiang, N. (2015). Provincial evaluation of vulnerability to geological disaster in China and its influencing factors: A three-stage DEA-based analysis. *Nat. Hazards (Dordr)* 79 (3), 1649–1662. doi:10.1007/s11069-015-1917-1

Li, S., Zhou, Z., Li, L., Lin, P., Xu, Z., and Shi, S. (2016). A new quantitative method for risk assessment of geological disasters in underground engineering: Attribute Interval Evaluation Theory (AIET). *Tunn. Undergr. Space Technol* 53, 128–139. doi:10.1016/j.tust.2015.12.014

Li, X., Liu, X., Li, J., Wang, Q., Liao, W., and Zhang, L. (2013). Factor analysis of earthquake-induced geological disasters of the M7. 0 Lushan earthquake in China. *Geodesy Geodyn.* 4 (2), 22–29. doi:10.3724/SP.J.1246.2013.02022

Lin, J., Chen, W., Qi, X., and Hou, H. (2021). Risk assessment and its influencing factors analysis of geological hazards in typical mountain environment. *J. Clean. Prod.* 309, 127077. doi:10.1016/j.jclepro.2021.127077

Lin, J., Lin, M., Chen, W., Zhang, A., Qi, X., and Hou, H. (2021). Ecological risks of geological disasters and the patterns of the urban agglomeration in the Fujian Delta region. *Ecol. Indic.* 125, 107475. doi:10.1016/j.ecolind.2021.107475

Liu, J., Jin, X., Xu, W., and Zhou, Y. (2022). Evolution of cultivated land fragmentation and its driving mechanism in rural development: A case study of jiangsu province. *J. Rural Stud.* 91, 58–72. doi:10.1016/j.jrurstud.2022.02.011

Liu, X., Yu, C., Shi, P., and Fang, W. (2012). Debris flow and landslide hazard mapping and risk analysis in China. *Front. Earth Sci.* 6 (3), 306–313. doi:10.1007/s11707-012-0328-9

Lv, L., Chen, T., Dou, J., and Plaza, A. (2022). A hybrid ensemble-based deep-learning framework for landslide susceptibility mapping. *Int. J. Appl. Earth Observation Geoinformation* 108, 102713. doi:10.1016/j.jag.2022.102713

Oliveira, S., Pereira, J. M. C., San-Miguel-Ayanz, J., and Lourenco, L. (2014). Exploring the spatial patterns of fire density in southern europe using geographically weighted regression. *Appl. Geogr* 51, 143–157. doi:10.1016/j.apgeog.2014.04.002

Pan, A. P. (2016). Study on mobility-disadvantage group' risk perception and coping behaviors of abrupt geological hazards in coastal rural area of China. *Environ. Res.* 148, 574–581. doi:10.1016/j.envres.2016.04.016

Pu, C., Xu, Q., Zhao, K., Chen, W., Wang, X., Li, H., et al. (2022). Spatiotemporal evolution and surface response of land subsidence over a large-scale land creation area on the Chinese Loess Plateau. *Int. J. Appl. Earth Observation Geoinformation* 111, 102835. doi:10.1016/j.jag.2022.102835

Qi, S., Xu, Q., Lan, H., Zhang, B., and Liu, J. (2010). Spatial distribution analysis of landslides triggered by 2008.5.12 Wenchuan Earthquake. China. *Eng. Geol* 116 (1), 95–108. doi:10.1016/j.enggeo.2010.07.011

Qin, Y., Wu, J., Zhan, H., Xiong, C., Jia, C., Bai, X., et al. (2021). Discussion on the correlation between active fault and geological disaster distribution in the Ganzi area, Western Sichuan province, China. *J. Geomechanics* 27 (3), 463–474. doi:10.12090/j.issn.1006-6616.2021.27.03.042

Qing, C., Guo, S., Deng, X., and Xu, D. (2021). Farmers' disaster preparedness and quality of life in earthquake-prone areas: The mediating role of risk perception. *Int. J. Disaster Risk Reduct* 59, 102252. doi:10.1016/j.ijdrr.2021.102252

Siddique, T., Haris, P. M., and Pradhan, S. P. (2022). Unraveling the geological and meteorological interplay during the 2021 Chamoli disaster, India. *Nat. Hazards Res* 2 (2), 75–83. doi:10.1016/j.nhres.2022.04.003

Smyth, C. G., and Royle, S. A. (2000). Urban landslide hazards: Incidence and causative factors in niterói, rio de Janeiro state, Brazil. *Appl. Geogr* 20 (2), 95–118. doi:10.1016/S0143-6228(00)00004-7

Song, W., and Li, H. (2020). Spatial pattern evolution of rural settlements from 1961 to 2030 in Tongzhou District, China. *Land Use Policy* 99, 105044. doi:10.1016/j.landusepol.2020.105044

Song, Y., Jarvis, D. I., Bai, K., Feng, J., and Long, C. (2020). Assessment of the resilience of a tartary buckwheat (fagopyrum tataricum) cultivation system in Meigu, southwest China. *Sustainability* 12 (14), 5683. doi:10.3390/su12145683

Tan, Q., Bai, M., Zhou, P., Hu, J., and Qin, X. (2021). Geological hazard risk assessment of line landslide based on remotely sensed data and GIS, 169. *Measurement* doi:10.1016/j.measurement.2020.108370

Tang, F., Lin, F., Jin, C., Deng, G., Zhao, H., Tie, Y., et al. (2020). Practical geological technologies facilitating poverty alleviation in Wumeng Mountain area. *China Geol.* 3 (3), 504–508. doi:10.31035/cg2020055

Tang, M., Liu, P., Chao, X., and Han, Z. (2021). The performativity of city resilience for sustainable development of poor and disaster-prone regions: A case study from China. *Technol. Forecast. Soc. Change* 173, 121130. doi:10.1016/j.techfore.2021.121130

Tselios, V., and Tompkins, E. L. (2020). Can we prevent disasters using socioeconomic and political policy tools? *Int. J. Disaster Risk Reduct* 51, 101764. doi:10.1016/j.ijdrr.2020.101764

van Westen, C. J., Soeters, R., and Sijmons, K. (2000). Digital geomorphological landslide hazard mapping of the Alpago area, Italy. *Int. J. Appl. Earth Observation Geoinformation* 2 (1), 51–60. doi:10.1016/S0303-2434(00)85026-6

Wan, F., Guo, H., Li, J., Gu, M., Pan, W., and Ying, Y. (2021). A scheduling and planning method for geological disasters. *Appl. Soft Comput* 111, 107712. doi:10.1016/j.asoc.2021.107712

Wang, H., Wang, X., Zhang, C., Wang, C., and Li, S. (2022). Analysis on the susceptibility of environmental geological disasters considering regional sustainable development. *Environ. Sci. Pollut. Res. Int*. doi:10.1007/s11356-022-22778-3

Wang, J., Zhu, S., Luo, X., Chen, G., Xu, Z., Liu, X., et al. (2020). Refined micro-scale geological disaster susceptibility evaluation based on UAV tilt photography data and weighted certainty factor method in Mountainous Area. *Ecotoxicol. Environ. Saf* 189, 110005. doi:10.1016/j.ecoenv.2019.110005

Wang, X., Zhang, C., Wang, C., Liu, G., and Wang, H. (2021). GIS-based for prediction and prevention of environmental geological disaster susceptibility: From a perspective of sustainable development. *Ecotoxicol. Environ. Saf* 226, 112881. doi:10.1016/j.ecoenv.2021.112881

Wang, Z., Lai, C., Chen, X., Yang, B., Zhao, S., and Bai, X. (2015). Flood hazard risk assessment model based on random forest. *J. Hydrology* 527, 1130–1141. doi:10.1016/j.jhydrol.2015.06.008

Wu, S., Zhang, R., Wang, C., and Feng, D. (2022). The impact of natural disasters on rural household wealth: Micro evidence from China. *Front. Environ. Sci* 10. doi:10.3389/fenvs.2022.993722

Xi, X., Wang, S., Yao, L., Zhang, Y., Niu, R., and Zhou, Y. (2021). Evaluation on geological environment carrying capacity of mining city – a case study in Huangshi City, Hubei Province, China. *Int. J. Appl. Earth Observation Geoinformation* 102, 102410. doi:10.1016/j.jag.2021.102410

Xiao, Y., Tang, X., Li, Y., Huang, H., and An, B.-W. (2022). Social vulnerability assessment of landslide disaster based on improved TOPSIS method: Case study of eleven small towns in China. *Ecol. Indic* 143, 109316. doi:10.1016/j.ecolind.2022.109316

Xu, D., Liu, E., Wang, X., Tang, H., and Liu, S. (2018). Rural households, livelihood capital, risk perception, and willingness to purchase earthquake disaster insurance: Evidence from southwestern, China. *Int. J. Environ. Res. Public Health* 15 (7), 1319. doi:10.3390/ijerph15071319

Xu, D., Peng, L., Liu, S., Su, C., Wang, X., and Chen, T. (2017). Influences of migrant work income on the poverty vulnerability disaster threatened area: A case study of the three gorges reservoir area, China. *Int. J. Disaster Risk Reduct* 22, 62–70. doi:10.1016/j.ijdrr.2017.03.001

Xu, F., Li, H., and Bao, H. (2018). Performance comparisons of land institution and land regulation systems on water area decrease. *Habitat Int.* 77, 12–20. doi:10.1016/j.habitatint.2017.12.009

Xu, G., Jiang, Y. H., Wang, S., Qin, K., Ding, J. C., Liu, Y., et al. (2022). Spatial disparities of self-reported COVID-19 cases and influencing factors in Wuhan, China. *Sustain. Cities Soc* 76, 103485. doi:10.1016/j.scs.2021.103485

Xu, Y., Qiu, X., Yang, X., Lu, X., and Chen, G. (2020). Disaster risk management models for rural relocation communities of mountainous southwestern China under the stress of geological disasters. *Int. J. Disaster Risk Reduct* 50, 101697. doi:10.1016/j.ijdrr.2020.101697

Yang, L., Chau, K. W., Szeto, W. Y., Cui, X., and Wang, X. (2020a). Accessibility to transit, by transit, and property prices: Spatially varying relationships. *Transp. Res. Part D Transp. Environ.* 85, 102387. doi:10.1016/j.trd.2020.102387

Yang, L., Chu, X., Gou, Z., Yang, H., Lu, Y., and Huang, W. (2020b). Accessibility and proximity effects of bus rapid transit on housing prices: Heterogeneity across price quantiles and space. *J. Transp. Geogr.* 88, 102850. doi:10.1016/j.jtrangeo.2020.102850

Yang, L., Liang, Y., He, B., Lu, Y., and Gou, Z. (2022). COVID-19 effects on property markets: The pandemic decreases the implicit price of metro accessibility. *Tunn. Undergr. Space Technol* 125, 104528. doi:10.1016/j.tust.2022.104528

Yang, Z., Wu, D., and Wang, D. (2021). Exploring spatial path dependence in industrial space with big data: A case study of Beijing, *Cities*, 108. doi:10.1016/j.cities.2020.102975

Yao, J., Zhang, X., Luo, W., Liu, C., and Ren, L. (2022). Applications of Stacking/Blending ensemble learning approaches for evaluating flash flood susceptibility. *Int. J. Appl. Earth Observation Geoinformation* 112, 102932. doi:10.1016/j.jag.2022.102932

Youssef, A. M., Pradhan, B., Sabtan, A. A., and El-Harbi, H. M. (2012). Coupling of remote sensing data aided with field investigations for geological hazards assessment in Jazan area, Kingdom of Saudi Arabia. *Environ. Earth Sci* 65 (1), 119–130. doi:10.1007/s12665-011-1071-3

Zeng, X., Guo, S., Deng, X., Zhou, W., and Xu, D. (2021). Livelihood risk and adaptation strategies of farmers in earthquake hazard threatened areas: Evidence from sichuan province, China. *Int. J. Disaster Risk Reduct* 53, 101971. doi:10.1016/j.ijdrr.2020.101971

Zhang, X., Zhang, B., Yao, Y., Wang, J., Yu, F., Liu, J., et al. (2022). Dynamics and climatic drivers of evergreen vegetation in the Qinling-Daba Mountains of China. *Ecol. Indic* 136, 108625. doi:10.1016/j.ecolind.2022.108625

Zhao, D., Lancuo, Z., Hou, G., Xu, C., and Li, W. (2021). Assessment of geological disaster susceptibility in the hehuang valley of qinghai province. *J. Geomechanics* 27 (1), 83–95. doi:10.12090/j.issn.1006-6616.2021.27.01.009

Zhao, Z., Chen, J., Xu, K., Xie, H., Gan, X., and Xu, H. (2021). A spatial case-based reasoning method for regional landslide risk assessment. *Int. J. Appl. Earth Observation Geoinformation* 102, 102381. doi:10.1016/j.jag.2021.102381

Zhou, W., Guo, S., Deng, X., and Xu, D. (2021). Livelihood resilience and strategies of rural residents of earthquake-threatened areas in Sichuan Province, China. *Nat. Hazards (Dordr).* 106 (1), 255–275. doi:10.1007/s11069-020-04460-4

Zhuang, L., He, J., Yong, Z., Deng, X., and Xu, D. (2020). Disaster information acquisition by residents of China's earthquake-stricken areas. *Int. J. Disaster Risk Reduct* 51, 101908. doi:10.1016/j.ijdrr.2020.101908

Zuo, R., Agterberg, F. P., Cheng, Q., and Yao, L. (2009). Fractal characterization of the spatial distribution of geological point processes. *Int. J. Appl. Earth Observation Geoinformation* 11 (6), 394–402. doi:10.1016/j.jag.2009.07.001

frontiers | Frontiers in Environmental Science

TYPE Original Research
PUBLISHED 24 November 2022
DOI 10.3389/fenvs.2022.1044600

Check for updates

OPEN ACCESS

EDITED BY
Jun Yang,
Northeastern University, China

REVIEWED BY
Hao Zhu,
Chengdu University of Technology, China
Fang Han,
Southwest Jiaotong University, China

*CORRESPONDENCE
Shuying You,
syouoo@163.com

SPECIALTY SECTION
This article was submitted to Land Use Dynamics,
a section of the journal
Frontiers in Environmental Science

RECEIVED 14 September 2022
ACCEPTED 07 November 2022
PUBLISHED 24 November 2022

CITATION
Chen K, Lin H, Cao F, Han Y, You S, Shyr O, Lu Y and Huang X (2022), Do hospital and rail accessibility have a consistent influence on housing prices? Empirical evidence from China. *Front. Environ. Sci.* 10:1044600. doi: 10.3389/fenvs.2022.1044600

COPYRIGHT
© 2022 Chen, Lin, Cao, Han, You, Shyr, Lu and Huang. This is an open-access article distributed under the terms of the Creative Commons Attribution License (CC BY). The use, distribution or reproduction in other forums is permitted, provided the original author(s) and the copyright owner(s) are credited and that the original publication in this journal is cited, in accordance with accepted academic practice. No use, distribution or reproduction is permitted which does not comply with these terms.

Do hospital and rail accessibility have a consistent influence on housing prices? Empirical evidence from China

Kaida Chen[1,2], Hanliang Lin[1], Fangxiao Cao[2], Yan Han[3], Shuying You[4]*, Oliver Shyr[1], Yichen Lu[2] and Xiaodi Huang[5]

[1]Department of Urban Planning, National Cheng Kung University, Tainan, China, [2]College of Landscape Architecture and Art, Fujian Agriculture and Forestry University, Fuzhou, China, [3]Department of Spatial Culture Design, Kookmin University, Seoul, South Korea, [4]International Digital Economy College, Minjiang University, Fuzhou, China, [5]Fujian Communications Planning and Design Institute CO.,Ltd., Fuzhou, China

This study investigates the interaction between the accessibility of various urban public facilities and the price of urban space by analysing the influence of urban hospitals and rail accessibility on housing prices. In recent years, with the development of social civilisation and the influence of COVID-19, people have become increasingly interested in the quality of hospitals in their living environment. This makes medical convenience (hospital accessibility) a crucial element in determining housing prices. At the same time, people regard rail as one of the important means to access hospitals. Therefore, demonstrating the intrinsic value of accessibility to hospitals and rail in residential areas is essential. As a point of reference, this paper presents an empirical analysis of Fuzhou, Fujian Province, China, a city in a developing nation with relatively widespread access to hospitals during a significant rail construction period. The study demonstrates the interaction between hospital and rail accessibility and their moderate influence on housing prices, which is geographically heterogeneous. The study also determines the optimal metric model for assessing geographical interaction based on the significance and stability of the interaction in geographic space. It concludes with a discussion of the findings and social recommendations.

KEYWORDS

housing prices, spatial economics, geographical heterogeneity, facility accessibility, interaction

1 Introduction

1.1 Background

In recent years, as the economy as a whole has risen, the problem of ageing has become more severe, and people have become increasingly concerned about their quality of life. Furthermore, in the context of COVID-19 over the past 2 years, people are becoming more health-conscious and aware of how to gain access to a high-quality hospital (Wu et al., 2013). As an integral part of the city's infrastructure, hospitals serve the diagnostic needs of residents and contribute to economic growth (Yang et al., 2022).

Consequently, people tend to consider the proximity of hospitals when purchasing houses (Baumont et al., 2003). The factors they consider include degree, ownership, type, scope and accessibility, which is one of the most important. Accessibility is a crucial concept in human geography for analysing the geographical arrangement of public service facilities (Yang et al., 2019). Western scholars have been concerned with accessibility since 1950. The accessibility of healthcare facilities largely impacts the convenience of getting healthcare services.

These concerns about hospital accessibility have also prompted a recent increase in research on the influence on housing prices. Li, Gong (Li et al., 2021) used the Gaussian-two step floating catchment area method to study the influence of accessibility to public services on housing prices in Beijing. The influence was strongly positive at a 1% significance level. A one-unit increase in the accessibility of hospitals is associated with an average increase of 1.1% in housing prices, all other variables being equal.

By contrast, when purchasing houses, people also consider the proximity of rail accessibility in addition to hospital accessibility (Yang et al., 2020a). As an efficient and environmentally friendly means of transportation, rail is an essential component of residential accessibility (Yang et al., 2020b). Numerous studies have demonstrated that rail stations have a significant influence on housing prices. Foreign scholars initiated their research in this field earlier than their counterparts in China. Alonso, for instance, proposed bid rent theory as early as 1964, arguing that accessibility has a direct influence on housing prices near transportation hubs (Alonso, 1964).

Collectively, the aforementioned studies indicate that hospital and rail station accessibility will affect housing prices. Given the potential correlation between hospital and rail accessibility, investigating the interaction between hospital and rail station accessibility on housing prices. This paper introduces the concept of interaction to the hedonic price model and develops a linear regression interaction regression model and a spatial regression interaction regression model for the continuous accessibility variables. It examines the mutual adjustment relationship between the accessibility variables of hospitals and that of rail stations on housing prices. A few scholars have conducted studies on the relationship between such two variables, but the studies are brief and do not provide a thorough overview of the relationship between the two. As a result, this paper will focus on the interaction between the two to supplement the research in this field.

The paper is structured into four components. The first part is the introduction and review, which explores the background of the study and a summary of previous research. The second part is the statistics and methodology, which introduces the subject of the study, the research framework, the research statistics sources and the research methodology. The third part is a report of the research statistics results. The fourth part is discusses and concludes.

2 Literature review

2.1 Influence of hospitals on housing prices

As a key element of urban infrastructure, hospitals have a significant influence on housing prices. Numerous international studies, such as Banzhaf and Farooque (2012), have confirmed this finding. The findings of Dziauddin (2014) also suggest that hospital accessibility can affect housing prices.

Scholars have occasionally discussed the varying effects of the different categories of hospitals on influencing housing prices. In a study of the influence of different categories of hospitals on housing prices, Baden (2013) used the hedonic price model to conduct a controlled experiment to examine the influence of medical centres and hospitals on retirement housing prices. They concluded that hospitals had a positive influence on retirement housing prices, whereas medical centres had a negligible influence. By incorporating different ecological sites into a feature analysis based on a spatial multilevel model, Liu et al. (2020) concluded that the proximity of a grade-A tertiary hospital plays a positive role in housing prices.

Previous scholars have evaluated the accessibility of hospitals, and their findings regarding the influence of hospitals are diverse. They can be divided into three broad perspectives: spatial distance, number of hospitals and density of hospitals. The findings can also be categorized as positive, negative or both. The section that follows provides a more in-depth analysis of the research conducted in these two areas.

2.1.1 Perspectives of hospital accessibility

One of the most common options is research based on the distance of houses to hospitals. Many scholars have conducted research from this perspective. For example, Using geostatistical methods and quantitative regression, Wang and Liu (2013) ascertained that the distance to hospitals and schools significantly decreased housing prices by 3.8% and 3.3%, respectively. Dziauddin et al. (2013) determined that for every

additional metre in a straight line and grid distance from the hospital in Malaysia, the housing prices would increase by about MYR 3. Dziauddin (2014) employed the hedonic price model to determine the influence of location characteristics on housing prices and determined that the housing prices would increase by approximately MYR 5.52 per metre of distance from the hospital. Peng and Chiang (2015) used quantile regressions to examine the spatial effects of hospitals in the Taipei metropolitan area at different housing prices scales. They found that hospitals were rated higher for their 'close but not too close' proximity to residential areas and that housing prices were unrelated.

Precedents for defining hospital accessibility based on the proximity of hospitals to a residence are numerous. Several Chinese scholars have also conducted the following research on the influence of the density of hospitals on housing prices. Wang and Gao (2014) investigated the spatial characteristics of housing prices using spatial statistics on average transaction prices in residential areas of Beijing in 2005 and 2012, revealing that housing prices in 2005 and 2012 increased by 10.7% and 7.5%, respectively, when one or more grade-A tertiary hospitals were within 1,000 m of a residential area. Yang et al. (2016) used a sample of 1,840 general residences on Xiamen Island to examine the direction and extent of capitalisation of public items in the residential market by constructing hedonic price equations, demonstrating that the walkability of grade-A tertiary/secondary hospitals had a negative influence on housing prices, with each additional grade-A tertiary/secondary hospital lowering the total housing prices by 2.8%.

A small number of scholars employed the density concept, which is derived by combining distance and quantity, as an indicator of hospital accessibility. Wang and Chen (2019) use a non-linear model of three property types, buildings, apartments and suites - a combination of upward and downward trends derived from the generalised additive model as an indicator of hospital accessibility. The study concluded that the residential-to-hospital distance pattern has a 'V' curve, with the lowest prices at 0.8 km to the hospital. The right number of hospitals will result in higher prices, and too many or too few will result in lower prices.

2.1.2 Variability in the results of the influence of hospital accessibility

The majority of scholarly research indicates that the proximity of hospitals has a positive influence on housing prices. The pertinent literature is compiled and summarized as follows: Guo et al. (2016) studied the spatially divergent status of housing prices and their factors in Jinan and concluded that key hospitals play a crucial role in housing prices, which were positively correlated with the distance to hospitals. According to Jabbar (2016) research, individuals are willing to pay more for a nearby hospital. Lan and Ye (2020) investigated the linear relationship between these factors and housing prices in Shanghai using linear regression on a large statistics set combining characteristics such as housing prices and location information. It concluded that hospitals have a positive influence on the price of surrounding houses. Liu et al. (2022) compared the multi-scale effects of accessibility to various facilities on housing prices and demonstrated that hospitals have a positive influence on housing prices, indicating that the closer the proximity, the higher the housing prices.

Nonetheless, some scholars have concluded that the influence of hospitals on housing prices is marginal. According to He et al. (2010), hospital proximity appears to have little influence on housing transaction prices. Cao et al. (2019) analysed the geographical variation of the public housing resale prices credited to the Housing Development Board (HDB) in Singapore and the various determinants of HDB resale condominium prices and concluded that the distance to the proximate general hospital was marginally correlated with HDB resale condominium prices in Singapore in 2011.

Some scholarly research even indicates that the presence of hospitals has the potential to result in lower housing prices. Using weighted least squares and a heteroskedasticity consistent covariance matrix estimator, Tan (2011) estimated the coefficients of the influence of the structure, location and neighbourhood characteristics of houses on housing prices. Li et al. (2013) used GIS techniques and the hedonic price model to determine the extent to which different spatial factors influence housing prices in Xiamen. They found that housing prices increased by CNY 1,190 for every kilometre away from the hospital. Peng et al. (2015) examined the spatial influence effect of grade-A tertiary hospitals on the neighbouring housing prices by harnessing the hedonic price model and multiple regression analysis, finding that grade-A tertiary hospital plays a negative role in housing prices in their vicinity. By contrast, Luo et al. (2010), who conducted a study on housing prices in the central area of Wuhan, discovered that greater accessibility to a hospital led to lower housing prices.

In addition, a body of research suggests that the influence of hospitals on housing prices is two-way. The first study by Waddell and Hoch (1993) investigated a non-linear housing prices gradient in a multi-node urban area and discovered that hospitals lower housing prices by 3% within half a mile, boost them by 2% between one and two miles and then decay to zero. Zhang et al. (2016) used the hedonic price model to examine the link between the prices of major hospitals and the surrounding residential communities, using Shandong Provincial Hospital as an example. In both the east–west and north–south within the study distance range, a significant cubic function relationship was observed between the weighted distance from the residential community to the major hospital and its price. In the east-west, within a 0.83 km radius of the key hospital, the price of housing decreases as the distance increases. Within 0.83–2.35 km of the key hospital, the price of housing increases as the distance increases. In the north–south,

within 1.03 km of the key hospital, the price of housing decreases as the distance increases. Within 1.03–2.46 km of the key hospital, the price of housing increases proportionally with distance. Febrita et al. (2017) concluded that housing prices increase gradually as the distance between hospitals and residences decreases, but that the most expensive residences may be located either far from or close to hospitals. Han et al. (2018) highlighted the importance of different geographical heterogeneity and concluded that the influence of hospitals on housing prices in Shenzhen is predominantly negative, meaning housing prices are lower near hospitals. Owing to the lack of hospitals and the increase in the elderly population, hospitals have a positive influence on Longgang and Yantian's housing prices. Lan et al. (2018) analysed service facilities in Xi'an, China and concluded that hospitals have varying effects on housing prices in different regions. In well-built residential areas in the south, the presence of hospitals exacerbates issues such as traffic jams and environmental pollution, and hospitals therefore have a detrimental influence on housing prices; in poorly built facilities in the city's periphery, hospitals have a beneficial influence on housing prices.

2.2 Influence of rail station proximity on housing prices

Rail is an essential component of urban infrastructure, and rail stations can have a substantial influence on housing prices in the vicinity. This subject has been researched by numerous scholars around the world. Foreign scholars initiated research in this field considerably earlier than their Chinese counterparts. In Almosaind et al. (1993), an empirical study of rail in Portland determined that proximity to a light rail station is advantageous for houses within 500 m walking distance, with a housing prices differential of nearly 10.6% and a distance decay effect.

Numerous studies and the vast majority of scholarly research have demonstrated that rail stations have a significant positive influence on housing prices. McDonald and Osuji (1995) compared land values in Chicago before and after the rail plan was announced and found a 17% increase within 1.5 miles of the station. Benjamin and Sirmans (1996) demonstrated that for every 0.1-mile increase in distance to a rail station, flat rents decrease by 2.5%. In addition, Agostini and Palmucci (2008) for Santiago, Chile; Bae et al. (2003) for Seoul, Korea; Hao and Chen (2007) for Shanghai and Li, Chen (Li et al., 2019) for Beijing all conclude that rail contributes to neighbourhood housing prices. Tan et al. (2019) conducted empirical analyses of rail in Wuhan and all concluded that rail can promote the growth of housing prices and that the two have a positive correlation. Zhang (2014) examined housing prices statistics near Nanjing Lines one and two from a distance-based research perspective and discovered that rail has a positive influence on housing prices, with the results indicating that the stimulative effect of rail on housing prices growth is greatest when the distance between rail and residential is less than 500 m. Once the distance between rail and residential reaches 2,000 m, the growth effect ceases to be significant. Im and Hong (2018) examined the difference in housing prices in Daegu, South Korea, before and after the opening of the rail transit line. They discovered that housing prices within 500 m of the proximate station on the new line increased by approximately USD 96.3 per square foot. Rohit and Peter (2018) used a characteristic price model analysis to demonstrate that rail in Bangalore substantially increased property values, with the influence of rail appearing to extend well beyond the traditional 500 m radius to encompass the entire city.

Alternatively, some studies have found that rail lessens the housing prices along the route. Teng et al. (2014) used the hedonic price model to study the influence of rail on housing prices along rail transit lines, using Tianjin metro line 1 as an example, and the analysis revealed that housing prices decreased with increasing distance from the proximate rail station. The average housing prices in non-central areas increased and then decreased with increasing distance from the proximate rail station, whereas the average housing prices in central areas increased and then decreased with increasing distance from the proximate rail station. However, once the distance exceeds 500 m, the change in housing prices is no longer statistically significant.

A few studies have also concluded that the influence of rail on housing prices along the route is negligible. In a study of the influence of transit improvements on housing premiums, Bajic (1983) determined that savings in commuting expenses were capitalised into housing values. Gatzlaff and Smith (1993) analysed statistics on housing prices along rail transit lines in Miami and determined no significant increase in condominium prices along rail transit lines. When contrasting commercial properties in Washington and Atlanta, Cervero and Landis (1993) came to comparable conclusions. Bae et al. (2003) and others examined the influence of the construction of the new rail transit line five in Seoul, Korea, on the influence of nearby housing prices and found that accessibility had a smaller influence on housing prices than other variables.

2.3 Interaction between hospital and rail accessibility

Less research has been conducted on the interaction between hospital and rail accessibility. The only available study, conducted by Tang et al. (2020), concludes that the interaction between hospitals and rail stations has no significant influence on housing prices.

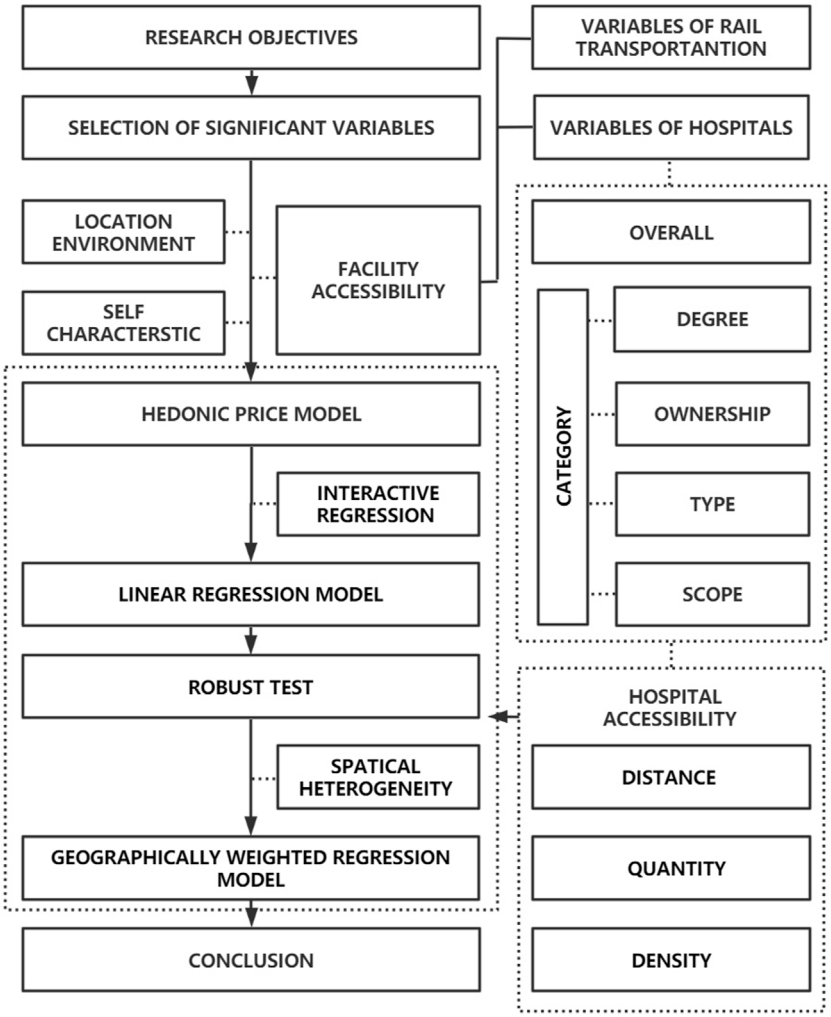

FIGURE 1
Framework diagram.

3 Methods

3.1 Research objective

The city of Fuzhou in China's Fujian Province was selected as the subject of this study. Fuzhou (E:119.28, N:26.08.) is located on the southeastern coast of China. It is one of the country's most prosperous regions, as well as the capital of Fujian Province. Fuzhou has abundant hospitals, a large population and a large sample size of housing, and its housing prices trends are generally consistent with those at the national level which is typically representative. In addition, it occurs at a time when the construction of urban rail is currently underway, so discussing the influence of hospital and rail accessibility on housing prices is interesting.

3.2 Research framework

Figure 1 depicts the framework of this paper, and the core of the research process is divided into three stages. The first stage is the hedonic price model to examine the presence of the hospital and rail accessibility variable among the significant variables affecting housing prices. The second stage is an interaction regression model to examine whether mutual moderation in the influence of hospital and rail accessibility on housing prices actually exists. In the third stage, the geographical heterogeneity in the interaction moderating effects was investigated using a spatial regression model. In addition, a robustness test was conducted on the findings of the second stage of the study prior to determining whether geographical heterogeneity exists in the interaction in the third stage, making the preconceived

TABLE 1 Descriptive statistics of the variables (N = 1,079).

Variables		Description	Mean	Std.Dev
Explained variables				
	Pri	**Housing prices (ten-thousand yuan/m^2)**	**2.810**	**1.081**
Explanatory Variables				
Variables of the Location environment				
	CityLC1	Dummy variable, 1 if the residence inside Second Ring Road, 0 else	-	-
	CityLC2	Dummy variable, 1 if the residence inside Third Ring Road, 0 else	-	-
	Pop20	The quantity of population in 2020 (n)	819,222.390	253,976.403
	PopD20	The density of population in 2020 (person/km^2)	11,173.178	8,231.573
	GDP21	Per capita GDP in 2021 (hundred million yuan)	567.270	266.461
Variables of the Self-characteristics				
	Pro2 C1	Dummy variable, 1 if the residence contain commercial housing	-	-
	Pro2 C2	Dummy variable, 1 if the residence contain housing placement	-	-
	Flo	Dummy variable, 1 for the residence is high-rise building, 0 else	-	-
	Age	Dummy variable, 1 for the residence built after 2000, 0 else	-	-
	PriS	Dummy variable, 1 for the residence with high-quality primary school, 0 else	-	-
	MidS	Dummy variable, 1 for the residence with high-quality middle school, 0 else	-	-
	ManF	Average property management fee per month (yuan/m^2)	1.153	0.664
	BuiD	Density of buildings (c)	2.372	1.226
	GreR	Greening rate of community (c)	0.330	1.282
Variables of the Facilities accessibility				
	Mar	Distance to the proximate market (m)	1,081.384	1,225.371
	Sce	Distance to the proximate scenic spot (m)	1,075.086	843.265
	Gre	Distance to the proximate green space (m)	720.815	1,512.736
	Wat	Distance to the proximate main water source (m)	1,150.353	726.864
	Fac	Distance to the proximate factory (m)	1,578.608	1,315.822
	Gas	Distance to the proximate closest gas station (m)	1,176.205	647.471
	Fun	Distance to the proximate funeral facility (m)	3,167.635	1,350.823
	Dum	Distance to the proximate dump (m)	9,562.531	3,546.301
	Sta	Distance to the proximate rail station (m)	1,369.524	1,440.691
	Hos	The accessibility of hospitals	Table 2	
	HosD	Distance to the proximate hospital(m)		
	HosB	Quantity of hospitals in butter zone (n/km^2)		
	HosK	Kernel density of hospitals(c)		
	Inter (Sta&Hos)	Interaction of Sta and Hos	-	-

notions of the pertinent study findings more convincing and trustworthy.

3.3 Statistics sources

In this study, 1,079 housing samples and other relevant geographical information statistics were selected in March 2021, when the rail construction in Fuzhou City was opened to traffic. These statistics were obtained from internet information crawling and field research, and the statistics of the variables are described in Table 1.

3.4 General variables

In this study, interception statistics variables that may influence housing prices were established, and the most significant ones were utilised in the final regression model through a screening regression procedure. This includes

TABLE 2 Statistics variables of hospitals (N = 1,079).

Category		Quantity	Average distance of hospitals (m)	Std. Dev	Search radius of butter zone (m)	Mean	Std. Dev	Search radius of kernel density (m)	Mean	Std. Dev
All hospitals		**97**	**910.304**	**911.965**	**900**	**2.151**	**2.254**	**1800**	**0.809**	**0.730**
Degree	grade-A tertiary hospital	22	1884.214	2094.828	1900	1.997	2.092	3,800	0.168	0.146
	grade-B tertiary hospital	11	2,273.896	2,389.647	2,300	1.264	1.023	4,600	0.072	0.045
	secondary hospital	22	1824.654	1779.746	1850	1.723	1.704	3,700	0.151	0.121
	class-I hospital	42	1,393.957	1,503.742	1,400	2.209	2.154	2,800	0.339	0.286
Ownership	public hospital	84	952.681	911.834	950	2.024	2.204	1900	0.685	0.638
	private hospital	13	2,130.476	2,349.810	2,150	1.490	1.226	4,300	0.095	0.059
Type	WM hospital	84	1,012.580	1,167.364	1,000	2.245	2.200	2000	0.690	0.595
	CM hospital	13	2080.572	1,670.765	2,100	1.295	1.273	4,200	0.089	0.069
Scope	general hospital	39	1,310.493	1,002.704	1,300	1.622	1.909	2,600	0.300	0.287
	special hospital	28	1711.745	1,674.344	1700	1.735	1.624	3,400	0.182	0.134
	medical center	30	1702.341	2094.818	1700	2.470	2.325	3,400	0.256	0.211

Note: "WM" is the abbreviation of "Western Medicine", "CM" is the abbreviation of "Chinese Medicine".

statistics on the explanatory variable, housing prices statistics for March 2021, as well as statistics on three other explanatory variables: location environmental, self characteristics and facilities accessibility.

3.5 Research and moderator variable

As shown in Table 2, the primary variable of this study is hospital accessibility. The investigation will be categorised from multiple vantage points. First, the study's objectives will be set at all hospitals in the city, without distinction between hospital categories; second, the study's objectives will be to investigate the influence of different degrees of hospitals on housing prices and their reliance on rail access. Given that different degrees of hospitals are differentiated by the level of equipment, the quantity of beds and specialists, there is a certain overlap in the function of demand for medical care between the different degrees of hospitals. To eliminate such covariance interferences, the study will use regressions with different degrees of hospitals independently. To investigate the variability of the influence of differences in the degree, ownership, type and scopes of hospitals on housing prices, as well as their reliance on rail access, a sub-study of the influence of different categories of hospitals was also conducted. Given no absolute non-substitutability of medical functions between hospitals with similar categorisation perspectives, the classified hospitals will continue to be fitted independently and separately in the regression analysis.

The study will establish a variety of accessibility indicators for hospitals. Given that hospitals are not like school district zoning

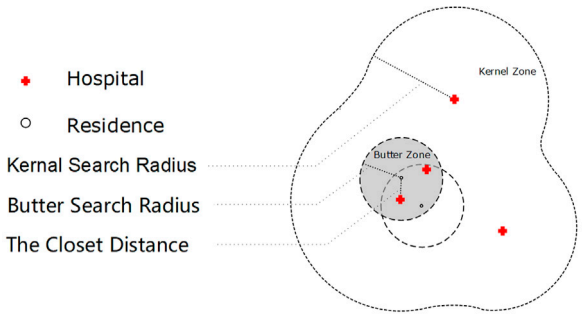

FIGURE 2
Categories of hospital accessibility index.

according to the residential grid but rather public facilities that are freely chosen by residents under market conditions, the accessibility of hospitals will be described by the Euclidean distance to the proximate hospital, the quantity of hospitals within the residential buffer zone and the urban hospital kernel density to which the residence belongs (Figure 2).

The various accessibility evaluation indicators for the residential hospital variable have distinct connotations. The Euclidean distance from hospitals explains, from a macroeconomic standpoint, the influence of hospital and rail accessibility on housing prices, as well as their mutually moderating effect. The quantity of hospitals within the residential buffer zone compensates for the absence of micro-

level characteristics of proximity to hospitals due to the moderating effects of macro-level distance to hospital and rail accessibility factors on housing prices, and the radius size of the buffer is set as the average distance between all hospitals of the same type in the city. The final urban hospital kernel density value describes the comprehensiveness of the city's macro healthcare system's backup coverage when the distance to the proximate hospital in a residence is estimated and the quantity of hospitals within a close residence is the same. The search radius of the kernel density is defined as double the average distance between all hospitals of the same type within a city.

In this study, the rail accessibility variable serves as a moderator variable, and the spatial linear distance to the proximate rail station will be used to characterise the accessibility of rail to a residence. In contrast to hospitals, which are distinct and unique, rail stations are viewed as homogeneous, and people typically choose the proximate rail station.

4 Research methods

4.1 Kernel density estimation

For determining surface densities and for conducting empirical analyses of aggregation, the kernel density estimation method is frequently employed. It is used to calculate and estimate the aggregation of statistics from sample statistics and to investigate the dispersion and properties of hotspots in a spatial area by gauging the change in study element density *via* a specified distance decay function. Kernel density estimation is the practice of interpolating through discrete point or line statistics, where the points dropping further into the search agent have different weights, using the distance decay function to monitor the difference in the local density of the event; the closer to the centre, the greater the weight of the points. The kernel density estimation can intuitively reflect the spatial layout characteristics of the studied object, whose specific calculation formula model is as formula 1.

$$f(x) = \frac{1}{Nh}\sum_{i=1}^{N} K\left(\frac{x - x_i}{h}\right) \tag{1}$$

In formula 1: f (x) is the kernel density function; $K(\frac{x-x_i}{h})$ is the kernel function; N is the quantity of known points; h is the finding radius; $x - x_i$ is the distance from the centre point to the known points.

4.2 Hedonic price model

The hedonic price model is a linear model function that is frequently applied to price forecasting, land value estimation and real estate transactions (Yang et al., 2018). The specific function model comes in a variety of shapes, including linear, semi-logarithmic and double-logarithmic. However, the double-logarithmic model is better able to convey the existence of significant marginal utility of the transaction price for residential characteristics when purchasing a residence, making the simulation process more realistic and reasonable. As a result, the hedonic price model used in this study adopts the double-logarithmic model frequently used by scholars. The explanatory variables and the housing prices are related as formula 2.

$$\ln Price(i) = \beta_0 + \sum_{i=1}^{i=n} \beta_k \ln x_{ki} + \varepsilon_i \tag{2}$$

Here, Price ln $Price(i)$ represents the housing prices, i refers to the statistics of the i-th property, $Price(i)$ stands for the average price per square metre of the i property, which includes the sum of the housing prices itself, the cost of decoration and other aspects of the costs, that is, the average transaction price of the i property. k is the characteristic factor; it represents the k-th characteristic influence factor among many attributes. Likewise, i also refers to the statistics of the i-th property, x_{ni} indicates the performance of the nth characteristic influencing factor in the i property. β_n represents the unstandardised coefficient of the k-th relevant characteristic influencing factor on housing prices. ε_i represents the stochastic error term. In addition to the coefficients embodied in the model itself, the regression analysis allows the strength of significance of the main positive or negative explanatory variables affecting housing prices to be derived.

4.3 Interactive regression model

The addition of an interaction term to a linear regression model in econometrics is a special case of a regression equation model where the interaction can be viewed as the outcome of the interaction of two or more contributing factors. This approach broadens the range of variables that can be understood and the depth to which they are influenced by various explanatory factors in the regression model to some amount. The two cases of additive and multiplicative interaction terms were separately considered during the study, but after comparing the significance of the pertinent statistics, the multiplicative interaction model with the best fit and significance was selected as the method for this interaction study. Its specific formula model is as formula 3.

$$y_i = \beta_i + \beta_u x_{ui} + \beta_v x_{vi} + \beta_{uv} x_{ui} x_{vi} + \varepsilon_i \tag{3}$$

$$\frac{\partial^2 y_i}{\partial x_{ui} \partial x_{vi}} = \frac{\partial\left(\frac{\partial y_i}{\partial x_{ui}}\right)}{\partial x_{vi}} = \beta_{uv} \tag{4}$$

The 'interaction effect' in the interaction model, or the relationship between an explanatory variable's effect and its magnitude, is represented by formula 4.

TABLE 3 Filtering statistics of the variables (N = 1,079).

Variables	Step 1		Step 2		Step 3		Step 4	
	Coefficients	t	Coefficients	t	Coefficients	t	Coefficients	t
(Constant)	-3.353***	-6.754	-3.270***	-6.730	-2.765***	-5.741	-2.645***	-5.569
CityLC1	0.124***	7.452	0.119***	7.534	0.089***	5.376	0.092***	5.567
CityLC2	0.177***	6.689	0.174***	6.667	0.172***	6.343	0.180***	6.776
Pop20	0.089***	3.317	0.097***	3.650	0.092***	3.430	0.081***	3.157
PopD20	0.066***	8.282	0.069***	8.659	0.064***	8.211	0.063***	8.107
GDP21	0.151***	8.014	0.148***	7.903	0.166***	8.901	0.170***	9.263
Pro2 C1	0.130	1.415	-	-	-	-	-	
Pro2 C2	0.156**	1.721	-	-	-	-	-	-
Flo	0.004	0.266	-	-	-	-	-	-
AgeC	0.074***	3.630	0.085***	4.213	0.082***	4.165	0.084***	4.226
PriS	0.281***	10.216	0.275***	10.182	0.256***	9.614	0.256***	9.612
MidS	0.240***	8.320	0.247***	9.013	0.229***	8.490	0.233***	8.684
ManF	0.162***	12.513	0.173***	13.964	0.185***	15.032	0.186***	15.114
BuiD	0.013	0.831	-	-	-	-	-	-
GreR	0.038***	2.489	-	-	-	-	-	-
Mar	-0.035***	-4.005	-0.031***	-3.628	-0.013	-1.470	-	-
Sce	0.007	0.613	-	-	-	-	-	-
Gre	-0.031***	-4.560	-0.028***	-4.327	-0.025***	-3.849	-0.025***	-3.794
Wat	-0.034***	-4.163	-0.034***	-4.236	-0.040***	-4.950	-0.040***	-4.891
Fac	0.012	1.307	-	-	-	-	-	-
Gas	0.002	0.208	-	-	-	-	-	-
Fur	0.042***	3.124	0.043***	3.234	0.040***	3.095	0.037***	2.861
Dum	0.148***	8.236	0.148***	8.325	0.142***	8.166	0.138***	8.028
Sta	-	-	-	-	-0.050***	-6.124	-0.053***	-6.735
HosD	-	-	-	-	-0.023***	-2.538	-0.025***	-2.726
R-squared	0.654		0.650		0.665		0.664	
Adjusted R-squared	0.647		0.645		0.660		0.660	

Note: ** Significant at the 10% level. *** Significant at the 5% level.

4.4 Geographically weighted regression model

In spatial analysis, the GWR model is frequently employed. On top of conventional global regression, it considers the spatial position of each variable and computes the local effects of variables at various places using a spatial weight function, which has higher fitting properties. The GWR, whose precise calculation formula is as formula 5, incorporates the geographic location of the sample point statistics into the regression parameters:

$$y_i = \beta_o(u_i, v_i) + \sum_{k=1}^{p} \beta_k(u_i, v_i) x_{ik} + \varepsilon_i \quad i = 1, 2, \ldots, n \qquad (5)$$

where (u_i, v_i) is the geographical coordinate of the i-th sample point; $\beta_k(u_i, v_i)$ is the k-th regression parameter of the i-th sample point; ε_i is the random error of the i-th sample point.

5 Analysis results

5.1 Linear regression model

Through the screening of significant variables and the R-squared test, the regression equation of STEP4 was chosen as the fitting function for the study, and the following results were found. The significant variables influencing housing prices are the location of residence (inside Second Ring Road or Third Ring Road), the quantity of population, the density of population and the GDP level in the variables of the location environment. In the variables of self-characteristics, the age of residence, high-quality primary and secondary school and property management fee are significant. The variables of facilities accessibility include distance to the closet green space, distance to the proximate main water source, distance to the proximate funeral facilities, distance

TABLE 4 Regression results of the Hos (N = 1,079).

Category		HosD		HosB		HosK	
		Coefficients	T	Coefficients	t	Coefficients	t
All hospitals		**-0.025*** **	**-2.726**	**0.002****	**1.947**	**0.006*** **	**3.684**
Degree	grade-A tertiary hospital	-0.035***	-3.451	0.004***	3.311	0.007***	3.277
	grade-B tertiary hospital	-0.027***	-2.455	0.002***	1.963	0.016***	5.511
	secondary hospital	-0.038***	-3.681	0.003***	2.626	0.008***	4.604
	class-I hospital	-0.019***	-2.226	0.002***	1.965	0.007***	3.815
Ownership	public hospital	-0.015	-1.590	0.001	0.770	0.005***	3.165
	private hospital	-0.041***	-3.738	0.003***	2.184	0.010***	3.831
Type	WM hospital	-0.028***	-3.130	0.002	1.445	0.005***	3.035
	CM hospital	-0.051***	-4.155	0.002***	2.067	0.005***	2.446
Scope	general hospital	-0.010	-1.005	0.002**	1.665	0.005***	2.782
	special hospital	-0.037***	-3.980	0.003***	2.500	0.009***	4.719
	medical center	-0.029***	-3.135	0.003***	2.621	0.009***	4.207

Note: ** Significant at the 10% level. *** Significant at the 5% lvel.

to dump area and distance to rail stations and hospitals, which are the study's primary concerns. The coefficients in Table 3 reveal the trends in the effects of each of these variables on housing prices. Negative coefficients are associated with the variables for distance to hospitals and rail stations.

The regressions were then fitted to different categorisations and hospital accessibility perspectives using a filtered functional model, yielding the following analysis (Table 4). The table depicts the level of significance of the influence on housing prices from a variety of hospital accessibility measurement vantage points.

5.2 Linear interaction regression model

The results of the interaction term analysis are presented in Table 5 by simulating the interactive regression results of the proximate hospital. The subsequent analysis outcomes contain linear and spatial interaction regression models. Moreover, the study demonstrates the robustness of the linear regression results before moving on to the spatial interaction regression model, demonstrating the dependability of the study's statistics.

The results of each model fit are presented in Table 5, one for each of the aforementioned hospital accessibility indicators. R-squares greater than 0.63 are displayed in each table containing interaction regression models for the various categories of hospital and rail accessibility. In the table, the core study variables: the hospital accessibility, the rail accessibility and its interaction, the significance and the coefficients are also described.

5.3 Robustness test spot check

To increase the dependability of the findings of this research, a robustness test spot check was conducted following the linear regression model. Different categories of hospitals were selected at random to conduct the sample check for the regression fit analysis from each of the three evaluative perspectives of the study variables. The outcomes are displayed in Table 6.

5.4 Spatial interaction regression model

The study regressed the linear regression case with significant spatial interactions using a geographically weighted model, yielding the statistics presented in Table 7.

The study compiles the spatial interaction effects of residential proximate hospitals and rail stations in Table 7. When all the impact variables are significant in an interactive regression function, the highest explained sample rate of 73.4% (792/1,079) was found for the regression model of the interaction between grade-A tertiary hospital distance and rail station distance with a positive spatial variance value. The next highest explained sample rates of 61.5% (590/1,079) was found for the regression model of the interaction between grade-B tertiary hospital distance and rail station distance with a negative spatial variance value. The third explained sample rates is 53.8% (580/1,079) for the interaction between distance to CM hospitals and distance to rail stations, with negative values of spatial variance. Fourth is 53.0% (572/1,079) for the interaction between distance to private hospitals and distance to rail stations, with negative values of spatial

TABLE 5 Interactive regression results of the hospital accessibility.

Category		Distance						Quantity						Density					
		Sta		HosD		Inter (Sta&HosD)		Sta		HosB		Inter (Sta&HosB)		Sta		HosK		Inter (Sta&HosK)	
		Coefficients	t	Coefficients	t	Coefficients	t	Coefficients	t	Coefficients	t	Coefficients	t	Coefficients	t	Coefficients	t	Coefficients	t
all hospitals		0.184***	3.656	0.215***	4.209	-0.035***	-4.77	-0.021**	-1.899	-0.028***	-4.176	0.004***	4.535	-0.033***	-3.322	-0.021***	-2.312	0.004***	3.04
Degree	grade-A tertiary hospital	0.272***	4.776	0.260***	4.952	-0.043***	-5.733	-0.024***	-2.254	-0.026***	-3.721	0.004***	4.317	-0.026***	-2.323	-0.025***	-2.436	0.004***	3.244
	grade-B tertiary hospital	0.285***	4.599	0.262***	4.867	-0.043***	-5.47	-0.028***	-2.499	-0.022***	-3.039	0.003***	3.407	-0.014	-1.158	-0.022**	-1.931	0.005***	3.373
	secondary hospital	0.257***	4.424	0.246***	4.586	-0.042***	-5.391	-0.022***	-2.066	-0.028***	-4.228	0.004***	4.727	-0.030***	-2.726	-0.025***	-2.408	0.005***	3.276
	class-I hospital	0.128***	2.501	0.154***	3.135	-0.025***	-3.59	-0.017	-1.582	-0.032***	-4.737	0.005***	5.14	-0.029***	-2.635	-0.019***	-2.121	0.004***	2.96
Ownership	public hospital	0.188***	3.544	0.230***	4.289	-0.035***	-4.629	-0.018**	-1.651	-0.032***	-4.719	0.005***	4.894	-0.034***	-3.374	-0.023***	-2.493	0.004***	3.126
	private hospital	0.300***	5.325	0.251***	5.166	-0.044***	-6.167	-0.018	-1.634	-0.031***	-4.205	0.005***	4.602	-0.013	-1.112	-0.030***	-2.834	0.006***	3.92
Type	WM hospital	0.183***	3.859	0.208***	4.349	-0.034***	-5.022	-0.017	-1.602	-0.033***	-4.895	0.005***	5.182	-0.032***	-3.207	-0.026***	-2.911	0.004***	3.573
	CM hospital	0.178***	2.467	0.155***	2.359	-0.030***	-3.184	-0.012	-1.014	-0.032***	-4.63	005***	5.034	-0.031***	-2.598	-0.022**	-1.934	0.004***	2.471
Scope	general hospital	0.238***	3.751	0.269***	4.417	-0.041***	-4.655	-0.021**	-1.886	-0.025***	-3.826	0.004***	4.118	-0.028***	-2.631	-0.029***	-2.939	0.005***	3.505
	special hospital	0.255***	4.664	0.244***	4.851	-0.042***	-5.689	-0.027***	-2.454	-0.024***	-3.353	0.004***	3.769	-0.031***	-2.798	-0.021***	-2.238	0.004***	3.242
	medical center	0.157***	3.212	0.161***	3.557	-0.028***	-4.287	-0.025***	-2.401	-0.023***	-3.335	0.004***	3.886	-0.023***	-2.101	-0.022***	-2.323	0.004***	3.366

Note: ** Significant at the 10% level. *** Significant at the 5% level.

10.3389/fenvs.2022.1044600

TABLE 6 Robust test (N = 1,079).

Variables	Distance to the closest hospital		Quantity of grade-A tertiary hospitals in butter zone		Kernel density of general hospitals	
	Coefficients	t	Coefficients	T	Coefficients	t
(Constant)	-3.204***	-7.909	-4.079***	-8.427	0.708***	2.103
CityLC1	0.107***	6.435	0.111***	6.173	0.085***	5.174
CityLC2	-	-	0.133***	4.547	0.318***	14.699
Pop20	-	-	0.169***	6.771	-0.091***	-4.317
Pop20D	0.085***	14.109	0.084***	10.709	-	-
GDP21	0.201***	11.430	-	-	0.259***	15.386
AgeC	0.100***	4.868	-	-	0.082***	3.958
ManF	0.184***	14.489	0.190***	15.143	0.191***	14.916
PriS	0.272***	9.757	-	-	0.292***	10.448
MidS	0.238***	8.498	0.350***	12.863	0.283***	10.094
Gre	-	-	-0.029***	-4.091	-	-
Wat	-0.038***	-4.831	-0.046***	-5.329	-0.058***	-7.420
Fur	0.040***	3.234	0.085***	6.317	0.009	0.710
Dum	0.094***	6.046	0.203***	12.159	-	-
Sta	0.203***	3.904	-0.028***	-2.581	-0.030***	-2.745
Hos	0.214***	4.061	-0.021***	-2.832	-0.040***	-3.945
Inter (Sta&Hos)	-0.038***	-4.982	0.004***	3.644	0.006***	4.260
Performance statistics						
R-squared	0.637		0.618		0.632	
Adjusted R-squared	0.633		0.614		0.628	

Note: ** Significant at the 10% level. *** Significant at the 5% level.

variance. Except for the spatial variances for secondary hospitals, which were positive, all other interaction regression equations had significance below 50% and negative spatial variances.

Table 8 shows the spatial relationship between the quantity of hospitals and the proximate rail station. Although it only has the explained sample rates of 14.7% (159/1,079) and a negative spatial variance value, the interaction regression model between medical centres and rail stations within the residential neighbourhood has the greatest explained sample rates of all the interaction regression equations. The explained sample rates for the other interaction regression models are even lower.

Table 9 displays the spatial coefficients and variance of the interactive function between the distance to the proximate rail stations and the hospital kernel density located in the residential area. Similar to the regression interaction model for the quantity of hospitals, the explained sample rates for each interaction model are relatively low, with the highest explained sample rates being 17.1% (184/1,079) for the interaction model for the density values of rail stations and general hospitals in the area, with a negative spatial variance value. The table also contains the proofs of the interaction regression models for the remaining categories.

6 Discussion and conclusion

6.1 Discussion

6.1.1 General and moderator variable

In the linear regression model (Table 3), the results of a city-wide statistics analysis led to the investigation of the following variables that affect the correlation of housing prices. Variables of environmental location are location of residence (inside Second Ring Road or Third Ring Road), the quantity of population, the density of population and the GDP level. Variables of self-characteristics are the age of residence, high-quality primary and secondary school and property management fee. Variables of facilities accessibility are rail accessibility (moderator variable), green space accessibility, main water source accessibility, funeral facilities accessibility and dump area accessibility. The variables that do not affect housing prices include the following. For self-characteristic variables, they are the residence containing commercial housing or housing placement, the residence with a high-rise building, the density of building and greening rate. For facilities accessibility variables, they are large shopping malls accessibility, scenic spots accessibility, factories accessibility and gas station accessibility. Of these significant variables, variables of

TABLE 7 Results of the geographically weighted regression analysis based on distance (N = 1,079).

	All hospitals		Gread-A tertiary hospital		Gread-B tertiary hospital		Secondary hospital		Class-I hospital		Public hospital		Private hospital		WM hospital		CM hospital		General hospital		Special hospital		Health center	
Variables	Coefficient	DIFF of criterion	Coefficient	DIFF of criterion	Coefficient	DIFF of criterion	Coefficient	DIFF of criterion	Coefficient	DIFF of criterion	Coefficient	DIFF of criterion	Coefficient	DIFF of criterion	Coefficient	DIFF of criterion	Coefficient	DIFF of criterion	Coefficient	DIFF of criterion	Coefficient	DIFF of criterion	Coefficient	DIFF of criterion
Intercept																								
Urban																								
Edu																								
Popu																								
PopDen																								
GDPG																								
GDP																								
Road																								
Fish																								
Bath																								
Tax																								
Tax																								
Fin																								
Hos																								
Bus																								
Road																								
Beta (Intelligent)																								
Statistical Significant Variables																								
Obs																								
Rsq2																								
Neighbors																								
AIC																								
Statistical Diagnostic																								
AICc																								
RSQRD																								
R-squared																								
Adjusted R-squared																								

Note: *All coefficient is based on standardisation of explanatory variables.

10.3389/fenvs.2022.1044600

TABLE 8 Results of the geographically weighted regression analysis based on quantity (N = 1,079).

	Gread-A tertiary hospital		Gread-B tertiary hospital		Secondary hospital		Special hospital		Medical center	
Variables	**Coefficient**	**DIFF of criterion**	**Coefficient**	**DIFF of criterion**	**Coefficient**	**DIFF of criterion**	**Coefficient**	**DIFF of criterion**	**Coefficient**	**DIFF of criterion**
Intercept	0.861–1.131	-0.947	0.876–1.127	-1.153	0.902–1.121	-1.169	0.883–1.152	-3.112	0.876–1.157	-1.308
CityLC1	-0.013–0.138	-8.183	-0.015–0.146	-6.716	-0.020–0.143	-9.004	-0.015–0.138	-6.124	-0.016–0.139	-7.819
CityLC2	-0.067–0.211	-5.668	-0.014–0.207	-7.832	-0.000–0.206	-4.240	-0.094–0.178	-5.120	-0.089–0.311	-5.140
Pop20	-0.168–0.108	-1.296	-0.164–0.129	-3.961	-0.165–0.131	-3.546	-0.183–0.111	-4.272	-0.172–0.124	-6.442
PopD20	-0.065–0.140	-52.891	-0.069–0.144	-65.760	-0.061–0.148	-81.311	-0.074–0.130	-82.854	-0.066–0.137	-52.497
GDP21	-0.008–0.248	-4.254	-0.012–0.246	-2.070	-0.009–0.247	-4.725	-0.012–0.258	-4.218	-0.025–0.251	-5.699
AgeC	0.002–0.043	3.149	0.002–0.049	3.126	0.003–0.052	2.971	0.002–0.051	3.146	0.003–0.052	3.155
ManF	0.068–0.117	0.826	0.068–0.116	1.467	0.068–0.113	2.074	0.067–0.114	2.315	0.068–0.115	1.391
PriS	0.028–0.089	-11.463	0.028–0.089	-11.418	0.026–0.088	-12.589	0.028–0.089	-11.409	0.028–0.089	-11.794
MidS	-0.012–0.111	-11.098	-0.012–0.113	-10.692	-0.012–0.112	-11.053	-0.012–0.112	-10.882	-0.012–0.105	-10.293
Gre	-0.072–0.036	-2.627	-0.076–0.045	-6.077	-0.078–0.035	-4.857	-0.077–0.041	-5.309	-0.077–0.034	-4.636
Wat	-0.133–0.023	-21.104	-0.115–0.025	-14.694	-0.116–0.022	-17.112	-0.124–0.024	-18.705	-0.115–0.024	-10.624
Fur	-0.059–0.097	-6.861	-0.066–0.113	-9.449	-0.060–0.132	-9.204	-0.060–0.106	-9.464	-0.061–0.111	-5.044
Dum	-0.239–0.275	1.379	-0.220–0.292	-0.487	-0.226–0.275	-1.702	-0.260–0.255	-1.960	-0.247–0.269	-1.121
Sta	-0.066–0.038	-4.687	-0.049–0.045	-9.093	-0.079–0.044	-8.155	-0.054–0.066	-8.456	-0.104–0.069	-7.718
HosB	-1.304–0.384	-1,652.915	-1.098–0.775	-450.342	-0.558–0.226	-28.632	-0.396–1.702	-200.218	-1.364–1.449	-1728.549
Inter (Sta&HosB)	-0.305–1.461	-143.952	-0.733–1.119	-193.557	-0.227–0.531	-3.024	-1.571–0.470	-41.799	-1.366–1.428	-64.772
Statistical of Significant Variables										
Sta	234/1,079		171/1,079		331/1,079		361/1,079		396/1,079	
HosB	415/1,079		459/1,079		267/1,079		326/1,079		237/1,079	
Inter (Sta&HosB)	519/1,079		502/1,079		326/1,079		349/1,079		309/1,079	
All	87/1,079		71/1,079		85/1,079		128/1,079		159/1,079	
Statistical of Regression										
AICc	-616.856		-612.368		-613.403		-621.107		-616.967	
BIC/MDL	-259.653		-254.427		-256.128		-262.665		-260.703	
R-square	0.741		0.740		0.740		0.742		0.741	
Adjusted R-square	0.716		0.715		0.715		0.717		0.716	

Note: *All coefficient is based on standardisation of explanatory variables.

10.3389/fenvs.2022.1044600

TABLE 9 Results of the geographically weighted regression analysis based on density (N = 1,079).

	All hospitals		Gread-A tertiary hospital		Secondary hospital		Class-I hospital		Public hospital		WM hospital		General hospital		Special hospital		Medical center	
Variables	**Coefficient**	**DIFF of criterion**	**Coefficient**	**DIFF of criterion**	**Coefficient**	**DIFF of criterion**	**Coefficient**	**DIFF of criterion**	**Coefficient**	**DIFF of criterion**	**Coefficient**	**DIFF of criterion**	**Coefficient**	**DIFF of criterion**	**Coefficient**	**DIFF of criterion**	**Coefficient**	**DIFF of criterion**
Intercept	0.444–1.124	-4.894	0.265–1.123	-11.694	0.328–1.170	-2.064	0.184–1.124	-1.541	0.483–1.124	-4.546	0.370–1.125	-5.637	0.549–1.129	-3.083	0.285–1.096	-4.501	-1.308	-0.748
CityLC1	-0.16	-3.553	-0.153	-5.683	-0.148	-2.064	-0.168	-5.862	-0.156	-3.75	-0.159	-4.717	-0.151	-8.493	-0.139	-3.755	-0.155	-7.425
CityLC2	-0.716	-3.976	-1.134	-2.907	-0.925	-4.294	-0.339	-4.774	-0.56	-5.165	-1.405	-3.734	-0.369	-7.21	-0.556	-0.927	-0.565	-3.185
LnPop20	-0.261	-21.86	-0.3	-5.822	-0.301	-6.013	-0.309	-6.183	-0.281	-21.691	-0.299	-9.195	-0.241	-1.484	-0.323	-10.368	-0.333	-8.545
PopD20	-0.191	-38.268	-0.214	-2.82	-0.197	-39.115	-0.211	-44.821	-0.184	-36.31	-0.203	-38.226	-0.201	-63.044	-0.225	-3.006	-0.234	-37.912
GDP21	-0.247	-7.348	-0.253	-8.024	-0.234	-12.096	-0.271	-5.547	-0.247	-8.859	-0.254	-6.896	-0.233	-5.887	-0.255	-11.738	-0.284	-6.828
AgeC	0.002–0.052	3.521	0.002–0.046	3.358	0.002–0.044	3.305	0.003–0.053	3.133	0.002–0.050	3.71	0.002–0.050	3.311	0.001–0.050	3.201	0.002–0.047	3.176	0.003–0.055	2.952
ManF	0.067–0.115	1.764	0.068–0.117	1.224	0.068–0.118	1.363	0.067–0.116	1.582	0.068–0.116	2.103	0.067–0.115	1.87	0.068–0.117	1.521	0.069–0.116	1.354	0.068–0.116	1.162
PriS	0.026–0.090	-12.38	0.025–0.089	-11.106	0.030–0.089	-11.509	0.027–0.088	-11.774	0.024–0.091	-12.463	0.026–0.090	-12.442	0.029–0.089	-11.243	0.025–0.089	-12.832	0.026–0.088	-10.833
MidS	-0.115	-5.275	-0.113	-9.308	-0.125	-9.537	-0.11	-5.388	-0.118	-6.221	-0.119	-7.937	-0.121	-9.573	-0.123	-10.55	-0.112	-7.058
Gre	-0.113	-6.104	-0.119	-2.886	-0.127	-6.414	-0.117	-6.835	-0.116	-6.514	-0.111	-4.972	-0.117	-7.065	-0.12	-5.565	-0.119	-7.059
Wat	-0.134	-18.079	-0.165	-27.135	-0.153	-18.465	-0.137	-10.596	-0.135	-20.299	-0.144	-19.519	-0.151	-21.81	-0.125	-15.215	-0.132	-9.925
Fur	-0.192	-7.494	-0.244	-14.242	-0.219	-8.735	-0.171	-9.194	-0.186	-7.058	-0.195	-8.609	-0.192	-7.748	-0.236	-10.124	-0.206	-9.472
Dum	-0.506	-5.306	-0.482	-2.397	-0.478	-3.335	-0.549	-4.162	-0.492	-2.581	-0.476	-5.421	-0.491	-1.382	-0.456	0.791	-0.543	-4.526
Sta	-0.124	-5.351	-0.313	-5.131	-0.293	-6.218	-0.204	-6.961	-0.123	-6.445	-0.128	-5.372	-0.156	-10.586	-0.258	-3.876	-0.297	-6.998
HosK	-3.779	-30.283	-6.551	-136.34	-9.674	-84.357	-6.602	-4.635	-4.016	1.012	-6.156	-97.924	-5.46	-260.868	-6.749	-31.256	-9.176	-5,448.431
Inter (Sta&HosK)	-4.188	0.3	-7.519	0.323	-9.901	1.242	-6.516	-4.729	-4.918	1.902	-5.967	-0.927	-6.327	-0.028	-7.465	3.171	-10.436	-46.949
Statistical of Significant Variables																		
Sta	379/1,079		399/1,079		343/1,079		358/1,079		396/1,079		434/1,079		329/1,079		287/1,079		400/1,079	
HosK	207/1,079		249/1,079		359/1,079		379/1,079		132/1,079		236/1,079		310/1,079		337/1,079		475/1,079	
Inter (Sta&HosK)	198/1,079		377/1,079		466/1,079		417/1,079		169/1,079		241/1,079		359/1,079		432/1,079		510/1,079	
All	61/1,079		120/1,079		158/1,079		107/1,079		39/1,079		125/1,079		184/1,079		116/1,079		143/1,079	
Statistical of Regression																		
AICc	-625.115		-634.912		-622.46		-617.99		-620.824		-630.83		-619.302		-626.837		-626.656	
BIC/MDL	-262.832		-280.138		-267.722		-261.664		-259.203		-270.119		-256.035		-271.855		-271.732	
R-square	0.744		0.745		0.742		0.741		0.742		0.745		0.742		0.743		0.743	
Adjusted R-square	0.718		0.72		0.717		0.716		0.717		0.72		0.717		0.718		0.718	

Note: *All coefficient is based on standardisation of explanatory variables.

10.3389/fenvs.2022.1044600

environmental location and self-characteristic are both positively correlated with housing prices. All the facilities accessibility variables, except for the funeral facilities variable and the dump areas variable, express a positive correlation between facilities accessibility and housing prices. This result is not much different from the results of previous related studies and can be understood in the context of people's life experience.

6.1.2 Research variable

On the basis of the results of the hospital accessibility regression model (Table 4) and the interaction regression model statistics (Table 5) with rail accessibility, a discussion will be developed regarding the influence of hospital accessibility on housing prices and that of accessibility interactions on housing prices. The discussion in the section on interaction studies will be divided into two: a linear regression section and a spatial regression section. Discussion of the former will be categorised in terms of hospital type and accessibility evaluation. In the spatial regression model discussion section, sample models where the interaction is generally spatially significant and stable will be discussed and analysed in a targeted manner.

6.1.3 Linear regression model

6.1.3.1 Distance

In the results of the model measuring residential accessibility by distance to the proximate hospital (Table 4–5), there is a positive value-added orientation of unclassified proximate hospital accessibility to housing prices, and there is a reciprocal moderating influence on housing prices with the accessibility of the proximate rail station. The greater the distance to the hospital, the smaller the influence of medical accessibility on housing prices. This suggests a spatially positive linear correlation between the perception of medical proximity and accessibility. Additionally, from a city-wide perspective, people's preference for the proximate hospital can be interpreted as a spatially substitutable effect of rail for transporting their medical needs. In other words, people will choose rail to get to the hospital due to its accessibility, and this preference for accessibility will be reflected in the price of housing.

People's preference for medical accessibility when purchasing a residence does not result in different outcomes based on the hospital's degree. People can access the proximate level of the hospital *via* rail, so the influence of hospital distance on houses also changes with the distance from the rail station to the residence and *vice versa*, that is, the distance from the proximate rail station has a different influence on the price of houses located at different levels of proximity to hospitals. The influence of proximity to the proximate rail station on residence values at varying distances from the hospital varies.

In the case of residential proximity to a public hospital, the convenience added by the public hospital is offset by its equally negative effects, so there is no direct proximity effect of the public hospital on housing prices. These negative factors may include the noise, the mixed traffic and the psychological rejection of hospitals in the minds of residents around public hospitals. Given that public hospitals encompass several degrees, including grade-A tertiary, grade-B tertiary, secondary and class-I hospitals, the findings for public hospitals as a whole are presented here. Although grade-A tertiary hospitals are public hospitals, their positive influence outweighs the negative influence; hence, the overall presentation of grade-A tertiary hospitals remains positively connected with the influence on housing prices. By contrast, other tiers of public hospitals fail to cancel the negative consequences by beneficial influences. As a result, the overall data results for public hospitals were distinct from those of grade-A tertiary hospitals. Furthermore, the proximity of the proximate public hospital to the housing stock can somewhat mitigate the reliance of the housing stock on rail and, with the accessibility of rail, can change the price influence of the proximate public hospital from a positive to a negative. Firstly, it is understandable that when no hospitals are nearby, people will demand rail access to hospitals, thereby increasing the reliance of houses on rail stations. Secondly, when houses are in close proximity to a rail station, the negative price influence of hospital proximity increases as people from other areas choose to travel *via* the nearby rail station, perhaps due to the need to travel to a hospital in close proximity to the residence. This makes the residence's surroundings susceptible to the combined noise of the nearby rail station and hospital. These are extremely undesirable environmental factors, so prices will naturally decrease. Private hospitals are not subject to the same limitations as public hospitals. Given that the negative influence of hospitals is due to the flow of people and psychological factors, private hospitals are generally not the first choice for people in China to visit, greatly reducing the negative influence resulting from the flow of people in private hospitals. Secondly, people dislike hospitals from the psychological factor, mainly because they dislike the inner feelings of life, death and illness that hospitals bring. Generally, the main place to experience life, death and illness in China remains public hospitals, so the negative influence of private hospitals is much less than that of public hospitals, which have more of a role of auxiliary medical support. The statistics conclude that people travel by rail to private hospitals and that the distance from the residence to the proximate private hospital lowers the price of housing because private hospitals do not have the negative life influence from public hospitals' high demand.

When hospital types are separated by Chinese and Western medicine (WM), these distinctions do not produce distinct outcomes due to hospital type. Similar to hospital categorisation, the positive price markup for housing decreases as the distance between the hospital and the residence increases, regardless of the type of hospital. In addition, the demand for proximate Chinese or Western

hospitals can be met by rail, so the influence of hospital distance on housing is amplified by the distance between the rail station and the residence.

A significant correlation is found between the proximity to the proximate speciality hospital and medical centre and housing prices, and a reciprocal moderating effect exists between the distance to the proximate special hospital and the influence of rail stations on housing prices. In essence, the reasons for both outcomes are the same as those for private hospitals, namely, the urgent need for medical coverage, and the influence on housing prices is a combination of the direct influence of proximity and the moderating effect of rail. However, a significant reciprocal moderating effect is found between the proximate rail station and the proximate hospital. This indicates that the proximity of the general hospital has some negative effects on the residential neighbourhood, thus offsetting the premiums associated with the general hospital's accessibility. Owing to the hospital's comprehensive nature, these negative influences may include the possibility of high levels of noise, traffic congestion, mixed traffic and psychological rejection of people. Their fundamental characteristics are comparable to those of public hospitals.

6.1.3.2 Quantity

In the regression model of hospital accessibility based on the quantity of hospitals in the residential neighbourhood (Table 4–5), the results of the study statistics for hospitals not classified indicate that when hospitals are not classified for regression fitting, the presence of a large number of medical centres, low-degree hospitals or hospitals where people do not frequently seek services renders this hospital accessibility evaluation criterion insufficient to fully reflect people's needs. The criterion only partially reflects this trend in hospital demand. Consequently, when the impact on housing prices is quantified on a scale based on the quantity of hospitals within 900 m of a residence, only marginal significant results are observed. Additionally, unclassified hospitals may have a moderating effect on rail station proximity, thereby reducing the extent to which they increase housing prices.

When hospitals are targeted and graded, a positive correlation is found between the quantity of hospitals at each degree and the housing prices within the proximate average distance to hospitals of varying degrees. The degree to which this positive correlation change is greatest in the presence or absence of the first hospital, indicates that hospitals have a significant marginal influence on housing prices. Simultaneously, the quantity of hospitals within an average distance of the proximate hospital and the distance between the residence and the proximate rail station has a reciprocal moderating influence on housing prices. This moderating effect can be explained in two ways. First, the quantity of hospitals in the immediate residential area already meets the need to some extent, thereby reducing the need for rail access to hospitals and reducing the influence of housing prices on rail accessibility. Second, no hospitals are present in the immediate residential area, but the need for rail access to hospitals remains because rail accessibility shares some of the need for hospital accessibility. Thus, there is an interaction term significant for the influence on housing prices.

Possible explanations for the insignificance of public hospitals include the presence of some of these medical centres and their low degree, rendering them neither routinely nor interactively significant in relation to rail. It may be able to moderate it in an interactive manner with the proximity of the rail stations, suggesting that the more alternatives people have for medical services, the less dependent their housing prices will be on rail accessibility. Private hospitals are not in the same position as public hospitals. The presence of private hospitals, due to their necessity to meet market demand, makes the number of hospitals in close proximity to residences provide an additional gain in value for medical care, showing a positive correlation between the number of hospitals in the area and housing prices. Similar to public hospitals, housing price dependence on rail accessibility decreases as the quantity of private hospitals increases.

As with type, the fact that WM hospitals encompass medical centres and the majority of lower-degree hospitals renders them insignificant in terms of the pattern. In relation to the distance of the rail stations, however, the quantity of options within its buffer zone can have a moderating effect, that is, the greater the quantity of options for WH, the lower the dependence on the rail stations. By contrast, CM hospitals, are not as highly valued by residents as their Western counterparts, as evidenced by the fact that they have a significant influence on housing prices. The non-essential modern medical demands and functional orientation of health care in CM hospitals provide an additional medical benefit. Consequently, the quantity of CM hospitals within the residential buffer zone is positively correlated with housing prices. In addition, a moderating effect appears to be associated with rail transport, suggesting that people use rail transport to travel to different CM hospitals, and that the greater the quantity of CM hospitals in the neighbourhood, the weaker the impact of distance change to the rail stations on housing prices.

Among the attribute-specific differences, the influence of general hospitals on housing price is marginally significant. However, a moderating effect is found in terms of distance from rail stations which is a very intriguing point to consider. Although general hospitals can provide strong medical services, the negative aspects of their strong services, such as congestion, noise, mixed traffic and psychological rejection, make the quantity of general hospitals in the buffer zone absolutely insignificant in terms of their hospital convenience, which has no positive additive influence on housing prices. If there are numerous general hospitals in the buffer zone, the approximate functional overlap between them due to the completeness of medical services precludes meeting the absolute significance

criteria for influencing housing prices. In the interaction regression model, the reliance on general hospital access is generally such that a portion of the population must choose rail. In the vast majority of instances, the interaction term between the distance to the proximate rail station and the quantity of hospitals within the residential buffer zone will be significant, as indicated by the fact that the further a residence is from the rail station, the more dependent its value is on the quantity of hospitals within the buffer zone. In buffer zones with more general hospitals, house price premiums are likely to be less affected by rail accessibility.

For the quantity of special hospitals and medical centres in the respective residential buffer zones, the complementary and additive functions of their positioning in the healthcare system enable them to have a direct positive additive influence on housing prices, similar to CM hospitals, and to interact significantly with the distance to the proximate rail station. In other words, an interaction between the accessibility of rail and the quantity of special hospitals and medical centres in terms of their influence on housing prices.

6.1.3.3 Density

In the density-based hospital accessibility evaluation system (Table 4–5), the results of the overall hospital density statistics illustrate the overall hospital density of the city of Fuzhou, which, when not categorised, has a premium added to residence. Differences in the overall healthcare system can have an influence on housing price appreciation when the proximity of the proximate hospital and the quantity of hospitals in the vicinity of a residence are the same. Where the overall medical system is more accessible, the influence of rail on housing prices is reduced. This can be interpreted as a reduction in the reliance on rail to access hospitals, which can be avoided in areas with better access to health services.

When degrees are developed for the level of hospital and the intensity of medical care is graded, the health care system of hospitals of all degrees can be favourably connected with housing prices. This indicates that the intensity of the healthcare system provides a positive price premium for housing, which is understood by most people. However, among the different levels of hospital density, all degrees of hospitals are able to interact with rail accessibility to moderate the effect on housing prices. However, a slight difference is perhaps observed in the reasons why the density of tertiary hospitals (grade-A and B), secondary hospitals and class-I hospitals can have a moderating influence on housing prices in relation to rail accessibility. The moderating effect of the density of tertiary hospitals (grade-A and B) is because areas with a low density of such hospitals are accessed by rail, while the density of class-I hospitals and secondary hospitals moderates the influence of rail on housing prices because they are more numerous and widely distributed. When people demand low-degree hospitals, they can access them by other, shorter means of transport, thus partially diluting the reliance on rail demand and making rail convenience less of an additive to housing prices.

The urban concentration of public and private hospitals can have a positive correlation with housing prices. This is largely in line with expectations and is typical of the influence of service amenities on housing prices. A similar interaction is observed between hospital density and rail accessibility in the regulation of housing prices for public and private hospitals. As a result, the density of both spaces tends to reduce the extent to which residence price is affected by rail stations.

Similar to the nature categorisation, the distribution density of WM and CM hospitals is positively correlated with housing prices from a type standpoint. Again, rail accessibility interacts with WM and CM hospitals on housing prices. In essence, the higher the density of WM or CM hospitals in a residential neighbourhood, the less the reliance on rail stations.

In the scope categorisation, the density of the distribution of general hospitals, special hospitals and medical centres has a positive correlation with housing prices, which is moderated by the proximity of houses to rail station. This demonstrates the relationship between the number of hospitals and the housing prices, irrespective of the scopes of the hospitals that offer residents hospital accessibility. This could be interpreted as a reduction in reliance on rail due to the accessibility of hospitals or as an increase in reliance on rail accessibility to hospitals due to the lack of hospital density in the area and the necessity of meeting medical needs. Conversely, the negative effects associated with high medical intensity, regardless of the hospital's scope, can be negatively correlated with housing prices when residences are closer to rail stations, consistent with the characteristics of public and WM hospitals.

6.1.4 Spatial regression model

The study confirms that the regression model of hospital accessibility (Table 6–8), based on the spatial distance to the proximate grade-A tertiary hospitals, fits better than the linear model (Adjusted R-square = 0.722) to the greatest extent possible. The geographic heterogeneity in the extent to which residential sample prices are spatially moderated by hospital accessibility and rail accessibility is explained. The moderating effect expressed by this spatial regression model demonstrates the explanatory rate of the sample, the spatial stability and the spatial geographical distribution of the explained sample, which is not captured by the linear regression model (Figure 3). In the geospatial distribution figure, the lighter the colour of the explained residential sample, the smaller the coefficient of the interaction term of its model and the weaker the mutual moderating effect of hospital and rail accessibility (distance from the residence to the proximate grade-A tertiary hospital) on the influence of housing prices; whereas the grey residential sample indicates that the spatial coefficients cannot be resolved by this regression function.

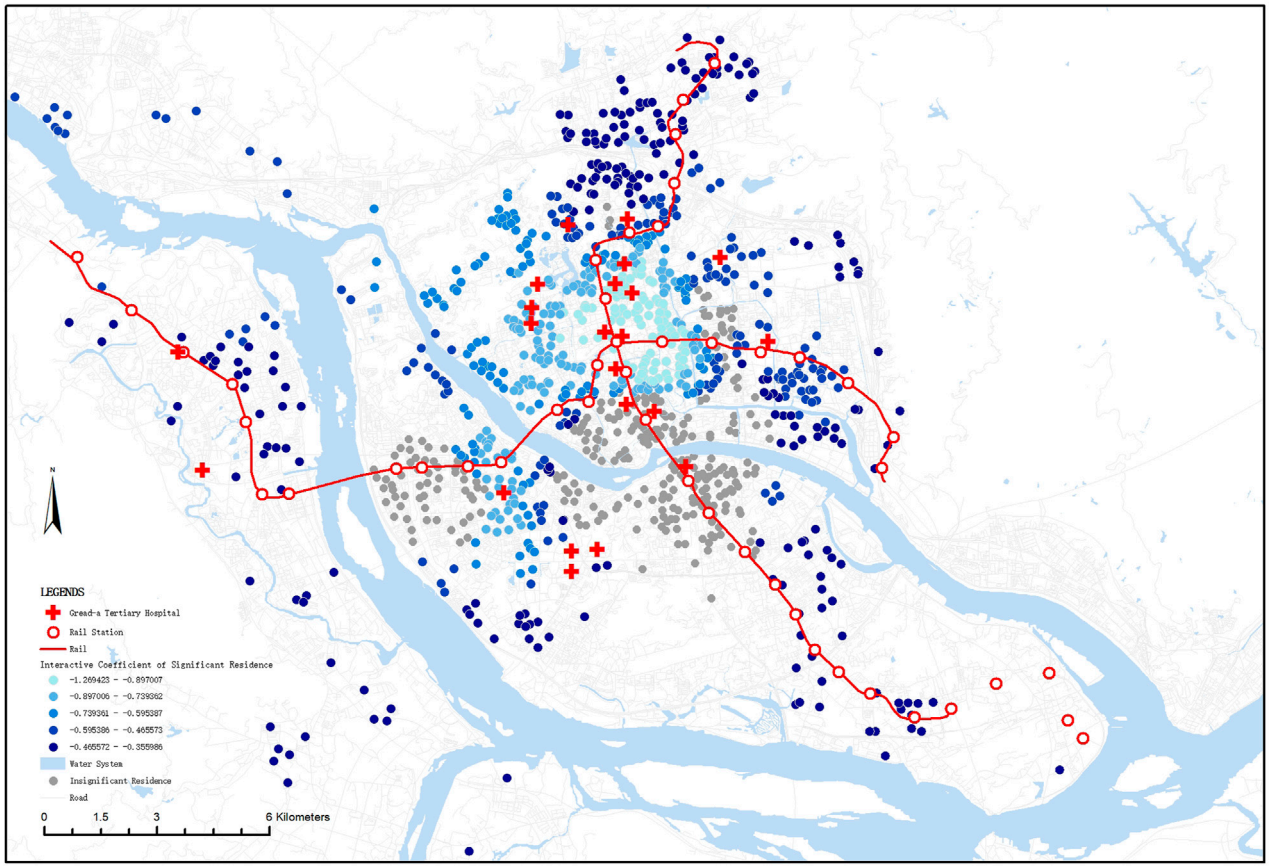

FIGURE 3
Geospatial distribution of interaction samples.

The subsequent paragraphs will discuss and analyse the reasons for the applicability of the aforementioned models and their explanation of the sample's geospatial distribution. Although other spatial interaction regression models can also reflect the influence of hospital and rail accessibility on housing prices to a certain extent and can compensate for other perspectives on hospital accessibility that are not captured by spatial distance scales, their explained sample rates are relatively low and the majority of interactions are spatially heterogeneous. In other words, the strength of the interactions cannot be summarised consistently as geographic space changes.

The excellent regression performance of the linear model, the linear interaction regression model, and the spatial interaction regression model for the distance to a grade-A tertiary hospital as a metric of residential hospital accessibility demonstrate its reliability. The reason is that in real life, the first choice for Chinese citizens for daily medical treatment is often grade-A tertiary hospitals, which often have a certain brand effect. As a Chinese saying goes: 'no need to consult for minor illnesses, and no need to see a doctor for a big one as well'. When most people need medical treatment, they will always habitually go to the proximate grade-A tertiary hospital, and most people will not consider hospital choices specific to their condition. This explains why the presence of a second hospital has no influence on the marginal effect of the real estate price when evaluating the quantity of hospitals' accessibility. Several key grade-A tertiary hospitals in the city centre of Fuzhou are simultaneously linked by passenger rail transit lines. When suburban houses are far from their own proximate grade-A tertiary hospital but close to a rail station, city dwellers typically choose rail as a quick and comfortable way to reach the city centre for medical care. Therefore, both the regression model for the distance to the proximate grade-A tertiary hospital and the regression interaction regression model has a high degree of general applicability. In addition, these innate understandings of grade-A tertiary hospitals and rail render the interactions underlying latent housing price models extremely spatially stable.

The discussion of the interpretation of the spatial interaction regression model will be divided into two parts: the significance causes and the interaction's strength. The significance of the

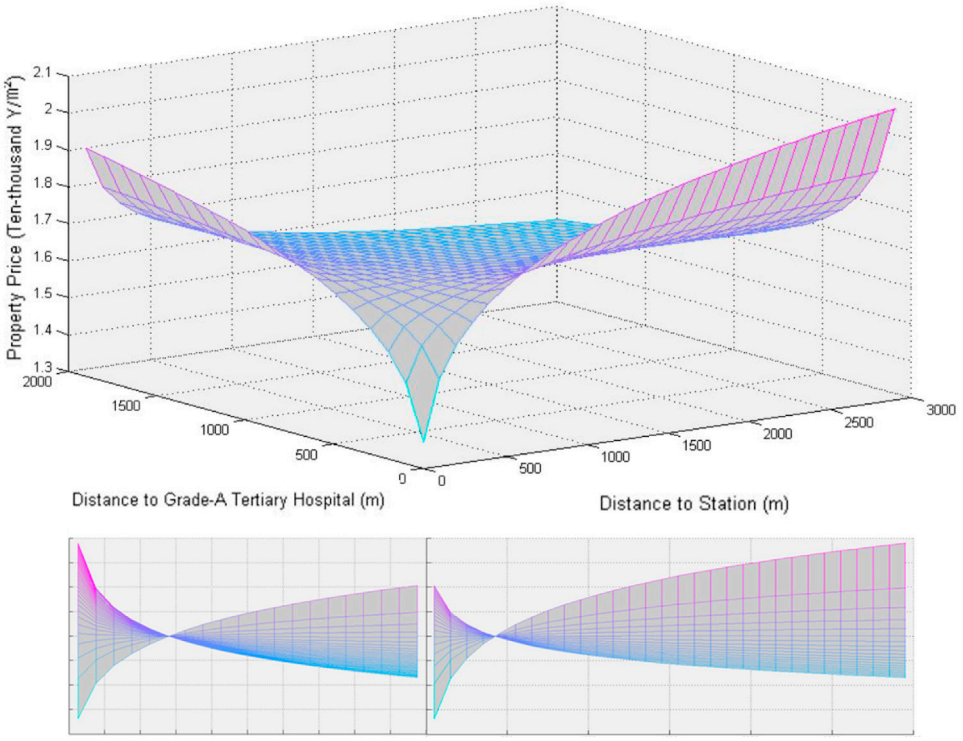

FIGURE 4
Spatial interactive regression model of housing prices.

sample implies that the prices of the residential sample conform to the pattern revealed by the regression model function. To some extent, housing prices are affected by the interaction moderation formed by their distance from the proximate grade-A tertiary hospital and the proximate rail station, the specific effects of which were discussed in the hospital distance section of the linear regression.

Furthermore, the presence of a small sample of insignificant residential interactions in the model can be explained by several reasons. 1) The proximity of residences to a grade-A tertiary hospital does not have a citywide core status and therefore does not attract other people to the residential proximity of the grade-A tertiary hospital *via* rail, avoiding the confusing and noisy crowd and poor psychological perceptions associated with the proximity of a grade-A tertiary hospital and a rail station at the same time, thereby preventing a downward trend in housing prices. 2) There is a reliable grade-A tertiary hospital in the immediate area, and the commute to this hospital does not rely on a rail at all. 3) Other, more significant housing prices influencing variables in the residential area were omitted from the study, thereby weakening the interaction between the grade-A tertiary hospital and rail.

The strength of the interaction and the geospatial distribution characteristics are described as follows. Although the presence of grade-A tertiary hospitals and rail stations in the proximity to housing does have a hurtful influence on housing prices, the distance of the negative influence will be reduced, and the extent to which housing prices will fall as a result of the negative influence will be less. Conversely, the weaker the interaction, the greater the dependence on the accessibility of grade-A tertiary hospitals and rail stations. Therefore, the geospatial distribution of the interaction's strength can be summarised as follows: the closer the grade-A tertiary hospital to the residence and the closer the residence is to the rail station, the weaker the interaction, and *vice versa*.

The final study was based on a spatial interaction regression model of residential proximate grade-A tertiary hospital and rail station distance (Table 6) with a randomly drawn image of the functional characteristics of a significant sample (Figure 4) to analyse the strength of the interaction effect and the characteristics of the pattern of change. The graph of the function for this sample indicates that when all other factors influencing housing prices are held constant, housing prices decrease with the decrease in spatial straight-line distance from the rail station when the residence is less than 550 m from the proximate grade-A tertiary hospital, and the reduction is greater the closer the residence is to the grade-A tertiary hospital. Similarly, when houses are less than 400 m

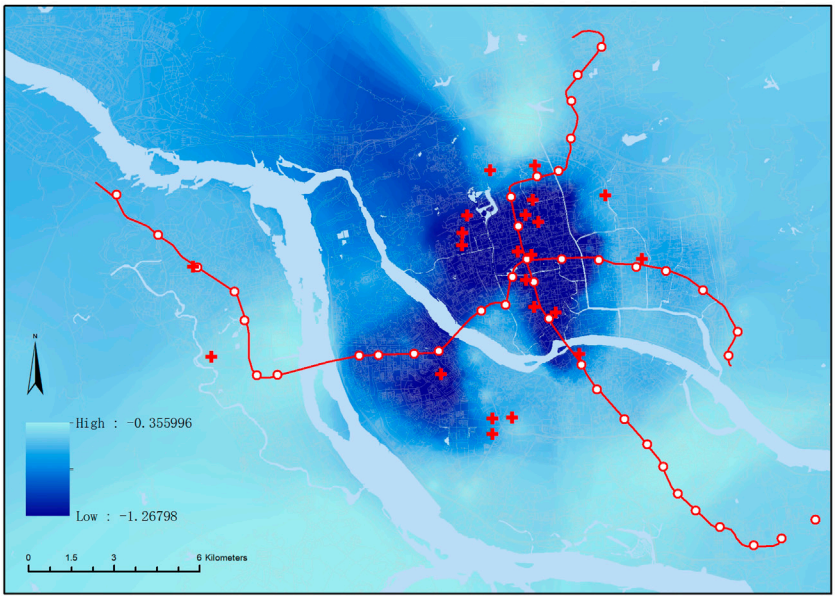

FIGURE 5
Interaction strength distribution.

from the proximate rail station, the price of houses decreases as the straight-line distance to the grade-A tertiary hospital decreases, and more so as the distance to the rail station decreases. When either the distance to the proximate grade-A tertiary hospital or rail station is 550 or 400 m, the other distance has no influence on housing prices, regardless of how it changes. When the distance to a grade-A tertiary hospital exceeds 550 m or the distance to a rail station exceeds 400 m, the other accessibility variable will have a positive influence on housing prices, and as the distance increases, housing prices will decrease. The distances of 550 m for a grade-A tertiary hospital and 400 m for a rail station can be interpreted as the distances at which people will accept a change of transport mode to reach the hospital by rail. If the distance is less than these, people will not be able to reach the hospital by rail, and if it is greater, they will not perceive the area as convenient. Similarly, when houses are 550 m from a grade-A tertiary hospital, residents are less reliant on the additional accessibility convenience of rail. Therefore, changes in rail station distance no longer affect housing prices. When the distance to the grade-A tertiary hospital is less than this, however, people from other areas will travel by rail to the grade-A tertiary hospital in the vicinity of the residence, and the traffic noise and congestion caused by the rail station become a factor in reducing the housing prices. Concurrently, the inconvenience of being 550 m away from the proximate grade-A tertiary hospital encourages people to travel to a grade-A tertiary hospital elsewhere by rail, thereby making the accessibility of the rail station a positive price variable.

7 Conclusion

This study confirmed that the variables influencing housing prices included a wide range of factors, including regional context, individual characteristics and facilities accessibility. The study's findings indicate that different variables exert varying degrees of influence and maintain continuity with prior research.

Regarding the amenity accessibility variables of interest, rail station accessibility and hospital accessibility have a significant influence on housing prices. The level of significance of the performance of the hospital accessibility variables on housing prices was found to be similar for different categories and different measures, and the overall analysis is consistent with the observed situation.

The Euclidean distance to the proximate grade-A tertiary hospital was used as a measure of hospital accessibility when analysing the interaction between hospital and rail accessibility on housing prices regulation. The interaction regression model had the highest explained sample rates and spatial stability. The study compared spatial interaction regression models from different hospital categorisation perspectives and accessibility perspectives and discovered that not all models had the same number of explained sample rates, heterogeneity of interactions, and spatial distribution patterns. The model that could explain sample prevalence and stability to the greatest extent was selected for detailed coefficient analysis and interpretation.

The existence of interactions indicates that the influence of hospital and rail accessibility on housing prices is not constant.

The influence of hospital accessibility on housing prices with differing rail accessibility is independent of all other variables (control variables). Rail accessibility has a different influence on housing prices with varying hospital accessibility. Using an image of the housing prices-relationship function, the study examined the reliance of residents on grade-A tertiary hospitals and rail station facilities.

Lastly, the distribution of the interaction between the city's grade-A tertiary hospitals and rail stations is plotted based on the strength of the model interaction (Figure 5). This predictive map for the city-wide interaction is an accurate representation of the geospatial distribution characteristics of the interaction in Fuzhou, and the interaction strength for each region can be determined by consulting the legend's coefficients. This distribution can be used to comprehend the regional strength of the interaction as well as the spatial distribution of its regional extent.

7.1 Implications

The findings of this study can be utilised by citizens to inform their house purchase decisions. For purchasers with a significant medical need for a residence, purchasing a residence with a medical package tailored to their specific medical requirements is possible. As the influence of different hospitals on housing prices varies, investing excessively in high-end hospitals, public hospitals, WM hospitals or general hospitals is not needed. In addition, the study discovered that when housebuyers consider hospital and rail accessibility, the straight-line distance to the proximate venue is the most effective reference point. Therefore, when people purchase a residence, they typically only need to consider the proximate hospital's spatial distance. Lastly, a price-moderating relationship is observed between the accessibility of grade-A tertiary hospitals and the accessibility of rail. Therefore, housebuyers who combine the need for medical care with the need for rail can purchase houses in appropriate areas based on the geospatial distribution of the interactions in the findings.

Using the study's findings, city planners can modify the urban distribution density of public facilities such as rail and grade-A tertiary hospitals, as well as their location in relation to residential areas. By doing so, they can better regulate the stability of urban housing prices, improve regional coordination and increase the overall effectiveness of hospitals and per capita access to a hospital.

This study's process of exploring variables from multiple perspectives can be used by future scholars and researchers to determine the optimal perspective for measuring model variables. A precise measurement perspective will maximise the reduction of covariance, increase the significance of variables and enhance the model's fit, allowing researchers to precisely identify the core reference factors and uncover the objective patterns underlying them.

7.2 Limitations

In the process of the study, the quantity of samples is insufficient and the angle of variable selection may still be inadequate, so some covariates are integrated into the present variables, resulting in an inadequate fit of the equation. Faced with such issues, in the future, the quantity of statistics sources is hoped to be expanded and the statistics' precision can be enhanced when variables are extracted.

In the case of hospital accessibility, a degree of inadequacy is identified in evaluating accessibility based on the Euclidean distance from the residence to the proximate hospital and rail station. This is because spatial distance does not fully express the accessibility of houses to different facilities and does not reflect the detailed variation in the influence on housing prices based on the distance measure, which is only linear at a macro level. Furthermore, the categorisation of hospitals can only be based on a fixed hospital unit standard, which is limited by the information available and therefore does not allow for a more precise evaluation of the distance to demand based on the proximate specialist hospital department. This makes our hospital categorisation subject to the problem of ignoring functional overlap.

In addition, a more rational evaluation model for a hospital in the buffer zone is required for all hospitals in the nearby residential area, due in part to the duplication of functions between hospitals. The model must be based on the quantity of hospitals and the ability to calculate comprehensive medical functions. Additionally, the quantity of hospitals in the buffer zone is the same, but the specific accessibility differences are not reflected, so a more accurate calculation process of accessibility in the buffer zone based on the quantity of hospitals is required.

In the design of the study on hospital kernel density, calculating a comprehensive medical kernel density system evaluation with area-weighted weights based on the frequency of demand for different hospital categories and age bracket preferences as a whole in their everyday lives was not possible due to a lack of statistics and information. Consequently, the evaluation of the medical system can only be conducted on the basis of distinct global and categorical categories, as well as an assessment of the moderating effect of hospitals on housing prices and rail accessibility under distinct categories.

The models based on geographical heterogeneity as a starting point for ideas that validate empirical conclusions have not been validated consistently in geographical models based on other ideas. Owing to the limitations of the model concept, a limited interpretation of the conclusions is therefore possible.

Data availability statement

The original contributions presented in the study are included in the article/supplementary material, further inquiries can be directed to the corresponding author.

Author contributions

KC, HL, SY and OS contributed to conception and design of the study. KC and YH organized the database. FC performed the statistical analysis. KC and SY wrote the first draft of the manuscript. KC, YH, SY, XH and YL wrote sections of the manuscript. All authors contributed to manuscript revision, read, and approved the submitted version.

Funding

This study was supported by the National Natural Science Foundation of China (No. 51808452) and the General Program of the Sichuan Federation of Social Science Associations (No. SC20B113).

Conflict of interest

Author XH was employed by Fujian Communications Planning and Design Institute CO.,Ltd.

The remaining authors declare that the research was conducted in the absence of any commercial or financial relationships that could be construed as a potential conflict of interest.

Publisher's note

All claims expressed in this article are solely those of the authors and do not necessarily represent those of their affiliated organizations, or those of the publisher, the editors and the reviewers. Any product that may be evaluated in this article, or claim that may be made by its manufacturer, is not guaranteed or endorsed by the publisher.

References

Agostini, C., and Palmucci, G. A. (2008). The anticipated capitalisation effect of a new metro line on housing prices. *Fisc. Stud.* 29 (2), 233–256. doi:10.1111/j.1475-5890.2008.00074.x

Almosaind, M. A., Dueker, K. J., and Strathman, J. G. (1993). *Light-rail transit stations and property values: A hedonic price approach*. Washington, DC: Transportation Research Record.

Alonso, W. (1964). *Location and land use*. Cambridge, MA: publications of the Joint Center for Urban Studies of the Massachusetts Institute of Technology and Harvard University Press.

Baden, U.R. (2013). *Retirement housing and medical facilities : Preference, proximity and price*.

Bae, C., Jun, M. J., and Park, H. (2003). The impact of Seoul's subway Line 5 on residential property values. *Transp. policy* 10 (2), 85–94. doi:10.1016/s0967-070x(02)00048-3

Bajic, V. (1983). *The effects of a new subway line on housing prices in metropolitan toronto*. Washington, DC: Urban Studies.

Banzhaf, S., and Farooque, O. (2012). *Interjurisdictional housing prices and spatial amenities: Which measures of housing prices reflect local public goods?* Cambridge, Massachusetts, United States: National Bureau of Economic Research, Inc.

Baumont, C., Ertur, C., and Le Gallo, J. (2003). *Spatial analysis of employment and population density: The case of the agglomeration of dijon, 1999*. Germany: University Library of Munich.

Benjamin, J. D., and Sirmans, G. S. (1996). Mass transportation, apartment rent and property values. *J. Real Estate Res.* 12 (1), 1–8. doi:10.1080/10835547.1996.12090830

Cao, K., Diao, M., and Wu, B. (2019). A big data–based geographically weighted regression model for public housing prices: A case study in Singapore. *Ann. Am. Assoc. Geogr.* 109, 173–186. doi:10.1080/24694452.2018.1470925

Cervero, R., and Landis, J. (1993). Assessing the impacts of urban rail transit on local real estate markets using quasi-experimental comparisons. *Transp. Res. Part A Policy Pract.* 27 (1), 13–22. doi:10.1016/0965-8564(93)90013-b

Dziauddin, M. F., Alvanides, S., and Powe, N. (2013). Estimating the effects of light rail transit (lrt) system on the property values in the klang valley, Malaysia: A hedonic house price approach. *J. Teknol.* 61 (1), 35–47. doi:10.11113/jt.v61.1620

Dziauddin, M. F. (2014). *The determinants of house prices in the klang valley, Malaysia*.

Febrita, R. E., Alfiyatin, A. N., Taufiq, H., and Mahmudy, W. F. (2017). "Data-driven fuzzy rule extraction for housing price prediction in Malang, East Java," in 2017 International Conference on Advanced Computer Science and Information Systems (ICACSIS), Bali, Indonesia, 28-29 October 2017. (Washington, DC: IEEE).

Gatzlaff, D. H., and Smith, M. T. (1993). The impact of the Miami metrorail on the value of residences near station locations. *Land Econ.* 69 (1), 54–66. doi:10.2307/3146278

Guo, J., Xia, T., and Li, J. (2016). Study on the spatial divergence of urban residential prices and the influencing factors. *Statistics Decis.* (08), 142–145. doi:10.13546/j.cnki.tjyjc.2016.08.039

Han, S., Ren, F., Wu, C., Chen, Y., Du, Q., and Ye, X. (2018). Using the tensorflow deep neural network to classify mainland China visitor behaviours in Hong Kong from check-in data. *ISPRS Int. J. Geoinf.* 7 (4), 158. doi:10.3390/ijgi7040158

Hao, Q., and Chen, J. (2007). Geospatial differences in distance to CBD, transport accessibility and residential prices in Shanghai. *World Econ. Pap.* 1 (01), 22–35. doi:10.3969/j.issn.0488-6364.2007.01.003

He, C., Zhen, W., Guo, H., Hu, S., Rui, Z., and Yang, Y. (2010). Driving forces analysis for residential housing price in beijing. *Procedia Environ. Sci.* 2 (1), 925–936. doi:10.1016/j.proenv.2010.10.104

Im, J., and Hong, S. H. (2018). *Impact of a new subway line on housing values in Daegu, Korea: Distance from existing lines*. Washington, DC: Urban Studies.

Jabbar, E. H. (2016). Willingness to pay for public park, waste disposal and wide roads. *Hedonic Price Model.* 5, 35–47.

Lan, F., Wu, Q., Zhou, T., and Da, H. (2018). Spatial effects of public service facilities accessibility on housing prices: A case study of xi'an, China. *Sustainability* 10 (12), 4503. doi:10.3390/su10124503

Lan, J., and Ye, Z. (2020). Factors affecting Shanghai housing prices. *Front. Econ. Manag. Res.* 1 (2), 59–62. doi:10.33969/twjournals.femr.2020.010214

Li, R., Gong, S., and Gao, Y. (2021). Accessibility of public service facilities in beijing and its impact on housing prices. *Acta Sci. Nat. Univ. Pekin.* 57 (05), 875–884.

Li, S., Chen, L., and Zhao, P. (2019). The impact of metro services on housing prices: A case study from beijing. *Transportation* 46 (4), 1291–1317. doi:10.1007/s11116-017-9834-7

Li, Y., Lang, H., Xu, W., Hui, W., and He, Z. (2013). Using GIS and Hedonic in the modelling of spatial variation of housing price in Xiamen city. *IRSPSD. Int.* 1 (4), 29–42. doi:10.14246/irspsd.1.4_29

Liu, L., Yu, H., Zhao, J., Wu, H., Peng, Z., and Wang, R. (2022). Multiscale effects of multimodal public facilities accessibility on housing prices based on mgwr: A case study of wuhan, China. *ISPRS Int. J. Geoinf.* 11 (1), 57. doi:10.3390/ijgi11010057

Liu, T., Hu, W., Song, Y., Zhang, A., and Cleveland, C. J. (2020). Exploring spillover effects of ecological lands: A spatial multilevel hedonic price model of the housing market in wuhan, China. *Ecol. Econ.* 170, 106568. doi:10.1016/j.ecolecon.2019.106568

Luo, X., Yue, B., Lin, A., and Chen, F. (2019). Impact of accessibility of public service facilities on housing price in central district of wuhan city: Based on analysis of tri-network transport system. *Areal Res. Dev.* 38 (02), 86–91+6.

McDonald, J. F., and Osuji, C. I. (1995). The effect of anticipated transportation improvement on residential land values. *Regional Sci. Urban Econ.* 25 (3), 261–278. doi:10.1016/0166-0462(94)02085-u

Peng, B., Shi, Y., Shan, Y., and Chen, D. (2015). The spatial impacts of class 3A comprehensive hospitals on peripheral residential property prices in Shanghai. *Sci. Geogr. Sin.* 35 (07), 860–866. doi:10.13249/j.cnki.sgs.2015.07.860

Peng, T-C., and Chiang, Y-H. (2015). The non-linearity of hospitals' proximity on property prices: Experiences from Taipei, Taiwan. *J. Prop. Res.* 32 (4), 341–361. doi:10.1080/09599916.2015.1089923

Rohit, S., and Peter, N. (2018). Does urban rail increase land value in emerging cities? Value uplift from Bangalore metro. *Transp. Res. Part A Policy Pract.* 117, 70–86. doi:10.1016/j.tra.2018.08.020

Tan, R., He, Q., Zhou, K., and Xie, P. (2019). The effect of new metro stations on local land use and housing prices: The case of Wuhan, China. *J. Transp. Geogr.* 79, 102488. doi:10.1016/j.jtrangeo.2019.102488

Tan, th (2011). Neighborhood preferences of house buyers: The case of klang valley, Malaysia. *Int. J. Hous. Mark. Analysis* 4 (4), 58–69. doi:10.1108/17538271111111839

Tang, K., Li, Q., Lu, H., and Yu, P. (2020). Accessibility of public service facilities and its impact on housing prices. *Geospatial Inf.* 18 (02), 90–93+8+8.

Teng, S., Yan, J., and Zhou, S. (2014). *Research on impact of urban rail transit on house price along the line: A case study on No. 1 line of Tianjin subway*. Berlin Heidelberg: Springer.

Waddell, P., and Hoch, B. I. (1993). Residential property values in a multinodal urban area: New evidence on the implicit price of location. *J. Real Estate Finance&Economics* 7 (2), 117–141. doi:10.1007/BF01258322

Wang, F., and Gao, X. (2014). The transitional spatial pattern of housing prices in beijing: Factors and implications. *IRSPSD. Int.* 2 (3), 46–62. doi:10.14246/irspsd.2.3_46

Wang, L., and Liu, G. (2013). "Spatial variation analysis of the housing price in multi-center city: A case study in chongqing city, China," in 2013 International Conference on Computational and Information Sciences: IEEE Computer Society, Shiyang, China, 21-23 June 2013, 450–453.

Wang, P-D., and Chen, M. (2019). The non-linear relationships of numeric factors on housing prices by using gam. *J. Data Sci.* 17 (1), 131–144. doi:10.6339/jds.201901_17(1).0006

Wu, W., Zhang, W., and Dong, G. (2013). Determinant of residential location choice in a transitional housing market: Evidence based on micro survey from Beijing. *Habitat Int.* 39, 16–24. doi:10.1016/j.habitatint.2012.10.008

Yang, L., Chau, K. W., Szeto, W. Y., Cui, X., and Wang, X. (2020). Accessibility to transit, by transit, and property prices: Spatially varying relationships. *Transp. Res. Part D Transp. Environ.* 85, 102387. doi:10.1016/j.trd.2020.102387

Yang, L., Chen, Y., Xu, N., Zhao, R., Chau, K. W., and Hong, S. (2020). Place-varying impacts of urban rail transit on property prices in Shenzhen, China: Insights for value capture. *Sustain. Cities Soc.* 58, 102140. doi:10.1016/j.scs.2020.102140

Yang, L., Liang, Y., He, B., Lu, Y., and Gou, Z. (2022). COVID-19 effects on property markets: The pandemic decreases the implicit price of metro accessibility. *Tunn. Undergr. Space Technol.* 125, 104528. doi:10.1016/j.tust.2022.104528

Yang, L., Wang, B., Zhou, J., and Wang, X. (2018). Walking accessibility and property prices. *Transp. Res. part D Transp. Environ.* 62, 551–562. doi:10.1016/j.trd.2018.04.001

Yang, L., Zhang, X., Hong, S., Lin, H., and Cheng, G. (2016). The impact of walking accessibility of public services on housing prices: Based on the cumulative opportunities measure. *South China J. Econ.* (1), 14. doi:10.19592/j.cnki.scje.2016.01.005

Yang, L., Zhou, J., Shyr, O. F., and Huo, D. (2019). Does bus accessibility affect property prices? *Cities* 84, 56–65. doi:10.1016/j.cities.2018.07.005

Zhang, X. (2014). An empirical study of the impact of metro station proximity on property value in the case of nanjing, China. *Asian Dev. Policy Rev.* 2, 61–71. doi:10.18488/journal.107.2014.24.61.71

Zhang, Z., Kong, F., Ni, H., Mo, Z., Wan, J. B., Hua, D., et al. (2016). Structural characterization, α-glucosidase inhibitory and DPPH scavenging activities of polysaccharides from guava. *Carbohydr. Polym.* 144 (21), 106–114. doi:10.1016/j.carbpol.2016.02.030

frontiers | Frontiers in Environmental Science

TYPE Original Research
PUBLISHED 25 November 2022
DOI 10.3389/fenvs.2022.1045959

Check for updates

OPEN ACCESS

EDITED BY
Jun Yang,
Northeastern University, China

REVIEWED BY
Yibin Ao,
Chengdu University of Technology, China
Wei Zhang,
Sichuan University, China

*CORRESPONDENCE
Xu Cui,
cuixu@swjtu.edu.cn

SPECIALTY SECTION
This article was submitted to Land Use Dynamics,
a section of the journal
Frontiers in Environmental Science

RECEIVED 16 September 2022
ACCEPTED 07 November 2022
PUBLISHED 25 November 2022

CITATION
Liang P, Cui X, Lin M, Yang T and Wu B (2022), High-speed rail effects on station area-level business commercial agglomeration: Evidence from 110 stations in China.
Front. Environ. Sci. 10:1045959.
doi: 10.3389/fenvs.2022.1045959

COPYRIGHT
© 2022 Liang, Cui, Lin, Yang and Wu. This is an open-access article distributed under the terms of the Creative Commons Attribution License (CC BY). The use, distribution or reproduction in other forums is permitted, provided the original author(s) and the copyright owner(s) are credited and that the original publication in this journal is cited, in accordance with accepted academic practice. No use, distribution or reproduction is permitted which does not comply with these terms.

High-speed rail effects on station area-level business commercial agglomeration: Evidence from 110 stations in China

Pengpeng Liang[1], Xu Cui[1]*, Mao Lin[2], Tian Yang[1] and Bo Wu[1]

[1]School of Architecture, Southwest Jiaotong University, Chengdu, China, [2]School of Design, Southwest Jiaotong University, Chengdu, China

As a critical transportation infrastructure, high-speed rail (HSR) greatly enhances accessibility and shortens the spatial-temporal distance among cities. It is well documented that HSR significantly impacts regions and cities' economic development and spatial structure. The proportion and frequency of business passenger trips are increasing yearly, and the demand for "station as the final destination" is becoming more and more prominent. Given the pivotal role of the design and construction of HSR station areas in achieving "station as the final destination," the study of their development characteristics and patterns has important implications for urban planning. Previous studies have focused extensively on the macro impact of the HSR operation on regional economies, urban industries, and tourism development, whereas only a few were conducted at the station level. Furthermore, the business-commercial agglomeration effects of the HSR operation on the development and construction of station areas have neither been studied nor accurately measured. To fill this gap, we first constructed a panel data set consisting of the point of interest (POI) data, China City Statistical Yearbook data, and the HSR station operation data from 2012 to 2017. Next, we developed difference-in-differences (DID) models to decipher the impact of the HSR operation on the station-level business and commercial agglomeration. The results show that the HSR operation has increased the business-commercial agglomeration index (BCAI), the commercial agglomeration index (BAI), and the business agglomeration index (CAI) by 28.3%, 29%, and 21.3%, respectively. In other words, the HSR operation has significant business-commercial agglomeration effects in the station area, and the agglomeration effect size of business is more extensive than that of commerce. Interestingly, the BCAI grew slowly in the first 3 years after the HSR operation but started to rise much faster from the fourth year, which HSR's catalytic effects can explain. The results also reveal that the business-commercial agglomeration effects have a clear spatial threshold as the BCAI tends to decrease from 1500 m to 3000 m away from HSR stations. The plausibility of the results has been confirmed by the parallel trend, placebo, and robustness tests.

KEYWORDS

high-speed rail, station areas, business-commercial agglomeration effects, business-commercial agglomeration index, difference-in-differences model, spatial distribution patterns

1 Introduction

Transportation infrastructure is generally considered one key factor in shortening travel time and promoting urban economic growth (Bhatta and Drennan, 2003; Hong et al., 2011; Diao, 2018; Deng et al., 2020). An efficient transportation system not only improves accessibility among cities but also plays a vital role in shaping urban spatial structure (Lakshmanan, 2011; Yu et al., 2013; Yang et al., 2019; Yang et al., 2020a; Zhou X. et al., 2022). Investments in transportation infrastructure can accelerate industrial agglomeration and meet people's demand for goods and high-quality services. Since the beginning of the 21st century, high-speed rail (HSR) has become a significant emerging inter-city transportation service. The rapid development of the HSR has reshaped the territory's spatial structure. In recent decades, the benefits of HSR can be characterized by high speed, high frequency, high accessibility, travel time reliability, low-carbon life, a greater chance of commuting between the two cities, and relatively low fares (compared with other transport modes, especially flights), have been widely acknowledged and emphasized (Givoni, 2006; Campos and de Rus, 2009; Zhou Y. et al., 2022). HSR weakens the absolute boundaries of natural barriers and spatial and temporal distances, creating positive spillover and agglomeration effects on cities and surrounding areas. China, Spain, Japan, Germany, France, and other countries are planning to or have already implemented large-scale HSR constructions. Among them, China's HSR mileage ranks first across the globe. In 2003, Qinhuangdao-Shenyang HSR was operated, which can be considered the first attempt at China's HSR. In 2008, the first real HSR in the history of China, the Beijing-Tianjin Intercity Railway, was operated. By the end of 2021, the operating mileage of China's HSR has reached 40,000 km. China's "four vertical and four horizontal" HSR corridors have been fully built, and the "eight vertical and eight horizontal" HSR corridors are being densely formed. As a new form of public transportation, HSR promotes urbanization and national economic growth.

As a high-quality transportation infrastructure (public social goods), HSR has various advantages. The most obvious advantage is that HSR improves the travel experiences between cities and shortens commuting time. Other advantages include, but are not limited to, enhancing train punctuality rates, providing comfortable and convenient services, increasing passenger capacity, creating a comfortable travel environment, stimulating urban economic development, promoting regional integration, and stimulating tourism development (Yang et al., 2020b; Gong and Li, 2022; Jiang et al., 2022). Thus, the government has increasingly invested in the construction of the HSR. Although the HSR has a tremendous spatial impact at the national, regional, and urban levels, HSR station areas have received the most direct spatial benefit (Meng, et al., 2018). Specifically, the development of HSR station areas brings opportunities for the construction of new cities and the renewal of old cities, offering possibilities for optimizing urban spatial structure (Dong et al., 2021; Chang et al., 2022). The design and development of HSR station areas is a long-standing topic. Scholars in planning, developers, and governments are all paying attention to the construction of HSR station areas. Corresponding research findings have significant theoretical relevance and positive practical implications.

By compressing the spatial-temporal distance and reducing travel costs, the HSR promotes the agglomeration of economic activities in station areas (Ribalaygua and Perez-Del-Cano, 2019; Cui et al., 2021; Du et al., 2021; Wang et al., 2022). The improved accessibility brings the station areas with the influx of people, logistics, capital, and information. The construction of the HSR has affected the demand for mixed land development, residence, employment, and transportation. In contrast to traditional railway stations' single transportation function, HSR station areas accommodate travel needs and various business and commercial activities. In other words, HSR station areas are not only transportation network nodes (reflecting transportation value and node value) but also urban public places (reflecting functional value and place value) (Gui et al., 2021; Cummings and Mahmassani, 2022). The HSR helps enhance the network externalities of cities, which can complement or replace the agglomeration externalities of localization. At the same time, the spillover of passenger flow brings development opportunities to station areas. To maximize the benefits created by HSR, urban planners have tried to connect the station area with the city center (or commercial center) to reach a station-city integration situation.

HSR has promoted the regionalization of economic activities and strengthened intercity exchanges. The growth of business ridership with the travel characteristics of short distance, high frequency, and high time value has given rise to the development and agglomeration of commercial, business, and transportation facilities around stations (Wang et al., 2018). It is because that business ridership is less sensitive to the cost of transportation but more sensitive to the cost of time. In other words, business passengers want to reach their destinations quickly. In this regard, "Station as the final destination" is the inherent and essential requirement and the ultimate goal for developing HSR station areas. People have planned many newly-built HSR stations with various commercial and business spaces in station areas, trying to transform the transportation nodes into high-quality urban places. In addition to the drivers of the business ridership demand, economic forces are another critical factor contributing to business and commercial agglomeration. The change in accessibility caused by HSR directly impacts land prices in the station area, resulting in higher land lease prices in areas closer to the station. Specifically, businesses and commerce (e.g., high-end restaurants and business offices) can afford higher land lease prices and tend to congregate in core areas closer to the site.

TABLE 1 Selected studies on benefit impacts of HSR.

Reference	Perspective	Samples	Method	Key finding
Shaw et al. (2014)	Region	China's HSR network 2008–2013	Timetable-based accessibility evaluation	The spatial distribution of HSR travel-time accessibility shows a corridor effect; and HSR travel cost and the spatial distribution of distance accessibility show a radial pattern.
Zhang et al. (2020a)	Region	China Railway Express (CR express)	Multiple attribute decision making (MADM)	The practicality of structural hole theory in complex networks is confirmed; Moscow ranks first in the importance of nodes in the CR express network.
Xu and Huang (2019)	Region	China's HSR network 2007–2030	Geographically weighted regression (GWR) model.	Small and medium-sized cities are more suitable for HSR investment than mega-cities; the central and western regions are gradually becoming the core areas for HSR construction.
Wang et al. (2018)	Region	the four HSR lines in Jiangsu	Spatial autoregressive (SAR) model	The HSR operation has a significant impact on trade volume with spatial differences in different regions of Jiangsu province.
Campos and de Rus (2009)	Urban	166 HSR projects across the world	International comparison	The article identifies the definition, different development, and operation models of the HSR economy.
Jia et al. (2017)	Urban	336 cities at the prefecture level	PSM-DID model	China's HSR construction has a positive impact on regional economic growth, and effects vary for different lines.
Tian et al. (2021)	Urban	160 HSR-connected cities	Panel model	The city location improvement in the HSR network may inhibit the agglomeration of the service industry in peripheral areas.
Carteni et al. (2017)	Urban	the 20 most domestic visited cities in Italy	Perceived choice model	The willingness to buy HSR tickets for travel is 40% higher than that of buying traditional train tickets.
Dong, et al. (2021)	Station area	180 HSR new towns	Instrumental variable and DID model	There are two key factors for the success of new towns, including the location and local market.
Geng et al. (2015)	Station area	896 housing samples	Hedonic model	In the range of 0.475 km–0.891 km, the closer distance to the HSR station is, the lower the price of housing presents; in the range of 0.891 km–11.704 km, the opposite is true.
Deng et al. (2020)	Station area	124 HSR station areas	Multiple linear regression	The main factors affecting the development of HSR station areas are the level of economic development of the city, city hierarchy and location.
Zheng et al. (2019)	Station area	97 cities operating HSR	DID model	The nighttime light intensity in HSR station areas has increased by an average of 27%.

Therefore, business and commercial agglomeration under the market mechanism will be generated in HSR station areas (Wang et al., 2014; Wang et al., 2021).

Previous studies regarding the impact of HSR have primarily focused on the city or regional-level urban economic development, land use, urban vitality, spatial changes in house prices, and tourism (Masson and Petiot, 2009; Chen and Haynes, 2017; He et al., 2018; Yang et al., 2020a; Yang et al., 2020c; Jin et al., 2020; Yang et al., 2021; Wenner and Thierstein, 2022). In contrast, only a few have analyzed the development pattern and formation mechanism of HSR station areas. Furthermore, most of the station-level HSR studies are qualitative case analyses or mainly focus on the impact of the HSR operation on housing prices and economic growth (Geng et al., 2015; Zheng et al., 2019). There is still a lack of quantitative, systematic, and national-level studies on the agglomeration effect of HSR station areas. In recent years, the development of new technologies and the rise of big data, such as points of interest from online maps, cell phone signaling data, etc., have provided solid support and opportunities for studying HSR station areas at a microscopic scale. However, some debate is whether HSR station areas can produce agglomeration effects. However, what is the degree of business and commercial agglomeration generated by HSR? Is there a difference between business agglomeration and commercial agglomeration? These issues are critical to the design and development of HSR station areas.

To address the above questions, based on the data from 2012 to 2017, namely the data on China's point of interest (POI), China City Statistical Yearbook data, and the HSR station operation data, difference-in-differences (DID) models were established to systematically examine the station-level business-commercial agglomeration effects of the HSR operation. The plausibility and validity of the model results were verified by the parallel trend test, placebo test, and robustness test. This paper contributes to the literature in the following ways: 1) enriching the current theory of the HSR station area development and adding new empirical evidence to the HSR operation; 2) estimating the business-commercial agglomeration effects of China's HSR station areas in recent years; 3) revealing the spatial distribution patterns of business and commerce land use across different buffers; 4) proposing innovative research directions. Our investigation intended to study the BCAI by using DID models. This paper may be one of the first research efforts and fills a gap in planning and design.

The rest of this paper is structured as follows. Section 2 reviews the study of the impact of the HSR operation on the

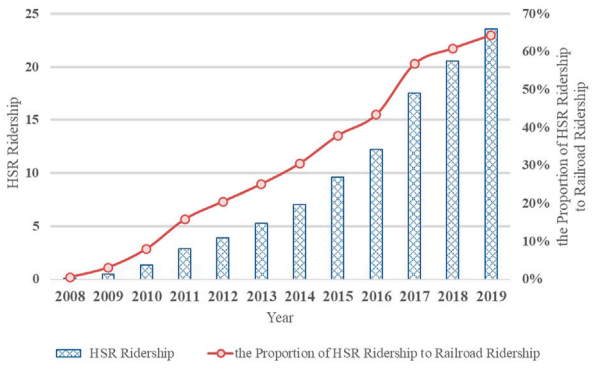

FIGURE 1
HSR ridership and the proportion of HSR ridership to railroad ridership from 2008 to 2019.

region, city, and station area. Section 3 describes the research object, the data sources for empirical analysis, and the DID model as the research methodology. Section 4 analyzes the spatial distribution of HSR stations and the business-commercial development in station areas. Section 5 presents the empirical model results and discusses the relationship between the HSR and business-commerce. Section 6 concludes and identifies future research directions.

2 Literature review

2.1 The impact of HSR at the regional and urban level

Extensive literature assesses the regional and urban impacts of the HSR (Table 1). At the regional level, many scholars have pointed out that the HSR operation brings about accessibility improvement (Zhu et al., 2016; Xu et al., 2018; Sahu and Verma, 2022), which facilitates the rapid movement of various factors across different regions. By making developed and peripheral regions closer, the HSR transforms the connectivity of peripheral regions, which provides opportunities for coordinated regional development. The HSR construction has increased the level of the transportation network and expanded the range of urban isochronous circles (Wang et al., 2020). In other words, the HSR has expanded the hinterland of the central city and triggered a spatial reshaping. Dong et al. (2020) have confirmed that the HSR can connect megacities with second-tier cities at the regional level, facilitating the flow and optimal allocation of resources. Specifically, the HSR operation can reduce the time cost of people flow and increase the spillover level of highly skilled people and knowledge.

At the urban level, the topic of the HSR has also received much attention (Garmendia et al., 2012; Long et al., 2018; Deng et al., 2019). Shao et al. (2017) showed that HSR has a positive impact on urban service agglomeration and has a significant impact on productive services. By studying the tourism industry in Spain for over 15 years, Albalate and Fageda (2016) showed that high-speed rail may positively impact tourism and be an alternative to air. Dai et al. (2018) studied 19 sub-sectors of industries in cities along the Beijing-Shanghai HSR line and found that the HSR has agglomeration and diffusion effects on tertiary industries. In general, the HSR has a positive effect on regions and cities (Garmendia et al., 2008; Shaw et al., 2014; Jia et al., 2017; Xu and Huang, 2019).

However, other studies hold a different view (Vickerman, 1997; Ortega et al., 2012; Geng et al., 2015; Mota et al., 2017; Li et al., 2019). These scholars have argued that the HSR has negatively affects regions and cities or that the impact mechanisms are complex and unclear. The HSR operation may cause traffic congestion, environmental damage, and noise and affect the development of other industries (such as the airline industry). Chen, et al. (2016) have found that the HSR operation leads to uneven regional economic development. The HSR enhances the agglomeration capacity of central nodes, while it may cause the loss of production factors in less developed areas. Chen et al. (2016) believed that the role of high-speed rail in affecting the economy was ambiguous. The economic impact of the HSR investment can be achieved by interacting with other factors, such as land use. This impact can be positive or negative. The impact may increase in the short term but may reduce economic growth in the periphery in the long term. It is worth noting that the HSR may have increased environmental costs (Givoni, 2006; Westin and Kageson, 2012).

2.2 The impact of HSR at station area level

The development of HSR station areas benefits from accessibility improvement. The HSR operation has caused changes in the land use of station areas, increasing people's social and economic activities. Diversified industries are clustering in HSR station areas, especially commerce, business, real estate, leisure and entertainment, tourism, etc. In Europe, the development of many HSR station areas plays an important role in urban regeneration (Bertolini, 2000; Hickman et al., 2021). De Wijs et al. (2016) saw many similarities between redeveloping HSR station areas and smart cities like digital parking systems, electronic schedules for public transportation, and sustainable energy buildings. In Asia, the construction of HSR station areas is often used as one of the critical factors in the construction of new towns. The HSR station is an essential catalyst for urban transformation in the new era. The success or failure of the development of HSR station areas can directly affect whether the city or region can successfully achieve new development (Zou et al., 2016).

FIGURE 2
The Study on the spatial distribution of HSR stations. Note: The original map (No. GS (2019)1686) was from the China National Natural Resources Standard Map Service website (http://bzdt.ch.mnr.gov.cn/). The authors mapped the spatial distribution of HSR stations based on it.

Commercial and business land space in HSR station areas has grown (Willigers and van Wee, 2011; Soria Caceres, 2018). Wang et al. (2014) have found that the station area development of the Beijing-Shanghai line is much greater than that of the Wuhan-Guangzhou line, and the proportion of commercial-type land use is also higher. According to the gravity model, distance affects the strength of commercial exchange. That is, the HSR shortens the time between cities, increases commercial activities, and expands the scope of the market. Beckerich et al. (2019) have argued that types of business and commerce differ between central and peripheral HSR stations. Companies in the peripheral HSR station areas want to be adjacent to the area's industrial bases, while companies in the central HSR station areas want to find more customers. Other scholars have shown that by promoting new construction or renewal of station areas, the HSR strengthens the public space attributes of station areas and enhances commercial and business activities in station areas (Halbert, 2004; Yin et al., 2015).

A consensus has been formed on the distribution characteristics of the HSR station area. It is generally believed that the first circle is mainly for distributing transportation services and business functions; the second is mainly for business-commercial and cultural entertainment; the third is mainly for residential, R&D, and other functions. However, scholars differ significantly in defining the scope of impact of HSR stations depending on different study perspectives and purposes. Lin. (2011) has shown that the HSR station impact area is the one accessible by a 20-min walk (about 1500 m) through a study of the walking endurance time of HSR passengers. Some other literature introduced the 2 km radius' scope around the HSR station as the core impact area (Zhao and Chen, 2015; Cao et al., 2020). To verify the model's validity, we estimated the model according to different circle ranges. Specifically, each HSR station area was divided into 500 m units for sensitivity tests with different distance (1500 m, 2000 m, 2500 m, 3000 m) thresholds.

2.3 Thrust of this study

As shown above, many studies have investigated the impact role of HSR in regions, cities, and station areas, mainly focusing on the impact of HSR on transportation, economy, and industry. Some research results in the station area have mainly addressed traffic accessibility, land use, housing prices, and business siting. The literature lacks a quantitative assessment of the commercial and business impact of the HSR operation on the station areas. Studying the business-commercial agglomeration effects in HSR station areas can provide an innovative and practical perspective to explain the impact of the HSR on station area development. We used POI data to evaluate the agglomeration effect of the HSR operation and to explore the differences between commercial and business characteristics in different circles.

3 Data and methodology

3.1 Study area

According to the "Medium-long-Term Railway Network Plan," the HSR is defined as a railroad system operating at a speed of over 200 km per hour. Since the HSR operation started, its ridership has progressively increased, with an average annual growth of 61.8% from 2008 to 2019 (Figure 1). The proportion of HSR ridership in railroad ridership also increased yearly to 70.7% of 2019 (http://www.china-railway.com.cn). The HSR ridership provides support for the developmental construction of station areas. Taking into account the difficulty of access to the data, we empirically investigated the business-commercial agglomeration effects of HSR station areas in China by using the panel data of 110 HSR stations from 2012 to 2017. Stations are mainly distributed along the high-speed railway lines of Chengdu-Chongqing, Nanning-Anqing, Hefei-Fuzhou, Xi'an-Chengdu, Naning-Guangzhou, Xiamen-Shenzhen, Shendan-Dandong, and some others (Figure 2).

3.2 Data and variables

The business-commercial agglomeration effects are the most basic and vital indicator of the place value in HSR station areas. Traditional data is mainly used to obtain business and commercial information by mapping site attributes through satellite maps. In short, it is more difficult to obtain data directly from the Natural Resources Bureau (due to security concerns). Mapping the land information of HSR station areas by hand drawing is enormous. Results are also subject to some inaccuracies due to the differences in the mappers. Fortunately, open access to big data in recent years has provided reliable data for research. Business-commercial agglomeration index (BCAI) is mainly reflected by the corresponding POI density of HSR station areas. POI data is typical of big geographic data, using location information to represent entity geographic attributes. POI information mainly includes latitude-longitude coordinates, names, types, address information, etc.

The data processing process is as follows. Firstly, we collected the city POI dataset from 2012 to 2017 (http://sdsp.ecnu.edu.cn/) and removed the data outside the 3 km buffer zone in HSR station areas (Shen et al., 2014; Wang and Gu, 2019; Deng et al., 2020; Wang et al., 2022). Secondly, we used ArcGIS software to extract the annual POI data of high-speed railway station areas. From a buffer of 1500 m, a dataset of HSR station areas was created for every 500 m increase. Finally, this study was to assess the changes in the BCAI that occurred before and after the HSR operation started. Therefore, we filtered the data from the HSR station area datasets for the types of catering services, shopping services, accommodation services, car sales, business residences, corporate enterprises, and financial and insurance services. These seven types of POI data measured the BCAI. The formula is as follows.

$$\boldsymbol{BCAI} = \boldsymbol{ln}\left\{\sum_{i=1}^{3}\left(\frac{\boldsymbol{N_i}}{\boldsymbol{S}}\right) + \sum_{j=1}^{4}\left(\frac{\boldsymbol{N_j}}{\boldsymbol{S}}\right)\right\} \quad (1)$$

where $BCAI$ is the business and commercial agglomeration index. N_i and N_j represent the number of POI for elements i and j of the station area. i stands for business residence, corporate enterprise, and financial and insurance services. j represents catering service, shopping service, accommodation service, and car sales. S represents the area of the HSR station area.

$$\boldsymbol{BAI} = \ln\sum_{i=1}^{3}\left(\frac{\boldsymbol{N_i}}{\boldsymbol{S}}\right) \quad (2)$$

Where BAI is the business agglomeration index. N_i represents the number of POI for element i of the station area. i stands for business residence, corporate enterprise, and financial and insurance services. S represents the area of the HSR station area.

$$\boldsymbol{CAI} = \ln\sum_{j=1}^{4}\left(\frac{\boldsymbol{N_j}}{\boldsymbol{S}}\right) \quad (3)$$

where CAI is the commercial agglomeration index. N_j represents the number of POI for element j of the station area. j represents food service, shopping service, accommodation service, and car sales. S represents the area of the HSR station area.

In general, the business and commercial agglomeration effects of the HSR station areas may be influenced by various factors. In addition to the BAI and the CAI, we collected the

TABLE 2 Definitions and units of variables.

Variable	Variable type	Description	Unit
BCAI_1500M	Explained variable	Business-commercial agglomeration index within 1500 m of HSR stations	pcs/km^2
BAI_1500M	Explained variable	Business agglomeration index within 1500 m of HSR stations	pcs/km^2
CAI_1500M	Explained variable	Commercial agglomeration index within 1500 m of HSR stations	pcs/km^2
POST_HSR	Dummy variable	1 for the operation of high-speed rail, 0 otherwise	—
POP	Urban economic and social development variable	Permanent population	10^4 persons
GDP2	Urban economic and social development variable	Secondary industry as percentage to GDP	—
GDP3	Urban economic and social development variable	Tertiary industry as percentage to GDP	—
AVE_INVESTMENT	Urban economic and social development variable	Real estate development investment per capita completed	10^4 yuan (per person)
ENTERPRISE	Urban economic and social development variable	Number of Industrial Enterprises	pcs
EMPLOYMENT	Urban economic and social development variable	Persons employed in urban units at year-end	10^4
AVE_WAGE	Urban economic and social development variable	Average Wage of Employed Staff and Workers	10^4 yuan (per person)
AVE_ROAD	Urban economic and social development variable	Urban road area per capita	10^4 m^2 (per person)

Note: *BCAI_1500M*, *BCAI_2000M*, *BCAI_2500M*, and *BCAI_3000M* denote the effect of different spatial distances respectively.

TABLE 3 Summary statistics of variables.

Variable	Mean	St. D.	Min	25%	50%	75%	Max
BCAI_1500M	2.34	2.25	−1.26	0.44	2.46	4.06	7.07
BAI_1500M	1.16	2.01	−1.96	−0.35	1.11	2.80	5.82
CAI_1500M	1.76	2.53	−1.96	−0.57	1.81	3.78	6.74
POST_HSR	53%	—	0	—	—	—	1
POP	561.63	544.96	39.24	254	384.34	724.01	3358.01
GDP2	47.76	8.5	19.76	43.05	47.38	52.7	73.44
GDP3	42.65	10.23	20.93	35.25	40.93	50.22	77.49
AVE_INVESTMENT	1.06	1.01	0.04	0.33	0.77	1.48	7.98
ENTERPRISE	1709.96	1558.8	21	583	1161	2207	7669
EMPLOYMENT	104.98	157.97	7.8	25.08	44.47	109.06	986.87
AVE_WAGE	5.38	1.37	2.61	4.37	5.34	6.21	10.15
AVE_ROAD	6.32	6.34	0.46	2.13	5.09	8.66	54.35

economic and social development indicators of the cities having the HSR as variables. These variables included urban resident population, the share of secondary and tertiary industries in GDP, real estate investment per capita, number of industrial enterprises, number of employed persons, average wages, and urban road area per capita. The data on urban economic and social development were obtained from China City Statistical Yearbook. The HSR construction data came from the National Railway Administration of the People's Republic of China (http://www.nra.gov.cn/), China State Railway Group Co., Ltd. (http://www.china-railway.com.cn/), and China Railway 12,306 website (https://www.12306.cn/index/). The high-speed trains in our study were those named with C, D, and G as the first letter. The latitude and longitude data of HSR stations were obtained through the API interface of Gaode Map (https://lbs.amap.com/tools/picker). Table 2 summarizes the definitions and units of the variables in this study, and Table 3 shows the descriptive statistics for all variables.

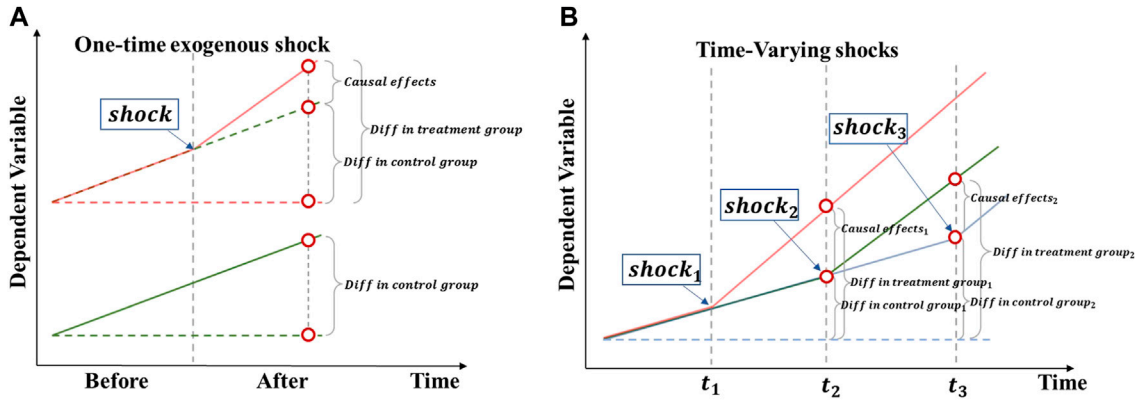

FIGURE 3
The graphical illustration of the traditional DID model and the multi-period DID model. **(A)** The traditional DID model. **(B)** The multi-period DID model.

3.3 Methodology

The natural experiment evaluation method, typically such as the DID model, can effectively identify causality and address the endogeneity of omitted variables (Zhang et al., 2020b; Yang et al., 2022). The DID model effectively identifies policy or exogenous shocks (e.g., HSR operation start) under the premise of controlling for other factors. The model can remove the time effect and separate the policy treatment effect. Therefore, the DID model is now commonly used in studies on the impact of the HSR operation on urban development. Figure 3 explains the basic ideas and differences between the traditional DID model and the multi-period DID model in diagrammatic language.

The different opening dates of the 110 HSR stations do not comply with the traditional DID requirement of the same policy implementation time point. To accurately assess the commercial and business impact of the HSR operation, we used a multi-period DID model to measure the time-averaged effects of different policy implementations. In the DID model, samples were divided into treatment and control groups. The control group provided a counterfactual analysis. However, this paper does not have a control group utterly untouched by the policy intervention, meaning that all sample areas began the HSR operation at different times. When we calculated the treatment effects, samples without the HSR were used as a control group for those already having the HSR. The model was established for time-fixed effects and urban-fixed effects.

$$BCAI_1500M_{i,t} = \gamma_0 + \gamma_1 \times POST_HSR + \sum \theta_{i,t} X_{i,t} + \lambda_t + \mu_i + \varepsilon_{i,t} \quad (4)$$

where $BCAI_1500M_{i,t}$ represents the standard agglomeration index of both business and commerce. $POST_HSR$ indicates a dummy variable for whether the sample areas run the HSR, and takes the value of one when the HSR is operational, and 0 otherwise. γ_1 is the interaction term coefficient, which is the main parameter of primary concern. We expected it to be significantly positive, indicating that the HSR operation has boosted the concentration of business and commerce in the station areas. i and t denote city and time, respectively. μ_i is an urban effect that does not vary over time and is used to control for unobserved characteristics of business and commerce that affect the entire city. λ_t is a time effect that does not change with individuals and is used to explain trends in business and commercial changes that follow time. Since other factors may influence the explanatory variables, we included a set of control variables ($X_{i,t}$) in the model. $\varepsilon_{i,t}$ is the error term.

$$BAI_1500M_{i,t} = \alpha_0 + \alpha_1 \times POST_HSR + \sum \theta_{i,t} X_{i,t} + \lambda_t + \mu_i + \varepsilon_{i,t} \quad (5)$$

where $BAI_1500M_{i,t}$ represents the business agglomeration index. $POST_HSR$ indicates a dummy variable for whether sample areas run the HSR and takes the value of one when the HSR is operational, and 0 otherwise. α_1 is the business agglomeration effect's regression coefficient and is the primary concern parameter.

$$CAI_1500M_{i,t} = \beta_0 + \beta_1 \times POST_HSR + \sum \theta_{i,t} X_{i,t} + \lambda_t + \mu_i + \varepsilon_{i,t} \quad (6)$$

where $CAI_1500M_{i,t}$ represents the commercial agglomeration index. $POST_HSR$ indicates a dummy variable for whether the sample areas run the HSR and takes the value of one when HSR is operational, and 0 otherwise. β_1 is the commercial agglomeration effect's regression coefficient and is the primary concern parameter.

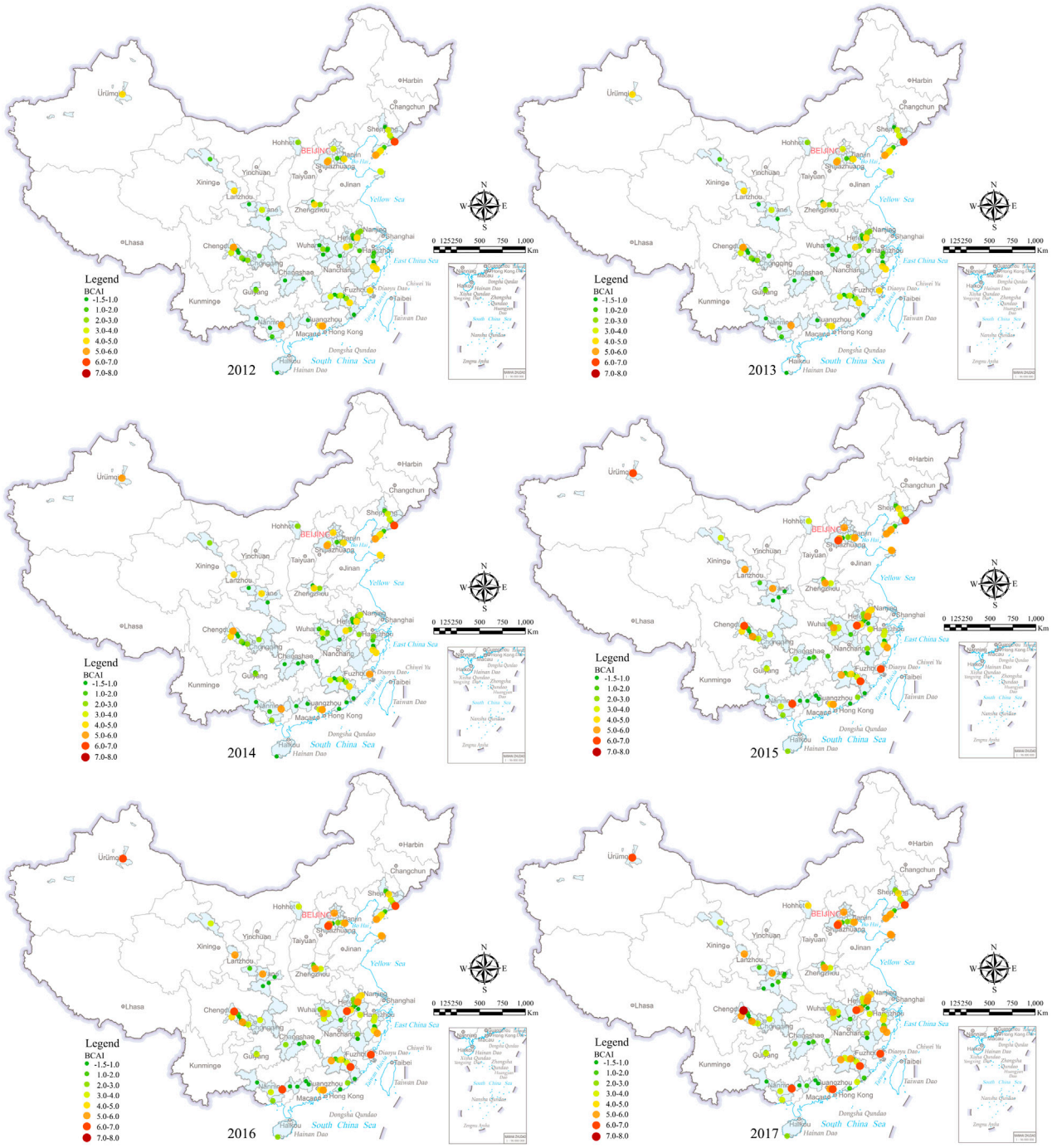

FIGURE 4
The spatial distribution of the BCAI in HSR station areas from 2012 to 2017.

4 The characteristics of the business-commercial agglomeration in HSR station areas

We sorted out the business and commercial POI data for all HSR station areas and then compared the BCAI for different years for analysis. Figure 4 illustrates the spatial distribution of the BCAI in HSR station areas from 2012 to 2017. First, the business and commerce in HSR station areas have changed considerably. Before the HSR operation, business and commercial development was low, and even some samples presented extremely low levels. Stations with high BCAI are

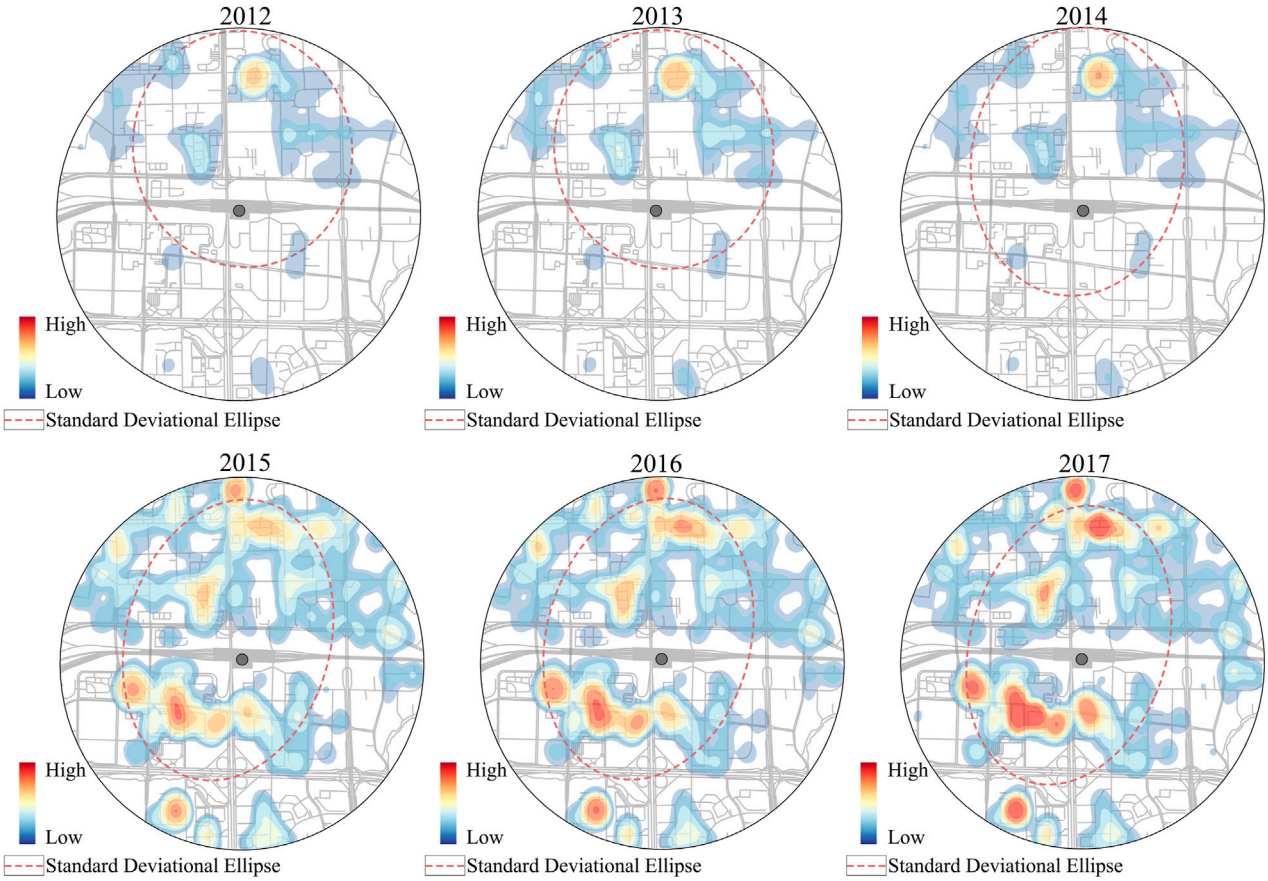

FIGURE 5
Typical case, chengdu south station business and commercial space distribution diagram.

mainly located in the eastern coastal region, most of which were upgraded to HSR stations. Many new HSR station areas were idle before the HSR operation, with much-undeveloped land to use. After the HSR started operation, the BCAI in HSR station areas grew faster. HSR stations in provincial cities have better infrastructure for rapid business and commercial development, such as Chengdu, Zhengzhou, Wuhan, Lanzhou, and other cities.

The BCAI varies significantly from one HSR station area to another. The spatial distribution results show heterogeneity in the growth of the BCAI in station areas. The BCAI in the eastern region was growing faster than that in the western and central regions, such as Yiwu Station, Nanning East Station, and Ma'anshan East Station, whose business and commercial growth rate reached 40%–60%. In addition, BCAI growth rates are higher for HSR stations closer to the city center in large cities than that for those in suburban or distant suburban areas. For example, the average growth rate of the BCAI at Chengdu South Station after the HSR operation in 2015 was 23.2% (Figure 5). The reason for this is that the excellent location of the city's south station provided favorable conditions for the rapid growth of the BCAI. Chengdu South Station is located 5.8 km from the traditional Chengdu city center and 2.7 km from the new city center (the Financial City). The HSR, as a catalytic point, has dramatically stimulated business and commercial development in the station areas.

Additionally, the spatial sectors of HSR station areas show considerable differences. For the development direction vertical to the HSR line, the business and commerce in the sectors with the direction close to the city center or the original built-up area of the city tends to develop better, and the business and commerce in sectors closer to the city center have a relatively balanced development. There is no significant difference in land value due to the slight difference in transport conditions between the two sides of the zone. The analysis based on the standard deviation ellipse can further illustrate the sector development pattern. For example, the center of the standard deviation ellipse of Chengdu South Station from 2012 to 2014 was located on the station's south side. From 2015 to 2017, the southern sector improved, and the center of the standard deviation ellipse started to move southward. Before the

TABLE 4 Baseline results.

Variable	Model 4: BCAI_1500 M		Model 5: BAI_1500 M		Model 6: CAI_1500 M	
	Coef.	t-statistic	Coef.	t-statistic	Coef.	t-statistic
POST_HSR	0.283***	3.060	0.213***	2.960	0.290**	2.300
lnPOP	0.175	0.670	−0.304	−1.420	0.390	0.940
lnGDP2	0.744	1.350	−0.160	−0.220	1.225*	1.670
lnGDP3	1.510**	2.330	0.176	0.230	2.009**	2.050
lnAVE_INVESTMENT	0.143	0.910	−0.023	−0.250	0.181	0.730
lnENTERPRISE	0.499**	2.350	0.532***	3.020	0.365	1.230
lnEMPLOYMENT	0.163**	2.060	0.084	0.970	0.332**	2.400
lnAVE_WAGE	0.611	1.520	0.209	0.650	1.196*	1.770
lnAVE_ROAD	−0.209	−1.520	−0.287**	−2.390	−0.298*	−1.780
Constant	−16.175***	−3.130	−0.434	-0.070	−27.047***	−3.310
City Fixed Effect	YES	YES	YES			
Year Fixed Effect	YES	YES	YES			
Observations	660	660	660	660	660	660

Note: *$p < 0.1$, **$p < 0.05$, ***$p < 0.01$.

HSR operation, the BCAI was low, mainly distributed in 1000–1500 m. With the HSR operation, the BCAI proliferates in the 500–1000 m range. The overall spatial evolution of the station area shows three stages: the slow development period, the rapid growth period, and the stable period. It indicates that during the evolution of business and commerce in HSR station areas, the HSR agglomeration effect has promoted changes in the functional distribution, spatial structure, and business composition in station areas.

In summary, the role of transportation infrastructure in the relative attractiveness to corporate businesses, catering, shopping, and accommodations is often considered critical. The HSR operation has reduced people's travel time costs and promoted population mobility. Low costs mean that people can overcome the spatial barriers between cities, which expands urban economic activity. As areas that benefit most directly from improved accessibility, HSR station areas tend to have agglomeration effects. The HSR station areas generate more significant attraction for catering services, shopping services, accommodation services, car sales, business residences, corporate enterprises, and financial and insurance services.

5 Results

5.1 Baseline results

We established three benchmark regression models by using the BCAI, the BAI, and the CAI as dependent variables to explain the "net effect" of the HSR operation on the business and commercial agglomeration in HSR station areas. Table 4 reports the regression results of three double difference models controlling for "city fixed effects" and "time fixed effects". First, the BCAI and the BAI are significant at 1%, the CAI is significant at 5%, and the POST_HSR coefficient estimates are all positive. The results show that the HSR operation has agglomeration effects on business and commerce in station areas. This finding is consistent with our expectations. Second, Model one shows that the BCAI improves by 28.3% after the HSR operation, which proves that HSR stations have a significant spillover effect. In other words, the HSR stations make accessibility greatly enhanced, creating favorable conditions for the development and construction of station areas. Finally, Model 2 and Model 3 indicate that the agglomeration effect of commerce is greater than that of business, with the BAI increase of 21.3% and the CAI increase of 29% after the HSR operation. It is because most customers demand commercial facilities, and business customers often favor business facilities. The high ridership creates significant commercial opportunities and development potential for the station areas.

The baseline regression model also shows that the share of the tertiary sector, the number of urban industrial enterprises, and the number of employees significantly contributes to the BCAE in general. The results of the control variables are consistent with our expectations and the previous studies on the influence on the development and construction of station areas. In models 4 and 6, the estimated coefficient of the tertiary sector share (lnGDP3) is significantly positive. In model 6, the estimated coefficient of the share of the secondary sector (lnGDP2) is significantly positive. It indicates that regions

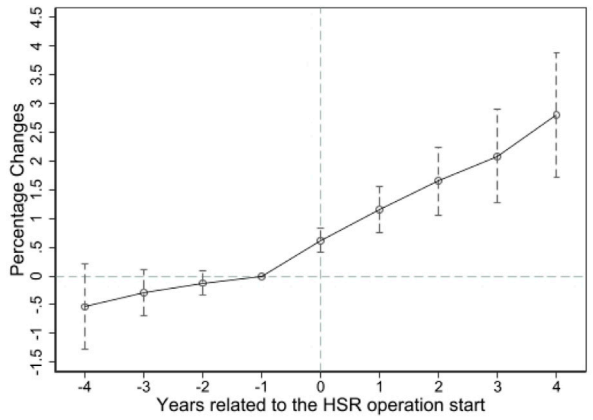

FIGURE 6
The diagram of the parallel trend test.

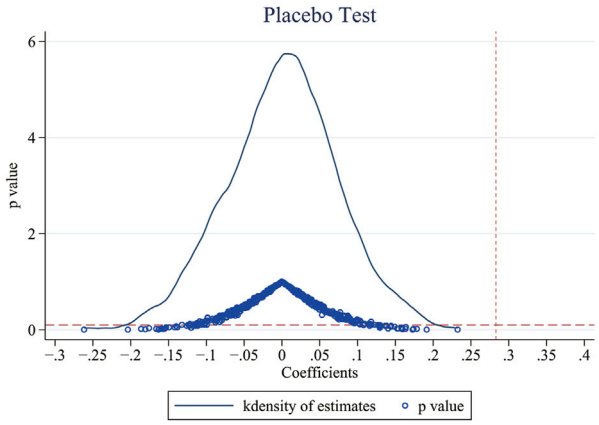

FIGURE 7
The kernel density distribution of the estimated coefficients.

with a larger share of the tertiary sector will have a higher BCAI based on the control for other variables. One possible reason is that cities with a high share of tertiary industries can provide more labor and production factors, generating more demand for transportation. With the improved accessibility of HSR stations, the population and elements in the city move to the station areas, promoting the construction of commercial development. The estimated coefficients of the number of urban industrial enterprises (lnENTERPRISE) in models 4 and 5 are significantly positive, indicating that cities with more employment opportunities have tremendous potential for development. Enterprises often look to expand revenue by reducing costs, and the HSR operation reduces time and transportation costs. That increases the opportunities for enterprises to be located in the station area, which in turn promotes the development of station areas. The estimated coefficients of urban employment (lnEMPLOYMENT) in models 4 and 6 are significantly positive, indicating that urban employment promotes business development in station areas. During the development of HSR station areas, the labor force begins to transfer to the station areas, which can support the pooling and development of resources.

5.2 Parallel trend test and dynamic effects

With the HSR operation, business and commerce in station areas have been developed to a certain extent. To test how the impact of HSR operation on the BCAI changes over time and the equilibrium trend assumption of the baseline regression model, we included dummy variables before and after the HSR operation started, respectively. In our study, the equilibrium trend test was divided into the test before the HSR operation and the test after the HSR operation started. If all the policy impact effects before the HSR operation show no correlation, the experimental and control groups will have the same trend. If the policy impact after the HSR operation start is relevant, it shows that the HSR operation makes the experimental and the control groups will have different trends. Therefore, we chose the base period 1 year before the HSR operation and established the following regression model.

$$\begin{aligned} \boldsymbol{BCAI_1500M_{i,t}} &= \boldsymbol{\beta_1} + \boldsymbol{\beta_2} \times \boldsymbol{POST_{HSR}}^{-2} + \boldsymbol{\beta_3} \times \boldsymbol{POST_{HSR}}^{-3} \\ &\quad + \boldsymbol{\beta_4} \times \boldsymbol{POST_{HSR}}^{-4} \\ &\quad + \boldsymbol{\alpha_0} \times \boldsymbol{POST_{HSR}}^{0} + \boldsymbol{\alpha_1} \times \boldsymbol{POST_{HSR}}^{1} \\ &\quad + \boldsymbol{\alpha_2} \times \boldsymbol{POST_{HSR}}^{2} + \boldsymbol{\alpha_3} \times \boldsymbol{POST_{HSR}}^{3} \\ &\quad + \boldsymbol{\alpha_4} \times \boldsymbol{POST_{HSR}}^{4} + \sum \boldsymbol{\theta_{i,t} X_{i,t}} + \boldsymbol{\lambda_t} + \boldsymbol{\mu_i} + \boldsymbol{\varepsilon_{i,t}} \end{aligned} \tag{7}$$

In the model, $POST_{HSR}{}^{-2}$, $POST_{HSR}{}^{-3}$, and $POST_{HSR}{}^{-4}$ denote the time dummy variables of 2, 3, and 4 years and above before the operation of HSR, respectively (1 year before the operation as the base period). $POST_{HSR}{}^{0}$, $POST_{HSR}{}^{1}$, $POST_{HSR}{}^{2}$, $POST_{HSR}{}^{3}$, and $POST_{HSR}{}^{4}$ portray the time dummy variables for the year of HSR operation start, 1 year, 2 years, 3 years, and 4 years and more after the start, respectively. α_0、 α_1, α_2, α_3, α_4, β_2, β_3, and β_4 are our estimated coefficients of interest, reflecting the dynamic effect of the HSR operation on the BACI.

The model regression results show that the estimated coefficients of the dummy variables are all insignificant before the HSR operation, and the estimated coefficients of the dummy variables are all positively significant after the HSR operation start. Our model satisfies the parallel trend assumption. Figure 6 depicts the estimated coefficients of our interest in Model 7, indicating that the BACI shows an increasing trend year by year after the HSR operation start. Interestingly, 4 years after the HSR operation started, the BACI has grown much faster than that in previous years. Overall, the HSR operation has a significant impact on the BACI.

TABLE 5 Robustness check for change in the distance threshold.

Variable	BCAI_1500M		BCAI_2000M		BCAI_2500M		BCAI_3000M	
	Coef.	t-statistic	Coef.	t-statistic	Coef.	t-statistic	Coef.	t-statistic
POST_HSR	0.283***	3.060	0.146*	1.760	0.140*	1.690	0.137*	1.730
lnPOP	0.175	0.670	0.073	0.310	0.152	0.690	0.105	0.480
lnGDP2	0.744	1.350	1.328**	2.250	1.586***	2.970	1.215**	2.430
lnGDP3	1.510**	2.330	1.559**	2.390	2.182***	3.320	1.722***	2.800
lnAVE_INVESTMENT	0.143	0.910	0.270*	1.870	0.234*	1.700	0.242*	1.770
lnENTERPRISE	0.499**	2.350	0.301*	1.780	0.294	1.630	0.245	1.500
lnEMPLOYMENT	0.163**	2.060	0.052	0.730	0.076	1.310	0.082	1.310
lnAVE_WAGE	0.611	1.520	0.374	1.030	0.396	1.140	0.414	1.140
lnAVE_ROAD	-0.209	−1.520	−0.255	−1.640	−0.261*	−1.930	−0.294**	−2.000
Constant	−16.175***	−3.130	−14.448**	−2.600	−17.404***	−3.200	−13.380**	−2.570
City Fixed Effect	YES	YES	YES	YES				
Year Fixed Effect	YES	YES	YES	YES				
Observations	660	660	660	660	660	660	660	660

Note: *$p < 0.1$, **$p < 0.05$, ***$p < 0.01$.

5.3 Placebo test

The purpose of the placebo test is for the presence of chance in the results of the DID model. We verified that the estimates were not biased by conducting a placebo test on the main results of this paper by randomly selecting HSR stations from samples. If the estimated coefficient of the regression of the placebo treatment variable remains significantly positive, it indicates that the original model is biased. That is, changes in the explanatory variables may be influenced by other factors. In contrast, the regression coefficients for the placebo treatment variables do not deviate significantly from zero if there is no significant omitted variable bias. We have repeated the above experiment 500 times to avoid small probability events. Figure 7 portrays the kernel density distribution of the estimated coefficients of the 500 placebo treatment variables and the distribution of corresponding *p*-values. The placebo test results indicate that the means of the estimated coefficients are around 0, and the vast majority of *p*-values are greater than 0.1 (horizontal red dashed line). Also, the true estimate of the DID model (vertical dashed line) is significantly larger than the maximum value of 500 random estimates. Overall, the model estimation results are not coincidental, and there is no serious bias due to omitted variables.

5.4 Robustness test

Some may argue that the current model evaluation results are based on the 1500 m station-area impact range, and the station-area impact range threshold setting may influence the true results. Thus, we decided to develop the model robustness test further. The level of urban economic development affects the agglomeration effects of HSR station areas and may lead to differences in the influence areas of different HSR station areas. As a result, we have conducted sensitivity tests with different thresholds to test the robustness of the DID model. Specifically, we re-estimated the impact of HSR operation on the BACI by establishing a model with thresholds for the impact range of different HSR station areas. Table 5 shows the model results for the 1500 m, 2000 m, 2500 m, and 3000 m thresholds. All the estimated coefficients are significantly positive, which corroborates the robustness of the model. Interestingly, the estimates for the different thresholds are 0.283, 0.146, 0.140, and 0.137, respectively. The BACI is lower as the distance from the HSR station becomes further, which also verifies the circle effect in HSR station areas.

6 Conclusion and discussion

The HSR in China is in a rapid construction phase, and many cities are looking to construct new cities with the enhancement of the HSR stations. The proportion of business passenger travel is increasing yearly, and the demand for “station as the final destination” is becoming more and more prominent. Therefore, the HSR station area has become one of the key development objectives in urban planning. Previous studies have focused extensively on the macro impact of the HSR operation on regional economies, urban industries, and tourism development, whereas only a few were conducted at the station level. Furthermore, how to accurately understand and evaluate the effect of the HSR operation and reveal the development rules of HSR station

areas is of great significance. The study presumed that the operation of HSR can bring business and commercial agglomeration effects in station areas. Given this, we collected POI data, China City Statistical Yearbook data, and the HSR station operation data from 2012-2017 and developed several DID models to verify our hypotheses. We measured business and commercial development in 110 HSR station areas in China. The empirical findings provide strong evidence and support the arguments that we have presented. The parallel trend, placebo, and robustness tests confirmed the results' plausibility and validity. Current studies tend to focus on the impact of the HSR operation on regional economic integration, urban industrial carbon emissions, tourism development, and station area economies. We specifically analyzed the agglomeration effects of the HSR operation on business and commerce in station areas and revealed the spatial distribution patterns of business and commerce land use across different buffers, which enriches the existing literature.

The development and construction of HSR station areas is an academic and fundamental practical issue. Many countries, such as Japan, Spain, Germany, and South Korea, have already built large-scale HSRs. Although the HSR has undergone extensive construction in China, the operation cycle is relatively short. Some scholars have pointed out that a mature HSR station area generally requires 25–30 years of development. Therefore, our findings are instructive for the HSR station areas under construction and for future HSR station areas. Specifically, the HSR operation has increased the BCAI, the BAI, and the CAI by 28.3%, 29%, and 21.3%, respectively. In other words, the HSR operation has significant business-commercial agglomeration effects in the station area, and the agglomeration effect of business is significantly more than that of commerce. These findings provide recommendations for practitioners and researchers to design and plan station areas. However, the purpose of this article is not to provide a detailed interpretation of the case but to highlight an innovative perspective and research framework. Our research results have specific theoretical and practical significance for the construction of HSR station areas and can provide a reference for the formulating future urban planning-related policies and government decisions.

We must acknowledge that this study is not without limitations. First, the HSR operation is not only beneficial to economic development and land development in station areas. Some other benefits and costs warrant further exploration. Second, we have mainly used POI data and China City Statistical Yearbook data. The recent emergence of new big data, such as Baidu heat data, cell phone signaling data, Tencent location data, and Weibo check-in data, has enabled us to analyze HSR station areas more comprehensively. Future research may leverage new types of big data and use more advanced machine learning techniques to explore the complex development dynamics of the HSR station areas.

Data availability statement

The raw data supporting the conclusion of this article will be made available by the authors, without undue reservation.

Author contributions

All authors contributed to the conception and design of the study. PL, XC, and ML: Methodology and models. PL conceptualization, supervision, and writing—original draft. XC: Questing for the funding support. ML, TY, and BW: Collecting the research data. TY and BW: Validation and writing.

Funding

This study was supported by the National Natural Science Foundation of China (No. U20A20330) and the National Natural Science Foundation of China (No. 51778530).

Conflict of interest

The authors declare that the research was conducted in the absence of any commercial or financial relationships that could be construed as a potential conflict of interest.

Publisher's note

All claims expressed in this article are solely those of the authors and do not necessarily represent those of their affiliated organizations, or those of the publisher, the editors and the reviewers. Any product that may be evaluated in this article, or claim that may be made by its manufacturer, is not guaranteed or endorsed by the publisher.

References

Albalate, D., and Fageda, X. (2016). High speed rail and tourism: Empirical evidence from Spain. *Transp. Res. Part A Policy Pract.* 85, 174–185. doi:10.1016/j.tra.2016.01.009

Beckerich, C., Benoit, S., and Delaplace, M. (2019). Are the reasons for companies to locate around central versus peripheral high-speed rail stations different? The cases of reims central station and champagne-ardenne station. *Eur. Plan. Stud.* 27 (3), 574–594. doi:10.1080/09654313.2019.1567111

Bertolini, L. (2000). Planning in the borderless city: A conceptualisation and an application to the case of station area redevelopment. *Town Plan. Rev.* 71 (4), 455–475. doi:10.3828/tpr.71.4.2883q121q1671185

Bhatta, S. D., and Drennan, M. P. (2003). The economic benefits of public investment in transportation. *J. Plan. Educ. Res.* 22 (3), 288–296. doi:10.1177/0739456x02250317

Campos, J., and de Rus, G. (2009). Some stylized facts about high-speed rail: A review of HSR experiences around the world. *Transp. Policy* 16 (1), 19–28. doi:10.1016/j.tranpol.2009.02.008

Cao, Y., Yu, L., and Li, S. (2020). Spatial evolution of high-speed railway station areas and planning response. *City Plan. Rev.* 44 (11), 88–96.

Carteni, A., Pariota, L., and Henke, I. (2017). Hedonic value of high-speed rail services: Quantitative analysis of the students' domestic tourist attractiveness of the main Italian cities. *Transp. Res. Part A Policy Pract.* 100, 348–365. doi:10.1016/j.tra.2017.04.018

Chang, Z., Zheng, L., Yang, T., and Long, F. (2022). High-speed rail, new town development, and the spatial mismatch of land leases in China. *Land Use Policy* 115, 106014. doi:10.1016/j.landusepol.2022.106014

Chen, Z., and Haynes, K. E. (2017). Impact of high-speed rail on regional economic disparity in China. *J. Transp. Geogr.* 65, 80–91. doi:10.1016/j.jtrangeo.2017.08.003

Chen, Z., Xue, J., Rose, A. Z., and Haynes, K. E. (2016). The impact of high-speed rail investment on economic and environmental change in China: A dynamic cge analysis. *Transp. Res. Part A Policy Pract.* 92, 232–245. doi:10.1016/j.tra.2016.08.006

Cui, X., Liang, P., and Fan, L. (2021). Study on the influence mechanism and planning strategy of population agglomeration effect in High-Speed railway station area based on the cases of beijing, shanghai, chongqing and chengdu. *J. Hum. Settlements West China* 36 (4), 19–28. doi:10.13791/j.cnki.hsfwest.20210403

Cummings, C., and Mahmassani, H. (2022). Does intercity rail station placement matter? Expansion of the node-place model to identify station location impacts on amtrak ridership. *J. Transp. Geogr.* 99, 103278. doi:10.1016/j.jtrangeo.2022.103278

Dai, X., Xu, M., and Wang, N. (2018). The industrial impact of the Beijing-Shanghai high-speed rail. *TRAVEL Behav. Soc.* 12, 23–29. doi:10.1016/j.tbs.2018.03.002

De Wijs, L., Witte, P., and Geertman, S. (2016). How smart is smart? Theoretical and empirical considerations on implementing smart city objectives – A case study of Dutch railway station areas. *Innovation Eur. J. Soc. Sci. Res.* 29 (4), 424–441. doi:10.1080/13511610.2016.1201758

Deng, T., Gan, C., Perl, A., and Wang, D. (2020). What caused differential impacts on high-speed railway station area development? Evidence from global nighttime light data. *Cities* 97, 102568. doi:10.1016/j.cities.2019.102568

Deng, T., Wang, D., Yang, Y., and Yang, H. (2019). Shrinking cities in growing China: Did high speed rail further aggravate urban shrinkage? *Cities* 86, 210–219. doi:10.1016/j.cities.2018.09.017

Diao, M. (2018). Does growth follow the rail? The potential impact of high-speed rail on the economic geography of China. *Transp. Res. Part A Policy Pract.* 113, 279–290. doi:10.1016/j.tra.2018.04.024

Dong, L., Du, R., Kahn, M., Ratti, C., and Zheng, S. (2021). Ghost cities" versus boom towns: Do China's high-speed rail new towns thrive? *Regional Sci. Urban Econ.* 89, 103682. doi:10.1016/j.regsciurbeco.2021.103682

Dong, X., Zheng, S., and Kahn, M. E. (2020). The role of transportation speed in facilitating high skilled teamwork across cities. *J. Urban Econ.* 115, 103212. doi:10.1016/j.jue.2019.103212

Du, J., Druta, O., and van Wesemael, P. (2021). Place quality in high-speed rail station areas: Concept definition. *J. Transp. Land Use* 14 (1), 1165–1186. doi:10.5198/jtlu.2021.1820

Garmendia, M., de Urena, J. M., Ribalaygua, C., Leal, J., and Coronado, J. M. (2008). Urban residential development in isolated small cities that are partially integrated in metropolitan areas by High Speed Train. *Eur. Urban Regional Stud.* 15 (3), 249–264. doi:10.1177/0969776408090415

Garmendia, M., Romero, V., Maria de Urena, J., Maria Coronado, J., and Vickerman, R. (2012). High-speed rail opportunities around metropolitan regions: Madrid and london. *J. Infrastruct. Syst.* 18 (4), 305–313. doi:10.1061/(asce)is.1943-555x.0000104

Geng, B., Bao, H., and Liang, Y. (2015). A study of the effect of a high-speed rail station on spatial variations in housing price based on the hedonic model. *Habitat Int.* 49, 333–339. doi:10.1016/j.habitatint.2015.06.005

Givoni, M. (2006). Development and impact of the modern high-speed train: A review. *Transp. Rev.* 26 (5), 593–611. doi:10.1080/01441640600589319

Gong, W., and Li, V. J. (2022). The territorial impact of high-speed rail on urban land development. *Cities* 125, 103581. doi:10.1016/j.cities.2022.103581

Gui, W., Zhang, X., and Wang, A. (2021). Research on spatial planning evaluation of Beijing Shanghai high speed railway station based on node-place model. *J. Intelligent Fuzzy Syst.* 40 (1), 733–743. doi:10.3233/jifs-200712

Halbert, L. (2004). The decentralization of intrametropolitan business services in the Paris region: Patterns, interpretation, consequences. *Econ. Geogr.* 80 (4), 381–404. doi:10.1111/j.1944-8287.2004.tb00244.x

He, Q., He, W., Song, Y., Wu, J., Yin, C., and Mou, Y. (2018). The impact of urban growth patterns on urban vitality in newly built-up areas based on an association rules analysis using geographical 'big data. *Land Use Policy* 78, 726–738. doi:10.1016/j.landusepol.2018.07.020

Hickman, R., Garcia, M. M., Arnd, M., and Peixoto, L. F. G. (2021). Euston station redevelopment: Regeneration or gentrification? *J. Transp. Geogr.* 90, 102923. doi:10.1016/j.jtrangeo.2020.102923

Hong, J., Chu, Z., and Wang, Q. (2011). Transport infrastructure and regional economic growth: Evidence from China. *Transportation* 38 (5), 737–752. doi:10.1007/s11116-011-9349-6

Jia, S., Zhou, C., and Qin, C. (2017). No difference in effect of high-speed rail on regional economic growth based on match effect perspective? *Transp. Res. Part A Policy Pract.* 106, 144–157. doi:10.1016/j.tra.2017.08.011

Jiang, C., Wang, K., Wang, Q., and Yang, H. (2022). The impact of high-speed rail competition on airline on-time performance. *Transp. Res. Part B Methodol.* 161, 109–127. doi:10.1016/j.trb.2022.05.004

Jin, S., Yang, J., Wang, E., and Liu, J. (2020). The influence of high-speed rail on ice-snow tourism in northeastern China. *Tour. Manag.* 78, 104070. doi:10.1016/j.tourman.2019.104070

Lakshmanan, T. R. (2011). The broader economic consequences of transport infrastructure investments. *J. Transp. Geogr.* 19 (1), 1–12. doi:10.1016/j.jtrangeo.2010.01.001

Li, Y., Yang, B., and Cui, Q. (2019). The effects of high-speed rail on air passenger transport in China. *Appl. Econ. Lett.* 26 (9), 745–749. doi:10.1080/13504851.2018.1494798

Lin, C. (2011). Research of impact factors of High-speed railways Hub area development in China. *Urban Plan. Int.* 26 (6), 72–77.

Long, F., Zheng, L., and Song, Z. (2018). High-speed rail and urban expansion: An empirical study using a time series of nighttime light satellite data in China. *J. Transp. Geogr.* 72, 106–118. doi:10.1016/j.jtrangeo.2018.08.011

Masson, S., and Petiot, R. (2009). Can the high speed rail reinforce tourism attractiveness? The case of the high speed rail between perpignan (France) and barcelona (Spain). *Technovation* 29 (9), 611–617. doi:10.1016/j.technovation.2009.05.013

Meng, X., Lin, S., and Zhu, X. (2018). The resource redistribution effect of high-speed rail stations on the economic growth of neighbouring regions: Evidence from China. *Transp. Policy* 68, 178–191. doi:10.1016/j.tranpol.2018.05.006

Mota, C., Lopez, M. A., and Martinez-Rodrigo, A. (2017). A mathematical study of accessibility and cohesion degree in a High-Speed rail station connected to an urban bus transport network. *Open Phys.* 15 (1), 160–174. doi:10.1515/phys-2017-0017

Ortega, E., Lopez, E., and Monzon, A. (2012). Territorial cohesion impacts of high-speed rail at different planning levels. *J. Transp. Geogr.* 24, 130–141. doi:10.1016/j.jtrangeo.2011.10.008

Ribalaygua, C., and Perez-Del-Cano, S. (2019). Assessing spatial planning strategy in high-speed rail station areas in Spain (1992-2018): Towards a sustainable model. *Eur. Plan. Stud.* 27 (3), 595–617. doi:10.1080/09654313.2018.1564189

Sahu, S., and Verma, A. (2022). Quantifying wider economic impacts of high-speed connectivity and accessibility: The case of the Karnataka high-speed rail. *Transp. Res. Part A Policy Pract.* 158, 141–155. doi:10.1016/j.tra.2022.02.011

Shao, S., Tian, Z., and Yang, L. (2017). High speed rail and urban service industry agglomeration: Evidence from China's Yangtze River Delta region. *J. Transp. Geogr.* 64, 174–183. doi:10.1016/j.jtrangeo.2017.08.019

Shaw, S., Fang, Z., Lu, S., and Tao, R. (2014). Impacts of high speed rail on railroad network accessibility in China. *J. Transp. Geogr.* 40, 112–122. doi:10.1016/j.jtrangeo.2014.03.010

Shen, Y., de Abreu e Silva, J., and Martinez, L. M. (2014). Assessing high-speed rail's impacts on land cover change in large urban areas based on spatial mixed logit methods: A case study of madrid atocha railway station from 1990 to 2006. *J. Transp. Geogr.* 41, 184–196. doi:10.1016/j.jtrangeo.2014.09.007

Soria Caceres, C. H. (2018). Nuevos usos espaciales en las estaciones ferroviarias de alta velocidad/New space use of high speed railway stations. *GEOGRAFARES* 26, 86–105. doi:10.7147/geo26.21000

Tian, M., Li, T., Ye, X., Zhao, H., and Meng, X. (2021). The impact of high-speed rail on service industry agglomeration in peripheral cities. *Transp. Res. Part D Transp. Environ.* 93, 102745. doi:10.1016/j.trd.2021.102745

Vickerman, R. (1997). High-speed rail in Europe: Experience and issues for future development. *Ann. Regional Sci.* 31 (1), 21–38. doi:10.1007/s001680050037

Wang, C., Meng, W., and Hou, X. (2020). The impact of high-speed rails on urban economy: An investigation using night lighting data of Chinese cities. *Res. Transp. Econ.* 80, 100819. doi:10.1016/j.retrec.2020.100819

Wang, L., and Gu, H. (2019). *Studies on China's high-speed rail new town planning and development*. Singapore: Springer.

Wang, L., Wang, C., Chen, C., and Gu, H. (2014). Development and planning of the surrounding area of High-Speed rail stations: Based on empirical study of Beijing-Shanghai line. *Urban Plan. Forum* 4, 31–37.

Wang, L., Yuan, F., and Duan, X. (2018). How high-speed rail service development influenced commercial land market dynamics: A case study of jiangsu province, China. *J. Transp. Geogr.* 72, 248–257. doi:10.1016/j.jtrangeo.2018.09.010

Wang, L., Zheng, W., He, S., and Wei, S. (2022). Assessing urban vitality and its determinants in high-speed rail station areas in the Yangtze River Delta, China. *J. Transp. Land Use* 15 (1), 333–354. doi:10.5198/jtlu.2022.2010

Wang, S., Mo, H., Lv, H., Xu, P., and Yin, H. (2021). Industrial structure of high-speed railway station areas under the influence of location: Empirical evidences from POI data. *Acta Geogr. Sin.* 76 (8), 2016–2031.

Wenner, F., and Thierstein, A. (2022). High speed rail as urban generator? An analysis of land use change around European stations. *Eur. Plan. Stud.* 30 (2), 227–250. doi:10.1080/09654313.2021.1946485

Westin, J., and Kageson, P. (2012). Can high speed rail offset its embedded emissions? *Transp. Res. Part D Transp. Environ.* 17 (1), 1–7. doi:10.1016/j.trd.2011.09.006

Willigers, J., and van Wee, B. (2011). High-speed rail and office location choices. A stated choice experiment for The Netherlands. *J. Transp. Geogr.* 19 (4), 745–754. doi:10.1016/j.jtrangeo.2010.09.002

Xu, W. A., and Huang, Y. (2019). The correlation between HSR construction and economic development - empirical study of Chinese cities. *Transp. Res. Part A Policy Pract.* 126, 24–36. doi:10.1016/j.tra.2019.05.017

Xu, W., Zhou, J., Yang, L., and Li, L. (2018). The implications of high-speed rail for Chinese cities: Connectivity and accessibility. *Transp. Res. Part A Policy Pract.* 116, 308–326. doi:10.1016/j.tra.2018.06.023

Yang, J., Yang, R., Chen, M., Su, C. J., Zhi, Y., and Xi, J. (2021). Effects of rural revitalization on rural tourism. *J. Hosp. Tour. Manag.* 47, 35–45. doi:10.1016/j.jhtm.2021.02.008

Yang, L., Chau, K. W., Szeto, W. Y., Cui, X., and Wang, X. (2020a). Accessibility to transit, by transit, and property prices: Spatially varying relationships. *Transp. Res. Part D Transp. Environ.* 85, 102387. doi:10.1016/j.trd.2020.102387

Yang, L., Chen, Y., Xu, N., Zhao, R., Chau, K. W., and Hong, S. (2020b). Place-varying impacts of urban rail transit on property prices in Shenzhen, China: Insights for value capture. *Sustain. Cities Soc.* 58, 102140. doi:10.1016/j.scs.2020.102140

Yang, L., Chu, X., Gou, Z., Yang, H., Lu, Y., and Huang, W. (2020c). Accessibility and proximity effects of bus rapid transit on housing prices: Heterogeneity across price quantiles and space. *J. Transp. Geogr.* 88, 102850. doi:10.1016/j.jtrangeo.2020.102850

Yang, L., Liang, Y., He, B., Lu, Y., and Gou, Z. (2022). COVID-19 effects on property markets: The pandemic decreases the implicit price of metro accessibility. *Tunn. Undergr. Space Technol.* 125, 104528. doi:10.1016/j.tust.2022.104528

Yang, L., Zhou, J., Shyr, O. F., and Huo, D. D. (2019). Does bus accessibility affect property prices? *Cities* 84, 56–65. doi:10.1016/j.cities.2018.07.005

Yin, M., Bertolini, L., and Duan, J. (2015). The effects of the high-speed railway on urban development: International experience and potential implications for China. *Prog. Plan.* 98, 1–52. doi:10.1016/j.progress.2013.11.001

Yu, N., de Jong, M., Storm, S., and Mi, J. (2013). Spatial spillover effects of transport infrastructure: Evidence from Chinese regions. *J. Transp. Geogr.* 28, 56–66. doi:10.1016/j.jtrangeo.2012.10.009

Zhang, X., Wu, W., Zhou, Z., and Yuan, L. (2020a). Geographic proximity, information flows and corporate innovation: Evidence from the high-speed rail construction in China. *Pacific-Basin Finance J.* 61, 101342. doi:10.1016/j.pacfin.2020.101342

Zhang, X., Zhang, W., and Lee, P. T. (2020b). Importance rankings of nodes in the China railway express network under the belt and road initiative. *Transp. Res. Part A Policy Pract.* 139, 134–147. doi:10.1016/j.tra.2020.07.003

Zhao, Q., and Chen, G. (2015). Influence of hsr station location on the development of surrounding areas: A case study of beijing-shanghai hsr and wuhan-guangzhou hsr. *City Plan. Rev.* 39 (7), 50–55.

Zheng, L., Long, F., Chang, Z., and Ye, J. (2019). Ghost town or city of hope? The spatial spillover effects of high-speed railway stations in China. *Transp. Policy* 81, 230–241. doi:10.1016/j.tranpol.2019.07.005

Zhou, X., Chen, S., and Zhang, H. (2022a). Travel on the road: Does China's high-speed rail promote local tourism? *Environ. Sci. Pollut. Res. Int.* 2022, 1–14. doi:10.1007/s11356-022-22114-9

Zhou, Y., Zhang, L., and Chiaradia, A. J. F. (2022b). Estimating wider economic impacts of transport infrastructure Investment: Evidence from accessibility disparity in Hong Kong. *Transp. Res. Part A Policy Pract.* 162, 220–235. doi:10.1016/j.tra.2022.05.014

Zhu, Y., Diao, M., and Fu, G. (2016). The evolution of accessibility surface of China in the high-speed-rail era. *Environ. Plan. A* 48 (11), 2108–2111. doi:10.1177/0308518x15619935

Zou, Z., He, Z., and Chen, H. (2016). Evaluating the development potential of areas surrounding high-speed railway stations:an empirical analysis for Wuhan-Guangzhou passenger corridor line. *J. Rail Way Sci. Eng.* 13 (11), 2125–2132. doi:10.19713/j.cnki.43-1423/u.2016.11.004

frontiers | Frontiers in Ecology and Evolution

TYPE Original Research
PUBLISHED 28 November 2022
DOI 10.3389/fevo.2022.1031678

Check for updates

OPEN ACCESS

EDITED BY
Jun Yang,
Northeastern University, China

REVIEWED BY
Fang Qiu,
The University of Texas at Dallas, United States
Decheng Zhou,
Nanjing University of Information Science and Technology, China
Zhi Qiao,
Tianjin University, China

*CORRESPONDENCE
Ziqi Chen
chenzq0227@163.com

SPECIALTY SECTION
This article was submitted to Environmental Informatics and Remote Sensing, a section of the journal Frontiers in Ecology and Evolution

RECEIVED 30 August 2022
ACCEPTED 01 November 2022
PUBLISHED 28 November 2022

CITATION
Hou G, Zhang H, Liu Z, Chen Z and Cao Y (2022) Historical reconstruction of aquatic vegetation of typical lakes in Northeast China based on an improved CA-Markov model. *Front. Ecol. Evol.* 10:1031678. doi: 10.3389/fevo.2022.1031678

COPYRIGHT
© 2022 Hou, Zhang, Liu, Chen and Cao. This is an open-access article distributed under the terms of the Creative Commons Attribution License (CC BY). The use, distribution or reproduction in other forums is permitted, provided the original author(s) and the copyright owner(s) are credited and that the original publication in this journal is cited, in accordance with accepted academic practice. No use, distribution or reproduction is permitted which does not comply with these terms.

Historical reconstruction of aquatic vegetation of typical lakes in Northeast China based on an improved CA-Markov model

Guanglei Hou[1], Haobin Zhang[1,2], Zhaoli Liu[1], Ziqi Chen[1,2]* and Yakun Cao[1]

[1]Northeast Institute of Geography and Agriculture, Chinese Academy of Sciences (CAS), Changchun, China, [2]College of Geo-Exploration Science and Technology, Jilin University, Changchun, China

Aquatic vegetation is an important marker of the change in the lake ecosystem. It plays an important supporting role in the lake ecosystem, and its abundance and cover changes affect the ecosystem balance. Collecting accurate long-term distribution data on aquatic vegetation can help monitor the change in the lake ecosystem, thereby providing scientific support for efforts to maintain the balance of the ecosystem. This work aimed to establish an improved CA-Markov model to reconstruct historical potential distribution of aquatic vegetation in the two typical lakes (Xingkai Lake and Hulun Lake) in Northeast China during 1950s to 1960s. We firstly analyzed remote sensing data on the spatial distribution of aquatic vegetation data in two lakes in six periods from the 1970 to 2015. Then, we built a transfer probability matrix for changes in hydrothermal conditions (temperature and precipitation) based on similar periods, and we designed suitability images using the spatial frequency and temporal continuity of the constraints. Finally, we established an improved CA-Markov model based on the transfer probability matrix and suitability images to reconstruct the potential distributions of aquatic vegetation in the two northeastern lakes during the 1950s and 1960s. The results showed the areas of aquatic vegetation in the 1950s and 1960s were 102.37 km^2 and 100.7 km^2 for Xingkai Lake and 90.81 km^2 and 88.15 km^2 for Hulun Lake, respectively. Compared with the traditional CA-Markov model, the overall accuracy of the improved model increased by

more than 50%, which proved the improved CA-Markov model can be used to effectively reconstruct the historical potential distribution of aquatic vegetation. This study provides an accurate methodology for simulating the potential historical distributions of aquatic vegetation to enrich the study of the historical evolution of lake ecosystem.

KEYWORDS

aquatic vegetation, improved CA-Markov model, transfer probability matrix, suitability images, historical reconstruction

Introduction

Lakes are an important foundation for economic development and ecological security in China. Northern Lakes account for 37% of the total lake area in China, providing significant strategic support services for ensuring the socioeconomic development and ecological security of China (Bu et al., 2013; Wang et al., 2015; Dai et al., 2021). Aquatic vegetation—including submerged vegetation, floating leaf vegetation, and emergent vegetation—can clarify water, decrease the rate of nutrient cycling, suppress waves, improve water quality, and provide food and habitats for many aquatic animals (Jeppesen et al., 1998; Horppila and Nurminen, 2003; Orth et al., 2006). Aquatic plants are also important regulators of the evolution and balance of the lake ecosystem, and they play an important role in maintaining lake ecosystems and waterfowl and phytoplankton communities (Roijackers et al., 2004; Bilton et al., 2006).

Since the 1950s, numerous studies have demonstrated that lake ecosystems have undergone a severe decline due to the combined effects of climate change and human activities (Sand-Jensen et al., 2000; Moss et al., 2011). Similarly, there has been a significant decline in aquatic vegetation of lakes; this has further exacerbated the loss of ecosystem services, resulting in severe ecological problems for lake ecosystems. Therefore, quantifying the historical distributions of aquatic vegetation—including its abundance and dynamics—not only helps reveal the response of lake ecosystems to climate change but also supports the conservation of lake biodiversity (Körner and Nicklisch, 2002; Liira et al., 2010; Kolada et al., 2014; Qing et al., 2020).

At present, there are two main ways to obtain information on the historical spatial distribution of aquatic vegetation in lakes. (1) *Historical field survey records*: Field surveys and monitoring of aquatic vegetation provide important original information on the distribution of aquatic vegetation, according to the literature. However, studies of the distribution, abundance, and dynamics of aquatic vegetation in lakes have focused on a few lakes in a small geographical area (Sand-Jensen et al., 2000; Körner and Nicklisch, 2002) and have covered a short historical period of field surveying data, mostly after the 1980s. In addition, most field surveys have recorded distributions in the form of points, rather than continuous spatial data, limiting the application of aquatic vegetation data in the geospatial model. (2) *Historical remote sensing image interpretation*: Remote sensing technologies have become the most effective methods for identifying and monitoring the historical spatial patterns of aquatic vegetation due to their ability to support large-scale, abundant, long-term observation based on spectral indices (Fornes et al., 2006; Laba et al., 2010; Luo et al., 2017; Song et al., 2019). Nevertheless, the earliest satellite image data date back to the 1970s (i.e., Landsat MSS satellite data), making it impossible to obtain information on the spatial distribution of aquatic vegetation in lakes before the 1970s. Considering the low levels of disturbance in the lakes caused by human activities during the 1950s and 1960s, aquatic vegetation was mainly affected by climate change. Therefore, the spatial distribution and dynamics of aquatic vegetation can be used to predict the response of aquatic vegetation to natural environmental change. However, no datasets on the distribution and changes in aquatic vegetation were obtained using the aforementioned methods during the 1950s and 1960s, which hinders a comprehensive and systematic assessment of aquatic vegetation for lakes.

The CA-Markov model, which incorporates the theories of Markov chain and cellular automata (Sang et al., 2011), is widely used to simulate the land surface type (Zhou et al., 2020; Fu et al., 2022). In addition to predicting temporal and spatial patterns of future changes in the land surface type, it also reconstructs historical land surface characteristics (Mondal et al., 2016; He et al., 2022). However, as changes in the land surface type are often affected by many factors, the common CA-Markov model cannot always accurately simulate historical surface type changes. In recent research, the integration of spatial information and decision conditions used in multi-criteria evaluations has demonstrated a powerful capability to control the comprehensive effects of many factors. The essence of this technique lies in the production of suitability images of land surface type to improve the predictive ability of the CA-Markov model (Getachew et al., 2021). The collection of suitability images is scored by each influential

factor, producing constraint conditions for the CA model (Ahmed, 2011). The factors used in the suitability images cover sociometric elements and environmental dimensions, and the images translate this information into manageable information or measurable parameters. The selection of factors is usually based on ranking results from the analytic hierarchy process (AHP) and principle component analysis (Lee and Chan, 2008), as well as scores assigned based on experience and literature reviews (Zavadskas and Antucheviciene, 2007). However, previous studies have faced a serious problem: the factor selection and suitability score assignment were unrelated to the land surface change for the given model. Therefore, establishing appropriate suitability images to improve the CA-Markov model is crucial for the high-accuracy historical reconstruction of land surface features.

As the land surface system has the same land cover (Yang et al., 2019), aquatic vegetation and the water body can be deemed two lake cover types in the lake ecosystem. In this study, we developed a novel calculation method for the previous transfer probability matrix based on the similarity of change in annual average temperature and the annual precipitation of different periods. Also, we developed a new collection of suitability images based on the constraints of the spatial frequency of occurrence and the temporal recency effect in the simulation process to improve the accuracy of the CA-Markov model. Then, by combining the transfer probability matrix and suitability images, we built an improved CA-Markov model to reconstruct the historical distribution of aquatic vegetation in Xingkai Lake and Hulun Lake during the 1950s and 1960s. We evaluated the model accuracy by comparing the results of the common CA-Markov model simulation and the remote sensing interpretation; the model simulation error rate (MSER) was used to evaluate model improvement. The research results provide scientific data for lake ecosystem research and lake responses to climate change while enriching the method of simulating and reconstructing aquatic vegetation in historical periods.

Materials and methods

Study area

Xingkai Lake and Hulun Lake, located in Northeast China, were selected to reconstruct the historical potential distribution of aquatic vegetation using the improved CA-Markov model (**Figure 1**) and are located in a temperate humid and a semi-humid monsoon climate zone, respectively. Precipitation is mainly concentrated in summer and autumn, with abundant water in the lakes during the information period, followed by a long freezing period in winter, with a low water level in the lakes. According to the literature, aquatic vegetation is rich in both lakes and has undergone dramatic changes in the past decades (Yuan et al., 2018; Mao et al., 2022).

Xingkai Lake is the largest freshwater lake in northeastern Asia. It is located on the border between China and Russia, with the geographical coordinates of 131°58'30"∼133°07'30 "E and 45°01'00"∼45°34'30 "N. Xingkai Lake is divided into big Xingkai Lake and small Xingkai Lake by Chinese people, with a total surface area of 4,190 km^2, an average water depth of 4.5 m, and a maximum depth of 10 m. The aquatic vegetation is mainly concentrated in small Xingkai Lake.

Hulun Lake is located in the western part of the Hulunbuir grassland, with geographical coordinates of 117°00'10"∼117°41'40 "E and 48°30'40"∼49°20'40 "N and a total area of 2,339 km^2. A total of four rivers empty into Hulun Lake, including the Kherlen, Hailar, Halaha, and Orxon rivers. The aquatic vegetation is concentrated in the estuary.

Because of the different sources of lake water replenishment, the two lakes exhibit different levels of variability in water storage. In addition, both the lakes are located in a mid-latitude region, where the lake ecosystems are sensitive to global climate change, and both lakes have experienced minimal human disturbance during the 1950s and 1960s. Therefore, the lakes are excellent research areas for exploring the historical distribution and changes in aquatic vegetation in relation to the response of lake ecosystems to climate change.

Data and processing

Landsat images of the two lakes during the 1970–2015 (1970s, 1980s, 1990s, 2000, 2010, and 2015) were downloaded from the Geospatial Data Cloud[1]. The images were processed by radiometric and geometric calibration (**Table 1**). Then, three indices (NDVI, SAVI, and NDWI), whose thresholds were determined by the Otsu algorithm, were calculated to gain 200 training samples of aquatic vegetation for each lake based on the decision tree model. A random forest model was adopted to obtain the distribution of aquatic vegetation using 150 training samples for each lake from imagery for the six periods. The remaining 50 samples were used to verify the model, and the total accuracy was over 85%.

The datasets acquired from the remote sensing imagery served as the basis for the reconstruction of the historical spatial distribution of aquatic vegetation in the 1950s and 1960s. Given the demarcation of the lake extent for reconstruction by the CA-Markov model, we downloaded Zhang Guoqing's 1960–2015 lake boundary datasets in China (Zhang et al., 2019) to restrict the extent of the simulation of aquatic vegetation. In order to analyze climatic changes in different historical periods, we downloaded meteorological datasets on the nearest meteorological stations of the two lakes from the National Meteorological Center[2]. Then, the annual average temperature and annual precipitation were calculated from the 1950 to 2021.

1 http://www.gscloud.cn/
2 http://data.cma.cn/

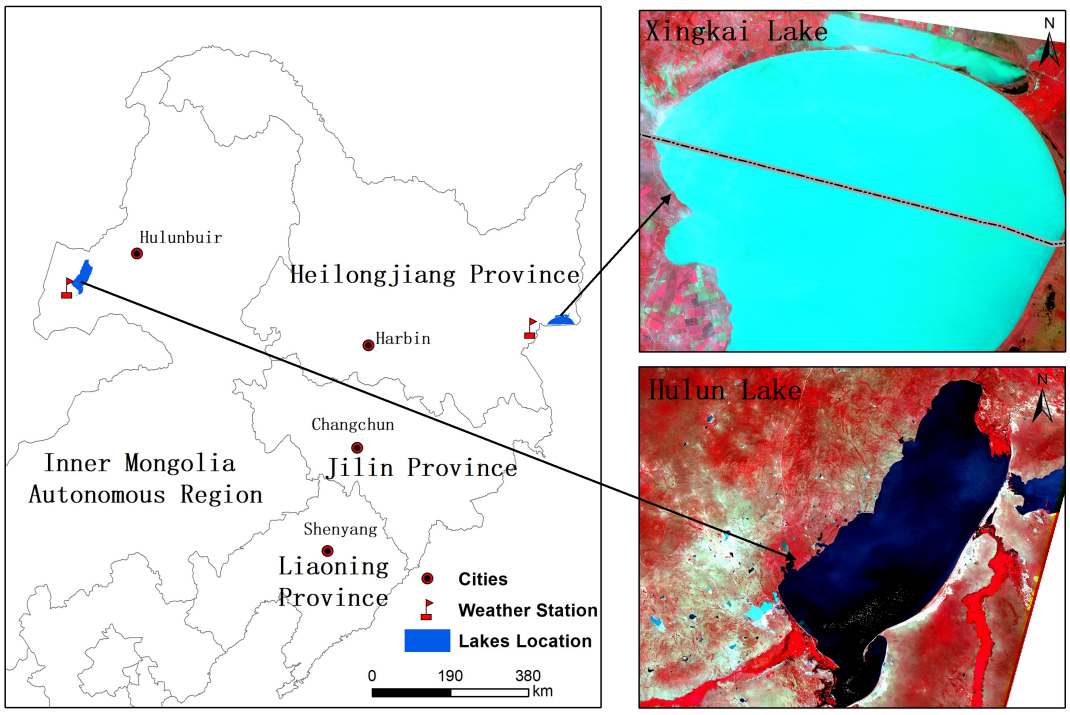

FIGURE 1
Location of lakes in the study area of Northeast China.

Methods

The CA-Markov model combines the ability of the CA model to simulate complex spatial changes with the advantages of the Markov model for temporal prediction (Yang et al., 2016, 2019). By adding continuous spatial distribution elements to Markov chains and using multiple constraints and limiting factors, the model can achieve spatial predictions for future features and accurately reconstruct historical states. This allows for the high-accuracy simulation of ecosystem changes.

The Markov chain model is a quantitative description of transfer states using the area transfer matrix and the area probability transfer matrix between the feature states in different periods. Its mathematical equation is as follows:

$$S_{ij} = \begin{bmatrix} s_{11} & s_{12} & \cdots & s_{1n} \\ s_{21} & s_{22} & & s_{2n} \\ \vdots & & \ddots & \vdots \\ s_{n1} & s_{n2} & \cdots & s_{nn} \end{bmatrix}$$

$$P_{ij} = \begin{bmatrix} p_{11} & p_{12} & \cdots & p_{1n} \\ p_{21} & p_{22} & & p_{2n} \\ \vdots & & \ddots & \vdots \\ p_{n1} & p_{n2} & \cdots & p_{nn} \end{bmatrix}$$

where i, j = 1,2,...,n represent the land-use types before and after transfer, S_{ij} is the land-use area transfer matrix, and P_{ij} is the land-use area transfer probability matrix.

The cellular automata (CA) model is a discontinuous spatiotemporal dynamics model characterized by discrete time, space, and state (Fu et al., 2018). Each cell in the CA system has discrete states, and each raster cell corresponds to a cell whose transformation rules are localized in time and space. These local rules interact to form a dynamic evolutionary system expressed by the following mathematical formula:

$$S_{t+1} = f(S_t, N)$$

where $S_{(t+1)}$ is the state of the tuple at the previous moment, S_t is the state of the tuple at the current moment, N is the tuple domain, and f is the local space tuple transfer rule.

The implementation of the CA-Markov model requires two important parameters: the transition probability matrix and suitability images. The transition probability matrix can be used to describe the transition probability of the land surface type transformation for two time intervals. The matrix is used to predict and simulate the land surface type transition areas for both future and historical periods. The suitability images are based on multiple criteria (transformation rules) that determine the state of the feature at the next moment. The prediction of spatial features is achieved computationally by adding continuous, spatially distributed features to the Markov chain using multiple constraints and limiting factors.

TABLE 1 Timelines, path, and row of Landsat imagery data.

Lakes		Parameters of landsat imagery					
Hunlun Lake	Date	1976.07.12	1986.06.17	1990.08.15	2000.09.27	2011.08.10	2015.07.27
	Path, Row	134/26	125/26	125/26	125/26	124/26	125/26
	Sensor	MSS	TM	TM	TM	ETM+	ETM+
	Satellite	Landsat2	Landsat5	Landsat5	Landsat5	Landsat7	Landsat7
	Bands	4	7	7	7	8	8
Xingkai Lake	Date	1973.07.07	1982.05.22	1990.09.03	2002.08.11	2010.08.17	2015.09.08
	Path, Row	122/29	123/28	114/28-29	114/28-29	114/28-29	114/28-29
	Sensor	MSS	MSS	TM	ETM+	ETM+	OLI
	Satellite	Landsat1	Landsat3	Landsat5	Landsat7	Landsat7	Landsat8
	Bands	4	5	7	8	8	11

TABLE 2 Impact factors of the suitability images.

Influencing factors	Factor descriptions
Spatial frequency of occurrence	If a pixel was occupied by aquatic vegetation with a higher frequency during the 1970–2015, it had a higher probability of being modeled as aquatic vegetation in the 1950s and 1960s
Temporal recency effect	If a pixel was occupied by aquatic vegetation in years closer to the 1950s and 1960s, it had a higher probability of being modeled as aquatic vegetation

Transfer probability matrix module

The transfer probability matrix is derived from the Markov chain and determines the transformation rule from the start status to the end status for the land surface types; it contains joint probabilities, which are the product of amplitude of the two states (Eberly and Carlin, 2000). It can also be considered as the transition rule for the CA model, which decides the cell number or probability of transformations between land surface types during the two periods. For the lakes, the distribution of the lake surface types (aquatic vegetation and water bodies) in the two time intervals can generate the transfer matrix of Markov probability. Considering the spatiotemporal correlation of the evolution of aquatic vegetation, more complex relationships between the changing pattern of aquatic vegetation and regional conditions were found. Moreover, the local climatic conditions directly affect the distribution and transformation probability of aquatic vegetation in the lake. Some research has shown that changes in aquatic vegetation are closely related to climate (Zhao et al., 2021), that is to say, if the change in climate conditions was similar for two periods, the transformation probability of aquatic vegetation is likely to be similar as well. For instance, assuming that the climate change scenario for 1960–1970 is similar to that for 1990–2000, we assigned similar transfer probability matrices for the two periods. Therefore, in this study, the changes in the annual average temperature and annual precipitation are selected as environmental factors to assist the Markov model for calculating the probability transfer matrix.

The dynamic evolution of aquatic vegetation is considered a transfer process. However, for the historical distribution of aquatic vegetation, reconstruction of the "possible states" was a reverse process in which past states are simulated from more recent states. To avoid the transferability of errors, we selected the aquatic vegetation in the 1970s as a baseline to simulate vegetation distribution in the 1950s and 1960s. Consequently, we used a 20-year step to simulate the spatial distribution of aquatic vegetation in lakes in the 1950s and a 10-year step to simulate the distribution in the 1960s.

Suitability image module

The probabilistic CA-Markov model is a potent simulator for predicting changes in the land surface type compared with other types of linear extrapolation models (Aaviksoo, 1993). The suitability images are based on multiple criteria (transformation rules) to determine the state of a cell at the next moment. The prediction of geomorphic elements is achieved scientifically by adding continuous, spatially distributed elements to the Markov chain using multiple limiting constraints. By incorporating the suitability images into the CA transformation rules and constraining the CA to change by itself, the defects of the cellular automata can be remedied and the simulation results can better reflect the complexity of the spatiotemporal evolution of land surface patterns.

Given the spatiotemporal succession of vegetation growth (Wang et al., 2020), the spatial occurrence frequency and temporal recency effect of aquatic vegetation growth in the historical period were selected as the two most important constraint factors to generate the suitability images. These images were then used to reconstruct the potential distribution

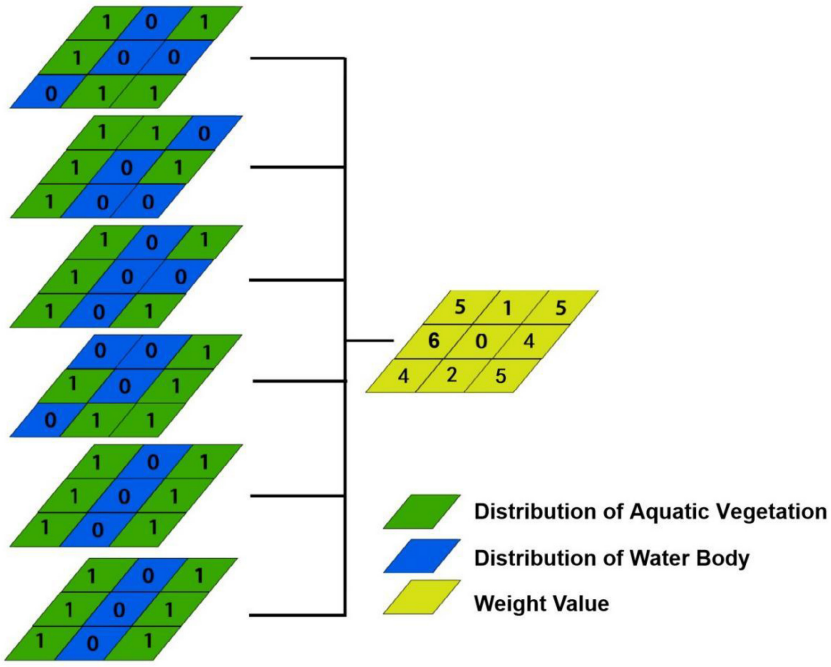

FIGURE 2
Spatial occurrence frequency weighting analysis map of aquatic vegetation.

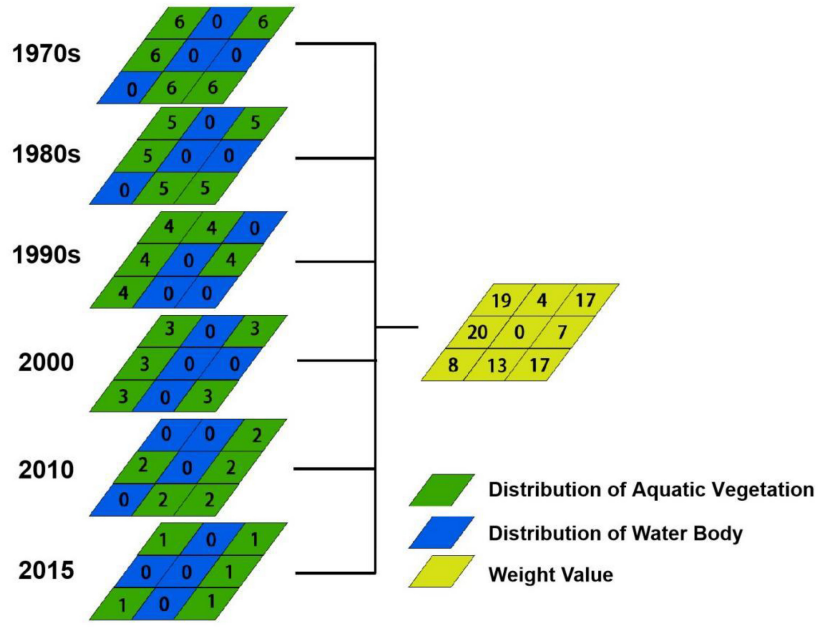

FIGURE 3
Temporal recency effect weighting analysis map of aquatic vegetation.

zones of aquatic vegetation in this study. Based on the aquatic vegetation dataset obtained from remote sensing data for six periods from 1970 to 2015, the potential distribution zones of aquatic vegetation in the 1950s and 1960s were simulated at the pixel scale using the restrictive conditions of the two suitability images. Table 2 shows the definition of the relationship between the influencing factors and aquatic vegetation for the construction of the suitability images.

Spatial frequency of occurrence

Without considering the influence of temporal succession on the simulation, we defined the pixel as the basic unit for aquatic vegetation simulation. The probability of emergence for the aquatic vegetation during the 1950s and 1960s was controlled by the spatial frequency of occurrence in the six periods (1970–2015) for each pixel. **Figure 2** shows the spatial occurrence frequency weighting analysis of aquatic vegetation. Pixels assigned a value of 1 represent aquatic vegetation, while pixels assigned a value of 0 represent a waterbody. The occurrence frequency of aquatic vegetation in the historical distribution data was superimposed to generate a judgment matrix. If the pixel value was larger in the judgment matrix, it was more likely to be simulated as aquatic vegetation. Finally, a spatial frequency weighting map of aquatic vegetation was generated (**Figure 2**).

Temporal recency effect

Given the influence of temporal succession on aquatic vegetation, there is a temporal recency effect for the simulation of aquatic vegetation. Periods closer to the simulated period were allocated a greater weight value. In this study, in the case of simulating the spatial distribution of aquatic vegetation in the 1960s, the image of 2015 was defined as the base weight, with a value of 1. The weight value increased by 1 every decade as the data approached the simulation periods. As a result, we constructed a linearly increasing weight matrix, where 2010 had a weight of 2, 2000 had a weight of 3, 1990 had a weight of 4, 1980 had a weight of 5, and 1970 had a weight of 6. If aquatic vegetation existed in multiple periods for the simulation target image pixel, the weight value was the sum of the weights of all the periods. For instance, if the input simulation pixel was aquatic vegetation in both the 1970s and 1980s, the weight was 11: the sum of weight 5 in the 1980s and weight 6 in the 1970s. Based on the temporal recency effect, pixels of the different periods were assigned differentiated weights calculated by overlay analysis. As a result, 15 different weight assignments occurred in the prediction distribution of aquatic vegetation in the 1960s. **Figure 3** shows a temporal recency effect weighting analysis map of aquatic vegetation, including the results of the weight assignments.

We normalized the weights of the spatial frequency of occurrence and the temporal recency effect and multiplied them to produce spatiotemporal restricted factor image datasets. Then, they were used to generate the transfer suitability image in the Markov process, which provided transfer rules for the reconstruction of the spatial distribution of aquatic vegetation through the CA-Markov model.

Validation of simulation accuracy

The simulation results were validated through the quantitative evaluation of the modeled results and the interpretation of remote sensing data. The kappa coefficient is an important metric for consistency testing, and it can often be used to assess the effectiveness of a measure of classification (Visser and de Nijs, 2006). Because the analysis was focused on aquatic vegetation, the lake water surface area is much larger than lake aquatic vegetation. The resulting high kappa coefficient for the waterbody reduces model accuracy. Therefore, the model simulation error rate (MSER) was used to validate the model accuracy. The calculation is as follows:

$$MSER = \left| \frac{D_o - D_s}{D_o} \right|$$

where D_o is the area of aquatic vegetation in the interpretation data and D_s is the area of aquatic vegetation in the simulation. Ideally, the value of MSER is 0, indicating that the simulated results are in agreement with the interpretation results.

In this study, a 5*5 filter was implemented in the improved CA-Markov model. This means that a rectangular space of 5*5 around a pixel was considered to have a significant influence on that the state change of the pixel (Zhao et al., 2011). The weight of each neighboring cell (i.e., pixel) was considered to have the same influence on the central cell. Since there were no spatial data on aquatic vegetation in Hulun Lake and Xingkai Lake in the 1950s and 1960s, it was difficult to validate the simulation results in these two periods. We used the improved CA-Markov model to simulate the distribution of the aquatic vegetation data in the 1990s and 1970s by 10-year steps and 20-year steps, respectively. Then, we validated the results of the simulation by comparing it with the interpretation of remote sensing data to calculate the kappa coefficient (He et al., 2020). The probability transfer matrix and the suitability image were two necessary parameters for the CA-Markov model to reconstruct the historical distribution. We considered the error transferability in order to simulate the spatial distribution of aquatic vegetation in the 1950s and 1960s, both of which were carried out based on the data from the 1970s. Moreover, the spatial distribution of aquatic vegetation in lakes in the 1950s and 1960s was reconstructed in 20-and 10-year steps, respectively. The CA-Markov model was implemented using IDRISI 17.0 software.

Results and analysis

Transfer probability matrix based on climate change consistency

The transfer probability matrix is a random matrix and is the basic quantity to characterize the Markov chain statistics,

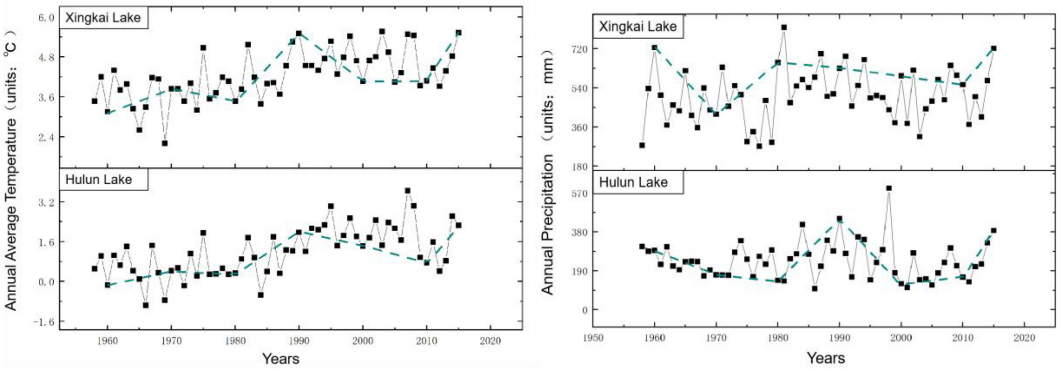

FIGURE 4
Variation trends per decade of annual average temperature **(left)** and annual precipitation data **(right)** during study periods.

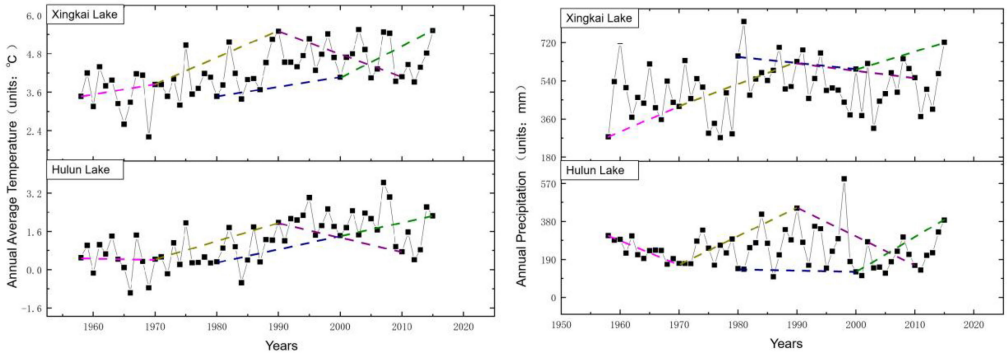

FIGURE 5
Variation trends per two decades of annual average temperature **(left)** and annual precipitation data **(right)** during study periods.

TABLE 3 Fitting equations for annual precipitation (AP) and annual average temperature (AAT) per decade.

Years	Factors	Xingkai lake	R^2	Hunlun lake	R^2
1960–1970	AP	y = −13.865x + 563.48	0.1713	y = −10.262x + 307.06	0.6599
	AAT	y = −0.0353x + 3.7399	0.0285	y = −0.0586x + 0.8353	0.0953
1971–1980	AP	y = −11.977x + 514.01	0.0637	y = 0.1776x + 227.17	0.00007
	AAT	y = 0.0105x + 3.799	0.0036	y = −0.0185x + 0.6431	0.0089
1981–1990	AP	y = −7.5564x + 630.64	0.0484	y = 15.642x + 187.7	0.1907
	AAT	y = 0.111x + 3.7441	0.0484	y = 0.0693x + 0.6246	0.0722
1991–2000	AP	y = −14.696x + 608.04	0.2035	y = -0.4624x + 273.07	0.00001
	AAT	y = 0.0063x + 4.6365	0.0021	y = −0.0049x + 2.0042	0.0007
2001–2010	AP	y = 19.998x + 399.44	0.311	y = 6.6315x + 152.63	0.0949
	AAT	y = −0.0618x + 5.0672	0.0909	y = −0.0498x + 2.2981	0.0282
2001–2010	AP	y = 77.48x + 282.2	0.7617	y = 61.87x + 71.03	0.9631
	AAT	y = 0.2499x + 3.6557	0.6528	y = 0.3157x + 0.3037	0.4405

and it represents the linkage from one spatial characteristic to another (Fu et al., 2018). As the matrix describes independent spatial characteristics, their joint probability is the product of the probability measures of the two spaces separately (Eberly and Carlin, 2000). Therefore, the change in spatial distribution of aquatic vegetation from one period to another must correlate with spatiotemporal succession.

Meanwhile, a complex relationship was found between the changing pattern of aquatic vegetation and climatic conditions, which directly affected the distribution probability

TABLE 4 Fitting equations for annual precipitation (AP) and annual average temperature (AAT) per two decades.

Years	Factors	Xingkai lake	R^2	Hunlun lake	R^2
1958–1970	AP	y = −3.1918x + 491.25	0.0111	y = −10.262x + 307.06	0.6599
	AAT	y = −0.0379x + 3.8412	0.0501	y = −0.0586x + 0.8353	0.0953
1971–1990	AP	y = 8.1737x + 432.79	0.1162	y = 5.3896x + 194.35	0.1247
	AAT	y = 0.0525x + 3.5544	0.2159	y = 0.0412x + 0.3406	0.1162
1981–2000	AP	y = −7.4126x + 635.98	0.179	y = 1.6426x + 254.88	0.0064
	AAT	y = 0.0384x + 4.11	0.1439	y = 0.0811x + 0.6405	0.337
1991–2010	AP	y = −0.6791x + 525.45	0.0016	y = −5.3572x + 286.07	0.0774
	AAT	y = −0.0027x + 4.7272	0.0009	y = 0.0811x + 0.6405	0.0007
2000–2015	AP	y = 5.6674x + 468.23	0.057	y = −0.0033x + 2.0352	0.3583
	AAT	y = −0.017x + 4.8274	0.0163	y = −0.0452x + 2.2244	0.0498

and transformation probability of aquatic vegetation in the lake. Therefore, the selection of suitable environmental factors can better simulate the dynamics of aquatic vegetation. According to related studies, there was a strong correlation between vegetation changes and meteorological factors in China, and the spatial distribution of aquatic vegetation also changed with climatic conditions. Consequently, we selected the annual average temperature and precipitation as environmental factors to assist the Markov model for calculating the probability transfer matrix.

Based on the meteorological data from the nearest weather stations around the lake during 1950–2015, the variation trends of annual average temperature and annual precipitation were analyzed at 20- and 10-year steps, respectively, to identify period with climate change trends similar to those of the 1950s and 1960s. Then, we used the Markov model to obtain the transfer probability matrix by superimposing the aquatic vegetation distribution map for those periods in the simulation reconstruction of aquatic vegetation in the 1950s and 1960s using IDRISI software. Figures 4–5 show the variation trends of annual mean temperature and annual rainfall in 20- and 10-year steps, respectively.

Considering the differences in the period of establishment of the weather stations and the period of acquiring the earliest meteorological data, we unified all the earliest meteorological data to 1958. Then, we fit the variation trends of annual mean temperature and annual rainfall in 20- and 10-year steps, respectively. Tables 3–4 show the fitted trends of temperature and precipitation for each period.

The variation trends of annual rainfall and average temperature of meteorological data of the two lakes were fitted by 10- and 20-year steps, respectively. Considering that temperature variation plays a key role in vegetation in North China, the period consistent with the temperature variation in the fitted time interval was selected as the basis for constructing the transfer probability matrix. For the simulation with a 10-year step, the variety of aquatic vegetation distribution data during 2001–2010 was selected as the calculated transfer probability matrix for the 1960–1970 fit. Uniformly, for the 20-year step, the change in aquatic vegetation distribution data from 2000 to 2015 was selected as the calculated transfer probability matrix for the 1950–1970 fit.

The reconstruction of historical data by the CA-Markov model is a reverse process that simulates past data using recent data. The calculation of the transfer probability matrix also occurs in the reverse direction. In order to simulate the distribution of aquatic vegetation in the 1960s with a 10-year step, we used the spatial distribution of aquatic vegetation from 2010 to 2000 to establish the transfer probability matrix extracted from the Markov model. Likewise, the transfer probability matrix for the 1950s with a 20-year step was established by the spatial distribution of aquatic vegetation from 2015 to 2000. The transfer probability matrices in the 1950s and 1960s were established using Markov models. Table 5 shows the parameters of transfer probability matrices in the CA-Markov model for predicting aquatic vegetation in the 1950s and 1960s.

Construction of suitability images based on spatial frequency of occurrence and temporal recency effect

Based on the spatial frequency and temporal recency effect maps discussed earlier, we obtained the suitability images for aquatic vegetation adaptation by combining the weight analysis maps. The weight analysis maps obtained in the Markov process were combined with the Collection Editor to generate the transfer suitability images, and they provided the transfer rules for the reconstruction of the spatial distribution of aquatic vegetation by the CA-Markov model. Figure 6 shows the weight maps made by the spatial frequency of occurrence and temporal recency effect in Xingkai Lake, and Figure 7 shows the suitability image of Xingkai Lake.

TABLE 5 Transfer probability matrices for predicting the 1950s and 1960s.

Transfer matrix	Transfer matrix for predicting 1960s		Transfer matrix for predicting 1950s	
	Waterbody	Aquatic vegetation	Waterbody	Aquatic vegetation
Waterbody	0.84	0.16	0.83	0.17
Aquatic Vegetation	0.51	0.49	0.41	0.59

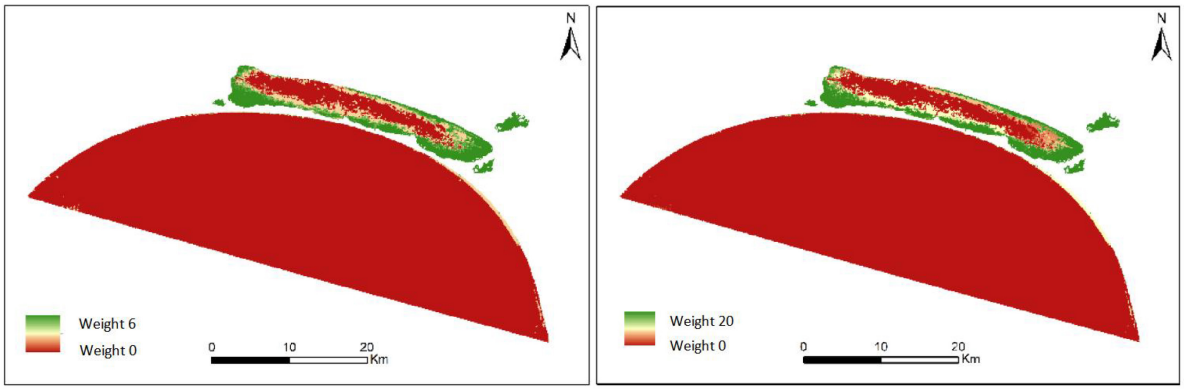

FIGURE 6
Weight analysis maps of the spatial frequency of occurrence **(left)** and temporal recency effect **(right)** in Xingkai Lake.

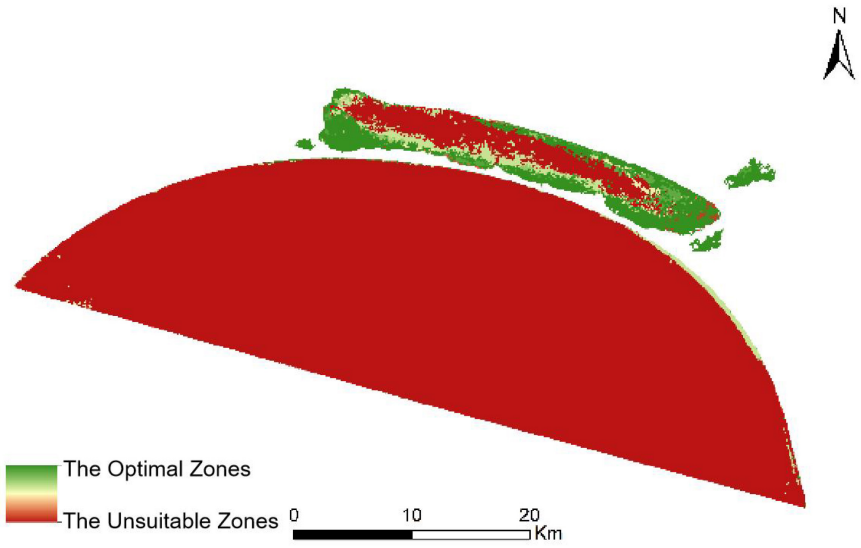

FIGURE 7
Suitability image of Xingkai Lake.

Simulation of the potential spatial distribution of aquatic vegetation in the 1950s and 1960s

Using the transfer probability matrix and suitability images, we implemented an improved CA-Markov model to reconstruct the potential spatial distribution of aquatic vegetation in the 1950s and 1960s with 20- and 10-year steps for Xingkai Lake and Hulun Lake. Figure 8 shows the spatial distribution of aquatic vegetation for the two lakes, while Table 6 shows the areas of aquatic vegetation in the lakes in the 1950s and 1960s.

The area of aquatic vegetation in Xingkai Lake was 102.37 km^2 in the 1950s, 100.70 km^2 in the 1960s, and 61.64 km^2 in the

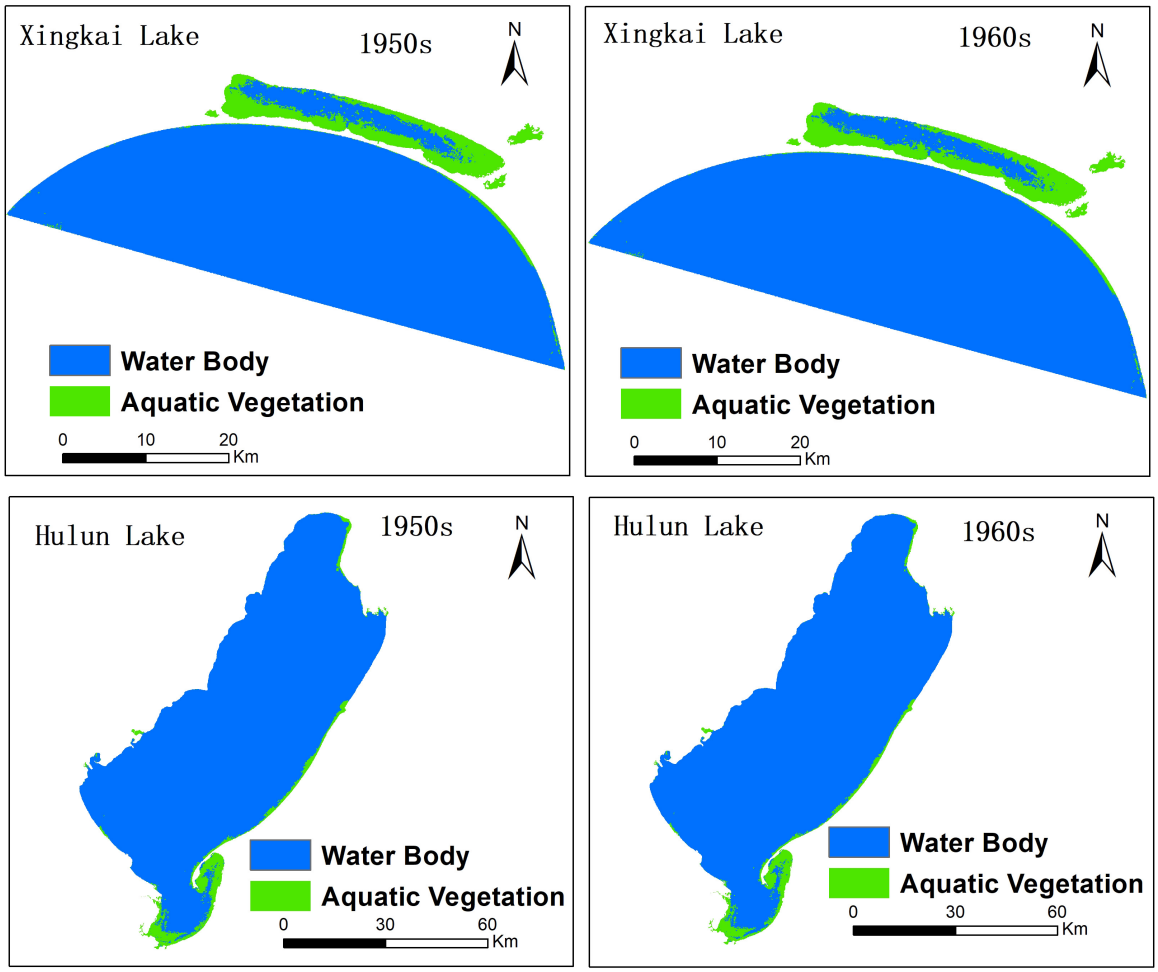

FIGURE 8
Potential spatial distribution of aquatic vegetation in Xingkai Lake and Hulun Lake in the 1950s and 1960s.

1970s, showing a decreasing trend in aquatic vegetation areas. For Hulun Lake, the area of aquatic vegetation was 90.81 km^2 in the 1950s, 88.15 km^2 in the 1960s, and 60.87 km^2 in the 1970s. This also shows a decreasing trend in the area of aquatic vegetation, which is consistent with the results of the study by Zhang et al. (2019).

TABLE 6 Areas of aquatic vegetation in Xingkai Lake and Hulun Lake in the 1950s and 1960s (km^2).

	1950s	1960s	1970s
Xingkai Lake	102.37	100.7	61.64
Hunlun Lake	90.81	88.15	60.87

Aquatic vegetation areas of the two lakes in the 1970s were calculated using remote sensing image data.

Discussion and conclusion

Discussion

Simulation accuracy

Due to the lack of ground survey data in the 1950s and 1960s and the absence of relevant thematic maps and remote sensing images, it was difficult to verify the simulated spatial distributions of aquatic vegetation in the two lakes. To determine the effect of the improved CA-Markov model, we compared the effects of the traditional CA-Markov model and the improved model (He et al., 2020). The spatial distribution of aquatic vegetation in the two lakes in the 1980s was simulated using the traditional and improved models in 10- and 20-year steps, respectively. Then, we compared the results of the two models with interpretations of the aquatic vegetation distribution from remote sensing images in order to evaluate the reliability and accuracy of the improved CA-Markov model.

TABLE 7 Comparison of results of the traditional CA-Markov model and improved CA-Markov model with 10-year steps.

Lake	Interpretation (km^2)	T CA-Markov (km^2)	MSER	I CA-Markov (km^2)	MSER	Improved accuracy
Xingkai Lake	96.11	149.98	0.56	114.38	0.20	64.86%
Hunlun Lake	76.9	100.46	0.08	83.17	0.31	28.73%

T CA-Markov is the result of the traditional CA-Markov model; I CA-Markov is the result of the improved CA-Markov model.

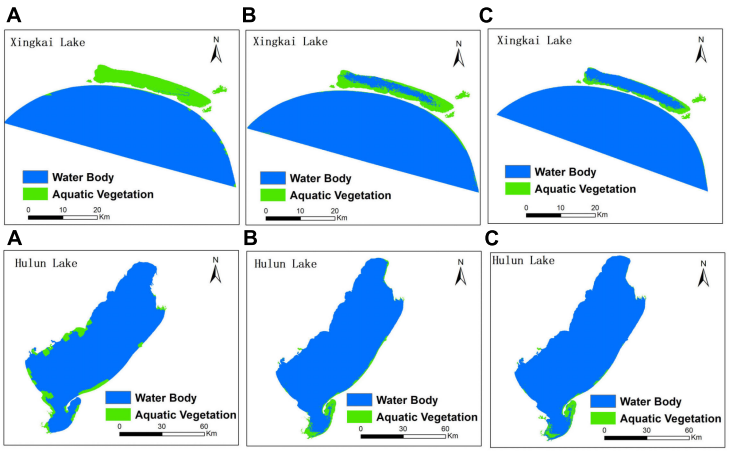

FIGURE 9
Comparison between the interpretation results and the simulation results of two models with a 10-year step (**A**: results of the traditional CA-Markov model; **B**: results of the improved CA-Markov model; **C**: results of interpretation remote sensing).

TABLE 8 Comparison of results of the traditional CA-Markov model and improved CA-Markov model with 20-year steps.

Lake	Interpretation (km^2)	T CA-Markov (km^2)	MSER	I CA-Markov (km^2)	MSER	Improved accuracy
Xingkai Lake	61.76	161.05	1.61	108.58	0.79	51.34%
Hunlun Lake	97.55	115.04	0.18	104.37	0.08	55.72%

T CA-Markov is the result of the traditional CA-Markov model; I CA-Markov is the result of the improved CA-Markov model.

First, we implemented the evaluation in 10-year steps. The distributions of aquatic vegetation of the two lakes in the 1990s were used as base data to simulate the probable distribution of aquatic vegetation in the 1980s by using the traditional and improved CA-Markov models. The traditional model was obtained from the transfer probability matrix based on the characteristics of aquatic vegetation changes in the lakes from 2000 to 1990; simulation directly applied the CA-Markov model method without considering geographical factors. We used the approach presented in this article to construct simulation rules for an improved CA-Markov model to simulate the distribution of aquatic vegetation in the 1980s. Table 7 shows the MSER of the accuracy comparison between the results of the two models and the interpretation result.

Table 7 shows that the improved CA-Markov model was used to simulate the distribution of the aquatic vegetation of Xingkai Lake in the 1980s, and the simulation accuracy was improved by 64.86% compared with that in the traditional CA-Markov model. However, the results of the improved CA-Markov model were inferior to the traditional CA-Markov model in MSER indicators in Hulun Lake. This is because the results of the traditional model simulated the distribution pattern of aquatic vegetation on the western shore of the lake, which is closer to the remote sensing extraction results. Figure 9 shows the comparison between the interpretation results and the simulation results of the two models.

We also implemented the evaluation with a 20-year step. The distribution of the aquatic vegetation of the two lakes in the 1990s was used as base data to simulate the probable distribution of the 1980s using the traditional and improved models. Table 8 shows the MSER of the accuracy comparison between the results of the two models and the interpretation results.

Table 8 shows the comparison of results of the traditional and improved CA-Markov models with 20-year steps. In the reconstructed historical data, the results of the improved CA-Markov model are significantly better for Xingkai Lake and Hulun Lake. The MSER value of the traditional CA-Markov

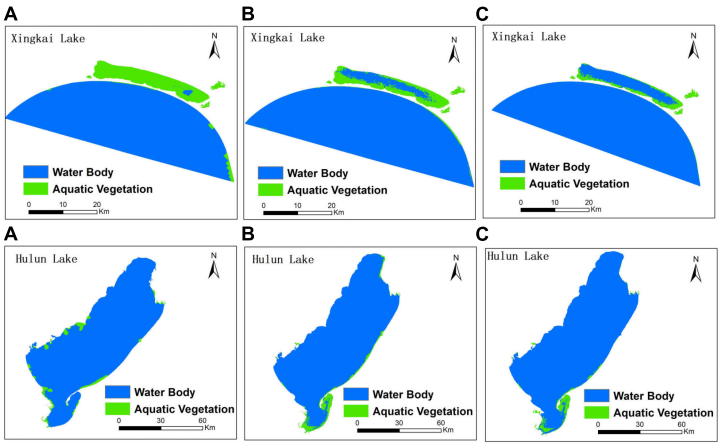

FIGURE 10
Comparison between the interpretation results and the simulation results of the two models with a 20-year step (**A**: results of the traditional CA-Markov model; **B**: results of the improved CA-Markov model; **C**: results of interpretation remote sensing).

model increased significantly: the MSER of the traditional model result of Xingkai Lake reached 1.61, while the MSER of the improved model was 0.79, improving by 51.34%. Overall model accuracy improved by more than 52% for the 20-year step with the improved CA-Markov model. Therefore, the improved CA-Markov model must be supported by geographical data for better simulation under longer term simulation conditions. Figure 10 shows the comparison between the interpretation results and the simulation results of the two models.

By improving the CA-Markov model, we provided a new simulation of the potential distribution of aquatic vegetation in the historical period. The results of the improved model had higher accuracy than the results of the traditional CA-Markov model. The transfer probability matrix of the improved CA-Markov model was constructed based on the consistency of changes in environmental conditions (meteorological factors), and then it was combined with a spatial frequency of occurrence and temporal recency effect to enhance the rules for suitability images. This improved model represents a rigorous method for the simulation and reconstruction of aquatic vegetation information in historical periods. In addition, it provided a reference for the reconstruction of the historical spatial distributions of other features.

Implications for reconstruction

To the best of our knowledge, the CA-Markov model has been widely used for the surface type changes in feature prediction and historical reconstruction (Yang et al., 2021; He et al., 2022). Although many studies have focused on qualitative methods for the suitability of images, it has not improved since the 1980s (Fu et al., 2018). Particularly, the selection of constraint factors for the suitability images neglected the connection to local historical spatiotemporal data, and we argued that the historical data were important factors for the inter-decadal succession of plant growth.

This study has made several innovative contributions to the literature. First, although the CA-Markov model has been widely used to reconstruct land cover patterns in historical periods (Yang et al., 2016), this is the first study to examine the historical distribution of the aquatic vegetation in lakes. In particular, our approach compensates for the difficulty of obtaining datasets due to the absence of historical remote sensing images and maps; such datasets are important for studying the evolution of lake ecosystems.

Second, we attempt to identify periods with similar climate change trends in different histories. We determine the transition probability matrix based on the distribution of aquatic vegetation in these periods. The aforementioned evaluation shows that our approach successfully improves simulation accuracy.

Third, historical reconstruction is a reverse process in which the past state is simulated from the current state. Therefore, the transfer probability matrix must be constructed from the current to the historical state. This finding provides new insights for the historical simulation of other relevant land surface types.

Fourth, the influencing factors of the spatiotemporal succession of vegetation growth were included as restrictive conditions in the model. Unlike the simulation of land-use types, human activities and policies have a large impact on prediction and reconstruction of land-use cover changes (Fu et al., 2018; Zhang et al., 2020), while the spatiotemporal succession of aquatic vegetation is important for sustainability over long timescales. In this study, we selected the spatial occurrence frequency and temporal recency effect of aquatic vegetation growth as the two most important constraint factors to generate the suitability images. These images, in turn,

controlled the transformation process of the cellular automata in the model.

Finally, we selected two typical lakes in Northeast China to reconstruct the historical distribution of the aquatic vegetation. Due to the large number of lakes in China, most of them lack historical records. Therefore, reconstructing the historical spatial distribution of aquatic vegetation is significant for studying the response of lake ecosystems to global climate change. The methodology and reconstruction process in this study can provide a reference model for other lakes.

Limitation for applicability

The improved CA-Markov model not only enriches the method of estimating historical aquatic vegetation but also provides a scientific basis for the response of lake ecosystems to climate change in China. Although we successfully reconstructed potential spatial distributions using the improved CA-Markov model, a few uncertainties and limitations remain. First, suitability images were constructed using spatial distribution data on aquatic vegetation in six periods (1970–2015). Because of the reconstruction of the historical spatial distribution of aquatic vegetation, the spatial distributions extracted from remote sensing data in all six periods were used in the simulation process. Thus, the results of the aquatic vegetation simulation were obtained in every possible distribution area. In addition, aquatic vegetation change is a complex process influenced not only by natural factors, such as climate change and natural disasters, but also by uncertain factors such as socioeconomic development and other human activities. The problem of setting the parameters of the CA-Markov model while considering such factors should be explored in future research.

Conclusion

This article proposes an improved CA-Markov model to reconstruct the spatial distribution of feature elements in historical periods. The model is based on the reverse transfer probability matrix derived from changes in meteorological factors and suitability images calculated from the spatial frequency of occurrence and the temporal recency effect. The main conclusions obtained are as follows:

(1) The transfer probability matrix is constructed based on the consistency of changes in meteorological elements and the cell conversion rules established from the climate-driven perspective, providing a theoretical basis for the simulation of the spatial distribution of aquatic vegetation.
(2) The suitability images are constructed from the spatial frequency of occurrence and the temporal recency effect, further standardizing the constraints and influences from the spatiotemporal correlation of geographic elements; this makes the simulation results of the model more convincing.
(3) The spatial distribution of aquatic vegetation in the 1990s is simulated and validated for consistency with the results of remote sensing image interpretation. The improved CA-Markov model has good generalizability for simulating the potential spatial distribution of historical aquatic vegetation.

Data availability statement

The original contributions presented in this study are included in the article/supplementary material, further inquiries can be directed to the corresponding author.

Author contributions

GH and HZ designed the study and completed the manuscript. ZL revised the manuscript. HZ, ZC, and YC contributed to the data collection and processing. All authors have read and agreed to the published version of the manuscript.

Funding

This work was financially supported by the National Key Research and Development Program of China (2019YFA0607101 and 2021YFD1500104) and the National Natural Science Foundation of China (41701494).

Conflict of interest

The authors declare that the research was conducted in the absence of any commercial or financial relationships that could be construed as a potential conflict of interest.

Publisher's note

All claims expressed in this article are solely those of the authors and do not necessarily represent those of their affiliated organizations, or those of the publisher, the editors and the reviewers. Any product that may be evaluated in this article, or claim that may be made by its manufacturer, is not guaranteed or endorsed by the publisher.

References

Aaviksoo, K. (1993). Changes of plant cover and land use types (1950's to 1980's) in three mire reserves and their neighbourhood in Estonia. *Landsc. Ecol.* 8, 287–301. doi: 10.1007/BF00125134

Ahmed, B. (2011). Modelling spatio-temporal urban land cover growth dynamics using remote sensing and GIS techniques: A case study of Khulna City. *J. Bangladesh Inst. Plann.* 4:43.

Bilton, D. T., Mcabendroth, L., Bedford, A., and Ramsay, P. M. (2006). How wide to cast the net? Cross-taxon congruence of species richness, community similarity and indicator taxa in ponds. *Freshw. Biol.* 51, 578–590. doi: 10.1111/j.1365-2427.2006.01505.x

Bu, H., Wan, J., Zhang, Y., and Meng, W. (2013). Spatial characteristics of surface water quality in the Haicheng River (Liao River basin) in Northeast China. *Environ. Earth Sci.* 70, 2865–2872. doi: 10.1007/s12665-013-2348-5

Dai, L., Liu, Y., and Luo, X. (2021). Integrating the MCR and DOI models to construct an ecological security network for the urban agglomeration around Poyang Lake, China. *Sci. Total Environ.* 754:141868. doi: 10.1016/j.scitotenv.2020.141868

Eberly, L. E., and Carlin, B. P. (2000). Identifiability and convergence issues for Markov chain Monte Carlo fitting of spatial models. *Stat. Med.* 19, 2279–2294. doi: 10.1002/1097-0258(20000915/30)19:17/18<2279::aid-sim569>3.0.co;2-r

Fornes, A., Basterretxea, G., Orfila, A., Jordi, A., Alvarez, A., and Tintore, J. (2006). Mapping *Posidonia oceanica* from IKONOS. *ISPRS J. Photogramm. Remote Sens.* 60, 315–322. doi: 10.1016/j.isprsjprs.2006.04.002

Fu, F., Deng, S., Wu, D., Liu, W., and Bai, Z. (2022). Research on the spatiotemporal evolution of land use landscape pattern in a county area based on CA-Markov model. *Sustain. Cities Soc.* 80:103760. doi: 10.1016/j.scs.2022.103760

Fu, X., Wang, X., and Yang, Y. J. (2018). Deriving suitability factors for CA-Markov land use simulation model based on local historical data. *J. Environ. Manage.* 206, 10–19. doi: 10.1016/j.jenvman.2017.10.012

Getachew, B., Manjunatha, B. R., and Bhat, H. G. (2021). Modeling projected impacts of climate and land use/land cover changes on hydrological responses in the Lake Tana Basin, upper Blue Nile River Basin, Ethiopia. *J. Hydrol.* 595:125974. doi: 10.1016/j.jhydrol.2021.125974

He, F., Yang, J., Zhang, Y., Sun, D., Wang, L., Xiao, X., et al. (2022). Offshore Island connection line: A new perspective of coastal urban development boundary simulation and multi-scenario prediction. *GIsci Remote Sens.* 59, 801–821. doi: 10.1080/15481603.2022.2071056

He, Z. S. Y., Xie, L., Liang, B. P., Deng, X. J., Yan, T. Q., Tong, Y. J., et al. (2020). Simulation of land use in Li River Basin based on CA-Markov model. *Ecol. Sci.* 39, 142–150. doi: 10.14108/j.cnki.1008-8873.2020.05.017

Horppila, J., and Nurminen, L. (2003). Effects of submerged macrophytes on sediment resuspension and internal phosphorus loading in Lake Hiidenvesi (southern Finland). *Water Res.* 37, 4468–4474. doi: 10.1016/S0043-1354(03)00405-6

Jeppesen, E., Lauridsen, T., Kairesalo, T., and Perrow, M. (1998). "Impact of submerged macrophytes on fish-zooplankton interactions in lakes," in *The structuring role of submerged macrophytes in lakes*, eds E. Jeppesen, M. Søndergaard, and K. Christoffersen (New York, NY: Springer).

Kolada, A., Willby, N., Dudley, B., Nõges, P., Søndergaard, M., Hellsten, S., et al. (2014). The applicability of macrophyte compositional metrics for assessing eutrophication in European lakes. *Ecol. Indic.* 45, 407–415. doi: 10.1016/j.ecolind.2014.04.049

Körner, S., and Nicklisch, A. (2002). Allelopathic growth inhibition of selected phytoplankton species by submerged macrophytes. *J. Phycol.* 38, 862–871. doi: 10.1046/j.1529-8817.2002.t01-1-02001.x

Laba, M., Blair, B., Downs, R., Monger, B., Philpot, W., Smith, S., et al. (2010). Use of textural measurements to map invasive wetland plants in the Hudson River National Estuarine Research Reserve with IKONOS satellite imagery. *Remote Sens. Environ.* 114, 876–886. doi: 10.1016/j.rse.2009.12.002

Lee, G. K. L., and Chan, E. H. W. (2008). The analytic hierarchy process (AHP) approach for assessment of urban renewal proposals. *Soc. Indic. Res.* 89, 155–168. doi: 10.1007/s11205-007-9228-x

Liira, J., Feldmann, T., Mäemets, H., and Peterson, U. (2010). Two decades of macrophyte expansion on the shores of a large shallow northern temperate lake–A retrospective series of satellite images. *Aquat. Bot.* 93, 207–215. doi: 10.1016/j.aquabot.2010.08.001

Luo, Z., Feng, W., Luo, Y., Baldock, J., and Wang, E. (2017). Soil organic carbon dynamics jointly controlled by climate, carbon inputs, soil properties and soil carbon fractions. *Glob. Chang. Biol.* 23, 4430–4439. doi: 10.1111/gcb.13767

Mao, P., Zhang, J., Li, M., Liu, Y., Wang, X., Yan, R., et al. (2022). Spatial and temporal variations in fractional vegetation cover and its driving factors in the Hulun Lake region. *Ecol. Indic.* 135:108490. doi: 10.1016/j.ecolind.2021.108490

Mondal, M. S., Sharma, N., Garg, P. K., and Kappas, M. (2016). Statistical independence test and validation of CA Markov land use land cover (LULC) prediction results. *Egypt. J. Remote. Sens. Space Sci.* 19, 259–272. doi: 10.1016/j.ejrs.2016.08.001

Moss, B., Kosten, S., Meerhoff, M., Battarbee, R. W., Jeppesen, E., Mazzeo, N., et al. (2011). Allied attack: Climate change and eutrophication. *Inland Waters* 1, 101–105. doi: 10.5268/IW-1.2.359

Orth, R. J., Carruthers, T. J. B., Dennison, W. C., Duarte, C. M., Fourqurean, J. W., Heck, K. L., et al. (2006). A global crisis for seagrass ecosystems. *Bioscience* 56, 987–996.

Qing, S., Runa, A., Shun, B., Zhao, W., Bao, Y., and Hao, Y. (2020). Distinguishing and mapping of aquatic vegetations and yellow algae bloom with landsat satellite data in a complex shallow lake, China during1986-2018. *Ecol. Indic.* 112:106073. doi: 10.1016/j.ecolind.2020.106073

Roijackers, R., Szabó, S., and Scheffer, M. (2004). Experimental analysis of the competition between algae and duckweed. *Arch. Hydrobiol.* 160, 401–412. doi: 10.1127/0003-9136/2004/0160-0401

Sand-Jensen, K., Riis, T., Vestergaard, O., and Larsen, S. E. (2000). Macrophyte decline in danish lakes and streams over the past 100 years. *J. Ecol.* 88, 1030–1040. doi: 10.1046/j.1365-2745.2000.00519.x

Sang, L., Zhang, C., Yang, J., Zhu, D., and Yun, W. (2011). Simulation of land use spatial pattern of towns and villages based on CA–Markov model. *Math. Comput. Simul.* 54, 938–943. doi: 10.1016/j.mcm.2010.11.019

Song, K., Shang, Y., Wen, Z., Jacinthe, P.-A., Liu, G., Lyu, L., et al. (2019). Characterization of CDOM in saline and freshwater lakes across China using spectroscopic analysis. *Water Res.* 150, 403–417. doi: 10.1016/j.watres.2018.12.004

Visser, H., and de Nijs, T. (2006). The map comparison kit. *Environ. Model. Softw.* 21, 346–358. doi: 10.1016/j.envsoft.2004.11.013

Wang, S., Meng, W., Jin, X., Zheng, B., Zhang, L., and Xi, H. (2015). Ecological security problems of the major key lakes in China. *Environ. Earth Sci.* 74, 3825–3837. doi: 10.1007/s12665-015-4191-3

Wang, Y., Shen, X., Jiang, M., and Lu, X. (2020). Vegetation change and its response to climate change between 2000 and 2016 in marshes of the Songnen plain, Northeast China. *Sustainability* 12:3569. doi: 10.3390/SU12093569

Yang, J., Guo, A., Li, Y., Zhang, Y., and Li, X. (2019). Simulation of landscape spatial layout evolution in rural-urban fringe areas: A case study of Ganjingzi District. *GIsci Remote Sens.* 56, 388–405. doi: 10.1080/15481603.2018.1533680

Yang, J., Yang, R., Chen, M.-H., Su, C.-H., Zhi, Y., and Xi, J. (2021). Effects of rural revitalization on rural tourism. *J. Hosp. Tour. Manag.* 47, 35–45. doi: 10.1016/j.jhtm.2021.02.008

Yang, X., Jin, X., Du, X., Xiang, X., Han, J., Shan, W., et al. (2016). Multi-agent model-based historical cropland spatial pattern reconstruction for 1661–1952, Shandong Province, China. *Glob. Planet. Change* 143, 175–188. doi: 10.1016/j.gloplacha.2016.06.010

Yuan, Y., Jiang, M., Liu, X., Yu, H., Otte, M. L., Ma, C., et al. (2018). Environmental variables influencing phytoplankton communities in hydrologically connected aquatic habitats in the Lake Xingkai basin. *Ecol. Indic.* 91, 1–12. doi: 10.1016/j.ecolind.2018.03.085

Zavadskas, E. K., and Antucheviciene, J. (2007). Multiple criteria evaluation of rural building's regeneration alternatives. *Build Environ.* 42, 436–451. doi: 10.1016/j.buildenv.2005.08.001

Zhang, G., Yao, T., Chen, W., Zheng, G., Shum, C. K., Yang, K., et al. (2019). Regional differences of lake evolution across China during 1960s–2015 and its natural and anthropogenic causes. *Remote Sens. Environ.* 221, 386–404. doi: 10.1016/j.rse.2018.11.038

Zhang, X., Zhou, J., and Li, M. (2020). Analysis on spatial and temporal changes of regional habitat quality based on the spatial pattern reconstruction of land use. *Acta Geogr. Sin.* 75, 160–178. doi: 10.11821/dlxb202001012

Zhao, G. W., Chen, Y. B., Chen, J. F., and Li, J. T. (2011). Spatial scale sensitivity of CA-Markov model. *Sci. Geol. Sin.* 31, 897–902. doi: 10.13249/j.cnki.sgs.2011.08.014

Zhao, Q. Q., Zhang, J. P., Zhao, T. B., and Li, J. H. (2021). Vegetation changes and its response to climate change in China since 2000. *Plateau Meteorol.* 40, 292–301. doi: 10.7522/j.issn.1000-0534.2020.00025

Zhou, L., Dang, X., Sun, Q., and Wang, S. (2020). Multi-scenario simulation of urban land change in Shanghai by random forest and CA-Markov model. *Sustain. Cities Soc.* 55:102045. doi: 10.1016/j.scs.2020.102045

frontiers | Frontiers in Environmental Science

TYPE Original Research
PUBLISHED 29 November 2022
DOI 10.3389/fenvs.2022.1068205

Check for updates

OPEN ACCESS

EDITED BY
Bing Xue,
Institute for Advanced Sustainability Studies (IASS), Germany

REVIEWED BY
Meng Zhang,
Xi'an Jiaotong University, China
Laing Zhou,
Lanzhou Jiaotong University, China
Chunlin Li,
Key Laboratory of Forest Ecology and Management, Institute of Applied Ecology (CAS), China

*CORRESPONDENCE
Li Wu,
wuli2009@yxnu.edu.cn

SPECIALTY SECTION
This article was submitted to Environmental Informatics and Remote Sensing,
a section of the journal
Frontiers in Environmental Science

RECEIVED 12 October 2022
ACCEPTED 11 November 2022
PUBLISHED 29 November 2022

CITATION
Zhou J, Yang M, Chai J and Wu L (2022), Evaluation on the urban green space layout in the central city of Yuxi based on big data.
Front. Environ. Sci. 10:1068205.
doi: 10.3389/fenvs.2022.1068205

COPYRIGHT
© 2022 Zhou, Yang, Chai and Wu. This is an open-access article distributed under the terms of the Creative Commons Attribution License (CC BY). The use, distribution or reproduction in other forums is permitted, provided the original author(s) and the copyright owner(s) are credited and that the original publication in this journal is cited, in accordance with accepted academic practice. No use, distribution or reproduction is permitted which does not comply with these terms.

Evaluation on the urban green space layout in the central city of Yuxi based on big data

Jing Zhou[1], Maoxiao Yang[2], Jing Chai[1] and Li Wu[1]*

[1]College of Geography and Land Engineering, Yuxi Normal University, Yuxi, China, [2]Yunnan Design Institute Group Engineering Investment Co., Ltd., Yuxi, China

As an important part of urban public infrastructure, urban green space plays an indispensable role in urban development and public physical, mental, and emotional health. By collecting open data such as POI, OSM, and ASTER GDEM and using spatial analysis software such as ARCGIS, QGIS, and Global Mapper, this study conducted thermal analysis of crowd activities, service pressure analysis, and demand evaluation for the layout of park green space in the central urban area of Yuxi City. The results show that there are great differences in the area and spatial layout of the thermal classes of crowd activity. Class II occupies the largest area, accounting for 60.73%, while class V occupies the least area, accounting for 2.04%. The thermal classes of crowd activity decrease from the center of the city to the periphery, and their area increases with the decrease of the thermal classes. With the increase in the level of green space service pressure, the proportion of the area decreased, among which the proportion of grade I was as high as 53.20%, while that of grade V was only 1.89%, which was mainly affected by the spatial location. The demand level and the area of park green space are obviously different, mainly concentrated in the first level, accounting for 69.68% of the total demand, and the large area is scattered in the periphery of the central urban area, followed by the fourth level, accounting for 10.46%. The area of other levels, especially the high level of demand, is less. Comprehensive analysis shows that the service level, type of green space, service pressure, and demand of green space have a strong correlation with the geographical location. In future planning, Yuxi City should combine the population distribution density and land development intensity and carry out reasonable layout and planning of park green space by reducing the low-demand area, increasing the green space area of high-demand area, improving public transportation, and improving accessibility.

KEYWORDS

urban green space, big data, geoinformation technology, layout evaluation, Yuxi City

Introduction

Under the background of ecological civilization construction, urban green space has become the current research hotspot (Danilina et al., 2021; Ye et al., 2022). As a basic element of urban green infrastructure, the urban green space system represents urban sustainability (Chen S. S. et al., 2021; Danilina et al., 2021). Urban green space is a green space open to the public, with recreation as the main function and ecology, beautification, and disaster prevention and is also an important part of the urban green space system (Wu et al., 2007; Jordan et al., 2022) and has significant social, ecological, cultural, and economic value (Zhou et al., 2020; Chen D. et al., 2021). Scientific research on the spatial distribution of urban green space services can provide theoretical and data support for evaluating the level and quality of urban services and guiding urban green space planning (Li and Lu, 2021).

The construction and development of urban green space has developed from a single urban park design to a multi-functional urban park system (Li et al., 2008; Chen, 2011). The evaluation index of urban green space has also developed from focusing on the quantity, area, shape, and structure level of urban park and other quantitative indicators (Li and Liu, 2009) to paying more attention to spatial distribution (Xue et al., 2019; Xue et al., 2020b), the visual analysis (Jinwon et al., 2022), and evaluation of the accessibility (Taleai et al., 2014; Tu et al., 2019; Addas, 2022) and the fairness (Tang and Gu, 2015; Wu and Peng, 2015; Kuang et al., 2021) of park services, and the exploratory appraisal beneficial or adverse effect (Mueller et al., 2022). With the wide application of big data in the field of urban planning (Donahue et al., 2018; Gao et al., 2021; Ma et al., 2022), the layout evaluation of urban green space tends to use urban big data for fine research (Zhai et al., 2017; Qi et al., 2018; Han and Wang, 2020), so as to achieve human-centered urban green space system planning.

All the time, the planning and design of urban green space requires first to meet the use requirements of people (Schindler et al., 2022; Wang et al., 2022). In the planning layout, according to the reasonable service radius of "300 m to see the green, 500 m to see the park" (Charlotte et al., 2022), the different types of green space are evenly distributed in the appropriate position in the city, and the service blind area of green space is avoided as far as possible. However, there is a disconnection between planning and reality in the practical application. For example, only the service radius of the planning is considered, but the real travel distance of the residents is ignored (Yoo and Roberts, 2022), or from the perspective of supply, only considering to meet the requirements of the balanced layout of green space, but ignoring the actual use of the residents' demand and frequency (Monika et al., 2022). At the same time, the relationship between the service capacity of the road traffic network and public transportation system and the layout of urban green space is ignored. According to a series of problems, the stock of high density in the city construction and development background, the city green space layout should be to "revitalize the stock, and optimize increment" as the guidance (Xue et al., 2016), in accordance with the green low carbon and intensive land economical utilization planning (Liu Q. et al., 2021) and development concept, based on the scientific research of big data in the city to explore a new update (Qi et al., 2018; Liu et al., 2022). It promotes the construction of urban green space from an extensive layout emphasizing "quantity" to smart optimization emphasizing both "quantity" and "quality" (Lennon, 2021; Xue et al., 2023), and guides the layout adjustment and function improvement of the different types of green space at macro, medium, and micro-levels. The spatial layout planning of urban green space lags far behind the current needs of efficient development of park green space in terms of refinement and systemization (Bai et al., 2022). The urban big data, especially the urban open data, provide a scientific basis for quantitative research on the precise placement of urban green space and the precise efficiency of resources (Wu and Peng, 2015; Liu et al., 2022). Therefore, it is urgent to explore the optimization path of the spatial layout of urban green space based on the support of urban big data, to construct fine planning, management, and regulation of urban green space and efficient ecological space creation.

Focusing on an ecological environment and livable and harmonious city construction, Yuxi City has proposed several special urban and rural habitat improvement actions and plans in the process of creating a national ecological garden city. The park system planning of Yuxi City is one of the important contents. Using big data such as Point of Interest (POI), outdoor hot spots, and thermal data of crowd activity, this study carried out cluster thermal analysis, park service pressure analysis, and demand analysis to comprehensively evaluate the spatial distribution, service level, and citizens' demand for urban green spaces. Through the support analysis of urban big data, the optimization mode of the planning and layout structure of the park system in Yuxi City was explored from the analysis of park service demand and service pressure, or accessibility and fairness, to further guide the construction of the urban green space system and improve the ecological environment of human settlements.

2 Materials and methods

2.1 Research scope

According to the information of the Yuxi Housing and Urban-Rural Development Bureau, by the end of 2020, the total area of urban built-up area in the central city of Yuxi is 38.70 km^2, covering Hongjiu Road in the north, Dongfang Reservoir in the east, Subi Mountain in the south, and Huixi Road in the west. According to the Yuxi Green Space System Planning (2011–2030), the research scope is comprehensively

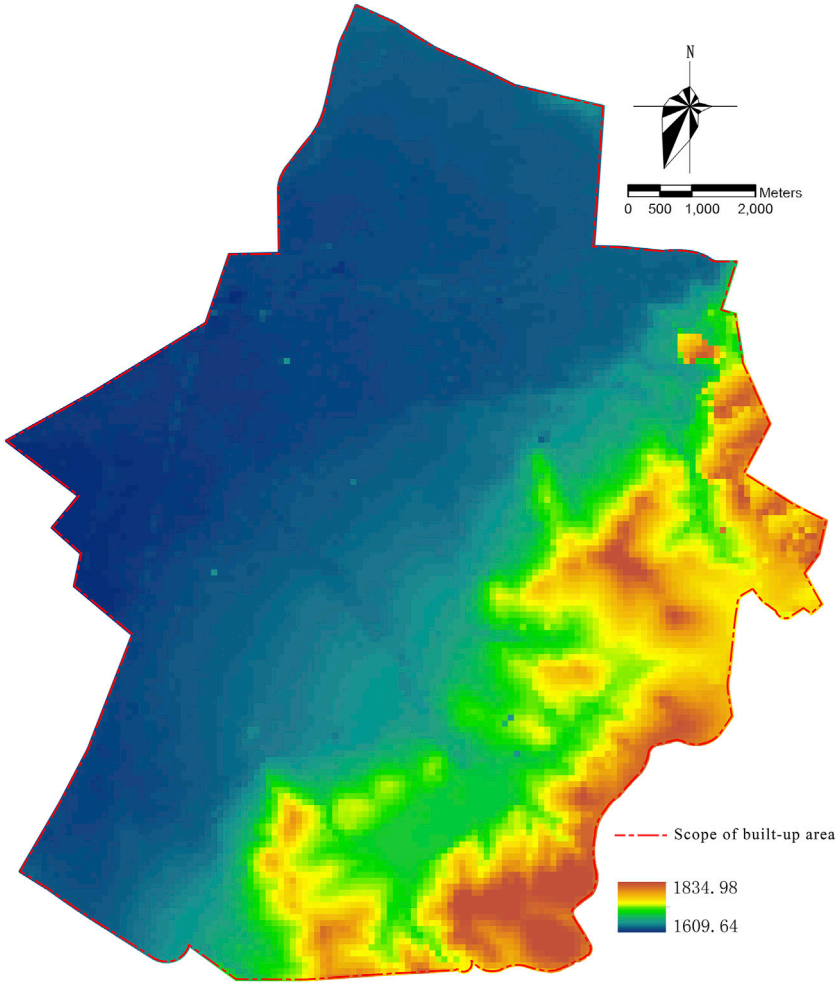

FIGURE 1
The DEM elevation of built-up area in Yuxi City.

defined, including Yudai Street, Fenghuang Street, Yuxing Street, and Liqi Street in Hongta District.

2.2 Data source and processing

The DEM elevation data of the central city of Yuxi (built-up area) (Figure 1) were obtained by using open data and tools (Li et al., 2022) from the web such as Global Mapper, Geospatial Data Cloud, and ArcGIS, and were processed by bid projection conversion, area cropping, and raster output. The vector data of roads (Figure 2), water systems, and park green areas (Figure 3) in the study area were obtained using Open-Source Neighborhood Map (OSM) and used for layout evaluation after coordinate projection conversion and manual calibration.

POI data were mainly obtained through urban open-source data. They mainly include 4,575 housing prices, 4,284 catering services, 9,427 shopping facilities, 987 transportation facilities, 1,881 companies and enterprises, 4,081 living services, 561 sports and leisure service facilities, 899 science, education, and culture facilities, 3,740 public service facilities (including medical treatment), and 1,056 residential area data within the study area, a total of 31,491 pieces of data (Table 1).

2.3 Technical methods

2.3.1 POI data collection

By referring to relevant literature reports (Tu et al., 2020; Liu H. L. et al., 2021; Qin et al., 2021), the influencing factors of various urban areas on people's activities, especially recreational activities, are divided into three categories: accessibility, population distribution, and social and

FIGURE 2
Current situation of urban roads in Yuxi City Center.

economic status of people. The obtained data are classified and combined, and seven factors, namely, bus traffic station density, cultural and entertainment facilities, office facilities, public service facilities, commercial service facilities, residential areas, and population income are finally selected. In the POI data obtained, the number of bus stops can reflect the traffic condition and the accessibility of the region. Cultural and entertainment facilities, office facilities, large public facilities, residential areas, and other POIs were selected as direct measurement factors to obtain regional population distribution information. Since the socioeconomic status of the population is difficult to be directly obtained, it is known that the housing price is positively correlated with the socioeconomic ability of the population. Therefore, the differentiation of the socioeconomic status of the population can be obtained by obtaining the housing price information on the Anjuke.

2.3.2 Evaluation and analysis of urban green spaces

First, the spatial distribution was analyzed for existing parks. The population thermal data processed by QGIS software were collected and input into the green land of the research area. The population thermal data within the green area were clipped, and population spatial distribution data were connected to the green area layer by using the spatial connection tool, which could reflect the spatial distribution of people's heat toward the park. The area with the highest use density of the park was extracted as the radiation center of the park, and the radiation range of the high-frequency use area of the park was obtained. The distribution characteristics and service scope of the park space in the urban built-up area were analyzed by adding the heatmap of the distribution density of people's outdoor activities in Yuxi City. Then, the data of the regional points with high density of human flow in the park were extracted for the radiation range analysis,

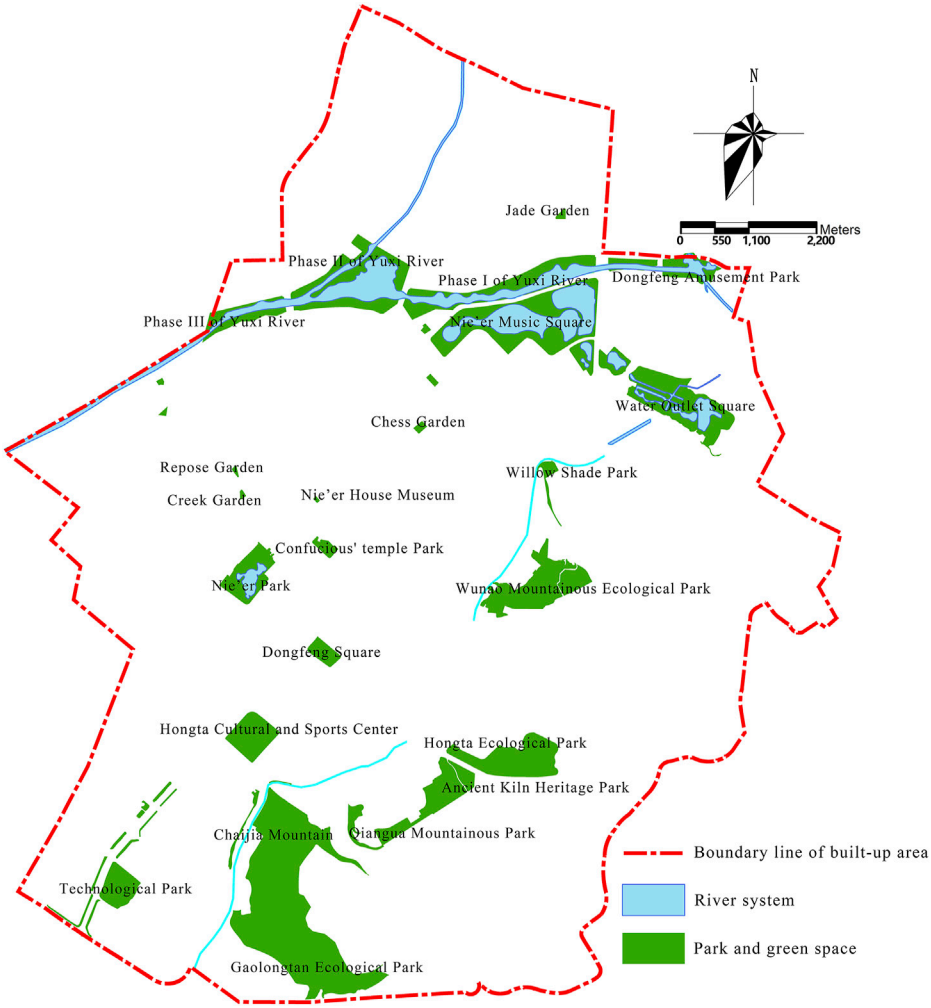

FIGURE 3
Spatial distribution of park and water in Yuxi City Center.

which reflected the spatial distance of the actual service people in the high-frequency use space of the park within the service radius of 500 m. In combination with the hotspots of urban economic vitality, the data of interest points of restaurants, shopping malls, office areas, and residential areas were selected. The density analysis tool of QGIS was used to conduct statistics on the outdoor activities of the urban population and obtain the heatmap analysis of the main activities (Figure 4).

Second, the service pressure can be quantitatively analyzed by the distribution characteristics and density of the people's activities within the service range of urban parks. Existing studies have shown that areas with high population activity distribution density do not necessarily have high population density, but often have high demand for urban parks. POIs that are closely related to people's activities and can reflect the intensity of people's activities are selected, such as POIs of residential areas, catering, shopping, entertainment, cultural and sports activities, and financial institutions. GIS software was used to spatialize and visualize them, and the existing park locations were further generated into the 500-m service range of each park. Then, the POIs corresponding to the service range of each park and the service pressure figure of green space were obtained (Figure 5). The service pressure is calculated by the following formula:

$$U = N/A, \quad (1)$$

where U is the service pressure (unit/km^2), A is the area of the urban park (km^2), and N is the number of POIs within the service range of the urban park (unit).

Third, the demand evaluation of people in different urban spaces for park green space was evaluated. According to the current investigation and reference to relevant studies (Yuan

TABLE 1 Description of POI data.

Name of data	Data attribute	Data types	Data sources
Green space	Statistics of the actual distribution of various types of parks in the current layout of urban space	Vector surface data	Investigation of existing situation, Global Mapper, and Geospatial data cloud
Elevation of built-up area	Reflects the basic terrain of the built-up area	Raster data	DEM of Geospatial Data Cloud
Traffic route	Current road distribution	Vector line data	Open street map
Traffic stop	Including bus station and parking lot facility distribution	Vector point data	Baidu Map
Cultural and recreational facilities	Including science, education and culture facilities, sports, and leisure service facilities	Vector point data	Baidu Map
Office facilities	Corporate class, including industrial, enterprise, and business office	Vector point data	Baidu Map
Public service facilities	Public service facilities, including administrative management at all levels (including community service centers), medical and health care, and important urban public buildings	Vector point data	Baidu Map
Commercial service facilities	Catering service, shopping, and life service	Vector point data	Baidu Map
Residential districts	Urban first- and second-class residential land and hotels	Vector point data	Baidu Map
Income of population	Unit price information of new houses and second-hand houses	Vector point data	Baidu Map

et al., 2021; Zhou et al., 2022), different urban space populations have different needs for park green space. The AHP method is used to determine the corresponding weights of influencing factors. By establishing the hierarchical structure model, constructing the judgment matrix, hierarchical single sorting, calculating the feature vector, consistency testing, and other steps, seven factors, namely, bus station density, cultural and entertainment facilities, office facilities, public service facilities, commercial service facilities, residential areas, and population income were selected. From the three aspects of accessibility, social, and economic status of the population and population distribution, this study evaluates the differences in the needs of people in different urban spaces for green spaces, and establishes a unified data information evaluation table. At the same time, the research area was divided into 30 m × 30 m spatial cell grids, and the grid size kept matching with the accuracy of DEM data (30 m resolution). The collected POI data related to each influencing factor were spatialized and rasterized through the geographic information system, and the raster superposition calculation was carried out according to the weight to obtain the demand evaluation of the park within the research scope (Figure 6).

3 Results and analysis

3.1 Spatial distribution of urban green spaces

The grid aggregation density analysis tool of QGIS was used to obtain statistics on the urban population's outgoings and obtain the crowd activity heatmap (Figure 4). On this basis, the thermal area of crowd activities is divided into six levels, and the ArcGIS 10.8 software is used to calculate the thermal area of crowd activities at all levels using a grid calculator. Heat class II of crowd activity occupies the largest area, 9.16 km^2, accounting for up to 60.73%, followed by class I, with an area of 2.49 km^2, accounting for 16.54%, and the area of class V is the least, only 0.31 km^2, accounting for 2.04%. Figure 4shows how the thermal level of crowd activities decreases from the center of the city to the surrounding areas in space, and its area increases with the decrease of the thermal level. However, the farther away the thermal level is from the center of the city after reaching a certain level, the area also decreases, as shown in Figure 4.

After years of construction and development, the central city of Yuxi has gradually formed an overall urban pattern of "one center, two cores, and four clusters," with the central city as the center and four clusters of Daying Street, Beicheng, Chunhe, and Yanhe in the periphery. As the central area of Hongta District, the central city basically forms a "centralized" overall layout with the old city as the core and gradually expands outward. The three areas included the central area of the old city as the main residential, commercial, and service comprehensive area; the eastern mountain area of tobacco industry production, new industrial park, as the main industrial, college, and secondary education area; and residential comprehensive area, the south and north of the residential, administrative, and commercial area, as the main urban new area.

However, it can be seen from Figure 4 that there are still two problems in Yuxi's urban green space. The central city green

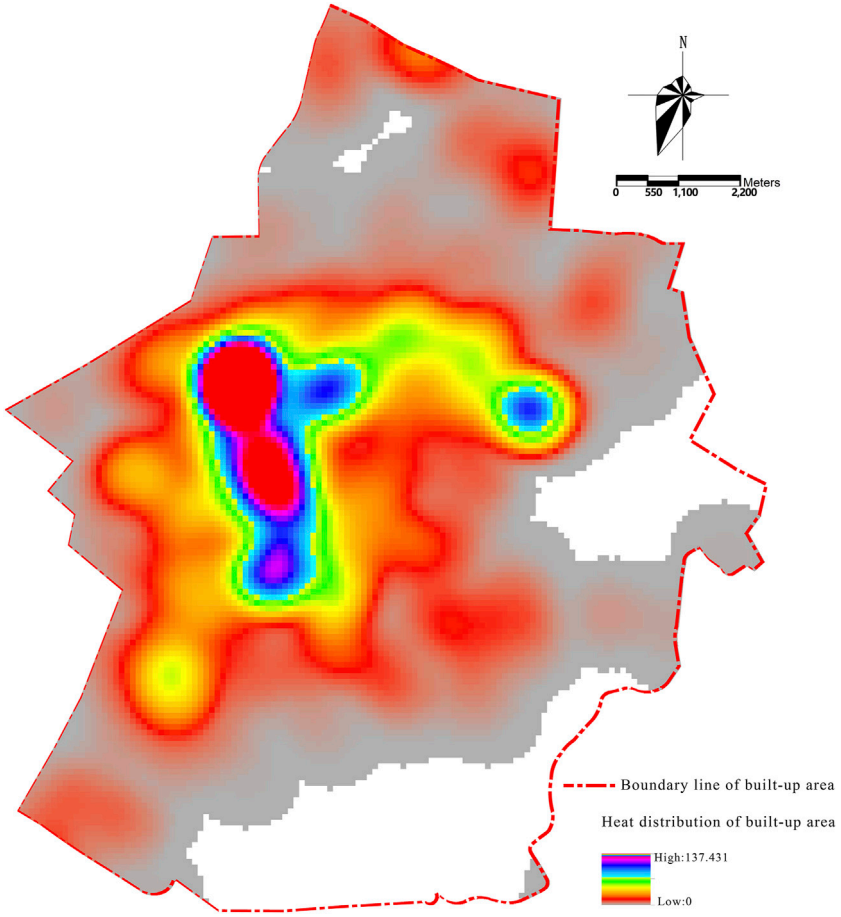

FIGURE 4
Thermal distribution of crowd activity in Yuxi City center.

system is not complete. As far as the whole urban area is concerned, a complete urban landscape green space system has not been formed yet, and there is no linear or ribbon-like connection between all kinds of green spaces. Although the background environment of mountains and the countryside around the city is good, it fails to form an organic whole. The combination of greening and urban culture is not high. The green investment in the core areas such as main entrances, urban trunk roads, and existing cultural facilities is insufficient, the theme is not prominent enough, and the cultural connotation is relatively weak. The distribution of public green space is uneven. From the perspective of urban outdoor hotspots, the heat and service pressure of the comprehensive area of living, trade, and service in the central area dominated by the old city are greater than those in other areas, indicating that the utilization rate of green space is higher, and the area of green space is smaller in this region. The plots show that public green space is mainly concentrated in the new urban areas, such as the north and southeast of the built-up area, while the central old city comprehensive area is obviously insufficient, and there is a big gap among all groups. The green space development in this area is difficult, the service radius of green space is insufficient, the building density is high, the traffic is crowded, and the ecological environment quality is declining.

3.2 Service level of urban green land

With the help of the service pressure formula, the ratio of the number of POIs within the service range of each park to the park area was calculated, and the service pressure of each park was obtained (Figure 5). By referring to relevant research results and combining the population and facility density of various interest points in Yuxi City, the expert consultation method was adopted to divide the urban park service pressure in the central urban area of Yuxi City into five levels successively. The higher the level, the greater will be the service pressure. As shown in Figure 5, the service pressure level is inversely proportional to the area. The

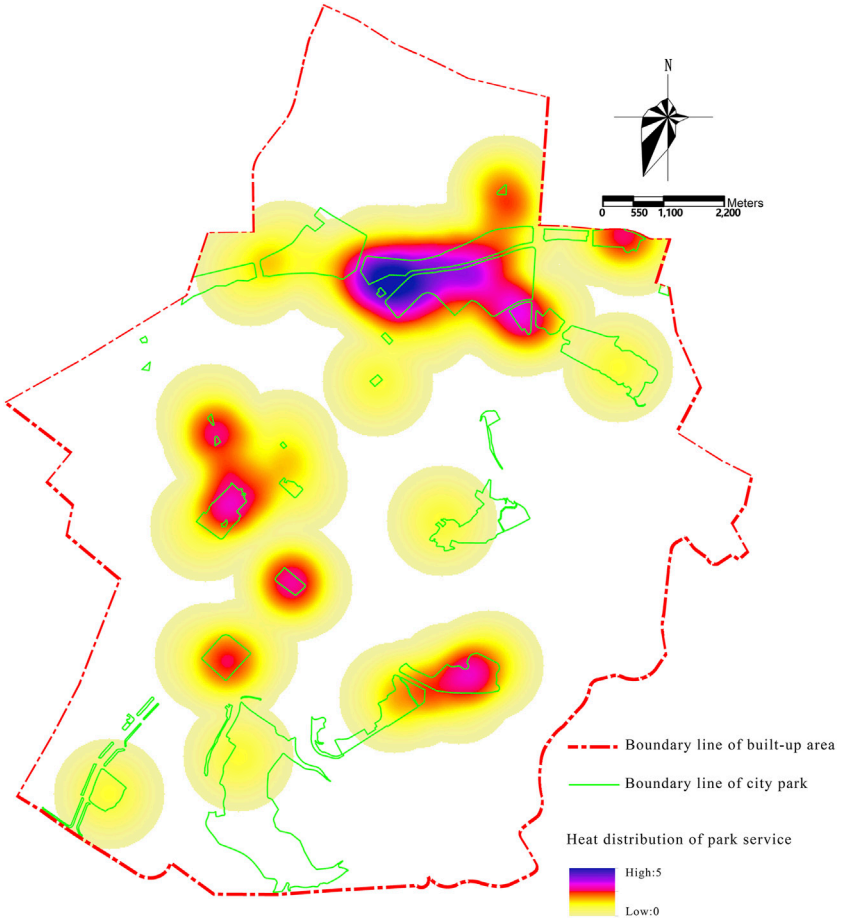

FIGURE 5
Distribution of park service pressure in Yuxi City center.

higher the pressure level, the smaller will be the area, and the lower the pressure level, the larger will be the area. The first-level area of service pressure is the largest, which is 7.68 km^2, accounting for 53.20% of the total area. The second is grade 2, with an area of 4.15 km^2, accounting for 28.75%. The smallest area is grade 5, accounting for only 1.89%, mainly distributed in the northeast of the central urban area (Table 2). Through the service pressure and cluster thermal analysis of the green space usage data in the central city of Yuxi City, it is found that the service level of the green space in the central city of Yuxi is strongly correlated with the type and geographical location of the urban green space (Figure 5).

Through comprehensive analysis, it is found that the use of comprehensive parks is affected by the type of recreation space, service facilities, and park transportation convenience. These parks are designed with diversified and characteristic recreation spaces and service entertainment facilities suitable for different users. The types of activities are also in line with the characteristics of the times and meet the recreation needs of modern people. For example, Nie Er Park and Nie Er Music Square (Yuhu area) have a large area of open squares, tree-lined walks, children's playgrounds, beaches, and perfect surrounding commercial facilities.

The use heat and service pressure of special parks are greatly influenced by the attraction of the park theme. We can plan regular events to form characteristic recreation space and popular science education activities to attract many people. For example, the "Lantern Festival" in the landscape belt of the State River, the Memorial Park of Revolutionary Martyrs, the Ancient Kiln Site Park, Nie Er Residence, East Wind Playground, and other popular science and education theme activities have become the cultural symbols of these parks, which effectively enhance the attraction and uniqueness of the special parks. However, there is little correlation between the heat of famous special parks and the number of traffic facilities around them. In recent years, the proportion of floating population in Yuxi City has increased year by year, and foreign tourists occupy a

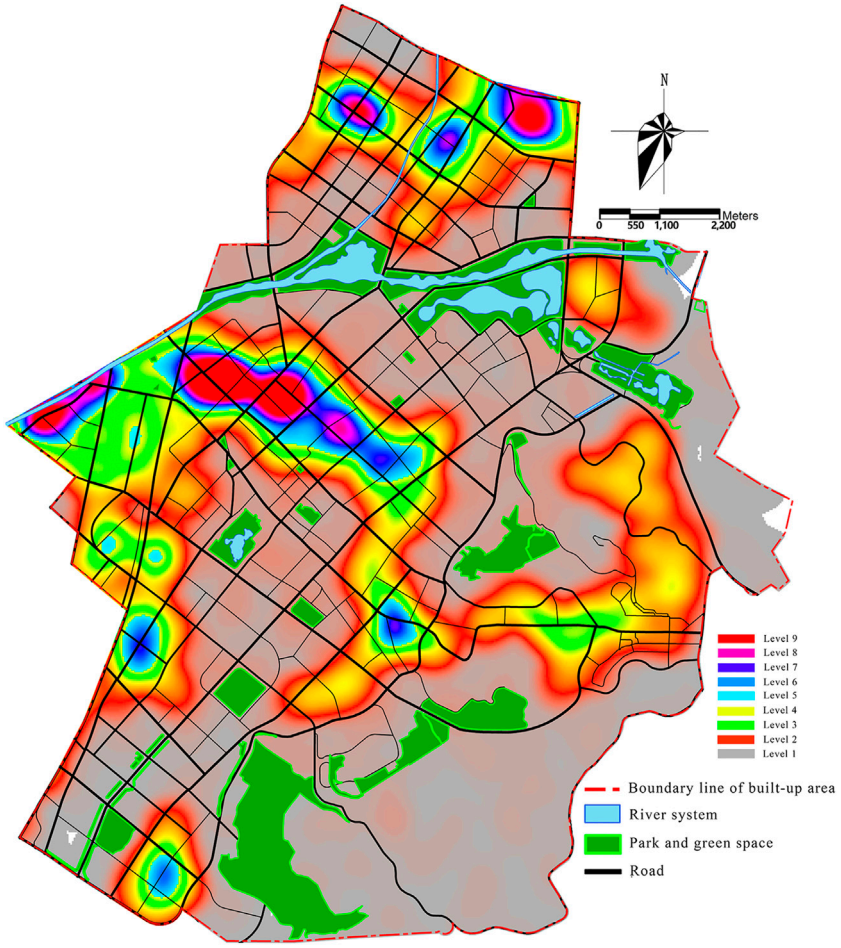

FIGURE 6
Spatial distribution of demand on urban green spaces in Yuxi City Center.

TABLE 2 Area of urban green space service pressure levels in Yuxi City.

Grade	Pressure value	Name and types of parks	Total area (km^2)
5	>10,000	Nie 'er Music Square—Square Area (comprehensive park), Yuxi River Phase I—Viewing Platform Area (comprehensive Park), Binhe Road Small Garden (garden)	7.68
4	7,500–10,000	Nie er Park (comprehensive Park), Dongfeng Square (community Park), Hongta Ecological Park (special Park)	4.15
3	5,000–7,500	Xiyuan (recreational park), Recreation Park (recreational park), Jade Garden (recreational park), Dongfeng Amusement Park (special park), Hongta Cultural and Sports Center (special park), Ancient Kiln Site Park (special park), Wenmiao Park (special park), Nie Er's Former Residence (special park), Yuxi Dahe Phase II (community park)	1.72
2	2,500–5,000	Science and Technology Park (comprehensive park), Chaijiashan Park (special park), Wunao Mountain Ecological Park (special park), Water Outlet Square (community park), Qiyuan Park (recreational park), Beiyuan Community Park (community park), Yuxi Dahe Phase III (community park)	0.61
1	<2,500	Golongtan Ecological Park (special park), Qianguashan Park (special park), Liuyin Park (special park), Purple Maple Park (community park)	0.27

certain proportion in the users of green space. The use of special parks is greatly affected by the popularity. Therefore, the attraction of well-known special parks to outsiders reduces the direct correlation between the use of green space and the convenience of public transport. However, special parks such as Gaolongtan Ecological Park, Qianguashan Park, Liuyin

TABLE 3 Weight of the influence factor.

Symbol	Impact factors	Weight
Accessibility	Density of bus stops	0.0317
Socioeconomic status of the population	House price	0.0252
	Cultural and recreational facilities	0.1032
	Office facility	0.0361
	Commercial service facilities	0.1568
	Public facilities	0.3269
Distribution of population	Residential area	0.3201

Park, Chaijiashan Mountain Park, and Wunaoshan Ecological Park, which are themed on mountain protection, water restoration, ecological recreation, and sports, are not well-known and mainly serve for the protection and restoration of the city's ecological environment. Therefore, its entertainment facilities and accessibility are poor, not attractive, and space heat and service pressure are relatively low. Among the influencing factors of the frequency of community parks and street parks, the location of the park and its opening degree were significantly greater than the size of the park. Although the larger the scale is, the more favorable it is for the construction of recreation space, and the usage heat and service pressure are not positively correlated with the size of the park. Although the green spaces beside the streets, such as Triangle Park, Chess Park, and Jade Garden, are small in size, they occupy a favorable position, with a high degree of open use for citizens, convenient transportation links by foot and bicycle, large crowds of people around them, high heat value of outdoor activities, and higher service pressure and use frequency than other green spaces. Although the scale of community parks is relatively large, the use of heat is relatively low and the service pressure is small. Except for the high use rate of a small number of community parks that are open to the public, such as Dongfeng Square and Dongfeng Amusement Park, the service pressure and heat of large community parks, such as Outlet Square and Yuxi Dahe Phase III, are relatively low. Purple Maple Garden is mainly used by residents inside the community, and its location is relatively secluded, with low awareness of openness and public, and the pressure and heat of park service are extremely low. The analysis results are also consistent with the actual use in the survey. However, due to the lack of data on the elders and children in the POI data, the use evaluation of community parks has certain limitations.

3.3 Demand analysis of urban green land

The hierarchical structure model is established according to the required evaluation method. When constructing the judgment matrix, the index quantification table was distributed to 20 industry experts. A total of 20 quantified index tables were recovered with a recovery rate of 100%. After hierarchical single sorting, feature vector calculation, consistency test, and other steps, the weight table of impact factors was obtained (Table 3), which was transformed into the score table of the GIS evaluation index (Table 4). The natural breakpoint method is a univariate classification method based on cluster analysis. By calculating data breakpoints between classes to determine a certain number of grades, the difference between classes can be minimized and the difference between classes can be maximized. The main advantage of this method is to distinguish similar values in the data most effectively (Cai et al., 2021). Therefore, the demand evaluation value of park green space was obtained through GIS calculation, and it was divided into nine levels (Figure 6). The ArcGIS 10.8 software was used to obtain statistics on the demand area of green space at all levels, and it was found that the demand for green space in Yuxi City was mainly concentrated in level 1, with an area of 29.62 km^2, accounting for 69.68% of the total demand, mainly including the peripheral and sporadic distribution in the central urban area. The next is grade 4, with an area of 4.45 km^2, accounting for 10.46%. The third is level 2, with an area of 4.26 km^2, accounting for 10.02%. The area of other demand levels is relatively low and has little difference.

As shown in Figure 6, regions with higher demand levels occupy smaller areas, while regions with lower demand levels occupy larger areas. In fact, ideally, the area with a higher rating should have denser and better-served community parks and recreation parks and be closer or more accessible to large regional or city-wide parks. The highest demand for parks in central urban areas is along Yuxing Road, Zhongwei area, to public rental housing. Another high point is the old railway station area and rainbow community, Bailong Road in Liqi Town, Kangjing Road line area, which is also relatively high demand. Most people in Yuxi live and work in this area, which not only brings traffic pressure but also produces high-pressure and high-demand areas in terms of park services (Figure 6).

TABLE 4 Index score of GIS evaluation.

Index	Grading value	Scoring value	Weight
Density of bus stops	Number of bus stops is divided into five levels: 1, 2, 3, 4, 5	1, 2, 3, 4, 5	0.0317
House price	Grading value of average house price (≤0.4 w, 0.6 w, 0.8 w, 1 w, ≥1.2 w)	1, 2, 3, 4, 5	0.0252
Cultural and recreational facilities	There are five levels according to the number of cultural and recreational facilities: 1, 2, 3, 4, 5	1, 2, 3, 4, 5	0.1032
Office facilities	There are five levels according to the number of office facilities: 1, 2, 3, 4, 5	1, 2, 3, 4, 5	0.0361
Public facilities	There are five levels according to the number of public facilities: 1, 2, 3, 4, 5	1, 2, 3, 4, 5	0.1568
Commercial service facilities	There are five classes according to the number of commercial service facilities: 1, 2, 3, 4, 5	1, 2, 3, 4, 5	0.3269
Residential area	There are five classes according to the number of residential areas: 1, 2, 3, 4, 5	1, 2, 3, 4, 5	0.3201

4 Discussion

4.1 Application of big data in urban green space evaluation

Urban big data, especially urban open data, provide a scientific basis for quantitative research on the precise placement of urban green space and the precise efficiency of resources (Wu and Peng, 2015; Chen S. S. et al., 2021). Therefore, it is urgent to explore the optimization path of the spatial layout of urban green space based on the support of urban big data (Ahas et al., 2010; Gao et al., 2021), so as to construct fine planning, management and regulation of urban green space, and efficient ecological space creation. Big data have the characteristics of huge data volume, comprehensive data coverage, and complex data types (Xue et al., 2020a; Jinwon et al., 2022; Liu et al., 2022). Therefore, when using big data to conduct relevant research, selecting appropriate data is crucial for the smooth development of the research (Xue et al., 2020b; Sim et al., 2020). This study innovatively used POI data to analyze the intensity of crowd activities and then evaluate and optimize the green space. The data are easy to obtain, the processing is relatively simple, and the results are also easy to visualize and visually present, which can avoid many influences brought by traditional planning, but there are still some problems and challenges.

On one hand, the existing big data acquisition and processing technology in the field of spatial planning is not yet mature, and there are technical blind spots in data validity, redundancy processing, stripping (Liu et al., 2022), and other aspects, and the lack of a perfect data security system (Ahas et al., 2010). At the same time, due to interests and confidentiality, it is difficult to achieve data integration and sharing between government departments and enterprises in a short period of time, which limits the breadth and depth of big data acquisition for planning and compilation (Huang et al., 2021). On the other hand, big data are more scientific in the simulation and analysis of the correlation of factors, but there are still imprecision problems in the study of causes and mechanisms (Zhang L. et al., 2022). How to integrate with traditional data analysis to avoid similar problems needs further exploration. In addition, the existing green space system planning results based on big data are still at the theoretical and methodological level, and a complete technical system has not yet been formed (Zabelskyte et al., 2022). How to promote in the industry to guide practical work and in what form to participate in the national statutory planning system will also become a challenge for future research.

But nonetheless, from the perspective of the data used, compared with the traditional spatial layout model, this study obtains the data of bus station density, housing price, cultural and entertainment facilities, office facilities, commercial service facilities, public facilities, and residential areas based on Baidu Map API, which has higher efficiency, lower cost, and more targeted experimental data. From the perspective of research methods, based on the principle of the original park layout planning, this paper introduces urban open data to quantitatively analyze the service level of urban parks and the evaluation of park green space needs from two aspects, providing a new perspective for the study of the spatial layout of urban green space.

4.2 Prospect of urban green space planning

Urban green spaces are a part of the social space and a vital part of the urban landscape and act as an environmental framework of the territory and a factor ensuring a more comfortable environment for humans (Morar et al., 2022). Since 1999, Greenbelt Park (Turf Park), Lotus Pond Park, and Yunxi Park (Triangle Park) have been rebuilt successively in the central city, and green parks such as Dongfeng Square Green Park, Highland Park, and Hongta Cultural and Sports Center have been added. In addition, the green space in front of the People's Hospital, Yun Yuan, Qin Yuan, Nie Er's former residence green garden, and other street green spaces are actively built. Nie Er Road, Yuhu Road, and Dongfeng South Road have become the model roads of urban greening. Qianguashan Park, Yuxi River Greenbelt Phase I, II, III Project, and Outlet Ecological Park set off the wave of

ecological city construction. Relying on its own natural resources and economic advantages, Daying Street Office has been more prominent in greening work in recent years, and has built green spaces such as Huixi Park, Yuquan Temple Park, and Huilong Ecological Park. After years of efforts, the landscape of Yuxi's central city has been fundamentally changed, and the green indicators have been greatly improved. It was awarded the title of "Provincial Garden City" in 2006 and "National Garden City" by the Ministry of Housing and Urban-Rural Development in 2010. But for a whole city, the level of construction is inadequate.

At present, Yuxi has started the compilation of Yuxi's Territorial Space Plan (2020–2035). Therefore, the author hopes to provide some suggestions for the planning of urban green space systems and the overall planning of territorial space from the perspective of citizens' green space use in the future, to make green space planning more scientific, reasonable, and targeted. The first is to improve public transport and the accessibility of green spaces in parks. There is a strong correlation between the green space of comprehensive parks and the distribution of public transport facilities. In the process of green space system revision, the site selection of new comprehensive parks and other green space types can rely on the location of public transport stations to improve the transportation convenience and accessibility of citizens to green space. By giving full play to the comprehensive functional benefits of urban green space, unified planning and comprehensive arrangement should be carried out.

The second is to reduce high-demand areas by rational layout of park green space. Combined with the aforementioned research results, from the perspective of the types and distribution of green space in central city parks, the distribution of green space in large parks in the north and southeast is relatively concentrated, but the use heat and service pressure are relatively low, and the frequency of green space use is low. Therefore, it is suggested that the existing park should be reconstructed, and the land use attributes should be transformed appropriately and reasonably, to enhance its vitality and attractiveness. At present, the park utilization rate in the comprehensive service area of the central old city is high, the distribution is uneven, and the service pressure is high. To increase the citizens' green space recreation and leisure activities, it is suggested to appropriately increase some of the conditionally attached green spaces along the street, share the pressure of the high utilization rate of green space, and make up for the current situation of regional green space tension. From the POI data, it can be seen that the spatial distribution and utilization rate of green space in the west of the central city are low, and the main reason is the lack of large comprehensive parks or special parks. Therefore, it is suggested that in the new round of urban general planning revision, appropriate consideration should be given to the conversion of land use types, balancing the distribution and types of green space in each area, so that green space can serve citizens more effectively.

Finally, the recreation space is rationally planned to provide diversified leisure experiences. The main functions of urban green space can be summarized into the following aspects: protecting the urban ecological environment (Slaev et al., 2022), improving urban microclimate (Muluneh and Worku, 2022), disaster prevention and reduction (Isabella et al., 2022), education (Mendoza et al., 2022), recreation (Zhang B. et al., 2022; Zhang S. N. et al., 2022), beautification (a beautiful urban environment is conducive to attracting investment) (Li and Lu, 2021), and so on. These functions are closely related to the life and production of the citizens, and directly affect the sustainable utilization and development of the city. In the process of building green space and transforming the park, the space with low attraction should be transformed to provide a space type more in line with the recreation needs of modern people in combination with the evolution of citizens' lifestyle.

5 Conclusion

In this study, the urban open data were used to analyze the service pressure and clustering heat of the existing park green space in Yuxi City, and the influencing factors and research paths of the optimal layout of urban green space were proposed. In terms of research methods, based on the original park layout planning principle, this paper introduces urban open data from two aspects to quantify the evaluation of the urban park service level and urban green space demand, which provides a new perspective for the study of urban green space layout. From the perspective of practice, this study can provide a certain reference for the planning and selection of park green space in Yuxi's central city and the formulation of relevant policies.

Combined with multi-source and heterogeneous urban open data, the park layout was studied. Community information from different platforms such as Homelink and Anjuke was used for cross-validation to obtain more detailed housing price information and other data, to improve the accuracy of the park service target population positioning experiment. Based on the current road network of the city, combined with the travel data of various transportation modes such as POI of urban public transportation stations, the travel modes and routes of citizens are considered from multiple perspectives, which enhances the objectivity of the experimental data and improves the credibility of the experimental results. The POI data of urban cultural and entertainment facilities, office facilities, commercial service facilities, public facilities, and residential areas obtained from Baidu API have a relatively comprehensive grasp of the spatial and geographical location of the population distribution in the central urban area, which improves the comprehensiveness of the experimental data analysis.

Because of the principle of urban green space layout planning, the following two aspects are further considered. First, the use heat and service pressure of various urban parks are classified according to the nature of park use, to analyze the service level and efficiency of parks. The service level of green space in the central city has strong correlation with the type and geographical location of park green space. The use of the comprehensive park is affected by the type of recreation space, service facilities, and the convenience of the park transportation. The comprehensive benefit and service level of the park are high. The popularity of special parks has little correlation with the distribution number of surrounding traffic facilities, but with the characteristic recreation space and popular science education activities. The location factors of community parks and street parks are obviously greater than the scale factors, so the layout should be combined with the areas with high population distribution density and high land development intensity. Second, the evaluation index and model were constructed through the influence factors of bus station density, housing price, cultural and entertainment facilities, office facilities, commercial service facilities, public facilities, and residential areas, and the evaluation results of urban green space demand were calculated. Through the demand evaluation analysis of park green space, it is concluded that the area with a higher evaluation level should have more dense community parks and street-side green space with a higher service level and be closer or more convenient to regional or city-wide large parks.

Data availability statement

The original contributions presented in the study are included in the article/Supplementary Material; further inquiries can be directed to the corresponding author.

Author contributions

JZ and JC contributed to the conception of this study. MY and JC carried out the design and production of some diagrams. JZ and LW contributed significantly to the analysis and manuscript preparation. JZ performed the data analyses and wrote the manuscript. MY and LW helped perform the analysis with constructive discussions. All authors contributed to the manuscript and approved the submitted version.

Funding

This study was supported by the National Natural Science Foundation of China (Grant No. 42161041) and the Youth Project of Science and Technology Agency in Yunnan Province (Grant No. 202101BA070001-275).

Conflict of interest

Author MY was employed by the company of Yunnan Design Institute Group Engineering Investment Co., Ltd.

The remaining authors declare that the research was conducted in the absence of any commercial or financial relationships that could be construed as a potential conflict of interest.

Publisher's note

All claims expressed in this article are solely those of the authors and do not necessarily represent those of their affiliated organizations, or those of the publisher, the editors, and the reviewers. Any product that may be evaluated in this article, or claim that may be made by its manufacturer, is not guaranteed or endorsed by the publisher.

References

Addas, A. (2022). Exploring the pattern of use and accessibility of urban green spaces: Evidence from a coastal desert megacity in Saudi arabia. *Environ. Sci. Pollut. Res.* 29 (37), 55757–55774. doi:10.1007/S11356-022-19639-4

Ahas, R., Silm, S., Järv, O., Saluveer, E., and Tiru, M. (2010). Using mobile positioning data to model locations meaningful to users of mobile phones. *J. Urban Technol.* 17 (1), 3–27. doi:10.1080/10630731003597306

Bai, H., Li, Z. W., Guo, H. L., Chen, H. P., and Luo, P. P. (2022). Urban green space planning based on remote sensing and geographic information systems. *Remote Sens.* 14 (17), 4213. doi:10.3390/RS14174213

Cai, Y. L., Cao, S. S., Du, M. Y., Li, S. F., and Chen, S. S. (2021). Estimation and analysis of driving factors of total AHF in prefecture-level of China. *J. Geo-information Sci.* 23 (3), 405–418. doi:10.12082/dqxxkx.2021.200097

Charlotte, C., Dagmar, H., Stefan, H., and Dnadja, K. (2022). Urban green space interaction and wellbeing – investigating the experience of international students in berlin during the first COVID-19 lockdown. *Urban For. & Urban Green.*, 127543. doi:10.1016/J.UFUG.2022.127543

Chen, D., Long, X., Li, Z. G., Liao, C., Xie, C. K., and Che, S. Q. (2021a). Exploring the determinants of urban green space utilization based on microblog check-in data in Shanghai, China. *Forests* 12 (12), 1783. doi:10.3390/F12121783

Chen, S. S., Haase, D., Xue, B., Wellmann, T., and Qureshi, S. (2021b). Integrating quantity and quality to assess urban green space improvement in the Compact City. *Land* 10 (12), 1367. doi:10.3390/LAND10121367

Chen, Y. S. (2011). Construction and application of suitability evaluation index system for urban park green space. *J. Northeast For. Univ.* 39 (7), 105–108. doi:10.13759/j.cnki.dlxb.2011.07.025

Danilina, N., Tsurenkova, K., and Berkovich, V. (2021). Evaluating urban green public spaces: The case study of krasnodar region cities, Russia. *Sustainability* 13 (24), 14059. doi:10.3390/SU132414059

Donahue, M. L., Keeler, B. L., Wood, S. A., Fisher, D. M., Hamstead, Z. A., and McPhearson, T. (2018). Using social media to understand drivers of urban park visitation in the Twin Cities, MN. *Landsc. Urban Plan.* 175 (5), 1–10. doi:10.1016/j.landurbplan.2018.02.006

Gao, Y. Y., Zhang, X. R., Zhang, Z. Q., and al, e. (2021). Research on urban spatial structure based on double constraints of POI big data and accessibility. *Geogr. Geo-Information Sci.* 37 (3), 59–64. doi:10.3969/j.issn.1672-0504.2021.03.009

Han, X. L., and Wang, L. H. (2020). Impact of built environmental on the vitality of micro public open space. *Planners* 36 (9), 64. doi:10.3969/j.issn.1006-0022.2020.09.009

Huang, Y. Y., Lin, T., Zhang, G. Q., Zhu, Y. G., Zeng, Z. W., and Ye, H. (2021). Spatial patterns of urban green space and its actual utilization status in China based on big data analysis. *Big Earth Data* 5 (3), 391–409. doi:10.1080/20964471.2021.1939990

Isabella, D. M., Claudia, B., Giulia, C. M., Alessandro, C., and Alessandro, P. (2022). Citizens' use of public urban green spaces at the time of the COVID-19 pandemic in Italy. *Urban For. Urban Green.* 77 (2022), 127739. doi:10.1016/J.UFUG.2022.127739

Jinwon, K., Jerry, L. K., and Brijesh, T. (2022). Visualizing fairness: Distributional equity of urban green spaces for marginalized groups. *J. Environ. Plan. Manag.* 65 (5), 833–851. doi:10.1080/09640568.2021.1915258

Jordan, P., Hoover, F. A., and Hopton, M. E. (2022). Leveraging ancillary benefits from urban greenspace-a case study of St. Louis, Missouri. *Urban Water J.* 19 (3), 314–323. doi:10.1080/1573062X.2021.2001544

Kuang, W., Li, S., and Zhou, H. D. (2021). Method of accurately evaluating spatial equity of urban park green space: A case study of haidian District, beijing. *J. Huazhong Agric. Univ.* 41 (11), 36–44. doi:10.13300/j.cnki.hnlkxb.2022.01.015

Lennon, M. (2021). Green space and the compact city: Planning issues for a 'new normal. *Cities Health* 5 (1), 212–215. doi:10.1080/23748834.2020.1778843

Li, B., Song, Y., and Yu, K. J. (2008). Evaluation method for measurement of accessibility in urban public green space planning. *Acta Sci. Nat. Univ. Pekin.* 44 (4), 618–624. doi:10.13209/j.0479-8023.2008.096

Li, K. Y., and Lu, L. (2021). Research on spatial distribution of urban green space service based on POI data: A case study of zhengzhou city, Henan Province. *Areal Res. Dev.* 40 (6), 75–80. doi:10.3969/j.issn.1003-2363.2021.06.013

Li, W., Wang, H., Zhang, S., Jiang, B., and Young, L. S. (2022). Spatial and temporal evolution of urban green space pattern based on GIS sensors and remote sensing information: Taking xi'an as an example. *J. Sensors* 2022, 1–8. doi:10.1155/2022/3648880

Li, X. M., and Liu, C. F. (2009). Accessibility and service of Shenyang's urban parks by network analysis. *Acta Ecol. Sin.* 29 (3), 1554. doi:10.3321/j.issn:1000-0933.2009.03.054

Liu, H. L., Zheng, T. M., and Nie, J. X. (2021a). On the spatial allocation of the quantity and diversity of basic urban public service facilities: A case study of Wuhan inner city. *City Plan. Rev.* 45 (2), 84. doi:10.11819/cpr20210211a

Liu, Q., Hou, L., Sana, S., Usman, T., Rabia, R., and Shahla, R. S. (2021b). Perceptions of spatial patterns of visitors in urban green spaces for the sustainability of smart city. *Int. J. Distributed Sens. Netw.* 17 (8), 155014772110340. doi:10.1177/15501477211034069

Liu, S., Su, C., Yang, R., Zhao, J., Liu, K., Ham, K., et al. (2022). Using crowdsourced big data to unravel urban green space utilization during COVID-19 in Guangzhou, China. *Land* 11 (7), 990. doi:10.3390/LAND11070990

Ma, Q., Wang, L. X., Gong, X., and Li, K. (2022). Research on the rationality of public toilets spatial layout based on the POI data from the perspective of urban functional area. *J. Geo-Information Sci.* 24 (1), 50. doi:10.12082/dqxxkx.2022.210331

Mendoza, H., Loureiro, L. R., Gadeyne, S., Lefebvre, W., Vanpoucke, C., and Casas, L. (2022). Urban green spaces and suicide mortality in Belgium (2001-2011): A census-based longitudinal study. *Environ. res.*, 114517. doi:10.1016/J.ENVRES.2022.114517

Monika, O., Michael, D., and Jennifer, D. (2022). Urban greenspace access, uses, and values: A case study of user perceptions in metropolitan ravine parks. *Urban For. Urban Green.*, 127522. doi:10.1016/J.UFUG.2022.127522

Morar, C., Lukić, T., Valjarević, A., Niemets, L., Kostrikov, S., Sehida, K., et al. (2022). Spatiotemporal analysis of urban green areas using change detection: A case study of kharkiv, Ukraine. *Front. Environ. Sci.* 10 (2022), 823129. doi:10.3389/FENVS.2022.823129

Mueller, W., Milner, J., Loh, M., Vardoulakis, S., and Wilkinson, P. (2022). Exposure to urban greenspace and pathways to respiratory health: An exploratory systematic review. *Sci. Total Environ.* 829 (2022), 154447. doi:10.1016/J.SCITOTENV.2022.154447

Muluneh, M. G., and Worku, B. B. (2022). Contributions of urban green spaces for climate change mitigation and biodiversity conservation in Dessie city, Northeastern Ethiopia. *Urban Clim.* 46 (2022), 101294. doi:10.1016/J.UCLIM.2022.101294

Qi, R. H., Yang, W. R., Wang, S. L., Xie, Q. Y., and Wang, Y. J. (2018). Study on evaluation and planning of urban parks based on Baidu POI data. *Chin. Landsc. Archit.* 34 (3), 32. doi:10.3969/j.issn.1000-6664.2018.03.006

Qin, S. W., Yang, J. Y., Feng, Y. R., and Yan, S. (2021). Spatiotemporal vitality and influencing factors of urban parks based on multi-source data: A case study of nanjing. *Chin. Landsc. Archit.* 37 (1), 68–73. doi:10.19775/j.cla.2021.01.0068

Schindler, M., Le, T. M., and Caruso, G. (2022). How far do people travel to use urban green space? A comparison of three European cities. *Appl. Geogr.* 141 (2022), 102673. doi:10.1016/J.APGEOG.2022.102673

Sim, J., Miller, P., and Swarup, S. (2020). Tweeting the high line life: A social media lens on urban green spaces. *Sustainability* 21 (12), 8895. doi:10.3390/su12218895

Slaev, A. D., Alexander, E. R., Zdravkov, Z., Ivanov, V., and Georgieva, S. (2022). Market tools for the provision of urban green spaces in post-socialist Sofia. *Land Use Policy* 122 (2022), 106377. doi:10.1016/J.LANDUSEPOL.2022.106377

Taleai, M., Sliuzas, R. V., and Flacke, J. (2014). An integrated framework to evaluate the equity of urban public facilities using spatial multi-criteria analysis. *Cities* 40, 56–69. doi:10.1016/j.cities.2014.04.006

Tang, Z. L., and Gu, S. (2015). An evaluation of social performance in the distribution of urban parks in the central city of Shanghai: From spatial equity to social equit. *Urban Plan. Forum* 48 (9), 48–56. doi:10.16361/j.upf.201502001

Tu, X. Y., Huang, G. L., Wu, D. F., and Guo, X. (2020). How do travel distance and park size influence urban park visits? *Urban For. Urban Green.* 52 (2020), 126689. doi:10.1016/j.ufug.2020.126689

Tu, X. Y., Huang, G. L., and Wu, J. G. (2019). Review of the relationship between urban green space accessibility and human well-being. *Acta eco. Sin.* 39 (2), 421–431. doi:10.5846/stxb201802030294

Wang, P. W., Han, L. R., and Mei, R. (2022). An impact asymmetry analysis of small urban green space attributes to enhance visitor satisfaction. *Int. J. Environ. Res. Public Health* 19 (5), 2922. doi:10.3390/ijerph19052922

Wu, D. F., Yang, R., and Liu, H. L. (2007). Minneapolis park system and its water space. *Chin. Landsc. Archit.* 23 (3), 24. doi:10.3969/j.issn.1000-6664.2007.03.006

Wu, H., and Peng, Z. H. (2015). Application of big data technology in urban planning. *City Plan. Rev.* 39 (9), 93–99. doi:10.11819/cpr20150916a

Xue, B., Xiao, X., and Li, J. Z. (2020a). Identification method and empirical study of urban industrial spatial relationship based on POI big data: A case of Shenyang city, China. *Geogr. Sustain.* 1 (2), 152–162. doi:10.1016/j.geosus.2020.06.003

Xue, B., Xiao, X., Li, J. Z., and Xie, X. (2020b). Analysis of spatial economic structure of Northeast China cities based on Points of Interest big data. *Sci. Geogr. Sin.* 40 (5), 691–700. doi:10.13249/j.cnki.sgs.2020.05.003

Xue, B., Xiao, X., Li, J. Z., Xie, X., Ren, W. X., and Lu, C. P. (2019). POI-based analysis on the affecting factors of property prices' spatial distribution in the traditional industrialarea. *Hum. Geogr.* 34 (4), 106–114. doi:10.13959/j.issn.1003-2398.2019.04.013

Xue, B., Xiao, X., Li, J. Z., Zhao, B. Y., and Fu, B. (2023). Multi-source data-driven identification of urban functional areas: A case of shenyang, China. *Chin. Geogr. Sci.* doi:10.1007/s11769-022-1320-2

Xue, B., Zhang, L., Geng, Y., Mitchell, B., and Ren, W. (2016). Extended land use categories in urban brownfield redevelopment of China: Case of Tiexi District, Shenyang of China. *J. Urban Plan. Dev.* 142 (3), 1. doi:10.1061/(ASCE)UP.1943-5444.0000309

Ye, J., Kang, S. Q., Fu, G. S., Lü, H. Y., Qian, W. Q., and Tang, X. H. (2022). Research progress of urban green space landscape pattern change based on satellite remote sensing. *Bull. Surv. Mapp.* (3), 23–27. doi:10.13474/j.cnki.11-2246.2022.0071

Yoo, E. h., and Roberts, J. E. (2022). Static home-based versus dynamic mobility-based assessments of exposure to uUrban green space. *Urban For. Urban Green.*, 127528. doi:10.1016/J.UFUG.2022.127528

Yuan, B., Zhou, L., Dang, X., Sun, D., Hu, F., and Mu, H. (2021). Separate and combined effects of 3D building features and urban green space on land surface temperature. *J. Environ. Manage.* 295, 113116. doi:10.1016/j.jenvman.2021.113116

Zabelskyte, G., Kabisch, N., and Stasiskiene, Z. (2022). Patterns of urban green space use applying social media data: A systematic literature review. *Land* 11 (2), 238. doi:10.3390/LAND11020238

Zhai, X. J., Sun, X. H., and Sun, Z. Y. (2017). Research on the quantity and distribution characteristics of public cultural facilities in central area of Zibo city based on POI data. *J. Shandong Normal Univ. Nat. Sci.* 32 (2), 73–79. doi:10.3969/j.issn.1001-4748.2017.02.013

Zhang, B., Xie, Z. X., Hao, L., and Gao, J. X. (2022a). The leisure service and its spatial differences of urban green space in Shanghai. *Ecol. Sci.* 41 (2), 114–123. doi:10.14108/j.cnki.1008-8873.2022.02.014

Zhang, L., Chen, P. F., and Hui, F. M. (2022b). Refining the accessibility evaluation of urban green spaces with multiple sources of mobility data: A case study in Shenzhen, China. *Urban For. Urban Green.* 70 (2022), 127550. doi:10.1016/J.UFUG.2022.127550

Zhang, S. N., Li, X. P., Chen, Z. L., and Ou, Y. Y. (2022c). A bibliometric analysis of the study of urban green spaces and health behaviors. *Front. Public Health* 10 (2022), 1005647. doi:10.3389/FPUBH.2022.1005647

Zhou, L., Yuan, B., Hu, F. N., Wei, C. Z., Dang, X. W., and Sun, D. Q. (2022). Understanding the effects of 2D/3D urban morphology on land surface temperature based on local climate zones. *Build. Environ.* 208 (2022), 108578. doi:10.1016/j.buildenv.2021.108578

Zhou, L., Zhou, C. H., Che, L., and Wang, B. (2020). Spatio-temporal evolution and influencing factors of urban green development efficiency in China. *J. Geogr. Sci.* 30 (5), 724–742. doi:10.1007/s11442-020-1752-5

frontiers | Frontiers in Environmental Science

TYPE Original Research
PUBLISHED 01 December 2022
DOI 10.3389/fenvs.2022.1071668

Check for updates

OPEN ACCESS

EDITED BY
Jun Yang,
Northeastern University, China

REVIEWED BY
Sihan Xue,
Zhengzhou University, China
Junyi Hua,
Ocean University of China, China

*CORRESPONDENCE
Xiao Liu,
xiaoliu@scut.edu.cn
Ying bao,
yingbaoscut@126.com

SPECIALTY SECTION
This article was submitted to Environmental Informatics and Remote Sensing, a section of the journal Frontiers in Environmental Science

RECEIVED 16 October 2022
ACCEPTED 14 November 2022
PUBLISHED 01 December 2022

CITATION
Li K, Liu X and Bao Y (2022), Evaluating the performance of different thermal indices on quantifying outdoor thermal sensation in humid subtropical residential areas of China. *Front. Environ. Sci.* 10:1071668. doi: 10.3389/fenvs.2022.1071668

COPYRIGHT
© 2022 Li, Liu and Bao. This is an open-access article distributed under the terms of the Creative Commons Attribution License (CC BY). The use, distribution or reproduction in other forums is permitted, provided the original author(s) and the copyright owner(s) are credited and that the original publication in this journal is cited, in accordance with accepted academic practice. No use, distribution or reproduction is permitted which does not comply with these terms.

Evaluating the performance of different thermal indices on quantifying outdoor thermal sensation in humid subtropical residential areas of China

Kunming Li[1], Xiao Liu[2,3,4,5]* and Ying Bao[2,3,4]*

[1]Department of Architecture, Henan University of Technology, Zhengzhou, China, [2]School of Architecture, South China University of Technology, Guangzhou, China, [3]State Key Laboratory of Subtropical Building Science, South China University of Technology, Guangzhou, China, [4]Architectural Design and Research Institute Co., Ltd, South China University of Technology, Guangzhou, China, [5]Faculty of Architecture, The University of Hong Kong, Hong Kong, Hong Kong SAR, China

Considerations of urban microclimate and thermal comfort are necessary for urban development, and a set of guidelines for a comfortable microclimate must be developed. However, to develop such guidelines, the predictive ability of thermal indices for outdoor thermal perceptions under different design decisions must be defined. The present study aimed to determine suitable indices for assessing outdoor thermal reaction in humid subtropical residential areas of China. Five criteria of coefficients of determination, Spearman's rho, percentage of correct prediction, percentage of thermal comfort indices' class predictions, and distribution of thermal comfort indices' class predictions per class of thermal sensation votes (TSV) were established to assess the performance of four thermal indices commonly used in outdoor thermal comfort research of China. The empirical thermal comfort index (TSV_{model}) had a better correlation with TSV, while the Universal Thermal Climate Index (UTCI) was the most successful, simulating 29.8% of TSV. The testability of Physiologically Equivalent Temperature (PET) and Standard Effective Temperature (SET*) were very low, with the correct predictive ability 16.5% and 24.4% respectively. In the selected indices, the UTCI reasonably approximated the observed data for this study and was recommended to assess the outdoor thermal comfort for evaluating the thermal comfort level under different design decisions. For all the indices, the systematic errors were

Abbreviations: PMV, Predicted Mean Vote [-]; SET*, Standard Effective Temperature [°C]; OUT_SET*, Outdoor Standard Effective Temperature [°C]; PET, Physiologically Equivalent Temperature [°C]; UTCI, Universal Thermal Climate Index [°C]; DI, Discomfort index [-]; CP, Cooling Power [W/m^2]; THI, Temperature-Humidity Index [°C]; Ts, Thermal Sensation [-]; TSV, Thermal Sensation Votes [-]; TSV_{model}, The empirical thermal comfort index [-]; T_{mrt}, Mean Radiant Temperature [°C]; Adu, Surface area of the unclothed body [m^2]; Ta, Air temperature [°C]; RH, Relative humidity [%]; G, Global radiation [W/m^2]; Tg, Globe temperature [°C]; D, Globe diameter [m]; ε, Globe emissivity [-]; M, Metabolic rates [W]; Clo, Clothing insulation [clo]; RMSE, Root mean square error [°C]; RMSEs, Systematic errors [°C]; RMSEu, Unsystematic errors [°C]; d, Index of agreement [-]; V_a, Wind speed at a height of 1.1 m above the ground [m/s]; V_{10m}, Wind speed at a height of 10 m above the ground [m/s].

generally higher than the unsystematic errors, indicating that the assessment scales do not adapt to humid subtropical residential areas of China. It is necessary to establish the thermal sensation ranges of humid subtropical areas of China.

KEYWORDS

humid subtropical area, thermal sensation votes, thermal comfort indices, assessment, performance

1 Introduction

Most of the world's population lives in cities and is continuously becoming more urbanized (United Nation, 2019). By the end of 2021, the urbanization rate of China was 64.7% (China Bureau of Statistics, 2021), indicating more than 914.2 million people lived in cities. In the context of Chinese reality, most urban population live in concentrated residential areas. The outdoor space of residential area is an organic part of the city, and their quality provides comfort and healthy surroundings to city dwellers (Du and Xia, 2018; He, 2022) and contributes to the energy efficiency of buildings (Yang et al., 2014; Li et al., 2021; Li et al., 2022). Consequently, the creation of attractive outdoor spaces is one of the main tasks of planning designer. However, at the design stage, planners and architects face difficulties in assessing the impact of different design concepts on people's perception. For the proposed difficulties, numerous thermal comfort indices have been developed to assess outdoor thermal comfort.

At present, commonly used thermal comfort indices for the valuation of outdoor thermal comfort could be divided into two groups of empirical and rational indices (Haghshenas et al., 2021). The former is derived from environmental variables and subjective estimates. One example is the correlation between subjective thermal sensation votes and measured microclimate parameters determined through multiple regression analysis. The rational indices are based on the heat balance equation of the human body. Common indicators for outdoor thermal comfort research are Predicted Mean Vote (PMV) (Fanger, 1970), Standard Effective Temperature (SET*) (Gagge et al., 1986), Outdoor Standard Effective Temperature (OUT_SET*) (Pickup and de Dear, 1999), Physiologically Equivalent Temperature (PET) (Höppe, 1999), and Universal Thermal Climate Index (UTCI) (Jendritzky et al., 2012). PMV, a heat balance model initially proposed by Fanger (1970), is more widely used for indoor conditions. SET* was developed by Gagge et al. (1986) based on Gagge's two-node model. PET based on the Munich energy-balance human body model–MEMI was introduced by Höppe (1999). To cover wider range of outdoor weather conditions, the UTCI index was designed based on Fiala's multi-node model (Jendritzky et al., 2012).

The existing standards and guidelines have no recommendations on which thermal comfort index is suitable for describing outdoor thermal comfort (Johansson et al., 2014; Fang et al., 2021; Haghshenas et al., 2021; Potchter et al., 2022). The choice of thermal index for outdoor thermal comfort evaluation has become a special research topic. In the Mediterranean climate, Tseliou et al. (2010) examined the ability of three indices, Discomfort index (DI), Cooling Power (CP), and PET, to describe the thermal sensation, illustrating that the performance of the three indices was limited. In an arid climate, Ruiz et al. (2015) demonstrated that there was a high contrast between subjective thermal sensation votes and the prediction results by six indices, including Temperature-Humidity Index (THI), Vinje's Comfort Index (PE), Thermal Sensation (TS), PMV, PET, and COMFA outdoor thermal comfort models, indicating that all models' testability was very low (below 25%). Pantavou et al. (2013) assessed the performance of numerous thermal indices to quantify the thermal sensation in Athens, Greece, demonstrating that the majority of the studied indices predicted approximately 35% of the thermal sensation votes. In severe cold area of China, Chen et al. (2020) compared the predictive ability of PET, SET*, and UTCI, demonstrated none of them applicable in predicting thermal perceptions. In cold region of China, Lai et al. (2014a) compared three different thermal comfort indices, PMV, PET, and UTCI, with the actual thermal reaction, proved that the UTCI provided a satisfactory outdoor thermal comfort prediction, while PMV overestimated it. In the hot-summer and cold-winter region of China, Wei et al. (2022) illustrated UTCI is better than PET for outdoor thermal comfort assessment. In Hong Kong, Ng and Cheng (2012) identified that PMV generally overestimated the thermal perception toward the warmer threshold in summer and *vice versa* in winter, recommended the use of PET as an alternative thermal index.

Residents in different regions have various thermal requirements due to climate adaptation (Lin, 2009). Furthermore, both psychological and physiological differences between ethnicities could influence human thermal perception (Lin, 2009). In addition, none of the mentioned thermal comfort models were built based on Chinese experimental studies. Furthermore, the yearly increase in the duration of hot weather in the humid subtropical areas of China (He et al., 2022; Yang et al., 2022) has a great impact on the use of outdoor space (Huang et al., 2022). Therefore, it is necessary to propose an adaptive model to quantify the correlations between urban microclimate and outdoor thermal sensation in humid subtropical residential areas of China and assess the effects of different design ideas on people's comfort. Therefore, the performances of different thermal indices for predicting thermal sensation in humid subtropical residential areas of China were evaluated.

2 Material and methods

2.1 Field surveys

2.1.1 Sites

The database of this study was conducted in Guangzhou, China. It has a humid subtropical climate under the Köppen climate classification. The monthly mean air temperature varied slightly throughout the year, with a range of 13–29°C (Figure 1), indicating a hot summer and a warm winter. The monthly mean relative humidity was higher, being more than 60% all year.

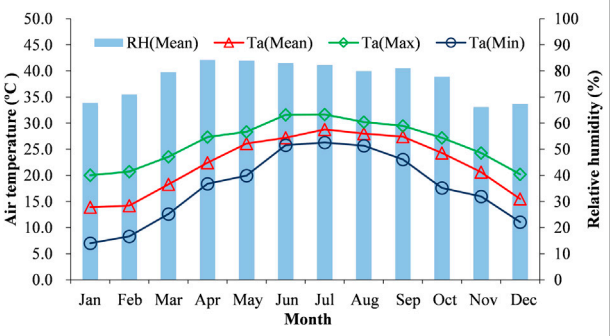

FIGURE 1
Monthly mean/maximum/minimum air temperature and mean relative humidity of Guangzhou based on the meteorological data from China Meteorological Administration and Tsinghua University (2005).

In order to obtain residents' thermal sensation votes under different urban microclimates, field survey sites were selected to capture a wide range of thermal environment level in humid subtropical residential areas of China. Wind environment, direct solar radiation, reflected solar radiation and long wave radiation were considered comprehensively. Finally, eight sites were selected. The site features are shown in Figure 2. There were different microclimate conditions in the eight survey sites (e.g., shaded, sunlit, windy, windless, *etc.*). Thus, the observational data covered a wide range of thermal environment that people may encounter in humid subtropical residential areas of China.

2.1.2 Questionnaire surveys

To obtain subjects' thermal comfort conditions in all possible weather conditions appeared in the hot and humid area of China, the questionnaire survey was designed from the cold season to the hot season. Table 1 summarized the questionnaire surveys schedule on 24 days. The questionnaire surveys were performed during the timeframes of 8:00–12:00 and 14:00–18:00 in cold season and shoulder season, and 7:00–12:00 and 15:00–19:00 in hot season, when the outdoor space was commonly used. Each activity site was visited once a day in each season. Two spots were not surveyed in shoulder season because of continuous rainy

FIGURE 2
Sites configurations. Sites A1, B3, and B4 are shaded and windless; Site C5 is shaded and windy; Sites A2 and D7 are sunlit and windy; Sites C6 and D8 are sunlit and windless.

TABLE 1 Surveys schedule.

Seasons	Month	Day	Questionnaires
Cold season	January	10, 17, 19, 22, 25, 28	305
	February	2, 8	
Shoulder season	April	4, 14, 16, 22, 23, 27	216
Hot season	June	20, 22, 27, 28	484
	August	2, 6, 19, 22	
	September	6, 11	

days, and two sites were surveyed twice in hot season. 1,005 valid questionnaires were obtained in this study: 305 in cold season, 216 in shoulder season, and 484 in hot season. The samples had a good balance of sex ratio (45.3% male and 54.7% female). The age of the survey subjects varied from 8 to 64 years old (mean age of 33.2 years old).

The questionnaire contained two parts. The first part was the subjects' personal information covered age, gender, height, weight, clothing worn, activity level, and reasons for visiting a particular place. The second section involved thermal perception related voting contained thermal sensation votes (TSV), thermal comfort votes (TCV), thermal acceptance vote and preference vote. The TSV in this study adopted the 9-point scale (i.e., "very cold" −4; "cold" −3; "cool" −2; "slightly cool" −1; "neutral" 0; "slightly warm" +1; "warm" +2; "hot" +3; "very hot" +4). The TCV was rated on a 4-point scale (i.e., "comfortable" 0; "slightly uncomfortable" +1; "uncomfortable" +2; "very uncomfortable" +3). The conventional 4-point scale (i.e., "clearly acceptable" +1; "just acceptable" +0.01; "just unacceptable" -0.01; "clearly unacceptable" -1) was used for thermal acceptability. The preference vote involved air temperature, relative humid, wind speed, and global radiation and was given on a 3-point scale (i.e., "decrease" −1; "not change" 0; "increase" +1).

2.1.3 Physical measurement

During the questionnaire survey, microclimatic variables (i.e., air temperature (Ta); relative humidity (RH); wind speed (V_a); globe temperature (Tg) and global radiation (G)) next to the interviewees were measured. Based on the recommended sensor height for standing subjects in ISO 7726 (ISO 7726, 1998), all instruments were placed at a height of 1.1 m above the ground. The accuracies of Ta sensor (HOBO Pro V2 U23-001), RH sensor (HOBO Pro V2 U23-001), V_a sensor (HD32.3), Tg sensor (HD32.3) and G sensor (LP 471 PYRA 02.5) were ± 0.20°C, ± 2.5%, ± 0.15 m/s, ± 0.50°C and ± 5 W/m^2, respectively. The ranges and accuracies of the instruments were all in accord with the ISO 7726 standard (ISO 7726, 1998). The Ta and RH sensors were shielded from solar irradiance with forced ventilation. On the measurement day, the thermal environment parameters were acquired at 1 min intervals.

2.2 Selected thermal indices and indices processing

In 2020, Li and Liu (2020) published a literature review article of 123 studies that investigated outdoor thermal comfort in China. The proportions of thermal indices applied in the reviewed publications are shown in Figure 3. The types of indices varied significantly among the studies. The most commonly used index was PET, followed by UTCI and SET*. In some outdoor thermal comfort studies of humid subtropical areas in China, local empirical thermal comfort index (TSV_{model}) have been developed through multiple linear regressions between actual thermal sensation votes and some microclimatic variables (Table 2). Therefore, the present study selected PET, SET*, UTCI, and TSV_{model} as the comparison indices.

Table 3 shows the selected thermal indices sorted by name and key parameters and the formulas or models for their calculation in the present study. The UTCI was calculated using "UTCI calculator" provided on the www.utci.org website (Bröde et al., 2012). PET was calculated using the RayMan software (Matzarakis et al., 2007). SET* was calculated using MATLAB code. All the thermal indices were calculated using the measured parameters 3-min average, as this was the estimated time for completing a questionnaire. The empirical thermal comfort index based on the annual data was selected as the TSV_{model}. The annual TSV_{model} in Guangzhou (Fang et al., 2021) was based on the voting of young college students. Therefore, the selected TSV_{models} was the empirical formula of Hong Kong (Cheng et al., 2012) located in the same climate zone as Guangzhou. The TSV_{model} (with RH) considered four microclimate variables, including air temperature, relative humidity, wind speed, and solar radiation, while the TSV_{model} (without RH) considered three microclimate variables, air temperature, wind speed, and solar radiation. The following equation was used to correct the wind speed at 10 m height.

$$V_m = V_a \times \left(\frac{H_m}{H_a}\right)^{0.22}$$

Where: V_m is the wind speed at the desired height (m/s), V_a is the measured wind speed (m/s), H_m is the desired height (m), and H_a is the measurement height 1.1 m.

The mean radiant temperature (T_{mrt}) is one of the most important variables for calculating PET, SET*, and UTCI. T_{mrt} is calculated from the measured globe temperature combined with measurements of wind speed and air temperature according to the following formula (Thorsson et al., 2007):

$$T_{mrt} = \left[\left(T_g + 273.15\right)^4 + \frac{1.10 \times 10^8 V_a^{0.6}}{\varepsilon D^{0.4}}\left(Tg\text{-}Ta\right)\right]^{0.25} - 273.15$$

where V_a is the measured wind speed (m/s), Ta is the air temperature (°C), Tg is the globe temperature (°C), D is the globe diameter (m), and ε is the globe emissivity.

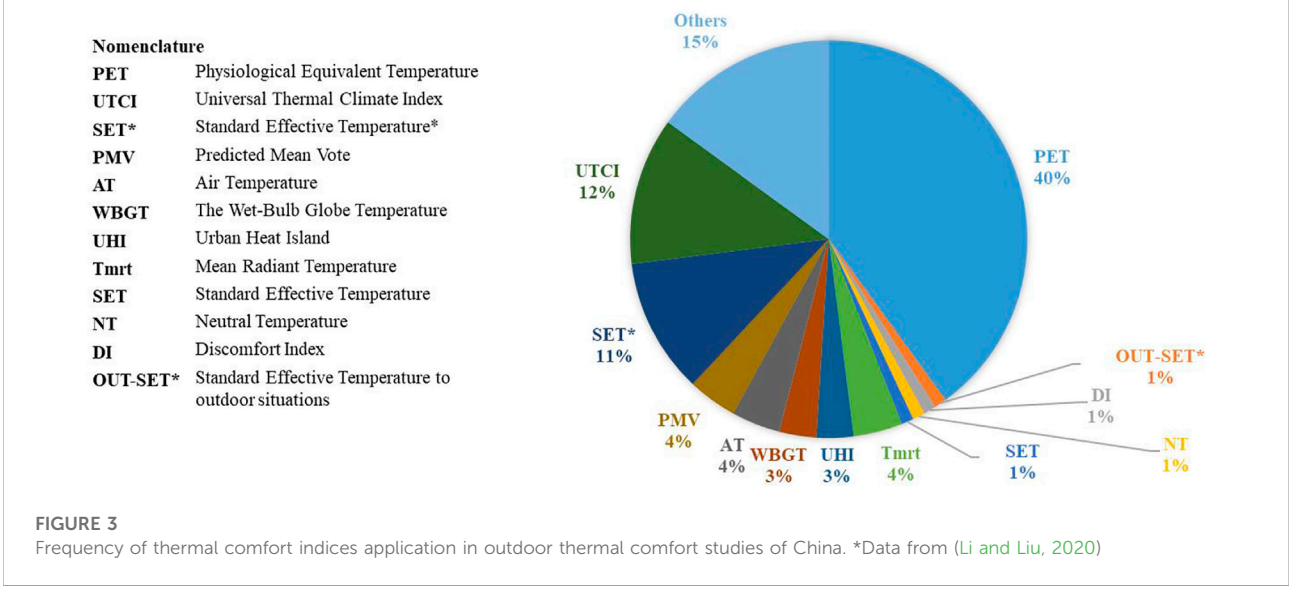

FIGURE 3
Frequency of thermal comfort indices application in outdoor thermal comfort studies of China. *Data from (Li and Liu, 2020)

TABLE 2 Thermal comfort regression models in humid subtropical areas of China.

References	Location	Empirical TSVmodel	R^2
Cheng et al. (2012)	Hong Kong, China	TSV_{model} (with RH) = 0.1185Ta − 0.6091V_a + 0.0025G + 0.1155RH − 4.77 (annual), TSV_{model} (without RH) = 0.1185Ta − 0.6091V_a + 0.0025G − 2.47 (annual)	0.91 0.90
Yang et al. (2013)	Changsha, China	TSV_{model} = 0.313Ta + 0.030T_{mrt} − 0.304V_a + 0.026RH − 11.622 (summer)	0.552
Lai et al. (2014b)	Wuhan, China	TSV_{model} = 0.0643Ta + 0.00076SR − 0.161V_a − 0.00376RH − 1.382 (summer and autumn)	0.670
Zhao et al. (2016)	Guangzhou, China	TSV_{model} = 0.245Ta + 0.059T_{mrt} − 0.457V_a + 0.013RH − 8.527 (summer)	0.598
Fang et al. (2021)	Guangzhou, China	TSV_{model} = 0.197Ta + 0.002RH − 0.373V_a + 0.014T_{mrt} + 0.161Clo + 0.141M − 4.741 (annual)	0.56

TABLE 3 Thermal indices along with the key parameters and the formulas or the models for their calculation.

Indices	Parameters	Formulas/models	References
PET	Ta, RH, V_a, T_{mrt}, M[a], Clo[a], Sex, Weight, Height	MEMI.model	Höppe (1999); Matzarakis et al. (2007)
SET[a]	Ta, RH, V_a, T_{mrt}, M, Clo, Adu[a], Weight	Gagge's two-node model	Gagge et al. (1986)
UTCI	Ta, RH, V_{10m}[a], T_{mrt}	6th order polynomial calculated by Ta, RH, V_{10m}[a], T_{mrt}	Jendritzky et al. (2012); Bröde et al. (2012)
TSV_{model}	Ta, RH, V_a, G	TSV_{model} (with RH) = 0.1185Ta − 0.6091V_a + 0.0025G + 0.1155RH − 4.77 (R^2 = 0.91), TSV_{model} (without RH) = 0.1185Ta − 0.6091V_a + 0.0025G − 2.47 (R^2 = 0.90)	Cheng et al. (2012)

[a]Note: M is the metabolic rates; Clo is the clothing insulation; Adu is the surface area of the unclothed body; V_{10m} is the wind speed at a height of 10 m above the ground.

2.3 Data analysis

2.3.1 Three statistical and two qualitative criteria

Three statistical and two qualitative criteria were selected and established to verify the performance of thermal indices for quantifying outdoor thermal sensations (Monteiro and Alucci, 2006): 1) the coefficient of determination between the thermal comfort indices' parameters and TSV, 2) the Spearman's rho correlation coefficient between the thermal comfort indices value and TSV, 3) the percentage of correct

TABLE 4 Assessment scales of selected thermal indices.

Thermal sensation	PET (°C)	SET* (°C)	UTCI (°C)	TSV_{model}
Hot +3	>42	>44	>34	>2.5
Warm +2	36–42	38–44	28–34	1.5–2.5
Slightly warm +1	30–36	32–38	22–28	0.5–1.5
Neutral 0	24–30	26–32	16–22	−0.5–0.5
Slightly cool -1	18–24	20–26	10–16	−1.5~ −0.5
Cool -2	12–18	14–20	4–10	−2.5~ −1.5
Cold -3	<12	<14	<4	<−2.5

predictions, 4) the percentage of thermal comfort indices' class predictions, and 5) the distribution of thermal comfort indices' class predictions per class of TSV, assessed by cross-tabulation analysis.

The first coefficient of determination illustrated the possible potential of the model, indicating how well the model variables vary in function with variations in thermal responses. The second correlation verified the sensibility of the indices, showing how well the results of thermal comfort indices vary in function to variations in thermal responses. It has been argued that the coefficient of determination and Spearman's rho correlation coefficient are often inappropriate or misleading when comparing model-predicted and observed variables (Potchter et al., 2022). The relationship between the coefficient of determination and Spearman's rho correlation coefficient and model performance was not always consistent. Therefore, other evaluation criteria must be introduced. The last three criteria were selected to indicate the performance of the indices, focusing on the compare of coincidence between the prediction by the selected thermal indices and the actual thermal sensation votes perceived by the interviewees.

2.3.2 Thermal comfort indices' assessment scales

To apply the last three criteria, assessment scales for thermal comfort indices should be established. Table 4 lists the assessment scales of the selected thermal comfort indices. The assessment scales were established on the basis of earlier comfort researches: reasonable estimate threshold on thermal perception and the neutral temperature of previous studies in humid subtropical areas of China (de Dear and Brager, 1998; Lin and Matzarakis, 2008; Lin et al., 2011; Huang et al., 2016). The neutral PET was 27.17°C (Lin and Matzarakis, 2008), suggesting the neutral range was from 27.17 − 3.00 to 27.17 + 3.00, or simply 24–30°C. Correspondingly, the range of feeling "slightly warm" +1 was obtained through a 6°C increase of the range of "neutral" 0; and "slightly cool" −1 was obtained through a 6°C decrease of the "neutral" 0 range. The neutral SET* values were 28°C and 29.3°C in the cool and hot seasons, respectively (Lin et al., 2011). The SET* assessment scales were calculated based on neutral SET* 29°C. The assessment scales of the UTCI were calculated based on the neutral UTCI 19°C (Huang et al., 2016). Finally, the TSV_{model}'s assessment scales were set by the values ± 0.5, ±1.5, and ±2.5.

The analysis was further performed using *IBM SPSS* software. All variables presented in the following paragraphs were statistically significant at a confidence level equal to or less than 0.05 (Sig. ≤ 0.05).

3 Results and discussion

3.1 Microclimate conditions

The minimum, maximum, means, and standard deviations of the measured variables (including Ta, RH, V_a, and T_{mrt}) as well as the calculated thermal indices PET, UTCI and SET* were summarized in Table 5. Ta ranged between 14.7 and 38.3°C, which indicates that Guangzhou was climatically characterized by a hot summer and a warm winter. The variations in RH and T_{mrt} were significant throughout the year, as indicated by their standard deviations, with 17.9% and 7.7, respectively. RH ranged between 15.7 and 99.4% with an average value of 62.6% indicating relatively high humidity during the surveys. The variation in V_a was also significant, ranging between 0.0 and 3.9 m/s.

3.2 Outdoor thermal sensation

In the present study, the 9-point scale (i.e., "very cold" −4; "cold" −3; "cool" −2; "slightly cool" −1; "neutral" 0; "slightly warm" +1; "warm" +2; "hot" +3; "very hot" +4) of ISO 10551 was used to record thermal sensations, especially extreme hot sensations in the hot season. However, in previous studies in humid subtropical areas of China, in which the assessment scales were established based on, thermal sensation was rated on the ASHRAE 7-point scale (i.e., "cold"−3; "cool"−2; "slightly cool"−1; "neutral" 0; "slightly warm" +1; "warm" +2; "hot"

TABLE 5 The statistical results of the microclimate parameters.

Seasons		Ta (°C)	RH (%)	V_a (m/s)	T_{mrt} (°C)	PET (°C)	UTCI (°C)	SET* (°C)
Cold season	Min.	14.7	15.7	0.1	11.6	13.1	10.2	20.4
	Max.	26.4	89.7	3.9	37.1	28.8	27.4	32.6
	Mean	19.5	49.6	0.8	23.9	19.7	19.7	27.2
	St.Dev.	1.7	20.7	0.7	7.1	2.9	2.7	2.3
Shoulder season	Min.	22.8	56.5	0.0	22.3	26.6	28.2	28.6
	Max.	32.6	87.3	2.0	41.6	41.2	36.8	37.4
	Mean	25.7	70.3	0.7	26.9	30.9	31.1	31.9
	St.Dev.	1.6	7.4	0.4	3.1	2.3	1.6	1.6
Hot season	Min.	26.2	23.8	0.0	25.2	25.5	27.7	28.6
	Max.	38.3	99.4	3.2	68.5	55.3	47.4	43.6
	Mean	31.7	66.4	0.7	34.8	33.3	34.6	33.7
	St.Dev.	2.6	15.8	0.6	6.3	4.3	3.2	2.4
Annual	Min.	14.7	15.7	0.0	11.5	13.1	10.2	20.4
	Max.	38.3	99.4	3.9	68.5	55.3	47.4	43.6
	Mean	27.9	62.6	0.7	30.1	29.0	29.7	31.5
	St.Dev.	5.7	17.9	0.6	7.7	6.8	6.9	3.5

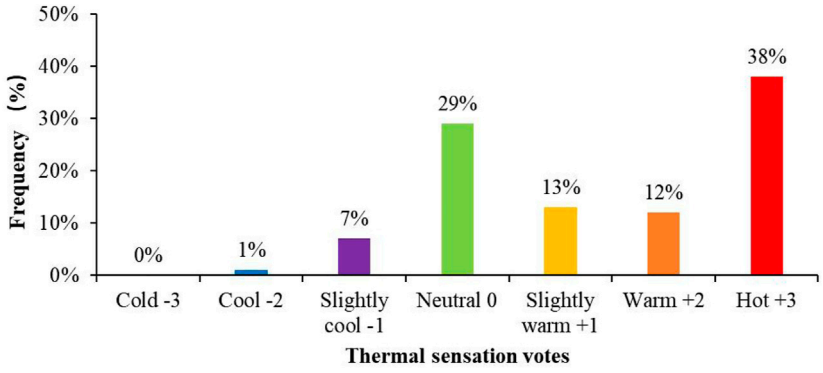

FIGURE 4
Frequency distributions of thermal sensation votes.

+3). To apply the last three criteria, comparing the prediction by the selected thermal indices with the actual thermal sensation indicated by the interviewees, the extreme categories such as "very hot" +4 and "very cold" −4 which rarely occurred with 4.1% and 0% respectively were merged to the categories of "hot" +3 and "cold" −3, respectively.

Figure 4 shows the frequency distribution of thermal sensation votes. The TSV ranged from "cool" −2 to "hot" +3. The highest frequencies of votes were "neutral" 0 and "hot" +3, with 29% and 38%, respectively. The "slightly warm" +1 and "warm" +2 votes were essentially the same, with 13% and 12%, respectively. While, the "slightly cool" −1 and "cool" −2 votes had few occurrences, for a total of 8%.

3.3 Comparison between selected indices' prediction and thermal sensation votes

3.3.1 Coefficient of determination and Spearman's rho correlation coefficient

The first two statistical criteria, the coefficient of determination between the thermal comfort indices' parameters and TSV and the Spearman's rho correlation coefficient between the results of the thermal comfort indices and TSV, were estimated, as shown in Table 6. The coefficients of determination were generally higher than Spearman's rho correlation coefficients. Moreover, strong associations were

TABLE 6 Coefficient of determination and Spearman's rho correlation coefficient.

Indices	Coefficients of determination	Spearman's rho correlation coefficient
TSV_{model} (with RH)	0.934	0.813
TSV_{model} (without RH)	0.942	0.833
PET	0.879	0.735
UTCI	0.880	0.761
SET*	0.752	0.665

found between coefficients of determination and Spearman's rho correlation coefficients, indicating that high coefficients of determination would predict high Spearman's rho correlation coefficients. This is because both coefficients have the same interpretation of prediction possibilities, and the coefficient of determination shows how well the model parameters vary in function to variations of thermal responses, while the Spearman's rho correlation coefficient verified how well the results of thermal comfort indices vary in function with variations in thermal responses.

TSV_{model} (with RH) and TSV_{model} (without RH) showed the highest coefficients, with coefficients of determination of 0.934 and 0.942 and Spearman's rho correlation coefficient of 0.813 and 0.833, respectively, followed by UTCI and PET, with 0.880 and 0.761, and 0.879 and 0.735, respectively; the lowest was observed in the case of SET* with 0.752 and 0.665.

3.3.2 Percentage of correct predictions and two qualitative criteria

According to the third criterion percentage of correct predictions, UTCI was the most successful index simulating 29.8% of thermal sensation votes (Table 7), followed by the TSV_{model} (with RH), TSV_{model} (without RH), and SET* simulating approximately 24.5%, while the lowest was observed in PET (16.5%).

The percentage of thermal index class predictions demonstrated significant differences compared with the original TSV, as shown in Figure 5. For all the selected thermal indices, discrepancies were mainly identified in the positive thermal sensation ("slightly warm" +1; "warm" +2; "hot" +3). The frequency of the original "hot" +3 was higher than the predictions of the selected thermal comfort indices, whereas the total frequencies of the original "slightly warm" +1 and "warm" +2 were lower than the predictions of the selected thermal comfort indices. Furthermore, PET overestimated the negative thermal sensation ("cool" −2 and "slightly cool" −1), while SET* overestimated the "neutral" 0. In contrast, UTCI showed better agreement with the primordial votes than the rest of the selected thermal comfort indices, indicating "hot" +3 and "neutral" 0 with 29% and 19%, respectively, compared with the original "hot" +3 with 38% and "neutral" 0 with 29%.

Cross-tabulation analysis was used to assess predictive ability of indices considering each class of TSV scale separately. Figure 6 shows the TSV cross-tabulation. The applicability of UTCI was also verified by cross-tabs. Approximately 57% of the UTCI's predictions were classified correctly as "hot" +3, while great success had also been observed in the case of class "neutral" 0 and "slightly cool" −1, at 40% and 48%, respectively. For the TSV_{model} (with RH), TSV_{model} (without RH) and PET, predictions were accurate only in the case of "hot" +3. All the SET*predictions were inaccurate.

3.3.3 Performance assessment

The average Spearman's rho correlation coefficient was evaluated as approximately 0.60, suggesting a moderate correlation (Willmott, 1982; Pantavou et al., 2013). For the selected thermal comfort indices, all indices correlated well with TSV, with coefficients greater than 0.60. In particular, the same better fits were found for TSV_{model} (with RH) and TSV_{model} (without RH), with coefficients larger than 0.80. Although all the selected thermal comfort indices had suitable applicability according to the first two statistical criteria, the last three criteria demonstrated limited performance; this proved that the coefficient of determination and the Spearman's rho correlation coefficient were often inappropriate or misleading when comparing model-predicted and observed variables (Willmott, 1982; Potchter et al., 2022). The relationships between the coefficient of determination and Spearman's rho correlation coefficient and model performance were not always consistent.

All the selected thermal indices had limited performance in the prediction of thermal sensation because the thermal sensation in the urban microclimate was a complex phenomenon with multiple factors of concern, the microclimate, physiological, psychological, and behaviors (Nikolopoulou et al., 2001; Nikolopoulou and Steemers, 2003; Chen and Ng, 2012). The microclimate in a certain region affects

TABLE 7 Percentage of indices' correct predictions.

Indices	TSV_{model} (with RH)	TSV_{model} (without RH)	PET	UTCI	SET*
Percentage of correct predictions	24.4%	24.3%	16.5%	29.8%	24.4%

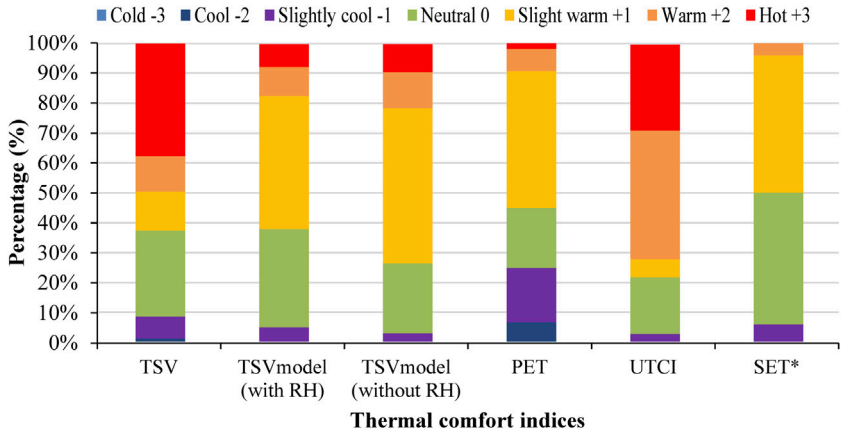

FIGURE 5
Percentage of thermal indices' class predictions.

TSV_{model} (with RH)	TSV	0%	1%	7%	29%	13%	12%	38%
		-3	-2	-1	0	1	2	3
0%	-3							
0%	-2							
5%	-1	4%	12%	**33%**	31%	6%	6%	8%
33%	0			8%	**36%**	17%	14%	25%
45%	1		1%	6%	30%	**10%**	10%	43%
10%	2			2%	13%	15%	**17%**	53%
8%	3			4%	11%	13%	9%	**63%**

SET*	TSV	0%	1%	7%	29%	13%	12%	38%
		-3	-2	-1	0	1	2	3
0%	-3							
0%	-2							
6%	-1	3%	5%	**36%**	31%	20%	2%	3%
44%	0		1%	8%	**36%**	14%	15%	26%
46%	1		1%	3%	21%	**12%**	10%	53%
4%	2		10%	7%	21%	14%	**10%**	38%
0%	3							

TSV_{model} (without RH)	TSV	0%	1%	7%	29%	13%	12%	38%
		-3	-2	-1	0	1	2	3
0%	-3							
0%	-2							
3%	-1	7%	17%	**32%**	27%	0%	7%	10%
23%	0			12%	**38%**	19%	13%	18%
52%	1		1%	5%	31%	**12%**	11%	40%
12%	2			5%	15%	11%	**18%**	51%
9%	3			3%	9%	15%	8%	**65%**

UTCI	TSV	0%	1%	7%	29%	13%	12%	38%
		-3	-2	-1	0	1	2	3
0%	-3							
0%	-2							
3%	-1	8%	12%	**48%**	16%	12%	0%	4%
19%	0		3%	14%	**40%**	21%	14%	8%
6%	1		3%	10%	18%	**13%**	28%	28%
43%	2			4%	34%	12%	**9%**	41%
29%	3		1%	4%	16%	10%	12%	**57%**

PET	TSV	0%	1%	7%	29%	13%	12%	38%
		-3	-2	-1	0	1	2	3
0%	-3							
7%	-2	3%	**9%**	24%	29%	28%	6%	1%
18%	-1		2%	**13%**	36%	35%	12%	2%
20%	0		1%	8%	**35%**	11%	15%	30%
46%	1		1%	4%	26%	**11%**	9%	49%
7%	2			3%	7%	15%	**10%**	65%
2%	3			6%	22%	17%	6%	**49%**

FIGURE 6
Distribution of thermal indices' class predictions per class of TSV (each row adds to 100%).

the thermal sensations directly (Chen and Ng, 2012), while psychological and behavioral factors play an important role in the determination of thermal evaluation of inhabitants (Brager and de Dear, 1998; Schweiker et al., 2013). The psychological and behaviors were not taken into consideration in the thermal comfort models of PET, UTCI, and SET*. In contrast, the TSV_{model} (with RH) and TSV_{model} (without RH) should have better performance because the equations were derived from the survey data implicit of the habits and customs of the residents. The limited performance of the TSV_{model} may be due to differences in habits and customs between Guangzhou and Hong Kong. In addition, the TSV_{models} were developed

TABLE 8 Quantitative measures of thermal indices' assessment scales performance with observed data.

Thermal indices	RMSE (°C)	RMSEs (°C)	RMSEu (°C)	*d*
TSV_{model} (with RH)	1.60	1.31	0.93	0.72
TSV_{model} (without RH)	1.54	1.23	0.93	0.77
PET	1.84	1.49	1.05	0.61
UTCI	1.43	1.09	1.08	0.84
SET*	1.68	1.56	0.82	0.59

based on the multiple linear regressions between the original thermal sensation votes and some local microclimatic parameters. Local microclimatic conditions play an important role in affecting thermal sensations of people (Chen and Ng, 2012). The varied microclimates under different topographic characteristics and urban morphologies led to various thermal sensations.

3.4 Adaptation analysis

The limited performance of the selected indices was examined using the last three criteria. The last three criteria were estimated based on the assessment scales of previous studies in the humid subtropical areas of China. The assessment scales may not have adapted to Guangzhou. A set of difference measures, including the root mean square error (RMSE), systematic error (RMSEs), unsystematic error (RMSEu), and an index of agreement (*d*), for model evaluation proposed by Willmott (1982) was used to quantitatively evaluate the adaptation of thermal comfort indices' assessment scales. The RMSE explains the extent of the average difference between the original and prediction. Both RMSEs and RMSEu derived from RMSE, explain how much of the RMSE is systematic in nature and what portion is unsystematic. As for a credible model, the magnitude of RMSEs should close to 0, while the result of RMSEu should approach RMSE. The index of agreement (*d*) is intended to be a descriptive measure of how a model predicts a variable with high accuracy. The *d* value of one represents a perfect prediction of the variable.

The difference measures are presented in Table 8. For UTCI, the RMSEs was relatively small, and the RMSEu approached the RMSE, indicating that the UTCI better conforms to the criteria of the systematic error. The *d* value for UTCI was 0.84, suggesting that the assessment scales of the UTCI reasonably approximated the observed data for this study. For all the other indices, the RMSEs were generally higher than the RMSEu, indicating that the assessment scales did not adapt in Guangzhou. The RMSEu was approximately one owing to the complexity of the outdoor thermal comfort evaluation.

4 Conclusion

The present study presented field survey results of outdoor thermal comfort, aiming to propose an adaptive model to quantify the correlations between urban climate and outdoor thermal sensations for humid subtropical residential areas in China. The paper presented the results of field thermal comfort survey focusing on the comparison between the prediction by thermal indices (i.e., PET, UTCI, SET* and TSV_{model}) commonly used in China and the actual thermal sensation expressed by interviewees. The main conclusions are as follows:

1. The TSV_{model} had a better correlation with TSV, while the UTCI was the most successful index, simulating 29.8% of TSV. The testability of PET and SET* were very low, with the correct predictive ability 16.5% and 24.4%, respectively.
2. For all the selected thermal comfort indices, the percentage of thermal comfort index class predictions demonstrated significant differences compared with the original TSV. In contrast, UTCI showed better agreement with the original, indicating 'hot' +3 and 'neutral' 0 with 29% and 19%, respectively, compared with the original +3 with 38% and 0 with 29%.
3. For all the indices, the RMSEs were generally higher than the RMSEu, demonstrating that the assessment scales did not adapt to Guangzhou. Therefore, it was necessary to establish the thermal sensation scales of Guangzhou. The RMSEu were approximately one owing to the complexity of the outdoor thermal comfort evaluation.
4. In the selected indices, the UTCI reasonably approximated the observed data for this study and was recommended to assess the outdoor thermal comfort in humid subtropical residentials of China to evaluate the thermal comfort level under different design decisions, thus creating a comfortable urban microclimate.

In our study, UTCI was calculated by 'UTCI calculator' provided on the www.utci.org website based on Ta, RH, V_{10m} and T_{mrt}. The 10 m high wind speed was required to calculate UTCI, as well as the mean radiant temperature (T_{mrt}) which was

derived from RayMan software. The UTCI would be difficult to use in the actual design process in a more convenient way by designers and urban planners. However, we could propose some outdoor thermal comfort design strategies base on evaluation indexes UTCI. The proposed strategies would provide a common basis for the creating guidelines to use in future studies regarding creating a comfortable microclimate in the humid and subtropical residential area of China.

Data availability statement

The original contributions presented in the study are included in the article/supplementary material, further inquiries can be directed to the corresponding authors.

Ethics statement

Ethical review and approval was not required for the study on human participants in accordance with the local legislation and institutional requirements. Written informed consent from the participants was not required to participate in this study in accordance with the national legislation and the institutional requirements.

Author contributions

KL: Conceptualization, methodology, software, validation, formal analysis, investigation, data curation, visualization, writing- original draft preparation, and writing-review and editing. XL: Conceptualization, methodology, visualization, software, writing- original draft preparation, writing-review and editing, and funding acquisition. YB: Conceptualization, resources, software, writing- original draft preparation, writing-review and editing, and funding acquisition.

Funding

This research is supported by the 2022 Guangdong Philosophy and Social Science Foundation (Grant No. GD22XGL02); the National Natural Science Foundation of China (Grant No. 52108011); the Fundamental Research Funds for the Henan Provincial Colleges and Universities in Henan University of Technology (Grant No. 2018QNJH11); Guangzhou Philosophy and Social Science Planning 2022 Annual Project (Grant No. 2022GZQN14); Department of Education of Guangdong Province (Grant No. 2021KTSCX004); Department of Housing and Urban–Rural Development of Guangdong Province (Grant No. 2021-K2-305243); the Fundamental Research Funds for the Central Universities (Grant No. QNMS202211); Science and Technology Program of Guangzhou, China (Grant No. 202102020302); State Key Laboratory of Subtropical Building Science, South China University of Technology (Grant No. 2021ZB16); China Postdoctoral Science Foundation (Grant No. 2021M701249).

Acknowledgments

Special thanks to the cultivation programme for young backbone teachers in Henan University of Technology and the key special projects of science and technology aid economy 2020 of the National Key R&D Program of China.

Conflict of interest

Authors XL and YB were employed by Architectural Design and Research Institute Co., Ltd.

The remaining author declares that the research was conducted in the absence of any commercial or financial relationships that could be construed as a potential conflict of interest.

Publisher's note

All claims expressed in this article are solely those of the authors and do not necessarily represent those of their affiliated organizations, or those of the publisher, the editors and the reviewers. Any product that may be evaluated in this article, or claim that may be made by its manufacturer, is not guaranteed or endorsed by the publisher.

References

Brager, G. S., and de Dear, R. J. (1998). Thermal adaptation in the built environment: A literature review. *Energy Build.* 27, 83–96. doi:10.1016/S0378-7788(97)00053-4

Bröde, P., Fiala, D., Błażejczyk, K., Holmér, I., Jendritzky, G., Kampmann, B., et al. (2012). Deriving the operational procedure for the universal thermal climate index (UTCI). *Int. J. Biometeorol.* 56, 481–494. doi:10.1007/s00484-011-0454-1

Chen, L., and Ng, E. (2012). Outdoor thermal comfort and outdoor activities: A review of research in the past decade. *Cities* 29, 118–125. doi:10.1016/j.cities.2011.08.006

Chen, X., Gao, L., Xue, P., Du, J., and Liu, J. (2020). Investigation of outdoor thermal sensation and comfort evaluation methods in severe cold area. *Sci. Total Environ.* 749, 141520. doi:10.1016/j.scitotenv.2020.141520

Cheng, V., Ng, E., Chan, C., and Givoni, B. (2012). Outdoor thermal comfort study in a subtropical climate: A longitudinal study based in Hong Kong. *Int. J. Biometeorol.* 56, 43–56. doi:10.1007/s00484-010-0396-z

China Bureau of Statistics (2021). *Statistical communique of the people's Republic of China on national economic and social development in 2021*. China: Natl. Bur. Stat. Available At: http://www.stats.gov.cn/tjsj/sjjd/202209/t20220929_1888798.html.

China Meteorological Administration and Tsinghua University (2005). *Meteorological data for built environmental analysis in China*. Beijing: China Architecture & Building Press.

de Dear, R. J., and Brager, G. S. (1998). Developing an adaptive model of thermal comfort and preference. *ASHRAE Trans.* 104 (1A), 145–167.

Du, W., and Xia, X. (2018). How does urbanization affect ghg emissions? A cross-country panel threshold data analysis. *Appl. Energy* 229, 872–883. doi:10.1016/j.apenergy.2018.08.050

Fang, Z., Zheng, Z., Feng, X., Shi, D., Lin, Z., and Gao, Y. (2021). Investigation of outdoor thermal comfort prediction models in South China: A case study in Guangzhou. *Build. Environ.* 188, 107424. doi:10.1016/j.buildenv.2020.107424

Fanger, P. O. (1970). *Thermal comfort - analysis and applications in environmental engineering*. New York, NY, USA: McGraw-Hill Book Company, 244.

Gagge, A. P., Fobelets, A. P., and Berglund, L. G. (1986). Standard predictive index of human response to the thermal environment. *ASHRAE Trans.* 92, 709–731.

Haghshenas, M., Hadianpour, M., Matzarakis, A., Mahdavinejad, M., and Ansari, M. (2021). Improving the suitability of selected thermal indices for predicting outdoor thermal sensation in Tehran. *Sustain. Cities Soc.* 74, 103205. doi:10.1016/j.scs.2021.103205

He, B.-J. (2022). Green building: A comprehensive solution to urban heat. *Energy Build.* 271, 112306. doi:10.1016/j.enbuild.2022.112306

He, B.-J., Wang, J., Zhu, J., and Qi, J. (2022). Beating the urban heat: Situation, background, impacts and the way forward in China. *Renew. Sustain. Energy Rev.* 161, 112350. doi:10.1016/j.rser.2022.112350

Höppe, P. (1999). The physiological equivalent temperature - a universal index for the biometeorological assessment of the thermal environment. *Int. J. Biometeorology* 43 (2), 71–75. doi:10.1007/s004840050118

Huang, H., Li, Y., Zhao, Y., and Zhai, W. (2022). Analysis of the impact of urban summer high temperatures and outdoor activity duration on residents' emotional health: Taking hostility as an example. *Front. Public Health* 10, 955077. doi:10.3389/fpubh.2022.955077

Huang, J., Zhou, C., Zhuo, Y., Xu, L., and Jiang, Y. (2016). Outdoor thermal environments and activities in open space: An experiment study in humid subtropical climates. *Build. Environ.* 103, 238–249. doi:10.1016/j.buildenv.2016.03.029

ISO7726 (1998). *Ergonomics of the thermal environment—instruments for measuring physical quantities*. Geneva: International Standard Organization.

Jendritzky, G., de Dear, R., and Havenith, G. (2012). UTCI-why another thermal index? *Int. J. Biometeorol.* 56, 421–428. doi:10.1007/s00484-011-0513-7

Johansson, E., Thorsson, S., Emmanuel, R., and Kruger, E. (2014). Instruments and methods in outdoor thermal comfort studies – The need for standardization. *Urban Clim.* 10, 346–366. doi:10.1016/j.uclim.2013.12.002

Lai, D. Y., Guo, D. H., Hou, Y. F., Lin, C. Y., and Chen, Q. Y. (2014a). Studies of outdoor thermal comfort in northern China. *Build. Environ.* 77, 110–118. doi:10.1016/j.buildenv.2014.03.026

Lai, D., Zhou, C., Huang, J., Jiang, Y., Long, Z., and Chen, Q. (2014b). Outdoor space quality: A field study in an urban residential community in central China. *Energy Build.* 68, 713–720. doi:10.1016/j.enbuild.2013.02.051

Li, B., Guo, W., Liu, X., Zhang, Y., and Caneparo, L. (2022). The third solar decathlon China buildings for achieving carbon neutrality. *Buildings* 12, 1094. doi:10.3390/buildings12081094

Li, B., Guo, W., Liu, X., Zhang, Y., Russell, P. J., and Schnabel, M. A. (2021). Sustainable passive design for building performance of healthy built environment in the lingnan area. *Sustainability* 13, 9115. doi:10.3390/su13169115

Li, J., and Liu, N. (2020). The perception, optimization strategies and prospects of outdoor thermal comfort in China: A review. *Build. Environ.* 170, 106614. doi:10.1016/j.buildenv.2019.106614

Lin, T. P., de Dear, R., and Hwang, R. (2011). Effect of thermal adaptation on seasonal outdoor thermal comfort. *Int. J. Climatol.* 31, 302–312. doi:10.1002/joc.2120

Lin, T. P., and Matzarakis, A. (2008). Tourism climate and thermal comfort in sun moon lake, taiwan. *Int. J. Biometeorol.* 52 (4), 281–290. doi:10.1007/s00484-007-0122-7

Lin, T. P. (2009). Thermal perception, adaptation and attendance in a public square in hot and humid regions. *Build. Environ.* 44, 2017–2026. doi:10.1016/j.buildenv.2009.02.004

Matzarakis, A., Rutz, F., Matzarakis, A., Rutz, F., and Mayer, H. (2007). Modelling radiation fluxes in simple and complex environments—Application of the RayMan model. *Int. J. Biometeorol.* 51, 323–334. doi:10.1007/s00484-006-0061-8

Monteiro, L., and Alucci, M. P. (2006). "Outdoor thermal comfort: Comparison of results of empirical field research and predictive models simulation," Louvain-la-Neuve, Belgium .*Proceedings of the comfort and energy use in buildings*

Ng, E., and Cheng, V. (2012). Urban human thermal comfort in hot and humid Hong Kong. *Energy Build.* 55, 51–65. doi:10.1016/j.enbuild.2011.09.025

Nikolopoulou, M., Baker, N., and Steemers, K. (2001). Thermal comfort in outdoor urban spaces: Understanding the human parameter. *Sol. Energy* 70 (3), 227–235. doi:10.1016/S0038-092X(00)00093-1

Nikolopoulou, M., and Steemers, K. (2003). Thermal comfort and psychological adaptation as a guide for designing urban spaces. *Energy Build.* 35, 95–101. doi:10.1016/S0378-7788(02)00084-1

Pantavou, K. G., Santamouris, M., Asimakopoulos, D., and Theoharatos, G. (2013). Evaluating the performance of bioclimatic indices on quantifying thermal sensation for pedestrians. *Adv. Build. Energy Res.* 7 (2), 170–185. doi:10.1080/17512549.2013.865557

Pickup, J., and de Dear, R. J. (1999). "An outdoor thermal comfort index (OUT_SET*)—Part I—the model and its assumptions," (Sydney, 279–283.*International congress of biometeorology and international conference on urban climatology.*

Potchter, O., Cohen, P., Lin, T.-P., and Matzarakis, A. (2022). A systematic review advocating a framework and benchmarks for assessing outdoor human thermal perception. *Sci. Total Environ.* 833, 155128. doi:10.1016/j.scitotenv.2022.155128

Ruiz, A., Maria, C., and Erica, N. (2015). Adaptive model for outdoor thermal comfort assessment in an Oasis city of arid climate. *Build. Environ.* 85, 40–51. doi:10.1016/j.buildenv.2014.11.018

Schweiker, M., Brasche, S., Bischof, W., Hawighorst, M., and Wagner, A. (2013). Explaining the individual processes leading to adaptive comfort: Exploring physiological, behavioural and psychological reactions to thermal stimuli. *J. Build. Phys.* 36 (4), 438–463. doi:10.1177/1744259112473945

Thorsson, S., Lindberg, F., Eliasson, I., and Holmer, B. (2007). Different methods for estimating the mean radiant temperature in an outdoor urban setting. *Int. J. Climatol.* 27, 1983–1993. doi:10.1002/joc.1537

Tseliou, A., Tsiros, I. X., Lykoudis, S., and Nikolopoulou, M. (2010). An evaluation of three biometeorological indices for human thermal comfort in urban outdoor areas under real climatic conditions. *Build. Environ.* 45 (5), 1346–1352. doi:10.1016/j.buildenv.2009.11.009

United Nation (2019). *World urbanization prospects: The 2018 revision ST/ESA/SER.A/420* (New York: United Nation.

Wei, D., Yang, L., Bao, Z., Lu, Y., and Yang, H. (2022). Variations in outdoor thermal comfort in an urban park in the hot-summer and cold-winter region of China. *Sustain. Cities Soc.* 77, 103535. doi:10.1016/j.scs.2021.103535

Willmott, C. J. (1982). Some comments on the evaluation of model performance. *Bull. Am. Meteorol. Soc.* 63 (11), 1309–1313. doi:10.1175/1520-0477(1982)063<1309:scoteo>2.0.co;2

Yang, J., Xin, J., Zhang, Y., Xiao, X., and Xia, J. C. (2022). Contributions of sea–land breeze and local climate zones to daytime and nighttime heat island intensity. *npj Urban Sustain.* 2, 12. doi:10.1038/s42949-022-00055-z

Yang, L., Yan, H., and Lam, J. C. (2014). Thermal comfort and building energy consumption implications - a review. *Appl. Energy* 115, 164–173. doi:10.1016/j.apenergy.2013.10.062

Yang, W., Wong, N. H., and Zhang, G. (2013). A comparative analysis of human thermal conditions in outdoor urban spaces in the summer season in Singapore and Changsha, China. *Int. J. Biometeorol.* 57 (6), 895–907. doi:10.1007/s00484-012-0616-9

Zhao, L., Zhoua, X., Li, L., Heb, S., and Chena, R. (2016). Study on outdoor thermal comfort on a campus in a subtropical urban area in summer. *Sustain. Cities Soc.* 22, 164–170. doi:10.1016/j.scs.2016.02.009

frontiers | Frontiers in Earth Science

TYPE Original Research
PUBLISHED 04 January 2023
DOI 10.3389/feart.2022.1024680

Check for updates

OPEN ACCESS

EDITED BY
Jun Yang,
Northeastern University, China

REVIEWED BY
Shaohua Wang,
Aerospace Information Research Institute (CAS), China
Dongxue Zhao,
The University of Queensland, Australia

*CORRESPONDENCE
Yanhong Zhang,
giswork@163.com

SPECIALTY SECTION
This article was submitted to Environmental Informatics and Remote Sensing, a section of the journal Frontiers in Earth Science

RECEIVED 22 August 2022
ACCEPTED 08 December 2022
PUBLISHED 04 January 2023

CITATION
Chen Z, Zhang Y, Zang P, Liu Z and Zhao W (2023), Mapping the grassland quality of the flooded plain based on Jilin-01 images with a red-edge spectral band.
Front. Earth Sci. 10:1024680.
doi: 10.3389/feart.2022.1024680

COPYRIGHT
© 2023 Chen, Zhang, Zang, Liu and Zhao. This is an open-access article distributed under the terms of the Creative Commons Attribution License (CC BY). The use, distribution or reproduction in other forums is permitted, provided the original author(s) and the copyright owner(s) are credited and that the original publication in this journal is cited, in accordance with accepted academic practice. No use, distribution or reproduction is permitted which does not comply with these terms.

Mapping the grassland quality of the flooded plain based on Jilin-01 images with a red-edge spectral band

Ziqi Chen[1,2], Yanhong Zhang[1]*, Peng Zang[1], Zhaoli Liu[2] and Wenbin Zhao[3]

[1]College of Geo-Exploration Science and Technology, Jilin University, Changchun, China, [2]Northeast Institute of Geography and Agriculture, Chinese Academy of Sciences, Changchun, China, [3]College of New Energy and Environment, Jilin University, Changchun, China

In response to the difficulties of flood plain quality assessment, red-edge spectral remote sensing data acquired from the Jilin-01 satellite were used. The Grassland Quality Index (GQI) was formed by the Normalized Difference Vegetation Index (NDVI) and Normalized Difference Red Edge Index (NDRE) related to the determination of grassland quality and the first principal component of the red-edge Chlorophyll Index obtained by principal component analysis. The GQI was applied to evaluate grassland quality in the flooded plain, which is an important grassland ecological-barrier area in the western area of Jilin Province, and was then verified using field measurement data. Results show that 1) 80% of grasslands in Xianghai Nature Reserve are of a medium quality, and the grasslands with good growth status account for approximately 15% and are mainly concentrated in the wetland and swamp areas in the central south part of the reserve and that 2) the correlation of the evaluation results was verified using the survey field biomass, and the coefficient of the empirical correlation model is 0.96, which indicates good consistency. This study is of practical significance for the timely and accurate monitoring of grassland growth, which is beneficial for the development of livestock husbandry and the protection of the ecological environment in northern China.

KEYWORDS

grassland quality index (GQI), normalized difference vegetation index (NDVI), red-edge spectrum band, principal component analysis, grassland quality evaluation

1 Introduction

With the synchronous improvement of high spatial and high spectral resolution of remote sensing technology, the quantitative evaluation capability of ground objectives has been further strengthened (Kanke et al., 2012; Das et al., 2014; Sibanda et al., 2017). This is especially true for surface vegetation, which is a very effective feature on the earth's surface due to its spatial position and its spectral sensitivity to radiation changes (Amy et al., 2014). The multi-spectral satellite payload in the traditional visible band occurs mainly in the blue band (450–520 nm), green band (520–590 nm), red band (630–690 nm), and

near-infrared band (770–890 nm) (Niemann et al., 2015; Zhou et al., 2021). Red-edge spectra are between the red band and the near-infrared band (Baranoski and Rokne, 2005; Cho et al., 2008; Shaokui et al., 2011).

Additionally, red-edge spectra have been used to estimate the plant nitrogen content, chlorophyll content, and biomass. This is due to the development of hyper-spectra remote sensing, which can be used to estimate the leaf nitrogen content and chlorophyll concentration more accurately (Eitel et al., 2009; Ramoelo et al., 2012; Clevers and Gitelson, 2013; Delegido et al., 2013; Vincini et al., 2014; Kanke et al., 2016). Red-edge data of Rapid-Eye and World-View satellites are mainly applied to the research of crops, woodlands, and land cover. These studies (Ma and Weiwei, 2015; Fang et al., 2017; Shu et al., 2018; Su et al., 2018) mainly focused on the following: 1) an evaluation of the overall quality of regional vegetation using red-edge spectra; 2) the study the index system of vegetation evaluation; and 3) usually single indicators, such as the nitrogen content of vegetation, chlorophyll content, or control of certain pests and diseases, are evaluated. In terms of single indices, Fang et al. (2017) evaluated the effectiveness of different red-edge indices on inverting the health level obtained in grasslands by comparison, and the results showed that NDRE can be applied to accurately and quickly monitor the health of grasslands with an accuracy of more than 80%. Li et al. (2014) studied various vegetation indices based on the performance of red-edge spectral indices of bandwidth and crop growth stage changes. Regarding integrated indices, Hu et al. (2017) proposed a new vegetation health index (VHI), which integrates three factors, namely, the normalized mountain vegetation index, the nitrogen reflectance index, and yellow light band reflectance, through principal component transformation. This is a way to reduce errors caused by the subjective weighted summation integration method and facilitate extensive and rapid evaluation and monitoring of vegetation health in soil erosion areas. From the perspective of the research and realization process, first, the evaluation index system is complex, which makes it difficult in many cases to obtain supporting data; second, the selection of indicators is too subjective, which is not conducive to promoting the method to other times and places. The main reason for the above problems is that sensors with red-edge spectra are still seldom, the transmission time is not long, and research on remote sensing using red-edge spectra still needs further study.

Jilin-1 is the first commercial satellite to be named after a province in China. Among data with a spatial resolution of 4 m acquired by 07 satellites launched in January 2018, B4 is a red-edge spectra and is based on the significant expression of B4 to the vegetation. In this study, the grassland quality index (GQI) was established using a principal component analysis (PCA) method, considering the vegetation-related NDVI, NDRE, and chlorophyll indexes that were integrated to evaluate the quality of grassland in the Xianghai Nature Reserve. Also, biomass data were used to confirm the performance for the grassland quality evaluation, especially in dispersed grassland habitat, to enhance its ability to quantitatively evaluate vegetation quality. This paper quickly and accurately judged the regional grassland growth conditions to improve the inverse accuracy of grassland quality by constructing a comprehensive vegetation index, which is of great significance for the protection and improvement of the ecological environment.

2 Materials and methods

2.1 Study area

The study area is located in the Xianghai Nature Reserve in the western Jilin province. The area occurs at a latitude and longitude of 122° 04′E–122° 30′E and 43° 59′N–48° 33′N and covers a total area of 1054.67 km^2 as shown in Figure 1. This area belongs to the continental monsoon climate of the north temperate zone with an annual average temperature of 5.1 °C and annual average precipitation of 408.3 mm. Most rainfall is concentrated in July and August. There are semi-arid grasslands embedded in this area, which show the landscape characteristics of a dune elm forest—vast grassland—reed grass field—lake water. However, marsh vegetation, meadow vegetation, and the saline-alkali vegetation community are more common. The plants belong to 537 species, 237 genera, 89 families, and 5 phyla. Grassland is not only the base of animal husbandry development but is also the main habitat for many waterfowl, especially for Grusgrus (see Table1). Thus, grasslands play an important role in local economic and ecological construction and require extra attention.

2.2 Data collection and processing

Figure 2 provides the overall methodological flowchart for the evaluation of grassland quality from Jilin-01 satellite images.

2.2.1 "Jilin-01" images and processing

"Jilin-01" is a high spatial resolution satellite platform that was independently developed by Changguang Satellite Technology Co., Ltd. The images are remote sensing image data of the 04–07 satellite of "Jilin No.01," and the 04–06 satellite was launched on 21 November 2017 while the 07 satellite was launched on 19 January 2018. Multi-spectral data were obtained by this satellite, which had a spatial resolution of 4 m while B4 carried the red-edge spectra information. This was a sensitive spectrum and indicated a growing status of green plants. The images used in this study were acquired on the 19th, 25th, 26th, and 27th of September 2018.

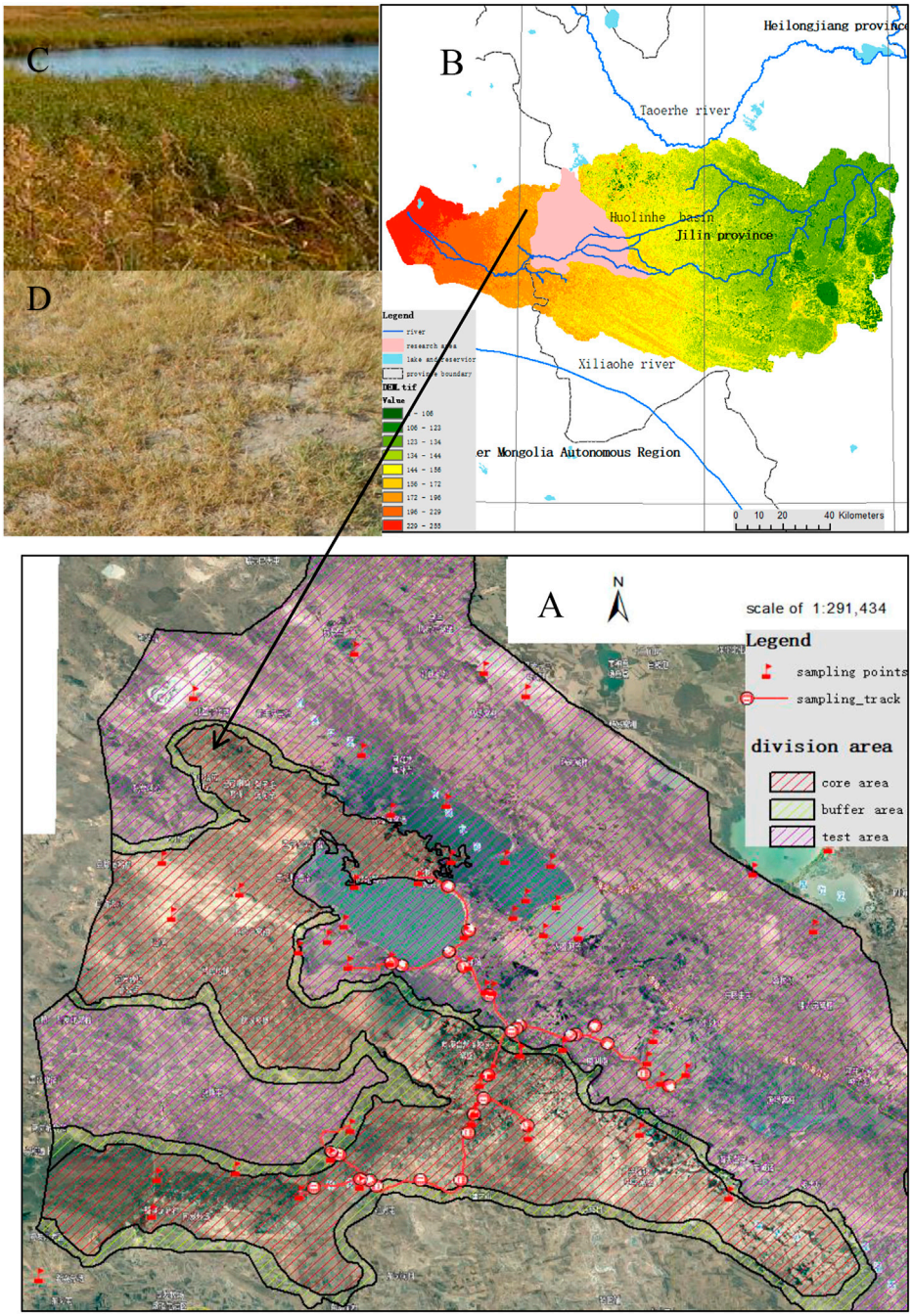

FIGURE 1
The location and condition map of the study area. **(A)** Image and surveying point from 2014 to 2018 in Xianghai nature reserve; **(B)** the location of Xianghai nature reserve in Jilin province; **(C)** the reed community; and **(D)** the meadow community.

First, the center wavelength value and bandwidth were input according to the 07-star image spectra information. The radiation gain and radiation offset were set using the absolute gain coefficient and absolute bias coefficient stored in the metadata. Then, the Flash atmospheric correction and radiometric calibration with a scaling factor of 1 were performed on the image using radiometric calibration parameters. To obtain a complete image of the tested area, the four images obtained at different times were processed with mosaic, feathered, and light evenness processing.

TABLE 1 Habitat types and population statistics of Grusgrus.

Habitat type		Shallow waters	Swamp	Meadow	Farmland
2017	Number	81	700	1627	235
	Frequency, %	9.86	8.45	32.39	5.63
2018	Number	1133	1824	2581	528
	Frequency, %	14.43	16.53	25.77	5.46

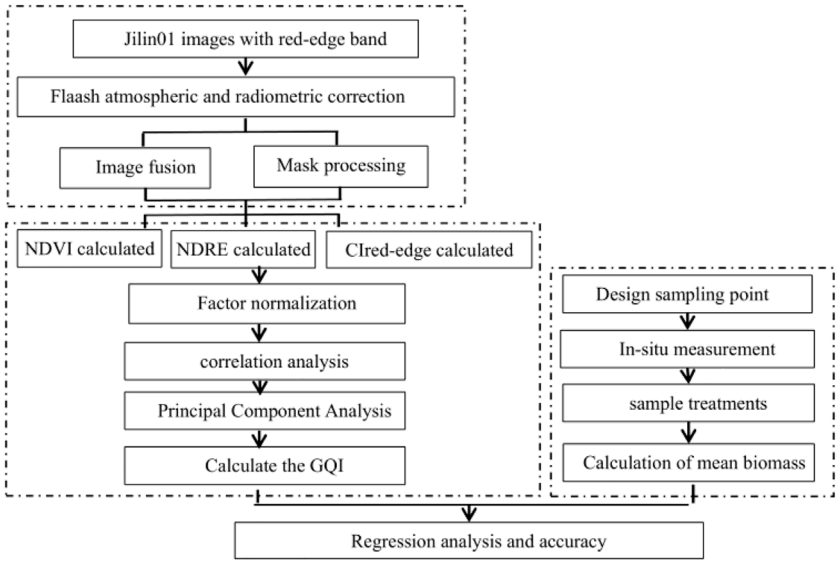

FIGURE 2
The overall methodological flowchart for evaluation of the grassland quality.

2.2.2 Field sampling data

To test the accuracy and applicability of GQI formed in this paper, 27 large plots, which cover the 3 photo communities, were selected with a slightly larger scope of 4.0 m × 4.0 m to ensure a pure pixel with a single species. Within each plot, small plots of 1.0 m × 1.0 m are set at the four corners and center of each quadrat to investigate the species and their abundance, height, and coverage. Then, all the above-ground parts of the five small quadrats at ground level were cut, and the soil, gravel, and other debris were removed after returning to the laboratory. The material was then dried at 65 ˚C to a constant weight. The mean weight of the five small plots is used as the biomass of the large quadrat.

2.3 Method

The differences in spectral characteristics reflect the differences in chlorophyll and leaf water content, which not only influenced each other, but were also closely related to grassland quality. The red-edge index is very sensitive to various physical and chemical properties of vegetation and can be used to identify the growing status of grasslands. The location, height, and slope of the “red edge” may vary with different vegetation and different growing conditions of the same vegetation (Yang et al., 2012). In this study and according to the spectral band characteristics of the Jilin-1 satellite image, the Normalized Difference Vegetation Index (NDVI), Normalized Difference Red Edge Index (NDRE), and Red Edge Chlorophyll Index are selected ($CI_{red-edge}$) to evaluate the grassland quality.

2.3.1 NDVI

NDVI can quantify the growth of grassland vegetation and has been widely used for grassland vegetation monitoring (Chen et al., 2023). One study showed that NDVI is sensitive to the change in soil background (Xu, 2013), and is linearly correlated with the vegetation distribution density. Additionally, it is a comprehensive reflection of vegetation types, cover forms, and

growth conditions in a unit pixel, and its size depends on the vegetation coverage and leaf area index. NDVI has a wide range of vegetation coverage detection and good temporal and spatial adaptability and it is therefore widely used.

The expression of NDVI is as follows:

$$NDVI = \frac{\rho_{NIR} - \rho_{Red}}{\rho_{NIR} + \rho_{Red}} \quad (1)$$

where ρ_{NIR} is the reflectivity of the near-infrared band and ρ_{Red} is the reflectivity of the red band.

2.3.2 NDRE

NDRE can be used to analyze the health of vegetation in the images obtained by multi-spectral sensors. Replacing the red band of NDVI with the red-edge band of NDRE provides a new measurement method and its calculation formula is as follows:

$$NDRE = \frac{\rho_{NIR} - \rho_{Red-edge}}{\rho_{NIR} + \rho_{Red-edge}} \quad (2)$$

where ρ_{NIR} is the reflectance of the near-infrared band and $\rho_{Red-edge}$ is the reflectance of the red-edge band. The intensity of light absorption at the top of the leaf is low, so the NDRE can be measured deep into the canopy and permits better and more permanent monitoring. The results show that NDRE is sensitive to chlorophyll content, leaf area variability, and soil background change. The higher the value, the higher the chlorophyll content; usually soils have the lowest, unhealthy plants have a medium amount, and healthy plants have the highest.

2.3.3 Chlorophyll index, $CI_{red-edge}$

$CI_{red-edge}$ was used to calculate the total chlorophyll content of leaves, and most vegetation is sensitive to small changes in chlorophyll content. The total chlorophyll content is linearly correlated with the reciprocal reflectance of the green/red sider band and the difference of the near-infrared band. Therefore, observations using the green band (570 nm) and the red-edge band (730 nm) are widely used in estimating the chlorophyll content of vegetation. In this study, the normalized difference index or proportional index using the red-edge band performed very well in estimating the chlorophyll or nitrogen content:

$$CI_{red-edge} = \frac{\rho_{NIR}}{\rho_{Red-egde}} - 1 \quad (3)$$

where ρ_{NIR} is the reflectance of the near-infrared band and $\rho_{Red-edge}$ is the reflectance of the red-edge band.

2.4 Grassland quality index (GQI)

Based on the above three planting indices, this study continuously experimented and explored and also proposed the grassland quality index (GQI) constructed by the combination of NDVI, NDRE, and $CI_{red-edge}$, which is expressed as follows:

$$GQI = 0.215*NDVI + 0.462*NDRE + 0.461*CI_{red-edge} \quad (4)$$

Because the subjective determination of the weight of each index usually affects the calculation results of the index, the current and common method is used to carry on the weighted sum of various indexes. When two or more indicators jointly contribute to ecological change, it is difficult to determine which indicator plays the main role in ecological change and then assign a specific weight to it. Previous studies have shown that use of a principal component analysis (PCA) can solve this problem (Hu et al., 2017). The PCA method maintains the low-order principal component and reduces the influence of the high-order principal component so that it can reduce the dimension of the dataset while maintaining the maximum variance contribution of the dataset. PCA was used to integrate the three variables into GQI

TABLE 2 Three indices of the principal component analysis.

Index	PC1 value
NDVI	0.591
NDRE	0.967
$CI_{red-edge}$	0.967

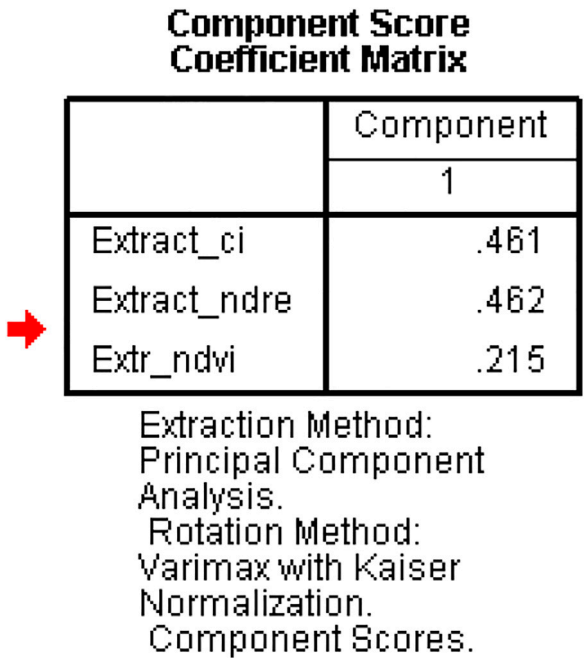

FIGURE 3
The component score coefficient matrix.

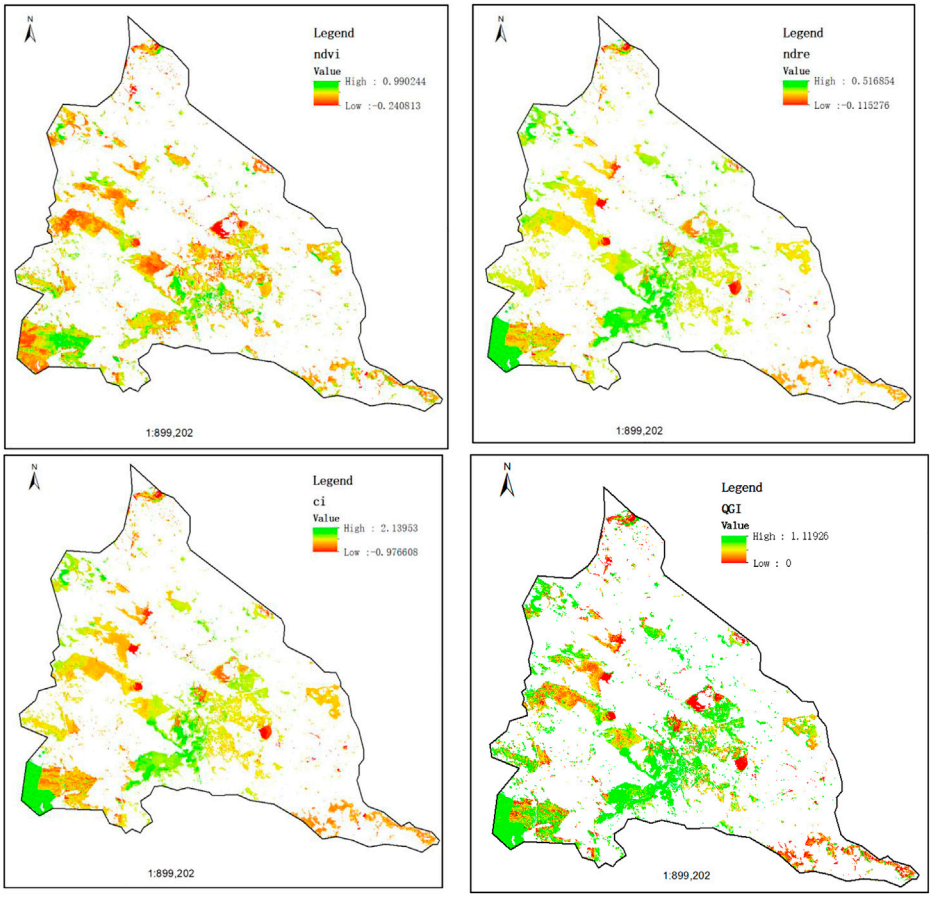

FIGURE 4
Results of study area NDVI, NDRE, and $CI_{red-edge}$ and the GQI.

through a linear transformation to avoid bias caused by subjective weighting due to the conventional weighted summation integration method.

PCA was conducted on three factors, and three principal component characteristic factor subsets were obtained as shown in Table 2. This shows that PC1 has concentrated most of the eigenvalues of the three factors. Among them, NDRE and $CI_{red-edge}$ introduce a red-edge band that has a high contribution value to PC1. The correlation analysis between the two also reached 0.967. PC1 concentrates the characteristics of each index to the maximum extent and can reasonably explain the grassland quality so it can be used as an effective evaluation. The score matrix of components is shown in Figure 3. From this, we can obtain the comprehensive index and grassland quality index (GQI) with the linear transformation of these three variables. The higher the value, the better the grassland quality. Otherwise, the quality is not good.

2.5 Error measurement

Biomass is an important index used to measure the quality of the ecological environment and the value of nature conservation (Qu et al., 2010). To verify the evaluation results, 15 random sites were arranged as sampling points within the scope of the study area, and the above-ground biomass of the sample points was measured using quadrate harvesting. Then, a correlation model was established using nine effective measuring sites. The larger the correlation index, the more reliable the evaluation result. To avoid individual differences, a buffer zone was delimited with each sample point as the center and at a radius of 4 m. Then, a square of 64 m^2 was made and GQI values were obtained from five points (a, b, c, d, and e) that were randomly selected in the square to calculate the average value, which is considered the quality index of the square.

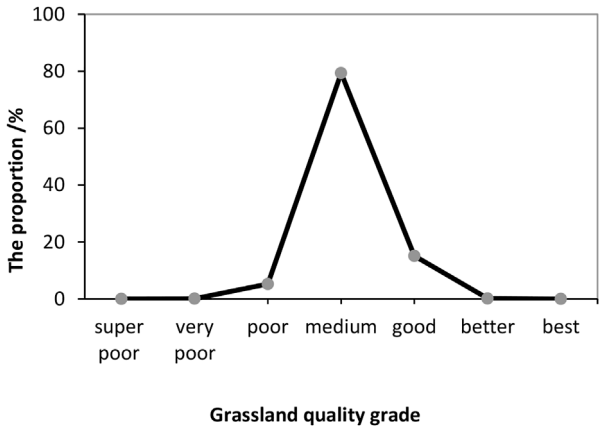

FIGURE 5
Classification statistics of the grassland quality index.

3 Results and analysis

3.1 The grassland quality map and grassland distribution

The GQI was applied to the Xianghai Nature Reserve. As shown in Figure 4, the overall grassland quality in the study area occurred at a medium level, and 15% of grasslands had good growth conditions and were mainly concentrated in the wetland and marsh areas in the south-central part of the reserve. This indicates that the environmental management in this area has achieved certain results and the vegetation health was in relatively good condition. A total of 80% of the grassland was of medium quality and was widely distributed in the study area. However, there are still a small number of scattered areas with poor grassland quality in approximately 5% of the region. These areas were mainly saline-alkali land and sandy land with an insufficient water supply and serious land degradation. In this study, 0.8 was used as the step length for each grade, and the grassland quality was divided into seven grades as follows: super poor (−2.6–−1.8), very poor (−1.8–−1), poor (−1–−0.2), medium (−0.2–0.6), good (0.6–1.4), better (1.4–2.2) and best (2.2–3.0). According to Figure 5, the grassland quality index is generally a normal distribution, which is more consistent with reality.

3.2 Error analysis

According to the data, the bi-coordinate longitudinal curve of above-ground biomass and grassland index of GQI was made as shown in Figure 6. The figure clearly shows that the two indices present the same trend and indicate that the established comprehensive index of grassland quality GQI is highly consistent with above-ground biomass. To quantify the relationship between the two variables, the least square

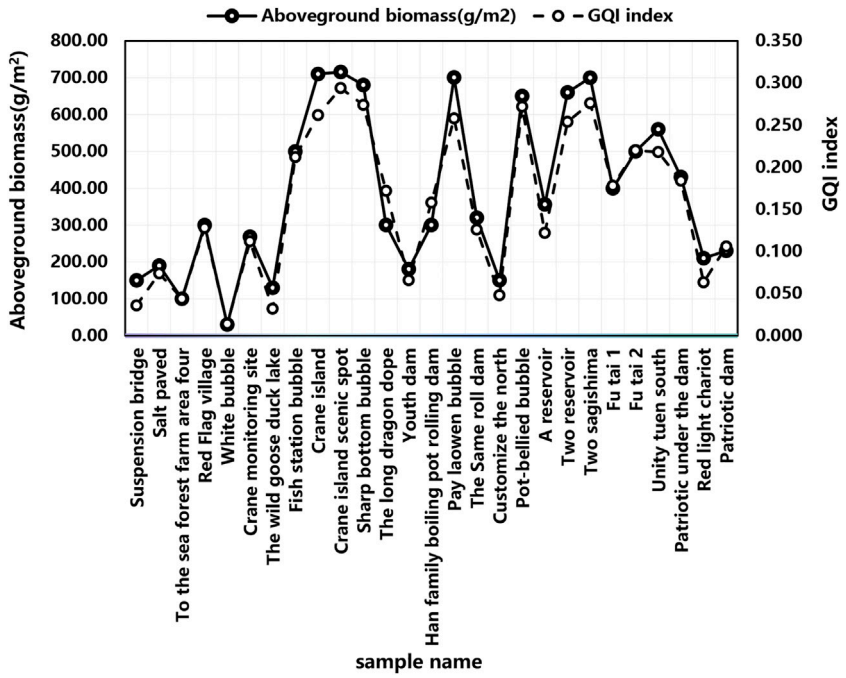

FIGURE 6
The graph of two vertical axis.

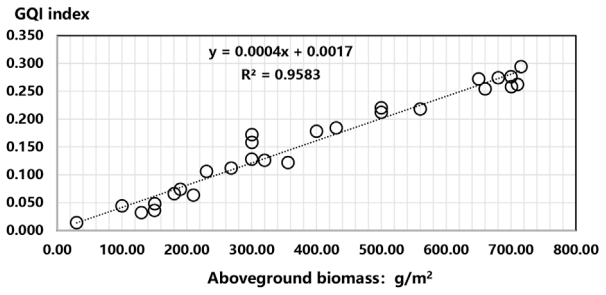

FIGURE 7
The two-index scatterplot.

method is further used to establish the correlation, the correlation model is y = 0.0004x + 0.0017, and R-squared is 0.96.

The scatter plot of the correlation is shown in Figure 7. This also quantitatively shows that the GQI is highly consistent with above-ground biomass, which further indicates that the comprehensive index of grassland quality GQI can reflect grassland quality.

4 Discussion and conclusion

4.1 Discussion

4.1.1 Analysis of factors influencing the grassland quality

The grassland quality in the south-central and southwestern parts of Xianghai Nature Reserve is good and the area is recharged by rivers and reservoirs and the marshland soil is relatively fertile, and so the growth conditions required for vegetation are at a high level. In contrast, the grassland quality in the central-western and southeastern areas is poor, especially in the NDVI, which reflects the low coverage of grassland in the area, which is mostly degraded to saline conditions. Currently, agriculture and animal husbandry in the protected areas are still blindly reclaimed, farmed, and overgrazed and are crudely operated at the cost of the environment and the destruction of resources.

4.1.2 Limitations of the grassland quality index

Previous studies mostly focused on the use of red-edge bands to evaluate the overall quality of regional vegetation, but often needed several indicators and only monitored a single situation of vegetation such as nitrogen and chlorophyll content. The selection of index factors is also often affected by individual factors. Based on the PCA of the normalized vegetation index (NDVI), normalized difference red-edge index (NDRE), and red-edge chlorophyll index (CI-red-edge), a new vegetation index-grassland quality index (GQI) is constructed. The integration of each index is not a weighted sum but is based on the contribution of each index to the first principal component. Therefore, the index can be objectively coupled with each index and reasonably represents the regional ecological quality. Compared with the single vegetation index, the comprehensive index can more comprehensively reflect the advantages and disadvantages of different indicators used to evaluate the grassland quality. The red-edge band adds more spectral information and therefore reflects the various physical and chemical properties of grasslands and improves the accuracy of the grassland quality index (GQI).

However, the index also has some shortcomings as follows: for the areas with sparse grassland coverage, the index has a large error with the actual situation. The NDRE and the red-edge band are affected by soil moisture and light intensity, and the sensitivity of the index to the changes in chlorophyll content is changed. Therefore, the grassland quality index (GQI) is not suitable for use in large areas of grassland.

4.1.3 The accuracy verification

Based on the "Jilin No.1" remote sensing image and using Jilin Xianghai Nature Reserve as the study area, this study analyzed the quantitative evaluation of grassland quality with the vegetation index extracted from satellite image "07." To verify the accuracy, field survey data of above-ground biomass were used to compare the GQI values from the inversion map one by one. It is not easy to ensure the exact correspondence between the field's measured points and the GQI map points. To improve and ensure the accuracy of the measured sample points corresponding to the position of the points taken on the map, and for the field measurement points this paper adopts the method of averaging five measuring points in the upper, lower, left, right, and center positions within the 4 m*4 m quadrate. For the GQI value of the inversion map, the averaging method is adopted to collect five measurement points at the upper, lower, left, and right positions and center positions with a 16 m*16 m quadrate. Although the corresponding correlation coefficient of the point values in this paper was as high as 0.9583, the determination of the quadrat size is very random and needs to be further studied and improved.

4.2 Conclusion

The grassland quality evaluation index (GQI) is formed by constructing NDVI and NDRE related to grassland quality and the first principal component of the red-edge Chlorophyll Index obtained by principal component analysis. Then, it is used for the evaluation of the grassland quality in the Xianghai Nature Reserve. Results show that 80% of grasslands in Xianghai Nature Reserve are of medium quality and widely distributed. The mean value of the GQI in the study area was 0.062. Approximately 15% of grasslands had good growth status and were mainly concentrated in the wetland and swamp areas in the central south part of the reserve. There are still scattered patches

with very poor grassland quality in the reserve area, where the water supply is insufficient and land degradation is serious (most of which are saline-alkali land and sandy land). The correlation of the evaluation results were verified using the survey field biomass, and the coefficient of the established empirical correlation model was 0.96, which indicated good consistency. The results also indicated that the GQI is an effective indicator of grassland quality growth.

Data availability statement

The datasets presented in this article are not readily available because they are not fully published. Requests to access the datasets should be directed to Zhangyanhong, giswork@163.com.

Author contributions

ZC and YZ designed the paper and completed the manuscript. ZL revised the paper. PZ and WZ contributed to data collection and processing. All authors read and agreed to the published version of the manuscript.

Funding

This research was supported by the Strategic Priority Research Program of the Chinese Academy of Sciences (Grant No. XDA28110503) and the National Key Research and Development China (Project No. 2021YFD1500104-3).

Acknowledgments

First, we would like to thank the Remote Sensing of Chang Guang Satellite Technology Co., Ltd., Changchun, who provided the remote sensing images and conducted the processing workshop. Then, we would like to thank the National Xianghai Nature Reserve Administration, who provided guidance for the sample site investigation. Third, we would like to thank the Wetland Center, Northeast Institute of Geography and Agroecology, and Chinese Academy of Sciences, which provided the identification of wetland plants and types. Last, we would like to thank the editor and the reviewers for their careful work and thoughtful suggestions that have substantially improved this paper.

Conflict of interest

The authors declare that the research was conducted in the absence of any commercial or financial relationships that could be construed as a potential conflict of interest.

Publisher's note

All claims expressed in this article are solely those of the authors and do not necessarily represent those of their affiliated organizations, or those of the publisher, the editors, and reviewers. Any product that may be evaluated in this article, or claim that may be made by its manufacturer, is not guaranteed or endorsed by the publisher.

References

Amy, E. F., Wang, L., and Chen, J. (2014). Two new hyperspectral indices for comparing vegetation chlorophyll content. *Geo-spatial Inf. Sci.* 17, 17–25. doi:10.1080/10095020.2014.889264

Baranoski, G. V. G., and Rokne, J. G. (2005). A practical approach for estimating the red edge position of plant leaf reflectance. *Int. J. Remote Sens.* 26 (3), 503–521. doi:10.1080/01431160512331314029

Chen, C., Li, G., and Peng, J. (2023). Temporal and spatial characteristics of Xinjiang grassland normalized vegetation index and its response to climate change from 1981 to 2018[J/OL]. *J. Ecol.* 2023 (04), 1–16. AvaliableAt: http://kns.cnki.net/kcms/detail/11.2031.Q.20220908.1607.002.html.

Cho, M. A., Skidmore, A. K., and Atzberger, C. (2008). Towards red-edge positions less sensitive to canopy biophysical parameters for leaf chlorophyll estimation using properties optique spectrales des feuilles (PROSPECT) and scattering by arbitrarily inclined leaves (SAILH) simulated data. *Int. J. Remote Sens.* 29 (8), 2241–2255. doi:10.1080/01431160701395328

Clevers, J., and Gitelson, A. A. (2013). Remote estimation of crop and grass chlorophyll and nitrogen content using red-edge bands on Sentinel-2 and -3. *Int. J. Appl. Earth Observation Geoinformation* 23, 344–351. doi:10.1016/j.jag.2012.10.008

Das, P. K., Choudhary, K. K., Laxman, B., Rao, S. K., and Seshasai, M. (2014). A modified linear extrapolation approach towards red edge position detection and stress monitoring of wheat crop using hyperspectral data. *Int. J. Remote Sens.* 35 (3-4), 1432–1449. doi:10.1080/01431161.2013.877616

Delegido, J., Verrelst, J., Meza, C. M., Rivera, J. P., Alonso, L., and Moreno, J. (2013). A red-edge spectral index for remote sensing estimation of green LAI over agroecosystems. *Eur. J. Agron.* 46, 42–52. doi:10.1016/j.eja.2012.12.001

Eitel, J., Long, D. S., Gessler, P. E., Hunt, E. R., and Brown, D. J. (2009). Sensitivity of ground-based remote sensing estimates of wheat chlorophyll content to variation in soil reflectance. *Soil Sci. Soc. Am. J.* 73 (5), 1715–1723. doi:10.2136/sssaj2008.0288

Fang, C. Y., Wang, L., and Xu, H. Q. (2017). Comparison of red edge index of different vegetation in urban grassland health discrimination [J]. *J. Geo-Information Sci.* 19 (10), 1382–1392. doi:10.3724/SP.J.1047.2017.01382

Hu, X. J., Xu, H. Q., Guo, Y. B., and Zhang, B. B. (2017). [Remote sensing detection of vegetation health status after ecological restoration in soil and water loss region]. *J. Appl. Ecol.* 1 (28), 250–256. doi:10.13287/j.1001-9332.201701.020

Kanke, R., Solie, S., and Taylor, R. (2012). Red edge as a potential index for detecting differences in plant nitrogen status in winter wheat[J]. *J. PLANT Nutr.* 35 (10), 1526–1541. doi:10.1080/01904167.2012.689912

Kanke, Y., Dalen, M., and Harrell, D. (2016). Evaluation of red and red-edge reflectance-based vegetation indices for rice biomass and grain yield prediction models in paddy fieldsEvaluation of red and red-edge reflectance-based vegetation indices for rice biomass and grain yield prediction models in paddy fields[J]. *Precis. Agric.* 17 (5), 507–530. doi:10.1007/s11119-016-9433-1

Li, F., Miao, Y. X., Feng, G. H., Yuan, F., Yue, S., C., Gao, X., W., et al. (2014). Improving estimation of summer maize nitrogen status with red edge-based spectral vegetation indices. *Field Crops Res.* 157, 111–123. doi:10.1016/j.fcr.2013.12.018

Ma and Weiwei (2015). *Research on remote sensing inversion methods for grassland types and their quality parameters [D]*. Shanghai: Graduate School of the Chinese Academy of Sciences Shanghai Institute of Technical Physics.

Niemann, K. O., Quinn, G., Stephen, R., Visintini, F., and Parton, D. (2015). Hyperspectral remote sensing of mountain pine beetle with an emphasis on previsual assessment. *Can. J. Remote Sens.* 41 (3), 191–202. doi:10.1080/07038992.2015.1065707

Qu, Y. Y., Gao, W., Guo, T. Y., and Chen, W. (2010). Migratory waterbirds in yeyahu wetland nature reserve of beijing[J]. *Wetl. Sci.* 8 (2), 144–150. doi:10.3788/HPLPB20102208.1780

Ramoelo, A., Skidmore, A. K., Cho, M. A., Schlerf, M., Mathieu, R., and Heitk? Nig, I. M. A. (2012). Regional estimation of savanna grass nitrogen using the red-edge band of the spaceborne RapidEye sensor. *Int. J. Appl. Earth Observations Geoinformation* 19, 151–162. doi:10.1016/j.jag.2012.05.009

Shaokui, G. E., Carruthers, R. I., Kramer, M., Everitt, J. H., and Anderson, G. L. (2011). Multiple-level defoliation assessment with hyperspectral data: Integration of continuum-removed absorptions and red edges. *Int. J. Remote Sens.* 32 (21), 6407–6422. doi:10.1080/01431161.2010.510492

Shu, M., Gu, X., Sun, L., Zhu, J., and Zhang, L. (2018). High spectral inversion of winter wheat lai based on new vegetation index[J]. *Sci. Agric. Sin.* 51, 3486–3496. doi:10.3864/j.issn.0578-1752.2018.18.005

Sibanda, M., Mutanga, O., and Rouget, M. (2017). Testing the capabilities of the new WorldView-3 space-borne sensor's red-edge spectral band in discriminating and mapping complex grassland management treatments. *Int. J. Remote Sens.* 38 (1-2), 1–22. doi:10.1080/01431161.2016.1259678

Su, W., Hou, N., Li, Q., Zhang, M. Z., Zhao, X. F., and Jiang, K. P. (2018). Inversion of corn canopy leaf area index based on sentinel-2 remote sensing image [J]. *Trans. Chin. Soc. Agric. Mach.* 49 (1), 151–156. doi:10.6041/j.issn.1000-1298.2018.01.019

Vincini, M., Amaducci, S., and Frazzi, E. (2014). Empirical estimation of leaf chlorophyll density in winter wheat canopies using sentinel-2 spectral resolution. *IEEE Trans. Geoscience Remote Sens.* 52 (6), 3220–3235. doi:10.1109/TGRS.2013.2271813

Xu, H. Q. (2013). Remote sensing evaluation index of regional ecological environment changes [J]. *China Environ. Sci.* 33 (5), 889–897. doi:10.3969/j.issn.1000-6923.2013.05.019

Yang, H. F., Li, J. L., Mu, S. J., Yang, Q., Hu, X. X., Jin, G. P., et al. (2012). Research on hyperspectral reflection characteristics of three main grassland vegetation types in xinjiang [J]. *J. Grassl.* 21 (6), 258–266. doi:10.11686/cyxb20120634

Zhou, W., Li, H., Xie, L., Nie, X., Yue, T., Du, Z., et al. (2021). Remote sensing inversion of grassland aboveground biomass based on high accuracy surface modeling. *Ecol. Indic.* 121, 107215. doi:10.1016/j.ecolind.2020.107215

frontiers | Frontiers in Earth Science

TYPE Original Research
PUBLISHED 05 January 2023
DOI 10.3389/feart.2022.974442

Check for updates

OPEN ACCESS

EDITED BY
Jianhong Xia,
Curtin University, Australia

REVIEWED BY
Huisheng Yu,
Northeastern University, China
Bao-Jie He,
Chongqing University, China

*CORRESPONDENCE
Xiao Xie,
xiexiao@iae.ac.cn

SPECIALTY SECTION
This article was submitted to Environmental Informatics and Remote Sensing,
a section of the journal
Frontiers in Earth Science

RECEIVED 21 June 2022
ACCEPTED 12 September 2022
PUBLISHED 05 January 2023

CITATION
Yang Z, Wu T, E C, Xie X, Tan L and Jiang X (2023), A quantitative enhanced assessment for ancient landslide reactivation risk considering cross-time scale joint response mechanism.
Front. Earth Sci. 10:974442.
doi: 10.3389/feart.2022.974442

COPYRIGHT
© 2023 Yang, Wu, E, Xie, Tan and Jiang. This is an open-access article distributed under the terms of the Creative Commons Attribution License (CC BY). The use, distribution or reproduction in other forums is permitted, provided the original author(s) and the copyright owner(s) are credited and that the original publication in this journal is cited, in accordance with accepted academic practice. No use, distribution or reproduction is permitted which does not comply with these terms.

A quantitative enhanced assessment for ancient landslide reactivation risk considering cross-time scale joint response mechanism

Zixi Yang[1], Tingchen Wu[2], Chao E[2,3], Xiao Xie[2,3]*, Leiqi Tan[1,4,5] and Xinxi Jiang[6]

[1]Faculty of Geomatics, Lanzhou Jiaotong University, Lanzhou, China, [2]Key Lab for Environmental Computation and Sustainability of Liaoning Province, Institute of Applied Ecology, Chinese Academy of Sciences, Shenyang, China, [3]Weifang Institute of Modern Agriculture and Ecological Environment, Weifang, China, [4]National-Local Joint Engineering Research Center of Technologies and Applications for National Geographic State Monitoring, Lanzhou, China, [5]Gansu Provincial Engineering Laboratory for National Geographic State Monitoring, Lanzhou, China, [6]Jiangshan Weiye Surveying and Mapping Co., Ltd., Jiangshan, China

Ancient landslide has strong concealment and disturbance sensitivity due to its special geotechnical mechanical characteristics, and it is the potential hazard that cannot be ignored in human activities and major engineering planning. The quantitative assessment of ancient landslide reactivation risk has become more necessary for pre-disaster scientific warning. However, because the mechanisms of deformation and damage during the evolution of ancient landslides are quite complex, traditional landslide risk assessment methods only select the single-time scale and relatively stable environmental factors for analysis, lacking consideration of dynamic triggering factors such as rainfall. Focusing on the complexity, a quantitative enhanced assessment for ancient landslide reactivation risk considering cross-time scale joint response mechanism is proposed. First, on the basis of systematic analysis of the implicit genesis mechanism and explicit characterization, an evaluation system of the cross-time scale joint characteristics of ancient landslide reactivation is constructed. Then, XGBoost algorithm and SBAS-InSAR are used to establish the long-time scale developmental evolution mechanism model and the short-time scale dynamical trigger model, respectively. Subsequently, we propose a cross-time scale joint response mechanism. The information entropy weight method is applied to calculate the contribution degree of long-short time scale assessment models for ancient landslide reactivation based on the constraints of quantitative interval thresholds, and the assessment processes of different time scales are dynamically and quantitatively correlated. Finally, the updated optimization of the assessment of ancient landslide reactivation risk is achieved. In this research, experimental analysis was carried out for ancient landslide groups in a geological hazard-prone area in Fengjie County, Chongqing, a typical mountainous region of China. The results of the comparative analysis validate the superiority of the method in this paper. It helps to accurately

assess the ancient landslide potential hazard in advance, providing scientific basis and technical support for the risk assessment of mountainous watershed geological hazards and major engineering projects.

KEYWORDS

ancient landslide, reactivation risk, quantitative assessment, cross-time scale joint response mechanism, SBAS-InSAR, China

1 Introduction

Ancient landslide is a slope that has suffered one or more slides which has the deformation trend and potential reactivation risk (Wang S. B. et al., 2021). The reactivation risk of ancient landslides is the probability of slide and occurrence again, due to the influence of environmental and human triggering factors. (Luo et al., 2021; Huang et al., 2022; Xu et al., 2022). Related works indicate a certain path dependency of the dynamic evolution of ancient landslides in time series, which implies a high probability of landslides re-occurring in unstable areas where landslides have occurred before, and these will produce more severe disasters (Samia, 2018; Hu et al., 2022). Therefore, early ancient landslides are potential hazards for human engineering activities, and the precise analysis of the stability condition of ancient landslides and the quantitative assessment of the risk of re-landslides are of vital significance for the safety of people's lives and properties and scientific disaster prevention and mitigation (Xu et al., 2019; Zhu et al., 2019).

Currently, many researches around landslide risk assessment have been mentioned and expected to be applied in reactivation risk assessment of ancient landslide. These studies can be classified into three categories according to the methodological focus: 1) the method of landslide risk assessment based on expert experience including fuzzy logic method (Zhu Q. et al., 2021), fuzzy comprehensive evaluation (Gu et al., 2012) and analytic hierarchy process (Das et al., 2022). Zhu T. T. et al. (2021) used fuzzy logic method to analyze landslides and obtained the results of landslide environmental factor characteristics and landslide susceptibility. However, such methods are susceptible to the influence by experts' subjective experience, the accuracy of the analysis results is difficult to guarantee. With the rapid development of earth observation technology, many scholars have proposed 2) the method of landslide risk assessment based on data. The method mainly applies rich observation data such as GNSS, remote sensing and In-SAR to extract information on the spatial and temporal variation of landslides, and then quantitatively analyzes the landslide risk (Li et al., 2021; Zhu Q. et al., 2021; Bondur et al., 2022). In-SAR technology has the advantages of all-day, high precision and large range, which can obtain continuous surface deformation information of a certain area at the scale of centimeter or even smaller (Bondur et al., 2021). Wang N. Y. (2019) used the In-SAR technique to extract landslide deformation points and calculate deformation rates based on multi-period data as a way to classify the degree of landslide susceptibility. Ciampalini et al. (2016) and Yhokha et al. (2018) capture the signal of accelerated surface deformation and the phenomenon of local slow deformation in the early stage of landslide, and then analyze the distribution and development pattern of landslide hazards and conduct risk assessment (Huang et al., 2020; Yan et al., 2021). Rott and Nagler (2006) and Dong et al. (2018) used In-SAR data to analyze landslides and have demonstrated that the In-SAR technique is a reliable approach to improve landslide identification and monitoring. Especially the small baseline subset interferometric synthetic aperture radar (SBAS-InSAR) proposed by Italian scholar Berardino et al. (2002), the precision of its surface deformation monitoring can reach millimeter level, which has a significant superiority in landslide deformation monitoring research ((Lanari et al., 2007; Zhao et al., 2019; Yang, 2020; Zhang et al., 2022). It has been proved that such observation data can well reflect the real state of landslide, but how to further analyze the deformation trend is still a problem. For this problem, 3) the method of landslide risk assessment based on Machine Learning (ML) is mentioned. The use of logistic regression, random forest (Liu et al., 2018; Sun, 2019), artificial neural network (Polykretis and Chalkias, 2018; Sevgen et al., 2019; Hua et al., 2021), support vector machine (Kalantar et al., 2018; Yu et al., 2019), BP (back propagation) neural network and decision tree (Wang N. 2019) for integrated analysis of multiple landslide causal factors to improve the accuracy of landslide assessment analysis. The machine learning method can support the comprehensive analysis of multiple influencing factors, which can more effectively solve the problem of non-linear relationship expression. Moreover, it might achieve better generalization capabilities due to powerful study strategies (Tien Bui et al., 2016). In particular, XGBoost is a type of decision tree model that optimizes classification performance by combining multiple weakly predictive models into a high-accuracy ensemble, following the steepest gradient along a differentiable loss function (Friedman, 2001; Friedman, 2002). The XGBoost algorithm has been preferred by many researchers to fit models with well-documented speed and high predictability for the training dataset, which has already achieved superior results in classification and regression prediction in several fields (Li and Liu, 2019; Pham et al., 2021; Wang R. et al., 2021). Furthermore, some scholars have also adopted it for landslide susceptibility mapping and surface deformation monitoring (Zhao et al., 2018; Stanley et al., 2020). Zhang et al. (2020) noted that the accuracy of XGBoost in identifying landslide

points was as high as 91.27%, well above the random forest algorithm, which indicates that the XGBoost algorithm has a high accuracy in landslide research. Chakraborty et al. (2019) used XGBoost to analyze the spatial distribution characteristics, genetic mechanisms and development environments of landslide hazard points in the study area, and demonstrated that it can support information mining of potential associations of landslide features (Chen and Guestrin, 2016), producing regular and generalizable results of landslide hazard environment characteristics.

However, the reactivation process of ancient landslides is very complex, it can be broadly divided into potential creeping and apparent activation process. In the creep process, the environmental conditions in which the ancient landslide is located remain relatively unchanged for a long time, as the basis for breeding hazards, its influence is impossible to ignore; when the ancient landslide is strongly triggered by rainfall or earthquake in short time, it will suddenly produce obvious deformation and reactivation. The existing methods fail to accurately and quantitatively assess the risk of ancient landslide reactivation due to a lack of comprehensive consideration of the environmental and triggering factors, which can easily lead to problems such as randomness, bias and blindness in the assessment results. Therefore, it is necessary to consider the effect of disaster-triggering factors in a short period of time on the basis of environment influence over a long time and then establish more stable and reliable risk assessment models.

Aiming at the above problems, this paper proposes a cross-time scale joint enhanced quantitative assessment method of ancient landslide reactivation risk. Firstly, a landslide factor system including long-time scale and short-time scale factor was established based on the reactivation process characteristics of ancient landslides. Then, XGBoost is used to analyze the long-scale factors and extract the deep environmental feature evolving for a long time, while SBAS-InSAR is used to extract the deformation feature of ancient landslide under the action of short time-scale factors. In particular, a cross-scale joint mechanism constrained by quantitative thresholds is proposed to fusion different scales features, and the results of the ancient landslides reactivation risk assessment using a single scale were updated. Finally, we analyzed the ancient landslides area in Fengjie, Chongqing, China, which can not only improve the assessment accuracy but also identify the potential risk. This method provides an effective way for prevention of ancient landslide reactivation. This paper is organized as follows. *Principle of Mechanism Section* presents the Principle of Mechanism of the study, including the cross-time scale joint quantitative enhanced assessment model, and its modeling and analyzing process. The study area and data for modeling on analytical framework are viewed in *Materials Section*, then presents the modeling process of study area in *Modeling Process Section* and *Results and Analysis Section* discusses the experimental results. Finally, the conclusions are presented in *Conclusion Section*.

2 Principle of mechanism

2.1 Overview

Regarding to the difficulty of traditional methods to comprehensively consider the characteristics of the disaster-causing factors at different time scales. This paper innovatively proposes a quantitative enhanced assessment mechanism of ancient landslide reactivation risk jointly across time scales, which can jointly analyze landslide evolution characteristics at long-time scale and dynamical trigger characteristics at short-time scale. The assessment of complex ancient landslide reactivation risk based on establishing a dynamic quantitative correlation between the two scale processes, and finally achieving a risk assessment results consistent with the ancient landslide reactivation mechanism. The schematic principle flowchart of this method is shown in Figure 1, and the specific steps include:

1. First, this paper constructs a cross-time scale joint feature evaluation system for ancient landslide reactivation. Divides the causing factors into different single-scale categories according to the temporal characteristics of the factors based on the full consideration of the short-term dynamical triggering process and long-term developmental evolution of ancient landslide deformation.
2. Then, the adaptation analysis model was determined based on the evaluation factors of different time scales, and the quantitative risk assessment of the ancient landslide area was carried out in long-short scales separately. In which, the XGBoost is used to excavate the deep-seated disaster-generating characteristics and deformation damage mechanism of the long-time scale factors and to calculate the spatial-temporal probability of landslide re-occurrence. The SBAS-InSAR technique is used to invert the landslide surface deformation state and intensity based on short-time scale dynamical triggers.
3. Particularly, a cross-time scale joint response mechanism based on quantitative interval thresholds is then proposed to dynamically and quantitatively correlate the assessment processes of different time scales to achieve the updated optimization of the reactivation riskiness of ancient landslides. The information entropy weight method is used to calculate the contribution degree of long-short time scale assessment models for ancient landslide reactivation based on the constraints of quantitative interval thresholds, and the optimal weights are assigned separately and the assigned assessment models are nonlinearly superimposed jointly to obtain updated results on the riskiness of ancient landslide reactivation.

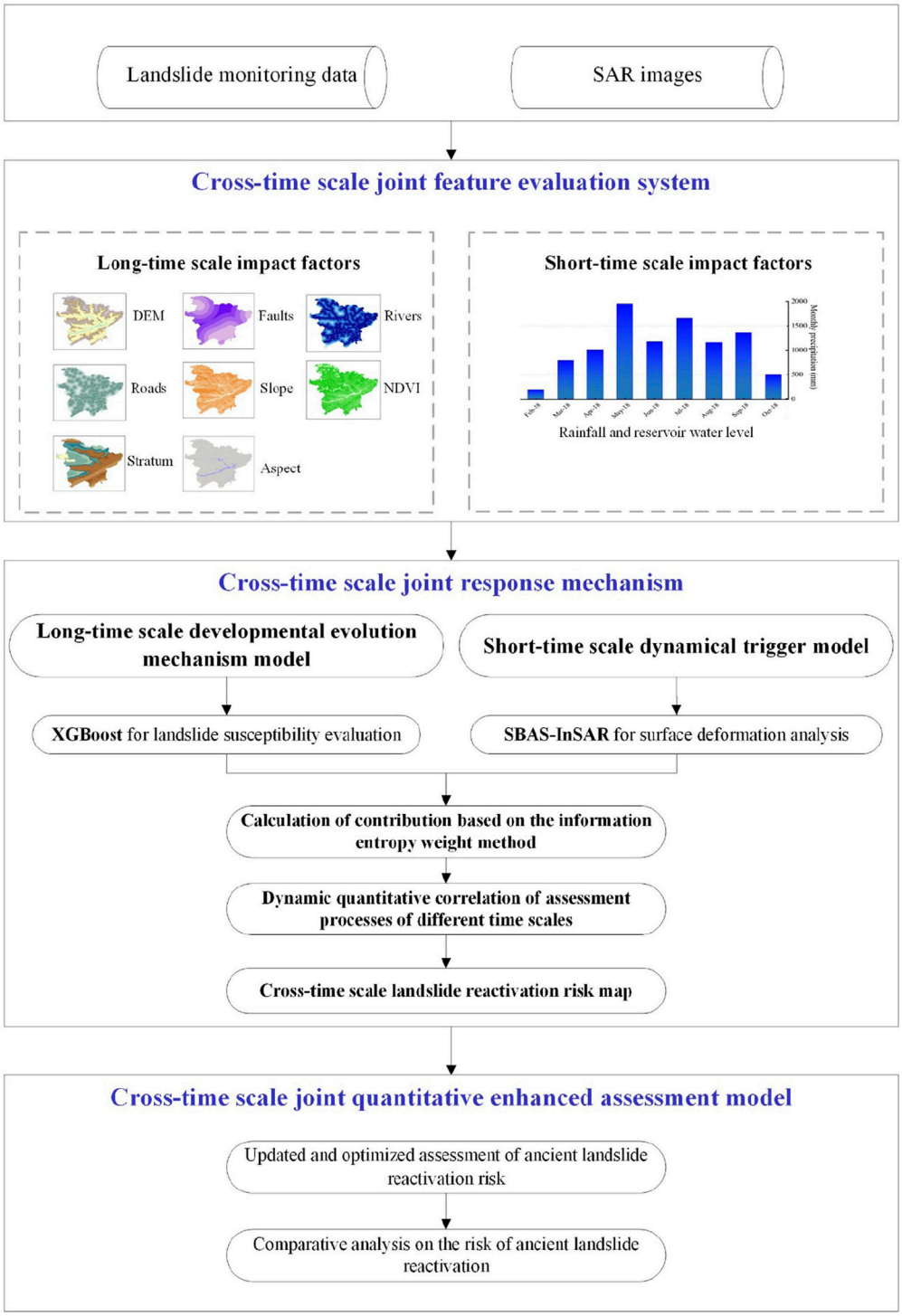

FIGURE 1
Overall flowchart of the cross-time scale joint quantitative enhanced assessment model.

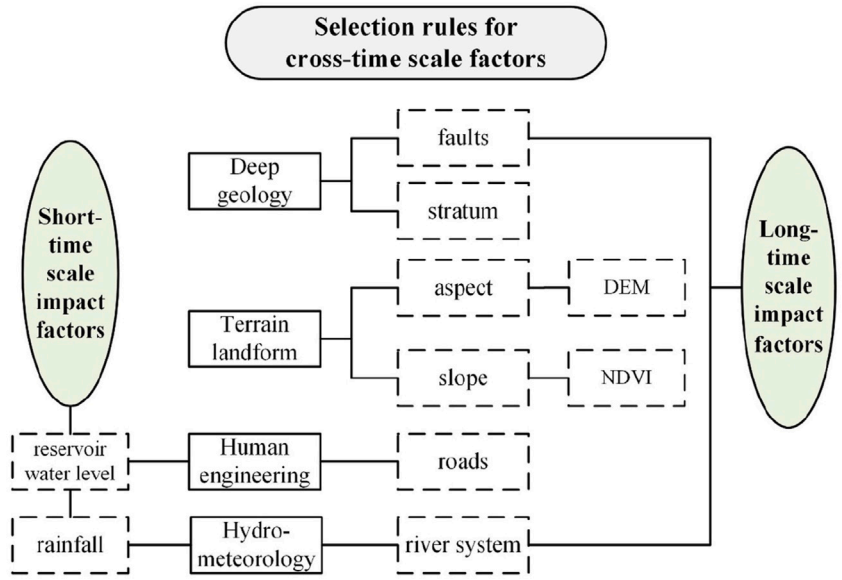

FIGURE 2
Selection rules for cross-time scale factors.

2.2 Cross-time scale joint feature evaluation system

The landslide reactivation mechanism is particularly complex, and the effect of the reactivation characteristic factors on the deformation and damage of the internal structure of the ancient landslide varies with spacetime, showing a nonlinear and unsteady character. Moreover, the ancient landslide is dramatically influenced by external dynamic triggers such as heavy rainfall and sudden changes in reservoir water level. The triggers that induce secondary disasters at key nodes are kinetic and strong, resulting in a dynamic and random short-term activation process of residual landslide deformation.

In this study, the spatial-temporal characteristics of ancient landslide disaster-causing environments were generalized by considering the economic applicability of factor data and historical geography. Based on the principles of systematicity, representativeness, hierarchy and operability, the cross-time scale joint feature evaluation system of ancient landslide reactivation is constructed (Figure 2).

1 long-time scale feature evaluation factor sets: the feature factors of the disaster-generating environment with low correlation are identified, including deep geological factors (faults, stratum), topographic and geomorphological factors (slope, aspect, DEM, NDVI), human engineering factors (roads), and hydrological factors (river systems), which can be used for the study of ancient landslide susceptibility in long-time scales.

2 short-time scale feature evaluation factor sets: for the dynamic triggers that induce reactivation and their characteristics, rainfall and reservoir water level changes were identified as the influencing factors on short-time scales. Among them, rainfall, as a force majeure contingency, is the most important factor to induce landslide deformation in the short term.

2.3 Cross-time scale joint response mechanism

Reactivation mechanisms and tendency are frequently correlated with historical disaster-causing environments strongly, leading to a trend for landslides to occur in areas where landslides have already occurred. And ancient landslides also show strongly reactivation characteristics under the combined effect of seasonal rainfall and periodic reservoir water level changes (Liao et al., 2016). Therefore, the assessment of the reactivation risk of ancient landslides requires the analysis of the response characteristics of the action of short-term dynamical triggers based on the full consideration of long-term regional environmental impacts. To address the above problems, this paper constructs a cross-time scale joint response mechanism based on quantitative interval thresholds. Combining the information entropy theory to correlate the assessment processes of different time scales dynamically and

TABLE 1 Constraints on the construction of the joint response mechanism.

Stability	WS	SD	LS	Constraints
ST	wet season	SD_1= {$\|V_{los}\|$≤10 mm/year}	LS_1 = {sus. ≤ Low}	C_1 = {WS, SD_1, LS_1}
IST	non-wet season	SD_2= {$\|V_{los}\|$>10 mm/year}	LS_2 = {sus. ≥ Moderate}	C_2 = {NWS, SD_2, LS_2}

quantitatively, which can systematically couple the implicit mechanism and explicit characterization of ancient landslide development and evolution. In-depth analysis of the temporal correlation characteristics existing between long-term disaster-inducing conditions and sudden dynamical triggers, finally achieve the updated optimization of ancient landslide reactivation riskiness.

Step1: Regional rainfall is seasonal, sudden and diverse, and different intensity of rainfall will lead to different degrees of surface deformation and landslide displacement, which will in turn affect the evolutionary process of ancient landslide reactivation in a sudden manner. Therefore, we screen the interval threshold of high intensity of surface deformation subject to rainfall effects with a high landslide susceptibility level based on the wet season for the construction of the joint response mechanism across time scales. To take into account factors at different scales and stages, the joint constraints are expressed formally by wet season (WS), surface deformation (SD) and landslide susceptibility (LS) triads:

$$C = (\{WS\}, \{SD\}, \{LS\})$$

The quantitative interval thresholds set in Table 1 are adopted as the constraints for optimizing the entropy method model. (Where, ST = stability threshold, IST = instability threshold, NWS= non-wet season, sus. = susceptibility, V_{los} denotes the surface deformation velocity in the line of sight direction).

Step2: This paper quantifies the degree of importance of long-short time scale evaluation models for ancient landslide reactivation based on information entropy theory combined with the above joint constraints, as a weighted joint basis for single scale models. Of which, it is crucial to abstract the long-short time-scale assessment model into information factors and use the information entropy weight model to quantitatively calculate the contribution of both. The optimized entropy weight method model was regarded as the basis for updating the risk of ancient landslide reactivation.

The information entropy weight method is a means to determine objective weights, which measures the weights of influencing factors of different scales according to entropy value and the degree of discreteness between evaluation indicators. The entropy value is negatively correlated with the information entropy, and the information entropy can reflect the amount of information among the indicators, which is suitable for the study of complex relationships and correlation characteristics among factors of different scales (Yang and Qiao, 2009). The information entropy weight method has been widely used to determine the weight index of natural hazards, including comprehensive environmental evaluation of natural processes such as landslides and debris flows (Yang and Qiao, 2010; Pourghasemi et al., 2012). The information entropy weight method is calculated by the following formula:

$$\begin{cases} WE_i = \dfrac{1 - E_i}{\sum_{i=1}^{n}(1 - E_i)} \\ E_i = -\dfrac{1}{\ln k}\sum_{j=1}^{k} p_{ij}\, ln\left(p_{ij}\right) \\ p_{ij} = \dfrac{FR_{ij}}{\sum_{j=1}^{k} FR_{ij}} \end{cases} \tag{1}$$

where WE_i is the weight, E_i is the information entropy, and FR_{ij} is the landslide frequency ratio of the jth graded category under the ith influencing factor. The larger value of weight WE_i, the greater the amount of information in the single-scale evaluation model, the greater the contribution of this evaluation model to the development of ancient landslide reactivation, and the condition is favorable to the occurrence of ancient landslide reactivation either.

Step3: The contribution of the single-scale model calculated by the optimized entropy weight method model is used as the weight, and the nonlinear weighted superposition of the long-short time scale evaluation results is carried out to achieve the cross-time scale joint assessment of the reactivation probability of ancient landslides.

3 Materials

3.1 Study area

The experimental area adopted in this study is the geographical range between 109°1′17″ and 109°45′58″ east longitude and 30°29′19″ and 31°22′23″ north latitude, which is located in the northern part of Fengjie County, Chongqing (Figure 3, China's administrative zoning map is derived from the

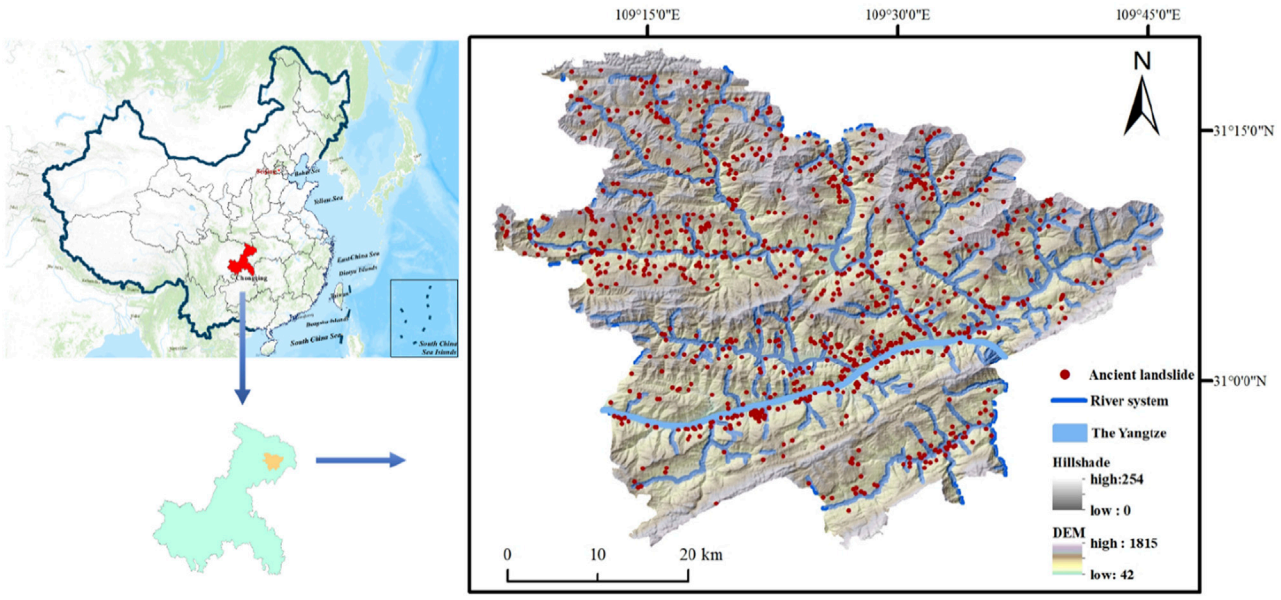

FIGURE 3
Location of the study area.

department of natural resources standard map service website (http://211.159.149.56/index.html), whose figure number is: GS (2020) 4632).

Fengjie County is a mountainous area in the eastern part of the Sichuan Basin, which is a geological disaster-prone area in the Three Gorges reservoir area of China. The terrain of Fengjie is undulating and the geological conditions are relatively fragile and it has abundant rainfall and high intensity of short-term storms. The entire area is severely affected by sudden changes in rainfall and reservoir levels throughout the year, leading to increasingly frequent landslide hazards caused. According to statistics, more than 1,000 landslides have occurred in the region since 1970, including 952 ancient landslides that were revived by the rainfall. Meanwhile, the relevant departments have deployed a large number of landslide monitoring instruments and obtained a large amount of data. Therefore, the conditions in the region are suitable for exploring the risk of ancient landslide reactivation at different time scales for research validation.

3.2 Data used for modeling

3.2.1 Dataset of influencing factors of ancient landslide reactivation

This paper collects the characteristic data on the disaster-causing factors of ancient landslides in Fengjie County, involving surface topography and geomorphology, deep geological structure, hydrology, and human engineering activities, for conducting risk assessment analysis of ancient landslide reactivation in the study area.

Data sources include:1) 30 m resolution DEM data 2) 2.5 m resolution slope and aspect data 3) 1:200,000 vector geological map for extracting information on stratum and faults 4) 1: 5,000 national geo-monitoring data for extracting data on roads and river systems 5) 30 m resolution Landsat 8 satellite digital products for extracting normalized difference vegetation index (NDVI) 6) Monthly precipitation generated by processing China Surface Climate Information Daily Value Dataset V3.0 7) 952 ancient landslide points, contained in the 2018 historical landslide dataset, for analysis of the distribution status and patterns of historical landslide sites. Other primary data information is shown in Table 2.

3.2.2 SAR images

Single Look Comple (SLC) SAR image data in Interferometric Wide (IW) mode from the Earth observation satellite Sentinel 1A are acquired in this study. 46 Sentinel-1A ascending orbital data covering the study area from January 2018 to December 2019 are selected for SBAS-InSAR processing to analyze the surface deformation characteristics ancient landslide at short time scales. In addition, Sentinel 1A has good baseline control and shorter revisiting times (12 days), which accumulates a large amount of high-precision radar image data in a relatively short period of time and can obtain time-domain continuous surface deformation characteristic information through its phase information (Huang et al.,

TABLE 2 Data and data sources.

Data	Data sources	Resolution
DEM	SRTM data	30 m
Slope	Chongqing Geomatics and Remote Sensing Center	2.5 m
Aspect		
Stratum	Chongqing Municipal Bureau of Land and Resources	1 : 200000
Faults		
Roads	National Geographic Monitoring Data	1 : 5000
River system		
NDVI	Landsat 8	30 m
Precipitation	China Surface Climate Information Daily Value Dataset V3.0	
Landslide inventory	Chongqing Geomatics and Remote Sensing Center	
SAR images	NASA Alaska Satellite Facility	20 m

2020). Sentinel 1A has been widely used in the fields of ground subsidence monitoring and landslide deformation monitoring. At the same time, the surface runoff and infiltration generated during the rainfall process are quite prone to the reactivation of larger-scale ancient landslide, so we specifically selected SAR image data containing before and after the wet season to extract information on the landslide surface deformation generated during this period.

4 Modeling process

4.1 Long-time scale developmental evolution mechanism model

Ancient landslide reactivation is generally the consequence of coupled deep-surface multi-factors. The deformation and damage mechanism during the long-term development and evolution of ancient landslides is relatively complex with numerous deformation influencing factors. This study combines the basic geographic conditions of the experimental area and the knowledge pattern of ancient landslides to summarize and analyze the response pattern of long-time scale feature evaluation factors to the regional disaster environment and the mechanism of ancient landslide development and evolution. By quantifying the influence of spatial-temporal effects of historical observation data on deep geological conditions (e.g. faults, geological rock formations, etc.) and topographic and geomorphological conditions (e.g. slope, aspect, NDVI, etc.) during the development of ancient landslides, we hierarchically quantify the magnitude of the probability of occurrence of the ancient landslide reactivation hazard. In this research, the XGBoost model was adopted to construct the long-time scale developmental evolution mechanism model for ancient landslide susceptibility evaluation.

4.1.1 Preparation of the sample dataset

In this research, landslide units and non-landslide units formed the sample dataset for the experiment, and the landslide units consisted of 952 historical landslide events. We finally chose a ratio of 1:10 to construct non-disaster negative sample points after several experiments (Sun et al., 2021). Moreover, in order to select truly "non-landslides" as closely as possible, the 500 m buffer zone of historical landslide points and major river system were avoided. Subsequently, the multi-source heterogeneous experimental data were pre-processed spatially, including data format and spatial reference unification. Since there were two types of continuous and discrete in the evaluation factors of ancient landslide reactivation features, they were quantified by classification or discretized by grading in order to unify the model inputs, respectively. The final processed sample data is a two-dimensional array of 10474×8 (10474 is the number of samples and 8 is the number of features) with element values of 0 or 1, where 1 is for landslide samples and 0 is for non-landslide samples.

4.1.2 XGBoost for landslide susceptibility evaluation

XGBoost is a high-efficiency integrated learning algorithm based on decision trees. In this algorithm, the stepwise forward additive model is adopted to reduce the risk of overfitting by optimizing the structured loss function, and multiple preferred weak learners (decision trees) are combined to accomplish the learning task and thus achieve a superior classification model (Sahin, 2020; Can et al., 2021; Stanley et al., 2021). With the addition of the regularization term, the algorithm will select a simple and well-performing model. The regularization term at the right end of the loss function is designed to suppress overfitting of the weak learner in each iteration, but is not involved in the integration of the ultimate model. The objective function of XGBoost is as follows:

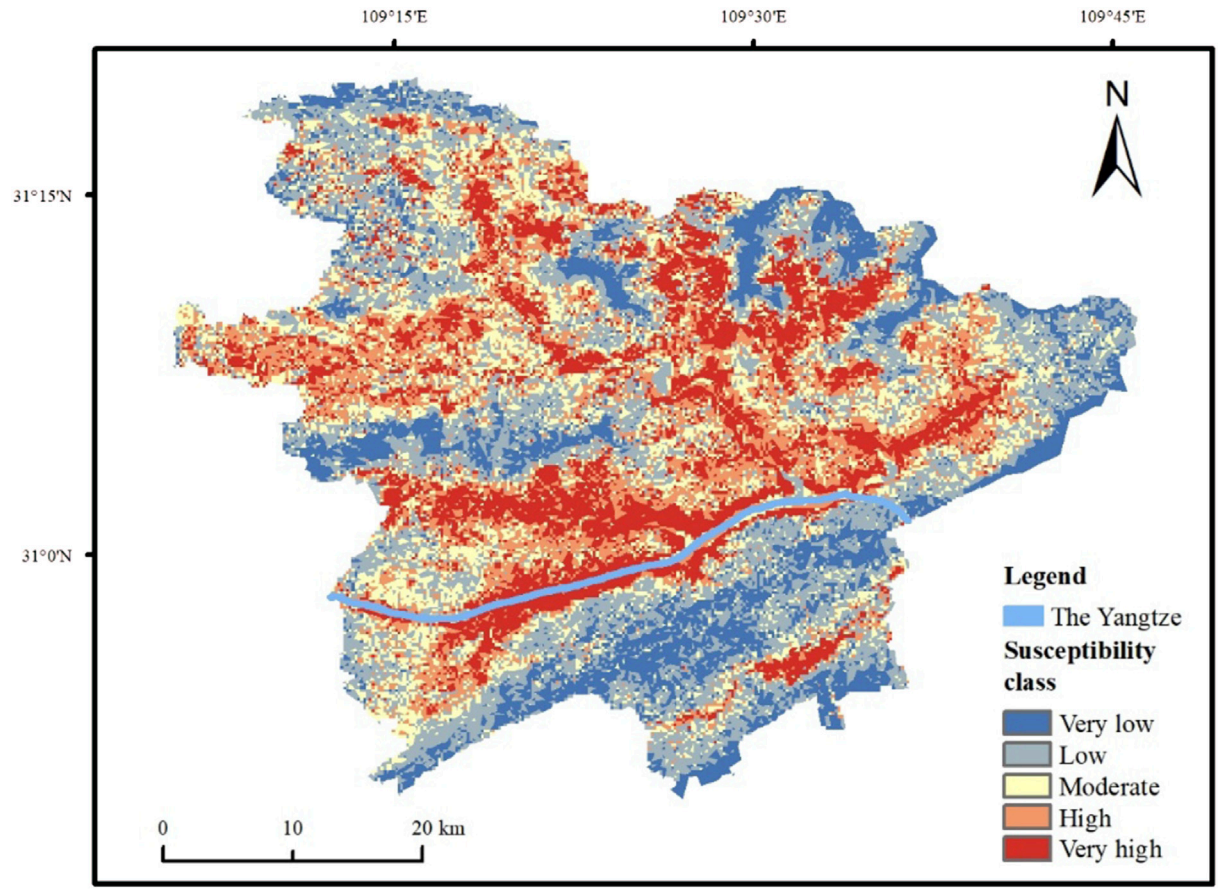

FIGURE 4
Landslide susceptibility map based on XGBoost.

$$L^{(t)} \tilde{=} \sum_{i=1}^{n}\left[l\left(y_i, y_i^{\Lambda(t-1)}\right) + g_i f_t(x_i) + \frac{1}{2}h_i f_t(x_i)^2\right] + \Omega(f_t) \quad (2)$$

Where t denotes the number of iterations, y_i represents the actual value, $y_i^{\Lambda(t-1)}$ is the predicted value in round $i-1$, $\sum_{i=1}^{n} l(y_i, y_i^{\Lambda(t-1)})$ represents the prediction error in round $t-1$, $f_t(x_i)$ is the weight of the ith sample classified to the leaf where it is located in the tth round, f_t denotes the tree model generated in the tth round. Optimal solution ω_j and objective function value O^t of the objective function in the form of a quadratic function:

$$\omega_j = -\frac{G_j}{H_j + \lambda} \quad (3)$$

$$O^t = -\frac{1}{2}\sum_{j=1}^{T}\left(\frac{G_j^2}{H_j + \lambda} + \gamma^T\right) \quad (4)$$

where j represents the leaf node, T represents the total number of leaf nodes, γ and λ denote the pre-designed hyperparameters. Let $\sum_{i\in I_j} g_i = G_i$, $\sum_{i\in I_j} h_i = H_i$, and I_j be the set of samples on the jth leaf. Substituting it into the optimized above equation. Then the loss function in the process of modeling the evolutionary mechanism of ancient landslides on long time scales is:

$$J(f)_t = \sum_{i=1}^{n}\left(y_i, y_i^{\Lambda(t-1)} + f_t(x_i)\right) + \Omega(f_t) + C$$

$$\Omega(f_t) = \gamma^{T_t} + \frac{1}{2}\lambda\sum_{j=1}^{T}\omega_j^2 \quad (5)$$

where x_i denotes each data point, T_t is the number of leaf nodes in the tth iteration, and w_j is the weight of leaf node j.

In this work, the processed long-time scale feature evaluation factor data are used as the input of the XGBoost model, and 70% of the sample data are extracted for training the model and 30% are applied for prediction to verify the model accuracy using the random selection and 5-fold cross-validation methods. Then, on the basis of XGBoost algorithm, a long-time scale evolution mechanism model was established to quantitatively calculate the spatio-temporal probability of the reactivation of the ancient landslide development process. Eventually, the

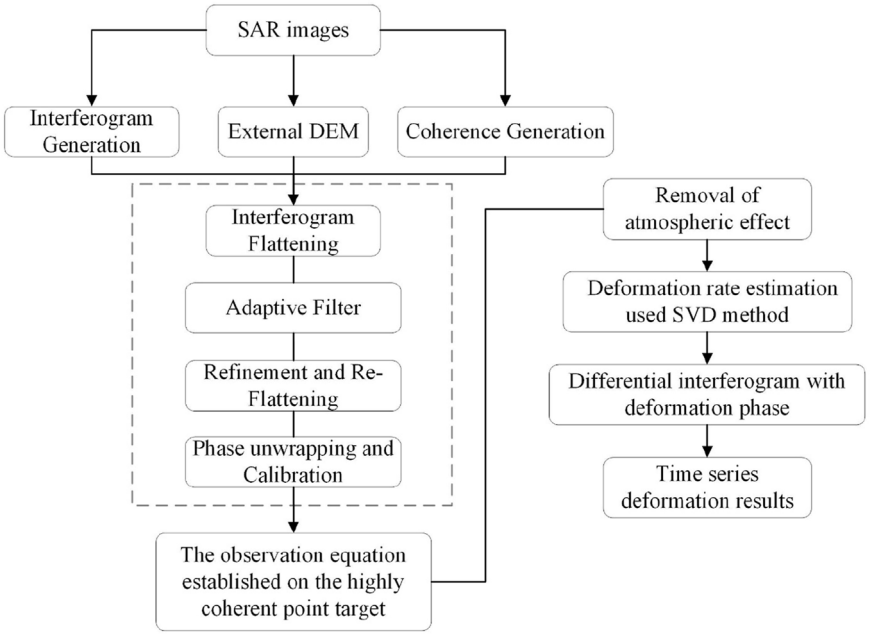

FIGURE 5
Processing flow of SBAS-InSAR technology.

obtained ancient landslide susceptibility maps were reclassified into five classes using the quantile method: very low susceptibility, low susceptibility, moderate susceptibility, high susceptibility, and very high susceptibility (Figure 4).

4.2 Short-time scale dynamical trigger model

Since the dynamic evolution of ancient landslide reactivation hazards are remarkably influenced by external dynamic-induced factors such as heavy rainfall and sudden changes in reservoir water level, the process of transforming ancient landslides from stable to unstable states is extremely short. However, the triggering factors do not simply obey the relevant laws of mathematical statistics in spacetime. When the ancient landslide has a tendency of peristaltic deformation in the long time series development and evolution, the cumulative displacement of the ground surface will show "stepwise" sudden changes in a short time series under the influence of external dynamics factors. Single-scale static long time series analysis is unable to simply obtain the correlation characteristics between dynamic triggers and landslide deformation. The amount of information on the spatial and temporal evolution of landslide hazards based only on data-driven landslide susceptibility analysis is relatively one-sided and lagging, and is prone to the problem of underfitting and overfitting of risk assessment analysis results, which directly affects the accuracy and reliability of ancient landslide reactivation risk assessment. Therefore, this study uses SBAS-InSAR technology to establish dynamic correlations of short-term kinetic trigger processes, and generalize and analyze the dynamic triggers (e.g., heavy rainfall, reservoir level changes) that induce the ancient landslide reactivation at key nodes of developmental evolution. To establish a short time-scale kinetic trigger model to cope with the shortage of short-term triggers such as suddenness and randomness. Finally, a short-time scale dynamical trigger model is established to overcome the shortage of short-term triggers such as suddenness and randomness.

4.2.1 SBAS-InSAR technique

SBAS-InSAR acquires the surface deformation time series by the least squares method and performs temporal fitting with singular value decomposition (SVD), which effectively improves the temporal resolution of monitoring. Further, the minimum-parametric least-squares value of the surface deformation rate between image sequences is sought (Berardino et al., 2002). The basic principle of SBAS-InSAR is as follows (Figure 5):

The M-scene SAR images of the same region are acquired in the time period from t_1 to t_M, and one of them is selected as the main image, and then the N-scene interferogram is generated according to the principle of interferometric combination, which satisfies the following relationship:

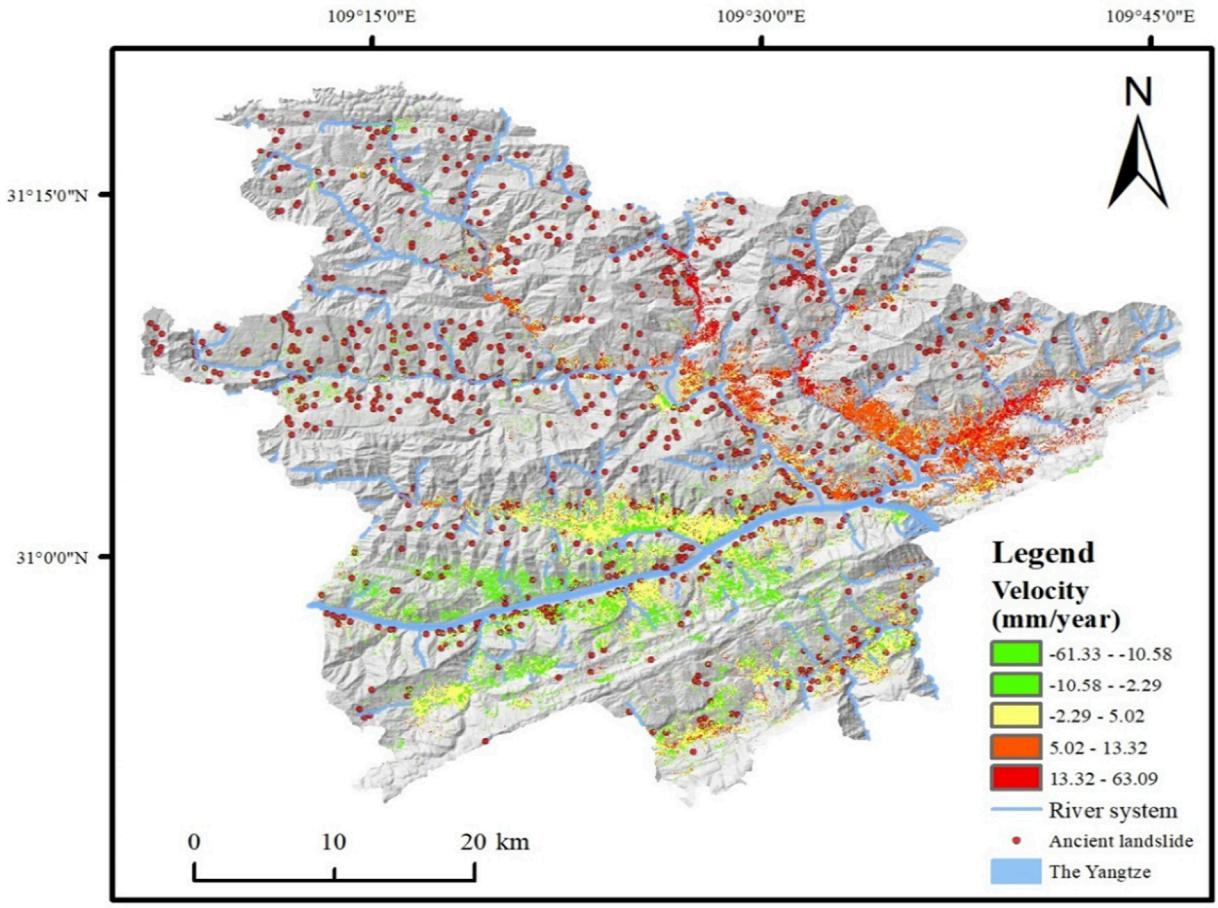

FIGURE 6
Average deformation velocity in the line of sight direction.

$$\frac{M}{2} \le \mathrm{N} \le \frac{M(M-1)}{2} \tag{6}$$

The interferometric phase produced at the point (x, r) for the i (i=1, 2, ..., N) view interferogram generated from the master image A and the image B can be expressed as:

$$\begin{aligned} \Delta\varphi_i(x,r) &= \varphi_A(x,r) - \varphi_B(x,r) \\ &\approx \Delta\varphi^i_{def}(x,r) + \Delta\varphi^i_{\varepsilon}(x,r) + \Delta\varphi^i_{\alpha}(x,r) \\ &\quad + \Delta\varphi^i_{noi}(x,r) \end{aligned} \tag{7}$$

where t_A, t_B ($t_A > t_B$) are the SAR image acquisition times corresponding to the ith interferogram, $\Delta\varphi^i_{def}(x,r)$ is the deformation on the slope distance corresponding to the moment from t_B to t_A, $\Delta\varphi^i_{\varepsilon}(x,r)$ is the topographic phase error, $\Delta\varphi^i_{\alpha}(x,r)$is the atmospheric phase error, $\Delta\varphi^i_{noi}(x,r)$ is the noise phase error. Supposing that the deformation rate between different interferograms is $v_{i,i-1}$, the cumulative deformation from t_B to t_A can be expressed as follows:

$$\Delta\varphi^i_{def}(x,r) = \frac{4\pi}{\lambda} \sum_{k=tB,i+1}^{tA,i} (t_k - t_{k-1}) v_{k,k-1} \tag{8}$$

Finally, the phase unwinding of the interferograms of N SAR images can obtain the deformation rates of different SAR images at the acquisition time.

4.2.2 Surface deformation analysis based on SBAS-InSAR

In this study, the surface displacement and deformation velocity in the line of sight direction (V_{los}) of the experimental area were finally measured by SBAS-InSAR technique using Sentinel1-A ascending orbit images through a series of processing such as connection graph generation, interferometric workflow, orbit refinement and re-flattening, deformation inversion and geocoding. The line-of-sight (LOS) direction average surface deformation velocity distribution map for Fengjie from January 2018 to December 2019 was classified

TABLE 3 Results of the information entropy weight method.

Information entropy weight method

Item	Information sEntropy value	Information utility value	Weights
Long time scale evaluation model	0.996	0.004	0.439
Short time scale evaluation model	0.995	0.005	0.561

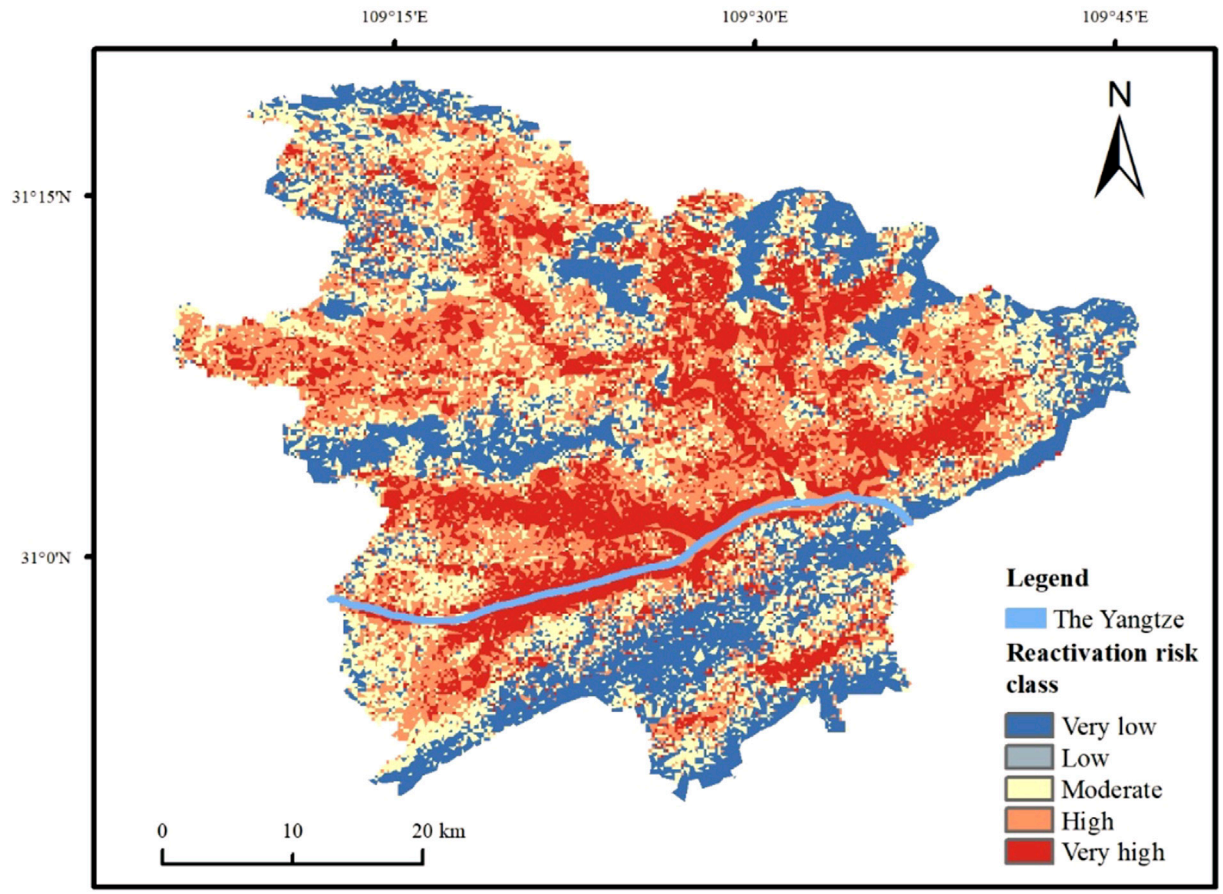

FIGURE 7
Landslide risk map based on joint response mechanism.

into five classes (Figure 6). The velocity here is obtained by dividing the total amount of deformation by the total time span. Related studies have shown that V_{los} between -10 and 10 mm/year indicates that the slope is in a state of weak deformation and the probability of landslide is smaller, when V_{los}>10 mm/year or V_{los}< -10 mm/year indicates that the slope is in a state of highly active deformation (Wang, 2021). Consequently, the threshold value for the quantitative interval of deformation velocity for the joint response mechanism across time scales in this study is $|V_{los}|$ >10 mm/year. A positive rate means that the surface is moving close to the satellite along the line of sight (LOS) direction of the radar satellite, which is usually considered as a surface uplift movement, on the contrary, a negative rate is considered as a landslide subsiding downward.

4.3 A cross-time scale joint quantitative assessment model for ancient landslide reactivation risk

In this section, based on the above joint response mechanism, a cross-time scale joint enhanced quantitative assessment model

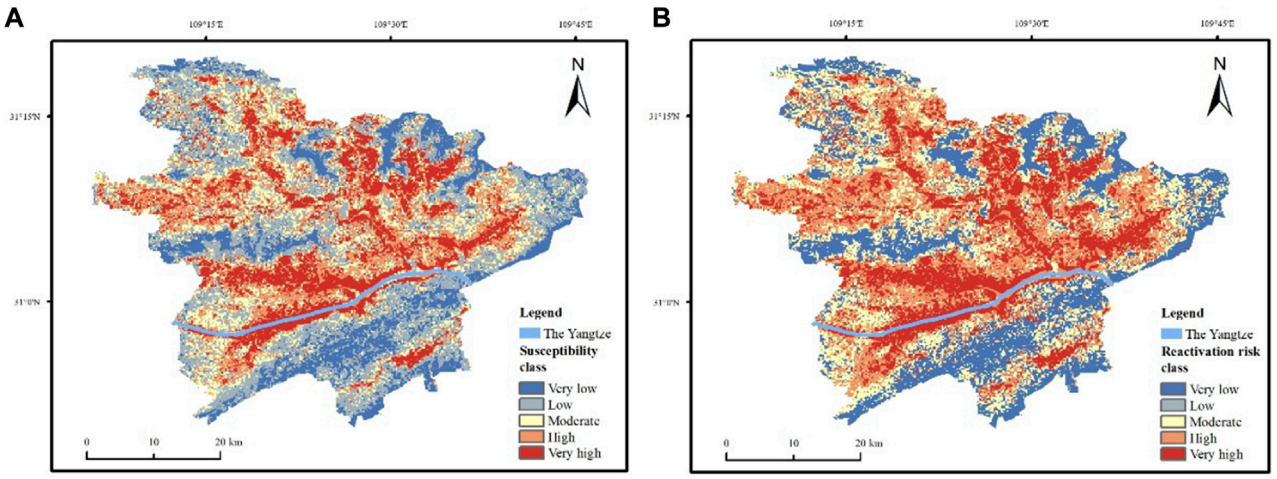

FIGURE 8
Landslide maps at different scales. **(A)** Long-time scale landslide susceptibility map **(B)** Cross-time scale landslide risk map.

for ancient landslide reactivation risk is developed. First, the single-scale quantitative assessment model was reclassified into five classes separately. In which, the interval threshold of surface deformation instability is $|V_{los}|$ >10 mm/year. Then, the entropy weighting method based on the joint constraints of quantitative interval thresholds was used to calculate the degree of contribution of the long-short time scale evaluation model for the ancient landslide reactivation, and a weight of 0.439 was assigned to the evaluation result of XGBoost model and 0.561 to the evaluation result of SBAS-InSAR model, respectively. The weighting results are shown in Table 3. The nonlinear joint mapping of the two assessment models with optimal weights was carried out in the GIS platform, and the optimized and update results of the ancient landslide reactivation risk were finally displayed, as shown in Figure 7.

5 Result and analysis

5.1 Experimental results

A cross-time scale riskiness map of ancient landslide reactivation based on the joint response mechanism with constraints is derived. After setting the quantitative interval threshold, the optimized entropy weight method calculates the optimal weight to minimize the density of historical landslides in very low and low susceptibility areas and maximize the density of historical landslides in high susceptibility areas. Compared with the landslide susceptibility map, the ancient landslide reactivation risk map is consistent with the geospatial characteristics of historical landslide occurrence, fixing the overfitting and underfitting that occurred in the data processing. The refinement of landslide susceptibility using surface deformation data enables the assessment results to be more realistic, objective and reliable, making the evaluation results of ancient landslide reactivation risk more reasonable (Figure 8). Consequently, the optimized landslide reactivation risk map has absolute stability and relatively high precision.

5.2 Analysis and discussion

5.2.1 Local comparison of evaluation models on long-time scale and cross-time scale

From the optimized riskiness map of ancient landslide reactivation, we found that the very-high-risk areas are mainly distributed in a band pattern on both sides of the Yangtze River and its major tributaries. This area has an extremely large number of ancient landslides, with 572 ancient landslides points, accounting for more than 60% of the ancient landslides in the study area. The ancient landslides occurring in the area are mainly influenced by the erosion of the Yangtze River and its tributaries by washing. The lithology is mainly soft rocks such as the Middle Triassic Badong Formation, and the joint action of stratum and geological structure has formed a penetrating soft zone, which provides favorable conditions for the occurrence of ancient landslide reactivation disasters. After the Three Gorges Reservoir was fully impounded, the long-term action of groundwater due to rainfall exacerbated the deep deformation of the reservoir bank slopes, leading to many apparent historical landslide events over a long time series. The high-risk area is mainly located on both sides of the river and on both sides of the very high-risk area, which is also distributed in a band pattern, with 278 landslide points. Other

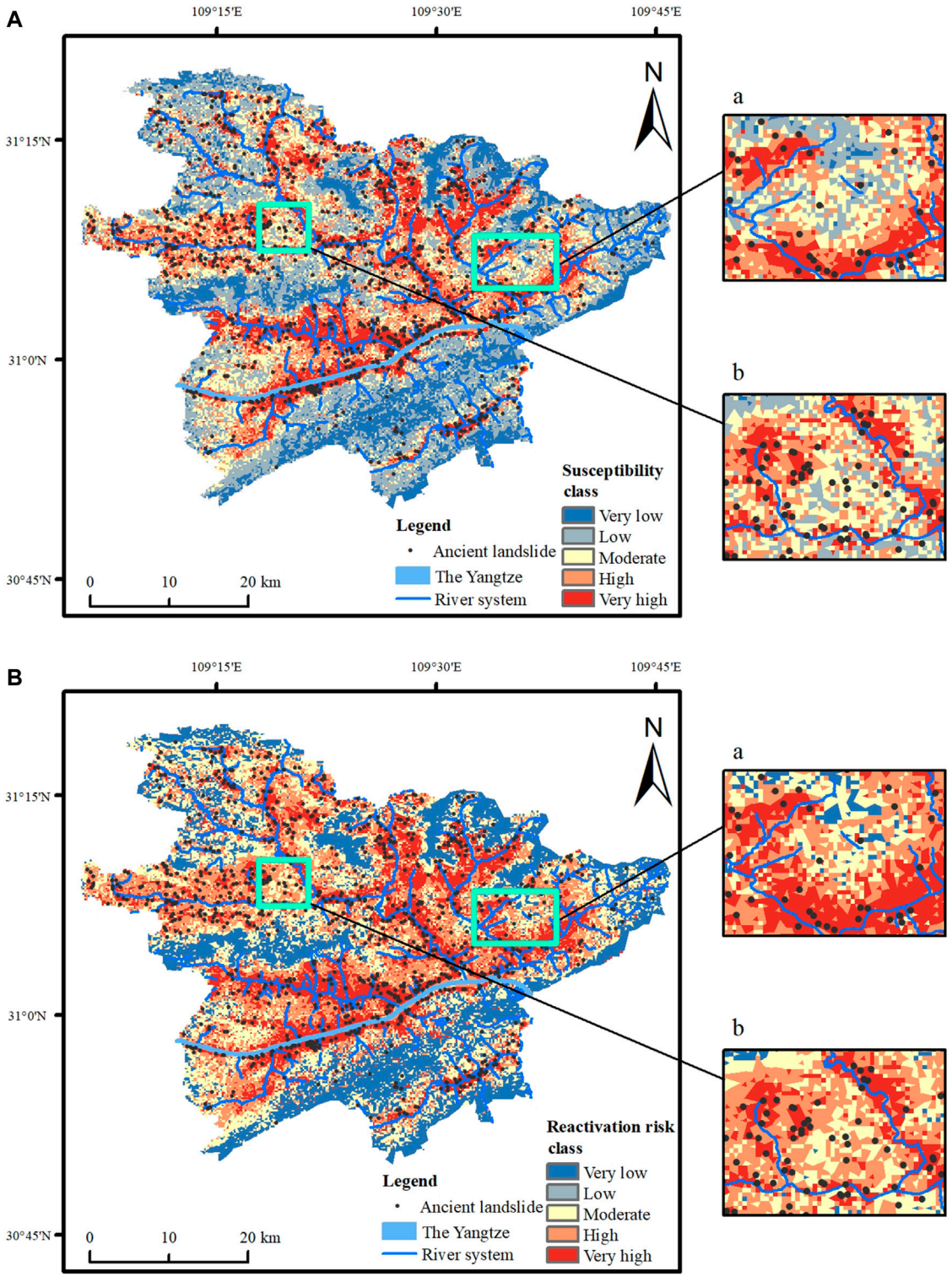

FIGURE 9
Comparative maps of typical areas at different scales. **(A)** Long-time scale landslide susceptibility map **(B)** Cross-time scale landslide risk map.

TABLE 4 Statistical results of landslide susceptibility zoning and risk zoning based on cross-time scale joint response mechanism.

Class	Susceptibility zoning			Risk zoning		
	L%	A%	FR	L%	A%	FR
Very low and low	7.47	42.59	0.17	1.79	23.51	0.08
Moderate	12.83	20.21	0.63	8.83	26.17	0.34
High	22.71	19.02	1.19	29.23	27.86	1.05
Very high	56.99	18.18	3.13	60.15	22.46	2.68

Where, L= Landslide ratio, A= Area ratio, FR (Landslide frequency ratio) = L/A.

risk areas are distributed in patches throughout the study area, and there are fewer landslides developed in these areas. The joint cross-scale landslide riskiness maps generally exhibited a higher degree of riskiness than the long-scale landslide susceptibility maps, which was caused by fusing SBAS-InSAR surface deformation monitoring results (Figure 9). As a result, this technique can effectively reduce the possibility of false negatives in long-scale models and extremely improve the precision of risk assessment.

Furthermore, in this section, the spatial superposition analysis of the optimized updated results of the ancient landslides reactivation risk and the distribution of historical landslide disaster points is carried out. Also making a comprehensive statistic of the area ratio, landslide ratio and landslide frequency ratio of zoning. From the statistical results (Table 4), it can be seen that the landslide ratio and landslide frequency ratio increase with the increase of zoning class. Among them, 92 and 98% of the historical landslide hazard points fall in the medium-risk area and above of the landslide susceptibility map and the cross-time scale landslide riskiness map, respectively. More of the occurred ancient landslide events fall in the medium-high risk area, indicating that the overall accuracy of the optimized and updated landslide riskiness map is greatly improved. Of these, 18.18% of the very high susceptible zone area covers 56.99% of the historical landslide hazard sites, and 22.46% of the very high-risk zone area covers 60.15% of the historical landslide hazard sites, with an increase in both the area of the zone and the number of ancient landslides that have occurred. The frequency ratio of landslides in the low-susceptibility area and the low-risk area are both less than 1. The updated landslide risk map only accounts for 1.79% of the ancient landslide hazard points and the density of ancient landslides is extremely low, indicating that ancient landslide hazard points are concentrated in the optimized medium-high risk zone. The results of landslide risk assessment in this experimental study area can better and realistically reflect the spatial distribution of the occurrence of ancient landslides, and fully verify the reliability and validity of the cross-time scale joint response mechanism.

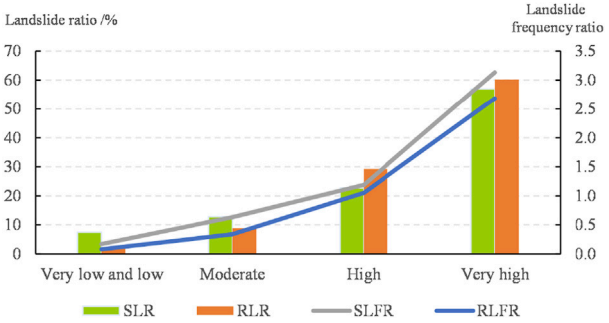

FIGURE 10
Statistical chart of area ratio, landslide ratio and landslide frequency ratio. Where, SLR = susceptibility landslide ratio, RLR = risk landslide ratio, SLFR = susceptibility landslide frequency ratio, RLFR = risk landslide frequency ratio.

However, the single-scale landslide susceptibility map has steep landslide frequency ratio curves in the high and very-high susceptibility areas with large leap order standard deviations, and the smoothness and reasonableness of the zoning results are insufficient. The ancient landslide reactivation risk map fixes the overly varying landslide frequency ratio of the susceptibility map, making the data more smooth and more stable and with higher preciseness (Figure 10). The experimental results indicated that the joint results of the SBAS-InSAR technology-based ground deformation evaluation model and the XGBoost model-based landslide susceptibility evaluation model obtained based on the cross-time scale joint response mechanism could indeed update and improve the sensitivity of ground deformation and optimize the final risk assessment results, making the evaluation results of the model more reasonable and convincing.

5.2.2 Overall analysis of evaluation models on short-time scale and cross-time scale

The experimental results showed that the average surface deformation and surface deformation velocity in the study area varied significantly in the short time series after the beginning of wet season (Figure 11). Before the wet season (Feb 2018–April 2018), the surface deformation changes were relatively stable, the deformation displacement of the slope was mainly within the range of −14.1–18.4 mm, and the minor deformation means lower probability of ancient landslide reactivation. However, by plotting of monthly precipitation and surface deformation against time for the study area in 2018 (Figure 12), we can clearly observe that: The monthly precipitation in May reached its peak throughout the year. Starting from the intense wet season (May 2018–September 2018), with the increase of accumulated rainfall, the geological environment was greatly affected by the change of water level, which led to an ever-increasing amount of both surface uplift and subsidence, and the magnitude of displacement increased with rainfall intensity. Particularly, the surface deformation increased to the range of −56.7–56 mm in

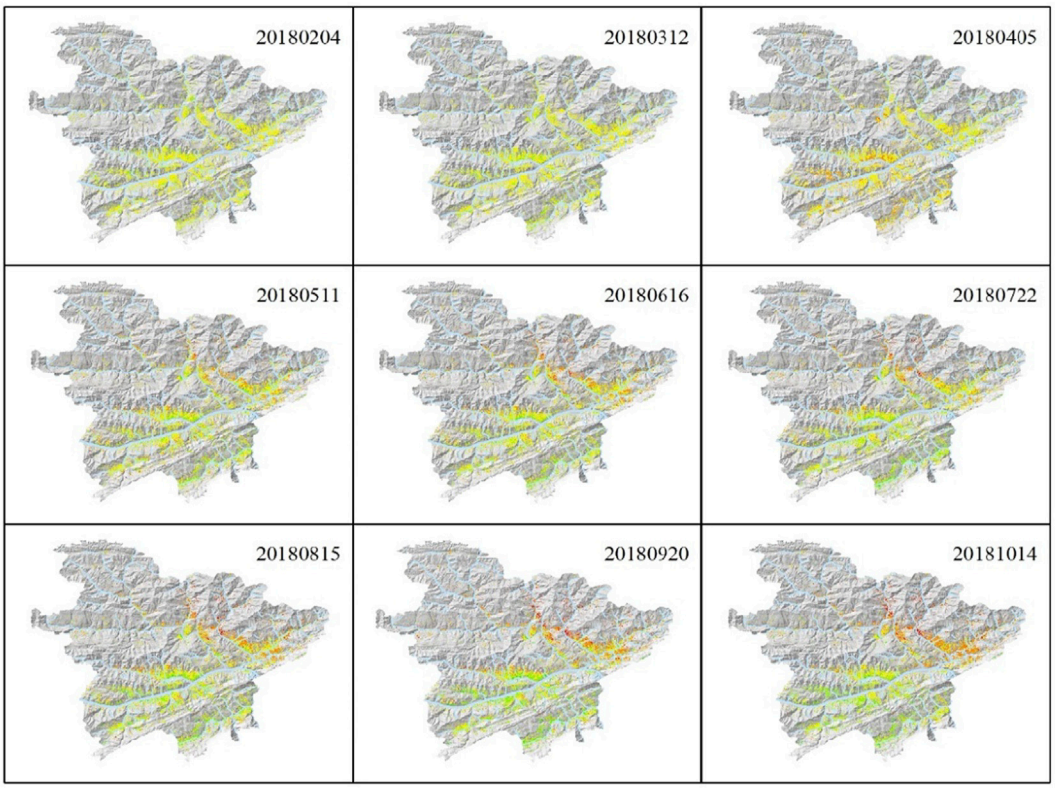

FIGURE 11
Partly surface deformation in short-time series in 2018.

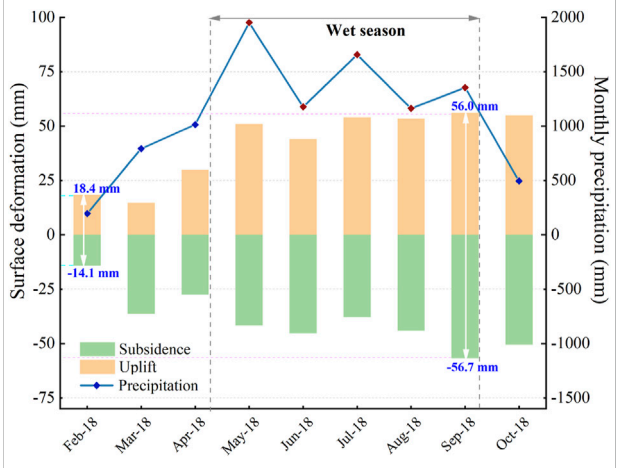

FIGURE 12
Monthly precipitation and surface deformation in the study area plotted against time in 2018.

September, and the accumulated deformation displacement added to the maximum. As a result, the risk of ancient landslide reactivation has also been increased throughout the region due to a sharp and extremely rapid increase in surface deformation triggered by major external triggering factors such as rainfall, resulting in a particularly large area of high and very-high risk areas.

Comparing the updated optimized cross-time scale model and short-time scale model in temporal and spatial dimensions, the following summary can be drawn: 1) Temporally, during the non-wet season, the surface deformation changes less and most areas should show non-sensitive characteristics. However, during the wet season, when cumulative rainfall increases from May to September, the surface deformation increases sharply and areas of increased risk are widely distributed over the study area, with a consequent enhancement in the probability of ancient landslide reactivation. 2) Spatially, the areas of surface deformation are mainly distributed around rivers and special geological formations. Especially after the rainfall, the sudden change of reservoir water level may also be an important influencing factor for the ancient landslide reactivation. As the reservoir water level rises, the rapid deformation of the reservoir bank landslide under the action of pore water pressure, and the influence range of reservoir water fluctuation increases accordingly, leading to the rising risk of reactivation of ancient landslide. At this point, the contribution of the long-time scale factor water system is relatively larger. The very-high risk area of the ancient landslide reactivation requires focused attention from decision makers.

6 Conclusion

In this study, the XGBoost algorithm is used to excavate the deformation damage mechanism during the long-term evolution of the ancient landslide, and the surface deformation inversion by SBAS-InSAR technique is used to clear the potential sensitivity of some area in landslide. Compared with the conventional model, the enhanced assessment based on cross-time scale joint response mechanism highlights the risk classes improved by the surface deformation velocity, and the classification of landslide riskiness is more accurate, realistic and reliable. It is specifically reflected in the follows:

1) From the perspective of extracting the significant hazard, the false negative of each landslide susceptibility class is reduced by more than 20% based on cross-time scale joint response mechanism. It indicated that t the cross-time scale joint response mechanism can effectively update the risk level and reduce misreporting and omission, which has outstanding advantages for avoiding false negatives.
2) From the perspective of extracting the potential hazard, the results of landslide risk assessment based on cross-time scale joint response mechanism show that about 18.18% of the area is updated to a high risk level. It indicated that the cross-time scale joint response mechanism can capture the signal of accelerated ground deformation before the ancient landslide reactivation, improve the risk level of landslides characterized by ground motion.
3) From the perspective of model scalability and migratability, the reactivation of ancient landslides is not only significantly associated with rainfall, but also with short-scale factors such as earthquakes and reservoir rise-fall. Combining this information based on cross-time scale joint response mechanism can make the assessment results more accurate in different environments.

Consequently, we believe that the cross-time scale joint enhanced quantitative assessment method of ancient landslide reactivation risk may be a more effective method to assess the potential riskiness of secondary landslides, and can be applied to landslide mapping and quantitative risk management on a regional scale, which is of great value for effective land use management and project planning.

Data availability statement

The original contributions presented in the study are included in the article/Supplementary material, further inquiries can be directed to the corresponding author.

Author contributions

Author Contributions: Conceptualization, XX; methodology, ZY, TW, and CE.; software, ZY, and CE; validation, TW and LT; formal analysis, XX, CE, and XJ; investigation, TW and XX; resources, XX; data curation, XX; writing—original draft preparation, ZY, TW, and XX; writing—review and editing, XX and CE; visualization, TW and ZY; supervision, XX; project administration, XX; funding acquisition, XX. All authors have read and agreed to the published version of the manuscript.

Funding

Supported by The Shenyang Young and Middle-aged Scientific and Technological Talents Program (RC210502); The Weifang Science and Technology Project (2021ZJ1134); The Support of Science and Technology for the Sichuan-Tibet Railway Special Project (XZ202101ZD0001G) and the LZJTU EP 201806.

Acknowledgments

We are grateful to Qing Zhu (Southwest Jiaotong University) and Tao Liu (Lanzhou Jiaotong University) for their guidance on this study. Zhu provided valuable professional advice both at the start of the study and during the refinement process.

Conflict of interest

XJ is employed by the company Jiangshan Weiye Surveying and Mapping Co., Ltd.

The remaining authors declare that the research was conducted in the absence of any commercial or financial relationships that could be construed as a potential conflict of interest.

Publisher's note

All claims expressed in this article are solely those of the authors and do not necessarily represent those of their affiliated organizations, or those of the publisher, the editors and the reviewers. Any product that may be evaluated in this article, or claim that may be made by its manufacturer, is not guaranteed or endorsed by the publisher.

References

Berardino, P., Fornaro, G., Lanari, R., and Sansosti, E. (2002). A new algorithm for surface deformation monitoring based on small baseline differential SAR interferograms. *IEEE Trans. Geosci. Remote Sens.* 40 (11), 2375–2383. doi:10.1109/tgrs.2002.803792

Bondur, V., Chimitdorzhiev, T., Dmitriev, A., and Dagurov, P. (2021). Fusion of SAR interferometry and polarimetry methods for landslide reactivation study, the bureya river (Russia) event case study. *Remote Sens. (Basel).* 13 (24), 5136. doi:10.3390/rs13245136

Bondur, V. G., Chimitdorzhiev, T. N., Dmitriev, A. V., and Dagurov, P. N. (2022). Assessment of the Bureya River landslide reactivation using the persistent scatterer interferometry. *Dokl. Earth Sci.* 502 (1), 31–36.

Can, R., Kocaman, S., and Gokceoglu, C. (2021). A comprehensive assessment of XGBoost algorithm for landslide susceptibility mapping in the upper basin of Ataturk dam, Turkey. *Appl. Sci. (Basel).* 11 (11), 4993. doi:10.3390/app11114993

Chakraborty, T., Alam, M. S., and Islam, M. D. (2019). "Landslide susceptibility mapping using XGBoost model in Chittagong District, Bangladesh," in Proceedings on International Conference on Disaster Risk Management, Dhaka, Bangladesh, 431–434.

Chen, T., and Guestrin, C. (2016). "XGBoost," in Proceedings of the 22nd ACM SIGKDD International Conference on Knowledge Discovery and Data Mining - KDD '16, New York, USA, 785–794. doi:10.1145/2939672.2939785

Ciampalini, A., Raspini, F., Lagomarsino, D., and Catani, F. (2016). Landslide susceptibility map refinement using PSInSAR dataLandslide susceptibility map refinement using PSInSAR data. *Remote Sens. Environ.* 184, 302–315. doi:10.1016/j.rse.2016.07.018

Das, S., Sarkar, S., and Kanungo, D. P. (2022). GIS-based landslide susceptibility zonation mapping using the analytic hierarchy process (AHP) method in parts of Kalimpong Region of Darjeeling Himalaya. *Environ. Monit. Assess.* 194 (3), 234–328. doi:10.1007/s10661-022-09851-7

Dong, J., Zhang, L., Li, M., Yu, Y., Liao, M., Gong, J., et al. (2018). Measuring precursory movements of the recent Xinmo landslide in Mao County, China with Sentinel-1 and ALOS-2 PALSAR-2 datasets. *Landslides* 15 (1), 135–144. doi:10.1007/s10346-017-0914-8

Friedman, J. H. (2001). Greedy function approximation: A gradient boosting machine. *Ann. Stat.* 29, 1189–1232. doi:10.1214/aos/1013203451

Friedman, J. H. (2002). Stochastic gradient boosting. *Comput. Stat. Data Anal.* 38 (4), 367–378. doi:10.1016/s0167-9473(01)00065-2

Gu, C. Z., Yang, H. F., Hu, X. F., Zeng, J. X., and Luo, G. (2012). Analysis of energy conversion of earthquake-induced landslide based on fuzzy synthetic evaluation. *Rock Soil Mech.* 33 (S1), 297–302.

Hu, S., Qiu, H. J., Wang, N. L., Wang, X. G., Ma, S. Y., Yang, D. D., et al. (2022). Movement process, geomorphological changes, and influencing factors of a reactivated loess landslide on the right bank of the middle of the Yellow River, China. *Landslides* 19 (6), 1265–1295. doi:10.1007/s10346-022-01856-0

Hua, Y., Wang, X., Li, Y., Xu, P., and Xia, W. (2021). Dynamic development of landslide susceptibility based on slope unit and deep neural networks. *Landslides* 18 (1), 281–302. doi:10.1007/s10346-020-01444-0

Huang, J. X., Xie, M. W., and Atkinson, P. M. (2020). Dynamic susceptibility mapping of slow-moving landslides using PSInSAR. *Int. J. Remote Sens.* 41 (19), 7509–7529. doi:10.1080/01431161.2020.1760398

Huang, X., Wang, L., Ye, R., Yi, W., Huang, H., Guo, F., et al. (2022). Study on deformation characteristics and mechanism of reactivated ancient landslides induced by engineering excavation and rainfall in Three Gorges Reservoir area. *Nat. Hazards (Dordr).* 110 (3), 1621–1647. doi:10.1007/s11069-021-05005-z

Kalantar, B., Pradhan, B., Naghibi, S. A., Motevalli, A., and Mansor, S. (2018). Assessment of the effects of training data selection on the landslide susceptibility mapping: A comparison between support vector machine (SVM), logistic regression (LR) and artificial neural networks (ANN). *Geomat. Nat. Hazards Risk* 9 (1), 49–69. doi:10.1080/19475705.2017.1407368

Lanari, R., Casu, F., Manzo, M., and Lundgren, P. (2007). Application of the SBAS-DInSAR technique to fault creep: A case study of the hayward fault, California. *Remote Sens. Environ.* 109 (1), 20–28. doi:10.1016/j.rse.2006.12.003

Li, X. E., Zhou, L., Su, F. Z., and Wu, W. Z. (2021). Application of InSAR technology in landslide hazard: Progress and prospects. *Natl. Remote Sens. Bull.* 25 (02), 614–629.

Li, Z. S., and Liu, Z. G. (2019). Feature selection algorithm based on XGBoost. *J. Commun.* 40 (10), 101–108.

Liao, H. B., Yin, K. L., and Wang, G. H. (2016). Dynamic mechanism of intermittent reactivation of deep-seated reservoir ancient landslide. *Rock Soil Mech.* 37 (09), 2645–2653. doi:10.16285/j.rsm.2016.09.029

Liu, J., Li, S. L., and Chen, T. (2018). Landslide susceptibility assesment based on optimized random forest model. *Geomatics Inf. Sci. Wuhan Univ.* 43 (7), 1085–1091.

Luo, G., Ren, G., Bao, X., Yang, X., and Liu, T. (2021). Stability analysis of the shiliushubao landslide based on deformation characteristics and external trigger factors in the three Gorges reservoir. *Adv. Civ. Eng.* 2021, 1–12. doi:10.1155/2021/2714918

Pham, Q. B., Achour, Y., Ali, S. A., Parvin, F., Vojtek, M., Vojteková, J., et al. (2021). A comparison among fuzzy multi-criteria decision making, bivariate, multivariate and machine learning models in landslide susceptibility mapping. *Geomat. Nat. Hazards Risk* 12 (1), 1741–1777. doi:10.1080/19475705.2021.1944330

Polykretis, C., and Chalkias, C. (2018). Comparison and evaluation of landslide susceptibility maps obtained from weight of evidence, logistic regression, and artificial neural network models. *Nat. Hazards* 93 (1), 249–274. doi:10.1007/s11069-018-3299-7

Pourghasemi, H. R., Mohammady, M., and Pradhan, B. (2012). Landslide susceptibility mapping using index of entropy and conditional probability models in GIS: Safarood Basin, Iran. *Catena* 97, 71–84. doi:10.1016/j.catena.2012.05.005

Rott, H., and Nagler, T. (2006). The contribution of radar interferometry to the assessment of landslide hazards. *Adv. Space Res.* 37 (4), 710–719. doi:10.1016/j.asr.2005.06.059

Sahin, E. K. (2020). Assessing the predictive capability of ensemble tree methods for landslide susceptibility mapping using XGBoost, gradient boosting machine, and random forest. *SN Appl. Sci.* 2 (7), 1308–1317. doi:10.1007/s42452-020-3060-1

Samia, J. (2018). Landslide path dependency and its impact on space-time modelling of landslide susceptibility, PhD Thesis. Wageningen University.

Sevgen, E., Kocaman, S., Nefeslioglu, H. A., and Gokceoglu, C. (2019). A novel performance assessment approach using photogrammetric techniques for landslide susceptibility mapping with logistic regression, ANN and random forest. *Sensors* 19 (18), 3940. doi:10.3390/s19183940

Stanley, T. A., Kirschbaum, D. B., Benz, G., Emberson, R. A., Amatya, P. M., Medwedeff, W., et al. (2021). Data-driven landslide nowcasting at the global scale. *Front. Earth Sci.* 378. doi:10.3389/feart.2021.640043

Stanley, T. A., Kirschbaum, D. B., Sobieszczyk, S., Jasinski, M. F., Borak, J. S., and Slaughter, S. L. (2020). Building a landslide hazard indicator with machine learning and land surface models. *Environ. Model. Softw.* 129, 104692. doi:10.1016/j.envsoft.2020.104692

Sun, D. L. (2019). Mapping landslide susceptibility based on machine learning and forecast warning of landslide induced by rainfall, PhD Thesis. East China Normal University.

Sun, D., Wen, H., Xu, J., Zhang, Y., Wang, D., and Zhang, J. (2021). Improving geospatial agreement by hybrid optimization in logistic regression-based landslide susceptibility modelling. *Front. Earth Sci.* 686. doi:10.3389/feart.2021.713803

Tien Bui, D., Tuan, T. A., Klempe, H., Pradhan, B., and Revhaug, I. (2016). Spatial prediction models for shallow landslide hazards: A comparative assessment of the efficacy of support vector machines, artificial neural networks, kernel logistic regression, and logistic model tree. *Landslides* 13 (2), 361–378. doi:10.1007/s10346-015-0557-6

Wan, D., Ding, Y., Lu, Y., Jiang, X., and Xiong, G. (2021). Study on the mechanism of Xiajiang Hydraulic Project landslide reactivation based on long-term *in situ* monitoring techniques. *IOP Conf. Ser. Earth Environ. Sci.* 861 (4), 042046. doi:10.1088/1755-1315/861/4/042046

Wang, N. (2019). Study on early warning of rainfall-induced landslide in bazhou district, Master's Thesis. University of Electronic Science and Technology of China.

Wang, N. Y. (2019). Study on evaluation of landslide susceptibility in the middle reaches of Bailongjiang Basin, Master's Thesis. Nanjing Normal University.

Wang, R., Zhang, K., Ning, Y., Xu, W., Wang, W., and Qin, J. (2021). Reactivation of ancient landslide deposits: Geological characteristics and deformation mechanism. *Adv. Civ. Eng.* 2021, 1–12. doi:10.1155/2021/6614180

Wang, S. B., Zhuang, J. Q., Zheng, J., Fan, H. Y., Kong, J. X., and Zhan, J. W. (2021). Application of Bayesian hyperparameter optimized random forest and XGBoost model for landslide susceptibility mapping. *Front. Earth Sci.* 617. doi:10.3389/feart.2021.712240

Wang, W. H. (2021). Landslide hazard identification based on SBAS-InSAR and machine learning -Taking Lanzhou City as an example, Master's Thesis. Lanzhou Jiaotong University. doi:10.27205/d.cnki.gltec.2021.001122

Xu, Q., Dong, X. J., and Li, W. L. (2019). Integrated space-air-ground early detection, monitoring and warning system for potential catastrophic geohazards. *Geomatics Inf. Sci. Wuhan Univ.* 44 (07), 957–966. doi:10.13203/j.whugis20190088

Xu, Q., Lu, H. Y., Li, W. L., Dong, X. J., and Guo, C. (2022). Types of potential landslide and corresponding identification technologies. *Geomatics Inf. Sci. Wuhan Univ.* 47 (03), 377–387. doi:10.13203/j.whugis20210618

Yan, Y. Q., Guo, C. B., Zhang, Y. S., Zhang, X. J., Zheng, Y. Z., Li, X., et al. (2021). Study of the deformation characteristics of the Xiongba ancient landslide based on SBAS-InSAR method, Tibet, China. *Acta Geol. Sin.* 95 (11), 3556–3570. doi:10.19762/j.cnki.dizhixuebao.2021195

Yang, G. (2020). Optimized regional landslide susceptibility evaluation in Maoxian based on SBAS-InSAR technique, Master's Thesis. Jilin University. doi:10.27162/d.cnki.gjlin.2020.005732

Yang, Z., and Qiao, J. (2009). "Entropy-based hazard degree assessment for typical landslides in the Three Gorges Area, China," in *Landslide dis. Mitigat. Three gor. Res*, 519–529.

Yang, Z., and Qiao, J. (2010). "Regional landslide zonation based on entropy method in Three Gorges area, China," in 2010 Seventh International Conference on Fuzzy Systems and Knowledge Discovery, 1336–1339.

Yhokha, A., Goswami, P. K., Chang, C. P., Yen, J. Y., Ching, K. E., and Aruche, K. M. (2018). Application of persistent scatterer interferometry (PSI) in monitoring slope movements in Nainital, Uttarakhand Lesser Himalaya, India. *J. Earth Syst. Sci.* 127 (1), 6–13. doi:10.1007/s12040-017-0907-y

Yu, L. B., Cao, Y., Zhou, C., Wang, Y., and Huo, Z. T. (2019). Landslide susceptibility mapping combining information gain ratio and support vector machines: A case study from wushan segment in the three Gorges reservoir area, China. *Appl. Sci. (Basel).* 9 (22), 4756. doi:10.3390/app9224756

Zhang, F. H., Zhu, Y. Y., Zhao, X. Z., Zhang, Y., Shi, L. H., and Liu, X. D. (2020). Spatial distribution and identification of hidden danger points of landslides based on geographical factors. *Geomatics Inf. Sci. Wuhan Univ.* 45 (08), 1233–1244. doi:10.13203/j.whugis20200126

Zhang, J., Gao, B., Huang, H., Chen, L., Li, Y., and Yang, D. (2022). SBAS-InSAR-based landslide susceptibility mapping along the north Lancang River, Tibetan Plateau. *Front. Earth Sci. (Lausanne).* 1169. doi:10.3389/feart.2022.901889

Zhao, F., Meng, X., Zhang, Y., Chen, G., Su, X., and Yue, D. (2019). Landslide susceptibility mapping of karakorum highway combined with the application of SBAS-InSAR technology. *Sensors* 19 (12), 2685. doi:10.3390/s19122685

Zhao, J., Liu, Y., and Hu, M. (2018). Optimisation algorithm for decision trees and the prediction of horizon displacement of landslides monitoring. *J. Eng.* 2018, 1698–1703. doi:10.1049/joe.2018.8305

Zhu, Q., Chen, L., Hu, H., Pirasteh, S., Li, H., and Xie, X. (2020). Unsupervised feature learning to improve transferability of landslide susceptibility representations. *IEEE J. Sel. Top. Appl. Earth Obs. Remote Sens.* 13, 3917–3930. doi:10.1109/jstars.2020.3006192

Zhu, Q., Zeng, H. W., Ding, Y. L., Xie, X., Liu, F., Zhang, L. G., et al. (2019). A review of major potential landslide hazards analysis. *Acta Geod. Cartogr. Sinica* 48 (12), 1551–1561.

Zhu, Q., Zhu, M. D., Ding, Y. L., Zeng, H. W., Wang, W., and Liu, F. (2021). Fuzzy logic approach for regional landslide susceptibility analysis constrained by spatial characteristics of environmental factors. *Geomatics Inf. Sci. Wuhan Univ.* 46 (10), 1431–1440.

Zhu, T. T., Shi, X. G., Zhou, C., Jiang, H. J., Zhang, L., and Liao, M. S. (2021). Stability monitoring and analysis of shuping landslidein three Gorges area with sentinel-1 images from 2016 to 2020. *Geomatics Inf. Sci. Wuhan Univ.*, 46(10), 1560–1568. doi:10.13203/j.whugis20210247

frontiers | Frontiers in Earth Science

TYPE Original Research
PUBLISHED 10 January 2023
DOI 10.3389/feart.2022.1032953

Check for updates

OPEN ACCESS

EDITED BY
Bing Xue,
Institute for Advanced Sustainability Studies (IASS), Germany

REVIEWED BY
Daniela Piazzese,
University of Palermo, Italy
Dafang Wu,
Guangzhou University, China

*CORRESPONDENCE
Chunliang Xiu,
xiuchunliang@mail.neu.edu.cn

SPECIALTY SECTION
This article was submitted to Geoscience and Society, a section of the journal Frontiers in Earth Science

RECEIVED 31 August 2022
ACCEPTED 30 September 2022
PUBLISHED 10 January 2023

CITATION
Xiu C and Li T (2023), Construction of the Hainan Free Trade Port from the perspective of regional cultural development.
Front. Earth Sci. 10:1032953.
doi: 10.3389/feart.2022.1032953

COPYRIGHT
© 2023 Xiu and Li. This is an open-access article distributed under the terms of the Creative Commons Attribution License (CC BY). The use, distribution or reproduction in other forums is permitted, provided the original author(s) and the copyright owner(s) are credited and that the original publication in this journal is cited, in accordance with accepted academic practice. No use, distribution or reproduction is permitted which does not comply with these terms.

Construction of the Hainan Free Trade Port from the perspective of regional cultural development

Chunliang Xiu[1,2]* and Tong Li[1]

[1]School of Humanities and Law, Northeastern University, Shenyang, China, [2]Jangho Architecture College, Northeastern University, Shenyang, China

This study summarizes the internal relationship and mechanism of industrialization, business culture, and higher education that affect the development of modern industrial and commercial culture, and consequently, the construction of free trade ports in Hainan. The cases of Hong Kong, Singapore, and Dubai free trade ports were considered as references. Based on immigration, naturalization, and education in Hainan's history, Hainan's cultural base map, which influences the construction of modern industrial and commercial culture, was proposed to be formed by splicing and overlapping of the free, guarding, farming-reading, farming-marine, and immigrant cultures. The development course of Hainan in the past 30 years indicated that although Hainan has always been at the forefront and highland of reform and opening up, it is still relatively backward despite the implementation of long-term policies; moreover, its development performance is not ideal. The existing problems and factors related to the present ideology mainly include the following: 1) The pursuit of "making quick money" has led to the ups and downs of Hainan's development. 2) Lack of innovation hinders functional improvement leading to poor sustainability. 3) The course of modern industrial civilization based on a cultural base map is short. 4) Although bottom-up industrialization plays a key role in the formation of modern industrial civilization, it is not followed by Hainan. Furthermore, the cultural development path of Hainan Free Trade Port construction should 1) strongly promote industrialization by overcoming the shortcomings of industrial development, 2) deepen the reform of the agricultural reclamation system, improve the business environment, and cultivate a healthy modern industrial and commercial culture, 3) standardize the tourism market, and build the most advanced tourism industry culture, 4) improve the basic education level and develop excellent higher education opportunities, 5) enhance the diversity of human resources structure, and 6) revitalize literature and art, and showcase and develop Hainan's fine culture. Overall, the construction of the Hainan Free Trade Port requires long-term upgrading and development. It is necessary to continue cultural construction, adapt to the requirements of the highest level of openness and realize the healthy development of the Hainan Free Trade Port.

KEYWORDS

cultural base map, modern industrial and commercial culture, industrialization, regional development, Hainan Free Trade Port

1 Introduction

Hainan has been established as the largest special economic zone in China since 1988. Since the past 30 years, Hainan has changed its poverty and social backwardness; additionally, its development has changed course from being special economic zones to international tourist islands and free trade zones. However, except for tropical agriculture, tourism, and real estate, other industries such as the internet, medicine, and building materials have not developed extensively, and their role in the overall national development is lower than expected. On 1 June 2020, the state issued an overall plan to construct the Hainan Free Trade Port, which resulted in another historic opportunity to promote Hainan's development. The Hainan Free Trade Port can not only develop free trade but is also a strategic arrangement for Hainan's comprehensive and high-quality development. A question that arises here is that "Can we seize and efficiently utilize new opportunities, transcend the limitations of previous development results, and realize a real leap in Hainan's regional development by constructing a free trade port?" This is a common concern across different sectors. However, related research has been mainly conducted on aspects, such as international experience, free trade port system innovation, open policy, government distribution service framework, and domestic and foreign markets that has focused on the historical lessons of Hainan's development in the past 30 years (Wan et al., 2014; Zhiyuan and Rui, 2020; Li S. et al., 2021; Fan et al., 2022; Ye et al., 2022). As the construction of the free trade port is still at its nascent stage in achieving high-level economic development by integrating elements and resources, the influence of people and their cultural factors that play a role in regional development has been receiving increasing attention. This study analyzed the Hainan development history from the perspectives of regional culture, discussed the existing problems, and proposed the development of a free trade port through the construction of modern industrial and commercial culture, with an aim to promote the efficient and continuous construction of the free trade port.

2 Regional culture and development

2.1 Culture and civilization

Several definitions of "culture" exist that originate from different research perspectives. As early as 1871, British anthropologist Taylor defined culture as "culture or civilization includes knowledge, belief, art, law, ethics, and customs, as well as all abilities and habits acquired by people as members of society" (Taylor, 2010). Moreover, Guiso believed that culture represents "the traditional beliefs and values passed down from generation to generation by ethnic, religious, and social groups" (Guiso, 2006). Castellani mentioned that culture can be summarized by three characteristics: 1) it is shared by a group of people and is spread through socialization, 2) it imposes informal constraints on interpersonal communication, and 3) it differs from knowledge or human capital (Castellani, 2019). Malinowski believed that culture includes three levels, namely, utensils, organizations, and values, which are inseparable and differ regionally or at different historical stages (Malinowski, 2013).

These definitions indicate that there is a consensus that culture is the social and historical precipitation of humans, way of life (production), spiritual value, and group consciousness, including social customs, religious beliefs, ways of thinking, values, aesthetic tastes, and spiritual totems.

"Civilization" is the same as culture, but the difference is that culture is a concrete topic, while civilization sums up cultures and has integrity. Therefore, civilization is occasionally used in discussions related to culture.

2.2 Cultural and regional development

The important role of culture in shaping regional society and economy has received widespread attention. Weber indicated that at the beginning of the last century, the Protestant Reform was one of the main driving forces in the development of capitalism by encouraging individuals to pursue their own wealth (Weber, 2016). Schumpeter believed that innovation is the source of economic development, and the ability of innovation depends on the cultural and psychological factor of entrepreneurship (Schumpeter, 2021).

In the 1990s, "Cultural turn" represented an important academic change in western social sciences. The role of non-economic factors, such as culture, in the evolution of the spatial pattern of economic activities has been receiving widespread attention. To understand the basic regional characteristics during the interaction of social culture and political economy, the essence of regional development should be captured and the local diversity and regional differences should be comprehensively and accurately understood (Scott, 2017; Liu and Yao, 2021; Zhan and Gu, 2022). The main concept connecting culture and economy is "embeddedness," which implies that the relationship network among the stakeholders of economic activity considerably affects the outcomes of economic activities (Yeung, 2003).

The relationship between culture and economic development has received the attention of some researchers. For example, Amin considered the development of cultural and economic geography, and highlighted the mutual construction and mutual shaping relationship between culture and economy (Amin and Thrift, 2007), while Gibson proposed two paradigms of "cultural economization" and "economic culturalization" for the development of cultural and economic geography wherein the

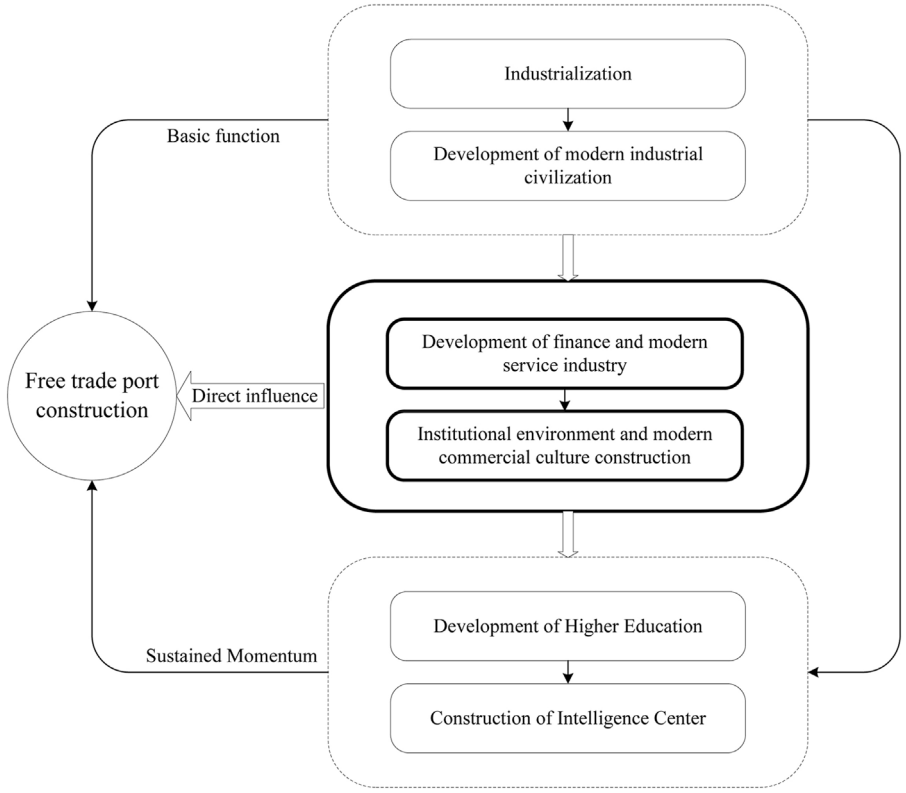

FIGURE 1
How industrial and commercial culture affects the construction of free trade ports.

former regards culture as a production factor (Gibson and Kong, 2005). Castellani divided the study of culture and economy into two categories; the first aimed to study cultural industry considering economic methods and theories, while the other regarded cultural factors as variables that affect economy; subsequently, these factors were included into economic research (Castellani, 2019).

Regional culture is the spatial projection of social culture, and exhibits regionality. It descriptively embodies the regional humanistic characteristics and spiritual outlook, and then becomes the internal factor fundamentally affecting the regional development trends and prospects. Scholars discussed the relationship between cultural factors and regional economic development, and conducted a preliminary analysis of the influence of a cultural model, cultural concept renewal, and cultural stereotypes on regional economic development (Johnson and Lenartowicz, 1998; Shi et al., 2014). Moreover, Scholars also discussed how regional cultural concepts affect regional development aspects across macro and micro levels and the regional development model with distinctive regional cultural characteristics formed through macro- and micro-level interactions (Huggins and Thompson, 2015; Lin et al., 2016). Considering the relatively good performance of economic and social development in areas dominated by the Protestant and Confucian civilizations, Zhang investigated the influence of Protestant and Confucian work ethics on the innovative behavior of employees in China (Zhang et al., 2012), and reported that the economic take-off of East Asia was highly evident in the late 20th century. Moreover, the emphasis of the Confucian culture on diligence, thrift, order, discipline, collectivism, knowledge, faith, and family responsibility was strongly related to this economic phenomenon (Yang, 2012; Tian et al., 2022). Since hundreds of years, owing to the prominent contradiction between man and land in the southeast coastal areas of China, the commercial and market culture was deeply rooted to ensure survival; therefore, it has achieved better development results under the background of reforms and opening up.

3 Modern industrial and commercial cultures and the construction of a free trade port

3.1 Modern industrial and commercial cultures and the significance of building a free trade port

Regional traditional culture and industrial and commercial traditions significantly influence the establishment of market

economy mechanisms and the development of modern industrial civilization. Regions rich in traditional commercial cultural resources have gained a broad belief foundation, rich knowledge sources, and strong power in market transformation, reform and opening up, and development performance (Li J. et al., 2021). Regional economic growth and social development and progress in many Chinese regions include the promotion of transformation from traditional farming civilization, with different characteristics, to modern industrial civilization, and the formation of a modern industrial and commercial culture that is conducive to opening up and innovative development.

Free trade port is a particular economic functional area in a country (region) that implements the policies associated with clearance of domestic customs, free entry and exit of personnel, goods, and funds, tariff exemption for most goods, and free and appropriate trade opportunities, all of which represent the highest level of economic openness in the world. Further, free trade port, which has high requirements for the legal system and contractual engagements, must have a competitive market environment with high openness and rigorous flow of factors. Hainan's status as a particular zone, unique location, good ecological environment, and conditions as an independent geographical unit is particularly suitable as a pilot field for national reform. The construction of the Hainan Free Trade Port will help to enhance the functional level of Hainan, make Hainan more internationally and regionally competitive, and further solve the problems that Hainan has been facing for decades, which is a significant initiative under the national overview. Under the guidance of this new goal, we should prioritize the role of cultural construction and promote the transformation of traditional regional culture to a form that meets the demands of modern industrial and commercial development to achieve the goal of high-level regional development and free trade port construction.

3.2 Experience of free trade port and its cultural environment construction

Presently, Hong Kong, Singapore, and Dubai are three free trade ports with high international recognition and successful operations. These three free trade ports and their cultural environment can be compared based on the following characteristics:

3.2.1 Industrialization process

Hong Kong and Singapore have experienced rapid industrialization, and their manufacturing industries were once extremely strong. The current industrial sectors in Dubai, including aerospace, marine equipment, biomedicine, and medical equipment, account for 11–14% of the gross domestic product (GDP). Further, Dubai is striving to promote diversified economic development, and the proportion of the oil industry in Dubai's GDP has dropped from 50% (30 years ago) to approximately 1% (present) (Dubai Statistics Center, 2020).

3.2.2 Business culture

Hong Kong, Singapore, and Dubai have well-established financial centers with advanced institutional environments and business cultures. Particularly, Singapore and Hong Kong ranked second and fourth, respectively, in the 2019 Global Business Environment Report (World Bank, 2018). Dubai is also an important financial center in the Middle East and in the world. All three regions have highly open money markets and capital markets, flawless credit systems, and advanced business cultures (Akhavan, 2017; Peng et al., 2018; Dong et al., 2019; Harrison et al., 2020).

3.2.3 Talent and education

Hong Kong and Singapore have many institutions for higher learning, advanced higher education, and excellent university resources. In Dubai, although the number of traditional institutions for higher learning is limited, Dubai vigorously supports the special education zone to attract overseas branches and establish the Dubai International Academic City, consequently, forming an agglomeration effect; additionally, the degree of internationalization of universities in Dubai is extremely high (Rottleb and Kleibert, 2022). Superior higher education is a fundamental requirement to ensure that human resources, scientific and technological achievements, and cultural environment are consistent with the functions of the free trade port.

3.3 Mechanism of modern industrial and commercial cultures affecting the construction of the free trade port

Using the abovementioned three areas as references, it is clear that the development of industrialization and modern industrial civilization plays a fundamental role, the development of a financial center and modern service industry has a direct impact, and the construction of a higher education and intellectual center promote sustainable development for the construction of the free trade port (Figure 1).

4 Modern industrial and commercial cultures of hainan and regional development performance and problem analysis

Hainan has experienced immigration since ancient times, and has consequently, formed an immigrant society with Han

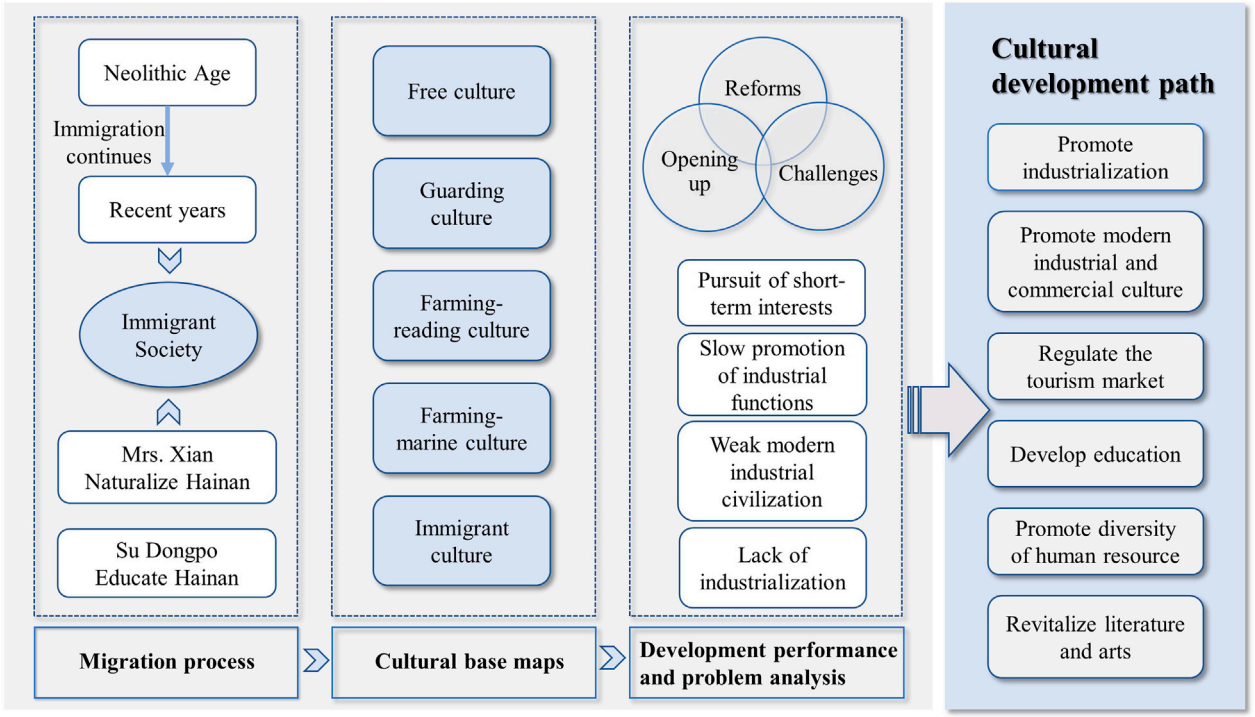

FIGURE 2
Cultural development path of Hainan free trade port.

nationality as the main body, including Li, Hui, Miao, and other ethnic minorities. Modern industrial and commercial cultures are closely related to regional development and immigration process (Figure 2).

4.1 Migration process

The ancestors of the Li nationality moved to Hainan Island in Neolithic Age and became the earliest residents. During the Qin and Han Dynasties, Lingao community crossed the Qiongzhou Strait and moved to the northern part of the island. Further, the Western Han Dynasty started establishing county governance, and until the Five Dynasties, immigrants from the Central Plains represented the main immigrant community, which was distributed in the northwest and northern coastal areas of the island. Later, Muslims began to enter Hainan Island in the Tang Dynasty and Muslims who settled in Song and Yuan Dynasties became the ancestors of Hui nationality in the island (Zhou and Tang, 2019). Since the Song Dynasty, trade in the South China Sea developed, and Hainan Island ultimately became an important landmark for sea routes. Many businessmen settled in Hainan, with most immigrants originating from Fujian, Guangdong, and Guangxi. They continued to immigrate during the Yuan and Ming Dynasties, reaching a peak in the Qing Dynasty, during which there was a simultaneous climax of overseas immigration from the late Qing Dynasty to the Republic of China. Most of the Miao immigrants on the island originated from the Jiajing and Wanli years of the Ming Dynasty, who transferred troops from Guangxi and settled in Hainan (Yan and Liu, 2011). After 1950, Hainan was populated by cadres from the north, soldiers and their families who entered the agricultural reclamation system, immigrants who entered various state-owned farms and returned overseas, Chinese intellectuals who were transferred due to construction, and educated youths who settled in Hainan while working in the countryside. After Hainan was established as a province, nearly 100,000 skilled personnel moved to Hainan (Qi, 2018). Subsequently, there was a constant influx of hundreds of thousands of migrant workers, and in recent years, a large number of retired citizens have migrated from the north.

Although Hainan was established as early as the first year of Han Yuanfeng (110 BC), the post-rebellion continued and Zhuya County was abolished; consequently, it was excluded from the effective jurisdiction for more than 500 years. During the Liang Wudi period of the Southern and Northern Dynasties, Mrs. Xian led her department to Hainan Island by crossing the Qiongzhou Strait to counter insurgency and conciliate the people. Simultaneously, Yazhou was built under her leadership. After decades of loyalty, Hainan politically unified with the mainland. Thus, Mrs. Xian could be mentioned as “the first person to

naturalize Hainan." Until the present day, Hainan conducts the "Noisy Military Slope" activity in February of the lunar calendar to commemorate Mrs. Xian[1].

During and after the Song Dynasty, numerous Han population moved into Hainan to make cultural connections, and the demotion of officials by the imperial court encouraged Hainan to attach importance to learning. Specifically, Su Dongpo was demoted to Hainan for 3 years, during which he conducted lectures and trained talented individuals; thus, he is referred to "the first person to educate Hainan." During the Ming and Qing Dynasties, academics, charitable schools, and community schools prevailed in Hainan, with many talented individuals appearing successively. Subsequently, Hainan began to disseminate talent, and was thus, referred to as "seaside Zou Lu" (Li, 2011)[2]. During the Ming Dynasty, Juren and Jinshi were in large quantities. Although the imperial examination results in the Qing Dynasty were inferior to those in the Ming Dynasty, the extent of cultural development and popularization advanced. Since modern times, Hainan culture has been greatly influenced by the western culture and overseas Chinese culture, consequently, resulting in modern education. After the foundation of New China, exceptional achievements were made in cultural popularization, and higher education and basic education was developed holistically. However, even now, Hainan's culture and education lag behind the national average level and people still do not give sufficient attention to culture and education (Liu and Gao, 2022).

4.2 Cultural base maps

Based on immigration, naturalization, and education in Hainan's history, along with the author's observations since several years, this paper attempted to comprehensively depict the cultural base map of Hainan. The different cultures were as follows:

Free culture: Individuals of the Li nationality were the first residents of Hainan, and there are millions of people at present; In the early days, these individuals dispersed across the entire island; subsequently, they migrated to the Wuzhishan and Limu mountains with the migration of mainland residents. The Li culture is characterized by naturalism and long-term stability of primitive culture. The social customs of matriarchal clans have been inherited in modern-day populations. Further, the primitive production system of "collective tillage system" continued in the central area of Wuzhishan until the early liberation, and the slash-and-burn land development mode was not completely eradicated even in the 1980s (Gao, 2011)[3]. Owing to the tropical conditions of this island, residents have become accustomed to a relaxed, slow, and simple life. In the past 30 years, the development process as a tourist center and a hotspot for health care and elderly care has also strengthened the regional characteristics of free culture.

Guarding culture: Hainan, an isolated island away from the national political center, has guarding problems before and after naturalization. As the Chinese culture was recognized, Lingao people adapted to naturalization and guarded the Hainan Island. During the later dynasties, garrison soldiers converted wastelands to cultivated lands with the assistance of farmers and businessmen to increase food production and generate revenue. Even now, coastal military dialect areas are scattered in the west and southwest of the island, which could be related to the sergeants who were recruited for guarding. From the end of the Yuan Dynasty to the beginning of the Ming Dynasty, Hainan was a pioneer in resisting the invasion of pirates; additionally, Hainan was also an important military center in modern times. Although the militarized agricultural reclamation system (Hainan Agricultural Reclamation), which was established after New China was founded, was not as large as Xinjiang Production and Construction Corps and Heilongjiang Agricultural Reclamation, it had a population of millions. It was once the main carrier of planned economy and significantly influenced Hainan society and its cultural composition. Since the foundation of the People's Republic of China as a national defense outpost, economic activities have been suppressed, and only primary products, such as grain, fishery, mined resources, and heat island crops, have been produced, without industrialization and without the influence of the corresponding industrial cultural process. The long-term guarding process and related functions have historically accumulated, and some characteristics, such as rugged publicity, bravery, and aggressiveness are related to this.

Farming-reading culture: Many Han people and demoted officials entered Hainan to develop agriculture in the low-level coastal areas around the island, with an aim to continue the activities of Central Plains and establish farming and reading traditions. Since the establishment of the Republic of China, basic education has gained popularity, but the development of high education quality at all levels has been slow. Farming-reading culture is aggressive. In the face of nature, a pragmatic view of heaven and man has been formed, and a social atmosphere of honesty, loyalty, and frankness has been formed through social interactions.

Farming-marine culture: Owing to the continuous progress of shipbuilding and navigation technology, marine fisheries and overseas trade are increasingly advancing. Hainan fishermen create a "Geng Lu Bu" for "farming-marine."[4] Fishermen believe in the oceans and are not afraid to take risks in life-

1 "Noisy Military Slope" refers to the Chinese Haikou Mrs. Xian Cultural Festival, a festival established in honor of Mrs. Xian.

2 "seaside Zou Lu" means the place where coastal culture flourishes.

3 "collective tillage system" is a system in which all members work together, and the products are distributed equally by household.

4 "Geng Lu Bu" is the knowledge of the route of navigation in the South China Sea that has been summed up by the people of Hainan in the practice process for thousands of years.

threatening environments to gain monetary profits. This attitude is an integral part of the farming-marine culture and has significantly contributed to developing the South China Sea Islands and their inclusion in China's territory. However, there is also some continuity in the value orientation of not sticking to rules and pursuing quick success.

Immigrant culture: Since a long time, local and foreign cultures have been blending, thus, forming a complex and diverse immigrant culture, which makes Hainan culture both diverse and inclusive (Zhu and Situ, 2001). The successive immigration and development of the Li, Miao, Hui, and Han nationalities in the Hainan Island is a result of continuous cultural integration. Even Han culture has many branches, including Minnan, Hakkas, and Chaoshan. After Qiongzhou was opened as a trading port in the late Qing Dynasty, several Hainan residents immigrated to Southeast Asia to earn livelihood, making Hainan an important hub of overseas Chinese population. Overseas technology, capital, and culture were transferred back to Hainan through various modes, which further increased the openness of Hainan culture. After the foundation of the People's Republic of China, especially since the foundation of the province, several new immigrants from all over the country engaged in tourism and other industrial activities and seasonal tourism immigrants entered Hainan, which further increased the diversity of regional culture and resulted in new challenges to upgrade functions.

Overall, the cultural base map in Hainan Island was formed by splicing and overlapping the free, guarding, farming-reading, farming-marine, and immigrant cultures. The characteristics of each of these cultures will fundamentally affect the regional development and modern industrial and commercial culture construction of Hainan in the future. Although realizing the development and evolution from "freedom" to participation in market competition, "guarding" to innovation and change, "farming-reading" to paying equal attention to business studies, and "farming-marine" to the development and evolution of accumulation is a challenging process, it is the key to building a vibrant modern industrial and commercial culture. However, the changes in immigration structure will directly affect the cultural characteristics of regional industry and commerce, and become an inevitable requirement to construct new functions.

4.3 Course of reform and opening up and the development of modern industrial and commercial culture

Hainan was mainly an agricultural region during its establishment. Despite its weak foundation and relatively backward economy, it has retained various policy advantages for more than 30 years and has become the frontier and highland of reform and opening-up.

4.3.1 Forefront in reforms

Hainan has always been at the forefront of national reforms, with nearly 100 reforms in total. Since the establishment of Hainan Province in 1988, the entire island has been designated as a special economic zone, thereby acting as a pioneer in reform. In recent years, the role of Hainan pioneers has expanded in several aspects. For example, in 1999, Hainan decided to build China's first ecological demonstration province (Zhang et al., 2019; Zhao and Jia, 2019; Qi et al., 2021). For more than 30 years, it adhered to the concept of green development and preserved the ecological environment of Hainan. In 2004 and 2005, policies to offset tax on special agricultural products and exempt agricultural tax, respectively, were implemented in Hainan, to promote agricultural development on the island. In 2014, Hainan was one of the first pilot provinces to implement a judicial system reform in China. Additionally, the reform related to the agricultural reclamation system is at the forefront of the country. In 2015, Hainan became the only provincial "multi-planning integration" reform pilot area in China, led to the practice of national "multi-planning integration" and institutional innovation. Other aspects, such as fiscal and taxation system, global tourism, and the reform of government functions, were also at the forefront. The status of reform pioneer positively influences the entire society to cultivate innovative consciousness and legal spirit and create a relaxed market environment.

4.3.2 Highland for opening up to the outside world

Hainan has always encouraged the idea of opening up to the outside world, and thus, it represents an open highland. In February 2001, to promote exchanges and cooperation between Asian countries and the world, Boao Forum for Asia was established. Hainan, representing the most open "Sky Special Zone" and the first pilot province in China, was the first to open the third, fourth, fifth, and seventh air rights (Civil Aviation Administration of China, 2020). Since May 2018, Hainan has followed a visa-free policy for inbound tourists of 59 countries, expanded the scope of visa-free countries, extended the visa-free residence time, and relaxed the number of visa-free people (People's Government of Hainan Province, 2018). The tax exemption policy for outlying passengers of Hainan implemented since July 2020 has further improved the tax exemption amount and the types of tax-free goods based on the pilot policy established in 2011 (Luo and Tian, 2016). Furthermore, Hainan, as the Frontier of maritime exchanges between China and Association of Southeast Asian Nations (ASEAN) countries, has continuously strengthened economic ties between the two parties by developing the "Belt and Road Initiative" and launching the China–ASEAN Free Trade Area, which promotes healthy relations between China and ASEAN countries. Moreover, Hainan integrated the "Pan-South China

Sea Economic Cooperation Circle" in the "Belt and Road Initiative" (Jin et al., 2021). This attitude of open highland has improved Hainan's integration with international mainstream market rules, and cultivated a cognizance of rules and an open vision of the entire society.

4.3.3 Challenges reflected through major events

The occurrence of several major events in Hainan over the years hindered its development course. Some of these events were the automobile smuggling incident before and after the establishment of the province, the storm in Yangpu, the real estate bubble, the second surge of the real estate market under the international tourism island strategy after 2010, and the real estate status across the island (Li, 2007; Tang et al., 2021). These events highlight the excessively high risk-taking and speculative orientations of some participants while pursuing economic development, as well as the lack of legal awareness and industrial outlook.

In addition to tropical agriculture, tourism and real estate, Hainan has attempted to transform and upgrade several other sectors. Some of these examples include the establishment of Hainan Airlines, the strategy of "one province and two places" (building China's emerging industrial province, tropical high-efficiency agricultural base, and tourism resorts, 1996), the establishment of Boao Forum for Asia (2001), the establishment of Yangpu Bonded Port Area (2007), and the establishment of Sansha City (2012). These measures have promoted Hainan's status and have comprehensively affected Hainan's regional development and modern industrial and commercial culture construction, but their role in developing foundation industries is not yet evident.

In 2018, on the occasion of the 30th anniversary of Hainan's establishment as a provincial special economic zone, the central government decided to support Hainan's establishment of an island-wide free trade zone (The State Council, 2018a). Simultaneously, Hainan Province announced the upgrading of real estate control measures, implemented the global purchase restriction, and proposed relatively strict restrictions on the payment of personal income tax or social insurance for non-registered families of this province. Subsequently, the regulation and control policies of the real estate market continued to overweigh, demonstrating Hainan's determination to de-real estate and transform and develop. In the second half of 2018, the overall plan of Hainan Pilot Free Trade Zone was proposed, and the construction of the free trade zone was comprehensively deployed from the aspects of economic system and service industry innovation and development (The State Council, 2018b). In November 2019, the Ministry of Commerce and other 18 governmental departments jointly issued a notice, proposing policies for improving the level of investment and trade facilitation, expanding the opening up of the financial sector, and accelerating the development of the shipping sector. In June 2020, the "Overall Plan for the Construction of Hainan Free Trade Port" was released, which proposed to develop Hainan into a high-level free trade port with strong international influence. In total, Hainan has 39 specific policies associated with free trade, investment, and cross-border capital flows in 11 areas (The State Council, 2020).

Thus, Hainan was again on the path of unprecedented development opportunities. However, we should learn from the previous experiences, expand the perspective of the new road of free trade port construction and regional healthy development, and construct modern industrial and commercial culture, including ideology and business concept. Moreover, as development performance has been unsatisfactory in the past, we should also reflect on the construction of industrial and commercial culture.

4.3.4 Development performance and problem analysis

In 2019, the GDP of Hainan Province was 530.893 billion yuan, the ratio of primary, secondary, and tertiary industries was 20.3:20.7:59.0, urbanization rate was 59.23% and the per capita GDP was 56,507 yuan, which was significantly lower than the national average of 70,892 yuan (People's Government of Hainan Province, 2020). Further, taxation and finance depended on real estate, and the income of residents, which depended on tourism was below the national level, despite the high cost of living. Moreover, the industrial development was weak, with the construction industry accounting for nearly half of the secondary industries.

The economic development of Hainan Province began late and had a poor foundation. However, with good resource conditions, unique ecological environment, and superior location facing the South China Sea, after more than 30 years of preferential policies, the economic development level represented by per capita GDP is still lower than the national average, and the quality of economic growth is not high; therefore, the performance of Hainan's economic development is not ideal. The analysis of existing problems and related ideological factors mainly includes the following factors:

4.3.4.1 The pursuit of "making quick money" has led to the ups and downs of Hainan's development

On observing Hainan's development since more than 30 years, we found that after several uncertainties, from the automobile incident and real estate bubble to the high interest rate of credit cooperatives and the construction of an international tourist island that boosted Hainan's housing prices, brought short-term dividends. This highlights the problems of excessive risk-taking, insufficient adherence to rules, and lack of industrial spirit. Thus, we can conclude that quick money is unreliable, and restoring normal conditions after the uncertainties that arise due to the pursuit of quick money demands more energy. If the tourism industry does not make long-term plans and make great efforts to standardize

management, it will easily become a quick money industry. Moreover, implementing any new favorable policy can be regarded as an opportunity to make quick money under the notion of quick success and benefit.

4.3.4.2 Lack of innovation leads to poor sustainability and slow improvements in functions

Hainan is not highly developed in the existing regional division of labor. In the public cognition, migratory bird pension, tourism, and tropical agriculture are the representative industries and functions of Hainan, which are not only far from the advanced nature of industrial structure, but also do not represent strategically emerging industries that are generally concerned by all localities. Moreover, the cultural environment and talent reserve required by industrial transformation and upgrading, and regional innovation and development are insufficient, resulting in fewer advanced functions and poor sustainability.

4.3.4.3 Short course of modern industrial civilization on the cultural base map

Intensive development of agriculture should be consistent with the modern artisan spirit in industrial culture. However, slash-and-burn farming has been a traditional agricultural practice in Hainan for a long time, and intensive cultivation production is gradually spreading from coastal areas to the central areas. Overall, the entire island lacks a common tradition of intensive cultivation.

Although Hainan's tradition of farming-reading is not short-term, its development on the island is highly non-uniform. Apart from values, such as honesty, courtesy, and pragmatic and enterprising natures, various complex and contradictory values still exist widely.

Hainan's daily life represents both slow and bold characteristics. This can be explained with the following example. "Old Papa Tea" represents the "slow life" of Hainan Island. Some friends can spend the entire day in hot summers with only a pot of tea[5]. "Old Papa Tea" is cheap and popular, and it is a comfortable lifestyle. "Chigongqi" completely reflects the hospitality and boldness of the Hainan people[6]. Whether the visitors are related to their hosts or not, "all guests are considered relatives" and should receive warm hospitality. However, these characteristics have some adverse effects on wealth and business principal accumulation, and participation in market competition.

The character and spirit of defying risks and seeking wealth in risks have considerable positive significance, but these may act as drivers of various short-term behaviors when formal channels are insufficient.

Furthermore, characteristic buildings also have certain cultural significance. The arcade is an architectural form that is supported by columns below, cantilevered from the second floor, and connected to multiple houses to form a pedestrian corridor (Zhao, 2020). Vendors can solicit business without any hindrance from wind and rain. The arcade in Hainan has a history of more than 100 years. It has a blend of Chinese and Western cultures, and conveys Hainan people's commercial ideology, which represents Hainan's modern urban commercial civilization. However, similar commercial civilization elements are not prominent in other regional cultural backgrounds.

4.3.4.4 Lack of industrialization process

Industrialization involves technology accumulation, changes in the economic structure and production mode, and social wealth surges. Bottom-up industrialization is also necessary to cultivate craftsman spirit, develop industrial civilization, and promote scientific, technological, and cultural progress. Hainan has long been a military center and a coastal defense outpost, focusing on reclamation and guarding; however, its industrial development is limited. Since the establishment of the province, the need for industrial development has been reconsidered several times. Consequently, industrialization has not been successfully achieved, and the process for developing industrial culture and industrial civilization is also lacking. Based on the current actual effect, promoting advanced industrial culture only through real estate and tourism is difficult, both of which may also have a "crowding out effect" on the development of new industries. Contrastingly, China's Yangtze River Delta and Pearl River Delta regions have faced complete industrialization since the reform and opening-up. The transformation of light industry to heavy chemical industry to high-tech industry and modern service industry is extremely coherent, and should be backed up by the development of industrial civilization. However, in some other areas, a long-term tradition of regulated economy exists, the development of a light industry with a high degree of marketization is lacking, the industrial structure relies heavily on tourism and other tertiary industries, or the economic development effectiveness is relatively poor for many years, which is worthy of vigilance.

5 Cultural development path of Hainan Free Trade Port construction

Based on the analysis of historical and cultural backgrounds, development performance, and international experience, this paper proposed the cultural development path of Hainan Free Trade Port, which mainly includes the following six aspects:

5.1 Promote industrialization

Regional culture develops after considerable accumulation over a certain period. On the one hand, promoting

5 "Old Papa Tea" is a kind of Hainan distinctive tea culture, economical, and is a good way of leisure and recreation for older people.

6 "Chigongqi" is a crucial folklore festival for the Hainan people.

industrialization assists in addressing the shortcomings of development, strengthening Hainan's economic strength, and supporting the construction of free trade port. On the other hand, industrialization is also necessary to cultivate healthy industrial and regional cultures, which Hainan should consider.

Presently, Hainan's industrial sectors include mainly petrochemical and related products, along with medicine, tropical agricultural product processing, automobile and equipment manufacturing, and information industry, but related industrial parks and enterprises are few, with no industrial scale and industrial chain. In 2020, Hainan's industry accounted for only 9.7% of the province's gross regional product, and it is urgent to promote industrialization. From the experience of other regional development, sustainable development can only achieve by decoupling economic growth from environmental pollution (Zhang et al., 2020). Hainan is also fully aware of the importance of environmental sustainability in developing regional industrialization and is making continuous efforts. In 1997, Hainan started promoting the "Information Smart Island" program, and has been committed to promote the informatization construction of Hainan Island for more than 20 years, paying great attention to the development of the information technology industry. For more than 30 years, Hainan has insisted on establishing an ecological province. In 2019, it established a negative list system for industries, and banned the development of industries having high energy consumption, high pollution, and high emission, along with low-end manufacturing industries (Hou et al., 2020). Hainan adheres to an environmentally sustainable new industrialization path, reduces the environmental risks faced by industrialization, and promotes industrial economic development based on protecting the ecological environment.

In the future, Hainan should strengthen leading industries, form industrial clusters, extend the industrial chain, and create high-value-added products based on environmental sustainability. For example, to develop a modern agricultural and sideline product processing industry featuring tropical crops, relying on excellent location conditions, relying on marine scientific and technological research and development institutions, and developing a blue ocean economy. Increase support for the Internet and artificial intelligence industries and actively integrate with tourism, agriculture, science, education, culture, health, and other industries. Additionally, broad industrial categories and related service industries of fine chemicals, equipment manufacturing, and new energy and materials should be promoted to ensure environmental conservation.

Thus, through the solid promotion of industrialization, Hainan could form an industrial culture that is proficient in craftsmanship, operates with integrity, adheres to rules, and is diligent in innovation.

5.2 Promotion of modern industrial and commercial culture

Modern industrial and commercial culture is also formed spontaneously through conscious promotion, with the cooperation among government, commercial subjects, and the public. Government departments can assist by improving their work methodology and enhancing their administrative efficiency and service level, industrial and commercial subjects can undertake the corresponding social and moral responsibilities, and the public can actively participate and supervise, thereby contributing to the formation and development of an advanced industrial and commercial culture in Hainan Free Trade Port.

The business environment directly affects the behavior of investors, which in turn affects the development and construction of free trade ports. The development of modern industrial and commercial culture should begin with improving the business environment, followed by advancing the reforms of "reform of government functions," simplifying market access, reducing interference with enterprise supervision and law enforcement, serving companies more accurately, and reducing enterprise costs.

The market-oriented reform of the Hainan Agricultural Reclamation, which has a pivotal position in the Hainan society and plays an important role in consolidating coastal defense and national security development, should be expanded. However, initially, social enterprises, government, and enterprises in the system and mechanism were not well distinguished; additionally, a single industry existed and vitality in the operation was lacking. In recent years, the reform in agricultural reclamation has been considerably promoted, but the market-oriented, socialized, and diversified reform is a long-term process. Weak market awareness and disregard for business rules under the long-term government-enterprise integration system should be changed while expanding the reform. Furthermore, executing the market-oriented reform of the Hainan Agricultural Reclamation will effectively solve the problem of slow development of the commercial culture in Hainan.

5.3 Standardization of the tourism market and construction of the most advanced tourism industry culture

Tourism industry is a crucial sector in Hainan. Although Hainan has sufficient experience in tourism development and management, implementing relatively stricter norms, exit mechanisms, and the most open credit system, improving the quality of tourism practitioners, upgrading traditional tourism through innovative cultural elements, and realizing the linkage and integration of culture and tourism is necessary to build the most advanced tourism industry culture in Hainan.

5.4 Improvement in the level of basic education and development of high-class higher education

Skilled personnel are largely required to construct the Hainan Free Trade Port. Additionally, education is an important part of the regional development environment that affects the skilled personnel's willingness to work. However, the present development level of basic education and higher education in Hainan cannot meet these requirements. The function of a high-level free trade port should be matched in various social fields, including education (Liu and Gao, 2022). High-quality basic education resources, such as renowned schools and teachers, should be introduced, cultural tradition of farming-reading in Hainan should be promoted, level of education awareness should be improved, and attention should be paid to improve the education level in backward areas of the central island. Further, the backward conditions of Hainan's higher education should be changed and high-class universities should be established as a strategic arrangement for Hainan's development and free trade port construction. Constructing high-class universities, collecting and developing skilled personnel, driving regional innovation, serving social needs, and leading social fashion are key links in Hainan's cultural and ecological construction.

5.5 Promotion of diversity of human resource structure

Immigrant culture is inclusive. However, due to the slow development of advanced industries, low wages, and increased brain drain since a long time, the existing tourism industry and human resource structure cannot strongly support the development of the free trade port. According to the construction requirements of the free trade port, the direction and structure of human resources should be regulated. While introducing a large proportion of human resources, attention should be paid to optimizing the combination of age and cultural background, and enhancing the regional industrial and commercial cultural characteristics by introducing a large number of skilled individuals having professional abilities. The restrictions on previously introduced small-sized commercial housing play a certain role in improving the utilization efficiency of scarce resources and optimizing the structure of population and human resources. Moreover, the new housing, employment, and social service policies and other policies can optimize the structure of human resources.

5.6 Revitalization of literature and art and development of Hainan's fine culture

Hainan's local culture is quite unique. Through the creation, revitalization, and development of literature and art, Hainan's culture will continue to prosper and contribute to the construction of free trade zone.

We should investigate the regional cultural characteristics, encourage literary and artistic creation under the background of Hainan, aggregate a series of literature and art characteristics, enrich the theme forms, support the development of Hainan opera and Lin opera, and protect and inherit local traditional culture. Moreover, media channels should be integrated, Hainan's fine cultural image should be promoted through different platforms, such as mobile phone applications, Internet, digital exhibitions, traditional media, and various tours, while retaining and enhancing its own cultural characteristics. Literature and art can endow Hainan culture with new vitality, and integrate it into the core of the mainstream culture.

6 Conclusion

The free trade port construction will greatly benefit Hainan and the country. Given Hainan's foundation and past development experiences and lessons, combined with the lessons learned from the development processes of Hong Kong, Singapore, and Dubai free trade ports, we believe that the construction of the Hainan Free Trade Port will be a long-term process. Moreover, the past mistakes of "speculating concepts," "making quick money," "misreading the classics," and "coveting fast and short-term effectiveness" should be avoided. "The nine-story platform starts from the base soil," which is based on the long-term process, lays a good foundation, and makes solid progress. Further, the requirements of the highest level of the open form should be improved from infrastructure and project construction hardware to legal system and humanistic environment software, and from the advancement of material form to the advancement of ideological values. Lastly, on analyzing the overall cultural and historical traits and characteristics of Hainan, we believe that the continuous construction of modern industrial and commercial culture will play a long-term role in the healthy development of the Hainan Free Trade Port.

Data availability statement

The original contributions presented in the study are included in the article/supplementary material, further inquiries can be directed to the corresponding author.

Author contributions

Conceptualization, CX; methodology, formal analysis, and writing-original draft, CX and TL; software, TL; writing-review

and editing, TL; project administration and funding acquisition, CX. All authors have read and agreed to published version of the manuscript.

Funding

This research study was supported by the National Natural Science Foundation of China (No. 41871162).

Acknowledgments

The authors are grateful to the editor and reviewers for their valuable comments and suggestions.

Conflict of interest

The authors declare that the research was conducted in the absence of any commercial or financial relationships that could be construed as a potential conflict of interest.

Publisher's note

All claims expressed in this article are solely those of the authors and do not necessarily represent those of their affiliated organizations, or those of the publisher, the editors and the reviewers. Any product that may be evaluated in this article, or claim that may be made by its manufacturer, is not guaranteed or endorsed by the publisher.

References

Akhavan, M. (2017). Development dynamics of port-cities interface in the Arab Middle Eastern world - the case of Dubai global hub port-city. *Cities* 60, 343–352. doi:10.1016/j.cities.2016.10.009

Amin, A., and Thrift, N. (2007). Cultural-economy and cities. *Prog. Hum. Geogr.* 31, 143–161. doi:10.1177/0309132507075361

Castellani, M. (2019). Does culture matter for the economic performance of countries? An overview of the literature. *J. Policy Model.* 41, 700–717. doi:10.1016/j.jpolmod.2018.06.006

Civil Aviation Administration of China (2020). Explanation on the "implementation plan for the pilot opening of the seventh freedom of traffic in hainan free trade port. Available at: http://www.caac.gov.cn/XXGK/XXGK/ZCJD/202006/t20200609_203003.html (Accessed August 30, 2022).

Dong, G., Zhu, J., Li, J., Wang, H., and Gajpal, Y. (2019). Evaluating the environmental performance and operational efficiency of container ports: An application to the maritime silk road. *Int. J. Environ. Res. Public Health* 16, 2226. doi:10.3390/ijerph16122226

Dubai Statistics Center (2020). National accounts. Available at: https://www.dsc.gov.ae/en-us/Themes/Pages/National-Accounts.aspx?Theme=24 (Accessed August 28, 2022).

Fan, G., Xie, X., Chen, J., Wan, Z., Yu, M., and Shi, J. (2022). Has China's Free Trade Zone policy expedited port production and development? *Mar. Policy* 137, 104951. doi:10.1016/j.marpol.2021.104951

Gao, H. (2011). *History of social development in hainan (volume 1)*. Beijing: Guangming Daily Publishing House. (in Chinese).

Gibson, C., and Kong, L. (2005). Cultural economy: A critical review. *Prog. Hum. Geogr.* 29, 541–561. doi:10.1191/0309132505ph567oa

Guiso, L., Sapienza, P., and Zingales, L. (2006). Does culture affect economic outcomes? *J. Econ. Perspect.* 20, 23–48. doi:10.1257/jep.20.2.23

Harrison, M., Hong, W., Lam, S., and Xiao, G. (2020). The promise of China's free trade zones – The case of hainan. *Asian Educ. Dev. Stud.* 9, 297–308. doi:10.1108/AEDS-11-2018-0173

Hou, S., Xu, B., Lin, L., Zhang, L., Zhao, X., Liu, J., et al. (2020). Research on construction of standard system for development of green economy in hainan province. *IOP Conf. Ser. Earth Environ. Sci.* 508, 012083. doi:10.1088/1755-1315/508/1/012083

Huggins, R., and Thompson, P. (2015). Culture and place-based development: A socio-economic analysis. *Reg. Stud.* 49, 130–159. doi:10.1080/00343404.2014.889817

Jin, F., Yao, Z., and Chen, Z. (2021). Development characteristics and construction prospects for an integrated economic zone in the South China Sea Region. *Dili Xuebao/Acta Geogr. Sin.* 76, 428–443. doi:10.11821/dlxb202102013

Johnson, J. P., and Lenartowicz, T. (1998). Culture, freedom and economic growth: Do cultural values explain economic growth? *J. World Bus.* 33, 332–356. doi:10.1016/S1090-9516(99)80079-0

Li, B. (2011). A probe into the performance and development of hainan culture in the ming dynasty and its causes. *J. Hainan Normal Univ. Sci.* 24, 111–119. (in Chinese). doi:10.16061/j.cnki.cn46-1076/c.2011.05.020

Li, J., Li, W., and Shi, Y. (2021a). The impact of regional culture on the psychological characteristics, startup behaviors and regional economy of modern Chinese business gangs. *Front. Psychol.* 12, 732377. doi:10.3389/fpsyg.2021.732377

Li, J. (2007). *One step ahead - a historical study of the early stage of Guangdong's reform and opening up*. (in Chinese).

Li, S., Liu, J., and Kong, Y. (2021b). Pilot free trade zones and Chinese port-listed companies performance: An empirical research based on quasi-natural experiment. *Transp. Policy* 111, 125–137. doi:10.1016/j.tranpol.2021.07.022

Lin, J., Cai, J., Han, Y., Zhu, H., and Cheng, Z. (2016). Culture sustainability: Culture quotient (CQ) and its quantitative empirical application to Chinese cities. *Sustainability* 8, 1235. doi:10.3390/su8121235

Liu, J., and Gao, Y. (2022). The role of education in regional repositioning: Experiences of hainan. *Asia Pac. Educ. Rev.* 23, 87–99. doi:10.1007/s12564-021-09717-6

Liu, W., and Yao, Q. (2021). Theorizing Belt and Road construction mode from institutional and cultural perspectives. *J. Geogr. Sci.* 31, 623–640. doi:10.1007/s11442-021-1862-8

Luo, C. D., and Tian, Y. Z. (2016). The measurement model construction and empirical study on the effects of offshore duty-free policy on Hainan tourism economy. *J. Discrete Math. Sci. Cryptogr.* 19, 569–590. doi:10.1080/09720529.2016.1178907

Malinowski, B. (2013). *A scientific theory of culture and other essays*. London: Routledge. doi:10.4324/9781315824109

Peng, P., Yang, Y., Lu, F., Cheng, S., Mou, N., and Yang, R. (2018). Modelling the competitiveness of the ports along the Maritime Silk Road with big data. *Transp. Res. Part A Policy Pract.* 118, 852–867. doi:10.1016/j.tra.2018.10.041

People's Government of Hainan Province (2018). Notice about visa free policy for 59 countries. Available at: http://en.hainan.gov.cn/englishgov/Policies/202201/c33e5a7ee5a0426cb933b900b044ab86.shtml (Accessed August 30, 2022).

People's Government of Hainan Province (2020). Statistical bulletin of national economic and social development of hainan province in 2019. Available at: https://www.hainan.gov.cn/hainan/ndsj/202003/a03a4d8c72184b6b867bea6e70aa25b3.shtml (Accessed August 29, 2022).

Qi, F., Wu, Y., Wang, J., and Wang, Q. (2021). China's hainan free trade port: Medical laws and policy reform. *Front. Public Health* 9, 764977. doi:10.3389/fpubh.2021.764977

Qi, Y. (2018). "New targets of hainan: From free trade zone to free trade port with Chinese characteristics." in Conference Proceedings of 2018 World Special Economic Zone Development(Shenzhen) Forum:Restarting Reform and Opening-up(Chinese & English). 53-54–381-383.

Rottleb, T., and Kleibert, J. M. (2022). Circulation and containment in the knowledge-based economy: Transnational education zones in Dubai and Qatar. *Environ. Plan. A* 54, 930–948. doi:10.1177/0308518X221077105

Schumpeter, J. A. (2021). *The theory of economic development*. London: Routledge. doi:10.4324/9781003146766

Scott, A. J. (2017). "A perspective of economic geography," in *Economy: Critical essays in human geography*, 3–23.

Shi, S., Huang, K., Ye, D., and Yu, L. (2014). Culture and regional economic development: Evidence from China. *Pap. Reg. Sci.* 93, 281–299. doi:10.1111/pirs.12114

Tang, Y., Hong, K., Zou, Y., and Zhang, Y. (2021). Impact of emotional perceived value on the uncertain evolution of the housing bubble. *Mathematics* 9, 1543. doi:10.3390/math9131543

The State Council (2018a). Guiding opinions of the central committee of the communist party of China and the state Council on supporting Hainan's comprehensive deepening of reform and opening-up. Available at: http://www.gov.cn/zhengce/2018-04/14/content_5282456.htm (Accessed August 29, 2022).

The State Council (2018b). Notice of the state Council on issuing the overall plan for the China (hainan) pilot free trade zone. Available at: http://www.gov.cn/zhengce/content/2018-10/16/content_5331180.htm (Accessed August 29, 2022).

The State Council (2020). The central committee of the communist party of China and the state Council issued the "overall plan for the construction of hainan free trade port. Available at: http://www.gov.cn/zhengce/2020-06/01/content_5516608.htm (Accessed August 29, 2022).

Tian, M., Rohlfer, S., Wu, Y., and Yan, H. (2022). Does confucian cdlture prom ote innmvation ? an empirical of a leading organization in the field**. *mrev.* 33, 82–107. doi:10.5771/0935-9915-2022-1-82

Tylor, E. B. (2010). *Primitive culture: Researches into the development of mythology, philosophy, religion, art, and custom*. doi:10.1017/CBO9780511705960

Wan, Z., Zhang, Y., Wang, X., and Chen, J. (2014). Policy and politics behind shanghai's free trade zone program. *J. Transp. Geogr.* 34, 1–6. doi:10.1016/j.jtrangeo.2013.10.015

Weber, M. (2016). "Die protestantische Ethik und der "Geist" des Kapitalismus," in *Neuausgabe der ersten Fassung von 1904-05 mit einem Verzeichnis der wichtigsten Zusätze und Veränderungen aus der zweiten Fassung von 1920. Herausgegeben und eingeleitet von Klaus Lichtblau und Johannes Weiß*. Editors K. Lichtblau and J. Weiß Wiesbaden (Springer Fachmedien). doi:10.1007/978-3-658-07432-6

World Bank (2018). *Doing business*. Available at: https://www.worldbank.org/en/programs/business-enabling-environment (Accessed August 7, 2022).

Yan, G., and Liu, D. (2011). *History of social development in hainan (volume I)*. Beijing: Guangming Daily Publishing House. (in Chinese).

Yang, B. (2012). Confucianism, socialism, and capitalism: A comparison of cultural ideologies and implied managerial philosophies and practices in the P. R. China. *Hum. Resour. Manag. Rev.* 22, 165–178. doi:10.1016/j.hrmr.2012.01.002

Ye, P., Zhang, H., Ma, S., Yang, F., and Li, Y. (2022). A knowledge map study of an application of a Smart land planning free-trade zone and China's contribution. *Land* 11, 909. doi:10.3390/land11060909

Yeung, H. W. (2003). Practicing new economic geographies: A methodological examination. *Ann. Assoc. Am. Geogr.* 93, 442–462. doi:10.1111/1467-8306.9302011

Zhan, Y., and Gu, R. (2022). Knowledge visualization analysis of international economic geography research. *Trop. Geogr.* 42, 706–715. doi:10.13284/j.cnki.rddl.003482

Zhang, L., Li, G., Zhu, L., and Guo, H. (2019). Construction and service demonstration of Hainan remote sensing big data platform. *Yaogan Xuebao/Journal Remote Sens.* 23, 327–335. doi:10.11834/jrs.20198193

Zhang, S., Liu, W., and Liu, X. (2012). Investigating the relationship between protestant work ethic and confucian dynamism: An empirical test in mainland China. *J. Bus. Ethics* 106, 243–252. doi:10.1007/s10551-011-0993-8

Zhang, X., Geng, Y., Shao, S., Song, X., Fan, M., Yang, L., et al. (2020). Decoupling PM2.5 emissions and economic growth in China over 1998–2016: A regional investment perspective. *Sci. Total Environ.* 714, 136841. doi:10.1016/j.scitotenv.2020.136841

Zhao, J. (2020). Influencing factors of urban architectural style in China: A case study of danzhou city, hainan province. *IOP Conf. Ser. Earth Environ. Sci.* 510, 062003. doi:10.1088/1755-1315/510/6/062003

Zhao, X., and Jia, P. (2019). Multi-planning integration advancing coastal zone management: A case study from hainan island, China. *J. Coast. Conserv.* 23, 869–875. doi:10.1007/s11852-018-0667-0

Zhiyuan, G., and Rui, H. (2020). Policy text analysis of hainan free trade zone (port) from the perspective of policy tools. *IOP Conf. Ser. Earth Environ. Sci.* 608, 012026. doi:10.1088/1755-1315/608/1/012026

Zhou, W., and Tang, L. (2019). *Compendium of hainan general history*. Beijing: People's publishing house. (in Chinese).

Zhu, H., and Situ, S. J. (2001). Areal diffusion and integration of the frontier pioneering culture in Hainan Island. *Dili Xuebao/Acta Geogr. Sin.* 56, 105–110.

frontiers | Frontiers in Earth Science

TYPE Original Research
PUBLISHED 17 January 2023
DOI 10.3389/feart.2022.1052117

Check for updates

OPEN ACCESS

EDITED BY
Jun Yang,
Northeastern University, China

REVIEWED BY
Jixiang Liu,
Xiamen University, China
Wei Lv,
Wuhan University of Technology, China

*CORRESPONDENCE
Wanqi Wang,
176540570@qq.com

SPECIALTY SECTION
This article was submitted to Geoscience and Society, a section of the journal Frontiers in Earth Science

RECEIVED 23 September 2022
ACCEPTED 31 October 2022
PUBLISHED 17 January 2023

CITATION
Song S, Xu G, Bao L, Xie Y, Lu W, Liu H and Wang W (2023), Classifying the surrounding rock of tunnel face using machine learning.
Front. Earth Sci. 10:1052117.
doi: 10.3389/feart.2022.1052117

COPYRIGHT
© 2023 Song, Xu, Bao, Xie, Lu, Liu and Wang. This is an open-access article distributed under the terms of the Creative Commons Attribution License (CC BY). The use, distribution or reproduction in other forums is permitted, provided the original author(s) and the copyright owner(s) are credited and that the original publication in this journal is cited, in accordance with accepted academic practice. No use, distribution or reproduction is permitted which does not comply with these terms.

Classifying the surrounding rock of tunnel face using machine learning

Shubao Song[1], Guangchun Xu[2], Liu Bao[1,2], Yalong Xie[1], Wenlong Lu[1], Hongfeng Liu[1] and Wanqi Wang[1]*

[1]China Academy of Railway Sciences Corporation Limited, Beijing, China, [2]Faculty of Geosciences and Environmental Engineering, Southwest Jiaotong University, Chengdu, China

Accurately classifying the surrounding rock of tunnel face is essential. In this paper, we propose a machine learning-based automatic classification and dynamic prediction method of the surrounding rocks of tunnel face using the data monitored by a computerized rock drilling trolley based on the intelligent mechanized construction process for drilling and blasting tunnels. This method provides auxiliary support for the intelligent decision of dynamic support at the construction site. First, this method solves the imbalance in the classification of the surrounding rock samples by constructing the Synthetic Minority Oversampling Technique (SMOTE) algorithm using 500 samples of drilling parameters covering different levels and lithologies of a tunnel. Second, it filters the importance of the characteristic samples based on the random forest method. Third, it uses the XGBoost algorithm to model the processed data and compare it with AdaBoost and BP neural network models. The results show that the XGBoost model achieves a higher accuracy of 87.5% when the sample size is small. Finally, we validate the application scenarios of the above algorithm/model regarding the key aspects of the tunnel construction process, such as surrounding rock identification, design interaction, construction supervision, and quality evaluation, which facilitates the upgrading of intelligent tunnel construction.

KEYWORDS

tunnel construction, digital twin, SMOTE, drill, machine learning

1 Introduction

The common methods of tunnel construction include drilling and blasting, shield construction, and immersed tube construction, among which over 80% of tunnel construction use the drilling and blasting method (Wang, 2010, 2020). Rock drilling rigs with hydraulic mechanical arms have been used in tunnels since the 1980s, which marks the beginning of mechanized tunnel construction. In the 21st century, as we entered the age of intelligence (Zhao et al., 2017), new opportunities and challenges for the development of technological innovation in railway tunnel construction has emerged (Yang et al., 2022), which has attracted the attention of the world's leading tunnel construction countries. In the future, the worldwide competition in railway tunnel

construction technology level directly depends on the breadth and depth of the application of intelligent technology in tunnel construction. Intelligent construction is an essential reflection of the level of intelligent construction technology. The number of mechanical tools used in the construction process and the depth of participation represent the technical level of railway tunnel construction. Intelligent equipment is the premise and core node of intelligent tunnel construction, and the full analysis and use of data generated by intelligent equipment is an important part of achieving the digital twin of the tunnel. More importantly, using the intelligent method to accurately identify the surrounding rock parameters of the tunnel working face and the application of the intelligent classification method of surrounding rock can provide timely geological condition feedback, which is conducive to the early detection and early warning of the adverse geology ahead.

At present, the cross-section of the railway tunnel excavation can reach 160 m^2, which is subject to faults, dense joints, local weathering, and stratigraphic divisions. Local optimization and adjustment of the design parameters must be made in time (Zhao, 2019). So far, we have been mainly relying on geologists to identify changes in the rock level *in situ*, which is subjective, time-consuming, and heavily affected by the technical level of the geologist (Liu et al., 2018). At this stage, intelligent rock drill trucks can carry out over-support drilling and anchor drilling and produce corresponding construction log information (Yu et al., 2018). However, although the truck has intelligent functions such as automatic positioning, automatic marking of drilling positions, and automatic data transmission, most of the information is discrete sensing data recording the operating status of the machine itself. Meanwhile, the data grows fast, with the structures varying greatly, and the representation forms are diverse. Besides, the data interaction format and data storage schemes differ greatly. Therefore, the collected data cannot be directly used for intelligent classification of the surrounding rock of tunnel face and guide the adaptive adjustment of support structure types and parameters. The dynamic control of the current state of construction at a later stage is mainly based on engineering experience and manual input of basic parameters and then matching. This will have a direct impact on the safety, speed, efficiency, and quality of the tunnel support measures and the cavern support measures in place, which in turn affects the stability of tunnel face and the quality of the tunnel construction.

Machine learning is a branch of artificial intelligence that is undergoing the most rapid development. Machine learning provides methods that can "learn" and uses sample data to make predictions or decisions and resolve complicated questions of reality without being explicitly "programmed." Machine learning technologies are used in various applications (Yang et al., 2021a; Liu et al., 2021; Xiao et al., 2021). Recently, machine learning technologies have undergone rapid advances.

Machine learning technologies have also been applied to a few rock quality analyses. Wedge et al. (2019) used convolutional neural networks and drilling parameters collected in mineral exploration to determine the lithology of strata and stratigraphic partitioning information and compare them with manual judgment results. Yi et al. (2021) used a support vector machine (SVM) and two neural network models to describe the identification of significant heterogeneity of surrounding rock on the face of large cross-section rock tunnels. Nishitsujiy and Exley (2019) compared the performance of SVM, deep learning, linear classifier, and Bayesian classifier in the classification of lithology. They concluded that deep learning might become the main method of lithology classification in the future. Valentin et al. (2019) used ultrasonic and micro-resistivity imaging logs as input to construct a classification model for borehole image data and identified four lithologies: calcareous, gabbro, shale, and siltstone, using a deep residual network. Cai (2002) selected seven types of parameters, such as rock strength, self-weight stress, rock integrity, and mining influence, as input to the neural network to identify the stability state of the surrounding rock of the roadway project. The research of the above scholars shows that it is feasible to use machine learning theory combined with drilling parameters to identify the geological structure information such as formation lithology, rock thickness, and joint development. However, it still requires intensive investigation on how to further quantitatively identify the surrounding rocks in different areas of tunnel face in practical engineering to guide the adjustment of design parameters.

In this paper, we selected tunneling sites with complex lithology for sample collection and focused on monitoring and analyzing the drilling parameters of computerized rock drill trucks. By using the random forest algorithm without significantly reducing the accuracy of the surrounding rock classification results or affecting the classification distribution, the correlation degrees between the surrounding rock and the drilling parameters–including propulsion speed, impact pressure, propulsion pressure, and rotary pressure–were obtained to be 82%, 63%, 50%, and 40%, respectively. This results in the ranking in order of the importance of each characteristic parameter with a strong correlation, affecting the classification results of the surrounding rock. for the selected tunnels, which mainly exhibit Class III, Class IV, and some Class V rock, the Synthetic Minority Oversampling Technique (SMOTE) algorithm was applied to analyze and simulate the few samples characterizing the mechanical parameters and add new samples to the data set. This solves the problem to some extent that the classifier emphasizes the majority classes and ignores the minority classes due to the differences in tunnel construction progress, the inconsistent number of surrounding rock grades, and the imbalance of samples. Third, we established a machine learning-based classification model for the surrounding rock of tunnel face. By drawing on the idea of integrated learning, we constructed the Back-Propagation Neural

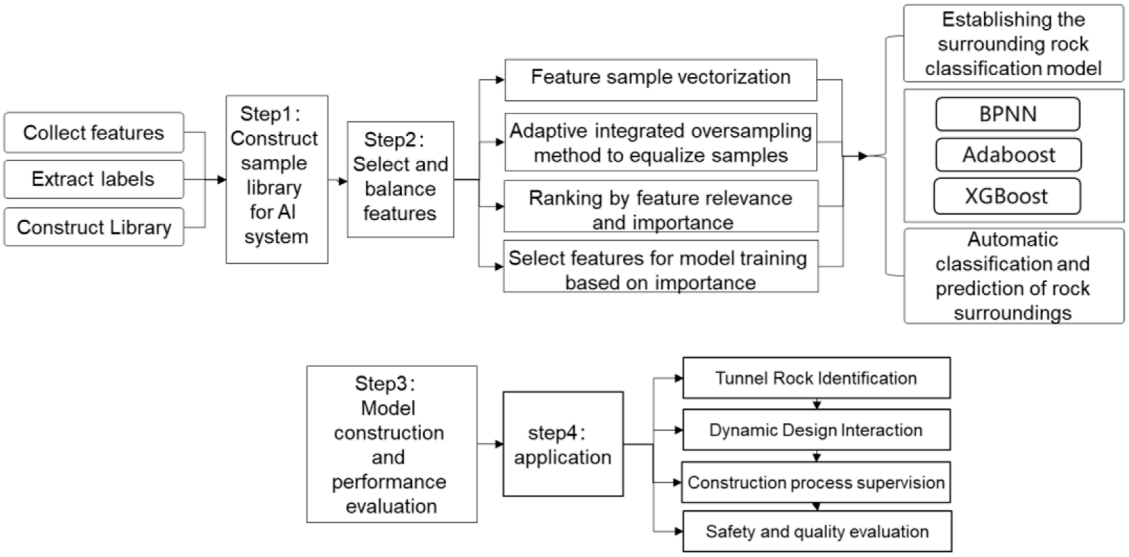

FIGURE 1
Research flow of this study.

Network, AdaBoost, and XGBoost algorithms to predict the processed data, respectively. It was found that with continuous adjustment of the learning rate and other hyperparameters, the prediction accuracy of the XGBoost algorithm (ensemble-tree-based) is the highest, reaching the optimal performance of 87.5%.

Figure 1 shows the research flow of this paper, which focuses on the key issues of perception, analysis, and decision-making of the drilling data acquired by intelligent equipment in real time. The investigation is to support the key aspects of the intelligent tunnel construction process, such as surrounding rock identification, design interaction, construction supervision, and quality evaluation, thus transforming and upgrading from the traditional working mode to the intelligent mode.

The contributions of this study are as follows: (1) establishing a prediction algorithm for automated surrounding rock classification based on the operation data of mechanical construction; (2) proposing a machine learning-based method for automatic classification and dynamic prediction of tunnel working face perimeter rock and (3) supporting the transformation and upgrading of the tunnel construction process from traditional working mode to intelligent working mode through machine learning technology.

2 Materials and methods

The classification of the tunnel surrounding rock is important for identifying the nature of the surrounding rock, determining the stability of the tunnel envelope, selecting the type of tunnel support, ensuring the safety and health of construction workers, and guiding safe construction. In general, the classification of surrounding rock is determined by a combination of two methods, namely qualitative classification and quantitative index. Qualitative classification refers to the use of an on-site geological sketch of the tunnel face to obtain a qualitative description of the rock hardness and rock integrity; while quantitative refers to the use of a rock rebound test, rock compressive strength test, rock wave velocity test, and rock body wave velocity test, and the introduction of groundwater, ground stress and the main structure of the surface production indicators, to obtain its surrounding rock classification index (Ranjbarnia et al., 2018).

In engineering practice, the determination of the surrounding rock level takes qualitative study as a primary tool and quantitative study as the secondary one. In this paper, we focus on the surrounding rock level data qualitatively obtained from the on-site tunnel face sketch results and use them as sample data for machine learning to solve classification problems. In addition, as the correctness of the surrounding rock level label will affect the accuracy of prediction, we verified the labeling of the surrounding rock level given by the field geological engineers through a small amount of rock rebound tests, rock compressive strength tests, rock wave velocity tests and rock body wave velocity tests.

Many factors influence the accurate identification of the surrounding rock of tunnel face, such as the geological analysis during the preliminary survey and design, advanced geological forecasting, the construction of the borehole camera, spectral imaging, 3D digital photography, laser scanning, and drilling measurement. They are of significance for reference to

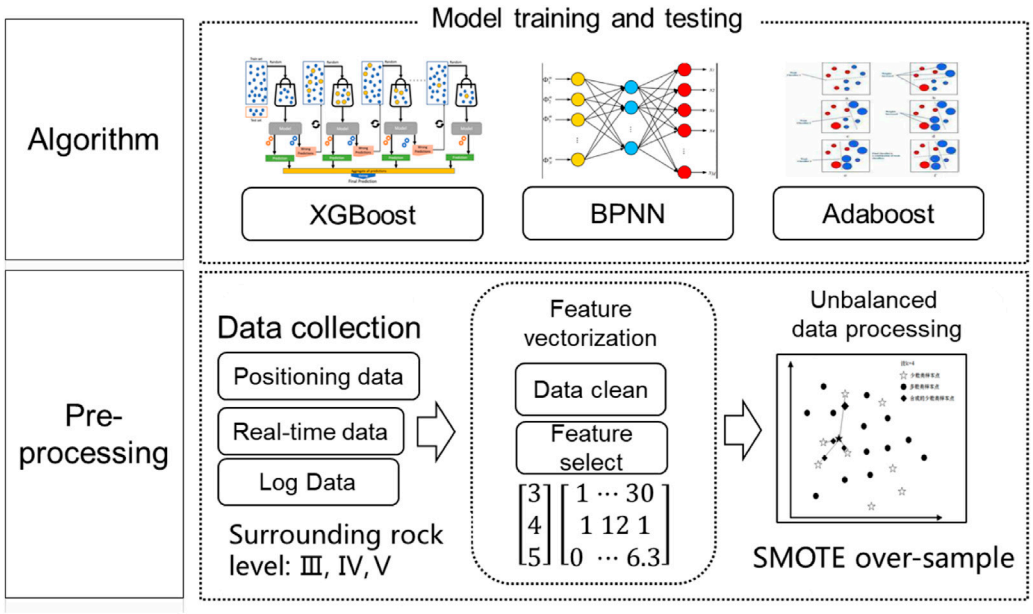

FIGURE 2
Process and methods for predicting the tunnel surrounding rock level.

the surrounding rock parameters evaluation. With the promotion of large supporting mechanized equipment, the real-time rock drilling parameters collected by the machine's self-awareness system can play a critical role and provide rapid response feedback (Zhao and Lu, 2018) for the determination of the surrounding rock level. Consequently, in this paper, we focus on the drilling parameters generated by a specific model of a computerized three-arm rock drilling rig during the rock drilling process in a tunnel with complex rock quality. The drilling parameters include propulsion speed, rotary pressure, propulsion pressure, rotary velocity, impact pressure, etc. A machine-learning sample library was then constructed using the above drilling parameters as well as the surrounding rock levels identified from the geological sketch of the tunnel face. The process and methodology for the prediction of tunnel surrounding rock levels are shown in Figure 2.

1) Data perception: The intelligent rock drilling trolley is used to collect drilling parameters such as the surrounding geological environment, operating conditions, and equipment information of the tunnel being constructed by the drill and blast method.
2) Data cleaning and collation: the collected raw data are cleaned and collated, and the data features are then vectorized. Finally, the data set is balanced using the SMOTE algorithm.
3) Model construction: The balanced dataset is used as the input of the XGBoost model for model training. XGBoost is an optimized distributed gradient boosting method that implements machine learning under the gradient boosting framework and solves numerous data-related problems in a rapid and accurate manner. It is an improvement over the gradient boosting decision tree with higher prediction accuracy and training efficiency.

The prediction accuracy and other aspects of the model are compared with that of the BPNN (Back propagation neural network) and AdaBoost models to find the model with the best prediction effect and stability.

2.1 Data pre-processing analysis

Due to the differences in geological conditions and construction progress of the tunnels, the number of collected tunnel surrounding rock level samples was inconsistent and disproportionate. According to the data collected from the test tunnel, the samples of the surrounding rock levels were mainly divided into three types: III, IV, and V. There were 162 samples of III, 278 samples of IV, and 60 samples of V. The imbalance of the categories was high. However, it is generally considered that the ratio of data samples should be kept around 1:1 to make the classification model better reflect the classification effect (Liu et al., 2020). For this reason, in this paper, we employ the SMOTE method for processing to solve the data imbalance problem.

SMOTE algorithm was proposed by Chawla in 2002 and has been adopted by both academia and industry (Kam and Dick,

TABLE 1 Main data set for computerized rock drill rigs.

Serial number	Data category	Data Content	
1	Trolley positioning data	Current stake of the dolly	
2	Real-time status data	Name of data	Normal operating range (HC110)
		Promoting pressure	−10-230 (bar)
		Speed of propulsion	−50-50 (m/min)
		Impact pressure	−10-210 (bar)
		Slewing pressure	−10-210 (bar)
		water pressure	0-50 (bar)
		water flow	0–180 (L/min)
		Current operating status, total current, and voltage of the whole machine	
3	Recurring log data	Positioning mileage, number of holes, total drilling distance, drilling start and stop time, jamming time, flushing/other time, feed rate, impact pressure, thrust pressure, rotary pressure, water pressure, water flow	

2006). The general idea of SMOTE is to interpolate between minority class samples to generate additional samples. The method generates new synthetic samples based on the k nearest neighbor samples of the minority samples, which are random points on a line segment with endpoints corresponding to the two nearest neighbor minority class samples.

$$x_{new} = x + rand(0,1) * ||\hat{x} - x|| \quad (1)$$

where x is a minority class sample, $\hat{x}$ is the nearest neighbor sample, and $\|\cdot\|$ denotes the distance formula.

Because the SMOTE algorithm has the problem of a lack of diversity, many improved algorithms have been proposed, such as BorderlineSMOTE proposed by Han et al. (2005) and adaptive synthetic (ADASYN) sampling proposed by He et al. (2008). BorderlineSMOTE will only generate synthetic data for minority class samples adjacent to the boundary, which leads to weaker model generalization. On the contrary, ADASYN generates minority-class data samples adaptively based on the distribution of minority-class data samples, and minority samples that are harder to learn will generate more synthetic data than minority samples that are easier to learn. In this paper, the ADASYN algorithm is adopted for data augmentation of the imbalanced sample data.

2.2 Feature selection

The drilling parameters of the intelligent rock drill rig reflect the response of the rock drill to different surrounding rocks under the action of constant impact energy. The intelligent rock drill trolley automatically collects a series of operating process data of the rock drill in real-time and records in detail the measured values and parameters, operating status, and other information during the operation of the intelligent construction equipment. The trolley has the characteristics of high collection frequency and a large amount of data. It possesses the most detailed process record data during the whole operation process. According to the operating characteristics of intelligent construction equipment, the data is sampled, quantified, and coded with a certain collection frequency by means of each data interface, and the data is cleaned according to some specific rules to form a data format that meets the needs of business functions such as real-time dynamic, intelligent grading of the surrounding rock.

The main data set information collected by the computerized rock drill rig is shown in Table 1.

The total energy output of the mechanical power system of the intelligent rock drill rig during the construction operation condition with normal main motor current and voltage can well reflect the quality and level of the surrounding rock (Jiang and Shen, 2018). It is generally believed that the lower the energy required to break the rock, the worse the quality of the surrounding rock and the higher the level of the surrounding rock; the higher the total energy output of the required drilling rig power system, the better the quality of the surrounding rock and the lower the level of the surrounding rock. Different mechanical arms of the multi-arm rock drill rig have different drilling parameters, and it is extremely difficult for us to consider all the influencing factors one by one in the actual engineering prognosis. On the one hand, too many parameters will bring trouble to the actual engineering site data collection. On the other hand, the excess parameters will make the construction of the neural network model complicated and prolong the training time. Meanwhile, the parameters of these influencing factors are not independent of each other, but there is a certain coupling relationship. Considering all of them may produce the problem of overfitting and be unfavorable to the prediction results.

TABLE 2 Feature name, description, and derived importance.

Feature name	Characterization	Importance
Propulsion pressure (bar)	Numerical type: feed pressure to the rock drill load-bearing mechanism to push the cylinder	0.50
Propulsion speed (m/min)	Numerical type: rock drill travel speed	0.82
Impact pressure (bar)	Numerical type: feed pressure to the rock drill impact hydraulic mechanism	0.63
Slewing pressure (bar)	Numerical type: oil feed pressure to the drilling tool rotation mechanism of the rock drill	0.40
Water pressure (bar)	Numerical type: rock driller inlet line pressure	0.20
Water flow rate (L/min)	Numerical type: rock driller inlet line flow	0.15

TABLE 3 List of hyperparameters of each classification model.

Model	List of Parameters
BPNN	batch=32, stddev=0.1(variance), lr=0.1 (learning rate), epochs=500 (number of rounds), hide_layer_num=3
XGBoost	base_score=0.5 (global bias), booster='gbtree' (base classifier model), learning_rate=0.05 (learning rate), max_depth=8 (maximum depth of tree), n_estimators=50 (number of trees)
AdaBoost	scoring='accuracy', cv=5-fold, error_score='raise'

In order to meet the research requirements and improve data quality, the raw data were cleaned with the goal of accuracy, completeness, and consistency.

Regarding duplicate values, since the ID is a unique identifier for each sample, no duplicate rejection operation is required after a duplicate lookup of the data. Regarding the missing values, for continuous variables, the missing values are filled with the mean value of the overall data on the variable; for discrete variables, the value with the highest frequency of the overall data on the variable is filled; when the number of missing variables is too large, the data is directly rejected.

The characteristic variables were initially filtered to see the distribution of values on the overall data for each variable, in turn, by the statistical function. In particular, the positioning mileage (current stake of the dolly) was removed because it does not provide useful information for the identification of the surrounding rock; the working status was removed because it only has a unique value on the whole data (normal working without warning status); and the variables such as the number of holes and the total length of the holes are not relevant to the output variable "surrounding rock level" and were removed; for The discrete variables with too many values for the four time values of drilling start/stop time, jamming time, and flushing/other time will produce a sparse matrix with too many dimensions, which will affect the effect of learning for classification, so they were also removed.

Second, the data was standardized to eliminate the effect of magnitude. Different variables often have different magnitudes and may differ in order of magnitude, and features with larger values tend to receive higher weights in the classification. In order to avoid the bias of the classifier among different features, the data was normalized to scale the value interval of the features to a specific range so that different feature variables would have the same weight in the classification and improve the efficiency of the model.

z-score normalization, also known as standard deviation normalization, is the most common method used in data normalization. The mean of each dimensional feature after processing is 0, and the standard deviation is 1. For each value v_i of the specific dimensional feature, the standardization formula is as follows.

$$v_i^{'} = \frac{v_i - mean}{std}$$

where *mean* is the mean of the original data in this dimension, and *std* is the standard deviation of the original data in this dimension.

After the dimensionality reduction of the data by eliminating the data of low relevance and redundant features, the size of the data set was reduced, which can effectively improve machine learning efficiency.

In addition to the above analysis, after data filtering of the original data, we then use the random forest algorithm (Yang et al., 2021b; Wei et al., 2022) to obtain the importance score of each attribute in the process of classifying and predicting the surrounding rock level, which can measure the value of the features in the model. The top six important features for the prediction model of the surrounding rock classification include propulsion speed, propulsion pressure, impact pressure, slewing pressure, water pressure, and water flow.

The list of features after completing feature selection is described in Table 2.

2.3 Training and testing of the classification model

To verify the applicability of the algorithms to different classification models and their influences on the effect of the surrounding rock level classification, we select several classification learning models commonly used in existing research for comparison experiments, including BPNN (Back

TABLE 4 Model training and testing results.

Surrounding rock level	Actual Sample Size/Sample	Number of Accurate Samples Identified by the Model/Sample			Accuracy/%		
		BPNN	XGBoost	AdaBoost	BPNN	XGBoost	AdaBoost
III	265	227	242	168	85.7%	91.3%	63.1%
IV	278	218	254	184	78.4%	91.4%	66.2%
V	257	188	213	153	73.2%	82.9%	59.5%

TABLE 5 The confusion matrix.

	Predicted condition		
	Positive (PP)	Negative (PN)	
Actual condition	Positive (P)	True Positive (TP)	True Negative (TN)
	Negative (N)	False Positive (FP)	False Negative (FN)

propagation neural network), XGBoost, and AdaBoost algorithmic models.

To ensure the stability of the experimental results, the model training process is based on k-fold cross-validation (Zhao et al., 2020, 2021). The data set is divided into five mutually exclusive equal subsets, and five rounds of training tests are conducted, with one subset taken as the test set and the other four subsets as the training set in each round without repetition. The evaluation index results after five rounds of training tests are averaged, and the final evaluation results are the output.

3 Results

The hyperparameters of each classification model are sought by GridSearchCV. The list of hyperparameters for each model is described in Table 3.

Adopting the training set and prediction set samples after pre-processing and feature selection mentioned above, the calculated prediction set discrimination results are shown in Table 4. In the case that the training set and prediction set were the same, XGBoost had the best prediction accuracy of 87.5%. The grading accuracy of the BP neural network for surrounding rock classification of the prediction set was 79.2%. AdaBoost had a much longer training time and was sensitive to the sample. Abnormal samples in the iteration may get higher weights, thus affecting the final prediction accuracy of strong learners. AdaBoost performed the worst this time, with an accuracy of 62.9%.

No matter how efficient a model we select, its prediction results will always be subject to some errors. Therefore, we analyze and evaluate the results and performance of these classification models on the test set based on a confusion matrix (Table 5). In this confusion matrix, four categories include TP (true positive), False Positive (FP), True Negative (TN), and False Negative (FN). TP case is a positive case that was correctly classified. FP case is a negative case that was incorrectly classified as positive. FN case is a positive case that was incorrectly classified as negative. TN case is a negative case that is correctly classified.

Precision is the proportion of true positive examples among all examples classified as positive. The closer its value is to 1, the better the classification performance for positive examples.

$$Precision = \frac{TP}{TP + FP}$$

Recall is the proportion of all true positive examples that are correctly classified as positive examples. The closer its value is to 1, the better the classification performance for positive examples.

$$Recall = \frac{TP}{TP + FN}$$

The F-measure (F) is the harmonic mean of *Precision* and *Recall*. The closer its value is to 1, the better the combined classification performance for positive samples. Its formula is shown below.

$$F = \frac{2}{Recall^{-1} + Precision^{-1}}$$

Or equivalently,

$$F = \frac{2Recall*Precision}{Recall + Precision}$$

TABLE 6 Classification model evaluation results.

Classifier	*Precision*	*Recall*	*F* value
BPNN	0.83	0.80	0.81
XGBoost	0.90act	0.88	0.89
AdaBoost	0.78	0.81	0.80

The evaluation results of the three classification models, namely BPNN, XGBoost, and AdaBoost, are depicted in Table 6. We find that our machine learning-based approach performs well in the studied problem.

With only the operating state of the machine itself known, the construction of the above-mentioned different classification models has well predicted the level of the surrounding rock with fast response. This also shows that the tunnel surrounding rock level is closely related to the drilling and blasting machinery construction parameters. By establishing a relationship between the drilling parameters of rock drilling machinery and the classification of the surrounding rock levels, the drilling parameters can be further optimized based on the predicted surrounding rock levels, which is of great significance for the study of intelligent visualization of tunnel construction.

4 Discussion

4.1 Discussion of the prediction results

The above predictions analyze the relationship between the change in the surrounding rock level and the mechanical drilling parameters during the construction of the rock drilling platform from different angles. Overall, the model meets the basic requirements for prediction accuracy. However, due to the lack of drilling parameter data and the inadequate classification of corresponding surrounding rock levels in practical analysis, the training data obviously cannot accurately fit the real surrounding rock level changes during the tunnel-boring process. The correlation between the construction drilling parameters and the parameters themselves has not been considered. In addition, we did not consider the differences in geological conditions and tunnel geometry. We think some improvements, such as optimizing the selection of input parameters, expanding the number of samples, diversifying the study area, and introducing more advanced and reasonable prediction methods, can be made to achieve better prediction results (Moore et al., 2022; Xu et al., 2022; Zhang et al., 2022). Furthermore, big data analysis based on heterogeneous monitoring data is suggested to help decision-making from the traditional construction method based on the

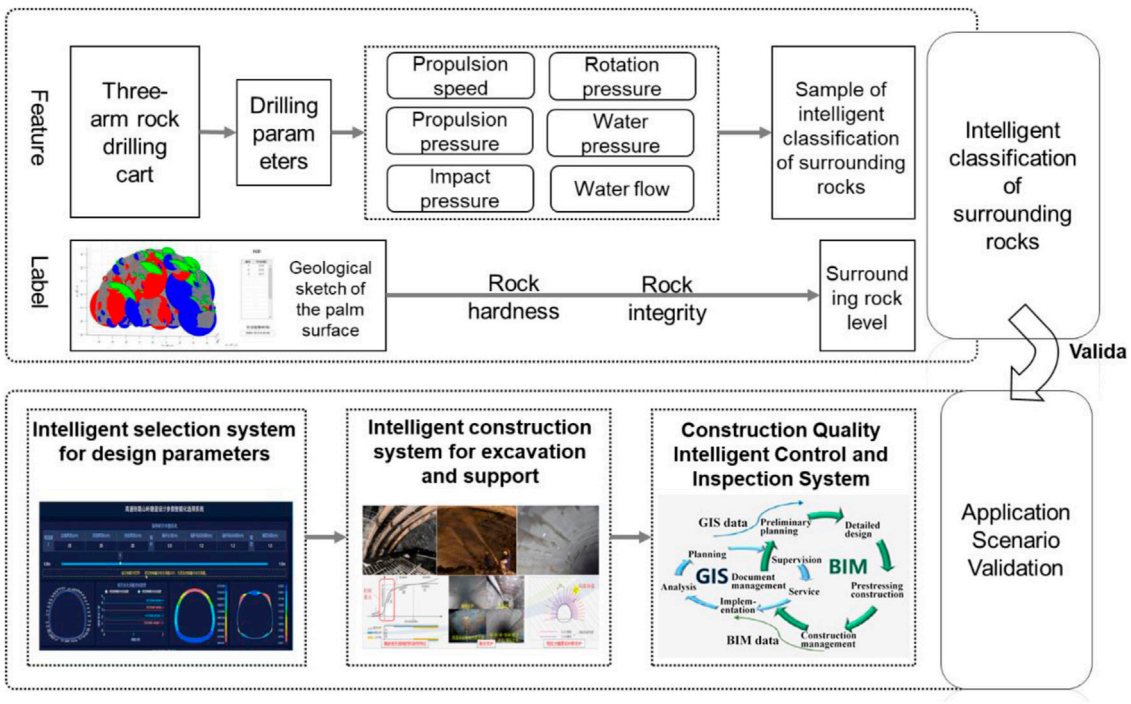

FIGURE 3
Intelligent classification of surrounding rocks and its application scenarios.

model of physical entities and the new decision model based on artificial intelligence.

4.2 Discussion of application scenarios

The research is based on machine learning and the design of algorithm models to achieve automatic collection, analysis, and classification of information from the complex geological environment of tunnels in difficult mountainous areas (Figure 3). The virtual simulation training model and the construction site can interact dynamically in the real-time field and share data with each other, leading to self-learning and self-optimization driven by the algorithm model. By using intelligent feedback analysis for forecasting and big data monitoring based on tunnel construction machinery, we can effectively identify the cases of poor stability of tunnel surrounding rock, including over-deformation, over-damage, and effectiveness for reinforcement. In addition, we will be able to assess the tunnel stability under the supporting system and evaluate the rationality of the supporting parameters so as to realize an intelligent, refined, and dynamic design of the tunnel supporting structure. The developed model will provide accurate, efficient, and comprehensive auxiliary decision-making for construction and management personnel, thus effectively strengthening the quality control and safety management of tunnel as well as improving the mechanization level of tunnel construction, accelerating the project progress and enhancing the construction efficiency under the premise of ensuring quality and safety.

5 Conclusion

In this paper, we established a prediction algorithm for automated surrounding rock classification based on the operation data of mechanical construction. Firstly, the data set was pre-processed, including missing value processing, outlier processing, data standardization processing, data normalization processing, and data sampling by the ADASYN algorithm to address the imbalance of data categories. Then, feature screening was carried out on the data set, and the importance of data features was sorted through the Random Forest algorithm so as to retain the features that have a larger impact on the prediction results and eliminate the features that have a smaller impact, hence enhance the model generalization ability and reduce the risk of overfitting. The model was divided into a training set and a test set, and the training data were fitted with different classifiers by the cross-validation method. The optimal classifier parameters were determined by the grid search method to adjust the parameters and evaluate the experimental results. Through the intelligent classification of "fast collection-real-time transmission-remote evaluation" of surrounding rock information, the intelligent connection between intelligent perception and intelligent equipment and background server is realized. The above-mentioned new artificial intelligence decision-making model from the original signal end of the equipment to the automated classification of tunnel envelope can be applied to key links and scenarios such as surrounding rock recognition, design interaction, construction supervision, and quality evaluation in the tunnel construction process. It supports the transformation and upgrading of the tunnel construction process from the traditional working mode to the intelligent one.

Data availability statement

The original contributions presented in the study are included in the article/supplementary material, further inquiries can be directed to the corresponding author.

Author contributions

SS: formal analysis, methodology, writing—original draft. GX: formal analysis, writing—review and editing. LB: validation, writing—review and editing. YX: validation and writing—review and editing. WL: validation and writing—review and editing. HL: validation and writing—review and editing. WW: conceptualization, supervision, and writing—original draft. All authors contributed to the article and approved the submitted version.

Conflict of interest

Authors SS, LB, YX, WL, HL and WW were employed by the company China Academy of Railway Sciences Corporation Limited.

The remaining author declare that the research was conducted in the absence of any commercial or financial relationships that could be construed as a potential conflict of interest.

Publisher's note

All claims expressed in this article are solely those of the authors and do not necessarily represent those of their affiliated organizations, or those of the publisher, the editors and the reviewers. Any product that may be evaluated in this article, or claim that may be made by its manufacturer, is not guaranteed or endorsed by the publisher.

References

Cai, S. (2002). *The stability classification for the wall rock in mining roadway dased on artificial neural network and the bolt supporting research*. Chongqing: Chongqing University.

Han, H., Wang, W. Y., and Mao, B. H. (2005). "Borderline-SMOTE: A new over-sampling method in imbalanced data sets learning," in International Conference on Intelligent Computing (Berlin, Heidelberg: Springer), 878.

He, H., Bai, Y., Garcia, E. A., and Li, S. (2008). "Adasyn: Adaptive synthetic sampling approach for imbalanced learning," in 2008 IEEE international joint conference on neural networks (IEEE world congress on computational intelligence), 1322

Jiang, Y., and Shen, B. (2018). Strengthened mechanized construction management and construction efficiency analysis of large cross-sectional tunnel. *Tunn. Constr.* 38 (8), 84

Kam, J., and Dick, S. (2006). Comparing nearest-neighbour search strategies in the SMOTE algorithm. *Can. J. Electr. Comput. Eng.* 31 (4), 203–210. doi:10.1109/cjece.2006.259180

Liu, D., Yao, M., and Zhang, X. (2018). Stability evaluation and control measures for tunnel face of large cross-sectional tunnel on Zhengzhou-Wanzhou high-speed railway. *Tunn. Constr.* 38 (08), 1311

Liu, J., Wang, B., and Xiao, L. (2021). Non-linear associations between built environment and active travel for working and shopping: An extreme gradient boosting approach. *J. Transp. Geogr.* 92, 103034. doi:10.1016/j.jtrangeo.2021.103034

Liu, Q., Wang, X., Huang, X., and Yin, X. (2020). Prediction model of rock mass class using classification and regression tree integrated AdaBoost algorithm based on TBM driving data. *Tunn. Undergr. Space Technol.* 106, 103595. doi:10.1016/j.tust.2020.103595

Moore, C., Scott, D., Burbery, L., and Close, M. (2022). Using sequential conditioning to explore uncertainties in geostatistical characterization and in groundwater transport predictions. *Front. Earth Sci. (Lausanne).* 10, 979823. doi:10.3389/feart.2022.979823

Nishitsuji, Y., and Exley, R. (2019). Elastic impedance based facies classification using support vector machine and deep learning. *Geophys. Prospect.* 67 (4), 1040–1054. doi:10.1111/1365-2478.12682

Ranjbarnia, M., Rahimpour, N., and Oreste, P. (2018). A simple analytical approach to simulate the arch umbrella supporting system in deep tunnels based on convergence confinement method. *Tunn. Undergr. Space Technol.* 82, 39–49. doi:10.1016/j.tust.2018.07.033

Valentin, M. B., Bom, C. R., Coelho, J. M., Correia, M. D., Márcio, P., Marcelo, P., et al. (2019). A deep residual convolutional neural network for automatic lithological facies identification in Brazilian pre-salt oilfield wellbore image logs. *J. Petroleum Sci. Eng.* 179, 474–503. doi:10.1016/j.petrol.2019.04.030

Wang, M. (2010). *Tunnelling and underground engineering technology in China*. Beijing: China Communications Press.

Wang, Z. (2020). *The construction technology of large cross-sectional tunnels in Zhengzhou-Wuhan high-speed railway with safety, rapidity and standardization*. Beijing: China Communications Press.

Wedge, D., Hartley, O., McMickan, A., Green, T., and Holden, E. J. (2019). Machine learning assisted geological interpretation of drillhole data: Examples from the Pilbara Region, Western Australia. *Ore Geol. Rev.* 114, 103118. doi:10.1016/j.oregeorev.2019.103118

Wei, D., Yang, L., Bao, Z., Lu, Y., and Yang, H. (2022). Variations in outdoor thermal comfort in an urban park in the hot-summer and cold-winter region of China. *Sustain. Cities Soc.* 77, 103535. doi:10.1016/j.scs.2021.103535

Xiao, L., Lo, S., Liu, J., Zhou, J., and Li, Q. (2021). Nonlinear and synergistic effects of TOD on urban vibrancy: Applying local explanations for gradient boosting decision tree. *Sustain. Cities Soc.* 72, 103063. doi:10.1016/j.scs.2021.103063

Xu, Z., Ding, Z., Gu, G., Jiang, J., Wang, L., and Niu, X. (2022). Deep exploration of Jiaodong type gold deposit, taking Shanhou gold deposit, southern part of Zhaoping fault as an example. *Front. Earth Sci. (Lausanne).* 10, 939375. doi:10.3389/feart.2022.939375

Yang, L., Ao, Y., Ke, J., Lu, Y., and Liang, Y. (2021b). To walk or not to walk? Examining non-linear effects of streetscape greenery on walking propensity of older adults. *J. Transp. Geogr.* 94, 103099. doi:10.1016/j.jtrangeo.2021.103099

Yang, L., Liang, Y., He, B., Lu, Y., and Gou, Z. (2022). COVID-19 effects on property markets: The pandemic decreases the implicit price of metro accessibility. *Tunn. Undergr. Space Technol.* 125, 104528. doi:10.1016/j.tust.2022.104528

Yang, L., Liang, Y., Zhu, Q., and Chu, X. (2021a). Machine learning for inference: Using gradient boosting decision tree to assess non-linear effects of bus rapid transit on house prices. *Ann. GIS* 27 (3), 273–284. doi:10.1080/19475683.2021.1906746

Yi, W., Wang, Mi., Tong, J., Zhao, S., Li, J., Gui, D., et al. (2021). Inhomogeneity identification method for surrounding rock of large-section rock tunnel face based on support vector machine. *China Railw. Sci.* 9 (5), 112

Yu, L., Wang, Z., and Yang, N. (2018). Study of measurement and distribution characteristics of surrounding rock stress of large cross-sectional high-speed railway tunnel with mechanized construction. *Tunn. Constr.* 38 (08), 1342

Zhang, L., Li, J., Wang, W., Li, C., Zhang, Y., Jiang, S., et al. (2022). Diagenetic facies characteristics and quantitative prediction via wireline logs based on machine learning: A case of lianggaoshan tight sandstone, fuling area, southeastern sichuan basin, southwest China. *Front. Earth Sci. (Lausanne).* 10, 1018442. doi:10.3389/feart.2022.1018442

Zhao, G., Yang, D., Liu, J., Jia, J., and Wu, H. (2019). High pressure behavior of crystal [2,2'-bi(1,3,4-oxadiazole)]-5,5'-dinitramide: A dft investigation. *J. Mol. Graph. Model.* 41 (1), 87–93. doi:10.1016/j.jmgm.2019.04.005

Zhao, H., and Lu, W. (2018). Application of triple-boom rock drilling jumbo to weak surrounding rock construction of Zhengzhou-Wanzhou high-speed railway tunnel. *Tunn. Constr.* 38 (8), 1342

Zhao, R., Yao, M., Yang, L., Qi, H., Meng, X., and Zhou, F. (2021). Using geographically weighted regression to predict the spatial distribution of frozen ground temperature: A case in the qinghai-tibet plateau. *Environ. Res. Lett.* 16 (2), 024003. doi:10.1088/1748-9326/abd431

Zhao, R., Zhan, L., Yao, M., and Yang, L. (2020). A geographically weighted regression model augmented by Geodetector analysis and principal component analysis for the spatial distribution of PM2.5. *Sustain. Cities Soc.* 56, 102106. doi:10.1016/j.scs.2020.102106

Zhao, Y., Tian, S. M., and Sun, Y. (2017). Development and planning of high-speed railway tunnels in China. *Tunn. Constr.* 37 (1), 11

frontiers | Frontiers in Earth Science

TYPE Original Research
PUBLISHED 18 January 2023
DOI 10.3389/feart.2022.1031098

Check for updates

OPEN ACCESS

EDITED BY
Jun Yang,
Northeastern University, China

REVIEWED BY
Shaohua Wang,
Aerospace Information Research Institute (CAS), China
Xiaoping Zhang,
Shandong Jianzhu University, China

*CORRESPONDENCE
Yanhong Zhang,
giswork@163.com
Xingchang Lu,
luxc@jlu.edu.cn

SPECIALTY SECTION
This article was submitted to Environmental Informatics and Remote Sensing, a section of the journal Frontiers in Earth Science

RECEIVED 29 August 2022
ACCEPTED 01 November 2022
PUBLISHED 18 January 2023

CITATION
Zang P, Zhang Y, Chen Z, Hou G, Liu Z and Lu X (2023), The inversion modeling and aboveground biomass mapping of withered grass changes in the western grassland of Northeast China. *Front. Earth Sci.* 10:1031098. doi: 10.3389/feart.2022.1031098

COPYRIGHT
© 2023 Zang, Zhang, Chen, Hou, Liu and Lu. This is an open-access article distributed under the terms of the Creative Commons Attribution License (CC BY). The use, distribution or reproduction in other forums is permitted, provided the original author(s) and the copyright owner(s) are credited and that the original publication in this journal is cited, in accordance with accepted academic practice. No use, distribution or reproduction is permitted which does not comply with these terms.

The inversion modeling and aboveground biomass mapping of withered grass changes in the western grassland of Northeast China

Peng Zang[1], Yanhong Zhang[1]*, Ziqi Chen[1,2], Guanglei Hou[2], Zhaoli Liu[2] and Xingchang Lu[1]*

[1]College of Geo-exploration Science and Technology, Jilin University, Changchun, China, [2]Northeast Institute of Geography and Agriculture, Chinese Academy of Science, Changchun, China

The aboveground biomass (AGB) of withered grass is an important early-warning indicator for grassland fire risk. Most grassland fires occur during the dry-grass season. In order to improve the fire-warning efficiency of withered AGB, it is essential to rapidly acquire the amount of withered-grass biomass. Remote-sensing data has been widely used in monitoring and estimating grassland yields during the growing season. However, applying remote sensing to the estimation of withered grass is still in need of exploration. The aim of this work was to try to establish a remote-sensing estimation model for withered AGB in the dry-grass season. The estimation of aboveground biomass can effectively prevent the occurrence of fire, protect the environment, facilitate local management and reduce economic losses. Our approach was to, first, calculate a dry-grass index based on Sentinel-2 image data and using ENVI, SNAP, and ArcGIS software. Second, a model to estimate the fuel quantity during the dry-grass season was established by regression analysis combined with field-measured data. Finally, the estimation model was used to predict the amount of fuel in different months of the dry-grass season, followed by the fire-defense elements, which were quantified and mapped in the Longzhao Marsh wetlands. It was found that: 1) the two indices were significantly correlated (0.678) with the amount of fuel; 2) the established model could accurately estimate the amount of fuel in the study area during the dry season, and accurate test results demonstrated that the correlation between the estimated results of the best model and the measured values was 0.863, indicating high accuracy; 3) the spatiotemporal variation of withered grass in the study area was obviously different, and the quantities of fuel predicted for the other months were more accurate, which may reflect monthly dynamic changes in actual fuel quantities; and 4) the establishment of a remote-sensing estimation model for fuel quantity in the Longzhao Marsh during the dry-grass season could provide important parameters for fire-risk warning in the western grassland of Jilin Province and Northeast China.

KEYWORDS

withered grass biomass, dry grass index, spatial-temporal variation, Sentinel-2 data, Northeast China

1 Introduction

Grassland resources play an important role in environmental protection, animal husbandry development, ecosystem balance, and carbon sequestration (Jiaxing Huang et al., 2021; Shuqing Feng et al., 2004; Hailiang Li et al., 2009). Aboveground biomass (AGB) is a key indicator of grassland growth and can be used to evaluate the regeneration ability of grassland ecosystems (Shuqing Feng et al., 2004; Hailiang Li et al., 2009). It is also the material basis for maintaining grassland ecosystem and fire research, and one of the most basic elements of grassland fires. Trees promote grass biomass in dry season (Ivan Raniero Hernández Salmerón et al., 2022). Rapid, accurate, and large-scale monitoring of grassland AGB is of great significance in determining the rational carrying capacity of grasslands and ensuring the safety of grassland ecosystems (Tarun K et al., 2021). Grassland fires are caused by the burning of AGB during the dry-grass season (Qingqing Li et al., 2013). Grassland vegetation is the main carrier of grassland fires. As an important part of grassland vegetation, the spatial distribution and quantity of combustible matter has a major impact on grassland fires (Wenyi Yang et al., 2001). Yellow grass in the grassland is the most important fuel, being the main component of, and basis for, combustion. The amount (weight, height, and continuity) of dry grass in a grassland not only changes with space, but also changes with time (Xinghua Li et al., 2007). At the same time, the species composition of grasslands is in constant flux. Changes in all prairie fuels determine or influence prairie fires (Batu Seyin 2007). Therefore, timely and accurate acquisition of grassland AGB data during the dry-grass season is of great significance to grassland fire-warning and fire-risk assessments (Yulong Bao et al., 2012). Moreover, estimating the biomass of withered grass can facilitate the management of local relevant departments. The sustainable utilization of withered grass resources can reduce economic losses and provide a basis for ecological restoration (Yujuan Zhai et al., 2021; Ziqi Chen et al., 2021; Ziqi Chen et al., 2022; Yanhong Zhang et al., 2021).

The most-combustible components in the dry-grass season are the leaves and branches of grassland vegetation, which do not easily decompose (Shan Yu et al., 2014). The main component of grassland fuel––the grass stock––constantly changes, posing a fire risk (Yi Zhuo et al., 2010). Remote-sensing data has been widely used in monitoring and estimating grassland yields during the growing season. After years of study, scholars have made different linear combinations of the band information extracted from remote-sensing images in order to obtain various vegetation indices. Among these, the normalized difference vegetation index can best reflect changes in the fuel coverage, biomass, and leaf-area index. It is mainly used for monitoring grass yields in the peak-grass season (Jianqing Zhou et al., 2019). Compared with the remote-sensing monitoring of vegetation growth and fuel yield in the peak-grass season, due to the influence of cold winters, the remote-sensing monitoring of fuel quantity in the dry-grass season can become more or less difficult. The dry-grass season usually starts in early October of 1 year and ends in early May of the next, which is also the fire-free season. Fires mainly occur in the grassland region of North China during the dry-grass season, so it is very necessary to be able to estimate the amount of fuel available during the dry-grass season. So far, there has been little domestic or foreign research on the use of remote sensing in the dry-grass season to estimate the amount of fuel, and related research on herbaceous vegetation has mainly focused on the cold season. The dry-grass index (DGI) is determined as DGI = 1/Ch1, where Ch1 is the relationship between Moderate Resolution Imaging Spectroradiometer (MODIS) data and the reflectivity of Channel 1 in National Oceanic and Atmospheric Administration (NOAA)/Advanced Very High Resolution Radiometer (AVHRR) data. Using the DGI to monitor fuel quantity during the dry-grass season is based on the principle that the lower the vegetation coverage, the higher the reflectivity of the ground (E. Chuvieco et al., 2002; Yeneayehu Fenetahun et al., 2022; Hao Pei et al., 1995). However, some case studies have indicated that its accuracy in hay estimation is not ideal. For example, Hao Pei et al. (1995) established a relationship between NOAA/AVHRR data and pasture-quantity data obtained quasisynchronously on the ground, producing a map of dry-grass quantity for the area around Xilinhot city. Using the Xilin Gol grassland as the research area, Qingdong Cui established estimation models for herbage stock in the cold season for four grassland types––meadow grassland, typical grassland, desert grassland, and sandy vegetation––using Earth Observing System (EOS)/MODIS and ground-survey data (Qingdong Cui 2009). Based on the EOS/MODIS data of Shan Yu et al. (2014) and using regression analysis, an estimation model for fuel quantity in the dry-grass season has been established, and the fuel quantity for Inner Mongolian grassland in the dry-grass season has been calculated. In recent years, some scholars have put forward a hay fuel estimation method based on spectral reflection characteristics. One of these––Zhengxiang Zhang––used field-measured spectra to create a new hay DGI and establish a model for predicting the

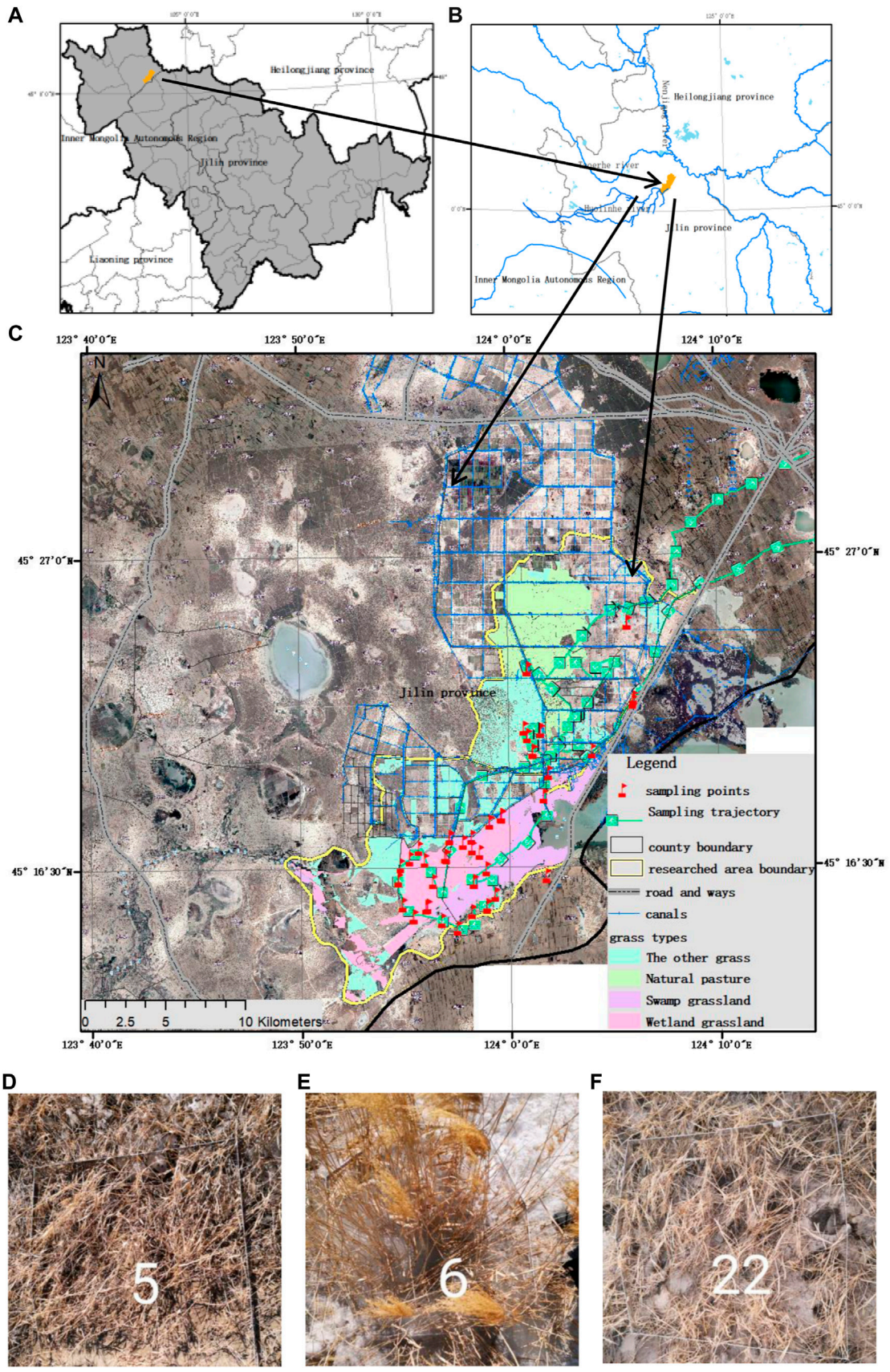

FIGURE 1
Schematic diagrams **(A,B)** and satellite images **(C–F)** showing the location of the study area and sampling points.

amount of fuel in the northeastern China grassland AGB, with the model also being applied to western Songliao; the accuracy of the calculation is relatively high (Zhengxiang Zhang 2010; Zhang et al., 2015). According to above researches, the estimation of withered grass biomass is usually based on low spatial resolution remote sensing images such as modis images, moreover the high spatial resolution remote sensing images are often used for the grassland in the growing season (Chao Liu et al., 2022; Lingxin Bu et al., 2022). The difference between grassland biomass in growing season and withered grass biomass using remote sensing methods is mainly due to the spectral reflection difference in modeling principles. Most studies use remote sensing data to model the grassland biomass in growing season, because the measured spectrum of grassland in growing season has a greater response to the bands of remote sensing images and commonly used indexes, and there is a higher correlation between grassland biomass and indexes. But it is difficult to find these characteristics in the withered grass. However, the discovery of DGI can well promote the estimation of biomass of withered grass and it is more convenient, practical and effective, which can be used for large area application of high-resolution remote sensing satellite in the estimation of withered grass biomass. Therefore, this study will use high spatial resolution remote sensing images to estimate the hay, in order to explore a new method for retrieving the amount of hay fuel. And establishing remote-sensing images with higher spatial resolutions and then calculating the hay biomass from these is a current important mission.

Determinations of the spatial distribution patterns and fuel loads of grasslands during the dry-grass season can not only be used to provide a practice basis of grassland fire safety management, soil carbon accumulation and remediation (Qixia Long et al., 2022), but can also provide a theoretical basis for fire prevention (Duwala et al., 2012; Hui Xu et al., 2015). This is of great importance for the management of grasslands and the formulation of fire-prevention measures (Shirong Chen et al., 2006). In this study, based on high-resolution Sentinel-2 data as the data source and results from previous studies, two kinds of fuel index were calculated, and a remote-sensing estimation model was established. This was done in combination with measured ground data in order to calculate the spatial variations in fuel quantity in the Longzhao Marsh during the dry-grass season, and in order to provide theoretical guidance and a scientific basis for local grassland fire prevention and soil carbon remediation. The study can promote the application of Sentinel-2 with high resolution in the estimation of large-scale grassland AGB, and provide methods and data support for the relevant departments in the study area to reasonably determine the balance of grass and livestock and use grassland resources.

2 Materials and methods

2.1 Overview of the study area

The study area was located in the ecological barrier area in western Northeast China (see Figure 1), within the area defined by 45°00′–45°28′N and 123°15′–124°13′E. The hydrological system comprised one main stream and two tributaries––the Taoer and Huolin Rivers. The abundant water resources in the area have resulted in a series of small brackish-water lakes and a brackish-water marsh. The rich river, lake, marsh, and marsh-meadow ecosystems in the region have given rise to high regional biodiversity. According to incomplete investigations and statistics, there are 239 species of plants in the Longzhao Marsh, belonging to 39 families and 132 genera. The vegetation mainly includes *Suaeda salsa* community, *Artemisia alkali* community, *Phragmites australis* community and *Cyperus sedge* community. The former two are typical salt-marsh communities, embedded in grasslands, meadows, and marshes, and widely distributed across this area. Suaeda salsa was the dominant species in those two communities, accompanied by *Artemisia suaeda*, *Swertia hydropiper*, *Polygonum polygonum*, and *Sibiricum plantarum*. Reed and sedge communities occurred in shallow water and around marshes. The dominant species in these was Phragmites communis, accompanied by cattails and small rushes. The dominant species in the sedge community was sedge, accompanied by shallots and *Scirpus mariqueter*. The dominant natural vegetation provides important habitats for a wide variety of animal populations, rich in 164 species––mainly birds, mammals, amphibians, reptiles, and fish. Abundant animal and plant resources and high quality ecosystems mean that this region has an important position in the ecological strategy of western Northeast China.

2.2 Data collection and processing

2.2.1 Sample plot selection and pretreatment

At total of 58 sample sites were set up in the study area in November 2019 and March 2020 based on geomorphic type and vegetation community. The different vegetation types included *Suaeda suaeda*, *Phragmites australis*, and sedge communities. Three 1 × 1-m subplots were set up in each sample plot. The locations––longitude and latitude, altitude, plant community composition, height, coverage, and frequency––of each sample site were recorded with the aid of the Global Positioning System (GPS). The location of the study area and the distribution of the sampling points are shown in Figure 1. The AGB harvesting method (Bingru Zhao et al., 2004; Qingdong Cui et al., 2009) was used to obtain direct measurements. The plots were mowed uniformly and the samples taken inside for natural air-drying in order to determine the quantity after finding the constant

TABLE 1 Description of downloaded Sentinel-2 image data.

Year	Date	Spacecraft ID	Level
2019	2019/09/12	Sentinel-2	L1C
2019	2019/10/24	Sentinel-2	L1C
2019	2019/11/15	Sentinel-2	L1C
2020	2020/03/12	Sentinel-2	L1C
2020	2020/04/24	Sentinel-2	L1C
2020	2020/05/12	Sentinel-2	L1C

weight (involving several weighings). The weight of hay (i.e., the measured amount of fuel) was obtained for each sample.

2.2.2 Image data source and preprocessing

Data was accessed *via* the European Space Agency's (ESA's) Copernicus data center website (https://scihub.copernicus.eu/dhus/). Surface reflectance products from the multi-temporal Sentinel-2B remote-sensing image were obtained. This is the only optical satellite with more than three red-edge bands (Yihan Pu et al., 2021). The wavelength distributions and spatial resolutions of the bands are provided in Table 1. Because Northeast China is completely covered in snow in December through February, continuous-time images were not selected. For this work, images from March 2020 that were consistent with the measured data from the ground were selected for modeling. Other data, reflecting changes in the quantity of fuel during the dry-grass season, were selected for predicting the amount of dry grass, including one scene image each from September, October, and November 2019 and one from April and May 2020 (see Table 2). For the downloaded images, first, we made radiometric calibration and atmospheric corrections (Fugen Jiang et al., 2021) using the Sen2cor tool in the Sentinel-2 software toolbox provided by the ESA. Then we applied SNAP software to resample the image at a 10-m spatial resolution for each pixel from a 20-m spatial resolution.

2.2.3 Calculation of the dry-grass index

The reflectance curves for soil and the subsoil are obviously different, with the reflectance of the subsoil layer being lower than that of soil in the visible and near-infrared bands. The reflectance differs with the amount of subsoil on the surface of the ground, with the reflectance reaching a maximum when the ground is completely bare and a minimum when the ground is completely covered by withered grass. When the ground is covered by subsoil, the reflectance is between the maximum and the minimum. The field spectroscopic measurements showed significant differences between the fuel spectra in these bands. In the short-wave infrared imagery bands (Zhengxiang Zhang 2010), the dominant features of all the reflectance spectra were two water-absorption bands, centered at 1,400 and 1,900 nm, and one reflection peak at 1,650 nm. In the 2,100-nm band, associated with cellulose and lignin, there was a significant absorption feature in the spectra of the dry-grass fuels. This feature was not visible in the soil spectrum. However, the contrast between the reflection peak and the absorption trough was marked. Based on variations in the spectral curve characteristics of the different vegetation types and the soil during the dry-grass season, and with reference to the dry-grass inversion model based on the other satellite images that the relevant MODIS data was based on (Zhenyu Xu et al., 2020; Suying Li et al., 2007), the 1,600-nm band represented a stable reflection peak

TABLE 2 Description of Sentinel-2 band information.

Band number	S2A	S2B	Spatial resolution (m)
	Central wavelength (nm)	Central wavelength (nm)	
B1	443.9	442.3	60
B2	496.6	492.1	10
B3	560.0	559.0	10
B4	664.5	665.0	10
B5	703.9	703.8	20
B6	740.2	739.1	20
B7	782.5	779.7	20
B8	835.1	833.0	10
B8a	864.8	864.0	20
B9	945.0	943.2	60
B10	1373.5	1376.9	60
B11	1613.7	1610.4	20
B12	2202.4	2185.7	20

in the spectral curve of the dry-grass fuel, and 2,100 nm represented the absorption characteristics of lignin and cellulose. In the short-wave infrared region of the electromagnetic spectrum, absorption characteristics associated with cellulose and lignin are usually observed at 2,100 nm in the subsoil spectrum (Zhengxiang Zhang 2010; Zhang et al., 2015). This absorption characteristic does not occur in the soil spectrum. This observation provided the basis for distinguishing dry grass from soil. Because the withered grass has a stable reflection peak at 1600 nm on its reflection spectrum curve, and has lignin absorption and cellulose absorption characteristics at 2100 nm, the B4, B11, B12 bands of the high-resolution remote sensing image Sentinel-2 data can be used to distinguish the withered grass, soil and other surface objects. And the index established between the bands should have a greater response to the biomass of withered grass. Therefore, the dry-grass fuel indices (DGI1 and DGI2), based on Sentinel-2 bands 4, 11, and 12, were significantly correlated with the field measurements of dry-grass fuel quality, and the contrast between the reflection peak and absorption trough was significant. From this, we progressed to determining DGI1 and DGI2 in order to calculate the amount of fuel in the withering-grass season. The specific calculations are as follows:

$$DGI1 = B4 \tag{1}$$

$$DGI2 = (B11 - B12)/(B11 + B12) \tag{2}$$

where B4 is the reflectance of the red band of the Sentinel-2 data, and B11 and B12 are the reflectances of the short-wave infrared band of the Sentinel-2 data.

2.2.4 Evaluation of the accuracy of the calculation

Based on the coordinates of the field survey quadrats, the straw index values of the corresponding pixels were extracted in order to generate datasets for the dry-weight biomass of the grassland. Then, correlation models for the dry weight biomass of the grassland and each straw index were established. Of the 58 measured samples, 45 were selected for establishing the model, while the remaining 13 were used to verify the model. Because the RMSE and R^2 are popular in various model evaluations, and the fitting effect is good. The accuracy of the model was evaluated using the root mean square error (RMSE) and coefficient of determination (R^2) (Jiaxing Huang et al., 2021; Zhang 2021). In order to make full use of the samples to improve the reliability of the model, the keep-one-cross method was used to verify the estimation results––that is, only one sample site was left as the test set each time, with the other sample sites being used as the training set. The final estimation results were determined after n repeated times (Qingdong Cui et al., 2009). The accuracy of the models were assessed using the R^2 and total RMSE values. The formula for calculating the accuracy of the evaluation index is as follows:

$$R^2 = 1 - \frac{\sum_{i=1}^{n}(X_i - \hat{X}_i)^2}{\sum_{i=1}^{n}\left(X_i - \bar{X}_{ii}\right)^2}$$
$$RMSE = \sqrt{\frac{\sum_{i=1}^{n}(X_i - \hat{X}_i)^2}{N}} \tag{3}$$

where, X_i and $\hat{X}_i$ represent the measured and calculated values, respectively, $\bar{X}_i$ represents the average measured values, n is the number of samples, and N is the number of reserved samples.

The smaller the RMSE, the better the fitting effect. The R^2 represented the degree of fitting between the predicted and measured values of the trend line of the regression analysis. When the R^2 trend line approached 1, the reliability was higher.

3 Results and analysis

3.1 Construction of the fuel quantity estimation model

Statistical analysis software was used to generate scatter plots of the DGI1 and DGI2 values for all the samples and the measured quantities of combustible matter in the grassland (see Figure 2). According to the scatter plots in Figure 2, there was a significant correlation between the two groups of data.

The two types of DGI values for all the samples used in the modeling were statistically analyzed, and the correlation between the grassland-fuel field data and the same quasisynchronous DGI was analyzed using SPSS software (Yingzhong Ma et al., 2012). Table 3 provides the correlation between the measured data and the calculated DGI based on Sentinel-2 data.

According to the statistical results, there was a correlation between the Sentinel-2B remote-sensing data and the measured data. The correlation was significant at the test level of 0.01, and the absolute value of the correlation coefficient was greater than 0.6. Therefore, based on the Sentinel-2B remote-sensing data, an estimation model for the dry season was established and can be used to calculate fuel quantity. By comparison, the DGI2 had a higher correlation with the actual fuel measurements.

A regression model for estimating fuel quantity and two kinds of DGI was established using SPSS statistical software. In this study, six models––unary linear regression, quadratic curve, cubic curve, logarithm, exponential, and power function––were set up, and all the established models passed the significance test (see Table 4).

The correlation coefficient and significance of each model in Table 4 showed that all the models established based on the two

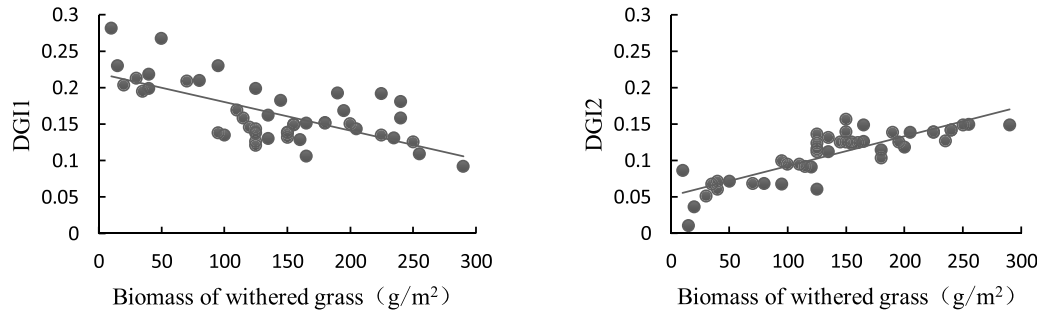

FIGURE 2
Scatter plots showing the amount of combustibles and the DGI values for construction of the dry-grass biomass model.

TABLE 3 Correlation between the dry weight of the combustible matter and the subsoil index derived from the Sentinel-2 remote-sensing data.

Indicator	DGI1	DGI2
Correlation	−0.630**	0.678**

**Correlation highly significant.

types of subsoil index were significantly correlated. Except for the cubic curve and logarithmic models, all the other R^2 values for the index model constructed using DGI2 were greater than for the model constructed using DGI1. The fitting degree of the exponential model based on DGI1 was the best, with R^2 = 0.639. The exponential model based on DGI2 also had the best-fitting degree, with R^2 =0.664, which was the highest among all the models.

Therefore, according to the significance of the model and the comparison of the fitting degree of R^2, the exponential model constructed using DGI1 and DGI2 can be used to estimate and calculate fuel quantities during the dry-grass season.

3.2 Evaluation of model accuracy

The 13 reserved randomly selected independent samples were used for model evaluation (Deng Pan 2017). Based on the two exponential models selected above, the correlation and RMSE between the actual measurements and estimations of fuel quantities were calculated using the cross-validation method to evaluate the model's accuracy. The accuracy evaluations of the two models are shown in Figures 3, 4. It can be seen from Figure 3 that the two DGI values of the samples used for verification were exponentially correlated with the actual fuel measurement, and can be used to verify the accuracy of the previously selected exponential model. As can be seen from the evaluation results in Figure 4, the correlation coefficient between the estimated measurement and the

TABLE 4 Model for estimating the amount of combustible matter during the dead-grass season.

DGI	Type	Fit model	R^2	Sig.
DGI1	Linear	Y=−0.205X+496.007	0.396	0.000
	Secondary	Y=0.207×10-4X2−0.941X+1100.995	0.532	0.003
	Third	Y=−(3.022E−7)X3+0.002X2−3.748X+2606.413	0.624	0.006
	Logarithmic	Y=−371.535lnX+2895.481	0.483	0.000
	Exponential	Y=1415.142e-0.002X	0.639	0.003
	Power	Y=X-2.481	0.631	0.000
DGI2	Linear	Y=2914.118X−155.718	0.460	0.014
	Secondary	Y=0.455×105X2-6579.54X+285.819	0.576	0.039
	Third	Y=0.103×107X3+0.002X2−3.748X+2606.413	0.661	0.031
	Logarithmic	Y=250.356lnX+732.281	0.382	0.000
	Exponential	Y=12.745e20.454X	0.664	0.000
	Power	Y=X1.902	0.646	0.000

Sig. < 0.01 was highly significant; Sig. < 0.05 was significantly correlated with Sig. > 0.01.

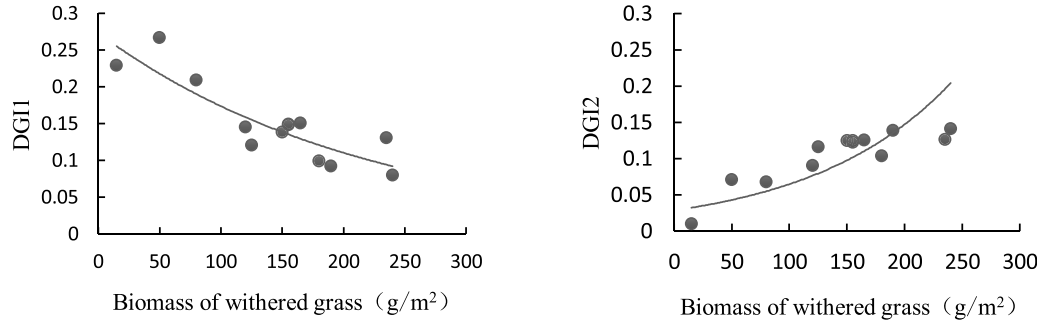

FIGURE 3
Correlations between the field-measured AGB data and the DGI index.

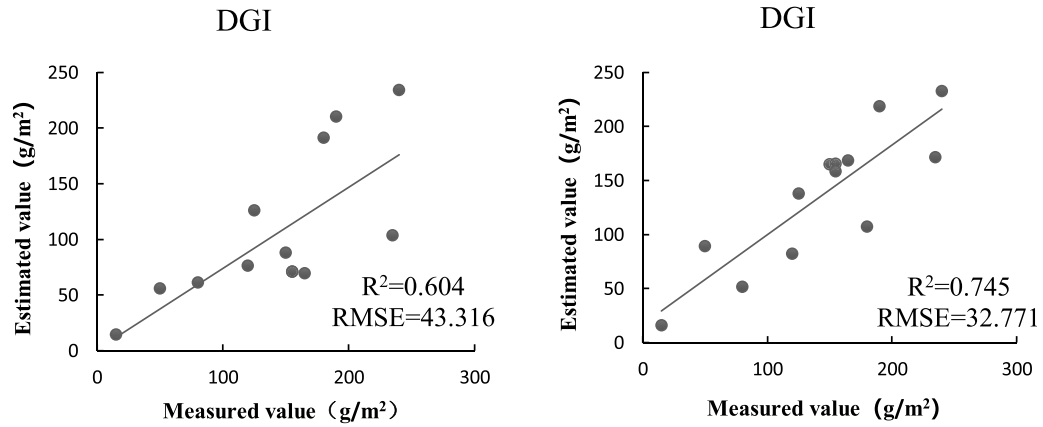

FIGURE 4
Correlations between the field-measured AGB data and the estimated values based on the DGI1 and DGI2 indices.

measured value established by the exponential model based on DGI1 was 0.777, whereas the correlation coefficient between the estimated measurement and the measured value established by the exponential model based on DGI2 was 0.863, with significant correlation, with the R^2 being 0.604 and 0.745, respectively. The RMSEs were 43.316 and 32.771 g/m^2, respectively, and the model's accuracy was 63% and 82%, respectively.

By comparison, based on the DGI1 exponential model, the simulation effect was mediocre, whereas the DGI2-based exponential model simulation effect was better. The correlation between the estimated and the measured values was high, and the relative minimum RMSE and model precision were the highest. So, this was chosen as the best option and the best model for calculating the amount of fuel in the dry grass in the study area.

3.3 Variation in the spatial characteristics of fuel quantity during the dry-grass season

The exponential model from DGI2 was used to calculate the amount of dry-grass fuel in September, October, and November 2019, and March, April, and May 2020 in the study area. The amount of dry-grass fuel and its spatial distribution are shown in Figure 5. As the map color gets darker, the number of grams of fuel per square meter goes from low to high (Qingqing Li et al., 2013). As can be seen from the spatial distribution of combustible matter in each month (Figure 5), there were significant differences across in the study area. In Figure 5, the aboveground biomass of grassland was the largest in October, and decreased in other months. The biological quantity value in the white

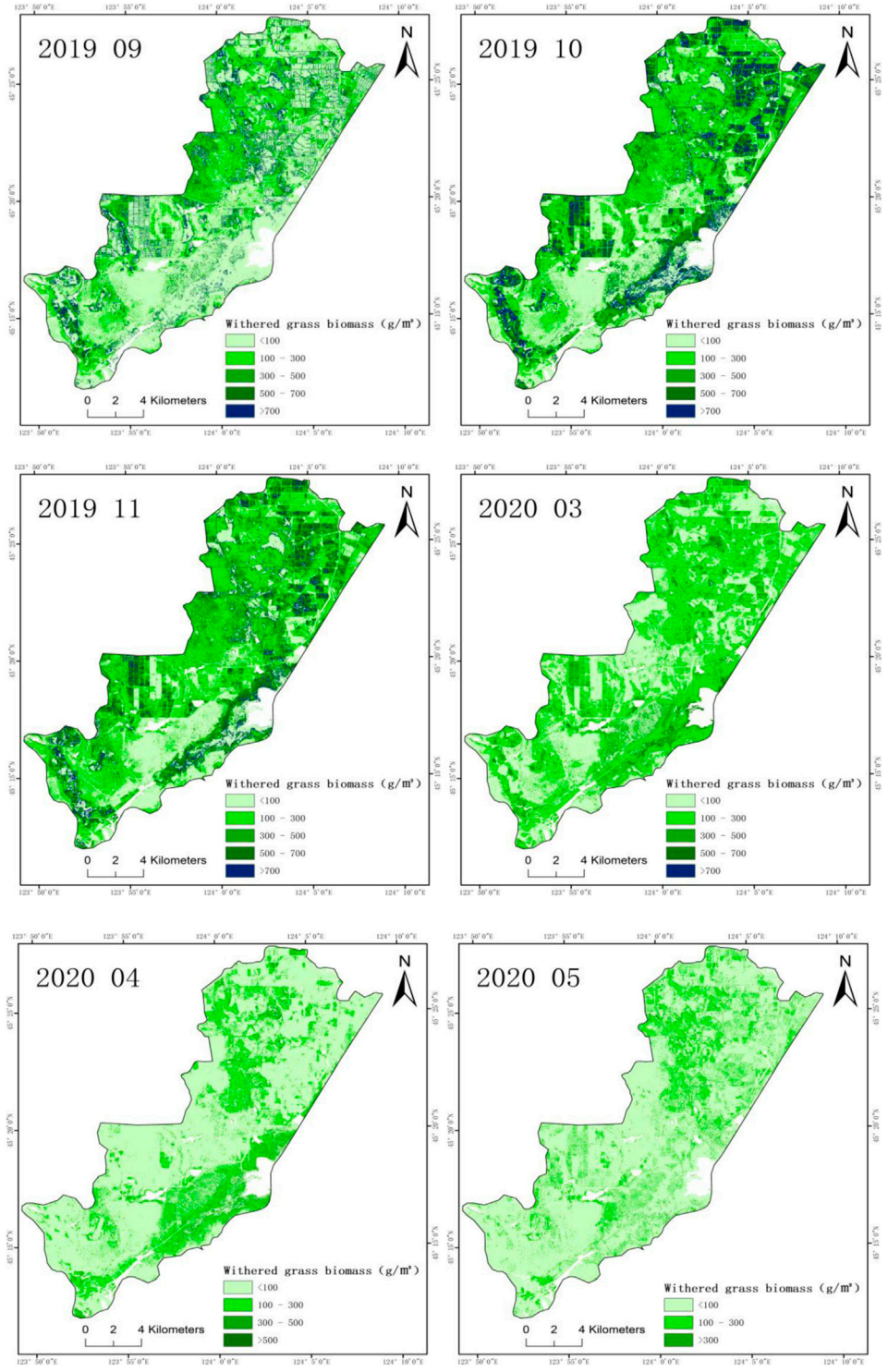

FIGURE 5
Spatial distribution of the dry-grass biomass.

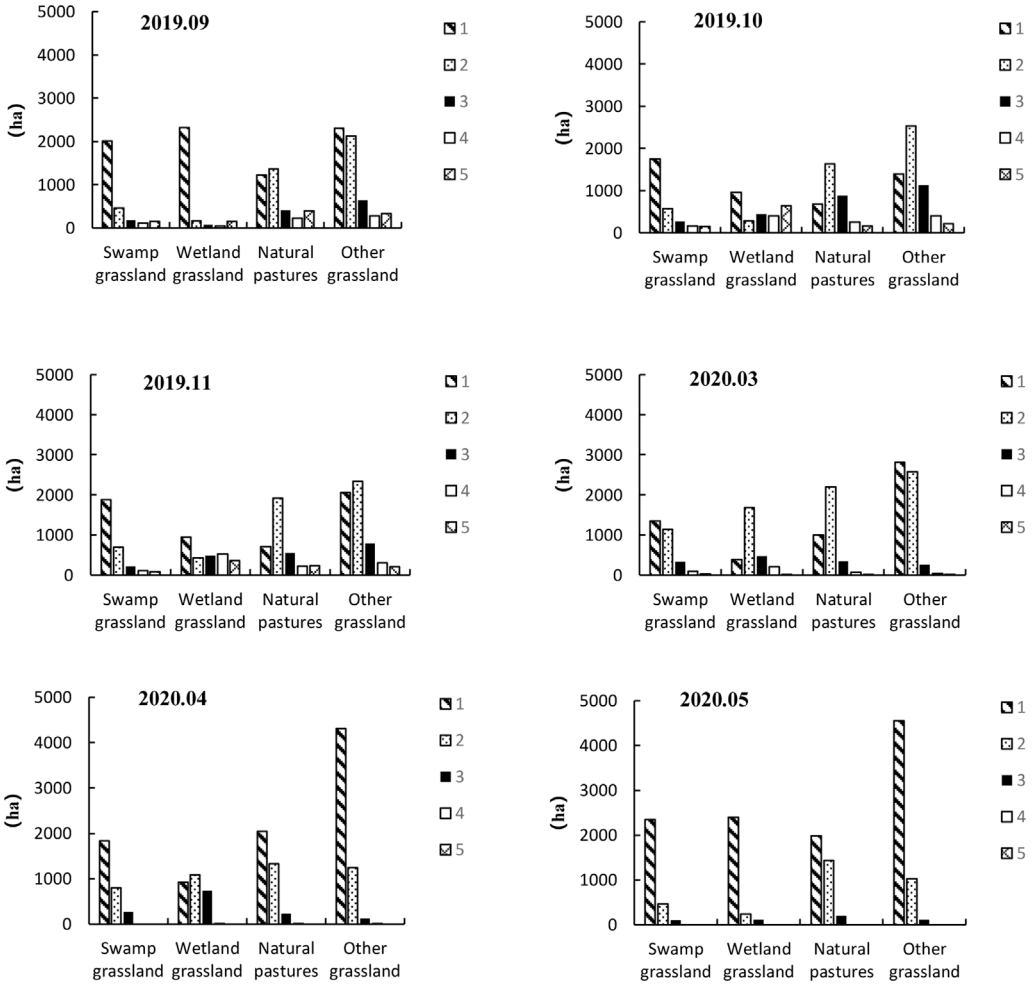

FIGURE 6
Monthly dynamic distributions showing the quantity of combustible grassland.

area is the lowest, being mainly covered by a water body, roads, residential zones, etc. The biomass of the area near Chagan Lake was higher in the southeast, which is dominated by wetland grasslands and swamp grasslands. The biomass was higher in most parts of the north and lower in saline–alkali land and paddy fields. The central and southwestern regions had less biomass, lower grassland density, and more saline land. The results showed that the aboveground biomass of grassland in the Longzhao Marsh increased gradually from southwest to northeast. Except in April and May, the aboveground biomass of grassland in northeast was generally above 200 g/m^2, which was significantly better than that in southwest. And the AGB of different grassland types varies greatly. In order to fully understand the cumulative difference in the combustibility of different vegetation types, including swamp grassland, wetland grassland, natural grassland, and other grasslands, all of which were included in the visual interpretation of the corresponding Sentinel-2B image, and based on the spatial distribution of combustible materials in each month, the combustibility of the four main vegetation types was calculated, as shown in Figure 6. In Figure 6, the grading of the biomass corresponds to the calculated map grade for the subsoil biomass. Levels 1–5 in the figure correspond to the biomass being less than 100, 100–300, 300–500, 500–700, and more than 700 g/m^2, respectively. From the statistical bar chart, across the entire study area, regardless of grassland type, most of the grassland biomass fell into Grades 1 and 2, indicating that the withered-grass biomass of various grassland types in the study area was relatively small, being mainly less than 100 and 100–300 g/m^2––equivalent to low coverage grassland. In particular, the less-than-100-g/m^2 type dominated, followed by 100–300 g/m^2. This challenges the protection of the western ecological barrier area.

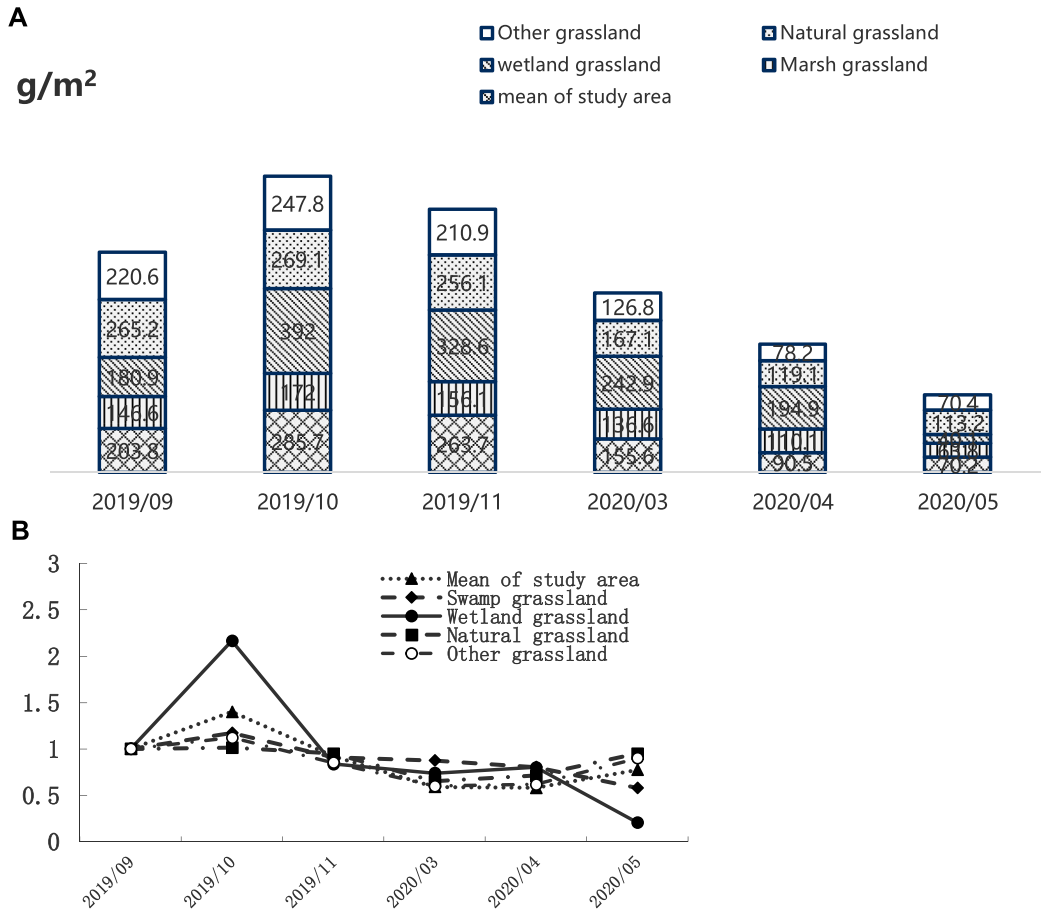

FIGURE 7
Monthly dynamic distribution chart **(A)** and variation curves **(B)** showing the amount of combustible matter in the dry season.

3.4 Dynamic temporal changes in fuel quantity during the dry-grass season

In order to explore the seasonal cumulative variation in fuel in the study area, based on calculations of the monthly fuel quantity and on the monthly dynamic distribution map of fuel quantity for the dry-grass season as shown in Figure 7A, the average value of available fuel per square meter was calculated and a curve showing the change in fuel quantity during the dry-grass season was drawn, as shown in Figure 7B. The average fuel volumes for the 6 months from October 2019 to May 2020 were 203.8, 285.7, 263.7, 155.6, 90.5, and 70.2 g/m^2, respectively. Using the area for September as the base, the ratio of the quantity for each subsequent month to the previous quantity was used as the fuel accumulation rate, as shown in Figure 7B. As can be seen from Figure 7A, the amount of fuel in the study area during the dry-grass season decreased month by month, changing significantly––that is, the amount of fuel present in October 2019 was the highest, and the amount in May 2020 was the lowest. The amount of fuel in March 2020 was significantly less than in November 2019, while the amount of fuel in April and May 2020 was significantly less than in March. It can also be seen from the average values for each month that the fuel stock had a decreasing trend, which is consistent with the change in fuel quantity in the actual dry-grass season. Note that the dry-grass AGB reached its maximum value in October, not the entire AGB of the grassland.

4 Discussion

The challenges involved in calculating remotely sensed grass AGB include a lack of effective and stable calculation models based on spectral indices from remote-sensing images that could be used to rapidly and accurately discriminate between grassland and acquire the state and quantity of grassland. Given the improvements required in various applications and the rapid development of high-resolution remote-sensing technology, the extraction and calculation of high-quality remote-sensing information is particularly urgent (Jinlong Gao et al., 2019).

In this regard, the aim of this study was to establish an effective model for estimating the biomass of dry grass based on new and high-resolution images from Sentinel-2B. Furthermore, the application of this model to the inversion of withered grass biomass can provide theoretical guidance and scientific basis for local grassland fire prevention, and this study can promote the application of high-resolution Sentinel-2 in the estimation of AGB of large grassland.

4.1 Advantages of using DGI2

In this work, two kinds of DGI were constructed from the Sentinel-2B image, and the calculation model was established using field-measured hay biomass data for the corresponding period. After evaluating the accuracy, the exponential model based on DGI2 had the best fitting effect, with $R^2 = 0.664$, and this was used to calculate the dry-grass biomass for different seasons across the research area. In addition, the spatial and temporal changes in the dry-grass biomass were explored. The significance of this study is that the rapid retrieval of biomass data from small and medium-scale grasslands can be achieved using Sentinel-2B remote-sensing images with high spatial resolution, and which are freely available for use. Compared with the grassland biomass calculation model based on hyperspectral field measurement data (Zhengxiang Zhang 2010; Jinlong Gao et al., 2019), the accuracy of the calculation model, based on an index obtained from images, may not be better (Weize Song et al., 2014; Y Zhang et al., 2019), but this method more convenient, practical, and efficient. Moreover, the construction of DGI index can also provide some theoretical support and reference for the research on the inversion of withered grass biomass with high spatial resolution remote sensing data.

4.2 Further improvements in the number and spatial distribution of sampling points

Different grassland types can be predicted for the AGB by applying the calculation model based on field sampling. According to the reference, the model's precision is affected by the field sampling, including the spatial distribution and number of sampling points (Sucharita Pradhan et al., 2021). The terrain of the study area was flat, so evenly distributed sampling points was helpful in improving the model's accuracy, while the principle of mathematical modeling indicates that a sufficient number of sample points is also be beneficial. So, enough spatially well-distributed field sampling points should be used in such studies. Further study of the grassland AGB in this region would be of great use for better understanding vegetation protection and fire-risk warning signs. In a more in-depth study, it would be useful to devise a better form of DGI (Hao Pei et al., 1995), in order to establish a more-representative and accurate monitoring model based on more field-measurement and remote-sensing data, and also to obtain a better understanding of the impact of terrain and other environmental factors (Qingqing Li et al., 2013; Shan Yu et al., 2014).

4.3 Improvement of spatiotemporal inconsistencies

There is a spatial inconsistency between the sampling plots of 1 x 1 m and the DGI pixel of 10 x 10 m, the latter obviously being significantly larger. This large disparity inevitably produces modeling errors (Sucharita Pradhan et al., 2021). Also, in the field, the sample plots were set up in relatively homogenous places, but this choice bias has led to errors in some heterogeneous regions (Shaoqin Yang et al., 2022). In the process of constructing the biomass calculation model, the accuracy was greatly affected by the location and quantity of the hay index value extracted from the image. In order to improve the accuracy of the biomass calculation model, so it better corresponds with the measured field data from GPS-located sample points, the location value could be gradually expanded on the image when the correlation coefficient has reached the maximum value.

There is no absolute synchronization in time between the sampling plots and the remote-sensing image, which will inevitably lead to uncertainty in the calculation model. To address this, we acquired data *via* the DGI, with data from the sampling sites coming from the same period, as far as possible, and this may have reduced the error in the model simulation to some extent. However, the number of AGB samples in this experiment was still insufficient. In the future, the number of sampling points should be appropriately increased to further improve the accuracy of the calculation model (Lati R.N et al., 2011; Unmesh Khati et al., 2021; Martin Paar et al., 2021).

5 Conclusion

Based on the need for a rapid and accurate remote-sensing model for estimating dry-grass AGB, and using field-measured AGB data from the Longzhao Marsh wetland in Da'an and applying ENVI, SNAP, and ArcGIS software, we established correlations between the AGB and two types of DGI. The two indices were significantly correlated (0.678) with the amount of dry-grass fuel. Six models of DGI fitting, based on Sentinel-2 remote-sensing data, were compared, and the optimal model was used to calculate and define the spatial distribution of the grass subsoil biomass across the study area. It was found that there was a significant

correlation between the measured dry AGB and the selected grass indices. The best model had a high calculation accuracy, with the fuel estimation models reaching the standard of macroscopic monitoring, the correlation between the calculated results for the best model and the measured values being 0.863. Therefore, the model for estimating grassland biomass by remote-sensing based on the DGI is feasible. According to the calculation, the fuel content in the Longzhao Marsh had a decreasing trend during the entire dry-grass season, and the decreasing trend was from October to May. Spatially, this equated to a decreasing trend from the northeast to southwest. These findings may provide a scientific reference for the early warning of grassland fires in western Jilin province, facilitate the management of grassland resources by local departments and promote economic development.

Due to the long, cold dry periods that affect the study area, it is difficult to collect field data, and so a model for estimating fuel quantitities would be enhanced by plenty of ground data. Calculations from the remote-sensing image using the model would also be affected by snow cover. In order to improve the accuracy of the estimation model of withered grass biomass and make it better correspond to the measurement data of gps positioning sampling points, the position value can be gradually expanded on the image when the correlation coefficient reaches the maximum value. The most important thing is to increase the number of ground sampling points and the location distribution of sampling points to find classical distribution points as far as possible to improve the accuracy of the estimation model. In future research, it is necessary to build a better DGI, so as to build a more representative and accurate monitoring model based on more field measurements and remote sensing data, and refer to more topographic and other environmental factors to eliminate errors.

Data availability statementt

The original contributions presented in the study are included in the article/Supplementary Material, further inquiries can be directed to the corresponding author:zangpeng1109@163.com.

Author contributions

PZ and YZ designed the paper and wrote the manuscript. ZC, XL and ZL revised the paper. YZ, GH, and PZ contributed to the data.

Funding

This research was funded by the National Key Research and Development Program of China (Project No. 2021YFD1500104-3), and the Strategic Priority Research Program of the Chinese Academy of Sciences (Grant No. XDA28110503).

Acknowledgments

First, thanks are given to the Remote-sensing Unit of the Changguang Satellite Technology Co. Ltd., Changchun, for providing the remote-sensing images and processing workshop. We would also like to thank the Gobi Energy Co. Ltd. for providing guidance in the sample site investigation. Third, thanks go to the Wetland Center, Northeast Institute of Geography and Agroecology, Chinese Academy of Sciences for identifying the wetland plants and plant types. Lastly, we would like to thank the editor and the reviewers for their careful work and thoughtful suggestions, all of which having improved this paper substantially.

Conflict of interest

The authors declare that the research was conducted in the absence of any commercial or financial relationships that could be construed as a potential conflict of interest.

Publisher's note

All claims expressed in this article are solely those of the authors and do not necessarily represent those of their affiliated organizations, or those of the publisher, the editors and the reviewers. Any product that may be evaluated in this article, or claim that may be made by its manufacturer, is not guaranteed or endorsed by the publisher.

References

Bao, Yulong, Zhang, Jiquan, Liu, Xingpeng, Chen, Peng, Liu, Xiaojing, Zhang, Qi, et al. 2012. Identification of grassland combustibles and estimation of hay content based on hyperspectral remote sensing [C]. Proceedings of the Innovative theoryof risk analysis and crisis response and Methods-Proceedings of the FifthAnnual Meeting of the Risk Analysis Professional Committee of China Disaster Prevention Association, Nanjing, China: Atlantis Press, 127–131.

Bu, Lingxin, Lai, Quan, and Liu, Xinyi. 2022. Study on the adaptability of different machine learning algorithms in grassland biomass estimation [J] *Acta Agrestia Sin.*: 1–12. http://kns.cnki.net/kcms/detail/11.3362.S.20220922.1407.002.html

Chen, Shirong. 2006. *Research on remote sensing monitoring and early warning method of grassland fire* [D]. Graduate School of Chinese Academy of Sciences (Remote Sensing Application Institute).Beijing China

Chen, Ziqi, and Zhang, Yanhong (2022). Quantitative identification of temporal-spatial variations of urban heat island (UHI) effects in Changchun, China. *IEEE J. Sel. Top. Appl. Earth Obs. Remote Sens.* 15, 3052–3060. doi:10.1109/JSTARS.2022.3167831

Chen, Ziqi, Zhang, Yanhong, Wang, Yongjie, and Ye, Li. 2021. Spatial variation and threshold analysis of the urban wetland cooling effect-a case study of Changchun city[J]. *IOP Conf. Ser. Earth Environ. Sci.*, 660(1):012136, doi:10.1088/1755-1315/660/1/012136

Chuvieco, E., Riano, D., Aguado, I., and Cocero, D. 2002. Estimation of fuel moisture content from multitemporal analysis of landsat thematic mapper reflectance data: Applications in fire danger assessment[J]. *Int. J. Remote Sens.*, 23, 2145, 2162, doi:10.1080/014311601006981811).

Cui, Qingdong, Liu, Guixiang, and Yi, Zhuo. 2009. Dynamic research on theconservation rate of pasture in Xilin Gol grassland in cold season [J]. *Chin. J. Grassl.*, 31(01): 102–108. https://kns.cnki.net/kcms/detail/detail.aspx?FileName=ZGCD200901019&DbName=CJFQ2009

Cui, Qingdong. 2009. *Research on the estimation technology of forage stock in natural grassland in cold season* [D]. Chinese Academy of Agricultural Sciences.Beijing.

Deng, Pan. 2017. *Research on the spatial distribution and potential fire behavior of combustibles in typical plantation forests in South subtropics*[D]. Central South University of Forestry and Technology.China.

Duwala, Guixiang Liu, Shan, Yu, and Li, Qingqing. 2012. Research on short-termforecast of fire danger level in Inner Mongolia grassland [J]. *Chin. J. Grassl.*, 34(04): 87–92, doi:10.3969/j.issn.1673-5021.2012.04.015

Fenetahun, Yeneayehu, Yuan, Y., Xu, X. W., and Wang, Y. D. 2022. Borana rangeland of southern Ethiopia: Estimating biomass production and carrying capacity using field and remote sensing data[J]. *Plant Divers.*, 2468–2659, doi:10.1016/j.pld.2022.03.003

Feng, Shuqing, Liu, Qingchun, Jin, Yi'an, and Zhang, Juan. 2004. Research on forage yield monitoring using EOS/MODIS [J]. *Qinghai Prataculture*, (03):6–10, doi:10.3969/j.issn.1008-1445.2004.03.002

Ivan Raniero Hernández SalmerónHolmgren, Milena. 2022. Global meta-analysis: Sparse tree cover increases grass biomass in dry pastures[J]. *Front. Environ. Sci.*, 10, doi:10.3389/fenvs.2022.949185

Huang, Jiaxing, Wu, Jing, Li, Chunbin, Qin, Gexia, Qian, Juanbing, and Li, Huaihai. 2021. Remote sensing inversion of aboveground biomass of grassland in Tianzhu County based on Sentinel-2 and Landsat 8 data [J]. *Acta Agrestia Sin.*, 29(09):2023–2030.doi:10.1016/j.ecolind.2020.107215

Jiang, Fugen, Sun, Hua, Li, Chengjie, Ma, Kaisen, Chen, Song, Long, Jiangping, et al. 2021. Combined GF-6 and Sentinel-2 red-edge band inversion of forest aboveground biomass [J]. *Acta Ecol. Sin.*, 41(20): 8222–8236.

Jinlong Gao, Baoping Meng, Liang, Tiangang, Feng, Qisheng, Ge, Jing, Yin, Jianpeng, Wu, Caixia, et al. (2019). Modeling alpine grassland forage phosphorus based on hyperspectral remote sensing and a multi-factor machine learning algorithm in the east of Tibetan Plateau, China. *ISPRS J. Photogrammetry Remote Sens.* 147, 104–117. doi:10.1016/j.isprsjprs.2018.11.015

Khati, Unmesh, Lavalle, Marco, and Singh, Gulab. 2021. The role of time-series L-band SAR and GEDI in mapping sub-tropical above-ground biomass[J]. *Front. Earth Sci. (Lausanne).*, 9, doi:10.3389/feart.2021.752254

Lati, R. N., Filin, S., and Eizenberg, H. (2011). Robust methods for measurement of leaf-cover area and biomass from image data. *Weed Sci.* 59 (2), 276–284. doi:10.1614/ws-d-10-00054.1

Li, Hailiang, and Zhao, Jun. 2009. Principles and methods of grassland remote sensing yield estimation[J]. *Pratacultural Sci.*, 26(03) 34–38.

Li, Qingqing, Liu, Guixiang, Duwala, Sachula, Chen, Xiaofei, Yun, Xiangjun, and Hasbagen.2013. Remote sensing monitoring of combustible matter in hay season in Ujimqin grassland[J]. *Chin. J. Grassl.*, 35(02): 64–68, doi:10.3969/j.issn.1673-5021.2013.02.012

Li, Suying, Li, Xiaobing, Ge, Ying, and Fu, Na. 2007. Biomass model of typical grassland area based on vegetation index: An example of Xilinhot city, inner Mongolia [J]. *Chin. J. Plant Ecol.*, 31(01):23–31, doi:10.17521/cjpe.2007.0004

Li, Xinghua. 2007. *Research on fire law and early warning of forest and grassland in northeastern Inner Mongolia* [D]. Chinese Academy of Agricultural Sciences.Beijing China.

Liu, Chao, Li, Ping, Wu, Yuntao, Pan, Shengnan, Zhou, Jia, and Liu, Lingli. 2022. An estimation method of grassland aboveground biomass based on digital camera images and community canopy structure survey [J] *Chin. J. Plant Ecol.*: 1–9 http://kns.cnki.net/kcms/detail/11.3397.Q.20221013.1623.010.html

Long, Qixia, Lan, Jiacheng, and Jiang, Yongxiang. 2022. The impact of ecological restoration on the accumulation characteristics and mechanism of soil organic carbon in rocky desertification areas [J]. *Acta Ecol. Sin.*, 42 (18): 7390–7402 https://kns.cnki.net/kcms/detail/detail.aspx?FileName=STXB202218010&DbName=CJFQTEMP

Ma, Yingzhong. 2012. Vegetation index and correlation analysis of natural grassland based on TM image and SPSS software [J]. *J. Anhui Agric. Sci.*, 40(23): 11693–11694, doi:10.3969/j.issn.0517-6611.2012.23.055

Paar, Martin, Berthold, Maximilian, Schumann, Rhena, Dahlke, Sven, and Blindow, Irmgard. 2021. Seasonal variation in biomass and production of the macrophytobenthos in two lagoons in the southern baltic sea[J]. *Front. Earth Sci. (Lausanne).*, 8, doi:10.3389/feart.2020.542391

Pei, Hao, Li, Yunpeng, and Fan, Yiyi. 1995. Preliminary study on monitoring foragestock in temperate grassland during the dry-weed season using meteorological satellite NOAA/AVHRR data [J]. *Grassl. China*, (06):44–47.

Pradhan, Sucharita, and Tiwari, Kamlesh Narayan. 2021. Evaluation of Sentinel 2 red edge channel for enhancing land use classification[J]. *Water Manag. Water Gov. Water Sci. Technol. Libr.*, 96:78–89, doi:10.1007/978-3-030-58051-3-6

Pu, Yihan, Zhang, Dong, Xu, Dandan, and Luan, Zhaoqing. 2021. Evaluation of Sentinel-2A red-edge band for vegetation classification in lakeside belts [J]. *For. Resour. Manag.*, (02): 131–139, doi:10.13466/j.cnki.lyzygl.2021.02.018

Seyin, Batu. 2002. Dynamic research on grassland combustibles[J]. *Grassl. China*, (05): 49–53, doi:10.3321/j.issn:1673-5021.2002.05.011

Shan, Yu, Duwala, and Liu, Guixiang. 2014. Research on remote sensing estimation model of combustible matter during subtilization period of grassland in Inner Mongolia [J]. *J. Arid Land Resour. Environ.*, 28(11): 145–151, doi:10.13448/j.cnki.jalre.2014.11.025

Song, Weize, Jia, Haifeng, Liu, Shujie, Liang, Shidong, Wang, Zheng, Hao, Lizhuang, et al. 2014. A remote sensing based forage biomass yield inversion model of Alpine-cold Meadow during grass-withering period in Sanjiangyuan area[J]. *IOP Conf. Ser. Earth Environ. Sci.*, 17, 012042, doi:10.1088/1755-1315/17/1/0120421).

Thakur, Tarun K., Patel, Digvesh K., Thakur, Anita, Kumar, Anirudh, Bijalwan, Arvind, Bhat, Jahangeer A., et al. 2021. Biomass production assessment in a protected area of dry tropical forest ecosystem of India: A field to satellite observation approach[J]. *Front. Environ. Sci.*, 9, doi:10.3389/fenvs.2021.757976

Xu, Hui. 2015. *Study on the hyperspectral biomass estimation method of subtilis in typical grassland of Xilingol League* [D]. Inner Mongolia Normal University.China.

Xu, Zhenyu, Li, Yingchang, Li, Mingyang, Li, Chao, and Wang, Lin. 2020. Regional forest biomass inversion based on Sentinel-1A and Landsat 8 data [J].*J. Central South Univ. For. Technol.*, 40(11):147–155, doi:10.14067/j.cnki.1673-923x.2020.11.018

Yang, Shaoqin, Wang, Xiang, Xu, Cheng, and Shang, Tianqi. 2022. Estimation of aboveground biomass of bamboo forest based on MODIS time series data [J] *J. Zhejiang Agric. For. Univ.*, 39 (04): 734–741, doi:10.11833/j.issn.2095-0756.20210431

Yang, Wenyi, Wang, Yingshun, and He, Junjie. 2001. Research on establishing a calculation model of grassland cold season stock carrying capacity using remote sensing information [J]. *Chin. J. Agrometeorology*, (01): 40–43.

Yi, Zhuo, Liu, Guixiang, and Cui, Qingdong. 2010. Research on the dynamic changesof combustibles in the dry season and remote sensing quantitative monitoring in Xilin Gol grassland pastoral area [C]. "Proceedings of the Risk Analysis and CrisisResponse from a Chinese Perspective"-Risk Analysis ProfessionalCommittee of China Disaster Prevention Association Proceedings of theFourth Annual Conference., 147–152.

Zhai, Yujuan, Hao, Libo, Zhang, Yanhong, Ye, Li, and Liu, Zhaoli. 2021. Wetland biodiversity disturbance evaluation induced by a water conservancy project in the flooded plain of the Huolin river lower reaches[J]. *Sustainability*, 13, 4476, doi:10.3390/su130844768).

Zhang, Jinqi.2021. *Study on surface dead combustible matter load and combustibility of different forest types in the southeastern foothills of theGreater Khingan Mountains in Inner Mongolia* [D]. Inner Mongolia Agricultural University.China.

Zhang, Y., Shu, Q., Wang, L., et al. July 2019. Estimation of fuel biomass for grasslands using data assimilation technique[C], IGARSS 2019- IEEE International Geoscience and Remote Sensing Symposium. IEEE, 9988–9991.Yokohama, Japan, doi:10.1109/IGARSS.2019.8898322

Zhang, Yanhong, Su, Sheng, Liu, Zhaoli, Hou, Guanglei, Chen, Ziqi, Han, Ying, et al. (2021). Ecological protection of the red area habitat risk assessment [J/OL]. *J. Jilin Univ. (Earth Sci. Ed.* 1–10. [2022-09-19]. doi:10.13278./.j.carol.carroll.nki.jjuese.20210190

Zhang, Zhengxiang. 2010. *Research on grassland fire status based on geographic information system and remote sensing* [D]. Northeast Normal University.Changchun, China.

Zhang, Zhengxiang, Zhang, Hongyan, Feng, Zhiqiang, Li, Xuedong, Bi, Yunzhi, Shi, Dongkai, et al. 2015. A method for estimating the amount of dead grass fuel based on spectral reflectance characteristics[J]. *Int. J. Wildland Fire*, 24(7):940–948, doi:10.1071/WF13149

Zhao, Bingru, Liu, Chuang, Wang, Jingjie, and Chen, Wenbo. 2004. Study on temporal and spatial variation of MODIS vegetation index in Xilin Gol grassland [J]. *Grassl. China*, (01):2–9, doi:10.3321/j.issn:1673-5021.2004.01.001

Zhou, Jianqing, Liu, Xiaodong, and Zhang, Siyu. 2019. Study on the distribution of surface combustibles in Xing'an larch plantation [J]. *For. Fire Prev.*, (01):19–23, doi:10.3969/j.issn.1002-2511.2019.01.005

Frontiers in Environmental Science

Explores the anthropogenic impact on our natural world

An innovative journal that advances knowledge of the natural world and its intersections with human society. It supports the formulation of policies that lead to a more inhabitable and sustainable world.

Discover the latest Research Topics

See more →

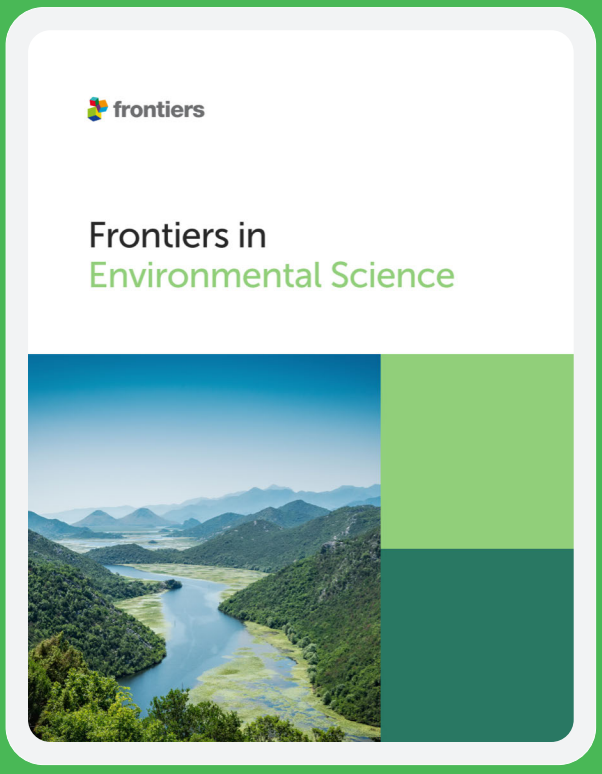

Frontiers

Avenue du Tribunal-Fédéral 34
1005 Lausanne, Switzerland
frontiersin.org

Contact us

+41 (0)21 510 17 00
frontiersin.org/about/contact